These proceedings of the Ninth International Conference on Permafrost (NICOP) extend the documented legacy of permafrost related research begun in 1963 when the first International Conference was held in West Lafayette, Indiana, USA. NICOP also marks the 25th anniversary of the Fourth International Conference on Permafrost that was convened in Fairbanks in July 1983. It is imperative that we continue this international and long-ranging dialogue of cooperation on permafrost, particularly during a period of overall global warming. At no time in the past has our overall interest level in permafrost been greater. The number of papers published in these proceedings substantiates this interest. In addition to climate change, development in regions of permafrost is contributing additional stress to this thermally sensitive environment. This recent increased growth is often associated with resource development such as oil and gas, and various mineral resources.

The papers presented in these proceedings are diverse in both time and space; they cover results from field and laboratory studies, remote sensing, analyses and modeling – or some combination of these. Both scientific and engineering aspects of various permafrost issues are presented, and are often intertwined with each other. We hope these proceedings provide one more positive step in our understanding of the permafrost environment that intrigues us as scientists and engineers.

2

NICOP 2008

Ninth International Conference on Permafrost

Edited by
Douglas L. Kane
and
Kenneth M. Hinkel

NICOP 2008

Ninth International Conference on Permafrost

2

Edited by Douglas L. Kane and Kenneth M. Hinkel

Ninth International Conference on Permafrost

Proceedings of the Ninth International Conference on Permafrost
University of Alaska Fairbanks
June 29–July 3, 2008

Ninth International Conference on Permafrost

Edited by Douglas L. Kane and Kenneth M. Hinkel

Volume 2

Institute of Northern Engineering
University of Alaska Fairbanks
2008

Ninth International Conference on Permafrost
Edited by Douglas L. Kane and Kenneth M. Hinkel

Printed in the United States of America

Elmer E. Rasmuson Library Cataloging in Publication Data
International Conference on Permafrost (9th : 2008 : Fairbanks, Alaska)
Ninth International Conference on Permafrost /
edited by Douglas L. Kane and Kenneth M. Hinkel.
— Fairbanks, Alaska : Institute of Northern Engineering,
University of Alaska Fairbanks, 2008.
2 v., : ill., maps ; cm.
Includes bibliographical references and index.
June 29–July 3, 2008
1. Permafrost–Congresses. 2. Frozen ground–Congresses.
I. Title. II. Kane, Douglas L. II. Hinkel, Kenneth M.

GB641.I6 2008

ISBN 978-0-9800179-2-2 (v.1)
ISBN 978-0-9800179-3-9 (v.2)

Cover Photo: Low-Centered Polygons, North Slope, Alaska

Production Editors: Thomas Alton and Fran Pedersen

Kane, D.L. & Hinkel, K.M. (eds). 2008. *Ninth International Conference on Permafrost.* Institute of Northern Engineering, University of Alaska Fairbanks (2 Vols.), 2140 pp.

Contents

Volume 1

Volume 2

Preface

Since the first International Permafrost Conference convened in 1963, we have sustained an international scientific and engineering collaborative effort until we now are immersed in this, the Ninth International Conference on Permafrost (NICOP). Considerable change has occurred over the past 45 years, resulting in heightened interest in the permafrost environment and understanding of its many aspects. Participation by engineers and scientists in advancing our knowledge of permafrost as a thermally impacted medium has continued to grow in the wake of both resource development and climate change.

The University of Alaska Fairbanks (America's Arctic University) is an excellent choice for the location of this conference. Permafrost is ubiquitous in Interior Alaska, and it influences many aspects of our society. Our local field trips are arranged around some of the most interesting phenomena here in the zone of discontinuous permafrost, including the world famous Permafrost Tunnel, the Trans Alaska Oil Pipeline, evidence of anthropogenic impacts on permafrost, and thermokarsting of warm permafrost. Fairbanks is also a good starting point for trips to other parts of Alaska, including the North Slope, Seward Peninsula, Denali National Park (Mount McKinley), and many other adventures. We have also taken this opportunity to offer courses related to the permafrost environment for high school and elementary teachers, advanced graduate students, and working professionals.

The University of Alaska Fairbanks hosted the Fourth International Conference on Permafrost in 1983. It was at this meeting that the International Permafrost Association (IPA) was formally established. IPA members are truly pleased with the strong international flavor of this year's conference, with approximately 30 countries participating. IPA's uninterrupted activities over the past 25 years are partially responsible for this concerted effort to expand our understanding of the permafrost environment, both spatially and temporally. It is also, however, abundantly clear that much of our current interest in this environment is driven by climate change.

Currently, many aspects of permafrost research are receiving considerable attention. These include carbon release into the atmosphere, discharge from catchments dominated with permafrost, the role of gas hydrates in cold environments, degrading permafrost and thermokarsting, infrastructure design in a changing environment, and the overarching issue of climate change on this thermally sensitive environment. It is essential that our scientific and engineering communities help our societies adapt to living and working on warming permafrost. Permafrost degradation will affect all aspects of life in the high latitudes and high elevations. We must anticipate the changes in ecology, hydrology, and infrastructure construction that will accompany degradation of permafrost with a warming climate. That is the challenge facing permafrost scientists and engineers. It is our hope that by sharing our knowledge and understanding, we may better serve our nations and people.

Enjoy the conference. We hope you will go home with increased knowledge and an invigorated appetite for expanding our understanding of the environment we call "permafrost."

—Douglas L. Kane
Water and Environmental Research Center, Institute of Northern Engineering
—Larry D. Hinzman
International Arctic Research Center

Acknowledgments

We, the organizers of the Ninth International Conference on Permafrost (NICOP), cannot sufficiently express our gratitude to those who have made NICOP both possible and successful. There are those who contributed financially by keeping the cost of the registration low, supporting young investigators, helping defer the cost of the proceedings, and sustaining many other behind-the-scenes activities. There are those who served on the numerous committees associated with this conference at the local, national, and international levels; we hope they found this exercise to be professionally rewarding. Finally, there are those who served as associate editors and reviewers of the more than 400 papers submitted. This conference is advertised as an International Conference; to be truly successful, much work must be done to overcome language barriers. While not always finding success in bringing a paper to publication, the associate editors and reviewers performed in a very commendable manner. Thank you all for your help.

—Douglas Kane, Larry Hinzman, and the Local Organizing Committee

NICOP Organizing Team Members

General Chair	Douglas Kane
Co-Chair	Larry Hinzman
Publications	Douglas Kane, Kenneth Hinkel, Thomas Alton, Fran Pedersen
Conference Facilitator	Elizabeth Lilly
Technical Program	Larry Hinzman
Short Courses	Larry Hinzman, Michael Lilly, Yuri Shur
Exhibits - Trade Show	Michael Lilly
Public Affairs	Marmian Grimes, Jenn Wagaman, Cherie Solie
Fundraising	Dave Norton, Jerry Brown, Larry Hinzman, Michael Lilly, James Rooney, Douglas Kane
Finance	Michael Lilly
Website	Gary Whitton
Special Events/Social	Elizabeth Lilly, Deborah Bennett, Melanie Jackson, Chris Lace
Young Researchers	Guido Grosse, Katey Walter, Andrew Balsar, Oliver Frauenfeld
ICOP-IPA-IPY Celebration	Jerry Brown, Jess Walker, John Zarling
Field Trip Guides	Deanne Stevens

U.S. Permafrost Association Board of Directors

Kenneth Hinkel, President
Yuri Shur, President-Elect
Oliver Frauenfeld, Secretary
Michael Lilly, Treasurer
Anna Klene, Member
Jennifer Harden, Member
Larry Hinzman, IPA Representative
Jon Zufelt, Past President

NICOP Program Committee

Larry Hinzman, Chair
Jerry Brown
Doug Goering
Jennifer Harden
Kenneth Hinkel
Douglas Kane
Frederick Nelson
Vladimir Romanovsky
Katey Walter
Jon Zufelt

Local Field Trip Organizers

James Begét
Deb Bennett
Nancy Bigelow
Patty Burns
Ed Clarke
Billy Connor
Charles Collins
Tom Douglas
Doug Goering
Jack Hébert
Melanie Jackson
Elden Johnson
Torre Jorgenson
Elizabeth Lilly
Michael Lilly
O.D. Odsather
Vladimir Romanovsky
Yuri Shur
Diana Solie
Katey Walter
Kenji Yoshikawa

Extended Field Trip Organizers

Donald “Skip” Walker
Tom Hamilton
Bill Streever
Chien-Lu Ping
Robert Gieck
Gary Michaelson
Torre Jorgensen
Jesse Walker
Caryn Rae
Kenneth Hinkel
Jerry Brown
Deanne Stevens
Jim Beget
Chris Burn
Antoni Lewkowicz
Tom Krzewinski
Phil Brease
Nel Caine
Koren Nydick
Elden Johnson
John Zarling
Ed Clarke
O.D. Odsather
Lee Schoen

Additional people who have assisted in NICOP Organization

Danielle Jamieson
Dan White
Michelle Bartlett
Wendy Warnick
Helga Wilm

U.S. National Committee

Jerry Brown, Chair
Roger Barry
Julie Brigham-Grette
Jody Deming
Craig Dorman
Kenneth Hinkel
Larry Hinzman
Douglas Kane
Frederick Nelson
Vladimir Romanovsky
Bill Streever
Rupert "Bucky" Tart
Patrick Webber
Jon Zufelt

International Organizing Committee

Antoni Lewkowicz, Chair
David Gilichinsky
Huijun Jin
Truls Mølmann
Marcia Phillips

NICOP Sponsors

Universities
University of Alaska International Polar Year (Gold plus)
University of Alaska President's Fund (Gold)
Alaska University Transportation Center (Gold)
University of Alaska Fairbanks Institute of Northern Engineering (Silver)
University of Alaska Fairbanks International Arctic Research Center (Silver)
University of Alaska Fairbanks Experimental Program to Stimulate Competitive Research (EPSCoR) (Bronze)
University of Colorado-National Snow and Ice Data Center (Contributor)

Government Agencies
Alaska Division of Geological & Geophysical Surveys, Fairbanks (Gold)
U.S. National Science Foundation (Silver)
U.S. Geological Survey (Silver)
U.S. Army Cold Regions Research and Engineering Laboratory (Bronze)
U.S. Department of Energy (Bronze)
U.S. Arctic Research Commission (Brass)
U.S. Bureau of Land Management (Brass)
Denali Commission (Brass)
North Slope Science Initiative (Brass)
U.S. Minerals Management Service (Contributor plus)
U.S. Fish & Wildlife Service, Fairbanks Field Office (Brass)

Corporate and Non-Governmental Organizations
Arctic Foundations, Inc., Anchorage (Gold)
Alyeska Pipeline Company, Anchorage (Silver)
BP Foundation (Bronze)
International Permafrost Association (Bronze plus)
GW Scientific, Fairbanks (Bronze)
Duane Miller & Associates, Anchorage (Bronze)
CH2MHILL Energy & Power, Anchorage (Brass)
ConocoPhillips Alaska (Brass)
EBA Engineering Consultants Ltd., Canada (Brass)
Golder Associates, Anchorage (Brass)
Shannon & Wilson, Inc. Seattle (Brass)
BeadedStream, LLC, Anchorage (Contributor)
Hawk Consultants, LLC, Anchorage (Contributor)
Houston Advanced Research Center (HARC) (Contributor)
Northern Engineering & Scientific (Contributor)
Northern Geotechnical Engineering, Inc., Anchorage (Contributor)
R&M Consultants, Inc., Anchorage (Contributor)
Tryck Nyman Hayes, Inc., Anchorage (Contributor)
Resource Data, Inc., Anchorage (Sustaining)
URS Corporation, Anchorage (Sustaining)
Usibelli Foundation (Sustaining)
Harley H. Hightower, FAIA, Anchorage (Sustaining)

ICOP Donor Circle (Contributor)
Jerry and Celia Brown
Edwin Clarke
Hugh M. French
Don W. Hayley
C.W. "Bill" Lovell
J. Ross Mackay (Honorary Member)
Michael C. Metz
Frederick E. Nelson
Jim and Florence Rooney
Rupert "Bucky" Tart
Ted B. Trueblood
H. Jess Walker
John Zarling

Individuals
Joe Malen

In-Kind Sponsors
ABR, Inc., Environmental Research and Services
Mountain Studies Institute
Pogo Mine, Teck Cominco Limited
University of Alaska Toolik Field Station
University of Cincinnati
University of Colorado, Institute of Arctic and Alpine Research
U.S. Army CRREL Permafrost Tunnel
U.S. Geological Survey
U.S. National Park Service

Associate Editors

Lukas Arenson, BGC Engineering, Canada
James Bockheim, University of Wisconsin, US
Julie Brigham-Grette, University of Massachusetts, US
Sherry Cady, Portland State University, US
Billy Connor, University of Alaska Fairbanks, US
Scott Dallimore, Geological Survey of Canada, CA
Claude Duguay, University of Waterloo, CA
Oliver Frauenfeld, University of Colorado, US
Hugh French, University of Ottawa, CA
Guido Grosse, University of Alaska Fairbanks, US
Stephan Gruber, University of Zurich, CH
Jennifer Harden, U.S. Geological Survey, US
Charles Harris, Cardiff University, UK
Christian Hauck, University of Karlsruhe, DE
Don Hayley, EBA Engineering Consultants, Ltd., CA
David Hik, University of Alberta, CA
Kenneth Hinkel, University of Cincinnati, USA
Hans-Wolfgang Hubberten, Alfred Wegener Institute, DE
Ole Humlum, University of Oslo, NO
Elden Johnson, Alyeska Pipeline Service Company, US
Torre Jorgenson, ABR Inc., US
John Kimble, Consulting Soil Scientist, US
Peter Kuhry, Stockholm University, SE
Philip Marsh, Environment Canada, CA
Chris McKay, NASA, US
James McNamara, Boise State University, US
Julian Murton, University of Sussex, UK
Frederick Nelson, University of Delaware, US
Mark Parsons, University of Colorado, US
Marcia Phillips, Swiss Federal Institute for Snow and Avalanche, CH
Volker Rachold, International Arctic Science Committee, SE
Vladimir Romanovsky, University of Alaska Fairbanks, US
Sharon Smith, Geological Survey of Canada, CA
Steve Solomon, Geological Survey of Canada, CA
Ted Vinson, Oregon State University, US
Daniel Vonder Mühll, ETH Zurich, CH
Patrick Webber, Michigan State University, US
John Zarling, Zarling Aero and Engineering, US

Reviewers

Clint Adler, Alaska DOT&PF, US
Thomas A. Ager, US Geological Survey, US
H. Jonas Akerman, Lund University, SE
Michel Allard, Université Laval, CA
Dale T. Andersen, NASA Ames, US
Lesleigh Anderson, US Geological Survey, US
Pat Anderson, University of Washington, US
Oleg A. Anisimov, State Hydrological Institute, RU
Lukas U. Arenson, BGC Engineering, CA
Arnold Arnoldusson, Norwegian Inst. of Land Inventory, NO
Valery Astakhov, National Research Inst. of Remote Sensing, RU
Tezera F. Azmatch, University of Alberta, CA
Megan Balks, University of Waikato, NZ
Andrew W. Balser, University of Alaska Fairbanks, US
Rene Barendregt, University of Lethbridge, CA
Brian Barnes, University of Alaska Fairbanks, US
David L. Barnes, University of Alaska Fairbanks, US
William Barr, University of Calgary, CA
Roger G. Barry, National Snow and Ice Data Center, US
Doug Benn, University Centre in Svalbard, NO
Bruce Bennett, Yukon Department of Environment, CA
Ivar Berthling, Norwegian University of Sci.and Tech., NO
Peter Blanken, University of Colorado, US
James Bockheim, University of Wisconsin, US
Xavier Bodin, University Paris/Joseph Fourier University, FR
Jan Boelhouwers, Uppsala University Uppsala, SE
Julia Boike, Alfred Wegener Institute, DE
W. Robert Bolton, Alfred Wegener Institute, DE
Christian Bommer, Swiss Fed. Inst. for Snow …, CH
Philip Bonnaventure, University of Ottawa, CA
Matthew T. Bray, University of Alaska Fairbanks, US
Alexander Brenning, University of Waterloo, CA
Gabriele Broll, University of Vechta, DE
Troy Brosten, Boise State University, US
Jerry Brown, International Permafrost Association, US
Bruce Brunette, Alaska DOT&PF, US
Margo M. Burgess, Geological Survey of Canada, CA
Christopher R. Burn, Carleton University, CA
Fabrice Calmels, University of Alberta, CA
Philip Camill, Carlton College, US
Iain B. Campbell, Land & Soil Consultancy Services, NZ
Sean K. Carey, Carleton University, CA
James W. Cassie, BGC Engineering Inc., CA
Beata Casto, University of Buffalo, US
Jessica E. Cherry, University of Alaska Fairbanks, US
Jens H. Christensen, Danish Meteorological Institute, DK
Hanne H. Christiansen, University Centre in Svalbard, NO
Evgenii Chuvilin, Moscow State University, RU
Graeme G.C. Claridge, Land & Soil Consultancy Services, NZ
Edwin S. Clark, Soils Alaska, US
Ian D. Clark, University of Ottawa, CA
Mark Clark, Natural Resources Conservation Service, US
Peter Cleall, University of Cardiff, UK
Gary D. Clow, US Geological Survey, US
Michael Cole, ABR Inc., US
Charles Collins, US Army, ERDC/CRREL, US

Jean Côté, Université Laval Québec, CA
Michelle Côté, Geological Survey of Canada, CA
Nicole Couture, McGill University, CA
Patrick Crill, Stockholm University, SE
Ronald P. Daanen, University of Alaska Fairbanks, US
Scott Dallimore, Geological Survey of Canada, CA
Debendra K. Das, University of Alaska Fairbanks, US
Simon Davies, Colorado School of Mines, US
Gregory P. De Pascale, William Lettis & Assoc. Inc., US
Reynald Delaloye, University of Fribourg, CH
Philip Deline, Université de Savoie, FR
Jack Dennett, EBA Engineering Consultants Ltd., CA
Alexander Derevyagin, Moscow State University, RU
Bernhard Diekmann, Alfred Wegener Institute, DE
Wojciech Dobinski, University of Silesia, PL
Yongtao Dong, University of Alaska Fairbanks, US
Guy Dore, Universite Laval, CA
D.S. Drozdov, Earth Cryosphere Institute, RU
Caroline Duchesne, Geological Survey of Canada, CA
Alejandra Duk-Rodkin, Geological Survey of, CA
Larry Dyke, Geological Survey of Canada, CA
Mark Ednie, Geological Survey of Canada, CA
Markus Egli, University of Zurich, CH
Olaf Eisen, Alfred Wegener Institute, DE
Wendy Eisner, University of Cincinnati, US
David Esch, Alaska DOT&PF (retired), US
Bernd Etzelmüller, University of Oslo, NO
Eugenie Euskirchen, University of Alaska Fairbanks, US
Zhaosheng Fan, University of Colorado, US
Herman Farbrot, University of Oslo, NO
Alexander N. Fedorov, Melnikov Permafrost Institute, RU
Michael G. Ferrick, US Army, ERDC/CRREL, US
Javier Fochesatto, International Arctic Research Center, US
Steven L. Forman, University of Illinois-Chicago, US
Daniel Fortier, University of Alaska Fairbanks, US
Richard Fortier, Université Laval, CA
Walter J. Fourie, University of Alaska Fairbanks, US
Pierre Francus, Inst. National de la Recherche Scientifique, CA
Oliver W. Frauenfeld, University of Colorado, US
Regula Frauenfelder, University of Oslo, NO
Barry M. Freifeld, Lawrence Berkeley National Laboratory, US
Hugh M. French, University of Ottawa, CA
Duane Froese, University of Alberta, CA
Rina Garcia, Stockholm University, SE
Gunther Ghysels, Ghent University, BE
I. Gidley, University of Calgary, CA
Robert E. Gieck, University of Alaska Fairbanks, US
Ted Goebel, Texas A&M University, US
Douglas J. Goering, University of Alaska Fairbanks, US
Jules M. Goldspiel, Cornell University, US
Michael Gooseff, Pennsylvania State University, US
Jacob Gorelik, Earth Cryosphere Inst. SB RAS, RU
Sergey Goryachkin, Geography Institute, Moscow, RU
Raoul Granger, National Hydrology Research Centre, CA
Mikhail N. Grigoriev, Permafrost Institute Yakutsk, RU
Guido Grosse, University of Alaska Fairbanks, US
Ed Grozic, EBA Engineering Consultants Ltd., CA
Jocelyn Grozic, University of Calgary, CA
Hansueli Gubler, AlpuG Davos, CH
Mauro Guglielmin, Insubria University Varese, IT
Steve D. Gurney, University of Reading, UK
Örjan Gustafsson, Stockholm University, SE
Spencer Guthrie, Brigham Young University, US
Wilfried Haeberli, University of Zurich, CH
Birgit Hagedorn, University of Alaska Anchorage, US
Tristram C. Hales, Cardiff University, UK
Svein-Erik Hamran, University of Oslo, NO
Chris Hanks, Alexco Resource Corp., US
Jennifer Harden, US Geological Survey, US
Charles Harris, University of Cardiff, UK
Robert N. Harris, Oregon State University, US
Stuart A. Harris, Calgary Alberta, CA
Bent Hasholt, University of Copenhagen, DK
Andreas Hasler, University of Zurich, CH
Steven Hastings, San Diego State University, US
C. Haththatowa, University of Calgary, CA
Christian Hauck, Karlsruhe Institute of Technology, DE
Helmut Hausmann, Technical University of Vienna, AT
Jennifer Heldmann, NASA Ames, US
Karen S. Henry, ERDC/CRREL, US
Rita Hermanns, Friedlipartner AG, CH
Thomas Herz, University of Giessen, DE
Ulrike Herzschuh, Alfred Wegener Institute, DE
Gloria Hicks, National Snow and Ice Data Center, US
Christin Hilbich, Friedrich-Schiller-Universität Jena, DE
Kenneth M. Hinkel, University of Cincinnati, US
Larry Hinzman, University of Alaska Fairbanks, US
Richard Hodgkins, Loughborough University, UK
Martin Hoelzle, University of Zurich, CH
Ed T. Hoeve, EBA Engineering Consultants Ltd., CA
Igor Holubec, I. Holubec Consulting Inc., CA
Anne Hormes, University Centre in Svalbard, NO
William T. Horne, EBA Engineering Consultants Ltd., CA
Hans-Wolfgang Hubberten, Alfred Wegener Institute, DE
Leroy Hulsey, University of Alaska Fairbanks, US
Ole Humlun, University of Oslo, NO
James Hunter, Geological Survey of Canada, CA
Atsushi Ikeda, University of Tsukuba, JP
Thomas Ingeman-Nielsen, Tech. University of Denmark, DK
Arne Instanes, Opticonsult Bergen, NO
Kenneth C. Irving, University of Alaska Fairbanks, US
Ketil Isaksen, Norwegian Meteorological Institute, NO
Mamoru Ishikawa, Hokkaido University, JP
Michel Jaboyedoff, University of Lausnne, CH
Matthias Jakob, BGC Engineering, CA
Richard Janowicz, Yukon Dept. of Environment, CA
Alexander Jarosch, University of British Columbia, CA
A. Jayasinghe, University of Calgary, CA
Margareta Johansson, Lund University, SE
Elden R. Johnson, Alyeska Pipeline Service Co., US
Ken Johnston, Earth Tech, CA
H. Jonas Akerman, Lund University, SE
Ben Jones, US Geological Survey, US
Kevin W. Jones, EBA Engineering Consultants Ltd., CA
Torre Jorgenson, ABR Inc., US
Håvard Juliussen, University Centre in Svalbard, NO
Andreas Kääb, University of Oslo, NO
Mikhail Kanevskiy, University of Alaska Fairbanks, US
Julian Kanigan, Indian and Northern Affairs, CA
Kumari Karunaratne, Carleton University, CA
Andreas Kellerer-Pirklbauer, University of Graz, AT
Martina Kern-Luetschg, Cardiff University, UK
Maureen Ketzler, US Forest Service, US
Alexander Kholodov, University of Alaska Fairbanks, US
John Kimble, Consulting Soil Scientist, US
Lorenz King, University of Giessen, DE

Kurt Kjær, University of Iceland, IS
Anna E. Klene, University of Montana, US
Michael Knapp, Alaska DOT&PF, US
Christof Kneisel Universität Würzburg, DE
Steven V. Kokelj, Indian and Northern Affairs, CA
Else Kolstrup, University of Uppsala, SE
Vladimir S. Kolunin, Earth Cryosphere Institute, RU
P.Y. Konstantinov, Melnikov Permafrost Institute, RU
Demitri Konyushkev, Docuchaev Soils Institute, RU
Michael Krautblatter, University of Bonn, DE
Thomas Krzewinski, Golder & Associates, US
Bernd Kulessa, Swansea University, UK
Anna N. Kurchatova, Tyumen State Oil and Gas University, RU
Denis Lacelle, Canadian Space Agency, CA
Branko Ladanyi, Polytechnique Montréal, CA
Christophe Lambiel, University of Lausanne, CH
Hugues Lantuit, Alfred Wegener Institute Potsdam, DE
David M. Lawrence, NCAR, US
Daniel Lawson, US Army, ERDC/CRREL, US
Marc Lebeau, Université Laval Québec QC, CA
Anne-Marie LeBlanc, Université Laval, CA
Jonah Lee, University of Alaska Fairbanks, US
Marina Leibman, Earth Cryosphere Institute, RU
Mathias Leopold, University of Jena, DE
David W. Leverington, Texas Tech University, US
Antoni Lewkowicz, University of Ottawa, CA
Xin Li, World Data Center for Glaciology Lanzhou, CN
Jenny Liu, University of Alaska Fairbanks, US
Shuhuang Liu, US Geological Survey, US
Jerónimo López-Martínez, University of Madrid, ES
Lorene A. Lynn, University of Alaska Fairbanks, US
Jacek Majorowicz, Northern Geothermal Consultants, CA
Galina Malkova, Russian Academy of Sciences, RU
Michael Manga, University of California Berkeley, US
Jan Mangerud, University of Bergen, NO
William F. Manley, University of Colorado, US
Gavin K. Manson, Natural Resources, CA
Sergei Marchenko, University of Alaska Fairbanks, US
Laurent Marescot, ETH Zuerich, CH
Margarita Marinonva, California Inst. of Technology, US
Philip Marsh, Nat. Hydrology Res. Centre Environment, CA
Irene Marzloff, Johann Wolfgang Goethe Univ., DE
Norikazu Matsuoka, University of Tsukuba, JP
Hansruedi Maurer, ETH Zurich, CH
Galina G. Mazhitova, Komi Science Centre, RU
William D. McCoy, Univ. of Massachusetts, US
Les McFadden, University of New Mexico, US
A. David McGuire, University of Alaska Fairbanks, US
Robert McHattie, Alaska DOT&PF (retired), US
Christopher McKay, NASA Ames Research Center, US
Fiona McLaughlin, Dept. of Fisheries and Oceans, CA
Malcolm McLeod, Landcare Research Hamilton, NZ
Nicola McLoughlin, University of Bergen, NO
Michael C. Metz, M.C. Metz Associates, US
Franz Meyer, Alaska Satellite Facility Fairbanks, US
Hanno Meyer, Alfred Wegener Institute, DE
Keith Meyer, Michael Baker Jr. Corp., US
Gary J. Michaelson, University of Alaska Fairbanks, US
Fred A. Michel, Carlton University Ottawa, CA
Nicole Mölders, University of Alaska Fairbanks, US
Jack D. Mollard, J.D. Mollard and Associates, CA
Dan Moore, University of British Columbia, CA
George Moridis, Lawrence Berkeley Laboratories, US
Thomas Moses, Alaska DOT&PF (retired), US
Michael Mungoven, USDA-NRCS, US
Julian B. Murton, University of Sussex, UK
Mark Musial, Golder Associates, US
Philippe Nater, GeoNum GmbH, CH
Frederick E. Nelson, University of Delaware, US
William G. Nelson, University of Alaska Anchorage, US
Heng Joo Ng, Schlumberger, CA
Derick Nixon, Nixon Geotech Ltd., CA
F. Mark Nixon, Geological Survey of Canada, CA
Jeannette Noetzli, University of Zurich, CH
Rune S. Ødegård, University of Gjovik, NO
Jonathan O'Donnell, University of Alaska Fairbanks, US
Stanislav Ogorodov, Moscow State University, RU
C. Ordonez, University of Calgary, CA
Kirk Osadetz, Geological Survey of Canada, CA
Thomas Osterkamp, University of Alaska Fairbanks, US
Jim M. Oswell, Naviq Consulting Inc., CA
Sam Outcalt, University of Michigan (retired), US
P. Paul Overduin, Alfred Wegener Institute, DE
Ron Paetzold, Geo-Watersheds Scientific, US
Michael Palmer, Indian and Northern Affairs, CA
Charles Paull, Monterey Bay Aquarium Research Inst., US
David Payer, US Fish and Wildlife Service, US
Rorik Peterson, University of Alaska Fairbanks, US
Richard Petrone, Wilfred Laurier University, CA
Eva-Maria Pfeiffer, University of Hamburg, DE
Marcia Phillips, Swiss Fed. Inst. for Snow …, CH
Ryan D. Phillips, C-CORE St John's Newfoundland, CA
Chien-Lu Ping, University of Alaska Fairbanks, US
Albert Pissart, Université de Liege, BE
Vladimir V. Pitulko, Inst. for History of Mat. Culture, RU
Lawrence J. Plug, Dalhousie University, CA
Stefan Pohl, Nat. Hydrology Res. Centre Environment, CA
Wayne Pollard, McGill University, CA
Olga Ponomareva, Earth Cryosphere Institute, RU
Anupma Prakash, University of Alaska Fairbanks, US
Jon Price, University of Waterloo, CA
William Quinton, Wilfred Laurier University, CA
Charles Racine, US Army, ERDC/CRREL (retired), US
Miguel Ramos, University of Alcala, ES
Gareth Rees, Scott Polar Research Institute, UK
J. Repelewska-Pękala, University of Maria Curie, PL
Anette Rinke, Alfred Wegener Institute, DE
Dan Riseborough, Geological Survey of Canada, CA
Armin Rist, Swiss Fed. Inst. for Snow …, CH
Stephen D. Robinson, St. Lawrence University, US
Isabelle Roer, University of Zurich, CH
Vladimir Romanovsky, University of Alaska Fairbanks, US
Bård Romstad, University of Oslo, NO
Vladislav Roujanski, EBA Engineering Consultants Ltd., CA
Stephan Saboundjain, Alaska DOT&PF, US
Torsten Sachs, Alfred Wagener Institute, DE
Kazuyuki Saito, University of Alaska Fairbanks, US
Michael Schirmer, Swiss Fed. Inst. for Snow …, CH
Lutz Schirrmeister, Alfred Wegener Institute, DE
Michael Schlegel, GeoEngineers Inc., US
Martin Schnebelli, Swiss Fed. Inst. for Snow …, CH
Edward A.G. Schuur, University of Florida, US
Georg Schwamborn, Alfred Wegner Institute, DE
Charles A. Schweger, University of Alberta, CA
Dmitry Sergeev, Institute of Environmental Geoscience, RU
Enrique Serrano, University of Valladolid, ES

Jack Seto, BGC Engineering Inc., CA
Natsagdorj Sharkhuu, Mongolian Academy of Sciences, MN
Nicolai I. Shiklomanov, University of Delaware, US
Yuri Shur, University of Alaska Fairbanks, US
Andrew G. Slater, University of Colorado, US
Lee Slater, Rutgers University, US
Chuck Slaughter, University of Idaho, US
Bruce Smith, Worley Parsons, CA
Orson P. Smith, University of Alaska Anchorage, US
Scott Smith, Research Branch Agriculture and Agri-Food, CA
Sharon Smith, Geological Survey of Canada, CA
Chris Spence, National Hydrology Research Centre, CA
Sarah M. Springman, ETH Zurich, CH
Blaire Steven, University of Wyoming, US
Christopher W. Stevens, University of Calgary, CA
De Anne Stevens, Alaska Dept. of Natural Resources, US
Marc Stiglitz, Georgia Institute of Technology, US
Vladimir Stolbovoy, Joint Research Centre of European …, IT
Dmity Streletskiy, University of Delaware, US
Robert Striegle, US Geological Survey, US
Tetsuo Sueyoshi, Hokkaido University, JP
Brad Sutter, NASA Ames Research Center, US
John Inge Svendssen, University of Bergen, NO
David Swanson, US Forest Service, US
Eors Szathmary, Eötvös Loránd University , HU
Pavel A. Tarasov, Free University of Berlin, DE
Charles Tarnocai, Agriculture and Agri-Food, CA
Rupert G. Tart, Golder Associates Ltd., US
Alan E. Taylor, ASL Environmental Sciences Inc., CA
Robert O. Taylor, Natural Resources, CA
Randi Thompson, BGC Engineering Inc., CA
Gennady S. Tipenko, Russian Academy of Sciences, RU
Horacio Toniolo, University of Alaska Fairbanks, US
J. Kenneth Torrance, University of Carleton, CA
Thomas P. Trainor, Univeristy of Alaska Fairbanks, US
Richard Trimble, EBA Engineering Consultants Ltd., CA
Dario Trombotto, Ianigla-Cricyt-Conicet, AR
Merritt R. Turetsky, Michigan State University, US
Craig Tweedie, University of Texas El Paso, US
William Ussler, Monterey Bay Aquarium Res. Inst., US
Jef Vandenberghe, Vrije Universiteit, NL
B. Van Vliet-Lanoë, Univ. Sciences et Tech. de Lille, FR
Yurij K. Vasilchuk, Moscow State University, RU
Alexander Vasiliev, Earth Cryosphere Institute, RU
Gonçalo Vieira, University of Lisbon, PT
Ted Vinson, Oregon State University, US
Jason G. Vogel, University of Florida, US
Daniel Vonder Mühll, ETH Zurich, CH
William Waite, US Geological Survey, US
Mark Waldrop, US Geological Survey, US
Donald Walker, University of Alaska Fairbanks, US
Katey Walter, University of Alaska Fairbanks, US
James Walters, University of Northern Iowa, US
B. Wang, Geological Survey of Canada, CA
KaiCun Wang, University of Maryland, US
Jeff Warburton, University of Durham, UK
Patrick J. Webber, Michigan State University, US
Matthias Wegmann, Institute of Safety and Security, CH
Malte Westerhaus, University of Karlsruhe, DE
Kimberly Wickland, US Geological Survey, US
Jacek Wierzchos, University of Lleida, ES
Cort J. Willmott, University of Delaware, US
William Winters, US Geological Survey, US
Stephen A. Wolfe, Geological Survey of Canada, CA
Ute Wollschlaeger, University of Heidelberg, DE
Ming-ko Woo, McMaster University, CA
Fred Wright, Geological Survey of Canada, CA
Yladimir Yakushev, VNIIGAZ, RU
Daqing Yang, University of Alaska Fairbanks, US
Edward Yarmak, Arctic Foundations, Inc., US
Shiqiang Ye, BC Hydro, CA
Kenji Yoshikawa, University of Alaska Fairbanks, US
Kathy Young, York University, CA
Dmitry Zamolodchikov, Ctr. for Ecol. and Prod. of Forests, RU
John P. Zarling, Zarling Aero and Engineering, US
Jay Zarnetske, Oregon State University, US
Aining Zhang, Natural Resources, CA
Gordon Zhang, EBA Engineering Consultants Ltd., CA
Tingjun Zhang, University of Colorado Boulder, US
Xiong Zhang, University of Alaska Fairbanks, US
Yu Zhang, Natural Resources, CA
Shu-ping, Zhao, CAREERI CAS, CN
Sergei Zimov, Northeast Science Station, RU
Jon E. Zufelt, US Army ERDC/CRREL, US

Experimental Research on Frost and Salt Heaving of Highway Foundation Soils in Seasonally Frozen Ground Regions in Gansu Province, Northwestern China

Guoyu Li
State Key Laboratory of Frozen Soil Engineering, CAREERI, Chinese Academy of Science, Lanzhou, Gansu 730000, China
Wenbing Yu
State Key Laboratory of Frozen Soil Engineering, CAREERI, Chinese Academy of Science, Lanzhou, Gansu 730000, China
Huijun Jin
State Key Laboratory of Frozen Soil Engineering, CAREERI, Chinese Academy of Science, Lanzhou, Gansu 730000, China
Yu Sheng
State Key Laboratory of Frozen Soil Engineering, CAREERI, Chinese Academy of Science, Lanzhou, Gansu 730000, China
Jilin Qi
State Key Laboratory of Frozen Soil Engineering, CAREERI, Chinese Academy of Science, Lanzhou, Gansu 730000, China
Lanzhi Lü
State Key Laboratory of Frozen Soil Engineering, CAREERI, Chinese Academy of Science, Lanzhou, Gansu 730000, China

Abstract

In the seasonally frozen ground regions in Gansu Province, Northwestern China, highway embankment and pavement have frequently been damaged due to the impacts of frost and salt heaving and thaw settlement, generally in the forms of pavement cracks and break-ups. Mechanisms and mitigative measures for these hazards have been puzzling geocryologists and road engineers. In this research repeated freeze-thaw experiments of saline soils sampled from the subgrade at highway segments with frequent and repeated damages, at periodically fluctuating temperatures, were conducted in order to investigate the relationship of freeze-thaw processes in saline foundation soils with the strengths and impacts of soil salinity on the stability of foundation soils. The experimental results showed that salinity and frost susceptibility had great impact on the deformation process in saline soils. The deformation of saline soil is accumulative within limited freeze-thaw cycles with sufficient water supply. Elevation of the embankment height, drainage, and salinity controls in subgrade and embankment fills were proposed to cost-effectively mitigate frost and salt heaving and subsequent thaw-weakening during highway design, construction, and maintenance periods in regions affected by seasonally frozen saline soils.

Keywords: frost action; frost heaving; highway foundations; saline soil; seasonally frozen ground; thaw-weakening.

Introduction

The area of salinized soils is 1.91 x 10^5 km^2, accounting for about 2.0% of the total land territory in China. It is distributed mainly in the arid, semi-arid, and cold regions. Gansu Province has a saline soil area of 1.16 x 10^4 km^2, one of the largest in China. The major centers for the distribution of saline soils, such as Dunhuang, Yumen, Jiuquan, Linze, Yongchang and Minqing, are located in the Hexi Corridor in Central and Western Gansu Province (Fig. 1) (Qiu et al. 1996, Xu et al. 1999). In addition, salts in the soil-water system can be partially crystallized and excluded, and migrate along the thermal, pressure, and moisture gradients.

Foundation soils can be significantly and differentially expanded from salt heaving, resulting in serious damages to roads and other buildings (Wu & Zhu, 2002). Studies on frost and salt heaving of saline soils have been intensively conducted both in laboratory tests and *in situ* observations in the field for many years. Xu et al. (1992) studied water and ion migration and its resultant deformation of soils in an experiment using the frozen Kaolin soil supplied with the NaCl solution. The result indicated that the deformation in the frozen Kaolin was mainly in the form of frost heaving. Qiu (1986) studied the processes of ion and water migration. He proposed that some ion types of salt for restraining frost heave. Fei et al. (1994) studied salt-heave characteristics of Xi'an Loess, and proposed that the salt-heave ratio was minimum for soils with 3% Na_2SO_4 and 1.8 g/cm^3 initial dry density. He further concluded that the salt heave of saline soil with Na_2SO_4 varied in a form of two parabolas with initial dry density and water content. Chen et al. (1988) suggested that the salt-heave ratio of silt with Na_2SO_4 changed exponentially with the cooling rate and the increasing overburden pressures. Xu et al. (1995, 1999) systemically studied frost and salt heave of soils, including changes of unfrozen water content, migration of moisture and ions, deformation due to salt heaving and its influencing factors, and coupled models for the prediction of frost and salt heaving. Wu & Zhu (2002) performed salt heave experiments of coarse-grained soil with Na_2SO_4 to analyze the processes of salt heave that affect the stability of building foundations. Results showed that the coarse-grained soil with a salt concentration layer could result in abrupt salt heaving that damaged engineering infrastructures. Liu et al. (2005)

Figure 1. Map of Gansu Province with main areas mentioned in paper.

carried out some experiments using soils with sulphates to measure the salt heave force and rate under a single factor and to study heave mechanisms. Other researchers mainly studied properties such as strength and deformation of saline soils, (Ogata et al. 1982, Sego et al. 1982), frost heave of saline soils (Chamberlian, 1983), the effect of salt enrichment on unfrozen water (Banin & Anderson, 1974), and water and ion migration in an open system (Ershov et al. 1989, 1991). In this paper, freeze-thaw experiments of typical soils, taken from the subgrade of highways where damages frequently occurred, have been conducted to study the characteristics of deformation processes due to the salt and frost heave and subsequent thaw weakening and settlement in Gansu Province. On the basis of this experimental study, some mitigative measures had been proposed to improve the stability of embankment and pavement soils in saline soil regions.

Experimental Process

Specimens for laboratory testing

Four soil specimens were studied in repeated freeze-thaw experiments in order to study deformation characteristics and processes caused by frost heave, salt expansion, and subsequent thaw settlement and weakening.

After careful field investigations on the damages of highway foundation soils in Gansu Province, northwestern China, three specimens of saline soils were sampled from road sections with severe damage in the embankment and pavement due to salt and frost heave. Sample No. 1 of silt was taken in Gaotai County along National Highway No. 109 (Fig. 1). Its field water content was 23.10% and salinity was very high. Salt crystals could be observed clearly. Numerous longitudinal and transverse cracks were found on the pavement where the specimen was taken. Sample No. 2 of silty clay was taken between Jiuquan to Jinta along National Highway No. 214. The climate is more arid in the area of Sample No. 2. The field water content was 5.18%. Sample No. 3 of fine silty sand was taken from the toe of the right side protection slope of National Highway No. 214 in the proximity of Jinta County, where visible white salt crystals

Table 1. Liquid and plastic limits, plastic index, and salinity of three saline soil specimens and the reference sample.

Sample	Liquid limit (%)	Plastic limit (%)	Plastic index	Salinity (%)
No. 1	21.1	13.8	7.3	9.1
No. 2	27.9	17.9	10	2.79
No. 3	19.9	10.3	6.6	6.14
No. 4	28.2	19.1	15	0.15

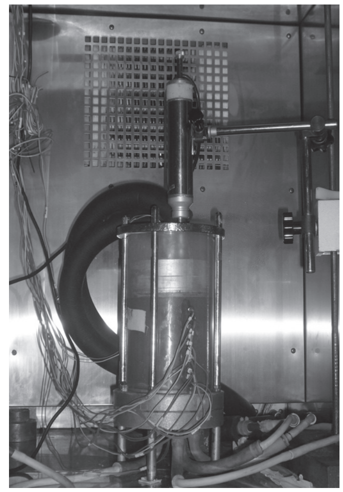

(a)

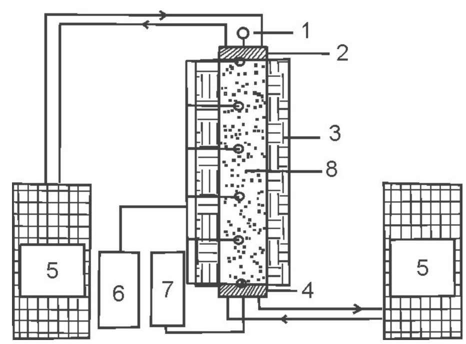

(b)

Figure 2. Diagram of experimental system for freeze-thaw testing of saline and reference soil specimens. Notes: (a) Photo of freeze-thaw experiment system; and (b) Simplified model of components in the experiment system. 1-Deformation sensor, 2-Top plate, 3-Insulation layer, 4-Bottom plate, 5-Cooling bath, 6-Temperature sensors, 7-Water supply, and 8-Testing sample.

occur on the adjacent ground surface. Field water content was 9.53%. In addition, another soil specimen, Sample No. 4 of clay, was obtained in the middle of the Maqü to Luqü section along National Highway No. 213, at an elevation of about 3500 m and with a cold climate. It was tested as a reference specimen because of very low salinity (Table 1).

The basic parameters, such as liquid and plastic limits, plastic index, and salinity, of the four specimens were measured in the State Key Laboratory of Frozen Soil Engineering, CAREERI, Chinese Academy of Science (Table 1). The ions in the tested saline soils mainly include Cl^-, NO^{3-}, SO_4^{2-}, Na^+, Ca^{2+}, Mg^{2+}, K^+.

Sample preparation

Soil samples taken and sealed in the field were placed in polymethyl methacrylate tubes, layer by layer, and compacted to a certain density. Soils were converted to testing specimens. Cylinder specimens were 100 mm high with a diameter of 101 mm. They were consolidated for 24 hours at room temperature for uniform moisture distribution. Then the repeated freeze-thaw tests were carried out.

Laboratory equipment

Laboratory equipment for performing repeated freeze-thaw tests on the four soil specimens was developed by the State Key Laboratory of Frozen Soils Engineering (Fig. 2).

The polymethyl methacrylate tube was filled with a soil specimen. The temperatures at the top and bottom plates were controlled by cooling baths. The temperature at the bottom plate remained at +1°C. The exterior of the tube was insulated. The experiment system was put into an insulated box with a constant temperature at +1°C.

Every 30 minutes, the temperature at each vertical interval of 10 cm in the tested soil columns was measured by thermal-susceptible resistance sensors with a precision of ±0.2°C. The deformation in the soil columns was measured by a deformation sensor with a precision of ±0.01mm at the top of the soil columns. The temperature at the top plate varied according to a sinusoidal function as follows:

$$T = -2.5 + 7.5\sin(\frac{2\pi}{72}t) \tag{1}$$

Water was sucked up into the soil columns through the bottom plate due to the temperature difference. A freeze-thaw cycle is 72 hours. Saline soil Sample Nos. 1, 2, and 3 experienced three freeze-thaw cycles. Sample 4 was subject to only one freeze-thaw cycle because it had low salinity, and the frost susceptibility was measured and used as a reference. The temperatures at different depths, and deformation of soil samples were measured and recorded automatically when the freeze-thaw experiments were carried out.

Results and Discussions

The test results for Sample No. 1 indicate that the deformation at the top plate increased at a sinusoidal variation of the top plate temperatures with the elapse of time (Fig. 3). The temperature at the top plate was negative, and the upper part of the soil sample was frozen at the beginning of the experiment. The relevant deformation had a quickly increasing trend during the first several hours. Then the deformation increased slowly until about 30 hours had elapsed, when the temperature at top plate was positive. Subsequently, the heave rate of the soil sample increased more pronouncedly when the temperature at the top plate became negative again. In addition, when the temperature at the top plate was in the range of 0°C to 2°C, the heave rate of the soil sample was still reasonably high, due to the salt heaving. No thaw settlement was observed during the entire deformation process, due to the high salinity of the soil sample. From the above analyses and discussions, it can be concluded that the deformation of Sample No. 1 mainly included frost and salt heaving.

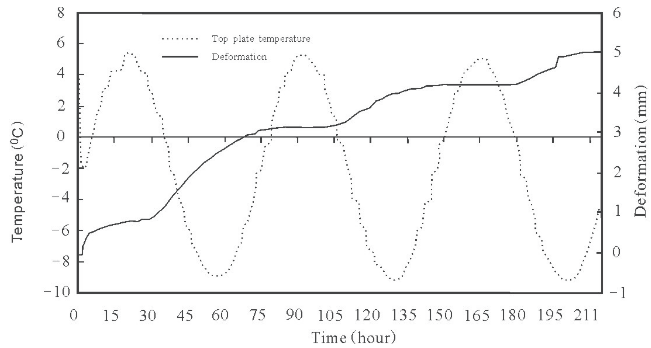

Figure 3. Temperature and the deformation processes of Sample 1

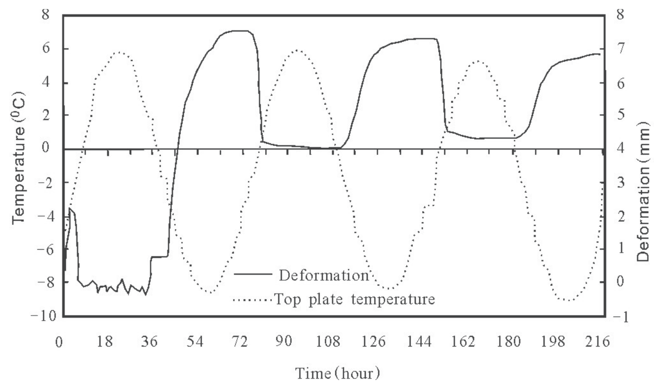

Figure 4. Temperature and the deformation processes of Sample 2.

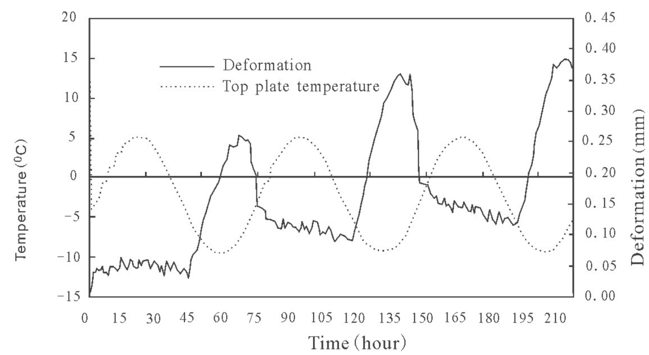

Figure 5. Temperature and the deformation processes of Sample 3

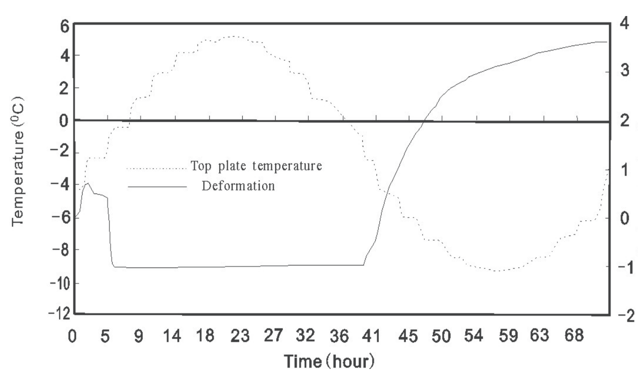

Figure 6. Temperature and the deformation processes of Sample 4.

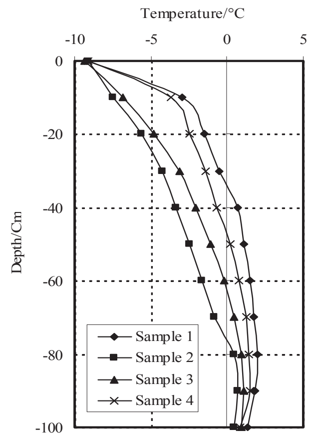

Figure 7. Temperature distribution curves in the tested soil columns when the top plate temperature reached -10°C, the minimum in the experiment.

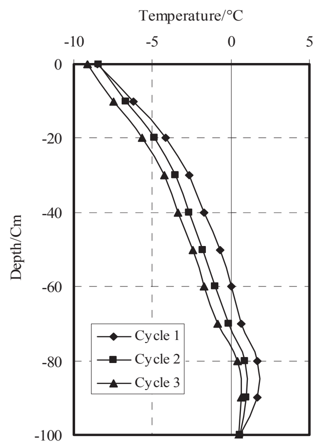

Figure 8. Temperature distribution curves of Sample No. 2 when the top plate temperature reached the minimum in different cycles.

Figure 4 is a diagram of the variation processes of the temperature and deformation at the top plate of Sample 2. The deformation of the soil sample gradually increased at the beginning when the temperature at the top plate was negative. A sudden decline of deformation of the soil sample occurred when the temperature at the top plate became positive, which mainly resulted from thaw settlement of the upper thawed soil. Slowly, the deformation kept almost steady, with only a slight decrease during the above-zero-temperature period. Subsequently, the deformation began to increase sharply when the temperature at the top plate was 2°C. It showed that salt heaving probably occurred. The deformation continued to rise sharply with the temperature becoming subzero and dropping continually. Meanwhile, it can be noted that the deformation was almost constant in the first few hours when temperatures dropped from 0°C to -2°C. That happened at each cycle. This indicates that there is a lag of deformation before cooling, due to insufficient time for deformation to occur. In the second cycle, the characteristics of the deformation process are similar to that of the first cycle. But the minimum amount of deformation of the soil sample corresponding to the positive temperature at the top plate was greater than that in the first cycle. It demonstrated

Table 2. Experimental results of four tested soil specimens.

Sample	Soil type	Salinity (%)	Deform-ation(mm)	Frozen depth(cm)	Water Uptake (ml)
No. 1	Silt	9.1	5	34	118
No. 2	Silty clay	2.79	7	76	89
No. 3	Silty sand	6.14	0.38	60	64
No. 4	Clay	0.15	3.6	47	45

that the deformation does not return to the initial position. There was a surplus heave deformation in Sample 2. The salt heave was not clear in the 2nd and 3rd cycles, probably because of a lack of salt after precipitation in the 1st cycle. From the above analyses and discussions, it can be seen that the deformation of Sample 2 was caused by frost heaving and thaw settlement, with possible salt heaving.

Figure 5 shows the variation processes of the temperature and the deformation at the top plate of Sample 3. The deformation of the soil sample began to increase when the temperature at the top plate was negative at the beginning. It was not clearer compared to that of Sample 2 (Fig. 4). When the top plate temperature became positive, the deformation was almost constant, with slight see-sawing decreases due to soil consolidation. When the temperature at the top plate decreased from a positive temperature to about -4.3°C, the deformation began to rise immediately and sharply. This showed that there was a longer lag of deformation compared to the temperature at the top plate, probably due to a high salinity (6.14%) and the soil type (silty sand), which are not favorable to soil freezing. Later, sudden settlement occurred in Sample 3 when the temperature increased to about -4.0°C. But it was still larger than that in the first cycle. This showed that the entire deformation was accumulative but smaller than Sample Nos. 1 and 2. It was difficult to determine the salt heave during the period of soil heave in Sample No. 3. So its deformation was mainly caused by frost heaving and thaw settlement, with possible salt heave, but the heave amount was smaller..

Sample No. 4, with low salinity, was tested for its frost-susceptibility. The deformation of the soil sample increased when the temperature at the top plate became negative at the beginning (Fig. 6). When the temperature reached the proximity of 0°C, sudden settlement of the soil sample occurred due to the thaw settlement of the upper part of the soil column. During the positive-temperature period at the top plate, the deformation kept stable. When the temperature decreased to about -0.6°C, the soil began to heave rapidly, until the temperature reached almost the minimum value of -9°C; then the increase of deformation slowed. However, even when the temperature rose within the subzero period, the frost heaving was still growing. This well confirmed that Sample No. 4 is a typical frost-susceptible soil.

Figure 7 shows the temperature distribution curves of the tested soil columns when the top plate temperature reached the minimum of -10°C during the 3rd cycle, except for Sample No. 4 in the 1st cycle. The frozen depth in Sample No. 2 was the maximum, while that of Sample No. 1 was the minimum. Sample No. 4, though subject to one freeze-thaw cycle, was frozen more deeply than Sample No. 1. Generally, the frozen depth in silty sand is greater than that in silty clay because of its greater thermal conductivity (Xu et al. 2001), but that in Sample No. 3 of silty sand was less than that in Sample No. 2. This indicates that salinity can effectively retard cold wave propagation.

Figure 8 shows the temperature distribution curves of Sample No. 2, as an example, when the top plate temperature reached the minimum of -10°C in different cycles. Note that the frozen depth rises with the increasing number of freeze-thaw cycles. The variation process of the frozen depth in Sample Nos. 1 and 3 is similar to that in Sample No. 2.

According to the above analyses and discussions based on the experimental results for four tested specimens, heave deformation is mainly influenced by soil type, salinity, freeze-thaw cycle numbers, and others. The heave deformation in Sample No. 2 of silty clay, with moderate salinity, is the maximum (Table 2). However, the heave deformation in Sample No. 3 of silty sand, with the greater salinity, is the minimum. Sample No. 4 expands to a higher level even after one cycle. The heave deformation in Sample No. 1, with the highest salinity, reached a higher level, and without thaw settlement. It can also be found that there are the different threshold values in salinity and freeze-thaw cycle for the different saline soils to lead to salt heave and salt hazards. To determine the threshold values need further investigations in detail.

Conclusions and Recommendations

According to the experiment results, analyses, and discussions mentioned above the following preliminary conclusions can be made:

(1) The deformation of saline soil is accumulative within limited freeze-thaw cycles with sufficient water supply, i.e., the minimum deformation increases gradually with the increasing number of freeze-thaw cycles.

(2) Salinity has great impact on the deformation process of saline soil. The deformation of soil with very high salinity was mainly caused by frost and salt heaving, without thaw settlement.

(3) Frost susceptibility strongly influences the deformation processes of saline soil. The heave deformation of non-frost susceptible saline soil, even with the higher salinity, is small.

(4) To determine the occurrence of salt heave is difficult for ordinal soils with moderate salinity because it happens together with frost heave.

(5) The heave deformation in saline soils is mainly influenced by soil type, salinity, freeze-thaw cycle number, water supply, and others. It is a complicated process with water, heat, and salt transfer subject to the repeated freeze-thaw cycles.

(6) Therefore, elevation of the embankment height from ground water table or surface standing water levels, subgrade and local drainage control, and stricter control of salinity of fills could be used to effectively mitigate frost and salt heaving, and subsequent thaw settlement and weakening for the design, construction, and maintenance of highway foundations in areas affected by saline soil.

Acknowledgments

This work was supported by the Chinese Academy of Sciences Knowledge Innovation Key Directional Project "Mechanisms and mitigation of frost heaving and thaw settlement of pipeline foundation soils in permafrost regions" (Grant No. KZCX2-YW-311), National Science Foundation of China Projects (Nos. 40401010, 40471023, and 40640420072), the Chinese Academy of Sciences 100 Talents Programs "Stability of linear engineering foundation in warm permafrost regions under a change climate" and "Deformation and stability of roadbed in permafrost regions", and the Open Fund of the State Key Laboratory of Frozen Soils Engineering (Grant No. SKLFSE200702). Generous assistance from the NICOP editors and reviewers is greatly appreciated and thus acknowledged.

References

Banin, A. & Anderson, D.M. 1974. Effects of salt concentration during freezing on the unfrozen content of porous materials. *Water Resources Research* 10(1): 124-128.

Chamberlaine, E.J. 1983. Frost heave of saline soils. *Proceedings of 4th International Conference on Permafrost*, 121-126.

Chen, X., Qiu, G. & Wang, Y. 1988. On salt heave of saline soil. *Proceedings of 5th International Symposium on Ground Freezing*, 35-39 (in Chinese).

Ershov, E.D., et al. 1989. Deformation of frozen soil under the action of solution. In: *Collections of Geocryological Study*. Moscow: Moscow University Publishing House, 202-210.

Ershov, E.D., Lebedenko, Yu.P. & Xu, X. 1991. Water and ion migration of frozen soil in open system. *Proceedings of 6th International Symposium on Ground Freezing*, 17-24.

Fei, X., Li, B. & Wang, J. 1994. Salt expansion law of different dried unit weight for sulphate salty soil. *Journal of Glaciology and Geocryology* 16(3): 245-251 (in Chinese).

Liu, P., Wang, J., Jiang, J. & Wang, C. 2005. Experimental researches and analysis of expansion characteristics of sulphate salty soil. *Journal of Jilin University (Earth Science Edition)* 35(1): 74-78.

Ogata, N., Yasuta, M. & Kataoka, T. 1982. Salt concentration effects on strength of frozen soils. *Proceedings of 3rd International Symposium on Ground Freezing*, 3-10.

Qiu, G. 1986. Ion and water migration and frost heave of Morin clay during freezing. *Journal of Glaciology and Geocryology* 8(1): 1-14 (in Chinese).

Qiu, G., Zhao, L., Wang, S., Zhang, X., Sheng, W., Yue, H. & Jin, H. 1996. *The Seasonally Freezing Halic Soils and Their Improvement-utilization in the Hexi Corridor, Gansu, China*. Laznhou, China: Lanzhou University Press, 1-115 (in Chinese with an extended English abstract).

Sego, D.C., Schultz, T. & Banasch, R. 1982. Strength and deformation behavior of frozen sand with a saline pore fluid. *Proceedings of 3rd International Symposium on Ground Freezing*, 11-18.

Wu, Q. & Zhu, Y. 2002. Experimental studies on salt expansion for coarse grain soil under constant temperature. *Cold Regions Science and Technology* 34(2): 59-65.

Xu, X., Lebedenko, Yu.P., Chuvilin, E.M., Kliuchikov & K. Yu. 1992. Experimental study on processes of heat-mass transfer and deformation in system of frozen Kaolin and salt solution. *Journal of Glaciology and Geocryology* 14(4): 289-295 (in Chinese).

Xu, X., Wang, J., Zhang, L., Deng, Y. & Tao, Z. 1995. *Mechanisms of Frost Heaving and Salt Expansion of Soils*. Beijing: Science Press, 1-126 (in Chinese).

Xu, X., Wang, J., Zhang, L. & Deng, Y. 1999. *Mechanisms of Frost Heave and Salt Expansion of Soils*. Beijing & New York: Science Press.

Xu, X., Wang, J. & Zhang, L. 2001. *Frozen Soil Physics*. Beijing: Science Press, 77-91.

The Effect of the Global Radiation Budget on Seasonal Frozen Depth in the Tibetan Plateau

Ren Li
Cold and Arid Regions Environmental and Engineering Research Institute, Chinese Academy of Sciences, 320 Donggang West Road, LanZhou 730000, China

Lin Zhao
Cold and Arid Regions Environmental and Engineering Research Institute, Chinese Academy of Sciences, 320 Donggang West Road, LanZhou 730000, China

Yongjian Ding
Cold and Arid Regions Environmental and Engineering Research Institute, Chinese Academy of Sciences, 320 Donggang West Road, LanZhou 730000, China

Abstract

In this study, monthly average daily global radiation of 22 radiometric stations across the Tibetan Plateau were utilized to determine the coefficients of the monthly Angström–Prescott model for estimating global solar radiation from sunshine duration. Using the model, global solar radiation of another 116 meteorological stations across the Tibetan Plateau were estimated. Combined with frozen ground data measurement at 75 stations, global radiation effects on the maximum frozen depth of the active layer were discussed. The result showed that global radiation in the cold season (from October to February the next year) had much influence on maximum frozen depth of the active layer. The relationship between them in three typical stations showed a marked negative correlation. As a whole, the maximum frozen depth of the active layer in nearly 80% of investigation stations had the same relationship with the global solar radiation, while the others showed a positive correlation. This indicated that the maximum frozen depth of the active layer was the result of combined effects of several factors other than global radiation. Of these influencing factors, such as global solar radiation, local latitude, longitude, altitude, air temperature in cold season, relative humidity, accumulation of precipitation in cold season, etc., only local latitude, altitude, global solar radiation, and air temperature showed high correlation with frozen depth. Essentially, the influences of local latitude and altitude can be regarded as the effects of global radiation indirectly. As the local latitude and altitude influenced the distribution of global radiation, so the global radiation was an important affecting factor on the maximum frozen depth of the active layer.

Keywords: active layer depth; global radiation; relative sunshine duration; Tibetan Plateau.

Introduction

Solar radiation is a main source of the Earth's energy and the basic driving force of the physical and biological processes on the earth surface. The processes respond to the seasonal variations in solar radiation fluxes in a complex manner. The distribution of solar radiation around the world determines the planet's mean climate variation resulting from the thermal balance of the Earth–atmosphere system, and establishes atmospheric and oceanic circulation patterns (Souza, et al. 2005). Topographic conditions effect the distribution of solar radiation.

As for China, its regional topography is complex and its surface condition is varied. This is especially conspicuous in the Qinghai-Tibetan Plateau (TP) with higher altitude and complex terrain. The TP is one of the most complex geographical features in the world, with an average elevation about 4 km or more. Such land surface features make much difference in solar radiation among different regions across the TP and result in unequal surface heating by solar radiation (Ye & Gao 1979). Non-uniform distribution of solar energy on the land surface has much effect on climate over the TP and its surrounding area, and even on the global climate. In addition, the TP, which is a huge land mass standing in the mid-altitude troposphere with high altitude and complex terrain, lies in the transition zone between the tropical and sub-tropical and also in the heart zone of the famous monsoon region in the Northern Hemisphere; its dramatic heating and its strong continental strongly impact the Asian monsoon, global atmospheric circulation and global climate change (Ye & Gao 1979, Tao et al. 1999).

Moreover, the distribution of solar radiation across the TP has a decisive effect on a decision on the characteristics of plateau glaciers, permafrost, and vegetation distribution.

Furthermore, due to its unique geographic environment, the TP developed a large area of permafrost, which is the result of the climate change, and it also has feedback effect on climate. As an important component of cryosphere, which is an important driving force of global change and a connection for interaction of other layers in the climatic system, the presence and changes of the permafrost can affect the energy and water exchanges of the land-atmosphere system and further affect the formation and development of regional climate (Yao et al. 2002, Zhang 2002). The active layer at the upper part of the permafrost is thawed in summer and frozen in winter. Permafrost changes, leading to changes in water and heat exchange characteristics between land and atmosphere, first by changing the water-heat states of the active layer, thereby causing changes and anomaly of the atmospheric circulation system (Wang et al. 2003), then affecting the weather system. Changes of the maximum frozen depth of the active layer are key indicators of climatic warming (Pavolv 1994). Thus, the maximum frozen depth of the active layer has a close relation with the climate.

As a product of climate change, features of permafrost are by the impacts of climate change, and global radiation in the TP is an important influencing factor on Plateau climate. Global radiation is the major source of ground heat in the TP. Fluctuations in global radiation will cause a corresponding impact to permafrost and its active layer (Kou et al. 1981). Study of the relationship between global radiation and frozen/thawed depth of the active layer do much to help us better understand the impact mechanism of the permafrost and its active layer. Relevant research work has been launched in the TP region and has achieved some results. In the early 1980s, Kou et al. (1981) studied the relationship between global radiation and the thawed depth of the active layer using the data measured at Fenghoushan at the TP. In their view, thawed depth of the active layer in the permafrost region was caused by solar radiant heat arriving at the surface and down into the ground, and the statistical relationship between them was established. The studies of Cheng et al. (1983, 1984, 1992) showed that the characteristics of the surface solar radiation latitudinal variation were important reasons for the permafrost zone. The variation of global radiation determined the annual mean temperature at the bottom of the freezing and thawing depth of the active layer (Zhou et al. 2000). Ding et al. (2000) discussed the relationship between the accumulative soil temperature at 4 cm depth below the surface and the freezing/thawing depth of the active layer of the TP. Research showed that the formation of permafrost and seasonal permafrost had a relationship with surface radiation-heat exchange. The structure of the radiation-heat balance had a decisive role in the formation and dynamics of frozen ground. The surface energy budget and the changing of the surface-air temperature were decided by the net radiation, which depends mostly on global radiation, surface condition, and net long-wave radiation (Zhou et al. 2000).

Those works mentioned above provided a basis for the mechanism research of permafrost in the TP; however, restricted by natural condition and outlay, those studies were only based on a single site and with a short-term dataset (Zhou et al. 2000). The work was small considering the large-scale and long-term dataset of the TP. For the whole TP, further works need to be done.

In this work, global radiation was estimated across the TP; its influence on the maximum frozen depth of the active layer was discussed. By multiple regression analysis method, several effect factors for the maximum frozen depth of the active layer were analyzed too.

Material and Method

Data used in this paper include frozen depth, global solar radiation, monthly accumulative precipitation, monthly average and extreme air temperatures, relative humidity, and relative sunshine duration. Frozen depth data in the cold season were collected in 75 meteorological stations from 1961–1998. Datasets of precipitation, monthly average air temperature and extreme temperatures, relative humidity, and relative sunshine duration were collected in 138 stations in the TP and its adjacent regions. These data were measured by corresponding observation criteria.

As for radiant data, there were only 22 radiometric stations in the TP and its adjacent regions; other meteorological stations are without radiation measurements, so global radiations in those stations was estimated. The AngstrÖm–Prescott model (APM) is the most convenient and widely used correlation for estimating global solar radiation (Liu & Ji 1985, Chegaar & Chibani 2001, Almorox & Hontoria 2004, Almorox et al. 2005), which is expressed by

$$Q / I_0 = a + bS_1 \tag{1}$$

where Q and I_0 are, respectively, the monthly mean daily global radiation (MJ.m-2.d-1) and daily extraterrestrial radiation on a horizontal surface (MJ.m-2.d-1); S_1 is relative duration of sunshine (the ratio between the number of hours of sunshine duration to the total number of daylight hours); a and b are empirically coefficients. Using the measured data of monthly average daily global solar radiation on horizontal surfaces and sunshine hours from 22 radiometric stations across the TP, as given in Table 1, coefficients a and b can be determined by the method of least squares. As a result, the APM over the TP can be written as (Li, et al. 2007):

$$Q / I_0 = 0.213 + 0.5691 S_1 \tag{2}$$

The performance of APM was evaluated by calculating the following statistical error test such as mean bias error (MBE), mean absolute error (MAE), root mean square error (RMSE), and mean relative error (MRE). These tests are fundamental measures of accuracy (Driesse & Thevenard 2002, Almorox & Hontoria 2004, El-Metwally 2004, Almorox et al. 2005, Tymvios & Jacovides 2005, Menges et al. 2006, Bulut & Büyükalaca 2007). They are defined as below:

$$MBE = \frac{1}{n}\sum_{i=1}^{n}\left(Q_{i,obs} - Q_{i,est}\right) \tag{3}$$

$$MAE = \frac{1}{n}\sum_{i=1}^{n}\left|Q_{i,obs} - Q_{i,est}\right| \tag{4}$$

$$RMSE = \sqrt{\frac{1}{n}\sum_{i=1}^{n}\left(Q_{i,obs} - Q_{i,est}\right)^2} \tag{5}$$

$$MRE = \frac{1}{n}\sum_{i=1}^{n}\left|\frac{Q_{i,obs} - Q_{i,est}}{Q_{i,obs}}\right| \tag{6}$$

The indexes (obs) and (est) identify observed and estimated values, respectively. Results of the APM, applied to the whole dataset available with 7400 samples from 22 radiometric stations across the TP, are illustrated in Figure 1. It can be seen from Figure 1 that the scattering of the data points was small. And the values of MBE, MAE, RMSE for the whole dataset result in -0.06, 1.22, 1.64 MJ.m-2.d-1, respectively. The value of MRE is 7.6%. Such results indicate that the agreement between the measured and estimated values is marked. It demonstrates that APM was acceptable for estimating monthly global solar radiation from relative sunshine duration over the TP. With Equation 2, the monthly average daily global radiation on a horizontal surface (Q) in MJ.m-2.d-1 from January 1961 to December 2000 at 116 meteorological stations can be estimated. Finally, its monthly total can be obtained too.

For convenience of analysis, the statistical variable, accumulative anomaly for Q and FD is introduced. It is defined as

$$x_j = \sum_{i=1}^{j}\left(x_i - \bar{x}\right) \qquad (j \le n) \tag{7}$$

where x_j is the accumulative anomaly value of Q or FD from first year to the j year, $\bar{x}$ is the average value of the whole dataset, and n is the length of the dataset.

Results and Discussion

EOF (Empirical Orthogonal Function) analysis results showed that Yushu (33°01′N, 97°01′E, 3682.2 m), Lenghu (38°45′N, 93°20′E, 2770.0 m) and Delingha (37°22′N, 97°22′E, 2982.4 m) were typical sites (Xu, et al. 1990, Wang et al. 2003), so the influence of global radiation on the maximum frozen depth of the active layer in these three typical sites is discussed at first.

Figure 2 shows the influences of the accumulative anomalies of global radiation on the maximum frozen depth of the active layer in three typical stations at the TP. It can

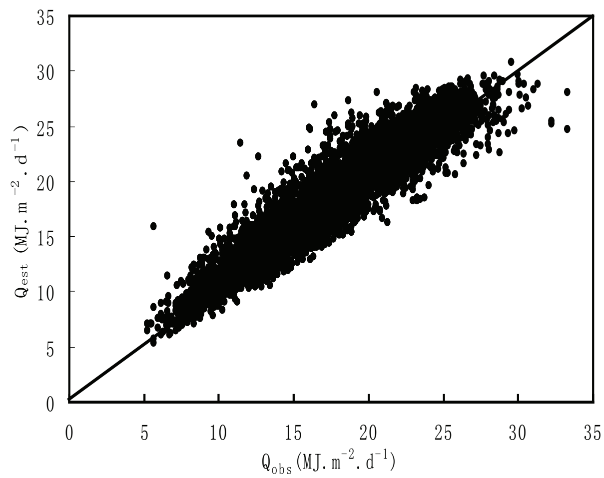

Figure 1. Results comparison between Q_{est} and Q_{obs} on the TP.

Table 1. Geographical location, annual mean air temperature (Ta) and period of the radiometric station used in regression analysis.

station	Latitude (N)	Longitude (E)	Altitude(m) (above sea level)	Ta(°C)	period
Kuche	41° 43′	83° 04′	1072.5	11.3	Jul 1957-2000
Ruojiang	39° 02′	88° 10′	888.3	11.6	Jun 1957-2000
Hetian	37° 08′	79° 56′	1374.5	12.4	Jun 1957-2000
Kashi	39° 28′	75° 59′	1288.7	11.8	Jul. 1957-2000
Erjina	41° 57′	101° 04′	940.5	8.7	1992-2000
Gangcha	37° 20′	100° 08′	3301.5	-0.4	1993-2000
Gerlmod	36° 25′	94° 54′	2807.6	4.9	Jul 1957-2000
Xining	36° 43′	101° 45′	2295.2	5.9	1959-2000
Yushu	33° 01′	97° 01′	3681.2	3.0	Apr1960-2000*
Guole	34° 28′	100° 15′	3719.0	-0.4	1993-2000
Dunhuang	40° 09′	94° 41′	1139.0	9.3	Jul 1957-2000
Jiuquan	39° 46′	98°29′	1477.2	7.2	1993-2000
Minqin	38° 38′	103° 05′	1367.0	7.3	1961-2000
Garze	31° 37′	100° 00′	4414.9	5.6	1994-2000
Hongyuan	32° 48′	102° 33′	3492.7	1.3	1994-2000
Panzhihua	26° 35′	101° 44′	1190.1	20.8	1992-2000
Changdu	31° 09′	97° 10′	3306.0	7.5	1961-2000*
Naqu	31° 29′	92° 04′	4507.0	-1.4	1961-2000*
Lahsa	29° 40′	91° 08′	3648.7	7.9	1961-2000*
Lijiang	26° 52′	100° 13′	2392.4	12.6	1961-2000*
Kunming	25° 01′	102°41′	1891.4	14.8	1961-2000
Tengchong	25° 01′	98° 30′	1654.6	14.9	1961-2000

* some missing in dataset.

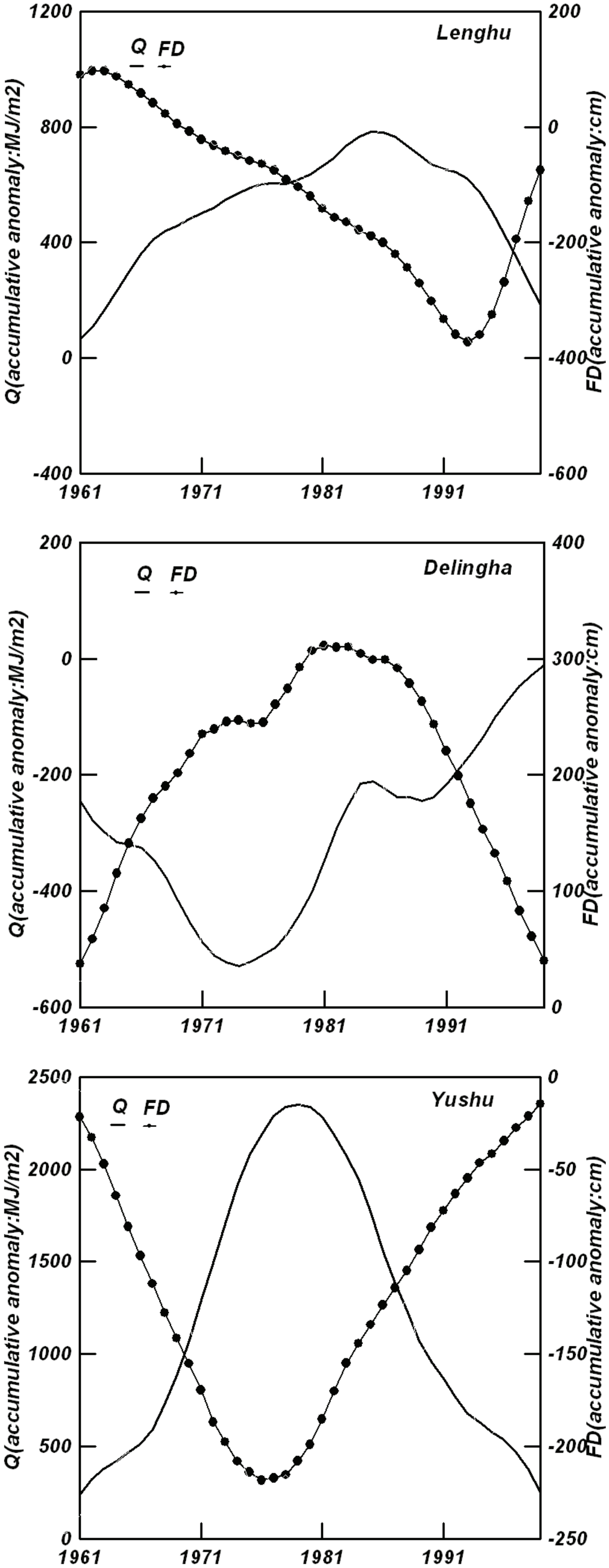

Figure 2. The influences of global radiation in three typical stations on the maximum frozen depth of the active layer.

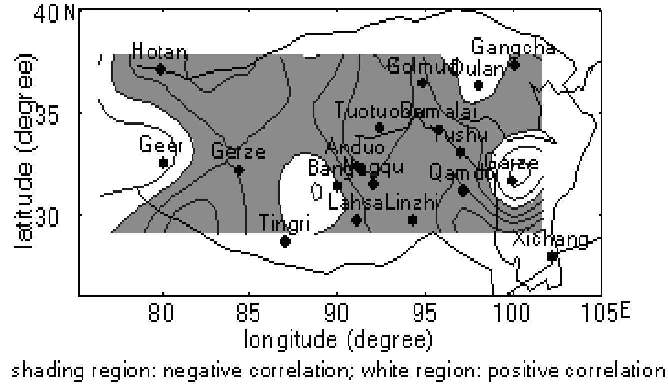

Figure 3. Distribution of the correlativity between global radiation and the maximum frozen depth of the active layer.

be seen from Figure 2 that the accumulative global radiation (Q) in cold season (from October to February of the next year) had much influence on FD. The relationship between them in three typical stations showed a marked negative correlation. How about the other stations across the TP? The relationships between global radiation and maximum frozen depth of the active layer in cold season across the TP for another 72 stations were also analyzed too. The results are illustrated in Figure 3.

Figure 3 shows the distribution of the correlativity between global radiation and maximum frozen depth of the active layer. In Figure 3, the shaded part stands for the negative correlation region, while the white part stands for the positive correlation region. As a whole, the maximum frozen depth of the active layer in nearly 80% of the investigation stations had the same relationship with global solar radiation as those typical stations, whereas the other 20% showed a positive correlation. It indicates that the maximum frozen depth of the active layer was influenced by other factors at the same time. In addition to global radiation, the maximum frozen depth of the active layer was the result of combined effects of other factors, such as soil water content, soil property, altitude and latitude, snowpack, vegetation, etc. But what is the importance among those factors mentioned above? Multiple regression analysis method was used here to answer the question. Factors such as global solar radiation, local latitude, longitude, altitude, average air temperature, relative humidity, and accumulation of precipitation in cold season were selected in the multiple regression analysis; among these factors only local latitude, altitude, global solar radiation and air temperature showed high correlation with frozen depth. The multiple regression equation could be written as

$$FD = -434.6 + 12.24\phi + 0.043H - 0.02Q - 6.74T_a \tag{8}$$

where Φ, H, Q, and Ta were the local latitude, altitude, global radiation, and air temperature at the station. The units of these variables were the same as those mentioned above.

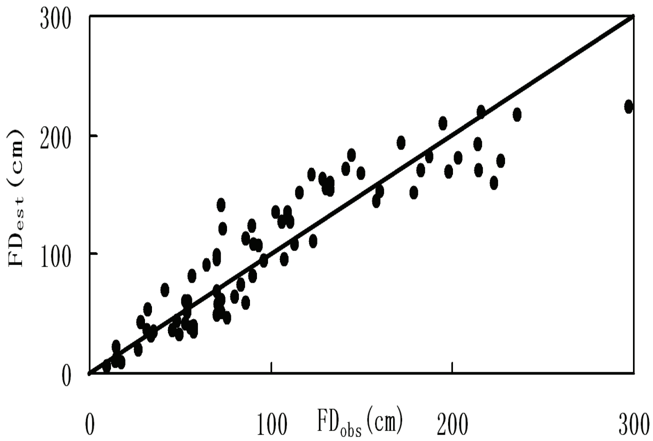

Figure 4. Comparison between the maximum frozen depth of the active layer values observed (FD_{obs}) and estimated (FD_{est}).

Global radiation was the amount from October to February of the next year. The air temperature, *Ta,* was the average value during the time range from October to February of the next year. The multiple correlation coefficient of Equation 8 was 0.90, the partial correlation coefficients for Φ, *H*, *Q* and *Ta* were 0.99, 0.98, 0.81, and 0.81, respectively. It indicated that the correlation between maximum frozen depth of the active layer and the four effective factors was good. The result between the observed and estimated frozen depth with Equation 8 is illustrated in Figure 4. It can be seen from Figure 4 that when the maximum frozen depth of the active layer is less than 300 cm, the agreement between the measured and computed values is good, and the scattering of the data points is small. It demonstrates that Equation 8 was acceptable for estimating the average of the maximum frozen depth of the active layer over the TP.

It can also be seen from Equation 8 that for the whole TP, the global ration showed a negative correlation with the maximum frozen depth of the active layer. The local latitude and altitude show positive correlation with the maximum frozen depth of the active layer. Essentially, the influences of local latitude and altitude can be regarded as the effects of global radiation indirectly. As the local latitude and altitude influence the distribution of global radiation, so the global radiation is an important affecting factor on the maximum frozen depth of the active layer.

Conclusions

From the above discussion, the following conclusions could be drawn:

(1) The APM was acceptable for the estimation of global solar radiation.
(2) Global radiation in the cold season greatly influenced the maximum frozen depth of the active layer. The relationship between them in three typical stations (Yushu, Lenghu, and Delingha) showed a marked negative correlation.
(3) For the whole TP, maximum frozen depth of the active layer in nearly 80% of all investigation stations had the same relationship with global solar radiation as the three typical stations; the others showed a positive correlation.
(4) The maximum frozen depth of the active layer was the result of combined effects of several factors except for global radiation. Among these influencing factors, local latitude, altitude, global solar radiation, and air temperature showed high correlation with the maximum frozen depth of the active layer.
(5) Global radiation was an important affecting factor on the maximum frozen depth of the active layer.

Due to a lack of data on soil properties of the TP, such as aspect was not considered in this work. Thus, further work needs to be done.

Acknowledgments

The authors thank the reviewers for their cogent suggestions. This work is supported by National Basic Research Project (973 Project), No.2007CB411504, National Natural Sciences Foundation of China, No. 40471026, 973 Project No. 2005CB422003, and the innovation project of CAREERI,CAS KZ2003111, KZ2003106.

References

Almorox, J. & Hontoria, C. 2004. Global solar radiation estimation using sunshine duration in Spain. *Energy Convers. Manage.* 45:1529–35.

Almorox, J. et al. 2005. Estimation of monthly Angstro¨m–Prescott equation coefficients from measured daily data in Toledo, Spain. *Renewable Energy* 30: 931–936.

Bulut, H. & Büyükalaca, O. 2007. Simple model for the generation of daily global solar-radiation data in Turkey. *Applied Energy* 84:477–491.

Chegaar, M. & Chibani, A., 2001. Global solar radiation estimation in Algeria. *Energy Conversion and Management* 42: 967-973.

Cheng, G.D. & Wu, B.J. 1983. Approach to the mathematical model of zonality of high-altitude permafrost. *Journal of Glaciology Cryopedology* 5(4):1-7.

Cheng, G.D. 1984. Problems on zonation of high-altitude permafrost. *ACT Geographica Sinica* 39(2):185-193.

Cheng, G.D. & Dramis, F. 1992. Distribution of mountain permafrost and climate. *Permafrost and Periglacial Process* 3(2):83-91.

Ding, Y.J. et al. 2000. The observational study on permafrost hydrology on large scale in the Qinghai-Tibetan Plateau. *Chinese Sciences Bulletin* 45(2): 208-214.

Driesse, A. & Thevenard, D. 2002. A test of Suehrcke's sunshine radiation relationship using a global data set. *Solar Energy* 72: 167–75.

El-Metwally, M. 2004. Simple new methods to estimate global solar radiation based on meteorological data in Egypt. *Atmos Res* 69: 217–39.

Kou, Y.G. et al. 1981. Investigation of solar radiation on Qinghai-Xizang Plateau and its neighboring districts and the relation between the radiation and permafrost on it. *Journal of Glaciology Cryopedology* 3(4): 25-32.

Li, R. et al. 2007. Global solar radiation estimation using sunshine duration over Tibetan Plateau. *Energy Conversion and Management* (under review).

Liu, Z.X. & Ji, G.L. 1985. The relation between global radiation and percentage of sunshine over the Qinghai Xizang Plateau and its contiguous zone. *Arid Land Geography* 8(4):51-58.

Menges, H.O. et al. 2006. Evaluation of global solar radiation models for Konya, Turkey. *Energy Conversion and Management* 47: 3149–3173.

Pavolv, A.V. 1994. Current change of climate and permafrost in the Arctic and Subarctic of Russian. *Permafrost and Periglacial Processes* 5: 101-110.

Souza, J.L., et al. 2005. Global solar radiation measurements in Maceió, Brazil. *Renewable Energy* 30: 1203–1220.

Tao, S. et al. 1999. *The Theory Research Advancement of TIPEX (part one)*. Beijing, China: Meteorological Press of China, in preface page.

Tymvios, F.S., et al. 2005. Comparative study of Angstro¨m and artificial neural networks methodologies in estimating global solar radiation. *Solar Energy* 78: 752–62.

Wang, C. et al. 2003. Study on relationship between frozen –thaw processes in Qinghai-Xizang Plateau and circulation in east Asia. *Chinese Journal of Geophysics* 46(3): 309-316 (in Chinese).

Xu, Guochang et al. 1990. The climatic characteristics of surface heating fields over the Qinghai-Xizang Plateau. *Plateau Meteorology* 9(1):32-43 (in Chinese).

Yao, T.D. et al. 2002. *The Dynamic Characteristics of Cryosphere in the Middle Part on the Qinghai-Tibetan Plateau.* Beijing China: Geological Press, in preface (in Chinese).

Ye, D. & Gao, Y. 1979. *Tibetan Plateau Meteorology.* Beijing: Science Press, 89-101 (in Chinese).

Zhang, T.J. 2002. A important landmark of representation on the Chinese permafrost study. *Journal of Glaciology Cryopedology* 24(3): 331-334 (in Chinese).

Tundra Soil-Water Content and Temperature Data in Support of Winter Tundra Travel

Michael R. Lilly
Geo-Watersheds Scientific, Fairbanks, Alaska
Ron F. Paetzold
Geo-Watersheds Scientific, College Station, Texas
Douglas L. Kane
University of Alaska Fairbanks, Fairbanks, Alaska

Abstract

Unfrozen soil-water content was monitored in the active layer of tundra soil, using TDR sensors at several locations on the North Slope of Alaska and in the Brooks Range foothills. In addition, soil temperature was monitored to a depth of 1.5 m at these locations using thermistors. Particular attention was paid to soil water and temperature behavior during freezing and thawing conditions. The upper organic layer of soil often exhibited very wet conditions and showed much greater temporal variability of soil moisture than the lower mineral soil layers. Permafrost acts as a barrier to water flow, so soils usually are wet as they thaw in the spring. Soil surface roughness and vegetation under tundra conditions make accurate placement of sensors almost impossible. Minor discrepancies between soil water freezing and thawing behavior must be tolerated. However, an overall picture of the processes still emerges. Results of this study may be useful in improving tundra travel guidelines. Currently, tundra travel is allowed if the soil temperature in the upper foot of soil is colder than -5°C. Soil-water content is not considered in the current management approach, though it can be used to help better describe the temperatures at which soil freezing is complete. The measured soil-moisture data indicates most of the soil-water freezing occurs above -2°C. This information indicates the -5°C temperature condition is very conservative and a warmer temperature management point should be considered.

Keywords: measurements; permafrost; soil moisture; soil temperature; tundra travel.

Introduction

A project was established in 2006 to gather data for use in addressing various surface transportation issues in northern Alaska. This report examines some of the results obtained thus far with respect to winter tundra travel. Current guidelines limit tundra travel to periods when the soil temperature at a depth of 30 cm is less than -5°C with snow cover depth minimums depending upon the type of tundra (Bader 2005). This criterion is based on the results of a three-year study (Bader & Guimond, 2004) and may be conservative.

Soil-temperature and water-content data are used in this paper to examine the possibility of using a slightly relaxed criterion that could result in longer periods of allowed tundra travel. This is based strictly on the freeze-thaw behavior of soil water. No measurements of soil strength were obtained. The objective is to examine the behavior of soil temperature and water content in tundra soils during the processes of freezing and thawing.

Materials and Methods

Twelve stations were installed in the fall of 2006. Eight of the stations are located on the coastal plain; the remaining four are in the northern foothills of the Brooks Range. The stations used in this report are located east of the Sagavanirktok River (Fig. 1).

Soil-water content was monitored at each station with Campbell Scientific, Inc. CS616 TDR-type sensors at depths of 10, 20, and 40 cm. The depths at some sites varied slightly due to soil conditions. The soil-water content sensors were installed horizontally with minimal soil disturbance. Factory calibration was used to convert raw readings to volume fraction soil-water content. TDR-type sensors respond to the soil dielectric constant, and since ice has a dielectric constant similar to dry soil, the sensor effectively responds to changes in unfrozen soil-water content. Hourly readings of unfrozen soil-water content were recorded.

Soil temperature was monitored at each station with YSI thermistors mounted in a string, at intervals to provide temperatures at 0, 5, 10, 15, 20, 40, 60, 80, 100, 120, 135, and 150 cm below the soil surface. The soil temperature string was placed into a hole drilled into the soil, and the evacuated soil was used to back-fill the hole. Hourly readings of soil temperature were recorded.

Other measurements include air temperature, relative humidity, net radiation, wind speed and direction, snow depth, and summer rain. Sensor readings at each station were measured and recorded with a Campbell Scientific, Inc CR1000 datalogger. Data were transmitted hourly to a central processing facility with FreeWave radios. Solar panels and a battery bank were used to provide power for each station throughout the year.

Results and Discussion

Ice formation within soil pores increases the bearing strength of freezing soils. Extremely dry soils, such as found in the Dry Valleys of Antarctica, or dry gravel or organic soils exhibit no increase in bearing strength when frozen.

As soil water freezes, it acts as an impediment to the movement of soil particles, thus increasing the bearing strength of the soil. Water freezing in soil pores acts as if solid particles were growing in the pores. A graph of frozen soil-water content versus soil bearing strength in water- saturated soil would be a typical S-shaped curve. As soil water starts to freeze, little strength is added. At some point, the increase in strength with water content is dramatic. As the freezing process goes to completion, the curve levels off, and little strength is added during the last stages of freezing. The bearing strength of frozen soil is greater than the maximum of the strength of ice or of unfrozen soil.

Similarly, for unsaturated soils, higher water content up to some maximum, will result in higher strength when the soil freezes. Very low soil-water content does little to increase soil strength when the soil is frozen. As soil-water content increases, soil strength increases upon freezing.

Soil water does not completely freeze at temperatures below 0°C. As heat is removed from water, the temperature lowers until the freezing point is reached. At this point, the temperature remains constant until the liquid water solidifies, or changes to ice, at which time the temperature will once again start to drop. In soils, however, water does not all freeze at the same temperature. Some freezes at or near 0°C, while some freezes at much lower temperatures. No unique freezing point exists for soil water (Koopmans & Miller 1966). There are two reasons for this. One, soil water contains solutes or salts which lower the freezing point. As the soil water freezes, the salts become more concentrated due to exclusion from the ice. And two, the "structure" of soil water becomes increasingly ordered closer to soil particles. This changes the free energy of the soil water and lowers the freezing point. A similar phenomenon can be observed in capillary tubes (Edlefsen & Anderson 1943).

Increasing the solute concentration of soil water produces a minor effect compared to the "structuring" of the soil water near soil particles.

The water next to soil particles is the last to freeze, and will do so only at extremely low temperatures, due to its molecular interaction with the soil particles (Anderson et. al. 1973). Water is a polar molecule, and soil particles, especially clay and organic matter, have associated negative charges. Water molecules tend to align in an ordered fashion or "structure" next to soil particles. The effect decreases with distance from the soil particle. The ordered molecules are more difficult to freeze than those in bulk solution or free water. The amount of unfrozen water present depends principally upon temperature for a given soil material. Except for very low water contents, it is virtually independent of the total soil-water volume. The unfrozen-water content at a given temperature is mainly dependent on specific surface area of the soil. The amount of unfrozen water at a given temperature increases as the specific surface area of a soil increases.

Data are presented from station DBM4 Sag Ivishak Met, which was chosen as representative for this project. The

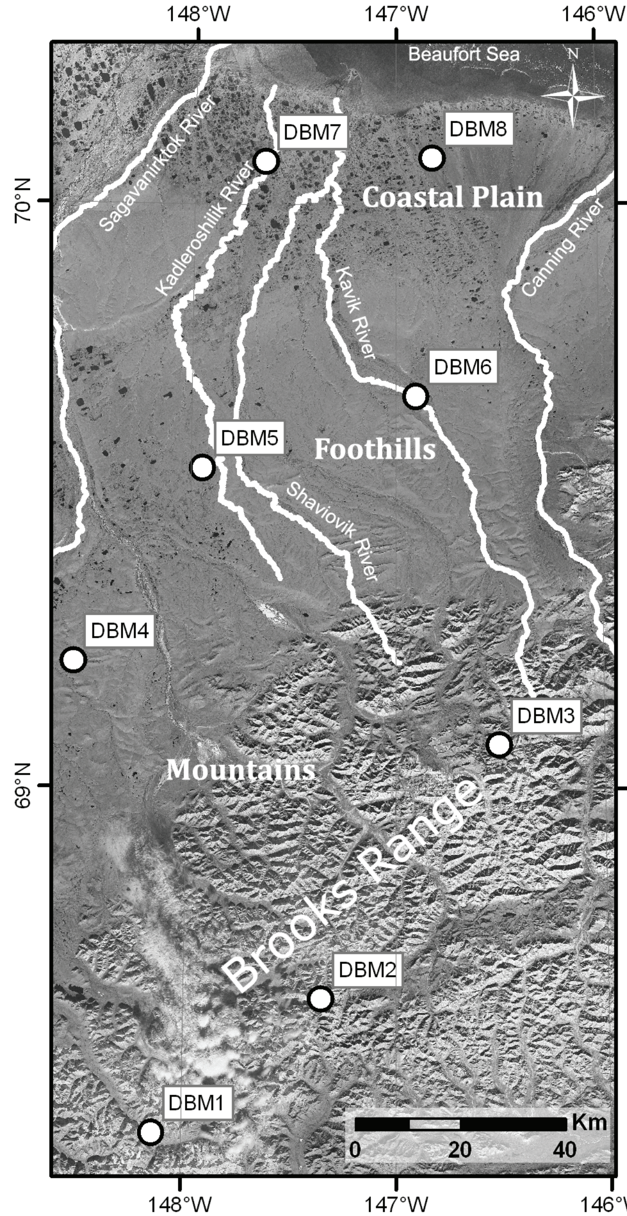

Figure 1. Study sites locations on the central North Slope, Alaska.

active layer thickness (Fig. 2) for this station, as determined by the point at which the maximum soil temperature line crosses the 0°C line, is approximately 60 cm for the period of measurement (October 1, 2006, to September 30, 2007). This is a fairly typical active layer thickness for the soils of this area. Active layer thickness varies from year to year depending on summer weather. The average soil temperature in the upper 150 cm was -4.15°C during the measurement period.

Other methods of active-layer strength determination may yield different results. Rod penetration is the most common method of determining active layer thickness. Problems with the rod penetration method include timing, presence of hard spots in the soil (ice lenses, rocks, compact areas, etc.), and operator consistency. It is also a labor-intensive method. An advantage of the penetration method is that it is usually

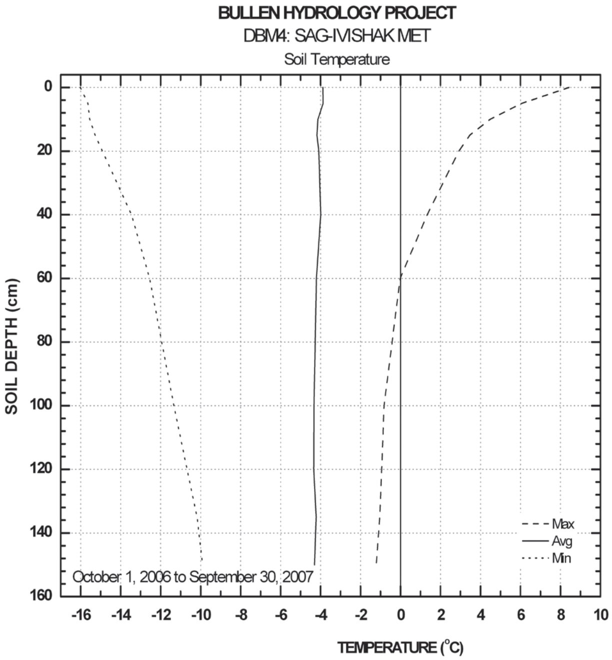

Figure 2. Average, maximum, and minimum soil temperature profiles for the DBM4 Sag Ivishak Met site.

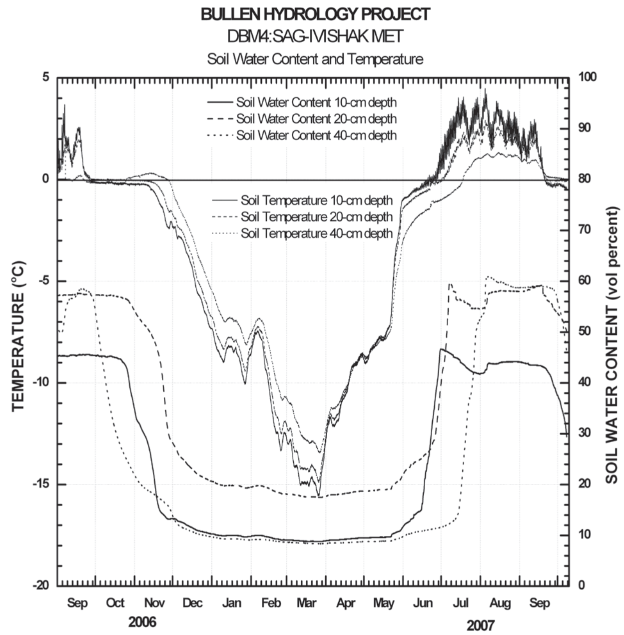

Figure 3. Soil-water content and temperature for the Sag-Ivishak (DBM4) meteorological station.

repeated over a relatively large area, resulting in an average, maximum, and minimum value for the area. One problem common to all methods is the location of the soil surface as a reference point for depth. This can be a very serious problem in tussock tundra.

Active layer thickness was generally a few centimeters less for the foothills stations than for those on the coastal plain. In addition, the soil at these sites remained frozen longer. Although soil temperatures vary among the stations, the relationship between soil temperature and soil water is consistent.

The soil-water content at the Sag Ivishak Met site was near saturation during the monitoring period from September 2006 to October 2007 (Fig. 2). This is typical of soils in this area. Often soils in northern Alaska are wetter in the spring and early summer, then dry out in the fall. During the summer, down-gradient drainage and evapotranspiration dry out the soils. The soil-water content at saturation in this soil is around 60% by volume. Normal mineral soils have a saturated-water content of around 40% to 45% by volume. The high-saturated water contents in the soils studied are attributed to high soil organic-matter content.

For greatest accuracy, the soil-water content sensors should be calibrated specifically to each soil, especially under conditions that depart from normal (Campbell Scientific, Inc. 2004). Although the absolute soil-water content may differ from that given by the factory calibration, the relative water contents and the behavior of phase change in relation to temperature should be accurate.

Freezing increases the complexity of the soil-water system. Water moves in response to various gradients, including thermal gradients. Water in soil moves from warm areas to cold areas. As water moves, in response to thermal gradients, it carries thermal energy or heat with it, thus modifying the thermal and hydraulic gradients.

Freezing of soil water changes its ionic concentration and thus its electrical properties, setting up new gradients and complicating water-content measurement based on electrical properties. The increase of solute concentration in soil water, due to solute expulsion from ice during freezing, can cause a minor decrease in the freezing point. This decrease is on the order of a few tenths of 1°C.

In spite of the complexity of determining soil-water content absolutely, much information may be extracted from the relative soil-water contents and the water-content curve shapes and positions.

Soil on Alaska's North Slope typically thaws from the top down, but freezes from both the top and bottom as shown in Fig. 3. These phenomena have been noted by others (Osterkamp & Romanovsky 1997, Romanovsky & Osterkamp 1997).

The unfrozen soil-water content curves indicate that water at the 40-cm depth began to freeze first, followed by that at the 10-cm depth. The water at the 20-cm depth was the last to freeze. As air temperature decreases and the days grow shorter in the fall, there is less heat transfer to the soil and it begins to freeze at the bottom of the active layer, just above the permafrost, depending on how cold the permafrost is. When the air temperature falls below freezing, water at the soil surface begins to freeze.

As the soil water freezes in the fall, the temperature remains near 0°C during the period of water-to-ice phase change. This phenomenon is often referred to as the zero curtain and is the result of the release of thermal energy during the phase change from water to ice.

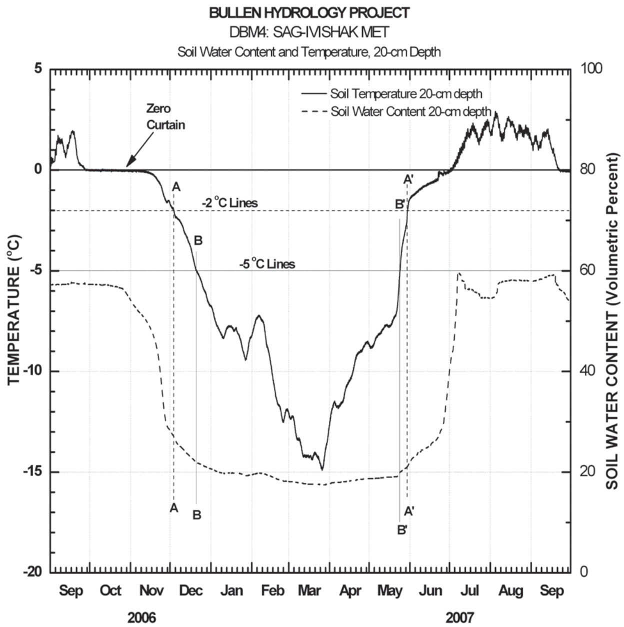

Figure 4. Soil temperature and water content for the 20-cm depth at Sag-Ivishak (DBM4) meteorological station.

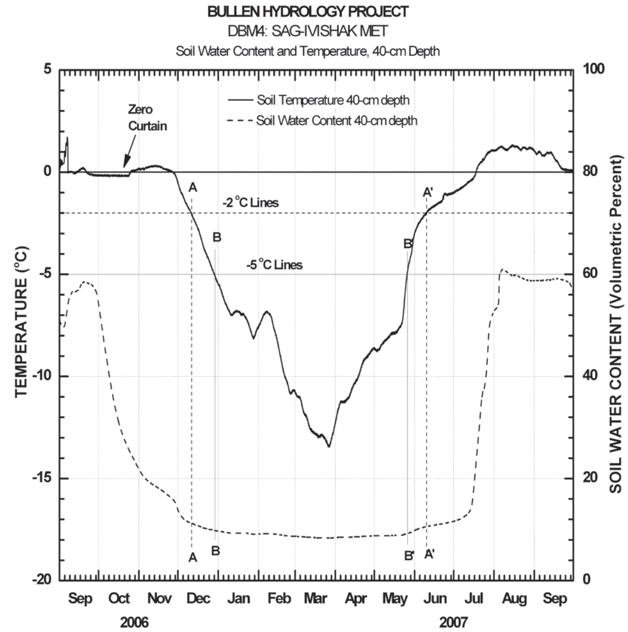

Figure 5. Soil temperature and water content for the 40-cm depth at Sag-Ivishak (DBM4) meteorological station.

The unfrozen-water content curve remains nearly constant during the initial period of the zero curtain. At some point, the soil water has lost most of its latent heat and rapid freezing occurs, as shown by the steep slopes of the curves in Figure 3. The unfrozen soil-water content curves then transition to a fairly constant unfrozen-water content, where very little further freezing occurs, even as the temperature markedly decreases. Sometimes this transition is rather abrupt, and sometimes it is more gradual.

Soil water at all sites studied thawed from the top down in the spring. In the spring, the days grow longer, air temperature increases, the snow begins to melt, and the soil thaws from the top down. Snowmelt water moves downward in response to gravity, warming the soil below.

Ice has a higher thermal conductivity than water, air, or soil. Thus ice is more efficient in transmitting thermal energy than water. This is another reason why soils thaw more quickly than they freeze.

In the spring, during thawing conditions, the soil temperature changes rapidly in response to liquid water moving into and through the soil. The temperature curve generally shows a slower rate of increase during the melting of the water at a particular depth. This is attributed to the latent heat required to thaw the ice. After the ice is thawed, the temperature resumes a rapid increase. The soil water generally thaws faster than it freezes. This may be attributed to the influence of liquid water moving through the soil, carrying thermal energy with it.

The phase-change period is shorter during the spring as the soil thaws and ice turns to liquid water. In addition, the temperature during this time usually is not constant at 0°C for any lengthy period of time. This may be attributed to meltwater carrying heat with it to underlying layers. During winter months, soils can desiccate and form thermal cracks. This increases the effective permeability of the soils, allowing more infiltration of water during snowmelt (Kane et. al. 2001).

Since no sensors were located at the 30-cm depth, data from 20 and 40 cm were used to approximate conditions there. Figures 4 and 5 show soil temperature and unfrozen-water content for the 20- and 40-cm depths, respectively.

Figures 4 and 5 show that soil water does not immediately begin to freeze at the onset of the zero curtain. Some time passes as the water is releasing latent heat while it starts to freeze. However, once started, the freezing process is relatively rapid.

Figure 5 shows a slight increase in soil temperature during the zero curtain during November. There is a corresponding decrease in the slope of the unfrozen-water content curve during this time. These features may be attributed to water moving into the soil layer at this point due to thermal gradients from the soil freezing above and below this depth. As the liquid water moves into this region, it carries heat or thermal energy with it, resulting in a slight increase in soil temperature.

Lines B and B' in Figures 4 and 5 indicate the time when the soil temperature drops below and rises above -5°C, respectively. During the time that the soil temperature is below -5°C, little additional unfrozen soil water will freeze even at soil temperatures well below -5°C. At these depths, the soil water is frozen to near its maximum level.

Lines A and A' show the conditions when the soil temperature is colder than -2°C. There is little difference in the frozen state of the soil water at these depths between -5°C and -2°C, particularly at the 40-cm depth. However, time that the soil is colder than -2°C is on the order of a month (Table 1), which is significant for tundra travel.

If we approximate the conditions at the 30-cm soil depth by the average of the 20- and 40-cm soil depths, Table 1

Table 1. Days soil temperature below certain levels for DBM4.

Soil temperature colder than	20-cm depth	40-cm depth	Avg of 20- and 40-cm depths
-1°C	195	209	202
-2°C	177	181	179
-3°C	169	165	167
-4°C	158	157	157
-5°C	154	148	151

shows that the soil was colder than 5°C during the winter of 2006–07 for approximately 151 days. During this time, the soil at the same depth was colder than -2°C for 179 days, four weeks longer. It was colder than -3°C for 167 days, 16 days longer. And the soil was colder than -4°C almost a week longer. Figures 3, 4, and 5 show steep curves for soil water freezing and thawing. When the soil reaches -2°C, the soil-liquid-water curve is near its minimum, and only minor freezing occurs at temperatures colder than this. Similar results were obtained for the foothills sites.

Again, no soil strength tests were performed, and the results indicate only the length of time that the soil was frozen at temperatures colder than indicated levels. However, it is known that the compressive (bearing) strength of the soils increases as the ice content increases.

Summary

Soil-water content and temperatures were monitored at twelve sites in northern Alaska from September 2006 through October 2007. Soil temperature and water behavior were observed during this time with particular attention paid to periods of freezing and thawing. Freezing started at the bottom of the active layer and proceeded from both the bottom and top of the active layer. During freezing, soil temperatures remained near zero while the soil water released its latent heat. This period is known as the zero curtain. At a point in the zero curtain, the soil water begins to freeze rapidly. When most of the water that was going to freeze had done so, a transition occurred to a nearly constant level of unfrozen soil-water content. Due to interaction with soil particles, soil water does not completely freeze. Soil temperatures colder than -2°C did not cause an appreciable increase in the amount of frozen soil water.

In the spring, the soils studied thawed from the top down. The thawing process was faster than freezing due to meltwater percolation. Also because of snowmelt, the soil-water content in the spring was at saturation. The difference in frozen soil-water content between -2°C and -5°C during the spring thaw was even less than it was in the fall during freezing.

A relaxation of the tundra travel guideline from a temperature of -5°C at a soil depth of 30 cm to a value between -2°C and -4°C could significantly increase the amount of time available for tundra travel. Further study needs to be undertaken to examine soil strength in the region between -2°C and -5°C before any changes in the guidelines are considered.

References

Anderson, D.M., Tice, A.R. & McKim, H.L. 1973. The unfrozen water and the apparent specific heat capacity of frozen soils. *Proceedings of the Second International Conference on Permafrost, Yakutsk, U.S.S.R., North American Contribution.* Washington, D.C.: National Academy of Sciences, 289-295.

Bader, H.R. & Guimond, J. 2004. *Tundra Travel Modeling Project.* Alaska Department of Natural Resources, 65 pp. http://www.dnr.state.ak.us/mlw/tundra/TundraModelReport.pdf

Campbell Scientific, Inc. 2004. *CS616 and CS65 Water Content Reflectometers.* Campbell Scientific, Inc.

Bader, H.R. 2005 *Tundra Travel Research Project: Validation Study and Management Recommendations.* Alaska Department of Natural Resources, 20 pp. http:www.dnr.state.ak.us/mlw/tundra/validation2005final_with_figures.pdf.

Edlefsen, N.E. & Anderson, A.B.C. 1943. Thermodynamics of soil moisture. *Hilgardia* 15: 31-298.

Kane, D.L., Hinkel, K.M., Goering, D.J., Hinzman, L.D. & Outcalt, S.I. 2001. Non-conductive heat transfer associated with frozen soils. *Global and Planetary Change* 29: 275-292.

Koopmans, R.W.R. & Miller, R.D. 1966. Soil freezing and soil water characteristic curves. *Soil Sci. Soc. Am. Proc*. 66: 680-685.

Osterkamp, T.E. & Romanovsky, V.E. 1997. Freezing of the active layer on the coastal plain of the Alaskan Arctic. *Permafrost and Periglacial Processes* 8: 23-44.

Romanovsky, V.E. & Osterkamp, T.E.. 1997. Thawing of the active layer on the coastal plain of the Alaskan Arctic. *Permafrost and Periglacial Processes* 8: 1-22.

The Effect of Snow Cover on Permafrost Thermal Stability

Erwin L. Long
Arctic Foundations, Inc.
Edward Yarmak, Jr.
Arctic Foundations, Inc.

Abstract

The investigation to determine a cause for differential settlement of a tower foundation at Glennallen that had been stable for over 40 years led to the derivation of formulae that reflected Osterkamp's measurements for depth to base of permafrost in the area and included snow depths, temperatures, and quantity of thermosyphon cooling.

Keywords: Alaska; foundation; permafrost; snow depth; thermosyphon; warming.

Background

Two towers were constructed in 1960 on permafrost, using thermosyphon technology for passive subgrade cooling for the first time. The two Alaska Communications Systems (ACS) towers are both located in the vicinity of the Gulkana Airport. The Glennallen Tower is located approximately 4½ mi (7.2 km) southwest of the Gulkana Airport along the Glenn Highway, and the Aurora Tower is located approximately 21 mi (34 km) northeast of the Gulkana Airport and ½ mi (0.8 km) off the Tok Cutoff Highway. The locations of the tower sites are shown on Figure 1. Both sites are underlain by lakebed colodial clay silts which include coarser soils with cobbles and boulders dropped from glacial icebergs. The weather station at the Gulkana Airport has operated continuously since 1949. The construction of the Glennallen tower was begun one year after the construction of the Alaska Road Commission (ARC) complex on the west side of the ACS site. The ARC complex was constructed as if on a non-permafrost site, and the ARC recognized the existence of permafrost only after their water well froze up and considerable differential settlement of the structures in the complex occurred. The Aurora tower was constructed on virgin stunted black spruce terrain underlain with permafrost.

The Gulkana Airport is at an elevation of 1580 ft (482 m). The Aurora tower site is at 1890 ft (576 m), and the Glennallen tower site is at 1455 ft (443 m). Both towers are four-legged with post and pad type foundations. The individual tower leg foundations are composed of three 12-in (300 mm) XH pipe thermosyphons 24 ft (7.3 m) in length with the base plates 18 ft (5.5 m) below finished grade and are described in detail by Long (1963).

The Glennallen site was evaluated in 1981, and a new transmitter and equipment building was constructed on thermosyphon piling to the east of the tower. The new structure replaced the original building that was originally constructed on-grade and later refrigerated to minimize thaw settlement.

Both tower foundations were evaluated and soil temperatures measured in 1988. Soil temperatures were found to be warmer than anticipated in the original design. As a result, 170 ft^2 (15.8 m^2) finned condensers were added to two of the waveguide thermosyphon piles at the turf-covered Glennallen tower facility in 1989. Temperature measurements at the Aurora facility indicated a depth of thaw of over 20 ft (6.1 m) in the area surrounding the most southern tower leg foundation. To reverse the thawing found at Aurora, 510 ft^2 (47.4 m^2) finned condensers were added to the NW, SW, and SE foundations and 170 ft^2 (15.8 m^2) finned condensers were added to each of the waveguide foundations in 1989. Foundation temperatures seemed to be affected more by summer surface conditions than by the winter snow cover or the winter air temperature.

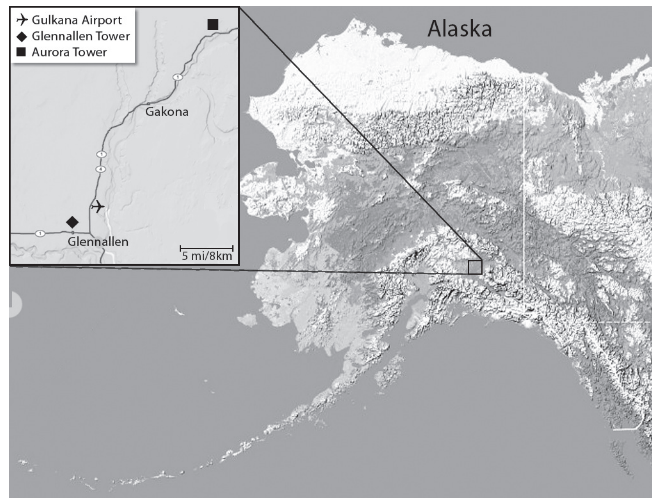

Figure 1. Location map.

In summer 2007, the foundations systems for each tower were inspected. Excessive settlement was found on two of the tower leg foundations at Glennallen. No settlement was found at Aurora. In order to prepare recommendations to stop the settlement at the Glennallen site, an in-depth evaluation was performed to determine the cause of the settlement. It was a goal to develop a method for better evaluation of permafrost stability with changing climate and to provide a means of pre-site evaluation.

Analysis

Osterkamp (2003) reported the depth to the base of permafrost at Gulkana for the period from 1985 to 2001. The depth to the base of permafrost is an excellent measure of the long-term thermal stability of permafrost. This measurement includes all the effects of climate change at a particular site.

Measured thermal conductivity of snow varies primarily with density and ranges from 0.02 btu/hr•ft•°F (0.034 W/M°K) to 0.29 btu/hr•ft•°F (0.503 W/M°K) for densities from 14.7 lb/ft^3 (0.236 g/cm^3) to 32.2 lb/ft^3 (0.515 g/cm^3) (Sturm et al. 2002). In comparison, a typical extruded polystyrene insulation used in civil construction has a thermal conductivity of approximately 0.02 btw/hr•ft•°F (0.03 W/M°K) (ASHRAE Fundamentals 2001). By the numbers, the insulating value of snow is very apparent. Of course, this is nothing new to the people who live in the Arctic and Subarctic, where a snow pile may be the difference between comfortable survival and freezing to death.

The authors have seen instances where snow drifting caused by man-made structures has insulated the ground to such a degree that the depth to the top of permafrost at the end of the thawing season increased from 5 ft (1.5 m) to 14 ft (4.3 m) in two years. An increase in the natural snow depth will have similar albeit more subtle consequences. In the region where the Glennallen and Aurora towers are located, a small change in the surface heat balance equals a large change in the foundation soil properties.

An empirical equation (Equation 1), which included snow depth, was developed to approximate the degree of surface freezing affecting the local permafrost. Weather data from the Gulkana Airport show an average accumulated snow depth of 26.6 in (676 mm) with an average Freezing Index of 4621 °F-days (2567 °C-days) and an average Thawing Index of 2970 °F-days (1650 °C-days) from 1960 through 2007. The end of December accumulated snow depth (DAS) was selected to approximate available seasonal surface snow conditions. Twenty inches (508 mm) was selected as an approximate mean snow depth at the end of December.

Accumulated degree days =

$$-\left(n_f\,{}^\circ d_f \,/\, \sqrt{\frac{DAS}{20}}\right) + \left(n_t\,{}^\circ d_t\right) \tag{1}$$

$°d_f$ = Degree days freezing (°F)
$°d_t$ = Degree days thawing (°F)
n_f = Winter air to surface temperature reference
n_t = Thawing air to surface reference
DAS = December accumulated snow depth (inches)
20 = Arbitrary snow depth reference (inches)

The results are shown as Figure 2 alongside a plot of the depth to the bottom surface of the permafrost presented by Osterkamp for Gulkana. Note that each plot fits the other well with a time offset to account for the depth to the base of the permafrost.

Equation 1 was then modified to represent the effect of the themosyphon cooling in a 70 ft (21 m) radius of the tower and building area. The work was done by trial and error so that the modified empirical equation would mimic the variation in the depth of the permafrost base over time.

The ground surface area being evaluated was selected as having a diameter approximately equal to the depth to the base of the permafrost. The magnitude of the supplemental cooling is a function of the thermosyphon radiator and is represented by its area (SF).

Accumulated degree days =

$$-\left(n_f\,{}^\circ d_f \,/\, \sqrt{\frac{DAS}{20}}\right) - \left({}^\circ d_f * \frac{SF}{A}\right) + \left(n_t\,{}^\circ d_t\right) \tag{2}$$

SF = Square feet of radiation surface
A = Square feet of 70-foot radius area

The plots of Equation 2 for each of the tower sites are shown in Figure 3. It is very apparent that 1976 was a pivotal year for the cooling of permafrost at Gulkana.

The permafrost cooling period from 1960 to 1976 reflects the greater Freezing Index (4935 °F-days (2742 °C-days)) and lesser Thawing Index (2906 °F-days (1614 °C-days)) with an average snow cover of 19.4 in (493 mm) at the end of December while the period from 1978 to 2007 reflects the lower Freezing Index (4416 °F-days (2453 °C-days)) and greater Thawing Index (3012 °F-days (1,673 °C-days)) combined with a heavier snow cover of 34.1 in (866 mm).

Figure 4 compares the Glennallen tower area accumulated degree-days with thermosyphon conditions with the conditions south and west of the tower. Figure 5 shows the Aurora tower area accumulated degree-days with thermosyphon conditions, compared with surrounding area conditions. The Glennallen tower area had a good surface turf cover, while Aurora had an exposed gravel surface which increased its summer thaw. Aurora had a greater thermosyphon heat removal capacity, which improved its frost conditions over Glennallen during years of heavy snow cover.

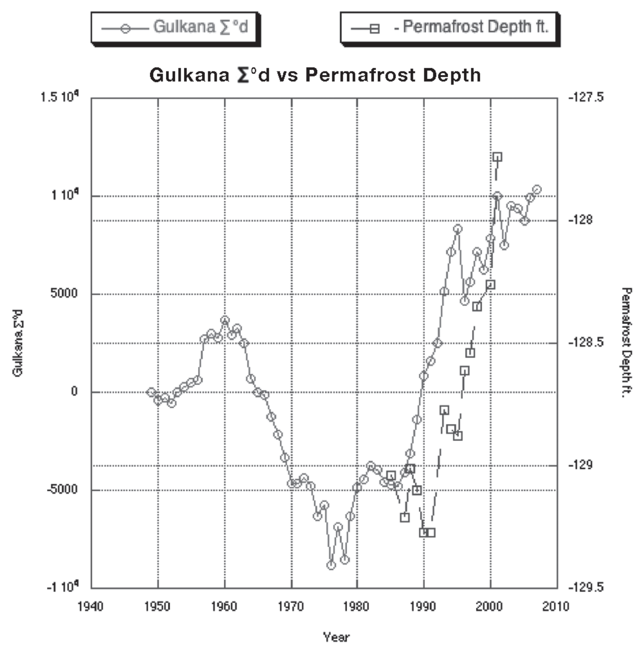

Figure 2. Equation 1 for Gakona airport

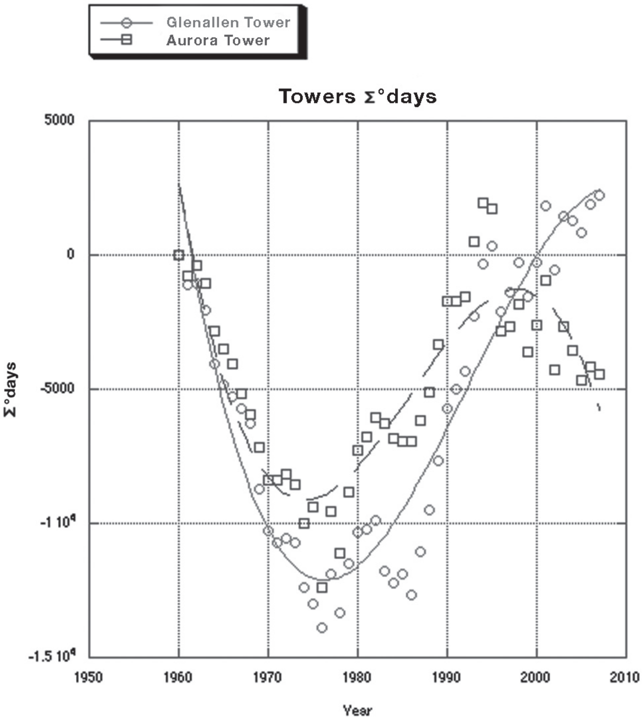

Figure 3. Equation 2 for Glennallen and Aurora towers.

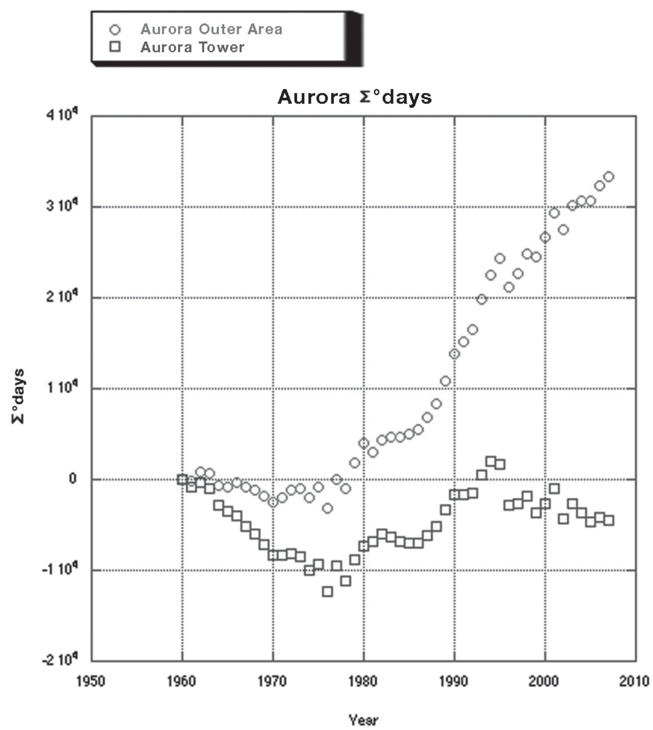

Figure 4. Glennallen tower thermosyphon effects.

With the prevalent colodial soil throughout the area, reduced temperatures will enhance ice lens formation as envisioned by Radd and Oevtle (1973), while warming will cause thawing and settlement (Nelson et al. 1983). By increasing the cooling capacity of the south and west foundations at Glennallen, ice lens formation and permafrost expansion below the foundation pads is expected to occur

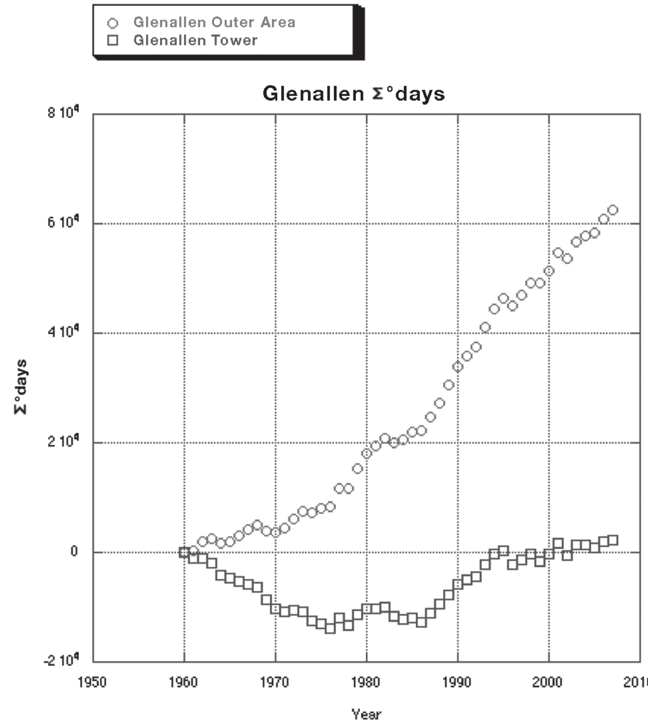

Figure 5. Aurora tower thermosyphon effects.

and help counteract the existing differential settlement and lateral thawing from the adjacent uncooled areas.

Conclusion

The data show that the greatest settlement occurred under the foundations with the least thermosyphon cooling capacity during periods of higher than normal snow cover. When analyzing the thermal conditions for a structure, the design should be area-wide and include snow conditions.

Recommendations

Increase the thermosyphon cooling of the foundations with the largest settlement at the Glennallen tower site.

References

ASHRAE Fundamentals. 2001. *Typical Thermal Properties of Common Building Insulating Materials.* American Society of Heating, Refrigeration and Air Conditioning Engineers, 25.5.

Long, E.L. 1963. The long thermopile. *Proceedings of the First International Conference on Permafrost, Lafayete, Indiana, USA:* 487-491.

Osterkamp, T.E. 2003. A thermal history of permafrost in Alaska. *Proceedings of the Eighth International Conference on Permafrost, Zurich, Switzerland*: 863-868.

Nelson, R.A.. Luscher, U., Rooney, J.W. & Stramler, A.A. 1983. Thaw strain data and thaw settlement predictions for Alaskan soils. *Proceedings of the Fourth International Conference on Permafrost, University of Alaska, National Academy Press*: 912-917.

Radd, F.J. & Oertle, D.H. 1973. Experimental pressure studies of frost heave mechanisms and the growth-fusion behavior of ice. North American Contribution, *Proceedings of the Second Second International Conference on Permafrost, Yakutsk, USSR*: 377-384.

Sturm, M., Perovich, D.K. & Holmgren, J. 2002. Thermal conductivity and heat transfer through the snow on the ice of the Beaufort Sea. *Journal of Geophysical Research* 107, American Geophysical Union.

Bibliography

Esch, David C. (ed.) 2004. *Thermal Analysis, Construction, and Monitoring Methods for Frozen Ground.* ASCE Technical Council on Cold Regions Engineering Monograph.

Kinney, Thomas C., Santana, Barry W., Hawkins, D. Michael, Long, Erwin L. & Yarmak Jr., Edward. *Foundation Stabilization of Gas Injection Facilities, Prudhoe Bay, Alaska*, 618-622.

Luscher, Ulrich & Afifi, Sherif S. *Thaw Consolidation of Alaskan Silts and Granular Soils*, 325-334.

North American Contribution. Second International Conference on Permafrost, Yakutsk, USSR, 1973.

Osterkamp, T.E. *Response of Alaskan Permafrost to Climate*, 145-152.

Proceedings of the Fourth International Conference on Permafrost. University of Alaska, National Academy Press, 1983.

Proceedings of the Sixth International Conference on Permafrost, South China University of Technology Press,1993.

Zhang, T. & Osterkamp, T.E. *Changing Climate and Permafrost Temperatures in the Alaskan Arctic*, 783-788.

Chronosequence of Forest Fire Effects on the Active Layer, Central Yakutia, Eastern Siberia

L. Lopez
The United Graduate School of Agricultural Sciences, Iwate University, Morioka 020-8550, Japan
G. Guggenberger
Martin Luther University, Halle-Wittenberg Institute of Agricultural and Nutritional Sciences, Soil Biology and Ecology Group Weidenplan 14 06108 Halle, Germany
E. Gerasimov
Permafrost Institute Siberian Branch, Ras, Yakutsk, Russia
R. Hatano
Graduate School of Agriculture, Hokkaido University, Sapporo, Hokkaido, 060-8589, Japan
A.N. Fedorov
Permafrost Institute Siberian Branch, Ras, Yakutsk, Russia

Abstract

Despite the large area that fire covers, its recurrent nature, and its ecological role in this boreal region, it has been poorly studied. This research was conducted in naturally burnt sites (five) with different post-fire periods; 4, 5, 15, 25, and 50 years and intact (*Larix cajanderi*) forest sites (three) that were considered as control sites. Sampled soil profiles included the active layer and the upper permafrost (0–1.7 m). The effect of fire on the aboveground can be clearly observed, but what happens in the belowground is not well understood in fire-prone eastern Siberia. Irreversible landscape changes occurred when the ice-rich and salty permafrost reached a degradation threshold. The results of this study show that the active layer of burnt sites older than 25 years does not differ significantly with the active layer of intact forests. On the other hand, the "younger" burnt sites showed a deepening of the active layer. The degrading and aggrading processes of the permafrost are apparently followed by hydro-geochemical processes supported by the poorly drained soil conditions of the active layer. In the intact forest sites, the soil ion profile shows increasing concentration downwards, especially in the permafrost layer. During the years of permafrost thawing, ions moved upward into the upper soil layers. Once the water balance of the site is balanced by the appearance of birch (*Betula platyphilla*), soil moisture in the lower layers starts accumulating, and this movement downward brings the ions back to the lower layers where, due to high water content and lower soil temperatures, they become trapped again in permafrost (aggrading). This process takes approximately 20 years. In conclusion, fires in central Yakutia are at present assimilated by the forest ecosystem and the drastic changes it experiences initially are temporal. The conditions necessary for a permanent change in this boreal forest ecosystem is the increase in fire frequency which would not allow forest regeneration.

Keywords: active layer; forest fires; global warming; permafrost regions; salinization.

Introduction

Forest fires in central Yakutia are recurrent phenomena that determine regeneration, carbon storage and temporal changes in land cover. The trigger for fire can be natural (lightning) or human caused (human activity), but the condition necessary for severe fire expansion is dry weather (long rainless periods), high temperatures and low relative humidity. Forest fires are a large source of both carbon dioxide and methane emissions. However, they are both a temporary source of carbon dioxide and usually a biogenic one (Radionow et.al. 2006). Under special circumstances, which are a combination of factors such as fire intensity and climatic cycles (Shender et al. 1999), its occurrence in ice-rich and shallow permafrost burnt sites can develop into thermokarst depressions (Czudek & Demek 1970, Brouchkov et al. 2004, Agafonov et al. 2004) or as is more general, forest can return to its former state (as before the disturbance occurs).

Forest fires in eastern Siberia are not crown fires which are more devastating in their effect (Harden et al. 2000), but surface fires (Mouillot & Field 2005) because of low tree density and because of the pyrophytic properties of larch trees (Nikolov & Helmisaari 1993, Tvsetkov 2004). Changes above ground can alter the movement of water and salts present in the lower part of the active layer and upper permafrost (Lopez et al. 2007a). The organic matter in the top layer cools the active layer, and its disappearance after severe fires results in active layer deepening. Forest fires in Siberia have been cited as large scale disturbances that can contribute to permafrost degradation if the soil thermal regime is altered by climatic change (Kasischke et al. 1995, Zimov et al. 1996). However, to our knowledge no study has focused on the long-term effect on the belowground after forest fires in eastern Siberia (several years after the fire occurrence). If climatic warming increases fire frequency or intensity, the increase in annual thaw depths could result in active layer salinization within areas of salt-rich permafrost (Kokelj & Lewkowicz 1999, Lopez et al. 2007a). Thus, the objective of this study is to assess the process by which the forest ecosystem, especially belowground, recovers after a forest fire,

Materials and Methods

Site description

Neleger Experimental Station is located 30 km north-northwest from the city of Yakutsk (62º05′N, 129°45′) and belongs to the Yakutsk Permafrost Institute. Mean annual air temperature is -10 to -11°C; amplitude of monthly temperatures is about 62°C. Snow cover is 30–40 cm, but it has recently reached 60 cm. Icy deposits are located at depths from 1.5 m to about 3 m; they occur over more than half of the territory, have thicknesses of up to 20–25 m and are distributed in 18% or 76,000 km^2 of the territory of central Yakutia (Fedorov et al. 1991). The area consists of a group of Lena River terraces with elevations of 200–220 m a.s.l.; it is a region of continuous permafrost up to 400–500 m thick. Quaternary deposits are from a few meters to 200 m thick. The bedrock predominantly consists of limestones and argillites. Disturbances that occurred around 10,000 years ago, and still continue, have changed the landscape of this area to grassland (thermokarst depressions). Precipitation during the snow-free growing season is on average 110 mm, which is about half the annual precipitation, whereas the corresponding potential evaporation rate is 370 mm (Muller 1982). Soils in this region are classified as Gelisols; they are predominantly silty-clay-loam (SiCL) to silty-clay (SiC) in 70% of the territory and sandy-loam (SaL) in the remaining part.

Sampling

The sites selected were three intact forests (F1, F2 and F3) and five chronologically burnt forests (B1, 4 years; B2, 5 years; B3, 15 years; B4, 25 years; and B5, 50 years). The soil texture at all sites was silty-loam. Three 1.7 m-long soil profiles were sampled at each location in May 2006. The sampling took place when the soil profile was still frozen and required a boring machine. The frozen layer (permafrost) was measured in late September when the thawing front reached its maximum. The core samples were sectioned in 10-cm intervals, logged, double-bagged, and returned to a laboratory. Soil texture was determined by observation and feel.

Soil moisture and chemical analysis

Soil moisture was determined gravimetrically by drying to a constant weight at 105ºC for 24 hours. A different set of soil samples taken next to the samples used for soil moisture measurements, in each of the profiles, was air dried and then analyzed for pH in a supernatant suspension of 1:5 soil:deionized water mixture (pH meter HORIBA) and electric conductivity in a supernatant suspension of 1:5 soil:deionized water mixture (Page et al. 1982) (EC meter TOA CM-30V) for each sampling site. Electric conductivity of saturated paste (EC_e), used to evaluate saline and alkaline soils, was estimated using soil water 1:5 suspension measurements and following the relation obtained by Slavich & Petterson (1993) for each soil texture. One soil profile at each of the sites was subjected to ion content analysis: cations were measured by atomic absorption spectrophotometer (Hitachi Z5010) and anions by ion chromatograph (Dionex).

Results

Soil texture in the profile was predominantly silty-loam at all locations down to 1.5 to 1.6 m. At site F1, pure ice was found from 1.5 m. The ice found in that particular sampling is part of ice wedges that can be 8 m long. It is this ice that if melted could form pools and cause ground subsidence. Pure ice was not found in burnt sites during sampling, but layers with high ice content were found below the active layer. By principle ice wedges are distributed in areas were the soil is predominantly silty loam and they are absent in sandy loam soils.

Soil moisture

Soil moisture in the active layer sampled at the forest sites revealed different moisture conditions depending on the time elapsed after the fire occurrence. For the period when the sampling was conducted, a common pattern is observed for the forest sites: higher soil moisture in the upper part of the active layer (0 to 60 cm) with high soil moisture content (40 to 60%). This same pattern was observed in the B1, B2 and B3 site. In these three sites and in the forest sites, there exists a layer of lower soil moisture at the bottom of the active layer. In contrast, in sites B4 and B5 (25 and 50 years after fire occurrence), there is a built up of an ice-rich layer in the upper permafrost where soil moisture ranged from 0.4 to 0.6 cm^3.cm^{-3}). Soil moisture in the active layer at the “younger” burnt sites ranged from .2 to .4 cm^3.cm^{-3} at the surface of the mineral soil layer (below 10 cm). At approximately 120 cm depth at all burnt as well as intact forest sites, soil moisture increased, signaling the boundary zone or “shielding layer” between the active layer and area where ice-rich permafrost concentrates (Shur 1988). In the burnt sites the active layer depth ranged from approximately 130 to 160 cm depending on the time elapsed after the fire event (Fig.1). In each site, vegetation differs in biomass with grasses and fireweed

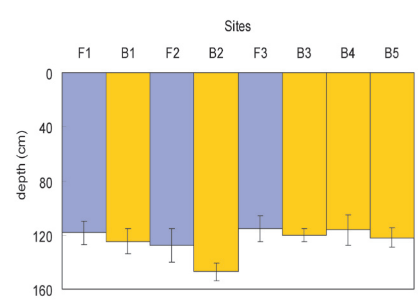

Figure 1. Soil thawing depth at the intact forest (F) and burnt (B) sites.

covering the recently burnt sites (B1 and B2) while birch dominates the sites burnt 15, 25 and 50 years ago (B3, B4 and B5). The size and age of trees differs accordingly but the most important characteristic is the vegetation succession. In B3, for instance, fireweed is non-existent and in B4 birch becomes dominant and its canopy covers the burnt site, while in the B5 site, larch trees are already present, although not still dominant.

Soil pH, EC_e and chemistry

Soil surface (0 to 15 cm) pH varies at the forest sites from 5.5 to 6.2 and then increases rapidly downwards. In the more recently burnt sites B1, B3 and B4, low pH values in the surface layer were observed, whereas pH in B2 and B5 were around 7. Regardless of the site, intact or burnt forest, pH shows a similar value of 8 from 50 cm downward. Despite significant differences observed in the total ion composition of the soil profile, no change was observed in the pH between the active layer and permafrost.

Electrical conductivity of the soil profile showed low values in the active layer (0.81±0.24) and high in the permafrost layer (1.0 to 3.0 $mS.cm^{-1}$) of the intact forest sites. In the burnt sites, EC_e is over 1.0 $mS.cm^{-1}$ and shows an increase in salt concentration in the active layer as compared to the intact forest site (Fig.2). Nevertheless, it is important to point out that EC_e in the B4 and B5 sites are similar to those in the intact forest. In general, the increase in salinity (using EC_e as a proxy) for the burnt sites in the active layer (1.03±0.19) is low in comparison to grasslands soil, for example. The most abundant ions in the active layer and upper permafrost are Cl^-, SO_4^{2-} and Na^+ (Lopez et al. 2007a). Of all these ions, it is the Na^+ that appears more mobile than the other two. As it was observed in the EC_e profile, ion concentration increases in the active layer as a result of fire disturbance. Na^+ moved upward in the B1, B2 and B3 sites, whereas in the B4 and B5 sites this was not observed and the concentration of Na^+ is similar to that in the active layer of the intact forest site. Cl^- appears to have decreased from the upper permafrost except for site B4, where the concentration in the permafrost was remarkably high. It was in the B2 and B3 sites that the increase of SO_4^{2-} was observed, while a decrease in the upper permafrost indicates that it was the source of this ion. Again, a remarkable concentration of SO_4^{2-} was observed in the upper permafrost layer of the B4 site as it was the case with Na^+.

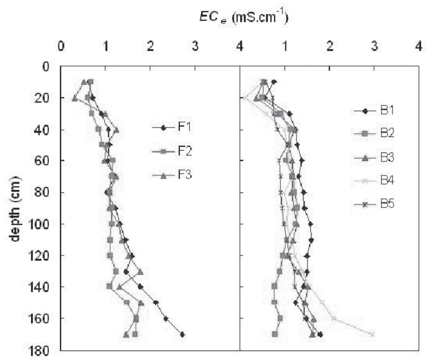

Figure 2. Electric conductivity in the intact forest (F) and burnt (B) sites. Each values are the mean of three samplings.

Discussion

Contrary to what has been suggested in previous studies, forest fires do not cause physical or chemical changes in the long-term that might bring changes in the landscape or specifically hinder the re-establishment of trees. These results, of course, do not suggest that thermokarst formations in the past were not triggered by forest fires. The conditions under which fires occurred at present differ from those during the early Holocene in which the landscape looks much different today than it did approximately 10,000 years ago. The thermokarst depressions intermingled within the forest and called "alas" are actually a drainage zone for the melting snow in early spring and the extreme precipitation events in summer (when the thawing layer is shallow and the storage capacity is low) that are characteristic in central Yakutia (Lopez et al. 2007b). Alas sites, where trees are not able to grow because of high salt content in the root zone (Desyatkin 1993, Lopez et al. 2007a) were caused by global climate changes that most probably triggered forest fires among several other climatic responses (Payette & Delwaide 2000). The results of this study suggest that at present, forests assimilate fires provided they keep the same frequency of occurrence to which they have been exposed during the Holocene. Unfortunately, fire frequency studies have been limited in Siberia, and other causes (political, social or economical) for fire have not been correctly addressed,

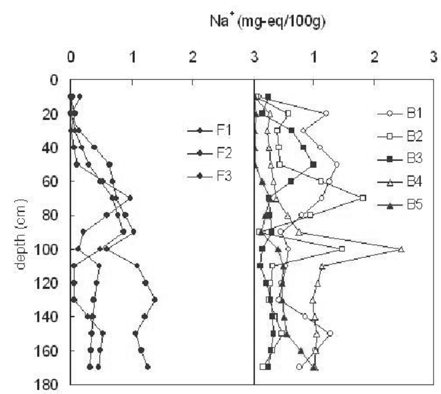

Figure 3. Na^+ profile in the soil profile (0-1.7 m) in the intact forest (F) and burnt (B) sites.

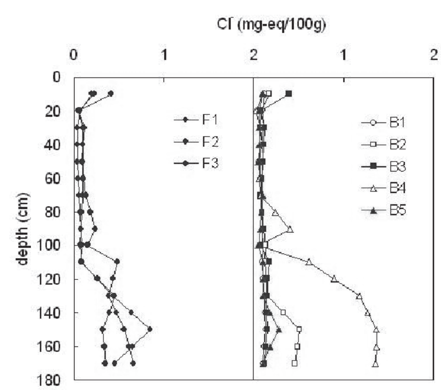

Figure 4. Cl^- profile in the soil profile (0-1.7 m) in the intact forest (F) and burnt (B) sites.

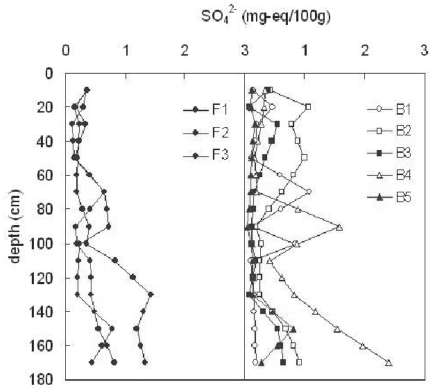

Figure 5. SO_4^{2-} profile in the soil profile (0-1.7 m) in the intact forest (F) and burnt (B) sites.

while global warming has been the most reasonable "pundit" to blame.

Soil moisture increased immediately in the active layer after clear-cut (Iwahana et al. 2005) sites in the same area whereas the cause for immediate increase of soil moisture in the active layer. In this experiment the same was not observed in the site more recently burnt (4 years) or in the other sites, suggesting that vegetation that appeared after severe forest fires (*Chamerion angustifolium*) transpired (2.6 mm d^{-1}, unpublished data) more than the vegetation that appears after clear-cuts. This transpiration rate is similar to the larch forest average transpiration of ~ 3 mm d^{-1} (Dolman et al. 2004, Ohta et al. 2001) in central Yakutia. After fires, the active layer is known to deepen in the first years and later recover to its former depth (Mackay 1995) following re-vegetation of the forest soil and thickening of the organic matter layer, factors that play an important role in keeping a thin active layer. Despite the spatiality of the sampling sites, recovery of the active layer has been also observed in this study. The difference of the above vegetation at each of the sites is thought to exert a strong influence on the water balance of the active layer, and thus cause movement of water that carries ions within its stream. The denser cover of birch trees 15 years after the fire occurrence is probably responsible for cooling of the active layer, as it can be observed from the active layer depth at each of the sites for the year when the experiment was conducted. The role of understory vegetation and the re-building of the organic mat cannot be set aside since they play an important role in keeping soil temperatures low in the soil (Harden et al. 2006). In the older burnt sites (25 years and 50 years) the depth of the active layer was found at around 110 cm depth which is similar to intact forest (Sawamoto et al. 2000). The B2 site had the deepest active layer (160 cm) in 2006. One of the explanation why B1 did not deepened as well could be that the fire in this latter site was light (not stand- replacing fire), and for that reason temperatures in this site were kept lower than in B2. As it has been observed in this study, deepening of the active layer has the potential to make soluble salts available for transport into the upper soil layers of the active layer. Elevated amounts of soluble salts in the root zone especially can affect negatively larch forest establishment because salinity affects plant growth and species diversity.

Between forest and thermokarst depressions in central Yakutia there is usually a belt of birch that marks a buffer zone where soil salt concentration is slightly higher than in the forest but lower than in the grassland soils (Lopez et al. 2007a). This spatial gradient of vegetation adaptability to soil conditions could be the explanation for chronological vegetation succession in fire-prone forest of eastern Siberia. According to information provided by local people, larch forest takes approximately 100 years to fully regenerate in this region.

The results of this study suggest that climate change, already observed in the form of increasing temperatures and increased precipitation in central Yakutia, have the potential to affect the boreal forest through forest fires but this will only happen if, prompted by higher summer temperatures, fire frequency increases prompted by higher summer temperatures, increases. Forest fires play a regeneration role that has been part of this boreal forest for centuries (Ivanova 1996) and has scarcely triggered thermokarst formations (Brouchkov et al. 2004). There should also be strong consideration of winter temperature and precipitation trends, since growing season hydrology and permafrost stability which is affected by winter conditions are strongly linked to the size and frequency of forest fires during the growing season (Ivanova. 1996, Harden et al. 2000) during the growing season.

Conclusions

The effects of forest fires in the boreal forest of central Yakutia are not permanent but are part of a regeneration cycle for the forest in this region. The steps leading to forest degradation (active layer continuous deepening, thawing of ice deposits, formation of pools on the forest soil, etc.) were not observed in the burnt sites in this study. On the contrary, forest fires appear as a temporal phenomenon that revitalizes the forest without affecting its stability.

Acknowledgments

The authors would like to thank the Ministry of Science, Culture and Education through Project RR2002. Our gratitude also goes to A. Cronin for making the English of this paper look "native."

References

Agafonov, L., Strunk, H. & Thomas, N. 2004. Thermokarst dynamics in Western Siberia: insights from dendrochronological research. *Palaeogeography, Palaeoclimatology, Palaeoecology* 209: 183-196.

Brouchkov, A., Fukuda, M., Fedorov, A.N., Konstantinov, P. & Iwahana, G. 2004. Thermokarst as a short-term permafrost disturbance, Central Yakutia. *Permafrost and Periglacial Processes* 15: 81-87.

Czudek, T. & Demek, J. 1970. Thermokarst in Siberia and its influence on the development of lowland relief. *Quaternary Research* 1: 103-120.

Desyatkin R.V. 1993. Syngenetic soil salinization during thermokarst alas formation. *Eurasian Soil Science* 25: 38-46.

Dolman, A.J., Maximov, T.C., Moors, E.J., Maximov, A.P., Elbers, J.A., Kononov, A.V., Waterloo, M.J. & Van der Molen, M.K. 2004. Net ecosystem exchange of carbon dioxide and water of far eastern Siberian larch (*Larix cajanderi*) on permafrost. *Biogeosciences* 1: 133-146.

Fedorov, A.N., Botulu, T.A. & Varlamov, C.P. 1991. Merzlotnie landshafti Yakutii (Poyacnitelnaya zapiska k "Merzlotna-Landshftnoi karte Yakutskoi ACCP masshataba 1:2,500,000. P.I. Melnikov (ed.), Moskow : GUGK, 2 pp.(in Russian).

Hamada, S., Ohta, T., Hiyama, T., Kuwada, T., Takahashi, A. & Maximov, T.C. 2004. *Hydrometeorological* behaviour of pine and larch forests in eastern Siberia. *Hydrological Processes* 18: 23-39.

Harden J.W., Trumbore, S.E., Stocks, B.J., Hirsch, A., Gower, S.T., O'Neill, K.P. & Kasischke, E.S. 2000. The role of fire in the boreal carbon budget. *Global Change Biology* 6: 174-184.

Harden J.W., Manies, K.L., Turetsky, M.R. & Neff, J.C. 2006. Effects of wildfire and permafrost on soil organic matter and soil climate in interior Alaska. *Global Change Biology* 12: 2391-2403.

Ivanova G.A. 1996. The extreme fire season in the central Taiga forest of Yakutia. In: J.G. Goldammer & V.V. Furyaev (eds.), *Fire in Ecosystems of Boreal Eurasia.* Dordrecht, the Netherlands: Kluwer Academic Publishers, 260-270.

Iwahana G.T., Machimura T., Kobayashi Y., Fedorov A.N., Konstantinov P.Y. & Fukuda M. 2005. Influence of forest clear-cutting on the thermal and hydrological regime of the active layer near Yakutsk, eastern Siberia. *J. Geophys. Research* 110: G02004, doi:10.1029/2005JG00039.

Kasischke E.S., Christensen N.L., Jr. & Stocks, B.J. 1995. Fire, global warming, and the carbon balance of boreal forests. *Ecological Applications* 5: 437-451.

Kokelj, S.V. & Lewkowicz, A.G. 1999. Salinization of Permafrost Terrain Due to Natural Geomorphic Disturbance, Fosheim Peninsula, Ellesmere Island. *Arctic* 52(4): 372-385.

Lopez, C.M.L., Brouchkov, A., Nakayama, H., Takakai, F., Fedorov, A.N. & Fukuda, M. 2007a. Epigenetic salinization and water movement in the active layer of Central Yakutia, Eastern Siberia. *Hydrological Processes* 21: 103-109.

Lopez, C.M.L., Saito, H., Kobayashi, Y., Shirota, T., Iwahana, G., Maximov, T.C. & Fukuda, M. 2007b. Inter-annual environmental-soil thawing rate variation and its control on transpiration from Larix cajanderi, Central Yakutia, Eastern Siberia. *Journal of Hydrology* 338: 251-260.

Mackay, J.R. 1995. Active layer changes (1968 to 1993) following the forest-tundra fire near Inuvik, N.W.T., Canada. *Arctic, Antarctic and Alpine Research* 27: 323-336.

Mouillot, F. & Field, C.B. 2005. Fire history and the global carbon budget carbon budget: a 1ºx1º fire history reconstruction for the 20th century. *Global Change Biology* 11: 398-430.

Nikolov, N. & Helmisaari, H. 1993. Silvics of the circumpolar boreal forest tree species. In: H.H. Shugart, R. Leemans & G. Bonan (eds.), *A Systems Analysis of the Global Boreal Forest.* Cambridge, England: Cambridge University Press, 111-132.

Ohta, T., Hiyama, T., Tanaka, H., Kuwada, T., Maximov, T.C., Ohata, T. & Fukushima., Y. 2001. Seasonal variation in the energy and water exchanges above and below a larch forest in eastern Siberia. *Hydrological Processes* 15: 1459-1476.

Page, A.L., Miller, R.H. & Keeney, D.R. 1982. *Methods of Soil Analysis, Second Edition.* Part 2-Chemical and *Microbiological Properties*, Second Edition. Madison, Wisconsin, 169 pp.

Payette, S. & Delwaide, A. 2000. Recent Permafrost Dynamics in a Subarctic Floodplain Associated with Changing Water Levels, Quebec, Canada. *Arctic, Antarctic and Alpine Research* 32: 316-323.

Radionow, A., Flessa, H., Kazansky, O. & Guggenberger, G., 2006. Organic matter composition and potential trace gas production of permafrost soils in the forest tundra in Northern Siberia. *Geoderma* 135: 49-62.

Sawamoto, T., Hatano, R., Yajima, T., Takahashi, K. & Isaev, AP. 2000. Soil respiration in Siberian Taiga Ecosystems with different Histories of Forest Fire. *Soil Science and Plant Nutrition* 46 (1): 31-42.

Shender, N.I., Romanovsky B.E. & Tetelbaum A.C. 1999. Prognoz estestbennoistoricheskih kolebanii klimata gorodov Yakutska i Ferbenska. *Nauka y Obrazobanie* 2: 24-29. (in Russian)

Shur, Y.L. 1998. *The Upper Horizon of Frozen Strata and Thermokarst.* Novosibirsk: Nauka, 212 pp.

Slavich, P.G. & Petterson, G.H. 1993. Estimating the Electrical Conductivity of Saturated Paste Extracts from 1:5 Soil:Water Suspensions and Texture. *Australian Journal of Soil Research* 31: 73-81.

Smith, M.W. 1975. Microclimatic Influences on Ground Temperatures and Permafrost Distribution, Mackenzie Delta, Northwest Territories. *Canadian Journal of Earth Science* 12: 1421-1438.

Tsvetkov, P.A. 2004. Pyrophytic properties of the Larch Larix gmelinii in Terms of Life Strategies. *Russian Journal of Ecology* 35: 224-229.

Zimov, S.A., Davidov, S.P., Voropaev, Y.V. & Prosiannikov, S.F. 1996. Siberian CO_2 efflux in winter as a CO_2 source and cause of seasonality in atmospheric CO_2. *Climatic Change* 33: 111-120.

Pedogenesis and Its Influence on the Structure of the Upper Layer of Permafrost

A.V. Lupachev
Institute of Physicochemical and Biological Problems in Soil Science of RAS
142290, Russia, Moscow Region, Pushchino, Institutskaya, 2

S.V. Gubin
Institute of Physicochemical and Biological Problems in Soil Science of RAS
142290, Russia, Moscow Region, Pushchino, Institutskaya, 2

Abstract

The structure of the upper layers of permafrost and their interaction with cryosols was studied. Cryogenic processes are widely distributed on loamy watersheds of North Jakutia's lowlands, where the active layer is relatively shallow. The upper layer of permafrost here is very complicated and its genesis is connected with the Holocene environmental conditions and pedogenic processes of that time. The authors propose the term "soil-cryogenic complex" that includes the soil profile, transient layer, and intermediate layer of permafrost. The role of the above-permafrost horizon of cryosols in forming structure, properties, and spatial differences of the transient layer was analyzed. Widely distributed lateral transition and accumulation of coarse organic matter between the elements of tundra microrelief were obtained.

Keywords: above-permafrost horizon; active layer; intermediate layer; lateral redistribution; soil organics; transition layer.

Introduction

In case of shallow thickness of the active layer (AL) (1 m and less), permafrost plays a great role in pedogenesis and determines the wide complex of signs and properties of cryosols. It is a significant physical and geochemical barrier that prevents vertical matter migration and determines its lateral redistribution (Shur 1988, Gubin 1994, Alekseev et al. 2003). The relatively high dynamics of AL thickness cause the formation of the complex structure of permafrost upper layers that reflect spatio-temporal interactions with pedogenesis.

Depending on climatic fluctuations, weather conditions, soil cover, and vegetation genesis, this zone of contact can appear as a component of the AL or as a component of permafrost (Shur & Jorgenson 1998, Shur et al. 2005).

The transient layer (TL) (the layer which thaws in the warmest conditions) and the intermediate layer (IL) (the layer of maximal Holocene thaw) are the upper layers of permafrost within this zone (Shur 1975, Shur 1988). The main properties and diagnostic signs of the TL, such as its thickness and the seasonal and long-term dynamics of being in a frozen or thawed state, are the significant factors that influence pedogenesis. It is well-known that the majority of pedogenic fieldwork in high-latitude areas is conducted in the summer, when the AL has not reached its maximum yet and the real above-permafrost soil horizon is still frozen. True thickness of the AL and the morphological structure of soils can be obtained only at the end of September–beginning of October, when surface freezing begins and snow cover becomes stable.

Methods

The moundy soil complex and TL were analyzed on loamy watershed sites of the Khomus-Yuriakh River (Indigirka lowland; 70°00′N, 153°36′E) and Sukharnaya River (Kolyma lowland; 69°30′N, 152°00′E). The basic deposits here are Late Pleistocene silty loams with the features of synlithogenic pedogenesis and with ice complex (yedoma formation). The IL thickness here is about 1–1.5 m. The vegetation cover is represented with moss-sedge-cotton-grass on the Indigirka site and with moss-sage-dryas on the Kolyma site. The mean gradients of the watershed slopes are about 2–3°. The Kolyma site has the features of steppe because of low thickness of snow cover and better drainage.

The structure of soils and the TL were analyzed at the beginning of autumn, when the AL had reached its relative maximum. On the Kolyma site, two trenches were dug through all microrelief elements (2 and 5 m long, 40 cm wide). The structure of soils, their horizon thickness, the AL thickness, and the TL structure (upper 20 cm) were studied. Near the trenches numerous additional soil pits ($n = 15$) were dug to obtain the variety of morphological properties of soils under the mounds of different height and types of vegetation and under the cracks of different depth.

On the Indigirka site, it was necessary to find two experimental, square sites because of more complete soil structure. The first (basic) site is on watershed (250 x 250 cm), and the second (additional) is on the top of a gentle slope (200 x 80 cm; 150 m from the first site; slope gradient, 3°). All of the microrelief elements were within these sites: low, middle, and high mounds with different vegetation, sedge-cotton-grass tussocks. Choosing the proper site, the maximal difference between mounds and crack surface was a concern. The majority of elements within the sites was similar; surface structure, size of mounds and cracks, soil and vegetation cover, and quantity of patchy mounds. The main difference was in relatively more ponding of the second (slope) site which was reflected in a greater distribution of tussocks.

On the first site (watershed), soil and permafrost surfaces were graded. The highest point of a site was taken as “zero,” with the precision of 1 cm and an interval of measure of 5 cm; 2500 measurements of each parameter were made. Measurements of soil horizon thickness (organogenic and above-permafrost) and the TL structure were made with an interval of 10 cm in 10 trenches, 25 cm wide.

After clearance of the site bottom, the lateral structure of the TL was analyzed. There are three main components of it: ice, ice-ground, and frozen coarse organics. Its ice saturation was estimated, and the cryogenic texture was obtained. Morphological analysis of soil profiles was made on the example of the most representative side of the trench, where samples were also taken. According to this data, schemes of soil and permafrost surface, TL structure, and vegetation-cover structure were made.

Additional soil pits (n = 15) were dug near the experimental sites and the TL structure was also studied to a depth of about 20 cm. The AL thickness was measured under the different types of mounds and cracks (n = 130).

The same measurements were made on the second site (slope), but the interval of measurements was 10 cm.

Results and Discussion

Comparison of the soil and permafrost surface schemes of the first Indigirka site (watershed) showed that the microelevations of the TL surface are under mounds and are represented by ice. The authors suggest that such structure of the TL surface can be determined by the previous history of soil-surface genesis, and propose the following model of ice formation.

At the earlier stages of nanorelief genesis (patchy mound with sparse vegetation), the AL thickness was more than under cracks. While thawed, water has accumulated here, and then with seasonal freezing, has turned to ice. This accumulation had a progressive tendency caused by ice forming on the one hand and by vegetation and organogenic horizon forming that has decreased the heat flux on the other hand. Heat absorption differences between ice, ice-ground, and frozen coarse organics determined different speeds of thaw, TL surface genesis, and structure formation (Mackay 1983).

The results of comparing soil surface and TL microrelief schemes of the second Indigirka site are a little bit different. Their topography is well expressed too, but the micro-depression zones of the TL surface are mainly distributed under the centers of mounds, and are presented by ice-grounds or coarse organics. The micro-elevations are under cracks filled with peat. Ice distribution in the TL is related to circumferential parts of mounds, and ice underlies 5–10 cm deeper than the TL surface. The same situation in the soil and the TL structure was obtained in numerous additional pits (n = 8) in microrelief and appears to be authentic for this region of the Indigirka lowland.

Another component of the above-permafrost horizon (AH) and TL formation was obtained in numerous soil pits and trenches. When the AL thickness reaches its relative maximum, the lower parts of soil profiles are over-saturated with water. The microdepressions of the TL surface microrelief become the channels, where the inrush of water is obtained. The scheme of possible fluxes, which was created by a method of relief plastic (Stepanov 2006) on data basis, coincided with the situation obtained in the field. Such water redistribution determines the coarse organic matter redistribution and discharge (Shuster et al, 2003, Mergelov 2006). The material is denuded from the microelevations of the TL surface and accumulates in the microdepressions. The obtained data show that the mean slope gradient is about 2–5°, and the maximal is 12–15° or even 20°. Such an active migration of small portions of wet peat along the microslopes can be forwarded by thaw of ice-ground with the reticulated cryotexture, which is distributed in negative microrelief forms.

The authors suppose that the difference in spatial structure of the TL and the AH is determined by the processes which occur in the lower parts of the soil profile and by the interaction of microrelief elements.

On the Indigirka site, in the majority of cryosols under mounds, the organogenic AH is forming. It consists of peat mixed with mineral material. Organic carbon content here is 4.7% (n = 6). These indexes are a little bit higher in the TL, but then they decrease with depth. Both horizons are spatially different. Zones which are extremely rich with organics are obtained here (23.4%). There are also flux-like zones in which the organic material is mixed with the mineral one (3.2%). As for the mean samples of coarse organic material, total organic carbon content is 10.1% for the first experimental site (n = 10) and 8.9% for the second (n = 6). The mean thickness of the AH is 7–12 cm, and the total thickness of this horizon with the TL is 25–32 cm. This data coincide with that of another author (Hinkel 2005).

The mean thickness of the peat (or duff) horizon is not more than 7–13 cm, and the quantity of organic carbon here is about 9%. So in some cases, the store of organic carbon in the system here (AH + TL) is even more than in the upper parts of soil profiles (except of peat soils in nanopolygonal cracks).

The given data allow us to single out the organogenic AH of Indigirka tundra soils that differs from similar horizons with cryoturbated organic material of the Kolyma lowland (Karavaeva 1969, Gubin 1994), other regions of North Jakutia (Elovskaya et al. 1979), and East European tundra (Ignatenko 1979). Soils with such an unusual lower horizon and TL were obtained earlier (in the 1980s–1990s) on watersheds of typical tundra in the Alazeya-Kolyma region. Distribution of such soils is limited, and the main requisition is the existence of cracks filled with peat that reach the surface of permafrost. So the possibility of such a system forming is determined by contemporary and previous (Holocene) conditions (AL thickness, processes of frost heaving and peat forming, etc.).

Conclusions

An analysis of loamy watershed deposits and cryosols of North Jakutia lowlands shows the existence of a complex system of layers with different properties on the border between the AL and permafrost. Its genesis and structure are determined by the bioclimatic situation of the Holocene. The authors propose to single out this system as a "soil-cryogenic complex." Its structure is the following: soil profile: TL (a layer which thaws in the warmest conditions) and IL (a layer of maximal Holocene thaw). The border between the AH and TL is the arena of active pedogenesis, where its most specific features are reflected. The spatio-temporal differences of this system show the mechanisms of soil-cover genesis and the interactions between its elements. Such well-expressed permafrost microrelief determines the wide lateral redistribution, migration, and accumulation of coarse organic matter within this complex.

Acknowledgments

The authors thank Yuri Shur for the inspiration for this work and for genuine interest in it.

References

Alekseev, A., Alekseeva, T., Ostroumov, V., Siegert C. & Gradusov B. 2003. Mineral transformations in permafrost-affected soils, North Kolyma lowland, Russia. *Soil Science Society of America Journal* 67: 596-605.

Elovskaya, L.G., Petrova, E.I. & Teterina, L.V. 1979. Soils of North Jakutia. Nauka, Novosibirsk (in Russian).

Gubin, S.V. 1994. Late Pleistocene soil formation on sea-lowlands of North Jakutia. *Pochvovedenie* 8: 5-14 (in Russian).

Hinkel, K.M. 2005. Characteristics and significance of the transition zone in drained thaw-lake basins of the Arctic Coastal Plain, Alaska. Published 01.12.2005 online in *Goliath*.

Ignatenko, I.V. 1979. Soils of East-European tundra and forest-tundra. Nauka, Moscow (in Russian).

Karavaeva, N.A. 1969. Tundra soils of North Jakutia. Nauka, Moscow (in Russian).

Mackay, J.R. 1983. Downward water movement into frozen ground, western arctic coast, Canada. *Canadian Journal of Earth Sciences* 20(1): 120-134.

Mergelov, N.S. 2006. Origin of organic carbon pools in Kolyma cryosols: Phenomenon of organic carbon impregnation in mineral horizons. In *Proceedings of 18th World Congress of Soil Science July 9-15, 2006, Philadelphia, Pennsylvania, USA*.

Shur, Y.L. 1975. On the transient layer. In: P.F. Shvetsov & L.V. Chistotinov (Eds.), *Methods of Geocryological Studies*, Shvetsov, USSR Institute of Hydrogeology and Engineering Ecology, Moscow: 82-85 (in Russian).

Shur, Y.L. 1988. Upper horizon of permafrost and thermokarst. Nauka, Moscow (in Russian).

Shur, Y.L. & Jorgenson, M.T. 1998. Cryostructure development on the floodplain of Colville River Delta, northern Alaska. *Proceedings of Seventh International Conference on Permafrost*. Centre d'Etudes Nordiques, Universite Laval: Quebec: 993-1000.

Shur, Y.L., Hinkel, K.M. & Nelson, F.E. 2005. The transient layer: implications for geocryology and climate-change science. Published online in *Wiley Interscience*. DOI: 10.1002/ppp.518.

Shuster, P.F., Reddy, M.M., Aiken J.R. & Shanley, J.B. 2003. What effect does permafrost have on dissolved organic carbon transport to streams during snowmelt? *U.S. Geological Survey, Water Resources Discipline.*

Stepanov, I.N. 2006. Relief plastics theory and new thematic maps. Nauka, Moscow (in Russian).

Soil Properties of the Eroding Coastline at Barter Island, Alaska

Lorene A. Lynn, Chien-Lu Ping, Gary J. Michaelson
Palmer Research Center, Agricultural & Forestry Experiment Station, University of Alaska Fairbanks, Palmer, AK, USA
M. Torre Jorgenson
Alaska Biological Research, Inc., Fairbanks, AK, USA

Abstract

Erosion along Alaska's Beaufort Sea Coast introduces substantial quantities of largely undecomposed organic matter into the Arctic Ocean annually. Three bluff exposures along the northern coastline of Barter Island revealed organic materials extending 1.5 meters below the surface. Peat deposits (12–80 cm thick) are in sediments that extend to 1.8 meters and overlay sands and gravels, under which are alluvial-marine sediments. The bluff exposures are composed of 10–20% ice wedges and moisture content of the soil ranged 2–80%. Total carbon content in the active layer averaged 10% and 14% in the frozen soil. Total nitrogen was less than 2% throughout the soil profiles. Soil pH and electrical conductivity show a relationship between mineral soils at depth and increased values.

Keywords: Arctic Alaska; coastal erosion; cryogenesis; cryoturbation; gelisols, patterned ground soils.

Introduction

Coastal erosion is a growing concern in northern Alaska. The apparent accelerated rate of erosion along the Beaufort Sea coast of Alaska (Brown et al. 2003) may have major implications for life and development along the coast. Several coastal Native Alaska villages are battling against increasing storm intensity and frequency (McCabe et al. 2001), a continuing loss in duration of the protective sea ice (Fetterer 2002, IPCC 2007), and increasing summer temperatures (Jorgenson et al. 2006). All of these are causing increased erosion and permafrost degradation. In Kaktovik, located on Barter Island, the current airport and an old landfill site are rapidly eroding into the sea (Robinson 2004). Erosion along the arctic coastline of northern Alaska has also been hypothesized to be a significant influence on global climate change due to the input of carbon-rich peat soils into the ocean and carbon dioxide to the atmosphere (Jorgenson et al. 2005). The result may be a positive feedback to an Arctic warming cycle.

On polygonal terrain along the coast, soil physical structure and chemical properties are strongly related to ice wedge polygon development (Shur and Jorgenson 2007). This interactive-formative process may span a period of five to eight thousand years. Soil stratifications and physical structures are mixed and warped, by cryoturbation, at the boundary of ice wedges due to freeze-thaw cycles and ice wedge formation and reformation (Bockheim 2007). This situation complicates the examination of soil morphology and characterization of the active layer and renders the systematic interpretation of permafrost soils a challenge.

In the past, tundra soils have been a significant carbon sink because primary production has been greater than the slow decomposition rate of organic matter in cold and frozen permafrost soils (Hobbie et al. 2000, Ovenden 1990). As a consequence, it is estimated that tundra soils have accumulated an estimated 25–33% of the world's soil carbon (Oechel and Vourlitis 1995). Soils along the Arctic coastline contain large quantities of mostly poorly decomposed organic materials (Ovenden 1990, Ping et al. 1997). As the coast erodes, there is a change in the thermal regime of the soil and the ice wedges degrade. Moisture content decreases while temperatures increase, and as a result the active layer thickens.

Likewise, warming temperatures can cause large scale permafrost and ice wedge degradation (Jorgenson et al. 2006) which can in turn cause substantial changes in surface hydrology (Hinzman 2005). In the last several decades, temperatures have been on the rise in the Northern Hemisphere, most notably in the Arctic and Sub-Arctic (IPCC 2007), and there is evidence that this warming trend will continue unabated (Chapman and Walsh 1993, Serreze et al. 2001). The current warming trend in the arctic is evidenced by increased erosion of the northern coast of Alaska (Semiletov 1999, Brown et al. 2003), permafrost degradation (Jorgenson and Kreig 1988, Jorgenson et al. 2001), and decreased extent and duration of sea ice and hydrological changes (Morrison et al. 2000).

The ability to make predictions about changes in the soil depends on an understanding of what alterations are taking place and what interactions may occur between various soil properties. To understand the complex changes that may occur due to erosion of coastal soils, a detailed study of soil morphology, as well as chemical and physical soil processes is required. In this study we examine properties of the soils that are eroding along the coastine exposures near Kaktovic Alaska in order to better understand the processes occurring and materials being transferred to nearshore waters.

Methods

Sites for intensive investigation were selected on the northern shore of Barter Island, west of the village of Kaktovik. Three bluffs sites were selected for excavation and sampling (GPS: 70.13393N, -143.65578W, 70.13393N, -143.65245W, and 70.1345N, -143.66083W). Polygons

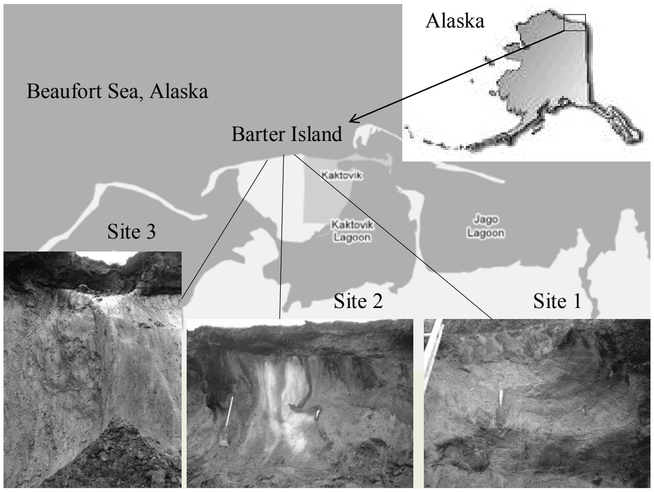

Figure 1. Site location and profile photos.

west of Kaktovik are very large and flat, measuring 12–20 m in diameter, indicating large ice wedge formation. Exposed ice wedges at the eroding bluff are indeed large, reaching 3–3.5 m in width. The large ice wedges and dense surface polygonal net in this area are consistent with high bluff alluvial-marine sediment landforms. Most of the vegetation cover along the northern Barter Island coastal bluff is sedge with some willow and small amounts of Dryas found on frost boils. Bluff exposures at three points located approximately 100 m apart (Fig. 1) were cleaned from the surface to a depth of 1.5 meters. Following removal of slumped and refrozen material, the soil layers were identified (Schoeneberger et al., 1998), dimensional samples were cut from the active layer, and dimensional core drilled with a SIPRE corer to a maximum depth of 1.5 m. All samples were kept frozen until time of analysis at the UAF-AFES Plant and Soils Laboratory at the Palmer Research Center. Soil bulk density and water contents were determined by weight difference of dimensional samples upon drying at 100°C. Total organic C (TOC) and N were determined using a LECO CHN analyzer and organic matter (%OM) by loss on ignition at 450°C. Exposure sediment, water, TOC, and N stocks were determined using the exposure description and analysis by the method of Kimble et al. (1993) to account for cryoturbation. Temperatures from near the surface soil and right above the permafrost table were measured with a thermometer.

Results and Discussion

Temperature

Soil temperatures in the first week of August, 2006, at the ground surface, measured from 5–7°C, and just above the permafrost 2–5°C. Surface temperatures are likely to vary based on weather conditions present.

Cryogenic features

Active layers along the northern coast of Barter Island averaged lower volumetric water at 38% compared to the permafrost which averaged 53% volumetric ice (Table 1).

Table 1. Soil properties for eroding shoreline at Barter Island, Alaska.

Property	Bluff Exposure 1	2	3
Bank height above water (m)	18	18	18
Mean thaw depth (cm)	45	36	54
Cumulative organic thickness (cm)	77	63	87
Maximum organic depth (cm)	133	78	127
Total amount of wedge ice volume (%)	21	20	18
Total organic carbon store in top 1m, excluding ice wedges, volumetric extrapolation from sample, (kg C/m²)	32	41	34

The high water content in active layers is positively related to organic matter which has high water holding capacity.

The high water (ice) content in permafrost is due to segregation of ice. The upper active layer is dryer than the permafrost due to exposure to warmer temperatures, drainage at the bluff face, and lateral movement to lower-lying thermo-erosion troughs nearby. In addition to buried organic layers holding water, ice lenses ranging in thickness from 1mm to 20mm were present in the permafrost cores. Vertically aligned ice bubbles in these ice lenses indicate that each lens is a former freezing front. In early winter, the thawed portion of the soil refreezes at two fronts: from the surface and from the underlying permafrost. Water in the active layer migrates toward these freezing fronts and low-lying water will migrate toward the lower freezing front. This vertical movement is evidenced in the bubble alignment. All three cores showed evidence of refreezing in the first 3 cm from a deeper thaw in a previous summer.

Ice wedge volume on Barter Island is higher compared to other portions of the Beaufort Sea coast. The high bluffs provide protection from direct ocean wave impact and erosion. Because of the volume of the large ice wedges, extensive cryoturbation is evident. As the ice wedges develop and expand, they squeeze the inter-laying soils, bending and distorting soil horizons, and altering bulk density and thus, moisture-holding capacity. This evidence of cryoturbation is strongest near the ice wedges and less in the center areas of polygons. Barter Island experiences short, cool summers and very cold winter temperatures. The severe cold can cause the surface soil layers to crack vertically. The combination of material falling or washing into these cracks, and the distortion imposed on soil layers by expanding ice wedges creates the cryoturbated features (Fig. 1).

Morphological properties

Depending on where the permafrost core is drilled in relation to the location of the ice wedges, great differences in soil stratigraphy are observed. For example, in the core at Site 1, a peat-filled crack extended from 125 to 133 cm below the surface, and vertically oriented layers of peat and sediments were found at a depth of 80–125 cm. The vertical

Table 2. Soil properties by horizon.

Exposure #	Horizon	Depth range (cm)	pH	EC ds cm²	Texture	Thermal State	Total OC (%)	Total N (%)	Total OM (%)
1	Oi/Oe	0-12	5.64	1.08	MK	AL	22.5	1.61	44.5
70.13393N	Bw	15-30	5.4	0.49	SIL	AL	2.47	0.148	3.99
-143.65578W	Oajj	30-45	4.98	0.58	MK	AL	14.7	0.810	30.2
	Oaf/Bgfjj	38-70	6.82	5.20	MK/SIL	Pf	7.21	0.498	14.4
	Bgf/Oafjj	70-99	6.79	11.25	SIL/MK	Pf	4.13	0.332	8.27
	Af/Oafjj	99-146	6.96	12.75	SI/MK	Pf	5.04	0.272	10.1
2	Oa	0-17	5.18	0.95	MK	AL	20.5	0.198	40.9
70.13393N	Bg	17-38	4.79	0.53	SIL (10% GR)	AL	19.9	1.15	39.8
-143.65245W	Oi/Bgjj	38-50	4.9	0.73	PTMK/SIL	AL	19.4	1.26	31.5
	Oaf/Bgfjj	50-75	4.93	2.35	MK/SIL	Pf	22.1	1.38	24.2
	Cf	79-94	7.04	2.37	S	Pf	0.770	1.52	1.54
3	Oa	0-19	6.58	0.86	MK	AL	14.4	0.00	28.9
70.1345N	Bw/Oajj	19-40	5.98	5.16	SIL	AL	19.7	1.34	20.0
-143.66083W	Oa	40-52	5.86	0.90	MK	AL	13.5	1.00	26.9
	Oa1/Bgf1	60-75	5.97	0.86	MK/SIL	Pf	14.7	0.953	35.4
	Oa2/Bgf2	80-85	6.53	1.15	MK/SIL	Pf	14.2	1.08	28.4
	Oa3/Bgf3	100-105	6.87	1.08	MK/SIL	Pf	6.50	1.05	13.0
	Oa4/Bgf4	117-127	6.78	1.65	MK/SIL	Pf	11.2	0.706	22.4
	Cf	140-155	7.36	2.52	S	Pf	1.13	0.0730	2.26

*AL=active layer; Pf=permafrost.

stratigraphy and high ice volume (50–70%) indicates that this core resides in close proximity to an ice wedge. Similar conditions existed at Site 3. The first attempt to drill a core at Site 2 resulted in a high ice volume sample with vertically oriented peat horizons, appearing as if cracks in the soil surface had filled with water, distorting the soil stratigraphy. At 97cm, gravel was encountered, drilling stopped, and a second, successful drilling, just 0.5m from the original site, resulted in the core used for analysis. The core at Site 2 had nearly horizontal soil layers with abrupt wavy boundaries. Layers of muck (sapric) alternated with mineral sediments, most likely deposited by eolian or alluvial processes. Organic-rich materials with lower ice volume (pore ice at 30%) were found from 50–70cm and below that marine-alluvial sand deposits were encountered.

All three sites followed similar general horizonation in the active layer. A thick organic layer (12–19cm) lay over silt, which lay over a more decomposed organic layer. Mixing of these layers due to cryoturbation was present in some cases, but the origin of the horizons could still be distinguished by texture (muck for organic materials and silt loam for Bg or Bw horizons). Organic matter was found cryoturbated deep into the permafrost to a depth of 133 cm. None of the bluff cores exhibited clear horizontal layering as the result of strong cryoturbation.

Redoximorphic features were observed in the root channels of the Bg and Bw horizons in the active layer (Fe-concentration 7.5 YR 5/8, matrix 2.5 Y 4/1). The saturated conditions created a reducing environment in which root channels become the source of oxygen in the redox process. Organic acids produced in the surface organic layers lower the pH and iron is reduced from Fe(III) to Fe(II). The reduced iron is water soluble and carried with water movement to the lower mineral layers. Roots extending into the mineral horizons exude oxygen where microbial activity facilitates oxidation and precipitation of the iron Fe(III) oxides resulting in the presence of reddish-brown soil mottling.

Soil physical properties

Thaw depth varied slightly among the 3 sites (45, 36, and 54 cm) most likely due to micro-topographical differences. Thaw depths are smallest in polygon troughs and deeper at the center of the polygon, and deeper again on the rim. Polygon troughs were generally avoided for pit excavation and coring, as they tend to have ice wedges (pure massive ice) below the surface. Thaw depths were not measured according to micro-topographical features, but in relationship to bluff excavations. Thaw depths of 25–50 cm are typical at bluff exposures along the Beaufort Sea coast, but varies somewhat based on annual climate at a particular site.

Soil textures at these locations were found to be fairly consistent. Muck layers (Oa) were found in the top 10–20 cm at all sites, followed by a silt loam horizon (Bg or Bw, 10–40 cm) and then a muck or muck/silt loam horizon (Oa/Bgjj) starting at 38 cm and extending to 100 cm in one site. Cores 2 and 3 had a Cf horizon of alluvial-marine sand at 79 and 140 cm respectively. This pattern of vertically stratified organics, mineral, organics, mixed organic/mineral, and sand gives a glimpse into the formation of the soils at the coast. The surface organic layer has likely been developing for many hundreds of years. The underlying thick silt layer is an indicator of a long-term event of eolian or alluvial deposit, which was preceded by a period of plant growth similar to current conditions. Cryoturbation has largely erased similar historical pattern in the permafrost layers, but the underlying sand layers are remnants from the end of the last ice age.

Chemical properties

Surface organic horizons and buried organic layers contained the highest quantity of organic carbon (OC) averaging 19.1% and 12.0%, respectively, and the silt dominant layers contained 7.6% OC on average. The total nitrogen (N) averaged 1% with no clear correlation between the values and the soil type, mineral or organic. This may be due in part to the difficulty in separating the mineral and organic components in cryoturbated layers. The pH at each site tended to increase with depth, as did the EC, especially in the mineral horizons. Additionally, there is an inverse relationship between the TOC%, pH and EC, which reflects the strong influence of the organic matter on soil properties. Organic acids produced by the OM decrease the pH values, but also act as a buffer, neutralizing the salt effects. Thus, the EC was lower in organic-rich layers, but higher in the mineral soil. The higher pH values found in deeper, mineral soils are due to the calcareous nature of the parent materials (Ca-rich deposits from the Brooks Range). At bluff Site 1, the EC values are significantly higher between 38–146 cm. This may be due to one of two reasons. One theory is that these soils represent an old surface, a thaw lake that had at one time been flooded with seawater. Another possibility is that the neighboring area, which was treated with bio-solids for 13 years, affected surrounding soils. The high salt content of the waste may have migrated and moved deep under the surface through frost cracks and cryoturbation.

Conclusions

Soils along the high bluffs of Barter Island are characterized by high ice volume, both in size of ice wedges and segregated ice within the depth measured. Cold temperature and the wet tundra on the coastal plain contribute to such ice formation. Cryoturbation was found in all exposed bluff faces and permafrost cores drilled inland. All active layers exhibited a similar pattern of horizonation: thick surface organic layer over a mineral B horizon, with a cryoturbated O horizon underneath. Redoximorphic features exhibited in pore linings and masses were common in the mineral B horizons. All profiles contained high organic carbon and increasing pH with depth.

Additional research is currently underway on the soil properties of similar soils inland from the bluff, those not impacted by erosion, in an effort to add to the understanding of the impacts of coastal erosion on soil properties.

Acknowledgments

This project is funded by a grant from the National Science Foundation #0436179. Fugen Dou, Daniel Fortier, B.J. Haggard, Mikhail Kanevskiy, and David Weindorf helped with field collection.

References

Bockheim, J.G. 2007. Importance of cryoturbation in redistributing organic carbon in permafrost-affected soils. *Soil Science Society of America Journal* 71:1335-1342.

Brown, J., Jorgenson, M.T., Smith, O.P. & Lee, W. 2003. Long-term rates of erosion and carbon input, Elson Lagoon, Barrow, Alaska. In Phillips, M., Springman, S.M. & Arenson, L.U. (Eds.), *ICOP 2003 Permafrost: Proceedings of the 8th International Conference on Permafrost.* Netherlands: A. A. Balkema Publishers, 101-106.

Chapman, W. L. & Walsh, J.E. 1993. Recent variations of sea ice and air temperature in high latitudes. *Bull. Amer. Meterol. Society* 74:33-47.

Fetterer, F., Knowles, K., Meier, W., and Savoie, M. 2002, updated 2007. Sea ice index. Digital media. National Snow and Ice Data Center. Boulder, CO.

Hinzman, L.D., Kane, D.L. & Woo, M. 2005. Permafrost Hydrology. *Encyclopedia of Hydrological Sciences.* Indianapolis, IN: John Wiley & Sons, Ltd.

Hobbie, S.E, Schimel, J.P., Trumbore, S.E., & Randerson, J.R. 2000. Controls over carbon storage and turnover in high-latitude soils. *Global Change Biology* 6(s1):196-210.

IPCC. 2007. Summary for Policymakers. In: *Climate Change 2007: Impacts, Adaptation and Vulnerability.* Contribution of Working Group II to the Fourth Assessment Report of the Intergovernmental Panel on Climate Change, Parry, M.L., Canziani, O.F., Palutikof, J.P., van der Linden, P.J. & Hanson, C.E., Eds. Cambridge, UK: Cambridge University Press 7-22.

Kimble, J.M., Tarnocai, C., Ping, C.L., Ahrens, R., Smith, C.A.S., Moore, J. & Lynn, W. 1993. Determination of the amount of carbon in highly cryoturbated soils. In Gilichinsky, D.A. Ed. *Post-Seminar Proceedings of the Joint Russian-American Seminar on Cryopedology and Global Change.* Pushchino, Russia, 15-16 Nov. 1992. Pushchino, Russia: Russian Academy of Science.

Jorgenson, M.T., & Kreig, R.A. 1988. A model for mapping permafrost distribution based on landscape component maps and climatic variables. *Proc. Fifth Int. Conf. on Permafrost.* Trondheim, Norway: TAPIR Publishers, 176-183.

Jorgenson, M.T., Racine, C.H., Walters, J.C. & Osterkamp, T.E. 2001. Permafrost degradation and ecological changes associated with a warming climate in central Alaska. *Climate Change* 48:551-579.

Jorgenson, M. T., Ping, C.L. Guo, L. Shur Y., and. Brown, J. 2005. A multi-scale approach to assessing the flux and transformation of organic carbon across the eroding coastline of northern Alaska. Berichte Zur Polarund Meeresforschung 506:65-68.

Jorgenson, M.T., Shur, Y.L., and Pullman, E.R. 2006. Abrupt increase in permafrost degradation in Arctic Alaska. *Geophysical Research Letters* 33, L02503, doi:10.1029/2005GL024960.

McCabe, G.J., Clark, M.P., Serreze, M.C. 2001. Trends in northern hemisphere surface cyclone frequency and intensity. *Journal of Climate* 14:2763-2768.

Morison, J., Aagaard, K. & Steele, M. 2000. Recent environmental changes in the Arctic: a review. *Arctic* 53:359-371.

Oechel, W.C, Vourlitis, G.L., Hastings, S.J. & Bochkarev, S.A. 1995. Change in arctic CO2 flux over two decades: effects of climate change at Barrow, Alaska, *Ecological Applications* 5(3):846-855.

Ovenden, L. 1990 Peat accumulation in northern wetlands. *Quaternary Research* 33:377-386.

Ping, C.L., Michaelson, G.J., & Kimble, J.M. 1997. Carbon storage along a latitudinal transect in Alaska. *Nutrient Cycling Agroecosystems* 49:235-242.

Robinson, R.A. 2004. Villages affected by flooding and erosion have difficulty qualifying for federal assistance. Highlights of GAO-04-895T, a testimony before the Committee on Appropriations, United States Senate.

Schoeneberger, P.J., Wysocki, D.A., Benham, E.C. & Broderson, W.D. 1998. Field book for describing and sampling soils. Natural Resource Conservation Service, USDA, National Soil Survey Center. Lincoln, Nebraska.

Semiletov, I.P. 1999. Destruction of the coastal permafrost ground as an important factor in biogeochemistry of the Arctic Shelf waters. Transactions (Doklady) of the Russian Academy of Sciences, 368(6):679-682.

Serreze. M.C., Clark, M.P., Etringer A.J., & D.H. Bromwich. 2001. Variability and trends in the hydro-climatology of the major Eurasian Arctic drainages. In *Second Wadati Conference on Global Change and the Polar Climate,* March 7-9, 2001. Tsukuba, Japan 83-86

Shur, Y.L., Jorgenson, M.T. 2007. Patterns of permafrost formation and degradation in relation to climate and ecosystems. *Permafrost and Periglacial Processes* 18:7-19.

Global Land Use Change and Its Specificity in Permafrost-Affected Regions: Consequences for Cryosols

Dmitry I. Lyuri
Institute of Geography, Russian Academy of Science, Moscow, Russia

Sergey V. Goryachkin
Institute of Geography, Russian Academy of Science, Moscow, Russia

Abstract

The most specific land use change in high latitudes is the dynamics of agricultural lands. Contrary to the global zonal trend (northward increase of agricultural land abandoning), there was the growth of agricultural areas in cold and permafrost-affected regions both of Eurasia and North America. But since the 1990s the dynamics of agricultural land became divergent in different parts of the North. Due to the system economic crisis in Russia, the area of agricultural lands in permafrost-affected regions shrank greatly; however, in Alaska and Norway, farmlands continued to grow. It proves that increasing of agricultural lands of the North is mostly related to social and economic reasons, but not to climate change. Consequences for cryosols induced by both socio-economic and climate changes are mostly similar. They provoke the deepening of the active layer, development of thermokarst, and change of organic matter quality (degradation of peat and increase of soil humus content).

Keywords: agricultural lands; cryosols; global change; land use; permafrost; socio-economic change.

Introduction

Global climate change and the following landscape and ecosystem transformations are the most popular topics in geosciences including geocryology and soil science. However, global change overwhelms not only climate, but also socio-economic processes as well. The shift of oil and gas mining to the north is a very well-known trend in the world. Socio-economic processes in the North usually have their specificity (Forbes 1999), but their influence on the trends of land use change in high latitudes is not the focus of recent studies. Less is known about the main trends of permafrost-affected landscapes and ecosystems change due to alteration of land use in the North, and only last year, the scientific community began to pay attention (Gutman 2007). As for permafrost and soils, something is known about how they are changed under such transformations of vegetation as clear-cutting (Iwahana et al. 2005) and forest fires (Yoshikawa et al. 2003, Lopez et al. 2006). Much less is known on the agricultural transformation of northern soils. However, the last decades were very crucial to agricultural lands of the world as the intensification of relevant technologies and the rise of productivity resulted in a drastic decrease of arable lands in many countries. Almost nothing is known about what the situation with the dynamics of agricultural areas is in northern (perma)frost-affected regions of the world.

The goal of this paper is to assess the main processes of land use change (primarily agricultural) in northern regions in comparison with the global trend and the consequences for (perma)frost-affected soils—cryosols. Analyses of national and world statistics, literature, and field observations are the main methods in the study.

Change of Agricultural Land Use

Global trends of agricultural land use

Contrary to the slow growth of total agricultural areas in the world, more than 80 countries demonstrate the stable decrease of them. From 1961 to 2002, about 2.3 mln km^2 were abandoned from agricultural use, mostly in Russia, Australia, the USA, and West Europe. Six types of abandonment of agricultural lands were distinguished (Lyuri et al. 2006). The first four types are associated with countries, where decreasing of agricultural lands is a result of agricultural intensification. *US-type*: the decrease of agricultural area as a result of agricultural intensification with the increase of agricultural production. Twenty-one countries (US, UK, West Europe, Australia, India, Thailand, etc.) have this type of agricultural lands dynamic, and they abandon about 1.0 mln km^2 of agricultural area (43.5% of the world value) (Fig. 1).

Japan-type: the decrease of agricultural area as a result of agricultural intensification with the decrease of agricultural production (the course for food import). Two countries, Japan

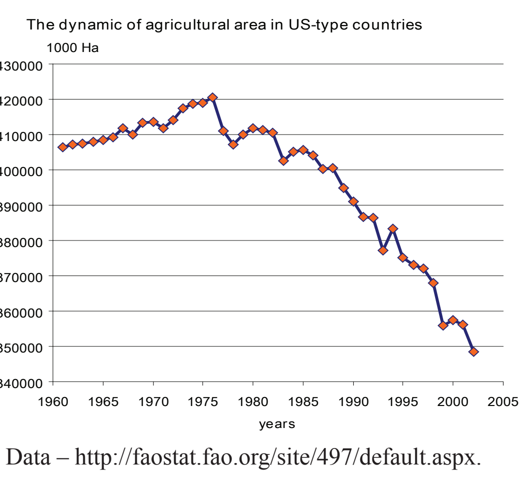

Figure 1. Data – http://faostat.fao.org/site/497/default.aspx.

and South Korea, abandoned 0.02 mln km^2 of agricultural area (<1% of the world value). *France-type*: the decrease of agricultural area as a result of agricultural intensification, then its increasing during last years with increasing of agricultural production (the course for food export). Six countries abandoned 0.1 mln km^2 of agricultural area (4%). *Hungary-type (transitional)*: the decrease of agricultural area as a result of agricultural intensification, then its decline as a result of deep economical crises. Nine countries (Poland, Hungary, and other countries of East Europe) abandoned 0.07 mln km^2 of agricultural area (3%).

Two other types of agricultural land abandonment are associated with countries where agricultural lands decrease as the result of crises, wars, revolutions, and other non-agricultural processes.

Russian-type: the enlargement of agricultural area, then its falling as a result of deep economical crises with the rise and then decrease of agricultural production. Seventeen countries (Russia, other countries of the former USSR, Bulgaria, and Romania) abandoned 0.85 mln km^2 of agricultural area (37.0% of the world value). *Miscellaneous-type*: the decrease of agricultural area with no relation to agricultural productivity and production. Twenty-one countries (Bangladesh, Cameroon, Lesotho, Nigeria, Swaziland, etc.) abandoned 0.25 mln km^2 of agricultural area (10.9%).

Abandoned agricultural area is substituted by two kinds of lands: (1) by settlements, infrastructure, industry, etc., and (2) by fallows. In the last case, fallows are usually a process of replacement by natural ecosystems.

Land use change in Russia and its northern regions

The dynamics of the areas of agricultural lands both in Russia as a whole and in its northern (perma)frost-affected regions is very specific. We have analyzed it separately for two essentially different periods: (1) for non-crisis 1960-1980, and (2) for the 1990s – system economic crisis in the country and afterwards. Figure 2 shows that the growth of the cropland areas has practically finished from the beginning of the 1960s for the whole territory of Russia. Cropland area expansion occurred only in the most southern regions; however, in boreal and temperate zones, it was stable or even diminishing.

The reverse situation took place in northern permafrost-affected areas. The intensive increase of the cropland area began from 1960-1970 and continued until the beginning of the crisis of 1990 (Fig. 3).

Similar patterns, but more complicated and controversial for northern territories, are characteristic for dynamics of arable lands and agricultural areas (Figs. 4, 5). Thus, the dynamics of the cultivated areas in permafrost-affected regions of Russia in the favorable 1960s-1980s was more similar to that of the most southern parts of the country, but not to adjoining boreal and temperate regions.

In the 1990s the system crisis had embraced all of the country, and in all regions of Russia there was a significant reduction of agricultural areas, including arable lands and crops (Figs. 6, 7).

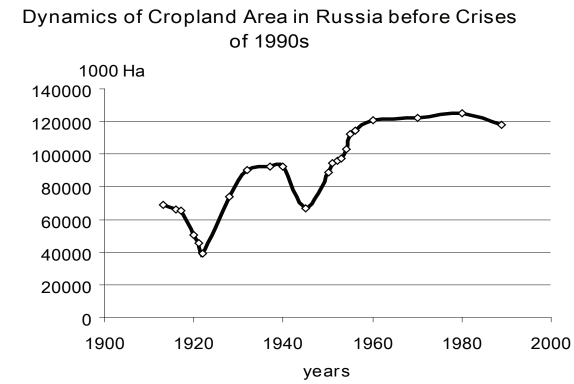

Figure 2. Data – State Committee 1985-1998.

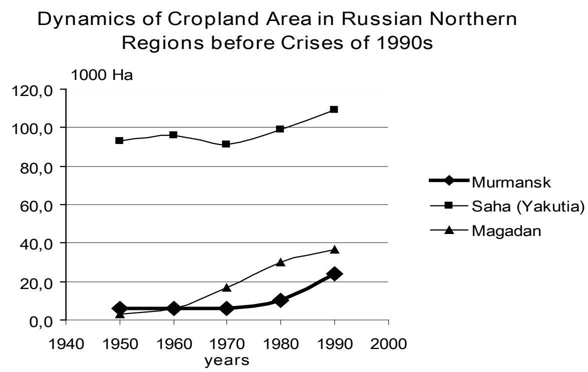

Figure 3. Data – State Committee 1985-1998.

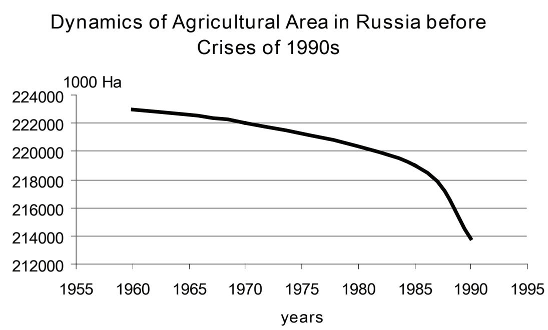

Figure 4. Data – State Committee 1985-1998.

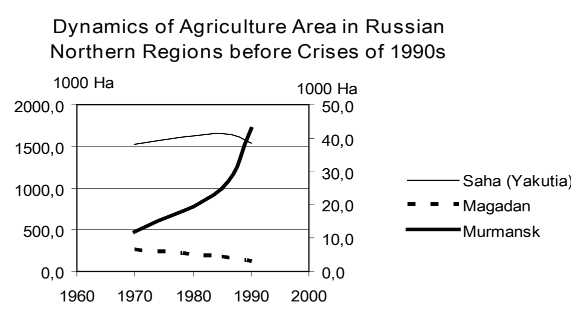

Figure 5. Left Y-axis is for Saha; right one, for others.. Data – State Committee 1985-1998.

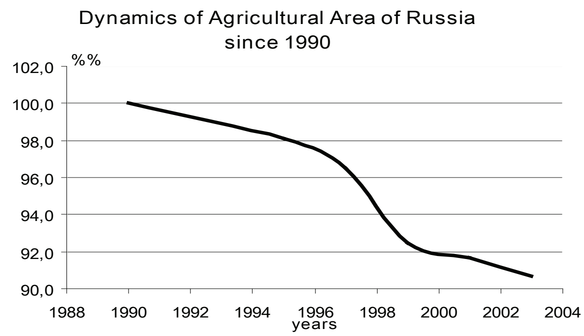

Figure 6. Data – State Committee 1985-1998, 2006.

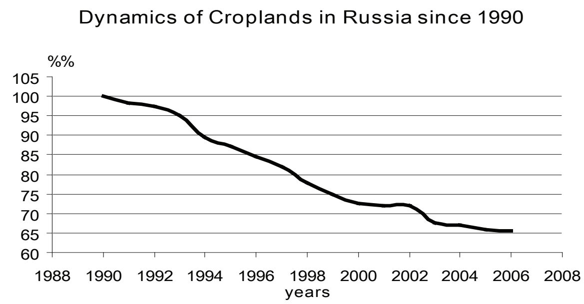

Figure 7. Data –State Committee 1985-1998, 2006.

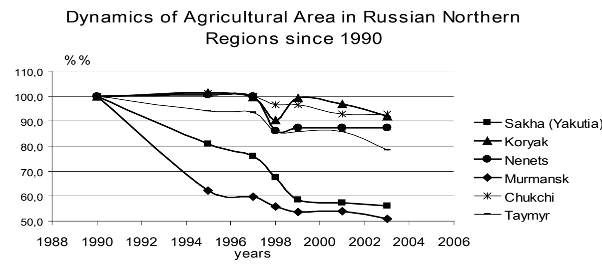

Figure 8. Data – State Committee 1985-1998, 2006.

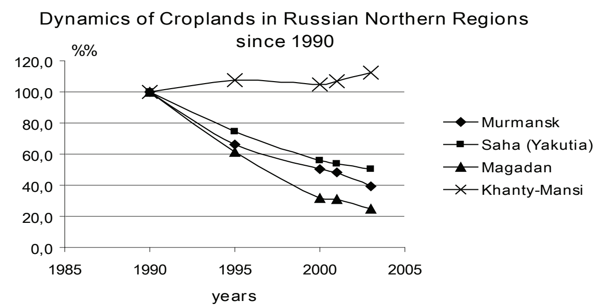

Figure 9. Data – State Committee 1985-1998, 2006.

Analogous processes took place in permafrost-affected regions of the country, though the unique subject of Russian Federation (Khanty-Mansi autonomous district), with some increase in the areas of croplands in crisis time, occurred namely in this zone. In all other northern regions, the agricultural areas were reduced, though this process had various rates. However, by the end of the 1990s in the majority of permafrost-affected regions the shrinkage of agricultural areas has practically stopped, and they were approximately stabilized. It is observed in the Murmansk area, Saha (Yakutia) (which has the greatest area of the agricultural lands in the permafrost-affected zone), in Nenets and Chukchi autonomous districts (Figs. 8, 9).

Such agricultural land stabilization has occurred more than in half of analyzed permafrost-affected regions. It is remarkable, but a similar effect of the termination of the shrinkage of agricultural areas takes place only in the most southern regions of the country, and in the boreal and temperate areas the process of croplands decrease proceeds with former intensity. Thus, the agricultural lands of permafrost-affected regions have reacted to the system crisis of the 1990s in a very specific form: Their dynamics even in these crisis years was more similar to dynamics in the most southern agriculturally productive areas of the country.

The effect of stabilization in cold regions, which in the south is related to the optimum for conducting agriculture by natural and demographic conditions, should be explained by other reasons. First, it is caused by the remoteness of these areas from the basic agricultural regions of the country; it makes the transportation of the foodstuffs here very expensive and focuses local producers and consumers on home resources. Secondly, it can be explained by the significant percentage in the population of local indigenous people for which the traditional agriculture is the core and even the only source of existence that forces them to stabilize the situation at a certain acceptable level as soon as possible. Besides that, a traditional economy is "economically isolated" and much more independent to financial cataclysms, legal problems, and other aspects of a system crisis than the modern economy.

Land use change in the north of Russia, US, and Europe

However, in spite of all specificity of the agriculture of permafrost-affected regions the general decrease of the agricultural areas in the north of Russia was very significant. So, arable lands of Russian northern regions in the period from 1990 until 2003 have decreased by 1.5 times (from 230,000 to 150,000 Ha) and reached practically the value of 1970 (Fig. 9).

However, the dynamics of Russian arable lands has a very severe pressure of economic crises. In this case it is very interesting what type of dynamics of agricultural lands was in other non-crisis permafrost-affected regions of the Northern Hemisphere. It was found out that in Alaska, the constant increase of the area of arable lands took place in the 1974-2004 period. It has extended practically in 5 times (Fig. 11). This Alaskan agricultural situation is principally contrary to the rest of the US, as the stable reduction of agricultural lands took place in the country at that time.

In another northern region—Norway—the other type of arable land dynamics takes place (Fig. 12). The expansion of arable lands from the middle of the 1990s was replaced by stabilization, and the last years, by insignificant reduction (approximately 3%). It essentially distinguishes Norway from all other countries of Western Europe, where from 1960-1980, there is a reduction of arable areas.

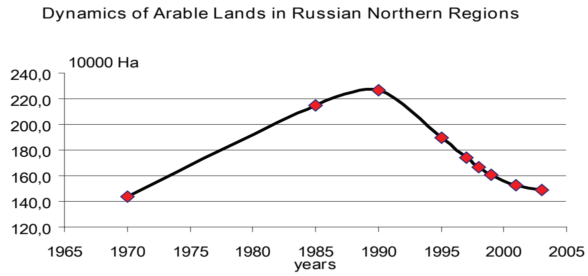

Figure 10. Data – State Committee 1985-1998, 2006.

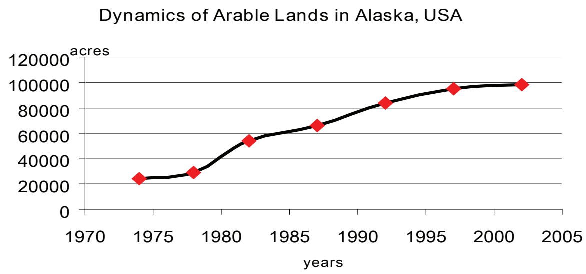

Figure 11. Data – USDA 2003.

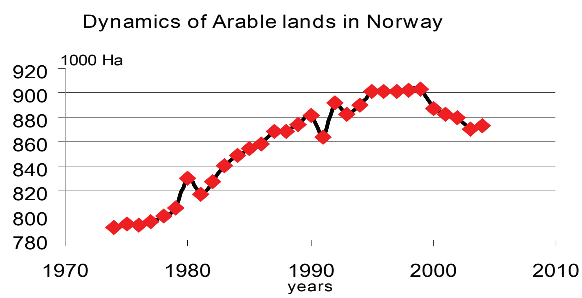

Figure 12. Data – http://faostat.fao.org/site/497/default.aspx.

Thus, the dynamics of arable lands in different cold regions of the Northern Hemisphere is essentially diverse. We see "growth-fall" in Russia, "growth" in Alaska and "growth-stabilization" in Norway. That allows the assumption that it is mainly defined by social and economic, but not by natural (changes of a climate) factors. Besides that, the dynamics of agricultural lands in permafrost-affected areas in different parts of the Northern Hemisphere are absolutely not similar to the mainland and neighbors: Alaska is different from the USA, and Norway, to all other countries of Western Europe. The Russian north is more likely similar to the Russian agriculturally productive south, than to the adjacent boreal and temperate regions.

Consequences of Land Use Change for Cryosols

Previous materials elucidated in the paper showed that agricultural use of soils in permafrost-affected regions of the world is growing or, at least, a stable factor of soil change. So, the influence of this type of land use on polar soils should be known as well as the other ones.

Figure 13. Total destruction of agricultural field after use of permafrost-affected soils for a cropland. Central Saha (Yakutia). Remnants of ploughed horizon proved the former tillage of these soils.

Our field studies in Central Saha (Yakutia) showed that the tillage of loamy soils resulted in occurrence of a humus horizon with a sharp lower boundary, as it is characteristic for all arable soils of the world. However, a specific tillage-induced feature is the lowering of the permafrost table often beneath 2 m (so after agricultural development, these permafrost-affected soils do not fit the criteria of Cryosols (WRB) and Gelisols (Soil Taxonomy) anymore).

But the most dangerous phenomena taking place after involvement of some permafrost-affected soils in agriculture is the total destruction of soil surface because of catastrophic development of thermokarst and thawing of underground ice wedges (Fig. 13).

Our data are in full correspondence with materials of Gavriliev (2004) who experimentally showed that after 12 years of agricultural use in Central Saha (Yakutia), ice wedges can thaw from a depth of 1.8 m to 3.2 m, and thermokarst holes can develop depths from 0 to 0.95 m.

The other data on tundra soils involved in agriculture from another part of the Eurasian cryosol area—northeast European Russia—also showed that they are characterized by development of sod and humus horizon instead of peaty litter and by occurrence of more contrast temperature regime with deep thawing of mineral horizons (Archegova et al. 2004).

Agriculture-induced soil change in permafrost areas has both similarity and difference with other types of land use and anthropogenic influence. As well as reindeer overgrazing, clear-cutting, and forest fires, it leads to active layer deepening (Broll 2000, Iwahana et al. 2005, Lopez et al. 2006). However, manure amendments for agriculture lead to an increase of carbon store in cryosols contrary to other types of land use. Anthropogenic change of cryosols has mostly the same trend as induced by global climate change, at least in some regions of the cryopedosphere—active layer increase (Mazhitova et al. 2004).

Conclusions

Agricultural land use change in permafrost-affected regions is very specific and has other trends than boreal and temperate regions of the world. Cold regions have different types of dynamic: (1) growth in Alaska, US, (2) growth and stabilization in Norway, and (3) growth and fall in Russia due to economic crises of the 1990s. Land use change is caused by socio-economic but not by climatic reasons. The local agricultural economy of remote northern areas is much smaller and more independent than that of central productive regions; that is why it will be saved by local communities, especially by indigenous people.

The consequences for cryosols induced by both socio-economic and climate changes are mostly similar. They provoke the deepening of the active layer, development of thermokarst, and change of organic matter quality (degradation of peat and increase of soil humus content).

Acknowledgments

This study was conducted within the framework of the IPY Cluster Project #262 “Response of Arctic and Subarctic soils in a changing Earth: dynamic and frontier studies.” Financial support was provided by the Presidium of Russian Academy of Sciences and its Department of Geosciences. The authors also acknowledge the Russian Foundation for Basic Research for the financial support of field investigation in Saha (Yakutia) and personally M. Zheleznyak, M. Grigoriev, R. Desyatkin, T. Maksimov, and P. Fedorov from Yakutsk for help in the organization of the expedition.

References

Archegova, I., Kotelina, N. & Mazhitova, G. 2004. Agricultural use of tundra soils in the Vorkuta area, Northeast European Russia. In: J. Kimble (ed.), *Cryosols. Permafrost-affected soils.* Springer: 661-676.

Broll, G. 2000. Influence of overgrazing by reindeer on soil organic matter and soil microclimate of well-drained soils in the Finnish Subarctic. In: R. Lal, J.M. Kimble & B.A. Stewart, *Global Climate and Cold Regions Ecosystems.* Boca Raton: CRC/Lewis Publ.: 163-176.

Forbes, B.C. 1999. Land use and climate change on the Yamal Peninsula of north-west Siberia: some ecological and socio-economic implications. *Polar Research* 18(2): 367-373.

Gavriliev, P.P. 2004. Classification of geocryological and soil processes on their danger for agricultural development. Permafrost-affected soil: diversity, ecology and conservation. *Proceedings of Russian scientific conference, June 28-30, 2004, Yakutsk.* Yakutsk: 149-154 (in Russian).

Gutman, G. 2007. Contribution of the NASA Land-Cover/Land-Use Change Program to the Northern Eurasia Earth Science Partnership Initiative: An overview. *Global and Planetary Change* 56(3-4): 235-247. http://faostat.fao.org/site/497/default.aspx

Iwahana, G., Machimura, T., Kobayashi, Y., Fedorov, A.N., Konstantinov, P.Y., & Fukuda, M. 2005. Influence of forest clear-cutting on the thermal and hydrological regime of the active layer near Yakutsk, eastern Siberia, *J. Geophys. Res.* 110::G02004, doi:10.1029/2005JG000039.

Lopez, M.L., Nakayama, H., Takakai, F., Argunov, R., Fedorov, A.N. & Fukuda, M. 2006. Forest fires, a permanent or a temporal disturbance in Permafrost Regions: Central Yakutia, Eastern Siberia? *Forest Ecology and Management* 234(1): S178.

Lyuri, D., Karavaeva, N., Nefedova, T., Konyushkov, B. & Goryachkin, S. 2006. Self-Restoration of Post-Agrogenic Soils: Recent Process of Late Antropocene. *Abstracts. 18th World Congress of Soil Science July 9-15 Philadelphia, Pennsylvania, USA.* CD-ROM, 27-2.

Mazhitova, G., Malkova, G., Chestnykh, O. & Zamolodchikov, D. 2004. Active-layer spatial and temporal variability at European Russian circumpolar-active-layer-monitoring (CALM) sites. *Permafrost and Periglacial Processes* 15(2): 123-139.

State Committee for Statistics. 1985-1998. Agriculture. Moscow, Goskomstat (in Russian).

State Committee for Statistics. 2006. Agriculture, Hunt and Forestry. Moscow, Goskomstat (in Russian).

USDA 2003. 2002 Census of Agriculture - State Data. National Agricultural Statistics.

Yoshikawa, K., Bolton, W.R., Romanovsky, V.E., Fukuda, M. & Hinzman, L.D. 2002. Impacts of wildfire on the permafrost in the boreal forests of Interior Alaska, *J. Geophys. Res.* 107, 8148, doi:10.1029/2001JD000438.

Control of Asymmetrical Subgrade Temperature with Crushed-Rock Embankments Along the Permafrost Region of the Qinghai-Tibet Railway

Wei Ma, Luxin Zhang, Qingbai Wu

State Key Laboratory of Frozen Soil Engineering, Cold and Arid Regions Environmental and Engineering Research Institute, 320 Donggang West Road, Lanzhou, 730000, China

Abstract

On the basis of in situ tests of embankments with different crushed rock structures, this paper studied methods for controlling asymmetrical subgrade temperature. It is found that these methods can slowly change the ground temperature regime, but cannot completely adjust the asymmetrical subgrade temperature. Small changes in thickness and grain size of crushed rock had only a limited effect on controlling asymmetrical temperature regime. Compared with the ground temperature regime under different structures of crushed rock slope protection of the same height, it is found that the ground temperature under the south shoulder of an embankment with full crushed rock coverage is lower than that under an embankment with partial coverage, and that the ground temperature under the north shoulder of an embankment with partial coverage is lower than that of a slope with full coverage. It is suggested, therefore, that the south-facing slope be fully covered with crushed rock with thicker structures, while the north-facing slope be partially covered with crushed rock and thinner structures.

Keywords: crushed rock structure embankment; permafrost region; Qinghai-Tibet Railway; south- and north-facing slope of the embankment; temperature regime.

Introduction

Using an active cooling embankment to protect the underlying permafrost, a lot of engineering measures were successfully applied in permafrost engineering construction, especially in the Qinghai-Tibet Railway (QTR) (Rooney 1997, Georing et al. 1996, 2000, 2001, 2003, Ma et al. 2002, Cheng 2003). For instance, they include crushed rock embankments, embankments with crushed rock slope protection, embankments with thermo-siphons and permafrost bridges etc. Their cooling effects have been studied (Georing et al, 1996, 2000, 2001, 2003, Wu et al. 2006, Sun et al. 2004). These measures have ensured that the QTR successfully passes through the warm permafrost regions with high ice contents. Long-term monitoring data along the QTR showed that these measures have different cooling effects in permafrost regions with different ground temperatures (Wu et al. 2005, Ma et al. 2006). In particular, no matter what embankment structure was used, there was a thermal difference between the south- and north-facing slopes of the embankment, an asymmetrical temperature regime was formed under the embankment -- the ground temperature under the south side shoulder is higher than that under the north side shoulder (Sun et al. 2004, Wu et al. 2005). This kind of temperature distribution can cause the potential instability of the embankment. It is therefore necessary to adjust the asymmetrical temperature distribution under embankments by using special measures.

Along QTR, on the basis of in situ tests and temperature monitoring of embankments with different crushed rock structures (3 embankments with the slopes fully covered by crushed rock, 3 embankments with the slopes partially covered with crushed rock with different grain sizes and 1 embankment with the slope partially covered with the filling soil of the embankment), this paper analyzed and compared the changes in the ground temperature regime under the embankment with different structures. Observations should provide fundamental data for preventing and fixing of the potential damage to embankments.

Test Sections and Schemes

The test site is in the Wudaoliang area along the QTR, which is a plateau with lacustrine deposits and thick ground ice area covered by 5%–6% vegetation, altitude of 4500–4700 m. The mean annual air temperature is -5.6°C and the mean annual range of air temperature is 22.3°C. The mean annual precipitation is 264.8 mm and the maximum snow depth is 14 cm.

DK1082+350–DK1082+500 was the test section of embankments with the slopes fully covered with crushed rock with different thicknesses; DK1082+650–DK1082+850 was the test section of embankments with the slopes partially covered by crushed rock with different grain size and an embankment with the slope partially covered with soil. Their details are shown in Table 1.

The original embankment in the test section is a common soil embankment built in 2002. The width of the track surface is 7.1 m, the height of embankment is 2.0–2.8 m and the gradient of embankment is 1:1.5. The widths of the south- and north-facing partial slope protection using soil are 3 m and 2 m.

For the requirements of the tests, we changed the original design. In the section DK1082+350–DK1082+500, we only fully covered crushed rock with different thickness on the slope of the original embankment (shown in Fig. 1). In the sections of DK1082+650–DK1082+750 and DK1082+800–DK1082+850, we use a partial coverage of crushed rock with

Table 1. Test schemes.

QTR kilometer post	T_{cp}* / °C	Mean height of embankment/m	Structure size of Slope protection of embankment	Structure type of embankment
DK1082+350-DK1082+400	-2.35	2.51	Thickness of the south/north-faced slope: 1.0 m/0.6 m ; Crushed rock size: 10 cm	Embankments with the slopes fully covered by crushed rock
DK1082+400-DK1082+450	-2.35	2.65	Thickness of the south/north-faced slope: 1.3 m/0.8 m; Crushed rock size: 10 cm	
DK1082+450-DK1082+500	-2.35	2.79	Thickness of the south/north-faced slope: 1.6 m/1.0 m ; Crushed rock size: 10cm	
DK1082+650-DK1082+700	-2.35	2.35	Width of the south/north-faced slope: 6.0/4.0 m Crushed rock size: 20 cm; Thickness: 1.5 m	Embankments with the slopes partially covered by crushed rock
DK1082+700-DK1082+750	-2.35	2.25	Width of the south/north-faced slope: 6.0/4.0 m; Crushed rock size: 30 cm Thickness: 1.5 m	
DK1082+800-DK1082+850	-2.35	2.76	Width of the south/north-faced slope: 5.0/3.0 m; Crushed rock size: 10 cm Thickness: 1.5 m	
DK1082+750-DK1082+800	-2.35	2.11	Width of the south/north-faced slope: 5.0/3.0 m; Thickness: 1.5 m	Embankment with the slope partially covered by soil

* T_{cp} is mean annual ground temperature at depth of 15 m from the original ground level down (shown in Fig. 4).

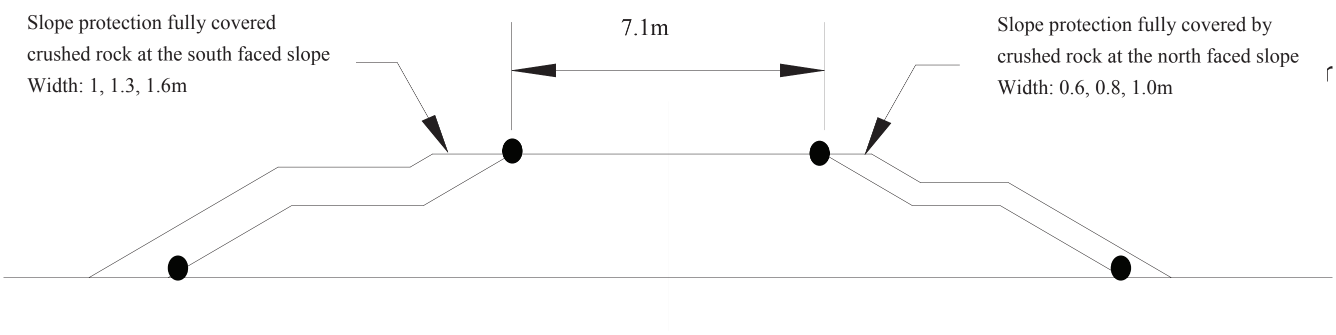

Figure 1. The cross section sketch map of embankment with the slope protection fully covered by crushed rock in DK1082+350–DK1082+500.

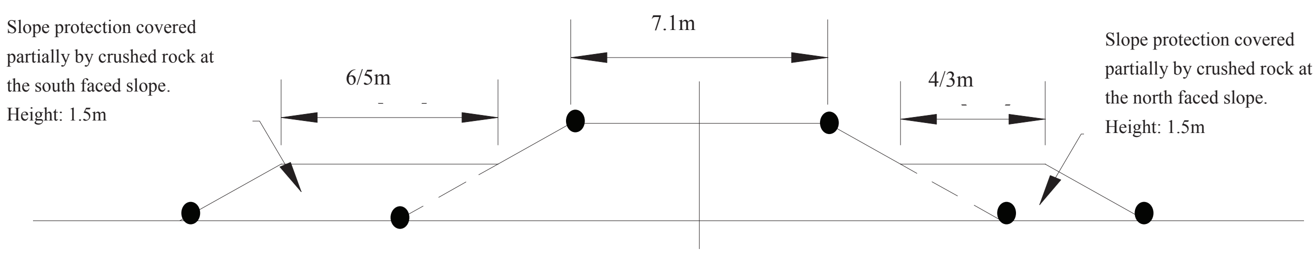

Figure 2. The cross section sketch map of embankment with the slope protection partially covered by crushed rock in DK1082+650–DK1082+850.

different widths and grain sizes to replace the original slope protection partially covered by soil (shown in Fig. 2). In the section of DK1082+750–DK1082+800, we only widened the original soil slope protection to 5.0/3.0m (shown in Table 1). Per test section, the length is 50 m, a lot of tests indicated that they are long enough to eliminate the thermal boundary effects from adjacent embankment sections (Wu et al. 2006, Sun et al. 2004, Ma et al. 2006).

DK1082+375, DK1082+425, DK1082+475, DK1082+675, DK1082+725, DK1082+775, and DK1082+825 respectively were chosen as monitoring profiles of ground temperature. In DK1082+375, DK1082+425, and DK1082+475, four boreholes were installed in each profile–on the south and north shoulder of the embankments and at the

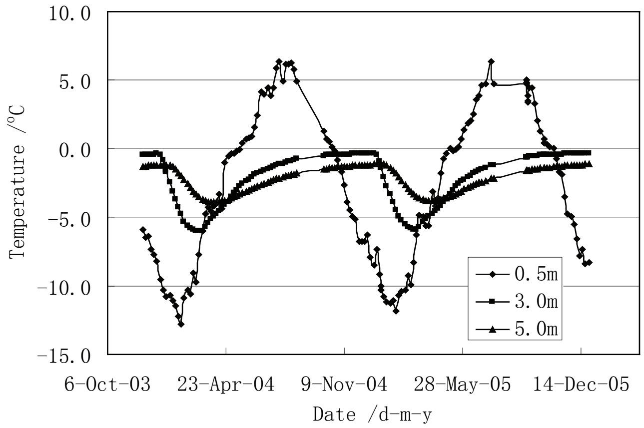

Figure 3. Ground temperature changes vs. time at different depths in the natural borehole (DK1082+600).

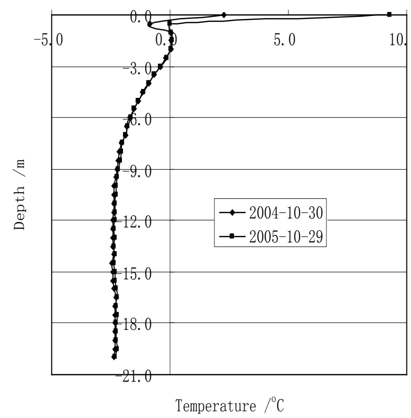

Figure 4. Ground temperature changes with depth when the thawing depth reached the maximum in the natural borehole (DK1082+600).

south and north toe for embankments with partial slope protection using soil (shown in Fig. 2 marked by "●"). In DK1082+675, DK1082+725, DK1082+775, DK1082+825, six boreholes were installed in each profile–the south and north shoulder and toe of embankment, the south and north toe of slopes partially covered by crushed rock, respectively (shown in Fig. 3 marked by "•"). Also a reference borehole 20 m deep was installed 20m away from the north slope toe of embankment at DK1082+600 to measure the natural ground temperatures.

A galvanized iron pipe was placed in each borehole. A thermometric string (the thermocouples placed at 0.5 m intervals) was installed in each pipe to record the temperatures at different depths.

The thermocouples were manufactured by the State Key Laboratory of Frozen Soil Engineering, Cold and Arid Regions Environmental and Engineering Research Institute, CAS, and the precision is ±0.05ºC. All data were collected using a Datataker 500 from Oct. 2003 to Dec. 2005.

Results and Analysis

Natural ground temperature changes

Figures 3 and 4 show the ground temperature changes with time at different depths and with depth when the thawing depth reached a maximum in the natural borehole. It is found that the permafrost table was at 2.0 m and the mean annual ground temperature was -2.35°C. It was also found there were little or no changes in the permafrost table or in the mean annual ground temperature. The air temperature therefore had very little effect on ground temperatures during the experimental years at the test site. So, we will not consider the effect of air temperature on temperature regime of embankment in following discussion.

Ground temperature changes under embankment with the slope protection partially covered by soil

Figure 5 shows the ground temperature changes with time at different depths and locations beneath the embankments. Compared with the slope shoulders and toes of embankment, it is found that the ground temperatures at the south shoulder and toe of the embankment were above -2°C and clearly higher than these under the north shoulder and toe. With increasing time, the minimum ground temperature at 0.4 m keeps slight increase, and under 0.4 m, they decrease slightly, and the decreasing range of ground temperature was about 0.2°C–0.3°C. Under the north shoulder of the embankment, the ground temperatures were about 1°C to -5.3°C. In the course of time, they decreased considerably, and the decreasing range of ground temperature is about 0.5°C to 1.1°C. Such developments would cause larger and larger ground temperature difference between the south and north slopes of the embankment and increase the potential instability of the embankment. So, this method can be put away first.

Ground temperature changes under the embankment with the slope protection fully covered by crushed rock

Figure 6 shows the typical ground temperature changes with time at different depths and positions under the embankments at DK1082+375. It can be seen that with the slope fully covered with crushed rock, the ground temperatures under embankment decrease noticeably, but the rate of decrease of ground temperature under the south side shoulder was less than that under the north side shoulder ground temperature difference, particularly under the toe of embankment. With increasing thickness of the crushed rock layer, the ground temperature difference decreases gradually under the south and north shoulders. Compared with embankments DK1082+425 and DK1082+475, the embankment structure with the thicknesses on the south/north-faced slopes of 1.6 m/1.0 m (DK1082+475) is better than the others. The difference exists mainly in the change of minimum ground temperature. The maximum ground temperature has no obvious relationship with thickness of the crushed rock layer. For the embankments with the thicknesses of crushed rock layer of 0.6 m and 1.0 m (DK1082+375), 0.8 m and 1.3 m (DK1082+425), 1.0 m and 1.6 m (DK1082+475), respectively, the differences in the minimum ground temperature at different depths under the south and north side shoulders were 1.29°C to 2.68°C, 0.98°C to 1.98°C, 0.90°C to 1.89°C, respectively. In addition,

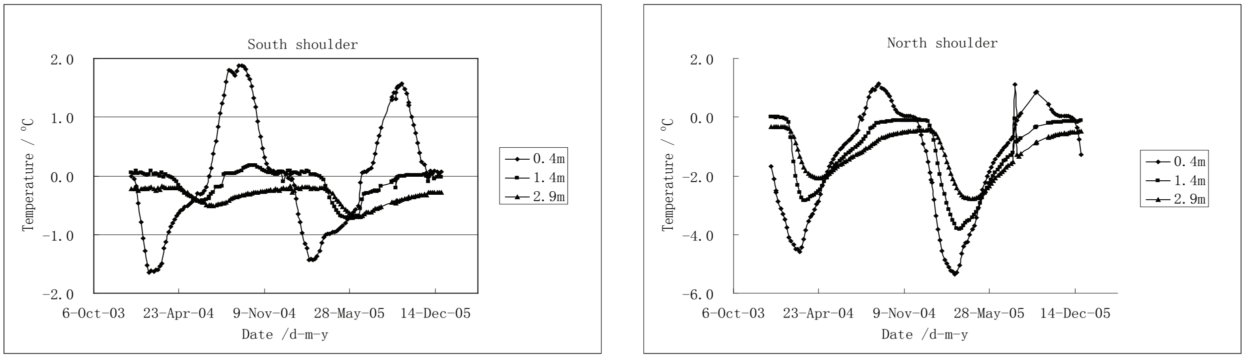

Figure 5 Ground temperature changes vs. time at different depths under embankment with the slope protection partially covered by soil (DK1082+775).

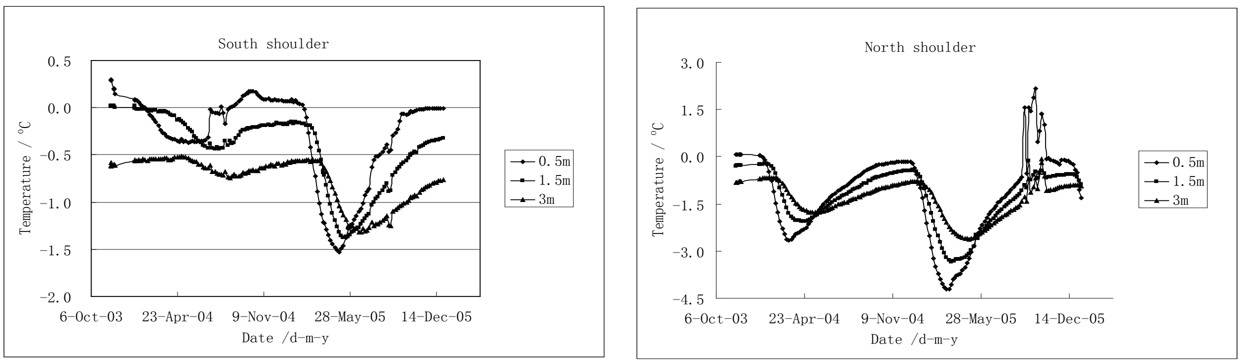

Figure 6. Ground temperature changes vs. time at different depths under the embankment with the slope protection fully covered by crushed rock (DK1082+375).

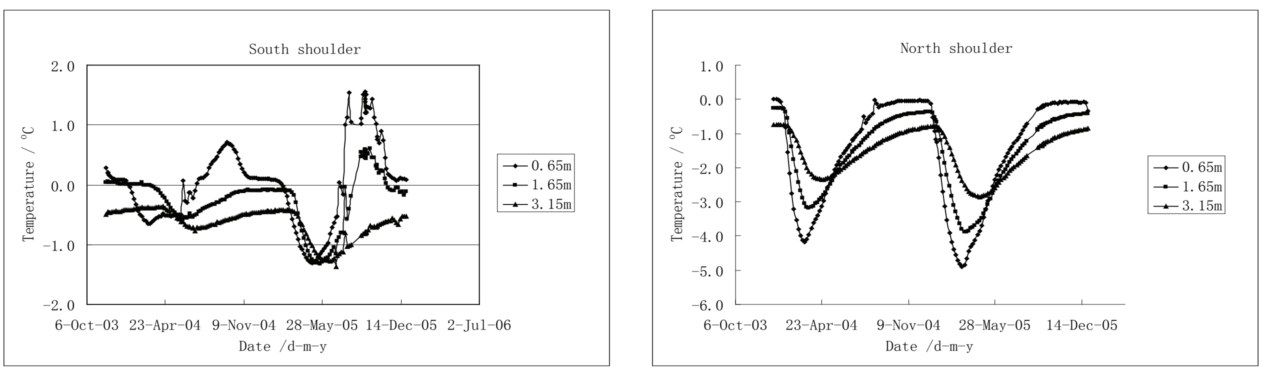

Figure 7. Ground temperature changes vs. time at different depths under the embankment with the slope protection partially covered by crushed rock (DK1082+675).

it is found that the minimum ground temperature in shallow layers under embankment had larger ground temperature differences than that in deeper layers.

Ground temperature changes under embankments with the slope protections partially covered by crushed rock

Figure 7 shows typical ground temperature changes with time at different depths and positions under the embankments at DK1082+675. It can be seen that with the slope partially covered by crushed rock, the ground temperature under the embankment decreased noticeably. Compared with minimum ground temperature, it was found that the rate of decrease of ground temperature under the south shoulder was larger than that under the north shoulder. The same was true for the south and north toes. However, a ground temperature difference still exists between the south-and north-facing slope of the embankment, particularly under the shoulders of the embankment. The ground temperature difference under the south and north shoulder and toe decreased gradually with time. Comparing with the ground temperature change under the shoulders and toes at DK1082+675, +725, +825, found that adjustment of the asymmetrical thermal regime under the embankment structure is best with the widths of the south/north-faced slopes of 4.0 m/6.0 m, using the crushed rock size of 30 cm (DK1082+725). Second best is the embankment with the widths of the south/north-faced slopes of 4.0m/6.0m and the crushed rock size of 20 cm (DK1082+675). The embankment with the widths

Table 2. Maximum thaw depth at the south and north shoulders of embankments.

Monitoring profile	Location	Height of embankment /m	Maximum thawing depth in 2003 /m	Maximum thawing depth in 2004 /m	Maximum thawing depth in 2005 /m	Structure type of embankment
DK1082+375	South shoulder	2.49	4.0	3.51	2.93	Embankments with the slopes fully covered by crushed rock
	North shoulder	2.53	3.25	2.48	2.46	
DK1082+425	South shoulder	2.59	4.0	3.41	3.82	
	North shoulder	2.71	3.6	3.33	3.29	
DK1082+475	South shoulder	2.76	4.0	3.66	3.36	
	North shoulder	2.81	3.5	2.62	3.00	
DK1082+675	South shoulder	2.28	4.1	3.62	3.43	Embankments with the slopes partially covered by crushed rock
	North shoulder	2.42	3.2	2.89	2.87	
DK1082+725	South shoulder	2.13	3.6	3.47	3.18	
	North shoulder	2.36	3.5	3.32	2.90	
DK1082+825	South shoulder	2.80	5.1	4.77	4.42	
	North shoulder	2.72	3.8	3.5	3.35	
DK1082+775	South shoulder	2.04	4.1	3.85	3.54	Embankment with the slope partially covered by soil
	North shoulder	2.17	3.8	3.54	2.96	

of the south/north-faced slopes of 3.0 m/5.0 m and the crushed rock size of 10 cm is the worst (DK1082+825). The difference of the minimum ground temperature at different depths under the south and north toe was 1.11°C to 1.27°C, 1.6°C to 2.26°C, 1.94°C to 3.2°C, respectively. In addition, the minimum ground temperature in shallow layers under embankment has larger ground temperature differences than that at deep layers.

Discussion and Suggestions

In general, choice of good embankment structure must consider both the ground temperature difference and the maximum thawing depth (permafrost table) between the south- and north-facing slopes of the embankments.

On the basis of observations, it is seen that except for the embankments with slope protection partially covered with soil, the other embankment structures achieved a certain adjustment of the asymmetrical thermal regime.

Compared with the thickness and size change of crushed rock, it is found that with full coverage using crushed rock, the ground temperature difference decreased gradually with increasing thickness of the crushed rock layer. For the slopes partially covered with crushed rock, the adjusting effect of the asymmetrical temperature distribution using larger grain sizes is better than the others. But, a small change in the thickness or grain size cannot completely adjust the asymmetrical temperature distribution in this test. Based on ground temperatures under the south and north shoulders, the ground temperature with full coverage with crushed rock under the south shoulder was lower than that using partial coverage with crushed rock, and the ground temperature of the partial coverage with crushed rock under the north shoulder is lower than that using coverage with crushed rock. For integrated effect of ground temperature regime, the asymmetrical temperature distribution adjustment using full coverage with crushed rock was better than partial coverage with crushed rock.

Table 2 shows the changes in the maximum thawing depth under the south and north shoulders for different monitoring profiles. Except for the monitoring profiles of DK1082+425 (south shoulder), DK1082+475 (north shoulder), and DK1082+825 (north shoulder) where the maximum thawing depth decreased from 2003 to 2004 and increased from 2004 to 2005, the others decreased from 2003 to 2005. Through in-situ investigation, we found that abnormal change of the maximum thawing depth in DK1082+425 (south shoulder), DK1082+475 (north shoulder), and DK1082+825 (north shoulder) were caused by rainwater massed at the slope toe of the embankment. The maximum thawing depth for full coverage with crushed rock under the south shoulder is less than that of using partial coverage with crushed rock, and the maximum thawing depth for partial coverage with crushed rock under the north shoulder is less than that of using full coverage. Compared with the difference of the maximum

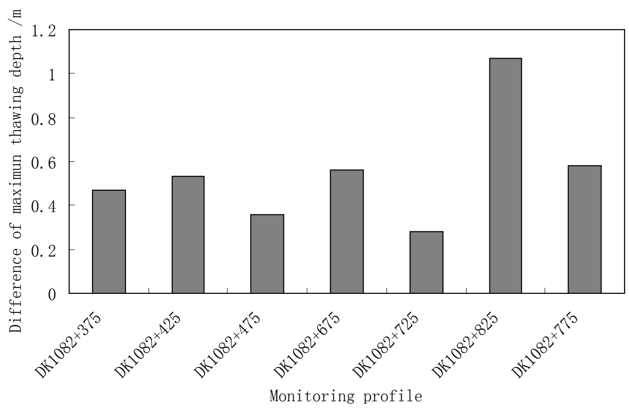

Figure 8. Difference of the maximum thawing depth between the south and north shoulder for different monitoring profiles in 2005.

thawing depth between the south and north shoulders in 2005, the differences at DK1082+475 and DK1082+725 are still less than the others, they are 0.36 m and 0.28 m, respectively (shown in Fig.8).

In other words, the better embankment structures for adjusting asymmetrical permafrost table were the embankments with slope protection using partial coverage with crushed rock with widths of the south/north-faced slope of 4.0 m/6.0 m and a crushed rock size of 30 cm (DK1082+725), as well as embankments with slope protection using full coverage with crushed rock and thickness of the south/north-facing slopes of 1.0 m/1.6m and the crushed rock size of 10 cm (DK1082+475).

Based on the above discussions, we can say that under the conditions of our test sections, these methods can slowly change the ground temperature regime but cannot absolutely adjust the asymmetrical temperature distribution under the embankments. In these testing programs the small change in thickness and grain size of the crushed rock had only a limited effect on adjusting and controlling the asymmetrical temperature regime. After integrated considering of the difference of ground temperature and the maximum thawing depth under the north shoulders and toes of the embankment, as well as economical cost, we suggest that the south-faced slope is better fully covered by crushed rock with wider and thicker structure. For the north-facing slope partial coverage with crushed rock that is narrower and thinner is better.

The above conclusions were drawn only based on three years of data and the lower temperature permafrost region; the effect of the warming climate was not considered. At present, we want to re-monitor these test sections and set up some new monitoring profiles in the higher temperature permafrost regions along the QTR and the Qinghai-Tibet Highway, and hope some new results can be found.

Acknowledgments

This work was supported in part by the grant of the Western Project Program of the Chinese Academy of Sciences (KZCX2-XB2-10) and the Natural Science Foundation of China (Grant No. 40401013 and 50534040).

References

Cheng, G.D. 2003. Impact of local factors to the permafrost distribution and its enlightenment to design of the Qinghai-Tibet Railway [J]. *Sciences in China* (Series D) 33(6): 602-607 (in Chinese with English abstract).

Georing, D.J. & Kumar P. 1996. Winter-time convection in open-graded embankments [J]. *Cold Regions Science and Technology* 24(1): 57-74.

Goering, D.J. 2001. Parks/Chena Ridge air convection embankment experimental feature. *Phase II Final Report*: *Oct. 1999 to Sept. 2000*. Report N. FHWA-AK-RD-01-02 (INE/TRC 02.21), Washington, DC: Federal Highway Administration.

Georing, D.J. & Kumar P. 2000. Convection heat transfer in railway embankment ballast[A]. *Ground Freezing 2000*[C], Rotterdam: Balkema: 31-36.

Georing, D.J. 2003. Passively cooled railway embankments for use in permafrost areas [J]. *Journal Cold Regions Engineering* 17(3): 119-133.

Ma, W., Cheng, G.D. & Wu, Q.B. 2002. Preliminary study on technology of cooling foundation in permafrost regions [J]. *Journal of Glaciology and Geocryology* 24(5): 579-587 (in Chinese with English abstract).

Ma, W., Wu, Q.B. & Cheng, G.D. 2006. Analyses of temperature fields under the embankment with crushed-rock structures along the Qinghai-Tibet Railway [J]. *Journal of Glaciology and Geocryology* 28(4): 586-595 (in Chinese with English abstract).

Rooney, J.W. 1997. Rock fill embankment applications for convective foundation cooling on BAM railway system [A]. *Proceedings of the 5th International Symposium on Cold Regions Development* [C], Anchorage, ASCE, 399-402.

Sun, Z.H., Ma, W. & Li, D.Q. 2004. Experimental study on cooling effect of air convection embankment with crushed rock slope protection in permafrost regions. [J]. *Journal of Glaciology and Geocryology* 26(4): 435-439 (in Chinese with English abstract).

Wu, Q.B., Cheng, G.D., Ma, W., et al. 2006. Technical approaches on ensuring permafrost thermal stability for Qinghai-Xizang Railroad construction [J]. *Geomechanics and Geoengineering* 1(2):119-128.

Wu, Q.B., Zhao, S.Y., Ma, W. et al. 2005. Monitoring and analysis of cooling effect of block-stone embankment for Qinghai-Tibet Railway. *Chinese Journal of Geotechnical Engineering* 27(12): 1386—1390.

Estimation of Frost Heave and the Stress-Strain State of the Buried Chilled Gas Pipeline

M.A. Magomedgadzhieva
State Engineering Designing Research Institute "Fundamentproject," Moscow, Russia
N.B. Kutvitskaya
State Engineering Designing Research Institute "Fundamentproject," Moscow, Russia
S.E. Grechishchev
State Engineering Designing Research Institute "Fundamentproject," Moscow, Russia

Abstract

It is well known that frost heave occurs in zones of thawed and non-anchored frost-susceptible soils under the effect of buried chilled gas pipelines. This phenomenon is due (related) to the specific stress-strained state of freezing soils. Simulation results revealed the following special features of the process: peak linear heave load increases with a decrease in permeability and with an increase in soil freezing rate; peak linear heave load increases in the following succession: sand–sandy loam–loam–clay; and peak linear heave load varies with time and achieves maximum values during the first year of operation of a gas pipeline. Appropriate thermal insulation can eliminate frost heave entirely. The technical decisions providing engineering protection are developed on the basis of soil thermal behavior simulations and strain calculations. These decisions will ensure the stability of the planned pipeline embedding during the whole operation period.

Keywords: buried pipeline; discontinuous permafrost; freezing rate; frost heave; heave load; stress-strained state; permeability.

Introduction

It is well known that frost heave occurs in zones of thawed (under ponds, lakes, bogs) non-anchored frozen soils under the effect of chilled gas pipelines. This phenomenon is related to the specific stress-strained state of freezing soils. Estimation of the displacement of a buried pipeline as a result of frost heave has been a problem because of the lack of appropriate theoretical analysis.

The phenomenon of the frost heave of chilled pipelines in unfrozen soils has been studied since the 1980s. The first approximate theoretical analysis of this phenomenon was undertaken by Grechishchev (1994). Experimental studies of the frost heave of chilled buried pipelines under natural conditions were carried out in France (Williams, 1986, 1989) and Alaska (Akagawa et al. 2004, Kanie et al. 2004).

The calculation of the theoretical peak heave force has remained the pri chilled pipeline on the surrounding soils, the theoretical peak frost heave force applied to a chilled pipeline, and the stress-strain state of the pipeline were evaluated.

Computation procedure was as follows. First, the anticipated thermal behavior of soil was estimated. Based on the obtained thermal behavior parameters (soil freezing above the pipe, soil freezing under the pipe, peak annual freezing rate under the pipe), maximum possible frost heave force applied to the chilled pipeline was estimated. Finally, the obtained linear pull-out force values were applied to the pipeline to estimate its stress-strained state.

Anticipated changes in the thermal conditions of soils underlying the pipeline during construction and operation periods were estimated using the specially developed PROGNOZ software (RSN 67-87), providing a possibility to make allowances for geological and geocryological section heterogeneity, soil physical and thermal properties, and the anthropogenic thermal effects. Mathematical simulation in this software is achieved by enthalpy finite-difference method on an explicit two-layer grid. Simulation was two-dimensional.

The applied calculation method (10) provided a possibility to estimate the values of normal heave forces applied to gas pipe or the confining force to be applied to the pipe to ensure its stability.

Software package Mathcad 2001 was developed for the numerical solution of model equations.

The stress-strained state of the gas pipeline was estimated using the Cosmos Works software based on the finite-element method. Normal frost heave force value was assumed to be equal to estimated heave load (shut-off pressure). Also, gas pipeline actual operating pressure and the subsoil and transmitted gas temperatures were assigned.

Initial Data

By way of a case study, given below are computation results for Olekmisk conditions. The pipeline diameter is 1400 mm, the pipe center depth is 1.5 m, and the operating pressure is assumed to be 10 MPa.

The frost heave of a buried chilled gas pipeline was estimated for the case of discontinuous permafrost with a roof foundering of 10 m and average annual soil temperature of minus 0.1°C at the annual zero amplitude depth. Calculations

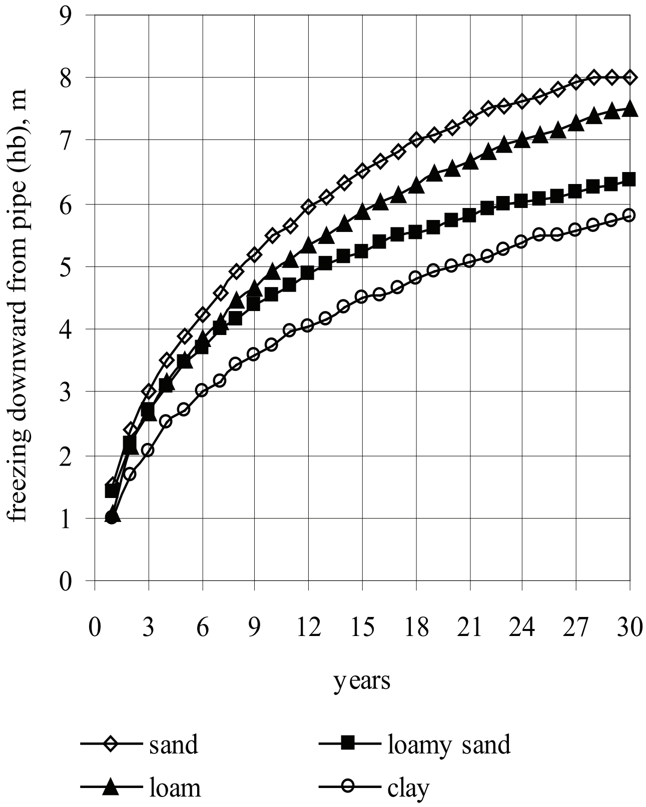

Figure 1. Change of depth freezing downwards from a chilled gas pipeline with time.

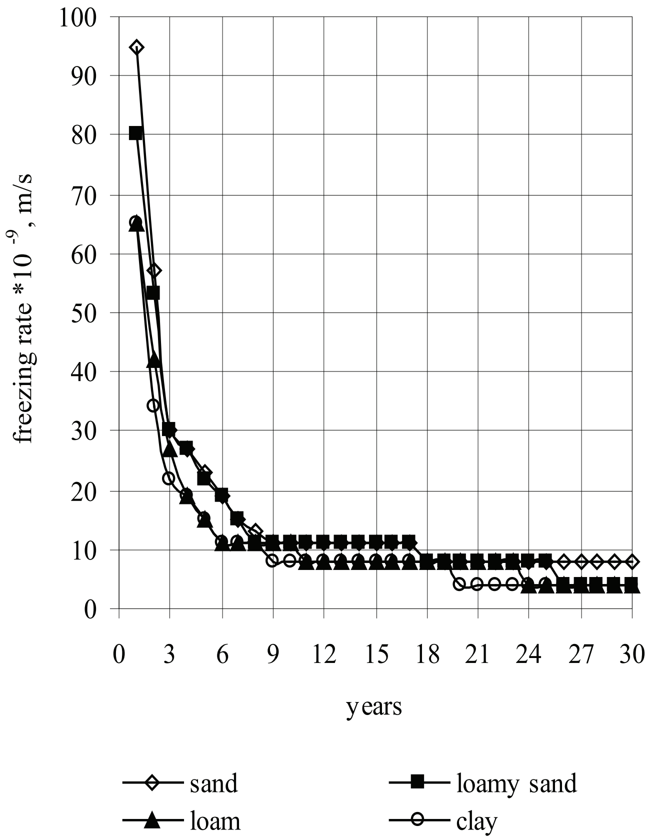

Figure 2. Change of freezing rate with time.

were performed for sand, loamy sand, loam and clay soils.

Calculations for the pipe-soil boundary were made for transmitted gas temperature varying in time from minus 7.5°C in winter to minus 2°C in summer. The following cases were studied: pipe without thermal covering and pipe with a thermal covering with a thermal resistance to heat transfer of 3.6 W/m^2×°C (with reference to clay soil).

Results

Thermal behavior calculation results are illustrated by Figure 1 and 2. The obtained data suggest that freezing depth (Fig. 1) and rate (Fig. 2) increase in the following succession: clay–loam–sandy loam–sand.

Peak linear heave load as a function of freezing rate is shown in Figure 3. As obvious from the figure, peak linear load value varies with time and is the highest during the first year of the gas pipeline operation period.

Data shown in Figure 3 also demonstrate the increase in peak linear heave load with an increasing soil freezing rate.

Peak heaving load as a function of soil permeability is shown in Figure 4. Analysis of data shown in Figure 4 suggests that the effect of soil permeability on linear heave load value is significant. Linear load value increases with a decrease in permeability.

Analysis of calculation results (Figs. 3 and 4) suggests that peak linear heave load increases in the following succession: sand–sandy loam–loam–clay.

The stress-strained state of pipeline under the estimated peak heaving load was estimated. Pipeline heave buckling (displacement), in this case, may be as large as 0.5 m.

Heat isolation restricts subsoil freezing. Heat isolation with a thermal resistance to heat transfer of 3.6 W/m^2×°C eliminates soil freezing under the pipeline completely. It follows that it is possible to select isolation thickness sufficient for the complete elimination of pipeline heave buckling.

Based on calculation results, engineering solutions can be worked out for stabilizing the planned chilled buried pipeline position: application of a heat insulation cover with a thickness determined by special calculations; application of ice-and-soil supports or chemically stabilized soils with screw-in anchors, to which pipeline is fastened by special heavy-duty belts. The calculated linear heave load values shall be borne by these anchors.

Conclusions

1. Simulation data analysis has revealed the following tendencies of the process: Peak linear heave load grows with a decrease in permeability and with an increase in soil freezing rate; peak linear heave load increases in the following succession: sand–sandy loam–loam–clay; and peak linear heave load varies with time and achieves maximum values during the first year of a gas pipeline operation period.

2. Integrated predictive estimation of the thermal and

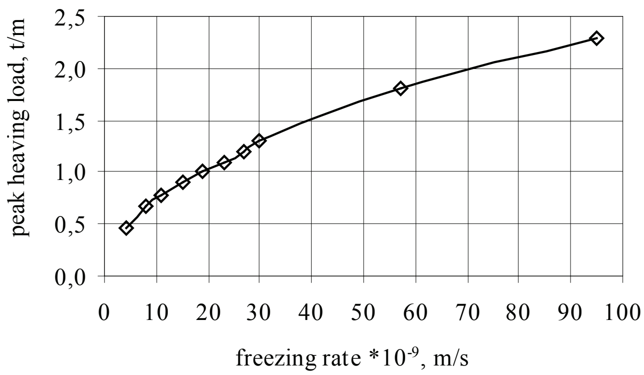

Figure 3. Variation of peak heaving load and freezing rate.

strain behavior of soils at the early stage of project designing provides the opportunity to identify and recommend the optimum temperatures of the piped product to minimize the thermal effect on the subsoil. At later stages of project designing (project design, detailed engineering), engineering protection solutions are developed on the basis of thermal behavior modeling and strain computation to ensure the stabilization of the planned pipeline position during the whole operation period.

References

Williams, P.J. 1986, 1989. Pipelines and Permafrost.

Grechishchev, S.E. 1994. Evaluation of Interaction of Buried Chilled Pipeline with Soils in Taliks Using thermodynamic model. *Proceeding of 7th International Cold Regions Engineering specialty conference*, *Canadian Society for civil Engineering, Edmonton*: 805-814.

Akagawa, S., Kim, K., Huang, S., Kanie, S. & Fukuda, M. 2004. Frost heave prediction of chilled gas pipeline in non-permafrost section of discontinuous permafrost. *Proceeding International Conference Cryosphere of Oil and Gas Bearing Provinces*, *Tyumen*: 43.

Kanie, S., Akagawa, S., Sato, M. & Mikami, T. 2004. Evaluation of interactive behavior between chilled gas pipeline and frost soil for structural design. *Proceeding International Conference Cryosphere of Oiland Gas Bearing Provinces*, *Tyumen*: 53.

Grechishchev, S.E., Magomedgadzhieva M.A. & Dmitrieva, S.P. 2005. Special features of frost heave of a buried chilled gas pipeline. *Proceedings of the Fifteenth International Offshore and Polar Engineering Conference, II, Seoul, Korea, June 19–24:* 57-62.

RSN 67-87. Engineering researches for construction. Drawing up of the forecast of changes of a temperature regime of soils by numerical methods.

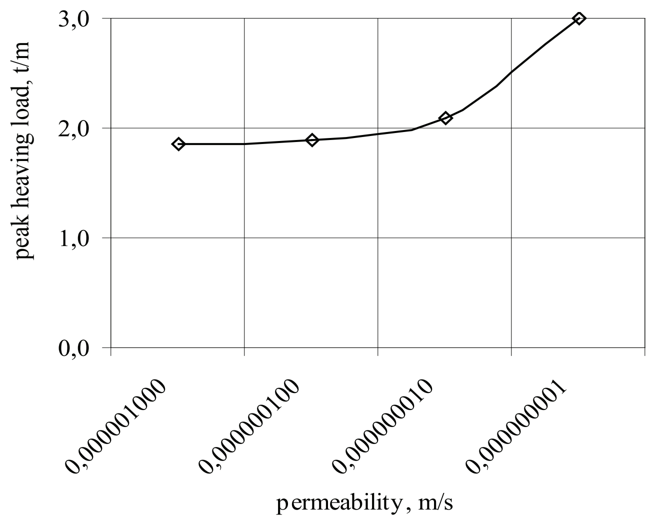

Figure 4. Variation of peak heaving load and permeability.

Analysis of Discharge Characteristics in a Region of Continuous Permafrost: Yana Basin in Siberia

Ipshita Majhi
WERC, University of Alaska Fairbanks
Daqing Yang
WERC, University of Alaska Fairbanks

Abstract

Yana basin was analyzed to understand the hydrology of the catchment, since it is situated in a continuous permafrost region with minimal human impact. The discharge analysis revealed the typical permafrost laid hydrograph with peak summer flood in June and minimum flow from November to April. Temperature and precipitation did not show any significant trend over 70 years. Statistical analysis showed a mixed trend for the stations examined, but there is no significant trend observed for winter months. There is a relationship between snow water equivalent and discharge, but further examination is needed to document the relation. Overall, a better understanding of hydrology was gained through this analysis.

Keywords: hydrology; permafrost; snow water equivalent; Yana.

Introduction

Rivers provide a vital link by integrating, spatially as well as temporally, atmospheric and land surface processes at catchment level, thereby providing a mechanism to detect climate change (Déry et al. 2005).

Significant changes have been observed in the large arctic river basins. For instance, Ye et al. (2003) and Yang et al. (2004) found Lena and Yenisei River discharges increase during the winter months and shift in peak discharge timing in Siberia mostly due to reservoir regulation. Small coastal rivers with no regulation and scarce population density provide an ideal medium to understand the effect of climatic variation on streamflow.

The emphasis of this research is to gain a better understanding of various parameters which affect the unregulated Yana River basin in Eastern Siberia. The basin was chosen for this analysis, since it is a non-regulated mid sized watershed, and streamflow response to snowmelt is direct without reservoir interference or other anthropogenic activities. This analysis will enhance our knowledge of discharge response to changes in precipitation, temperature and snow cover.

Study area, data, and method

The Yana basin is one of the large rivers in northeast Asia with a basin area of 238,000 km^2. The river flows north for 879 km, passing through subarctic and arctic region, and finally discharges into the Laptev Sea at 72°N .The Yana River lies between the East Siberian lowland and the Verkhoyano range. In the lowlands the elevation does not exceed 150 m. The climate in this region is continental. Precipitation ranges from 200–400 mm/year in the lowlands to 400–500 mm/year on the ridges. Continuous permafrost with infrequent taliks as well as widely developed taliks occurs everywhere.

Hydrological observations in the Siberian regions, such as discharge, stream water temperature, river-ice thickness, and dates of river freeze-up and break-up, have been carried out since the mid 1930s by the Russian Hydro Meteorological Services (Shiklomanov et al. 2000). The discharge data are now available from the R-Arctic Net (v.3.)-(www.r-arcticnet.sr.unh.edu/main.html) online.

In addition, subbasin mean monthly temperature and precipitation were obtained from University of New Hampshire (http://rims.unh.edu) along with the Special Sensor Microwave/Imager (SSM/I), remote sensing snow water equivalent data (SWE). As part of our preliminary analysis we defined the natural climatic variation through temperature and precipitation interannual variability, mean, standard deviation, and linear trend. Second, we analyzed monthly and annual discharge records along the main stream to quantify discharge change. Third, we compared snow water equivalent, precipitation, temperature, and discharge as a function of time to assess their relationship.

Result and Discussion

Climate-hydrology

Annual temperature during 1930–2000 ranged from -16°C to -12°C; the cold temperature is characteristic of a region with continuous permafrost (Fig. 1). The basin is characterized by a long cold season of eight months, with temperatures ranging from -10°C in September to around -2.5°C in May. The brief warm season has a temperature range of 9°C in June to 3°C in August, with July being the warmest month (mean temperature of 13°C). The coldest month is January with a mean monthly temperature of -40°C.

Mean annual precipitation over the basin ranges from 145 mm to 300 mm, with an average value of 220 mm (Fig. 1). There is minimal precipitation ranging around 5 mm in January, February, and March. Peak precipitation is in the months of July and August with an average rain depth of 45 mm. Monthly mean value of precipitation for September,

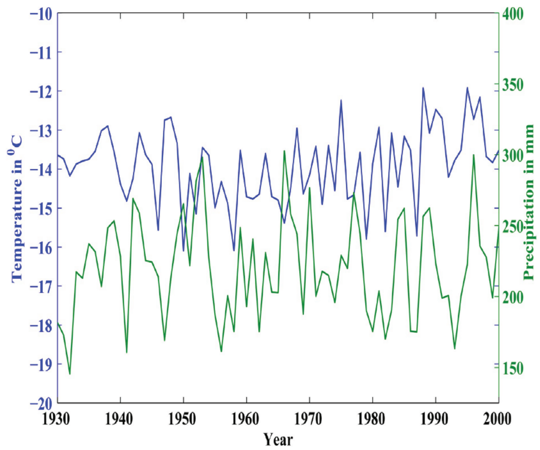

Figure 1. Interannual variability for temperature and precipitation at Yana basin from 1930–2004.

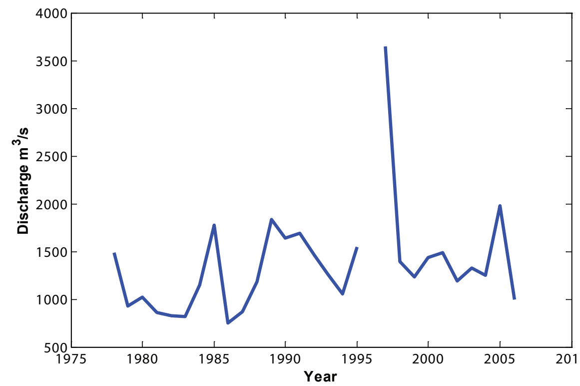

Figure 2. Interannual variability for discharge at Yana basin from 1976–2006.

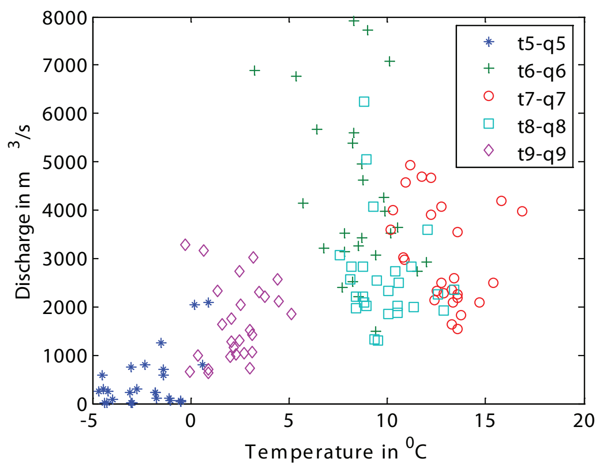

Figure 3. Discharge (*q*) and temperature (*t*) comparison from May to September with no lag.

October, November, and December are 25 mm, 15 mm, 10 mm, and 7 mm.

Temperature and precipitation interannual variability (standard deviation) did not show any significant upward trend from 1930–2000. The highs and lows of precipitation and temperature show consistency, indicating with higher annual temperature there is higher annual precipitation. To understand the basin hydrology, annual flow, monthly flow and variation (standard deviation) and trend are analyzed

It was found that basin discharge is typical of continuous permafrost region (Kane 1997) with peak flow in June and low flow dominating from October to April. Trend analysis shows mixed results for all the stations, but negligible or no change is observed during the cold season from October to April.

Discharge, temperature, precipitation, and Special Sensor Microwave/Imager (SSMI) SWE analysis

The discharge regime at the outlet shows interannual variation from 1600 m^3/s to 800 m^3/s with a tendency towards decreasing trend from 1988–2000 (Fig. 2). The variation in monthly streamflow is generally small for the cold season (October to April) and large in summer months, mainly due to floods associated with snowmelt and storm activities.

Correlation between temperature and discharge was examined to understand the effect of higher or lower temperature fluctuation on mean discharge. Statistical analysis of annual mean discharge at the basin outlet and temperature annual mean showed a positive correlation (R = 0.30). There is no consistent relationship for warm and cold season for zero time lag, which could be due to no flow for most of the cold season in the Yana basin (Fig. 3). The only statistically significant month was May with a strong positive correlation (R = 0.48). Yang et al. (2002), observed a similar relationship for Lena basin, emphasizing that higher temperature in May will lead to larger snowmelt floods. This relationship shows that during transition period, as the watershed warms up, snow cover disappears and evaporation starts to dominate (Yang et al. 2002). Since this is a smaller basin compared to other large Siberian rivers, even one month lag does not show any significant relationship except a high positive correlation between November to December (R = 0.47); that is, higher temperature in November leads to more discharge in December.

Statistical analysis for correlation between precipitation and discharge showed a positive relationship for interannual comparison (R = 0.24), indicating that some years with higher precipitation showed higher average discharge. The winter months of January (R = 0.43) and March (R = -0.32) showed a negative relationship for zero lag, and other months from October to April showed no significant relationship. This could be because cold months are characterized by snow cover accumulation, and discharge is mostly base flow or no flow (Yang et al. 2002).

Discharge and SWE follow an inverse relationship, with the advent of snowmelt at about day 86 (last week of March), and it finally disappears at day 150 day around the last week of May on average (Fig. 5). The discharge subsequently peaks on day 160. This is typical of arctic regions underlain with continuous permafrost. The time series of discharge and snow water equivalent emphasizes the inverse relationship. High value of snow water equivalent does not always lead to high peak discharge; this could be due to different ablation

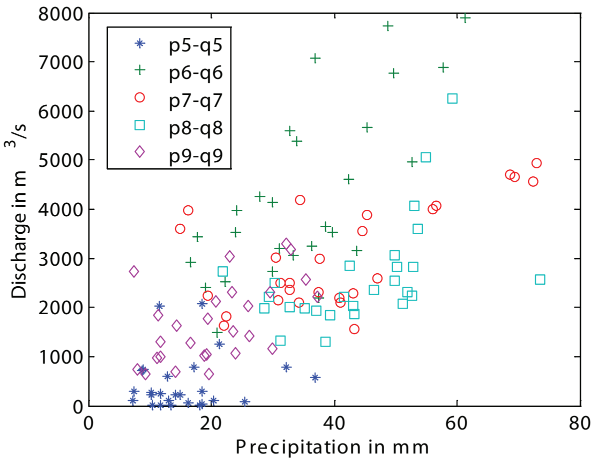

Figure 4. Discharge(q) and precipitation (p) comparison from May to September with no lag.

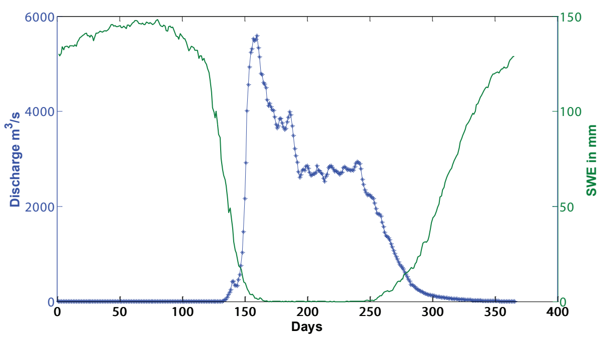

Figure 5. Daily mean discharge and SWE relationship.

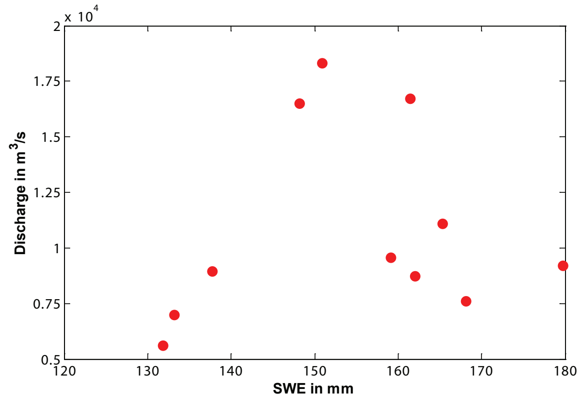

Figure 6. Daily maximum discharge and SWE relationship.

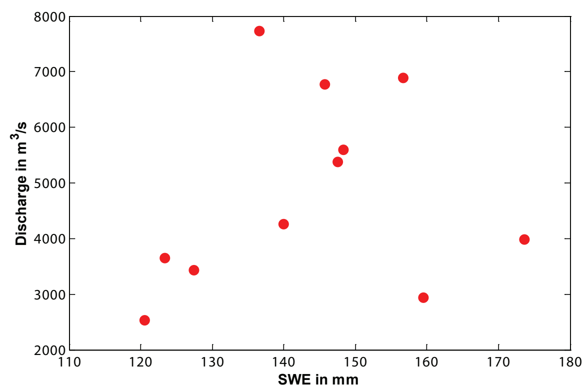

Figure 7 Monthly maximum discharge and SWE relationship.

rates, which are variable from year to year. We calculated the ablation rate around mid May to the first week of June and it varies from as low as 2 mm/day to as high as 16 mm/day at the start of snowmelt; the rates change with increase in temperature.

Highest daily value of SWE and discharge are compared, and their relationship (Fig. 6) follows a Gaussian curve. Increase in discharge is associated with increase in snow water equivalent (SWE), but there are some discrepancies for some years.

There is a lot of missing data for some years, and the mean value could be shifted to the month of August resulting in a lower peak. On looking at mean monthly maximum discharge in June and mean maximum SWE in March, the relationship is more linear with two outliers at the high end of SWE, which is similar to the daily maximum SWE and discharge relationship. The result indicates that on average, a year of higher precipitation in winter will lead to higher peak discharge.

The dates for maximum snow and discharge for each year are analyzed (Fig. 7), and no major change or shift is found in the timing of peak discharge and maximum snow water equivalent.

Conclusion

Significant changes have been observed in the large arctic river basins. For instance, Ye et al. (2003) and Yang et al. (2004) found Lena and Yenisei River discharges increase during the winter months and shift in peak discharge timing in Siberia mostly due to reservoir regulation. In our study of the Kolyma basin, we also found significant increase in winter discharge by as much as 522%-3157% downstream of the dam from December to April (Majhi et al. in press). Our results indicate that the Yana basin does not show any significant change in discharge.

Temperature and precipitation interannual variability (standard deviation) did not show any significant upward trend from 1930–2000. The peaks and lows of precipitation and temperature show consistency, indicating with higher annual temperature there is higher annual precipitation. Most of the precipitation falls in the summer months from June to September. Temperature shows a basin high of around 15°C in summer and a low of -40°C in January. Basin discharge is typical of continuous permafrost region with peak flow in June and low flow dominating from October to April. Trend analysis shows mixed results for all the stations, but negligible or no change is observed during the cold season from October to April.

The only statistically significant month for temperature and discharge was May with a strong positive correlation . Yang et al (2002), observed a similar relationship for the Lena basin, emphasizing that higher temperature in May will lead to larger snowmelt floods. Correlation between precipitation and discharge showed a positive relationship for interannual comparison, indicating that some years with higher precipitation showed higher average discharge. The winter months of January and March showed a negative relationship for zero lag, and other months from October to April showed no significant relationship, while there was significant relationship from June to September for no lag. This could be due to quick response of discharge to rain events, since the Yana is comparatively a medium-sized basin.

Overall there is a need to better understand discharge dynamics to further the hydrological cycle and its implications. Monitoring snow pack variability for the arctic region has implications in the context of global change, since it is fundamental to estimate the change in freshwater flux. Moreover, changes in snow depth and timing alter the surface albedo, resulting in feedbacks at both regional and global scale. The analysis reported may be very useful in improving the snow and discharge relationship in hydrological models.

References

Déry, S.J. & Wood, E.F. 2005. Decreasing river discharge in northern Canada. *Geophys. Res. Lett.* 32: L10401, doi:10.1029/2005GL022845.

Déry, S.J., Stieglitz, M., McKenna, E.C. & Wood, E.F. 2005. Characteristics and trends of river discharge into Hudson, James and Ungava Bays, 1964–2000. *Journal of Climate* 18: 2540-2557.

Kane, D.L. 1997. The impact of arctic hydrologic perturbations on arctic ecosystems induced by climate change. *Ecological Studies* 124: 63-81.

Shiklomanov, I.A. & Shiklomanov, A.I. 2003. Climatic change and the dynamics of river runoff into the Arctic Ocean. *Water Resources* 30: 593-601.

Yang, D., Kane, D.L., Hinzman, L., Zhang, X., Zhang, T. & Ye, H. 2002. Lena River hydrologic regime and recent change. *Journal of Geophysical Research Atmosphere* 107(D23): 4694, doi.

Yang, D., Ye, B. & Shiklomanov, A. 2004a. Streamflow characteristics and changes over the Ob River watershed in Siberia. *Journal of Hydrometeorology* 5: 69-84.

Ye, B., Yang, D. & Kane, D.L. 2003: Changes in Lena River streamflow hydrology: Human impacts versus natural variations. *Water Resour. Res.* 39: 1200, doi:10.1029/2003WR001991.

Modeling Temperature Profiles Considering the Latent Heat of Physical-Chemical Reactions in Permafrost and Gas Hydrates: The Mackenzie Delta Terrestrial Case

Jacek A. Majorowicz
NGC EDMONTON, 105 Carlson Close, Edmonton, Canada, T6R 2J8

Kirk Osadetz
Geological Survey of Canada, 3303 - 33rd St. NW, Calgary, Canada, T2L2A7

Jan Safanda
Geophysical Institute, Czech Academy of Sciences, 141-31 Praha 4, Czech Republic

Abstract

To understand better the formation and history of petroleum gas hydrates in terrestrial permafrost regions, we have performed numerical temperature profile modeling in response to surface forcing due to both the glacial-interglacial history and future climate change, where atmospheric CO_2 has doubled due to climate change. The models are constrained by heat flow from deep wells, thermal conductivity, latent heat, and the observed permafrost and gas hydrate thicknesses. The models consider the pressure–depth dependence of ice and gas hydrate thawing points over the entire gas hydrate and permafrost intervals, in contrast to previous models that considered only a thin layer using a constant dissociation temperature. In areas of thick permafrost, results show that a thinned gas hydrate layer persisted through previous interglacials, and that future warming before the "natural" end of the current interglacial will not destabilize the gas hydrate layer significantly. Therefore, present changes in temperature gradient reflect transient conditions, and they should not be used to derive thermal conductivity in permafrost regions using a constant heat flow assumption. We also find that the ratio of temperature gradients within and below the permafrost has very little to do with the thermal conductivity ratio of the permafrost, although this is less appropriate in the sub-permafrost layers due to the buffering effects of overlying ice-bearing permafrost. Models with unfrozen-frozen thermal conductivities of 2.4–3.6 W/(m.K), and with an unfrozen-frozen conductivity ratio of 2.1–3.4 W/(m.K), (that is, very similar conductivity ratios 1:1.5 and 1:1.6) give dramatically different thermal gradient ratios 1:5.4 and 1:2.9, respectively.

Keywords: climate change; gas hydrate; latent heat; permafrost.

Introduction

To understand better the formation and history of petroleum gas hydrates (GHs) in terrestrial permafrost regions, we have performed numerical modeling of the surface forcing due to both glacial-interglacial history and future climate change. Persistent GH layers in a terrestrial environment of thick permafrost in cold regions sequester methane and impede its migration into the atmosphere. The Mallik site in the Mackenzie Delta (MD) is an excellent example of such GH deposits (Dallimore & Collett 2005, Smith & Judge 1995, Judge et al. 1994, Judge & Majorowicz 1992). We examine this hypothesis by modeling terrestrial MD GH thickness variations below an ice-bearing permafrost (IBP) layer in response to past and future surface temperature changes, using a 1D thermal model that assumes no water or gas flow. Past surface forcing uses a detailed Holocene glacial-interglacial history compiled from other sources (Taylor et al. 2005). We also consider the implications of a warmer future based on a doubling of atmospheric CO_2 resulting in a local mean surface temperature increase of 2°C/100 yrs.

Method

Solving the transient heat conduction equation gives the temporally dependent subsurface temperature change in response to surface forcing:

$$C_v \, \partial T/\partial t = \partial[K(\partial T/\partial z)]/\partial z + A \qquad (1)$$

where T is the temperature, K is the thermal conductivity, C_v is the volumetric heat capacity, A is the rate of heat generation per unit volume, z is the depth, and t is the time in a one-dimensional layered geothermal model. We employed a computer code to simulated temporal subsurface temperature changes in response to surface forcing (Safanda et al. 2004). Within the model, Equation 1 is solved numerically by an implicit finite-difference method similar to that described by Galushkin (1997). The upper boundary condition is the temporally varying surface temperature, and the lower boundary condition is a constant heat flow density at 15 km depth. The depth grid steps are: 2, 5, 10, 50, 100, 250, and 500 m deep; model layers are defined between: 0–100, 100–1500, 1500–2000, 2000–2500, 2500–5000, 5000–10,000, and 10,000–15,000 m deep. Time steps vary between 0.5 yr to 50 yr, depending on the amplitude of surface temperature changes.

The finite-difference scheme of Equation 1 on the depth and time grids, together with the upper and lower boundary conditions, leads to a system of difference equations for unknown values T_{k-1}^{n+1}, T_k^{n+1}, T_{k+1}^{n+1} (where the subscript k and the superscript n denote a value at the k-depth step and the n-th time step) within a tri-diagonal matrix, which was solved by the forward method (Peaceman & Rachford 1955).

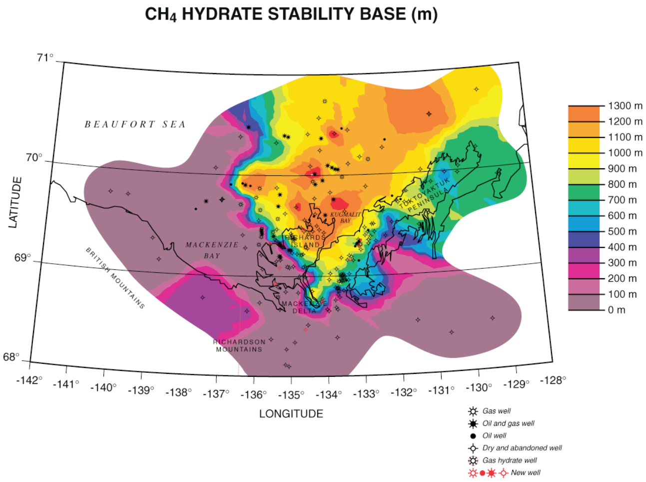

Figure 1. Depth to GH base of Type I stability in the BMB based on the interpretation of measured temperature logs, bottom hole temperature data (Fig. 2) and T-z calculations (modified from Majorowicz and Hannigan 2000) that are constrained additionally by both deep heat flow and base of the IBP. Modelling undertaken here is for northern Richards Island (near centre of figure).

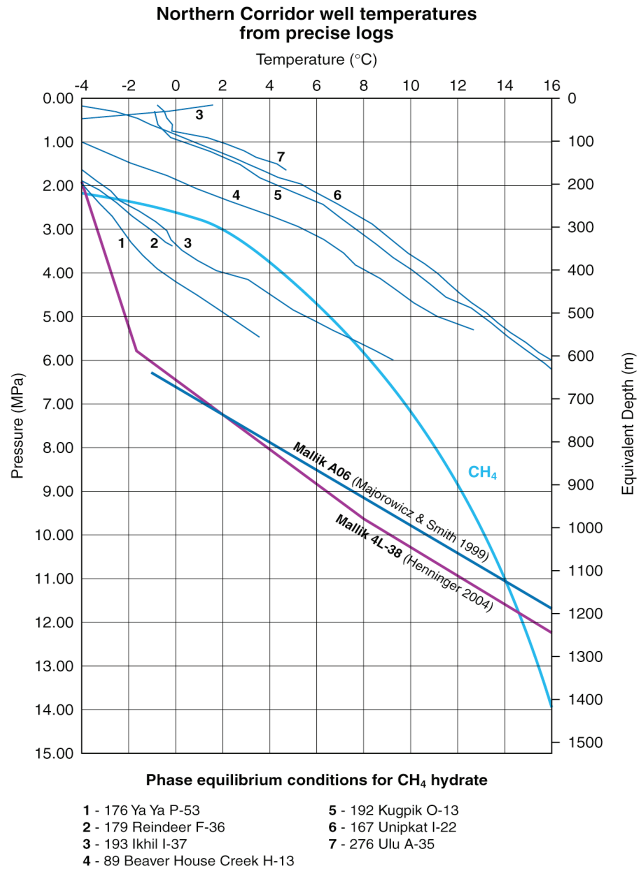

Figure 2. Example of temperature-depth profiles vs. the equilibrium GH stability curve. Examples of precise logs observed in wells years after the end of the drilling disturbance are from Taylor et al. (1982).

To estimate effective thermal conductivity values and volumetric heat capacity, it was necessary to consider the respective geometric and arithmetic averages of the constituent values for the rock matrix, water, ice, and GH in proportion to their volumetric fractions (Galushkin 1997, Nixon 1986). A consumption or release of the latent heat, L, in water/ice (334 kJ.kg^{-1}) and GH (430 kJ.kg^{-1}) accompanying either thawing or freezing was included. The effects of interstitial ice and GH were accounted for using apparent heat capacity (Carslaw & Jaeger 1959), when the volumetric heat capacity is increased in the depth sections of the model where the thawing and freezing occurs; that is, where the temperature is within the thawing range between the temperature of solidus T_S, and liquidus, T_L, at the actual simulation time step.

The liquidus and solidus temperatures of water/ice and GH are depth and hydrostatic pressure dependent (Galushkin 1997) and solidus temperatures were 0.2°C lower than liquidus temperatures. A contribution to the heat capacity from the latent heat = $\rho\Phi L/(T_L\text{-}T_S)$ was considered, where ρ is the density of either ice or GH, and Φ is a fraction of the total volume occupied by these phases. In the IBP zone, we infer the 30% rock matrix porosity to be fully occupied by water at temperatures above T_L, and by ice at temperatures below T_S. Within the GH stability zone, the GH saturation in matrix porosity was inferred to be 60%. For the model to be tractable, the model IBP and GH stability zones are assumed not to overlap, which follows common observation in the study area that GHs are not generally found within the IBP (Dallimore & Collett 2005). The salt concentration 9 g/L was considered constant with depth, and the p-T phase curves were adjusted to this value.

Numerical code performance was tested by comparing model results against the analytical solidification problem solution (Carslaw & Jaeger 1959), where the molten half-space at liquidus temperature, 1300°C, is in contact with a solid half-space at zero temperature and releases the latent heat of 477 kJkg^{-1} in the temperature range 1100°C–1300°C. Comparison of the differences between the numerical and analytical temperature profiles found them to be within about 20°C. If we assume that the magnitude of the difference is proportional to the temperature range, that is, to the contrast at the contact of the molten and solid half-spaces, the error expected for the IBP and GH numerical simulations should be about 100 times smaller (i.e., tenths of a °C) because of the scale of both the temperature range and surface temperature variations that are used in our simulations. A similar error range was estimated by halving the time and/or depth steps.

Our model uses deep heat flow, thermal conductivity, present IBP and Type I GH thicknesses, and a surface melting temperature (-0.576°C) that considers groundwater salinities (9 g/L). It employs latent heat effects throughout the IBP and GH layers, which improves upon previous models (e.g., Taylor et al. 2005). The models are constrained by deep heat flow from bottom hole temperatures in deep wells (Majorowicz et al. 1990) and thermal conductivity, latent heat, present IBP thickness, and present Type I GH thicknesses (Henniges et al. 2005). The models consider the pressure–depth dependence of ice assuming hydrostatic (e.g., Lachenbruch et al. 1982) and GH thawing points over

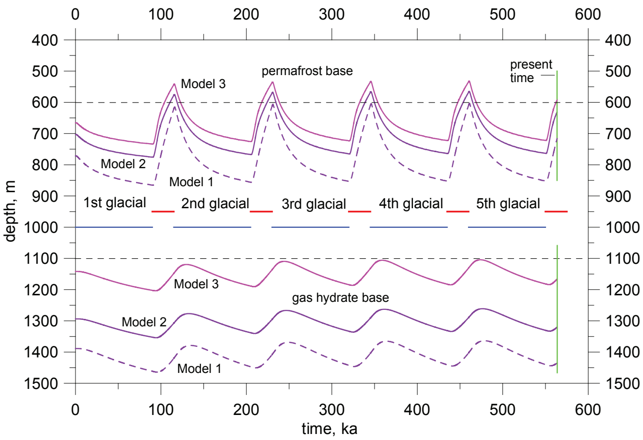

Figure 3. Simple test results of glacial-interglacial surface forcing upon permafrost and GH (Models 1–3 are described in the text). (Time scale shown is 600 ka. Dotted lines show the present base of permafrost and GH. Glacial-interglacial timing and temperature magnitudes are based on Muller & MacDonald (2000) and Taylor et al. (2005).

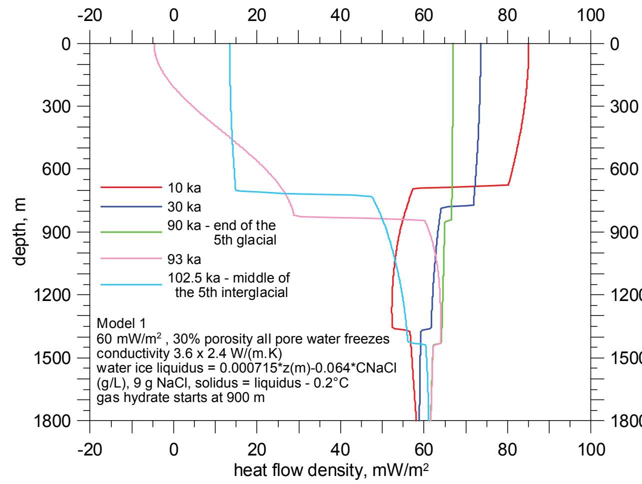

Figure 4. The heat flow and depth profiles for different phases of the glacial cycle for Model 1.

the entire expected extent of the IBP and GH layers (Sloan 1998). Previously published models have considered only a thin layer using a constant dissociation temperature (Taylor et al. 2005).

Current Gas Hydrate Stability Zone

The GH stability zone is currently widespread both in the onshore and offshore BMB, especially to the east of Mackenzie Bay (Fig. 1). There the GH stability zone base reaches 1.5 km deep, where the IBP is thick and the heat flow is low (Figs. 1, 2).

Modeling Results

We have simulated the downward propagation of the surface warming and cooling attending the cyclical glacial and interglacial models for a Richards Island location (Fig. 1). The dependence of the thermal conductivity on water/ice content and the specific heat of the rock section on the porosity and the proportion of interstitial water and ice are important. Accounting for the effect of the latent heat necessary to thaw the interstitial ice in the IBP layer is crucial for matching observations at realistic time rates. In the absence of this heat sink provided by thawing ice in the IBP, the subsurface warming would proceed much faster.

Models of the past history of permafrost and GH layers

Individual computational models use the characteristics of IBP and GH formation and dissipation as functions of temperature history, constrained by present temperature observations and current IBP and GH layer thicknesses. The surface climate history for the end of the Wisconsinan and Holocene is after Fig. 3b in Taylor et al. (2005); Pleistocene surface history of glacials and interglacials is after Muller and MacDonald (2000). Forward modeling of the past history for the IBP and GH layers on Richard's Island in the vicinity of the Mallik well (Dallimore et al. 1999, Dallimore & Collett 2005) can be calibrated against present-day observed IBP and GH zones, which have bases at about 600 m and about 1100 m, respectively.

The numerical solution of the transient heat conduction equation (eq. 1) was applied to model time vs. temperature, depth, IBP characteristics using latent heat effects (Galushkin 1997). This new model employs the pressure–depth dependence of ice and GH thawing points and considers latent heat effects in subsurface heat transport modeling and their impact on paleo-temperature reconstructions across the entire GH layer and not just its boundaries. All models account for latent heat by means of the apparent specific heat, which is a standard treatment. The model also considers diffusive heat flow related to surface-subsurface coupling.

Figure 3 shows three models of the surface temperature forcing effect on IBP and GHs, which currently have observed bases at about 600 m and about 1160–1170 m, respectively:

Model 1 is a simple test of glacial-interglacial forcing upon IBP and GH layers, where the GH zone is constrained to be 900 m deep or deeper. Results show that the model base of IBP and GH is much deeper than the currently observed values, despite a high heat flow value of 60 mW/m^2 (Majorowicz et al. 1990, Henniges et al. 2005). We infer that the frozen IBP conductivity, 3.6 W/(m.K), is lower than that used in this model, which is based on a measured GH layer conductivity of 2.4 W/(m.K), where the pore space of 30% is filled with water and adjusted using the geometric mean to the pore space filled with water ice. We considered glacial-interglacial cycle lengths of 115 ka, of which 90 ka are glacial and 25 ka are interglacial. The present day is 13.5 ka after the last glacial interval. In Model 1, the mean temperature during glacial intervals was -17°C (Allen et al. 1988) and the mean temperature during interglacials was -4°C, which is slightly higher than the present -6.5°C at the Mallik site.

Model 2, like Model 1, considers the climatic history proposed by Taylor et al. (2005, Fig. 3b). We note that in

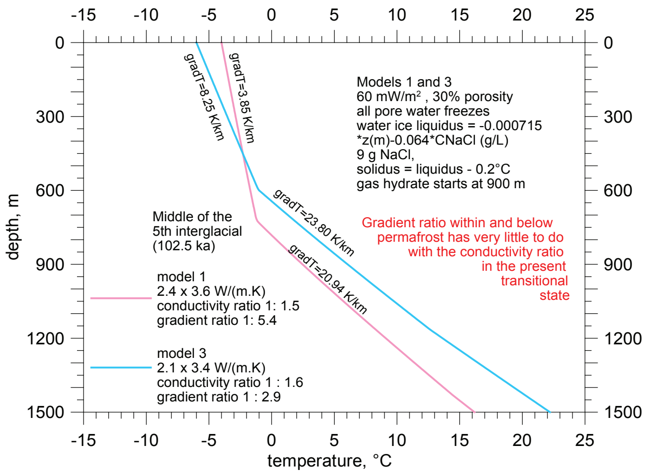

Figure 5. Thermal gradient for the frozen-unfrozen system vs. thermal conductivity ratio (Models 1 vs. 3).

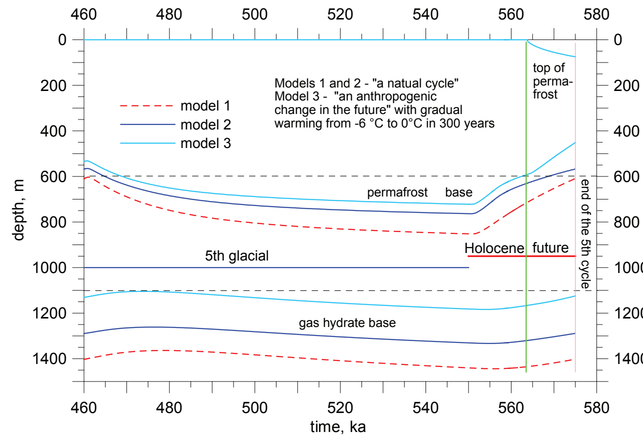

Figure 6. Consequences of the global climate change model that considers 6°C gradual warming projected 300 years into the future. Present time is marked by a green line.

Model 2 the base of both the IBP and the GH layers occurs ~100 m shallower than that calculated by Model 1, mainly due to higher average temperatures during glacial intervals (-15°C, rather than -17°C). In Model 2 the predicted current base of IBP, 13.5 ka after the onset of Holocene warming, is 657 m (-1.04°C) while the base of the GH layer is 1262 m (13.45°C), both of which are slightly too deep for observed values (Fig. 3).

Model 3 is a model that employs a surface warming like that of Model 2. However, Model 3 employs a frozen-thawed conductivity varying from 3.4 (frozen) to 2.1 (unfrozen) W/(m·K) compared with 3.6 (frozen) to 2.4 (unfrozen) W/(m·K) used in Models 1 and 2. This results in an appreciable improvement of the fit to observations. Figure 7 illustrates the position of the current base of the IBP. The calculated present base of IBP is very close to the observed depth of 600 m and the GH layer base is at ~1.17 km (Fig. 3).

All the models indicate generally similar thickness variations of the IBP and GH layers during glacial-interglacial cycles. Both the IBP and GH layers increase in thickness during glacial intervals and decrease in thickness during interglacial intervals. For Model 3 these variations are about 190 m for the IBP and about 80–90 m for the GH layer.

Model 2 predicts that the base of both IBP and GH layers are 100 m higher than those predicted in Model 1, mainly due to a higher average temperature mainly due to assumed warmer glacial, -15°C instead of -17°C. Yet, the predicted current IBP and GH layer bases were still slightly deeper than observed values. Model 3 improves the fit between the observed and predicted current IBP and GH layer characteristics as a result of changes to the frozen-thawed conductivities resulting in an appreciably improved fit to observed values. Today, 13.5 ka after the end of the last glacial interval, Model 3 predictions are very close to the observed IBP base (600 m) while the predicted current base of the GH layer is just slightly deeper (1160–1170 m) than the observed depth (1100 m).

Models of IBP and GH layer characteristics that are based on historical surface temperature forcing are both robust and informative. The predicted heat flow-depth profiles for Model 1 (Fig. 4) illustrate the different phases of the glacial cycle (Fig. 3, Model 1). For example, at 10 ka after the onset of the glacial interval, the base of the IBP, at 700 m, is moving downward, with an attendant heat release, while simultaneously the base of the GH, at 1350 m, is moving upward and consuming heat. The thermal inertia impact on sub-permafrost GH layer thinning is delayed and responsive to surface forcing, rather than leading and causative, due to the buffering effect of the overlying permafrost layer.

Models indicate that heat flow at depths above 1.5 km is in a transient state. Heat flow below that depth is stable, within the measurement error. The simple glacial-interglacial model also indicates that the ratio of temperature gradients within and below the IBP has very little to do with the conductivity ratio of the permafrost and sub-permafrost layers, such that even current temperature profiles are transient. Models with an unfrozen-frozen conductivity ratio = 2.4/3.6 W/(m.K), and models with an unfrozen-frozen conductivity ratio = 2.1/3.4 W/(m.K) give very similar conductivity ratios 1:1.5 and 1:1.6, but are characterized by dramatically different thermal gradient ratios: 1:5.4 and 1:2.9 (Fig. 5).

Below the buffering effects of the IBP the estimated conductivity, K, in the GH zone (Wright et al. 2005; Henninges et al. 2005) is based on both temperature gradients from a precise temperature profile (Henninges et al. 2005) and the deep heat flow, Q = 60 mW/m² (Majorowicz & Smith 1999). The estimates employ the equation:

$$Q/GradT=K \tag{2}$$

This is a correct assumption for steady state situations only, such as non-ice bearing permafrost areas with constant surface *T*. The resulting conductivity estimates are correct below the IBP, within the heat flow measurement error of 10%–15%, (Fig. 4).

The impact of future warming

Surface temperature will change dramatically accompanying the projected doubling of atmospheric CO_2

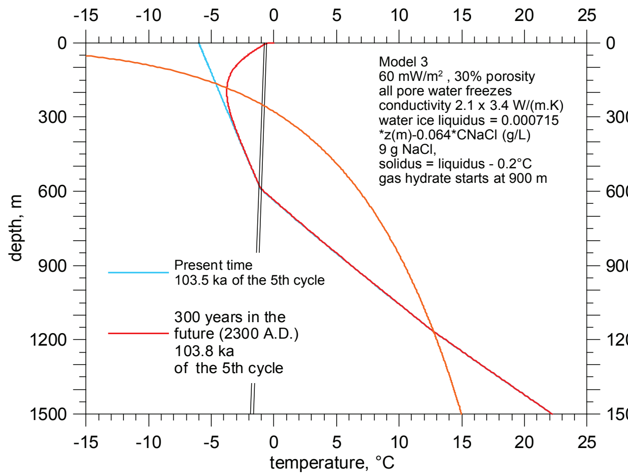

Figure 7. T-z profile corresponding to the expected future warming since present warming by a rate of 2°C/century from -6°C to 0°C.

resulting in future climate warming during the next 300 years. We predict the consequences of such a mean surface temperature change, from -6°C to 0°C, considering past history followed by gradual warming, at a rate of 2°C per century. The future predictions are shown in Figures 6 and 7. Hypothesizing a time corresponding to the "natural" end of this interglacial about 11.5 ka in the future, the model predicts that the IBP will have thawed by ~150 m from below and 70–80 m from the surface. The predicted accompanying GH layer thinning is very small and within the range of previous natural cycle variations (Fig. 3), in spite of the accelerated surface warming accompanying climate change.

Conclusions

Model results that consider latent heat effects of water/ice and GH formation and dissipation show that:

1. Historical and future surface temperature forcing implications for both IBP and GHs can be modeled successfully using available Pleistocene glacial-interglacial and Holocene surface temperature histories. Model GH layer thickness generally increases during colder intervals (i.e., glacial) and decreases during warmer intervals (i.e., interglacial). For Model 3, which most closely resembles observed values, these variations are ~190 m for the IBP and about 80–90 m for the GH layer. Where the IBP layer is thick it is unlikely that sub-permafrost GHs disappeared entirely during previous interglacial intervals, nor are they expected to disappear prior to the "natural" end of the current interglacial. In regions of thick terrestrial permafrost like the Mackenzie Delta, GH layers can act as a persistent sink for and barrier to the migration of methane.

2. Models that consider the consequences of current climate warming trends indicate that, when the current interglacial interval ends "naturally" ~11.5 ka from now, the study area IBP will have thawed ~150 m from below and 70–80 m from the top. The attending GH disassociation inferred is very small and comparable to that of model natural variations accompanying preceding glacial-interglacial cycles.

3. Temperature gradient ratios within the IBP are not strongly dependent on the conductivity ratio between permafrost and sub-permafrost layers, as the current temperature profile is a transient one. A model with an unfrozen-frozen conductivity of 2.4–3.6 W/(m.K) and a model with an unfrozen-frozen conductivity ratio 2.1–3.4 W/(m.K) result in very similar conductivity ratios, 1:1.5 and 1:1.6, but these two alternatives have dramatically different thermal gradient ratios of 1:5.4 and 1:2.9, respectively.

4. The hypothesis that links sudden glacial terminations to major methane emissions from large, rapid GH destabilization events (Nisbet 1990, 2002, Kennett et al. 2003) presumes that GHs destabilize rapidly in response to environmental change late in glacial intervals, and that they serve at other times as a sink for and barrier to the migration of methane into the atmosphere. This hypothesis applies mainly to marine GHs, which may be more easily destabilized than are the terrestrial sub-permafrost GHs we modeled.

Our study shows that terrestrial GHs below thick IBP vary in thickness in response to surface temperature history changes, but that terrestrial thermal inertia conserves both IBP and sub-permafrost GHs delaying and reducing methane release. Terrestrial thermal inertia also imposes a phase-delay between surface temperature warming and the subsequent onset of GH dissociation, making it unlikely that terrestrial GHs below thick permafrost could rapidly reinforce climate warming events, consistent with the hypothesis. The implications of latent heat effects and thermal inertia for submarine gas hydrates remain to be determined; however, our model results appear consistent with recent observations of methane isotopic compositions from ice cores (Sowers et al. 2006).

References

Allen, D., Michel, F. & Judge, A. 1988. The permafrost regime in the Mackenzie Delta-Beaufort Sea Region, N.W.T. and its significance to the reconstruction of the paleoclimatic history. *Journal of Quaternary Science*, INQUA Volume, June 1988: 3-13.

Carslaw, H.S. & Jaeger, J.C. 1959. *Conduction of Heat in Solids*, 2nd ed. Oxford University Press.

Dallimore, S.R., Uchida, T. & Collett, T.S. (eds.) 1999. *Scientific Results from JAPEX/INOC/GSC Mallik 2L-38 GH Research Well, Mackenzie Delta, Northwest Territories.* Canada. Geol. Surv. Canada, Bull. 544: 403 pp.

Dallimore, S.R. & Collett, T.S. (eds.) 2005. *Scientific Results from the Mallik 2002 Gas Hydrate production Research Well Program, Mackenzie Delta, Northwest Territories, Canada.* Geol. Surv. Canada Bull. 585: 140p. CD and Charts.

Galushkin, Yu. 1997. Numerical simulation of permafrost evolution as a part of sedimentary basin modeling: permafrost in the Pliocene-Holocene climate history of the Urengoy field in the West Siberian basin, *Can. J. Earth Sci*. 34: 935-948.

Henniges, J., Huenges, E. & Burkhard, H. 2005. In situ thermal conductivity of gas hydrate bearing sediments of the Mallik 5L-38 well. *J. Geophys. Res*. 110: B11206

Judge, A.S. &. Majorowicz, J.A. 1992. Geothermal conditions for gas hydrate stability in the Beaufort-Mackenzie area-the global change aspect. *Paleogeography Paleoclimatology and Paleoecology, Global & Planetary Change Section*, 98: 251-263.

Judge, A.S., Smith, L.S. & Majorowicz, J.A. 1994. The current distribution and thermal stability of natural gas hydrates in the Canadian Polar margin. *Proceedings of the IVth International Offshore and Polar Engineering Conference, Osaka.* The International Society of Offshore Polar Engineering, v. V I: 307-314.

Majorowicz, J.A. & Hannigan, P.K. 2000. Stability zone of natural gas hydrates in a permafrost – bearing region of the Beaufort–Mackenzie basin: Study of a feasible energy source. *Nat. Res. Res.* 9: 3-25.

Majorowicz, J.A. & Osadetz, K.G. 2001. Basic geological and geophysical controls bearing on gas hydrate distribution and volume in Canada. *AAPG Bulletin*, 85(7): 1211-1230.

Majorowicz, J.A., Judge, A. & Jones, F.W. 1990. Deep subpermafrost thermal regime in the Mackenzie Delta basin, northern Canada-analysis from petroleum bottom-hole temperature data. *Geophysics* 55: 362-371.

Majorowicz, J.A. & Smith, S.L. 1999. Review of ground temperatures in the Mallik field area: a constraint to the methane hydrate stability. In: S.R. Dallimore, T. Uchida & T.S. Collett (eds.), *Scientific Results from JAPEX/JNOC/GSC Mallik 2L-38 Gas Hydrate Research Well, Mackenzie Delta, Northwest Territories, Canada.* Geological Survey of Canada Bulletin 544: 45-56.

Muller, R.A. & MacDonald, G.J. 2000. *Ice Ages and Astronomical Causes: Data, Spectral Analysis, and Mechanisms.* Berlin: Springer Praxis, 318 pp.

Nisbet, E.G. 1990. The end of the ice age. *Can. J. Earth Sci*. 27: 148-157.

Nisbet, E.G. 2002. Have sudden large releases of methane from geological reservoirs occurred since the Last Glacial Maximum, and could such releases occur again? *Phil. Trans. R. Soc. Lond*. A 360: 581-607.

Nixon, J.F. 1986. Thermal simulation of subsea saline permafrost, *Can.J.Earth Sci.* 23: 2039-2046.

Peaceman, D.W & Rachford, H.H 1955. The numerical solution of parabolic and elliptic differential equations. *Journal of the Society for Industrial and Applied Mathematics* 3: 28-41.

Safanda, J., Szewczyk, J. & Majorowicz, J.A. 2004. Geothermal evidence of very low glacial temperatures on the rim of the Fennoscandian ice sheet. *Geophys. Res. Lett.* 31: L07211.

Sloan, E.D. 1998. *Clathrate Hydrates of Natural Gases*, 2nd ed., New York: Marcel Dekker Inc., 705 pp.

Smith, S.L. & Judge, A.S. 1995. *Estimate of Methane Hydrate Volumes in the Beaufort Mackenzie Region, Northwest Territories.* Geological Survey of Canada Current Research 1995, Part B: 81-88.

Sowers, T. 2006. Late Quaternary atmospheric CH_4 isotope record suggests marine clathrates are stable. *Science* v. 311: 838-840.

Taylor, A.E., Burgess, M., Judge A. &. Allen, V.S. 1982. Canadian Geothermal Data Collection Ä Northern Wells 1981, *Geothermal Series, Earth Physics Branch, E.M.R., Canada* 13: 153 pp.

Taylor, A.E., Dallimore,S.R., Hyndman, R. & Wright, J.F. 2005. Comparing the sensitivity of permafrost and marine gas hydrate to climate warming. In: S.R. Dallimore & T.S. Collett (eds.), *Scientific Results from the Mallik 2002 Gas Hydrate Production Research Well Program, Mackenzie Delta, Northwest Territories, Canada.* Geological Survey of Canada, Bulletin. 585: p. 130 and paper 52.

Wright J.F., Nixon, F.M., Dallimore, S.R., Henninges, J. & Cote, M.M. 2005. Thermal conductivity of sediments within the gas hydrate bearing interval at the Mallik 5L-38 gas hydrate production well. In: S.R. Dallimore & T.S. Collett (eds.), *Scientific Results from the Mallik 2002 Gas Hydrate Production Research Well Program, Mackenzie Delta, Northwest Territories, Canada.* Geological Survey of Canada, Bulletin. 585: 129-130.

The Last Twenty-Five Years of Changes in Permafrost Temperature in the European Russian Arctic

G.V. Malkova
Earth Cryosphere Institute, Russian Academy of Sciences, Moscow, Russia

Abstract

The 24-year-long permafrost temperature records from the long-term permafrost monitoring station Bolvansky are presented in this paper and analyzed in relation to climatic changes. The results of this analysis show that changes in mean annual ground temperatures generally follow the mean annual air temperatures. The warming trend in the air temperatures for the entire period of measurement at this site is 0.04°C/yr. Observed trends in mean annual permafrost temperatures vary from 0.003°C/yr to 0.02°C/yr in different natural landscapes. The warming trend in permafrost temperature for the entire period of measurement in anthropogenic landscapes is 0.04°C/year. A weak negative trend is observed in thawed boreholes (-0.012°C/year). For the last 10 years, an increase in climatic variability and an interchange of extremely cold and extremely warm years were observed, that led at first to a considerable increase in permafrost temperature. In 2007, a weak decrease in temperature was observed in most of the monitored boreholes.

Keywords: air temperature; climate change; permafrost temperature; thermal monitoring; trend.

Introduction

The geocryological observations show a general increase in permafrost temperatures during the last several decades in Alaska (Clow & Urban 2003, Osterkamp & Romanovsky 1999, Osterkamp 2003, Romanovsky 2006, Romanovsky et al. 2002) and northwest Canada (Smith et al. 2005, Burgess & Smith 2003). At some locations near the southern boundary of permafrost in Alaska, this warming has already resulted in permafrost thawing from the top down (Jorgenson et al. 2001, Osterkamp et al. 2000).

The cryolithozone of the European part of Russia extends predominantly just north of the Arctic Circle. Permafrost in this region is well studied. During the 1970s and 1980s, due to oil and gas field exploration and development, many drilling and geophysical surveys were carried out in the European North. State engineering-geological mapping (1:200,000 scale) was also accomplished. These activities provided important information on permafrost extent, thickness, and temperature regime. In order to investigate in detail the geocryological conditions of this region, several long-term permafrost-monitoring stations were established, in both natural settings and in settings disturbed by human activities. During the 1980s, there were 14 geocryological long-term monitoring stations where the ground temperature was measured in several dozens of boreholes. During the last ten years, the development of oil and gas fields in the European North has progressed rapidly. The building of oil-shipping terminals was accomplished in the coastal zone of the Barents Sea and Pechora Bay (Varandey et al.). With all these developments, current data on changes in geocryological conditions have turned out to be insufficient. Today, regular temperature measurements in boreholes are carried out only at Vorkutinsky and Bolvansky long-term monitoring stations. In 2006 and 2007, after an 11-year time gap, permafrost temperature measurements were conducted successfully in several reference boreholes at two more former long-term monitoring stations, Rogovoy and Korotaikha. Results of these geocryological studies are cited in the scientific literature (Kakunov & Sulimova 2005, Kakunov et al. 2006, Oberman 1998, 2001, 2006, 2007, Malkova 2005, 2006, 2007, Mazhitova et al. 2004, Oberman & Mazhitova 2001). The locations of the active stations are shown in Figure 1.

According to the mentioned publications by Kakunov and Oberman, the considerable increase in mean annual permafrost temperatures during the last two to three decades is typical for southern regions of the permafrost in the Russian European North (Vorkutinsky, Rogovoy and Korotaikha stations). This increase resulted in partial permafrost thawing, from the top down, and in a reduction in size of permafrost islands in the sporadic permafrost zone. New closed taliks appeared in the areas of high-temperature permafrost; the thickness of the existing closed taliks has increased. In areas directly affected by the human activity, the increase of permafrost temperature at the depth of zero annual amplitude varied from 0.2°C to 1.6°C during the period of observation. Fewer changes in permafrost were observed at the Arctic coast of the Barents Sea where the Bolvansky long-term observation station is situated on undisturbed landscape. In this paper the changes in permafrost that have occurred at the Bolvansky monitoring station during the last 25 years and their relation to observed climatic changes will be examined.

Methods of Measurements

The long-term permafrost monitoring station, Bolvansky, was established in 1983 at the location of the Bolvansky Cape weather station which has existed since 1935 (Fig. 1). Within the region (total area of 10 km²) twenty-five 12–15 m deep and 65–87 mm diameter boreholes were drilled in various landscape conditions. Each borehole was equipped

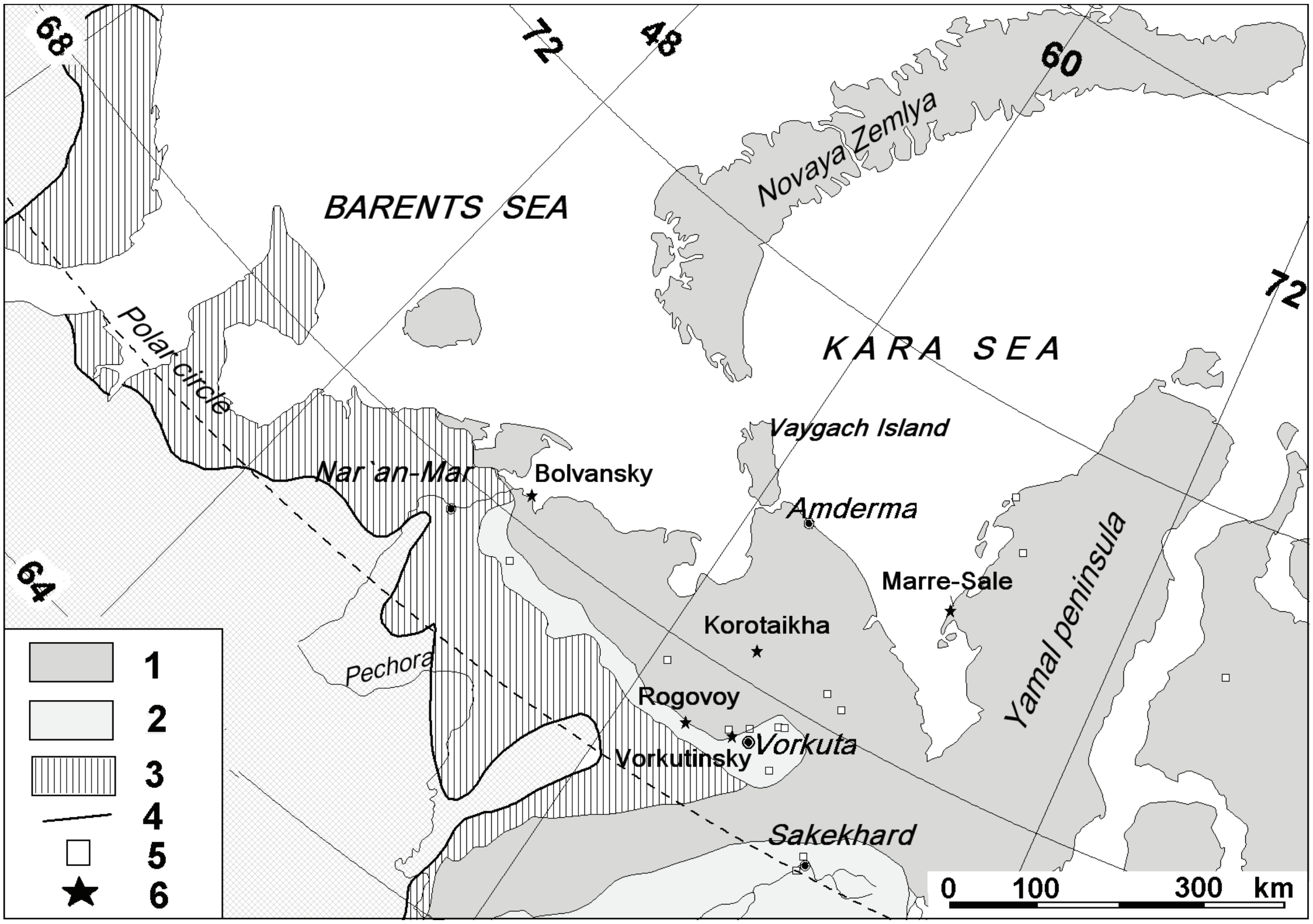

Figure 1. Location of long-term permafrost monitoring stations and permafrost spatial continuity in the European Russian Arctic: 1 – continuous permafrost, 2 – discontinuous permafrost, 3 – sporadic permafrost, 4 - southern boundary of permafrost distribution, 5 – closed permafrost monitoring stations, 6 – stations still in operation.

with steel casing to the depth of 3–5 meters, and was closed with a metal cap. A wooden box filled with sawdust was built around the aboveground portion of the casing to provide thermal insulation. Temperature measurements were taken three times a month using a string of mercury thermometers. The thermometers were located at depths of 1–6, 8, 10, 12, and 15 m. From 1983 until 1993, year-round studies were performed at this station. After 1993, observation sites and boreholes were abandoned for technical and organizational reasons. The results of the first ten years of geocryological study were archived as survey reports at the Russian Geological Data Center and have never been published in scientific literature.

In 1999, after a six-year break in measurements, 10 boreholes again were prepared for temperature measurements. Until 2005, ground temperature measurements were conducted there once a year at the end of the summer. LPC data loggers and strings of sensors in rubber cable were used in these measurements. The sensors were positioned at the same depths as in the previous period of measurements. Besides temperature measurements in boreholes, annual observations of temperature in the active layer have been carried out at the Circumpolar Active Layer Monitoring (CALM) project site. Soil temperatures are obtained with thermistor sensors inserted in the ground at various depths in the active layer and near-surface permafrost. The active layer depth at this site varies from 1–1.2 m. Therefore, the sensors in the active layer are installed at depths of 0.05, 0.25, 0.5, 0.75, 1, and 1.25 m. Readings are recorded at a regular time interval by battery-operated multi-channel data loggers (Brown et al. 2000).

In 2006, with technical support from the international project TSP, 4-channel automated HOBO U12 sets were installed in four key boreholes situated in various landscape conditions. Temperature is recorded automatically 4 times year-round. The first collection of data from the equipped boreholes was carried out at the end of summer 2007. At the same time four more HOBO U12 sets were installed in additional boreholes. Since 2007, all measurements are carried out every 6 hours; that is, four times a day. The sensors in the boreholes are installed at depths of 1 (or 3 m), 5, 7, and 10 m. This has permitted monitoring of permafrost temperature dynamics both in time and depth at each borehole. Through the entire time of measurements, we used three different types of thermometers. However, the error associated with the instrumentation was insignificant (<0.1°C) and corrections to the data were made accordingly.

The obtained information was processed in accordance with

Table 1. Mean annual permafrost temperature at the Bolvansky long-term monitoring station.

Borehole #	Landscape characteristics	Range of interannual fluctuations of the mean annual permafrost temperature, °C	Fluctuation amplitude, °C	Standard deviation	Long-term trend, °C /year (see Figure 2)
51	Edge of a drained lake, tundra	-1.0…-1.4	0.4	0.13	0.013
53	Gentle ridge, tundra	-1.7…-2.1	0.4	0.12	0.003
54	Gentle ridge, tundra	-1.8…-2.4	0.6	0.17	0.009
55	Edge of a ravine, tundra	-1.3…-1.9	0.6	0.21	0.015
56	Upper reaches of a ravine, peatland	-0.5…-0.8	0.3	0.10	0.011
59	Apex of a gentle ridge, tundra	-1.6…-2.3	0.7	0.21	0.023
60	Apex of a gentle ridge, disturbed tundra	-1.4…-2.4	1.0	0.36	0.040
61	Bottom of a drained lake, bog	+0.3…+0.8	0.5	0.17	-0.012
65	Gentle hillslope, tundra	-1.2…-1.7	0.5	0.15	0.011
83	Apex of a gentle ridge, tundra	-2.1…-2.5	0.4	0.17	0.007

prescribed protocol. Daily mean, monthly mean and mean annual ground temperatures were calculated. Calculation of trends and the regression equations were performed using the Microsoft Excel program. Climate data from the main weather stations (Nar'an-Mar, Vorkuta, Amderma, Fig. 1) of the European North were collected from the meteorological Internet site (http://meteo.infospace.ru/wcarch/html/r_index.sht) and processed similarly.

General Characteristics of the Research Region

The long-term permafrost monitoring station, Bolvansky, (68°17.3′N, 54°30.0′E) is located at the Pechora River Delta, on the northernmost extremity of Bolvansky Cape, which juts out into Pechora Bay (Barents Sea basin). The Bolvansky Cape weather station operated from 1935 to 1998. Long-term mean annual air temperature is -4.4°C, and precipitation is 404 mm. The area is represented by undulating marine plain with numerous lake depressions and large flat-bottomed valleys, some with permanent creeks. Elevations range from 20 to 35 m a.s.l. Quaternary deposit, a boulder sandy loam, is more than 100 m thick. Polygonal peatlands and fens with peat thickness ranging from 0.5–5 m occupy the inter-hill areas and depressions. The area is geocryologically unstable due to its location at the western extremity of the continuous permafrost zone in Europe and the near proximity of the discontinuous and sporadic permafrost zones. Permafrost exists just below the active layer under elevated and flat surfaces, whereas a deep position of the permafrost table is typical for valley bottoms, both dry and with flowing water. Open taliks occur under the Pechora valley, under Pechorskaya and Bolvanskaya Bays, and under many lakes (Mazhitova et al. 2004). The thickness of permafrost in this area is 100 to 200 m (Oberman & Mazhitova 2001).

The mean annual permafrost temperature at 10–12 m depth depends on landscape conditions and varies from -0.5°C to -2.5°C (according to measurements in 25 boreholes). In elevated areas and on hilltops the permafrost temperature varies between -2.0°C and -2.5°C. Within polygonal peatlands, on the slopes, and in the cols of hills with tundra vegetation the permafrost temperature varies from -1.5°C to -2.0°C. For the edges of lakes and terraces and also for the headstreams of small creeks, typical permafrost temperatures are in the range of -0.6°C to -1.4°C. On the bottoms of ravines and lakes, the permafrost surface is lowered in the depth from several meters to dozens of meters, and temperature of the thawed ground at the depth of 10 m is from +0.3°C to +1.0°C. The range of permafrost temperatures observed during the research period from 1983 to 2007 in presently operational boreholes are shown in Table 1 and Figure 2.

The mean annual air temperature in Bolvansky Cape according to the data from the weather station (until 1998) and from our data loggers (1999–2007) is shown in Figure 3. During the last decades, the two coldest periods, from 1985–1987 and from 1997–1999, are easily noticeable. Since the mid-1980s, two periods of warming were observed. The first one was from the mid-1980s to the mid-1990s and the second one in 2000–2005. According to the data from the Institute of Global Climate and Ecology (Rosgidromet and RAS), a general gradual increase of precipitation (5%–10% per 10 years) was observed. The years with maximum amount of precipitation (including snow) were 1990–1991, 1995–1996, and 2001–2002. The maximum snowfall occurred in 1981–1982 (snow accumulation was about 380 mm). The winters of 1985–1986, 1994–1995, and 2000–2001 had little snow accumulation (about 150 mm).

Results and Discussion

During the period between 1984 and 2007, a weak positive trend in the mean annual permafrost temperatures

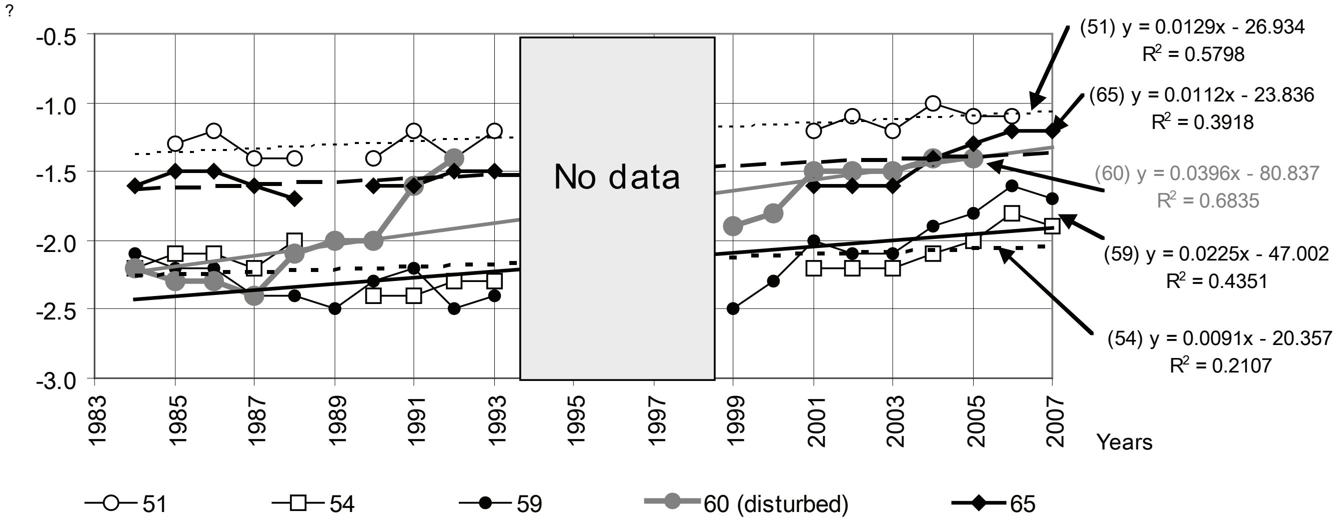

Figure 2. Mean annual permafrost temperatures and the long-term trends (from 1983 to 2007) in their variations measured in boreholes 51, 54, 59, 60, and 65 at the depth of 10 m.

(from 0.003°C/year to 0.02°C/year in the various landscape conditions) has been observed. During the same period, the trend of air temperature change of 0.04°C/year was much more pronounced (Fig. 3). An undoubted synchronism in soil and air temperature changes has been typical for all boreholes. During this period, the standard deviation of permafrost temperature interannual variability in the undisturbed landscapes has varied in rather narrow limits from 0.10 to 0.21. The standard deviation for disturbed conditions was 0.36.

During the last 8 years, the permafrost temperature has undergone especially considerable changes due to the greater interannual variations in the mean annual air temperature. Subsequent to anomalously severe 1998, we observed a noticeable decrease of the permafrost temperature in 1999. On the contrary, a warm 2000 as well as 2005 caused the increase in mean annual ground temperature in 2001 and its substantial increase in 2006. After relatively cold 2006 (the mean annual air temperature decreased by 2°C) some decrease (by 0.1°C to 0.2°C) of the permafrost temperature was observed in the boreholes at the end of the warm season.

Borehole #59 is the key for this long-term monitoring station. It is situated on the top of a gentle ridge in landscape conditions typical for this region. A CALM site where active layer monitoring is also performed is co-located with this borehole. The most complete set of observations of natural parameters is available for this borehole location. Besides the permafrost temperature measurements in the borehole (down to 10 m to 15 m in different years), the year-round active layer temperature data (with some gaps) and the maximum thawing depth are available for this location.

Figure 3 shows the mean annual air temperature variations at the Bolvansky station and the active layer and permafrost temperatures during the period of instrument measurements in the boreholes. During the last 10 years, the mean annual air temperature has undergone the greatest changes. The absolute minimum of the mean annual air temperature (-9.1°C) during the entire period of measurements started in 1935 was observed in 1998. Only 3 months in 1998 posted monthly mean temperatures above 0°C. At the same time, 2005 was the warmest on record with the mean annual temperature at -0.8°C. The duration of the period with positive monthly air temperatures was 6 months during that year.

The mean annual active layer temperature at a depth of 1.2 m ranged from -3.5°C to -0.5°C or 1°C to 2°C higher than the air temperature (due to the combination of a warming effect of snow and a negative thermal offset in the active layer). In general, the active layer temperature changes followed the changes in the air temperature, though within a smaller range. Especially significant decrease in the active layer temperatures was observed in the years with the low-snow winters. More frequently, the active layer temperatures ranged between -2°C and -3°C. As evident from Figure 3, the mean annual active layer temperature recently has a tendency towards increase. Since 2005, the active layer temperature has been increasing, staying in the range between -1°C and -2°C. In order to switch from seasonal thawing to seasonal freezing, the mean annual temperature at the bottom of the active layer is required to rise above 0°C. However, our data show that, up to the present day, the state of permafrost in the research region within each landscape type has been rather stable.

During the period of observations, the variations in the mean annual permafrost temperature in the Borehole 59 at the depth of zero amplitude have been relatively small. A decrease in ground temperature by 0.1°C or 0.2°C usually happens one or two years after a decrease in mean annual air temperature. The lowest permafrost temperature (-2.4°C) was observed in 1999 after a period of climatic cooling. Then, the permafrost temperature began to increase persistently following an increase in air temperature. However, the warming trend in the permafrost temperature was considerably smaller than the trend in the air temperature.

Borehole #60 was drilled on the same gentle ridge where the CALM site is situated, 100 m away from Borehole #59.

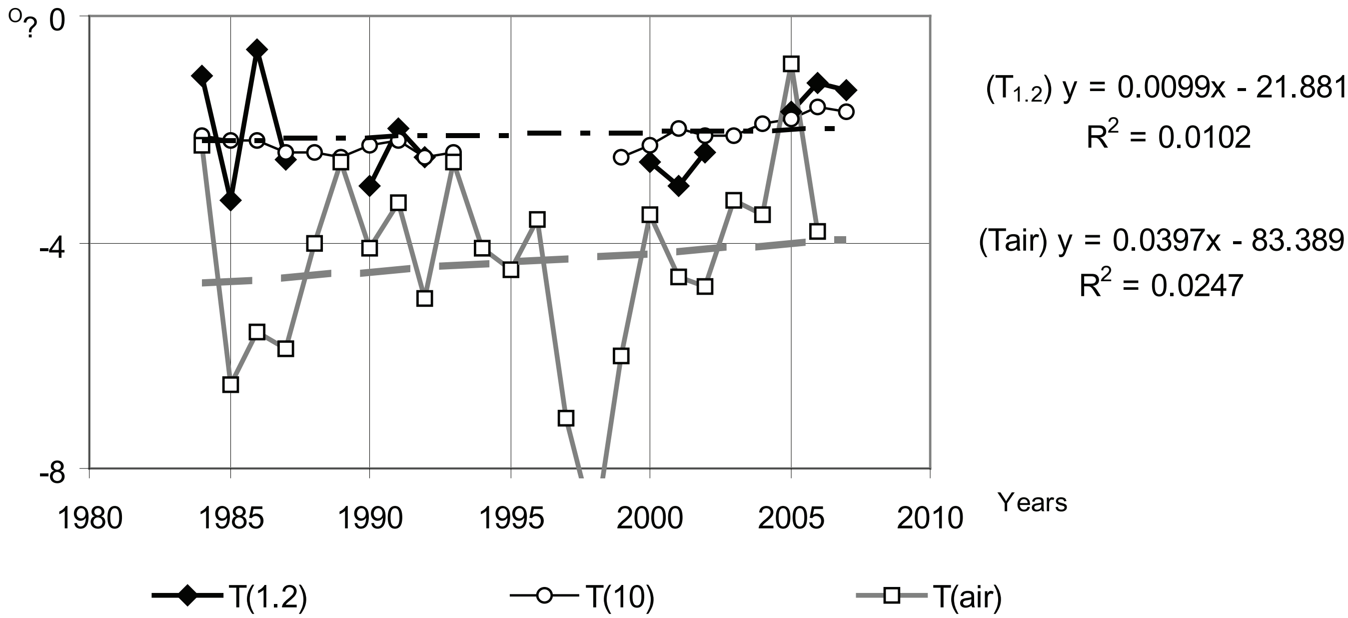

Figure 3. Mean annual temperatures of air, active layer (at the depth 1.2 m) and permafrost (at the depth 10 m) at the Bolvansky geocryological station, Borehole # 59. Grey dashed line is a linear trend of average annual air temperature.

This site was intentionally disturbed by removal of vegetation and organic soil layer. Figure 2 shows that during the first several years after the disturbance, after a small delay, a sharp increase in the mean annual ground temperature by 1°C occurred. During the first 15 years, a partial re-vegetation occurred at this site and, as a result, a decrease of permafrost temperature took place, by 1999–2000, but not to the initial values. The thickness of the snow cover did not change significantly at this disturbed site as compared with the undisturbed sites. In summer time, the amount of absorbed radiation was enlarged due to the stripping of the heat-insulating layers (vegetation and organic soil horizon). It resulted in the warming of the permafrost upper horizons. As the disturbed site gradually, naturally re-vegetated, a progressive decrease in mean annual permafrost temperature began (during 1992–1999 permafrost temperature at the depth of 10 m decreased from -1.4°C to -1.9°C) despite the observed increase in mean annual air temperature during this period (Pavlov & Malkova 2005, Malkova-Ananieva 2005). Further increase of the mean annual air temperature in 2000, 2003, and especially in 2005 again resulted in further ground warming by 0.3°C. According to our observations, the average long-term positive trend in permafrost temperature in the disturbed conditions was the largest for this long-term monitoring station and was equal to 0.04°C/year (Table 1).

Unfortunately, during the anomalously warm season of 2005, the thawing depth increased significantly within the limits of the disturbed site and Borehole #60 was filled with water and froze through the entire depth. Further temperature measurements are impossible.

Perennial observations of ground temperature in the thawed borehole situated in a drained lake basin (Borehole #61) have demonstrated a rather high long-term variability of ground temperature at the depth of 10–12 m (0.5°C) and a slightly negative temperature trend (-0.012°C/year). So, even under conditions of contemporary increase in mean annual air temperature, conditions for some decrease of ground temperature can be created at the bottom of drained lakes. Most likely, this is the result of changes in hydrological regime of the bog situated within the drying/drained lake bottoms. Namely, the lowering of the water level, due to the development of the erosion network, may explain these observations.

Conclusions

Conducted studies have demonstrated that the state of continuous permafrost of the coastal areas of the European North is still stable under the conditions of the recent increase in mean annual air temperature.

The permafrost temperature is a sensitive indicator of climatic changes, but the amplitudes of its variations were in a range between 0.3°C and 0.6°C, whereas the mean annual air temperature varied within 5°C during the same time period. Temperature changes at a depth of 10 m were observed in one or two years after the air temperature change.

The trends in the mean annual permafrost temperature increase are 2 to 10 times smaller than the trends of the increase in mean annual air temperature in various landscape conditions. For a significant change in the permafrost temperature regime, a combination of climate warming and surface disturbances is required.

The active layer temperature is determined both by the air temperature and by the snow cover thickness affecting the winter cooling rate under tundra conditions. The occurred climatic changes are not yet enough for the long-term thawing of the permafrost and for the transformation of the seasonally thawing layer into seasonally freezing layer in the studied area, which is located within the continuous permafrost zone.

Acknowledgments

This research was funded by the Polar Earth Science Program, Office of Polar Programs, National Science Foundation (ARC-0632400 and ARC-0520578) and CALM II project. Help in the fieldwork and in preparation and equipment of the boreholes was provided by D.S. Drozdov and A.B. Malkov.

References

Brown J., Hinkel, K.M. & Nelson, E.F. 2000. The Circumpolar Active Layer Monitoring (CALM) program: Research designs and initial results. *Polar Geography* 24(3): 165-258.

Burgess, M.M. & Smith, S.L. 2003. 17 years of thaw penetration and surface settlement observations in permafrost terrain along the Norman Wells pipeline, Northwest Territories, Canada. In: M. Phillips, S. Springman & L.U. Anderson, (eds.), *Permafrost, Eighth International Conference, Proceedings* Lisse, Netherlands: Balkema, Vol. 1: 107-112.

Clow, G.D. & Urban, F.E. 2003. GTN-P Monitoring network: detection of a 3 K permafrost warming in northern Alaska during the 1990's, *First Study of Environmental Arctic Change (SEARCH) Open Science Meeting, 27-30 October 2003, Seattle, WA*.

Jorgenson, M.T., Racine, C.H., Walters J.C. & Osterkamp, T.E. 2001. Permafrost degradation and ecological changes associated with a warming climate in central Alaska. *Climatic Change* 48(4): 551-571.

Kakunov, N.B. & Sulimova, E.I. 2005. Results of the observations of the ground temperature on the European North-East in the period of climatic warming 1970–2003 *Materials of the Third Conference of Russian Geocryologists* (2): 84-90. (in Russian).

Kakunov, N.B. & Sulimova, E.I. 2006. Methods of reconstructing the dynamics of southern boundary of permafrost and their temperature conditions in the European north-east of Russia for the last 230 years. *Earth Cryosphere Assessment: Theory, Applications and Prognosis of Alterations* (1): 76-78.

Malkova-Ananjeva, G.V. 2005. Frozen ground response to recent climate changes in the European North *2nd European Conference on Permafrost, Potsdam, Programme and Abstracts*: 137.

Malkova, G.V. 2006. Estimation of changes of geocryological characteristics in top horizons of permafrost in conditions of a varying climate and technogenesis. *Earth Cryosphere Assessment: Theory, Applications and Prognosis of Alterations* 1: 82-86.

Malkova, G.V. 2007. Generalization of the temperature measurement results at the Bolvansky geocryological steady-state-station. Cryogenic recourses of the Polar regions. *Materials of the International Conference. Salekhard, V.1*: 140-143 (in Russian).

Mazhitova, G.G, Malkova-Ananjeva, G.V, Chestnykh, O.L. & Zamolodchikov, D.D. 2004. Active layer spatial and temporal variability at European Russian Circumpolar-Active Layer-Monitoring (CALM) sites. *Permafrost and Periglacial Processes* 15: 123-139.

Oberman, N. G. 1998. Permafrost and cryogenic processes in the East-European Subarctic. *Eurasian Soil Science* 5: 540-550.

Oberman, N. G. 2001. Interdecadal dynamics of permafrost on the European North-East of Russia. *Materials of the Second Conference of Russian Geocryologists* (2): 212-217. (in Russian).

Oberman, N.G. & Mazhitova, G.G. 2001. Permafrost dynamics in the northeast of European Russia at the end of the 20th century. *Norsk Geografisk Tidsskrift–Norwegian Journal of Geography* 55(4): 241–244.

Oberman, N.G. 2006. Long-term tendencies of natural cryolithozone evolytion the north-east *Earth Cryosphere Assessment: Theory, Applications and Prognosis of Alterations* 1: 93-96.

Oberman, N.G. 2007. Some peculiarities of current degradation of permafrost in the Pechora-Ural region. *Cryogenic Resources of Polar Regions*: 95-99.

Osterkamp, T.E. 2003. A thermal history of permafrost in Alaska. In: M. Phillips, S. Springman and L.U. Anderson, (eds.), *Permafrost, Eighth International Conference, Proceedings* Lisse, Netherlands: Balkema, vol. 2: 863-868.

Osterkamp, T.E. & Romanovsky, V.E. 1999. Evidence for warming and thawing of discontinuous permafrost in Alaska. *Permafrost and Periglacial Processes* 10(1): 17-37.

Osterkamp, T.E., Viereck, L., Shur, Y., Jorgenson, M.T., Racine, C., Doyle, A. & Boone, R.D. 2000. Observations of thermokarst and its impact on boreal forests in Alaska, U.S.A. *Arctic, Antarctic and Alpine Research* 32; 303-315.

Pavlov, A.V. & Malkova, G.V., 2005. *Contemporary changes of climate in northern Russia*.: Album of small-scale maps: 54. (in Russian).

Romanovsky, V.E. 2006. Thermal state of permafrost in Alaska during the last 20 years. *Earth Cryosphere Assessment: Theory, Applications and Prognosis of Alterations* (1): 96-101.

Romanovsky, V.E., Burgess, M., Smith, S., Yoshikawa, K. & Brown, J. 2002. Permafrost temperature records: indicator of climate change. *EOS* 83(50): 589, 593-594.

Smith, S.L., Burgess, M.M., Riseborough, D. & Nixon, F.M. 2005. Recent trends from Canadian permafrost thermal monitoring network sites. *Permafrost and Periglacial Processes* 16: 19-30.

Numerical Modeling of Spatial Permafrost Dynamics in Alaska

Sergei Marchenko
Geophysical Institute, University of Alaska Fairbanks, USA
Vladimir Romanovsky
Geophysical Institute, University of Alaska Fairbanks, USA
Gennady Tipenko
Institute of Geoecology, Russian Academy of Science, Russia

Abstract

The Geophysical Institute Permafrost Laboratory model (GIPL) simulates soil temperature dynamics and the depth of seasonal freezing and thawing by solving 1D non-linear heat equations with phase change numerically. In this model the process of soil freezing/thawing is occurring in accordance with the unfrozen water content curve and soil thermal properties, which are specific for each soil layer and for each geographical location. At the present stage of development, the GIPL 2.0 model is combined with ArcGIS to facilitate preparation of input parameters and visualization of simulated results in the form of digital maps. The future climate scenario was derived from the Massachusetts Institute of Technology MIT-2D climate model output for the 21st century. This climate scenario was used as a driving force in the GIPL model. Initial results of calculations show that by the end of the current century widespread permafrost degradation could begin everywhere in Alaska southward from the Brooks Range.

Keywords: active layer thickness; ground temperature; numerical modeling; thawing permafrost.

Introduction

Many components of the cryosphere, particularly sea ice, glaciers, and permafrost, react sensitively to climate change. Climatic changes and changes in permafrost were reported recently from many regions of the Northern Hemisphere (Jin et al. 2000, Oberman & Mazhitova 2001, Harris & Haeberli 2003, Sharkhuu 2003, Romanovsky et al. 2002, Marchenko et al. 2007). Significant changes in permafrost temperatures were observed in Alaska. Ground temperature data from Alaska available for the last 30 years demonstrate an increase in permafrost temperatures by 0.5°C–3°C (Osterkamp & Romanovsky 1999, Osterkamp 2005). Recent observations show that the warming of permafrost has continued into the 21st century in Alaska (Clow & Urban 2002, Romanovsky et al. 2002, Romanovsky et al. 2003). While the increase in permafrost temperature may change many of its physical properties, the major threshold occurs when permafrost starts to thaw from its top down. The thawing and freezing of soils in arctic and sub-arctic regions is affected by many factors, with air temperature, vegetation, snow accumulation, and soil moisture among the most significant. To investigate how observed and projected changes in these factors influence permafrost dynamics in Alaska, we developed a numerical Geophysical Institute Permafrost Laboratory (GIPL) model. In this paper we will first describe this model. Then we will show how this model should be calibrated and validated before being used for projections of future changes in permafrost as a result of changes in climatic and other environmental conditions. After validation, the model was used to develop one possible scenario of the permafrost dynamics in Alaska during the current century.

Previous spatial modeling of permafrost

Recently, there have been a number of experiments to simulate soil temperature and permafrost dynamics on regional and global scales (Anisimov & Nelson 1997, Stendel & Christensen 2002, Sazonova & Romanovsky 2003, Oelke & Zhang 2004, Lawrence & Slater 2005, Zhang et al. 2006, Saito et al. 2007). There are two major approaches to spatial modeling of permafrost. One of them is to include a permafrost module directly into GCM. The second one employs the use of stand-alone equilibrium or transient permafrost models. These models are forced by the climatic outputs produced by GCMs. There were a few examples of simulations and forecasts of permafrost dynamics using coupled global climate models (Stendel & Christensen 2002, Lawrence & Slater 2005, Nicolsky et al. 2007, Saito et al. 2007), but some of the modeled results generated a significant controversy (Burn & Nelson 2006, Delisle 2007). The simplified treatment of subsurface thermal processes and problematic settings of the soil properties and lower boundary conditions precluded proper representation of the future permafrost dynamics in these GCMs (Burn & Nelson 2006).

In this research we used the GIPL-2.0 model, which is a numerical simulator of the temporal and spatial transient response of permafrost to projected changes in climate.

Methods

GIPL-2.0 model

A previous version of this model (GIPL-1.0) is an equilibrium, spatially distributed, analytical model for computation of the active layer thickness and mean annual ground temperatures (Sazonova & Romanovsky 2003). The GIPL-2.0 model simulates soil temperature dynamics and the depth of seasonal freezing and thawing by solving 1D non-linear heat equations with phase change numerically. In this model the process of soil freezing/thawing is occurring

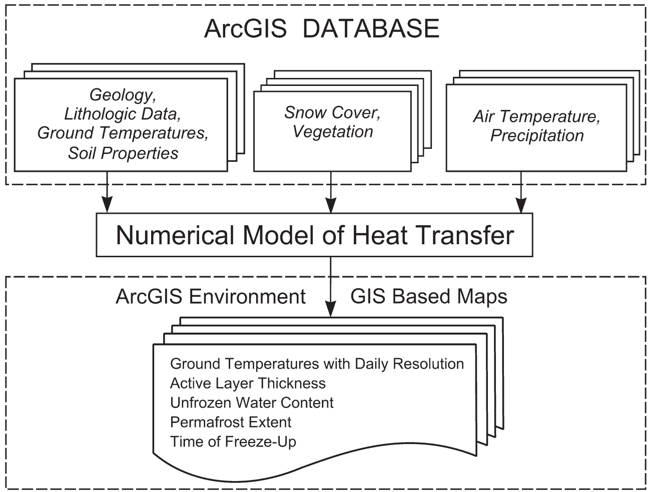

Figure 1. The GIPL-2.0 model schematic diagram.

in accordance with the unfrozen water content curve and soil thermal properties, which are specific for each soil layer and for each geographical location. The Special Enthalpy formulation of the energy conservation law makes it possible to use a coarse vertical resolution without loss of latent heat effects in the phase transition zone even in case of fast temporally and spatially varying temperature fields. At the present stage of development, the GIPL model is combined with ArcGIS to facilitate preparation of input parameters (climate forcing from observations or from Global or Regional Climate Models) and visualization of simulated results in the form of digital maps. The input data are incorporated into GIS and contain the information on geology, soils properties, vegetation, air temperature, and snow distribution (Fig. 1).

The soil characterization used in the GIPL-2.0 model is based on extensive empirical observations conducted in representative locations that are characteristic for the major physiographic units in Alaska.

The numerical solution of heat transfer is implemented in the extended program module, which can be called from the GIS environment. GIS allows visualization of input and output parameters and their representation in the form of digital maps. The new version of GIPL 2.0 simulates soil temperature and liquid water content fields for the entire spatial domain with daily, monthly, and yearly resolution. The merge of the new GIPL and the GIS technique provides a unique opportunity to analyze spatial features of permafrost dynamics with high temporal resolution.

Mathematical model

The basic mathematical model in our approach is the Enthalpy formulation of the one-dimensional Stefan problem (Alexiades & Solomon 1993, Verdi 1994). We used the quasi-linear heat conduction equation, which expresses the energy conservation law:

$$\frac{\partial H(y,t)}{\partial \tau} = div(\lambda(y,t)\nabla t(y,\tau)),\ y \in \Omega,\ \tau \in \Psi \tag{1}$$

where $H(y, t)$ is the enthalpy

$$H(y,t) = \int_0^t C(y,s)ds + L\Theta(y,t) \tag{2}$$

where $C(y, t)$ is the heat capacity, L is the latent heat, $\lambda(y, \tau)$ is thermal conductivity and $\Theta(y, t)$ is the volumetric unfrozen water content. The Equation (1) is complemented with boundary and initial conditions. The computational domain $0 \le \Omega \le 1000$ is extended to 1000 m in depth, and the time interval Ψ is 200 years with an initial temporal step of 24 hours.

Dirichlet's conditions $t(\tau)$ were set at the upper boundary. An empirical method of geothermal heat flux estimating (Pollack et al. 1993) in each grid point was applied for the lower boundary conditions.

$$\frac{\partial t}{\partial \tau}\Big|_{y=0} = t(\tau), \qquad \frac{\partial t(\tau)}{\partial y}\Big|_{y=1000} = g \tag{3}$$

where g is a geothermal gradient at the lower boundary.

A fractional step approach (Godunov splitting) was used to obtain a finite difference scheme (Marchuk 1975). The idea is to divide each time step into two steps. At each step, the spatial dimension (in the depth) is treated implicitly:

$$\frac{H(t_i^{n+1}) - H(t_i^{n+1/2})}{\Delta\tau_n} = \frac{2}{(\Delta h_{i+1} + \Delta h_i)} \times \left(\lambda_{i+1/2}^{n+1} \frac{\left(t_{i+1}^{n+1} - t_i^{n+1}\right)}{\Delta h_{i+1,y}} - \lambda_{i-1/2}^{n+1} \frac{\left(t_i^{n+1} - t_{i-1}^{n+1}\right)}{\Delta h_{i,y}} \right) \tag{4}$$

where $\Delta h_{i,y}$ is the spatial steps on the non-uniform grid.

The resulting system of finite difference equations is non-linear, and to solve it Newton's method was employed at each time step. On the first half step (4) in a case when a non-zero gradient of temperature exists, we use the difference derivative of enthalpy:

$$\frac{\partial H(t_i)}{\partial t} = 0.5\left[\frac{H(t_i) - H(t_{i-1})}{(t_i - t_{i-1})} + \frac{H(t_{i+1}) - H(t_i)}{(t_{i+1} - t_i)} \right] \tag{5}$$

The analytical derivative of representation (2) has to be used in the case of zero-gradient temperature fields. The second half step (4) is treated similarly. Thereby, we can employ any size spatial steps without any risk of losing any latent heat effects within the phase transition zone for fast temporally and spatially varying temperature fields.

Model validation and calibration

Ground temperature measurements of a very high quality (precision generally at 0.01°C) in shallow boreholes were used for initial model validation. More than 15 shallow boreholes (1–1.2 m in depth) across Alaska from north to south were available for validation (Romanovsky & Osterkamp 1997). The temperature measurements in the shallow holes were performed with vertical spacing of 0.08–0.15 m. At most of these sites, soil water content and snow depth also were recorded. In addition, more than 25 relatively deep boreholes from 29 m to 89 m in depth (Osterkamp & Romanovsky 1999, Osterkamp 2003) along the same transect were available for model validation in terms of permafrost temperature profiles and permafrost thickness.

Different earth's materials have varying thermal properties. The soil thermal conductivity and heat capacity vary within the different soil layers, as well as during the thawing/freezing cycles, and depend on the unfrozen water content that is a certain function of temperature. The method of obtaining these properties is based on the numerical solution for a coefficient inverse problem, and on minimization locally on the misfit between measured and modeled temperatures by changing thermal properties along the direction of the steepest descent. The method used and its limitations are described in more detail elsewhere (Nicolsky et al., in review).

There are two basic approaches to the calibration of modeled permafrost temperatures against the observed data, which can be distinguished by their use of temporal or spatial relationships. With the temporal approach, the quality of the modeling series is assessed by time series regression against measured data. The quantitative relationship between simulated and measured data is then determined for a ‘‘calibration'' period with some instrumental data withheld to assess the veracity of the relationship with independent data. Figure 2 illustrates the results of the model calibration for the specific site, West Dock (70°22'28.08"N, 148°33'7.8"W).

In the spatial approach, assemblages of the observed data from a number of different geographic locations with different landscape settings determine the quality of the modeling results. To achieve geographic correspondence between the scale of observation and modeling, we utilized a regional-scale permafrost characterization based on observations obtained from representative locations. Additional comparison of model-produced ground temperatures, active layer thickness, and spatial permafrost distribution with measured ground temperatures at the Alaskan sites shows a good agreement.

Input data set

In order to assess possible changes in the permafrost thermal state and the active layer depth, the GIPL-2.0 model was implemented for the entire Alaskan permafrost domain for the 1900–2100 time interval. For this study we used an input data set with grid boxes size 0.5° × 0.5°. Input parameters to the model are spatial datasets of mean monthly air temperature and snow water equivalent (SWE), prescribed soil thermal properties and water content, which are specific for each soil layer and for each geographical location. Initial distribution of temperature with depth was derived from the borehole temperature measurements obtained in Alaska by different researchers during the last several decades (Brewer 1958, Lachenbruch & Marshall ti

For climate forcing we used two data sets. For the period of

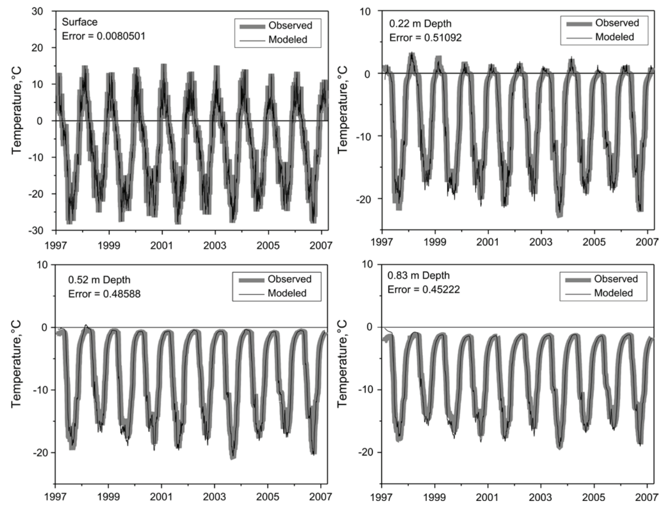

Figure 2. Example of the temporal model calibration for specific site.

1900–2000 climatic conditions, the CRU2 data set with 0.5° × 0.5° latitude/longitude resolution (Mitchell & Jones 2005) was used. The future climate scenario was derived from the MIT-2D integrated global system model (IGSM) developed at the Massachusetts Institute of Technology (MIT), which is a two dimensional (zonally averaged) atmospheric model coupled with a diffusive ocean model that simulates the surface climate over the land and ocean for 23 latitudinal bands globally (Sokolov & Stone, 1998). Snow data for the entire simulated period 1900–2100 were derived from the terrestrial ecosystem model (TEM) (Euskirchen et al. 2006). We used the MIT-2D output for the 21st century with a doubling, gradual increase of atmospheric CO_2 concentration by the end of the current century that corresponds to the IPCC SRES emission scenario A1B.

Results and Discussion

We compared ground temperatures at the depths of 2 m, 5 m, and 20 m for three snapshots of 2000, 2050, and 2100 (Fig. 3). If compared with present-day conditions, the greatest changes in temperatures for the 2050 and 2100 snapshots will occur at 2 m depth (Figs. 3 A, B, C). Results of calculation show that by the end of the current century, the mean annual ground temperatures (MAGT) at 2 m depth could be above 0°C everywhere southward of the sixty-sixth latitude, except for the small patches at the high altitudes of the Alaska Range and the Wrangell Mountains (Fig. 3C). The area of about 850,000 km^2 (about 57% of the total area of Alaska) will be involved in the widespread permafrost degradation and could contain both areas with completely disappeared permafrost and areas where thawing of permafrost is ongoing. It should be noted that by the term "thawing permafrost" we understand a situation when the permafrost table is lowered and a residual thawed layer (talik) between the seasonally frozen layer and the permafrost table continuously exists throughout the year.

According to calculations, the modern extent of the area with MAGT at 5 m depth above 0°C is about 125,000 km^2.

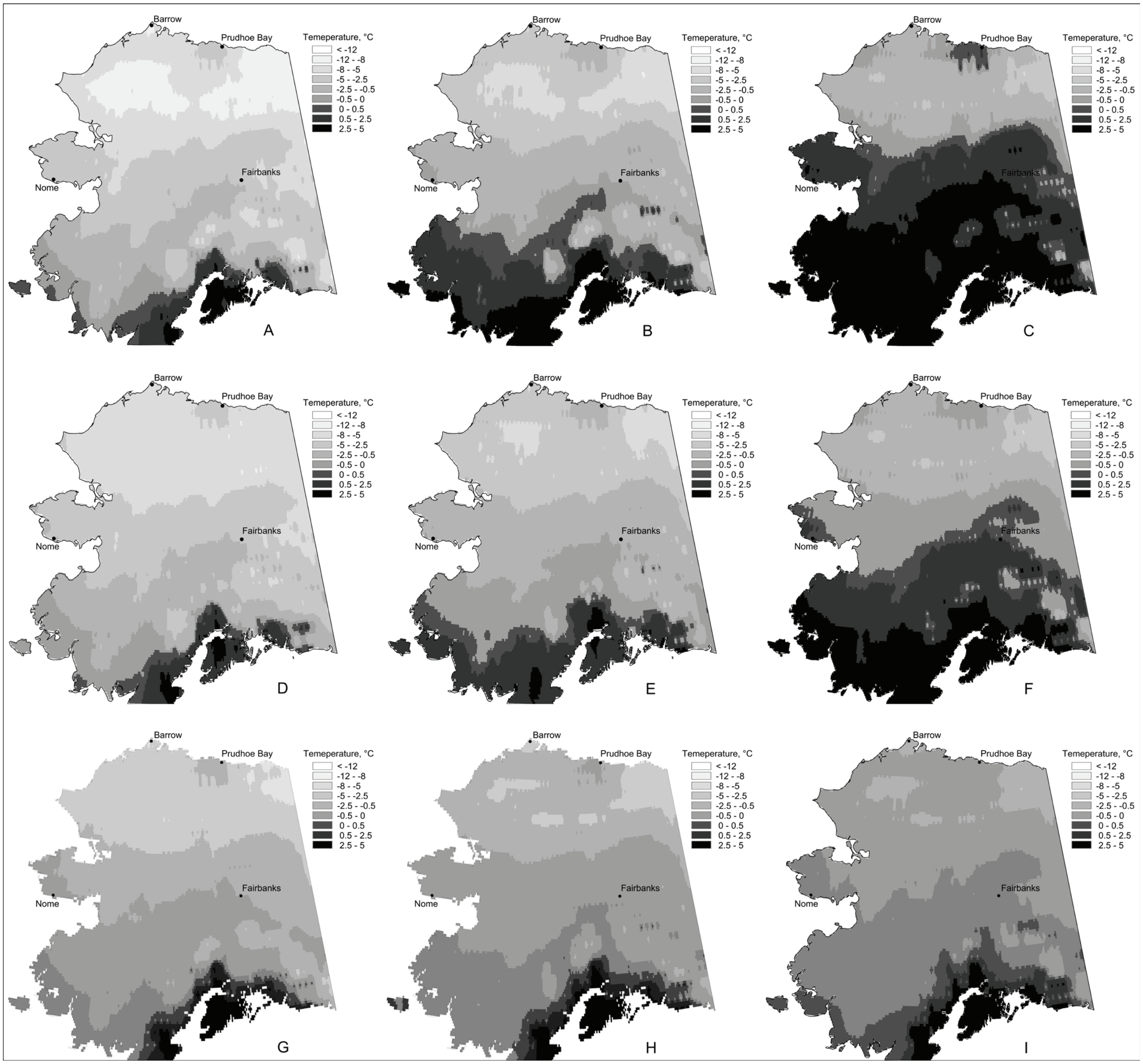

Figure 3. Projected mean annual ground temperatures at 2 m (A, B, C), 5 m (D, E, F), and 20 m (G, H, I) depths on 2000 (A, D, G), 2050 (B, E, H), and 2100 (C, F, I) using climate forcing from MIT-2D output for the 21st century.

The model-produced ground temperatures with positive MAGT at 5 m depth could occupy approximately 659,000 km^2 (about 45% of the total area of Alaska) by the end of the current century and could extend into the Interior of Alaska (Fig. 3F).

While the permafrost temperatures at 20 m depth could change significantly within a range of negative temperatures, the area with MAGT above 0°C at 20 m depth would not expand too much, even by 2100 (Figs. 3 G, H, I). The difference between these areas in 2000 and in 2100 does not exceed 100,000 km^2 (Figs. 3 G, I). Changes in permafrost temperatures will be much more pronounced within the areas with colder permafrost in comparison with areas where the permafrost temperature is presently close to 0°C. Also, it will not increase significantly in the areas of peat lands with a sufficiently deep organic layer. Projected changes in areas of MAGT above 0°C at the different depths and for the different times according to the MIT-2D climate change scenario are presented in Table 1.

Table 2 presents the statistics of modeled MAGT variables for the three snapshots obtained from 34,434 grid cells within the entire Alaskan domain. While the mean value and sums of MAGT at the depths of 2 m and 5 m turned to above 0°C by the end of the current century, the same characteristics for 20 m depth remain below 0°C (Table 2).

Statistics on active layer thickness (ALT) also have shown significant response to the scenario of climate change. The simulated mean values of ALT for the whole Alaskan permafrost domain are 0.78 m, 1.33 m, and 2.4 m for 2000, 2050, and 2100 respectively.

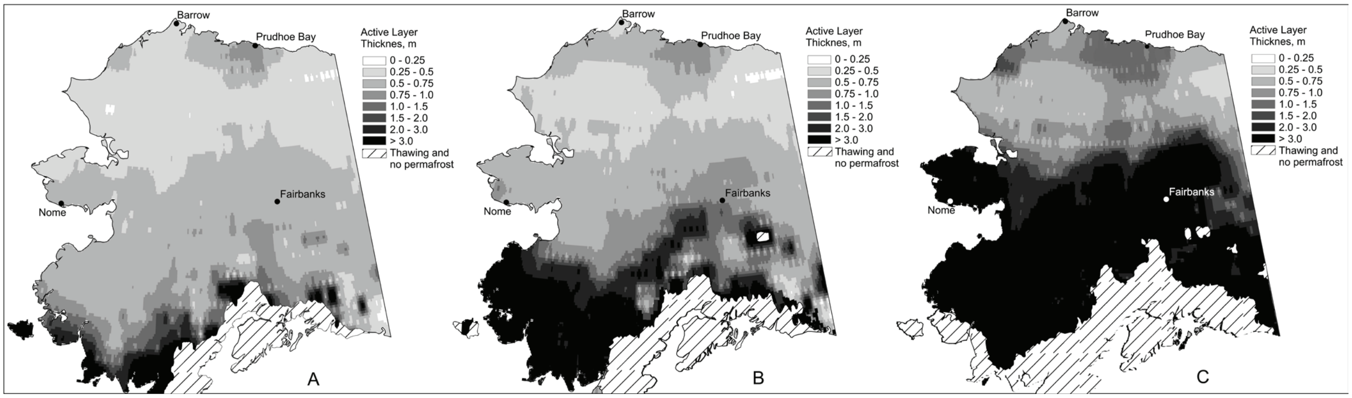

Figure 4. Projected active layer thickness and extent of thawing permafrost area in 2000 (A), 2050 (B), and 2100 (C) using climate forcing from MIT-2D output for the 21st century.

The area of thawing permafrost (permafrost table located deeper than 3 m) also increased according to our model from 65,000 km^2 in 2000, to 240,000 km^2 by 2050, and to 720,000 km^2 by 2100 (Fig. 4).

Conclusions

According to the future climate scenario derived from the MIT-2D climate model and the TEM output for the 21st century, widespread permafrost degradation could be observed everywhere in Alaska southward from the Brooks Range by the end of the current century. It means that the permafrost table in this region will be lowered down to 3–10 m in depth, and some small and thin patches of permafrost at the southernmost regions of Alaska could disappear completely. Nevertheless, permafrost thicker than 15–20 m in depth could still survive deeper than 10–15 m, even in the regions with widespread long-term thawing of permafrost. In the regions with ice-rich permafrost, the thawing processes will extended for a long time, especially in the regions with undisturbed surfaces. Modeling results show the Alaskan North Slope will not be experiencing a substantial widespread permafrost thawing and degradation during the present century.

Acknowledgments

This research was funded by the ARCSS Program and by the Polar Earth Science Program, Office of Polar Programs, National Science Foundation (OPP-0120736, OPP-0352957, OPP-0352958, ARC-0632400, ARC-0520578, ARC-0612533, IARC-NSF CA: Project 3.1 Permafrost Research), by a NASA Water and Energy Cycle grant, and by the State of Alaska. We would like to thank Dr. N. Shiklomanov from the University of Delaware for helpful discussions. We would also like to thank two anonymous reviewers for very helpful suggestions that were used to improve the manuscript.

Table 1. Areas of simulated MAGT above 0°C at the different depths and for the different times (thousands km^2/percent of the total area of Alaska).

Depth	2000	2050	2100
2 m	138.8/9.4	410.3/27.8	850.5/57.6
5 m	126.7/8.6	280.2/18.9	658.9/44.6
20 m	103.2/6.7	133.5/9.03	196.4/13.3

Table 2. Statistics of modeled MAGT variables within the entire calculated Alaskan spatial domain (34,434 grid cells).

Statistics	2000	2050	2100
2 m Depth			
Min	-12.52	-8.74	-5.44
Max	4.72	7.30	11.62
Mean	-4.32	-1.47	1.58
5 m Depth			
Min	-8.45	-6.62	-5.43
Max	3.71	5.00	10.46
Mean	-3.69	-1.68	0.54
20 m Depth			
Min	-9.86	-7.74	-5.38
Max	4.85	6.46	8.53
Mean	-3.32	-1.86	-0.62

References

Anisimov, O.A. & Nelson, F.E. 1997. Permafrost zonation and climate change in the northern hemisphere: results from transient general circulation models. *Climatic Change* 35: 241–258.

Alexiades, V. & Solomon, A.D. 1993. *Mathematical Modeling of Melting and Freezing Processes.* Washington: Hemisphere, 325 pp.

Brewer, M.C. 1958. Some results of geothermal investigations of permafrost in northern Alaska. *Transaction, AGU* 39: 19-26.

Burn, C.R. & Nelson, F.E. 2006. Comment on ''A projection of severe near-surface permafrost degradation during the 21st century'' by David M. Lawrence & Andrew G. Slater. *Geophysical Research Letters* 33, L21503, DOI:10.1029/2006GL027077.

Clow, G.D. & Urban, F.E. 2002. Largest permafrost warming in northern Alaska during the 1990s determined from GTN-P borehole temperature measurements. *EOS, Transactions of the AGU* 83(47), F258.

Delisle, G. 2007. Near-surface permafrost degradation: How severe during the 21st century? *Geophysical Research Letters* 34, L09503, DOI:10.1029/2007GL029323

Euskirchen, E.S., McGuire, A.D., Kicklighter, D.W., Zhuang, Q., Clein, J.S., Dargaville, R.J., Dye, D.G., Kimball, J.S., McDonald, K.C., Melillo, J.M., Romanovsky, V.E. & Smith, N.V. 2006. Importance of recent shifts in soil thermal dynamics on growing season length, productivity, and carbon sequestration in terrestrial high-latitude ecosystems. *Global Change Biology* 12: 731-750.

Harris, C. & Haeberli, W. 2003. Warming permafrost in European mountains. *World Meteorol. Org. Bull.* 52(3): 6 (See also *Global and Planetary Change* 39: 215–225).

Jin, H., Li, S., Cheng, G., Shaoling, W. & Li, X. 2000. Permafrost and climatic change in China. *Global and Planetary Change* 26(4): 387-404.

Lachenbruch, A.H. & Marshall, B.V. 1986. Changing climate: Geothermal evidence from permafrost in the Alaskan Arctic. *Science.* 234: 689–696.

Lawrence, D.M.& Slater, A.G. 2005. A projection of severe near surface permafrost degradation during the 21st century. *Geophys. Res. Lett*. 32, L24401, doi:10.1029/2005GL025080.

Marchenko, S., Gorbunov, A. & Romanovsky, V. 2007. Permafrost warming in the Tien Shan Mountains, central Asia. *Global and Planetary Change* 56: 311-327.

Marchuk, G.I. 1975. *Methods of Numerical Mathematics (Applications of Mathematics).* New York: Springer-Verlag, 316 pp.

Mitchell, T.D. & Jones, P.D. 2005. An improved method of constructing a database of monthly climate observations and associated high-resolution grids. *International Journal of Climatology* 25(6): 693-712.

Nicolsky, D.J., Romanovsky, V.E. & Tipenko, G.S. 2007. Estimation of thermal properties of saturated soils using in-situ temperature measurements. *The Cryosphere* 1: 41–58.

Nicolsky, D.J., Romanovsky, V.E., Alexeev, V.A. & Lawrence, D.M. 2007. Improved modeling of permafrost dynamics in a GCM land-surface scheme, *Geophys. Res. Lett.* 34, L08501, doi:10.1029/2007GL029525.

Oberman, N.G. & Mazhitova, G.G. 2001. Permafrost dynamics in the northeast of European Russia at the end of the 20th century. *Norwegian Journal of Geography* 55: 241-244.

Oelke, C. & Zhang, T. 2004. A model study of circum-arctic soil temperatures. *Permafrost Periglacial Processes* 15: 103–121.

Osterkamp, T.E. & Romanovsky, V.E. 1999. Evidence for warming and thawing of discontinuous permafrost in Alaska. *Permafrost and Periglacial Processes* 10: 17-37.

Osterkamp, T.E. 2003. Establishing long-term permafrost observatories for active-layer and permafrost investigations in Alaska: 1977–2002. *Permafrost and Periglacial Processes* 14: 331–342.

Osterkamp, T.E. 2005. The recent warming of permafrost in Alaska. *Global and Planetary Change* 49: 187–202.

Pollack, H.N., Hurter, S.J. & Johnson, J.R. 1993. Heat flow from the earth's interior: analysis of the global data set. *Reviews of Geophysics* 31(3): 267-280.

Romanovsky, V.E. and Osterkamp, T.E. 1997. Thawing of the active layer on the coastal plain of the Alaskan Arctic. *Permafrost and Periglacial Processes* 8(1): 1-22.

Romanovsky, V., Burgess, M., Smith, S., Yoshikawa, K. & Brown, J. 2002. Permafrost temperature records: indicators of climate change, *EOS, AGU Trans.* 83(50): 589-594.

Romanovsky, V.E., Sazonova, T.S., Balobaev, V.T., Shender, N.I. & Sergueev, D.O. 2007. Past and recent changes in permafrost and air temperatures in Eastern Siberia. *Global and Planetary Change* 56: 399-413.

Saito, K., Kimoto, M., Zhang, T., Takata, K. & Emori, S. 2007. Evaluating a high-resolution climate model: Simulated hydrothermal regimes in frozen ground regions and their change under the global warming scenario. *J. Geophys. Res*. 112: F02S11.

Sazonova, T.S. & Romanovsky, V.E. 2003. A model for regional-scale estimation of temporal and spatial variability of the active layer thickness and mean annual ground temperatures. *Permafrost and Periglacial Processes* 14(2): 125-139.

Sharkhuu, N. 2003. Resent Changes in permafrost of Mongolia. *Proceedings of the 8th International Conference on Permafrost, Zurich, Switzerland, July 2*: 1029-1034.

Sokolov, A.P. & Stone, P.H. 1998. A flexible climate model for use in integrated assessments. *Climate Dynamics* 14: 291-303.

Stendel, M. & Christensen, J.H. 2002. Impact of global warming on permafrost conditions in a coupled GCM. *Geophysical Research Letters* 29(13): 1632, 10.1029/2001GL014345.

Verdi, C. 1994. *Numerical aspects of parabolic free boundary and hysteresis problems. Lecture Notes in Mathematics.* New York: Springer-Verlag, 213-284.

Zhang, Y., Chen, W. & Riseborough, D.W. 2006. Temporal and spatial changes of permafrost in Canada since the end of the Little Ice Age. *J. Geophys. Res.* 111: D22103, doi:10.1029/2006JD007284.

Development of Frost-Crack Polygonal Relief in the Central Part of Tazovskiy Peninsula

Sergey Marchenko
Moscow State University, Geographical Faculty, Moscow, Russia

Dinara Abliazina
Moscow State University, Geographical Faculty, Moscow, Russia

Frederick Arnold
University of Hamburg, Soil Studies Institute, Hamburg, Germany

Abstract

On the Tazovskiy Peninsula (north of West Siberia) patterned ground is spread on considerable territory. In July 2007 different aspects of the process in the central part of the peninsula were explored. Descriptions and measurements of contemporary and ancient polygonal structures and certain parts of them were done near the Yubileinoe gas field and the town of Yamburg. On this basis we retraced the development of polygonal relief from ice wedges of first generation to ice-wedge casts. In contemporary climate conditions in the central part of Tazovskiy Peninsula, the process of frost wedging and development of polygonal relief takes place on peat grounds. The most typical dimensions of blocks are 10–15 m, and very often they are poorly expressed in relief. Ancient ice wedging of the Pleistocene period had much greater scales and was spread on mineral grounds as well. The thickness of ice wedges evidently reached 1–2 m.

Keywords: frost cracking; ice wedges; polygonal relief.

Introduction

One of the distinctive features of the cryolithosphere is patterned ground. North of western Siberia the phenomena is well spread on considerable territories, where severe climate in combination with ground conditions leads to frost cracking and formation of polygons. In July 2007 different aspects of the process in the central part of Tazovskiy Peninsula were explored. The exploration took place near the Yubileinoe gas field and the town of Yamburg. On the basis of certain examples, we retraced development of polygonal relief: from ice wedges of the first generation to the ice wedge casts.

Study Area

Exploration was carried out in the eastern and southern parts of Tazovskiy Peninsula (West Siberia, Russia). The territory is tectonic plate with Palaeogenic basement covered with a thick layer of sediments (Popov 1989). In the upper part, the sediments have marine, alluvial, and lacustrine genesis of different epochs of Pleistocene and are made up with loam, clay sand, and sand. The territory in general has poor vertical disarticulation caused mainly by cryogenic and fluvial processes. The vegetation is mainly tundra and forest tundra: *carex*, shrubs and bushes *betula nano, salix, ledum, eriophorum*; moss and lichens are widely spread: *cetraria islandica, sphagnum balticum*; very often they form polygonal peatlands. The main climate features are big yearly and weekly amplitudes of temperature with very cold winters. Mean January temperatures are -28°C; mean July temperatures are -12°C. Descriptions and measurements were done in two spots: forest-tundra territories near the Yubileinoe Gas Facility (65°57′N, 75°42′E) and tundra territories near the town of Yamburgh (68°00′N, 74°50′E).

Methods

To study the processes of frost-cracking and polygonal-relief formation, we made descriptions and measurements on spots that were selected to provide grounds, vegetation, and landscape diversity. Ice wedges and ice wedge casts were described in an exposure and in pits. Measurements were done with tape, ruler, and compass. To estimate the climatic parameters from the point of frost cracking (and

Table 1. Meteorological data for Noviy Urengoi and Noviy Port, 2005–2007.

	Period	Novii Urengoi	Period	Novii Port
Mean Yearly temperatures, dgr C	2005 after 23.06	2.291	2005 after 05.03	-1.285
	2006	-9.407	2006	-8.74
	2007	-8.738	2007	-4.91
Mean January temperatures, dgr C	2006	-30.493	2006	-36.19
	2007	-14.418	2007	-13.719
Mean July temperatures, dgr C	2005	13.085	2005	16.719
	2006	13.688	2006	16.651
	2007	16.5	2007	19.666
Annual precipitation, mm	2005 after 23.06	636.6	2005 after 05.03	392
	2006	912.9	2006	548
	2007	548	2007	499
Dates of stable temperature transition over/below 0 dgr C	2005 after 23.06	nd/15.10	2005 after 05.03	13.05/15.10
	2006	31.05/28.09	2006	30.05/29.09
	2007	15.06/14.10	2007	02.06/14.10
Quantity of negative degree*days after stable temperature transition below 0 dgr C	2005 after 23.06	nd	2005 after 05.03	nd
	2006	-4391.247	2006	-4514.08
	2007	-3136.67	2007	-4915.312
Quantity of positive degree*days after stable temperature transition above 0 dgr C	2005 after 23.06	nd	2005 after 05.03	1578.034
	2006	990.831	2006	1364.45
	2007	1132.924	2007	1399.004

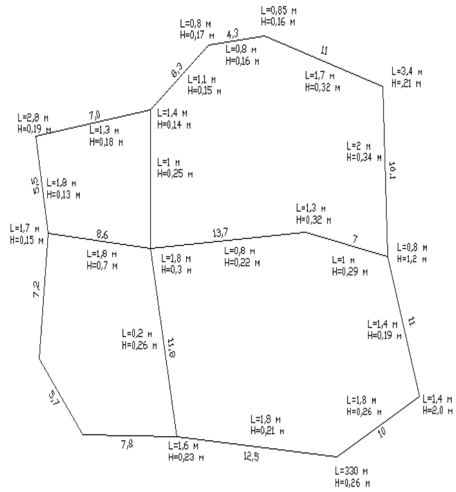

Figure 1. Results of measuring of a typical group of polygons near Ngarka-Poilovo-Yakha River (all values are in m).

Figure 2. A growing gully on the bank of Ngarka-Poilovo-Yakha River.

consequently polygonal system formation), we collected and analyzed meteorological data from Internet archives. We used meteorological data from the weather stations of Noviy Urengoi town and the village Noviy Port. The first town lies 40 km to the east of Yubileinoe and has nearly the same geographical conditions. Noviy Port and Yamburg are situated on the different banks of Obskaya Guba Bay, but have approximately the same latitude; the distance is 88 km. Thus a high correlation between meteorological conditions on the named weather stations and corresponding research sites is expected.

Site 1

The first place of exploration was situated in the valley of the Ngarka-Poilovo-Yakha River (67°53′40″N, 75°45′25″E). It is a wet territory with hummocks. During the Sartan time (22,000–18,000 years ago), strong cryogenesis led to formation of huge ice wedges in the lagoon sediments of Kargin time (40,000–22,000 years ago). During the Holocene the wedges partially degraded and formed ice wedge casts, overlain by

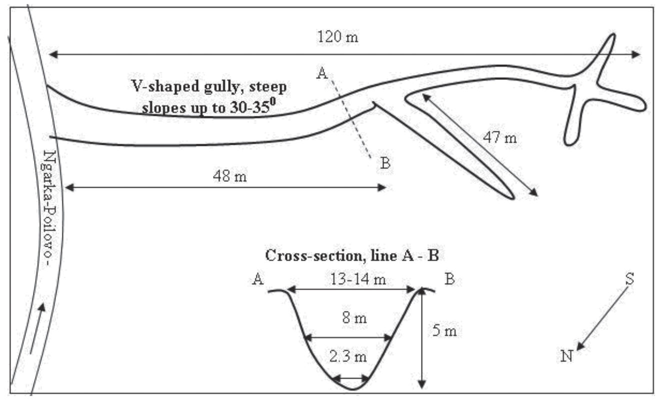

Figure 3. Gully scheme (67°53′40″N, 75°45′25″E).

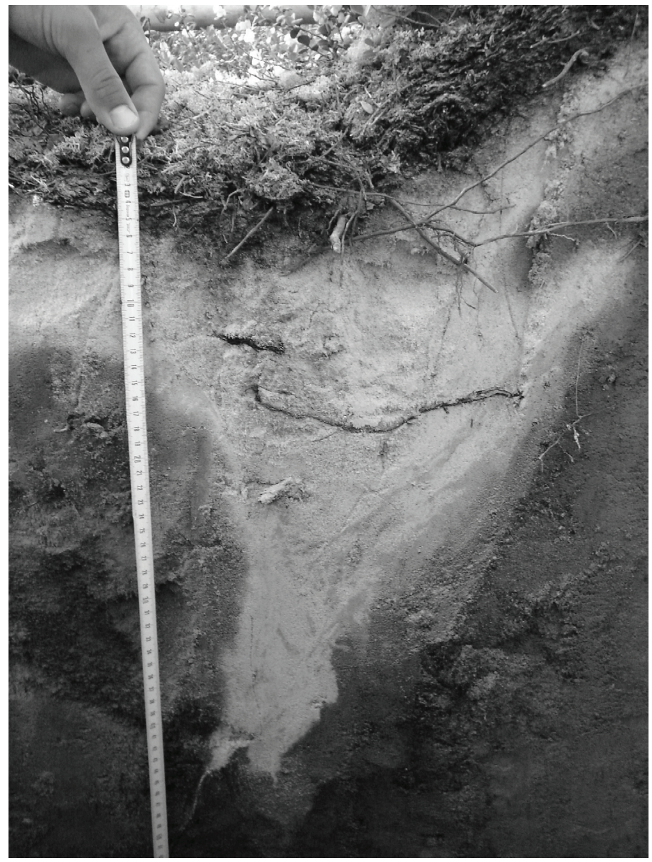

Figure 4. Sandy ice-wedge cast near the source of one of minor watercourses in the southern part of the Tazovskiy Peninsula.

peat up to 50 cm thick. On the surface of a small polygonal peat plateau, we sighted ice veins of the first generation. They are vein-like vertical ice inclusions up to 3 cm thick in the body of peat in different phases of decomposition. The peat plateau is a formed polygonal structure; typical dimensions of the blocks are 8–10 m in diameter. Judging by the considerable spreading of values, the polygons seem to be old enough as they reveal several generations of frost-cracking. In places where tensions in winter due to some reasons were higher, the peat is divided into polygons of smaller dimensions. Polygons are divided by depressions up to 0.4 m deep, in the depressions V-shaped ice wedges are detected. We have measured a group of polygons; the

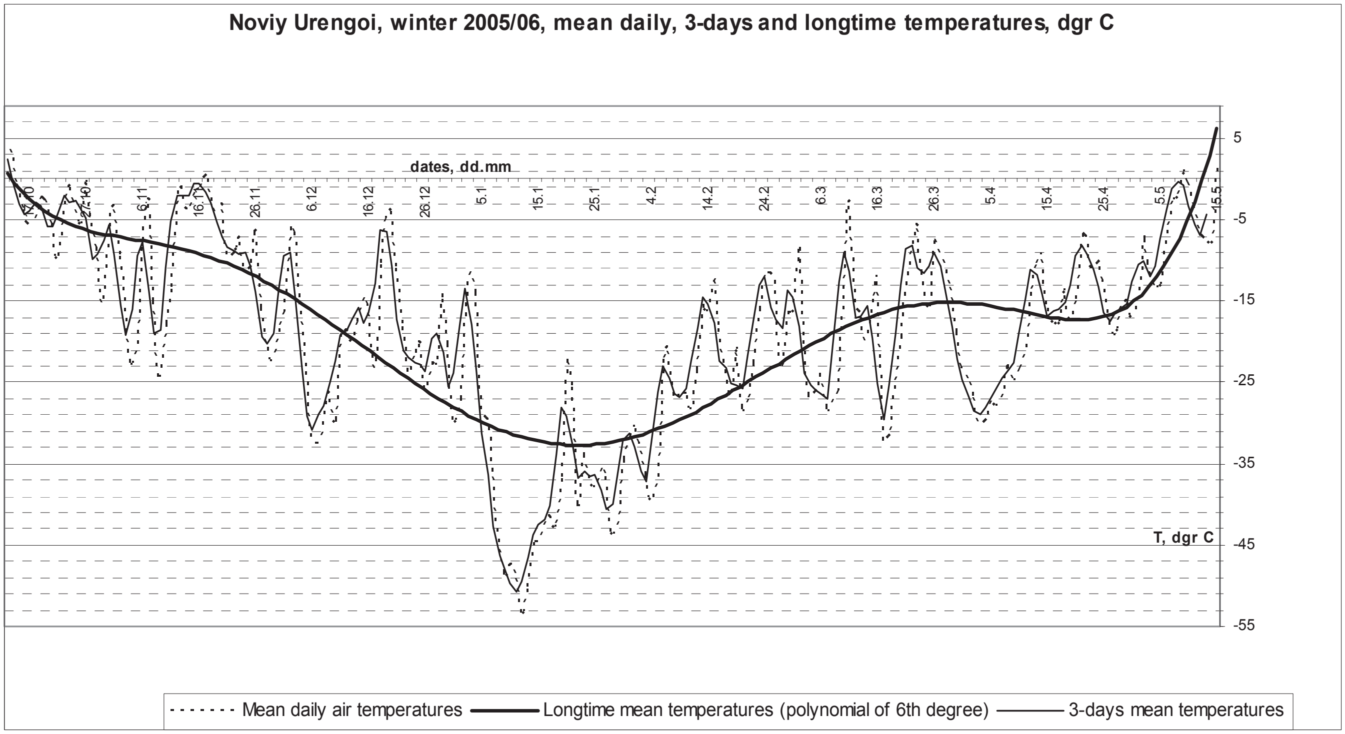

Figure 5.

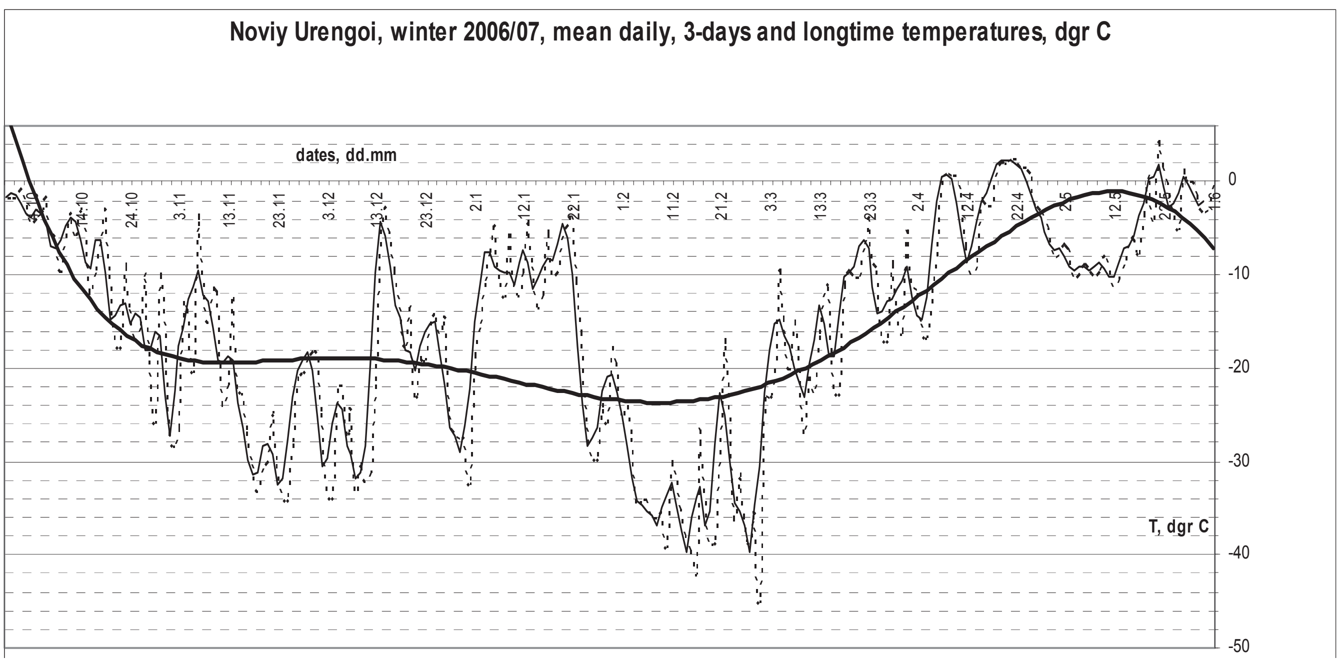

Figure 6.

results are shown on the Figure 1. The wedges separating the blocks open in the exposure on precipitous bank of the river Ngarka-Poilovo-Yakha; they can be retraced up to the depth of 2–2.5 m. Their complicated genesis is seen in the form: the bottom of a wedge is usually in the mineral sandy sediments where it developed as an epigenetic ice wedge, the part of wedge is almost strictly V-shaped; but in peat horizon which overcovers the mineral sediments from the depth of 1.5 it loses the strictness of form and is a syngenetic ice wedge. It is obvious that with the development of the peat plateau the conditions of heat exchange process changed, resulting in frost cracking and development of polygonal structures.

What is important about the ice wedges when they are revealed on banks of rivers, seas, and even minor

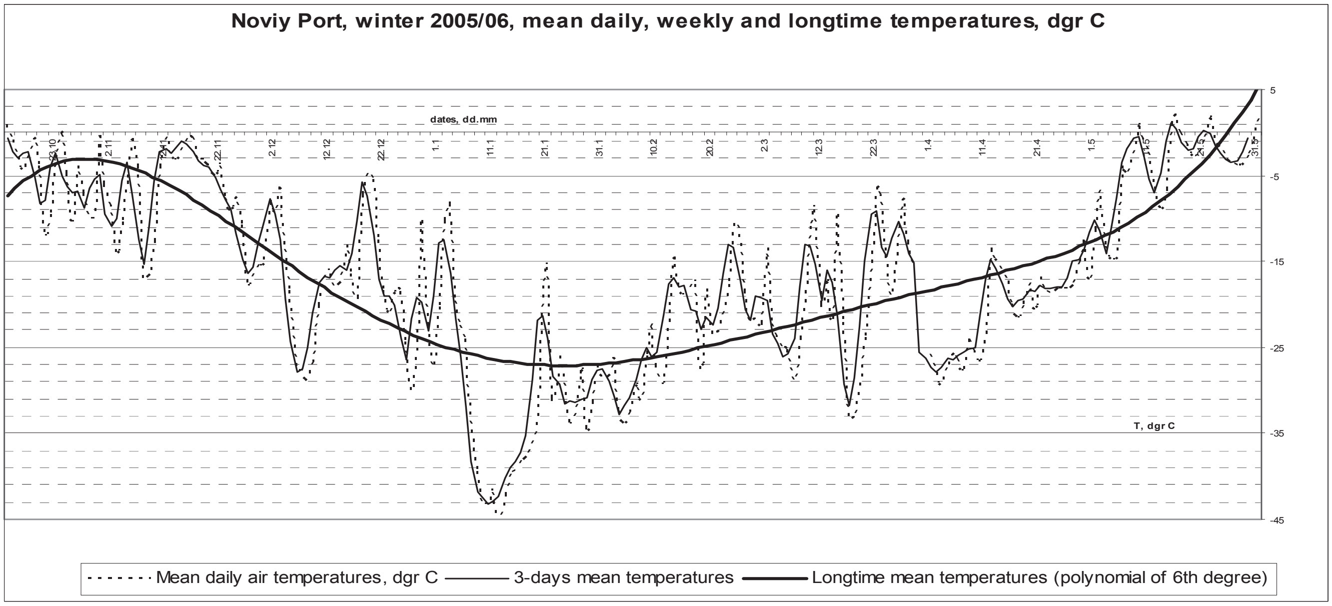

Figure 7.

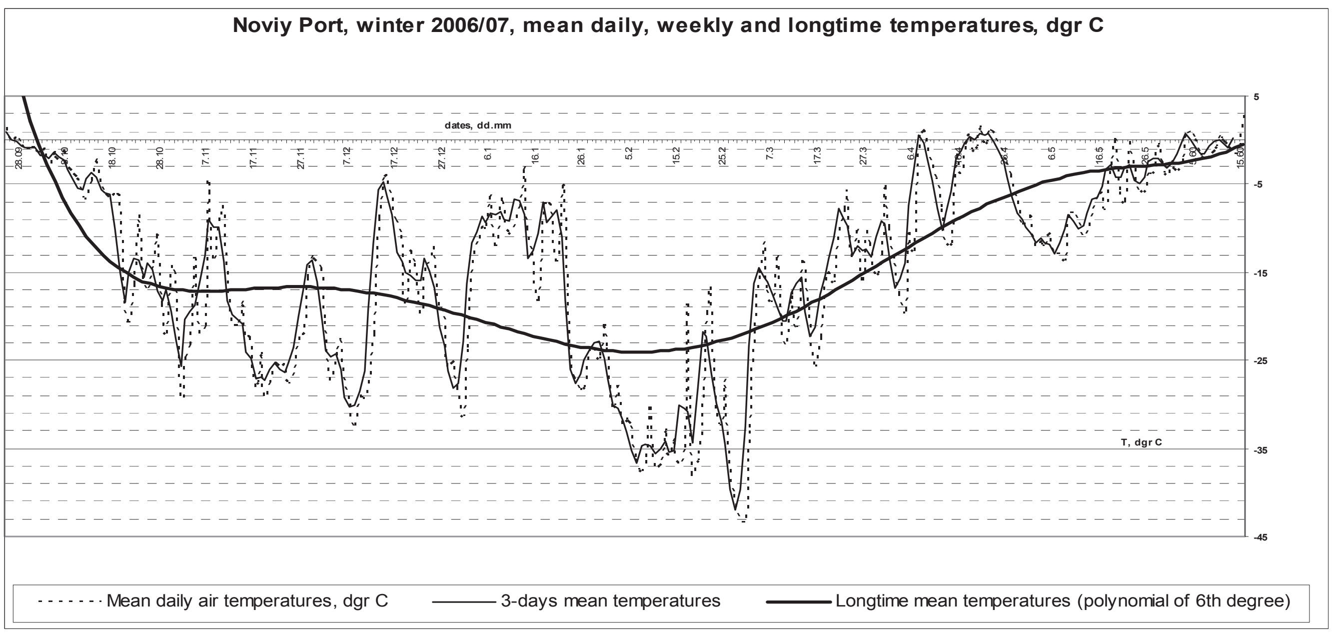

Figure 8.

watercourses is that while degrading they can advantage development of thermal erosion. Very often the forming gullies endanger different buildings, roads, plants, etc. And near the river Ngarka-Poilovo-Yakha vivid examples of the process can be detected (Figs. 2, 3).

The gullies form thermo-erosional outlets up to 8 m deep. One of them cuts through the right steep slope of the river and grows every year in the southwestern direction with speeds up to 4 m/year, thus endangering a gas cleaning and piping facility. The gully has a sophisticated formation with a number of tributaries; the tributaries inherit the polygonal form of wedges. Degrading, the wedges form linear depressions and during the spring seasons melting waters form watercourses in the depressions which hastens the gully growth. There was an attempt to stop the process - a unique construction of concrete and steel designed to help the melting waters in spring to flow faster and to prevent the banks from thermo-erosion was erected. But unfortunately the process of gully growing was not stopped completely. Another gully situated in 100 m to the south was detected (Fig. 3). Equal processes takes place on the bold shore of the Obskaya Guba Bay (Kara sea).

Site 2

On the bank of a thermokarst lake near the Yubileinoe gas field, northward of the previous spot, another small polygonal peat plateau is detected (67°57′01″N 75°52′13.3″E). It is

Table 2.

Decrease of T, °C	Number of fast (<10 days) decreases of air temperatures, mean daily temperatures in comparison with 3-days mean temperatures	
	Winter 2005/06	Winter 2006/07
5 to 10	14	10
11 to 15	4	11
16 to 20	4	2
21 to 25	2	1
25 to …	1	0
5 to …	25	24

Number of long decreases (>10 days) of air temperatures, mean daily temperatures in comparison with 20-days mean temperatures

	Winter 2005/06	Winter 2006/07
	3	4

Table 3.

Decrease of T, °C	Number of fast (<10 days) decreases of air temperatures, mean daily temperatures in comparison with 3-days mean temperatures	
	Winter 2005/06	Winter 2006/07
5 to 10	12	13
11 to 15	5	6
16 to 20	1	3
21 to 25	1	0
25 to …	1	0
5 to …	20	22

Number of long decreases (>10 days) of air temperatures, mean daily temperatures in comparison with 20-days mean temperatures

	Winter 2005/06	Winter 2006/07
	3	4

on the next stage of development, the polygons are uneven blocks usually pentahedral. The ice-wedges are on the stage of degradation – they do not reveal clearly in the upper 40 cm, while the wedges in the previous spot could easily be opened in the upper 30 cm. The depressions in between polygons are also poorly expressed. Measurements of a group of polygons were done. It was found out that apart from rather old polygons formed in the Sartan time, there were also new ones of smaller dimensions. The wedges and depressions dividing the old polygons are much more vividly expressed in the relief. Typical values for the first are 16–20 m in diameter. The latter are 8–12 m. and seem to have appeared after a fire that took place on the spot in 2005. The fire was quenched soon after it started, thus it did not spread on the nearby territories. Nevertheless it annihilated all the vegetation on the territory of about 30 by 30 m and now its spread is marked by poor vegetation and rests of ash. In winter 2005/06, that turned out to be extremely cold, frost polygons of a new generation developed on the territory limited by the edges of the fire spread.

Site 3

On the watershed near the source of one of the minor watercourses on the south of Tazovskiy Peninsula (66°0′35.6″N, 75°46′33.6″E), ancient polygonal structures were detected. They form characterful "avenues" up to 3–4 m wide, crossing with almost regular angles of 90 degrees. The "avenues" are also marked by vegetation: it varies from larch shaws on top of the polygons to lichens in the depressions. Typical dimensions of polygons are 17–20 in diameter. In about 500 m to the west the remains of a polygonal plateau were found. Ancient blocks are marked by relief features and vegetation. Differences are similar to those on the previous spot. In a dug prospect hole a sandy ice-wedge cast reveals itself in the loamy bearing strata (Fig. 4) Under the whitish sandy horizons there is a fine brownish horizon width, where the contents of organic material is increased. Below there are clear spots of ferritization on the contact with containing ground. The cast has the width of 30 cm in its upper part and 17 cm in the middle, while the depth is 50 cm.

Site 4

Near the valley of Halmer-Yakha River (65°58′45.8″N, 75°46′11.6″E) ancient polygonal structures on mineral grounds are detected, the surface is covered with larch shaws. Measurement of typical dimensions of polygons were made: the values for a typical group of polygons is 12.5 m by 12.5 m; 18.5 m by 11.5 m; 6.5 m by 9 m; 11 m by 9.5 m. The blocks are separated by depressions of considerable size: typical values of width are: 6.6 m; 5 m; 4.5 m; 5.7 m; they are up to 1 m deep.

Analysis of Meteorological Data

Frost cracking strongly depends on climatic conditions. Cracks appear when thermal tensions in the ground exceed the ground's tenacity. The tensions depend on thermal gradients and in general temperature increases with depth and temperature amplitudes decrease with depth. Thus thermal tensions that cause frost cracking depend on decreases of air temperature, especially when they reach considerable values in a short time. (Kudriavtsev 1978). According to the field research carried out by Mackay. (1974) north of Canada and by Podborniy (1976) in the lower reach of Yenisei River, frost cracking takes place when air temperatures lower below the average meaning for winter months. According to the research results near Ust'-Port (Yenisei delta, 69°39′45″N, 84°24′36″E) frost cracks can open both in the beginning and in the end of a rather long (1–2 months) cold period. The research also showed that even short (1–2 days) cold periods can lead to frost cracking. (Podborniy 1978). We tried to analyze meteorological data from the point of frost crack and consequently polygonal blocks formation. The results are given in the Figures 5, 6, 7, and 8 and in Tables 2 and 3.

Conclusions

According to the recent research done by Pavlov and Malkova (2005), the increase of annual air temperature relative to the norm in the region (calculated as mean in 1951–1990) of Tazovskiy Peninsula is 1.2°C, and in relation to the cold 1950s the value is about 1.6°C and the amplitude contraction owing to climate warming is 2°C. (Pavlov & Malkova 2005). On the basis of the data and of the descriptions and measurements done the following conclusions can be made. In contemporary climate conditions in the central part of Tazovskiy Peninsula, the process of frost wedging and development of patterned grounds takes place mainly on peat grounds with considerable humidification. In other cases degradation of frost-crack relief prevails. The factor of vegetation has a significant influence on the process, removing of destruction of vegetation can facilitate the development of polygonal structures. The most typical dimensions of blocks are 10–15 m, very often they are poorly expressed in relief. Development of polygons starts with formation of narrow ice wedges of the first generation, which slowly year after year grow and cross. While crossing they separate the polygonal blocks usually pentahedral or hexahedral. Ancient ice wedging of the Pleistocene period had much greater scales and spread on mineral grounds as well. The thickness of ice wedges evidently reached 1–2 m. Nowadays we can estimate the scale of cracking and development of polygons by investigating numerous ice wedge casts, forms of relief, vegetation, soils and other components of landscape.

Acknowledgments

The authors are grateful to the following persons for help and support in the project, both in the field works and in the process of article preparation: V.I. Grebenets (Moscow State University, Geographical faculty, Department of Cryolithology and Glaciology, Russia); Professor Eva-Maria Pfeiffer (University of Hamburg, Soil Studies Institute, Hamburg, Germany); V.V. Rogov (Moscow State University, Geographical Faculty, Department of Cryolithology and Glaciology, Russia); and A.N. Kurchatova (T'umen State Oil and Gas University, Russia).

References

Kudriavtsev, V.A. 1978. *General Geocryology.* Moscow: publishing house of Moscow State University, 456 p.

Pavlov, A.V. & Malkova, G.V. 2005. *Contemporary Changes of Climate in Northern Russia: Album of Small-scale Maps*. Novosibirsk: publishing house "Geo", 54 pp. (in Russian).

Podbornii, E.E. 1978. Time and intensity of frost crack formation. *Problems of Cryolithology VII*. Moscow: publishing house Science, 239 pp.

Popov, A.I. 1989. *Regional Cryolithology*. Moscow: publishing house of Moscow State University, 256 pp. (in Russian).

Popov, A I., Rozenbaum G.E. & Tumel' N.V. 1985 *Cryolithology*. Moscow: publishing house of Moscow State University, 239 pp.

New Insights into Spatial Uncertainty in Predictive Periglacial Modeling

Mathieu Marmion
Department of Geography, University of Oulu, P.O. Box 3000, 90014 Oulu, Finland
Thule Institute, University of Oulu, P.O. Box 7300, 90014 Oulu, Finland
Miska Luoto
Department of Geography, University of Oulu, P.O. Box 3000, 90014 Oulu, Finland
Jan Hjort
Department of Geography University of Helsinki, P.O. Box 64, 00014 Helsinki, Finland
Miia Parviainen
Department of Geography, University of Oulu, P.O. Box 3000, 90014 Oulu, Finland

Abstract

In this study, we produced maps of the uncertainty of predictions, provided by eight state-of-the-art modeling techniques for sorted (SP) and non-sorted (NSP) patterned ground, in subarctic Finland, at a 1.0 ha resolution. Five uncertainty classes (UC) represent the agreement between the different modeling techniques. The resulting uncertainty maps reflect the reliability of the estimates for the studied periglacial landforms in the modeled area. Our results showed a significant negative correlation between the uncertainty classes and the accuracy of the modeling techniques. On average, when all models agreed, the mean AUC values were 0.891 (NSP) and 0.886 (SP), and 0.494 (NSP) and 0.510 (SP) when only four models agreed. Mapping of the uncertainty of predictions in geomorphology can help scientists to improve the reliability of their data and modeling results.

Keywords: predictive accuracy; uncertainty classes; uncertainty mapping.

Introduction

Various modeling techniques are increasingly used in geomorphology in order to predict the spatial distribution of earth surface processes and landforms (Guzzetti et al. 1999). The development of spatial modeling in geomorphology is based on three trends: growth in the availability of remote sensed (RS) data and development of GIS techniques integrated with novel statistical methods (Walsh et al. 1998). Among several other applications, spatial modeling is used to assess the stability of terrain (Ermini et al. 2005) and to map glaciated landscapes (Brown et al. 1998) and periglacial processes (Hjort & Luoto 2006). In geomorphology, numerous areas have a lack of data, particularly in remote areas where field investigations are difficult to acquire. The predictions are used to fill these shortcomings in order to create more complete geomorphological maps (Vitek et al. 1996).

The used modeling techniques do not always provide robust predictions (Luoto & Hjort 2005). The reliability of the predictions can be improved by reducing the uncertainty of the models by using consensus methods (Thuiller 2004) or choosing a method which predicts most robustly a certain landform type (Luoto & Hjort 2005). However, these two approaches deal with the modeling uncertainty at a global scale (e.g., the whole modeled area). In this study, we propose a new approach, which does not aim to reduce the modeling uncertainty at a global scale, but to map it at a local scale.

Eight explanatory variables of 6998 grid squares were used as input into eight state-of-the-art modeling techniques to model the spatial distribution of sorted (SP) and non-sorted (NSP) patterned ground in subarctic Finland, at a 1.0 ha resolution. The eight modeling techniques are based on regression, machine learning, and classification algorithms. The accuracy of the models was evaluated using an independent test dataset (2999 grid squares) by the area under the curve (AUC) of a receiver operating characteristic (ROC) plot.

Material and Methods

Material

A dataset of 9997 grid squares at a 1.0 ha resolution was randomly divided into two subsets. The first subset (70%, 6998 grid squares) was used to calibrate the models, and the second subset (30%, 2999 grid squares) was used to evaluate the predictive performance of the models. In the whole study area, the prevalence of NSP and SP was 0.228 and 0.167, respectively. The prevalence was 0.227 (NSP) and 0.167 (SP) for the calibration dataset, 0.229 (NSP) and 0.167 (SP) for the evaluation dataset. Patterned ground was mapped *in situ* and it was located with a GPS-device in the whole study area of 100 km^2 during the field investigation in summer 2002. In total, eight explanatory variables were calculated for all of the grid squares to reflect the studied environmental conditions. The mean altitude (m), the mean slope angle (°), the wetness index, and the proportion of concave topography (%) were derived directly from a digital elevation model (DEM) at 20 m resolution. The proportions of four soil types, namely peat, glacigenic deposit, sand (and gravel), and rock terrain were derived from the digital soil map. More information about the record presences of the patterned grounds and the explanatory variables can be found in the study by Luoto & Hjort (2005).

Methods

The eight modeling techniques belong to three main categories of methods: three regression methods: Generalized Linear Model (GLM), Generalized Additive Model (GAM), and Multivariate Adaptive Regression Splines (MARS); two classification methods: Classification Tree Analysis (CTA) and Mixture Discriminant Analysis (MDA); and three machine learning methods: Artificial Neural Network (ANN), Random Forest (RF), and Generalized Boosting Methods (GBM).

GLMs are mathematical extensions of linear models (McCullagh & Nelder 1989) and have the ability to handle non-linear relationships and different types of statistical distributions characterizing spatial data. In this study, GLMs were built based on third order polynomial functions. GAMs are non-parametric extensions of GLM, using a smoothing spline with four degrees of freedom. GAM combines linear and additive response shapes within the same models (Hastie & Tibshirani 1990). MARS combines classical linear regression, mathematical construction of splines and binary recursive portioning producing linear or non linear models (Friedman 1991). These three regression methods are frequently used, and one example of utilization can be found in Luoto & Hjort (2005).

CTA is a binary based classification method and is an alternative to regression techniques (Breiman et al. 1984). At each node of the tree, a true/false decision is taken considering only one environmental parameter. Then the node separates a class into two different sub-classes whose purity level increases. CTA has been frequently used in geomorphology (Luoto & Hjort 2005). MDA is an extension of linear discriminant analysis (Venables & Ripley 2002). The environmental parameters form classes, for which density distribution is a mixture of Gaussian distributions. A set of environmental parameters is classified into the class with the maximum probability to belong to this class. MDA was used in geomorphology by Meritt & Wohl (2003).

ANNs, machine learning methods, are rule-based methods which have the ability to build accurate models when the functional form of the underlying equations is unknown (Lek & Guegan 1999). A network contains three different kinds of layers: the input layer, the intermediate layer, and the output layer. Each layer contains "neurons." The output of the previous layer of neurons is added, using weighted factors. This process is done until processing of the output layer. Examples of utilization of ANN can be found in Ermini et al. (2005). RF is based on multiple trees methods, generating several hundreds of random trees (Breiman 2001). Each tree is grown by selecting randomly a training dataset as many times as there are observations among the whole set of observation, with replacement from the original dataset. To be classified, vectors of environmental variables are input into each tree. Each tree gives a classification. The classification which appears the most often is attributed. GBM is the third implemented machine learning method and is also based on binary trees (Ridgeway 1999). To classify a vector, it is possible to use a CTA. A prior single tree classification can be improved as long as there is an estimate residual. This residual can be used as input into a second CTA, used to improve the prior classification. The sequence is repeated as long as necessary, decreasing step by step the estimate residual. To our knowledge, RF and GBM have not been used in geomorphological research.

All implemented modeling techniques except ANN were run in R environment (R Development Core Team 2004) under the BIOMOD framework (Thuiller 2003). ANN was run using the nnet library in S-plus.

The probability values of presence for SP and NSP provided by the modeling techniques were combined using a mean function as suggested by Johnson & Omland (2004). The outputs of the eight modeling techniques were then binarized using the prevalence of both landforms as a classification threshold (Liu et al. 2005). Each grid square of the modeled area was classified into five uncertainty classes (UC), reflecting the modeling agreement between the different modeling techniques (UC0 when all models agreed, UC4 when only four models agreed).

The predictive accuracy of the modeling techniques was assessed measuring the area under the curve (AUC) of a receiver operating characteristic (ROC) plot. This is a graphical method assessing the agreement between the observed presence/absence records and the model predictions, by representing the relationship between the false positive fraction and the true positive fraction of the related confusion matrix of the evaluated model (Fielding & Bell, 1997). The range of AUC is from 0.0 to 1.0, and a model providing excellent prediction has an AUC higher than 0.9; a fair model has an AUC in between 0.7 and 0.9, and a model is considered poor when the AUC is below 0.7 (Swets 1988).

Results

The performance of all eight modeling techniques is presented in Table 1. ANN was the most robust modeling technique, with mean AUC values of 0.861 and 0.859 for SP and NSP, respectively. On the contrary, MDA and RF had the lowest modeling performances with mean AUC values of 0.806 and 0.819, respectively. The AUC values of the mean projections were 0.898 for SP and 0.893 for NSP.

The mean AUC values were 0.891 and 0.886 for NSP and SP when all eight modeling techniques agreed, whilst 0.494 and 0.510 when only four models agreed. Furthermore, for all the models, there was a significant negative correlation between the uncertainty classes and the accuracy of the modeling technique (Table 1). The decrease of mean AUC values is the highest from the UC0 to the UC1, with a mean difference of 0.252 (NSP) and 0.219 (SP). ANN disagreed the most with the other modeling techniques, with 669 cases out of 1622 (amount of UC1 grid squares) for NSP and with 955 out of 1687 for SP (UC1).

Spatial distributions based on mean predictions of the eight modeling techniques and uncertainty maps of SP and NSP are presented in Figure 1. The majority of grid squares had a null

Table 1. AUC values based on of the eight different modelling techniques for non-sorted (NSP) and sorted (SP) patterned ground. Additionally, the correlation between uncertainty classes and AUC values are presented, as well as the false positive (FP; proportion of negative observations that were erroneously predicted as positive) and the false negative (FN: proportion of positive observations that were erroneously predicted as negative) fractions for each model and both landform types.

	ANN	**CTA**	**GAM**	**GBM**
	NSP – SP	NSP - SP	NSP - SP	NSP - SP
Calibration	0.844 – 0.860	0.833 – 0.824	0.834 – 0.839	0.839 – 0.852
Evaluation	0.859 – 0.861	0.826 – 0.825	0.837 – 0.840	0.834 – 0.849
Uncertainty class				
0	0.923 – 0.906	0.888 – 0.877	0.886 - 0.885	0.886 – 0.885
1	0.600 – 0.695	0.659 – 0.650	0.668 – 0.682	0.664 – 0.705
2	0.515 – 0.637	0.584 – 0.689	0.596 – 0.653	0.531 – 0.724
3	0.540 – 0.510	0.499 – 0.569	0.481 – 0.437	0.528 – 0.487
4	0.405 – 0.489	0.519 – 0.403	0.478 – 0.647	0.432 – 0.487
Correlation coef.				
	-0.886 ;-0.958	-0.903 ; -0.940	-0.943 ; -0.717	-0.939 ; -0.939
1-specificity (FP)	0.266 ; 0.338	0.144 ; 0.119	0.166 ; 0.191	0.155 ; 0.135
1-sensitivity (FN)	0.225 ; 0.146	0.283 ; 0.300	0.269 ; 0.219	0.279 ; 0.267

Table 1 continues.

	GLM	**MARS**	**MDA**	**RF**	***Mean***
	NSP - SP	NSP - SP	NSP - SP	NSP – SP	*NSP - SP*
Calibration	0.833 – 0.835	0.836 – 0.845	0.810 – 0.819	0.976 – 0.988	*0.851 – 0.858*
Evaluation	0.833 – 0.839	0.838 – 0.849	0.820 – 0.806	0.819 – 0.813	*0.833 – 0.835*
Uncertainty class					
0	0.884 – 0.885	0.882 – 0.885	0.893 – 0.876	0.885 – 0.885	*0.891 – 0.886*
1	0.657 – 0.681	0.665 – 0.658	0.566 – 0.589	0.635 – 0.676	*0.639 – 0.667*
2	0.556 – 0.678	0.551 – 0.730	0.542 – 0.573	0.581 – 0.489	*0.557 – 0.647*
3	0.512 – 0.383	0.699 – 0.644	0.614 – 0.535	0.578 – 0.486	*0.556 – 0.506*
4	0.499 – 0.589	0.537 – 0.627	0.569 – 0.317	0.515 – 0.519	*0.494 – 0.510*
Correlation coef.					
	-0.908 ; -0.775	-0.727 ; -0.790	-0.642 ; -0,930	-0.875 ; -0.848	*-0.853 ; -0.862*
1-specificity (FP)	0.163 ; 0.201	0.211 ; 0.199	0.126 ; 0.154	0.040 ; 0.086	*0.159 ; 0.178*
1-sensitivity (FN)	0.276 ; 0.221	0.211 ; 0.197	0.351 ; 0.291	0.271 ; 0.086	*0.271 ; 0.216*

uncertainty for SP and NSP, representing 68.5% and 67.8% of the whole area, respectively. For the different uncertainty classes these indices were for SP and NSP 16.9% and 16.2% (UC1), 6.7% and 8.1% (UC2), 5.0% and 5.4% (UC3), and 3.0% and 2.6% (UC4). In addition, the prediction of NSP seemed to be underestimated by most of the models. On average, the false negative fraction (FN = 0.271; proportion of positive observations that were erroneously predicted as negative) is higher than the false positive faction (FP = 0.159; proportion of negative observations that were erroneously predicted as positive).

Discussion

Statistical modeling techniques are increasingly used to map earth surface processes and landforms (Gruber & Hoelzle 2001, Hjort 2006, Brenning et al. 2007). In general, geomorphological data are sparse, and the utilization of modeling techniques can help to gather new spatial information (Vitek et al. 1996). Nevertheless, predictive modeling is only relevant if the accuracy of the predictions is known. Several studies have focused on the predictive accuracy of the models (Gruber & Hoelzle 2001, Luoto & Hjort 2005, Hjort & Luoto 2006). The spatial uncertainty of the models has commonly been reduced by combining the output of several models (e.g., consensus methods) or by selecting the most robust modeling techniques for a given landform. However, both these strategies reduce the predictive uncertainty of the models in the modeled area as a whole, whereas the mapping of the spatial uncertainty at a local scale would improve our understanding of the behavior of the models in individual grid squares.

The strong negative correlation between the uncertainty classes and the predictive accuracy of the models underlines the relevance of the multi-model approach. Grid squares in which all models agreed had high modeling accuracy. However, when the predictions disagreed, the predictive accuracy of the models decreased significantly. These results are confirmed by Nilsson et al. (2000), who used a multi-model approach in cell biology.

In this study, the mean probability values of the predictions based on all eight modeling techniques were more robust than the probability values based on single modeling techniques (see Johnson & Omland 2004). This improvement of accuracy is global. The uncertainty maps presented in Figure 1 delineate that the uncertainty is the highest on the edges of the clumped presences. These areas are transitional zones between suitable and non-suitable environments for both SP

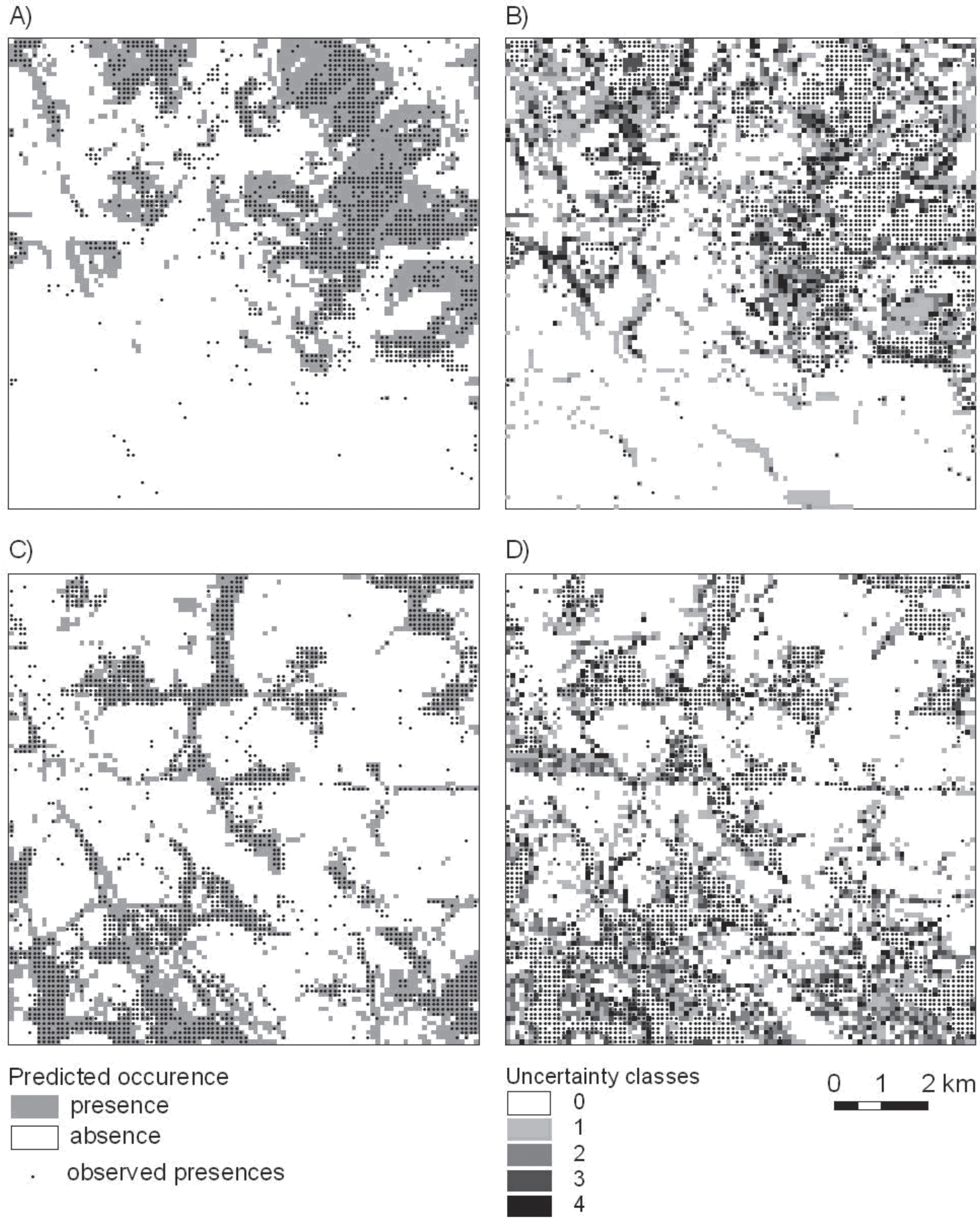

Figure 1. Spatial distribution based on mean predictions of the eight modeling techniques of sorted (A) and non-sorted (C) patterned ground and their uncertainty maps (B and D, respectively).

and NSP. As a consequence, the models have difficulty in differentiating the occurrence of the studied landform types in those areas. The fact that only few spots are predicted with a low accuracy is an asset for scientists who desire to improve the reliability of their data. In this case, the uncertainty analysis indicated that ca. 70% of the study area was accurately modeled for both landforms, thus the field investigations should be focused on the remaining 30% of the study area. It also confirms the assumption that models based on different mathematical algorithms provide rather similar predictions for most of the study area. Moreover, the fact that the NSP are underestimated by the models is partly due to the prevalence used as threshold to convert the output of the models to presences/absences.

Conclusion

Mapping of the uncertainty of predictions is a novel approach to representing the spatial reliability of predictions. It does not improve predictive accuracy of the models, but it provides a consistency map of the predictions. As a consequence, predictive maps can be interpreted simultaneously with uncertainty information, improving the understanding of potential pitfalls of the modeling exercise. We conclude that uncertainty mapping should be taken into account to deepen the understanding of the modeling procedure and to optimize field investigations to gather new field data.

Acknowledgments

MM and MP were funded by the Academy of Finland (project grant 116544). JH was funded by the Finnish Cultural Foundation. The comments of two unknown referees helped greatly in improving this paper.

References

Breiman, L., Friedman, F., Olshen, F. & Stone, C. 1984. *Classification and regression trees.* Pacific Grove, USA: Wadsworth.

Breiman, L. 2001. Random Forests. *Machine Learning* 45: 5-32.

Brenning, A., Grasser, M. & Friend, D.A. 2007. Statistical estimation and generalized additive modeling of rock glacier distribution in the San Juan Mountains, Colorado, United States. *Journal of Geophysical Research* 112.

Brown, D., Lusch, D. & Duda, K. 1998. Supervised classification of types of glaciated landscapes using digital elevation data. *Geomorphology* 21: 233-250.

Ermini, L., Catani, F. & Casagli, N. 2005. Artificial natural networks applied to landslide susceptibility assessment. *Geomorphology* 66: 327-343.

Fielding, A. & Bell, J. 1997. A review of methods for the assessment of prediction errors in conservation presence/absence models. *Environmental Conservation* 24: 38-49.

Friedman, J. 1991. Multivariate adaptive regression splines. *Annals of Statistics* 19: 1-141.

Gruber, S. & Hoelzle, M. 2001. Statistical modelling of mountain permafrost distribution: local calibration and incorporation of remotely sensed data. *Permafrost and Periglacial Processes* 12: 69-77.

Guzzetti, F., Carrara, A., Cardinali, M. & Reichenbach, P. 1999. Landslide hazard evaluation: a review of current techniques and their application in a multi-scale study, Central Italia. *Geomorphology* 31: 181-216.

Hastie, T. & Tibshirani, R. 1990. *Generalized additive models.* London: Chapman and Hall, 335 pp.

Hjort, J. 2006. *Environmental factors affecting the occurrence of periglacial landforms in Finnish Lapland: a numerical approach*. Shaker Verlag, Aachen, 162 pp.

Hjort, J. & Luoto, M. 2006. Modelling patterned ground distribution in Finnish Lapland: an integration of topographical, ground and remote sensing information. *Geografiska Annaler* 88A: 19-29.

Johnson, J.B. & Omland, K.S. 2004. Model selection in ecology and evolution. *Trends in Ecology & Evolution* 19: 101-108.

Lek, S. & Guegan, J. 1999. Artificial neural networks as a tool in ecological modelling, an introduction. *Ecological Modelling* 120: 65-73.

Liu, C., Berry, P.M., Dawson, T.P. & Pearson, R.G. 2005. Selecting thresholds of occurrence in the prediction of species distributions. *Ecography* 28: 385-393.

Luoto, M. & Hjort, J. 2005. Evaluation of current statistical approaches for predictive geomorphological mapping. *Geomorphology* 67: 299-315.

McCullagh, P. & Nelder, J.A. 1989. *Generalized linear models.* New York: Chapman & Hall.

Merritt, D.M. & Wohl, E.E. 2003. Downstream hydraulic geometry and channel adjustment during a flood along an ephemeral, arid-region drainage. *Geomorphology* 52: 165-180.

Nilsson, J., Persson, B. & von Heijne, G. 2000. Consensus prediction of membrane protein topology. *FEBS Letters* 486: 267-269.

Ridgeway, G. 1999. The state of boosting. *Computing Sciences and Statistics* 31: 172-181.

Swets, K. 1988. Measuring the accuracy of diagnostic systems. *Science* 240: 1285-1293.

Team, R.D.C. 2004. *R: A language and environment for statistical computing.* Vienna, Austria. R Foundation for Statistical Computing. http://www.R-project.org.

Thuiller, W. 2003. BIOMOD – Optimizing predictions of species distributions and projecting potential future shifts under global change. *Global Change Biology* 9: 1353-1362.

Thuiller, W. 2004. Patterns and uncertainties of species' range shifts under climate change. *Global Change Biology* 10: 2020-2027.

Venables, W.N. & Ripley, B.D. 2002. *Modern applied statistics with S.* Berlin: Springer-Verlag, 495 pp.

Vitek, J.D., Giardino, T.R. & Fitzgerald, J.W. 1996. Mapping geomorphology: a journey from paper maps, through computer mapping to GIS and virtual reality. *Geomorphology* 16: 233-249.

Walsh, S.J., Butler, D.R. & Malanson, G.P. 1998. An overview of scale, pattern, process relationships in geomorphology: a remote sensing and GIS perspective. *Geomorphology* 21: 183-205.

Modeling Discharge During the Rapid Drainage of Thaw Lakes in the Western Canadian Arctic

Philip Marsh
Environment Canada, National Water Research Institute, Saskatoon, Canada
Mark Russell
Environment Canada, National Water Research Institute, Saskatoon, Canada
Cuyler Onclin
Environment Canada, National Water Research Institute, Saskatoon, Canada
Heather Haywood
Environment Canada, National Water Research Institute, Saskatoon, Canada

Abstract

A large number of thaw lakes in the Western Canadian Arctic are prone to rapid or catastrophic drainage, with 41 lakes draining over a 57-year period in the study area. These lakes range in size up to 560 ha in area and up to 5 m in depth. Evidence suggests that such lakes may drain in less than 24 hours and the resulting drainage from even small lakes may have a peak discharge that is much larger than that experienced during normal spring snowmelt from small headwater basins. As a result, these drainage events play an important role in landscape evolution and may pose a significant threat to proposed pipelines in the study area. This paper will present information on the size and volume of lakes that have drained in the past, and provide order-of-magnitude estimates of discharge during lake drainage.

Keywords: discharge; lakes; rapid drainage; permafrost.

Introduction

The Arctic Coastal plain of northwest Canada is extremely lake rich. At the scale of approximately 10 km x 10 km, lake coverage varies from 15% to 50% of the total surface area. These lakes developed in an ice-rich permafrost environment during a postglacial warm period between 13,000 BP and 8,000 BP (Mackay 1992). Many of these lakes formed due to thawing of ice-rich permafrost that resulted in the settlement of the ground surface (Mackay 1992). Since that time, lake drainage, and disappearance of lakes from this landscape, has occurred at a rate of 1 to 2/year for Richards Is. and the Tuktoyaktuk Peninsula (Mackay 1992, Marsh & Neumann 2001). Such drainage occurs due to the melting or erosion of drainage channels through the ice-rich permafrost (Marsh & Neumann 2001). Similar thaw lake formation and drainage processes occur in the Alaskan Coastal Plain (Brewer et al. 1993) and Banks Island (Harry & French 1983), as well as the Yukon Coastal Plain, the Hudson Bay Lowland, and Siberia.

Mackay (1988, 1992) suggested that lake drainage occurs as underground tunnel flow through interconnecting ice wedge cracks, or by sustained flow through ice wedge troughs. Although drainage is often initiated as tunnel flow, the roof of the tunnel typically collapses during drainage, resulting in an open channel. Observations after drainage (Mackay 1988, 1992, Brewer et al. 1993), and through modeling of outflow (Marsh & Neumann 2001) suggest that lake drainage is often rapid or catastrophic, with partial or complete lake drainage occurring in less than 24 hours.

Through the application of an ice-dammed lake model, Marsh & Neumann (2001) demonstrated that the rate of drainage of permafrost-dammed lakes was at least partially explained by rapid melting of ground ice due to warm water flowing through the channel. They also demonstrated that the maximum discharge during drainage from a small lake (8.1 ha) was similar in magnitude to the spring peak discharge from a drainage basin of 6000 ha in area.

The rapid drainage of lakes modifies the landscape by decreasing lake area and deepening of lake outlet channels. Such events, with drainage channels up to 5 to 10 m in width and 5 m in depth and hundreds of m in length, may pose a significant hazard to pipelines proposed in the area north of Inuvik, NWT. In addition, the high discharge from these events may pose a danger to downsteam infrastructure related to pipeline development.

Marsh & Neumann (2001) estimated the discharge from two drained lakes north of Inuvik, NWT. However, there is no information on the size or volume of a wider range of drained lakes in the study area or of the possible discharge from these lakes. Since there are a large number of lakes in the area north of Inuvik where rapid lake drainage occurs, and since no approach has yet been described to predict which lakes are more prone to drainage, there are no observations of discharge from rapidly draining lakes. In addition, there is only a very small chance of obtaining such discharge measurements in the near future. As a result, the only method available to provide order-of-magnitude estimate of discharge for a lake drainage event is to apply a model such as tested by Marsh & Neumann (2001).

In order to provide order-of-magnitude estimates of discharge during lake drainage events, this paper will (1) evaluate the range of lake size and volume found in the study area and characterize the drainage channel dimensions for

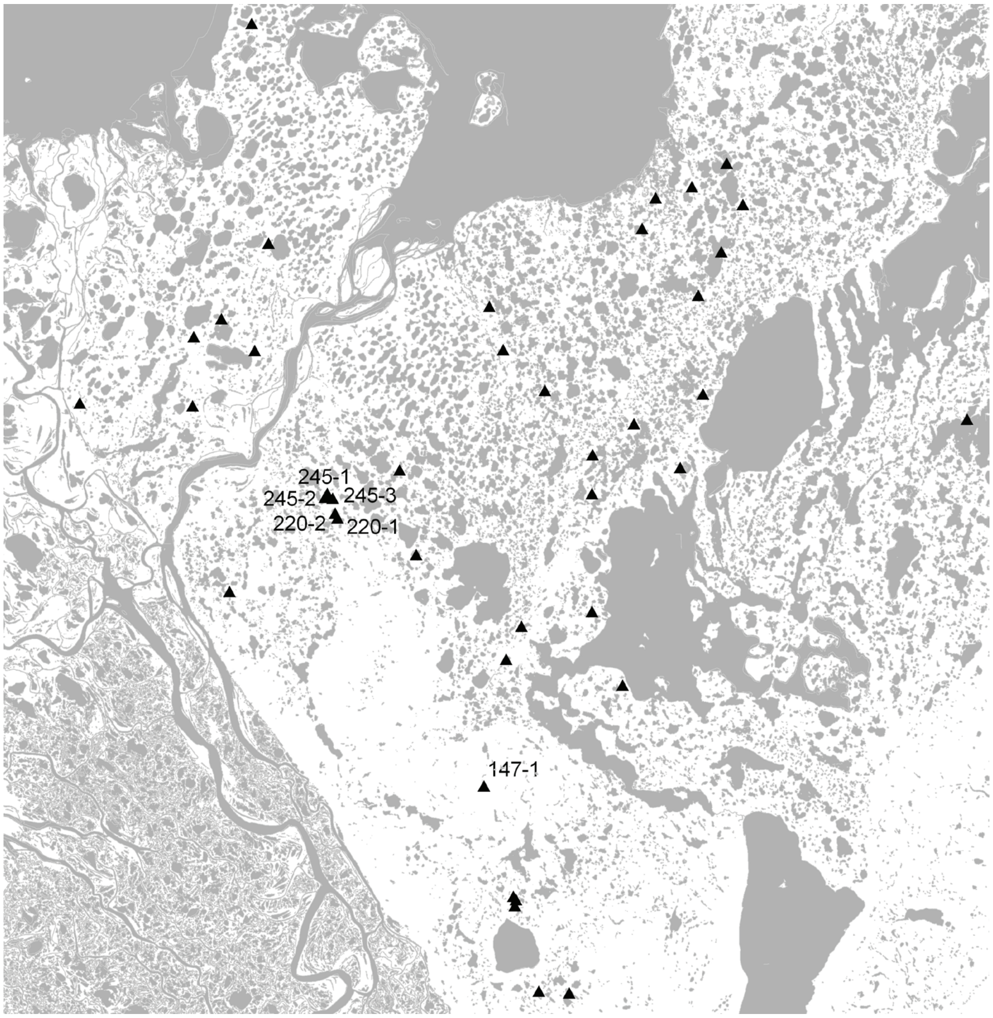

Figure 1. Study area north of Inuvik, NWT, and to the immediate west of the Mackenzie Delta. The 41 lakes that drained between 1950 and 2004 are shown by black triangles. Lakes studied in detail are numbered on the map. Lake number 147-1 is also called TVC Lake.

drained lakes in an area north of Inuvik, NWT, and (2) utilize a simple model to consider the range of possible discharge from these lakes.

Study Area and Methods

The study area includes the area north of Inuvik to the Beaufort Sea, and east from the Mackenzie Delta to near Tuktoyaktuk, NWT. There are 14,457 lakes, covering 19% of the 11,000 km^2 study area. Marsh et al. (2005) mapped drained lakes in this area (Fig. 1), using a combination of aerial photographs from 2000, topographic maps based on 1950 aerial photographs, and field observations. The present paper extends the size of the study area. For this expanded area, there are 41 lakes that drained between 1950 and 2000. The area of these lakes prior to lake drainage was determined from topographic maps and aerial photographs.

The area, volume, and average depth for 6 lakes (numbered in Fig. 1) in the study area was estimated from a high resolution digital elevation model (DEM) obtained from airborne LiDAR flown in August 2004. This DEM has 2 m pixels, with a vertical accuracy of 0.3 m and a horizontal accuracy of 0.6 m. Discharge from these 6 drained lakes was estimated using the methodology of Marsh & Neumann (2001), who applied an ice-dammed lake model from Clarke (1982).

Marsh & Neumann (2001), using discharge data estimated for Illisarvik Lake as derived from Mackay (1981), showed that modeled discharge for Illisarvik Lake was similar to observed for the first 3.5 hr of the modeled 5 hr discharge period. After this time, actual discharge was lower than modeled, with the observed peak being approximately 45% of observed. Marsh & Neumann (2001) suggested that this was due to the fact that channel enlargement by ice melt dominated the first portion of the melt period, while sediment erosion dominated the last portions of the lake drainage event. Following these results, modeled discharge estimates provided in this paper should be considered maximum possible discharge, with actual discharge likely being less.

Lake temperature, as required by the Marsh & Neumann (2001) model, was measured along a vertical profile from the lake surface to lake bed at a typical lake in the study area. Temperatures were measured from late June to early September, a period when many drainage events occur.

Results

Observations of a recent lake drainage channel

During the summer of 2006, a small lake in the study area drained. Although the lake was not observed during the drainage event, observations of the drainage channel soon after lake drainage, demonstrated two features typical of lake drainage as suggested by Mackay (1992) and Marsh & Neumann (2001). First, significant amounts of ground ice were observed along the walls of the drainage channel. Secondly, a surface vegetation mat extended across one portion of the channel, clearly suggesting that at least during the early portion of the event, drainage occurred by subsurface flow through a tunnel. At some point during the event, much of the tunnel collapsed, creating an open channel. Both of these observations further support the hypothesis that lake drainage occurs as tunnel flow through areas of high ground ice concentration, and provide further justification to use an ice-dammed lake model to estimate discharge from rapidly draining lakes (Marsh & Neumann, 2001).

Modeled discharge during lake drainage

Marsh & Neumann (2001) showed the sensitivity of lake discharge during rapid draining events to variations in lake water temperature, channel roughness, and ground ice content. However, due to a lack of data, they did not consider other factors affecting discharge, including lake volume, the length of the drainage channel, and the vertical drop along the drainage channel.

Lake area, volume, channel length, and vertical drop along the channel was obtained from LiDAR data for a series of 5 lakes within the study area and for TVC Lake discussed by Marsh & Neumann (2001). These data show a wide range of lake volumes, with average depth varying from 1.7 to 5.7 m. In addition, channel lengths varied from 8 m to over 500 m, and vertical drop varied between near zero and 14 m (Table 1).

In order to estimate discharge from these lakes during a period of rapid drainage, we used standard values for channel roughness and ground ice content from Marsh & Neumann (2001). Marsh & Neumann (2001) also showed that lake discharge is very sensitive to water temperature, with discharge increasing in magnitude with rising water temperature. The measured average water temperature for one year, from late June to early September, was 13°C at a typical lake in the study area. This temperature was used for all model runs. As noted by Marsh & Neumann (2001), modeled lake discharge increases with water temperature.

Figure 2. shows the discharge vs. time since start of discharge for each of the lakes in Table 1. Note the gradually rising discharge as the channel tunnel increases in cross-sectional area due to ice melting. Discharge continues to increase until the peak value is reached, after which the discharge rapidly drops to zero as the lake volume goes to zero, with maximum discharge ranging from 60 to 370 m^3/s.

As Marsh & Neumann (2001) suggested, however, it is likely that the peak value is less than shown in Figure 2, with the only example from Marsh & Neumann (2001) being 45% of modeled. In that example, discharge peaked,

Table 1. Lake area, volume, channel length, and vertical drop along the lake outlet channel for 6 study lakes as derived from LiDAR.

Lake #	Area ha	Volume m^3	Channel Length m	Vertical drop along lake outlet channel m
245-1	39.5	790,340	540	1
245-2	21.8	435,668	111	1
245-3	50.0	999,904	240	2
220-2	36.0	770,502	318	5
220-1	82.5	1,650,594	8	0.1
147-1 (TVC)	8.5	112,500	450	14
220-2 + 220-1	118.6	2,421,096	318	5

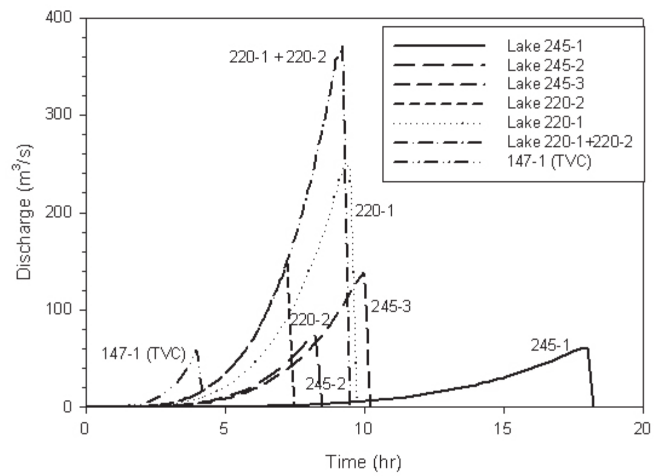

Figure 2. Modeled discharge during rapid lake drainage events. Time is in hours since the start of drainage. Note that Marsh & Neumann (2001) suggested that actual maximum discharge may be less than modeled as the regime changes from melt dominated to erosion dominated.

and then gradually decreased instead of rapidly dropping as shown in Figure 2. Even if discharge peaked at a value of 45% of that shown in Figure 2, it would be extremely high for such small headwater lake basins. For the larger lakes, it is likely that peak discharge would be orders of magnitude higher than the spring peak runoff.

Lake discharge compared to lake area

A total of 41 lakes drained in the study area during the period 1950 to 2007. These lakes varied in area from a minimum of 0.36 ha, to a maximum of 561 ha, with the majority of lakes less than 100 ha in area (Fig. 3). Since the 6 detailed study lakes described above, are within the size range typical of the study area, they allow us to consider the range of discharges that may occur from the majority of rapidly draining lakes.

Using measured lake volume, channel length, and vertical drop along the channel, the modeled discharge increases linearly with area (Fig. 4). The lack of scatter is surprising

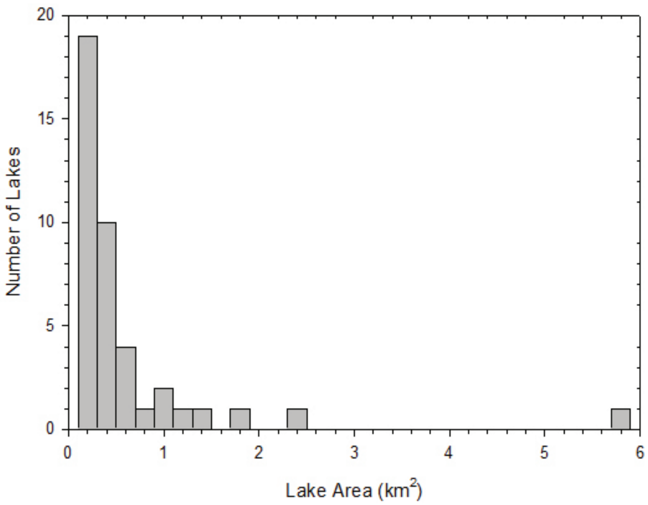

Figure 3. Histogram showing number of lakes within each area group. Note that of the 41 lakes in total, most lakes are in the range from 0 to 100 ha (0 to 1 km^2), a similar range to the 6 lakes in the detailed study area with LiDAR data.

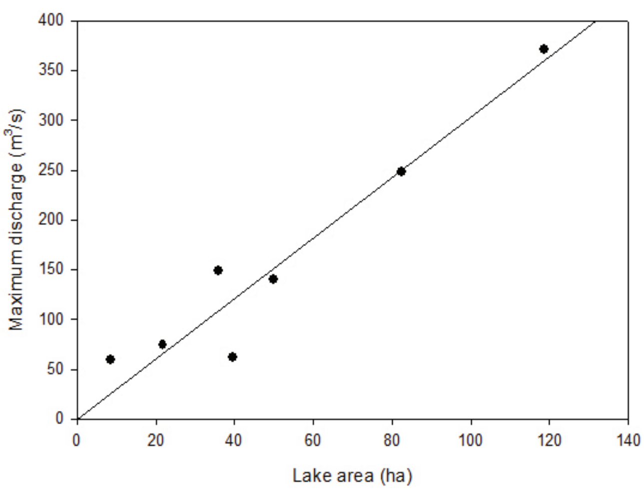

Figure 4. Relationship between lake area and modeled maximum discharge, showing a good linear relationship between the two. However, Marsh & Neumann (2001) suggested that actual maximum discharge is often less than modeled as the regime changes from melt dominated to erosion dominated.

given the range of lake depths (and therefore volume for lakes of any given size) and the variations in channel parameters (Table 1). However, it does suggest that lake size alone, may be used to provide order-of-magnitude estimates of lake discharge.

Although Figure 4 suggests a reasonable relationship between lake area and discharge for a small number of lakes, it would be expected that variations in average depth and channel length and vertical drop along the channel would result in a large variation in discharge for any lake of a given size. Given the data in Table 1, it is possible to estimate the range of possible discharges from rapidly draining lakes, of any given size.

Figure 5 shows possible discharge for increasing lake area, each with a range of lake conditions found in the study area (Table 1). As expected, there is a wide range of possible

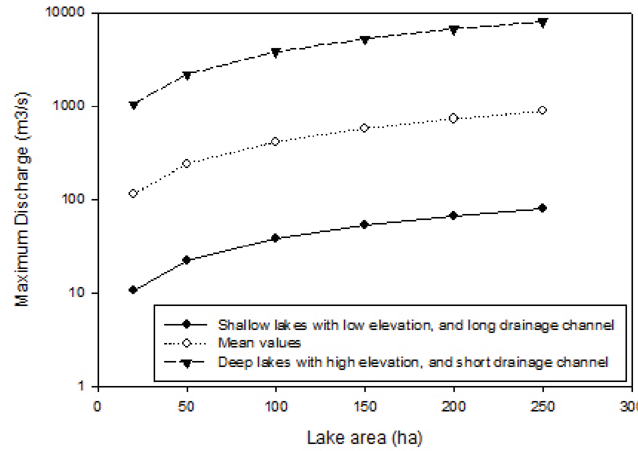

Figure 5. Discharge for lakes with average depth, channel length, and channel slope. Also shown, are maximum expected discharge for deep lakes, with short, steep drainage channels, and for shallow lakes with long, gentle drainage channels.

discharges, with higher discharge for deep lakes with short, steep drainage channels, and lower discharge for shallow lakes, with long, gradual drainage channels.

Grouping of drained lakes

Many drained lakes appear in groups, extending downstream along a drainage path. This is the case with lakes 245-1 to 220-1 shown in Figure 1. It is unknown if such groupings occur due to larger amounts of ground ice and ice wedge occurrence at these sites, or whether drainage occurred in an upstream lake with resulting higher downstream lake levels resulting in drainage of subsequent downstream lakes.

However, for the groupings of lakes 245-1 to 220-1, if drainage first occurred in the furthest upstream lake, we can estimate the maximum rise in water level for each downstream lake from our knowledge of lake areas and volumes.

In this case, drainage of the uppermost two lakes, followed by drainage of each subsequent lake would result in an increase in lake level by approximately 5 m, 14 m, and 34 m in the downstream 3 lakes. The increase in lake level is obviously an over-estimate, as it is assumed that all lake water would be added instantaneously to each downstream lake with no additional outflow from each lake. A complete and more accurate analysis of such a combined drainage event is not possible without additional information. However, it clearly indicates that if an upstream lake drained first, it would result in a very rapid rise in water levels in the downstream lakes. As Mackay (1991) noted, lake drainage can occur in ice-rich terrain under a number of conditions, including high water levels over topping ice wedges, with subsequent melting of ice wedges. Another possibility is that downstream drainage was initiated by mechanical erosion of the existing lake outlet channels and subsequent exposure of ground ice in the channel walls. Once ground ice was exposed, it would likely be prone to rapid melting of ice, channel enlargement, and increased discharge.

Conclusions

Previously drained lakes in the study area north of Inuvik, NWT, range in size up to 560 ha in area, with depths between 1.7 and 5.7 m. Previously published studies and observations in a recently drained lake suggest that lake drainage occurs over a short time, due to melting of ice-rich permafrost, and that flow often occurs within a subsurface tunnel. Detailed information on lake volume, channel length, and vertical drop along the drainage channel from LiDAR, are available for 6 lakes in the study area. Based on these data, as well as measured lake water temperature, and standard values for other parameters from Marsh & Neumann (2001), discharge from these 6 lakes would vary from 60 to 370 m^3/s. Using data for these lakes to estimate a range of possible lake discharge suggests that for shallow lakes with a long, low-slope outlet channel, discharge could range from 10 to 80 m^3/s, while for deep lakes with short, steep outlet channel, the discharge could vary from 1,000 to nearly 10,000 m^3/s. However, as noted by Marsh & Neumann (2001), it is likely that ice melting dominates only the initial rise to a peak, with actual peak discharge being roughly half of that suggested by the ice-dammed lake model. Even with this, model results suggest that discharge from a large, deep, rapidly draining lake could be orders of magnitude higher than that which would occur during spring snowmelt from such small headwater basins.

Acknowledgments

We would like to acknowledge funding from the Program for Energy R&D – Pipelines, from the Environment Canada Northern Energy Project, and from Environment Canada, National Water Research Institute. In addition, fieldwork in such northern locations would not be possible without support from the Aurora Research Institute and Polar Continental Shelf Project.

References

Brewer, M.C., Carter, L.D. & Glenn, R. 1993. Sudden drainage of a thaw lake on the Alaskan Arctic coastal plain. *Proceedings of the Sixth International Conference on Permafrost, Beijing, China.* , Guangzhou, China: University of Technology Press: 48-53.

Clarke, G.K.C. 1982. Glacier outburst floods from “Hazard Lake,” Yukon Territory, and the problem of flood magnitude prediction. *Journal of Glaciology* 28(98): 3-21.

Harry, D.G. & French, H.M. 1983. The orientation and evolution of thaw lakes, Southwest Banks Island, Canadian Arctic. *Proceedings of the Fourth International Conference on Permafrost.* Washington, DC: National Academy Press: 456-461.

Mackay, J.R. 1981. *An Experiment in Lake Drainage, Richards Island, Northwest Territories: A Progress Report.* Current Research, Part A, Geol. Surv. Canada, Paper 81-1A, 63-68.

Mackay, J.R. 1988. *Catastrophic Lake Drainage, Tuktoyaktuk Peninsula Area, District of Mackenzie*. Current Research, Part D, Geol. Surv. Canada, Paper 88-1D, 83-90.

Mackay, J.R. 1992. Lake stability in an ice-rich permafrost environment: Examples from the western Arctic coast. In: R.D. Robarts & M.L. Bothwell (eds.), *Aquatic Ecosystems in Semi-Arid Regions: Implications for Resource Management*. NHRI Symposium Series 7. Environment Canada: Saskatoon, Saskatchewan. 1-26.

Marsh, P. & Neumann, N.N. 2001. Processes controlling the rapid drainage of two ice-rich permafrost-dammed lakes in NW Canada. *Hydrological Processes* 15: 3433-3446.

Marsh, P., Russell, M. & Onclin, C. 2005. The hydrology of lakes in the Western Canadian Arctic – implications to proposed natural gas development. *15th International Northern Research Basins Symposium and Workshop Luleå to Kvikkjokk, Sweden, 29 Aug.–2 Sept. 2005,* 131-140.

Ice Wedge Polygon Dynamics in Svalbard: High-Resolution Monitoring by Multiple Techniques

Norikazu Matsuoka
Geoenvironmental Sciences, University of Tsukuba, Tsukuba, Japan
Hanne H. Christiansen
The University Centre in Svalbard, UNIS, Longyearbyen, Norway

Abstract

Techniques were combined to detect the timing and magnitude of thermal contraction cracking and to associate cracking with seasonal soil deformation in low-centered polygonal ground. An ice wedge trough rimmed by ramparts was instrumented with extensometers, breaking cables, shock loggers, thermistors, moisture sensors and an automatic camera. Three years (2004–2007) of monitoring highlighted, in general, symmetrical horizontal movements between the trough and ramparts. The ramparts extended in winter and shrank in summer mainly associated with frost heave and thermal deformation within the active layer. The trough showed the opposite movements, with winter shrinkage and summer extension, except for extension during mid to late winter. The frozen active layer cracked significantly in a very cold period in the late winter of 2006. Following the generation of superficial cracking, the trough began extending when the surface temperature rapidly lowered below -20°C. A major cracking event occurred when the permafrost top temperature reached -10°C, although the crack did not reach the permafrost.

Keywords: field monitoring; ice wedge; periglacial; permafrost; Svalbard; thermal contraction cracking.

Introduction

Thermal contraction cracking and associated ice wedge formation in frozen ground have been studied by theoretical considerations (e.g., Lachenbruch 1962, Plug & Werner 2001) and by field observations (e.g., Mackay & Burn 2002, Fortier & Allard 2005, Kokelj et al. 2007). In particular, long-term monitoring in the Canadian Arctic has provided data on cracking frequency, spatiotemporal variability of cracking activity and seasonal deformation of ice wedge polygons (Mackay 1992, 2000; Mackay & Burn 2002). A notable result is that not only thermal contraction in winter, but also seasonal soil expansion and contraction contribute to the development of the surface morphology and subsurface structure around the polygons. However, the detailed processes of soil deformation and cracking, as well as thermal conditions at which the ground cracks, are still uncertain, because of the lack of continuous recording of soil movement, cracking and contributing parameters.

This paper proposes a synthetic automatic monitoring system allowing year-round, concurrent monitoring of soil dilatation and cracking across a polygon trough, soil temperature, moisture, and snow conditions. Data for the first three years (2004–2007) are combined with data from manual observations of new-crack distribution and soil movement to discuss the timing and detailed processes of soil deformation and cracking.

The Study Site

The monitoring site is located on a fluvial, loess-covered terrace in the Adventdalen valley, Svalbard, Norway (Fig.

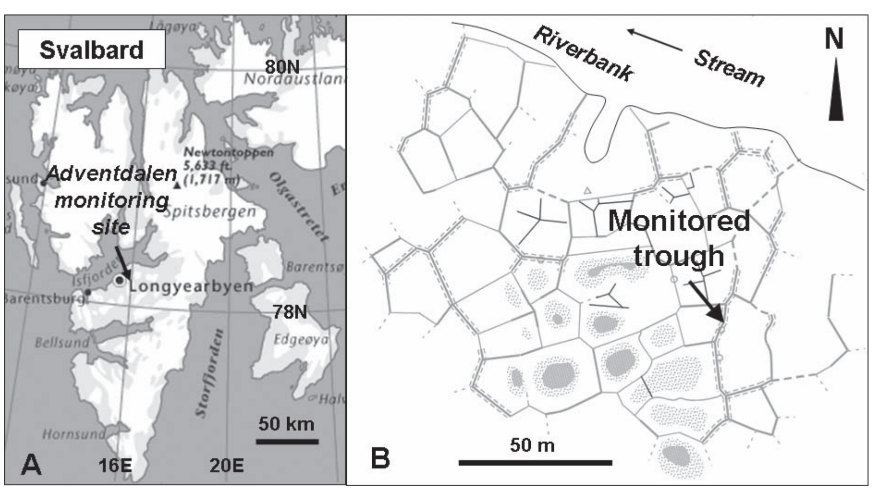

Figure 1. (A) Location map. (B) Polygonal patterns at the monitoring site. Thick solid line: major crack (trough). Thin solid line: secondary crack. Single broken line: tertiary crack. Solid line surrounded by broken lines: trough with well-defined ramparts. Dotted area: bog. Dark area: pond in July 2006.

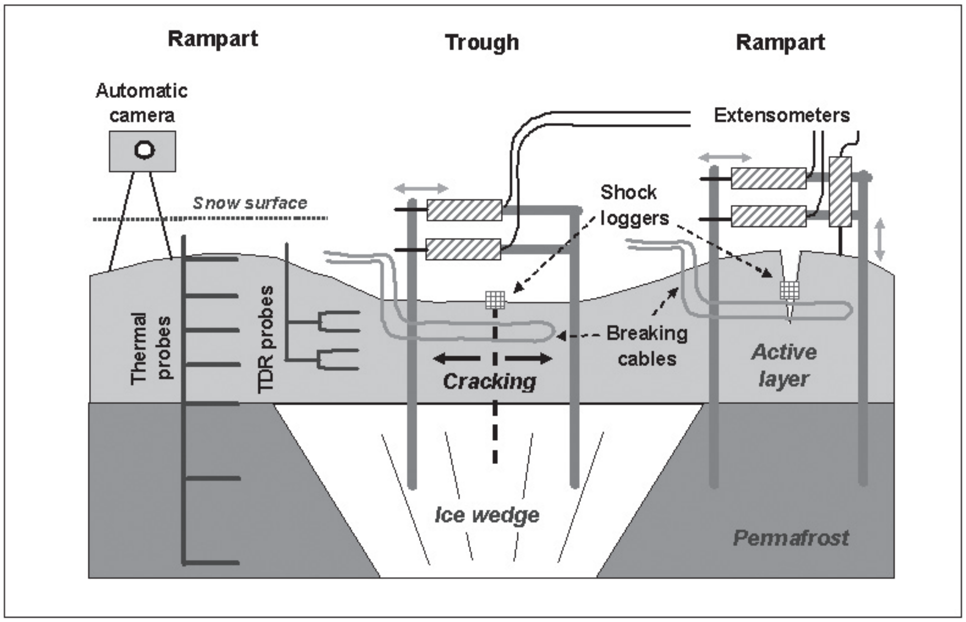

Figure 2. The schema of the automated monitoring system in a section (ca. 5 m wide and 2 m high) across an ice wedge trough with associated ramparts.

1A), where previous investigations report active ice wedge cracking (Christiansen 2005), and field measurements are carried out regularly throughout the year. Low-centered polygons (quadrangles to hexagons) 10–30 m in diameter dominate the ground (Fig. 1B). They are subdivided in places by secondary or tertiary cracks (troughs). The top 1.0 m of the soil consists of fine-grained loess, with the upper 0.5 m rich in organic material. The monitored ice wedge trough is 2.5 m wide and 0.3 m deep, with a rampart on each side. Open cracks develop at the top of the ramparts. Boreholes drilled across the trough showed that the maximum active layer depth (given by the top of the ice wedge) is about 0.95 m, and the ice wedge is about 2.5 m wide at the top.

The mean annual air temperature is -5.3°C and annual precipitation is 192 mm (1986–2006) at the Longyearbyen Airport meteorological station 10 km west of the monitoring site (www.met.no). Large fluctuations in air temperature between 0°C and -20°C to -30°C are common in winter due to the maritime setting with alternations in air masses between low-pressure system coming from the south and polar high-pressure conditions, contrasting with rather stable temperatures (5°C–8°C) in summer.

Instrumentation

Figure 2 illustrates the automatic monitoring system installed in the ice wedge trough and associated ramparts. Soil movements and cracking are monitored with three kinds of instruments. Kyowa extensometers attached to two vertical stakes anchored in permafrost measure horizontal movements across the trough and one of the ramparts at a resolution of 0.04 mm (cf. Matsuoka 1999). The base of the stakes is located at 20–40 cm below the permafrost table. Two extensometers at different heights (0.2 and 0.4 m above the ground) document tilting of the stakes. A vertical extensometer measures frost heave and thaw settlement on the rampart surface. The timing of cracking is monitored hourly by subsurface breaking cables made of very thin copper wires (cf. Mackay 1992) installed at 0.2 and 0.5 cm depth across the trough and in one rampart. Miniature 1-D accelerometers (Tinytag shock loggers, TGP-0605) placed in the top of thermal contraction cracks in the trough (3 loggers), and in the bottom of cracks in the ramparts (4 loggers), provide continuous hourly registration of impacts (e.g., cracking) given by the magnitude of acceleration up to 49 m/s2 at a resolution of 0.2 m/s2. Thermistors measure soil temperatures at 0.02, 0.2, 0.6, 1.0, 1.5 and 2.0 m depths below the top of a rampart every hour. The two deeper thermistors provide temperatures in permafrost and the one at 1.0 m nearly represents the TTOP (temperature at the top of permafrost). Campbell time domain reflectometry (TDR) probes measure the volumetric liquid moisture of the soil at 0.2 and 0.4 m depths below the rampart every six hours. An automatic camera photographs the monitoring site daily to display the snow depth, ground and snow surface conditions.

Following the monitoring of active layer temperatures and snow depth from 2002 (Christiansen 2005), the multi-technique monitoring started in the summer of 2004 (monitoring of the horizontal movement on the rampart started in the 2005 summer). Three years of data have been obtained by the summer of 2007. Most of the sensor-logger systems provided continuous data for the three years. However, problems with data loggers or sensors interrupted data acquisition of permafrost temperatures and vertical soil movement on the rampart in the first year (2004–05), cable breaking on the rampart in the second year (2005–06) and shock events from spring to summer of 2007. A year period is defined here as 365 days from 1 August.

Manual distance measurements have also been carried out since the 2003 summer. Distances between benchmark rods lined across the polygons were periodically measured. The occurrence of new cracks (or recurrence of old cracks) and snow depths are visually inspected all year round.

Results and Interpretations

Soil temperature and moisture

Ground surface temperatures showed significant fluctuations in winter, following air temperatures with minimum time lag (Fig. 3A, B). Such a correlation results from the shallow snow cover, the maximum depth being 5 cm over the ramparts and 30 cm in the troughs. The mean annual TTOP was coldest (-5.2°C) in the first year, followed by the third (-4.2°C) and second (-3.7°C) years.

The first year (2004–05) experienced cold periods in late November with a minimum surface temperature of -25°C and in early March with surface cooling to -33°C. TTOP fell below -10°C only during these two periods, which were separated by a long, relatively warm period.

Figure 3 summarizes results for the later two years (2005–2007), when nearly all datasets were available. The 2005-06 winter on the whole experienced mild climate. However, following a rise to nearly 0°C in mid-January 2006, the ground surface was cooled below -20°C (minimum -23°C) several times in February and March, during which TTOP fell below -10°C (Fig. 3B). The 2006–07 winter was also mild: the surface temperature fell below -20°C only briefly in late January (minimum -23°C) and in early April, and TTOP reached -10°C only in late February.

Water content in the active layer varied seasonally. The unfrozen soil in summer had high and variable contents, whereas the frozen soil in winter had low and stable values (Fig. 3C). The thawed soil at 0.2 m depth showed more varying water contents than at 0.4 m depth. In the 2006 summer, for example, the former experienced a period with relatively low volumetric water contents of 32%–35% from late July to early August, which was preceded and followed by periods with higher water contents of 38–45%, while the water content at 0.4 m depth was nearly stable at 33%–37%. The water content at 0.2 m depth temporarily rose to 62% in the early summer of 2007, reflecting rapid thawing of the soil (cf. Fig. 3B).

Soil deformation and cracking

In the first winter, the horizontal extensometers showed minor seasonal movement (<5 mm) with trough extension in early winter and shrinkage in early summer. Shock loggers located in the trough recorded frequent acceleration events from late February to middle March, when rapid ground cooling resulted in TTOP below -10°C. However, no breaking cables were cut, indicating the absence of cracking in the active layer below the monitored trough. Thus, the shock loggers probably sensed only superficial cracking.

The vertical extensometer recorded frost heave activity within the active layer for the later two years (Fig. 3D). The seasonal frost heave apparently amounted to about 20 mm, but this value probably underestimated the actual amount by about 40 mm, because the lowered level after the annual freeze-thaw cycle in 2005–06 implies upfreezing of the anchored stakes in winter. The lowering was possibly enhanced by deep thaw into the top of ice-rich permafrost during summer. Seasonal thawing was accompanied by two-step settlements in May and August, which presumably originated from thawing of ice-rich layers near the top and bottom of the active layer, respectively (cf. Matsuoka and Hirakawa 2000).

The horizontal extensometers showed, on the whole, opposite movement directions between the trough and rampart (Fig. 3E, F). The trough shrank in early winter and extended in early summer, while the rampart did the opposite at the same time. The symmetrical movements were also confirmed by the manual distance survey of the inter-benchmark distances across several parts of the ice wedge trough and ramparts. The repetition of seasonal movements resulted in interannual expansion of the rampart and contraction of the trough, and the former was about 50% greater than the latter (Fig. 3E, F).

A comparison between horizontal and vertical movements suggests that the crack in the rampart opened during frost heaving in winter and closed during thaw consolidation in summer (Fig. 3D, F). The correspondence was disturbed in early August 2006, during which the rampart crack extended by about 20 mm, while the ground gradually settled. Continuous records of cable breaking were missing, but a manual check of the cable continuity revealed that the two cables in the rampart were cut between 8 July and 16 August, probably due to the crack extension. The crack extension synchronized with the trough shrinkage by about 10 mm. The horizontal movements at both the rampart and trough were nearly stabilized in late August, while the ground significantly settled until seasonal frost heave began.

The horizontal extensometers also indicated temporary tilting of the stakes, as the upper extensometers (0.4 m in height) at both the rampart and trough showed wider annual ranges of horizontal movements than the lower ones (0.2 m) (Fig. 3E, F). The rampart experienced a maximum outward tilting of 1.8° during the third winter, and the trough had a maximum inward tilting of 0.2° during the second winter. Although the direction of tilting changed seasonally, the net outward tilting across the rampart and net inward tilting across the trough cumulated interannually. The former was greater than the latter, which corresponded to the difference in the net rampart extension and trough shrinkage.

The symmetrical movements between the trough and rampart were, however, disturbed in both late winters, during which only the trough extended in response to intensive cooling (Fig. 3E). This movement probably reflected thermal contraction in the frozen soil. The breaking cables in the trough detected cracking only in the second winter (Fig. 3I), although the shock loggers in the trough indicated increasing acceleration when the ground surface cooled rapidly below -15°C in all winters (Fig. 3G). The rampart shock loggers showed significant events which started when the ground

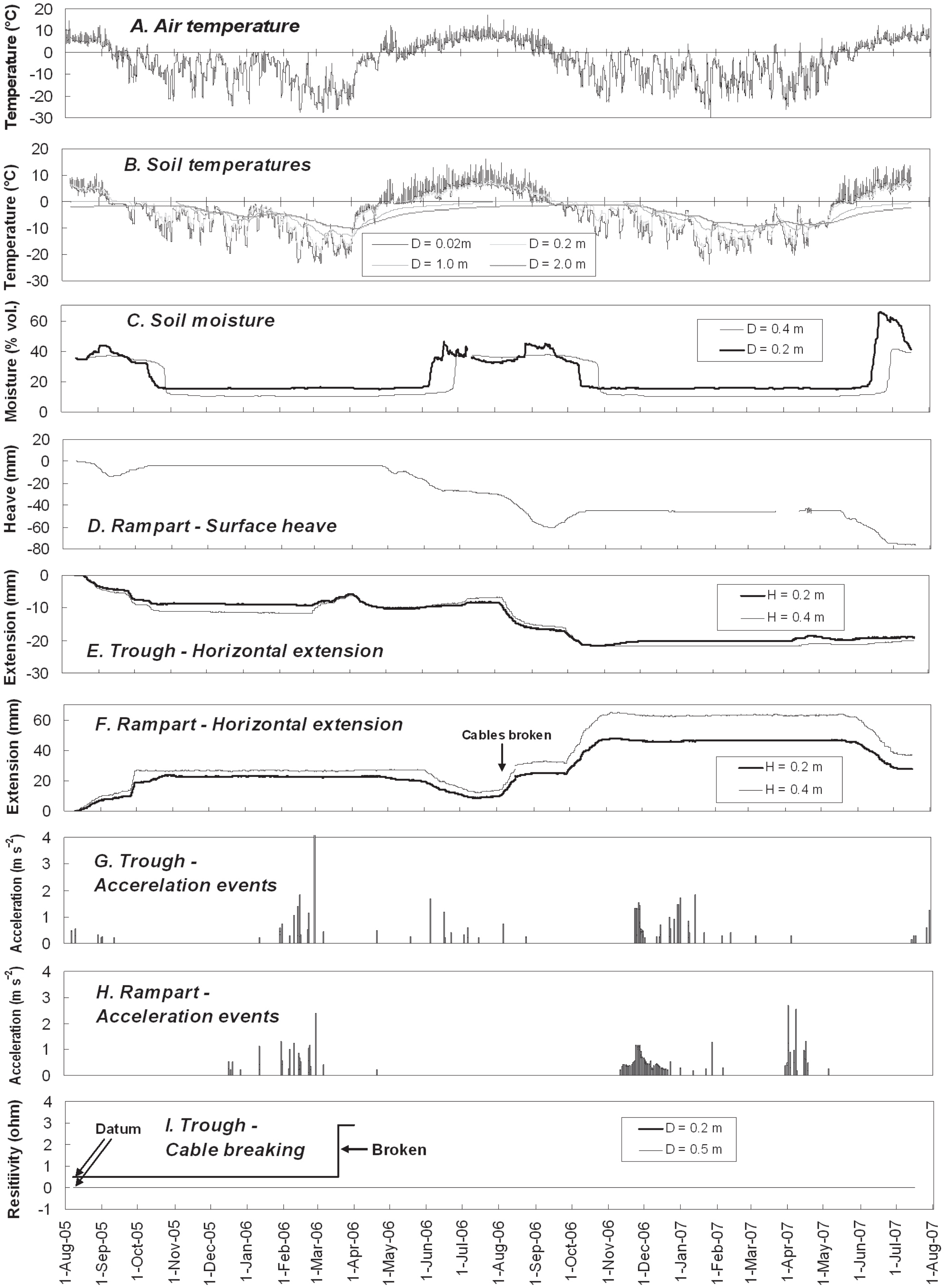

Figure 3. Summary of data from August 2005 to July 2007. The acceleration values in G represent averages of three loggers installed along the monitored trough and those in H averages of four loggers along the rampart. Acceleration values below 0.2 m s^{-2} are removed.

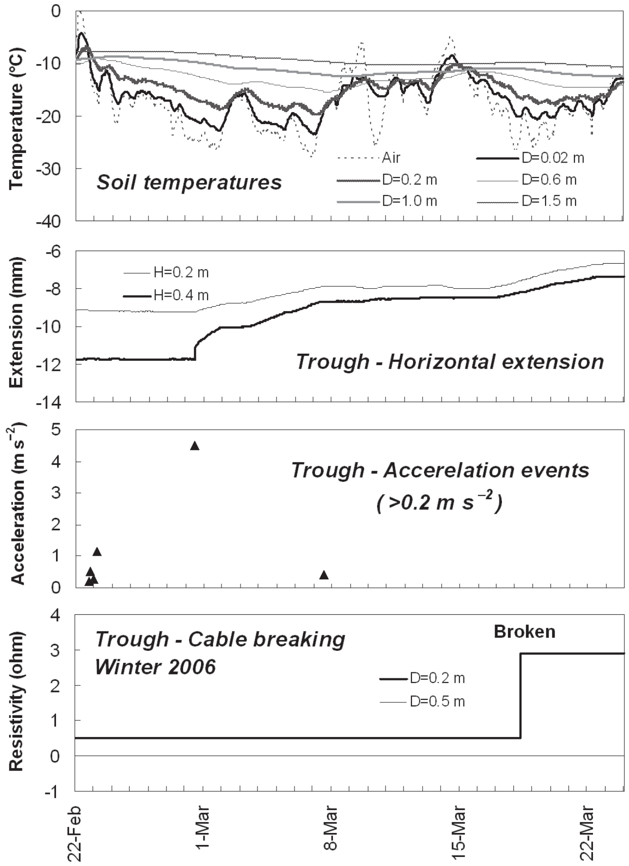

Figure 4. Close-up data in Winter 2006. The acceleration values represent averages of three loggers installed along the monitored trough.

cooled to around -10ºC in mid-December and terminated when the surface temperature became more stable cold around -20ºC in 2006 (Fig. 3H).

All sensors detected cracking in March 2006 (Fig. 4). First, the three shock loggers in the trough recorded frequent and intensifying acceleration events from mid February to early March, which probably indicated increasing superficial cracking starting when the ground had cooled below -10ºC. Next, the horizontal extensometers recorded gradual extension of the trough from 28 February to the end of March, with a relatively stable period in mid March. The copper cable at 0.2 m depth in the trough broke on 18 March, while the deeper cable at 0.5 m depth never broke during the winter. The shock loggers recorded maximum size events on 28 February, but did not record any events on 18 March. The shrinkage of the extensometers in early April (Fig. 3E) indicated the closure of the thermal contraction crack, when the ground started warming significantly (Fig. 3B).

The ground thermal data and visual observations of cracks on the snow surface suggest that a major crack was initiated most likely at the ground surface on 28 February, when the surface temperature fell below -20°C. The crack seems to have propagated gradually into the ground, and up through the snow pack, as the horizontal extension increased, quickest in the beginning (Fig. 4). Interrupted by a warmer and fairly isothermal period in the ground, the crack propagation recurred by rapid cooling and reached below 20 cm depth on 18 March. However, the subsequent termination of the cold period probably prevented further propagation of the crack into the permafrost.

The visual inspection also showed high spatial frequency of new cracks in the second winter. A new crack was actually found on the bottom of the snow-filled monitored trough on 9 April 2006, which supported the cable breaking. Thus, the thermal conditions in March 2006 were favourable for thermal contraction cracking.

In the third winter, similar horizontal movements were reproduced, but only minor late winter extension of the trough was recorded (Fig. 3E). The copper cables did not break. The shock loggers were not operating when the small horizontal extension in the trough occurred, but they did record activity, when ground temperatures first cooled below -10ºC in December. Visual inspection showed the generation of many fewer cracks than in 2006.

Discussion and Perspectives

Distance changes recorded with the vertical and horizontal extensometers and the benchmark poles are likely to reflect, primarily, seasonal thermal deformation and frost heave activity in the polygon and ice wedge trough system. In fact, the crack on the rampart opens during frost heaving in winter and closes during consolidation in summer (Fig. 3D, F). This relation is temporarily disturbed in mid summer, when opening of the rampart crack coincides with ground settlement. Corresponding to the highest near-surface temperatures, this movement appears to originate from thermal expansion in the rampart. The effect of soil moisture change is unclear but can not be ruled out, because the crack extension and subsequent stabilization in summer correspond, respectively, to relatively low water content and to raised water content at 0.2 m depth (Fig. 3C, E): the former possibly indicates crack opening by desiccation.

The symmetrical movements between the rampart and the trough indicate that the seasonal deformation within the active layer below a pair of ramparts basically constrains the deformation of the intervening trough. Before opening of thermal contraction cracks, superficial cracking is generated when the ground cools below around -10ºC, as recorded with the shock loggers. During mid to late winter, however, rapid ground cooling leads to intensive thermally-induced contraction in the frozen ground which has already cooled below -10ºC. The ground contraction induces extension of the trough when the surface temperature falls below -20°C, and crack activity is intensified when TTOP cools below -10°C. If the cold period is lasting for three weeks, a crack will propagate down below 0.2 m and possibly deeper into the ground. During the observed three years, however, the monitored trough did not experience intensive and long-lasting cooling enough to permit cracking into the permafrost. As a result, the ice wedge did not grow. Cracking reaching the ice wedge in the monitored trough most likely requires more rapid and/or intensive cooling, for instance, TTOP below -15°C (e.g., Allard & Kasper 1998, Matsuoka

1999, Fortier & Allard 2005). These results, however, do not exclude the possible occurrence of ice wedge cracking in other troughs at the study site. In fact, excavation of troughs with a number of new cracks in early summer displayed an ice veinlet on the frost table at 0.3–0.5 m depth.

The combination of various techniques presented here enables us to detect seasonal soil deformation and winter thermal contraction cracking activities, including superficial cracking, pre-cracking tensional soil deformation and major, deeper cracking. The observations show that, even in an overall warm winter, temporary intensive cooling can induce significant thermal contraction cracking of the active layer. However, the three years seem to have lacked large-magnitude cooling in combination with long-lasting cold periods which could cause ice wedge growth. This may be due to the recent relatively warm winters, in addition to the maritime Svalbard climate preventing long-lasting cold periods. Acquisition of the detailed critical thermal conditions for ice wedge growth probably requires widely distributed monitoring systems, as well as long-term, continuous monitoring over a decade or more.

The presented ice wedge monitoring system forms part of the project on "standardizing field techniques and constructing a global monitoring network for periglacial processes" that are involved in the activities of the International Permafrost Association Working Group "Periglacial Landforms, Processes and Climate." It will also form part of the periglacial process monitoring in the permafrost observatories that are being established in Svalbard during the International Polar Year in the "Permafrost Observatory Project: A Contribution to the Thermal State of Permafrost" IPY project.

Acknowledgments

The study was financially supported by the Grants-in-Aid for Scientific Research (grant no. 17300294, 19650220) from the Japan Society for the Promotion of Science and by funding from the University Centre in Svalbard. Some of the ice wedge measurements from 2007 are part of the International Polar Year project, "Permafrost Observatory Project: A Contribution to the Thermal State of Permafrost in Norway and Svalbard," supported by the Research Council of Norway (grant no. 176033/S30). We acknowledge field assistance by Ole Humlum, Andreas Kellerer-Pirklbauer, Michael Avian, Lene Kristensen, Mamoru Ishikawa, Atsushi Ikeda, and Tatsuya Watanabe. Thanks to the two anonymous reviewers and the review editor for constructive comments.

References

Allard, M. & Kasper, J.N. 1998. Temperature conditions for ice-wedge cracking: field measurements from Salluit, Northern Québec. *Proceedings of the Seventh International Conference on Permafrost, Yellowknife, Canada, June 23–27, 1998*: 5-12.

Christiansen, H.H. 2005. Thermal regime of ice-wedge cracking in Adventdalen, Svalbard. *Permafrost and Periglacial Processes* 16: 87-98.

Fortier, D. & Allard, M. 2005. Frost-cracking conditions, Bylot Island, eastern Canadian Arctic archipelago. *Permafrost and Periglacial Processes* 16: 145-161.

Kokelj, S.V., Pisaric, M.F.J. & Burn, C.R. 2007. Cessation of ice-wedge development during the 20th century in spruce forests of eastern Mackenzie Delta, Northwest Territories, Canada. *Canadian Journal of Earth Sciences* 44: 1503-1515.

Lachenbruch, A.H. 1962. Mechanics of thermal contraction cracks and ice-wedge polygons in permafrost. *Geological Society of America,* Special Paper 70: 1-69.

Mackay, J.R. 1992. The frequency of ice-wedge cracking (1967–1987) at Garry Island, western Arctic coast, Canada. *Canadian Journal of Earth Sciences* 29: 236-248.

Mackay, J.R. 2000. Thermally induced movements in ice-wedge polygons, western Arctic coast: a long-term study. *Géographie Physique et Quaternaire* 54: 41-68.

Mackay J.R. & Burn, C. 2002. The first 20 years (1978–1979 to 1998–1999) of ice-wedge growth at the Illisarvik experimental drained lake site, western Arctic coast, Canada. *Canadian Journal of Earth Sciences* 39: 95-111.

Matsuoka, N. 1999. Monitoring of thermal contraction cracking at an ice wedge site, central Spitsbergen. *Polar Geoscience* 12: 258-271.

Matsuoka, N. & Hirakawa, K. 2000. Solifluction resulting from one-sided and two-sided freezing: field data from Svalbard. *Polar Geoscience* 13: 187-201.

Plug, L.J. & Werner, B.T. 2001. Fracture networks in frozen ground. *Journal of Geophysical Research* 106: 8599-9613.

Recent Decade Thaw-Depth Dynamics in the European Russian Arctic, Based on the Circumpolar Active Layer Monitoring (CALM) Data

Galina Mazhitova
Komi Science Center, Russian Academy of Sciences, Syktyvkar, Russia
Galina Malkova
Earth Cryosphere Institute, Russian Academy of Sciences, Moscow, Russia
Olga Chestnykh
Dmitry Zamolodchikov
Center for Ecology and Productivity of Forests, Russian Academy of Sciences, Moscow, Russia

Abstract

Nine-to-twelve-year-long records of thaw-depth monitoring from three 100x100-meter grids in the European Russian Arctic are discussed. The grids belong to the Circumpolar Active Layer Monitoring (CALM) network. In agreement with a warming trend in air temperatures, thaw depths increased almost continuously in the discontinuous permafrost zone and fluctuated with an increasing trend in the continuous permafrost zone. The increases in thaw depth were followed by changes in seasonal thaw patterns. Of climatic indices, the thawing index was best correlated with thaw depths. Differential ground subsidence, as measured at one of the grids, constituted 43% of the thawed permafrost layer and visibly changed the site topography. Statistical analyses highlighted moss and the soil organic layer as limiters of thaw depth with their effect weakening as the thaw increases.

Keywords: active layer; climate warming; ground subsidence; permafrost; thawing index.

Introduction

Numerous publications show climate warming in the Arctic including its Russian sector (e.g., Pavlov & Ananjeva 2004). Circumpolar Active Layer Monitoring (CALM) was organized to trace changes in the active layer (thaw) depth induced by the warming and to study climatic controls over the thaw depth. Over 100 CALM grids employ a common measurement protocol ensuring statistical reliability of results. Ground subsidence, as a hazardous consequence of the active layer thickening, is monitored at many grids.

Three 100x100-m grids operate in the European Russian Arctic with the record length from 9 to 12 years. Intermediate monitoring results were published elsewhere (Mazhitova et al. 2004). In this paper, we discuss longer-term trends based on the CALM measurements.

Materials and Methods

Site descriptions

The Bolvansky grid (68°17.3′N, 54°30.0′E) is located in the continuous permafrost zone, whereas Ayach-Yakha (67°35.4′N, 64°09.0′E) and Talnik (67°19.8′N, 63°44.0′E) are in the discontinuous permafrost zone (Fig. 1). By fall 2007, records were 9-, 12-, and 10-years long, respectively. Soils are upland loamy with 5- to 21-cm thick organic horizons. Altitudes range within 5 m at each grid. Permafrost temperatures at the depth of zero annual temperature amplitude range from -0.6 to -2.5°C. End-of-season thaw depths averaged for the period of observation were 110 cm at Bolvansky, 116 cm at Talnik, and 74 cm at Ayach-Yakha. At Bolvansky and Talnik, local closed taliks occur, occupying a few grid nodes and fluctuating in area from year to year.

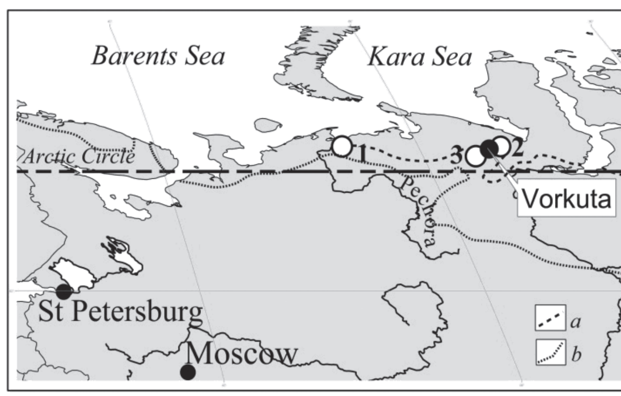

Figure 1. Location of Bolvansky (1), Ayach-Yakha (2), and Talnik (3) CALM grids in the European Russian Arctic. Southern borders of the continuous (a) and the discontinuous (b) permafrost zones are shown.

Field procedures

The European Russian CALM sites employ the standard systematic sampling design recommended under the CALM program (Brown et al. 2000). Permanent grids have been established with 10-m intervals between grid nodes. Grid dimensions are 100 x 100 m at Talnik and Bolvansky and 100 x 90 m at Ayach-Yakha. The nodes are marked with permanent stakes. Thaw depths are determined through 4 replicated measurements at each grid node. Measurements are conducted annually at the end of the warm season with the use of a graduated steel rod. Permafrost at all sites is cemented by ice, and hard enough to avoid errors due to rod penetration into it.

Besides the standardized measurements, additional datasets have been obtained for each grid. These sets differ depending on accessibility and other site-specific characteristics. At Talnik and Ayach-Yakha, seasonal thaw-depth dynamics are monitored through several measurements during the warm season. The same operations are performed at Bolvansky with a lesser number of field sessions due to difficulty of access. At Ayach-Yakha, snow depths are measured at each grid node annually in April. Volumetric water content in the surface soil horizon is determined for each grid node annually at the end of the warm season. At Ayach-Yakha and Talnik, where the portable Vitel Hydra® probe is used for the purpose, water content is determined several more times during the season. Air temperatures at a height of 2 m, as well as soil and upper-permafrost temperatures are recorded at all sites with the use of miniature Onset® data loggers. Permafrost temperatures at the depth of zero annual amplitude are measured in 3 boreholes at Bolvansky. Ground subsidence and/or heave are determined at Ayach-Yakha for each grid node annually at the beginning and at the end of the warm season with the use of a 2H-10KL leveling instrument (Russia) providing for 4 mm accuracy. A benchmark of the national geodetic network located near the grid is used as a base. At the same grid, angular displacement of several permanent pegs is measured to trace downslope ground movements. Moss and soil organic layer thicknesses at each grid node, vegetation maps, and soil descriptions are available for each grid.

Analytical procedures

The thawing index DDT (°C days) was calculated by summing average daily air temperatures for the period, beginning with positive daily averages and ending either with negative daily averages or on the day of grid probing, depending on the purpose. The freezing index FDD (°C days) was calculated by summing negative daily averages. ANOVA was conducted using the General Linear Models module of STATISTICA, version 7.2, software (©StatSoft, Inc).

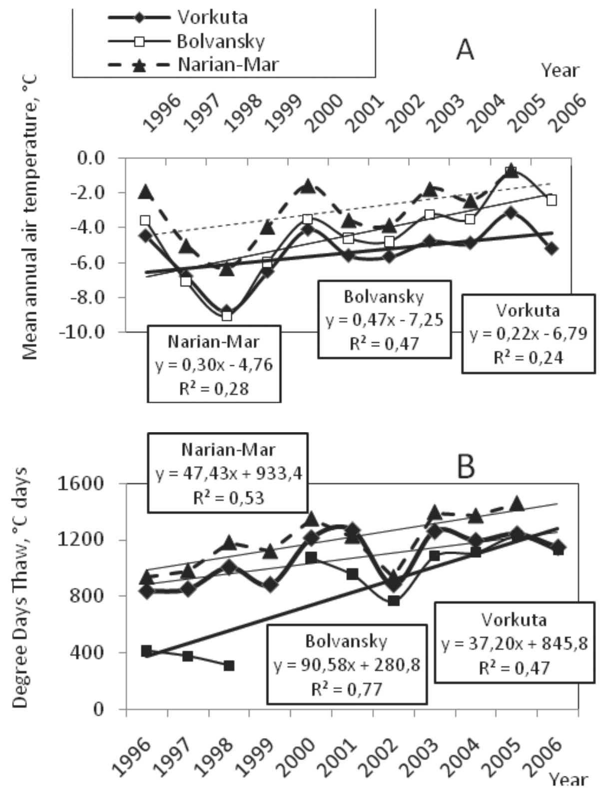

Figure 2. Mean annual air temperature (A) and Degree Days Thaw (B) dynamics during the period of CALM observations at the weather stations nearest to the grids. For Bolvansky, where the weather station was closed in 1999, the values measured at the CALM site are given for 1999–2007.

Results

Climate dynamics

Mean annual air temperature in the European Russian North rhythmically fluctuated during the 20th century, whereas in 1980–2006, showed an increasing trend with 0.02–0.05°C year^{-1} increments (Fig. 2, A). The increments were smaller than those registered in Siberia, where they amounted to 0.08°C year^{-1} (Pavlov & Ananjeva 2004). Mean annual air temperature dynamics during the period of CALM observations at the weather stations nearest to the grids is shown on Figure 2, A. During the same period, increasing trends in the thawing index were observed also (Fig. 2, B). Increases in permafrost temperature at the depth of zero annual temperature amplitude ranged from 0.003 to 0.06°C year^{-1} (Oberman & Mazhitova 2001, Pavlov et al. 2002).

Thaw-depth dynamics

At Ayach-Yakha and Talnik, grid-averaged end-of-season thaw depths showed almost continuous increase during the observation period with average annual increments of 2.3 and 5.5 cm, respectively. At Bolvansky, an increase in thaw depth was not continuous, yet had an increasing trend significant at p = 0.01 level with 1.7-cm annual increments (Fig. 3). Linear trend parameters were as follows: Ayach-Yakha y = 2.32x + 58.52, R^2 = 0.91; Talnik y = 5.51x + 74.38, R^2 = 0.94; Bolvansky y = 1.69x + 97.87, R^2 = 0.66.

Correlation between thaw depths and climatic indices

Thaw-depth dynamics duplicated dynamics of no one climate index; however, the increasing trends in thaw depths agreed with also-increasing, though less-significant, trends in mean annual air temperatures. Regressions of grid-averaged thaw depths by DDT$^{0.5}$ representing a form of Stefan solution (Boyd 1973) were widely used in the active layer modeling. The approximations are highly reliable for all 3 grids with R^2 equal to 0.87–0.92 when not only end-of-season thaw-depth values are used, but also those obtained earlier in the warm season (Fig. 4, A). With only end-of-season values considered (Fig. 4, B), the approximation reliability is obviously higher (significant at $p < 0.01$) for the Bolvansky grid located in the continuous permafrost zone than for the 2 grids located in the discontinuous permafrost zone ($p < 0.05$ for Ayach-Yakha and $p < 0.10$ for Talnik). No significant correlation was found with annual precipitation, liquid precipitation, snow depth, or freezing index. For example,

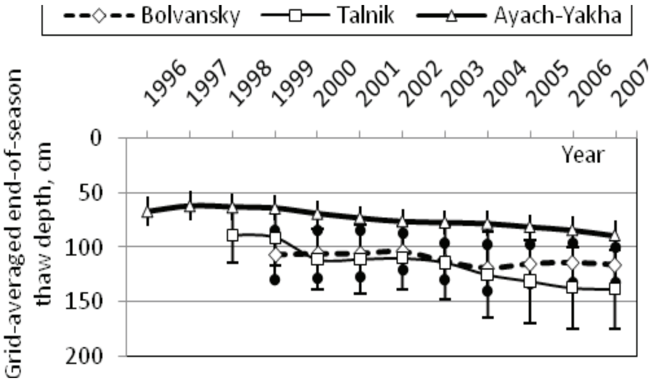

Figure 3. Statistical representation of the end-of-season thaw-depth dynamics at the CALM grids. Values are averages of 484 measurement points at Bolvansky and Talnik, and of 396 measurement points at Ayach-Yakha. One standard deviation extends in either direction.

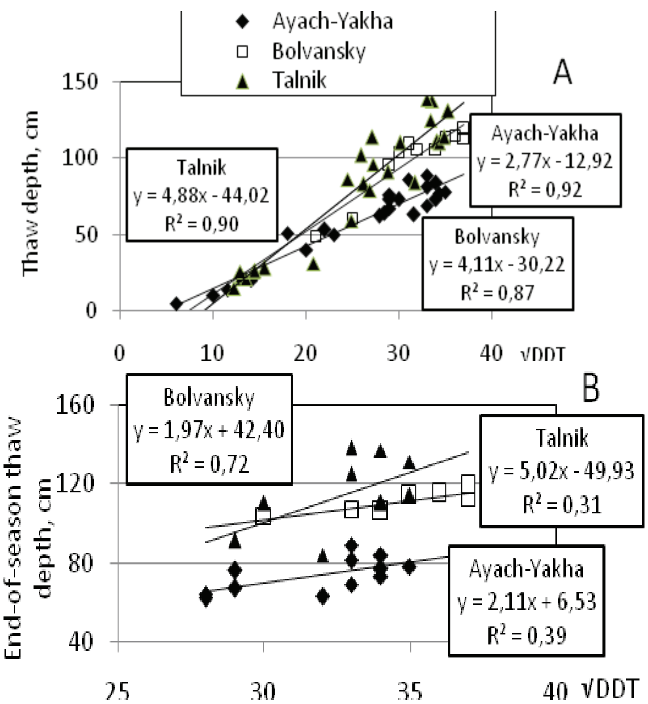

Figure 4. Thaw depth (A) and end-of-season thaw depth (B) plotted against the square root of the thawing index at the three European Russian CALM grids.

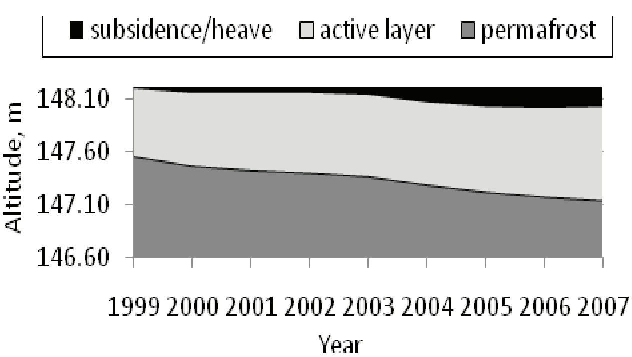

Figure 5. Inter-year dynamics of permafrost table, soil surface subsidence/heave, and active layer thickness at the Ayach-Yakha CALM grid. Grid-averaged altitudes are given for each year.

correlation between freezing index and thaw depth was insignificant ($p > 0.10$) for both Ayach-Yakha with its longer record (correlation coefficient R = 0.64) and Bolvansky with a shorter record (R = 0.01). Node-specific snow depths averaged for the period of observations at Ayach-Yakha showed no significant correlation with node-specific thaw depths averaged for the same period (R = -0.19, $p > 0.10$); similarly, annual site-averaged snow depths were not correlated with annual site-averaged thaw depths (R = 0.52, $p > 0.10$).

Ground heave/subsidence

Thawed or active layer thickness is a function of the permafrost table dynamics and ground heave/subsidence. Interrelations between the 3 indices were studied at the Ayach-Yakha grid. From 1999 to 2007, when these indices were monitored, the permafrost table sank annually at most grid nodes so that the decrease in its grid-averaged altitudes totaled 40 cm (StD 20 cm) by the end of the observation period (Fig. 5). The permafrost layer which had thawed seemed a transient-layer thawing and refreezing under long-term climatic fluctuations (Shur et al. 2005). It had volumetric ice content of 40–50%, higher pH values than those in the active layer, and relatively high organic matter content due to cryoturbations. Because of high ice content in the uppermost permafrost, the permafrost table sinking was followed by ground subsidence. In 1999–2006, the subsidence compensated for winter heave, and in most years its values were nearly proportional to the thickness of the newly thawed permafrost layer (Mazhitova et al. 2004). In 2007, however, though the permafrost table sank farther down, subsidence, for the first time, did not compensate for winter heave at most grid nodes and on grid-average. In that year, thaw at many grid nodes reached the contact between the superficial loess-like loam and the underlying till, and for the first time during the observation period, minor downslope movements of the ground were registered. Three of five reference pegs were found to move 2 cm downslope. In total, from 1999 to 2007, the grid subsided an average of 17 cm (StD 9 cm), with annual increments varying from 7-cm subsidence to 2-cm heave. Grid-averaged end-of-season thaw depth increased by 23 cm (StD 11 cm). Given 40 cm of permafrost table sinking, if we assess the latter based on the increase in thaw depth, only without considering subsidence, it would be 43% underestimated (23 cm instead of 40 cm).

Topographic changes

At Ayach-Yakha, changes in soil-surface and permafrost-table topography due to multi-year differential subsidence/heave were monitored in 1999–2007. Initial surface topography was represented by a 3° slope with a shoulder in the middle part of the grid. Smaller landforms were local rises, dips, and a hollow with several transverse partitions crossing the grid. Permafrost table topography mostly duplicated the soil surface topography; however, the range of altitudes was 30 to 40% wider. Only slightly heaved active frost boils occupying 3% of the grid area demonstrated the opposite pattern with the permafrost table mirroring soil-surface to-

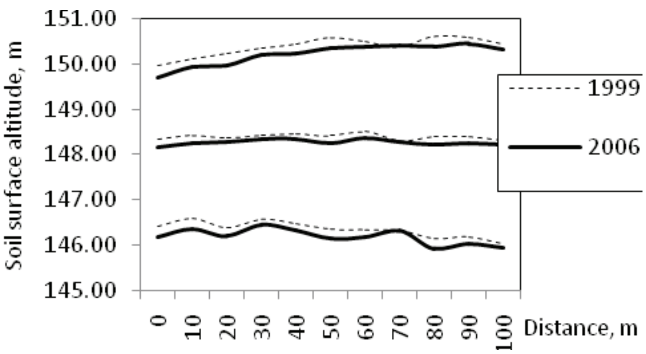

Figure 6. Changes in soil surface topography due to differential subsidence/heave as exemplified by three cross-sections through the Ayach-Yakha CALM grid.

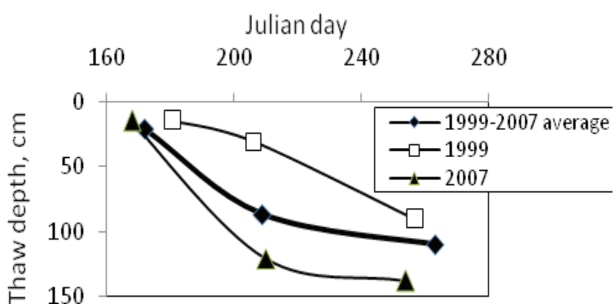

Figure 7. Inter-annual changes in seasonal thawing pattern at the Talnik CALM grid.

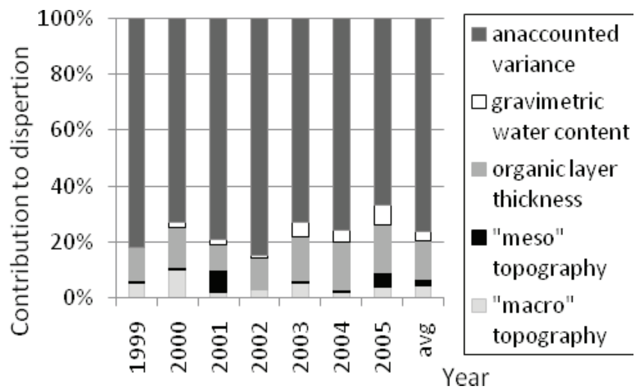

Figure 8. Components of the end-of-season thaw-depth variance at the Ayach-Yakha CALM site.

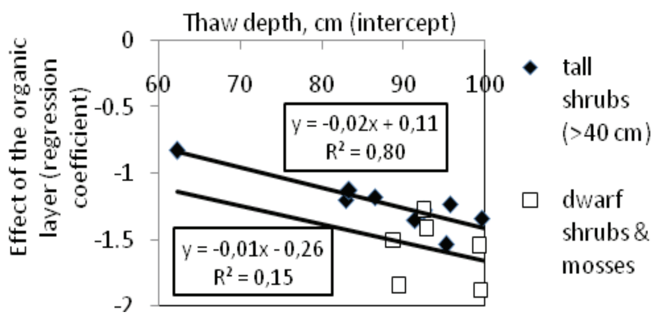

Figure 9. Moss/peat layer effect on thaw depth versus actual thaw depth expressed as the intercept and the coefficient of multiple linear regression, respectively. The independent variables included in the regression were the same as on Figure 8.

pography under them. In total, node-specific deviations of permafrost-table and soil-surface altitudes from the corresponding 2-dimentional linear surfaces modeled with the use of the least square regressions were correlated with R = 0.91. From 1999 to 2007, spatially-differential permafrost sinking changed the permafrost table topography. As the node-specific sinking values were well-correlated with subsidence values, soil surface topography changed accordingly (Fig. 6).

Changes in seasonal thawing pattern

Climate-induced intensification of the thawing process led to evident changes in seasonal patterns. As an example, seasonal thaw-depth dynamics in years with contrast weather conditions are presented for the Talnik grid (Fig. 7).

In 1999 (shallow thaw), thaw depth in late July was only 34% of the end-of-season value. The same value in 2007 (deepest thaw) was 87%. Late July thaw depth, averaged for the period of observations, was 75% of the end-of-season value. The displacement of maximal seasonal thawing rates to the earlier part of the warm season can be concluded.

Components of the thaw depth spatial variance

For the Ayach-Yakha grid, ANOVA under the General Linear Model approach was performed to reveal landscape predictors of thaw depth. Analyzed was the 1999–2005 period, since 1999 altitudes of all grid nodes were measured annually; the 2006–2007 data were not yet processed. Continuous independent variables were (1) surface "macro" topography (altitudes of grid nodes, range width 5 m); (2) surface "meso" topography (deviations of grid node altitudes from the 2-dimentional linear slope approximating the site surface, range width 1.2 m); (3) end-of-season volumetric water content in the upper soil layer, values from 10 to 82 %; and (4) organic (dense moss + peat) layer thickness, values from 4 to 21 cm. A categorical variable was (5) vegetation class (dwarf-shrub/moss versus tall shrubs). Sample size was 396 thaw depth; i.e., dependent variable, values (4 at each of 99 grid nodes) measured annually during 7 years; 99 annual measurements of dynamic independent variables 1–3, and 396 measurements of the organic layer thickness (4 at each of 99 grid nodes) conducted once.

In different years the examined factors explained in total from 18 to 33% of the end-of-season thaw-depth variability, with the organic-layer thickness explaining the largest portion of the latter compared to other variables (Fig. 8).

The effect of the organic layer was sensitive to thaw depth; it weakened as the latter increased, showing a linear trend significant at $p = 0.01$ for the vegetation class of tall (>40 cm) shrubs typical of the southern tundra (Fig. 9).

Discussion

Three European Russian CALM grids demonstrated increasing trends in the depth of thaw during the recent decade. In 2007 compared to 1999, the latter being the first year when all 3 grids were in operation in the discontinuous permafrost zone, thaw depths increased by 40% at Ayach-Yakha with its shallow thaw and by 51% at Talnik with deep thaw. The Bolvansky grid in the continuous permafrost zone, also with a deep thaw, showed only 9% increase, but still a high level of the trend significance: R^2 0.7 versus 0.9 at the 2 other grids. Given synchronous air temperature dynamics over the region as shown by weather stations, grid locations in dominant upland landscapes, and the maximum distance between the grids as large as 400 km, it is likely that the 3 records represent the main regional trend in thaw depth.

In the region under discussion, permafrost monitoring is conducted by the geological service. Thaw depths are mostly estimated indirectly based on ground temperature measurements at several depths. Only selected monitoring data were published. It was reported that from 1975–1995, thaw depths increased all over the region with exceptions registered at drained lake beds and technogenic sites (Oberman & Mazhitova 2001). For 1980–2003, data from 3 boreholes located at the Vorkuta field station 60 km south-west from the city of Vorkuta (see Fig. 1) were published (Pavlov et al. 2004). The authors, however, mentioned that more sites had been monitored during the same period and that, on average, a slightly increasing trend in thaw depths was observed. Still, the 3 selected records show different thaw-depth trends from 1999–2003: stability, increase, and decrease. Surprisingly, in the preceding 19 years the same sites demonstrated synchronous dynamics. On the whole, the bulk of our and other authors' data suggest that the increase in thaw depth was the dominant, though not universal, trend in the region during the recent 3 decades.

Correlation between thaw depth and climatic indices is widely discussed in the literature. As was shown above, at the 3 European Russian CALM grids end-of-season thaw depths were correlated with the thawing index at significance levels from $p = 0.01$ to $p = 0.10$. The R^2 values of corresponding linear regressions were 0.31–0.39 for the 2 sites located in the discontinuous permafrost zone. The value reported from the aforementioned Vorkuta field station located in the same zone is 0.44, based on the 1988–2003 period and a larger number of sites (Pavlov et al. 2004). During the period of our observations, the range of thawing index values composed 70% of its long-term range displayed by the 1947–2006 record of the Vorkuta weather station. Not represented were extremely cool summer seasons, whereas the extremely warm seasons responsible for thaw-depth jumping (Shur et al. 2005) were fully represented. The range of annual precipitation composed 80% and liquid precipitation 60% of the corresponding long-term ranges. These estimates show that the observation period covered most, though not all, of the long-term variability of climate indices. Still, thaw depths showed no statistically significant correlation with precipitation, snow depth, freezing index, or water content in the uppermost soil layer. Thawing index then seems to be the major control on thaw depth at present though under climatic warming. As other indices exceed the bounds of their natural variability, their effect on thaw depths can strengthen.

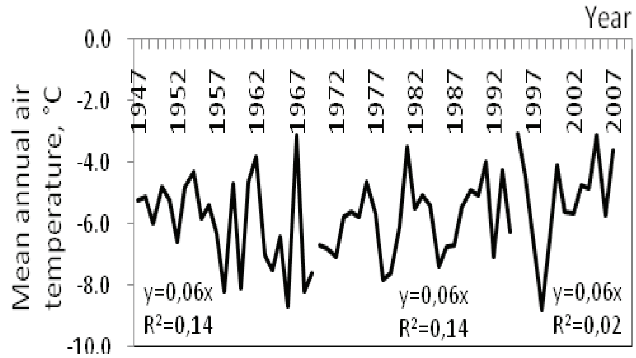

Figure 10. Trends in mean annual air temperature at the Vorkuta weather station. From left to right: a cooling branch of the assumed half-century climatic cycle, a warming branch of the same cycle, and the trend of recent 12 years.

Correlation between thaw depths and thawing index was confirmed by a large number of regressions based on long-term meteorological records from Siberia (Frauenfeld et al. 2004). Monitoring results from numerous CALM grids located in the Kolyma lowland in East Siberia (Fedorov-Davydov et al. 2004) showed that thaw depths were correlated with mean summer temperatures at upland landscapes and were not at intra-zonal landscapes. It is possible that the transitional position of most monitored sites explains the absence of the thawing index–thaw-depth correlation in Yakutia (Pavlov et al. 2004). North American data (Hinkel & Nelson 2003) suggest that thaw-depth response to air temperature forcing is best described by Markovian algorithm with a leading role of extremely warm or cool summer seasons in thaw-depth dynamics.

It is known that the lack of reliable climatic scenario impedes a climate change impacts assessment. Pronounced effects of natural climatic variability on permafrost conditions in the study region were reported. The monitoring conducted by the geological service showed effects of the warming branch of about a half-century climatic cycle (Oberman & Kakunov 2002, Oberman & Mazhitova 2003). A cooling branch, which onset was expected since the mid-1990s, did not show; however, instead, an insignificant ($p > 0.10$) warming trend was observed (Fig. 10).

A climatic scenario was developed for the study region by P. Kuhry using the HadCM2S750 model (Mazhitova et al. 2004). The modeling took into account a natural climatic variability signal and assumed gradual CO_2 increase in the atmosphere during the 21st century with stabilization at the 750 ppm level. The outcome was a lack of trend during the first quarter of the 21st century with further rapid warming by 3°C by 2085. Thaw depths, as modeled based on this scenario (V. Romanovsky in the same paper), were characterized by 30%-of-the-mean fluctuations during the first quarter of the 21st century, followed by an increase with talik formation in the mineral soil and peatland in 15 and in 70–75 years after the start of warming, respectively. During the recent decade, our observations and those of other authors agreed better with the modeled trend than with the trend expected under the superiority of natural climatic variability.

CALM design ensures high precision of major indices determination. At Ayach-Yakha, thaw depth was correlated with thawing index with the grid-averaged correlation coefficient (R) value of 0.36. However, R values were above the average (up to 0.6) at grid nodes located at even and convex micro-sites, whereas below the average and often negative (-0.6 to 0.2) at concave micro-sites. From the CALM grids in Yakutia, higher inertance of the thaw depth was reported for concave compared to convex micro-sites (Fedorov-Davydov et al. 2004). These examples highlight advantages of the CALM statistical approach and warn about possible errors of point measurements.

Conclusions

A climate warming signal in the European Russian Arctic, though weaker than that in Siberia, exerts itself on the sensitive high-temperature permafrost. Depths of seasonal ground thaw show increasing trends especially clear in the discontinuous permafrost zone. Potential increases in active layer thickness which could result from the sinking of permafrost table are partly consumed by ground subsidence. Thawing index correlates with seasonal and inter-annual thaw-depth dynamics in the greatest degree compared to other climatic indices. At present, permafrost is still protected from rapid thaw by a high-icy transient layer and the insulating effect of moss/peat layer. Regressions obtained, however, show that the latter effect weakens with the active layer thickening. Together with passing the threshold of the transient layer, this can lead to acceleration of thaw in the nearest future if the warming trend persists. Continuation of the monitoring with special regard to developing proper up-scaling methods is highly desirable.

Acknowledgments

The study was funded by the NSF through the grants OPP-9732051 and OPP-0352958. Help in the fieldwork and with data processing was provided by Drs. D. Drozdov, D. Karelin, D. Kaverin, and E. Vanchikova, and Mr. A. Kalmykov. Dr. J. Kimble upgraded the English.

References

Boyd, D.W. 1973. Normal freezing and thawing degree-days for Canada: 1931-1960. *Environment Canada.* Atmospheric Environment Service, Downsview, Ontario, Publication CLI 4-73, 1973, 38 p.

Brown, J., Hinkel, K.M. & Nelson, E.F. 2000. The Circumpolar Active Layer Monitoring (CALM) program: Research designs and initial results. *Polar Geography* 24(3): 165-258.

Fedorov-Davydov, D.G., Davydov, S.P., Davydova, A.I., Zimov, S.A., Mergelov, N.S., Ostroumov, V.E., Sorokovikov, V.A., Kholodov, A.L. & Mitroshin, I.A. 2004. Spatial-temporal patterns of seasonal soil thaw in the north of the Kolyma lowland. *Kriosfera Zemli* VIII(4): 15-26 (in Rusian).

Frauenfeld, O.W., Zhang, T., Barry, R.G. & Gilichinsky, D. 2004. Interdecadal changes in seasonal freeze and thaw depths in Russia. *Journal of Geophysical Research* 109, D05101, doi:10.1029/2003JD004245.

Hinkel, K.M. & Nelson, F.E. 2003. Spatial and temporal patterns of active-layer thickness at Circumpolar Active-Layer Monitoring (CALM) sites in Northern Alaska, 1995-2000. *Journal of Geophysical Research* 108(102) (D2).

Mazhitova, G., Malkova (Ananjeva), G., Chestnykh, O. & Zamolodchikov, D. 2004. Active layer spatial and temporal variability at European Russian Circumpolar-Active-Layer-Monitoring (CALM) sites. *Permafrost and Periglacial Processes* 15: 123-139.

Mazhitova, G., Karstkarel, N., Oberman, N., Romanovsky, V. & Kuhry, P. 2004. Permafrost and infrastructure in the Usa basin (Northeast European Russia): Possible impacts of Global Warming. *Ambio* 33(6): 289-294.

Oberman, N.G. & Mazhitova, G.G. 2001. Permafrost dynamics in the northeast of European Russia at the end of the 20th century. *Norsk Geografisk Tidsskrift–Norwegian Journal of Geography* 55(4): 241-244.

Oberman, N.G. & Kakunov, N.B. 2002. Monitoring of ground waters of the cryolithozone in the European part of Russia and the Urals. In: V.G. Balobaev & V.V. Shepelev (eds.), *Monitoring of Ground Waters of the Cryolithozone.* Institute of Geocryology, Yakutsk, 18-43 (in Russian).

Pavlov, A.V., Ananjeva, G.V., Drozdov, N.G., Moskalenko, N.G., Dubrov, V.A, Kakunov, N.B., Minailov, G.P., Skachkov, Y.B. & Skriabin, P.N. 2002. Monitoring of the active layer and permafrost temperatures in the north of Russia. *Kriofera Zemli* VI(4): 30-39 (in Russian).

Pavlov, A.V. & Ananjeva, G.V. 2004. Assessment of recent air temperature changes in the territory of the cryolithozone of Russia. *Kriosfera Zemli* VIII(2): 3-9 (in Russian).

Pavlov, A.V., Skachkov, A.B. & Kakunov, N.B. 2004. Inter-relations between multi-year changes in seasonal ground thaw and meteorological factors. *Kriosfera Zemli* VIII(4): 3-11 (in Russian).

Shur, Y., Hinkel, K.M. & Nelson, F.E. 2005. The transient layer: Implications for geocryology and climate-change science. *Permafrost and Periglacial Processes* 16: 5-17.

The Degradation of Ice Wedges in the Colville River Delta and Their Role in Pond Drainage

Molly McGraw
Southeastern Louisiana University, Hammond, LA USA

Abstract

A 58-year record of aerial photographs was used to examine bank retreat, the thermoerosion of ice wedges, and subsequent tapping of the ponds in the Colville River delta, Alaska, USA. The photographic record consists of aerial photographs acquired during seven different years between 1948 and 2006. ArcGIS was used to determine the rate of bank erosion and melting of the interconnecting ice wedges. The riverbank has eroded approximately 38 meters during the 58-year study period. This erosion is equal to a rate of about 0.7 m/year. Most of the bank erosion (29 m) occurred since 1971. The rate of degradation of the ice wedges, as reflected in trough size, coincides with the rate of bank erosion. The tapping of the first lake—that is, the one closest to the river—occurred between 1992 and 2002, while the other lakes drained between 2002 and 2006.

Keywords: Colville; degradation; ice wedge; lake drainage.

Introduction

The Colville River is the largest river north of the Brooks Range, Alaska, USA. The 600-km-long river is located entirely within the zone of continuous permafrost. The river flows through three physiographic provinces: the Arctic Mountains, the Arctic Foothills, and the Arctic Coastal Plain (Wahrahaftig 1965), before discharging into the Arctic Ocean 75 km west of Prudhoe Bay (Fig. 1). The Colville River delta is 600 km^2 in size, and the head of the delta lies 40 km south of the Arctic Ocean.

Both high-centered and low-centered polygons are found in the delta. High-centered polygons are generally found on river bluffs, adjacent to large thermokarst lakes. Low-centered polygons are the most common type of polygon and are found throughout the delta. The low-centered polygons frequently convert to high-centered polygons due to thermal erosion (Walker 1983). When low-centered polygons are located adjacent to a riverbank that contains a high concentration of peat, the ice wedges undergo faster thermoerosion than the peat. This disproportionate thermoerosion of the riverbank results in an uneven or serrated form of the bank (Fig. 2).

Lakes and ponds occupy roughly 16% of the delta (Walker 1978). This concentration of lakes is similar to other areas of Alaska's Arctic Coastal Plain, where lakes occupy approximately 20% of the area (Black 1969, Sellman et al. 1975, Frohn et al. 2005). Oriented lakes occur near the mouth of the west or Nechelik channel; channel lakes are found in abandoned river channels; and seasonal point bar lakes, in the ridge-swale systems of point bars. However, the most common lakes in the Colville Delta are ice wedge polygon and thaw lakes (Walker 1983).

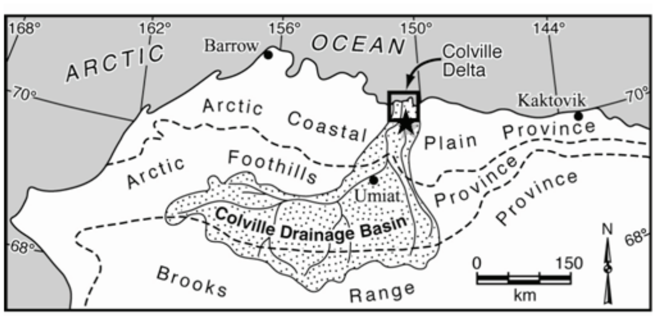

Figure 1. Location of the Colville River. The black star indicates the location of the study site.

The formation, degradation, and reformation, i.e., thaw cycle, of thermokarst lakes, has been the subject of much research (Britton 1958, Black 1969, Hopkins 1949, Lord et al. 1974, Billings & Peterson 1980, Everett 1980, Jorgensen & Osterkamp 2005, Jorgenson & Shur 2007). Thaw ponds form over ice wedge troughs and in the center of low-centered polygons. Low-centered polygons have shallow circular depressions that are completely enclosed by a low ridge or dyke. These depressions fill with meltwater and form ponds and lakes.

The ponds/lakes may expand laterally from mechanical erosion due to wave action and/or thermoerosion. During the summer months, the low albedo of lake water may absorb up to seven times the solar radiation of the surrounding soil (Harris 2002), contributing to the thawing of the surrounding

Figure 2. An example of a serrated riverbank along the Colville River. Photograph courtesy of H.J. Walker.

Figure 3. Peat overhanging the river. Photograph courtesy of H.J. Walker.

permafrost and ice wedge nets. In addition to albedo, lateral expansion rates also depend upon soil texture and ice content and the thickness of the overlaying organic mat (Jorgenson & Osterkamp 2005). Occasionally expansion taps into an adjacent lake. This is one of the main mechanisms for the coalescence of tundra lakes.

Catastrophic drainage of the ponds/lakes is common and may be triggered by tapping, bank overflow, stream piracy, and ice wedge degradation (Mackay 1988, Walker 1978). The Colville River is frozen for up to eight months of the year. During this period, snowdrifts protect the riverbanks from erosion. As temperatures rise in the spring, meltwater begins to accumulate on the surface of the river ice, and water begins to flow. The flowing water melts the snowdrifts and begins to undercut the riverbank producing a thermoerosional niche. The niche widens and deepens with increased water velocity and increasing water temperatures. If the niche deepens enough, the overlying peat will overhang the river and eventually slough into the river (Williams & Smith 1989, Jorgenson & Osterkamp 2005) (Fig. 3). During flood stage, the material that has sloughed off of the bank during the previous season is transported downriver exposing ice wedges. The ice wedges begin to progressively melt away from the riverbank (Fig. 4) and may lead to the eventual tapping and draining of adjacent thaw ponds (Walker 1983).

After drainage, organic matter begins to accumulate in the center of the drained lake basin. Eventually the ice wedges will regenerate and form low-centered polygons and the cycle will repeat its self.

Remote sensing has been extensively used to classify and study morphologic features on Alaska's Arctic Coastal Plain and the Colville River delta. Dawson (1975) used aerial photographs to analyze the distribution of landforms in the Colville River delta. During the 1980s, both Mossa (1983) and Roselle (1988) examined landforms within the delta using aerial photographs. Mossa (1983) compared the use of aerial photographs to satellite imagery to classify and determine the distribution of ice wedge polygons in the delta. Roselle (1988) examined lake tapping using aerial photographs.

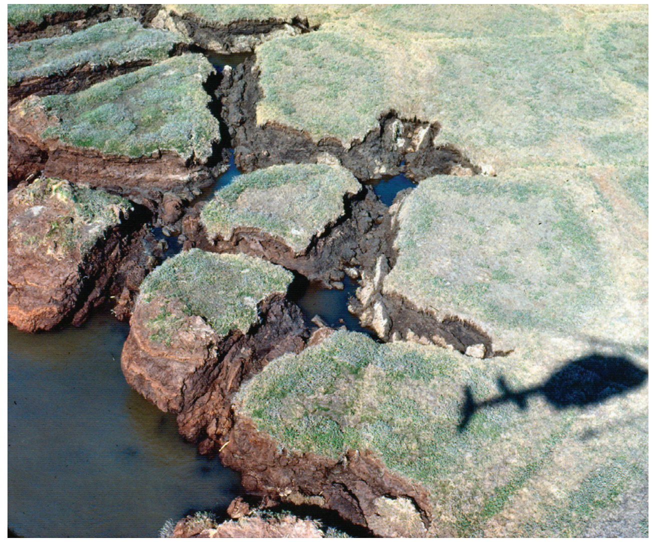

Figure 4. Progressive melting of polygons. Photograph courtesy of H.J. Walker.

Recent studies by Frohn et al. (2005), Hinkel et al. (2007), and Riordan et al. (2006), employed both aerial photographs and satellite imagery to examine the temporal change in several large thaw lakes near Barrow, Alaska. Jefferies et al. (2005) explored the use of various types of remotely sensed imagery, including aerial photographs, satellite imagery, synthetic aperture radar (SAR), and passive microwave, to study the behavior of ice on frozen tundra lakes. Aerial photographs have also been used to examine temporal change in ice wedge degradation in northern Alaska (Jorgenson et al. 2006).

This paper examines the interconnection between riverbank erosion, the degradation of an ice wedge net, and the draining of several small thaw lakes in the Colville River delta using a temporal series of aerial photographs. The photographic record spans a period of 58 years and provides excellent documentation of geomorphic change.

Study Site

The study site, consisting of three small thaw ponds, is located on the right bank at the head of the delta (70°10′20″N, 150°54′31″W). The shallow drained ponds are located on the apex of a cutbank and are aligned roughly perpendicular to the river (Fig. 5). The ponds are roughly 2+ m deep and range in size from 500 m^2 to 1500 m^2. Pond A, the largest of the three ponds, is situated approximately 108 m (as measured from the center of the pond) from the riverbank. The pond is oblong shaped and appears to be the result of the coalescence of 2 or more smaller ponds. Ponds B and C are small, 500 m^2, circular ponds located 30 m and 64 m, respectively, from the riverbank. A well-developed melted ice wedge trough system connects the 3 ponds and the river.

The tundra surface in the vicinity of the pond is flat to gently sloping and is occupied by non-orthogonal polygons and numerous small-to-medium thaw lakes. The soils are silty loam and overlain with a thick layer of peat. The peat

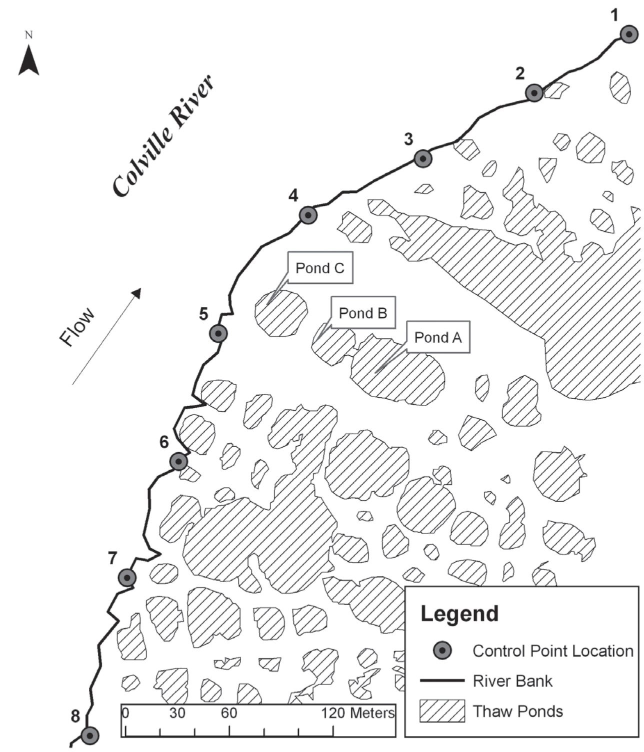

Figure 5. Study site.

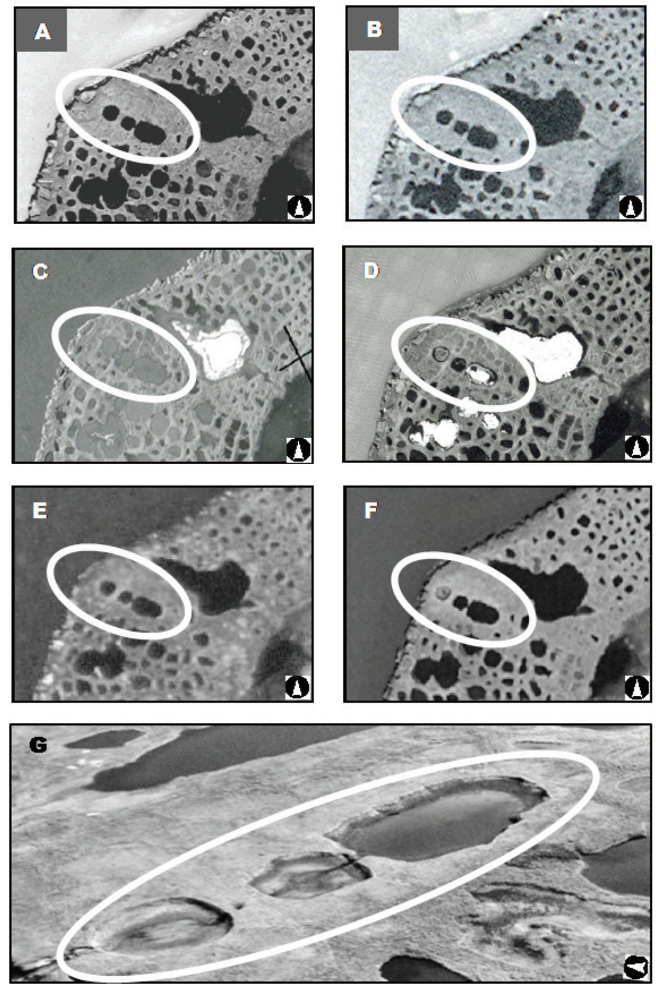

Figure 6: Imagery Dataset 1948–2006: A) 1948 photograph, B) 1955 photograph, C) 1966 photograph, D) 1971 photograph, E) 1992 photograph, F) 2002 photograph, and G) 2006 oblique photograph.

acts as a thermal regulator, moderating thermal erosion of the underlying soil. The serrated riverbank is an active cutbank and is approximately 4 m high at this location. Ice-shove ridges are present.

Methods

Aerial photography was used to examine bank retreat, the thermoerosion of the ice wedges, and subsequent tapping of the ponds. The photographic record consists of 7 sets of high-resolution aerial photographs made between 1948 and 2006 (Fig. 6). The pre-1992 imagery was scanned at a resolution of 600 dots per inch (dpi) and georectified to a 2002 Digital Orthophoto Quarter Quadrangle (DOQQ) of the Colville River delta, obtained from the United States Geological Survey (USGS) Alaska Science Center. Because the distinctive character of ice wedge polygons allows the precise identification of specific locations (Walker et al. 1987), the intersection of ice wedges were selected as ground control points (GCPs) for each scanned image. The rectification process of each image produced a Root Mean Square (RMS) of less than 1. Rectification and subsequent analysis was performed using ArcGIS 9.2. The 2006 photograph (Fig. 6g) is oblique and was not georectified; therefore, it was not used in the bank retreat calculations. Instead, the 2006 oblique image was used to ascertain spatial change in the ponds and ice wedge net.

In order to determine the rate of bank retreat, 3 sets of feature class shapefiles were produced for each image. First, a shapefile containing control points was created. The control points were established at roughly equal intervals parallel to the riverbank (Fig. 7). Next, a guideline shapefile was generated. The guideline file contained lines extending out from the control points to the riverbank; these lines intersected the riverbank at 90-degree angles. Finally, a reference point shapefile was created for each image. Reference points were placed at the intersection of the guidelines and the riverbank. The difference between the control points and the reference points was calculated for each image using Hawth's Analysis Tools. The cumulative change in the distance was graphed in Excel (Fig. 8).

The thermoerosion of the ice wedges and lake tapping was explored by comparing the photographs. The integrity of the 3 study ponds and the ice wedges adjacent to and connecting the ponds was examined and noted for each photographic dataset. The datasets were then compared to earlier and later datasets, and a chronology of morphologic change occurring at the site was developed.

In addition to the photographic record, a ground and aerial survey of the thaw ponds was conducted by the author. The ponds were visited during the summer of 2006.

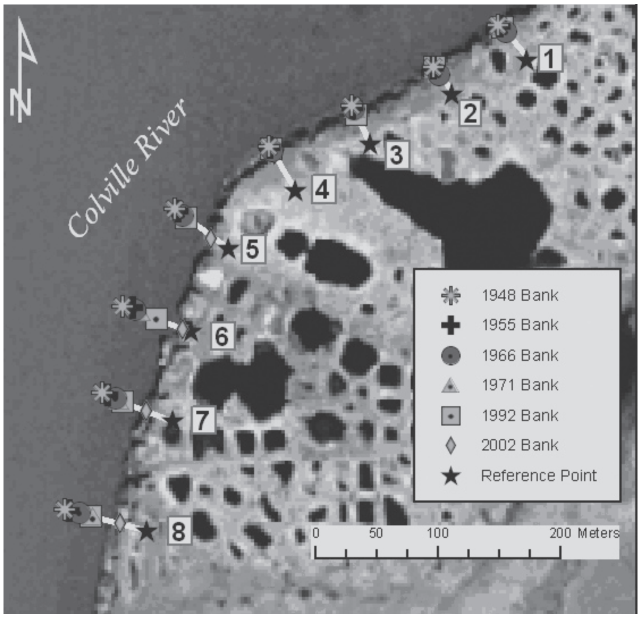

Figure 7. Bank retreat during the period 1948–2002.

Results

A comparison of the 1948 aerial photograph to subsequent aerial photographs traces the bank retreat, thermoerosion of adjacent ice wedges, and tapping of the 3 ponds. The cutbank, where the study site is located, has experienced differential retreat since 1948, with the southern or upstream bank experiencing the most retreat (Fig. 8). In 1948, Ponds A, B, and C are clearly visible, and the remnants of a fourth drained and partially eroded pond (Pond D) is evident adjacent to the riverbank (Figs. 6a, 9). Ponds A and B are joined by a well-defined 3-m long by 4-m wide trough created from the melting of an ice wedge. A longer 16 m by 2 m trough is present linking Pond C to the partially eroded pond.

By 1955 the entire bank has experienced a fairly steady retreat. The southern bank eroded about 5.7 m and the northern bank, approximately 3.7 m. The bank near Pond D had eroded ~3 m during this 7-year period (Fig. 6b).There appears to be no spatial change in the ice wedge net or in Ponds A, B, and C during this time.

Between 1955 and 1971, significant differential bank erosion occurred, with the southern bank experiencing almost 5 times more retreat than the northern bank. The southern bank retreated an average of 24 m compared to 5 m of retreat in the northern end (Fig. 8). Other than the almost-complete disappearance of Pond D by 1966 (Fig. 6c), there appears to be little spatial change in Ponds A, B, and C and in the adjacent ice wedge net during this time frame (Figs. 6b, c, d).

Similar to the previous time period, the 21-year period between 1971 and 1992 showed dramatic differential riverbank erosion, the southern bank retreating approximately 39 m compared to an average retreat of 4 m on the northern bank (Fig. 8). This steady, continuous bank erosion allowed thermoerosion of the ice wedge connecting the river to Pond C and the subsequent draining of Pond C by 1992 (Fig. 6e). This ice wedge, being perpendicular and adjacent to the river, was subjected to the annual thermoerosion of river floodwater and from thermoerosion and possible wave action of the surface water in Pond C. Additionally, Jorgenson et al (2006) suggests that the degradation of massive ice wedges has increased in northern Alaska since the early 1980s. He attributes this increase in degradation to the increase in regional summer temperatures. This multipronged erosion resulted in increased widening and deepening of the ice wedge trough as shown in subsequent photographs of this period.

The rapid bank retreat and thermoerosion of the ice wedge connecting Pond C to the riverbank continued during the next 10 years. A comparison of the 1992 and 2002 aerial photographs (Figs. 6e, f) shows uniform bank retreat along the entire riverbank. The southern bank retreated about 4 m during this time compared to 5 m for the northern bank. Additionally, an ice wedge trough between Ponds B and C has appeared by 2002, indicating degradation of the ice wedge linking Ponds C and B.

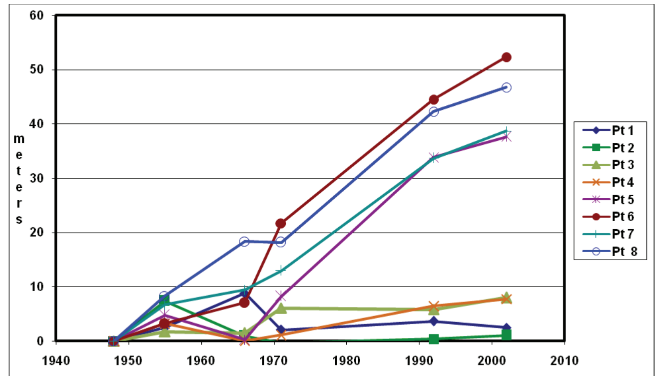

Figure 8. Calculated bank erosion rates from 1948–2002.

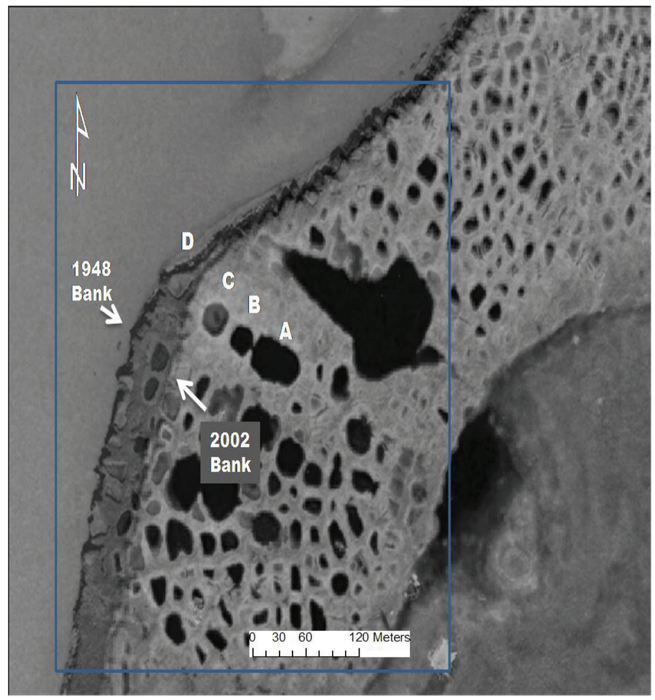

Figure 9. Figure showing the overall bank erosion from 1948 to 2002. Note the presence of a partially eroded polygon (D).

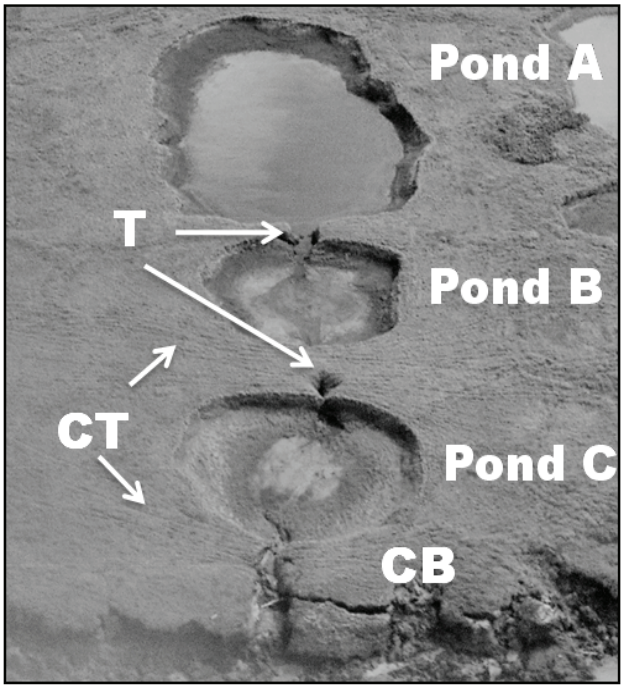

Figure 10. 2006 oblique aerial photograph of the thaw ponds. Note the melted ice wedge tunnels (T), caribou trails (CT), and collapse block (CB).

By 2006, vegetation is becoming established in Pond C, Pond B has drained and Pond A is partially drained (Figs. 6g, 10). The partial draining of Pond A suggests that the ponds were tapped during the 2006 flood. A partially collapsed melted ice wedge tunnel appears between Ponds B and C. Ice wedges which are oriented perpendicular to the river melt faster than ice in the surrounding peat, and may create a tunnel under the peat layer (Fig. 10). As evidenced by linear trails, the land bridges over the tunnels are used by caribou moving across the tundra.

Conclusion

In summary, the 58-year photographic record provides an excellent look into the sequential morphologic changes of an ice wedge net and associated thaw lakes. The photographic record clearly shows thermoerosion of an ice wedge net from both river floodwater and surface pond water. The riverbank adjacent to the study site has experience differential retreat for most of the study period. The greatest difference in the upstream or southern bank retreat and the downstream or northern bank retreat occurred from 1955 to 1992, when the southern bank was eroding as much as 10 times more than the northern bank.

The rate of ice wedge melt is tied to the local bank erosion. The degradation of interconnected ice wedges, all of which are perpendicular to the river, increased with the increasing riverbank erosion. The thermoerosion from river floodwater and surface water in the ponds, have degraded the ice wedges enough to allow the sequential drainage of each of the 3 ponds.

Acknowledgments

I would like to thank Jess Walker for his words of encouragement. I would also like to acknowledge ConocoPhillips, the Michael Baker Corporation, the USGS-Alaska Science Center, the Department of Geography and Anthropology at Louisiana State University and Southeastern Louisiana University for their support, and to two anonymous reviewers for their constructive comments.

References

Billings, W.D. & Peterson, K.M. 1980. Vegetational change and ice-wedge polygons through the thaw-lake cycle in arctic Alaska. *Journal of Arctic and Alpine Research* 12(4): 413-432.

Black, R.F. 1969. Thaw depressions and thaw lakes-a review. *Biuletyn Peryglacjalny* 19: 131-150.

Britton, M.E. 1957. Vegetation of the arctic tundra. In: H.P. Heansen (ed.), *Arctic Biology*. Corvallis, Oregon: Oregon State University Press, 67-113.

Dawson, A.G. 1975. *Landforms of the Colville River delta, Alaska, as interpreted from aerial photographs*. Unpublished M.S. Thesis. Baton Rouge, LA: Louisiana State University, 93 pp.

Everett, K.R. 1980. Landforms. In: D.A. Walker, K.R. Everett, P.J. Webber, & J. Brown (eds.), *Geobotanial Atlas of Prudhoe Bay Region, Alaska*. CRREL Report 80-14. Hanover, NH: US Army Cold Regions Research and Engineering Lab, 14-19.

Frohn, R.C., Hinkel, K.M. & Eisner, W.R. 2005. Satellite remote sensing classification of thaw lakes and drained thaw lake basins on the North Slope of Alaska. *Remote Sensing of Environment* 97(1): 116-126.

Harris, S.A. 2002. Causes and consequences of rapid thermokarst development in permafrost or glacial terrain. *Permafrost and Periglacial Processes* 13: 237-242.

Hopkins, D.M. 1949. Thaw lakes and thaw sinks in the Imuruk Lake area, Seward Peninsula, Alaska. *Journal of Geology* 57(2): 119-131.

Hinkel, K.M., Jones, B.M. Eisner, W.R. Cuomo, C.J. Beck, R.A.& Frohn, R. 2007. Methods to assess natural and anthropogenic thaw lake drainage on the western Arctic coastal plain of northern Alaska. *Journal of Geophysical Research-Earth Surface* 112: F02S16.

Jefferies, M.O., Morris, K. & Kozlenko, N. 2005. Ice characteristics and processes, and remote sensing of frozen rivers and lakes. In: C.R. Duguay & A. Pietroniro (eds.), *Remote Sensing of Northern Hydrology*. Washington, D.C.: American Geophysical Union, 63-90.

Jorgenson, M.T. & Osterkamp, T.E. 2005. Response of boreal ecosystems to varying modes of permafrost degradation. *Canadian Journal of Forestry Research* 5: 2100-2111.

Jorgenson, M.T. & Shur, Y. 2007. Evolution of lakes and basins in northern Alaska and discussions of the thaw lake cycle. *Journal of Geophysical Research* 112: F02S17.

Jorgenson, M.T., Shur, Y.L. & Pullman, E.R. 2006. Abrupt increase in permafrost degradation in Arctic Alaska. *Geophysical Research Letters* 33: L02503.

Lord, N.W., Atwater, M.A. & Pandolfo, J.P. 1974. Influence of the interaction between tundra thaw lakes and surrounding land. *Arctic and Alpine Research* 6(2): 143-150.

Mackay, R. 1988. Ice wedge growth in newly aggrading permafrost, western Arctic coast, Canada. *Proceedings of the Fifth International Conference on Permafrost. Trondheim, Norway,* 809-814.

Mossa, J. 1983. *Interpretation of the ice-wedge polygons of the Colville River Delta, Alaska, using aerial photography and Landsat digital imagery*. Unpublished M. S. Thesis. Baton Rouge, LA: Louisiana State University, 180 pp.

Riordan, B.D., Verbyla, D. & McGuire, A.D. 2006. Shrinking ponds in subarctic Alaska based on 1950-2002 remotely sensing images. *Journal of Geophysical Research* 111: G040002.

Roselle, D.L. 1988. *Morphology and sedimentation of Arctic tapped lakes*. Unpublished M. S. Thesis. Baton Rouge, LA: Louisiana State University, 109 pp.

Sellman, P.V., Brown, J., Lewellen, R.I., McKim, H. & Merry, C. 1975. *The Classification and Geomorphic Implications of Thaw Lakes on the Arctic Coastal Plain, Alaska*. CRREL Report 344.

Wahrhaftig, C. 1965. *Physiographic Divisions of Alaska*, USGS Professional Paper 482. Washington D.C.: US Geological Survey, 52 pp.

Walker, H.J. 1978. Lake tapping in the Colville River Delta, Alaska. *Proceedings of the Third International Conference on Permafrost. Edmonton, Canada, July 10-13, 1978*: 233-238.

Walker, H.J. 1983. Guidebook to permafrost and related features of the Colville River Delta Alaska. *Guidebook, Fourth International Conference on Permafrost, Fairbanks, Alaska*, *July 18-22, 1983.*

Walker, H.J., Arnborg, J.L. & Peippo, J. 1987. Riverbank erosion in the Colville Delta, Alaska. *Geografiska Annaler* 69: 61-70.

Williams, P.J. & Smith, M.W. 1989. *The Frozen Earth: Fundamentals of Geocryology*. New York: Cambridge University Press.

Managing Ice-Rich Permafrost Exposed During Construction

Robert L. McHattie
GZR Engineering, Fairbanks, Alaska, USA
Ted S. Vinson
Department of Civil Engineering, Oregon State University, Corvallis, Oregon, USA

Abstract

In northern Alaska ice-rich permafrost is often encountered during the construction of roads and other projects. When ice-rich permafrost is exposed during late spring through early fall, the potential for thawing is great. Ice-rich permafrost, typically silts with segregated ice or massive ground ice, experiences a substantial reduction in strength owing to the exceedingly high water content and lack of drainage and consolidation during thaw. The result can be a quagmire that "bogs down" equipment or, if the exposure is a cutslope, slope failure. In addition to stability and trafficability problems, environmental oversight increasingly focuses on particulate-rich effluent and poor aesthetics which are common by-products of the thaw process. In future scenarios, even visually-clear effluent produced during thawing could be classified as biologically toxic and require treatment before release from the project site. This study presents several construction projects in northern Alaska where problems due to thawing permafrost became a significant environmental concern. Several techniques now used (or proposed) for mitigating the problems are briefly discussed.

Keywords: construction; environment; excavation; ice-rich permafrost; management; thawing.

Introduction

Thawing of ice-rich permafrost has produced a number of problems on Alaskan projects including substantially reduced equipment mobility, uncontrolled erosion and runoff, and slope failures. The consequences of thawed ice-rich permafrost are environmental distress, project delays, change orders, and claims. Well-defined procedures are lacking to handle ice-rich permafrost and manage a site with exposed ice-rich permafrost. In the context of this paper, the definition of "ice-rich" permafrost is *any* permafrost material with a water content sufficiently high to cause "problems" upon thawing. Given this context, and the recent advancement of environmental regulations, monitoring, and enforcement, the definitions of "ice-rich" and "problem" can be expected to change with time.

Unfortunately, various types of construction problems related to thawed ice-rich permafrost, documented more than one-half century ago, still occur. In many instances the mitigation strategies employed to reduce the consequences of thawing permafrost only met with partial success or were completely unsuccessful. Newer environmental laws have defined as unacceptable some of the techniques that were recognized as "best practice" for many years.

At present, the construction engineer charged with the successful completion of a project in a permafrost environment has few, if any, resources available to identify a suitable mitigation strategy, particularly in an era of increasingly stringent and challenging environmental regulations. Environmental pressures continue to increase the trend to make long-accepted Alaska Department of Transportation and Public Facilities (ADOT&PF) methods for dealing with ice-rich permafrost either undesirable or unacceptable.

This study examines several construction projects in northern Alaska where problems caused by thawed ice-rich permafrost were of major concern. Techniques employed or proposed to mitigate the problems are described. The purpose of the study is to promote awareness of changing environmental concerns with respect to construction in a permafrost environment and encourage practices that will satisfy the increasing oversight of resource/regulatory agencies.

Problem Background

In northern Alaska exposure of ice-rich permafrost during construction of roads and other projects is an all too common occurrence (Fig. 1). Ice-rich permafrost exposed during late spring through early fall has a very high potential to thaw. Permafrost excavated in winter will cause severe problems if it is not properly disposed of prior to spring thaw. When thawed, ice-rich permafrost, typically silts with segregated ice or massive ground ice, experiences a substantial reduction in strength owing to the exceedingly high water content and lack of drainage and consolidation during the thawing process. The result can be a quagmire in which construction equipment is "bogged down" or, if the exposure is on a cutslope, a slope failure will result (Fig. 2). Aside from stability and trafficability problems, serious environmental issues arise when thawed particulate-laden fluids (sometimes dense slurries) must be controlled. In future scenarios, even visually clear effluent collected from thawed permafrost may have to be treated prior to release from the project site.

Thawing of ice-rich soils has posed problems since the first construction projects in permafrost environments. During the summer of 1954, the Alaska Road Commission exposed

Figure 1. Road cut in ice-rich permafrost (ADOT&PF file photo).

Figure 2. Thaw degradation of cutslope in ice-rich permafrost inducing slope failure (ADOT&PF file photo).

ice-rich permafrost (lake silts) two miles north of Paxson (Fig. 3). Upon thawing, the material actually started to flow. Problems associated with thawing of ice-rich permafrost occurred on a number of North American road projects over the next half-century and have been reported for a number of international projects as well. Slumping of thawed material was noted on several cutslopes in ice-rich permafrost along the Qinghai-Tibet railroad. Chinese researchers report a close correlation relating thaw damage to the orientation of the cutslope (which has been noted by a number of other professionals). Specifically, failures on south-facing slopes were usually more common and dramatic than failures on north-facing slopes. The south-facing slope has a warmer mean annual ground temperature below the sliding mass due to more intense solar heating when compared to the north-facing slope.

A recent example (from 2005 to 2007) of thaw-related problems is provided by the Dalton Highway, just north of Milepost 35. Figure 4 shows a cut that extended about 300 m (1000 ft) in total length. During drilling exploration, the cut volume was judged to be bedrock and weathered bedrock. The cut was designed to have a stepped backslope and also incorporated an interceptor ditch for collecting water along the top of the slope (to prevent erosion of the slope face). The cut design was appropriate for the expected fairly competent weathered bedrock. However, much of the bedrock cut material was not only highly weathered but also ice-rich. There was no special containment berm used for the excavated material. It was simply stockpiled (see Fig. 4b). Fortunately, the stockpile of excavated material didn't "run" as it thawed as might have occurred. However, there were cutslope failures and maintenance issues that required attention as shown in Figure 5.

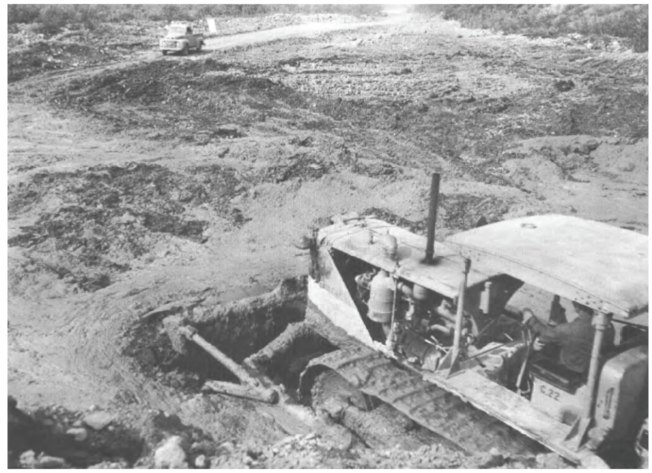

Figure 3. Thawed ice-rich permafrost flowing around a bulldozer blade. Ice-rich permafrost (lake silts) were exposed during the construction of the Richardson Highway (Photograph by Pewe 1954).

Disposal of excavated material is one of the most common problems associated with exposing ice-rich permafrost. It is no longer acceptable to simply waste the excavated permafrost at a convenient location without regard to the environmental consequences of failure or runoff from the eventually thawed material. One solution to the disposal of excavated permafrost is to construct retention berms and place the permafrost inside the berms as shown in Figures 6 and 7. When the ice-rich permafrost eventually thaws, it is restricted to the area inside the berms. The berm shown in Figure 6 allowed the thaw water to escape and cause other environmental concerns. Future retainment schemes may be complicated if excess water generated during thawing needs treatment prior to release from the containment area.

Finally, a problem in western Alaska, also related to permafrost degradation, is the use of excavated permafrost to construct road and airfield embankments. This unusual practice is necessary owing to the scarcity of suitable embankment fill at some locations. Permafrost is excavated in the winter and placed in the location of the required embankment (similar to the waste embankment shown in Fig. 7). Over a period of several years, the permafrost fill progressively thaws and becomes increasingly stable and viable as a runway embankment. If the thawed material is restrained from lateral spreading and flow, it eventually settles and drains and can be shaped and compacted to form the final load-supporting embankment. Snow berms can be placed adjacent to the embankment sideslopes to retain

(4a) Newly-constructed cutslope in ice-rich permafrost. Note interceptor ditch at slope top and stepped cut face.

(4b) View across permafrost waste pile at newly cutslope face in ice-rich permafrost. The volume of waste exceeded the boundary limits of the permitted area.

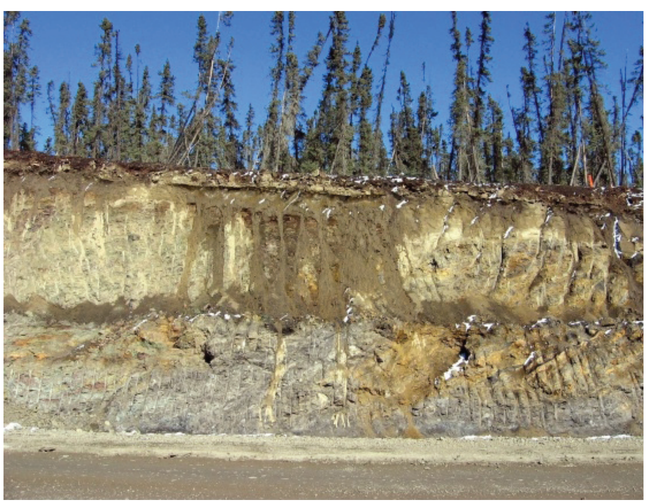

(4c) Ice-rich permafrost cutslope just starting to thaw.

Figure 4. Dalton Highway cut in ice-rich permafrost–before thaw (all photographs from ADOT&PF file courtesy of S. Lamont & J. Russell).

the thawing permafrost. Thawed soil, initially retained by the snow berm, drains and forms its own soil berm that continues to contain the spread of additional thawed material after the snow disappears. In the future, with all containment schemes, excess water collected behind the berms may need to be processed before release.

Mitigation Strategies for Ice-Rich Cutslopes

Documented concern for the instability of cutslopes in ice-rich permafrost and massive ground ice was presented in the 1969 design guidelines for the 123-km (56-mile) Livengood to Yukon River initial segment of the Trans Alaska Pipeline System (TAPS) haul road (Rooney 2006). The original engineer's sketch of the procedure to be employed is shown in Figure 8.

Anecdotal and published sources of information suggest that several techniques have been employed, with varying degrees of success, to mitigate problems related to thawing ice-rich permafrost. A few examples are:

- Berg and Smith (1976), based on observations along the TAPS haul road, presented the procedure shown in Figure 9. At the time of construction, trees are cleared (by hand to minimize environmental damage) for a distance equal to 1½ H_{CUT}. The cut is nearly vertical (1/4H:1V). The road grade is undercut approximately 1.5 m (5 ft) before placement of the gravel embankment. Wide ditches that will accommodate slumpage, while facilitating drainage flow and "cleanout," are constructed at the toe of the slope. During the first summer, the slope degrades rapidly. Hydraulic seeding is applied late in the thaw season (for best results). The lateral ditch is cleaned as necessary. The rate of degradation of the backslope decreases over a number of years. After 5 or 6 years, the slope usually becomes relatively stable and covered with surface vegetation that restores thermal equilibrium.
- Cutslopes may be protected with insulation to ensure stability and prevent slump material from reaching the drainage system.
- Cover the cutslope with a vegetation mat (closed netting) to provide minor insulation plus shading.
- Reduce the slope inclination to 1½H or 2H:1V; place topsoil on the slope; seed at 2 to 3 times the "normal" application rate (best suited to non-ice-rich permafrost)
- Cut the ice-rich permafrost slope about 1½H:1V and place a gravel berm adjacent to the slope face (berm height = cutslope height). The horizontal width of the berm is approximately 8 ft to facilitate construction, and the berm sideslope is approximately 1½H:1V

(5a) Pockets of thaw failure along cut face. —A gravel drainage blanket (left side of photo) was installed to slow thawing, retard slumping of thawed material, and provide drainage during the thawing process.

(5b) Advanced thaw condition along ice-rich permafrost cutslope shows ditch filling with saturated silt.

(5c) Advanced thaw degradation of cutslope shows block failures and runoff of highly fluid silt into ditch.

(5d) Advanced cutslope thaw with silty runoff flowing in ditch and general slumping of coarser material.

Figure 5. Dalton Highway cut in ice-rich permafrost—after thaw. (All photographs from ADOT&PF file courtesy of S. Lamont & J. Russell.). Each photograph shows damage that occurred as thawing progressed. The photos emphasize four major types of damage and associated environmental problems created during thawing: (1) damage above the cutslope, (2) damage on the cutslope, (3) ditch damage, and (4) high-particulate runoff. The damage creates and/or exacerbates the runoff problem. With much (and long-term) attention to ditch maintenance, such problems have "healed' themselves in the past when thawing progressed to a depth at which additional slumping and runoff finally ceased. Today, however, environmental-concerns/laws and close agency attention no longer permit creation of a problem that may continue for years. Methods must be devised to minimize, or hopefully eliminate, the types of damage shown in the photographs. Photograph 5a (left side) shows an example of a gravel drainage blanket used to slow thawing, retard slumping of thawed material, and provide drainage during the thawing process.

Figure 6. Containment structure for excavated permafrost on the North Slope of Alaska (photograph courtesy of G. Griffin).

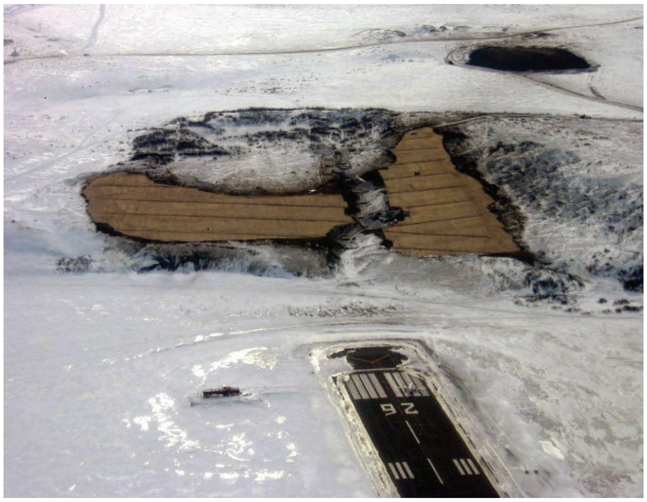

(7a) The top of a hill that extended into aircraft glidepaths was excavated to improve the approach to the runway. Synthetic matting (center brown areas) was placed on exposed permafrost to retard thaw and erosion and promote stabilizing plant growth.

(7b) Snow berm surrounding right side of ice-rich permafrost waste pile (shown in upper right of photograph [7a]).

(7c) Close-up view of newly-placed snow berm and ice-rich permafrost waste material behind snow berm.

(7d) Organic material contained in snow berm that remains after berm thaw (spring).

(7e) Organic remnants from thawed snow berm (summer). Note vegetation growth on waste pile.

Figure 7. Kotzebue runway improvement, April through August 2006 (all photographs from ADOT&PF file courtesy of S. Lamont). The purpose of project was to excavate the top of a hill that extended into the glidepath of aircraft (7a). During wintertime excavation of ice-rich materials in western Alaska, nearby snow may be the only choice of material available that can be piled up to provide retainment for excavated permafrost. Photographs 7b and 7c show the newly-constructed snow berm. The "snow" berm is actually composed of snow plus miscellaneous vegetation, soil, and rock detritus unavoidably included as the snow is collected. Photographs 7d and 7e show the berm after it progressed through a spring and summer's thawing. The vegetative matter in the berm is exposed and remains as the snow thaws. During thaw, the increasingly exposed vegetation and other non-snow materials helps shade and insulate the underlying remaining frozen berm. The retained (thawing) permafrost tended to stay in place as it and the berm thawed, suggesting the berm may not have provided appreciable retainment as expected.

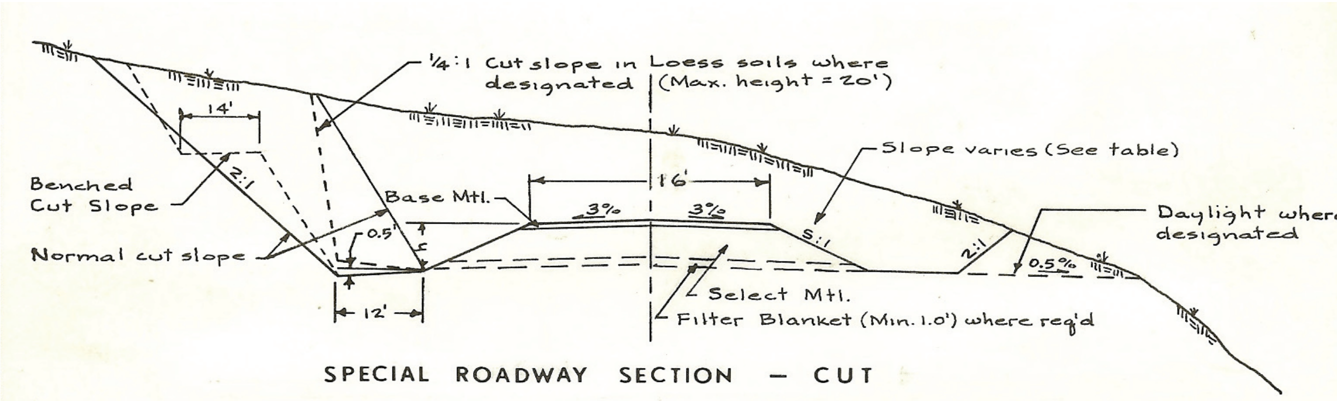

Figure 8. Original 1969 engineer's sketch of the procedure to be employed in a "special roadway section" defined as ice rich or massive ice cutslopes (after Rooney, pers. com.).

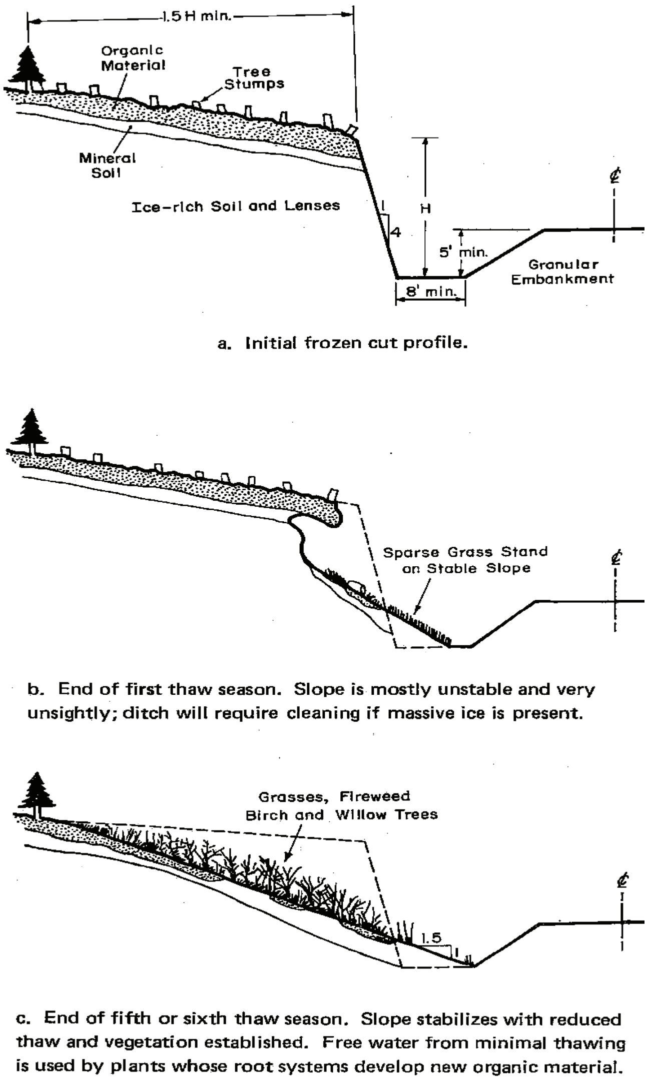

Figure 9. Idealized development of stability in ice rich cut (after Berg & Smith 1976).

Summary and Conclusions

At the present time engineers in Alaska do not possess a synthesis of design and construction methods to deal with the following:

- exposed and thawing ice-rich permafrost
- disposal of excavated ice-rich permafrost
- the use of permafrost to construct an embankment.

Increasing resource agency oversight requires evaluating all methods previously employed to address these problems, a number of which are reported herein, with respect to their environmental acceptability in addition to their engineering/constructability attributes. Best construction management practices will develop after a balance between reasonably attainable environmental goals and economical/practical engineering solutions is achieved.

Acknowledgments

Sam Lamont, John Ryer, Guan Griffin, Jesse Reinikainen, and Jeff Russell, ADOT&PF, Northern Region-Construction Section, provided the photographs and valuable insights into the history of the projects and issues described herein. Clint Adler, chief of research, ADOT&PF, provided the funding for the study through his office. The contribution of these individuals is gratefully acknowledged.

References

Berg, R. & Smith, M. 1976. *Observations along the Pipeline Haul Road between Livengood and the Yukon River.* US Army CRREL Special Report 76-11. Oct. 1976.

Rooney, J.W. 2006. Personal communication, Nov. 2006. Anchorage, AK: R & M Consultants, Inc.

Dissociation of Methane and Propane Gas Hydrates Formed on Water Droplets, at T<270 K

Vladimir P. Melnikov
Institute of Earth's Cryosphere SB RAS, Tyumen, Russia
Anatoly N. Nesterov
Institute of Earth's Cryosphere SB RAS, Tyumen, Russia
Aleksey M. Reshetnikov
Institute of Earth's Cryosphere SB RAS, Tyumen, Russia
Vladimir N. Feklistov
Institute of Earth's Cryosphere SB RAS, Tyumen, Russia

Abstract

Methane and propane hydrate formation on 0.15–2.0 mm water droplets and dissociation of the hydrate droplets were studied optically at 243–275 K. The instrument setup and the experimental procedure have been described. For the first time, the formation of liquid (supercooled) water during the hydrate dissociation was reliably detected in the temperature range of 253–270 K. The induction time for recrystallization of the metastable liquid water into ice varied from tens of hours at 270 K to a few seconds at 253 K. The dissociation pressure of the hydrates was measured, and the molar enthalpy of hydrate dissociation was calculated. In the temperature range of 253–270 K the molar enthalpy of dissociation for hydrates formed on the water droplets agrees well with the molar enthalpy of the bulk hydrate dissociation into water (liquid) and gas at T>273 K.

Keywords: dissociation; gas hydrates; ice; self-preservation, supercooled water.

Introduction

Detection of anomalously low rates of gas hydrate dissociation below the ice point (Davidson et al. 1986, Stern et al. 2001, Yakushev & Istomin 1992) is one of the most significant results on the kinetics of hydrate dissociation obtained in recent years. First observed under specific laboratory conditions, the gas hydrate dissociation rate decreased in some cases to zero, so the phenomenon was named the gas hydrate self-preservation effect (Yakushev & Istomin 1992). The effect is interesting not only from the viewpoint of basic research on the thermodynamics and mechanism of this phenomenon, but also from a practical perspective. Because of the effect, it is possible to store and transport natural gas in the gas hydrate form at a pressure of 1 atm and temperatures of 253–268 K (Gudmundsson et al. 2000). At present, such technologies are being developed in some countries, primarily in the USA, Norway, Japan, and England (Rogers et al. 2005). It is suggested also that due to the self-preservation effect, gas hydrates can exist in the upper layers of permafrost (at depths of 150–200 m) outside their thermodynamic field of stability as metastable (relic) gas hydrates (Dallimore & Collett 1995, Ershov & Yakushev 1992). Gas hydrate accumulations in permafrost can also cause incidents associated with drilling and production operations in the northern hydrocarbon fields. Because of permafrost thawing in response to global warming, there is a possibility that shallow, self-preserved gas hydrates could liberate methane gas to the atmosphere when they are decomposed.

It is supposed by some authors (Davidson et al. 1986, Yakushev & Istomin 1992) that the anomalously low hydrate dissociation rate is caused by the formation of an impermeable ice coating on the surface of hydrate particles, which develops in the initial stage of hydrate dissociation. However, the mechanism of ice formation and development of an impermeable ice coating on the hydrate surface is still poorly understood. We previously reported (Melnikov et al. 2003a, b) that during propane hydrate dissociation at 1 atm and T>270 K, metastable (supercooled) liquid water was formed initially, and then the water transformed into ice. Formation of the supercooled liquid during propane hydrate dissociation and its crystallization was visually observed. An indirect conclusion about methane hydrate dissociation into liquid (supercooled) water and gaseous methane was made, based on calculated data on the activation energy of methyl radical decay during isothermal annealing of γ-irradiated methane hydrates at 235–260 K (Takeya et al. 2005). It should be noted that Makogon (1981) first proposed the scheme of gas hydrate dissociation at T< 273 K as hydrate $\rightarrow$ liquid water $\rightarrow$ ice + gas, but reliable evidence for the process was not presented.

The purpose of this study is to obtain direct evidence of the formation of metastable (supercooled) water during gas hydrate dissociation at temperatures below 273 K. To do this, a special procedure of optical observation of hydrate dissociation was developed.

Experimental Apparatus and Procedure

A schematic of the experimental apparatus is shown in Figure 1. Its main element is a high-pressure reactor, within

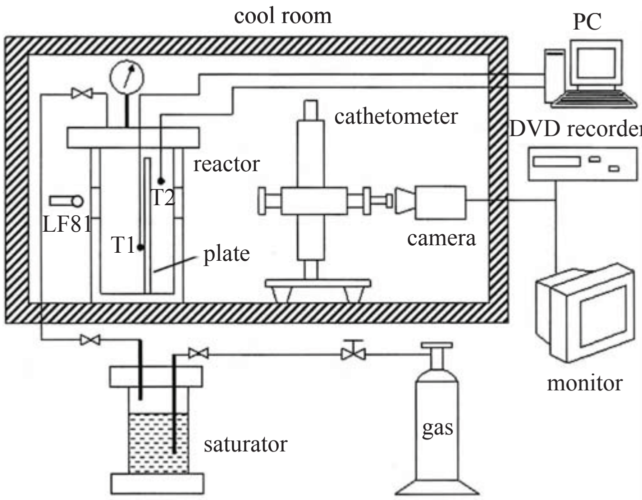

Figure 1. Experimental apparatus for study of hydrate formation/dissociation on water droplets. LF 81 – LED; T_1, T_2 – copper-constantan thermocouples.

which hydrates are formed and dissociate under controlled conditions. A reactor with a working volume of 100 cm^3 was made of stainless steel and equipped with quartz viewing windows on the side surface to facilitate visual observation of processes occurring within the reactor. The reactor was placed into the cool room (air thermostat) with a volume of 8 m^3 (2m x 2m x 2m). The temperature in the reactor was maintained to an accuracy of $\pm$0.1 K. A cathetometer was used for optical observation of hydrate formation/dissociation within the reactor. The ocular of the cathetometer telescope was joined with a Nikon Coolpix 995 digital camera. The image from the camera was displayed in parallel on the screen of a monitor and recorded by a DVD recorder. In this way we were able to make discrete pictures and a video film in a real time mode. Video capture and image analysis were performed using Pinnacle Studio Plus® v.10 and PhotoFinish® 4.0 software. Pure methane (99.9 mol.%) and propane (mol.%: C_2H_6 – 1.23, C_3H_8 – 94.27, C_4H_{10} – 4.13, $C_{5+higher}$ – 0.02, CO_2 – 0.35) were used as the hydrate forming gases.

The procedure to prepare the hydrate samples was as follows. Distilled water in the amount of 1.5–2.5 g was sprayed in the form of small droplets 0.15–1.5 mm in size on the surface of a transparent Plexiglas plate previously cooled to 253 K. It is well known that the hydrate formation induction time decreases when crushed ice or thawed ice is used for hydrate formation (Sloan 1998). Moreover, our numerous attempts to form propane hydrate directly from water droplets failed. Therefore, to obtain hydrates, we used the ice formed by freezing water droplets. All activities related to the assembly of the reactor, its evacuation and charging with hydrate-forming gas (about 3 atm for propane and 40 atm for methane) were carried out in the cool room at temperatures of 258–263 K. To increase the rate of hydrate formation, the reactor with pressurized gas and the frozen water droplets was heated above the ice melting point, because slow melting of the ice facilitates the hydrate forming reaction (Stern et al. 1996).

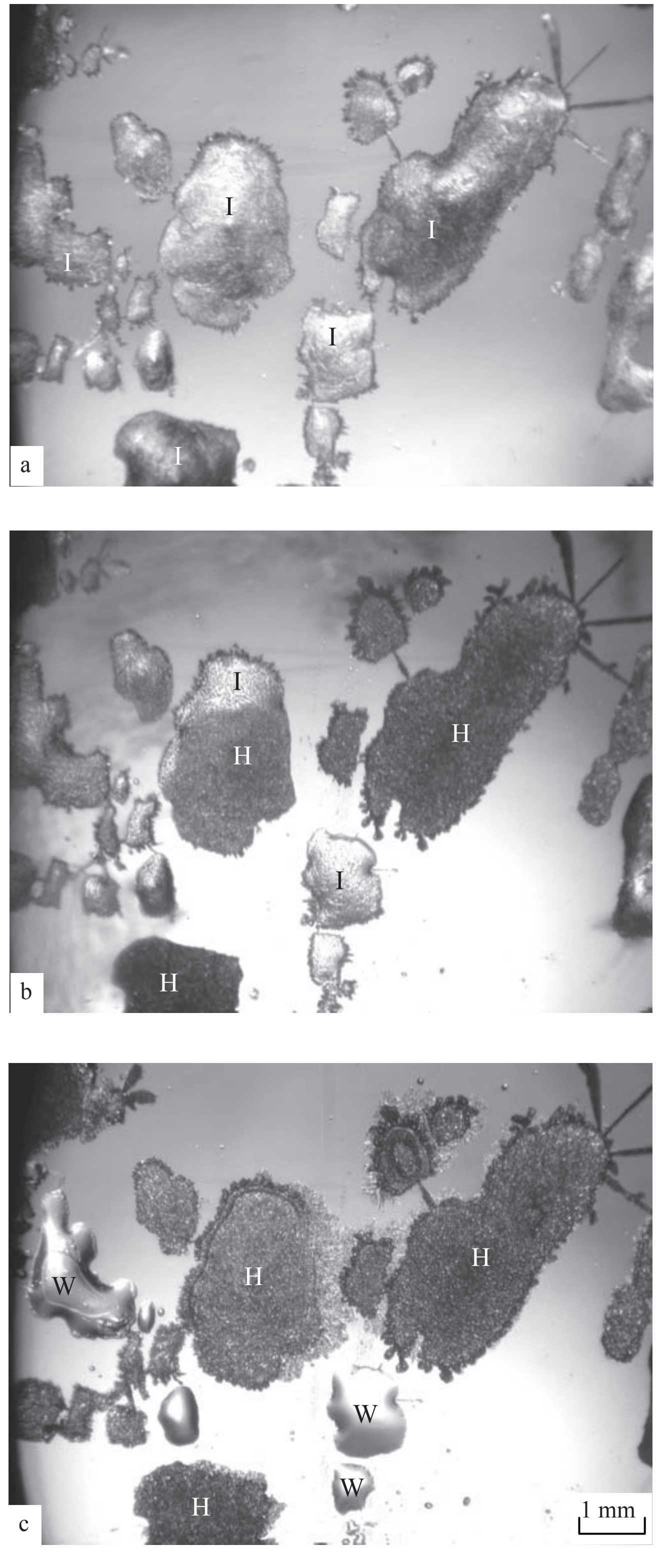

Figure 2. Propane hydrate growth on the ice surface (a-b) and appearance of water during melting of ice (c): a – 0 min(just before pressurization), *P*= 0 atm, *T*=258 K; b – 42 min, *P*=2.1 atm, *T*=270.0 K; c – 214 min, *P*=2.1 atm, *T* = 273.2 K. I-ice, H – hydrate, W –water.

Hydrate, ice, and water phases were distinguished by surface roughness and color (Fig. 2). The sample history and *P-T* conditions within the reactor were taken into account in addition to visual observation to identify the different phases observed in hydrate formation/ dissociation. Only the ice is presented in Figure 2a, where T=258 K, P=0 (just before the reactor was charged with propane). In Figure 2b (P=2.1 atm, T=270 K) the ice and propane hydrate, as well as the ice-hydrate boundary, are observed. On the monitor screen the hydrate surface looked rougher and darker. The ice-hydrate boundary corresponds to the propagation front of the gas hydrate film at the ice surface. Different mechanisms of ice surface coverage by a gas hydrate film were discussed by Genov et al. (2004). Monitoring movement of the ice-hydrate boundary at the ice surface, we were fortunate to measure the rate of the propane hydrate film propagation along the gas-ice interface. It was about 1 µm/s at P = 2.1 atm, T = 270 K, ΔT = 4 K. Here ΔT is supercooling, $\Delta T = T_{eq} - T$, where T_{eq} is the hydrate equilibrium temperature at the given pressure in the reactor. For comparison, the growth rate of the methane hydrate film along the methane-liquid water interface was about 40–100 µm/s at the same supercooling of ΔT = 4 K (Freer et al. 2001, Tailor et al. 2007). No data on the growth rate of a gas hydrate film at the ice surface have come to our notice.

Sometimes not all ice particles transformed into the hydrate, and when the temperature in the reactor increased above 273 K, the ice melt and water droplets appeared (Fig. 2c). At the same time an elevated pressure within the reactor provides the hydrate stability and additional hydrate formation. Because we used a small amount of water within the reactor, the pressure drop during the gas hydrate formation was insufficient to reliably estimate the amount of water converted into hydrate. Therefore the freezing/melting procedure (cooling of the reactor to 265 K and its heating to 273.5K) was repeated 4–5 times to provide a maximum of water conversion into gas hydrates.

To observe the dissociation of gas hydrates, a specified temperature was set in the cool room, and the reactor was kept at this temperature for another 2 h. Then, the pressure in the reactor was slowly reduced (0.05 atm/min for propane hydrate and 0.1 atm/min for methane hydrate). The dissociation of the hydrates was judged from the visually observed collapse of the rough surface of the hydrates, the appearance of smooth islands of the liquid phase on hydrate particles, and evolution of gas bubbles from the liquid. The pressure at which the first changes in hydrate particles were visually observed was taken as the hydrate dissociation pressure P_d at the given temperature. Once the hydrates begin to dissociate, the reactor valve was closed, and the pressure drop in the reactor was stopped.

Results and Discussion

Results describing the dissociation pressure for methane and propane hydrates formed on water droplets are shown in Figure 3. For comparison, the equilibrium pressure of

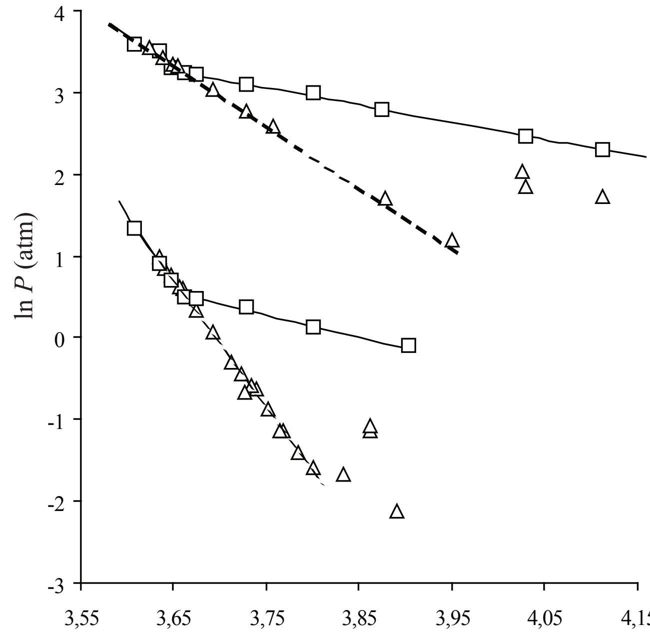

Figure 3. Dissociation pressure of gas hydrates, formed on water droplets (triangle), and equilibrium pressure of formation of bulk hydrates (square). The solid line is calculated data by the CSMHYD program. The dash line is the extension of the calculated water-hydrate-gas equilibrium curve into the metastable area.

hydrate formation for methane and propane bulk hydrates, P_{eq}, obtained in the control experiments and calculated by the CSMHYD program (Sloan 1998) are presented as well. In ln P – 1/T coordinates, the curve of the equilibrium pressure of gas hydrate formation $P_{eq} = P_{eq}(T)$ consists of two intersecting straight lines corresponding to water–hydrate–gas and ice–hydrate–gas equilibrium. The slope of these lines to the inverse temperature axis characterizes the molar enthalpy of hydrate dissociation into water and gas ΔH_{hwg} (hydrate (h) = water (w) + gas (g)) at T > 273 K and into ice and gas ΔH_{hig} (hydrate (h) = ice (i) + gas (g)) at T < 273 K (Sloan 1998)

$$\Delta H_{hwg(hig)} = - zR \frac{d(\ln P_{eq})}{d(1/T)} \tag{1}$$

where z is the compressibility factor for gas and R is the universal gas constant.

At temperatures above 273 K, the hydrate dissociation pressure P_d coincides with the equilibrium pressure of gas hydrate formation P_{eq} (Fig. 3). At 263 K<T<273 K for propane hydrate and 253 K<T<273 K for methane hydrate the values of ln P_d fall on a straight line (the regression coefficient is r^2=0.995) which coincides with the extension of the water–hydrate–gas equilibrium curve in the metastable area of supercooled water. This means that, at T <273 K the molar enthalpy of dissociation for hydrates formed on water droplets is equal to the molar enthalpy of hydrate dissociation into water(liquid) and gas for bulk hydrate. The experimental data on P_d and Equation 1 were used to calculate the molar enthalpy for the dissociation of methane

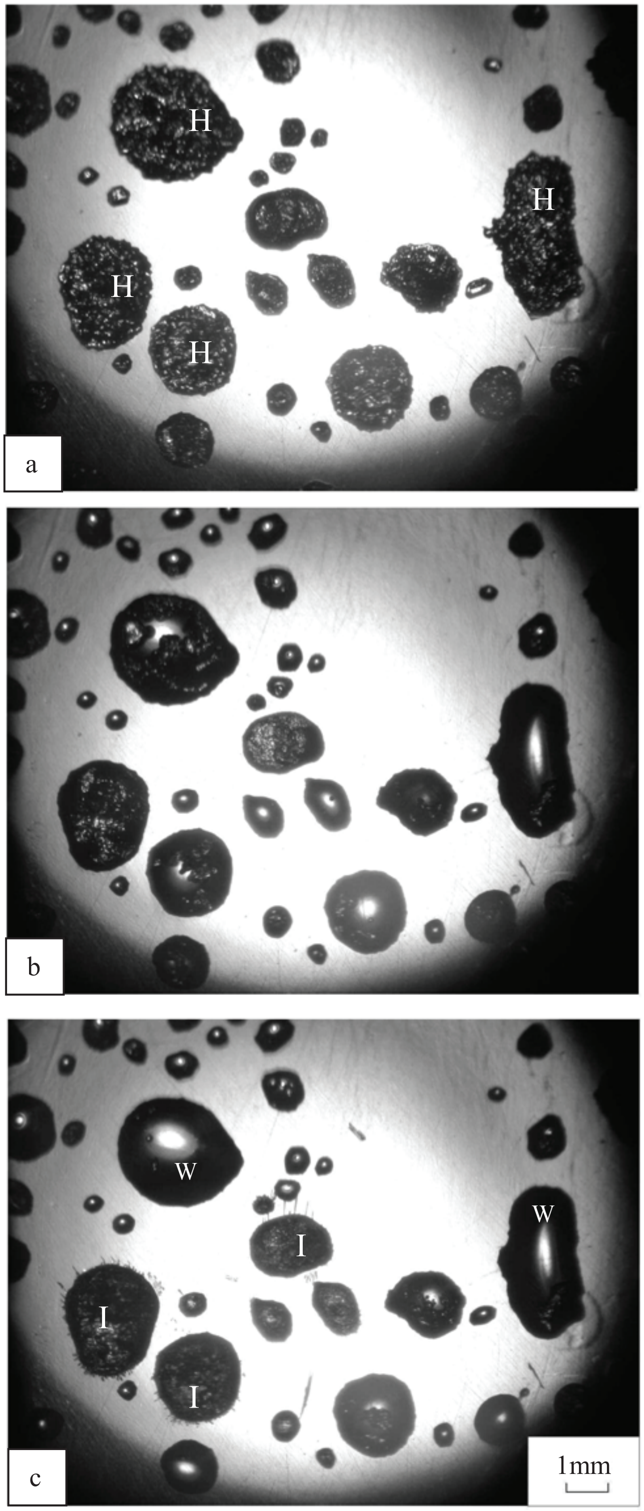

Figure 4. Dissociation of propane hydrates formed on water droplets. P_d = 0.54 atm, T = 267.9 K. a – 0 min (at the beginning of dissociation); b – 62 min; c – 89 min.

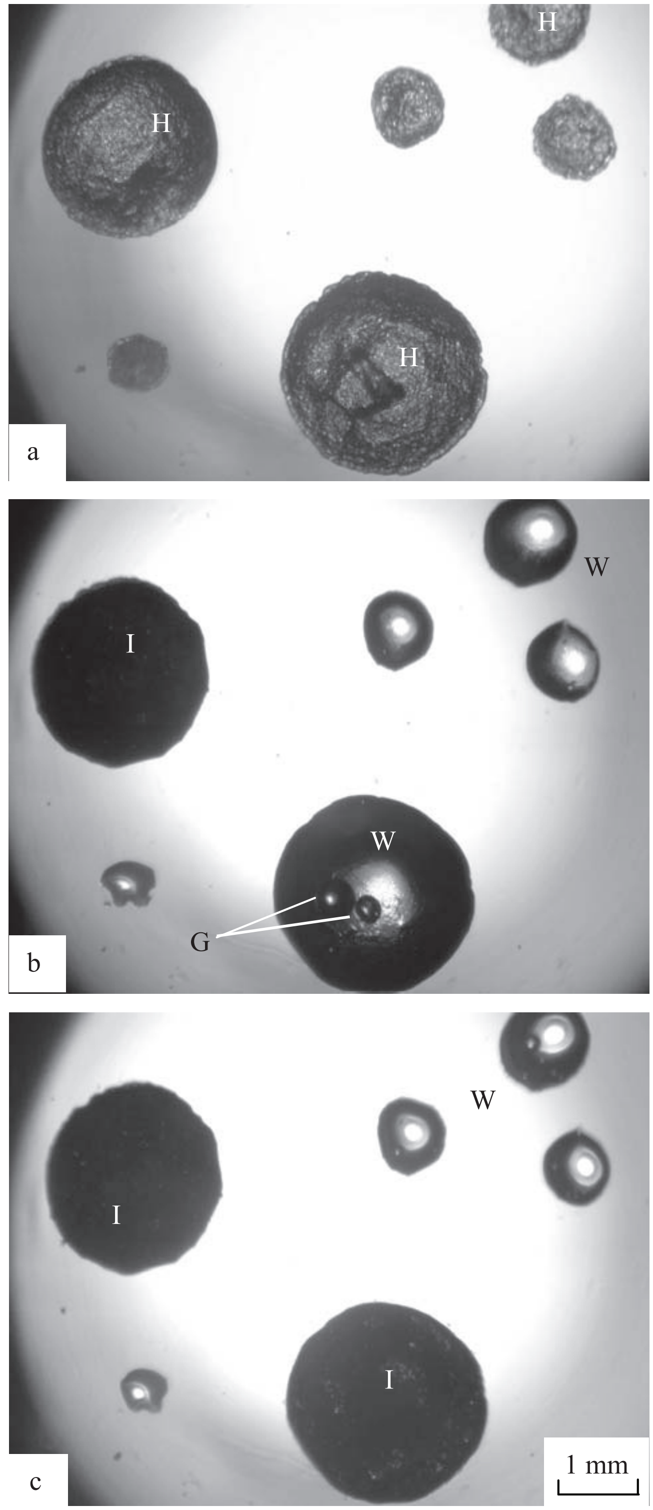

Figure 5. Dissociation of methane hydrates formed on water droplets. P_d = 9.9 atm, T = 263.15 K. a – 0 min (at the beginning of dissociation); b – 1 min; c – 115 min. G – gas bubble.

and propane hydrates formed on water droplets, into supecooled water and gas at T<273 K. The compressibility factor z was calculated with the Peng-Robinson equation of state (Peng & Robinson 1976). The calculated values are: ΔH_{hwg} = 54.6 kJ/mol for the methane hydrate dissociation into supercooled water and methane gas and ΔH_{hwg} = 128.9 kJ/mol for the propane hydrate dissociation into supercooled water and propane gas. The calculated values agree well with the molar enthalpy of hydrate dissociation into water and gas for bulk methane hydrate ΔH_{hwg} = 54.6 kJ/mol and bulk propane hydrate ΔH_{hwg} = 129.2 kJ/mol (Handa 1986). Hence the liquid phase detected visually in our experiments at $T < 273$ K during dissociation of hydrates formed on water droplets is nothing more nor less than supercooled water.

The consecutive series of visually detected changes occurring at 267.9 K during dissociation of propane hydrates formed on water droplets is shown on Figure 4. The zero time (Fig. 4a) immediately precedes the first changes of the image observed. By this time the pressure in the reactor had decreased to 0.54 atm and remained steady at that value. Only the hydrate phase is present in Figure 4a. After one hour of observation (Fig. 4b) small water droplets(size 0.2–0.3 mm) had formed on the hydrate as well as large droplets (1–2 mm) composed of both the liquid water phase and hydrates. It is interesting to note that the presence of the hydrate within the water droplets did not stimulate heterogeneous crystallization of the supercooled water. Only after 67 minutes from the onset of the hydrate dissociation, some (but not all) of the larger water droplets transformed into ice. In this case we observed that the droplets froze instantly in contradistinction to the terminal growth rate of hydrate on the ice surface (Fig. 2). However, the greater number of the small water droplets and some of the large water droplets did not freeze even 1.5 hours after the onset of the hydrate dissociation (Fig. 4c). When the reactor was heated above 273 K, the melting of the recrystallized water droplets was observed at 273.1$\pm$0.1 K.

The formation of metastable (supercooled) water during propane hydrate dissociation was reliably detected between 263 K and 273 K. In this temperature range, the transformations observed within the reactor were analogous to those presented in Figure 4, and values of the hydrate dissociation pressure P_d in all cases fell on the extension of the water–hydrate–gas equilibrium curve into the metastable area of the supercooled water at T<273.15 K, (Fig. 3).

Similar transitions were observed during methane hydrate dissociation at 253.15–273.15 K, (Fig. 5). Based on the P-T sample history (before cooling to 263.15 K, the reactor was heated to 274 K at 40 atm and no water droplets were observed, only the solid droplets) we can advocate that only the hydrates are presented in Figure 5a. The small liquid droplets along with the large droplet composed of the liquid phase, the solid and the gas bubbles, as well as the large dark solid droplet are observed in Figure 5b. In Figure 5c we can see the liquid droplets and two dark solid droplets. When we heated the reactor, we observed the melting of the dark solid droplets at the ice melting point. It follows that the dark solid droplets in Figures 5b and 5c were the ice.

A detailed study on the influence of the hydrate dissociation temperature on the induction time for the crystallization of supercooled water released during hydrate dissociation was not conducted in this work. Nevertheless, it follows from the data obtained that the induction time decreases with the decreasing temperature. For example, at temperatures close to the freezing point (269–270 K) none of the water droplets formed during hydrate dissociation had crystallized to ice within 24 hours of the observation.

Below 263 K for propane hydrates and 253 K for methane hydrates, the dissociation pressures P_d were higher than the P_d values corresponding to extension of the equilibrium

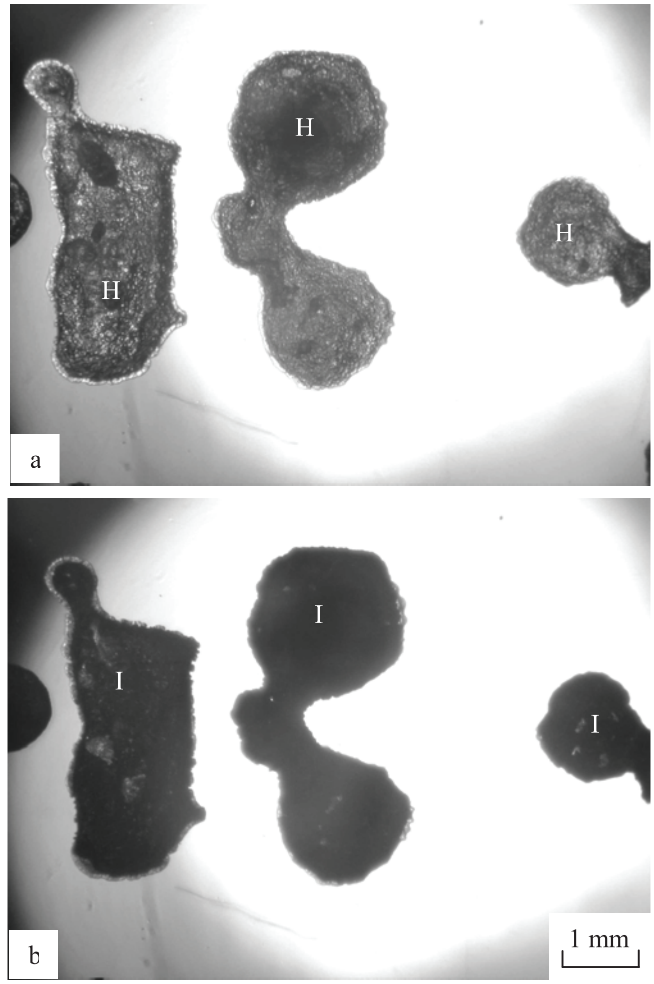

Figure 6. Dissociation of methane hydrates formed on water droplets. P_d = 5.64 atm, T = 243.15 K. a – 0 min (at the beginning of dissociation); b – 8 min.

curve for water–hydrate–gas in the metastable area of supercooled water (Fig. 3). The reasons for this deviation are still unclear. Appearance of the liquid phase was observed during propane hydrate dissociation below 263 K, however the induction time for its subsequent solidification did not exceed a few seconds. In the experiments with methane hydrates, only changes in the color of the hydrate samples were observed during the hydrate dissociation at T<253 K, whereas a distinct liquid phase was not observed (Fig. 6). Eight minutes from the beginning of the dissociation, no changes were observed within the reactor at 5.64 atm and 243.15 K. Because the dark solid droplets, formed during the methane hydrate dissociation (Fig. 6b) melted to liquid at 273.15 K, we have concluded that they were composed of water ice.

Conclusions

Visual observations of gas hydrate formation on water droplets and their dissociation at temperatures below 270 K were made. Direct optical evidence of the formation of metastable(supercooled) water during hydrate dissociation (between 257–270 K for propane hydrates and between

253–270 K for methane hydrates) were obtained for the first time. The induction time for recrystallization (freezing) of this supercooled water ranged from tens of hours at 270 K to a few seconds at 257 K. The dissociation pressures of gas hydrates formed on water droplets were measured. Molar enthalpies for the dissociation of these hydrates (into supercooled water and gas) were calculated based on the experimental pressure data. In the range of 263–273 K for propane hydrates and 253–273 K for methane hydrates, the calculated molar enthalpies are in good agreement with the enthalpies of dissociation of bulk propane hydrates and methane hydrates into water and gas at T>273.15 K. The data obtained supplement our knowledge about the mechanism of the gas hydrates self-preservation effect and the possibility of the existence of metastable (relict) gas hydrates within permafrost due to this effect.

Acknowledgments

This work was supported by the Russian Foundation for Basic Research (project no. 07-05-00102) and the Program for Basic Research of the Presidium of the RAS (project no.16.4.2). The authors are very grateful to Fred Wright from the Geological Survey of Canada and to an anonymous reviewer, who have improved the paper.

References

Dallimore, S.R. & Collett, T.S. 1995. Intrapermafrost gas hydrates from a deep core hole in the Mackenzie Delta, Northwest Territories, Canada. *Geology* 23(6): 527-530.

Ershov, E.D. & Yakushev, V.S. 1992. Experimental research on gas hydrate decomposition in frozen rocks. *Cold Region Sciences and Technology* 20: 147-156.

Freer, E.M., Selim, M.S. & Sloan, E.D. 2001. Methane hydrate film growth kinetics. *Fluid Phase Equilibria* 185: 65-75.

Davidson, D.W., Garg, S.K., Gough, S.R., Handa, Y.P., Ratclife, C.I., Ripmeester, J.A., Tse, J.S. & Lawson, W.F. 1986. Laboratory analysis of a naturally occurring gas hydrate from sediment of the Gulf of Mexico. *Geochimica et Cosmochimica Acta* 50: 619–623.

Genov, G., Kuhs, W.F, Staykova, D.K., Goreshnik, E. & Salamatin, A.N. 2004. Experimental studies on the formation of porous gas hydrates. *American Mineralogist* 89: 1228-1239.

Gudmundson, J.S., Andersson, V., Levik, O.I. & Mork, M. 2000. Hydrate technology for capturing stranded gas. *Annals of the New York Academy of Sciences* 912: 403-410.

Handa, Y.P. 1986. Compositions, enthalpies of dissociation, and heat capacities in the range 85 to 270 K for clathrate hydrates of methane, ethane, and propane, and enthalpy of dissociation of isobutene hydrate, as determined by heat-flow calorimeter. *Journal of Chemical Thermodynamics* 18: 915-921.

Makogon, Yu.F. 1981. *Hydrate of Natural Gas*. Tulsa: PennWell Books, 237 pp.

Melnikov, V.P., Nesterov, A.N. & Reshetnikov, A.M. 2003a. Kinetic of hydrate dissociation at a pressure of 0.1 MPa. In: M. Phillips, S.M. Springman & L.U. Arenson (eds.), *Permafrost.* Lisse: Swets & Zeitlinger, 753-757.

Melnikov, V.P., Nesterov, A.N. & Reshetnikov, A.M. 2003b. Mechanism of gas hydrate decomposition at a pressure of 0.1 MPa. *Doklady Earth Sciences* 389A: 455-458.

Peng, D. & Robinson, D.B. 1976. A new two-constant equation of state. *Industrial & Engineering Chemistry Fundamentals* 15: 59-64.

Rogers, R.E., Zhong, Y., Arunkumar, R., Etheridge, J.A., Pearson, L.E., McCown, J. & Hogancamp, K. 2005. Gas hydrate storage process for natural gas. *GasTIPS* 11: 14-19.

Sloan, E.D. 1998. *Clathrate Hydrates of Natural Gases*. Sec. ed. New York: Marcel Dekker, 705 pp.

Stern, L.A., Kirby, S.H. & Durham, W.B. 1996. Peculiarities of methane clathrate hydrate formation and solid-state deformation, including possible superheating of water ice. *Science* 273: 1843-1848.

Stern, L.A., Circone, S., Kirby, S.H. & Durham, W.B. 2001. Anomalous preservation of pure methane hydrate at 1 atm. *Journal of Physical Chemistry. B.* 105: 1756-1762.

Takeya, K., Nango, K., Sugahara, T. & Ohgaki, K. 2005. Activation energy of methyl radical decay in methane hydrate. *Journal of Physical Chemistry. B.* 109: 21086-21088.

Taylor C.J., Miller, K.T., Koh, K.A. & Sloan, E.D. 2007. Macroscopic investigation of hydrate film growth at the hydrocarbon/water interface. *Chemical Engineering Science* 62: 6524-6533.

Yakushev, V.S. & Istomin, V.A. 1992. Gas-hydrate self-preservation phenomenon. In: N. Maeno & T. Hondoh (eds.), *Physics and Chemistry of Ice.* Sapporo: Hokkaido University Press, 136-139.

Experimental Research on Physical-Mechanical Characteristics of Frozen Soil Based on Ultrasonic Technique

Qingzhou Meng
State Key Laboratory of Frozen Soil Engineering, CAREERI, CAS, Lanzhou 730000, Gansu, China
Dongqing Li
State Key Laboratory of Frozen Soil Engineering, CAREERI, CAS, Lanzhou 730000, Gansu, China
Jin Chen
State Key Laboratory of Frozen Soil Engineering, CAREERI, CAS, Lanzhou 730000, Gansu, China
Anhua Xu
Highway Research and Survey Design Institute of Qinghai Province, Xining, 810008, Qinghai, China
Shijing Huang
Highway Research and Survey Design Institute of Qinghai Province, Xining, 810008, Qinghai, China

Abstract

The research on frozen soil physical and mechanical characteristics has become a gradual focus in recent years. Traditionally, researchers take soil samples from the field and test their physical-mechanical characteristics in a laboratory using traditional universal testing apparatus. Although much useful data can be gained in this way, it is still time-intensive and uneconomical. The ultrasonic technique is an effective method to test physical-mechanical characteristics and is less expensive than traditional methods. According to the classical wave theory, there is a clear correlation between wave velocity and the medium characteristics. If we know the behavior of ultrasonic pulses in frozen soil, we will be able to obtain its physical-mechanical characteristic. In this article, the authors tested the ultrasonic pulses behavior in Lanzhou loess by RSM-SY5 ultrasonic apparatus. The results show clear correlation between frozen soil characteristics and ultrasonic behavior. From the results, the velocity of ultrasonic energy clearly increases with the decrease of temperature, and the change is especially prominent when the temperature exceeds -5°C. We also observed that the ultrasonic velocity increases with an increase in water content at the same temperature for the reason that ice content in frozen soil changes along with the water content. Based on the elasticity and laboratory test results, the dynamic properties of frozen soil can be determined. We conclude that the ultrasonic technique is a promising method that can substitute for traditional apparatus to test frozen soil characteristics.

Keywords: elastic modulus; frozen soil; physical characteristics; Poisson's ratio; shear modulus; ultrasonic velocity.

Introduction

The investigation on the physical-mechanical characteristics of frozen soil, along with the freezing consolidation in geotechnical engineering applications and the extensive development of the cold region, is currently a hot topic in the field of frozen soil. The present methodology, however, is labor-intensive because the researcher usually takes soil specimens from the field site and then tests them in the lab. According to classical wave theory, there is a close affinity between wave velocity and the physical-mechanical parameters of the propagating medium. Thus, if we can adopt ultrasonic detection, a simple and speedy method, to determine characteristics of frozen soil, it would be a significant work. In this article, in order to meet the need of rapid detection at the field site, the authors use the domestic RSM-SY5 ultrasonic apparatus to test the physical and mechanical properties of frozen soil. The results tend to summarize the relationship between wave velocity and the physical-mechanical properties of frozen soil.

Theory Basis of Ultrasonic Measurement

A certain point in the elastic medium is initially vibrated using an external or internal force. The vibration leads to wave formation and transmission in the medium. As an elastic wave, the process of a sonic wave transmission in the medium is a course of the transmission of the particle's elastic vibration. According to elastic mechanics, in an infinite medium, when the body force is neglected, we get the Lamei–Navier equation as follows:

$$Gu_{i,jj} + (\lambda + G)u_{j,ji} = \rho\ddot{u}_i \tag{1}$$

where ρ is the medium density, u represents the particle's displacement, and λ and G are Lamei coefficient.

When x_m is demanded to make partial derivative in Equation (1), we have:

$$Gu_{i,jjm} + (\lambda + G)u_{j,jim} = \rho\ddot{u}_{i,m} \tag{2}$$

In Equation (2), we contract the tensor's subscripts, i and m, and we note that volumetric strain θ is equal to $u_{i,i}$, so we have:

$$V_p{}^2\theta_{,jj} = \ddot{\theta} \tag{3}$$

where

$$V_p = \sqrt{\frac{\lambda + 2G}{\rho}} \tag{4}$$

Equation (3) is a wave equation, and it means that the velocity of volumetric strain in the medium is V_P; Equation (4) is the expression of transmission's velocity. If the coefficients λ and G are substituted by E and μ, we obtain:

$$V_p = \sqrt{\frac{E(1-\mu)}{\rho(1+\mu)(1-2\mu)}} \tag{5}$$

Exchanging the subscripts in Equation (2), we have:

$$Gu_{m,jji} + (\lambda + G)u_{j,jmi} = \rho\ddot{u}_{m,i} \tag{6}$$

According to strain analysis, the expression for the rotated tensor is:

$$\Omega_{im} = \frac{1}{2}(u_{m,i} + u_{i,m}) \tag{7}$$

Subtracting Equation (7) from (6), we obtain the expression of the rotated tensor that should meet the equation below:

$$V_s^2\Omega_{im,jj} = \ddot{\Omega}_{im} \tag{8}$$

$$V_s = \sqrt{\frac{G}{\rho}} \tag{9}$$

Equation (8) is the rotation part of the strain and means that, in the medium, strain transmission velocity is V_s. Equation (9) is the expression for the transverse waves. Employing E and μ to express Equation (9), we obtain:

$$V_s = \sqrt{\frac{E}{2\rho(1+\mu)}} \tag{10}$$

When the characteristic of the transmission of supersonic in the medium is obtained, we could measure the dynamical coefficients of the medium, such as E, G, μ and :

$$\left.\begin{aligned} E &= \frac{\rho V_s^2(3V_p^2 - 4V_s^2)}{V_p^2 - 2V_s^2} \\ G &= \rho V_s^2 \\ \mu &= \frac{V_p^2 - 2V_s^2}{2(V_p^2 - V_s^2)} \end{aligned}\right\} \tag{11}$$

where E is elastic modulus, G is shear modulus, and μ is Poisson's ratio.

From Equations (4) and (9), we know that the elastic wave velocity is determined by the characteristic of the medium and that, when the medium changes, the velocity is also changed. On the contrary, if the medium density and the characteristic of sonic transmission are known, we can derive the dynamic coefficients of the medium. Thus, we can employ the material's ultrasonic characteristics to analyze the medium's physical characteristics and to measure the material's dynamical coefficients such as the dynamic elastic modulus and the Poisson ratio. Although frozen soil cannot be considered as a completely elastic material, its elastic characteristic improves under comparative low temperature and, under the same stress level, the strain decreases with a reduction of the environmental temperature. The elastic strain is the most part one when the temperature is deceasing and therefore we can obtain the physical-mechanical characteristic of frozen soil by analyzing the transmission characteristics of supersonic in the frozen soil.

Table 1. Physical parameters of Lanzhou loess.

Grain component (%)			ω_p (%)	ω_L (%)
> 0.075mm	0.025 ~0.075	< 0.025mm		
10.04	48.17	41.58	14.92	29.36

Experimental Methodology

Specimen preparation

The material used in the experiment was Lanzhou loess; its main physical parameters are as follows:

In order to ensure sample uniformity, which can ensure the comparability of the experimental results, we employ a remodeling artificial freezing method to produce the sample. First, undisturbed soil is dried, pulverized, and sifted. We then test the initial water content and subsequently beat up loess uniformly. After that, we load the soil sample into a columned mould with a diameter of 61.4 mm and height of 125 mm and then compact the sample. Second, we put the soil sample into a temperature-controlled refrigerator and remove the mould after 24 hours of freezing. The quantity, height, and diameter of each sample is precisely tested. Last, we place the sample in a temperature-controlled refrigerator and freeze it under required temperature. In addition, in the course of producing the sample, we reassure that at least three samples with the same water content are made.

The introduction of the ultrasonic system

The ultrasonic system used in this experiment consists of ultrasonic transducers and ultrasonic apparatus. The transducer, with a working frequency of from 20 kHz to 50 kHz, is a ceramic transducer. The ultrasonic apparatus, made in the Institute of Rock and Soil Mechanics, Chinese Academy of Science, is a RSM-SY5 digital unit. It has a visualized interface and is easy to operate. Meanwhile, the data can be accessed and refreshed, and the transmit time and amplitude can be identified.. A picture of the ultrasonic system is showed in Figure 1.

Figure 1. Ultrasonic system.

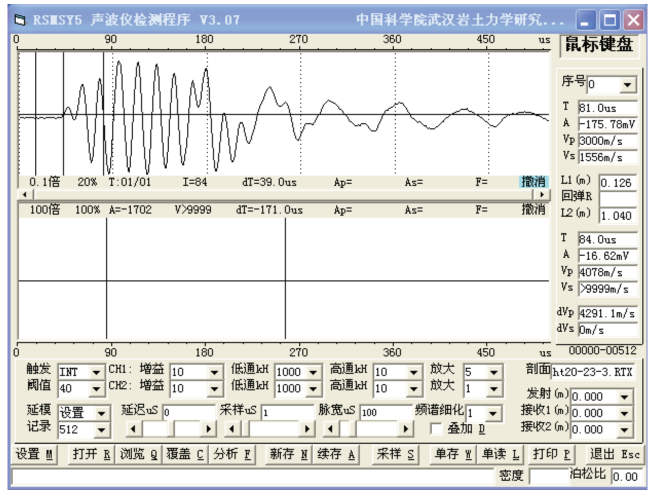

Figure 2. Screen shot of the ultrasonic software display.

Ultrasonic measurement procedure

At first, specimens were held for about 24 hours under a given testing temperature in the temperature-controlled refrigerator before it was tested. It was then placed into a thermostat tank, where the transmitting transducer and the receiving transducer were firmly pressed onto the end of the specimen. We should note here that good acoustical coupling between the soil sample surface and the face of the transducers is essential, as the ultrasonic waves cannot pass through air gaps between the transducer and the specimen. In this study, petroleum jelly was used as coupling media to improve the bonding between the transducers and the frozen soil specimen for compression wave and shear wave transmission. Finally, it sends an electric pulse (using a pulse generator) at a desired interval to both the transmitter on the end of the sample and the computer. This signal simultaneously triggers the computer to record and excites the transmitting transducer to vibrate at a frequency of 50 kHz. The vibration propagates through the frozen soil sample and arrives at the other end, where it is reconverted into an electrical signal by the receiving transducer. The operation is repeated many times. The wave travel time is determined by the time of the wave application and the time of wave arrival at the opposite end of the sample. The velocities of the waves were obtained as the quotient of the travel path to the wave travel time.

Experimental Results and Analysis

Both temperature and water content are important factors influencing the strength of frozen soils. In this research, the ultrasonic wave velocity in frozen soil at seven different temperatures and four different water contents was tested. From this experiment, we can infer the relationship between them.

Dilatational and shear wave velocity

The test results were shown in Figures 3 and.4 as follow. From the results, the velocity of ultrasonic wave was clearly increased with the decrease of temperature, and the change is especially prominent when the temperature exceeds -5°C. The reason is that the unfrozen water content became progressively smaller with the gradual reduction in temperature and the simultaneous increase of close-contact ice, intensified ice itself. From these figures we also can see that the ultrasonic velocity increased with the increase in water content at the same temperature; the reason is that the ice content in frozen soil changes along with the water content. If the water content is small, the ultrasonic velocity is largely determined by the contact condition of the soil grains; however, when the water content is large, the increased density of frozen soil will be helpful to the transmission of ultrasonic energy.

Dynamical parameters

If we take the frozen soil as an isotropic medium, dynamic modulus may be determined for frozen soil from a knowledge of the velocities of dilatational and shear waves. Hence, the dynamic elastic modulus E, dynamic shear modulus G and Poisson's ratio μ can be calculated as follows:

$$\begin{cases} E = \dfrac{\rho V_s^2 (3V_p^2 - 4V_s^2)}{V_p^2 - 2V_s^2} \\ G = \rho V_s^2 \\ \mu = \dfrac{V_p^2 - 2V_s^2}{2(V_p^2 - V_s^2)} \end{cases}$$

where V_p is velocity of the dilatational wave, V_s is velocity of the shear wave, ρ is density of the specimen.

Based on the formulas mentioned above and the laboratory test results, the dynamic properties of frozen soil can be determined. The results are presented in the following figures.

As seen in the figures, the dynamic elastic modulus and the dynamic shear modulus increase with a reduction in temperature. The variation trend of the dynamic modulus with the temperature reduction is in agreement with results

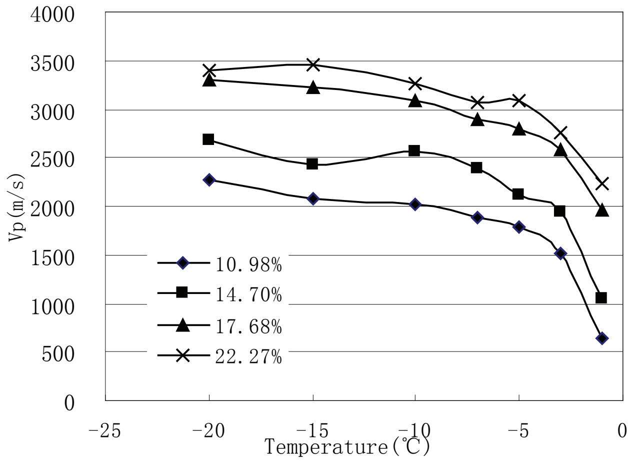

Figure 3. Relationship between temperature and compression wave velocity.

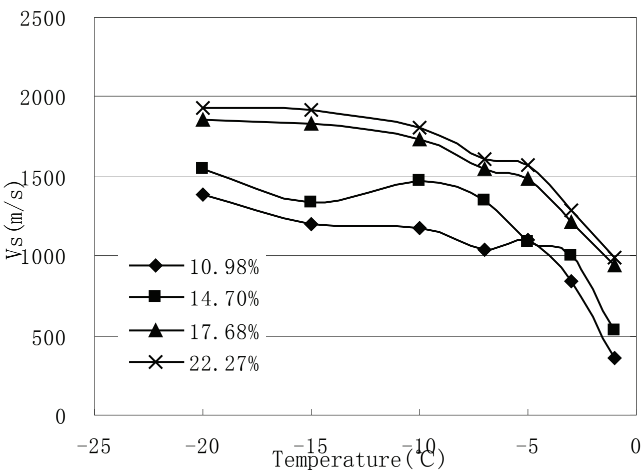

Figure 4. Relationship between temperature `and shear wave velocity.

obtained by a traditional universal test machine. The dynamic modulus has a close relation with water content such that the larger the water content, then the bigger the dynamic modulus. Compared with a universal material test machine, Poisson's ratio can be easily obtained by the ultrasonic apparatus. We can see from Figure 7 that, when the temperature increases, Poisson's ratio increases accordingly.

Conclusion

The wave velocity of ultrasonic energy in frozen soil decreases with temperature rising and increases with water content rising. Such velocity reflects the dynamical properties of frozen soil. Thus, using ultrasonic technology, we can instantly detect the dynamical coefficients of frozen soil. Furthermore, by this investigation method, we find that ultrasonic parameters can be used to estimate the mechanical properties of frozen soil. Therefore, in freezing consolidation and engineering construction in cold regions, in order to provide a powerful guarantee to such engineering, we can promptly test the mechanical properties of frozen soil at the site by ultrasonic techniques.

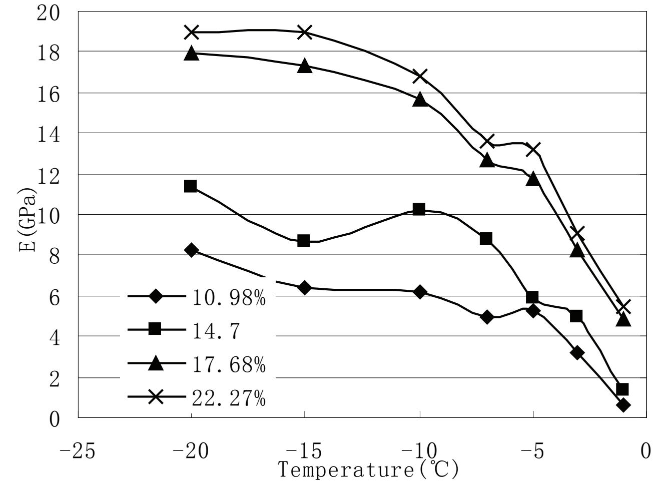

Figure 5. Relationship between temperature and dynamic elastic modulus.

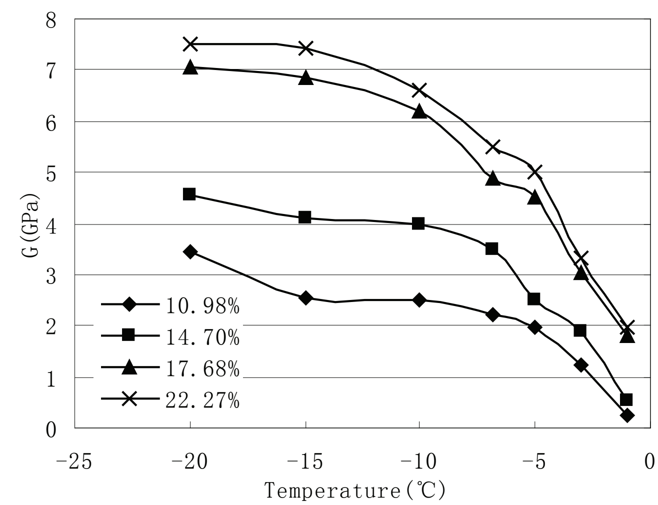

Figure 6. Relationship between temperature and dynamic shear modulus.

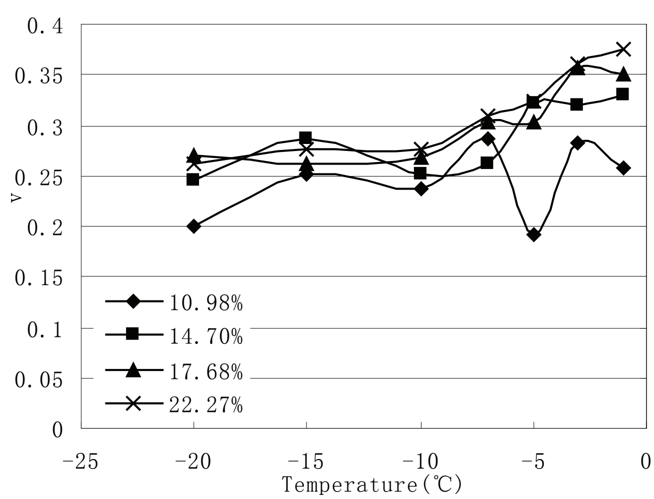

Figure 7. Relationship between temperature and Poisson's ratio.

Acknowledgments

This research was supported by the National Natural Science Foundation of China (No.40671039), the talent project of Cold and Arid Regions Environmental and Engineering Research Institute (No.2004122), the grant of the Knowledge Innovation Program of the Chinese Academy of Sciences (No.KZCX3-SW-351) and the key project of NSFC (No.40730736).

References

Lu Mingwan & Luo Xuefu. 2001. Foundations of Elasticity [M]. Beijing: Tsinghua University Press.

Ma Qin-Yong. 1998.Wave Velocity and Blast Ability Test on Artificially Frozen Soils [J]. *Journal of Glaciology and Geocryology.*

Sheng Yu, Fukuda Masami, Kim Hakasam & Imamura Tohru. 2000. Effect of unfrozen water content on the ultrasonic velocities in tire-mixed frozen soils [J]. *Chinese Journal of Geotechnical Engineering*.

Wu Shiming & Chen Longzhu.1989. Propagation velocities of elastic waves in saturated soils [J]. *Applied Mathematics and Mechanics.*

Effects of Retrogressive Thaw Slumps on Sediment Chemistry, Submerged Macrophyte Biomass, and Invertebrate Abundance of Upland Tundra Lakes

P.S. Mesquita
Water and Climate Impacts Research Centre, Department of Geography, University of Victoria, Victoria, Canada
F.J. Wrona
Water & Climate Impacts Research Centre, Environment Canada, Department of Geography, University of Victoria, Canada
T.D. Prowse
Water & Climate Impacts Research Centre, Environment Canada, Department of Geography, University of Victoria, Canada

Abstract

Global warming is forecasted to cause significant thawing of the permafrost that surrounds lakes and rivers across the Arctic, with wide-scale effects on the water quality and biotic characteristics of these water bodies. The benthic environment is believed to be especially sensitive to permafrost-induced ecological change, and this has been the focus of recent field-intensive research. Five lakes affected and three lakes not affected by retrogressive thaw slumps were sampled during late summer of 2006 to assess the potential effects of slumping on benthos. Water quality parameters, submerged macrophytes, benthic invertebrates, and sediment were collected. GLM, Kruskal-Wallis, and ANOVA were used to test for differences between both groups, as well as for possible interaction effects from sample depth. A significant difference (p<0.05) between disturbed and undisturbed lakes was found for macrophyte, invertebrates, underwater light attenuation, and some sediment variables. The results suggest that thaw slumps can affect the freshwater food-web through an increase in benthic production.

Keywords: invertebrates; macrophytes; permafrost retrogressive thaw slumping; sediment chemistry; tundra lakes.

Introduction

The arctic region has been predicted to be especially sensitive to the impacts of global warming (ACIA 2005). It is forecasted that warming will cause significant thawing of the permafrost that surrounds the lakes and rivers that dominate much of the arctic landscape.

Permafrost terrains in non-bedrock areas commonly have an ice-rich zone at the top of the permafrost table that are formed from downward moisture movement from the active layer at the end of summers and upward moisture movement from permafrost at winter. The seasonal leaching from thawed soils and ionic movement resultant from thermal induced moisture migration contribute to the solute enrichment encountered at the near-surface permafrost (Kokelj & Burn 2003, 2005).

Deepening of the active layer in a warmer climate can lead to the release of these solutes at near-surface permafrost increasing nutrient input to freshwater bodies, which in conjunction with a raise in solute-rich runoff from the landscape will probably affect primary production (Wrona et al. 2005, Hobbie et al. 1999). It is further predicted these changes will consequentially be reflected in modification of food-web structures and biogeochemical cycles (Wrona et al. 2005).

Considering that benthic production can be an important part of the overall primary and secondary production in arctic lakes (Sierszen et al. 2003, Rautio & Vincent 2007) a more comprehensive understanding of the effects of permafrost slumping on the benthic compartment is warranted. Among the benthic biota, a special focus should be placed on macrophytes as they contribute significantly to primary production, increase habitat heterogeneity (being beneficial to benthic invertebrates and fishes), and are involved in other important in-lake processes (Vadebouncoeur et al. 2003, Kalff 2001).

Many variables have been considered important for macrophyte production, such as underwater light availability, water nutrient content, lake morphology, littoral slope, sediment composition, and organic matter content. Lake sediment, besides acting as a base for physical attachment, has been recognized as an important source of nutrient supply to submerged macrophytes (Barko et al. 1991).

Some studies have already documented differences in lake water chemistry related to permafrost retrogressive thaw slumps (e.g., Kokelj et al. 2005) in a number of lakes in the area between Inuvik and Richards Island, Northwest Territories, Canada. However, the role of such landscape-related slumping on sediment loading, chemistry, and benthic biota still remains unclear and is predicted to be more frequent in a warmer climate (Wrona et al. 2005). This study focused on investigating the hypothesis that retrogressive slumping can produce significant differences in sediment and water chemistry, submerged macrophyte biomass, and benthic invertebrate abundance between undisturbed (U) and disturbed (D) lakes in a similar geographical region.

Lake Selection and Sampling Methodology

To test the above hypothesis, a set of lakes were selected between Inuvik and Richards Island (N.W.T). Based on lake/catchment characteristics and water quality data from a 60-lake survey (Thompson, unpubl.) and field logistics, a final subset of 3 lakes not affected by retrogressive slumping

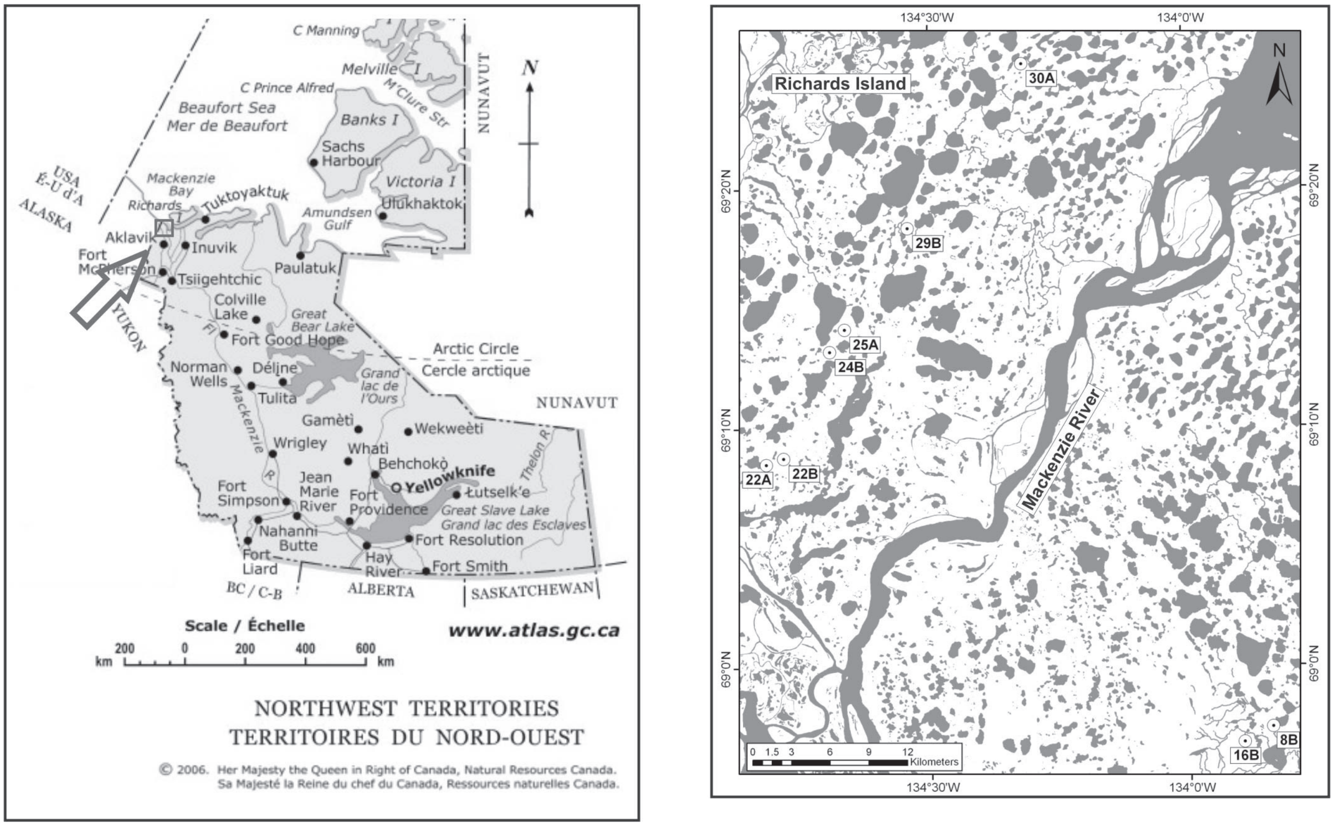

Figure 1. Geographic location of studied lakes. Source: Natural Resources Canada/CanVec (www.geogratis.gc.ca).

(undisturbed or *U* lakes) and 5 lakes affected (disturbed or *D* lakes) were selected for detailed study (Fig 1, Table 1). Disturbed lakes were sampled in two areas: one located at the opposite side (*Do*) of the physical disturbance caused by the slump, and another one in an area adjacent (*Da*) to the slump and thus directly physically affected by the disturbance. This allowed for testing whether undisturbed lakes are similar in their physical, chemical, and biological properties to disturbed systems (particularly with areas in disturbed lakes that are physically removed from the slump (*Do*).

Stratified radial transects starting from the shoreline towards the center of the lake were used as the main sampling unit (replicate) in the present study, and were distributed in order to encompass the different areas of each lake. Taking into consideration the focus on the littoral benthos, sampling points were randomly placed in 1 m, 2 m, and 3 m deep strata along the transects, yielding a maximum of 9 replicates (3 depths x 3 transects) in undisturbed lakes and a maximum of 18 replicates in disturbed lakes (9 in each disturbance zone - *Do* and *Da)*. However, due to logistical constraints in the field, some variables could not always be sampled at all strata depths in all lakes.

Between the end of August and the beginning of September 2006, samples of sediment, submerged macrophytes, benthic invertebrates, and pelagic water were taken from the selected lakes. In addition, interval measurements of underwater photosynthetic active radiation (PAR) (Li-cor LI-192) were taken at each of the transect points from the near surface to the maximum depth of one meter or before reaching the top of macrophytes. The results were used to calculate the light underwater attenuation coefficient (K_d) at each point in accordance with Kalff (2001).

Submerged macrophytes were collected at 1 m, 2 m, and 3 m deep strata with a telescopic macrophyte sampler (Marshal & Lee 1994) that covered an area of 0.164 m^2. The macrophytes were subsequently separated, washed, and oven-dried to a constant weight at 60°C for dry weight determination, and then extrapolated to represent a total biomass per m^2.

Sediment samples were collected with a sediment corer at 1 m and 3 m depths. Samples from the top 15 cm were transported to the laboratory, homogenized, and separated into two fractions. One fraction was frozen, freeze-dried, and sent for analysis of recoverable metals (i.e., environmentally available) and nutrients at the Environment Canada National Laboratory for Environmental Testing (NLET), Burlington, ON (Table 2).The remaining fraction was oven-dried and burned for calculations of loss of ignition (as a measure of organic matter content) in accordance with Hakanson & Jansson (1983).

Sediment samples for estimating invertebrate abundance were collected at 1 m, 2 m, and 3 m depths. Samples from the top 5 cm were washed through a 250 µm sieve, and the invertebrates were subsequently sorted, counted, and extrapolated to 1 m^2. Water physico-chemical parameters were collected at the deepest point in each lake previously determined from a bathymetric survey. A handheld

Table 1. Lake attributes summary table. Lake area (La), catchment area: lake area (Ca:La) ratio, catchment area: lake volume (Ca:Lv) ratio, maximum depth (Zmax), mean depth (Zmean), lakes (*U*= undisturbed, *D*= disturbed), number of lakes (N), mean, standard deviation (S.D), minimum and maximum values (Min and Max).

Lakes		La (m^2)	Ca:La	Ca:Lv	Zmax	Zmean
U lakes	Mean	40100	4.78	1.77	7.30	2.88
N= 3	S.D	19419	0.44	0.14	2.88	0.92
	Min.	18700	4.28	1.61	4.20	1.92
	Max.	56600	5.11	1.88	9.90	3.76
D lakes	Mean	76380	3.99	1.15	9.54	3.48
N= 5	S.D	40514	1.18	0.63	4.33	0.80
	Min.	35500	2.41	0.66	5.30	2.44
	Max.	142900	5.04	2.01	16.80	4.52

multiparameter Y.S.I was used to collect pH, temperature, and conductivity data. In addition, water samples were collected and sent to the NLET lab for analysis of particulate organic carbon (POC), dissolved phosphorus (DP), orthophosphate (OP), total phosphorus (TP), ammonium (NH_3N), nitrite-nitrate (NO_3NO_2), total dissolved nitrogen (TDN), particulate organic nitrogen (PON), and total nitrogen (TN).

Statistical analyses

All the variables were tested for normality using a Kolmogorov-Smirnov (K-S) test ($p<0.05$) and, when necessary, $\log_{10}$ transformed to fit the assumptions of parametric testing. General Linear Model (GLM) regressions were performed to test for differences in sediment chemistry and invertebrate abundance between undisturbed (*U*) and disturbed (*D*) lakes, using depth as a co-variate.

In cases where a significant difference (p<0.05) between disturbed and undisturbed lakes was found, a subsequent GLM with a Bonferroni simultaneous *a posteriori* test between lake/disturbance location (*U, Do* – opposite to slump, *Da* – adjacent to slump) and depth was performed. These analyses were used to ascertain whether the differences were related to in-lake processes (*Do* vs. *Da*) versus between lake (*U* vs. *Da*, *U* vs. *Do*) processes and physical proximity to the slump.

Since some sediment variables and macrophyte biomass data were not normally distributed even after transformation, the non-parametric Kruskal-Wallis test was used in these cases. As water nutrient data were only collected at one station per lake system, differences between undisturbed and disturbed lakes were analyzed using one-way Analysis of Variance (ANOVA). All the analyses were performed with MINITAB 13.1 (Minitab Inc. 2000).

Results

ANOVA tests for water nutrient data between undisturbed and disturbed lakes revealed no significant differences ($p>0.05$) for all measured constituents (POC, DP, OP, TP, NH_3N, NO_3NO_2, TDN, PON, TN). However, pH (mean = 7.6 in *U* vs. 8.19 in *D*) and specific conductivity (mean = 128.6 µS/cm in *U* vs. 516.7 µS/cm in *D*) were significantly different ($p<0.05$).

Table 2. List of key nutrient, metals and metalloids analyzed from sediment samples.

Carbon (organic/inorganic)	Sodium (Na)	Potassium (K)	Arsenic (As)
Nitrogen (organic)	Zinc (Zn)	Calcium (Ca)	Beryllium (Be)
Phosphorus (inorganic)	Cooper (Cu)	Magnesium (Mg)	Bismuth (Bi)
Phosphorus (P)	Nickel (Ni)	Iron (Fe)	Cadmium (Cd)
Manganese (Mn)	Molybdenum (Mo)	Cobalt (Co)	Gallium (Ga)
Antimony (Sb)	Lanthanum (La)	Chromium (Cr)	Aluminum (Al)
Thallium (Tl)	Lithium (Li)	Strontium (Sr)	Rubidium (Rb)
Uranium (U)	Lead (Pb)	Vanadium (V)	Barium (Ba)

GLM tests revealed significant differences (p<0.05) in only seven sediment variables between *U* and *D* lakes. Mg and Ca means showed highly significant differences, (p<0.01) with higher values in *D* lakes (Ca= 4.85 g/Kg in *U* vs. 9.44 g/Kg in *D*, and Mg= 5.74 g/Kg in *U* vs. 7.35 g/Kg in *D* (Fig. 2)).

Organic N and C, As, Ni, and Zn were also significantly different between *U* and *D* lakes ($p<0.05$). However, the highest mean values for these variables consistently occurred in undisturbed (*U*) lakes. The mean values of each of the variables for *U* and *D* were 7.29% and 4.90% of organic C, 0.61% and 0.34% of organic N, 0.02 g/Kg and 0.015 g/Kg of As, 0.052 g/Kg and 0.041 g/Kg of Ni, and 0.137 g/Kg and 0.106 g/Kg of Zn, respectively (Fig 2).

Bonferroni *a posteriori* testing revealed no significant differences (p>0.05) between in lake disturbance regions (*Da* and *Do*) and between disturbed regions and *U* lake comparisons for As, Ni, and Zn.

Mg and Ca were not significantly different between *Da* and *Do*, but were different between these regions and undisturbed lakes. In contrast, organic N content in *Da* (0.24%) was significantly different (p<0.05) from *Do* (0.24% vs. 0.44%), and highly significantly different (p<0.01) to undisturbed lakes (0.61%). Organic C was only significantly different (p<0.05) between *Da* and *U* lakes. These indicated that *Do*, a region within the disturbed systems, was similar to a "control" undisturbed lake for the variables organic N and C.

Kruskal-Wallis tests on Mn, Co, Sr, and ignition loss showed a significant difference ($p<0.05$) between *U* and *D* lakes. Median Mn concentrations varied from 0.83 g/Kg in *U* versus 0.42 g/Kg in *D*-lakes; Co ranged from 0.015 g/Kg on *U* to 0.013 g/Kg on *D*; ignition loss varied from 13.26% on *U* to 9.67% on *D*; and Sr, the only of these variables with

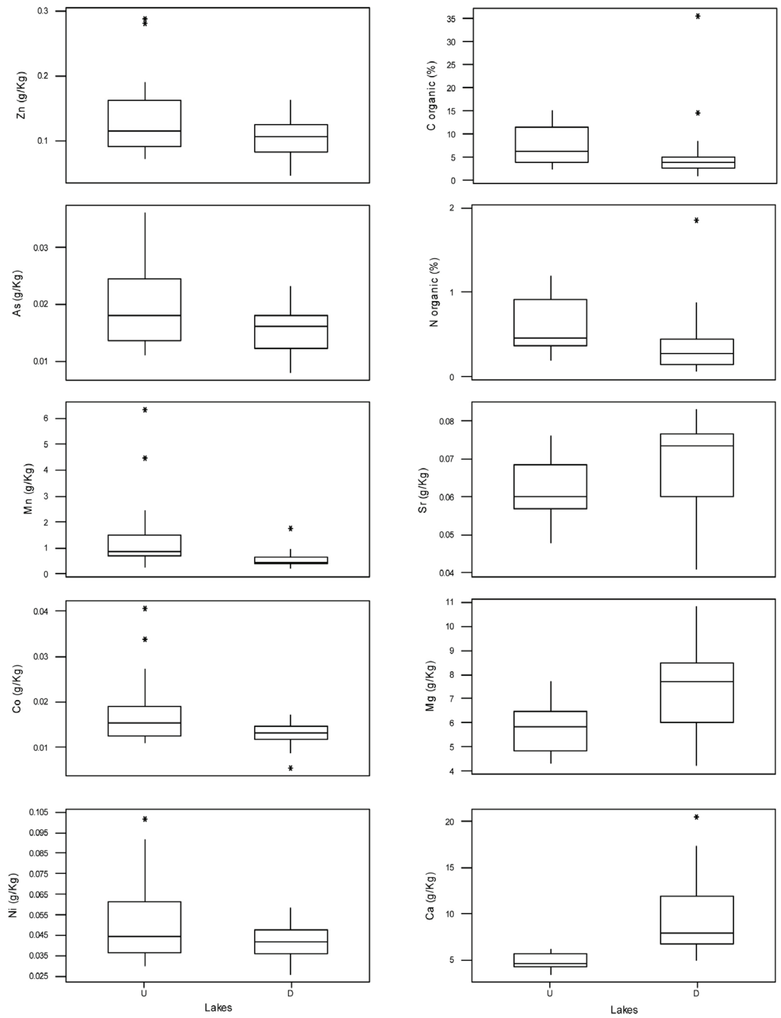

Figure 2. Box plots for sediment chemistry variables that were significantly different between undisturbed (*U*) and disturbed (*D*) lakes. All variables in g/Kg with the exception of C and N in %.

higher values in *D*, varied from 0.06 g/Kg on *U* versus 0.073 g/Kg on *D* (Fig2).

Mn, Co, and Sr were not significantly different between *Do* and *Da* regions ($p>0.05$) but were different to the undisturbed lakes. Ignition loss results had a similar pattern as found from the Bonferroni test for organic C. The K-W test revealed that only *Da* was significantly different from *U* ($p<0.05$). Correlation analysis showed a strong positive association between organic C and ignition loss ($r = 0.947$, $p<0.01$).

Although the median values for macrophyte biomass were the same (zero) at *U* and *D* lakes, the distributions were significantly different ($p<0.01$) according to Kruskal-Wallis test, with higher values on *D* lakes. This can be explained by the fact that macrophytes were more frequently found in *D* lakes (44%) than in *U* lakes (11%). The biomass present on *Do* was significantly different from *Da* and *U* lakes ($p<0.01$), while differences between *U* lakes and *Da* were not significant ($p>0.05$) (Table 3).

The difference in invertebrate abundance between *U* and *D* lakes was highly significant ($p<0.01$), with higher abundance values in *D* lakes. Differences between *U*, *Do* and *Da* were also significant, with *Da* having the highest abundance and being different from *U* ($p<0.01$), and from D*o* ($p<0.01$). Also, the interaction between *U/D* lakes and depth was significant ($p<0.05$), indicating a covariation between these two variables (Table 4).

Discussion and Conclusions

Significant differences were found between disturbed and undisturbed lakes for a variety of environmental variables. In general, disturbed lakes exhibited higher mean values of Mg, Ca, and Sr in sediments, and pH and conductivity in the water column. Undisturbed lakes had higher levels of organic C and N, As, Ni, Zn, Mn, Co, and organic matter in the sediment, and higher values of littoral underwater light coefficient of attenuation (K_d). The conductivity pattern is in accordance with previous observation by Kokelj et al. (2005), where lakes with catchments disturbed by thermokarst slumping had higher water ionic content and conductivity than undisturbed lakes in the same geographic area.

Macrophyte biomass and invertebrate abundance were higher in disturbed lakes, being postulated that this difference

Table 3. Macrophyte biomass (g/m^2) summary data from all lake, *U*, *D*, *Do*, and *Da*. Number of sample points (N), number and percentage of cases where macrophytes were present (N_p), minimum and maximum biomass (Min., Max.), median, and first and third quartiles (Q1, Q3).

Lakes/Areas	N	N_p and % presence	Min.	Max.	Median	Q1	Q3
All lakes	90	31 (34%)	0	705.5	0	0	19.21
Undisturbed lakes (*U*)	27	3 (11%)	0	24.268	0	0	0
Disturbed lakes (*D*)	63	28 (44%)	0	705.5	0	0	55.9
Opposite region (Do)	33	24 (72%)	0	705.5	28.7	0	104.1
Adjacent region (Da)	30	4 (13%)	0	76.22	0	0	0

is related to higher water transparency and concentrations of key chemical elements originated from the slump and transferred to the sediment. Thus, it is expected that a higher availability of nutrients for the growth and maintenance of macrophyte community produce a structurally more complex benthic habitat, having a positive effect on benthic invertebrates.

Previous studies have suggested that the sediment is the primary source of N, P, Fe, Mn, and other micronutrients necessary for macrophyte metabolism (Barko et al. 1991). However, the present study did not find macrophytes predominant at lakes with higher levels of organic N and Mn (undisturbed lakes). A possible explanation is that higher amounts of organic matter found in the sediment of undisturbed lakes could be affecting nutrient availability and uptake processes (Barko & Smart 1986).

In addition to decreased nutrient availability due to complexation with organic matter in organic sediments, macrophyte growth can be disrupted by the presence of phytotoxic compounds produced during anaerobic decomposition (Barko et al. 1991) For instance, accumulation of large quantities of refractory organic matter in sediments are shown to decrease nutrient availability and the growth of rooted submerged macrophytes, while additions of low quantities of labile organic matter in sediments may benefit macrophytes, especially on coarse textured sediments in oligotrophic systems (Barko et al. 1991).

With the exception of organic N, all the sediment variables and the light attenuation coefficient values were not significantly different within disturbed lakes, leading to the question of what factors might be influencing the absence of macrophytes in areas adjacent to the actual slump (*Da*). Since submerged macrophyte biomass is documented to be related more to underwater substrate slope at depths where irradiance is not the primary limiting factor (Kalff 2001), slope and related substrate stability is postulated to be the major factor influencing the almost complete absence of macrophytes in *Da* areas.

Based on preliminary results of bathymetric surveys and field observations, the underwater substrate slope near the slump disturbance is consistently higher than observed in opposite areas in the same lake or in undisturbed lakes. More detailed field analyses need to be conducted to determine the possible causal physical mechanism for this observation. It is possible that macrophyte colonization in disturbed areas is being constantly subjected to burial by soil and vegetation from the lakeshore slump.

Table 4. Invertebrate abundance (individuals/m^2) summary table from *U*, *D*, *Do,* and *Da*. Number of samples (N), minimum and maximum abundance (Min., Max.), mean, and standard deviation (S.D).

Lakes/Areas	N	Min.	Max.	Mean	S.D
Undisturbed lakes (*U*)	26	3215	39460	13232	8786
Disturbed Lakes (*D*)	68	2037	119549	28630	24482
Opposite region(Do)	35	2037	97334	22247	22818
Adjacent region (Da)	32	4584	119549	35631	25055

The observed water transparency and related light penetration values (PAR) in the littoral zone of disturbed lakes also contradicts what would be expected in a scenario of higher suspended sediments and color (dissolved organic carbon) arising from the input of landscape material into the lake water.

Two possible mechanisms could be operating individually or jointly to produce these observed patterns. First, higher ionic concentrations supplied to the lakes from the enriched slump runoff as those shown in Kokelj et al. (2005) could be adsorbing to organic compounds on the water column, causing them to precipitate and "clearing" the water. Secondly, adsorption of organic substances to the exposed mineral soils could be producing runoff with low concentration of colored material in disturbed catchment, while in undisturbed ones colored runoff would be a result of water flux through the shallow organic soils (Carey 2003, Kokelj et al. 2005). Further process-based research is necessary to elucidate the relative importance of these two possible processes and some preliminary experiments examining possible causal mechanisms can be found in Thompson et al. (2008).

In general, benthic invertebrates were found to be more abundant in disturbed lakes. However, while it was expected that areas with more macrophytes would support higher number of invertebrates, areas adjacent to slumps were found to have the highest mean abundance. Other factors, such as periphyton and bacterial abundance, pH, and oxygen, could be influencing benthic invertebrate communities and this needs to be further explored.

In summary, a warmer climate regime accompanied by enhanced seasonal thawing of the active layer will significantly affect benthic macrophyte and invertebrate communities of upland tundra lakes. The present work shows that in addition to the changes in water column characteristics already documented in previous studies (Kokelj et al. 2005), thermokarst retrogressive slumping also affects sediment chemistry and water transparency relationships in upland tundra lakes. In addition to influences related to input of enriched runoff, deposition of landscape material (i.e., soil and terrestrial vegetation) at the littoral zone can have an impact in macrophyte colonization rates and littoral complexity, affecting benthic invertebrates and upper level consumers.

Complementing the mentioned processes, other environmental changes need to be taken into consideration when projecting the effects of a warmer climate on upland tundra lakes. Active layer deepening could act synergistically with higher temperatures, higher UV penetration in lakes, changes in biota composition/ metabolism, and changes in runoff input due to alterations of biogeochemical cycles at landscape level which could all ultimately lead to a variety of different balances. Contrary to the expected increase in pelagic productivity and decreased transparency associated with permafrost degradation (Wrona et al. 2005), it is suggested that at an earlier stage, increases in the macrophyte biomass associated with higher transparency could be a possibility, being later followed by greater disturbance of littoral zone and decrease of macrophyte communities.

Acknowledgments

This work was supported by the Water-Climate Impact Research Centre (W-CIRC), Environment Canada (E.C), University of Victoria (UVic), Natural Sciences and Engineering Research Council, Polar Continental Shelf Project, and Aurora Research Institute. We would like to thank Megan Thompson (UVic), Tom Carter (NHRC, E.C), and Daniel L. Peters (W-CIRC, E.C) for their helpful participation during field data collection, Patricia Chambers (E.C) for aiding in macrophyte identification, John Mollison (NHRC, E.C) for manufacturing the macrophyte sampler, Kristie S. Heard (U. of New Brunswick) for helping with invertebrate sample work, and Thiago S. F. Silva (UVic) for assistance in reviewing the manuscript.

References

ACIA. 2005. *Arctic Climate Impact Assessment.* Cambridge University Press, 1042 pp.

Barko, J.W., Gunnison, D. & Carpenter, S.R. 1991. Sediment interaction with submersed macrophyte growth and community dynamics. *Aquatic Botany* 41: 41-65.

Barko, J.W. & Smart, R.M. 1986. Sediment-related mechanisms of growth limitation in submersed macrophytes. *Ecology* 67(5): 1328-1340.

Carey, S.K. 2003. Dissolved organic carbon fluxes in a discontinuous permafrost subarctic alpine catchment. *Permafrost Periglac. Process.* 14: 161-171.

Hakanson, L. & Jansson, M. 1983. *Principles of Lake Sedimentology*. New York: Springer-Verlarg, 316 pp.

Hobbie, J.E., Peterson, B.J., Bettez, N., Deegan, L., O'Brien, W.J., Kling, G.W., Kipphut, G.W., Bowden, W.B. & Hershey, A.E. 1999. Impact of global change on the biogeochemistry and ecology of an Arctic freshwater system. *Polar Research* 18: 207-214.

Johnson, R.K. & Ostrofsky, M.L. 2004. Effects of sediment nutrients and depth on small-scale spatial heterogeneity of submersed macrophyte communities in lake Pleasant, Pennsylvania. *Can. J. Fish. Aquat. Sci*. 61: 1493-1502.

Kalff, J. 2001. *Limnology: Inland Water Ecosystems.* Prentice-Hall, 592 pp.

Kokelj, S.V & Burn, C.R. 2003. Ground ice and soluble cations in near-surface permafrost, Inuvik, Northwest Territories, Canada. *Permafrost and Periglacial Processes* 14: 275-289.

Kokelj, S.V. & Burn, C.R. 2005. Geochemistry of the active layer and near-surface permafrost, Mackenzie Delta region, Northwest Territories, Canada. *Can J. Earth. Sci.* 42: 37-48.

Kokelj, S.V., Jenkins, R.E., Milburn, D., Burn, C.R. & Snow, N. 2005. The influence of thermokarst disturbance on the water quality of small upland lakes, Mackenzie Delta Region, Northwest Territories, Canada. *Permafrost and Periglacial Processes* 16: 343-353.

Marshall, T.R. & Lee, P.F. 1994. An inexpensive and lightweight sampler for the rapid collection of aquatic macrophytes. *J. Aquat. Plant Manage.* 32: 77-79.

Minitab v.13.1. 2000. State College, PA.

Rautio, M. & Vincent, W.F. 2007. Isotopic analysis of the sources of organic carbon for zooplankton in shallow sub-arctic and arctic waters. *Ecography* 30: 77-87.

Sierszen, M.E., McDonald, M.E. & Jensen, D.A. 2003. Benthos as the basis for arctic food webs. *Aquatic Ecology* 37: 437-445.

Thompson, M.S., Kokelj, S.V., Prowse, T.D. & Wrona, F.J. 2008. The impact of sediments derived from thawing permafrost on tundra lake water chemistry: an experimental approach. *Proceedings of the Ninth International Conference on Permafrost, Fairbanks, Alaska, June 29–July 3, 2008* (this proceedings).

Vadeboncoueur, Y., Jeppesen, E., Vander Zanden, M.J, Schierup, H, Christoffersen, K. & Lodge, D.M. 2003. From Greenland to green lakes: cultural eutrophication and the loss of benthic pathways in lakes. *Limnol. Oceanograph*. 48: 1408-1418.

Wrona, F.J., Prowse, T.D. & Reist, J.D. 2005. Freshwater ecosystems and fisheries In: *Arctic Climate Impact Assessment*. Cambridge University Press, 354-452.

The Vault Creek Tunnel (Fairbanks Region, Alaska): A Late Quaternary Palaeoenvironmental Permafrost Record

Hanno Meyer
Alfred Wegener Institute for Polar and Marine Research, Research Unit Potsdam, Potsdam, Germany
Kenji Yoshikawa
Water and Environmental Research Center, Institute of Northern Engineering, University of Alaska Fairbanks, Alaska
Lutz Schirrmeister, Andrei Andreev
Alfred Wegener Institute for Polar and Marine Research, Research Unit Potsdam, Potsdam, Germany

Abstract

The Vault Creek (VC) gold mining tunnel north of Fairbanks, Alaska, is the deepest and longest permafrost tunnel ever made available for periglacial research. The VC tunnel sedimentary profile includes loess and fluvial gravels above bedrock and is, thus, comparable to the famous Fox permafrost tunnel. AMS ^{14}C dates from the VC tunnel indicate that loess accumulation took place around 40–50 ka BP, whereas the fluvial sediments show mostly infinite ^{14}C ages, confirmed by IRSL dates around 55–85 ka. However, the pollen record of the VC tunnel reflects very warm and unambiguously interglacial climate conditions with the occurrence of *Abies* and *Tsuga* in large parts of the spectra. The stable isotope composition of ice wedges also reflects warm climatic conditions in the lower part of the profile. Consequently, a very warm phase occurred in Central Alaska, whose timing is uncertain due to conflicting age determinations and proxy indications.

Keywords: Central Alaska; climate reconstruction; ground ice; permafrost dating; Quaternary environment.

Introduction

Permafrost consists of sediment and ground ice preserving suitable signals for the reconstruction of Late Quaternary environment and climate. Thermokarst, thermoerosion, and slumping often prevent the possibility of resampling a permafrost outcrop. Therefore, underground excavations and permafrost tunnels such as the Fox and Vault Creek (VC) tunnels, may serve as three-dimensional natural laboratories for permafrost studies including dating techniques.

Especially in Central Alaska, where the chronology of sediments is still insufficiently known for the interval between 25 and 100 ka BP (Berger 2003), such revisitable sites are valuable for regional environmental reconstruction. Dating of deposits in this region is based upon a variety of methods including thermoluminescence (TL), infrared or optical stimulated luminescence (IRSL, OSL), fission track (FT), and ^{14}C, which led (and may further lead) to a substantial improvement of the knowledge on timing and duration of Late Quaternary warm and cold phases in Central Alaska. Here we present new data from the Central Alaskan Vault Creek permafrost tunnel near Fairbanks.

Study Area

The Fairbanks area is characterized by discontinuous permafrost and a continental climate with mean annual air temperatures of about -3.0ºC and precipitation of 263 mm (at Fairbanks airport, 1971–2000). Presently, spruce-birch-aspen taiga dominates the vegetation. Permafrost may reach a thickness of up to 120 m and is relatively warm with ground temperatures about -0.8°C at 2 m below ground surface at the tunnel site. The active layer reaches about 0.3 to 0.4 m.

Figure. 1. Study site: The Vault Creek tunnel north of Fairbanks. Additionally, an open pit near Fox was sampled.

Permafrost usually dominates valley bottoms and north slopes, but is largely absent on south-facing slopes. The VC tunnel is situated on a north-facing slope. Frost cracking activity is presently reduced in Interior Alaska. In Wisconsin times, when mean air temperatures were 4°C lower, ice wedge formation was a more common process. In the

Fairbanks region, permafrost is generally considered to have thawed and reset after Sangamon interglacial (Pewe 1975).

The VC tunnel is situated about 40 km north of Fairbanks, Alaska. It was established in 1990 by a local private gold miner and is, to our knowledge, the deepest (>40 m) and longest permafrost tunnel (>200 m) for periglacial research. The entrance of the VC tunnel is secured by a 30 m long steel tube, which makes the uppermost part of the section inaccessible (Fig. 1). This part has been sampled in a 3.0-m-deep auger hole (26 inches or 0.65 m in diameter) located about 50 m ENE of the tunnel's entrance (Fig. 2).

Results

The methodological approach applied to the permafrost sequence of the VC tunnel includes different dating techniques, sedimentology, and palynology, as well as stable isotope geochemistry ($\delta^{18}O$ and δD) of ground ice.

Sedimentology

The sedimentary and geocryological sequence is similar to that of the Fox research tunnel constructed in 1963 by the US Army Corps of Engineers (CRREL). About 40 m of Quaternary deposits overlie weathered schistose bedrock ("Birch-Creek schist"). The Quaternary deposits are: **(1)** at the bottom, 17.5 m of fossiliferous ice-bonded fluvial gravels with several sand and peat lenses, as well as numerous wood remains (depth: 22.5–40.05 m). No ice wedges occur in the gravel horizon; **(2)** in the upper part, about 12 to 15 m of ice-rich silty sediments are found (depth: 3–15 m). These are loess-like, organic-rich, and contain fossil bones, as well as relatively large ice wedges. The silt horizon has a very uniform unimodal grain size distribution (mean 52 µm). Between these two units: **(3)** a 7.5 m thick transition horizon of fluvial gravels interbedding with loess-like silt and relatively small ice wedges was distinguished (depth: 15–22.5 m).

The general sequence is characterized by mean total organic carbon (TOC) content of about 3%. Two horizons of higher TOC content (of up to 18%) are found at about 7.5 m and 23.5 m depth, respectively. C/N ratios are around 8, but significantly higher (reaching 20) at the TOC-enriched horizons. Carbonate contents (Cc) are, in general, below 1.5% (mean Cc 1.1%), but reach a maximum of up to 4.3% at 22.5 m depth. The mass-specific magnetic susceptibility (MS) is low in the transition and gravel horizons (mean MS: 24 and 30.10^8 SI, respectively), whereas the silt displays higher mean MS of almost 70.10^8 SI. The ice contents are significantly higher in the silt (up to 60 wt%) as compared to the gravels (max. 20 wt%). Both ground ice and sediments were significantly deformed by post-depositional slope processes, especially in the upper part of the sequence.

Two 1 to 3 mm thick layers of tephra were detected in the tunnel at about 2 m depth and at about 15.4 m depth. These white ash layers are yet unidentified. Especially the upper tephra is disturbed by creeping or sliding of slope material. At 15.7 m, three up to 20 cm thick ice bands intersect with sediments and ice wedges. Contacts between ice wedges and

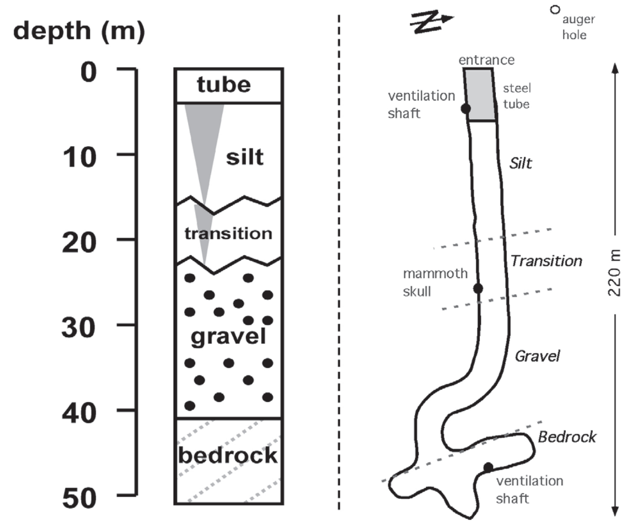

Figure 2. Schematic sedimentary profile of the VC tunnel and top view of the VC tunnel (schematic).

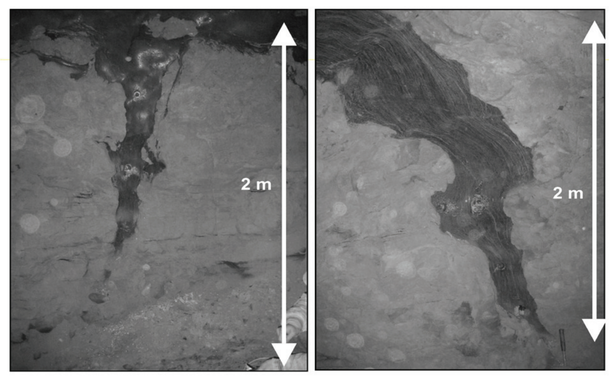

Figure. 3. Ice wedges of the VC tunnel of the silt horizon (left) and transition horizon (right). Note: deformation structures.

ice bands are similar to features interpreted as thermokarst-cave ice in the Fox tunnel (Shur et al. 2004) following melt and erosion of a part of an ice wedge by running water. No frost cracking occurred after refreezing of meltwater, so ice wedges were or became inactive after the melt event.

Geocryology

The different types of ground ice in the VC tunnel include massive ice such as: **(1)** ice wedges, the most important type of ground ice in the VC tunnel. These are associated only with the silt and transition horizons (Fig. 3).

They are wider (up to 3 m) and more strongly deformed in the upper section than in the transition horizon, where only small, vertically oriented ice wedges of 0.1-0.4 m in width were observed. Ice wedges in the silt horizon show signs of syngenetic growth. The inclination of ice wedges is stronger at the topmost part of the profile reaching up to 45–50° from the vertical line. This indicates a post-depositional transport of material e.g., by slumping or, more likely, by creeping without melting the wedge ice, which reacted plastically. Tops of ice wedges are visible in several cases, especially in the transition horizon; (2) thermokarst cave ice as also recognized in the Fox tunnel (Shur et al. 2004); and (3) a strange type of clear ice is observed at the wall with huge

Table. 1. Summary of all Radiocarbon and IRSL dated sediment and ice wedge samples of the VC tunnel, Fairbanks, Alaska

Sample ID	Depth (m)	Radiocarbon age (a BP)	Type of organic, Stratigraphic position	Lab number
FAI 4/7	0.75	2505 +/-25	wood remains in soil horizon (auger hole)	KIA 31128
FAI 4/5	1.35	3445 +/-35	soil horizon (auger hole)	KIA 31127
FAI 3/20	2.7	25,320 +/- 240	peat inclusion, topmost sample in VC tunnel (silt unit)	KIA 31125
FAI-1/42	2.8	45,120 +3300/-2330	grass roots (silt unit)	KIA 25271
FAI-1/40	4.6	44,220 +1700/ - 1400	wood, organic remains (silt unit)	KIA 28133
FAI-IW-4	5.0	46,120 +4080/ -2690	organic matter in wedge ice (silt unit)	KIA 25660
FAI-1/39	6.4	43,670 + 1480/ -1250	plant remains, leached residue (silt unit)	KIA 28132
FAI-IW-8	7.5	>40,970	organic matter in wedge ice (silt unit)	KIA 25661
FAI-1/37	8.4	49,930 + 3800/ -2570	wood, organic remains Z(silt unit)	KIA 28131
FAI-1/36	9.3	52,390 +2210/ - 1730	wood, organic remains (silt unit)	KIA 28130
FAI-1/34	10.9	42,090 +3410/-2380	silt. organic-rich.	KIA 24873
FAI-IW-12	12.0	34,400 +4390/-2820	organic matter in wedge ice (silt unit)	KIA 25275
FAI-1/30	13.3	> 52,440	wood, organic remains (silt unit)	KIA 28128
FAI-1/33	14.7	42,170 +3480/-2420	organic remains (silt unit)	KIA 28129
FAI mammoth	16.7	> 50,920	small fragments of mammoth skull, collagen, (transition horizon)	KIA 31124
FAI-1/26	19.6	49,550 +2190/-1720	wood remains (transition horizon)	KIA 25270
FAI-1/19	21.7	> 51,130	peat lens (transition horizon)	KIA 24872
FAI-1/2	34.8	> 52790	wood remains (gravel horizon)	KIA 24871
FAI-IW-18	open pit	3615 +/- 45	peat in wedge ice	KIA 25276
FAI-2-1	open pit	4625 +/- 50	small twig	KIA 25272
Infrared-stimulated optical luminescence (IRSL)				
FAI-OSL-2	20.4	75,000+/-10,000	middle sand (transition horizon)	
FAI-OSL-1	21.0	57,000 +/-4400	middle sand (transition horizon)	

crystals of several cm in diameter, most likely related to mining activity. These locations were avoided while sampling in the tunnel. Intrasedimental ice includes segregated ice, as thin layers of ice often bound upward near ice wedges, and finely dispersed pore ice, as well as ice lenses.

Dating

To assess the stratigraphic position of the VC tunnel, several dating techniques were applied (AMS ^{14}C, IRSL, U/Th). The results are summarized in Table 1 and Figure 4. Radiocarbon analyses were carried our at Leibniz laboratory in Kiel, IRSL dating at the Technical University of Freiberg and U/Th dating at GGA Institute in Hannover, Germany. A first stratigraphic scheme is mainly based upon ^{14}C dates.

Samples taken from the auger borehole show a Late Holocene sediment accumulation and soil development around 2.5 to 3.5 ka ^{14}C BP. These dates are similar to those of an open pit near Fox, where peat and ice wedges grew in the second half of the Holocene. The uppermost sample in the VC tunnel (silt horizon) was dated to 25.3±0.2 ^{14}C ka BP. Seven finite ^{14}C dates were measured in the sediments of the silt unit, all between 40,000 and 50,000 ^{14}C BP with a relatively large error bar. Two radiocarbon ages in the silt horizon are beyond dating range. One ice wedge of the silt unit was dated to 34,400+4,390/-2,820 ^{14}C BP. Ice wedges are vertical features, thus, younger organic remains might reach deeper parts of the profile, if the ice wedge was active after sediment accumulation.

From the transition and gravel horizons, three infinite ^{14}C ages of older than 50 ka BP were retrieved, among them one age from a mammoth skull. Only one finite age of 49,550 +2,190/-1,720 ^{14}C BP was measured in the transition horizon. Two IRSL ages in the transition horizon of 57±4.4 ka and 75±10 ka were measured between 20 and 21 m depth confirm the hypothesis of a Wisconsin age of transition and silt horizons. The fluvial gravel might be even older. The attempt to date peat material from the gravel unit by means of U/Th failed due to open system conditions and the subsequent loss of uranium and only an unreliable age (of 360–460 ka) was obtained.

Palynology

Pollen spectra from the VC tunnel can be subdivided into 5 main pollen zones (PZ-I to PZ-V). Oldest pollen spectra (PZ-I, below 27 m) reflect that spruce-birch forest with dwarf birch and shrub alder dominated at the site during that time. The climate was wet and warm, and the studied pollen spectra are unambiguously pointing to “interglacial environmental conditions” similar to Holocene ones.

Pollen spectra of PZ-II (17.5-27 m) are composed of Cyperaceae, *Picea*, *Betula*, Ericales and *Sphagnum* spores showing that spruce forest with some birch trees dominated

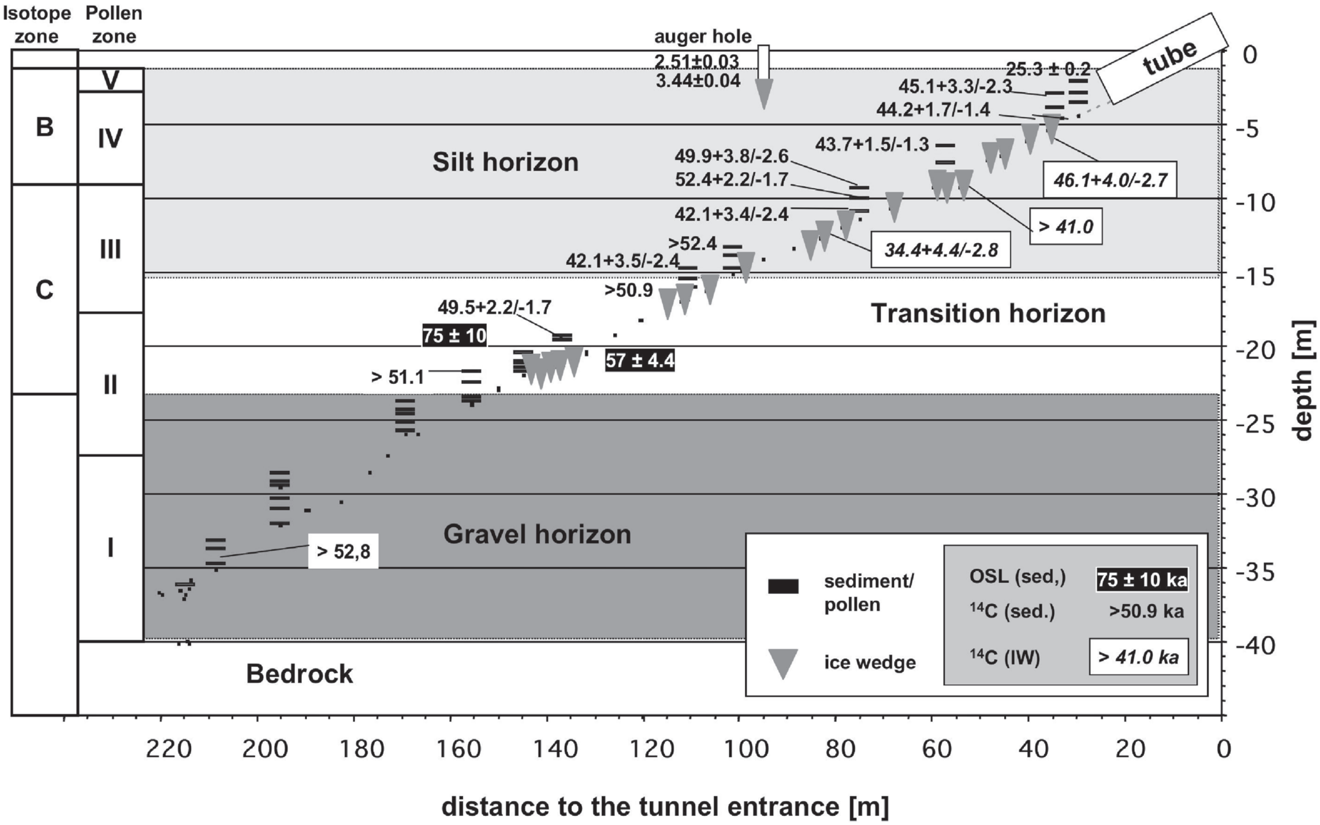

Figure. 4. Stratigraphic position of all sampled sediment profiles and ice wedges as well as their respective sedimentary horizon, pollen zone and isotope zone. Results of all IRSL and radiocarbon AMS ^{14}C dated samples are positioned at their right depth.

at the site during that interval. The find of relatively heavy pollen not readily transported by wind, such as hemlock (*Tsuga*) and fir (*Abies*) may reflect their presence in the local vegetation. The pollen spectra of PZ-III (8–17.5 m) are dominated by *Picea* and Cyperaceae pollen reflecting that spruce forest still dominated at the site. The permanent presence of hemlock and fir in the spectra reflects, most likely, that these trees grew around or not far from the site. Nowadays, these taxa occur in Alaska only in the rather moist coastal areas, where annual precipitation reaches at least 600 mm and winter and summer temperatures range from -6°C to -2°C and 13°C to 16°C, respectively (Viereck & Little 1972). Thus, during the PZ-III interval, climate conditions were probably wetter and warmer than today, e.g., such as in a warm stage of an interglacial. It should be stressed that redeposition seems unlikely due to the good preservation of pollen grain, even though both taxa are known from Tertiary deposits in Alaska (Ager et al. 1994).

A decrease of *Picea* and an increase of Cyperaceae pollen content in the pollen spectra of PZ-IV (depth: 2.8–8 m) may reflect a slight deterioration of the environmental conditions. However, spruce forest still dominated in the local vegetation. The presence of few hemlock and fir pollen shows, however, that climate conditions were still wet and warm during the PZ-IV interval. In pollen zones PZ-I to PZ-IV, typical cold indicators are missing.

Pollen zone PZ-V includes two samples from the uppermost part of the VC tunnel (2.0–2.7 m, near the entrance) reflecting a treeless environment and a significant deterioration of the climate conditions, which were extremely dry and cold during this time. A radiocarbon age of 25,320±240 a BP reflects a Late Wisconsin age of PZ-V.

Stable isotope geochemistry

Ice wedges are periglacial features giving information about winter temperatures which may be derived by stable oxygen and hydrogen isotopes (e.g,, Vaikmäe, 1989, Vasil'chuk 1992, Meyer et al. 2002). Ice wedges are fed by snowmelt or snow directly entering frost cracks, and thus are directly linked with atmospheric moisture. The isotopic composition of single ice wedges and other types of ground ice has been measured with a Finnigan Delta-*S* mass spectrometer using equilibration technique with a precision of ±0.1‰ for $\delta^{18}O$ and ±0.8‰ for δD. Significant differences have been observed in the isotopic composition of single ice wedges as well as in the other types of ground ice. Ice wedges have been subdivided into main isotope zones (A), (B), and (C).

The ice wedge of an open pit near Fox (A), directly dated to 3.6 ka ^{14}C BP, shows a mean $\delta^{18}O$ and δD of -21.8‰ and -172‰, respectively. This is a typical isotopic signature for ice wedges of Holocene age and may therefore be used as equivalent for interpretation of ice wedges in the VC tunnel.

The stable isotope composition of ice wedges in the tunnel displays two zones of varying winter temperatures: (B) 2.8–8 m depth. Ice wedges are characterized by lowest respective mean $\delta^{18}O$ and δD of about -26.5‰ and -210‰, thus, by relatively coldest winters. This estimate is based upon 8 single ice wedges with mean oxygen isotopic composition between

-29.3‰ (at 2.8 m, auger hole) and -23.6‰ (at 6.3 m). This indicates a certain degree of variability of winter climatic conditions, but nonetheless glacial conditions especially in the uppermost part, where lightest (most negative) isotopic composition is reached.

(C) 8–22 m depth. A much higher mean $\delta^{18}O$ and δD of about -22‰ and -175‰, respectively, is observed in the 14 ice wedges of isotope zone C. Mean oxygen isotopic composition in single ice wedges varies from -24.2‰ (at 10.2 m) and -20.5‰ (at 21 m). This could reflect winter temperatures similar to the present ones or, in parts, even warmer as today. Especially in the transition horizon, relatively heavy isotopic composition in ice wedges between -20‰ and -21‰ are common. This relatively clear subdivision is possible despite the fact that ice wedges, predominantly vertical features, propagate downward into older sediments. Between 13.5 and 15 m depth, ice wedges might have a limited climatic relevance. In this depth range, low d excess (below -2‰) points to secondary fractionation. This might be caused by evaporation/sublimation of snow or the participation of reprecipitated water. Therefore, the relatively variable isotopic composition of ice wedge in this depth range is considered with caution.

The mean isotopic composition of thermokarst-cave ice is $\delta^{18}O$ = -22.1‰, and is thus similar to that of ice wedges in isotope zone C. This points to an event of local melt of ground ice, which was subsequently refrozen as thermokarst-cave ice. Intrasedimental ice (both pore and segregated ice) displays highly variable isotopic composition all over the permafrost sequence due to the fact that this type of ice includes not only winter precipitation. Consequently, the isotopic composition of intrasedimental ice is heavier ($\delta^{18}O$ = -19.8‰, N = 23), with lightest values observed at the top of the silt horizon and heaviest values at the bottom.

Discussion

The environmental history reconstructed from sediments and ground ice of the Vault Creek tunnel revealed a series of new results for Central Alaska. The youngest part of the regional history was derived from samples of an auger hole (as well as of an open pit near Fox) and dated to the 2nd half of the Holocene, where peat accumulation took place, ice wedge growth was common and the climate was relatively wet and warm according to palynology and isotope geochemistry of ice wedges. Obviously, the top of the VC tunnel reveals a part of the environmental history around 25 ka ^{14}C BP. Pollen indicate a cold and glacial climate and treeless vegetation. Lightest isotopic composition in ice wedges (and in intrasedimental ice), also point to coldest climatic conditions for the whole sequence. This section was dated to an interval just some thousand years before Late Glacial Maximum. It also states clearly that at VC tunnel, loess accumulation continued at least until 25 ka BP. At the Fox tunnel, a hiatus was observed between about 14–30 ka BP (Hamilton et al., 1988).

The organic remains in fluvial gravels at the bottom of the sequence show infinite ^{14}C ages, which is also supported by the IRSL dates in the transition horizon. Consequently, fluvial activity must have been strong in Early Wisconsin or even before. At this time, summers must have been warm and wet, leading to the intensification of fluvial activity in the area.

Conflicting dates and proxy indications are especially related to the silt unit, which was AMS ^{14}C dated between 40 and 50 ka BP. Unfortunately, these dates are not always in the right order with increasing ages with depth and display relatively large error bars. Hence, it raises the question how the ages around 40 - 50 ka BP correlate with the extremely warm temperatures derived from pollen analyses (especially PZ-II and PZ -III).

This interval has not been known as very warm until now, whereas around 30 to 40 ka BP, interstadial conditions have been described for various sites. For instance, thaw unconformities in the Fox tunnel (the so called ”Fox thermal event”) have been dated to 30 to 35 ka BP (Hamilton et al., 1988). In northwest Canada, a mid-Wisconsin Boutellier non-glacial interval with temperatures similar to the present ones has been dated to between 30 and 38 ka BP (Schweger and Janssens, 1980). Three ^{14}C dates from ice wedges fall into this time interval (two from Fox, one from VC tunnel), confirming that in the region, frost cracking was active at that time. For about the same interval, temperatures similar to the present ones have been derived by pollen analysis for a sediment record of the Isabella basin, near Fox (Matthews et al. 1974). In Matthews' study, pollen zone Ab indicates climatic conditions as warm as today around 32 ka BP.

There are only few examples for Alaskan climate records extending beyond this interstadial phase. For instance, pollen spectra at Imuruk Lake, Seward Peninsula were interpreted differently by various authors. Pollen zone i was dated to >37 ka and >34.4 ^{14}C BP and attributed to the Sangamon by Colinvaux (1967). However, Shackleton (1982) assumed a Mid Wisconsin interstadial for this pollen zone. This re-estimate is based, among other methods, upon the assumption that the Old Crow (OC) tephra (predating pollen zone i) is about 80 ka old. New data yield an age for the OC tephra of about 142.3±6.6 ka BP (Berger 2003). Therefore, the pollen spectra at Imuruk Lake must be re-interpreted and at the moment, pollen zone i is more likely interglacial (Sangamon) than interstadial.

Nonetheless, in no other palynological study in Interior Alaska have such warm climatic conditions as in the VC tunnel been derived by means of pollen analyses (Ager & Brubaker, 1985). This is not only valid for a small part of the VC tunnel, but for almost the complete periglacial sequence. This reflects the difficulty of interpreting environmental data beyond radiocarbon dating range and the need to understand more about the environmental history in Alaska. This makes the VC tunnel exceptionally valuable for a more detailed study of this time interval.

To summarize, there are three possibe interpretations of our data: (1) trust the radiocarbon ages. In favor of this hypothesis is the high number of similar and finite ages of the silt horizon, as well as two IRSL ages from the transition horizon predating the loess. This points to a Wisconsin age of both transition and silt horizons. Additionally, the AMS method applied at Leibniz laboratory in Kiel, expanded the dating range back to about 50–70 ka BP (Nadeau et al. 1997, 1998). This assumption would lead to a very warm and as yet unknown interval in mid-Wisconsin times.

The fact that trees grew close to the site allows a second (hypothetical) interpretation, that (2) a small forest existed in the Vault Creek area due to locally different climate conditions (e.g., close to a hot spring) and survived through Wisconsin times. Finally, we can (3) disbelieve the ages, which are near the dating limit, and assign the whole sequence to the Sangamon (or other) interglacial based on interpretation of pollen spectra. A warm phase is supported by relatively heavy isotope composition of the ice wedges. Acceptance of this hypothesis would contradict Pewe's ideas of no ground ice surviving the Sangamon interglacial in Interior Alaska. In any case, winter temperatures must have been cold enough for frost cracking, and summers not so warm as to melt ground ice. This paradox of extremely warm summer temperatures at a presently discontinuous and relatively warm permafrost site, with predominantly loess accumulation in which ground ice was formed and survived, cannot be solved completely. It is likely that sediment transport downslope, redeposition, and burial of ground ice played a key role for the pre-existence of permafrost. At least once, melting influenced the sequence when thermokarst-cave ice was formed after lateral melting of ground ice. This displays the vulnerability of these deposits, but also the possibility of contaminating older deposits by younger organic material.

Conclusions

The late Quaternary record of the Vault Creek permafrost tunnel near Fairbanks spans more than 75 ka and indicates varying environmental conditions from rather fluvial (gravelly) to aeolian (silty) environmental conditions.

Fluvial activity was intensive in the Vault Creek area in or before Early Wisconsin, leading to the deposition of 17.5 m of fluvial gravels. Climate conditions were warm and wet during that time. There are no signs of frost cracking activity at that time.

AMS ^{14}C dates point out that silt accumulation and ice wedge growth took place in the vicinities of the VC tunnel from 40 to 50 ka BP to at least 25 ka BP. A very warm phase with spruce forest environment occurred in Central Alaska, whose timing and duration is still uncertain due to conflicting age determinations and proxy indications. However, a climate deterioration is evident at the top of the section (around 25 ka BP), when the climate was colder than today and a treeless tundra environment prevailed as indicated by pollen and ice wedge isotope geochemistry. During the second half of the Holocene, peat accumulation and ice wedge growth took place.

Acknowledgments

We thank Mr. Sam Skidmore for the field support and valuable suggestions. We also thank Melanie Sierralta from the GGA Institute in Hannover for U/Th dating and Matthias Krbetschek from Freiberg Technical University for providing two IRSL dates.

References

Ager, T.A. & Brubaker, L.. 1985. Quaternary palynology and vegetational history of Alaska. In: V.M Bryant. & R.G. Holloway (eds.), *Pollen records of Late Quaternary North American Sediments*. 353-384.

Ager, T.A., Matthews, J.V. & Yeend, W. 1994. Pliocene terrace gravels of the ancestral Yukon River near Circle, Alaska: Palynology, paleobotany, paleoenvironmental reconstruction and regional correlation. *Quaternary International* 22/23: 185-206.

Berger, G.W. 2003. Luminescence chronology of late Pleistocene loess-paleosol and tephra sequences near Fairbanks, Alaska. *Quaternary Research* 60: 70-83.

Hamilton, T.D., Craig, J.L. & Sellmann, P.V. 1988. The Fox permafrost tunnel: a late Quaternary geologic record in central Alaska. *Geological Society of America Bull.* 100: 948-969.

Matthews, J.V., Jr. 1974. Wisconsin Environment of Interior Alaska: Pollen and Macrofossil Analysis of a 27 Meter Core from the Isabella Basin (Fairbanks, Alaska). *Canadian Journal of Earth Sciences* 11(6): 828-841.

Meyer, H., Dereviagin, A.Yu., Siegert, C., Schirrmeister, L. & Hubberten, H.W. 2002. Paleoclimate reconstruction on Big Lyakhovsky Island, North Siberia – Hydrogen and oxygen isotopes in ice wedges. *Permafrost and Periglacial Processes* 13: 91-105.

Nadeau, M.J., Schleicher, M., Grootes, P.M., Erlenkeuser, H., Gottdang, A., Mous, D.J.W., Sarnthein, J.M. & Willkomm, H. 1997. The Leibniz-Labor facility at the Christian-Albrecht-University, Kiel, Germany. *Nuclear Instruments and Methods in Physics Research* 123: 22-30.

Nadeau, M.J., Grootes, P.M., Schleicher, M., Hasselberg, P., Rieck, A. & Bitterling, M. 1998. Sample throughput and data quality at the Leibniz-Labor AMS facility. *Radiocarbon* 40: 239-245.

Péwé, T.L. 1975. Quaternary Geology of Alaska. *US Geological Survey Prof. Paper* 835: 145pp.

Sellmann, P.V. 1967. Geology of the USA. CRREL permafrost tunnel, Fairbanks, Alaska. Technical Report 199, US Army CRREL. Hanover, New Hampshire, 22 pp.

Schweger, C.E. and Janssens, J.A. 1980. Paleoecology of the Boutellier non-glacial interval, St. Elias mountains, Yukon territory, Canada. *Arctic and Alpine Research* 12. 309-317.

Shur, Y., French, H.M.,Bray, M.T. & Anderson D.A. 2004. Syngenetic Permafrost Growth: Cryostratigraphic Observations from the CRREL Tunnel near Fairbanks, Alaska. *Permafrost and Periglac. Process*. 15: 339-347.

Vaikmäe, R. 1989. Oxygen isotopes in permafrost and ground ice – A new tool for paleoclimatic investigations. *5th Working Meeting Isotopes in Nature, Proceedings, Leipzig, September 1989:* 543-553.

Vasil´chuk, Yu.K. 1992. Oxygen isotope composition of ground ice—application to paleogeocryological reconstructions, Vol. 1, Moscow, Russia: 420 pp.

Viereck, L.A. & Little Jr., E.L. 1972. Alaska Trees and Shrubs. Agriculture Handbook No. 410, Forest Service US Department of Agriculture. Washington DC, 265 pp.

Properties of Eroding Coastline Soils Along Elson Lagoon Barrow, Alaska

G.J. Michaelson, C.L Ping, L.A. Lynn
University of Alaska Fairbanks, AFES-Palmer Research Center, Palmer, Alaska
M.T. Jorgenson
Alaska Biological Research Inc., Fairbanks, Alaska
F. Dou
International Arctic Research Center, University of Alaska Fairbanks, Alaska

Abstract

We studied eroding coastline soils at 6 points along the beach exposure of Elson Lagoon near Barrow, Alaska. Exposures consisted of an average 37 cm of thawed soil and 103 cm of permafrost soil. Sediments were Holocene in origin with basal organic matter dating from 4,820 to 6,650 ybp. Exposures contained large amounts of organic carbon and nitrogen (45–112 kgOC m^{-2}, 2.5–6.1 kgN m^{-2}). These amounts are among the highest found for exposures of similar heights across the north coast of Alaska. We estimate large amounts of water, sediment, organic C and N (1,144, 1,002, 98, and 6 kgx10^3 km^{-1}, respectively) are exposed to erosion each year along the lagoon. Methane released from the thawing exposure soils ranged from 0.06–1.66 gCH_4 m^{-2}, and soil horizons nearest to the top of the permafrost and bottom of the active layer released the largest amounts in all exposures.

Keywords: Alaska; coastal erosion; sediment transfer; methane; trace gases; soil organic carbon.

Introduction

Changing wind and sea ice conditions along the Alaskan arctic coast have been associated with increases in observed rates of coastal erosion. Brown et al. (2003) reviewed previous erosion rate studies of the arctic Alaska coastline. Long-term rates for the Beaufort Sea coast calculated for the latter part of the 20th century (1951–1983: Reimnitz et al. 1988, Barnes et al. 1992) showed that the finer sediments of the coastline in the Barrow region are eroding most rapidly at an average rate of 5.4 m yr^{-1} compared with an average rate of 1.4 m y^{-1} for the coarser-based sediments of the eastern two-thirds of the Alaska coastline. A more detailed photogrammetric study for one area of the Elson Lagoon near Barrow for the period 1979–2000 revealed erosion rates for different exposures varying from 0.69 to 2.75 m yr^{-1} with an average rate of 1.27 m yr^{-1} for the whole lagoon (Brown et al. 2003). The Brown et al. study found that the 1979–2000 erosion rates along lagoon segments had increased up to 47% over the previous 40-year period. These increases were for the exposures with fine-grained sediments, whereas the erosion rates of gravel beach segments of the lagoon remained lower at 0.5 m yr^{-1}. Sediment and carbon transfer rates along Elson Lagoon were estimated by Brown et al. (2003) using the erosion rate determined in the study combined with soils data from the 1957 soils map of the area. We studied actual soils profiles of exposures along Elson Lagoon and detail the soil materials exposed as they vary along the lagoon in order to characterize load and range of materials that are being released to the near-shore lagoon environment. Work at Elson Lagoon was part of a larger study to assess the fate and transformation of soil carbon eroding into the Beaufort Sea (Jorgenson et al. 2005).

Methods

Sites

Study sites were located along beach segments identified by Brown et al. (2003) for sites 1–4 and extending further southeast along the coastline for sites 5 and 6 (Fig. 1).

The soils at the exposures (Table 1) represent those of the major mapping units that covered over 80% of the area near Barrow, including south of Elson Lagoon as reported by Bockheim et al. (1999). Exposures sampled were typical in morphology for each respective beach segment.

Sampling and analysis

Soil profiles were excavated from the surface down to sea level to remove slumped and refrozen materials at each of the 6 beach exposure sites along Elson Lagoon (Fig. 1). Soil layers were identified (Schoeneberger et al. 1998) and sampled using cut blocks in the active layer and drill cores in permafrost. These dimensional samples were at regular depths to include all soil horizons identified down to sea level. Samples in permafrost were kept frozen and all samples were stored frozen until analysis at the UAF-AFES Plant and Soils Laboratory at the Palmer Research Center. Soil bulk density and water contents were determined by weight difference upon drying at 100°C of dimensional samples. Total organic C (TOC) and N were determined using a LECO CHN analyzer with carbonates removed by acid pretreatment. The sediment, water, TOC, N, nutrient contents, and gas contents of the exposures were determined using the exposure description and analysis by the method of Kimble et al. (1993) to account for cryoturbation. Available soil N, P, and K were extracted by 2M KCl, Mehlich-3, and neutral 1M ammonium acetate solutions respectively (Soil Survey Staff 1996). Methane and carbon dioxide gases evolved from

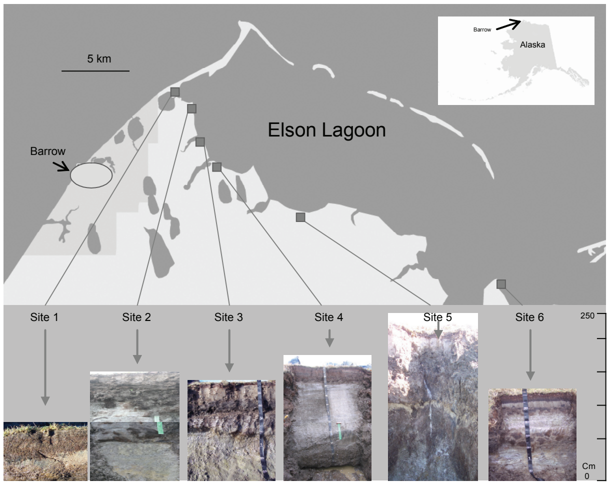

Figure 1. Study site locations and exposure profiles.

samples were determined by thawing dimensional samples for 5–10 hours in a sealed chamber attached to a Columbus Instruments Micro Oxymax respirometer. Radiocarbon dating was performed at NOAMES Laboratory, Woods Hole Massachusetts.

Results and Discussion

Soil characteristics

Exposure soils were either in alluvial-marine (sites 1 and 3) or drained lake (sites 2 and 4–6) deposits that contained inter-bedded peat and fine minerals of sandy loam to silty clay in texture (Fig. 1 and Table 1). The two alluvial marine exposures (sites 1 and 3) and one of the drained lake basins (site 5), showed little cryoturbation of organics within the layers and were Orthels while the majority of drained lake exposures had significant cryoturbation or frost mixing of organic matter and mineral materials and were Turbels under the U.S. soil classification system (Soil Survey Staff 1998). But all soils had uneven distribution of organic matter throughout their profiles (%OC in Table 1) contributing to increase OC stores to depth. Turbels are common to the area around the southern lagoon, as Bockhiem et al. (1999) mapped over 70% of the area as Turbels. Basal peat ages at sites 2 and 6 were 6650 ybp (125 cm) and 4820 ybp (60 cm), respectively.

Materials eroding at the exposures

Coastline exposures averaged 74% water and ice by volume ranging from 51% at site 4 to 90% at site 6 (site data in Fig. 2). An average of 69% was reported by Michaelson et al. (2006) for 29 exposures along the coast east to Colville River delta. Active layers along Elson Lagoon averaged lower at 67% volumetric water compared to the permafrost that averaged 77% volumetric ice. This is consistent with higher water holding capacities of organic horizons that elevate water contents in the active layer and the permafrost-encased organic horizons along with additional water in permafrost stored as ice lenses and massive ice. Water contents found in this study are generally higher than the 50% estimate used by Brown et al. (2003) to calculate erosion volume transfers along the lagoon. The mass of water in exposures studied here ranged from 431 to 1735 kg m^{-2} (average: 901 kg m^{-2}). The average mass of water in the Elson exposures tends to be somewhat lower than the average of 1200 kg m^{-2} found for 29 exposures along the coast from Barrow to the Colville River delta reported by Michaelson et al. (2006). However the 29 exposures across the larger coastal section averaged 175 cm in height compared to 140 cm in this study (Table 2). There is less than a 10% difference if considered on a per–cm-exposure height basis.

The mass of sediments available for transfer from the Elson Lagoon exposures were somewhat lower than that of water and ranged from 395–1032 kg m^{-2} (average 789 kg m^{-2}, Table 2). These sediment amounts encompass a greater range than found for three study-transects along the Beaufort Lagoon in the northeastern North Slope of Alaska, but the average of 789 kg m^{-2} is within the range of 871–998 kg m^{-2} found there (Jorgensen et al. 2003).

Carbon and nutrients at the exposures

Organic carbon (OC) and nitrogen transfer from the coastal tundra to the nearshore environment is of particular interest for terrestrial-aquatic carbon partitioning and budget analysis. Even with this interest, there are little data on carbon and very little on nitrogen in coastal tundra especially to depth (Ping et al. 2007). The soils of the coastal plain have been found to hold high amounts of organic carbon compared to the foothills region on average about 50% more (Michaelson et al. 1996). Exposure soils at sites 1–6 along Elson Lagoon ranged from 45 to 112 kgOC m^{-2} (Table 2), averaging 78 kgOC m^{-2}. Jorgensen et al. (2003) found similarly high stocks ranging from 54 to 136 kgOC m^{-2} in coastal exposures of the Beaufort Lagoon on the northeastern coastal plain. Exposures studied there averaged 240 cm in height compared to the Elson sites average of 140 cm, and average OC stocks there were 85 kgOC m^{-2} compared to 78 kgOC m^{-2} for the Elson Lagoon sites. Still, on average, the Elson exposures held about 60% more OC cm^{-1} of exposure height (0.56 compared to 0.35 kgOC cm^{-1} of exposure height) compared to the Beaufort Lagoon. When 29 exposure sites were considered from Barrow to the Colville River delta (Michaelson et al. 2006) exposures averaged 175 cm in height and contained on average 69 kgOC m^{-2} (0.39 kgOC cm^{-1} of exposure height,).

More OC data for the area is available for soils to a 100-cm depth in a study by Bockheim et al. (1999). They estimate the average Barrow area soils (around Elson Lagoon) to hold 50 kgOC m^{-2} to a depth of 100 cm with soils in mapping units containing from 27 to 73 kgOC m^{-2}. When OC stocks were calculated to only 100 cm for each site (including site 1 with only a 63 cm exposure measured) Elson sites 1–6 of this study averaged 63 kgOC m^{-2}. This average is the same as estimated as average for coastal plain soils by Michaelson et al. (1996).

The major organism-available nutrients nitrogen (NH_4+NO_3-N), phosphorus (PO_4-P), and potassium (K^+)

Table 1. Location, soil classification, surface characteristics, and selected soil properties for soil profiles at the exposure sites. Thermal state: AL = active layer and Pf = permafrost.

Site USDA Soil Classification	Unit:Terrain Surface Subsurface	Horizon	depth	pH	EC	USDA Texture	Thermal State	Organic C
			cm		*ds cm²*			---%--
1	-Alluvial-Marine	Oi	0-6	5.88	21.4	peat	AL	25.7
Typic	-Inactive Tidal Flat	Bg/Oa	6-11	5.63	18.7	loam	AL	9.0
Aquorthel	-Drained Lake Basin,	Oa/Bg	11-27	5.56	13.5	muck	AL	10.5
71°20.193'N	(Ice-poor Center)	Cg	27-53	7.27	23.5	Scl	AL	1.7
156°35.574'W		Cg	53-63+	7.58	24.8	Scl	Pf	2.1
2	-Drained Lake Basin,	Oi	0-8	4.91	0.43	Peat	AL	40.0
Typic	(Ice-rich Center)	Bg	8-22	5.07	0.77	S loam	AL	4.6
Aquiturbel	-Organic Fen	Oa/Bgjj	22-54	4.99	0.60	muck	AL	24.0
71°19.4496'N	-Thaw Basin, Ice-rich	Bg/Oajj	54-87	4.89	0.59	muck	AL	23.4
156°34.106'W		Oa/Bgf1jj	87-105	5.35	1.16	muck	Pf	25.0
		Cf	105-145	7.30	5.89	S loam	Pf	1.0
		Cf1	145-150+	7.29	3.80	S loam	Pf	0.9
3	-Alluvial-Marine	Oi	0-5	5.15	0.33	peat	AL	37.3
Fluventic	-Organic Fen	Bw	5-28	4.87	0.48	loam	AL	2.8
Historthel	-Alluvial-Marine	A/Oejj	28-40	5.45	0.70	Mucky sil	AL	16.7
71°18.237'N		A/Oijj	40-55	5.53	0.96	Peaty sil	AL	16.6
156°32.634'W		Bw/Oefjj	55-85	5.61	4.08	Sl	Pf	6.7
		Cf	85-125+	6.96	13.6	Scl	Pf	1.3
4	-Drained Lake Basin	Oi	0-4	4.91	2.96	peat	AL	39.9
Terric	Ice-rich Center	Oe	4-16	4.21	6.82	mk pt	AL	33.3
Hemistel	-Organic Fen	Oi	16-29	4.37	4.10	peat	AL	18.4
71°16.974'N	-Thaw Basin, Ice-rich	Oa	29-45	4.85	0.99	muck	AL	10.4
156°25.760'W	Margin	Oa1/Af1	45-60	5.1	0.78	silt loam	Pf	9.4
		Oa2/Af2	60-105	4.98	0.91	silt loam	Pf	9.3
		A3/Oaf1	105-120	5.31	1.75	silt loam	Pf	5.3
		A4/Oaf2	120-135	5.46	3.83	silt loam	Pf	9.7
		A5/Oaf3	135-155	5.82	4.65	silt loam	Pf	11.9
		A6/Oaf4	155-170+	6.12	8.16	silt loam	Pf	9.0
5	-Drained Lake Basin,	Oi	0-9	4.46	0.81	peat	AL	40.9
Typic	(Ice-rich Center)	Ajjj	9-23	4.92	1.11	loam	AL	9.6
Histoturbel	-Organic Fen	Oi/Bgjj	23-45	5.03	1.26	muck	AL	16.1
71°15.5658'N	-Thaw Basin, Ice-rich	Oi/Bgfjj	45-65	4.74	0.66	muck	Pf	18.9
156°20.131'W	(Margin)	Cf	65-75	4.62	0.53	S loam	Pf	2.2
		Oifjj	75-110	4.97	0.26	pt muck	Pf	35.6
		2Cf	110-200	6.42	4.79	Si Cl	Pf	4.6
		3Cf	200-220+	7.06	18.8	silt loam	Pf	3.9
6	-Drained Lake Basin,	Oi	0-16	4.87	1.73	Peat	AL	46.2
Typic	(Ice-rich Center)	Oa	16-45	4.77	0.87	mk peat	AL	27.0
Histoturbel	-Thaw Basin, Ice-rich	Bg	45-50	5.43	0.77	silt loam	AL	6.5
71°12.6912'N	(Margin)	Oafjj	50-85	5.48	0.42	mk peat	Pf	35.7
155°55.584'W	-Alluvial-Marine Deposit	Cgf	85-110+	6.98	0.69	S loam	Pf	1.9

(Table 2) are important for organisms to utilize carbon energy sources in coastal waters as well as on land. They have been little-studied in relationship to coastal erosion transfer in the Arctic. We found considerable variation in amounts across the 6 exposures. Nitrogen was high at site 4, phosphorus at site 2, and potassium in the intertidal site (site 1). Average organic or Total N transferred per km of coast was over 100 times the magnitude of the available NH_4+NO_3-N form (bottom Table 2). Although the amounts of OC and N available at the exposures were considerably higher on Elson Lagoon (over 80%) than the Alaska Barrow to Canada coastal averages found by Dou et al. (2007), the C:N ratios were the same at 17.7, an indication of similar average organic matter quality. Potassium was in the highest in magnitude of the three nutrients for all 6 sites.

Gas content of eroding soils

Trace gas release from eroding coastline is of particular interest because it could serve as a positive feedback to climate change with increased methane and carbon dioxide emissions. Tundra is known to release significant amounts of methane upon melting as has been measured in thermokarst lakes (Walter et al. 2006). Similar thawing of permafrost is occurring along the coastline. Warming and thawing of soils already containing methane under saturated conditions can be expected to release trace gasses. We measured methane and carbon dioxide released from frozen samples taken from the Elson Lagoon sites 1–6 (Fig. 2). Site exposures released an average of 0.61 gCH_4 m^{-2} exposure (range 0.06–1.66 gCH_4 m^{-2}) and 67 gCO_2 m^{-2} (range 43–78 gCO_2 m^{-2}). For the 29 sites along the coast to Colville River delta, Michaelson

Table 2. Height and load of sediment, water, total organic carbon, nitrogen, and extractable nutrients for exposures.

Site #	Bank Height	Sediment	H_2O	TOC	TN	NH_4+NO_3-N	PO_4-P	Exch.-K
Exposure stores								
	cm	---------*kg m*$^{-2}$---------				---------*g m*$^{-2}$---------		
1-BSC01	63	709	431	45.0	2.5	19	4	216
2-BLUFF	150	753	1104	80.5	5.3	36	14	57
3-ACS-9	125	1032	732	61.1	3.6	23	4	37
4-ACS13	170	870	663	112.1	6.1	97	7	136
5-BSC02	220	977	1735	99.3	5.2	47	6	106
6-BSC03	110	395	743	66.9	3.8	17	2	43
ave	139.7	789	901	77.5	4.4	40	6	99
stdev	53.8	300	462	25.0	1.3	30	4	69
Mass transfer estimate per km coastline with one meter of eroded bank								
		---------*kgx10*^{3} *km*$^{-1}$---------				---------*kg km*$^{-1}$---------		
average Sites 1-6		1002	1144	98	6	51	8	126

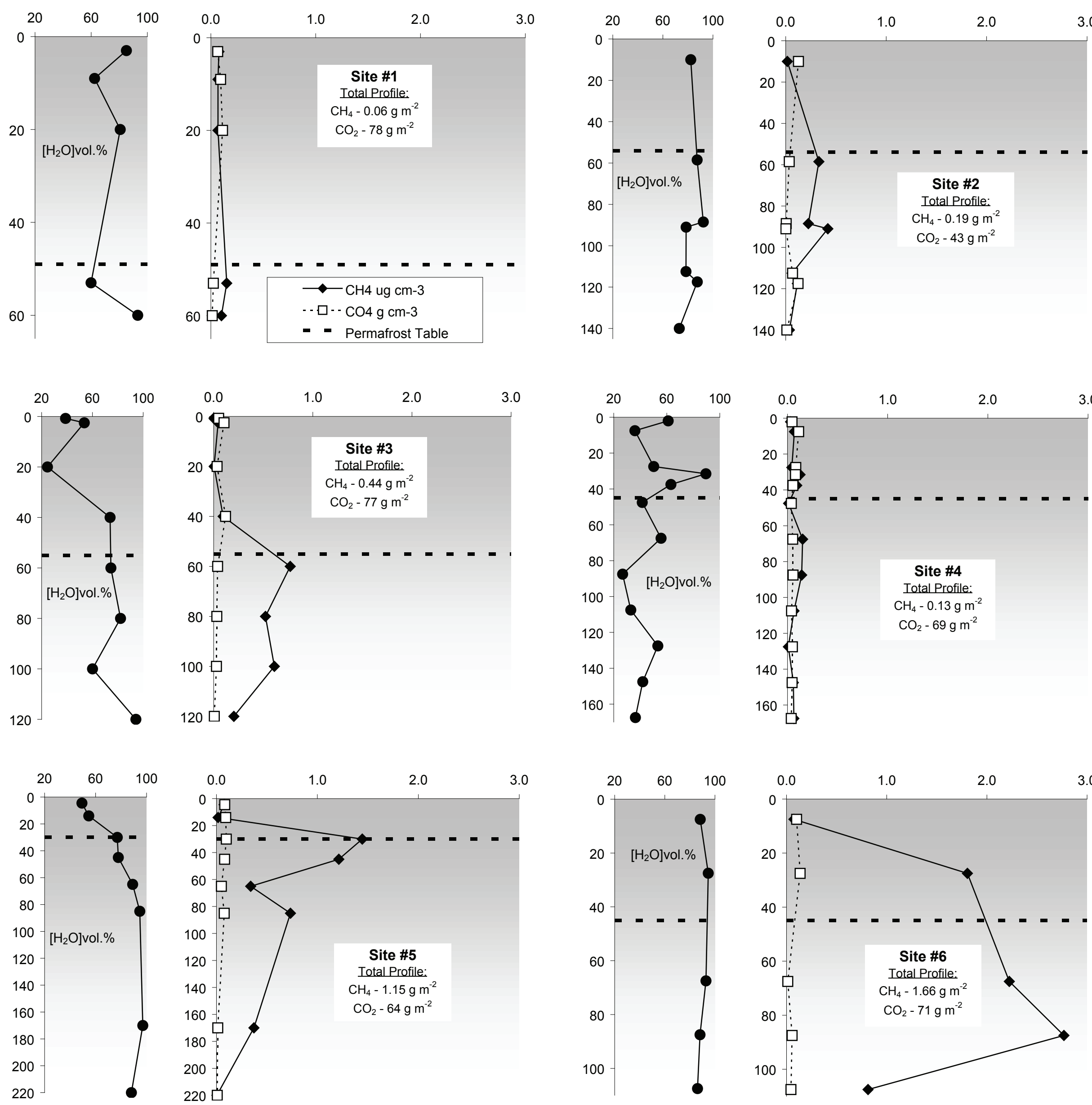

Figure 2. Volumetric water content ([H_2O]$_{vol.}$%) and methane/carbon dioxide gas release of soil profiles (lines are measured for cubic centimeters along the profile and totals are given as contained in a square meter of profile).

et al. (2006) reported average releases of 1.1 gCH_4 m^{-2} and 89 gCO_2 m^{-2} with an average exposure of 175 cm. The average methane release of the Elson sites was 0.43 gCH_4 m^{-1} of exposure height compared to the 29 sites to the east that averaged 0.63 gCH_4 m^{-1} of exposure height that is within the range found for the Elson sites (0.04–1.19 gCH_4 m^{-1} of exposure height). Carbon dioxide released had less variation with an average of 48 gCO_2 m^{-1} of exposure height for Elson sites. This compares closely to an average of 51 gCO_2 m^{-1} of exposure height found for 29 sites to the east by Michaelson et al. (2006).

As could be expected, methane releases tended to be higher in the permafrost and near permafrost (lower active layer, Fig. 2), while carbon dioxide release tended to be higher in the active layer. This is consistent with methane formation conditions more favorable in the saturated or frozen saturated organic horizons with limited contact to the atmosphere, while carbon dioxide would be favored in aerated near-surface layers. These relationship trends can be observed for nearly all site-exposure profiles. Methane increases at or near the top of the permafrost table, reaches a maximum in the permafrost, and decreases again at depth. Sites with the greatest water contents (sites 5 and 6) had the greatest methane contents. On an aerial basis the releases of methane are on the order of one-tenth those observed for wet tundra on the North Slope (Vourlitis et al. 1993).

Conclusions

Exposure heights along Elson Lagoon are near average for the North Slope, Alaska, coastline. However, Elson exposures contain larger OC stores than the average for the whole North Slope, Alaska, coastline. These larger OC stores are due to the presence of soils with both cryoturbated organic matter and layered peat or muck horizons. These OC rich horizons are a result of the drained-lake sequence history and the medium-textured soils of the lagoon's nearshore area. The history of the tundra, alternating from moist to aquatic conditions, allows for cryoturbation causing an increase in the OC storage in the moist condition, while peat development and sedimentary accumulation increases OC during wet or aquatic conditions. There is more OC eroding from exposures than would be predicted from the currently available local soil survey map of Bockheim et al. (1999).

The TN of exposures can also be expected to be higher than for other North Slope shore areas, as most of the nitrogen is associated with the eroding organic matter. The higher TN of eroding organic matter can be expected to positively affect the nutrient status and biotic activity of the nearshore area with N often limiting activity.

The stratification of peat by cryoturbation and by aquatic-sedimentary accumulation has resulted in layers of organic-enriched materials near the surface of the present-day permafrost table and just above it in the lower active layer. Both layers are under water-saturated conditions that favor accumulations of methane as organic matter decomposes. In exposures with these saturated organic layers, methane has accumulated presumably from subzero-temperature soil respiration and/or encasement of gases produced under previously thawed conditions with permafrost table fluctuation. Carbon dioxide present will be released along with methane upon thaw due to thermal erosion at the shoreline. This release upon thaw is in relatively small amounts, but could become a significant amount with increased rates of erosion and or with increased methane production due to changing soil thermal regimes.

Acknowledgments

This study was conducted as part of NSF grant OPP Grant #0436179. Field work was through the assistance of Yuri Shur, Mikial Kavansky, Daniel Fortier, Vladimir Tumskoy, Sabine Fiedler, Prothap Kodeal, and BASC staff at the Barrow Ilisagvik College.

References

Barnes, P.W., Reimnitz, E. & Rollyson, B.P. 1992. Map showing Beaufort Sea coastal erosion and accretion between Flaxman Island and the Canadian border northeastern Alaska (1:82,000). *U.S. Geological Survey Miscellaneous Investigations Series* Map I-1182-H, 22 pp. plus map.

Bockheim, J.G., Everett, L.R., Hinkel, K.M., Nelson, F.E. & Brown, J. 1999. Soil organic carbon storage and distribution in arctic tundra, Barrow, Alaska. *Soil Science Society of America Journal* 63: 934-940.

Brown, J., Jorgenson, M.T., Smith, O. & Lee, W. 2003. Long-term rates of arctic coastal erosion, Elson Lagoon, Barrow, Alaska. In: Phillips & Arenson (eds.), *Permafrost*: 101-106.

Dou, F., Xu, Y., Ping, C.L., Michaelson, G.J., Guo, L. & Jorgenson, M.T. 2007. Modeling spatial variations of tundra soil organic carbon along the coastline of northern Alaska. Manuscript in review.

Jorgenson, M.T, Macander, M., Jorgenson, J.C., Ping, C.L. & Harden, J. 2003. Ground ice and carbon characteristics of eroding coastal permafrost at Beaufort Lagoon, northern Alaska. In: Phillips & Arenson (eds.), *Permafrost*: 495-500.

Jorgenson, M.T., Ping, C-L., Guo, L., Shur, Y. & Brown, J. 2005. A multi-scale approach to assessing the flux and transformation of organic carbon across the eroding coastline of northern Alaska. *Berichte Zur Polarund Meeresforschung* 506: 65-68.

Kimble, J.M., Tarnocai, C., Ping, C.L., Ahrens, R., Smith, C.A.S., Moore, J. & Lynn, W. 1993. Determination of the amount of carbon in highly cryoturbated soils. In: D.A. Gilichinsky (ed.), Post-Seminar *Proceedings of the Joint Russian-American Seminar on Cryopedology and Global Change*. Pushchino, Russia, 15-16 Nov. 1992. Russian Academy of Science, Pushchino, Russia.

Michaelson, G.J., Ping, C.L., Jorgenson, M.T., Dou, F., Shur, Y. & Guo, L. 2006. Methane and carbon dioxide release from eroding coastline of North Slope, Alaska. World Congress of Soil Science Meeting, Philadelphia, July 2006, Abstracts.

Michaelson, G.J., Ping, C.L. & Kimble, J.M. 1996. Carbon storage and distribution in tundra soils of arctic Alaska, U.S.A. *Arctic and Alpine Research* 28(4): 414-424.

Ping, C.L., Michaelson, G.J., Jorgenson, M.T., Kimble, J.M., Epstein, H., Romanovsky, V.E. & Walker, D.A. 2007. High stocks of organic carbon in North American arctic region. *Geonature*, in review.

Reimnitz, E., Graves, M. & Barnes, P.V. 1988. Beaufort Sea coastal erosion, sediment flux, shoreline evolution and the erosional shelf profile. U.S. Geological Survey Map I-1182-G.

Schoeneberger, P.J., Wysocki, D.A., Benham, E.C. & Broderson, W.D. 1998. *Field book for describing and sampling soils.* Natural Resources Conservation Service, USDA, National Soil Survey Center, Lincoln, Nebraska.

Soil Survey Staff 1996. Soil survey laboratory methods manual, *Soil Survey Investigations Report No. 42*, Version 3.0.

Soil Survey Staff 1998. Keys to soil taxonomy, 8th edition. USDA Natural Resources Conservation Service, Washington, D.C.

Vourlitis, G.L., Oechel, W.C., Hastings, S.J. & Jenkins, M. 1993. The effects of soil moisture and thaw depth on CH4 flux from wet coastal tundra ecosystems on the north slope of Alaska. *Chemosphere* 26: 329-337.

Walter, K.M., Zimov, S.A., Chanton, J.P., Verbyla, D. & Chapin II, F.S. 2006. Methane bubbling from Siberian thaw lakes as a positive feedback to climate warming. *Nature* 443: 71-75.

The Application of Tritium in Permafrost Ground-Ice Studies

F.A. Michel
Dept of Earth Sciences, Carleton University, Ottawa, Canada

Abstract

Tritium, a radiogenic isotope of hydrogen with a half-life of 12.43 years, can be utilized as a natural tracer in water (ice) investigations. Anthropogenic tritium released into the atmosphere during nuclear testing from the 1950s to 1970s created peak monthly concentrations as high as 10,000 T.U. Recent values for Arctic Canada monitoring stations are below 30 T.U. Seasonal variations indicate higher tritium values occur during summer. Infiltration of precipitation into the thawed active layer during the summer produces elevated tritium concentrations within the soil profile. Elevated tritium levels also occur in ground ice below the permafrost table and have been interpreted previously as indicative of downward migration of water into the permafrost along a thermal gradient. Re-evaluation of data suggests that this tritium within the permafrost may in part represent the preservation of active layer water within a zone of aggrading permafrost during climatic cooling in the 1950s to 1980s.

Keywords: climate change; ground ice; permafrost; tritium.

Introduction

Although permafrost refers strictly to a thermal ground condition, many investigations of permafrost consider the distribution of water and ice in the soil as an important component due to their effects on the soil structure and stability. The accumulation of ice in the near surface can cause frost heave, while melting of excess ice can lead to thaw settlement; either can result in severe geotechnical problems. In addition, over time landforms and landscapes can be altered due to the freezing and melting of excess ice (e.g. pingos, palsas, ice wedges, patterned ground, thaw lakes, and excessive shoreline erosion) caused by changing climatic conditions. As the climate at any site changes, the seasonally frozen and thawed active layer can increase or decrease in thickness (CALM 2008) and as a result the position of the permafrost table will fluctuate.

Tritium, a radiogenic isotope of hydrogen that was produced in large quantities during atmospheric testing of nuclear devices in the 1950s and early 1960s, has been utilized by several researchers to investigate the incorporation of modern precipitation (since the 1950s) into ice contained within the active layer, the upper permafrost, and permafrost related features, such as ice wedges and frost blisters. Michel (1982, 1986) and Michel & Fritz (1978, 1982) first identified the presence of tritium within permafrost in northern Canada, while Russian investigations in Siberia were reported by Chizhov et al. (1983, 1985) and Chizhov & Dereviagin (1998). Other studies include reports by Livingstone (1988), Burn & Michel (1988), and Lewkowicz (1994). In these studies tritium has been employed as a marker to identify the presence of young water (ice) and to investigate the mechanisms for transferring this water into the permafrost from the active layer. The purpose of this paper is to examine the effects of climate change on the distribution of tritium in permafrost.

Distribution of Tritium in Precipitation

Tritium is naturally produced in low concentrations in the upper atmosphere through the interaction of cosmic radiation with ^{14}N and has a radiogenic half-life of 12.43 years. The distribution of this natural tritium in the stratosphere of the northern hemisphere is poorly understood, but is expected to be higher toward the poles; the natural concentration is considered to be in the range of 10 to 20 tritium units (T.U.; 1 T.U. = 1 atom of tritium in 10^{18} atoms of hydrogen). Testing of nuclear devices injected large quantities of anthropogenic tritium into the atmosphere, primarily in the northern hemisphere, with peak concentrations in precipitation occurring in 1963. Figure 1 displays the 1963 average monthly concentration data from North American monitoring stations. Average tritium concentrations over the polar region in 1963 (5000 T.U.) were 2 to 3 times that of the southern part of the continent and the highest recorded monthly values reached 10,000 T.U. in Whitehorse, Yukon and Nord, Greenland (IAEA 2007). Since 1963, the concentration in precipitation has decreased so that typical values today are in the range of 10 to 25 T.U. (Figure 2). At some localities, new sources of radiogenic emissions, such as nuclear facilities, may periodically give rise to increases in the tritium concentration of local precipitation.

There is also a seasonal variation at any given locale that is related to the ‘leakage’ of tritium from the stratosphere into the troposphere during the spring (Payne 1972). This causes the tritium concentration in precipitation to rise during the spring, peak in the summer and decline during the fall and winter, as shown in Figure 3 for the monitoring station at Alert.

The tritium concentration in precipitation peaks during the warmest part of the summer (July) when the active layer is rapidly thawing. The summer months also receive the highest amount of precipitation.

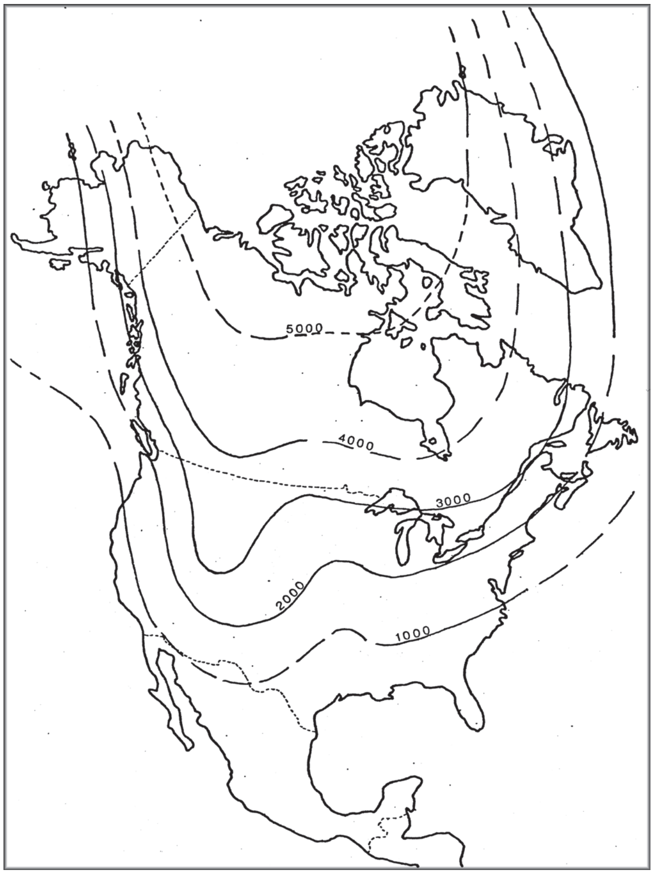

Figure 1. Distribution of average monthly tritium concentrations (in T.U.) for precipitation in North America during 1963. Dashed lines indicate uncertainty due to lack of station data (Michel 1977).

Distribution of Tritium in the Active Layer and Upper Permafrost

Tritium concentrations, for water (ice) contained within the active layer and upper permafrost, have been measured since the 1970s. Chizhov & Dereviagan (1998) summarize over 250 tritium data from a number of sample sites throughout Siberia, with measurements as high as 352 T.U. in the active layer and 323 T.U. in the upper permafrost. The author has measured numerous samples from cores collected along the various proposed pipeline routes in northern Canada and from a detailed study site (Illisarvik) in the outer Mackenzie Delta (Michel 1982). The highest concentration measured at Illisarvik was at a depth of 30 to 40 cm (269 T.U.), while the highest overall tritium value (370 T.U.) was measured from a site south of the Baker Lake community in Nunavut. Peak concentrations throughout the Canadian arctic are generally in the range of 200 to 250 T.U. for samples collected in the mid to late 1970s and early 1980s and are usually found in the lower portion of the active layer or the upper 30 to 50 cm of permafrost. These concentrations are higher than the contemporary average annual precipitation values shown in Figure 2 and must either represent older precipitation recharged during the late 1960s to early 1970s, or summer precipitation recharge that was not mixed (diluted) with snowmelt from winter precipitation. Many active layer tritium concentration values are similar to the average precipitation values.

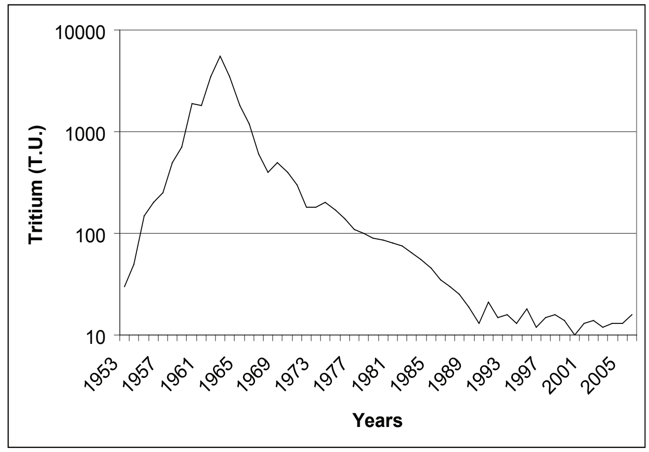

Figure 2. Estimated average tritium concentration for precipitation in the Canadian Arctic. Modeled on data from Ottawa, Canada, plus shorter term records from various Canadian (1955-1969), Greenland (1962-1971), and Alaska (1962-1971) stations (IAEA 2007). Also includes author's spot data from 1975 to 1989 and the author's arctic precipitation network data from 1989 to 2006.

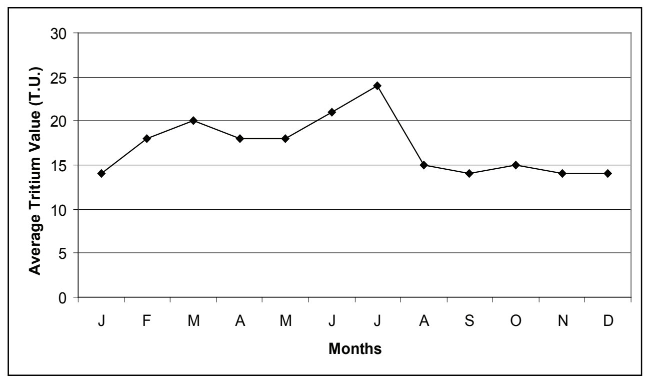

Figure 3. Average monthly tritium concentration in precipitation at Alert, Canada, for the period 1990-1999. Note the spring and summer increase.

Chizhov et al. (1983) and Chizhov & Dereviagan (1998) concluded from their investigations that the presence of tritium in the upper permafrost indicates that extensive moisture exchange takes place between the active layer and permafrost. A study by Burn & Michel (1988), where test plots were irrigated with water containing elevated tritium concentrations, also concluded that the transport of tritiated water into the upper permafrost was due to mass flow rather than molecular diffusion. In all of these studies, the transport of water into the upper permafrost was considered to be due to water migration along a thermal gradient. Most of these investigations involved the collection of spot samples from shallow pits or cores.

Detailed profiling was conducted in May 1979 for two cores at Illisarvik; one within the limits of the lake drained in 1978 (79-4) that subsequently froze to a depth of 2.45 m during the winter of 1978-79, and the other just outside the lake basin (79-3) (Figures 4a and b, respectively). Tritium in

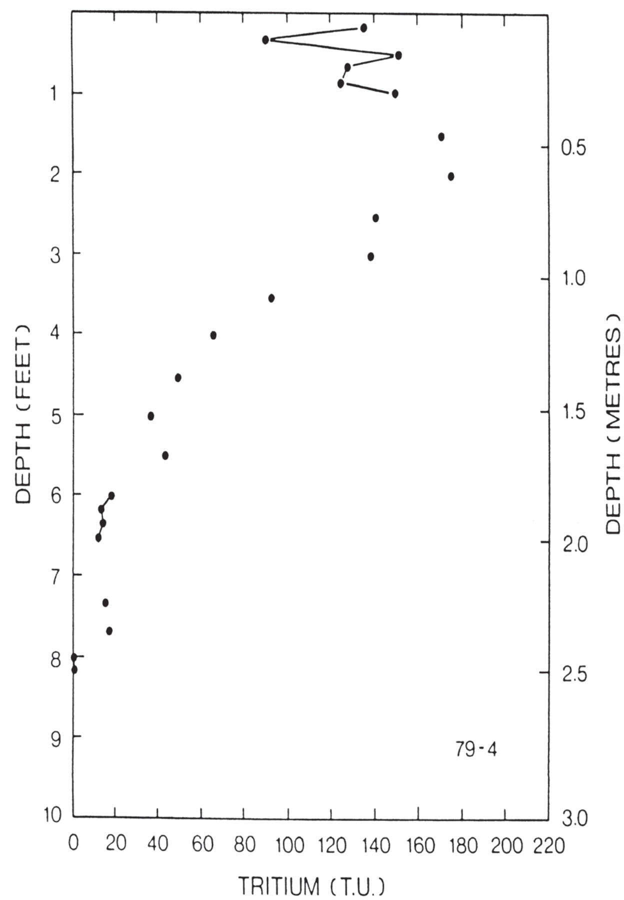

Figure 4a. Tritium concentration profile for lake-bottom sediments at Illisarvik in the Mackenzie Delta (Michel & Fritz 1982).

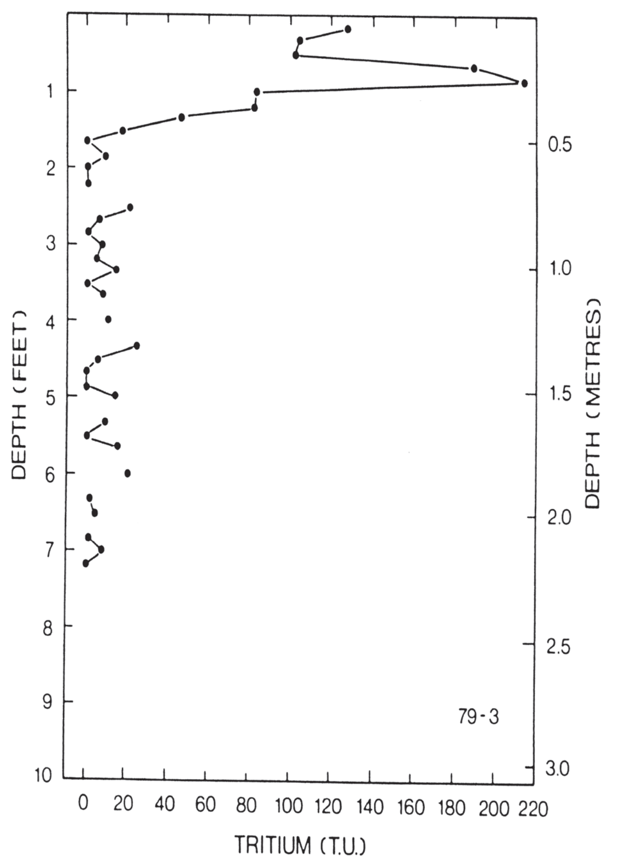

Figure 4b. Tritium concentration profile for frozen ground adjacent to the drained lake at Illisarvik in the Mackenzie Delta (Michel & Fritz 1982).

water from the shallowest lake sediment sample (136 T.U.) in core 79-4 closely reflects the tritium concentration of the lake water just prior to drainage (141 T.U.), while deeper samples display a gradual increase in tritium concentration to 177 T.U. at a depth of 40 cm. Below 40 cm the tritium profile displays a gradual decline to background concentrations at a depth of approximately 2 m. This profile is what would be expected for downward diffusion from a point source (the lake) and developed while the lake sediments were unfrozen (as a lake talik). Since the lake had no discharge creek and was surrounded by ground containing permafrost, there was little if any hydrologic gradient within the unfrozen sediments and thus little physical water migration within the lake sediments. The relatively low peak concentration of 177 T.U. is only on the order of 10% of the expected 1963 peak value (accounting for radiogenic decay) that would occur if the tritium were moving downward as plug (mass) flow. Therefore, through the diffusion process, the tritium concentration is reduced.

In contrast, tritium concentrations for core 79-3 waters peak at a depth of 25 cm (214 T.U., Figure 4b) which corresponds to the base of the active layer as determined from the stable isotope fractionation pattern measured for the pore water profile (Michel 1982). The tritium concentrations drop rapidly to 83 T.U. immediately below 25 cm and reach background values by a depth of 50 cm. Moisture contents throughout this 50 cm interval averaged 300% by weight, with the 20-25 cm interval the lowest at 125%. The sediments in the upper 50 cm of core 79-4 were also saturated, with moisture contents exceeding 500% by weight. This excess water resulted in the formation of ice lenses throughout the depth profiles of both cores.

Another core (NWD-1), collected near Norman Wells in the Mackenzie Valley, was sampled in detail to study its stable isotope (^{18}O) distribution, but was also analysed for tritium. As shown in Figure 5, elevated tritium concentrations were detected more than 50 cm below the level of maximum thaw. Furthermore, the stable isotope profile displays evidence of isotope fractionation generated at the time that the pore water froze.

Infiltration of young tritiated water after this ground was frozen, either by diffusion or mass flow along a temperature gradient, would have altered the stable isotope profile and thus the tritium must have been incorporated prior to permafrost forming in this soil. Since the tritium is related to anthropogenic sources, the presence of tritium in the permafrost indicates that this particular section of ground froze within the previous decade as a result of permafrost aggradation. Livingstone (1988) also found tritium within a section of aggrading permafrost that was caused by the continued deposition of sediments at his study site.

Tritium analysis of other ground ice bodies in Siberia

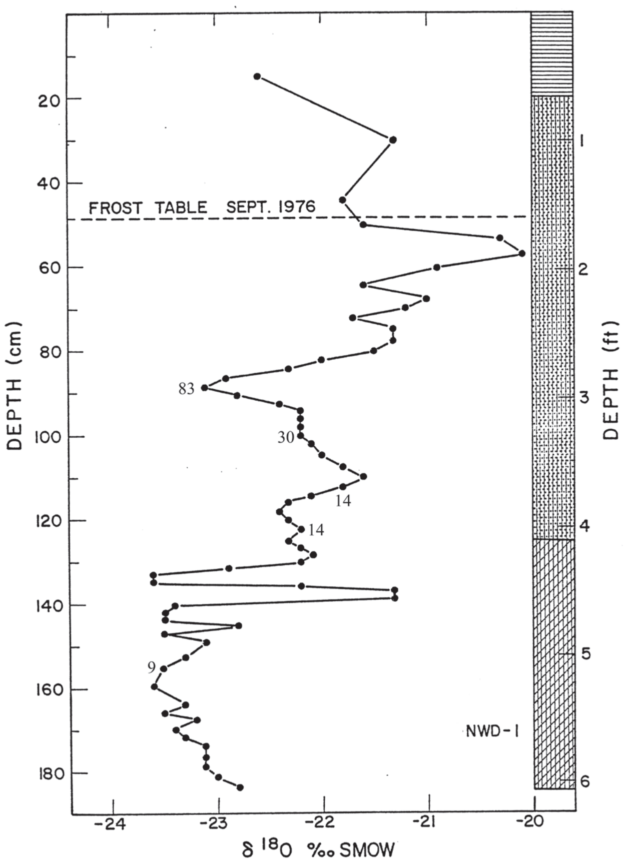

Figure 5. ^{18}O profile for frozen and unfrozen sediments near Norman Wells with spot tritium concentrations (in T.U.) shown below the frost table. Soil profile from top down consists of peat, sandy silt, and silty clay. (Modified from Michel & Fritz 1978.)

and in northern Canada also have been successful in identifying ice formed within the latter half of the 20th century. Identification of active ice wedge growth has been demonstrated in several studies, including Lewkowicz (1988) and Chizhov & Dereviagan (1998). It must be remembered that the source water for ice wedges, winter snowmelt, will contain tritium concentrations that are below the annual average precipitation value. Chizhov & Dereviagan (1998) have also reported tritium data for massive ice from a variety of settings and have been able to determine whether the ice is young (tritium bearing) or relict (pre-1953).

Tritium concentrations for local surface waters will reflect average precipitation values while groundwater retains a tritium signature from precipitation at the time of recharge (Michel 1977) and thus can be useful in distinguishing water sources. Michel (1986) found that the tritium concentration of massive ice within frost blisters at a site in Yukon reflected the age of the source water (local springs) rather than direct precipitation at the site. The tritium concentration within the ice core was considerably higher than water (ice) contained within the overlying organic cover and active layer. The tritium did not appear to have undergone fractionation during freezing of the ice as had been observed for the stable isotopes of the water. Without a clear understanding of how the massive ice formed, an incorrect age could have been assigned to the frost blister. It is important therefore to be careful with the age interpretation of tritium data.

Effect of Climate Change on Tritium Distribution

The active layer only begins to thaw once the snow cover has disappeared and solar radiation is absorbed by the darker ground surface. Excess water, frozen into the active layer during the previous winter as pore ice or ice lenses, will gradually drain down slope through the active layer and enter the local surface water system. Relatively warm summer rains can run off over the ground surface or infiltrate into the unfrozen portion of the active layer and enhance the rate of thaw. By the time the active layer begins to refreeze in the fall, there has been considerable drainage and flushing of the water originally in the active layer, as well as some mixing with the summer precipitation. This will result in a tritium signature for water in the unfrozen active layer that reflects a combination of the tritium concentrations found in the summer precipitation and that of water retained from previous years.

During the fall as the active layer refreezes, unfrozen tritiated water within the active layer will migrate along thermal gradients, both upward toward the ground surface and downward toward the permafrost table, leaving a relatively moisture deficient central zone within the active layer as observed at Illisarvik. If the following summer is cooler and the active layer does not thaw to the same depth as the previous year, some of the tritiated water will be retained in ice formed at or immediately below the permafrost table. Successive years of cooler temperatures would result in an aggrading permafrost table and the preservation of tritiated ice, while a series of warmer summers with greater active layer thaw would result in the formation of a thicker active layer and melting of ice previously accumulated at the permafrost/active layer boundary.

Average annual air temperatures have varied throughout the 20th century. From the 1910s to the early 1940s global temperatures rose such that the highest temperatures of the 20th century were recorded in the 1940s. A cooling trend followed, during the period from the late 1940s to the early 1980s, which has been followed in turn by another warming trend through the 1990s (Hardy & Bradley 1996). The cooling trend in the middle of the 20th century led some scientists to predict the start of a new ice age, while the latest warming trend has spurred the recent global warming debate.

All of these sustained periods of cooling and warming will have an impact on the depth of thaw and the thickness of the active layer. Maximum thaw depths should have been attained during the 1940s. The first part of the subsequent cooling trend corresponds to the period of atmospheric nuclear testing (1953 to 1962). During this period of cooling, the thickness of the active layer should have been decreasing and the permafrost table should have been aggrading upward. Precipitation infiltrating the active layer would have contained significant concentrations of tritium, which would then be preserved within the aggrading permafrost. Of course, variations in the active layer thickness also will occur due to site-specific microclimate effects that could differ from regional climate trends.

Although significant downward diffusion of tritium can occur at unfrozen sites, such as the Illisarvik lake sediments, and moisture migration along thermal gradients can aid in the transport of tritium into the upper permafrost, much of the tritium preserved in the upper 30 to 50 cm of permafrost is probably due to permafrost aggradation under a cooling climate regime. This preservation of tritiated water (ice) in the upper permafrost provides an independent estimate of the maximum active layer thickness developed since the 1950s with which to compare changes occurring in the active layer today due to the current warming trend. Many of the samples analysed for tritium were collected during the last cooling trend when active layers were thinning and therefore tritium was preserved within the upper permafrost. Calculated tritium decay rates for older precipitation from the 1960s and 1970s indicates that preserved precipitation from this period of aggrading permafrost should still have a higher radiogenic signature compared to modern precipitation; however, dilution and mixing with older tritium-free water may have lowered the concentrations to near background levels.

Conclusions

Previous studies have demonstrated that tritium can be utilized as a natural tracer in permafrost investigations and can help to distinguish between water sources of different ages. The presence of tritium in ground ice is indicative of water that recharged into the subsurface during the last half of the 20th century when significant anthropogenic tritium was injected into the atmosphere due to nuclear testing.

Although downward migration of moisture along thermal gradients or due to diffusion is possible, the majority of tritium detected within the upper 30 to 50 cm of permafrost is most likely the result of aggrading permafrost due to climatic cooling during the 1950s to 1980s. The identification of thaw depths caused by warming climatic conditions earlier in the 20th century will permit comparison with modern active layer development caused during the current warming trend.

References

Burn, C.R. & Michel, F.A. 1988. Evidence for recent temperature-induced water migration into permafrost from the tritium content of ground ice near Mayo, Yukon Territory, Canada. *Canadian Journal of Earth Sciences* 25: 909-915.

Chizhov, A.B., Chizhova, N.I., Morkovkina, I.K. & Romanov, V.V. 1983. Tritium in permafrost and in ground ice. In: *Proceedings 4th International Conference on Permafrost, Fairbanks, Alaska. Washington D.C.: National Academy Press,* 147-150.

Chizhov, A.B., Chizhova, N.I., Romanov, V.V., Morkovkina, I.K. & Boyarskiy, O.G. 1985. Tritium analysis in geocryological research. *International Geology Review* 27: 1370-1377.

Chizhov, A.B. & Dereviagan, A. Yu. 1998. Tritium in Siberia's permafrost. In: *Proceedings 7th International conference on Permafrost, Yellowknife,* NWT.: 151-156.

Circumpolar Active Layer Monitoring (CALM). 2008. www.udel.edu/Geography/calm/data/data-links.html.

Hardy, D.R. & Bradley, R.S. 1996. Climate change in Nunavut. *Geoscience Canada* 23(4): 217-224.

International Atomic Energy Agency (IAEA) 2007. *Global Network for Isotopes in Precipitation, Database.* http://www.iaea.or.at:80/programs/ri/gnip/gnipmain.htm.

Lewkowicz, A.G. 1994. Ice-wedge rejuvenation, Fosheim Peninsula, Ellesmere Island, Canada. *Permafrost and Periglacial Processes* 5: 251-258.

Livingstone, S.J. 1988. *Examination of permafrost aggradation using environmental isotope geochemistry, Victoria Island, NWT.* B.S. Thesis. Ottawa, Ontario: Dept. of Earth Sciences, Carleton University, 41 pp.

Michel, F.A. 1977. *Hydrogeologic studies of springs in the central Mackenzie Valley, Northwest Territories, Canada.* M.S. Thesis. Waterloo, Ontario: Dept. of Earth Sciences, University of Waterloo, 185 pp.

Michel, F.A. 1982. *Isotope investigations of permafrost waters in northern Canada.* Ph.D. Thesis. Waterloo, Ontario: Dept. of Earth Sciences, University of Waterloo, 424 pp.

Michel, F.A. 1986. Isotope geochemistry of frost-blister ice, North Fork Pass, Yukon, Canada. *Canadian Journal of Earth Science* 23: 543-549.

Michel, F.A. & Fritz, P. 1978. Environmental isotopes in permafrost related waters along the Mackenzie Valley corridor. In: *Proceedings 3rd International Conference on Permafrost, Edmonton, Alberta.* Vol. 1: 207-212.

Michel, F.A. & Fritz, P. 1982. Significance of isotope variations in permafrost waters at Illisarvik, NWT. In: *Proceedings 4th Canadian Permafrost Conference, Calgary, Alberta, March 2-6, 1981. National Research Council of Canada*: 173-181.

Payne, B.R. 1972. Isotope hydrology. In: *Advances in Hydroscience,* Vol. 8. New York: Academic Press, New York, 95-138.

Twenty Years of Permafrost Research on the Furggentälti Rock Glaciers, Western Alps, Switzerland

Dragan Mihajlovic
Institute of Geography, University of Bern, Switzerland
Flotron AG Engineers, Meiringen, Switzerland
Benno Staub, Anina Nussbaum
Institute of Geography, University of Bern, Switzerland
Bernhard Krummenacher
Geotest AG, Davos, Switzerland
Hans Kienholz
Institute of Geography, University of Bern, Switzerland

Abstract

Since 1988, long-term monitoring of the Furggentälti rock glaciers (Western Alps, Switzerland) has revealed significant changes in process dynamics. The changes include large seasonal and interannual variations of rock glacier activity, superimposed by an exponential increase of overall rock glacier creep velocity. During the monitoring period, the largest of the rock glaciers (located at 2450 m a.s.l.) developed signs of decay, with some parts of the rock glacier becoming inactive and others showing patterns of collapse. Analysis of local climate data suggests a strong and surprisingly low-latency link between rock glacier activity and weather patterns. Even though some of the long-term developments in the kinematics of the Furggentälti rock glaciers are also influenced by other factors, such as topography and process feedback, the short-term response to climate signals points at ever warmer permafrost conditions at the site as the major cause for the changes observed.

Keywords: climate change; ground surface temperature; long-term monitoring; rock glacier activity; Switzerland; warm permafrost.

Introduction

Background

During the 2003 summer heat wave, the many rock fall events in the Swiss Alps—the most prominent one affecting the well known Matterhorn—have demonstrated the very immediate and very obvious impact of rising temperatures on permafrost present in rock walls.

Though slower and less obvious, the thawing of perennially frozen debris typically found in rock glaciers is now becoming visible at the lower limit of alpine permafrost.

For the last 20 years, the Institute of Geography of the University of Bern has been closely monitoring a small rock glacier located in the western parts of the Swiss Alps. During the monitoring period, the rock glacier has undergone rapid changes in shape and process dynamics, which are coupled with the development of the local climate.

Situated at the lower limit of Alpine permafrost, the Furggentälti rock glacier is a textbook scenario for the impact of a warmer climate on rock glacier activity and evolution.

The project site

The Furggentälti (46°24.5′N, 7°38′E), a small valley near the Gemmi pass, is located in the western part of the Bernese Alps between Kandersteg and Leukerbad (Switzerland). The valley stretches over a range of approximately two square kilometers from west to east, from an altitude of approx. 2450 m to approx. 2850 m a.s.l.

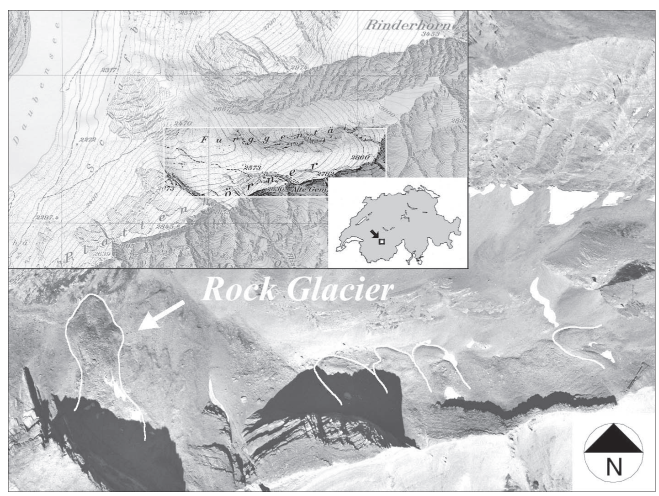

Figure 1. Geographic location and aerial view of the Furggentälti Valley (© Swiss Federal Office of Topography).

Most of the surface of the valley is covered by vast layers of periglacial debris, forming large talus cones on the foothills of the steep northern slope.

The Furggentälti Valley is home to many periglacial forms, including solifluction lobes and several small active and inactive rock glaciers on the north exposed slope. Typical periglacial patterned ground is also present in a flat region of the valley.

The focus of interest lies on an approximately 250 m long tongue-shaped rock glacier in the lower western part of the valley (Fig.1). The rock glacier is situated on a slope of about 20° of northern aspect, its front protruding into the bottom of the valley, at an altitude of approx. 2450 m a.s.l.

The research project

Initiated in 1988, the long-term monitoring project consists of several measurement programs recording meteorological data, ground temperatures, ground surface temperatures (GST, recorded by ultra miniature temperature loggers UTL, www.utl.ch), and rock glacier activity data through aerial and terrestrial survey. The time series recording air and ground surface temperatures represent the longest such measurement series in a periglacial environment in the Alps.

The project is funded by the Institute of Geography of the University of Bern (www.giub.unibe.ch), the PRO GEMMI foundation of Bern, and by the PERMOS program (Permafrost Monitoring Switzerland, www.permos.ch).

Changes in Rock Glacier Activity

Multi-decadal trends

Photogrammetric survey of the Furggentälti rock glacier spans over nearly five decades, the first set of small scale aerial photographs dating back to 1960. Since 1990, large scale aerial imagery was flown at five year intervals, and since 2001 in a two year interval.

A first photogrammetric assessment of the Furggentälti rock glacier in 1996 (Krummenacher et al. 1998) revealed unusually high surface velocities and a rapid increase during the late eighties and early nineties. Further photogrammetric surveys (Mihajlovic et al.2003) confirmed this multi-decadal trend, which was also observed in neighboring rock glaciers in the valley. The survey also found indications for a slowdown in surface velocities in the peripheral parts on the left and right side of the rock glacier (Fig. 2).

The latest data (Mihajlovic et al., in prep.) confirm both trends, with increased surface velocities found along the centerline of the rock glacier and a slowdown on the sides. The data have also detected the inactivation of peripheral parts of the rock glacier (Fig 3).

Interannual variations

Since 1994, terrestrial survey campaigns provide a more detailed picture of the development of rock glacier activity and process dynamics.

Annual survey campaigns have uncovered interannual variations in the activity of the rock glacier, showing a clear pattern of thermally induced acceleration and deceleration of surface velocities (Fig. 4).

The pattern clearly reflects the development of the warming conditions at the site, with some attenuation during 2005 to 2007.

Seasonal activity pattern

A seasonal activity pattern was detected during a series of repeated survey campaigns from August 1998 to October 1999 (Mihajlovic et al. 2003). After a continuous slowdown during winter, the permafrost creep process accelerates rapidly at the beginning of the Zero Curtain phase in spring, when water infiltrates into the frozen active layer and rock glacier material, triggering an instant warm-up of the thermal conditions there (Fig. 5).

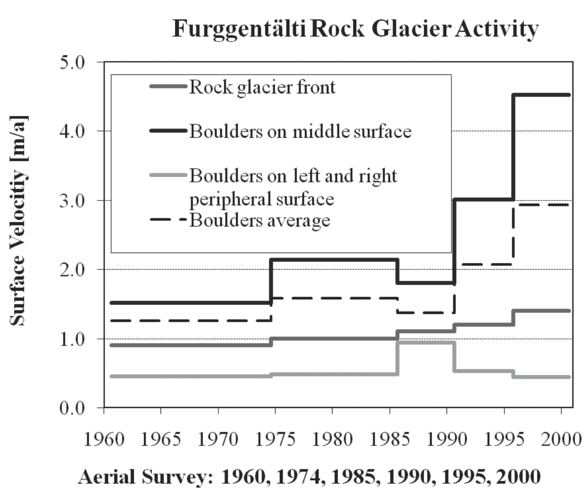

Figure 2. Multi-decadal trend. Rock glacier surface velocities derived from aerial survey 1960–2000.

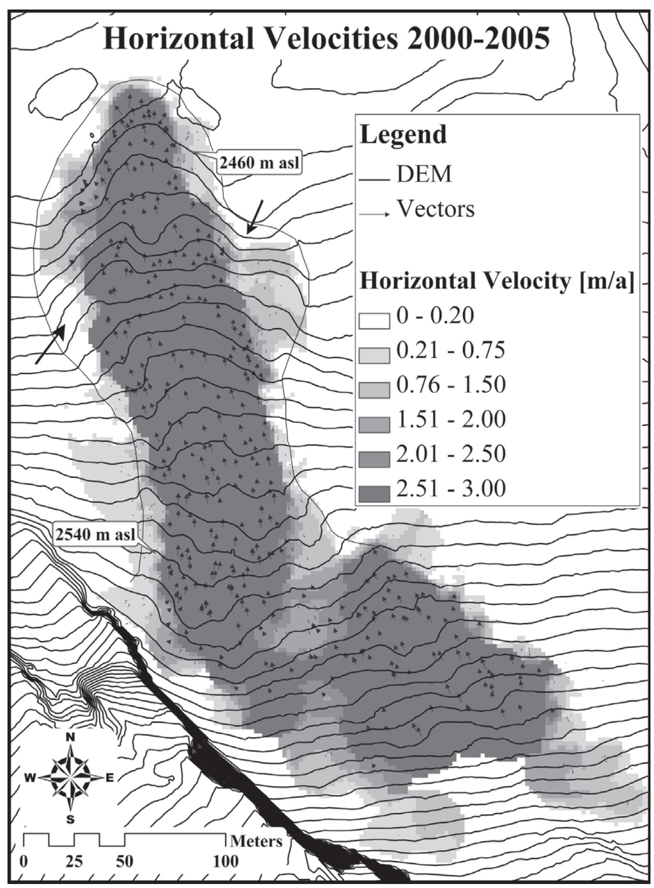

Figure 3. Velocity field of the Furggentälti rock glacier surface. Aerial survey, 2000–2005; arrows: parts inactivated during the monitoring period.

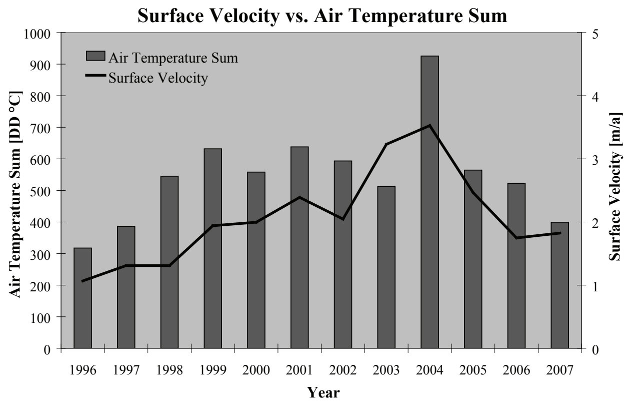

Figure 4. Interannual variations of surface velocities (terrestrial survey) vs. air temperature sum; period: September of the preceding year to August.

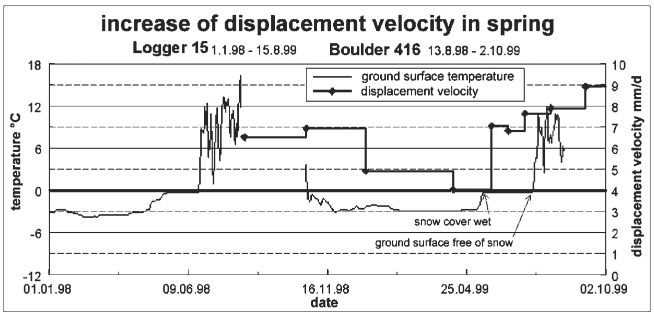

Figure 5. Seasonal variation of rock glacier activity compared with ground surface temperatures measured nearby.

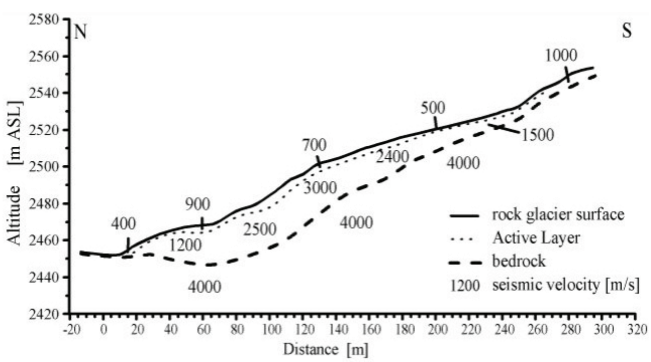

Figure 6. Seismic profile of the Furggentälti rock glacier; dashed line: estimation of bedrock surface (Nussbaum 2008).

New clues

The results (Nussbaum 2008) of geophysical soundings (GPR and refraction seismic) in 2007 are providing new clues for the unusual shape and rheology of the Furggentälti rock glacier, which are also affected by the special arrangement of rock glacier material on the underlying bedrock topography (Fig. 6).

The observed long-term acceleration of rock glacier activity could be partly the result of this arrangement or of process feedbacks such as the increasing surface area exposed to irradiation due to the extending rock glacier footprint. However, similar findings on neighboring rock glaciers in the Furggentälti, together with the thermally induced short-term variations, point at the warmer climate as the main cause for the long-term development.

Similar developments across the Alps

During the last years, similar observations on other rock glaciers have provided a clearer picture of changes in rock glacier activity in different parts of the Alps. Delaloye et. al. (2008) gives an overview of data from 17 rock glaciers. Several studies mention a similar increase of rock glacier surface velocities during the past decades (e.g., Roer 2005), as well as interannual variations (e.g., Ikeda et al. 2003).

Impact of a Warmer World

Ice temperature and permafrost creep

Lab experiments using centrifuges to assess the mechanical stability of rock glacier material have shown that the plasticity of rock glacier material increases rapidly with ice temperatures approaching 0°C (Arenson 2003). The reason for this non-linear behavior was found in the exponential increase in the presence of liquid water in the material, when increasing from approximately -2.5°C to 0°C.

Ice temperatures in the Furggentälti rock glacier cannot be measured directly, as the high surface velocity of several meters per year prevents the installation of a borehole or the retrieval of other (wired) equipment. Instead, the winter equilibrium temperature (WEQT) is used as an estimation for the permafrost temperature at its coldest state in the year. The WEQT is derived from continuously recorded ground surface temperatures (GST), which are measured by ultra miniature temperature loggers at several locations on the rock glacier surface.

During most of the 13 year monitoring period, winter equilibrium temperatures recorded on the Furggentälti rock glacier were within the range of -2.5°C to -1.5°C, with the exception of two distinct cooling events that led to a significantly lower WEQT in early 1996 and 2006.

Influence of weather patterns and snow cover

A comparison of ground surface temperatures of several years (Fig. 7) shows the broad variation of the atmospheric influence on the active layer.

The GST monitoring period (1994 to 2007) contains both positive and negative interannual WEQT fluctuations, which coincide with positive and negative variations of rock glacier activity. In the positive case, atmospheric conditions during the preceding year led to a general increase of ice temperatures, whereas in the negative case an overall cooling occurred. This information can be used as a simple pointer to assess the direction of the energy flux integral at the ground surface, for the corresponding interval.

The main factor controlling direction and magnitude of the energy flux is the snow cover (Keller 1994, Krummenacher et al. 1998, Mittaz et al. 2002) which acts both as a shortwave radiation shield and as a thermal insulator. Timing, duration and depth of the snow layer modulate the energy balance of the ground surface, and as a consequence the thermal conditions in the active layer.

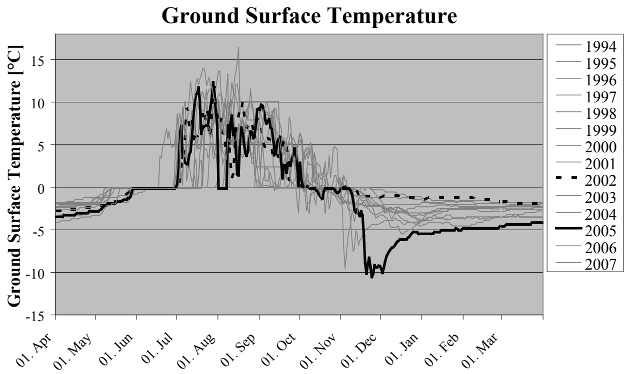

Figure 7. Bandwidth of fluctuations in ground surface temperatures from 1994–2006. Dotted line: 2002/2003; black line: 2005/2006. Recorded by UTL data logger #3 on the Furggentälti rock glacier surface.

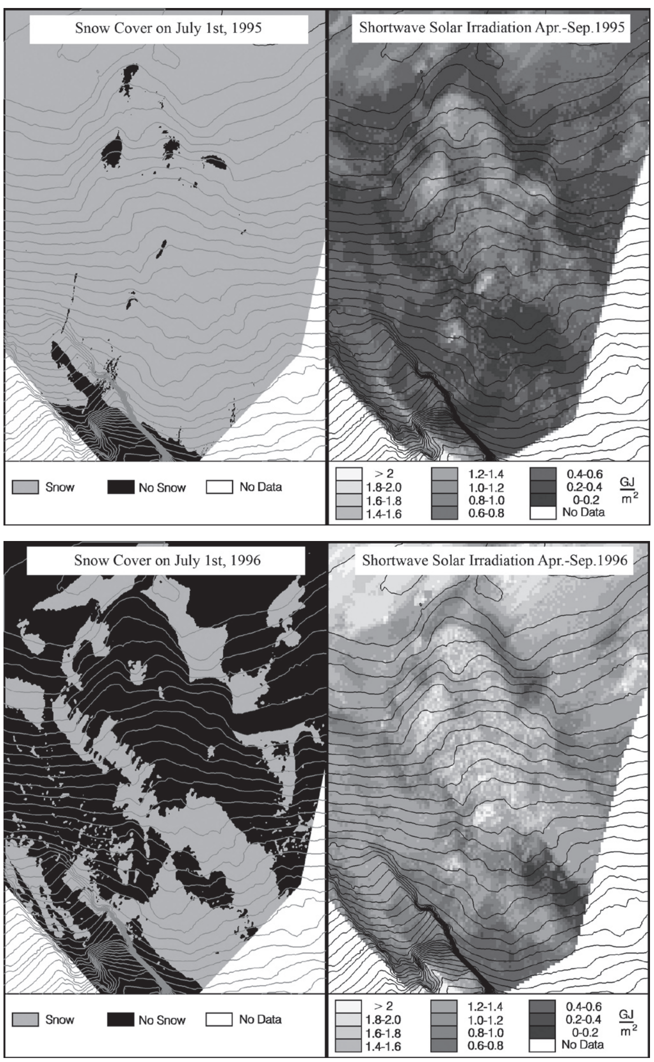

Figure 8. Snow cover variations (July 1 1995 and 1996) (derived from terrestrial orthophotos) and net shortwave solar irradiation April to September 1995 and 1996 on the Furggentälti rock glacier. Based on daily snow cover maps and shortwave radiation (1-hour interval), high resolution elevation model.

A study (Mihajlovic et al. in prep.) using local shortwave irradiation data and snow cover maps (derived from digital orthophotos of an automated camera taking daily photographs of the site) assessed the total shortwave irradiation on the rock glacier surface during the summer of 1995 and of 1996, which corresponds with the distinct positive variation between the WEQT in 1996 and 1997 (Fig. 6). During the period from April 1 to September 30, 1995 the average net shortwave irradiation on the true surface of the rock glacier amounts to 38 W/m^2, compared to 108 W/m^2 during the same period in 1996 (Fig. 8). This enormous difference is in large part caused by the different duration of the snow cover during spring and summer, whereas the total shortwave irradiation sum only differed by approximately 9%.

Analyzing the influence of the snow cover in GST data

In order to get a better picture of how different temporal patterns of snow cover occurrence influence permafrost temperature variations, a simple method was developed which allows extracting more specific parameters from existing GST measurement series. The basic idea is to skip from looking at GST time series in fixed intervals (e.g., annual intervals like MAGST Mean Annual GST, or monthly intervals etc.) to intervals which take into consideration the different states of thermal insulation properties of the snow cover.

For this, the annual cycle of snow cover ablation and development is divided into four phases, where each represents a different role of the snow cover on the energy flux between ground surface and atmosphere:

- Phase Z: Zero Curtain (springtime); GST shows 0°C, direct energy flux between atmosphere and ground surface is suppressed.
- Phase N: No Attenuation; during the absence of snow, GST shows big daily temperature fluctuations while the energy flux between atmosphere and ground surface is unhindered.
- Phase L: Low Attenuation; in this phase, a snow cover of limited depth is present. Energy flux between atmosphere and ground surface is attenuated, but not suppressed. Daily temperature fluctuations are still visible in the GST, but clearly attenuated.
- Phase H: High Attenuation; in this phase, the ground surface is covered by a thick and thermally insulating layer of snow, through which the energy flux is highly attenuated and therefore only minimal. No daily temperature fluctuations visible in GST.

To extract the beginning and end of these phases, the GST data is processed through a series of simple signal processors which act as band pass filters on the daily fluctuations showing up in the data. While the *Zero Curtain* (no daily fluctuations and 0°C) and the *No Attenuation* phase (large daily fluctuations) are easily distinguishable, the *Low Attenuation* phase (daily fluctuations below a certain threshold value) is less clearly defined and can vary by a few days, depending on the actual filter settings (Mihajlovic, in prep.). Figure 9 shows a typical arrangement of the phases.

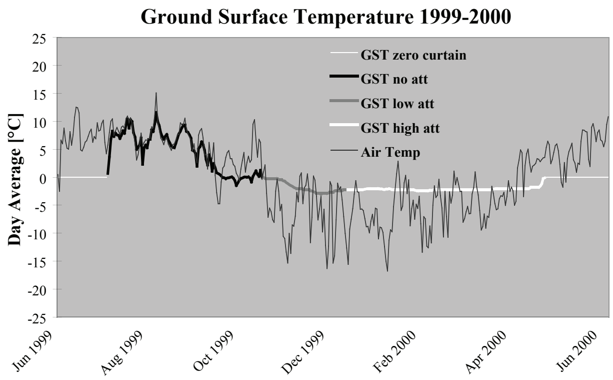

Figure 9. GST data divided into four phases which roughly represent different states of the thermal insulation properties of the snow cover; thin white line: Zero Curtain (phase Z); black: no attenuation of the atmospheric signal by the snow cover (phase N); gray: low attenuation phase (phase L); thick white line: high attenuation phase (phase H); thin gray line: air temperature (2 m).

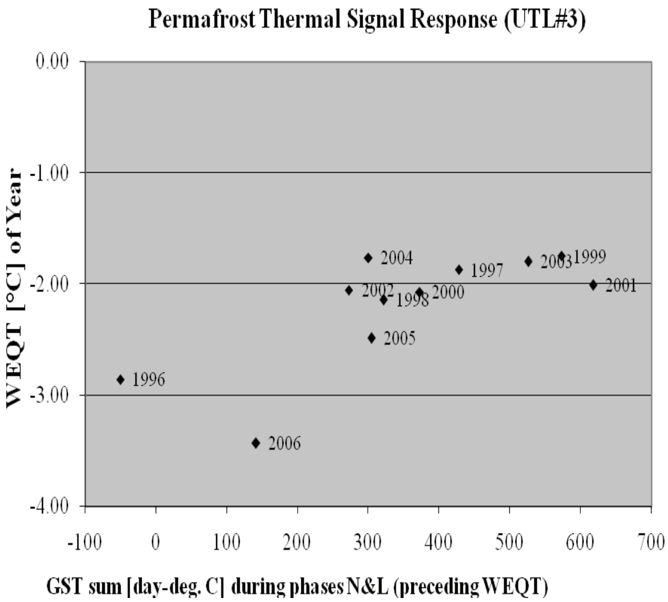

Figure 10. WEQT compared to the ground surface temperature sums of the preceding *No Attenuation* and *Low Attenuation* phases.

During Phase N and L, the ground surface temperature recorded is influenced by the energy flux between atmosphere and active layer, whereas during the *Zero Curtain* the temperature recorded is that of the snow cover. During the *High Attenuation* phase H, the data reflects the thermal "response" of the permafrost to the thermal "signal" applied to the surface of the active layer during the preceding phases N and L.

Comparing different years of GST data by adding temperatures sum for N and L phases only, the relation between thermal "signal" and the thermal "response" becomes more obvious (Fig 10).

The non-linearity in the relation shows how the thawing of ice in the rock glacier material is acting as a thermal buffer in warmer years with a high energy input. Doubling the thermal signal from, for example, 300 day-degrees C to 600 will not lead to substantial increase of the WEQT (and,

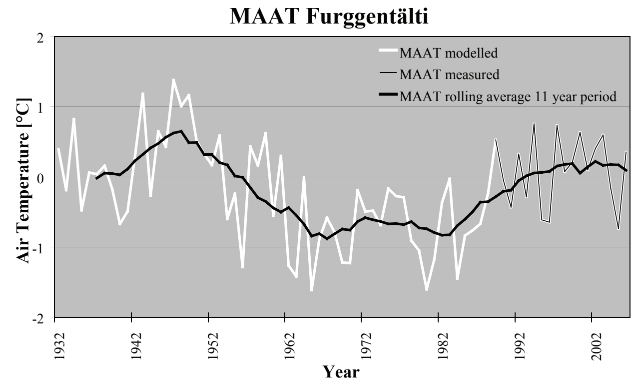

Figure 11. Modeled and measured air temperature in the Furggentälti; based on data of the nearby MeteoSwiss (www.meteoswiss.ch) meteorological station Montana 1932 to 1988, local measurements since 1988.

therefore, permafrost temperature), as the excess energy input of the warm season is leaving the rock glacier system as melt water. In contrast to this, reducing the thermal signal to 150 day-degrees C leads to a significant drop in permafrost temperature.

Long-term trend

Between 1988 and 2007, the trend in the air temperature data measured at the site shows a clear rise in average air temperatures during the first decade of measurements, which is then followed by a series of both extremely high and low temperatures during recent years. Long term temperature records of the nearby Meteoswiss meteorological station of Montana have been used to model air temperatures for the preceding decades (Fig. 11). The data suggest a general increase in air temperatures since the mid-1960s, preceded by a significantly warmer period during the forties and fifties.

One of the changes witnessed during the monitoring period is the increasing lack of snow. The clustered occurrence since the early nineties of winters with only little snow did not lead to a general cooling of the permafrost present in the rock glacier, as could be expected in higher regions with MAAT<<0°C. At the comparably low altitude of the site (average air temperature 1988–2006 = 0.1°C), the importance of the snow cover acting as a radiation shield during early summer is exceeding the "cooling effect" of the absence of snow during the cooling phase in early winter, as typical winter temperatures and the typical timing of snow falls do not a allow a profound cooling of the thermal conditions in the early winter of an average year.

The two WEQT cooling events recorded in the 13 year GST series (Fig. 10) find their explanation in abnormalities in the occurrence of snow; while an unusually long duration of a thick layer of snow on the Furggentälti rock glacier during the cold summer of 1995 led to the cold WEQT recorded in early 1996, the 2006 negative WEQT variation was caused by a lack of snow combined with exceptionally cold air temperatures during the preceding weeks of early winter.

Preliminary results based on long term snow depth and air temperature data of Montana station suggest that the depth and timing of snow cover in combination with air temperatures did not lead to a significant cooling of the permafrost conditions in the Furggentälti rock glacier during most of the past 75 years (Mihajlovic, in prep.).

Conclusions

The 20-year period of monitoring has amassed a large amount of scientific data about the sensitive environment in the Furggentälti Valley. The rather low cost methods used in the monitoring program such as the UTL data logger, which was especially developed for the project by B. Krummenacher (Krummenacher et al. 1998), have allowed uninterrupted data series over many years, despite limited funds.

The monitoring data is offering clues to a deeper understanding of the link between seasonal weather patterns on permafrost temperatures and subsequently on rock glacier activity.

The changes in shape and activity of the rock glacier during the last five decades reflect the development of the local climate during that period, which follows a general trend to warmer air temperatures and an increasing lack of snow. The changes also confirm the scenario of increased rock glacier activity before the onset of inactivation.

The findings of the monitoring program provide a graphic example for the impact of a warmer climate on the lower limit of alpine permafrost.

References

Arenson, L.U. 2003. *Unstable Alpine Permafrost: A Potentially Important Natural Hazard – Variations of Geotechnical Behavior with Time and Temperature.* Zürich: Publications of the Institute for Geotechnical Engineering (IGT), Swiss Federal Institute of Technology Vol. 218.

Delaloye, R. 2008. Recent interannual variations of rock glaciers creep in the European Alps. *Proceedings of the Ninth International Conference on Permafrost, Fairbanks, Alaska, June 29–July 3, 2008* (this proceedings).

Ikeda, A., Matsuoka, N. & Kääb, A. 2003. A rapidly moving small rock glacier at the lower limit of the mountain permafrost belt in the Swiss Alps. *Proceedings of the Eighth International Conference on Permafrost* 1: 455-460.

Keller, F. 1994. *Interaktionen zwischen Schnee und Permafrost.* Zürich: Mitteilungen der VAW/ETH Zürich, 127.

Krummenacher, B., Budmiger, K., Mihajlovic, D. & Blank B. 1998. *Periglaziale Prozesse und Formen im Furggentälti, Gemmipass.* Davos: Mitteilungen des Eidgenössisches Institut für Schnee- und Lawinenforschung Davos Nr. 245.

Mihajlovic, D., Krummenacher B. & Imhof, M. 2003. Developing new methods for monitoring periglacial phenomena. *Proceedings of the Eighth International Conference on Permafrost* 1: 455-460.

Mihajlovic, D. in prep. *Blockgletscheraktivität und Klima im Furggentälti, Gemmipass*. Bern: Institute of Geography, University of Berne.

Mittaz, C., Imhof, M. Hoelzle, M. & Haeberli, W. 2002. Snowmelt evolution mapping using an energy balance approach over an alpine terrain. *Arct. Antarct. Alp. Res.* 34(3): 274-281.

Nussbaum, A. 2008. *Geophysikalische Untersuchungen am Blockgletscher Furggentälti, Gemmi (VS)*. Berne: Institute of Geography, University of Berne (unpublished).

Roer, I. 2005: *Rockglacier kinematics in a high mountain geosystem*. Bonn: Department of Geography, University of Bonn.

Convective Heat Exchange Between Rivers and Floodplain Taliks

V.M. Mikhailov
North-Eastern Research Station of the Melnikov Permafrost Institute, SB RAS, Magadan, Russia

Abstract

The results discussed are estimates of convective heat exchange between rivers and floodplain taliks. Heat balance calculations were made for large sections of six rivers of northeastern Asia. Heat flux from rivers peaks in June, rarely in July, 100–200 W/m^2. Total heat transfer during summer is 700–1000·10^6 J/m^2; thus taliks obtain larger amounts of heat from rivers than from soil surface. In autumn, heat flux changes its sign, and rivers begin to receive heat back. This slows down their cooling, detains water freezing (for up to 10 days or even more), and sustains numerous glades in winter. These features demonstrate that convective heat exchange is not just capable of upholding floodplain taliks; it is far excessive for this task even in the coldest region of the Northern Hemisphere. Obviously, climatic conditions are not a limiting factor for geographical distribution of such taliks.

Keywords: convective heat exchange; floodplain taliks; heat balance; rivers; seasonal dynamics; thermal regime.

Introduction

Concerning the origin of floodplain taliks, the majority of authors agree that they exist due to convective heat exchange with rivers, though until recently no attempts were made to obtain quantitative characteristics of this process. Based on traditional approaches this problem is virtually unsolvable. The only practical way is to calculate a river heat balance. Accounting for all commonly considered components, the residual is convective heat flux into the ground. Using this approach, a number of estimates of this quantity were made for streams of III–IV orders (Mikhailov 2003); the data for calculations were received by *in situ* observations. Since the study process is highly dynamic and strongly dependant on hydrometeorological conditions, these results represent only short periods of time. Besides, it remained unclear whether it is possible to extrapolate them to larger watercourses. Dealing with such rivers, the investigated reaches should be several kilometers long or more, depending on water discharge. In such cases, it is usually impossible to obtain adequate data on the channel width for a given time span; that is why previous calculations could have been made only for one river during one ten-day period (Mikhailov 1998).

Profound research of convective heat exchange is not feasible without studying its seasonal dynamics. The most appropriate way is by using long-term means. While such hydrological and meteorological data are provided in reference books, the average width of extensive river sections can be estimated only for the date of the aerial mapping used to make the corresponding sheet of a topographic map. A special research program was carried out in order to solve this problem (Mikhailov & Ushakov 2002). It turned out that in braided rivers, correlation between channel width and water discharge is close enough to fulfill heat balance calculations with sufficient accuracy. Such rivers prevail in mountainous areas of northeastern Asia and are also associated with floodplain taliks (Mikhailov 1995).

The aim of this work is to investigate the main regularities of seasonal dynamics of convective heat exchange between floodplain taliks and rivers of medium and higher orders and its influence on a number of hydrological processes and phenomena.

Materials and Methods

The general pattern of estimations is the same as in the previous study (Mikhailov 1998): the intensity of heat exchange between rivers and adjoining grounds was calculated using stepwise approximation, so as to achieve identity of the simulated and actual river temperatures in the studied river sections. The calculations of temperature increments were carried out successively from one confluence node to another, with presumed instant water mixing in nodes.

Methods of calculations

The heat balance equation for a river segment, dx, under considered conditions is as follows (Vasilyev & Voyevodin 1975):

$$\Omega \frac{\partial T}{\partial x} + \frac{\partial}{\partial t}(sT) - \frac{B}{C}\sum q_i = 0 \qquad (1)$$

where x and t are distance downstream and time, respectively; Ω and T are, accordingly, water discharge and temperature; B and s are river channel width and cross-sectional area, respectively; C is water volumetric heat capacity; $\sum q_i$ is the sum of all heat fluxes influencing water temperature. Hereafter all dimensions are in SI if not specified otherwise.

The sum $\sum q_i$ includes the resultant of energy exchange on water surface (q_s); the heat of dissipation of kinetic energy of the flow (q_{diss}); the heat of thawing solid precipitation (q_m); and total heat flux into ground (q_{gr}), which is the sought quantity. Thermal influence of liquid precipitation is negligible; in large rivers; the same is true for the dispersed inflow. The working equation for estimations of river temperature increments between outfalls of tributaries is as follows:

$$T = T_0 + \frac{B\Delta x}{C\grave{U}}(q_s + q_{diss} - q_m - q_{gr}) - \frac{\Delta x}{\grave{U}\Delta t}\left(s\Delta T + T\Delta s\right) \qquad (2)$$

Hereafter the symbol « Δ » stands for the finite increment of the according quantity; index «0» implies that the labeled quantity is related to the upstream cross-section of the segment Δx. In calculations by formula (2) made with a specially designed computer algorithm, the step Δx was specified as approximately equal to the river width and so, as the number of steps to the next node, was an integer.

The constituents of q_s are generally known, e.g. (Pavlov 1984):

$$q_s = S\left(1 - A\right) + I_a - I_s - P - LE \qquad (3)$$

where S is total shortwave radiation; A is albedo of water surface; I_a and I_s are long-wave radiation of air and water surface, respectively; P and LE are sensible and latent heat fluxes accordingly. The methods of estimations of all these quantities are minutely elaborated and well-known. Though somewhat diverse empiric formulae are in use, the results obtained differ but a little (Mikhailov 1998).

The quantity q_{diss} is usually defined as the product $\rho gIVH$, where ρ is water density; g is gravitational acceleration; I is river inclination; H and V are mean values of the river velocity and depth, respectively. In calculations it is more appropriate to use the equivalent formula $q_{diss} = \rho gI\,\Omega/B$. Finally, q_m is evaluated by the dependency $q_m = L_m p/n$, where L_m is specific heat of ice thawing; p is monthly solid precipitation in millimeters; and n is the number of seconds in a given month.

Studied river sections and time span

The most suitable river sections for heat balance estimations are those between two stations, where full-scale hydrological and meteorological observations are implemented. It is essential, of course, that the river has a floodplain talik. Despite a fairly well-developed monitoring network and an abundance of such taliks, the first requirement is fulfilled only for one of six chosen sections. Besides, some necessary information is absent in principle. The lacking data were compensated using interpolations and various kinds of empirical dependences discussed in the next subsection.

The general information on the sections is given in Table 1. The first three are situated on the largest rivers of northeastern Asia; the others, in the Upper Kolyma basin (Fig. 1). All of them belong to the subarctic zone characterized by a severe, extremely continental climate. Those characteristics, which are the most important for the aim of the research, vary in close limits; thus the July mean air temperature ranges from 13.7 C to 15.6 C, and the total shortwave radiation ranges from 218 to 228 W/m^2.

In the selected sections, the rivers have braided channels and vast floodplains covered with mixed forest, which is a generally accepted indicator of floodplain taliks. The only exception is the Debin River, which is degrading over almost one-third of the section length and has no accumulative floodplain. In computations, convective heat exchange in such segments was specified as zero. Thus, the final result for this river, q_{gr} value, relates only to the reaches with floodplain taliks.

Table 1. Overview information on the studied river sections.

River	Length, km	Drainage area, km^2	Mean July discharge in the upper cross-section, m^3/s
Kolyma	190	11000	2210
Indigirka	113	32100	842
Anadyr	100	3400	964
Debin	89	2300	27.0
Detrin	63	2140	81.6
Berelekh	50	2180	119

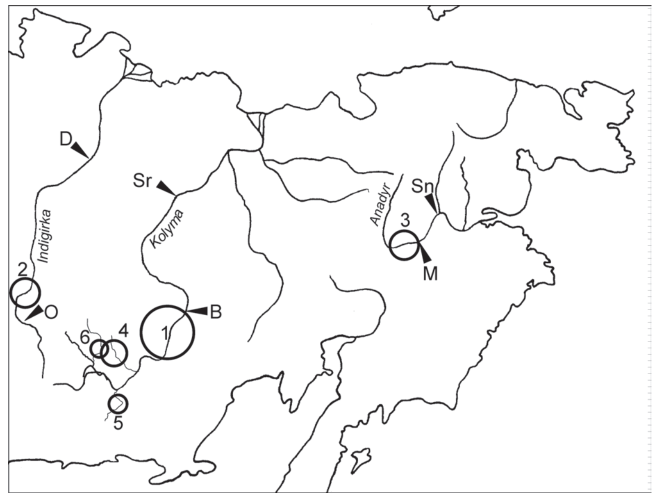

Figure 1. Locations of the studied river sections (circles) and gauging stations (triangles). Rivers: 1–Kolyma; 2–Indigirka; 3–Anadyr; 4–Debin; 5–Detrin; 6–Berelekh. Gauging stations: B–Baligichan; Sr–Srednekolymsk; M–Markovo; Sn–Snezhnoye; O–Oimyakon; D–Druzhina.

In May and October, the thermal regime of the studied rivers is considerably affected by freeze-thaw processes, which cannot be taken into account because of the lack of data. This limits the study period to four months.

Basic data

The values used in computations were monthly means in summer and ten-day means in September. The latter, except for water temperatures, were obtained via interpolation (using smoothed seasonal change curves). In this month, which is of particular interest for this study, a monotone decrease occurs of all quantities affecting water temperature; therefore such technique could not cause significant errors.

Most of the necessary information was obtained from reference books (Reference Book 1966; Long-Term Data 1985, 1987). The lacking data were acquired in the following ways.

Water discharges in the studied river sections were estimated using the data from the nearest gauging-stations, corresponding values of unit discharges, and increments of drainage areas. In five cases out of six, the upstream cross-sections were provided with discharge data, which minimized errors. The exception is the Kolyma River, but there the drainage area over the whole section increases less than 8%; this reduces the errors originating from the next discussed approximation.

Water discharges and temperatures of tributaries: The former quantities were calculated using drainage areas (measured on topographic maps) and unit discharge means estimated for each river section. To compute water temperatures, as well as in the previous study (Mikhailov 1998), empirical dependences "discharge–temperature" were derived via statistical treatment of data from 59 gauging-stations belonging to the investigated watersheds. All of these formulae were of the form $T = a\lg\Omega + b$ with a and b parameters calculated separately for each summer month and each ten-day period of September. When using long-term data, the correlation between temperatures and discharges is closer than in the case studied earlier, when the estimations were made for a short time span. While in that period 70% of T values were beyond the interval of ±1 C from the regression line; for mean July temperatures, the relation is inverse. In June, the range of temperatures is a little wider, but by the end of the season, it becomes sufficiently more narrow.

Climatic data used were obtained at the weather stations located, as a rule, in close vicinity to the gauging-stations, or not more than 100 km away from them. All weather stations, as well as gauging-stations, are situated in wide river valleys where local peculiarities are minimal. As it was mentioned above, the values of climatic characteristics vary within close limits all over the vast territory embracing the studied river sections, so the differences within short distances are negligibly small.

River channel width and cross-sectional area: To estimate B, traditional empirical formulae $B = \alpha\Omega^{\beta}$ were used (Park 1977). Values of a and β for braided rivers had been obtained earlier (Mikhailov & Ushakov 2002). Due to similarity in relations of B and H to water discharge (Park 1977), s values obey the dependence of the same form: $s = s_0\left(\Omega/\Omega_0\right)^{\beta}$, where s_0 is the cross-sectional area at the upstream station determined by hydrologic yearbook data. The β values were evaluated by analysis of information from the reference book (*Atlas of the Kolyma River* 1931) based on previously obtained results (Mikhailov & Ushakov 2002).

Discussion

The ultimate results of computations are shown in Table 2. To evaluate their reliability, a series of additional computations were made in which the values of quantities not provided with precise data differed from those used in the main version. Deviations were specified so as to be the maximum reasonable possible. If it is assumed that all errors do not compensate each other and affect the final result in the same direction, then it might change most significantly in June by 25 W/m² on average; in the Debin River, by 33 W/m². Further on, absolute values of errors decrease monotone,

Table 2. Mean monthly and ten-day period values of q_{gr}, W/m² and total heat transfer into ground over the study period (Q_{gr}), 10⁶J/m².

River	June	July	August	September 1	September 2	September 3	Q_{gr}
Kolyma	166	109	101	47	−23	−71	1033
Indigirka	152	111	95	36	−19	−65	906
Anadyr	171	207	145	69	−3	−81	1445
Debin	150	113	77	42	−7	−49	934
Detrin	99	101	55	17	−28	−62	689
Berelekh	111	147	86	22	−24	−70	931

and in the first ten-day period of September, respective values are 9 and 13 W/m². Relative errors are minimal in July (12 and 18%, correspondingly).

In fact, as the fluctuations in values of each of the said quantities are governed by combinations of numerous independent factors, and furthermore, an impact of each individual fluctuation is not overwhelming; their net effect most likely does not exceed a few W/m².

The quantity q_{gr} includes convective and conductive components. According to Braslavsky & Vikulina (1954), monthly means of the latter in shallow reservoirs decrease from June to August from 15 to 4 W/m² and become negative in September. As seen from Table 2, seasonal changes of both components are qualitatively similar, conductive one's share being mostly less than 10%. Actually, its contribution is still smaller, because in watercourses, cooled by both convective heat exchange and by inflow of tributaries, water temperatures are lower than in such reservoirs. In the Kolyma River, the difference in July is more than 3 C, and in the Debin River, it increases to 6 C. Obviously, this reduces conductive heat flux into the river bottom, and q_{gr} may be regarded as a close estimate of convective heat flux.

For further discussion, it is important to emphasize that convective heat transfer develops as a result of groundwater flow along a general valley slope, and so concentrates in a slightly inclined plane. Of course, in this flow a vertical circulation develops as well, but its role is limited because, as a rule, not deep under river thalwegs, the ground is either bedrock or immobile silted sediment having very low permeability. Therefore, first, it is warmed virtually by conductive heat transfer alone; second, groundwater flow cannot substantively influence heat flux from the soil surface.

Total heat transfer from rivers to floodplains: Obviously, the values in the last column of Table 2 are lower estimates of this quantity (some amount of heat adds up in May). As it is known, mature rivers in mountainous territories have floodplains which are 5–10 times wider than their channels. Accounting for river sinuosity, the relation of surface areas is at most 10:1. Therefore, during warm periods, taliks receive from rivers no less than $70–100·10^6$ J/m^2 (the lower margin being more likely atypical). Judging by the available data, it is more than the amount of heat supplied from soil surface. In the open woodlands of Central Yakutia, where the climate is warmer, the last-named quantity does not exceed $80·10^6$ J/m^2 (Pavlov 1984). In floodplain taliks, the soil surface is cooler due to the thick vegetation cover and subsurface, undoubtedly, warmer; both differences diminish heat supply from the surface. Also, some of this heat is spent on "useless" (for a talik existence) warming up of an aeration zone. Therefore, convective heat exchange with rivers is not only a unique factor of floodplain talik formation, it is also the major income source of their heat balance.

The value of Q_{gr} in the Anadyr River is almost 1.5 times greater than the maximum of all other such quantities (see Table 2). The reason is that in the Markovo Depression (to which the lower half of the studied section belongs) the river is aggrading and has an outstandingly large talik, up to 7 km wide (Vtyurin 1964). For comparison, the Kolyma River has twice as large July discharge, but its talik is approximately twofold narrower. This is why convective heat transfer from the Anadyr River to its floodplain is maximal. Since the results obtained are mean values over the whole river section, then in the depression itself heat flux is still greater.

The Detrin River, on the contrary, stands out against all others by substantially less intensive heat exchange with its floodplain. Based on the data available, there is not an adequate explanation for this phenomenon; one of the possible reasons may be degradation of the talik.

Heat flux direction change occurs, on average, within a short period of time, September 5–15, irrespective of a river size. The rivers begin to receive heat back while still having comparatively high temperatures (4–7°C); i.e., their thermal potential is not fully used. In other words, convective heat exchange with rivers is excessive in relation to sustaining floodplain taliks even under extremely severe climatic conditions. Summarizing all of the above-said, climate can hardly limit both the size of floodplain taliks and their geographical distribution.

The floodplain talik of the Anadyr River not only accumulates the largest amount of heat, but also spends it at a maximal rate: the third part of September q_{gr} is again the greatest by absolute value.

Convective heat exchange with floodplain taliks causes a number of peculiarities of thermal and ice regimes of rivers which earlier could not be adequately explained (Table 3). The most striking of them were first noticed by Shvetsov (1952) in the Indigirka River and named thermal anomalies. In summer, maximum river temperatures are observed not in places with the warmest air, but far downstream, while in autumn, temperature increments (of both water and air) change signs.

"Anomalies" (actually a pattern) are due to the fact that in all pairs of gauging-stations shown in Table 3, the upstream stations (see Fig. 1) are located on floodplain taliks which downstream pass away. In summer an intensive heat exchange with taliks decreases river temperature; in autumn it delays its cooling and ice phenomena, despite low air temperatures. Noteworthy, these peculiarities are best manifested in the Anadyr River.

Notwithstanding huge energy expenditures in autumn, the remnants of heat accumulated in taliks earlier are sufficient to sustain numerous glades during the whole winter. They are very typical for rivers of northeastern Asia, quite often stretching, one after another, for tens and hundreds of kilometres (Kuznetsov 1961); as this author rightly pointed out, these phenomena could not be explained by discharges of subpermafrost water. Obviously, such sequences of glades reveal plentiful and abundant outlets of groundwater from floodplain taliks.

General dynamics of convective heat exchange: On the whole, during the study period, a monotone decrease of q_{gr} values prevails. This is readily explained by the thawing of the seasonally frozen layer, which consumes very large amounts of heat even at low water temperatures. Also, energy flux to water surface diminishes during the warm season. Since during most of May the rivers remain covered with ice, q_{gr} as a rule reaches a maximum in June. The exceptions are the Anadyr and Berelekh Rivers, which

Table 3. Characteristics of thermal regime and freezing processes in the studied rivers.

River	Gauging station	Mean water temperature, °C		Average dates of:			
		July	October 1–10	drop of water temperature below 0.2 C	beginning of freezing process	beginning of ice drifting	beginning of freezing-up
Kolyma	Baligichan	14.5	1.4	Oct 11	Oct 7	Oct 9	Oct 17
	Srednekolymsk	15.4	0.8	Oct 6	Oct 5	Oct 10	Oct 13
Anadyr	Markovo	11.1	2.7	Oct 16	Oct 8	Oct 13	Oct 22
	Snezhnoye	15.1	1.4	Oct 7	Oct 6	Oct 7	Oct 10
Indigirka	Oimyakon	11.7	1.2	Oct 7	Oct 4	Oct 9	Oct 23
	Druzhina	15.1	0.3	Oct 3	Sept 30	Oct 3	Oct 12

display maximal values in July and require a more thorough analysis.

Convective heat exchange between rivers and taliks is due to intensive water exchange; the latter, in its turn, to concentration of groundwater flow in networks of preferential pathways with extremely high water-transmitting capacity (Mikhailov 1999). Experiments on indicator injections into observation wells have shown that after ice drifting in spring, a partial blocking of these pathways occurs resulting in a substantial decrease of alluvium effective permeability. The blocking was observed mainly at the beginnings of pathways and most probably is caused by entrainment of small ice particles. The research was carried out in the Kolyma River floodplain, which is covered with mixed forest. The studied sections of the Anadyr and Berelekh Rivers are distinguished by relatively sparse vegetation and an abundance of bare ground. In the former case, it is caused by frequent inwash of fresh sediment, the river being at the aggrading stage; in the latter case, by forest clearing and placer exploitation (Fig. 2). In both cases, the result is deep winter freezing, promoting the blockage of preferential pathways and diminishing convective heat transfer in early summer. After recovery of alluvium permeability, heat flux sharply increases and peaks in mid-summer.

As strong land disturbances, such as in the Berelekh River floodplain, are infrequent, there is an even smaller number of aggrading watercourses. In other studied rivers, the July values of q_{gr} , despite large differences in water discharges (almost by two orders of magnitude), are quite similar; in this month, even the Detrin River does not stand out. Taking into account the results of numerous observations in the valleys of smaller streams (Mikhailov 2003), in northeastern Asia these values in all typical floodplain taliks fall in the narrow range, probably not wider than 100–120 W/m^2; this opens up a possibility to estimate the distributions of such taliks over large river basins.

Conclusion

Based on heat balance calculations made for representative sections of six rivers of northeastern Asia, the main regularities of seasonal dynamics of convective heat exchange in river valleys have been ascertained. Usually heat flux is maximal at the beginning of summer, ranging from 100–170 W/m^2, but under conditions causing deep winter freezing of soil, the peak is shifted to July. The warming up of floodplains continues with decreasing strength up to and including the first ten-day period of September, on average. As a result, taliks receive from rivers very large amounts of heat; only since June, not less than 70–100 10^6 J/m^2 related to soil surface area. Comparison with published data demonstrates that heat exchange with rivers is not only crucial for the existence of taliks, it is a main income source of their heat balance (at least under climatic conditions close to the extreme ones).

The reverse side of intensive summer warming of floodplains is their rapid pre-winter cooling. In early autumn,

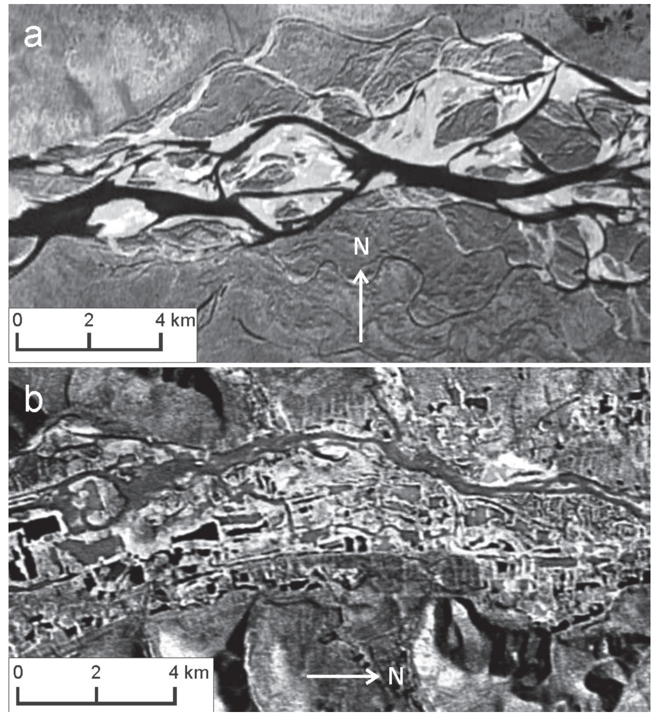

Figure 2. Satellite photographs of the valleys of Anadyr (a) and Berelekh (b) Rivers.

at relatively high temperatures of river water, heat flux changes its sign, and taliks start returning the accumulated heat to rivers. This process continues till the spring flood.

Convective heat exchange with taliks causes a specific distribution of water temperatures along the rivers ("thermal anomalies"); considerable delay of freezing-up and preceding ice phenomena (up to 10 days or even more) sustains numerous glades and successions of glades.

The results obtained lead to the conclusion that climatic conditions can hardly be a limiting factor for geographical distribution of floodplain taliks or their size. For further research, it is very important that in rivers at grade, which prevail in northeastern Asia, and in the absence of heavy soil-cover damage, mean July values of heat flux into taliks lie in a narrow range of 100–120 W/m^2, the same as in small streams or very close to it.

Acknowledgments

I am grateful to two anonymous referees for their useful advice which helped to improve the paper.

References

Atlas of the Kolyma River 1931. Irkutsk: Knizhnoye izdatelstvo, 432 pp. (in Russian).

Braslavsky, A.P. & Vikulina, Z.A. 1954. *Rates of Evaporation from the Surface of Water Reservoirs*. Leningrad: Gidrometeoizdat, 212 pp (in Russian).

Kuznetsov, A.S. 1961. Icings and glades in the north-east of the USSR. In: *Collected Works on Hydrology* 2: Leningrad: Gidrometeoizdat, 72-86 (in Russian).

Long-term data on the regime and resources of surface waters. *State Water Cadastre 1985, 1987*. Issues 16, 17. Leningrad: Gidrometeoizdat (In Russian).

Mikhailov, V.M. 1995. On the prevailing river channel pattern in the North-Eastern Russia and its relation to permafrost conditions in river valleys. *Kolyma* 7-8: 16-20 (in Russian).

Mikhailov, V.M. 1998. Development of taliks in the Kolyma River valley and water temperature. *Geoekologiya (Geoecology)* 6: 100-110 (in Russian).

Mikhailov, V.M. 1999. Preferential pathways for groundwater movement in coarse-grained alluvial deposits. *Kolyma* 4: 21-28 (in Russian).

Mikhailov, V.M. 2003. Hydro-thermal regime of watercourses as an indicator of ground-filtration taliks (on the results of in-situ research). *Kriosfera Zemli (Cryosphere of Earth)* 7: 57-66 (in Russian).

Mikhailov, V.M. & Ushakov, M.V. 2002. On some Morphological Correlations for Rivers of the North-Easternern Russia and Criteria of their Application. *Transactions of the Far-Eastern Hydro-meteorological Research Institute* 150: 177-187 (in Russian).

Park, C.C. 1977. World-wide variations in hydraulic geometry exponents of stream channels: an analysis and some observations. *Journal of Hydrology* 33: 133-146.

Pavlov, A.V. 1984. *Energy exchange in the Landscape Sphere of Earth*. Novosibirsk: Nauka, 256 pp (In Russian).

Reference Book on the Climate of the USSR. 1966. Issues 24, 33; parts 1-6. Leningrad: Gidrometeoizdat (in Russian).

Shvetsov, P.F. 1952. Anomalies in thermal regime of the Indigirka River in two characteristic cross-sections and the origin of them. In: *Research of Permafrost in the Yakutia Republic* 3. Moscow: Izdatelstvo AN SSSR, 106-108 (in Russian).

Vasilyev, O.F. & Voyevodin, A.F. 1975. Mathematical modeling of water quality in systems of open channels. In: *Dynamics of Continuous Medium* 22. Novosibirsk: Mining Institute of SB RAS, 73-87 (in Russian).

Vtyurin, B.I. 1964. Permafrost conditions of the Markovo Depression. In: *Permafrost Conditions of Western Siberia, Yakutiya and Chukotka*. Moscow: Nauka, 115-133 (in Russian).

Geophysical Study of Talik Zones, Western Yakutia

Svet Milanovskiy
Institute Physics of the Earth, RAS, Moscow
Sergey Velikin
Viluy Permafrost Station of the Permafrost Institute RAS Siberian Branch, Chernishevskii
Vyatcheslav Istratov
Radionda Ltd Company, Moscow

Abstract

For the last decade at a number of Hydro Units in Western Yakutia, we have observed subsurface seepage processes that compromise their structural stability. A number of geophysical techniques are discussed for verification of the permafrost state near Sitikan and Viluy Hydro Units, including electric, electromagnetic, ground penetrating radar, hydro location, thermal, and radiowave down-hole measurements. Ground-level and down-hole geophysical surveys focused on detecting thawing zones (talik) in dams, dam flanks, and tail-water zones. Long-term geophysical monitoring shows the spatio-temporal permafrost evolution and talik development in the flank shore of the Sitikan dam. Detection of the inflow zone and seepage velocity was performed for the right-bank contiguity of Viluy HPS-1. Numerically analyzed conditions causing the initiation and development of the talik near the reservoir are discussed.

Keywords: cold regions; dams; geophysical monitoring; permafrost; talik; thermal field.

Introduction

Permafrost covers about 70% of the territory of Russia, most of the territory of Alaska, as well as a significant part of Canada and mountain Alpine regions. Regular water and energy supplies in permafrost areas are vitally important conditions for inhabitants of the large northern territories of Russia, Canada, the U.S., and Alpine areas of China. Artificial reservoirs in permafrost terrain create the formation and development of talik zones in the adjacent flanks. Dam and flank shore stability is the key consideration in reservoir safety (power pool, water supply, tailing pit, etc.). Similar problems may also occur with natural basins in cold regions; climate change may activate lake drainage and changes in permafrost.

To avoid water loss and ensure the Hydro Unit stability in the permafrost zone, we need to use geophysical tools, including long-term monitoring for the detection of talik development. Along with required temperature control, different geophysical methods give information about variations in rock physical properties caused by thawing-freezing effects. Integrated geophysical monitoring allows observing time-space variability of the physical fields that reflect the evolution of frozen-thawed dam bed and flank shores.

Geophysical Observations

Study area

This study was conducted in the Aichal-Mirni region of Western Yakutia, which is an area of potential development of different types of anthropogenic development (Fig.1). They are connected with the exploitation of kimberlitic pipes, construction and operation of hydro facilities, injection and dumping of underground waters, underground storage facilities for toxic waste, and tailing dumps. Permafrost is very sensitive to natural and human-caused influences. In consequence of these circumstances, thawing-filtration processes were observed in a number of hydro technical projects in Western Yakutia: Marha, Irelyah, Viluy, Anabar, Sitikan, Kieng, and Iyraaas-Yuryah. We present two examples of geophysical observations from the Sitikan Hydro Unit and the Viluy Hydroelectric Power Station.

The Sitikan Hydro Unit (frozen type dam) provides the water supply for the city of Successful (near the diamond pipe "Udachnaya"). An underflow talik-zone developed in the dam basement in 1995 after 20 years of reservoir operation (Kronik 1999). As a result, there is currently significant water loss from the reservoir and a serious problem with water management.

Construction of the Viluy Hydroelectric Power Station (VHPS-1) was finished in 1967. It was the world's first large Hydro Unit with a rock fill dam on permafrost. More information about Viluy Hydro Units Cascade can be found at http://regtime.spb.ru/lenhydroproject/e_vil01_02.html. In August 1996, a temperature jump was observed in the right-bank contiguity of VHPS-1. During a few days, seepage was formed (Velikin & Snegirev 2004). This seepage continues to the present time despite special antifiltration efforts. For the last 15 years, various geophysical investigations were carried out on many engineering constructions in Western Yakutia by Viluy Permafrost Station (VNIMS). Priority interest was connected with the methodology of geophysical surveys of the permafrost state and its change near the hydro units. Some examples of this work are presented below.

Methods

Geophysical surveys focused on several main tasks: (1) eliciting and checking the position of inflow seepage near the dam and boundaries of dams, and detecting the location of most intensive thawing and seepage from the reservoir; (2) investigation of talik geometry in the frozen earth fill;

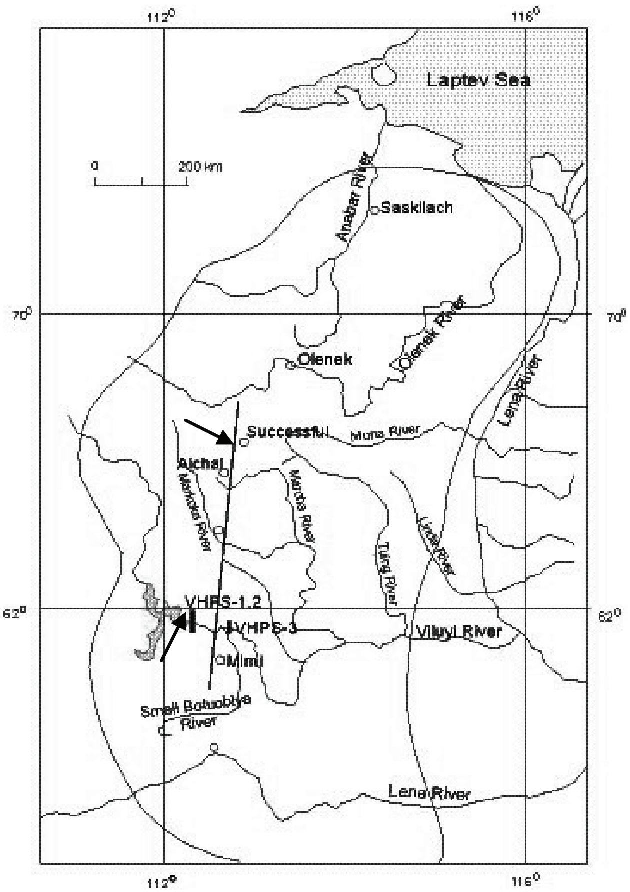

Figure 1. Case study areas: Sitikan Hydro Unit near Successful (Pipe Udachnaya) and Viluy HPS-1, 2 (shown by arrows).

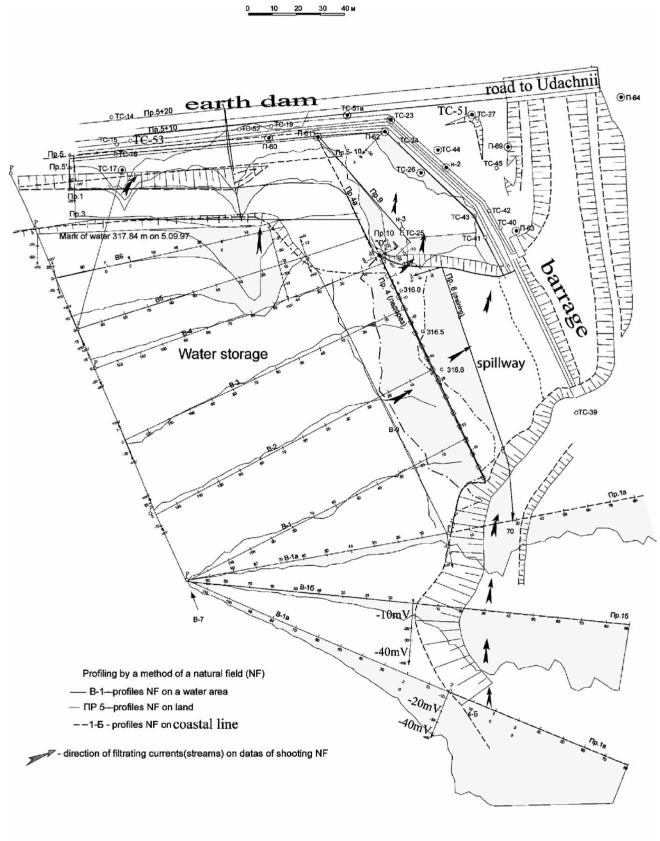

Figure 2. Natural Field profiles on water, land, and coastal zone of Sitikan Hydro Unit; negative NF anomalies indicate inflow seepage zones.

and (3) monitoring the progressive seepage dynamics in space and time.

From the many surface-based geophysical methods (Zikov 1999), the most useful for solving these tasks were selected including the Natural Field method (Semenov 1968) or Self Potential method (Erchul & Slifer 1989), Capacitive-Coupled Resistivity profiling or VCHEP method (Timofeev 1980, Hunter & Douma 2007), and Ground Penetrating Radar (GPR) (Arcone et al. 1998).

Down-hole observations near hydro units included long-term temperature measurements. Logging systems (electrical, flow meter survey, gamma logging, neutron-gamma logging, caliper measurement) (Zikov 1999) were used for petrophysical studies. The Radio Wave Geo-Introscopy (RWGI- ORWP) method (Istratov & Frolov 2003) with thermometrical data provided the opportunity to monitor talik development.

Talik detecting and monitoring

Natural field (Self-Potential) method: In this case, the natural field (NF) technique has an electrokinetic nature resulting from the transportation of charges by flowing water. Inflow zones correspond to negative values of electrical potential, while outflow zones have positive values of the NF (Semenov 1968, Zikov 1999, Erchul & Slifer 1989). A network of profiles (observation step of 2.5 m along profile) was established, covering the lower toe and upper heel, the adjacent banks, and the crust of the earth dam of the Sitikan Unit (Fig.2). Measurements were made relative to one of two stationary reference electrodes in the head race. In particular, NF data obtained in the head race of Sitikan detected (by negative anomalies) infiltration zones in the earth dam, below the spillway and along the boundary of the right bank.

Among the many applied surface geophysical studies, the Capacitive-Coupled Resistivity profiling method (VCHEP) and Natural Field (Self-Potential) methods were the main source of information about propagation of inflow zones and talik identification. The theory governing the VCHEP method has been discussed by Timofeev (1980). Advantages of the VHCEP method are high productivity and simplicity of measurements in cold region. There is no need for direct electrical contact between the transmitter and the ground (Hunter & Douma 2007). Specially-developed optional equipment VCHEP was used for the survey. This capability allowed us to determine effective resistivity (ρ_{ω}) values directly during field observations via conversion of measured electric field parameters for ω = constant and the selected unit configuration (Timofeev 1980, Zikov 1999). Later on, this approach was realized in the development of the “Ohm Mapper” device (Hunter & Douma, 2007). The VCHEP survey on the Sitikan Unit was done in April 1997 with two frequencies (8 and 12 kHz) and a square

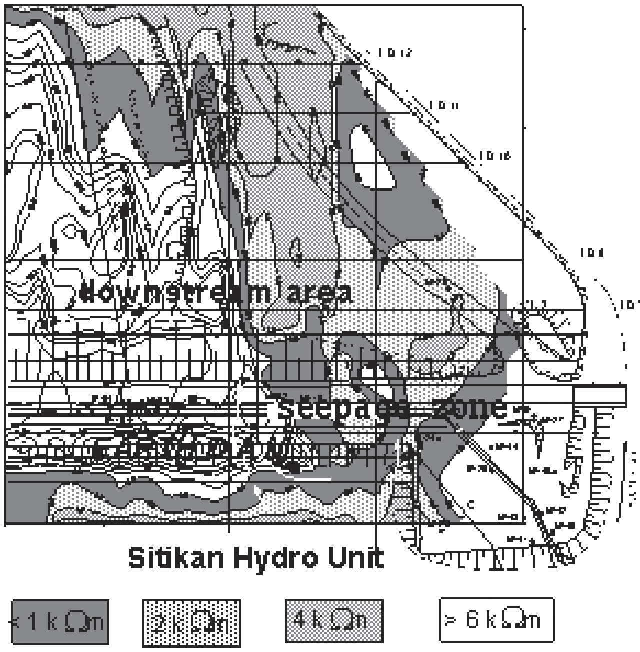

Figure 3. Spatial distribution of effective resistivity, ρ_ω kΩm (dipole length = 10 m, dipole-dipole spacing = 20 m, sampling step = 2.5m, ω = 8 kHz). Thawed zone determined with Capacitive-Coupled Resistivity profiling method (VCHEP) on Sitikan dam and tailwater. Shaded zones (low effective resistivity) correspond to talik's contour.

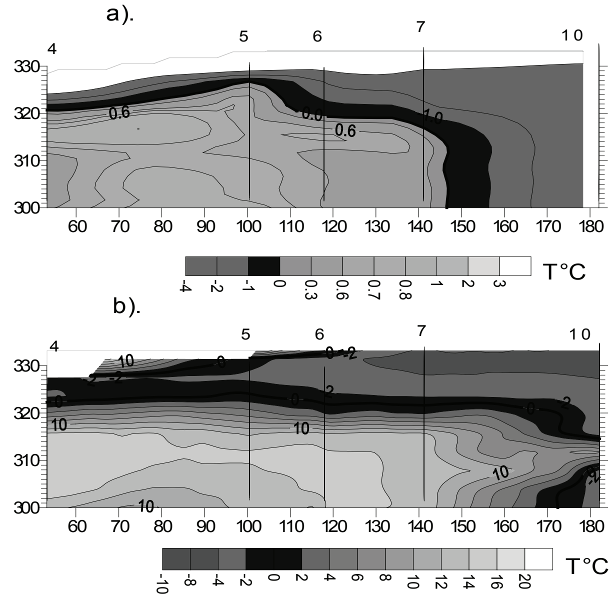

Figure 4. Dynamics of the ground temperatures within the reservoir flank of the Sitikan dam along boreholes (4-5-6-7-10) in (a) March 2001 and (b) August 2001.

waveform signal. At that time, snow cover and frozen rocks did not permit the use of any galvanic ground connection. Boundaries between frozen and thawed zones—the shaded zones in Figure 3—are reflected in the effective resistivity (ρ_ω) field for ω=8 kHz.

The Self Potential (NF method) survey was conducted with the "ERA-MAX" instrument along the water profile in the Viluy HPS-1 head race and on its bank. Several years of observations along these profiles showed significant changes in form and amplitude of the natural field associated with different water levels in the head race and discrepancy of observation lines. Nevertheless, in the zone adjoining the right-bank contiguity, the abnormal part was well detected by signal form and amplitude. As a rule, seepage originates from structure and head race contact. It would be logical to suppose that just this anomaly was caused by seepage processes. Later on, test methods proved this to be true.

Two contactless surveys were performed on water with the use of inflatable boat in a head race of VHPS-1 using Ground Penetrating Radar (Arcone et al. 1998): above-water GPR survey with "SIR2000" and at the Side Plan Hydro location (Velikin & Snegirev 2004) using the "GBO" instrument. Both methods confirmed the anomalous zone that was distinguished using the self-potential data in the head race area. GPR- reflecting boundaries associated with water-filled cracks, typically horizontal and vertical cracks, can be recognized on the radargram. On bottom-surface images obtained with hydrolocation, the anomalous site was distinguished by the occurrence of small depressions (slots) perpendicular to the shore. In the geological structure of the berm adjoining the head race, a number of similarly-oriented (orthogonal to shore zone) cracks were also marked. It is important that close spatial coincidence of anomalous zones found by Self-Potential, GPR, and Side Plan Hydro location methods was established. Detected zones at 242–238 m elevation, coinciding with the depth interval of intensive seepage, was established also by thermometry (Velikin & Snegirev 2004).

Borehole observations: The first warning information (in 1995) about talik nucleation at the base of Sitikan dam was from long-term temperature measurements initiated in 1990. Seasonal temperature field dynamics for the flank of Sitikan dam with active talik zone are presented in Figure 4. The network density of thermometric holes and the irregularity of observations have hampered estimation of the spatial distribution of the talik and seepage development. For processing, all previous available temperature data were used.

In addition, measurements were conducted in piezoborehole and on a water area, where earlier temperature observations were lacking. This has allowed us to "fill in" the missing periods of observations in individual holes, and to derive the general evolution of the talik zone. An example of the active stage of talik evolution for the period 2000–2006 is shown in Figure 5. Without going into details of the contingency of the Sitikan dam, it is necessary to say that for the last decade many efforts (grouting, air and kerosene cooling, enrockment, etc.) were implemented to prevent the consequences of seepage. Some results are shown in Figure 5 on the left part of the earth dam. We also can see the progressing talik in the right bank contiguity due to development of bypass filtration (Figures 4 and 5). For controlling the in situ situation in the seepage zone, tracer techniques (with colorings and electrolytes) were used to determine the flow rate (Velikin & Snegirev 2004). NaCl solution was used as a tracer. Resistive potentiometers installed in observation boreholes on a particular selected

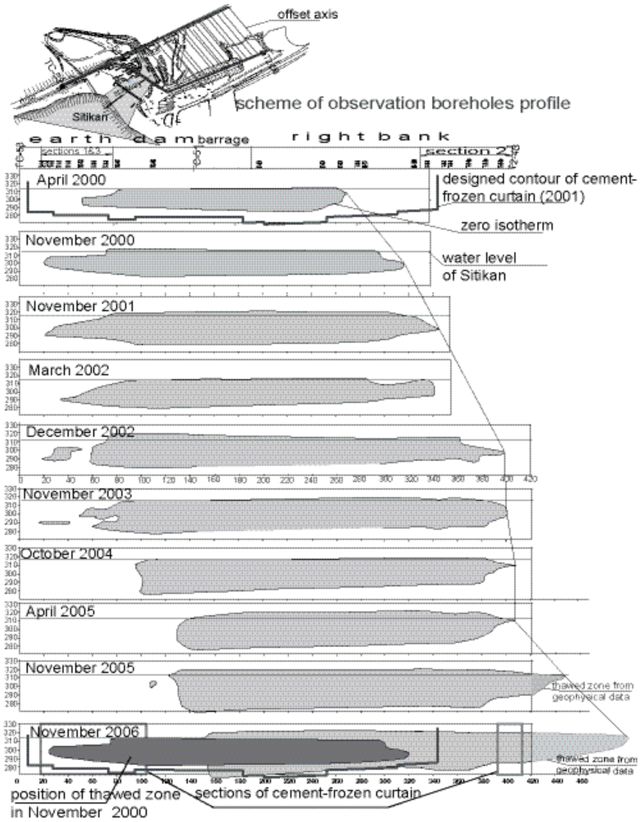

Figure 5. Dynamics of thawed zone (talik) contour along borehole profile (solid line on the upper schematic) for the Sitikan Hydro Unit over the period 2000–2006 (mainly by thermal data).

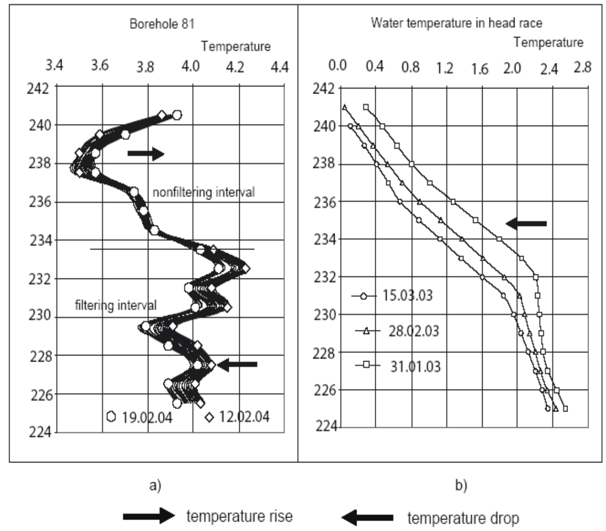

Figure 6. Revelation of percolation layers by logger measurements: (a) temperature measurements in piezometric borehole No. 81; (b) water temperature in head race.

interval were used as a recorder for continuously measuring water resistance filling the borehole.

Observations were carried out in two ways: (1) injecting a tracer into piezoborehole No. 80 and then measuring in piezoborehole No. 81 downstream; (2) injecting a tracer near the shore of the head race of the right-bank abutment and collecting measurements in piezoborehole No. 80. According to obtained data, the flow rate was estimated at approximately 50–60 m per hour. This is a fairly significant value and should be considered when developing anti-seepage measures.

Automatic temperature measurements in the boreholes using loggers are of special interest, insofar as they permit us to obtain information about the position of seepage horizons and their characteristics. Figure 6 illustrates logger measurements in piezometric borehole № 81 of the right-bank abutment in comparison to water temperature dynamics in the head race of the dam. Figure 6 shows that a general reduction of reservoir water temperature determines a temperature decrease in the filtration zone (236-232 m) of the embankment. In the upper part of the borehole, the logger data indicate a null or small temperature increase. The analysis of available data shows the high information content of logger temperature measurements. They may help to reveal reservoir intervals in thermometric boreholes based on analysis of temperature dynamics, identify the intervals where, despite the presence of positive temperatures, filtration flows are absent, and also to study the interaction peculiarities between the rocks and water.

For geophysical monitoring in a permafrost zone, the Radio Wave Geo-Introscopy (RWGI) profiling and cross-borehole measurement method, as well as the One-hole Radio Wave Profiling (ORWP) method, was used. Theory, tools and measuring techniques are described in Istratov & Frolov (2003). The purpose of radio wave investigations was as follows: First, to control the frozen rock thawing within the coastal zone of the reservoir and to assess the dynamics of the process; and second, to identify and locate the places of most intensive thawing and seepage from the reservoir. Thawing processes lead to a decrease of electrical resistivity (ρ); the saturation of the filtering layer must be reflected as an increase of relative dielectric permittivity (ε) within the same interval. If measurements are taken repeatedly at two frequencies along the borehole profile, the lower frequency data can give a picture of the rock electrical resistivity changes with space and time, thus providing insight into the process of frozen rock mass thawing under the influence of the reservoir. Measurements performed at high frequency permit the calculation of effective values of relative dielectric permittivity (ε); the higher values will indicate layers of most active filtration from the reservoir.

Monitoring in the Sitikan area began in 2000 and continues today (the last measurements were in March 2007). As an example, we consider the data obtained in 2001–2002 near the Sitikan Hydro Unit in Figure 7. In March and August 2001 and in March 2002, temperature measurements (Fig. 4) were made in boreholes 4 to 10, oriented perpendicular to the embankments of the Sitikan water resevoir. In additon, gamma logging and one-hole radio wave profiling (RWGI-ORWP) with the frequencies 1.25 and 31 MHz were conducted. Repeated ORWP data were interpolated between the holes (Fig. 7). The holes are 35 m to 45 m deep, with polyethylene casing and inside diameter of 65 mm. Sections based on repeated temperature measurements of

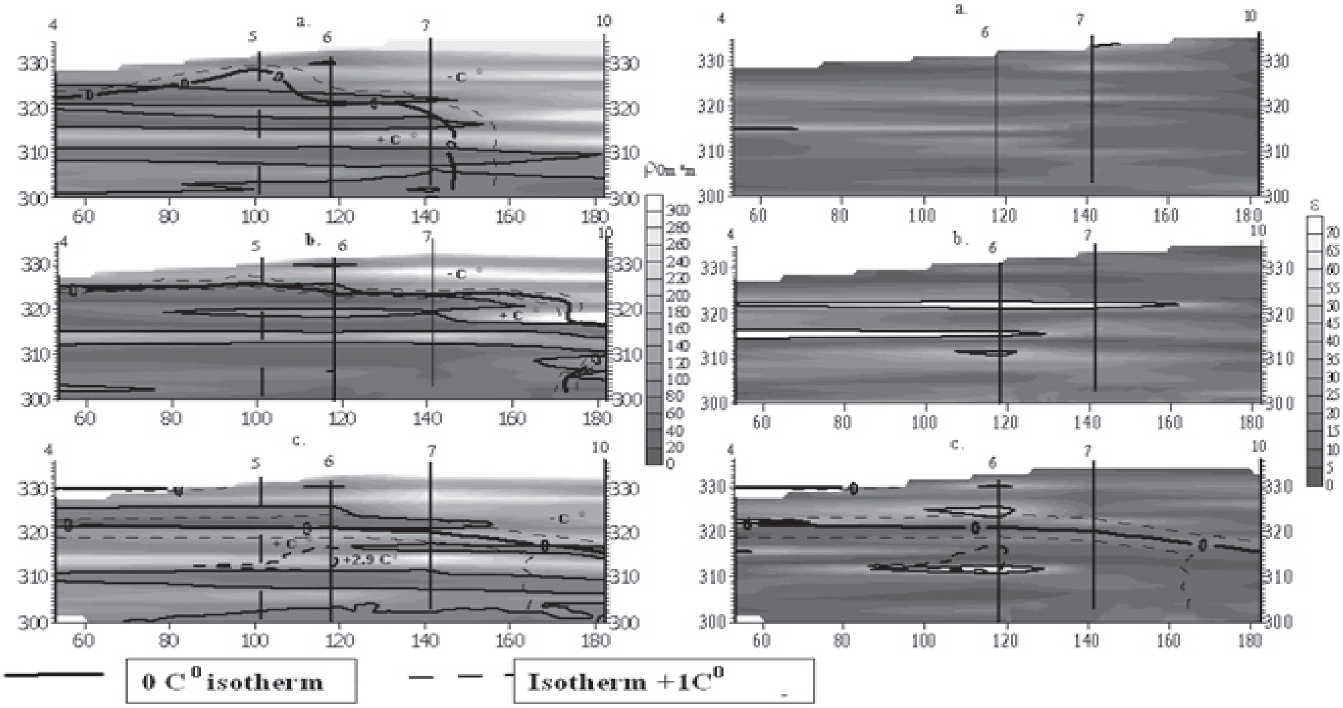

Figure 7. Examples of geoelectric sections of (left) effective electric resistivity (ρ) and (right) relative dielectric permittivity (ε) along boreholes profile (4 -5 -6 -7 -10) in a frozen embankment crosswise shoreline of the Sitikan Hydro Unit (Western Yakutia, Siberia). Replicated RWGI-ORWP observations in (a) March 2001; (b) August 2001; and (c) March 2002.

the fractionally thawed coastal frozen embankment in March and August 2001 show the dynamics of ground temperatures within the reservoir flank (Figs. 4 and 7). The geological section consists of carbonate rocks (limestone, dolomites and marbles) varying in fissured zones and clay content.

Comparing the results from March and August 2001, it is possible to see not only the general propagation of the "front" of lowered specific electric resistivity in the direction of borehole 10, but also to identify horizons at 309–311 m, 314–317 m, and 321–324 m, in which these changes occur most intensively. In August, a sharp decrease of resistivity was observed in these layers, and the first positive values of temperature were observed. Apparent on Figure 7 is the zero degree isotherm passage of 324–326 m on a sub-face of stratum of high resistivity. High resistivity gradient here marks the border of frozen and thawed rocks. In the section of effective dielectric permittivity, layers with the highest values of ε (intervals 311–314 m and 317–319 m, and near hole 6 at 306–309 m) correspond to a high gradient zone of positive temperature. Along these permeable layers, water from Sitikan penetrates deep into the coastal embankment, working over time like a "secondary" heat source by distributing heat and accelerating thaw of frozen rocks. However, in March 2002 (Fig. 7), the resistivity of rocks in a section increased. This phenomenon is connected with maximum freezing (frost penetration) of rocks, and minimum water temperature in Sitikan storage. Visually, it is tracked between holes 4 and 7 in a layer (314– 317 m) in which there is a relative increase of resistivity (ρ); below 314 m a reduction of ρ is observed. In March 2002 (at the time of minimal temperature of the entire rock embankment), the areas with heightened ε values are narrowed and located near borehole 6 at horizons 310–312 m and 322–325 m. This is connected with seasonal freezing of the embankment. However, the presence of local zones with heightened values of dielectric permittivity (ε) suggests the existence of "year-round" liquid water at the non-percolating level (322–325 m) and with bypass seepage from the water storage through the originally frozen embankment at level 310–312 m, corresponding to the Sitikan water level in March of 314 m.

The good correlation of geoelectric sections with the temperature data shows not only the direct dependence of electric properties on the frozen-thawed state of the embankment, but also the essentially higher sensitivity and resolution of electric methods for detecting the liquid water phase. Accurate interpretation of these data must also take into account the seasonal water level change of Sitikan.

Thermal Modeling

In the case of water storage, we have pressure headwaters constrained by a frozen dam with a set of engineered constructions. The non-steady problem of heat-mass transfer in fractured and porous saturated frozen Stratum (II) (Fig. 8), situated between frozen impermeable adjacent Stratam (I, III) is discussed. There is a pressure head acting from the Aquifer, explicating in thawing saturated Stratum (II) with allowance for seasonal variations of air-water temperatures on ground-water surface and within the Aquifer (Fig. 8). According to Petrunin & Milanovskiy (2005), from numerical analysis it follows that the process of thermal evolution of the frozen strata can conditionally be separated

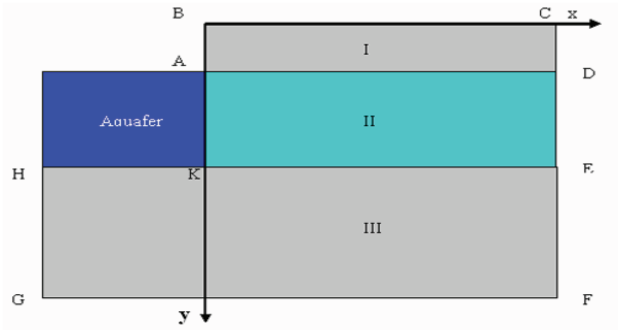

Figure 8. Schematic geometry of the model.

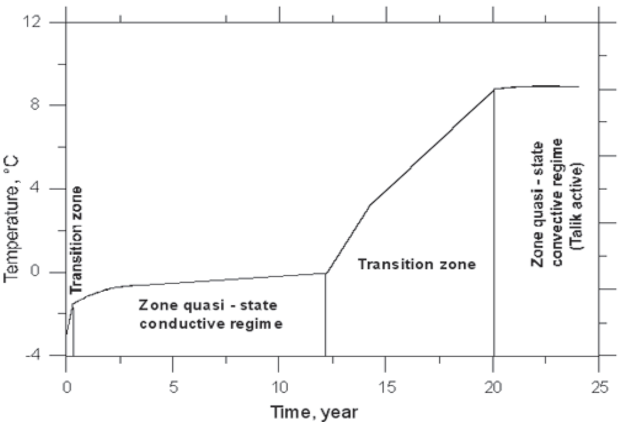

Figure 9. Variation of seasonal T-maximum in the mark-point situated in the middle of the top of permeable zone (talik zone) with time (from Petrunin & Milanovskiy 2005).

into two basic and two transient stages (Fig. 9). The first stage starts from the moment of water storage infill and represents initiation of thermodynamic equilibrium in the absence of convection. If it is quick enough; for 2–3 years it exhibits a quasi-state conductive heat regime in which seasonal variations in the thermal field quickly damp with depth according to Fourier's Law.

From Figure 9, the maximum seasonal temperature at the top of Stratum II (middle of AD) between 2–12 years ranges from -1°C up to 0°C, when the pore ice begins to thaw and permeability becomes distinct from zero. In this case, if there is hydraulic head, convective heat-mass transfer is initiated which is much more effective than pure conduction. This is the governing factor in our model for talik origination The results (Petrunin & Milanovskiy 2005) of 2-D thermal modeling indicate that talik development depends on specific thermal and hydraulic material parameters, water head, thickness of the frozen layer covering the talik, winter snow blanket insulating ground rocks, the seasonal temperature trend as well as on the presence of fractures in the frozen media. The observed evolution of the temperature field in the talik zone of the border part of the Sitikan Unit is in general agreement with the calculated temperature field.

Conclusion

Geophysical data testify about different types of talik zones. Nevertheless, they have a very common characteristic feature—the presence of a triggering mechanism for talik initialization. For identification of this mechanism, we need the pre-talik temperature history that leads to pre-heating of the strata, the existing fractures or pore channels (partly-open or ice cemented), and the reservoir water head. For example, in the Sitikan Unit case, the pre-talik history was about 20 years. An important factor for the stability of long-existing constructions like a Hydro Unit or waste confinement in the permafrost zone is global climatic change. The proposed simple model can be used for analyzing more complex situations. The results presented show the efficiency of a number of key geophysical methods for the study of permafrost peculiarities associated with talik formation and its development near Hydro Units in Western Yakutia. The proposed long-term geophysical monitoring of the permafrost state can be used for emergency situation prediction.

Acknowledgments

The authors express their true thanks to the anonymous reviewer for helpful comments.

References

Arcone, S., Lawson, D., Delaney, A., Strasser, J.C. & Strasser J.D. 1998 Ground-penetrating radar reflection profiling of groundwater and bedrock in an area of discontinuous permafrost. *Geophysics* 63(5): 1573-1584.

Erchul, R.A. & Slifer, D. 1989. The Use of Self Potential to Detect Ground-Water Flow in Karst. *Technical Report REMR-GT-6*, U.S. Army Engineer Waterways Experiment Station, Vicksburg, MS.

Hunter, J.A. & Douma, M. 2007. Development of a Capacitive-Coupled Resistivity Method for Permafrost Surveys in North America: Melinki Russkas (A Little Russian Tale*) Fast TIMES* 12(4): 23-26.

Istratov, V.A. &. Frolov, A.D. 2003. Radio wave borehole measurements to determine *in situ* the electric property distribution in a massif. *J. Geophys. Res. – Planets* 108(E4): 8038-8043. doi:10.1029/2002JE001880

Kronik, A.A. 1999 Hydraulic structures. In: L.N. Khrustalev & E.D. Ershov (eds.), *Permafrost Engineering,* V5. Moscow: MGU, 413-445.

Petrunin, A.G. & Milanovskiy, S.Yu. 2005. Talik formation in the flank shore of water-storage reservoir in permafrost area. *Abstract UCOP*, *Potsdam, June 12–16*: 189.

Semenov, A.S. 1968. *Electro prospecting by natural field method,* Leningrad: Nedra, 391 pp. (in Russian).

Timofeev, V.M. 1980. *Application of electro profiling with magnetic capacitor antenna for engineering survey*. Abstract of Ph.D. Thesis, Moscow, VSEGINGEO, 24 pp. (in Russian).

Velikin, S.A. & Snegirev, A.M. 2004. Study of the right-bank contiguity of the dam at the Viluy hydroelectric power plant: Complex of techniques. *Journal of Glaciology and Geocriology* 26: 142-150.

Zikov, Y.D. 1999. Geophysical Methods for Cryosphere Zone Investigations. Moscow: MGU, 244 pp. (in Russian)

Seasonally Frozen Ground Effects on the Dynamic Response of High-Rise Buildings

Rys Miranda
School of Engineering, University of Alaska Anchorage, Anchorage, AK, USA
Zhaohui (Joey) Yang
School of Engineering, University of Alaska Anchorage, Anchorage, AK, USA
Utpal Dutta
School of Engineering, University of Alaska Anchorage, Anchorage, AK, USA

Abstract

It is well-known that temperature variation can impact the properties and performance of various materials utilized in civil structures. Much work has been performed to evaluate these impacts; however, limited work has been performed to evaluate the seismic performance of civil structures embedded in or surrounded by seasonally frozen ground. This paper presents a comparison study of seasonally frozen ground effects on two high-rise buildings in Anchorage, Alaska. The dynamic properties of a 14-story building have been evaluated under winter and summer conditions, and then correlated with frost depths quantified from temperatures recorded at a nearby airport. Further, these results have been compared with that of a nearby 20-story building. Discussions and conclusions are provided with regard to the impact of seasonally frozen ground on buildings with different configurations, specifically with or without a basement. These findings will provide insight into frozen ground effects on high-rise building design.

Keywords: dynamic response; earthquake engineering; frozen ground; soil-structure interaction.

Introduction

Even though the concept of frozen soil dynamic properties has been around for decades, very little work has been conducted to evaluate the seismic performance of civil structures with respect to frozen ground conditions, seasonally, or permafrost. Early investigations of frozen soil dynamics are rooted back in the 1940s as a by-product of the search for oil in permafrost-laden regions (Vinson 1978). Considerable changes in mechanical properties take place between unfrozen soil and frozen soil. Notably, the Young's Modulus, E, of frozen soils are larger, in magnitudes of tens and hundreds, than that of unfrozen soil (Tsytovich 1975). Experiments conducted by Tsytovich (1975) have concluded that the compressibility of frozen soils is so miniscule that it can be disregarded for engineering purposes. Other experiments, involving ultrasonic pulses, have revealed that the wave velocity of soil increased as the temperature decreased (Finn et al. 1978). Vinson (1978), by means of cyclical triaxial testing, determined that the dampening ratio of soil diminished with decreasing temperatures. All these parameters play a crucial role in evaluating seismic response and the soil-structure interaction of frozen ground versus unfrozen ground.

This paper will investigate the impacts of such changes in soil parameters to the dynamic response of a 14-story reinforced concrete office building in Anchorage, Alaska. Furthermore, findings from this building will be compared to those of a nearby 20-story building obtained in a recent study (Yang et al. 2007).

Project location and description

The subject, a 14-story office building known as the Frontier Building, is located in mid-town Anchorage, Alaska (61°11′15″N latitude, 149°53′05″W longitude). Anchorage, Alaska is an ideal setting for this project, since it is located within a seismically active region and is exposed to subarctic conditions with considerable annual frost penetration. The environment of the project site is that of a typical urban setting with asphalt concrete paved roads and concrete sidewalks surrounding the building. Minimal tree or vegetative cover can be observed around the general area. The topography is consistently flat and relatively level. The local climate has an average annual temperature varying from -1.6°C to 6.2°C and average frost penetration of 2.0 m (WRCC 2007).

Anchorage is located on one of the most seismically active regions of southcentral Alaska. According to national seismic hazard maps, the probabilistic peak ground acceleration of the Anchorage metropolitan area is around 0.4 g with 10% exceedance in 50 years (Wesson et al. 1999). The subduction of the Pacific plate underneath the North American plate, causes intense seismic activities in and around Anchorage. The Prince William Sound earthquake of 1964 (M_w=9.2) was one of the prominent examples of such subduction zone seismic activities which caused widespread damage in the Anchorage area. In addition to the subduction zone earthquakes, some prominent surface faults (Haeussler & Plafker 2003) surrounding the region, also contribute to the seismic hazard of the region. The Castle Mountain Fault is in the vicinity of the Anchorage area and has the potential to generate 6–7 magnitude earthquakes (Woodward-Clyde 1982).

Geologically, the soils underneath the project area consist of glaciofluvial, glaciodeltaic, and alluvial fan deposits (GF, sand and gravel) (Combellick 1999). The area is located on seismic site class C/D (Dutta et al. 2000; Martirosyan et al. 2002) with average site amplification around 2.5 times at 1 Hz. (Dutta et al. 2001)

The Frontier Building

The Frontier Building is a reinforced concrete building constructed in the early 1980s under the 1979 edition of the Uniform Building Code (UBC). The building is founded on a series of reinforced concrete strip footings running in the east-west direction. The footings on the north and south edges are 2.7 m wide and 1.4 m thick, while the interior footings are 3.4 m wide and the same thickness as the edge footings. Stemming from the footings are 1.2 m (north and south edges) and 0.9 m (interior columns) diameter reinforced concrete columns. A total of 14 columns make up the entire building. The typical floor level construction is 0.2–0.3 m thick reinforced concrete diaphragm. The first floor of the building is essentially a slab-on-grade atop the backfill of the strip footings. The bottom of the foundation is at a depth of 1.7 m below ground. The roof of the building is set at 50.6 m above ground level (first floor). The plan dimension of the building is 59.4 x 32.6 m in the E-W and N-S edges, respectively.

Geotechnical Characteristics

Site geotechnical properties

Existing soils investigation reports were utilized to assist with the determination of frost/thaw penetration. The soil characteristics down to 21.3 m are available from the boring report, conducted during the design and construction of the Frontier Building, which reveals the presence of a peat stratum of about 0.6 m thick overlying 2.4 m thick of very dense, damp, gray, slightly gravelly, fine to coarse sand (Combellick, pers. com.). The deeper formation consists of stiff sandy silts, but these layers are of no concern for the present study, since frost penetration is not expected to exceed 3 m in the area. The soil properties such as unit weight/density, moisture content, and groundwater level are taken from the boring reports of DOWL Engineers and Alaska Testlab (pers. com.) from a nearby site. The report showed a mass density, ρ, of 2002 kg/m^3 and a moisture content, ω, of 20% with the groundwater level at approximately 4.0 m below the surface.

Frost/thaw penetration

The Modified Berggren Equation, developed by Aldrich and Paynter, is a reliable method for quantifying frost/thaw penetration. The modified equation simply applies a correction coefficient, λ, to the widely used Steffan Equation (Andersland & Ladanyi 2004).

The surface freezing and thawing indices, I_{sf} and I_{st} respectively, were derived from air freezing (I_{af}) and air thawing (I_{at}) indices by relation of the surface *n*-factor values for the site environment as shown in equations (1) and (2).

$$I_{sf} = n_f \cdot I_{af} \text{ Freezing} \tag{1}$$

$$I_{st} = n_t \cdot I_{at} \quad \text{Thawing} \tag{2}$$

The air freezing and air thawing indices were calculated using daily average air temperatures from the Ted Stevens International Airport, approximately 4.8 km from the subject building. The I_{af} was calculated for each day starting from October 24, 2006 (the first day of freezing), to April 2, 2007 (day of maximum frost penetration or last day of freezing), and the obtained values were multiplied by the n_f-factor of 0.9 (pavement free of snow and ice) to determine the I_{sf}. The n_f-factor is consistent with the surrounding environment of paved roads and sidewalks. The daily I_{sf} values were added cumulatively to generate a day-by-day index, which was then used to quantify a day-by-day frozen ground thickness. A similar procedure was used to numerically track I_{st} into the frozen ground. The air thawing index, I_{at}, was calculated for each day starting from April 3, 2007 (the first day of thawing), all the way to June 24, 2007 (day of complete ground thaw out). The I_{at} value for each day was multiplied by the n_t-factor of 1.775 (average factor for asphalt pavement and concrete pavement) to produce I_{st}. The I_{st} values were then added cumulatively to generate a day-by-day index which, in turn, was used to quantify the day-by-day thaw penetration. The daily thaw penetration was added cumulatively until the summation was equal to or greater than the calculated frost penetration, which meant the frozen ground had completely thawed out.

The value of I_{sf} and I_{st} obtained above can then be used to numerically determine the depth (X) of frost and thaw penetration by means of the Modified Berggren Equation expressed as:

$$X = \lambda \cdot \left(\frac{172{,}800 \cdot k_{avg} \cdot I}{L} \right)^{1/2} \tag{3}$$

where X (m) is the depth of frost/thaw penetration, k_{avg} (J/(sec·m·°C)) is the soil thermal conductivity, L (MJ/m^3) is the soil latent heat, I (°C·days) is the absolute value of the surface freezing index or surface thawing index, and λ is the dimensionless correction coefficient.

We will numerically calculate the value of k_{avg}, L, and λ of equation. (3) as follows: To determine the soil thermal conductivity, k, we assumed that the peat layer was completely removed and replaced with excavated material displaced by the strip footing. This assumption will provide consistent soil properties down to 3.1 m. Applying the soil's mass density of 2002 kg/m^3 and moisture content of 20%, values of k_f (frozen) and k_u (unfrozen) were found to be 3.25 J/(sec·m·°C) and 2.00 J/(sec·m·°C), respectively, for an average k_{avg}, of 2.63 J/(sec·m·°C).

The volumetric latent heat, L, can be calculated by the equation:

$$L = \rho_d \cdot L' \cdot \left(\frac{\omega - \omega_u}{100} \right) \tag{4}$$

where L' = 333.7 kJ/kg is the mass latent heat for water, ω_u, is the unfrozen water in the frozen soil which is generally so small that it is considered to be at 0%, and the other variables are as before. Inserting the soil properties ρ_d and ω into equation (4) yields a latent heat value of 111,389 kJ/m^3.

The correction coefficient, λ, can be derived from the thermal ratio, α, and the fusion parameter, μ. The thermal ratio and fusion parameter can be expressed by the following equations, respectively:

$$\alpha = \frac{v_o}{v_s} = \frac{v_o \cdot t}{I_{sf}} \tag{5}$$

$$\mu = \frac{c_v}{L} \cdot v_s = \frac{c_v \cdot I_{sf}}{L \cdot t} \tag{6}$$

where c_v (kJ/m^3·°C) is the soil volumetric heat capacity, t is the time or duration of the freezing period, and v_o and v_s (°C) are surface temperatures initially above freezing and below freezing respectively.

Volumetric heat capacity, c_v, is the average of the unfrozen volumetric heat capacity, c_{vu}, and the frozen volumetric heat capacity, c_{vf}, which are expressed by the following equations:

$$c_{vu} = \frac{\rho_d}{\rho_w} \cdot \left(0.17 + 1.0\frac{\omega}{100}\right) \cdot c_{vw} \tag{7}$$

$$c_{vf} = \frac{\rho_d}{\rho_w} \cdot \left[\left(0.17 + \frac{\omega_u}{100}\right) + 0.5 \cdot \left(\frac{\omega - \omega_u}{100}\right)\right] \cdot c_{vw} \tag{8}$$

where ρ_w represents the density of water at 1,000 kg/m^3, c_{vw} represents the volumetric heat capacity of water at 4.187 MJ/m^3·°C, and all others are as before. Inserting the soil properties into equations (8) and (9) yields the values of 0.62 MJ/m^3·°C and 0.45 MJ/m^3·°C, respectively, for an average value, c_v, of 0.54 MJ/m^3·°C.

The time of freezing, t, is the number of days starting from October 24, 2007 to April 2, 2007, which comes out to 160 days. Average surface temperature, v_o, is derived by multiplying the average air temperature for the year by the average *n*-factor. This value was found to equal 4.35°C.

The thermal ratio and fusion parameter can then be solved by inserting the appropriate values into equations (6) and (7). In doing so, α equaled approximately 0.6 and μ, 0.04. These values are then inputted into the chart in Figure 1 to determine a correction coefficient, λ, of 0.94.

With all the variables determined, frost and thaw penetrations can be calculated via equation (3). The calculated seasonal frost depth was calculated for the days corresponding to dynamic data collection. The geothermal gradient for this area was examined to see if it had any substantial influence on the frost penetration. Without empirical data to determine the geothermal gradient, a rule of thumb approximation proved by Brown (1963) was used and determined the gradient to be 1.8 x 10^{-2} °C/m. This gradient was deemed negligible.

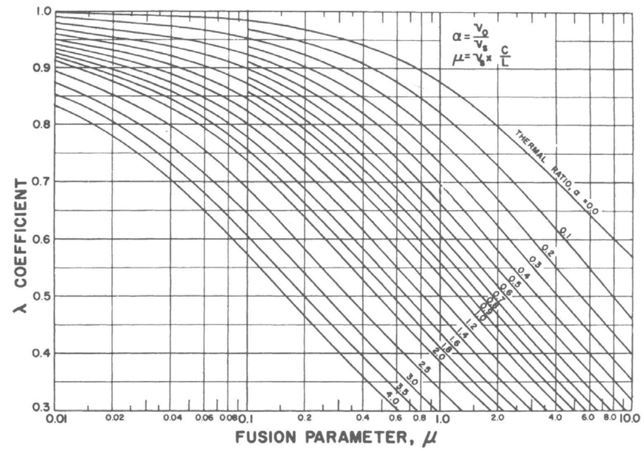

Figure 1. Correction coefficient (Andersland & Ladanyi 2004).

Strong Motion Instrumentation

Strong motion sensors

Installation of seismic sensors in the Frontier Building took place in early 2007. The seismic sensors used to measure the structural response of the building were the Kinematrics EpiSensor (Force Balance Accelerometer Model FBA ES-T, ES-U). Each sensor has a bandwidth of DC to 200 Hz and is capable of reading a user-defined acceleration spectrum of ±0.25 - ±4.0 g's with 1.25 V/g sensitivity (Kinemetrics 2005). A ±4.0 g range was selected for the sensors on this project. Three Altus K2 Strong Motion Accelerographs serve as the digital data recorders with 12 channels per data recorder. The recorders are located on the fourteenth floor of the building, within the communications closet. Thirty channels monitor lateral movement in 10 of the 14 floors of the building. Of the 30 channels, 20 channels are dedicated to the E-W direction and 10 channels to the N-S direction. The remaining 6 channels are set up for monitoring in the vertical direction. The vertically-oriented sensors are located only on the first and fourteenth floors. Nodes designated for biaxial sensitivity were composed of two ES-U2 sensors, with one oriented in the N-S direction and the other in the E-W direction. Uniaxial sensors oriented vertically were used for vertical measurements. Each of the sensors was installed on either the floor or the ceiling of the representative level of the building. The GPS antenna is installed on the rooftop of the building for accurate time (±0.5 ms) synchronization of the data recording devices (Kinemetrics 2002).

Data collection

We have measured the earthquake, as well as the ambient vibration, data of the building. In case of earthquake, the seismic system is preset to record any event that produces 1 gal acceleration at the base of the building (first floor) for a duration of 120 s. For the ambient vibration data, the recording duration was changed to 4–7 minutes. In both cases, the data were sampled at the rate of 200 samples/s and were processed in the same manner.

Data Analysis, Results, and Discussion

Data analysis

The recorded data from each sensor, after correcting for the baseline and instrument response, were filtered between 0.01–45.0 Hz using a fourth order bandpassed Butterworth filter. ARTeMIS Extractor was used to analyze the dynamic characteristics of the Frontier Building based on collected data. ARTeMIS Extractor is an Operational Modal Analysis (OMA), or output-only modal analysis software (Structural Vibration Solutions A/S 2007), and is a widely used program for strong motion dynamic analysis.

In ARTeMIS, a configuration file was first generated describing the structural geometry of the building. The generated model is shown in Figure 2. The arrows in the nodes represent the direction of sensor orientation. In the next step, the recorded time histories from each sensor were applied to the model and Spectral Density Matrix (SDM) were computed.

The generated SDM can then be decomposed into Singular Value Density (SVD) systems apparent to individual modes by means of either Frequency Domain Decomposition (FDD) or the Enhanced Frequency Domain Decomposition (EFDD) (Bai 2007). The dynamic characteristics of interest were the first and second modal frequencies (when available) and the corresponding mode shape. The data generated by ambient noise were enough to clearly depict the first two modes in the weak direction (E-W), the strong direction (N-S), and torsional direction. The data generated by the earthquake events had clear peak picking for only the first two modes in the weak direction (E-W) for the April 25, 2007, event and the first mode in the weak direction (E-W) and first mode in the strong direction (N-S) for the May 22, 2007, event. This was due to the direction of the earthquake's epicenter being mainly in the E-W direction relative to the building.

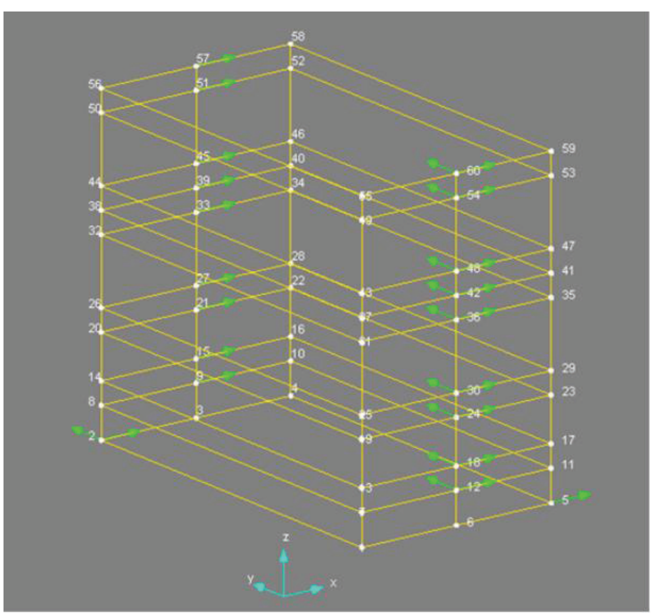

Figure 2. Geometric model of the Frontier Building generated by ARTeMIS.

The analyzed modal frequencies were then correlated with the calculated seasonal frost penetration. The relation between the first and second modal frequencies and frost depth can be seen tabulated in Table 1 and graphically in Figure 3. The data revealed minimal variation in the first and second modes with respect to varying frozen ground thickness. All fundamental frequencies for the weak axis were within 2% of one another and 3% for the second mode frequencies.

Discussion

The tabulated results do not reveal similar trends found in similar past projects conducted by Qi et al. (2006), Yang et al. (2007, 2008), and Bai (2007). These past projects, involving a pile foundation bridge, a 20-story office building (the Atwood Building) with an unheated parking garage basement, and an open, unheated, four-level parking garage yielded increases in the fundamental frequencies ranging from 4% up to 50% from summer to winter season. All these projects are anticipated to differ from the Frontier Building in that they all have foundation designs that allowed for the surrounding ground to freeze, whereas, the design of the Frontier Building allowed heat from the inside of the building to migrate to the foundation and prevent any ground freezing in the vicinity of the building. A thermal finite element model was generated for the Frontier Building, as well as for the Atwood Building, to examine and compare the two buildings' thaw bulbs.

It is appropriate to compare these two buildings, in that they are similar in shape and size, and they are relatively close to one another, and therefore, exposed to similar climate, as well as geotechnical, characteristics. They do, however, differ in configuration with respect to their foundations. As mentioned before, the Frontier Building has a footing foundation with the first floor directly on top of the foundation backfill. The Atwood building, on the other hand, has an unheated underground garage beneath the first floor of the building.

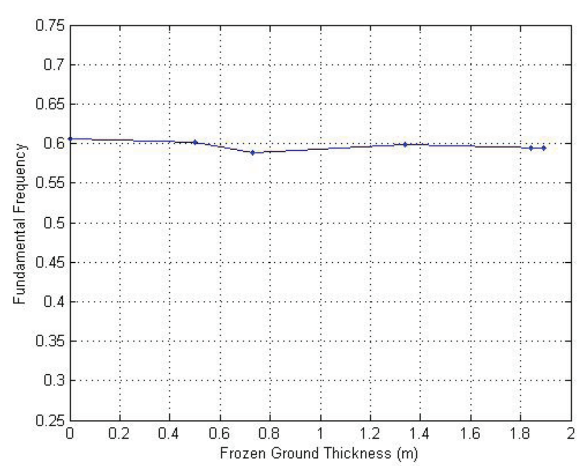

Figure 3. Frozen ground vs. fundamental frequency for the Frontier Building.

Table 1.

Event Date	Frozen Ground Thickness (m)	EFDD Frequency (Hz)					
		1st Mode			2nd Mode		
		E-W[b]	N-S	Torsion	E-W[b]	N-S	Torsion
03/01/2007	1.84	0.5945	0.6773	0.9183	1.861	2.059	2.736
04/05/2007	1.89	0.5936	0.6665	0.9012	1.845	2.025	2.698
04/25/2007[a]	1.34	0.5994	--	--	1.836	--	--
05/22/2007[a]	0.73	0.5888	0.6718	--	1.833	--	--
06/01/2007	0.50	0.6020	0.6766	0.9067	1.870	2.019	2.709
08/17/2007	0.00	0.6060	0.6733	0.9080	1.889	2.048	2.709

[a] Actual Recorded Earthquake Events
[b] E-W Direction Represents the Weak Axis of the Building

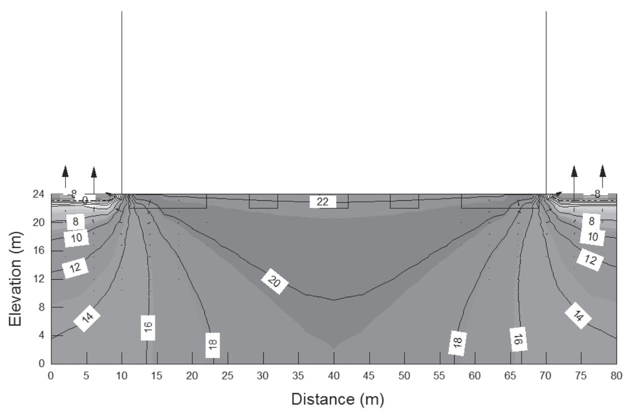

Figure 4. Thermal FE modeling results of the Frontier Building.

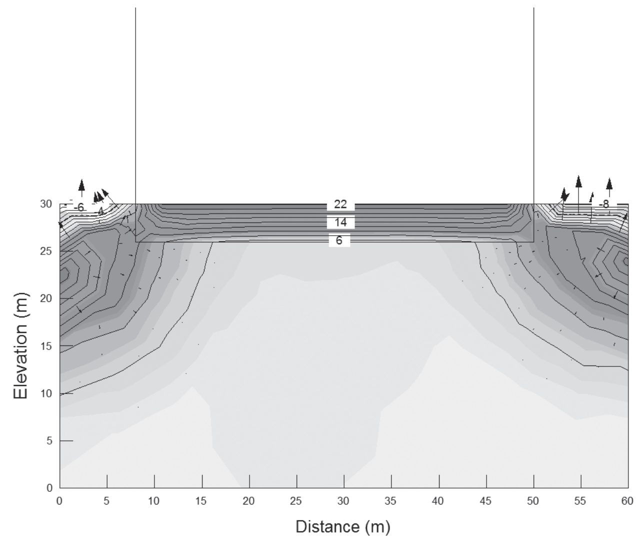

Figure 5. Thermal FE modeling results of the Atwood Building.

The Temp/W Module of Geo Studio 2004, Finite Element modeling software, was used to examine the thaw bulb of each building to compare thaw bulbs as a result of the foundation configuration. The average temperature of the interior of both buildings was assumed to be 22.2°C, and the average outside air temperature during the freezing period was found to be -8.2°C, from the temperature data obtained from a nearby airport described earlier. Soil properties such as thermal conductivity and heat capacity were inputted into the program, and the thaw bulb for each building was generated as shown in Figures 4 and 5.

The thermal contour lines are labeled with their appropriate temperature while the 0°C line (signifying the freezing front) is delineated with a bold dashed line. The arrows in the diagrams represent heat flow vectors. The direction of the arrow represents the direction of heat flow, and the size of the arrow determines the magnitude. Regional shading also relates to the thermal gradient. These two models could be refined to produce more accurate results (e.g., freezing front) by including details of the wall and openings in the basement. However, they are good enough to show that (1) sufficient heat migration was allowed from the building into the foundation, thus preventing frozen ground to develop in the Frontier Building; (2) the unheated parking garage/basement in the Atwood Building acts as a thick insulating layer preventing heat from infiltrating the surrounding soil, thus allowing frozen ground to develop.

Conclusions

After comparing the thermal analysis of the two buildings, the following conclusions were determined:

- Decreasing ambient air temperature did not impact the dynamic properties of the Frontier Building. This was due to the fact that the building's foundation design allowed for a large enough thaw bulb to prevent significant frost penetration.
- The Atwood Building's dynamic properties were impacted by seasonal frost due to its foundation design creating enough of an insulating layer to inhibit heat migration.
- Foundation design, with respect to heated or unheated, plays a crucial role in whether or not the structure's foundation will be influenced by frozen ground leading to potential impact on dynamic properties.

Acknowledgments

The strong-motion instrumentation was sponsored by the Advanced National Seismic System Program of U.S. Geological Survey. This study is partially supported by Chancellor's Research Funds of the University of Alaska Anchorage. We want to thank the management of the Frontier Building for their support to this project.

References

Anderland, O.B. & Ladanyi, B. 2004. *Frozen Ground Engineering*. New Jersey: The American Society of Civil Engineers & John Wiley & Sons, Inc., 363 pp.

Bai, F. 2007. *Effects of Seasonally Frozen Ground on Dynamic Properties of UAA Parking Garage Soil-Structure System*. University of Alaska Anchorage, School of Engineering, Civil Engineering Graduate Project.

Brown, W.G. 1963. *The Temperature Under Heated or Cooled Areas on the Ground Surface. National Research Council Canada,* Division of Building Research, Research Paper No. 208.

Combellick, R.A. 1999. *Simplified Geologic Map of Central and East Anchorage, Alaska. Alaska* Department of Natural Resources, Division of Geological & Geophysical Surveys, Preliminary Interpretive Report 1999-1.

Combellick, R.A., Mayer, J.L., Sink-Blair, K.D. & Weems, S.M. 2001. *Geotechnical Borehole and Well-Log Database for Anchorage, Alaska.* Alaska Department of Natural Resources, Division of Geological & Geophysical Surveys, Miscellaneous Publication 40.

Combellick, R.A. Personal Communication. Transcribed Notes of Boreholes for the Frontier Building.

DOWL Engineers and Alaska Testlab. Personal Communication. Log of Boring for Test Boring 3.

Dutta, U., Biswas, N., Martirosyan, A., Nath, S., Dravinski, M., Papageorgiou, A. & Combellick, R. 2000. Delineation of spatial variation of shear wave velocity with highfrequency Rayleigh waves in Anchorage, Alaska. *Geophys. J. Int.* 143: 365-375.

Dutta, U., Martirosyan, A., Biswas, N., Papageorgiou, A., Dravinski, M. & Combellick, R. 2002. Estimation of S-wave site response in Anchorage, Alaska, from weak motion data using generalized inversion method. *Bull. Seism. Soc. Am.* 91: 335-346.

Finn, W.D.L. & Yong, R.N. 1978. Seismic Response of Frozen Ground. *American Society of Civil Engineers, Journal of the Geotechnical Engineering Division* 104: 1225-1241.

Haeussler, P. & Plafker, G. 2003. *Earthquakes in Alaska.* U.S. Department of the Interior, U.S. Geological Survey, Publication No. 95-624, ver. 1.1.

Kinemetrics, Inc. 2005. *EpiSensor Force Balance Accelerometer Model FBA ES-U2 User Manual*. Document 301929, Revision D.

Martirosyan, A., Dutta, U., Biswas, N., Papageorgiou, A. &. Combellick, R. 2002. Determination of site response in Anchorage, Alaska on the basis of spectral ratio methods. *Earthquake Spectra* 18: 85-104.

Qi, J., Ma, W., Sun, C. & Wang, L. 2006. Ground Motion Analysis in Seasonally Frozen Regions. *Cold Regions Science and Technology* 44: 111-120.

Structural Vibrations Solutions A/S. 2007. ARTeMIS Product Information. http://www.svibs.com.

Tsytovich, N.A. 1975. *The Mechanics of Frozen Ground*. Washington D.C.: Scripta Book Co., 426 pp.

Ventura, C.E., Laverick, B., Brinker, R. & Andersen, P. 2003. Comparison of Dynamic Characteristics of Two Instrumented Tall Buildings. *Proceedings of the Twenty-first International Modal Analysis Conference*, *Kissimee, Florida.*

Vinson, T.S. 1978. Parameter effects on dynamic properties of frozen soils. *American Society of Civil Engineers, Journal of the Geotechnical Engineering Division*, 104: 1289-1306.

Wesson, R., Frankel, A., Mueller, C. & Harmsen, S. 1999. Probabilistic Seismic Hazard Maps of Alaska, USGS Open-File Report, 99-36.

Western Region Climate Center (WRCC). 2007. http://www.wrcc.dri.edu.

Woodward-Clyde Consultants. 1982. Anchorage Office Complex, Geotech. Invest. Report to Alaska Dept. of Trans. and Public Facilities, Vol. I-III, Anchorage, AK.

Yang, Z., Dutta, U., Xiong, F., Zhu, D., Marx, E., and Biswas, N. 2007. Seasonal Frost Effects on the Soil-Foundation-Structure Interaction System. *American Society of Civil Engineers, Journal of Regions Engineering* 21(4): 108-120.

Yang, Z., Dutta, U., Xiong, F., Biswas, N. & Benz, H. 2008. Seasonal Frost Effects on the Dynamic Behavior of a Twenty-Story Office Building. *International Journal of Cold Regions Science and Engineering* 51: 76-84

Seasonal Thermal Regime of a Mid-Latitude Ventilated Debris Accumulation

Sébastien Morard
Geography Unit, Geosciences Department, University of Fribourg, Switzerland
Reynald Delaloye
Geography Unit, Geosciences Department, University of Fribourg, Switzerland
Jonathan Dorthe
Geography Unit, Geosciences Department, University of Fribourg, Switzerland

Abstract

The internal and reversible mechanism of air circulation throughout a porous debris accumulation-like talus slope, relict rock glacier, and rockfall deposit acts as an efficient advective conveyor of heat, which strongly influences the ground surface thermal regime during the whole year. Combining the detection of visual evidences and ground surface temperature (GST) measurements (continuous logging, winter mapping) has proved to be relevant for identifying areas affected by internal ventilation and for characterizing the spatial pattern of the seasonal ground surface temperature anomalies. Five types of specific annual ground thermal regime can be defined. Vegetation, soil, and micro-fauna appear to be related to these different thermal regimes. The distribution of vegetal associations is closely linked to the ground temperature in summertime.

Keywords: air circulation; ecosystems; seasonal thermal regimes; Swiss Alps and Prealps; talus slopes.

Introduction

The mechanism of deep air circulation (the so-called chimney effect or wind tube) is known to be a process of ground overcooling in the lower and, presumably, deeper parts of porous talus slopes (e.g., Wakonnig 1996, Delaloye et al. 2003, Sawada et al. 2003). It occurs frequently in mid-latitudes, where it can generate and/or preserve extrazonal permafrost conditions up to more than 1000 metres below the regional lower limit of discontinuous mountain permafrost (Gorbunov et al. 2004, Sone 2005, Delaloye & Lambiel 2007). The process plays, moreover, a decisive role in the conservation of specific terrestrial ecosystems (Gude & Molenda 2003).

Detailed investigations on the thermal regime of talus slopes and other porous debris accumulations (relict rock glaciers, rockfall deposits) have been carried out since 1997 in western Switzerland (Jura mountains, Prealps, and Valais Alps) in several sites located between 650 and 2000 m a.s.l. with a corresponding mean annual air temperature (MAAT) ranging from +8 to +2°C, respectively (Fig. 1) (e.g., Delaloye 2004, Lambiel 2006). They demonstrate that internal air circulation is a mechanism common to almost all prospected sites causing a significant annual negative anomaly of the ground surface temperature (GST) (up to more than 7°C below MAAT) at the bottom of the debris accumulation, independent of the slope orientation.

The present paper describes the seasonal spatial pattern of the ground surface thermal regime in porous debris accumulations, which are affected by the air circulation mechanism. It provides some key methods for detecting and assessing both the occurrence of a ventilation mechanism and its spatial influence. It also gives a preliminary overview on the related specific terrestrial ecosystems, in particular on the development and spatial extent of vegetal associations and soils.

Background

Cold airflow blowing out of the ground in summertime in the lower parts of scree slopes was used for centuries in mountainous or volcanic mid-latitude areas as natural refrigerators for the conservation of food (e.g., DeSaussure 1796). Several assumptions have been advanced to explain the origin of ground cooling (Harris & Pedersen 1998). Recent studies (Wakonnig 1996, Delaloye et al. 2003, Sawada et al. 2003) and our analysis of several tens of sites investigated in Switzerland demonstrate that a deep reversible air circulation process (the so-called "chimney effect") acting throughout the whole of an accumulation of blocky material (Delaloye & Lambiel 2007) is likely to be the main factor controlling the ground surface thermal regime on these sites. The cooling effect of air circulation in a porous medium has also been used artificially in embankments to preserve permafrost conditions under highway and railway infrastructure in high-latitude or high altitude (e.g., Goering & Kumar 1996, Niu & Cheng 2005).

The reversible air circulation

Variations of both the direction and the velocity of the air circulation throughout an accumulation of loose sediments are primarily controlled by the thermal contrast between the outside and inside (ground) air causing a gradient of driving pressure (Delaloye et al. 2003). The flow direction reverses seasonally. During winter, an ascent of relatively warm light air tends to occur in the upper part of the debris accumulation. It leads to a dynamic low (a depression) in the lower part, causing a forced aspiration of cold external air deep inside the ground even through a thick—but porous—snowpack. A gravity discharge of relatively cold dense air occurs during summer in the lowermost part of the debris accumulation, preventing the GST to rise significantly above 0°C in this

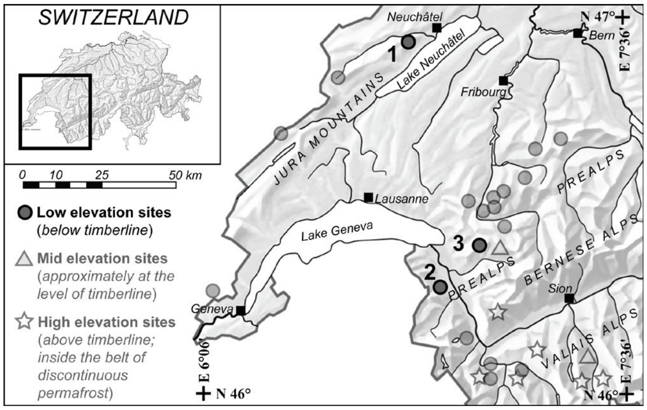

Figure 1. Location map of investigated areas with ventilated terrain in western Switzerland (after Delaloye 2004, Lambiel 2006, Dorthe & Morard 2007). Main sites: 1: Creux-du-Van; 2: Dreveneuse; 3: Bois des Arlettes.

section. As a consequence, a diffuse aspiration of external warm air occurs in the upper part of the slope.

An internal "cold reservoir" is built up during winter by the advection of external air (Sone 2005). The efficiency of the process depends on the intensity and duration of cold weather periods. The "frigories" are supposed to be "stored" by groundwater freezing (latent heat) and by conduction in the rocky materials and/or in the underlying finer ground (Delaloye & Lambiel 2007). The thermal conditions observed at the ground surface and in the shallow sub-surface in summertime are mainly influenced by the intensity of winter cooling and the recharge of the cold reservoir.

Specific ecosystems

The lower parts of ventilated talus slopes usually shelter specific ecosystems, whose typical distribution areas are located at higher latitude and/or higher elevation (e.g., Rist et al. 2003, Gude & Molenda 2003). Besides the occurrence of boreo-alpine species, significant differences in phenological development (like dwarfing of trees, early yellowing, or shorter developmental staging of vegetation) have also been highlighted between flora growing in the cold ventilated areas and those located outside (Ruzicka 1999, Körner & Hoch 2006).

Sites Characteristics

Data from the three main sites of investigation in western Switzerland (Creux-du-Van, Dreveneuse-du-Milieu, Bois des Arlettes) are used in this paper. The sites are located between 500 and 1200 metres below the estimated elevation of the regional lower limit of discontinuous mountain permafrost (about 2200–2400 m a.s.l. on northern slopes) (Fig. 1, Table 1).

Sites description

The Creux-du-Van (Cr) north-facing talus slope consists of limestone pebbles in the uppermost part transiting gradually to metric boulders downwards. The lower part of the slope is covered by an organic soil, and several patches of dwarf red spruces (*Tofieldio-Picetum* association) are occurring. The thickness of the blocky layer was estimated by geophysics to be about 20 m with the possible existence of a frozen body (Marescot et al. 2003). The site has been intensively studied since 1997 (Delaloye et al. 2003, Delaloye 2004).

Table 1. Topo-climatic characteristics of the investigated sites.

N°	Sites	Elevation	MAAT	Orientation
1	Creux-du-Van	1170-1290	+ 5.4°C*	N
2	Dreveneuse	1600-1800	+ 3.8°C**	E
3	Bois des Arlettes	1650-1900	+ 3.9°C***	NW

Locations are displayed on Figure 1. MAAT (Oct. 2004 to Sept. 2005) measured at: *1210 m a.s.l.; **1700 m a.s.l. (derived from Moléson, 2000 m a.s.l.); ***1740 m a.s.l.

The Dreveneuse-du-Milieu (Dr) east-facing talus slope consists of limestone pebbles and angular decimetric blocks. It is connected to a 200 m long relict rock glacier extending downward in a forested area. A few dwarf red spruces are found in the lower part of the slope as well as locally on the relict rock glacier. The thickness of the blocky layer was estimated by geophysics to be about 20 m for the talus slope and about 15 m for the relict rock glacier.

The large Bois des Arlettes (Arl) talus slopes face to the northwest and also consist of limestone debris. They dominate several sizeable relict rock glaciers. The thickness of the blocky layer was estimated to be about 25 m for the talus slope and 15–20 m for the relict rock glacier. Vegetation is almost lacking on the talus slope. The relict rock glaciers are conversely covered by a thin organic soil and a mixed forest, including some patches of azonal vegetation (*Salicetum Retuso-Reticulatae*) with alpine species such as *Pritzelago alpina* or *Dryas octopetalia*.

Meteorological conditions of the year 2004–2005

Data presented in the paper date from the hydrological year 2004–2005 (Fig. 2).

Relatively warm conditions occurred from October to mid-January in comparison to the climatic norm 1961–1990, interspersed with a cold phase by mid-November. Two successive persistent cold periods were then recorded until mid-March, separated by a short spell of milder weather in the first days of February. Afterwards, air temperatures remained warmer than the norm, except for August.

Winter 2004–2005 was also characterized by relatively late snowfalls, the snow cover remaining thin (less than about 50 cm) until mid-February. The snow cover reached its maximal thickness (1.5 m at Creux-du-Van and probably as much on the two other sites) by mid-March.

Methods

According to Delaloye (2004) and Morard et al. (2008), the observation of visual evidences (like "snowmelt windows" in the upper part of a slope in winter or ground-ice occurrences in early summer in the lower part) was used to point out the activity of a ventilation mechanism through a debris accumulation (Figs. 4, 5). In addition, ground temperature measurements were carried out to assess the spatio-temporal variability of the ventilation system.

Several single-channel dataloggers (UTL-1) were installed

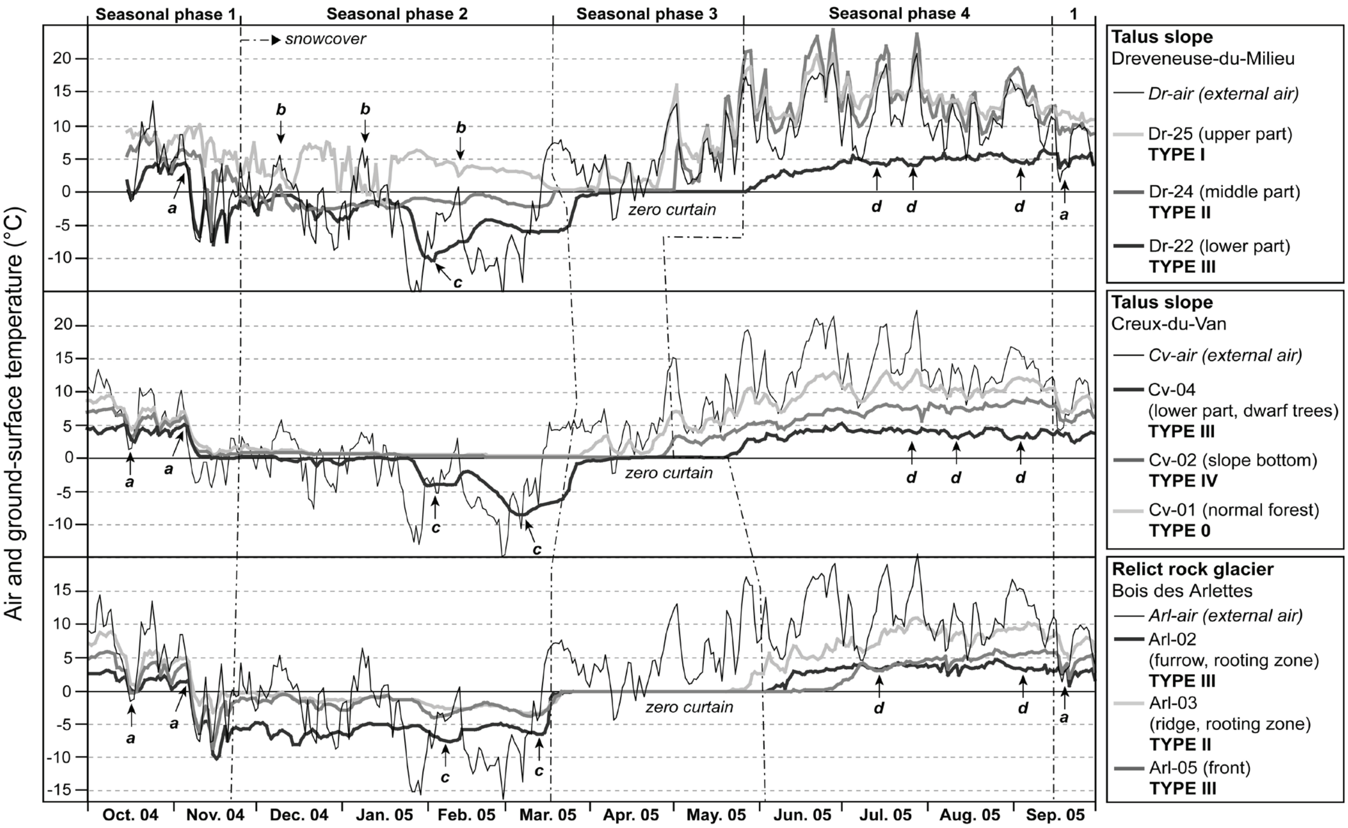

Figure 2. Thermal behaviors of the different parts of a ventilated talus slope–relict rock glacier complex. Data are daily air and ground-surface temperature. Locations of the dataloggers are shown in Figures 4 and 5. Arrows: a) inversion of the air flow direction; b) mild weather events; c) colder ground-surface temperature in January-–March 2005; d) coldest ground temperature in summertime.

on the different sites, mostly along a longitudinal profile crossing the whole debris accumulation. They recorded the ground surface temperature at a depth of about 10–20 cm every two hours. Atmospheric air temperatures were measured in situ (Creux du Van, Bois des Arlettes), or derived from official meteorological stations of the Federal Office of Meteorology and Climatology network using an altitudinal gradient of -0.58°C/100 m (Dreveneuse).

The comparison between ground and surrounding air temperature provides information about both the direction and intensity of the airflow. A similar relationship corresponds to an aspirating regime, while an inverse relationship indicates an expelling phase reflecting partially the thermal state of the ventilated system at a given moment (Lismonde 2002). A close non-delayed relationship between air and ground temperatures is assumed to be related to a higher intensity of the air flow.

To determine both the efficiency and the spatial pattern of a ventilation system, the winter temperature at the ground/snow interface was also mapped after a long period of cold weather in February 2005 using the BTS (bottom temperature of the snow cover) technique.

Results

Time series reported in Figure 2 and summed up in Table 2 illustrate the annual behavior of the GST for the three main sites of investigation along a slope profile. Four seasonal phases (1–4) can be distinguished for describing the thermal regime of the various parts of a ventilated debris accumulation, paying attention to the thermal anomalies in regard to the outside air temperature.

Seasonal phase 1: Autumn and early winter conditions

The fall–early winter phase until the onset of a thick snow cover is characterized by the frequent reversibility of the ventilation system. The air flows downwards in mild weather, whereas aspiration occurs in the lower parts of the ventilated terrain when the weather becomes colder. Not only the foot of talus slopes suffers an intense cooling of the ground, but also the relict Bois des Arlettes rock glacier (arrows "a" in Fig. 2). In all these places, this seasonal phase 1 is characterized by a negative thermal anomaly.

In November 2004, the GST in the upper part of the Dreveneuse talus slope (Dr-25) remained permanently above the freezing point, with variations inversely related to those of the external air temperature. Snowmelt windows, hoarfrost, wet blocks, basal icing of a thin snow cover, and condensation fog are visual evidences of the outflow of "warm" air during this phase.

During the phase 1, the lower part of the Dreveneuse talus slope (Dr-22) cooled from +4°C to -6.8°C between 6–10 November 2004, whereas the GST in the upper part of the slope remained as high as +8°C. At Bois des Arlettes, a rapid decrease of the GST from +1.5°C to -6.4°C and from +4°C to -6°C was also observed in a furrow in the rooting zone (Arl-02), and on the front (Arl-05) of the relict rock glacier, respectively. Where the soil is thicker and damper as in the Creux-du-Van lower talus slope (dwarf trees area), a zero curtain period can start (Cv-04).

Table 2. Temperature characteristics of the investigated sites.

UTLs	MAGST (°C)	ATA (°C)	GFI (°C)	NFD (day)	ZCD (day)
Dr-air	*3.76**	*0*	*-613*	*105*	*0*
Dr-25	7.94	+4.18	-6.5	8	0
Dr-24	5.54	+1.78	-204	114	42
Dr-22	-0.01	-3.77	-601	205	48
Cv-air	*5.35**	*0*	*-441*	*85*	*0*
Cv-04	0.74	-4.91	-336	171	34
Cv-02	3.29	-2.06	0	63	63
Cv-01	4.96	-0.39	0	0	0
Arl-air	*3.96**	*0*	*-614*	*109*	*0*
Arl-02	-0.92	-4.88	-789	210	74
Arl-03	2.54	-1.41	-213	194	58
Arl-05	0.68	-3.28	-311	222	87

Location on Figures 4 and 5. * Mean annual air temperature (°C). MAGST: mean annual ground surface temperature (°C); ATA: annual thermal anomaly (°C); GFI: ground freezing index (°C); NFD: number of frozen days; ZCD: zero curtain duration (day).

Seasonal phase 2: winter conditions

Winter is often characterized by a thicker (more than 1 m) and continuous snow cover as well as by colder weather conditions. The ascending air circulation regime is prevailing.

According to the elevation, the ground surface or its close subsurface should normally not freeze under the thicker snow cover, as it was recorded at the terminal edge of the Creux du Van talus slope (Cv-02) and in the surrounding area (Cv-01).

In the upper part of a talus slope, as in Dreveneuse (Dr-25), the GST remained warm for the whole winter, but dropped strongly for a short time by mild air temperatures (arrows "b" in Fig. 2). The only temperature below freezing point was registered during the mildest weather period in January 2005. The GST tended however to decrease gradually from about +7°C in the beginning of November to +2°C in March. An inverse relationship to the outside air temperature is also observed. Warm air outflow is easily perceptible as well as associated phenomena like snow funneling with hoarfrost, snowmelt windows, and vaulted spaces at the base of the snowpack.

GST was at or below freezing point during the whole winter in the middle and lower parts of the talus slopes (Dr-24, Dr-25, Cv-04), as well as on the relict rock glacier (Arl-02, Arl-03, Arl-05). The GST mapped in February illustrates the spatial geometry of the colder areas (Fig. 3). The thermal regime is mainly controlled by the evolution of the external air temperature (arrows "c" in Fig. 2) with a time lag of a few days which seems to increase by the end of the winter.

Seasonal phase 3: Snowmelt period

At the onset of the snowmelt phase in March, the GST rose suddenly to 0°C in the lower parts of the ventilated terrains and remained stable for 42 days at Dr-24 to 87 days at Arl-05 (Table 2). In the upper part of a talus slope (Dr-25), the snowmelt phase provoked a temperature drop to about 0°C. This non-constant zero curtain phase lasted for a few days only.

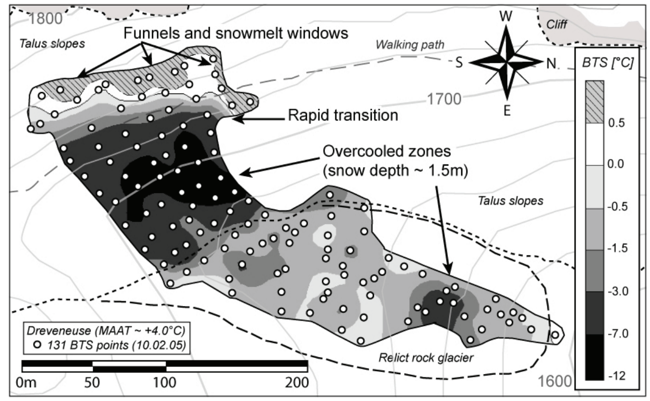

Figure 3. Ground surface winter temperature mapping (Dreveneuse-du-Milieu, 10 February 2005). Note the overcooled zone in the middle/lower part of the talus slope, the cold areas on the relict rock glacier, and the rapid transition in the uppermost zone to warmer ground temperature.

Seasonal phase 4: summer conditions

The gravity discharge of cold dense air prevents the GST to increase above +6°C in the lower parts of the debris accumulations as at Dr-22, Cv-04, Cv-02, Arl-02, and Arl-05. There is a more or less well-established inverse relationship between the airflow temperatures and those of the external air (as indicated by arrows "d" in Fig. 2). At these places, cold air outflow, azonal vegetation, ground ice, or late-lying residual snow patches can be observed.

In the upper and middle parts of talus slope (Dr-25, Dr-24), the GST varies in close correspondence with the evolution of the surrounding air temperature. In the marginal ridges of the relict rock glacier (Arl-03) and in the areas outside the porous debris accumulations (Cv-01), this GST regime can be considered as normal: the fluctuations are smooth and depend directly on the air temperature.

Synthesis and Discussion

Annual thermal regime of a ventilated system

Air circulation throughout a porous debris accumulation produces major differences in the thermal regime of areas only a few (tens of) meters from each other. Temperature anomalies occur and vary seasonally, depending both on the location on the landform and the meteorological factors (external air temperature and snow cover). Indeed, five types of annual thermal regime can be defined on the basis of the four seasonal phases described above:

- Type I: positive anomaly in autumn, winter, and summer. This behavior concerns the upper part of a ventilated system, where in particular the GST remains significantly higher than 0°C during winter due to the expelling of internal warm air. A positive annual thermal anomaly will result in such places (+4.18°C at Dr-25). A spell of mild weather in winter may cause the weakening or the end of the ascending airflow and consequently an episodic decrease of the GST.
- Type II: slight negative anomaly possible in winter, positive anomaly in summer. This kind of thermal regime affects the section located immediately above the coldest

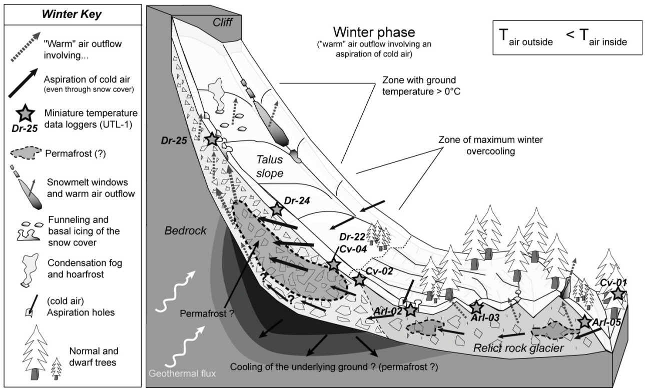

Figure 4. Model of winter ascending air circulation (in talus slope relict rock glacier system). The stars indicate the general position of the dataloggers presented in Figure 2.

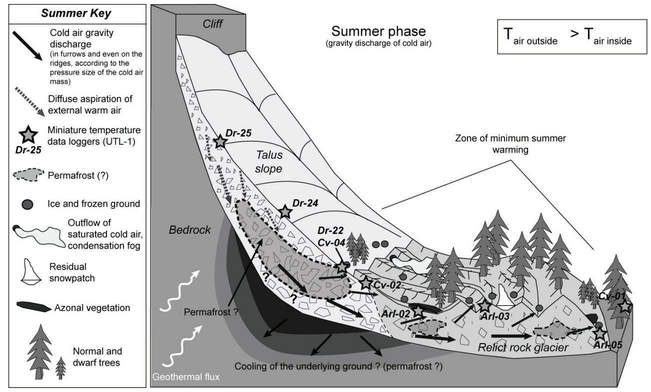

Figure 5. Model of summer descending air circulation (in talus slope/relict rock glacier system). The stars indicate the general position of the dataloggers presented in Figure 2.

area. Air aspiration occurs in late fall and winter but there is no influence of the summer gravity discharge. The annual thermal anomaly is slightly positive (Dr-24) or slightly negative (Arl-03), probably due to different ground surface properties (blocky material directly exposed to solar radiation in summer at Dr-24, thick soil and shady forest at Arl-03).

- Type III: negative anomaly in fall, winter, and summer, late lying of snow. This annual type is associated to the coldest part of the system, permanently frozen during winter due to the aspiration of external air (even through the snow cover) and remaining cool in summer because of the gravity discharge of internal cold air. Such areas are located in the lower part of the talus slope as well as locally on the connected relict rock glacier–if existing. The annual thermal anomaly reached -3.28°C to -4.91°C at Dr-22, Cv-04, Arl-02 and Arl-05 (Table 2).
- Type IV: slight negative anomaly possible in winter, negative anomaly in summer less pronounced than in type III, late-lying snow. This area is located under the coldest zone at the bottom of a talus slope and is partially affected by the summer gravity discharge. The annual thermal anomaly is slightly negative (CV-02).
- Type 0: no seasonal anomaly. During winter and in the presence of snow, the ground temperature does not drop below 0°C. This behavior concerns mainly sectors which are not affected by the air circulation and, where the heat fluxes are only conductive. The mean annual temperature is close to MAAT (CV-01).

Dissymmetry of seasonal overcooled zones

A spatial shift can be identified between the zones of maximum winter overcooling and those of minimum summer warming (Figs. 4, 5). The seasonal contrast between types II and IV shows that in a talus slope, the area affected by the winter aspiration of cold air, is shifted upwards compared to the cold summer area, the seasonal gravity discharge concentrating in the lowermost parts of the slope. Such a shift has not so far been observed on the downward relict rock glaciers. However, the occurrence of thermal regimes of type III and the lack of warm areas on these landforms indicate that internal ventilation is occurring as far as the front of a relict rock glacier and should be connected to those of the upper talus slope. Figures 4 and 5 illustrate the resulting concept of air circulation throughout a talus slope–relict rock glacier complex and the possible location of permafrost within the system.

Spatial implication on related terrestrial ecosystems

Temperature is one of the key factors (with moisture) controlling the distribution of organisms and primary production (such as pedological processes) in ecosystems. The spatial distribution of vegetation and soils on a ventilated system often indicates different GST conditions.

The seasonal asymmetrical position of cold zones plays an important role on the vegetal distribution. The thermal regime of type II is not associated with azonal vegetation. At Arl-03, for instance, the presence of *Rhododendro-Vaccinetum Juniperetosum* Ass. indicates normal ground thermal conditions during the vegetation period in summer. Conversely, a cold summer ground surface thermal regime of types III and IV is associated with alpine species like *Pritzelago alpina* and *Dryas octopetalia* (for instance at Arl-02) and limits the growth of tree roots (Körner et al. 2006) (Dr-22, Cv-04). The phenological development is strongly conditioned by the summer ground temperature.

Soils found in overcooled sectors evolve differently from the general pedoclimatic trend (Gobat et al. 2003). Furthermore, cold summer temperature directly influences the development of humus. Spatial variations in pH, organic texture, and kind of macrorests is clearly dependent on the location of ventilated systems (Rossel et al. 2004) and the GST regime.

A strong thermal stability is observed in summertime, but also from year to year (Delaloye 2004), where the cold air outflows occur. It would also provide possible favorable long-term abiotic conditions for azonal and less-competitive species. Genetic DNA-analyses carried out on different separated populations of wingless beetles found in cold scree slopes have shown on the one hand an own genetic evolutionary way (island-like character of this biotope), and on the other hand the existence of true faunal relicts from glacial periods (Gude et al. 2003).

Conclusion

The main conclusion of our study is that thermal anomalies induced by advective heat fluxes ("chimney effect") are observed in many porous debris accumulations located below the regional lower limit of discontinuous permafrost in the Swiss mountains. An interconnection in the airflow between a talus slope and a relict rock glacier located immediately downstream has also been identified.

The combination of visual and thermal measurements has proved to be a relevant method for detecting and characterizing heterogeneous ground surface thermal regimes of a ventilated debris accumulation.

A succession of negative seasonal anomalies is typical in the lower part of a ventilated area, while in the upper part the GST regime presents usually a positive anomaly during the whole year. Other differentiated types of seasonal thermal regimes occur in the upper and lower margins of the coldest places of a debris accumulation. Moreover, the occurence, development, and spatial pattern of distribution of specific "cold" terrestrial ecosystems are directly influenced by the internal circulation of air.

Acknowledgments

Special thanks are due to Walter Leimgruber for editing the English text, and to numerous students and other people for their precious help in the fieldwork.

References

Delaloye, R. 2004. *Contribution à l'étude du pergélisol de montagne en zone marginale.* PhD Thesis. University of Fribourg, Switzerland. *GeoFocus* 10, 240 pp.

Delaloye, R. & Lambiel, C. 2007. Drilling in a low elevation cold talus slope (Dreveneuse, Swiss Prealps). *Geophysical Research Abstracts* 9: 10907.

Delaloye, R., Reynard, E., Lambiel, C., Marescot, L. & Monnet, R. 2003. Thermal anomaly in a cold scree slope (Creux-du-Van, Switzerland). *Proceedings of the Eighth International Conference on Permafrost, Zurich*: 175-180.

DeSaussure, H.-B. 1796. Voyages dans les Alpes, précédés d'un essai sur l'histoire naturelle des environs de Genève. *Tome troisième, Neuchâtel, S.-Fauche*.

Dorthe, J. & Morard, S. 2007. Ventilation des éboulis froids et des glaciers rocheux fossiles des Préalpes suisses romandes. Master's Thesis. Univ. Fribourg, 166 pp.

Gobat, J-M, Aragno, M. & Matthey, W. 2003. Le sol vivant. Bases de pédologie, biologie des sols. *Presses Polytechniques et Universitaires Romandes, Collection Gérer l'Environnement* 14, 568 pp.

Goering, D.J. & Kumar, P. 1996. Winter-time convection in open-graded embankments. *Cold Regions Science and Technology* 24(1): 57-74.

Gorbunov, A.P., Marchenko, S.S. & Seversky, E.V. 2004. The thermal environment of blocky materials in the mountains of central Asia. *Permafrost and Periglacial Processes* 12: 69-77.

Gude, M. & Molenda, R. 2003. Felsen, Block- und Schutthalden, Blockmeere. *Handbuch Naturschutz und Landschaftspflege, Landsberg*, XI-2.27: 181-192.

Harris, S.A. & Pedersen, D.E. 1998. Thermal regimes beneath coarse blocky materials. *Permafrost and Periglacial Processes* 9: 107-120.

Körner, C. & Hoch, G. 2006. A test of treeline theory on montane permafrost island. *Arctic, Antarctic and Alpine Research* 38: 113-119.

Lambiel, C. 2006. *Le pergélisol dans les terrains sédimentaires à forte déclivité: distribution, régime thermique et instabilités.* Thèse, Université de Lausanne, Institut de Géographie, Coll. «Travaux et Recherches» 33, 260 pp.

Lismonde, B. 2002. Climatologie du monde souterrain : Vents des ténèbres. *Edition du Comité Départemental de Spéléologie de Isère, 1ère édition, Tome 1*, 168 pp.

Marescot, L., Loke, M.H., Chapellier, D., Delaloye, R., Lambiel, C. & Reynard, E. 2003. Assessing reliability of 2D resistivity imaging in mountain permafrost studies using the depth of investigation index method. *Near Surface Geophysics*: 57-67.

Morard, S., Delaloye, R. & Dorthe, J. (2008). Indices de fonctionnement de la ventilation des éboulis froids. *Proceedings of the Swiss Geomorphological Society (SSGm) Annual Meeting 2007, 12–14 July, Samedan.*

Niu, F. & Cheng, G. 2005. Field experiment study on effects of duct-ventilated railway embankment on protecting permafrost of the Qinghai-Tibet Plateau. *Terra Nostra, Second European Conference on Permafrost, Potsdam*: 187.

Rist, A., Phillips, M. & Auerswald, K. 2003. Undercooled scree slopes covered with stunted dwarf trees in Switzerland–abiotic factors to characterize the phenomenon. *Proceedings of the Eighth International Conference on Permafrost, Zurich, Switzerland*: 135-136.

Rossel V., Weber G. & Gobat J.-M. 2004. Humus forms on permafrost in a cold scree slope (Creux du Van). *Eurosoil, 4–12 September 2004, Freiburg, Germany*.

Ruzicka, V. 1999. The freezing scree slopes and their arachnofauna. *Decheniana–Beihefte, Bonn* 37: 141-147.

Sawada, Y., Ishikawa, M. & Ono, Y. 2003. Thermal regime of sporadic permafrost in a block slope on Mt. Nishi-Nupukaushinupuri, Hokkaido Island, Northern Japan. *Geomorphology* 52: 121-130.

Sone, T. 2005. Extra-zonal permafrost and ground air circulation at a slope along the Kanoko-dam, Oketo town, Hokkaido, Japan. *Terra Nostra, Second European Conference on Permafrost, Potsdam*: 80.

Wakonigg, H. 1996. Unterkühlte Schutthalden. *Beiträge zur Permafrostforschung in Osterreich. Arbeiten aus dem Inst. f. Geogr. Karl-Franzens-Universität, Graz* 33: 209-223.

Genetic, Morphological, and Statistical Characterization of Lakes in the Permafrost-Dominated Lena Delta

Anne Morgenstern
Alfred Wegener Institute for Polar and Marine Research, Research Unit Potsdam, Potsdam, Germany
Guido Grosse
Geophysical Institute, University of Alaska Fairbanks, Fairbanks, Alaska, USA
Lutz Schirrmeister
Alfred Wegener Institute for Polar and Marine Research, Research Unit Potsdam, Potsdam, Germany

Abstract

This study provides a detailed inventory of lakes in the Lena Delta, northern Siberia. The inventory is based on Landsat-7 ETM+ image data and spatial analysis in a Geographical Information System (GIS). Several morphometric lake attributes were determined from the resulting dataset and statistically analyzed with respect to the lakes' association with one of the three geomorphological main terraces of the Lena Delta. Significant differences in the morphometric lake characteristics allowed the distinction of a mean lake type for each main terrace. The lake types reflect the special lithological and cryolithological conditions and geomorphological processes prevailing on each terrace. Special focus was laid on the investigation of lake orientation and the discussion of possible mechanisms for the evolution of the second terrace's oriented lakes.

Keywords: GIS; lake morphometry; Lena Delta; oriented lakes; remote sensing; thermokarst lakes.

Introduction

Numerous lakes occur as characteristic landforms throughout the Lena Delta. They are of importance to the contemporary ecology and geomorphology in this sensitive Arctic environment as well as for the reconstruction of the delta's environmental history. So far, only general descriptions of the lake population were available (e.g., Grigoriev 1993). They suggest that several lake types of different genesis can be distinguished and that the western delta is characterized by oriented lakes. However, a detailed inventory of the Lena Delta lakes did not exist. Such an inventory potentially provides a base dataset essential to a variety of research conducted in this region. This study was aimed to create a lake dataset of the Lena Delta including morphometric and spatial characteristics using remote sensing and GIS techniques to analyze the dataset regarding a morphometric lake classification, and to investigate possible hypotheses of the morphogenesis of the lakes in this periglacial delta environment.

Regional Setting

The Lena Delta in northern Siberia is the largest Arctic river delta (Walker 1998). It is situated in the zone of continuous permafrost and is widely affected by thermokarst. It is characterized not only by alluvial sediments and active fluvial processes, but also by large non-deltaic units. Three main terraces can be distinguished by their geomorphology (e.g., Are & Reimnitz 2000, Schwamborn et al. 2002) (Fig. 1). The first main terrace, which represents the modern active delta, is comprised of the lower and upper floodplains and the first terrace above the floodplain. It forms most of the eastern Lena Delta and is characterized by alluvial Holocene sands with silts and peat. The second terrace captures broad parts of the western Lena Delta. It consists of Late Pleistocene to Early Holocene sands of fluvial genesis, but is hardly influenced by modern fluvial processes. The third main terrace is the relic of a Late Pleistocene accumulation plain with fine-grained and ice-rich deposits.

Materials and Methods

Remote sensing

A mosaic of three Landsat-7 ETM+ scenes taken in the summers 2000 and 2001 covering 98 % of the Lena delta (Schneider et al., in prep.) was used as a basis for lake extraction using the software ENVI™ 4.1. First, we conducted a gray-level thresholding on the mid-IR band 5 to separate open water from land, as water bodies are strong absorbers in these wavelengths and easily distinguishable from other land cover classes. Second, the water class was subjected to a segmentation algorithm to differentiate standing water from rivers and the sea. This method creates separate classes for coherent pixels with the same value. As rivers and estuaries are connected with the sea, they form one single class and were deleted. Some lakes along the coastline that have broad (in the range of several pixels) connections to the sea were thereby also removed from the dataset. They experience a strong marine influence; for example, during storm floods, which can lead to major changes in lake morphometry and lagoon formation. Thus, these lakes were not considered for morphometric and further analysis.

GIS and morphometric analysis

The resulting raster dataset of all remaining lakes was imported into ArcGIS™ 9.0 and converted into vector format

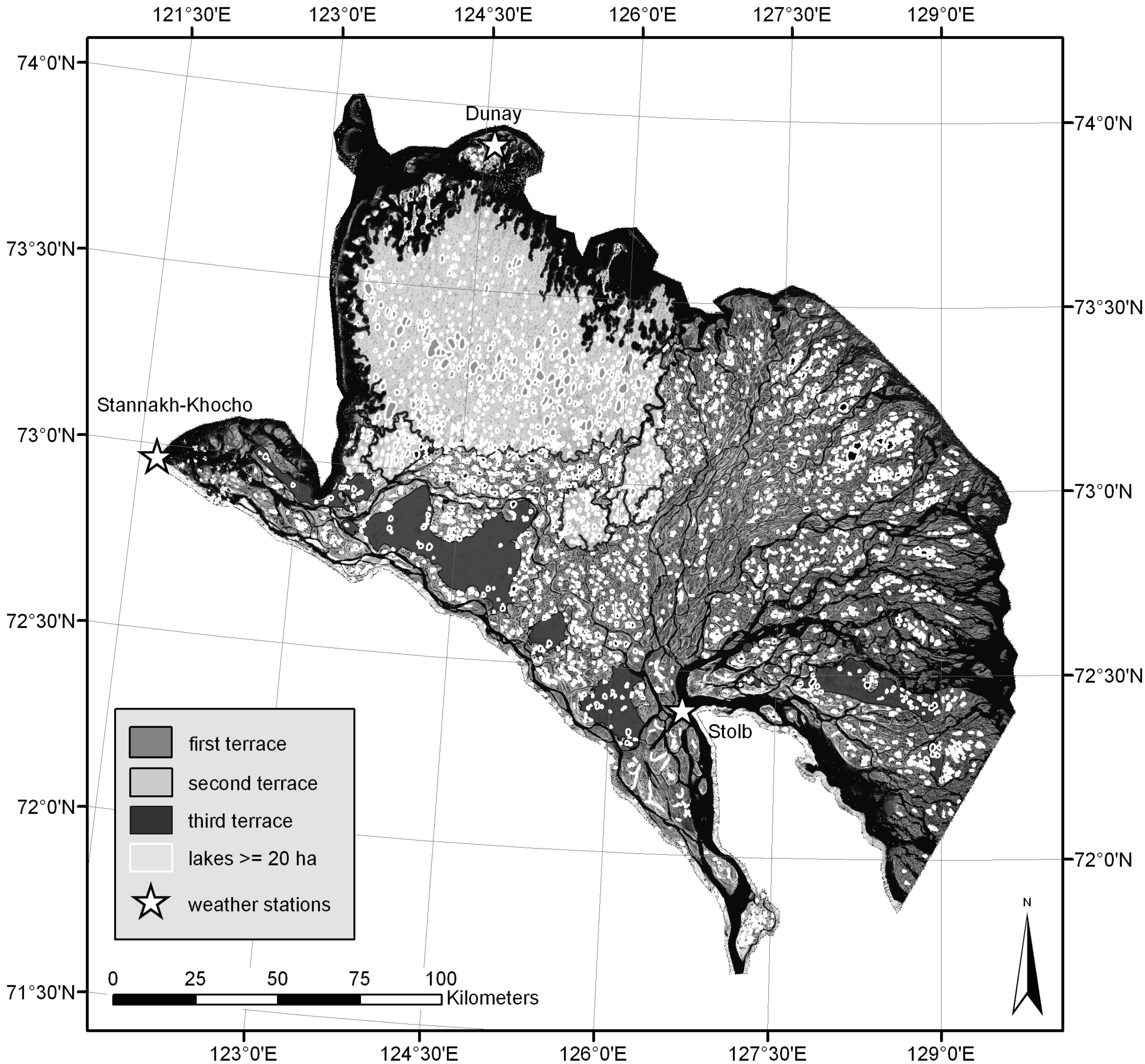

Figure 1. Landsat-7 ETM+ mosaic of the Lena Delta (Band 2) with analyzed lakes and main terraces, and meteorological stations.

where each lake is represented by a polygon. Shape metrics like *area*, *perimeter*, *circularity index* ($4\times\pi\times area/perimeter^2$), *elongation index* (main axis/minor axis), *orientation of main axis* (reference axis is E-W, value range is [0.1;180]°), and *degree of deviation from mean orientation* were calculated. The *circularity index* (values between 0 and 1, with 1 being a perfect circle) is not simply a counterpart to the *elongation index*, but also reflects the smoothness of the shoreline.

As the spatial resolution of the Landsat imagery is 30 m, minimum lake size for analyses was set to 20 ha to ensure reasonable results for reckoning the shapes of the lakes. The lake dataset was manually checked for errors due to misclassification caused by light cloud cover in some places.

On the second terrace in the western Lena Delta, several coalesced lakes occur, which is obvious in the red spectrum from deep basins divided by flat underwater ridges, some of them cut by deeper channels beneath the present lake water level. As our analyses were aimed on lake genesis, we manually divided the coalesced lakes (n=51) along the middle line of the ridges into their single basins and treated each basin as an individual lake (n=120 of which n=17 < 20 ha were excluded from further analysis). The final lake dataset contained 2669 lakes.

Another vector layer was created for the second and third geomorphological main terraces of the Lena Delta by manually digitizing their boundaries based on the Landsat image data, where they are visually easily distinguished. At places of uncertainty, results of field observations were used to determine terrace affiliation. The lake dataset was then divided into three subgroups according to the lakes' association with one of the geomorphological main terraces. The subgroup for the first terrace lakes was created by subtraction of the second and third terrace lakes from the whole lake population.

The variables described above were statistically analyzed for these subgroups using the software SPSS™ 12.0. Several statistics were calculated for the variables within an explorative data analysis (EDA). Variables were tested for normal distribution using the *Kolmogorov-Smirnov test* and for homogeneity of variance using the *Levene test*. In case of non-normal distribution skewness was minimized by data transformation and subsequent tests were performed with the transformed data. To test significant differences in the means of the variables between the three terraces analysis of variance (ANOVA) was performed. Non-parametric *Median test* and *Kruskal-Wallis test* (rank-based) were used with the non-transformed data for validation. Furthermore, multiple comparative tests (*Games-Howell*) were applied to identify terraces between which significant differences in the mean values occur at the 5% level. Bivariate correlations were calculated for the variables *area*, *circularity*, *elongation*, and *degree of deviation from mean orientation* using the rank-based *Spearman's Rho* correlation coefficient.

Results

The total area of lakes ≥ 20 ha is 1861.8 km², which corresponds to 6.4 % of the delta area, as the delta area within the extent of the mosaic was calculated to be 29,000 km² (Schneider et al., in prep.). Table 1 shows the area calculations for the three geomorphological main terraces. The results show great differences in lake occurrence, density, and area. The first terrace shows the highest number of lakes in total, but lake density and the ratio of lake area to the area of the corresponding terrace are highest on the second terrace. For the third terrace, all calculated values are the lowest.

Major results of the EDA are the following (see also table 2). Means, medians and percentiles for *area* show that comparatively larger lakes occur on the second terrace and rather smaller lakes on the first. The frequency distributions are strongly skewed towards lower values on all terraces, so smaller lakes are in general much more abundant than larger ones. Maximum values for the *circularity index* are well below 1 (< 0.7), i. e. throughout the delta no nearly circular lakes occur. Lakes with values of nearly 1 for the *elongation index* (which means almost equal major and minor axes) therefore have complex shorelines at the image resolution. Values for *circularity index* and *elongation index* show generally the largest deviation from perfect circularity for the first terrace and the smallest for the third terrace. Mean *orientation* of all lakes is 90.0°, the median is 80.2°. Means (medians) are 94.9° (95.9°) on the first main terrace, 78.6° (75.9°) on the second terrace, and 90.7° (82.0°) on the third terrace, respectively. Figure 2 shows the frequency distributions of *orientation*. The percentage of lakes with a deviation from the *orientation* mean (median) of ≤ 10° of the according terrace are 9.6 % (9.5 %) for the first terrace, 63.0 % (66.2 %) for the second, and 24.7 % (35.8 %) for the third terrace, respectively. Also the means and medians of *degree of deviation from mean orientation* show that lakes on the second terrace deviate the least and lakes on the first terrace the most from the according mean orientation.

The results of the ANOVA as well as of the non-parametric tests show significant differences in the parameter values between the three main terraces for all variables. Multiple comparative tests revealed the following results at the 5% level. The lakes of the first terrace significantly differ from the second terrace lakes in all variables. No significant differences were found between the first and the third terraces regarding *orientation*, and between the second and the third regarding *orientation* and *area*. On the first terrace, lakes are smaller on average than on the second and third terraces. Nearly circular lakes are more abundant on the third than on the other terraces.

In the context of our analyses we defined oriented lakes as lakes with little deviation from mean orientation and with a deviation from circularity. Deviation from mean orientation is significantly smaller on the second terrace than on the other two terraces, it is highest on the first terrace. Thus, lakes on the second terrace can be statistically characterized as oriented lakes with their main axes tending in NNE-SSW directions.

Of the 18 tests for correlations ten were significant at the 5% level. These include medium negative correlations (r = -.444 to -.465) between *circularity* and *elongation* on all terraces as expected from the design of the variables. All other significant correlations are very small ($|r| \leq .186$) except for the correlation between *area* and *degree of deviation from mean orientation* on the third terrace (r = -.415, p = .01).

Discussion

For all analyzed morphometric lake variables we found significant differences between the three geomorphological main terraces of the Lena Delta. From these differences we deduce one mean lake type for each terrace:

1. Lakes on the first terrace are on average small and elongated, with irregular shapes and strong deviations from mean orientation.
2. On the second main terrace, large elongated lakes with a NNE-SSW orientation of their major axes prevail. Lake density is highest here.
3. The third terrace lakes are mainly characterized by regular shorelines and little deviation from circularity.

These results imply that the forming of a lake's shape towards one of these mean lake types is linked to the according delta main terrace, i. e. lake morphometry is influenced differently on the different main terraces. Different lake morphometries can be caused primarily by diverse lake genesis or by secondary processes subsequently altering the lake's primary shape. The different conditions and processes prevailing on each terrace of the Lena Delta are used to explain the development of the mean lake types found.

The first main terrace is the only one with widespread recent and Holocene fluvial and deltaic activity. The genetic lake type

Table 1. Area calculations for the three geomorphological main terraces of the Lena Delta.

		First terrace	Second terrace	Third terrace
Terraces	Area in km²	15,840.1	6098.6	1711.6
	Percentage of delta area	54.6	21.0	5.9
Lakes ≥ 20 ha	Number	1796	792	81
	Number per 1000 km²	113.4	129.9	47.3
	Percentage of total lake number	67.3	29.7	3.0
	Total area in km²	997.0	808.1	56.7
	Percentage of terrace area	6.3	13.3	3.3
	Percentage of delta area	3.4	2.8	0.2

* Differences from 29,000 km² and 100% total delta area arise from the percentage of sea and river area, respectively, in the mosaic.

Table 2. Descriptive statistics for the analyzed morphometric lake variables.

		Delta	First terrace	Second terrace	Third terrace
Area (in m²)	Mean	697,579	555,124	1,020,382	699,922
	Median	409,500	372,600	557,100	442,800
	Standard deviation	956,500	634,463	1,410,506	566,554
	Interquartile range	452,700	339,075	757,800	598,500
Circularity	Mean	0.31	0.28	0.36	0.46
	Median	0.31	0.27	0.36	0.48
	Standard deviation	0.14	0.14	0.12	0.11
	Interquartile range	0.22	0.22	0.15	0.18
Elongation	Mean	2.11	2.26	1.83	1.49
	Median	1.75	1.85	1.66	1.37
	Standard deviation	1.20	1.37	0.64	0.45
	Interquartile range	0.92	1.12	0.55	0.36
Orientation (in °)	Mean	90.0	94.9	78.6	90.8
	Median	80.2	95.9	75.9	82.0
	Standard deviation	47.1	54.3	21.4	38.2
	Interquartile range	65.94	94.8	12.3	44.4
Degree of deviation from mean orientation (in °)	Mean	38.6	47.5	12.9	29.1
	Median	31.5	48.3	6.8	21.4
	Standard deviation	27.0	26.3	17.0	24.5
	Interquartile range	48.1	45.3	11.7	33.5

typical for such environments is abandoned lakes. Walker (1983) differentiates between abandoned-channel lakes resulting from channel braiding and abandoned meanders or oxbow lakes resulting from meandering. They are predominantly small, often elongated and/or crescent-shaped because they occupy former river branches or meanders, and do not show any particular orientation as the fluvial system shows no clear directional pattern itself at a small scale. Thus, the morphometric characteristics for these lakes are consistent with the mean lake type deduced for the first terrace of the Lena Delta. Further lake types described for the first terrace are polygon ponds and small circular thermokarst lakes (e.g., Grigoriev 1993). Polygon ponds were generally not considered in this study because of their small size. As for the circular thermokarst lakes no area range is reported in the literature, but we assume that they mostly have areas below 20 ha and were therefore not treated in our analyses. Their characteristics, such as smooth shorelines and approximate circularity, are not reflected in the mean lake type of the first terrace.

The morphometry of the lakes on the second terrace and their formation will be discussed in the following section on lake orientation.

Characteristics of the lake shapes on the third main terrace are typical for thermokarst lakes in ice-rich permafrost. The results are therefore consistent with landscape descriptions given in the literature (e.g., Grigoriev 1993). The shape of the lakes is controlled by their thermokarst genesis and is not significantly changed by other factors during further evolution.

In comparing morphometric lake characteristics in the Lena Delta with other arctic deltas like the Colville or the Mackenzie River deltas, only the first geomorphological main terrace should be considered, as it represents an actual deltaic environment. Lake types described for the Colville Delta are abandoned lakes, point-bar lakes, and thermokarst lakes (e.g., Fürbringer 1977, Walker 1983). In the Colville Delta, remnants of oriented lakes also occur, but these were not a part of the delta originally until a river branch cut through an area with oriented lakes (Walker 1983). For the Mackenzie Delta, typical lakes are described as irregular in outline with indented shorelines, and genetic lake types are primarily abandoned channel lakes, point-bar lakes,

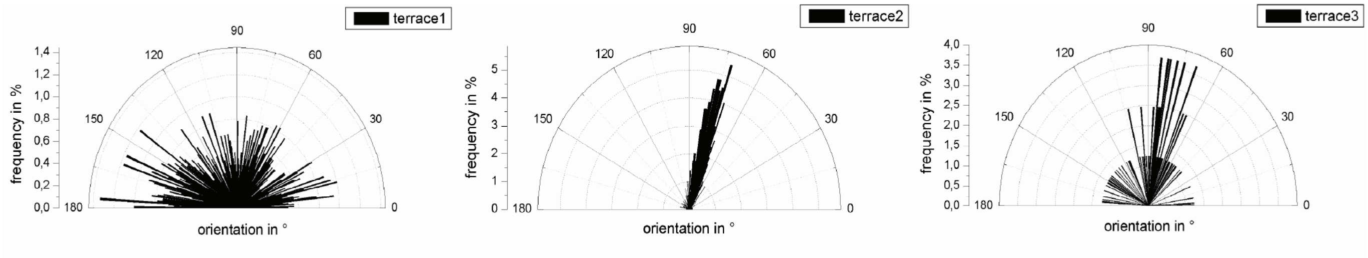

Figure 2. Frequency distribution of *orientation* of the Lena Delta lakes (intervals = 1°).

floodplain lakes, and thermokarst lakes (Mackay 1963). Lake types described for these deltas are thus comparable to the first terrace lakes of the Lena Delta.

Lake orientation

The character of lake orientation as expressed by the variables *degree of deviation from mean orientation* and *circularity* differs significantly between the three main terraces as described above. The process of lake orientation is long term and requires stability of exogenous orienting factors. Active fluvial processes prevailing on the first terrace may overlay tendencies of lake orientation there. Existing discrepancies between the second and the third terraces, however, must be discussed in detail.

Thermokarst lake evolution on both terraces reaches back at least to the early Holocene warming period (Schirrmeister et al. 2003, Schwamborn et al. 2002). Exogenous factors that have been discussed as causing or influencing lake orientation; for example, prevailing wind directions, solar radiation, etc. (e.g., Livingstone 1954, Mackay 1956, Carson & Hussey 1959), therefore, have affected both terraces in the same way for several thousand years. The different character of lake orientation implies a dependence of further endogenous; i.e., terrace-specific factors.

Lithology and cryolithology of the second and third main terraces differ considerably. Sediments on the second main terrace are Late Pleistocene fluvial sediments that consist of homogeneous fine- and medium-grained sands with massive cryogene structures. Large ice wedges are absent, and the ground ice content is generally rather low (15–25 wt%) (Schirrmeister et al. 2007). The sediments are comparable to those in the North American Arctic Coastal Plain where oriented lakes occur. The homogeneity of the sands allows for a uniform distribution of forces driving orientation processes. If these forces operate directionally, orientation can clearly develop. Sediments on the third main terrace, however, are mainly composed of the Yedoma Suite, with peat, sands, and silts with high ground-ice content (30–80 wt%) and inhomogeneous ice distribution (huge ice wedges and intrapolygonal sediments with segregated ground ice in the form of ice bands and small ice lenses) (Schirrmeister et al. 2003). This heterogeneity prevents a continuous distribution of external effects because of the different physical characteristics of the sediments; for example, bulk density or thermal conductivity. Orienting factors, therefore, cannot operate uniformly, and the development of a clear orientation is strongly impeded. The negative correlation between the lake *area* and the *degree of deviation from mean orientation* of

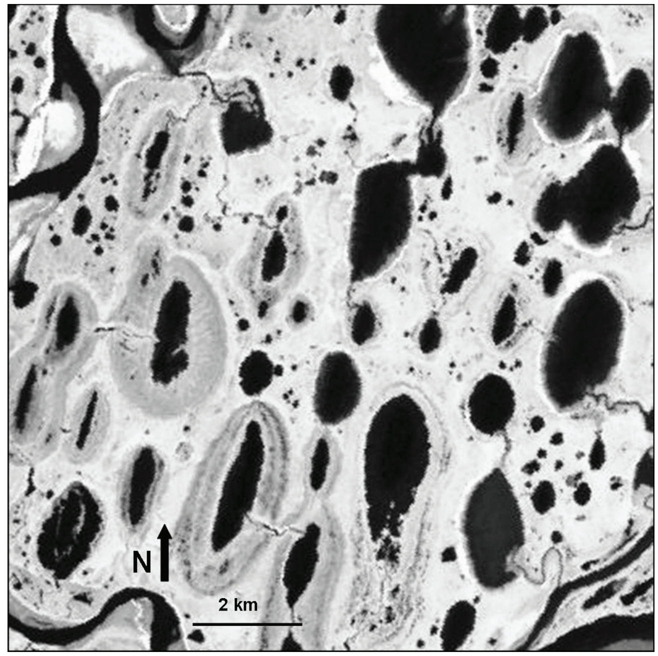

Figure 3. Section of oriented lakes in the western Lena Delta (subset of the Landsat-7 ETM+ mosaic).

the third terrace lakes may still implicate a tendency towards lake orientation in the course of lake growth. The mean NNE-SSW orientation of the poorly elongated third terrace lakes is consistent with that of the second terrace.

As for the cause of lake orientation in the Arctic Coastal Plain, several hypotheses have been discussed. The theory supported by most authors supposes preferential erosion of the lake shores at right angles to prevailing summer wind directions due to wind-driven currents and wave activity (e.g., Livingstone 1954, Mackay 1956, Côté & Burn 2002, Hinkel et al. 2005). The literature reports northern to northeastern main wind directions for the entire Lena Delta in the summer, and southern to southwestern in the winter (e.g., Grigoriev 1993, Gukov 2001). However, wind data of several meteorological stations scattered throughout the delta area show great differences in prevailing directions. Unfortunately, there is no station in the western Lena Delta close to the oriented lakes. Of the three stations closest to the western Lena Delta lakes (Fig. 1), two are situated directly at the Laptev Sea coast. On Dunay Island (73.9°E 124.6°N, data from 1955–1994), wind blows mainly from eastern directions; the Stannakh-Khocho station (73.0°E 121.7°N, data from 1981–1994) registered prevailing winds from southern directions with a minor peak from eastern directions for the whole time span, and from eastern directions at times of positive air temperatures, respectively. The third station is located in the central southern delta on Stolb Island (72.4°E 126.5°N, data from 1955–1991) and shows pronounced southern wind directions. All three stations may not reflect the actual wind situation of the second main terrace, as climate on Stannakh-Khocho and Stolb Island is supposedly influenced by the mountain ranges flanking the Lena Delta in the south. On the Island Dunay, which is a few kilometers off from the mainland of the second terrace, the marine influence has an impact on weather conditions. It can be suggested though, that, because of the flat relief of the second terrace, major wind directions in the inner part of the terrace do not differ much from the situation at its margins; thus wind data from Dunay Island might be the most suitable for assessing the situation on the second terrace. Assuming that the eastern prevailing wind direction measured over the forty-year time span was consistent throughout the lake orientation process, the wind hypotheses proposed for North American oriented lakes might also be applicable for the oriented lakes of the Lena Delta. However, little is known about the detailed conditions and factors that might be involved in lake-orientation processes in the Lena Delta or the stability of wind regimes over Holocene time scales. Further research is necessary to prove or reject any particular orientation theory for this unique Arctic environment.

Conclusions

The three main terraces of the Lena Delta vary largely in the occurrence of morphometric lake characteristics. This led to the deduction of one mean lake type for each terrace. The first main terrace, which represents the modern active delta, is characterized by small lakes of irregular shape, like abandoned lakes. Large oriented lakes with their major axes tending in NNE directions dominate on the second terrace, which consists of Late Pleistocene to Early Holocene homogeneous sands. On the third terrace, which is represented by relics of a Late Pleistocene accumulation plain with heterogeneous fine-grained and ice-rich deposits, typical thermokarst lakes with regular, circular shorelines prevail. Mean morphometric lake characteristics are consistent with the lithological and cryolithological conditions and geomorphological processes prevailing on each terrace. Wind hypotheses proposed for North American oriented lakes might also explain the orientation of lakes on the second terrace of the Lena Delta, but the detailed conditions and mechanisms of the evolution of the oriented lakes in the Lena Delta remain to be investigated.

Acknowledgments

We thank Thomas Kumke for helpful assistance with statistical analyses, Mikhail N. Grigoriev, Georg Schwamborn, and Hartmut Asche for fruitful discussions and Pier Paul Overduin for grammar and spell check. We are grateful to Alexander Brenning and another anonymous reviewer for constructive comments on the manuscript.

References

Are, F. & Reimnitz, E. 2000. An overview of the Lena river delta setting: geology, tectonics, geomorphology, and hydrology. *Journal of Coastal Research* 16(4): 1083-1093.

Carson, C.E. & Hussey, K.M. 1959. The multiple-working hypothesis as applied to Alaska's oriented lakes. *Iowa Academy of Sciences Proceedings* 66: 334-349.

Côté, M.M. & Burn, C.R. 2002. The oriented lakes of Tuktoyaktuk Peninsula, western arctic coast, Canada: a GIS-based analysis. *Permafrost and Periglacial Processes* 13: 61-70.

Fürbringer, W. 1977. About the sedimentology of an arctic delta (Colville delta, North Alaska). *International Journal of Earth Sciences* 66(1): 577-614.

Grigoriev, M.N. 1993. *Cryomorphogenesis in the Lena Delta*. Yakutsk: Permafrost Institute Press, 176 pp.

Gukov, A.Yu. 2001. *Hydrobiology of the Lena Delta mouth area*. Moscow: Scientific World, 288 pp.

Hinkel, K.M., Frohn, R.C., Nelson, F.E., Eisner, W.R. & Beck, R.A. 2005. Morphometric and spatial analysis of thaw lakes and drained thaw lake basins in the western arctic coastal plain, Alaska. *Permafrost and Periglacial Processes* 16: 327-341.

Livingstone, D.A. 1954. On the orientation of lake basins. *American Journal of Science* 252: 547-554.

Mackay, J.R. 1956. Notes on oriented lakes of the Liverpool Bay area, Northwest Territories. *Revue Canadienne de Geographie* 10: 169-173.

Mackay, J.R. 1963. *The Mackenzie Delta area, N.W.T.* Ottawa: Geographical Branch Memoir 8, Mines and Technical Surveys, 202 pp.

Schirrmeister, L., Kunitsky, V.V., Grosse, G., Schwamborn, G., Andreev, A.A., Meyer, H., Kuznetsova, T., Bobrov, A. & Oezen, D. 2003. Late Quaternary history of the accumulation plain north of the Chekanovsky Ridge (Lena Delta, Russia): A multidisciplinary approach. *Polar Geography* 27: 277-319.

Schirrmeister, L. (ed.) 2007. Studies of periglacial landscape dynamics and surface characteristics studies in the western Lena Delta. *Reports on Polar and Marine Research* 550: 83-195.

Schneider, J., Grosse, G. & Wagner, D. Land cover classification of tundra environments in the Arctic Lena Delta based on Landsat-7 ETM+ data and its application for upscaling methane emissions. Submitted to *Remote Sensing of Environment*.

Schwamborn, G., Rachold, V. & Grigoriev, M.N. 2002. Late quaternary sedimentation history of the Lena delta. *Quaternary International* 89: 119-134.

Walker, H.J. 1983. *Guidebook to permafrost and related features of the Colville River delta, Alaska*. Guidebook 2, Fourth International Conference on Permafrost. Fairbanks, Alaska: Alaska Division of Geological and Geophysical Surveys, 34 pp.

Walker, H.J. 1998. Arctic deltas. *Journal of Coastal Research* 14: 718-738.

Vegetation and Permafrost Changes in the Northern Taiga of West Siberia

Nataliya Moskalenko
Earth Cryosphere Institute SB RAS, Moscow, Russia

Abstract

The goal of this ongoing study is to examine the impact and indicators of climate change and disturbance from natural gas pipeline construction on vegetation and permafrost conditions in various northern bioclimatic zones. The results of 37 years of observations (1970–2006) from one site near Nadym, an area of sporadic permafrost, are reported. Field methods include landscape and vegetation mapping, and permanent fixed transects across natural complexes and at plots established both in natural and disturbed conditions. Transect and plot measurements were focused on labile components of vegetation and permafrost such as species composition, active layer thickness, and ground temperature. Impacts and interactions were assessed through regression and autocorrelation of frequency of plant species and active layer thickness. Undisturbed plots show an increase of woody plants, presumably due to climate warming, and disturbed sites showed thermokarst and changed soil moisture regime and, during recovery, an increase in the frequency of succession species.

Keywords: climate change; human-induced disturbances; landscape; permafrost; vegetation.

Introduction

Vegetation and permafrost changes in natural northern environments have been studied by Koloskov (1925), Gorodkov (1932), Sumgin (1937), Tyrtikov (1969, 1979, 1980). They demonstrated that freezing and thawing conditions change in response to vegetation dynamics. Increases in moss and lichen cover thickness result in the reduction of seasonal thaw depths and decreases in soil and ground temperatures.

The work reported here is part of a large, long-term, ongoing program on vegetation and environment interactions at seven sites in the Yamal-Gydan region of northern West Siberia. The sites span the gamut of bioclimatic zones, permafrost conditions, and intensity of human disturbances. The program also includes a Circumpolar Active Layer Monitoring (CALM) program site established in 1997 (see Brown et al. 2003). The results from the Nadym site are reported.

Description of the Observation Site

The site is located near the town of Nadym and the natural gas pipeline Nadym-Punga (Burgess et al. 1993). It is in the northern taiga with sporadic permafrost (Melnikov 1983) on the III fluvial-lacustrine plain with altitude ranging from 25–30 m above sea level. The plain is composed of sandy deposits interbedded with clays, with an occasional covering of peat (Melnikov et al. 2004). Patches of permafrost are closely associated with peatlands, tundras, mires, and frost mounds.

At Nadym, records have been made since 1972. Annual geobotanical censuses are made on 28 permanent fixed plots (10 x 10 m) in natural and disturbed conditions. The structure, average height, phenological and vital condition, frequency, and coverage of plant species on 50 registered 0.1 m^2 plots were recorded. In addition, soil descriptions, microclimatic supervisions, and measurements of ground temperature in boreholes at depths up to 10 m (Dubrovin et al. 1996), and seasonal thaw depths were kept.

Table 1. Thawing depths (h_{th}) on two peatland types.

Vegetation	h_{th} in cm	*K
Rubus chamaemorus-Ledum palustre-Cladina rangiferina	67.1±17.1	-0.71 (0.5-0.8)
Carex rotundata-Sphagnum lindbergii	173.7±28.2	0.58 (0.5-0.7)

*K - Coefficient of correlation (confidence level).

Analysis of Results

The measurements of the active layer thickness plots show that the smallest values of seasonal thaw depth are observed under *Rubus chamaemorus-Ledum palustre-Sphagnum-Cladina rangiferina* cover on flat peatland (Table 1). This type of peatland serves as an indicator of depths of seasonal thaw. Areas with deepest thaw are confined to large sedge-moss pools within peatlands and to bogs.

There has been marked an increase in air temperature at Nadym. Figure 1A shows the trend from 1970–2006 that amounts to 0.04°C per year. The air and soil temperature increase on the peatland is the likely cause for the appearance of tree species (*Betula tortuosa*, *Pinus sibirica*) and the rise in frequency of shrubs (*Ledum palustre, Betula nana*). For the investigated period the ground temperature on undisturbed palsa peatland has increased from -1.8 up to -0.5°C (Fig. 1B(1)). On a flat peatland the rise in ground temperature was less (Fig. 1B(2)). The active layer thickness on palsa peatland has increased by 35% for the 37-year period (Fig. 1C).

In the first years following vegetation removal in 1972 cotton grass/cloudberry groupings covering only 20% of

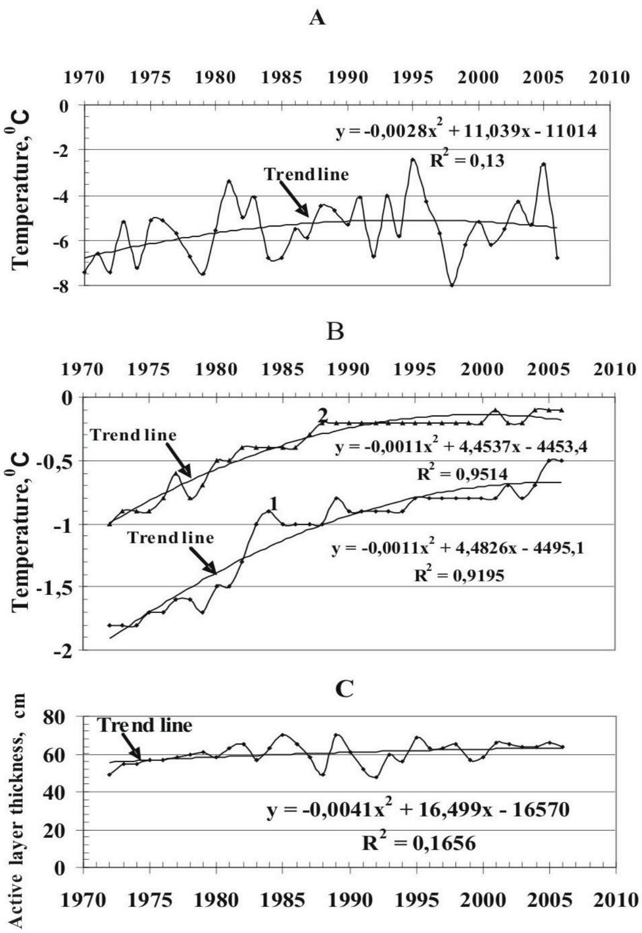

Figure 1. Mean-annual temperature (A), ground temperature at the depth 10 m (B) on palsa peatland (1) and flat peatland (2) and active layer thickness (C) on palsa peatland.

the surface had formed on the disturbed peatland plots. In four years these were replaced by cotton grass/cloudberry/*Polytrichum* groupings. The coverage of the surface by sedge and mosses in 7 years had increased up to 40%, and in 10 years up to 60%. At this time the amount of cloudberry (*Rubus chamaemorus*) had decreased, the role of cotton grass (*Eriophorum scheuchzeri, E. vaginatum*) had increased, and occasional shrubs and lichens appeared on rare moss hummocks, although the latter made no appreciable contribution to the vegetation cover. Also significant moss cover developed with *Polytrichum* species and peat mosses. In 15 years the disturbed plots had a continuous cloudberry/cotton grass/*Polytrichum*/*Sphagnum* cover. In 30 years the surface and the permafrost table had lowered with the development of thermokarst and bogs, and it was covered with cotton grass/peat moss.

The resulting fragment of cotton grass/peat moss bog continues 33 years after disturbance, although this bog community radically differs from the initial tundra (Table 2) community in appearance, structure, frequency, coverage of dominant species, and ecological condition. The undisturbed tundra has also changed; for example, the frequency of *Ledum palustre* on a natural plot has clearly increased. This is most likely in response to a rise in air temperature (Fig. 2).

Table 2. Species composition of *Rubus chamaemorus*-*Ledum palustre*-*Sphagnum*-*Cladina* community.

Species	Height, cm	Coverage, %	Frequency, %
1. Andpol	20	1.5	46
2. Betnan	50	1	22
3. Carrot	30	<1	<1
4. Chacal	30	1	6
6. Erisch	25	<1	2
6. Erivag	45	1.5	38
7. Ledpal	45	16	86
8. Oxymic	2	1	14
9. Pinsib	90	<1	6
10. Rubcha	10	6	92
11.Vaculi	35	<1	<1
12. Vacvit	10	4	76
13. Cetcuc	7	2	48
14. Cetisl	5	1	12
15. Claran	11	22	64
16. Claste	11	28	76
17. Claama	6	<1	8
18. Clacoc	5	<1	6
19. Diccon	2	<1	2
20. Plesch	2	<1	4
21. Polcom	3	1	14
22. Sphang	4	5	12
23. Sphfus	4	25	36
24. Sphlin	4	<1	<1
25. Tomnit	2	<1	<1

Key to first column: Andpol – Andromeda polifolia, Betnan – Betula nana, Carrot – Carex rotundata, Chacal – Chamaedaphne calyculata, Erisch – Eriophorum scheuchzeri, Ledpal – Ledum palustre, Oxymic – Oxyccocus microcarpus, Pinsib – Pinus sibirica, Rubcha – Rubus chamaemorus, Vaculi – Vaccinium uliginosum, Vacvit – Vaccinium vitis-idaea, Cetcuc – Cetraria cucullata, Cetisl – Cetraria islandica, Claama – Cladonia amaurocraea, Clacoc – Cladonia coccifera., Claran – Cladina rangiferina, Claste – Cladina stellaris, Diccon – Dicranum congestum, Plesch – Pleurozium schreberi, Polcom – Polytrichum commune, Sphang – Sphagnum angustifolium, Sphfus – Sphagnum fuscum, Sphlin – Spagnum lindbergii, Tomnit – Tomenthypnum nitens.

The ITEX (International Tundra Experiment) program has reported similar increases of shrub forms from plot warming experiments (see Hollister et al. 2005, Walker et al. 2006).

On the disturbed plots the frequency response of *Ledum palustre* is different. First it increased in dry years, and then after 1990 it decreased in connection with the increase in precipitation and the development of bogging; but during all periods of observation its frequency is less than on undisturbed plots. The *Rubus chamaemorus* frequency on undisturbed plots shows no clear trend (Fig. 3A) compared to the increase of *Ledum palustre*. However on the disturbed plots *Rubus chamaemorus* frequency decreases and mirrors the changes seen for of *Ledum palustre.* The frequency of *Rubus chamaemorus* has decreased considerably in recent years in connection with increased precipitation and development of bogging. However in the first years after disturbance, in contrast to *Ledum palustre,* the frequency of

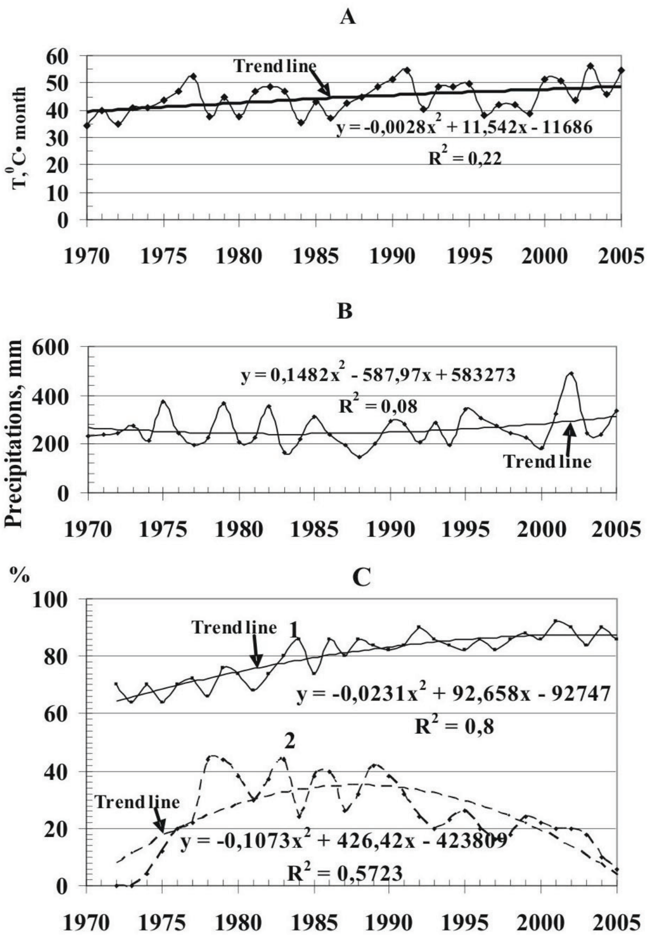

Figure 2. Thawing index of air temperature (the sum monthly mean air temperatures above 0°C) (A), summer precipitation (B) and frequency of *Ledum palustre* (C) in natural (1) and disturbed (2) conditions.

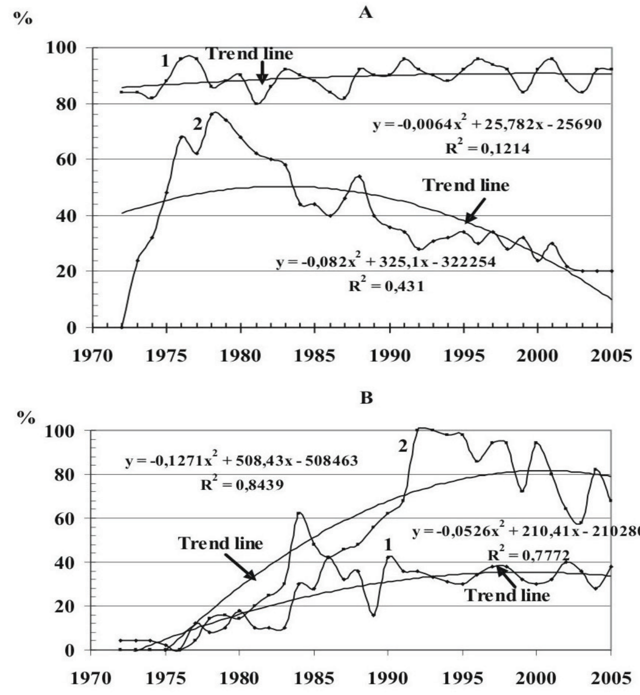

Figure 3. Frequency of *Rubus chamaemorus* (A) and *Eriophorum vaginatum* (B) in natural (1) and disturbed (2) conditions.

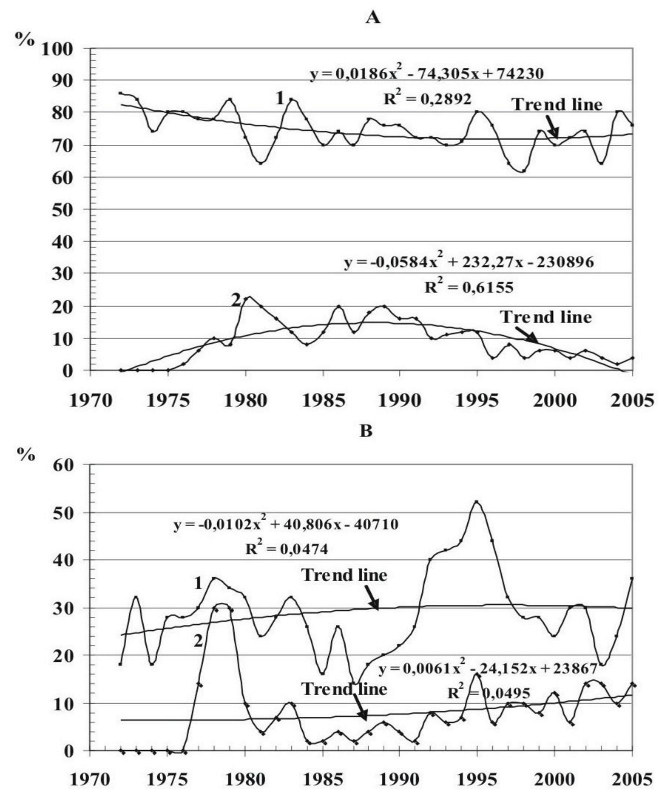

Figure 4. Frequency of *Cladina stellaris* (A) and *Sphagnum fuscum* (B) in natural (1) and disturbed (2) conditions.

Rubus chamaemorus increases while under little competition from other species, and has almost returned to its initial condition. The frequency of *Eriophorum vaginatum* in natural sites increased and this is correlated with increased precipitation. In disturbed sites the *Eriophorum* was twice that of undisturbed sites and is the result of development of wetter soil conditions and bogginess (Fig. 3B).

The frequency of *Cladina stellaris* in natural conditions has a weak negative downward trend (Fig. 4A) while on disturbed sites the negative trend is more pronounced and similar to the trend for *Ledum palustre*, namely an increase till 1990, and then, in connection with activation of increased precipitation and bogging, it began to decrease to 40 times less than in the natural condition.

The frequency of *Sphagnum fuscum,* both in natural and in the disturbed condition shows a small positive trend with the maximum on both plots falling in the same years which were warm and had adequate summer precipitation (Fig. 4B).

Thus, the fragment of cotton grass/peat moss bog, formed in 33 years after removal of *Rubus chamaemorus-Ledum palustre-Sphagnum-Cladina* plant community, differs from initial tundra community in appearance, structure, frequency, and coverage of dominant species.

These long-term records of species frequency on disturbed and undisturbed permanent plots were processed using a method of autocorrelation (Vasilevich 1970). As a result, all species were divided in three groups based on various

Table 3. Coefficients of autocorrelation between interannual values of frequency of plant species for flat peatland in natural (above a line) and disturbed (under the line) conditions, according to descriptions for 1972–2002 using "Statgraph."

Species	Years														
	1	2	3	4	5	6	7	8	9	10	11	12	13	14	15
Andpol	0.53	0.2	0.0	0.21	0.32	0.34	0.07	-0.2	-0.2	-0.1	0.0	0.0	-0.2	0.35	-0.1
	0.81	0.6	0.36	0.21	0.15	0.61	0.03	0.0	-0.1	-0.1	-0.1	-0.1	-0.1	-0.1	-0.1
Betnan	0.23	0.14	0.22	-0.2	-0.1	-0.1	0.06	0.0	0.0	-0.1	0.01	-0.3	0.13	0.0	0.05
	0.37	0.35	0.03	0.0	-0.1	-0.1	0.02	-0.1	0.0	0.0	0.05	0.05	0.0	0.0	-0.5
Erisch	0.64	0.58	0.51	0.43	0.31	0.18	0.08	0.0	-0.1	-0.2	-0.4	0.16	0.19	0.36	0.33
	0.63	0.34	0.14	-0.1	-0.1	-0.1	-0.1	-0.1	-0.1	-0.1	-0.2	-0.3	-0.2	-0.2	-0.2
Erivag	0.73	0.67	0.49	0.45	0.29	0.27	0.21	0.0	-0.1	-0.2	-0.3	-0.4	-0.4	-0.5	-0.5
	0.86	0.72	0.57	0.41	0.31	0.22	0.14	0.1	0.0	-0.1	-0.2	-0.2	-0.2	-0.2	-0.2
Ledpal	0.64	0.58	0.51	0.43	0.31	0.18	0.08	0.0	-0.1	-0.2	-0.2	-0.2	-0.2	-0.3	-0.3
	0.67	0.4	0.27	0.06	-0.1	-0.2	-0.1	-0.1	-0.1	-0.1	-0.1	0.46	0.06	-0.4	-0.4
Oxymic	0.03	0.0	-0.3	0.06	-0.1	-0.1	-0.3	0.0	0.3	0.2	0.0	-0.1	-0.1	-0.3	0.11
	0.52	0.32	0.25	0.04	0.0	0.0	-0.2	-0.2	-0.1	-0.1	-0.2	-0.2	-0.3	-0.3	-0.3
Rubcha	0.34	-0.1	-0.1	-0.3	-0.2	0.04	0.11	0.2	0.0	-0.3	-0.2	0.09	-0.5	-0.4	0.38
	0.7	0.48	0.21	0.0	-0.1	-0.2	-0.2	-0.2	-0.2	-0.2	-0.2	-0.3	-0.3	-0.26	-0.3
Vacvit	0.34	-0.1	0.11	0.02	0.0	0.08	0.16	-0.1	-0.3	-0.1	-0.1	0.03	0.2	0.0	0.08
	0.73	0.44	0.2	0.16	0.0	-0.1	-0.2	-0.2	-0.2	-0.2	-0.2	-0.2	-0.2	-0.3	-0.3
Cetcuc	0.35	0.13	0.35	0.36	0.03	0.18	0.19	-0.1	-0.2	-0.2	-0.1	0.25	0.13	-0.1	0.0
	0.54	0.35	0.33	-0.1	-0.1	-0.1	-0.2	0.0	0.1	-0.1	-0.1	-0.3	-0.5	-0.3	-0.3
Cetisl	0.27	0.32	0.2	0.0	-0.2	-0.2	-0.1	-0.3	-0.2	-0.1	-0.1	-0.4	0.0	-0.1	0.0
	0.18	0.04	0.24	0.05	0.0	-0.1	-0.2	0.2	0.0	-0.2	-0.1	-0.1	-0.2	-0.2	-0.2
Claama	0.25	-0.1	0.41	0.28	-0.1	0.09	0.14	-0.2	-0.3	0.0	-0.1	0.65	0.28	0.0	0.0
	0.0	0.04	0.0	-0.1	0.17	-0.1	0.01	-0.2	-0.1	-0.2	-0.2	0.26	-0.4	0.06	-0.1
Clacoc	0.0	0.04	0.0	-0.1	0.17	-0.1	0.01	-0.2	-0.1	-0.2	-0.2	0.26	-0.1	0.06	-0.1
	0.77	0.6	0.5	0.33	0.14	0.0	-0.3	-0.3	-0.4	-0.5	-0.5	-0.5	-0.4	-0.4	-0.4
Claran	0.14	-0.2	-0.3	0.0	0.28	0.19	0.08	-0.3	-0.2	0.1	0.1	-0.2	0.15	-0.4	-0.3
	0.67	0.41	0.3	0.18	0.08	0.02	-0.1	-0.1	0.0	-0.2	-0.3	-0.3	-0.3	-0.3	-0.3
Claste	0.26	-0.3	-0.1	0.23	0.16	0.17	0.13	-0.3	-0.3	0.1	0.23	0.13	-0.2	-0.23	0.15
	0.68	0.51	0.31	0.08	0.0	-0.1	-0.1	-0.1	-0.1	-0.1	-0.1	-0.2	-0.3	-0.3	-0.3
Polcom	0.45	0.42	0.3	0.14	0.09	0.04	0.0	-0.1	0.1	0.0	0.05	0.47	0.0	-0.2	-0.1
	0.63	0.46	0.27	0.17	0.13	0.1	0.01	-0.1	-0.1	-0.1	-0.2	-0.2	-0.3	-0.3	-0.3
Sphang	0.63	0.39	0.28	0.04	0.08	0.13	0.08	0.1	0.0	-0.2	-0.2	-0.2	0.29	0.0	0.0
	0.5	0.55	0.42	0.43	0.36	0.38	0.16	0.1	-0.1	-0.1	-0.2	-0.2	-0.2	-0.3	-0.3
Sphfus	0.37	0.2	0.0	-0.1	-0.3	-0.3	-0.2	-0.3	-0.1	0.0	-0.1	0.63	0.18	0.02	-0.1
	0.62	0.05	-0.18	-0.2	-0.2	-0.3	-0.3	-0.2	-0.1	-0.1	0.0	0.0	0.0	-0.1	-0.1
Sphlin	0.6	0.29	0.33	0.32	0.19	0.09	0.06	0.0	-0.1	-0.1	-0.1	-0.1	-0.1	-0.1	-0.1
	0.63	0.1	-0.15	-0.2	-0.2	-0.2	-0.2	-0.2	-0.2	-0.2	-0.2	-0.2	-0.3	-0.3	-0.3

Key to first column see in Table 2.

characteristics of interannual frequency changes: (1) the group with succession frequency changes (autocorrelation coefficient, K decreases with time throughout entire period of observations); (2) the group with cyclic frequency changes (K decreases and increases with certain periodicity); (3) the group with irregularly cyclic frequency changes (observed, different periodicity in changes of K values).

This analysis has shown (Table 3) that species with succession changes of frequency play a greater role in vegetation cover formed after disturbance, while participation of species with cyclic and irregular cyclic changes in frequency decreases.

In *Rubus chamaemorus-Ledum palustre-Sphagnum-Cladina* vegetation, species with cyclic behaviour form the most cover (48%). Nine species from this group are chamaephytes (low shrub-*Andromeda polifolia, Chamaedaphne calyculata, Vaccinium vitis-idaea*; lichens-*Cladina rangiferina, C. stellaris, Cladonia amaurocraea* and mosses-*Dicranum congestum, Pleurozium schreberi, Polytrichum commune*).

A smaller number of species (39% cover) have irregular cycles of frequency. This group of species contains 5 chamaephytes (3 species of lichens-*Cetraria cucullata, C. islandica, Cladonia coccifera;* 2 species of mosses-*Sphagnum fuscum, Tomenthypnum nitens)*; 2 phanerophytes (*Pinus sibirica, Betula nana*); and 2 cryptophytes *(Carex rotundata, Eriophorum scheuchzeri*). Only three species (2 chamaephytes-*Ledum palustre, Sphagnum angustifolium,* and 1 hemicryptophyte-*Eriophorum vaginatum*) show succession changes of frequency. Correlation coefficients over the sampling period permanently decrease for these species.

The frequency of these species has increased in undisturbed sites. For example, *Eriophorum vaginatum* has increased from 4% up to 42%, *Ledum palustre* from 64% up to 90%, and at *Sphagnum angustifoliu*m from 2% up to 24%. Probably the increase in frequency of these species is typical of the *Rubus chamaemorus-Ledum palustre-Sphagnum-Cladina* stage of flat peatland as it develops toward the final *Eriophorum-Ledum-Dicranum-Cladina* stage.

The analysis of developmental stages of vegetation on flat peatland following disturbance shows, as one would expect, a greater number (52%) of characteristic succession species. Of these 12 species, 8 are chamaephytes (low shrub-*Andromeda polifolia and Vaccinium vitis-idaea*; lichens-*Cladina stellaris, Cladonia coccifera* and mosses-*Polytrichum commune, Sphagnum angustifo1lium, S. lindbergii);* 3 species-hemicryptophytes (*Eriophorum vaginatum, Rubus chamaemorus* and *Oxyccocus microcarpus*) and 1 species-cryptophyte (*Eriophorum scheuchzeri*).

Species associated with mature surfaces have both cyclic and irregularly cyclic frequencies and contribute only half as much to the cover in disturbed plots compared to succession species. All species with irregularly cyclic frequency changes are chamaephytes (low shrub-*Vaccinium uliginosum;* lichens-*Cetraria islandica, Cladina rangiferina;* and mosses-*Sphagnum fuscum* and *Sphagnum lindbergii)*. *Cetraria cucullata, C. islandica,* and *Sphagnum fuscum* have the same character of frequency changes both in disturbed and natural conditions.

The group with cyclic frequency changes on disturbed sites includes chamaephytes (shrub-*Ledum palustre, Chamaedaphne calyculata*; lichen-*Cladonia amaurocraea*; moss-*Pleurozium schreberi*); and phanerophyte (*Betula nana*).

Conclusion

This research has determined the impact of climatic changes and human-induced disturbances on vegetation and permafrost conditions in West Siberia North. It has demonstrated the interactions between permafrost and vegetation and has identified plant communities that can be used as indicators of seasonal thaw depths.

The stages of vegetation recovery after the termination of human-induced disturbances were revealed at the sites with removed vegetation, located in different landscape conditions.

Changes in the frequency of plant species in undisturbed sites are correlated with the thaw index of air temperature and amount of precipitation.

During the study the appearance of tree species (*Betula tortuosa*, *Pinus sibirica*) and rise in frequency of shrubs (*Ledum palustre, Betula nana*) are related to a warming trend.

Natural plant communities are dominated by species with cyclic and irregular cyclic changes of frequency over the study period. For plant communities in disturbed and unstable conditions, considerable participation by species with succession changes of frequency is observed.

Acknowledgments

I thank Vladimir P. Melnikov, Elena A. Slagoda, Dmitry S. Drozdov, and Alexandr A. Vasiliev from the Earth Cryosphere Institute for logistic support. An anonymous reviewer is acknowledged for his very useful comments in improving the paper.

This study was made possible through financial support from the grant of the Tyumen governor and the U.S. National Science Foundation (Grants OPP-9732051 and OPP-0225603).

References

Brown, J., Hinkel, K. & Nelson, F. (compilers) 2003. Circumpolar Active Layer Monitoring (CALM) Program network: description and data. In: *International Permafrost Association Standing Committee on Data Information and Communication. 2003. Circumpolar active-layer permafrost system, version 2.0.* Edited by M. Parsons & T. Zhang. Boulder, CO: National Snow and Ice Data Center/World Data Center for Glaciology. CD-ROM.

Burgess, M.M., Gretchitschev, S.E., Kurfurst, P.I., Melnikov, E.S. & Moskalenko, N.G. 1993. Monitoring of engineering-geological processes along pipeline routes in permafrost terrain in Mackenzie River Valley, Canada and Nadym Area, Russia. *Permafrost VI International Conference. Proced. Vol. 1, July 5-9, Beijing China*: 54-59

Dubrovin, V.A., Kulikov, A.I., Fedoseev, A.V. & Fedoseeva, A.R. 1996. The development of computerized observation techniques in the system of geocryological monitoring. *Fundamental Research of Earth Cryosphere in Arctic and Sub-Arctic.* Pushchino: 81-82.

Gorodkov, B.N. 1932. Permafrost and vegetation. In: *Permafrost*. Leningrad, izd-vo Akad. Nauk USSR: 48-60.

Hollister, R.D., Webber, P.J. & Tweedie, C.E. 2005. The response of Alaskan arctic tundra to experimental warming: differences between short- and long-term responses. *Global Change Biology* 11: 1-12.

Koloskov, P.I. 1925. *Climatic Foundations of Agriculture in the Amur Area.* Blagoveshensk, Soviet for Eastern Meteorological Service, 152 pp.

Melnikov, E.S. (ed.) 1983. *Landscapes of Permafrost Zone of the West Siberian Gas Province.* Novosibirsk, Nauka, 166 pp.

Melnikov, E.S., Leibman, M.O., Moskalenko, N.G. & Vasiliev, A.A. 2004. Active Layer Monitoring in West Siberia. *Polar Geography*, v. 28, № 4: 267-285.

Moskalenko, N.G. 1999. *Anthropogenic Vegetation Dynamics in the Permafrost Plains of Russia*. Novosibirsk, Nauka, 280 pp.

Moskalenko, N.G. (ed.) 2006. *Anthropogenic Changes of Ecosystems in West Siberian Gas Province*. Moscow, Earth Cryosphere Institute, 358 pp.

Sumgin M.I., 1937. *Permafrost in the USSR.* Moscow, Izd-vo Akad. Nauk USSR, 379 pp.

Tyrtikov, A.P. 1969. *Impact of the Vegetation Cover on Ground Freezing and Thawing*. Moscow, Mosk. Gos. Univ., 192 pp.

Tyrtikov, A.P. 1979. *Vegetation Cover Dynamics and Evolution of Permafrost Elements of Relief.* Moscow, Nauka, 115 pp.

Tyrtikov, A.P. 1980. Impact of the vegetation cover on ground temperature in the West Siberia North. *Natural Conditions of West Siberia.* Moscow, Mosk. Gos. Univ.: 112-118.

Vasilevich, V.I. 1970. Method of autocorrelation with study of vegetation dynamics. *Trudy MOIP*. Dep. biol. 38: 17-23.

Walker, M.D., Wahren, C.H., Hollister, R.D., Henry, G.H.R., Ahlquist, L.E., Alatalo, J.M., Bret-harte, M.S., Calef, M.P., Callaghan, T.V., Carroll, A.B., Epstein, H.E., Jónsdóttir, I.S., Klein, J.A., Magnússon, B., Molau, U., Oberbauer, S.F., Rewa, S.P., Robinson, C.H., Sshaver, G.R., Suding, K.N., Thompson, C.C., Tolvanen, A., Totland, Ø., Turner, P.L., Tweedie, C.E., Webber, P.J. & Wookey, P.A. 2006. Plant community responses to experimental warming across the tundra biome. *Proceedings of the National Academy of Science of the United States of America (PNAS)* 103(5): 1342-1346.

Experimental Study of Thermal Properties for Frozen Pyroclastic Volcanic Deposits (Kamchatka, Kluchevskaya Volcano Group)

R.G. Motenko
Department of Geocryology, Geological Faculty, Moscow State University, Moscow, Russia
E.P. Tikhonova
Department of Geocryology, Geological Faculty, Moscow State University, Moscow, Russia
A.A. Abramov
Institute of Physicochemical and Biological Problems of Soil Science, Puschino, Russia

Abstract

New data about thermal properties of volcanic deposits is presented together with a short review of permafrost conditions in the study area. This data is necessary for estimation of primary permafrost characteristics (thickness, active layer depth), yet pyroclastic volcanic deposits have not been sufficiently studied. Measurements were made across a wide range of densities and humidity, in the frozen and thawed state. These deposits have a low ability to transfer heat and can act as efficient insulators. According to our results, dry (*W*=0%) cinder and ash (both frozen and unfrozen) have a similar thermal conductivity of about 0.15-0.18 $Wm^{-1}K^{-1}$. At *W*=35%, the thermal conductivity is about 1 $Wm^{-1}K^{-1}$.

Keywords: cinder; permafrost; thermal properties; volcanic ash.

Introduction

The main goal of our work was to study the thermal properties of pyroclastic volcanic deposits in the frozen and thawed states. This data is necessary for the estimation of primary geocryological characteristics (thickness, active layer depth), but pyroclastic volcanic deposits have been inadequately studied to date. Furthermore, these deposits can play an important role in permafrost aggradation during eruptions (Kellerer-Pirklbauer et al. 2007) and in the prevention of permafrost thaw beneath lava flows.

Study Area

The Klyuchevskaya volcano group (Fig. 1) is situated in the Central Kamchatka Depression (55-56°N, 160-161°E) and consists of the active volcanoes Klyuchevsky (~4800 m a.s.l.), Bezymianny (2900 m a.s.l.), Ushkovsky (3900 m a.s.l.), and Plosky Tolbachik (3100 m a.s.l.), as well as ten others that are not active today and numerous small forms like cinder cones and extrusive domes (Braitseva et al. 1995). Here, the Large Fissure Tolbachik Eruption (LFTE) took place in 1975 and 1976, during which about 500 km² were covered by scoria and ash, and three new cinder cones and lava fields were formed (Fedotov & Markhinin 1983).

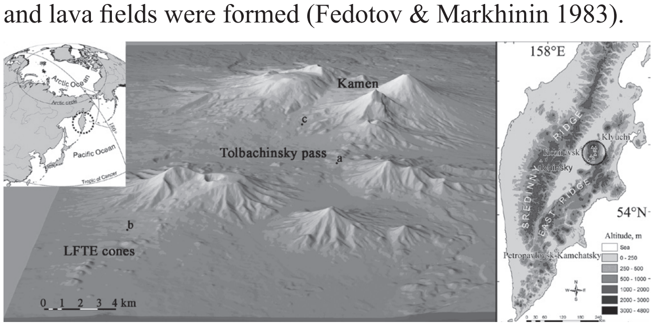

Figure 1. Study area.

Vegetation zones are largely controlled by altitude and eruptions; foliage forest occurs up to 200 m a.s.l., fir forest to 400 m a.s.l., stone birch forest to 800 m a.s.l., shrubs and elfin woods to 1200 m a.s.l., mountain tundra to 2000 m a.s.l., and isolated patches of grass and lichen are found up to 2500 m a.s.l. Around cinder cones of LFTE there are dead forest areas where vegetation has been damaged during the eruptions.

Geocryological Conditions

Permafrost and periglacial processes are widespread in the study area; permafrost covers about 2000 km². The lower boundary of permafrost in the study area is 750-900 m a.s.l. for north-facing slopes and 650-800 m a.s.l. for south facing slopes without forest vegetation, according to our data. The measured MAGTs vary from -2.8°C at 1330 m a.s.l. to -7°C at 2500 m a.s.l. Numerous solifluction lobes, clay cryoturbation spots, polygonal structures, and areas of sorted ground occur between 1000 and 1700 m a.s.l.

Glaciers occupy about 240 km² in the study area, and many of them are covered by debris and pyroclastic deposits, especially the terminus region. This can preserve ice from summer ablation. The equilibrium line altitude (ELA) is situated between 2000 and 2700 m a.s.l. The mean ice thickness is about 30-60 m for valley glaciers, and 100-250 m for glaciers in calderas. Large fields of dead ice exist near Klyuchevsky volcano (Muravyev 1999).

The thickness of the active layer decreases with altitude. Measurements of active layer depth have been conducted at several places (at elevations 800-2700 m a.s.l.) by wire probe (5 mm in diameter) or in pits. The maximal seasonal thaw depth is up to 2.5 m at 900 m a.s.l. and 50 cm at 2500 m a.s.l. Below the lower boundary of permafrost, in forested zone, the seasonal freezing is up to 2-2.5 m thick.

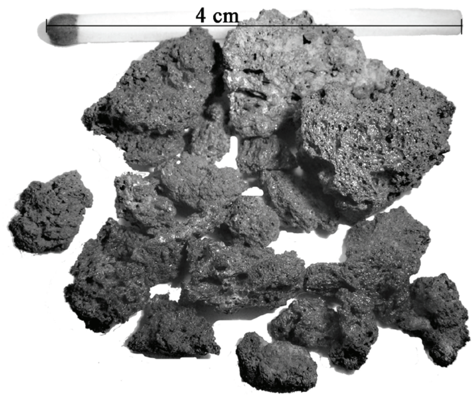

Figure 2. Volcanic cinder particles.

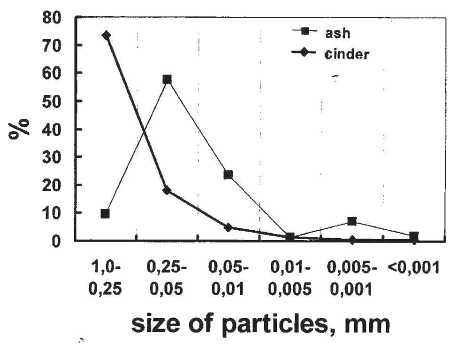

Figure 3. Granulometric composition of volcanic cinder and ash.

We studied the dynamics of the active layer on 100 m x 100 m grids in the framework of the CALM program (point a and b on Figure 1); measurements were made at the end of the warm season. The sites are situated at altitudes of 1330 m and 1630 m asl. The surface is composed of volcanic cinder with no vegetation. Active layer depth at CALM sites did not show significant changes in the last five years.

Physical Properties of Samples

Samples for this study were collected near Tolbachik and Kamen volcanoes (Fig. 1). Volcanic ashes from different sites were investigated at natural humidities (only sample 2 was studied for a range of humidities) (Table 1). Volcanic cinder (Fig. 2) was collected near LFTE cones only, and investigated at several humidities for unsorted particles (size <1 cm) and those sifted through 1 mm and 2 mm sieves. Mean granulometric composition for ash and cinder are shown on Figure 3. These deposits are ultra pure, their pH is neutral (6-8), and total organic carbon content (TOC) is very low (0%-2%). The freezing temperature of these coarse grained deposits is about 0°C.

Methods

Field data about thermal conductivity for thawed deposits was collected using a needle probe with constant power. The accuracy of the measurements is about 12%. These data are available only for volcanic ashes. Deposits at these locations have been sampled for density and humidity, and for laboratory investigations.

Table 1. Volcanic ash samples list. [a]-collected near Tolbachinsky pass, [b]-collected near LFTE cones, [c]-collected near Kamen volcano.

Sample	Depth, m	Age, years	ρ, gr/cm^3	ρ_d, gr/cm^3	Humidity W, %
1[a]	0.2	1475±50	1.50	1.07	38
2[b]	0.2	30	1.40	1.20	30
3[a]	0.55	1475±50	1.44	0.88	64
4[c]	0.15	-	1.60	1.32	21
5[a]	0.75	1475±50	1.67	1.26	33
6[c]	0.4	-	1.47	1.47	13

In the laboratory we use the I-type regular mode method (α-calorimeter) (Ershov 2004). Thermal diffusivity (a) was detected by heating and cooling the ground in an environment with constant temperature (outside of area with intensive phase changes). The temperature range was 0ºC to +20ºC and -22ºC to -12ºC. All measurements were made two times. The accuracy of measurements is about 10%.

Specific heat capacity (C) is calculated as the sum of ground components (rock matrix, water, ice). Thermal capacity was set to 4200 Jkg^{-1}K^{-1} for water and set to 2100 Jkg^{-1}K^{-1} for ice. Thermal capacities for the rock matrix were measured on an ITC-400 by monotonous heating. The accuracy of measurements is about 10% (Platunov 1972).

Thermal conductivity (λ) was calculated as: $\lambda = C\rho\, a$.

The analysis of chemical and granulometric composition, pH, and TOC (total organic carbon) were made in the laboratories of the Institute of Physicochemical and Biological Problems of Soil Science, using standard techniques.

The preparation and processing of the material for radiocarbon dating was carried out by the ^{14}C laboratory of the Department of Geography at the University of Zurich (GIUZ). The dating itself was done by AMS (accelerator mass spectrometry) with a tandem accelerator at the Institute of Particle Physics at the Swiss Federal Institute of Technology Zurich (ETH).

Results and Discussion

Results on thermal conductivity are presented in Figures 4 and 5.

Figure 4 shows data for volcanic ashes. Sample 2 was investigated at two rock matrix densities and several humidities. At ρ_d=1.2 gr/cm^3, λ increased with an increase in humidity (from 0% to 38%) from 0.17 to 0.67 Wm^{-1}K^{-1} in the thawed state and to 0.78 Wm^{-1}K^{-1} in the frozen state. At ρ_d=1.0 gr/cm^3, the increase was smaller (up to 0.53 and 0.63 Wm^{-1}K^{-1}, respectively). All other ash samples were investigated at natural humidities and densities. For dry samples, λ was set

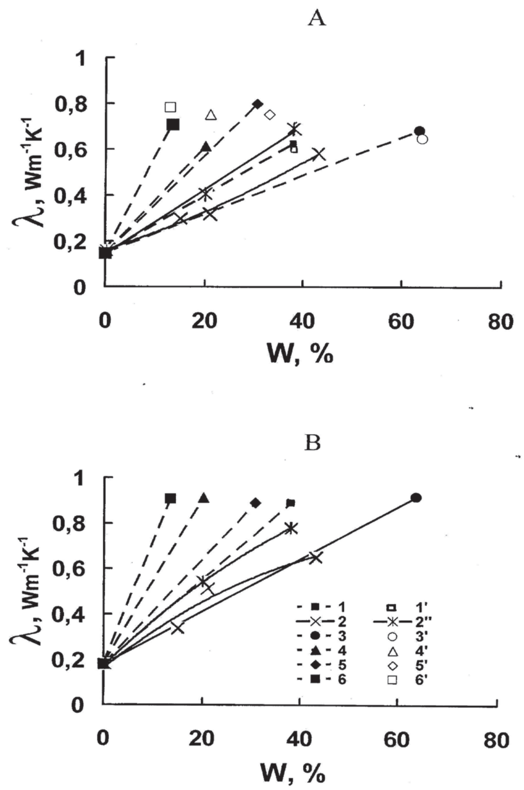

Figure 4. Correlation between thermal conductivity (λ) and humidity (W) for thawed (A) and frozen (B) volcanic ash at different densities (ρ_d): 1 – 1.1 gr/cm³, 2 – 1 gr/cm³, 2″ – 1.2 gr/cm³, 3 – 0.88 gr/cm³, 4 – 1.32 gr/cm³, 5 – 1.33 gr/cm³, 6 – 1.47 gr/cm³; 1′, 3′, 4′, 5′, 6′ – field data (ρ_d are the same).

to 0.17 Wm⁻¹K⁻¹ as in sample 2. The dotted lines on Figure 4 show the estimated correlation of λ to humidity. The lower the density, the lower the λ, but the relation is clearer with samples from one site. We believe that this is due to different age and mineral composition. Field data is presented only for thawed ash samples (1', 3', 4', 5', 6'); the divergence with laboratory data is about 12%.

According to our results, the thermal conductivity of dry (W=0%) ash and cinder (both frozen and thawed) is similar at about 0.15-0.18 Wm⁻¹K⁻¹. The dependence of λ on density and humidity is similar for volcanic cinders to that in ashes. Unsorted cinder is non-homogeneous and does not fit the method requirements, so that data for cinder sample 3 is only an estimate. This cinder is very porous, resulting in a lower λ value.

The dependence of thermal diffusivity (a) on humidity and density is similar to that for λ. For volcanic cinders with W = 0%–35%, a = 0.17 to 0.30–0.54×10⁻⁶m²s⁻¹ in the frozen state, and up to 0.21–0.33×10⁻⁶m²s⁻¹ in the thawed state. For volcanic ashes at natural humidities and densities, a = 0.20×10⁻⁶m²s⁻¹ (sample 3) – 0.36×10⁻⁶m²s⁻¹ (sample 6) for frozen material, and 0.392×10⁻⁶m²s⁻¹ – 0.580×10⁻⁶m²s⁻¹ for thawed material.

The C from the ITC-400 for volcanic cinder is 750 Jkg⁻¹K⁻¹ and for volcanic ash is 750–800 Jkg⁻¹K⁻¹. Only for ash sample 3 is it 1000 Jkg⁻¹K⁻¹.

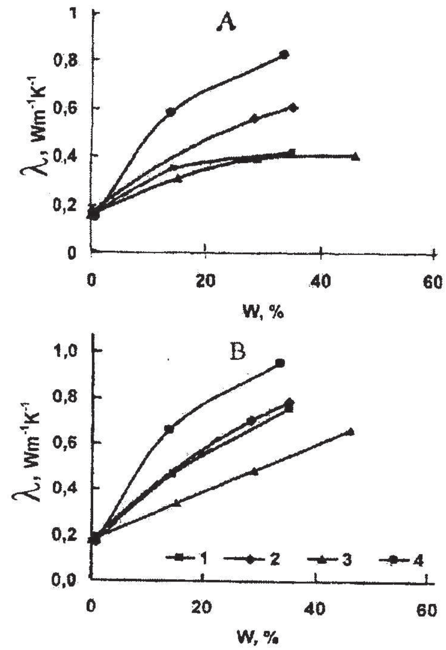

Figure 5. Correlation between thermal conductivity (λ) and humidity (W) for thawed (A) and frozen (B) volcanic cinder at different densities (ρ_d): 1 – 1.1…1.2 gr/cm³) (≤1 mm), 2 – 1.1 gr/cm³ (≤2 mm)), 3 – 0.9 – 1.0 gr/cm³ (≤1 cm), 4 – 1.3 - 1.4 gr/cm³) (<1 mm).

Conclusions

New thermal conductivity data were collected for pyroclastic deposits in both the thawed and frozen states. Results show that thermal conductivity is very low under dry conditions and increases as the humidity and density of the deposit increases. The thermal conductivity of dry cinder and ash, according to our measurements, is about 0.15-0.18 Wm⁻¹K⁻¹. The maximum thermal conductivity is about 1 Wm⁻¹K⁻¹ with an ice content 35%-40%. Field measurements for thawed ashes compare well with laboratory data.

The low heat transfer rate in these deposits can play an important role in the formation and preservation of permafrost. The formation of permafrost during eruptions is in relation to active layer thickness and thickness of deposited volcanic deposits. Pyroclastic volcanic deposits can preserve underlying permafrost layers from thawing due to its effective insulation properties and thermal offset effects. In the case of large explosive eruptions, permafrost can aggrade in surrounding terrain, especially during a winter eruption when the falling cinder has subzero temperatures and buries large quantities of snow and ice.

Acknowledgments

The authors want to express their thanks to all who helped in this study, especially D.A. Gilichinsky and Y.D. Muravyev.

Thanks are due to the NAI for financial support during these years.

References

Braitseva, O., Melekestsev, I., Ponomareva, V. & Sulerzhitsky, L. 1995. Ages of calderas, large explosives craters and active volcanoes in the Kuril-Kamchatka region, Russia. *Bull. Volcanol.* 57: 383-402.

Ershov, E.D. (ed.) 2004. *Methods of Geocryological Research*. Moscow: MSU, 306 pp.

Fedotov, S.A. & Markhinin, Y.K. 1983. *The Great Tolbachik Fissure Eruption: Geological and Geophysical Data 1975-1976.* Cambridge: Cambridge University Press, 355 pp.

Kellerer-Pirklbauer, A., Farbrot, H. & Etzelmuller, B. 2007. Permafrost aggradation caused by tephra accumulation over snow-covered surfaces: examples from the Hekla-2000 eruption in Iceland. *Permafrost and Periglacial Processes* 18: 269-284. doi:10.1002/, 596 pp.

Muravyev, Y.D. 1999. Present-day glaciation in Kamchatka-distribution of glaciers and snow. *Cryospheric Studies in Kamchatka* II: 1-7.

Platunov, E.S. 1972. *Thermo Physical Measurements at Monotonous Regime*. Moscow: Energy, 205 pp.

Spatial Analysis of Glacial Geology, Surficial Geomorphology, and Vegetation in the Toolik Lake Region: Relevance to Past and Future Land-Cover Changes

C.A. Munger, D.A. Walker, and H.A. Maier

Institute of Arctic Biology, University of Alaska Fairbanks, AK 99775, USA

T.D. Hamilton

U.S. Geological Survey, 4200 University Drive, Anchorage, AK 99508-4667, USA

Abstract

Vegetation succession on different age glacial surfaces may provide clues to how tundra regions will respond to future climate and land-use changes. In the Toolik Lake region, of Alaska, three major glacial advances occurred during the middle to Late Pleistocene. Here we use a new group of maps of the upper Kuparuk River region to examine the interrelationships between glacial history, surficial geomorphology, vegetation, and spectral properties. Older surfaces in the region have greater amounts of shrub- and moss-rich vegetation and higher values of the Normalized Difference Vegetation Index (NDVI), an index of vegetation greenness. Younger surfaces have a higher proportion of disturbance-related features such as non-sorted circles and areas with warmer soils. Landscape responses to climate change are likely to be heterogeneous and may be most easily detected in areas where there are already high amounts of shrubs or areas with high disturbance regimes.

Keywords: climate change; ecosystems; GIS; glacial history; NDVI; patterned ground; vegetation.

Introduction

The Toolik Lake region is situated in close proximity to several major Late Cenozoic glacial surfaces (Hamilton 1986). In this cold region, landscape evolution proceeds more slowly than in temperate regions, so that differences in geomorphology and vegetation are evident on surfaces spanning hundreds of thousands of years. These surfaces have not been altered by agriculture or other anthropogenic influences, so the region is an excellent laboratory to examine the effects of geological processes on ecosystem function. Such studies can help us understand how arctic systems change over long periods of time and provide insights regarding how they might change in the future in response to climate change. This paper focuses on the linkage between glacial geology, surficial geomorphology, and vegetation in the upper Kuparuk River region, where the glacial history has been shown to be a defining characteristic for a wide variety of terrestrial and aquatic ecosystems characteristics (Jorgenson 1984a, Walker & Walker 1996, Oswald et al. 2003). We use mapped information that is part of a hierarchical geographic information system (HGIS), which has been assembled for the University of Alaska's Toolik Lake Field Station and an Arctic Geobotanical Atlas (Walker et al. 2008 this volume)

Glacial geology

The complex topography of the Toolik Lake region results from glacial deposits that flowed into the region during three major glacial advances. Glacial deposits within the Toolik Lake region are assigned to Sagavanirktok (middle Pleistocene), Itkillik I, and Itkillik II (Late Pleistocene) glaciations of the central Brooks Range glacial succession (Detterman et al. 1958, Porter 1964, Hamilton & Porter 1975, Hamilton 1986, Hamilton 2003) (Fig. 1a). A simplified version of Thomas Hamilton's glacial geology map of the upper Kuparuk River region (Hamilton 2003) was used for this analysis.

The Sagavanirktok glaciation consisted of several separate glacial events dating broadly from middle Quaternary time (about 780,000 to 125,000 yr B.P.). During the initial (maximum) advances, large valley glaciers flowed north along the Itkillik River, Sagavanirktok River, and Kuparuk River drainages. Most of the upper Kuparuk River watershed, including the Imnavait Creek watershed, is on drift of older Sagavanirktok-age deposits. The surfaces of the Sagavanirktok River glaciation have massive gently sloping moraines that rise about 100 m from the valley bottoms to the crests trending SSE to NNW (Hamilton 1986). These moraines are well represented in the Imnavait Creek watershed. The hills formed by these moraines are rounded by gelifluction and heavy loess cover and are topped with 20 cm to 40 cm of peat. Occasional glacial erratics protrude up to 1 m above the tundra surface.

Itkillik I glaciers abutted divides (west, east, and south of the upper Kuparuk drainage) but overflowed those divides only locally. The subsequent Itkillik II glaciers advanced between about 25 and 11.5 kya ^{14}C and formed extensive ice-stagnation features around Toolik Lake. Glacial flow patterns during the Itkillik II advance were generally similar to those of the present-day river drainages. Other features on the glacial geology map include bedrock, river deposits, lacustrine deposits, fan deposits, colluvial deposits, and shales and siltstones of the Chandler Formation (along the north boundary of the map), Toruk Formation (middle-eastern portion of the map), and Fortress Mountain Formation (north side of the Atigun River).

Surficial geomorphology

The landscapes in the Toolik Lake region have been

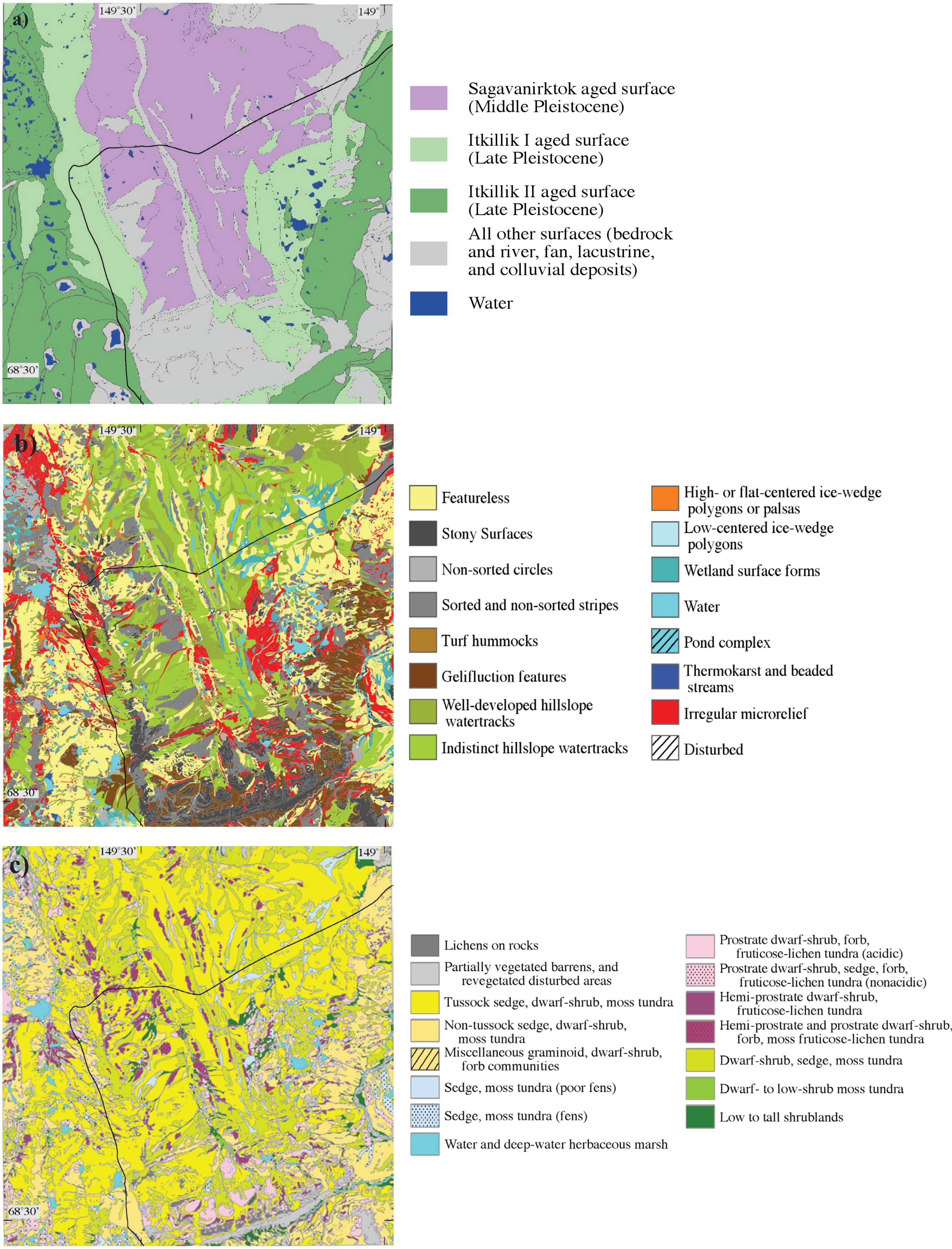

Figure 1. a) Glacial geology, b) surficial geomorphology, and c) vegetation of the Toolik Lake region.

modified by a variety of geomorphological processes including alluviation, colluviation, and periglacial processes (Fig. 1b). Common surficial geomorphological map units described for the Imnavait Creek region (Walker & Walker 1996) include sorted and nonsorted circles (frost boils), turf hummocks, gelifluction lobes and terraces, water tracks, high- and low-centered ice-wedge polygons, wetland features (strangmoor, aligned hummocks, palsas), and thermokarst features.

Vegetation

The vegetation of the region (Fig 1c) was studied and mapped as part of the Arctic Long-Term Ecological Research (LTER) project at Toolik Lake (Walker et al. 1994, Walker & Walker 1996), and the Department of Energy R4D (Response, Resistance, Resilience and Recovery of vegetation from Disturbance) project at Imnavait Creek (Walker & Walker 1996). Fifty plant communities and land-cover types were recognized during the mapping of the upper Kuparuk River region, and they are designated by numeric codes in the GIS database. These were grouped into the 14 physiognomic map units shown on Fig. 1c. (For more details on the vegetation mapping, see Walker et al. 2008)

NDVI

The Normalized Difference Vegetation Index (NDVI) is an index of vegetation greenness that can be linked to plant biomass and other biophysical properties of the vegetation (Shippert 1995). The NDVI = (NIR – R)/(NIR + R), where NIR is the spectral reflectance in the Landsat Thematic Mapper in the near-infrared channel (0.76–0.9 µm) and R is the reflectance in the red channel (0.63–0.69 µm). Four images were used in the analysis (3 Aug 1985, 8 Aug 1995, 4 Aug 1999, and 21 Jul 2001). The NDVI was calculated for each 30-m pixel in each image, and a composite average NDVI was calculated for each pixel using the mean value for the four years. To examine how plant production varies with glacial history, we examined the distribution of the Normalized Difference Vegetation Index (NDVI) on the three glacial surfaces.

Analysis of the Maps

The surficial geomorphology, vegetation, and NDVI maps were stratified according to the glacial units in Figure 1a. Results of the analysis are shown in Figures 2 and 3.

Effects of glacial history on surficial geomorphology

Terrain evolution associated with the glacial history of the region was noted by Hamilton (Hamilton & Trexler Jr. 1979). Our analysis extends Hamilton's earlier observations to surface forms that are superimposed on the larger landforms of the regions (Fig. 2). The broad hill-slope deposits of the Sagavanirktok-age surfaces are dominated by indistinct and well-developed water-track patterns (55% on Sagavanirktok surfaces, 13% on Itkillik-I, and 9% on Itkillik-II surfaces). The older Sagavanirktok surfaces also have more peaty wetlands (3% on Sagavanirktok surfaces and 2% on Itkillik-I

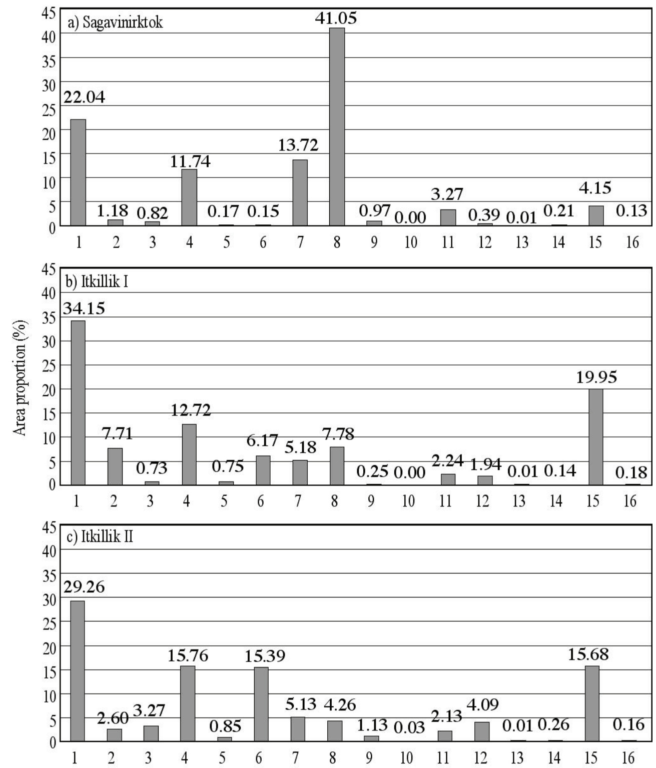

1. Featureless
2. Stony surfaces
3. Non-sorted circles
4. Sorted and non-sorted stripes
5. Turf hummocks
6. Gelifluction features
7. Well-developed hill-slope water tracks
8. Indistinct hill-slope watertracks
9. High- or flat-centered ice-wedge polygons and palsas
10. Low-centered ice-wedge polygons
11. Wetland surface forms
12. Water
13. Pond Complex
14. Thermokarst and beaded streams
15. Irregular microrelief
16. Disturbed

Figure 2. Proportion of surficial geomorphologic types on a) Sagavanirktok-aged, b) Itkillik I-aged, and c) Itkillik II-aged glacial surfaces.

and Itkillik-II surfaces). Stripes and nonsorted circles are more abundant on the younger surfaces, especially the Itkillik II surfaces. Stripes cover 12% of Sagavanirktok surfaces, 13% of Itkillik-I, and 16% of Itkillik-II surfaces. Non-sorted circles cover 1% on Sagavanirktok surfaces, 1% on Itkillik-I, and 3% of Itkillik-II surfaces. Lakes are also more abundant on the younger surfaces (less than 1% on Sagavanirktok surfaces, 2% on Itkillik-I, and 5% on Itkillik-II surfaces).

Effects of glacial history on vegetation and plant production

The Sagavanirktok age surfaces have a dominance of acidic tussock tundra (61% tussock-sedge, dwarf-shrub, moss tundra cover, compared to 38% on Itkillik I, and 24% on Itkillik II surfaces) and relatively high percentages of

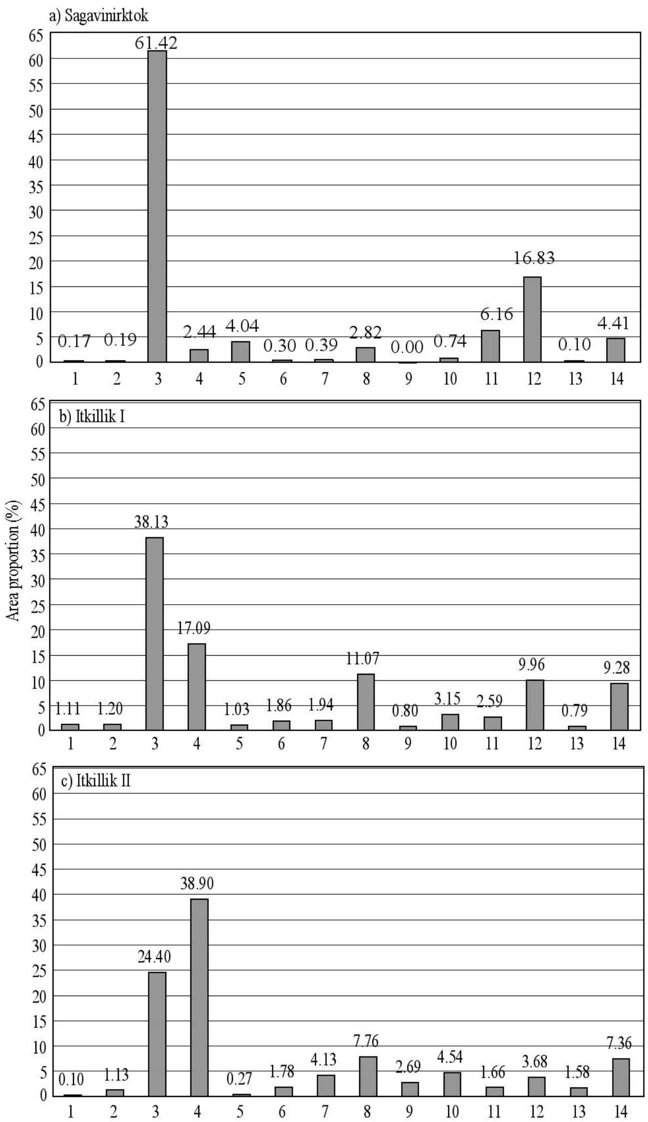

1. Lichens on rocks
2.Partially vegetated vegetated barrens and revegetated disturbed areas.
3. Tussock sedge, dwarf-shrub, moss tundra
4. Non-tussock sedge, dwarf-shrub, moss tundra
5. Sedge, moss tundra (poor fens)
6. Sedge, moss tundra (fens)
7. Water and deep-water herbaceous marsh
8. Prostrate dwarf-shrub, forb, fruticose-lichen tundra (acidic)
9. Prostrate dwarf-shrub, sedge, forb, fruticose lichen tundra (nonacidic)
10. Hemi-prostrate dwarf-shrub, fruticose-lichen tundra
11. Hemi-prostrate and prostrate dwarf-shrub, forb, moss fruticose-lichen tundra
12. Dwarf-shrub, sedge, moss tundra
13. Dwarf- to low-shrub moss tundra
14. Low to tall shrublands

Figure 3. Proportion of vegetation types on a) Sagavanirktok aged, b) Itkillik I aged, and c) Itkillik II aged glacial surfaces.

erect-dwarf shrub tundra types (21% on Sagavanirktok-age surfaces, 20% on Itkillik-I, and 13% on Itkillik-II surfaces) and poor-fen wetlands (4% on Sagavanirktok surfaces, 1% on Itkillik-I surfaces, and 0% on Itkillik-II surfaces) (Fig. 3). In contrast, the much younger Itkillik II surfaces have a dominance of nonacidic tundra (nontussock-sedge, dwarf-shrub, moss tundra, 2% on Sagavanirktok surfaces, 17% on Itkillik-I surfaces, and 39% on Itkillik-II surfaces) and are more vegetatively diverse with relatively high percentages of snowbed vegetation (hemi-prostrate-dwarf-shrub vegetation types, less than 1% on Sagavanirktok surfaces, 3% on Itkillik-I, and 5% on Itkillik-II surfaces), rich fens (0% on Sagavanirktok surfaces and 2% on Itkillik-I and Itkillik-II surfaces), and dry nonacidic tundra (prostrate dwarf shrub, sedge, forb, lichen tundra, 0% on Sagavanirktok surfaces, 1% on Itkillik-I and 3% on Itkillik-II surfaces.

Landscape age at Toolik Lake is also linked to biomass and the Normalized Difference Vegetation Index (NDVI) (Fig. 4). Older landscapes have higher NDVI and greater amounts of standing biomass (Shippert et al. 1995). The higher NDVI values of the older landscapes are due in part to relative proportions of dry, moist, and wet vegetation types on different aged surfaces. Generally, drier vegetation with lower NDVI is dominant on younger surfaces, as shown in the area analysis of vegetation on the different age glacial surfaces (Fig.3). Of greater regional significance is the difference in biomass and NDVI of vegetation growing on moist upland surfaces. The biomass of the *Sphagno-Eriophoretum vaginati* tussock tundra, which grows on the older acidic surfaces, is about 25% greater than its nonacidic counterpart *Dryado integrifoliae-Caricetum bigelowii* (512 g m^{-2} vs. 403 g m^{-2}). These types also have different key ecosystem properties, including active layer depths (Nelson et al. 1997) (Walker et al. 2003 submitted), trace gas fluxes (Oechel et al. 2000), species composition (Gough et al. 2000), abundance of frost boils (Bockheim et al. 1998), and soil carbon (Bockheim et al. 1996).

Implications with Respect to Land-Cover Change

The difference in shrub cover on the different glacial surfaces is of particular interest because of relevance to the issue of shrub expansion associated with climate warming (e.g., Sturm et al. 2001). While the older surfaces have overall greater cover of erect dwarf-shrub tundra types, as noted above, the younger surfaces have greater cover of taller riparian shrubs (4% on Sagavanirktok surfaces, 9% on Itkillik-I, and 7% on Itkillik-II surfaces). This is possibly due to the greater abundance of rocky and gravelly stream channels on the younger surfaces and steep south facing slopes with relatively warm, nutrient-rich soils.

Area analysis of the vegetation units occurring on the different age glacial surfaces shows that the older landscapes have more acidic tundra, less dry nonacidic tundra, fewer snowbeds, more dwarf-shrub tundra, much less moist nonacidic tundra, fewer rich riparian shrublands, fewer rich fens, more poor fens, and fewer lakes. Torre Jorgenson noted differences in the abundance of plant communities on the different glacial surfaces (Jorgenson 1984b), and soil heat flux was higher on the younger surfaces (Jorgenson

1984a). Others have linked Hamilton's glacial units to a hypothesis of vegetation succession, whereby peat formation (paludification) and ice aggradation on older surfaces lead to restricted drainage, a general acidification of the soils, and the introduction of *Sphagnum* mosses to wet hill slopes. Thicker moss carpets change the soil chemistry, hydrology, and soil thermal properties, resulting in peat formation and acidic mires in colluvial basins, extensive water-track development, and tussock tundra on gentle hill slopes (Jorgenson 1984a, Walker et al. 1989, Walker & Walker 1996, Mann et al. 2002).

Variation in the degree of paludification is a primary factor controlling the distribution of acidic tussock tundra, *Sphagno-Eriophoretum vaginati* and its non-acidic counterpart *Dryado integrifoliae-Caricetum bigelowii* (Walker et al. 1994). The plant association *Dryado integrifoliae-Caricetum bigelowii* is included within the "non-tussock sedge, dwarf-shrub, moss tundra" unit on the vegetation map (Fig. 1c) and occurs most abundantly on younger surfaces, often with high disturbance regimes, including Itkillik-age glacial surfaces, loess deposits, solifluction features, frost-boil complexes, and alluvial terraces; whereas well-developed tussock tundra (included in the "tussock-sedge, dwarf shrub, moss tundra" unit) forms under conditions of long-term site stability. The *Dryado integrifoliae-Caricetum bigelowii* and related associations found on younger landscapes are also floristically much more diverse than tussock tundra, and important with respect to regional biodiversity. These associations have the highest species diversity of any of the communities sampled in the region (Walker et al. 1994). Several authors have noted the affect of soil pH on tundra plant diversity (Walker 1985, Gough et al. 2000); however, the effects of landscape age on other aspects of biodiversity such as upon total regional plant community and animal diversity have not been studied in any detail.

Paleoecological studies from lakes on the Itkillik II and Sagavanirktok-age surfaces near Toolik Lake indicate that the onset of moist conditions between the early and middle Holocene triggered processes of plant succession leading up to the current conditions (Oswald et al. 2003). Soil moisture appears to have been better retained by fine-textured soils and more gently sloped landforms on the Sagavanirktok surfaces, promoting greater plant cover, thicker organic soil horizons, shallower active layers, aggradation of permafrost, and acidic soils; whereas the better-drained Itkillik surfaces continued to support relatively xeric, sparse, non-acidic vegetation.

Our study found the older Sagavanirktok-age surfaces have a greater abundance of shrubby vegetation types than the younger surfaces. These were dominated by communities with dwarf-shrubs and large areas of shrubby watertracks. We also found that the best developed (tall) shrub communities were most common on the younger Itkillik-age surfaces, suggesting that the higher disturbance regimes, warmer soils, and higher nutrient regimes in certain microsites promoted the development of well-developed shrub communities. Future changes of the regional vegetation will be in response to both

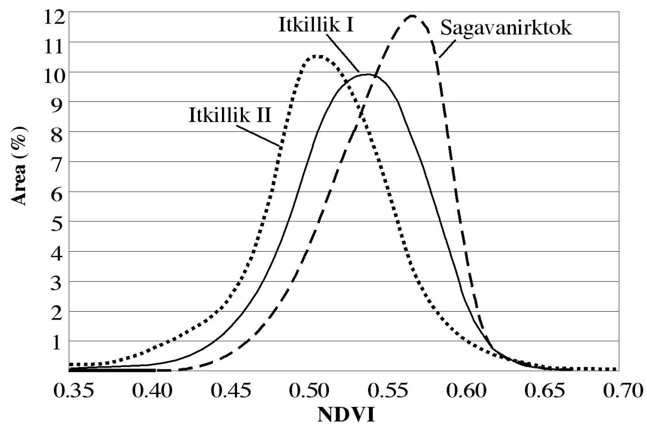

Figure 4. Distribution of NDVI on different aged glacial surfaces.

altered climate and changes in natural and anthropogenic disturbance regimes. We are currently conducting a more detailed study of the greening response of these surfaces during the period of Landsat satellite-observations (1981 to present) (Munger 2007), which will yield further insights regarding the past and future land-cover changes in these landscapes.

Acknowledgments

Funding for this study was provided by the National Science Foundation (ARC-0425517 and ARC-0531180). The Alaska Geobotany Center is located within the Institute of Arctic Biology, University of Alaska Fairbanks, Fairbanks, Alaska 99775-7000.

References

Bockheim, J.G., Walker, D.A. & Everett, L.R. 1996. Soil carbon distribution in nonacidic and acidic soils of arctic Alaska. In: R. Lal, J.M. Kimble, R.F. Follett & B.A. Stewart (eds.), *Advances of Soil Science. Proceedings of the International Symposium on Carbon Sequestration in Soil. Ohio State University.* Columbus: CRC Press, 143-155

Bockheim, J.G., Walker, D.A., Everett, L.R., Nelson, F.E. & Shiklomanov, N.I. 1998. Soils and cryoturbation in moist nonacidic and acidic tundra in the Kuparuk river basin, arctic Alaska, U.S.A. *Arctic and Alpine Research* 30: 166-174.

Detterman, R. L., Bowsher A.L. & Dutro, J.T., Jr. 1958. Glaciation on the arctic slope of the Brooks Range, northern Alaska. *Arctic* 11: 43-61.

Gough, L., Shaver, G.R., Carrol, J., Royer, D.L. & Laundre, J.A. 2000. Vascular plant species richness in Alaskan arctic tundra: the importance of soil pH. *Journal of Ecology* 88: 54-66.

Hamilton, T.D. 1986. Late Cenozoic glaciation of the Central Brooks Range. In: T.D. Hamilton, K.M. Reed, & R.M. Thorson (eds.), *Glaciation in Alaska: the Geologic Record.* Alaska Geological Society, 9-49.

Hamilton, T.D. 2003. *Glacial Geology of the Toolik Lake and Upper Kuparuk River Regions, Institute of Arctic Biology*. Biological Papers of the University of Alaska. No. 26, Fairbanks, AK.

Hamilton, T.D. & Porter, S.C. 1975. Itkillik glaciation in the Brooks Range, northern Alaska. *Quaternary Research* 5: 471-497.

Hamilton, T.D. & Trexler Jr., J.H. 1979. Analyses of surficial deposits, central Brooks Range, Alaska. *Open-File Report*. U.S. Geological Survey, 79-228.

Jorgenson, M.T. 1984a. *Controls of the Geographic Variability of Soil Heat Flux near Toolik Lake, Alaska.* M.S. Thesis. University of Alaska Fairbanks.

Jorgenson, M.T. 1984b. The response of vegetation to landscape evolution on glacial till near Toolik Lake, Alaska. In: *Inventorying Forest and Other Vegetation of the High Latitude and High Altitude Regions, Proceedings of an International Symposium, Society of American Foresters Regional Technical Conference, Fairbanks, AK,* 134-141.

Mann, D.H., Peteet, D.M., Reanier, R.E. & Kunz, M.L. 2002. Responses of an arctic landscape to Late-glacial and early Holocene climatic changes: the importance of moisture. *Quaternary Science Reviews* 21: 997-1021.

Munger, C.A. 2007. *Spatial and Temporal Patterns of Vegetation, Terrain, and Greenness in the Toolik Lake and Upper Kuparuk River Region.* M.S. Thesis. University of Alaska Fairbanks.

Nelson, F.E., Shiklomanov, N.I., Mueller, G.R., Hinkel, K.M., Walker, D.A. & Bockheim, J.G. 1997. Estimating active-layer thickness over a large region: Kuparuk River Basin, Alaska. *Arctic and Alpine Research* 29: 367-378.

Oechel, W.C., Vourlitis, G.L., Verfaillie, J., Jr., Crawford, T., Brooks, S., Dumas, E., Hope, A., Stow, D., Boynton, B., Nosov, V. & Zulueta, R. 2000. A scaling approach for quantifying the net CO2 flux of the Kuparuk River Basin, Alaska. *Climate Change Biology* 6: 160-173.

Oswald, W.W., Brubaker, L.B., Hu, F.S. & Kling, G.W. 2003. Holocene pollen records from the central Arctic Foothills, northern Alaska: testing the role of substrate in the response to climate change. *Journal of Ecology* 91: 1034-1048.

Porter, S.C. 1964. Late Pleistocene glacial chronology of north-central Brooks Range, Alaska. *American Journal of Science* 262: 446-460.

Shippert, M. M., Walker, D.A. & Auerbach, N.A. 1995. Biomass and leaf-area index maps derived from SPOT images for Toolik Lake and Imnavait Creek areas, Alaska. *Polar Record* 31: 147-154.

Sturm, M., McFadden, J.P., Liston, G.E., Racine, H. & Holmgren, J. 2001. Snow-shrub interactions in arctic tundra: a hypothesis with climatic implications. *Journal of Climate* 14: 336-344.

Walker, D.A. 1985. *The Vegetation and Environmental Gradients of the Prudhoe Bay Region, Alaska.* In: U.S. Army Cold Regions Research and Engineering Laboratory, Hanover, NH.

Walker, D.A., Jia, G.J., Epstein, H.E., Raynolds, M.K., Chapin, F.S., III, Copass, C.D., Hinzman, L.D., Kane, D., Maier, H.A., Michaelson, G.J., Nelson, F., Ping, C.L., Romanovsky, V.E., Shiklomanov, N. & Shur, Y. 2003 submitted. Vegetation-soil-thaw-depth relationships along a Low-Arctic bioclimate gradient, Alaska: synthesis of information from the ATLAS studies. *Permafrost and Periglacial Processes.*

Walker, D.A., Maier, H.A. & Barbour, E.M. 2008. A web-based arctic geobotanical atlas and new hierarchy of maps of the Toolik Lake region, Alaska. *Proceedings of the Ninth International Conference on Permafrost, Fairbanks, Alaska, June 29–July 3, 2008* (this proceedings).

Walker, D.A., & Walker, M.D. 1996. Terrain and vegetation of the Imnavait Creek Watershed. In: J.F. Reynolds & J.D. Tenhunen (eds.), *Landscape Function: Implications for Ecosystem Disturbance, a Case Study in Arctic Tundra.* Springer-Verlag, New York, 73-108.

Walker, M.D., Walker, D.A. & Auerbach, N.A. 1994. Plant communities of a tussock tundra landscape in the Brooks Range Foothills, Alaska. *Journal of Vegetation Science* 5: 843-866.

Walker, M.D., Walker, D.A. & Everett, K.R. 1989. Wetland soils and vegetation, Arctic Foothills, Alaska. *U.S. Fish and Wildlife Service* 89 (7).

Choosing Geotechnical Parameters for Slope Stability Assessments in Alpine Permafrost Soils

Philippe Nater
GeoNum GmbH, Zurich, Switzerland

Lukas U. Arenson
BGC Engineering Inc. Vancouver, BC, Canada

Sarah M. Springman
Institute for Geotechnical Engineering, ETH Zurich, Zurich, Switzerland

Abstract

The shear strength of alpine permafrost soils can be expressed in terms of internal friction ϕ' and cohesion *c* utilizing a Mohr-Coulomb failure criterion as for many other soils. The challenges lie in the correct parameterization, in other words the assignment of realistic values for the chosen parameters ϕ' and *c*. Because the strength of frozen soils depends on the temperature, a correlation of the effective angle of internal friction ϕ' and cohesion *c* with temperature-dependent parameters, such as the volumetric ice content w_i, is proposed. The correlations are based on laboratory tests carried out on undisturbed samples of alpine permafrost soils. Utilizing an example calculation, this paper provides guidance in dealing with limit equilibrium slope stability analysis and assistance in selecting appropriate soil parameters.

Keywords: alpine permafrost soil; failure; limit equilibrium analysis; shear strength parameters.

Introduction

When assessing the stability of permafrost slopes, engineers are often faced with the challenge of selecting appropriate soil parameters and model. Only a limited number of laboratory test results are available from which such parameters could be extracted. Based on published data and interpretation of laboratory tests on undisturbed samples of alpine permafrost soils presented by Arenson et al. (2004) and Arenson and Springman (2005a, 2005b), reassessing the strength of those soils for the use in limit equilibrium analysis was carried out. The chosen strength model for describing the shear resistance is a Mohr-Coulomb failure criterion with a frictional and a cohesive component. The idea is based on presentations by Ting et al. (1983) and Goughnour and Andersland (1968) which suggest different mechanisms for different ice contents. The parameters to select are the effective angle of friction ϕ', representing the structural hindrance of the mass of the soil particles, and the cohesion *c,* representing the bonding effect of the ice between the soil particles. The Mohr-Coulomb criterion will be adapted to frozen soils found in warm alpine permafrost. Water in the soil pores changes phase as temperature reaches the freezing point. Four different states can therefore be distinguished (Fig. 1):

(1) In a frozen state, single soil grains may have no contact with other grains in the ice matrix. The soil fraction does not add frictional contribution to the resistance so that only the cohesive component is active. The cohesive component can be described with the variable *c*, which depends on temperature and strain rate.

(2) In a transient process with increasing temperature, the volume of the ice phase decreases allowing for soil grain contacts. This effect causes the formation of a frictional component with a simultaneous decrease of the cohesional bonding effect. No liquid water is present.

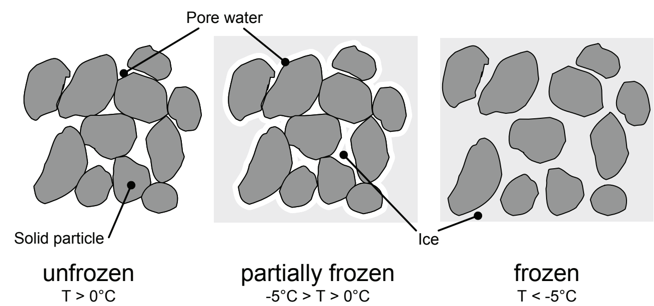

Figure 1. Different states that may be encountered in an alpine permafrost soil.

(3) In a different state, both frozen and unfrozen water are present in parallel in the voids between the particles and on the particle edges. The bonding effect of the ice present in some voids provides a cohesive component *c* to the soil strength, and at the same time the full granular friction can be mobilized.

(4) In the unfrozen state, all pore water is in the liquid phase. The soil behaves as any unfrozen soil. Taking into account the drained long-term behavior of soil, the cohesive component is set to zero; *c* = 0 kPa. Most soils in alpine environments have only little fines, and therefore the assumption of drained conditions is realistic.

The concept will be followed that the drained loading of a completely dry or fully saturated soil will lead to a state where no cohesion appears (*c* = 0 kPa). Unsaturated conditions where significant apparent cohesion can be observed will not be discussed here but are not in contradiction to the described model. It is not the aim to show a material description based on physically manifest relations but to show the potential of the approach.

Literature Review

A brief literature review was performed to complement test results of Arenson et al. (2004) and Arenson and Springman (2005a, 2005b) and to enlarge the database of known shear strength parameters of frozen soils in order to increase confidence in the proposed interpretation of the Mohr-Coulomb model. They conducted a series of triaxial compression tests on undisturbed permafrost soil samples, including controlled temperature and volumetric ice content ,together with an interpretation of the test results towards a definition of an effective angle of internal friction ϕ' and cohesion *c*. From the test series it can be observed that the effective angle of internal friction decreases with the volumetric ice content, whereas the cohesion increases (Fig. 2).

One of the key parameters for describing a warm permafrost soil in order to assess the shear strength is the unfrozen water content, hence the volumetric ice content w_i. These relationships are unique for each individual soil and control the attribution of the effective angle of internal friction ϕ' and cohesion *c*. The effective angle of internal friction ϕ' at a temperature $T > 0°C$ defines the initial conditions for the decrease.

In addition, the strength of the ice is temperature dependent. Therefore it is important to quantify the effective angle of internal friction, the cohesion at a given volumetric ice content in function of the temperature or vice versa for each frozen soil individually. This can be done with temperature controlled triaxial or simple shear tests. However, due to practical difficulties, such tests are rarely carried out in practice, and only limited data are available for comparison.

As for temperature colder than about -5°C, results of unconfined compression tests on frozen soil and ice samples are presented in the literature, from which the uniaxial strength and therefore cohesion can be derived. However no information about the effective angle of internal friction ϕ' can be derived. At the given temperatures it can be assumed that all the water is frozen for all sandy and silty soils. The samples are mostly not tested at temperatures above 0°C, therefore no information about the effective angle of internal friction ϕ' is available.

Some tests on sand (e.g., Tsytovich 1975) can be interpreted to define both effective angle of internal friction and cohesion with defined temperature, whereas the volumetric ice content is not shown explicitly. The calculated cohesion *c* of the samples tested at temperatures above 0°C indicates an unsaturated state, but information about saturation is not available.

Ladanyi (1990) shows tests with a measured unfrozen angle of effective friction of ϕ' = 35°. The frozen sand samples were tested at temperatures below and equal to -5°C. At these temperatures all the pore water is basically frozen. The effective angle of friction is assumed to be negligible at this stage.

Goughnour and Andersland (1968), Sego et al. (1982), as well as Sego and Chernenko (1984) present additional values for triaxial compression strength of frozen sands at low

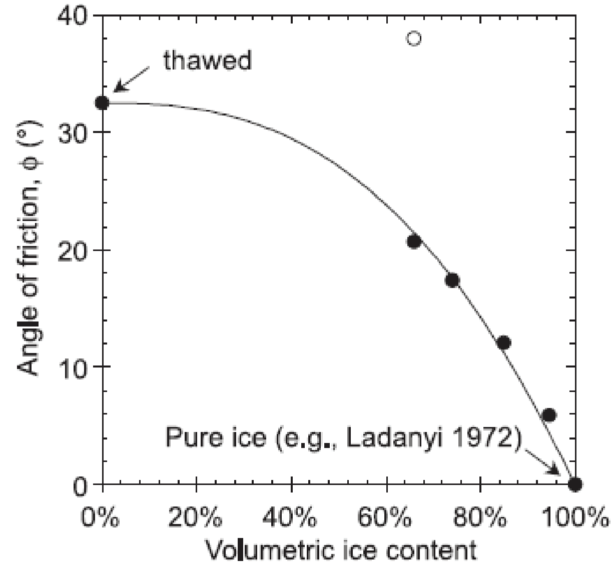

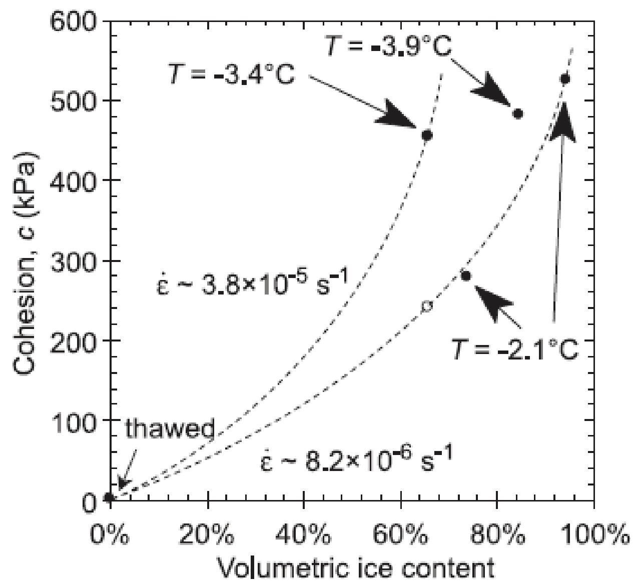

Figure 2. Effective angle of internal friction ϕ' and cohesion *c* as function of the volumetric ice content (Arenson & Springman 2005b).

temperatures. Hivon and Sego (1995), Sego and Chernenko (1984), Sego et al. (1982) and Stuckert and Mahar (1984) take into account the impact of salinity on the strength parameters of frozen soils. However, for comparison, tests were carried out on non-saline samples.

Yuanlin and Carbee (1984) have conducted unconfined compression tests with a constant strain rate and a variation of temperature on frozen silts. The effective angle of internal friction at temperatures above 0°C is not known and assumed to be in the order of ϕ'_{cv} =,32°, which is reasonable for a silty soils. No information about the volumetric ice content is provided. It was assumed that the samples are completely frozen at T = -5°C. The same is true for the results published by Stuckert and Mahar (1984).

In summary, the number of available test data from triaxial compression testing on frozen soils compared to

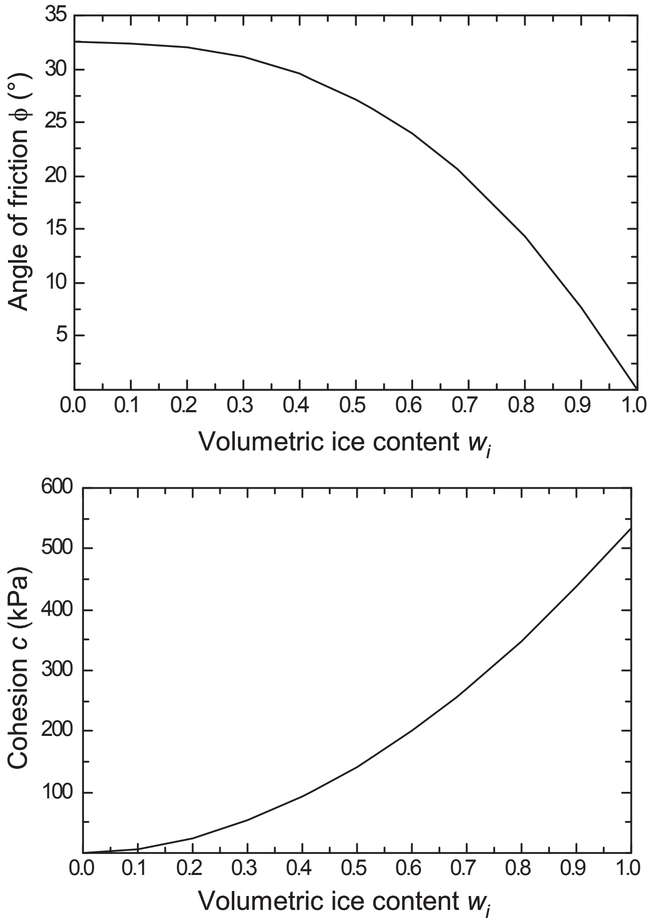

Figure 3. Effective angle of internal friction ϕ' and cohesion c as a function of the volumetric ice content w_i for $\phi'_{initial}$=32°. ϕ' and c are calculated according Equations 1 and 3, respectively.

the number of unconfined compression tests is very limited. In consequence the aim of adding test results to the data produced by Arenson (2005a) was not successful. This reduces the statistical base for the proposed interpretation of the Mohr-Coulomb failure criterion, but nevertheless the concept is worth being followed.

Model

Because of the limited test data available, the approach presented is mainly based and fitted to the data of Arenson and Springman (2005a). The test results have been reevaluated in respect of the two main components of shear strength, i.e. the effective angle of internal friction ϕ' and the cohesion c, as well as for the volumetric ice content w_i and the temperature T. With the given database it was appropriate to normalize the results for a specific temperature and then give a correlation for alternative temperatures. All the relations are curve fits with power law.

As a first input variable the effective angle of internal friction ϕ' of the dry or saturated unfrozen material is needed. For design purposes it is suggested to neglect the dilatancy effects (ψ=0). Unfortunately it is not explicitly stated if a critical, constant volume angle of internal friction, ϕ'_{cv}, or a peak value, ϕ'_{peak}, is presented for most publications where an unfrozen effective angle of internal friction is available.

With increasing volumetric ice content the effective angle of internal friction ϕ' decreases from ϕ'= $\phi'_{initial}$ to ϕ'=0. Arenson and Springman (2005b) suggest the following relationship:

$$\phi' = \phi'_{initial} - \phi'_{initial} \bullet w_i^{2.6} \tag{1}$$

with

ϕ' (°)	effective angle of internal friction,
$\phi'_{initial}$ (°)	initial effective angle of internal friction,
w_i (-)	volumetric ice content.

It is important to note that the angle of internal friction is unaffected by the temperature.

The second input variable is the cohesion c (here not defined as effective or total cohesion). In contrast to the effective angle of internal friction ϕ', the value of cohesion rises with the volumetric ice content w_i. The cohesive strength of the ice matrix is dependent on the temperature represented by two steps of calculation. Firstly the cohesive strength will be calculated for a reference temperature (e.g. -2.1°C) to relate the calculated values to Arenson and Springman (2005b). Secondly cohesion is adapted to any given temperature with a linear correlation. The formulas are given with:

$$c_{(T=-2.1°C)} = 534.93kPa \bullet w_i^{1.91} \tag{2}$$

$$c = -\frac{c_{(T=-2.1°C)}}{2.1} \bullet T \tag{3}$$

with

c (T = -2.1°C) (kPa)	cohesion at reference temperature,
c (kPa)	cohesion,
T (°C)	temperature.

Using these two formulae (Fig. 3) it is possible to set individual strength profiles to a soil stratum for any given temperature profile according to the initial effective angle of internal friction ϕ' and the volumetric ice content w_i of the material. It is now obvious that with the variation of the soil temperature profile provoked by seasonal change of the surface temperature, a redistribution of the strength parameters occurs with time. With higher soil temperatures the frictional component of the shear strength gains importance and vice versa.

The correlations were counterchecked with the few test results described in the literature review section. Effects of the variation of the strain rate are not discussed within this contribution. The significance of the strain rate rises with the volumetric ice content of the sample, whereas the aim of the parameterization is the description of the behavior of temperate alpine permafrost soils; that is, close to zero centigrade. Where not explicitly described, the volumetric ice content w_i was calculated using a power law function neglecting exact knowledge of the soil composition and volumetric water content. The function was chosen as

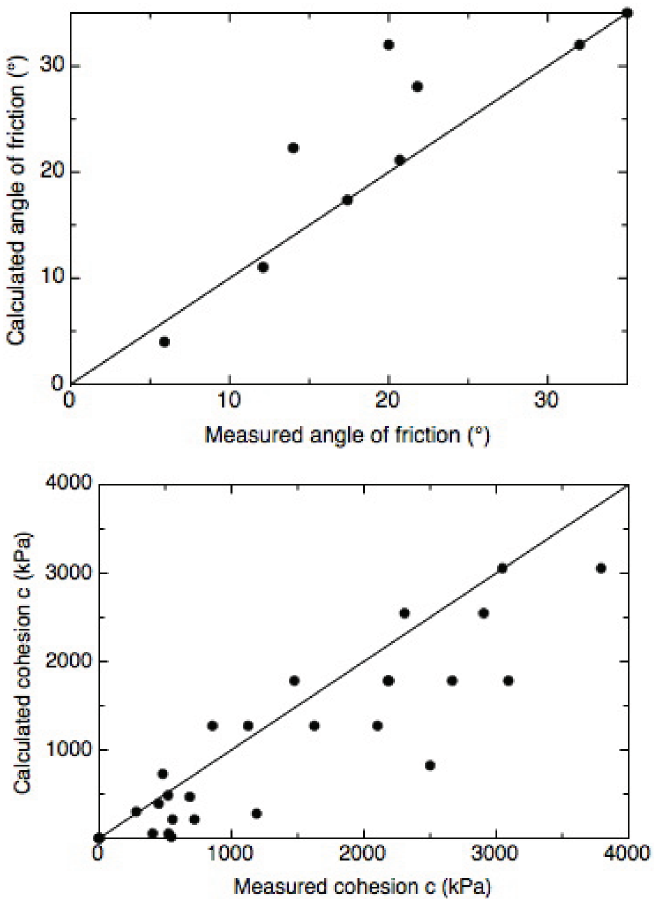

Figure 4. Calculated versus measured angle of friction ϕ' and calculated versus measured values for cohesion *c*.

$$w_i = \left(-\frac{1}{5} \bullet T\right)^{\frac{1}{2}} \quad (4)$$

Equation 4 is based on test results available and has similar form to the unfrozen water content function suggested by Tice et al. (1976). It further inherits the assumption that all soils are completely frozen at T = -5°C. This seems low but includes the variability in the permafrost soil composition even concerning certain clay size particle contents. Such an assumption is on the conservative side.

Figure 4 shows the measured against the calculated values obtained with the proposed strength model. In these figures all the evaluated data is shown, even though some of the tests were conducted at temperatures below to T = -5°C. The inserted diagonal line represents the ideal case of *calculated=measured* values.

The linear correlation with an inclination of 1.1, instead of the drawn ideal line of 1.0 (R^2=0.77) for the effective angle of internal friction ϕ' (Fig. 4), indicates an overestimation of the calculated values, whereas an inclination of 0.8 (R^2=0.80) stands for a more conservative prediction for the cohesion. Some of the scatter can be explained with the variation of the strain rates that have not been considered in the analysis presented.

Table 1 shows the evaluated data for the tests and calculations on material with a temperature T above -5°C.

Table 1. Measured against calculated strength properties of frozen soils.

T °C	w_i -	$\phi'_{measured}$ °	$\phi'_{calculated}$ °	$c_{measured}$ kPa	$c_{calculated}$ kPa	Authors -
-2.1	1.0	5.9	4.0	520	485	A. & S. 2005
-3.9	0.9	12.1	11.0	480	728	
-2.1	0.7	17.4	17.4	280	301	
-3.4	0.7	20.7	21.1	450	392	
		32.0	32.0	0	0	
-1.0	0.5	21.8	28.1	525	55	T. 1975
-2.0	0.6	14.0	22.3	720	212	
		20.0	32.0	0	0	
		35.0	35.0	0	0	L. 1990
-5.0	1.0			1126	1274	
-5.0	1.0			1626	1274	H.&S. 1995
-2.3	0.7			1190	279	
-5.0	1.0			2103	1274	S. &M. 1984
-4.0	0.9			2500	823	G. & A. 1968
-0.5	0.3			545	14	Y. & C. 1984
-1.0	0.5			405	55	
-2.0	0.6			555	212	
-3.0	0.8			685	469	
-5.0	1.0			857	1274	

Example Application

To get a brief overview on the impact of a temperature dependent parameterization of an alpine permafrost soil, a profile from the Muragl rock glacier in Switzerland was chosen for a limit equilibrium analysis using the numerical program Slope/W (GeoStudio2004). Even though rock glacier materials represent special and unique conditions, the concept can be applied to any other frozen soil, assuming soil properties are available. Details and an overview of the Muragl rock glacier can be found in Arenson (2002). The modeled slope has a length of approximately 500 m and a height of approximately 235 m, which results in an overall inclination of about 25°. Bedrock can be found at an average depth of 33 m.

Two measured temperature profiles were applied on the section with a temperature resolution of ΔT = 1.0°C and a geometrical resolution of Δy = 0.5 m. The profiles represent typical conditions with the first temperature profile representing the summer maximum surface air temperature of 12.2°C and the second, the winter minimum surface air temperature of -6.0°C from a one year measurement cycle (Fig. 5). The two states do not implicitly represent coldest or warmest conditions for the interpretation of a global safety factor.

The geotechnical parameters have been set on the basis described above with a resolution according to the temperature profile. The initial effective angle of internal friction was set to ϕ' = 33°, and bedrock was assumed to be impenetrable by a failure mechanism. The limit equilibrium approach follows the Morgenstern-Price method. Neither water flow nor possible unsaturated strength in the unfrozen active layer has been accounted for during the analysis.

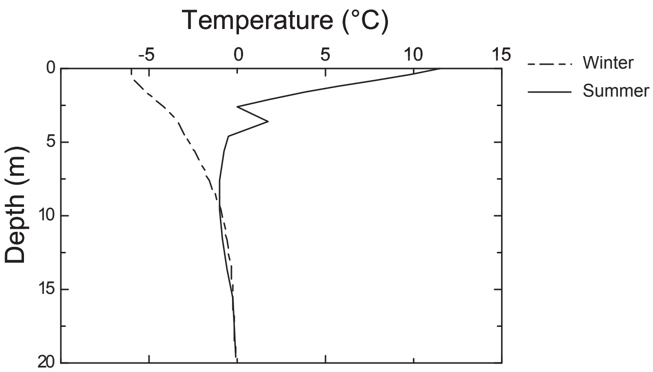

Figure 5. Temperature profile from borehole measurement on the Muragl rock glacier.

Table 2. Data of the temperature profile show in Figure 5.

Y	T_{winter}	T_{summer}
m	°C	°C
0.0	-6.0	11.6
0.4	-6.0	9.8
0.8	-5.8	7.8
1.2	-5.5	5.7
1.6	-5.2	3.9
2.1	-4.7	1.8
2.6	-4.2	0.0
3.6	-3.4	1.8
4.6	-2.9	-0.5
5.6	-2.4	-0.7
7.6	-1.5	-1.0
9.6	-0.9	-1.0
11.6	-0.5	-0.8
13.6	-0.3	-0.6
15.6	-0.2	-0.2
19.6	-0.1	-0.1

Table 3 shows the parameters for each temperature layer. The correlations follow the rules presented above.

Figures 6 and 7 show the results of the limit equilibrium calculations on the Muragl rock glacier cross sections.

The global factor of safety varies between 1.22 and 1.48 from summer to winter, which is a change of 21%. The calculated critical mechanisms show significant differences in size and depth. This is due to the difference in the contribution of friction and cohesion to the global shear resistance. An increase in the frictional component of the shear resistance causes the failure mechanism to shift towards the surface, whereas an increase in cohesion results in a deeper lying failure surface.

These preliminary analyses show minimum safety factors relatively close to a critical value of 1. However, such a result is expected for slopes that form under natural conditions. Nevertheless, the results allow for the possibility of large deformations. It is interesting to note that the failure planes for the winter conditions (Fig. 7) are located approximately at similar depths than the shear zone observed in the active Muragl rock glacier (Arenson et al. 2002). These deformations may therefore be interpreted as the main deformation mechanism observed in active rock glaciers

Table 3. Input parameter for limit equilibrium analysis.

$\phi'_{initial}$	T	w_i	ϕ'	$c'_{(-2.1°C)}$	c
°	°C	-	°	kPa	kPa
33	-5.5	1	0	535	1401
33	-4.5	0.95	4	484	1037
33	-3.5	0.84	12	381	634
33	-2.5	0.71	20	276	329
33	-1.5	0.55	26	169	121
33	-0.5	0.32	31	59	14
33	0 +	0	33	0	0

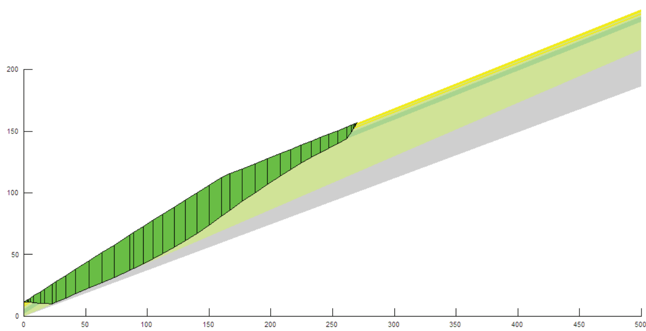

Figure 6. Failure mechanism for a summer temperature profile with a global factor of safety of 1.22.

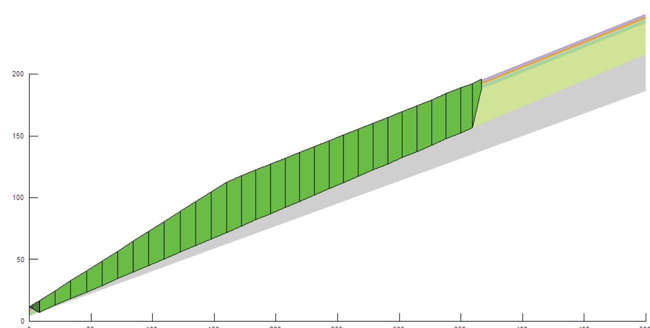

Figure 7. Failure mechanism for a winter temperature profile with a global factor of safety of 1.48.

referred to as creep. Creep is not considered directly during the stability analysis presented. The parameters included in the analysis were chosen as large strain parameters, i.e. large creep deformations are included to a certain extent.

Conclusions

Engineers often struggle with assessing slope stability for temperate frozen slopes. By selecting the appropriate shear strength parameters it is possible to give realistic temperature dependent assessment of the stability of alpine permafrost slopes. A simple approach is presented to incorporate seasonal temperature changes, allowing calculation of slope stabilities in an environment of temperature increase due to global warming. In such a case the model proposes an increasing contribution of the friction component and a decreasing amount of cohesion in the mobilization of shear strength. This leads towards shallower failure surfaces with a lower probability of failure, due to the fact that the angle of effective friction is far less subjected to variability than the cohesive portion of the general shear resistance. In a transient process alpine permafrost slopes with inclinations higher than the sum of the effective angle of friction ϕ'_{cv} and the angle of dilatancy ψ will be subjected to local failures due to the decrease of the bonding effect of the ice matrix. After reaching a new long-term equilibrium the former alpine permafrost slopes will reach a state as observed for the majority of natural slopes with an inclination at about the effective angle of friction.

The major problem with using the presented approach for warm frozen slopes is the lack of test data. Even though results from triaxial compression are standard in geotechnical engineering, only a few data are available for temperate coarse-grained permafrost soils. In addition, it is recommended that interaction between thermal modeling and slope stability calculations utilizing temperature dependent strength parameters should be employed in slope stability analysis. As such numerical tools become available it is still crucial to carry out proper geotechnical laboratory tests for an accurate soil characterization.

Acknowledgments

The authors would like to thank the two anonymous reviewers for their valuable comments on the initial version of the manuscript.

References

Arenson, L.U. 2002. *Unstable Alpine Permafrost: a Potentially Important Natural Hazard*. Ph.D. Dissertation. Institute for Geotechnical Engineering Technische Wissenschaften ETH, Zurich.

Arenson, L.U., Hoelzle, M. & Springman, S.M. 2002. Borehole deformation measurements and internal structure of some rock glaciers in Switzerland. *Permafrost and Periglacial Processes* 13: 117-135.

Arenson, L.U., Johansen, M.M. & Springman, S.M. 2004. Effects of volumetric ice content and strain rate on shear strength under triaxial conditions for frozen soil samples. *Permafrost and Periglacial Process*es 15: 261-271.

Arenson, L.U. & Springman, S.M. 2005a. Triaxial constant stress and constant strain rate tests on ice-rich permafrost samples. *Canadian Geotechnical Journal* 42: 412-430.

Arenson, L.U. & Springman, S.M. 2005b. Mathematical descriptions for the behavior of ice-rich frozen soils at temperatures close to 0°C. *Canadian Geotechnical Journal* 42: 431-442.

Goughnour, R.R. & Andersland, O.B. 1968. Mechanical properties of sand-ice system. *ASCE Journal of the Soil Mechanics and Foundations Division* 94: 923-950.

Hivon, E.G. & Sego, D.C. 1995. Strength of frozen saline soils. *Canadian Geotechnical Journal* 32: 336-354.

Ladanyi, B. & Morel, J.-F. 1990. Effect of internal confinement on compression strength of frozen sand. *Canadian Geotechnical Journal* 27(1): 8-18.

Sego, D.C. & Chernenko, D. 1984. Confining pressure influence on the strength of frozen saline sand. *Cold Regions Engineering Specialty Conference*, *Edmonton, AB*. Montreal: Canadian Society for Civil Engineering, 565-578.

Sego, D.C., Schultz, T. & Banasch, R. 1982. Strength and deformation behavior of frozen saline sand. *3rd International Symposium on Ground Freezing*. Hanover, NH: 11-17.

Stuckert, B. & Mahar, L. 1984. Role of ice content in the strength of frozen saline coarse grained soils. Proceedings, *Cold Regions Engineering Specialty Conference*, *Edmonton, AB*. Montreal: Canadian Society for Civil Engineering, 579-587.

Tice, A.R., Anderson, D.M. & Banin, A. 1976. *The Prediction of Unfrozen Water Contents in Frozen Soils from Liquid Limit Determinations*. CRREL Report 76-8. Hanover, NH.

Tsytovich, N.A. 1975. *The Mechanics of Frozen Ground*. New York, NY: McGraw-Hill Book Company.

Yuanlin, Z. & Carbee, D.L. 1984. Uniaxial compressive strength of frozen silt under constant deformation rates. *Cold Regions Science and Technology* 9: 3-15.

A Permafrost Observatory at Barrow, Alaska: Long-Term Observations of Active-Layer Thickness and Permafrost Temperature

F.E. Nelson, N.I. Shiklomanov, and D.A. Streletskiy
Department of Geography, University of Delaware, Newark, DE, 19716, USA
V.E. Romanovsky and K. Yoshikawa
Geophysical Institute, University of Alaska, Fairbanks, AK, 99775, USA
K.M. Hinkel
Department of Geography, University of Cincinnati, Cincinnati, OH, 45221, USA
J. Brown
International Permafrost Association, P.O. Box 7, Woods Hole, MA, 02543, USA

Abstract

Barrow, Alaska, has a long heritage of permafrost research. The area's initial permafrost temperature measurements were made during the First International Polar Year (1882-83). In the mid 1940s, the U.S. Geological Survey initiated a program of geothermal measurements. In the early 1960s the U.S. Army's Cold Regions Research and Engineering Laboratory established a series of plots for active layer measurements. In the 1990s, National Science Foundation projects expanded the active layer measurement program as part of the emerging Circumpolar Active Layer Monitoring network. A program of borehole temperature measurements was initiated in 2000, when two deep boreholes were drilled and equipped with thermistor cables and data loggers. These sites, located within and adjacent to the Barrow Environmental Observatory, and several other long-term projects on erosion and plant phenology, contribute to this permanent, protected permafrost observatory. Long-term permafrost monitoring programs at Barrow have contributed substantially to development of geocryological theory.

Keywords: active layer; Alaska; Barrow; borehole monitoring; permafrost; thermal regime.

Introduction

The Barrow, Alaska, area has a long history of permafrost observation and research. The initial permafrost temperature observations at Barrow were made during the First International Polar Year (1882–83) in a meat cellar with an average February temperature of -11°C at a depth of 11 m. Beginning in the mid 1940s and continuing into the 1950s, the U.S. Geological Survey (USGS) conducted a wide range of permafrost investigations, including geothermal measurements in many boreholes and shallow measurements in association with construction and exploration activities (Brewer 1958, Lachenbruch & Marshall 1986). In the early 1960s the U.S. Army's Cold Regions Research and Engineering Laboratory (CRREL) established twenty 10×10 m grids on which active layer measurements were made seasonally throughout most of that decade (Brown & Johnson 1965, Brown 1969). Many of these investigations were made in cooperation with, or supported by, the former Naval Arctic Research Laboratory (NARL) in Barrow. Beginning in the early 1990s, a series of National Science Foundation (NSF) projects expanded the active layer measurement program to a 1×1 km grid under what was to become a site within the Circumpolar Active Layer Monitoring (CALM) network. Active layer measurements have been made annually on the CRREL and CALM grids since 1992 (Brown et al. 2000). A program of borehole temperature measurements on the same USGS boreholes was initiated in 2000 and in April 2001. Under this program, two new 50 m deep boreholes were drilled and equipped with thermistor cables, a micrometeorological station, and data loggers (Yoshikawa et al. 2004).

The CALM grids and the deep permafrost observatory boreholes are located within the Barrow Environmental Observatory (BEO), 7500 acres of privately owned land that has been designated for research and long-term observations by the Ukpeagvik Iñupiat Corporation (UIC) landowners and the regional North Slope Borough government (Fig. 1). Several other long-term observational projects are located within the BEO, including the Arctic Coastal Dynamics key sites along Elson Lagoon (Aquirre et al. 2008), and the International Tundra Experiment located within the CALM grid (Hollister et al. 2006, 2008).

The initiatives mentioned above are approved projects of the present International Polar Year (2007–2009). The International Permafrost Association's legacy for the IPY is to establish a permanent network of permafrost observatories on protected lands. The Barrow permafrost observatory is an excellent example of a long-term monitoring site. It is also part of the Global Terrestrial Network for Permafrost (GTN-P) (Brown et al. 2000). As a follow-up to the First International Polar Year measurements, temperatures are being monitored with miniature data loggers in several active meat cellars in the Barrow communities.

Earlier papers by the present authors have reported on previous results for these active layer and permafrost temperature sites (Nelson et al. 1998, Romanovsky et al.

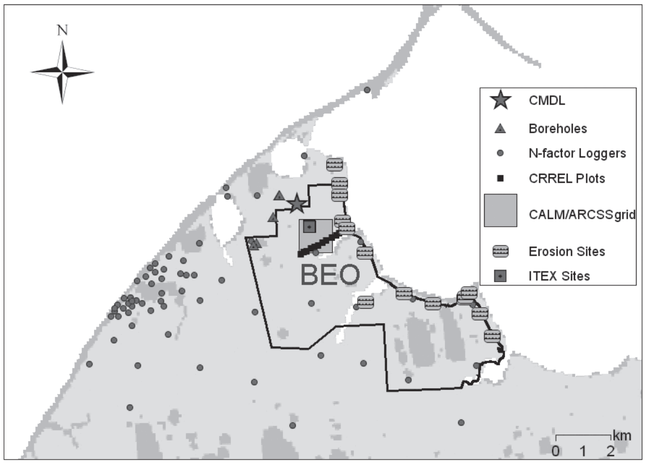

Figure 1. Map of the Barrow Environmental Observatory, showing main research sites mentioned in the text.

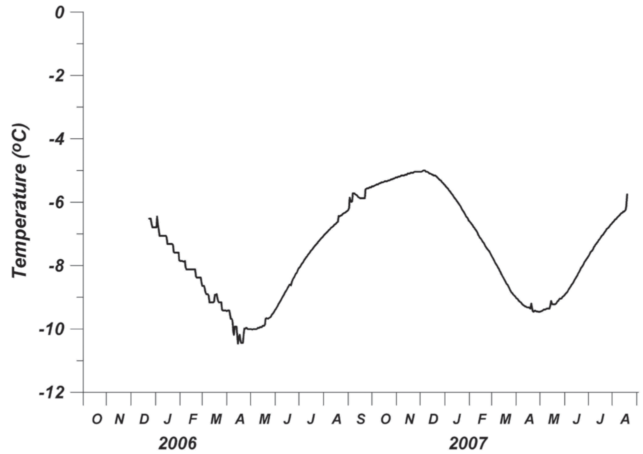

Figure 2. Temperature (hourly readings) in the meat cellar of a Barrow resident (Richard Glenn), from late 2005 through summer 2007. Instrumentation was changed in March 2006.

2002, Hinkel & Nelson 2003, Yoshikawa et al. 2004). This paper updates the earlier results from continuing projects, adds to their interpretations, and documents the existence of this permafrost observatory. A complete history of permafrost research at Barrow remains to be written.

Local Environment

Barrow, Alaska (71.3°N, 156.5°W, population 4600) is situated at the confluence of the Beaufort and Chuckchi Seas. Although Barrow's climate is influenced by its proximity to the Arctic Ocean, mean annual temperature in the village is -12°C, and the annual range of mean monthly temperature is about 31°C. Precipitation averages 106 mm yr^{-1}, with about 63% falling as rain during the brief summer. Topography is dominantly level, the area's primary relief being produced by the juxtaposition of drained thaw lakes and intervening "upland" tundra (Hinkel et al. 2005). Soils, developed on the unconsolidated Gubik Formation of Late Pleistocene age (Black 1964), show considerable variation (Bockheim et al. 2001). Permafrost underlies the entire area and reaches depths of more than 400 m. The upper permafrost contains abundant excess ice, with combined pore and lens ice averaging 50-75% in the upper 2 m (Sellmann et al. 1975). Ice-wedge networks are ubiquitous in the Barrow area.

Data Collection

The Circumpolar Active Layer Monitoring (CALM) program has operated in Barrow since 1991. Initially developed under the auspices of the International Tundra Experiment (ITEX), CALM acquired its own funding base from the U.S. National Science Foundation in 1998. The CALM protocol is well documented in published papers and on the CALM web site (Brown et al. 2000, Nelson et al. 2004a, 2004b; <http://www.udel.edu/ Geography/calm/>). At Barrow, thaw depth is measured at each of the 121 grid nodes on the CALM/ARCSS 1 km^2 grid; nodes are spaced 100 m apart. Using a graduated steel probe, thaw depth measurements are typically made in mid-August, when the active layer is at its maximum thickness. Active-layer thickness data continue to be collected annually on the 10×10 m "CRREL Plots" established in the early 1960s (Brown & Johnson 1965, Brown 1969).

Soil temperatures have been monitored hourly since 1993 at two sites near the CRREL study area. Measurements are recorded to depths of 1.2 m using Campbell data loggers reading Measurement Research Corporation (MRC) thermistor probes, and yield data comparable to those obtained during CRREL's programs at Barrow in the early 1960s. Several other shallow (0.0 to 1.2 m) ground temperature installations are maintained in cooperation with the U.S. Department of Agriculture's Natural Resources Conservation Service and the National Oceanic and Atmospheric Administration.

High-precision frost heave and thaw settlement measurements are made on the BEO using differential global positioning system (DGPS) technology (Little et al. 2003). Several of the former CRREL sites are monitored via DGPS, as is a series of nearby geomorphic forms, primarily frost boils. These observations continue a series of measurements first implemented at Barrow in the early 1960s (Lewellen 1972).

As part of the International Polar Year 2007–2008 initiative, the program of thermal measurements in Barrow meat cellars, first instituted in 1882-83 (Ray 1885), has been resumed. Data are recorded in the meat cellars of several Barrow residents at 1 hr intervals, using miniature two-channel data loggers (Fig. 2). Peak annual temperature lags several months after its July peak in the Barrow air-temperature record. Temperature is recorded at a depth of approximately 7 m in the cellar.

Snow surveys are conducted each spring by measuring snow depth at the 121 grid nodes on the 1 km^2 CALM/ ARCSS grid. Typically, two measurements are made at each grid node using a graduated steel probe. Snow depth measurements are made in April or May.

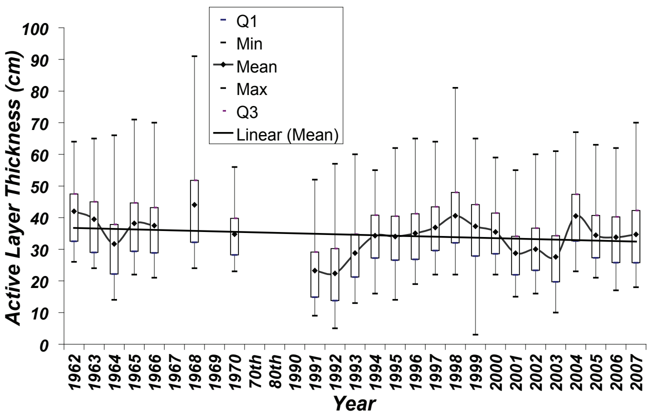

Figure 3. Box plots (Tukey 1977) of active-layer thickness on the CRREL plots at Barrow for the period 1962–2007. Maximum, minimum, and mean values are indicated, as are quartile (Q) locations and a linear fit to annual mean values.

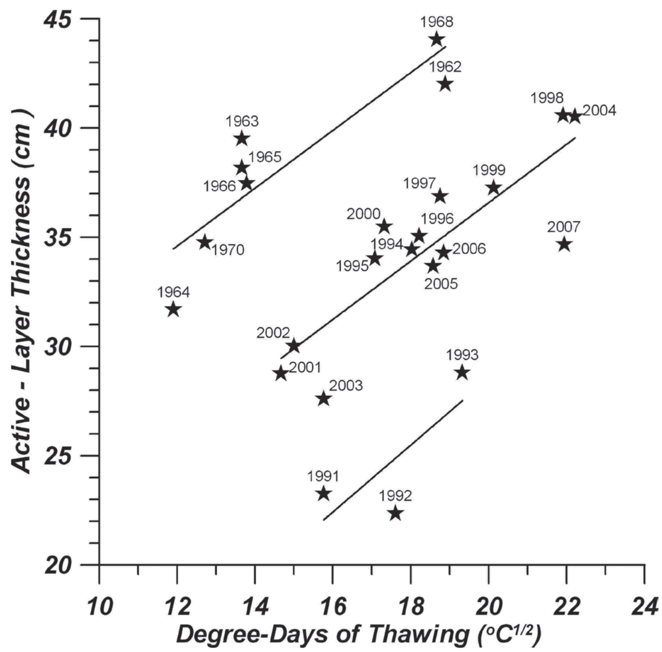

Figure 4. Active-layer thickness vs. thawing index at Barrow, Alaska, 1962–2007.

Four boreholes are being monitored under the Thermal State of Permafrost (TSP) program (Romanovsky et al. 2002), using Campbell data loggers. Two boreholes are the original USGS holes (Lachenbruch & Marshall 1986), with new cables and the two new ones were drilled in 2001. New thermistor cables were installed in several of the 1950s USGS boreholes to depths of 9, 14, and 24 m.

Long-term air-temperature measurements began at the National Weather Service site in Barrow in 1922, and data from this ongoing program are available through the archives of the U. S. National Climate Data Center (<http://www.ncdc.noaa.gov/oa/ncdc.html>). A geographic-ally extensive data set was also collected at hourly intervals between 2001 and 2005 within a 150 km^2 area surrounding Barrow, including sites within the BEO, using a network of approximately 70 data loggers recording air and near-surface soil temperature, as part of the Barrow Urban Heat Island Study (Hinkel et al. 2003; Hinkel & Nelson 2007).

Data from NSF-supported sites are reported annually to the University Consortium for Atmospheric Research, and are ultimately deposited in the National Snow and Ice Data Center's Frozen Ground Data Center (<http://nsidc.org/fgdc/>). Data sets are made available periodically on CDs issued by the Global Geocryological Data system (Parsons et al. 2008). CALM data are also available through the CALM program's web site at the University of Delaware.

Results

Active layer

For the last decade (1998–2007), CALM active-layer thickness (ALT) data, averaged over the grid, have remained close to the range of values from the 1960s (Fig. 3). ALT values in the early 1990s were substantially less than in the 1960s and early 2000s. Maximum values were recorded in 1998 and 2004 (42 cm); these values coincide with the warmest summers. The 2003 minimum (29 cm) was similar to 1993 but deeper than the shallowest thaws of 1991 and 1993 (24 cm).

Based on statistical analysis of ALT values from the Barrow CRREL plots, Nelson et al. (1998) argued that the active layer in ice-rich terrain displays "Markovian behavior," i.e., it tends to remain within a tightly constrained range of depths until a climatic, anthropogenic, or other perturbation causes it to shift to a new datum, where it remains until another perturbation causes it to become "set" at another new level (Fig. 4).

Average active-layer thickness from the Barrow CRREL plots is plotted against the square root of the thawing index (annual thawing degree days) for all years of record in Figure 4. The additional data collected over the past decade appear to confirm the hypothesis advanced by Nelson et al. (1998). Three distinct curves have emerged, each consisting of a series of sequential years.

Nelson et al. (1998) advanced a series of hypotheses to explain the apparently sudden changes in ALT, concluding that they most likely result from penetration of thaw into the ice-rich layer in the upper permafrost. Subsequently, Shur et al. (2005) provided a theoretical explanation for such behavior, involving the "transient layer," an intermediate layer of ground that cycles between permafrost and non-permafrost status at decadal to millennial time scales. Bockheim & Hinkel (2005) found abundant cryostratigraphic evidence for fluctuations in the transient layer ("transition zone") in the Barrow area.

Thaw settlement

The transient layer concept advanced by Shur et al. (2005) also helps to explain why data from mechanical probing of the active layer may not show long-term correspondence with climatic warming. Penetration of thaw into or through the transient layer can result in pronounced differential settlement at the surface. Besides jeopardizing structures at the surface, this phenomenon may obscure the record of climate-induced changes in ice-rich permafrost environments (Streletskiy et al. 2008).

The Barrow site was used to evaluate long-term trends in terrain first surveyed in the early 1960s (Lewellen 1972). DGPS and ALT measurements were performed in June and August of every year for the period 2001–2006. All sites were equipped with temperature loggers measuring air and ground surface temperature at hourly intervals. Winter heave (Hw) was assumed as the difference in elevation of the ground surface between June of a specified year and August of the previous year. Summer subsidence (Hs) was estimated as the difference in ground surface elevation between August and June of the same year.

On average, winter heave did not compensate for summer ground subsidence at most of the North Slope landscapes investigated during the 2001–2006 observation period (Streletskiy et al. 2008). Comparison of our data at Barrow with the historical record there (Lewellen 1972) shows that significant changes in the elevation of the ground surface have occurred over the past four decades. The survey of 1964 was made in July, while our measurements were made in June and August. Comparison of elevation data from August of 2006 with those from July of 1964 shows that total elevation change (Ht) for three sites is -21.4 to -23.6 cm, while one site shows Ht = 30.6 cm. This produces an average value of -8.9 cm in 42 years, or -0.2 cm/year. Comparison of the July 1964 data with those from June of 2006 yields an average for the four sites of -6.2 cm or -0.15 cm/year. Average Hs over the last four years at the four sites is -2.2 cm, while Hw is 1.4 cm, The average elevation change at the four sites between June of 2006 and June 2003 is 1.1 cm, while the difference between August elevations for the same period is -7 cm. Long term subsidence and frost heave almost compensate for each other, while over the short term the amplitude of both Hs and Hw varied greatly. Long-term ground elevation change is less than that over the short term. The amplitude of surface elevation changes may, however, have increased during the last 40 years.

Interpolation/validation procedures

Owing to logistical constraints, "end-of-season" active-layer thickness is measured on a different date virtually every year. Variations in year-to-year weather dictate that the active layer may not have reached its maximum extent in late August in some years, while in other years upfreezing from the base of the active layer may have begun by this time. In both situations an underestimate of maximum ALT is obtained. Figure 5 shows results from a form of interpolation, used to describe the dynamics of thaw penetration at Barrow by comparing data derived from two techniques for measuring ALT: direct measurements using a metal probe at the CRREL plots and those interpolated from MRC temperature probes. Only summers in which ALT was measured more than three times were used (1963, 1964, 1966, 1994, and 2004). The polynomial fit is based on 42 sets of measurements from

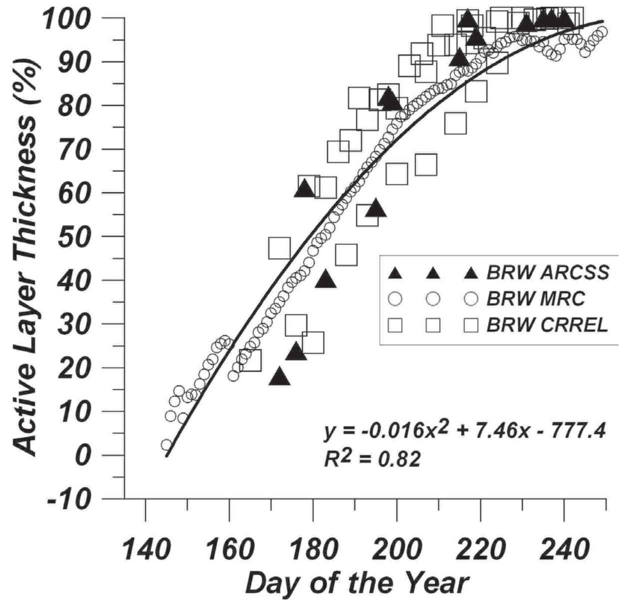

Figure 5. Active-layer depth measurements from the CALM grid, CRREL plots, and nearby Campbell/MRC installation. Statistical relation in the figure were obtained by fitting a polynomial to the probed data. The solid line was produced by fitting a polynomial equation to the MRC data, yielding an R^2 value of 0.96.

these years, where maximum thaw depth was assumed to have been reached. An independent data set, measured at the neighboring 1 km^2 CALM grid (BRW ARCSS), was included (years 1995, 1996, 2001, and 2006); these were also believed to show maximum thaw. Finally, daily interpolated values of ALT from the MRC probes for 1993-2001 period (BRW MRC) were plotted. Despite differences in measurement techniques, sampling design and date of observation, the points fall very close to the fit produced from the Barrow CRREL plots (BRW CRREL). This procedure accounts for about 80% of the variation in thaw depth at the Barrow sites. This technique, based on Pavlov's (1984) methodology, can be used to estimate percent of thaw penetration on a particular day of the year or to adjust a measured thaw depth to maximum ALT (Streletskiy et al. 2008).

Permafrost temperature

Figure 6 shows permafrost temperatures from the several newly instrumented boreholes. The upper graph shows the first year's results for the new 50 m borehole. The lower graph compares the 1950 annual profile with current measurements. These initial results, for this specific site at the 14 m depth, indicate warming of about 1.2°C. This small increase over such a long period is consistent with a previous analysis of long-term permafrost temperature variations at Barrow for the period 1924–1997 (Romanovsky et al. 2002).

Those results implied that the observed 1.2°C difference at 14 meters in permafrost temperatures between 1950 and current temperatures is due to very recent warming during the late 1990s. Much colder permafrost temperatures at the permafrost table (up to 2 to 3°C colder) were typical for Barrow during the 1970s.

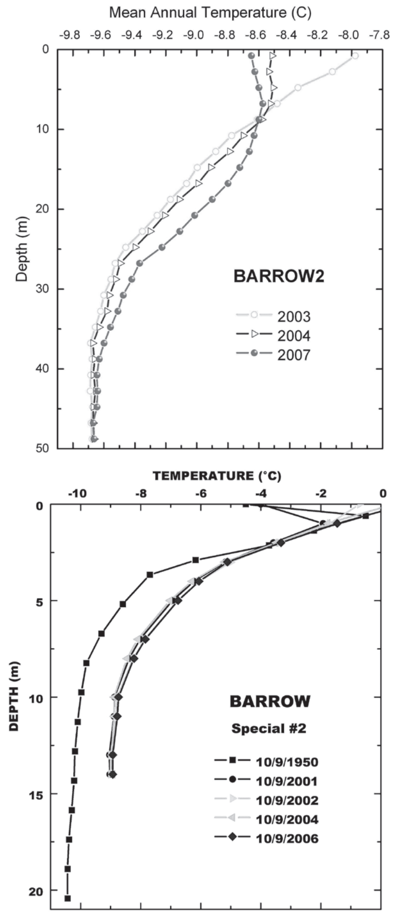

Figure 6. Upper: Annual permafrost temperatures at the new North Meadow Lake permafrost observatory, Barrow, Alaska. Lower: Comparison of 1950 and 2000s permafrost temperatures at the nearby Special 2 site.

Conclusions

Barrow has served as a permafrost observatory for more than a century, and the geocryological data record produced in the Barrow vicinity is unrivaled in Alaska in terms of length, diversity, and depth. The Barrow area played host to many pioneering studies on the roles that permafrost plays in global-change science, and the BEO continues to provide data important to those efforts. Because the Barrow Environmental Observatory is adjacent to an urbanized area there is abundant opportunity for local applications of the information obtained within BEO confines. The village of Barrow generates a significant urban heat-island effect (Hinkel et al. 2003, Hinkel & Nelson 2007), and the BEO is therefore an excellent location to attempt discernment between the geocryological impacts of anthropogenic factors and climatic variations (Nelson, 2003).

Barrow's geocryological data records illustrate the importance and effectiveness of sustained, well-organized monitoring efforts supported by adequate logistical arrangements. Sustained monitoring programs contribute much to the often subtle interplay between theory, application, and observation. Monitoring programs can reveal relationships that become apparent only decades after measurement programs are begun.

Acknowledgments

The permafrost investigations described in this paper were carried out within the Barrow Environmental Observatory, private land designated for research and long-term observation by the Ukpeagvik Iñupiat Corporation (UIC). The Barrow Arctic Science Consortium (BASC), a not-for-profit organization dedicated to scientist/community collaboration, was designated by UIC to manage the BEO with support from the U.S. National Science Foundation. We are grateful to both UIC and BASC for the opportunity to establish and maintain these observatories. Individual projects are supported by NSF grants in support of CALM (OPP-9732051 to the University of Cincinnati and OPP-0352958 to the University of Delaware) and TSP (ARC-0632400 and ARC-0520578 to the University of Alaska Fairbanks). Opinions, findings, conclusions, and recommendations expressed in this paper are those of the authors, and do not necessarily reflect the views of the National Science Foundation. We are grateful to four anonymous reviewers for criticism and suggestions that led to significant improvements in this paper. This paper is a contribution to both the present International Polar Year, and to the Permafrost Young Researchers Network (PYRN) through the efforts of the junior author (DAS).

References

Aguirre, A. et al. 2008. Erosion of the Barrow Environmental Observatory coastline 2003-2008, northern Alaska. (*this proceedings*).

Black, R.F. 1964. Gubik Formation of Quaternary age in northern Alaska. *U. S. Geological Survey Professional Paper302-C*: 59-91.

Bockheim, J.G. & Hinkel, K.M. 2005. Characteristic and significance of the transition zone in drained thaw lake basins of the Arctic Coastal Plain. *Arctic* 58: 406-417.

Bockheim, J.G., Hinkel, K.M. & Nelson, F.E. 2001. Soils of the Barrow region, Alaska. *Polar Geography* 25(3): 163-181.

Brewer, M.C. 1958. Some Results of Geothermal Investigations of Permafrost in Northern Alaska. *Transaction, AGU*, 39, 19-26.

Brown, J. 1969. Soil properties developed on the complex tundra relief of Northern Alaska. *Builetyn Peryglacjalny* 18, 153–167.

Brown, J. 2006. Permafrost and the International Polar Year. *Proceedings of the 13th International Conference: Cold Regions Engineering 2006, Current Practices in Cold Regions Engineering*. July 23-26, 2006, Orono, Maine, 9 pp.

Brown, J, Hinkel, K.M. & Nelson, F.E. 2000. The Circumpolar Active layer Monitoring (CALM) Program: Research Designs and Initial Results. *Polar Geography* 24 (3) 165-258 (published in 2002).

Brown, J. & Johnson, P.L. 1965. Pedo-ecological investigations at Barrow, Alaska. U.S. Army Cold Regions Research and Engineering Laboratory, *CRREL Technical Report 159*, 32 pp.

Brown, J., Jorgenson, M. T., Smith, O.P. & Lee, W. 2003. Long-term rates of erosion and carbon input, Elson Lagoon, Barrow, Alaska. In *ICOP 2003 Permafrost: Proceedings of the 8th International Conference on Permafrost*. M. Phillips, S.M. Springman, and L.U. Arenson, eds.) A.A. Balkema Publishers, Netherlands, 101-106.

Hinkel, K.M., Frohn, R.C., Nelson, F.E., Eisner, W.R., Beck, R.A. & Bockheim, J.G. 2005. Morphometric and spatial analysis of thaw lakes and drained thaw lake basins in the western arctic coastal plain, Alaska. *Permafrost and Periglacial Processes* 16(4): 327-341.

Hinkel, K.M., Nelson, F.E., Shur, Y., Brown, J. & Everett, K.R. 1996. Temporal changes in moisture content of the active layer and near-surface permafrost at Barrow, Alaska, U.S.A., 1962-1994, *Arctic and Alpine Research* 28(3): 300-310.

Hinkel, K.M., Nelson, F.E., Klene, A.E & Bell, J.H. 2003. The urban heat island in winter at Barrow, Alaska. *International Journal of Climatology*, 23, 1889-1905.

Hinkel, K.M. & Nelson, F.E. 2007. Anthropogenic heat island at Barrow, Alaska, during winter: 2001-2005. *Journal of Geophysical Research-Atmospheres*, 112, D06118, doi:10.1029/2006JD007837.

Hollister, R.D., Webber, P.J., Nelson, F.E. & Tweedie, C. E. 2006. Soil thaw and temperature response to air warming varies by plant community: Results from an open-top chamber experiments in northern Alaska. *Arctic, Antarctic, and Alpine Research* 38(2): 206-215.

Hollister, R.D., Webber, P.J., Slider, R.T., Nelson, F.E. & Tweedie, C.E. 2008. Soil temperature and thaw response to manipulated air temperature and plant cover at Barrow and Atqasuk, Alaska (*this proceedings*).

Lachenbruch, A.H. & Marshall, B.V. 1969. Heat flow in the Arctic. *Arctic* 22: 300-311.

Lachenbruch, A.H. & Marshall, B.V. 1986. Changing climate: Geothermal evidence from permafrost in the Alaskan Arctic *Science* 234: 689-696.

Lewellen, R.I. 1972. *Studies on the Fluvial Environment: Arctic Coastal Plan Province, Northern Alaska* (2 vols.) Palmer, AK: Lewellen Arctic Research.

Little, J., Sandall, H., Walegur, M. & Nelson, F.E. 2003. Application of differential GPS to monitor frost heave and thaw settlement in tundra environments. *Permafrost and Periglacial Processes* 14(4): 349-357.

Nelson, F.E. 2003. (Un)frozen in time. *Science* 299: 1673-1675.

Nelson, F.E. (ed.). 2004. Special Issue: Circumpolar Active Layer Monitoring (CALM) Workshop. *Permafrost and Periglacial Processes* 15(2): 99-188.

Nelson, F.E. (ed.). 2004. Eurasian Contributions to the Circumpolar Active Layer Monitoring (CALM) Workshop. *Polar Geography* 28(4): 253-340.

Nelson, F.E., Outcalt, S.I., Brown, J., Shiklomanov, N.I. & Hinkel, K.M. 1998. Spatial and temporal attributes of the active-layer thickness record, Barrow, Alaska. *Proceedings, Seventh International Conference on Permafrost, 23-27 June 1998, Yellowknife, Canada*, Antoni G. Lewkowicz and Michel Allard (eds.), Universite Laval, Centre d'etudes nordique, Collection Nordicana No. 57, 797-802.

Pavlov, A.V. 1984. *Energy Exchange in Earth's Land-scapes.* Novosibirsk: Nauka, 256 pp. (in Russian).

Parsons, M.A., Romanovsky, V.E., Shiklomanov, N.I. Christiansen, H.H., Overduin, P., Zhang, T., Balks, M. & Brown, J. 2008. Managing permafrost data: Past approaches and future directions (*this proceedings*).

Ray, P.H. (ed.). 1885. *Report of the International Polar Expedition to Point Barrow, Alaska*. Washington, DC: Government Printing Office.

Romanovsky, V.E., Burgess, M., Smith, S, Yoshikawa, K. & Brown, J. 2002. Permafrost temperature records: Indicator of climate change. *Eos* 83 (50): 589, 593-594.

Sellmann, P.V., Brown, J., Lewellen, R.I., McKim, H. & Merry, C. 1975. The classification and geomorphic implications of thaw lakes on the Arctic coastal plain, Alaska. *U. S. Army Cold Regions Research and Engineering Laboratory Research Report 334*.

Shiklomanov, N., Nelson, F.E., Streletskyi, D.A., Hinkel, K.M. & Brown, J. 2008. The Circumpolar Active Layer Monitoring (CALM) program: data collection, management, and dissemination Strategies (*this proceedings*).

Shur, Y., Hinkel, K.M. & Nelson, F.E. 2005. The transient layer: implications for geocryology and global-change science. *Permafrost and Periglacial Processes*, 16(1), 5-17.

Streletskiy, D.A., Shiklomanov, N.I. & Nelson, F.E. 2005. Monitoring of thaw settlement using a differential global position system approach. In: *Proceedings of the Third Russian Conference on Geocryology*, vol. 2, 163-169.

Streletskiy, D., Shiklomanov, N.I., Nelson, F.E. & Klene, A.E. 2008. Long-term active layer and ground surface temperature trends: 12 years of observations at Alaskan CALM sites (*this proceedings*).

Tukey, J. 1977. *Exploratory Data Analysis*. Reading, MA: Addison-Wesley Publishing Company, 499 pp.

Wood, K. & Streletskiy, D.A. 2008. Soil and Permafrost Temperature Data Obtained During the First International Polar Year (*this proceedings*).

Yoshikawa, K., Romanovsky, V., Duxbury, N., Brown, J. & Tsapin, A. 2004. The use of geophysical methods to discriminate between brine layers and freshwater taliks in permafrost regions. *Journal of Glaciology and Geocryology* 26:301-309.

—*Plenary Paper*—

Decadal Results from the Circumpolar Active Layer Monitoring (CALM) Program

Frederick E. Nelson and Nikolay I. Shiklomanov
Department of Geography, University of Delaware, Newark, DE 19716, USA
Kenneth M. Hinkel
Department of Geography, University of Cincinnati, Cincinnati, OH 48221, USA
Jerry Brown
International Permafrost Association, P.O. Box 7, Woods Hole, MA, 02543, USA

Abstract

The Circumpolar Active Layer Monitoring (CALM) program was established in the early 1990s to observe temporal and spatial variability of active layer thickness, active layer dynamics, near-surface permafrost parameters, and the response of these factors to changes and variations in climatic conditions. The CALM network involves 15 participating countries and is comprised of 168 sites distributed throughout the Arctic, parts of Antarctica, and several mountain ranges of the mid-latitudes. Groups of sites are used to create regional maps of active layer thickness. Data obtained from the network are used to validate permafrost, hydrological, ecological, and climatic models at a variety of geographic scales. Several sites have records of frost heave and thaw subsidence that are contributing to a reconceptualization of the role of the active layer in global-change studies.

Keywords: active layer; climate change; mapping; monitoring; permafrost; thaw subsidence.

Introduction

Although formal monitoring programs incorporating measurements of depth to permafrost were in existence in the nineteenth century (Richardson 1839, Yachevskyi & Vannari 1912, Shiklomanov 2005) they generally lasted only a few years. Until the early 1990s, the majority of data describing and measuring the thickness, variability, and thermal regime of the active layer were collected in support of specific ecological, geomorphic, or engineering investigations and programs. The limited duration of most field measurement programs yielded only short data records, providing an inadequate basis for analyzing long-term trends. Sampling designs and data-collection procedures were not standardized, making inter-site and inter-regional comparisons problematic. The prospects for using information about the active layer in larger geographic and systems contexts were limited further by the lack of a suitable archive for such information.

Increasing recognition of the active layer's importance in the context of global climate change (e.g., Kane et al. 1991) provided much of the impetus for creating a long-term monitoring program focusing on the active layer and shallow permafrost. This paper provides a sketch of the CALM program's history, including a review of its benchmark objectives and achievements. As the CALM II program nears the end of its second five-year term of financial support, it is appropriate to take stock of accomplishments and to project future directions.

Early History of CALM

Following discussions at an international symposium held in West Siberia in 1989 (Melnikov 1990), the concept of the Circumpolar Active Layer Monitoring (CALM) program was developed to observe the long-term response of the active layer and near-surface permafrost to changes in climatic parameters. Initial foci of the program included "data rescue" activities and creation of a data archive (Barry 1988, Barry et al. 1995), building an alliance of field scientists willing to share data (Brown et al. 2000), execution of critical field experiments (Mueller 1996, Nelson et al. 1998a), and development of a data-collection protocol (Nelson et al. 1996). By the middle of the decade, many of these tasks had been implemented (Brown et al. 1995, 1997) and most of the components necessary to implement a comprehensive international network of CALM stations were in place.

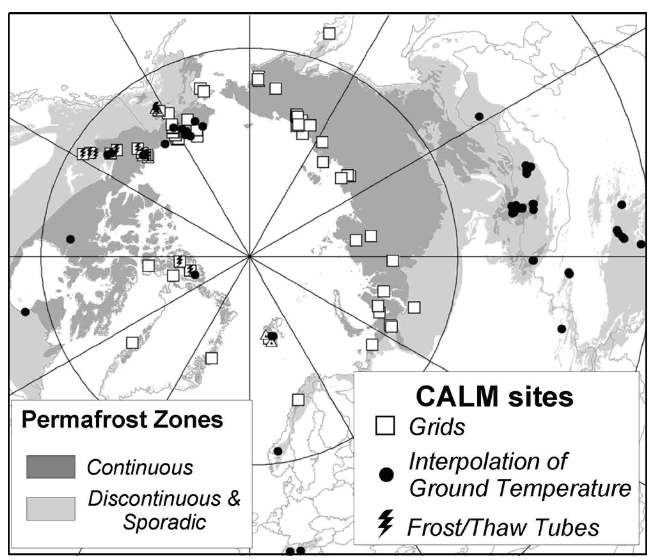

Figure 1. Permafrost distribution and location of CALM sites in the Northern Hemisphere as of 2008. Sites are grouped according to active layer monitoring methods. After Shiklomanov et al. (2008).

During this early period, considerable emphasis was placed on developing monitoring and sampling methodologies. In association with the Arctic Flux Program in northern Alaska (Weller et al. 1995), a grid-based sampling framework was developed and tested extensively (Fagan 1995) for obtaining data with manual probes. Experiments were also conducted with frost/thaw tubes (Nixon & Taylor 1998, Nixon et al. 2003) and monitoring of the shallow thermal regime (Paetzold et al. 2000, Hinkel et al. 2001). Results indicated that the various techniques were complementary and that no single data-collection strategy could achieve adequate results at all sites. Accordingly, CALM has maintained a variety of measurement techniques to the present time (Fig. 1).Until 1998, no formal funding mechanism for CALM was in place, and the initial CALM protocol was published as part of a manual (Molau & Molgaard 1996) developed for the International Tundra Experiment (ITEX) program, which formed an organizational umbrella for CALM during the early and mid-1990s.

CALM I

To implement CALM as a quasi-independent global-change monitoring program, the U.S. National Science Foundation's (NSF) Office of Polar Programs provided a five-year grant (1998–2002) to the University of Cincinnati. The proposal addressed the clear and pressing need to integrate Russian monitoring sites into the CALM network. An organizational meeting at the Seventh International Conference on Permafrost, held in Yellowknife NWT in July 1998, provided a forum for implementing CALM's goals, field instrumentation, sampling designs, and data-handling procedures.

Under the NSF-sponsored *Arctic Transitions in the Land-Atmosphere System* (ATLAS) program, the CALM network expanded by developing additional Alaskan sites. Existing or newly developed sites in Canada, China, Greenland, Kazakhstan, Mongolia, Norway (Svalbard), Sweden, Switzerland, and Antarctica were brought into the program, mostly on a voluntary basis, making it both bipolar and circumpolar. The CALM I project provided a variety of field instruments, data loggers, and standardized protocols for active layer measurements. A web site was established and metadata and data were maintained at this location, with periodic transfer to the Joint Office of Scientific Studies (JOSS) and the National Snow and Ice Data Center (NSIDC) in Boulder, Colorado. CALM data became an integral part of the CDs produced by NSIDC for the 7th and 8th International Conferences on Permafrost (Parsons & Zhang 2003).

Measurements conducted under CALM I represented a distillation of knowledge about the active layer and its behavior as understood at the time the NSF proposal was written in 1997. The proposal focused on five interrelated hypotheses that guided field and analytic work from 1998 to 2003. Several of these hypotheses have been confirmed by subsequent work, while others were in need of refinement from both theoretical and observational standpoints. Brief statements of these hypotheses are summarized in the following paragraphs.

(1) One of CALM I's central hypotheses specified that "the thickness of the active layer will increase in concert with climatic warming," noting that this concept is one of the basic tenets of global-change science in cold regions. Intervening years of monitoring and analytic activities under CALM have confirmed that refinement of this straightforward hypothesis is in order. Although sites in tundra environments show strong correlation between cumulative summer warmth (thawing degree days) and ALT, this relation is much weaker at boreal sites (Brown et al. 2000). Ecological changes, (e.g., non-acidic to acidic tundra (Walker et al. 1998) or development of shrubs (Sturm et al. 2001) may create sufficient insulation at the surface to offset or even counteract a simple temperature-ALT relation. Subsequent work under CALM II has shown that consolidation accompanying penetration of thaw into an ice-rich stratum at the base of the active layer can result in subsidence of the surface but little or no apparent thickening of the active layer, as traditionally defined.

(2) A complementary but very general hypothesis held that nonlinearities in the ALT-temperature relation are introduced by the multiplicity of variables involved. This hypothesis has been confirmed by subsequent work, and both modeling (e.g., Oelke & Zhang 2004, Anisimov et al. 2007, Shiklomanov et al. 2007) and field experiments (e.g., Hinkel & Nelson 2003) continue to address the issue.

(3) Work on the 1 km^2 ACRSS/CALM grids in northern Alaska in the mid 1990s indicated that ALT would show significant spatial and temporal autocorrelation. Subsequent work, which included formal sampling designs and statistical evaluation (Nelson et al. 1998a, 1999, Gomersall & Hinkel 2001, Shiklomanov & Nelson 2002, Hinkel & Nelson 2003, Shiklomanov & Nelson 2003), has confirmed this hypothesis. The strength of the autocorrelation function shows extreme variation in different localities; where the wavelength of important influences is large (e.g., in terrain containing abundant drained thaw lakes) ALT exhibits a large degree of spatial structure. Conversely, where local influences show considerable variation (e.g., in tussock terrain) ALT exhibits little discernable spatial structure, except over very small areas (Mueller 1996). Progress was also achieved under CALM I in the temporal domain. Several studies (Nelson et al. 1998b, Shiklomanov & Nelson 2002, Hinkel & Nelson 2003, Walker et al. 2003) found that, when stratified by vegetation/soil association ("landcover units"), ALT clearly shows a response to variation in summer climatic parameters, particularly temperature, in a predictable fashion. As a result, spatial patterns of ALT remain relatively constant, independent of thaw magnitude (i.e., whether it is a "hot" or "cold" summer). The implications of these findings are large, both for scaling to larger regions and for purposes of prediction via climate scenarios.

(4) A fourth, very general, hypothesis suggested that increased ALT and associated hydrological disruptions will lead to adverse societal effects, particularly damage to infrastructure. Considerable evidence exists in support

of this hypothesis, but the issue is awash with nuance and requires a substantial amount of further investigation. Thaw of ice-rich permafrost in many northern locations is causing substantial environmental change and problems for human occupants (Nelson 2003, U. S. Arctic Research Commission 2003, Hinzman et al. 2005). At issue, however, is whether increased ALT, *sensu stricto*, is behind these issues. Again, consolidation accompanying penetration of thaw into underlying ice-rich materials may or may not be reflected by ALT as it is traditionally measured.

(5) The fifth of the 1997 hypotheses represented a "geographic integration" of the first three: *ALT varies regionally in concert with climatic trends*. This hypothesis was verified forcefully in north-central Alaska using CALM data over a period of more than a decade. As elaborated under (3) above, stratification by vegetative/edaphic landcover units facilitates both empirical and predictive mapping of ALT and can yield highly accurate representations of average thaw depth. This hypothesis has been verified through work involving (a) compositionally diverse landcover associations in 1 ha units, distributed over an extensive region (Nelson et al. 1997); (b) integrated 1 km^2 landscape units distributed over the region (Nelson et al. 1998a, Hinkel & Nelson 2003); and (c) regional maps at high spatial resolution over a 13-year time series (Shiklomanov & Nelson 2002). The latter study included validation using a large data set collected on a week-long helicopter survey (Muller et al. 1998).

The CALM workshop

At the close of CALM I field activities, an NSF-funded international CALM workshop was held in November 2002 at the University of Delaware's campus in Lewes, Delaware. The workshop provided an opportunity for CALM scientists to present data and site histories, review methodologies, discuss progress and problems in the network, implement unified data-analytic procedures, and plan future activities. Discussions and collaborations arising from the Lewes workshop resulted in a series of regional papers and poster abstracts addressing the spatial and temporal variation of active layer thickness at a large number of Eurasian and North American and other sites (Nelson 2004a, 2004b). A series of posters, published as extended abstracts, were presented in Zurich, Switzerland, in July 2003 at the 8th International Conference on Permafrost (Haeberli W. & Brandová 2003), where almost all CALM sites were represented.

After the conclusion of funded CALM I field activities in 2002, limited support for fieldwork at Alaskan and Eurasian sites was made possible in 2003 through a one-time contribution from the University of Delaware's Center for International Studies.

CALM II

The achievements of CALM I provided impetus for continuing the network on a long-term basis, and set the stage for a more comprehensive and integrated system of observations. The proposal to NSF for a second five-year support period focused on several objectives based, in turn, on a series of interrelated themes and hypotheses. CALM II's initial objectives, discussed in detail by Nelson et al. (2004b), were: (1) to maintain and expand programs of long-term, active layer observations in existing regional networks; (2) to **c**ontinue to develop CALM's web-accessible database and provide data management and archiving support; (3) to develop standardized active layer data sets for use in validating hydrologic, ecosystem, permafrost, and climate models; and (4) to integrate active layer and thaw settlement observations over seasonal, inter-annual, and decadal time scales and across a range of geographic scales. These topics are addressed at length in other papers in these proceedings (and publications cited therein), and only brief summary statements with key references are given here.

Accompanying the launch of the CALM II program was a revised and expanded data-collection protocol (Nelson & Hinkel 2003).

Observation network

CALM's network of observation sites continues to expand, having grown from 125 at the close of the CALM I program to 168 at the beginning of 2008. One of the most significant developments in this regard was the creation of a formal program of CALM observations on the Antarctic continent and in the maritime sub-Antarctic islands (Bockheim 2005, Boelhouwers et al. 2003, Vieira et al. 2006, Ramos 2007, 2008). The Antarctic Permafrost and Soils (ANTPAS) program (Parsons et al. 2008) incorporates several sites, known collectively as the CALM-South (CALM-S) network. Ground temperatures are monitored at several sites in South Victoria Land on Livingston Island/South Shetland Islands (Hauck et al. 2007). The CALM-S program is being developed to investigate conditions across environmental gradients from the Andes to the sub-Antarctic islands and through the Antarctic Peninsula and Transantarctic Mountains to the McMurdo Dry Valleys.

Detailed descriptions of ongoing research at many other CALM sites are provided elsewhere in these proceedings (Christiansen & Humlum 2008, Fyodorov 2008, Hollister et al. 2008, Nelson et al. 2008, Riseborough 2008, Smith et al. 2008, Streletskiy et al. 2008, Vasiliev 2008, Viereck 2008, Zamolodchikov 2008). Regional summaries are contained in Shiklomanov et al. (2008). Some concerns about the existing geographic distribution of sites were discussed by Anisimov et al. (2007), and this topic is under investigation (Streletskiy, in progress).

CALM database

The CALM II program is administered through the University of Delaware (UD). Analysis, archiving, and distribution of CALM's long-term observations are integral components of the project. Field data are provided by participants on an annual basis to the CALM office at UD, where they are incorporated into several databases. The data are distributed through the CALM web site (www.udel.edu/Geography/calm), which has been revised extensively and expanded under CALM II. CALM data products are also produced and distributed by the Frozen Ground Data Center at the University of Colorado. Further information is provided elsewhere in this volume by Shiklomanov et al. (2008).

Model validation

Active layer observations and auxiliary information from the CALM network provide a circumpolar database, which has been used extensively to validate process-based geocryological (e.g., Oelke & Zhang, 2004, Shiklomanov et al. 2007) and hydrological (Rawlins et al. 2003) models. Further discussion of the use of CALM data for model validation is contained in Shiklomanov et al. (2008).

Because CALM investigators adhere to a standardized, well-documented protocol, data from the program are useful for validating modeling efforts at a variety of geographic scales. CALM was identified as a model program with respect to data harmonization in the recent U.S. National Research Council report *Toward an Integrated Arctic Observing Network* (Committee on Designing, 2006, p. 82),

Integration

Integration of data, spatial interpolation, and creation of regional representations of active layer thickness were of vital concern early in the CALM program. Nelson et al. (1997) created a map of active layer thickness for a 27,000 km^2 area of north-central Alaska, and conducted validation studies by helicopter survey (Muller et al. 1998, Shiklomanov & Nelson 2002). A spatial time series extending over 1.5 decades now exists for this region

A second regional map is the detailed digital landscape and active layer map created at the Earth Cryosphere Institute (Russian Academy of Sciences). This regional compilation embraces a hierarchy of data layers, including landscape units, organic layer thickness, lithology, and landscape-specific characteristic values of active layer thickness in the northern part of West Siberia. At present, the map is being refined and extended.

Several other regions contain large assemblages of sites and are representative of high-latitude climatic/landscape gradients, making them suitable candidates for spatial data integration. These include the Lower Kolyma River, the Barrow Peninsula on Alaska's North Slope, the Mackenzie River region (Canada), and the North Atlantic region. Each of these regions has been the subject of extensive geocryological research and contains enough information to undertake regional-scale mapping.

Toward an integrated theory of the active layer and upper permafrost

Research treating permafrost-climate interactions has traditionally been based on a two-component conceptual model involving a seasonally frozen active layer and underlying perennial frozen materials. Analysis of data obtained from some of the CALM sites indicated, however, that this conceptualization is inadequate to explain the behavior of the active layer/permafrost system, particularly in ice-rich terrain. To an observer measuring active layer thickness using traditional methodology (e.g., mechanical probing) thaw penetration into the ice-rich layer may not be apparent, owing to thaw consolidation and net subsidence of the surface. This phenomenon has contributed to the view that active layer thickness may not follow climatic trends closely (e.g., Hinzman et al. 2005).

The apparent stability of active layer thickness in many Arctic landscapes, suggested by CALM records, indicates the existence of self-regulating mechanisms that contribute a robustness to the upper permafrost with respect to external climatic forcing. In many regions an ice-rich layer exists below the base of the active layer (e.g., Brown 1967, Mackay 1972, Shur 1988a). Owing to latent-heat effects, such ice-rich layers resist thaw and tend to promote interannual stability in the position of the base of the active layer. During unusually warm summers, however, thaw may penetrate well into this ice-rich layer. Conversely, following colder summers ice may be added to the upper permafrost, possibly resulting in a subsequent decrease of ALT. Although the magnitude, frequency, and variability of these processes are not well documented, Nelson et al. (1998b) hypothesized that they may be responsible for abrupt, long-lasting ("Markovian") changes in ALT at Barrow.

Shur (1988a, b) reconceptualized the active layer/permafrost system, accounting for these factors explicitly. Basing his formulation on earlier Russian work, Shur noted the existence of a *transient layer* that alternates in status between seasonally frozen ground and permafrost over multi-decadal periods. This layer serves as a buffer between the active layer and permafrost. Significant ice segregation can occur within this layer during "cold" years, due predominantly to freezing from below during the autumn and winter. During most "warm" years, this ice-rich layer protects underlying permafrost from thawing, although extreme summers may reduce its vertical extent significantly. Its existence explains the fact that wedge ice and other massive ice formations are located frequently *beneath* the transient layer, as observed for example at Barrow (Brown 1969). Incremental segregation or melting of ice within the transient layer can, however, result in substantial heave or subsidence at the surface over decadal time scales. The thickness of the transient layer plays a crucial role in evaluating the potential response of the active layer/permafrost system to climatic change, and for development of thermokarst processes. For well-developed thermokarst terrain to evolve, the long-term maximum thaw depth should be achieved consistently from year to year during the thawing season.

Shur et al. (2005) discussed the characteristics and behavior of a three-tier system containing a transient layer. The primary characteristics of such a system are the different periodicities at which the constituent layers cycle through 0˚C and the relative abundance, morphology, and distribution of ice contained in each. Although the ice-rich character of the transient layer acts to retard its rate of degradation, progressive thaw under monotonic climate warming would lead to its destruction, with attendant thaw consolidation and

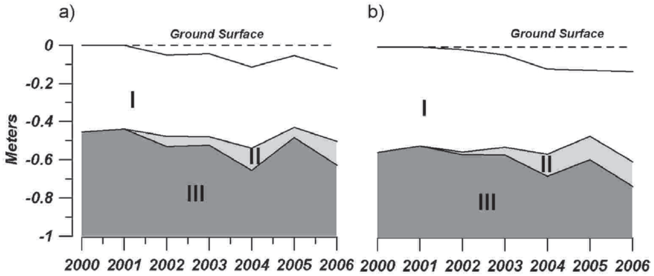

Figure 2. Annual changes in position of ground surface and ALT, as measured by mechanical for representative coastal plain (a) and foothills (b) CALM sites. I- ALT measured by probing; II- ALT, corrected for ground subsidence; III-permafrost. From Streletskiy et al. (2008).

differential subsidence at the surface. Elimination of the most ice-rich parts of the transient layer may be accompanied by an abrupt and long-lasting increase in the thickness of the active layer. Thaw penetration into spatially heterogeneous ground ice in the underlying permafrost triggers differential thaw settlement at the surface.

Simultaneous monitoring of active layer thickness and thaw subsidence have been undertaken at several ice-rich CALM sites in Alaska and Russia (Little et al. 2003, Mazhitova & Kaverin 2008, Streletskiy et al. 2008). To account for ground subsidence in the active layer record at several CALM sites in northern Alaska, annual changes in the position of the ground surface, relative to the level at the beginning of the measurements in the year 2000, were added to the active layer measurements produced by mechanical probing (Fig. 2). Results from two sampling locations in northern Alaska indicate a monotonic increase in thaw penetration over the period of measurement. Similar results were obtained by Overduin & Kane (2006) elsewhere on Alaska's North Slope and in Russia by Mazhitova & Kaverin (2008). Bockheim & Hinkel (2005) found widespread stratigraphic evidence for fluctuations in the position of the transient layer in northern Alaska. Taken together, these results indicate that the CALM program should install instrumentation to monitor thaw subsidence at any site containing abundant ground ice at shallow depth.

Conclusion

CALM is, in the first instance, a global-change program. Its change-detection function remains a critically important part of its mission. As part of this charge, the program is also concerned with differentiating between the impacts of long-term climate change and more localized anthropogenic effects (Nelson, 2003).

CALM data have proven useful in many contexts. Owing to the limited observational record at most sites, however, it is not yet possible to arrive at definitive conclusions about long-term changes or trends in the temperature and thickness of the active layer. The few long-term data sets available from high-latitude sites in the Northern Hemisphere show very substantial interannual and interdecadal fluctuations. The spatial variability of active layer thickness is large, even within geographic areas of limited extent (e.g., 1 km^2). Most sites in tundra environments show a strong, positive relation between summer temperature and the thickness of the active layer. This relation is weaker in boreal environments, but these are understudied and require more investigations (e.g., Hinkel & Nicholas 1995, Viereck 2008). Increases in thaw penetration, subsidence, and development of thermokarst terrain have been observed at some sites.

CALM II continues existing partnerships and collaborations with other international organizations and programs, including GCOS/GTOS, CEON, CliC, ITEX, ICARP, IASC, and the ongoing IPY and IUGS Year of Planet Earth programs (Brown et al. 2000, U.S. Arctic Research Commission Permafrost Task Force 2003). CALM is making significant contributions to International Polar Year 2007–08 as a major component of the *Thermal State of Permafrost* IPY project.

Reflecting its open, community-based structure, CALM II holds annual meetings and round-table discussions in connection with major scientific conferences. The second CALM Workshop is being held in Alaska during June 2008, immediately preceding the Ninth International Conference on Permafrost in Fairbanks. The workshop will focus on creating a research agenda for the CALM III program, with particular attention paid to monitoring in the boreal regions and on instrumentation suitable for extending thaw-subsidence measurements to all CALM sites in ice-rich terrain.

Acknowledgments

A program such as CALM could not exist without the cooperation, ideas, and efforts of a large group of researchers from around the world. CALM investigators, many of whom contribute on an entirely voluntary basis, have created a network of permafrost observatories and databases that has helped to revolutionize permafrost science in ways that could only be hinted at just two decades ago (Barry 1988).

CALM projects in Kazakhstan, Mongolia, Russia, and the United States have been supported by grants from the U.S. National Science Foundation (OPP-9732051 to the University of Cincinnati and OPP-0352958 to the University of Delaware). The University of Delaware provided funding for limited field operations during 2003. Opinions, findings, conclusions, and recommendations expressed in this paper do not necessarily reflect the views of the National Science Foundation. This paper is a contribution to the present International Polar Year, and the Permafrost Young Researchers Network.

References

Anisimov, O.A., Lobanov, V.A., Reneva, S.A., Shiklomanov, N.I., Zhang, T. & Nelson, F.E. 2007. Uncertainties in gridded air temperature fields and effects on predictive active layer models. *Journal of Geophysical Research: Earth Surface* 112(F2): F02S14, doi:10.1029/2007JF000593.

Barry, R.G. 1988. Permafrost data and information: status and needs. In Senneset, K. (ed.), *Proceedings of the Fifth International Conference on Permafrost*, vol. 1. Trondheim, Norway: Tapir Publishers, 119-122.

Barry, R.G., Heginbottom, J.A. & Brown, J. 1995. *Workshop on Permafrost Data Rescue and Access*. Boulder, CO: World Data Center A for Glaciology, 132 pp.

Bockheim, J. 2005. *International Workshop on Antarctic Permafrost and Soils: Final Report*. November 14-18, 2004, University of Wisconsin, Madison, WI., (http://erth.waikato.ac.nz/antpas/pdf/FIN_REP_Ant_Wk3.pdf), 84 pp.

Bockheim, J.G. & Hinkel, K.M. 2005. Characteristics and significance of the transition zone in drained thaw lake basins of the Arctic Coastal Plain, Alaska. *Arctic* 58: 406-417.

Boelhouwers, J., Holness, S. & Sumner, P. 2003. The maritime Subantarctic: a distinct periglacial environment, *Geomorphology* 52: 39-55.

Brown, J. 1967. An estimation of the volume of ground ice, coastal plain, arctic Alaska. *CRREL Technical Report,* 22 pp.

Brown, J. 1969. Soil properties developed on the complex tundra relief of northern Alaska. *Biuletyn Peryglacjalny* 18: 153-167.

Brown, J. 1997. Disturbance and recovery of permafrost terrain. In Crawford, R.M.M. (ed.), *Disturbance and Recovery in Arctic Lands: An Ecological Perspective*. Dordrecht, The Netherlands: Kluwer Academic Publishers, 167-178.

Brown, J., Nelson, F.E. & Walker, D.A. 1995. Circumarctic Active Layer Monitoring (CALM): an international contribution to ITEX. *Proceedings of the 6th ITEX Workshop, 7-11 April, 1995*. Ottawa, (abstract).

Brown, J., Taylor, A.E., Nelson, F.E. & Hinkel, K.M. 1997. The Circumpolar Active Layer Monitoring (CALM) program: structure, current status. *Abstracts of the 27th Arctic Workshop*. Ottawa: University of Ottawa, Department of Geography.

Brown, J., Hinkel, K.M. & Nelson, F.E. 2000. The Circumpolar Active Layer Monitoring (CALM) program: historical perspectives and initial results. *Polar Geography* 24(3): 165-258.

Christiansen, H.H. & Humlum, O. 2008. Monitoring and modeling climatic control on maritime active layer thickness and top permafrost temperatures in loess sediments in the UNISCALM site, Adventdalen, Svalbard (this proceedings).

Committee on Designing an Arctic Observing Network, 2006. *Toward an Integrated Arctic Observing Network*. Washington, DC: National Research Council of the National Academies, 116 pp.

Fagan, J.D. 1995. *Sampling Designs for the Measurement of Active-Layer Thickness*. M.S. thesis, Rutgers University-New Brunswick, 118 pp.

Fyodorov, D. 2008. Seasonal thaw of soils in the North Yakutian ecosystems (this proceedings).

Gomersall, C. & Hinkel, K.M. 2001. Estimating the variability of active-layer thaw depth in two physiographic regions of northern Alaska. *Geographical Analysis* 33: 141-155.

Haeberli W. & Brandová, D. (eds), 2003. *8th International Conference on Permafrost: Extended Abstracts on Current Research and Newly Available Information*,. Glaciology and Geomorphodynamics Group, Geography Department, University of Zurich: Zurich, Switzerland

Hauck, C., Vieira, G., Gruber, S., Blanco, J. & Ramos, M. 2007. Geophysical identification of permafrost in Livingston Island, maritime Antarctica. *Journal of Geophysical Research* 112, F02S19, doi:10.1029/2006JF000544.

Hinkel, K.M. & Nicholas, J.R.J. 1995. Active layer thaw rate at a boreal forest site in central Alaska, U.S.A. *Arctic and Alpine Research* 27: 72-80.

Hinkel, K.M., Paetzold, R., Nelson, F.E. & Bockheim, J.G. 2001: Patterns of soil temperature and moisture in the active layer and upper permafrost at Barrow, Alaska: 1993-1999. *Global and Planetary Change* 29: 293-309.

Hinkel, K.M. & Nelson, F.E. 2003. Spatial and temporal patterns of active layer thickness at CALM sites in northern Alaska, 1995-2000. *Journal of Geophysical Research-Atmospheres*, 108(D2): 10.129/2001JD000927.

Hinzman, L., Bettez, N., Bolton, W.R., Chapin, F.S., Dyurgerov, M., Fastie, C., et al. 2005. Evidence and implications of recent climate change in northern Alaska and other Arctic regions. *Climatic Change* 72, 251-298.

Hollister, R.D., Webber, P.J., Slider, R.T., Nelson, F.E. & Tweedie, C.E. 2008. Soil temperature and thaw response to manipulated air temperature and plant cover at Barrow and Atqasuk, Alaska (this proceedings).

Kane, D.L., Hinzman, L.D. & Zarling, J.P. 1991. Thermal response of the active layer to climatic warming in a permafrost environment. *Cold Regions Science and Technology* 19 (2): 111-122.

Little, J., Sandall, H., Walegur, M. & Nelson, F.E. 2003. Application of differential GPS to monitor frost heave and thaw settlement in tundra environments. *Permafrost and Periglacial Processes* 14(4): 349-357.

Mackay, J.R. 1972. The world of underground ice. *Annals of the Association of American Geographers* 62: 1-22.

Mazhitova, G. & Kaverin, D. 2008. Coupled monitoring of active layer depth and soil surface subsidence at a Circumpolar Active Layer Monitoring (CALM) site, European Russian Arctic *Earth Cryosphere* (in press).

Melnikov, P.I. 1990. *Proceedings of the International Symposium on Geocryological Studies in Arctic Regions, Yamburg, USSR, August 1989*. Moscow: Nauka, 80 pp.

Molau, U. & Molgaard, P. 1996: *ITEX Manual*. Copenhagen: Danish Polar Center, 53 pp.

Mueller, G.R. 1996. *A Multiscale GIS Analysis of Active Layer Thickness and Vegetation Type on Alaska's North Slope*. M.A. Thesis, SUNY-Albany, Albany, New York, 132 pp.

Muller, S.V., Walker, D.A., Nelson, F.E., Auerbach, N.A., Bockheim, J., Guyer, S. et al. 1998. Accuracy assessment of a land-cover map of the Kuparuk River basin, Alaska: considerations for remote regions. *Photogrammetric Engineering and Remote Sensing* 68(6): 619-628.

Nelson, F.E. 2003. (Un)frozen in time. *Science* 299: 1673-1675.

Nelson, F.E. (ed.) 2004a. Eurasian Contributions to the Circumpolar Active Layer Monitoring (CALM) Workshop. *Polar Geography* 28(4): 253-340.

Nelson, F.E. (ed.) 2004b. Special Issue: Circumpolar Active Layer Monitoring (CALM) Workshop. *Permafrost and Periglacial Processes* 15(2): 99-188.

Nelson, F., Brown, J., Lewkowicz, T. & Taylor, A. 1996. Active layer protocol. In: Molau, U. & Molgaard, P. (eds.) *ITEX Manual*, second edition. Copenhagen: International Tundra Experiment, pp. 14-16 + data forms.

Nelson, F.E., Shiklomanov, N.I., Mueller, G.R., Hinkel, K.M., Walker, D.A. & Bockheim, J.G. 1997. Estimating active-layer thickness over a large region: Kuparuk River basin, Alaska, U.S.A. *Arctic and Alpine Research* 29(4): 367-378.

Nelson, F.E., Hinkel, K.M., Shiklomanov, N.I., Mueller, G.R., Miller, L.L. & Walker, D.A. 1998a, Active-layer thickness in north-central Alaska: systematic sampling, scale, and spatial autocorrelation. *Journal of Geophysical Research-Atmospheres* 103(D22): 28,963-28,973.

Nelson, F.E., Outcalt, S.I., Brown, J., Shiklomanov, N.I. & Hinkel, K.M. 1998b, Spatial and temporal attributes of the active-layer thickness record, Barrow, Alaska U.S.A. In Lewkowicz, A. and Allard, M. (eds.), *Proceedings of the Seventh International Conference on Permafrost*. Québec: Centre d'Etudes Nordiques, Université Laval, 797-802.

Nelson, F.E., Shiklomanov, N.I. & Mueller, G.R. (1999). Variability of active-layer thickness at multiple spatial scales, north-central Alaska, U.S.A. *Arctic, Antarctic, and Alpine Research*, 31(2), 158-165.

Nelson, F.E., Shiklomanov, N.I., Hinkel, K.M. & Brown, J. 2003. The Circumpolar Active Layer Monitoring (CALM) program: recent developments. In: *8th International Conference on Permafrost: Extended Abstracts on Current Research: Newly Available Information*, Haeberli W, Brandová D (eds). Glaciology and Geomorphodynamics Group, Geography Department, University of Zurich: Zurich, Switzerland, 113-114.

Nelson, F.E., Shiklomanov, N.I., Christiansen, H.H. & Hinkel, K.M. 2004a. The Circumpolar Active Layer Monitoring (CALM) Workshop: Introduction. *Permafrost and Periglacial Processes 15(2)*: 99-101.

Nelson, F.E., Shiklomanov, N.I., Hinkel, K.M. & Christiansen, H.H. 2004b. Introduction: The Circumpolar Active Layer Monitoring (CALM) Workshop and the CALM II Program. *Polar Geography* 28(4), 253-266.

Nelson, F.E., Shiklomanov, N.I., Streletskiy, D.A., Romanovsky, V.E., Yoshikawa, K., Hinkel, K.M. & Brown, J. 2008. A permafrost observatory at Barrow, Alaska: long-term observations of active-layer thickness and permafrost temperature (this proceedings).

Nelson, F.E. & Hinkel, K.M. 2003. Methods for measuring active-layer thickness. In: Humlum, O. and Matsuoka, N. (eds.) *A Handbook on Periglacial Field Methods.* Longyearbyen, Norway: University of the North in Svalbard, currently online at: <http://www.unis.no/RESEARCH/GEOLOGY/Geo_research/Ole/PeriglacialHandbook/ActiveLayerThicknessMethods.htm>.

Nelson, F.E., Shiklomanov, N.I., Streletskiy, D.A., Romanovsky, V.E., Yoshikawa, K., Hinkel, K.M. et al. 2008. A permafrost observatory at Barrow, Alaska: Long-term observations of active-layer thickness and permafrost temperature (this proceedings).

Nixon, F.M. & Taylor, A.E. 1998. Regional active layer monitoring across the sporadic, discontinuous and continuous permafrost zones, Mackenzie Valley, northwestern Canada. In Lewkowicz, A.G. and Allard, M. (eds.). *Proceedings of the Seventh International Conference on Permafrost*. Québec: Centre d'Etudes nordiques, Université Laval, 815-820.

Nixon, M., Tarnocai, C. & Kutmy, L. 2003. Long-term active layer monitoring: Mackenzie Valley, northwest Canada. In Phillips, M., Springman, S.M. & Arenson, L.U. (eds.), *Proceedings of the Eighth International Conference on Permafrost*, vol. 2. Lisse: A.A. Balkema, 821-826.

Oelke, C. & Zhang, T. 2004. A model study of Circum-Arctic soil temperatures. *Permafrost and Periglacial Processes* 15: 103-121.

Overduin, P.P. & Kane, D.L. 2006. Frost boils and soil ice content: field observations. *Permafrost and Periglacial Processes* 17: 291-307.

Paetzold, R.F., Hinkel, K.M., Nelson, F.E., Osterkamp, T.E., Ping, C.L. & Romanovsky, V.E. 2000. Temperature and thermal properties of Alaskan soils. In: Lal, R. and Kimble, J.M. (eds.) *Global Climate Change: Cold Regions Ecosystems*, Boca Raton: CRC Press, pp. 223-245.

Parsons, M. & Zhang, T. 2003. *CAPS: The Circumpolar Active-Layer and Permafrost System, Version 2.0.* Boulder, CO: National Snow and Ice Data Center/World Data Center for Glaciology, 3 compact disks.

Parsons, M.A., Smith, S., Romanovsky, V.E., Shiklomanov, N.I., Christiansen, H.H., Overduin, P., Zhang, T.J., Balks, M.R. & Brown, J. 2008. Managing permafrost data: past approaches and future directions (this proceedings).

Ramos, M. 2007. Permafrost and active layer monitoring in the maritime Antarctic. First results from CALM sites in Livingston and Deception Islands. *Geophysical Research Abstracts*, 9: 1607-7962/gra/EGU2007-A-01816.

Ramos, M. 2008. Thermal active layer monitoring in two different sites on Livingston Island during the last seven years: a comparative study (this proceedings).

Rawlins, M.A., Vorosmarty, C.J., Lammers, R.B., Frolking, S. & Fekete, B.M. 2003. Simulating pan-Arctic runoff with a macro-scale terrestrial water balance model. *Hydrological Processes* 17(13): 2521-2539.

Richardson, J. 1839. Notice of a few observations which it is desirable to make on the frozen soil of British North America; drawn up for distribution among the officers of the Hudson's Bay Company. *Journal of the Royal Geographical Society* 9: 117-120.

Riseborough, D.W. 2008. Modeling of active layer and talik formations: implications for permafrost monitoring (this proceedings).

Shiklomanov, N.I. 2005. From exploration to systematic investigation: Development of geocryology in 19th- and early-20th-century Russia. *Physical Geography* 26 (4): 249-263.

Shiklomanov, N.I., Anisimov, O.A., Zhang, T., Marchenko, S., Nelson, F.E. & Oelke, C. 2007. Comparison of model-produced active layer fields: Results for northern Alaska. *Journal of Geophysical Research: Earth Surface* 112(F2); F02S10, doi:10.1029/2006JF000571.

Shiklomanov, N.I. & Nelson, F.E. 2002. Active-layer mapping at regional scales: a 13-year spatial time series for the Kuparuk region, north-central Alaska. *Permafrost and Periglacial Processes* 13(3): 219-230.

Shiklomanov, N.I. & Nelson, F.E. 2003. Statistical representation of landscape-specific active-layer variability. In: Phillips, M., Springman, S.M., and Arenson, L.U. (eds.) *Proceedings of the Eighth International Conference on Permafrost*, vol. 2. Lisse: A. A. Balkema, 1039-1044.

Shiklomanov, N.I., Nelson, F.E., Streletskiy, D.A., Hinkel, K.M. & Brown, J. 2008. The Circumpolar Active Layer Monitoring (CALM) program: data collection, management, and dissemination strategies (this proceedings).

Shur, Y.I. 1988a. The upper horizon of permafrost soils. In Senneset, K. (ed.). *Proceedings of the Fifth International Conference on Permafrost*, vol. 1. Trondheim, Norway: Tapir Publishers, 867-871.

Shur, Y.I. 1988b. *Upper Horizon of Permafrost and Thermokarst*. Moscow: Nauka. 208 pp. (in Russian).

Shur, Y., Hinkel, K.M. & Nelson, F.E. 2005. The transient layer: implications for geocryology and global-change science. *Permafrost and Periglacial Processes* 16(1), 5-17.

Smith, S.L., Burgess, M.M. & Riseborough, D.W. 2008. Ground temperature and thaw settlement in frozen peatlands along the Norman Wells Pipeline corridor, NWT Canada: 22 years of monitoring observations (this proceedings).

Sturm, M., Racine, C. & Tape, K. 2001. Climate change: increasing shrub abundance in the Arctic. *Nature* 411: 546-547.

Streletskiy, D.A., in progress, *Spatial and Temporal Variability of Active-layer Thickness at Regional and Global Scales.* Ph.D. dissertation, Department of Geography, University of Delaware.

Streletskiy, D.A., Shiklomanov, N.I., Nelson, F.E. & Klene, A.E. 2008. Thirteen years of observations at Alaskan CALM sites: long-term active layer and ground surface temperature trends (this proceedings).

U.S. Arctic Research Commission Permafrost Task Force, 2003. *Climate Change, Permafrost, and Impacts on Civil Infrastructure*. Washington, D.C.: U.S. Arctic Research Commission, 62 pp.

Vasiliev, A. 2008. Active layer monitoring in West Siberia under the CALM program (this proceedings).

Vieira, G., Hauck, C., Gruber, S., Blanco, J.J. & Ramos, M. 2006. Geophysical surveying for permafrost research in the maritime Antarctic. First results from Livingston and Deception Islands. *Geophysical Research Abstracts* 8: 1607-79621/gra/EGU06-A-09446.

Viereck, L. 2008. Effect of wildfire and fireline construction on the annual depth of thaw in a black spruce permafrost forest in interior Alaska: a 36-year record of recovery (this proceedings).

Walker, D.A., Bockheim, J.G., Chapin, F.S. III, Eugster, W., King, J.Y., McFadden, J.P. et al. 1998. A major arctic soil pH boundary: implications for energy and trace-gas fluxes. *Nature* 394: 469-472.

Walker, D.A., Epstein, H.E., Gould, W.A., Kelley, A.M., Kade, A.N. et al. 2003. Frost-boil ecosystems: complex interactions between landforms, soils, vegetation and climate. *Permafrost and Periglacial Processes* 15: 155-188.

Weller, G., Chapin, F.S., Everett, K.R., Hobbie, J.E., Kane, D.L., Oechel, W. C. et al. 1995. The Arctic Flux Study: a regional view of trace gas release. *Journal of Biogeography* 22: 365-374.

Yachevskyi, L.A. & Vannari, P.I. 1912. *Instructions for Studying Permafrost in Soils*, second edition, St. Petersburg: Russian Imperial Geographical Society (in Russian).

Zamolodchikov, D. 2008. Recent climate and active layer changes in Northeast Russia: regional output of Circumpolar Active Layer Monitoring (CALM) (this proceedings).

Modeling Observed Differential Frost Heave Within Non-Sorted Circles in Alaska

D.J. Nicolsky, V.E. Romanovsky
Geophysical Institute, University of Alaska Fairbanks PO Box 757320, Fairbanks, AK 99775, USA
G.S. Tipenko, D.A. Walker
Institute of Environmental Geosciences, Russian Academy of Science, PO Box 145, 101000 Moscow, Russia

Abstract

We investigate bio-geophysical processes causing differential frost heave in non-sorted circles north of Alaska's Brook Range. The main question to be addressed is, "How doest heterogeneity in soil properties and ground surface conditions cause the differential frost heave observed within the non-sorted circle?" We address this question by developing a numerical thermo-mechanical model of a non-sorted circle. A sensitivity study of predicted differential frost heave, with respect to soil physical properties and vegetation characteristics, shows that hydrological and thermal properties, as well as the local heterogeneity in distribution of surface vegetation, have a decisive role in formation of differential frost heave. We applied this model to simulate differential frost heave at the Franklin Bluffs site and obtained a good quantitative agreement with observed soil temperatures, water content, and frost heave. For other locations, such as at the Sagwon Bluffs and Howe Island sites, we obtained qualitative agreement with frost heave measurements.

Keywords: freezing and thawing; frost heave; numerical modeling; patterned ground**;** permafrost.

Introduction

Extensive areas of the Arctic landscape are characteristically patterned into small-scale ground features called non-sorted circles. Non-sorted circles are 0.5–3.0 m diameter patches of barren or sparsely vegetated soil formed by frost action (van Everdingen 2002) and ordinarily develop on poorly drained tundra sites (Fig. 1).

Changes to these features in relation to changes in climate could affect energy and carbon mass exchange at the tundra surface with possible feedbacks to the climate. However, formation, development, and maintenance of such ground patterns and their interaction with vegetation is poorly understood (Walker et al. 2004). The objective of this study is to numerically model observed frost heave in non-sorted circles and gain an understanding of interactions between water fluxes, temperature dynamics as influenced by the plant canopy and the motion of soil particles resulting from the heave of ground surface.

As part of the biocomplexity of the patterned-ground project (Walker 2004), we observed non-sorted circles at several locations near the Dalton Highway in Alaska. We instrumented several non-sorted circles at these sites with sensors that measure soil temperature, moisture content, and the maximum frost heave (Walker et al. 2004). Our measurements revealed that the maximum frost heave in a circle interior was 2–8 times greater compared to frost heave surrounding the circle tundra. This phenomenon is referred to as the differential frost heave.

Our field observations support the idea that the frost heave of saturated soil very often cannot be explained solely by the expansion of liquid water transforming into ice crystals. In this study,we apply a general thermo-mechanical model (Mikkola & Hartikainen 2001) of frost heave to simulate the observed frost heave in non-sorted circles. In this work, we assume that the soil is a homogeneous mixture of liquid water, ice, and soil skeleton. We assume that the skeleton and ice undergo small deformations described by linear elasticity, and the linear momentum conservation principles can be exploited in the quasi-static form. In our model, we also neglect ice flow relative to the soil skeleton. The liquid water is an incompressible and non-viscous fluid that changes its phase and is always in thermodynamical equilibrium with ice. The chemical potential of the liquid water is modified due to adsorption to the soil skeleton.

Based on observations from field experiments and results of our numerical simulations, we conclude that heterogeneity in surface characteristics and soil properties (due to the presence of a heterogeneous plant canopy together with presence of waterlogged conditions) are among the primary requirements necessary for occurrence of differential frost heave observed in non-sorted circles.

Physical Description

In this section, we highlight key physical processes and mechanisms presumably causing the differential frost heave in non-sorted circles. The area surrounding the circle is called the inter-circle area and has a relatively thick mat of vegetation as well as a layer of organically enriched soil (Fig. 1). Incorporation of the organic material into soil leads to heterogeneity in thermal properties, structure, and water-holding capacity of soil. For example, different soil textures indicate distinctive thermal conductivities, soil porosity, and dependence of the unfrozen liquid water content on temperature. Besides variances in thermal and hydrological properties, the non-sorted circle has heterogeneous rheological properties due to structural change that takes place during annual freeze-thaw cycles. This structural change is caused by freezing water that creates a microscopic structure in the form of a sequence of ice lenses.

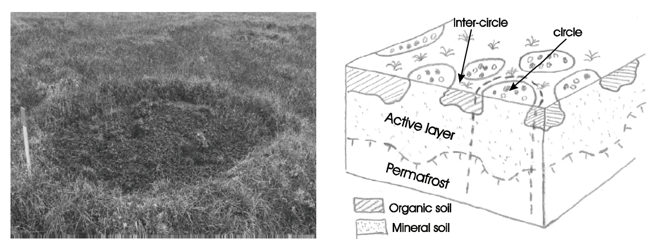

Figure 1. A photography (left) and schematic description (right) of the non-sorted circle.

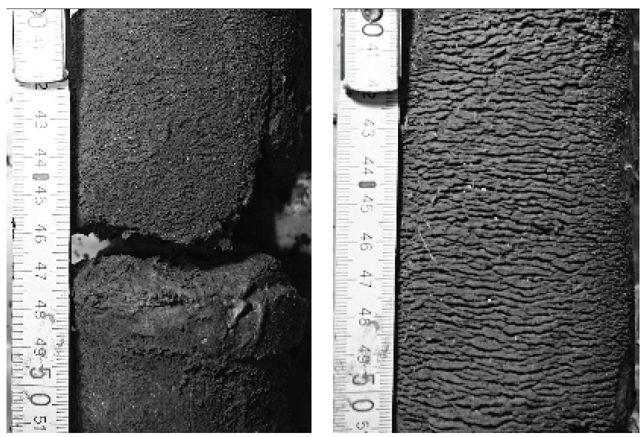

Figure 2. Core samples obtained from the inter-circle area (left photo) and circle (right photo) at the Franklin Bluffs site during winter. On the right photograph, a sequence of horizontally oriented ice lenses can be observed. The vertical scale is in centimeters.

Figure 2 shows the ice lenses in soil core samples from a non-sorted circle at the Franklin Bluffs site, Alaska. Each ice lens separates soil particles, causes the observed lenticular soil structure, and hence lessens structural solidity of soil. In Graham & Au 1985 and Qi et al. (2006), it was shown that soil has a long-term memory of its previous freeze/thaw cycles, which in particular reduces bonding between soil particles. To account for reduction in the bonding, we assume that soil is more structurally solid if it has fewer ice lenses. From a soil core obtained by drilling in winter, we observed that the circle has many more ice lenses than in the inter-circle area, and these lenses can be found even at the significant depth of 0.5 m (Fig. 2). Therefore, we assume that soil in the inter-circle is more structurally solid than in the circle. Despite these heterogeneities, the difference between observed active layer depths (maximum depth of summer thaw) of the circle and inter-circle does not exceed 0.3 m in the majority of cases.

It is well known that frost heave is caused by volumetric water expansion during freezing. However, as mentioned earlier, the observed frost heave heights do not seem to be exclusively dependent on the active layer depth, and on volumetric water content in the soil before freezing. From field observations at the Franklin Bluffs site, we know that the active layer thicknesses for the circle and inter-circle areas are 0.9 and 0.8 m, respectively, and volumetric water content in these areas during summer is almost the same. Thus, if water does not migrate, the frost heave is computable and its height is about 3.0–3.5 cm for both circle

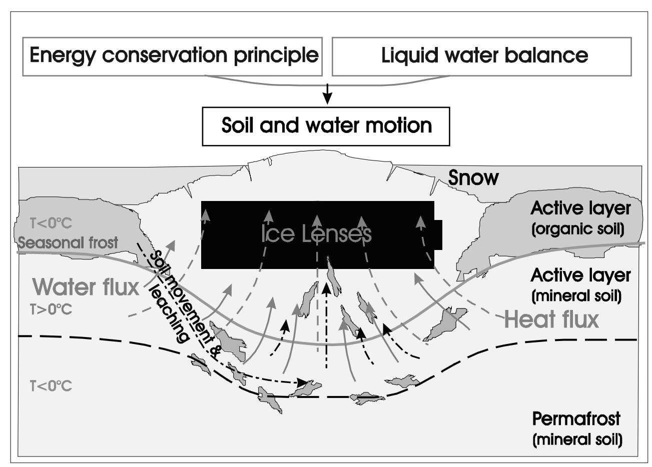

Figure 3. A diagram of fundamental physical processes taking place in a non-sorted circle when it freezes during the fall. Directions of the water flow, heat flux, and soil displacement are marked by solid, dashed, and dot-dashed lines, respectively. Location of the upper 0ºC isotherm is marked by the solid line, whereas location of the permafrost table by the dashed line.

and inter-circle areas. The latter values of the frost heave contradict observations at Franklin Bluffs site, at which the ground heaves by 15 cm in the center of a circle and only by 3 cm in the inter-circle. This significant variation on the local-scale frost heave is called the differential frost heave. We hypothesize that the key physical process responsible for the differential frost heave within non-sorted circles is water redistribution between the circle and inter-circle. The water redistribution is caused by lateral components in the cryogenic suction that pulls water from thawed soil to partially frozen soil. The lateral components in the cryogenic suction are due to heterogeneity in soil properties and in ground surface conditions, first of all in vegetation cover. Figure 3 shows fundamental physical processes occurring in the non-sorted circle in the fall when it freezes.

We describe the nature of these processes and their implications to the observed values of the differential frost heave as follows. When the ground surface temperature becomes lower than 0ºC, water trapped in soil pores starts to freeze. In Figure 3, the direction of the heat flux during freezing is shown by dashed arrows. In several classical works, it was demonstrated that temperature gradients in the freezing ground create cryogenic suction, inducing flow of water towards a freezing region along the temperature gradient (O`Neill & Miller 1985). Since the circle lacks an organic layer, the frost propagates through it faster, causing stronger water migration into the circle, consequently resulting in more intensive ice lens formation and thus higher frost heave in the circle. Over a period of time, the circle heaves significantly higher than the inter-circle area. A secondary consequence of the heave is the reduced thickness of the snowpack above the circle compared to the inter-circle area (Fig. 3). The heterogeneous snow distribution further enhances the thermal heterogeneity of the soil surface. An absence of a vegetation mat within the heaving areas in conjunction with difference in the snow thickness results in

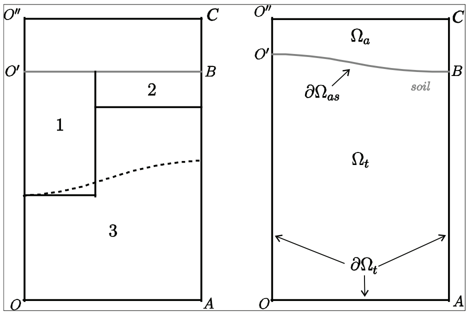

Figure 4. Schematic cross section (left) of the non-sorted circle and its computational domain (right). Segment OO″ is the axis of rotation, AB is the external boundary, and the dotted line on the left shows the upper permafrost boundary.

observed lower winter soil temperatures in the circle than in the inter-circle. The thermal difference between the circle and inter-circle areas creates cryogenic suction and drives water from the inter-circle to the circle (the direction of liquid water motion is shown by solid arrows). Reaching a freezing region, water forms ice lenses, which exert uplifting forces causing deformation of the soil skeleton. We highlight directions of soil particle velocities by dash-dotted arrows (Fig. 3). In our model we exploit a simple rheological model of the soil skeleton and assume that its deformations are well simulated by linear elasticity theory in which the soil stiffness takes into account structural differences and loss in soil bonding caused the ice lenses.

Besides the thermal differences, which cause liquid water migration towards the circle, hydraulic properties of the soil also determine water flux affecting the liquid water migration. One of the key hydraulic parameters is a coefficient of hydraulic conductivity and its dependence on liquid water content, θ_w, for partially frozen ground. According to Konrad & Duquennoi (1993), the hydraulic conductivity increases with an increase of unfrozen water content that is a function of both temperature and porosity. Another hydrological aspect that is important in sustaining water migration is the availability of water inside the non-sorted circle or at its boundary. We note that observations reveal higher values of frost heave that have been measured at poorly drained sites. Hence, lateral boundary conditions play an important role in allowing water to migrate into the circle due to cryogenic suction and to create ice lenses. In our model, we simulate the non-sorted circles either as hydrologically opened or closed systems by setting to zero either the water flux or pressure, respectively, on external boundaries. In the next section, we will briefly describe a general thermo-mechanical model of freezing soil. An interested reader can consult Mikkola & Hartikainen (2001), where the theory is discussed in detail.

Numerical Model

We consider a mixture of several constituents—water, ice, and soil particles—occupying a change in time region. Since a non-sorted circle has an axial symmetry, we solve governing equations in an axisymmetrical domain. In Figure 4, we show the cross-section of the computational domain consisting of three regions. Soil properties for each region are listed in Table 1.

Table 1. Description of soil properties for non-sorted circles along the Dalton Highway in Alaska.

Domain	Soil	Ice lenses	Unfrozen water
1	Mineral	Many	High content
2	Organic	Many	Low content
3	Mineral	Few	High content

We solve the energy conservation principle for the mixture by using two mass conservation principles for soil particles and liquid water, and a quasi-elasticity principle for the soil particles.

Based on the energy conservation principle, we compute the soil temperature T. The temperature consecutively defines the magnitude of the cryogenic suction, f, that forces liquid water from a thawed region towards the partially frozen one. The flux of liquid water, F, is defined such that

$$F \approx \nabla\left(p + \rho_w L \frac{T}{T_0}\frac{\partial f}{\partial \theta_w}\right) + \rho_w L \frac{T}{T_0}\nabla f, \qquad (1)$$

where L is the latent heat of fusion, ρ_w is the water density, and $T_0 = 273.15$ºC. Consequently, the flux F is used in the water conservation principle, i.e., Darcy's Law, and to calculate the pressure, p (Mikkola & Hartikainen 2001). The latter is used to define a force in the quasi-linear elasticity law in order to compute displacement of soil particles. The system is coupled, since the soil particle displacement is used to compute the temperature and the pore pressure. We note that the system pore pressure/soil displacement (up to the coefficients) is common in the poro-elasticity theory. On the ground surface, we specify the temperature and zero pressure. On the lateral boundary, we set zero heat flux, zero pressure/water flux (open/closed system). At some depth (in our case 2.0 m), we set zero heat and water flux.

The system of equation is discretized by a finite element method in a fixed-in-time domain that embeds ground material OABO′ in a heaving non-sorted circle (Fig. 4). The fictitious domain method is used to set physically realistic boundary conditions on the moving ground surface O′B, lateral boundaries AB, OO′ and bottom OA of the non-sorted circle.

In nature, we observe that the maximum frost heave is larger at sites where near-surface ground water is abundant (Walker et al. 2004). To explain this phenomena, we show that liquid water migration towards the partially frozen region as well as the unlimited water supply are both essential to simulate the observed frost heave. Hence, we model two cases. In the first case, we model the zero-pressure boundary condition on AB, and hence water is allowed to pass through this boundary. In the second case, the zero-flux boundary condition is placed on the segment AB, resulting in a hydraulically isolated system.

Due to presence of the cryogenic suction, during freezing there is an induced flow of liquid water from the thawed

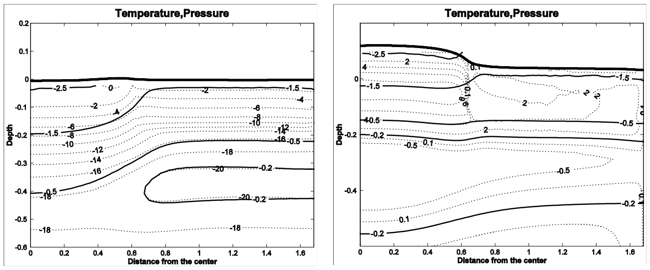

Figure 5. Contours of the temperature in ºC (solid lines) and pressure in 10^5Pa (dotted lines) at the 30th days after beginning of freezing, for hydraulically closed and open systems, in the left and right plots, respectively.

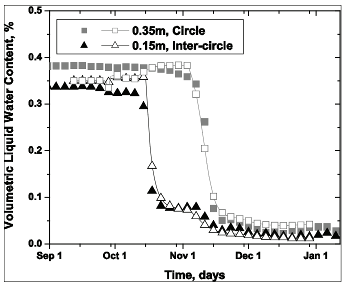

Figure 6. Dynamics of the measured (filled symbols) and calculated (hollow symbols) liquid water content at the Franklin Bluffs site in the center of the circle and in the inter-circle.

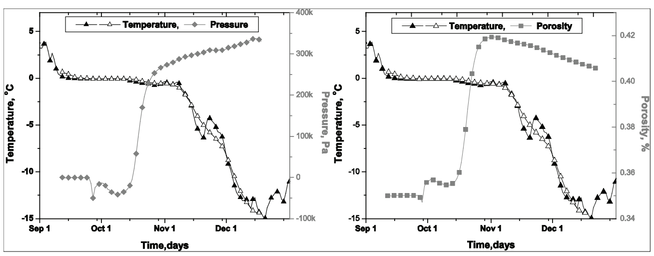

Figure 7. Dynamics of the measured (filled triangles) and calculated (hollow triangles) temperature at 0.35 m depth in the circle. The dynamics of pressure and porosity are marked by filled squares in the left and right plots, respectively.

region to the partially frozen zone. As a result, the pressure in the thawed region decreases. In the hydraulically closed system without internal sources of water, the boundaries are not water-permeable, and hence no additional water can appear in the non-sorted circle. Consequently, the pressure can decrease (Fig. 5).

In the hydraulically open systems with suction, the cryogenic suction creates similar effects as in the closed systems. Namely, it forces the flow of water and creates a low pressure zone in the thawed region. However, unlike the closed systems, the pressure on the external boundary is equal to zero, and water can flow through the boundary and compensate deficiency in water volume and, associated with it, negative pressure. Therefore, in the hydraulically open systems, the pressure in the thawed region is slightly negative compared to the closed system (Fig. 5). We observe that the positive-pressure increase exists in the partially frozen region and it creates the uplifting forces which produce the frost heave.

We conclude that the cryogenic suction forces create water flow. The pressure dynamics and the uplifting forces strongly depend on the pressure boundary condition. These results show that the model qualitatively predicts typical physical behavior of hydraulically closed and open systems occurring in nature. An interested reader is referred to Nicolsky et al. (in review) and to references therein, where the governing system of equations is described.

Frost Heave Modeling at the Franklin Bluffs Site

In this section, we apply the general model to a non-sorted circle located at the Franklin Bluffs site (148.7°W, 69.6°N) on the Dalton Highway in Alaska. The non-sorted circle is approximately 0.6 m in radius and is developed in waterlogged non-acidic tundra. In the inter-circle, the organic layer is 0.2 m in depth (Walker et al. 2004). An array of sensors measuring temperature and moisture dynamics in time are installed at several depths and at several locations across it.

The cryogenic suction is calibrated by matching the simulated unfrozen water content to the observed one at 0.35 m depth in the circle and 0.15 m depth in the inter-circle, respectively. Thermal conductivities of the frozen mineral and organically enriched soil are set to be 1.9 and 0.9 W/(mK), respectively. The Young's modulus for the mineral soil inside and outside the circle is $2 \cdot 10^6$ and $2 \cdot 10^7$ Pa, respectively, which are typical values for weakly consolidated and consolidated silt-clay mixture. Since the non-sorted circle is located in a waterlogged area, we model it as a hydraulically open system. Initial soil temperature distribution with depth was approximated by measured temperature on September 12, 2002, and the soil porosity was set to be 0.35. On this day the active layer depths in the center of the non-sorted circle and in the surrounding tundra were 0.80 and 0.60 m, respectively.

We simulated the soil freezing from September 12, 2002, through December 18, 2002, when the temperature in the non-sorted circle became less than -5ºC. On the circle and inter-circle ground surface, we prescribed a 5-day-running average of the corresponding measured ground surface temperature. The calculated liquid water content at 0.35 m depth in the circle and 0.15 m depth in the inter-circle is compared to the measured data (Fig. 6). The difference in freeze-up timing between the observed and modeled ground is less than three days.

In general, the discrepancy between the measured and computed temperature at the depth of 0.35 m in the circle is less than 1ºC (Fig. 7).

In addition to comparing the measured and computed soil temperatures, we show the calculated pressure dynamics at the same point; i.e., at the depth of 0.35 m. Note that initially when the ground surface temperature was above 0ºC, the pressure was zero (we assume there is no gravity and that the pressure on the lateral boundary is zero). However, as soon as ground freezing begins, the cryogenic suction starts

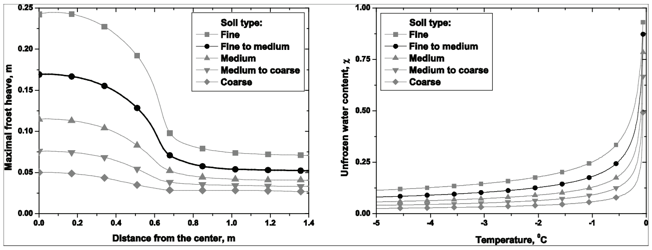

Figure 8. Sensitivity of the frost heave (left) on parametrization of the unfrozen water content (right).

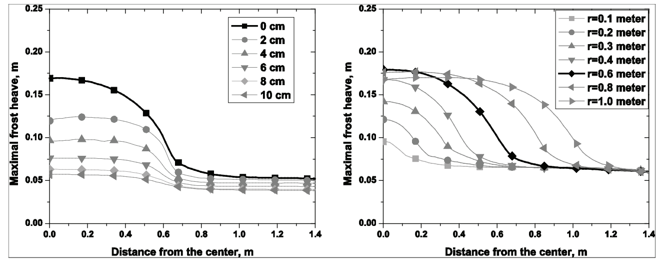

Figure 9. Sensitivity of the maximum frost heave to an addition of organically enriched soil (left) and to the radius (right) of the non-sorted circle.

to force water migration from a still-unfrozen part of the active layer to a partially frozen one. Therefore, the pressure lowers in the entire thawed part of the active layer, and the pressure dynamics have slightly negative pressure at this time (Fig. 7).

When the freezing front reaches the depth/region at which the pressure and temperature dynamics are shown (0.35 m), the cryogenic suction starts to force water migration into this still partially frozen region. Soil porosity consecutively increases (Fig. 7). Due to an increase of the water mass, and due to its expansion while freezing, the pressure continues to increase (Fig. 7). Note that the increased porosity is associated with formation of ice lenses and development of the frost heave (the small decrease in soil porosity is due to numerical regularization of the soil mass conservation principle). The value of the computed frost heave in the center of the non-sorted circle is approximately 0.18 m, whereas in the inter-circle it is 0.045 m. These computed values are in a good agreement with field observation circles heave by 0.15–0.2 m.

Sensitivity Analysis

In this section, we present results from the sensitivity study of the frost heave with respect to unfrozen water content, changes in the organic layer, and geometric dimensions. We define the calculated maximum frost heave at the Franklin Bluffs site as a reference point against which we compare a series of numerical experiments. To simplify comparison, we show the calculated frost heave for the Franklin Bluffs site by a line with circle symbols.

In the first series of experiments, we analyze dependence of the maximum frost heave on the unfrozen water content for the mineral soil. Note that parameterization of unfrozen water content depends on mineralogy, solute concentration, texture, and other factors. For example, the high unfrozen water content is associated with fine-grained ground material. For coarse-grained materials, such as sand, the unfrozen water content depends sharply on temperature near 0ºC (Fig. 8). For each shown parameterization, we simulate freezing of the non-sorted circle and compute the maximum frost heave (Fig. 8). In these numerical experiments, all model parameters except for the parameterization of the unfrozen water content were fixed and equal to the values related to the Franklin Bluffs site.

From the computed results, we observe that the largest frost heave occurs when the soil has a high unfrozen water content. This effect has the following explanation. Hydraulic conductivity of the partially frozen soil increases if the unfrozen water content θ_w becomes higher, and hence more water migrates through the partially frozen region due to cryogenic suction flow F (non-linearly dependent on θ_w) and forms ice lenses. The above-mentioned dependence of the frost heave on unfrozen water content is commonly observed in nature; i.e., that sand and gravel are not frost-heave susceptible soils whereas silt is. Note that clays, which have an even higher unfrozen water content, are typically not capable of developing significant frost heave since they have very small hydraulic conductivity.

In our field experiments, we observe that a thin organic layer is typical on top of some circles. From the physical point of view, this layer represents an additional thermal resistance and changes mean temperatures in the soil. Therefore, in the third series of experiments, we analyze dependence of the maximum frost heave on presence of organically enriched soil in the non-sorted circles. We consider several configurations of organic layers varying in their thicknesses. We additionally place on top of the non-sorted circle an organic layer, which uniformly covers the circle and inter-circle. The soil thermal, hydraulic, and rheological properties of this additional layer are identical to the properties of the original organically enriched soil in the inter-circle for the Franklin Bluffs site. Note that an increase in insulation layer causes a decrease in the active layer thickness. From our field studies, we observed that each additional 0.02–0.03 m of the organic material results in 0.04–0.05 m decrease of the active layer. In the left plot in Figure 9, we show the maximum frost heave developed for various thicknesses of the additional organic layer.

We emphasize that observed results are in agreement with observations at non-sorted circles along the Dalton highway in Alaska. For example, the scarcely vegetated circles at the Franklin Bluffs area heave by 0.15–0.2 m, whereas moderately vegetated circles at the Happy Valley site develop only 0.07–0.1 m of heave during winter. Also, field experiments (Kade et al. 2006, Kade & Walker, in press) at Sagwon Bluffs involved both the removal and addition of vegetation on non-sorted circles. The removal of vegetation at this location resulted in a 1.4ºC increase in mean summer mineral soil surface temperature compared to control, a 6%

increase in the depth of the thaw layer, and a 26% increase in frost heave. The addition of a 0.1 m thick moss layer results in the opposite effect; i.e., a 2.8ºC decrease in the mean summer mineral soil surface temperature, a 15% reduction in the thaw layer, and a 52% decrease in heave. Despite the fact that the numerical model is focused on non-sorted circles at the Franklin Bluffs site, and the field experiments were conducted at the Sagwon Bluffs site, results from these studies show qualitative agreement, and almost similar quantitative behavior of frost heave reduction.

In the fourth series of experiments, we investigate sensitivity of frost heave to the radius of the non-sorted circles. We calculate the frost heave for circles which have 0.1, 0.2, ... 1.0 m radius. Our calculations support observations which reveal that small-scale non-sorted circles heave less compared to the large-diameter ones. The maximum computed frost heave is for circles with the radius of 0.6 m (Fig. 9). For circles with a radius larger than 0.6 m, the maximum frost heave decreases slightly, since liquid water has to migrate to the center of the non-sorted circle longer from the lateral boundary where water is abundant. Smaller values of frost heave computed in the center of the non-sorted circle with a large radius can promote development of live vegetation as observed in nature.

Conclusions

We present a numerical thermo-mechanical model of differential frost heave with special emphasis on simulating biocomplexity of non-sorted circle ecosystems. Unlike many other models that study 1-D ice lens formation, we are concerned with 2-D effects of soil freezing. Heterogeneity in soil properties and surface conditions results in curved frost penetration and 2-D temperature fields. Therefore, the cryogenic suction results in horizontal water redistribution inside the non-sorted circle.

The model was tested using observational data obtained from several sites within the Permafrost/Ecological North American Arctic Transect. We obtained a good comparison between simulated and observed dynamics of physical processes in the non-sorted circle at the Franklin Bluffs. The model also qualitatively represents “non-heaving” non-sorted circles at the Howe Island site.

The simulated frost heave is sensitive to hydrological soil properties, and to changes in the vegetative insulation layer within the circle and inter-circle areas. The results of our sensitivity analysis, with respect to addition/removal of vegetation layer to/from the surface of a circle, are well correlated with field observations where a layer of organic material was either added or removed from the non-sorted circle.

The most active development of differential frost heave takes place for non-sorted circles within waterlogged areas with strong upper-soil-layer heterogeneity caused by living vegetation. The most important driver of the non-sorted circle ecosystem is the presence of vegetation that, over a significant time, changes the soil mineralogy and thermal and hydrological soil properties. This then changes the amount of differential frost heave and reduces or enhances all bio-geophysical processes responsible for the formation and evolution of the non-sorted circles.

Acknowledgments

We thank J. Hartikainen and J. Stroh for their advice along the way. This research was funded by ARCSS Program and by the Polar Earth Science Program, Office of Polar Programs, National Science Foundation (OPP-0120736, ARC-0632400, ARC-0520578, ARC-0612533, IARC-NSF CA: Project 3.1 Permafrost Research), by NASA Water and Energy Cycle grant, and by the State of Alaska.

References

Fremond, M. & Mikkola, M. 1991. Thermomechanical modeling of freezing soil. *The Sixth International Symposium on Ground Freezing, Rotterdam*.

Graham, J. & Au, V.C.S. 1985. Effects of freeze-thaw and softening on a natural clay at low stresses. *Canadian Geotechnical Journal* 22(1): 69-78.

Kade, A., Romanovsky, V.E. & Walker, D.A. 2006. The N-Factor of Nonsorted Circles Along a Climate Gradient in Arctic Alaska. *PPP* 17: 279-289.

Kade, A. & Walker, D.A. 2007. Experimental alternation of vegetation on non-sorted circles: effects on cryogenic activity and implications for climate change in the Arctic. *AAAR* (in press).

Konrad, J.M. & Duquennoi, C. 1993. A model for water transport and ice lensing in freezing soils. *Water Resources Research* 29(9): 3109-3124.

Mikkola, M. & Hartikainen, J. 2001. Mathematical model of soil freezing and its numerical application. *Inter. J. Num. Meth. in Engineering* 52: 543-557

Nicolsky, D.J., Romanovsky, V.E., Tipenko, G.S. & Walker, D.A. 2008. Modeling biogeophysical interactions in non-sorted circles in the Low Arctic. *JGR, Biogeosciences*. (accepted).

O`Neill, K. & Miller, R.D. 1985. Exploration of a rigid ice model of frost heave. *Water Resources Research* 21: 281-296.

Qi, J., Vermeer, P.A. & Cheng, G. 2006. A Review of the Influence of Freeze-thaw Cycles on Soil Geotechnical Properties. *PPP* 17: 245-252.

Van Everdingen, R. 2002. Multi-Language Glossary of Permafrost and Related Ground-Ice Terms.

Walker, D.A., Epstein, H.E., Gould, W.A., Kelley, A.M., Kade, A.N., Knudson, J.A., Krantz, W.B., Michaelson, G., Peterson, R.A., Ping, C., Raynolds, M.K., Romanovsky, V.E. & Shur, Y. 2004. Frost-Boil Ecosystems: Complex Interactions Between Landforms, Soils, Vegetation and Climate. *PPP* 15: 171-188.

Engineering-Induced Environmental Hazards in Permafrost Regions of the Qinghai-Tibet Plateau

Fujun Niu
State Key Laboratory of Frozen Soil Engineering, Cold and Arid Regions Environmental and Engineering Research Institute, CAS, Lanzhou, China 730000

Jian Xu
State Key Laboratory of Frozen Soil Engineering, Cold and Arid Regions Environmental and Engineering Research Institute, CAS, Lanzhou, China 730000

Zhanju Lin
State Key Laboratory of Frozen Soil Engineering, Cold and Arid Regions Environmental and Engineering Research Institute, CAS, Lanzhou, China 730000

Ping Wang
The First Railway Survey and Design Institute of China, Xi'an, China 710043

Abstract

The permafrost in the Qinghai-Tibet Plateau is characterized by massive ground-ice and high ground temperature. Under the influence of global warming, the permafrost is degrading. At the same time, many linear structures, including highways, gas pipelines, cable lines, electrical transfer lines, and railways, have been constructed during the past 50 years. Such engineering activities along with the rising air temperature have changed the permafrost environment along the Qinghai-Tibet Corridor. Field investigation shows that the main environmental hazards related to permafrost changes have widely developed, such as thaw slumping, thawing settlement, thermokarst, icing, frost mound, etc. The main factors causing these hazards include changes of conditions of the ground surface, the groundwater, and natural slope stability. Engineering treatment for preventing the hazards needs to be based on a good understanding of possible changes of ground thermal regime and water movement, along with their processes.

Keywords: engineering activity; hazard; linear structure; permafrost; Qinghai-Tibet Plateau.

Introduction

Permafrost covers 1,500,000 km^2 of area on the Qinghai-Tibet Plateau (Zhou et al. 2000). On the plateau, many linear structures such as highways, railways, gas pipelines, electricity-transmitting lines, and optical fiber cables have been constructed since the 1950s. The permafrost was initially discovered during construction of the Qinghai-Tibet Highway. Though permafrost was encountered at that time, no special engineering treatment was adopted, and the road embankment was just paved with side soils. During the construction, possible changes to the permafrost were not considered, and the seed for roadbed engineering problems was planted thereby. Environmental change caused by engineering activities can lead to environmental hazards, which simultaneously affect engineering stability. These hazards include thawing settlement, thaw slumping, thawing grooves, thermokarsts, frost heave, etc. The purpose of this paper is to introduce the permafrost situation in the Qinghai-Tibet Plateau, to describe some main thawing hazards and frost hazards along the Qinghai-Tibet Highway (QTH) and the Qinghai-Tibet Railway (QTR), to analyze formations of the hazards, and to discuss their treatments.

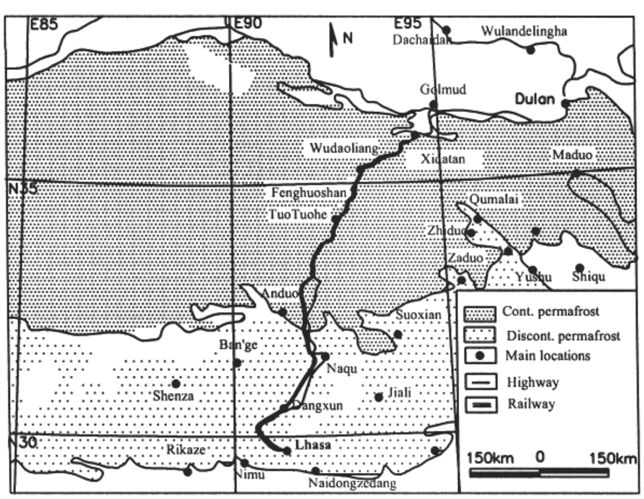

Figure 1. Permafrost distribution and the position of the highway and railway on the Qinghai-Tibet Plateau.

Permafrost and Engineering Activities in the Qinghai-Tibet Plateau

Permafrost comprises 75% of the total land of the plateau; its distribution is shown in Figure 1. The figure shows that along the highway and railway from Golmud to Lhasa, the northern limit of the permafrost is located in the Xidatan Basin north to the Kunlun Mountains. The southern limit is located in the Anduo Basin south to the Tanggula Mountains. The permafrost of the plateau features rich ice and high ground temperature. Take the 550-km-long continuous permafrost along the railway, for example. The section of

Figure 2. Thaw slumping at K3035 mileage of QTH.

permafrost with volume ice content higher than 20% is 221 km. The section with mean annual ground temperature (MAGT) higher than -1.0ºC (warm permafrost) is 221 km. On the whole, the warm and ice-rich permafrost is 124 km long (Liu et al. 2000, Wu et al. 2004).

As the permafrost of the plateau is warm and rich in ground-ice, it is sensitive to global warming and engineering activities. Monitored data from boreholes in the natural ground along the highway showed that the ground temperature at the permafrost table increased by a value of 0.08ºC/a from 1996 to 2001. The table was lowered 2.6 to 6.6 cm/a. According to investigations in past 30 a, the MAGT of the seasonal frozen ground, and the island permafrost along the QTH increased 0.3 to 0.5ºC from the 1970s to 1990s. The MAGT of the continuous permafrost increased 0.1 to 0.3ºC within the period. Under natural conditions, the permafrost area shrunk 0.5 to 1.0 km at the north edge and 1 to 2 km at the south edge. While affected by highway construction, it shrunk 5 to 8 km at the north edge and 9 to 12 km at the south edge (Wang & Mi 1993, Zhu et al. 1995, Nan et al. 2003). Therefore, the degradation influence of engineering activities on the permafrost was much more serious than that of natural forces.

To engineering projects, thawing settlement is the first response to degradation, and some phenomena related to the thawing easily occur, such as thaw slumping and thermokarst. On the other hand, in some cases when the hydrological conditions are changed in permafrost regions, other environmental hazards related to freezing can also occur, such as icing and frost heaving. On the plateau, all projects including highway, railway, cable line and pipe line are near parallel and concentrated in a region called the Qinghai-Tibet Corridor. The earliest project was the Qinghai-Tibet Highway. It was constructed in the 1950s, and repaired in large scale three times, mainly for treating problems caused by permafrost. From 1973 to 1977, a gas pipeline was constructed. The pipeline crossed 560 km of permafrost regions. In 2001, the Qinghai-Tibet Railway began to be constructed after nearly 30 years of intermittent planning, discussion, and investigation. The construction was finished in 2006, and the railway was opened to service in 2007. The electricity-transmitting line was constructed along the railway in 2006. We know that the highway has many problems in the permafrost section, but the railway, in service for one year, was constructed based on cooling-roadbed principles and cost much more than the highway. The railway's roadbed was stable according to our investigation from July to September in 2007. However, some environmental hazards along the railway related to construction activities in the permafrost section have occurred and might influence the roadbed stability in future. Here in this paper, some typical environmental hazards caused by engineering activities were introduced.

Main Environmental Hazards Along the Highway and the Railway

Thawing induced hazards

(1) Thaw slumping

Thaw slumping is commonly caused by slope toe disturbance in ice-rich permafrost regions. On the plateau, well-developed thaw slumping exists on the west side of the highway at K3035 mileage (Fig. 2) in the Kekexili Hill Region between Wudaoliang and the Fenghushan Mountains. In the slope, massive ground-ice with thickness of about 1 m was well developed and buried 2 m deep. The slumping was initially caused by cutting for embankment of the highway during 1990–1992. The failure showed as detachment of the active layer, and consisted of sand and silty clay. After years of repetition of the thawing-collapse-slide, the current 110 m long and 72 m wide landslide area was formed.

To survey the retrogressive process of the landslide area, some monitoring points and boreholes for monitoring the ground temperature, as shown in Figure 3, were installed in 2002. Monitored data of the 8 points near the back wall indicated that, from 2002 to 2006, the longest retrogressive distance at point 1 was 8.0 m. The collapse mainly occurred within a period from July to September, which is the main thawing period of a year. As the grass surface and the soil layers were destroyed when collapse occurred, the ground thermal status was also changed. Figure 4 was drawn with annually averaged ground temperature data obtained from borehole A in the undisturbed natural ground, and borehole B, in the failed zone. The figure shows that the temperature of natural ground at a depth of 0.0 m to 4.5 m was lower than that of the failed zone. Also, the thermal gradient in borehole B was very low, indicating that thermal exchange between the atmosphere and the ground in the failed zone was very limited. This might lead the permafrost in the zone to degrade.

As slope failure of thaw slumping is strikingly influenced by frozen soil, temperature, and groundwater, engineering treatments should fully consider these factors. Reasonable methods should be based on decreasing thermal energy entering the soil and draining groundwater, such as covering the collapsing zone with crushed stone, stacking grass bags filled with earth, re-vegetation, and so on.

(2) Thawing groove

A thawing groove is normally caused by linear cutting or

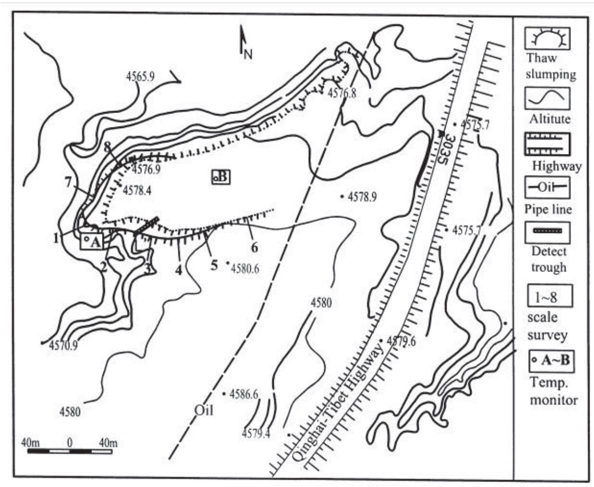

Figure 3. Relief map of the thaw slumping and the monitored positions.

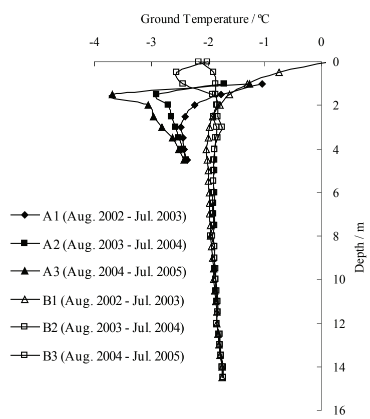

Figure 4. Annually averaged ground temperatures in borehole A and B.

even ground surface disturbance by truck or car driving in wet land in permafrost regions. Figure 5 shows a thawing groove developed along the QTR at K980 mileage south to the Kunlun Mountain. The strata here consisted of 10 m thick fine sand with gravels and the underlying silty clay. The permafrost table was 1.5 m in depth and the permafrost was ice-rich or ice-saturated. The embankment was constructed in 2003, and the slopes were covered with crushed stone in 2006. On the west side a 1.5 m high water barrier and drainage ditch were constructed in 2003. But in 2006, as surface water was gathered between the barrier and the embankment, the barrier was removed and the ditch was covered. According to our investigation, a 180 m long thawing groove along the former ditch developed with a depth of 20 cm in July 2007 (Fig. 5[a]) and then subsided to 40 cm in September (Fig. 5[b]). The gathered water shown in Figure 5(a) was mainly from ground-ice melting according to pit investigations, indicating that the subsidence was caused by thawing of the underlying frozen soils. Figure 6 shows the cross- section of the groove and its relative position to the embankment. Because of the settlement in the groove, many parallel fissures developed along the groove. The nearest fissure

(a)

(b)

(Figure 5. Thawing groove developed on the west side of QTR: (a) Status in July 2007; (b) Status in September 2007.

was 3.5 m from the embankment. Such a hazard needs to be remedied soon, otherwise it continues to develop and even worsen when surface water moves into the fissures and the groove. As it has laterally thermal erosion to the roadbed of the railway, its long existence ultimately affects roadbed stability.

The thawing grooves in some sections along the railway mainly resulted from insufficient understanding of the interaction among the earth surface, ground temperature regime, ground-ice, and melted water. To avoid such problems, engineering construction should be restricted so as not to disturb the surrounding environment. When thawing grooves occur, earth refilling, grass sheet covering, and even sunshine shielding, along with efficient drainage, can be adopted to stop groove development. Basically, the objective is to stop melting of the ground-ice

(3) Thermokarst

Thermokarst results from the thawing of ice-rich permafrost or the melting of massive ice. On the plateau, normal thawing or melting is caused by change or disturbance of the ground surface, as that makes the surface absorb more energy than before. We mentioned above that the embankment of the QTH was initially just stacked with
two side soils. That not only changed the original ground surface, but also left many pits along the way. Now many of the pits show as small thermokarst lakes or where water

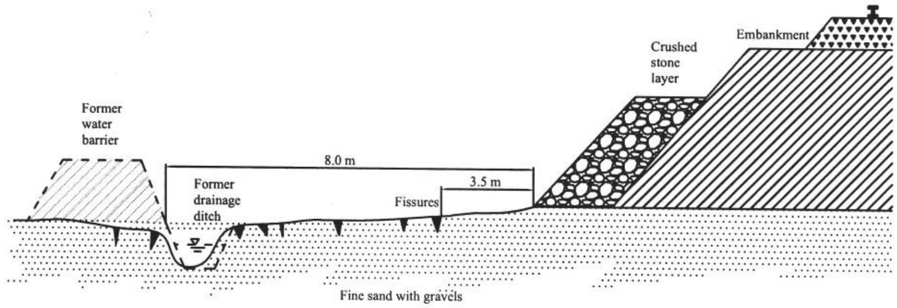

Figure 6. Cross-section of the thawing groove and the embankment

Table 1. Surface waters on the two sides of the QTH within 150 km in the permafrost regions.

Region	Mileage of the QTH /km	Kind of permafrost	MAGT / ºC	Small thermokarst lake		Accumulated water pit	
				Number	Area / m²	Number	Area /m²
Xidatan Basin	K2886~K2895	Icy soil	-3.0~-1.5				
Kunlun Mountain	K2895~K2910	Ice-saturated soil and massive ice	-3.0~-1.5	1	1,200	15	949
Unfrozen Spring Valley	K2810~K2920	Ice-rich soil and seasonal frozen soil	-3.0~-1.5; >0			3	400
Xieshuihe Plateau	K2920~K2941	Ice-saturated soil and massive ice	-1.5~-0.5	11	2,405	25	1,134
Xieshuihe Plateau	K2941~K2946	Ice-rich soil	-1.5~-0.5				
Qingshuihe Basin	K2946~K2956	Massive ground-ice	>-0.5	14	2,710		
Qingshuihe Basin	K2956~K2959	Icy soil and ice-saturated soil	-1.5~-0.5				
Chuma'erhe Plateau	K2959~K2963	Ice-saturated soil	-1.5~-0.5	5	2,700	3	21
Chuma'erhe Plateau	K2963~K2970	Massive ground-ice	-1.5~-0.5	4	790	21	721
Chuma'erhe Plateau	K2970~K2978	Massive ground-ice and ice-saturated soil	-1.5~-0.5			20	1,655
Chuma'erhe Plateau	K2978~K2983	Massive ground-ice	-1.5~-0.5	5	610	13	468
Chuma'erhe Plateau~Wudaoliang Hill	K2983~K3006	Icy soil and massive ground-ice	-1.5~-0.5	1	100	27	364
South Wudaoliang Hill region	K3006~K3017	Ice-rich soil and ice-saturated soil	-1.5~-0.5	10	685	20	814
Kekexili Hill region	K3017~K3027	Massive ground-ice	-3.0~-1.5	11	1,120	30	420
Honglianghe Hill region	K3027~3036	Ice-saturated soil	-1.5~-0.5	7	1,015	57	1,488

accumulates. Thermokarst lakes with characteristic collapses of the shore land were different to surface accumulated water. We investigated the surface waters along the two sides of the highway and classified them into small thermokarst lakes and accumulated water in Table 1. The statistical data in the table show that 69 small thermokarst lakes developed mainly in the regions with ice-saturated permafrost or massive ground-ice. In the regions with low ice content permafrost, no thermokarst lake developed within the investigated 150 km zone. At the same time, surface water did not readily accumulate either.

To intensively investigate the thermal regime of the ground under a thermokarst lake, we drilled boreholes in a lake near the Fenghuoshan Mountain region, where permafrost is rich in ground-ice. The lake shown as Figure 7 was approximately elliptic, 150 m long and 120 m wide. The water in the lake was 2.0 m deep. Figure 7 shows that the shore edge collapsed during thawing time, which is a characteristic of a thermokarst lake. Six boreholes were drilled in the lake and in the shore land, and temperature probes were installed in 2006. Figure 8 shows positions of the boreholes and the local strata. Borehole investigation revealed that the permafrost table was buried 2.1 m deep. Under the table, the massive ground-ice existed with a thickness of about 3 m, which supplied a water source for the formation of the lake by melting.

Figure 9 shows the temperatures of the water and the humus deposits in the lake. The curves in the figure indicate that the lake water at a depth of 0.5 m processed phase change between water and ice. In fact the maximum ice thickness in winter was 0.7 m. The temperatures at other depths were all above 0ºC. The ground temperatures of the six boreholes at maximum-thawed-depth time were drawn in Figure 10. The figure indicates that the ground temperature in borehole 6, which was in the center of the lake, was higher than 0ºC. The permafrost table in boreholes 3–6 was 2.0 m deep, while in borehole 2, it was 7.2 m deep, as the borehole was in the lake area. The figure also shows that the ground temperature decreased from the lake to the land. Also, the ground thermal gradients were different. Such a situation was the same with the lakes studied by Burn at the west Arctic coast, Canada (Burn 2005). In that region, if lake ice freezes to the bottom sediments, it may be underlain by permafrost. Otherwise the thermal talik may penetrate through permafrost. Here, the thermokarst lake was somewhat similar to lakes in the Arctic region. Table 2 lists the calculated thermal gradient and estimated depth of the permafrost base in the different boreholes. The data in the table indicate that no permafrost existed, and there was a negative thermal gradient under the center area of the lake, hinting that the lake water provided a heat source to the underlying sediments. In the other boreholes, the temperature gradients were positive as normal. The permafrost base in the lake near the bank was 32.2 m deep, while far from the lake, the base depth lowered. Such differences revealed that the thermokarst lake has greatly influenced the existence of local permafrost. It also seriously laterally eroded neighboring permafrost. Therefore, if thermokarst existed near a roadbed, with time it would influence the thermal stability of the roadbed along permafrost regions. Engineering experience in permafrost regions of the plateau shows that good drainage systems and no-excavation are effective ways to avoid thermokarst.

Figure 7. Thermokarst lake near Fenghuoshan Mountain.

Freezing induced hazards

In the engineering constructions in the permafrost regions of the plateau, thaw settlement was paid much more attention than frost problems. As the permafrost degraded in the past years and the degradation continues, thaw settlement problems are becoming more serious than frost heave problems. However, when the groundwater seepage conditions are changed, outflow or new movement of the groundwater might cause frost heave problems.

Figure 11 shows an icing incorporated with a frost mound along the QTH in the Unfreezing Spring region (Budongquan region), where both permafrost and seasonal frozen ground exist. Springs are widely distributed and are the main

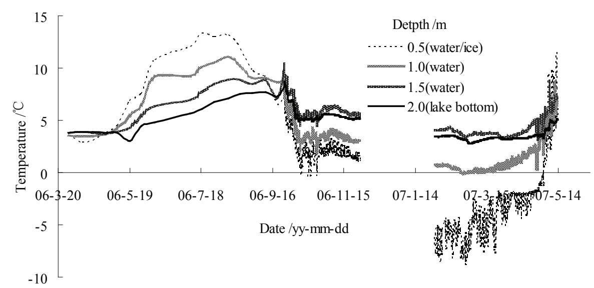

Figure 9. Temperature of the water and shallow depth of the thermokarst lake.

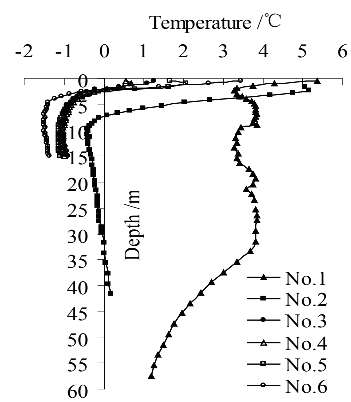

Figure 10. Ground temperatures in the six boreholes at beginning of October, 2006.

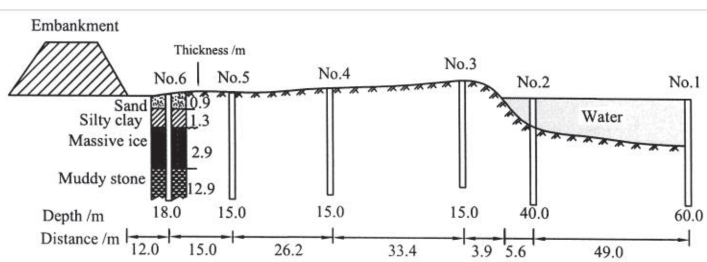

Figure 8. Borehole distribution and the local strata around the thermokarst lake.

Table 2. Thermal gradient and estimated permafrost base depth in different boreholes.

Hole number	Thermal gradient / ºC/100m	Depth of permafrost base /m	Depth range for calculation /m
No.1	-6.3		45~60
No.2	1.8	32.2	30~40
No.3	3.2	52.7	11~15
No.4	2.0	64.3	11~15
No.5	1.8	75.5	11~15
No.6	1.8	89.7	11~15

Figure 11. Icing and frost mound along the QHT.

source of the local river. After the QTH embankment was constructed and some of the groundwater discharge was blocked, icings along with frost mounds resulted. Every winter several icings formed at the two sides of the highway within a 3 km section. Some of them even covered the road surface shown as Figure 11. At the same time, when icings and frost mounds thawed, the roadbed subsided unevenly. To solve such a hazard, groundwater migration routes need to be investigated, and seepage structures are necessary. In a road structure, sometimes a bridge is the final choice.

Conclusions

(1) Permafrost in the Qinghai-Tibet Plateau is in degradation under the influence of global warming. Moreover, in the narrow Qinghai-Tibet corridor, dense engineering projects have intensified the degradation and caused secondary hazards. These hazards mainly show as thawing settlement, thaw slumping, thawing grooves, thermokarst, frost heave, etc.

(2) Thaw slumping is commonly caused by slope toe disturbance in ice-rich permafrost regions. Well-developed thaw slumping along the QTH has developed to about 7500 m^2 in scale in the past 15 years. The permafrost in the slumping zone is under degradation, characterized by ground-ice melting and temperature-rising.

(3) Thawing grooves are mainly caused by linear cutting or even ground surface disturbance. A thawing groove which exists along the QTR subsided 40 cm in 2 years. Long-time development of the groove finally affects the roadbed stability by parallel cracks and lateral thermal erosion.

(4) Thermokarst results from the thawing of ice-rich permafrost or the melting of massive ice. There were 69 small thermokarst lakes in an ice-saturated permafrost section within 150 km along the QTH. Permafrost under a typical thermokarst lake near the Fenghuoshan region has totally thawed. Therefore, lateral thermal erosion of a thermokarst lake needs to be considered if it is near an engineering project.

(5) An icing incorporated with a frost mound along the QTH was cause by embankment blocking of groundwater discharge. The road surface was hard to keep even because the roadbed suffered frost heave and thaw settlement every year.

(6) Restricting ground surface disturbance and excavation, ensuring an efficient drainage system, and keeping the ground frozen are suggested ways to avoid the secondary hazards in permafrost regions of the plateau.

Acknowledgments

This work was supported in part by the Chinese Natural Science Fund (No. 40471023), the grant of the Knowledge Innovation Program of the CAS (No.KZCX1-SW-04, KZCX-XB-10) and the National Science Supporting Project of the Ministry of Science and Technology of China (2006BAC07B02).

References

Burn, C.R. 2005. Lake-bottom thermal regimes, western Arctic coast, Canada. *Permafrost and Periglacial Progresses* 6: 355-367.

Liu, Y.Z., Wu, Q.B., Zhang, J.M. et al. 2000. Study on ground temperature field in permafrost regions of Qinghai-Tibet Plateau. *Highway* 2: 4-8.

Nan, Z.T., Gao Z.S., Li, S.X. et al. 2003. Permafrost Changes in the Northern Limit of Permafrost on the Qinghai-Tibet Plateau in the Last 30 Years. *ACTA Geographic SINICA* 586): 817-823.

Wang, S.L. & Mi, H.Z. 1993. The Change of Permafrost under Roadbed with Asphalt Pavement along the Qinghai-Tibet Highway. *Journal of Glaciology and Geocryology* 15(4): 566-573.

Wu, Q.B., Cheng, G.D. & Ma, W. 2004. The impact of climate warming on Qinghai-Tibetan Railroad. *Science in China, Series D* 47 (Supp.I): 122~130.

Zhou, Y.W., Cheng, G.D., Qiu, G.Q. et al. 2000. *Permafrost in China*. Beijing: Science Press, 403-404.

Zhu, L.N., Wu, Z.W. & Liu Y.Z. 1995. Permafrost Degeneration in the East of Tibetan Plateau. *Journal of Glaciology and Geocryology* 17(2): 120-124.

Comparison of Simulated 2D Temperature Profiles with Time-Lapse Electrical Resistivity Data at the Schilthorn Crest, Switzerland

Jeannette Noetzli
Glaciology, Geomorphodynamics, Geochronology, Geography Department, University of Zurich, Switzerland
Christin Hilbich
Department of Geography, University of Jena, Germany
Christian Hauck
Institute for Meteorology and Climate Research, University of Karlsruhe/Forschungszentrum, Karlsruhe, Germany
Martin Hoelzle
Glaciology, Geomorphodynamics, Geochronology, Geography Department, University of Zurich, Switzerland
Stephan Gruber
Glaciology, Geomorphodynamics, Geochronology, Geography Department, University of Zurich, Switzerland

Abstract

The Schilthorn Crest in the Bernese Alps, Switzerland, is a prominent permafrost research site. Topographic and transient effects influence the temperature field below the east-west oriented crest. Measured T(z)-profiles in boreholes, however, do not provide sufficient information for a comprehensive description of the subsurface temperature distribution. We combine ground temperature measurements, electric resistivity tomography (ERT) monitoring, and numerical modeling to investigate the 3-dimensional thermal regime below the crest. The modeled temperature field of a north-south oriented cross section agrees well with ERT results along the same profile. The simulated thermal regime below the Schilthorn is characterized by generally warm permafrost, with the coldest zone below the upper part of the north-facing slope, and permafrost a little below the surface on the south-facing slope. The combination of temperature modeling and measurements and geophysical monitoring bears potential to improve simulation and validation strategies.

Keywords: alpine permafrost distribution; electrical resistivity; thermal modeling; tomography monitoring; transient and topographical temperature effects.

Introduction

Permafrost was first found on Schilthorn summit, Switzerland, when the facilities for the cable car were built between 1965 and 1967. During the construction of the buildings, several ice lenses with a thickness of up to 1 m were encountered. Since then, extensive research has taken place on Schilthorn (e.g., Imhof 2000, Vonder Muehll et al. 2000, Hauck 2001, Mittaz et al. 2002, Hilbich et al. 2008), making it to one of the most intensively investigated permafrost sites in the European Alps. Three boreholes in perennially frozen ground were drilled within the PACE-project between 1998 and 2001 (Harris 2001). These boreholes provide the basis for monitoring and quantification of changes in the permafrost thermal regime.

In mountain areas, the interpretation of T(z)-profiles measured in boreholes with respect to climate signals is complicated by topographic effects (Gruber et al. 2004). The Schilthorn represents an east-west oriented ridge with a warm south-facing and a colder north-facing slope. Even though measured temperature profiles in boreholes enable an initial assessment of topography related and transient effects, they are only representative of isolated local spots. A comprehensive analysis of permafrost distribution and evolution below the crest can only be achieved by integrating additional subsurface data

Figure 1. View of the Schilthorn Crest in the Bernese Alps looking eastward. The ERT-Profile starts just below the meteo station in the northern slope and reaches across the crest approximately to the southern border of the photo.

In this paper, we combine measurements of surface and subsurface temperatures, electric resistivity tomography (ERT), and numerical modeling of a subsurface thermal field for a 2-dimensional investigation of permafrost conditions below the Schilthorn crest. A 2D heat transfer model is forced by measured near-surface temperatures at the upper boundary to simulate the thermal field of a north-south cross section of the ridge. An ERT monitoring system was installed across the same profile, which provides additional information on subsurface conditions, and enables comparison of modeling results for a qualitative validation.

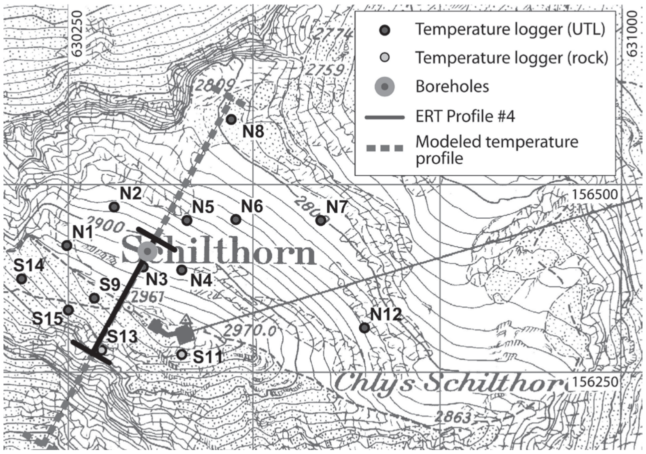

Figure 2. Overview of the field site Schilthorn Crest showing the locations of the near-surface temperature loggers, the boreholes, the measured ERT profile, and the modeled north-south cross section. Map: Swisstopo.

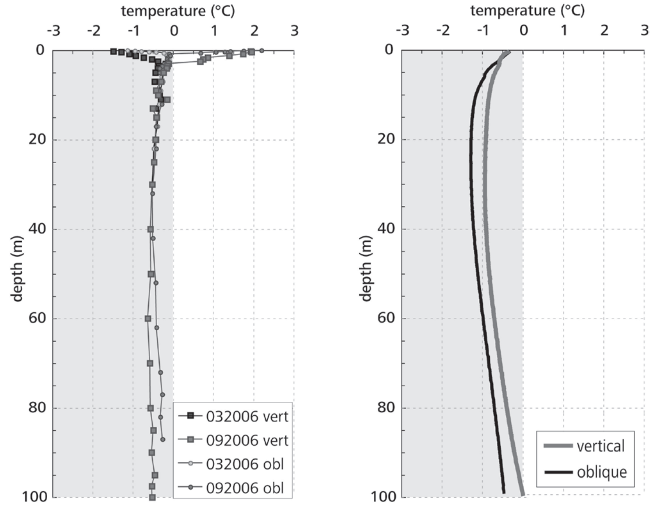

Figure 3. T(z)-profiles for the 101 m vertical (vert, black) and oblique (obl, gray) boreholes on the Schilthorn for spring and autumn 2006 (left). Modeled T(z)-profiles extracted from the temperature field in Fig. 4 at the locations of the two boreholes (right; colored illustration available on CD-Rom).

The Field Site

The Schilthorn (2970 m a.s.l., 46.56°N/7.83°E, Figs. 1, 2) is located in the Bernese Oberland in the Northern Swiss Alps. The three boreholes are located on a small plateau on the north-facing slope approximately 60 m below the summit. Air temperatures recorded at the meteo station close to the boreholes indicate an annual mean of -2.8 °C for the years 1999–2007 (Hoelzle and Gruber 2008). The annual precipitation is estimated to 2700 mm and about 90% of it falls as snow (Imhof 2000). As the precipitation maximum occurs during summer and due to additional snow input through wind transport, the snow cover on the northern slope usually persists from October until June or even July (Hauck 2001). The average snow depth since the beginning of measurements at the meteo station in 1999 is around 80 cm. The Schilthorn consists of dark micaceous shales that weather to form a fine-grained debris layer of up to several meters in thickness covering the entire summit region. The ice content of the subsurface material is assumed to be generally low (around 5–10% in the upper meters, as reported from direct observations, Imhof et al. 2000, Vonder Mühll et al. 2000).

Temperature Measurements

Boreholes

In the scope of the PACE project, a 14 m borehole was drilled in 1998 and complemented by two 101 m boreholes in 2000. Today, these boreholes are part of the Permafrost Monitoring Switzerland (PERMOS). The deeper boreholes were drilled vertical and with an angle of 60° to the vertical in order to account for topography-related effects. Temperatures measured in these boreholes point to warm permafrost conditions with temperature values between -1 and 0°C below depth of the zero annual amplitude (ZAA) at approximately 20 m, and to a very small temperature gradient with depth (Fig. 3, left). The temperature gradient in the oblique borehole is slightly greater than in the vertical borehole. Ground temperatures are considerably higher compared to other sites at similar altitude and exposition, which is probably due to the low bedrock albedo, thick snow cover, and low ice content at the site (Hauck 2001).

Ground surface temperatures

In addition to the borehole measurements, 14 temperature loggers were distributed on both sides of the crest in summer 2005 and 2006 to measure near surface-temperatures (see Fig. 2). The loggers were installed at a depth of 30 cm (UTL mini loggers) and 10 cm (rock temperature loggers), respectively, and temperatures are recorded every 2 hours. The accuracy of the temperature loggers is given as ±0.25°C and ±0.1°C, respectively. As the lower parts of the steep southern slope are difficult to access, loggers were only placed in the upper part of the slope. These near-surface temperature measurements provide the upper boundary condition for the numerical heat transfer model presented in the following section. In addition, they can be used to constrain the interpretation of the geophysical results concerning the subsurface thermal regime.

Numerical Modeling of Subsurface Temperatures

General approach

We considered a purely conductive transient thermal field under variable topography in an isotropic and homogeneous medium according to Carslaw and Jaeger (1959). In steep topography, heat transfer at depth mainly results from conduction, driven by the temperature variations at the surface. Processes such as fluid flow are not included in this first step. Subsurface temperatures are calculated for conditions in the hydrological year 2006/2007 (i.e., 1 Oct. to 30 Sept.) based on mean annual conditions at the surface. That is, seasonal variations at the surface are not included, and temperature variations above the ZAA are not simulated.

Ice contained in the pore space and crevices delays the response to surface warming by the uptake of latent heat during warming. This is addressed in our finite-element heat transport model by apparent heat capacity, which substitutes the volumetric heat capacity in the heat transfer equation and includes energy consumed during phase change. We used the approach described by Mottaghy & Rath (2006).

The resulting temperature pattern is expected to be similar for any north-south oriented cross crest profile. Hence, simulations are conducted for a 2D section across the crest and the borehole site on the northern slope. The assumption of symmetry in an east-west direction is supported by first results of a quasi-3D geoelectrical investigation including four parallel and two orthogonal ERT-profiles in the Schilthorn summit area (Krauer 2008). The selected profile was extracted from a digital elevation model (DEM) with 10 m horizontal resolution (Data Source: Swissphoto). The finite element (FE) mesh was generated for this geometry with corresponding 10 m resolution at the surface, and lower resolution at greater depth. The mesh consists of 1468 elements. The software package COMSOL Multiphysics was used for forward modeling of subsurface temperatures.

Boundary conditions

For all near-surface temperature loggers the mean annual temperature for the hydrological year 2006/2007 was calculated and set as an upper boundary condition at the corresponding elevation and side of the modeled profile. The measured thermal offset between the ground surface and TTOP is small at Schilthorn (about 0.3°C; cf. Hoelzle & Gruber 2008) and is, hence, neglected in the simulations.

The years 2006 and 2007 were very warm and clearly above the long-term average. Therefore, measured near-surface temperatures are not representative for the thermal conditions at the surface during the past decades and century. Transient effects are likely to occur and, therefore, initialization of the heat conduction model is required in order to perform a realistic simulation of the current subsurface temperature field. Based on the assumption that surface temperature fluctuations mainly follow air temperatures, we used mean annual air temperatures (MAAT) from the meteo station on Jungfrauoch (3576 m a.s.l., Data source: MeteoSwiss) some 10 km east of Schilthorn to describe the evolution of the upper boundary. For Jungfraujoch, air temperature data is available back to 1933. The total difference in MAAT between 2006 and the mean of the period 1933–1950 is +1.52°C. We additionally assumed a difference in air temperature of +0.5°C between the start of the data recordings and the Little Ice Age (ca. 1850). The model initialization was started in 1850, and daily time steps were taken. A uniform lower boundary heat flux of 0.08 W m^{-2} was set at sea level, and thermal insulation was assumed for the lateral boundaries of the geometry.

Subsurface properties

Subsurface material properties were assigned on the generated FE mesh. In purely diffusive and transient simulations, thermal conductivity, volumetric heat capacity,

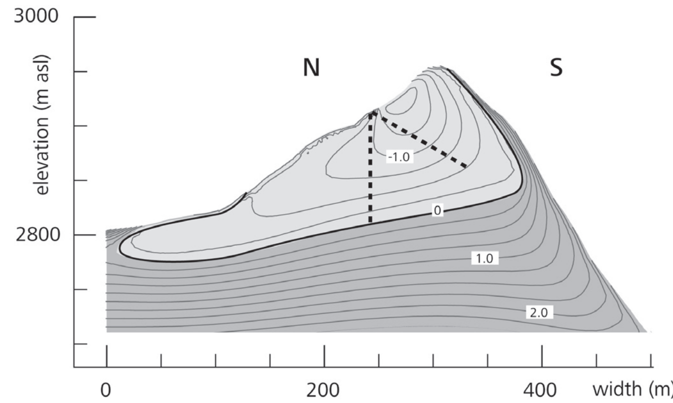

Figure 4. Isotherms of the modeled subsurface temperature field for a north-south cross section of the Schilthorn crest. The 0°C isotherm is depicted in black, and the dashed black lines indicate the boreholes. Light gray areas are permafrost, darker shaded areas are outside permafrost (colored illustration available on CD-ROM).

and the ice/water content are the petrophysical parameters of importance. However, only little is known on the subsurface characteristics below steep topography and the parameters were set based on published values: Thermal conductivity was assumed as 2.5 W K^{-1} m^{-1}, and heat capacity to 2.0 x 10^6 J m^{-3} K^{-1} for the bulk material (Cermák & Rybach 1982).

Based on estimations from geophysical measurements (cf. Hauck et al. 2008) for the upper layers, a uniform ice content of 5% for the entire profile was assumed in the model simulations. The unfrozen water content is described by an exponential function, and the steepness factor was set to 0.2 (cf. Mottaghy & Rath 2006).

Modeling results

The resulting temperature field for the Schilthorn profile is depicted in Figure 4. Maximum permafrost thickness amounts to roughly 100 m below the northern slope and the top of the crest. Isotherms are steeply inclined in the top part, and a lateral heat flow exists from the warm south to the colder north face. Simulated permafrost temperatures are higher than -2°C for the entire profile.

The coldest temperatures exist below the northern and central part of the ridge. The reason is that coldest surface temperatures are found in the steep part of the northern slope (mainly due to reduced solar radiation and longer snow cover duration), and that surface temperatures are higher on the small plateau where the boreholes are located, as well as on the southern side. The southern slope is mainly permafrost-free at the surface. However, due to the cold, northern slope permafrost can be found below the surface. In addition, this is caused by the fact that 20th century warming has not yet penetrated to greater depth in the model, which lowers the temperatures a few tens of meters below the surface compared to present-day steady-state conditions. Similarly, permafrost remains below the surface at the foot of the northern slope. These results point to the importance of transient 2D/3D modeling, as such transient and topography related effects could not be detected using steady state 1D models.

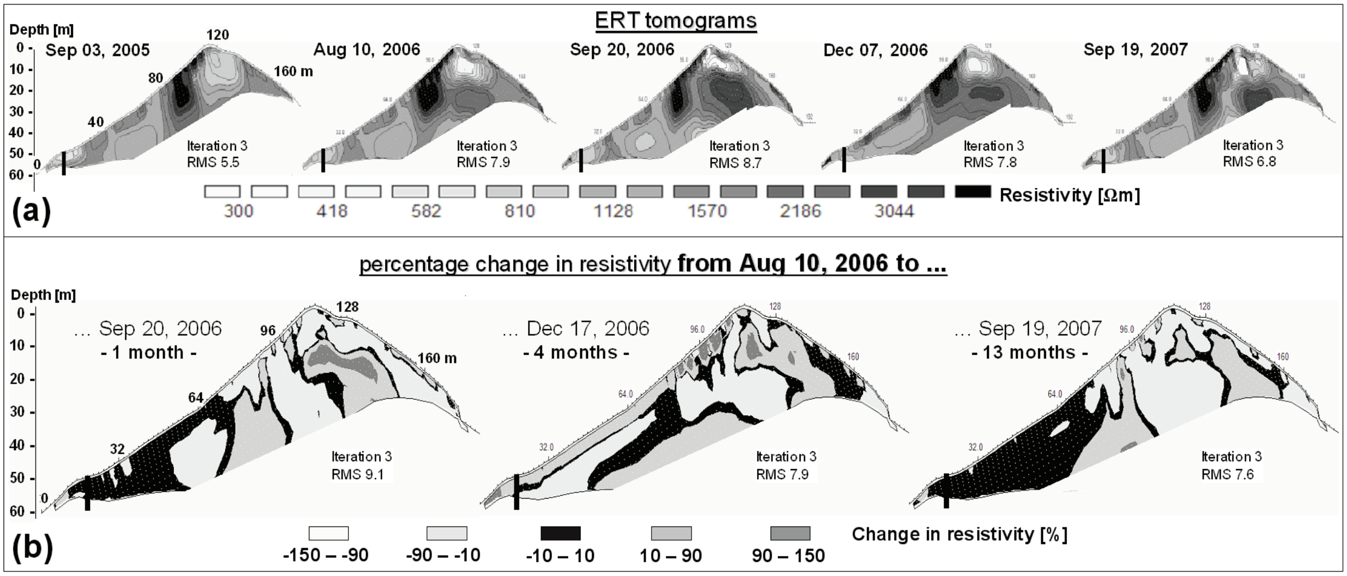

Figure 5. ERT monitoring data illustrated as individual resistivity tomograms for subsequent measurements (a), and as calculated change in resistivity based on the reference profile from August 10, 2006 over one, four, and 13 months (b; colored illustration available on CDRom).

In contrast to ERT profiles (c.f. next section), which mainly allow for a qualitative validation of the general pattern of temperature distribution, comparison with extracted T(z)-profiles at the locations of the boreholes shows the accuracy of the modeled temperature values (Fig. 3). In general, the modeled profiles correspond to the measured data in Figure 3 as temperatures are below -1.5°C for the entire profile, and temperature gradients with depth are small. For both measured and modeled profiles, the oblique borehole shows a slightly more curved profile. However, temperatures of the modeled profile average about 0.2°C colder than the measured values, but range up to 1°C in the upper half of the profile. Further, in the lower parts, the oblique profile is warmer than the vertical profile, which could not be reproduced in the simulation. The results are encouraging given the model error sources, which include: (1) subsurface properties (i.e., ice content, thermal conductivity) are assumed as homogenous for the entire profile and are hardly known at depth; (2) the temperature evolution at the surface may be influenced by effects of solar radiation and snow cover, and, hence, not exactly follow air temperature. In addition, the higher ice content in the limestone scree in the upper meters can slow down the reaction of the subsurface to changing surface temperatures by the uptake of latent heat; (3) small scale variability at the site may cause random errors in logger measurements, and (4) processes such as heat transport by convection are not taken into account.

Geophysical Measurements

Electrical Resistivity Tomography (ERT)

In 1999, a semi-automatic ERT monitoring system was installed on a 60 m line close to the three boreholes in the north facing slope to observe subsurface resistivity changes with respect to ground ice and water content (Hauck 2001, Hilbich et al. 2008). In summer 2005, a second ERT monitoring line (188 m) was installed across the crest, complemented by a quasi-3D ERT survey along four transects across the crest in 2006. Datasets across the crest can be used to analyze the 3D permafrost distribution.

The measured signal is sensitive to temporally variable properties such as temperature, via the unfrozen water, and ice content, as well as unchanging material characteristics, such as lithology and porosity. Repeated ERT measurements, therefore, yield information on the changes occurring in the physical properties of the ground with changing temperature and time (Fortier et al. 1994).

ERT monitoring data of the cross-crest profile (Fig. 2) are available on different time scales: (a) annual measurements in late summer (August/September) for 2005, 2006, and 2007, and (b) seasonal-scale measurements between August and December 2006. Whereas the annual resolution provides interannual resistivity changes between 2005 and 2007, the seasonal scale helps to identify zones with pronounced resistivity changes to delineate ice-free from ice-rich regions. ERT data were processed with the software RES2DINV (Loke & Barker 1995). Besides a qualitative comparison of individual tomograms, a so-called time-lapse inversion of time series of ERT data allows for a quantitative assessment of the resistivity changes.

Results

Figure 5 shows the results of the ERT monitoring across the Schilthorn Crest. In general, measured resistivities are quite low compared to other permafrost sites and do not exceed 4000 Ωm. This is mainly due to the thick fine-grained debris layer covering the summit region. Outcrops of the underlying bedrock also indicate strongly weathered conditions of the micaceous shales with crevices, where water can percolate. In addition to the comparably conductive host material, the low ice content is in accordance with the low resistivity values.

A number of features can be observed in all tomograms (cf. Fig. 6): (A) a relatively homogeneous zone with resistivities between 700 and 1600 Ωm in the lower part of the northern slope, (B) a high resistive zone (>3000 Ωm) in the upper part of the northern slope, (C) a homogeneous intermediary zone in the southern slope with resistivities from 1200 to 1700 Ωm, and (D) a very low resistive anomaly (<500 Ωm) with an underlying high resistive anomaly (>2300 Ωm) at the summit.

The high resistive anomaly in the northern slope (B) may indicate the presence of ground ice and/or firm bedrock. Both possibilities would result in increased resistivity values compared to regions with lower ice contents or more weathered bedrock occurrences, respectively. The low resistive anomaly at the crest (D) is difficult to interpret. In comparable terrain, such low resistivity values are normally associated with very high amounts of unfrozen water or conductive man-made structures (e.g., cables). The presence of such a large amount of water is very unlikely since the crest consists of firm bedrock without a superficial debris cover, whereas metallic remnants from the construction of the summit station (e.g., anchors) are found all over the crest. A man-made low resistive anomaly can therefore, not be excluded. The high resistive anomaly directly below this feature is believed to be an inversion artifact, which is often generated during inversion below a zone of anomalously high or low resistivity values (Rings et al. 2007).

Apart from the high and low resistive anomalies close to the crest, the characteristics of the northern (A) and southern (B) slope seem to be similar. From the qualitative analysis of the individual tomograms no clear indication of differences in permafrost occurrence and ice content between the two slopes is apparent. Calculating the percentage change of resistivities between subsequent measurements (Fig. 6), the tomograms can be transferred into information on seasonally changing properties. From this, zone (A) in the northern slope can be seen as a region with little change in the deeper parts but with pronounced resistivity changes within the upper 4–5 m. This clearly indicates the presence of permafrost with active layer freezing in winter. The deeper parts tend to exhibit slightly lower resistivities in winter, which we interpret as delayed advance of the summer heating (increasing unfrozen water content and therefore decreasing resistivities) into the ground. Zone (B) only yields systematic resistivity changes near the surface, that can be attributed to thawing (decreasing resistivities) between August and September and freezing (increasing resistivities) processes until December. Both processes are similar to the features in zone (A) but seem to be more pronounced. Zone (C) is characterized by a homogeneous resistivity decrease during summer, but shows almost no changes between August and December, i.e., no active layer freezing can be observed. In contrast to the very similar absolute resistivity values, seasonal changes are different in the northern and southern slope. This can be related to differences in subsurface material properties, i.e., permafrost or ice content.

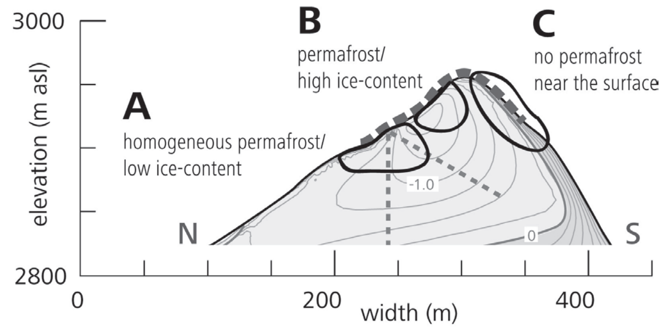

Figure 6. Three features that are addressed in the discussion section are highlighted by black circles: (A) A homogeneous permafrost zone in the lower northern slope with low ice content, (B) a cold zone in the north slope with a high ice content, and (C) no permafrost near the surface on the southern slope. Additionally, grey dashed lines indicate the boreholes and the extent of the ERT profile (colored illustration available on CD-ROM).

Discussion

In both the modeled temperature field and the ERT profiles, three zones in the investigated cross section of the Schilthorn Crest can be distinguished that are particularly interesting (Fig. 6). Cross validation of the results of the two complementary approaches enables an interpretation as follows.

(A) In the lower part of the northern slope, a zone of homogeneous temperatures and resistivities exits. The small variations in temperature in this area may be explained by the fact that temperature values are only little below the melting point and the energy input of the recent warming is consumed by latent heat. Also, the results from ERT monitoring suggest high amounts of unfrozen water and only little ice content (Hauck et al. 2008).

(B) In the upper part of the northern slope a zone of cold temperatures exists. The corresponding zone of high resistivity in the ERT profile is, hence, probably caused by higher ice content rather than by geological characteristics. This is also supported by the larger seasonal resistivity changes pointing to higher contents of ice and unfrozen water than in the lower part of the northern slope.

(C) The permafrost boundary on the southern slope is likely situated only a little below the surface, an effect that can be mainly attributed to surface warming of the past century that has not yet affected greater depths. Seasonal resistivity changes support the hypothesis that there is no permafrost near the surface in the southern slope.

The results of this qualitative validation corroborate the assumption that the general pattern of the subsurface temperature field can be modeled using diffusive and transient 2D and 3D simulations. Using such an approach enables the simulation of temperature fields at greater depths that cannot be reached by geophysical measurements or direct measurements in boreholes. Additionally, the numerical model can be used to calculate scenarios of the evolution of subsurface temperatures and of future permafrost occurrence below the Schilthorn Crest by prescribing the evolution of the upper boundary condition or by coupling the model to a surface energy balance model and/or using regional climate model output (cf. Noetzli et al. 2007).

Conclusions and Perspectives

The subsurface thermal field of a 2D-section across the Schilthorn was modeled assuming a purely conductive and homogenous underground in a first approach. Comparison with measured ground temperatures and ERT profiles leads to the following conclusions:

- The subsurface thermal regime of the Schilthorn Crest is predominantly influenced by both topography and transient effects. The cold northern slope and the recent 20th century warming induce permafrost on the southern side of the crest only a little below the surface.
- The thermal regime of the profile can be characterized by a cold zone below the upper part of the northern slope, permafrost occurrence only a little below the surface on the southern slope and in the lowest part of the northern slope, and rather homogeneous conditions at and below the area of the boreholes.
- The modeled temperature field agrees with the results from ERT monitoring. The three zones mentioned above can be distinguished in the results of both methods.

ERT monitoring on Schilthorn is being continued in the scope of PERMOS. The combination of thermal modeling, temperature measurements in boreholes and geophysical surveys bears potential to further improve modeling and validation strategies. These may include (1) quantitative comparison of numerical results and measured data to estimate model performance, (2) extending single point temperature data to larger scales using 2D or 3D resistivity values, and (3) improving the representation of the subsurface physical properties in the model by incorporating subsurface information (e.g., geological structures, water/ice content) detected by geophysical surveys.

Acknowledgments

We are indebted to Michael Krauer for making available the ERT data measured within his M.S. thesis. Further, we'd would like to thank the motivated students that helped us in the field and the Schilthornbahnen AG for generous logistic support. Part of this study (JN) was financed by the Swiss National Science Foundation as part of the NF 20-10796./1 project, and geophysical fieldwork (CH) was partly financed by PERMOS.

References

Carslaw, H.S. & Jaeger, J.C. 1959. Conduction of heat in solids. In *Oxford Science Publications*. Oxford: Clarendon Press, 510 pp..

Cermák, V. & Rybach, L. 1982. Thermal conductivity and specific heat of minerals and rocks. In G. Angeneister, (ed.), *Landolt-Börnstein Zahlenwerte und Funktionen aus Naturwissenschaften und Technik, Neue Serie, Physikalische Eigenschaften der Gesteine*. V/1a. Berlin: Springer Verlag, 305-343

Gruber, S., King, L., Kohl, T., Herz, T., Haeberli, W. & Hoelzle, M. 2004. Interpretation of geothermal profiles perturbed by topography: The Alpine permafrost boreholes at Stockhorn Plateau, Switzerland. *Permafrost and Periglacial Processes* 15(4): 349-357.

Fortier, R., Allard, M. & Seguin, M.K. 1994. Effect of physical properties of frozen ground on electrical resistivity logging. *Cold Regions Science and Technology* 22: 361-384.

Harris, C., Haeberli, W., Vonder Muehll, D., & King, L. 2001. Permafrost monitoring in the high mountains of Europe: The PACE project in its global context, *Permafrost and Periglacial Processes* 12: 3-11.

Hauck, C. 2001. *Geophysical methods for detecting permafrost in high mountains*. Ph.D. Thesis. Zürich, Switzerland: ETH-Zürich, 204 pp.

Hauck, C., Bach, M. & Hilbich, C. 2008. A 4-phase model to quantify subsurface ice and water content in permafrost regions based on geophysical datasets. *Proceedings of the Ninth International Conference on Permafrost, Fairbanks, Alaska, June 29–July 3, 2008* (this proceedings).

Hilbich, C., Hauck, C., Hoelzle, M., Scherler, M., Schudel, L., Völksch, I., Vonder Mühll, D. & Mäusbacher, R. 2008. Monitoring of mountain permafrost evolution using electrical resistivity tomography: A seven-year study of seasonal, annual and long-term variations at Schilthorn, Swiss Alps. *Journal of Geophysical Research* 113:F01S90, doi:10.1029/2007JF000799.

Hilbich, C., Hauck, C., Delaloye, R. & Hoelzle, M. 2008. A geoelectric monitoring network and resistivity-temperature relationships of different mountain permafrost sites in the Swiss Alps. *Proceedings of the Ninth International Conference on Permafrost, Fairbanks, Alaska, June 29–July 3, 2008* (this proceedings).

Hoezle, M & Gruber, S. 2008. Borehole measurements and ground surface temperatures and their relationship to meteorological conditions in the Swiss Alps. *Proceedings of the Ninth International Conference on Permafrost, Fairbanks, Alaska, June 29–July 3, 2008* (this proceedings).

Imhof, M. 2000. Permafrost investigation in the Schilthorn massif, Bernese Alps, Switzerland. *Permafrost and Periglacial Processes* 11(3): 189-206.

Krauer, M. 2008. Versuch einer 3-dimensionalen Erfassung des Peramfrosts in der Gipfelregion des Schltohrns mittels Geoelektrik, M.S. Thesis. University of Zurich, 112 pp.

Loke, M.H. & Barker, R.D. 1995. Least-squares deconvolution of apparent resistivity. *Geophysics* 60: 1682-1690.

Mottaghy, D. & Rath. V. 2006. Latent heat effects in subsurface heat transport modeling and their impact on paleotemperature reconstructions, *Geophysical Journal International* 164: 236-245.

Noetzli, J., Gruber, S., Kohl, T., Salzmann, N. & Haeberli, W. 2007. Three-dimensional distribution and evolution of permafrost temperatures in idealized high-mountain topography. *Journal of Geophysical Research* 112: doi:10.1029/ 2006JF000545.

Rings, J., Preko, K., Scheuermann, A. & Hauck, C. 2007. Soil water content monitoring on a dike model using electrical resistivity tomography. *Near Surface Geophysics* (in press).

Stocker-Mittaz, C. 2002. *Permafrost distribution modeling based on energy balance data*. Ph.D Thesis. Zurich, Switzerland: University of Zurich, 122 pp.

Vonder Mühll, D., Hauck, C. & Lehmann, F. 2000. Verification of geophysical models in Alpine permafrost by borehole information. *Annals of Glaciology* 31: 300-306.

The Effect of Fines Content and Quality on Frost Heave Susceptibility of Crushed Rock Aggregates Used in Railway Track Structure

Antti Nurmikolu and Pauli Kolisoja
Tampere University of Technology, Tampere, Finland

Abstract

The high smoothness requirement of rails does not allow frost action in the structural layers of the track. Long-term experience with the use of crushed rock aggregates in the uppermost layer of the track, the ballast bed, indicates that the aggregates degrade substantially with accumulating traffic loading. In Finland, the use of crushed rock aggregates has recently extended to the lower structural layers (subballast). For the purpose of setting optimal material requirements for crushed rock aggregates, their degradation and its impacts on frost susceptibility have been studied at TUT. Sampling, a total of 132 frost heave tests, and a large number of laboratory index tests revealed that in certain crushed rock aggregate the frost susceptibility at under 15% fines content was directly proportional to the fines content. In the combined analysis of various aggregates, the observation of quality of fines improved the correlation.

Keywords: ballast; crushed rock aggregate; fines; frost heave test; frost susceptibility; pore size distribution.

Introduction

The smoothness requirement of railway tracks is extremely high and is tightening along with increasing train speeds. Even relatively small deviations in track geometry limit the competitiveness of environmentally friendly rail traffic, as travel times increase and traffic capacity diminishes. In cold climates frost action is an essential factor behind the vertical deviations of track geometry. Because structural layers are generally considered to be built of "non-frost-susceptible" materials, the frost action of traffic routes is commonly associated with problems in the frost-susceptible subgrade. However, in the severe loading environment of the track structure, crushed rock aggregates degrade as a consequence of traffic loading, maintenance operations, and environmental loadings. The tendency towards higher axle loads and train velocities further increases the loading applied to structural layers.

Coarse-grained and uniformly graded crushed rock aggregate, ballast (Fig. 1), is traditionally used in the uppermost structural layer of a track. A literature review by Nurmikolu (2005) showed that many studies dealing with the degradation of ballast have been published. As a result of ballast degradation, its water retention, frost susceptibility, and deformations increase. Finally, the effectiveness of the maintenance performed to keep the track geometry at an acceptable level decreases to the extent that the most economical alternative is to clean the ballast with a special sieving machine in the field. Published research data dealing directly with the frost susceptibility of ballast are scarce, though at least in Finland, maintenance operators have distinct experiences of frost action in ballast causing deviations in track geometry. In a recent field study Akagawa (2007) found that degraded ballast causes significant frost heave in a track. Studies dealing with the frost susceptibility of other coarse-grained materials, such as the base course aggregates of roads, have been published in recent years, perhaps due to the increased smoothness requirements, for example, by Guthrie & Hermansson (2003) and Konrad & Lemieux (2005). It is obvious that the frost susceptibility criteria for the crushed rock aggregates of modern railway track structure cannot be determined on the basis of that literature.

Unlike in the case of ballast, there is no experience of the long-term behavior of crushed rock aggregates in the structural layers below the ballast bed. The use of crushed rock aggregates in the intermediate and frost protection layers (subballast) started in Finland with the 74 km Kerava-Lahti double track line finished in 2006. From the degradation point of view, the stress levels in the lower parts of the structure are of course lower than in the ballast but, on the other hand, cleaning of the lower layers in the same manner as the ballast bed is practically impossible. Therefore, a 100-year service life is required of the substructure (Finnish Rail Administration 2005). In order to distribute the loading applied to the subgrade, to diminish deformations and to prevent convective heat transfer (Goering et al. 2000), the material of the frost protection layer must be more fine grained and more broadly graded than ballast. Consequently, the material can become frost susceptible as a result of lesser degradation than ballast.

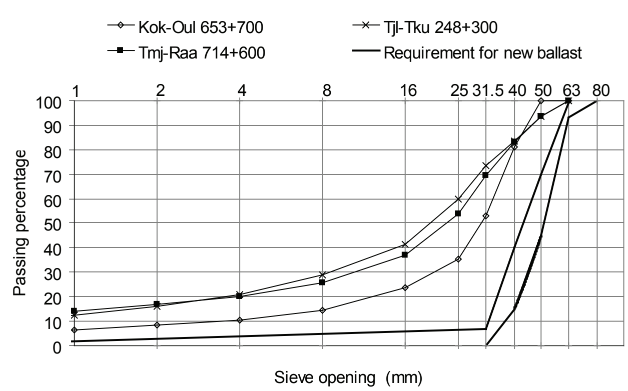

Figure 1. Finnish grading requirement for fresh ballast and examples of degraded samples taken from track structure.

Experimental Studies

Test materials and methods

The degradation of the crushed rock aggregates used in the structural layers of tracks and the quality of the produced fines was studied by long-term cyclic loading tests, ballast bed sampling, and laboratory tests of the samples. The studies concerning degradation have been described elsewhere (Nurmikolu et al. 2001, Nurmikolu 2005) as well as those dealing with the evaluation of the ballast bed's degradation stage by GPR (e.g., Silvast et al. 2007). The samples of the degradation examinations were utilized also in frost susceptibility studies.

The fines generated from ballast in an actual loading environment of a track structure were considered to be the best approximation of the quality of fines possibly produced by degradation of crushed rock aggregates in the lower structural layers. Frost susceptibility examinations were focused on 36 degraded ballast bed samples that had been in service without cleaning for a long time (mainly over 30 years or subject to 40–340 million gross tons of train loading). The sampling points were also decentralized geographically across as much of the rail network as possible to ensure a comprehensive sample of different parent rocks. Also, seven fresh, unused crushed rock aggregates from the quarries and eight natural gravels and sands, mostly from the substructure of the track, were examined. Of the fines of the samples, grain-size distribution (Sedigraph equipment), mineralogy (X-ray diffraction), specific surface area (nitrogen adsorption), pore size distribution (mercury porosimeter), water adsorption, humus content (ignition method), and surface texture (Scanning Electron Microscope) were examined. Of the coarse particles several properties were studied, too, water adsorption being the most important in terms of frost action. A total of 132 frost heave tests were done with the samples with various fines contents and grain-size distributions in the arrangement described next.

Frost heave test arrangement

The frost heave test method has not been internationally standardized. Thus, the results yielded by various arrangements, some of them listed (e.g., by Chamberlain 1981) are difficult to compare. Based on a literature review of the test methods (Nurmikolu 2005), the step freezing test arrangement was considered the most suitable for this research and was set up. In this arrangement the specimens were prepared by the Intensive Compactor Tester (ICT 150RB) into a PVC pipe (inside diameter 150 mm) which served as the specimen mould in the test. The intention was to achieve sample height of 150 mm but, due to fixed compaction effort, specimen heights varied mainly from 145–155 mm. The key decision with regard to minimizing technical testing constraints was to use a cut-up mould pipe (Fig. 2) in the test arrangement, as also recommended by ISSMFE (1989). The frictional force operating at the interface between the mould walls and the aggregate, which is increased by the freezing of water, limits the occurrence of frost heave. Different solutions have been sought for the problem such as discussed by Kujala (1991). In the cut-up mould pipe individual mould rings can separate from each other during frost heave. Then, there is movement between the mould and aggregate only within part of one mould ring, whereby the frictional force resisting frost heave is considerably less compared to a continuous mould pipe. This was obvious also based on the experimental results which showed the frost heave in a cut-up mould pipe to be 2- to 4-fold compared to a continuous pipe using identical sample materials.

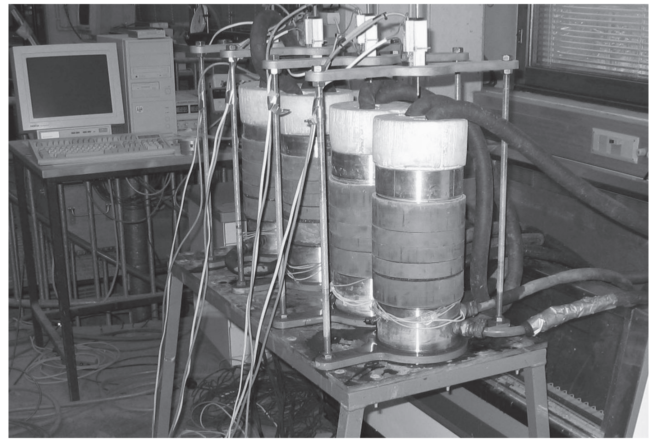

Figure 2. Frost heave test arrangement at TUT.

The equipment built for frost heave testing enabled freezing four samples simultaneously. Before starting the test, seven thermocouples were attached to a specimen at 25 mm intervals. At the beginning of the test the specimens were saturated by keeping them submerged in water for a day. At the same time the specimens were cooled to 1°C–2°C. Then the water level was lowered to about 12 mm above the bottom level of the specimen material, and the specimens were thermally insulated in order to minimize radial heat flows. The specimens were frozen in the natural freezing direction from top to bottom. The temperature of the top surfaces of specimens was controlled by circulation of a cooling agent to -3°C, and the bottom surfaces of specimens with water circulation to +1°C. The supply of additional water for specimens was secured during freezing in line with the view of Konrad and Lemieux (2005), who considered free water flow important in testing the materials of traffic routes. Frost heave was measured during the test by displacement transducers attached to specimen frames. The freezing phase was continued for a minimum of four days. The only load resisting frost action in the tests was the 3 kPa pressure from the caps.

The frost heave specimens made from ballast layer samples were, for the most part, made by proportioning the grain-size distributions (Fig. 3) from sieved fractions as desired to allow comparing the impact of fines quality. The selection of frost heave specimen grain-size distributions was tied to the typical grain-size distributions of degraded ballast bed samples and the recommended grain-size distribution of subballast material and likely progress of degradation (Nurmikolu 2005). Due to the test scale, the maximum grain

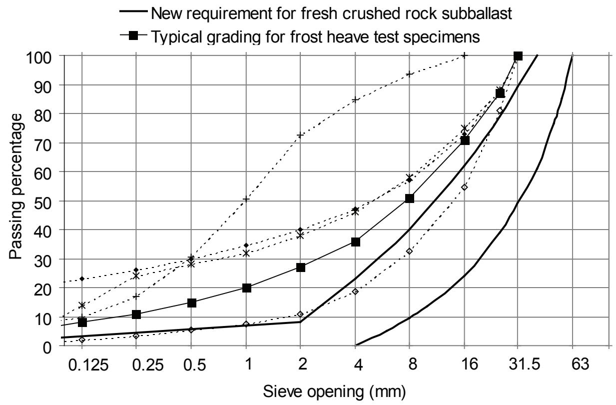

Figure 3. Typical grading curves of crushed rock samples proportioned for frost heave test specimens. Dashed curves depict variation range of tested gradings. New Finnish requirement for grading of fresh crushed rock subballast is presented, too.

size of frost heave specimens was limited to 31.5 mm. Frost heave tests on gravel and sand samples, as well as some of ballast bed samples, were done using their natural grain-size distribution of under 31.5 mm.

Parameters depicting frost susceptibility

Several parameters depicting frost susceptibility were among the analyzed results of the frost heave tests, such as accumulated frost heave, frost heave ratios, and frost heave rates after various freezing periods. A parameter independent of freezing conditions, the segregation potential (presented by Konrad 1980), was not determined, because the flow rate of the additional water into the sample was not measured. Instead, the "frost heave coefficient," which is similar in principle and is used commonly in Finland in frost dimensioning of road structures, was determined. The frost heave coefficient, *SP*, (mm/Kh) is determined from Equation 1, where *v* is the frost heave rate (mm/h) and *gradT_* is the average temperature gradient in the frozen sample section (K/mm).

$$SP = \frac{v}{gradT\_} \tag{1}$$

The primary difference in principle between the frost heave coefficient and segregation potential is that the *v* in Equation 1 indicates the flow-rate of water into the freezing zone instead of the frost heave rate when determining segregation potential (Konrad 1980). Thus, in water saturated material the frost heave coefficient can, in principle, be considered about 1.09-fold compared to segregation potential with the assumption that all the water flowing to the freezing zone ends up thickening the ice lens. However, the in situ frost heave occurring in completely or nearly water-saturated material is accounted for in the frost heave coefficient but not in the segregation potential, which increases the above-mentioned difference in water-saturated material. In an unsaturated state the difference is more difficult to assess since, according to Guthrie and Hermansson (2003), ice segregation may take place due to a material's internal water flow in the absence of external additional water. This kind of frost action cannot be depicted based on the flow rate of additional water into the material, but it is considered by the frost heave coefficient. Another difference in principle between the concepts is that when determining the segregation potential, the temperature gradient should be observed in the partly frozen zone at the frost front, not throughout the frozen layer, which is easier to measure.

As suggested by Konrad (1980) for the segregation potential, the reference value for the frost heave coefficient was determined at the moment the transient freezing phase changes into the stationary freezing phase, that is, as the frost front stops migrating in the sample. Due to the large variations in the frost heave coefficient during the test, it is highly important to follow a systematic practice, although sometimes the moment is hard to determine, as the frost front continues migrating very slowly.

Test Results and Discussion

The impact of grain-size distribution on frost susceptibility

The amount of fine-grained material coarser than fines (>0.063 mm) was observed to have an insignificant effect on the frost susceptibility of crushed rock aggregates within the range of variation normally occurring in the case of materials of the track structure. The impact of the other features of grain-size distribution on frost heave was also found insignificant in practical terms with the examined crushed rock aggregates and the grain-size distribution variation range allowed by the test method (Fig. 3). Observations (e.g., by Konrad 1999) suggest that the frost susceptibility of uniformly graded material may be lower than that of broadly-graded material containing an equal amount of fines. In crushed rock aggregates, however, especially in the case of uniform grain-size distribution and large maximum grain size which allow internal sorting, as with ballast, the finest fraction accumulates at the bottom of the material layer. In fact, internal sorting may result in a non-frost-susceptible material becoming locally frost-susceptible.

The impact of fines content on frost susceptibility

It is natural to start an analysis of the effect of fines content on frost susceptibility with test results on a specific aggregate with different fines contents. Figure 4a shows that after 4 days of freezing (h_{96h}), the frost heave of a specific fresh crushed rock aggregate is fully linearly dependent on the amount of fines in the material within the estimated repeatability limits of the test (Nurmikolu 2005). This applies to fines contents below 15%. The dependence is about the same as regards the frost heave coefficient (SP_o) (the subindex indicates the unloaded nature of the tests) in Figure 4b. Based on all the tests with fines content below 15%, the mutual correlation coefficient (R) between h_{96h} and SP_o was as high as 0.95, but yet h_{96h} correlated generally slightly more closely with the fines content, which is why the following figures only include h_{96h}.

When the analysis of Figure 4a is widened by including

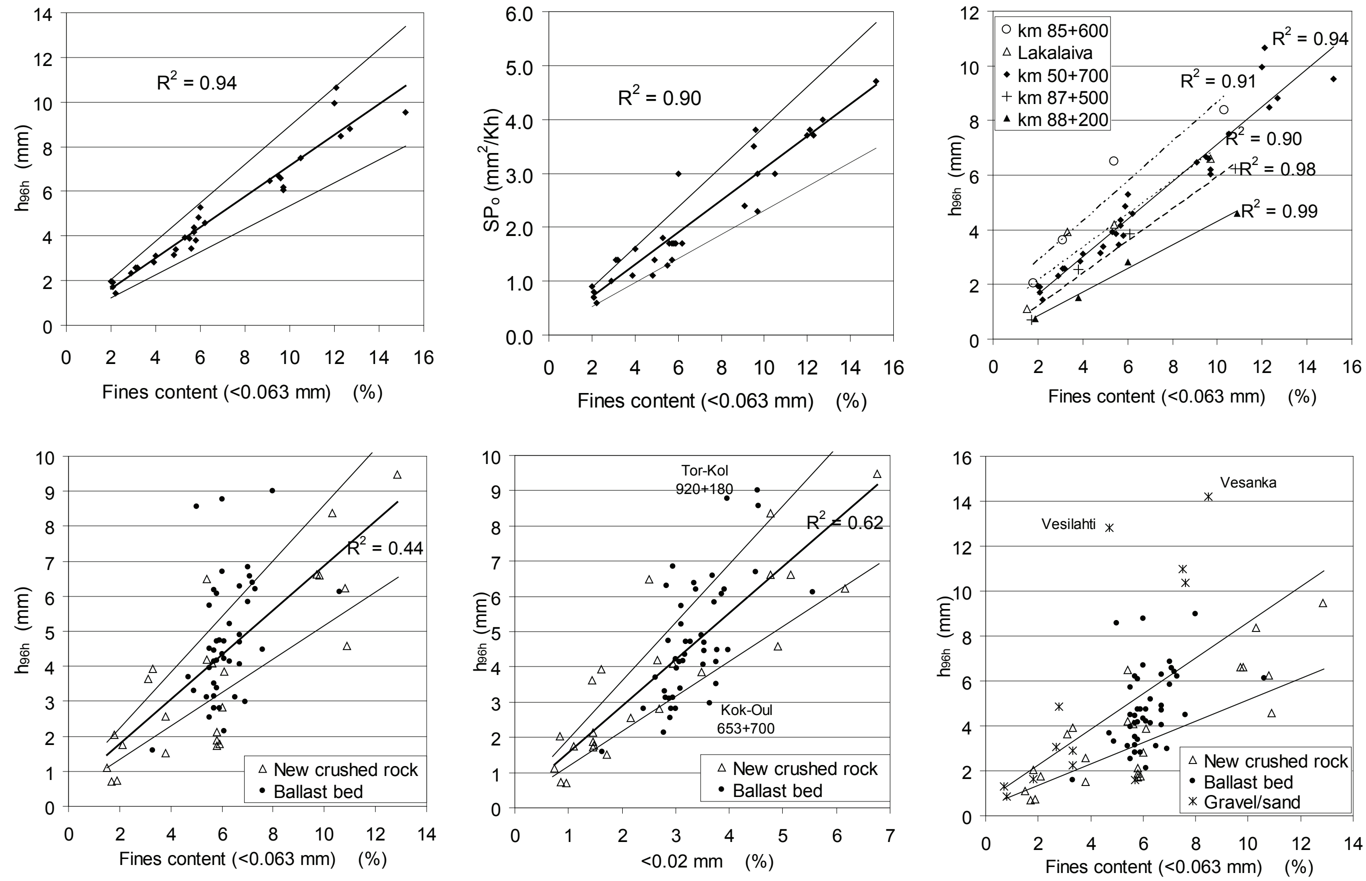

Figure 4. Correlation of parameters depicting frost susceptibility (h_{96h}, SP_o) with fines (or under 0.02 mm material) content applied to: (a & b) only tests on specific (km 50+700) aggregate, (c) different unused crushed rock aggregates, (d & e) all new crushed rock aggregates and degraded ballast bed samples from track, and (f) new crushed rock aggregates, ballasts as well as gravel and sand materials.

the corresponding results for four other fresh crushed rock aggregates, we find that the correlations between h_{96h} and fines content were strong with each aggregate as shown by Figure 4c. The location of the correlation line varied slightly depending on the aggregate, indicating slight qualitative differences in aggregates or their fines.

Figure 4d also includes the results from the tests on degraded ballast bed samples. The large number of observations made during tests on the material of Figure 1 was reduced in order to eliminate its excessive weighting. The correlation between h_{96h} and fines content is clearly weaker than in the above examinations of individual aggregates. This is explained partly by the different internal grain-size distribution of fines as seen in Figure 4e, where the correlation of h_{96h} is much stronger in the content of the finer portion of fines (<0.02 mm). This view is also supported by observations on the frost susceptibility of natural soils by, for example, Kujala (1991) and Vinson et al. (1987). Regression Equations 2 and 3, where $P_{0.02mm}$ is the content of under 0.02 mm material, could be obtained from this combined analysis of all tested crushed rock aggregates.

$$h_{96h} = 1.32 \cdot (P_{0.02mm}) + 0.24 \qquad (R^2=0.62) \qquad (2)$$

$$SP_o = 0.57 \cdot (P_{0.02mm}) + 0.14 \qquad (R^2=0.53) \qquad (3)$$

In Figure 4f the results from the tests on natural gravel and soil materials were added to show that if frost heave is assessed on the basis of fines content, there seems to be considerably more deviation in the case of gravels and sands than with crushed rock aggregates. The frost susceptibility of some gravels and sands was remarkably higher than that of crushed rock aggregates with a corresponding fines content. This can only partly be explained by the internal grain-size distribution of fines.

The impact of particle quality on frost susceptibility

The frost susceptibility of some crushed rock aggregates in Figures 4d and 4e and especially that of gravels and sands (Fig. 4f), which deviated from that evaluated on the basis of fines content, can be largely explained by divergent surface properties of particles. For example, the water adsorptions of the fines of the most divergent materials in Figure 4f (Vesilahti gravel and Vesanka sand) were almost 3-fold compared to the average level of crushed rock aggregates (Nurmikolu 2005). Corresponding differences could be noted, for example, in relation to the specific surface area or pore size distribution of fines as shown by Figure 5. The differences are clearly revealed by the SEM images in Figure 6.

The porosity and water retaining properties of some gravel and sand materials that deviated clearly from those

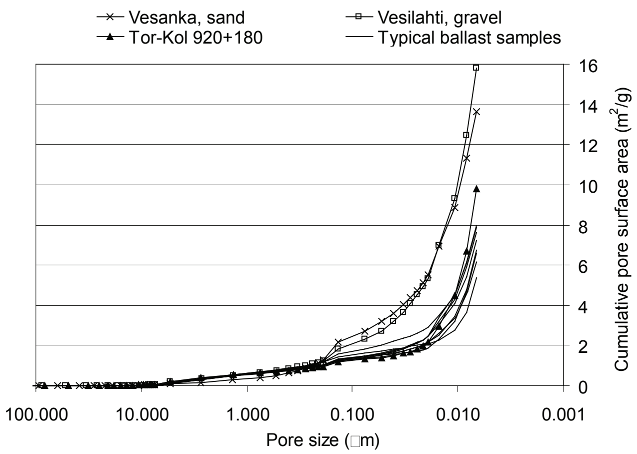

Figure 5. Cumulative pore surface areas in relation to pore size with regular ballast samples and with samples diverging the most from the analyzed fines.

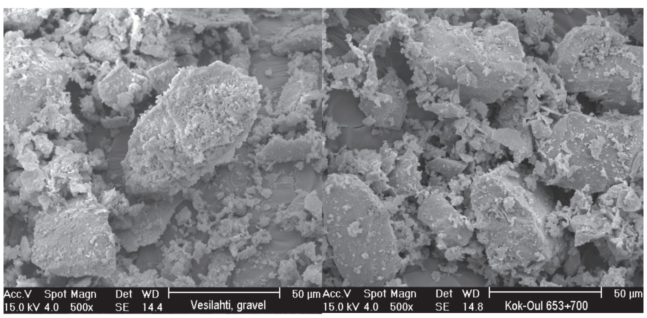

Figure 6. SEM images of the fines of (a) non-frost-susceptible ballast bed sample and (b) weathered, highly frost-susceptible gravel.

of crushed rock aggregates indicate their slight weathering. As a result, their frost susceptibility was higher than that of the examined crushed rock aggregates with corresponding fines content. The environmental loading on the particles of naturally sorted coarse-grained soils over millennia is of a different magnitude than the loading on crushed rock aggregate particles over the few decades since their crushing.

Distinct chemical weathering after crushing could be observed only in one ballast bed sample, where opaque minerals and mica had weathered, causing deposits of iron compounds on grain surfaces. In general, most of the fines in the ballast samples consisted of the most common rock minerals, quartz, feldspars, and amphiboles, whose average share in the mineral fines of the samples was established at about 80% (Fig. 7). This was a positive finding as it proved that despite the thousands of times larger specific surface area of fines compared to coarse grains, hard minerals appear to be resistant to chemical weathering in the structure even in the form of fines. The findings support the idea (Nurmikolu 2005) that degradation of ballast aggregates in the Finnish railway network is mainly the result of mechanical fragmentation and attrition caused by traffic loads and tamping (maintenance), or in a few cases possibly by frost weathering.

The significance of particles' quality on frost heave

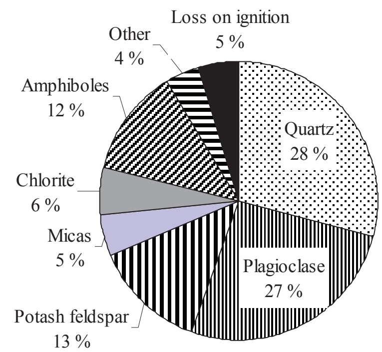

Figure 7. Indicative average mineral content of the fines of 36 ballast samples based on X-ray diffraction analyses.

susceptibility was examined statistically with stepwise regression analysis. The examined determining variables alongside the amounts of fines fractions (<0.063 mm, <0.02 mm and <0.002 mm) were water adsorption, specific surface area, total pore volume and total pore area of fines, as well as water absorption of coarse particles. The outcome of the stepwise regression analysis was clear. Based on the index properties of aggregate particles, the predictability of each parameter depicting frost susceptibility could be improved significantly compared to examinations based solely on the contents of fines fractions. The best correlation was achieved by using as independent variables the content of under 0.002 mm material, $P_{0.002mm}$, water absorption of coarse particles, WA_{24}, and total pore volume of fines measured with the mercury porosimeter, V_{tot}. Both water absorption and total pore volume clearly improved the coefficient of determination. In the case of parameters h_{96h} and SP_o this yielded regression Equations 4 (R^2=0.86) and 5 (R^2=0.80), which explained frost susceptibility in this combined analysis of aggregates nearly as well as fines content in the analyses of individual aggregates. Other independent variables did not improve the attained coefficients of determination.

$$h_{96h} = 6.9 \cdot P_{0.002mm} + 15.8 \cdot WA_{24} + 10.6 \cdot V_{tot} - 8.0 \quad (4)$$

$$SP_o = 2.8 \cdot P_{0.002mm} + 10.0 \cdot WA_{24} + 4.6 \cdot V_{tot} - 3.8 \quad (5)$$

Concluding Remarks

Degradation of the crushed rock aggregates used in the track structure affects their frost susceptibility. Some problems due to frost action can therefore be explained by frost heave in the structural layers instead of the freezing of frost-susceptible subgrade.

The results obtained from various frost heave test arrangements are hard to compare. The test method should be internationally standardized and made rather easy to perform while yet minimizing the technical restraints preventing frost heave from occurring. The arrangement with cut-up mould pipes worked well in this study.

The frost susceptibility of a certain crushed rock aggregate was found to be at the examined under 15% fines contents directly proportional to its fines content. In the combined analysis of various crushed rock aggregates, frost susceptibility correlated better with the very finest, under 0.02 mm and under 0.002 mm, fractions of fines than with the total fines content.

Because significant chemical weathering could not be observed even in ballast bed samples that had been in service for a long time except in one case, the surface properties of mineral particles of crushed rock aggregates varied relatively little with a few exceptions. With the rock types typically used in Finland, the impact of fines on the performance of the ballast bed can, thus, be largely assessed on the basis of their amount.

The porosity and water retaining properties of some gravel and sand materials, clearly more disadvantageous than those of crushed rock aggregate, indicated their weathering and caused their higher frost susceptibility compared to crushed rock aggregates with the same fines content.

Of the examined qualitative properties of particles, water absorption of coarse particles and total pore volume of fines correlated best with frost susceptibility. The regression model building on the under 0.002 mm material content, the water absorption of coarse particles and the total pore volume of fines explained frost susceptibility in the combined analysis of aggregates nearly as well as fines content in the analyses of individual aggregates.

The concept of the non-frost susceptibility of aggregate is mainly theoretical, since minor frost heave, not explained by in-situ frost heave, actually occurs in many materials generally assumed to be non-frost-susceptible. Therefore, it would be more important to deal with the concept of practical non-frost susceptibility. Establishing the limits of it would require field observations or large-scale tests. In their absence, and as a result of the investigations and consideration of the high smoothness requirement of railway tracks, it is suggested that a frost heave coefficient of 1.0 mm^2/Kh and frost heave of 2.2 mm after four days, attained in the described test, be applied to the track structure as the limits of practical non-frost susceptibility. In fines content-based frost heave models of crushed rock aggregates, the suggested limits corresponded to an under 0.02 mm fraction content of 1.5%. In the case of typical crushed rock aggregate this corresponded to a fines (<0.063 mm) content of 2.7%.

Acknowledgments

The authors want to thank the Finnish Rail Administration for financing the research and participating in its steering. Thanks go also to the Academy of Finland for their partial funding (Finance decision 73664).

References

Akagawa, S. 2007. Frost heave susceptibility of ballast containing fines. *Proceedings of 8th International Symposium on Cold Region Development (ISCORD 2007), Tampere, Finland, September 25–27, 2007.*

Chamberlain, E.J. 1981. *Frost Susceptibility of Soil, Review of Index Tests.* Hanover, New Hampshire: CRREL Monograph 81-2, 110 pp.

Finnish Rail Administration 2005. *Track Technical Regulations and Instructions (RAMO) Part 3, Track Structure.* Helsinki, Finnish Rail Adminstration, 44 pp. (in Finnish).

Goering, D.J., Instanes, A. & Knudsen, S. 2000. Convective heat transfer in railway embankment ballast. *Ground Freezing 2000, Louvain-La-Neuve, Belgium, September 11–13:* 31-36.

Guthrie, W.S. & Hermansson, Å. 2003. Frost heave and water uptake relations in variably saturated aggregate base materials. *Transportation Research Board 82nd Annual Meeting, Paper No. 03-4391, Washington, DC, January 12–16*: 22 pp.

ISSMFE Technical Committee on Frost, TC-8 1989. Work report 1985–1989. *VTT Symposium 94, Frost in geotechnical engineering, Saariselkä, Finland, March 13–15, 1989, Vol 1:* 15-70.

Konrad, J.-M. 1980. *Frost Heave Mechanics.* Ph.D. Thesis. Edmonton, University of Alberta, 405 pp.

Konrad, J.-M. 1999. Frost susceptibility related to soil index properties. *Canadian Geotechnical Journal* 36: 403-417.

Konrad, J-M. & Lemieux, N. 2005. Influence of fines on frost heave characteristics of well-graded base-course material. *Canadian Geotechnical Journal* 42: 515-527.

Kujala, K. 1991. *Factors Affecting Frost Susceptibility and Heaving Pressure in Soils.* Ph.D. Thesis. ACTA Universitatis Ouluensis Series C 58, 99 pp.

Nurmikolu, A., Uusinoka, R., Niskanen, P. & Kuula-Väisänen, P. 2001. Effects of aggregate strength on the life cycle of railway ballast. *Proceedings of Aggregate 2001 – Environment and Economy, Helsinki, August 6–10, 2001, Vol. 1:* 213-218.

Nurmikolu, A. 2005. *Degradation and Frost Susceptibility of Crushed Rock Aggregates Used in Structural Layers of Railway Track.* Doctoral Thesis. Publication 567. Tampere University of Technology.

Silvast, M., Nurmikolu, A., Kolisoja, P. & Levomäki, M. 2007. GPR technique in the analysis of railway track structure. *Proceedings of 14th European Conference on Soil Mechanics and Geotechnical Engineering, Madrid, Spain, September 24–27, 2007.*

Vinson, T.S., Ahmad, F. & Rieke, R. 1987. Factors important to the development of frost heave susceptibility criteria for coarse-grained soils. *Transportation Research Record* 1089: 124-131.

Contemporary Permafrost Degradation of Northern European Russia

Naum Oberman
Mining Geological Joint-Stock Company MIREKO, Syktyvkar, Russia

Abstract

This paper discusses the results of permafrost temperature monitoring. Temperatures were recorded over recent decades at a depth of zero annual amplitude at eight geocryological field stations located between the Ural Mountains and the lower reaches of the Pechora River. It is shown that almost all permafrost within this region has been warming. Permafrost temperature increases during the last 20 to 30 years ranged from 0.22°C to 1.56°C. Regional patterns of mean annual permafrost temperature dynamics are analyzed. During the period of observations, new closed taliks appeared, and those existing prior to climate warming increased in thickness by 0.6 to 6.2 m depending on a number of factors. Data presented in this paper suggest that permafrost of this region is more vulnerable to recent climate warming than that in Central Yakutia and West Siberia.

Keywords: monitoring; northern European Russia; permafrost; taliks; temperature; warming.

Introduction

Global climate warming leads to increases in permafrost temperature in many northern regions (Gravis et al. 1988, Haeberli et al. 1993, Pavlov 1994, Osterkamp et al. 1994, Romanovsky & Osterkamp 2001). A number of publications were devoted to the impacts of this warming on permafrost in northern European Russia (Oberman 1996, Pavlov 1997, Kakunov 1999, Oberman 2001, Oberman & Mazhitova 2003, Kakunov & Sulimova 2005, Pavlov & Malkova 2005). Most of the cited publications analyze long-term permafrost monitoring records that were obtained from one or two long-term geocryological field stations in operation during the last two to three decades. The stations are located near the city of Vorkuta in the eastern part of the studied region (Fig. 1, Station #2) and close to the Pechora River delta at Cape Bolvansky in its western part (Fig. 1, Station #11). Data obtained from these two areas are rather different. In the Vorkuta area a rapid warming of permafrost was observed while the permafrost temperatures at Cape Bolvansky remained relatively stable. Given this difference, the interpolation of these data onto the entire region is hardly possible. It was necessary to include in the analysis additional data from other sites within the region where permafrost had been monitored over recent decades.

Therefore, in 2006-2007, the MIREKO Stock Company resumed measurements at six geocryological field stations where measurements were conducted in the past. As a result, the number of field stations where 20 to 38 year-long records are available increased to eight (Fig.1). In this paper we discuss the data from these eight stations. Shorter (10 to 12 years) records from other stations that have not been published before are also included in this analysis. Original observational data used in the paper are from (Kakunov et al. unpublished, Glavatskikh et al. unpublished, Karpovich et al. unpublished, Malkova & Vasiliev unpublished, Romenskaya et al. unpublished, Oberman unpublished).

Study Area and Methods

The study region (Fig.1) is characterized by rather diverse environmental conditions. The Pechora lowland (Bolshezemelskaya Tundra), bordered by the Ural and Pai-Khoi Mountains and their foothills to the east, occupies most of the region. The geological section is represented mostly by Quaternary loam, loamy sand, and sand often overlain with peat. Landscapes with various geneses have different ages that vary from Middle Pleistocene to Holocene. They are dominated by one of these types of deposits or by the combination of different types. Climatic conditions vary within the region. Mean annual air temperature averaged over 1950-2005 declines from -2.4°C in the southwest to -7.5°C in the northeast of the region. Annual precipitation increases from 300-400 mm at the seacoast to 400-500 mm in the continental part of Bolshezemelskaya Tundra and to 500-600 mm and more in the Ural foothills. The long-term means of annual maximum snow depths increase in the same direction from 44 cm at the coast to 59 cm in Bolshezemelskaya Tundra and 78 cm in the Ural foothills. Recent trends in the mean annual air temperature are characterized by higher rates of warming in continental areas and lower rates towards the coast. In the continental areas the rates also decline from east to west (Pavlov & Malkova 2005). Our analysis showed that trends in precipitation and snow depths were similar to those in air temperature, yet better expressed. Excessive humidity is typical for the entire region. Climate is responsible for the region belonging mostly to the tundra zone. Permafrost spatial distribution ranges from isolated patches to continuous permafrost. In the 1970s, permafrost temperatures at the depth of zero annual amplitude varied mostly from -1°C to -3°C, reaching in some places -5.5°C, and permafrost thickness varied from 10 to 700 m, rarely more.

Long-term changes in permafrost temperatures were monitored using mercury thermometers with a scale factor from 0.05°C to 0.1°C. The thermometers were put in cases

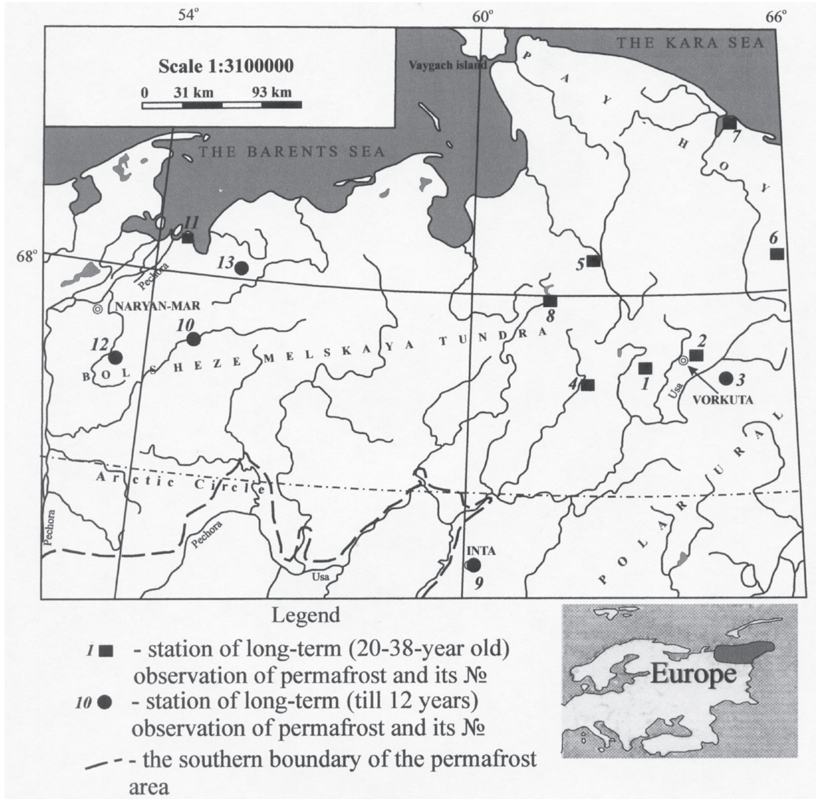

Figure 1. Survey map of the region.

filled with an inert material such as, for example, grease. In 2007, together with a representative from the Geophysical Institute, University of Alaska Fairbanks, temperatures were measured simultaneously with mercury thermometers and dataloggers. Readings differed in average by 0.05°C. Since 2007, boreholes are being equipped with temperature dataloggers. In the past, measurement frequency varied from one to three times monthly to four times annually.

Long-Term Permafrost Dynamics

Multi-year trends in permafrost characteristics were derived from 20-and-more-year-long monitoring records. The record lengths allowed averaging the short-term (decadal) temperature fluctuations (for example, Boreholes ZS-124/124a and ZS-14/227 in Figure 2). These relatively long-term records showed that permafrost temperatures at the depth of zero annual amplitude increased during the period of observations at all eight reference field stations in the region (data from most of them are given in Table 1). At the beginning of monitoring, only one of eight stations (#2) was located in the sporadic permafrost zone, two stations (#1 and #4) were in the discontinuous permafrost zone and the rest of the boreholes were in the continuous permafrost zone (Fig.1).

Permafrost warming over the recent 20 to 50 years has been reported by a number of authors who conducted occasional repeating temperature measurements on certain topographic surfaces in 10 areas within the studied region. The reported rates of warming were similar to those registered at our reference field stations. All available data suggest that permafrost warming from 1950-2000 took place mostly in the second half of this period.

The total increase in the mean annual permafrost temperature varies for different stations from 0.22°C to 1.56°C (Table 1) and depends first of all on the length of observational period. To overcome the effect of different record lengths, the average annual warming rates were calculated. These rates range from 0.01°C to 0.08°C per year. At each field station the maximum rates were usually observed in peatlands and minimum rates were typical for loamy deposits, with sand deposits showing intermediate values.

Generally, the rates of increase in mean annual permafrost temperatures decrease towards the seacoast. In loamy deposits that dominate the region, the rates were 0.031°C to 0.034°C per year at the distance of 165-170 km from the Barents Sea coast. At the same time, these rates were only 0.02°C to 0.028°C per year in the area located 80-85 km from the coast (Fig.1, Table 1: Stations #4 and #1, and Stations #5 and #8, Boreholes KT-5 and 37-6). Similarly, the rates were higher in the continental east of the region and lower in the coastal west, decreasing from 0.031°C-0.034°C per year at Stations #4 and #1 to 0.01°C per year in Borehole 49 (Table 1). The rates of increase in mean annual permafrost temperature (calculated for 1982-1993 at Station #10) decreased from the eastern continental Station #1 to the western continental Station #10, from 0.034°C to 0.013°C per year. Both stations are located at about the same latitude. Owing to the tendencies, the permafrost warming is most

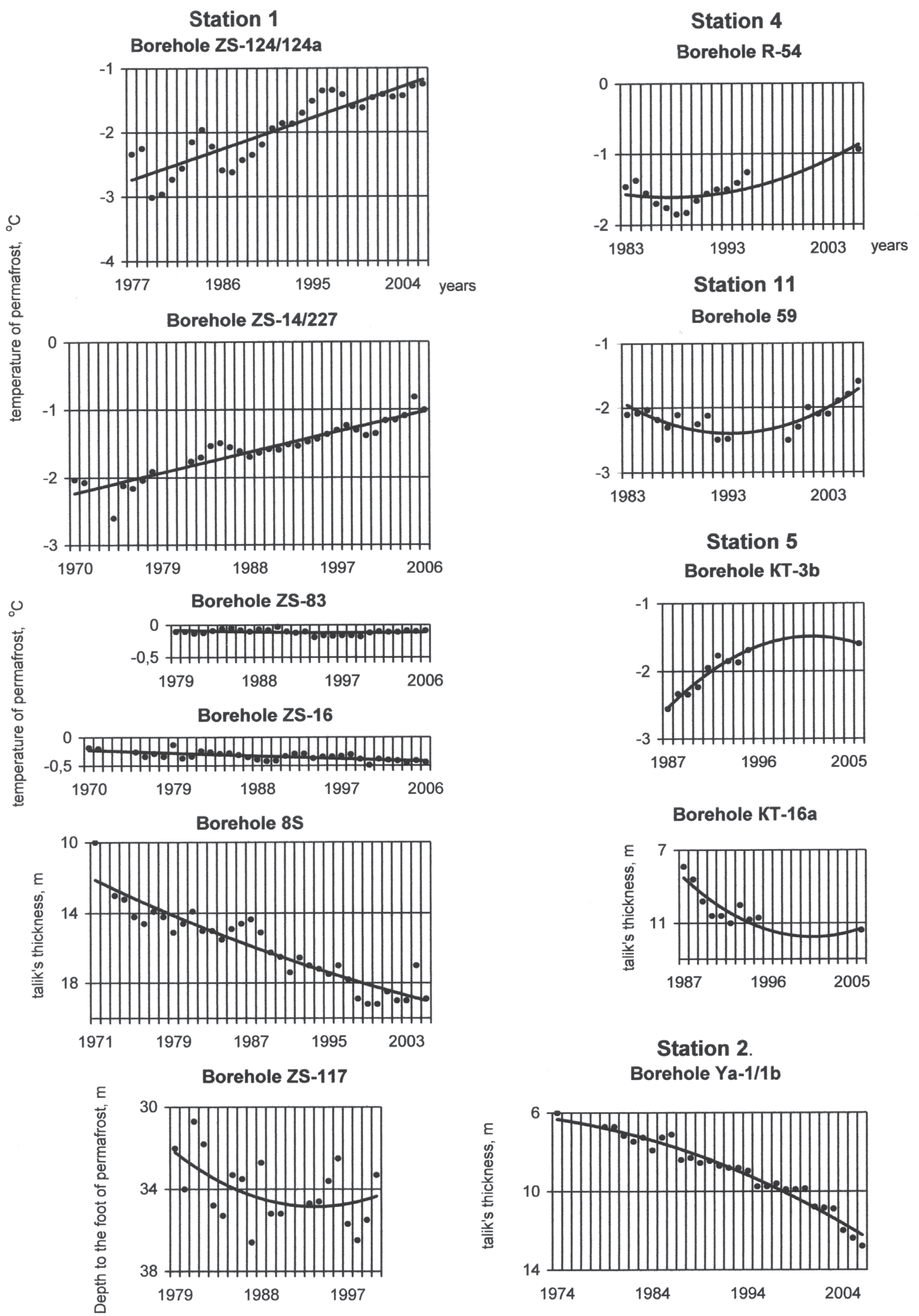

Figure 2. Long-term trends in permafrost characteristics.

pronounced in the eastern continental areas and least in the western coastal regions. The least significant permafrost warming was observed at the westernmost coastal Station #11 (Cape Bolvansky) and was due to the later initiation of climatic warming in this area compared to the rest of the region (Oberman 2007).

The regional pattern of permafrost warming correlates closely with the above discussed pattern of recent trends in major meteorological parameters.

While permafrost warming was a dominant process, permafrost cooling was observed locally, mostly in the areas of complete or partial drainage of thermokarst lakes. Cooling

Table 1. Long-term changes of permafrost in the region.

Landscape*	№ of the station; borehole	Relief; microrelief at the start of observations	Rock's lithology	Period, years	Depth, m	Ground temperature, ^{o}C: initial	changes during the period	changes $^{o}C/yr$
1	1; ZS-124/124a	slope; polygonal	peat, loam, sandy loam	1977-2006	10	-2.78	+1.56	0.054
	1; ZS-14/227	watershed; spot-medallion	loamy sediments	1970-2006	15	-2.23	+1.20	0.034
1a	11; 59	ridge's crest; spot-medallion	loams	1983-2006	12	-1.95	+0.22	0.01
2	8; 100-6	slope; polygonal	peat, sands, loams	1987-2007	10	-4.30	+1.56	0.078
	8; 35-6	watershed; polygonal	sands, gravel	1987-2007	15	-2.85	+1.09	0.055
	8; 37-6	foot of slope	loams	1988-2007	14	-2.10	+0.52	0.028
3	4; R-54	side of the stream's valley	loam, sand, varved clay	1983-2006	10	-1.56	+0.71	0.031
4	5; KT-5	by watershed; bog	loamy sediments	1986-2006	15	-2.87	+0.41	0.021
	5; KT-3b	I above flood-plain terrace	sands, gravel	1987-2006	15	-2.55	+0.95	0.05
5	2; UP-35	slope's foot; frost small mound	peat, loam	1986-2006	10	-1.72	+0.69	0.035
	7; K-2	marine terrace	sand, loam	1982-2007	10	-3.93	+0.97	0.039
Closed taliks								
		Talik's type				Talik's thickness, m: initial	changes during the period	changes m/yr
1	1; EK-67	snow-made talik	loams, sandy loams, pebble	1980-2006		0	+15.8	0.61
	1; ZS-83	ground water transient talik	loams, sands	1976-2006		0	+8.6	0.29
	1; 8S	snow-made talik	loamy sediments	1971-2005		12.1	+6.7	0.20
3	4; R-53	near-channel talik	sandy loam, varved clay	1983-2006		8.8	+0.6	0.03
4	5; KT-8	near-channel talik	loams, sandy loam	1986-2006		13.2	+2.8	0.14
	5; KT-16a	snow-made talik	loamy sediments	1987-2006		8.6	+2.8	0.15
5	2; UP-34	ground water made talik	loams, limestones	1975-2006		43.5	+24.8	0.80
	6; 23	snow-made talik	sandy loam, gravelly sandy loam	1978-2007		4.9	+6.1	0.21
	6; 32	lake talik	sands, sandy loams	1977-2007		5.0	+6.2	0.21
	7; K-41	snow-made talik	sands, loam	1982-2007		5.3	~ +3.7	0.15

Note: * - plains: 1 and 1a – glacial-marine of Middle Pleistocene age (continental areas and sea coast); 2 – marine, Middle Pleistocene; 3 – lacustrine-alluvial, Late Pleistocene; 4 – lacustrine-alluvial, alluvial-marine, Late Pleistocene; 5 – piedmont areas.

with the rate of 0.006°C per year (during 1970-2006) was observed in the frozen basal peat layer below the floor of one of the lakes that drained before 1969; i.e., before the onset of pronounced warming (Fig. 2, Borehole ZS-16). Cooling rates observed in the thawed peaty sediments of the lakes drained during the climatic warming were much higher. At an initial mean annual ground temperature of 1.5°C, the rates were -0.042°C per year during 1974-2005 and, at an initial temperature of 2.87°C, they were -0.082°C per year during 1980-2006 (Stations #1 and #4, respectively). The duration of periods of thawed lake sediments rapid cooling prior to relative stabilization was equal for both lakes and totaled 14 years. This similarity in temperature regime between these two lakes occurred in spite of different drainage dates and significant differences in the initial enthalpy of bottom deposits. Similar permafrost temperatures in the surrounding terrain of both lakes can possibly explain the phenomenon.

Anomalous permafrost temperatures that persist during the time of recent climatic warming were observed at the sites where permafrost degradation resulted in the development of closed taliks (Fig. 2, Borehole ZS-83, Table 1). Here, the permafrost table lowered to 8.6 m in 30 years. It lowered even deeper, to almost 16 m, in an area where a newly developed closed talik coalesced with a preexisting lateral talik (Table 1, Borehole EK-67). Taliks existing prior to the recent climatic warming also increased in thickness, though to a smaller degree than newly developed taliks. Reduced rates of ground temperature changes in these taliks were probably due to a deeper permafrost table position and, hence, weakened effects of air temperatures on ground temperatures. Total increases in thickness of the closed taliks developed in Quaternary deposits ranged from 0.6 to 6.7 m (Table 1) depending on the geographical location, genetic type of the particular talik, ice content and lithological characteristics of the bearing sediments, hydrological, hydrogeological and other factors. The thickness of newly-developed taliks decreases northward (towards the sea coast), in accordance with the increasing severity of geocryological conditions and in accordance with already mentioned regional distribution of the recent climatic trends (see the Borehole pairs 8S & KT-16a and 23 & K-41, in Table 1). Thawing of the very ice-rich varved clays (Station #4, Borehole R-53) is accompanied by high heat consumption, and therefore total increases in thickness of closed taliks were minimal (only around 0.5 m) in this kind of deposit. On the other hand, a ground-water-formed closed talik in bedrock with practically zero ice content demonstrated a 25-meter increase in thickness in 31 years (Station #2, Borehole UP-34).

As a result of climatic warming, permafrost patches 10 to 15 m thick (Stations #1 and #2) thawed completely. In the patches where Quaternary deposits were perennially frozen to a depth of around 35 m, the base of the permafrost tended to rise (Fig. 2, Borehole ZS-117). Comparison of small-scale maps based on 1950-1960 data with those based on 1970-1995 data shows a shift of the southern limit of permafrost by several tens of kilometers northwards (Oberman 2001). This also indicates that permafrost is degrading in the southernmost part of the region.

At the same time, newly formed permafrost developed within the bottom of completely or partially drained lakes. This new permafrost was confined either by the elevated parts of the lake floor or by the bottom sections adjoining the frozen lakeshores. At one such site, permafrost developed from 1974 to 2001 to a depth of 14.5 m. To assess the extent of new permafrost formation, an analysis of satellite remote sensing data was performed by I.O. Smirnova (Research Institute for Cosmo-Aero-Geological Methods) for the entire region under discussion. According to her results, the area of lakes drained between 1988 and 2000 comprises only a fraction of a percent of the total area. Moreover, only an insignificant part of the drained area has been freezing recently and forming permafrost. Hence, on a regional scale, the significance of the formation of new permafrost is very limited compared to the predominant permafrost degradation.

Finally, the material presented indicates that permafrost dynamics could be very different within different Russian permafrost regions. Recent long-term increases in mean annual air temperature were several-fold smaller in northern European Russia than in Central Yakutia and West Siberia (Pavlov & Malkova 2005). However, an increase in permafrost temperatures at the depth of zero annual amplitude was several-fold larger than those in Central Yakutia and comparable to those in West Siberia. One reason for these differences could be the two-fold increase in atmospheric precipitation in the discussed region. This, in turn, was associated with an increase in the warming effect of ground waters on permafrost (Oberman 2006a, b). The maximum snow depth increase in recent decades was also reported for the western part of the Russian Arctic (Bulygina & Razuvaev 2007). This increase also contributed to the observed warming of permafrost. Taken together with the relatively high temperatures of permafrost in northern European Russia, all the above-discussed evidence indicate that this region is one of the most vulnerable to further warming. A large extent of permafrost degradation can be expected in this region in the foreseeable future.

Conclusions

In all geocryological zones and major landscapes of northern European Russia, the long-term (20 to 38 years) warming trend in permafrost temperatures at the depth of zero annual amplitude were recently observed. Short-term permafrost temperature fluctuations are superimposed on this trend. Total temperature increases vary from 0.22°C to 1.56°C with annual rates ranging between 0.01°C and 0.08°C per year. The observed warming rates decrease from continental areas towards the coast, and from eastern regions toward the west of the study area. These tendencies correlate closely with the recent intra-regional trends in mean annual air temperature, annual precipitation, and snow depth. Permafrost warming led to formation of new closed taliks and to an increase in thicknesses of pre-existing taliks. The increase in thickness of these taliks range from 0.6 to 6.7 m and depend on the location and genesis of the talik, as well as on ice content in the bearing deposits and other factors. Some thin permafrost patches completely thawed.

Excessive humidity and a recently observed steep increasing trend in snow depths, together with relatively high permafrost temperatures, cause higher vulnerability of permafrost to climate warming in this region as compared to Central Yakutia and, to a lesser degree, to West Siberia.

Acknowledgments

This investigation became possible due to financial support coming from the Russian Federal Agency for Mineral Resources Management (№AM-18/35 pr, 30.01.2006) and, since 2007, from the Geophysical Institute, University of Alaska Fairbanks, USA (the Polar Earth Science Program, Office of Polar Programs, National Science Foundation; ARC-0632400, ARC-0520578).

I wish to thank Prof. Vladimir Romanovsky and Dr. Galina Mazhitova for translating the paper into English and Roman Makov for computer design and formatting of this manuscript.

References

Bulygina, O.N. & Razuvaev, V.N. 2007. Recent snow cover variability in Northern Eurasia. *Proceedings of the International Conference "Cryogenic resources of polar regions", Salekhard, Russia, June 17-21, 2007* 1: 201-204.

Gravis, G.F., Moskalenko, N.G. & Pavlov, A.V. 1988. Perennial changes in natural complexes of the cryolithozone. *Proceedings of the Fifth International Conference on Permafrost, Trondheim, Norway, August 2-5, 1988* 1: 165-169.

Haeberli, W., Cheng, G., Gorbunov, A.P. & Harris, S.A. 1993. Mountain permafrost and climate change. *Permafrost and Periglacial Processes* 4: 165-174.

Kakunov, N.B. 1999. Monitoring of the active/seasonally frozen layer and upper layers of cryolithozone during the ongoing half-century climatic cycle in the European northeast of Russia. *Abstracts of the International Conference "Monitoring of Cryosphere", Pushchino, Russia, April 20-23, 1999*: 120-121.

Kakunov, N.B. & Sulimova, E.I. 2005. The results of observing grounds temperatures in the European Northeast of Russia during the 1970-2003 warming-up period. *Proceedings of the 3rd Conference of Geocryologists of Russia, Moscow, Russia, June 1-3, 2005* 2: 84-90.

Oberman, N.G. 1996. Geocryological specificity and current trends in natural and anthropogenic dynamics of the cryolithozone of the East-European Subarctic. *Proceedings of the 1st Conference of Geocryologists of Russia, Moscow, Russia, June 3-5, 1996* 2: 408-417.

Oberman, N.G. 2001. Intra-century dynamics of the permafrost zone in the European Northeast of Russia. *Proceedings of the 2nd Conference of Geocryologists of Russia, Moscow, Russia, June 6-8, 2001* 2: 212-217.

Oberman, N.G. & Mazhitova, G.G. 2003. Permafrost mapping of Northeast European Russia based on the period of climatic warming 1970-1995. *Norwegian Journal of Geography* 57, No. 2: 111-120.

Oberman, N.G. 2006a. Long-term tendencies of natural cryolithozone evolution the European Northeast. *Proceedings of International Conference "Earth cryosphere assessment: theory, applications and prognosis of alterations", Tyumen, Russia, May 29-31, 2006* 1: 93-96.

Oberman, N.G. 2006b. Permafrost monitoring. In: I.S. Zektser (ed.), *Geology and Ecosystems*. Boston/Dordrecht/London: Springer. Kluwer Academic Publishers, 341-354.

Oberman, N.G. 2007. Some peculiarities of current degradation of permafrost in the Pechora-Ural region. *Proceedings of the International Conference "Cryogenic resources of polar regions", Salekhard, Russia, June 17-21, 2007* 1: 96-99.

Osterkamp, T.E., Zhang, T. & Romanovsky, V.E. 1994. Evidence for a cyclic variation of permafrost temperatures in Northern Alaska. *Permafrost and Periglacial Processes* 5: 137-144.

Pavlov, A.V. 1994. Current changes of climate and permafrost in the Arctic and Sub-Arctic of Russia. *Permafrost and Periglacial Processes* 5: 101-110.

Pavlov, A.V. 1997. Geocryological-climatic monitoring in Russia: methodology, results and forecast. *Cryosfera Zemli (Earth Cryosphere)* 1: 47-58.

Pavlov, A.V. & Malkova, G.V. 2005. *Contemporary changes of climate in northern Russia: Album of small-scale maps*. Novosibirsk: Academic Publishing House "Geo", 54 pp.

Romanovsky, V.E. & Osterkamp, T.E. 2001. Permafrost monitoring system in Alaska (structure and results). *Cryosfera Zemli (Earth Cryosphere)* 4: 59-68.

MAGST in Mountain Permafrost, Dovrefjell, Southern Norway, 2001–2006

Rune Strand Ødegård
Gjøvik University College, P.O.Box 191, NO-2802 Gjøvik, Norway
Ketil Isaksen
Norwegian Meteorological Institute, P.O.Box 43 Blindern, NO-0313 Oslo, Norway
Trond Eiken, Johan Ludvig Sollid
Department of Geosciences, University of Oslo, P.O.Box 1047 Blindern, NO-0316 Oslo, Norway

Abstract

A monitoring program to measure ground and air temperatures was started in autumn 2001 in Dovrefjell (62°15′N, 9°20′E), a mountainous area in southern Norway. Ground temperatures are measured in a transect from deep seasonal frost at 1039 m a.s.l. to discontinuous mountain permafrost at 1505 m a.s.l. in 11 boreholes 9 m deep. This is the first transect of this type set up in Scandinavia. Preliminary results are presented including measurements at 0.2 m and 8.5 m depth. The collected ground surface temperatures (GST) show pronounced fluctuations and large interannual variability. A simple normalization procedure is suggested to relate the observed GST to the reference period 1961-1990. The results suggest that even with an averaging period of 5 years the MAGST could deviate more that 1°C from the 30-year average. The period 2001–2006 is generally found to be warmer than the reference period, suggesting thawing permafrost at sites with discontinuous or thin snow cover.

Keywords: MAGST; monitoring; mountain permafrost; Norway.

Introduction

Permafrost is known to be widespread in the world mountain ranges, but scientific investigations only started during the past few decades (Haeberli 1973, Haeberli & Patzelt 1982, Ødegård et al. 1992, Haeberli et al. 1993). The focus of these investigations has been on degrading permafrost and reduction in the stability of mountain slopes (e.g. Harris et al. 2001). Slow thaw of deeper subsurface materials may provoke larger-scale instability on steeper slopes in areas previously considered stable (Dramis et al. 1995). Other studies are related to buildings and other installations directly affected by ground thawing (Haeberli 1992, Haeberli et al. 1993). Permafrost is sensitive to changes in surface energy exchange; it is therefore important to investigate the marginal permafrost areas. Equally important is an understanding of the dominant processes for permafrost development and degradation in mountain areas.

The use of miniature temperature data loggers (MTDs, Fig. 1) for mountain permafrost studies has greatly increased during the last decade. Large amounts of ground surface temperature data now exist from many mountain areas. Continuous temperature recordings make it possible to determine, for example, the mean monthly and annual ground surface temperature (MMGST and MAGST) at selected sites.

This paper presents preliminary results from a monitoring program to measure ground and air temperatures in Dovrefjell (62°15′N, 9°20′E), a mountainous area in southern Norway (Fig. 2). Ground temperatures are measured in a transect from deep seasonal frost at 1039 m a.s.l. to discontinuous mountain permafrost at 1505 m a.s.l. in 11 boreholes 9 m deep in the period 2001–2006. This is the first transect of this type set up in Scandinavia. The analysis includes measurements at 0.2 m and 8.5 m depth. The collected ground surface temperatures (GST) show pronounced fluctuations and large interannual variability. A simple normalization procedure is suggested to relate the observed GST to the reference period 1961–1990.

Figure 1. Miniature temperature datalogger (MTD) used in this study. This tool is especially designed for rough field conditions. The thermistor in the MTDs is a TMC-1T with a temperature range of −30°C to +40°C and with accuracy given by the manufacturer to be ±0.13°C. The loggers are available from GEOTEST in Switzerland.

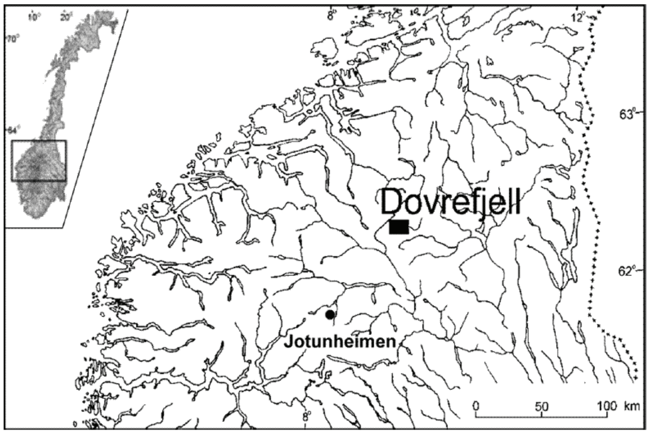

Figure 2. The research area in central southern Norway.

Table 1. Mean ground temperatures 2001–2006, column 2 shows normalized temperatures described in the next section.

BH-nr	Mean 2001-2006 0.2m depth	Normalised 0.2m depth	Mean 2001-2006 8.5m depth
DB1	-1.1	-1.9	-0.2
DB2	-1.0	-2.1	-0.3
DB3	0.7		0.2
DB5	-0.8	-1.7	0.6
DB6	-0.7	-1.7	-0.3
DB7	0.5		1.4
DB8	0.8		2.0
DB10	1.5	0.9	2.6
DB11	1.4	0.8	2.1

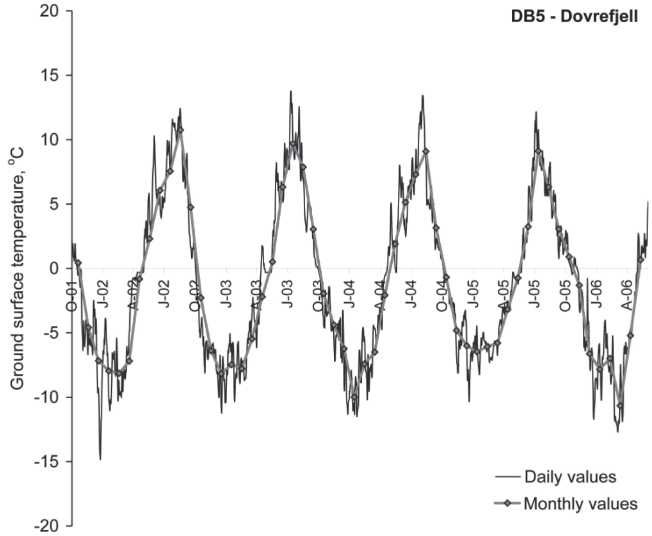

Figure 3. Daily and monthly time series of ground surface temperature at monitoring site DB5 in Dovrefjell, 2001–2006. The temperature series shows large interannual variability.

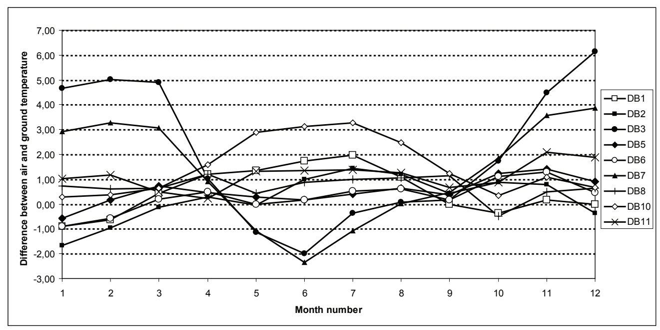

Figure 4. Difference between air temperatures and observed MAGST at the monitoring sites (0.2 m depth–averages 2001–2006).

Research Area and Previous Studies

The setting and overall scope of the monitoring program in Dovrefjell were presented by Sollid et al. (2003). Key information from the boreholes like position, altitude, surface material, and snow depth are described in this paper.

Ground temperatures are correlated with elevation. The lower limit of the mountain permafrost in Dovrefjell is about 1500 m a.s.l., mapped using the BTS (Bottom Temperature of Snow) method (Ødegård et al. 1996, Isaksen et al. 2002). This limit is representative for areas with a stable snow cover of 1–2 m. Sporadic permafrost is present at elevations down to 1000 m a.s.l. in some palsa bogs (Sollid & Sørbel 1998)

Regression based on 18 climate stations in the vicinity (Aune 1993) indicates that the 0°C isotherm is located at 910 m a.s.l. The mean temperature lapse rate is 0.44°C/100 m (Tveito et al. 2000). The average yearly precipitation is 600 mm (Østrem et al. 1988). Unstable and stormy weather are common in winter, and the dominant wind direction is from the southwest.

Field Data

This study is based on analysis of a subset of the observations including monthly averages from 9 boreholes at 0.2 m depth and 8.5 m depth (Table 1, Figs. 3, 4). DB1, 2, and 6 are located at exposed sites, at main ridge-crest or plateau locations, where winter snow accumulation is minimal. Sites DB5, DB10, and DB11 have discontinuous snow cover in the vicinity of the boreholes. DB 3, 7 and 8 have a maximum snow cover between 0.3 m and 1.0 m as measured in late winter. DB1, DB2, and DB6 are in permafrost; the other boreholes have deep seasonal frost.

Normalization Procedure

In the normalization procedure the monthly scale was selected. The monthly scale improves the correlation between air and ground temperatures (Fig. 5), and captures the overall seasonal variations (Fig. 4). The World Meteorological Organization (WMO) established a standard for a "normal" period to ensure that calculations of climate averages (the "normals") are calculated on a consistent period. A 30-year period is considered long enough to calculate a representative average, and to reduce the impact that one-off, extreme events have on the average. Thus, in this study the official standard normal period 1961–1990 is used.

The normalization procedure starts with the calculation of the MMGST from MTDs by averaging the observations. The second and more complicated step is to obtain mean

Table 2. Difference between observed and normalized air temperatures at Fokstugu (1961–1990).

	JAN	FEB	MAR	APR	MAY	JUN	JUL	AUG	SEP	OCT	NOV	DEC	JUN-AUG	OCT-APR	YEAR
2002	3.2	2.1	1.4	3.9	2.2	1.2	1.1	4.7	1.9	-3.8	-3.4	-3.1	2.3	0.0	1.0
2003	2.1	2.2	3.1	2.2	-1.0	1.1	3.3	0.6	0.8	-2.5	2.0	1.8	1.7	1.6	1.3
2004	-1.6	2.5	1.7	3.5	0.5	-1.1	-0.2	2.0	1.1	-0.5	0.5	3.0	0.2	1.3	1.0
2005	4.3	0.8	0.0	2.2	-2.0	-2.4	2.4	-0.2	1.5	2.0	3.4	0.8	-0.1	1.9	1.1
2006	2.4	1.1	-4.0	-0.3	-0.6										
Average	2.1	1.7	0.4	2.3	-0.2	-0.3	1.7	1.8	1.3	-1.2	0.6	0.6	1.0	1.2	1.1

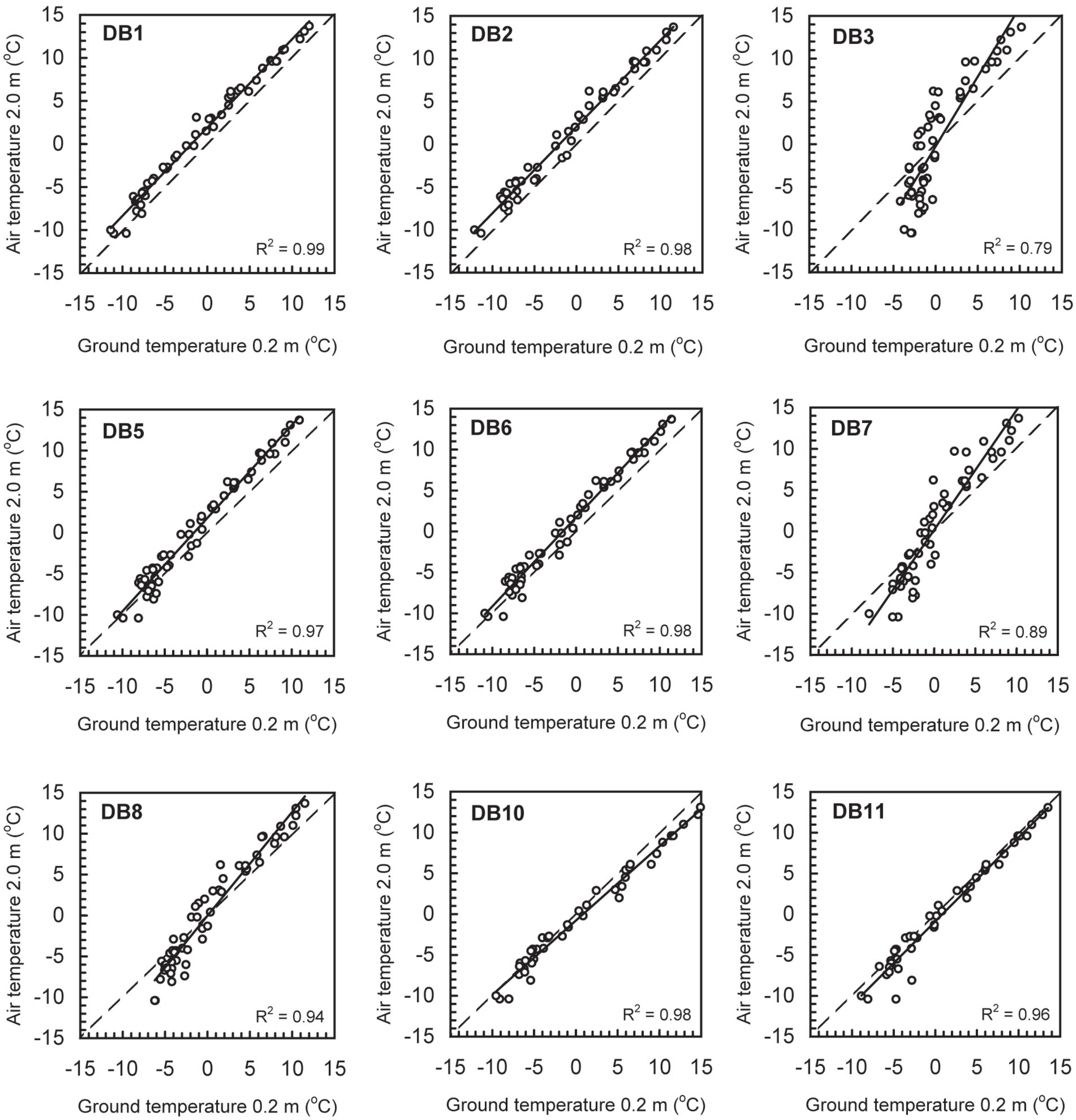

Figure 5. Recorded monthly ground surface temperature for monitoring sites in Dovrefjell vs. monthly air temperature for the weather station at Fokstugu. The snow thickness at several of the monitoring sites is low and for DB1, DB2, and DB6 most of the time snow is completely absent, due to redistribution by wind. Monitoring sites DB3, DB7, and DB8 are highly influenced by snow.

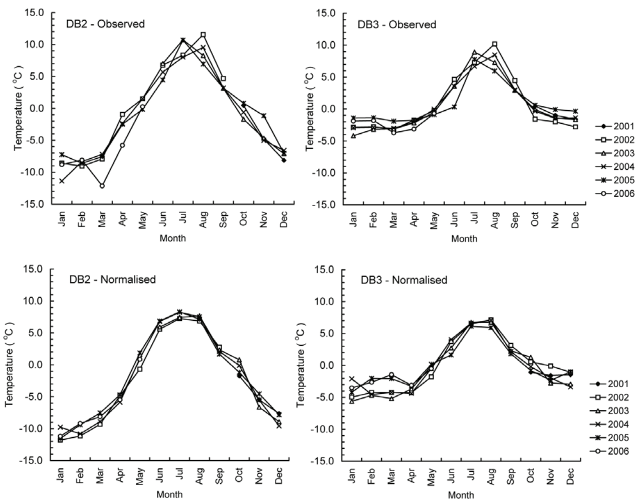

Figure 6. The upper graphs show observed ground surface temperature at selected monitoring sites DB-2 (left) and DB-3 (right). The lower graphs show normalized values for the ground surface temperatures at the same two sites.

monthly air temperature maps and monthly anomaly maps of the air temperature with reference to a standard normal period, in this study 1961–1990.

In Norway 1 km gridded temperature maps and anomaly maps are available from the Norwegian Meteorological Institute (Tveito et al. 2000). The spatial analyses were based on 1247 stations in Fennoscandia using residual kriging. The trend components were defined by a stepwise linear regression.

One alternative method is to obtain air temperature data from a nearby meteorological station having a long time series (e.g. 30-year period or more). A monthly mean temperature anomaly field in a radius of, for example, 30–50 km tends to be quite homogenous, typically within in the range of ±0.3°C.

A high correlation between air and ground temperatures suggests low influence of snow and latent heat effects, which suggests a strong coupling between the air temperatures and the ground surface temperatures. At these sites the monthly air temperature anomalies are simply applied to the MMGST to obtain a normalized estimate.

Results

The normalization procedure outlined above was applied to 6 boreholes (DB1, DB2, DB5, DB6, DB10, and DB11) to obtain the first estimate of MAGST based only on a few years of measurements. The normalization procedure reduces the monthly and interannual variability in the dataset (Fig. 6), especially during summer. At exposed sites with a thin snow cover, the variability in the normalization results during autumn and winter is mainly due to problems with the extrapolation of data obtained from the meteorological stations. For some time periods during autumn and winter, the air temperature in valleys is often lower than in the surrounding mountains because of temperature inversions. This is the case at the Fokstugu meteorological station approximately 15 km from the research area.

For the monitoring period autumn 2001 to spring 2006 the MAGST at exposed sites are on the range 0.6ºC to 1.1°C higher than the 1961–1990 average (Table 1, column 1 and 2).

For determination of MAGST for sites having a thick snow cover the suggested method is not applicable during winter due to the insulating effect of the snow (DB3, DB7, and DB8).

Except DB3 the average ground temperatures observed at 8.5 m depth are higher than MAGST at 0.2 m depth. The averages during the monitoring period range from 0.4°C to 1.2°C higher than MAGST. At DB3 the average at 8.5 m depth is 0.5°C colder than MAGST. This is a good illustration of the complexity of the ground thermal regime in mountain permafrost/deep seasonal frost. The distance between DB2 and DB3 is only 55 m.

Discussion and Conclusions

Observations in 9 shallow boreholes, in warm permafrost (3 boreholes) and deep seasonal frost (6 boreholes), in the period from autumn 2001 to spring 2006 show the limitations of surface measurements in the validation of mountain permafrost models. The results suggest that even with an averaging period of 5 years the MAGST could deviate more that 1°C from the 30-year average (1961–1990). This study shows that a simple normalization procedure based on air temperature anomaly maps could be applied at some sites with a good coupling between air and ground temperatures. A more general normalization procedure would require more sophisticated methods.

The period 2001–2006 is generally found to be warmer than the reference period, suggesting thawing permafrost at sites with discontinuous or thin snow cover.

The ground temperature averages at 8.5 m depth are generally found to be higher than the averages at 0.2 m depth. This is surprising because the conductivity ratio between unfrozen and frozen surface material (Kt/Kf) will cause an offset between the MAGST and the ground temperature at the top of the permafrost. The thermal offset is caused by different thermal properties in the thawed and frozen states (Romanovsky & Osterkamp 1995). These conductivity controlled models show good performance in arctic low-land applications when compared with borehole data (Smith & Riseborough 2002, Wright et al. 2003).

In mountain terrain the surface is often covered with blocks, introducing a top surface layer where non-conductive heat transfer mechanisms are important. Another complication is the redistribution of snow due to wind drift, resulting in a highly variable snow cover, even on scales of just a few meters. This is definitely the case at the observed boreholes and needs to be considered in order to obtain modeling results that can be compared with borehole data. There is also a possibility for lateral heat transfer in a complex soil-water system, but conclusive statements cannot be made based on this study.

The plan is to continue the monitoring for several decades, for the study of permafrost temperatures under future climate development and probable accelerated warming in the mountains of southern Norway.

Acknowledgments

The monitoring program was initiated by J.L. Sollid, University of Oslo, in co-operation with K. Isaksen, Norwegian Meteorological Institute, R.S. Ødegård, Gjøvik College and T. Eiken, University of Oslo. Forsvarsbygg at Hjerkinn by O.E. Martinsen partly financed the drilling operation and assisted in organizing the field work. The authors give their thanks to Mr. Martinsen and to the institutions involved.

References

Aune, B. 1993. Temperaturnormaler, normalperiode 1961–1990. DNMI. Report 2/93 *Klima.* 63 pp.

Dramis, F., Govi, M., Guglielmin, M. & Mortara, G. 1995. Mountain permafrost and slope instability in the Italian Alps: the Val Pola Landslide. *Permafrost and Periglacial Processes* 6: 73–81.

Haeberli, W. 1973. Die Basis Temperatur der winterlichen Schneedecke als möglicher Indikator für die Verbreitung von Permafrost. *Zeitschrift für Gletscherkunde und Glazialgeologie* 9: 221–227.

Haeberli, W. 1992. Construction, environmental problems and natural hazards in periglacial mountain belts. *Permafrost and Periglacial Processes* 3: 111–124.

Haeberli, W. & Patzelt, G. 1982. Permafrostkartierung im Gebiet der Hochebenkar – Blockgletscher , Obergurgl, Ötztaler Alpen. *Zeitschrift für Gletscherkunde und Glazialgeologie* 18: 127–150.

Haeberli, W., Guodong, C., Gorbunov, A.P. & Harris, S.A. 1993. Mountain permafrost and climate change. *Permafrost and Periglacial Processes* 4: 165–174.

Harris, C., Davies, M.C.R. & Etzelmüller, B. 2001. The assessment of potential geotechnical hazards associated with mountain permafrost in a warming global climate. *Permafrost and Periglacial Processes* 12: 145–156.

Isaksen, K., Hauck, C., Gudevang, E., Ødegård, R.S. & Sollid, J.L. 2002. Mountain permafrost distribution in Dovrefjell and Jotunheimen, southern Norway, based on BTS and DC resistivity tomography data. *Norwegian Journal of Geography* 56: 122-136.

Ødegård, R.S., Sollid, J.L. & Liestøl, O. 1992. Ground temperature measurements in mountain permafrost, Jotunheimen, southern Norway. *Permafrost and Periglacial Processes* 3: 231–234.

Ødegård, R.S., Hoelzle, M., Johansen, K.V. & Sollid, J.L. 1996. Permafrost mapping and prospecting in southern Norway. *Norsk Geografisk Tidsskrift* 50: 41–53.

Østrem, G., Dale Selvig, K. & Tandberg, K. 1988. Atlas over breer in Sør-Norge. *Meddelser nr. 61 fra Hydrologisk avdeling* . Norwegian Water Resources and Energy Directorate (NVE). Oslo. 45 pp.

Romanovsky, V.E. & Osterkamp, T. E. 1995. Interannual variations of the thermal regime of the active layer and near-surface permafrost in Northern Alaska. *Permafrost and Periglacial Processes* Vol. 6.: 313-335.

Smith, M.W. & Riseborough, D.W. 2002. Climate and the Limits of Permafrost: A Zonal Analysis. *Permafrost and Periglacial Process* 13: 1-15.

Sollid, J.L. & Sørbel, L. 1998. Palsa bogs as a climate indicator – examples from Dovrefjell, southern Norway. *Ambio* 27: 287-291.

Sollid, J.L., Isaksen, K., Eiken, T. & Ødegård, R. 2003. The transition zone of mountain permafrost on Dovrefjell, southern Norway. M. Phillips, S.M. Springman & L.U. Arenson (eds.), *Proceedings Eighth International Conference on Permafrost*: 1085-1089.

Tveito, O.E., Førland, E., Heino, R., Hanssen-Bauer, I., Alexandersson, H., Dahlström, B., Drebs, A., Kern-Hanssen, C., Jónsson, T., Vaarby Laursen, E. & Westman, Y. 2000. *Nordic Temperature Maps*. DNMI-report 09/00. 54 pp.

Wright, J.F., Duchesne, C. & Côté, M.M. 2003. Regional-scale Permafrost Mapping using the TTOP Ground Temperature Model. *Proceedings Eighth International Conference on Permafrost*: 1241-1246.

Effects of Changing Climate and Sea Ice Extent on Pechora and Kara Seas Coastal Dynamics

S.A. Ogorodov
Lomonosov Moscow State University, Faculty of Geography, Moscow, Russia

Abstract

About half of the Eurasian Arctic coastline consists of ice-rich deposits. The dynamic response of this coastal type is forced mainly by thermal and wave-energy mechanisms. The role of the thermal factor increases with ground ice content. Low ice content makes the wave-energy factor more significant. We present a comparison of the changing influence that wave energy and temperature regimes can exert on coastal dynamics for two types of Pechora and Kara seas coasts. The first type is represented by barriers and spits, which are expressed by sandy deposits with low ice content. For such coasts, a clear dependence between the seasonal wave energy magnitude directed landward and the coastal retreat rate was found. The second type represents the typical thermo-erosion bluff coast composed of sandy and clayey deposits with medium ice content. The dynamic regime of this type of coast is determined by both thermal and wave-energy factors.

Keywords: climate change; coastal dynamics; sea ice; wave energy.

Introduction

The evolution of Arctic coasts over the coming decades will be governed by changes in the natural environment caused by the effects of climate warming. Rising temperatures are altering the Arctic coastline by reducing sea ice and thawing permafrost, and larger changes are projected to occur as this trend continues. In September, 2007, the area of sea ice in the northern hemisphere achieved its historical minimum for the period of satellite observation (since 1978; http://arctic.atmos.uiuc.edu/cryosphere). Less extensive sea ice creates more open water, allowing stronger wave generation by winds, thus increasing wave-induced erosion along Arctic coasts. Therefore, the acceleration of erosion and thermo-abrasion of the coast is attributable to both an increase of air and water temperatures and a possible intensification of wind-generated wave activity. This is an important topic to pursue given the direct impacts to human communities and infrastructure already being felt along Arctic coasts.

In spite of a short active period, dynamic processes in the coastal zone of the Arctic seas are characterized by a very high intensity. The intensity is due to low coastal stability, which is composed of frozen dispersive sediments and is evolving under the influence of thermal-erosion process. About half of the Eurasian Arctic coastline is exposed to coastal erosion processes and undergoes coastal destruction at rates of 1–5 m per year. In general, which processes

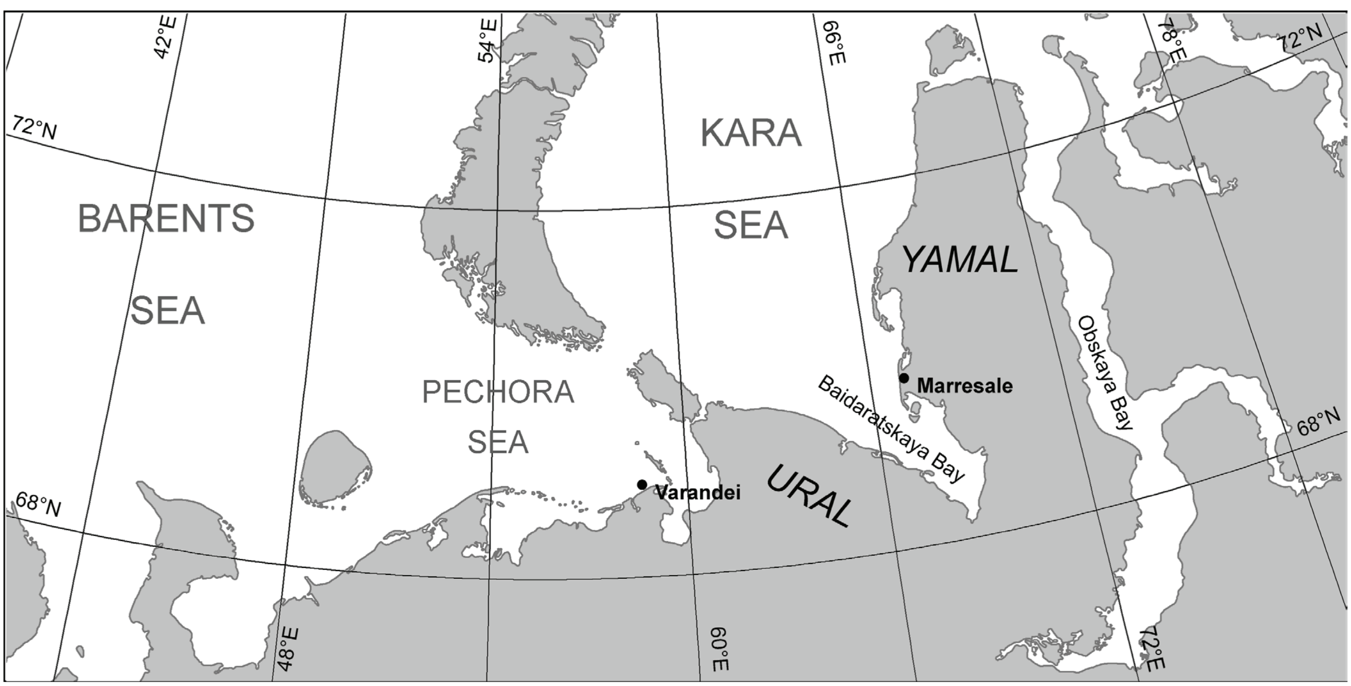

Figure 1. The research area.

affect thermal-erosion coasts, and with what intensity, is determined by a combination of and interaction between thermal and wave-energy factors.

The thermal influence shows itself as energy transmission to the coast, which is composed of frozen sediments, via radiative and sensible heat fluxes from air and water. Accordingly, higher air and water temperatures, together with a longer ice-free period and longer period with positive air temperature, affect the stability of frozen coasts. The role of the thermal factor usually increases with increasing ice content in coastal deposits. In turn, low ice content renders the wave-energy factor more significant.

The wave-energy factor acts via the direct mechanical impact of sea waves on the shore. Correspondingly, the effectiveness of this factor is determined by storm-driven sea surge intensity, as well as by the length of the stormiest period. Conversely, surge intensity substantially depends on the fetch, which is intrinsically linked to sea ice extent since less extensive sea ice creates more open water, allowing stronger wave generation by wind.

We present a comparison of the changing influence of wave energy and temperature regimes on coastal dynamics for two types of coast. These results are drawn from work conducted along the Barents (Pechora) and Kara Sea coasts (Fig. 1), but have much broader implications to coastal regions throughout the Eurasian Arctic.

Methods

Microsoft Excel was used for statistics and correlation analysis. Wave energy flux was calculated using the Popov-Sovershaev (1981, 1982) wind-energy method (Ogorodov 2002). The method is based on the theory of wave processes and takes established correlations between wind speed and parameters of wind-induced waves into account.

For deep-water conditions, when the sea floor does not influence the wave formation, the wave energy flux per second (for 1 m of wave front) at the outer coastal zone boundary is calculated by the equation similar to the one used in Longinov's method (1966):

$$E_{0dw} = 3\times 10^{-6} V_{10}^{3} x \qquad (1)$$

where V_{10} is the real wind speed measured by anemometer at 10 m above sea level [*m/s*], x is the real or extreme distance of wave racing [*km*];, and the dimension of the coefficient 3×10^{-6} corresponds to the dimensions of ρ/g, where ρ is density [g/m^3], g is gravitational acceleration [m/s^2], i.e., $\frac{t/m^3}{m/s^2}$. Thus, E_{0dw} has dimensions, $\frac{tm}{ms}$ or *t/s*, as is the convention in coastal dynamics.

The same equation for the shallow sea zone appears in the following form:

$$E_{0sw} = 2\times 10^{-6}\left(\frac{gH}{V_{10}^{2}}\right)^{1.4} V_{10}^{5} \qquad (2)$$

where E_{0sw} has the same dimensions as in equation (1). Equation (2) is valid under two conditions: for shallow sea basins, i.e., for most of the arctic seas, wave energy is determined in accordance with kinematic index of shallowness, $\frac{gH}{V_{10}^{2}}$, between water depth H along the wind direction and wind speed V_{10}. At $\frac{gH}{V_{10}^{2}} \leq 3$ water depth hampers formation of wind-induced waves.

Another condition is determined by the following: a wave starts to interact with the sea floor when it becomes high enough after it has covered a certain ideal distance without touching the sea floor, when it has developed in the deep-sea basin where equation (1) is valid. Hence, at the boundary between deep-sea and shallow zones both equations should be valid. From this it follows that the ratio between the minimum wave fetch at which the interaction between waves and sea floor begins and the water depth at the distance of that wave fetch is:

$$\frac{x_{\min}}{H} \geq 6.5\left(\frac{gH}{V_{10}^{2}}\right)^{0.4} \qquad (3)$$

where $x_{\min}$ is expressed in kilometers, and H is in meters.

At $\frac{gH}{V_{10}^{2}} = 3$ equation (3) becomes

$$\frac{gx_{\min}}{V_{10}^{2}} \geq 30 \qquad (4)$$

From (4) we can get the value of the extreme wave fetch for deep-sea conditions equal to the value obtained by other means:

$$x_{\lim} = 3V_{10}^{2} \qquad (5)$$

This value could be neglected if other factors limiting wave fetch are absent, for example by sea ice or islands.

To calculate the sum of wave energy of a certain direction from the energy flux per second, E_0 calculated for all wind speeds by wind direction is multiplied by the overall wind duration, for wind of a certain speed range on a monthly or monthly ice-free period, expressed in seconds. The values obtained are summarized for each rhumb line. The rhumb fluxes of wave energy, E_r, are represented by the wave energy sum for all wind speed gradations within a certain rhumb during the dynamically active period.

For delimitation of an ice extent boundary and determination of duration ice-free period http://arctic.atmos.uiuc.edu/cryosphere data are used.

Figure 2. Pesyakov Island, the first type coast.

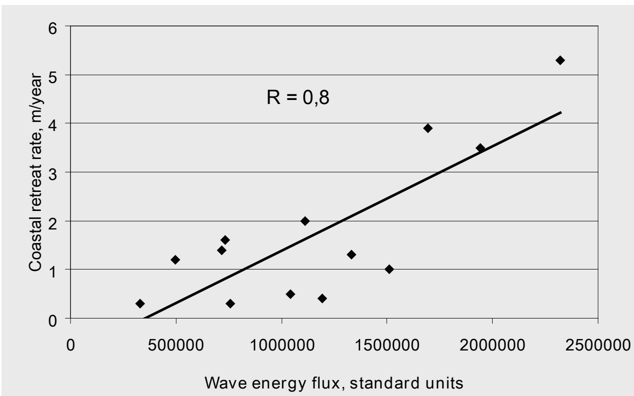

Figure 3. Correlation between wave energy and coastal retreat rate.

Results and Discussion

The Varandei Coast, Barents Sea example

It is a wide-spread opinion that sea coasts consisting of frozen deposits must develop as thermoerosion (thermoabrasion) type coasts. At the same time, coastal bluffs formed of frozen deposits with low ice content (*the first type*) are not subject to thaw slumping, permafrost creep (solifluction), gully thermoerosion, and thermokarst (Fig. 2). Periodicity of extreme storm surges and the total wave energy activity in the coastal zone during the active dynamic period are the main factors which determine the dynamics of coasts with low ice content. Based on the Actualism method, we can suppose that, in the case of climate warming, low ice content coastal dynamics will have similar features to those which they have in the warmest years and decades at the present. Thus, to forecast the dynamics of similar coasts under conditions of climate change, it is only necessary to predict changes in the regional wind-wave regime. As basic coastal retreat values, one may use the values obtained by direct stationary observations during the period with certain wind-wave parameters.

To substantiate this hypothesis, we performed correlation analysis of the results of stationary observations on coastal dynamics and hydrometeorological data. For Varandei area (Pechora Sea), wave energy fluxes at the external border of the coastal zone were calculated using wind direction and speed for each year between 1981 and 2002. The total

Figure 4. Ural Coast of Baidaratskaya Bay, the second type coast.

value of the wave energy flux from the all wave-dangerous rhumbs for dynamically active period (from July to October) was obtained. Then we calculated correlation indices between the value of the wave energy flux and temperature characteristics, and the value of coastline retreat near the Varandei settlement.

The obtained results permit us to conclude that for coasts of *the first type*, consisting of low ice content deposits (Varandei site), there is a clear dependence between the wave energy volume at the external border of the coastal zone and the coastal retreat rate. The correlation index (R) is 0.8 (Fig. 3).

At the same time, a significant correlation between the temperature regime and the coastal retreat rate was not observed (Ogorodov 2005). There was no determined interrelationship between average temperatures of active dynamic period and wave activity.

Thus, the conditions of the climate change dynamics of coasts formed by deposits with low ice content will be determined more by wind-energetic than temperature regimes.

The Baidaratskaya Bay and Marresale Coasts, Kara Sea example

The second coastal type represents the typical, thermo-erosion bluff coast composed of sandy and clayey deposits with medium ice content (Baidaratskaya Bay and Marresale Coasts, Kara Sea; Fig. 4). The dynamic regime of coasts of *the second type* is defined by both thermal and wave-energy factors. Thermodenudation processes, caused by the thawing of frozen deposits, result in the mass-wasting of unconsolidated sediments that are loosely deposited at the foot of the coastal bluff. This material is easily washed away by the waves and water-level surges that accompany storm events. In the absence of significant melting, a given wave energy level cannot act with the same efficiency on the coastal bluff to remove material, and hence should result in lower coastal retreat rates. Correspondingly, the persistence of the thawed, loose material at the base of the bluff when wave activity is low should reduce the rate of the thermodenudation processes and also coastal bluff retreat.

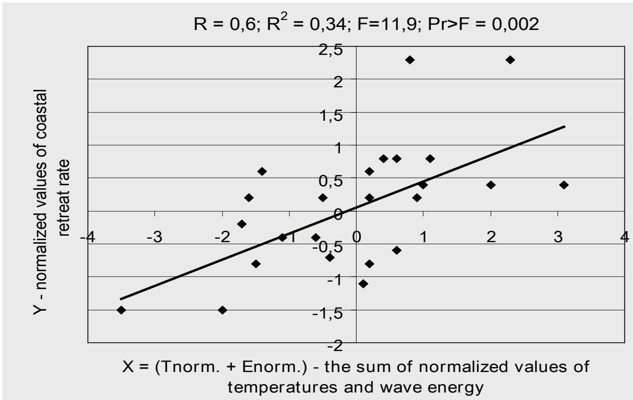

Figure 5. Seasonal erosion response at the second type coast, 1977–2004, with respect to an index combining a representation of seasonal thermal and wave energies (their normalized seasonal values were added and plotted against the normalized erosion response). Results considering the influence of temperature and wave action together showed superior explanatory capacity than temperature or wave energy alone.

For a region with the *second type* of coast (Baidaratskaya Bay and Marresale sites, Kara Sea), we have calculated the sums of temperatures averaged monthly for the mild season (from June to September) for the period from 1977 to 2004, as well as the total value of the wave energy flux. We performed correlation analyses of these data and the results of monitoring of the coastal dynamics. We observed that both factors influence the coastal retreat rate equally. Seasonal indicators of temperature and wave energy returned correlation coefficients (against seasonal erosion) of 0.41 and 0.39, respectively, while together they returned 0.6 (Fig. 5). The maximal coastal retreat rate (2.0–3.5 m/year) corresponds to the years when both average temperature and wave-energy flux approach the maximum values. Such behavior corresponds to the years 1982, 1983, 1988, 1989, 1994, and 1995 (Vasiliev et al. 2005), in particular. The coincidence of minima of these parameters corresponds to the lowest rates of coastal recession (0.5 m/year, for example, during the years 1978 and 1999).

The combined analysis of coastal retreat rate and hydrometeorological parameters specifying the temperature and wave regime seems to be difficult because of the discreteness of monitoring of coastal dynamics. For example, the measurement of the position of the brow of the coastal bluff is usually performed at the end of August and beginning of September, while the high wave energy activity occurs at the end of September and in October. As a result, these measurements give information on the retreat rate of the brow of coastal bluff under the action of thermodenudation processes during the summer of a given year and wave erosion during autumn of the previous year.

Dynamics of coasts consisting of frozen deposits is mainly caused by the two environmental forcing factors, namely, by the thermal and wave-energy mechanisms. As a rule, the role of the thermal factor increases with the ground ice content of the coastal deposits. In turn, low ground ice content renders the wave-energy factor more significant.

Conclusions

Thus, temperature regime and waves, as the major environmental forcing agents determining dynamics of arctic coastal margins have been considered. Rising temperatures are altering the arctic coastline and much lager changes are projected to occur during this century as a result of reduced sea ice, thawing permafrost. Less extensive sea ice creates more open water, allowing stronger wave generation by winds, thus increasing wave-induced erosion along arctic shores. Therefore, the acceleration of erosion and thermo-abrasion of the coast can be caused by both increase of the air and water temperature and possible increasing of wind-wave activity.

Acknowledgments

I am grateful to Dr. David Atkinson (International Arctic Research Center, University of Alaska) for wind data and scientific assistance, and also to the Russian Foundation of Basic Research, projects 07-05-12072, for financial support.

References

Longinov, V.V. 1966. Energetic method of estimating alongshore sediment drift in coastal zone. Proceedings of SoyuzmorNIIproekt, 12 (8): 13-28. (in Russian).

Ogorodov, S.A. 2002. Application of wind-energetic method of Popov-Sovershaev for investigation of coastal dynamics in the Arctic. In: V. Rachold et al. (eds.), *Arctic Coastal Dynamic. Report of an International Workshop. Potsdam (Germany) 26–30 November 2001, Reports on Polar and Marine Research*. Bremerhaven. 413: 37-42.

Ogorodov, S.A. 2005. Peculiarities of Dynamics of Barents Sea Coasts Formed by Deposits with Low Ice Content, TERRA NOSTRA: *2nd European Conference on Permafrost, Potsdam, Germany, June 12–16, 2005:* 164.

Popov, B.A., Sovershaev, V.A. 1981. Principles in distinguishing data for calculating wave energy fluxes. Beregovaya zona morya (Coastal zone). Moscow, Nauka, 47-53 (in Russian).

Popov, B.A., Sovershaev, V.A. 1982. Nekotoryie cherty dinamiki arkticheskikh beregov Azii (Some features of the coastal dynamics in arctic Asia). Voprosy geografii, 119. Morskie berega (Sea coasts). Moscow, Mysl', 105-116 (in Russian).

Vasiliev, A., Kanevskiy, M., Cherkashov, G., Vanshtein, B. 2005. Coastal dynamics at the Barents and Kara Sea key sites. In: *Geo-Marine Letters. An International Journal of Marine Geology*. Vol. 25, N 2-3, 110-120.

Solifluction Lobes in Sierra Nevada (Southern Spain): Morphometry and Palaeoenvironmental Changes

Marc Oliva
Department for Physical and Regional Geography and Landscape Research Laboratory, University of Barcelona, Spain
Lothar Schulte
Department for Physical and Regional Geography and Landscape Research Laboratory, University of Barcelona, Spain
Antonio Gómez Ortiz
Department for Physical and Regional Geography and Landscape Research Laboratory, University of Barcelona, Spain

Abstract

This paper presents a morphometric and spatial approach, the aim of which is to classify solifluction lobes in Sierra Nevada in southern Iberian Peninsula, to understand the involved geomorphic processes, and to reconstruct their evolution during the Late Holocene. Under the present climatic conditions, solifluction is inactive to weakly active in this massif. According to our findings, water availability in the semiarid environment of Sierra Nevada is the main factor controlling solifluidal dynamics. Only lobes near water channels and those influenced by water supply from late-lying snow patches show displacements. By contrast, thermal and topographic monitoring of a solifluction lobe in the Rio Seco Valley showed that, despite a seasonal frozen layer of 70 cm thickness, solifluction processes remain inactive. However, sedimentological studies on solifluction lobes indicate that during the Late Holocene, periods of increased solifluction processes (e.g., Little Ice Age) alternated with periods of geomorphic stability (e.g., Medieval Warm Period). Present climate may not be cold and/or wet enough to trigger important solifluction processes from 2500 to 3000 m altitude.

Keywords: Late Holocene; seasonal frozen layer; Sierra Nevada; solifluction lobes.

Introduction

Solifluction has been defined as the slow mass wasting associated with freeze–thaw action (Andersson 1906, Ballantyne & Harris 1994). During the last decades, research on present and past solifluction processes was undertaken mostly in high-latitude (polar and subpolar regions) and in mid-latitude mountain environments, where periglacial processes affect settlements, infrastructures, and equipment (Matsuoka 2001).

By contrast, solifluction features in the Mediterranean region have attracted less attention from geomorphologists and geophysicists due to the reduced extension of the periglacial belt and lower demographic pressure at high altitudes. However, studies on present solifluction dynamics in Spanish mountains were carried out by Gómez Ortiz et al. (2005) in Sierra Nevada, by Grimalt & Rodríguez (1994) on the Balearic Islands, by Palacios et al. (2003) in the Peñalara massif, and by Chueca & Julián (1995) in the Central Pyrenees**.**

Since the beginning of the research on solifluction phenomena, studies focused on morphometry and spatial pattern of the lobes (Andersson 1906, Rapp 1960, Washburn 1979), but during the last years, research turned towards the active layer, particularly on chronostratigraphy, processes, sediment flux, and ground temperature monitoring (Harris et al. 1997, Matsuoka 2001, Jaesche et al. 2003). In order to understand the nature of mechanisms, processes, and evolution of solifluction landforms, it is crucial to deal with the causes of solifluction being active in some periods and inactive in others (Gamper 1983, Veit 1988, Matthews et al. 2005).

The purpose of the present paper is to examine the morphometry and palaeoenvironmental changes of solifluction lobes in two study areas on the northern and southern slopes of Sierra Nevada.

Regional Setting

Sierra Nevada, the highest massif in the Iberian Peninsula (Mulhacén, 3478 m), is located at latitude 37ºN between the subtropical high-pressure belt and the mid-latitude westerlies. Mean annual temperature at 2500 m records 4.4ºC, and annual precipitation reaches only 702 mm^{-1}yr

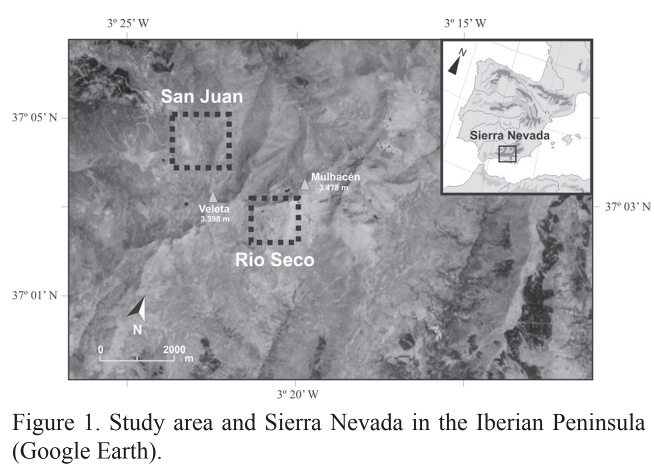

Figure 1. Study area and Sierra Nevada in the Iberian Peninsula (Google Earth).

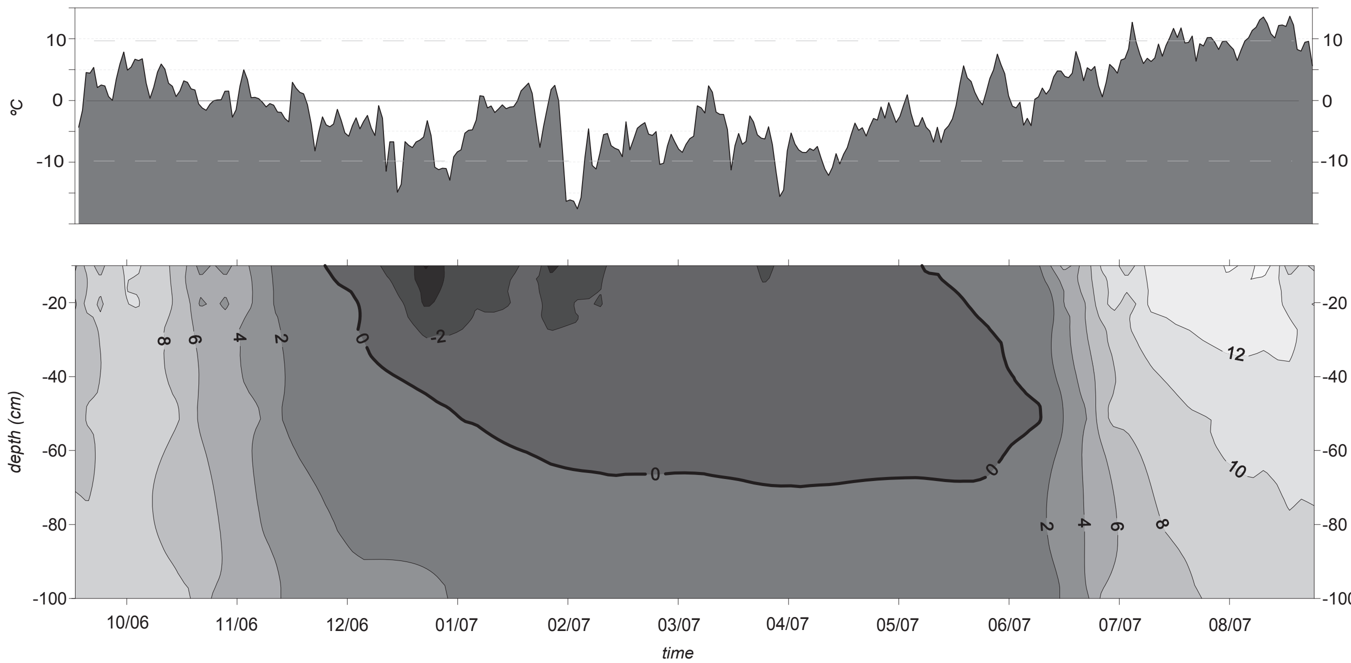

Figure 2. Mean daily air temperature at Veleta Peak, 3398 m (figure above), and ground temperatures of a solifluction lobe of the Rio Seco cirque at 3001 m (figure below) from September 2006 to August 2007.

(1965–1992). 80% of the total precipitation falls between October and April, mainly as snow.

As a consequence of global warming since the end of the Little Ice Age (LIA), the southernmost glacier of Europe located in the Veleta cirque disappeared (Schulte 2002). However, local discontinuous permafrost and active rock glacier dynamics are closely related to remnants of dead ice located in the highest northern cirques of the massif (Gómez Ortiz et al. 2001, Schulte et al. 2002, Gómez Ortiz et al. 2005).

The vegetation cover of the alpine belt in Sierra Nevada is very low, but includes a large number of endemic species (Molero Mesa & Pérez Raya 1987). This sparse vegetation and the low resistance schist, the dominant bedrock in the highest part of Sierra Nevada, enhance solifluction and erosion processes, hence the headwaters of Rio Seco and San Juan valleys show frequent solifluction lobes. In the Rio Seco cirque (southern slope), they are located between 2930 and 3005 m a.s.l. and in the U-shaped valley of San Juan (northern slope) between 2474 and 2911m. Vegetation cover ranges from 1.6% in the Rio Seco cirque to 3.8% in the San Juan valley.

Materials and Methods

More than two hundred solifluction lobes were morphometrically analysed according to the nomenclature of Hugenholtz and Lewkowicz (2002) and Matsuoka et al. (2005), considering 8 variables: altitude, slope, orientation, typology, vegetal cover, length, width, and front height. Universal Temperature Loggers (UTL-1) were installed to measure the ground temperatures continuously every two hours at different depths (2, 10, 20, 50, and 100 cm).

Table 1. Mean stake displacements of monitored solifluction lobes from August 2006 to August 2007.

Valleys	Heights (m a.s.l.)	n	Moving stakes (%)	Horizontal ($cm^{-1}yr$)	Vertical ($cm^{-1}yr$)
San Juan	2793–2911	47	61.8	0.31	0.41
Rio Seco	2935–3001	40	11.8	0.05	0.14

Sedimentological laboratory standard methods were carried out on soil samples extracted from several lobes. Organic carbon was determined with a CN Elemental Analyzer and grain size was measured according to Scheffer & Schachtschabel (2002).

Thermal and Dynamic Control of Solifluction Lobes

From August 2005 to August 2007, displacements of 16 solifluction lobes at different heights were monitored by up to 9 wooden stakes each (50 cm long x 3 cm wide), inserted 45 cm into the lobes. The measurements of the stakes at the lobe fronts and sides may provide sensitive records of active solifluction processes nowadays in Sierra Nevada.

In San Juan, 38.2% of 47 installed stakes did not show any horizontal displacement, reaching 88% out of 40 in the Rio Seco cirque. Furthermore, grass cover, intact root network, soil formation (thin A horizons), and micro-scale geomorphology (clearly defined, steep-sloping lobe fronts) support the interpretation of the inactivity pattern of these lobes.

The rest of the stakes indicate horizontal movement of less than 0.5cm/yr (Table 1) indicating solifluction processes.

Table 2. Different types and characteristics of solifluction lobes in Sierra Nevada.

Type	Characteristics	Nº of lobes (monitorized lobes)	Active / stable	Length (m)		Width (m)		Front height (m)		Slope (º)	
				Range	Mean	Range	Mean	Range	Mean	Range	Mean
Stone-banked lobe-1 STL-1	Abundance of gravels/ rocks > 50%	6 (1)	1 / 0	3-10	5,1	2-5	3,4	0,6-1	0,39	9-19	13,0
Stone-banked lobe-2 STL-2	Abundance of gravels/ rocks < 50%	34 (2)	1 / 1	2-8	5,4	2-8	4,5	0,3-0,9	0,52	7-16	10,3
Low solifluction lobe LSL	Dominance of turf with a frontal height < 80 cm.	104 (4)	2 / 2	1,5-6	4,4	1-5	3,6	0,2-0,7	0,47	7-15	9,8
High solifluction lobe HSL	Dominance of turf with a frontal height ≥ 80 cm	32 (5)	1/ 4	2-10	6,6	2-10	5,3	0,8-1,2	0,9	6-18	11,5
Solifluction terrassettes ST	Low solifluction terrasses	3 (2)	0 / 1	0,6-2	1,1	0,3-1	0,8	0,2-0,3	0,24	6-18	10,0
Stone-mantled lobes MSS	Stone-dominance large lobe ≥ 8 m length	11 (0)	0 / 0	9-15	9,9	8-13	9,5	0,6-1,4	0,86	7-19	14,0
Turf-mantled lobes MST	Turf dominance large lobe ≥ 8 m length	6 (1)	0 / 1	10-18	13,3	10-19	12,7	0,5-1,5	0,78	9-19	13,1
Block STL (block)	Lobe with a rock above	4 (1)	1 / 0	3,5-6	5,0	2-3,5	2,8	0,5-0,9	0,67	6-10	8,0
Mudflow-affected solifluction lobes MSL	Irregular-shaped lobes with muddy matrix	2 (1)	0 / 1	1-6	5,5	5-10	7,5	0,2-0,7	0,67	8-9	8,5

The higher vertical movement rates are due to freeze-thaw uplift. However, the measured surface velocity of the Sierra Nevada lobes is relative slow compared with rates recorded in polar and subpolar regions (Matsuoka 2001).

According to our findings, water availability in the semiarid environment of Sierra Nevada is the main factor controlling solifluidal dynamics. Only lobes near water channels and those influenced by water supply from late-lying snow patches show displacements. Therefore, we expect higher displacement rates during periods of moister climate conditions.

Figure 2 shows mean daily air temperature of Veleta Peak (3398 m a.s.l.) and ground temperature at 10, 20, 50, and 100 cm depth of an inactive solifluction lobe in the Rio Seco cirque at 3001 m a.s.l. from September 2006 to August 2007. The Universal Temperature Logger (UTL-1) at 2 cm depth failed, and no data were obtained.

The formation of the 70 cm thick frozen layer started at the end of November and persisted until the beginning of June. Increased frost penetration was recorded during mid December, the end of January, and the end of March.

This relatively sensitive response of the ground temperature at 10 and 20 cm depth results mainly from reduced snow cover during the winter of 2006–2007. Nevertheless, the persistent conservation of the seasonal frozen layer is due to quite cold late-spring temperatures and a continuous snow cover until the end of May. In contrast to the local permafrost detected in the 3000 m high Veleta (Gómez Ortiz et al. 2005) and Mulhacén cirques (Schulte et al. 2002), the observed pattern of the ground temperature in Figure 2 does not indicate any permafrost regime at the key site of the southern exposed Rio Seco cirque (3001 m a.s.l.).

Morphometry of Solifluction Lobes

In the San Juan valley, 156 lobes were mapped, and 46 were mapped in the Rio Seco Valley. This difference in numbers results from the different amount of water supply and tectonically-influenced valley topography, which explains why there are no solifluction lobes between 2550–2750 m a.s.l. (Fig. 3).

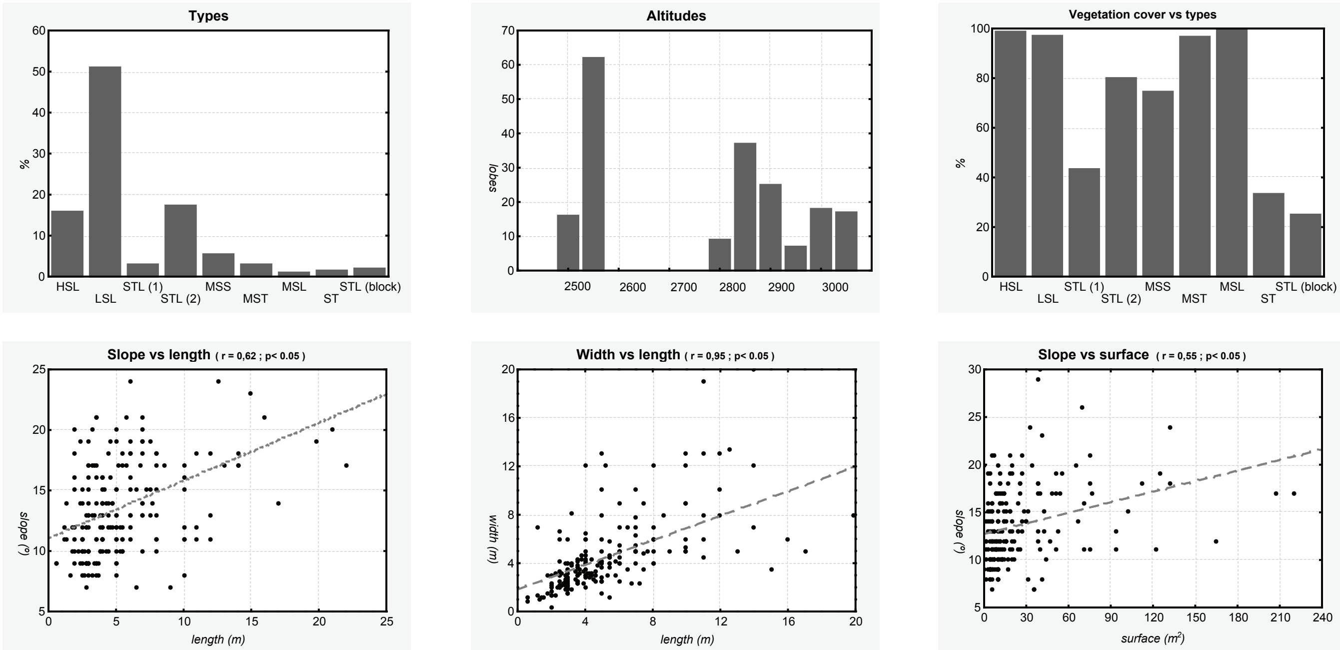

Figure 3. Relations between lobe morphometry, topography and vegetation cover in Sierra Nevada..

In general, a wide range of solifluction lobes can be observed in Sierra Nevada. Types with principal morphometrical and pedological characteristics are listed in Table 2 and can be integrated into two main groups: peat-topped lobes and uncovered stone and block-rich lobes.

There is no evidence that lobe size or other features such as front height, slope gradient, orientation, etc. listed in Figure 3, are related to present solifluction processes. Neither external factors (altitude, slope, and orientation), nor internal characteristics of solifluction lobes correlate with active lobes.

Only vegetation cover may explain the stability or mobility of solifluction lobes, with positive correlations with stable lobes (r = 0.58). Although two well-vegetated LSL also show small horizontal displacements, vegetation seems to impede movement in peat lobes but not in block-rich lobes, which tend to show higher displacement rates**.**

A correlation matrix for lobe morphometry, topography and vegetation cover of solifluction lobes from Sierra Nevada is given in Table 3.

Regarding the lobe morphology, the matrix shows a positive correlation between length and width with slope (r = 0.63; r = 0.54). The height of the riser also shows good correlation with length (r = 0.74) and width (r = 0.71). The surface area is mainly controlled by slope gradient (r = 0.63) and vegetation cover (r = 0.46).

However, orientation does not seem to be an important criterion explaining lobe morphology in Sierra Nevada (r between -0.26 and 0.32). Vegetation cover is mostly controlled by drainage and temperature, showing negative correlations with slope (r = -0.70): the steeper solifluction lobes are, the sparser vegetation cover they have.

Solifluidal Activity During the Late Holocene

Several solifluction lobes in both study areas were examined by macroscopic soil description and geochemical laboratory standard analysis. Figure 4 shows the lithostratigraphy, water content, grain size, and organic carbon content (OC) of a HSL lobe in the Rio Seco cirque at 2945 m a.s.l.

The stratigraphy of the lobe is defined by the alternation of coarse grained stone-rich layers with peat and organic-rich (OC up to 30%). The aggradation of the lobe finished with the development of an organic A horizon. The coarse-grained and sometimes cryoturbated layers are interpreted as solifluidal deposits, whereas the organic-rich horizons represent soil formation under stable geomorphic conditions. Several solifluction lobes in Rio Seco and San Juan valley show a similar lithostratigraphy.

Based on tentative correlations with a solifluction lobe, radiocarbon-dated by Esteban (1994) from 1100 ± 120 yr BP (basal organic layer) to 170 ± 120 yr BP (uppermost organic horizon), we argue that our profile could cover the Late Holocene, from the Medieval Warm Period at the bottom, to the 20th century warming at the top.

The two solifluction layers could correlate with the two main cooler climate pulses of the Little Ice Age reconstructed by Schulte (2002) from ^{210}Pb-dated glacier advances at the nearby Veleta cirque. Historical climate research from documentary data undertaken by Rodrigo et al. (1999) considers that the coldest and wettest phase of the LIA occurred from 1590 to 1650. Radiometric dating and further research is needed to support our chronological model.

Conclusions

This paper presents a morphometric and spatial approach, the aim of which is to classify solifluction lobes in Sierra Nevada in

Table 3. Correlation matrix for lobe morphometry, topography, and vegetation cover of solifluction lobes from Sierra Nevada ($p < 0.05$).

	Orientation	Slope	Vegetation cover	Length	Width	Front height	Surface area	L/W
Orientation								
Slope	0.03							
Vegetation cover	0.31	0.18						
Length	0.05	0.63	0.49					
Width	0.32	0.54	0.61	0.95				
Front height	-0.09	0.29	0.52	0.74	0.71			
Surface area	0.29	0.63	0.46	0.96	0.95	0.62		
L/W	-0.26	-0.22	-0.83	-0.59	-0.74	-0.49	-0.54	

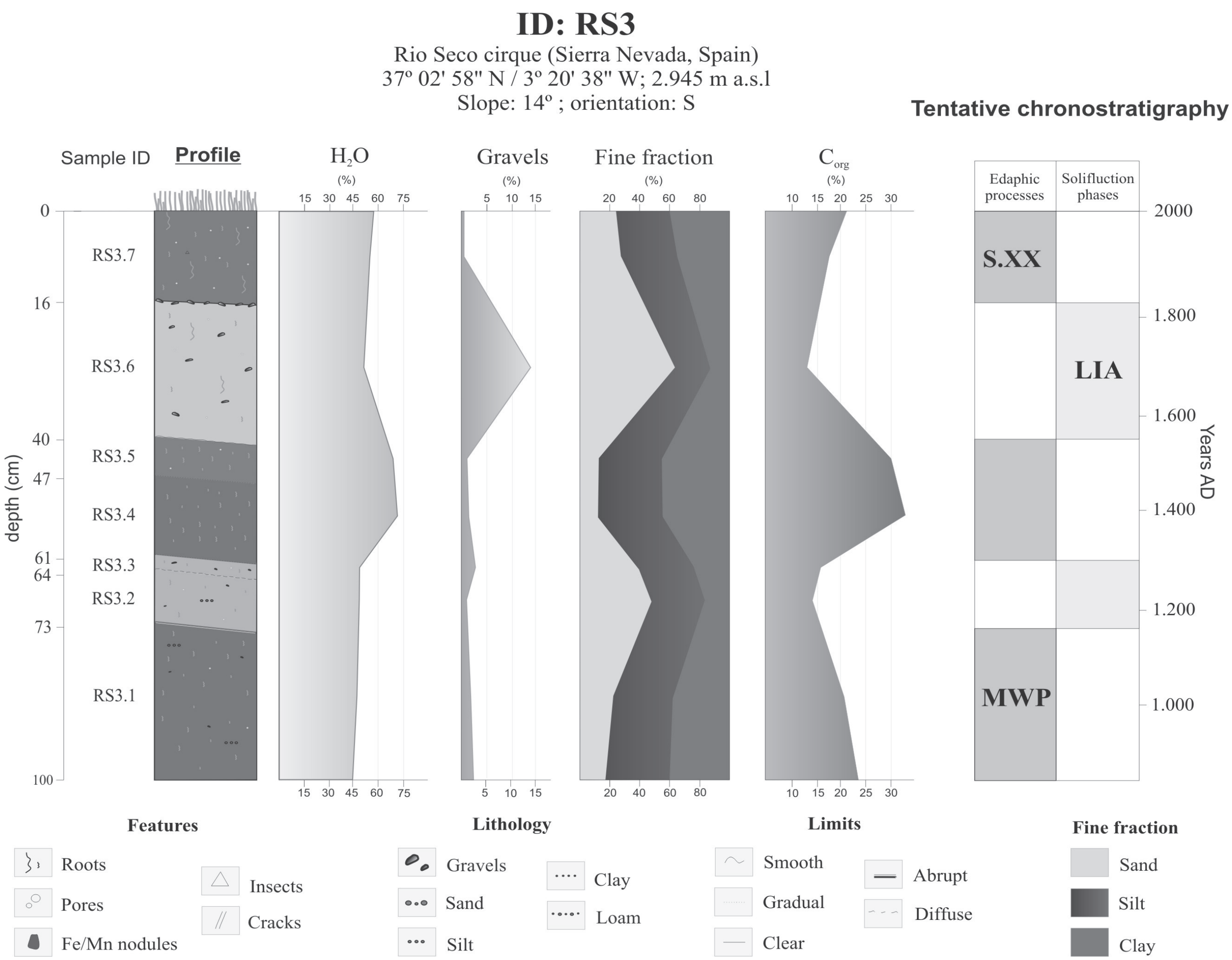

Figure 4. Lithostratigraphy and soil properties of a solifluction lobe of the Rio Seco cirque

southern Iberian Peninsula. Under the present climatic conditions, solifluction is mostly inactive, and only some lobes present small displacements. Thermal and topographic monitoring in the Rio Seco Valley showed that, despite a seasonal frozen layer of 70 cm thickness, solifluction processes were inactive. However, sedimentological studies on solifluction lobes indicate that during the Holocene, periods of increased solifluction processes (e.g., Little Ice Age) alternated with periods of geomorphic stability (e.g., Medieval Warm Period).

We assume that cooler periods in Sierra Nevada could promote solifluction, whereas warmer periods induce soil formation. Present climate may not be wet and/or cold enough to trigger important solifluction processes from 2500 to 3000 m altitude. Future radiocarbon dating will improve our solifluction chronostratigraphy and provide data to precisely identify the timing and environmental conditions of solifluction processes in the alpine belt of Sierra Nevada.

Acknowledgments

This research was financially supported by the Spanish Ministry of Education, project AP-2004-4548 and the Fluvalps-3000 Project (CGL2006-01111). Sedimentological analyses were undertaken at the laboratory of the Department of Geography, University of Berne.

References

Andersson, J.G. 1906. Solifluction, a component of subaerial denudation. *Journal of Geology* 14: 91-112.

Ballantyne, C.K. & Harris, C. 1994. *The Periglaciation of Great Britain.* Cambridge: Cambridge Univ. Press.

Chueca, J. & Julián, A. 1995. Cuantificaclón de movimientos en masa lentos en medios de montaña: Pirineo Central. *Lurralde* 18:173-196.

Esteban, A. 1994. *Evolución del paisaje durante los útimos 10.000 años en las montañas del Mediterráneo occidental: ejemplos del Pirineo Oriental y Sierra Nevada*. University of Barcelona, Master Thesis.

Gamper, M.V. 1983. Controls and rates of movement of solifluction lobes in the eastern Swiss Alps. *Proceedings of the Fourth International Permafrost Conference, Fairbanks, Alaska, July 18–22, 1983:* 328-333.

Gómez Ortiz, A., Palacios, D., Ramos, M., Tanarro, L.M. & Salvador Franch, F. 2001. Location of permafrost in marginal regions: Corral Del Veleta, Sierra Nevada, Spain. *Permafrost Periglac. Process.* 12(1): 92-110.

Gómez, A., Schulte, L., Salvador, F., Palacios, D., Sanz de Galdeano, C., Sanjosé, J.J., Tanarro, L.M. & Atkinson, A. 2005. Field trip to Sierra Nevada Massif Glacial Geomorphology and Present Cold Processes. *Sixth International Conference on Geomorphology. September 7–11, 2005 Zaragoza (Spain)*. Field trip guides, Vol. II: 309-354.

Grimalt, M. & Rodríguez, A. 1994. El modelado periglacial en Baleares. Estado de la cuestión. *Periglaciarismo en la Península Ibérica, Canarias y Baleares*. Servicio de Publicaciones Universidad Granada: 189-201.

Harris, C., Davies, M. & Coutard, J.P. 1997. Rates and processes of periglacial solifluction: an experimental approach. *Earth Surface Processes and Landforms* 22: 849–868.

Hugenholtz, C.H. & Lewkowicz, A.G. 2002. Morphometry and environmental characteristics of turf-banked solifluction lobes, Kluane Range, Yukon Territory, Canada. *Permafrost and Periglacial Processes* 13(4): 301-313.

Jaesche, P., Veit, H. & Huwe, B. 2003. Snow cover and soil moisture controls on solifluction in an area of seasonal frost, Eastern Alps. *Permafrost Periglac. Proces.* 14: 399-410.

Matsuoka, N. 2001. Solifluction rates, processes and landforms: a global review. *Earth-Science Reviews* 55: 107-134.

Matsuoka, N., Ikeda, A. & Date, T. 2005. Morphometric analysis of solifluction lobes and rock glaciers in the Swiss Alps. *Permafrost Periglac. Process* 16: 99-113.

Matthews, J.A., Seppälä, M. & Dresser P.Q. 2005. Holocene solifluction, climate variation and fire in a subartic landscape Al Pippokangas, Finnish Lapland based on radiocarbon-dated buried charcoal. *Journal of Quaternary Science* 20: 533-548.

Molero Mesa, J. & Pérez Raya, F. 1987. *La flora de Sierra Nevada*. Granada, Spain. University of Granada.

Palacios, D., Andrés, N. de, Luengo, E. 2003. Distribution and effectiveness of nivation in Mediterranean mountains: Peñalara (Spain). *Geomorphology* 54, 157-178.

Rapp, A. 1960. Recent development of mountain slopes in Kärkevagge and surroundings, Northern Scandinavia. *Geografiska Annaler* 42a: 65-200.

Rodrigo, F.S., Esteban-Parra, M.J., Pozo-Vázquez, D. & Castro-Diaz, Y. 1999. A 500-year precipitation record in Southern Spain. *International Journal of. Climatology* 19: 1233-1253.

Scheffer, F. & Schachtschabel, P. (2002). Lehrbuch der Bodenkunde. *Spektrum Akademischer Verlag*, 462 pp.

Schulte, L., 2002. Climatic and human influence on river systems and glacier fluctuations in southeast Spain. *Quaternary International* 93-94: 85-100.

Schulte, L., Marcos Garcia-Blanco, J. de, Gómez Ortiz, A, Palacios Estrema, D., Tanarro Garcia, M., Fernández Fernández, A. & Ramos Sainz, M. 2002. Evolución Glaciar y periglaciar del Circo del Mulhacén (Sierra Nevada, Península Ibérica). Publicaciones del Instituto Geológico y Minero de España. *Serie Geología* 1: 491-499.

Veit, H.. 1988. Fluviale und solifluidale morphodynamik des spät- und postglazials in einem zentralalpinen flusseinzugsgebiet (Südliche Hohe Tauern, Osttirol). *Bayreuther Geowissenschaftliche Arbeiten* 13:1-167.

Washburn, A. 1979. *Geocryology: a survey of periglacial processes and environments*. London: Arnold, 406 pp.

Cyanobacteria Within Cryptoendolithic Habitats: The Role of High pH in Biogenic Rock Weathering in the Canadian High Arctic

Christopher R. Omelon
Department of Geological Sciences, The University of Texas at Austin, Austin, Texas, USA
Wayne H. Pollard
Department of Geography, McGill University, Montréal, Québec, Canada
F. Grant Ferris
Department of Geology, University of Toronto, Toronto, Ontario, Canada
Philip C. Bennett
Department of Geological Sciences, The University of Texas at Austin, Austin, Texas, USA

Abstract

Cryptoendolithic microorganisms are widespread in the Canadian High Arctic and show differences in microbial community composition and pH conditions. Laboratory experiments measuring changes in pH and DIC of 15 strains of phototrophic microorganisms (both cyanobacteria and algae) representative of species found in High Arctic cryptoendolithic habitats show clear differences in their ability to generate high pH conditions and uptake HCO_3^- during photosynthesis. Surveys of cryptoendolithic habitats show that microorganisms capable of producing high pH conditions are found within sandstone outcrops that experience rapid exfoliative weathering under water-saturated conditions, suggesting that these microorganisms play a direct role in chemical erosion of the host rock. This is possibly the only known chemical weathering mechanism directly related to photosynthesizing microorganisms in terrestrial silicate rocks, and may have a profound impact on landscape evolution in polar desert environments such as the Canadian High Arctic.

Keywords: biogenic weathering; carbon concentrating mechanism; cyanobacteria; pH shifting; silica dissolution.

Introduction

The abundance and diversity of microorganisms in the subsurface reflect not only their ability to grow under a wide range of natural conditions, but also their capacity to harvest energy from light as well as organic and inorganic substrates. The complexity of these microbial communities depends upon the suitability of a given habitat for colonization, which in many cases exhibit extremes in physical and/or chemical conditions to effectively limit the number of species that can exist within any given ecological niche. An example of this natural selection is found in cryptoendolithic habitats, where microbial colonization is restricted to those organisms able to acquire the necessary resources for growth within the physical confines of pore spaces of rocks. Communities are normally found directly beneath the rock surface (Fig. 1) that consist of primary producers such as algae and/or cyanobacteria as well as consumers and decomposers, including fungi and heterotrophic bacteria (Friedmann et al. 1980, Friedmann et al. 1981, Friedmann 1982, Friedmann & Ocampo-Friedmann 1984, Hirsch et al. 1988, De La Torre et al. 2003, Selbmann et al. 2005, Omelon et al. 2007). They are found in both hot and cold deserts around the world (Friedmann et al. 1987, Bell 1993, Cockell et al. 2003, Bungartz et al. 2004, Omelon et al. 2006) and local areas in temperate regions where climatic extremes limit epilithic colonization (Bell et al. 1986, Ferris & Lowson 1997, Gerrath et al. 2000, Casamatta et al. 2002, Sigler et al. 2003).

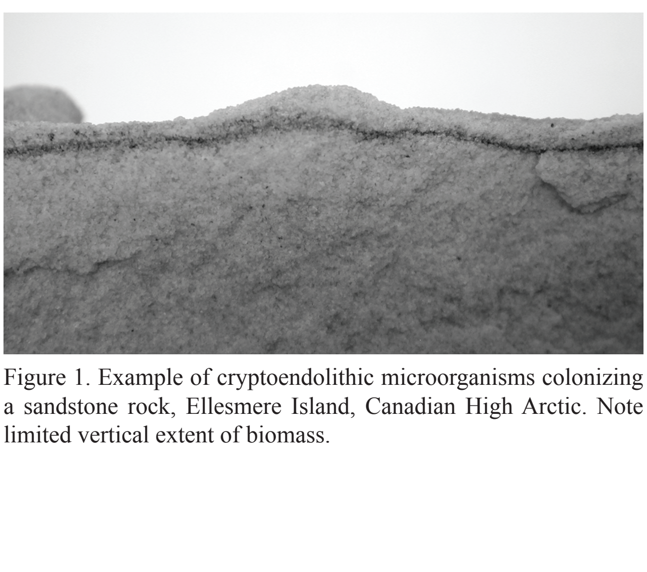

Figure 1. Example of cryptoendolithic microorganisms colonizing a sandstone rock, Ellesmere Island, Canadian High Arctic. Note limited vertical extent of biomass.

Location and site characteristics

Cryptoendolithic colonization of sandstone outcrops are found around Eureka, Ellesmere Island, Nunavut in the Canadian High Arctic (80°00′N, 85°55′W). Microbial communities show marked differences in composition and diversity despite similarities in microclimate, pore space availability, and host rock mineralogy (Omelon et al. 2006). More recently, Omelon et al. (2007) showed that cyanobacteria-dominated communities exist under higher pH conditions in contrast to communities dominated by fungi and algae that are characterized by lower pH conditions, suggesting that the activity of the dominant microorganism(s) controls the pH of the surrounding environment.

It is believed that differences in pH within these cryptoendolithic habitats control weathering rates of the

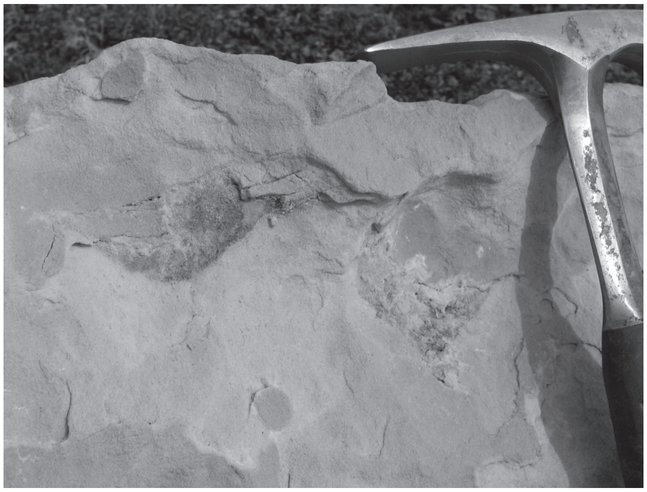

Figure 2. Exfoliative weathering of sandstone rock, with the detachment boundary occurring along the horizon of microbial colonization.

host rock (Omelon et al. 2007). Outcrops dominated by the cyanobacterial species *Leptolyngbya* sp. and *Gloeocapsa* sp. exhibit exfoliated rock weathering through flaking off of surface material, with the origin of detachment occurring along the colonized boundary (Fig. 2). This is in contrast to uncolonized sandstones and those dominated by algae and fungi, which do not exhibit these weathering patterns. This study attempts to relate these observations to cryptoendolithic microbial community structure by examining how microbial activity influences pH, and therefore how cyanobacteria and algae are involved in biogenic weathering of silicate rocks in this polar desert environment.

Biogenic weathering: background

The traditional view of biogenic weathering of sedimentary rocks links the solubilization of cementing minerals to the production of inorganic and organic acids by cryptoendolithic lichens (Friedmann 1982, Hirsch et al. 1995, Wierzchos & Ascaso 1996, Ascaso et al. 1998, Burford et al. 2003, Gaylarde & Gaylarde 2004). Decreasing pore water pH accelerates dissolution of primary silicates and increases solubility (Knauss & Wolery 1986, Knauss & Wolery 1988), while organic acids complex aluminum, and in some cases silica (Bennett & Siegel 1987, Bennett & Casey 1994, Stillings et al. 1996). The net result is the removal of both framework silicates and cements, with the mobilization of nutrients that benefit the microbial community (Bennett et al. 2001).

Bioalkalization

In contrast, cyanobacteria are not known to produce organic acids or acid pore water environments but rather may contribute to silicate dissolution via *bioalkalization* (Budel et al. 2004), whereby high pH conditions are generated in pore waters during cyanobacterial photosynthesis. As with acidic environments, high pH conditions also increase both quartz and feldspar solubility and dissolution kinetics (Brady & Walther 1989, Bennett 1991), resulting in accelerated mineral dissolution that leads to enhanced cycling of elements and nutrients within cryptoendolithic habitats (Johnston & Vestal 1989, Johnston & Vestal 1993, Ferris & Lowson 1997, Blum et al. 2002), and influences residence times of these microbial communities (Omelon et al. 2007).

Cyanobacteria have adapted to changes in temperatures and atmospheric CO_2 and O_2 levels over the past 2.5 billion years (Giordano et al. 2005), which enables them to survive under a wide range of environmental conditions (Badger et al. 2006). Most notable is the evolution of a carbon concentrating mechanism (CCM) to maintain high rates of CO_2 fixation for photosynthesis under conditions of low dissolved CO_2 concentrations (<15 µM) normally found in aquatic habitats (Kaplan & Reinhold 1999, Price et al. 2002, Badger & Price 2003).

The CCM consists of active transport systems to accumulate dissolved inorganic carbon (DIC) within the cell. Specifically, the CCM involves distinct modes of DIC uptake as either HCO_3^- or CO_2 by transporters (Omata et al. 1999, Shibata et al. 2001, Price et al. 2002, Price et al. 2004), to accumulate HCO_3^- within the cell for carbon fixation. A consequence of activation of HCO_3^- transporters for carbon fixation is the production of excess OH^- that is expelled from the cell, resulting in a high pH in the surrounding environment as shown in the equation:

$$HCO_3^- + H_2O \rightarrow (CH_2O) + O_2 + OH^- \quad (1)$$

In the case of silica-rich cryptoendolithic habitats, this mechanism can lead to accelerated weathering of the lithic substrate (Chou & Wollast 1985, Knauss & Wolery 1986, Knauss & Wolery 1988, Brady & Walther 1989, Budel et al. 2004). Observations of pH values >9 in cultures of cyanobacteria from High Arctic cryptoendolithic habitats suggest that these microorganisms use HCO_3^- transporters and are therefore capable of bioalkalization.

Materials and Methods

Cyanobacterial and algal species

Experiments were conducted on a total of 15 species of phototrophic microorganisms; these include 2 species cultured from field samples as well as cultures obtained from the Culture Collection of Algae at the University of Texas at Austin (Table 1) that correspond to the same genus' as those found in the High Arctic cryptoendolithic habitats as described by Omelon et al. (2007). Despite the fact that many algae and cyanobacteria are cosmopolitan in nature, an attempt was made to select cultures from similar habitats (i.e., cold and/or desert conditions) as these species may have adapted their mode of DIC uptake to specific climate and/or microenvironmental conditions. Species were cultured in designated liquid media, aerated with normal air and continuously illuminated at ~60 µmol·m^{-2}·s^{-1} at 20°C.

Table 1. Phototrophic microorganisms (cyanobacteria and algae) used for pH drift and DIC experiments. Field samples in bold.

Taxa	Origin
Cyanobacteria	
***Leptolyngbya* sp.**	**Ellesmere Island, Canada**
Gloeocapsa sp.	N/A
Synechococcus sp.	Atacama Desert, Chile
Aphanothece sp.	Great Salt Plains, Oklahoma, USA
Leptolyngbya sp.	Great Salt Plains, Oklahoma, USA
Eukaryotic Algae	
***Cladophorella* sp.**	**Ellesmere Island, Canada**
Stichococcus sp.	Battleship Promontory, Antarctica
Chlorella antarctica	Antarctica
Chlorosarcinopsis negevensis	Negev Desert, Israel
Bracteacoccus minor var. desertorum	Negev Desert, Israel
Chlorococcum aegyptiacum	El Tahir, Egypt
Botrydiopsis alpina	Unterengadin, Switzerland
Cladophora kosterae	Jarden des Plantes, Paris, France
Tetracystis sp.	Ganzu, Wuwei City, China
Chroococcus turgidus	Bloomington Indiana, USA

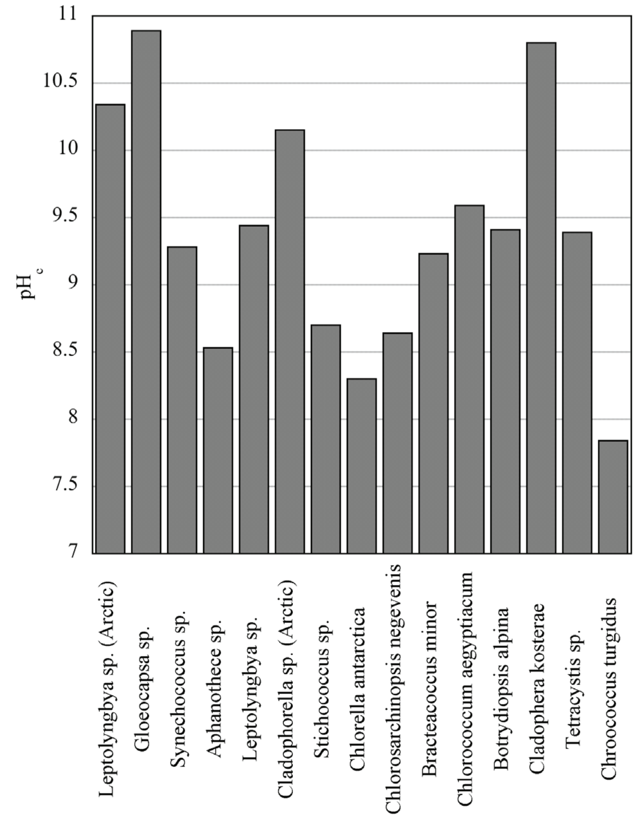

Figure 3. pH compensation points for 15 phototrophic microorganisms. Cultures were incubated at 100 µmol·m^{-2}·s^{-1} and 20°C; pH was monitored until values stabilized.

pH drift experiments

Experimental liquid medium contained 0.25 mmol $CaCl_2$, 0.15 mmol $MgSO_4$, 1 mmol NaCl, 50 µmol KCl, and 1 mmol $NaHCO_3$. Cells were harvested and washed three times in experimental medium by centrifugation at 1000 g for 5 minutes to remove culture media, resuspended in 30 ml of experimental medium in 50 ml Erlynmeyer flasks double-sealed with Parafilm, and incubated at 20°C under saturated photosynthesis light levels (~100 µmol·m^{-2}·s^{-1}) and constant stirring. The pH of the medium was measured periodically, concurrent with the removal of 1 ml subsamples for DIC measurements that were analyzed using a Dohrmann DC-180 carbon analyzer. Experiments were monitored until pH values stabilized, which corresponded to only small changes in DIC concentrations.

Results and Discussion

pH drift

In all cases, the pH of the solution increased from initial pH values (~7–8) as a result of microbial uptake of CO_2 or HCO_3^- for photosynthesis until the pH compensation point (pH_c) was reached, normally within 24 hours of initiation of experiments (Fig. 3). The highest pH_c value recorded was 10.89 by the coccoid cyanobacteria *Gloeocapsa* sp., followed by a pH_c of 10.80 by the filamentous alga *Chladophera kosterae*; similarly high pH_c values were associated with High Arctic cryptoendolithic filamentous cyanobacterial and algal species *Leptolyngbya* sp. (10.34) and *Cladopherella* sp. (10.02). Six species produced pH_c values ranging between 9–10 (two cyanobacteria, four algae), with the remaining five species (one cyanobacteria, four algae) reaching pH_c values <9 that rose only slightly from initial pH values.

DIC measurements

As with pH, uptake of HCO_3^- or CO_2 led to decreases in DIC concentrations in all samples (Fig. 4), with the same species that generated high pH_c values removing the largest amount of available DIC. Uptake by *Gloeocapsa* sp. was the most dramatic, with the removal of 98.9% of DIC, followed by *Cladophera kosterae* (80.2%), the High Arctic *Leptolyngbya* sp. (66.0%), and the High Arctic *Cladopherella* sp. (60.1%). The remaining species removed less that 50% of available DIC from the experimental solution.

A pH_c >9 is the suggested lower limit for activation of a CCM (Kevekordes et al. 2006), however a more definitive value may be a pH of 10, as the concentration of CO_2*(aq)* at this level is <0.06% of total DIC (Banares-Espana et al. 2006) and suggests the use of HCO_3^- transporters over CO_2 transporters.

Based on these guidelines, all species in the current study are able to activate a CCM and therefore utilize HCO_3^- during photosynthesis. *Gloeocapsa* sp., *Cladophera kosterae*, *Leptolyngbya* sp. and *Cladopherella* sp. were the most efficient at removing HCO_3^- from solution with concurrent generation of high pH conditions; in all cases, changes in pH and DIC concentrations occurred within 24 hours. In contrast, the remaining species showed initial increases in pH corresponding to uptake of CO_2 followed by slow changes in pH and lower final pH_c values, suggesting these microorganisms are less efficient in their ability to uptake HCO_3^-.

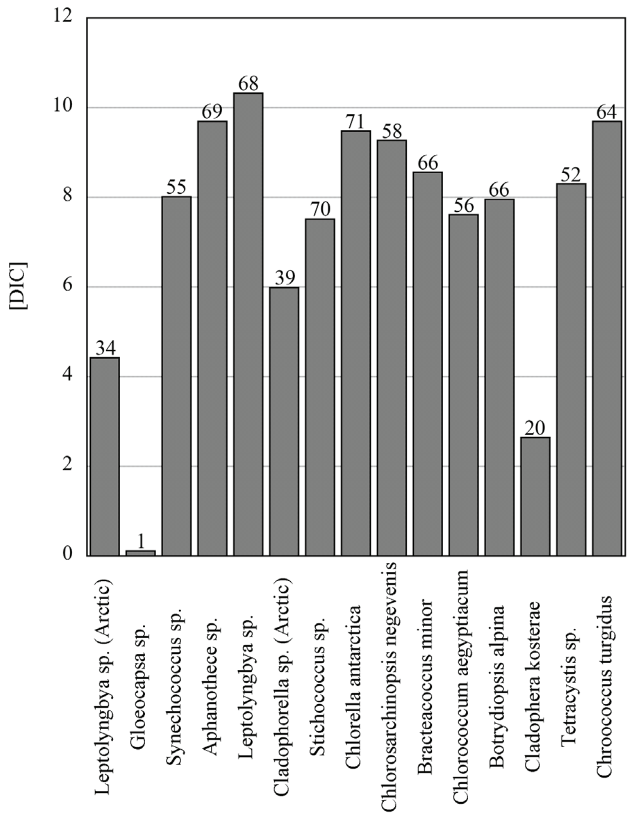

Figure 4. DIC concentrations remaining for 15 phototrophic microorganisms. Cultures were incubated at 100 μmol·m^{-2}·s^{-1} and 20°C; DIC was measured until no further changes occurred. Numbers above columns represent % DIC remaining.

A comparison of these results to the microbial survey of cryptoendolithic communities around Eureka, Nunavut (Omelon et al. 2007) shows that the dominant microorganisms found at sites with high rates of weathering through exfoliation of the overlying rock surface (*Leptolyngbya* sp. and *Gloeocapsa* sp., and to a lesser extent *Cladophorella* sp.) are the same microorganisms capable of producing high pH conditions in laboratory experiments. In contrast, sites with the lowest measured pH values in the field were populated by microorganisms that produced pH_c values <10 (*Chlorella antarctica*, *Bracteacoccus minor var. desertorum*) as well as limited removal of DIC in the current study, suggesting that these microorganisms do not readily uptake HCO_3^- for photosynthesis through a CCM. Although the majority of microorganisms used in this study were not cultured directly from cryptoendolithic habitats in the Canadian High Arctic, many of these microorganisms are widely distributed in nature and likely possess similar physiological traits, such as the presence or absence of a CCM. It is interesting to note, however, differences in pH_c and DIC uptake between the two *Leptolyngbya* spp., suggesting that microorganisms may evolve to adapt to conditions within their specific environment.

Silicate weathering in the cryptoendolithic environment

Although high pH conditions can be generated in aquatic habitats where cyanobacteria and algae consume all available $CO_2(aq)$ and must therefore use HCO_3^- for photosynthesis, there is little knowledge or understanding of the impact of high pH-generated conditions in terrestrial habitats. The data presented here provides information that, when coupled with an understanding of microenvironmental conditions within cryptoendolithic habitats, can explain observations of exfoliative weathering of rocks colonized by microorganisms generating high pH conditions. Previous work by Omelon et al. (2006) showed that High Arctic cryptoendolithic habitats experience warmer temperatures and wetter conditions than the exposed outcrop surface. Temperatures can reach up to 30°C within the cryptoendolithic habitat and were found to exceed 10°C and 20°C for substantial periods of time (753 and 93 h·yr^{-1}, respectively) during summer months, which is likely correlated to substantial net growth in these environments (Omelon et al. 2006). Furthermore, evidence of water infiltration into the subsurface resulting from rainfall or snowmelt and subsequent retention of this moisture in pore spaces leads to increased rates of photosynthesis due to increased light penetration and continuous irridation. The combination of these microenvironmental conditions generates elevated pH within pore waters, whereby rates of OH^- production by cyanobacteria and algae with an effective CCM exceeds rates of diffusion of $CO_2(g)$ into the water-saturated microenvironment. These high pH conditions greatly enhance silicate and quartz dissolution rates—for example, at pH 9.8, the solubility of quartz doubles, and at pH 10.8 it is almost five times the solubility at pH 7—resulting in the solubilization of the rock matrix near these photosynthesizing organisms. In contrast, sites dominated by microorganisms that do not produce high pH conditions experience increased rates of photosynthesis but with apparently negligible production of OH^-.

The sporadic nature of this rock exfoliation highlights the fact that generation of high pH conditions within these habitats requires the presence of liquid water that effectively limits CO_2 diffusion from the atmosphere, thereby requiring activation of microbial CCMs. Given the low number of precipitation events that occur in this region of the Canadian High Arctic, rapid solubilization of intergranular silica-rich cements is restricted to those periods of moisture infiltration into the subsurface. In contrast, during periods of arid conditions, all photosynthesizing microorganisms uptake atmospheric CO_2, resulting in little change in pH in the cryptoendolithic environment.

Direct evidence for silica dissolution through bioalkalization has been found in preliminary ESEM observations of etch pits on quartz grain surfaces overlain by cyanobacterial communities. Further documentation of such features will provide additional evidence for chemical weathering of silica-rich intergranular cements through the generation of high pH conditions by these microorganisms, and will be of interest to studies focusing on mechanisms that lead to the creation of terrestrial biosignatures.

Conclusions

The global ubiquity of cyanobacteria and algae in cryptoendolithic habitats and the generation of high pH conditions by those microorganisms with efficient CCMs suggests that bioalkalization could play a fundamental role in the chemical weathering of silica minerals (Schwartzman & Volk 1989). In addition, this pH shift has important implications for porosity development, release of essential nutrients, and mobilization of metals under high pH conditions. Understanding the biogeochemical dynamics of cryptoendolithic microorganisms is an important step towards a broader understanding of how phototrophic microorganisms control silica dissolution in terrestrial landscapes.

Acknowledgments

The authors wish to thank Canada's Atmospheric Environment Service and the Polar Continental Shelf Project for lodging and logistical support during field seasons. This work is supported by the Jackson School of Geosciences at the University of Texas at Austin, the Natural Sciences and Engineering Research Council of Canada, and the Canadian Space Agency. We sincerely thank the staff of the Eureka Weather Station for their dedicated field support, and Lisa Nguyen of UT Austin's Culture Collection of Algae for laboratory assistance.

References

Ascaso, C., Wierzchos, J. & Castello, R. 1998. Study of the biogenic weathering of calcareous litharenite stones caused by lichen and endolithic microorganisms. International *Biodeterioration and Biodegradation* 42: 29-38.

Badger, M.A., Price, G.D., Long, B.M. & Woodger, F.J. 2006. The environmental plasticity and ecological genomics of the cyanobacterial CO_2 concentrating mechanism. *Journal of Experimental Botany* 57: 249-265.

Badger, M.R. & Price, G.D. 2003. CO_2 concentrating mechanisms in cyanobacteria: molecular components, their diversity and evolution. *Journal of Experimental Botany* 54: 609-622.

Banares-Espana, E., Lopez-Rodas, V., Salgado, C., Costas, E. & Flores-Moya, A. 2006. Inter-strain variability in the photosynthetic use of inorganic carbon, exemplified by the pH compensation point, in the cyanobacterium *Microcystis aeruginosa*. *Aquatic Botany* 85: 159-162.

Bell, R.A. 1993. Cryptoendolithic algae of hot semiarid lands and deserts. *Journal of Phycology* 29: 133-139.

Bell, R.A., Athey, P.V. & Sommerfeld, M.R. 1986. Cryptoendolithic algal communities of the Colorado plateau. *Journal of Phycology* 22: 429-435.

Bennett, P.C. 1991. The dissolution of quartz in organic-rich aqueous systems. *Geochimica et Cosmochimica Acta* 55: 1781-1797.

Bennett, P.C. & Casey, W.H. 1994. Organic acids and the dissolution of silicates. In: E.D. Pittman & M. Lewan (eds.), *The Role of Organic Acids in Geological Processes*. Springer-Verlag.

Bennett, P.C., Rogers, J.R., Hiebert, F.K. & Choi, W.J. 2001. Silicates, silicate weathering, and microbial ecology. *Geomicrobiology Journal* 18: 3-19.

Bennett, P.C. & Siegel, D.I. 1987. Increased solubility of quartz in water due to complexation by dissolved organic compounds. *Nature* 326: 684-687.

Blum, J.D., Klaue, A., Nezat, C.A., Driscoll, C.T., Johnson, C.E., Siccama, T.G., Eagar, C., Fahey, T.J. & Likens, G.E. 2002. Mycorrhizal weathering of apatite as an important calcium source in base-poor forest ecosystems. *Nature* 417: 729-731.

Brady, P.V. & Walther, J.V. 1989. Controls on silicate dissolution rates in neutral and basic pH solutions at 25 C. *Geochimica et Cosmochimica Acta* 53: 2823-2830.

Budel, B., Weber, B., Kuhl, M., Pfanz, H., Sultemeyer, D. & Wessels, D. 2004. Reshaping of sandstone surfaces by cryptoendolithic cyanobacteria: bioalkalization causes chemical weathering in arid landscapes. *Geobiology* 2: 261-268.

Bungartz, F., Garvie, L.A.J. & Nash III, T.H. 2004. Anatomy of the endolithic Sonoran Desert lichen *Verrucaria rubrocincta* Breuss: implications for biodeterioration and biomineralization. *The Lichenologist* 36: 55-73.

Burford, E.P., Fomina, M. & Gadd, G.M. 2003. Fungal involvement in bioweathering and biotransformation of rocks and minerals. *Mineralogical Magazine* 67: 1127-1155.

Casamatta, D.A., Verb, R.G., Beaver, J.R. & Vis, M.L. 2002. An investigation of the cryptobiotic community from sandstone cliffs in southeast Ohio. *International Journal of Plant Science* 163: 837-845.

Chou, L. & Wollast, R. 1985. Steady-state kinetics and dissolution mechanisms of albite. *Amer. J. Sci.* 285: 963-993.

Cockell, C.S., McKay, C.P. & Omelon, C. 2003. Polar endoliths - an anti-correlation of climate extremes and microbial diversity. *International Journal of Astrobiology* 1: 305-310.

de la Torre, J.R., Goebel, B.M., Friedmann, E.I. & Pace, N.R. 2003. Microbial diversity of cryptoendolithic communities from the McMurdo Dry Valleys, Antarctica. *Applied and Environmental Microbiology* 69: 3858-3867.

Ferris, F.G. & Lowson, E.A. 1997. Ultrastructure and geochemistry of endolithic microorganisms in limestone of the Niagara Escarpment. *Canadian Journal of Microbiology* 43: 211-219.

Friedmann, E.I. 1982. Endolithic microorganisms in the Antarctic cold desert. *Science* 215: 1045-1053.

Friedmann, E.I., Friedmann, R.O. & McKay, C.P., 1981. Adaptations of cryptoendolithic lichens in the Antarctic desert. In: P. Jouventin, L. Masse &

P. Trehen (eds.), *Colloque sur les Ecosystemes Subantarctiques*. Paris: Comite National Francais des Recherches Antarctiques.

Friedmann, E.I., Kappen, L. & Garty, J. 1980. Fertile stages of cryptoendolithic lichens in the dry valleys of Southern Victoria Land. *Antarctic Journal of the United States* 15: 166-167.

Friedmann, E.I., McKay, C.P. & Nienow, J.A. 1987. The cryptoendolithic microbial environment in the Ross Desert of Antarctica: satellite-transmitted continuous nanoclimate data, 1984 to 1986. *Polar Biology* 7: 273-287.

Friedmann, E.I. & Ocampo-Friedmann, R. 1984. Endolithic microorganisms in extreme dry environments: Analysis of a lithobiontic habitat. In: M.J. Klug & C.A. Reddy (eds.), *Current Perspectives in Microbiology.* Washington, DC: American Society of Microbiology.

Gaylarde, P. & Gaylarde, C. 2004. Deterioration of siliceous stone monuments in Latin America: Microorganisms and mechanisms. *Corrosion Reviews* 22: 395-415.

Gerrath, J.F., Gerrath, J.A., Matthes, U. & Larson, D.W. 2000. Endolithic algae and cyanobacteria from cliffs of the Niagara Escarpment, Ontario, Canada. Canadian *Journal of Botany-Revue Canadienne De Botanique* 78: 807-815.

Giordano, M., Beardall, J. & Raven, J.A. 2005. CO_2 concentrating mechanisms in algae: mechanisms, environmental modulation, and evolution. *Annual Reviews of Plant Biology* 56: 99-131.

Hirsch, P., Eckhardt, F.E. W. & Palmer, R.J. 1995. Fungi active in weathering of rock and stone monuments. *Canadian Journal of Botany-Revue Canadienne De Botanique* 73: S1384-S1390.

Hirsch, P., Hoffmann, B., Gallikowski, C.C., Mevs, U., Siebert, J. & Sittig, M. 1988. Diversity and identification of heterotrophs from Antarctic rocks of the McMurdo Dry Valleys (Ross Desert). *Polarforschung* 58: 261-269.

Johnston, C.G. & Vestal, J.R. 1989. Distribution of inorganic species in two Antarctic cryptoendolithic microbial communities. *Geomicrobiology Journal* 7: 137-153.

Johnston, C.G. & Vestal, J.R. 1993. Biogeochemistry of oxalate in the Antarctic cryptoendolithic lichen-dominated community. *Microbial Ecology* 25: 305-319.

Kaplan, A. & Reinhold, L. 1999. CO_2 concentrating mechanisms in photosynthetic microorganisms. *Annual Rev. Plant Physiol. Plant Mol. Biol.* 50: 539-570.

Kevekordes, K., Holland, D., Haubner, N., Jenkins, S., Koss, R., Roberts, S., Raven, J.A., Scrimgeour, C. M., Shelly, K., Stojkovic, S. & Beardall, J. 2006. Inorganic carbon acquisiton by eight species of *Caulerpa* (Caulerpaceae, Chlorophyta). *Phycologia* 45: 442-449.

Knauss, K.G. & Wolery, T.J. 1986. Dependence of albite dissolution kinetics on pH and time at 25°C and 70°C. *Geochim. Cosmochim. Acta* 50: 2481-2497.

Knauss, K.G. & Wolery, T.J. 1988. The dissolution kinetics of quartz as a function of pH and time at 70°C. *Geochimica et Cosmochimica Acta* 52: 43-53.

Omata, T., Price, G.D., Badger, M.R., Okamura, M., Gohta, S. & Ogawa, T. 1999. Identification of an ATP-binding cassette transporter involved in bicarbonate uptake in the cyanobacterium *Synechococcus* sp. strain PCC 7942. *Proceedings of the National Academy of Sciences of the United States of America* 96: 13571-13576.

Omelon, C.R., Pollard, W.H. & Ferris, F.G. 2006. Environmental controls on microbial colonization of High Arctic cryptoendolithic habitats. *Polar Biology* 30: 19-29.

Omelon, C.R., Pollard, W.H. & Ferris, F.G. 2007. Inorganic species distribution and microbial diversity within High Arctic cryptoendolithic habitats. *Microbial Ecology.*

Price, G.D., Maeda, S.-i., Omata, T. & Badger, M.A. 2002. Modes of active inorganic carbon uptake in the cyanobacterium, *Synechococcus* sp. PCC7942. *Functional Plant Biology* 29: 131-149.

Price, G.D., Woodger, F.J., Badger, M.A., Howitt, S.M. & Tucker, L. 2004. Identification of a SulP-type bicarbonate transporter in marine cyanobacteria. *PNAS* 101: 18228-18233.

Schwartzman, D.W. & Volk, T. 1989. Biotic enhancement of weathering and the habitability of Earth. *Nature* 340: 457-460.

Selbmann, L., de Hoog, G.S., Mazzagalia, A., Friedman, E. I. & Onofri, S. 2005. Fungi at the edge of life: cryptoendolithic black fungi from Antarctic desert. *Studies in Mycology* 51: 1-32.

Shibata, M., Ohkawa, H., Kaneko, T., Fukuzawa, H., Tabata, S., Kaplan, A. & Ogawa, T. 2001. Distinct constitutive and low-CO_2-induced CO_2 uptake systems in cyanobacteria: genes involved and their phylogenetic relationship with homologous genes in other organisms. *PNAS* 98: 11789-11794.

Sigler, W.V., Bachofen, R. & Zeyer, J. 2003. Molecular characterization of endolithic cyanobacteria inhabiting exposed dolomite in central Switzerland. *Environmental Microbiology* 5: 618-627.

Stillings, L.L., Drever, J.I., Brantley, S.L., Sun, Y. & Oxburgh, R. 1996. Rates of feldspar dissolution at pH 3-7 with 0-8 mM oxalic acid. *Chemical Geology* 132: 79-90.

Wierzchos, J. & Ascaso, C. 1996. Morphological and chemical features of bioweathered granitic biotite induced by lichen activity. *Clays and Clay Minerals* 44: 652-657.

—Plenary Paper—

Thermal State of Permafrost in Alaska During the Fourth Quarter of the Twentieth Century

T. E. Osterkamp
Geophysical Institute, University of Alaska, Fairbanks, Alaska, U.S.A.

Abstract

Permafrost temperatures in Alaska increased during the fourth quarter of the twentieth century at sites north of the Brooks Range from the Chukchi Sea to Canada, south along a transect from Prudhoe Bay to Gulkana, and at other sites. Tentative results are presented concerning the characteristics of the warming. Meteorological records, permafrost temperature measurements, thermokarst studies, and modeling efforts suggest the warming occurred statewide. Its magnitude along the transect was 3 to 4°C for the Arctic Coastal Plain, 1 to 2°C for the Brooks Range, and 0.3 to 1°C south of the Yukon River. The warming was seasonal, primarily in winter. Active layer thicknesses on the Arctic Coastal Plain did not increase. Thawing at the permafrost surface and base is occurring and new thermokarst terrain has developed. Probable causes of the warming and thawing include changes in air temperatures, snow cover effects, and combinations of these.

Keywords: borehole temperatures; climate warming; permafrost; thermokarst

Introduction

Air temperatures in Alaska warmed from the late 1800s until near the end of the second quarter of the twentieth century (Hansen & Lebedev 1987). There was a cooling during the third quarter and, in the permafrost regions of Alaska, a step-like increase in air temperatures during the fourth quarter (1976/1977, Hartmann and Wendler 2003). This warming peaked in the early 1980s and was followed by decreased air temperatures into the mid-1980s. Temperature trends from the late 1970s to the end of the 20th century were sometimes warmer although many sites had little or no warming or a cooling. From the cooler mid-1980s to the end of the century, most sites showed a warming trend. The first 6 years of the 21st century have been consistently warm, typically about the same as the period around 1980. Snow covers were generally thick during the third quarter and relatively thin during the early 1980s. Snow cover thicknesses during the 1990s were typically much greater than during the 1980s. The recent warming may be the continuation of the long term warming or a new unrelated warming event.

The thermal state of Alaskan permafrost has responded to these climatic changes and perhaps to other factors. It appears there were two permafrost warming events; a long-term warming that was initiated in the early 1900s and a recent warming (since 1976/1977).

Past international conferences on permafrost have examined climate-permafrost interactions and have documented permafrost warming in Alaska. This paper reiterates, updates, and extends reviews of the thermal state of permafrost in Alaska by the U.S. Geological Survey and University of Alaska (Lachenbruch et al. 1982, Lachenbruch & Marshall 1986, Osterkamp et al. 1984, 1987, Lachenbruch et al. 1988, Clow et.al 1991, Lachenbruch 1994, Osterkamp & Romanovsky 1999, Romanovsky et al. 2003, Osterkamp 1983, 2003a, b, 2005, & 2007a, b). The data used herein are from the U.S. Geological Survey studies (Lachenbruch & Marshall 1986, Clow & Urban 2002) and the University of Alaska studies (Fig.1). (See Osterkamp (2003b) for methods and site information.) The paper is primarily concerned with the characteristics, impacts, and causes of permafrost warming during the last quarter of the twentieth century and attempts to provide at least tentative answers to questions regarding this warming. The effort is hampered by the lack of data even in the northwest and along a north-south transect of Alaska where most of the data are concentrated. This makes it difficult to arrive at definitive conclusions about the thermal state of the permafrost. However a better understanding of permafrost conditions is emerging from efforts that combine modeling, weather data, and thermokarst studies with temperature measurements.

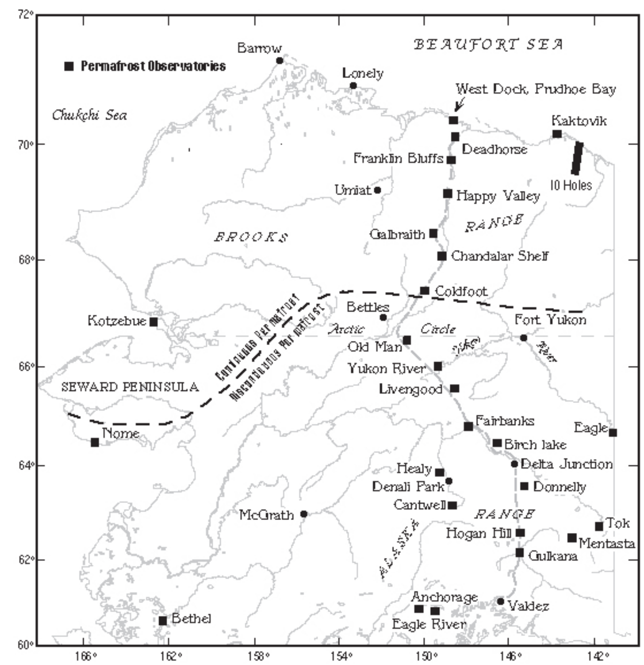

Figure 1. Location of the Alaskan transect and other sites. USGS sites are primarily in northwest Alaska.

Review and Discussion

Effects of climate on permafrost

The effects of climate (here the averaged weather, primarily air temperature and precipitation) on permafrost are difficult to determine because of sparse data and a multitude of non-climatic factors that can influence the thermal state of permafrost. These factors include terrain (topography, slope, aspect, geomorphology), hydrology (surface drainage, site wetness, proximity of nearby water bodies, presence of underground water), vegetation (succession, insulation, insolation, snow interception), geology (type of soil and rock, tectonic setting and geothermal heat flow), and disturbances (human, animal, fire, and flooding events) (Osterkamp & Jorgenson, in press). The factors operate at different time scales (days to millennia) and spatial scales (local to continental). The effects of changes in some of them (e.g., geomorphology, vegetation (succession), disturbances) have the potential for being mistaken for changes in climate as do other related factors (e.g., rapid sedimentation at the ground surface, three dimensional heat flow, and vertical variations in thermal conductivity).

The permafrost surface is separated from effects of air temperatures and other climatic factors by vegetation, snow cover in winter, and an active layer that freezes and thaws annually. Heat and mass transport processes, including coupled and advective processes, and phase change in these materials influence the surface temperature of the permafrost (Outcalt et al. 1975, Goodrich 1982, Smith & Riseborough 1983, Lachenbruch 1994, Zhang et al. 1996, 1997). There are also intricate thermal feedback effects such as the effects of air temperature and moisture on vegetation, the ensuing effects of vegetation and wind on snow cover, and the effects of the resulting snow cover on permafrost surface temperatures. Consequently, the relationships between climate and permafrost surface temperature are exceedingly complex. Even the case of air temperature is not straightforward. Warming of annual mean air temperatures can be a result of a general change in all seasons or seasonal changes such as warmer or longer summers (defined here as the period when the ground is snow free) or warmer or shorter winters (when snow is on the ground). Since winters are longer than summers in permafrost areas, cooler summer temperatures can be offset by warmer winter temperatures resulting in a net warming.

The net result of a snow cover is that it increases mean annual ground surface temperatures. The magnitude of the warming depends on the timing and duration of the snow cover, its accumulation (thickness) and melting history, and the effects of macrostructure (wind slab, depth hoar) on its properties (Goodrich 1982, Goodwin et al. 1983, Zhang et al. 1996, Zhang 2005). Interactions of wind, microrelief, and vegetation with the snow cover also influence the surface temperature of permafrost (Zhang et al. 1997).

The above considerations suggest that, when permafrost warms, the warming cannot be automatically attributed to increasing air temperatures and/or the effects of changes in snow cover thickness. Nevertheless, modeling studies confirm the primary role of air temperatures and the effects of changes in snow cover on the surface temperature of permafrost (Outcalt 1975, Goodrich 1982). Applications of models to field conditions show that, using measured daily air temperatures and snow cover thicknesses as input data to drive calibrated site specific conductive numerical models that include phase change and use realistic thermal parameters taking into account site conditions (wetness and others), typically produces remarkable agreement between calculated and measured active layer and permafrost temperatures (Zhang et al. 1997, Osterkamp & Romanovsky 1997, Osterkamp and Romanovsky, 1999; Romanovsky and Osterkamp 2000). While mass transport, advective, and coupled processes are known to occur in the snow cover, vegetative mat, and active layer, they appear to be of secondary importance in influencing long-term permafrost surface temperatures except in certain settings. The reasons for this are not known but may include cancellation of effects, shortness of their duration, and others.

Characteristics of the warming

For the long-term event, temperature profiles in deep boreholes generally indicate an increase at the permafrost surface of 2 to 4°C in northwest Alaska. Warming did not begin synchronously at all sites, not all sites showed a warming, and the results were not readily contourable (Lachenbruch & Marshall 1986, Lachenbruch et al. 1988, Clow et al. 1991).

For the recent warming during the last quarter of the twentieth century, observations show that permafrost in warmed north of the Brooks Range from the Chukchi Sea Coast to the Alaska-Canada border, south along a transect from Prudhoe Bay to Gulkana and up to 300 km from the transect (Fig. 1, Clow & Urban 2002, Osterkamp 2003a, 2005, 2007a, Osterkamp & Jorgenson 2005). Borehole temperatures at Prudhoe Bay (Fig. 2), thermokarst observations, basal thawing measurements, and modeling investigations elsewhere suggest that permafrost temperatures increased statewide coincident with the increase in air temperatures that began in 1976/1977 in Alaska (Osterkamp 2007a). The initial permafrost warming peaked in the early 1980s and then cooled into the mid-1980s. Arctic sites began warming again about 1986 and Interior sites about 1988 (Fig. 2). The timing of this warming was somewhat later in the western Arctic (Chukchi Sea to the Colville River), not long before 1989 (Clow, personal communication, 2006). Warming generally continued through the 1990s although some sites leveled off or cooled near the end of the century while some continued to warm. The magnitude of the total warming at the permafrost surface through 2003 falls into three latitudinal groups; an average of 3°C for the western Arctic and a range of 3 to 4°C for the Arctic Coastal Plain near Prudhoe Bay, 1 to 2°C along the transect through the Brooks Range including its northern and southern foothills, and 0.3 to 1°C south of the Yukon River (Osterkamp 2005). On the Arctic Coastal Plain, the magnitude of the recent warming is comparable to that of the long term warming but it occurred over a much shorter time period.

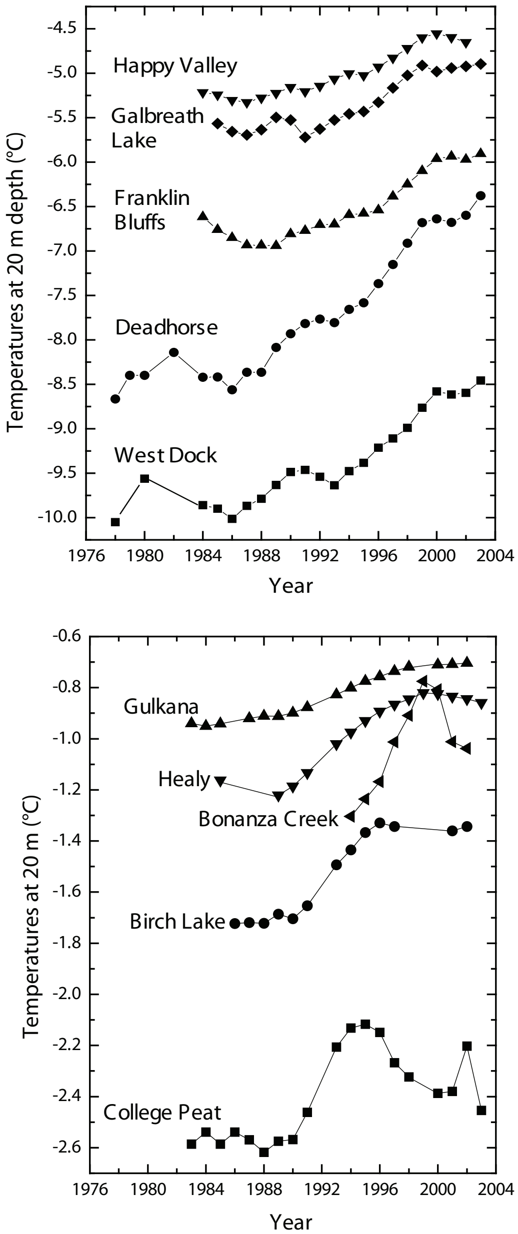

Figure 2. Temperatures (20 m depth) for selected sites.

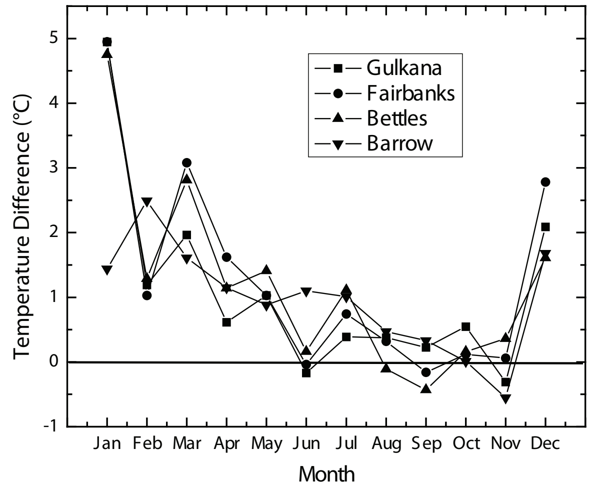

Figure 3. Increases in mean monthly air temperatures for the period after (1977-1996) compared to before (1957-1976) the recent warming.

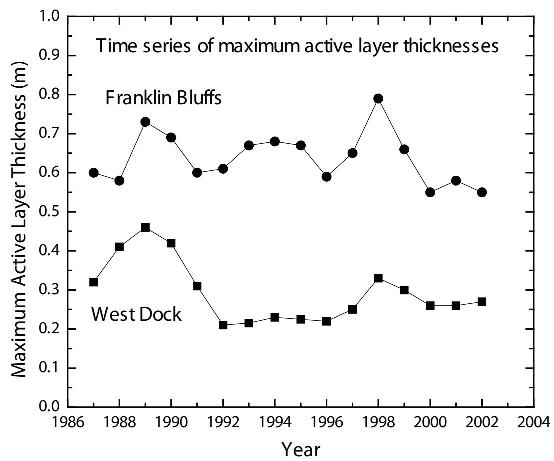

Figure 4. Time series of maximum active layer thicknesses for two sites on the Arctic Coastal Plain.

Measurements show that permafrost warmed north of Kotzebue, near Cantwell, and at Eagle River; sites that are 300 km or more from the transect (Osterkamp 2007a). These observations from widely separated areas coupled with weather data and other observations suggest that the scenario developed above for northern Alaska and the transect may also hold, with some differences in timing and magnitude, in other permafrost areas in the state (Osterkamp 2007a). However, some sites cooled over the same period and a site near Eagle had not warmed by 1994 indicating that there may be other areas that are exceptions to the warming.

The regime shift that occurred in 1976/1977 was seasonal, characterized by increased air temperatures for mid to late winter months (Hartmann & Wendler 2003). There was little change in summer and early winter air temperatures (Fig. 3). This seasonality also occurred in permafrost surface temperatures at the Deadhorse and Franklin Bluffs sites. Again, the general nature of the warming (Fig. 3) suggests a similar statewide seasonality for the permafrost warming with possible exceptions (Osterkamp 2005).

While the permafrost warmed 3 to 4°C, maximum active layer thicknesses at nearby sites on the Arctic Coastal Plain did not show increasing trends from 1987 to 2002 (Fig. 4, Osterkamp 2005). This is a direct result of the observed seasonality in air temperatures. Since the warming occurred primarily in winter, active layer thicknesses would not be expected to be significantly influenced by the warming and cannot be used as an indicator of the warming. The widespread seasonality of the air temperature increases (Fig. 3) suggests that statewide active layer thicknesses may not have been generally influenced significantly by the warming.

Natural thawing of the permafrost from the top downward has been observed to occur in a tundra and a forest site at a rate of about 0.1 m/yr in response to the permafrost warming (Osterkamp 2005). Basal thawing is occurring at four sites with shallow (<40 m thickness) discontinuous permafrost.

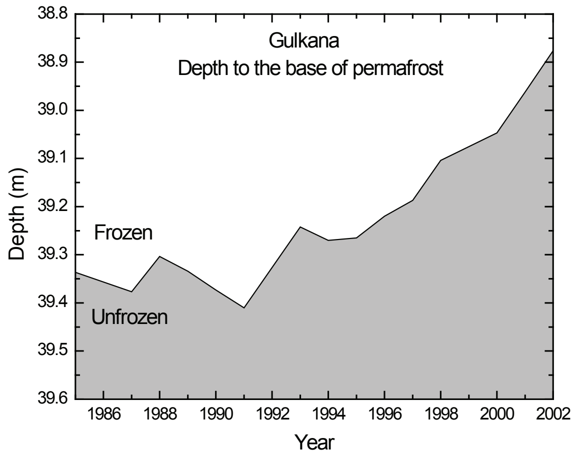

Figure 5. Thawing at the base of the permafrost at Gulkana.

Sites with thicker permafrost (>60 m) are generally warming at depth. At Gulkana, thawing at the base of the permafrost began about 1992 and proceeded at a mean rate of ~ 0.04 m/yr until 2000 when it accelerated to ~ 0.09 m/yr (Fig. 5, Osterkamp 2005). These basal thawing rates are much greater than predicted theoretically. If basal thawing at Gulkana was the result of a step change in permafrost surface temperature, the change would have occurred in 1976 coincident with the statewide warming of air temperatures. Thawing at the boundaries of unfrozen ground with permafrost (taliks in the continuous permafrost and isolated permafrost masses elsewhere) as a result of permafrost warming is predicted (Osterkamp 2003, 2005) but has not been investigated.

Thermokarst terrain was absent at a site near Healy, when the site was established (1985) but now exists in several places throughout the area (Fig. 6). Maximum thaw settlement was about 1.1 m in a pit at the borehole pipe and up to about 1½ m in the surrounding area (Osterkamp et al., submitted). New thermokarst terrain, formed by thawing ice-rich permafrost, has been observed, not only in Interior Alaska, but also in Northern Alaska where old ice wedges have been thawing since 1989 (Osterkamp et al. 2000, Jorgenson et al. 2001, Jorgenson et al. 2006).

Causes

For the recent warming, the data reviewed above suggest that permafrost generally warmed statewide coincident with increasing air temperatures in 1976/1977. There was not a pattern of corresponding changes in snow cover at this time suggesting this initial warming may have been primarily a result of increased air temperatures. Increasing permafrost temperatures in the late 1980s and into the 1990s may have been in response to a series of winters with thick snow covers (Osterkamp & Romanovsky 1999). This appears to be the case for Healy (Osterkamp 2007b) and Gulkana (Fig. 7) and, at least partially, for other sites. At some sites, air temperatures increased less than permafrost surface temperatures implicating snow cover effects in the observed warming. At Barrow, modeling results have shown that snow cover effects were involved in the century-long warming and the recent warming (Zhang & Osterkamp 1993). Stieglitz et al. (2003) have shown that about half the recent warming there was due to air temperature changes and half due to snow cover effects.

Figure 6. Photos showing thermokarst and changes in surface mophology over two decades at the Healy site.

Since new thermokarst was observed at Healy coincident with warming permafrost, it appears that permafrost thawing and development of thermokarst terrain was also a result of snow cover effects there (Osterkamp et al. submitted).

Summary

This paper uses borehole temperature measurements, basal thawing measurements, thermokarst observations, modeling results, and weather data in an attempt to reconstruct the thermal state of permafrost in Alaska during the last quarter of the twentieth century. This effort is hindered by the sparsity of long-term permafrost temperature data and the lack of interpretive studies which make the conclusions tentative.

During the last quarter of the twentieth century, permafrost warmed north of the Brooks Range from the Chukchi Sea to the Alaska-Canada border, south along a transect from Prudhoe Bay to Gulkana and up to 300 km from the transect. Sporadic measurements also show that permafrost warmed at other widely separated sites including north of Kotzebue, near Cantwell, and at Eagle River. It appears likely that permafrost temperatures increased statewide coincident with the statewide increase in air temperatures that began in 1976/1977. Some sites did not warm indicating there may be other sites that are exceptions to the warming.

The initial permafrost warming peaked in the early 1980s

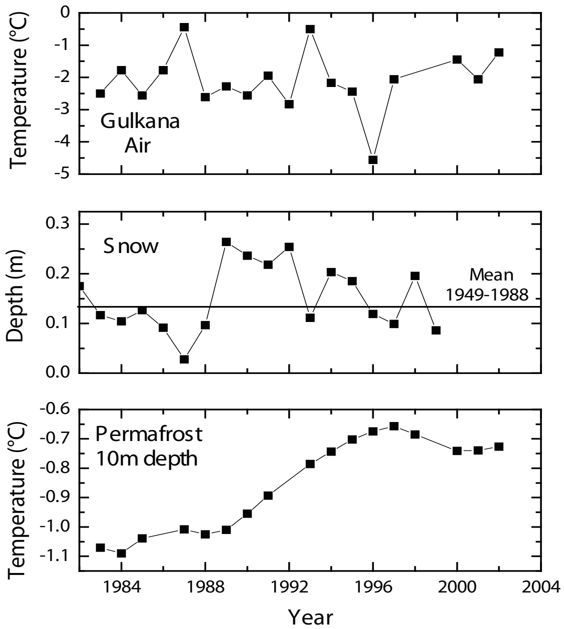

Figure 7. There was a trend of increasing permafrost temperatures at the Gulkana site (1989-1997) while air temperatures decreased and snow covers were thicker than the long term average.

and then cooled into the mid-1980s. Arctic sites began warming again about 1986 (Western Arctic prior to 1989) and Interior sites about 1988. Warming generally continued through the 1990s although some sites leveled off or cooled near the end of the century while some continued to warm.

The magnitude of the total warming at the permafrost surface was up to 4°C for the Arctic Coastal Plain, 1 to 2°C along the transect through the Brooks Range including its northern and southern foothills, and 0.3 to 1°C south of the Yukon River.

Increased air temperatures in the two decades after 1976/1977 were seasonal, a result of warmer winter temperatures with little change in summer conditions. This seasonality also occurred in permafrost surface temperatures at the Deadhorse and Franklin Bluffs sites. It is suggested that this was likely the case for other areas of the state. While permafrost temperatures increased by 3 to 4 °C, maximum active layer thicknesses did not show an increasing trend.

Thawing at the permafrost table and base has been observed in shallow permafrost and new thermokarst terrain has been observed.

Warming of the permafrost in the Arctic Coastal Plain in the late 1970s was probably caused primarily by increased air temperatures and, in Interior Alaska during the late 1980s and into the 1990s, primarily by increased snow cover thicknesses. At a few sites in Interior Alaska and for certain time periods, the permafrost warmed entirely because of snow cover effects. Generally, both air temperatures and snow cover effects appear to have contributed to the permafrost warming.

A thorough study of the effects of past snow conditions is needed. However, due to the complex and non-linear nature of snow cover effects, calibrated site-specific numerical models are required to quantify the relative contributions of snow and air temperatures to warming and thawing of the permafrost.

Acknowledgments

This research was supported by the Arctic Natural Sciences Program (most recently #0520578) and ARCSS, Office of Polar Programs at NSF, Army Research Office, U. S. Dept. of Energy, NIGEC (Western Regional Center), Asahi Beer Company, NSF and USDA Long Term Ecological Research Program and by the State of Alaska. The data are available on-line for use by other researchers at http://nsidc.org/data/arcss034.html and http://nsidc.org/data/arcss106.html. The data, through 2003, are of high quality with a resolution of 3 to 5 mK and an accuracy better than 10 mK. Contact the author if you need further information (ffteo@uaf.edu).

References

Clow, G.D., Lachenbruch, A.H. & McKay, C.P. 1991. Inversion of borehole temperature data for recent climatic changes: Examples from the Alaskan Arctic and Antarctica. *Proc. Int. Conf. on the Role of Polar Regions in Global Change*, 11-15 June, ed. by G. Weller, C.L. Wilson, and B.A.B. Serverin, Geophysical Institute, Univ. of Alaska, Fairbanks, AK.

Clow, G.D. & Urban, F.E. 2002. Largest permafrost warming in northern Alaska during the 1990s determined from GTN-P borehole temperature measurements. *EOS, Trans. AGU*, 83, (47): F258.

Goodrich, L.E. 1982. The influence of snow cover on the ground thermal regime. *Can. Geotech. J.*, 19: 421-432.

Goodwin, C.W., Brown, J. & Outcalt, S.I. 1983. Potential responses of permafrost to climatic warming. *Conf. Proc.: Potential effects of carbon dioxide-induced climatic changes in Alaska, Misc. Pub*. 83-1: 92-105, edited by J.H. McBeath, Univ. of Alaska, Fairbanks, AK.

Hansen, J. & Lebedev, S. 1987. Global trends of measured surface air temperatures. *J. Geophys. Res*., 92(D11): 13,345-13,372.

Hartman, B. & Wendler, G. 2003. Manifestation of the Pacific decadal oscillation shift of 1976 in Alaskan climatology. *Proc. AMS 7th Conf. Polar Meteorology and Oceanography and Joint Symp. on High-Latitude Climate Variation*, 12-16 May, Hyannis, MA.

Jorgenson, M.T., Racine, C.H., Walters, J.C. & Osterkamp, T.E. 2001. Permafrost degradation and ecological changes associated with a warming climate in central Alaska. *Climatic Change*, 48(4): 551-579.

Jorgenson, M.T., Shur, Y.L. & Pullman, E.R. 2006. Abrupt increase in permafrost degradation in Arctic Alaska. *Geophys. Res. Letters*, 33, (L02503): doi:10.1029/2005GL024960.

Lachenbruch, A.H. 1994. Permafrost, the active layer, and changing climate. *Open file report* 94-694, U.S. Geological Survey, Menlo Park, CA, 43 pp.

Lachenbruch, A.H., Sass, J.H., Marshall, B.V. & Moses, T.H. 1982. Permafrost, heat flow and the geothermal regime at Prudhoe Bay, Alaska, *J. Geophys. Res*., 87(B11): 9301-9316.

Lachenbruch, A.H. & Marshall, B.V. 1986. Changing climate: Geothermal evidence from permafrost in the Alaskan Arctic. *Science* 234: 689-696.

Lachenbruch, A.H., Cladouhos, T.T. & Saltus, R.W. 1988. Permafrost temperature and the changing climate. *Proc. 5th Int. Conf. on Permafrost*, 3: 9-17, 2-5 August, edited by K. Senneset, Tapir Publishers, Trondheim, Norway.

Osterkamp, T.E. 1983. Response of Alaskan permafrost to climate, *Final Proc., 4th Int. Conf. on Permafrost,* p. 145-152, 17-22 July, NAS, Washington D.C.

Osterkamp, T.E. 1994. Evidence for warming and thawing of discontinuous permafrost in Alaska, *EOS, Trans. AGU*. 75(44): 85.

Osterkamp, T.E. 2003a. A thermal history of permafrost in Alaska, *Proc. 8th Int. Conf. on Permafrost*, 2: 863-868, edited by M. Phillips, S.M. Springman, L.U. Arenson, A.A. Balkema, Lisse, The Netherlands.

Osterkamp, T.E. 2003b. Establishing long-term permafrost observatories for active layer and permafrost investigations in Alaska: 1977-2002. *Permafrost and Periglacial Proc.* 14 (4): 331-342.

Osterkamp, T.E. 2005. The recent warming of permafrost in Alaska. *Global and Planetary Change*, 49: 187-202.

Osterkamp, T.E. 2007a. Characteristics of the recent warming of permafrost in Alaska. *J. Geophys. Res*., 112, F02S02, doi:10.1029/2006JF000578.

Osterkamp, T.E. 2007b. Causes of warming and thawing permafrost in Alaska. *EOS*, 88(48): 3-4, 27 November.

Osterkamp, T.E. & Payne, M.W. 1981. Estimates of permafrost thickness from well logs in northern Alaska. *Cold Regions Science and Technology* 5: 13-27.

Osterkamp, T.E. & Romanovsky, V.E. 1997. Freezing of the active layer on the Coastal Plain of the Alaskan Arctic. *Permafrost and Periglacial Proc*. 8: 23-44.

Osterkamp, T.E. & Romanovsky, V.E. 1999. Evidence for warming and thawing of discontinuous permafrost in Alaska. *Permafrost and Periglacial Proc*. 10: 17-37.

Osterkamp, T.E. & Jorgenson, J.C. 2005. Warming of permafrost in the Arctic National Wildlife Refuge. *Permafrost and Periglacial Proc*. 16: 1-5.

Osterkamp, T.E. & Jorgenson, M.T., in press, Permafrost conditions and processes, *Geological Monitoring Manual*, Geological Society of America.

Osterkamp, T.E., Gosink, J.P. & Kawasaki, K. 1984. Permafrost temperature measurements in an Alaskan transect: Preliminary results. *Workshop on Permafrost Geophysics*, Spec. Rept. 85-5, U.S. Army CRREL, Hanover, NH.

Osterkamp, T.E., Gosink, J.P. & Kawasaki, K. 1987. Measurements of permafrost temperatures to evaluate the consequences of recent climate warming. Final report, Contract 84 NX 203 F 233181, Alaska Dept. of Transportation and Public Facilities, Fairbanks, Alaska.

Osterkamp, T.E., Viereck, L., Shur, Y., Jorgenson, M.T., Racine, C.H., Doyle, A.P. & Boone, R.D. 2000. Observations of thermokarst in boreal forests in Alaska. *Arctic, Antarctic, and Alpine Res*. 32(3): 303-315.

Outcalt, S.I., Goodwin, C., Weller, G. & Brown, J. 1975. Computer simulation of snowmelt and soil thermal regime at Barrow, Alaska. *Water Resour. Res*. 11(5): 709-715.

Romanovsky, V.E. & Osterkamp. T.E. 1997. Thawing of the active layer on the coastal plain of the Alaskan Arctic. *Permafrost and Periglacial Proc*. 8(1): 1-22.

Romanovsky, V.E. & Osterkamp, T.E. 2000. Effects of unfrozen water on heat and mass transport processes in the active layer and permafrost. *Permafrost and Periglacial Proc.* 11: 219-239.

Romanovsky, V.E., Sergueev, D.O. & Osterkamp, T.E. 2003. Spatial and temporal variations in the active layer and near-surface permafrost temperatures in Northern Alaska, *Proc. 8th Int. Conf. on Permafrost*, 2: 989-994, edited by M. Phillips, S.M. Springman, L.U. Arenson, A.A. Balkema, Lisse, The Netherlands.

Shur, Y.L., Hinkel, K.M. & Nelson, F.E. 2005. The transient layer: Implications for geocryology and climate change science. *Permafrost and Periglacial Proc.* 16: 5-17.

Smith, M.W. & Riseborough, D.W. 1983. Permafrost sensitivity to climate change. *Proc.4th Int. Conf. on Permafrost*, pp. 1178- 1183, NAS, Washington, D.C.

Stieglitz, M., Dery, S.J., Romanovsky, V.E. & Osterkamp, T.E. 2003. The role of snow cover in the warming of arctic permafrost. *Geophys. Res. Letters* 30(13): 1721, doi:10.1029/2003GL017337.

Zhang, T. 2005. Influence of the seasonal snow cover on the ground thermal regime: An overview. *Rev. Geophys*. 43, RG4002, doi:10.1029/2004RG000157.

Zhang, T. & Osterkamp, T.E. 1993. Changing climate and permafrost temperatures. *Proc. 6th Int. Conf. on Permafrost*, p. 783-788, 5-9 July, South China University of Technology Press, Wushan, Guangzhou, PRC.

Zhang, T., Osterkamp, T.E. & Stamnes, K. 1996. Influence of the depth hoar layer of the seasonal snow cover on the ground thermal regime. *Water Resour. Res*. 32(7): 2075-2086.

Zhang, T., Osterkamp, T.E. & Stamnes, K. 1997. Effects of climate on the active layer and permafrost in Alaska north of the Brooks Range. *Permafrost and Periglacial Proc*. 8(1): 45-68.

Field Trials of Surface Insulation Materials for Permafrost Preservation

James M. Oswell
Colt Worley Parsons Ltd./Naviq Consulting Inc., Calgary, Canada
Jack R. Everts
Exxon Mobil Development Company./Imperial Oil Resources Ventures Limited, Calgary, Canada

Abstract

Two test sites were initiated to examine the use of several insulating-type materials for potential use as thermal mitigation strategies on the Mackenzie Gas Project. The Woodenhouse test site, located northeast of Slave Lake, Alberta, was constructed in March 2005. The Norman Wells, Northwest Territories, test site was constructed in March 2006. At both sites, flax straw bales and white reflective surfaces were being tested. A test cell of shredded wood was also tested at the Woodenhouse test site. Each test cell was approximately 20 m by 20 m in plan area. A control cell was also present. Temperatures were measured at the ground surface and at selected depths to 10 m. All temperatures were recorded on dataloggers. The performance of the test materials was examined from several perspectives including thermal performance, degradation/deterioration, and imported weed growth. Compared to the control cell, straw bales provided the best thermal protection, followed by shredded wood. The reflective surface was marginally better than the control.

Keywords: monitoring; pipeline; surface insulation; thermal mitigation.

Introduction

The Mackenzie Gas Project (MGP) is intended to transport natural gas from the Mackenzie Delta area in northern Canada through the Northwest Territories to connect with distribution pipelines in northern Alberta. The proposed pipeline will have an initial capacity of about 0.8 billion cubic feet per day (bcfd), with a fully expanded capacity of nearly 1.8 bcfd. Along the route, the pipeline will traverse approximately 200 km of continuous permafrost and about 1000 km of discontinuous permafrost. The pipeline will be designed as a fully buried system.

Right-of-way clearing and pipeline construction will alter the geothermal character of the permafrost within the right-of-way, which if not mitigated, will inevitably result in permafrost warming, deepening of the active layer and other effects. For sloping terrain along the route, these geothermal changes could result in instability of the slopes, if not mitigated. There are approximately 160 identified slopes along the route that may require mitigation to ensure long-term stability.

Slope stability issues along pipeline routes underlain by permafrost have been addressed in the past. Perhaps the most important case history for mitigation of the effects of thawing permafrost on slope stability was the Norman Wells oil pipeline, owned and operated by Enbridge Pipelines (NW) Inc. This pipeline is fully buried in discontinuous permafrost along its 868 km route that somewhat parallels the proposed Mackenzie gas pipeline between Norman Wells and Alberta. To address the thawing of permafrost on slopes and related instability that could result, a layer of wood chips was installed on approximately 33% of Norman Wells pipeline slopes. The design and performance of the wood chip-covered slopes was documented by Hanna and McRoberts (1988), Hanna et al. (1994) and Oswell et al. (1998).

Given the design, construction and operational differences between the Mackenzie gas project and the Norman Wells pipeline project (for example, right-of-way width, pipeline operating temperatures, diameters, ground temperatures), the MGP decided to conduct field tests to assess the thermal properties of several surface insulation materials that may be useful in mitigating permafrost degradation.

Surface Insulation Field Trials

Test materials

The field trials tested the following three different materials:

- Shredded wood
- Straw bales
- Reflective surface (geotextile)

The shredded wood material consists of well-graded wood fibers ranging in lengths from about 200 mm to about 50 mm. This material differs from the wood chips used on the Norman Wells pipeline, which were typically flat wood particles being circular to elongated and up to about 25 mm to 40 mm in diameter.

The straw bales were standard rectangular flax straw bales sized at about 0.4 m high, 0.51 m wide and 1.1 m long, and weighing about 30 kg. Flax was selected because it was very slow to decompose and it was of low palatability to animals such as moose and caribou.

The reflective surface material consisted of a white geotextile, intended to reflect the summer solar radiation from the ground surface while allowing the cold winter temperatures to penetrate the ground. Reflective materials have been used to reduce snow and ice ablation (Poplin et al. 1991).

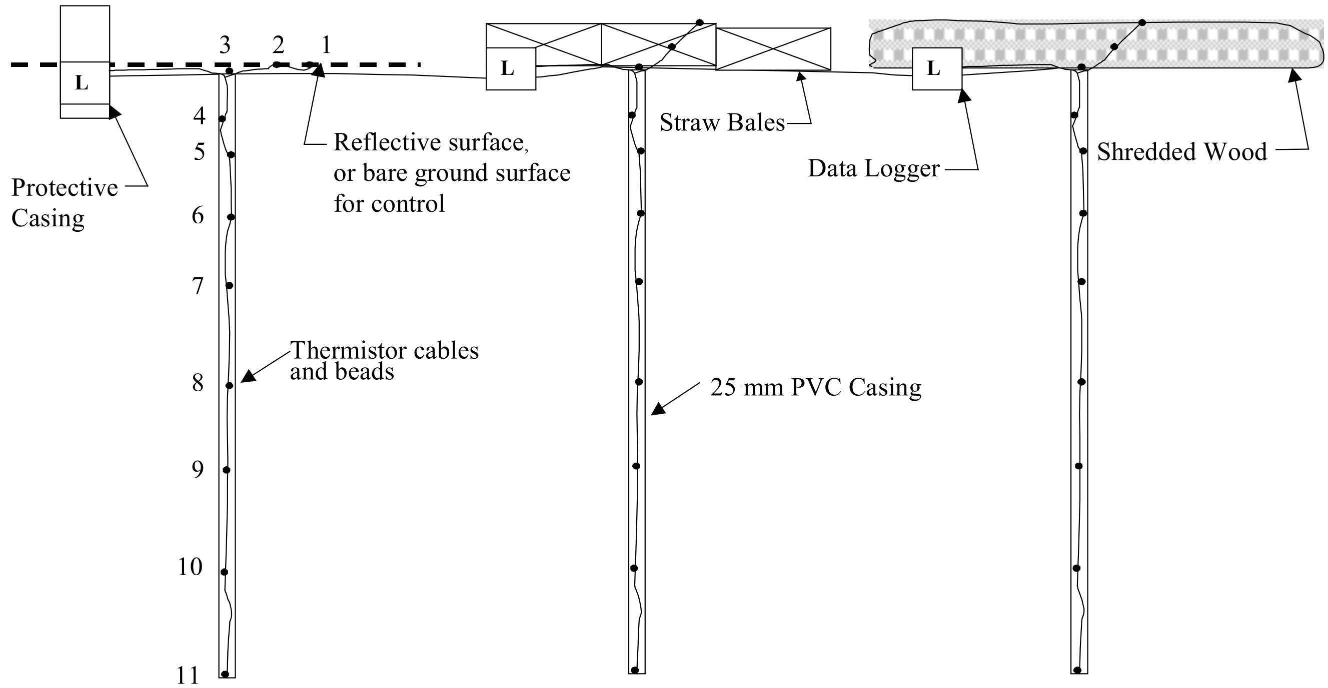

Figure 1. Layout of test cells (not to scale) and associated instrumentation.

Test site and set-up

Two test sites were established; the first site was in northern Alberta, near the community of Slave Lake, at a compressor station site named Woodenhouse. The mean annual air temperature was about +1.3°C. The test site area was previously cleared of all vegetation and the ground surface consisted of granular fill over unfrozen mineral soil. The second test site was in Norman Wells, Northwest Territories, which has a mean annual air temperature of about -5.5°C. This site was initially forested with sparse spruce trees, but was cleared of trees at the start of the test program. The ground surface consisted of the native organic mat underlain by mineral soils that was frozen, but considered to be warm permafrost.

The Woodenhouse test site consisted of three test cells plus a control. The test cells were straw bales, shredded wood and a reflective surface, each 20 m by 20 m in plan dimensions. A control cell was installed to provide baseline data for comparison. The Norman Wells test site was the same as the Woodenhouse site except that there was no shredded wood test cell.

The ground temperatures were monitored using an eleven bead thermistor cable attached to a data logger, recording temperatures at 12-hour intervals. The temperatures were measured at the following depths: 0 m, 0.5 m, 1.0 m, 2.0 m, 3.0 m, 4.5 m, 6.0 m, 8.0 m, and 10.0 m. In addition, two thermistor beads were attached to a "pig-tail" that would monitor the temperatures at the mid-point and top surface of the straw bales and shredded wood layers. Air temperatures were monitored at 1.0 m above the ground surface at the control cell.

The Woodenhouse site was installed in February 2005 and the Norman Wells site was installed in February 2006. The sites were prepared by site clearing, including snow clearing, installing the test cells and then drilling boreholes to install the thermistor cables. Figure 1 presents the typical test cell and thermistor cable lay-out showing the thermistor bead numbering.

Initial thermal performance

This paper only reports initial results from the Woodenhouse test site in northern Alberta. Data collection from the Norman Wells site has experienced a number of challenges, and as a result full analysis of these datahas not been completed. For the Woodenhouse test site, temperature data has been regularly downloaded since testing began.

Thermistor beads 3 (0 m), 4 (0.5 m depth) and 5 (1.0 m depth) provided the most representative data on the near surface geothermal reaction of the surface cover. Bead 9 (6.0 m depth) provided ground temperatures at a moderate depth.

Figure 2 shows ground surface temperatures for all of the test cells at Woodenhouse. The ground surface temperatures at the control test cell and the reflective surface test cell were similar to each other. The ground surface temperatures for the straw bales and shredded wood materials were dampened compared to the atmospheric temperatures. That is, the effect of the straw bale and shredded wood layers was to reduce the day-to-day temperature variation in ground temperature compared to the air temperatures. Furthermore, the straw bales and shredded wood materials experienced a time lag in responding to atmospheric variations. This time lag was about one month, although more data is necessary to more accurately quantify the lag-period.

The time lag experienced for temperatures under the straw bale and shredded wood test cells compared to the control test cell was more apparent at depths of 0.5 m (see Fig. 3)

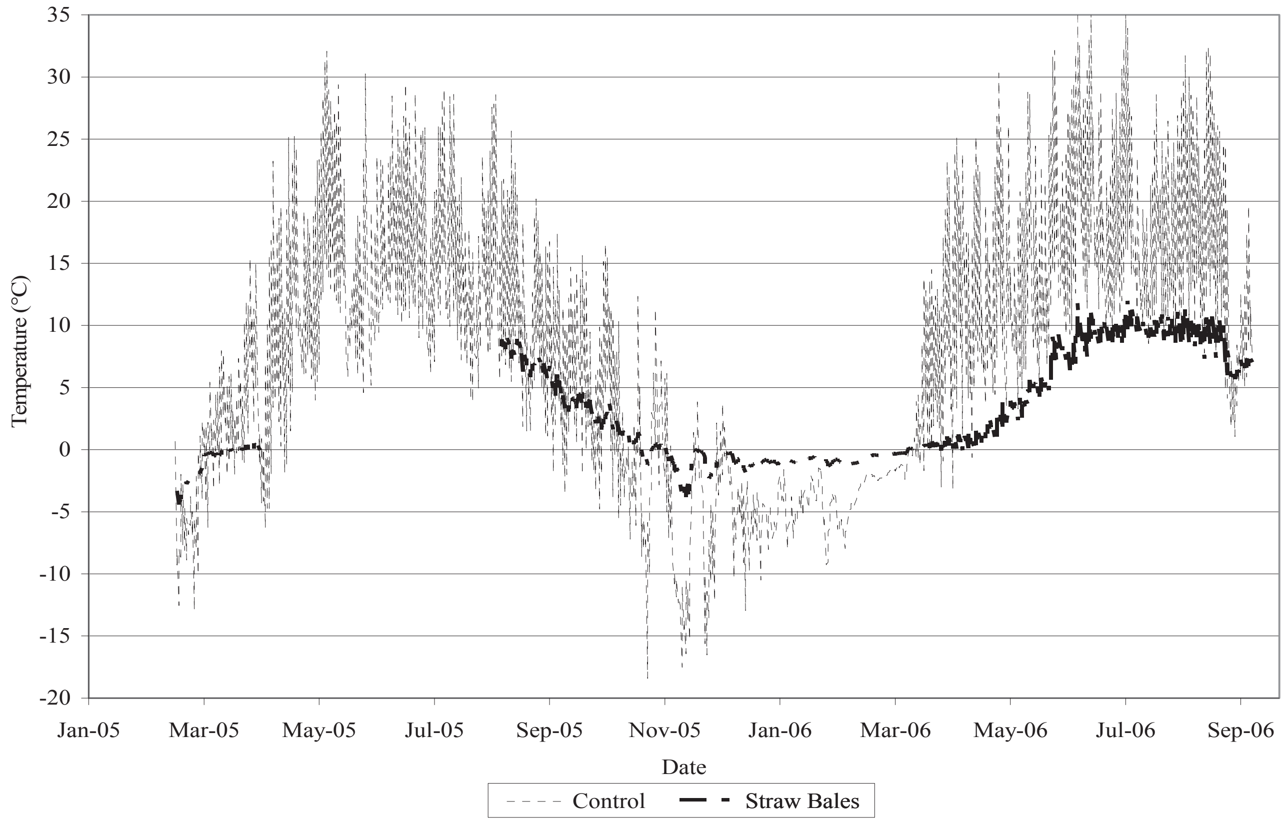

Figure 2a.

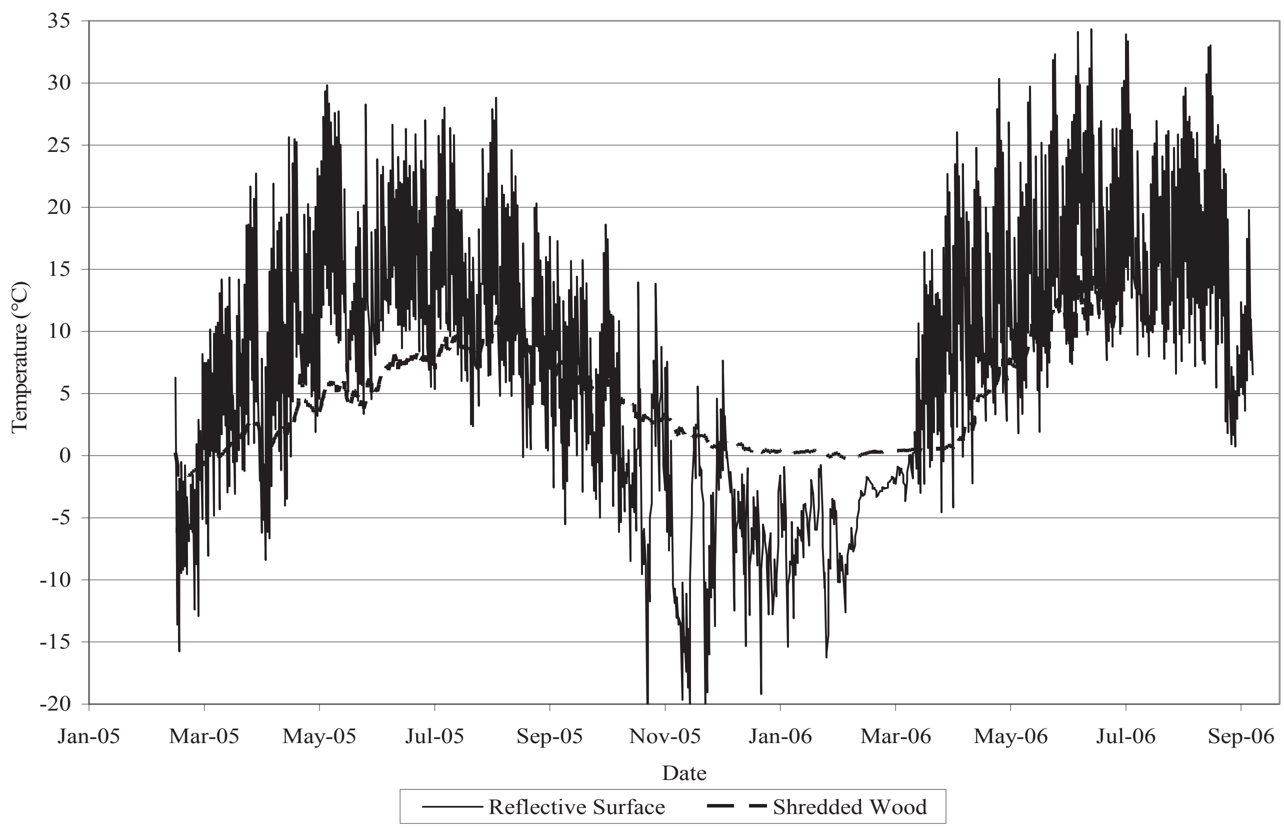

Figure 2b.

Figure 2. Temperature data from Woodenhouse test site, at ground surface.

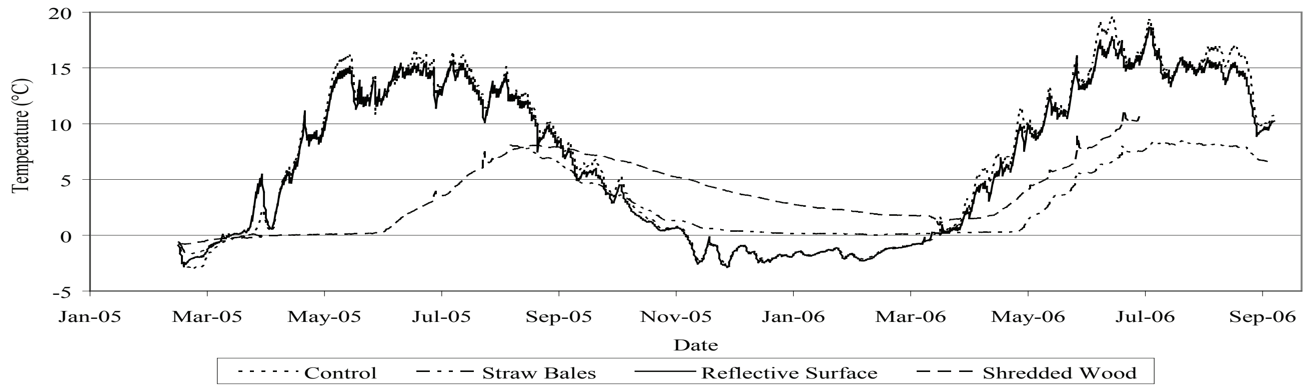

Figure 3. Temperature data from Woodenhouse test site, at 0.5 m below ground surface.

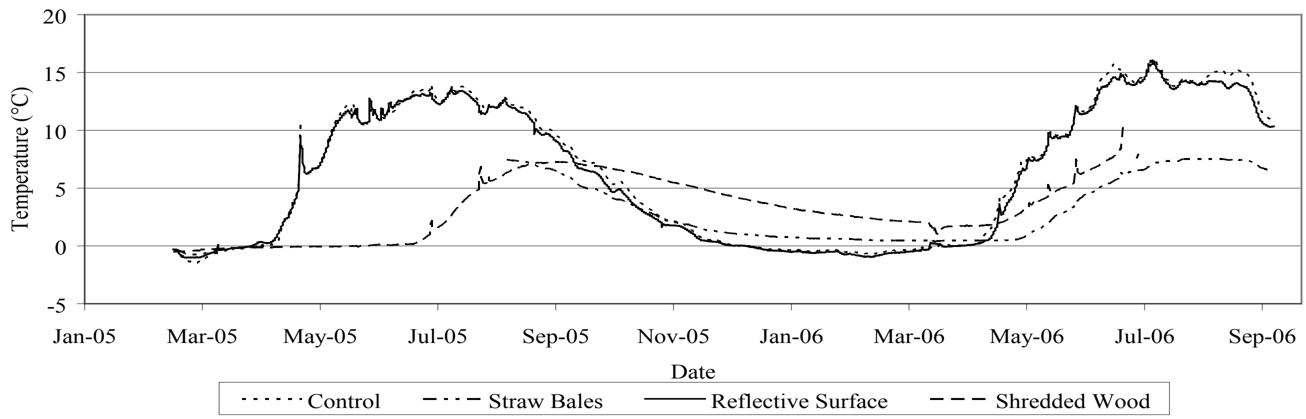

Figure 4. Temperature data from Woodenhouse test site, at 1.0 m below ground surface.

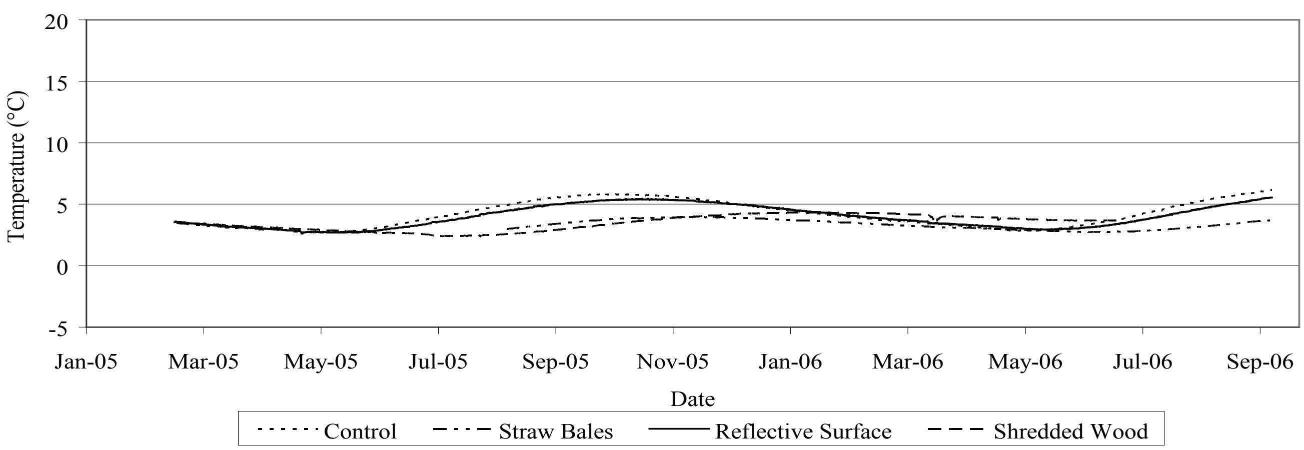

Figure 5. Temperature data from Woodenhouse test site, at 6.0 m below ground surface.

Table 1. Annual degree-day analysis of Bead 3, ground surface temperatures at Woodenhouse.

Test Cell Section	Analysis Period	Calculated Annual °C-Days	Percent of Control	Efficiency Compared to Control
Control	August 31, 2005 – August 30, 2006	2,174	100	1.0
Straw bales	August 31, 2005 – August 30, 2006	1,090	50	2.0
Reflective surface	August 31, 2005 – August 30, 2006	1,945	89	1.1
Shredded wood	July 17, 2005 – July 16, 2006	1,711	79	1.3

and 1 m (see Fig. 4). The time lag was particularly evident during the summer of 2005 and 2006 and lasted about one month. At the end of the winter of 2006, the shredded wood test cell showed a minimal time lag in May 2006 in terms of responding to warmer air temperatures, while the straw bales experienced a time lag of about two weeks before the ground started to warm.

With depth, all ground temperature responses to air temperature changes are dampened. This dampening is a result of the thermal resistance of the mineral soil. Based on the temperature data from thermistor Bead 9 at a depth of 6 m (see Fig. 5), it appears that the influences of the surface insulation material are nearly completely moderated by the overlying soil cover. That is, the temperature response at 6 m depth for each of the test cells and the control are nearly the same.

There were only small differences in the average winter temperatures for any of the test cell materials at Woodenhouse, compared to the control cell temperatures. Between November 2005 and April 2006 winter temperatures measured as follows:

• Under the straw bale and shredded wood test cells, ground temperatures were several degrees warmer than the temperatures under the control cell.

• In the cell containing the reflective surface material, ground temperatures were slightly colder than the temperatures under the control cell.

The warmer average winter temperatures experienced by the shredded wood test cell was because of the long time lag in the response of the ground temperature to the seasonal change in air temperature. This was most apparent in thermistor Bead 5 at 1 m depth (see Fig. 4) and thermistor Bead 9 at 6 m depth (see Fig. 5). In summer 2005, the ground temperatures under the shredded wood lagged behind the ambient temperatures by at least one month. The warmer ground temperatures developed in the summer and early fall of 2005 were carried well into the late fall and early winter 2005–2006, which caused an overall warmer average winter soil temperature.

Ground temperature responses in the summers of 2005 and 2006 also showed differences between the straw bale and shredded wood test cells, and the control cell. The ground temperatures under the reflective surface test cell during the summer of 2005 and 2006 appeared to be close to those of the control cell. Both the straw bales and shredded wood cells recorded average ground surface and near surface (0.5 m depth) temperatures that were less than one-half of those measured in the control cell.

The effectiveness of the test materials could be further examined by a degree-day analysis using Bead 3, which measured the ground surface temperature. This analysis is shown in Table 1.

The data from the degree-day analysis reinforced the observations from the temperature plots. The straw bales achieved one-half the number of annual degree-days of the control section, whereas the shredded wood achieved only 79% of the annual degree-days. The reflective surface material had a minimal effect on the ground temperatures.

Physical performance of test materials

The examination of physical performance of the test materials focused on degradation and loss of integrity of the materials, as these issues will ultimately affect the long-term suitability of the insulation materials used. Observations from the Woodenhouse and Norman Wells test sites were both considered.

Visual examination of the straw bales at both the Woodenhouse and Norman Wells test sites revealed that the bales had shrunk since their initial installation. This shrinkage was first identified at the Woodenhouse test site in the summer of 2005. Consequently, for the Norman Wells straw bale test cell, a thin layer of loose straw was spread over the test cell prior to placement of the bales so that if shrinkage occurred, bare earth (or the organic mat) would not be exposed.

The shrinkage of the straw bales probably resulted from moisture loss from the straw. It would be reasonable to expect that drying would cause the straw bales to shrink in height and length, but less in width because of the anisotropic structure of the straw stalks.

One concern expressed in the planning phase of the study was that foraging by animals, particularly ungulates, would damage the straw bales. However, visual observations at the Woodenhouse and Norman Wells test sites indicated that animals were not eating the straw bales.

The physical performance of the reflective surface materials at the Woodenhouse and Norman Wells test sites appeared to be good. Inspection of the material in the fall of 2006 did not reveal any substantive deterioration of the geotextile reflective material. Some discolouration at the Woodenhouse site had occurred likely associated with airborne dust from adjacent exposed areas. The Norman Wells test site did not have exposed mineral soil near the test cells. Consequently, this site provided a good contrast to the Woodenhouse test site in terms of darkening of the reflective fabric.

Visual observations at Woodenhouse indicated that animal traffic, if any, had not damaged the reflective surface material. No evidence of animal traffic has been found at the Norman Wells test site.

Importation of noxious weeds at test sites

The importation of noxious weeds to sites in the Northwest Territories should be avoided. As part of the initial program to establish the test sites, the straw bales were tested for weeds by an agricultural laboratory. The test results for noxious weeds were negative.

Plants have started to grow on and between the straw bales at Woodenhouse. The weeds observed at the site were stinkweed and tartary buckwheat, species that were common in Alberta, but were not on the noxious weed list. These plants were annuals that were reproducing from seed on new surface disturbances. However, they are not expected to persist more than a few years on the bales at Woodenhouse. If these weeds were imported to the Mackenzie Valley, they would not likely produce seed because of the short growing season and would likely die out after the first year.

Plants were also observed to be growing through seams of the reflective surface material at the Woodenhouse test site. These plants are likely the result of airborne seeds or regeneration of rootstocks that were present on the ground surface when the reflective surface material was installed.

Observations and Conclusions

From the preliminary field testing and analysis, one can conclude the following:

• Although the straw bales shrunk in volume during testing, further temperature measurement and analysis is necessary to determine whether this shrinkage is sufficient to materially affect their thermal insulation properties when used as an insulation system.

• The anchoring system proposed by the manufacturer of the reflective surface material was inadequate for the application at the Woodenhouse test site, where there was exposed mineral soil. However, a revised anchoring system was successfully implemented at the Woodenhouse site but was then found to be inadequate for the Norman Wells test site, which consists of an organic layer overlying hard or frozen mineral soil. The “third generation” anchoring system used at Norman Wells appears to be performing well.

• As measured in terms of ground surface annual degree-days, a single layer of straw bales provided the best thermal performance compared to the control, being about twice as effective as the control cell. The 0.5 m layer of shredded wood performed about 1.3 times better than the control cell. Both materials showed value as ground surface insulation materials.

• Both the shredded wood and straw bales experienced a time lag in response to seasonal ambient temperature changes. In the case of the shredded wood test cell, this time lag appears to help increase the average winter temperature of the ground surface above the average air temperatures measured.

• In comparing the ground surface temperatures of the reflective surface material to the control cell, the reflective material experienced a small, but measurable reduction in ground surface temperature during the thawing period compared to the control cell at the Woodenhouse test site. A reduction of about 10% in ground surface annual degree-days was achieved by the reflective surface compared to the control cell. However, additional monitoring from one or more thaw seasons is needed to confirm the effectiveness. If long-term reduction in ground surface heating can be confirmed, then the applicability of reflective surfaces can be evaluated from a cost-benefit perspective.

Acknowledgments

The authors acknowledge the assistance of their colleagues at Colt Worley Parsons Limited, Imperial Oil Resources Ventures Limited and ExxonMobil Development Company who worked on the Mackenzie Project. Permission to publish this paper has been granted by Imperial Oil Resources Ventures Limited and ExxonMobil Development Company.

References

Hanna, A.J. & McRoberts, E.C. 1988. Permafrost slope design for a buried oil pipeline. *Proceedings of the Fifth International Conference on Permafrost, Trondheim, Norway, August 2–5, 1988*. Volume 2: 1247-1252

Hanna, A.J., Oswell, J.M., McRoberts, E.C., Smith, J.D. & Fridel, T.W. 1994. Initial performance permafrost slopes: Norman Wells pipeline project, Canada. *Proceedings of the Seventh International Cold Regions Engineering Specialty Conference, Edmonton Alberta, March 7–9, 1994*: 369-395.

Oswell, J.M., Hanna, A.J. & Doblanko, R.M. 1998. Update of performance of slopes on the Norman Wells pipeline project. *Proceedings, Seventh International Conference on Permafrost, Yellowknife, Canada.*

Poplin, J.P., Weaver, J.S., Gulati, K.C., Lord, S. & Sisodiya, R.G. 1991. Experimental field study of spray ice ablation. *Proceedings, International Conference on Port and Ocean Engineering under Arctic Conditions, POAC*. Volume 1: 259-272.

The State of Subsea Permafrost in the Western Laptev Nearshore Zone

P.P. Overduin
Alfred Wegener Institute for Polar and Marine Research, Potsdam, Germany
V. Rachold
International Arctic Science Committee, Stockholm, Sweden
M.N. Grigoriev
Permafrost Institute Siberian Branch, Russian Academy of Sciences, Yakutsk, Russia

Abstract

Permafrost in the nearshore zone is affected by sea bottom temperatures, formation of bottom-fast ice, ice movement, formation of brines through freezing, and diffusion of salt water into the sediment. Subsea permafrost drilled on- and offshore along a north-south transect in the Laptev Sea yields sediment temperature, state and pore-water salinity to show salt diffusion into the sediment and its effect on phase state. Since inundation, the permafrost has been separated from atmospheric temperature and radiation fluctuations by a 0 to 6 m water column and, in winter, by sea ice. Nearshore development of bottom-fast ice concentrates brines at the sea bottom and leads to the penetration of a saline front that exceeds seawater salinity by a factor of at least 2. Subsea permafrost pore space can contain a mix of ice and pore-water solution that is primarily determined by salinity.

Keywords: brine; coastal zone; continental shelf; permafrost; subsea.

Introduction

Permafrost beneath the ocean floor is the result of relative sea level rise inundating the land surface. Inundation changes the heat flux at the upper boundary of the permafrost, generally leading to warming and eventual degradation. Nearshore seabed temperature records covering the annual cycle are rare, but measured temperatures are usually negative. Sufficiently saline pore waters can thaw subsea permafrost at negative temperatures. Methods of estimating permafrost distribution include bathymetric delineation (Brown et al. 1998) and heat transfer modeling (Romanovskii et al. 2005). Modeling uses inferred climate histories and simplified heat transfer. Models of permafrost evolution after inundation have been refined by including salinity effects (Swift & Harrison 1984, Hutter & Straughan 1999, Outcalt 1985), but these have not resulted in improvements to regional or global permafrost distribution estimates. Unknowns affecting distribution include regional glacial and sea level histories, the effect of spatial heterogeneity in terrestrial permafrost (esp. thermokarst) on subsequent degradation, and processes affecting sea bottom temperature and salinity (esp. bottom-fast ice). Based on the consequent spatial variability (Overduin et al. 2007b), public domain direct observations of the distribution of ice-bearing subsea

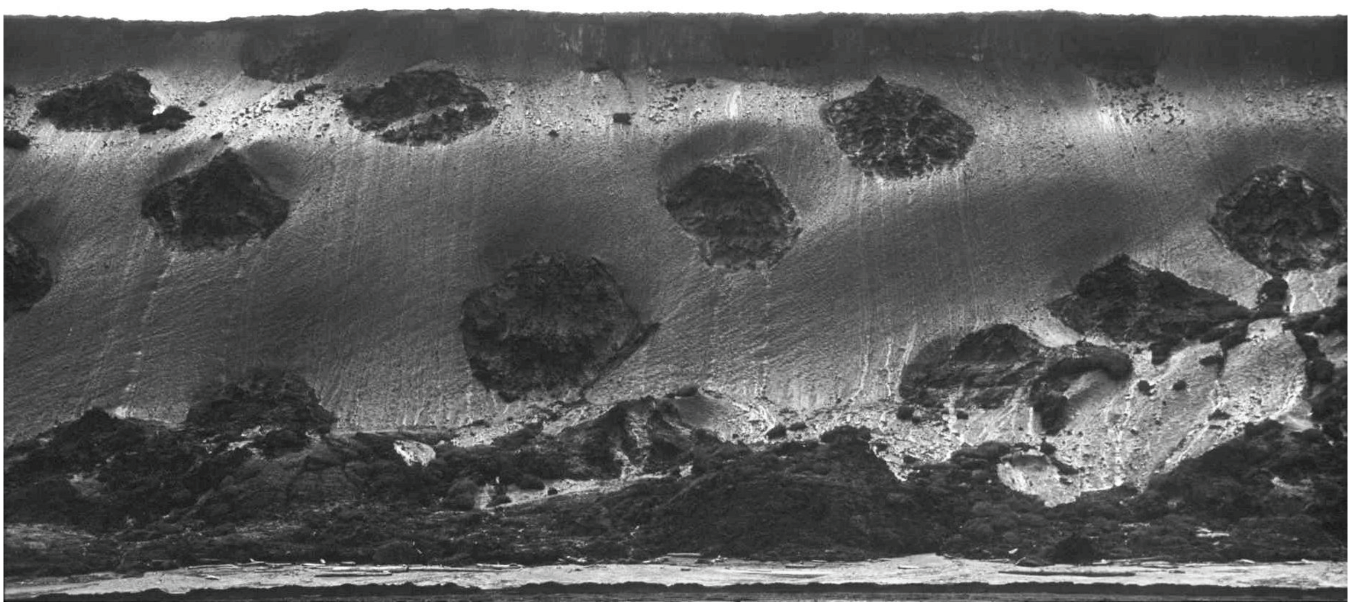

Figure 1. A straight-on view of the eroding Laptev Sea coastal bluff at Cape Mamontov Klyk. The bluff is about 20 m high and is composed mostly of ice with inclusions of organic-rich soil (photograph by Hanno Meyer, 2003).

Figure 2. Map showing the location of Cape Mamontov Klyk (above) in the Western Laptev Sea.

permafrost, particularly at water depths shallower than 10 m, provide poor predictive capability for regions where no observations have been made.

In this study, sediment from the Laptev Sea is examined to determine changes in permafrost following submergence. Modeled subsea permafrost is thick (700-1000 m) and ice-bearing and extends over 400 km from the modern coastline (Romanovskii et al. 2005). The shallow inclination of the shelf and the absence of localized glaciation during the last glacial interval create a suitable test bed for subsea permafrost studies. We seek to identify processes determining the rate and distribution of permafrost degradation in the nearshore zone.

Site Description

Located midway between the Anabar and Olenek Rivers, Cape Mamontov Klyk was named for the discovery of mammoth tusks emerging from its thawing coastal bluffs (Figs. 1, 2), which currently reach over 25 m in height with a ground ice content up to over 80% by volume. The bluff stratigraphy is part of the Siberian ice complex deposits formed during the Late Pleistocene (Romanovskii 1993). The coastal bluff contains mostly silty sand, with relatively high organic content (Schirrmeister et al. submitted). The coastal plain stretches from the Pronchishev Ridge about 30 km to the south of the coast, lies 25 to 55 m a.s.l. and inclines to the north-northeast at 0.1°-0.2° at the cape. Thermokarst depressions and lakes up to several km across cover about 50% of the coastal plain in the region (Grosse et al. 2006). The coastline bisects some of these features, and they likely affect the bathymetry and subsea permafrost table (Romanovskii 2000). Available nearshore bathymetry is not precise enough to show these features, but the seafloor continues at less than 0.05° for at least 13 km from shore (Fig. 3). Modeling of permafrost development suggests that thermokarst terrain extends out to at least the 55 m isobath, and probably much further (Romanovskii & Hubberten 2001). Based on bathymetry from Russian maps and field data, the sea level rise inundated the shelf from a point over 200 km north of Mamontov Klyk over the past 11 ka (Bauch et al. 2001). Sea level rise over the past 2 ka was less than 2 mm a^{-1}, but there is little information on recent changes in coastline position, which is currently retreating at about 4.5 m a^{-1} (Arctic Coastal Dynamics Project Team 2008), and average erosion rates of ice complex coastlines in the Laptev Sea are about 2.5 m a^{-1} (Grigoriev & Rachold 2003).

Methods

In April 2005, a coastal and offshore drilling program drilled five cores along a north-south transect (Overduin et al. 2007a). Coring sites extended from onshore (core C1) to 12.5 kilometers offshore (cores C2-C5) and 6 m water depth (Fig. 3). A dry, hydraulic, rotary-pressure drilling technique was used and a borehole casing prevented infiltration. Depths of penetration are shown in Figure 3 and listed in Table 1, along with the state of the sediment as determined upon recovery. Recovered sediment material remained frozen during transport and storage.

Sediment temperature was measured using calibrated thermistors. Measurements were made from 1 to 11 days after drilling at the depths shown in Figure 4 (Junker et al. accepted). The dry drilling technique allowed temperature equilibration within 3 days at the bottom of C2. A thermistor string was permanently installed at the onshore site (C1). Mean annual temperatures for C1 were calculated using hourly measurements for the time period June 1, 2005-June 1, 2006 (Fig. 4). The temperature profiles for C2, C3 and C4 were measured at least 96 hours after drilling, C5 was measured one day later.

Pore water salinity was measured by thawing the sediment and extracting pore water using small suction lysimeters with 0.2 µm pores. Thawing and extraction took up to three days, depending on sample grain-size. The extracted pore water salinity was measured to a reference temperature of 25°C. Uncertainty in salinity depended on the measurement range with an upper limit of ±0.1‰.

At low salinity, the ice content in cryotic sediment mostly depends on grain-size and temperature. At higher salinities, however, the salinity of the pore water is more important. For low-salinity samples (<5‰), we used the total water content of frozen samples as a proxy for volumetric ice content (θ_i). For high-salinity samples (≥5‰), volumetric ice content was estimated as the difference between total (θ_{tot}) and liquid water content (θ_l). Total volumetric water content (ice and water) was measured using the weight (w_{fr}) and water displacement (V_{tot}) of sealed frozen samples and the weight of the sample after freeze-drying (w_{dry}).

Uncertainties were ±5 x 10^{-5} kg in weight and ±5 x 10^{-5} m^3 in volume. The error introduced by ignoring liquid water content in fresh water samples is small for these sediments (<5%) relative to absolute variations in ice content between samples, since grain sizes are not small and segregated ice is present in much of the profile.

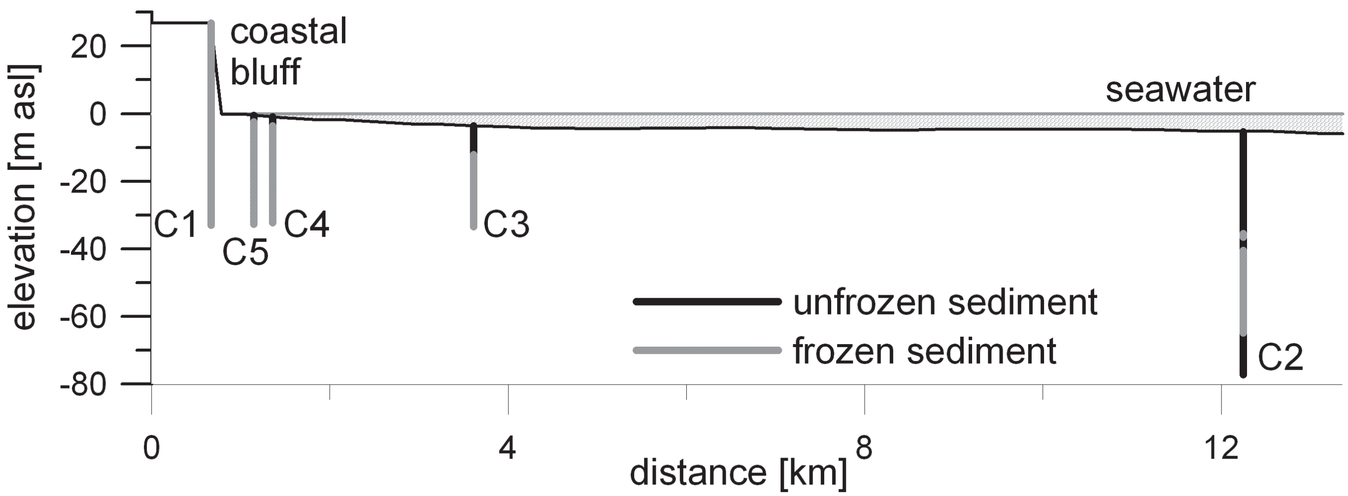

Figure 3. The locations and elevations (in meters relative to sea level) of cores along the transect are shown, along with the field-determined state (frozen/unfrozen) of the sediment (adapted from Overduin et al. 2007a).

Sediment liquid water content lay between 4 and -25°C in the laboratory using 7 cm time domain reflectometry (TDR) sensors in a 100 mL cell, which had been calibrated in air and deionized water. A Campbell Scientific TDR100 was used to generate waveforms, which were analyzed for bulk relative dielectric permittivity. Liquid water content was estimated using a mixing model for the relative dielectric permittivity of a porous medium. We assume that the sediment may be represented as a rigid three-component medium (ice, soil, water). The mixing model gives the composite relative dielectric permittivity (ε_c) based on the volumetric fractions and dielectric permittivities of the components:

$$\varepsilon_c = \left[(1-\eta)\varepsilon_s^{\ \alpha} + (\eta-\theta_l)\varepsilon_i^{\ \alpha} + (\theta_l)\varepsilon_l^{\ \alpha}\right]^{1/\alpha} \tag{1}$$

where η is the porosity, and the subscripts, *i*, *s* and *l* refer to ice, soil and liquid, respectively (Roth et al. 1990). The exponent, α, is related to the geometry of the components in the mixture. Soil and ice relative dielectric permittivities are assumed to be similar at the frequency of measurement ($\varepsilon_m = \varepsilon_s \approx \varepsilon_i$), leading to an expression for the liquid water content that is equivalent to a two-component model:

$$\theta_l = \left[\varepsilon_{comp}^{\ \alpha} - \varepsilon_m^{\ \alpha}\right]\left[\varepsilon_l(T)^\alpha - \varepsilon_m^{\ \alpha}\right]^{-1} \tag{2}$$

Changes in pore solution dielectric permittivity as a result of changes in solute concentration are ignored, as are temperature dependencies of the soil and ice dielectric permittivity. Temperature was varied using an external cooling bath and a pump, which circulated the cooling fluid around the sample cell. Liquid water content was measured during multiple warming and cooling cycles. Temperature was monitored in the sediment sample using PT100s with an accuracy of better than ±0.1°C.

Table 1. Borehole and sediment characteristics for each drill site.

	C2	C3	C4	C5	C1
Distance to coast [km]	11.5	3	1	0.5	0.1
Water depth [m]	6.0	4.4	2.2	1.5	--
Ice thickness [m]	1.35	1.85	2.1	1.5	--
Core depths [m relative to sea level]	to -77	to -31	to -32	to -31	+26.2 to -34
Bottom water salinity [‰]	29.2	30.0	32.2	>100	--
Bottom water temp. [°C]	-1.5	-1.6	-1.7	-6	--
Frost table depth [m]	35	12	3.9	2.8	--

Results

The exposed coastal profile is described in Schirrmeister et al. (submitted), and consists of silty sand, organic-rich ice complex deposits overlying silty sand to fine sand deposits. The subsea sediment is composed of silty sands to fine sands. Based on available analyses, we cannot distinguish between unfrozen sediment that has been redeposited and sediment that has thawed in place. The upper thawed subsea sediment shows weakly layered structure, and has probably been reworked in its upper portion by redeposition and wave action. Below the frozen-unfrozen interface, the presence of freshwater ice, ice wedges, composite ice wedges, ataxitic layers indicating the presence of an active layer with seasonal thawing and layers of organic debris and twigs suggest terrestrial and shallow water environments. These features were found in C1 (25.5-12.8 m r.s.l.), C5 (2.8-14.5 m r.s.l.), C4 (3.9-14 m r.s.l.) and C2 (40.3-64.7 m r.s.l.), roughly corresponding to the upper portion of the frozen sediments for the subsea cores in Figure 3. In each core, these sediments are underlain by sandier, cryotic sediments without significant segregated ice.

Water depth decreased gradually with distance from the shore (1.5, 2.2, 4.4, 6.0 m at C5, C4, C3 and C2, resp.). C5

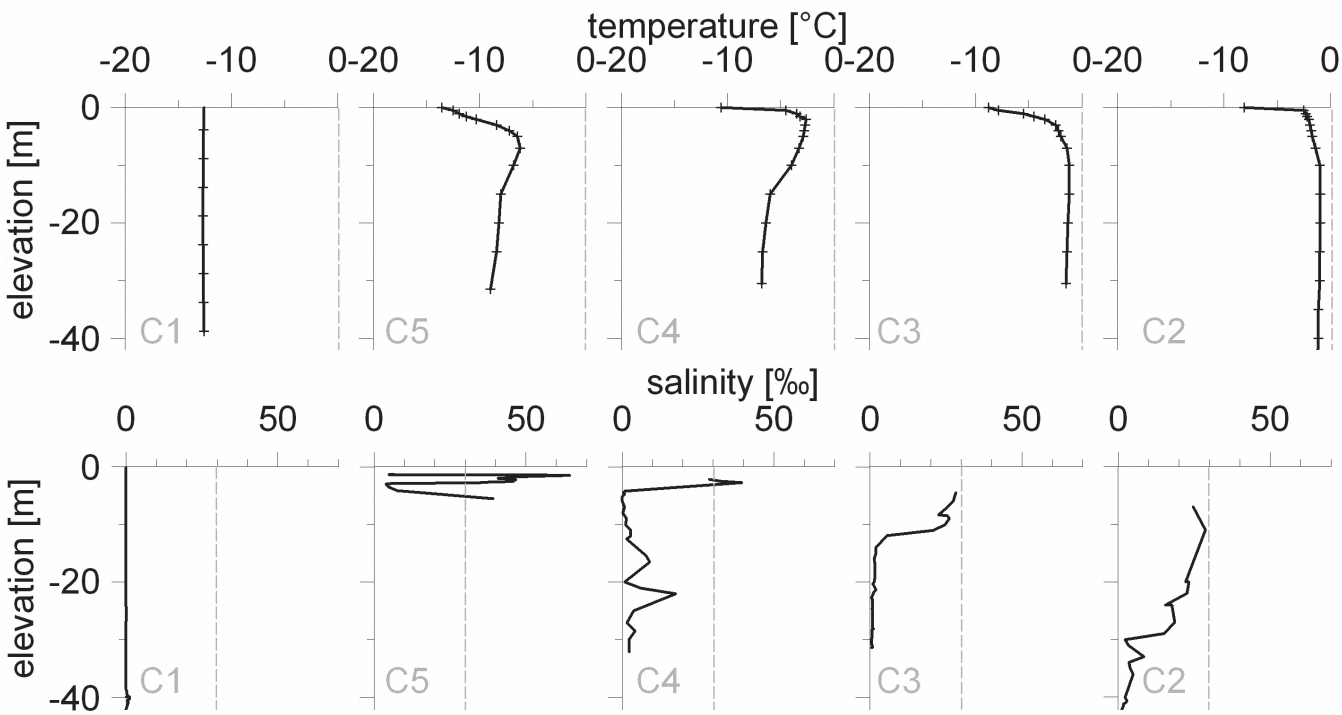

Figure 4. Profiles of sediment temperature (top) and pore water salinity (bottom) from onshore (at left) to furthest offshore (at right; some data taken from Rachold et al. 2007). Available data for the depths from 0 to 42 m below sea level are presented for all cores.

was therefore located in the bottom-fast ice zone. Bottom water salinities decreased with distance from shore, while temperatures increased (Table 1). The interface between unfrozen and frozen sediment was located at successively lower depths within the sediment column with increasing distance from the coastline (2.8, 3.9, 12 and 36 m at C5, C4, C3 and C2, respectively). Sediment temperatures at 20 m below sea level increased from an almost constant mean

Annual value of -13°C onshore (C1), to -8°C, -6°C, -1.5°C and -1°C with increasing distance from the coast (Fig. 4). The temperature gradient over depth in C2 was almost flat over the upper 40 m of the sediment profile. The temperatures at the frozen/unfrozen interface were -8.4, -2.8, -1.2 and -1.1 in C5, C4, C3 and C2, respectively. The salinity of pore water extracted from the sediment varied between 0 and 65‰ (Fig. 4). Salinities exceeding that of bottom water measured in August 2003 (17.3‰ to 20.7‰) and below the ice in April 2005 (29.2‰ to over 100‰) were found in C5 and C4. In C3 and C2, a saline pore water front was observed at depths of about 12 and 36 m, respectively. Frozen sediment generally had pore water salinity less than 5‰. Higher salinity found below the uppermost salt water front in C4 (around 16 and 22 m), and the variability in C5 salinity, suggest irregular brine production or migration.

Figure 5 shows the ice content as a function of temperature for four sediment samples. The sediment samples vary in terms of grain-size, sediment composition, and pore-water salinity. Differences in salinity are large enough (12, 25, 45 and 65‰) to make grain-size differences negligible in determining volumetric liquid water content at temperatures less than about -2°C. Increasing salinity decreases the sediment volumetric ice content. Ice content is shown for both cooling and warming temperature histories of all four samples. Hysteresis is clearly visible for the two lower salinity samples, but results in no more than a 4% ice content difference between warming and cooling at 45‰, and negligible differences at 65‰. For the latter, warming and cooling curves are superimposed. For the lowest salinity sample, the rate of change of state with temperature is low at temperatures below -5°C. At higher salinities, any addition or removal of heat results in significant phase change (around 2% K^{-1}), rather than temperature change.

Measured total volumetric water contents in core C2 range from 14% to 100%. Ice content in C2 increased with depth from a low value of 3% (based on temperature and pore-water salinity) to a maximum of 20% in the unfrozen zone. In the frozen sediment, ice contents ranged from 17% to 100%. Values in excess of 40% (based on core volume and weight loss on drying) corresponded to depths which were identified as frozen in the field and contained segregated ice. Segregated ice occurred as ice lenses, injection ice, ice wedges, and composite ice wedges. Values determined by weighing dried samples match to within 15% of adjacent freshwater samples.

Discussion

Previous results from this campaign were based on field observations (Overduin et al. 2007a+b, Rachold et al. 2007). In this paper, we add laboratory analyses performed on pore water and sediment samples to describe the position and temperature of the frozen-unfrozen interface in the subsea

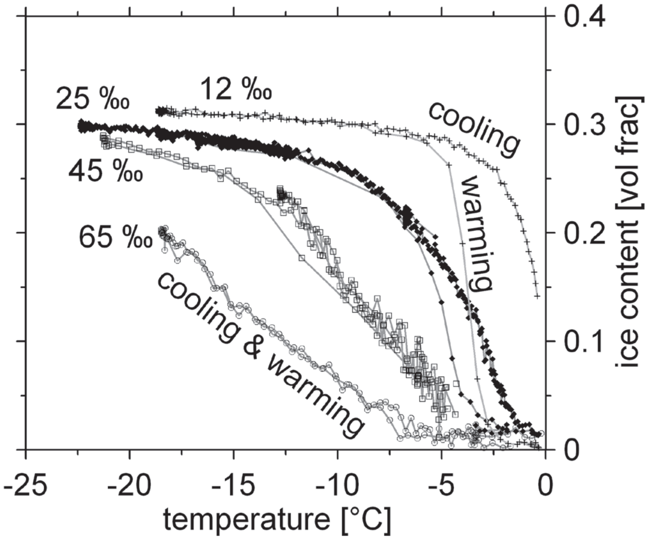

Figure 5. The volumetric ice content of four sediment samples (salinities: 12, 25, 45, and 65‰) as a function of temperature. Data were collected during cooling and warming for all four samples.

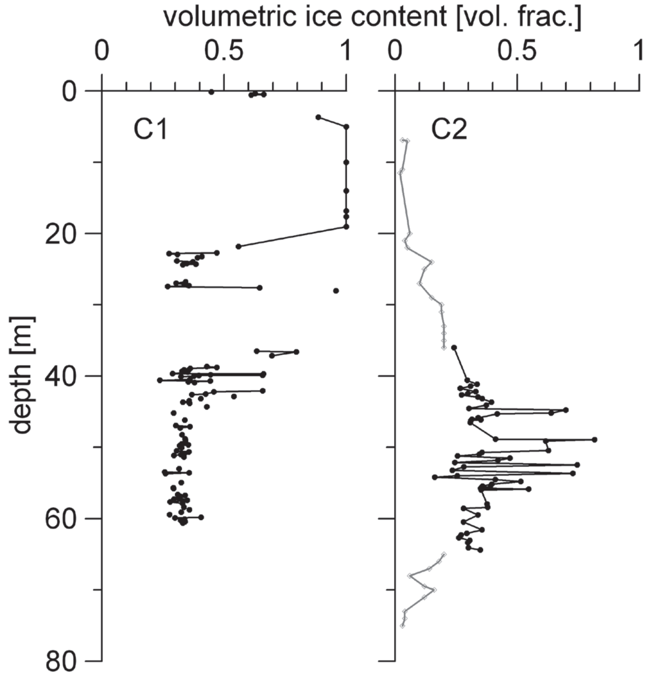

Figure 6. The volumetric ice content of the cores C1 and C2.

sediment. Coastal erosion and the subsequent inundation of the land at Cape Mamontov Klyk result in a large geomorphologic change in the upper permafrost, including thermoerosion, reworking of the eroded material, transport and redeposition offshore. These processes currently result in the thawing, removal, and redeposition of about the upper 25 m of permafrost. Redeposited and underlying unredeposited (in-situ) sediment is considered permafrost, as it remains cryotic. The boundary between the two is not yet clear, but must lie at or above the frozen/unfrozen interface. The actions of thermoerosion, thermokarst basin flooding, and wave action on the shallow sea bottom (Are et al. 2001), will have attenuated any topographic reflections of the previous thermokarst topography in the transition from terrestrial to marine.

The depth within the sediment of the frozen/unfrozen interface is difficult to determine. The classification of sediment as frozen or unfrozen in the field is highly subjective, since it rests upon a determination of plasticity. The determination is generally made by examining core sections at the surface, after they have been subjected to drilling and passage through the borehole. In some studies, the sea bottom was probed, akin to a permafrost probe, until sufficient resistance was encountered (Osterkamp et al. 1989). The temperatures at the interface observed here ranged from -1.1°C to -8.4°C, with inferred ice contents between 5% and over 25%, based on salinity and temperature. The transition from ice-free to ice-bearing to ice-bonded is likely to be gradual in most settings. Sediment ice and liquid water content depends strongly on pore water salinity over a wide temperature range (from 0°C to -20°C). As a consequence of this and the low temperature gradient, the phase boundary (the zone between ice-free sediment and sediment unaffected by saline solution) in C2 is almost 30 m thick, and covers a range of ice contents from 3% to over 20% by volume. Detection methods sensitive to step-like transitions in material properties over a short depth range, such as seismic or geoelectric methods, are thus confronted with a poor reflector.

The high salinities observed in the uppermost sediment at C5 (Fig. 4) strongly suggest that salt exclusion during sea ice formation results in brine formation. In this case, the brine formed was under positive pressure, and flooded and flowed out of the borehole 8-10 hours after drilling (Rachold et al. 2007). The salinity profile for C5 suggests the diffusion of at least one brine front down a strong concentration gradient into the sediment, which may be due to the formation of a seasonal active layer (Osterkamp et al. 1989). The progressive diffusion of the brine front into the sediment pore water is evident from the salinity graphs of Figure 4. Applying a mean ice thickness of 1.7 m, the bottom-fast ice (BFI) zone extends over 2 km from shore. Under current coastline retreat (4 to 4.5 m a^{-1}), this translates to seasonal brine production over a period of 440 to 500 years. The low inclination of the seabed in the western Laptev suggests that even longer periods are common, since coastal retreat for the Laptev Sea is 2 to 2.5 m a^{-1}. Both coastal retreat rates and the nearshore shore face profile will be important in determining the rate of descent of the salt front into the sediment, and differences may help to explain the variability observed in the position of the frozen/unfrozen interface. Provided that sediment could be removed from the shoreface effectively enough to account for increased erosion, increases to sea level rise will lower the rate of permafrost degradation by seawater penetration.

Conclusions

The saline-freshwater interface in the sediment column was identified in cores drilled off the coast of Mamontov Klyk in the Laptev Sea. Bottom-fast ice results in highly concentrated sea water being produced at the ice-sediment interface, and probably accelerates the degradation of subsea permafrost. Saltwater diffusion into the sea bottom results in the presence of ice-free sediment at sub-zero temperatures down to a depth of 40 m in subsea sediments, 12 km offshore. The transition from ice-free to ice-bonded sediment occurs over a depth range of about 30 m 2.6-6.0 ka after inundation. The energy requirements for the permafrost to become near-isothermal are reduced by the diffusion of salt water into the sediment. Changes in phase as a result of salt water intrusion and warming change the effective thermal properties of the sediment and affecting the rate of further degradation.

Acknowledgments

We gratefully acknowledge the help of all those involved in the field and lab work, including Alexander Derevyagin, Antje Eulenburg, Katja Hockun, Viktor Kunitsky, Franziska Merker, Gunter Stoof, and Maria Winterfeld. This work was supported by the German Ministry for Education and Research (BMBF). We thank Dmitry Melnichenko, director of the Tiksi Hydrobase, for providing logistic support. Improvements to the paper were suggested by two reviewers and William R. Bolton.

References

Arctic Coastal Dynamics Project Team, 2008. The Arctic Coastal Dynamics (ACD) Circumpolar Coastal Classification.

Are, F.E., Grigoriev, M.N., Rachold, V., Hubberten, H.-W., Rasumov, S.O. & Schneider, W. 2001. Shoreface profiles of the central and western Laptev Sea coast. *Reports on Polar Research* 388: 60-64.

Bauch, H.A., Mueller-Lupp, T., Taldenkova, E., Spielhagen, R.F., Hassens, H., Grootes, P.M., Thiede, J., Heinemeier, J. & Petryashov, V.V. 2001. Chronology of the Holocene transgression at the North Siberian margin. *Global and Planetary Change* 31: 125-139.

Brown, J., Ferrians Jr., O.J., Heginbottom, J.A. & Melnikov, E.S. 1998. Digital Circum-Arctic Map of Permafrost and Ground-Ice Conditions. In: International Permafrost Association, *Circumpolar Active-Layer Permafrost System (CAPS) version 1.0.*

Grigoriev, M.N. & Rachold, V. 2003. The degradation of coastal permafrost and the organic carbon balance of the Laptev and East Siberian Seas. In: M. Phillips (ed.), *Proceedings of the 8th International Conference on Permafrost, Zürich, Switzerland, 21-25 July 2003*, 319-324.

Grosse, G., Schirrmeister, L. & Malthus, T. 2006. Application of Landsat-7 satellite data and a DEM for the quntification of thermokarst-affected terrain types in the periglacial Lena-Anabar coastal lowland. *Polar Research* 25(1): 51-67.

Hutter, K. & Straughan, B. 1999. Models for convection in thawing porous media in support of the subsea permafrost equations. *Journal of Geophysical Research* 104(B12): 29 249-29 260.

Junker R., Grigoriev, M.N. & Kaul, N. Non-contact infrared temperature measurement in dry permafrost boreholes, accepted for publication in the *Journal of Geophysical Research*.

Osterkamp, T.E., Baker, G.C., Harrison, W.D. & Matava, T. 1989. Characteristics of the active layer and shallow subsea permafrost. *Journal of Geophysical Research* 94(C11): 16227-16236.

Outcalt, S. 1985. A numerical model of subsea permafrost. In: D.M. Anderson & P.J. Williams (eds.), *Freezing and Thawing of Soil-Water Systems*. New York: American Society of Civil Engineers, 58-65.

Overduin, P.P., Grigoriev, M.N., Junker, R., Rachold, V., Kunitsky, V.V., Bolshiyanov, D.Yu. & Schirrmeister, L. 2007a. The Expedition COAST I: COAST Drilling Campaign 2005: Subea permafrost Studies in the near-shore zone of the Laptev Sea. *Reports on Polar Research* 550: 1-40.

Overduin, P.P., Hubberten, H.-W., Rachold, V., Romanovskii, N.N., Grigoriev, M.N. & Kasymskaya, M. 2007b. The evolution and degradation of coastal and offshore permafrost in the Laptev and East Siberian Seas during the last climatic cycle. In: J. Harff, W.W. Hay & D.M. Tetzlaff (eds.), *Coastline Changes: Interrelation of Climate and Geological Processes, Geological Society of America*, Special Paper 426, Boulder, USA.

Rachold, V., Bolshiyanov, D.Yu., Grigoriev, M.N., Hubberten, H.-W., Junker, R., Kunitsky, V.V., Merker, F., Overduin, P.P. & Schneider, W. 2007. Near-shore Arctic subsea permafrost in transition. *EOS: Transactions of the American Geophysical Union* 88(13): 149-156.

Romanovskii, N.N. 1993. Osnovy Kriogeneza Litosfery, Izdatelstvo Moscow State University, Moscow.

Romanovskii, N.N. & Hubberten, H.-W. 2001. Results of permafrost modeling of the lowlands and shelf of the Laptev Sea region, Russia. *Permafrost and Periglacial Processes* 12: 191-202.

Romanovskii, N.N., Hubberten, H.-W., Gavrilov, A.V., Tumskoy, V.E. & Kholodov, A.L. 2005. Permafrost of the east Siberian Arctic shelf and coastal lowlands. *Quaternary Science Reviews* 23: 1359-1369.

Roth, K., Schulin, R., Flühler, H. & Attinger, W. 1990. Calibration of time domain reflectometry for water content measurement using a composite dielectric approach. *Water Resources Research* 26(10): 2267-2273.

Schirrmeister, L., Grosse, G., Kunitsky, V.V., Magens, M., Meyer, H., Derivyagin, A.Yu., Kuznetsova, T., Andreev, A.A., Kienast, F., Grigoriev, M. & Preusser, F. submitted. Periglacial landscape evolution and environmental changes of Arctic lowland areas during the Late Quaternary (Western Laptev Sea coast, Cape Mamontov Klyk). submitted to *Polar Research.*

Swift, D.W. & Harrison, W.D. 1984. Convective transport of brine and thaw of subsea permafrost: Results of numerical simulations. *Journal of Geophysical Research* 89(C4): 2080-2086

Sources of Discrepancy Between CCSM Simulated and Gridded Observation-Based Soil Temperature Over Siberia: The Influence of Site Density and Distribution

Debasish PaiMazumder
University of Alaska Fairbanks, Geophysical Institute & College of Natural Science and Mathematics
Nicole Mölders
University of Alaska Fairbanks, Geophysical Institute & College of Natural Science and Mathematics

Abstract

Soil-temperature climatologies determined at different depths from simulations with the Community Climate System Model version 3 (CCSM), capture the annual phase of gridded soil-temperature climatologies based on observations for 1951–1980, 1961–1990, and 1971–2000, but not the amplitude; some of these discrepancies can be attributed to simulated forcing (PaiMazumder et al. 2007). By using soil-temperature data simulated by the Weather Research and Forecasting (WRF) model, it is shown that some of the discrepancies between CCSM-derived and gridded observed climatologies may result from the interpolation required for gridding and/or network design (density and distribution of sites).

Keywords: climate simulation; network design; soil-temperature evaluation; Siberia; uncertainty.

Introduction

Accurate simulation of soil temperature in Climate System and Earth System Models is essential because soil temperature influences high-latitude hydrology, biochemical processes, and ecosystems. Soil temperatures are mostly controlled by the surface water and energy balance, which explains the strong connection and feedback between soil and near-surface atmospheric conditions. In the Arctic and Subarctic, the onset, duration, thickness, density, and structure of seasonal snow cover strongly influence soil temperatures (e.g., Zhang et al. 1996, Mölders & Romanovsky 2006).

Soil temperatures simulated at different depths by the Community Climate System Model version 3 (CCSM) (Collins et al. 2006a) are evaluated over Siberia for three climatologies (1951–1980, 1961–1990, 1971–2000) by means of observational data (PaiMazumder et al. 2007) provided by the National Snow Ice Data Center (NSIDC) (Zhang et al. 2001). PaiMazumder et al. (2007) also evaluated CCSM-derived climatologies of near-surface temperature, cloud fraction, precipitation, and snow depth with those from ERA40 reanalysis, the International Satellite Cloud Climatology project (ISCCP), the Global Precipitation Climatology Center (GPCC), and the NSIDC, respectively, to examine the sources for discrepancies between simulated and observed soil-temperature climatology. Inaccurate simulation of near-surface temperature, cloud fraction, precipitation, and snow depth may have some influences on discrepancies between CCSM-derived and observed soil-temperature climatology, but do not explain all discrepancy found. Sensitivity studies with slightly altered plant functional types and percentage of sand attributed marginal discrepancies from incorrect percentages of sand and/or plant types (PaiMazumder et al. 2007).

Typically, climate models like CCSM provide soil temperatures that represent a volume average of several hundred square kilometers in horizontal extension of several centimeters in thickness. It is obvious that soil temperatures simulated for such a volume are difficult to compare to measurements at a site (point measurements). Therefore, it has become common practice to interpolate available measurements to the grid of the climate model (e.g., Li et al. 2007). It is obvious that such interpolation may introduce uncertainty into the grid-cell averages; hence, the evaluation. Since the gridded soil-temperature climatologies are based on measurements projected onto the CCSM3 grid by Cressman interpolation (PaiMazumder et al. 2007), some discrepancies between CCSM-derived and gridded observed climatologies may result from interpolation and/or network density and distribution. Observational networks are often designed with accessibility and ease of maintenance in mind. Most of the Siberian soil-temperature sites are long-term agricultural monitoring stations. Consequently, the observational network follows agricultural-used land along major haul ways and is not uniformly distributed. Hence, the density and/or design of network may bias the regional averages estimated therefrom. Mitchell et al. (2004) assessed accuracy and reliability of gridded data and concluded that observed gridded data (1901–2000) are not appropriate for climate change. They also describe the development of high resolution (0.5°) of gridded dataset (Climate Research Unit [e.g., CRU TS 2.0] data) for the globe derived from climatological observations and transient coupled atmosphere-ocean general-circulation-model (GCM) simulations. The gridded dataset depends on the applied interpolation algorithms, and always has to be associated with an assessment of the accuracy of the grid point values. Therefore, it is essential to assess the uncertainty in regional averages resulting from the density and/or design of an observational network. The aim of our case study is to exemplarily investigate this uncertainty to further assess the discrepancies between CCSM-derived and observed soil-temperature climatologies found by PaiMazumder et al.

(2007). In doing so, the Weather Research and Forecasting (WRF) (Skamarock et al. 2005) model is used to provide a dataset of soil temperatures that will be considered as "reference" for determination of regional averages to which data from a real network and artificial networks are compared to assess the accuracy of gridded datasets based on station data, and to develop recommendations for network design to optimize their use for model validation.

Experimental Design

Brief model description

The CCSM is a fully coupled climate model to simulate the Earth system over broad ranges of spatial and temporal resolutions. It consists of the Climate Atmospheric Model, version 3 (CAM3) (Collins et al. 2006b), the Community Land Model version 3 (CLM3) (Dai et al. 2003, Oleson et al. 2006), the Community Sea Ice Model version 5 (CSIM5) (Briegleb et al. 2004), and the Parallel Ocean Program version 1.4.3 (POP) (Smith et al. 1992). These four components exchange data via a coupler without flux correction.

CCSM is run with 26 vertical layers at a spectral truncation of T42 corresponding to a spatial resolution of ≈2.8° x 2.8°. CCSM is started with the ecliptic conditions of 1-1-1950 and CO_2 concentration of 355 ppmv. Each model component is spun up separately. Based on these simulations, we determine three climatologies, 1951–1980, 1961–1990, and 1971–2000.

The WRF is a mesoscale non-hydrostatic model. Out of the variety of physical options, we use the following model setup: Cloud formation and precipitation processes at the resolvable scale are considered by Thompson et al.'s (2004) five-water class (cloud-water, rainwater, ice, snow, graupel) mixed-phase bulk-microphysics parameterization. The Grell-Devenyi (2002) ensemble parameterization considers subgrid-scale convective clouds. The Goddard shortwave-radiation scheme and the Rapid Radiative Transfer Model (Mlawer et al. 1997) are applied. The Yonsei University scheme (Skamarock et al. 2005) is used for simulating atmospheric boundary layer processes. Monin-Obukhov similarity theory is applied for surface-layer physics. Soil temperature, volumetric ice and water content, snow temperature and density and the exchange of heat and moisture at the land-atmosphere interface are determined by a modified version of the Rapid Update Cycle land-surface model (Smirnova et al. 1997, 2000).

The WRF domain encompasses Siberia by 70 x 150 grid-points with a grid-increment of 50 km and 31 vertical layers from the surface to 50 hPa. Soil conditions are determined at six levels. In the presence of snow, five snow layers are considered. The time step is 200s. The National Centers for Environmental Prediction (NCEP) 1.0° x 1.0° and 6h-resolution global final analyses (FNL) serve as initial and boundary conditions. For our case study, we perform simulations for July and December 2005. They start daily at 1800 UT for 30 hours of integration. We discard the first six hours as spin-up time.

Analysis

To estimate uncertainty due to network density and design, WRF-simulated soil temperatures serve to represent data from an optimal, dense, and equally distributed observational network. Regional averages of soil temperatures determined from the WRF output for July and December 2005 are considered to be the "reference."

Regional averages of soil temperature are determined for the 411 sites of the actual historic observation network used in PaiMazumder et al.'s (2007) CCSM soil-temperature evaluation. Herein, the soil temperature simulated for a WRF grid cell wherein a site falls is taken as the soil temperature for that site. This procedure is common practice in mesoscale modeling (e.g., Narapusetty & Mölders 2005). Four artificial networks are assumed with 500, 400, 200, and 100 arbitrarily taken WRF grid cells as "sites." These networks are denoted 500-, 400-, 200-, and 100-site networks hereafter. Soil temperatures obtained from WRF simulations at the 500, 400, 200, and 100 sites are used to calculate the regional averages for these networks. These regional averages are compared with the reference regional averages to assess the contribution of network density and design to uncertainty in gridded data used for evaluation of climate model data.

Since systematic and nonsystematic errors can contribute to any simulation result, as well as to regional averages obtained from different networks, performance measures like bias, standard deviation of errors (SDE), root mean square errors (RMSE), and correlation coefficients (e.g., Anthes 1983, Anthes et al. 1989) are calculated at different spatial and temporal scales for the various networks. The performance measures and correlation coefficients are determined to evaluate the discrepancies between the regional averages obtained from the "reference" and those of a network. They are calculated for all networks for the daily and monthly course.

To estimate the uncertainties in regional averages resulting from the density and design of networks, we compare the regional averages of soil temperature obtained from the WRF simulation ("reference") and various site networks (500-, 400-, 200-, 100-site network and historic networks). In this case study, we consider the accuracy of soil temperature measurements to be within ±0.5 K for the reasons discussed in PaiMazumder et al. (2007). The regional averages of soil temperature estimated from the "reference" and the different networks will be considered to be in good agreement if regional averages obtained from the different networks lie within the above-mentioned uncertainty range to the "reference."

In a next step, we compare the uncertainty determined as described above with the discrepancies found between CCSM-derived and gridded-observation-derived climatologies by PaiMazumder et al. (2007) to assess how much the network design may explain some of these discrepancies.

Results

Impact of network design on regional averages

Regional averages of soil temperature obtained from the artificial networks are highly correlated with those of the reference (>0.972) at all depths in both months. Regional averages of soil temperature obtained from the historic network are more highly correlated with the "reference" in December (R = 0.921) than in July (R = 0.732) at 00 UT, 06 UT, 12 UT, and 18 UT at all depths.

In both months, the daily spatial standard deviations of soil temperatures obtained from the historic network are higher than those of all other networks. The standard deviations of soil temperature obtained from the various networks are higher at all depths in December than in July. In December, in general, soil temperatures vary strongly in space due to the large horizontal differences in snow cover and/or thickness. Thus, taking measurement along the haul ways leads to larger standard deviations of the regional averages in winter than summer because of snow conditions and terrain height of the site. In July, for given insolation and soil type, soil heating/cooling varies less in space than in December, when differences in snow cover/thickness may strongly affect soil temperatures. Consequently, taking the measurement along a haul way has less impact on the regional average and its standard deviation for Siberia in summer than winter.

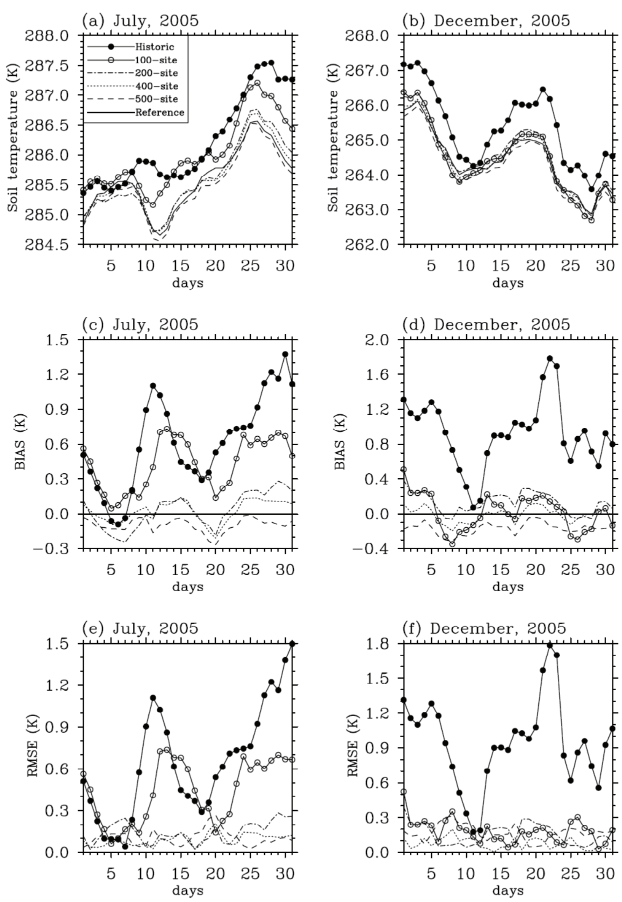

Figure 1. Temporal behavior of (a) regionally averaged soil temperature at 0.2-m depth obtained from the "reference," 500-, 400-, 200-, 100-site network and the historic network for July 2005 and (b) December 2005. Biases for (c) July and (d) December and RMSE for (e) July and (f) December between the "reference" and 500-, 400-, 200-, 100-site network and the historic network. Note that in (c) to (f), labels on the y-axis differ. In (c) and (d), the thick line serves to better visualize the positive and negative bias.

At 0.2-m depth, soil temperatures obtained from the historic network overestimate the reference average by up to 1.5 K and 1.8 K in July and December, respectively (Fig. 1). The historic network also fails to capture the timing of the soil-temperature maxima and minima represented in the reference average. For example, on July 11 and 26, upper soil temperatures from the historic network average do not reflect the warm periods seen in the reference average (Fig. 1). These differences in timing of extremes between the regional averages of the historic network and "reference" occur due to a frontal system passing Siberia. The non-equal distribution of sites of the historic network therefore gets "biased" to the time when the system passes the majority of the sites. In December, the high bias found for the historic network may partly be explained by the fact that the sites of the historic network may not well represent the regional differences in snow cover and/or thickness. The 100-site network also fails to capture the regional soil-temperature averages obtained from the "reference" with 0.8-K bias in July (Fig. 1), while in December, the 100-site network captures the reference average well. Obviously, a randomly distributed 100-site network represents soil conditions in winter well when the soil is partly insulated by snow. However, in summer, convection may lead to spatial differences in soil heating due to shading by clouds and/or heat input by precipitation that a 100-site network cannot capture appropriately. Regional averages of soil temperature obtained from 500-, 400-, and 200-site networks provide acceptable results in comparison to the reference average at all depths in both months. The historic network shows higher biases and RMSEs than all other networks in both months (Fig. 1, Table 1). This means that the historic network introduces some bias into regional averages and any evaluation study therewith.

Higher systematic bias may have occurred due to the difference in landscape and terrain elevations between the regional averages derived from the "reference" and historic network. At 0.2-m depth (0.4 m and 1.6 m), RMSEs for the historic network reach up to 1.5 K (1 K and 1.9 K) and 1.8 K (1.3 K and 1.1 K) in July and December, respectively (Fig. 1). Errors in regional soil-temperature averages based on the historic network are also high for the upper soil layer, and errors decrease at 0.4-m depth and increase again for deeper soil layers in both months. The high diurnal variability close

Table 1. Monthly averages of bias and RMSE for the historic and 200-site networks for upper and deeper soil.

Networks		Historic network		200-site network	
Month	Layer	bias	RMSE	bias	RMSE
July	Upper	0.6	0.7	0.02	0.1
	Deeper	1.7	1.9	0.3	0.3
December	Upper	1	1	0.1	0.2
	Deeper	1.2	1.2	0.2	0.3

to the surface may cause the high errors in the upper soil (Table 1). The increase found for deeper soil layers may be related to the constant lower boundary condition used in WRF. These soil-temperature values are from climatologies which differ notably in space. Thus, the historic network cannot represent the "reference" because the sites are not randomly distributed to capture the regional pattern.

Evaluation of CCSM by gridded data

As reported by PaiMazumder et al. (2007), CCSM captures well the phase of the 30-year average annual soil temperature curves at all depths, but not the amplitude. CCSM overestimates the 0.2-m soil temperature for the majority of the grid cells over Siberia from December to March for the first climatology (1951–1980) (Fig. 2). Similar is true for 0.4-m and 1.6-m depths, but with marginally decreasing frequency with increasing depth, whereas at 0.8 m and 3.2 m, CCSM overestimates soil temperature throughout the year (Fig. 2). In April, soil temperature will be overestimated for most of the grid cells at all depths if soil temperature is below freezing and underestimated otherwise, leading to overall overestimation. In May and June, the general pattern shifts towards underestimation at all depths except 3.2 m (Fig. 2). In July and August, CCSM tends to underestimate soil temperature by up to 1.2 K at 0.2 m, and overestimates them by up to 0.5 K at 0.4-m and 0.8-m depth. At 1.6 m, the tendency to overestimate soil temperature is obvious for the colder (<275 K), but less obvious for the warmer (>285 K) end of the temperature range. In September, soil temperatures are underestimated at 0.2-m and 0.4-m depth by up to 0.6 K and 0.4 K for most grid cells (Fig. 2). At 0.8 m and 1.6 m, CCSM overestimates soil temperatures by up to 0.4 K and 1.1 K, respectively, for most grid cells. In October, the general pattern again shifts towards overestimation by up to 2.5 K (Fig. 2). In November, simulated soil conditions are too warm for soil temperatures below the freezing point at all depths. PaiMazumder et al. (2007) also found that biases and RMSEs decrease with increasing depth because most variability occurs near the surface. RMSEs are higher in winter than in the other seasons for all three climatologies. Mean annual soil temperatures are over-estimated by 2.5 K, on average.

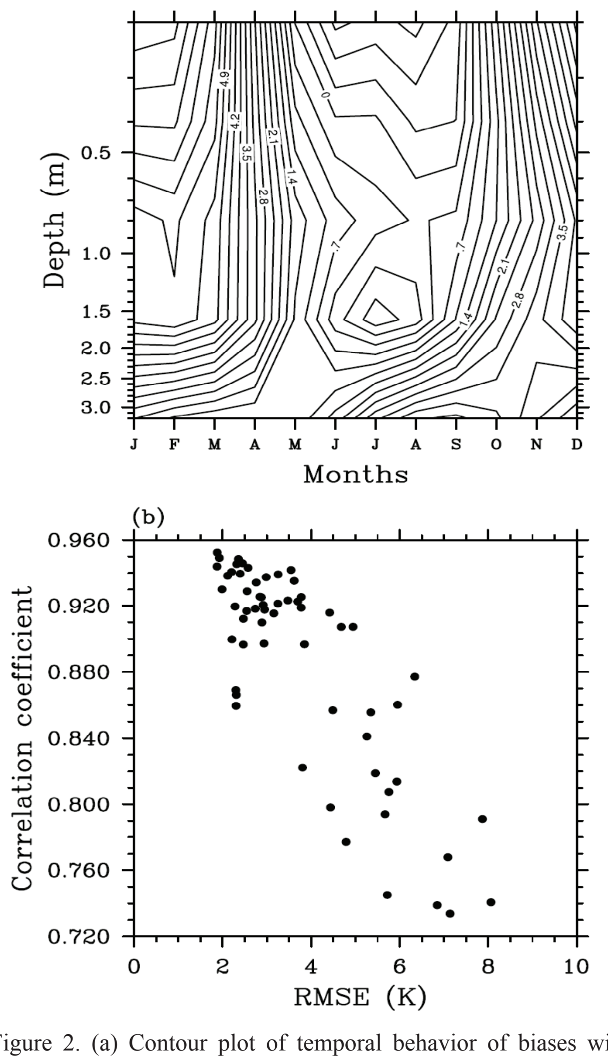

Figure 2. (a) Contour plot of temporal behavior of biases with depths for the first climatology (1951–1980). (b) RMSE vs. correlation coefficient for the first climatology for all 12 months at 0.2-m, 0.4-m, 0.8-m, 1.6-m, and 3.2-m depth.

Overall, CCSM simulates the annual average soil temperature reasonably well, though its performance is better in summer than in winter. Due to acceptable RMSEs and high correlations (cf. Fig. 2), PaiMazumder et al. (2007) concluded that the fully coupled CCSM acceptably simulates soil temperature. As pointed out by these authors, CCSM also has some difficulties in capturing near-surface temperature, cloud fraction, precipitation, and snow depth with biases (RMSEs) -1.0 K (3 K), 0.32% (0.52%), 7.6 mm/month (19.9 mm/month), and 0.04 m (0.09 m), respectively (for further details see Table 1 in PaiMazumder et al. 2007). Hence, the inaccurate simulation of near-surface temperature, cloud fraction, precipitation, and snow depth may contribute to the discrepancies between CCSM-derived and observed soil temperature climatology. Difference in plant functional types between model and real world and decreasing and increasing sand percentage in the model may marginally affect soil temperature. Thus, incorrect assumptions on the mineral soil type cannot explain the discrepancies found. Another source of these discrepancies may be that CCSM only considers mineral soils. However, large areas of Siberia have organic soils at least in the upper soil layers. The thermal and hydraulic properties of mineral and organic soils differ strongly and yield to appreciable differences in soil temperature and soil-water freezing behavior (cf. Mölders & Walsh 2004, Lawrence & Salter 2007). Nicolsky et al. (2007) showed that incorporating organic matter in CLM3 significantly changes the soil temperature simulation. Thus, providing gridded data of organic material distribution and consideration of organic material in CCSM are essential future steps for the scientific community to take.

Discussion and Conclusions

PaiMazumder et al. (2007) found that CCSM tends to overestimate soil temperature in winter and underestimate in summer, with better performance in summer than winter. In spring and fall, simulated and observed climatologies agree the best. Therefore, we performed a case study with WRF for December and July 2005 to further examine reasons for discrepancies in CCSM-derived and observed soil-temperature climatologies. In this case study, we assume the soil temperatures simulated by WRF as a reference dataset from which we determine the "reference" regional averages. These reference averages are compared to the regional averages determined from WRF data at the sites of the network used in PaiMazumder et al. (2007) and to four randomly but spatially even distributed artificial networks to assess exemplarily potential contribution of the historic network to the discrepancies found by these authors.

The high differences (1.8 K) between regional averages of soil temperature obtained from the historic network and "reference" in December suggest that the network design may affect gridded observational averages more in December than in July. This means that the high discrepancies between CCSM-derived and observation-based gridded soil-temperature climatologies can be explained by the network design in winter.

PaiMazumder et al. (2007) also showed that in December, biases between simulated and observed soil temperature reach up to 6 K at 0.2-m depth; about 2.5 K bias may result from incorrect simulation of observed forcing. Our study shows that about 2-K bias may be explained by uncertainties due to network density in winter. This means that about 1.5-K bias may result from measurement errors and/or model deficiencies.

In July, biases caused by the historic network are higher than biases in CCSM found by PaiMazumder et al. (2007). Hence, we have to conclude that in summer, CCSM performs well for simulating soil temperature. On the contrary, in winter, biases in CCSM can only partially be explained by uncertainties due to network density.

Similar results are found for RMSE and SDE in winter, whereas in summer, RMSEs for the historic network are lower than RMSEs in CCSM by 1 K on average. Hence, the discrepancies between CCSM-simulated and observation-based gridded soil-temperature climatologies in winter can be explained by incorrect simulation of atmospheric forcing as well as network design. Thus, improvement of soil-model physics is essential for better winter soil temperature simulation.

From this case study, it can also be concluded that the historic network always fails to capture the "reference" regional soil temperature averages with high biases, RMSEs, and SDEs in both months. On the contrary, the randomly distributed 500-, 400-, and 200-site networks capture the "reference" regional soil-temperature averages well at all layers. These networks also capture well the diurnal variation of soil temperature in the upper soil. Hence, our case study suggests that randomly distributed networks of 200 sites or more reliably reproduce acceptable regional averages of soil temperatures for Siberia. However, maintenance of such networks may be expensive because many of the sites would not be easily accessible in a remote area like Siberia. Future studies should examine the general robustness of the influence of the network density and design.

Acknowledgments

We thank U.S. Bhatt, M.E. Brown, G. Kramm, S.E. Porter, J.E. Walsh, and the anonymous reviewers for fruitful comments; C. Swingly for help with the ERA40 data; B. Rudolf for access to the precipitation data; T. Zhang, A. Etringer, and J. McCreight for providing the gridded soil-temperature and snow-depth data; and J. Miller for installing CCSM3 at ARSC. This research was supported by the International Arctic Research Center, UAF, under the auspices of the NSF cooperative agreement OPP-0327664, and from EPSCoR grant 0701898. ARSC and NCAR provided computational support.

References

Anthes, R.A. 1983. Regional models of the atmosphere in middle latitudes. *Mon. Wea. Rev.* 111: 1306-1335.

Anthes, R.A., Kuo, Y.H., Hsie, E.Y., Low-Nam, S. & Bettge, T.W. 1989. Estimation of skill and uncertainty in regional numerical models. *Quart. J. Roy. Meteorol. Soc.* 111: 763-806.

Briegleb, B.P., Bitz, C.M., Hunke, E.C., Lipscomb, W.H., Holland, M.M., Schramm, J.L. & Moritz, R.E., 2004. Scientific description of the sea ice component in the Community Climate System Model, version three. NCAR Technical Note NCAR/TN463-STR, 70 pp.

Collins, W.D., Bitz, C.M., Blackmon, M.L., Bonan, G.B., Bretherton, C.S., Carton, J.A., Chang, P., Doney, S.C., Hack, J.J., Henderson, T.B., Kiehl, J.T., Large, W.G., McKenna, D.S., Santer, B.D. & Smith, R.D. 2006a. The Community Climate System Model: CCSM3. *J. Climate* 19: 2122-2143.

Collins, W.D., Rasch, P.J., Boville, B.A., Hack, J.J., McCaa, J.R., Williamson, D.L., Briegleb, B.P., Bitz, C.M., Lin, S.J. & Zhang, M. 2006b. The formulation and atmospheric simulation of the Community Atmosphere Model: CAM3. *J. Climate* 19: 2144-2161.

Dai, Y., Zeng, X., Dickinson, R.E., Baker, I., Bonan, G., Bosilovich, M., Denning, S., Dirmeyer, P., Houser, P., Niu, G., Oleson, K., Schlosser, A. & Yang, Z.L. 2003. The Common Land Model (CLM). *Bull. Amer. Meteor. Soc.* 84: 1013-1023

Lawrence, D.M. & Slater, A.G. 2007. Incorporating organic soil into a global climate model. *Clim. Dyn.* doi: 10.1007/s00382-007-0278-1.

Li, Z., Bhatt, U.S. & Mölders, N. 2007. Impact of doubled CO_2 on the interaction between the regional and global water cycle in four study regions. *Clim. Dyn.* doi 10.1007/s00382-007-0283-4.

Mitchell, T.D., Carter, T.R., Jones, P.D., Hulme M. & New, M. 2004. A comprehensive set of high-resolution grids of the monthly climate for Europe and the globe: the observed record (1901-2000) and 16 scenarios (2002-2100). Tyndall Centre for Climate Change Research, 55 pp.

Mlawer, E.J., Taubman, S.J., Brown, P.D., Iacono, M.J. & Clough, S.A. 1997. Radiative transfer for inhomogeneous atmospheres: RRTM, a validated correlated-k model for the longwave. *J. Geophys. Res.* 102D: 16663-16682.

Mölders, N. & Walsh, J.E. 2004. Atmospheric response to soil-frost and snow in Alaska in March. *Theor. Appl. Climatol.* 77: 77-105.

Mölders, N. & Romanovsky, V.E. 2006. Long-term evaluation of the Hydro-Thermodynamic Soil-Vegetation Scheme's frozen ground/permafrost component using observations at Barrow, Alaska. *J. Geophys. Res.* 111: D04105, doi: 10.1029/2005JD005957.

Narapusetty, B. & Mölders, N. 2005. Evaluation of snow depth and soil temperature predicted by the Hydro-Thermodynamic Soil Vegetation Scheme (HTSVS) coupled with the PennState/NCAR Mesoscale Meteorological Model (MM5). *J. Appl. Meteor.* 44: 1827-1843.

Nicolsky, D.J. & Romanovsky, V.E. 2007. Improved modeling of permafrost dynamics in a GCM land-surface scheme. *Geophys. Res. Lett.* 34: L08501, doi:10.1029/2007GL029525.

Oleson, K.W., Dai, Y., Bonan, G.B., Bosilovich, M., Dickinson, R., Dirmeyer, P., Hoffman, F., Houser, P., Levis, S., Niu, G.Y., Thornton, P., Vertenstein, M., Yang, Z.L. & Zeng, X. 2004. Technical description of Community Land Model (CLM). Technical Report NCAR/TN-461+STR, National Center for Atmospheric Research, Boulder, CO. 80307-3000, 174 pp.

PaiMazumder D., Miller, J., Li, Z., Walsh, J.E., Etringer, A., McCreight, J., Zhang, T. & Mölders, N. 2007. Evaluation of Community Climate System Model soil temperatures using observations from Russia. *Theor. Appl. Climatol.* doi: 10.1007/s00704-007-0350-0.

Skamarock, W.C., Klemp, J.B., Dudhia, J., Gill, D.O., Baker, D.M., Wang, W. & Powers, J.G. 2005. A description of the advanced research WRF version 2. NCAR Technical Note, NCAR/TN-468+STR, 88 pp.

Smirnova T.G., Brown, J.M. & Benjamin, S.G. 1997. Performance of different soil model configurations in simulating ground surface temperature and surface fluxes. *Mon. Wea. Rev.* 125: 1870-1884.

Smirnova T.G., Brown, J.M., Benjamin, S.G. & Kim, D. 2000. Parameterization of cold season processes in the MAPS land-surface scheme. *J. Geophys. Res.* 105D: 4077-4086.

Thompson G., Rasmussen, R.M. & Manning, K. 2004. Explicit forecasts of winter precipitation using an improved bulk microphysics scheme. Part I: Description and sensitivity analysis. *Mon. Wea. Rev.* 132: 519-542.

Zhang, T., Osterkamp, T.E. & Stamnes, K. 1996. Influence of the depth hoar layer of the seasonal snow cover on the ground thermal regime. *Water Resour. Res.* 32: 2075-2086.

Zhang, T., Barry, R.G. & Gilichinsky D. 2001. Russian historical soil temperature data. National Snow and Ice Data Center, Boulder, CO, http://nsidc.org/arcss078.html/.

Remote Sensing-Based Study of Vegetation Distribution and Its Relation to Permafrost in and Around the George Lake Area, Central Alaska

Santosh K. Panda
Geophysical Institute, University of Alaska Fairbanks, Fairbanks, USA
Anupma Prakash
Geophysical Institute, University of Alaska Fairbanks, Fairbanks, USA
Diana N. Solie
Alaska Division of Geological & Geophysical Surveys, Department of Natural Resources, Fairbanks, USA

Abstract

We employed remote sensing techniques in combination with in situ measurements to investigate the presence/absence of permafrost in and around the George Lake area, central Alaska. The complex interrelationship between vegetation, topography, local geology, and permafrost in a discontinuous permafrost setting was examined. We used SPOT multi-spectral data to generate a land cover map for the study area. Eleven land cover classes were mapped including eight vegetation classes in a maximum likelihood classifier. Correlative relationship between surface parameters and permafrost was used to gain a preliminary understanding of permafrost distribution in the study area. In situ measurements in different vegetation and topographic settings disclosed that scattered short black spruce with thick moss layer is a potential indicator of permafrost with shallow active layer depth. Integrated analysis of vegetation map, equivalent latitude values, and field observations suggests that equivalent latitude greater than 63° is permissive of permafrost in the study area.

Keywords: Interior Alaska; mapping; permafrost; remote sensing.

Introduction

This study integrates remotely sensed (SPOT multispectral) data with field data for the area near George Lake, central Alaska, to understand the complex interrelationship between vegetation, topography, local geology, and permafrost in a discontinuous permafrost setting. It is a part of the Alaska Division of Geological & Geophysical Surveys (DGGS) project on the proposed Alaska gas pipeline corridor that aspires to identify the associated geohazards along the Alaska Highway corridor (such as areas underlain by permafrost, areas with highest potential for active faulting, liquefaction, landslides) (Solie & Burns 2007).

In order to make informed decisions regarding alignment and design of future infrastructure development, and assess the impact of climate change, a precise understanding of near-surface permafrost conditions is critical. Direct field investigation of permafrost or detection by indirect geophysical technique is limited to small areas due to the huge extent, extreme climate, and limited fieldwork time, and poor accessibility to most parts of arctic and sub-arctic Alaska. In such a situation, remote sensing techniques can be of great help. Many environmental factors that reflect the permafrost condition and indicate its presence/absence (like vegetation, topography, snow cover) can be mapped fairly from remote sensing data. The correlative relationship between these environmental factors and permafrost is exploited to get indirect information about subsurface permafrost (e.g., Etzelmuller et al. 2001, 2006, Frauenfelder et al. 1998, Jorgenson & Kreig 1988, Leverington & Duguay 1996, 1997, Morrissey et al. 1986, Peddle 1991, Peddle & Franklin 1993). Distribution of permafrost in discontinuous permafrost zones is strongly influenced by local climate, topography (elevation, slope, and aspect), local hydrology, vegetation cover, geology, and seasonal snow cover (e.g., Smith 1975, Goodrich 1982). Vegetation cover is one of the best indicators of spatial distribution of permafrost and relative thickness of active layer in discontinuous permafrost zones (Duguay et al. 2005). Hence, detailed vegetation mapping is critical in mapping near-surface permafrost.

Methods

Fieldwork was carried out during summer 2007 along the Alaska Highway between Lisa Lake and Dot Lake (Fig. 1). We visited different vegetation, topographic, and geologic settings, and collected data on active layer depth, soil type, moss layer thickness, and vegetation type. We sampled a total of 155 locations using a frost probe for active layer depth measurements and a soil auger to reveal the soil profile in the top 1.5 m.

The most widely accepted definition of permafrost is “any ground that remains frozen for at least two consecutive years” (French 2007). However, in this study, we adopted the permafrost definition by Brown (1967) and French (1976) that define “ground remaining frozen (at or below 0°C) throughout at least one summer” as permafrost. We also assume the depth to frozen ground measured using a frost probe in the field as active layer depth.

Absence of ice in well-drained sandy soil makes it impossible to measure active layer depth using a frost probe. In such situations, soil temperature is the only criteria

Table 1. Classification accuracy totals. For a brief description of classes (superscript 1-11), please refer to text.

Class Name	Reference totals	Classified totals	Number correct	Producer's accuracy (%)	Kappa statistics
[1]Thick spruce	15	15	15	100	1.00
[2]Spruce	64	63	62	96.88	0.98
[3]Spruce & Willow	43	41	35	81.4	0.82
[4]Birch & Spruce	34	31	31	91.18	1.00
[5]Deciduous	22	22	16	72.73	0.70
[6]Aspen	20	25	19	95	0.74
[7]Alpine Vegetation	5	6	5	100	0.83
[8]Grassland	16	11	10	62.5	0.90
[9]Turbid river water	13	13	13	100	1.00
[10]Lake	15	15	15	100	1.00
[11]Exposed surface	5	10	4	80	0.38
Totals	252	252	225	89.29	0.87

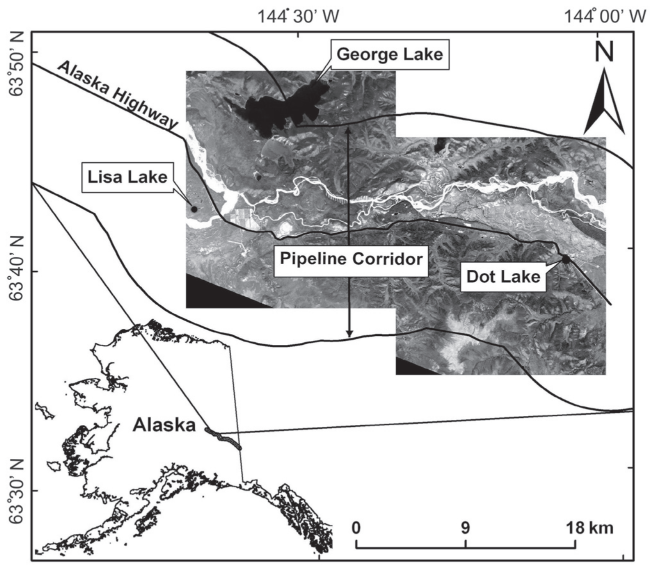

Figure 1. Study area extends from Lisa Lake to Dot Lake along the Alaska Highway. It is a small section of DGGS' proposed gas pipeline corridor study.

to define active layer depth. Hence, we installed Hobo temperature data loggers at 14 selected locations to record soil temperature. The temperature loggers are logging in their first year, and we have not used temperature data in the analysis. These temperature data will be used to estimate thetemperature at any depth and eventually to estimate the active layer depth (Williams & Smith 1989).

We used SPOT 5 multispectral data that has four spectral bands in visible and near infrared (IR) range (Green: 500–590 nm; Red: 610–680 nm; NearIR: 780–890 nm; SWIR: 1580–1750 nm) for land cover classification. Two rectangular scenes covering the study area were clipped from original SPOT scene (acquired on June 30, 2003) that was ortho-rectified and fused with the 2.5 m panchromatic band to improve the spatial resolution of multispectral data (Pohl & Van Genderen 1998). Classification was done using a combination of both unsupervised and supervised signature in a maximum likelihood classifier using ERDAS Imagine, a commercially available image processing software package (Schowengerdt 1983, ERDAS Imagine 2005). We classified the SPOT scenes into eleven land cover classes. These include 1) very dense stands of both black spruce and white spruce; 2) relatively less dense than thick spruce stands; 3) mostly observed in valleys, where spruce is widespread and willows generally grow near small water channel or creek; 4) mix of birch and spruce, generally observed in north facing slope, most prominent forest type in interior Alaska; 5) mix stands of deciduous trees including balsam poplar, willow, alder and birch; 6) stands of aspen vegetation only; 7) small alpine plants (e.g., mountain avens, dryas, sage, etc.); 8) open areas filled with grass; 9) flowing river water with heavy sediment loads; 10) standing water body; and 11) includes different types of bare surfaces (bed rock surfaces, bare surfaces on steep slopes, cut slopes surfaces on foot hills, soils, gravel quarry). Reference totals are the reference pixels selected randomly on the classified image for which actual classes are known. Classified totals are the pixels classified as a particular class by the classification process. Two hundred fifty-two randomly generated points were used to assess the classification accuracy. The superscripts 1–11 in Table 1 refer to the eleven land cover classes described above.

We generated an equivalent latitudes map of the study area from slope and aspect images using 60 m (pixel size) Digital Elevation Model (DEM). Equivalent latitude is an index of long-term potential solar beam irradiation on a surface (Lee 1962). A close relationship exists between equivalent latitude and presence or absence of permafrost, vegetation assemblages, and thaw depth (Dingman 1970, Koutz & Slaughter 1973).

We used the following equation to calculate equivalent latitude (Okanoue 1957):

$$\theta' = \sin^{-1}(\sin k \cdot \cos h \cdot \cos\theta + \cos k \cdot \sin\theta) \tag{1}$$

where k is the slope of the surface, h is the aspect of the surface, θ is the actual latitude of the area, and θ' is the equivalent latitude of the area.

Results and Discussion

The study area is classified into eleven land cover classes, including eight vegetation classes using a combination of both unsupervised and supervised signatures in a maximum likelihood classifier (Fig. 2). For classes 1, 2, 3, 4, 5, and 9, signatures obtained from unsupervised classification were used. For classes 6, 7, 8, 10, and 11, the following numbers of training areas were used in classification 120, 46, 214, 76, and 44, respectively (Table 1). We assessed the classification results using field records, field photographs and in consultation with DGGS scientists. A team of geologists from DGGS did a detailed geologic mapping of the study area as part of the "Alaska Gas Pipeline Corridor" project. Classification results yield an overall accuracy of 89.29% and overall Kappa statistics (Congalton 1991) of 0.87 (Table 1). Classification results of four land cover classes (thick spruce, alpine vegetation, turbid river water, and lake) show 100% accuracy whereas grassland class shows lowest accuracy (62.5%) owing to overlap of spectral signature of grassland and exposed surface classes in visible and near IR bands. Both the grassland and exposed surfaces classes have high digital number (DN) values in all the visible bands. High DN values for exposed surfaces in all the visible bands are obvious, but high DN values for grassland is most likely due to the summer timing of image acquisition (June 30, 2003). During field survey we found that grasslands are mostly dominant in open drained lake beds, and towards the middle of summer lot of grass stems became dry. At the same time the upper soil surface was also very dry. Therefore, the high digital values of grasslands in all the visible bands might be due to the combined effect of dry soil and dry grass stems.

Field sampling in different vegetation settings during summer 2007 revealed that tussocky areas with short, scattered black spruce were characterized by permafrost with shallow active layer depth (less than 50 cm); birch, tall black spruce, and white spruce were found in areas characterized by deeper active layer (greater than 50 cm); and aspen and mixed deciduous vegetation dominated where the upper 1.5 m was unfrozen.

Dividing the classified vegetation map into two elevation units reveals that valleys and floodplain deposits of the low elevation unit (<500 m a.s.l.) are dominated by spruce trees and tussocks. Analysis of the high elevation unit (>500 m a.s.l.) with respect to slope and aspect reveals the dominance of mixed birch and tall spruce on north- and west-facing slopes. Aspen and mixed deciduous trees are generally found in south- and east-facing slopes in well-drained conditions.

On the basis of equivalent latitude values, we classified the study area into three distinct zones. All south-facing slopes have equivalent latitudes less than 60°. Relatively flat floodplain, moraine, and eolian deposits have equivalent latitudes between 63–65°. All north-facing slopes are characterized by equivalent latitudes greater than 65°. The result of integrated analysis of vegetation map, equivalent latitude map and field observation is summarized in Table 2.

Table 2. Interpretation of integrated analysis of vegetation map, equivalent latitude map, and field observations.

Topography	Equivalent latitude (°)	Vegetation	Depth to frozen ground (Summer 2007)
Valleys and flood plain deposits (<500 m asl)	63 – 65	Scattered and/or drunken short black spruce	Less than 50 cm.
North facing slopes (>500 m asl)	Greater than 65	Tall black and white spruce, birch	Greater than 50 cm
South facing slopes (>500 m asl)	Less than 60	Deciduous (aspen, poplar, willow etc.)	None/deeper than 1.5 m

Our findings suggest that equivalent latitude greater than 63° is permissive of permafrost in the study area. This is in close agreement with the findings of Dingman (1970) and Koutz & Slaughter (1973). Dingman (1970) showed that in the elevation range of 256–494 m for Glenn Creek watershed, the permafrost/non-permafrost boundary lay between the 60° and 65° equivalent latitude isopleth lines. Koutz & Slaughter (1973) found a marked correspondence between soils with permafrost and the area above 65° equivalent latitude; and soils without permafrost with equivalent latitude isopleths below 60°.

In the prevailing climatic conditions the high variability of active layer depth

$$(\overline{X} \pm s = 65.61 \pm 19.72 \text{ cm};$$

where $\overline{X}$ is sample mean; s is standard deviation of sample is attributed to difference in soil types, moss layer thickness, and local geology. Thus, even though the equivalent latitude of north-facing slopes is more northerly than that of the valleys and flood plains, the active layer tends to be deeper due to soils which are generally less silt-rich and well drained.

Conclusions

The applied remote sensing technique in combination with *in situ* measurements has considerable potential for use as a tool in regional-scale permafrost mapping. We exploited the correlative relationship between surface parameters and permafrost to gain a preliminary understanding of permafrost distribution in the study area. Tussock land with scattered short black spruce tree and a thick moss layer is a potential indicator of permafrost with shallow active layer depth. At the higher elevation unit (>500 m a.s.l.) birch, tall black spruce and white spruce are dominant in north- and west-facing slopes characterized by a relatively deeper active layer. Broad-leaved, deep rooted deciduous vegetation in south- and east-facing slopes in well-drained soil condition

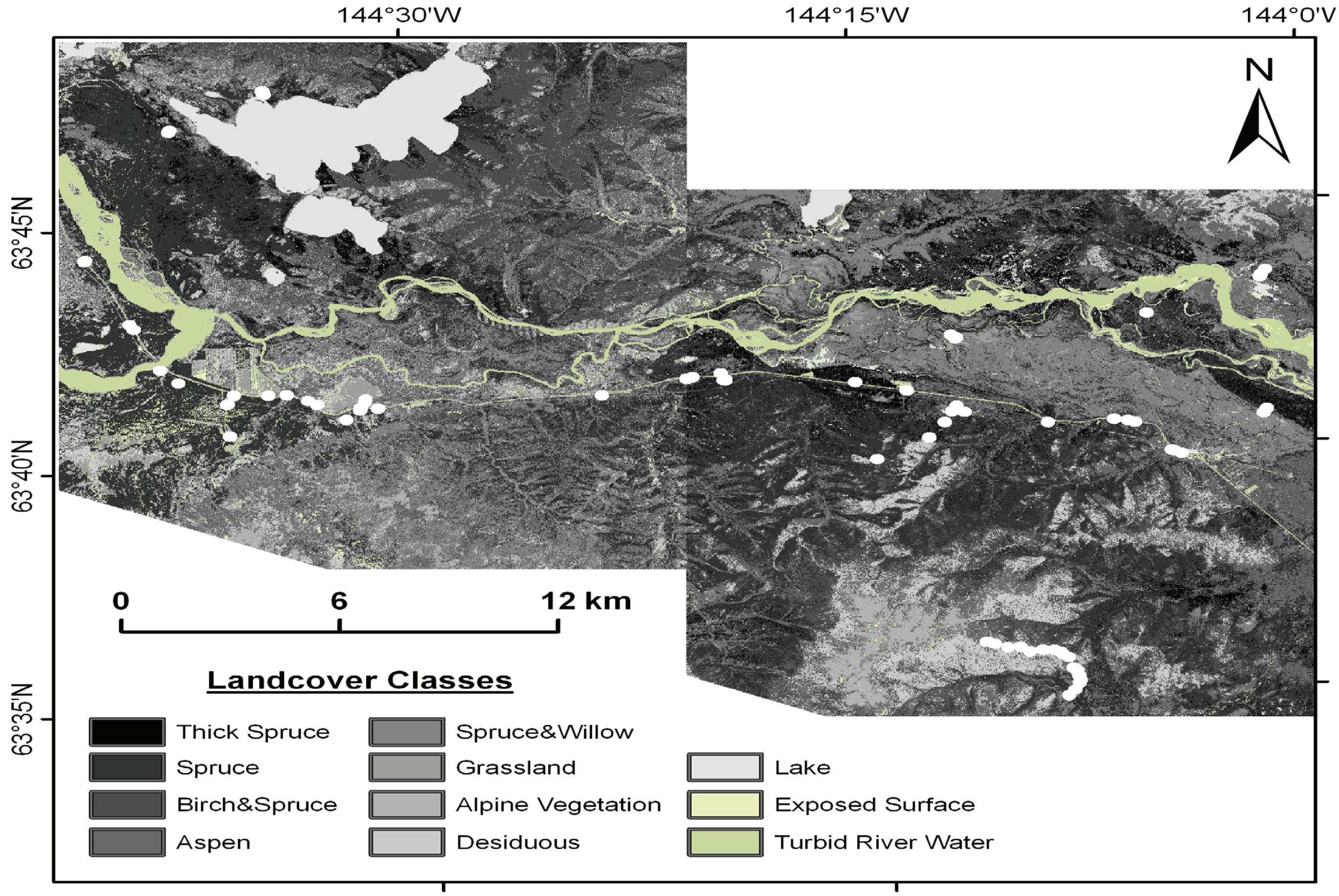

Figure 2. Land cover classification map of George Lake area. Eleven land cover classes including eight vegetation classes were mapped from SPOT multispectral data (acquired on June 30, 2003) in supervised maximum likelihood classifier. White dots represent the sampled locations for permafrost investigations, vegetation distribution, and field data collection.

indicates absence of near-surface permafrost. Equivalent latitude values for the permafrost and non-permafrost portion of the study area also supports the accepted generalization that near-surface permafrost is present under north-facing slopes and absent under south-facing slopes. However, we do not rule out the possibility of deeper permafrost in south-facing slopes. In the prevailing climate conditions, high variance of active layer depth is attributed to different soil types and moss layer thickness.

Acknowledgments

Field support and partial funding for this research was provided through DGGS as part of an on-going project to map bedrock and surficial geology and identify geohazards along the proposed natural gas pipeline corridor from Delta Junction, Alaska, to the Canadian border. We acknowledge additional support from the Alaska Space Grant Program. (ASGP). The authors acknowledge Dr. Richard D. Reger and De Anne Stevens for guidance and help in taking measurements in the field. Special thanks to Dr. Vladimir Romanovsky for advice regarding the various aspects of this study and providing temperature data loggers.

References

Brown, R.J.E. 1967. *Permafrost in Canada.* Canada Geological Survey Map 1246A. National Research Council publication NRC 9769.

Congalton, R. 1991. A review of assessing the accuracy of classifications of remotely sensed data. *Remote Sensing of Environment* 37: 35-46.

Dingman, S.L. 1970. *Hydrology of the Glenn Creek Watershed Tanana River Drainage, Central Alaska.* Ph.D thesis. Cambridge, Massachusetts: Harvard University, 122 pp.

Duguay, C.R., Zhang, T., Leverington, D.W. & Romanovsky, V.E. 2005. Satellite remote sensing of permafrost and seasonally frozen ground. In: C.R. Duguay & A. Pietroniro (eds.), *Remote Sensing in Northern Hydrology: Measuring Environmental Change.* Washington, DC: American Geophysical Union, 91-118.

ERDAS Imagine. 2005. Norcross, GA, USA: Leica Geosystem Geospatial Imaging, LLC.

Etzelmuller, B., Heggem, E.S.F., Sharkhuu, N., Frauenfelder, R., Kaab, A. & Goulden, C. 2006. Mountain permafrost distribution modeling using a multi-criteria approach in the Hovsgol area, Northern Mongolia. *Permafrost and Periglacial Processes* 17: 91-104.

Etzelmuller, B., Hoelzle, M., Heggem, E.S.F., Isaksen, K., Mittaz, C., Vonder Muhll, D., Odegard, R.S., Haeberli, W. & Sollid, J.L. 2001. Mapping and modeling the occurrence and distribution of mountain permafrost. *Norsk Geografisk Tidsskrift–Norwegian Journal of Geography* 55: 186-194.

Frauenfelder, R., Allgower, B., Haeberli, W. & Hoelzle, M. 1998. Permafrost investigations with GIS - A case study in the Fletschhorn area, Wallis, Swiss Alps. *Proceedings of the Seventh International Conference on Permafrost*, *Yellowknife, Canada*: 291-295.

French, H.M. 1976. *The Periglacial Environment* (First edition). London: Longman Group Limited, 309 pp.

French, H.M. 2007. *The Periglacial Environment* (Third edition). John Wiley and Sons, 458 pp.

Goodrich, L.E. 1982. The influence of snow cover on the ground thermal regime. *Canadian Journal of Earth Sciences* 19: 421-432.

Jorgenson, M.T. & Kreig, R. A. 1988. A model for mapping permafrost distribution based on landscape component maps and climatic variables. *Proceedings of the Fifth International Conference on Permafrost, Trondheim, Norway, August 2–5, 1988*: 176-182.

Koutz, F.R. & Slaughter, C.W. 1973. *Equivalent Latitude (Potential Insolation) and a Permafrost Environment: Caribou-Poker Creeks Research Watershed, Interior Alaska.* Unpublished report. U.S. Army Cold Region Research and Engineering Laboratory, 31 pp.

Lee, R. 1962. Theory of the "Equivalent Slope". *Monthly Weather Review* 90: 165-196.

Leverington, D.W. & Duguay, C.R. 1996. Evaluation of three supervised classifiers in mapping depth to late-summer frozen ground, central Yukon Territory. *Canadian Journal of Remote Sensing* 22(2): 163-174.

Leverington, D.W. & Duguay, C.R. 1997. A Neural network method to determine the presence or absence of Permafrost near Mayo, Yukon Territory, Canada. *Permafrost and Periglacial Processes* 8: 205-215.

Morrissey L.A., Strong, L. & Card, D.H. 1986. Mapping permafrost in the boreal forest with thematic mapper satellite data. *Photogrammetric Engineering and Remote Sensing* 52: 1513-1520.

Okanoue, M. 1957. A simple method to compute the amount of sunshine on a slope. *Journal of Japanese Forest Society* 39(11): 435-437.

Peddle, D.R. 1991. Evidential classification of land cover and permafrost from multisource remote sensing imagery in mountainous terrain, Yukon. Calgary: Department of Geography, University of Calgary, 178 pp.

Peddle, D.R. & Franklin, S.E. 1993. Classification of permafrost active layer from remote sensed and topographic evidence. *Remote Sensing of Environment* 44: 67-80.

Pohl, C. & Van Genderen, J.L. 1998. Multisensor image fusion in remote sensing: concept, methods and applications. *International Journal of Remote Sensing* 19(5): 823-854.

Schowengerdt, R.A. 1983. *Techniques for Image Processing and Classification in Remote Sensing*. Academic Press, 249 pp.

Smith, M.W. 1975. Microclimate influences on ground temperatures and permafrost distribution, Mackenzie Delta, Northwest Territories. *Canadian Journal of Earth Sciences* 12: 1421-1438.

Solie, D.N. & Burns, L.E. 2007. Alaska Highway corridor geology and geophysics. *Alaska GeoSurvey News* 10(1): 1-5.

Williams, P.J. & Smith, M.W. 1989. *The Frozen Earth: Fundamentals of Geocryology*. Cambridge: Cambridge University Press, 306 pp.

Electrical Freezing Potentials During Permafrost Aggradation at the Illisarvik Drained-Lake Experiment, Western Arctic Coast, Canada

V.R. (Sivan) Parameswaran
Department of Geography and Environmental Sciences, Carleton University, Ottawa, Canada, and Institute for Research in Construction, National Research Council Canada, Ottawa, Canada

C.R. Burn
Department of Geography and Environmental Studies, Carleton University, Ottawa, Canada

Abstract

A probe containing a series of electrodes spaced at regular intervals was used to monitor electrical potentials developed across the freezing front during permafrost aggradation at depth in the talik of the Illisarvik drained lake bed. Data were collected from 2000 to 2007. The electrode located at the freezing interface showed a peak electrical potential, commonly of tens of mV, when measured with respect to reference electrodes in the unfrozen or the completely frozen region. The location of the freezing front was consistent with temperature measurements using thermistors installed at these depths. This experiment suggests that, with proper electrode probes and frequent measurements, electrical freezing potentials can be used for monitoring the movement of the freezing front in permafrost areas.

Keywords: freezing potential; Illisarvik; permafrost aggradation.

Introduction

The development of electrical freezing potentials across freezing interfaces in aqueous solutions and moist soils has been studied for the past five decades (e.g., Workman & Reynolds 1950). The potentials arise due to charge separation during phase change of water and selective incorporation in the frozen and unfrozen regions of H^+ and OH^- ions in pure water and other cations and anions in solutions and soils. Early measurements of freezing potentials in water and dilute solutions, as well as in soils, have been reviewed by Parameswaran (1982) and Parameswaran et al. (2005). Field measurements of such potentials developed during permafrost aggradation were presented by Parameswaran & Mackay (1983, 1996), during thawing of the active layer by Parameswaran et al. (1985), and during freezing of lake water by Burn et al. (1998).

During freezing, liquid water migrates to the freezing interface, especially in fine-grained silty and clayey soils (Williams & Smith 1989). An electrical field developing at the freezing front will enhance the drift of unfrozen water, leading to accumulation of ice at the freezing interface (Hoekstra & Chamberlain 1963, Nersesova & Tsytovich 1966). Such geo-electrical potentials may also affect the cathodic protection of buried pipelines and other utilities. The purpose of this paper is to present recent measurements of electrical potentials made at depth during freezing of the talik at the Illisarvik drained-lake experiment, near the western Arctic coast of Canada (Figs. 1, 2).

Illisarvik

A field experiment to drain a lake and to study the aggradation of permafrost in a natural arctic environment was conceived by Professor J.R. Mackay in the 1960s

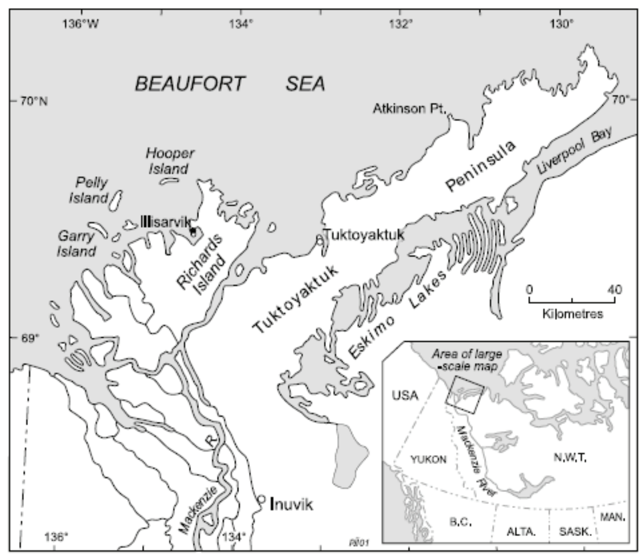

Figure 1. Location of Illisarvik (Mackay & Burn 2002a, Fig. 1, reproduced with permission of NRC Research Press).

(Mackay 1997). Illisarvik Lake, on the west coast of Richards Island, Northwest Territories, was 600 m long and 300 m wide, with a depth mostly between 2 and 3 m, and at the deepest point, over 5 m. Most of the lake bottom remained unfrozen throughout the year, and at the midpoint, the depth of the sublake talik was 32 m (Hunter et al. 1981). The lake was drained on 13 August 1978. After drainage, permafrost started to grow downwards and from the sides of the talik into the lake sediments, and since then, permafrost has been aggrading at the center of the lake by gradual freezing of the ground (Mackay 1997). Field studies have been conducted at the site on a continuing basis into several topics including growth of permafrost, development of ground ice, development of the active layer, pore-water

Figure 2. Aerial view of Illisarvik (Mackay & Burn 2002b, Fig. 2, reproduced with permission of NRC Research Press).

expulsion, electrical freezing potentials developed during permafrost growth, and other geophysical effects (see Burn & Burgess 2000).

By 1995 the talik was at -0.2°C or below, but surface evidence of pore-water expulsion, in the form of an annual ice dome on the residual pond near the center of the lake bed, has indicated that the talik is not frozen (Mackay 1997). The top of the ice dome has been up to about 1 m higher than the surrounding pond ice between 1995 and 2007. Water collected from beneath the ice dome in late winter 2000 may be indicative of the solute concentrations in the groundwater of the unfrozen talik. Measured concentrations of major ions were (mg/L): Na^+ 1000; Cl^- 2000; Ca^{++} 460; Mg^{++} 470; K^+ 51. The total dissolved solids were measured at 6700 mg/L. The conductivity of the water was 6 mS/cm. Similar data are presented by Mackay (1997).

Freezing Potentials at Illisarvik

The deposits in the lake bed consist of 2 to 4 m of fine-grained, organic-rich lake sediments over medium- to fine-grained sand. Permafrost was established in these deposits during the first winter following drainage, and by 1981 the ground had frozen to a depth of about 5.65 m. In June 1981, an electrode probe, about 10 m long, was installed at the center of the lake, with 21 ring electrodes placed around the bottom 3 m of the probe and spaced 150 mm apart. While the freezing front advanced downwards, a small electrical potential (a few hundred mV up to 1 V) developed at each electrode, as the freezing front crossed that location. These measurements, carried out over 15 months, were reported by Parameswaran & Mackay (1983).

The conclusion from this early field measurement, during relatively rapid ground freezing, was that progress of the freezing front could be monitored with suitable electrodes installed at regular intervals. Between March 1981 and August 1982, the freezing front advanced from electrode location 15 down to electrode location 11, about 0.6 m downwards. This was confirmed by temperature measurements near the electrode locations. It is important to note that at this stage of the field experiment, the temperature gradient in the frozen ground was relatively steep, and there was little temperature depression below 0°C within the talik (Mackay 1997). As a result, the freezing front was relatively well-defined in physical terms. The thermo-physical conditions were quite different by 1998 when the investigation reported here began (e.g., Mackay 1997).

Field Methods

Drilling in the center of Illisarvik in August 1998 indicated that the ground was at least partially frozen to a depth of 13.5 m. In August 1999, a hole was drilled by water jet in the center of the drained lake bed, and an electrode probe was inserted to a depth of 16 m. Water-jet drilling does not provide undisturbed samples from the hole, but it is possible to interpret a generalized stratigraphy from the soil materials returned uphole, the behavior of the pipe during drilling, and the resistance of the ground to the drill. A thermistor cable was placed in a second hole, approximately 3 m from the first. The cable was installed in a casing of 1-in steel pipe. We have found that near the ground surface the steel pipe is sufficiently robust to withstand environmental stresses in a field context, while PVC pipes we have installed have lasted only a few years before being damaged.

The stratigraphy at the site comprised the active layer, about 0.8 m thick, lying on top of hard frozen organic lake sediments. Below 4.3 m depth the ground was not as well bonded, and below 13.5 m the ground was unfrozen. Temperature profiles from August 2000 and 2005 for the upper 18 m at the lake center are presented in Figure 3.

Probe Design

Figure 4 presents a schematic diagram of the electrode probe. The top 2 segments of the probe consisted of 1-in steel pipe, each 2 m long. Below that were 6 schedule 80 PVC pipes, each also 2 m long. All the pipes were threaded at both ends to fit joining couplings. Below these 8 lengths was a 1-m long PVC pipe with a conical plug at the bottom.

Ten ring electrodes made of gold-plated copper strips, 12.5 mm wide and about 1 mm thick, were placed around the PVC tubes at various intervals. Most of the electrodes were located in the unfrozen zone below 13.5 m on the PVC pipe #6, but 1 electrode (E1) was located in the hard frozen zone (on PVC pipe #1), and 2 (E2 and E3) were in the partially frozen ground, E2 on PVC pipe #2 and E3 on pipe #4. Electrodes E4 to E10 were on pipe #6 (Fig. 4).

Coaxial cables of sufficient length were soldered to the ring electrodes and fed through the hollow center of the tube assembly. The ends were stored above ground in a pipe nipple connected to the top of the uppermost steel pipe.

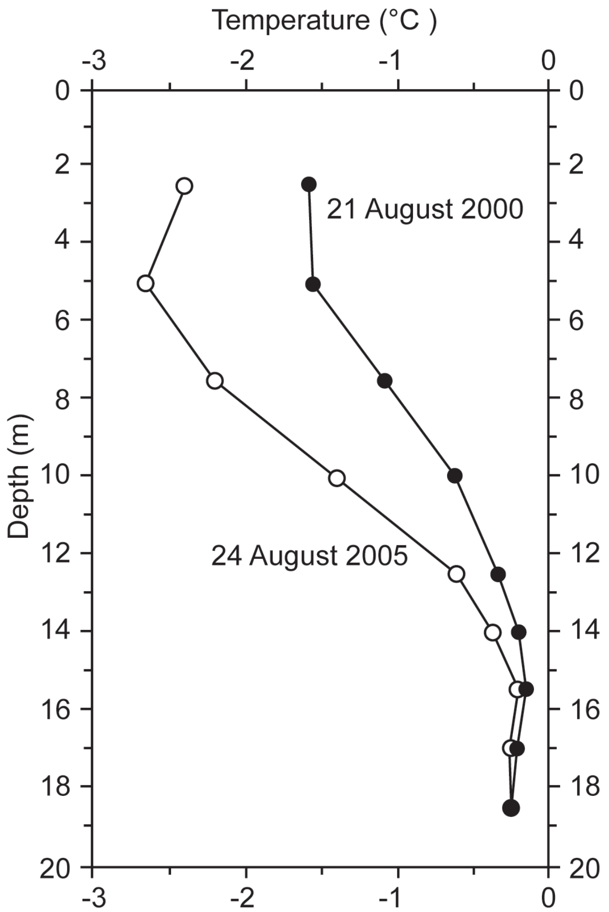

Figure 3. Ground temperature profiles at the center of Illisarvik, 21 August 2000 and 24 August 2005, showing evolution of the ground thermal regime during the study period.

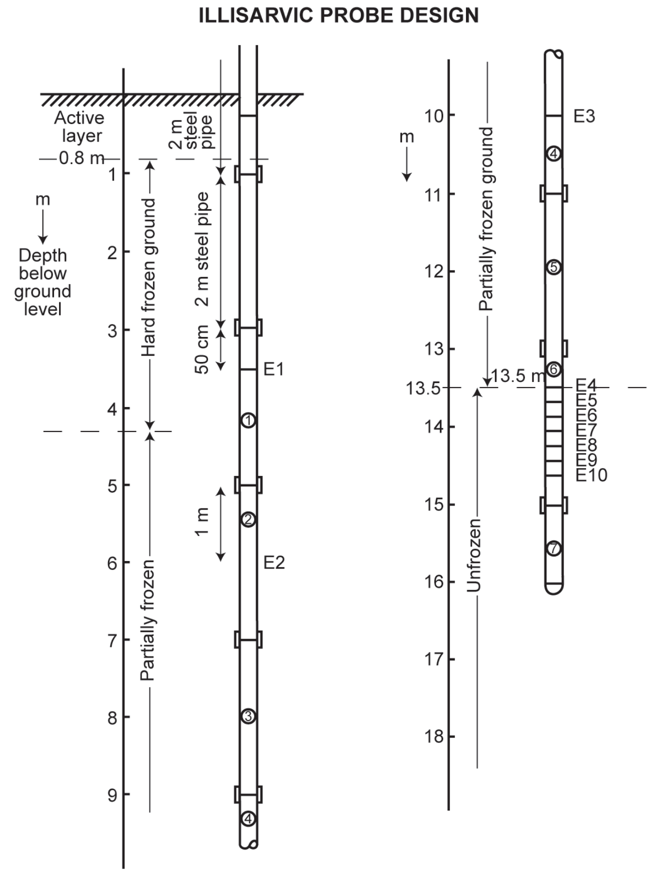

Figure 4. Probe design.

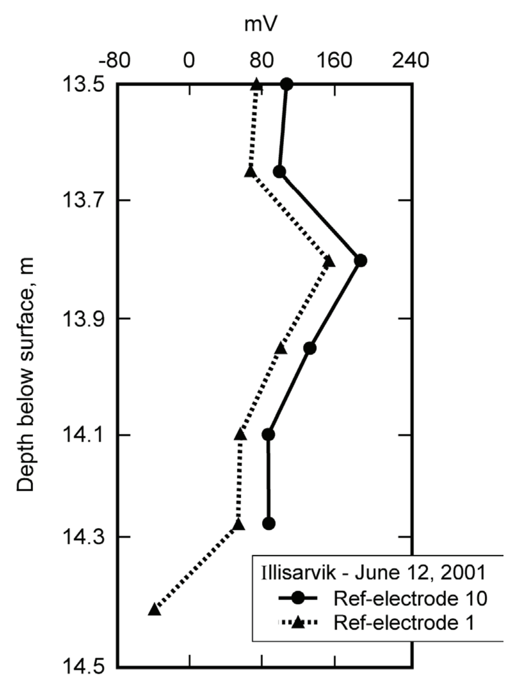

Figure 5. Electrical potential profiles from 12 June 2001.

During field visits throughout the year between 1999 and 2007, the electrical potentials developed at each electrode were measured with respect to the unfrozen ground at electrode E10 as well as the frozen ground at electrode E1. The potentials (in mV) were measured by multimeter with a sensitivity of 0.01 mV.

Results

Data collected up to March 2006 indicated a peak potential within the interval between E4 (13.5 m depth) and E10 (14.4 m depth). After this date, in August 2006 and April, June, and August 2007, the measurements provided no trend with depth, and the potentials at most electrodes tended to 0 mV shortly after connection.

Figure 5 presents data from 12 June 2001, showing a typical set of measurements for E4 to E10. In general, the potential at E1 was positive with respect to E10 throughout the period of measurement. The plot shows the potentials at each electrode as a function of depth.

A peak is observed at electrode E6, at a depth of 13.8 m below the ground surface, indicating the location of the freezing front. Both curves, with reference to E1 or E10, follow the same trend and show the peak at the same location. Figure 6 shows similar measurements from 20 August 2001, when, again, the peak was recorded at electrode E6.

Figure 7 shows the readings taken on 14 April 2003. The peak potential had advanced to electrode E9, at a depth of 14.25 m below the ground surface. This suggests that between June 2001 and April 2003, the locus of electrical potential advanced downwards from 13.8 m to 14.25 m.

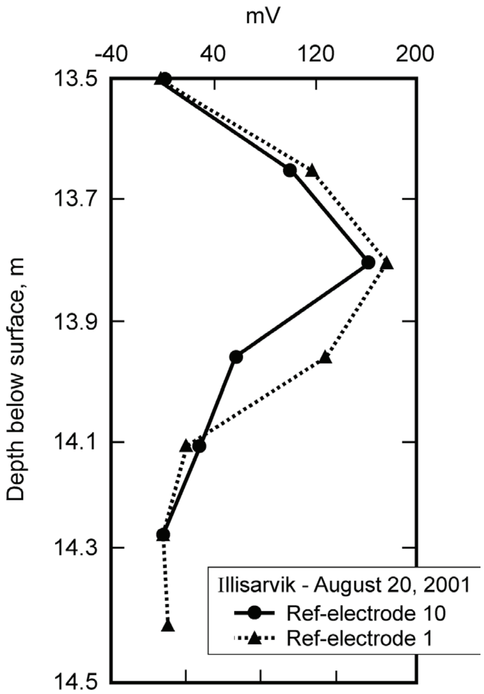

Figure 6. Electrical potential profiles from 20 August 2001.

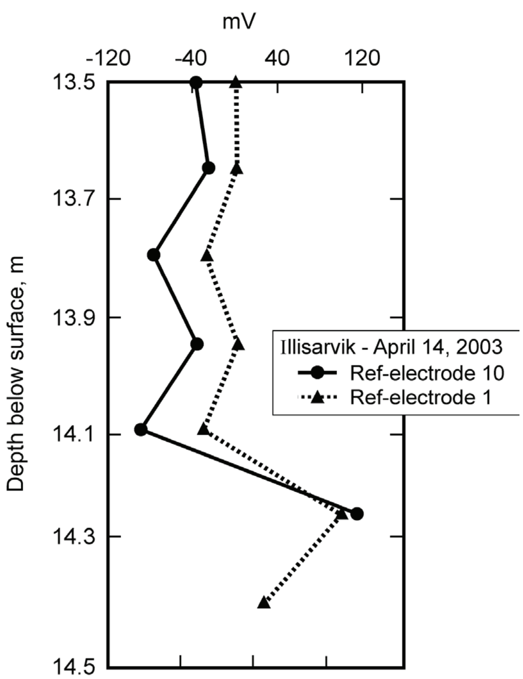

Figure 7. Electrical potential profiles from 14 April 2003.

However, measurements taken on 20 June 2004 showed considerable variation of potentials at the electrodes at different depths (Fig. 8), with the peak occurring at electrode E9 at a depth of 14.25 m below the ground surface. During the period of measurement, data similar to the profile in Figure 8 were collected on several occasions, but normally the profiles presented one distinct peak potential. The peak potential was measured at E8 or E9 between April 2002 and March 2006.

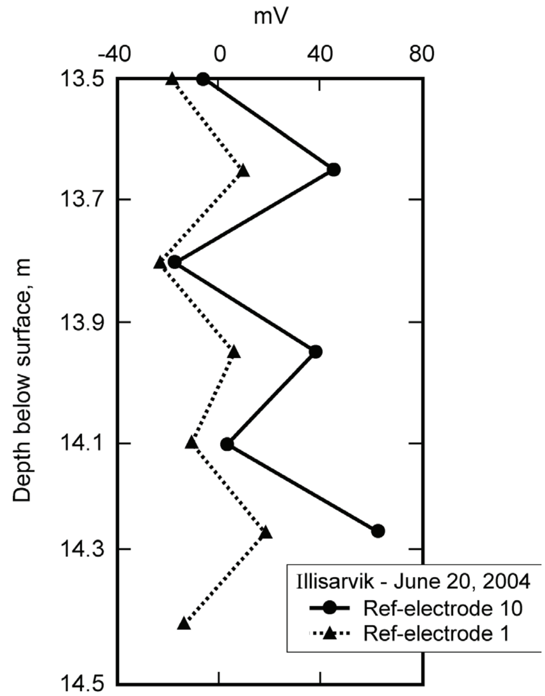

Figure 8. Electrical potential profiles from 20 June 2004.

Figure 9 is a plot of the location of the freezing front with time (as estimated from the peak electrical freezing potentials measured on the electrodes) and the variation of the temperature of the ground between 2000 and 2005. The lower curve shows the temperatures at a depth of 14.0 m and the upper one at 15.5 m. The peak potential in June and August 2001 was at electrode location E6, at a depth of 13.8 m. The temperatures measured by the thermistors installed in this region of the ground were -0.29°C to -0.30°C at a depth of 14 m and -0.20°C to -0.22°C at a depth of 15.5 m. In April 2002, the temperature at 14 m depth was -0.34°C and the peak potentials were observed on electrodes E8 and E9, at depths of 14.1 and 14.25 m, respectively. The temperature at the depth of 15.5 m was -0.18°C, in the unfrozen region of the ground. These data suggest that the peak potential developed at a temperature of about -0.3°C, for the temperature at 14 m, was between -0.3°C and -0.4°C when the peak was measured at depths between 14.1 m and 14.25 m. The pattern illustrated in Figure 8 and the persistence of potentials in the profile lower than the peak value, both above and below the location of the peak, indicate that the freezing front is not a distinct feature at the scale of these measurements (intervals of 15 cm). Instead, there is likely a freezing zone, with some temperature depression, within which the potentials develop. The stratigraphic interpretation from the drilling record indicated partially frozen ground from depths of 4.3 m to 13.5 m (Fig. 4). The measurements presented here suggest that there is a concentration of solutes close to the temperature of ice nucleation in the soil, leading to development of a potential by charge separation. In turn, this suggests that there is a relatively restricted area where solute effects are focused, in comparison with the 9 m of partially frozen ground.

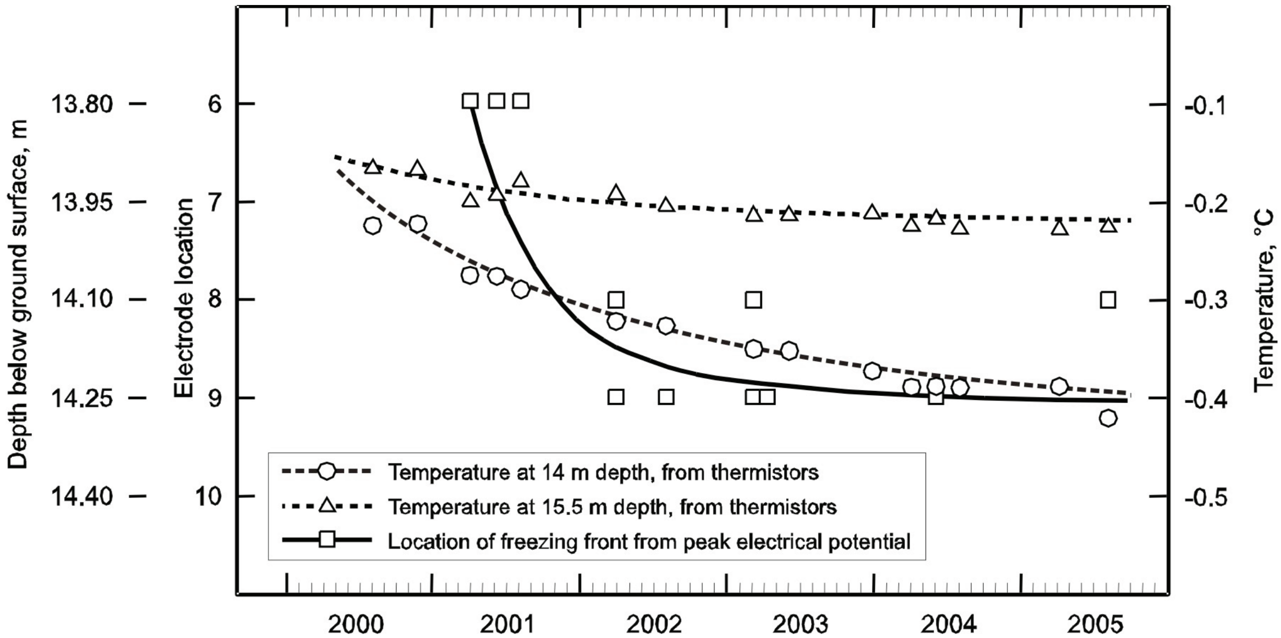

Figure 9. Location of the freezing front interpreted from peak potentials and proximal ground temperatures at depth in the talik at Illisarvik, 2000–2005.

Assuming a freezing point depression of about 0.2°C to 0.25°C due to the solutes present in the groundwater at these depths, we can assume electrode E8 is at the freezing front, and the electrode potential measurements indicate this. By January 2003, the temperature at 14 m depth was less than -0.35°C. The peak freezing potentials were observed on electrode E9, at a depth of 14.25 m. As shown by the upper curve in Figure 9, the temperature at the depth of 15.5 m was still around -0.2°C, the temperature measured after drilling, when it was determined to be unfrozen.

Measurements after March 2006 showed considerable oscillations in the profile, and very low absolute voltages, indicating probably that the freezing front had advanced below the lowest electrode in the assembly. Similar patterns in the measured profile were also observed in the measurements reported by Parameswaran & Mackay (1983), when all the electrodes were embedded in the frozen soil. This could be the effect of shorting the circuit, as the measuring electrode and the reference electrode were both embedded within the same frozen system. Laboratory observations of the shorting potentials were reported by Parameswaran et al. (2005).

Conclusions

Electrical freezing potentials were observed at electrodes positioned at the freezing interface in the talik of the Illisarvik drained lake. The location of the peak electrical potential indicated its development at a temperature of about -0.3°C. The principal results are:

(1) Electrical potentials can be measured during permafrost aggradation. The potential is permafrost positive.
(2) The potential is on the order of tens of mV.
(3) The potential may develop below 0°C, perhaps indicating the nucleation temperature of ice in groundwater.

With proper electrode probes and with more frequent measurements, electrical potential probes can be used for monitoring the movement of the freezing front in permafrost areas.

Acknowledgments

The research has been supported by the Natural Sciences and Engineering Research Council of Canada, the Polar Continental Shelf Project of Natural Resources Canada, and the Aurora Research Institute. We thank Larry Boyle for manufacturing the probe, and A. Burn, D. Riseborough, and J.R. Mackay for assistance during installation. D. Esagok and L. Kutny have provided assistance with measurements throughout the project. We also thank Don Hobbs, Peter Richards, and Michelle Gagnon of the Institute for Research in Construction, National Research Council Canada, for preparation of Figures 3 through 9. The National Research Council of Canada Research Press kindly gave permission to reproduce Figures 1 and 2. This paper is Polar Continental Shelf Project contribution number 00808.

References

Burn, C.R. & Burgess, M.M. 2000. The Illisarvik Bibliography. www.nwtresearch.com/illisarvik

Burn, C.R., Parameswaran, V.R., Kutny, L. & Boyle, L. 1998. Electrical potentials measured during growth of lake ice, Mackenzie Delta area, N.W.T. *Proceedings of the Seventh International Conference on Permafrost, Yellowknife, N.W.T., June 23-27, 1998*: 101-106.

Hoekstra, P. & Chamberlain, E. 1963. Electro-osmosis in frozen soils. *Nature* 203: 1406.

Hunter, J.A., MacAulay, H.A., Gagné, R.M., Burns, R.A., Harrison, T.E. & Hawkins, J.P. 1981. Drained lake experiment for investigation of growth of permafrost at Illisarvik, Northwest Territories – initial geophysical results. *In* Current research, part C. Geological Survey of Canada, Paper 81-1C, 67-76.

Mackay, J.R. 1997. A full-scale field experiment (1978-1995) on the growth of permafrost by means of lake drainage, western Arctic coast: a discussion of the method and some results. *Canadian Journal of Earth Sciences* 34: 17-33.

Mackay, J.R. & Burn, C.R. 2002a. The first 20 years (1978/79 to 1998/99) of ice-wedge growth at the Illisarvik experimental drained lake site, western Arctic coast, Canada. *Canadian Journal of Earth Sciences* 39: 95-111.

Mackay, J.R. & Burn, C.R. 2002b. The first 20 years (1978/79 to 1998/99) of active-layer development, Illisarvik experimental drained lake site, western Arctic coast, Canada. *Canadian Journal of Earth Sciences* 39: 1657-1674.

Nersesova, Z.A. & Tsytovich, N.A. 1966. Unfrozen water in frozen soils. *Permafrost, Proceedings of the First International Conference*, *Lafeyette, Indiana, November 11-15, 1963*: 230-234.

Parameswaran, V.R. 1982. Electrical freezing potentials in water and soils. *Proceedings of the Third International Symposium on Ground Freezing, Hanover, NH, June 22-24, 1982*: Vol. 2, 83-89.

Parameswaran, V.R. & Mackay, J.R. 1983. Field measurements of electrical freezing potentials in permafrost areas. *Proceedings of the Fourth International Conference on Permafrost, Fairbanks, Alaska*, *July 17-22, 1983*: Vol. 1, 962-967.

Parameswaran, V.R. & Mackay, J.R. 1996. Electrical freezing potentials measured in a pingo growing in Western Canadian Arctic. *Cold Regions Science and Technology* 24: 191-203.

Parameswaran, V.R., Johnston, G.H. & Mackay, J.R. 1985. Electrical potentials developed during thawing of frozen ground. *Proceedings of the Fourth International Symposium on Ground Freezing*, *Sapporo, Japan, August 5-7, 1985*. Vol. I, pp. 9-16.

Parameswaran, V.R., Burn, C.R., Profir, A. & Ngo, Q. 2005. A note on electrical freezing and shorting potentials. *Cold Regions Science and Technology* 41: 83-89.

Williams, P.J. & Smith, M.W. 1989. *The Frozen Earth: Fundamentals of Geocryology*. Cambridge: Cambridge University Press, 360 pp.

Workman, E.J. & Reynolds, S.E. 1950. Electrical phenomena occurring during the freezing of dilute aqueous solutions and their possible relationship to thunderstorm electricity. *Physical Review* 78: 254-259.

Managing Permafrost Data: Past Approaches and Future Directions

Mark A. Parsons
World Data Center for Glaciology, Boulder, USA

Sharon L. Smith
Geological Survey of Canada, Ottawa, Canada

Vladimir E. Romanovsky
University of Alaska Fairbanks, USA

Nikolai I. Shiklomanov
University of Delaware

Hanne H. Christiansen
The University Centre in Svalbard, UNIS, Norway

P. Paul Overduin,
Alfred Wegner Institute, Potsdam, Germany

Tingjun Zhang
National Snow and Ice Data Center, Boulder, USA

Megan R. Balks
University of Waikato, Private Bag 3105, Hamilton, New Zealand

Jerry Brown
International Permafrost Association, Woods Hole, USA

Abstract

The International Permafrost Association (IPA) has a long history of data management. Notable achievements include the establishment of a Global Geocryological Data (GGD) system and the publication of the Circumpolar Active-layer Permafrost System (CAPS) compilations. At the same time, the IPA has struggled to maintain continual stewardship of permafrost and related data with sustained support. Activities as part of the International Polar Year will significantly increase data holdings and will required renewed emphasis on data description, preservation, and integration with other disciplines.

Keywords: data management; frozen ground; GGD; IPA; IPY; permafrost.

Introduction

Permafrost and seasonally frozen ground data and information are critical for fundamental process understanding, environmental change detection, impact assessment, model validation, and engineering applications. The International Permafrost Association (IPA) has long emphasized the importance of these data and has encouraged ongoing data sharing and management through the Global Geocryological Data (GGD) system. The GGD is an internationally distributed system linking investigators and data centers around the world and was proposed by Barry et al. (1995). The World Data Center (WDC) for Glaciology at Boulder has historically acted as central node of the GGD and has published two compendiums of permafrost related data: *Circumpolar Active-Layer Permafrost System* (CAPS) Version 1 and the substantially updated Version 2 (IPA DIWG 1998, IPA SCDIC 2003).

Data advertised through the GGD and published on CAPS include information on borehole parameters, soil temperature, cryosols, and climatology as well as maps, metadata, and bibliographies. Data come from diverse international sources, but data produced by IPA projects have always been prominent in the collections. These products include benchmark maps such as the *Circum-Arctic Map of Permafrost and Ground-Ice Conditions* (Brown et al. 1998) as well as data and metadata from ongoing IPA programs such as the Global Terrestrial Network for Permafrost (GTN-P), the Arctic Coastal Dynamics (ACD) program, and the Antarctic Permafrost and Soils (ANTPAS) project. These IPA programs continue to produce important data with a burst of new activity in the International Polar Year (IPY). Another area of potential data growth is through satellite remote sensing.

While the GGD has succeeded in capturing and describing many important data resources, it has been an ad hoc activity without sustained support for ongoing data collection and stewardship. There is a critical need to sustain data stewardship activities throughout the entire data lifecycle. Note, data stewardship is a broader concept than data management. It can be defined as "all activities that preserve and improve the information content, accessibility, and usability of data and their associated metadata" (NRC 2008). Correspondingly, the concept of a data lifecycle reflects how data are continually evaluated, improved, and maintained for archiving until retired or discarded.

The GGD is linked to the broader IPY Data and Information Service (IPYDIS), which works with the Scientific Committee on Antarctic Research (SCAR) and International Arctic Science Committee (IASC) to establish a lasting polar data infrastructure. The IPA seeks to contribute to this international effort by capturing the burst of permafrost data collection during IPY, and ensuring the preservation of past data in a new CAPS Version 3 compilation. The IPA also seeks to develop a more sustainable data collection and stewardship strategy through linkages to other relevant international programs including the intergovernmental Group on Earth Observations (GEO).

Global Geocryological Data

The need for a consistent and comprehensive permafrost data management has long been recognized. In 1983, the U.S. National Research Council called for greater coordination and a specialized permafrost data clearinghouse (NRC 1983). In 1988, the WDC for Glaciology at Boulder organized a workshop in Trondheim, Norway in conjunction with the Fifth International Conference on Permafrost (Barry & Brennan 1989). This workshop, coupled with a paper presented by Roger Barry (1988), led to the establishment of a Data and Information Working Group within the IPA and established the overall IPA data strategy. The strategy was refined based on an international survey of permafrost data holdings (Barry & Brennan 1993) and culminated in the establishment of the GGD and the first CAPS compilation for the Seventh International Conference on Permafrost, SICOP, in 1998. Furthermore, delegates to the SICOP International Conference recognized the importance of continuity in data and information activities, and the existing Working Group was reestablished as a permanent Standing Committee on Data Information and Communication (SCDIC) during the Twelfth IPA Council Meeting at SICOP in Yellowknife, Canada.

The 1998 CAPS1 included 56 datasets and an additional 89 metadata descriptions for products held elsewhere around the world. In late 2002, the newly established Frozen Ground Data Center (FGDC) at the WDC for Glaciology at Boulder in collaboration with the International Arctic Research Center published the contents of CAPS online at the FGDC web site and began updating and adding to the CAPS collection to create CAPS Version 2. CAPS2 expanded the scope of CAPS by including data and information for seasonally frozen ground regions from in-situ measurements, satellite remote sensing, and model outputs and included data and metadata for more than 200 datasets. More comprehensive data documentation was also written.

Since the publication of CAPS2, the FGDC has published several other datasets. These additions include important historical data (Oberman & Kakunov 2004), maps (Sodnom & Yanshin 1990), and long-term, broad-scale time series of seasonally frozen soil parameters (Zhang et al. 2005). These products are available through the FGDC web site. Data will remain available until the next major media migration or system upgrade at the WDC, at which point the FGDC distribution will need to be retired, unless continued funding can be identified.

In many ways, the history of the GGD parallels the evolution of digital data management in general. Initial bibliographic efforts grew into data compilation and recording efforts. Standard metadata formats were created and implemented. Central catalogs describing distributed data were created. Media and distribution methods evolved.

In some ways the GGD was at the forefront of developments in data management. For example, CAPS1 included specific citations for all datasets and urged investigators to formally cite data use as they would any other publication. This practice is just now gaining wide spread acceptance as is evident in the IPY Data Policy and increasing acceptance of data citations by leading journals.

On the other hand, the GGD has been largely an ad hoc effort punctuated by intense activity around the CAPS compilations. This contrasts with the increasing recognition of the importance of continual data stewardship and full lifecycle data management (USGCRP 1999, NRC 2008). For example, part of the effort of updating CAPS was to try and contact the investigators and institutions holding the 89 GGD products described but not contained on CAPS1. Unfortunately, 45 of the 89 products were not readily accessible and may no longer be available. The potential loss of these data highlights the need for continued support of data management for the permafrost community.

The IPA through its SCDIC needs to evolve its data strategy and the general GGD system to more actively acquire current datasets, rescue data at risk of loss, ensure the planned migration of investigator held data to more permanent archives, and address the growth of data resulting from the burst of IPA activity as part of the IPY.

IPA Programs and the IPY

A summary of the major IPA activities since its formation in 1983 is presented in these proceedings (Brown et al. 2008). In addition to mapping, bibliographic, and terminology projects, the main IPA focus has been on broad, coordinated international field programs. Individual national sponsors fund each program, but the field efforts are unified through IPA coordination of site documentation, data collection methods, and metadata descriptions. Each program has its own data management structure that can be considered a node of the GGD, while metadata should be broadly shared to facilitate discovery across the GGD. IPA programs include:

- The Global Terrestrial Network for Permafrost (GTN-P), which includes both boreholes and active layer sampling protocols.
- The Arctic Coastal Dynamics (ACD) project.
- Northern Circumpolar Soil Carbon Database (NSCD) (Tarnocai et al. 2007).

• Each IPA program is linked to IPY approved and coordinated projects including "Permafrost Observatory Project: A Contribution to the Thermal State of Permafrost" (IPY project #50), "Arctic Circum-Polar Coastal Observatory Network (ACCO-Net)" (IPY 90), "Antarctic and sub-Antarctic Permafrost, Periglacial and Soil Environments" (IPY 33), "Carbon Pools in Permafrost Regions" (IPY 373), and the Russian project, "Response of Arctic and Subarctic soils in a changing Earth: dynamic and frontier studies" (IPY 262).

Global Terrestrial Network for Permafrost

The GTN-P consists of two components: the Thermal State of Permafrost (TSP) and the Circumpolar Active Layer Monitoring Network (CALM) (Burgess et al. 2000). Together they are contributing to the Global Earth Observation System of Systems and the UN Framework Convention on Climate Change through the Global Terrestrial Observing System.

The TSP component of GTN-P consists of a network of boreholes, in which permafrost temperatures are measured. The network currently consists of over 300 boreholes with many new sites to be established during IPY. This network is built on a number of regional networks. Boreholes range in depth from a few meters to greater than 100 m with record lengths of up to three decades. Data collected from this network has provided important information on the change in permafrost temperature over time and are important contributions to major regional and global assessments (ACIA 2004, IPCC 2007, UNEP 2007).

TSP borehole metadata (site descriptions) and summary permafrost temperature data are accessible through the GTN-P web site hosted by the Geological Survey of Canada (GSC). A major goal for IPY is to provide a "snapshot" that describes the thermal state of permafrost for a specific time period. This snapshot can serve as a baseline for the assessment of the rate of change of permafrost conditions and can be used to validate climate model scenarios and to support process research to improve our understanding of permafrost dynamics.

Two national programs within the TSP project illustrate the project scope and its data management challenges. The TSP Norway project plans to establish the North Scandinavia Permafrost Observatory around 70°N, covering a transect from maritime northern Norway into northwestern Sweden and Finland. The Svalbard Nordenskiöld Land Permafrost Observatory around 78°N is already being established. Both observatories deliver borehole temperatures, active layer thickness, meteorological, and periglacial process data from different permafrost landforms. All these data will be organized in the NORPERM database located at the Norwegian Geological Survey. The aim is to also include earlier permafrost and periglacial data from all of Norway and Svalbard in the database. Data from NORPERM shall also be available to others through the GTN-P.

The Canadian Permafrost Monitoring Network coordinated by the GSC consists of over 100 monitoring sites maintained by government agencies and universities. Sites are largely concentrated in the western Arctic (Mackenzie Valley and Delta), northern Quebec, with a few sites in the high Arctic. During IPY, scientists intend to establish new monitoring sites in northern Manitoba, Yukon and Nunavut Territories as part of the TSP project.

The Canadian network maintains a web site that links to the GTN-P web site and provides access to metadata for both active layer and permafrost thermal monitoring sites and summary data. Linkages with the Canadian cryospheric community are through the Canadian Cryospheric Information Network. Canada's contribution to the IPY will be a standardized set of permafrost temperatures collected during IPY that will be compiled into a digital database to be released through the web site and as a CD publication.

The other major component of GTN-P, CALM, monitors active layer thickness and shallow ground temperature, and coordinates field experiments. The CALM network currently consists of more than 150 sites distributed throughout the Arctic and several mountain ranges of the mid-latitudes. Efforts to expand the number and capabilities of sites in the Southern Hemisphere (CALM-S) are underway through ANTPAS. Instrumentation and data-acquisition methods include monitoring the soil thermal and moisture regimes with automatic data loggers, mechanical probing of the seasonally thawed layer at specified spatial and temporal intervals, frost/thaw tubes, and a variety of instruments for measuring frost heave and thaw subsidence.

Data are transferred to the CALM data repository at the University of Delaware for archive and distribution through the CALM web site, which is linked to the GTN-P site and FGDC (Shiklomanov et al. 2008).

Arctic Coastal Dynamics

The ACD project of IASC and the IPA was created in 1999 to improve understanding of circum-Arctic coastal dynamics under the influence of environmental changes and geologic controls. ACD's international and ongoing effort to segment and classify the entire circum-Arctic coastline has resulted in a scalable GIS database of coastal geomorphological characteristics evaluated by regional experts. This detailed evaluation has been compiled into a geographic information system (GIS), which contains data on coastal morphology, composition, dominant processes, ground ice, and environmental forcing parameters such as wind speed, storm counts, melt season, and wave energy.

This information is available for over 1300 segments, covering the coastline of all eight regional seas of the Arctic Ocean. The coasts of the Barents, Kara, Laptev, East Siberian, Chukchi, and Beaufort Seas have been segmented, as has the coastline of Svalbard. The length of individual segments varies (median length is 38 km), but the segmentation format is scalable, allowing the adoption of future digital coastlines and the integration of additional, higher-resolution data. The data are available via an Internet map server and as a downloadable geodatabase at the ACD web site. Others with complementary datasets are encouraged to contribute to this growing data resource. Future development will include the incorporation of remote sensing into the geodatabase.

ACD represents the coastal component of the ongoing international effort to integrate existing and planned Arctic observatories into a coherent Sustained Arctic Observatory Network (SAON). In addition, ACD's IPY activity, ACCO-Net, integrates 17 Arctic coastal observatory projects with 24 ACD key sites into an extended network.

Antarctic Permafrost and Soils

The overall objective of ANTPAS is to develop an internationally coordinated, web-accessible, database and monitoring system on Antarctic permafrost and soils. Specific objectives are to:

1. Develop a web-accessible repository for permafrost and soils data.
2. Prepare thematic maps on Antarctic permafrost and soils.
3. Develop a system of boreholes providing data on permafrost and soils properties, past environmental change, and responses to climate change.
4. Develop a monitoring system recording active layer and periglacial process responses to climate change along selected environmental gradients.

With no centralized funding, ANTPAS progress is restricted to member activity within existing research programs. ANTPAS has developed a web site for publications and links to relevant databases (Objective 1).

Progress has been made on developing soil and permafrost maps (Objective 2), particularly for the Antarctic Peninsula and the Trans-Antarctic Mountain regions. The soil and permafrost data are to be stored, and made available through the web sites of the individual investigators with links to each database from the ANTPAS web site. ANTPAS Objectives 3 and 4 compliment the TSP and CALM projects in the Northern Hemisphere.

Other Geocryological Data

Satellite remote sensing

Satellite remote sensing data are increasingly used for permafrost and seasonally frozen ground studies (Zhang et al. 2004, Duguay et al. 2005). Remote sensing of permafrost terrain and near-surface soil freeze/thaw cycles typically uses a combination of imaging in optical and thermal wavelengths, passive microwave remote sensing, and active microwave remote sensing using scatterometer and Synthetic Aperture Radar (SAR). Consequently, large amounts of valuable data can be generated.

Images and data from the orbiting visible and near-infrared sensors can be used to infer permafrost distribution (e.g., Anderson et al. 1984), active layer thickness, and various periglacial features (Leverington & Duguay 1996). LANDSAT data provide a high-resolution (15 m to 80 m), long (1972–present) time-series, useful to investigate changes in land surface morphology such as in rock glaciers, thaw lakes, and other periglacial phenomena. Land surface temperature is a key parameter for permafrost and seasonally frozen ground studies. The potential application of using land surface temperature products derived from visible and infrared sensors from 1980 to the present can be substantial (Zhang et al. 2004, Duguay et al. 2005). Remotely sensed land surface temperatures can be used to drive numerical models simulating the development of the active layer and thermal regime of permafrost or to estimate thawing index, which can be used to estimate active layer thickness.

SAR data has been used to map bottom fast ice that controls the preservation and development of subsea permafrost (Solomon et al. 2005). Data from passive microwave sensors dating from 1978 can be used to detect near-surface soil freeze-thaw status based on the spectral sensitivity of brightness temperatures to the state of water (liquid or solid) in soils. Zhang and Armstrong (2003) have provided the near-surface (<5 cm) soil freeze/thaw status derived from passive microwave satellite remote sensing data over the Arctic terrestrial drainage basin. Other near-surface soil freeze/thaw data products are also available but have not yet been archived.

Scatterometery can also be used to detect near-surface soil freeze/thaw status with relatively high spatial resolution. Attempts have been made to apply the differential interferometric synthetic aperture radar technique to monitor the surface deformation (frost heave and thaw settlement) due to the annual freeze/thaw cycle of the active layer over permafrost (Wang & Li 1999).

As satellite remote sensing techniques improve, more and better products will continue to be generated. It is essential to archive and distribute such data products.

Periglacial process data

Information on the movement and activity of different periglacial landforms derived from many different techniques including remote sensing, geophysical data such as resistivity and georadar, direct movement measurements, and snow distribution data are increasingly being collected; yet they are lacking coordinated data management arrangements. For example, the TSP Norway project is collecting significant periglacial process data. In another example, the FGDC at WDC for Glaciology at Boulder has received several offers of data on rock glaciers from independent investigators. Because these data are not part of a formal funded program at the WDC, it is difficult for the WDC to acquire the data.

Historical and other data

There are a variety of other important geocryological data sources. Various national programs continue to produce important data outside the bounds of formal IPA programs. While some of these data are well managed and readily available, others need to be better described through formal metadata protocols, converted to digital formats, or migrated to new media. Some data are at risk as investigators retire or research programs end. Some data even need to be "rediscovered", such as those datasets advertised on CAPS that are no longer readily available.

Models are also increasingly important in characterizing and predicting geocryological processes, especially in a changing climate regime (e.g., Marchenko et al. 2008).

Preservation and distribution of significant model outputs will be a growing concern.

Finally, the IPA has often produced specialized bibliographies and these have also been featured on CAPS. The Cold Regions Bibliography Project continues this work with the *Bibliography on Cold Regions Science and Technology* (Tahirkheli 2008).

Future Directions

The increased IPY field data collection, the increased application of remote sensing methods, and the growing need to integrate data across disciplines challenge the ad hoc nature of the GGD. To achieve the IPY goals of greater international collaboration and interdisciplinary research, it is insufficient to simply share basic metadata. Data must be provided in more consistent formats through more interoperable data exchange protocols. Open Geospatial Consortium (OGC) standards and technologies provide one approach to interoperable data sharing. Several information portals such as the Arctic Research Mapping Application and the Arctic Portal build off OGC technologies. Already, within the GGD, the ACD is providing its coastal segment database through an OGC map server, while the WDC for Glaciology provides the *Circum-Arctic Map of Permafrost* and other cryospheric data through several OGC protocols (WMS, WCS, WFS) (Maurer 2007). Users can then use these data and services to prepare their own maps, view regions and variables of interest, and compare data from different sources.

Another goal of IPY is to leave a legacy for future generations. This challenges the SCDIC and the GGD to develop a more continuous and sustainable data stewardship and preservation strategy. This applies not only to publicly available databases, but sufficient resources must also be committed for active data rescue activities. We should also recognize the value of the past CAPS compilations in providing data snapshots at periodic intervals. These snapshots can act as archival records that are, in essence, preserved simply through their broad and public distribution. IPY marks an important milestone for the IPA with a pulse of new data, and much of that data will be presented at the Ninth International Conference on Permafrost. The SCDIC hope to use this opportunity to create a new CAPS3 compilation. An excellent deadline and opportunity for broad distribution of CAPS3 is the large IPY closing conference in Oslo, Norway in June 2010. Table 1 summarizes some of the potential content.

As the SCDIC develops CAPS3, it must consider how CAPS can evolve as a preservation medium, as well as what data and information it will contain. Is it still appropriate to create physical media for public distribution (e.g., DVDs), or are other strategies such as the peer-to-peer based LOCKSS (Lots of Copies Keeps Stuff Safe) Program more appropriate? Documentation on CAPS3 should evolve to comply with the ISO standard Open Archival Information System Reference Model (CCSDS 2002, cf. Duerr et al. 2006). Finally, quality control procedures for the data compiled need to be determined. Historically, quality control was the responsibility of individual investigators and national programs, but CAPS3 compilers will want to ensure data are in suitably preserveable formats with adequate description of data uncertainties. CAPS3 can serve as benchmark in the development of a lasting polar data system.

Table 1. Initial CAPS3 data sources.

Source	Description or Activity
GTN-P TSP	Temperature data from 300 designated boreholes
GTN-P CALM	Active layer data from 150 sites
ACD	1331 coastal segments described in a geodatabase.
ANTPAS and TSP	Maps, thousands of soil profiles, and periglacial process data
NCSCD	Database of thousands of polygons with soil properties and carbon stocks
CAPS1 and CAPS2	Updates to key products Rescue of lost products
National programs	Identification, description, and acquisition of important products
Remote sensing & model output	Identification, description, and acquisition of important products
Other projects and investigators	Historical data and value added products such as maps, graphical presentations, analyses, etc.
Bibliographies	Monthly updates to the Cold Regions Bibliography

Acknowledgments

Work discussed in this paper is supported by the U.S. National Science Foundation Office of Polar Programs, the Canadian IPY programme, and the Norwegian Research Council's IPY programme.

References

ACIA (Arctic Climate Impacts Assessment). 2005. *Impacts of a Warming Arctic, Arctic Climate Impacts Assessment.* Cambridge University Press.

Anderson, D.M. et al. 1984. Applications of ERTS-1 imagery to terrestrial and marine environmental analysis in Alaska. *Proceedings of the 3rd Earth Resources Technology Satellite-1 Symposium, Washington, DC, V. 1: Technical Presentations, Section B, 1984*: 1,575-1,606.

Barry, R.G. 1988. Permafrost data and information: Status and needs. In: K Senneset (ed.), *Proceedings of the Fifth International Conference on Permafrost,. Trondheim, Norway, 2–5 August 1988*. Tapir Publishers, 119-122.

Barry, R.G. & Brennan, A.M. (eds.) 1989. Workshop on Permafrost Data and Information, Trondheim, Norway, 2 August 1988. *Glaciological Data. GD-23*.

Barry, R.G. & Brennan, A.M. 1993. Towards a Permafrost Information and Data System. *Proceedings of the Sixth International Conference on Permafrost, Wushan, China, 5–9 July 1993.* South China University of Technology Press.

Barry, R.G., Heginbottom, J.A. & Brown, J. 1995. Workshop on Permafrost Data Rescue and Access. 3-5 November 1994, Oslo, Norway. *Glaciological Data. GD-28*.

Brown, J., Ferrians, O.J. Jr., Heginbottom, J.A. & Melnikov, E.S. 1998. revised February 2001. *Circum-Arctic Map of Permafrost and Ground-Ice Conditions.* Boulder, CO: National Snow and Ice Data Center/WDC for Glaciology. Digital Media.

Brown, J., French, H.M. & Guodong, C. 2008. History and Accomplishments of the International Permafrost Association on its 25th Anniversary. *Proceedings of the Ninth International Conference on Permafrost, Fairbanks, Alaska June 29–July 3, 2008* (this proceedings).

Burgess, M.M., Smith, S.L., Brown, J., Romanovsky, V. & Hinkel, K. 2000. Global Terrestrial Network for Permafrost (GTNet-P): permafrost monitoring contributing to global climate observations. *Geological Survey of Canada, Current Research.* 2000-E14: 8.

CCSDS (Consultative Committee for Space Data Systems). 2002. *Reference Model for an Open Archival Information System (OAIS) CCSDS 650.0-B-1 Issue 1* Washington, DC: CCSDS Secretariat.

Duerr, R., Weaver, R. & Parsons, M. 2006. A New approach to preservation metadata for scientific data: A real world example. *Geoscience and Remote Sensing Symposium, IGARSS 2006 IEEE International Conference,* 305-308.

Duguay, C.R., Zhang, T., Leverington, D.W. & Romanovsky, V.E. 2005. Satellite remote sensing of permafrost and seasonally frozen ground. In: C.R. Duguay & A. Pietroniro (eds.), *Remote Sensing in Northern Hydrology.* Geophyiscal Monograph 163, Washington, D.C.: American Geophysical Union, 91-118.

IPA DIWG (International Permafrost Association Data and Information Working Group) (comp.). 1998. *Circumpolar Active-Layer Permafrost System* Boulder, CO: National Snow and Ice Data Center/WDC for Glaciology. CD-ROM.

IPA SCDIC (International Permafrost Association Standing Committee on Data Information and Communication) (comp.). M.A. Parsons & T. Zhang (eds.) 2003. *Circumpolar Active-Layer Permafrost System Ver. 2.* Boulder, CO: National Snow and Ice Data Center/WDC for Glaciology. CD-ROM.

IPCC. 2007. *Climate Change 2007: The Physical Science Basis. Contribution of Working Group I to the Fourth Assessment Report of the Intergovernmental Panel on Climate Change. S.* Solomon et al. (eds.) Cambridge University Press, 996 pp.

Leverington, D.W. & Duguay, C.R. 1996. Evaluation of three supervised classifiers in mapping 'depth to late-summer frozen ground', central Yukon Territory. *Canadian J. of Remote Sensing* 22(2): 163-174.

Marchenko, S.S. et al. 2008. Numerical Modeling of Spatial Permafrost Dynamics in Alaska. *Proceedings of the Ninth International Conference on Permafrost, Fairbanks, Alaska June 29–July 3, 2008* (this proceedings).

Maurer, J. 2007. *Atlas of the Cryosphere* Boulder, CO: National Snow and Ice Data Center. Digital Media.

NRC (National Research Council). 1983. *Permafrost Research: An Assessment of Future Needs* Washington, DC: National Academy Press.

NRC (National Research Council). 2008. *Environmental Data Management at NOAA: Archiving, Stewardship, and Access*. Washington, DC: National Academies Press.

Oberman, N.G. & Kakunov, N.B. 2004. *Ground Temperatures from Deep Boreholes in the Ob River Valley, Russia (VK-1615 and Zs-124/124A).* Boulder, CO: National Snow and Ice Data Center/WDC for Glaciology. Digital Media.

Shiklomanov, N.I. et al. 2008. The Circumpolar Active Layer Monitoring (CALM) Program: Data Collection, Management, and Dissemination Strategies. *Proceedings of the Ninth International Conference on Permafrost, Fairbanks, Alaska June 29–July 3, 2008* (this proceedings).

Sodnom, N. & Yanshin A.L. (eds.) 1990. *Geocryology and Geocryological Zonation of Mongolia*. Digitized 2005 by M.A. Parsons. Boulder, CO: National Snow and Ice Data Center/WDC for Glaciology. Digital Media.

Solomon, S., Manson, G. & Fraser, P. 2005. Remote sensing of bottom-fast ice in the Mackenzie Delta region, Northwest Territories, Canada. *Report of the 5th International Arctic Coastal Dynamics workshop, Montreal, Canada, Oct. 13-16, 2004.*

Tahirkheli, S.N. 2008. Permafrost in the Bibliography on Cold Regions Science and Technology. *Proceedings of the Ninth International Conference on Permafrost, Fairbanks, Alaska June 29–July 3, 2008* (this proceedings).

Tarnocai, C., Swanson, D., Kimble, J. & Broll, G. 2007. *Northern Circumpolar Soil Carbon Database* Ottowa, Canada: Research Branch, Agriculture and Agri-Food Canada. Digital Media.

UNEP (United Nations Environment Program). 2007. *Global Outlook for Ice and Snow.* Birkeland, Norway: Birkeland Trykkeri A/S.

USGCRP. 1999. *Report of the USGCRP Workshop 28-30 Oct. 1998.* US Global Climate Research Program.

Wang, Z. & Li, S. 1999. Thaw deformation of permafrost active layer near Toolik Lake, Alaska, imaged by DINSAR technique during summer time. *Eos, Trans. of the American Geophysical Union* 80.

Zhang, T. & Armstrong, R. 2003 updated 2005. *Arctic Soil Freeze/Thaw Status from SMMR and SSM/I, Version 2*. Boulder, CO: National Snow and Ice Data Center/WDC for Glaciology. Digital Media

Zhang, T., Barry, R.G. & Armstrong, R.L. 2004. Application of satellite remote sensing techniques to frozen ground studies. *Polar Geog*. 28: 163-196.

Zhang, T., Frauenfeld, O.W., McCreight, J. & Barry, R.G. 2005. *Northern Hemisphere Ease-Grid Annual Freezing and Thawing Indices, 1901–2002.* Boulder, CO: National Snow and Ice Data Center/WDC for Glaciology. Digital Media.

Regional Geocryological Dangers Associated with Contemporary Climate Change

A.V. Pavlov
Earth Cryosphere Institute, Russian Academy of Sciences, Moscow, Russia
G.V. Malkova
Earth Cryosphere Institute, Russian Academy of Sciences, Moscow, Russia

Abstract

Contemporary climate plays an important role both in the evolution of frozen strata and in genesis of the cryogenic processes. The activation of seasonal thawing, thermokarst, and solifluction is specified by the perennial changeability of the climate characteristics during the warm period of the year. The activation of seasonal freezing, cryogenic cracking, frost heave, and partly of icing formation is specified by the winter ensemble of the climate factors. The small-scale map of the geocryological hazards in the north of Russia has been fulfilled. Western Siberia, the Taimyr Peninsula, southern Yakutia and the Trans-Amur territories are among the unstable regions. The most stable conditions have been registered in the European part of the Russian cryolithozone, in northeastern Siberia and on the Chukot. The climate warming has brought about the increase of the mean annual ground temperature, some displacement (towards north) of the boundary of the types of permafrost, and the 15% reduction of the area of the continuous permafrost.

Keywords: climate warming; cryogenic processes; geocryological hazards; permafrost temperature.

Introduction

During the last hundred years, the climate warming has become distinctly apparent and has been widely discussed in scientific literature and in press (Anisimov et al. 1999, Douchkov & Balobaev 2001, Izrael et al. 1999, 2002, Klimenko et al. 2001, Malevsky-Malevich et al. 2001, Obzor 2003, Pavlov & Ananieva 2005, Pavlov et al. 2002, Pavlov 2001, Fotiev 2000, Gavrilova 2005, Nelson et al. 1993, Osterkamp 2003, Zhang & Osterkamp, 1993).

The meteorological data revealed that the global climate warming which had begun in the 1960–1970s was most distinctly registered in subarctic and middle latitudes. For the end of the 20th Century, the rise in air temperature in the north of Russia made up on average 1.1–1.2°C whereas the rise in global temperature was about two times less (0.6°C). The greatest rate of global warming fell in the 1980s. The centers of contemporary warming in Russia were central Yakutia and Transbaikalia, where the air temperature increase amounted to 2–4°C during 1965–2000. In the arctic regions the increase made up not more than 0.5–0.7°C during the same period. Since the second half of the 1990s, the tendency towards the delay in climate warming has exhibited in some northern Russian regions (towns: Turukhansk, Olerkminsk, Aldan, and Yakutsk).

In 2001–2005 the air temperature rise all over the north of Russia has been estimated as very weak (about +0.1°C) (Pavlov et al. 2007). In northwestern Siberia the mean annual air temperature rise of 1/3 part has occurred due to the warm period, whereas in central Yakutia it has been less than of 1/3 part. Only since the middle of the 1990s the contribution of the warm period to the formation of the total climate warming has had a 15–16% increase in central Yakutia.

Methods

The researches are based on the accumulation, classification and analysis of data on the air temperature for more than 80 weather stations with the observation time up to 150–165 years. The data on each weather station have been presented in Excel format in order to make the carrying out of the computerized mode of the statistical assessment of the observation results easy to use. The data smoothing with 3, 5 and 10–year periods has been executed.

The correlation and regression analysis of the observational series have been used (Pavlov et al. 2007). The deviations of the moving mean 10–year air temperature values from climatic norm have been estimated as very weak, weak, moderate and strong. The spatial regularities of the contemporary changes in climate have been revealed by means of the small-scale electronic mapping (Pavlov & Malkova 2005).

The investigations have demonstrated the high performance of the electronic maps' application for regional assessments of the climate changes and for identification of the geocryological dangers under these changes. The electronic version of these maps allows the on-the-fly registration of the necessary refinements when new data are obtained.

Contemporary Increase in the Mean Annual Air Temperature during Warm and Cold Periods

In 2005–2007 the authors of this paper have worked out the maps of the contemporary increase in air temperature during the warm and the cold periods. In order to make the comparative assessment of the air temperature rise in the summer period, the coefficient n_s (relative thawing index) has been inserted. This coefficient is equal to the ratio of the summer air temperature sum in 1991–2000 to the climatic norm.

The regularities of this coefficient's change in the north of Russia are represented as isolines (Pavlov & Malkova 2005). For the most part in northern regions the rise in n_s makes up 1.05÷1.1 (Fig. 1). The north of central and eastern Siberia is remarkable for stable (in the perennial cycle) summer air temperatures (n_s is approximately 1.0). The air temperature rises in summer period are greater only for the Gydansky and Taimyr Peninsulas (1.1÷1.25). On the whole, the map characterizes the potential of seasonal thawing depth increase under the contemporary climate warming. The perennial decrease of n_s has been registered nowhere, and that's why the contemporary climate changes do not promote the thawing depth decrease in the north of Russia.

For the most part of the Russian cryolithozone we predict the weak increase of the ground seasonal thawing depth (up to 5%). The increases of seasonal thawing depth for 5–10% are to be expected only in western Siberia and in the Far East, and the greatest ones (10–20%) on the north of the Gydansky and Taimyr Peninsulas. In these regions, the massive and wedge ground ice beds are widely spread, and therefore the increase of seasonal thawing depth can contribute to activation of the thermokarst, thermodenudation and thermo-abrasion.

Our colleagues (Gravis & Konchenko 2007) also have executed in the short term a forecast of activization of cryogenic processes the nearest years, using other methods. By their estimations, significant activization of cryogenic processes of the Russian cryolithozone is expected on the arctic islands of the Kara Sea and on Taimyr. These researches have confirmed authentically our forecast estimations.

In order to make the comparative assessment of the air temperature change in the winter period, the coefficient n_w (relative freezing index) has been inserted. This coefficient is equal to the ratio of the winter air temperature sum in 1991–2000 to the climatic norm (Pavlov et al. 2007). The regularities of this coefficient's change in the north of Russia are represented as isolines. For the various regions of Russian cryolithozone the change of n_w makes up 0.85÷1.0 (Fig. 2). This fact testifies to the warming in the cold period of the year. According to the meteorological observation data all over the territory, the fall of temperature in the winter period has not been registered during the last decades. Thus, the existing climatic situation does not promote the increase of seasonal freezing and the activation of cryogenic cracking but contributes to the intensification of the cryogenic heave and of the icing formation, and sometimes to the kurum activation. The greatest dynamics of these processes is to be expected in Transbaikalia and in southern Siberia, where recently the East Siberia–Pacific Ocean trunk pipelining has been started.

Elaboration of the Small-Scale Map of the Geocryological Hazards under Contemporary Climate Warming

The elaboration of the map of geocryological hazards under contemporary climate warming is based on the maps of the contemporary air temperature increase during warm and cold periods. For that, the territories with the relative

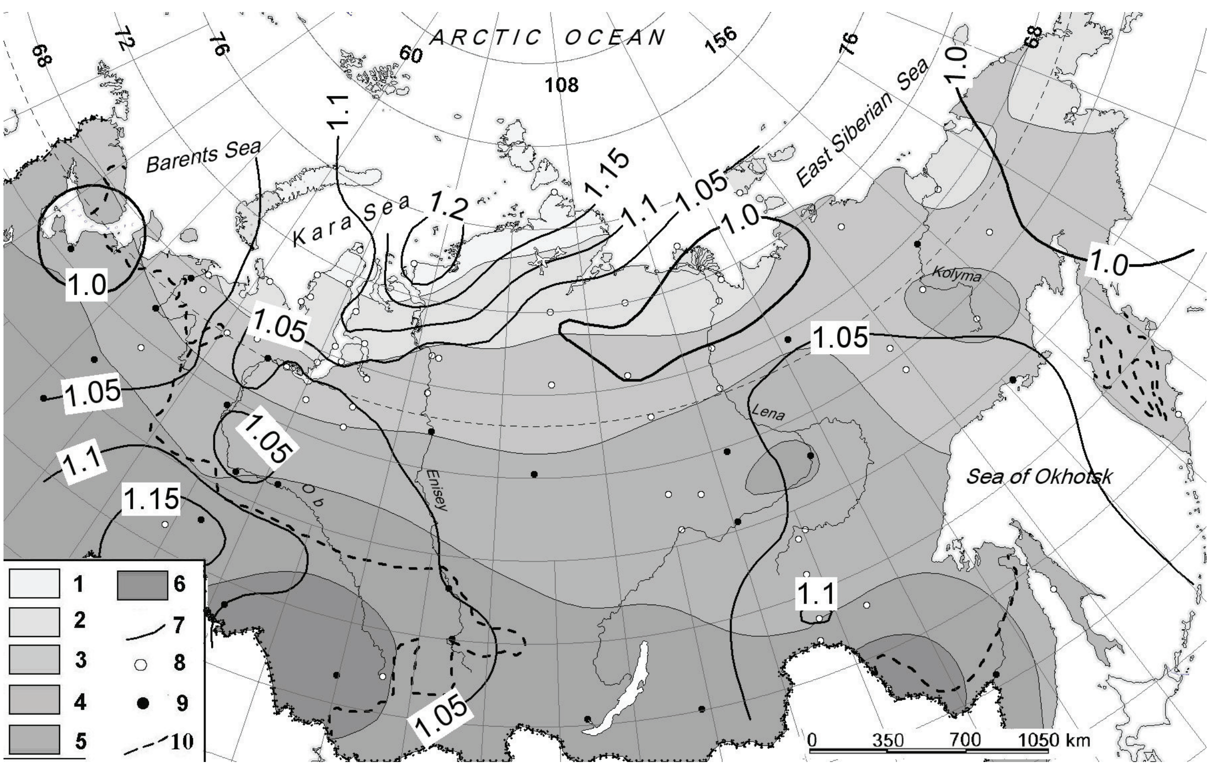

Figure 1. A map of the contemporary increase in air temperature during the warm period. The norm of sums of air temperature in warm season, °C•month: (1) less than 15, (2) 15 to 30, (3) 30 to 45, (4) 45 to 60, (5) 60 to 75, (6) >75, (7) isolines of the relative thawing index, (8) weather stations with observations made for <100 years, (9) weather stations with observations made for >100 years, and (10) the southern limit of permafrost.

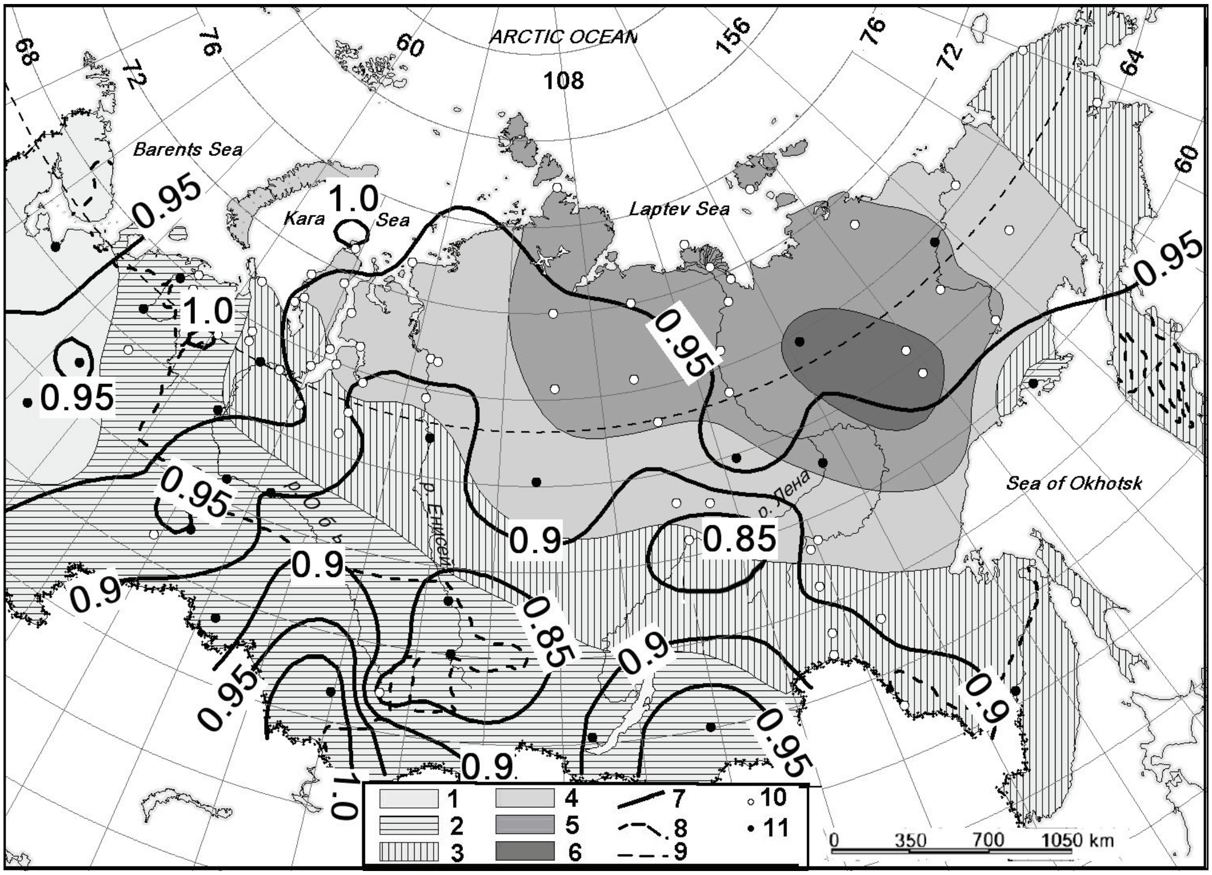

Figure 2. A map of the contemporary increase in air temperature during the cold period. The norm of sums of air temperature in cold season, °C•month: (1) > -60, (2) -60 to -100, (3) -100 to -140, (4) -140 to -180, (5) -180 to -220, (6) < -220, (7) isolines of the relative freezing index, (8) the southern limit of permafrost, (9) Arctic Circle, (10) weather stations with observations made for <100 years, and (11) weather stations with observations made for >100 years.

index n_s more than 1.1, within 1.1 and 1.05, and less 1.05 have been marked out on the map of the relative warming of summer period. The data of the territory are characteristic for strong, moderate and weak degree of the activation of cryogenic processes during summer period, respectively. The territories with the relative index n_w less than 0.9, from 0.9 to 0.95, and more than 1.05 have been marked out on the map of the relative warming of winter period. The singled-out territories characterize the degree of the potential activation of the cryogenic processes (strong, moderate and weak) during the summer period.

The superposition of the two transformed maps makes it possible to make up the map of the geocryological hazards under the climate warming (Fig. 3), depicting on the whole the extreme warming of the summer and winter periods.

The superposition of maps doesn't result in the coincidence of territories with strong activation of the cryogenic processes both in warm and in cold periods simultaneously. But there occurs the combination of strong activation of the processes in the warm period and the moderate one in the winter period (Taimyr Peninsula), as well as the strong activation in the winter period and the moderate one in the warm period (southern Siberia and the Trans-Amur territories). Besides, the intersection of the territories with moderate activation of the cryogenic processes both in warm and in cold periods has been noted (western Siberia, eastern Russia and Transbaikalia). During the perennial cycle the stable geocryological conditions have been registered on the most part of northern Europe, on northeastern Siberia and on the Chukot.

Within the ranges of the Russian cryolithozone, the stable climate conditions and hence the weak manifestation of the geocryological hazards are maintained for 1/4 of the area. The most unfavorable combination of the climate factors, and hence the greatest manifestation of the geocryological hazards, are characteristic for 10% of the territory. The moderate degree of the geocryological hazards is typical for the rest of the area.

Forecast of the Ground Temperature Change and Permafrost Extent

The predictive estimations of the increase of the temperature of the upper horizons of the permafrost on the territory of the Russian cryolithozone have been carried out taking into account the contemporary warming and change of air temperature during summer and winter periods (Malkova 2006). The approximate solutions of the Stephen's problem

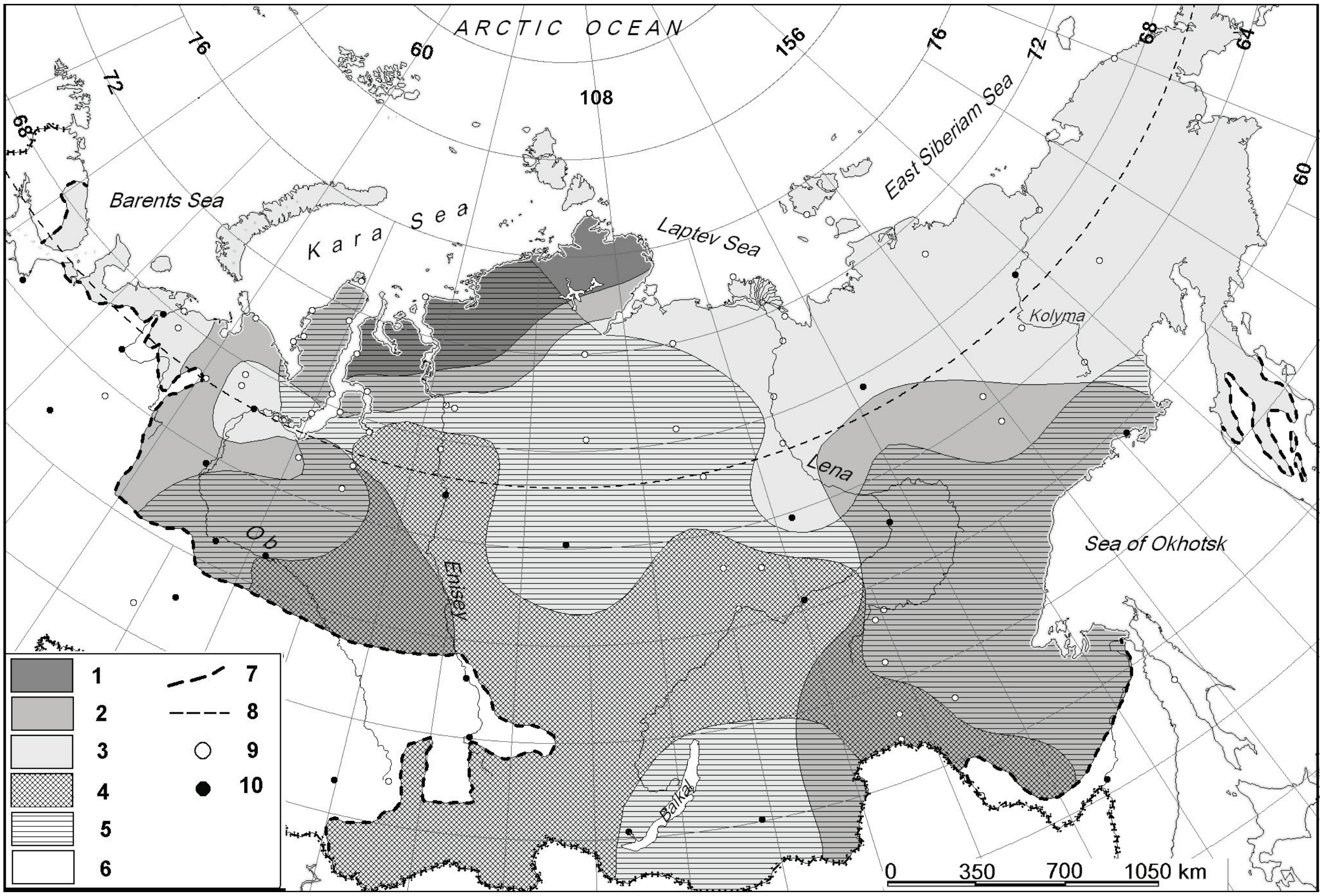

Figure 3. A map of geocryological hazards under the contemporary climate warming in the Russian cryolithozone. Potential activation of the cryogenic processes during the summer period: (1) strong, (2) moderate, (3) weak potential activation of the cryogenic processes during the cold period, (4) strong, (5) moderate, (6) weak, (7) the southern limit of permafrost, (8) Arctic Circle, (9) weather stations with observations made for <100 years, and (10) weather stations with observations made for >100 years.

and the on-line technique of calculation of the mean annual ground temperature have been used for the predictive estimates of the cryolithozone's evolution (*Recommendations*... 1989, *Geocryological forecast*... 1983).

According to the predictive estimates (during the last 30 years) the zone with the transient type of ground temperature (-1 to +1) under the influence of contemporary warming has moved towards north for 100–120 km in western Siberia, for 20–50 km in the European part, for 50–80 km in central Siberia and in eastern Russia. The adduced estimates of the changes of the mean annual temperature of the active layer are well agreed with the field data of the geocryological steady-state stations in the plains of western Siberia and northern Europe but are to be verified in the eastern regions of the country.

In the situation of the contemporary warming, the favorable conditions for permafrost thawing from the top and for replacement of seasonal thawing by seasonal freezing have occurred on the south of the Russian cryolithozone. The data of the recently drilled holes witness that the total thawing of the whole permafrost strata (both contemporary and relict) has not yet taken place. On the whole the area of the island permafrost has been reduced by a factor of 2 (for 1.3 million km^2) throughout Russia. As a result, the continuous and discontinuous permafrost limits have moved towards the north, and the area of the discontinuous permafrost extent has changed insignificantly whereas the area of the continuous permafrost diminished by 15% (for 1 million km^2).

Conclusions

During the last 30–40 years climate warming has been registered all over the territory of north of Russia due to the air temperature rise in summer and winter periods. The greatest increase of the mean annual air temperature is typical for subarctic and adjacent regions. The carried out researches demonstrate the possibility of using meteorological data for the assessment of the development of the dangerous cryogenic processes and the manifestation of the regional geocryological hazards. The conditions for some moving of the permafrost extent limits towards the north have been created due to the peculiarities of the contemporary warming. The tendency toward reduction of the island and continuous permafrost areas has been marked. The researches are proposed to be continued involving the fulfillment of verification of the results on data of the immediate observations on the development of the cryogenic geological processes and ground temperature.

Acknowledgments

This research was supported by RFBR grants 05-05-64215, 08-05-00421 and CALM II-project.

References

Anisimov, O.A., Nelson, F.E. & Pavlov, A.V. 1999. Predicting scenarios of the cryolithozone evolution under the global climate changes in XXI century. *Kriosfera Zemli* 3(4): 15-25.

Gavrilova, M.K. 2005. Climate change throughout the permafrost area in Eurasia during the XX century. *Materials of the Third Conference of the Russian Geocryologists* 2: 45-50 (in Russian).

Geocryological forecast for the West-Siberian gas-bearing province. 1983: 183. (in Russian).

Gravis, G.F. & Konchenco, L.A., 2007. Cryogenic geological processes: problems of the short–term forecast. *Cryogenic Resourses of Polar Region* 2: 131-133.

Douchkov, A.D.& Balobaev, V.T. 2001. Evolution of the thermal and phase state of the Siberian cryolithozone. *Global Changes of the Environment*: 79–104.

Izrael, Yu.A., Pavlov, A.V, & Anokhin, Yu.A. 2002. Cryolithozone's evolution under the contemporary changes of global climate *Meteorologiya i gidrologiya*, *2002, N.*1:10-18 (in Russian).

Klimenko, V.V., Mikushina, O.V. & Larin, D.A. 2001. Temperature trends of the Taimyr region in the conditions of the global climate change. *Geoecologiya: ingenernaya geologiya, gidrogeolgiya, geocryologiya* 1: 195-203 (in Russian).

Malevskii-Malevitch, S.P., Molkentin, E.K. & Nadiozhina, E.D. 2001. Modelling of contemporary and predicted distributions of ground temperature in the permafrost zone throughout the Russian territory. *Materials of the Second Conference of the Russian Geocryologists* 2: 189-196 (in Russian).

Malkova, G.V. 2006. An assessment of the geocryological changes in the upper permafrost horizons in the conditions of the varying climate and technogenesis. *Theory and practice of the assessment of the Earth cryosphere state and the forecast of its changes* 1: 82-86.

Nelson, F.E., Lachenbruch, A.H., Woo, M.-K., Koster, E.A., Osterkamp, T.E., Gavrilova, M.K.. & Cheng, G. 1993. Permafrost and Changing Climate. *Proceedings of the Sixth International Conference on Permafrost, Beijing, China.* Beijing: South China University of Technology Press, 987-1005.

Osterkamp, T.E. 2003.A thermal history of permafrost in Alaska. In: M. Phillips, S. Springman & L.U. Anderson (eds.), *Permafrost, Eighth International Conference Proceedings.* Lisse, Netherlands: Balkema, 863-868.

Pavlov, A.V. 2001. Response of the Permafrost to contemporary Climate Change. In: *Permafrost Response on Economic Development, Environmental Security and Natural Resources*. Kluver Academic Publishers, 277-292.

Pavlov, A.V. 2002. Secular anomalies of the air temperature in the Russian North. *Kriosfera Zemli*. *VI* 2: 75-81 (in Russian).

Pavlov, A.V. & Malkova, G.V. 2005. Contemporary changes of climate in northern Russia: Album of small-scale maps: 54 (in Russian).

Pavlov A.V., Malkova G.V. & Skachkov, Yu.B. 2007. Modern tendencies in the evolution of thermal state of cryolithozone under the climate changes. *Cryogenic Resources of the Polar Regions* 1: 34–38.

Recommendations on the forecast of the thermal state of the frozen ground. 1989: 73 (in Russian).

Zhang, T. & Osterkamp, T. 1993. Changing Climate and Permafrost Temperatures in the Alaskan Arctic. *Proceedings of the Sixth International Conference on Permafrost, Beijing, China*. Beijing: South China University of Technology Press, 783-788.

Wedge Structures in Southernmost Argentina (Rio Grande, Tierra del Fuego)

Augusto Perez-Alberti
Department of Geography, University of Santiago de Compostela, Spain

Andrea Coronato
CADIC. *Conicet., Argentine*

Manuela Costa Casais
Instituto Padre Sarmiento. CSIC. Santiago de Compostela, Spain

Marcos Valcarcel-Diaz
Department of Geography, University of Santiago de Compostela, Spain

Jorge Rabassa
CADIC. Conicet., Argentine

Abstract

Wedge-like structures occur in raised beach gravels near Rio Grande, eastern Tierra Del Fuego (latitude 53°50′S; longitude 67°5′W). They vary in dimension, being approximately 1.0–1.5 m deep and 0.3–0.8 m in apparent width. Some are closely spaced, while others are as much as 5.0–8.0 m apart. The infill is predominantly fine and coarse sand, together with silt, all of local provenance. There is little evidence of secondary infill. It is unclear whether these structures are soil wedges, sand wedges, or composite wedges. Their significance as regards the possible previous occurrence of perennially-frozen ground in the lowlands of Tierra del Fuego has yet to be determined.

Keywords: frozen ground; periglacial; soil wedges; Tierra de Fuego, Argentina.

Introduction

This paper documents the occurrence of wedge-like sedimentary structures in the lowlands of eastern Tierra del Fuego. The morphology of the wedges and the nature of the wedge infill are described.

The critical question is whether these structures are relict permafrost phenomena (i.e., ice wedge casts, sand wedges, or composite wedges), or whether they are simply soil (i.e., "ground") wedges and, as such, merely reflect deeper seasonal frost conditions than today. The recent literature that discusses the significance of these various phenomena includes Ghysels and Heyse (2006), Murton and Bateman (2007), and French (2007, 117–118, 127, 327).

Study Area

Tierra del Fuego is located between 52°40′S and 55°7′S and 65°05′W and 68°40′W. Its Atlantic coastline is about 330 km long and runs from northwest to southeast. The dominant feature is steep cliffs, in part formed on sediments, fronted by wide sedimentary intertidal surfaces developed under paraglacial conditions.

The study area near Cape Peñas (Fig. 1) is located at 53°50′S and 67°35′W. The present climatic conditions are temperate-cold, semi-arid, with a mean annual temperature of 5°C. The mean temperature during the coldest month, June, is 0°C while that of the warmest month, January, is 9°C. Rainfall is distributed throughout the year, diminishing between August and October. Total annual rainfall is 380 mm, and snow is generally scarce. The prevailing winds are westerly and to a lesser extent northwesterly and southwesterly. They reach their maximum intensity during the spring and summer months. The wedge-like sedimentary structures are developed on raised beach deposits and were first described by Coronato et al. (2004).

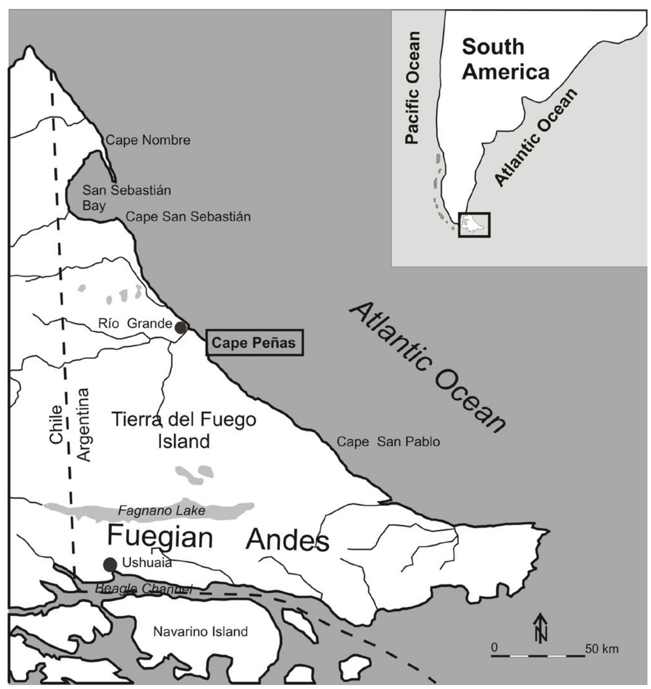

Figure 1. Location of Cape Peñas.

Codignoto (1983, 1984) obtained a radiocarbon age for the beach deposit that was older than 43 ky B.P., and amino-acid racemization on shells of *Pilar rostrata* gave a DL-aspartic acid ration of 0.36 (Rutter et al. 1989). The beach deposits

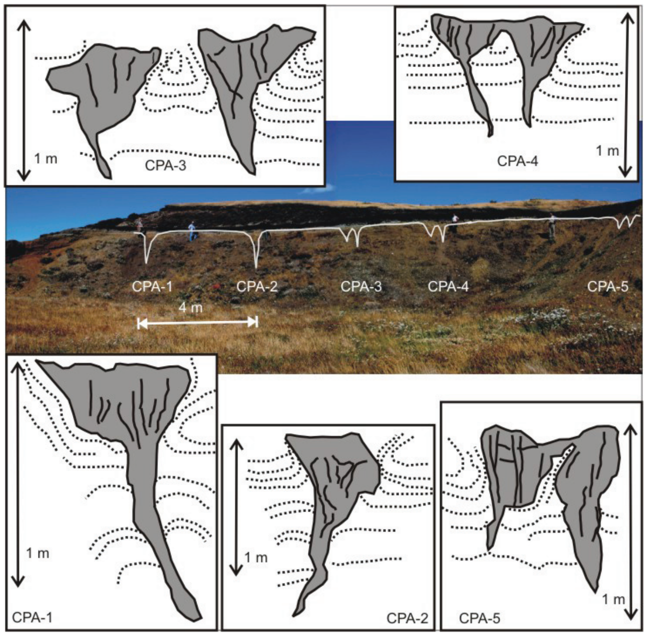

Figure 2. Morphological characterization of sector CPA.

were assigned therefore, to marine oxygen-isotope stage 5e (Meglioli 1992).

The depositional sequence consists from bottom to top of alternating layers about 12 cm in thickness, composed of gravel, pebbles, and sand. The pebbles are rarely more than 8 cm long. Near the coastline there are thick layers of gravels, while further inland there are alternating layers of gravel and sand. The gravel is covered by organic deposits rich in aeolian sand.

Wedge structures attributed to cold-climate conditions have been described previously from southern Argentina (Corte 1968, Auer 1970, Abrahan de Vazquez & Garleff 1984, Grosso & Corte 1989, Vogt & del Valle 1994).

The Permafrost Context

Several authors (e.g., Burn 1990, Murton & Kolstrup 2003, Lemcke & Nelson 2004) refer to the difficulty of determining the type of climatic environment that causes the formation of wedges. Polygonal networks may occur in temperate as well as cold (i.e., periglacial or permafrost) environments. Wedges that occur in non-periglacial environments rarely exceed a few meters in depth. In contrast, those formed in periglacial and permafrost environments are larger and may form polygons 10+ m in diameter. As a rule the polygons that develop in the absence of permafrost are smaller and usually measure between 0.5–2 m in diameter.

There appears to be little difference in the spacing of ice wedge and sand wedge networks. For example, in Siberia and Arctic North America ice and sand wedges are typically separated by distances of between 10–30 m. However, Gozdzik (1986) indicates that in Poland the distance between Pleistocene-age sand-wedge casts is usually much smaller, and the modal size of the dimensions of sand-wedge polygons is about 3.3 m.

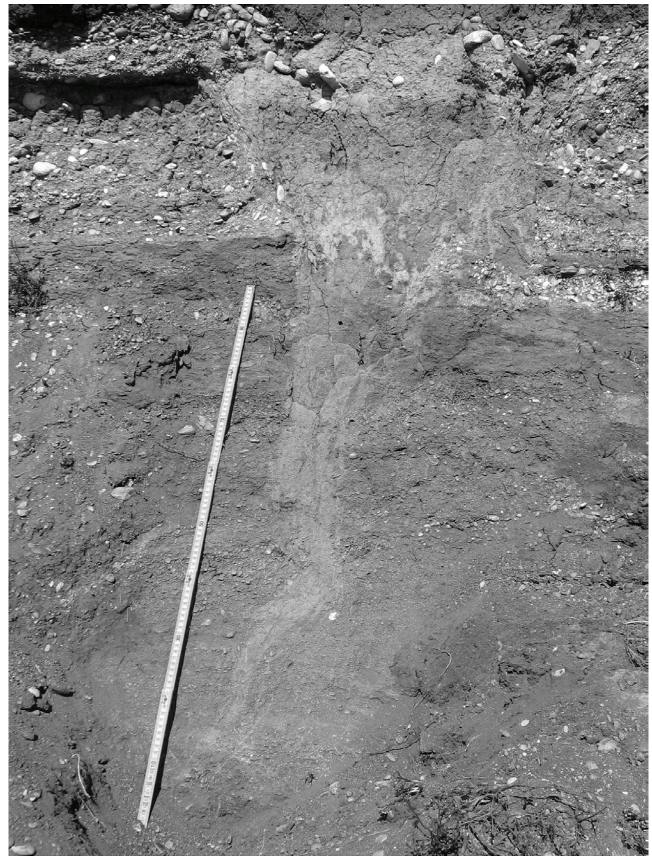

Figure 3. Wedge structure CPA-2.

It is increasingly understood that the mechanism underlying the formation of polygonal structures is related to fast and marked drops of temperature to below -15°C to -20°C. Also, the geometry and size of fissures is related to the type of material affected.

Another consideration is the material infill of the cracks and the thaw-modification that results as the permafrost degrades. Usually there is a slumping of the enclosing sediments and formation of sets of miniature faults. The fissure infill is regarded as secondary. In contrast sand wedges, even when thawed, constitute wedges of primary infill. Thus the resulting sedimentary structures are quite different between the two types of wedges.

The occurrence of cold-climate wedge structures always gives rise to the question of the climatic conditions under which they were formed.

Both sand and ice wedges form under conditions of continuous permafrost. Péwé (1966) indicated that ice wedges only exist where mean annual air temperature (MAAT) is in the -6°C to -8°C range, while Romanovskii (1985) pointed out that, on a substrate of sand or gravel, cracking commonly occurs at MAAT of around -7°C, but in silt the MAAT is slightly higher, -2.5°C.

Wedge Structures

At Cape Penas, a number of wedge structures are exposed in a gravel quarry. The wedges are elongate in shape, reaching up to 1.50 meters in depth and 85cm in width, separated by distances ranging from 1.5 to 9m. One exposure (CPA) is parallel to the coast and nine well-defined forms were identified (Fig. 2).

Wedge structure CPA-1 is slightly inclined seawards and measures 120 cm in depth. The upper section is concave, funnel-shaped, and 85 cm deep and 40 cm wide. The wedge gradually narrows downwards. In the lower section of the wedge layers of sand and gravel dip toward the bottom. In the upper section rounded clasts are turned upwards. The wedge is covered by a level of pebbles and peaty-sandy materials.

CPA-2 (Fig. 3) is located 4m west of CPA-1 and is 140 cm deep. The upper section increases its width from 40 cm to 50 cm. The lower section narrows from 20 cm to 5 cm in width. Upturning of enclosing sediment is evident. CPA-3, located at a distance of 4 m from CPA-2, is smaller and more diffuse in shape. It has an open V-structure for a depth of 92 cm. It has a width of 32 cm in the upper section and 10 cm in the lower part. As in the previous wedge structures, pebbles in adjacent sediments are imbricated or tilted upwards.

CPA-4, located 4 m from CPA-3, shows a double wedge structure with a width of 58 cm and 73 cm. The smaller of the two structures is 47 cm wide at its head, while the bigger one (CPA-4a) is between 46 cm and 73 cm. The first narrows in depth whilst the second shows well differentiated segments: an upper one 25 cm deep and 13 cm wide, and a lower one of scarcely 5 cm.

Wedge structure CPA-4b shows the best example of adjacent pebbly strata being deformed upwards. The pebble layers trace perfect arches with clasts oriented in an upwards direction. Another double structure is found in CPA-5, about 9 m away from CPA-4. It is composed of two fissures measuring 80 cm and 68 cm in depth and 42 cm and 34 cm across their upper sections respectively. They also show evidence of upward deformation of enclosing beds.

CPA-6 is located about 3 m from CPA-5. It measures 70 cm in depth. Its width is 30 cm in the upper section and 19 cm in the middle. CPA-7 is 2.20 m away from CPA-6, and is 130 cm deep, with the top section being 80 cm wide. It also shows signs of upward thrusting of adjacent clasts. CPA-8 is at distance of 2.4 m from CPA-7. It is 140 cm deep and its upper section is 78 cm wide, decreasing to 18 cm in the middle part. The upper section shows some clast upturnings. CPA-9 is about 3.40 m from CPA-8. It is 90 cm long, 46 cm wide at the top, and 24 cm in the middle section. As in the previous cases, the infill is well defined with regard to the surrounding deposit.

Granulometry of Wedge Infill

In an attempt to understand the genesis of the wedge infill, samples of wedge infill material were taken from three wedges: CPA-2, CPA-4, and CPA-5. Samples were extracted from soil horizons that were common to each wedge: A, E, Bg_1, Bg_2, and BCg. Grain-size analysis was applied to the fine fraction (<2 mm) using the pipette method following

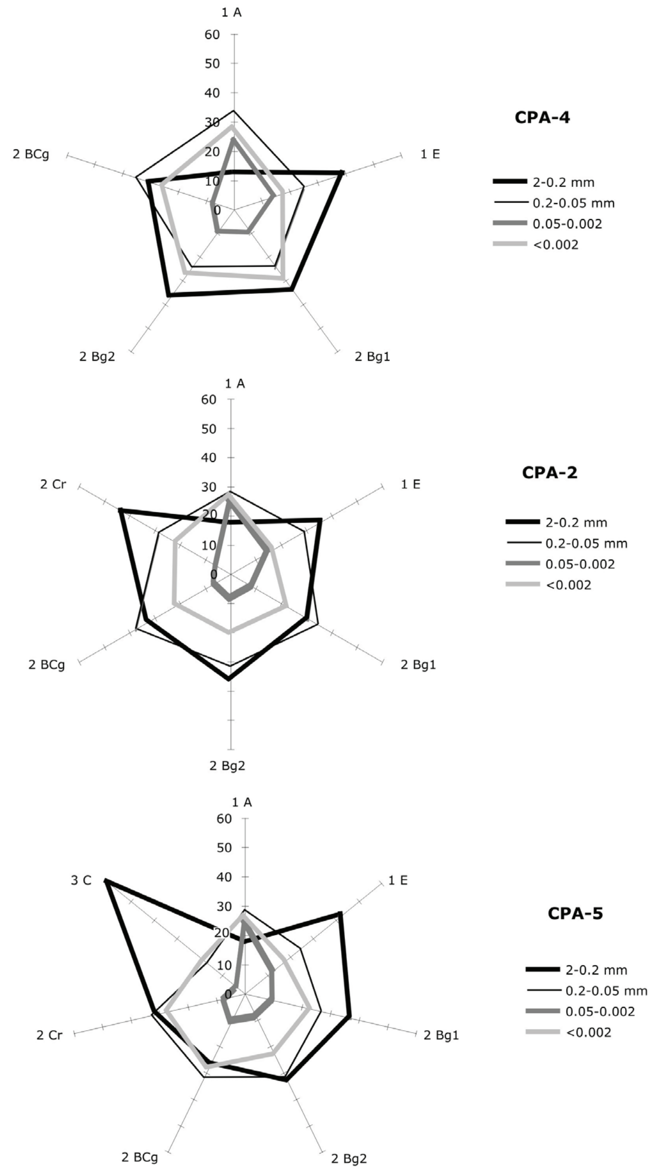

Figure 4. Granulometry of wedge infill.

dispersion with sodium hexametasulphate. The granulometric descriptions of the samples from each horizon are illustrated in Figure 4. The results for all wedges are similar except for the presence or absence of horizons Cr and C, the former being present in wedge CPA-2 and both in CPA-5.

Sand prevails in the three profiles analyzed, with mean values ranging from 46% to 77%. The lowest percentages of sand occur in horizons 1A (46%), while the highest values (between 64% and 77%) appear in 2Cr and 3C. These are in contact with the beach sediments. In horizon 2B, mean percentages ranges from 59% to 70%, increasing towards the lower subhorizon BCg with the exception of wedge CPA-5, which shows a tendency to decrease in this subhorizon.

In the three wedges analyzed there is a size-sorting reflected in the horizons. For example, in the 1A horizons the proportion of fine sands is greater (34% fine sands and 12% coarse in CPA-4), as it is in subhorizon BCg, although the difference is not so marked (37% fine sands, 33% coarse sands in CPA-2). In the remaining 2B subhorizons the values of the fine and coarse fractions are very similar. This tendency changes towards the bottom of the wedges in horizons 2Cr and 3C. For example, the percentage of coarse sands tends to increase (with minimum values of 64% and maximum values of 77% in horizon 3C of CPA-5).

Clay is the second most important fraction. Maximum values occur in horizons A (28% in CPA-4), BCg (29% in CPA-5), and Cr (28% in CPA-5). This fraction decreases in horizons E (17% in CPA-2) and C, the latter at the base of the wedge (18%). The decrease is irregular.

The percentage of silt is never greater than 30%. The highest values are reached in horizon 1A (26%), diminishing progressively until horizon 3C (4%). Fractional analysis reveals a higher content in coarse silt than in fine sediment (9% fine silts as opposed to 17% coarse silts in horizon A of CPA-2).

Mineralogical Analyses

Study of the coarse and fine sand fraction was undertaken for the infill of wedge CPA-2 with the aim of describing the degree of weathering and roundness.

It was found that the mineral fragments are dominated by quartz and by rock fragments in which metamorphic rocks predominate. In general it is possible to classify the mineral fragments into three groups. The first group includes horizons 1A, 1E, and $2Bg_1$; the second group, the horizons $2Bg_2$ and 2BCg; and the third group includes the 2Cr and 3C horizons.

In the first group, rock fragments are predominant in the larger fraction, while monomineral particles prevail in the smaller one. There are rounded rock fragments, some of them spherical, with unpolished surfaces showing impact marks indicative of wind-dominated transportation. The quartz particles on the other hand generally show polished surfaces, with V-shaped impact pits that reveal that they were worked in a marine environment. The clearest marine features appear in the coarse sand, while the fine sand shows aeolian features.

The second group (from horizons $2Bg_2$, 2BCg) shows a smaller number of fragments of both rock and spherical minerals and a progressive increase in the number of sub-rounded and non-spherical fragments. The latter are highly polished and bear impact pits. There are some signs of contact with the upper horizon, evident in the existence of some unpolished, spherical, and rounded fragments in the fine fraction of subhorizon $2Bg_2$. The third group, composed of horizons 2Cr and 3C, reveals a more heterogeneous character. Rock fragments predominate in the coarse sand, and monomineral particles in the fine sand. The quartz particles are polished, ranging from rounded to subrounded, and show impact pits on their surface. There are traces of oxidization on the external faces of all grains, producing a highly characteristic shiny dark-brown patina.

X-ray diffraction analysis of the clay present in the wedge infill revealed the presence of illite and smectite, and the total absence of kaolinite.

Discussion and Conclusions

The origin of these wedge-like structures is not clear. They may or may not reflect cryogenic processes. If they are cold-climate phenomena, it is uncertain whether they formed in seasonally or perennially frozen ground.

Several generalizations can be made. First, it is clear that the wedge structures are not isolated phenomena but occur at regular intervals throughout the section studied. Second, the adjacent enclosing sediments frequently show upward deformation adjacent to the wedge. Third, fine or very fine sand is the predominant infill material, although other size fractions are also present. Fourth, the reworking of the sand-size material suggests an autochthonous contribution. Fifth, the surface characteristics shown by the majority of the sand particles indicate that they were modeled in a marine environment. However, some sand in horizons A, E, Bg_1 possess aeolian features that suggest transport into the wedge by wind.

If the wedges are cryogenic in origin, they appear to have been generated in two phases. In the first phase, thermal-contraction cracking would have occurred in a cold and arid environment marked by an intense temperature drop during the winter months. Such climatic conditions do not exist today on the coast of Tierra del Fuego. In the second phase, more humid conditions would have seen the incorporation of coarse sand and fine gravel into the wedge, presumably during episodes of deep seasonal frost.

The heterogeneous nature of the infill suggests the wedges are of a composite origin However, the possibility that they are soil or ground wedges and formed under conditions of deep seasonal frost rather than permafrost cannot be eliminated. Their age has yet to be determined.

Acknowledgments

Research in Tierra del Fuego is being supported by Spanish International Polar Year Program (POL2006-PC091) and the Spanish Ministerio de Educacion y Ciencia research project CGL2004-03380/BOS. The authors wish to acknowledge the constructive comments of two anonymous reviewers. They also wish to thank Professor Hugh French for help with the original manuscript and for his editorial assistance in rewriting the paper following review.

References

Abraham de Vazquez, E.M. & Garleff, K. 1985. Fossil phenomena in the central and southern part of the Piedmont of Mendoza Province, Argentina. *Zbl. Geol. Paläont.* Teil I, H. 11-12: 1709-1719, Stuttgart.

Auer, V. 1970. The Pleistocene of Fuego-Patagonia. Part. V: Quaternary problems of southern South America. *Ann. Acad. Sci. Fennicae* A. III: 100: 194.

Burn, C.R. 1990. Implications for palaeoenvironmental reconstruction of recent ice-wedge developement at Mayo, Yukon Territory. *Permafrost and Periglacial Processes* 1: 3-4.

Codignoto, J. 1983. Depósitos elevados y/o acreción del Pleistoceno-Holoceno en la costa fueguino-patagónica. *Simposio Oscilaciones del nivel del mar durante el último hemiciclo deglacial en la Argentina*. 12-16. Mar del Plata.

Codignoto, J. 1984. Estratigrafía y geomorfología del Pleistoceno-Holoceno costanero entre los paralelos 52º30′S y 42º00′S, Argentina. *IX Congreso Geológico Argentino*. Actas III: 513-519. San Carlos de Bariloche.

Coronato, A., Bujalesky, G., Pérez Alberti, A. & Rabassa, J. 2004. Evidencias criogénicas fósiles en depósitos marinos interglaciarios de Tierra del Fuego, Argentina. *X Reunión Argentina de Sedimentología, San Luis, September 2004*, Abstracts: 48-49.

Corte, A. 1968. Informe preliminar del progreso efectuado en el estudio d elas estructuras de crioturbación pleistocenicas fosiles en la provincia de Santa Cruz. *Terceras Jornadas Geologicas Argentinas*. Tomo II: 9-19.

French, H. 2007. *The Periglacial Environment. Third Edition.* Chichester: J. Wiley & Sons, Ltd., 458 pp.

Ghysels, G. & Heyse, I. 2006. Composite-wedge pseudomorphs in Flanders, Belgium. *Permafrost and Periglacial Processes* 17 : 145-162.

Gozdzik, J.S. 1986. Structures de fentes de remplissage primaire sableaux du Vistulien en Pologne et leur importance paléogéographique. *Biuletyn Peryglacjalny* 31: 71-105.

Grosso, S.A. & Corte, A.E. 1989. Pleistocene Ice Wedge Cast at 34 degrees S Eastern Andes Piedmont, South America. *Geografiska Annaler* 71A: 125-136.

Lemcke, M.D. & Nelson, F.E. 2004. Cryogenic Sediment-Filled Wedges, Northen Delaware, USA. *Permafrost and Periglacial Processes* 15: 319-326.

Meglioli, A. 1992. *Glacial Geology of Southernmost Patagonia, the Strait of Magellan and Northern Tierra del Fuego.* Ph.D. Dissertation. Bethlehem, USA: Lehigh University.

Murton, J.B. & Kolstrup, E. 2003. Ice-wedge casts as indicators of palaeotemperatures: precise proxy or wishful thinking? *Progress in Physical Geography* 27: 155-170.

Murton, J.B. & Bateman, M.D. 2007. Syngenetic sand veins and anti-syngenetic sand wedges, Tuktoyaktuk Coastlands, Western Arctic Canada. *Permafrost and Periglacial Processes* 18*:* 33-47.

Péwé, T. 1966. Paleoclimatic significance of fosil ice wedges. *Biuletyn Peryglajalny.* 15: 65-73.

Rutter, N., Schnack, E, del Río, J., Fasano, J., Isla, F. & Radke, U. 1989. Correlation and dating of Quaternary littoral ones along the Patagonian coast, Argentina. *Quaternary Science Review* 8: 213-234.

Romanovskii, N.N. 1985. Distribution of recently active ice and soil wedges in the USSR. In: Church, M. Slaymaker, O. eds., *Field and Theory: Lectures in geocryology.* Vancouver: University of British Columbia Press, 154-165.

Vogt, T. & del Valle, H. F. 1994. Calcretes and Cryogenic Structures in the Area of Puerto Madryb (Chubut, Patagonia, Argentina). *Geografiska Annaler* 76A: 57-75.

Modeling Interaction Between Filterable Solutions and Frozen Ground

G.Z. Perlshtein
Institute of Environmental Geoscience, Russian Academy of Sciences, Moscow, Russia
G.S. Tipenko
Institute of Environmental Geoscience, Russian Academy of Sciences, Moscow, Russia

Abstract

Research of interactions between filterable solutions and frozen ground are very important for many problems of contemporary basic and applied geocryology. In thaw zones, heat and salt transport by groundwater often proves to be more significant than transport by means of a molecular-diffusion mechanism. For the case of water movement in permeable frozen ground, quantitative description of convective heat and mass transfer is insufficiently devised. The presented model consists of the conventional equations set for convective heat and salt transfer. It is supplemented by an ice melting equation. Phase equilibrium ice-solution is expressed by dependency of the crystallization temperature upon concentration. The heat sink is prescribed in direct proportion to the difference between solution temperature and the eutectic point. Modeling results accord entirely to the modern view on the physical essence of the processes under consideration. The obtained method is planned for practical use, in particular, diamond mining in Yakutia.

Keywords: eutectic point; groundwater flow; ice melting; mathematical modeling; permeable frozen ground.

Introduction

The interaction between salts and frozen ground has increasingly drawn the attention of permafrost scientists and engineers. Salt and heat transfer with groundwater flow plays a significant role in forming the frozen massif structure, thermal regime, and ground characteristics in the cryolithozone. Solution appearance in ice-containing ground changes the phase equilibrium conditions: the temperature derived at the point of contact with the frozen zone corresponds to the eutectic point at a given concentration. For that reason, the temperature field dynamics of saline ground is highly dependent on the solute diffusion.

Understanding the essence and quantitative regularities of the process is very important for solving such problems as contemporary basic and applied geocryology : as an evaluation of salted ground state,; palaeoreconstructions and prediction of coastal and offshore permafrost behavior,; cryopeg dynamics,; thawing frozen ground by the use of salts, etc. A number of works (Ershov 1990, Komarov 2003, Permyakov & Romanov 2000, and others) are devoted to theseis problems. These works consider heat and salt transport only by means of a molecular-diffusive mechanism.

Quantitative research of heat and mass transfer induced by groundwater movement is of great interest. In the case of forced convection, energy and substance fluxes often prove to be much more intensive than those conditioned by molecular-diffusive forces.

It should be noted that the theory of convective diffusion started to develop rapidly about the middle of the last century (Bear 1961, Veriguin 1962, and others). In many respects, it was associated with leaching and other geotechnological method problems. (Kalabin 1981).

Existing quantitative theories of the interaction between groundwater flow and frozen ground have been developed in connection with solving practical problems such as hydraulic thawing of frozen ground and hydraulic engineering in permafrost regions (Bogoslovsky 1959, Goldtman et al. 1970, and others). These works consider movement of fresh water only, in the thaw zone.

However, it is not uncommon in nature that, when pores and fissures of frozen soils and rocks are only partially filled with ice, they keep an essential permeability and can not be considered as aquifuges. The movement of saliferous water in such a medium has some important features. Knowledge of them is important for general theory as well as for solving practical problems of drainage waters burial (in particular, at diamond mining in Yakutiya) and other technological challenges.

Short Review of Existing Models

There are two approaches to quantitative description of interrelated processes of heat and salt transfer: (1) the model of phase change on the mobile interphase surface that is well known as Stefan's problem, and (2) models of phase change in some temperature range. In the case of a classical (front) approach to the problem, diffusion occurs only in a thawed zone. The models with unfrozen water also take into account the salt transport in the frozen zone through the films of unfrozen water. In either case, the equations of heat transfer and diffusion use the dependency of the solution thermodynamic potential from its solute concentration (for instance, functional dependency of solution concentration on eutectic point).

As a rule, both approaches are realized in the frames of one-dimensional calculating schemes.

In equations, a heat-mass transfer with moving water is factored in through an additional item summand that is proportionate to the water flow velocity. The latter is found through solving groundwater dynamics equations.

Methods for calculating thaw rate are well-developed for the cases of water moving in thawed zones along an impermeable boundary with frozen ground. They were used widely, for example, for designing mining works at the permafrost placers of northeastern Russia.

When deriving an equation, the assumption is used that the temperatures of matrix solid material and moving water are equal. Owing to that, the temperature fields of the ground components are described by one common equation.

It should be noted that coarse-grained ground and fissured rocks could have a significant permeability in the frozen state. It is obvious that this assumption noticeably conflicts with studied processes when water moves in permeable frozen ground that has some amount of ice in it. The simplest case of heat transfer during fresh water movement through permeable frozen zone has been analyzed by one of the authors (Perlshtein & Jiltsov 1984) and was distinguished into a special type of convective heat transfer in thawing ground. To date, however, the processes of joint convective transfer of heat and salts in permeable frozen rocks are very poorly explored and studied.

Main Assumptions and Mathematical Statement of the Problem

This paper offers a quantitative description of heat-mass transfer during solution movements, not only in the thaw zone, but also in permeable frozen massif. This model reflects the following features of the process:

1. salt diffusion occurs in the part of a fissured-pored space that is not filled with ice;
2. when solution gets in contact with frozen rocks, the temperature on the contact instantly settles to the crystallization temperature at a given concentration;
3. in every elementary volume of the area of study, moving solution and matrix solid material with ice inclusions can have different temperatures (at least, until the ice completely melts).

The source, brought into equations of convective heat and salt transfer, is defined by heat flux density from solution into solid phase for temperature fields, and by the water influx due to ice melting for concentration fields. The value for this source is included in a boundary condition for ice and matrix solid material temperature fields. In the first approximation, it is assumed that in both solid and liquid phases, the heat fluxes normal to solution flow are negligible in comparison to energy absorption on a melting front, and that right after ice melt-out, temperatures of medium components equalize.

The stated assumptions lead to the following system of heat-mass transfer equations:

$$\rho_w c \frac{\partial T}{\partial t} = \nabla(\lambda \nabla T + c\rho_w T k_f \nabla \varphi) + n\rho_i L \frac{\partial \theta}{\partial t}, \qquad (1)$$

$$\frac{\partial \theta}{\partial t} = W_\theta(T, \theta, M), \qquad (2)$$

$$\frac{\partial M}{\partial t} = \nabla(D\nabla M + Mk_f \nabla \varphi) + W_M(T, \theta, M) \qquad (3)$$

$$\nabla(k_f \nabla \varphi) + nW_\theta = 0 \qquad (4)$$

where $W_\theta(T, \theta, M)$ – rate of ice saturation changes, units:

$$W_\theta(T, \theta, M) = \frac{\beta(V, \theta)}{n}\left(T^*(M) - T\right) \qquad (5)$$

and $W_M(T, \theta, M)$ –rate of dissolution due to ice melting:

$$W_M(T, \theta, M) = \frac{M}{(1-\theta)} W_\theta(T, \theta, M); \qquad (6)$$

T = temperature, K; M = concentration, kg/kg; t = time, s; ρ_w, ρ_i = water and ice density, kg/m^3; c = specific heat, J/(kg ·K); λ= heat conductivity, W/(m ·K); L = specific latent heat of ice melting, J/kg; k_f = hydraulic conductivity, m/s; V = water flow velocity, m/s; D = diffusion coefficient, m^2/s; φ = hydraulic pressure head, m; β = the volumetric coefficient of convective heat transfer, 1/s ·K; T^* = eutectic point, K; θ = ice saturation in pores, m^3/ m^3; n = porosity.

Modeling Results

A modeling objective was to study ice melt-out processes with $CaCl_2$ solution being injected into the layer of permeable highly fissured frozen rocks. Temperature and concentration fields had an axial symmetry. The characteristics of permeable zone and country rocks are given in Table 1.

Surface rock temperature was equal to -4° with 0.01 K/m gradient. The brine injected in the borehole had constant temperature (7°C) and concentration (6 and 20% in two model runs).

Main calculation results are presented on the graphs. It shows that energy and material flow has a high propagation rate around the borehole. It is explained by the very high permeability of rocks that was specially set in calculations for evaluating an extreme impact of convective heat-mass transfer to frozen rocks.

Just as was expected, in the first model run (M_0 = 6%) salt concentration is monotonously increasing in the whole area studied and quickly approaches the concentration of injected solution. In the distance from the borehole, temperatures and concentrations very quickly equalize with eutectics of injected solution.

The temperature pattern of change is somewhat more complicated (Fig.1).

It is interesting to note that, in the second model run, the temperature is even decreasing in the beginning. The reason for it is the fast brine propagation, when the eutectic

Table 1. Characteristic of massif under consideration.

№ of layer	Depth	n	k_f	θ	λ	c
1	0–250	0	0	0	3.0	836
2	250–300	0.1	$3\cdot10^{-5}$	0.5	3.0	836
3	300–1000	0	0	0	3.0	836

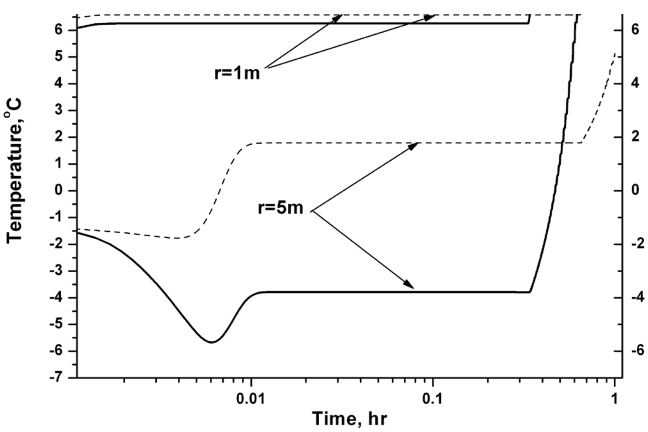

Figure 1. The temperature changes at different distance from borehole with mass transfer (solid line) and with initial concentration (dash line).

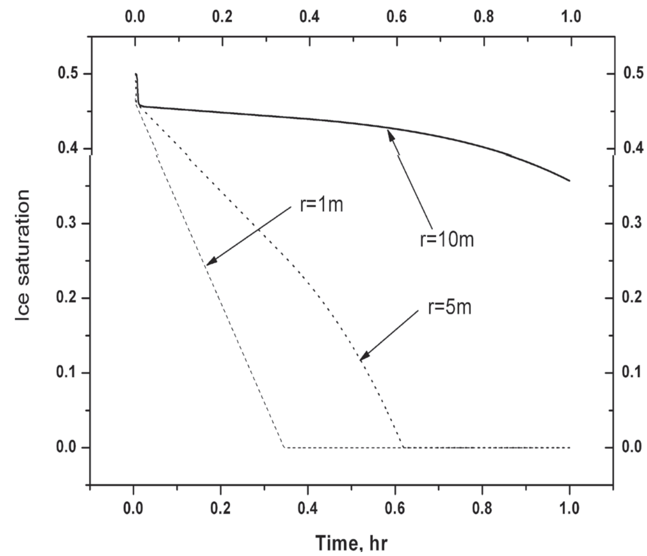

Figure 2. Ice content dynamics at different distances from the borehole.

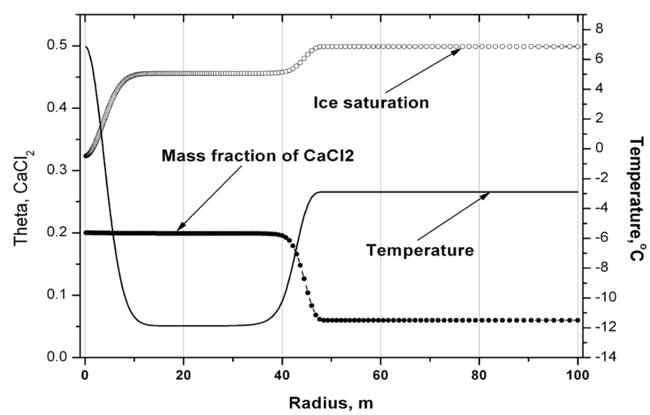

Figure 3. Spatial variation of the ice content, salt mass fraction, and temperature (time: 6 minutes).

point of the brine is lower than the beginning temperature of the area studied. Its growth is obviously suppressed by heat consumption for melting the ice.

Quite interesting are the peculiarities of ice content dynamics in different parts of area studied (Fig.2)

High and constant thawing speed is registered close to the injection well because of a significant solution influx that has practically an initial temperature. A clearly defined jump in an ice-melting rate is traced on some distance from the borehole, and the value of this “step” does not change with the further distance increase. It indicates that thawing at this point happens at the expense of heat released due to rock cooling, provided that the solution temperature does not change much at all. It is to be recalled that the initial temperature in the permeable zone was significantly higher than the eutectic point. After that, the process happens with increasing speed due to the solution temperature that increases in time, arriving at every point.

Spatial variation of studied parameters is presented in Figure 3.

Conclusions

The most interesting of all the obtained results is the pattern of ice content change in space and time. For the first time ever, this paper gives a mathematical statement of a problem for temperature and concentration fields, which is determined by high rates of solution flow in permeable frozen massif. Model calculations are in good agreement with a general concept about the physics of studied processes of convective diffusion and heat transfer. It proves that it is a working model. It seems likely that the described calculation method could be used for solving practical problems associated with burial of drainage brines in permafrost. This is an acute problem for commercial development of diamond mining in Yakutia. The authors see the main object of further research in conducting laboratory and field experiments to verify the model and to develop methodology for experimental determination of volumetric (intra-pore) heat transfer coefficient. This coefficient needs to be determined for rocks of different composition, porosity (fissuring), and level of ice saturation.

Acknowledgments

The authors thank their colleagues F.G. Atrotschenko, A.N. Vlasov, V.P. Merzlyakov, and Marina Tishkova for participation in discussions regarding this research. This work has been supported by the RFBR (the Russian Foundation for Basic Research).

References

Bear, J. 1961. Some experiments on dispersion. *J. Geophys. Res*. 66(8): 2455-2467.

Bogoslovsky, P.A. 1959. On thermal calculation of filtering earth dams. *Proceedings of Gorky Building Engineer Institute.* Gorky: 86-112 (in Russian).

Chizhov, A.B., Buldovich, S.N. & Chizhova, N.I. 1975. Hydrogeological condition of Chulman Depression. In: *Southern Yakutia*, MGU Publ.: 291-311 (in Russian).

Ershov, E.D. 1990. *General Geocryology.* Moscow: Nedra, 119-157 (in Russian).

Goldtman, V.G., Znamensky, V.V. & Chistopolsky, S.D. 1970. *Hydraulic Thawing Frozen Ground.* Magadan: 450 pp. (in Russian).

Kalabin A.I. 1981. *Minerals Extraction by Underground Leaching and Other Geotechnical Methods.* Moscow: Atomizdat, 303 pp. (in Russian).

Komarov, I.A. 2003. *Thermodynamics and Heat-Mass Transfer in Dispersed Frozen Ground.* Moscow: Publishing Scientific World, 406-428.

Perlshtein, G.Z. & Jiltsov, V.D. 1984. Approximate formulae for calculating Hydraulic Thawing Duration of Permeable Frozen Ground. *Proceedings of VNII-1 Institut,* Magadan: 99-104 (in Russian).

Permyakov, P.P. & Romanov, P.G. 2000. *Heat and Salt Transport in Frozen Unsaturated Ground*. Yakutsk: 126 pp. (in Russian).

Veriguin, N.I. 1962. Foundations of salts dilution theory at water movement in ground. In: *Engineering Geological Properties of Ground and Methods of Their Study.* Moscow: AS USSR, 89-117.

—Plenary Paper—

Russian Approaches to Permafrost Engineering

Georgy Perlshtein
Institute of Environmental Geoscience, Russian Academy of Sciences, Moscow, Russia

Abstract

The basic goals and problems that permafrost engineers and scientists are facing presently remain almost the same as they were 20 years ago. Nevertheless, the contemporary stage of cold regions development has specific features. One of the most important is permafrost response to global climate changes. In this report, some new technical solutions are described concerning construction, mineral mining, and development of oil and gas fields, environmental protection, surveys, and other related activities. Among them, a foundation on sandy back-filled ground in Yakutsk is exemplified. Most erected buildings here have not undergone any dangerous deformations over a 20-year period of operational experience. The methods of roadbed operation were improved for the railroad lines Obskaya-Bovanenkovo, Chara-Cheena, and others. Some new features of thermokarst, frost heave and other dangerous cryogenic processes have been revealed in connection with pipeline construction. This has induced the development of permafrost monitoring. In any event, the main principle of Russian specialists is to apply such scientific-technical decisions that utilize the site's natural conditions. This helps alleviate the negative influence of permafrost and uses favorable features of the territory

Keywords: discontinuous permafrost; frozen ground; monitoring of cryogenic processes; permafrost engineering; pipeline; oil and gas field development.

Introduction

During long years of exploring and developing the large territories of Siberia, the Far East and the European North, Russians have gained considerable experience on living and working with permafrost conditions. At the end of the last century, the old system of scientific-technical maintenance of the economy proved to be obsolete, and the new one is in the process of being developed. The problems of development within the permafrost regions that engineers and scientists presently face remain the same as they were 20 years ago.

In the last few years, because of some positive shifts in the economic and political atmosphere, the demand for scientific and technical support of human activities in the permafrost zone has increased. New approaches for implementing innovative engineering solutions and improving survey and monitoring systems of permafrost terrains are important in relation to the economy.

Methodological approaches for operating on frozen ground state formed the basis of the natural-technical systems concept (Epishin 1985).

Permafrost response to climate change has received much attention. Research follows such directions as observations at permafrost stations and using specially equipped geothermal wells; improving methods for long-term geocryological forecast and modeling the permafrost thermal regime for different scenarios of climate changes; and comparative analysis of geocryological maps prepared at different times.

In spite of all obvious difficulties in the economic transitional period, the potential of Russian geocryology has remained high. Thus the modern approaches used by Russian specialists for solving permafrost engineering problems are of value.

Construction

Stability of construction in frozen ground is one of the most responsible and important goals in permafrost engineering. Existing federal construction norms and regulations (SNIP 2.02.04-88) specify two construction methods for permafrost territories: 1) preserving the ground in the frozen state, and 2) keeping the ground under foundations in a thawed state. The choice of method and particular technological scheme occurs at the design stage and depends on the engineering-geocryological conditions of a given construction site. However, in the area of continuous permafrost, the first methodology is usually preferred.

For example, in Central Yakutia (Yakutsk, Mirny), pile foundations are used widely, usually with a ventilated crawl space. The preference is for cast-in-place piles. Unfortunately, this method is expensive. Costs related to foundations can amount to 3 to 5 times as much as foundations outside of the permafrost zone and can be 40% of the total cost of building. Such construction does not prevent the subsidence of ground caused by water leakages, departure from recommended maintenance programs, and other factors. In the near future, these problems may increase due to global warming.

In conditions of discontinuous, warm permafrost, construction is usually carried out according to the second method, with the preliminary thawing of frozen ground to a depth no less than the thaw bulb. Most engineering constructions in the Central Transbaikalia, close to the southern limit of the permafrost zone, were built in the 1950s using the first method, and since then have undergone catastrophic deformation. Recommendations for foundation reconstruction have been developed, taking into consideration the fact that the major part of thaw settlement has already occurred. These recommendations suggested

Figure 1. Housing estate erected in Yakutsk on back-filled ground.

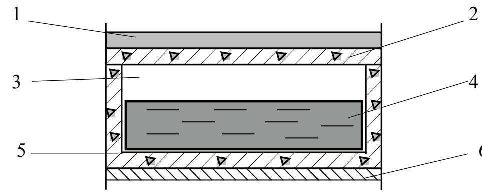

Figure 2. Scheme of foundation equipped with the cold accumulator: 1 – insulation; 2 – ceiling slab; 3 – ventilated channel; 4 – cold accumulator filled with water; 5 – concrete case; 6 – ground surface.

allowing thawing of ground (Recommendations… 1988). The resulting economic impact exceeded 100 million rubles (Institute of Natural Resources, Ecology and Cryology SB RAS).

A particularly interesting form of construction employed in Yakutsk has been to utilize sandy back-filled ground (Fig. 1).

Both permafrost construction methodologies were used in this case. Buildings with pile foundations were erected using the first methodology with ventilated crawl space. Meanwhile, the placement of sandy ground up to the design reference level was carried out after installing bearing posts of 4 m in height. Ground freezing occurred during the preparation of construction, construction itself, and at exploitation stages. The buildings have remained in satisfactory condition except for the kindergarten, which was dangerously deformed because of hot-water leakage under the building. A substantial number of the buildings are constructed on raft foundations without taking any special measures to regulate the foundations' temperature regime. Twenty years of operational experience have shown that none of these buildings has undergone any dangerous deformations, and they have sustained structural stability (Tseeva & Egorov 2005, Polishchuk et al. 2008).

The new method for assessment of foundation reliability is beginning to be applied. It is based upon statistical analysis of meteorological factors that change randomly (Khrustalyov & Pustovoit 1988). A characteristic feature of modern construction on permafrost is increased attention to maintaining a predetermined temperature regime, or ground thermal stabilization. There are active and passive stabilization methods. Active thermal stabilization involves refrigerating ground to a given depth by means of special equipment and technology. The most popular are seasonal refrigerating devices, especially two-phase thermosyphons (Dolgikh et al. 2005). In recent years, devices working year-round have become more and more common. During the summer period, their above-ground condensers are chilled by special devices that work using the Peltier effect (Bayasan et al. 2005).

Building reliability analysis using probabilistic methods brought us to the conclusion that, in many cases, use of thermal stabilizers drastically decreases the influence of chance meteorological factors on ground temperature. This approach gives the opportunity to determine the safety factor correctly, thereby preventing the damages caused by construction breakdown.

The original type of surface foundation on frozen ground deserves attention (Fig. 2). Here, the crawl space is equipped with a special device that acts as zero curtain (Khrustalev 2005).

Heat pump applications in permafrost engineering are important. New research on this subject has been carried out since the late 1980s (Goodrich & Plunkett 1990, Guly & Perlshtein 1998, Instanes 2000). Unfortunately, in Russia, research on the subject did not go beyond purely theoretical studies. Nevertheless techno-economic evaluations were accomplished, assisted by computer modeling for the temperature fields of foundations. They indicate that the cost of installing a heat pump to cool the foundation can be compensated for by using the heat produced by the building itself (Perlshtein et al. 1998). Heat pumps also can be successfully used in other engineering applications in cold regions; for example, in frozen food depots as conceived and constructed by Krylov (1951), which received wide recognition. To increase the storage life of perishables, it is necessary to maintain a low interior storage temperature, which in warm seasons requires artificial cooling. Heat pump cooling may frequently be the most economic way to achieve the necessary thermal regime. The design concept of such refrigerated ice storage, combined with a heated greenhouse, was worked out by the Northeastern Permafrost station for the native company Oyary. The results of this work were reported at the Seventh International Conference on Permafrost (Guly & Perlshtein 1998).

It should be noted that the considered examples do not exhaust all possibilities of heat pump usage in northern engineering. It is of great interest to study combinations such as warm and cold food depots; underground mine and surface domestic complexes; and a tailings impoundment and ore-dressing plant. Heat collection from solar heating in summer is considered to be especially prospective. Heat pump usage combined with the simplest solar collectors (synthetic hose) will allow for the reduction of 90% of hot water cost in the period June through August. Finally, in the global warming context, applying heat pumps is a unique technical solution which may make it possible to prevent catastrophic thawing of ground under foundations, practically without additional expense. Investments are needed to develop further research in this new direction of applied geocryology.

Valuable experience on the design, construction, and management of railroads on permafrost was accumulated in Russia during the twentieth century, and continues to increase. Measures are systematized that include control

Figure 3. Impoundment of the road surroundings, northwestern Siberia.

of the ground surface heat exchange, combined usage of thermosyphons and heat insulation for stabilizing frozen foundations, and roadbed monitoring (Kondratiev 2005).

Rock fills have wide application in roadbed construction (Minailov 1979, Goering 1998). The physical effect consists in ground cooling at the expense of air convection. Rock fills are employed not only for road construction, but also in other branches of industry; for example, in pipeline installation.

The monitoring system of the railway on permafrost soils is based on the allotment of potentially hazardous sections with establishing the control on their deformation (Ashpiz 2005).

The methodology of roadbed operation was developed for projects of the railroad lines Obskaya-Bovanenkovo, Chara-Cheena, and others. Full-scale experiments and theoretical studies (Passek et al. 2005) were conducted on the temperature regime of the road foundations under conditions of flooded lands (Fig. 3). The impoundment depth was found that induces permafrost degradation in different climatic conditions.

A new algorithm and programs for numerical modeling have been developed at St. Petersburg State University of Means of Communication (Kudryavtsev 2004). These allow the calculation of 3-dimensional temperature and moisture fields of the ground in the roadbed base. The procedure for correct assignment of the bottom boundary condition was worked out (Danielyan & Tkachenko 2005).

Oil and Gas Field Development

In the last few decades, oil and gas field development has become more active in northwestern Siberia, especially on the Yamal Peninsula. Yamal is a unique place in regard to its natural wealth of resources and the difficulty of their development, which is caused by the complexity of natural geocryological conditions and by a particular vulnerability of this territory to technogenic pressure. As a result, there was a need to strengthen the geocryological service and organize monitoring of territories under development.

"Nadymgazprom" specialists, in collaboration with leading Russian scientific, design, and exploration organizations, conducted a geoecological evaluation of the territory and obtained several important results from the scientific point of view (Remizov et al. 2001). For the first time, the connection between cryogenic processes, not only related to

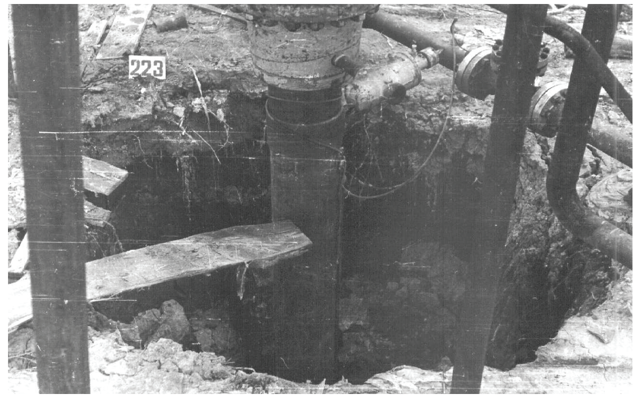

Figure 4. The thermokarst funnel around production wellhead.

climatic changes but also to tectonic sensitivity of the region, was documented. Also, the influence of surface subsidence as a result of hydrocarbon extraction at significant depths has been analyzed. These data are interesting for future statistical analysis of established quantitative characteristics of thermokarst and landslides-earthflow for understanding these cryogenic processes.

Local standards and environmental protection measures have been developed taking into account the prognosis of cryolithozone reaction to modern climate changes.

The stability of producing wells is one of serious technical-ecological difficulty to an oil and gas complex (Fig. 4). Heat exchange in the ground around an operational well has been modeled for the Bovanenkovo field. A new system of preventing "wellhead funnel" formation has been developed on the basis of this model. It includes radially positioned thermosyphons and thermal insulation (Bereznyakov et al. 1997).

The expansion of pipeline construction in the cryolithozone is due to Russia's increasing demands on hydrocarbon fuel for domestic and foreign markets. Unfortunately, an accelerated rate of construction negatively influences the quality of surveying and design solutions. Thermokarst subsidence and frost heave uplift of above-ground pipe foundations are among the common cryogenic processes (Fig. 5). Extremely intensive frost heave uplift of the tube support was recorded during Urengoy pipeline operation—up to 1.5 m in one year (Pazinyak 2001). Quite an attractive option is to install underground pipes; However, for safe operation, a proactive geotechnical monitoring service that can anticipate dangerous situations is a necessity.

Difficulties in the development of Yamal natural resources are induced not only by building and operating industrial structures. Conventional permafrost regions problems are connected with activity of the all local infrastructure.

Institute Fundamentprojekt (Institute of Foundation Design) has devised the main engineering solutions on foundations for the facilities of the Bovanenkovo and Harasavey gas fields (Yamal Peninsula) and also for the gas pipeline from Yamal to the central regions of Russia. These include frozen ground stabilizing with heat shields and thermosyphons, reinforcing ground surface on the slopes with geogrids and geocells (Grechichshev et al. 2005).

Figure 5. Deformations of the pipes due to thermokarst subsidence and frost heave processes.

Figure 6. Fissured rocks of the cryogenic weathering zone (gold-bearing ore deposit Troitskoje, Transbaikalia).

Mineral Mining

In many sites of eastern Siberia and the Far East that are located within the permafrost zone, mining plays an important part in the regional economy.

Open-pit mining of ore deposits has special features in most sites. It is known that the cryogenic weathering zone usually has significant thickness (Slagoda 2005). The fissured rocks of this zone have low ice content (as a rule, no more than 30–50 kg/m^3); however, it predetermines a loss of strength when thawing (Fig. 6).

That is the reason why, in the summer, miners thaw rocks layer by layer using natural heat. This minimizes and sometimes completely avoids the more expensive and dangerous drill-and-blasting operations. The calculation of the open-pit slope takes into account that the warm-season thawing penetrates several meters into rock massif. The placer mining with open-pit method occurs in the warm season, and earth is moved primarily with bulldozers. To make sense of using them, it is necessary to thaw frozen ground. The heat required to melt the ice consumes the main part of the overall energy spent on thawing the ground. Hence, the main goal of an engineering survey is to detect and show the borders of the frozen ground and determine its ice content. As for the ground temperature regime, there is no need to study it carefully.

One of the constant difficulties in placer mining is flushing out frozen sands from open-pit and underground mining. Deposits of the productive horizon, extracted by explosives and deposited in piles at the beginning of the summer, do not have enough time to thaw. And at the end of the flushing season, the ground quickly freezes. This leads to a tremendous loss of metal. This problem, however, is easily solved by using sprinkling thawing. The approximate analytic formulas for it were derived 25 years ago (Perlshtein & Giltsov 1984). The numerical model is described in a paper submitted for this conference.

The simplest methods of thermal melioration of frozen soils are applied to permafrost placers (for example, removal of plant-moss-peat cover). However, under new economic conditions, it is often necessary to use powerful excavators and prolong the season for overburden removal. This brings about hydraulic thawing and deposits drainage. In turn, this requires studying the permeability and other mass transfer properties.

Underground mining of gold placers is used when the burial depth is more than 20 m. It requires breaking gold-bearing deposits during the winter and processing them on the surface during the summer. In this case, the primary goal of the survey is to study permafrost thickness and its temperature. Also sub-permafrost waters must be detected to prevent their ingress into the mine. If the frozen massif temperature is warm (minus 1–2ºC), that predetermines reduced strength of the ground, and mining work is usually conducted in the winter. It is possible to harden the ground significantly at the expense of ventilation with cold air. This should be thoroughly examined in the course of underground-mine planning. Also a hard winter in the permafrost zone allows for the use of ice filling of underground workings. It provides stability when excavating the pillars (bearing blocks).

Hazards and Environmental Protection

For abatement against impact of dangerous cryogenic processes, Russian specialists try to take advantage of the local natural features (severe climate, specific properties of the frozen ground, etc.).

For example, burial of mining toxic waste poses a serious threat to the vulnerable environment. In any tailings disposal method, the seepage-control measures must be designed in such a way to exclude contaminating surface and ground water within the adjacent areas. It is possible to install dams with an impervious frozen core, as used widely in the permafrost zones of Canada, Russia, and Alaska. A new method of tailings management is planned for use at some ore deposits. Its essence consists in dividing the entire area of the tailings disposal facility into several cells. The winter ones (at the periphery of the tailings facility) are filled with successive layers of tailings each of them being permitted to freeze under natural cold conditions prior to the placement of the next layer. The winter regime of slurry discharge must provide for tailings settlement, mill-water return, and complete freezing of sediments. This method makes it possible to turn the inclement climate into a helpful factor for mining in permafrost regions. Storage of the mine wastes in the frozen state reduces the risk of seepage losses of the toxic solutions. As a result, the construction cost of the tailings disposal facility considerably decreases, and the level of the environmental safety rises.

The method of keeping nuclear waste underground in artificially frozen ground was considered (Khrustalev et al. 2004; 2005). A facility for underground water storage also uses impermeability of frozen soils and ice walls (Kuzmin 2005).

Important data was collected by analyzing catastrophic shifts on the Kolka Glacier, where a huge ice block collapsed on September 20, 2002. The resulting giant ice-water-rock stream was 18 km in length and 80–100 m in height, and flowed at a speed of 150 km/hour. Over 120 lives were lost, the Verkhny Kardamon settlement was buried, the Verkhnaya Saniba village was flooded, and all communication systems were destroyed. After studying the consequences of the Kolka Glacier collapse, it has been determined that this catastrophe as a natural event most resembles a snow-rock-ice avalanche. Based on field research and satellite image analysis, the ice volume involved in this catastrophic shift was 80 ±15 million m^3. Part of the glacier could still remain in its bed. New data made it possible to refine the prognosis of how events could develop in the catastrophe zone. In the next 10–20 years, new catastrophic processes in the Kolka Glacier cirque are unlikely to occur. The main part of the ice body in the Karmadonskaya depression will melt in 2–3 years, but its full degradation will take not less than 10 years [include a reference].

Surveying, Mapping, and Monitoring

The Russian school of engineering-geological survey is traditionally based upon complex geosciences assessment of explored territories involving a wide range of information. Heightened attention is given to methods of mapping. Thus Fundamentprojekt has investigated natural conditions for major industrial facilities on the Barentz Sea coast. Maps at different scale and functions have been prepared and reflect frozen-ground properties (temperature, salinity, strength) and also the results of geocryologic prognosis.

The team at the Earth Cryosphere Institute SB RAS (ECI SB RAS) has drawn up a series of medium-scale GIS maps for permafrost territories with intensive economic activity, such as northwestern Siberia, central Yakutia, the northern variant of pipeline eastern Siberia-Pacific Ocean, and others. These maps present the clearest available information on permafrost conditions in these regions (Drozdov et al. 2007).

Geophysical methods of prospecting are widely practiced. The ECI SB RAS has developed an original methodology of high performance seismic prospecting on lateral SH waves.

Figure 7. Deformations of the railroad bed (Chara-Cheena).

Among the most significant practical implementations are surveying for the third traffic-ring road for Moscow, and research on the factory MFFR-R site to utilize weapon-grade plutonium in the Tomsk region, which was conducted in 2004 within the framework of the Intergovernmental Russian-American Agreement.

Monitoring of cryogenic processes was conducted for the Novaya Chara-Cheena Railroad (northern Transbaikalia). It has been determined that anthropogenic impact, along with climate change, in the foothills of the Udokan Ridge has caused thawing massive ice and ice-wedges as well as catastrophic subsidence of the railroad base (Fig. 7). Under the influence of earthquakes and cryogenic destruction, catastrophic landslides and flow slides occurred in the mid-elevation mountain zone. In the areas of rock streams (kurums) development, these processes led to a railroad slide (Institute of Natural Resources, Ecology and Cryology SB RAS).

Data from integrated monitoring was used to study the natural dynamics of vegetation and its changes under the influence of oil and gas development for northwestern Siberia. It is interesting to note that according to a second grading of peat-mineral hummocks, which took place 30 years after laying the pipeline, the surface had undergone subsidence, heave, and stabilization, but had never returned to its original position, remaining 8–80 cm lower. The intensity of subsidence decreases, moving further away from the pipeline (Institute of the Earth Cryosphere SB RAS).

Conclusions

Permafrost influences the development of northern territories (oil and gas production, mining placers and ore deposits, open-pit and underground operations, etc.). Applied technological methods must use advanced scientific-technical solutions according to the natural conditions of the site. This allows alleviation of the negative influence of permafrost and also uses favorable features of the territory. Accordingly, engineering services must determine necessary and sufficient volume of geocryological information to provide for the success of prospecting, design, and operational activities.

Exchange of experience and analysis of design errors are very helpful in solution of such problems. Round-table discussions on permafrost engineering problems take place at the annual Russian permafrost conferences.

I think that, presently, the main tasks for Russian applied geocryology are:

- Arrange monitoring of cryolithozone for the most economically important regions;
- Enhance the theoretical basis and determine unified methods of quantitative geocryological prognosis;
- Develop a complex of quantitative models of permafrost-geological processes on the basis of combining deterministic and probabilistic approaches;
- Develop further explorative-investigational work around the use of nontraditional resources of natural heat and cold of the cryolithozone;
- Actively participate in and closely coordinate research within the framework of the International Polar Year;
- Equip laboratory, stationary and fieldwork with modern control and measurement instrumentation.

Acknowledgments

The author thanks S.E. Grechishchev, L.N. Khrustalev, V.P. Melnikov, M.A. Minkin, L.T.Roman, V.N. Zaitsev and R.V. Zhan for their proposals on selecting initial materials for the report. I appreciate the participation of my colleagues D. Sergueev and M. Tishkova in discussing and preparing this text. Especially I would like to express my thanks to IPA President Dr Jerry Brown, who reviewed and suggested revisions to this paper.

References

Ashpiz, E.S. 2005. The monitoring system of the railway bed situated on the permafrost soils. *Proceeding of III Conference of Geocryologists of Russia*, *June 1-3, 2005.* Moscow State University Publishing, vol. 4: 12-19 (in Russian).

Bayasan, R.M., Korotchenko, A.G., Lobanov, A.D. & Pustovoit, G.P. 2005. Technique for thermal stabilization of soils at bases of structures in permafrost regions. *Journ. of Glaciology and Geocryology* 26: 27-32.

Bereznyakov, A.I., Griva, G.I., Osokin, A.B., Popov, A.P., Salikhov, Z.S., Smolov, G.K. & Chugunov, L.S. 1997. *The Problems of Production Wells' Stability within the Gas-Condensate Fields of Yamal Peninsula.* Moscow: IRC Gazprom, 159 pp. (in Russian).

Danielyan, Yu.S. & Tkachenko, E.I. 2005. Resolution of the engineering geocryology problems in the limited areas. *Proceeding of III Conference of Geocryologists of Russia*, *June 1-3, 2005*. Moscow State University Publishing, vol. 4: 94-100 (in Russian).

Dolgikh, G.M., Okunev, S.N., Osokin, A.B., Popov, A.P., Smolov, G.K. & Galaktionov, E.Y. 2005. *Proceeding of III Conference of Geocryologists of Russia, June 1-3, 2005.* Moscow State University Publishing, vol. 4: 100-104 (in Russian).

Drozdov D.S., Korostelev Yu.V., Malkova G.V., Melnikov E.S., Soromotin A.V., Ukraintseva E.A. & Chekrygina, S.N. 2007. Preliminary geocryological and environmental mapping of the areas of perspective economic activity. *Cryogenic Resources of Polar Regions: International Conference, Vol. II, Salekhard, June, 2007*: 264-266.

Epishin, V.K. 1985. Natural-technical systems. In: *Theoretical Basis of Engineering Geology. Social and Economic Aspects.* Moscow: Nedra: 36-45 (in Russian).

Goering, D.J. 1998. Experimental investigation of air convection embankments for permafrost-resistant roadway design. *Proceeding of the Seventh International Conference on Permafrost*, *Yellowknife, NWT, Canada*: 319-326.

Goodrich, L.E. & Plunkett, J.C. 1990. Performance of heat pump chilled foundations. *Proceeding of the Fifth Canadian Permafrost Conference*. Centre d'Etudes Nordiques, Universite Laval: 409-418.

Grechichshev, S.E., Korobkov, N.F., Pavlov, Ark,V. & Sheshin, Yu.B. 2005. The optimum two-layered insulation composition in the embankment structure. *Proceeding of III Conference of Geocryologists of Russia*, *June 1-3, 2005*. Moscow State University Publishing, vol. 4: 72-79 (in Russian).

Guly, S.A. & Perlshtein, G.Z. 1998. Ice food depot cooled with the heat pump: Pre-feasibility study. *Proceedings of the Seventh International Conference on Permafrost*, *Yellowknife, Canada:* 383-390.

Instanes, B. 2000. Permafrost engineering on Svalbard. *International Workshop on Permafrost Engineering, Longyearbyen, Svalbard, Norway*: 1-23.

Khrustalev, L.N. 2005. *Geotechnical Fundamentals for Permafrost Regions.* Moscow: MSU, 82-97 (in Russian).

Khrustalev, L.N., Erchov, E.D., Parmuzin, S.Yu., Vorotyntseva, T.V., Barinov, A.S., Prosorov, L.B. & Tkachenko, A.V. 2005. Underground keeping of the nuclear waste in the artificially creating permafrost soil. *Proceeding of III Conference of Geocryologists of Russia*, *June 1-3, 2005*. Moscow State University Publishing, vol. 4: 214-218 (in Russian).

Khrustalyov, L.N. Erchov, E.D., Parmuzin, S.Y. & Dmitriyev S.A. 2004. Reinforced concrete depot of radioactive waste. *Patent of Russia* No. 242813, Bulletin No. 35, 2004 (in Russian).

Khrustalyov, L.N. & Pustovoyt, G.P. 1988. Probabilistic-statistical calculations of the building basements in cryolithozone. Novosibirsk: Nauka, 253 pp. (in Russian).

Krylov, M.M. 1951. *Isothermal Ice Storages.* Academy of Sciences of the USSR, 101 pp. (in Russian).

Kudryavtsev, S.A. 2004. Numerical modeling the processes of freezing, frost heave and thawing ground. *Basements, Foundations & Soil Mechanics* 4: 21-26 (in Russian).

Kondratiyev, V.G. Problems and ways of stabilization of railway and highway embankment on the icy permafrost. *Proceeding of the Third Conference of Geocryologists of Russia*, vol.4. Moscow: MSU: 144-149 (in Russian).

Kuzmin, G.P. 2005. Estimation of thawing-freezing dynamics in the walls of underground water storages. *Proceeding of III Conference of Geocryologists of Russia*, *June 1-3, 2005.* Moscow State University Publishing, vol. 4: 177-183 (in Russian).

Minailov, G.P. 1979. Experimental study of rock fill cooling impact on the underlying ground temperature. *Workshop "Improvement of Design and Construction Methods for Railroads in Siberia," November 20-22, Moscow,* Proceeding: 129-130 (in Russian).

Passek, V.V., Jusupov, S.N. & Nevmerghitskaya, L.I. 2005. Variation of permafrost ground temperature conditions as partial flooding of area located near earth bed. *Third Conference of Geocryologists of Russia*, vol.4. Moscow: MSU, 209-214 (in Russian).

Pazinyak, V.V. 2001. Frost heave as a destabilization factor of oil-and-gas industry objects. *Proceedings of International Conference: Conservation and Transformation of the Matter and Energy in Earth Cryosphere*. Pushino: 171-172 (in Russian).

Perlshtein, G.Z. & Giltsov, V.D. 1984. Approximate formulas for calculating the duration of hydraulic thawing permeable frozen ground. *Technique and Technology for Permafrost Placers Mining*, Magadan: VNII-1, 99-104 (in Russian).

Perlshtein, G.Z., Buiskih, A.A., & Guly, S.A. 1998. Some prospects for heat pump applications in permafrost engineering. *Proceedings of the International Workshop "Permafrost Response on Economic Development, Environmental Security and Natural Resources."* Novosibirsk: Kluwer Academic Publishers, Netherlands, 425-435.

Polishchuk V.L., Roman L.T., Tseeva A.N., Tsernant A.A. & Livanov, N.I. 2008. Construction on back-filled ground in cryolithozone. Moscow, "Economika, stroitel'stvo, transport," 350 pp. (in Russian).

Recommendations on the control of structures stability on the thawing ground. 1988. Yakutsk, Permafrost Institute SB RAS, 32 pp. (in Russian).

Remizov, V.V., Kononov, V.I., Bereznyakov, A.I., Glukhenkiy, A.G., Dyomin, V.M., Mikhaylov, N.V., Osokin, A.B., Popov, A.P., Rechetnikov, L.N. & Smolov, G.K. 2001. *Nadymgzprom: Geotechnical Monitoring in Cryolithozone*. Moscow: IRC Gazprom, 149 pp. (in Russian).

Slagoda, E.A. 2005. The reconstruction of the cryolithozone with using the micro-morphological traces of cryogenesis in the Upper Neozoic deposits. *Abstract of the doctor thesis,* Tyumen, 48 pp. (in Russian)

SNIP 2.02.04-88.1988. Basements and foundations on the permafrost. Gosstroy USSR (in Russian).

Tseeva, A.N. & Egorov, G.E. 2005. Experience of the use of surface slab foundations in Yakutsk. *Proceeding of III Conference of Geocryologists of Russia, June 1-3, 2005.* Moscow State University Publishing, vol. 4: 219-228 (in Russian).

Numerical Modeling of Differential Frost Heave

Rorik A. Peterson
Mechanical Engineering, College of Engineering and Mines, University of Alaska Fairbanks, Fairbanks AK, USA

Abstract

Differential frost heave (DFH) is laterally non-uniform heave. DFH occurs near buried chilled pipelines, leads to roadway and foundation damage, and also causes some types of patterned ground. Several recent advances in numerically modeling multi-dimensional frost heave at two different spatial scales are discussed. Coupled heat and liquid water transport in a partially frozen saturated soil is modeled at the millimeter scale. Individual ice lens formation is shown to occur when the effective interparticle pressure becomes zero at a finite distance below the nearest existing lens. Liquid water velocity is time dependent, and initially increases quickly and then decreases more gradually until subsequent lens initiation. Velocity also appears to be temporally unstable, occurring in pulses balanced by heat flux. DFH is also spatially unstable on the meter-scale and strongly dependent on the frozen soil mechanical properties. A three dimensional model on the meter-scale shows pattern ground development that depends on soil modulus.

Keywords: frost heave; ice lens; numerical modeling; patterned ground.

Introduction

Differential frost heave (DFH) is laterally non-uniform (i.e., multi-dimensional) heave. The spatial irregularity of DFH causes out-of-plane stresses that result in bending, compaction, dilation, and failure of both the frozen and unfrozen soil. DFH occurs at buried chilled pipelines, leads to roadway and foundation damage, and also causes some types of patterned ground. Analytic and numerical frost heave modeling has progressed significantly as our fundamental understanding of its origins has improved and computational techniques and resources continue to advance. The problem remains complex, however, due to the wide range of length scales from micron-scale unfrozen water films, to the millimeter-scale frozen fringe, to meter-scale soil deformation.

Some of the early numerical models of frost heave that attempted to account for individual ice lens formation are due to O'Neill and Miller (1985) and Gilpin (1980). These models were one-dimensional, which made them both more numerically tractable at the time and also directly applicable to laboratory frost heave experiments. Over the next few decade several numerical variations were developed for the one-dimensional solution, but the underlying physics remained essentially the same.

More recently, Rempel (2007) has shown that an assumption in the previous models concerning local ice pressure is unnecessary and probably incorrect, and provided both an analytical and numerical solution to the one-dimensional frost heave problem. Quantitatively, this solution is not drastically different than those previous when reproducing laboratory frost heave scale experiments. However, it may have more profound implications when describing frost heave with greater overburden pressure as would occur below glaciers and ice sheets.

Multi-dimensional solutions of frost heave are less prevalent, perhaps due to the complicating factor of describing the unfrozen and frozen soil deformation that one-dimensional solutions need not address. Michalowski and Zhu (2006) have recently addressed this issue numerically by introducing a "porosity rate function". The effect of frozen soil elastic modulus on the spontaneous initiation of DFH has been demonstrated analytically by Peterson and Krantz (2003) using a linear stability analysis.

Several recent advances in numerically modeling DFH at two different spatial scales are discussed here. The formation of discrete ice lenses occurs on a roughly millimeter scale in a region of partially frozen soil. The coupled heat and liquid water transport is modeled in two dimensions. The formation of a new ice lens at a discrete location below the nearest existing lens is shown, and its dependence on a spatially variable overburden pressure is demonstrated. The flux of liquid water to the growing ice lens is shown to vary in time. Flux initially increases rapidly as the frost heave pressure increases, but then quickly subsides due to decreasing permeability as pore ice increases. Additionally, the velocity appears to be temporally unstable when the heat flux from the lens is held constant. Pulses of water on an approximately one-second scale occur, and are balanced by the constant heat flux and slowing decreasing temperature at the lens boundary.

During freeze up of a natural soil such as the active layer in permafrost regions, hundreds of individual ice lens can form, and modeling at the millimeter scale rapidly becomes complex due to discontinuities in water flux as each new lens forms and the liquid water pressure adjusts nearly instantaneously. Scaling analysis (Fowler & Krantz 1994) indicates that the process can be recast into a more continuous problem by applying jump boundary conditions at the frozen fringe. This reduced model still accounts for discrete lens formation but does not directly solve for the temporally evolving temperature, pressure and liquid water profile within the frozen fringe. Analytic solutions to this reduced model are currently known only in one dimension. A multi-dimensional numerical solution can be used to investigate the effects of surface variability in temperature

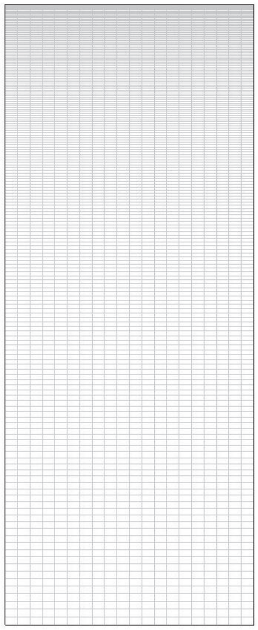

Figure 1. The finite element grid with a logarithmic vertical element size distribution.

and pressure, due to ground vegetation cover or engineering infrastructure, for example.

Here a three-dimensional solution demonstrates that patterned ground can form due to a positive feedback mechanism when small perturbations in the ground surface are randomly distributed as an initial condition. The elastic modulus of the frozen soil provides a stabilizing mechanism once perturbations reach a moderate size, resulting in larger patterns in more stiff soils. This may have implications for changes in natural patterned ground size when soil properties and/or ice content are spatially variable. The soil elastic modulus is only one of several properties than may be spatially and temporally variable, and conclusive model predictions will likely have to consider the combined effect of them all.

Model Description

The two-dimensional model of the partially frozen, saturated soil beneath an ice lens includes transient heat and liquid water transport. The transient energy balance equation is

$$\rho_{eff} C_{eff} \frac{\partial T}{\partial t} = \nabla \bullet \left(k_{eff} \nabla T \right) \tag{1}$$

where T is temperature, C is heat capacity, ρ is density, and k is thermal conductivity. The subscript *eff* denotes effective properties that are volume averages of the three phases: liquid water, ice, and soil. The soil volume fraction is assumed constant. The water transport equation is Darcy's Law for a saturated soil

$$\nabla \bullet \left(\frac{\rho_w \kappa}{\eta} \nabla p_w \right) = 0 \tag{2}$$

where κ is permeability, η is viscosity, and p_w is water pressure. The permeability is a non-linear function of the ice content, W, which is also a non-linear function of the temperature

$$\kappa = \kappa_0 W^{\gamma} \tag{3}$$

where the exponent γ=8 and κ_0 is the unfrozen permeability. Here an exponential function is also used to describe the unfrozen water content.

$$W = \exp[\alpha T] \tag{4}$$

where α = 5 and T is in °C. The exponent depends on the soil type and is usually in the range of 2–10. The results discussed here are general for any value of the exponent, although the exact numerical values will vary.

A two-dimensional finite element mesh consisting of quadrilateral elements was created in a 1-cm wide by 2.5 cm tall domain. The third dimension is not modeled a this scale. The temperature, pressure, and their dependent properties are highly non-linear just below the top boundary. Therefore, element size follows a log space distribution in the vertical direction with evenly spaced elements in the horizontal. The resulting 20 by 200 element grid is shown in Figure 1. The smallest element at top is 2.9 microns by 0.5 millimeters.

Frost susceptible soils are usually silty clays, with relatively wide particle size distributions spanning 1.0 to several hundred microns. This model makes a continuum assumption that material properties are continuous throughout each numerical element, and therefore mass transport can be modeled using Darcy's flow equation. Although the smallest elements in this analysis are of the order of some particle dimensions, it is assumed that micron-scale heterogeneities will average out and the continuum assumption is valid. An attractive alternative would be to use a Discrete Element (DEM) or Material Point Method (MPM), but they are not investigated here.

Initial and Boundary Conditions

The initial conditions are 0°C for temperature and zero gage pressure throughout the domain. The pressure boundary conditions are zero gage pressure at the bottom and $P_{load}(x)$ at the top. Gravitational effects on the pressure distribution are negligible at this scale compared to flow resistance and thermomolecular pressure. The functional form of P_{load} is discussed below. The thermal boundary conditions are 0°C at the bottom and constant heat flux at the top; the flux value is discussed below. The side boundaries have a no-energy-flux condition for the thermal problem, and no mass flux for pressure.

The numerical problem is solved using Comsol Multiphysics version 3.2, a commercial finite element package that is tailored to coupled physical problems. The non-linear solver uses an adjustable time step based on the temporal dynamics of the transient solution.

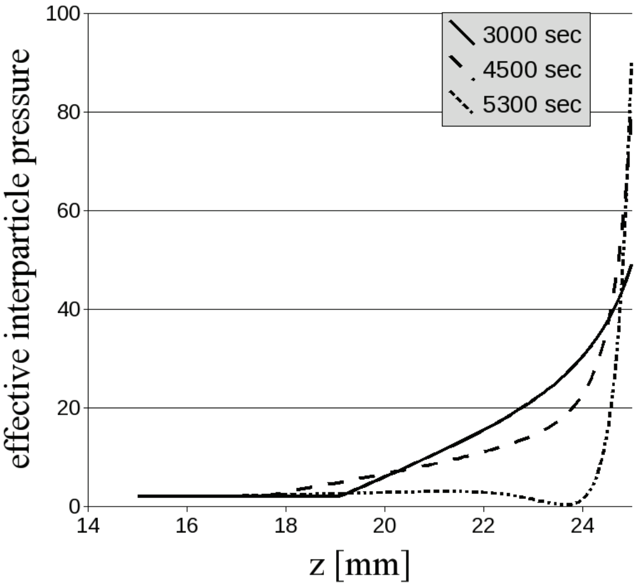

Figure 2. Interparticle pressure in kPa as a function of the vertical location below the existing ice lens.

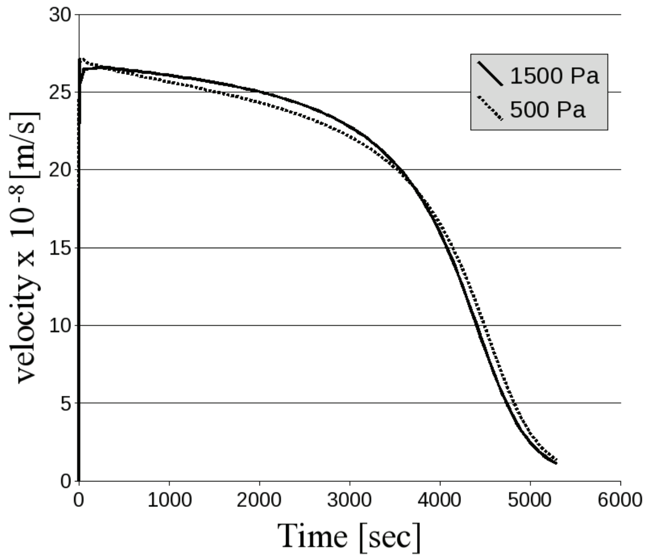

Figure 3. Water flux to the upper boundary for two extremes of the overburden pressure. Len initiation occurs at about 5300 seconds.

Small-Scale Fringe Behavior

All results discussed here used a constant heat flux from the top surface of 100 watts (W) per square meter. During natural soil freezing in autumn when snow depth is relatively thin, the rate of heat flux would be on the order of 10-–100 W/m^2. This estimate assumes a snow thermal conductivity of 0.1 W/m·K (Sturm et al., 2002) a snow depth of 1-–10 cm, and an air temperature of negative 10°C. The higher range of this flux estimate is used to expedite the numerical solution, and a preliminary sensitivity investigation indicates that the overall trends discussed here are general for the entire range of heat flux values.

The energy flux is balanced by thermal conduction to the boundary and latent heat of fusion for the water flux advecting to the boundary and freezing. The interparticle effective pressure is calculated at each time step within the domain and initiation of a new lens begins whenever this function reaches zero. Using a sinusoidal varying surface pressure on the top boundary, p_{load}=1000+500[cos(πx/0.01] Pa, the effective pressure is less on the right hand side and a new lens will initiate on that side first. Figure 2 shows the computed interparticle effective pressure at three different times on the right-hand side of the domain.

The *x*-axis of Figure 2 only shows the upper 1 cm of the domain where the effective pressure is changing most dramatically. Note that the major pressure variation is occurring on the scale of 1 mm, which is one to two orders of magnitude larger than the smallest particle dimensions, and lends support to the continuum assumption when using the Darcy flow equation. Initially the effective pressure increases from the base value because of cryostatic suction. In an unconsolidated soil, compaction may occur during this time with a loss of porosity. These effects are not considered at this point and the porosity is held constant. The suction region extends further downward as time progresses and the ice content increases.

As time nears 5300 seconds, the effective pressure begins to decrease below its base value as the thermomolecular force increases and begins to accommodate a larger fraction of the overburden pressure. As the ice content increases at a particular depth, the unfrozen water film thickness decreases and the dispersion force will increase. Eventually, this force is great enough to push between the soil particles and the effective pressure becomes zero. At this point, a new ice lens will form at this location. This is shown in Figure 2 at about 1-mm below the previous ice lens.

The flux of liquid water to the top boundary freezes and causes the existing ice lens to thicken. The velocity is a function of the cryostatic suction and is therefore spatially varying due to the pressure boundary condition at the top surface. The velocity as a function of time is shown in Figure 3 at the left and right sides of the domain where the pressure is largest and smallest, respectively. The *y*-axis is shown in m/s and scaled by 10^{-8}, so the maximum velocity is 0.25 microns per second. There is an initial rapid rise in the velocity followed by a more gradual decrease until subsequent lens initiation. The initial rise occurs as the ice content initially becomes non-zero and the thermomolecular force is greater than the overburden pressure. The decline is due to increasing ice content that decreases the permeability. The magnitude of velocity throughout the domain is similar, and the two curves span the entire range. From about 200 to 3700 seconds, the larger overburden results in greater water flux by about 3%. At times greater than 2700 seconds, the lower pressure results in a greater velocity. This can be seen where the lines cross in Figure 3 near 3700 seconds. The total increase in lens thickness is spatially varying, and can be determined by integrating the velocity with time and is equal to the area underneath the curves. For the data shown

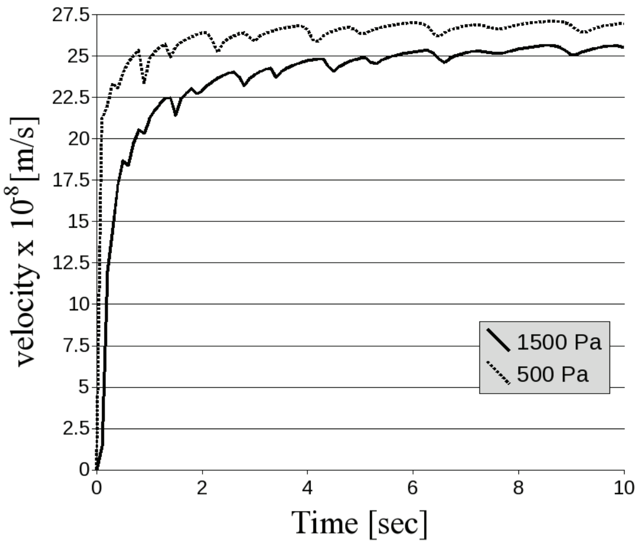

Figure 4. Water flux to the upper boundary during the initial 10 seconds. Pulses occur on a scale of one second.

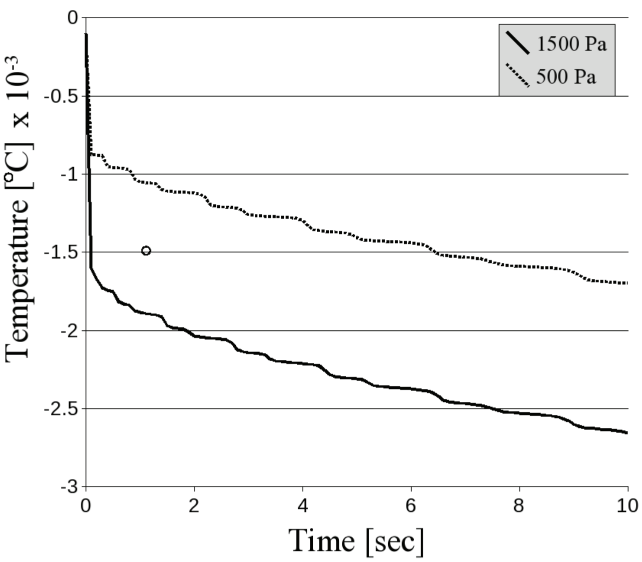

Figure 5. Temperature of the upper lens boundary during the initial 10 seconds. Fluctuations correspond to pulses in the liquid water velocity.

in Figure 3, this results in a thickness of 1.047 mm when P=1500 Pa, and 1.043 mm when P=500 Pa.

The rapid increase in velocity occurs during the first 10 seconds and is shown in Figure 4. There is a slight delay for the greater pressure on the left-hand side because it takes longer for the thermomolecular pressure to balance the greater overburden. A larger ice content is required for water flux to begin and is controlled by the finite energy flux at the top surface. Because the overburden pressures in this simulation are relatively small at only 0.5–1.5 kPa, the delay is less than 1 second. The velocity reaches its maximum value by 5 seconds, and already begins to decline around 10 seconds.

There are obvious fluctuations in the velocity that occur with a periodicity on the order of 1 second. These fluctuations are not due to numerical time stepping and are reproducible with changes in the time stepping protocol. For the results shown in Figure 4, the time step was adaptive and on the order of 0.001 seconds during the first 10 seconds. The fluctuations appear to be due to a temporal instability where a small increase in water flux temporarily slows the rate of ice formation below. Because the heat flux from the top boundary is fixed at 100 W/m^2, it is balanced by the combination of thermal conduction and latent heat of fusion for the liquid water. An increase in velocity means that more lens ice is formed, and therefore less pore ice is formed below the lens. It is the increase in pore ice that eventually slows the liquid water flux. There is a corresponding negative feedback when the water flux decreases slightly. The combination of these two effects results in pulses of water reaching the growing ice lens.

The temperature at the top boundary also shows fluctuations on the 1-second time scale, corresponding to these pulses of liquid water. Figure 5 shows the temperature at the upper boundary for the high and low pressure sides. Overall, the temperature slowly decreases, but there are periods of quick decline that correspond directly with when the liquid water flux is at a minimum. During these short periods more pore ice is formed. When the temperature decline is nearly flat, the corresponding water flux is at a maximum and lens ice formation is at a maximum. These short-term fluctuations become damped as time progresses, and are not readily apparent at times greater than a few hundred seconds.

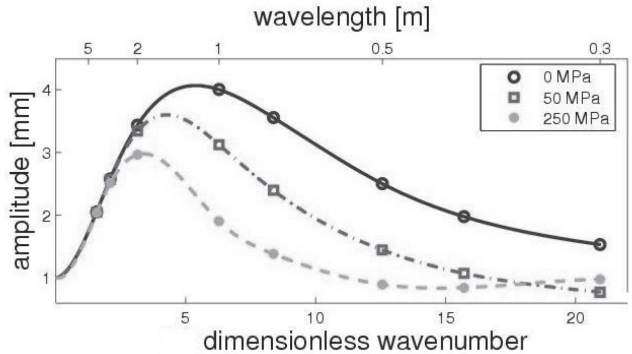

Figure 6. Amplitude of the surface perturbations after one freeze cycle to a depth of 1 meter.

Large-Scale Pattern Formation

The larger scale frost heave problem is solved using the generalized model equations of Fowler and Krantz (1994). An additional description of how the frozen soil deforms must be added to their model, and here it is assumed to behave as a thin plate with Young's Modulus E. The bending of a thin plate of thickness h can be described by

$$P_b = \frac{Eh^3}{12\left(1-\nu^2\right)} w \tag{5}$$

where P_b is the additional pressure (force per area) required (or resulting from) the bending on the plate, w is the deflection of the plate mid-plane, and ν is Poisson's ratio. A

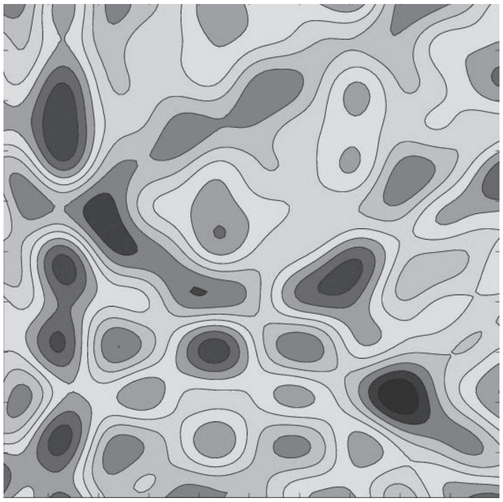

Figure 7. Initial random ground surface perturbations with a maximum amplitude of 1 millimeter.

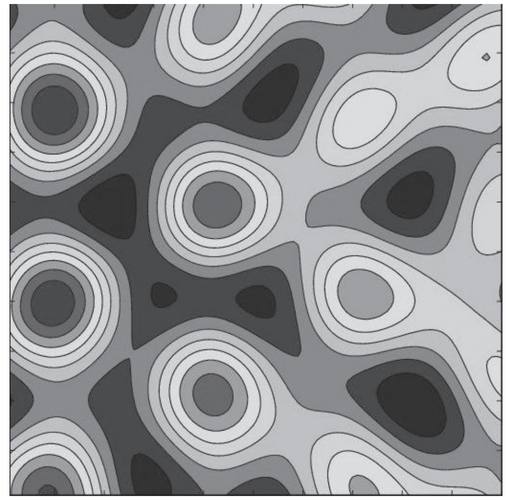

Figure 9. Final ground surface topography after 16 freeze cycles to one meter. Young's modulus is 50 MPa.

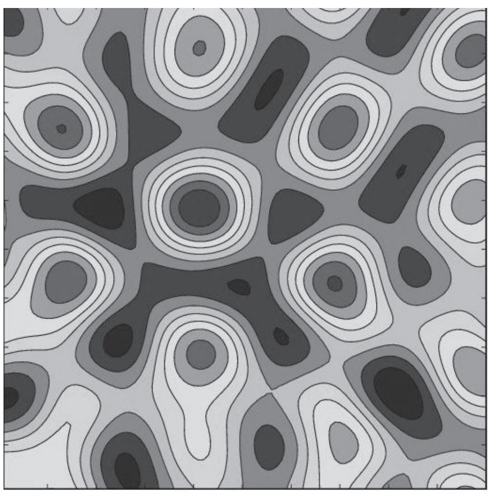

Figure 8. Final ground surface topography after 16 freeze cycles to one meter. Young's Modulus is zero.

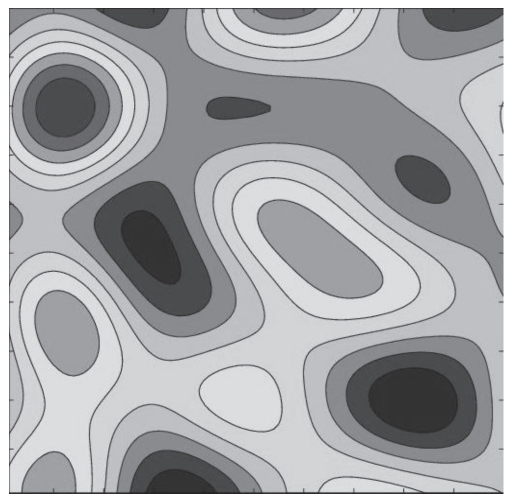

Figure 10. Final ground surface topography after 16 freeze cycles to one meter. Young's modulus is 250 MPa.

two dimensional model for freezing with a constant surface temperature of -10°C was solved using small, sinusoidal varying ground surface perturbations of 1-millimeter amplitude. Because of a singularity when the thickness of frozen soil is zero, an initial frozen thickness of 10 cm was used. The model was run until the depth of freezing reached 100 cm, which is typical of the active layer in permafrost regions.

The final amplitude of the surface perturbations is shown in Figure 6. The top *x*-axis shows the dimensional wavelength of the perturbations, and each curve represents three different values of the Young's Modulus. The symbols show the numerical results of different simulations and the curves are a cubic spline fit to the results. There is a maximum in each curve which indicates the wavelength pattern that is most likely to evolve in the long term from an otherwise homogeneous system that experiences only random perturbations. Even when the modulus is zero, short wavelength patterns do not tend to grow significantly.

Each of the simulations that generated the results shown in Figure 6 involved a perturbation with only a single wavelength. The development of a pattern with a characteristic wavelength can be demonstrated by solving the frost heave model in three dimensions. Random perturbations are once again imposed on the top surface with maximum amplitude of 1 millimeter. In order to approximate the "white noise" of naturally occurring perturbations in nature, a linear superposition of 25 randomly chosen three-dimensional patterns with varying frequencies and spatial offsets was generated. A contour plot of this initial condition is shown in Figure 7, where eight equally-spaced contours represent the range from 0 to 1 millimeter.

Using the same initial conditions, the three-dimensional model was solved for 16 sequential freeze cycles. At the end of each freeze cycle, the final surface topography was used as the initial surface topology for the subsequent year. In this way, the thaw process is not explicitly modeled, and it is assumed that any topography changes due to differential ice formation are maintained. This likely leads to an overestimation of the final pattern amplitude, and probably favors patterns of a shorter wavelength that would otherwise be mitigated by solifluction or other melt-related processes.

Figures 8, 9, and 10 show contour plots of the final surface topology when the modulus is 0 MPa, 50 MPa, and 250 MPa, respectively. Eight equally-spaced contours are shown, and the lateral dimension is $2\pi = 6.28$ meters. Because of the simplifying assumptions concerning the thaw process, the final magnitude of the pattern is of less consequence than the spatial characteristics. It is readily apparent that when the modulus of the frozen soil increases (Figs. 8–10), the dominant pattern that evolves has a characteristically larger size. All other conditions are identical including the initially perturbed surface. This general conclusion has been postulated before based on linear stability analysis (Peterson & Krantz 1994) and a numerical model for stone circle development (Kessler et al. 2001). However, this model solves for the time-dependent evolution of the pattern, and also explicitly accounts for differential soil movement that depends on the mechanical properties of the frozen soil.

Conclusions

Differential frost heave is a complicated process to model due to important processes that occur over a wide range of spatial scales, ranging from micron-scale liquid water films, to millimeter-scale partially frozen fringe, and to meter-scale soil deformation. Results from numerical modeling of differential frost heave in multiple dimensions at the two larger spatial scales have been discussed. Discrete ice lens formation is predicted to occur on the scale of 1-millimeter below an existing lens, which is in agreement with laboratory measurements and field observations of freezing soils under similar conditions. Spatial variability in the time and location of new ice lens formation is shown by solving for when the interparticle effective pressure becomes zero.

The velocity of liquid water to a thickening ice lens is shown to vary in time, with an initially rapid increase followed by a more gradual decrease as the pore ice content increases. The total amount of lens ice that forms is the time integral of this velocity, and is shown to spatially vary with variations in the overburden pressure. Similar behavior would be expected with a spatially varying surface temperature or thermal flux due to variations in surface ground cover. The liquid water velocity also appears to be temporally unstable, resulting in pulses on a scale of one second. The lens temperature also fluctuates on a similar scale because the total heat flux is balanced by the rate of heat conduction from below and the latent heat of fusion of liquid water. These fluctuations eventually dampen long after the liquid water velocity has reached a maximum and are not apparent at the time of subsequent lens initiation.

The larger scale frost heave problem is solved to demonstrate pattern growth that is dependent on the frozen soil mechanical properties. Patterns of a different characteristic wavelength will develop depending on the elastic modulus, with more still soils resulting in patterns of a larger size. The characteristic pattern size is on the order of 1–2 meters, which is in the range of naturally occurring patterns. A more complete model of pattern generation and evolution must more properly account for the dynamics of thawing soil, which will likely lead to favoring of larger patterns.

References

Fowler, A.C. & Krantz, W.B. 1994. A generalized secondary frost heave model. SIAM *J. Appl. Math.* 54: 1650-1675.

Gilpin, R.R. 1980. A model for the prediction of ice lensing and frost heave in soils. *Water Resour. Res.* 16(5): 918-930.

Kessler, M.A., Murray, A.B. & Werner, B.T. 2001. A model for sorted circles as self-organized patterns. *J. Geophys. Res.* 106(B7): 13287-13306.

Michalowski, R.L. & Zhu, M. 2006. Frost heave modeling using porosity rate function. *Int. J. Num. and Anal. Methods in Geomechanics* 30(8): 703-722.

O'Neill, K. & Miller, R.D. 1985. Exploration of a rigid ice model of frost heave. *Water Resour. Res.* 21: 281-296.

Peterson, R.A. & Krantz, W.B. 2003. A mechanism for differential frost heave and its implications for patterned-ground formation. *J. Glaciology* 49(164): 69-80.

Rempel, A. 2007. Formation of ice lenses and frost heave. *J. Geophys. Res.* 112: F02S21, doi: 10.1029/2006JF000525.

Sturm, M., Perovich, D. K. & Holmgren, J. 2002. Thermal conductivity and heat transfer through the snow on the ice of the Beaufort Sea. *J. Geophys. Res.* 107: (8043,) doi: 10.1029/2000JC000409.

Energy Balance Response of a Shallow Subarctic Lake to Atmospheric Temperature and Advective Persistence

Richard M. Petrone
Cold Regions Research Centre, Wilfrid Laurier University, Waterloo, Ontario, Canada
Wayne R. Rouse
School of Geography & Geology, McMaster University, Hamilton, Ontario, Canada
L. Dale Boudreau
National Archives & Data Management, Environment Canada, Downsview, Ontario, Canada

Abstract

This paper examines two hypotheses that apply to the energy balance of shallow subarctic lakes. These are other factors remaining constant, evaporation and sensible heat fluxes will increase with increasing air temperature, and the influence of mesoscale advection on latent and sensible heat fluxes decreases with increasing wind directional frequency. The data used to examine these hypotheses are derived from a shallow subarctic lake in the Hudson Bay Lowland coastal area near Churchill, Manitoba. They represent two separate years with differing weather and wind directional frequencies. Directional frequencies are divided into onshore (from Hudson Bay) and offshore (from the continental interior). For the former, the air masses are generally cool and moist, and for the latter, they are relatively warm and dry. Analysis of these data indicates that both hypotheses are valid within the framework of this study.

Keywords: advective persistence; Hudson Bay.

Introduction

There are a plethora of small, shallow freshwater lakes and ponds in the North American subarctic. Rouse (1973) estimates that small lakes cover ~3% of the Hudson Bay Lowlands in Ontario, while Dredge (1986) estimates lakes to cover 50% of the Hudson Bay Lowlands in Manitoba. These subarctic freshwater systems, which are dominated by low energy environments and cold region processes, play important hydrological and biogeochemical roles (Pienitz 1995). Hydrologically, these lakes are an important link between the regional hydrology and climate via their evaporative processes, while biogeochemically they can be significant from a nutrient cycling and biological perspective (Schertzer et al. 2003, Nagarajan et al. 2004, Boudreau & Rouse 1995, Macrae et al. 2004). Thus, lakes are an important component of the landscape in this environment and are worthy of consideration in hydrologic and climatologic studies. However, the pronounced warming predicted by global climate models may alter the surface energy balance of these lakes, thereby directly and indirectly altering their hydrological and/or biogeochemical function. Thus, an understanding of the energy regimes of these lakes, and how they are influenced by their regional climate, is required. The goal of this paper is to compare the surface energy fluxes of a shallow tundra lake between a normal wet and warm wet year to gain a better understanding of the potential interactions of these systems with their surrounding environments.

Shallow water bodies have been shown to be especially sensitive to warmer temperatures depending on the amount and timing of regional precipitation (Hondzo & Stefan 1991, Smol et al. 1991, Hondzo & Stefan 1993, Douglas et al. 1994, Nagarajan et al. 2004, Binyamin et al. 2006). Due to their distinctively small size, northern lakes are generally thoroughly mixed with a uniform temperature distribution and may become ephemeral (Bello & Smith 1990). Thus, if global climate models are accurate in their predictions of pronounced warming in high latitudes, the susceptibility of these lakes to ephemeral behaviour, or complete disappearance, is increased. The surface energy fluxes of these shallow tundra lakes have also been shown to be very responsive to advective effects, especially in the Churchill, Manitoba region, where Hudson Bay is seen to have a strong influence on the surface energy balance of the adjacent land up to 65 km inland (Rouse & Bello 1985). In order to investigate this influence on the region's abundant lakes, measurements were taken during the snow free period over Golf Lake, located east of the town of Churchill, Manitoba.

Churchill, a high subarctic wetland region in northern Manitoba, is an area that has been studied in detail. Many shallow lakes and ponds are dispersed throughout this region, most of which are less than 0.5 m deep, and less than 200 m in diameter (Bello & Smith 1990). The smaller ponds are generally poorly defined, very shallow, and frequently flood and dry up. Like most lakes in the subarctic tundra, Golf Lake is shallow (average depth of ~0.88 m) promoting thorough mixing and a uniform temperature distribution >95% of the time (Stewart & Rouse 1976, Binyamin et al. 2006).

The specific objectives of this paper are to study the atmospheric influence on Golf Lake from the surrounding land and adjacent bay, and to examine how the partitioning of the lake energy balance responds to changing mesoscale climatic conditions.

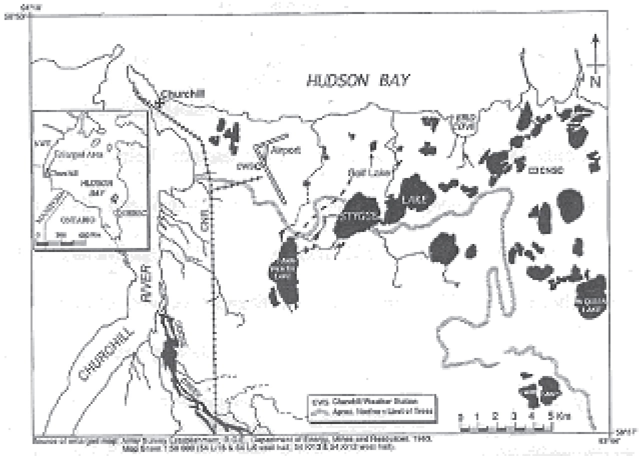

Figure 1. Study map illustrating the location of the town of Churchill, Manitoba and position of Golf Lake relative to the town and Hudson Bay.

Methods

Study area

Golf Lake is located in a wetland-dominated area, 11 km east of Churchill, Manitoba (58°46′N, 94°09′W) (Fig. 1). This region is classified as a high subarctic wetland region (N.W.W.G., Wetland Regions of Canada 1987). Hudson Bay exerts a strong influence on the climate of the area, causing Churchill to have high subarctic conditions, such as long, cold winters, short, cool summers, and low annual precipitation. This strong regional influence of Hudson Bay has been shown to extend at least 65 km inland, enhancing the flux of sensible heat and suppressing the fluxes of both latent and ground heating when winds originate offshore over Hudson Bay (Rouse 1991). This suppression of temperatures by the bay in the Churchill region causes the treeline and region of continuous permafrost to extend relatively far south in the Hudson Bay Lowland when compared to the rest of northern Canada.

Golf Lake is oval in shape with its long axis oriented approximately northeast–southwest (Fig. 1). The lake is approximately 550 m long by 350 m wide, 0.88 m deep on average, and is 1.2 m at its deepest point (Boudreau & Rouse 1995). The lake is surrounded by treeless upland heath to the east and sedge fens to the south, north, and west, with only a few larch (*Larix larcina*) and white spruce trees (*Picea glauca*) two to three meters in height. The immediate perimeter of the lake is dominated by various *Carex* species.

Measurements

An instrumented meteorological tower was located in the centre of the lake in 1.2 m of water. Air temperature, vapor pressure, and wind speed were measured at heights of 0.55, 1.05 and 1.55 m above the water surface. Lake temperatures were taken at the water surface, and at seven depths within the water column, with the bottom two sensors located within the loose organic bottom sediment. The heat flux through the bottom of the lake was measured using a Middleton heat flux plate.

Table 1. Mean precipitation (P), incident solar radiation (K↓) and air temperature (TAir) for Golf Lake, Churchill, Manitoba, 1991 and 1995.

	P (mm)	K↓ (W m^{-2})	T_{Air} (°C)
1995	224	182	10.4
1995	224	182	10.4

Table 2. Mean precipitation (P), incident solar radiation (K↓), air temperature (Ta), water temperature (Tw) Bowen ratio (β), the frequency of temperature inversion and lapse conditions (T-Inv. and T-Lapse, respectively), and the frequency of vapour pressure inversion and lapse conditions (e-Inv. and e-Lapse, respectively) for on and offshore winds, Golf Lake, Churchill, Manitoba, Canada, 1991 and 1995. n denotes the number of days with ON and OFF shore wind directions.

	1991		1995		COMBINED	
	ON	OFF	ON	OFF	ON	OFF
P(mm)	10	24	74	72	84	96
K↓(W/m^2)	209	226	198	164	203	195
Ta (°C)	9.7	15.7	10.1	14.9	9.9	15.3
Tw (°C)	14.9	16.1	12.9	16.4	13.9	16.3
β	0.5	0.1	0.7	-0.5	0.6	-0.2
T-Inv.	7	40	3	23	5	31.5
T-Lapse	93	60	97	77	95	68.5
e-Inv.	0	0	0	0	0	0
e-Lapse	100	100	100	100	100	100
n	10	12	26	14	36	26

Measurements yielded all components of the lake's energy balance via,

$$Q^* = Q_W + Q_E + Q_H \qquad (1)$$

where Q^* (W m^{-2}) is the net radiation, Q_W is the lake heat storage and Q_E and Q_H are the fluxes of latent and sensible heat, respectively.

The partitioning of the available energy between the sensible and latent heat fluxes is described by the Bowen ratio (β),

$$\beta = \frac{Q_H}{Q_E} \qquad (2)$$

Substitution of the flux equations for sensible and latent heat into equation (2) yields the following expression for the Bowen ratio,

$$\beta = \gamma \frac{\Delta T}{\Delta e} \qquad (3)$$

where γ is the psychrometric constant (0.0662 kPa °C^{-1}), ΔT is the vertical change in air temperature, and e is the vertical change in vapor pressure (kPa). β is a useful term to examine the relative importance of the sensible and latent heat fluxes, and the importance of cold air advection.

The heat storage within the lake (Q_W) is calculated from the sum of the series of lake layers, using the mean temperature and thickness of each layer giving,

$$Q_W = \sum C_W \left(\frac{\Delta T_W}{\Delta t} \right) \Delta z \tag{4}$$

where C_W is the volumetric heat capacity, $(\Delta T_W / \Delta t)$ is the water temperature change over time, and Δz is the depth increment of the volume of water in question, usually from the surface to the lake bottom.

The latent heat flux Q_E is derived using the energy balance approach in which,

$$Q_E = \frac{(Q^* - Q_W)}{1 + \gamma \dfrac{\Delta T_a}{\Delta e}} \tag{5}$$

where $\gamma(\Delta T_a/\Delta e)$ is the Bowen ratio. After determining Q_E, the sensible heat flux Q_H is derived as a residual in equation (1). Measurements are then grouped according to wind direction (with 360° representing true north) according to the following criteria: 315°–45° are referred to as *Onshore winds* (originating over Hudson Bay); 225°–315°and 45°–135° are referred to as *Along shore winds*, and 135°–225° are referred to as *Offshore winds* (originating over the interior tundra). The surface energy balance terms are then normalized as a ratio of the net radiation.

Results and Discussion

The two study seasons differed significantly in their seasonal weather. 1991 was on average about 5°C warmer than 1995, and was wetter and sunnier (Table 1). The air temperature and precipitation for 1991 and 1995 were greater than the observed normals for the region (9.7°C and 112 mm, respectively, Rouse et al. 1987), with 1991 being notably warmer and wetter than normal. The impact of differences in the summer weather on the energy balance of Golf Lake for these two seasons was substantial (Fig. 2). In both years, Q_H followed the same trend as Q*, reaching maximum in late June or early July and decreasing subsequently. Q_E reached maximum values around the first week of July, but remaining high through the measurement periods. There was little lake net heat storage (Q_w) in either year.

Lake and air temperature trends help to understand observed trends in the surface energy balance. In both years, onshore winds were associated with cooler temperatures and offshore winds with warmer temperatures (Table 2). In 1991, onshore winds were less frequent, and also less frequently associated with increased precipitation than in 1995. Inversion periods with negative sensible heat flux were frequent in 1991 (Fig. 2). In contrast, 1995 experienced lapse conditions (air temperature less than lake temperature) for the bulk of the season, with a resulting enhanced sensible heat flux (Table 2). Onshore winds always corresponded with lapse conditions in both years. $\beta = Q_H/Q_E$ generally showed large fluctuations from day to day, but over the season averaged out near zero (Table 3). β was higher for onshore than for offshore winds in both years.

Since the surface fluxes are strongly coupled with the net

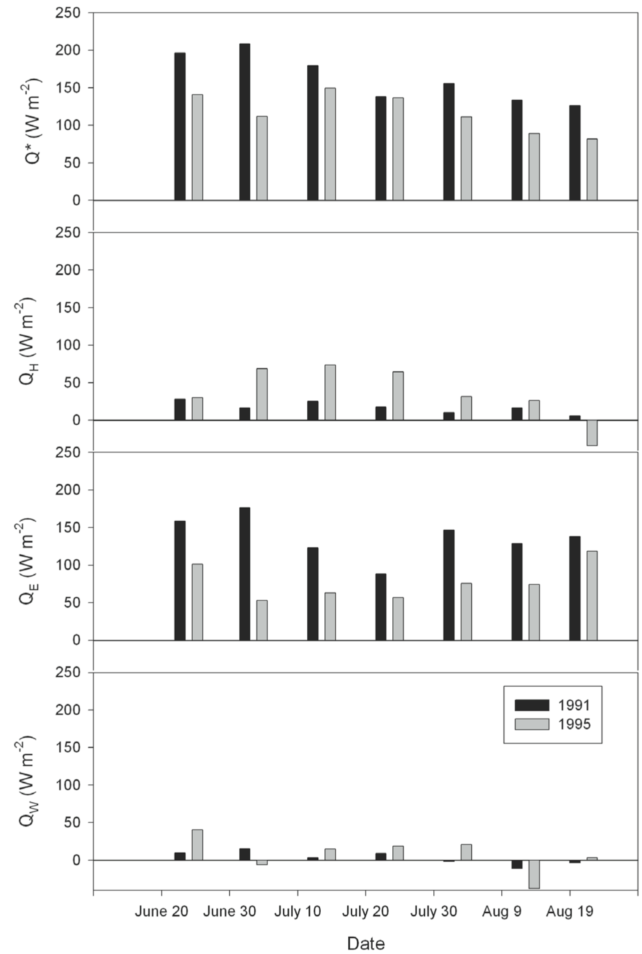

Figure 2. Surface energy balance for Golf Lake, Churchill, Manitoba, 1991 and 1995. Net radiation (Q*), sensible heat flux (Q_H), latent heat flux (Q_E) and lake heat storage (Q_W) data are expressed as 10-day running averages.

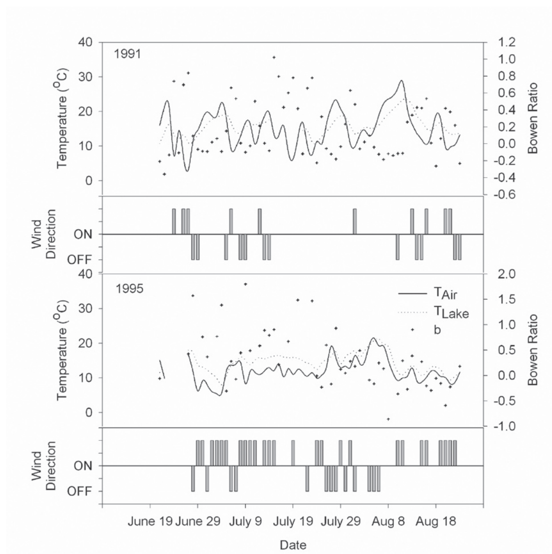

Figure 3. Air and lake temperatures (T_a and T_W, respectively), and Bowen ratio (β) for onshore and offshore winds, Golf Lake, Churchill, Manitoba, 1991 and 1995. All variables are expressed as daily averages.

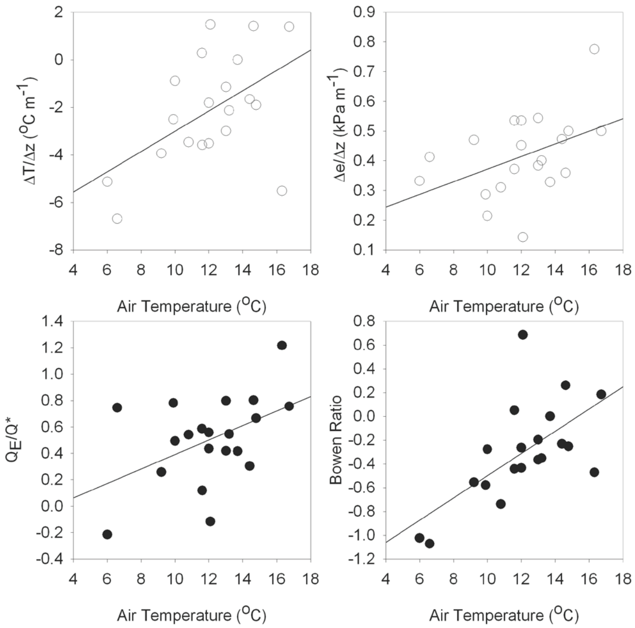

Figure 4. Relationship of vertical temperature ($\Delta T/\Delta z$) and vapour ($\Delta e/\Delta z$) gradients, relative latent heat (Q_E/Q^*) flux, and Bowen ratio (β) to air temperature. Data are plotted for both On and Offshore winds for both 1991 and 1995, for $Q^* = 200 \pm 40$ W m^{-2}. The lines are best-fit regression lines.

Table 3. Seasonal averages of the relative sensible (Q_H/Q^*) and latent heat (Q_E/Q^*) fluxes, relative lake heat storage (Q_W/Q^*), lake (T_W) and air (T_a) temperatures, and air temperature gradient (dT/dz). Golf Lake, Churchill, Manitoba, Canada, 1991 and 1995. Values are for Onshore and Offshore winds and standardized for $Q^* = 200 \pm 40$ Wm^{-2}.

		Q_H/Q^*	Q_E/Q^*	Q_W/Q^*	T_a (°C)	T_w (°C)	dT/dz (°C/m)
1991	ON	0.35	0.85	-0.30	11.5	15.8	2.2
	OFF	0.03	0.75	0.23	16.9	16.1	0.4
1995	ON	0.29	0.63	0.10	9.9	13.5	-1.8
	OFF	0.42	0.79	0.01	15.3	16.2	-0.4

radiation, to better understand their dynamics, it is useful to normalize them as a ratio of the net radiation, to give relative latent and sensible heat fluxes (Table 3). This brings out yearly contrasts. In 1995, all offshore flows produced large relative evaporation, and most onshore flows produced large relative sensible heat fluxes (Table 3). In 1991, onshore winds frequently resulted in larger relative evaporation than offshore winds (Table 3). By eliminating Q* as a variable, it is evident that $\Delta T/\Delta z$, $\Delta e/\Delta z$, Q_E/Q^* and β all increase with increasing atmospheric temperatures (Fig. 4). The rapid increase in β with increasing Ta arises because the rate of increase in Q_H substantially exceeds that in Q_E.

Many of the differences seen in the 1991 and 1995 data are due to differences in the directional persistence of winds. These have a substantial impact on $\Delta T/\Delta z$ and $\Delta e/\Delta z$. $\Delta e/\Delta z$ over the lake resulting from the differing response of lake and air temperatures. Even a shallow lake's response to changing atmospheric conditions requires periods of time

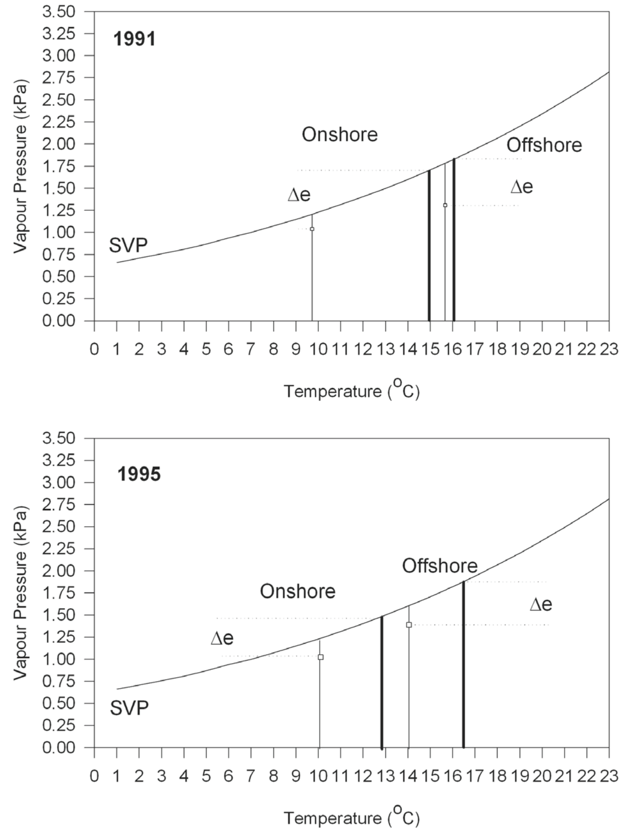

Figure 5. Vapour pressure-temperature relationships, during On and Offshore conditions, Golf Lake, Churchill, Manitoba, 1991 and 1995. Squares represent seasonal vapour pressures; thick lines represent seasonal lake temperatures; and fine lines represent seasonal air temperatures.

ranging from several hours to days, due to its relatively large heat capacity compared with the atmosphere. The large increases in $\Delta e/\Delta z$ and Q_E for onshore conditions in 1991 were due both to the increased temperatures and lesser persistence of onshore winds, which never persisted for longer than two days. (Fig. 3, Table 3). In 1995, there was substantially greater persistence in wind direction (Fig. 3). In 1991, lake temperatures were very close for both onshore and offshore winds, due to the much lower frequency and persistence of onshore winds compared with 1995 (Fig. 3). During offshore winds, larger differences between air and lake temperature generated large vapor pressure gradients. The relationship became stronger as lake temperature increased, due to physical principles dictated by the slope of the saturated vapor pressure-mean temperature curve (Fig. 5). The warmer conditions in 1991 stimulated greater vapor pressure gradients over the lake (Fig. 4), which resulted in greater Q_E. This is similar to the results in Rouse et al. (1987) who reported on a similar increase in evaporation with increasing air temperature for a sedge fen in the Churchill region. The enhancement of the latent heat flux for warmer conditions could also be due to the greater suppression of the sensible heat flux during the frequent inversion conditions of 1991 (Strub & Powell 1987).

Conclusions

Within the context of this study, our evidence indicates that both hypotheses appear valid. With a control on interacting variables, the vertical temperature and vapor pressure gradients increase with increasing air temperatures which, in turn, results in increased sensible and latent heat fluxes. With increasing atmospheric temperatures, sensible heat fluxes increase more rapidly than latent heat fluxes. Thus, shallow lakes respond fairly rapidly to atmospheric temperature changes, especially in the direct heating of the atmosphere. However, this response in advective situations depends on wind directional frequencies. Where wind directions change frequently, the response is greater than when they change less frequently.

Acknowledgments

The authors wish to thank M. Macrae and the staff of the Churchill Northern Studies Centre for their assistance in the field. Funding was provided by the Natural Science and Engineering Research Council of Canada, and the Northern Science Training Program.

References

Bello, R.L. & Smith, J.D. 1990. The effect of weather variability on the energy balance of a lake in the Hudson Bay Lowlands, Canada. *Arctic and Alpine Research* 22(1): 98-107.

Binyamin, J., Rouse, W.R., Davies, J.A., Oswald, C.J. & Schertzer, W.M. 2006. Surface energy balance calculations for small northern lakes. *International Journal of Climatology* 26: 2261-2273.

Boudreau, L.D. & Rouse, W.R. 1995. The role of individual terrain units in the water balance of wetland tundra. *Climate Research* 5: 31-47.

Douglas, M.S.V., Smol, J.P. & Blake Jr., W. 1994. Marked post-18th Century environmental change in high Arctic ecosystems. *Science* 266: 416-419.

Dredge, L.A. 1986. *Surficial Geology, Northeastern Manitoba*. Geological Survey of Canada, Map 1517A. 1:500,000.

Hondzo, M. & Stefan, H.G. 1993. Regional water temperature characteristics of lakes subjected to climate change. *Climatic Change* 24: 187-211.

Hondzo, M. & Stefan, H.G. 1991. Three case studies of lake temperature and stratification response to warmer climate. *Water Resources Research* 27(8): 1837-1846.

Macrae, M., Bello, R.L. & Molot, L. 2004. Intermittent Hydrologic Pathways in Tundra Ponds and Implications for Carbon Dynamics in the Hudson Bay Lowland. *Hydrological Processes* 18(11): 2051-2069.

Nagarajan, B., Yau, M.K. & Schuepp, P.H. 2004. The effects of small water bodies on the atmospheric heat and water budgets over the MacKenzie River Basin. *Hydrological Processes* 18: 913-938.

N.W.W.G., The Canadian Wetland Classification System, National Wetlands Working Group of the Canada Committee on Ecological Land Classification, 1987: *Ecological Land Classification Series*, No. 21, Lands Conservation Branch, Canadian Wildlife Service, Environment Canada, Ottawa, Ontario, 18 pp.

Pienitz, R., Smol, J.P. & Birks, H.J.B. 1995. Assessment of freshwater diatoms as quantitative indicators of past climatic change in the Yukon and Northwest Territories, Canada. *Journal of Paleolimnology* 13: 21-49.

Rouse, W.R. 1991. Impacts of Hudson Bay on the terrestrial climate of the Hudson Bay Lowlands. *Arctic and Alpine Research* 23: 24-30.

Rouse, W.R. 1973. The microclimate of different terrain units in the Hudson Bay Lowlands. In B.D. Kay (ed.), *Proceedings: Symposium of the Physical Environment of the Hudson Bay Lowlands: March 30-31, 1973.* University of Guelph, pp. 69-82.

Rouse, W.R., Hardill, S.G. & Lafleur, P.M. 1987. The energy balance in the coastal environment of James Bay and Hudson Bay during the growing season. *Journal of Climatology* 7: 165-179.

Rouse, W.R. & Bello, R.L. 1985. Impact of Hudson Bay on the energy balance in the Hudson Bay Lowlands and the potential for climatic modification. *Atmosphere-Ocean* 23(4): 375-392.

Schertzer W.M., Rouse, W.R., Blanken, P. & Walker, A. 2003. Over-lake meteorology and estimated bulk heat exchange of Great Slave Lake in 1998 and 1999. *Journal of Hydrometeorology* 4: 649-659.

Smol, J.P., Walker, I.R. & Leavitt, P.R. 1991. Paleolimnology and hindcasting climatic trends. *Verh. Internat. Verein. Limnol.* 24: 1240-1246.

Stewart, R.B. & Rouse, W.R. 1976. A simple method for determining evaporation from shallow lakes and ponds. *Water Resources Research* 12: 623-628.

Strub, P.T. & Powell, T.M. 1987. The exchange coefficients for latent and sensible heat flux over lakes: dependence upon atmospheric stability. *Boundary-Layer Meteorology* 40: 349-361.

Numerical Analysis of Forced and Natural Convection in Waste-Rock Piles in Permafrost Environments

Hoang-Nam Pham
Department of Civil and Environmental Engineering – University of Alberta, Edmonton, AB, Canada
Lukas U. Arenson
BGC Engineering Inc., Vancouver, BC, Canada
David C. Sego
Department of Civil and Environmental Engineering – University of Alberta, Edmonton, AB, Canada

Abstract

Mine waste-rock material is often a highly porous medium and it is an ideal environment to analyze the effect of natural and forced air convections on the waste-rock pile temperatures in permafrost regions. Two-dimensional finite element method is utilized to examine the behavior of different waste-rock piles. Forced convection as a function of air velocity is solved by applying the Navier-Stokes momentum equation and the continuity equation. Coupled thermal and air flow modeling of waste-rock piles is carried out for a period of 10 years. The cooling effect of the closed waste-rock piles mainly relies on gravity driven natural convection within the porous waste-rock layer, which is controlled by the thermal boundary condition. The cooling effect of the open waste-rock piles, on the other hand, is controlled by the cold temperature air flow that penetrates the pile. Preliminary results indicate that the center of the waste-rock piles will form a frozen core and an active layer of about 5 meters in approximately 2.2 years.

Keywords: convective heat transfer; natural convection; numerical simulation; waste-rock piles.

Introduction

Natural convection in fluid saturated porous media plays a key role in a wide range of technical applications, such as fluid flow in geothermal reservoirs, insulations, dispersion of chemical contaminants and migration of moisture in grain storage system. A comprehensive literature survey focusing on this subject is given by Nield & Bejan (1998).

Research on natural convection in permafrost regions has seen increasing attention by many researchers. Goering & Kumar (1996) investigated the characteristics of natural convection in porous rock embankments and showed significantly enhanced cooling effects in winter beneath these porous rock embankments. A large number of numerical models showed that natural convection during winter time can lower the foundation soil temperature by as much as 5°C on an annual average basis in comparison with standard sand or gravel embankments. In addition, researchers at the State Key Laboratory of Frozen Soil Engineering at the Chinese Academy of Sciences in Lanzhou have performed numerical and experimental studies on natural convection for the railway project on the Qinghai-Tibetan Plateau. Yu et al. (2003) investigated the cooling effect of coarse rock layers and fine rock layers under open-top and windy boundary in a laboratory investigation. Lai et. al. (2003) proposed the ripped-rock embankment structure on the Qinghai-Tibet railway under climatic warming by numerical simulation. Arenson et al. (2007) presented the results of numerical simulation of natural convection of waste-rock material, where the temperature at the base decreased from -4°C (conduction only) to -6°C due to convection.

In this work, numerical simulation of convection in waste-rock pile will be performed to evaluate the parameters that affect the convective heat transfer in coarse materials, namely wind, snow cover (boundary conditions), and internal intrinsic permeability of the waste-rock.

Governing Equations and Material Properties

Governing equations

Consider a fluid-saturated porous media with constant physical properties except for the density in the buoyancy force term, which is satisfied by the Boussinesq's approximation, thermal conductivity and volumetric heat capacity which are variation with temperature. Local thermal equilibrium is taken into consideration; e.g., the temperature of the fluid phase is equal to the temperature of the solid phase. The porous media is homogenous and isotropic. The flow of fluid within the porous media is governed by Darcy's law and the flow of fluid over the waste-rock pile is controlled by Navier-Stockes law with a Darcy term account

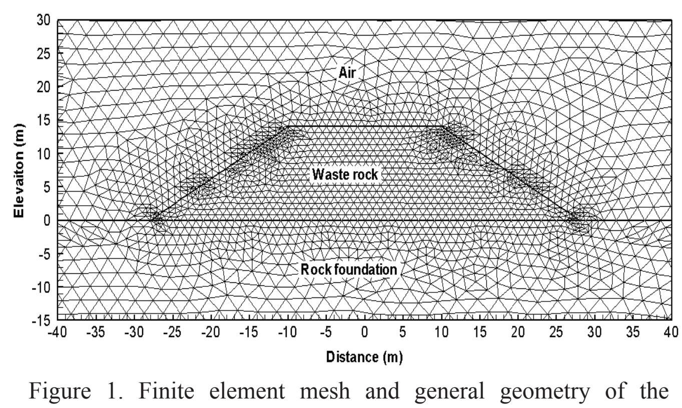

Figure 1. Finite element mesh and general geometry of the simulation.

for the effects of forced convection into the pile. Figure 1 shows the computational domain and mesh.

Conservation of mass:

$$\frac{\partial u}{\partial x}+\frac{\partial v}{\partial y}=0 \tag{1}$$

Conservation of momentum

- Fluid in porous media

Darcy's law

$$u=-\frac{K}{\mu}\frac{\partial P}{\partial x} \tag{2a}$$

$$v=-\frac{K}{\mu}\left[\frac{\partial P}{\partial y}-\rho_o g\beta(T-T_o)\right] \tag{2b}$$

- Free fluid flow

Navier-Stokes equation with Darcy's term

$$\rho\left(u\frac{\partial u}{\partial x}+v\frac{\partial u}{\partial y}\right)=-\frac{\partial P}{\partial x}+\mu\left(\frac{\partial^2 u}{\partial x^2}+\frac{\partial^2 u}{\partial y^2}\right)-\frac{\mu}{K}u \tag{3a}$$

$$\rho\left(u\frac{\partial v}{\partial x}+v\frac{\partial v}{\partial y}\right)=-\frac{\partial P}{\partial y}+\mu\left(\frac{\partial^2 v}{\partial x^2}+\frac{\partial^2 v}{\partial y^2}\right)-\frac{\mu}{K}v+\rho g\beta(T-T_o) \tag{3b}$$

Conservation of energy

$$\left(C_S+L\frac{\partial W_u}{\partial T}\right)\frac{\partial T}{\partial t}+C_a\left(u\frac{\partial T}{\partial x}+v\frac{\partial T}{\partial y}\right)= =\frac{\partial}{\partial x}\left(\lambda_x\frac{\partial T}{\partial x}\right)+\frac{\partial}{\partial y}\left(\lambda_y\frac{\partial T}{\partial y}\right) \tag{4}$$

where u and v are velocity in x, y direction; K is the intrinsic permeability; μ: dynamic viscosity; P: air pressure; ρ_O: air density; C_S: volumetric heat capacity of the waste-rock; C_a: volumetric heat capacity of air; L: latent heat of water; W_u: unfrozen water content; λ_x, λ_y: thermal conductivity in x, y direction; β: thermal expansion of air; T is temperature of solid and fluid.

We introduce the stream function ψ, expressed as:

$$u=\frac{\partial\psi}{\partial y} \tag{5a}$$

$$v=-\frac{\partial\psi}{\partial x} \tag{5b}$$

By substituting Equations (5a, 5b) into Equations (2a, 2b), and eliminating the pressure term, we obtain:

$$\frac{\partial}{\partial x}\left(\frac{\mu}{K}\frac{\partial\psi}{\partial x}\right)+\frac{\partial}{\partial y}\left(\frac{\mu}{K}\frac{\partial\psi}{\partial y}\right)=\rho_o\beta g\frac{\partial T}{\partial x} \tag{6}$$

By introducing the stream function, the conservation of mass in the porous media is automatically satisfied.

One of common methods to solve Equations (3a, 3b) is to eliminate the pressure terms through the penalty parameter γ. The method is called the penalty finite element method (Reddy & Gartling 2000).

$$P=-\gamma\left(\frac{\partial u}{\partial x}+\frac{\partial v}{\partial y}\right) \tag{7}$$

where $\gamma = 10^4 Re$ to $10^{12} Re$; Re is the Reynolds number.

To determine the effects of heat transfer, the local Nusselt number and Rayleigh number are defined as following:

The local Nusselt number on the base of the waste-rock

$$Nu_b=\frac{1}{L_b}\int_0^{L_b}\frac{\partial T}{\partial y}dx \tag{8}$$

The Rayleigh number of waste-rock

$$Ra=\frac{\rho_o g\beta C_a KH\Delta T}{\mu\lambda} \tag{9}$$

where L_b is the length of the base of the waste-rock pile; H is the height of the waste-rock pile.

The average Nusselt number on the base is defined as.

$$\overline{Nu}=\frac{\left(\frac{1}{L_b}\int_0^{L_b}\frac{\partial T}{\partial y}dx\right)_{convection}}{\left(\frac{1}{L_b}\int_0^{L_b}\frac{\partial T}{\partial y}dx\right)_{conduction}} \tag{10}$$

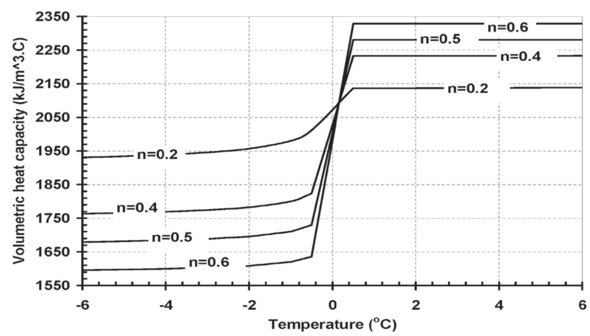

Figure 2. Relation between volumetric heat capacity and temperature with degree of saturation S = 0.6 and porosity n of the waste-rock material at the Diavik mine.

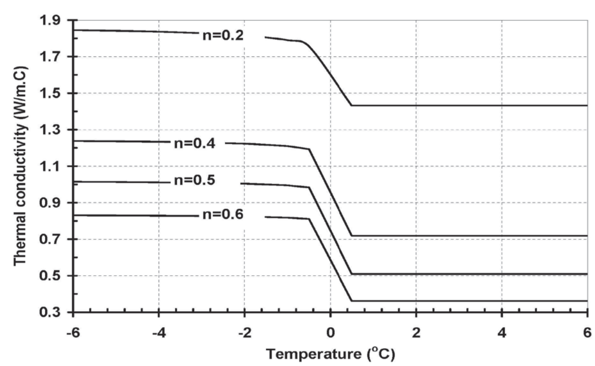

Figure 3. Relation between thermal conductivity and temperature with degree of the saturation S = 0.6 and porosity n of waste-rock material at the Diavik mine.

Material properties

The intrinsic permeability of the waste-rock material varies from 10^{-8} to $3x10^{-7}m^2$, based on calculation from grain size distribution resulting porosity between 0.3 and 0.5 and the degree of saturation is 0.6. A porosity n = 0.4 was chosen for this study.

Figure 2 shows a sharp change in volumetric heat capacity around the freezing point due to phase change of pore water. Similarly, the thermal conductivity changes with temperature as shown in Figure 3.

Additional parameters used are air density ρ_o = 1.293kg/m^3, dynamic viscosity μ = 1.49kg/mday, thermal expansion of air $\beta = 3.6710^{-3}$(C^{-1}), and volumetric heat capacity of air C_a = 1.3 kJ/m^{3}C.

Temperature variation with time is governed by the following equation with a mean average surface temperature of -4.8°C.

Ground temperature:

$$T = -4.8 + 17\sin\left(\frac{-2\pi t}{365} + \frac{17\pi}{180}\right) \tag{11}$$

Air temperature:

$$T = -9.5 + 28\sin\left(\frac{-2\pi t}{365} + \frac{17\pi}{180}\right) \tag{12}$$

Figure 4 shows that the wind velocity varies from 3m/s to 10m/s. Thus, this range was used to analyze the influence of forced convection on heat transfer in the waste-rock piles.

Numerical Results and Discussions

The strength and pattern of the convective heat transfer within a waste-rock depends mainly on geometry, intrinsic permeability of the waste-rock and the ambient temperature on the ground surfaces (Nield & Bejan 1999).

With impermeable surfaces (snow cover during winter), the influence of wind velocity is negligible and the motion of air is governed by natural convection.

With permeable surfaces during summer, the magnitude of the air velocity inside a waste-rock due to wind blow (forced convection) is mainly controlled by the intrinsic permeability of the waste material.

Table 1 and 2 show how the air velocity at the center axis of a waste-rock pile is strongly influenced by the intrinsic permeability based on the modeling in this study.

Results for impermeable surfaces of waste-rock piles

Figure 5a, b, c, and d show temperature distributions 10 years after construction. Figure 5a and b give similar temperature contours and the lowest temperature is -5.5°C. This can be explained by the fact that, under small intrinsic permeabilities ($1x10^{-8}$ and $3x10^{-8}$), heat transfer in waste-rock material is dominated by conduction; e.g., only dependent on the thermal conductivity of the material with small Rayleigh and Nusselt number. Furthermore, a 5-m active layer is formed normal to surface of the waste-rock and ground. In Figure 5c, temperatures at the base of the waste-rock pile are colder than in Figure 5a and 5b. This indicates an increase in the Rayleigh numbers and heat transfer via convection is developing. Figure 5d shows a significant change in temperature at the base in comparison with those shown in Figure 5a, b, and c. Temperatures drop from -5.5°C down to -8°C. This results from the increasing permeability. Furthermore, the unfrozen zone at the toe of the waste-rock decreases substantially.

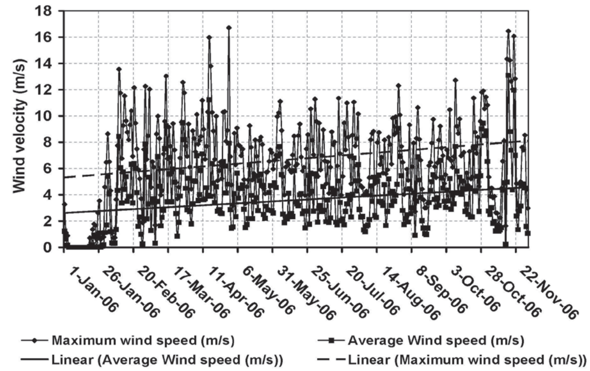

Figure 4. Wind velocity measured at the Diavik mine site.

Table 1. Air velocity inside waste-rock with $K = 1x10^{-8}m^2$.

Wind velocity (m/s)	Range of air velocity (m/s)
4	$3.13x10^{-5}$ – $3.59x10^{-5}$
5	$3.88x10^{-5}$ – $4.40x10^{-5}$
6	$4.51x10^{-5}$ – $5.21x10^{-5}$
8	$6.25x10^{-5}$ – $6.94x10^{-5}$
10	$7.75x10^{-5}$ – $8.68x10^{-5}$

Table 2. Air velocity inside waste-rock with $K = 3x10^{-7}m^2$.

Wind velocity (m/s)	Range of air velocity (m/s)
4	$9.38x10^{-4}$ – $1.05x10^{-3}$
5	$1.16x10^{-3}$ – $1.31x10^{-3}$
6	$1.40x10^{-3}$ – $1.57x10^{-3}$
8	$1.88x10^{-3}$ – $2.11x10^{-3}$
10	$2.31x10^{-3}$ – $2.60x10^{-3}$

Figure 6a, b, c, and d indicate the variation in temperature with time for selected points within the pile. Those points are used to determine when a 5-m active layer forms.

With $K = 1x10^{-8}$ and $3x10^{-8}$, there is no difference in time as conduction dominates the heat transfer and this process is controlled by thermal conductivity. A frozen core forms after 800 *days* following construction as shown in Figure 6a and b. In addition, heat transfer approaches nearly steady state after around 2000 *days*.

In Figure 6c, the time required to form a frozen core is about 780 *days;* i.e., 20 *days* earlier than shown in Figure 6a, 6b. These 20 *days* reduction are due to convective heat transfer, however, conduction still dominates the heat transfer in the waste-rock with $K = 1x10^{-7}$.

Four hundred and fifty *days* is the time required to form this frozen core as with $K = 3x10^{-7}m^2$ (Fig. 6d). Note that the temperature at the base drops rapidly, and after about 200 *days*, it is below the freezing point (0°C). Convective heat transfer dominates with high Rayleigh and Nusselt numbers.

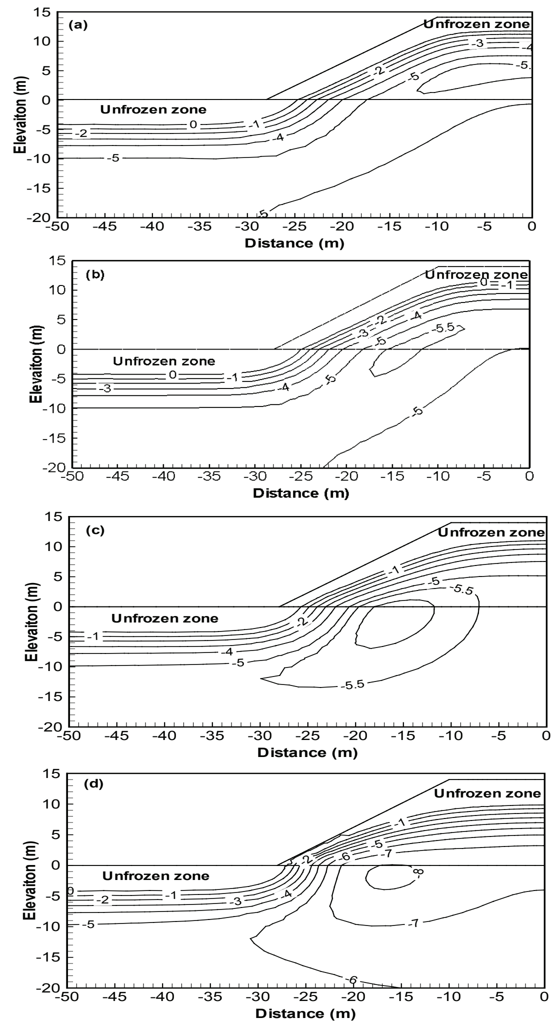

Figure 5. Temperature distribution after 10 *years*, impermeable boundary surfaces with (a) K = 1x10^{-8}, (b) K = 3x10^{-8}, (c) K = 1x10^{-7}, (d) K = 3x10^{-7}.

Just a small change in permeability K = 1x10^{-7} to 3x10^{-7} changes the temperature at point H from -4°C to -6°C after 1.5 *years* (Fig. 7). This establishes the importance of the Rayleigh being greater than a critical value; the convective heat transfer accelerates changing the temperatures. In Figure 7, measured temperatures from the Diavik mine site match the temperature for K = 3x10^{-7}.

The measured temperature from the site shows that the heat transfer in the waste-rock is dominated by convection and the selected intrinsic permeability, thermal conductivity and volumetric capacity are close to the in situ values. However, long-term measurements at the base and inside of the waste-rock pile are needed to confirm these.

They are small at low values of K = 1x10^{-8} – 3x10^{-8}, thus conduction dominates the heat transfer (Fig. 8). The amount of heat extracted from the base is small, and temperatures at the base change slowly. There is a "jump" in the Nusselt number by changing K from 1x10^{-7} to 3x10^{-7}. Therefore, it can be concluded that a small variation in K, assuming the corresponding Rayleigh number is larger than a critical value, will produce significant changes in Nusselt number which controls the heat transfer rate.

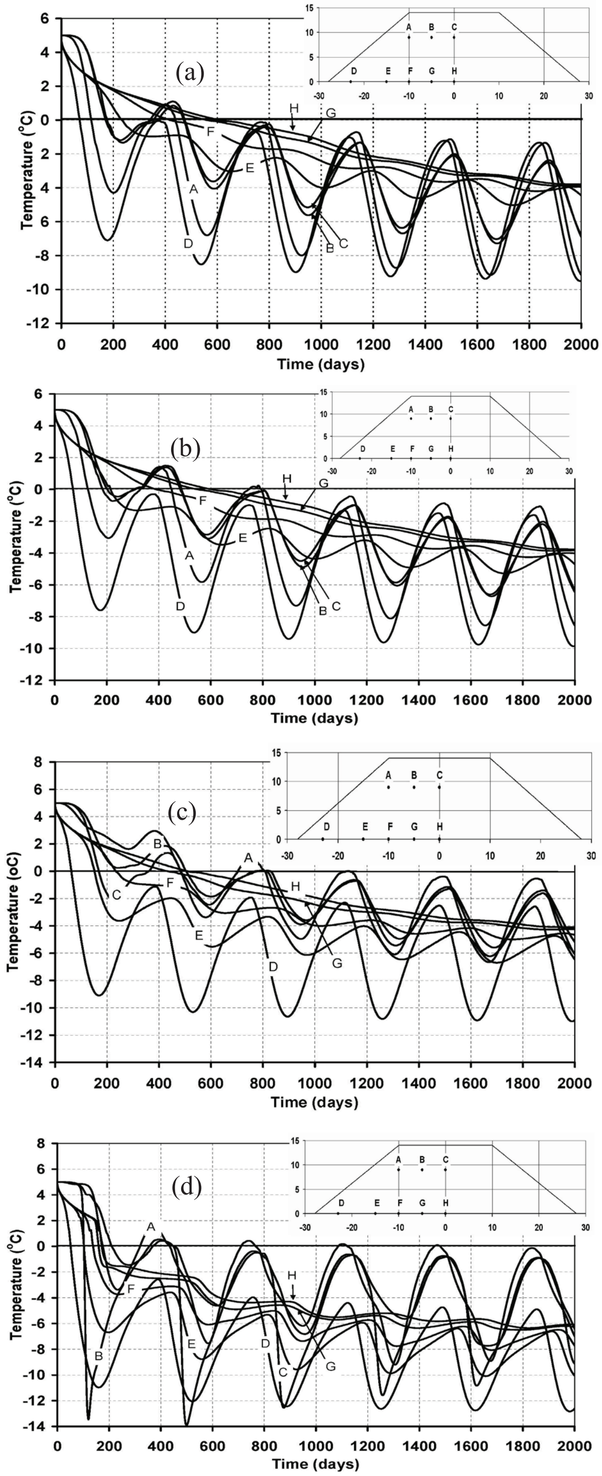

Figure 6. Temperature with time at particular points for K = 1x10^{-8} (a), 3x10^{-8} (b), 1x10^{-7} (c), 3x10^{-7} (c), respectively.

There is a significant change in Rayleigh number when K varies from 1x10^{-7} to 3x10^{-7} and thus the heat transfer rate as indicated in Figure 9. However, there is no significant change in Rayleigh numbers when K changes from 1x10^{-8} to 3x10^{-8} because these values produce a Rayleigh number smaller than the critical value. Zero values of Rayleigh number with K = 1x10^{-7} and 3x10^{-7}m^2 happen during summer when conduction dominates. Critical Rayleigh number is

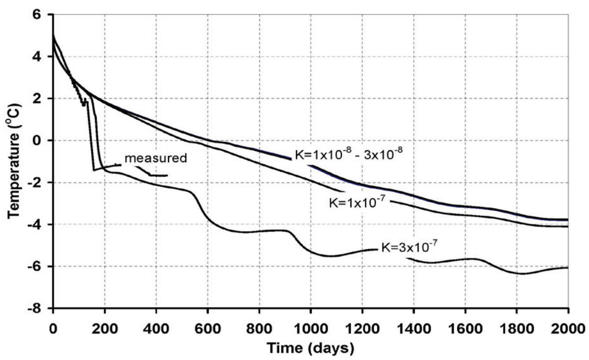

Figure 7. Temperature variation at point H (central point waste-rock pile).

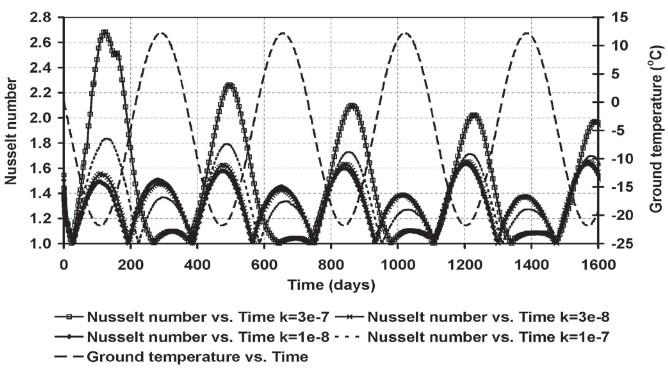

Figure 8. Variation of local Nusselt number (Eq. 8) versus time with K = 1x10^{-8}, 3x10^{-8}, 1x10^{-7} and 3x10^{-7}.

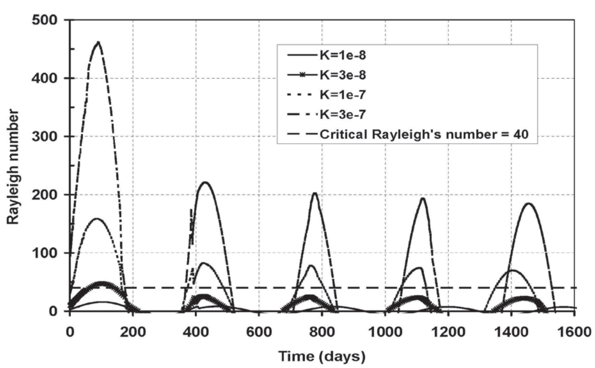

Figure 9. Variation of Rayleigh number with time.

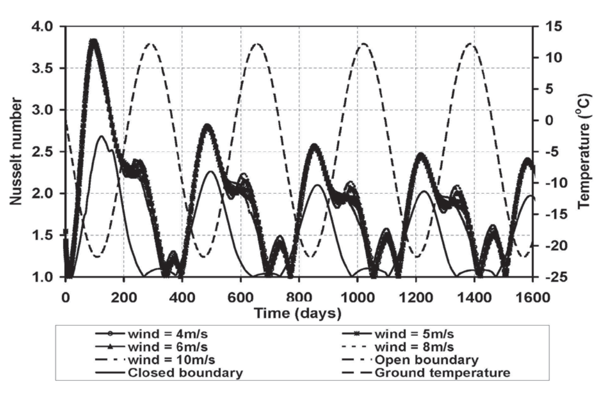

Figure 10. Variation of local Nusselt number with time in the case of open boundary with K = 3x10^{-7}.

defined as $Ra_{cr} = 4p^2$ when the conduction state is unstable or an average Nusselt number larger than 1 (Nield & Bejan 1999).

Results for permeable surfaces of waste-rock pile

With permeable surfaces, the heat transfer rate, which is represented by the Nusselt number, does not change for wind velocity up to 10m/s with K = 3x10^{-7}m^2 (Fig. 10). However, there is a large change in the Nusselt number when moving from a closed to an open boundary. Thus, with open surfaces, heat transfer rate into the waste-rock pile does not change due to change in wind velocity of the environment with K up to 3x10^{-7}.

With a small value of K = 1x10^{-8}m^2, there is only a very small change in the local Nusselt number when the wind velocity changes up to 10 m/s in the case of an open boundary condition or a closed boundary condition. Because with small values of K, the air velocity due to forced convection and natural convection is very small, and thus, convective heat transfer is not significant compared to conductive heat transfer.

Conclusions

Heat transfers in the waste-rock pile are investigated using numerical modeling for two-dimensional momentum, continuity, and energy equations. The results are compared to measured temperatures at the Diavik mine site.

The following conclusions can be drawn from the analysis presented:

- The value of intrinsic permeability has a large impact on the heat transfer in waste-rock materials with Rayleigh's number larger than a critical value. However, with small Rayleigh numbers (conduction dominates), heat transfer does not depend on the intrinsic permeability. With K = 3x10^{-7}m^2 (convection dominates), temperature at the base of a 14-m-high waste-rock pile is about -6°C instead of -4°C for K below 1x10^{-8} to 1x10^{-7}m^2.
- When the Rayleigh number is larger than a critical value, a small increase in K results in a significant increase in the Nusselt and Rayleigh number and thus, heat transfer rates due to convection also increase rapidly.
- Heat transfer becomes steady after 6 years for these studies independent on K. A frozen core with a 5-m active layer is formed after 800 days with K = 1x10^{-8} to 1x10^{-7}m^2 and 450 *days* with K = 3x10^{-7}m^2.
- The influence of the wind velocity on the heat transfer in waste-rock piles with open boundary conditions is not significant when the value of K is below 3x10^{-7} m^2. However, there is a rapid change in the heat transfer due to the conditions of the surface of a waste-rock pile (open or closed boundary) at high values of K.
- A comparison with measurements from the Diavik mine site confirmed the convection within the waste-rock pile, and good agreement was achieved by using an intrinsic permeability of 3x10-7 m^2. However, more data are required to confirm this initial comparison.

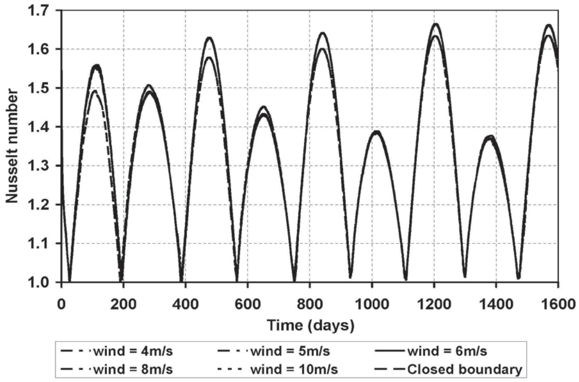

Figure 11. Variation of local Nusselt number with time in the case of open boundary with $K = 1x10^{-8}$.

The results presented clearly confirm reports on convective heat transfer made for arctic waste-rock piles, where temperatures measured within these coarse piles cannot be explained by conduction alone. Numerical modeling showed that once a critical Rayleigh number is reached, significant cooling at the base occurs. However, additional modeling and field data are required to study the combination in parameters and boundary conditions necessary to further convection in waste-rock piles.

Acknowledgments

This research is made possible through funding provided by Diavik Diamond Mines Inc. (DDMI), the Canada Foundation for Innovation (CFI), the Natural Science and Engineering Research Council of Canada (NSERC), the International Network for Acid Prevention (INAP), and the Mine Environment Neutral Drainage (MEND) program. In-kind support provided by Environment Canada is greatly appreciated. We thank Carol Ptacek (Environment Canada), and FDA Engineering for their technical support and patience during the construction phase.

References

Arenson, L.U., Pham, H.N., Klassen, R. & Sego, D.C. 2007. Heat convection in coarse waste-rock piles. *Canadian GeotechnicalCconference, Ottawa, Ontario, Canada. October –21-24, 2007.* In press

Arenson, L.U., Chen, J.F., Pham, H.N. & Sego, D.C. Laboratory investigations on air convection in porous media. Canadian *Geotechnical Conference, Ottawa, Ontario, Canada. October 21 - 24, 2007*. In press

Goering, D.J. & Kumar, P. 1996. Winter-time convection in open-graded embankments. *Cold Regions Science and Technology* 24(1): 57-74.

Lai, Y.M., Li, J.J., Niu, F.J. & Yu, W.B. 2003. Nonlinear thermal analysis for Qing-Tibet railway embankments in cold regions. *Journal of Cold Regions Engineering* 17(4): 171-184.

Lai, Y.M., Zhang, S.J., Zhang, L.X. & Xiao, J.Z. 2004. Adjusting temperature distribution under the south and north slopes of embankment in permafrost regions by the ripped-rock revetment. *Cold Regions Science and Technology* 39(1): 67-79.

Nield, D.A. & Bejan, A. 1999. *Convection in Porous Media.* New York: Springer.

Reddy, J.N. & Gartling, D.K. 2000. *The Finite Element Method in Heat Transfer and Fluid Dynamics*. New York: CRC press.

Effects of Ground Temperature and Slope Deformation on the Service Life of Snow-Supporting Structures in Mountain Permafrost: Wisse Schijen, Randa, Swiss Alps

Marcia Phillips
Swiss Federal Institute for Snow and Avalanche Research WSL-SLF
Stefan Margreth
Swiss Federal Institute for Snow and Avalanche Research WSL-SLF

Abstract

Modifications of ground temperature are of special interest in alpine permafrost regions, as the thermal properties of the permafrost influence the geotechnical characteristics of the ground and thus the stability and service life of mountain infrastructure. Air temperatures have been particularly warm in the past decade in the Swiss Alps, leading to various occurrences of slope and structure instability. The case of snow-supporting structures (snow nets) located on a steep slope in alpine permafrost is presented. Some of the structures have undergone such strong deformation that they must be replaced after only 17 years, as opposed to a service life of ~80 years under normal conditions. Borehole temperature and deformation measurements and surveys of the positions of the snow nets show that creep is particularly pronounced during hot summers in steep slope sectors. Technical solutions include the use of floating foundations and of construction techniques specially adapted to permafrost conditions.

Keywords: creep; floating foundations; mountain permafrost; service life; snow nets; technical solutions.

Introduction

Modifications of permafrost conditions and in particular warming and thawing of near-surface ground ice and active layer thickening can have devastating effects on the stability and service life of infrastructure in mountain permafrost regions (Haeberli 1992, Harris et al. 2001). Thaw subsidence, differential settlement, or heave and enhanced creep rates are particularly problematic for alpine infrastructure that is partly or completely anchored in sediments or bedrock containing ice (Phillips et al. 2007), especially in steep terrain. Alpine infrastructure typically includes structures such as cable-car stations, pylons, water pipes, shelters, and snow-supporting structures—many with high safety requirements. The service life of snow-supporting structures in creeping permafrost is the focus of this paper.

The past decade was characterized by a number of abnormal climatic events in the Swiss Alps. Seven of the last 10 years were among the 10 warmest registered since 1900. The warming was generally more pronounced in summer than in winter. The most extreme event was summer 2003, which was 4–5.5°C warmer than average and was the hottest measured since 1753 (MeteoSchweiz (annual reports), North et al. 2007). Mean annual snow depths varied strongly, with some very snow-rich winters (e.g., 1998/1999, 2000/2001) or winters with very little snow (e.g., 2001/2002, 2004/2005). It is not yet possible to determine trends in snow depth at altitudes where permafrost occurs (Marty et al. 2007).

In parallel to observations of slope and rock wall instability (Gruber et al. 2004, Gruber & Haeberli 2007, Springman et al. 2003), reports of structure instability in permafrost in the Alps during this warm decade have increased (e.g., Personal communications P. Feuz, C. Danioth, M. Walser, H.-R. Keusen). Alongside direct monitoring of the structures themselves (Phillips et al. 2003, Steiner et al. 1996, Vonder Mühll & Keusen 1995), the long-term monitoring of ground temperatures and deformation rates is essential to understand the current and future nature of these developments and the influence of factors such as climate fluctuations, construction activity, or the very presence of infrastructure. Improvements of design and service life are consequently the aim of such observations.

This paper presents borehole data (temperatures and deformation) and displacement data for snow-supporting structures (snow nets) that have undergone such strong creep-induced deformation that partial reconstruction is planned for 2008, only 17 years after their construction.

Site Description

The study site Wisse Schijen is a steep east-northeast-oriented slope located between 3010 and 3140 m a.s.l. in the Mattertal, above Randa (Canton Valais, Switzerland). Permafrost occurs in almost the entire slope (Keller 1995, Phillips et al. 2003). Slope angles range between 37 and 42°. The blocky scree is 2.5 m thick (gneiss, quartzite and marble), underlain by approximately 0.5 m of ice-rich sediments and finally by bedrock. There are narrow bands of bedrock visible in places and these are subject to flexular toppling, causing rockfall.

Wisse Schijen is an avalanche-starting zone, equipped with snow nets to protect Randa. There are several rows of snow bridges (rigid avalanche defense structures) below the area protected with snow nets, which would be destroyed if the latter were damaged or removed, and consequently, avalanches would break loose (Fig. 1).

Eight horizontal rows of snow nets between 24.5 and 45.5 m long and with a structure height of 4.0 m were built at Wisse Schijen in 1990 (upper rows 1–4) and 1991 (lower rows 5–8). The snow nets consist of triangular wire rope

Figure 1. The study site Wisse Schijen with 8 rows of snow nets is located in the upper part of the slope (outlined). Row 2 is shown inset. Several rows of snow bridges are visible in the slope sector below.

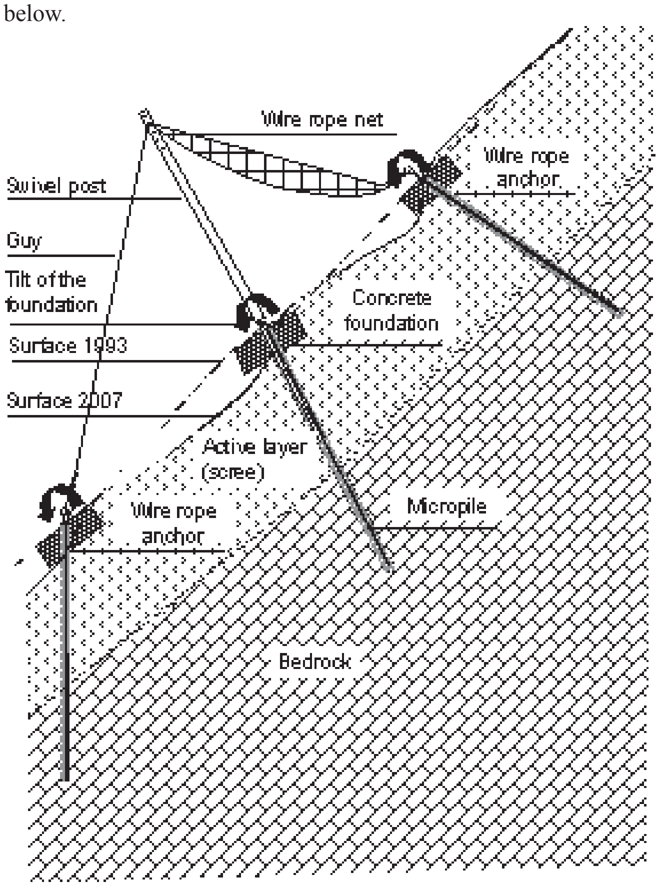

Figure 2 Configuration of the snow nets used. The location of the ground surface in 1993 and 2007 and the direction of tilt of the foundations are shown.

nets, which are attached to swivel supports with a ball joint at the contact to the base plate (Fig. 2).

The support and anchor spacing distance is 3.5 m. The structures are anchored with micropiles consisting of steel tubes (Ø 76 mm, length 1.5 m) and anchor bars (Ø 32 mm) under the supports and with wire rope anchors for the up- and downslope anchors. Concrete foundations were built to facilitate drilling and to stabilize the anchor heads. The anchor boreholes (Ø 100 mm) were drilled through these foundations rather than directly into the unstable scree.

Anchor lengths are 5 m and the anchors penetrate the bedrock. Large amounts of anchor grout were used (up to 30 kg m^{-1} (Personal communication, R. Bumann)) due to the large voids in the scree.

Snow nets were chosen for this sector of the slope (as opposed to snow bridges) because they are better adapted to rockfall. No specific construction methods were applied for permafrost conditions (e.g., the preheating of anchor grout to prevent freezing during the curing process as recommended by Margreth (2007)) or creep.

Two boreholes (B1 and B2) were drilled in 1998 when it became obvious that there were permafrost-related stability problems on the site. B1 is between net rows 5 and 6 (3046 m a.s.l.), B2 is between rows 7 and 8 (3019 m). A third, B3 is located between the top two rows of snow bridges (2953 m a.s.l.), where there is no occurrence of permafrost. All three boreholes are equipped with inclinometer tubes and borehole temperatures are measured in B1 and B2. The boreholes are shallow (6 m) due to various technical problems that arose during drilling.

Methods

Air temperatures and snow depth

Air temperatures and snow depth were measured by an automatic weather station (STN 2, Oberer Stelligletscher) located at 2910 m a.s.l., above St. Niklaus, 8 km away from the study site, on the same side of the valley. There is no weather station on the site itself. The snow data in particular therefore only gives a rough indication of the conditions in the area (e.g., if a winter was snow-rich or not).

Ground temperatures

Universal Temperature Loggers (UTL/Hobo) were used to measure borehole temperatures at five depths (0.5, 1, 2, 3, 4 m) in B1 and B2 (precision 0.25°C). Measurements were carried out hourly and were started in 2001.

Borehole deformations

The boreholes are equipped with inclinometer tubes, and measurements are effected using a Sinco Digitilt inclinometer (precision ±0.15 mm m^{-1}). The measurements were made at 1-m intervals and were carried out once a year (summer 1999–2007), which implies that data covers the second half of the previous summer period and the first half of the current one. Permanent borehole deformation measurements effected at a similar site in the eastern Swiss Alps (Rist 2007, in press) have shown that no deformation whatsoever occurs in winter; all movement ceases when the active layer freezes and only recommences when the latter thaws due to snowmelt infiltration in spring.

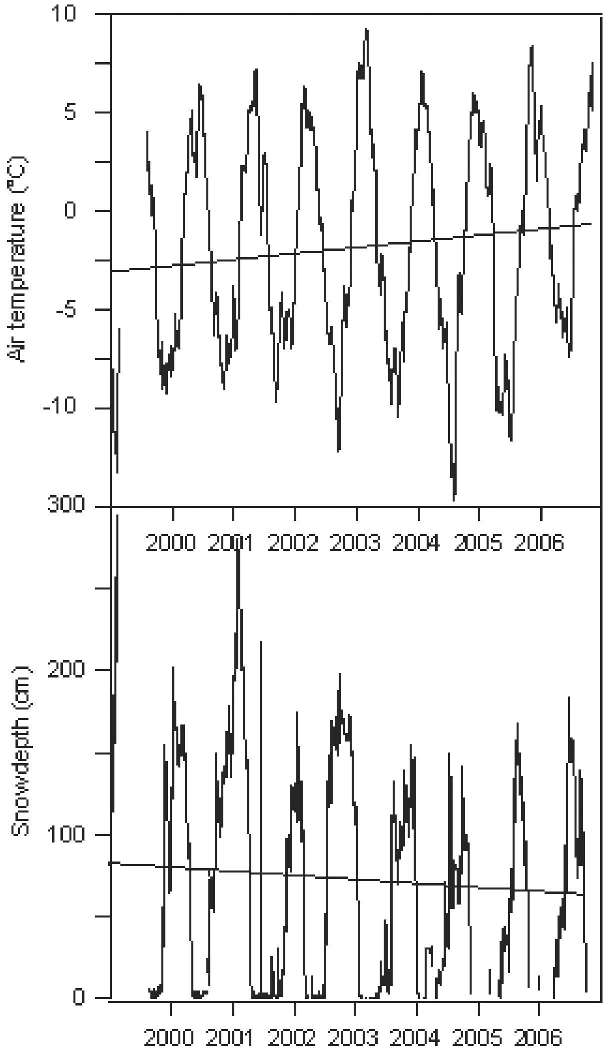

Figure 3. Air temperature (30-day running means) (top) and snow depth measured (bottom) by the automatic weather station STN2 (Stelligletscher, 2910 m, 1999–2007). Trends are shown.

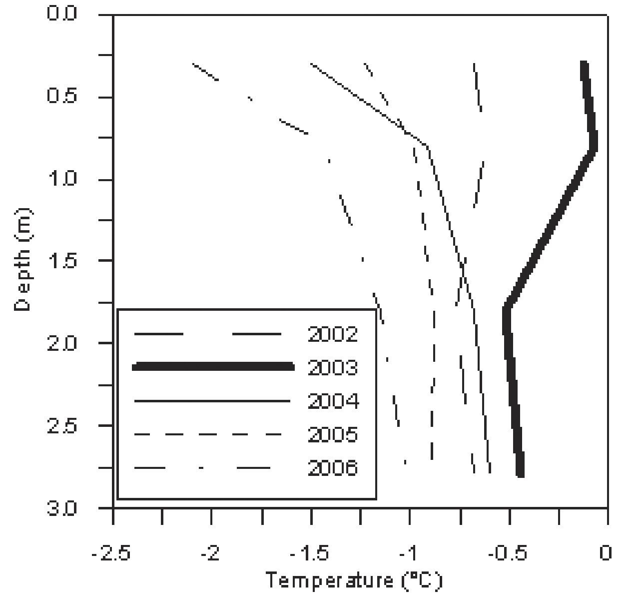

Figure 4a. Mean annual vertical temperature distribution in borehole B1.

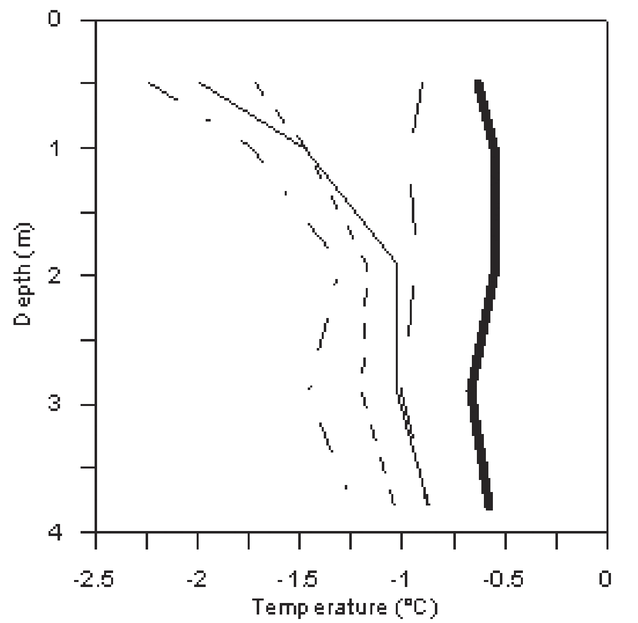

Figure 4b. Mean annual vertical temperature distribution in borehole B2 (same legend as Fig. 4a).

Structure stability

The position of 48 anchor heads was surveyed (1999–2007) using a Wild TC 1610 theodolite (precision ±2 mm). Both horizontal and vertical displacements were measured. The measurements were carried out once a year (summer), which implies that data covers the second half of the previous summer period and the first half of the current one and that the influence of the previous winter (e.g., particularly large snow loads on snow nets, meltwater in spring) must be taken into account.

Visual inspection

The 8 rows of nets were systematically inspected and photographed every summer, and problems recorded and reported. The visual observations include the inspection of row geometry, of the state of the foundations and of the superstructure. Any damage induced by differential creep or settlement, rockfall and surface erosion is assessed according to Margreth (2007).

Results

Air temperature and snow depth

Mean annual air temperature measured by the automatic weather station STN2 during the period 1999–2006 was -1.9°C. Figure 3 (top) shows the 30-day running means for air temperature. Summers 2003 and 2006 were particularly warm, with high thawing degree-days during the snow-free period (744 and 654, respectively, as opposed to a mean of 428 for all other years, see Fig. 5).

Mean snow depth during the period 1999–2006 was 70 cm. Winter 2000–2001 was snow-rich, with snow depths up to 270 cm. In contrast, shallow snow covers characterized winters 2004–2005 and 2005–2006 (Fig. 3, bottom).

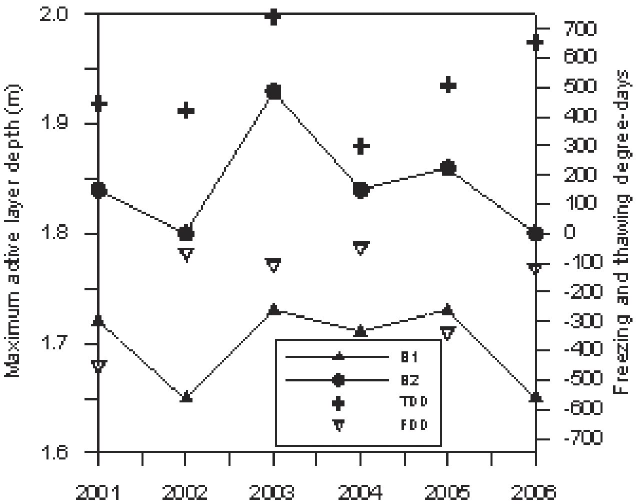

Figure 5. Maximum annual active layer depths measured in B1 and B2 (2001–2006) and thawing- (TDD) and freezing degree-days (FDD) during the annual snow-free period (right y axis).

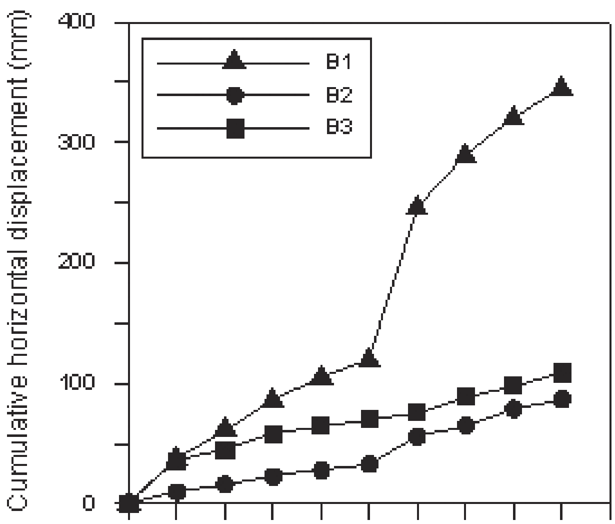

Figure 6. Cumulative displacement (mm) at 1 m depth in boreholes B1, B2, and B3 (1998–2007).

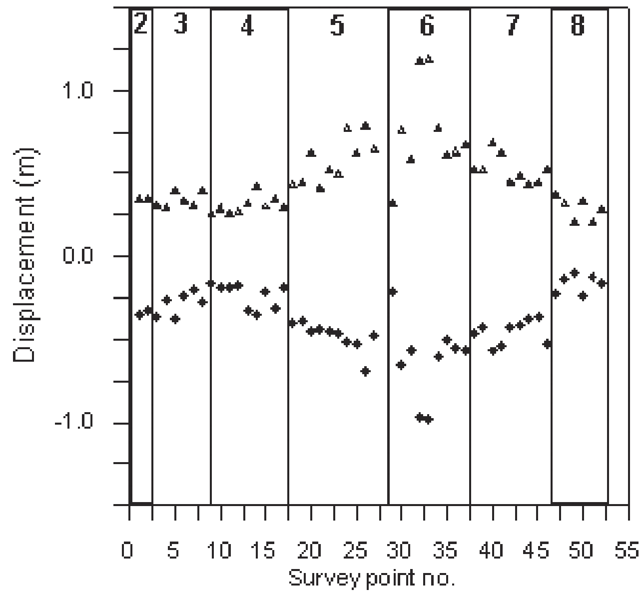

Figure 7. Mean horizontal (triangles) and vertical (diamonds) displacements of 52 anchor heads between 1999 and 2007. The snow net row numbers are indicated in bold.

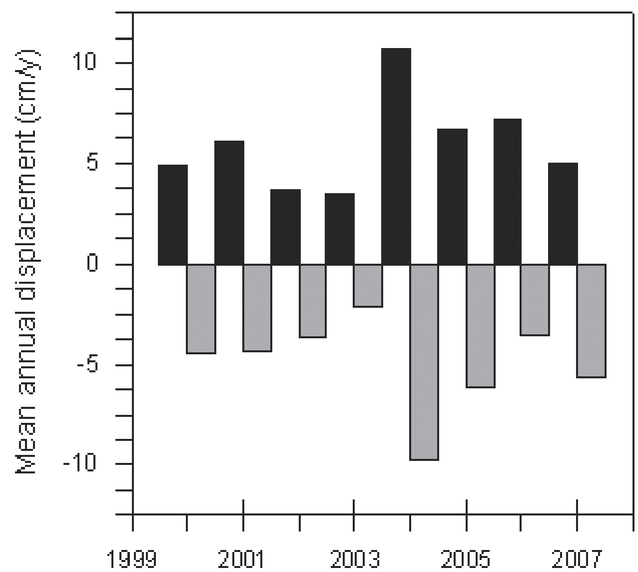

Figure 8. Mean annual horizontal (black) and vertical (grey) displacement of the anchor heads.

Ground temperatures

Borehole temperatures measured in B1 and B2 indicate that B1 is slightly warmer, despite being at a higher altitude. The mean annual temperature was warmest in 2003 in both boreholes (Figs. 4a, b). Shallow snow covers probably cause the slight cooling trend after 2003.

Maximum annual active layer depths are shown in Figure 5. The base of the active layer is defined here as being the depth of maximum seasonal penetration of the 0°C isotherm into the ground (Burn 1998). Mean active layer depth in B1 is 1.70 m and 1.85 m in B2. Active layer depths remained fairly constant throughout the measurement period, with a slight deepening in B2 (9 cm deeper than average) in summer 2003.

Borehole deformations

The cumulative horizontal displacements measured at 1 m depth (Fig. 6) indicate that the yearly displacements were quite regular, with the exception of the measurement period 2003–2004, during which a pronounced deformation of 126 mm occurred in B1 and a slight increase is also visible in B2. It should be noted that B1 is located between the damaged snow net rows 5 and 6. From 2005 onwards, it was no longer possible to measure deeper than 1.8 m in B1, as the inclinometer tube was too strongly deformed.

Structure stability

During the measurement period 1999–2007, the horizontal displacements of the anchor heads varied between 0.2 and 1.2 m (average 0.47 m) and the vertical displacements between -0.1 and -0.97 m (average -0.38 m). Displacements exceeding 0.5 m occurred in the net rows 5, 6 and 7 (Fig. 7). Mean

Figure 9a. Dislocated swivel support (left). Fig. 9b. Tipped concrete foundation (right) in the damaged snow net rows 5 and 6.

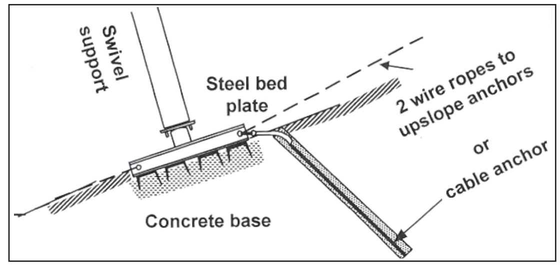

Figure 10. Floating foundation for snow nets in creeping permafrost conditions: steel bed plate on a base of lean concrete.

annual displacement velocities of the anchor heads varied from year to year. In the measurement period 2003–2004, they were particularly pronounced with mean displacements of 10.7 cm and -9.7 cm, respectively (Fig. 8).

Visual inspection

The problems observed at the study site include:

- Disturbed geometry of entire rows of nets, which can lead to uneven snow loading and to elevated constraints in the superstructure.
- Tipping of the base plates, leading to a blockage of the ball joint and to dislocation of swivel supports (Fig. 9a).
- Downslope tipping of the concrete foundations (Fig. 9b).
- Surface erosion and settlement of several decimeters causing anchor tendon exposure, which can lead to buckling or failure.
- Rockfall into the nets.

It is not known whether the anchor tendons are deformed or have undergone failure.

The assessment of the state of the snow nets has shown that all rows with the exception of rows 5 and 6 are in Condition Class 2 ("Damaged"). This implies that repairs are moderately urgent (within 1–3 years), and there is no immediate impairment for the serviceability of the structures. Rows 5 and 6 are, however, in Condition Class 3 ("Poor") (Margreth 2007) and repairs are very urgent, as there is a danger of collapse and their supporting function is no longer warranted.

Discussion

State of the permafrost, slope, and structure stability

As the deformation and displacement measurements occur in mid-summer, it is difficult to attribute movements to a particular cause. However, borehole deformations (in B1) and structure movements were significantly higher in the measurement period 2003–2004. They cannot be attributed to a significant deepening of the active layer or to a snow-rich winter. The mean annual borehole temperatures (January 1 to December 31) show that 2003 was the warmest year at all depths (Figs. 4a, b), and this seems to have influenced the creep rates. Creep rates remained constant in B3 where creep is not temperature-dependant (non-permafrost).

Not only the thickness of the active layer can vary, but also its position relative to the underlying stratigraphy (e.g., downward extension of the active layer into finer, ice-rich sediments due to warming or to settlement), which can augment the potential for slope instability (Rist 2007, in press). The degree of exposure of the micropiles and foundations (up to 0.4 m) indicates that settlement has occurred in places due to loss of permafrost ice. The exact amount and rate of settlement is difficult to quantify however, because scree is constantly eroded and replaced from upslope.

The presence of 300 foundations in the slope may have a slight stabilizing effect at a very local scale, as is shown by the accumulation of material directly above the foundations. However, this may be countered by the fact that there is more snowmelt water in spring due to the artificial retention of snow on the slope. The slope, therefore, cannot be characterized as being more stable due to the presence of the snow nets.

Technical solutions

The anchor heads have undergone substantial displacement from the start—in the first year after construction-isolated damages were visible (Stoffel 1995). Two rows of snow nets (5 and 6, located in the steepest sector) have now been subjected to such intense creep-induced deformation that their replacement is planned for 2008.

Under normal conditions snow nets have an expected service life of 80 years. The mid- and long-term service life of the structures are however not assured with creep rates exceeding 5 cm/year (Margreth 2007). The data presented above helps to explain the remarkably short service life of the snow nets at the study site. Whereas various problems are visible in the superstructure, the current state of the anchors is unknown. It is possible that deformation or failure of the micropiles and wire rope anchors has occurred in places and that collapse may be imminent. In order to ensure protection against avalanches, it is therefore necessary to replace the most badly damaged rows of nets (5 and 6) as soon as possible and to monitor the remaining rows carefully.

In order to improve the service life of the new structures in this highly unstable terrain, floating foundations will be used under the swivel posts, rather than fixed ones (Fig. 10). Steel bed plates on a base of lean concrete have been tested in similar terrain and proved to be well-adapted (Phillips 2006). If necessary, they can be readjusted relatively easily, whereas the replacement of fixed anchors is hardly possible. In addition, specially adapted construction techniques will be used, as recommended for permafrost terrain (Margreth 2007).

As a result of the experience gained with the snow nets in the Wisse Schijen sector, the neighboring avalanche slopes are triggered artificially. Special reinforcement measures against snow avalanches will be met for potentially affected infrastructure in the valley.

Conclusions

Wisse Schijen is a site with particularly difficult conditions for snow-supporting structures. The creep rates in the steep permafrost slope can exceed 5 cm/year, particularly in hot summers, implying that mid- and long-term service life is not ensured. In such cases the construction of snow-supporting structures is only advisable if no alternatives are available (Margreth 2007). In this particular case, it is not possible to build an avalanche retention dam to protect the village due to lack of space at the base of the avalanche slope. In addition, there are snow bridges below that must be protected. It is necessary, therefore, to replace the most strongly damaged structures (rows 5 and 6) as soon as possible and to use floating foundations rather than fixed ones under the supports. In addition, permafrost-specific construction methods must be used (Margreth 2007). It is advisable to continue monitoring ground temperature, slope deformation and the position of the snow nets in order to determine the effects of short- and long-term climate fluctuations on the stability and service life of the structures. The state of the snow nets on the study site is surprisingly good in view of the difficult conditions; rigid steel snow bridges would probably have had much more severe damages and an even shorter service life.

Acknowledgments

The authors would like to thank the Swiss Canton Valais for the financial support of the project and in particular Charly Wuilloud, Head of Natural Hazards in Valais and Leo Jörger, mayor of Randa. Klaus Aufdenblatten and his team carried out the surveys of the snow nets, and Herman Rovina and Damian Gitz carried out the borehole inclinometer measurements—all under difficult terrain conditions, for which they are sincerely thanked. Christian Bommer and two anonymous reviewers provided useful comments.

References

Burn, C.R. 1998. The active layer: two contrasting definitions. *Permafrost and Periglacial Processes* 9: 411-416.

Gruber, S., Hoelzle, M. & Haeberli, W. 2004. Permafrost thaw and destabilization of Alpine rock walls in the hot summer of 2003. *Geophys. Res. Lett*. 31 (L13504): 1-4.

Gruber, S. & Haeberli, W. 2007. Permafrost in steep bedrock slopes and its temperature-related destabilization following climate change. *Journal of Geophysical Research* 112, F02S18, doi:10.1029/2006JF000547.

Haeberli, W. 1992. Construction, environmental problems and natural hazards in periglacial mountain belts. *Permafrost and Periglacial Processes* 3: 111-124.

Harris, C., Davies, M. & Etzelmüller, B. 2001. The assessment of potential geotechnical hazards associated with mountain permafrost in a warming global climate. *Permafrost and Periglacial Processes* 12: 145-156.

Keller, F. 1995. *Permafrost in Lawinenanrisszonen. Bericht über BTS-Messungen zur Kartierung von Permafrost in Lawinenanrisszonen*, Report 500.7.

Margreth, S. 2007. *Defense structures in avalanche starting zones*. Technical Guideline as an aid to enforcement. FOEN, SLF, Bern and Davos.

Marty, C., Phillips, M. & Lehning, M. 2007. Klimaänderung und Naturgefahren. *Bündner Wald* 60(3): 35-42.

MeteoSchweiz (annual reports). *Witterungsberichte*.

North, N., Kljun, N., Kasser, F., Heldstab, J., Maibach, M., Reutimann, J. & Guyer, M. 2007. *Klimaänderung in der Schweiz. Indikatoren zu Ursachen, Auswirkungen, Massnahmen*. Report Umwelt Zustand Nr. 0728, Bern.

Phillips, M., Margreth, S. & Ammann, W. 2003. Creep of snow-supporting structures in alpine permafrost. *Proceedings of the Eighth International Conference on Permafrost, Balkema July 21-25*: 891-896.

Phillips, M. 2006. Avalanche defence strategies and monitoring of two sites in mountain permafrost terrain, Pontresina, Eastern Swiss Alps. *Natural Hazards* 39: 353-379.

Phillips, M., Ladner, F., Muller, M., Sambeth, U., Sorg, J. & Teysseire, P. 2007. Monitoring and reconstruction of a chairlift midway station in creeping permafrost terrain, Grachen, Swiss Alps. *Cold Regions Science and Technology*.

A Selection of papers presented at the International Snow Science Workshop, Jackson Hole, Wyoming, September 19-24, 2004, 47(1-2): 32-42.

Rist, A. 2007 (in press). *Hydrothermal processes within the active layer above alpine permafrost in steep scree slopes and their influence on slope stability*. PhD Thesis, Swiss Federal Institute for Snow and Avalanche Research SLF and University of Zurich.

Springman, S.M., Jommi, C. & Teysseire, P. 2003. Instabilities on moraine slopes induced by loss of suction: a case history. *Geotechnique* 53: 3-10.

Steiner, W., Graber, U. & Keusen, H.-R. 1996. Construction in rock at 3550 meters elevation (Jungfraujoch, Switzerland), In: G. Barla (ed.), *Eurock 96*. Torino, Italy: A.A. Balkema, 543-550.

Stoffel, L. 1995. *Bautechnische Grundlagen für das Erstellen von Lawinenverbauungen im alpinen Permafrost*. SLF, Davos.

Vonder Mühll, D. & Keusen, H.-R. 1995. Bauen auf kriechendem Eis. *Schweizerische Technische Zeitschrift* 10: 45-48.

Classification of Arctic Tundra Soils Along the Beaufort Sea Coast, Alaska

C.L Ping, L.A. Lynn, G.J. Michaelson
Palmer Research Center, Agricultural & Forestry Experiment Station, University of Alaska Fairbanks, Palmer, AK
M.T. Jorgenson
Alaska Biological Research, Inc., Fairbanks, AK
Y.L. Shur, M. Kanevskiy
Department of Civil & Environmental Engineering, University of Alaska Fairbanks, Fairbanks, AK

Abstract

The Study of Northern Alaska Coastal Systems project provided the opportunity to examine cryogenic soils and permafrost features using exposed bluffs along the coastline. More than 50 study sites were selected along the 1,957 km coastline of the Beaufort Sea. The soil exposures that were sampled represent the soils and permafrost in similar landforms with similar microtopography and permafrost features 20–50 miles inland. Nearly all the soil profiles described along the exposed bluffs and drilled cores from deltas were classified in the Histel, Turbel, and Orthel suborders of the Gelisol order. The presence and depth of ice wedges, cryturbation features, gleyed horizons, and the abundance of organic matter differentiated the soils into great groups and subgroups. Soil morphological features suggest the multigenic origin of soil carbon. Classification of soils associated with different microtopography will facilitate soil mapping on the Arctic Coastal Plain.

Keywords: arctic tundra; coastal erosion; Gelisols; soil classification.

Introduction

A soils map is an important tool needed for land resource management. A detailed soils map is greatly needed for ecosystem/land management, land-based research, and most recently, accurate estimation of terrestrial carbon stock and other major and minor nutrients levels. The currently existing soils map of arctic Alaska was based on an exploratory survey (Reiger 1979) and was mapped at a scale of 1:1,000,000, much too crude for site-specific resource management. Thus, the National Cooperative Soil Survey in Alaska is planning a soil project for arctic Alaska which involves the cooperation and partnership of federal and state, the University of Alaska Fairbanks and all other interested parties. Most soils in the arctic tundra are cryoturbated. To correctly describe and classify the soils it is necessary to observe the soil profile under the whole cycle of patterned ground (Agriculture Canada Expert Committee on Soil Survey 1998, Kimble et al. 1993). However, based on past experience (Ping et al. 1998), soil inventory in the permafrost regions is time consuming and usually limited to shallow depths due to logistical limitations. Because of the nearly flat or very gentle slopes of the Arctic Coastal Plain (Brown & Kreig 1983), the landforms at different segments of the coast extend inland for 10s of km. Thus, the soils information gained from the coastal bluffs can be extrapolated to similar landforms inland.

The study of arctic coastal erosion and the fate and transformation of soil carbon, which is a component of the Study of Northern Alaska Coastal Systems (Jorgenson et al. 2005), provided pedologists with the opportunity to study the soils on wide and deep coastal exposures along the Beaufort Sea coast. The project was designed to study the carbon flux and transformation and material transfer across the land-sea boundary across 1,957 km of coastline of the Beaufort Sea (Jorgenson & Brown 2005, Jorgenson et al. 2005).

Along the Beaufort Sea coast, there are five types of coastal exposure identified by Jorgenson & Brown (2005): deep bays and inlets, deltas, exposed bluffs, lagoons, and tapped basins. Deep bay and inlets are composed of ice-rich marine silt and are most common in the western portion of the coast. The landforms resulted from coalescence of large lakes and subsequent flooding during sea level rise in mid-late Holocene. The bluff heights are 2–3 m. Large and small deltas are found across the Beaufort Sea coast. Exposed bluffs occur primarily along the western and eastern portion of the study area. Bluff heights range from 2–4 m. The reworked marine silt of early Holocene to late Pleistocene on the western part is ice-rich, about 20% ice wedges by volume. The late Pleistocene sand deposit in the middle part is ice-poor. Lagoons are bordered seaward by barrier islands, thus the erosion rates are lowest among the above-mentioned coastal types. The lagoons have the same exposures as that of the exposed bluffs. Tapped basins occur in ice-rich marine silt in the western portion of the coast. This type is characterized by large thaw lakes with raised ridges between them. Ice wedge contents increase with age up to 20% in older surfaces.

Methods

A total of 50 extensive study sites were systematically distributed along the 1,957 km of Beaufort Sea mainland coast. The sites included all five coastal types. At each site, geomorphic characteristics, surface cryogenic features, shoreline morphology, and land cover types were recorded. A vertical face along the coastal bluffs was cleaned to expose the soil profile and the ground ice stratigraphy. At

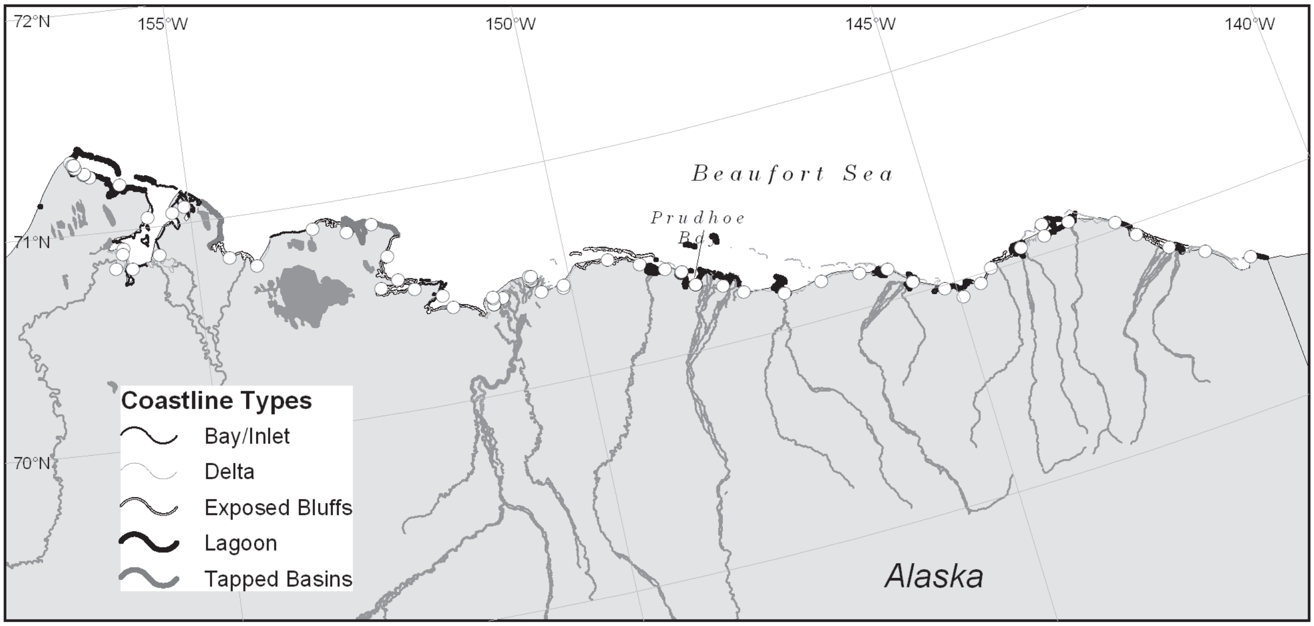

Figure 1. Five types of coastal exposure along the Beaufort Sea Coast.

sites along the thawed lake sequence, which were nearly all sea-level deltas, soil pits were excavated to the top of seasonal frost then a 7.5 cm diameter SIPRE core was used to drill the frozen cores, usually to 2 m. Geomorphic units were classified according to standard engineering geology terminology developed for Alaska. Soil morphological properties were described according to Schoeneberger et al. (1988) and soil classification according to Soil Survey Staff (2006). Ground ice structure and cryogenic features were described based on Shur & Jorgenson (1998).

Result and Discussion

Morphology and classification

The patterned ground type, cryogenic process involved, and soil classification of the study sites were summarized in Table 1. The deep bay/inlet coast type has mixed surface morphology of tapped basin and lagoon, but with fewer ice wedges (<20%). Thus there are both low- and high-centered polygons and thaw lake sequences. Ruptic Histoturbels and Typic Aquiturbels dominate the high-centered polygons with frost boils, Typic Histoturbels and Histic Aquiturbels dominate the low-centered polygons, whereas Fibric Glacistels and Glacic Historthels dominate the very poorly drained troughs between polygons.

In newly formed river deltas, the permafrost table is generally below 1 m and there are no diagnostic horizons with little or no cryoturbated features. Since these soils were frequently inundated by tidal or flooding waters, they were classified in the Aquic suborder of Entisols, i.e., Aquents. The mean annual soil temperature (MAST) at 50 cm was estimated to be below freezing; thus all soils found in recently formed deltas are Typic Gelaquents. However, where the deltas were vegetated with mostly sedges, and the deltas become estuaries, the repeated inundation and deposition of fine textured minerals on the vegetation mat caused repeated burial of thin vegetation layers. In addition, there were large areas of deltas and estuaries with sulfur-rich fluvial deposits. The surface had patches of bare ground with a thin crust of rusty red color over black mud, indicative of quick oxidation of ferrous Fe. These soils had subsurface horizons rich in iron sulfite (pyrite), which has a characteristic color of 4/N according to the Munsell Color Chart. They keyed out as Sulfuric Aquorthels. Those soils had stratified organic and reduced mineral horizons, a combined thickness of organic horizons generally greater then 6 cm within the top 50 cm, a permafrost table within 1 m, lacked cryoturbation, and were keyed out as Fluvaquentic Historthel. Both the Sulfuric and the Fluvaquentic Historthels had strong H_2S odor when the pits were opened.

Exposed bluffs and lagoon coastal types have similar morphology except the prevalence to the open ocean. In the eastern and western portions of the coast, high bluffs contained massive ice wedges occupying more than 20% of the exposed face. The surface of these coastal types is characterized by flat polygons and high-centered polygons dotted with frost boils. The troughs between the polygons were wide, generally 3–4 m due to deterioration of the underlying ice wedges. The ice wedges were usually within 1 m of the surface; thus the soils were classified as Sapric Glacistels and Glacic Histoturbels. Soils formed in the high-centered polygons were highly cryoturbated, and the continuity of the surface organic horizons were interrupted by frost boils; Ruptic-Histic Aquiturbels become the dominant soil type. In the flat polygons, Typic Histoturbels were the dominant soil type. In the ice-poor sand sheet in the mid-coastal zone, there was less cryoturbation, existing only at the margin of the polygons. The drainage in this area was moderately well to somewhat poor and the soils contained dark organic-rich mineral surface horizons; thus the dominant soil types were Aquic Molliorthels.

Table 1. Coastal type, patterned ground, cryogenesis, and soil classification of selected studied sites along the Beaufort Sea coast.

Coast type/ Site #	Patterned ground	Thcickness OM in top 50 cm	Cryogenic processes	Glacic (Wf) horizon , cm	Degree of cryoturbation	Thaw depth, cm	Soil classification
Bay/Inlet							
BSC-2	High-center polygon/ frost boils	9	Small ice wedge, Ojj, O/Bgjj	not present	High	38	Histic Aquiturbels
BSC-4	flat polygon/ polygon rim	19	Ice lens, ataxitic structure, Ojj, O/Bgjj	not present	high	44	Ruptic Histoturbels
Delta							
BSC -	River delta	0	not present	none	none	>100	Typic Gelaquents
BSC-37	Coastal marsh	24	not present	none	minimal	71	Typic Historthels
CAHA-T1-02	Estuary	12	ice lens, ice wedge, microataxitic	39-182 cm	medium	39	Glacic Aquorthels
Exposed bluff							
BSC-22	Flat polygon, deep trough	23	Ice lens, reticulate structure, Oe/Bgjj,Oajj	not present	high	42	Typic Histoturbels
BSC-36	Low-center polygon	90	Ice wedge, ice lens	76	low	43	Fibric Glacistels
Lagoon							
BSC-25	high-center polygon	8	hummocky surface, frsot cracks	Not present	low	49	Aquic Molliturbels
BSC-40	flat polygon/frsot boil	6 - 26	Oe/Bgjj, Oejj, Oa/Cgjj	not present	high	45	Ruptic Histoturbels
			highly cryoturbated	60	medium	50	Glacic Histoturbels
ELS-3	flat polygon	7	horizon, Oa/Bgjj	not present	minimal	28	Typic Historthels
			Ice lens,				
Taped Basin							
CAHA-T1-05	Flat basin floor	14	Cryogenic fabrics, Oa/Bg	not present	high	26	Typic Histoturbels
CAHA-T1-06	low-center polygon	47	Ice belt, reticulate fabric	39-44, 47-49	low	34	Typic Sapristels
CAHA-T1-08	flat sedge meadow	6	Ice lens, ice belt	Not present	minimal	55	Typic Aquorthels
CAHA-T1-09	high-center polygon/ frost boil	27	Ice wedge, Oa/Bgjj, Oejj	90	high	51	Glacic Histoturbels
CAHA-T1-E4	high-center polygon polygon trough	40	Ice wedge, Bgjj, Oa/Bgjj	40	high	38	Hemic Glacistels

In the tapped basin/thaw lake basins, a microtoposequence formed following the lake draining. In the recently drained lake beds, there was a continuous organic horizon under sedge vegetation that was generally more than 14 cm thick over stratified reduced mineral and organic horizons. They lacked cryoturbation. Most of these soils have ice wedges or ground ice within 1 m and thus keyed out as Glacic Historthels. Soils without a glacic horizon within 1 m keyed out as Typic Historthels. Where the surface-organic layer was thin the soils keyed out as Ruptic-Histic Aquorthels and Glacic Aquorthels. Toward the slightly elevated edge of the drained-lake basin flat-polygons formed which have observable cryoturbation around 20–40 cm. These soils had thin organic horizons and some have ice wedges within 1 m, and thus keyed out as Typic Aquiturbels and Glacic Aquiturbels, respectively. Between the drained lakes there were raised broad ridges with high-centered polygons formed from ice wedge deterioration in the troughs. There was a high degree of cryoturbation under the polygon center in that the surface organic layers were broken and the underlying reduced mineral horizons were mixed with cryoturbated organics (Bg/Ojj or Ojj/Bg). Thus, these soils keyed out as Ruptic-Histic Aquiturbels. Glacic Aquiturbels appear as a minor component in this microtopography. In the troughs, the thick organic horizon sits on top of ice wedges, and thus the soils keyed out as Fibric Glacistels.

Mode of carbon accumulation

The arctic tundra soils are known to accumulate and sequester organic carbon (Michaelson et al. 1996). In most soils examined in the five coastal types, cryturbation was prevalent throughout most landform types except deltas. In the deltas, organic carbon accumulated through burial by fluvial sedimentation by the rivers. Organic horizons only formed after the establishment of sedge marsh vegetation.

In the tapped basins, organic carbon accumulated when marsh vegetation grows in the drained-lake basins, followed by mixing and burial from bank erosion/collapsing and flooding. Once the lakes were drained and the land surface was raised due to ice wedge formation, there was increased cryoturbation evident that churned the surface organic matter down into the lower active layer and upper permafrost. Carbon sequestration reached the maximum in the high-center polygons formed in between the drained lakes due the increased surface age and cryoturbation. In the exposed bluffs and lagoons, carbon accumulated and was sequestered through two main mechanisms. First, through the commonly known near-surface cryoturbation associated with patterned-ground formation that churns surface organic matter generally within the top 1 m. (Bockheim et al. 1998, Ping et al. 1998, 2008). Second, this field investigation found that ice wedge formation also plays an important role in carbon sequestration because the pressure from the expanding ice wedge deforms the surface organic matter down as far as 3 m deep, as seen in both sites 2 and 40.

Summary

In landforms dominated by high-centered polygons, Ruptic Histoturbels and Typic Histoturbels are the main soil types with Histic Aquiturbels and Glacic Histoturbels as minor components. In landforms dominated by flat and low-centered polygons, Typic Histoturbels and Typic Historthels are the main soil types with Glacic Historthels as minor components. In landforms dominated by thaw lake basins, Typic Historthels and Glacic Aquorthels are the main soil types and Ruptic Histurbels and Glacistels are minor components. In deltas, Typic Aquorthels and Typic Historthels are the dominant soil types with Glacic and Sulfuric Historthels as minor components. As found in this study, soil types were more related to microtopography rather than the physiographic classification of the coastal types, with the exception of delta. Also found in this study, organic-carbon accumulation and sequestration in arctic Alaska as examined from the exposed Beaufort Sea coast are multigenic and not just the result of cryoturbation.

Acknowledgments

This study was supported by National Science Foundation Arctic System Science Program, Collaborative Research: Flux and transformation of organic carbon across the eroding coastline of northern Alaska (NSF-0436179).

References

Agriculture Canada Expert Committee on Soil Survey. 1998. *The Canadian System of Soil Classification, Third Edition.* Ottawa: NRC Research Press.

Bockheim, J.G., Walker, D.A., Everett, L.R., Nelson, F.E. & Shiklomanov, N.I. 1998. Soils and cryoturbation in moist nonacidic and acidic tundra in the Kuparuk River Basin, arctic Alaska, U.S.A. *Arc. Alp. Res*. 30: 166-174.

Brown, J. & Kreig, R.A. 1983. Elliott and Dalton Highway, Fox to Prudhoe Bay, Alaska. In: *Guidebook 4: Guidebook to Permafrost and Related Features.* Fairbanks: Alaska Div. of Geol. and Geophys. Surv., 230pp.

Jorgenson, M.T. & Brown, J. 2005. Classification of the Alaskan Beaufort Sea coast and estimation of carbon and sediment inputs from coastal erosion. *Geo-Mar Lett.* 25: 69-80.

Jorgenson, M. T., Ping, C.L., Guo, L., Shur Y. & Brown, J. 2005. A multi-scale approach to assessing the flux and transformation of organic carbon across the eroding coastline of northern Alaska. *Berichte Zur Polarund Meeresforschung* 506: 65-68.

Kimble, J.M., Tarnocai, C., Ping, C.L., Ahrens, R., Smith, C.A.S., Moore, J. & Lynn, W. 1993. Determination of the amount of carbon in highly cryoturbated soils. In: D.A. Gilichinsky (ed.), *Post-Seminar Proceedings of the Joint Russian-American Seminar on Cryopedology and Global Change, Pushchino, Russia, 15-16 Nov. 1992.* Pushchino, Russia: Russian Academy of Science.

Michaelson, G.J., Ping, C.L. & Kimble, J.M. 1996. Carbon storage and distribution in tundra soils of arctic Alaska, U.S.A. *Arctic and Alpine Research* 28(4): 414-424.

Ping, C.L., Bockheim, J.G., Kimble, J.M., Michaelson, G.J. &. Walker, D.A. 1998. Characteristics of cryogenic soils along a latitudinal transect in arctic Alaska. *Journal of Geophysical Research* 103(D22): 28,917-28,928.

Ping, C.L., Michaelson, G.J., Jorgenson, M.T., Kimble, J.M., Epstein, H., Romanovsky, V.E. & Walker, D.A. 2008. High stocks of organic carbon in North American arctic region. *Nature Geoscience* (in review).

Rieger, S., Schoephorster, D.B. & Furbush, C.E. 1979. *Exploratory Soil Survey of Alaska.* Washington, D.C.: U.S. Dept. of Agriculture, Soil Conservation Service, U.S. Government Printing Office.

Schoeneberger, P.J., Wysocki, D.A., Benham, E.C. & Broderson, W.D. 1998. *Field Book for Describing and Sampling Soils*. Lincoln, Nebraska: Natural Resources Conservation Service, USDA, National Soil Survey Center.

Shur, Y. & Jorgenson, M.T. 1998. Cryostructure development on the floodplain of the Colville River delta, northern Alaska. In: A.G. Lewkowicz & M. Allard (eds.), *Proceedings Seventh International Conference on Permafrost, Yellowknife, Canada*. Universite Laval. Nordicana 57: 993-999.

Soil Survey Staff 2006. *Keys to Soil Taxonomy, 10th edition.* Washington, D.C.: USDA Natural Resources Conservation Service.

Thermal Diffusivity Variability in Alpine Permafrost Rock Walls

P. Pogliotti
GEOSITLAB, Department of Earth Sciences, University of Turin, Italy
ARPA Valle d'Aosta, Climate Change Div., Aosta, Italy
E. Cremonese
ARPA Valle d'Aosta, Climate Change Div., Aosta, Italy
U. Morra di Cella
ARPA Valle d'Aosta, Climate Change Div., Aosta, Italy
S. Gruber
Glaciology and Geomorphodynamics Group, Department of Geography, University of Zurich, Switzerland
M. Giardino
GEOSITLAB, Department of Earth Sciences, University of Turin, Italy

Abstract

Permafrost degradation has been hypothesized as being one of the main causes of rockfalls and rock wall instability in the recent past in high mountain areas. Ongoing rock wall permafrost evolution remains poorly understood because of the lack of systematic measurements; models are often validated and driven by few existing instrumented sites. In rock wall subsurface temperature modeling, thermal diffusivity (κ) is one of the main parameters to be considered. In this study, thermal diffusivity data series were inferred from rock temperature data in order to understand their annual variation, their distribution in different temperature ranges, and their relation to atmospheric conditions. A harmonic analysis was performed to define amplitude and phase of the daily temperature waves at different depths by means of a least square minimizing optimization procedure. The analysis conducted shows that changes in κ values are influenced by different factors such as depth, season, rock temperature, aspect, and snowfall.

Keywords: rock wall temperature; thermal diffusivity.

Introduction

Steep bedrock slopes in high mountain areas are subjected to permafrost action. During the very hot summer of 2003, many rockfalls occurred in the European Alps, and sometimes massive ice was visible in the exposed detachment zone (Gruber et al. 2004b). These observations suggest that permafrost degradation may be one of the main causes of rock wall instability observed in recent years in high mountain areas (Dramis et al. 1995, Noetzli et al. 2003, Gruber et al. 2004a).

Thawing and degradation of rock wall permafrost is very fast if compared to permafrost in gentle morphology because of the lesser amount of ice content and the absence of a debris insulation layer (Gruber et al. 2004b); moreover, steep bedrock morphologies are abundant in many cold mountain regions and contain a significant proportion of permafrost (Gruber & Haeberli 2007).

Present and future global warming (IPCC 2007) will likely lead to a significant increase in frequency and intensity of rockfall events caused by variations in rock wall thermal regimes (Davies et al. 2001). Consequently, its degradation is spatially a widespread problem (Gruber & Haeberli 2007) which causes an increment in risks for people and infrastructures in high mountain areas (Harris et al. 2001).

In order to obtain a better understanding of rockfall trigger mechanisms and processes linking slopes warming and their local destabilization, an increase in knowledge on rock wall temperature regimes and their evolution is very important (Gruber & Haeberli 2007). Quantitative understanding and models of surface temperature distribution within steep rock faces in complex topography exist and have been validated with near-surface measurements (Gruber & Hoelzle 2001, Gruber 2005). However, many questions about active layer and sub-surface rock wall permafrost evolution remains poorly understood because of the lack of deeper systematic measurements and models.

In purely diffusive and stationary state models, thermal diffusivity is considered the only petrophysical parameter of importance (Yershov 1998), and in permafrost modeling, it is often considered as constant. Nevertheless, the continuous variability of water content linked to environmental conditions (Saas 2005), together with the latent heat effect associated with thawing and freezing (Mottaghy & Rath 2006), may cause great variability in thermal diffusivity in the active layer. These mechanisms may affect deeper temperature regimes and cause a probable "thermal offset" (Gruber & Haeberli 2007) between the rock surface and the top of permafrost.

The main purpose of this work is to evaluate the annual course of thermal diffusivity on some alpine permafrost rock walls and its variability related to environmental conditions. Using rock wall temperature data series measured at different depths of the active layer, a harmonic analysis was used to define amplitude and phase of daily temperature waves by means of a least square minimization procedure. Optimized amplitude values at each depth were used to obtain hourly data of rock thermal diffusivity κ. These data series were analysed in order to understand their annual variation, their distribution in different temperature ranges, and their relation to atmospheric conditions inferred from in situ meteorological collected data.

Research Strategy

Field measurements

All data series were collected within the international project PERMAdataROC started in March 2006, during which several measurement sites were equipped on high steep slopes in six different areas in the western European Alps. For this study, two of the six areas were selected because they are characterized by long data series and by a higher number of measured variables. One is the SW ridge of the Matterhorn, and the other is the peak of the Aiguille du Midì in the Mont Blanc massif (Fig. 1).

In each area the measured variables are: rock wall temperature at depths of 3, 30, and 55 cm; air temperature and relative humidity (10 cm from the rock surface); and solar radiation, wind speed, and wind direction, measured by means of an automatic weather station (MAWS), installed on the rock wall with sensors parallel to the rock surface (Table 1).

Measurements started in November 2005 at the Matterhorn site, and at the end of December 2006 at the Aiguille du Midì site. For this study, a total of eight data series were used; data series characteristics are shown in Table 2.

In order to identify snow events, daily albedo values were calculated from radiation data, and a snow index (S_i) was defined as the ratio between daily and mean albedo: snow index values greater than 1.25 are caused by snow events. Since some problems in snow index definition may occur, mainly in winter due to snow deposition on MAWS's sensors during snowfalls events, sonic anemometer, air temperature, and humidity data series were also used as further confirmation of snow events.

Table 1. Instrumentation

Parameter	Instrument	Log. interval
Rock temp.	Geoprecision - M-Log 6	60 min
Air temp. & hum.	Geoprecision - M-Log 5	60 min
Radiation	Kipp&Zonen - CNR-1	10 min
Wind	Vaisala - WMT50	10 min

Thermal diffusivity evaluation

Rock temperature data were used for thermal diffusivity evaluation. Signal detrending using running-mean was performed on rock temperature data series in order to remove low frequency oscillations as seasonal and annual ones. Assuming that temperature variation at any depth is sinusoidal, the thermal diffusivity of rock, κ ($m^2\ s^{-1}$), can be calculated with the following equation (1) (Matsuoka 1993):

$$\kappa = \frac{\pi}{P}\left[\frac{Z_1 - Z_2}{\ln(A_1 / A_2)}\right]^2 \tag{1}$$

where P is the period of one complete harmonic oscillation (24 hours) given in seconds, A_1 and A_2 are the amplitude of temperature waves (°C) at depth Z_1 (i.e., 0.03 m) and Z_2 (i.e., 0.3 m).

A harmonic analysis of rock temperature data was performed to define amplitude A_1 and A_2 of daily temperature waves at different depths using the following equation which describes a general harmonic oscillation:

$$T_{(z,t)} = A_{(z)} \sin(\omega t + \phi) \tag{2}$$

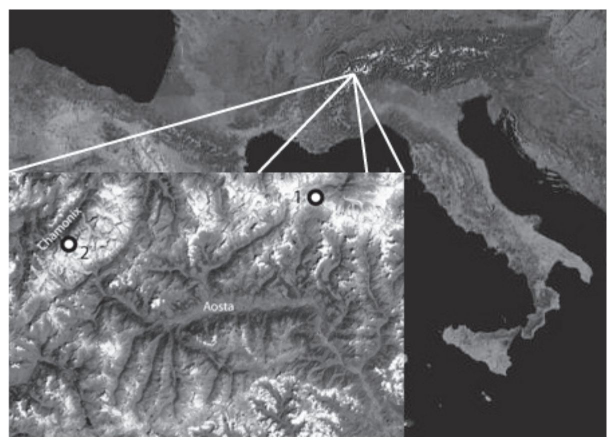

Figure 1. Research site localization. 1: Matterhorn. 2: Aiguille du Midì.

Table 2. Data series characteristics

Site	Series name	Aspect	Elevation (m a.s.l.)	Length (days)	Season	Mean rock temp. (°C) -55cm	-30cm	-3cm
Matterhorn	CCS_Tr	N158-90	3820	126	sum	3.12	3.70	4.14
	CCS_Ta	N158-90	3820	126	sum			
	CCS_Rad	N158-90	3820	370	sum			
	CHEM_Tr	N180-90	3750	744	win-sum	0.58	0.90	1.28
Aig. du Midì	ADMS_Tr	N160-85	3820	209	win-sum	0.56	0.98	1.05
	ADMN_Tr	N335-80	3825	209	win-sum	-7.20	-7.16	-7.03
	ADMS_Ta	N160-85	3820	209	win-sum			
	ADMS_Rad	N160-85	3820	209	win-sum			

Abbreviations: Tr: rock temperature; Ta: air temperature and relative humidity; Rad: solar radiation.
Lithology: Matterhorn, gneiss; Aiguille du Midì, granite.

Table 3. Mean values and standard deviations of κ data series at Cheminèe site (Matterhorn).

Depth interval	Entire series		Warm Period		Cold Period	
	κ mean	standard deviation	κ mean	standard deviation	κ mean	standard deviation
(cm)	$x10^{-6}$ (m^2 s^{-1})	$x10^{-6}$ (m^2 s^{-1})	$x10^{-6}$ (m^2 s^{-1})	$x10^{-6}$ (m^2 s^{-1})	$x10^{-6}$ (m^2 s^{-1})	$x10^{-6}$ (m^2 s^{-1})
3 - 30	2.401	0.175	2.505	0.189	2.298	0.065
30 - 55	1.524	0.041	1.517	0.029	1.530	0.050
3 - 55	1.898	0.072	1.932	0.077	1.865	0.048

Warm period: summary of all springs and summers; cold period: summary of all autumns and winters.

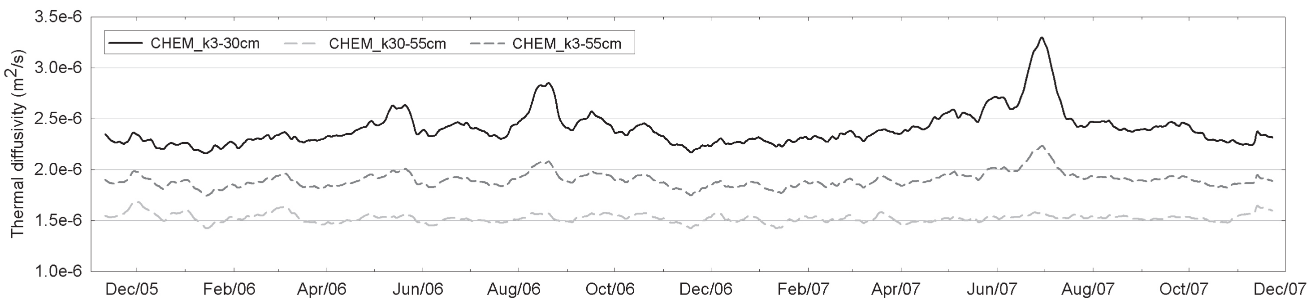

Figure 2. Annual course of computed thermal diffusivity at the Cheminèe site (Matterhorn) smoothed over 15 days.

where ω is the angular frequency of the oscillation (i.e, for daily cycles ω=(2π/24) h^{-1}), $A_{(z)}$ is the amplitude of temperature oscillation at depth z, and Φ is the phase angle.

A least-square minimization procedure was applied using equation 2 in order to obtain estimates of unknown parameters A(z) and Φ. A(z) is the parameter chosen for thermal diffusivity evaluation. Amplitude values at different depths were used in equation 1 to obtain hourly data of rock thermal diffusivity κ. As rock temperature data at three different depths were available, three different couples of amplitude data series were used: 3÷30cm, 30÷55cm, and 3÷55cm. The fitting procedure was computed on every series using a three-day running-window, moving with an hourly step. The standard error of computed thermal diffusivity values was evaluated using a bootstrap resampling technique. In the bootstrap procedure, the original dataset is randomly resampled N times (in this study N=500); in this way, for each hourly step, 500 synthetic thermal diffusivity datasets were generated. Instead, as described in Efron and Tbshirani (1993), the standard deviation of the distribution of these 500 values is a good measure of the parameter's standard error. The parameter standard error was used as an indicator of the reliability of amplitude values. Finally, the resulting thermal diffusivity data series was smoothed with a median filter of three hour's width, to avoid rapid fluctuations.

Results and Discussion

Annual course of thermal diffusivity

In order to show the annual variations in thermal diffusivity at each depth, the longer available data series (CHEM) is considered in Figure 2. Table 3 shows mean values of κ and standard errors of the whole data series and for cold (autumn plus winter) and warm (spring plus summer) periods.

The first 30 cm of rock show a mean value of about 2.4×10^{-6} m^2s^{-1} and great annual variability, with values generally below the mean during the cold season, and above the mean during the warm season. This observed variability decreases with depth: oscillations of deeper thermal conductivity data series are strongly reduced, and the seasonal behaviour underlined for the shallower rock layer cannot be seen. These differences are probably due to the different variability in water content during the year: greater in the first centimetres of rock and lesser at depth. Moreover, mean κ values of 30–55cm depth interval are significantly reduced, probably because of the different degree of saturation in comparison to the shallower rock layer.

To gain an understanding of the reliability of the diffusivity values presented, laboratory measurements of thermal conductivity were performed on gneiss samples collected at the Matterhorn study site. The results give a mean value of thermal conductivity equal to 2.7 $Wm^{-1}K^{-1}$. Using a mean tabled value of volumetric heat capacity for granitic rock equal to 1.75×10^6 $Jm^{-3}K^{-1}$ (Yershov 1998), the resulting value of thermal diffusivity is 1.54×10^{-6} m^2 s^{-1}, a value which is very similar to the mean of the whole series calculated for the 30–55cm depth interval (1.52×10^{-6} m^2 s^{-1}).

These results seem to suggest that significant differences in thermal diffusivity values can be obtained by considering the first centimetres rather than the deeper rock layers. This matter should be taken into account when thermal diffusivity values are applied to heat conduction models for the projection in depth of rock wall temperature.

Distribution of κ values in different rock temperature ranges

Figure 3 show the distribution of 3–55cm thermal diffusivity values above and below 0°C both at the north and south Aiguille du Midì sites.

The 30 cm depth data series was used as the rock temperature reference at each site. In the period considered, on the northern site only 10% of rock temperature data were

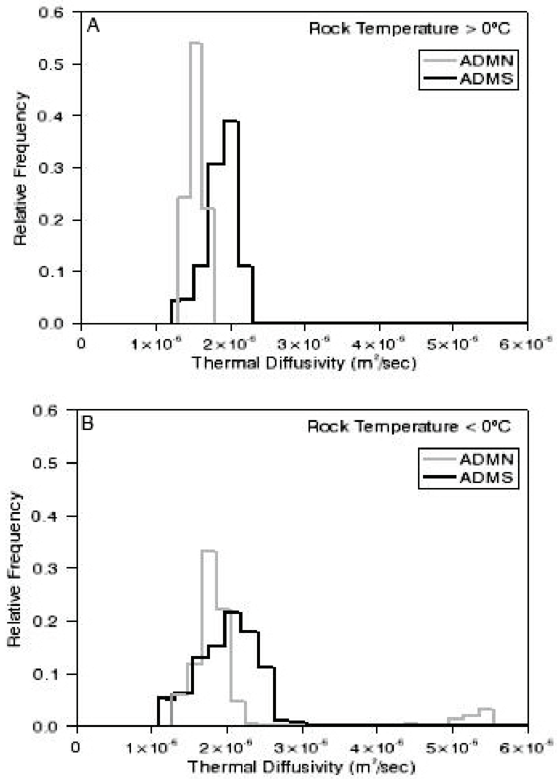

Figure 3. Distribution of thermal diffusivity values (3–55cm depth interval) below and above 0°C at ADM northern and southern sites.

above 0°C, whereas in the south, this proportion was around 50%. Moreover, minimum north and south values were -17.97°C and -14.06°C respectively, while the maxima were 3.97°C and 16.4°C, respectively.

The histograms in Figure 3 show the effect of rock wall aspect and different conditions on thermal diffusivity.

Regarding aspect, the northern site showed values lower than the southern one and less dispersed around the mean. Lower values suggest that northern exposures may be more saturated than southern exposures, as indicated in previous studies (Saas 2005). On both aspects, κ values are generally greater below 0°C; this is probably due to the substitution of water by ice in the pore space and fractures of frozen rock (Williams & Smith 1989).

Thermal diffusivity variations caused by snow events and rock wall temperature

Evaluation of the effect of snow events on thermal diffusivity was conducted by choosing some meaningful summer and winter events in the Matterhorn and Aiguille du Midì data series. Using a smoothed (24-hour) thermal diffusivity normalized deviation index κ_{di} (defined as κ/κ_{mean}), the temporal evolution of the CCS and ADM thermal diffusivity data series was analysed, considering 3–55cm depths.

In the CCS data series, an intense summer snow event (2nd half of August 2006) was considered. As shown in Figure 4, when the snow index increases, κ_{di} decreases (maximum

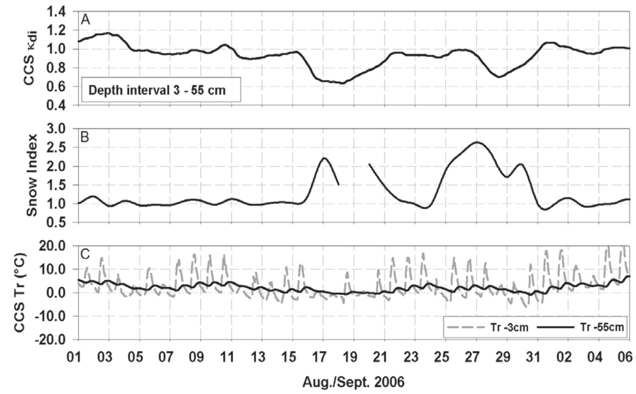

Figure 4. Comparison between CCS thermal diffusivity deviation index, snow index, and rock temperature.

reduction of about 40% of the mean value) and vice-versa: as the S_i starts decreasing κ_{di} rises closer to the mean value. During snowy days, shallower rock (-3 cm) temperature crosses above and below 0°C several times, while the deeper one (-55 cm) is closer to zero. In such a condition, phase changes may occur in the active layer: thus the consumption and release of latent heat due to thawing and freezing of percolating water cause the variation in apparent heat capacity. This variation affects κ which is inversely proportional to apparent heat capacity (Mottaghy & Rath 2006). The decrease in thermal diffusivity shown in Figure 4a during snow events is probably linked to water phase changes.

Similar considerations can arise from the observations of thermal diffusivity data series at ADM northern and southern sites (Fig. 5). During the spring-summer period κ_{di} temporal evolution, and the magnitude of its variation during snow events, are similar to what is observed in CCS data series. The southern face shows thermal diffusivity reduction related to snow events starting from the end of March (Fig. 5c); the same behaviour is observed on the northern side (Fig. 5a) only at the end of spring, when rock temperature rises toward 0°C (Fig. 5b), suggesting a possible role played by rock temperature on water availability.

On the other hand, during winter, κ_{di} variations related to snow events show an opposite behaviour: a strong increase in κ_{di} is observed on both faces, with a general higher intensity on the northern one, where a doubling of thermal diffusivity value occurred.

On the southern face, a strong increase of κ_{di} values, comparable to those in the north, occurred at the end of February. During this event, the southern face rock temperature showed values of about -10°C at the depth of 55 cm: a value closer to annual minima and similar to northern face rock temperature in the same period (-13°C). This means that the thermal conditions of the south wall were very similar to those experienced by a northern wall, suggesting, once again, that rock temperature may influence thermal diffusivity variability. However, further investigations are needed in order to understand the reliability of these winter increases.

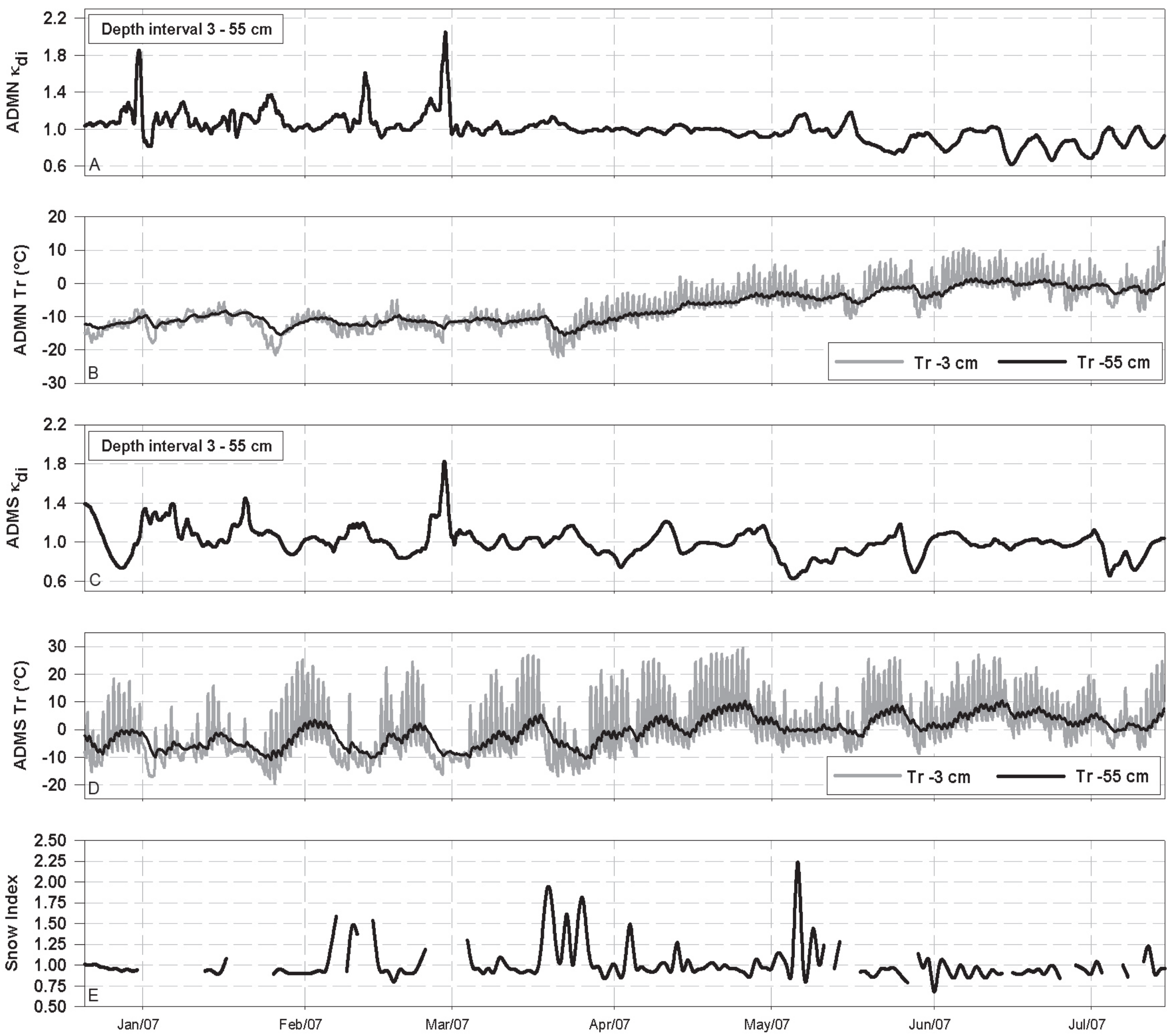

Figure 5. Temporal variation of thermal diffusivity deviation index at Aiguille du Midì northern (A) and southern (C) face. Rock temperature data at Aiguille du Midì north (B) and south (D) at depths of 3 and 55 cm. Snow Index value (S_I) used to identify snow events (E). All data series are smoothed with a 24-hour moving average, with the exception of the Snow Index (daily data).

As outlined in Figure 5d, periods of strong rock wall warming can be followed by thermal diffusivity reductions: κ_{di} variations observed at the end of April on the ADM southern face may have been caused by the previous 10 days of rock temperature above 0°C.

This reduction is more likely related to this rock warming period, rather than to the snow event which occurred during the first days of May, when the κ_{di} reduction had already reached its maximum value. A similar situation can be observed at the end of May. Moreover, on the northern face, a late May κ_{di} reduction occurred when rock temperature was above 0°C (Fig. 5b).

These observations suggest that thermal diffusivity variability may be influenced both by snow events and rock temperature and their interactions. Summer κ_{di} reductions can be explained by an increase in water circulating in the rock heap resulting from snow melting, and from ice-filled discontinuities melting due to warming periods. Winter thermal diffusivity increases, which occur during snow events, appear to be related to cooling intensity rather than to water supply as discussed in Williams & Smith (1989).

Conclusions and Outlook

The analysis conducted in this study leads to the following conclusions:

The estimation of thermal diffusivity variability, from rock temperature data measured at different depths, is possible, and the applied methodology gives reliable values. Changes in thermal diffusivity values are influenced by different factors such as depth, season, rock temperature, aspect, and snowfall. Thermal diffusivity variability decreases with depth, and its mean values in deeper layers are significantly reduced with respect to shallower ones. This should be taken into account when using heat conduction models on the whole rocky heap.

Mean northern κ values are lower than southern ones: this difference may be related to the higher degree of saturation experienced by northern exposures. κ values are greater below 0°C because of the substitution of water by ice in the pore space and fractures of frozen rock.

Reductions in thermal diffusivity related to snow events were observed both on southern and northern faces during warm periods and are probably linked to water phase changes. Winter thermal diffusivity increases, which occur during snow events, appear to be related to cooling intensity rather than to water supply. Thermal diffusivity variations seem to be related to rock temperature, as well: warming periods may result in strong reductions in κ values, likely due to an increase in water circulating in the rock wall.

Such behaviours were observed on both monitoring sites: they, therefore, appear to be independent of system variables such as lithotype, degree of fracturing, and aspect.

In order to test the reliability of these first observations, it is necessary to wait for the results of the PERMAdataROC project: longer data series are needed in order to better understand the behaviour of thermal diffusivity variability.

A first application of computed thermal diffusivity values can be found in energy balance estimation. k values. and rock temperature data at different depths allow calculation of heat conduction which, coupled with net radiation measurements, may allow estimation of the ratio of available energy dissipated through turbulent fluxes. This information may be useful in heat conduction modeling.

References

Davies, M.C.R. Hamza, O. & Harris, C. 2001. The effect of rise in mean annual temperature on the stability of rock slope containing ice-filled discontinuities. *Permafrost Periglac. Process.* 12: 137-144.

Dramis, F. Govi, M. Guglielmin, M. & Mortara, G. 1995. Mountain permafrost and slope instability in the Italian Alps: the Val Pola landslide. *Permafrost Periglac. Process*. 6: 73-82.

Efron, B.B. & Tbshirani, R.J. 1993. *An Introduction of the Bootstrap*. New York: Chapman & Hall.

Gruber, S. & Hoelzle, M. 2001. Statistical modelling of mountain permafrost distribution—local calibration and incorporation of remotely sensed data. *Permafrost and Periglac. Process*. 12: 69-77.

Gruber, S., Hoelzle, M. & Haeberli, W. 2004a. Rock-wall temperature in the Alps: modelling their topographic distribution and regional differences. *Permafrost and Periglac. Process*. 15: 299-307.

Gruber, S., Hoelzle, M. & Haeberli, W. 2004b. Permafrost thaw and destabilization of Alpine rock walls in the hot summer of 2003. *Geophysical Research Letters* 3 1:L13504,doi:10.1029/2004GL020051.

Gruber, S. 2005. *Mountain permafrost: transient spatial modelling , model verification and use of remote sensing*. Ph.D. Thesis. Zurich, Switzerland: University of Zurich, 121 pp.

Gruber, S. & Haeberli, W. 2007. Permafrost in steep bedrock slopes and its temperature-related destabilization following climate change. *J. Geophys. Res*. 112:F02S18, doi:10.1029/2006JF000547.

Harris, C., Davies, M.C.R. & Etzelmüller, B. 2001. The assessment of potential geotechnical hazards associated with mountain permafrost in a warming global climate. *Permafrost and Periglac. Process*. 12(1):145-156.

IPCC. 2007. Summary for Policymakers. In*: Climate Change 2007: The Physical Science Basis. Contribution of Working Group I to the Fourth Assessment Report of the Intergovernmental Panel on Climate Change*. Cambridge, U.K. & N.Y., N.Y.: Cambridge University Press, 18pp.

Matsuoka, N. 1994. Diurnal freeze-thaw depth in rock walls: field measurements and theoretical considerations. *Earth Surf. Process. Landforms* 19: 423-435.

Monteith, J.L. & Unsworth, M. 1990. *Principles of Environmental Physics* (2nd ed). London: Edward Arnold, 307pp.

Mottaghy, D. & Rath, V. 2006. Latent heat effect in subsurface heat transport modeling and their impact on palaeotemperature reconstructions. *Geophys. J. Int.* 164: 236-245.

Noetzli, J., Hoelzle, M. & Haeberli, W. 2003. Mountain permafrost and recent alpine rock-fall events: a GIS-based approach to determine critical factors. *Proceedings of the 8th International Conference on Permafrost, Zurich, Switzerland*: 827-832.

Saas, O. 2005. Rock moisture measurements: techniques, results and implications for weathering. *Earth Surf. Process. Landforms* 30: 359-374.

Williams, P.J. & Smith, M.W. 1989. *Frozen Earth: fundamentals of geocryology*. Cambridge, U.K.: Cambridge University Press, 306 pp.

Yershov, E.D. 1998. *General Geocryology.* Cambridge: Cambridge University Press, 604 pp.

Massive Ground Ice in the Eureka Sound Lowlands, Canadian High Arctic

Wayne H. Pollard, Nicole Couture
Department of Geography, McGill University

Abstract

This paper documents the nature and significance of massive ground ice and thermokarst in the Eureka Sound lowlands in central Ellesmere and Axel Heiberg Islands in the Canadian High Arctic. We characterize the stratigraphic, ice content, and distribution patterns of ground ice, estimate potential thaw, and document recent trends in the rate and pattern of thermokarst. The Eureka area (~80°N) is characterized by cold polar desert conditions (mean air temperature of -19.7ºC) and permafrost up to 600 m thick. A total of 189 natural exposures of massive ice were mapped between 1991 and 2007, including 91 that were active in 2007. Most of these exposures are in the headwall of retrogressive thaw slumps. Repeated surveys of headwall positions have provided both short- and long-term retreat rates. Since 2004 there has been a detectable increase in thermokarst activity, including retrogressive thaw slumps, development of new thaw ponds, and degraded ice wedges.

Keywords: cryostratigraphy; ground ice; High Arctic; polar desert; thermokarst.

Introduction

Ground ice plays a major role in the evolution of landscapes underlain by continuous permafrost. Thawing permafrost, widespread terrain instability and resulting infrastructure problems are often cited as serious problems facing polar regions in response to global warming (ACIA 2005, IPCC 2001). Information about ice content and distribution is extremely variable across the Arctic. For example, there is considerable detailed information about the nature and distribution of ground ice for parts of Siberia (Astakov 1986, Astakov & Isayeva 1988, Streletskaya & Leibman 2003), the Alaskan coastal plain (Lawson 1986), and the western Canadian Arctic (Mackay 1971, 1989, Mackay & Dallimore 1992, Murton & French 1994), but by comparison, ground ice occurrence in the High Arctic has received limited attention (Robinson 1993, 2000, Pollard 1991, 2000a, 200b, Pollard & Bell 1998). Several studies have alluded to increased thermokarst as an outcome of climate change (Lawrence & Slater 2005, Nelson et al. 2001, Zimov et al. 2006). However, little is known about its anticipated pattern or the potential magnitude of thermokarst because it is entirely dependent on information about near-surface ground ice. Detailed information about the active layer is also needed before a realistic prediction about thaw subsidence can be made. Areas where the active layer is relatively thin, like the High Arctic, are more vulnerable to even small increases in summer temperature and the duration of the thaw season because the buffering capacity of the active layer is limited.

This paper documents massive ground ice, ice-rich sediments and thermokarst for the Eureka area in central Ellesmere and Axel Heiberg Islands in the Canadian High Arctic (Fig. 1). Recent data on the nature and distribution of ground ice conditions, ice content, and potential thaw are presented along with observations on the rate and pattern of thermokarst. The objectives of this paper are (i) to describe the nature and distribution of ground ice in the Eureka Sound Lowlands; (ii) to describe permafrost stratigraphy and ice contents, and (iii) to describe current patterns in thermokarst activity in this area. Preliminary findings on massive ice in the Eureka area were presented in Pollard & Bell (1998) and Couture & Pollard (1998), the current paper presents new findings, is based on new data and focuses more on thermokarst.

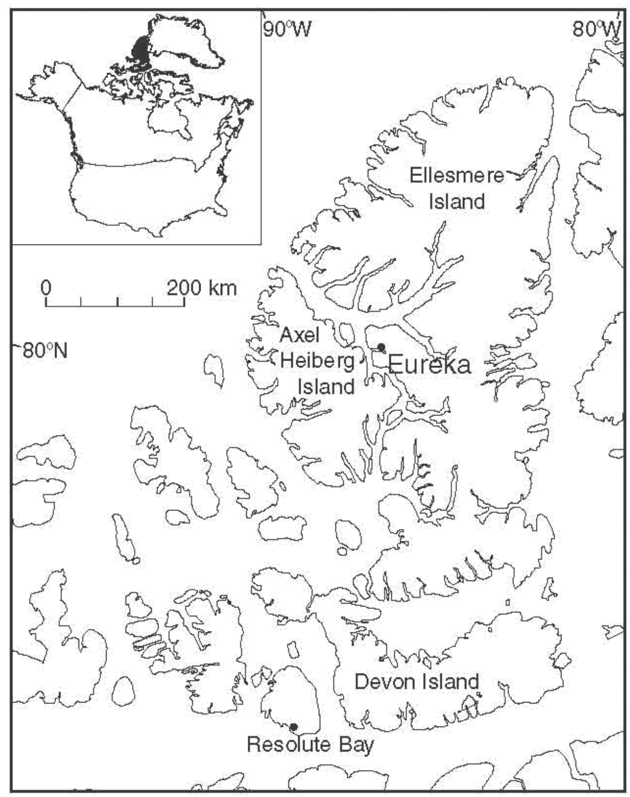

Figure 1. Map showing the location of Eureka in the Eureka Sound lowlands.

Ground ice remains one of the most problematic aspects of permafrost and a major obstacle to development in arctic regions. Knowledge about ground ice, particularly massive ice and ice-rich sediments, is necessary not only to understand the Late Quaternary landscape evolution of this region, but also to assess the potential geomorphic response of the landscape to natural and anthropogenic disturbances of permafrost regimes. Thermokarst and erosion associated with the Eureka weather station and the Panarctic Gemini E-10 well site reflect the sensitive nature of surficial sediments and icy permafrost in this part of the Arctic (Couture & Pollard 2007). Concern that global warming will not only cause a shift in the pattern of permafrost distribution but will also induce widespread thermokarst (Lawrence et al. 2005) in areas underlain by ice-rich sediments provides additional impetus for ground ice investigation. Ground ice studies may also provide useful proxy information on paleoclimates and paleogeomorphology.

Study Area

This study focuses on massive ground ice located in the Eureka Sound lowlands on west-central Ellesmere Island and east-central Axel Heiberg Island (Fig. 2). Eureka Sound is bordered by gently rolling lowlands surrounded by glacierized mountains rising to elevations of more than 500 m a.s.l.

The landscape is incised by several short river channels and dotted by numerous tundra ponds. Ice wedge polygons are ubiquitous over most of the area and active layer detachment and retrogressive thaw slump scars are common. This area is underlain by poorly lithified Mesozoic and Cenozoic clastic rocks of the Savik, Awingak, Deer Bay, Isachsen, Christopher, Hassel, Kangkuk and Eureka Sound Formations (oldest to youngest). Outcrops of weathered bedrock are widespread at elevations above marine limit and resistant sandstones of the Heiberg Formation form steep ridges in excess of 500 m a.s.l. Fosheim Peninsula lies east of (beyond) a glacial drift belt that marks the Late Pleistocene glacial limit (Bell 1996). Approximately 30% of the peninsula lies below the Holocene marine limit, which is approximately 140–150 m a.s.l. (Bell 1996). Below this elevation a blanket of thinly laminated sandy silt and silty clay from <1 to ~15 m thick covers most surfaces.

Pollard & Bell (1998) developed an emergence history for the Fosheim Peninsula (from dates for articulated bivalves of marine origin) that constrain the age of ground ice deposits for different elevations. A fine-grained till and diamicton overlying bedrock is described by Hodgson (1985) for the northern part of Fosheim Peninsula. The Quaternary history and the extent of Pleistocene glaciation in this area are still poorly understood (Bell 1996, Pollard & Bell 1998) and could have a strong bearing on the interpretation of massive ground ice origin, in particular its age and the possible preservation of buried glacier ice. Thus, a particular concern of field mapping and section description is the identification of fine till or diamicton units and their association with massive ice.

The study area is characterized by cold polar desert conditions (the Eureka weather station has a mean air temperature of -19.7°C based on a 50-year record) and permafrost up to 600 m thick (Pollard 2000b). Preliminary studies indicate that the marine sediments are extremely ice-rich (Pollard 1991, 2000a). Of particular interest is the widespread occurrence of massive ice in the lowlands surrounding Eureka Sound, Slidre Fiord and the Slidre River Valley, where it frequently occurs as extensive bodies of massive tabular ice (Couture & Pollard 1998, Robinson 1993, Pollard 1991, Pollard & Bell 1998, Pollard 2000a).

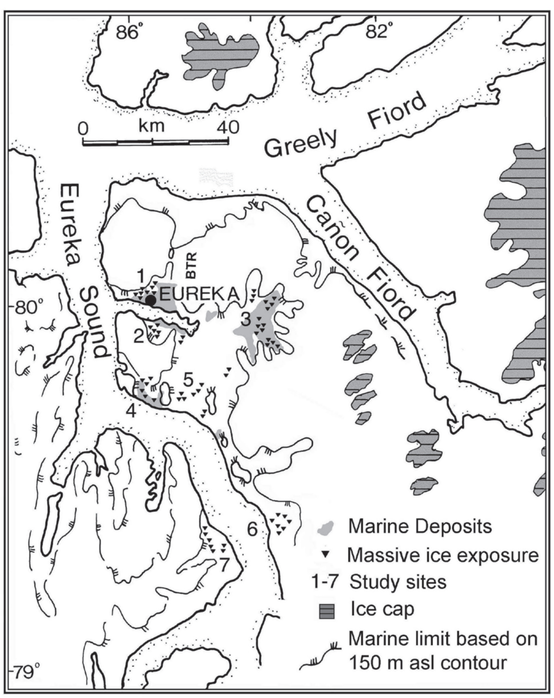

Figure 2. Map of the Eureka Sound Lowlands showing the location of ice-rich permafrost, massive ground ice exposures and study sites 1–7 (see text for details). BTR refers to Black Top Ridge.

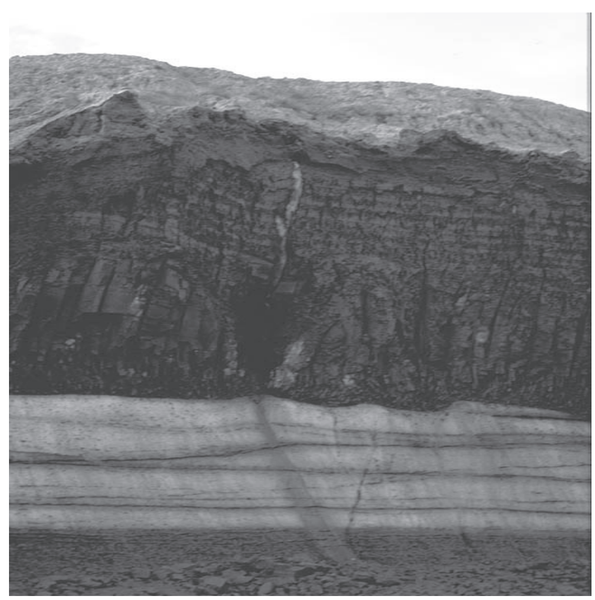

Figure 3. Massive ground ice (~3 m thick) conformably overlain by 5+ m of laminated marine sediments containing reticulate ice veins.

Ground Ice Conditions

Ground ice conditions

Fieldwork on massive ground ice in this area began in 1991 by examining natural exposures (retrogressive thaw slumps, river banks and block failures), but since 2001 has included coring (~40 cores <5 m and 5 cores between 5–17 m) and geophysical investigations (GPR and resistivity).

Ground ice distribution

Seven ice-rich areas characterized by numerous ground ice exposures with massive ice as well as both active and inactive thermokarst features and tundra ponds have been identified (Fig. 2). Study sites include: (1) Eureka, (80°00′N, 85°57′W); (2) South Slidre Fiord (79°56′N, 86°05′W & 79°54′N, 85°30′W), (3) Slidre River, (79°55′N, 84°14′W) including Hot Weather Creek (79°59 & 84°28′W) and Gemini (79°58′N, 84°10′W) (4) Blue Man Cape, (79°44′N, 85°57′W) (5) Eureka Sound (79°43′N, 84°30′W) (6) South Fosheim (79°28′N, 84°20′W) and (7) May Point (79°25′N, 84°29′W). The Romulus Lake (79°52′N, 84°55′W) and the Depot Point (79°22′N, 86°24′W & 79°24′N, 86°00′W) areas also display widespread thermokarst, but only a few exposures of massive ice. A number of isolated massive ice exposures and retrogressive thaw slumps have also been mapped. Retrogressive thaw slumps frequently contain relatively large bodies of massive ice and ice-rich permafrost (excess ice). The distribution of massive ice corresponds closely with the distribution of fine-grained marine sediments identified by Bell (1996), in fact 181 exposures (96%) occurred in marine sediments. The nature of the ice is also stratigraphically controlled by these and other surficial materials. The most significant ice exposures occur where marine deposits >7 m thick form flat to gently dipping plateaus.

Of the 189 natural exposures containing massive ice and ice-rich sediments 88% are retrogressive thaw slump head walls, 8% river cuts and 4% block failures. These data are supplemented by 20 core holes.

Cryostratigraphy

Most exposures include horizontally layered massive ice several meters thick conformably overlain by 1–7 m of massive to weakly laminated marine sediment (Fig. 3). The ground surface is often littered with cobble to boulder-sized clasts and a fine gravel lag deposit in areas of wind erosion. A typical section includes a thin surface layer 5–20 cm thick of massive fine sand with a few large sub-rounded clasts (gravel to cobble sized) that grades into a massive fine silty sand. The fine sand unit varies in thickness between 1–3 m. This unit grades into a finely laminated silt and silty sand. Layers (laminae) 1–1.5 cm thick of well sorted silt and fine sand are interpreted as rythmites associated with episodic glacial melt water deposition into a shallow marine (brackish) system (Bell 1996). Soil salinities range between 0.2%–0.5%. The active layer is typically 30–70 cm deep.

Ice contents are initially high immediately below the base of the active layer. This unit grades into 0.5–2.0 m of faintly laminated to massive silty clay. It is extremely ice-rich, ice occurs in a regular to irregular reticulate cryotextures with vertical fissures initially predominating. Salinities are between 0.4%–0.6%. Ice content tends to increase with depth forming a network of vertical and horizontal segregated ice lenses which grades into massive ice with angular blocks of silty clay 2–5 cm in diameter. The contact between the silty clay unit and the massive ice is abrupt but conformable. Sediments in the ice are similar to the sediments in the overlying silty clay unit. There is also chemical continuity in the major ions and environmental isotopes.

The massive ice unit ranges from 2–10 m plus in thickness. Given that basal contacts are rarely observed in natural exposures the total thickness is inferred from geophysical surveys and a few deep core holes. Massive ice displays horizontal to gently dipping bands of sediment and sediment-rich ice. Ice color varies between white (bubble rich) and clear (appears black). Ice petrofabrics range from strong preferred vertical c-axes with large (1–3 cm long) euhedral crystals in the middle of the unit to random c-axis orientations and small anhedral crystals near sediment bands and at the upper contact. The basal contact is observed in 3 core holes from the Eureka area. In all 3 cases the ice grades into ice-rich bedrock (poorly lithfied sandstone). Technically this is an unconformity however there is chemical continuity between the massive ice and ice retrieved from 10 cm into the bedrock.

In the Eureka Sound Lowlands the pattern in ground ice content is closely linked to the thickness of marine sediments, and although considerable variation exists both locally and regionally, the presence of terraced marine deposits has proven to be an extremely good indicator of massive ice. Several sections at each massive ice site were analyzed for ice content. For convenience, ice content values are expressed as percent volume although most of the measurements

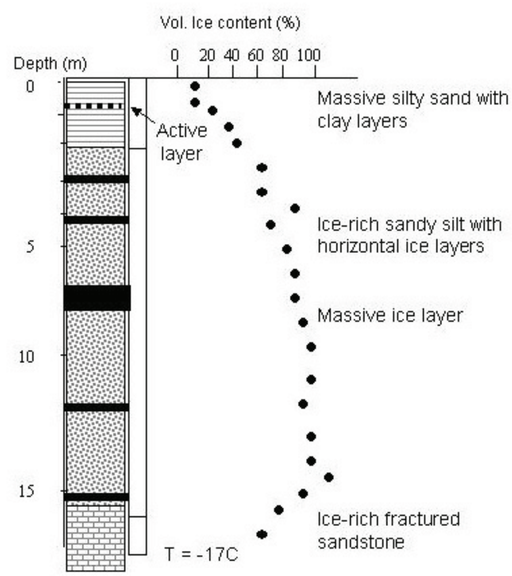

Figure 4. Typical cryostratigraphic profile through a massive ice body, based on a 17 m core taken near Eureka obtained using a modified seismic drill.

were done gravimetrically. Gravimetric ice contents were converted to volumetric ice contents following a procedure outlined in Pollard & French (1980). The base of the active layer formed the top of most measured profiles. Active layer depths display considerable variation ranging from 60–70 cm for dry south-facing surfaces to 30–40 cm for damp north facing or shaded locations. For much of Fosheim Peninsula, particularly above marine limit where surficial materials are coarse, the permafrost is quite dry and ice contents average between 3–10% by volume.

Ice content profiles

In the ice-rich areas below marine limit three patterns in ice content profile occur (Fig. 5). The first is marked by moderately high ice contents (20%–30%), occurring as pore ice and thin discontinuous ice lenses and layers near the base of the active layer. Beneath the active layer, ice contents increase sharply so that at depths of roughly 1.0–1.3 m they reach 60%–99% where layers of pure ice and muddy ice predominate; the sediment in the ice is mainly silt or clay sized. In this pattern, high ice contents extend between 2–7 m to depths of up to 8–9 m. In only a few instances is it possible to obtain data below the base of the massive ice zone, and in such cases the ice contents drop dramatically (10%–30%).

Pore and lens ice occur where the lithology changes to coarse sandy material or weathered bedrock. The second pattern includes a layer of weakly laminated sandy silt 5–7 m thick with ice contents ranging from 8%–15% near the base of the active layer, to 12%–17% at depths of 2–3 m. Near the base of this unit, ice contents increase to 30%–40% as the clay and silt contents increase. Pore and lens ice grade into more regular vertical and reticulate patterns of ice veins. At depths ranging from 7–10 m, faintly laminated silty clay materials abruptly change to massive ice with fragments or layers of silty clay (60%–70% ice) to pure horizontally foliated massive ice (90%–100% ice). The third pattern is intermediate between the first and second patterns. In this case, ice contents increase gradually (15%–30%) with depth usually reflecting a rise in silt content. At a depth of roughly 4–5 m, interbedded layers of silty ice and icy silt with ice

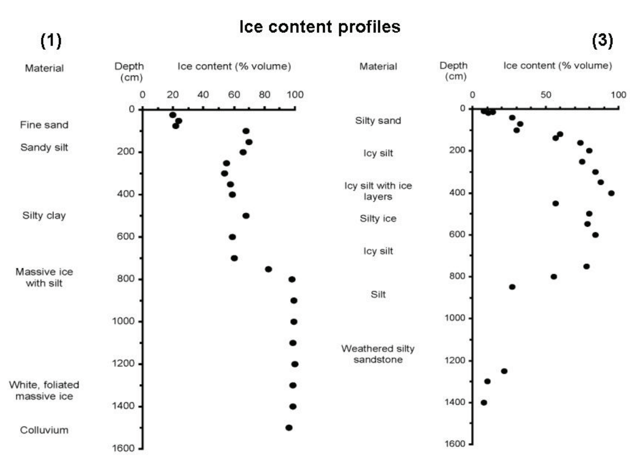

Figure 5. Ice content profiles, patterns 1 & 3.

contents of 65%–78% (sometimes higher) predominate for up to 5 m. At a depth of 9–10 m ice contents decrease to 50%–60% and below this depth, they drop off dramatically (5%–10%) as materials grade into a weathered bedrock substrate.

Various forms of ground ice occur in the surficial materials in the Eureka Sound Lowlands. Pore ice occurs in virtually all perennially frozen unconsolidated sediments and in places is a source of excess ice. Similarly, ice-wedge polygons occur on most surfaces except resistant bedrock outcrops and ridges (e.g., Black Top Ridge). High centered polygons are most common and polygon dimensions are highly variable, ranging from 7–20 m in diameter depending on setting and materials. In low-lying areas ice-wedge troughs are usually well developed, but at higher elevations and in coarse-grained materials they are poorly defined. Ice wedge dimensions are also highly variable and depend on a combination of setting, age and water supply. In the Eureka area, for example, ice wedges range from small fissures 10–30 cm wide and 100–200 cm deep, to classic V-shaped wedges 100–200 cm wide and 350 cm deep. The average ice wedge trough width based on the measurement of 350 wedges in 5 different areas (70 x 5) is 130 cm. Following the method described in Pollard & French (1980, Equation 8), it is estimated that ice-wedge ice comprises approximately 10%–12% of the upper 5 m of permafrost; this is comparable with estimates from the Mackenzie Delta and Yukon Coast. Segregated ice ranges through a full spectrum of forms from thin discontinuous ice lenses, to fully developed reticulate textures, to thick tabular bodies of massive ice (Fig. 3). It is particularly significant in fine-grained marine silts, silty clays and sandy silts that were deposited during the late Quaternary and have subsequently been exposed to cold subaerial permafrost conditions (Bell 1996). Roughly 25%–30% (~4000 km^2) of the Eureka Sound lowlands lie below the Holocene marine limit (150 m a.s.l.). Above this elevation, dry, weathered coarse-grained Tertiary deposits are widespread. Apart from large, widely spaced ice wedges (Lewkowicz 1994), areas above marine limit do not seem to contain significant amounts of ground ice. Elevated, more resistant bedrock surfaces display no evidence of ground ice, but at Hot Weather Creek thick layers of pure ice were observed at depth in consolidated rock strata of the Eureka Sound Formation. Buried ice is present in relatively small quantities as buried snow bank deposits in the stabilized headwalls of retrogressive thaw slumps. Buried glacier ice could be present in various till deposits but to date has not been observed. These studies have shown that pore ice and wedge ice form a significant contribution to the total volume of ground ice in the upper 10 m of permafrost (Couture & Pollard 1998). Buried snow bank ice is present in small amounts in areas of active thermokarst and buried glacier ice occurs in association with moraines formed by modern ice caps and glaciers.

Following a methodology presented in Pollard & French (1980) and modified in Couture and Pollard (1998) we attempt a first approximation of ground ice in the top 7 m of permafrost in the Eureka Sound Lowlands, an area of roughly 12,000 km^2. The total volume of ground ice is calculated by estimating the areal extent of various types of ice-rich terrain in the study area. We establish percentages of ice content by volume for each type of terrain unit. This study considers the top 7.5 m of soil because this was the lower limit of most of our sample data, and because the immediate effects of surface disturbance are unlikely to penetrate to much greater depths. Our estimates concern only the volume of permafrost, or frozen materials, so we subtract the average active layer thickness of 0.6 m, so that the thickness of materials actually used in calculations is 6.9 m. Ice content profiles were used to calculate the average volumetric ice content associated with pore ice and massive ice based on terrain type. A combination of air photo analysis and field data were used to estimate the volume of ice associated with ice wedges. The highest ice volumes (65%) were associated with marine terraces. Below marine limit, pore ice segregated ice comprise 45% by volume of frozen sediment while in areas underlain by bedrock they account for 9.5%. Ice wedges comprise only 5% of the volume of frozen sediments. This low value reflects the relatively small size of ice wedges. Ground ice in all forms makes up approximately 30% of the upper 6.9 m of permafrost.

Thermokarst

Thermokarst is an important erosional process unique to areas underlain by ice-rich permafrost and refers to landforms resulting from the thawing of ground ice. The importance of thermokarst is often discussed in terms of its potential occurrence as an impact on human activity (e.g., as a response to construction of pipelines and highways) or global warming; however, it should not be forgotten that thermokarst is a naturally occurring erosional process. The nature and magnitude of thermokarst is directly related to two important variables, (i) the thermal stability of the upper part of permafrost, including the depth of the active layer, and (ii) ground ice contents. Retrogressive thaw slumps (also called retrogressive thaw flow slides) are one of the more spectacular forms of backwearing thermokarst and also involve thermal erosion (Fig. 6). Preliminary observation on thermokarst in the Eureka area are presented in Robinson (2000).

Most of the 189 natural massive ice exposures were in retrogressive thaw slumps. In comparison with similar landforms in the Mackenzie Delta-Yukon Coastal Plain area the retrogressive thaw slumps in the Eureka Sound Lowlands are relatively small. The average length of exposed headwall was <80 m (the largest was 158 m) and average headwall height was 5–7 m. The highest head wall was 12 m but heights around 4–5 m were common. Through the course of this study the headwall position of 3–4 slumps in each of the study areas was monitored by a combination of DGPS, total station surveys and tape surveys. In addition late July thaw depths (active layer) were also monitored in the vicinity of the headwall. Climate data from the Eureka weather station and an automatic weather station in the Eureka area allowed

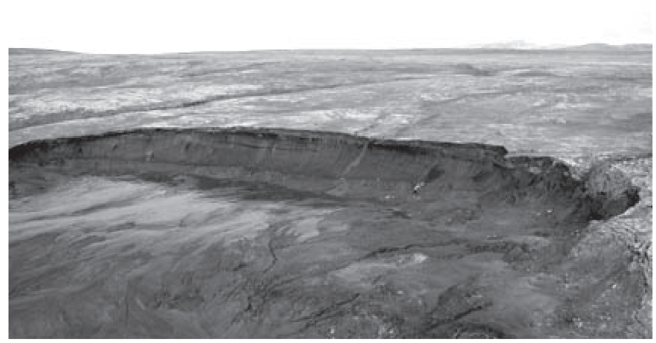

Figure 6. A retrogressive thaw slump near Depot Point. The exposed headwall is approximately 80 m long.

us to compare retreat rates with air temperature. The average mean daily temperature for July (the warmest month) was +5.7°C and the average number of thawing degree-days for July was 176.7.

July 1998 and 2003 were the two warmest Julys during this study. Through the course of this study 30 slumps were surveyed. In some cases sites were measured annually, but most were surveyed every second or third year. With the exception of two slumps that remained active through the entire study (one at South Slidre and one at Blue Man Cape—sites 2 and 4 respectively) most (70%) stabilized after 7–8 years, (20%) after 10 years and (4%) stabilized only 2–3 years after their initiation. Slumps stabilized very quickly following 1–2 years with of rapid retreat. Stabilization occurs when the sediment from the active layer is not removed (by viscous flow) fast enough and buries the head wall. Retreat rate varies across the headwall of every slump; maximum retreat at a point along the headwall can be misleading so we took the average of the most active 10 m section. Over 17 years of observation the average retreat for all sites is 6.9 m/yr, the highest annual retreat was 21 m. A comparison between average annual retreat based on all the slumps and mean July temperature does not show a particularly strong relationship although the highest single retreat rates occurred in years with warmer than average July temperatures. The number of active slumps seems to correspond with years with warm mean July temperatures. Between 1990 and 1995, there were 85–90 active slumps, from 1995–2000 the number dropped to 67–70, from 2000–2005 the number of slumps went back up to 75–77, but since 2005 the number has risen to 91–93. There is a close relationship between July thaw depth and mean July temperature. In 1998, 2003 and 2006 mean July temperatures were 3°C–4°C warmer than average and July thaw depths we 10% higher than average. Since 2000 many of the ice wedge polygons in the vicinity of the monitoring sites exhibited significant thaw degradation and deepening of ice wedge troughs. Numerous new thaw ponds have formed with ice wedge troughs and intersections.

Conclusions

This paper summarizes 15 years of observations on massive ice in the Eureka Sound Lowlands. Three main conclusions can be drawn from this research. First, massive ground ice is a significant component of surficial sediments in the Eureka Sound Lowlands, which represents one of the more ice-rich regions in the Canadian Arctic. Second, the nature and distribution of massive ice is closely linked to the presence of marine sediments and sea level history. And thirdly, shallow massive ice and ice wedges are highly vulnerable to thermokarst. Prior to 2005 there appeared to be little relationship between warmer-than-normal July temperatures and thermokarst, but from 2005–2007 the number of thermokarst features and the amount of thermokarst has been increasing.

Acknowledgments

The authors wish to acknowledge the following sources of funding NSERC Discovery Grant (W. Pollard), ArcticNet NCE, and DIAND's NSTP Program (Couture). Logistical support from NRCan's Polar Continental Shelf Project and the Eureka Weather Station (EC) are gratefully acknowledged. The authors also wish to acknowledge the useful comments of two anonymous reviewers.

References

Arctic Climate Impact Assessment (ACIA). 2005. Arctic Climate Impact Assessment. Cambridge University Press. 1042 pp.

Astakhov, V.I. 1986. Geological conditions for the burial of Pleistocene glacier ice on the Yenisey. *Polar Geography and Geology* 10: 286-295.

Astakhov, V.I. & Isayeva, L.L. 1988. The Ice Hill: an example of retarded deglaciation in Siberia. *Quaternary Science Reviews 7*: 29-40.

Bell, T. 1996. Later Quaternary glacial and sea level history of Fosheim Peninsula, Ellesmere Island, Canadian High Arctic. *Canadian Journal of Earth Sciences* 33: 1075-1086.

Couture, N.J. & Pollard, W.H., 2007 Modelling geomorphic response of a high Arctic polar desert to climatic change. *Climatic Change,* doi: 10.1007/s10584-007-9309-5.

Couture, N. & Pollard, W. 1998. An assessment of ground ice volume near Eureka, Northwest Territories. In: *Proceedings, Seventh International Permafrost Conference,* Centre d' études nordiques, Collection Nordicana, No 57: 195-200.

International Panel on Climate Change (IPCC). 2001a. Climate Change 2001: impacts, adaptation, and vulnerability. Third Assessment Report, Cambridge University Press, Cambridge, UK. 1032 pp.

Lawrence, D.M. & Slater, A.G., 2005. A projection of severe near surface permafrost degradation during the 21st century. *Geophysical Research Letters* 32, L22401, doi:10.1029/2005GL025080.

Lawson, D. 1986. Ground ice in perennially frozen sediments, northern Alaska. *Proceedings of the Fourth International Conference on Permafrost.* Washington, DC: National Academy Press, 695-700.

Lewkowicz, A. 1994. Ice wedge rejuvenation, Fosheim Peninsula, Ellesmere Island, Canada. *Permafrost and Periglacial Processes* 5: 251-268.

Mackay, J.R. 1971. The origin of massive icy beds in permafrost, western Arctic, Canada; *Canadian Journal of Earth Sciences* 8: 397-422.

Mackay, J.R. 1989. Massive ice some field criteria for the identification of ice types. *in Current Research, Part G;* Geological Survey of Canada, Paper 89-1G, 5-11.

Mackay, J.R. & Dallimore, S.R. 1992. Massive ice of the Tuktoyaktuk area, western Arctic coast, *Canada. Canadian Journal of Earth Sciences* 29: 1235-1249.

Murton, J.B. & French, H.M. 1994. Cryostructures in permafrost, Tuktoyaktuk coastlands, western Arctic *Canadian Journal of Earth Sciences* 31: 737-747.

Nelson, F., Anisimov, O. & Shiklomonov, N. 2001 Subsidence risk from thawing permafrost. *Nature* 410: 889-890.

Pollard, W.H. & French, H.M. 1980. A first approximation of the volume of ground ice, Richard Island, Pleistocene Mackenzie Delta, NWT *Canadian Geotechnical Journal* 17: 509-516.

Pollard, W. & Bell, T. 1998. Massive ice formation in the Eureka Sound Lowlands: A landscape model. In: *Proceedings, Seventh International Permafrost Conference*, Université Laval, Centre d'etudes nordiques, Collection Nordicana, No 57: 903-908.

Pollard, W.H. 1991. Observations on massive ground ice on Fosheim Peninsula, Ellesmere Island, Northwest Territories; *in Current Research, Part E, Geological Survey of Canada, Paper 91-1E*, 223-231.

Pollard, W.H. 2000. Distribution and characterization of ground ice on Fosheim Peninsula, Ellesmere Island, Nunavut, *in Environmental Response to Climate Change in the Canadian High Arctic,* Geological Survey of Canada, Bulletin 529: 207-233

Pollard, W.H. 2000. Ground ice aggradation on Fosheim Peninsula, Ellesmere Island, Nunavut, *in Environmental Response to Climate Change in the Canadian High Arctic, Geological Survey of Canada, Bulletin* 529: 325-333.

Robinson, S.D. 1993. Geophysical and Geomorphological Investigations of Massive Ground Ice, Fosheim Peninsula, Ellesmere Island, Northwest Territories. M.Sc. thesis, Queen's University, Kingston, Ontario, 171 pp.

Robinson, S.D. 2000. Thaw-slump-derived thermokarst near Hot Weather Creek, Ellesmere Island, Nunavut. *Geological Survey of Canada* 529: 335-345.

Streletskaya, I.D. & Leibman, M.O. 2003 Cryogeochemical model of tabular ground ice and cryopegs, Yamal Peninsula, Russia. *Proceedings of the Eighth International Conference on Permafrost*, *Zurich, Switzerland, 21-25 July 2003*: 1111-1115.

Zimov, S., Schur, E. & Chaplin, F. 2006. Permafrost and global carbon budget. *Science* 5780: 1612-1613.

Long-Term Monitoring of Frost Heave and Thaw Settlement in the Northern Taiga of West Siberia

Olga Ponomareva
Earth Cryosphere Institute, Russian Academy of Sciences, Siberian Branch, Moscow, Russian Federation
Yuri Shur
University of Alaska Fairbanks, Department of Civil and Environmental Engineering, Fairbanks, Alaska USA

Abstract

Monitoring of frost heave and thaw settlement has been carried out for 37 years in the discontinuous permafrost zone of West Siberia. Long-term frost heave is a modern process in the natural condition of the discontinuous permafrost zone. The rise of old frost mounds and the formation of new ones has been observed. Old mound development occurs non-uniformly in time and is associated with cold winters. The rate of frost heave is maximum in the central part of frost mounds and minimal at the margins. Long-term frost heave in flat peatland has also been observed; it occurs at about the same rate but is more spatially uniform. The exception is represented at peripheral sites in flat peatland with a lowered permafrost table. Contemporary thermokarst is inactive in natural conditions. Thaw settlement is very intensive after the removal of a vegetative cover and part of the soil layer. The subsidence rate decreases substantially after 2–3 years. The maximum observed thermokarst subsidence reached 1 m during the period of monitoring.

Keywords: climate; human-induced disturbances; long-term frost heave; thermokarst.

Introduction

Frost heave and thermokarst-related features occur widely in the northern taiga of Western Siberia (Melnikov et al. 1983) where permafrost is discontinuous. Frost heave forms are represented by individual mounds, ridges (with length many time greater then width and height), and vast flat elevated areas. Heights vary from 0.5 to 10 m (Veisman et al. 1976). These forms develop both in natural and disturbed areas (Fig. 1)

Contemporary forms related to thermal subsidence occur primarily in disturbed areas along the Nadym-Punga gas pipeline. Their depth reaches 1 m. There are different opinions on the contemporary activity of these cryogenic processes. According to Evseyev (1976), frost mounds in the region are relic and degrading forms. Nevecherja (1980) described modern frost mounds and has evaluated the growth rate in the northern taiga of Western Siberia. However, he believed that the majority of frost mounds, ridges, and frost-heaved areas were formed long ago, and do not currently grow, and some mounds degrade in the contemporary environment. According to Nevecherja (1980), frost mound growth stops after the frozen nucleus reaches about 10 m. Recently, changes in vegetation on old frost mounds associated with their rise was described by Moskalenko & Ponomareva (2004).

Study Site

A long-term monitoring program was established by N. Moskalenko, V. Nevecherja, and Y. Shur in 1971 to study the impact of pipeline construction on permafrost stability, and on the development of permafrost-related processes in the pipeline right-of-way and surrounding terrain. In this paper, we present data from the Nadym site to demonstrate contemporary dynamics of frost heave and thermokarst in natural areas and those impacted by pipeline construction.

Figure 1. Disturbed frost mounds.

The Nadym monitoring station is located 30 km to the south from the city of Nadym (Fig. 2), in a subzone of northern taiga. It encompasses three geomorphological levels: the third lacustrine-fluvial plain, the flood plain of the Hejgi-Jaha River, and the second fluvial terrace of the Nadym River. The relief is nearly flat with numerous lakes and mires.

The studied region is characterized by two layers of permafrost, which can be defined as surface permafrost and deep permafrost. The surface permafrost is discontinuous and sporadic on the lacustrine-fluvial plain and the flood plain of the Hejgi-Jaha River. Patches of permafrost are confined to peatlands, tundra, and frost mounds. On the terrace of the Nadim River, the permafrost table is lowered and does not merge with the bottom of the active layer.

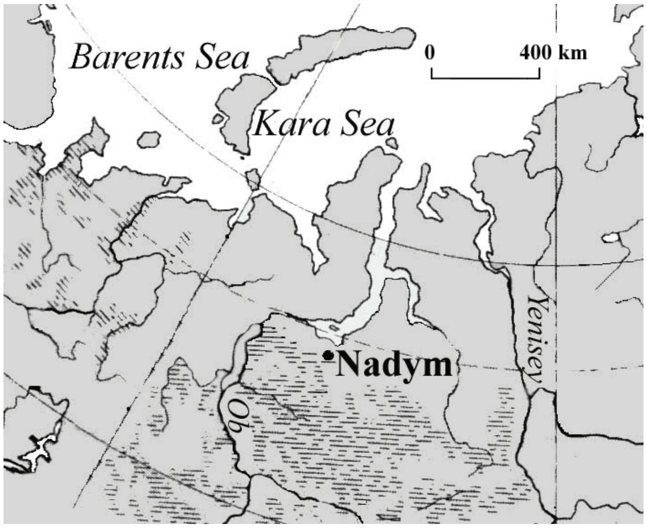

Figure 2. Study site near Nadym.

Depending on terrain conditions, mean annual permafrost temperature varies from 0 to -2°C. The warmer permafrost temperature is typical for dry forest-covered sandy soils. Extensive peatlands have the coldest permafrost temperature. The active layer varies from 0.5–0.7 m on peatlands, and up to 4 m on blowout sand.

The depth of seasonal freezing varies from 0.3 to 0.8 m in peatland, and from 1.5 to 2.5 m in forest with well-drained sandy soil. Recently the permafrost temperature and seasonal thaw depth has increased in both natural and disturbed settings, which is reflected in the dynamics of natural processes (Moskalenko 1998)

Research Objectives and Methods

The analysis of climatic conditions is based on long-term observations at the Nadym weather station.

Observations of long-term frost heave and thaw subsidence were conducted along four transects that cross the gas pipeline right-of-way, the surrounding disturbed zone, and the terrain unaffected by construction that has remained in a natural state. Measurements of frost heave and thaw settlement were made relative to deeply anchored reference bench marks. Elevation surveys and vegetation descriptions were carried out yearly at the end of August. The active layer thickness and permafrost temperature were measured in September.

Analysis of Results

The analysis of the climatic data

According to long-term data, air temperatures and the precipitation amount in in the study region vary markedly from year to year (Fig. 3). The long-term mean annual air temperature is -5.6°C; the difference between annual mean temperatures of the coldest and warmest years reached 5.69° during last 40 years. Despite such fluctuations, a 10-year moving average of annual mean air temperature shows an increase in the period from 1966 to 1997, and small variations

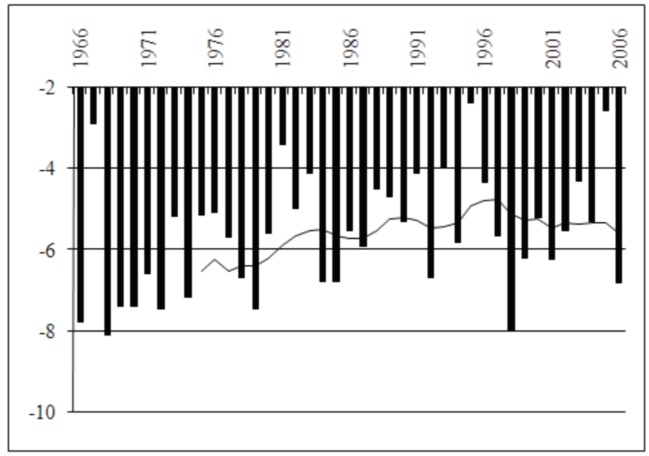

Figure 3. Annual mean temperatures with a 10-year moving average, °C.

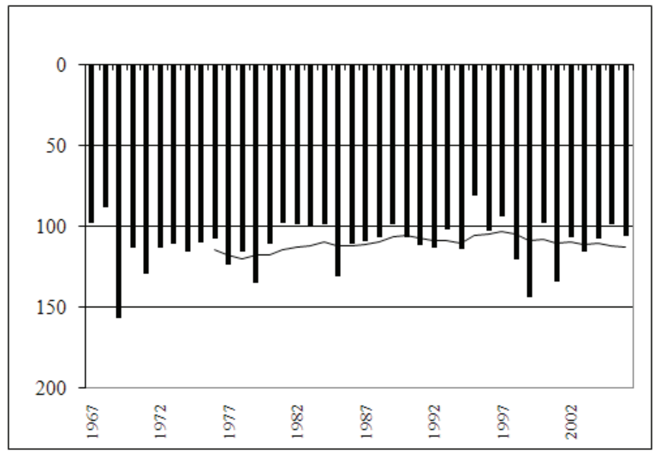

Figure 4. Freezing indices (in °C months) with a 10-year moving average. One degree-month is equal to 30 degree-days.

from 1998 to 2006 (Fig. 3).

Figure 4 shows the freezing Iindices and Figure 5, the thawing indices for the same period. The winter of 1995 had the smallest freezing index for the entire observation period. It was equal to 80.5°C-month, and occurred at the end of the period of warming. The most severe winters occurred in 1999 and 2001 following the warm period, with freezing indices of 144 and 134° C-months. An exception was the cold winter of 1985. Freezing and thawing indices in this paper are presented in °C-months because they were evaluated from available information on monthly mean air temperatures. Their presentation as °C-days would create the wrong impression about the data, but can be estimated by multiplying °C-months by 30.

Thawing indices (Fig. 5) show continuous increase; with time, this will lead to a steady deepening of the active layer and thawing of the ice-rich upper layer of permafrost. However, thermokarst activation under natural conditions has not been detected so far.

The annual mean precipitation is shown in Figure 6. Winter and summer precipitation for the same period is shown in Figure 7 and Figure 8.

It was expected that the abundance of precipitation during

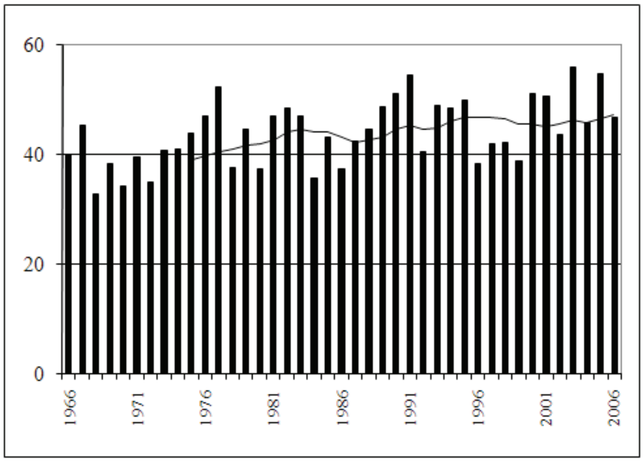

Figure 5. Thawing indices (in °C-months) with a 10-year moving average. One degree month is equal to 30 degree-days.

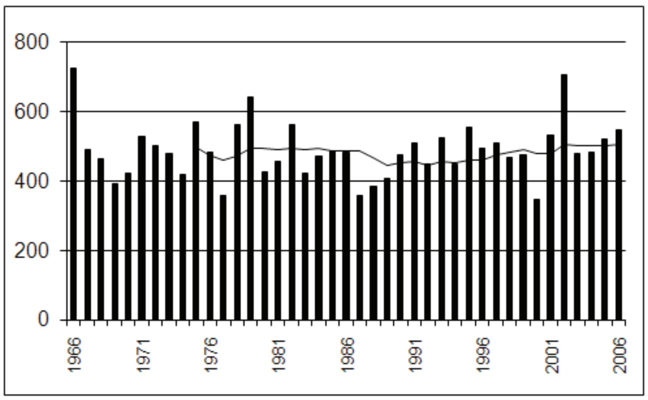

Figure 6. Annual mean precipitation (mm) with a 10-year moving average.

the period with negative air temperatures would lead to a decrease in the intensity of frost heave, and the amount of precipitation for the period with positive temperatures would impact bog development. According to the data presented in Figure 6, the total amount of yearly precipitation increases after 1987, as did the summer precipitation (Fig. 7). The increase in summer precipitation after 1987 has caused an expansion of the bog and lake area, as revealed by 1989 and 2004 satellite images. There is no visible trend in winter precipitation (Fig. 8).

Long-term frost heave of soils of third lacustrine-fluvial plain

Frost heave of soils in the third lacustrine-fluvial plain was studied at 327 points along four transects. Transects were located across various landscapes. The survey of surface elevation was conducted once a year, at the end of August or beginning of September, when seasonal thaw depth had reached its maximum and surface elevation reflected the effects of long-term frost heave processes with minimum seasonal effects. The survey was performed with reference to deep permanent benchmarks.

Transect I-I (Fig. 9) crosses a series of peat-mineral and mineral frost mounds that are surrounded by mires. A survey of frost mounds surfaces shows that frost heave is not

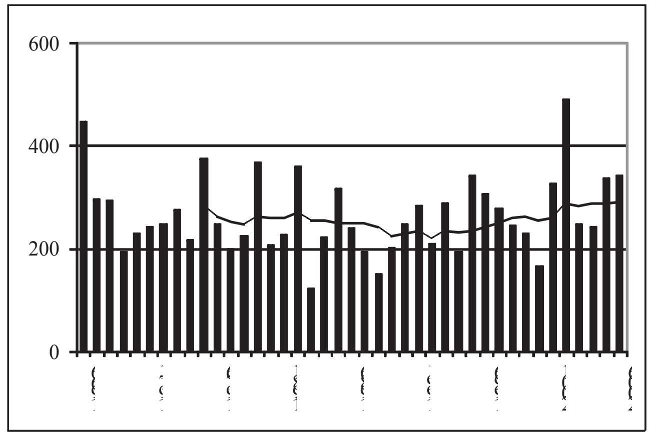

Figure 7. Summer precipitation (mm) with a 10-year moving average.

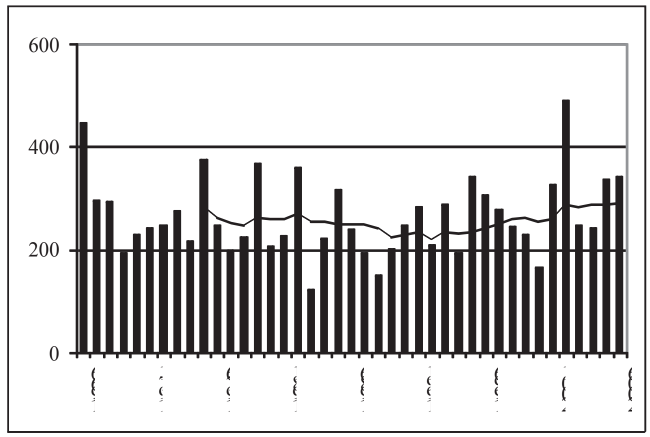

Figure 8. Winter precipitation (mm) with a 10-year moving average.

uniform; there is a steady rise of mound tops and sporadic rise of slopes which is intermittent with subsidence. They rise in the coldest winters;. dDuring the monitoring period, maximal rise occurred in the most severe winter of 1999. During the last 26 years, the central part of one peat-mineral frost mound rose 70 cm, while a mineral frost mound rose 30 cm. For the analysis of frost heave intensity, it is important to note that a thin snow cover occurred nine9 times, including 1985, 1995, 2000, and 2001, during which intensive frost heave took place. The winters of 1985 and 2001 were especially severe. The snow thickness impact on frost heave was obvious in the warm winter of 1995 with low snow thickness. The rise of frost mounds tops with subsidence of their slopes was observed in 2005.

Maintenance work along the gas pipeline in 2004 initiated new surface disturbances and changes in the drainage conditions, which led to the formation of small lakes and widespread flooding (Fig. 10). It decreased the growth of frost mound tops and led to subsidence of their slopes in 2005 and 2006.

Transect II-II was established on the flat peatland and bogs of the third lacustrine-fluvial plain (Fig. 11). The thickness of peat along transect II-II varies from several centimeters to 1.75 m. To a depth of 5 m, peat is underlain by fine and

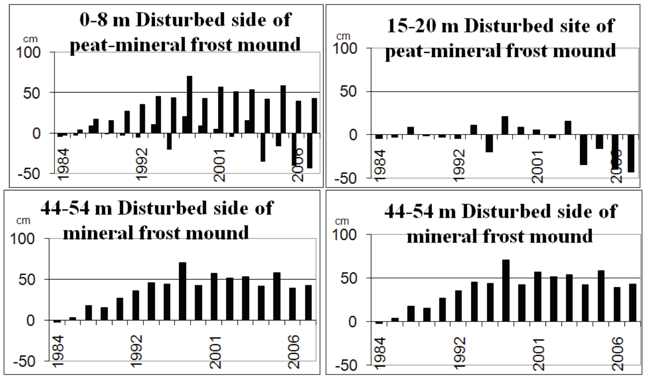

Figure 9. Changes in surface elevation (cm) along transect I-I relative to surface elevation in 1980. Annual values represent averages for that segment of the transect.

Figure 10. Flooding of the area adjacent to the pipeline in the vicinity of transect I-I. View from the gas pipeline.

Figure 11. Flat peatland along transect II-II.

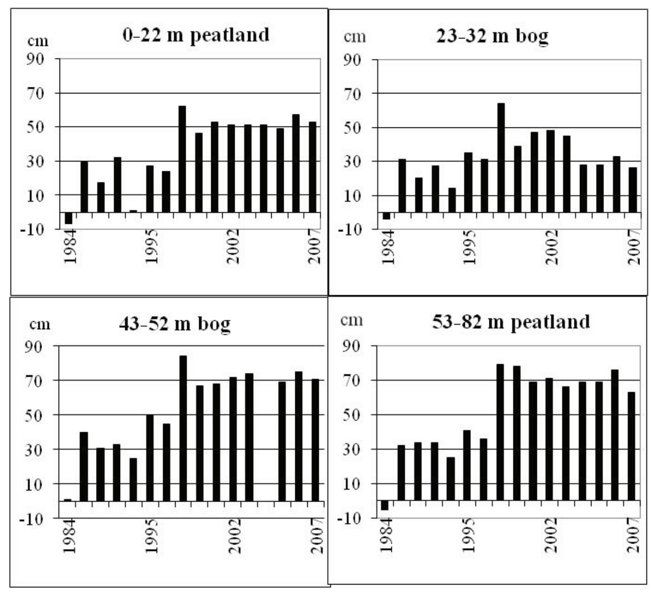

Figure 12. Deviation of surface elevation (cm) along transect II-II from elevation in 1980. Annual values represent averages for labeled segments of the transect.

silty sands and seams of sandy loam with some gravel and pebbles. The layer of sandy loam continues to a depth of 7 to 8 m, where it is underlain by sand. The layer of surface permafrost associates with flat peatlands here.

It was found that the surface along transect II-II experienced a rise in the severe winters of 1985 and 1999 , and in 32 years has became higher by 67 cm than it was in 1980. Frost heave of the flat peatland is uniform in the study area. After 1999, surface rise has slowed down. (Fig. 12).

Transect III-III includes flat peatland and hummocky tundra. Peat, which varies in thickness from several to 80 cm, is underlain by loamy sand to a depth of 3 to 8 m, with loam below. The permafrost table here is lowered to a depth of 3.5 to 4 m. Pereletoks are formed in some years above it. (aA pereletok is a layer of frozen ground which formed as a part of seasonally frozen ground and remained frozen for several summers ([van Everdingen 1998)]). Frost heave on transect III-III (Fig. 13) in one year is intermittent with thermal settlement in another, and the accumulated surface rise for the monitoring period is only 12 cm. The maximal rise of the surface occurred in the cold winter of 2001, with a thin snow cover in the previous winter.

Transect IV-IV is located on a peat-mineral frost ridge, disturbed in 1971 during construction of the gas pipeline. Removal of the vegetation cover triggered thermokarst, an increase in permafrost temperature, and a lowering of the permafrost table (Shur 1981). Vegetation recovery reverses these processes and is favorable to frost heave, although its intensity is very low. It is possible to identify two periods in the direction of processes on the soil surface. The period 1972–1977 is characterized by surface subsidence following construction, and the period which began in 1978 is the period of slow rise of the surface (Fig. 13). During the first period, the surface subsidence was 104 cm on average. The slow rise of the surface (by 50 cm on average) during the second period did not compensate for the earlier subsidence.

Thaw subsidence

In natural conditions, inactive thermokarst forms associated with thawing ice-wedges are typical for peatlands (Fig. 14). Ice-wedge pseudomorphs are also widespread in the region (Fig. 15). Distinguishing forms which could be attributed to contemporary thermokarst in natural conditions are rare, local, and occur on the margins of flat peatlands mainly in association with thermal erosion. Observation show that,

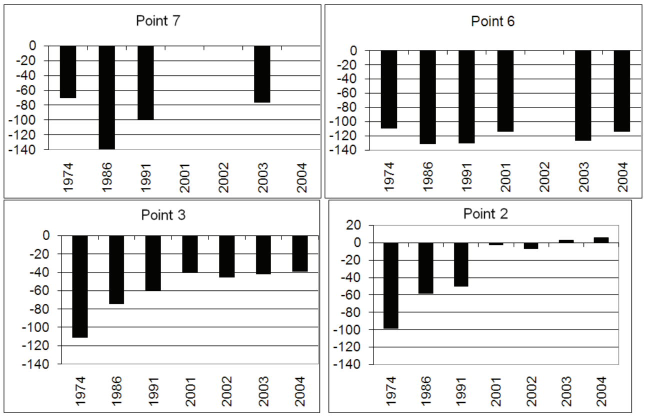

Figure 13. Deviation of surface elevation (cm) along transect IV-IV from elevation in 1972. Annual values represent deviations for every point along the transect.

Figure 14. Inactive thermokarst forms in the vicinity of transect III-III.

Figure 15. Ice-wedge pseudomorphs in the vicinity of transect I-I

despite the lack of notable thermokarst forms, uniform thermal settlement takes place. From 2000 to 2005, the rise of frost mounds and peatlands slowed down, and thermal settlement increased. It reached 31 cm on a peat-mineral frost mound, 47 cm on a mineral frost mound, and up to 64 cm on flat peatland. However, settlement has not led to formation of prominent thermokarst features. Our observations confirm Vejsmana's (1976) conclusion about weak development of modern thermokarst features under natural conditions. This conclusion is correct for natural, undisturbed terrestrial complexes. Presumably, thermokarst will develop at the margins of lakes as their area increases. We expect that our ongoing studies will reveal this.

Conclusions

1. The formation of frost mounds in the discontinuous permafrost zone of West Siberia is a contemporary process on lacustrine-fluvial plain and flood plains in the northern taiga of West Siberia. During the last 30 years, their height has increased from 30 to 70 cm, with a maximal rise occurring in the coldest winters of 1999 and 2001.
2. In areas disturbed during pipeline construction, peat frost mounds occur in three stages: thaw settlement, surface stabilization, and frost heave. The last two stages largely depend on vegetation recovery.
3. Thermokarst is not active under natural conditions. It is triggered by construction work, and is very active in the first several years. The total thaw settlement in the study area reached 100 cm during the period of observation.

Acknowledgments

This research was partly funded by the Polar Earth Science Program, Office of Polar Programs, National Science Foundation (ARC-0632400 and ARC-0520578). Natalia Moskalenko has been our long-term companion in the field and our mentor on terrain analysis. Comments by reviewers and their advice were very helpful. Ken Hinkel provided valuable suggestions that improved the manuscript.

References

Evseev, V.P. 1976. Migration pingos in the northeast of the European part of the U.S.S.R. and in Western Siberia. *Problems of cryolitology*, Vol. V. MGU: 95-160 (in Russian).

Melnikov, E.S., Veisman, L.I., Moskalenko, N.G., Tagunova, L.N., Ukraintzeva, N.G., Chekrigina, S.N., Ananieva, G.V., Goralchuk, M.I., Krizuk, L.N., Lazareva, N.A., Merkushenkova, R.I., Slavin-Borovsky, V.B. & Shirshikova, A.S. 1983. *Terrain Units of Permafrost Region of the West Siberian Gas Province*. Novosibirsk: Nauka, 164 pp. (in Russian).

Moskalenko, N.G. 1998. Impact of vegetation removal and its recovery after disturbance on permafrost. *Proceedings of the Seventh International Conference on Permafrost*, *Yellowknife:* 763-769.

Moskalenko, N.G. & Ponomareva, O.E. 2004. Changes of frost mounds, disturbed by construction work in northern taiga of West Siberia. *Earth Cryosphere* II(8): 10-16 (in Russian).

Nevecherya, V.L. 1980. Cryogenic heave at long-term freezing of grounds in the north of Western Siberia. *Geocryological Research*: M. VSEGINGEO: 45-49 (in Russian).

Shur, Y.L. 1981. The thermokarst forecast. In: *Methodical Recommendations Under the Forecast of Development Cryogenic Physical – Geological Processes in the Mastered Regions of the Far North)*. M. VSEGINGEO: 18-37 (in Russian).

van Everdingen, R. (ed.) 1998. Multi-language glossaryof permafrost and related ground-ice terms. International Permafrost Association

Veisman, L.I. et al. 1976. Contemporary geologocal processes and their occurrence in the middle course of Nadym r. and Pur-Taz einterfluve. *Abstract collection TSINIC*, Series II, RELEASE 2(43б), Moscow, 50-54 (in Russian).

The Permafrost of the Imuruk Lake Basaltic Field Area (Alaska) and Astrobiological Implications

O. Prieto-Ballesteros
D.C. Fernández-Remolar
J. Torres Redondo
M. Fernández-Sampedro
M.P. Martín Redondo
J.A. Rodriguez-Manfredi
J. Gómez-Elvira
Centro de Astrobiología-INTA-CSIC, 28850 Torrejón de Ardoz. Spain
D. Gómez-Ortiz
Rey Juan Carlos University, 28933 Móstoles, Spain
F. Gómez
Centro de Astrobiología-INTA-CSIC, 28850 Torrejón de Ardoz. Spain

Abstract

We have studied the permafrost in the Imuruk Lake volcanic field area (Alaska) from an astrobiological perspective. Our main goal was to test in terrestrial permafrost the type of instrumentation designed to search for biosignatures in this environment to obtain a performance baseline, should the instrument be used on a future space mission to explore Mars. Permafrost characterization was performed using geophysical sounding and drilling, and different levels of the rock cores were analyzed to determine the mineralogy, geochemistry, and microbiology. Thirteen lines of electric tomography from the Imuruk Lake coast up to the hill of the Imuruk formation were analyzed. Three perforations were made at strategic locations along the slope of the hill. Samples were collected at several depths in the three holes for mineralogical, geochemical, and biological analysis. Here we present the results of the subsurface mapping performed to locate the permafrost and of the analyses of the core samples.

Keywords: Alaska; astrobiology; electrical tomography; Imuruk Lake; permafrost.

Introduction

The study of terrestrial permafrost has become a priority for planetary missions focused on Mars. The main reason is that the martian permafrost likely represents the current main water reservoir of the planet (Clifford & Parker 2001). From an astrobiological perspective, permafrost is important not only because of the role of the water in the planet's hydrological cycle and the fact that it may hold a direct record of the planet's paleoclimatic record, but also because it may be a potential habitat for microorganisms (or preserve biomolecular tracers of past life) since it (a) acts as a thermally stable shelter, (b) is a source of moisture, and (c) is a shield against incoming radiation (Gomez et al. 2004). Consequently, robotic exploration of permafrost on Mars is being considered for future missions by the international suite of space agencies (Smith & McKay 2005, Shotwell 2005). At present, direct study of the martian permafrost has not been possible due to technical limitations and uncertainties. However, terrestrial analogues to Mars' permafrost are currently being investigated from novel perspectives that include space technology and astrobiology. The results are being used to develop instrumentation for future space missions focused on the search for life.

Some characteristics of martian permafrost have been modeled by using data from planetary exploration missions. At the present time, this dataset is continuous at circumpolar latitudes, where an active layer (the top layer of permafrost that seasonally thaws) is absent. At middle latitudes, permafrost is continuous although a thin active layer may exist, especially if salts are present to depress the melting point. In the tropical zone, ground temperatures exceed 273 K during the summer, and annual mean temperatures indicate that continuous permafrost exists, but ice is absent or patchy at best due to hyperaridity (Squyres et al. 1992). Recently, *Mars Odyssey* mission data have defined the periennial underground ice stability zone from latitudes higher than 60º (Feldman et al 2002, Mellon et al. 2004).

The Alaskan permafrost now serves as a martian analogue for the planetary science community. The permafrost of the Imuruk Lake area (Seward Peninsula, Alaska) offers a valuable and relatively accessible location for testing instruments for remote mapping and searching for life in the water underground. There are few studies about this area, though some report the general geology (Hopkins 1963) or different analyses of cores from several drill sites in the area, which were cored to constrain the climatic events that have occurred in the area (Colinvaux 1964, Colbaugh 1968, Marino 1977, Shackleton 1982, Hamilton 1991). None of the reports, however, covers permafrost mapping, mineralogy, geochemistry, and biology simultaneously. Nor do any reports consider the recent interest in the permafrost as an analogue environment of Mars. The permafrost on this area is considered continuous (Péwé 1975), and it extends in some parts to more than 50 m thick (Hopkins 1963). Ice wedges and polygons are frequent in the Imuruk Lake area. It has been suggested from analyses of the stratigraphy that certain ice wedges in frozen ground are at least from the early Wisconsinan glacial period.

We show here the results of a field campaign performed during the summer of 2005 in the Imuruk Lake area. With the intent to develop future instrumentation for remote life detection systems, we pursued three main objectives: (1) permafrost localization by geophysical techniques and drilling the permafrost, (2) microbial diversity analysis, with special interest on the deeper part of the cores given the older age of this permafrost (i.e., the preservation pattern of biosignatures in cold environments is of extraordinary astrobiological interest), and (3) understanding of the cold ecosystem for the purpose of detecting and mapping permafrost niches. Geophysical sounding for mapping the permafrost was made before we sampled it. Three cores in the mapped area were taken. Clean drilling techniques were used, following planetary protection rules. Geochemical and biological analyses were made in the laboratory, though they were previously prepared in situ.

Regional Setting

The Imuruk Lake area is on the Seward Peninsula, a few kilometers above the polar circle. It is north of the Bendeleben Mountains in a Cenozoic lava plain. Landscape heights of the surrounding area vary from 45 to 600 m, with the highest topography caused by Mesozoic granitoid intrusions and Paleozoic metamorphic rocks, which constitute the geological rock basement. The central part of the area is characterized by monogenetic volcanoes, active from the late Paleogene. Five volcanic formations have been distinguished in the Imuruk Lake area, among which mantles of windblown silt with different extent and thickness have been deposited (Hopkins 1963). Volcanism is basaltic to andesitic, mainly with pahoehoe lava flows, although locally there are some dome structures. Permafrost in these materials is especially interesting with regard to the interaction between rocks and ice, from which we derive analogies to important martian landforms and materials. Ice-rich permafrost is primarily continuous—tens of meters thick, except under and near the major lakes and rivers. In addition, parts of the lava flows interrupt the permafrost, thus allowing groundwater circulation.

The Imuruk Lake occupies a basin configured by a distorted northwest trending graben. Tectonics during the Cenozoic formed several fracture systems in three different stages. The lake area was uplifted to the northwest, as well as bent, as shown by the study of the terraces. Three levels of terraces have been identified: The low level is presently occupied by active beaches on the east shores of the lake; intermediate terraces are cover by peat and silt; and the higher terrace is a wave cut not associated with sediments.

Current climate in the Imuruk Lake area is cold, with a mean temperature of 266 K and minimum values during winter of 213 K. Annual precipitation is 20 cm, from which 50% is between July and September, and 25% is as snow.

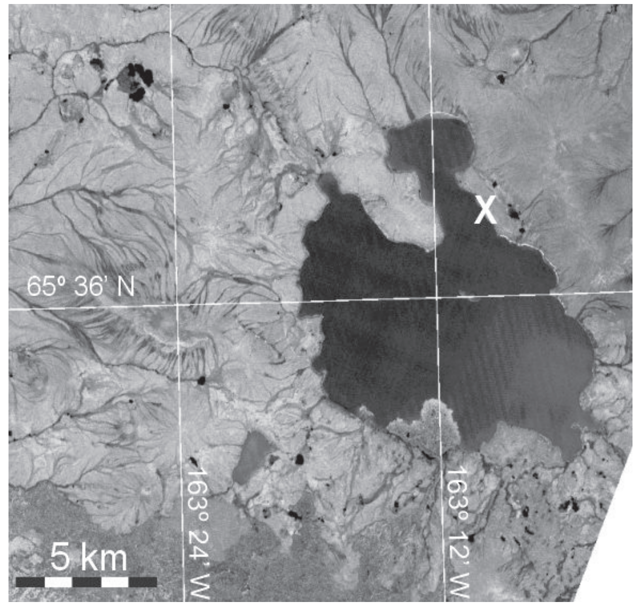

Figure 1. Imuruk lake area. Field work of 2005 campaign was made at the east shore of the lake (X).

Glaciations have affected the Imuruk area from lower Pleistocene: Nome River, Salmon Lake and Mount Osborn glaciations altered the successive volcanic rocks, which were erupted and produced eolic silts that covered them.

Considering the bad accessibility of the area, some analysis of ASTER images was performed in order to constrain the study area before the fieldwork campaign. The selection of the study area was made among the most ancient volcanic formations, where surface materials showed a low brightness temperature during summer and the topography is smooth enough to facilitate the drilling. Fieldwork performed during the 2005 expedition was made in the eastern part of the Imuruk Lake between Nimrod Hill and the lake itself (Fig. 1). This area was mapped by Hopkins (1963) as the named Imuruk volcanic formation, which is dominated by basalts and basaltic andesite lava flows overlain by 1–6 m of windblow silt. A cover of peat is present at the top. Surrounding the volcanic hill, some lake sediments, gravel, sand, silt, and peat of intermediate terraces have been mapped already (Hopkins 1963).

Geophysical Survey

To map the permafrost underground, electrical resistivity tomography (ERT) sounding was performed. ERT is a geophysical prospecting technique designed for the investigation of areas of complex geology. The principal applications of this technique are (Telford et al. 1990, Reynolds 1997, Hauck & Mühll 2003, Kneisel 2004; Šumanovac 2006) mapping stratigraphy and aquifer boundary units, such as aquitards, bedrock, faults and fractures, delineation of voids in karstic regions, mapping saltwater intrusion into coastal aquifers, identification of contaminated groundwater plumes, mapping of mineralization zones, exploration of

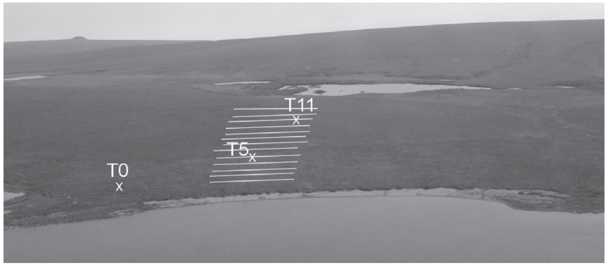

Figure 2. Image of the area where the 13 ERT lines were done. T0, T5, and T11 are the locations of the drill sites.

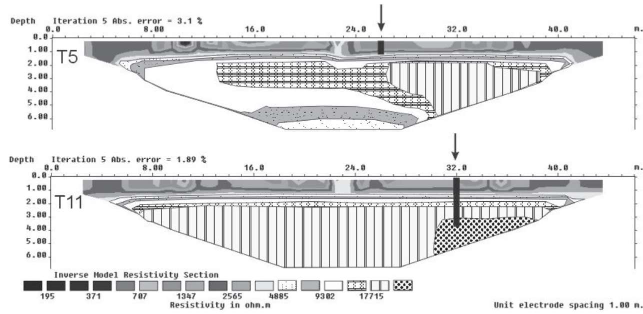

Figure 3. Tomographic profiles 5 and 11. Black arrows indicate the drilling sites.

sand and gravel deposits, as well as mapping permafrost in mountainous regions, among others.

Several standard electrode arrays are available, such as Wenner, dipole-dipole, and pole-dipole arrays, with different horizontal and vertical resolution, penetration depth, and signal-to-noise ratio. The Wenner array provides good vertical resolution, though it also gives reasonable horizontal resolution (Sasaki 1992). This method has a greater signal-to-noise ratio than others (e.g., the dipole-dipole method) because the potential electrodes are placed between the two current electrodes. These features provide greater depth of investigation.

Syscal KID Swich-24 equipment was used for taking the measurements. Thirteen parallel lines from the Imuruk lake coast up to the hill of Imuruk formation were accomplished (Fig. 2). Each ERT line was 48 m long, with 2 m between each pair of electrodes. The space between lines was around 15 m, depending on the difficulty of the topography for settling the electrical lines.

The resistivity field dataset comprises resistance measurements between various electrodes and related geometry information. An apparent resistivity value is calculated, which depends only on the resistance measurements and the array geometry. These data are plotted as a pseudosection, which is a plot of the apparent resistivity values based on the geometry of the electrodes. These pseudosections, which are difficult to work with, are then converted into sections with true resistivity values and depths via a data inversion procedure that helps in the interpretation process. An inversion of the data produces a plot that shows a resistivity value for each horizontal and vertical node. This resistivity inversion section is then used to interpret the subsurface lithology. The data are inverted with RES2DINV software. Data processing steps include removing bad data points, selecting the inversion method, and then interpreting the data.

The resulting ERT data for our study indicated that permafrost in the region analyzed is at a mean depth of 0.50 m under the surface, sometimes even shallower. The presence of peat materials at the top of the stratigraphic column acts as an insulator layer, maintaining very effectively the low temperature below.

From the analysis of the 13 ERT profiles, 2 clearly distinctive units were identified (Fig. 3): an upper unit that extended from the surface to 0.5–1 m depth, characterized by resistivity values ranging from 130 to 680 ohm·m, and a lower unit that reached 6 m depth (the maximum depth of investigation), defined by a resistivity that ranged from 12,400 to 30,000 ohm·m. Taking into account the in situ drilling observations, the study area was comprised by silt overlain by a thin level of peat.

Typical resistivity values for silt and peat are 10–200 ohm·m (Telford et al. 1990, Reynolds 1997, Comas et al. 2004), a value that depends mainly on the water content and ionic concentration. Permafrost resistivity values are typically greater than 10^3–10^4 ohm·m (Reynolds 1997, Hauck & Mühll 2003, Kneisel 2004) due to the strong resistance of the ice. Bearing this in mind, the upper low-resistivity unit could be related to the presence of peat and silt material with unfrozen water, whereas the lower high-resistivity unit represents the permafrost developed in silt materials. Vertical heterogeneities in electrical resistivity were observed in the upper part of all the profiles, which have been interpreted as the edges of the polygonal terrains (Fig. 3). Thus, the lower resistivity values in the upper unit correspond to finer grained and higher water content materials of the polygonal terrains, whereas higher resistivity values are associated with the coarser materials (i.e., at the edges of the polygonal terrains).

The high resistivity in the lower unit represents the permafrost developed in silt materials, which reached a thickness of at least 5–5.5 m in all the profiles. At first glance, this unit is much more homogeneous than the upper unit, although some spatial variations were measured. ERT profiles 1 to 8 exhibited resistivity values for permafrost that ranged from 12,500 to 21,000 ohm·m, with higher values at the end of the profiles than at the center. In addition to this, ERT profiles 6 and 7 showed resistivity values at 6 m depth (about 5,000 ohm·m), similar to the ones that defined the top of the permafrost at 0.5–1 m depth. This fact makes evident that the base of the permafrost in these profiles is located near the maximum depth of investigation. The resistivity values for the permafrost in ERT profiles 9 to 13 ranged from 24,000 to 30,000 ohm·m, being much more homogeneous than in profiles 1 to 8. The resistivity did not decrease in depth, so the lower boundary of the permafrost must be below 6 m depth. Only profiles 12 and 13 showed a spatial variation in the resistivity of the permafrost, with higher values to the western end.

Drilling Survey

A Cardi E-400 driller—small, portable, and fuel-operated—was employed in this expedition. By connecting 0.5 m bits, a maximum 5 m long drill was obtained. The diameters of the bit and the recovered core were 50 mm and 40 mm, respectively. No refrigerant substances were applied to preserve the area from contamination.

Drilling points were selected on the basis of the permafrost depth known from the ERT data analysis. Three perforations were done along the hill (Fig. 2). The first core obtained, which was placed in the ERT line 5 (T5), was about 1 m long. It consisted of peat and brown silt with abundant organic matter. The permafrost started at 0.3 m underneath the surface. The second core, drilled at ERT line 11 (T11), reached 3.6 m depth. Permafrost was found at 0.55 m. The peat cover above it was smaller. Below it, brown silt with organic matter was observed to a depth of 3.0 m. The sand fraction of the silt was composed of quartz and plagioclases (albite and anorthite), while the fine fraction was composed of clinochlore, montmorionite, illite, and vermiculite. From this point to the core bottom, the materials were green-yellowish silt, almost free of organic material (Fig. 4). The third core was drilled out of the study area by tomographic lines closer to the lake, and penetrated a 2 m depth (T0). Permafrost was at 0.50 m, at the same depth as the peat cover. Below that level, we found the green-yellowish silt with transversal lenses of both clean ice and organic silt. The silt found in this core was free of quartz. The sand fraction was made by anorthite, labradorite, and microcline as plagioclases, with diopside, augite, and acmite as pyroxenes. From 1.5 m down, the materials are basaltic-andesitic pebbles inlayed in a silt matrix (Fig. 5).

Samples were collected at several depths in the three holes for mineralogical, geochemical, and biological analysis. They were fixed in situ with formaldehyde to maintain them until biological laboratory analyses were developed. Several types of fresh growth media were inoculated with samples from different depths in the field for microbial enrichment. The mineralogy of the core samples was analyzed by XRD, FTIR, petrographic microscope, and SEM.

Laboratory Analysis

Core sampling for further laboratory analyses was performed in all 3 cores, starting at 50 cm from the surface. Geochemical analysis of selected samples of the melted ice and sediment along the cores was run by ICP- MS Perkin Elmer Elan 9000 and an elemental analyzer LECO CHNS-932. Mineralogical studies were performed with XRD and microscope thin sections analysis.

Dating and correlation with other cores

Samples from cores 11 and 5 were taken for age analysis. The C^{14} dating analyses were done in the Angström Laboratory of Uppsala University (Sweden). Measurements were performed on the sediments after the roots and carbonates were removed. Our analysis indicated that the age of the silt sediment at 2.0 m in the T11 drill site is 11155±75 BP, and 12705±90 BP at the bottom of the core (3.6 m). We found that the T0 core ages are 13450±100 at 1.5 m and 20250±225 years BP at 2 m depth.

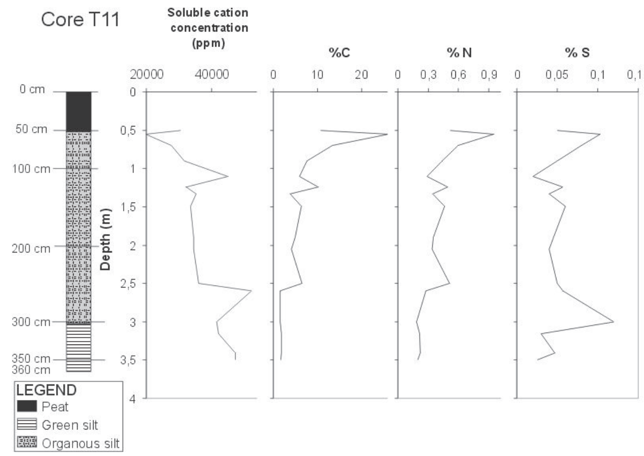

Figure 4. Lithology and distribution of soluble cation concentration, %C, %N, and %S in core T11.

Some other drilling studies, which included C^{14} dating analysis, are available in the bibliography. All of the cores in our study were obtained from the lake floor. Colinvaux (1964) reported the results from some cores, named cores I and V, made in Imuruk Lake between the east shore and the Gull Islands. Core I is the more relevant and longest one (8 m long). It consists of layers of mud from the weathering of the volcanic rocks, as well as sand layers that were transported from the beach in low-water-level episodes of the lake. The mud layers are enriched with montmorillonite and kaolinite. Dating of this core was problematic because: (a) two of the youngest dates were measured near the core base (probably due to tectonics), and (b) there are some gaps in the sediment record (possible erosion occurred during the lower-water-level episodes). Later revisions of the core data were done by Colbaugh (1968), Shackleton (1982), and Hamilton (1991) to constrain the climatic events that occurred in the area. Marino (1977) studied the paleomagnetism of the cores. It is worth noting that no detailed petrologic descriptions of the core sections are published, so we are unable to correlate the cores we collected with any others.

Geochemistry.

In cold areas, the mineralogy of the sediment is made up of many chemical elements, though some soluble ions are commonly removed or concentrated, depending on the availability of liquid water (Chegue-Goff & Fyfe 1997, Kokelj & Burn 2003, 2005). These soluble elements can indicate the depth of the active layer of the permafrost. CHNS elemental analysis is useful for delimiting the peat and organic-rich layers in the sediment cores. The entire core T5 is peat, with a carbon content that ranged from 34.7 to 40.9 %. In core T11, the concentration of carbon had a maximum peak of 26% at 0.55 m, though it decreased with depth. The peat should end at 0.6 m. The silt from 0.6 to 2.5 had an average of 7% C, and from 2.5 to 3.6 m, the green silt had an average of 1.6% C (Fig. 4). Samples taken from below the T0 core (Fig. 5) had a very low carbon concentration, except

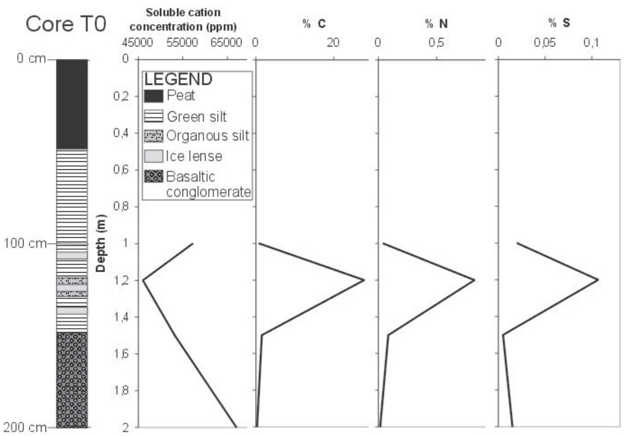

Figure 5. Lithology and distribution of soluble cation concentration, %C, %N, and %S in Core T0.

in a thin layer at 1.2 m. In the three cores, the trend of H, N, and S are well correlated to C, except for S in core T11, where there was a positive anomaly at 3 m.

Soluble cations (Na, Mg, Ca, K) are good indicators of permafrost active layer fluctuation. These elements are mobilized when liquid water is present and they are concentrated above the ice table (Fig. 4 and 5). Note the lack of data from the upper centimeters of the T11 and T0 cores. The T11 core data showed a positive anomaly at 1.1 m and 2.6 m. The anomaly at 1.1 m is mostly due to Na and K, which are probably related to an enrichment of feldspars in the sediment. In the 2.6 m anomaly, the presence of all four cations in the mineralogy of the silt contributed to the change. The T0 core was found to be enriched in Ca and Mg in the upper part, and there was a negative anomaly at 1.2 m due to the organic rich and clean ice water layers at this level. The total content of cations increased at the bottom of the core as a result of the presence of K and Na in the feldspars and clays.

Biology

In situ hybridization techniques were used to document the distribution of targeted microorganisms in the study area. Samples were fixed in the field with formaldehyde (4% v/v) and refrigerated for 2 h. After incubation, samples were washed twice with PBS and filtered. Filters were stored under frozen conditions in PBS-ethanol (1:1). Samples from several depths were chosen for further study with different DNA-specific probes. Cell counts were measured using the optical microscope.

The abundance of cells per mg of sample was analyzed in the first 60–70 cm of the column (the permafrost active layer). Elemental chemical analyses determined an active layer of 50–70 cm (according to the microbiological studies; see Gomez et al. 2008).

Hybridization with DNA-specific probes determined a high presence of bacteria in the upper part of the T11 column. In contrast, lower concentrations of active cells of bacteria were found deeper in the sample. From 2.1 m to 3.6 m depth, we found that the Archaea were the most abundant cell types in the samples.

Discussion

Our ERT survey in the Imuruk Lake area revealed the occurrence of two units: an upper low-resistivity unit that consists of peat and silt with unfrozen water, which was vertically heterogeneous due to the structure of the polygonal terrains; and a lower unit of higher resistivity, which was found associated with the development of permafrost in silt materials. Variations in resistivity in this lower unit revealed that permafrost in the southern part has a higher content of liquid water that decreased in thickness towards the central part of the study area, where the base could be located at around 6 m depth. In contrast, we found that permafrost in the northern zone contains a lesser volume of liquid water and/or reaches a greater thickness. Geophysical sounding by ERT or GPR (Corbel et al. 2006) could be useful in a planetary mission for mapping the stratigraphy, structure, and position of ice-rich permafrost on Mars before deploying the complex instrumentation needed to drill on Mars.

When ice-rich permafrost is drilled on Mars, in situ analyses should (a) confirm the presence of the liquid phase and its movements, for example, by following the salts; (b) characterize the environment, for example, by recording the temperature and pH; and (c) search for biosignatures. Mineral analysis would reveal elements that might be used by some microorganisms. The changes in the oxidation state of the elements and the pH of the liquid phase would affect the state of the organic matter (Vogt & Larqué 2002). The secondary mineralogy that would result from this type of interaction could be detected by space missions, and might indicate the presence of life. Microbial activity may be traced by direct or indirect fingerprints on the minerals. Mineral biosignatures may be distinguished by textural and chemical changes due to dissolution and the growing kinetics variation shifted by metabolism, such as the formation of nanometric particles of iron oxyhydroxides during the iron-oxidizing bacterial enzymatic catalysis, or the reorganization of mineral paragenesis when equilibrium is perturbed biologically.

Given the thermal stability of permafrost (at temperatures less than 0ºC), such a deposit could harbor extinct organisms. Living organisms could thrive if they are able to extend the adaptation processes because of the slower metabolism at low temperatures. However, sudden changes of activity due to the seasonal melting of ice could occur inside the active layer of the permafrost. The metabolic state and the biochemistry of permafrost organisms have not been well studied to date. Microorganisms living in the permafrost could survive frozen during long periods of time (Gilichinsky et al. 2007) and could be activated instantaneously as indicated by some biogeochemical manifestations (for instance, enzymes suddenly working, presence of metastable iron sulfides and nitrates, or lipids, protein, and ADN synthesis) (Rivkina et al. 2004, Vorobyova et al. 1997). Moreover, the study of biosignature preservation in permafrost environments will reveal whether they might be useful places to search for evidence of life in future missions to Mars.

Conclusions

We are studying the permafrost in the Imuruk Lake volcanic field area (Alaska) from an astrobiological perspective. Terrestrial permafrost is an essential reference for potential habitable environments on Mars.

Studies like this will help guide future planetary explorations and guide the interpretation of their data by providing directions on how to (1) develop new instrumentation for detecting and mapping the permafrost on Mars; the current or ancient (but now frozen) active layer could be search with geophysical methods such as the ERT used in this study, though more fieldwork is needed to be capable of interpreting data from Mars; (2) define preservation patterns of biosignatures in cold environments that may be used in future missions; and (3) develop new instrumentation for detecting life, in situ and remotely. The extreme environment in which this kind of work was accomplished entails a suitable testbed for developing robust and effective techniques that warranty the success of the mission.

Acknowledgments

We would like to thank to Jeffrey S. Kargel, the U.S. National Park Bering Land Preserve, Rosalyn Grimes, NASA-JPL, Juan Perez-Mercader, and INTA for the support.

References

Chegue-Goff, C. & Fyfe, W.S. 1997. Effect of the permafrost on geochemistry in a Canadian peat plateau bog. *Applied Geochem*. 12: 465-472.

Colbaugh, P.R. 1968. *The environment of the Imuruk Lake area, Seward Peninsula, Alaska during Wisconsin time.* Masters thesis. Dept. of Zoology, Ohio State University, Columbus.

Colinvaux, P.A. 1964. Environment of Bering land bridge. *Ecological Monographs* 34: 297-329.

Comas, X. & Slater, L. 2004. Low-frequency electrical properties of peat. *Water Resources Res.* 40: W12414.

Corbel, C. et al. 2006. WISDOM: An UHF GPR on the Exomars Mission. *Eos Trans. AGU* 87(52): P51D-1218.

Clifford, S.M. & Parker, T.J. 2001. The evolution of the Martian hydrosphere: Implications for the fate of a primordial ocean and the current state of the northern plains. *Icarus* 154: 40-79.

Feldman, W.C. et al. 2002. Global distribution of neutrons from Mars: Results from Mars Odyssey. *Science* 297: 75-78.

Gilichinsky, D.A. et al. 2007 Microbial Populations in Antarctic Permafrost: Biodiversity, State, Age, and Implication for Astrobiology. *Astrobiol.* 7*:* 275-311.

Gomez et al. 2004. UV radiation effects over microorganisms and study of protective agents. *ESA SP*-545: 21-25.

Gomez, F. et al. 2008. Microbial diversity in a permafrost environment of a volcanic-sedimentary Mars analog: Imuruk Lake, Alaska *Proceedings of the Ninth International Conference on Permafrost, Fairbanks, Alaska, June 29–July 3, 2008* (this proceedings).

Hamilton, T.D. & Brigham-Grette, J. 1991. The last interglaciacion in Alaska: Stratigraphy and paleoecology of potential sites. *Quat. Int*. 10–12: 49-71.

Hauck, C. & Mühll, V.D. 2003. Inversion and interpretation of two-dimensional geoelectrical measurements for detecting permafrost in mountainous regions. *Permafrost and Periglac. Process*. 14: 305-318.

Hopkins, D.M. 1963. Geology of Imuruk Lake area, Seaward Peninsula, Alaska. *USGS Bulletin 1141*-C, 98 pp.

Kneisel, C. 2004. New insights into mountain permafrost occurrence and characteristics in glacier forefields at high altitude through the application of 2D resistivity imaging. *Permafrost and Periglac. Process.* 15: 221-227.

Kokelj, S.V. & Burn, C.R. 2003 Ground ice and soluble cations in near-surface permafrost, Inuvik, Northwest Territories, Canada. *Permafrost and Periglac. Process.* 14: 275-289.

Kokelj, S.V. & Burn, C.R. 2005. Geochemistry of the active layer and near-surface permafrost, Mackenzie delta region, Northwest Territories, Canada. *Canadian J. of Earth Sci.* 42: 37-48.

Marino, R.J. 1977. *Paleomagnetism of two lake sediment cores from Seaward Peninsula, Alaska.* M.S. Thesis, Ohio State Univ., 183 pp.

Mellon, M.T. et al. 2004. The presence and stability of ground ice in the southern hemisphere of Mars. *Icarus* 169(2): 324-340.

Péwé, T.L. 1975. Quaternary geology of Alaska. *Geological Survey Prof. Paper* 835.

Reynolds, J.M. 1997. *An Introduction to Applied and Environmental Geophysics.* John Wiley and Sons, 796 pp.

Rivkina et al. 2004. Microbial life in permafrost. Space life sciences: Search for signatures of life, and space flight environmental effects on the nervous system. *Advances in Space Research* 33(8): 1215-1221.

Sasaki, Y. 1992. Resolution of resistivity tomography inferred from numerical-simulation. *Geophys. Prospecting* 40: 453-463.

Smith, H.D. & McKay, C.P. 2005. Drilling in ancient permafrost on Mars for evidence of a second genesis of life. *Planet. and Space science* 53(12): 1302-1308.

Shotwell, R. 2005. Phoenix –the first Mars Scout mission. *Acta Astronautica* 57: 121-134.

Squyres, S.W. et al. 1992. In: H.H. Kieffer (ed.), *Mars*. University of Arizona Press.

Šumanovac, F. 2006. Mapping of thin sandy aquifers by using high resolution reflection seismics and 2D electrical tomography. *J. Appl. Geophys.* 58: 144-157.

Shackleton, J. 1982. Paleoenvironmental histories from Whitefish and Imuruk lakes, Seaward Peninsula, Alaska. *Inst. Polar Studies Report* 76.

Vogt, T. & Larqué, P. 2002. Clays and secondary minerals as permafrost indicators: examples from the circum-Baikal region. *Quaternary Internat.* 95-6: 175-187.

Vorobyova, E. et al. 1997. The deep cold biosphere: facts and hypothesis. *FEMS Microbiol. Rev.* 20: 277-290.

Telford, W.M. et al. 1990. *Applied Geophysics*. Cambridge University Press, 770 pp.

What Dictates the Occurrence of Zero Curtain Effect?

Jaakko Putkonen
Department of Earth and Space Sciences, University of Washington, Seattle, WA 98195, USA.

Abstract

Zero curtain effect refers to the persistence of ground temperatures at or close to 0°C during annual ground freezing or thawing. This phenomenon is related to both active layer underlain by permafrost and seasonally frozen ground. Zero curtain effect in the permafrost areas is traditionally contributed to the ground water freezing in the fall and resulting release of the latent heat. If the phase change of water to ice or vice versa is the primary reason then the zero curtain should be found in the fall and spring in both the active layer and seasonally frozen soils, which is not the case. Through thermal modeling it is shown that the annual evolution of the subsurface thermal field leads into the establishment of isothermal soil near 0°C between two phase change fronts only in special cases. The modeled occurrence and timing of zero curtain effect corresponds well with the observations.

Keywords: active layer; ground ice; permafrost; thermal modeling; unfrozen water; zero curtain.

Introduction

Zero curtain is defined in the *Glossary of Permafrost and Related Ground-ice Terms* as the persistence of a nearly constant temperature, very close to the freezing point, during annual freezing (and occasionally during thawing) of the active layer (van Everdingen 2005). Outcalt et al. (1990) provide a good history of the definition and related research, and a suggestion of the correct usage of the term which is followed here.

Figure 1A shows prominently the modeled zero curtain in the fall that is a characteristic feature of active layer annual thermal regime and has important implications to water migration in soil and related ice lensing and frost heave (e.g., Hallet et al. 2004). For good examples of zero curtain in natural soils see Washburn (1979, Figure 3.34) and French (1996, Figure 4.5). This phenomenon is explained to result of the latent heat that is released through the phase change of water into ice (Washburn 1979, Williams & Smith 1991, French 1996, Osterkamp & Romanovsky 1997, van Everdingen 2005). A careful examination of the evolution and maintenance of the zero curtain has revealed mass and heat fluxes in the forms of water and vapor in some cases (Hinkel et al. 1990, Outcalt et al. 1990, Hinkel & Outcalt 1994) and only heat conduction and phase change in others (e.g., Osterkamp & Romanovsky 1997).

The release of latent heat through freezing of water is generally found to be the primary explanation for the occurrence of the zero curtain effect that is often seen in the fall in the thermal record of active layer underlain by permafrost. Therefore it is intriguing that those same thermal records often show no zero curtain in the spring, when the same amount of soil ice melts. Simplistically one would expect to see approximately similar zero curtain in the spring as is seen in the fall at a given field site. Yet, typical field observations show active layer temperatures at any given level in the soil to cross 0°C in the spring at a steady rate. This is also well represented in Figure 1B.

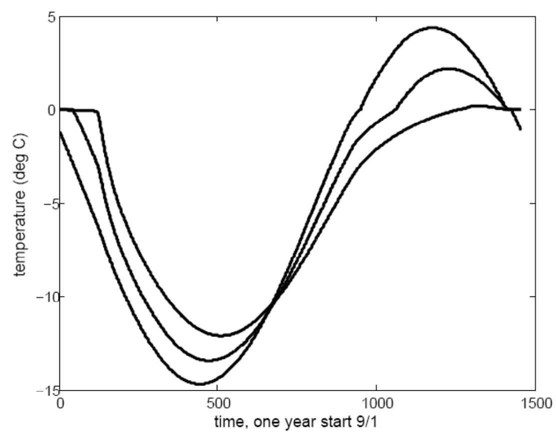

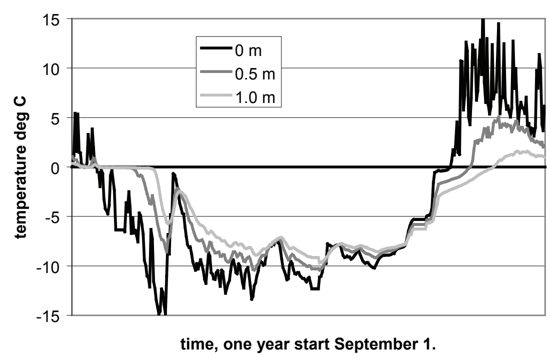

Figure 1. A. Modeled soil temperatures over one year at 0.1 (largest amplitude), 0.5, and 1.0 m (smallest amplitude) below ground surface. Mean annual temperature of the surface forcing is -5°C. B. Measured soil temperatures over one year at a field site in Spistbergen (Putkonen, 1997). Note prominent zero curtain in the fall in both model and observations and the lack of zero curtain in the spring.

No clear explanation has been given in the literature for the intriguing lack of the zero curtain in the spring in the permafrost areas or the intriguing reversal of zero curtain effect occurring in the spring and no zero curtain effect in the fall in seasonally frozen ground.

This apparent contradiction between observations and the simplistic phase change governed explanation motivated the analyses that are presented here.

The purpose of this paper is not to model or explain all the possible soil thermal processes such as non-conductive heat transfer that potentially contribute to the maintenance and longevity of the zero degree curtain. However, the objective of this analysis is to provide a clear explanation for the characteristic occurrence (fall or spring) of the zero curtain effect and the intriguing contrast in timing of zero curtain effect between permafrost and seasonally frozen soils.

It is suggested here that the occurrence of zero curtain is primarily controlled by the soil thermal regime rather than just the existence of the water or ice and related phase change at or near 0°C. In the case of the soil that is underlain by permafrost where the mean annual soil temperature is below 0°C, the time lag in the penetration of the annual thermal wave into the soil will make the soil almost isothermal close to 0°C at the beginning of the fall freeze up regardless of the water content. Because of the almost vanishing thermal gradient at shallow subsurface (~0.5 m), and the presence of water in the soil, the temperatures are changing only near the surface and at depth. This explains why the soil is retained for a prolonged period at the 0°C. On the other hand, in the spring the time lag in the penetration of the annual surface thermal wave enhances the steepness of the thermal gradient near 0°C, the isothermal soil domain is too cold to be affected by phase change of ice to water, and therefore the energy is effectively transferred through the whole soil column. This results in slow but steady temperature increase at all levels in the soil. Therefore the soil temperatures increase at a steady rate through the spring at all levels without any significant slowing in the warming rate at or near 0°C.

In some instances the soil surface temperature may be held at 0°C for weeks due to the melting of the snow and resulting ice/water bath at soil surface. However, this will only modify the driving temperature and potentially slow the overall warming of the soil, but it will not result in zero curtain effect.

The above suggestion that the occurrence of zero curtain effect is dictated by the annual evolution of the soil thermal profile leads to three robust and testable predictions: 1) in soils that are underlain by permafrost and where mean annual soil temperature is <0°C, the zero curtain effect occurs in the fall and there is no significant zero curtain effect in the spring, 2) in areas of seasonally frozen ground (mean annual soil temperature >0°C) the zero curtain effect occurs in the spring rather than in the fall and remarkably there should be no significant zero curtain effect in the fall, and 3) in the areas where the mean annual soil surface temperature is close to 0°C, there should be a short and weak zero curtain effect at both fall and spring.

To study the annual evolution of the thermal regime of soil that contains ice and water, a soil thermal model is used. Finally the model results are qualitatively compared to representative soil temperatures from three field sites that correspond to the above mentioned three soil thermal regimes.

Soil Thermal Model

A one-dimensional thermal model (Putkonen 1998, Putkonen et al. 2003, Putkonen & Roe 2003) is used where soil heat flux (Eq. 1), q is given as

$$q = k\frac{dT}{dx} \tag{1}$$

where k is thermal conductivity [W/m K], and dT is the temperature difference [K] at two points separated by dx, the distance in x direction [m]. When the soil heat flux (Eq. 1) is combined with an expression for the conservation of energy, they lead to the differential equation that describes the time dependent soil thermal evolution (Eq. 2)

$$\frac{dT}{dt} = \frac{dq}{dx} \tag{2}$$

where dt is time difference [s]. This leads to the general formulation of thermal diffusion (Eq. 3):

$$\frac{dT}{dt} = K\left(\frac{d^2T}{dx^2}\right) - dT \cdot LE\left(V_{ufwater}\left(T_{t=t-1}\right) - V_{ufwater}\left(T_{t=t}\right)\right) \tag{3}$$

where $V_{ufwater}(T_{t=t-1})$ is the volume of unfrozen water [kg/m^3] at the temperature $T_{t=t-1}$ [K] at the time step t = t − 1, and K (Greek Kappa) is the thermal diffusivity [m^2/s].

In the model the phase change of water is distributed over a wide temperature range rather than occurring sharply at 0°C. This formulation is based on direct determination of unfrozen water content of a representative frozen soil sample at varying temperatures (Putkonen 1997). The initial soil water content is 295 kg/m^3.

To achieve maximum clarity in the model results the soil surface temperature is forced by a simple sinusoidal thermal wave with annual amplitude of 20°C. The initial soil thermal state is generated by running the model with five consecutively repeated annual cycles that carry over the soil moisture and temperatures from the end of previous year to the beginning of the following. After this initializing sequence the maximum difference between soil temperatures at the end of model years 4 and 5 is less than 0.02°C.

The lower boundary condition in the model is adiabatic (no flux across the boundary) at 20 m below ground surface where the initial temperature is the mean of the annual surface forcing (-5°C, 5°C, or 0°C depending on the case).

Soil thermal properties and surface thermal forcing that are used in the model are representative of general permafrost soils and are inspired by actual measurements at a field site in Spitsbergen (Putkonen 1997). However, these model runs do not attempt to reproduce any actual observations. The mean annual temperature of the forcing corresponds to the three climatic cases.

Soil thermal conductivity of a frozen soil with all water frozen is 3.0 W/m K; thawed soil thermal conductivity is 2.6 W/m K. The frozen soil thermal conductivity that contains unfrozen water scales between the completely frozen and completely thawed stages with the unfrozen water content. The thermal conductivity of the bedrock is 5.0 W/m K. The heat capacity of the soil mineral matter is 1.7x10^6 J/m^3 K. The heat capacities of water and ice are 4.18x10^6 J/m^3 K and 1.92x10^6 J/m^3 K respectively. The soil bulk heat capacity is a sum of the constituent heat capacities and therefore varies continuously as the water is freezing or thawing in the soil.

The internal consistency of the thermal model was tested by contrasting the modeled soil surface heat flow over a given time period (W/m^2) against the energy involved in the water phase change and soil temperature change. These two independent calculations of the soil energy were within 2% of one and other. This is probably as close as a finite difference formulation can be expected to be.

Results

As shown in Figure 1A, the model reproduces the zero curtain effect in the fall and does not reproduce a zero curtain effect in the spring exactly as reported for typical active layer underlain by permafrost (Washburn 1979, Williams & Smith 1991, French 1996). This same pattern is also seen in the field data obtained in Spitsbergen (Putkonen 1997) and shown for comparison in Figure 1B.

When the same model is run for the seasonally frozen ground (mean annual soil temperatures >0°C) a zero curtain effect is seen only in the spring (Figure 2A), which is also seen in the field data. And finally when the model is run for the case where mean annual soil temperature is exactly 0°C, short and weak zero curtain effect is seen both in the spring and fall (Figure 3A).

Discussion

It is counterintuitive that the soil temperatures from a given field site show a distinct zero curtain in the fall (Fig. 1, mean annual soil temperature is -5°C) and no zero curtain in the spring, although same amount of water is freezing in the fall as ice is melting in the spring. To illustrate the reasons for this phenomenon it is useful to consider the soil thermal gradient and the annual evolution of the soil vertical thermal profile (temperature vs. depth below surface).

It is well known that the original amplitude of the thermal wave at the soil surface decreases as it penetrates into the soil and that there is a time lag that increases with depth for a thermal perturbation to travel into the soil (e.g., Turcotte & Schubert 1982). For those reasons the soil thermal gradient in the spring when the surface starts to thaw is almost constant, which makes the soil temperatures at all levels to increase slowly but at steady rate (Fig. 4). Even though the ice is melting in the soil no sections of the soil profile remain persistently at or near 0°C.

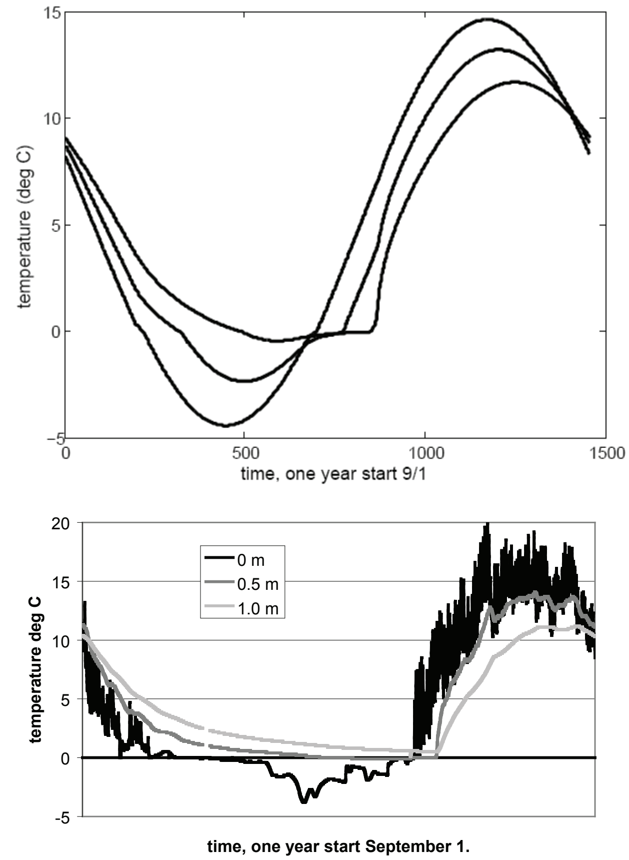

Figure 2. A. Modeled soil temperatures over one year at 0.1, (largest amplitude) 0.5, and 1.0 m (smallest amplitude) below ground surface. Mean annual temperature of the surface forcing is 5°C. B. Measured soil temperatures over one year at the Bonanza Creek Experimental Forest's primary upland weather station LTER1 (Hollingsworth et al. 2005). Note prominent zero curtain in the spring in both model and observations and the lack of zero curtain in the fall.

In the fall the soil temperatures between about 0.5–1.0 m below surface are above freezing but already close to 0°C. A moderate amount of cooling at the surface and at the depth below 1.0 m suffices to bring the soil temperatures to freezing point in the layer 0.5–1.0 m below surface. At that point the thermal gradient in this middle layer approaches 0°C/m and consequently the temperature in that domain do not change until a thermal gradient is re-established.

For these reasons it is clear that two conditions have to be met for the zero curtain to develop in the soil: 1) the active layer has to contain ice or water, and 2) the thermal gradient in the soil has to become 0°C/m at or near 0°C.

Since water and ice are common in the natural soils the soil thermal gradient near 0°C appears to dictate the timing and presence of zero curtain effect.

Although present at some field areas, the non-conductive heat transfer processes (Outcalt et al. 1990) do not appear to be necessary for the zero curtain effect to develop because the zero curtain effect is seen both at the sites without non-conductive heat transfer and it is also well developed in the model without non-conductive heat transfer.

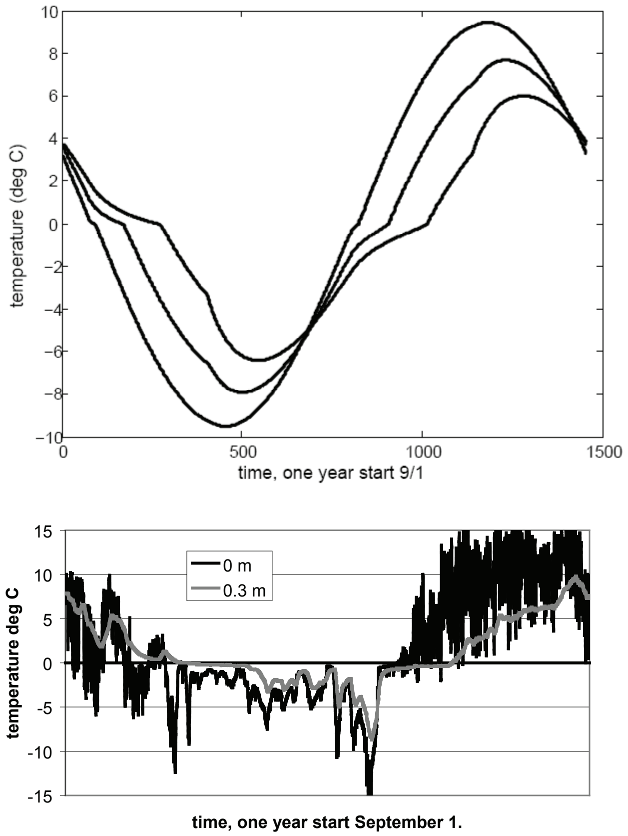

Figure 3. A. Modeled soil temperatures over one year at 0.1, (largest amplitude) 0.5, and 1.0 m (smallest amplitude) below ground surface. Mean annual temperature of the surface forcing is 0°C. B. Measured soil temperatures over one year at the USDA SCAN site #2065, Aniak, AK, USA (USDA, 2007). Note the absence of the zero curtain in the fall and spring in both model and observations.

Two phase change boundaries in close proximity bracket the domain of the soil where zero curtain effect is seen (Osterkamp & Romanovsky 1997). However, as shown in this paper the first order explanation for both the presence of the two phase change boundaries, and the zero curtain effect is the annual evolution of the soil thermal profile which clearly predicts the timing (fall and/or spring) of the zero curtain effect.

When soil temperatures from real field sites are studied it is important to keep in mind that seasonal snow cover may affect the soil thermal forcing and render the annual soil surface temperature cycle significantly different from the modeled sinusoidal annual thermal wave.

Conclusions

If zero curtain effect was caused only by release or consumption of the latent heat in the soil then there should be symmetrically a zero curtain both in the fall and spring. Or at the least there should be a zero curtain effect present in the fall in both permafrost underlain and seasonally frozen soil which is not the case.

For the clear conceptual description of the occurrence of the zero curtain effect let's assume that the soil surface thermal forcing follows a simple sinusoidal pattern that repeats itself in the annual time scale. When the forcing temperature at the soil surface crosses 0°C and approaches the mean annual soil temperature, the near surface soil thermal profile becomes inverted and a section of the soil just below it becomes nearly isothermal near 0°C. Two separate phase change fronts develop in the soil as pointed out by Osterkamp & Romanovsky (1997). The soil domain in between of the two phase change fronts quickly approaches 0°C and the zero curtain effect develops. However, when the forcing temperature at the soil surface crosses 0°C again approximately six months later in the following transitional season (either spring or fall depending on the case) and diverges further from the mean annual soil temperature, the near surface soil temperature inversion underlain by a nearly isothermal soil domain develop again, but at this time the isothermal soil is thermally far from 0°C and no phase change is present. Without phase change the isothermal soil quickly develops a monotonic thermal gradient and consequently only one phase change front develops. Therefore no zero curtain effect is present.

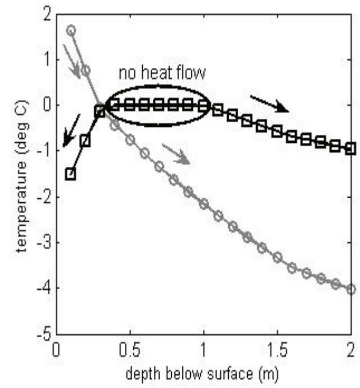

Figure 4. Modeled soil vertical thermal profiles for spring (gray) and fall (black) for a soil with mean annual thermal forcing of -5°C. The segment of the profile marked with black oval represents the zero curtain. As is illustrated by the spring (gray) profile the presence of significant thermal gradient at this time ensures that all levels of the soil are warming in concert and zero curtain can not develop. In the fall the soil at 0.5–1.0 m below surface quickly reaches freezing point and the thermal gradient vanishes. Therefore no heat flows through this segment of soil and the temperatures remain at or near 0°C until all the water has frozen. The black and gray arrows show the direction of heat flow during fall and spring respectively.

The above explanation highlights the importance of the soil thermal regime and annual thermal evolution in determining the timing and occurrence of the zero curtain effect. The phase change of water to ice or vice versa is necessary as well but it fails to explain the timing and the lack of zero curtain effect in fall in seasonally frozen soil.

It is also important to notice that the zero curtain is not only limited to condition where water is freezing (fall). In the case of seasonally frozen ground (mean annual soil temperature >0°C), the zero curtain appears in the spring when the soil ice is melting.

Acknowledgments

The author is grateful to the dynamic group of colleagues in the Quaternary Research Center, University of Washington, who have stimulated innovative research over the years. The manuscript was improved by the comments of two anonymous reviewers and an associate editor.

References

French, H.M. 1996. *The periglacial environment.* Harlow: Addison Wesley Longman Limited, 341 pp.

Hallet, B., Putkonen, J., Sletten, R. & Potter, N., Jr. 2004. Permafrost process research in the United States since 1960. In: A.R. Gillespie, S.C. Porter & B.F. Atwater (eds.), *The Quaternary period in the United States.* San Francisco: Elsevier, 584 pp.

Hinkel, K.M. & Outcalt, S.I. 1994. Identification of heat-transfer processes during soil cooling, freezing, and thaw in Central Alaska. *Permafrost and Periglacial Processes* 5: 217-235.

Hinkel, K.M., Outcalt, S.I. & Nelson, F.E. 1990. Temperature variation and apparent thermal diffusivity in the refreezing active layer, Toolik Lake, Alaska. *Permafrost and Periglacial Processes* 1: 265-274.

Hollingsworth, J., Downing, J. & Charlton, B. 2005. *BNZ-LTER Data Catalog, Bonanza Creek Experimental Forest: Hourly Soil Temperature at varying depths from 1988 to Present.* http://www.lter.uaf.edu/.

Osterkamp, T. & Romanovsky, V. 1997. Freezing of the Active Layer on the Coastal Plain of the Alaskan Arctic. *Permafrost and Periglacial Processes* 8: 23-44.

Outcalt, S.I., Nelson, F.E. & Hinkel, K.M. 1990. The Zero-curtain effect: Heat and mass transfer across an isothermal region in freezing soil. *Water Resources Research* 26(7): 1509-1516.

Putkonen, J. 1997. *Climatic control of the thermal regime of permafrost, northwest Spitsbergen*. Ph.D Dissertation Thesis. Seattle: University of Washington, 121 pp.

Putkonen, J., Sletten, R.S. & Hallet, B. 2003. Atmosphere/ice energy exchange through thin debris cover in Beacon Valley, Antarctica. In: M. Phillips, S.M. Springman & L.U. Arenson (eds.), *Eighth International Conference on Permafrost, Zurich, Switzerland, July 21–25, 2003*. Zurich, Switzerland: Swiss Federal Institute for Snow and Avalanche Research, Davos, Switzerland (CHE), 913-915.

Putkonen, J.K. 1998. Soil thermal properties and heat transfer processes near Ny Alesund, Northwestern Spitsbergen, Svalbard. *Polar Research* 17: 165-179.

Putkonen, J.K. & Roe, G. 2003. Rain on snow events impact soil temperatures and affect ungulate survival. *Geophysical Research Letters* 30(4): 200-204.

Turcotte, D.L. & Schubert, G. 1982. *Geodynamics, Applications of Continuum Physics to Geological Problems.* New York: John Wiley & Sons, 450 pp.

USDA, 2007. USDA, Soil Climate Analysis Network (SCAN) web page. http://www.wcc.nrcs.usda.gov/scan/.

van Everdingen, R. (ed.), 2005. *Multi-language glossary of permafrost and related ground-ice terms.* Boulder, CO: National Snow and Ice Data Center/World Data Center for Glaciology.

Washburn, A.L. 1979. *Geocryology: A survey of periglacial processes and environments.* Norwich: Fletcher & Sons Ltd, 406 pp.

Williams, P.J. & Smith, M.W. 1991. *The Frozen Earth: Fundamentals of Geocryology*. Oxford: Alden Press, 306 pp.

Definition of Warm Permafrost Based on Mechanical Properties of Frozen Soil

Jilin Qi
State Key Laboratory of Frozen Soil Engineering, Cold and Arid Regions Environmental and Engineering Research Institute, Chinese Academy of Sciences, 320 Donggang West Road, Lanzhou 730000, China

Jianming Zhang
State Key Laboratory of Frozen Soil Engineering, Cold and Arid Regions Environmental and Engineering Research Institute, Chinese Academy of Sciences, 320 Donggang West Road, Lanzhou 730000, China

Abstract

This paper attempts to give a definition of "warm frozen soil" according to the mechanical behavior of frozen soils with K_0 compression. K_0 compression tests were carried out on ice-rich frozen silty clay to investigate its straining properties. Three groups of samples were tested, with ice contents of 40%, 80% and 120%, respectively. The samples were compressed under a constant load and with stepped temperature rising from about -1.5°C to -0.3°C. Strain rates at different temperatures were examined. It was found that the strain rate at around -0.6°C increased abruptly. At the same time, strain rates under temperatures higher than -0.6°C were not as temperature-sensitive as was generally understood. Analysis of compressive coefficients was made on the data both from our own testing program and from the literature, which showed that at about -1°C was a turning point in the compressive coefficient against temperature. Based on both our work and taking into account the unfrozen water content vs. temperature, the range of -1°C to -0.5°C seems to be the temperature where the mechanical properties change greatly. For convenience, -1.0°C can be defined as the boundary for warm frozen soils.

Keywords: compressive coefficient; K_0 compression; strain rate; warm frozen soil.

Introduction

The mechanical properties of soils have been extensively studied in the last century. For unfrozen soils, various strength criteria and constitutive models have been proposed and applied to practice in geotechnical engineering. On the other hand, due to their sensitivity to temperature and ice content, the mechanical properties of frozen soils are more complicated, and many investigations have been carried out to study these properties (Jessberger 1980, Landanyi 1981, Morgenstern 1981, Sayles 1988). However, many of these studies were carried out on frozen soils at relatively low temperatures. When the temperature of frozen soil is close to 0°C, its plastic deformation must also be taken into consideration (Landanyi 1999), especially with high ice contents (Phukan 1983). Monitored temperatures of the soil layers underneath the embankments of the newly built Qinghai-Tibet railway on the Tibetan Plateau show that a warmer frozen zone formed after a certain period of time (Fig. 1). In this case, neither the theories for unfrozen soils nor those for cold frozen soils are suitable for describing the soils' mechanical properties. This kind of frozen soil can be named *warm frozen soil*.

In the literature, the term *warm frozen soil* is often used to describe a frozen soil at a relatively high temperature. However, what "warm" really means has not been clearly and logically defined. It is generally accepted that a warm frozen soil has higher unfrozen water content and therefore has less ability to resist loads and is more temperature-sensitive (Tsytovich, 1975). For these materials, the mechanical properties should be used to define the temperature boundary between "warm" or "cold" frozen soils. Tsytovich (1975) defined temperature boundaries for stiff and plastic frozen soils for different soil classifications according to their failure characteristics, for instance, -0.3, -0.6, -1.0 and -1.5°C for fine sand, silty sand, silty clay, and clay. This is reasonable because the fine grains lower the freezing temperature to a certain degree. However, these definitions are difficult to apply to engineering practice. On the one hand, failure is only the ultimate stage of loading for the safety of engineering constructions. On the other hand, from the point of view of engineering practice, a simple boundary may be convenient for engineers to follow, as long as it is reasonably accepted.

During construction of the Qinghai-Tibet railway on the Qinghai-Tibetan Plateau, a preliminary rule was made where *warm permafrost zone* was defined as the region with a mean annual ground temperature higher than -1°C. This was mainly based on the investigation of damage to embankments of the Qinghai-Tibetan highway. It is a rather geographical definition (Preliminary Regulations for Design of the Qinghai-Tibet Railway in Permafrost Regions, 2002). Where the frozen soil is concerned, it would be more rational to take into account the mechanical properties to define what a warm frozen soil really is. In this field, much confusion can be found from previous studies. For instance, Shields et al. (1985) studied the creep behavior of sand at a temperature between -2.5°C and -3.0°C, and called that warm permafrost. Foster et al. (1991) studied permafrost with a temperature of about -1°C which was regarded as warm permafrost. It is recognized that the term *warm* is a rather relative definition without a clear and reasonable basis.

In this paper, silty clay obtained from the Qinghai-Tibetan plateau along the newly constructed railway was

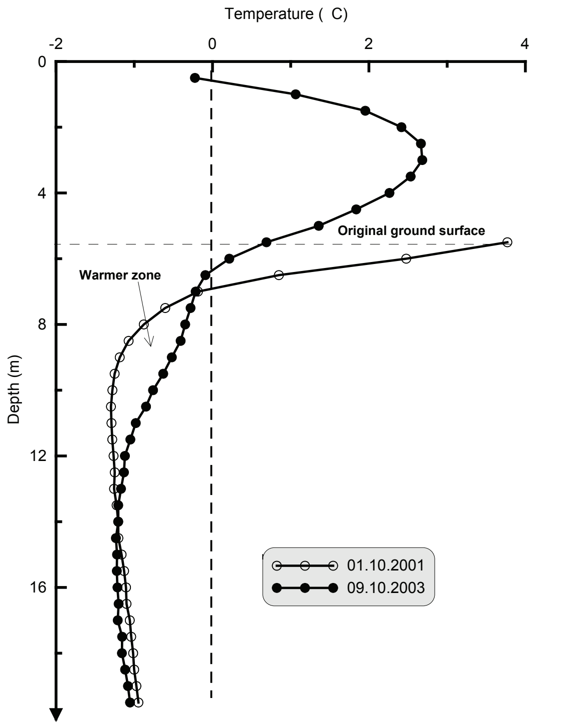

Figure 1. A warmer frozen zone formed in the layers underneath the embankment of the Qinghai-Tibet railway.

studied using K_0 compression under constant load and stepped temperature. The strain rate at each temperature step was studied. Data from the literature on the relationship between the compressive coefficient and temperature were re-analyzed. Based on these two testing programs, the temperature boundary for warm frozen soils as a material will be defined.

Description of the Testing Program

In the study of the mechanical properties of warm frozen soils, the temperature must be controlled precisely. To meet this demand, a new apparatus was designed, where a refrigerator was combined with a fan to control the temperature. An oedometer was placed in the box of the refrigerator for K_0 compression tests, as is shown in Figure 2. From the results, it can be seen that the temperatures could be controlled very well, and temperatures showed only small variations as will be seen in the next section of this paper.

The soil obtained along the Qinghai-Tibet Railway has a plastic limit and liquid limit of 18.8% and 36.5%, respectively. Its grain size distribution is shown in Figure 3. The freezing temperature of the soil is -0.2°C. Soil samples were prepared with ice contents of 40%, 80% and 120%. The dimensions of the samples were 61.8 mm in diameter and 40 mm in height. Loads of 0.1, 0.2 and 0.3 MPa were applied. Altogether 9 tests were carried out on samples with different ice contents and different loads.

The samples were installed in the oedometer and then placed in the refrigerator box. The desired temperature of about -1.5°C in the box was kept constant for 24 h, then

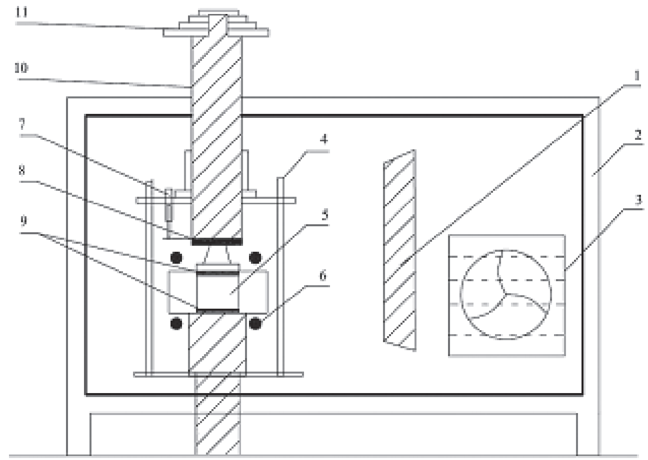

1、Heater 2、Refrigerator box 3、Fan 4、Support frame
5、 Soil sample 6、Temperature sensor 7、Displacement sensor
8、Stress sensor 9、Permeable disc 10、Plunger
11、Standard poise

Figure 2. Sketch of the apparatus for precise temperature controlled K_0 testing.

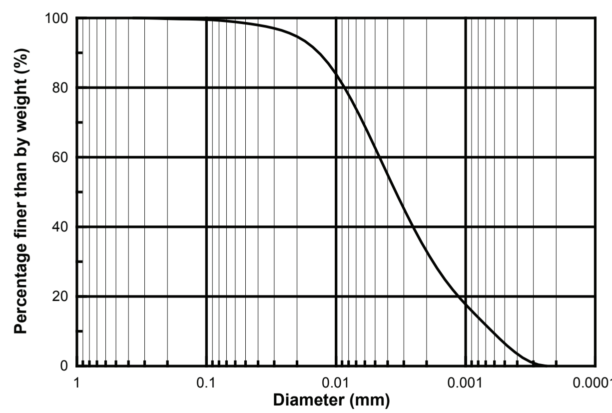

Figure 3. Grain size distribution of the tested soil.

a load was applied to the sample. When the strain became constant, the next higher temperature was adjusted and new strain occurred. In all, 5 temperature steps were applied in each test, approximately -1.5, -1.0, -0.6, -0.5 and -0.3°C.

Test Results and Discussion

Strain rate vs. temperature in this testing program

Figure 4 shows the development of strain against time with change in temperature for the soil with an ice content of 40%. It can be seen that at every step the temperature was controlled quite well, even at higher than -0.5°C. From the three tests shown in Figure 4, it seems that when the temperature rose above a certain value, the strain developed more quickly. This phenomenon was also found in the other 6 tests. In this paper, the strain rate at each temperature step was used for analysis. The strain rate is defined as the inclination of the tangent line at the starting point of the new strain-time curve when the temperature rose to a new step, as is shown in Figure 4 (a).

Five strain rates corresponding to the five temperature steps were obtained from each test, allowing a curve of strain rate against temperature to be plotted. Nine curves were obtained from the 9 tests in the whole program. These are all shown in

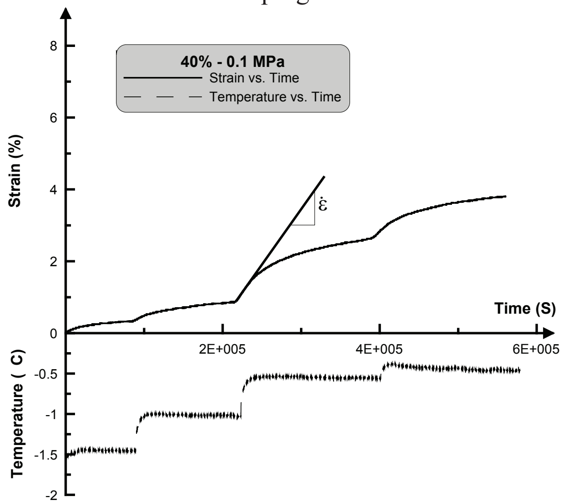

a. Ice content 40% and load of 0.1 MPa.

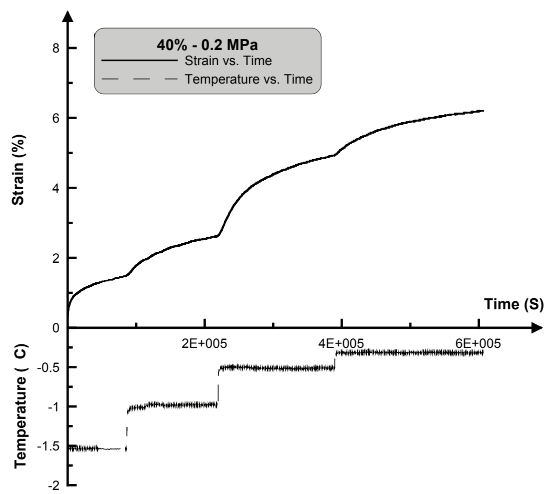

b. Ice content 40% and load of 0.2 MPa.

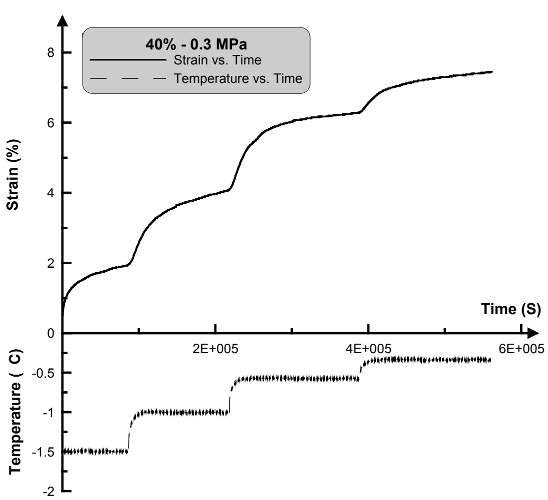

c. Ice content 40% and load of 0.3 MPa.

Figure 4. Temperature change with time and the corresponding strain development for the soil with water content of 40% and loads of 0.1, 0.2, and 0.3 MPa.

Figure 5. It can be seen in Figure 5 that the strain rate increased with the increase in temperature up to about -0.6°C, then decreased dramatically. In previous studies it was thought that, with a small increase in temperature, the mechanical properties for the warm frozen soils would change greatly. However, this is not found (see Fig. 4). The strain rates increased again when the temperature rose to about -0.2°C, which was very close to the freezing point of the soil.

It should be pointed out that the data corresponding to the first temperature step (about -1.5°C) were excluded in order to get rid of the influence induced by the experiment setup.

Compressive coefficient

Another mechanical property, the compressive coefficient (C), was examined in this work. This parameter was defined as the ratio of the strain to the corresponding load range by the following formula:

$$C = \frac{\Delta \varepsilon}{\sigma_2 - \sigma_1} \tag{1}$$

In this paper, C is the change in strain when stress increases from 0 to 0.2 MPa. Figure 6 shows that for the soil used in this testing program, C decreases with the decrease in temperature, and -0.6°C seems to be the turning point.

Confined compression of frozen soils was also studied by Zhu et al. (1982). In their testing program, a silty clay from the Qinghai-Tibet plateau and a medium-grained sand from Lanzhou were tested under different temperatures with stepped load. For the silty clay, different water content ranges were also investigated The temperatures investigated were in a relatively wide range from -0.5°C to -7.0°C, and the applied load was up to 0.8 MPa.

The relationship between the compressive coefficient of the silty clay and temperature at different water content range is shown in Figure 7. It can be seen that with the decrease in temperature, the compressive coefficient decreases. The turning points are all near a temperature of about -1°C. The frozen Lanzhou sand showed similar results.

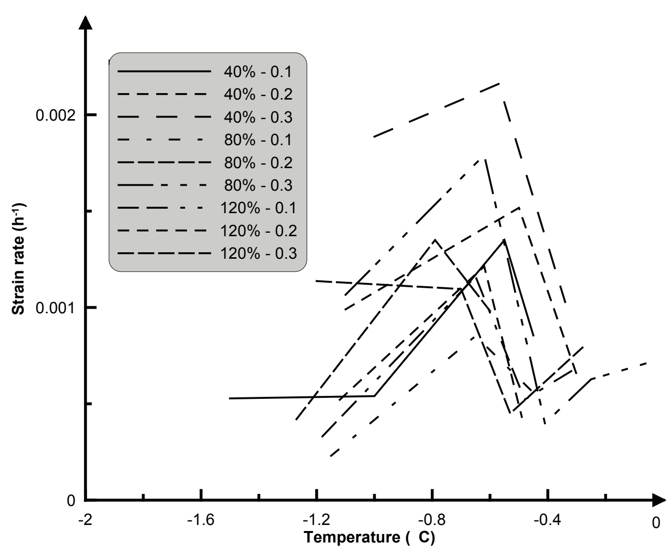

Figure 5. Strain rate against temperature (40% – 0.1: 40% refers to the water content, and 0.1 in MPa is the applied load).

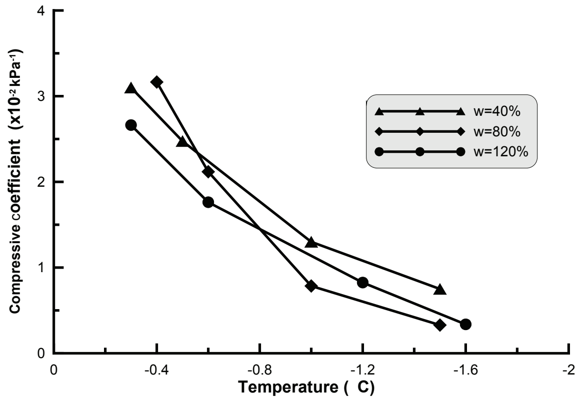

Figure 6. Compressive coefficient against temperature for silty clay in own testing program.

Unfrozen water content vs. temperature

It is widely accepted that changes in mechanical properties of frozen soils are due to changes in unfrozen water content with temperature. Loads also lower the freezing point of water in frozen soils, but this is only noticeable under loads of tens of MPa (Chamberlain et al. 1972). In the loading range discussed in this paper, this effect can be ignored.

The unfrozen water content of the soil in the tests carried out for this investigation was measured using Nuclear Magnetic Resonance (NMR) in a separate testing program. Figure 8 shows the relationship between unfrozen water content and temperature of the soils in these tests and in the work by Zhu et al. (1982). Both soils show that the unfrozen water content increases with an increase in temperature. For both soils, the most rapid change of unfrozen water content occurs within the temperature range of about 0～-1.0 °C. Considering that both testing programs showed that the mechanical properties changed more rapidly at temperatures between -0.6°C and -1.0°C, it seems reasonable that the temperature boundary for warm frozen soils should be -1.0°C. This is also in accordance with the temperature boundary for the warm permafrost zone in permafrost engineering.

This temperature boundary is based on testing data on sand and silty clay which are often encountered in engineering practice in permafrost regions on the Qinghai-Tibet plateau. On rare occasions variations can be expected. For instance, Tsytovich (1975) pointed out that for clayey soils with montmorillonite minerals, the temperature boundary for stiff and plastic frozen soil could be as low as -5.0°C.

Conclusions

As a material, the temperature boundary of warm frozen soils should be defined by mechanical properties. According to the tests carried out and the testing program in the literature on sand and silty clay, it can be concluded that -1.0°C should be defined as the temperature boundary for warm frozen soils. This seems reasonable taking into consideration the relationship between unfrozen water content and temperature. It is also convenient for the engineers because it coincides with the temperature boundary for the "warm permafrost

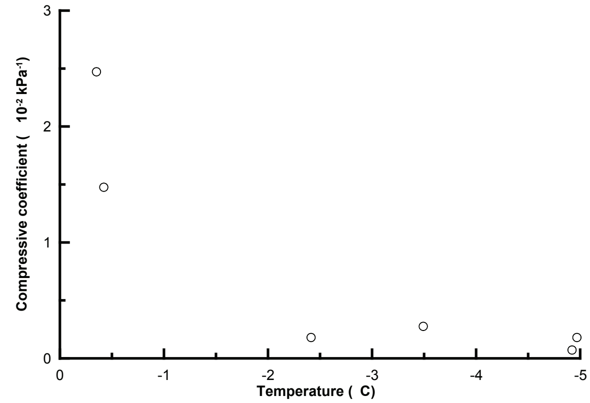

a. Water content of less than 17%.

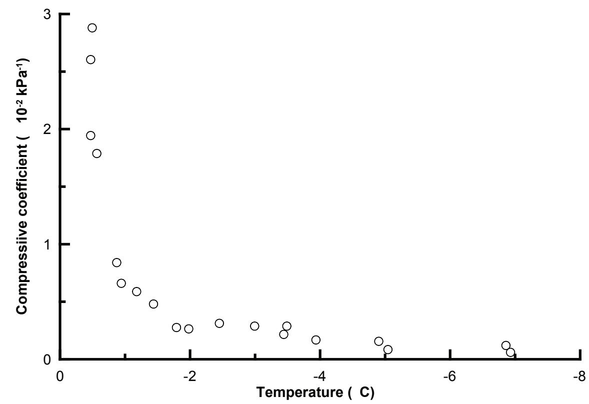

b. Water content of 18%-28%.

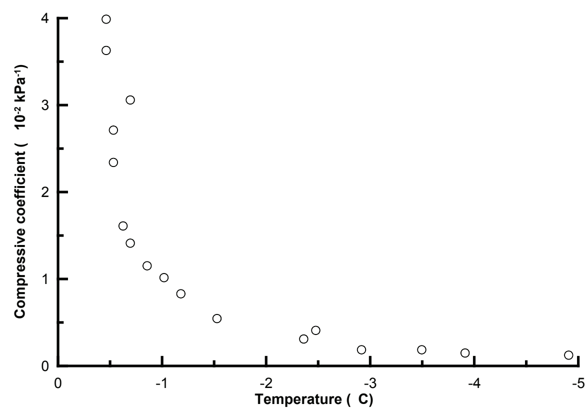

c. Water content of 30%-40%.

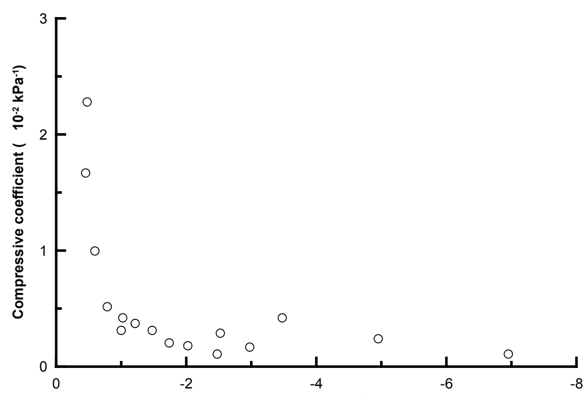

d. Water content of 50%-90%.

Figure 7. Compressive coefficient vs. temperature for the silty clay at different water content range (after Zhu et al. 1982)

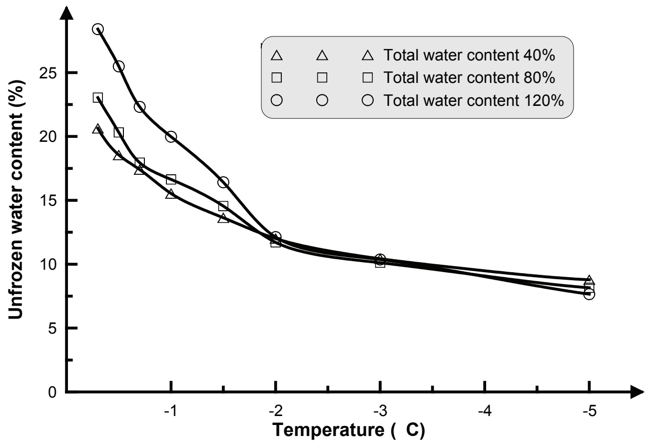

a. Soil tested in this program.

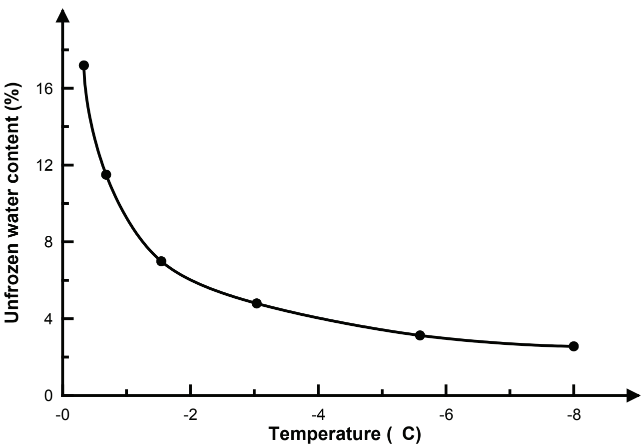

b. Soil tested by Zhu et al. (1982).

Figure 8. Unfrozen water content against temperature.

zone." Previous ideas that the mechanical properties of frozen soils would change dramatically with any small change in temperature was not found in the relationship between the strain rate and temperature.

Acknowledgments

This work was supported by the Hundred Young Talented Scientists Program of the Chinese Academy of Sciences granted to Dr. Jilin Qi. The authors thank Mr. Bo Zheng for his great efforts in performing the testing program.

References

Chamberlain E, Groves C. & Perham J. 1972. The mechanical behavior of frozen earth materials under high pressure triaxial test conditions. *Geotechnique* 22(3): 469-483.

First Survey and Design Institute of the Chinese Railway Ministry. 2001. Preliminary Regulations for Design of the Qinghai-Tibet Railway in Permafrost Regions. (unpublished).

Foster, M.L., Washburn, D.S. & Foote, D.S. 1991. OTH-backscatter power plant foundation design for warm, ice-rich permafrost soils. *Proceedings of the International Arctic Technology Conference. Anchorage, AK, USA, May 29–31, 1991*: 471-480.

Jessberger, H.L. 1980. State-of-the-art report - Ground freezing, mechanical properties, processes and design. *Engineering Geology* 18(1-4): 5-30.

Ladanyi, B. 1999. Creep behaviour of frozen and unfrozen soils: A comparison. *Proceedings of the Tenth International Conference, Lincoln, NH, USA, August 16-19, 1999*: 173-185.

Landanyi, B. 1981. Mechanical behavior of frozen soils (A). *Proceedings of the International Symposium on the Mechanics Behavior of Structure Media. Ottawa, Canada, May 18–21, 1981*: 205-245.

Morgenstern, N.R. 1981. Geotechnical engineering and frontier resource development. *Geotechnique* 31(3): 305-365.

Phukan, A. 1983. Long-Term creep deformation of roadway embankment on ice-rich permafrost. *Proceedings of the Fourth International Conference on Permafrost*, *Fairbanks, AK, USA, July 17–22, 1983*: 369-373.

Sayles, F.H. 1988. State of the art: Mechanical properties of frozen soil, mechanical properties of frozen soil. *Proceedings of the Fifth International Symposium on Ground Freezing, Nottingham, England, July 26-28, 1988* (1): 143-165.

Shields, D.H., Domaschuk, L., Man, C-S. & Kenyon, R.M. 1985. Deformation properties of warm permafrost. *Strength Testing of Marine Sediments: Laboratory and In-Situ Measurements*. San Diego, CA, January 26–27, 1984: 473-486.

Tsytovich, N.A. 1975. *The Mechanics of Frozen Ground.* Washington, DC: McGraw-Hill, Scripta Book Company, 426 pp.

Zhu, Y.L., Zhang, J.Y. & Wu, Z. W. 1982. Elastic and compressive deformation of frozen soils. *Proceedings of the Third International Symposium on Ground Freezing*. U.S. Army Corps of Engineers Cold Regions Research and Engineering Laboratory, Hanover, NH, USA, June 22–24, 1982: 65-77.

Active Layer Temperature Monitoring in Two Boreholes in Livingston Island, Maritime Antarctic: First Results for 2000–2006

M. Ramos
Department of Physics, University of Alcalá, Spain
G. Vieira
Centre for Geographical Studies, University of Lisbon, Portugal
J.J. Blanco
Department of Physics, University of Alcalá, Spain
S. Gruber
Glaciology and Geomorphodynamics Group, Department of Geography, University of Zurich, Switzerland
C. Hauck
Institute for Meteorology and Climate Research, Forschungszentrum Karlsruhe/University of Karlsruhe, Germany
M.A. Hidalgo and D. Tomé
Department of Physics, University of Alcalá, Spain

Abstract

This paper describes the active layer thermal regimes in two shallow boreholes, Sofía 275 m a.s.l. and Incinerador 35 m a.s.l., for which the ground temperature series has been recorded continuously from 2000 to 2006. The monitoring sites are located in Livingston Island, South Shetland Archipelago, Antarctica. This is one of the most sensitive regions of Earth to climate change, with a major warming trend over the last 50 years, of ca. +2.5ºC in the Mean Annual Air Temperatures (MAAT). This region is located near the climatic limit of permafrost, since MAAT at sea level is close to -2ºC. Lineal fits of the ground temperatures series for the study period at different depths in these boreholes show positive slopes. An outcome from the analysis of freezing and thawing indexes is that most of the ground warming seems to concentrate in the summer.

Keywords: active layer; freezing index; shallow boreholes; ground temperatures.

Introduction

The climate of the Antarctic Peninsula region has experienced a major warming trend over the last 50 years with annual mean air temperatures at Faraday/Vernadsky station having increased at a rate of 0.56ºC/decade and 1.09ºC/decade during the winter (King 1994, Turner et al. 2005).

Several factors contributing to the anomalous warming in the Antarctic Peninsula and the Weddell Sea region have been proposed, some of them related to the increase in westerlies observed over the last 30 years (Marshall 2002).

Increasing air temperatures and precipitation may cause the degradation or even the disappearance of permafrost in the sporadic permafrost zone, where current climatic conditions produce near-zero annual air temperatures, like in the South Shetlands Islands, north of the Antarctic Peninsula.

The energy exchange between the ground surface and the atmosphere depends on the radiation balance, ground heat fluxes and turbulent heat fluxes at the ground and snow surfaces. These are especially complex in the alpine or polar maritime areas, where the relief is mountainous and snow cover influence is particularly strong (Van Lipzig et al. 2004, King & Turner 1997, King et al. 2003). The seasonal snow cover, which presents a barrier to ground heat loss in winter, is a leading factor in the ground thermal regime and active layer depth (Romanosky & Osterkamp 2000, Ling & Zhang 2004). Snow has a high surface albedo and high emissivity, inducing cooling of the snow surface, while its low thermal conductivity makes it a good insulator. The ground heat flux is another important magnitude in the energy balance and the main factors that control it in permafrost terrain are: (i) moisture content in the active layer, (ii) thaw effects at the free boundary, and (iii) non-conductive heat transfer effects (variable thermal diffusivity).

The active layer thickness and dynamics are extremely important factors in polar ecology. Since most exchanges of energy, moisture, and gases between the atmospheric and terrestrial systems occur through the active layer, its thickening has important effects on physical, geomorphic, hydrologic and biological processes (Nelson & Anisimov 1993). Furthermore, the issue of active layer response to climate change is of increasing concern, particularly in what respects to its degradation and consequent physico-chemical influences on the biogeochemical cycle of carbon and on global change modeling (Anisimov et al. 1997, Osterkamp 2003).

Compared to the Arctic, very little is known about Antarctic permafrost (Bockheim 1995). In 2004 only 4 active layer boreholes were being monitored in the Antarctic Peninsula Region and a number as small as 21 in the whole Antarctic region (Bockheim & Hall 2004). Complex logistical and maintenance problems and the remoteness of the Antarctic are the main causes for this scarcity. The limited knowledge of the ground temperature conditions led to a recent effort in order to increase active layer and permafrost research in the Antarctic under the framework of international programs. Two core projects of the International Polar Year 2007–08 where Antarctic permafrost plays a central role are under way: ANTPAS – Antarctic and Sub-Antarctic Permafrost, Soils and Periglacial Environments and TSP – Permafrost Observatory Project - Thermal State of Permafrost (Guglielmin 2006, Bockheim & Hall 2004). The present research is integrated in these projects and intends to monitor and model the active layer temperature regime in two shallow boreholes in Livingston Island (South Shetland Islands, Antarctic Peninsula) (Ramos & Vieira 2003, Ramos et al. 2007).

The study's ultimate aim is to document the influence of climate change on permafrost degradation in this area which has a very strong influence on the regional climate warming.

Study Area

Livingston Island is located in the South Shetlands Archipelago at (62º39′S, 60º21′W) (Fig. 1). The climate at sea level is cold oceanic, with frequent summer rainfall in the low areas and a moderate annual temperature range. The climate reflects the strong influence of the circum-Antarctic low-pressure system. Meteorological conditions in summer are dominated by the continuous influence of polar frontal systems (Simonov 1977, Styszynska 2004). Relative humidity is very high, with average values ranging from 80 to 90%.

Data from different stations in King George Island (South Shetlands Archipelago) show a mean annual air temperature of -1.6ºC near sea level and an annual precipitation of about 500 mm. Data that we collected in Livingston Island at 15 m a.s.l. show a MAAT from -3.2ºC to -1.5ºC. From April to November, average daily temperatures at sea level generally stay below 0ºC and from December to March they are generally positive. The MAAT (2003 to 2006) at 275 m a.s.l. in Reina Sofia Hill, near the Sofía borehole, was -4.2ºC. This corresponds to a lapse rate of -0.8ºC/hm and to an air freezing season about 1 month longer than at sea level.

Permafrost in the South Shetland Islands is widespread above the Holocene raised-beaches (ca. 30 m a.s.l.) (Serrano & López-Martinez 2000). Meteorological and geophysical data indicate that environmental conditions close to sea-level are marginal for the maintenance of permafrost (Hauck et al. 2007).

Figure 1. Location of the study area in Livingston Island. Black areas represent glacier free terrain (SAS – Spanish Antarctic Station).

Table 1. Freezing season length (in days) in Incinerador and Sofia boreholes from 2000 to 2006. Temperatures at 15 cm depth at 30 min intervals.

Year	INC	SOFIA	Sofia-INC
1999		273	
2000	197	238	41
2001	211	294	83
2002	201	294	93
2003	225	332	107
2004	211	290	79
2005	176	246	71
2006	197	262	65
Mean	203	279	76

Methodology

Shallow boreholes

Borehole sites are in the vicinity of the Spanish Antarctic Station Juan Carlos I in Livingston Island. One of them is located at Reina Sofia hill (275 m a.s.l., 0.9 m active layer thickness) in a diamicton with a water content of 22.1% in saturation conditions. The other borehole is located at Incinerador point (35 m a.s.l., 2.4 m of seasonal frost, with possible permafrost below) in quartzite bedrock with negligible interstitial water content. Both boreholes were drilled in 2000, providing a 7-year series of active layer temperatures.

Thermal diffusivity, calculated by analyzing cuasi-stationary sinusoidal temperature signals using inverse modeling (Blanco et al. 2007), has a mean winter value in the Incinerador borehole of 1.5 10^{-6} ms^{-2} . In Sofía borehole, in winter the value is 0.55 10^{-6} ms^{-2} (Ramos & Vieira 2003).

In the Incinerador borehole a chain composed of six data loggers measures temperatures at 5, 15, 40, 90, 150, and 230 cm depth. At Sofia borehole, four temperature dataloggers are installed at 5, 15, 40, and 90 cm. The logging interval is 30 min and the accuracy of the data loggers (Tiny Talk Gemini Co.) is 0.2ºC. Due to data logger limitations during the first years the series present a short period with lack of data for the thawing season in both boreholes.

At the monitoring sites there is no vegetation and in the islands, mosses and grasses are very sparsely distributed.

Following the Berggren equation, active layer thickness is a square root function of the freezing index (Andersland & Ladany 1994). Freezing and thawing indexes have been calculated for different depths in Sofía and Incinerador boreholes and these are used to estimate the evolution of the active layer thickness.

Results and Discussion

The analysis of the ground temperatures is based on the comparison of the temperatures at 15 and 90 cm depths in both boreholes. Temperatures at 230 cm from the Incinerador borehole complement the analysis. In the Sofía borehole the mean ground temperatures at 15 and 90 cm, from 2000 to

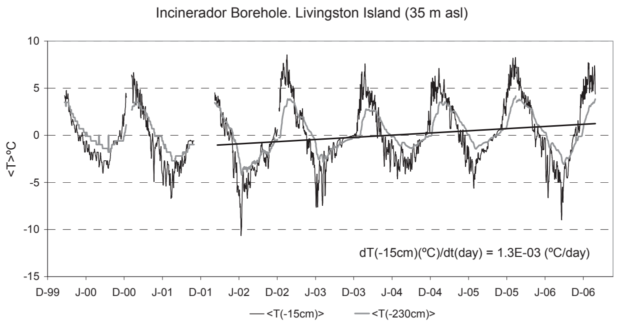

Figure 2. Temperatures at the Incinerador borehole from 2000 to 2006 at 15 and 230 cm depth. The lineal fit corresponds to the 15 cm sensor for the period of 2002–2006.

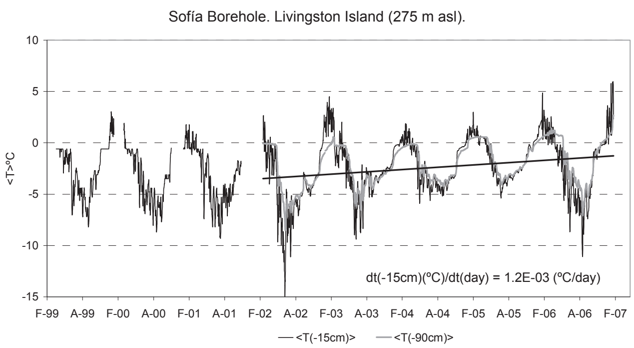

Figure 3. Temperature series at the Sofia borehole from 1999 to 2006 at 15 and 90 cm depth. The lineal fit corresponds to the 15 cm position sensor for the period of 2002–06.

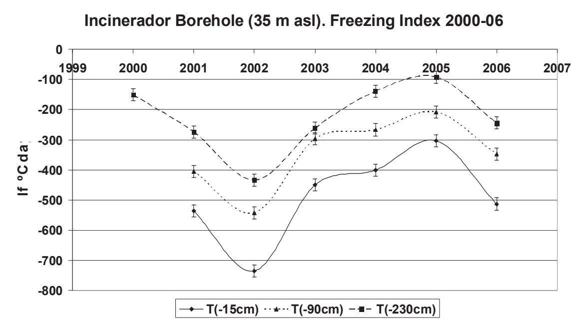

Figure 4. Incinerador freezing index evolution in the periods 2000 to 2006 at 15, 90, and 230 cm depth.

2006, were -2.6ºC and -2.1ºC respectively. In the Incinerador borehole (35 m a.s.l.) at the same depths, values of -0.1ºC and 0.2ºC were recorded for the same period. The differences between both places are close to the regional atmospheric lapse rate that has a value of -0.8ºC/hm (Ramos & Vieira 2003). The mean length of the freezing season in the Sofia site is 279 days per year, which is roughly two months longer than at the Incinerador site (see Table 1).

During the 7-year period the thermal regime in the Incinerador borehole showed the behavior of a typical annual period wave within a dry homogeneous material. Figure 2 shows the temperature oscillations around 0ºC at 15 and 230 cm. Signals at 15 and 230 cm are delayed more or less 5 days as a function of the ground thermal inertia.

Table 2. Lineal best-fit slopes (dT/dt x 10^{-3} ºC/day) of the daily ground temperatures in Sofía and Incinerador boreholes from 2002 to 2006.

depth (cm)	15	90	230
Incinerador	1.3	0.8	0.8
Sofía	1.2	1.2	--

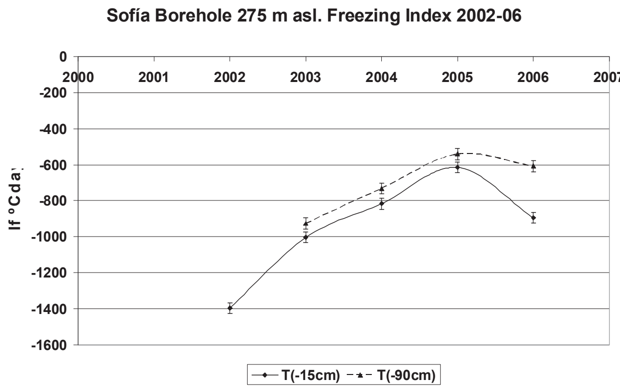

Figure 5. Sofía freezing index evolution in the periods 2002 to 2006 at 15 and 90 depth.

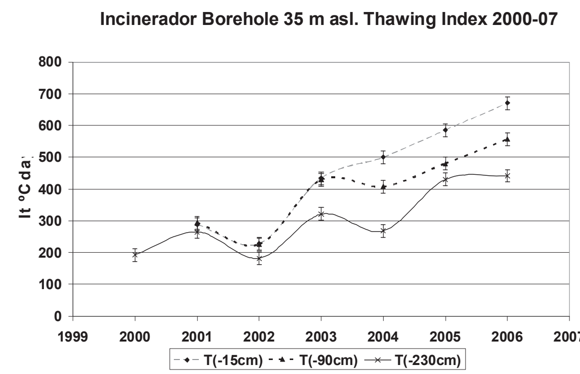

Figure 6. Incinerador thawing index evolution during the periods 2000 to 2006 at 15, 90, and 230 cm depth.

The lineal fit for the period with a complete data series for both boreholes (2002 to 2006) shows a warming trend at all depths, with similar values in both of them (see Table 2).

Direct observations in pits and temperature data show that from 1999 to 2002 the top of the permafrost table in Sofía borehole was at 90 cm, but since 2003 its depth increased.

Figure 4 shows the freezing index evolution in Incinerador borehole at 15, 90, and 230 cm depth. The curve shows a wave shape with a 5-year period and amplitude of more or less 300ºC-day. The mean at 15 cm depth for the period of 2002 to 2006 is -480ºC-day. In Sofía borehole (Fig. 5) the value for the same period, at the same depth is -945ºC-day.

Figure 6 shows the thawing index evolution from 2000 to 2006 at 15, 90, and 230 cm in the Incinerador borehole. In this period a very significant warming trend is observed at all depths, with, almost, a doubling of the thawing index. It changes from 300ºC-day at 15 cm depth in the summer of 2001, to more than 600ºC-day in the summer of 2006. Despite the short time-series, this trend seems to support a significant warming during the summer.

Conclusions

The scarcity of ground temperature data in the Maritime Antarctic has driven us to install shallow boreholes in Livingston Island. Theses are used for monitoring the impact of climate change on the active layer temperatures and on permafrost.

Lineal fits of the ground temperatures at different depths in Sofía (275 m a.s.l.) and Incinerador (35 m a.s.l.) boreholes show positive slopes. This confirms that the climate warming trend identified by other authors is contributing to ground warming. The similar positive slopes in both boreholes indicate that they are probably more influenced by a regional signal, than by local site-specific influences. The increase in active layer thickness at Sofia borehole has been confirmed by the direct observations of permafrost thaw at 90 cm depth. The short period of the data series limits the conclusions and therefore no absolute trends in the climate signal are presented here. An outcome from the analysis of freezing and thawing indexes is that most of the ground warming seems to concentrate in the summer. This is in agreement with climatological data for the Antarctic Peninsula region published by various authors.

Acknowledgments

We acknowledge the support from the MEC, Office of Spanish Polar Programs through the grant: CGL2005-25112-E/ANT. We thank the field support of the staff from UTM and Spanish Army in the Spanish Antarctic Station Juan Carlos I. This paper is integrated in IPY projects ANTPAS (ID. 33) and TSP (ID.50).

References

Andersland, O.B. & Ladany, B. 1994. *Frozen Ground Engineering.* Chapman & Hall, 352 pp.

Anisimov, O.A., Shiklomanov, N.I. & Nelson, F.E. 1997. Global warming and active layer thickness: results from transient general circulation models. *Global and Planetary Chang.* 15: 61-67.

Blanco, J.J. Tomé, D. Ramos, M. Vieira, G. Gruber, S. Hauck, C. & Hidalgo, M.A. 2007. *Active layer apparent thermal diffusivity and its dependence on atmospheric temperature (Livingston Island, Maritime Antarctic)*. U.S. Geological Survey and the National Academies, USGS OFR-2007, Extended Abstract, 1-4.

Bockheim, J. 1995. Permafrost distribution in Southern circumpolar region and its relation to the environment: a review and recommendations for further research. *Permafrost and Periglacial Processes* 6: 27-45.

Bockheim, J.G. & Hall, K.J. 2004. Permafrost, active layer dynamics and periglacial environments of continental Antarctica. *South Afr. J. Sci.* 98: 82-90.

Guglielmin, M. 2006. Ground surface temperature (GST), active layer, and permafrost monitoring in continental Antarctica. *Permafrost and Periglacial Processes* 17(2): 133-143.

Hauck, C., Vieira, G., Gruber, S. Blanco, J. & Ramos, M. 2007. Geophysical identification of permafrost in Livingston Island, maritime Antarctica. *J. Geophys. Res.* 112, (F02S19) doi:10.1029/2006JF000544.

King, J.C. 1994. Recent climate variability in the vicinity of Antarctic Peninsula. *Int. J. Climatol*. 14(4): 357-369.

King, J.C. & Turner, J. 1997. *Antarctic Meteorology and Climatology.* Cambridge: Cambridge University Press: 114-120.

King, J.C., Turner, J., Marchall, G.J., Connolley, W.M. & Lachlan-Cope, T.A. 2003. Antarctic Peninsula variability and its causes as revealed by analysis of instrumental records. In: E. Domack et al., *Antarctic Peninsula Climate Variability.* Antarctic research series, AGU, 79: 17-30.

Ling, F. & Zhang, T. 2004. A numerical model for surface energy balance and thermal regime of the active layer and permafrost containing unfrozen water. *Cold Regions Science and Technology* 38: 1- 15.

Marshall, G.J. 2002. Analysis of recent circulation and thermal advection change in the northern Antarctic Peninsula. *Int. J. Climatol.* 22(12): 1557-1567.

Nelson, F.E. & Anisimov, O.A. 1993. Permafrost zonation in Russia under anthropogenic climate change. *Permafrost and Periglacial Processes* 4(2): 137-148.

Osterkamp, T.E. 2003. Establishing long-term permafrost observatories for active-layer and permafrost investigations in Alaska: 1977-2002. *Permafrost and Periglacial Processes* 14: 331-342.

Ramos, M. & Vieira, G. 2003. Active layer and permafrost monitoring in Livingston Island, Antarctic. First results from 2000 to 2001. *Proceedings of the Eighth International Conference on Permafrost, Lisse, Zurich*: 929-933.

Ramos, M., Vieira, G., Gruber, S., Blanco, J.J., Hauck, C., Hidalgo, M.A., Tomé, D., Neves, M., & Trindade, A 2007. *Permafrost and active layer monitoring in the Maritime Antarctic: Preliminary results from CALM sites on Livingston and Deception Islands*. U.S. Geological Survey and the National Academies, USGS OF-2007-1047, Short Research Paper 070, doi:10.3133/of2007-1047.srp070.

Romanovsky, V.E. & Osterkamp, T.E. 2000. Effects of unfrozen water on heat and mass transport processes in the active layer and permafrost. *Permafrost and Periglacial Processes* 11: 219-239.

Serrano, E. & López-Martínez, J. 2000. Rock glaciers in the South Shetland Islands, Western Antarctica. *Geomorphology* 35: 145-162.

Simonov, I.M. 1977. Physical geographic description of Fildes Peninsula (South Shetland Islands). *Polar Geography* 1: 223-242.

Styszynska, A. 2004. The origin of coreless winters in the South Shetlands area (Antarctica). *Polish Polar Research* 25: 45-66.

Turner, J., Colwell, S.R., Marshall, G.J., Lachlan-Cope, T. A., Carleton, A.M., Jones, P.D., Phil, V.L., Reid, A. & Iagovkina S. 2005. Antarctic climate change during the last 50 years. *Int. J. Climatol.* 25: 279-294.

Van Lipzig., N.P.M., King J.C. & Lachlan-Cope. T.A. 2004. Precipitation, sublimation, and snow drift in the Antarctic Peninsula region from a regional atmospheric model. *J. Geophys. Res.* 109: 24106-24132.

Circumpolar Relationships Between Permafrost Characteristics, NDVI, and Arctic Vegetation Types

Martha K. Raynolds and Donald A. Walker
University of Alaska Fairbanks

Abstract

An understanding of the distribution and characteristics of vegetation found on different types of permafrost is necessary input for modeling permafrost response to climate change. Interactions between climate and soil thermal regime are modified where vegetation exists, and >75% of permafrost on land in the Arctic is covered by non-barren vegetation types. A circumpolar spatial analysis was conducted to compare mapped permafrost characteristics with the Normalized Difference Vegetation Index (NDVI), mapped vegetation types, and environmental characteristics. A General Linear Model (GLM) analysis found that, when added to a model that included climate and lake cover, permafrost characteristics accounted for an additional 11% of the variation in NDVI. High ice content in permafrost had the strongest effect, lowering NDVI. Over 65% of areas with thin overburden is vegetated by low-stature, low-cover, low-biomass vegetation types that have little impact on thermal regimes. This climbs to >82% for areas that also have high ice content permafrost. Over 83% of areas with thick overburden have vegetation types with denser, taller vegetation, which alters the interaction between climate and permafrost. Including vegetation characteristics in permafrost models will be particularly important in areas with thick overburden and medium or high ice content.

Keywords: arctic vegetation; Circum-Arctic Map of Permafrost and Ground Ice Conditions; Circumpolar Arctic Vegetation Map; NDVI; permafrost.

Introduction

Permafrost, its characteristics, and its vulnerability to change are increasingly in the public eye as a result of attention focused on climate change and the Arctic. Climate change is occurring at a faster rate in the Arctic than other biomes and is resulting in an increase in temperatures in almost all parts of the Arctic (Comiso 2006, Hassol 2004). The effects on the Arctic Ocean have resulted in dramatic loss of summer sea ice, especially in the summer of 2007 (Comiso et al. 2008). The effects on land, both to permafrost and vegetation, are a focus of on going research, particularly during the 2008 International Polar Year.

Most permafrost, even in the Arctic, is covered with vegetation, and the interactions between the permafrost and the vegetation affect both the growing environment for arctic plants and the thermal environment of the permafrost. Permafrost strongly affects vegetation by affecting landscape and soil characteristics. Permafrost underlying the annually-thawed active layer limits soil drainage and results in cryogenic features such as polygons, gelifluction lobes, circles, and mounds (Washburn 1980). Permafrost ice content can raise surface elevations through aggradation or lower it due to degradation (Jorgenson et al. 2001). Permafrost affects the characteristics of the active layer, such as its depth, soil temperatures, and soil moisture (Schuur et al. 2007).

Vegetation affects permafrost by changing the thermal characteristics of the soil. Vegetation shades and insulates the soil, reducing the transfer of summer warmth (Kade et al. 2006, Shur & Jorgenson 2007). Vegetation also cools the surface through evapotranspiration. Vegetation has the opposite effect in winter; well-vegetated areas are insulated by the plants and the snow they trap, while unvegetated soils are more exposed to winter temperatures (Kade et al. 2006). The types and strength of the effect of vegetation on the climate-soil interactions vary with vegetation type and depend on the amount of total plant biomass, plant lifeforms, and continuity of plant cover (Kade et al. 2006, Walker et al. 2003).

In order to understand the effects of climate change on permafrost, it is important to understand the distribution of vegetation types in permafrost areas and the characteristics of those vegetation types that affect the thermal regime of the soil. This study compares vegetation distribution in the Arctic, the area north of the treeline, with permafrost characteristics. The vegetation was characterized using both a vector vegetation map and satellite raster data of the normalized difference vegetation index (NDVI). This spatial comparison of arctic vegetation types and NDVI with permafrost distribution help define areas where vegetation has the strongest influence on permafrost, with implications for the possible effects of climate change.

Methods

The permafrost map

The extent and ground ice content of permafrost and depth of overburden in the Northern Hemisphere (20°N to 90°N), were mapped on the Circum-Arctic Map of Permafrost and Ground-Ice Conditions (Brown et al. 1997, http://nsidc.org/data/ggd318.html), and summarized by Zhang et al. (1999). The map was printed at 1:10,000,000 scale, and the digital format at 12.5-km pixel resolution was used for this study. Permafrost extent was mapped as continuous (94% of Arctic land area), discontinuous (3%), sporadic (2%), or isolated (1%). Ground-ice content was divided into low

Table 1. Vegetation types of the Circumpolar Arctic Vegetation Map (CAVM Team 2003).

Code	Vegetation Type
B1	Cryptogam, herb barren
B2	Cryptogam barren complex (bedrock)
B3	Noncarbonate mountain complex
B4	Carbonate mountain complex
G1	Rush/grass, forb, cryptogam tundra
G2	Graminoid, prostrate dwarf-shrub, forb tundra
G3	Nontussock sedge, dwarf-shrub moss tundra
G4	Tussock-sedge, dwarf-shrub, moss tundra
P1	Prostrate dwarf-shrub, herb tundra
P2	Prostrate/Hemiprostrate dwarf-shrub tundra
S1	Erect dwarf-shrub tundra
S2	Low-shrub tundra
W1	Sedge/grass, moss wetland
W2	Sedge, moss, dwarf-shrub wetland
W3	Sedge, moss, low-shrub wetland

(54%), medium (15%), and high (31%) categories, referring to the volume of visible ice in the upper 10–20 m. Two landscape categories were mapped. Lowlands, highlands, and intra- and inter-montane depressions characterized by thick (>5–10 m) overburden (any soil or other material that lies above the bedrock horizon in a given area) cover 36% of Arctic land areas. Mountains, highlands, ridges, and plateaus characterized by thin (<5–10 m) overburden cover and exposed bedrock cover 64% of the Arctic.

Satellite data (AVHRR NDVI)

The normalized difference vegetation index (NDVI) is a measure of relative greenness calculated as: NDVI = (NIR -R) / (NIR + R*),* where NIR is the spectral reflectance in the near-infrared where reflectance from the plant canopy is dominant, and R is the reflectance in the red portion of the spectrum where chlorophyll absorbs maximally. NDVI has a theoretical maximum of 1 and its relationship to vegetation characteristics such as biomass, productivity, percent cover, and leaf area index is asymptotically nonlinear as it approaches 1. As a result, NDVI is less sensitive to ground characteristics at higher values and essentially saturates when leaf area index >1 (van Wijk & Williams 2005). This is not a severe problem in the Arctic where vegetation is often sparse and patchy; the mean NDVI for arctic land areas in the data set used in this study was 0.32, well below the saturation point (Raynolds et al. 2006).

NDVI values in the Arctic increase with the amount of vegetation as measured by leaf area index (LAI), phytomass, and productivity (Riedel et al. 2005, Shippert et al. 1995). NDVI values correlate well with ground characteristics of arctic vegetation and can be used to distinguish between vegetation types (Hope et al. 1993, Stow et al. 2004).

A 1-km-resolution maximum-NDVI data set was used for this study. These data were derived from the U.S. Geological Survey EROS AVHRR polar composite of NDVI data for 1993 and 1995 (CAVM Team 2003, Markon et al. 1995). Daily data were collected by AVHRR sensors onboard NOAA satellites for channel 1, red (0.5 to 0.68 μm) and channel 2, near-infrared (0.725–1.1 μm). Satellite measurement of NDVI is affected by a variety of conditions, especially cloud cover, viewing angle and seasonal variation, that can be compensated for by compositing data over time (Goward et al. 1991, Riedel et al. 2005). Daily NDVI values were composited into 10-day maxima. The maximum values of these composited data during two relatively cloud-free summers (11 July–31 August in 1993 and 1995) were used to create an almost cloud-free data set of maximum NDVI for the circumpolar Arctic in the early 1990s.

The vegetation map

The third data set used in this analysis was the Circumpolar Arctic Vegetation Map (CAVM Team 2003, http://www.arcticatlas.org/atlas/cavm). The map extent includes all land areas north of the northern limit of trees. The map was created at 1:7,500,000 scale with minimum polygon diameter of 8 km and is available digitally as a vector map. The integrated vegetation mapping approach used to create the vegetation map was based on the principle that a combination of environmental characteristics controls the distribution of vegetation. Vegetation-type boundaries were based on existing ground data and vegetation maps, bioclimate (Tundra Subzones A–E), floristic regions, landscape categories, elevation, percent lake cover, substrate chemistry, and surficial and bedrock geology, drawn on an AVHRR false-color infrared base map. The distribution of 15 arctic vegetation types (Table 1) was mapped and described on the CAVM, using a unifying circumpolar legend which enables analysis of the entire Arctic (CAVM Team 2003, Walker et al. 2005).

Analysis

In each of the permafrost categories the area of different vegetation types and average NDVI values were tabulated. Spatial-distribution characteristics were analyzed using GIS software. The CAVM was mapped at finer resolution than the permafrost map, so the most common permafrost category for each CAVM polygon was determined. Results of the analysis were summarized graphically, showing vegetation types occurring on different types of permafrost, using symbols proportional to area. The NDVI raster data were analyzed by calculating the average NDVI value for different categories within the permafrost map and summarizing these results using bar graphs. This analysis of over 7 million 1-km^2 pixels represents the true mean of the classes, so comparative statistical tests based on sampling were not appropriate.

General linear models (GLM) (R Development Core Team 2006) were run to determine the importance of permafrost variables in accounting for variation in NDVI in the Arctic. Attributes mapped as characteristics of the CAVM polygons, weighted by area, were used as input data. A basic model including variables known to be important in controlling NDVI (Raynolds et al. 2006) was run first, using the CAVM classes for bioclimate zone and percent lake cover. These variables accounted for the latitudinal variation in NDVI due to climate, and for the reduction in NDVI due to cover of water (NDVI of water is essentially zero). Variables from the permafrost map: extent, ice content, overburden, and the combined code (a unique number for each combination of extent, ice content, and overburden) were added to the model one at a time to evaluate their effect on the model. The amount of variation accounted for by the different variables in each model and the significance of the variable in the model were tabulated.

Interdependence of data sets

Climate and landscape characteristics including slope, elevation, geologic and glacial history have important effects on all three variables: NDVI, permafrost and vegetation. In some cases these characteristics will vary together, especially in extreme conditions. For example, steep, high elevation mountains will generally have low NDVI, continuous, low ice-content permafrost with little overburden, and barren vegetation types. In more moderate terrain the type of vegetation which will grow on a given type of permafrost varies. In these areas the vegetation map and the NDVI data provide valuable information about the distribution of vegetation on different types of permafrost.

Results

Most of the Arctic has continuous permafrost underlying 4.68 million km^2 of land surface (excluding ice and water). Arctic areas without continuous permafrost include southern Greenland, European Arctic Russia, and in Alaska the Seward Peninsula and southern parts of the Kuskokwim River Delta. Continuous permafrost in the Arctic supports a mix of vegetation types. Over 83% of areas with thick overburden commonly is vegetated by erect shrub tundras (S1, S2), graminoid-shrub tundra (G3, G4), or low-shrub wetlands (W3) (Fig. 1). All of these vegetation types have relatively high stature, high biomass, and complete cover (Walker et al. 2005). Over 65% of areas with thin overburden have barren vegetation types (B1-B4), sparse graminoid (G1, G2), or prostrate dwarf-shrub (P1, P2) vegetation types with low stature, low biomass, and partial ground cover (Walker et al. 2005). Areas with thin overburden and high ice content are likely to be vegetated with either cryptogam, herb barrens (B1), graminoid, prostrate dwarf-shrub (G2), or prostrate dwarf-shrub herb tundra (P1), with >82% of these areas vegetated by vegetation types that have low-stature, low cover, and low biomass.

In areas of discontinuous permafrost, tussock tundra (G4) and erect-shrub (S1, S2) vegetation types are common. Areas with sporadic permafrost support mostly low-shrub vegetation (S2) and sedge, moss, low-shrub wetland (W3). Areas with isolated permafrost are dominated by non-carbonate mountain vegetation complexes (B3).

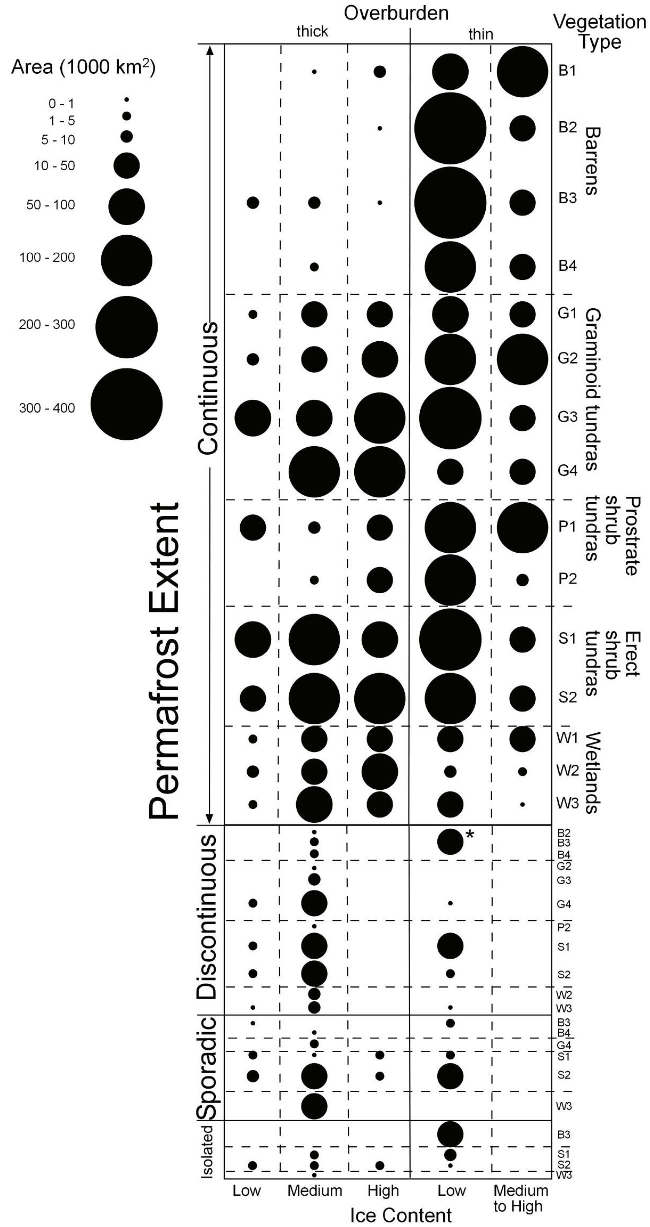

Figure 1. Area of Arctic in different types of permafrost categories (Brown et al. 1997) and different vegetation types (CAVM Team 2003). * The area represented by this symbol was all vegetation type B3.

Low ice-content permafrost is characterized by barren types (B2, B3) and shrub types (S1, S2). Medium ice-content permafrost supports graminoid- (G4) and shrub-dominated (S1, S2) vegetation, as well as wetlands (W3). High ice-content permafrost is most commonly vegetated by graminoid-dominated vegetation types (G2, G3, G4), prostrate dwarf-shrub (P1), or cryptogam barrens (B1).

Examination of the types of permafrost that characterize vegetation types reveals that only three vegetation types have <90% continuous permafrost: non-carbonate mountain complex (B3); low shrub tundra (S2); and sedge, moss, low-shrub wetland (W3). Vegetation types that occur mostly on low ice content permafrost include the barren types (B2,

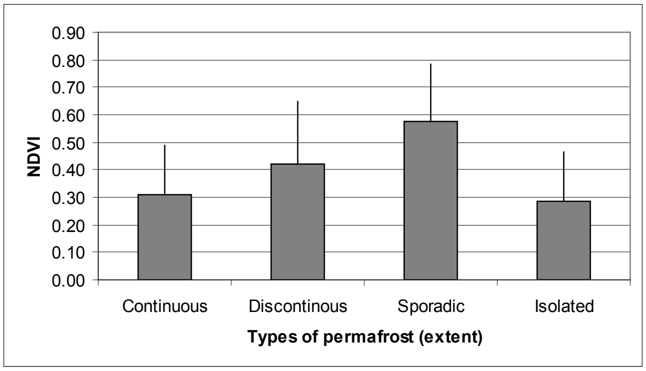

Figure 2. Average NDVI of Arctic areas with differing extent of permafrost (lines = s.d.).

B3, B4) and types common on the Canadian Shield (P2, S1). Cryptogam herb barrens (B1) characteristic of the High Arctic and wetland vegetation types (W1, W2, W3) occur mostly on medium or high ice content permafrost. Tussock sedge, dwarf-shrub, moss tundra (G4) occurs mostly on areas with thick overburden and medium or high ice content.

NDVI varied inversely with permafrost extent, increasing from continuous to discontinuous to sporadic (Fig. 2), as would be expected, following the climate gradient from colder to warmer (Raynolds et al. 2006). NDVI was lowest for isolated permafrost, which occurred mostly in the mountainous areas of southern Greenland, where steep slopes and exposed bedrock limit plant cover.

The largest differences in NDVI values occurred between overburden categories; NDVI was much greater in areas with thick overburden than with thin (Fig. 3). Thin overburden occurs in glaciated areas such as the Canadian Shield, on mountains, ridges, and plateaus. Thick overburden is less common in the Arctic and occurs at lower elevations and in depressions where sediments can accumulate. Areas with thick overburden are more commonly vegetated by graminoid (G3, G4) or erect-shrub (S1, S2) vegetation types with high NDVI values, while areas with thin overburden often have sparse vegetation with low NDVI values (B1, B2, B3, Fig. 1).

NDVI values varied less by ice content within overburden types (Fig. 3). High and medium-to-high ice-content permafrost had lower NDVI than average. Areas with thick overburden and high ice-content permafrost are largely covered with graminoid vegetation types, while medium ice-content permafrost areas are more commonly vegetated by shrub-dominated types (Fig. 1). Areas with thin overburden and medium-to-high ice-content permafrost mostly occur in high-latitude areas (such as the Canadian Arctic Islands), and have barren or sparse, prostrate vegetation (B1, P1, G2).

Permafrost characteristics accounted for 11.9% of the variation in arctic NDVI in a general linear model that included bioclimate zone, percent lake cover, and permafrost characteristics (Table 2). The CAVM variables accounted for 54.9% of the variation, with bioclimate zone responsible for 38.6% and percent lake cover for 16.3%. Permafrost ice content accounted for more of the remaining variation than either extent or depth of overburden.

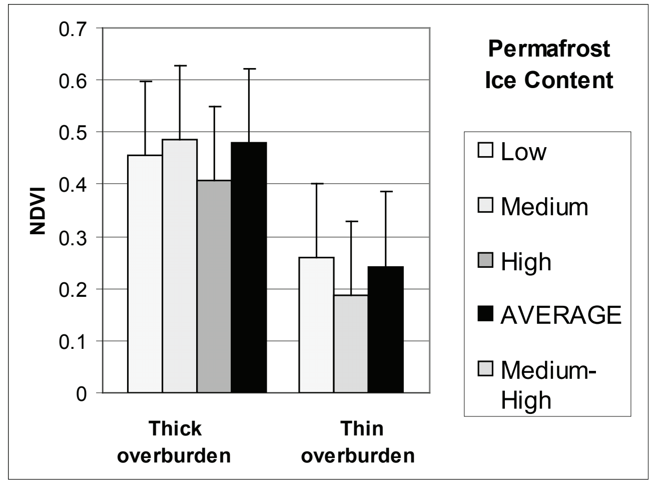

Figure 3. Average NDVI of Arctic areas with shallow vs. deep overburden over bedrock, and different levels of ice content (lines = s.d.).

Discussion

The comparison of the Circum-arctic Map of Permafrost and Ground Ice Conditions, the Circumpolar Arctic Vegetation Map, and satellite NDVI values emphasized the importance of the difference between areas with thick overburden (>5–10 m) and thin overburden (<5–10 m). The thick overburden areas had NDVI values almost twice as high as those of the thin overburden areas, indicating a much greater amount of vegetation cover (Shippert et al. 1995). NDVI would be expected to be lower in areas with thin soils, but the distinction between overburden <5 m and >5 m occurs far below the rooting depth of arctic plants. GLM models showed that once climate and percent lake cover were accounted for, overburden depth was much less important. Areas with thin overburden had more lake cover (especially on the Canadian Shield) and a more northerly distribution than areas with thick overburden, both effects reducing the average NDVI.

The model results showed that ice content correlated with variation in NDVI, and the map summaries showed that medium-high ice-content permafrost with thin overburden has especially low NDVI values. These conditions occurred mainly in the northern areas of the Arctic: the Canadian Arctic Islands and Novaya Zemlya.

About one quarter of the Arctic land area is covered by barren vegetation types. In these areas the vegetation plays a minimal role in the soil thermal regime, and the permafrost is climate-driven. The rest of the continuous permafrost in the Arctic would be considered climate–driven, ecosystem-modified permafrost, according to Shur & Jorgenson (2007). The effect of the vegetation modification is to reduce soil temperatures in summer and to increase them in winter (Kade et al. 2006). Vegetation types that have the most plant cover, thickest moss layers, and deepest organic soils insulate the soil most from summer warming (Kade et al. 2006). Types with the tallest vegetation trap the most snow in winter and

Table 2. Results of GLM analysis of variation in NDVI. Models included 3 variables, bioclimate subzone and percent lake cover plus one of the other variables. Results are from the Type 1 sums of squares, with terms added sequentially.

Model variables	% of variation in NDVI accounted for by variables	Significance (p)
Bioclimate zone	38.6	$< 2 \times 10^{-16}$
Percent lake cover	16.3	$< 2 \times 10^{-16}$
+ Permafrost ice content	6.1	$< 2 \times 10^{-16}$
+ Permafrost extent	4.2	$< 2 \times 10^{-16}$
+ Overburden	1.4	$< 2 \times 10^{-16}$
+ Permafrost combination	11.9	$< 2 \times 10^{-16}$

insulate the soils from winter cooling (Sturm et al. 2001).

The net effect of vegetation on soil thermal regimes depends largely on the thickness of the moss/peat layer and the height of the vegetation. For example, tussock tundra (G4) at Happy Valley on the North Slope of Alaska has a thick peat layer (12 cm) developed from dead tussocks and mosses, a relatively thick layer of live moss (5 cm), and also a dwarf-shrub layer (25 cm tall) (Walker et al. in press). The vegetative factors in tussock tundra decreasing absorption of summer warmth by the soil outweigh the factors warming the soil in winter, resulting in thinning of the active layer and aggradation of ice at the top of the permafrost (Shur & Jorgenson 2007). This process had been recognized by arctic researchers as paludification, a process whereby soils become progressively wetter and more acidic as reduced thaw depth restricts soil drainage (Mann et al. 2002, Walker et al. 2003). The shallower thaw and saturated soils in turn favor peat-producing species like sphagnum mosses and tussock sedges in a positively reinforcing cycle.

The vegetation types with characteristics resulting in the greatest effect on the soil thermal regime are graminoid-erect dwarf-shrub (G3, G4, W3) and erect-shrub (S1, S2) types (Walker et al. in press). These vegetation types are common in areas with thick overburden and medium or high ice-content permafrost, which occur mostly in the foothills and coastal plains of the southern Arctic. These vegetation types are also common in areas with thin overburden and low ice-content permafrost, which occur mostly on the Canadian Shield and mountainous areas.

Areas with thin overburden and low-ice content permafrost are shown as having mostly low to medium risk of subsidence due to climate change in a study that modeled IPCC climate predictions, soils, and permafrost data (Nelson et al. 2001). Risk of subsidence increases with ice-content, and areas with medium and high ice content permafrost on deep overburden are more commonly mapped as having medium or high risk of subsidence (Nelson et al. 2001).

Medium ice-content permafrost extends into discontinuous and sporadic permafrost where the permafrost is preserved by the effects of the vegetation (climate-driven, ecosystem-protected, Shur & Jorgenson 2007). Although researchers have recognized the importance of predicting the effects of climate change on permafrost in these areas because of the high risk of subsidence (Nelson et al. 2001), the complex interactions between the climate, the vegetation, and the soil are difficult to quantify. Vegetation cover varies from shrub- (42% S2, 13% S1) to graminoid-dominated (14% G4, 5% G3), and 20% of the area is wetlands (W3), in a mosaic of vegetation types with differing thermal attributes. Not surprisingly, different models project either thawing or persistence of this permafrost (Anisimov & Reneva 2006). Spatially detailed models that include vegetation data will be required to understand the effects of climate change on permafrost in these areas.

An additional complicating factor is that vegetation is not a static characteristic but will in many cases change in response to changes in permafrost. Changes in surface elevation and stability due to subsidence and erosion will change vegetation, usually to wetter types (Jorgenson et al. 2006). Increases in active layer depths in southern tundra are likely to increase shrubbiness (Schuur et al. 2007). Complete thawing of permafrost that allows previously saturated soils to drain will improve conditions for tree-line advance (Lloyd et al. 2003).

Conclusions

This study highlights both the effects of permafrost on vegetation, and conversely, the effects of vegetation on permafrost. A GLM analysis found that when added to a model that included climate and lake cover, permafrost characteristics accounted for an additional 11% of the variation in NDVI. High ice-content permafrost with shallow overburden was most strongly correlated with lower NDVI.

Over 75% of permafrost on land in the Arctic is covered by non-barren vegetation types, resulting in some degree of ecosystem-modification of the permafrost. Vegetation insulates the soil from both summer warmth and winter cold, with the net effect depending on vegetation characteristics. Thick moss layers and erect shrubs have the greatest effects on soil thermal regimes, and vegetation types with both occur in areas with medium to high ice-content permafrost and in areas of non-continuous permafrost. Including thermal characteristics of vegetation and the spatial distribution of different vegetation types, though complex, will be important for predicting the effects of climate change on permafrost in these areas.

Acknowledgments

Research for this publication was supported in part by a Univ. of Alaska International Polar Year (IPY) graduate fellowship through the Cooperative Institute for Arctic Research (CIFAR) with funds from NOAA under cooperative agreement NA17RJ1224, and NSF grants ARC-0531180 and ARC-0425517. Comments from three anonymous reviewers were very helpful in revising and focusing the paper.

References

Anisimov, O.A. & Reneva, S. 2006. Permafrost and changing climate: the Russian perspective. *Ambio.* 35(4): 169-175.

CAVM Team. 2003. *Circumpolar Arctic Vegetation Map*, scale 1:7,500,000, Conservation of Arctic Flora and Fauna (CAFF) Map No. 1. U.S. Fish and Wildlife Service, Anchorage, Alaska.

Comiso, J.C. 2006. Arctic warming signals from satellite observations. *Weather* 61(3): 70-76.

Comiso, J.C., Parkinson, C.L., Gersten, R. & Stock, L. 2008. Accelerated decline in the Arctic sea ice cover. *Geophysical Research Letters* 35: L01703.

Goward, S.N., Markham, B., Dye, D.G., Dulaney, W. & Yang, J. 1991. Normalized Difference Vegetation Index measurements from the Advanced Very High Resolution Radiometer. *Remote Sensing of Environment* 35: 257-277.

Hassol, S.J. (ed.) 2004. *Impacts of a Warming Arctic, Arctic Climate Impact Assessment*. Cambridge, UK: Cambridge University Press, 146 pp.

Hope, A.S., Kimball, J.S. & Stow, D.A. 1993. The relationship between tussock tundra spectral reflectance properties, and biomass and vegetation composition. *International Journal of Remote Sensing* 14(10): 1861-1874.

Jorgenson, M.T., Racine, C.H., Walters, J.C. & Osterkakmp, T.E. 2001. Permafrost degradation and ecological changes associated with a warming climate in Central Alaska. *Clim. Change* 48: 551-579.

Jorgenson, M.T., Shur, Y.L. & Pullman, E.R. 2006. Abrupt increase in permafrost degradation in Arctic Alaska. *Geophysical Research Letters* 33: L02503.

Kade, A.N., Romanovsky, V.E. & Walker, D.A. 2006. The *n*-factor of nonsorted circles along a climate gradient in arctic Alaska. *Permafrost and Periglacial Processes* 17: 279-289.

Lloyd, A.H., Yoshikawa, K., Fastie, C.L., Hinzman, L. & Fraver, M. 2003. Effects of permafrost degradation on woody vegetation at arctic treeline on the Seward Peninsula, Alaska. *Permafrost and Periglacial Processes* 14: 93-101.

Mann, D.H., Peteet, D.M., Reanier, R.E., & Kunz, M.L. 2002. Responses of an arctic landscape to Late Glacial and Early Holocene climatic changes: the importance of moisture. *Quaternary Science Reviews* 21: 997-1021.

Markon, C.J., Fleming, M.D. & Binnian, E.F. 1995. Characteristics of vegetation phenology over the Alaskan landscape using AVHRR time-series data. *Polar Record* 31(177): 179-190.

Nelson, F.E., Anisimov, O.A. & Shiklomanov, N.I. 2001. Subsidence risk from thawing permafrost. *Nature* 410: 889-890.

R Development Core Team 2006. *R: A language and environment for statistical computing*. R Foundation for Statistical Computing, Vienna, Austria.

Raynolds, M.K., Walker, D.A. & Maier, H.A. 2006. NDVI patterns and phytomass distribution in the circumpolar Arctic. *Remote Sensing of Environment* 102(2006): 271-281.

Riedel, S.M., Epstein, H.E., Walker, D.A., Richardson, D.L., Calef, M.P., Edwards, E.J. & Moody, A. 2005. Spatial and temporal heterogeneity of vegetation properties among four tundra plant communities at Ivotuk, Alaska, U.S.A. *Arctic, Antarctic and Alpine Research* 37(1): 25-33.

Schuur, E.A.G., Crummer, K.G., Vogel, J.G. & Mack, M.C. 2007. Plant species composition and productivity following permafrost thaw and thermokarst in Alaskan tundra. *Ecosyst.* 10:280-292.

Shippert, M.M., Walker, D.A., Auerbach, N.A. & Lewis, B.E. 1995. Biomass and leaf-area index maps derived from SPOT images for Toolik Lake and Imnavait Creek areas, Alaska. *Polar Record* 31: 147-154.

Shur, Y. & Jorgenson, M.T. 2007. Patterns of permafrost formation and degradation in relation to climate and ecosystems. *Permafrost & Periglac. Proc.* 18: 7-19.

Stow, D.A., Hope, A., McGuire, D., Verbyla, D., Gamon, J., Huemmrich, F., Houston, S., Racine, C., Sturm, M., Tape, K., Hinzman, L., Yoshikawa, K., Tweedie, C., Noyle, B., Silapaswan, C., Douglas, D., Griffith, B., Jia, G., Epstein, H., Walker, D., Daeschner, S., Petersen, A., Zhou, L. & Myneni, R. 2004. Remote sensing of vegetation and land-cover change in arctic tundra ecosystems. *Remote Sensing of Environment* 89(3): 281-308.

van Wijk, M.T. & Williams, M. 2005. Optical instruments for measuring leaf area index in low vegetation: application in arctic ecosystems. *Ecological Applications* 15(4): 1462-1470.

Walker, D.A., Epstein, H.E., Gould, W.A., Ping, C.-L., Romanovsky, V.E., Shur, Y., Tarnocai, C.T., Daanen, R.P., Gonzalez, G., Kade, A.N., Kelley, A.M., Krantz, W.B., Kuss, H.P., Matveeva, N.V., Michaelsen, G.J., Munger, C.A., Nicolsky, D.J., Peterson, R.A., Raynolds, M.K. & Vonlanthen, C.M. 2007 (in press). Arctic patterned-ground ecosystems: a synthesis of studies along a North American Arctic Transect. *Journal of Geophysical Research - Biogeosciences.*

Walker, D.A., Jia, G.J., Epstein, H.E., Chapin, F.S., Copass, C., Hinzman, L.D., Knudson, J.A., Maier, H.A., Michaelson, G.J., Nelson, F.E., Ping, C.L., Romanovsky, V.E. & Shiklomanov, N. 2003. Vegetation-soil-thaw-depth relationships along a low-arctic bioclimate gradient, Alaska: synthesis of information from the ATLAS studies. *Permafrost and Periglacial Processes* 14: 103-123.

Walker, D.A., Raynolds, M.K., Daniels, F.J.A., Einarsson, E., Elvebakk, A., Gould, W.A., Katenin, A.E., Kholod, S.S., Markon, C.J., Melnikov, E.S., Moskalenko, N.G., Talbot, S.S., & Yurtsev, B.A. 2005. The Circumpolar Arctic Vegetation Map. *Journal of Vegetation Science* 16: 267-282.

Washburn, A.L. 1980. *Geocryology*. New York: John Wiley & Sons, 406 pp.

Zhang, T., Barry, R.G., Knowles, K., Heginbottom, J.A. & Brown, J. 1999. Statistics and characteristics of permafrost and ground-ice distribution in the northern hemisphere. *Polar Geogr.* 23(2): 132-154.

Rock Glacier Distribution and the Lower Limit of Discontinuous Mountain Permafrost in the Nepal Himalaya

Dhananjay Regmi
Central Department of Geography, Tribhuvan University, Kathmandu, Nepal

Abstract

This study, by dealing with the distribution of rock glaciers as an indicator landform for mountain permafrost occurrence, estimated the existence of permafrost in five different study areas of the Nepal Himalaya (from east to west): Kangchenjunga, Khumbu, Langtang, Annapurna, and Sisne). Rock glaciers were identified by aerial photographs at all five sites, and they were checked in the field at the three sites Kangchenjunga, Khumbu, and Langtang. First, periglacial as well as glacial rock glaciers were mapped. Glacial rock glaciers were observed only in eastern Nepal, which may be attributed to the high amount of precipitation. In a second step, only periglacial rock glaciers were extracted and analyzed within a GIS by considering area, altitude, and aspect. The results show that: (1) the size of the rock glaciers tends to decrease from east to west, (2) the mean altitude of rock glaciers decreases towards the west, and (3) the aspects of the rock glaciers are variable, but southerly aspects are most common.

Keywords: glacial rock glaciers; Nepal Himalaya; periglacial rock glaciers; permafrost; rock glaciers.

Introduction

Rock glaciers, known and studied in high altitudes as well as high latitude regions, are considered to be one of the indicators of the presence of permafrost (Haeberli 1985, Barsch 1996). The spatial distribution of rock glaciers reflects climatic conditions, particularly the mean annual air temperature (MAAT) and mean annual precipitation (MAP) (Humlum 1998). The calculated critical conditions for the presence of active rock glaciers in the Central European Alps are MAAT of less than -1/-2°C and MAP of less than 2000 mm. These landforms are typical of regions with a cold, dry continental climate (Barsch 1996, King 1986).

Mountain permafrost in low and mid latitudes is considered to be sensitive to climate changes due to the fact that its temperature is close to the melting point (e.g., Haeberli 1985). Warming and degradation of permafrost have been reported in many mid latitude mountains: air and borehole temperatures have shown apparent warming trends in recent years in European mountains (Vonder Mühll et al. 1998, Harris et al. 2001, Isaksen et al. 2001, Harris et al. 2003). This may lead to an increase of natural hazards in high alpine environments. Slope failures, rockfalls, landslides and debris flows, all of which are assumed to be influenced by changes in the permafrost conditions, are known from numerous locations in high mountains, especially in the Alps (Haeberli et al. 1999, Harris et al. 2001). Therefore, proper knowledge of the permafrost distribution becomes highly significant.

Permafrost in Nepal has received very little scientific attention, despite the fact that Nepal is a country known for the Himalaya. The number of studies in the Nepal Himalaya is comparatively few and the knowledge of permafrost distribution is very limited. The distribution of permafrost was evaluated in the Nepal Himalaya initially by Fujii and Higuchi (1976) using ground temperatures. They indicated the possibility of permafrost occurrence above 4900 m in the Khumbu valley and above 5000 m in the Hidden valley. Since then, the zonation of mountain permafrost has been attempted based on the distribution of rock glaciers (Jacob 1992, Ishikawa et al. 2001), and the lower limit of discontinuous mountain permafrost zone was predicted to be at around 4800 to 5500 m.

This study examines the distribution of rock glaciers in the Nepal Himalaya in terms of size, altitude and slope orientation by focusing on five study areas. Furthermore, on the basis of active and inactive rock glaciers in these five areas of the Nepal Himalaya, the study describes the distribution of discontinuous permafrost. The relationship between the altitudinal distribution of rock glaciers and precipitation is also discussed.

Study Area

This study focuses on five study areas of the Nepal Himalaya: Kangchenjunga, Khumbu, Langtang, Annapurna, and Sisne Himal (Fig. 1). The easternmost area, Kangchenjunga, is located around 700 km from the Bay of Bengal, whereas the westernmost area, Sisne Himal, lies approximately 1100 km from Kangchenjunga. The climate in the east is strongly influenced by the southwest monsoon of the Indian sub-continent, whereas the one in the west is dominantly influenced by the mid-latitude westerlies (Asahi 2004). Hence, a substantial decrease in the MAP occurs across the Himalaya from the east to the west (Fig. 1). The selected study areas described here provide an opportunity to examine rock glaciers within different climatic and geomorphological settings. A brief description of all five study areas is given below and summarized in Table 1.

Kangchenjunga Himal (size of study area: 260 km²)

Kangchenjunga Himal, which includes peaks higher than 8000 m in altitude including the third highest peak in the world (Mount Kangchenjunga, 8586 m a.s.l.), lies in

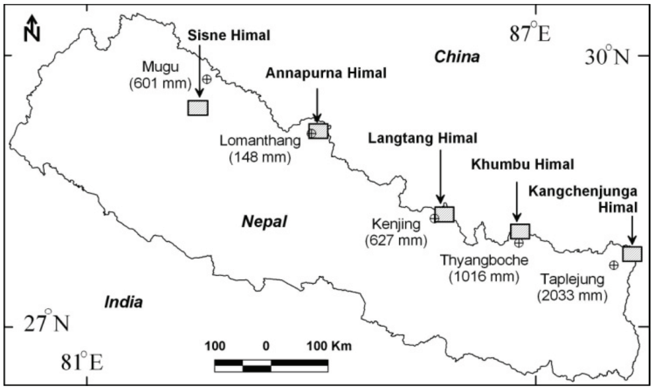

Figure 1. Location of the study area (shaded rectangles) and mean annual Precipitation (MAP) at relevant meteorological stations.

Table 1. Name and location of the five study areas, its coverage by aerial photograph interpretation and number of used aerial photographs at each site.

Name	Lat.	Long.	Area (km²)	Number of aerial phot.
Kangchenjunga Himal	27°45	88°05	260	41
Khumbu Himal	27°55	86°50	345	55
Langtang Himal	28°10	85°35	396	63
Annapurna Himal				
(a) Damodar Himal	*29°10*	*83°50*	*199*	*32*
(b) Mustang Himal	*29°10*	*84°10*	*161*	*24*
Sisne Himal	29°25	82°20	293	46
Total			1654	261

the easternmost part of the Nepal Himalaya (Fig. 1). The climate of this area is strongly influenced by maritime air masses (Ishikawa et al. 2001). The recorded MAP between 1987 and 1998, at the nearest permanent meteorological station (Taplejung: 1732 m a.s.l., about 60 km southwest of the study area), was 2033.4 mm, approximately 70% of which occurred during the summer monsoon period between June and September (DHM 1991, 1997, 2000). The study area receives less rainfall than the Taplejung area due to its leeward location further inland.

Khumbu Himal (size of study area: 345 km²)

Khumbu Himal is located in the eastern part of the Nepal Himalaya and includes Mount Everest and other peaks higher than 8000 m a.s.l. The climate in Khumbu is dominated by strong seasonality. A rainy season occurs between June and September; similar to the Kangchenjunga study area. Precipitation generally falls as snow above 5600 m a.s.l. The recorded MAP between 1967 and 1979 at the nearest permanent meteorological station (Thyangboche: 3867 m a.s.l., about 10 km southwest of the study area), was 1016 mm (DHM 1976, 1980).

Langtang Himal (size of study area: 396 km²)

Langtang Himal is located about 60 km north of Kathmandu (Fig. 1). The Langtang valley is surrounded by the high mountain ranges of Langtang Himal and Jugal Himal. Langtang Himal, with summit altitudes of about 6500 to 7200 m a.s.l., makes the northern and eastern divides, bordering Nepal and Tibet (China). Jugal Himal, with the peak altitudes of about 6800 m a.s.l., makes the southern divide. The MAP in the period 1987 to 1997 at the nearest permanent meteorological station (Kenjing: 3920 m a.s.l.) was 626 mm (DHM 1991, 1997, 2000).

Annapurna Himal - Upper Mustang area (size of study area: 360 km²)

Upper Mustang lies in the northern part of Mustang. It borders Tibet to the northeast, Dolpa District to the west. The highest peaks to the south exceed 6000 m in elevation. In 1992, Upper Mustang was included as one of the seven sectors of the Annapurna Conservation Area, the largest protected area in Nepal. The study area is subdivided into Damodar Himal to the south-east, and the Mustang Himal to the south-west of Lo Manthang, the largest settlement of Upper Mustang. The climate of Upper Mustang can be characterized as a rain shadow desert, desiccated by strong winds and high solar radiation. The region falls under the Dhaulagiri–Annapurna mountain rain-shadow zone (Asahi 2004). The recorded MAP for the neighboring station Lomanthang: 3705 m a.s.l. in the period 1976 to 1996 was only 148 mm (DHM 1980, 1986, 1991, 1997). Rainfall varies within Mustang with southern areas receiving slightly more rain than the north (Kunwar 2002).

Sisne Himal (size of study area: 293 km²)

Sisne Himal lies in the central southern part of western Nepal, with its highest peak of 5582 m a.s.l. The major parts of the mountain ridges do not exceed 5000 m in elevation and only some small glaciers exist. The recorded MAP between 1973 and 1996 at the nearest permanent meteorological station (Mugu: 3803 m a.s.l.) was 601 mm (DHM 1976, 1980, 1986, 1991, 1997).

Methodology

Permafrost, usually a subsurface phenomenon, and its presence is difficult to identify on the surface. Therefore, rock glaciers were used as a landform indicating permafrost by applying aerial photograph interpretation in all five study areas. Vertical aerial photographs of each study area in its entirety were interpreted using a stereoscope. The 1:50,000 scale aerial photographs were taken by the Survey Department, Government of Nepal in 1992 for eastern Nepal (Kangchenjunga, Khumbu, Langtang) and in 1996 for western Nepal (Annapurna and Sisne). More than 250 photographs were investigated for this study. Rock glaciers were carefully delineated on the aerial photographs and drawn onto analog topographic maps of 1:50,000 scale published by Survey Department, Government of Nepal.

Prior to the interpretation of aerial photographs, field observations were made to check the distribution of rock glaciers in three areas of Kangchenjunga, Khumbu, and

Langtang. The field observations allowed for accurate and more detailed interpretation of the aerial photographs.

The front and side slopes of rock glaciers appear "lighter" than their upper surface on aerial photographs, reflecting the exposure of "fresh" (unweathered) materials and the lack of lichen cover. Such characteristics enabled identification of the location of active and inactive rock glaciers using aerial photographs. Inactive rock glaciers having darker frontal and marginal slopes are observed and mapped in the field.

In order to delineate the discontinuous mountain permafrost zone based on rock glacier distribution, it is important to distinguish the type and origin of rock glaciers (Barsch 1978). Based on origin and geographical locations, rock glaciers are divided into two categories: glacial-origin and periglacial-origin rock glaciers (Humlum 1996). However, the terms glacier rock glacier and periglacial rock glacier are used in this study following Benn and Evans (1998). The origin of rock glaciers was identified on the basis of the rock glacier initiation line altitude (RILA) as suggested by Humlum (1988).

Based on these approaches, periglacial and glacial rock glaciers were mapped by aerial photograph interpretation with field verification. The analog maps with detail field and aerial photograph interpretation results were scanned and digitized in ArcView 3.2. After that, size, altitude, and aspect of each of the periglacial rock glaciers were analyzed using the ArcView Spatial Analyst.

Results

Distribution of periglacial and glacial rock glaciers in the five study areas

A total of 140 rock glaciers were identified by interpretation of aerial photographs in the five study areas of Nepal, covering a total area of 1654 km². Glacial rock glaciers were only found in the eastern Nepal Himalaya, i.e., Kangchenjunga and Khumbu Himal (Table 2).

A total of 22 rock glaciers were identified above 4800 m a.s.l. in Kangchenjunga Himal (Fig. 2a), covering an area of 259.6 km². Eight were recognized as glacial and 14 were periglacial rock glacier.

A total of 58 rock glaciers were identified in Khumbu Himal (Fig. 2b), covering an area of 345.4 km². Four rock glaciers were recognized as glacial and 54 were periglacial rock glacier.

Table 2. Summarized results at each of the five study areas.

Name	r.g. gla. (n)	r.g. perigl. (n)	r.g. all (n)	Total r.g. area	Mean r.g. area
Kangchenjunga Himal	8	14	22	2.45	0.11
Khumbu Himal	4	54	58	5.56	0.09
Langtang Himal	0	13	13	0.89	0.07
Annapurna Himal	0	18	18	1.32	0.07
(a) Damodar Himal	*0*	*9*	*9*	*0.63*	*0.07*
(b) Mustang Himal	*0*	*9*	*9*	*0.09*	*0.07*
Sisne Himal	0	29	29	1.35	0.04
Total	12	128	140		

In Langtang, Annapurna, and Sisne Himal with the examined area of 396.2, 359.7, and 293.1 km², a total of 13, 18, and 29 rock glaciers were identified, respectively (Figs. 2c; 2d; 2e). All rock glaciers in Langtang, Annapurna and Sisne Himal were identified to be of periglacial rock glacier.

The mean size of the rock glaciers (including glacier rock glaciers) is 0.11, 0.09, 0.07, 0.07, and 0.04 km² in Kangchenjunga, Khumbu, Langtang, Annapurna, and Sisne Himal, respectively.

Difference in the size of the periglacial rock glaciers in the Nepal Himalaya

The size comparisons show that the periglacial rock glaciers become smaller from eastern Nepal towards western Nepal although the size of the rock glaciers substantially varies among the study areas (Fig. 3).

In Kanchenjunga Himal, the size of the rock glaciers ranges between 0.03 km² and 0.19 km² with the average of 0.09 km². It ranges between 0.01 km² and 0.29 km² with the average of 0.09 km² in Khumbu Himal. Similarly, in Langtang, the size of rock glaciers ranges between 0.009 km² and 0.028 km², with the average of 0.07 km². In Annapurna, the size of the rock glaciers ranges between 0.04 km² and 0.14 km², with the average of 0.07 km² (Fig. 3). The size of the rock glaciers is substantially decreased in the western Nepal and it ranges between 0.009 km² and 0.107 km², with the average of 0.046 km² in Sisne Himal (Table 3).

Altitudinal variations in periglacial rock glacier distribution from east to west of Nepal

The mean lower limit of periglacial rock glaciers shows a decreasing trend from eastern Nepal (5239 m a.s.l) to western Nepal (4513 m a.s.l.) although the altitude of the rock glaciers significantly varies (Fig. 3). The lowest altitude of all 128 mapped periglacial rock glaciers is 5300 m a.s.l. on the south- to east-facing slopes, and 4800 m a.s.l. on the north to west-facing slopes (Fig. 2a; 3). Rock glaciers are located at the altitude ranging from 4800 m to 5640 m Kangchenjunga Himal. They are located at altitudes ranging from 4440 m to 5400 m, with the mean altitude of 4996 m in Khumbu. Similarly, in Langtang Himal they are located at altitudes ranging from 4600 m to 4920 m, with the mean altitude of 4722 m (Fig. 3). In Annapurna Himal they are

Table 3. Summarized result of altitudinal distribution and mean area of periglacial rock glaciers in five study areas.

Name	Altitudinal range (m a.s.l)	Mean altitude (m a.s.l)	Mean r.g. area
Kangchenjunga Himal	4800-5640	5239	0.09
Khumbu Himal	4440-5400	4996	0.09
Langtang Himal	4600-4920	4722	0.07
Annapurna Himal	4450-5120	4746	0.07
(a) Damodar Himal	*4480-4960*	*4681*	*0.07*
(b) Mustang Himal	*4450-5120*	*4810*	*0.07*
Sisne Himal	4200-4800	4513	0.04

located at altitudes ranging from 4450 m to 5120 m, with the mean altitude of 4746 m, whereas in Sisne Himal they are located at altitudes ranging from 4200 m to 4800 m (Table 3).

Orientational variations in periglacial rock glacier distribution from east to west of Nepal

The aspects of the periglacial rock glaciers from all Nepal Himalaya are shown in Figure 4. The rock glaciers are orientated toward the different directions, but they are mostly found on the south-, southeast-, and southwest-facing slopes.

In Kanchenjunga Himal, aspectual distribution suggests that most rock glaciers are oriented toward the east, south, and southwest directions (Fig. 2a). In Khumbu, rock glaciers are mostly found to be oriented toward the southeast, south and west directions (Fig. 2b). Similarly, rock glaciers are mostly found to be oriented toward the southwest directions in Langtang Himal (Fig. 2c). In Annapurna Himal, rock glaciers are mostly found to be oriented toward the southeast and south directions (Fig. 2d). Likewise, rock glaciers are mostly found to be oriented towards the southeast in Sisne Himal (Fig. 2e).

Discussion

King (1986) and Haeberli et al. (1993) indicated that the total amount of annual precipitation plays an important role in determining a mountain permafrost zone. The altitudinal range of the mountain permafrost zone in general decreases

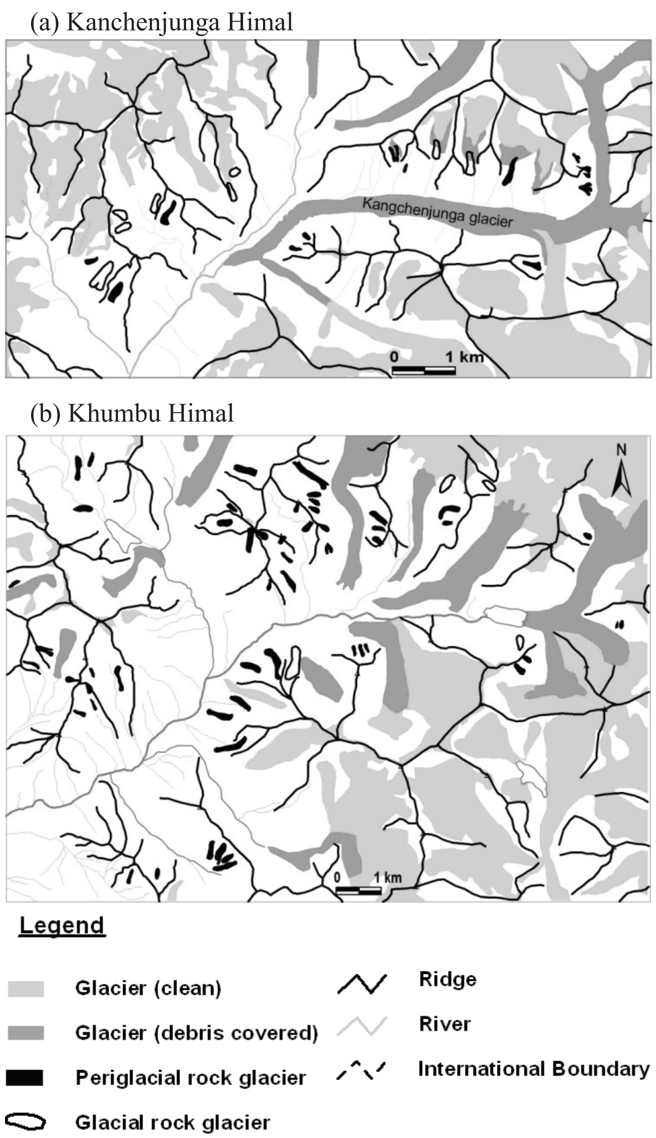

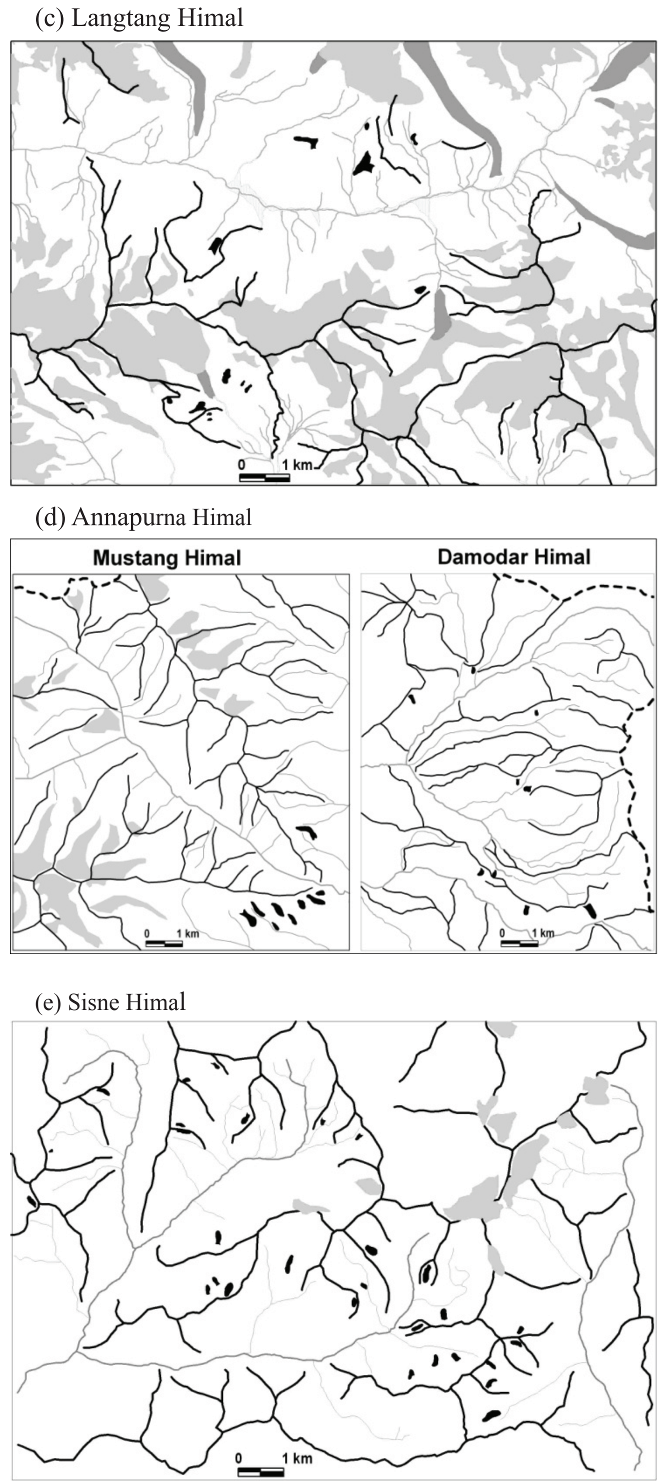

Figure 2. Rock glacier distribution and other landforms in the five study sites (a, b, c, d, and e) in the Nepal Himalaya.

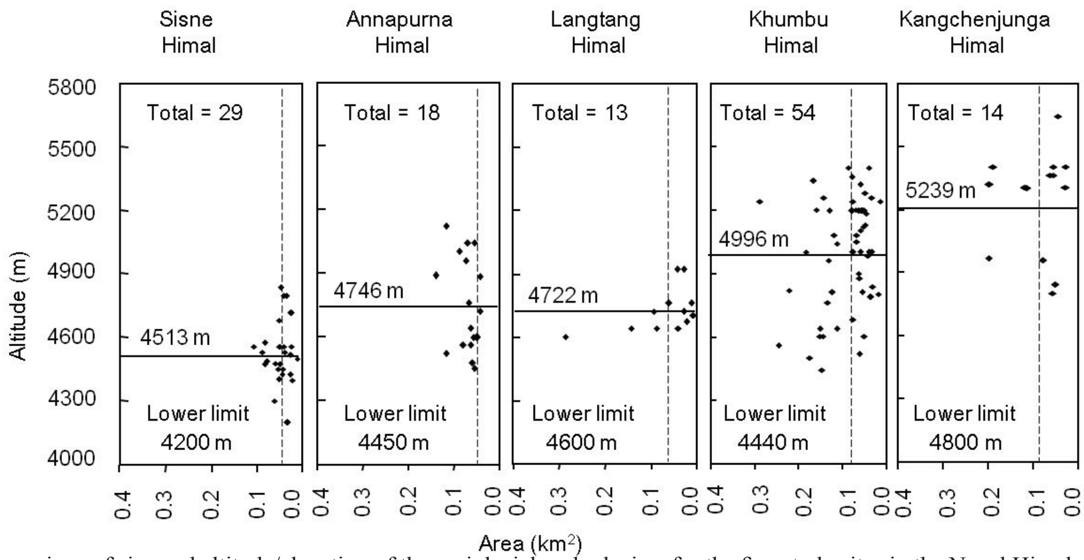

Figure 3. Comparison of size and altitude/elevation of the periglacial rock glaciers for the five study sites in the Nepal Himalaya. Horizontal line indicates the mean altitude of the rock glacier front of all rock glaciers of the given study area. Vertical dotted line indicates the mean area of each region.

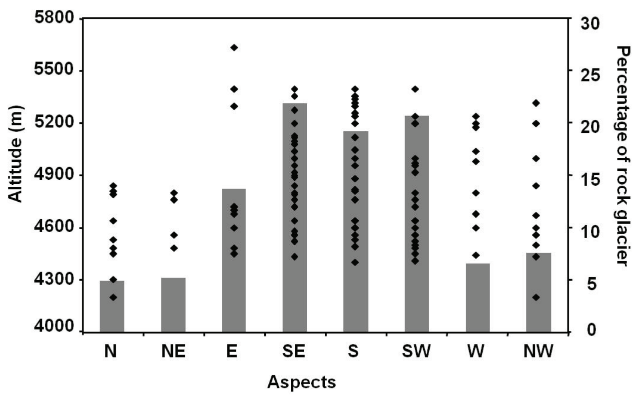

Figure 4. Altitudes and aspects of the periglacial rock glaciers in the Nepal Himalaya (n=128). Each dot shows the altitude of a rock glacier by slope aspect. The bar shows the percentage of the rock glaciers in a given aspect class.

with increasing annual precipitation. MAP substantially decreases from east to west in the Nepal Himalaya. Discussion focuses mainly on the effect of the decrease in precipitation from east to west Nepal Himalaya.

Due to its location in the easternmost part of the Nepal Himalaya, Kangchenjunga Himal is strongly influenced by monsoon winds coming from the Bay of Bengal, which provides high precipitation. MAP at the nearest meteorological station (Taplejung, 1732 m) in the Kangchenjunga region is approximately 2400 mm. Dhar and Nandargi (2000) reported a MAP of 1167 mm at Kambachen (4100 m altitude). This indicates that the permafrost in Kangchenjunga Himal belongs to an oceanic type of mountain permafrost. In contrast, the small amount of MAP in western Nepal (472 mm, in Sisne) indicates that the permafrost in Sisne belongs to a continental type.

The mean lower limit of periglacial rock glacier occurrence is 5239 m a.s.l. in Kangchenjunga Himal and 4996 m in Khumbu Himal (Fig. 3). These altitudes are considerably higher than those in the western Himalaya, which are under dry continental climatic conditions, e.g., 4513 m for Sisne Himal. Owen and England (1998) indicated that rock glaciers in the Pakistan Himalaya are restricted to regions with an MAP of less than 1000 mm and altitudes above 4000 m a.s.l. The decrease in the lower limit of rock glaciers from east to west coincides with the decrease in annual precipitation. This suggests that the MAP may cause the altitudinal difference in the lower limit of discontinuous mountain permafrost zone within the Nepal Himalaya.

Conclusions

The distribution of rock glaciers in five selected study areas in the Nepal Himalaya was mapped by applying aerial photograph interpretation and field observations. Based on this, the distribution of mountain permafrost was assessed. The following conclusions can be drawn from this study.

1. High amount of precipitation in eastern Nepal is most likely to lead to the development of glacial rock glaciers. However, further investigations are recommended considering temperature, snow cover, weathering rates, bedrock type and topography.
2. Periglacial rock glaciers in the eastern Nepal Himalaya tend to be larger than those of the western Nepal Himalaya.
3. The mean altitude of the periglacial rock glaciers decreases towards the western Nepal Himalaya.
4. Aspect of the periglacial rock glaciers is inhomogeneous, but they are mostly found in southern aspects.

Acknowledgments

I would like to thank Dr. Teiji Watanabe for his valuable comments on this manuscript. Special thanks are due to Dr. Yuki Sawada for his suggestions. The Japan Science Society is gratefully acknowledged for the Sasagawa Scientific Research Grant which partly supported this research.

References

Asahi, K. 2004. *Late Pleistocene and Holocene glaciations in the Nepal Himalaya and their implications for reconstruction of paleoclimate*. Ph.D. Thesis. Japan: Graduate School of Environmental Earth Science, Hokkaido University.

Barsch, D. 1978. Rock glaciers as indicators of discontinuous Alpine permafrost. An example from the Swiss Alps. In: *Proceedings, Third International Conference on Permafrost*. Ottawa: National Research Council, 349-352.

Barsch, D. 1996. *Rockglaciers. Indicators for the Permafrost and Former Geoecology in High Mountain Environments.* Berlin: Springer, 331 pp.

Benn, D.I. & Evans, D.J.A. 1998: *Glaciers and Glaciation*. London: Arnold, 734 pp.

Dhar, O.N. & Nandargi, S. 2000. An appraisal of precipitation distribution around the Everest and Kanchenjunga peaks in the Himalayas. *Weather* 55: 223-234.

DHM 1976. *Precipitation Records of Nepal,* 1971-1975. Department of Hydrology and Meteorology (DHM), Ministry of Science and Technology, HMG Nepal, Kathmandu.

DHM 1980. *Precipitation Records of Nepal,* 1976-1979. Department of Hydrology and Meteorology (DHM), Ministry of Science and Technology, HMG Nepal, Kathmandu.

DHM 1986. *Climatological Records of Nepal,* 1980-1985. Department of Hydrology and Meteorology (DHM), Ministry of Water Resources, HMG Nepal, Kathmandu.

DHM 1991. *Precipitation Records of Nepal,* 1987-1990. Department of Hydrology and Meteorology (DHM), Ministry of Science and Technology, HMG Nepal, Kathmandu.

DHM 1997. *Precipitation Records of Nepal,* 1991-1994. Department of Hydrology and Meteorology (DHM), Ministry of Science and Technology, HMG Nepal, Kathmandu.

DHM 2000. *Precipitation Records of Nepal,* 1994-1998. Department of Hydrology and Meteorology (DHM), Ministry of Science and Technology, HMG Nepal, Kathmandu.

Fujii, Y. & Higuchi, K. 1976. Ground temperature and its relation to permafrost occurrences in the Khumbu Himal and Hidden Valley. *Seppyo* Special Issue 38: 125-128.

Haeberli, W. 1985. Creep of mountain permafrost: internal structure and flow of Alpine rock glaciers. *Mitteilungen der Versuchsanstalt fur Wasserbau, Hydrologie und Glaziologie.* Eidgenossische Technische Hochschule, Zurich 77: 142 pp.

Haeberli, W., Guodong, C.H., Gorbunov, A.P. & Harris, S.A. 1993. Mountain permafrost and climatic change. *Permafrost and Periglacial Processes* 4: 165-174.

Haeberli, W., Kääb, A., Hoelzle, M., Bösch H., Funk, M., Vonder Mühll, D. & Keller, F. 1999. Eisschwund und Naturkatastrophen im Hochgebirge, *Schlussbericht*, NFP, Zürich 31.

Harris, C., Davies, M.C.R. & Etzel Müller, B. 2001. The assessment of potential geotechnical hazards associated with mountain permafrost in a warming global climate. *Permafrost and Periglacial Processes* 12: 145-156.

Harris, C., Vonder Muhll, D., Isaksen, K., Haeberli, W., Sollid, J.L., King, L., Holmlund, P., Dramish, F., Guglielmin, M. & Palacios, D. 2003. Warming permafrost in European mountains. *Global and Planetary Change* 39: 215-225.

Humlum, O. 1988. Rock glacier appearance level and rock glacier initiation line altitude: a methodological approach to the study of rock glaciers. *Arctic and Alpine Research* 20: 160-178.

Humlum, O. 1996. Origin of rock glaciers: Observation from Mellemfjord Disko Island, Central West Greenland. *Permafrost and Periglacial Processes* 7: 361-380.

Humlum, O. 1998. The climatic significance of rock glaciers. *Permafrost and Periglacial Processes* 9: 375-395.

Isaksen, K., Holmlund, J., Solid, L. & Harris, C. 2001. Three deep alpine-permafrost boreholes in Svalbard and Scandinavia. *Permafrost and Periglacial Processes* 12: 13-25.

Ishikawa, M., Watanabe, T. & Nakamura, N. 2001. Genetic differences of rock glacier and the discontinuous mountain permafrost zone in Kanchenjunga Himal, eastern Nepal. *Permafrost and Periglacial Processes* 12: 243-253.

Jacob, M. 1992. Active rock glacier and the lower limit of discontinuous alpine permafrost, Khumbu Himalaya, Nepal. *Permafrost and Periglacial Processes* 3: 253-256.

King, L. 1986. Zonation and ecology of high mountain permafrost in Scandinavia. *Geografiska Annaler* 68: 131-139.

Kunwar, P.B. 2002. *Fuel Energy Research in Upper Mustang of Annapurna Conservation Area*. King Mahendra Trust for Nature Conservation/Annapurna Conservation Area Project. Upper Mustang Biodiversity Conservation Program NEP/99/G35 (GEF) & NEP/99/021(TRAC).

Owen, L.A. & England J. 1998. Observations on rock glaciers in the Himalayas and Karakoram Mountains of northern Pakistan and India. *Geomorphology* 26: 199-213.

Vonder Mühll, D., Stucki, T. & Haeberli, W. 1998. Borehole temperatures in alpine permafrost: a ten year series. In: A.G. Lewkowicz & M. Allard (eds.), *Proceedings of the Seventh International Conference on Permafrost.* Collection Nordicana, vol. 57. Quebec: Universite´ Laval: 1089-1095.

Frost-Protected Shallow Foundation Design Issues: A Case Study

Charles H. Riddle
R&M Consultants, Inc., Anchorage, Alaska, USA

James W. Rooney
J&F Rooney, LLC, Anchorage, Alaska, USA

Gregory W. Carpenter
U.S. Army Corps of Engineers, Anchorage, Alaska, USA

Abstract

As part of the Housing Privatization Project at Elmendorf Air Force Base, Alaska, a design/build contract was implemented for the construction of 372 housing units and all associated site improvements. Adverse weather conditions including heavy rainfall with early freezing temperatures and limited snow cover during the fall and early winter period produced conditions conducive to excessive ground frost heaving. The building appurtenances adjacent to the vertical insulation and above the horizontal insulation were exhibiting excessive and unacceptable upward movement. These adverse impacts included heaving stoops, patio slabs, driveways, and uplifting of the protective perimeter vertical insulation board. A plan to repair the damaged work product was developed and implemented. The repair efforts involved removal of all damaged items. Either excavation of the silt layer or placement of additional horizontal insulation board was determined on a site-specific basis. It is important to critically assess the potential for differential movement associated with building perimeter appurtenances.

Keywords: building appurtenances; foundation insulation; frost heave.

Introduction

As part of the Housing Privatization Project at Elmendorf Air Force Base, Alaska, a design/build contract was implemented for the construction of 372 housing units and all associated site improvements. Figure 1 provides an aerial photograph of the site and completed project. The housing units consisted of 93 four-plex buildings of two-story wood frame structure constructed on frost-protected, thickened-slab shallow foundations. The project is located near the Boniface gate entrance, east of Vandenberg Avenue and immediately north and south of Provider Drive. The project owner is Aurora Military Housing, LLC, and construction was completed by Osborne Construction Company and Davis Constructors and Engineers, Inc., in a joint effort with the Hunt Building Corporation.

During the spring of 2001, "fast track" construction was initiated on the Boniface Housing Project. It continued through the following winter period and into the next 2002 full season, with the intent of allowing early occupancy as each of the four phases were completed. The first phase was completed and occupied in early fall 2001 while work continued on the remaining three phases. Adverse weather conditions including heavy rainfall with early freezing temperatures and limited snow cover during the fall and early winter period produced conditions conducive to excessive ground frost heaving. Adverse impacts to building unit perimeter entrances became visually apparent through the winter months. These impacts included heaving stoops, patio slabs, driveways, and uplifting of the protective perimeter vertical insulation board with consequent distortion of cover flashing. The authors were retained to evaluate site conditions and assist in developing remedial solutions for the contractors.

Investigation of soil conditions and perimeter appurtenances revealed frost penetration to depths of 0.9 to 1.2 m and the presence of a saturated frozen silt layer, having a variable thickness ranging from 0.3 to 1.2 m, interspersed in a sandy gravel and gravelly sand outwash deposit. It was apparent that the buildings' shallow foundation perimeter insulation was limiting frost penetration below the slabs in accordance with design requirements; however, the building appurtenances adjacent to the vertical insulation and above the horizontal insulation were exhibiting excessive and unacceptable upward movement, up to as much as 75 to 100 mm. In many instances, the larger movement resulted from a "cantilevered" lifting of the frozen material overlying the horizontal insulation board.

After review of all the conditions, a plan to repair the damaged work product was developed and implemented. The repair efforts involved removal of all damaged items. Either excavation of the silt layer or placement of additional horizontal insulation board was determined on a site-specific basis. Additional efforts were made to control roof drainage and to improve drainage away from the building perimeter. The vertical insulation board was removed and reattached in a more positive manner in those areas where excessive movement had occurred. For the 192 housing units involved, the required repairs included 111 front entry stoops, 98 patios, 92 back stoops, 80 driveways, and 82 sidewalks.

As with most structures founded on soils that are subjected to frost heave effects, it is important to critically assess the

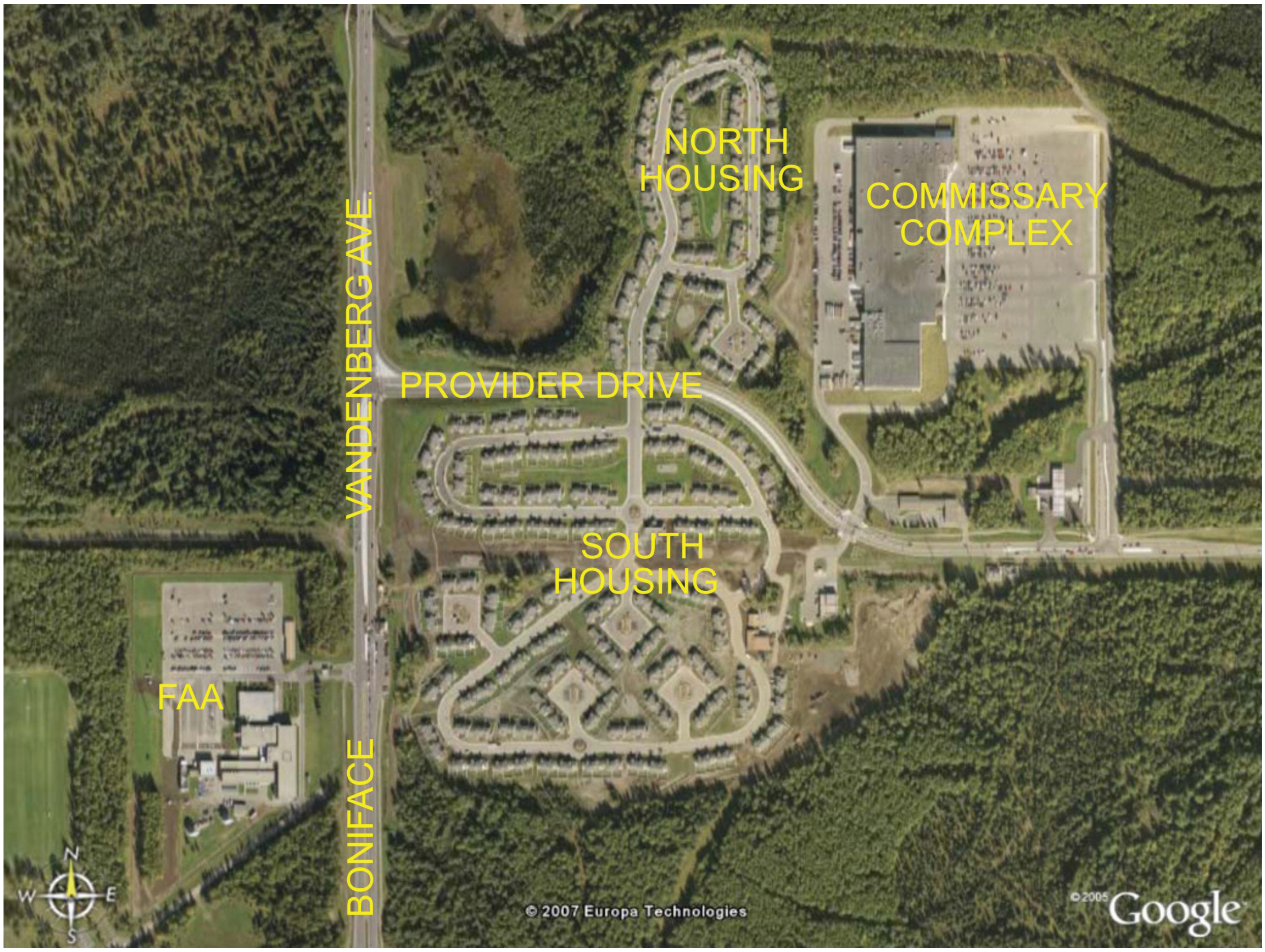

Figure 1. Aerial photograph showing Boniface Housing Project and adjacent commissary complex.

potential for differential movement associated with building perimeter appurtenances. In this case, a combination of circumstances created conditions that caused excessive differential frost heaving.

Historical Use of Frost-Protected Shallow Foundations

Some of the earliest reported work on the use of frost-protected foundations dates back to the late 1960s and early 1970s (Woodworth & Krzewinski 2002, Robinsky & Bespflug 1973, Thue 1974). Since that time, a number of technical papers have identified the effectiveness of this shallow foundation solution when appropriate design measures are implemented. It has also been utilized for remedial applications in repairing frost heave affected foundation systems such as documented in a prior case study (Woodworth & Krzewinski 2002). The Boniface Housing Project utilized the "Design Guide for Frost-Protected Shallow Foundations" (U.S. Dept. of Housing & Urban Dev. 1994). At this point in time, the principle guidelines provided in "Design of Frost-Protected Shallow Foundations" serve as an American Society of Civil Engineers (ASCE) practice standard in the United States.

While all of these documents fully address concerns with building structure foundation performance, little to no information is provided on the treatment of building perimeter appurtenances and the potential adverse effects of transitions at the outer edge of the horizontal insulation boards. This paper is presented for the purpose of identifying some of the adverse impacts that occurred when excess frost heave and unanticipated climate conditions developed during the Boniface Housing Project construction period.

Site Conditions

Elmendorf AFB is located within the Cook Inlet-Susitna Lowland physiographic province and is immediately adjacent to the northern boundary of Anchorage, Alaska. The area is characterized as a glaciated lowland containing areas of ground moraine and stagnant ice topography, drumlin fields, eskers, and outwash plains, with rugged mountains located immediately to the east. This region of Alaska is considered to be generally free of permafrost. One exception is where isolated masses of permafrost occur in lowland areas with high ground insulation, such as peat bogs and swamps. Soils at the site are interpreted as generally coarse-grained alluvial deposits of well-bedded and well-sorted gravel and sand overlying glacio-marine clay deposits of the Bootlegger Cove formation. The alluvial material is commonly overlain by 0.3 to 1.5 m of silt (R&M Engineering Consultants 2001). Bedrock was encountered at a depth of approximately 136 m in a nearby water well.

Lying between Cook Inlet and the Chugach Mountains, Elmendorf AFB has a transitional climate which may be characterized as variable, with the influence of both maritime and continental climates. Elmendorf AFB receives about 398 mm of precipitation per year. The temperature ranges from extremes of about -36ºC to 29ºC with an annual mean of 2.2ºC. The mean monthly temperature ranges from about -11ºC in January to 14ºC in July.

The undeveloped site was relatively flat, having a gentle southward slope. Much of the site was wooded with spruce and birch trees. Soil conditions within the site were defined by 20 test borings drilled to a depth of about 8.2 m by the Corps of Engineers in September 1998. The surficial soils consisted of silts and silty sand extending to a depth of 0.9 to 1.2 m, overlying sand and gravel that continued to the bottom of the test borings. Groundwater was only encountered in three test holes and was at a depth of 6 m or greater. Moisture content of the silty soil varied from 8% to 33% and averaged about 18%. Average moisture content for the granular soil was less than 4%.

Foundation Design and Building Perimeter Insulation Details

The buildings were constructed with slab-on-grade floor systems and bearing foundations consisting of a thickened perimeter edge, as shown in Figure 2. An air freezing index of 1905ºC-days, corresponding to a 100-year return period, as identified in the "Design Guide for Frost-Protected Shallow Foundations" was utilized. The insulation requirements for preventing frost heave of the thickened edge and spread footings are presented in Table 1.

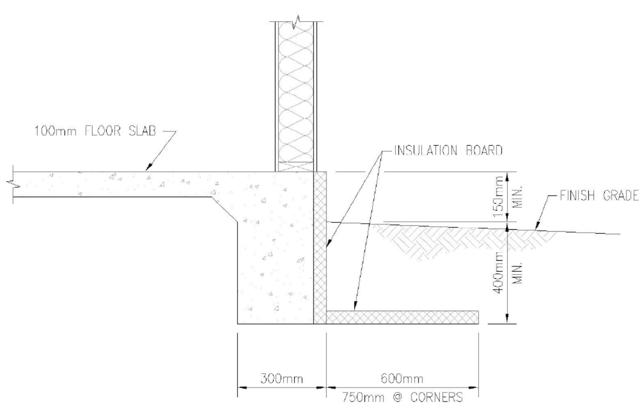

Figure 2. Thickened-slab edge foundation.

Table 1. Project insulation requirements.

Insulation	Thickness	R-Value	Required R-Value
Vertical	38 mm	1.1 k • m^2/w	1.0 k • m^2/w
Horiz. (walls)	76 mm	2.3 k • m^2/w	1.4 k • m^2/w
Horiz. (corners)	76 mm	2.3 k • m^2/w	2.0 k • m^2/w

Freezing temperatures were not observed below any of the foundation insulation board, and the building foundations have remained stable.

The design procedures were based on those required for heated buildings utilizing Anchorage, Alaska, climatic data, and assumed no insulating ground vegetation or snow cover. Since construction continued through the winter months without full building heat effects, it is likely that requirements for an unheated building would have been more appropriate. However, in either case, it seems that the adverse frost heave impacts on perimeter appurtenances would have been the same. With this in mind, an attempt has not been made to evaluate the climate and thermal conditions that actually occurred, but only to address the adverse building perimeter appurtenance impacts.

Frost Heave Impacts on Building Appurtenances

The adverse frost heave impacts resulted from both vertical and horizontal volumetric expansion of the soil, and also from a "cantilevered" lifting of the soil overlying the insulation board. Horizontal forces exerted against the vertical insulation board caused upward movement of the boards as the soil beyond the edge of horizontal board continued to heave. This resulted in sufficient vertical board movement that 1) displaced building perimeter flashing, 2) lifted stoop and patio slabs against door jambs, and 3) raised driveway pavement well above the garage door floor slab surfaces. Some of these conditions are shown in Figures 3a, 3b, 4, 5a, and 5b.

As can be seen in the test pit photograph (Fig. 6), an air gap of over 25 to 30 mm was found above the top of insulation board and the overlying soil cover. An interpretation of the forces and movements that occurred is shown in Figure 7.

When problems with the building perimeter appurtenances became visually apparent, the project contractors initiated efforts to evaluate the causes and to implement corrective

Figure 3a. Ponded water against building between driveway in insulated area that did not heave.

Figure 3b. Garage door and driveway entry with pavement fracture above outside edge of buried horizontal insulation board. Note temporary tapered wood spacer between uplifted asphalt pavement and garage door.

Figure 4. Uplifted concrete patio slab. Door sill and jambs were lifted by patio slab.

Figure 5a. Displaced vertical insulation board with flashing partially removed.

Figure 5b. View of perimeter base flashing covering vertical insulation board. Flashing has been slightly distorted by upward board movement.

actions. Such factors as project schedules, costs, and disruption of occupied building units needed to be considered in developing appropriate corrective action. The project contractors, owner/developer, and involved governmental agencies all worked together to implement necessary corrective measures.

Many driveways that had been constructed experienced significant frost heaving during the period of sub-freezing temperatures. Surface heaving of up to 63 mm was measured between the driveway surface and top of garage floor slab. Heaving of the concrete door stoops and patio slabs was also experienced to the point where door sills and jambs were distorted and impacting door swings and closures. Heaving soil conditions on the outer side of the insulation were also blocking drainage from roof snowmelt during thawing periods and, thus, compounding soil moisture and icing conditions.

Corrective actions for driveways included the following efforts and are shown in Figure 8.

• Removal of all asphalt and underlying silty soil down to gravelly soil or to a depth of 1.5 m.

• Extension of 76 mm horizontal insulation out to 1.8 m from the building edge within the driveway limits.

• Backfill excavation with F2 soil or better up to the insulation level and overlay with 450 mm of non-frost susceptible (NFS) material, 50 mm of crushed aggregate base course, and 50 mm of asphalt.

• Pave driveway to an elevation 12 mm below garage slab floor surface.

Corrective action for concrete stoops and patio slabs included the following efforts and are shown in Figure 9.

• Break up and remove concrete.

• Excavate and remove underlying soil down to the top of horizontal insulation board.

Figure 6. Test pit exposing horizontal insulation board. Air gap was found between insulation board and overlying frozen soil that was lifted by adjacent deeper frozen ground.

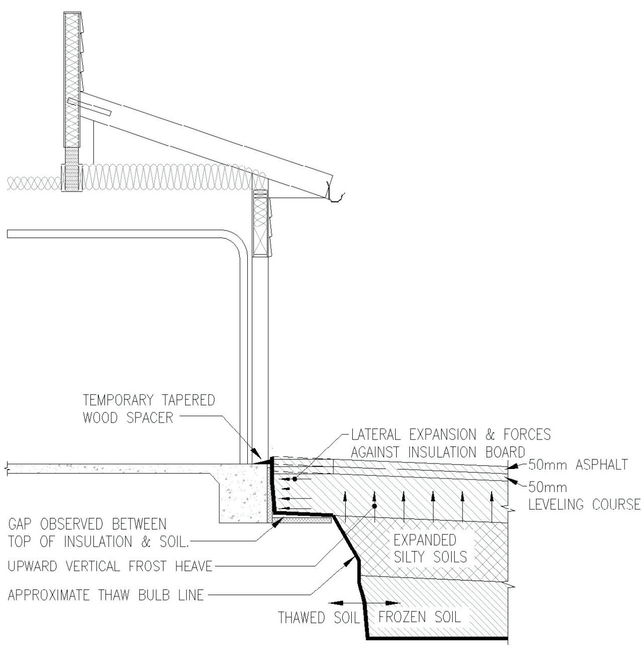

Figure 7. Interpreted ground heaving conditions and consequent expansion forces that caused vertical movement of pavement, stoops, patio slabs, and vertical insulation boards.

• Extend horizontal insulation coverage under entire slab area.

• Backfill with approximately 28 mm of NFS material.

• Remove and replace vertical base flashing using a modified flashing detail.

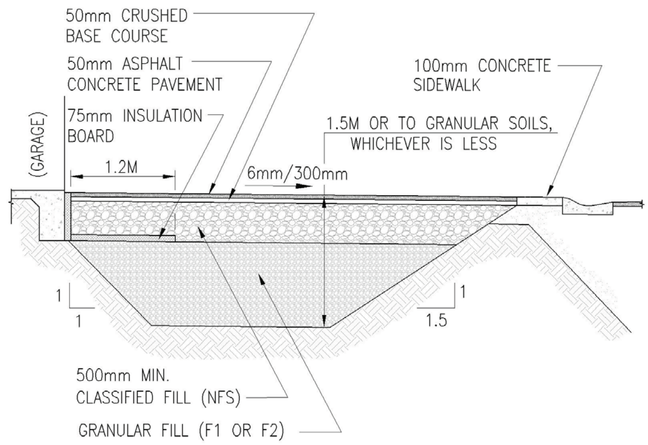

Figure 8. Profile of revised driveway improvement to reduce frost heave effects.

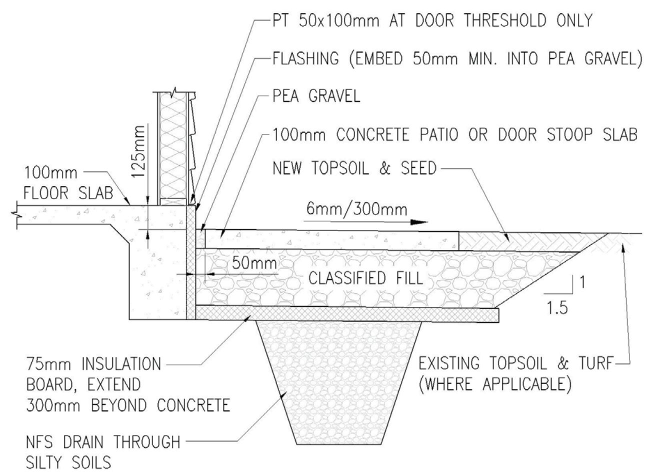

Figure 9. Profile of patio and stoop slab improvements to reduce frost heave effects.

• Re-pour new concrete patio/stoop 125 mm to 150 mm below finish floor elevation using a modified patio/stoop detail.

Corrective action for perimeter base flashing involved some limited total replacement of flashing, but in most cases consisted of cutting off existing flashing and installing new flashing using a two-piece flashing detail, as shown in Figure 10.

Roof drainage collection and disbursement modifications involved the following:

• Revising gutter location over garages to drain to center of driveways and install downspouts to improve drainage away from the building.

• Extension of gutters over front entries to reduce drainage and ice buildup on stoop.

Repairs and modifications for the project were completed by late 2002, and it is apparent that the contractor's efforts to address the frost heave-related problems were successful. Brief visual investigations have been made at those areas

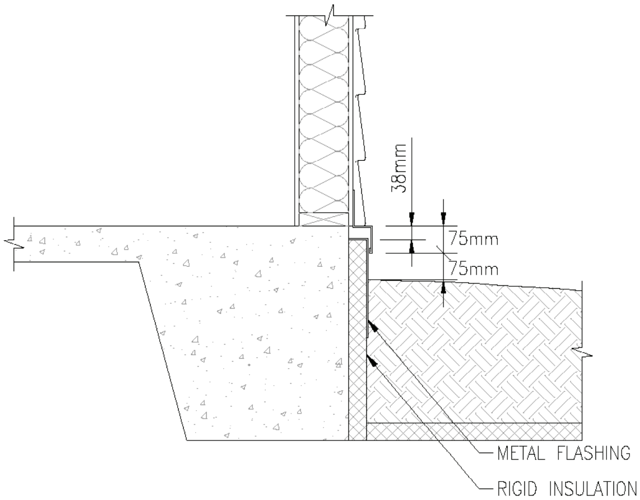

Figure 10. Foundation flashing detail modification to reduce frost jacking effects.

where the more significant frost heave impacts occurred. No evidence of adverse effects have been observed through the summer of 2007.

Closure

As with most structures founded on soils that are subjected to frost heave effects, it is important to critically assess the potential for differential movement associated with building perimeter appurtenances. In this case, a combination of circumstances created conditions that caused excessive differential frost heaving. Adverse weather conditions, including heavy rainfall with early freezing temperatures and limited snow cover during the fall and early winter period, produced conditions conducive to excessive ground frost heaving.

After review of all the conditions, a plan to repair the damaged work product was developed and implemented. The repair efforts involved removal of all damaged items. Either excavation of the silt layer or placement of additional horizontal insulation board was determined on a site-specific basis. Additional efforts were made to control roof drainage and to improve drainage away from the building perimeter.

Problems with building structure perimeter frost heave effects are not unique to just frost-protected shallow foundation structures. There are far too many examples of frost heave and jacking of driveways, decks, patios, and seasonally ponded drainage around buildings constructed on other foundation systems. This paper has been prepared for the purpose of identifying a condition that can occur with any foundation system that has the potential for vertical ground movement adjacent to the perimeter of a fixed structure. It is important for project designers to fully assess the potential for such movement and to develop details that can accommodate anticipated movements.

References

R&M Engineering Consultants. 2001. Soils and Foundation Evaluation, Boniface Gate Housing Development, Elmendorf AFB, Alaska.

Robinsky, E.I. & Bespflug, K.E. 1973. Design of Insulated Foundations, *ASCE Journal of the Soil Mechanics and Foundations Division* Sept.: 649-667.

Thue, J.V. 1974. Thermal Design of Shallow Foundations, *Frost I Jord (Frost Action in Soil)* 13: 5-21.

U.S. Department of Housing and Urban Development, Office of Policy Development Research. 1994. Design Guide for Frost-Protected Shallow Foundations.

Woodworth, J.R. and Krzewinski, T.G. 2002. Case Study: Townhouse Complex Failure Due to Frost Action: Investigation and Repair. *Proceedings of the 11th International Conference Cold Regions Engineering, ASCE.*

Estimating Active Layer and Talik Thickness from Temperature Data: Implications from Modeling Results

D. W. Riseborough
Geological Survey of Canada

Abstract

Projected permafrost warming and degradation due to climate change will make it difficult to continue with current monitoring protocols at some sites, as the top of permafrost descends to depths beyond the reach of active layer probes and thaw tubes. In this paper, thermal modeling results were used to evaluate the accuracy of active layer and talik depths estimates obtained using temperature cable data. The thermal regime of degrading permafrost was simulated using a fine-mesh 1-dimensional finite element model, while active layer and talik depths were estimated using model output at the coarse spacing typical of thermistor cable strings. Results show that estimates of annual active layer and talik depths obtained by extrapolation from above (the unfrozen side of the 0°C isotherm) were more accurate than those obtained by interpolation, or by extrapolation from below, especially where the soil thermal properties were significantly temperature-dependent. Estimates of active layer depth obtained using the annual temperature envelope were no more accurate than those obtained using individual temperature profiles, while estimates of talik depths were more accurate than estimates of active layer depth.

Keywords: active layer; ground temperature; models; talik; permafrost monitoring.

Introduction

Projected permafrost warming and degradation due to climate change will make it difficult to continue with current monitoring protocols at some sites, as the top of permafrost descends to depths beyond the reach of some methods for active layer monitoring. The standard methods for determining active layer thickness include probing, frost tubes, and estimation from soil temperature profiles (Nelson & Hinkel 2004). Probing is limited by field logistics to less than 1.5 m, while thaw tubes as currently designed are limited to about 2.4 m depth (Mark Nixon, personal communication). Estimating active layer and talik depth from temperature profiles is a common practice, but is subject to errors that are the subject of this paper.

Nelson & Hinkel (2004) suggest that the accuracy of the active layer thickness estimates from temperature profiles depends on the distance between measurement depths and the data-collection interval, and indicate that simple linear interpolation between measurements is used to determine calculate the position of the 0ºC isotherm.

Estimating the position of the 0ºC isotherm is also a problem in geothermal modeling, since most numerical models calculate changes in temperature at finite intervals along a profile, and do not calculate the position of the 0ºC isotherm directly. Calculating active layer depths by interpolation in a coarse grid usually produces a time series that follows a scalloped pattern, with slow descent before and rapid descent after the front passes points in the calculation mesh (Fig. 1). This effect depends on the interpolation method, and occurs here because linear interpolation does not account for the change in thermal properties as ice forms at 0ºC, causing an abrupt change in temperature gradient (Fig. 2). Estimating the position of the 0ºC isotherm in profiles such as in Figure 2 could be improved by using extrapolation from the grid temperatures above or below the frost front. The analysis presented in this paper is an attempt to determine whether this is generally true, by examining the magnitude of errors in 0ºC isotherm depth estimates from temperature profiles. Active layer thickness and depth of taliks were both examined, and depth estimates by extrapolation from above, by interpolation, and by extrapolation from below were compared. The effect of the distance between temperature points was also examined. This approach to error analysis could also be applied to other interpolation methods (such as cubic spline or other more sophisticated methods that account for the change in properties across the phase boundary), which are not considered here.

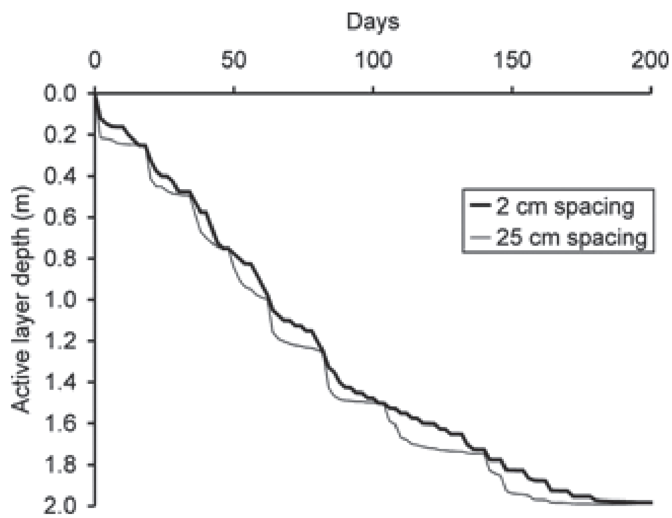

Figure 1. Example of active layer depth estimates from evenly-spaced node temperatures. Note the "scalloped" shape as node depths are approached.

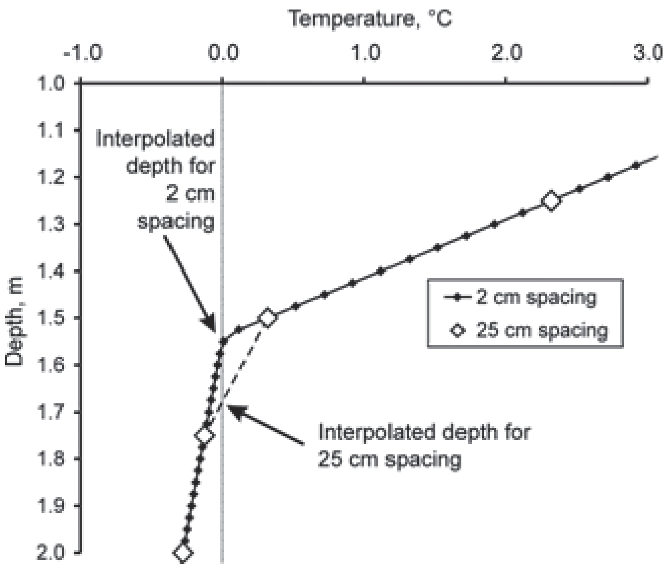

Figure 2. Typical temperature profile detail near the base of the active layer. The scalloping observed in Figure 1 is an effect of the interpolation method, as shown.

Method

Thermal modeling results were used to evaluate the accuracy of active layer and talik depth estimates obtained using temperature cable data. The multi-year thermal regime of degrading permafrost was simulated using a fine-mesh 1-dimensional finite element model, while active layer and talik depths were estimated using model output at the coarse spacing typical of thermistor cable strings. Using the fine-mesh output from the numerical model (spacings of 0.02 to 0.025 m for active layers, and 0.1 m for taliks), the "true" position of the 0ºC isotherm depth could be known to reasonable accuracy (within about 0.01m for active layers, and 0.05 m for taliks). Comparisons with active layer and talik depth estimates by extrapolation or interpolation from temperature data at coarser spacing allowed an evaluation of the relative accuracy of the estimation methods.

For active layer estimates, two different kinds of data were used. The *profile* method applied the estimation methods to instantaneous temperature profiles, allowing the tracking of seasonal progression of the active layer, as in Figure 1. The *envelope* method used annual temperature envelopes (depth profiles of the warmest and coldest ground temperatures experienced in a year) to estimate the annual maximum depth of thaw, applying the estimation methods to the profile of annual maximum temperature.

To evaluate the relationship between accuracy and sensor spacing, thermistor string data were simulated by selecting model output temperature corresponding to the depths appropriate for each spacing evaluated. For the analysis of active layer estimates, spacings of 0.1, 0.2, 0.3, 0.4, 0.5, 0.6, 0.75, and 1.0 m were used; for talik depth estimates, spacings of 0.2, 0.4, 0.6, 0.8, 1.0, 1.5, and 2.0 m were used.

This method was applied to simulations of similar climates, with two distinct substrates yielding somewhat different thermal regimes. The simulated surface climates included daily and inter-annual variability, with a long-term climate trend. Both simulation substrates included a 0.2-m thick saturated surface organic layer, overlying 20 m of saturated soil with 50% volumetric moisture content. For one substrate ("Bimodal"), all phase change was assumed to occur at 0ºC, with thermal properties having frozen and thawed values. The second ("Temperature dependent") substrate material had a substantial unfrozen water characteristic (using the freezing characteristic of Fairbanks silt), with phase change occurring over a broad range of freezing temperatures, resulting in temperature-dependent thermal properties at temperatures below freezing.

Model details

Simulations were made using Goodrich's discontinuous element model TONE (evaluated in Bouchard 1990 and Riseborough 2004). In each time step, the thermal conductivity and apparent heat capacity within each element were averaged based on the temperature profile, improving accounting for the total latent heat. This formulation should produce better results in soils that exhibit strong temperature dependence in thermal properties due to the freezing characteristic, as it accommodates the distribution of thermal properties across each element. Significant transitions over small temperature changes are not lost between points in the calculation mesh. However, this averaging results in a softer transition between frozen and thawed conditions in simulations where phase change is more abrupt.

Simulations

An initial 100-year simulation with a stationary climate was first performed for each substrate to establish an equilibrium initial temperature profile for subsequent simulations For each substrate, a 50-year active layer simulation and a 150-year talik simulation were performed with approximately the same surface climate (with initial mean annual temperature of -6.4, with a 1ºC per decade warming trend). Simulated climates included a 0.4-m deep annual snow cover with a parabolic accumulation function (Zhang 1993) and a density of 350 kg m^{-3}, inter-annual temperature variability (simulated by specifying standard deviations of 10% to the freezing and thawing indices, as described in Riseborough 2007), and daily variability with a standard deviation of 3ºC.

For both substrates, active layer simulations were performed with a fine mesh (0.02 and 0.025 cm spacing) in the upper 3 m (for analysis of active layer estimates) and 32 time steps per day, while talik simulations had a mesh of 0.1 m over the upper 15 m and 8 time steps per day. All simulations extended to 20 m, with a constant heat flux prescribed at the base of the mesh.

In bimodal simulations, talik depths reached 3 m depth after 68 years, and thawed to 15 m by year 118. In the simulations with temperature-dependent thermal properties, thaw depths reached 3 m by year 78, but the earliest were deep active layers, and a persistent talik did not form until year 89. Thaw depth extended to 15 m in year 137.

Analysis

Model outputs consisted of instantaneous temperature profiles at 10-day intervals and annual temperature envelopes, with results recorded for all nodes in the finite element mesh (node spacings of 0.02 and 0.025 m for active layer simulations, and 0.1 m for talik simulations). Once the simulations were complete, node temperatures (simulated "sensors") were used to construct coarser temperature profiles by sampling results at the appropriate depth intervals.

For all analyses, active layer depths were estimated in the same way, using temperature profile and temperature envelope results. Using either the instantaneous profiles or the profile of annual maximum temperature from the envelope, the node depths bounding the 0ºC isotherm were determined, and the appropriate node pairs were selected for the active layer estimate: for interpolation, the bounding nodes were used; for extrapolation, the first two nodes above or below the 0ºC position were used. Using the temperature gradients determined from these pairs, the position of the 0ºC isotherm was determined as the depth-intercept of the line defined by the sampled depth and temperature data.

Initial results showed that extrapolation methods were unreliable once freezeback had been initiated, due to the nearly isothermal conditions present between the freezing fronts bounding the unfrozen active layer. As a result, active layer estimates for instantaneous temperature profiles were not evaluated once freezeback had begun.

Talik depth estimates were obtained as for active layers, except that only one instantaneous temperature profile per year was evaluated. For the analysis of talik depths, only nodes between 3 m and 15 m were examined, in order to exclude active layers from the analysis, and to limit results to the part of the simulated profile with the smaller node spacing. For the cases with bimodal thermal properties, no active layers exceeded 3 m. In the cases with temperature dependent properties, deep active layers developed for several years before the establishment of a persistent talik.

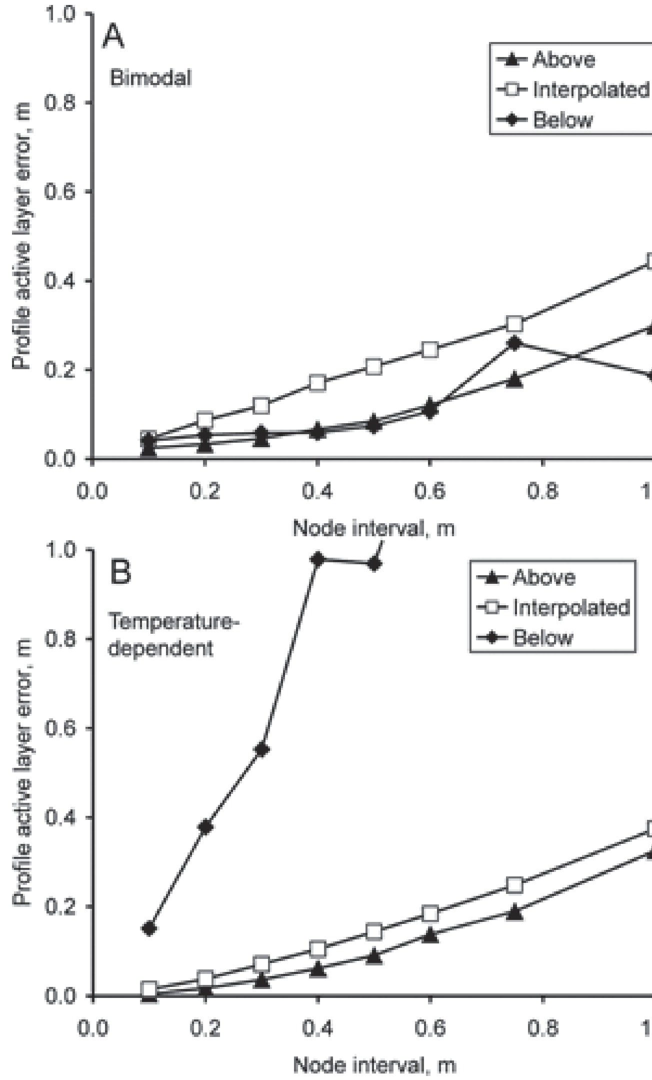

Figure 3. Average error in active layer depth estimated from instantaneous temperature profiles, as a function of selected node interval. A: simulations with bimodal (frozen/unfrozen) thermal properties and all phase change at 0ºC. B: simulations with temperature dependent thermal properties and unfrozen water.

Results and Discussion

Results for all interpolation methods were evaluated using the same procedure: for each profile or envelope, active layer or talik estimates with coarse temperature spacings were compared to estimates obtained with the fine mesh model output, and the average absolute value of all errors for each spacing calculated. Results are presented in Figures 3–5, and show that for all cases, errors increase as the node spacing increases, generally at a rate more than proportional to the increase in spacing. Errors in active layer estimates are not smooth functions of spacing, due to the variability imposed in the simulations.

Active layers from temperature profiles

Figure 3 shows the average error in active layer depth estimated from instantaneous temperature profiles. For the bimodal case, extrapolation yields more accurate active layer depth estimates, for all spacings. Up to a spacing of 0.6 m, the error in active layer depth with either extrapolation method is about half that of the error for interpolation. For the case with temperature dependent thermal properties, estimates based on extrapolation from below are very poor (exceeding the node spacing), while interpolation and extrapolation from above are better than for the bimodal case. The significant difference in errors when extrapolating from below is due to the effect of temperature dependent thermal properties on the temperature gradient, resulting in curvature in the temperature profiles that would make linear extrapolation through the frozen soil unreliable. This same effect is responsible for the improvement in the depth estimates using interpolation, as curvature in the frozen part of the temperature profiles reduces the rate of change of temperature gradient in the upper part of the frozen soil.

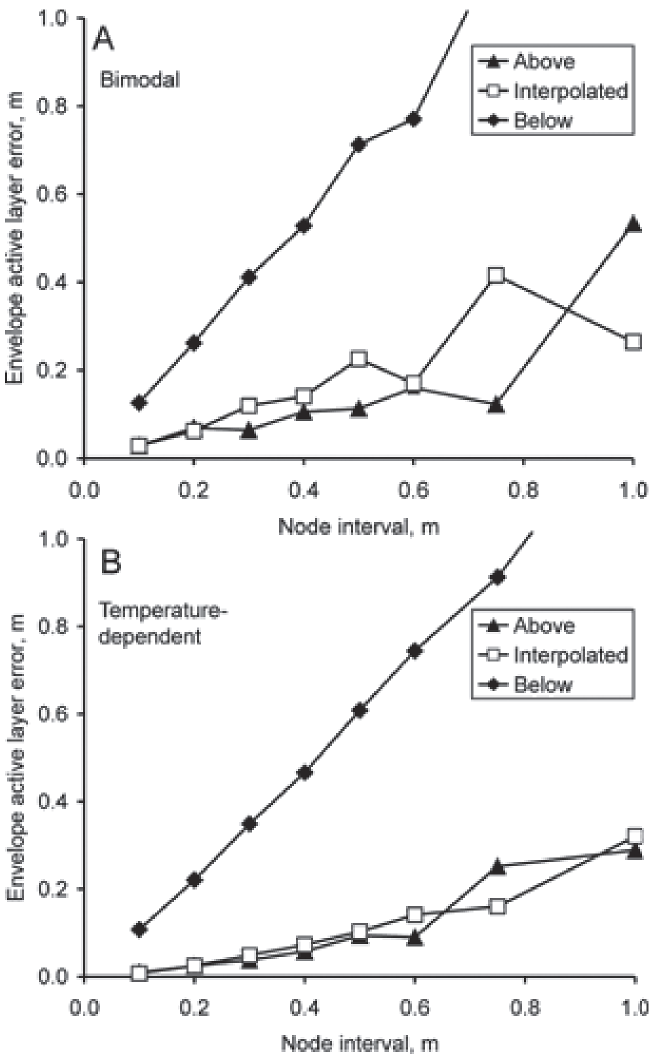

Figure 4. Average error in active layer depth estimated from annual temperature envelopes, as a function of selected node interval. A: simulations with bimodal (frozen/unfrozen) thermal properties and all phase change at 0ºC. B: simulations with temperature dependent thermal properties and unfrozen water.

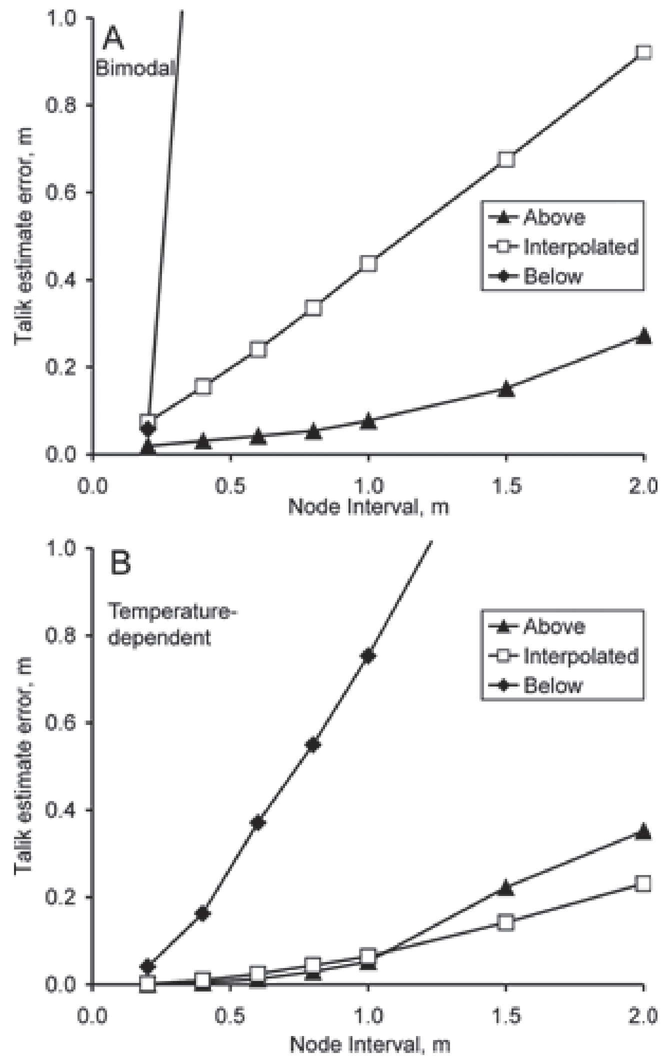

Figure 5. Average errors in estimated talik depth, as a function of selected node interval. A: simulations with bimodal (frozen/unfrozen) thermal properties and all phase change at 0ºC. B: simulations with temperature dependent thermal properties and unfrozen water.

Active layers from temperature envelopes

Figure 4 shows the average error in active layer depth estimated from annual temperature envelopes. These results represent the kinds of estimates that could be obtained using cable temperatures from a data acquisition system, from which a reliable temperature envelope could be derived. Results suggest that the errors in active layer estimates for extrapolation from above is similar to those for instantaneous profiles (Fig. 3), while estimates by extrapolation from below in soils is poor in both soil types (again exceeding the node spacing), and errors in estimates by interpolation are only slightly greater than with estimates by extrapolation from above.

Taliks

Figure 5 shows the average error in talik depth, estimated from instantaneous temperature profiles. Errors are a relatively smooth function of node spacing, due to the more steady thermal conditions within the talik compared to thermal conditions within the active layer. The accuracy of depth estimates by interpolation is similar to that for active layer estimates by instantaneous profiles (Fig. 3), while the error magnitudes when extrapolating from above are much smaller (less than half). For both soil types, extrapolation from below is unreliable, with estimation errors up to nine times the node spacing. This is due to the nearly isothermal conditions present in the permafrost degrading beneath the talik.

Conclusions

Results are summarized in Figure 6, in which the errors presented in Figures 3–5 are expressed as a proportion of the node spacing, shown as averages for all spacings:

1. Extrapolation from above is the most accurate method in all cases, and especially in cases with bimodal thermal properties.

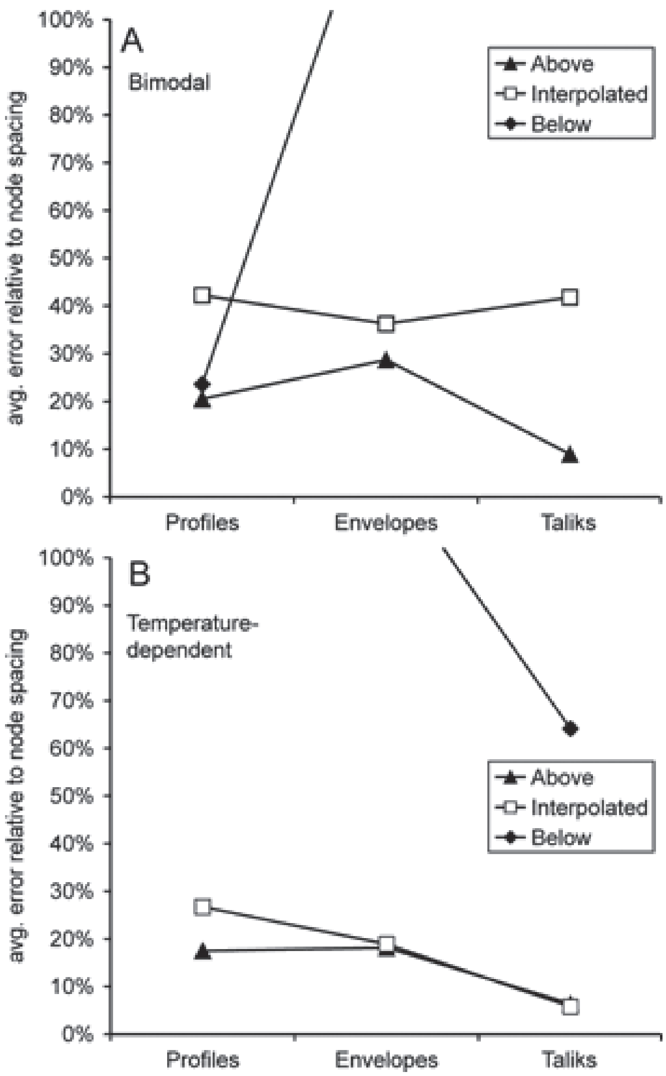

Figure 6. Average active layer/talik depth-estimate errors, expressed as a percentage of the node interval. A: simulations with bimodal (frozen/unfrozen) thermal properties and all phase change at 0ºC. B: simulations with temperature dependent thermal properties and unfrozen water. Results are truncated at 100%, as errors for extrapolation from below approached 900%.

2. For profiles, envelopes, and taliks, soils with bimodal thermal properties (and therefore an abrupt change in gradient at 0ºC), interpolation yields average errors of about 40% of the node spacing.

3. Estimation of active layer thickness from temperature envelopes is less accurate than estimates from profiles. This is likely due to the nature of the envelope data, which combines the effects of the phase transition and of diffusive extinction, yielding a profile that is not as simple to analyze as an instantaneous profile. Given that the average error for all methods exceed 25% of the node spacing when applied to envelope data in soils with bimodal thermal properties, estimates of active layer depth using temperature data from an acquisition system might be improved using sensor thawing indices (Riseborough 2003); alternately, the nearly continuous data would make it possible to select the best instantaneous profiles for estimating the active layer depth, although profiles may not capture the maximum active layer depth.

4. Except for active layer estimates from instantaneous temperature profiles in soils with bimodal thermal properties, extrapolation from below is not a reliable estimation method.

5. Talik depth can be estimated with greater relative precision than active layer depth, as deeper temperature profiles are less influenced by short term perturbations.

The extrapolation results presented here were used without a check to ensure that the 0ºC isotherm estimate was between the bounding sensors. The overall accuracy of active layer or talik estimates could be increased when used in an automated procedure by checking for this condition and reverting to estimation by interpolation where it is not met.

Results for the idealized conditions presented here may be considered a lower limit on the estimation errors investigated, since the precision of modeled temperatures exceeds that of most measurement and recording systems; Spatial and temporal variations in surface thermal conditions and in thermal properties along the soil profile will introduce additional variations not present in the smooth temperature profiles generated by the model.

While the results presented here may be applied to any temperature cable data, they also suggest a cable design strategy for optimizing 0°C isotherm depth estimates. Use of data acquisition systems typically limits the number of sensors to about 10.. Where talik depth or active layer depth is a key parameter in a monitoring program, an optimum cable design would concentrate sensors, with a relatively small spacing, close to the position of the front. A cable design with an extended lead would permit cable repositioning with the evolving thermal regime.

Acknowledgments

The ideas for the analysis presented in this paper developed from conversations with Caroline Duchesne. The comments of the anonymous reviewers were very helpful in improving the quality of the paper.

References

Burn, C.R. 1998. The active layer: two contrasting definitions. *Permafrost and Periglacial Processes* 9: 411-416

Bouchard, C. 1990. Simulation du régime thermique des sols pergélisolés: essai du modèle TONE. Université Laval, Département de Géographie, Mémoire de Maîtrise, 137 pp.

Nelson, F.E. & Hinkel, K.M. 2004. Methods for measuring active-layer thickness. In: Humlum, O. & Matsuoka, N. (eds.), *A Handbook on Periglacial Field Methods* Version 20040406. available on-line at: http://www.unis.no/RESEARCH/GEOLOGY/Geo_research/Ole/PeriglacialHandbook/HandbookMain.htm.

Riseborough, D.W. 2003. Thawing and freezing indices in the active layer. *Proceedings of the Eighth International Conference on Permafrost, Zurich, Switzerland*.

Riseborough, D.W. 2004. *Exploring the Parameters of a Simple Model of the Permafrost: Climate Relationship*. Unpublished PhD dissertation, Carleton University, Ottawa, Canada, 328 pp.

Riseborough, D.W. 2007. The effect of transient conditions on an equilibrium permafrost model. *Permafrost and Periglacial Processes* 18: 21-32.

Zhang, T.J. 1993. *Climate, Seasonal Snow Cover and Permafrost Temperatures in Alaska North of the Brooks Range.* PhD dissertation, University of Alaska, Fairbanks, 232 pp.

Mesoscale and Detailed Geocryological Mapping as a Basis for Carbon Budget Assessment (East European Russian Arctic, CARBO–North Project)

F.M. Rivkin, J.V. Vlasova, A.P. Popova
Fundamentprojekt Institute, Russia
G. Mazhitova
Komi Science Centre, Russian Academy of Sciences, Russia
P. Kuhry
Stockholm University, Sweden
I.S. Parmuzin, I.V. Chehina
Fundamentprojekt Institute, Russia

Abstract

A landscape-geocryological map is considered to be an important basic resource for comprehensive carbon budget studies under the international EU-funded CARBO-North project. The project is aimed at assessing the carbon balance at northern latitudes. The mesoscale and more detailed landscape-geocryological maps were produced for the intensive study sites using an integrated geosystem approach and landscape features indicative of permafrost conditions. The maps actually suggest a model showing spatial patterns of numerous landscape factors responsible for local and regional carbon budgets. The key issue of the mapping technique applied was the development of matrix legends arranged as tables. In general, the structure and content of such tables are variable and depend on study purposes, scale, and environmental conditions of particular areas. Under this study, a mesoscale landscape-geocryological map was produced for the Khoseda–Khard intensive site and a detailed map for the Seida intensive site, both sites located in the forest-tundra life zone.

Keywords: carbon budget; geocryological mapping; landscape; permafrost; zoning.

Introduction

Interannual climate dynamics and the ongoing rise of air temperature in the Arctic induce changes in geocryological conditions: increases in ground temperature and changes in its seasonal dynamics, increases in depth of seasonal thaw, partial degradation of thin permafrost, etc. As the permafrost is an enormous reservoir of organic matter, these changes in its upper layers bear the potential of producing a significant effect on the greenhouse gas balance at northern latitudes. Climate warming and the associated differential settlement of the soil surface can increase the thickness of the seasonally thawed (active) layer. This may substantially change conditions in the upper part of the geological section which, in turn, may lead to changes in drainage patterns and overall regional hydrology. The latter, meanwhile, is one of the major controls on regional carbon balance. In particular, the spatially differential settlement of soil surface may change the ratio of drained to wet areas. It is extremely difficult to forecast the dynamics and scope of such changes. Permafrost degradation is a complicated process associated with numerous feedbacks. Thus, it normally leads to enhancement of wet areas; however, such enhancement causes larger heat losses for the phase transition of water in a seasonal freeze-thaw cycle slowing down the progression of permafrost thaw, and, in some cases, even inducing the formation of new permafrost.

Permafrost is considered a “preserved greenhouse gases reservoir” (Samarkin et al. 1994), while the cryogenic landscapes are deemed a productive environment for this gas generation. The CARBO-North project includes as an important task the development of comprehensive landscape-geocryological maps to be used in the regional carbon budget studies for interpretation, upscaling, modeling, and forecast purposes. While developing the maps, we widely employed a technique related to the use of landscape indicators of permafrost conditions (Armand 1975). This insured common formatting of the maps of different intensive study sites and permitted the mapping of major controls on carbon budgets.

Study Area and Methods

Landscape-geocryological maps were produced for two sites, Khoseda-Khard and Seida (Fig.1).

The Khoseda-Khard site is located at 67°08′N, 59°30′E (center coordinates) and is considered in CARBO-North as a mesoscale intensive study site for assessment of the carbon budget. The site area is about 200 km^2.

Information available in achived databases, analysis of major environmental controls over geocryological conditions at the regional, landscape, and local levels, and results of a field survey we conducted earlier in this area were used for developing a map of the site.

The Seida site is located at 67°03′18″N, 62°56′06″E (center coordinates) and is considered a detailed intensive study site. The mapping area is around 4 km^2. Mapping was performed using satellite images and the results of the field surveys we conducted earlier in adjacent areas.

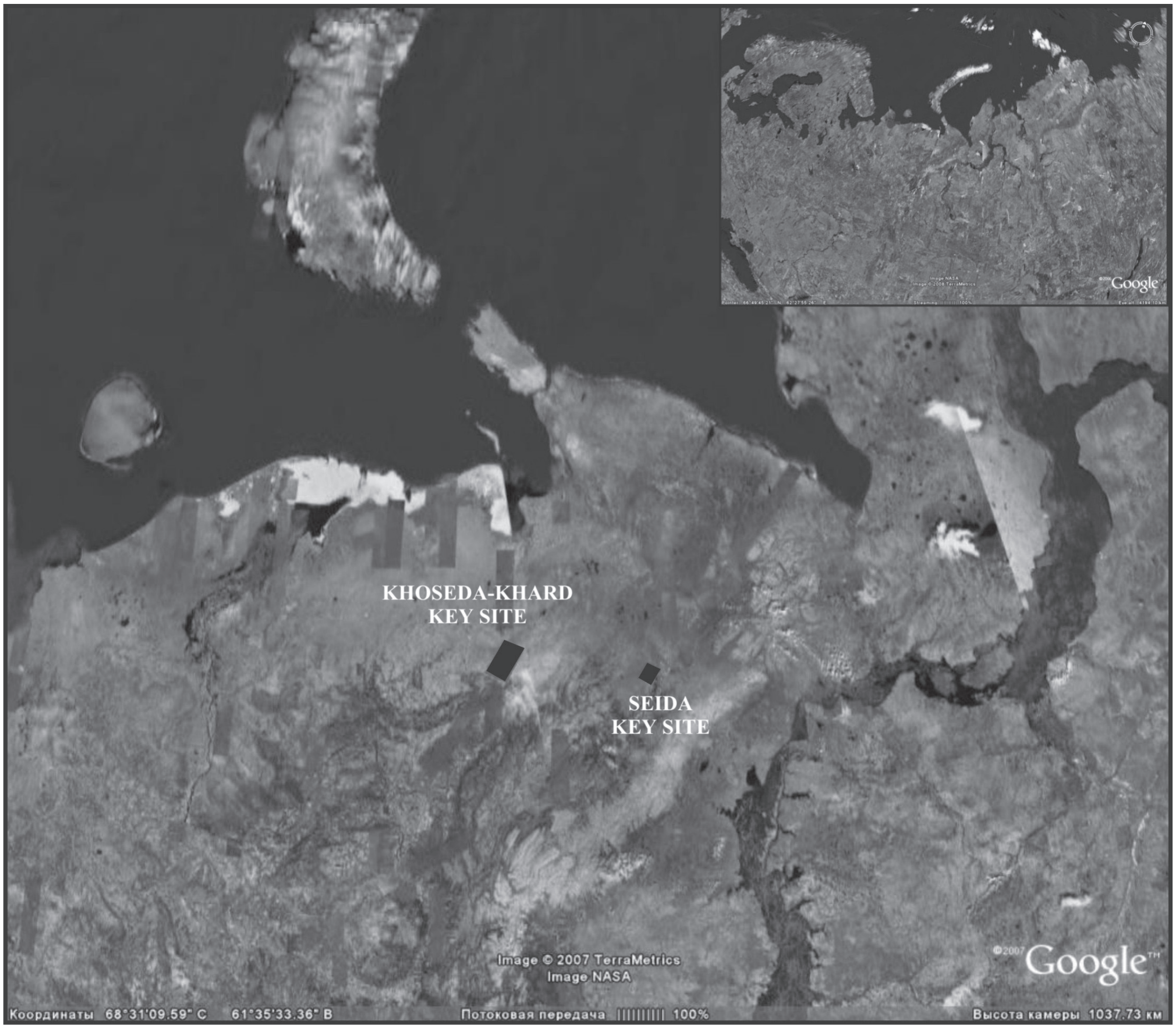

Figure 1. The location map of study sites.

The landscape-geocryological mapping technique we employed has been repeatedly used recently for compiling electronic atlases aimed at the assessment of the environment and human impacts upon it. The technique allows for mapping complex interrelations within the environment, in particular those between soil surface conditions and frozen ground distribution, or between ground lithological composition and temperature.

Accordingly, our landscape-geocryological mapping was based on revealing interrelations between the landscape features on the one hand, and the geological structure and geocryological conditions on the other. Information was summarized in matrix-format tables. Such tables are much more than just a form of data organization. They can serve for the purposes of system analysis, and at the same time they are the main component of map legends (Rivkin et al. 2004). Actually, the matrix schemes are regional geocryological classifications of an area, and accordingly, the GIS maps based on these schemes are spatial models of the classification. The combination of matrix schemes and GIS maps makes it possible to upscale rather accurately upscale point data on soil and vegetation carbon stocks and fluxes. Besides, various gradient and other spatial analyses become possible, as well as the assessment of partitioning of carbon between various landscape components, for example, active layer and permafrost, or permafrost-affected and permafrost-free soils. Moreover, the maps supplied with the matrix schemes are highly valuable for modeling changes in carbon budget induced by the climate change.

Results and Discussion

Mesoscale landscape-geocryological map of the Khoseda-Khard intensive study site

The Khoseda-Khard site is located in the southeastern part of the so-called Bolshezemelskaya Tundra and is stretched out along the Khoseda-Yu River. The vegetation represents a transition from the forest-tundra to the tundra life zone. The site altitudes vary from 60–70 m at the Khoseda-Yu water line to 130–175 m at the interfluve summits.

Most elevated parts of the interfluves represented by ridges and hills are composed of Middle Quaternary ice-marine deposits and dissected by numerous flow paths conveying surface water runoff. These flow paths are 5–100 meters wide and 0.5–3 meters deep. Away from the ridges and hills, the interfluve's surfaces are mostly represented by gentle slopes with altitudes of 90-120 m composed of Middle Quaternary lacustrine-alluvial deposits. This altitudinal level is characterized by large areas of peatlands and lakes.

The Khoseda-Yu River runs from south to north crossing the study site. The river is up to 50-60 m wide and 2–3 m deep with an average flow velocity of 0.8 m s^{-1}. The river valley is up to 30 m deep with steep (10°,-30°) slopes scarred by landslides and gullies. The I, II and III river terraces are clearly distinguishable above the flood plain. Smaller rivers are 5-20 m wide and up to 2 m deep. Their relative cut-in is 5-10 m. In the valleys of these rivers, the first and, less frequently, the second river terrace can be distinguished.

The site is rich in lakes. The lakes are mainly (except for the Neryta lake) shallow with depths of 1-3 m and small in size, less than 200 m across. They are of thermokarst origin and are located at peatlands. Many lakes are gradually draining.

The site location at the transition from tundra to forest-tundra provides for the diversity of plant associations. In a geocryological sense, the area is close to the southern boundary of the permafrost region. A characteristic feature of the area is that the permafrost distribution and temperatures are strongly controlled by landscape factors. Vegetation types and surface conditions are therefore reliable indicators of permafrost distribution. For example, in forest patches with tall understory and in shrub thickets the near-surface permafrost is typically absent, whereas in tundra it occurs at shallow depths. The high indicative value of landscape factors allowed for their use to map geocryological conditions.

The spatial analysis of environmental controls over present geocryological conditions was performed in a matrix format. The geomorphological and geological-genetic conditions of the terrain were plotted against the horizontal axis of the matrix. Identified were 8 successive geomorphological levels, within which 11 more geological-genetic complexes of deposits were distinguished, and within these complexes another 12 typical cryolithological sections were identified (Table 1). This subdivision was performed using the hierarchical approach. First of all, we identified the large geomorphological elements: interfluves and river valleys. After that we considered meso- and micro-relief, drainage, and vegetation type. Finally, the major types of cryological sections as well as exogenetic processes and associated landforms were identified.

The Middle Pleistocene ice-marine deposits of the Rogovaya suite ($gmII^{2-4}$) consist of clay loam and dark gray clay interbedded with layers and lenses of sand and sandy loam with inclusion of pebbles, gravel, and boulders. The Middle Pleistocene lacustrine-alluvial deposits of the Dozmer age ($laII^4$) are made up of loam interbedded with layers and lenses of sand and loamy sand. The Upper Pleistocene deposits of the Kazantsev age ($laIII^1$) are mainly formed by sand interbedded with layers and lenses of loamy sand and loam. All of the above deposits are classified as deposits with low ice content.

The floodplain alluvial deposits (aIV) and the deposits of the first river terrace consist mainly of gravel and pebbles, sand, and loamy sand. The alluvial deposits of the second ($aIII^{3-4}$) and the third ($aIII^{2-3}$) river terraces are made up of loam, loamy sand, and sand.

In peatland areas the bog-lacustrine deposits (lbIII-IV) with a 0.5–5 m thick peat layer overlap the ice-marine and lacustrine-alluvial deposits. When in a frozen state, peat has a high ice content, while the underlying mineral ground, frequently rich in peat admixture, has a medium to high ice content. The bog-lacustrine deposits are distributed at different geomorphological levels. They are not thick (3–7 m), and at each level there are various types of ground underlying these deposits.

On the landscape-geocryological map and in the matrix legend a specific digital code and color are assigned to each of the identified geological-genetic types of deposits and their typical cross-sections.

The landscape and geocryological conditions of the terrain are plotted along the vertical axis of the matrix. With consideration for surface topography, patterned grounds, vegetation, drainage, and depth to ground water, a total of 12 landscape sub-regions were identified:

- Spruce/birch forests and thin forests with dense understory (willow, dwarf birch) on flat plain surfaces and gentle (up to 6°) slopes, irregularly drained.
- Spruce/birch forests and thin forests with dense understory (willow, dwarf birch) on slopes more than 6° steep, well drained.
- Spruce/birch thin and sparse forests with sparse understory on flat plain surfaces and gentle (up to 6°) slopes, well drained.
- Hummocky dwarf-shrub/lichen tundra with patches of spruce/birch thin forests and shrub thickets on slopes more than 6° steep, well drained.
- Dwarf-shrub/moss/lichen tundra with low and medium hummocks on flat plain surfaces and gentle (up to 6°) slopes, well drained.
- Shrub/- and shrub/moss/lichen tundra (willow, dwarf birch up to 1 m high) on flat plain surfaces and gentle (up to 6°) slopes, irregularly drained.
- Willow, rarely dwarf birch thickets (willow up to 2 m and dwarf birch up to 1 m high) with grass/moss/sedge ground cover on flat depressed surfaces, gentle (up to 6°) slopes and along water lines, irregularly or poorly drained.
- Polygonal peatlands with hummocky dwarf-shrub/moss/lichen communities at drained polygon centers and sedge/moss communities in waterlogged dips, thermokarst depressions and subsided sites along thawing ice wedges.
- Palsa peatlands (degrading) with dwarf-shrub/moss/lichen communities on drained palsas and sedge/moss communities in waterlogged thermokarst depressions.
- Sedge/moss fens on depressed flat surfaces.
- Sedge/grass/moss meadows, in places hummocky, on large rivers flood plains, moderately drained.
- Small river and creek valleys with sedge/grass/moss communities on moderately drained flood plains and shrub/-

or dwarf- shrub/grass/moss communities on well drained terrace risers.

The map of a given scale allowed for identifying six types of permafrost sub-regions according to the degrees of permafrost spatial discontinuity:

1. discontinuous (sporadic) permafrost (covering 50%–90% of the area, of which 10%–50% has a permafrost table at 2–10 m depth);
2. massive-island permafrost (covering 20%–50% of the area, of which 10%–50% has a permafrost table at 3–10 m depth);
3. sparse island permafrost (covering <10% of the area, whereas >90% of the area is thawed grounds);
4. thawed ground underlain by the permafrost table at a depth of 3–8 m;
5. thawed ground with pereletoks and new formations of permafrost 1–3 m thick;
6. thawed ground.
7. The mean annual ground temperatures range from >0°C in the forested areas in the south of the site under survey to –1.5°C in the mineral tundra soil and polygonal peatlands in the north of the site.

Table 1. Geological-genetic complexes and cryolithological sections of Quaternary deposits at the Khoseda-Khard intensive study site.

Geomorphological level	Geological-genetic complex of deposits			Cryolithological section
Rogovskaya ice-marine plain	Bog-lacustrine	Late Pleistocene-Holocene	lb III-IV	One-to-three meters of peat underlain by loamy sand and sand. Ground is either thawed, or permanently frozen. Ice content in the frozen ground is medium or high in the upper 2-4 m layer and low in the deeper layers.
		Middle Pleistocen	gm II $^{2-4}$	Loam with layers and lenses of sand and loamy sand. Ground is either thawed, or frozen with low ice content.
Dozmer lacustrine-alluvial plain	Ice-marine	Late Pleistocene-Holocene	lb III-IV	Two-to-four meters of peat underlain by the interbedded loam, sandy loam and sand. Ground is either thawed, or permanently frozen. Ice content in the frozen ground is medium or high in the upper 3-7 m layer and low in the deeper layers.
	Bog-lacustrine	Middle Pleistocene	la II ^{4}	Loam with layers and lenses of sand and loamy sand partly overlain by a peat layer up to 0.5 m. Ground is either thawed, or permanently frozen with medium or low ice content.
Kazantsev lacustrine-alluvial plain	Lacustrine-alluvial	Late Pleistocene-Holocene	lb III-IV	Three-to five meters of peat underlain by interbedded sand, loamy sand and loam. Ground is either thawed or permanently frozen. Ice content in the frozen ground is medium to high in the upper 3-7-m layer and low in the deeper layers.
	Bog-lacustrine	Late Pleistocene	la III ^{1}	Sand with layers and lenses of sandy loam and loam partly overlain by a peat layer up to 0.5 m thick. Ground is thawed or permanently frozen with low ice content.
III river terrace	Alluvial	Late Pleistocene	a III $^{2-2}$	One-meter thick peat layer underlain by interbedded sand, loamy sand and loam. Ground is either thawed, or permanently frozen. Ice content in the frozen ground is medium in the upper 1-2 m layer and low in the deeper layers.
II river terrace	Bog-lacustrine	Late Pleistocene-Holocene	lb III-IV	One-meter thick peat layer underlain by interbedded sand, loamy sand and loam. Ground is either thawed, or permanently frozen. Ice content in the frozen ground is medium in the upper 1-2 m layer and low in the deeper layers.
	Alluvial	Late Pleistocene	a III $^{3-4}$	Sand with layers and lenses of loamy sand and loam. Ground is either thawed, or permanently frozen with low ice content.
I river terrace		Pleistocene-Holocene	a III-IV	Loam underlain by sand. Ground is either thawed, or permanently frozen with low ice content.
Floodplain and I river terrace (non-denudative)				Loam underlain by sand. Ground is either thawed, or permanently frozen with low ice content.
Floodplain	Alluvial	Holocene	a IV	Thawed sand underlain by thawed loam.

On the produced map and in the attached matrix legend, alphanumeric codes are assigned to combinations of landscape features, permafrost sub-regions, and ground temperatures; combinations are hatched differently on the map.

Within the identified permafrost sub-regions there are thus unique combinations of geological and physiographic factors: climatic, edaphic, botanical, lithologic, geomorphologic, hydrologic, hydro-geologic, and others, i.e. the entire spectrum of factors responsible for geocryological conditions. By combining the identified landscape and geocryological sub-regions (the vertical axis of the matrix) and the typical geological-genetic complexes (the horizontal axis of the matrix) we succeeded in identifying 64 typological areas at the Khoseda-Khard site.

The fact that the site is located at the transition between the tundra and the forest-tundra provides for diversity and contrast of the surface conditions, which in its turn results in spatial and temporal instability of seasonal thaw and freezing depths. The shallowest thaw depths, those of 0.3–0.8 m, are characteristic for peatlands. In mineral grounds at well drained interfluves, depths of seasonal thaw vary from 0.6 to 2.0 m depending on a ground lithological composition. Depths of seasonal thaw in loamy soils rich in peat admixture are 0.4–1.0 m, and in the loamy sand and sand deposits 0.8–2.0 m.

Cryogenic processes and landforms are highly characteristic of the area; they differ depending on the geocryological conditions of particular sites: composition, structure, physical properties, and temperature range of frozen or thawed ground. The most common are frost mounds of various shapes and sizes formed as a result of multi-annual and seasonal freezing of the ground. The seasonally thawed layer in the northern part of the site is associated with the patterned ground: non-sorted circles and hummocks. Cryogenic (frost) cracking occurs both in peatlands and mineral soils and is associated with large-block surfaces and residual polygonal relief. Ancient thermokarst lakes are numerous in peatlands. Present-day thermokarst manifests itself in the form of melting of repeatedly-wedge ice. Erosion, including thermal erosion is of limited occurrence and is confined to river valleys and thawing ice wedges with erosive gullies developing along the latter. Landslide accumulation areas can be found at the foot of steep slopes of river valleys. The ongoing paludification is limited to peatlands and wet interfluve depressions.

Detailed landscape-geocryological map of the Seida intensive study site

The site is located on the left bank of the Sediakha River, 6 km west of the Seida village. The site is the floor of a large, drained, ancient lake currently occupied by a peatland and scarred with water runoff paths and creek valleys. The perimeter of the lake basin is framed by a glacier spur with altitudes of 120–130 m. The site has a block-polygonal relief; well drained elevated blocks with shrub/moss/lichen vegetation are separated by erosive gullies differing in depth and width and overgrown by shrubs. The near-surface permafrost at the site can be subdivided into two sub-regions: discontinuous (sporadic) and massive-island. In peatlands and in the relatively elevated areas occupied by tundra with frost boils or low hummocks, the permafrost table is located directly under the active layer. In wet depressions, erosive gullies, at footslopes, and on smooth shrubby hillslopes the permafrost table is located at depths of 5 or more meters. Over 10 m deep continuous thawed ground is located under the lakes and in the large wet depressions with open water bodies.

The Seida site map indicates comprehensive information on geocryological features of the upper ground layers (down to 10 m depth). Geocryological mapping was performed on the basis of landscape subdivision of the area with the use of high-resolution satellite images.

Similarly to the mesoscale mapping of the Khoseda-Khard site, the spatial analysis of the environmental factors responsible for present-day geocryological conditions was performed in the matrix format. The structure of the detailed mapping matrix is, to a great extent, similar to that developed for the mesoscale mapping. Such consistency allows one to better correlate different types of terrain when working with maps of various scales and detail. Besides, it provides for more accurate upscaling of gas fluxes determined and estimated at various scales.

The geomorphologic and geological-genetic conditions of the area are plotted along the horizontal axis of the matrix. The whole site is located within one (non-segmented) geomorphological level (glaciofluvial lowland and II river terrace), within which are distinguished 3 geological-genetic complexes of deposits, within which another 4 typical cryolithological sections are identified (Table 2).

The landscape and geocryological conditions of the area are plotted against the vertical axis of the matrix. With consideration for surface topography, vegetation, depth to ground water, permafrost temperature and other characteristics, and thickness of seasonally frozen or seasonally thawed layers a total of 7 landscape sub-regions were identified:

- Dwarf-shrub/moss/lichen tundra, moderately drained, with small hummocks, occasionally with frost boils, groundwater at a depth of 1–3 m, discontinuous permafrost (occurs at 50%–90% of the area, and at 10%–50% of the area the permafrost table is at a depth of 3–5 m);
- Shrub/moss/lichen tundra, shrubs up to 1 m high, medium and large hummocks, irregularly drained, ground water at 0–1 m, permafrost surface at a depth of 3–6 m;
- Peatland, irregularly drained, with dwarf-shrub/moss/lichen communities on mounds and moss/sedge in hollows, ground water at 0–0.5 m, discontinuous permafrost (occurs at 70%–90% of the area, and at 10%–30% of the area the permafrost table is at a depth of 2–5 m);
- Palsa peatland, strongly eroded, with dwarf-shrub/moss/lichen tundra on palsas and sedge/moss communities in inter-palsa depressions, ground water at 0–0.5 m, massive-island permafrost (covering 50% of the area and within 50% of that area the permafrost surface is at a depth of 2–10 m);
- Sedge/moss mire with residual palsas occupied with dwarf shrub/moss/lichen communities, ground water at 0–0.3

Table 2.Geological-genetic complex of deposits and cryolithological sections of Quaternary deposits at the Seida intensive study site.

Geomorphological level	Glaciofluvial lowland and II river terrace			
Geological-genetic complex of deposits and their age	alluvial, glaciofluvial	bog-lacustrine		alluvial deposits of river channels and small water channels
	late Pleistocene	late Pleistocene-Holocene		Holocene
	a,fg III^2	lbIII-IV		alV
Cryolithological section	thawed or frozen sand and loamy sand with pebble interbeds and low ice content	peat layer up to 1 m thick underlain by interbedded sand, loamy sand, and loam, thawed grounds or frozen grounds with a low ice content below a depth of 1-3 m	peat later from 1 to 4 m thick underlain by interbedded sand and loamy sand, rarely loam, frozen with medium or high ice content below a depth of 4 m	peat layer up to 1 m thick underlain by interbedded sand, loamy sand, and pebble

m, island permafrost (covering 20%–30% of the area and within area 70%–80% the depth of the permafrost table is 5–10 m);

- Water lines and bogged depressions with herb/sedge/moss and shrubs of varying coverage up to 2 m high, poorly drained, ground water at 0–1 m, thawed ground with possible pereletoks and new formations of permafrost;
- Creek valleys, irregularly drained, herb/sedge/moss communities, occasionally willow thickets up to 2 m high, ground water at 0–1 m, thawed grounds.

By combining the identified landscape sub-regions and the typical sections of geological-genetic complexes (the horizontal axis of the matrix) we managed to identify 8 typological areas at the Seida site, which in its turn allows for mapping the whole spectrum of the existing geocryological and landscape conditions.

The landscape-geocryological maps of the two intensive sites differ in the degree of detail. Variability within map polygons in permafrost conditions, ground temperatures, soil, vegetation, and degree of drainage is much higher on the Khoseda-Khard than on the Seida map. Attribution of a polygon to the particular typological area on the Khoseda-Khard map is based on generalization, so that for the local-level carbon budget assessment further detailization of the map is needed. The latter, in a large degree, can be done using the typological units defined and deliniated on the mesoscale map. On the contrary, on the detailed map of the Seida site, characteristics of the ground including ground temperatures, as well as degrees of drainage, soil and plant communities defined in the legend precisely correspond to each polygon shown on the map. This makes it possible to accurately enough determine landscape-geocryological features necessary to estimate and interprete local carbon budgets.

It should be stressed once again that the landscape-geocryological units identified during the mesoscale mapping, if necessary for carbon studies, can be subjected to further sequential detailization in the course of detailed field mapping. From the technical viewpoint it can be done in a form of sequential detailization of the spatial analysis matrix. It is important to keep the detailed-scale matrix in compliance with the medium-scale matrix, so that the detailed-scale matrix r would suggest more detail within the mapping units and, correspondingly, map polygons which were defined on the medium-scale map.

Conclusions

The matrix schemes of landscape-geocryological subdivision developed under the CARBO-North project represent regional classifications of landscape and geocryological conditions. They reflect the system of environmental controls over the geocryological situation, as well as major controls over carbon budget components at the studied areas. On the one hand, sequential detailed geocryological mapping of an area allows for sequential detailed assessment of the carbon budget components and, on the other hand, makes it possible to integrate and upscale the detailed carbon data to assess a regional carbon budget using mesoscale cartographic models.

Acknowledgments

The authors of this paper would like to thank all their colleagues for advice and proofreading.

References

Armand, D.A. 1975. *Landscape Science (Theoretical Basics and Logical-Mathematical Methods)*. Moscow, 288 pp.

Rivkin, F.M., Kuznetsova, I.L., Ivanova, N.V. & Suhodolsky, S.E. 2004. Engineering-geocryological mapping for construction purposes in permafrost regions. In: *Engineering Geology for Infrastructure Planning in Europe.* Berlin Heidelberg: Springer-Verlag, 172-178.

Samarkin, V.A., Fedorov-Davydov, D.G., Vecherskaya, M.S. & Rivkina, E.M. 1994. CO_2 and CH_4 emission from cryosols and subsoil permafrost and possible global climate changes. In: *Soil Processes and Greenhouse Gas Emission.* US National Soil Survey Centr. Nebraska, V. 3: 55-71.

Permafrost Degradation and Influx of Biogeogases into the Atmosphere

E. Rivkina
Institute of Physicochemical and Biological Problems in Soil Science, Pushchino, Russia
G. Kraev
Institute of Physicochemical and Biological Problems in Soil Science, Pushchino, Russia

Abstract

The data on methane content and pattern of its distribution across permafrost of different age and origin on late Cenozoic permafrost of Northeastern Arctic are summarized. We have found that methane is present in the epycryogenic Holocene and early Pleistocene layers and is absent in the syncryogenic late Pleistocene ice complex. Incubation under anaerobic conditions triggered the process of methane formation in Holocene and early Pleistocene layers and did not initiate it in the ice complex sediments. Based on the analysis of microbial community, organic matter, and potential for methane formation in various genetic types of permafrost sediments, we concluded that ice complex sediments, and to a lesser extent than epycryogenic ones, have the potential to produce methane in consequence of permafrost degradation.

Keywords*:* permafrost; methane production; methanogenic arhaea; isotopic composition.

Introduction

In the framework of global change studies in the last decades, attention has been given to CO_2 and CH_4 emission from high-latitude ecosystems (Whalen & Reeburgh 1990, Christensen, 1993, Fyodorov-Davydov 1998, Reeburgh et al. 1998, Worthy et al. 2000, Zamolodchikov & Fyodorov-Davydov 2004, Wagner et al. 2003, van Huissteden et al. 2005). However, significant amounts of these greenhouse gases have been isolated from biogeochemical cycling and conserved in permafrost (Rivkina et al. 1992,) together with organic matter (Schirrmeister et al. 2002, Kholodov et al. 2004) and viable anaerobic microorganisms (Rivkina et al. 1998, Gilichinsky 2002). Thus, permafrost is a huge deposit and potentially, a large source of old organic carbon. It is important to assess the consequences of permafrost degradation because at least four pathways of carbon moblilization are influenced by permafrost thaw:

1. The reservoir of carbon dioxide and methane bound in upper permafrost horizons that, unlike the deep high-pressure gas hydrates, could be easily liberated in the case of thawing in the polar regions.

2. The paleomicrobial community of viable methanogens expected to retain activity and be anew involved in biogeochemical processes, including generation of greenhouse gases (Rivkina et al. 2006).

3. Labile organic matter conserved in permafrost will be consumed by these microorganisms as an energy source for greenhouse gas production.

4. Increased production of methane in the active zone. This is in fact observed on northeastern Arctic exposures under present conditions with associated release methane, which is of similar magnitude to the direct production in Arctic tundra (Rivkina et al. 2001).

Recent studies have provided a new impetus to such discussion, as they forecast high gas emission in response to permafrost degradation (Walter et al. 2006, Zimov et al. 2006). These papers, describing the flux of greenhouse gases from thermokarst ponds, have stimulated significant public and scientific interest. Quantification of methane release from thawing permafrost is of prime importance in climate research.

Our objective is to clearly recognize the concentration and features of distribution of carbon sources in permafrost, based on its history (Sher 1974, Schiermeister et al. 2002). The present paper, based on the analysis of microbial community, organic matter and content of CO_2 and CH_4, as well as on the possibility of methane formation and oxidation in various genetic types of permafrost sediments, will discuss the potential of greenhouse gases emission to the atmosphere in response to permafrost degradation and specifically, the late Pleistocene Icy Complex thawing upon which most activities are now focused.

Study Area and Object of Investigation

Investigations were carried out in continuous permafrost area in tundra and forest tundra zone landscapes on north-eastern Arctic coastal lowlands (125–162°E, 68–72°N), located between the Lena and Kolyma River deltas (Fig. 1). Sites were located outside the oil and gas basins, and were characterized by different Quaternary deposits (early Pleistocene to Holocene) and permafrost of both syn- and epicryogenic origin (Kaplina et al. 1984, Schirrmeister et al. 2002). Permafrost here had begun to form 3 million years ago and until now has not been deeply affected by global thawing.

Studies were carried out down to 100 m depths on fine dispersed late Cenozoic stratotypes, which have been well described by many authors (Kaplina et al. 1981, 1988, Sher et al. 2005) on the bases of radiocarbon, palynological, paleontological, paleomagnetic, cryolithological, and physicochemical data.

Distribution, thickness and area of the following strata

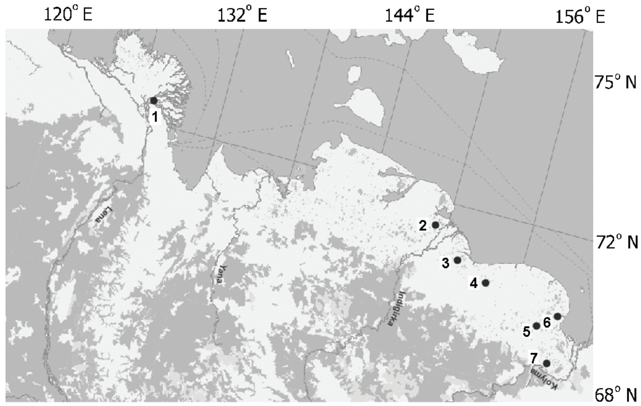

Figure 1. Arctic study sites: 1–Bykovskii Peninsula, Lena River; 2–Low basin of Indigirka River; 3– Khomus-Yuryakh River; 4–Alazeya River; 5–Chukochya River; 6– East Siberian Sea coast; 7–Khalarchinskaya tundra sandy plain.

were calculated, tested for microorganisms, organic matter, CO_2, and CH_4 presence:

- Thomus-Yar Suite, the lowermost (15–20 m below sea level) sediments in the middle Chukochya and Alazeya Rivers (Kolyma lowland) dated back to the second half of the Pliocene, 2–3 million years.
- Overlying Olerian Suite, the stratotype of late Pliocene.
- Early Pleistocene age (1.8–0.6 million years). The upper part of the suite is represented by epicryogenic horizons with pseudomorphoses, and the lower one, by syncryogenic layers.
- Middle Pleistocene syncryogenic sediments and ice wedges belong to buried Icy Complex, named as Jukagir Suite on Cape Svyatoy Nos (Laptev Sea coast), Allaikha Suite on the left channel inflow of Indigirka River, and Maastakh Suite on the right bank of the middle Chukochya River.
- Predominantly syncryogenic middle to upper Pleistocene cross-sections on Bolshoy Homus-Yuryah River (Kolyma lowland): three Ice Complex units with interbedded epicryogenic horizons. Age of deposits varied from >50 ka in the late Pleistocene Ice Complex to 200–600 ka in the middle Pleistocene.
- Marine sediments of Kon'kovaya Suite (East Siberian Sea coast), frozen after sea level dropped at the end of the middle Pleistocene 120 ka ago.
- Late Pleistocene (10–60 ka old) syncryogenic Ice Complex deposits known as Edoma Suite that compose the upper part of cross sections of remains of a late Pleistocene accumulative plane between Lena and Kolyma Rivers.
- Late Pleistocene epigenetically frozen river bed sands of Khalerchinskaya tundra region on the left bank of lower Kolyma River, overlain by Holocene eolian sands.
- Holocene (6–8 ka) syncryogenic alluvial deposits of water meadows on the modern flood-lands and epicryogenic alas horizon and "covering" layer on the top of the Icy Complex, formed by refreezing of the sediments that have melted and drained.

Methods

The data presented are based on 2000 tested samples. Thirty cm-long permafrost cores (diameter 68–107mm) were sampled from boreholes (step-interval 1 m). The strict protocols for drilling and the subsequent handling of cores are designed to ensure uncontaminated material. For microbiological studies the cores were split into c. 5-cm long segments, placed into sterile boxes or bags, stored in the field within a hole in the permafrost at a natural temperature of -10°C, and transported frozen to the laboratory.

Gas samples were collected in the field by degassing 50 g of frozen cores in a 150-mL syringe under a nitrogen atmosphere (Alperin & Reeburgh 1985). The gas mixture was then transferred through a needle to the rubber septa sealed vials filled with salt water. At that point, brine was substituted by gas with the excess water flowing out through the second needle. Gas samples were kept in the vials until further analysis in the lab. CH_4 and CO_2 concentrations were measured using KhPM gas chromatograph (Russia) equipped with katharometer (for carbon dioxide) and hydrogen-flame ionization detector (for methane). Hydrogen was used as a carrier gas in both cases. The same samples were analyzed for $\delta^{13}C$ methane and carbon dioxide using GC Combustion Thermo Finnigan interface and Delta XL mass spectrometer (Germany). To estimate methanogenesis, samples were incubated for 3 weeks at temperatures -16.5, -10, -5, -1.8, and 5°C as described by Rivkina et al. (2007). At the end of the incubation, newly formed radioactive CH_4 was removed from the experimental vials by an air flow (50 ml/min). It was passed through a drexel bottle with a solution of 200 g/l NaCl and 1N KOH and combusted to $^{14}CO_2$ at 700–800°C with cobalt oxide as a catalyst. At the final stage $^{14}CH_4$, oxidized to $^{14}CO_2$, was absorbed in the vial with a mixture of 2 ml β-phenylethylamine and 10 ml of Universal LSC cocktail (Sigma). Vials were counted on an LS 5000 TD liquid scintillation counter (Beckman). Archaea were cultivated according the Hungate anaerobic technique (1969).

The total organic matter was estimated by wet and dry incineration methods. Redox potential was measured in the field immediately after melting, using an "Ecotest-120" (Russia) potentiometer with a platinum electrode and a silver chloride electrode as reference.

Results

Methane and carbon dioxide content and distribution

Unlike CO_2, which is found in all layers below the permafrost table (in various concentrations up to 20 ml of gas per 1 kg of frozen ground), CH_4 shows a distinct and alternating pattern with depth. In a generalized geological cross-section, in which all the geological layers exist in chronological order, CH_4-containing layers would be sandwiched between layers free of methane (Fig. 2). The CH_4 concentration (0.4 to 30.0 ml/kg) does not appear to be correlated to any textural or chemical characteristics of the sediments, age, or the depth of burial. Methane is found primarily on a present-day floodplain bog, in the "covering" layer, alas horizons, marine deposits, late Pliocene-early Pleistocene and Pliocene suites. The lowest concentrations of CH_4 (<0.01 ml/kg) are present in modern alluvial plains in virtually all the river valleys of the area, in Holocene eolian and late Pleistocene river-bed sands, and in the mid and late Pleistocene Icy Complexes in different locations in the region.

For at least several hundreds of thousands years, methane has not diffused from the methane-rich layers into adjacent layers, which are devoid of methane, which implies that there is negligible diffusion of methane in the permafrost under both present and past conditions. We can estimate an upper limit on the diffusion of methane by using the profile shown in Fig. 2 (sites 4 and 5). The methane profile in sediments that are 0.6 to 3 million years old retain structure over length scales of about 3 m. The relationship between time (T), and distance diffused (x), is given by $T = x^2/D$, where D is the diffusion coefficient. From this relationship we calculate that D must be less than 10^{-13} m^2/s; i.e., the upper limit on the diffusion of methane through permafrost is surprisingly low.

Evidence from the West Siberian natural gas fields and gas-hydrate bearing fields in Mackenzie Delta (Dallimore & Colett 1995) further supports the conclusion that methane is in a bound form and not able to diffuse through the near-surface fine dispersed frozen sediments with negligible lithostatic pressure. It suggests that the methane is held in a clathrate form within the sediments (Rivkina et al. 2001).

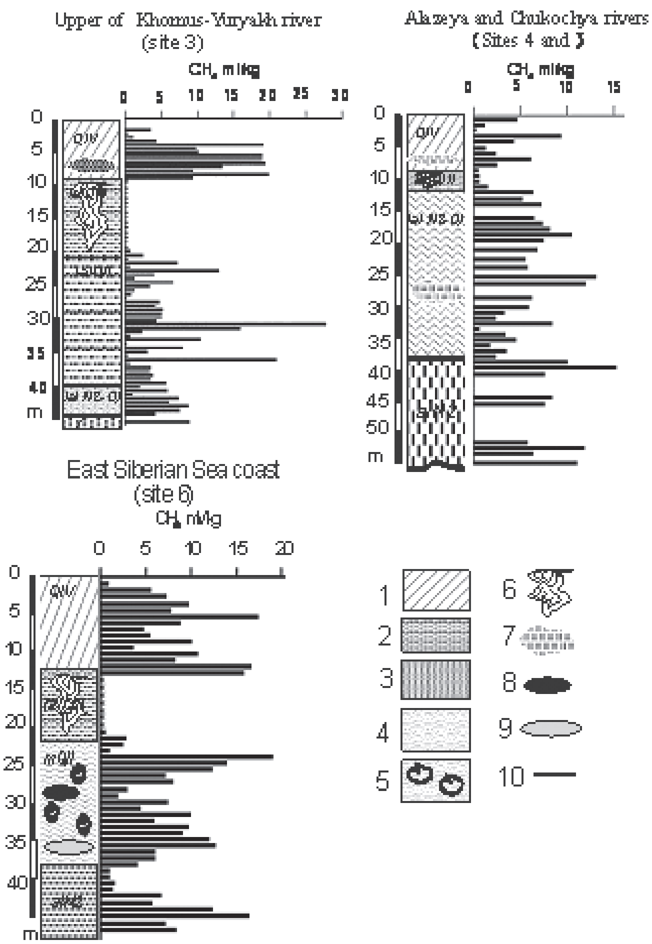

Figure 2. Methane content in permafrost: 1–loam, 2–sandy loam, 3–sand, 4–loamy sands, 5–marine sediments, 6–ice wedges, 7–peat, 8–methane hydrate, 9–lenses of cryopegs, and 10–methane concentration.

One possible way to reconcile the methane hydrate formation at low pressures with the theoretical requirement for stability only at high pressures is to assume that, within the pore spaces of the permafrost, high pressures are created by the freezing process and that it is within these zones of high pressure that the methane hydrate is located. The matrix formed by the sediment grains in permafrost may be crucial to the formation of these intrapore high-pressure zones. In the pore spaces, methane concentration is possibly much higher than it was measured in these samples. The possibility that methane-hydrate may exist in fine-grained sediments of the upper permafrost horizons was confirmed experimentally (Ershov et al. 1991, Chuvilin et al. 2005).

However, strong diffusion of methane from below was observed if the borehole crossed the fine dispersed sediments and reached the pebbles horizon (Fig. 3). Despite the fact that methane content in fine dispersed sands and sandy loams did not differ from typical value, the methane concentration in the borehole gas phase reached 90%. It means that methane in the borehole came from a different source (e.g., from a deeper strata). The same situation is often obtained if the borehole reached CH_4-lenses buried in near surface marine sediments (Fig. 2, site 6).

From the isotopic composition of C-CH_4 (Fig. 4) CH_4-containing layers can be separated into two groups: a main group containing horizons of different origin and age, late Pliocene to Holocene, with $\delta^{13}C$ values ranging -64 to -80 per mil and a minor group represented by mid Pleistocene epicryogenic soils with $\delta\,^{13}C$ value varying 90 to 100 per mil.

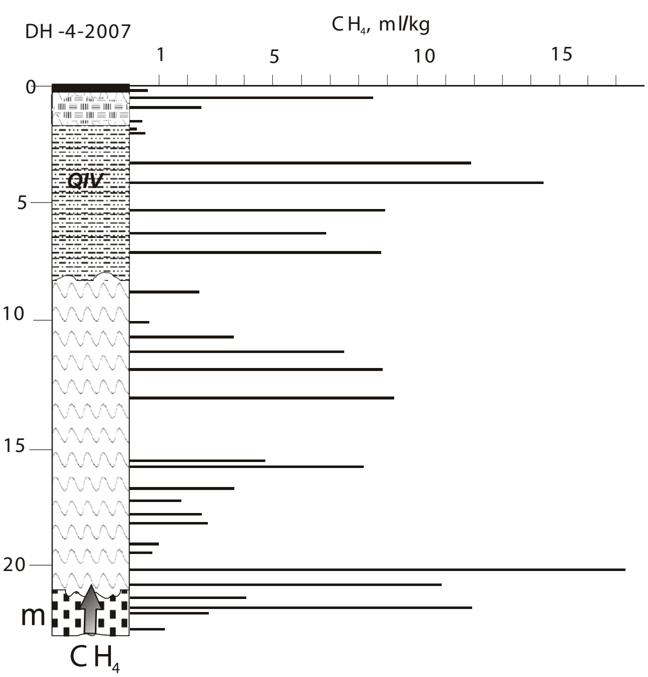

Figure 3. Methane entry in borehole from pebble horizon.

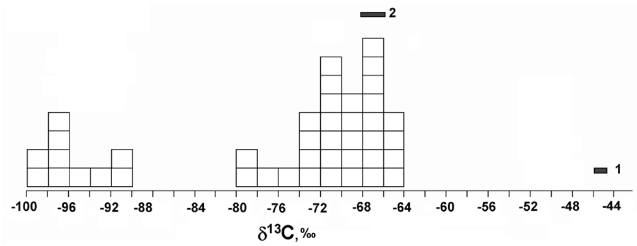

Figure 4. δ [13]C of methane from permafrost. 1–atmospheric methane, 2–methane from gas fields, 3–methane hydrate from permafrost, Mackenzie River delta (Dallimore et al. 1995)

The isotopic composition of methane produced by methanogenic bacteria in natural ecosystems ranges from -50 to -70‰, while abiogenic methane is substantially more enriched in ^{13}C, with values ranging from -45 to -50‰ (Fig. 4). The isotopic composition of CH_4 carbon in permafrost (δ ^{13}C -64 to -99‰) confirms its biological origin and, along with discrete bedding, suggests *in situ* formation of this biogenic gas. The extremely low value of δ ^{13}C methane in some samples (-90 to -99‰) allows us to conclude that CH_4 mainly formed as a result of CO_2 reduction, and a portion of this methane could be formed at subzero temperatures, which was accompanied by significant fractionating of carbon isotopes.

Permafrost also contains viable methanogenic bacteria, but only in epigenetically frozen sediments, and not in the eastern Arctic sincryogenic Icy Complexes. In contrast, viable methanotrophic (methane-oxidizing) psychrophilic bacteria are present in both, epi- and syngenetically frozen layers (Khmelenina et al. 2002).

Incubation of thawed permafrost samples in anaerobic conditions with CO_2+ H_2 showed methanogenic activity in Holocene and late Pliocene-early Pleistocene epicryogenic sediments only. In the samples of Icy Complex this process was not observed (Fig. 5). At the same time, methanotrophic bacteria were able to oxidize and assimilate methane in samples from both, epi- and syncryogenic horizons with the maximum rate of methane oxidation was observed at permafrost table (Khmelenina et al. 2002).

The content of total organic carbon in epicryogenic layers and Icy Complex is similar and varied 1.5–2 to 5% (Fig. 6). But for all that the Icy Complex contains more labile organic matter than epicryogenic sediments: range of ulmification is 15 and 20%, respectively (Kholodov et al. 2006).

Discussion

Greenhouse gases of biological origin excluded during frozen state from biogeochemical turnover are a variety of geogases inherent to cryolithosphere only. Unlike the deep high-pressure gas hydrates, this reservoir of ancient biogeogases in the upper horizons of the cryolithosphere could be easily liberated into the atmosphere and reinvolved in the present-day turnover, should the permafrost degrade as a result of warming. However, this reservoir of organic carbon and methane has been very poorly quantified. Recent research has shown that considerable variation exists in the

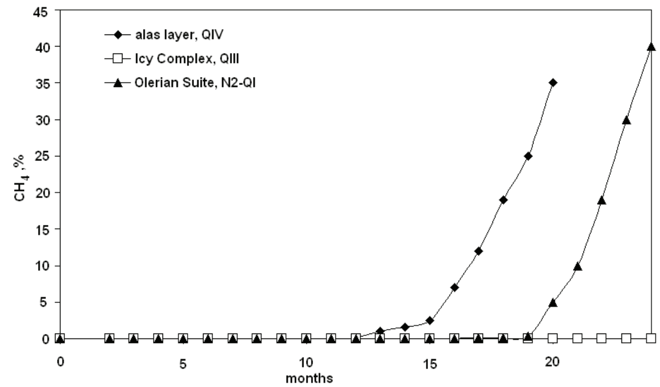

Figure 5. Increase of methane concentration (percentage by volume) in headspace of jars with different permafrost sediments incubated at 22°C in anaerobic condition

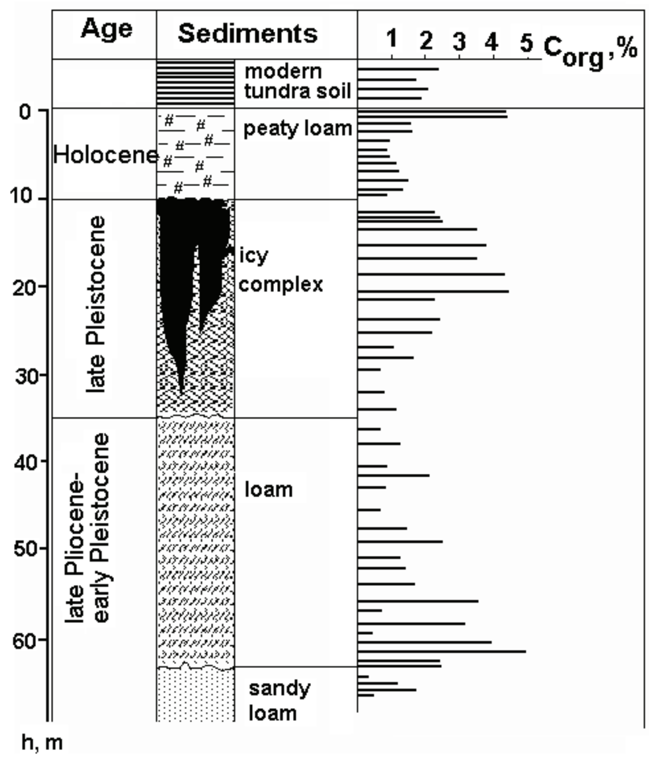

Figure 6. Content of organic carbon in late Cenozoic frozen suites (sites 4 and 5, Figs.1, 2).

amount of methane stored in frozen deposits (Rivkina et al. 2007). This strongly affects estimates of the amount of greenhouse gases that may be released from these deposits upon warming, and forecasting the contribution of these gases to atmosphere. To answer the question, does the release of bound methane and carbon dioxide and activation of CH_4 and CO_2 formation lead to dramatic effects on climate, it is necessary to understand the response of permafrost to climate warming in the past. The Holocene optimum, which was accompanied by widespread permafrost degradation, can be used as models of future warming.

Methane content in the Earth's atmosphere during the Pleistocene and Holocene was affected by the climate changes, varying between 0.35 to 0.7 ppm, reaching the maximum concentrations during optima and minimum in cryochrones. This could be demonstrated by the high methane content in alas layers, formed during the Holocene optimum. Nevertheless, permafrost thawing during the Holocene optimum, which destroyed at least half of the Icy Complex in the eastern Arctic, did not lead to dramatic warming of air temperatures, probably because methane generation took place simultaneously with methane oxidation, and smoothly gave way to new cooling and refreezing of thawed sediments. Anthropogenic effects became more prominent during the last 270 years. During this time, atmospheric methane content has increased sharply to 1.8 ppm, independently of century cryo- and thermochrones.

Our data established several important findings:

1. Methane is present in the epicryogenic Holocene and late Pliocene-early Pleistocene sediments and is absent in the late Pleistocene Icy Complex.

2. Incubated under anaerobic conditions, Holocene and late Pliocene-early Pleistocene sediments, but not sediments of the Icy Complex, exhibited methane formation.

3. Permafrost contains viable paleomicroorganisms, including methane-producing archaea. Nevertheless, viable methanogenic bacteria were isolated from epicryogenic layers only, and never found in Icy Complexes.

4. The isotopic composition of CH_4 carbon in permafrost confirms its biological origin as a result of CO_2 reduction.

On the basis of these findings we can conclude that climate warming and, as a consequence, permafrost thawing, undoubtedly trigger biological activity, including the microorganisms of the carbon cycle. In this case the methane content, microbial community, organic matter, and methane production, show that Icy Complex have less potential as a methane producer than epicryogenic sediments. Thawing of the Icy Complex will not add methane to the atmosphere because 1) the Icy Complex does not contain bound methane, and 2) the Icy Complex does not contain methanogenic bacteria. An additional CH_4 flux is possible also in cases when the talik zone under thermokarst lakes penetrates through the Icy Complex and reaches the underlying methane-containing horizons (as shown on Fig. 3).

We calculated the possible additional greenhouse gases flux to atmosphere in the case of thawing 50-m thick CO_2 and CH_4-containing epicriogenic sediments under square 1 km^2. The sum of C (CO_2+CH_4) store in such volume is ~ 150 tons (without calculation of possible methane oxidation or production). Even the amount is not very significant; this flux of biogeogases bound in permafrost to atmosphere has to be taken into consideration even now. For example, the average abrasion rate of the Arctic coast consisting of frozen sediments is 3 m/year. Destruction of each kilometer of coast 25 m high is accompanied by the release of 3 tons of methane and carbon dioxide. Given the minimal length of the Arctic coastline, the total quantity of C (CO_2+CH_4) being annually released into the atmosphere today is 12 thousand tons. The same order of gases, likely due to the coastal abrasion, came from the river-banks and lakesides in the cryolithozone.

The other way is emission to atmosphere of the gases newly formed in thawed permafrost. In recent years, methanogenic archaea have been isolated from permanently cold lake and marine sediments (Franzmann et al. 1997; Von Klein et al. 2002; Kendall et al. 2007), as well as culture-independent methods, and have demonstrated that the active layer of arctic soils is a natural habitat of a diverse archaeal community (Ganzert et al. 2007). Even though there is limited data regarding microbial processes in thawed permafrost sediments, we can forecast that microbial activity in thawed layers and themokarst lakes is increasing, but not more than in the existing lakes and seasonally thawing soils.

Conclusion

One can expect that due to permafrost thawing and the accessibility of organic matter, the paleomicrobial community would become involved in the biogeochemical processes, including production of greenhouse gases. The ultimate goal of the current investigation is to estimate the sum effect of these processes, taking into account their outcomes in the past optima.

Acknowledgments

This research was supported by the Russian Fund for Basic Research (grants: 04-04-48257, 08-05-00268).

References

Alperin, M.J. & Reeburgh, W.S. 1985. Inhibition experiments on anaerobic methane oxidation. *Appl. Environ. Microbiol*. 50: 940-945.

Christensen, T. 1993. Seasonal emission of methane from the active layer of organic tundra soil scale and controlling factors. *Proc. of Joint Russia-American Seminar on Cryopedology and Global Change, Puschino, Russia*, pp. 325-341.

Chuvilin, E.M., Perlova, E.V. & Yakushev, V.S. 2005. Classification of gas compound in rocks of permafrost zone. *Kriosfera Zemli* 3: 73-76. (in Russian).

Dallimore, S.R. & Colett, T.S. 1995. Intrapermafrost gas hydrates from a deep core hole in the Mackenzie Delta, Northwest Territories, Canada. *Geology* 23(6): 527-530.

Ershov, E.D., Lebedenko, Yu.P, Chuvilin, E.M., Istomin, V.A. & Yakushev, V.S. 1991. Peculiarities of gas hydrates existence in cryolithozone. *Dokl. Akad. Nauk* 321:788-791.

Fedorov-Davydov, D.G. 1998, Respiration activity in tundra biocenoses and soils of the Kolyma Lowland. *Eurasian Soil Science* 31(3): 263-274.

Franzmann, P.D, Liu, Y, Balkwill, D.L., Aldrich, H.C., Conway de Macario, E. & Boone, D.R. 1997, Methanogenium frigidum sp. nov., a psychrophilic, H2-using methanogen from Ace Lake, Antarctica. *Int J Syst Bacteriol* 47(4): 1068-1072.

Ganzert, L, Jurgens, G, Munster, U. & Wagner, D. 2007. Methanogenic communities in permafrost-affected soils of the Laptev Sea coast, Siberian Arctic, characterized by 16S rRNA gene fingerprints. *FEMS Microbiol Ecol*. 59: 476-488.

Gilichinsky, D. 2002. Permafrost as a microbial habitat. In : G. Bitton (ed.), *Encyclopedia of Environmental Microbiology*. New York: Wiley, 932-956.

Hungate, R.E. 1969. A roll tube method for cultivation of strict anaerobes. In: J.B. Norris & D.W. Ribbons (eds.), *Methods in Microbiology*. New York: Academic Press, 116-132.

Kaplina, T.N., Lakhtina, O.V. & Rybakova, N.O. 1981. Cainozoic sediments of Alazeya river midstream (Kolyma lowland) *Izves. of USSR Academy of Sciences, series geol*. 8: 51-63

Kaplina, T.N. & Lozhkin A.V. 1984. Age and history of accumulation of the "Ice Complex" of the Maritime Lowlands of Yakutia. In: A.A. Velichko, H.E. Wright Jr. & C.W. Barnosky (eds.), *Late Quaternary Environments of the Soviet Union*. The University of Minnesota Press. London: Longman, 147-151.

Khmelenina, V.N., Makutina, V.A., Kalyuzhnaya, M.G., Rivkina, E.M., Gilichinsky, D.A. & Trotsenko, Yu.A. 2002. Viable methanotrophic bacteria findings in permafrost sediments of North-Eastern Siberia. *Dokl. Biol. Sci.* 384: 235-237. Translated from Dokl. Akad. Nauk 384: 283–285.

Kholodov, A.L., Rivkina, E.M., Snytin, P.S., & Borisov, R.R. 2004. Quaternary deposits of Laptev Sea coast as a source of organic matter and biogenic gases. *Rep. on Polar Res*. 482: 117–124.

Kholodov, A.L. , Zolotareva, B.N. & Shirshova L.T. 2006. Organic matter in the main types of frozen quaternary deposits of the Bykovsky peninsula: Total content and group composition of the humus. *Earth Cryosphere*. X(4): 29-34.

Kendall, M.M., Wardlaw, G.D., Tang, C.F., Bonin, A.S., Liu, Y. & Valentine, D.L. 2007. Diversity of archaea in marine sediments from Skan Bay, Alaska, including cultivated methanogens and description of *Methanogenium boonei* sp. nov. *Appl Environ Microbiol*. 73: 407-414.

Rivkina, E.M., Samarkin, V.A. & Gilichinsky, D.A. 1992. Methane in the permafrost soils of Kolyma-Indigirka Lowland. *Dokl.Akad. Nauk* 323(3): 559-563. (in Russian).

Rivkina, E., Gilichinsky, D., Wagener, S., Tiedje, J. & McGrath, J. 1998. Biogeochemical activity of anaerobic microorganisms from buried permafrost sediments. *Geomicrobiol. Journ.* 15: 187-193.

Rivkina, E, Gilichinsky, D., McKay, C. & Dallimore, S. 2001. Methane distribution in permafrost: Evidence for an interpore pressure methane hydrate. In: R. Paepe & V. Melnikov (eds.), *Permafrost Response on Economic Development, Environmental Security and Natural Potential*, NATO series, Kluver Academic Publishers, 487-496.

Rivkina, E.M., Kraev, G.N., Krivushin, K.V., Laurinavichus, K.S., Fyodorov-Davydov, D.G., Kholodov, A.L., Shcherbakova, V.A. & Gilichinsky, D.A. 2006. Methane in permafrost of Northeastern Arctic. *Earth Cryosphere*. X(3): 23-41.

Rivkina, E., Shcherbakova, V., Laurinavichius, K., Petrovskaya, L., Krivushin, L., Kraev, G., Pecheritsina, S. & Gilichinsky, D. 2007. Biogeochemistry of methane and methanogenic archaea in permafrost. *FEMS Microbiol Ecol*, 61: 1-15.

Schirrmeister, L., Siegert, C., Kuznetsova, T., Kuzmina, S., Andreev, A., Kienast, F., Meyer, H. & Bobrov, A.A. 2002. Paleoenvironmental and paleoclimatic records from permafrost deposits in the Arctic region of Northern Siberia. *Quaternary International.* 89: 97-118.

Sher, AV. 1974. Pleistocene mammals and stratigraphy of the Far Northeast USSR and North America. *International Geology Review* 16(7-10): 1-282 (Book Section), American Geological Institute.

Sher, A.V., Kuzmina, S.A., Kuznetsova, T.V. & Sulerzhitsky, L.D. 2005. New insights into the Weichselian environment and climate of the East Siberian Arctic, derived from fossil insects, plants, and mammals. *Quaternary Science Reviews* 245: 533-569.

van Huissteden, J. 2004, Methane emission from northern wetlands in Europe during Oxygen Isotope Stage 3. *Quaternary Science Reviews* 23: 1989-2005.

van Huissteden, J., Maximov, T.C. & Dolman, A.J. 2005. High methane flux from an arctic floodplain (Indigirka lowlands, Eastern Siberia). *J. of Geophys. Res.* 110, G02002, doi:10.1029/2005JG000010.

Von Klein, D., Arab, H., Volker, H. & Thomm, M. 2002. Methanosarcina baltica sp. nov.: A novel methanogen isolated from the Gotland Deep of the Baltic Sea. *Extremophiles* 6: 103-110.

Wagner, D., Kobabe, S., Pfeiffer, E-M. & Hubberten, H-W. 2003. Microbial controls on methane fluxes from a polygonal tundra of the Lena Delta, Siberia. *Perm. Perigl. Proc.* 14: 173-185.

Walter, K.M., Zimov, S.A., Chanton, J.P., Verbyla, D. & Chapin III, F.S. 2006. Methane bubbling from Siberian thaw lakes as a positive feedback to climate warming. *Nature* 443: 71-75.

Whalen, S. & Reeburgh, W. 1990. Consumption of atmospheric methane by tundra soils. *Nature* 346: 160-162.

Zamolodchikov, D., Fyodorov-Davydov, D. 2004. The biological cycles in terrestrial Polar ecosystems and its influence on soil formation. In: J. Kimble (ed.), *Cryosols: Permafrost-Affected Soils,* Section 4, Chapter 2. Springer, 479-508.

Zimov, S.A., Schuur, E.A.G. & Chapin III, F.S. 2006 Permafrost and the global carbon budget. *Science* 312: 1612-1613

Observations and Considerations on Destabilizing Active Rock Glaciers in the European Alps

Isabelle Roer, Wilfried Haeberli
Glaciology, Geomorphodynamics & Geochronology; Geography Department, University of Zurich, Switzerland
Michael Avian, Viktor Kaufmann
Institute of Remote Sensing and Photogrammetry, Graz University of Technology, Austria
Reynald Delaloye
Department of Geosciences, Geography, University of Fribourg, Switzerland
Christophe Lambiel
Institute of Geography, University of Lausanne, Switzerland
Andreas Kääb
Department of Geosciences, University of Oslo, Norway

Abstract

In many high mountain regions, warming of perennially frozen ground in both coarse debris and rock walls has a major influence on slope stability. In this context, indications of destabilizing active rock glaciers, such as high horizontal velocities (up to 4 ma^{-1}), front advance rates of up to 4 ma^{-1}, and development of crevasse-like cracks (up to 14 m deep), have been documented and monitored in the Alps for a few years. Beside the limited knowledge of rock glacier dynamics, our principle hypothesis is that the primary factors controlling the development of cracks and the destabilization of rock glacier tongues are the rheological properties of warming ice. In addition, we postulate that hydrological effects of unfrozen water within the active layer, the permafrost body, or at its base may contribute to the initiation of the slide-like mass wasting.

Keywords: European Alps; kinematics; rock glacier; slope destabilization.

Introduction

In the context of recent climatic changes and their impact on the cryosphere, high-mountain environments play a key role due to their sensitivity to thermal changes. The indicative role of rock glaciers in these geosystems was emphasized only recently (e.g., Harris & Haeberli 2003, Haeberli et al. 2006), but was up to now mainly restricted to temperature variations within the permafrost body and variations in active layer thickness. Within the last decade, an increasing number of studies monitored and quantified the creep behavior of rock glaciers in the European Alps and observed increasing surface displacements since the 1990s (Schneider & Schneider 2001, Ikeda et al. 2003, Lambiel & Delaloye 2004, Kääb et al. 2007, Roer 2007). In this context it is described that the Alpine rock glaciers show a rather synchronous behavior and respond sensitively to recent temperature increase (Roer et al. 2005a, Roer et al. 2005b, Kääb et al. 2007, Delaloye et al. 2008). In 2003, Kääb et al. stated that the correlation between the velocity field (e.g., speed, creep direction, strain rates) and the present day three-dimensional geometry indicates that most active rock glaciers have not undergone significant dynamic changes in the past. But recently, distinct changes in surface topography are described for a number of active rock glaciers in the Alps, indicating the landslide-like behavior and destabilization of these landforms.

Based on these observations, the study aims at identifying primary factors controlling the development of cracks and causing the landslide-like behavior of the landforms. Furthermore, possible natural hazards due to rock glacier instabilities are discussed.

Observations

The destabilization of active rock glaciers is indicated by distinct changes in their kinematics, geometry and strongly modified topography. These phenomena are investigated qualitatively by field inspection and by interpretation of terrestrial and aerial photographs. In addition, horizontal velocities, advance rates of the rock glacier front, as well as the growth and depth of cracks, are measured and quantified by the use of digital othophotos and by differential GPS measurements in the field. Also, recently the remote sensing technique InSAR (Interferometric Synthetic Aperture Radar) has been applied to detect landform changes (Delaloye et al. in prep., Lambiel et al. 2008). Once indications for destabilizations are detected, the rock glaciers have been surveyed regularly and monitored in detail. Examples are provided from different regions of the European Alps:

(1) rock glacier Hinteres Langtalkar, Carinthia, Austria
(2) rock glacier Grueo1, Valais, Switzerland
(3) rock glacier Furggwanghorn, Valais, Switzerland
(4) rock glacier Petit-Vélan, Valais, Switzerland
(5) rock glacier Tsaté-Moiry, Valais, Switzerland

First, observations on variations in velocity fields accompanied by the development of transverse cracks were described for the rock glaciers Äusseres Hochebenkar and Hinteres Langtalkar, both situated in Austria (Kaufmann &

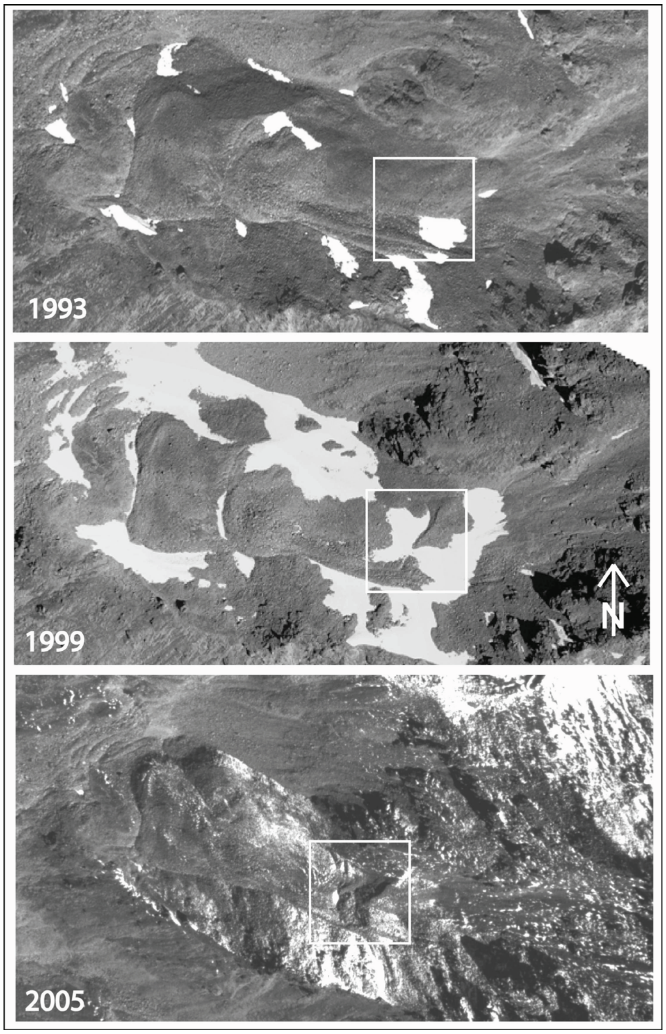

Figure 1. Development of cracks cracks phenologically similar to crevasses occurring on glaciers, in the rooting zone of rock glacier Furggwanghorn (Valais, Switzerland). A small crack started to grow between 1993 and 1999 and evolved into two 14 m deep cracks until 2005. In parallel, the former stable front of the rock glacier advanced about 1.55 ma^{-1} during this time. Orthoimages of 1993, 1999, and 2005 © Swiss Federal Office of Topography (Swisstopo).

Ladstädter 2003, Avian et al. 2005). The strong deformation of the lowest part of the rock glacier Hinteres Langtalkar was interpreted as expression of enhanced strain due to movement of the landform over a terrain ridge into steeper terrain. Thus, the sudden change in slope inclination seemed to cause this specific dynamic response. Later, further rock glaciers showing similar creep instabilities accompanied by the formation of surface ruptures were detected in the Valais, Switzerland.

Rock glacier topography

At the scale of an entire rock glacier, its typical topography is characterized by a relatively smooth and unstructured surface in the upper part (with sometimes longitudinal ridges) and a distinct pattern of ridges and furrows in the lower part, indicating compressive flow. Thus, the surface structure of a rock glacier depicts the complex strain history

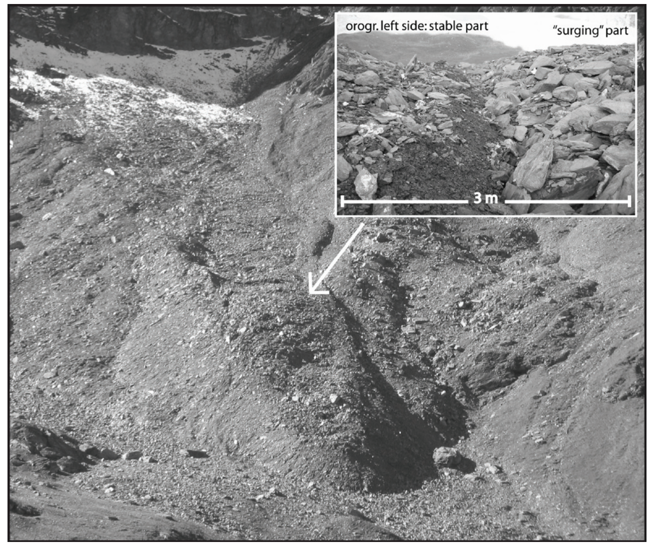

Figure 2. Rock glacier Tsaté-Moiry, Valais, Switzerland. Several scars, developing since the 1980s, are found all over the landform. Velocities at the front were about 7 ma^{-1} between 2006 and 2007. In the field, stable and surging parts can easily be differentiated due to stability (wedged or loose blocks) as well as sorting of the material at the rock glacier surface (Photos: C. Lambiel, 2007).

of the landform (Haeberli 1985, Kääb & Weber 2004). Normally, even if the horizontal velocities are high, the geometric change of the creeping permafrost body is very small (Kääb & Vollmer 2000, Roer 2007).

Most of the rock glaciers investigated here show a smooth morphology prior to the sliding behavior (e.g., rock glacier Furggwanghorn 1993, Fig. 1). In addition, those landforms featuring failures at the front in parallel, indicate smooth surfaces with continuous horizontal displacements in their rooting zones (Kaufmann & Ladstädter 2003, Roer 2007). In the case of rock glacier Tsaté-Moiry, indications for destabilization are not restricted to one part, but affect the whole landform (Fig. 2). Most of the rock glaciers show a collapse behavior in the lowermost part of their tongue. Such failures are indicated by the rugged topography due to the crack formation and by the strong advance of the tongue which is accompanied by a lowering of the surface.

Horizontal velocities and advance rates

As mentioned before, the morphological change of the rock glaciers studied here is caused by distinct high horizontal velocities over the entire landforms, between 1.00–3.76 ma^{-1} (Table 1). These velocities indicate strong spatial variations. In general, deformation rates of the investigated rock glaciers are very small in the rooting zone and at the margins of the landform; the highest movement rates are found in the central flow field. On most of the destabilizing rock glaciers, highest velocities are measured at the front, where most of the morphological changes occur (e.g., Fig. 3). For some of these rock glaciers, measurements of velocities were even inhibited on the destabilized parts of the tongue, due to a loss in corresponding features in the repeated orthophotos. In such cases, the surface is not slowly changing anymore,

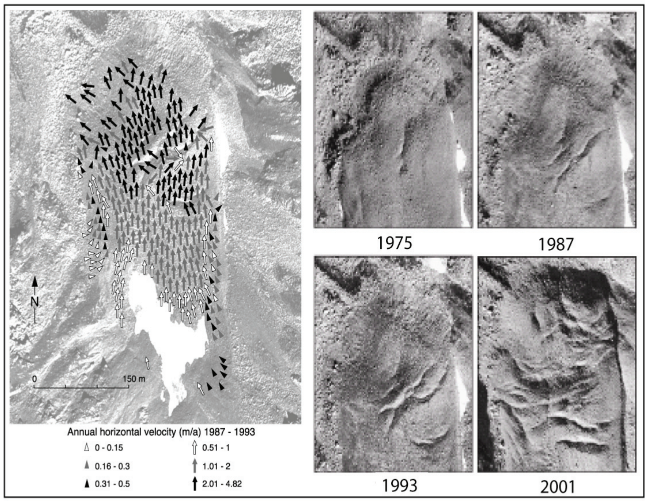

Figure 3. Collapsing tongue and development of deep cracks of rock glacier Grueo1 (Valais, Switzerland) between 1975 and 2001. The cracks started to develop on the orographic right side, while later (between 1993 and 2001) the landslide-like failure extended over the entire tongue. Between 1975 and 2001 the rock glacier advanced about 60 m (~ 2.3 ma^{-1}). (See also Roer 2007, Kääb et al. 2007). Orthoimages of 1975, 1987, and 1993 © Swiss Federal Office of Topography (Swisstopo). Orthoimage of 2001 © RTG 437, Department of Geography, University of Bonn.

but is rather characterized by tilting and toppling of blocks into the forming cracks.

In addition to the high displacement rates, all rock glaciers considered here indicate extraordinary changes at their fronts. Regarding typical rock glaciers, even if different advance mechanisms occur (Kääb & Reichmuth 2005), the annual rates are very small (0.1- 0.4 ma^{-1} in the Alps (Roer 2007)). In contrast, rock glaciers showing a landslide-like behavior, feature extraordinary advances of several meters per year (see Table 1, Fig. 5). Due to that fact, the shape of the terminal fronts changed significantly. Hence, they are not stable anymore, and often show a high rockfall frequency.

Formation of cracks

Caused by the high horizontal velocities and the pronounced advance of the fronts, cracks that are –phenologically similar to crevasses which occur on glaciers –developed on all rock glaciers in this study. These cracks are mostly found in the lower part of the tongues; rock glacier Furggwanghorn is the only one with cracks in the rooting zone after 1993 (Fig. 1). They are up to 14 m deep and feature lengths of 150 meters and more. An interesting fact is that, on most of the rock glaciers investigated, first indications of the existence and growth of cracks go back for over 20 years (Table 1). The formation of cracks on the rock glaciers Grueo1 (Fig. 3) and Hinteres Langtalkar (Fig. 4), expanded and accelerated in the 1990s. This is in accordance with observations on rock glacier Furggwanghorn, which show a more recent crack formation (between 1993 and 1999, Fig. 1). In the case of rock glacier Tsaté-Moiry, the phenomena is instead described by the occurrence of scars (which are less deep than cracks, and therefore seem to affect the active layer only) occurring all over the landform.

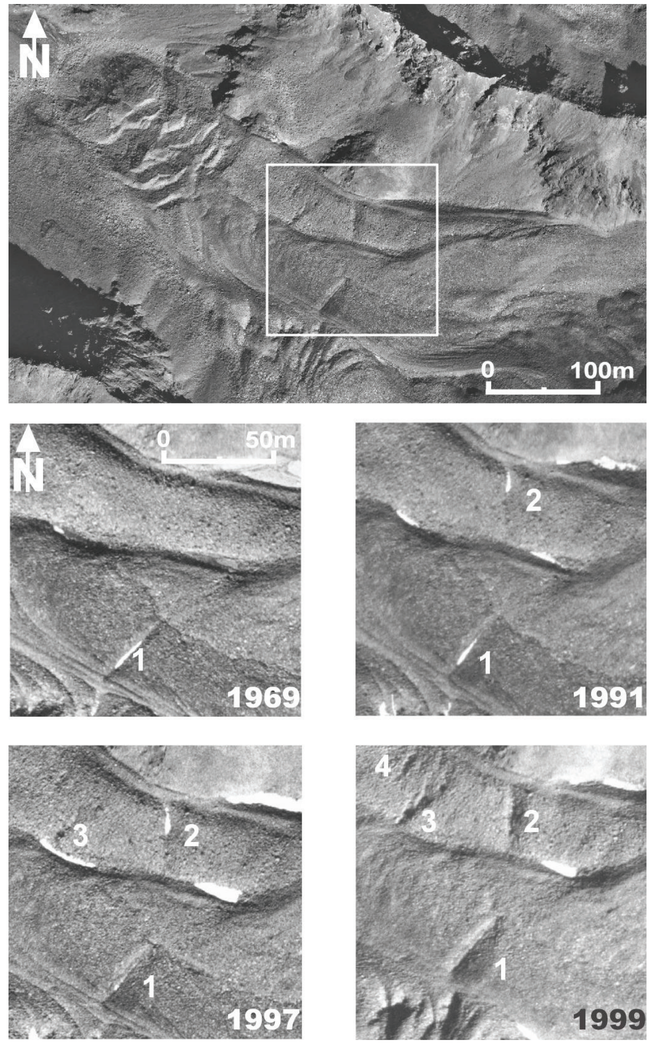

Figure 4. Rock glacier Hinteres Langtalkar (Carinthia, Austria): formation of cracks (1–4) between 1969 and 1999 in the middle part of the landform (square in uppermost image). Aerial photographs of rock glacier Hinteres Langtalkar for 1969, 1991, 1997, and 1999 © Austrian Federal Office of Metrology and Survey (BEV), Vienna, 2001.

Inspections and investigations of these cracks in the field offered more questions than answers. In most of the cracks, neither ice nor evidence of water was found during the summer months, hinting at a well-developed drainage through and/or underneath the creeping permafrost bodies. However, on rock glacier Hinteres Langtalkar (Fig. 4), two of the cracks were filled with water during summer.

Destabilization of rock glacier tongues

A destabilization of the rock glacier tongues happens in those cases where deep cracks form in the lower part of the landforms (i.e., rock glaciers Hinteres Langtalkar, Grueo1, and Tsaté-Moiry). The cracks indicate deep shear-zones similar to those known for rotational landslides (Dikau et al. 1996). Also, the movement of the tongue, which is characterized by a massive downslope displacement of the mass accompanied by a distinct lowering of the surface (see Fig. 5), is analagous to sliding processes. Hence, a change

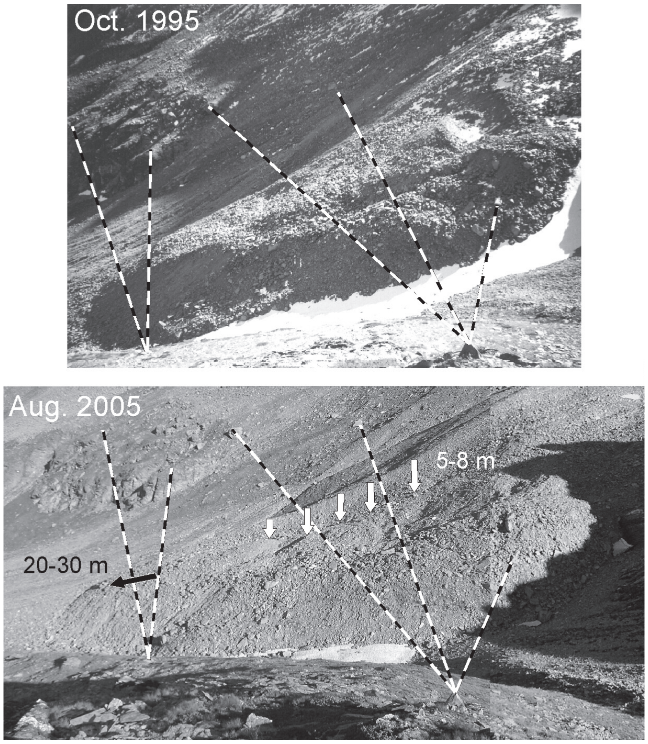

Figure 5. Instability of the tongue of rock glacier Petit-Vélan (Valais, Switzerland). The dashed lines connect the fixed points in stable terrain outside the rock glacier and provide the basis for the photo analysis. Between October 1995 and August 2005, this landform advanced about 20–30 m (approx. 2.5 m per year). Due to that shift of mass, vertical lowering of 5–8 m occurred (Photos: R. Delaloye)

in process regime is indicated. Related to the landslide-like mass wasting, the lowermost part of the tongues changed from a formerly convex to a more concave morphology.

Hazards

The changes described before can affect all parts of rock glaciers: the active layer, the permafrost body, the rooting zone, or the front. Arenson (2002) stated that instabilities within the active layer seem to be most probable due to the effect of unfrozen water during summer. The accelerated horizontal velocities, as well as the sliding processes, strongly influence the stability of the rock glacier front. Here, enhanced rockfall activity (frequency and magnitude) was recognized on several rock glaciers. In general, the position of the landform (especially the slope angle) is decisive for its hazard potential.

Considerations

The interpretation of the presented observations is, up to now, strongly limited due to the complexity of the phenomenon and the lack of information on the thermal state and internal structure of the rock glaciers considered here. Borehole data (internal deformation, temperatures) or data delivered by geophysical soundings from adjacent landforms can not be consulted, since the dynamics of individual rock glaciers cannot be readily compared. Therefore, only the given information on rock glacier kinematics can be analysed. Since these data provide a cumulative signal reflecting all components of the creep process (internal deformation, sliding in shear horizons, and deformation at the base), the processes below the surface can be considered to some degree. The key question is which of the creep components increased by certain changes, i.e., whether the internal deformation, the sliding in shear horizons, or the basal sliding increased significantly (Fig. 6).

Table 1. Summary of characteristics of the investigated rock glaciers. The numbers refer to the rock glaciers listed on page 1.

rockgl.	mean annual velocity (ma^{-1})	front advance (ma^{-1})	crevasses in lower part	crevasses in rooting zone	beginning of crevasse formation
1	2.80 (mean 1997 - 1998)	-	x	-	before 1954
2	2.79 (mean 1993 - 2001)	2.30 (1975-2001)	x	-	before 1975
3	1.46 (mean 1993 - 2001)	1.55 (1975-2001)	-	x	between 1993 and 1999
4	1.24 (mean 2005 - 2007)	2.50 (1995-2005)	x	-	between 1988 and 1995
5	1.50 (mean 2005 - 2007)	4.00 (1999-2005)	x	x	before 1988

Under constant temperatures, stresses, and strain rates, rock glaciers show long-term steady-state (secondary) creep behaviour (Haeberli 1985). The flow results from the plastic deformation of the ice inside the supersaturated permafrost body in response to gravity and is controlled mainly by its internal structure (Barsch 1992). Sliding in shear horizons, where reduction in viscosity enables higher deformations, plays an additional role (Wagner 1992, Arenson et al. 2002). Hence, different factors or a combination thereof, may lead to the observed geomorphic changes: changes in ice content or ice characteristics; changes in the shear horizons (e.g., number, position, frictional behaviour, occurrence of unfrozen water); or changes in the internal structure of the permafrost body leading to changes in deformation. Another creep component, which could have led to the observed changes, might be the deformation of subpermafrost sediments (Fig. 6).

All those effects may result from a change in ground temperature regime. The significance of a rise in air temperature for a change in the strength of ice-rock mixtures has been demonstrated by Davies et al. (2001) in laboratory tests. They proved that a rise in air–and consequently ground–temperature leads to a reduction in shear strength of ice-bonded discontinuities and thus may induce slope failures. In addition, Kääb et al. (2007) conclude from modeling and field investigations, that the creep of perennially frozen granular material close to 0°C is significantly more sensitive to climate forcing than the creep of colder material. Their modeling results also stress the importance of a deeper understanding of shear horizons in rock glaciers, since they appear to be the most sensitive parts in the response of the permafrost bodies to atmospheric and ground warming.

The analysis of the observed development of cracks indicates that strain rates increased significantly. It is not clear whether this formation is a gradual process (as indicated by the slow growth of most of the cracks, Figs. 3, 4) or sudden exceeding of a threshold (as given by the acceleration of crack formation in the 1990s). In addition, this development may differ between rock glaciers. The related changes at the rock glacier surface (e.g., thinning of the protecting debris cover) might enhance the process by positive

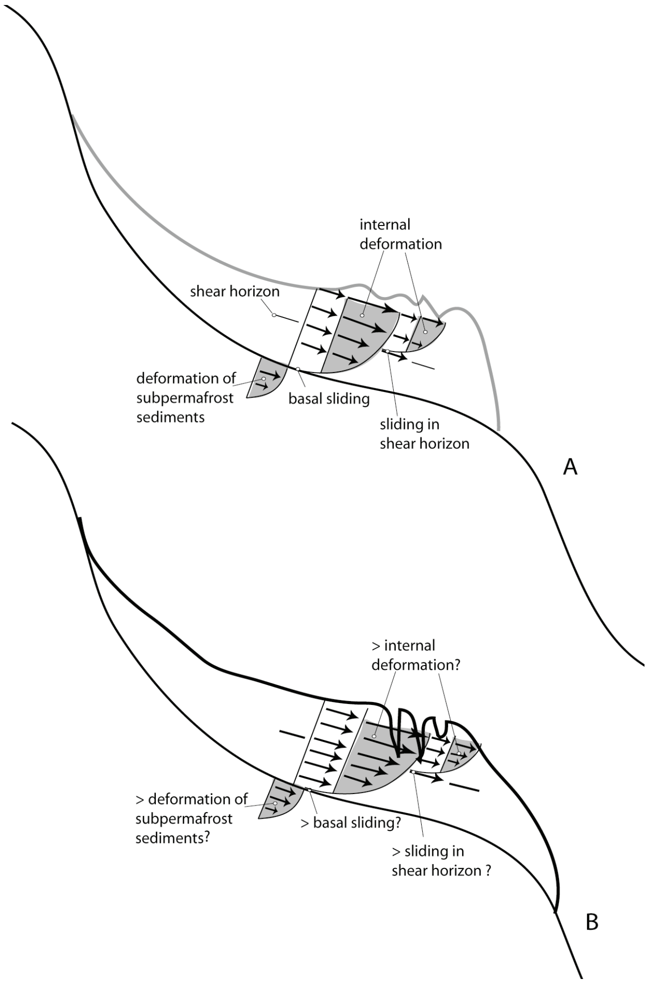

Figure 6. Schematic profile of a typical rock glacier for steady-state conditions (A), and a destabilized rock glacier with crack formation in the lower part of the tongue (B). A deformation profile showing the single creep components is depicted for both cases; it is not clear which component is decisive for the destabilization of the tongue

feedback mechanisms (Kääb et al. 2007). Due to the cracks, latent heat can easily penetrate into the permafrost body, and thus may lead to a warming of the ice (thermokarst phenomena).

The observed changes at the front of the rock glaciers' are probably not exclusively related to permafrost creep processes alone. The analysis of the morphological changes indicates a mass wasting similar to landslides.

Conclusions and Perspectives

Our principle hypotheses are that the primary factors controlling the development of cracks and the destabilization of rock glacier tongues are the rheological properties of warming ice and the resulting changes in the stress-strain relation. In addition, and related to the before mentioned, hydrological effects (unfrozen water) within the permafrost body or at its base may contribute to the initiation of rapid flow acceleration into tertiary creep. Unfrozen water ponding on the permafrost surface could lead to surface instabilities and trigger landslides (Arenson 2002). Another component in this context might be the deformation of subpermafrost sediments. In some cases, topographic influences due to movement onto steep slopes (>25-30°) and/or convex terrain can initiate the destabilization of the landform. Generally, the interpretation of those exceptional rock glaciers is limited, due to the little knowledge of rock glacier dynamics.

The challenge in the investigation of destabilized active rock glaciers lies in the ongoing monitoring of these landforms, for research purpose as well as for hazard assessments. In addition, more data related to internal characteristics are needed in order to develop a process model that couples creep and sliding mechanisms. The coupled analysis will allow for an assessment of how changes in subsurface characteristics will be translated into a rheological response. These goals fit into the key questions of future permafrost research addressing spatio-temporal changes of surface and subsurface processes in response to atmospheric forcing.

Acknowledgments

The photogrammetric analyses of Furggwanghorn rock glacier were conducted in collaboration with Patrick Thee, Swiss Federal Institute for Forest, Snow, and Landscape Research. We gratefully acknowledge the valuable comments of two anonymous reviewers.

References

Arenson, L.U. 2002. Unstable alpine permafrost: a potentially important natural hazard–variations of geotechnical behaviour with time and temperature. Doctoral thesis No. 14801, ETH Zurich.

Arenson, L.U., Hoelzle, M. & Springman, S. 2002. Borehole deformation measurements and internal structure of some rock glaciers in Switzerland. *Permafrost and Periglacial Processes* 13: 117-135.

Avian, M., Kaufmann, V. & Lieb, G.K. 2005. Recent and holocene dynamics of a rock glacier system: The example of Langtalkar (Central Alps, Austria). *Norwegian Journal of Geography* 59(2): 149-156.

Barsch, D. 1992. Permafrost creep and rockglaciers. *Permafrost and Periglacial Processes* 3: 175-188.

Davies, M.C.R., Hamza, O. & Harris, C. 2001. The effect of rise in mean annual temperature on the stability of rock slopes containing ice-filled discontinuities. *Permafrost and Periglacial Processes* 12: 137-144.

Delaloye, R., Perruchoud, E., Avian, M., Kaufmann, V., Bodin, X., Hausmann, H., Ikeda, A., Kääb, A., Kellerer-Pirklbauer, A., Krainer, K., Lambiel, C., Mihajlovic, D., Staub, B., Roer, I. & Thibert, E. 2008. The short-term response of rock glaciers creep to recent warm periods in the European Alps (2002–2007). *Proceedings of the Ninth International Conference on Permafrost, Fairbanks, Alaska, June 29–July 3, 2008* (this proceedings).

Delaloye, R., Strozzi, T., Lambiel, C. & Perruchoud, E. in prep. Landslide-like development of rockglaciers detected with ERS-1/2 SAR Interferometry. *Proceedings ESA FRINGE Symposium 2007*.

Dikau, R., Brunsden, D., Schrott, L. & Ibsen, M.L (eds.). 1996. *Landslide recognition. Identification, movement and causes.* Wiley. Chichester: 251.

Haeberli, W. 1985. Creep of mountain permafrost: internal structure and flow of alpine rock glaciers. *Mitteilungen der Versuchsanstalt für Wasserbau, Hydrologie und Glaziologie* 77: 139.

Haeberli, W., Hallet, B., Arenson, L., Elconin, R., Humlum, O., Kääb, A., Kaufmann, V., Ladanyi, B., Matusoka, N., Springman, S. & Vonder Mühll, D. 2006. Permafrost creep and rock glacier dynamics. *Permafrost and Periglacial Processes* 17: 189-214.

Harris, C. & Haeberli, W. 2003. Warming permafrost in the mountains of Europe. *Bulletin of the World Meteorological Organization* 52, 3: 1-6.

Ikeda, A., Maatsuoka, N. & Kääb, A. 2003. A rapidly moving small rock glacier at the lower limit of the mountain permafrost belt in the Swiss Alps. *Proceedings of the Eighth International Conference on Permafrost, Zürich, Switzerland, June, 2003*. Balkema, 1: 455-460.

Kääb, A. & Vollmer, M. 2000. Surface geometry, thickness changes and flow fields on creeping mountain permafrost: automatic extraction by digital image analysis. *Permafrost and Periglacial Processes* 11: 315-326.

Kääb, A., Kaufmann, V., Ladstädter, R. & Eiken, T. 2003. Rock glacier dynamics: implications from high-resolution measurements of surface velocity fields. *Proceedings of the Eighth International Conference on Permafrost, Zürich, Switzerland, June, 2003*. Balkema, 1: 501-506.

Kääb, A. & Weber, M. 2004. Development of transverse ridges on rock glaciers: field measurements and laboratory experiments. *Permafrost and Periglacial Processes* 15: 379-391.

Kääb, A. & Reichmuth, T. 2005. Advance mechanisms of rock glaciers. *Permafrost and Periglacial Processes* 16: 187-193.

Kääb, A., Frauenfelder, R. & Roer, I. 2007. On the response of rockglacier creep to surface temperature increase. *Global and Planetary Change* 56: 172-187.

Kaufmann, V. & Ladstädter, R. 2003. Quantitative analysis of rock glacier creep by means of digital photogrammetry using multi-temporal aerial photographs: two case studies in the Austrian Alps. *Proceedings of the Eighth International Conference on Permafrost, Zürich, Switzerland, June, 2003*. Balkema, 1: 525-530.

Lambiel, C. & Delaloye, R. 2004. Contribution of real-time kinematic GPS in the study of creeping mountain permafrost: Examples from the Western Swiss Alps. *Permafrost and Periglacial Processes* 15: 229-241.

Lambiel, C., Delaloye, R., Strozzi, T., Lugon, R. & Raetzo, H. 2008. ERS InSAR for assessing rock glacier activity. *Proceedings of the Ninth International Conference on Permafrost, Fairbanks, Alaska, June 29–July 3, 2008* (this proceedings).

Roer, I. 2007. Rockglacier kinematics in a high mounain geosystem. *Bonner Geographische Abhandlungen* 117: 217.

Roer, I., Kääb, A. & Dikau, R. 2005a. Rockglacier acceleration in the Turtmann valley (Swiss Alps) – probable controls. *Norwegian Journal of Geography* 59(2): 157-163.

Roer, I., Avian, M., Delaloye, R., Lambiel, C., Bodin, X., Thibert, E., Kääb, A., Kaufmann, V., Damm, B. & Langer, M. 2005b. Rockglacier "speed-up" throughout European Alps—a climatic signal? *Proceedings of the Second European Conference on Permafrost, Potsdam, Germany, June 2005*: 101-102.

Schneider, B. & Schneider, H. 2001. Zur 60jährigen Messreihe der kurzfristigen Geschwindigkeits-schwankungen am Blockgletscher im Äusseren Hochebenkar, Ötztaler Alpen, Tirol. *Zeitschrift für Gletscherkunde und Glazialgeologie* 37(1): 1-33.

Wagner, S. 1992. Creep of alpine permafrost from borehole deformation at Murtèl rock glacier, Grison (Swiss Alps). *Permafrost and Periglacial Processes* 3:157-162.

—Plenary Paper—

Thermal State and Fate of Permafrost in Russia: First Results of IPY

V.E. Romanovsky, A.L. Kholodov, S.S. Marchenko
Geophysical Institute, University of Alaska Fairbanks

N.G. Oberman
MIRECO Mining Company, Syktivkar, Russia

D.S. Drozdov, G.V. Malkova, N.G. Moskalenko, A.A. Vasiliev
Institute of Earth Cryosphere, Tyumen, Russia

D.O. Sergeev
Institute of Environmental Geoscience, Moscow, Russia

M.N. Zheleznyak
Melnikov Permafrost Institute, Yakutsk, Russia

Abstract

To characterize the thermal state of permafrost, the International Permafrost Association launched its International Polar Year Project #50, Thermal State of Permafrost (TSP). Ground temperatures are measured in existing and new boreholes within the global permafrost domain over a fixed time period in order to develop a snapshot of permafrost temperatures in both time and space. This data set will serve as a baseline against which to measure changes of near-surface permafrost temperatures and permafrost boundaries, to validate climate model scenarios, and for temperature reanalysis. The first results of the project based on data obtained from Russia are presented. Most of the observatories show a substantial warming during the last 20 to 30 years. The magnitude of warming varied with location, but was typically from 0.5 to 2°C at the depth of zero annual amplitude. Thawing of Little Ice Age permafrost is ongoing at many locations. There are some indications that Late Holocene permafrost has begun to thaw at some undisturbed locations in northeastern Europe and in northwest Siberia. Projections of future changes in permafrost suggest that by the end of the 21st century, Late Holocene permafrost in Russia may be actively thawing at all locations and some Late Pleistocene permafrost could start to thaw as well.

Keywords: dynamics of permafrost; long-term thaw; modeling; temperature regime.

Introduction

Permafrost has received much attention recently because surface temperatures are rising in most permafrost areas of the Earth, which may lead to permafrost thaw. Thawing of permafrost has been observed at the southern limits of the permafrost zone; thawing can lead to changes in ecosystems, in water and carbon cycles, and in infrastructure performance. If the current trends in climate continue, warming of permafrost will eventually lead to widespread permafrost thawing in the colder permafrost zones. There is, however, uncertainty concerning where this thawing will occur first, the rate of thaw, and the consequences for arctic, subarctic, and global natural systems. Hence, it is critically important to organize and sustain continuous observations of the thermal state of permafrost in various locations and for various natural settings within the entire Earth permafrost domain. To characterize the thermal state of permafrost, the International Permafrost Association launched its International Polar Year Project #50, Thermal State of Permafrost (TSP). Ground temperatures are measured in existing and new boreholes within the global permafrost domain over a fixed time period in order to develop a snapshot of permafrost temperatures in both time and space (Brown & Christiansen 2006). The resulting data set will serve as a baseline against which to measure changes of near-surface permafrost temperatures and permafrost boundaries, to validate climate model scenarios, and for temperature reanalysis.

More than half of Russia is occupied by permafrost, constituting a significant portion of the entire Northern Hemisphere permafrost area. Hence, without comprehensive understanding of permafrost dynamics in Russia it will be very difficult to draw any general conclusions about the state and fate of permafrost in the Northern Hemisphere. Permafrost research in Russia has a long, rich history. Many historically active institutions are still active in permafrost research today, though there is a strong need to develop an integrated network of permafrost research stations to improve the efficiency and sustainability of these efforts. The Russian-US TSP project funded by the US National Science Foundation (NSF) was established to initiate the process of collaborating and integrating US (mainly Alaskan) and Russian permafrost observing stations into an International Network of Permafrost Observatories (INPO) within the framework of the International Polar Year (IPY). Several institutions from the universities and the US Geological Survey and more than ten Russian institutions and organizations are involved in this project. This project is open to new participants, both individual and institutional. The first results of this project based on both currently measured and historical data from several permafrost regions in Russia (Fig. 1) are presented in this paper.

Examination of past trends in permafrost conditions and

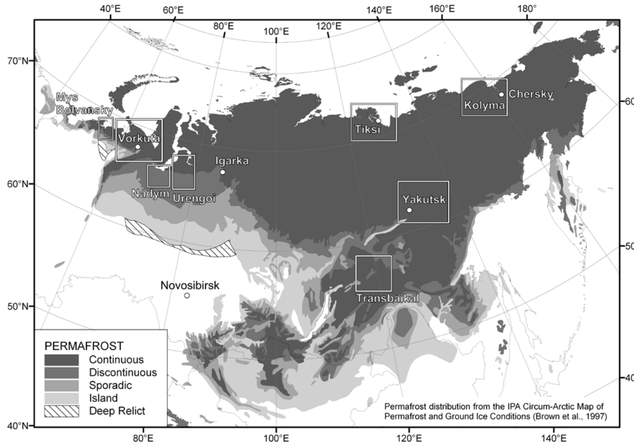

Figure 1. Location of selected Russian TSP research areas discussed in this paper.

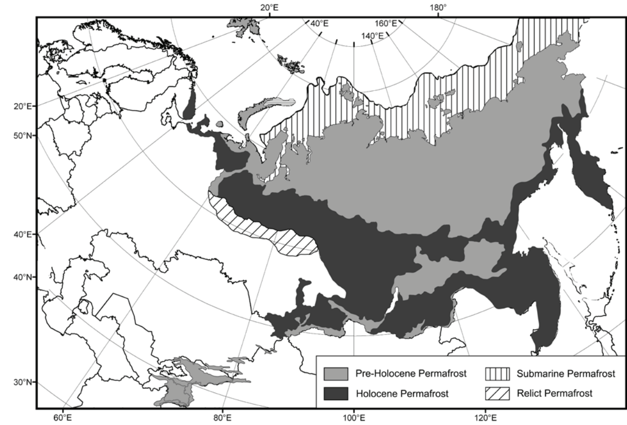

Figure 2. Present-day distribution of permafrost of different ages in Russia (after Lisitsyna & Romanovskii 1998).

distribution (especially during the last glacial-interglacial cycle) can also facilitate better understanding of the possible rates and pathways of permafrost degradation in the future. The primary reasons for this are: 1) many present-day features in permafrost distribution both vertically and laterally were formed during the last 100,000 years, and 2) we can expect that with persistent future climate warming, the first permafrost to thaw will be the youngest Little Ice Age permafrost, followed by Mid and Late Holocene permafrost, and last to thaw will be the Late Pleistocene permafrost. Thawing of the Little Ice Age permafrost is ongoing at many locations. There are some indications that Late Holocene permafrost has started to thaw at some specific undisturbed locations in northeastern Europe, in northwestern Siberia, and in Alaska. In this paper we will briefly describe our knowledge of permafrost development in Russia during the last glacial-interglacial cycle and provide currently available information about recent long-term permafrost thawing in this region.

Permafrost History in Russia During the Last Glacial-Interglacial Cycle

Permafrost distribution changed during the last glacial-interglacial cycle in response to changes in climate. During the last glacial maximum (ca. 20ky BP), permafrost underlay more land area than today. Significant portions of non-glaciated territory of Europe, northern Eurasia, and North America were affected by permafrost. With the termination of the last glacial epoch during the transition from glacial to interglacial climate, permafrost started to thaw rapidly both from the top and from the bottom at the southernmost limits of its Late Pleistocene maximum distribution. With climate warming in progress, more and more permafrost in this area became involved in rapid degradation. As a result, by the time of the Holocene Optimum (5-9 ky BP), permafrost had completely disappeared from most of the territory of deglaciated Europe, from northern Kazakhstan, and from a significant portion of West Siberia in northern Eurasia (Yershov 1998). In areas where the upper several hundred meters of permafrost was ice-rich, such as in the Pechora River basin and in the northern and central parts of West Siberia, permafrost had not disappeared completely; it is still present at greater depths (200 m and deeper). Permafrost on land was generally stable and did not experience any widespread thaw during the Holocene Optimum within the northern part of Central Siberia and within the entire continuous permafrost zone in East Siberia and in the Russian Far East (Fig. 2). However, numerous thermokarst lakes have rapidly developed during this period causing localized thawing of permafrost under lakes that were sufficiently deep.

Climate cooling during the Middle and Late Holocene resulted in a reappearance of permafrost in many areas of the present-day discontinuous permafrost zones (Fig. 2). In some areas, permafrost aggradation was accompanied by an accumulation of new sediments resulting in so-called syngenetic permafrost formation. More commonly, this new Holocene permafrost was formed by refreezing of already existing sediments and bedrock (termed epigenetic permafrost). In the areas where the Late Pleistocene permafrost was still in existence at some depth, two-layered permafrost was formed. The number of newly formed thermokarst lakes significantly declined within the continuous permafrost area.

Generally, Holocene climate has been much more stable than during the Late Pleistocene. However, several relatively warm and cold several-centuries-long intervals can be traced in the Middle and Late Holocene (Velichko & Nechaev 2005). During these intervals, new, fairly shallow, short-lived permafrost appeared and disappeared several times in some specific landscape types found within the sporadic and discontinuous permafrost zones near the southern boundary of present-day permafrost distribution. The last and probably the coldest of such intervals was the Little Ice Age, which dominated most of the Northern Hemisphere climate between ca. 1600 and 1850. During this period, shallow permafrost (15 to 25 m, e.g. Romanovsky et al. 1992) was established within the sediments that were predominantly unfrozen during most of the Holocene. Present-day warming initiated the Little Ice Age permafrost thawing that has been documented for several regions in North America (Jorgensen et al. 2001, Payette et al. 2004).

A Short Description of Selected Research Areas and Methods of Measurements

A large number of borehole temperature measurements at different depths were obtained for the Eurasian permafrost regions starting in the 1960s. Only a small fraction of these data became available for analysis during the initial implementation stage of the Russian TSP project. Comparing retrospective data with results of modern observation allows estimation of the trends in thermal state of permafrost during the last few decades. During the first year of this project (2007), some data from the European North of Russia, north of the western Siberia and Yakutia regions were collected. New temperature monitoring instruments were installed in more than 100 already existing and newly drilled boreholes at various locations within the Russian permafrost domain. This instrumentation allows automatic continuous collection of temperature data with sub-daily time resolution.

The longest permafrost temperature time series from Russia in our records are from northeast European Russia and from northwest Siberia. Permafrost temperatures at various depths have been measured since the early 1970s in the Nadym and Urengoy research areas, since the late 1970s in the Vorkuta research area, and since the early 1980s near the Mys Bolvansky meteorological station located near the shore of the Barents Sea (Fig. 1). At each location the specially designed temperature-monitoring boreholes were established in different natural landscape settings within these research areas.

Permafrost temperatures in more than 200 boreholes were measured in the mid-1980s in the Transbaykal Chara research area (Romanovskiy et al. 1991). This area is characterized by extremely high variability in landscape and permafrost conditions. Temperature measurements were re-established in the 2000s in a very limited number of selected boreholes as a part of the Russian TSP activities.

Temperatures in permafrost boreholes have been measured in the Yakutsk research area (Fig. 1) since the 1960s; however, most collected data are not readily available. In this paper we present permafrost temperature data for 1990–2006 collected by scientists from the Melnikov Permafrost Institute at their long-term monitoring station in Yakutsk. A permafrost temperature time series similar in length was obtained from the Tiksi research station as a collaborative effort between the Melnikov Permafrost Institute and Hokkaido University, Japan (Prof M. Fukuda).

Since the 1970s, the researchers from the Institute of Physical-Chemical and Biological Problems of Soil Science (Russian Academy of Science, RAS) have obtained occasional temperature measurements within the network of boreholes on the Kolyma lowland (Fig. 1). However, many of these boreholes are abandoned now and only a few are still available for further observations. Recently, temperatures in four boreholes established in the 1990s were re-measured. During the 2007 field season, as a part of the Russian TSP project, three boreholes were reconstructed by drilling new boreholes next to the old ones for continuity of temperature measurements. The first results of these activities will be presented in this paper.

Most of the boreholes at the Russian permafrost research stations were equipped with permanently installed thermistor strings and temperatures were measured periodically. In some boreholes thermistor strings were inserted into the boreholes only for the short period during which measurements were performed (but long enough to equilibrate thermistor temperature with ambient borehole temperature). The accuracy of the measurements using calibrated thermistors was typically at or better than 0.1°C. In the Vorkuta region temperatures were monitored using mercury thermometers with a scale factor from 0.05 to 0.1°C. The thermometers were placed in cases filled with an inert material such as, for example, grease. The frequency of measurements varied at different locations from once per year to monthly measurements. Starting in 2006, boreholes are being equipped with HOBO U-12-008 temperature data loggers and TMC-HD temperature sensors (www.onsetcomp.com/products/data-loggers/u12-008). Ice bath testing of these sensors and loggers always shows an accuracy of 0.1°C or better. Time resolution of these measurements is typically at four-hour intervals.

The diversity of past measuring techniques could lead to uncertainty when comparing data obtained using these different sensors. Special field experiments were performed during the 2007 field season to address this concern. Temperatures were measured simultaneously with mercury thermometers and data loggers in a borehole within the Vorkuta research area (Oberman 2008). In the Urengoy research area, data logger and thermistor string measurements were performed simultaneously in the same borehole. Readings in both cases differed on average by 0.05°C. These experiments assure the comparability of all measurement techniques at an overall accuracy of 0.1°C. The high temporal resolution of data obtained by the newly installed sensors and data loggers also demonstrates that the depths of zero annual amplitude at the Urengoy, Nadym, Vorkuta, and Mys Bolvansky research areas are relatively shallow, not exceeding 7 to 8 m.

Long-Term Changes in Permafrost Temperatures

At the Urengoy research area in northwest Siberia (Fig. 1) permafrost temperature at the depth of zero seasonal amplitude increased during 1974–2007 in all landscape units (Fig. 3A). An increase of up to 2°C was measured at colder permafrost sites (e.g., borehole UR1503, Fig. 3A). Up to 1°C warming for the same period was observed in warmer permafrost. A 2°C warming was observed in warm permafrost in a borehole that was situated in deciduous forest (not shown). A similar increase was characteristic of marshes with standing water at the surface (borehole

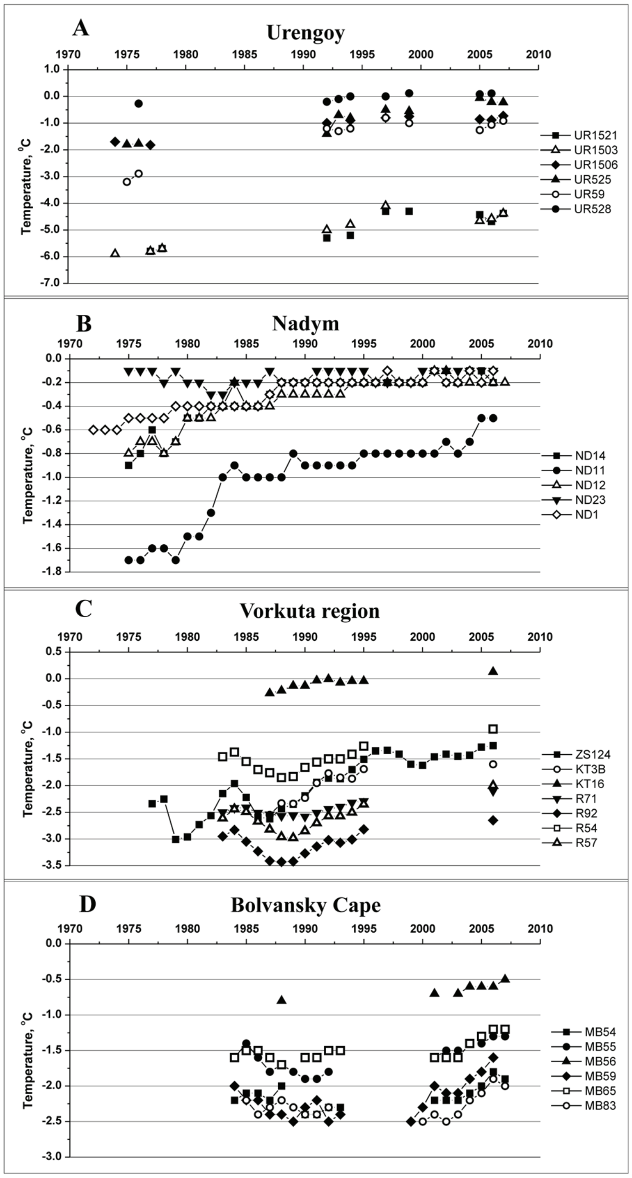

Figure 3. Decadal trends in permafrost temperatures at selected sites in Russia.

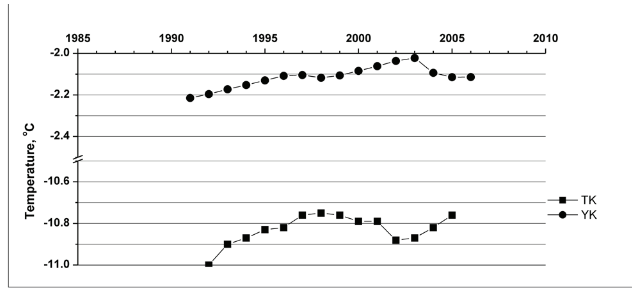

Figure 4. Time series of mean annual permafrost temperatures at 30 m depth at the Yakutsk (YK; circles) and Tiksi (TK; squares) sites.

UR59, Fig. 3A) Generally, the most significant changes in permafrost were measured in the forested and shrubby areas; often the formation of taliks up to 10 m thick were observed. In undisturbed tundra, permafrost is still generally stable (Drozdov et al. 2008). It was also observed that most warming occurred between 1974 and 1997. At the majority of locations permafrost temperatures did not change, or even cooled between 1997 and 2005. A slight warming has occurred since then at sites characterized by temperatures colder than -0.5°C (Fig. 3A).

In the Nadym research area (Fig. 3B) the most significant permafrost warming occurred before 1990, by about 1°C at a colder site and by up to 0.5°C at the warmer sites (Moskalenko 2008). At the warmest site (borehole ND23) permafrost temperature was -0.1 to -0.2°C and did not change for the entire measurement period (1975–2007). Since the temperature reached the same values at the rest of the warm sites in the late-1980s or early-1990s, it appears that permafrost temperature has not changed at the depth of zero annual amplitude at these sites (boreholes ND14, ND 12, and ND1, Fig. 3B). High temporal resolution data obtained with new data loggers show that all annual variations in temperature have occurred in the upper 2 meters of soil, indicating that permafrost has already begun to thaw internally at these sites.

Relative cooling occurred in the Vorkuta region in the late 1970s, mid to late 1980s, and in the late 1990s (Fig. 3C). The most significant warming occurred between the late 1980s and late 1990s. The total warming since 1980 was almost 2°C at the Vorkuta site (Oberman 2008).

At the Bolvansky station in northwest Russia the warming trend in air temperature for the last 25 years is 0.04°C/yr; observed trends in mean annual permafrost temperatures vary from 0.003 to 0.02°C/yr in various natural landscapes (Malkova 2008). For the last 10 years, an increase in climatic variability and alternation of extremely cold and extremely warm years has been observed. These changes initially led to a considerable increase in permafrost temperature, followed in 2007 by a small decrease in temperature in most boreholes (Fig. 3D).

Continuous 15-year permafrost temperature time series were obtained in Tiksi and Yakutsk by researchers from the Melnikov Permafrost Institute in collaboration with scientists from Hokkaido University in Japan. Permafrost temperatures at 30 m depth show a slight positive trend for the 1990–2005 time period (Fig. 4). In contrast, permafrost temperatures apparently did not change significantly in the Kolyma research area (Fig. 1) in the eastern Siberian Arctic during the last 10 to 20 years (Kraev et al. 2008). However, further study is needed to test this conclusion, which was based on recent temperature measurements in or near the historical boreholes that were recently re-occupied as a part of the TSP program.

Permafrost temperatures obtained from the Transbaikal research area (Fig. 1) generally increased during the last 20 years. Borehole #6 was established in the mid-1980s by researchers from Moscow State University and is located in the upper belt of the Udokan Range; temperatures re-measured at this site show a 0.9°C increase between 1987 and 2005 at 20 m depth (Fig. 5). Since 2006, temperatures in this borehole have been recorded at 4-hour time intervals.

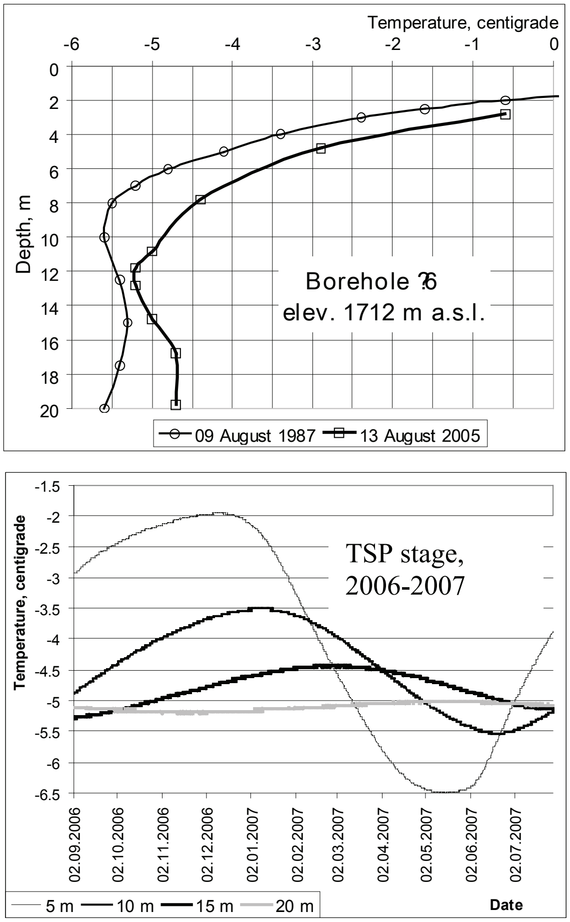

Figure 5. Upper graph: Temperature profiles from the Transbaikal research area obtained in 1987 and 2005. Lower graph: Continuous temperature records at four different depths.

Evidence of Long-Term Thawing of Permafrost

Recently observed warming in permafrost temperatures have resulted in thawing of natural, undisturbed permafrost in areas close to the southern boundary of the permafrost zone. Most observed thawing of long-term permafrost has occurred in the Vorkuta and Nadym research areas. At several locations in the Vorkuta area, long-term thawing of permafrost has led to the development of new closed taliks (Oberman 2008). At one of these locations, the permafrost table lowered to 8.6 m in 30 years. It lowered even more, to almost 16 m, in an area where a newly developed closed talik coalesced with an already existing lateral talik. Permafrost thawing during the last 30 years also resulted in the deepening of previously existing closed taliks. The total increase in depth of the closed taliks developed here ranged from 0.6 to 6.7 m depending on the geographical location, genetic type of a particular talik, ice content and lithological characteristics of the bearing sediments, hydrological, hydrogeological, and other factors.

As a result of recent climatic warming, permafrost patches 10 to 15 m thick thawed out completely in this area (Oberman 2008). In deposits perennially frozen to a depth of about 35 m, the permafrost base has been slowly rising. Comparing small-scale maps based on 1950–1960 data with maps based on 1970–1995 data shows a shift of the southern limit of permafrost by several tens of kilometers northwards (Oberman 2001). This also indicates that permafrost is mostly degrading in the southernmost part of the region.

Permafrost is also degrading in the Nadym and Urengoy research areas. Temperature records from five of a total of seven boreholes in the Nadym area show that cold winter temperatures do not penetrate deeper than 2 m into the ground and that permafrost became thermally disconnected from seasonal variations in air temperature. This also indicates that the constituent ice is already actively thawing in the upper permafrost although the permafrost table (based on the formal 0°C definition of permafrost) is still located just below the active layer. In Urengoy, permafrost is thawing in the forested and shrubby areas, developing closed taliks (Drozdov et al. 2008).

Permafrost degradation in natural undisturbed conditions not associated with surface water bodies has not been reported from the other research areas discussed in this paper. There are numerous occasions of long-term permafrost thawing in Central Yakutian areas around the city of Yakutsk, but all are directly related to natural (forest fire) or anthropogenic (agricultural activities, construction sites) disturbances (Fedorov 1996, Fedorov & Konstantinov 2003).

Permafrost Temperature Reanalysis and Modeling of Past and Future Changes in Permafrost Temperatures

Two levels of permafrost modeling are implemented in our research: a "permafrost temperature reanalysis" and spatially-distributed physically based permafrost modeling. The first level of modeling is the "permafrost temperature reanalysis" approach (Romanovsky et al. 2002). At this level, a sophisticated numerical model (Sergueev et al. 2003, Marchenko et al. 2008), which takes into account the temperature-dependent latent heat effects, is used to reproduce active layer and permafrost temperature field dynamics at the chosen sites. The input data are prescribed specifically for each site and include a detailed description of soil thermal properties and moisture for each distinct layer, surface vegetation, snow cover depth and density, and air temperature. In this modeling approach variations in air temperature and snow cover thickness and properties are the driving forces of permafrost temperature dynamics. The second level of permafrost modeling involves the application of a spatially distributed physically based model that was recently developed in the University of Alaska Fairbanks (UAF) Geophysical Institute Permafrost Lab (GIPL, Sazonova & Romanovsky 2003).

Permafrost temperature reanalysis was successfully applied to several locations within the Russian permafrost domain (Marchenko & Romanovsky 2007, Romanovsky et al. 2007). The model has been calibrated (Nicolsky et al. 2007) for each specific site using several years of measured

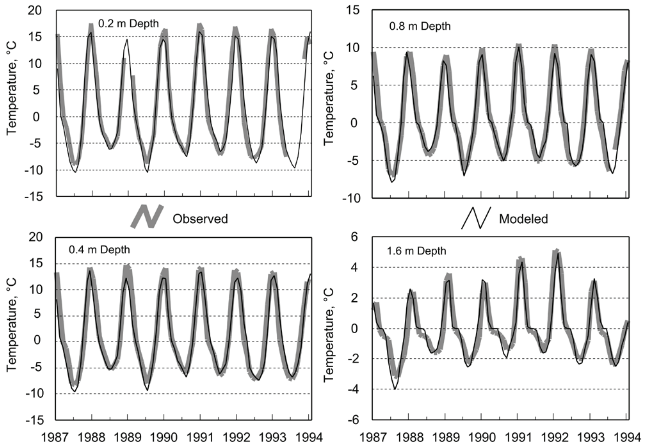

Figure 6. Observed (thick gray line) and calculated (thin black line) ground temperatures at the Yakutsk meteorological station at several depths.

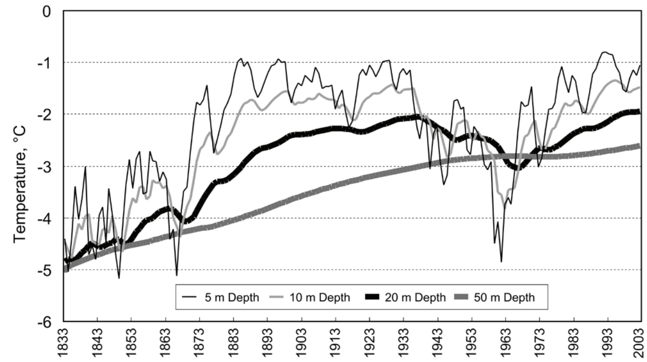

Figure 7. Calculated permafrost temperature time series at several depths for a specific location at the Yakutsk meteorological station.

permafrost and active layer temperature data and climatic data from the closest meteorological station for the same time interval. After validation on measured data that were not involved in the calibration process, the calibrated model can then be applied to the entire period of meteorological records at each station, producing a time series of permafrost temperature changes at various depths. Figure 6 shows the results of calibration of the permafrost model using climate and soil temperature data from the meteorological station in Yakutsk. The differences between measured and modeled temperatures are typically less than 0.5°C and rarely exceed 1°C. Deviation of modeled from measured temperatures decreases with depth (Fig. 6).

The calibrated model was then used to calculate the permafrost temperature dynamics during the transition period from the Little Ice Age up to the present (Fig. 7). Climate forcing includes the air temperature and snow cover dynamics for the period 1833–2003. Air temperature was reconstructed by using observed temperature records from 1834–1853 and 1887–2003 and a spectral analysis technique (Shender et al. 1999). It was also assumed that there were no long-term trends in the snow cover characteristics.

The initial (1833) temperature profile was derived from permafrost temperatures observed by Prof. Middendorf in 1844–1846 in the Shergin's mine in Yakutsk (Sumgin et al. 1939). All measurements were made in narrow horizontal holes in the walls of the mine. The length of each hole was about 2 m. Independent boreholes near Shergin's mine confirmed the characteristic permafrost temperature. Another independent method to test the choice of initial conditions is comparing calculated with measured temperatures for the time intervals when both are available. Such a comparison shows a satisfactory agreement (e.g., compare Figs. 4 and 7).

The results of calculations shown in Figure 7 indicate that the most rapid permafrost warming in the Yakutsk area occurred during the second half of the 19th century. Mean annual temperatures at the shallow depths (5 and 10 m) were already at the present-day level by the 1880s and 1890s, while deeper temperatures continued to increase up to the 1930s. A colder period in the 1940s and especially in the 1960s interrupted this warming trend. Only by the year 2000, permafrost temperatures at the 20 m depth had returned to the pre-cooling level. However, permafrost temperature at greater depths (e.g., 50 m in Fig. 7) continued to increase, although at a slower rate.

The spatially distributed permafrost model GIPL1 that was developed at the Permafrost Lab of the Geophysical Institute, UAF (Sazonova and Romanovsky 2003, Sazonova at al. 2004) was applied for the entire permafrost domain of northern Eurasia (Fig. 8). For present-day climatic conditions, the CRU2 data set with 0.5° x 0.5° latitude/longitude resolution (Mitchel & Jones 2005) was used. The future climate scenario was derived from the MIT 2D climate model output for the 21st century (Sokolov & Stone 1998).

Due to this model's spatial resolution (0.5 x 0.5 latitude/longitude) it is practically impossible to reflect the discontinuous character of permafrost in the southern permafrost zones. That is why we choose the ground surface and soil properties for each cell that will produce the coldest possible mean annual ground temperatures within the cell. This choice means that all results produced by this model reflect permafrost temperatures only in the coldest landscape types within this area. It also means that if our results show thawing permafrost somewhere within the domain, we should interpret this to mean that permafrost is thawing in practically all locations within the area. It also means that in the stable permafrost area identified in Figure 8, partial thawing of permafrost may occur at some specific locations.

According to this model, by the end of the 21st century permafrost that is presently discontinuous with temperatures between 0 and -2.5° C will have crossed the threshold and will be actively thawing. In Russia, the most severe permafrost degradation is projected for northwest Siberia and the European North. This model also shows that by the mid-21st century most of the Late Holocene permafrost will be actively thawing everywhere except for the south of East Siberia and the Far East of Russia.

By the end of 21st century, practically all Late Holocene permafrost will be thawing and some Late Pleistocene permafrost will begin to thaw in the European North and in Siberia (compare Figs. 2 and 8).

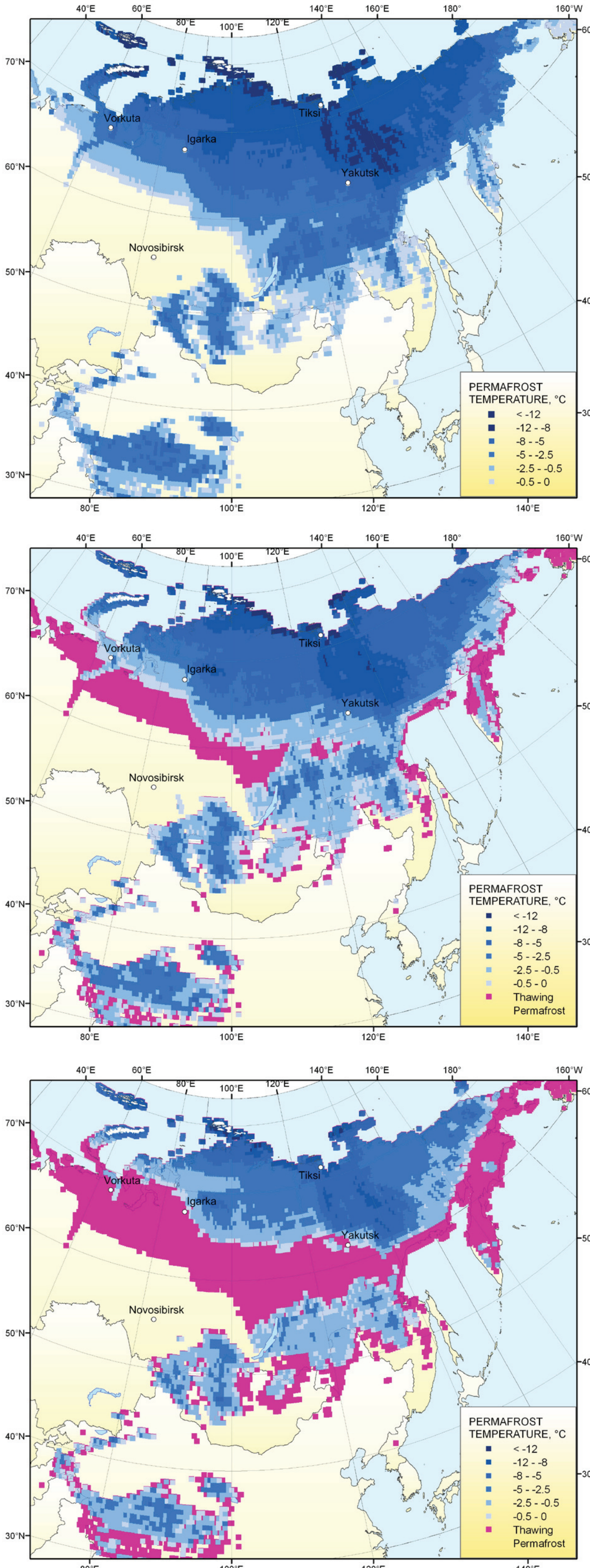

Figure 8. Calculated distribution of mean annual ground temperatures at the bottom of the active layer in Northern Eurasia averaged for three time intervals: 1990-2000 (upper graph), 2040-2050 (middle graph), and 2090-2100 (lower graph). The area with widespread permafrost thawing from the top down is shown in pink.

Conclusions

- Most of the permafrost observatories in Russia show substantial warming of permafrost during the last 20 to 30 years. The magnitude of warming varied with location, but was typically from 0.5 to 2°C at the depth of zero annual amplitude.
- This warming occurred predominantly between the 1970s and 1990s. There was no significant observed warming in permafrost temperatures in the 2000s in most of the research areas; some sites even show a slight cooling during the late-1990s and early-2000s. Warming has resumed during the last one to two years at some locations.
- Considerably less or no warming was observed during the same period in the north of East Siberia.
- Permafrost is already thawing in specific landscape settings within the southern part of the permafrost domain in the European North and in northwest Siberia. Formation of new closed taliks and an increase in depth of pre-existing taliks has been observed in this area during the last 20 to 30 years.
- Permafrost temperature reanalysis provides a valuable tool to study past changes in permafrost temperature, which helps to place recent changes into a long-term perspective.
- An implemented spatially-distributed permafrost model shows that if warming in air temperatures continues to occur, as predicted by most climate models, widespread thaw of Late Holocene permafrost may be in progress by the mid-21st century. If warming continues, some Late Pleistocene permafrost will begin to thaw by the end of the 21st century.

Acknowledgments

This research was funded by the Polar Earth Science Program, Office of Polar Programs, U.S. National Science Foundation (ARC-0632400, ARC-0520578), by the Russian Foundation for Basic Research, by the Russian Federal Agency for Mineral Resources Management (№AM-18/35 pr, 30.01.2006), by a NASA Water and Energy Cycle grant, by the State of Alaska, and in cooperation with several earlier and on-going Russian activities. We would like to thank Drs. Jerry Brown, Kenneth Hinkel, and Candace O'Connor for their valuable suggestions, which improved the quality of this paper.

References

Brown, J. & Christiansen, H.H. 2006. Report of the International Permafrost Association. *Permafrost and Periglacial Processes* 17: 377-379.

Drozdov, D.S., Malkova, G.V. & Melnikov, V.P. 2008. Recent advances in Russian geocryological research: a contribution to the international polar year. *Proceedings of the Ninth International Conference on Permafrost*, Fairbanks, Alaska, June 29-July 3 (this proceedings).

Federov, A.N. 1996. Effects of recent climate change on permafrost landscapes in central Sakha. *Polar Geography* 20: 99-108.

Federov, A. & Konstantinov, P. 2003. Observations of surface dynamics with thermokarst initiation, Yukechi site, Central Yakutia. *Proceedings of the Eighth International Permafrost Conference*, Switzerland, July 21-25, pp. 239-243.

Jorgenson, M.T., Racine, C.H., Walters, J.C. & Osterkamp, T.E. 2001. Permafrost degradation and ecological changes associated with a warming climate in central Alaska. *Climatic Change*, 48(4): 551-571.

Kraev, G.A., Abramov, Bykhovets, S., Fyodorov-Davydov, D., Kholodov, A., Lupachev, A., Mamykin, V., Ostroumov, V., Sorokovikov, V., Gilichinsky, D., Zimova, G. & Zimov, S. 2008. Thermal state of permafrost in the eastern Arctic. *Proceedings of the Ninth International Conference on Permafrost*, Fairbanks, Alaska, June 29-July 3 (this proceedings).

Lisitsyna, O.M. & Romanovskii, N.N. 1998. Dynamics of permafrost in Northern Eurasia during the last 20,000 years. *Proceedings of the Seventh International Permafrost Conference*, Yellowknife, Canada, June 23-27, pp. 675-681.

Malkova, G.V. 2008. Last twenty-five years of changes in permafrost temperature of the European north of Russia. *Proceedings of the Ninth International Conference on Permafrost*, Fairbanks, Alaska, June 29-July 3 (this proceedings).

Marchenko, S.S. & Romanovsky, V.E. 2007. Modeling the effect of organic layer and water content on permafrost dynamics in the Northern Hemisphere. *Eos Trans. AGU*, 88(52): Fall Meet. Suppl., POSTER, Abstract GC23A-0985.

Marchenko, S.S, Romanovsky, V.E. & Tipenko, G.S. 2008. Numerical modeling of spatial permafrost dynamics in Alaska. *Proceedings of the Ninth International Conference on Permafrost*, Fairbanks, Alaska, June 29-July 3 (this proceedings).

Mitchell, T.D. & Jones, P.D. 2005. An improved method of constructing a database of monthly climate observations and associated high-resolution grids. *International Journal of Climatology* 25(6): 693-712.

Moskalenko, N.G. 2008. Vegetation and permafrost changes in West Siberia northern taiga. *Proceedings of the Ninth International Conference on Permafrost*, Fairbanks, Alaska, June 29-July 3 (this proceedings).

Nicolsky, D.J., Romanovsky, V.E. & Tipenko, G.S. 2007. Using in-situ temperature measurements to estimate saturated soil thermal properties by solving a sequence of optimization problems. *The Cryosphere* 1: 41-58.

Oberman, N.G. 2001. Intra-century dynamics of the permafrost zone in the European Northeast of Russia. *Proceedings of the 2nd Conference of Geocryologists of Russia*, Moscow, Russia, June 6-8, 2001 2: 212-217.

Oberman, N. 2008. Contemporary permafrost degradation of the European north of Russia. *Proceedings of the Ninth International Conference on Permafrost*, Fairbanks, Alaska, June 29-July 3 (this proceedings).

Payette, S., Delwaide, A., Caccianiga, M. & Beauchemin, M. 2004. Accelerated thawing of subarctic peatland permafrost over the last 50 years. *Geophysical Research Letters* 31: L18208, doi:10.1029/2004GL020358.

Romanovskiy, N.N., Zaitsev, V.N., Volchenkov, S.Yu., Zagryazkin, D.D. & Sergeyev, D.O. 1991. Alpine permafrost temperature zonality, northern Trans-Baikal region, USSR. *Permafrost and Periglacial Processes* 2: 187-195.

Romanovsky, V.E., Garagula, L.S. & Seregina, N.V. 1992. Freezing and thawing of soils under the influence of 300- and 90-year periods of temperature fluctuation. *Proceedings of the International Conference on the Role of Polar Regions in Global Change*, University of Alaska Fairbanks 2: 543-548.

Romanovsky, V.E., Burgess, M., Smith, S, Yoshikawa, K. & Brown, J. 2002. Permafrost temperature records: Indicator of climate change. *EOS* 83(50): 589-594.

Romanovsky, V.E., Sazonova, T.S., Balobaev, V.T., Shender N.I. & Sergueev, D.O. 2007. Past and recent changes in permafrost and air temperatures in Eastern Siberia. *Global and Planetary Change* 56: 399-413.

Sazonova, T.S. & Romanovsky, V.E. 2003. A model for regional-scale estimation of temporal and spatial variability of the active layer thickness and mean annual ground temperatures. *Permafrost and Periglacial Processes* 14(2): 125-139.

Sazonova, T.S., Romanovsky, V.E., Walsh, J.E. & Sergueev, D.O. 2004. Permafrost dynamics in 20th and 21st centuries along the East-Siberian Transect. *Journal of Geophysical Research* 109: D01108, doi:10.1029/2003JD003680.

Sergueev, D., Tipenko, G., Romanovsky, V. & Romanovskii, N. 2003. Mountain permafrost thickness evolution under influence of long-term climate fluctuations (results of numerical simulation). In: *Permafrost*, Phillips, M., S. Springman, and L.U. Arenson (eds.), Swets & Zeitlinger, Lisse, 1017-1021.

Shender, N.I., Romanovsky, V.E. & Tetelbaum, A.S. 1999. A forecast of the natural variability of climate in Yakutsk and Fairbanks (in Russian). *Science and Education* 2: 24-29.

Sokolov, A.P. & Stone, P.H. 1998. A flexible climate model for use in integrated assessments. *Climate Dynamics* 14: 291-303.

Sumgin, M.I., Kachurin, S.P., Tolstikhin, N.I. & Tumel, V.F. 1939. *General Geocryology* (in Russian), Soviet Academy of Science Publishing, 340 pp.

Velichko A.A. & Nechaev, V.P. (eds.). 2005. *Cenozoic climatic and environmental changes in Russia*, edited by H.E. Wright Jr., T.A. Blyakharchuk, A.A. Velichko & O. Borisova. Special Paper 382. *The Geological Society of America*, 226 pp.

Yershov, E. 1998. *General Geocryology*. Cambridge: Cambridge University Press, 580 pp.

Soil Climate and Frost Heave Along the Permafrost/Ecological North American Arctic Transect

V.E. Romanovsky, S.S. Marchenko, R. Daanen
Geophysical Institute, University of Alaska Fairbanks
D.O. Sergeev
Institute of Environmental Geoscience, Moscow, Russia
D.A. Walker
Institute of Arctic Biology, University of Alaska Fairbanks

Abstract

Soil climate data were collected during a recent biocomplexity study along a bioclimatic gradient in the North American Arctic tundra. The measurements were made from south to north at Happy Valley, Sagwon Hills, Franklin Bluffs, Deadhorse, West Dock, Howe Island, Green Cabin, Mould Bay, and Isachsen research sites. Mean annual air temperature changes from around -10°C at the Happy Valley and Sagwon Hills sites to -16°C at Mould Bay and Isachsen. Mean annual ground surface temperature has an even larger range, changing from -2°C to -15.5°C in the same direction. Mean annual ground temperature at the permafrost table changes from -3.5°C at Happy Valley to -15.5°C at Mould Bay and -14.7°C at Isachsen. Snow depth generally decreases from south to north, and snow density generally increases in the same direction. Measured maximal frost heave within the nonsorted circles in patterned ground vary between 18–20 cm at the Deadhorse and Franklin Bluffs sites and less than 1 cm at West Dock.

Keywords: active layer; frost heave; patterned ground; permafrost; snow cover; temperature regime; thermal offset.

Introduction

Recent warming in permafrost temperatures has been reported from many locations in the Circumpolar North (Harris & Haeberli 2003, Isaksen et al. 2000, Pavlov & Moskalenko 2002, Oberman & Mazhitova 2001, Osterkamp 2003a, Osterkamp & Romanovsky 1999, Romanovsky et al. 2002, Romanovsky et al. 2007b, Smith et al. 2005). At some of these locations that lay near the southern boundary of permafrost, this warming has already triggered long-term permafrost thawing. These changes in permafrost inevitably affect northern ecosystems, making them evolve rapidly. Some of these changes could be advantageous, but most of them have negative consequences for the natural and anthropogenic systems. Because of a wide variety in permafrost conditions in the Arctic and Subarctic, different regions experience different rates or even different directions of this change during the same time period. To document the temporal changes and spatial variability of permafrost in Alaska, a number of permafrost observatories were established in the late 1970s and early 1980s by the Geophysical Institute, University of Alaska Fairbanks, along the International Geosphere-Biosphere Program (IGBP) Alaska Transect, which spans the entire permafrost zone in Alaska (Osterkamp 1986, Osterkamp & Romanovsky 1999, Romanovsky & Osterkamp 2001, McGuire et al. 2002, Osterkamp 2003a, b, Romanovsky et al. 2003).

The recent Biocomplexity Project of the University of Alaska Fairbanks, which investigates small pattern-ground features that occur along a North American Arctic Transect (NAAT), has been funded by the National Science Foundation, USA, and is now in the final stage of its accomplishment (Walker et al. 2004, 2008). This project made it possible to extend the IGBP Alaska Transect into low- and high-Arctic regions in western Canada (Fig. 1). This extension was a valuable addition to the Transect because it adds sites where permafrost temperatures are some of the coldest in the Northern Hemisphere. Also, a reduced vegetative cover and high ice content make permafrost in this region extremely vulnerable to recently observed and projected changes in climate.

There are two types of natural gradients that will be discussed in this paper. One is the regional north to south gradient in air and soil temperatures, snow, and active layer thickness. Another is the local gradient in soil moisture and temperature, active layer thickness, and ground surface heave that is governed mostly by the surface vegetation distribution. The local gradients are the cause and, at the same time, affected by nonsorted circle formation and evolution. The regional gradients in the atmospheric climate, soil climate, and vegetation also modulate the formation and development of patterned ground and are responsible for the specific morphological features of the patterned ground in the arctic landscapes. The morphology and origination of these features have been discussed in the scientific literature for many years (e.g., Washburn 1980). Soil and permafrost climate data, together with air temperature, snow depth, and seasonal frost heave data collected at the sites along the Permafrost/Ecological North American Arctic Transect during the lifetime of the Biocomplexity Project, together with some previously collected temperature data, will be discussed in this paper. First, we will provide a brief description of natural settings at the research sites and provide some information on measuring technique and the equipment used. Further, using long-term data from several sites, we will show how relatively short records from the

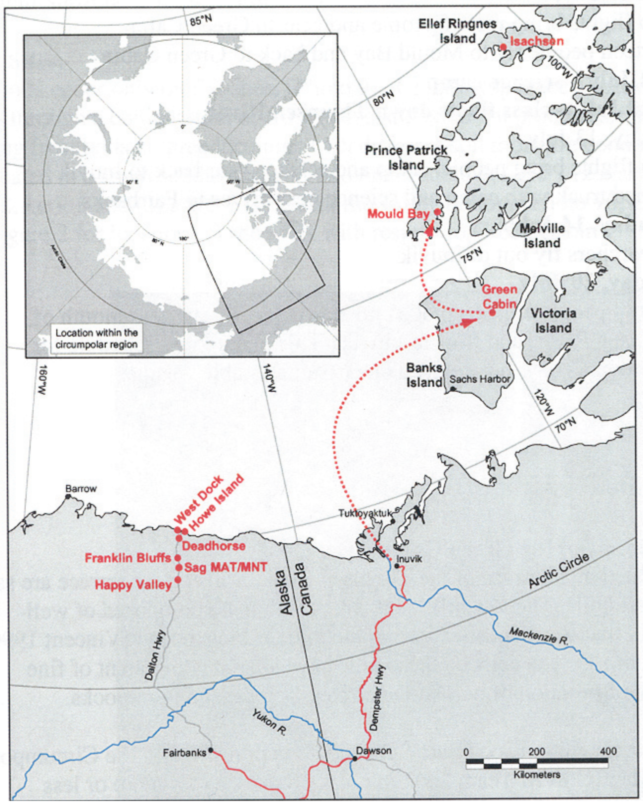

Figure 1. Location of research sites along the Permafrost/Ecological North American Arctic Transect.

biocomplexity project (2001–2006) fit a more general picture of temperature changes during the last 20 years. Then we will present data on soil climate and seasonal frost heave for the entire transect during the years of 2004–2006. Discussions based on these data lead to several important conclusions.

A Short Sites Description

Temperature, moisture, and snow measurement stations were installed from south to north at: Happy Valley, Sagwon Hills, Franklin Bluffs, Deadhorse, West Dock, Howe Island, Green Cabin (Banks Island), Mould Bay, and Isachsen (Fig. 1). All these sites are located in the continuous permafrost zone with a relatively cold climate. Climatic conditions determine type of vegetation along this transect. All sites are within the tundra biome and represent all types of tundra from subzone A (or arctic desert) at Isachsen to subzone E (or southern tundra) at Happy Valley. The specific locations were chosen as representative of zonal conditions within each of five Arctic bioclimate subzones (A through E) (Walker et al. 2005). All the studies were located on fine-grained sediments conducive to the formation of nonsorted patterned-ground features and zonal vegetation. The Sagwon MAT and Happy Valley locations had acidic soils (pH < 5.5), and all the others had nonacidic soils. Several sites (Howe Island, Green Cabin, Deadhorse, Franklin Bluffs) had soil pH values exceeding 8.0. The zonal vegetation varied from nearly barren surfaces with scattered mosses, lichens, and very small forbs in subzone A to knee-high shrub-dominated

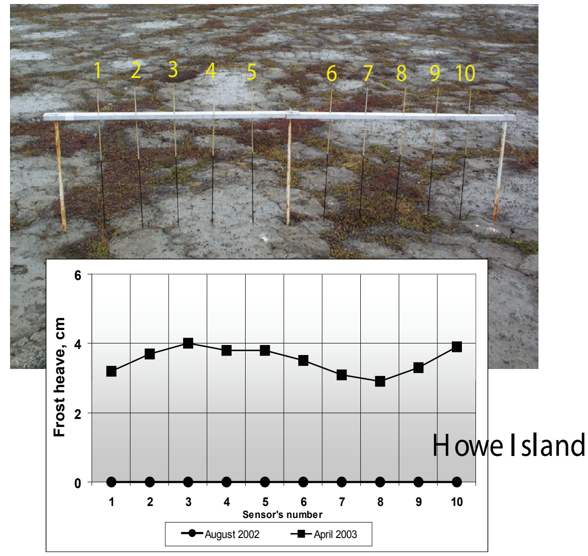

Figure 2. Frost heave measurements across a nonsorted circle at the Howe Island site.

tundra with thick moss carpets in subzone E. A more comprehensive description of natural settings at the study sites can be found in (Walker et al. 2008).

Methods of Measurements

Small climate stations were established at each location. The air and ground-surface temperatures at each location were recorded using standard Campbell Scientific L107 thermistors. Two ground surface thermistors and two 1-m long arrays of thermistors (with approximately 10 cm distance between thermistors) were located about six meters apart: one in an unsorted circle and the other between the circles. After pre-installation calibration, the precision of the sensors is better than 0.04°C. All measurements were made with one-hour time interval. The stations were operated and data were stored by Campbell Scientific CR10-X data loggers. A 20-watt regulated solar panel coupled with a 12-volt battery was used for power supply. The installations are also part of the Permafrost Observatory Network (Osterkamp 2003, Osterkamp & Romanovsky 1999, Romanovsky & Osterkamp 2001, Romanovsky et al. 2003). Snow depth was measured continuously with one-hour resolution at most of the sites using a Campbell Scientific SR50 Sonic Ranging Sensor that was connected to the Campbell data logger at the climate stations. Also, the maximum snow depth was measured every year manually at the Alaskan sites during spring (late April) field trips. At the Canadian sites, maximum snow depth was measured manually once in early May 2006. The ground moisture (including the unfrozen water content in winter) was measured at two depths within the unsorted circle and at two depths in the inter-circle space. SDI-12 volumetric water content sensors (http://www.stevenswater.com/catalog/stevensProduct.aspx?SKU=%2793640%27) were used. Each of the sensors was pared with an additional L107 temperature probe. Moisture content was recorded hourly during the entire year.

Frost heave was monitored on and off the unsorted circles at all sites using two types of specially designed heave meters. Along the Alaskan portion of the NAAT, a ten-pin heave instrument described in (Walker et al. 2004) was used (Fig. 2). In the High Arctic, heave scribers were used. Each of these instruments consisted of a 2-m x 1.5-cm solid copper grounding rod that was driven 1.5 m into the ground, anchoring it in the permafrost. A steel plate and sleeve with an attached sharp steel scriber was placed on the rod, with the plate resting on the ground. The steel plate and scriber slid freely on the rod, rising with the frost heave in the winter and allowing the scriber to scratch a line on the copper rod. The length of the scratched line above a reference scribe determined the amount of heave.

Long-Term Changes in the Air, Active Layer, and Permafrost Temperatures

When we describe atmosphere and soil climatic conditions for some period of time, it is always important to have information on how this period looks compared to longer-term patterns of these parameters. It is especially important now when the climate experiences significant changes within short time intervals. Fortunately, we have long-term (more than 20 years) continuous temperature records for three sites within the NAAT: West Dock, Deadhorse, and Franklin Bluffs. Data from the West Dock site are shown in Figure 3. This figure clearly shows a significant long-term warming trend in mean annual temperatures at all levels: air, ground surface, and permafrost at 20 m depth. A linear trend in air and ground surface temperatures was 3°C for the last 20 years, and an increase in permafrost temperature at 20 m depth was 2°C. This figure also shows that during the period of the Biocomplexity Project (2001–2006), soil climate was the warmest on average for the last 20 years. Also, during this period the soil climate was relatively stable except for an anomalously warm year, 2003.

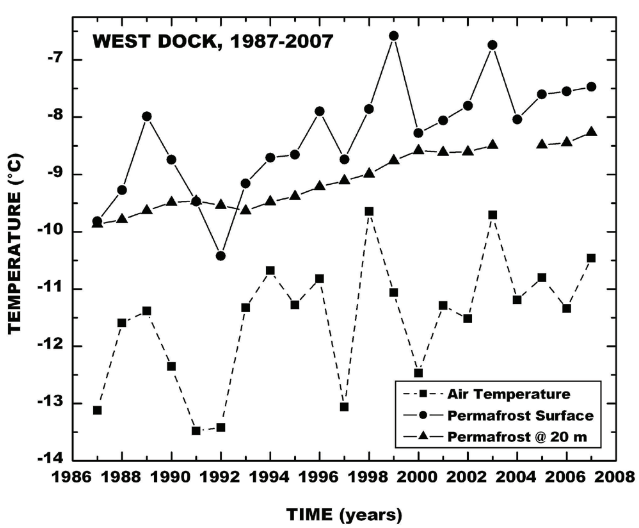

Figure 3. Time series of mean annual air (squares), permafrost surface (circles), and permafrost at 20 m depth (triangles) temperatures at the West Dock site.

Figure 3 also shows that the interannual variations in the surface temperature can differ significantly from the interannual changes in the air temperature. However, on a longer time scale (five years and longer), the match in these trends is very good. Similar results were obtained from the Deadhorse and Franklin Bluffs sites. We came to similar conclusion analyzing long-term data from the East Siberian Transect (Romanovsky et al. 2007b).

Snow Conditions and Air and Soil Temperatures Along the NAAT Transect

All our sites are within the continuous permafrost area. However, there is a significant range of air and soil temperatures along this transect. Mean annual air temperature (MAAT) changes from around -10°C at the Happy Valley and Sagwon Hills sites to -16°C at Mould Bay and Isachsen (Fig. 4), while mean July air temperatures vary in the range from 10°C at Happy Valley to 3°C at Isachsen (not shown). Elevated temperatures at Isachsen are an artifact, because only temperatures for 2005–2006 were available for this station (it was established in the summer of 2005) and the 2005–2006 year was substantially warmer in this region than 2004–2005. Data from the Mould Bay station show that MAAT in 2005–2006 was warmer by almost 2°C than in 2004–2005. Mean annual ground surface temperature (MAGST) was by more than 1°C warmer as well.

All Alaskan sites show very similar MAAT in the range between -9.7°C (Sagwon MNT) and -11.3°C (Franklin Bluffs). All Canadian sites are much colder with MAAT at or colder than -16°C. The spatial variability in MAGST is much more pronounced along NAAT. The warmest sites are all located in the inland part of the transect, with temperatures as warm as -2°C (Happy Valley) and just below -4°C (Deadhorse and Franklin Bluffs). Relatively colder temperatures were observed at Sagwon Hills (-5°C and -6°C). All coastal sites in Alaska have lower MAGST with -7.2°C at West Dock and -8.8°C at Howe Island. The coldest MAGST were observed in the Canadian Arctic with MAGST typically at or below -14°C. It was shown in previous publications (Kade et al. 2006, Walker et al. in review) that summer temperatures at the ground surface within the unsorted circles are significantly warmer than in inter-circle areas. As it can be seen from Figure 4, it is not true for the mean annual surface temperatures, which are generally very similar for both circle and inter-circle areas. A possible explanation is that differential frost heave within the circles decreases snow depth here and decreases surface temperatures during the winter. Colder winter temperatures compensate summer warmer temperatures within the circles with a net effect close to zero.

Snow cover is the major factor that determines the difference between MAGST and MAAT. Our data show that this difference is much larger at the inland sites than at the sites close to the Arctic coasts. Snow depth is generally decreasing from the south to the north, and snow density is generally increasing in the same direction. The maximum

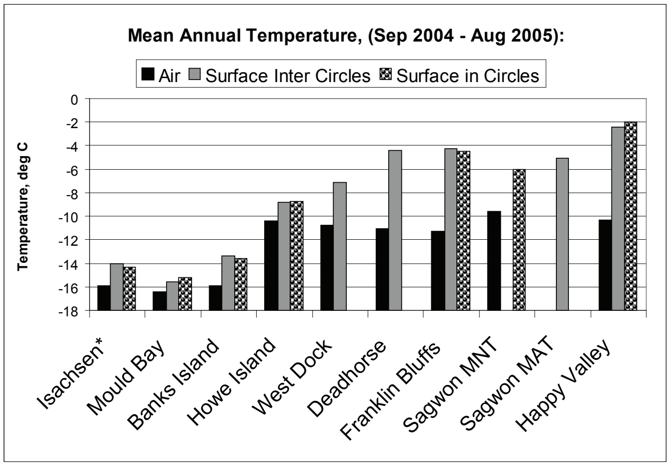

Figure 4. Mean annual temperatures (September 2004–August 2005, except for Isachsen where temperatures were measured in 2005–2006) in the air (black) and at the ground surface within inter-circles (gray) and circles (polka-dot) along NAAT.

snow thickness decreases from 60–70 cm at Happy Valley to 20 cm and less at the Banks Island and Mould Bay sites (Fig. 5). Accordingly, the warming effect of snow on MAGST is decreasing from 8°C at Happy Valley to only 1°C at the Mould Bay site (Fig. 4). Mean annual soil temperature near the permafrost table changes from -3.5°C at Happy Valley to -15.3°C at Mould Bay (Fig. 6). There is no noticeable difference in this parameter between circle and inter-circle areas.

Comparing Figures 4 and 6 we can see that the mean annual temperatures at the permafrost table are always colder than MAGST. This effect is very well-known as a "thermal offset" (Burn & Smith 1988, Romanovsky & Osterkamp 1995). Thermal offset for most of the sites along NAAT in 2004–2005 was less than -1°C, with the smallest number for Mold Bay (-0.1°C) and Banks Island (-0.15°C). For Isachsen, West Dock, Deadhorse, Franklin Bluffs, and Sagwon MNT, the thermal offset was in the range between -0.3 and -0.75°C. Significantly larger thermal offset was measured at the Howe Island site (-1°C), and for the acidic tundra sites Sagwon MAT (-1.3°C) and Happy Valley (-1.2°C). Increased thermal offset at the acidic tundra sites directly related to increased thickness of the organic soil layer that has a significantly larger ratio of the thermal conductivities in the frozen and thawed states. This ratio is the most important parameter responsible for thermal offset (Romanovsky & Osterkamp 1995).

Active Layer Depth

Active layer depth does not have a pronounced latitudinal trend and has a significant local variability, depending on the soil type and on the structure and density of the surface vegetation cover (Fig. 7). At the localities with dense vegetation, the active layer depth could be from 20 to 40% less than within the nonsorted circles with much less or no vegetation. For example, the mean depth of thaw at the end of August 2005 in the vegetated tundra between the nonsorted

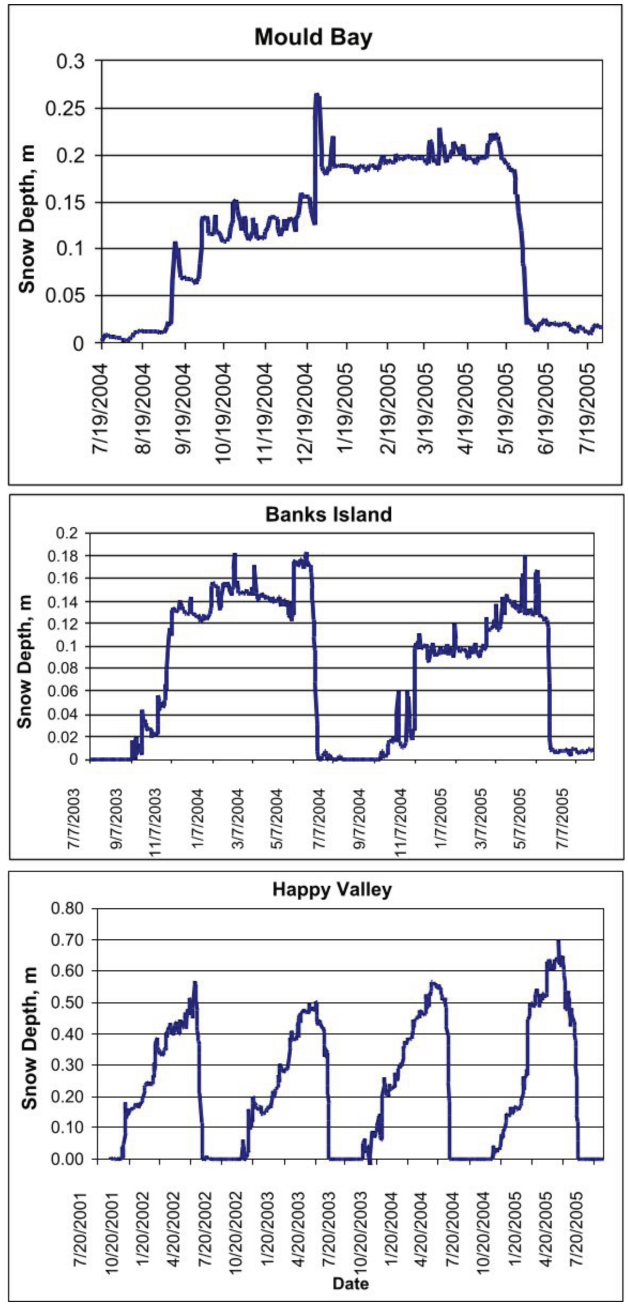

Figure 5. Hourly recorded snow cover depth at three sites: Mould Bay (A), Banks Island (B), and Happy Valley (C).

circle features was less at Happy Valley, the site with the warmest soil-surface temperatures (active layer = 30 cm), than it was at Isachsen, the coldest site (almost 50 cm). Maximum active layer thickness was observed in the middle part of the transect at the sites Franklin Bluffs, Deadhorse, Howe Island, and Banks Island.

A large difference in the active layer thickness between the nonsorted circles and inter-circle areas was observed in better vegetated sites Franklin Bluffs, Sagwon Hills, Happy Valley (Fig. 7), and Deadhorse (not shown). This difference was much less at the sites with less vegetation (Howe Island, Banks Island, Mould Bay, and Isachsen). Because of this local variability in the active layer thickness and because of

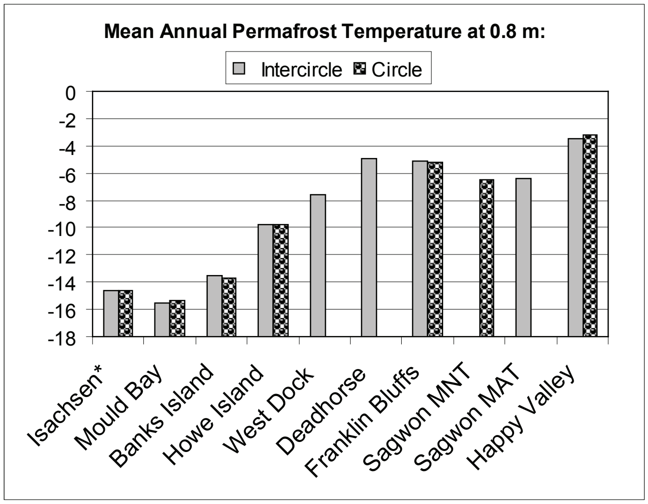

Figure 6. Mean annual soil temperatures (September 2004–August 2005, except for Isachsen, where temperatures were measured in 2005–2006) at 0.8 m depth at different sites along NAAT.

the differences in the timing of freezing, the ground surface experiences a significant differential frost heave, which is mostly responsible for nonsorted circle development.

Frost heave

Measured maximum frost heave within the circles vary between 18–20 cm at the Deadhorse and Franklin Bluffs sites and less than 3 cm at the Green Cabin site on Banks Island (Fig. 8). Frost heave in inter-circle areas was typically less than 3 cm and very seldom reached 5 cm. Frost heave was greatest in the centers of nonsorted circles on silty loess soils at Deadhorse, Franklin Bluffs, and Sagwon MNT (20, 19, and 15 cm, respectively) (Fig. 8). Intermediate amounts of heave occurred on the clay soils at Isachsen, and the acidic tundra sites at Sagwon MAT (9 cm) and Happy Valley (9.5 cm). Heave was least at West Dock (0.4 cm), where there was a thick organic soil layer and no patterned ground. Differential heave (difference in the heave on the circles and between circles) was also greatest at Deadhorse and Franklin Bluffs (17 cm), where there was strong contrast in the vegetation on and between the patterned ground features. Differential heave was least (0 cm) at Isachsen, where the zones between patterned ground features are very narrow. Generally low amounts of heave occurred in the sandier soils at Mould Bay, Howe Island (Fig. 2), and Green Cabin on Banks Island. Measured heave also varies significantly along the local topographical gradients illustrating the dependence of this process on local water availability. More information on governing physical processes responsible for frost heave and nonsorted circles formation and on numerical modeling of these processes can be found in (Nicolsky et al. 2008).

Conclusions

• A strong regional gradient exists in the air and soil temperatures along the North American Arctic Transect. Mean annual air temperature ranges between -10°C and

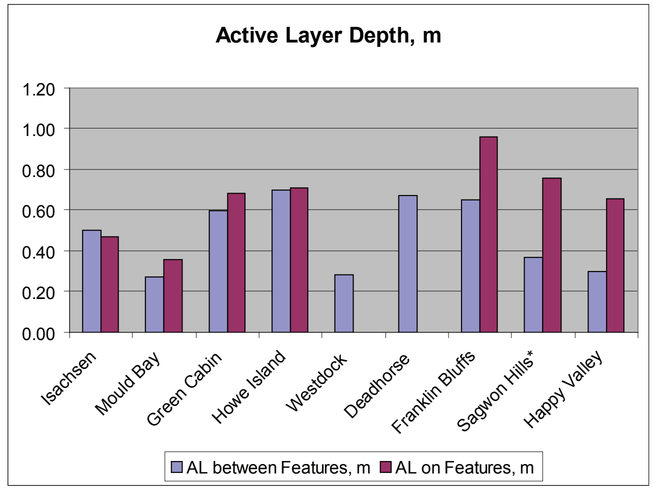

Figure 7. Maximum summer thaw (active layer depth) at the sites along NAAT.

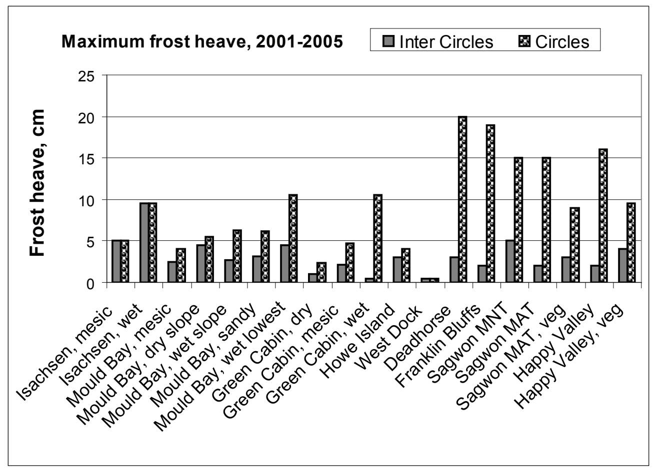

Figure 8. Maximum frost heave observed during period of measurements (2001–2005) at different sites along NAAT.

-16°C, while the mean annual soil temperatures are in the range between -2°C and -14°C.

• Snow cover differs significantly between the inland sites (Happy Valley, Franklin Bluffs), where the maximum snow depth is typically at 45–65 cm, and the coastal sites (Howe and Banks Islands, Mould Bay, and Isachsen) with 15–25 cm.

• Local differences in surface conditions (vegetation and snow cover, and soil physical properties, etc.) are associated with the nonsorted circles, which produce significant local differences in the active layer depth, soil freezing rates, soil ice formation (Nicolsky et al. 2008) and, as a result, a significant differential frost heave.

• The amount of seasonal heave is governed by the degree of these differences and by the water availability that changes along the local topographic gradients. The measured differential frost heave ranges between a few cm at mesic and dry sites to almost 20 cm at wet sites on the Alaskan Arctic Plain.

Acknowledgments

This research was funded by ARCSS Program and by the Polar Earth Science Program, Office of Polar Programs, National Science Foundation (OPP-0120736, ARC-0632400, ARC-0520578, ARC-0612533, IARC-NSF CA: Project 3.1 Permafrost Research), by NASA Water and Energy Cycle grant, and by the State of Alaska.

References

Burn, C.R. & Smith, C.A.S. 1988. Observations of the "thermal offset" in near-surface mean annual ground temperatures at several sites near Mayo, Yukon Territory, Canada. *Arctic* 41(2): 99-104.

Harris, C. & Haeberli, W. 2003. Warming permafrost in European mountains. *World Meteorol. Org. Bull*. 52(3): 6 (see also *Global and Planetary Change* 39: 215–225).

Isaksen, K., Vonder Mühll, D., Gubler, H., Kohl, T. & Sollid, J.L. 2000. Ground surface temperature reconstruction based on data from a deep borehole in permafrost at Janssonhaugen, Svalbard. *Annals of Glaciology* 31: 287–294.

Kade, A., Romanovsky, V.E. & Walker, D.A. 2006. The N-factor of nonsorted circles along a climate gradient in Arctic Alaska. *Permafrost and Periglacial Processes* 17: 279-289.

McGuire, A.D. et al. 2002. Environmental variation, vegetation distribution, carbon dynamics, and water/energy exchange in high latitudes. *Journal of Vegetation Science* 13: 301-314.

Nicolsky, D.J., Tipenko, G.S., Romanovsky, V.E. and Walker, D.A. 2008. Modeling observed differential frost heave within nonsorted circles in Alaska. *Proceedings of the Ninth International Conference on Permafrost, June 29–July 3, 2008, Fairbanks, Alaska,* submitted.

Oberman, N.G. & Mazhitova, G.G. 2001. Permafrost dynamics in the northeast of European Russia at the end of the 20th century. *Norwegian Journal of Geography* 55: 241-244.

Osterkamp, T.E. 1986. Observations of shallow permafrost temperatures in Arctic Alaska. *EOS, Trans. AGU* 67(44).

Osterkamp, T.E. 2003a. A thermal history of permafrost in Alaska, *Proceedings of the Eighth International Conference on Permafrost, July 21-25, 2003, Zurich, Switzerland:* 863-868.

Osterkamp, T.E. 2003b. Establishing long-term permafrost observatories for active layer and permafrost investigations in Alaska: 1977-2002. *Permafrost and Periglacial Processes* 14: 331-342.

Osterkamp, T.E. & Romanovsky, V.E. 1999. Evidence for warming and thawing of discontinuous permafrost in Alaska. *Permafrost and Periglacial Processes* 10(1): 17-37.

Pavlov, A.V. & Moskalenko, N.G. 2002. The thermal regime of soils in the north of Western Siberia. *Permafrost and Periglacial Processes* 13: 43-51.

Romanovsky, V.E. & Osterkamp, T.E. 1995. Interannual variations of the thermal regime of the active layer and near-surface permafrost in Northern Alaska. *Permafrost and Periglacial Processes* 6(4): 313-335.

Romanovsky, V.E. & Osterkamp, T.E. 2001. Permafrost: changes and impacts. In: R. Paepe & V. Melnikov (Eds.), *Permafrost Response on Economic Development, Environmental Security and Natural Resources.* Kluwer Academic Publishers: 297-315.

Romanovsky, V.E., M. Burgess, Smith, S., Yoshikawa, K. & Brown, J. 2002. Permafrost temperature records: Indicator of climate change. *EOS* 83(50): 589, 593-594.

Romanovsky, V.E., Sergueev, D.O. & Osterkamp,T.E. 2003. Temporal variations in the active layer and near-surface permafrost temperatures at the long-term observatories in Northern Alaska. In: M. Phillips, S. Springman & L.U. Arenson (Eds.), *Permafrost.* Lisse: Swets & Zeitlinger: 989-994.

Romanovsky, V.E., Gruber, S., Instanes, A., Jin, H., Marchenko, S.S., Smith, S.L., Trombotto, D. & Walter, K.M 2007a. Frozen ground (Chapter 7). In: *Global Outlook for Ice and Snow, Earthprint*. UNEP/GRID, Arendal, Norway: 181-200.

Romanovsky, V.E., Sazonova, T.S., Balobaev, V.T., Shender, N.I. & Sergueev, D.O. 2007b. Past and recent changes in permafrost and air temperatures in Eastern Siberia. *Global and Planetary Change* 56: 399-413.

Smith, S.L., Burgess, M.M., Riseborough, D. & Nixon, F.M. 2005. Recent trends from Canadian permafrost thermal monitoring network sites. *Permafrost and Periglacial Processes* 16: 19-30.

Walker, D.A. et al. 2004. Frost-boil ecosystems: Complex interactions between landforms, soils, vegetation, and climate. *Permafrost and Periglacial Processes* 15: 171-188.

Walker, D.A. et al. 2005. The circumpolar Arctic vegetation map. *Journal of Vegetation Science* 16: 267-282.

Walker, D.A. et al. 2008. Biocomplexity of small patterned-ground features along the North American Arctic Transect. *Journal of Geophysical Research* (accepted).

Washburn, A.L. 1980. *Geocryology: A Survey of Periglacial Processes and Environments*. New York: Halsted Press, John Wiley and Sons, 406 pp.

The Davidson Ditch – A Historical Review

James W. Rooney
J&F Rooney, LLC, Anchorage, Alaska, USA
Charles H. Riddle
R&M Consultants, Inc., Anchorage, Alaska, USA

Abstract

In the early 1920s, the Davidson Ditch project was initiated because of the need to develop an adequate water supply for placer mining properties on Cleary and Goldstream Creeks just north of Fairbanks, Alaska. The project, extending over a distance of 155 km along the Chatanika River drainage, was started in 1925 and completed in 1928. The water intake structure was located at the headwaters of the Chatanika River. Most of the project traversed permafrost terrain, and much of the ditch placement was located on sidehill terrain. There are still some remnants of the long-abandoned project some 80-plus years after construction. It is interesting that very little information has been provided through the years on the technical issues and facility performance, nor has any environmental assessment of the project's impact on terrain, vegetation, or regional infrastructure been addressed with regard to ground disturbance and continued climate-warming trends.

Keywords: Davidson Ditch; Fairbanks Exploration Company; global warming; permafrost; water supply.

Introduction

In the early 1920s, the Davidson Ditch project was initiated due to the need for developing an adequate water supply for the Fairbanks Exploration Company's (FE Company) placer mining properties on Cleary and Goldstream Creeks just north of Fairbanks, Alaska (Boswell 1979). James M. Davidson conceptually defined a plan and then surveyed a ditch route for collecting water along a major portion of the Chatanika drainage expected to supply water for development of the Fairbanks area dredge operations. Norman C. Stines, who believed in the application of cold water thawing of frozen gravels and who overcame considerable skepticism, with the support of the U.S. Smelting Refining and Mining Company (USSR&M), was the overall driving force that led to the Fairbanks area dredge mining activities. The Davidson Ditch was the key solution for attaining a sufficient water supply to support the planned development of the targeted placer mining areas (Stines 2006). In 1969, the senior author, while working on initial Trans Alaska Pipeline System (TAPS) route studies, had the opportunity to participate in a review of the Davidson Ditch project files at the FE Company's Fairbanks office and was impressed with the level of technical effort and some of the similarities between it and the proposed TAPS project.

Location and Concerns

The Davidson Ditch project, extending over a distance of 155 km along the Chatanika River drainage (as shown in Fig. 1), was started in 1925 and completed in 1928. The water intake structure, a small metal-faced dam, was located at the headwaters of the Chatanika River, just below the confluence of Faith and McManus Creeks. Most of the project traversed permafrost terrain. Because of the need to maintain a gradual flow gradient, much of the ditch placement was located on sidehill terrain facing south to reduce exposure to those soils having highly variable ice content. Even with the passage of more than 80 years following construction, there are still some remnants of the long-abandoned project. It is interesting that very little geotechnical and environmental information has been provided through the years on project issues and facility performance. Nor has much, if any, environmental assessment of the project's impact on terrain, vegetation, or regional infrastructure been assessed with regard to both current concerns and making future projections on manmade and climatic warming impacts. It seems apparent that both positive and negative impacts identified with this project could provide some relevant insight for our attempts to evaluate related climate-warming issues.

Project Infrastructure

This project involved construction of a 3.6 m wide main excavated ditch with a downslope fill berm. The main ditch had a gradient of 0.4 m/km and was 134 km in length. Two feeder ditches added another 9.7 km to the system. There were 15 valley-crossing siphons that had a total length of 9.8 km of steel lock-bar pipe with an inside diameter ranging from 1,168 to 1,422 mm. These siphons had a capacity to carry up to 212,340 liters of water at a maximum head pressure of 1,550 kPa. The length of the valley siphons extended from a minimum of 30 m to 1,128 m. Penstocks and flumes added an additional 0.6 km. Also, a 2.1 m square tunnel 1,128 m long was constructed between Vault and Fox Creeks.

Design Features

The project was designed by J.B. Lippincott, a consulting engineer from Los Angeles, California, who had prior experience on projects in areas with permafrost. His reports describe excavation of frozen muck containing pure ice

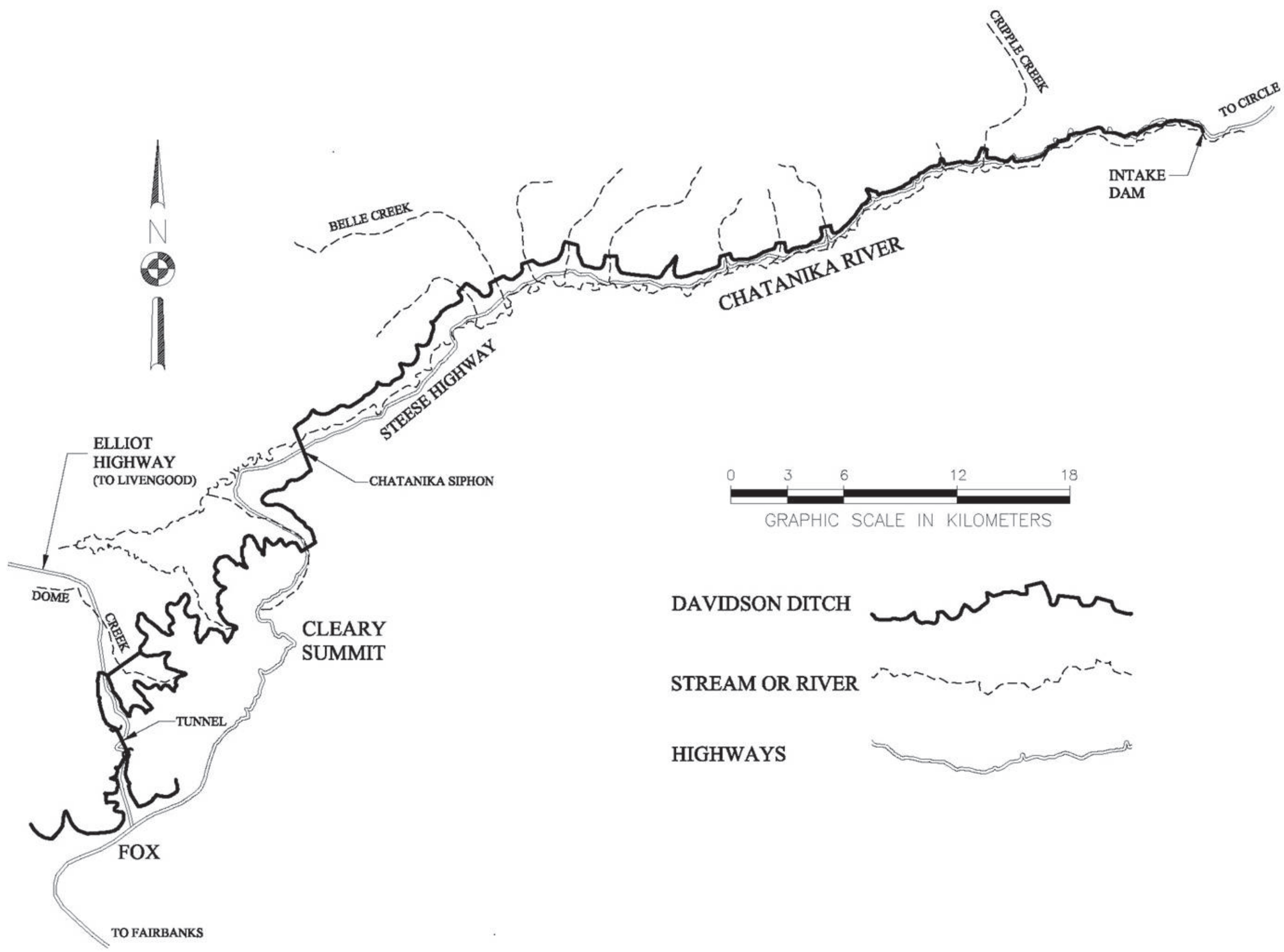

Figure 1. Davidson Ditch route map.

and silt soils having from 150 mm to 600 mm of organic mat overburden. The valley bottoms were described as containing soils with much higher ice content. Preference was given to the south-facing slopes to minimize exposure to the valley slopes that have higher ice content and face north. Concerns were also expressed with accomplishing the valley crossings on timber pile supported trestles with pile bents being spaced at 6 m. The timber piles were installed using steam jets and allowing pile freezeback, or were driven into competent soils to obtain pile support. Valley icing was a significant concern because of the possibility of pile flotation with spring breakup and flooding. The extreme effects of large temperature variation on the siphons were also considered. Temperature extremes of plus 37ºC to minus 57ºC and a full range of 94ºC were utilized to address expansion and contraction concerns along the siphons. Insulation of the pipe anchors to reduce ground warming was also addressed. Anchor systems were employed at the siphons to resist both anticipated vertical and horizontal forces associated with the potential for flotation, water flow, and temperature extremes. The anchors were installed midway between expansion joints.

A typical cross-section of the Davidson Ditch is shown in Figure 2. The construction zone width including the edge of clearing limits extended to over 15 m. Lippincott's evaluation of soil and permafrost conditions along the route, as quoted by Boswell (1979), in one of his reports follows:

> The material through which the ditch was excavated consisted of frozen muck, ranging from almost pure ice to almost solid silt, and covered with from six inches to two feet of moss; heavy slide rock, also covered with heavy moss; decomposed schist slide, usually covered with light moss; rock in place, but shattered so as not to require blasting; solid schist… The northern slopes of the hills are much more frozen than the southern ones… In this report, frozen ground is considered as distinct from the ancient glacial ice which contains but 20 to 30 percent of earth. Such ice is found usually in the valley flats.

The extent of earthwork involved in ditch construction, as summarized by Boswell, was:

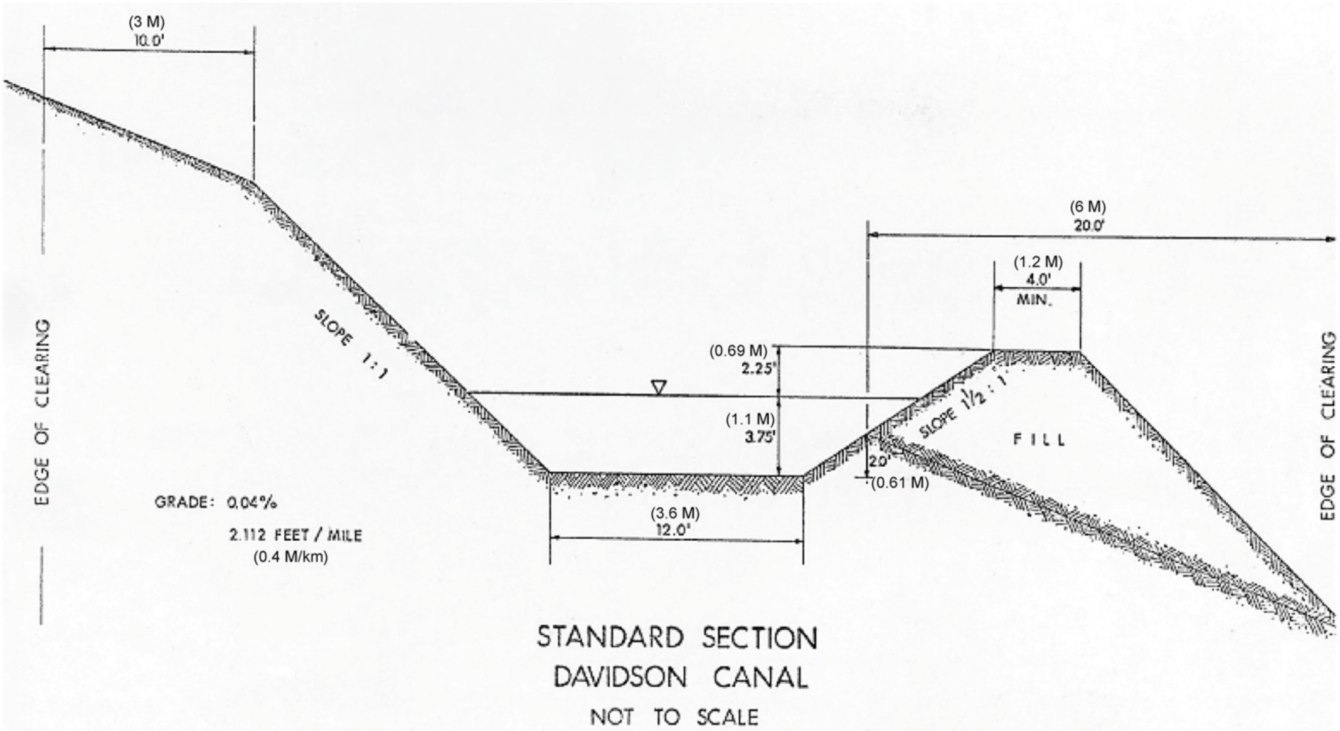

Figure 2. Davidson Canal standard section.

Soil and loose rock	1,455,324 y^3 (1,112,675 m^3)
Solid rock	118,401 y^3 (90,524 m^3)
Total:	1,573,725 y^3 (1,203,199 m^3)

The valley siphon crossings were accomplished through the frozen soils, noted in the above quote, using the pile bents to support the siphon pipe above flood flow levels and anticipated surface icing conditions. Other than comments on evident frost-jacking of the timber piles, little information has been provided on the overall performance of these pile supports. Each siphon crossing was restrained at the center point by a weighted and braced anchor system for restraining excessive siphon pipe movement. This restraint system was placed in an excavation of the frozen soil and supported as shown on Figure 3. While long-term performance of the anchor system appears to have been acceptable, it would be interesting to learn what ground conditions now exist after over 80 years.

Operation Issues

Operation of the ditch required considerable maintenance efforts as a result of ground deformation, soil and ice thaw instability, and berm washouts. Ditch tending personnel were utilized along the grade to maintain and repair the ditches throughout the summer. The ditches and siphons were drained each fall under controlled conditions in order to minimize potential sudden drawdown or freeze damage to the siphon pipe. The extent of ground thawing below and around the ditch construction zone over the period does not appear to have been documented and the current thermal state after over thirty years of abandonment is unknown. It would seem worthwhile to review current ground conditions, past climate as well as site-specific history in order to develop a better understanding of our modeling capabilities and improve our ability to define potential future project impacts.

The Davidson Ditch operated until it was closed in 1942, due to the closing of major placer mining during World War II. It was reopened in 1945. The Davidson Ditch was again in operation until 1952. At that time, the system was acquired by the Chatanika Power Company which utilized the water supply head, at approximately 1,068 N of pressure, to generate an average 9,000 MJ of electricity. The Davidson Ditch continued to function until August, 1967 when major flooding took out the arch bridge supporting the siphon and also collapsed over 213 m of uphill pipe.

Some project photographs taken during early operations, and shown in Figures 4 through 8, identify: the intake and diversion dam, siphon pipe, a typical siphon pipe support, anchor and outlet penstock, and the Chatanika River bridge that supported the siphon pipe.

Closure

Evidence of the ditch and some pile bents may still be observed along segments of the route. Photos of the abandoned project, taken by the senior author in the fall of 1970, are included as Figures 9 through 13. These identify some selected features that remained at that time. These include: the ditch itself, siphon pipe penstock inlet and outlet structures, and a siphon pipe valley crossing. The siphon pipe was salvaged in 1974 and many features of the project were obliterated (Fradley 1974). Consideration was given to making the Davidson Ditch a national historical site that would have

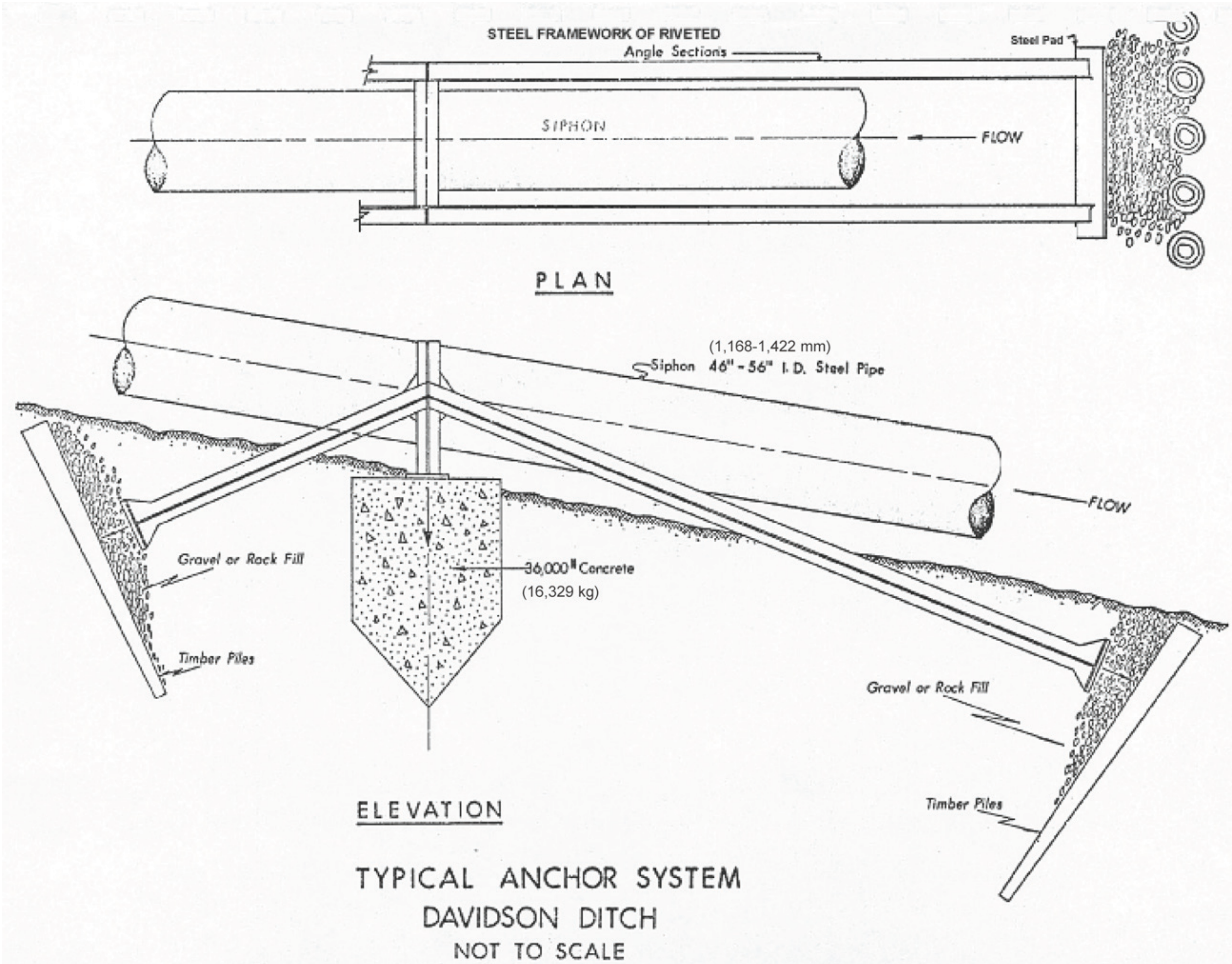

Figure 3. Davidson Ditch typical anchor system.

Figure 4. Intake and diversion dam at headwaters of Chatanika River.

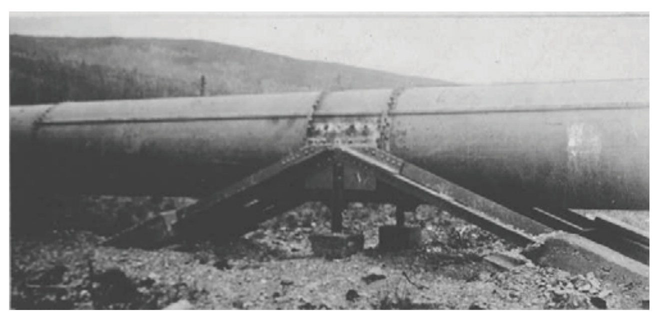

Figure 5. Typical siphon pipe anchor.

included a trail system along the route. Unfortunately, property ownership issues did not allow this to happen.

Details associated with the FE Company's earthwork effort and the economic impact of the Davidson Ditch because of its capability to deliver water to the Fairbanks mining region was documented by Boswell (1979) and Deyos (1925) as follows:

Est. stripping of overburden	7,000,000 y^3 (5,351,884 m^3)
Est. dredging of gravel	5,500,000 y^3 (4,205,052 m^3)
Est. initial investment	$10,000,000
(included cost of Davidson Ditch at $1,773,800)	
Est. total payroll 1926 to 1969	$50,552,175
Est. total gold value recovery (at $35/oz.) from all dredges in the Fairbanks area	$125,000,000

Most of the areas dredged by the FE Company were generally covered by frozen, relatively unstable soils that were totally modified by the mining operations. Much of the

Figure 6. Typical siphon pipe support on timber pile trestle bent.

impacted areas have since been developed and are now the site of both residential and business activities.

In closing, it seems the total socio-economic and environmental impact of the FE Company's Davidson Ditch operations should be reviewed and assessed for both historical value, its possible modeling value, and with regard to estimating any potential future impacts associated with climate-warming trends.

References

Boswell, J.C. 1979. *History of Alaskan Operations of United States Smelting, Refining and Mining Company*. University of Alaska, Fairbanks: Minerals Industries Research Laboratory, Special Publications, Spring 1979, 126 pp.

Davidson, J.M. 2006. *Alaska Mining Hall of Fame Foundation (1853–1928)*.

Deyos, M.C. 1925. Waste Gold, *Fairbanks Daily News Miner*, Fairbanks, Alaska Dec. 24, 1925.

O'Donnell, H.W. 1970. *Report on the Davidson Ditch*, Fairbanks, Alaska: Trans Alaska Pipeline System, June, 1970.

Stines, Norman C. 2006. *Alaska Mining Hall of Fame Foundation (1881–1955)*.

Fradley, Dennis. 1974 Davidson Ditch Pipe Salvaged, *Fairbanks Daily News Miner*, Fairbanks, Alaska, April 18, 1974.

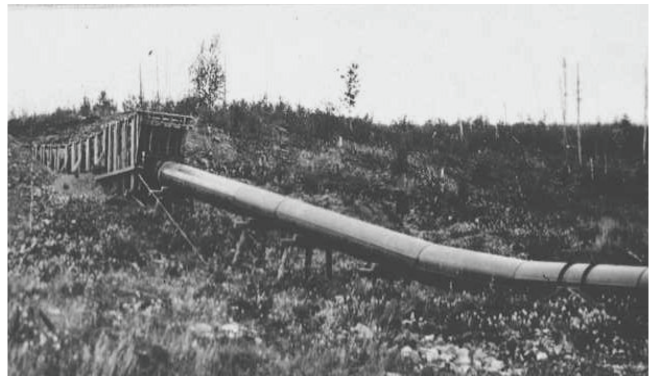

Figure 7. Typical outlet penstock at siphon valley crossing.

Figure 8. Chatanika River siphon and steel arch bridge crossing.

Davidson Ditch – Early Project Photos

Figure 9. Abandoned ditch, fall, 1970.

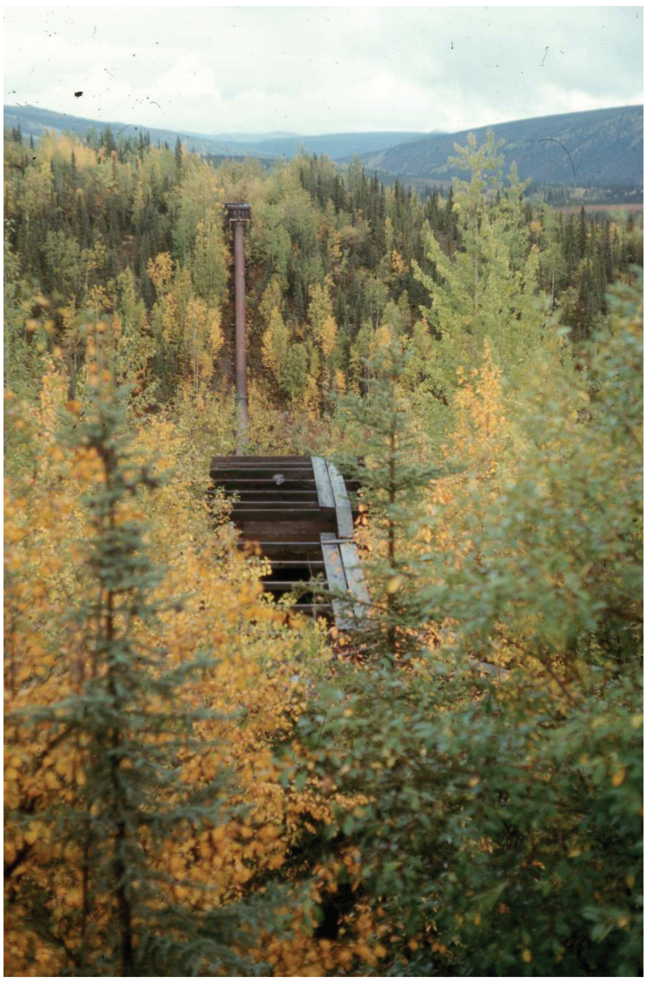

Figure 10. Siphon intake and outlet structures, at a valley crossing, fall, 1970.

Figure 11. Siphon pipe valley crossing, fall, 1970.

Figure 12. Inlet structure and siphon pipe, fall, 1970.

Figure 13. Wood outlet structure at siphon valley crossing, fall, 1970.

Davidson Ditch – Photos of Abandoned Project

Periglacial Landscape Evolution at Lower Mid-Latitudes on Mars: The Thaumasia Highlands

Angelo Pio Rossi
International Space Science Institute, CH-3012, Bern, Switzerland
Stephan van Gasselt
Institut für Geologische Wissenschaften, Freie Universität Berlin, Germany
Monica Pondrelli
IRSPS, Universita' d'Annunzio, Pescara, Italy
Tanja Zegers
RSSD of ESA. ESTEC, NL 2200 AG, Noordwijk, The Netherlands
Ernst Hauber
DLR, Institute for Planetary Research, Berlin, Germany
Gerhard Neukum
Institut für Geologische Wissenschaften, Freie Universität Berlin, Germany

Abstract

We report on the detection of periglacial landforms at high mid-latitudes in the Thaumasia Highland (Mars) that are characterized by lobate to tongue-shaped flow and creep morphologies and which have a close resemblance to terrestrial landforms found in mountainous permafrost regions. It appears that pristine ice-related landforms are best described by small-scale protalus lobes, with few to no distinct impact craters at both HRSC and MOC NA scale. Exposure to solar insulation seems to control the distribution of rock glacier-like landforms, with a preferred occurrence on south-facing slopes. Older, less pristine lineated crater fills, which are commonly considered to represent landforms related to the viscous deformation of ice and debris, show, however, a less systematic distribution of flow directions. Both relatively young landforms are likely related to climatic variations on Mars orbital variations in its recent past and form the youngest witnesses of high obliquity.

Keywords: climate change; Mars; mid-latitudes; periglacial landforms; protalus lobes.

Introduction

Several landforms on Mars have been suggested to be related to the presence of ground ice (Mangold 2003, Squyres 1978, Squyres & Carr 1986), including lobate debris aprons, concentric and lineated crater fill and fretted terrain (Colaprete & Jakosky 1998, Lucchitta 1984, Squyres 1978). These landforms are commonly related to the creep of ice and debris as documented from various latitudes and in a varying geologic context (Crown et al. 2003, Head et al. 2005, 2006, Mangold 2001, Mangold & Allemand 2001, Squyres 1979, van Gasselt et al. 2007).

Large-scale features at the Martian fretted terrain and so-called lobate debris aprons have been primary candidates for periglacial landforms, but the availability of high resolution image and topography data over increasingly large portion of the Martian surface has allowed discovery and exploration of smaller features, comparable in size to terrestrial rock glacier systems. Recent landforms interpreted as glacial or periglacial have been described extensively also at tropical to equatorial latitudes on Mars (Head et al. 2006, Rossi et al. 2000, van Gasselt et al. 2007, 2008) during the last decade.

Also, the presence of ground ice has been indirectly assessed on Mars with non-image data by instruments such as the Neutron Spectrometer onboard 2001 Mars Odyssey spacecraft (Feldman et al. 2004): the large-scale inventory of potential ice-rich deposits in Martian soil indicates regional high abundances of thick bodies of ground ice, especially at mid to high northern latitudes.

Data and Methods

In the present work we used image and topographic data from different sources: MGS (Mars Global Surveyor) MOLA (Mars Orbiter Laser Altimeter) topographic data, MEX (Mars Express) HRSC (High Resolution Stereo Camera), and 2001 Mars Odyssey THEMIS (Thermal Emission Imaging System). In selected areas, we also used THEMIS visible (VIS) and MGS MOC (Mars Orbiter Camera) narrow angle (NA) images. HRSC-derived digital elevation models have been used as well (Gwinner et al. 2005). HRSC data, with their high spatial resolution and large swath, are well complemented by very high resolution MOC NA data. MOLA topography has been used mostly in the form of single profiles (Precision Experiment Data Records, PEDR), in order to avoid any resampling effect introduced during data gridding, because of the small scale (few km) of several of the studied landforms; gridded MOLA Mission Experiment Gridded Data Records (MEGDR) data were used in areas where profiles could not be extracted.

The nomenclature used here is descriptive, trying to avoid genetic terms or implications whenever possible. The

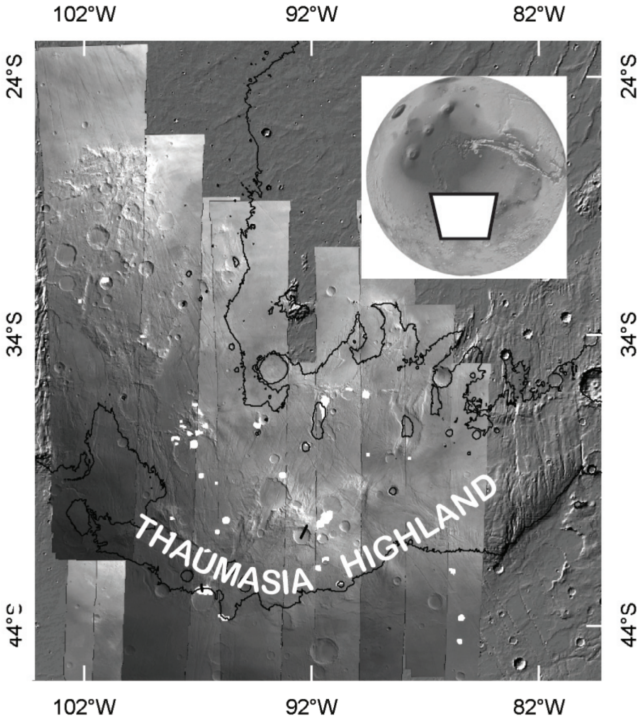

Figure 1. Location of possible periglacial landforms outlined in white, on top of HRSC Nadir Mosaic (Nadir channels from orbits 266, 279, 292, 344, 357, 380, 420, 431, 442, 453, 486, 497, 508, 530, 563) of Thaumasia Highland. The 4000 m altitude contour line is indicated in black; the background is a MOLA topography-based shaded relief.

terminology is similar to the one used by Whalley & Azizi (2003).

Thaumasia Geology and Geomorphology

The Thaumasia region on Mars located in the eastern hemisphere near 35° latitude is well known for its primarily volcanic and complex tectonic history (Fig. 1).

The Thaumasia region on Mars has a rich and complex geological history (Dohm et al. 2001, Dohm & Tanaka 1999). It comprises a tectonic plateau, characterized by high plains and dissected by various graben systems (Grott et al. 2007). In addition several smaller-scaled compressional tectonic features, such as wrinkle ridges (Dohm & Tanaka 1999) indicative of the volcano-tectonic history are observed frequently.

Among younger water-related surface features (Ansan & Mangold 2006), there is also an abundance of geomorphic evidence for cold-climate resurfacing processes such as a variety of periglacial landforms or glacial-like flows. Low latitude glacial or glacial-like morphologies have been described mostly from the northern hemisphere (Head et al. 2006), and recently also from the southern one (Dickson et al. 2006, Rossi et al. 2006),

The Thaumasia region was one of the areas on Mars where work on periglacial and glacial landforms is relatively sparse (Dickson et al. 2006, Rossi et al. 2006) which is predominantly caused by a substantial lack of high resolution data coverage (e.g., MOC) at the time when large-scale mapping efforts were started (Dohm et al. 2001).

Description of Study Area and Landforms

The study area spans in latitude from 25°S to 45°S. The altitude of identified ice-related landforms is more constrained, being in general higher than 4000 m above Mars MOLA datum with elevations as high as 5000 m. (Fig. 1).

Three main kinds of possible ice-assisted creep-related landforms have been found in Thaumasia Highland: lineated crater (and valley) fills, debris aprons, and protalus lobes.

Lineated crater fills

This group of features appears to be very widespread in the study area and was described initially from the northern dichotomy boundary and the southern-hemispheric impact basins (Squyres 1978, 1979).

There is a high abundance of impact craters larger than a few kilometers in diameter that show this peculiar surface texture in Thaumasia Highland.

Lineated crater and valley fills are usually associated to each other and form curvilinear ridges and saddles, usually arranged with slightly concentric to transversal geometries (Figs. 2A, 2C). Longitudinal ridges, similar to the ones present in fretted terrains (Squyres 1978) are usually not observed. Lineations appear as ridges and furrows arranged transversally with respect to the inferred flow direction. The surface texture of lineated fills is relatively rough. Circular to sub-circular features, possibly being degraded small impact craters (Fig. 2C) are visible within the infill. The lack of high-resolution data (e.g., in Fig. 2C) does not allow generalizations over the complete population of lineated craters. Circular to irregular depressions with unclear impact origin are also abundant in crater fills: they show a certain resemblance with thermokarst features (Costard & Kargel 1995).

Lineated and/or curvilinear crater fills on Mars have been interpreted as related to ice flow (Squyres & Carr 1986), or were alternatively attributed to eolian erosion (Zimbelman et al. 1989).

Most lineated fills are showing general slopes consistently with flow directions derived from morphology (Figs. 2A, 2B). The direction of flows in these crater fills shows a correlation to regional slope orientation but little to no connection to local exposure, unlike protalus lobes features as described below.

The actual thickness of these fills in not well constrained, since they appear completely contained within crater rims and no cross-section cuts are visible in the study area.

Debris aprons

Certain craters in the Thaumasia Highland are showing features with a strong resemblance with debris aprons (Colaprete & Jakosky 1998, Squyres 1978, Squyres & Carr 1986) (Fig. 3B). They are isolated or appear superimposed on lineated crater fills. These landforms often show concave upward profiles

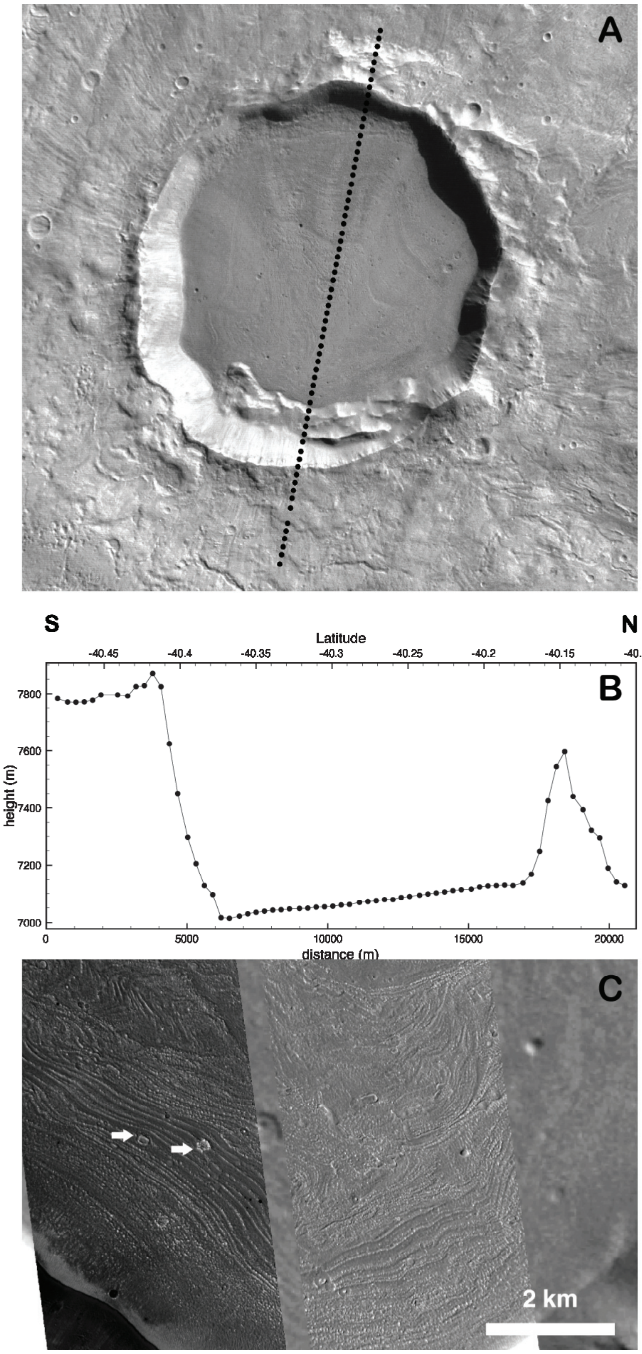

Figure 2. A) HRSC nadir from orbit 442 (north is up), the footprints of MOLA PEDR shots are indicated by black dots; the scene is about 20 km wide. The flow-like lineated crater fill is mainly emanating from the northern part of the crater. B) Portion of MOLA profile from orbit 19873: the lineated crater fill has an almost constant slope of about 0.5° southwards. C) Detail of the morphology of a lineated crater fills at MOC scale (HRSC orbit 508, MOC NA E1200147 and E0501814). Arrows indicate sample deformed (compressed) crater-like features embedded in the crater fill.

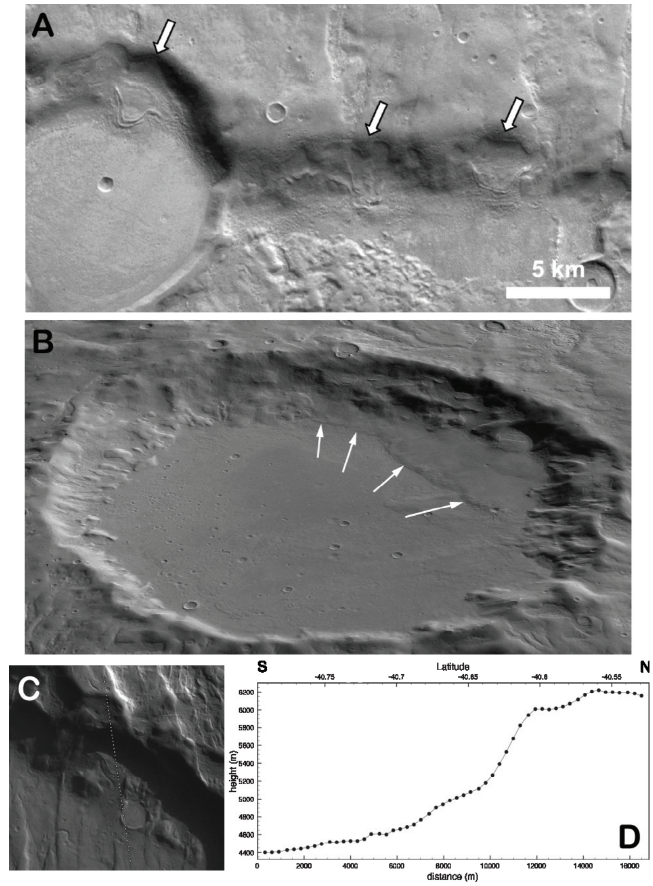

Figure 3. A) Example of well-developed protalus lobes, indicated by arrows (HRSC nadir band from orbit 292, north is up). These lobate forms are developed on crater floors or fills and linear slopes. B) perspective view of HRSC nadir from orbit 453 draped on HRSC stereo-derived DTM (Gwinner et al. 2005). Arrows indicate the edge of a concave debris apron. Small, apparently younger protalus lobes are located on the highest part of the rim, well above the debris apron. C) HRSC nadir from orbit 508, the footprints of MOLA profile shown in 3-D are indicated; the protalus lobe is facing southward and it's largely in shadow; the image is about 25 km wide; the lobate feature is about 5 km long; north is up D) Portion of MOLA PEDR profile from orbit 13002: The protalus lobe in 3C shows a convex upward profile, unlike some debris aprons such as the one in 3B. The inferred thickness for this particular lobe is about 200 m.

on MOLA and HRSC DTM (Gwinner et al. 2005) contrasting to large-scale features observed at the dichotomy boundary which usually are convex upward (Chuang & Crown 2005, Mangold & Allemand 2001, Squyres 1978, van Gasselt et al. 2008). They are characterized by smooth to moderately rough surface texture. Both in term of scale, apparent chronology, and degradation level, they appear to be transitional between larger, older lineated crater fills and smaller protalus lobes. They tend to emanate from south-facing slopes, but with a less clear correlation to the general direction of exposure when compared to protalus lobes.

Protalus lobes

Protalus lobes (Whalley & Azizi 2003) are the most common possible periglacial landform which could be found in the study area. They are characterized by multiple lobate concentric ridges. Their width usually exceeds their length (Figs. 3A, 3C), thus forming broad features along footslopes. Their total length is in most cases limited to few kilometers and few of them are just 2 to 3 km long (Fig. 3A).

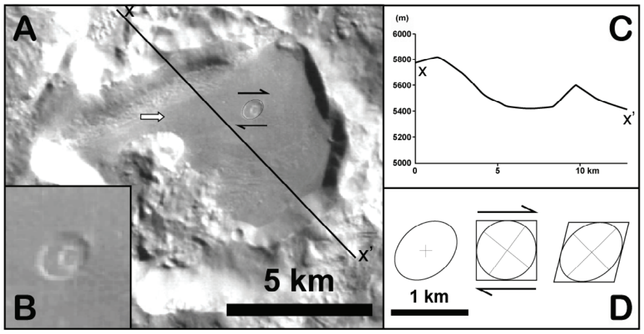

Figure 4. A) Example of possible finite strain of an originally circular impact crater. The black arrows symbolize the simple shear direction, and the white one indicates the directions of linear features in the crater fill with an azimuth consistent with the simple shear inferred by the elliptical crater-like feature; HRSC orbit 497. B) Enlargement of the apparently deformed circular feature (impact crater?) C) Topographic profile across the valley fill imaged in 4A from MOLA gridded topography: the local slope is consistent with the inferred direction of movement and the observed finite strain. D) Strain of a supposed originally circular impact crater under simple shear, hypothesized in this case.

Their texture is moderately rough as observed at scales of HRSC (~15–20 m/pixel resolution) and MOC (~3–5 m/pixel resolution): where high-resolution MOC image data are available, their surface even appears blocky.

Protalus lobes develop preferentially on south-facing slopes, both in case of linear south-facing scarps and northern impact crater rims. The apparent flow direction is from north to south. The correlation between exposure and development for protalus lobes is much stronger than for any other landforms discussed herein.

The impact crater density on these lobate landforms is very scarce: it is the lowest among all morphologies described here. This is also consistent with the observed geometrical relationship between all the different possible periglacial landforms in Thaumasia.

The thickness of protalus lobes can be evaluated using MOLA PEDR profiles: thicknesses range from a few tens of meters up to approximately 200 m (Fig. 3D).

In addition, features similar to protalus ramparts (Whalley & Azizi 2003) have been observed in various parts of Thaumasia Highland (Fig. 3). They appear less widespread than lobes. They tend to develop on top of other larger flow features, such as lineated valley fills.

Morphometric aspects—finite deformation of fills

Both MOLA altrimetric data (single profiles) and HRSC-derived DTM data have been used to characterize the morphology and morphometry of landforms in the Thaumasia Highland.

Crater fills are characterized by very gentle slopes, consistent with the flow direction that could be derived from morphological observations (Fig. 2). The slopes are usually less than one degree. The slopes of crater fills imaged in Fig. 2 are averaging at 0.6 degrees dipping southward. The more convex portion of protalus lobes shows a slope inclination of up to about 7 degrees (Fig. 3D).

Apart from the local disruption and deformation (Fig. 2C), some lineated crater fills show evidence of horizontal deformation/movement. In one case (Fig. 4), it was possible to measure finite deformation of a presently elliptical feature, interpreted as a deformed impact crater (Fig. 4B). Linear features in the crater fill units (Fig. 4A) show a direction consistent with horizontal simple shear, as deduced from the deformation of an original circular impact crater (Fig 4B). The simple shear deformation assumes area conservation on the surface of the fill, which appears to be a reasonable assumption. The assumption of an original circularity of the structure in Fig. 4B is also consistent with the observed crater features (at available resolution), which are ruling out an oblique impact event (an alternative explanation for such an oblique structure), because a hypothetical projectile with a 5–10 degrees incidence angle, needed to produce such an elliptical crater (Gault & Wedekind 1978), would impact on the outer rim before reaching its interior (Fig. 4C).

The finite maximum linear deformation (and linear movement within the fill) of the crater is of about 200 meters. The timescale is not well constrained. Also, the thickness of the deformed fill (and the vertical component of the deformation) is not well constrained.

Relative chronology

Lineated valley/crater fills appear to be the oldest feature among the ones described in the present study. Debris aprons and, later, protalus lobes are characterizing the most recent landscape evolution in the Thaumasia Highland area.

The relative chronology of the landforms in the study area indicates progressive shrinking of landforms confirming the ideas of ice-assisted creep and flow. This view is consistent with considerations of the preservation of morphologies and the local stratigraphic relationships (protalus lobes are clearly postdating lineated crater fills.).

Lineated crater fill units appear often from poorly to slightly altered by crater impacts. At several places, these units have a slightly deflated appearance, which suggests that the present fretted appearance is related partially to erosive effects, also suggesting again an older age of lineated crater/valley fills when compared to protalus ramparts and lobes.

Discussion and Conclusions

Our analysis shows distinct landform development through time in Thaumasia Highland. A generic sequence of periglacial landform development in the study area includes, in chronological order:

a) Large lineated crater fills (areas of ~150–170 km^2), containing possible thermokarst features.
b) Moderate debris aprons (areas of several tens of km^2), with a general “deflated” appearance.
c) Small protalus lobes with little to no impact craters visible at available image resolutions (lengths of ~2–5 km).

d) Locally very small protalus ramparts (several hundred meters to few kilometers in size).

Crater-size frequency analyses to deduce absolute ages will produce unreliable absolute ages due to high degradational effects as well as due to flow deformation of surfaces. The very small size of discovered protalus lobes makes absolute dating even more difficult. Geometrical and stratigraphic relationships are in any case showing a sensibly more recent age of small protalus lobes with respect to lineated crater/valley fills.

Also, the size of these two main groups of landforms is very different: lineated (and sloping) crater fills are large, up to more than 100 km^2, while protalus lobes are usually covering areas of not more than 5–10 km^2.

The flow direction inferred from lineated crater fills show little to no correlation with slope orientation, being more correlated with local and regional topography. On the other hand, mostly concave-upward debris aprons and mostly convex-upward protalus lobes are developed preferentially on south-facing slopes, suggesting a stronger and temporarily closer role of morpho-climatic conditions during their development. This is consistent with previous observations on glacial/periglacial features at mid to low-latitudes (Head et al. 2005).

In the Thaumasia highlands, the dominant concave-upward profile of debris aprons (Mangold & Allemand 2001, Squyres 1978), where present, is indicative of a past scenario involving the melting of ice-cored rock glaciers or debris-covered glaciers (Clark et al. 1994). Contrasting to this, protalus lobes mostly show clear convex-upward profiles (Fig. 3D), which together with their apparent relatively young age is indicating that they might have been active recently or might even be active today.

Although the nature and evolution of such landforms are often controversially discussed, there is observational evidence that the existence and evolution of such landforms is related to climatic variations controlled by the orbital configuration of Mars (Forget et al. 2006, Laskar et al. 2004, Murray et al. 1973, Ward 1974), which was responsible for the deposition of equatorial ice during high-obliquity phases and depletion of an ice reservoir during periods of low obliquities.

The Thaumasia highlands provide the geomorphologic settings necessary for formation of creep-related landforms due to an abundance of high-relief slopes and tectonically dissected terrain allowing accumulation and supply of wall-rock debris at footslopes.

We identified flow and creep morphologies exhibiting a lobate to tongue-like shape and which are characterized by linear to curvilinear ridges and furrows closely resembling large-scale gelifluction lobes or terrestrial rock glaciers and protalus landforms indicative of periglacial environments.

The general lack of impact craters suggests young surface ages. Although water ice is not considered to be stable at equatorial latitudes on Mars today, there are morphologic indicators suggesting re-activation and/or even initial formation of such landforms in the transitional belt between equatorial latitudes and mid-latitudes on Mars during geologically recent times.

Acknowledgments

We thank the HRSC Experiment Teams at DLR Berlin and Freie Universitaet Berlin, as well as the Mars Express Project Teams at ESTEC and ESOC, for their successful planning and acquisition of data as well as for making the processed data available to the HRSC Team. We acknowledge the effort of the HRSC Co-Investigator Team members and their associates who have contributed to this investigation in the preparatory phase and in scientific discussions within the Team.

References

Ansan, V. & Mangold, N. 2006. New observations of Warrego Valles, Mars: Evidence for precipitation and surface runoff. *Planetary and Space Science* 54: 219-242.

Chuang, F.C. & Crown, D.A. 2005. Surface characteristics and degradational history of debris aprons in the Tempe Terra/Mareotis fossae region of Mars. *Icarus* 179: 24-42.

Clark, D.H., Clark, M.M. & Gillespie, A.R. 1994. Debris-covered glaciers in the Sierra Nevada, California, and their impications for snowline reconstructions. *Quaternary Research* 41: 139-153.

Colaprete, A. & Jakosky, B.M. 1998. Ice flow and rock glaciers on Mars. *Journal of Geophysical Research* 103: 5897.

Costard, F.M. & Kargel, J.S. 1995. Outwash plains and thermokarst on Mars. *Icarus* 114: 93-112.

Crown, D.A., McElfresh, S.B.Z., Pierce, T.L. & Mest, S.C. 2003. Geomorphology of debris aprons in the Eastern Hellas region of Mars. *Lun. Planet. Sci. Conf. Abs.* League City, Houston, Tex., USA: Lun. Planet. Inst., 1126. CD-ROM.

Dickson, J.L., Head, J.W., Kreslavsky, M.A. & Marchant, D.R. 2006. Linear Lobate Debris Aprons, Piedmont-like Lobes, and Crater Fill in the Acheron Fossae Graben Region, Mars: Evidence for Debris-covered Glacier Formation and Flow. *37th Annual Lunar and Planetary Science Conference, Volume 37*: 1321.

Dohm, J.M. & Tanaka, K.L. 1999. Geology of the Thaumasia region, Mars: plateau development, valley origins, and magmatic evolution. *Planetary and Space Science* 47: 411-431.

Dohm, J.M., Tanaka, K.L. & Hare, T.M. 2001. *Geologic Map of the Thaumasia Region, Mars.* Map I-2650, Geologic Investigation Series. U.S. Department of the Interior, U.S. Geological Survey.

Feldman, W.C., Prettyman, T.H., Maurice, S., Plaut, J.J., Bish, D.L., Vaniman, D.T., Mellon, M.T., Metzger, A.E., Squyres, S.W., Karunatillake, S., Boynton, W.V., Elphic, R.C., Funsten, H.O., Lawrence, D.J. & Tokar, R.L. 2004. Global distribution of near-surface hydrogen on Mars. *Journal of Geophysical Research (Planets)* 109: 09006, doi: 10.1029/2003JE002160.

Forget, F., Haberle, R.M., Montmessin, F., Levrard, B. & Head, J.W. 2006. Formation of Glaciers on Mars by

Atmospheric Precipitation at High Obliquity. *Science* 311: 368-371.

Gault, D.E. & Wedekind, J.A. 1978. Experimental Studies of Oblique Impact. *Lunar and Planetary Institute Conference Abstracts* 9: 374-376.

Grott, M., Kronberg, P., Hauber, E. & Cailleau, B. 2007. Formation of the double rift system in the Thaumasia Highlands, Mars. *Journal of Geophysical Research (Planets)* 112: 06006, doi: 10.1029/2006JE002800.

Gwinner, K., Scholten, F., Spiegel, M., Schmidt, R., Giese, B., Oberst, J., Jaumann, R., Neukum, G. & Team, H.C.-I. 2005. Hochauflösende Digitale Geländemodelle auf der Grundlage von Mars Express HRSC-Daten: *Photogrammetrie– Fernerkundung–Geoinformation* 5: 387-394.

Head, J.W., Neukum, G., Jaumann, R., Hiesinger, H., Hauber, E., Carr, M., Masson, P., Foing, B., Hoffmann, H., Kreslavsky, M., Werner, S., Milkovich, S., van Gasselt, S. & Co-Investigator Team, T.H. 2005. Tropical to mid-latitude snow and ice accumulation, flow and glaciation on Mars. *Nature* 434: 346-351.

Head, J.W., Marchant, D.R., Agnew, M.C., Fassett, C.I. & Kreslavsky, M.A. 2006. Extensive valley glacier deposits in the northern mid-latitudes of Mars: Evidence for Late Amazonian obliquity-driven climate change. *Earth and Planetary Science Letters* 241: 663-671.

Laskar, J., Correia, A.C.M., Gastineau, M., Joutel, F., Levrard, B. & Robutel, P. 2004. Long term evolution and chaotic diffusion of the insolation quantities of Mars. *Icarus* 170: 343-364.

Lucchitta, B.K. 1984. Ice and debris in the fretted terrain, Mars. *Journal of Geophysical Research* 89: 409.

Mangold, N. 2001. Lobate Debris Aprons as Potential Targets for Ground Ice Detection Analogs to Terrestrial Rock Glaciers. *Conference on the Geophysical Detection of Subsurface Water on Mars*, 7009.

Mangold, N. 2003. Geomorphic analysis of lobate debris aprons on Mars at Mars Orbiter Camera scale: Evidence for ice sublimation initiated by fractures. *Journal of Geophysical Research (Planets)* 108: 8021.

Mangold, N. & Allemand, P. 2001. Topographic analysis of features related to ice on Mars. *Geophysical Research Letters* 28: 407-410.

Murray, B.C., Ward, W.R. & Yeung, S.C. 1973. Periodic insolation variations on Mars. *Science* 180: 638-640.

Rossi, A.P., Komatsu, G. & Kargel, J.S. 2000. Rock Glacier-like Landforms in Valles Marineris, Mars. *Lunar and Planetary Institute Conference Abstracts* 31: 1587.

Rossi, A.P., Chicarro, A.F., Pacifici, A., Pondrelli, M., Helbert, J., Benkhoff, J., Zegers, T., Foing, B. & Neukum, G. 2006. Widespread Periglacial Landforms in Thaumasia Highland, Mars. *37th Annual Lunar and Planetary Science Conference*, *Volume 37*: 1568.

Squyres, S.W. 1978. Martian fretted terrain–Flow of erosional debris. *Icarus* 34: 600-613.

Squyres, S.W. 1979. The distribution of lobate debris aprons and similar flows on Mars. *Journal of Geophysical Research* 84: 8087-8096.

Squyres, S.W. & Carr, M.H. 1986. Geomorphic evidence for the distribution of ground ice on Mars. *Science* 231: 249-252.

van Gasselt, S., Hauber, E. & Neukum, G. 2007. Cold-climate modification of Martian landscapes: A case study of a spatulate debris landform in the Hellas Montes Region, Mars. J*ournal of Geophysical Research (Planets)* 112: 09006, doi: 10.1029/2006JE002842.

van Gasselt, S., Hauber, E., Rossi, A.P. & Neukum, G. 2008. Emplacement of lobate rock glacier landforms and landscape modifications, Mareotis Fossae, Mars. *Proceedings of the Ninth International Conference on Permafrost, Fairbanks, Alaska, June 29–July 3, 2008* (this proceedings).

Ward, W.P. 1974. Climate Variations on Mars, 1, astronomical theory of insulation. *Journal of Geophysical Research* 79: 3375-3386.

Whalley, W.B. & Azizi, F. 2003. Rock glaciers and protalus landforms: Analogous forms and ice sources on Earth and Mars. *Journal of Geophysical Research (Planets)* 108d, doi: 10.1029/2002JE001864.

Zimbelman, J.R., Clifford, S.M. & Williams, S.H. 1989 Concentric crater fill on Mars – an aeolian alternative to ice-rich mass wasting. *19th Lunar and Planetary Science Conference, Houston, TX*. Houston, TX Lunar and Planetary Institute, 397-407.

Stone Frost Mounds in Shallow Bedrock Depressions at Lady Franklin Point, Victoria Island, Nunavut, Canada

Vladislav E. Roujanski
EBA Engineering Consultants Ltd.

Abstract

Unusual terrain features that resemble partially collapsed miniature pingos or stone rings have been recently observed at Lady Franklin Point, Victoria Island, Canada. These features tend to occur in clusters within shallow partially water-filled depressions underlain by frost-shattered flat-lying dolostone bedrock. The mounds are round or oval in shape, 0.5 m to 3 m in diameter, and up to 0.6 m in height. The origin of these mounds is likely associated with frost action. A distinctive central hollow portion of the mounds, partially filled with water, observed in summer at one of the two studied sites is indicative of the seasonal occurrence of an ice core that forms in winter and melts away the following summer. The seasonal formation of an ice core results in doming of the horizontally-lying flat rock fragments. The mounds observed at this site appeared active, and were characterized by loose frost-heaved flat rock fragments and a lack of vegetation. The mounds at another site resembled miniature pingo remnants with a collapsed central portion and well-defined low circular ridge composed of cobble to silt-sized material covered with vegetation. The center was marked by a small shallow depression. At first glance, these features may be viewed as a variety of a frost blister, i.e., a seasonal frost mound. However, unlike a frost blister, which usually develops in finer grained soils and collapses when its ice core melts out, the Lady Franklin Point stone frost mounds remain prominent micro terrain features for a relatively long time because the flat angular fragments of rock do not readily settle back upon melting of the ice core in summer. Therefore, morphologically speaking, the Lady Franklin Point stone frost mounds are a perennial geocryogenic phenomenon.

Keywords: dolostone bedrock; frost action; frost blister; pingo; stone frost mound; stone ring.

Introduction

Lady Franklin Point is an east-west oriented peninsula located on the southwest end of Victoria Island, in the Canadian Arctic (Fig. 1). The peninsula is about 11 km long by 4.5 km wide. The low-lying coastal landscape (the highest point is approximately 15 m above sea level) is dominated by raised beach ridges composed predominantly of gravel- and cobble-sized material with boulders disseminated throughout. Individual ridges are separated by swales or broad level areas dotted with shallow lakes and dry lake depressions. Complexes of the raised beach ridges found in the central part of the peninsula mark former strandlines (Fig. 1).

Over half the peninsula area, mainly the northern portion, is underlain by partially exposed Early Palaeozoic dolostone bedrock: flat-lying and jointed, locally frost-shattered, fractured, frost-jacked, or blanketed by recent marine sediments (mainly gravel and sand) up to 3 m thick. A veneer of glacial clay approximately 0.3 m thick covered by a blanket of marine sand and gravel was encountered at the top of shallow bedrock in one location just north of the existing airstrip. The southern portion of the peninsula consists of low-lying areas underlain by recent lacustrine deposits.

Unusual terrain features that resemble partially collapsed miniature pingos or stone rings were observed in water-filled or partially dried depressions underlain by weathered bedrock. This paper discusses the suggested origin of these landforms and other terrain features found at Lady Franklin Point.

Methods

The descriptions of the permafrost terrain features discussed in this paper are based on ground observations combined with aerial photography and satellite imagery (Google Earth and IKONOS) interpretation.

Stone Frost Mounds

Small distinct mounds were observed at two locations visited by the author of this paper in summers of 2003 and 2004 referred to as Site 1 and Site 2 (Fig. 1). These landforms tend to occur in clusters within shallow, partially water-filled depressions underlain by frost-shattered flat-lying dolostone bedrock (Figs. 2, 3).

The mounds are round or oval in shape, 0.5 m to 3 m in diameter, and up to 0.6 m in height. They resemble partially collapsed miniature pingos (Photos 1 and 2) or stone rings (Photo 3). The formation of pingos is explained in great detail by Mackay (1973, 1979, 1985), Washburn (1973) and others. The origin of stone rings and sorted circles is thoroughly discussed by Washburn (1973), Williams & Smith (1989) and others. The mounds found at Lady Franklin Point are also associated with frost action; however, the mechanism of their formation is different from either pingos or stone rings.

A distinctive central hollow portion of the mounds, partially filled with water, observed in summer of 2003 at Site 1 (Fig. 2, Photos 1 and 2), suggests the seasonal occurrence of an ice core that forms in winter and melts away the following

Figure 1. Location of study sites, Lady Franklin Point, Victoria Island.

summer. The mounds observed at this site appeared active and were characterized by loose frost-heaved flat rock fragments and a lack of vegetation.

A cluster of stone mounds observed at Site 2 in 2003 and 2004 (Fig. 3, Photo 3) is located in a shallow lake depression. The mounds at this site resemble stone rings or miniature pingo remnants with a collapsed central portion and well-defined low circular ridge composed of cobble to silt-sized material. Stones comprising the ridge are lichen-covered with vegetation present both on the ridge and in the central concave area (Photo 3). According to Washburn (1973), the presence of vegetation indicates that the mounds are inactive, which may be associated with drying out of the lake at Site 2.

The formation of the Lady Franklin Point stone mounds is likely the result of frost action. The seasonal formation of an ice core results in doming of the horizontally-lying flat rock fragments. Loose angular pieces of the underlying frost-shattered bedrock are displaced upward by frost jacking and thrusting and undergo some frost sorting. At first glance, these landforms may be viewed as a variety of a frost blister, i.e., a seasonal frost mound. However, unlike a frost blister, which usually develops in finer-grained soils and collapses when its ice core melts out, the Lady Franklin Point stone frost mounds remain prominent micro terrain features for a relatively long time because the flat angular fragments of rock do not readily settle back upon melting of the ice core the following summer. Therefore, morphologically speaking, the Lady Franklin Point stone frost mounds are a perennial geocryogenic phenomenon.

Other Frost-Modified Terrain Features

Linear fractures several hundred meters long and up to 0.5 m wide were observed in several locations within the flat surface of partially exposed dolostone bedrock. The appearance of the fractures suggests that frost action plays an important role in their formation: frost-shattered rock blocks near the ground surface, which form the edges of the fractures, appeared tilted upward by frost jacking and spread out by ice wedging and frost thrusting (Photo 4). The edges of the fractures are slightly raised above the surrounding flat-lying bedrock surface covered by mossy tundra.

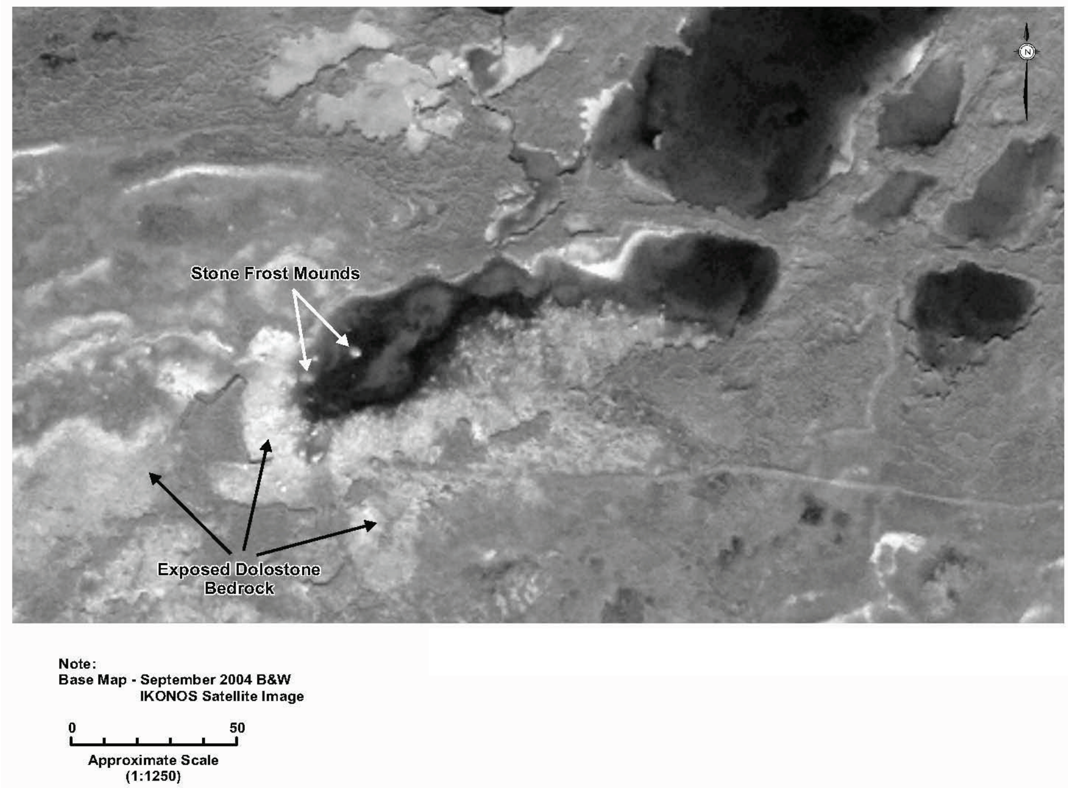

Figure 2. Occurrence of stone frost mounds at Site 1, Lady Franklin Point, Victoria Island.

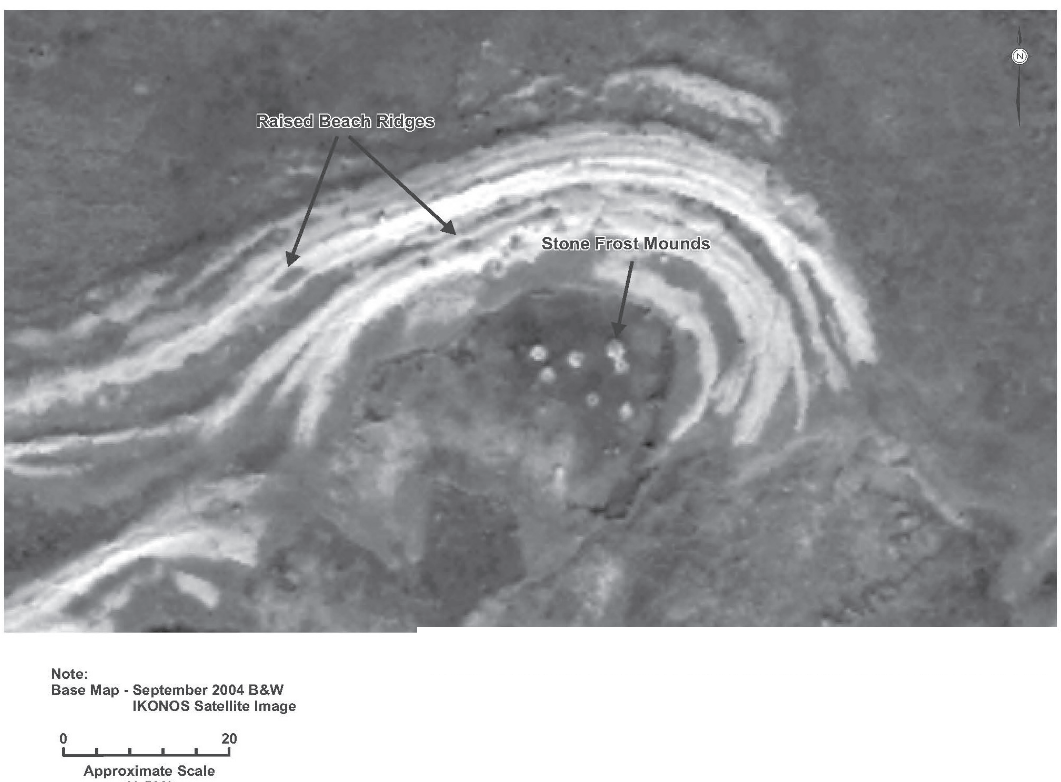

Figure 3. Occurrence of stone frost mounds at Site 2, Lady Franklin Point, Victoria Island.

Photo 1. Site 1. A stone frost mound developed in a shallow water-filled dolostone bedrock depression. Notice hollow central portion of the mound filled with water and a field book for scale. Lady Franklin Point, south Victoria Island. Photo taken August 31, 2003.

Photo 2. Site 1. A stone frost mound developed in a shallow water-filled dolostone bedrock depression. More stone frost mounds in the background. Lady Franklin Point, south Victoria Island. Photo taken August 31, 2003.

Photo 3. Site 2. A cluster of stone frost mounds located in a shallow water-filled dolostone bedrock depression. A raised beach ridge in background. Lady Franklin Point, south Victoria Island. Photo taken August 27, 2003.

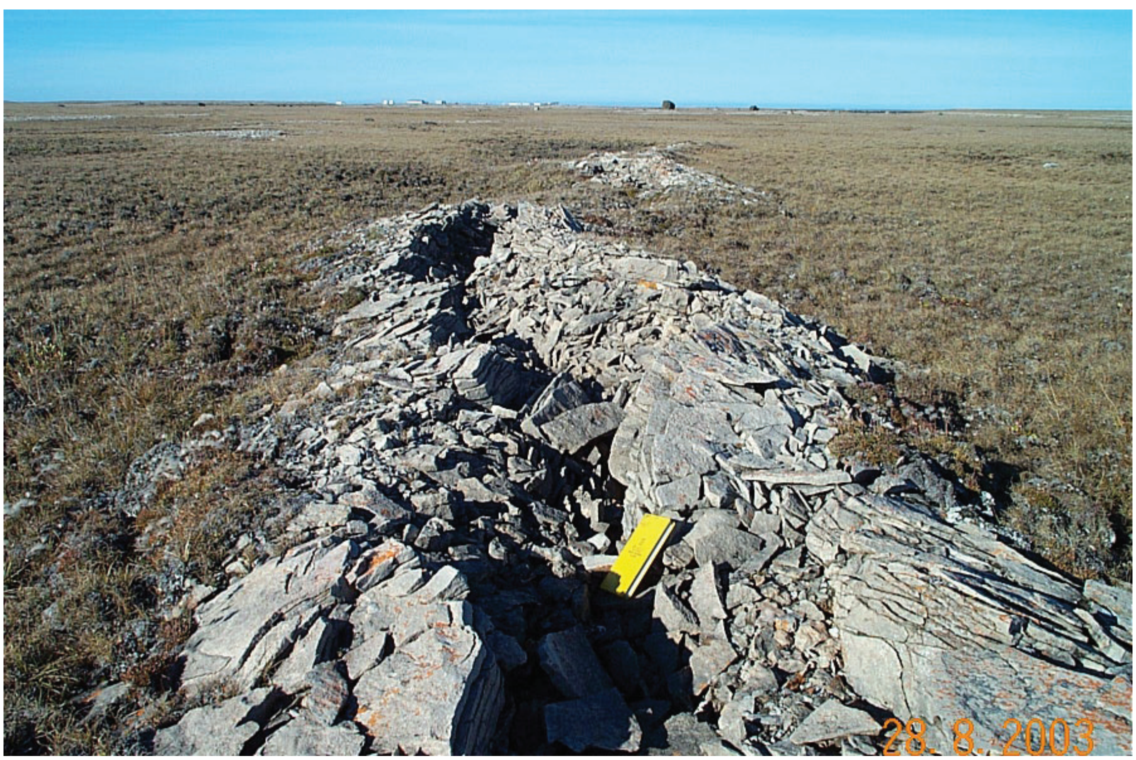

Photo 4. A frost-modified fracture in partially exposed dolostone bedrock. Lady Franklin Point, south Victoria Island. Photo taken August 28, 2003.

Conclusions

Frost action is an important geomorphic process at Lady Franklin Point resulting in unusual terrain features: stone frost mounds and frost-modified fractures in exposed bedrock.

The Lady Franklin Point stone frost mounds result from cycles of seasonal thawing and freezing in the saturated frost-shattered uppermost layer of the flat-lying dolostone bedrock. Thus, they can be considered a seasonal feature. However, morphologically speaking, they are perennial landforms that remain prominent micro terrain features for a relatively long time.

References

Mackay, J.R. 1973. The growth of pingos, western Arctic coast, Canada. *Canadian Journal of Earth Sciences* 10(6): 979-1004.

Mackay, J.R. 1979. Pingos of the Tuktoyaktuk Peninsula area, Northwest Territories. *Geographie Physique et Quaternaire* 33(1): 3-61.

Mackay, J.R. 1985. Pingo ice of the western Arctic coast, Canada. *Canadian Journal of Earth Sciences* 22(10): 1452-1464.

Washburn, A.L. 1973. *Periglacial Processes and Environments* London: Edward Arnold Ltd., 320 pp.

Williams, P.J. & Smith, M.W. 1989. *The Frozen Earth: Fundamentals of Geocryology.* Cambridge: Cambridge University Press, 360 pp.

Arctic Road Research Program: Experiences and Implementation

Seppo M.I. Saarelainen
Senior Research Scientist, Technical Research Centre of Finland VTT, Espoo, Finland

Abstract

In the Arctic Road Research Program, experimental construction was carried out on the Main Road 21 in Kilpisjarvi, Northern Finland, in the years of 1986–87. The aim was to reduce or mitigate various problems caused by cold climate. The themes of test construction were as follows: control of frost-heave damage, reduction of thaw settlements of a road on permafrost, reduction of snow accumulation on the pavement, and control of icing on the pavement. According to the experience gained, frost protection at frost heave sites had functioned according to the design, and the tested materials can be used in the frost protection of road pavements, at least in the conditions of Main Road 21, Kilpisjarvi. The rate of thaw settlement of the road on permafrost had been markedly reduced. Snow accumulation on the pavement had been reduced significantly. Ice accumulation on the pavement was not observed after the experimental repair of the worst sites. The methodical experience and knowledge was seen necessary to implement and apply in the guidelines of pavement planning and design in Finland.

Keywords: design; frost heave; naled control; pavements; permafrost; snow accumulation; test construction.

Introduction

Finland is located between latitudes 60 and 70°N, and the annual mean air temperature varies between +4°C in the south and -3°C in the north. Discontinuous permafrost is found only in Northern Lapland, mainly on peatlands and fjell plateaus. Precipitation is about 350 mm/year, and the terrain is treeless tundra.

The problems are mostly manifested of the maintenance of main roads from Finland to Norway, where winters are long enough to cause problems with excessive frost heaving and naled formation, causing pavement damage and traffic safety problems (Saarelainen & Vaskelainen 1988). Permafrost, lying and thawing under the road, causes settlements, and the open terrain with high wind speeds benefits snow accumulation on the pavement. Further, indications of deficient stability of thawing fjell slopes were detected.

To find a better solution to pavement structures, a test construction program was carried out at Kilpisjarvi, Northern Lapland, at 67°N in the years of 1986–87. (Saarelainen 1993a, 1993b, 1993c, Saarelainen & Vaskelainen 1995, Saarelainen & Onninen 2000). The sites were selected according to the investigations, test pavements were designed according to the site conditions, and after construction, test pavements and structures were monitored, primarily over two years, and later in longer intervals (Fig. 1).

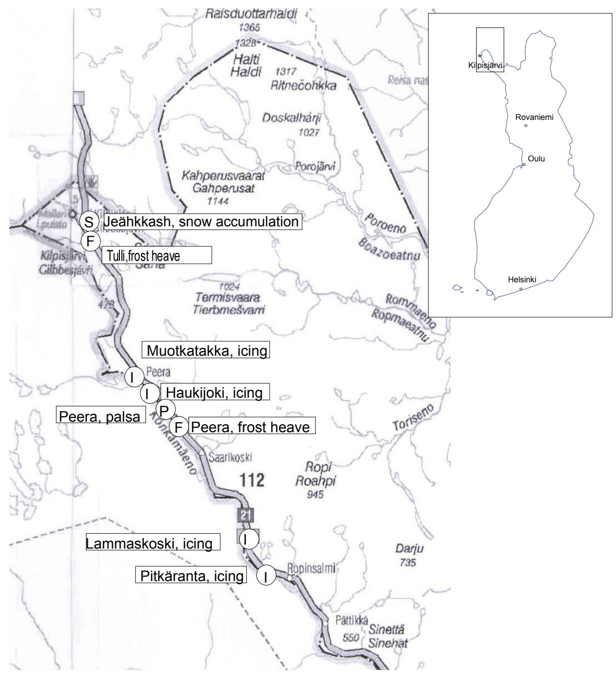

Figure 1. Arctic Road, Kilpisjarvi. Site locations.

Outline of the Problems

Frost heaving

Pavement damage and roughness, resulting from large and uneven frost heaving were found at some road stretches constructed on subgrades of silts and silty tills. The measured normal heaves varied up to 300 mm with seasonal frost penetration up to 3–4 m. At the Kilpisjärvi meteorological station in the period of 1931–1960, the annual average air freezing index was about 43,000 Kh (deg-hours), and the maximum freezing index, occurring once in 10 years, has been about 55,000 Kh (deg-hours).

Thaw settlements

Settlements due to thawing permafrost were found at some peatland sites, which also were characterised with palsa-mounds. The road line, crossing a palsa, had settled about 1.8 m since it was paved in 1982 with a settlement rate of 80 mm/y. The depth of permafrost at the site was about 7–8 m. The frozen subgrade consisted of frozen peat, that was compressed about 70% based on thaw-compression testing. The old road surface prior to paving was dark oiled gravel.

Snow accumulation

Excessive snow accumulation had been met during years in the pavement maintenance in an open mountainous terrain, where wind speed may rise considerably. The snow densities were low due to cold, continuous winters. Accumulation was most severe in road-cuts along the hill slopes. Snow plowing was normally started in December. The traffic suffered also from reduced visibility (white-out) during severe winds and storms. Along the test road, snow depths along the road profile and in transverse sections were measured. The recorded maintenance of snow accumulation started when the measured wind speed exceeded about 5 m/s or after a snowfall of 50 mm.

Naled formation

In cold winters, like in the late 1980s, ice accumulation had been observed, causing expensive maintenance work. Problematic sites were located either on a road section along a hill slope or on a road crossing a watercourse, stream, or river. Indicated problems resulted from disturbance in the winter drainage. Groundwater continued flowing during the winter in the ground below the seasonal frost. If the frost penetrated to or below groundwater level, groundwater was forced onto the ground and snow surface where it froze. In a local natural watercourse, water flow froze from bottom up and formed ice dams that forced the water onto the surface to freeze. In more southern regions, road culverts are filled with ice in wintertime. Ice-filled side ditches and bridge or culvert openings may flood over during quick snowmelt in spring and cause erosion damage and traffic risks on the road.

Solution of the Problems

Frost heaving

At selected sites, test pavements were designed so that the frost heaving in a design winter (maximum once in 10 years) was less than 50 to 70 mm. The design was done applying “Segregation potential concept” (Konrad & Morgenstern 1981)

$$\frac{\partial v_w}{\partial t} = SP\frac{\partial T}{\partial z} \tag{1}$$

where $\frac{\partial v_w}{\partial t}$ is flow of water from unfrozen soil to the freezing zone, $\frac{\partial T}{\partial z}$ is the thermal gradient in the freezing zone, SP is the coefficient of proportionality, segregation potential.

The frost heave was calculated using a layered finite-difference program SSR that solves, in time intervals, a balance equation of heat at the freezing front (Saarelainen 1992). This is based on the surface temperature and thermal properties of the layered horizon and results in calculating the frost penetration and frost heave in time. With the same procedure, the segregation potential (SP) was back-estimated and compared with the estimated frost penetration and levelled frost heaving of the old pavement during the winter of 1985–86. The back-estimated segregation potential varied between 0 and 7 mm^2/Kh.

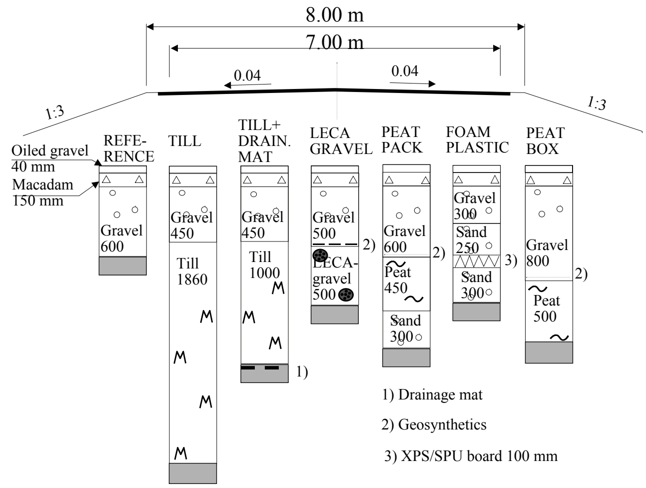

Figure 2. Tulli. The material layers of different frost-protected test pavements.

The aim of the test pavements was to study the applicability of different frost protection materials, like extruded polystyrene (XPS), LECA-gravel (lightweight expanded clay aggregate), prepacked and dried peat, local dried peat, and a slightly frost-susceptible sandy till. The layer thickness needed in frost protection was determined in the individual design. The frost heaving as well as SP varied along the line greatly, and the structures are not quite comparable with each other. The mechanical design of the pavement was carried out according to the actual road standards (minimum surface modulus during thaw more than about 170 MPa).

Structures with layer thicknesses are illustrated in Figure 2.

The test pavements were constructed in summer 1987. The frost protection materials were transported from southern-central Finland except for the local till and local peat.

Thaw settlements

Permafrost could be seen in the terrain in the form of frost mounds and palsas on peatlands. The average annual air temperature according to long-term climatic observations was about −3°C, and the elevation is about +400 m above sea level. The area is in the discontinuous alpine permafrost zone.

According to temperature profiling and electric soundings, the thickness of palsa below the test site was about 7–8 m. The top layer below the old pavement consisted of frozen peat with ice content about 50–95% by volume and thaw-compression of more than 70% under compressive stress of 25 kPa.

The test pavement contained, besides an overlay of 700 mm of gravel and asphalt, insulation of XPS, underlain with a gravel layer of 500 mm. The thickness of XPS (100 mm) was analysed using an analytic thermal FEM program, ADINA-T. The analysis with a given insulation thickness was conducted over three calendar years with the objective

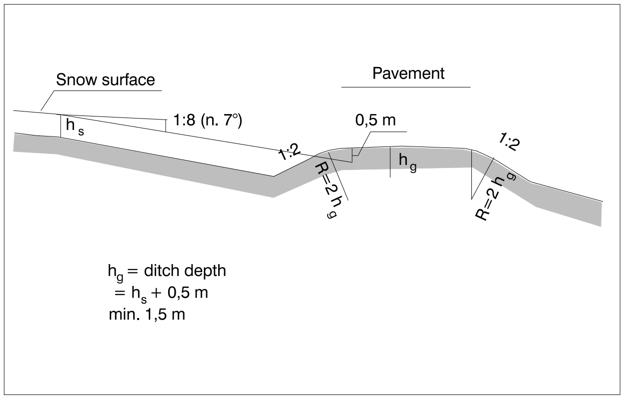

Figure 3. Type transverse profile to prevent snow accumulation on pavement in a sloping terrain.

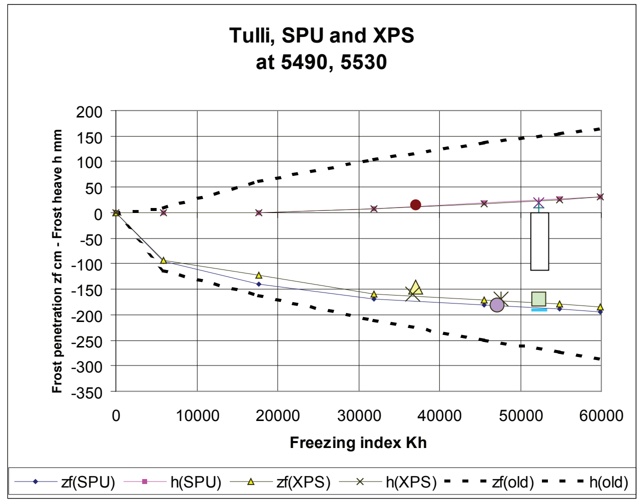

Figure 4. Tulli, the estimated and observed frost penetration (zf) and frost heaving (h) of polyurethane (SPU), and polystyrene (XPS) insulated test pavements.

that the thaw should not penetrate to the underlying frozen and thaw-sensitive subgrade.

The old pavement was removed in autumn 1986, and the new pavement with insulation was constructed in May 1987. The test section was paved in the next summer.

Snow accumulation

To reduce snow accumulation, the new pavement grade was raised above the estimated maximum snow level. The snow level was measured during the previous winter along the road. (Because the observed snow thickness at the Kilpisjärvi meteorological station was maximum occurring once in 10 years, the measured snow surface level at the site corresponded also to a maximum snow level, occurring once in 10 years, see Byalobzhenskiy 1983). Applying the observation statistics of snow thickness from a neighbouring observation station, this interpretation can be done for snow depth observations at a road site. The pavement surface was set 0.2–0.5 m higher than the estimated design snow level. Because the test road was located along a mountain slope, the transverse profile of the road was smoothed with curved shoulders and the upslope ditch was widened to provide a storage area for the accumulation of snow (Fig. 3).

The snow fences installed previously were removed.

Naled formation

Improvement of winter drainage was tested at four sites, two of which were slopes with groundwater icing problems and two with watercourse icing.

The principal improvement at groundwater icing was to collect the water into subsurface drains in the upper terrain below the estimated frost penetration and to drain it into a deep insulated pipe across the road.

The principal improvement at the watercourse icing site was to lead the upstream water flow through the road into a deep insulated pipe installed below the seasonal frost depth.

The drainage installations were constructed in 1987, and no pavement icing needing maintenance measures has been observed since then. Tested approaches have been successfully applied in road maintenance operations in Finnish Lapland since then (Kaitala et al. 2007).

Experiences after Construction

Frost heaving

The calculated frost heaving and frost penetration vs. freezing index are illustrated in Figure 4 for the test pavement with frost insulation boards. Observed frost heaves and frost penetration of different winters (1987/88, 1988/89, and 1989/90) have also been marked. A reasonable match can be seen that the applied calculation model SSR reasonably estimated actual frost heave and frost penetration, and that the material characteristics applied in the analysis were of correct magnitude.

For different frost protection materials, the following estimated characteristics were summarized in Table 1.

According to the observations, the frost heaving and frost penetration corresponded well to the calculated values. This confirmed the validity of the calculation model, the back-estimated frost-heave parameters (segregation potential), and the insulation properties of the applied materials. A more comprehensive presentation of the test pavements is included in the site reports (Saarelainen 1993, 2002).

Thaw settlements

The settlements were observed along the road centerline. Observations are illustrated in Figure 5. During the first years, the pavement surface was light-coloured, and the maximum annual settlement was about 10 to 20 mm/y. After the road was paved with dark asphalt pavement, the rate of settlement increased to a maximum 30 mm/y.

It is obvious that in these marginal permafrost conditions, thaw can be decreased with thermal insulation and light-coloured surface. For further reduction, active cooling might be useful. The rate of settlement in this actual case was reduced to a level that could be maintained by normal road maintenance.

Table 1. Characteristics of applied frost insulation materials (Saarelainen 2002).

Material	Dry density kg/m³	Moisture content w_{vol}, %	Frozen thermal conductivity λ_f, W/Km Estim.	Obs.
LECA-gravel	300	7	0.2	0.2
Packed peat	300	10	0.5	0.7
SPU	40	4	0.035	0.035
XPS	38	0,4	0.035	0.035
Local peat	200	60	1.0	1.0

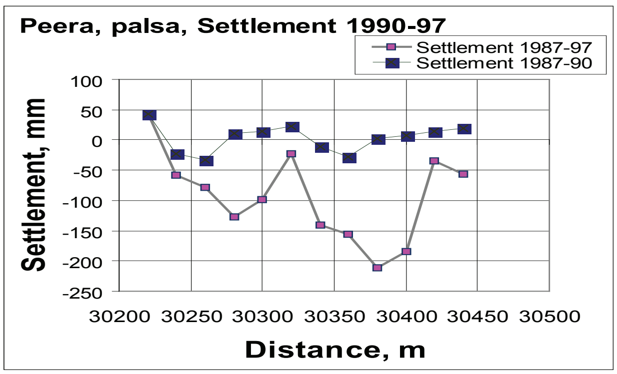

Figure 5. Peera, palsa. Pavement settlements since construction in 1987 until 1990 and 1997.

Snow accumulation

Before repair, snow and ice removal was needed by December. After the road was raised, the wind was observed to keep the pavement free from snow over the winter. In most severe winters with a very thick snow cover, heavy maintenance was still necessary as late as March.

The following recommendations to reduce snow accumulation were seen as appropriate:

- the pavement surface should be raised more than 0.5 m above the maximum design snow level,
- in a sloping terrain, a spare space for snow accumulation should be planned in the cut upslope,
- the pavement shoulders should be rounded to minimize wind turbulence on the road, and
- snow fences may still be necessary to maintain visibility during snowstorms

Naled formation

Ice accumulation in the road ditches was monitored after the repair. The ice accumulation was clearly reduced, and it did not cause any further maintenance effort, although winter temperatures were still severe.

In conclusion, the following recommendations are appropriate:

- Groundwater icing can be reduced with deep drainage in the upper terrain, and draining the water through the road in a deep thawed pipe.
- Surface water icing can be reduced or prevented by leading the water flow in the watercourse into a thermally-insulated deep culvert across the road line. During snowmelt and summer season, water then flows in the open watercourse.
- Icing can be reduced and water flow can be maintained by local heating. The electrical energy needed for heating cables can be produced with a wind generator.

It was also observed that icing problems are induced when a natural watercourse is treated and disturbed by excavation.

Conclusions

The described test construction revealed some extreme road maintenance problems in Finland. The approaches applied in the design and construction were seen as efficient, and they have been later applied elsewhere in Northern Finland. The results in the form of design models and approaches, as well as the design characteristics of insulation materials, may be useful also in other regions in cold climates.

References

Bjalobzenskij, G.V. 1983. Determination of snow cover thickness for snow accumulation design of pavements. *Avtomobilnye dorogi*, 1983, No. 10 (in Russian).

Kaitala, E. & Saarelainen, S. 2007. Improvement of de-icing on the roads at Kittila, Muonio, Enontekio, Inari and Utsjoki. *Proceedings of the Eighth International Symposium on Cold Region Development ISCORD 2007, Sept. 25–27. 2007, Tampere, Finland*, 2 pp.

Konrad, J.-M. & Morgenstern, N.R. 1981. The segregation potential of freezing soil. *Can Geot. Journal* 17: 473-486.

Saarelainen, S. & Vaskelainen, J. 1988. Problems of Arctic road construction and maintenance in Finland. *Proceedings of the Sixth International Conference on Permafrost.* Trondheim: Tapir Publishers, 1466-1471.

Saarelainen, S. 1992. *Modelling frost heaving and frost penetration at some observation sites in Finland. The SSR model.* Espoo: VTT Publications 95, 121pp, http://www.vtt.fi/inf/pdf/publications/1992/P95.pdf

Saarelainen S. 1993a. Repair of a road built on permafrost at Kilpisjarvi, Northern Finland. *Proceedings of the Sixth International Conference on Permafrost, Beijing, China, June 1993*: 539-543.

Saarelainen, S. 1993b. Use of frost insulation in the repair of frost heave damages. *Proc. Int. Symp. on Frost in Geotechnical Engineering, Anchorage, Alaska, June 28th–July 1st 1993:* 113-116.

Saarelainen, S. 1993c. Arctic road construction. Final report of Kilpisjarvi-project in Finnish with English summary. Helsinki. *Tielaitoksen tutkimuksia* 5/1993, 62 pp.

Saarelainen, S. & Kivikoski, H. 1995. Preventing snow accumulation on road pavements. *PIARC, Proc. of International Winter Road Conference, Lulea, Sweden, 1995.*

Saarelainen, S. & Onninen, H. 2000. Long term settlement of a road built on permafrost at Kilpisjarvi, Northern Finland. *Proceedings of the International Workshop on Permafrost Engineering, Longyearbyen, Svalbard, Norway 18–21 June 2000.* Oslo: Norwegian Geotechnical Institute, 129-138.

Saarelainen, S. 2002. *Arctic Road Research Program 1985–1990. Final report.* Helsinki: Finnish Road Administration, Report 21, 89 pp.

Methane Emission from Siberian Wet Polygonal Tundra on Multiple Spatial Scales: Vertical Flux Measurements by Closed Chambers and Eddy Covariance, Samoylov Island, Lena River Delta

Torsten Sachs

Alfred Wegener Institute for Polar and Marine Research, Telegrafenberg A43, 14473 Potsdam, Germany

Michael Giebels

Institute of Geoecology, Technical University Braunschweig, Germany

Christian Wille

Institute of Botany and Landscape Ecology, Ernst Moritz Arndt University of Greifswald, Germany

Lars Kutzbach

Institute of Botany and Landscape Ecology, Ernst Moritz Arndt University of Greifswald, Germany

Julia Boike

Alfred Wegener Institute for Polar and Marine Research, Telegrafenberg A43, 14473 Potsdam, Germany

Abstract

Ecosystem-scale measurements and investigations of the small-scale variability of methane emission were carried out in northern Siberian wet polygonal tundra using the eddy covariance technique during the entire 2006 growing season. Simultaneous closed chamber flux measurements were conducted daily at 15 plots in four differently developed polygon centers and a polygon rim from July–September 2006. Our study site was located in the southern part of the Lena River Delta, characterized by arctic continental climate and comparatively cold, continuous permafrost. Controls on methane emission were identified by applying multi-linear and multi-nonlinear regression models. We found a relatively low growing season average methane flux of 18.7 ± 10.2 mg m^{-2} d^{-1} on the ecosystem scale and identified near-surface turbulence, soil temperature, and atmospheric pressure as the main controls on the growing season variation methane emissions. On the micro-site scale, fluxes showed large spatial variability and were best described by soil surface temperature.

Keywords: closed chambers; eddy covariance; flux; methane; Siberia; tundra.

Introduction

Introduction

Arctic tundra ecosystems cover an area of about 7.34 x 10^{12} m^2 (Reeburgh et al. 1998) and are underlain by permafrost. Despite increased research, especially in connection with the much stated concern of potential increased emission of climate-relevant trace gases from warming or thawing tundra areas, these sensitive high-latitude ecosystems with their complex network of interconnected processes and controls are far from being understood. Vegetation, state of the permafrost, soil texture, hydrology, and many other relevant parameters and consequently also processes controlled by these parameters vary greatly on small spatial scales. This is especially valid for methane emission on various scales from arctic wetlands (Christensen et al. 2000, Kutzbach et al. 2004, Whalen & Reeburgh 1992).

To our knowledge, only four studies reported methane flux data from Arctic tundra on the ecosystem scale using eddy covariance techniques, namely Fan et al. (1992) from western Alaska, Harazono et al. (2006) from northern Alaska, Friborg et al. (2000) from Greenland, and Hargreaves et al. (2001) from Finland. Manuscripts by Wille et al. (2008) and Sachs et al. (2008) reporting data from the Lena River Delta, Siberia, are currently in press.

On the other hand, many studies are available reporting point data using closed chamber methods (Christensen et al. 2000, Kutzbach et al. 2004, Whalen & Reeburgh 1992). While closed chamber methods have multiple inherent problems, such as the exclusion of atmospheric parameters and induced alteration of concentration gradients underneath the chamber, resulting in disturbed fluxes, they are widely used to investigate the small scale variability of methane fluxes. The eddy covariance method does not allow for a spatial resolution high enough to investigate that kind of variability in heterogeneous areas.

We conducted intensive field studies on the ecosystem (1 ha to 1 km^2) and micro-site scales (0.1–100 m^2) using eddy covariance and closed chamber methods simultaneously in order to investigate the temporal and spatial variability of methane emissions. For the first time, methane flux measurements on the ecosystem scale in Arctic Siberian tundra were carried out during an entire growing season from the beginning of June–September 2006, and measurements on the micro-site scale were conducted within the eddy covariance footprint from July–September 2006.

Material and Methods

Study site

The study site was located on Samoylov Island, 120 km south of the Arctic Ocean in the southern central Lena River

Delta (72°22′N, 126°30′E) and is considered representative of the active delta landscape. Over the past ten years, Samoylov Island has been the focus of a wide range of studies on surface-atmosphere gas and energy exchange, soil science, hydrobiology, microbiology, cryogenesis, and geomorphology (Boike et al. 2003, Kutzbach et al. 2004, 2007, Liebner & Wagner 2007, Schwamborn et al. 2002, Wille et al. 2008, Sachs et al. 2008).

Samoylov Island covers an area of about 7.5 km². The western part of the island (3.4 km²) is a modern floodplain with elevations from 1–5 meters above sea level (a.s.l.). The study site is located in the center of the Late-Holocene eastern part (4.1 km²) with elevations from 10–16 meters a.s.l. The surface of the terrace is characterized by wet polygonal tundra with a flat but regular micro-relief caused by the development of low-center ice wedge polygons. The typical elevation difference between depressed polygon centers and elevated polygon rims is up to 0.5 m (Kutzbach 2006). The poorly drained and hence mostly inundated centers are characterized by *Typic Historthels*, while *Glacic* or *Typic Aquiturbels* dominate at the dryer but still moist polygon rims (Soil Survey Staff 1998, Kutzbach et al. 2004). As the summer progresses, these soils typically thaw to a depth of 30–50 cm.

Hydrophytic sedges, as well as mosses, dominate the vegetation in the wet polygon centers (Kutzbach et al. 2004). Polygon rims are dominated by mesophytic dwarf shrubs, forbs, and mosses. Surface classification of aerial photographs taken in 2003 shows that elevated and dryer polygon rims cover approximately 60% of the area surrounding the study site, while depressed and wet polygon centers and troughs cover 40% of the area (G. Grosse pers. comm.. 2005).

The climate in the region is arctic continental climate characterized by very low temperatures and precipitation. Mean annual air temperature at the meteorological station on Samoylov Island was -14.7°C and mean precipitation was 137 mm, ranging from 72–208 mm in a period from 1999–2005 (Boike et al. 2008). Snowmelt and river break-up typically start in the first half of June, and the growing season lasts from mid-June through mid-September. The continuous permafrost in the delta reaches depths of 500–600 m (Grigoriev 1960) and is characterized by very low temperatures between -13°C and -11°C (Kotlyakov & Khromova 2002).

Ecosystem scale flux measurements

In situ ecosystem scale methane fluxes were measured using the eddy covariance (EC) method with a tunable diode laser spectrometer (TGA 100, Campbell Scientific Ltd., USA) for CH_4 analysis. A more detailed description of the technical set-up can be found in Sachs et al. (2008).

The EC system was set up in the center of the eastern part of Samoylov Island and was surrounded by a relatively homogenous fetch of wet polygonal tundra. Larger lakes were located at the periphery of a 600 m radius around the tower. Successful measurements were conducted for 103 days from June 9–September 19, 2006, covering an entire growing season (Sachs et al. 2008).

Additional parameters measured at the eddy covariance system and an automated long-term monitoring station 700 m south of the EC tower include air temperature, relative humidity, incoming and outgoing solar and infrared radiation, photosynthetically active radiation (PAR), barometric pressure, precipitation, and soil temperature data at various depths. Additional daily manual measurements at five sites in close proximity to the tower included thaw depth using a steel probe, soil temperatures in 5 cm depth intervals, water level, and soil moisture using a Theta Probe type ML2x (Delta-T Devices Ltd., Cambridge, UK) where no standing water was present.

The area from which 80% of the cumulative methane flux originated was calculated using a footprint analysis according to Schuepp et al. (1990). The upwind distance of this flux contribution was on average 518 m, the maximum contribution originated from an average distance of 116 m.

Small scale flux measurements

For small-scale flux measurements, five different micro-sites characteristic of the prevalent surface and vegetation features within the eddy covariance fetch were established in close proximity to the flux tower (Fig. 1).

Polygon 1 was a low-center polygon with standing water in the center. The northern side of the polygon rim showed signs of beginning degradation, which might serve as a hydraulic connection to surrounding polygon troughs. Vegetation in the center is dominated by *Drepanocladus revolvens* (100% coverage) and *Carex chordorrhiza* (8% coverage).

Polygon 2 was a high-center polygon with no standing water in the center due to drainage into surrounding thermokarst cracks and troughs. The vegetation was dominated by *Hylocomium splendens* (85% coverage) and *Tomentypnum nitens* (10% coverage).

Polygon 3 was a low-center polygon with a massive rim on the western side and a completely degraded rim on the eastern side, where a large thermokarst crack of more than 2

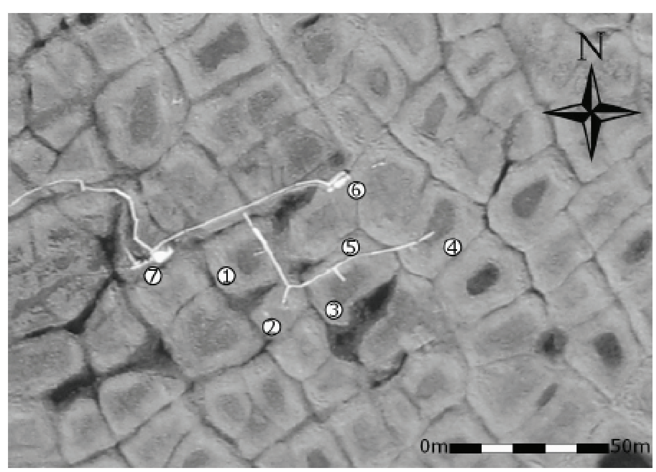

Figure 1. Aerial view of investigation site: 1 – low-center polygon, 2 – high-center polygon, 3 – low-center polygon, 4 – low-center polygon, 5 – rim, 6 – eddy covariance system, 7 – tent for equipment (Photo: J. Boike).

m depth was located. There was standing water in the polygon center and the vegetation was dominated by *Drepanocladus revolvens* (90% coverage), *Carex chordorrhiza* (10% coverage), and *Carex concolor* (10% coverage).

Polygon 4 was a low-center polygon with no apparent rim degradation and no apparent hydraulic connection to surrounding cracks or troughs. It usually maintained the highest water level and was dominated by *Scorpidium scorpidioides* (100% coverage), *Carex chordorrhiza* (8% coverage), and *Carex concolor* (3% coverage).

The polygon rim micro-site was underlain by a massive ice wedge and draining into polygon 3 to the east and the polygon crack to the west. Vegetation was dominated by *Hylocomium splendens* (60% coverage), *Rhytidium rugosum* (30% coverage), and *Carex concolor* (4% coverage).

In each of the four polygon centers and along the rim, three 50 cm x 50 cm PVC chamber collars with a water-filled channel as a seal were inserted 10–15 cm into the active layer. Chambers were made of opaque PVC and clear PVC, respectively, for light and dark measurements. Chamber volume was 12.5 l at the high-center and rim micro-sites and 37.5 l at the other sites, where higher vegetation did not allow for the use of small chambers.

Chamber measurements at all 15 plots were made daily from July 12–September 19, 2006 with both clear and opaque chambers. Sample air was drawn from a port on top of the chamber every 45 s for 8–10 minutes for simultaneous analysis of CO_2, CH_4, and water vapor using a photo-acoustic infrared gas spectrometer Innova 1412 with optical filters UA0982 for CO_2, UA0969 for CH_4, and SB0527 for water vapor (INNOVA AirTech Instruments, Denmark). A membrane pump was connected to two other ports and circulated chamber headspace air through perforated dispersive tubes for mixing.

Due to water interference with the CH_4 optical filter sample air was dried prior to entering the analyzer using 0.3 nm molecular sieve (beads, with moisture indicator; Merck KGaA, Darmstadt, Germany). Temperature and pressure inside the chamber were logged continuously by a MinidanTemp 0.1° temperature logger (Esys GmbH, Berlin, Germany) and the Innova 1412, respectively.

Flux modeling

We used multiple linear regression, as well as regression tree analysis, to identify the main controls on eddy covariance methane fluxes. All analyses were based on daily averages of measured and quality-controlled fluxes and are reported elsewhere in detail (Sachs et al. 2008). A multiplicative exponential regression model modified and extended after Friborg et al. (2000), was set up and fitted to the in situ data for small-scale flux modeling. It can be written as

$$FCH_4 = a \cdot b^{((T-\bar{T})/10)} \cdot c^{(u*-\overline{u*})} \cdot d^{(p-\bar{p})} \quad (1)$$

where a, b, c, and d are fitted parameters, T is the soil temperature at 10 cm depth in a polygon center, u_* is the friction velocity, p is the air pressure, and horizontal bars denote the mean values of the respective variables. A weighting factor of σFCH_4^{-2} was applied during the fitting process, with σFCH_4 being the daily mean of the noise estimates of the hourly flux data points.

For closed chamber measurements, we used multiple linear regression analyses to identify statistically significant controls on methane flux. Data was first tested for multi-collinearity following Schuchard-Ficher (1982) and for parameter significance using a t-test. The regressors were discarded in a stepwise procedure until only independent and significant parameters remained.

Results

Ecosystem-scale methane flux

Mean daily ecosystem methane flux was 18.7 ± 10.17 mg m^{-2} d^{-1} during the study period and showed relatively small seasonal variation (Fig. 2). However, strong variations could be observed, which coincided with pronounced decreases in air pressure and higher wind speed after calm periods.

In the first two weeks of measurements, average daily methane fluxes were already 13.8 mg m^{-2} d^{-1}, with high variability from 5.7 mg m^{-2} d^{-1} to 22.0 mg m^{-2} d^{-1}. Soil temperature was still below 0 °C when measurements started and showed very little variation in the early part of the thawing period. The lowest methane flux was observed during days with relatively high air pressure and low wind speed. Methane fluxes increased to an average of 25.0 mg m^{-2} d^{-1} in the third week. However, this increase was mainly due to an extreme peak on June 27, which coincided with the lowest observed air pressure during the summer and high wind speeds. The last ice from the bottom of ponds and smaller lakes surfaced and melted around this time.

Methane fluxes dropped to an average of 12.3 mg m^{-2} d^{-1} during the calm period at the end of June, and then steadily increased to the highest measured fluxes of on average 35.1 mg m^{-2} d^{-1} in the first week of August, roughly following variations in soil temperature and closely following variations in wind speed. Throughout July, above-average methane fluxes frequently correlated with rapid decreases in air pressure. Until the third week of August, fluxes remained between 17.0 and 20.0 mg m^{-2} d^{-1} and then decreased to less than 13.0 mg m^{-2} d^{-1} during a longer calm high-pressure period at the end of August.

During the first and second week of September, which were characterized by steadily decreasing air pressure, partly strong winds, and rain or snow events, methane fluxes increased to an average of 18.2 mg m^{-2} d^{-1} and 21.6 mg m^{-2} d^{-1}, respectively, despite a decrease in soil temperature and refreezing of the top soil layers and water bodies. By mid-September, all water bodies, except for the large thermokarst lakes, were covered with ice up to 8 cm thick. During the calm high-pressure period after September 13, methane fluxes decreased markedly to below 10.0 mg m^{-2} d^{-1} at the end of the measurement period.

All approaches showed that variation in methane fluxes could best be explained by friction velocity u_* and soil

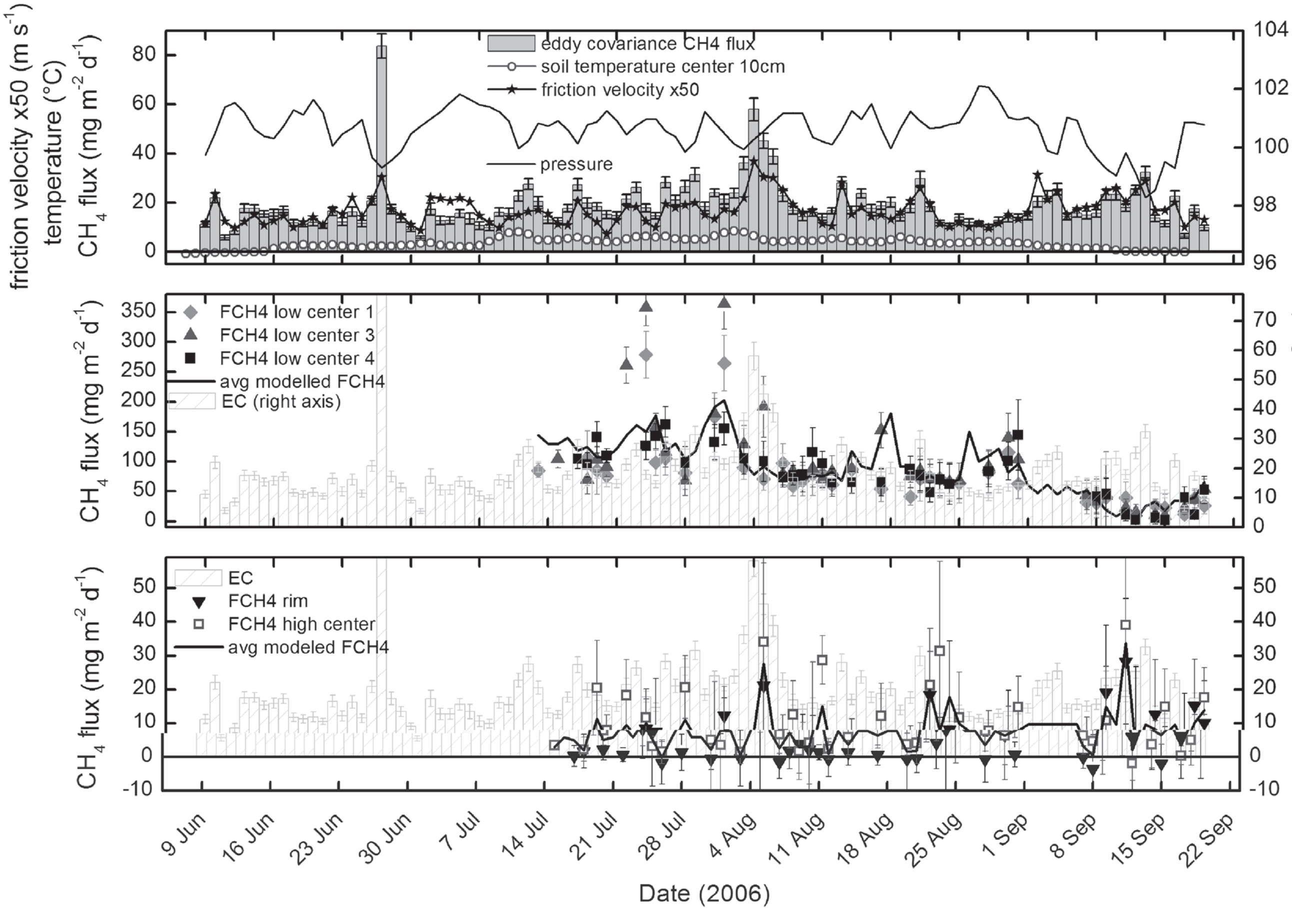

Figure 2. Top panel: Daily averages of eddy covariance methane fluxes and environmental controls during the 2006 growing season. The error bars of the eddy covariance data indicate the daily average noise level. Middle panel: Closed chamber methane fluxes from low center polygons and average modeled chamber flux. Each point represents the average of six flux measurements in the respective polygon. Bottom panel: Closed chamber methane fluxes from a polygon rim and a high center polygon and average modeled chamber flux. Each point represents the average of six flux measurements at the respective site. The error bars of the chamber data indicate the mean standard errors of the flux estimates. In the middle and bottom panel, the eddy covariance fluxes are given as light-grey columns for comparison. Note the different scale of the two y-axes in the middle panel!

temperatures at 10 cm depth in a polygon center and 20 cm depth in a polygon rim, respectively. Friction velocity alone accounted for 57% of the variance in methane emissions and another 3% could be explained by wind speed, which is closely correlated with friction velocity. Soil temperatures on the other hand only explained about 8% of the variance. The best agreement ($r^2_{adj} = 0.68$) of modeled and measured data was obtained by a model which included an exponential term that accounts for the observed influence of air pressure.

Thaw depth, which increased gradually and without variation throughout the season, did not improve the model, nor did water level, which remained above the soil surface at all times in the polygon centers.

The cumulative methane emission during the 2006 growing season was 1.93 g m^{-2}, which agrees well with the cumulative flux during the same period of a combined 2003 and 2004 dataset that amounted to 1.87 g m^{-2} (Wille et al. 2008). The model underestimated the cumulative measured flux by less than 5%.

Small-scale methane flux

Small-scale methane emission was similar among low-center polygons (Fig. 2) and differed strongly from fluxes at the high-center and rim micro-sites (Fig. 2).

At all three low-center micro-sites, mean daily fluxes in July and August were around 100 mg m^{-2} d^{-1} and decreased at the beginning of September to less than 50 mg m^{-2} d^{-1}, closely following variations in air temperature. When snow started to accumulate between September 10 and 15 during a period of below-zero temperatures, emissions fluctuated below 20 mg m^{-2} d^{-1}. At polygon 4, the seasonal course was less pronounced and variability was less extreme than at polygon 1 and 3, where peak fluxes exceeded 350 mg m^{-2} d^{-1} and were associated with spatial standard deviations of up to ±300 mg m^{-2} d^{-1}, demonstrating a large spatial variability even within micro-sites. These extreme emissions were generally associated with high temperatures.

It was not possible to construct a multidimensional regression model with independent and significant parameters. The predictor variable with the highest explanatory power within the final one-dimensional model was surface temperature.

At polygon 2 (high center) and at the polygon rim, very low methane concentrations in the closed chamber system frequently caused the analyzer to reach its detection limit, resulting in noisy data and a high exclusion rate during flux calculation. Fluxes that could be calculated were very low throughout the campaign and rarely exceeded 10 mg m^{-2} d^{-1}, which is about 10% of the average fluxes from low-center polygon micro-sites. No seasonal course is evident from the data and no statistically significant correlation with any of the observed environmental parameters was found. Gaps in the time series were filled with monthly average flux values, accounting for the small positive fluxes that were present.

Averaging closed chamber methane fluxes from wet polygon centers and drier sites, respectively, and weighing them according to the distribution of wet (40%) and drier (60%) surfaces classes results in an up-scaled closed chamber flux of 39.11 mg m^{-2} d^{-1}, which is double the eddy covariance flux during the same time period.

Discussion

Discussion

Results from eddy covariance measurements differ from closed chamber data both in terms of the seasonal variation and the identified controls on methane emissions. While ecosystems scale fluxes do not show much of a seasonal course, results from low-center polygon closed chambers show a pronounced decrease of methane emission towards the end of the season, which is more in agreement with most studies and results from deterministic process-based models used for larger scale modeling (Kirschke et al. 2008).

Emission peaks also do not match on the different scales. While ecosystem scale emission peaks usually coincide with high wind speed, low air pressure, and generally "bad weather" conditions, the largest emission from polygon centers as measured by closed chambers occurred during warm and dry days. However, the very weak peaks visible in closed chamber data from the rim and high-center micro-site tend to be more in agreement with eddy covariance emission peaks.

These differences in the seasonal dynamics may partly be explained by the very different hydrological conditions of the investigated micro-sites in combination with the importance of plant-mediated transport of methane (Kutzbach et al. 2004): in the wet polygon centers, water levels were always at or above the soil surface. Here, higher water levels could lead to decreased methane emission, as more vegetation becomes submerged and plant-mediated transport decreases. In addition, higher temperatures likely increase microbial methane production close to the surface. Hence, warm weather and falling water levels could actually increase emissions as long as the water table remains above the surface. At "drier" micro-sites, on the other hand, storm systems with strong precipitation events lead to a temporary increase in anaerobic soil volume and an increase in methane production, while lower temperatures have a negative effect on the activity of methane oxidizing microbes in the upper horizons of the active layer.

However, a large influence on the ecosystem methane flux can also be ascribed to open-water surfaces such as polygon ponds and thermokarst cracks, which were not covered by the closed chamber measurements but were present in the eddy covariance footprint. Diffusive and turbulent gas transfer between water and atmosphere is known to be proportional to the third power of the wind speed (Wanninkhof & McGillis 1999) and observation of methane ebullition (Walter et al. 2006) in the field indicates that water bodies are an important contributor to ecosystem methane efflux. These micro-sites must be included in future small-scale measurements within the eddy covariance footprint in order to more accurately scale chamber flux measurements to larger areas. A more detailed analysis of the small-scale variability and the scaling problems is in preparation.

The discrepancies in the results on the different scales also highlight the need for more non-intrusive and spatially integrating measurements from high-latitude ecosystems to verify and understand the results produced by the eddy covariance method. Larger scale methane emission models that have previously been developed on the basis of closed chamber data only, should incorporate new findings from eddy covariance or other non-intrusive techniques.

Our findings raise the question to which extent methane fluxes in permafrost ecosystems are controlled by near-surface controls including atmospheric boundary layer conditions and vegetation, or by soil characteristics and processes in the deeper active layer including microbial community structure and activity.

Acknowledgments

We would like to thank the members of the joint Russian-German expedition LENA-2006, especially Waldemar Schneider (AWI), Dmitry Yu. Bolshianov (AARI, St. Petersburg), Mikhail N. Grigoriev (Permafrost Institute, Yakutsk), Alexander Y. Derevyagin (Moscow State University), and Dmitri V. Melnitschenko (Hydro Base, Tiksi) for all logistical, travel, and administrative arrangements. We are also grateful to Günther "Molo" Stoof for technical support in the field and to Barnim Thees for valuable input regarding the statistical analysis.

References

Boike, J., Hinzman, L.D., Overduin, P.P., Romanovsky, V., Ippisch, O. & Roth, K. 2003. A comparison of snow melt at three circumpolar sites: Spitsbergen, Siberia, Alaska. *Proceedings of the Eighth International Conference on Permafrost, Zürich, Switzerland*: 79-84 pp.

Boike, J., Wille, C. & Abnizova, A. 2008. The climatology and summer energy and water balance of polygonal tundra in the Lena River Delta, Siberia. *J. Geophys. Res.* (in press).

Christensen, T. R., Friborg, T., Sommerkorn, M., Kaplan, J., Illeris, L., Soegaard, H., Nordstroem, C. & Jonasson, S. 2000. Trace gas exchange in a high-arctic valley 1. Variations in CO_2 and CH_4 flux between tundra vegetation types. *Global Biogeochem. Cycles* 14(3): 701-714.

Fan, S.M., Wofsy S.C., Bakwin P.S., Jacob D.J., Anderson S.M., Kebabian P.L., McManus J.B., Kolb C.E. & Fitzjarrald D.R. 1992. Micrometeorological measurements of CH_4 and CO_2 exchange between the atmosphere and subarctic tundra. *J. Geophys. Res.* 97(D15): 16,627-16,643.

Friborg, T., Christensen T.R., Hansen B.U., Nordstroem C. & Soegaard H. 2000. Trace gas exchange in a high-arctic valley: 2. Landscape CH_4 fluxes measured and modeled using eddy correlation data. *Global Biogeochem. Cycles*, 14(3): 715–724.

Grigoriev, N.F. 1960. The temperature of permafrost in the Lena delta basin – deposit conditions and properties of the permafrost in Yakutia. *Yakutsk*, 2: 97-101.

Harazono, Y., Mano, M., Myiata, A., Yoshimoto, M., Zulueta R.C., Vourlitis G.L., Kwon H. & Oechel W.C. 2006. Temporal and spatial differences of methane flux at arctic tundra in Alaska. *Mem. Natl. Inst. Polar Res.*, Spec. Issue 59: 79-95.

Hargreaves, K.J., Fowler, D., Pitcairn, C.E.R. & Aurela M. 2001. Annual methane emission from Finnish mires estimated from eddy covariance campaign measurements. *Theor. Appl. Climatol.*, 70: 203-213.

Kirschke, S., Guenther, K.P., Wisskirchen, K., Sachs, T. & Dech, S. 2008. Methane Emission from Siberian Wet Polygonal Tundra on Multiple Spatial Scales: Process-based Modeling of Methane Fluxes on the Regional Scale, Lena Delta. (this proceeding)

Kotlyakov, V. & Khromova T. 2002. Permafrost, snow and ice. In: *Land Resources of Russia*. CD-ROM. V. Stolbovoi & I. McCallum (eds.), International Institute of Applied Systems Analysis and the Russian Academy of Science, Laxenburg, Austria.

Kutzbach, L., Wagner D. & Pfeiffer E.-M. 2004. Effect of microrelief and vegetation on methane emission from wet polygonal tundra, Lena Delta, Northern Siberia. *Biogeochemistry* 69: 341-362.

Kutzbach, L. 2006. The exchange of energy, water and carbon dioxide between wet arctic tundra and the atmosphere at the Lena River Delta, Northern Siberia. *Reports on Polar and Marine Research* 541.

Kutzbach, L., Wille, C. & Pfeiffer, E.-M. 2007. The exchange of carbon dioxide between wet arctic tundra and the atmosphere at the Lena River Delta, Northern Siberia. *Biogeosciences* 4: 869-890.

Liebner, S. & Wagner, D. 2007. Abundance, distribution and potential activity of methane oxidizing bacteria in permafrost soils from the Lena Delta, Siberia. *Environmental Microbiology* 9(1): 107-117.

Reeburgh, W.S., King J.Y., Regli S.K., Kling G.W., Auerbach N.A. & Walker, D.A. 1998. A CH_4 emission estimate for the Kuparuk River basin, Alaska. *J. Geophys. Res.* 103(D22): 29,005-29,014.

Sachs, T., Wille, C., Boike, J. & Kutzbach, L. 2008. Environmental controls on ecosystem-scale CH_4 emission from polygonal tundra in the Lena River Delta, Siberia. *J. Geophys. Res.* in press.

Schuchard-Ficher, C., Backhaus, K., Humme, U., Lohrberg, W., Plinke, W. & Schreiner, W. 1982. *Multivariate Analysemethoden. Eine anwendungsorientierte Einführung*. Berlin, Heidelberg, New York: Springer-Verlag, 346 pp.

Schuepp, P.H., Leclerc M.Y., MacPherson J.I. & Desjardins R. L. 1990. Footprint prediction of scalar fluxes from analytical solutions of the diffusion equation. *Boundary-Layer Meteorology* 50(1-4): 355-373.

Schwamborn, G., Rachold, V. & Grigoriev, M.N. 2002. Late Quaternary sedimentation history of the Lena Delta. *Quaternary International* 89: 119-134.

Soil Survey Staff. 1998. *Keys to Soil Taxonomy 8th Edition*. Blacksburg, Virginia: Soil Conservation Service.

Walter, K.M., Zimov, S.A., Chanton, J.P., Verbyla, D. & Chapin III, F.S. 2006. Methane bubbling from thaw lakes as a positive feedback to climate warming. *Nature* 443: 71-75.

Wanninkhof, R. & McGillis, W.R. 1999. A cubic relationship between air-sea CO_2 exchange and wind speed. *Geophysical Research Letters* 26(13): 1889-1892.

Whalen, S.C. & Reeburgh, W.S. 1992. Interannual variations in tundra methane emission: A 4-year time series at fixed sites, *Global Biogeochem. Cycles* 6(2): 139-159.

Wille, C., Kutzbach, L., Sachs, T., Wagner, D. & Pfeiffer, E.-M. 2008. Methane emission from Siberian arctic polygonal tundra: Eddy covariance measurements and modeling. *Global Change Biology* (in press).

Refinement of Physical Land Scheme for Cold-Region Subsurface Hydrothermal Processes and Its Impact on High-Latitude Hydroclimate

Kazuyuki Saito
International Arctic Research Center (IARC), University of Alaska Fairbanks, Fairbanks, USA
Frontier Research Center for Global Change, Japan Agency for Marine-Earth Science and Technology (JAMSTEC), Yokohama, Japan

Abstract

Sensitivity experiments on subsurface and atmospheric hydroclimate were conducted to examine different levels of complexity in a physical terrestrial scheme in a coupled global climate model (GCM). In one-dimensional off-line experiments local impacts were examined for (1) snow cover and the organic layer, (2) soil column depth, and (3) hydrothermal parameterization in which effects of ground ice and unfrozen water under the freezing point are taken into account. The results reaffirmed the crucial role of snow and the organic layer for subsurface thermal regime. A total depth of 20 m was needed for physically-consistent simulation in the cold regions. An on-line simulation coupled with the atmospheric GCM showed the importance of the refined parameterization for better climatology and seasonality of the active layer and the high-latitude hydroclimate. The findings provide a basis for better physical representations in GCMs to investigate the hydroclimate of the Arctic, and on the larger spatial scales.

Keywords: frozen ground; global climate model; hydroclimate; physical land surface scheme.

Introduction

Global climate models (GCMs) are a useful tool to investigate large-scale permafrost and seasonally frozen ground (frozen ground, hereafter), and its impacts on the climate system, where the multiple feedbacks and interactions connect different components within the system. However, the current implementation and performance of physical terrestrial schemes in the state-of-the-art regional/global models still need substantial improvement and optimization on the resolved local physical (and biogeochemical) processes and properties, networking between different climate components, the initial and boundary conditions, and others, to be fully used.

Previous studies have pointed out the importance of a number of factors: (1) snow cover and top organic layer (e.g., Saito et al. 2007, Beringer et al. 2001), (2) total resolved depth of the soil column (Saito et al. 2007, etc.), (3) hydrothermal parameterization of the soil property, namely consideration of both solid and liquid water under the freezing point (e.g., Romanovsky & Osterkamp 2000, Flerchinger & Saxton 1989). Recently, several studies have appeared to examine the importance of those factors using the National Center for Atmospheric Research Land Surface Model (NCAR LSM) (Alexeev et al. 2007, Nicolsky et al. 2007, Yi et al. 2007). In this study, sensitivity experiments were conducted to evaluate the impact of the aforementioned factors using a land surface scheme in a Japanese-developed coupled global climate model. One-dimensional off-line experiments were intended to examine local subsurface hydrothermal impacts. On-line experiments coupled with the atmospheric component investigated the impacts on the high-latitude hydroclimate both below the surface and in the atmosphere.

Methods

Model and data

The numerical model used in the present study was CCSR/NIES/FRCGC MIROC3.2 coupled Atmosphere-Ocean global climate model (K-1 developers 2005), and the physical terrestrial scheme, MATSIRO (Takata et al. 2003). On-line experiments were performed at the horizontal resolution of Triangular 42 truncation (T42; ca. 2.5° by 2.5°).

For the off-line experiments, two different observational forcing datasets, both from the arctic tundra climate zones, were used; one taken at Barrow, AK, for 1990 through 2003 (soil temperatures were available only for the limited periods) provided by the Permafrost Laboratory, Geophysical Institute, University of Alaska Fairbanks (Mölders & Romanovsky 2006), and the other taken at Tiksi, Russia, for 1999 through 2005, provided by the Institute of Observational Research Center for Global Change, Japan Agency for Marine-Earth Science and Technology (JAMSTEC), Japan (H. Yabuki, personal communication). The period analyzed in this paper is from August 2002 to July 2003, since it is the only period during which Barrow and Tiksi observations overlapped.

Experimental conditions of the off-line experiments are summarized in Table 1. In off-line experiments (s4, g4, m4, n4, and o4) impact of snow cover and the top organic layers were examined in a 4 m soil column. Snow amount is prognostically calculated in the model, thus different amounts of precipitation were applied. Organic soil was specified by prescribing different values of thermal conductivity in the top layer. The original hydrothermal parameterization (C) does not consider the effect of either ground ice or unfrozen water on thermal properties under the freezing point. The refined parameterization (R) took both into account. Detailed explanation of the hydrothermal parameterization is found in Saito (2008). In another set of experiments (C4, C10, C50;

Table 1. Summary of the settings and conditions for the off-line experiments.

Name	Total depth (m)	Depth of soil layer boundaries (m)	Spin-up (year)	Precipitation	Thermal conductivity of top organic layers (W/m/K)[a)]	Thermal param. [b)]
s4	4	0.05, 0.25, 0.50, 1.0, 2.0, 4.0	30	5 times larger than observed	N/A	C
g4				As observed		
m4				No snow		
n4					0.1	
o4					0.025	
C4	4	0.05, 0.25, 0.50, 1.0, 2.0, 4.0	100	As observed	0.1	C
R4						R
C10	10	0.05, 0.25, 0.50, 1.0, 2.0, 3.5, 6.0, 10	100	As observed	0.1	C
R10						R
C50	50	0.05, 0.25, 0.50, 1.0, 2.0, 3.5, 6.0, 9.0, 14, 21, 30, 40, 50	100	As observed	0.1	C
R50						R

a) Specified only in the top layer (5 cm thick). Default value is that of mineral soil. b) Parameterization methods for soil thermal conductivity and heat capacity. C: Conventional, R: Ground ice and unfrozen water. See text for details.

R4, R10, R50), difference in total soil column depth was examined at three different depths (Table 1.).

Four integrations were performed online for combinations of presence/absence of the top organic soil layers in taiga and tundra zones (TOS/NoTOS), and the hydrothermal parameterization in the conventional (C) or refined (R) form. The top organic layer was prescribed only in tundra and taiga regions. The soil column depth was set to 4 m in all cases to focus on the above effects. The model was forced by monthly climatological sea surface temperatures and sea ice concentrations for the period between 1980 and 2000. Ten year outputs after 20-year spin-up were used for analysis.

Results

Near-surface conditions

Annual soil temperature range is shown with depth in Figure 1. Similarly, the seasonal evolution in the near-surface hydrothermal regime is shown in Figure 2. For both sites, Barrow and Tiksi, excessive snow cover led to a smaller annual amplitude and warmer soil temperatures for all layers; in Tiksi, the zero curtain was found below 2.5 m (s4; Figs. 1, 2).

When the snow amount and, therefore, the snow-covered period were more realistically simulated (g4), the thermal regime was closer to the observed. When snow cover was removed, cooling in winter was expectedly enhanced, whereas summer temperatures showed little impact (m4). On the contrary, inclusion of the top organic layer exerted a larger impact in summer than in winter for both areas (n4 and o4). The wetness of the upper soil layers was different with and without the top organic layer; it was kept close to saturation when the organic layer was present (Fig. 2c). With a stronger organic layer effect (o4), freezing and thawing at 20 cm depth occurred at a later time and proceeded more slowly.

Total depth and thermal parameterization

Examination of different total soil column depths showed that 15 m or below that annual amplitude is almost zero so that the zero heat flux condition at the lower boundary should be justified (Fig. 3). The refined parameterization (solid lines) simulated larger annual amplitude (warmer maximum) of soil temperature between 2 and 10 m. The equilibrated temperature below 15 m was warmer for the R runs by about one degree.

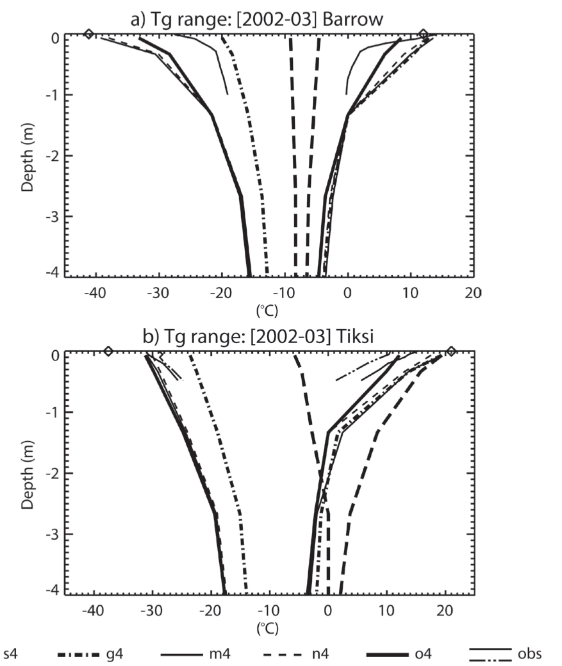

Figure 1. Annual range of soil temperature with depth, simulated for a one-year period from August, 2002 to July, 2003 for a) Barrow and b) Tiksi. Thin lines down to 1 m at Barrow and .48 m (two locations) at Tiksi are the observed values. Thick dashed lines are for experiment s4, and similarly, the thick dot-dashed for g4, the thin solid for m4, the thin dashed for n4, and the thick solid for o4.

On-line experiments

Figure 4 shows the latitudinal profile of atmospheric and hydrological variables in January and July, averaged over

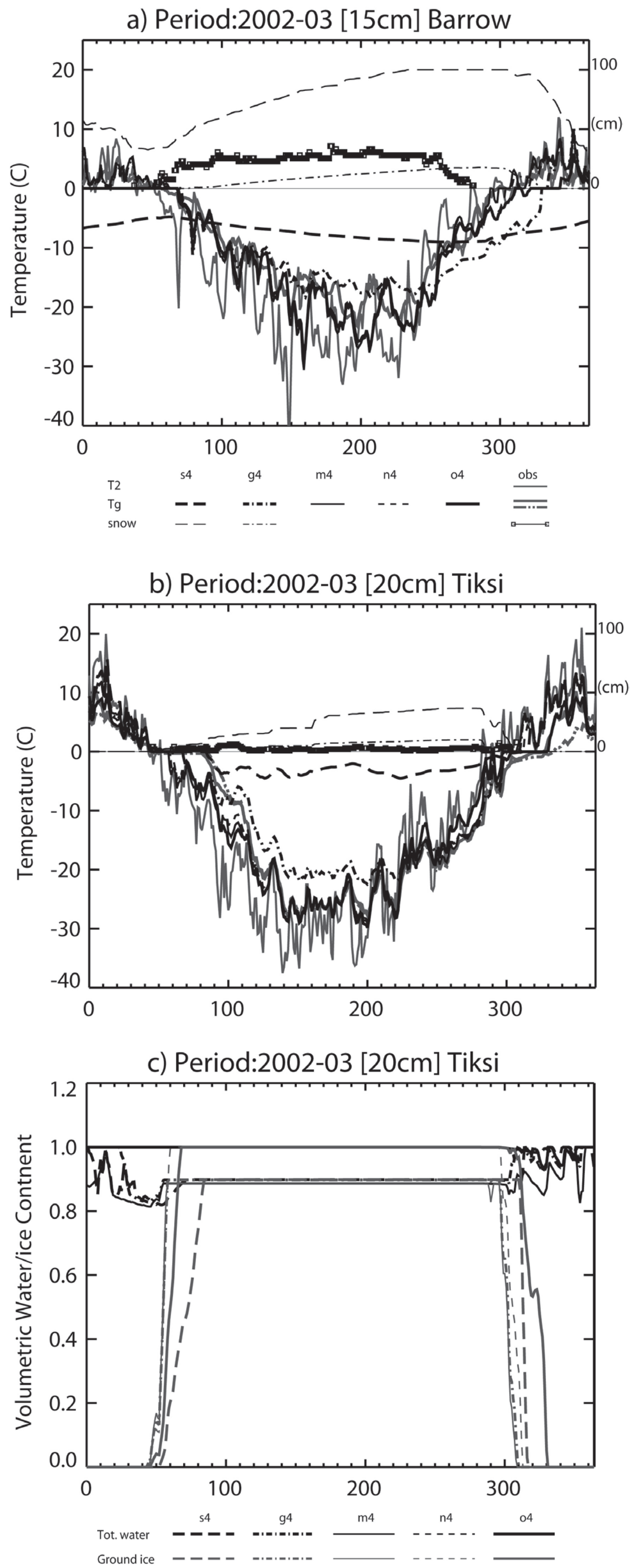

Figure 2. Seasonal evolution of soil temperature at (a) Barrow at the depth of 15 cm, (b) Tiksi at 20 cm depth. Line styles are the same as in Figure 1, except the thin solid gray line for surface air temperature at 2 m [forcing data]. Thinner lines above the 0 level are snow depth, and observed snow depth is shown with box symbols. (c) Seasonal evolution of soil moisture (thick lines) and ground ice content (thin gray lines), both relative to the saturation, at Tiksi; no observations were available for the period.

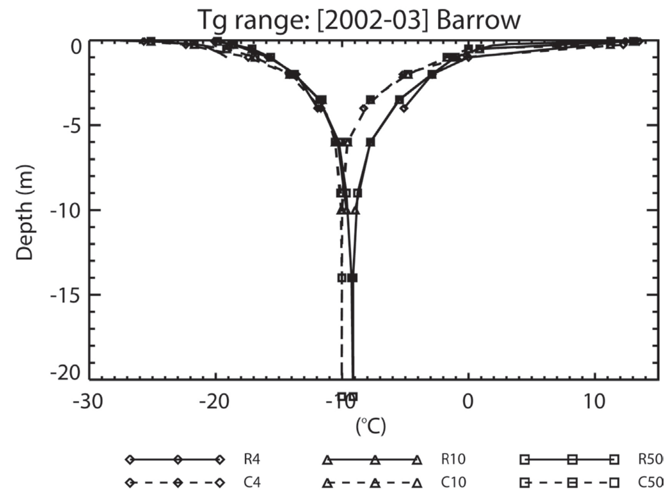

Figure 3. Annual range of soil temperatures, against depth, for different soil column depths (4 m, 10 m, and 50 m), and for the different thermal parameterizations. Dashed lines show the result of the conventional parameterization (C), while solid lines show that of the refined one (R).

land grids (excluding ice-covered areas) in each zonal band. Near-surface hydrologic conditions (i.e., soil moisture content) showed little difference between the four runs in all months (not shown), but subsurface thermal regimes (and ground ice content) differed to a substantial degree by the thermal parameterization (Figs. 4e, 4g). In the R4 runs it was cooler and a substantial amount of ice was retained in the summertime.

As for the atmospheric impact, surface air warmed faster and greater from spring to summer in R4 (Fig. 4a), and, similarly, cooled faster and greater in winter (Fig. 4b). The difference was most apparent in high latitudes. This led to an earlier and larger snow accumulation in winter (not shown), although precipitation did not vary much between the four simulations (Figs. 4c, 4d) in the high-latitudes. It was in the lower latitudes during summer monsoonal period that large precipitation differences were found; wetting of the Tibetan Plateau and drying of coastal China (not shown). The differences were canceled when taking the zonal average in Figure 4d. Land-average total annual runoff did not vary greatly between integrations; however, its seasonal distribution did change between the R4 and C4 runs. During the high-latitude melting season, runoff was greater for the R4 runs due to shallower active layer depth (Fig. 4g). On the contrary, it was smaller in summer because a larger amount of soil moisture was removed to the atmosphere by evapotranspiration (Fig. 4h, cf. Fig. 4b).

Distributions of frozen ground depended on both the organic soil and the hydrothermal parameterization (Fig. 5). The classification of the frozen ground followed the same methodology used in Saito et al. (2007). *Near-surface permafrost* is defined as an area with the maximum active layer thickness shallower than the model soil depth, in this case 4 m, for two consecutive years. Similarly, *seasonally-frozen ground* is defined as an area with its soil experiencing

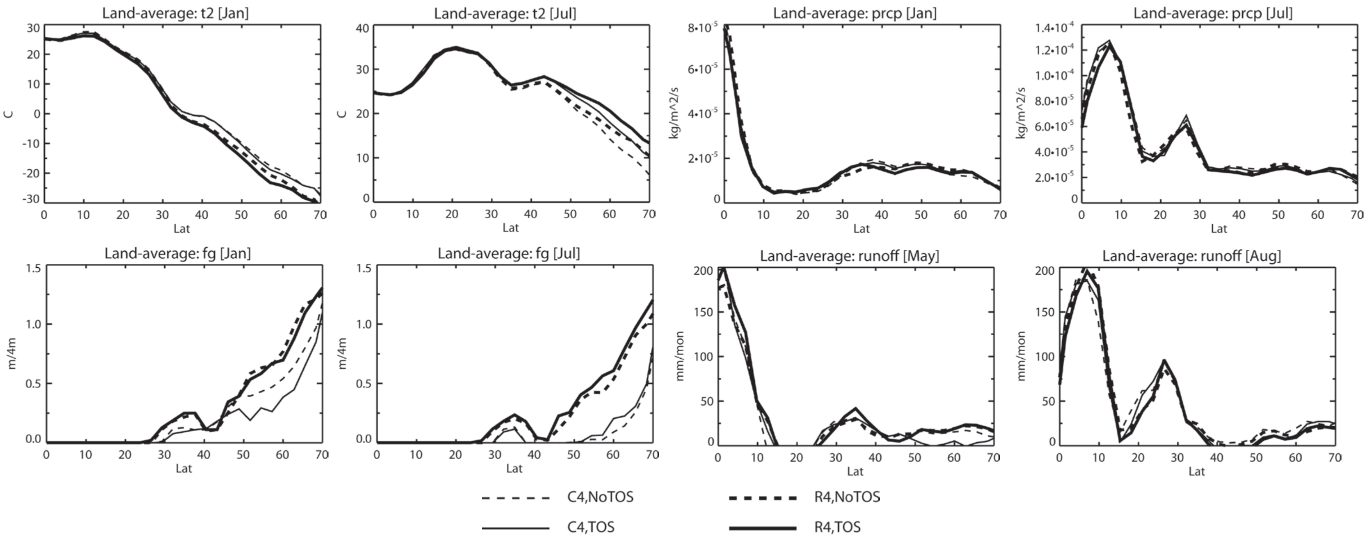

Figure 4. Latitudinal profiles of the a) surface air temperatures (T2), c) precipitation (total of liquid and solid), e) total ground ice amount in the 4 m column, averaged over land grids (except for permanently ice-covered areas) in January. Thick lines show the results by the refined thermal parameterization, whereas the thin lines show the conventional one. Solid lines denote the top-organic-soil (TOS) runs, and dashed lines the no-top-organic-layer (NoTOS) runs. Except for July b), d), and f) are same as a), c), and e). Except for runoff in May and August g) and h) are same as a) and b), respectively.

subfreezing at any time of a year. Distribution of near-surface permafrost (dark shades) is surprisingly different between R4 and C4; in the C4 runs it is very scarce largely due to excessive warming and thawing in summer (Fig. 4f). In contrast the R4 runs overestimated, when compared to the present-day observational estimate (e.g., Fig. 5c in Saito et al. 2007). Seasonally-frozen ground distribution did not differ much between runs and the observations (again, cf. Fig. 5c in Saito et al. 2007) for it is largely determined by surface air temperatures, which did not vary south of 30°N between runs (Figs. 4a, 4b).

Discussion

Weather-regime difference

The impact of snow cover appeared differently in Barrow and Tiksi, although both sites are located in arctic tundra, (Figs. 1, 2). The exaggerated warming in the s4 case for Tiksi likely resulted from warmer summer surface air temperatures (T2), which led to complete thawing down to 4 m in summer and to shallower snow cover climatology in winter. Tiksi's annual T2 range was -37.6°C to 21.0°C, while it was -41.2°C to 12.0°C for Barrow, for the examined period. Average snow depth was 6.7 cm for Tiksi and 23.0 cm for Barrow, although snow covered both sites for about 63% of the period (63.5% for Tiksi, and 62.4% for Barrow). Therefore, snow cover greater than observed had a larger insulation impact in Tiksi than in Barrow. There we also found seasonal differences affected the quality of the simulations: for the early snow accumulation period in Tiksi (days 50–85 in Fig. 2b) soil temperature was simulated best by the g4 run, whereas it was the no snow cover cases (m4, n4 and o4) that simulated the thermal regime best. In Barrow, discrepancies between the simulated and observed thermal regime are large during the snow melt season. Delayed snow melt led to slower subsurface warming (days 260–320 in Fig. 2a). These discrepancies, however, may be due in part to improper snow calculation in the model; it is prone to slower accumulation in the early cold season, greater insulation effects in midwinter, and slower melting in the warming season (Figs. 2a, 2b).

Another source of discrepancy from the observed thermal regime was the depth of the top organic layer. It is about 30 cm in Barrow and more than 50 cm in Tiksi, as inferred by the observed soil temperature profiles (cf. Figs. 1a, 1b). Hence, the prescribed organic layer of 5 cm may have been insufficient.

The experiments showed similar outcomes in Barrow and Tiksi, but also gave different responses in some variables or in different seasons, although both sites are located in the same arctic tundra climate zone. Similar evaluations with observations taken at places with varying weather and bio-climate regimes (not only arctic tundra, but also arctic taiga, high-altitude areas, etc.) will be instrumental to verify the findings in the present study, confirm the generality, and understand the heterogeneity between the regions more quantitatively. Similarly, knowledge of the geographical distribution of depth and physical/ biogeochemical properties of the organic layers, for example, will also be beneficial for more plausible future climate predictions.

Interactions with the atmosphere

Implementation of the physically-based parameterization of the soil hydrothermal properties impacted not only the subsurface but also the near-surface atmosphere. Surface air temperature in high latitudes decreased by about 5°C in winter (zonal average, only over land), and increased about 2°C in summer (Figs. 4a, 4b). Takata (2002) and

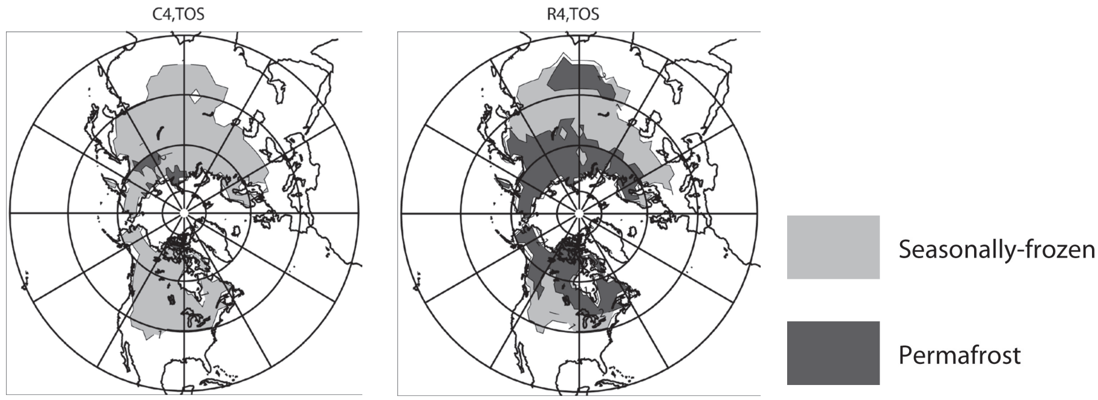

Figure 5. Distribution of near-surface permafrost (dark shades) and seasonally-frozen ground (light shades) simulated with a) the conventional thermal parameterization and b) the refined thermal parameterization. Near-surface permafrost is defined as the areas in which some layers are frozen for more than two consecutive years. Seasonally-frozen ground is defined as the areas in which soil temperatures in any layer is below 0°C at least once a month.

Takata and Kimoto (2000) have previously examined the impact of land processes (including freezing/thawing, but with "conventional" parameterizations) on the atmospheric hydroclimate. They showed changes in the regional-scale atmospheric circulations, and argue that the warming of high-latitude land in summer and the cooling in winter enhance the thermal contrast between the continents and oceans, leading to a stronger monsoonal circulation.

In high latitudes, surface heat fluxes were different between C4 and R4 runs. In the R4 runs, both sensible and latent heat fluxes to the atmosphere were stronger from spring to early summer due to a higher conductivity of heat with ground ice present, and to the near-surface moisture abundance resulting in a warmer near-surface air. From autumn to winter, again because of a higher heat conductivity, downward sensible heat flux (i.e., from the atmosphere to the ground) was stronger in the R4 runs, leading to a cooler air.

Inclusion of the top organic soil (50 cm for taiga and 20 cm for tundra, shown as difference between solid and dashed lines in Fig. 4) further added to the annual amplitude of surface air temperature, but stabilized the annual change in the subsurface ground ice content. This is a reasonable response because the organic layers tend to thermodynamically decouple the atmosphere and the subsurface more efficiently.

Overestimation of the near-surface permafrost in the R4 runs likely resulted from prescribed organic layers being too thick in Central to Western Eurasia, Central to Southern Canada, and the Tibetan Plateau (Fig. 5). On the contrary, the near absence of near-surface permafrost in the C4 runs was primarily due to the warmer T2 in winter with the prescribed sea surface temperature experiments as compared to the coupled ocean runs (Saito et al., 2007). The cause of these differences needs to be investigated further.

Summary and Implications

A series of sensitivity experiments performed off- and on-line in the present study showed the importance of representing complexity for frozen ground simulations. Of crucial importance in the physical terrestrial schemes is physically-based hydrothermal parameterization; that is, consideration of ground ice and unfrozen water under the freezing point. It affects not only subsurface hydrothermal regimes, but also the exchange of energy and water between the soil and the atmosphere. For a physically consistent thermal simulation, a soil column of 20 m or deeper was found necessary. Implementation of these components should be seriously considered when impact of atmospheric warming on frozen ground and its feedback to the atmosphere are to be investigated.

Snow conditions and soil properties (such as top-layer organic soil) need more localized attention. Snow calculations still require a considerable amount of elaboration, on both the atmospheric (cloud formation, advection, radiation, atmospheric thermal and hydrological conditions, etc.), and terrestrial (snow microphysics, radiative properties, thermodynamics, and their regional differences) sides of the GCM. In the current version of the model, the organic soils are only prescribed and do not vary in the course of integrations. This may suffice for short-term simulations, for example, for 30 years. However, one of the anticipated targets in the next Assessment Report of the Intergovernmental Panel for Climate Change (IPCC), is to consider a timescale where the residence timescale of subsurface organic contents in the cold regions matter. For such longer-term simulations, in which 100 or 300 years are targeted, adaptation strategy will be needed to reflect biogeochemical changes in time.

Acknowledgments

This work was partly supported by (1) the Global Environment Research Fund (B-061) of the Ministry of the Environment, Japan, (2) Ministry of Education, Culture, Sports, Science and Technology (MEXT), Japan, and (3) the National Science Foundation under Agreement No. ARC-0327664, USA. All numerical integrations were run on the NEC SX-8 supercomputer at JAMSTEC. The author would like to thank the Permafrost Laboratory at the Geophysical Institute, University of Alaska Fairbanks, and also the Institute of Observational Research for Global Change, JAMSTEC, for providing observational data.

References

Alexeev, V.A., Nicolsky, D.J., Romanovsky, V.E. & Lawrence, D.M. 2007. An evaluation of deep soil configurations in the CLM3 for improved representation of permafrost. *Geophys. Res. Lett.* 34: L09502, doi:10.1029/2007GL029536.

Beringer, J., Lynch, A.H., Chapin, F.S., III, Mack, M. & Bonan, G.B. 2001. The representation of Arctic soils in the land surface model: the importance of mosses. *J. Climate* 14: 3324-3335.

Flerchinger, G.N. & Saxton, K.E. 1989. Simultaneous heat and water model of a freezing snow-residue-soil system I. Theory and development. *Trans. ASAE* 32: 565-571.

K-1 Model Developers. 2004. K-1 coupled GCM (MIROC) description. Tech. Rep. 1. H. Hasumi & S. Emori (eds.), Cent. for Clim. Syst. Res., Univ. of Tokyo, Kashiwa, Japan. 34 pp.

Molders, N. & Romanovsky, V.E. 2006. Long-term evaluation of the hydro-thermodynamic soil-vegetation scheme's frozen ground/permafrost component using observations at Barrow, Alaska. *J. Geophys. Res.* 111: D04105, doi:10.1029/ 2005JD005957.

Nicolsky, D.J., Romanovsky, V.E., Alexeev, V.A. & Lawrence, D.M. 2007. Improved modeling of permafrost dynamics in a GCM land-surface scheme. *Geophys. Res. Lett.* 34: L08501, doi:10.1029/ 2007GL029525.

Romanovsky, V.E. & Osterkamp, T.E. 2000. Effects of unfrozen water on heat and mass transport processes in the active layer and permafrost. *Permafrost Periglacial Processes* 11: 219-239.

Saito, K., Kimoto, M., Zhang, T.J., Takata, K. & Emori, S. 2007. Evaluating a high-resolution climate model: Simulated hydrothermal regimes in frozen ground regions and their change under the global warming scenario. *J. Geophys. Res.* 112: F02S11, doi:10.1029/ 2006JF000577.

Saito, K. 2007. Cold-region subsurface hydro-thermal sensitivity of physical land scheme in global climate model: idealized off-line evaluation. *Geophys. Res. Lett.* In preparation.

Takata, K. 2002. Sensitivity of land surface processes to frozen soil permeability and surface water storage. *Hydrol. Processes* 16: 2155-2172.

Takata, K. & Kimoto, M. 2000. A numerical study on the impact of soil freezing on the continental-scale seasonal cycle. *J. Meteorol. Soc. Jpn*. 78: 199-221.

Takata, K., Emori, S. & Watanabe, T. 2003. Development of the minimal advanced treatments of surface interaction and runoff. *Global Planet. Change* 38: 209-222.

Yi, S., Woo, M.K. &Arain, M.A. 2007. Impacts of peat and vegetation on permafrost degradation under climate warming. *Geophys. Res. Lett.* 34: L16504, doi:10.1029/2007GL030550.

Zhang, T., Barry, R.G., Knowles, K., Ling, F. & Armstrong, R.L. 2003. Distribution of seasonally and perennially frozen ground in the Northern Hemisphere, in *Proceedings of the 8th International Conference on Permafrost, 21–25 July, 2003, Zurich, Switzerland*, vol. 2, M. Phillips, S.M. Springman & L.U. Arenson, (eds.), Brookfield, VT: A.A. Balkema, 1289-1294.

Portable Shallow Drilling for Frozen Coarse-Grained Material

Tohru Saito
International Arctic Research Center, University of Alaska Fairbanks
Kenji Yoshikawa
Water and Environmental Research Center, University of Alaska Fairbanks

Abstract

We are drilling boreholes for a permafrost outreach program that involves schools in arctic regions. The purpose of the project is to establish permafrost-monitoring stations at schools and have students and teachers participate in gathering data. We drill a 6 m deep borehole for the monitoring stations to measure ground temperatures. There are more than 50 sites established, and many of the schools are located in remote villages in Alaska and Canada. This created a great opportunity and necessity to develop a portable, lightweight, small-diameter drill system. However, permafrost conditions and local geology vary greatly. A portable drill system is strongly affected by the grain size of the frozen materials. The design for the auger and coring bits (mechanical properties) for fine-grained, frozen soils are already well developed. However, frozen gravel, boulders, and glacial sediments are extremely difficult to drill, even when using heavier track-mounted hydraulic drill systems. In our outreach project, we tried to develop a method of drilling through frozen gravel using a portable drill system. This study presents our experiments and an introduction to different techniques for a portable drill system.

Keywords: auger; frozen gravel; percussion drill; portable drill; rotary percussion system.

Introduction

Portable drilling systems were probably developed as percussion systems to find shallow groundwater. Sample percussion systems were established and widely used in Japan as 'Kazusa-hori' in the early 18th century. After the industrial revolution, rotary-type drilling systems became more popular than the traditional percussion systems. Today, there are many more different types of drill systems widely available. Table 1 lists the classification of various drilling systems.

Drilling systems should meet the following conditions to be useful for the permafrost outreach program:

1. Lightweight: All systems should be compact and light enough to carry on a small airplane, helicopter, snowmobile, and small boat to reach remote villages.
2. Portable: The operation should only require one or two persons to start and complete all work to establish the monitoring station.
3. Small diameter hole: The hole should be as small as possible to minimize site disturbance, and the borehole only needs to be large enough to install a 1-inch (25 mm) PVC casing.
4. Versatile: The drill should be able to penetrate different types of frozen ground (materials). Most sites consist of widely different types of sacrificial geology. It is important to be able to adapt to any kind of ground condition to successfully drill at each school.

Drilling techniques for fine-grained soils, such as frozen silt and sand, are well researched and developed, especially by the US Army Corps of Engineers Cold Regions Research and Engineering Laboratory (CRREL) (e.g., Mellor 1976, Lawson & Brockett 1980, Sellmann & Brockett 1986, 1988, Calmels et al. 2005). Sellmann & Mellor (1986) summarized extraordinary work on drill-bit design for frozen fine-grained soils. They concluded that for best performance, the drill bits should (1) stay sharp as long as possible, (2) resist damage from impact with any coarse-grained material, and (3) be large enough to allow penetration at the maximum feasible design rates. Lack of adequate clearance angle between bits and flute is a common problem.

This study focuses on attributes of a portable drilling system for frozen, coarse-grained materials, such as frozen gravel, because this material is one of the most difficult materials to drill and is very common around the study sites. We also need to be able to drill boreholes through these materials in many remote villages.

Table 1. Popular drilling systems used today. Experiments on prototype portable drilling systems are indicated.

type	system	in this study
percussion	rope drill	no
	rod drill	yes
	hammer drill	yes
	down-hole drill (in line drill)	yes
rotary	spindle drill	yes
	rotary table drill	no
	drive head drill	yes
	power swivel drill	yes
	bit rotation (turbo drill, dyne drill, electro drill)	no
other	earth auger	yes
	push casing	yes

Figure 1. Hot water jet system employed for old borehole (left) and prototype lightweight compact disassembled rotary drill with air swivel (right).

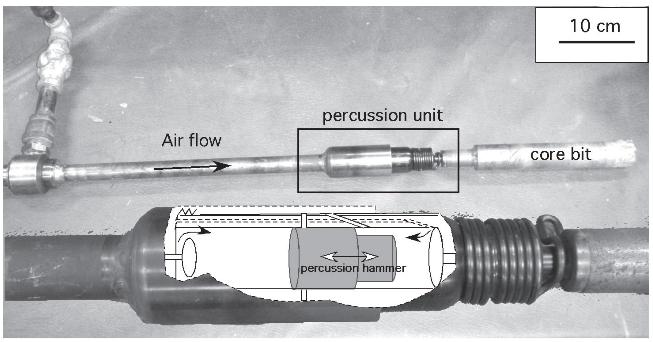

Figure 2. Prototype down-hole drill unit (in-line percussion drill)

Methods

Drilling system
Water jet drill

Water jet (hot water jet) systems (Fig. 1) are widely used for glaciological investigations. This method is definitely effective for boreholes on glaciers, sea ice, and ice rich permafrost. We used a Honda 5HP pressure jet pump with a custom-made nozzle and also tested a hot water jet unit from Kovacs Enterprise Ltd.

Jackhammer

A jackhammer is a powerful tool to break hard, solid material such as rock or ice, but limited drill depth is a weak point of this tool. Usually jackhammers can only dig 1–3 m or less. However, we used a gas-powered Swedish rotation jackhammer (Pionjar 120) that could drill a hole 6 m deep to bedrock, even through granite. The jackhammer was capable of producing two actions: percussion and rotation. By design, percussion is the primary action and rotation is the secondary action. Problems occur when the ground material melts from the drilling. The borehole becomes wet from the thawing silt, and the rotating driving shaft starts to stick to the mud and eventually stops rotating. The wet silty material and melt water generated by the action also absorb the percussion power of the jackhammer. As a result, jackhammers work wonderfully in dry bedrock but not in frozen silty gravel.

Figure 3. Portable hydraulic spindle (rotary) drill with air swivel. This is lightweight unit compared with track rig machine, but it is still heavy (more than 100 kg) to carry around.

Down-hole drill (in-line percussion drill)

It is generally known that shock and vibration action is very efficient for gravel or bedrock drilling to separate each grain (Borisovich 1990). We tried to employ this action in an adaptation with our portable drilling system. We modified the in-line shock actions using an air hammer tool (Aircoworld air hammer: bore diameter 19.05 mm, 4500 blow per minute (RPM), average air consumption 143 cubic meter per minute) (Fig. 2). This unit has about 100 g of weight moving up and down in the cylinder 4500 times per minute controlled by pressurized air. Air is supplied by the air compressor through the ¾-inch steel rod.

Rotary drill and earth auger

Both rotary drills and earth augers use rotation action for drilling. We used three different types of rotary drills: (1) Electric drills are easiest to use and work well in cold temperatures. (2) Mechanical (gasoline powered?) drills (Fig. 1) are probably the most commonly used portable drills, because they are relatively lightweight and strong, but they can be hard to start in colder temperatures. (3) Hydraulic drills are best for deeper boreholes. They are easy to handle and strong, which is why most commercial drillers use this method. Hydraulic systems, however, require many different heavy components that prevent them from converting into a portable system (Fig. 3). Also the hydraulic fluid needs to be kept warm during operation.

Percussion drill

The electric percussion/rotation drill is one of the best portable drill systems. We tried the heavy-duty, electric percussion drill to see if we could drill in permafrost (Fig. 4).

Figure 4. Electric percussion drill with water swivel. This hammer drill has 14A/120V power with 120–250 RPM rotation with impact (energy: 13.3 ft/lb)

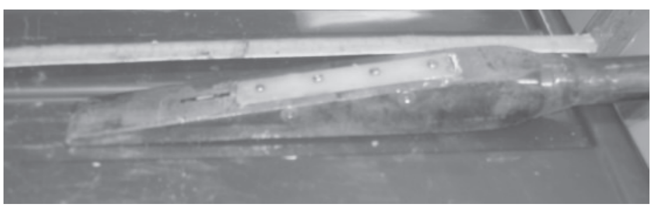

Figure 5. Prototype percussion drill bit with thermistor and electric resistivity contact points (Wenner configuration).

Drill bits

Drill bits are one of the most important components of drilling. We tested many different bits for this experiment. Auger bits with a rotating system are faster and easier to drill. However, this is difficult in a gravel layer. In general, core bits are used for core sampling but can also be used for drilling in gravel layers. We used several different shapes of core bits with carbide or diamond chips.

Drill bit experiment

The drill bit comparison experiment was carried out in an outdoor laboratory using a controlled frozen soil medium, comparing the drill speed in fine-grained soil and coarse-grained material. Auger bits and drills were tested on artificially frozen blocks of frozen ground about 50 cm x 50 cm and 30 cm deep. Time was recorded every 10 cm to compare the speed of the drill with different drill bits.

Figure 6. 30 mm diameter core bit for gravel (negative rake angle) (on left) and for silt (positive rake angle) (on right).

Figure 7. Fifty mm-wide auger bit for multi-grained (no rake angle [left]) and for silt (positive rake angle [right]).

Results

In general, the in-line percussion method worked better than just using the rotational drill. Figure 8 shows results from the experiment with the rotational drill using the in-line percussion and without it, in fine and coarse-grained materials. This figure shows that the inline system works well for both (fine- and coarse-grained) materials. However, the benefit of the percussion action is clearer in coarse gravel. The in-line percussion drill system performs 2.2 times more efficiently than using a rotation drill alone (Fig. 8, open dots).

Using water/air is a great way to remove materials (chips) from the borehole and also keep the bit tip clean. The water/air swivel allows pressurized water or air to flow through the tips of the drill bit while the drill is rotating. The chips are then blown out of the borehole. The system requires a large air compressor (>100 CFM) or high-pressure water pump (2 GPM), and it worked great with our portable drill system. This drilling system, therefore, includes three major components when digging the ground: (1) rotation action, (2) high pressure forced water/air - pushing action to remove chips, (3) impact (percussion) action. The swivel effectively blows chips out of the borehole, but working with permafrost

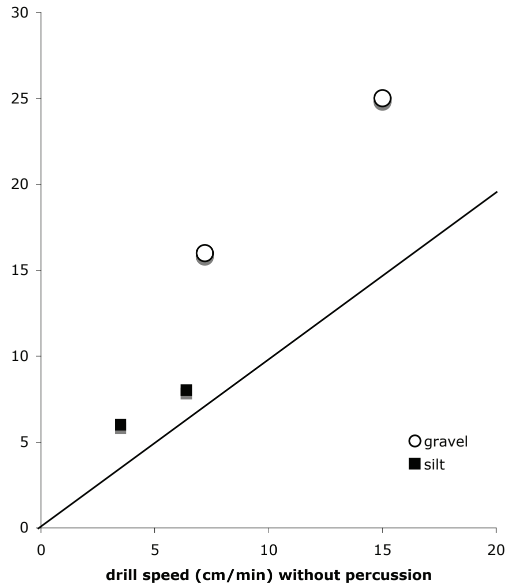

Figure 8. Drill speed performance with/without percussion action (inline) for frozen silt and gravel.

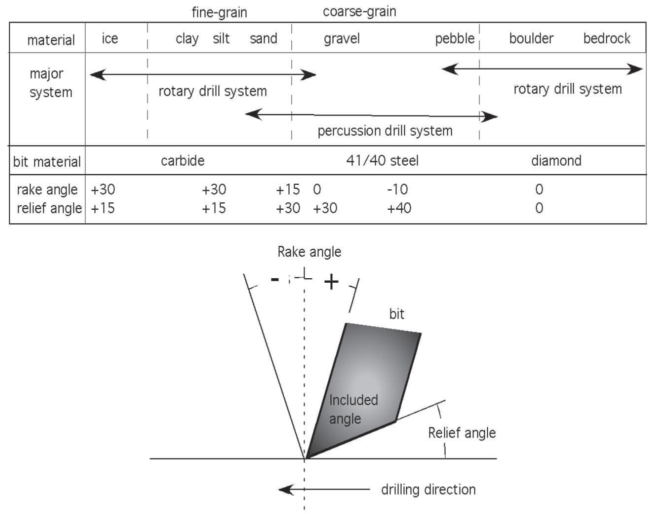

Figure 9. Ideal main drill system and bit properties of portable drill system for different frozen materials. Rake and relief angles for ice and fine-grained soil is after Sellmann & Mellor (1986). The rake and relief angle is the angle between the surface of the permafrost to the carbide bit. The relief angle is to prevent the land from rubbing on the surface of the work being cut.

we would like to keep the study site frozen while we drill. Therefore, a cooling system is needed for the water or air sent through the swivel. If supercooled water or chilled air is used, the system will cause minimal disturbance.

In general, physical theory for effective drilling depends on three major functions: rotation of the bit, down loading, and chip removal. When one of these functions does not work properly, drill speed slows down significantly or even stops. Using the portable drill system in a graveled area, the depth of the cutting blade is significantly smaller than the grain size of the gravel restricting rotation. Also, removing the chips requires water, air, or auger flights to establish a large enough flow pathway. The velocity of the flow pathway is related to the grain size of the chips. Maximum grain size (G:mm) is calculated by the following equation (Mori 1981).

$$G = 0.0055v^2\, G_w/(G_s - G_w)$$

where v = velocity(cm/sec), G_s = density of grain, and G_w = density of water. Using this equation, 6–10 mm diameter grains require 40–60 cm/sec of velocity using water. Although this is not an impossible pressure to create, it makes it unlikely to easily convert a portable drill system. Drilling through coarse-grained material clearly exceeds the limit of the physical theory for drilling, and our experience suggests the following conclusions for drilling frozen, coarse materials:

1. Rotation systems do not work properly.
2. Percussion systems aid in removing grain particles
3. Pyramid shaped bits (zero apparent rake) (Fig. 9) work well for removing pebbles, especially when very fine grain material content is present in the matrix.
4. Bentnite works well to keep the wall stable.
5. Diamond core bits work great to drill through any kind of gravel, rock, and boulder, but take longer and generate heat.

Figure 10. Human-powered traditional percussion system using steel rod.

Table 2 shows a summary of our experiments. Percussion action helps to separate each grain and remove the gravel

Table 2. Summary of the portable drilling operation for fine- and coarse-grained frozen materials.

type	system	for fine-grained materials	for coarse-grained materials	benefit	weakness	remarks
percussion	jackhammer	Fair	fair	portable	need weight	Pionjar 120
	jackhammer with rotation	Fair	good	portable	requires 2 people	Pionjar 120
	rod drill	Fair	good	simple	heavy depend on weight of hammer	handmade
	hammer drill	Fair	fair	very portable	weak action	Bosch 14A
	down-hole drill (in-line drill)	Fair	good	efficient	needs air compressor	modified from air hammer
rotary	spindle drill	Good	fair	strong hydraulic system	heavy	hydraulic system
	spindle drill with air	Excellent	good	strong hydraulic system	heavy, need air compressor >100CFM	hydraulic system
	spindle drill with water	Excellent	good	strong hydraulic system	heavy, need water pump and water source	hydraulic system
	drive head drill	Good	fair	portable	weaker action	
	drive head drill with air	Excellent	good	portable	weaker action	
	drive head drill with water	Excellent	good	portable	weaker action	
other	earth auger	Good	fair	portable	only fine grained materials	little beaver
	push casing	Fair	bad	strong hydraulic system	unlike success???	hydraulic system
	water jet	Good	fair	portable	needs water pump and water source	5HP Honda

from the frozen matrix allowing it to move. However, the chips (grain) could not be removed from the borehole because of the grain size. A smaller diameter driving-rod is an essential parameter to successfully drill through coarse-grained material.

Percussion power simply depends on the weight of the hammer (Borisovich 1990). Heavier weights on the driving rod generate greater percussion energy. However, the reality of drilling in remote villages limits the size of a human-powered percussion system to about 30 kg (Fig. 10). Using a smaller diameter rod (12 mm) instead of using heavy weights for percussion can reduce weight and still allow effective drilling. Because of the smaller diameter, the speed of drilling was increased, and the borehole is small enough that the grainy materials can be pushed to the inside wall of the borehole.

Conclusion

The rotating drill is highly effective for fine-grained materials and even in coarse-grained material if the pore space is filled with silt or clay. The percussion system creates an effective action for drilling in coarse grain materials. This is illustrated in Figure 9. Heavier weights on the driving rod generate better percussion energy. However, the reality of drilling in remote villages limits the transport of heavier weights. Using a smaller diameter rod for percussion reduces weight, yet allows effective drilling.

The inline percussion (down-the-hole) drill improved drilling performance with the combination of percussion action and bit rotation. The combined actions are important systems for drilling through the coarse grain permafrost. We still need to design and build an inlinein-line percussion system for heavy-duty use and stronger impact energy in the future.

Acknowledgments

This project was funded by the National Science Foundation EPSCoR program (#0346770, #0701898) and the State of Alaska. We would like to thank the UAF Mechanical Engineering machine shop (Ned Manning and Eric Johansen) for building the prototype in-line percussion system, and Jon Holmgren and Sam Skidmore for developing many prototype bits, and VECO Polar Resources for logistical support.

References

Borisovich, B. 1990. *Drilling in the Permafrost.* pPublished for the Office of Polar Programs, New Delhi: National Science Foundation by Amerind Pub. Co., 318 pp.

Calmels, F., Gagnon, O. & Allard, M. 2005. A portable earth-drill system for permafrost studies. *Permafrost and Periglacial Processes* 16(3): 311-315. DOI: 10.1002/ppp.52

Lawson, D. & Brockett, B. 1980. *Drilling and Coring of Frozen Ground in Northern Alaska.* US Army Cold Regions Research and Engineering Laboratory, CRREL Special Report 80-12, 14 pp.

Mellor, M. 1976. *Mechanics of Cutting and Boring. Part II: Kinematics of Axial Rotation Machines.* US Army Cold Regions Research and Engineering Laboratory, CRREL Report 77-7, 85 pp.

Mori, H. 1981. *Study on the properties of soils in the northern coast of Tokyo Bay using a self-boring pressuremeter.* Soils and Foundations, Japanese Society of Soil Mechanics and Foundation Engineering.

Sellmann, P.V. & Brockett, B. 1986. *Auger Bit for Frozen Fine-grained Soil.* US Army Cold Regions Research and Engineering Laboratory, CRREL Special Report 86-36.

Sellmann, P.V. & Brockett, B. 1988. *Evaluation of Several Auger Bits in Frozen Fine-Grained Soils, Asphalt, and Concrete.* US Army Cold Regions Research and Engineering Laboratory, CRREL Special Report 88-8, 10 pp.

Sellmann, P.V. & Mellor, M. 1986. *Drill Bits for Frozen Fine-gGrained Soil.* US Army Cold Regions Research and Engineering Laboratory, CRREL Special Report, 86-27.

Detection and Enrichment of Ammonia Oxidizers from Permafrost Soils of Siberia

Tina Sanders, Claudia Fiencke
Institute of Soil Science, University of Hamburg, Germany
Eva Spieck
Biocenter Klein Flottbek, University of Hamburg, Germany
Eva-Maria Pfeiffer
Institute of Soil Science, University of Hamburg, Germany

Abstract

Permafrost soils cover about a quarter of the Earth's land surface. The soils are continuously frozen throughout the year, and only the active layer thaws near the surface during the short vegetation period. Microbial life of the polygonal Siberian tundra is influenced by extreme gradients of temperature and moisture. During nitrification, ammonia is oxidized by chemolithoautotrophic nitrifiers, the ammonia (AOB) and nitrite oxidizers (NOB), in two steps via nitrite to nitrate. Cell numbers of nitrifiers and potential activities of AOB were determined in geochemical characterized soil samples of the active layers. Results obtained by MPN-counts showed clearly that higher cell numbers of AOB and activities were found in the upper part of the dryer polygon rims compared to the waterlogged polygon centres. Our results reveal the existence of AOB in permafrost soil, which are well-adapted to the extreme environment.

Keywords: ammonia-oxidizing bacteria; Lena Delta; nitrifiers; nitrification; permafrost; Siberia.

Introduction

Since artic wetland soils are the most important natural source of the climate-relevant trace gas methane, many investigations focused on the microbial C-cycle of permafrost soils. But despite a close connection between C-cycle and N-cycle, the N-cycle is mostly unexplored.

Nitrogen as well as carbon cycling in arctic ecosystems is dominated by physical and biogeochemical controls which are unique to the generally cold-dominated environment. Drastic seasonal fluctuations in temperature, a short growing season, cold soil temperature, and the occurrence of permafrost are some of the obvious physical controls on nitrogen cycling and biological activity. Most of the nitrogen accumulates in the organic substance in response to low soil temperatures, excessive soil moisture, and low soil oxygen concentration (Gersper et al. 1980, Marion & Black 1987, Nadelhoffer et al. 1991, Schimel et al. 1996). Standing crops in tundra vegetation store about two times more nitrogen than temperate grasslands (Van Cleve & Alexander 1981). But through the low N-mineralization rates and lack of N-input by N-fixation and N-pollution, the soils are nitrogen deficient and rely to a large extent on internal recycling (McCown 1978).

N-cycling in the soil is crucial for growth of plants and microorganisms. Imbalances in N-cycling are due to nitrate leaching, nitrogen oxide release, and increase the methane emission (Adamsen & King 1993, Carini et al. 2003). Most of the N-transformations were catalyzed by microorganisms (Fig. 1, Fiencke et al. 2005). Nitrification, the microbiological oxidation of ammonia to nitrate via nitrite, occupies a central position within the terrestrial nitrogen cycle. Aerobic chemolithoautotrophic ammonia (AOB) and nitrite oxidizing (NOB) bacteria represent the most important group of nitrifying bacteria (Fiencke et al. 2005). As a result of nitrate and acid formation, the nitrification process has various direct and indirect implications of soil systems. It increases the loss of soil nitrogen due to leaching of nitrate and volatilization of nitrogen gases directly or by denitrification and therefore, influences the nitrogen supply to plants.

Beside ammonia oxidizing Proteobacteria, it has been mentioned that Archaea (AOA) participate in ammonia oxidation and have been found in different soils and habitats. (Nicol & Schleper 2006, Leininger et al 2006). Some representative of the AOA were enriched and described (Könneke et al. 2005, Hatzenpichler et al. 2008). In some habitats, more archaeal than bacterial genes were detected. (Leininger et al. 2006), but at this moment it is not clear which group of microorganisms dominate in the N-cycle.

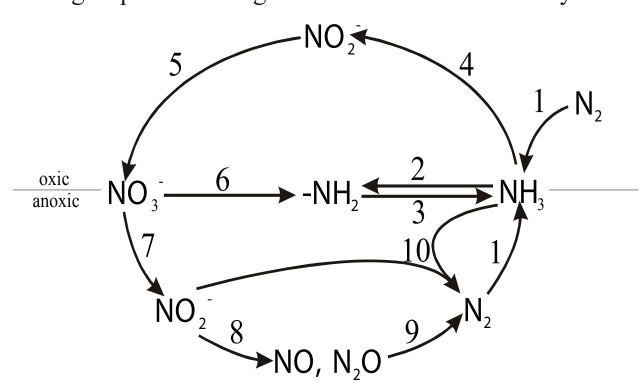

Figure 1. Nitrogen cycle. (1) dinitrogen (N_2) fixation, (2) assimilation of ammonia (NH_3) to amino group ($-NH_2$) of protein, (3) ammonification, (4) ammonia oxidation, (5) nitrite (NO_2^-) oxidation, (6) assimilation of nitrate (NO_3^-), (7, 8, 9) denitrification via nitrite, nitric oxide (NO) and nitrous oxide (N_2O), (10) anaerobic ammonia oxidation.

Nitrifying bacteria are found in the upper layer of soils, like the rhizosphere, where organic matter is mineralized, and ammonia and oxygen are present. The slow growth rates and difficulties in recovering pure cultures have hampered cultivation-dependent approaches to investigating the number, community composition, and dynamics of nitrifiers in soil. The number and turnover rate is, therefore, determined by traditional methods like most-probable-number (MPN) technique and activity tests.

During the *Expedition to the Lena Delta* in Summer 2005 and 2007, microbial nitrification was investigated by field experiments. Furthermore, soil and gas samples were taken for further ecological, molecular, and soil analyses.

Investigation Area

The study site is located on Samoylov Island (72°22′N, 126°28′È) in the southern part of the Lena Delta on the north coast of Siberia (Fig. 2).

The climate is true-arctic, continental, and characterized by low annual temperatures (-13,6°C) and low annual precipitation (319 mm) (ROSHYDROMET 2007). The main soil unit of Island Samoylov is covered mainly by the soil-plant-complex consisting of Glacic Aquiturbels and Typic Historthels (Fig. 3b).

The Typic Historthels are Gelisols that have in 30% or more of the pedon more than 40% by volume, organic materials from the surface to depth of 50 cm (Soil Survey Staff 2006). They formed in the depressed centers of low-centered ice wedge polygons characterized by water saturation to the soil surface and organic matter accumulation due to anaerobic condition. The Glacic Aquiturbels formed at the elevated borders of the polygons, are characterized by prolonged inundation, but with less organic matter accumulation and pronounced cryoturbation.

Materials and Methods

The investigations of nitrification were carried out on Samoylov in August 2005 and July 2007. Soil samples were taken from the active layer of two low-centered polygons, at the polygon rim and polygon center, at 3 depths (0–5, 5–15, 15–25 cm) (Fig. 3). Samples were analyzed freshly on-site and after transportation (frozen or unfrozen at about 6°C) lasting for two months to our institute in Hamburg, Germany.

On-site and after transportation, nitrification was determined by enrichment and ammonia oxidizing activity tests. Therefore, ammonia (AOB) and nitrite oxidizing bacteria (NOB) were enriched for further quantification by MPN-technique in media with 1 mM ammonium and 0.3 mM nitrite for three months at about 6°C. The ammonia oxidizing activities were measured at different temperatures (6°C, 12°C, 17°C, 20°C, 28°C, 37°C) and 0.75 mM ammonium sulfate using ISO/DIN 15685:2001 standard tests. The activities were measured by ammonia consumption and nitrite formation up to a period of 6 weeks in the field and eight weeks in the laboratory. Samples for the test were taken twice a week.

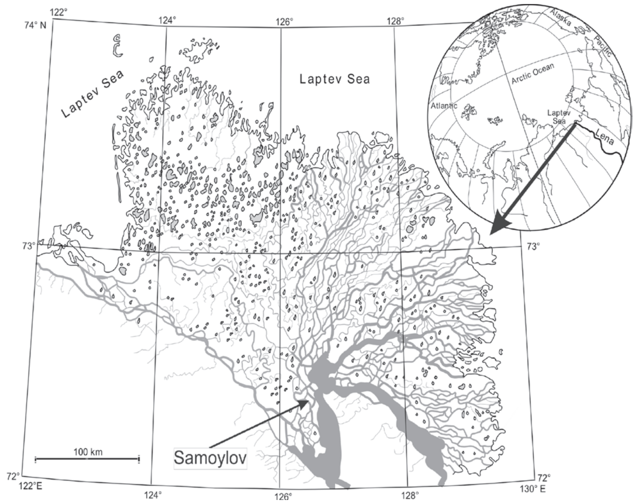

Figure 2. Map of the Lena Delta with location of Samoylov Island.

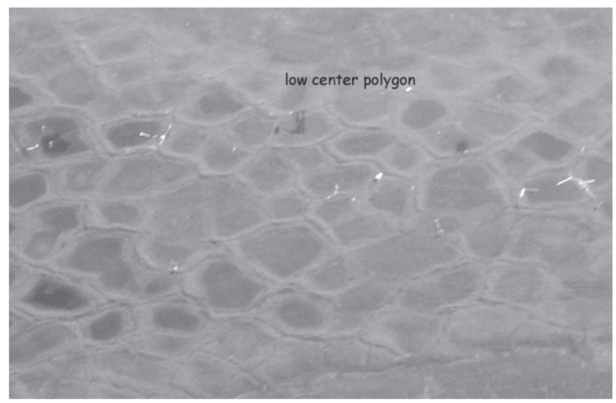

Figure 3a. Low-center polygon landscape on the island Samoylov.

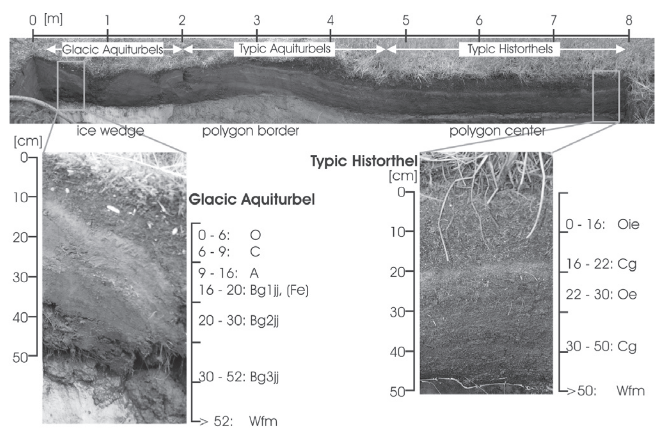

Figure 3b. Soil cross-section of a low-centered polygon and investigated soil-profiles (Classification U.S. Soil Taxonomy).

Chemical characterization of soils was done after transportation. For pH determination, soil suspensions with dest. water were measured after an equilibration of one hour. C/N was analyzed after oven drying (105°C) and grinding by Vario MAX element analysator. For ammonium, nitrite, and nitrate detection, soil samples were extracted with 0.0125 M $CaCl_2$ and were analyzed by spectral photometer tests. Methane was measured in situ by gas chromatography.

Results and Discussion

Chemical parameters

The chemical characterization of the soil samples shows that ammonium accumulates in the moist, anaerobic, and methane-containing Typic Historthel of the polygon center, and only low concentrations of nitrite and nitrate were found (Fig. 4a). In contrast to the moist polygon center, in the Glacic Aquiturbel of the dryer polygon rim, high nitrate concentrations were found in the oxic top soil (Fig. 4b).

Ammonia oxidation

Ammonia oxidation was measured by MPN-counts and ammonia oxidizing activity tests. Highest cell numbers of nitrifiers (AOB and NOB) were found at depths of 5–15 cm in the Glacic Aquiturbel of the polygon rim ($2 \cdot 10^5$ cells/g dw, data not shown).

During the field survey in August 2005 and July 2007, all soil samples were tested for ammonia oxidation activity. Additionally, all soil samples were tested again after two months of transportation.

In the field experiments of 2005 and 2007, ammonia-oxidizing activity was only detected in soil samples in depths 5–15 cm of the Glacic Aquiturbel of the polygon rim. In July 2007, activities of 22,56 ng N-Nitrit per g dry weight and hours were found.

After two months of unfrozen transportation, the same samples were analyzed again. After that time, the activities in the 5–15cm polygon rim sample increased, and few activities were found in the surface sample (0–5 cm) of the polygon center (Fig 5a). In soil samples which were taken one and a half months later (August 2007), ammonia oxidizing activity was also detected in upper layers of the polygon rim and center (Fig. 5b). Higher activities in the upper parts of the center in August might be due to lower water content (July 412 %, August 173%) due to decrease of water level in the polygon center.

The results indicate that small-scale differences in soil hydrology have significant impact on the N-cycle. Better drained, reduced acidity and methane concentration of oxic soil samples of the polygon rim favor nitrification, and therefore, lead to the accumulation of nitrate. Nitrate was possibly not degraded in dry sites, owing to lack of denitrification in these more aerated micro-environments. Instead, in the moist polygon center, nitrification was inhibited by oxygen deficiency, and therefore the ammonium formed by mineralization accumulated. In the moist anoxic environment, nitrate was possibly quickly reduced by denitrification.

Furthermore, the activity of the most active soil sample was analyzed at different temperatures. As shown in Table 1, activities depend on transportation of soil samples and temperature used for activity tests. Generally, higher activities were found in the soil samples after an unfrozen

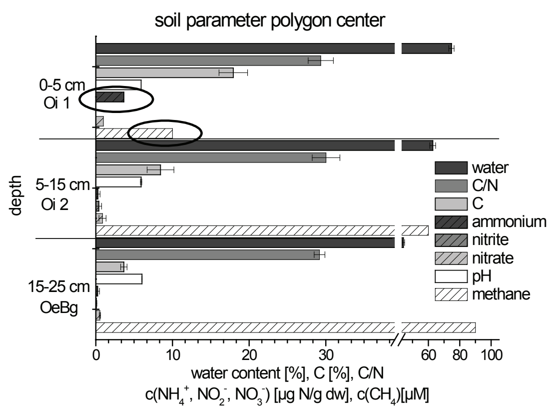

Figure 4a. Chemical soil parameters of the Typic Historthel of the polygon center. Soil samples were taken in August 2005. Error bars represents 4 parallels.

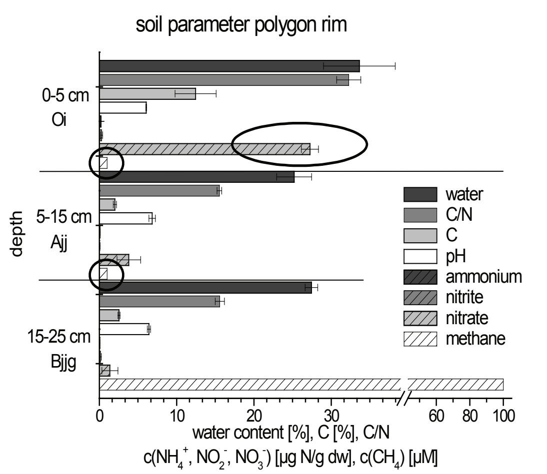

Figure 4b. Chemical soil parameters of the Glacic Aquiturbel of the polygon rim. Soil samples were taken in August 2005. Error bars represents 4 parallels.

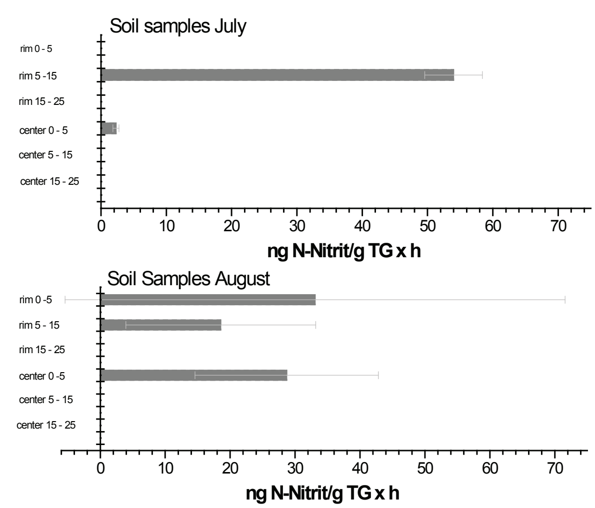

Figure 5. Ammonia-oxidizing activities measured by formation of nitrite in Typic Historthel of the polygon center and Glacic Aquiturbel of the polygon rim. Samples were taken in July (5a) and August (5b) 2007 and activities were measured over a period of 8 weeks at 6 °C. Error bars represent 4 parallels.

Table 1. Activity of the ammonia-oxidizing bacteria at the polygon rim of the depth of 5 to 15 cm at temperatures between 6°C and 37°C. Frozen and unfrozen transported samples were analyzed after two months of transportation.

Temperature [°C]	Ammonia-oxidizing activity [ng N-nitrite/g dw·h]	
	unfrozen	frozen
6	23.4	0.6
12	6.6	1.3
20	60.5	12.0
28	9.1	2.5
37	0.2	0.2

transport of the samples from the field to the laboratory. In frozen transported soil samples, ammonia oxidizing activity is obviously lower. Highest activity was found at tests conducted at 20°C, second highest at 6°C. Therefore, two peaks of activity were found independently of frozen or unfrozen transportation. An explanation for the two peaks could be that two different ammonia-oxidizing communities got different temperature optima.

Summary

The results indicate that small-scale differences in soil hydrology of the polygonal tundra have significant impact on the N-cycle. In the dryer, aerobic Glacic Aquiturbel of the polygon rim, high nitrate and low inhibitory methane concentrations correlated with high cell numbers and activities of ammonia oxidizing bacteria. In contrast, in the moist, anaerobic, methane-containing Typic Historthel polygon center, lower cell numbers and activities of ammonia-oxidizing bacteria were detected. The ammonia-oxidizing activities depended on the temperature. Highest activities were found at 6 and 20°C.

Conclusions

This paper show preliminary results on one special part of the nitrogen cycle. Further investigation will consider unstudied processes and fluxes of the N-cycle like mineralization and denitrification. It should also be clarified which group of ammonia-oxidizing organisms, Proteobacteria or Archaea, take part in the activities in that environment. First results may help to understand how predicted climate changes influence the N-cycle in soils of the polygonal tundra.

Acknowledgments

We thank the Russian–German parties of Expedition Lena 2007 for the pleasant teamwork in the field. Special thanks go to the staff of the Alfred Wegener Institute, Research Unit Potsdam for making the expedition to the Lena Delta possible. Thanks, also, to the University of Hamburg and the Institute of Soil Science for advice in the planning of the work.

References

Adamsen, A.P.S. & King, G.M. 1993. Methane consumption in temperate and subarctic forest soils: rates, vertical zonation, and responses to water and nitrogen. *Appl. Env. Microbiol.* 59: 485-490.

Carini, S.A., Orcutt, B.N. & Joye, S.B. 2003. Interactions between methane oxidation and nitrification in coastal sediments. *Geomicrobiology Journal* 20: 355-374.

Fiencke, C., Spieck, E. & Bock, E. 2005. Nitrifying bacteria. In: D. Werner & W. E. Newton (eds.), *Nitrogen Fixation in Agriculture, Forestry, Ecology, and the Environment.* Springer, The Netherlands, Dordrecht. 12: 255-276.

Gersper, P.L., Alexander, V & Barkley, S.A. 1980. The soils and their nutrients. In: J. Brown, P.C. Miller, L.L. Tieszen, F.L. Bunnell (eds.), *An Arctic Ecosystem. The coastal Tundra at Barrow, Alaska.* Stoudsburg: Dowden, Hutchinson & Ross, 219-254.

Hatzenpichler, R., Lebedeva, E.V., Spieck, E., Stoecker, K., Richter, A., Daims, H. & Wagner, M. 2008. A moderately thermopholic ammonia-oxidizing crenarchaeote from a hot spring. *PNAS* 105(6): 2134-2139.

Könneke, M., Bernhard, A. E., de la Torre, J. R., Walker. C. B., Waterbury, J. B. & Stahl, D. A. 2005. Isolation of an autotrophic ammonia-oxidizing marine archaeon. *Nature 437*: 543-546.

Leiniger, S., Urich, T., Schloter. M., Schwark, L., Qi, J., Nicol, G.W., Prosser, J.I., Schuster, S.C. & Schleper, C. 2006. Archaea predominate among ammonia-oxidizing prokaryotes in soils. *Nature Letters 442: 806- 809.*

Marion, G.M.,& C.H. Black. 1987. The effect of time and temperature on nitrogen mineralization in Arctic tundra soils. *Soil Science Society of America Journal* 51: 1501-1508.

McCown, B.H. 1978. The interactions of organic nutrients, soil nitrogen and soil temperature and plant growth and survival in the arctic. In: L.L. Tieszen (ed.), *Vegetation and production ecology of an Alaskan arctic tundra*. New York: Springer, 435-456.

Nadelhoffer, K.J., Giblin, A.E., Shaver, G.R., and G.R. Laudre. 1991. Effects of temperature and substrate quality on element mineralization in six arctic soils. *Ecology* 72: 242-253.

Nicol, G.W. & Schleper, C. 2006. Ammonia-oxidizing Crenarchaeota: important players in the nitrogen cycle? *Trends in Microbiology 14*: 207-212.

ROSHYDROMET.2007.10.10. Russian Federal Service for Hydrometeorology and Environmental Monitoring. Weather Information for Tiksi. http.//www.worldweather.org/107/c01040.htm.

Schimel, J.P., Kielland, K & Chapin, F.S. 1996. Nutrient availability and uptake by tundra plants. In: J.F. Reynolds & J.D. Tenhunen (eds.), *Landscape function and disturbance in arctic tundra. Ecological Studies 120.* Berlin: Springer, 203-221.

Soil Survey Staff. 2006. Keys to Soil Taxonomy. 10th ed., Washington, D.C.: United States Department of Agriculture 6 Natural Resources Conservation Service, 332pp.

Van Cleve, K., & Alexander, V. 1981. Nitrogen cycling in tundra and boreal ecosystems. In: E.E. Clark, & T. Rosswall (eds.), *Terrestrial nitrogen cycles. Ecol. Bull. Stockholm.* 33: 375-404.

Bending Characteristics of Pipe-in-Pipe Systems

Motohiro Sato
Graduate School of Engineering, Hokkaido University
Kenta Shimazaki
Graduate School of Engineering, Hokkaido University
Shunji Kanie
Graduate School of Engineering, Hokkaido University
Satoshi Akagawa
Graduate School of Engineering, Hokkaido University
Takashi Mikami
Graduate School of Engineering, Hokkaido University

Abstract

Structural pipe-in-pipe cross sections have significant potential for application in oil and gas production systems because of their property that combines insulation performance with structural strength in an integrated way. By making use of such excellent structural properties, however, we consider that this pipe-in-pipe system can be also applicable to pipelines in cold or permafrost regions. In this case, bending characteristics become one of the most important factors for the structural design of the pipelines. The purpose of this research is to investigate the bending characteristics of such pipe-in-pipe systems analytically by considering the Brazier effect. Results are presented to show the variation of the degree of ovalization and the Brazier moment with the relative elastic modulus of the filler and pipe materials, the filler thickness, and the thicknesses of the inner and outer pipes.

Keywords: Brazier effect; pipe-in-pipe; pipeline; pure bending.

Introduction

Structural pipe-in-pipe cross sections have significant potential for application in oil and gas production systems because of their property that combines insulation performance with structural strength in an integrated way. Such cross sections comprise inner and outer thin walled pipes with the annulus between them fully filled by a selectable thick filler material to impart an appropriate combination of properties. The technology of the pipe-in-pipe system has developed in the field of offshore engineering. One of the authors investigated the elastic buckling behaviour of pipe-in-pipe cross sections under external hydrostatic pressure (Sato & Patel 2007). By making use of such excellent structural properties, however, we consider that this pipe-in-pipe system can be also applicable to pipelines in cold or permafrost regions, such as chilled gas pipeline systems installed under ground. In this case, bending rigidity or flexibility near the boundary between permafrost and non-permafrost areas become one of the most important factors for the structural design of the pipelines.

In pure bending, the cross sections of a hollow cylindrical pipe ovalize, and this reduce the flexural stiffness of the pipe as the curvature increases. This is known as *the Brazier effect* (Brazier 1927), and it is quite important to evaluate this effect accurately in order to understand the bending behaviour of the pipe-in-pipe system.

From this point of view, the purpose of this research is to investigate the bending characteristics of such pipe-in-pipe systems analytically by considering the Brazier effect. The *Brazier moment*, which is the maximum moment carrying capacity of the ovalized cross section, can be calculated by introducing the strain energy per unit length of the pipe in terms of the degree of ovalization for outer and inner pipe curvature. The total strain energy of the pipe-in-pipe system is the sum of the strain energy of the outer and inner pipes and the compliant core. It is also clear that the moment of inertia of the cross section is increased by the presence of the core compared with single wall pipes.

Results are presented to show the variation in degree of ovalization and the Brazier moment with the relative elastic modulus of the core and outer/inner pipes materials, the core thickness, and the thicknesses of the inner and outer pipes.

Analytical Model

Figure 1 shows the configuration of a perfectly cylindrical pipe-in-pipe cross section that is analyzed here. The pipe-in-pipe cross sections under consideration have an annulus fully filled with a material that provides continuous structural support to both the thin-walled outer and inner pipes with Young's modulus E_P and Poisson's ratio ν_P. The geometric variables are the thickness of the outer pipe, t_1, that of the inner pipe, t_2, the middle surface of the outer pipe, a_1, and that of the inner pipe, a_2. In the following formulation, the subscripts 1 and 2 correspond to the outer and inner pipes, respectively.

As shown in Figure 2(b), in pure bending the cross sections of a hollow circular cylindrical pipe-in-pipe ovalize and this reduces the flexural stiffness of the pipe as the curvature increases.

Formulation

Strain energy associated with ovalization of the core

The strain energy U_1 per unit length in the ovalized core is expressed as

$$U_1 = \frac{1}{2}\int_0^{2\pi}\int_{a_2}^{a_1}(\sigma_r\varepsilon_r + \sigma_\theta\varepsilon_\theta + \tau_{r\theta}\gamma_{r\theta})rdrd\theta \tag{1}$$

where σ_r, σ_θ, $\tau_{r\theta}$ and ε_r, ε_θ, $\varepsilon_{r\theta}$ are the core stresses and strains in the radial, circumferential, and shear directions, respectively. As shown in Figure 2(b), the radial and tangential displacement, u_i and v_i, respectively, of outer and inner pipes ovalized by ζ_i are (Calladine 1983)

$$u_i = a_i\varsigma_i\cos 2\theta = \delta_i\cos 2\theta \tag{2a}$$

$$v_i = -\frac{1}{2}a_i\varsigma_i\sin 2\theta = -\frac{1}{2}\delta_i\sin 2\theta \tag{2b}$$

The basic equation for the core is expressed by the stress function $\phi(r,\theta)$ in polar coordinates as (see Timoshenko & Goodier 1970)

$$\left(\frac{\partial^2}{\partial r^2} + \frac{1}{r}\frac{\partial}{\partial r} + \frac{1}{r^2}\frac{\partial^2}{\partial\theta^2}\right)^2\phi(r,\theta) = 0 \tag{3}$$

The normal stresses in the radial and circumferential directions σ_r, σ_θ and the shear stress $\tau_{r\theta}$ are determined from

$$\sigma_r = \frac{1}{r}\frac{\partial\phi(r,\theta)}{\partial r} + \frac{1}{r^2}\frac{\partial^2\phi(r,\theta)}{\partial\theta^2} \tag{4a}$$

$$\sigma_\theta = \frac{\partial^2\phi(r,\theta)}{\partial r^2} \tag{4b}$$

$$\tau_{r\theta} = -\frac{\partial}{\partial r}\left(\frac{1}{r}\frac{\partial\phi(r,\theta)}{\partial\theta}\right) \tag{4c}$$

In the problem considered here, the two displacement components for the core, the radial displacement $u(r,\theta)$ and the circumferential displacement $v(r,\theta)$, are assumed to have circumferentially periodic forms written as:

$$u(r,\theta) = u_C(r)\cos 2\theta \tag{5a}$$

$$v(r,\theta) = v_C(r)\sin 2\theta \tag{5b}$$

Therefore, $\phi(r,\theta)$ should be expressed as follows:

$$\phi(r,\theta) = f(r)\cos 2\theta \tag{6}$$

The general solutions of Equation 3 are as follows:

$$f(r) = Ar^{-2} + B + Cr^4 + Dr^2 \tag{7}$$

where *A*, *B*, *C*, *D* are arbitrary constants. In this case, the corresponding stress components are

$$\sigma_r = -(6Ar^{-4} + 4Br^{-2} + 2D)\cos 2\theta \tag{8a}$$

$$\sigma_\theta = (6Ar^{-4} + 12Cr^2 + 2D)\cos 2\theta \tag{8b}$$

$$\tau_{r\theta} = (-6Ar^{-4} - 2Br^{-2} + 6Cr^2 + 2D)\sin 2\theta \tag{8c}$$

The strain components for the plane strain problem are derived by

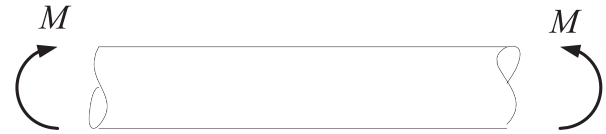

Figure 1. Pipe-in-pipe system in pure bending.

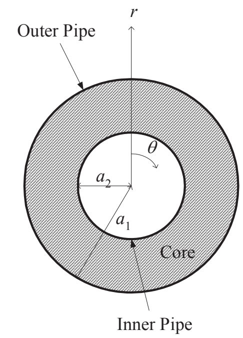

Figure 2. Pipe-in-pipe cross section.

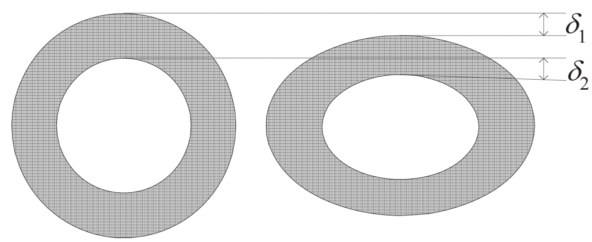

(a)Before bending (b) After bending

Figure 3. Ovalization for pipe-in-pipe cross sections. (The degree of ovalization is $\zeta_i = \delta_i / a_i$ (i = 1, 2).)

$$\begin{Bmatrix}\varepsilon_r\\ \varepsilon_\theta\\ \gamma_{r\theta}\end{Bmatrix} = \frac{1}{E_C}\begin{bmatrix}1-\nu_C^2 & -\nu_C(1+\nu_C) & 0\\ -\nu_C(1+\nu_C) & 1-\nu_C^2 & 0\\ 0 & 0 & 2(1+\nu_C)\end{bmatrix}\begin{Bmatrix}\sigma_r\\ \sigma_\theta\\ \tau_{r\theta}\end{Bmatrix} \tag{9}$$

The corresponding displacements in the radial and circumferential directions $u(r,\theta)$ and $v(r,\theta)$ can be obtained from Equations 8 and 9, and the following displacement-strain relationship is derived:

$$u(r,\theta) = \int\varepsilon_r dr = \frac{1+\nu_C}{E_C}\left\{\frac{2A}{r^3} + \frac{4B(1-\nu_C)}{r} - 4\nu_C Cr^3 - 2Dr\right\}\cos 2\theta + P \tag{10a}$$

$$v(r,\theta) = \int(r\varepsilon_\theta - u)d\theta = \frac{1+\nu_C}{E_C}\left\{\frac{2A}{r^3} + \frac{2B(2\nu_C-1)}{r} + 2C(3-2\nu_C)r^3 + 2Dr\right\}\sin 2\theta + Q \tag{10b}$$

where *P* and *Q* are constants of integrations. For the problem considered here, the outer and inner pipes are assumed to be perfectly bonded to the core. The middle surface outer pipe displacements (u_1, v_1) and inner pipe displacements (u_2, v_2) are taken to have circumferentially periodic forms written as:

$$u(a_i, \theta) = u_i \tag{11a}$$

$$v(a_i, \theta) = v_i \tag{11b}$$

From Equations 2, 10, and 11, we can obtain the constants A, B, C, D as functions of δ_1 and δ_2. This fact indicates that the strain energy associated with ovalization of the core (Eq. 1) can be expressed by the displacements of the outer and inner pipes. Substituting the constants in the stresses and strains, we obtain the strain energy which is the function of δ_1 and δ_2.

In addition to this, we find the strain energy of the outer and inner ovalized pipes is (Calladine 1983)

$$U_2 = \sum_{i=1}^{2} \frac{3}{8} \pi E_P \frac{t_i^3}{a_i \sqrt{1-\nu_P^2}} \zeta_i \tag{12}$$

Strain energy associated with bending of the pipe-in-pipe system

The strain energy per unit length to bend a pipe of flexural rigidity $(EI)_{PIP}$ to a curvature C is

$$U_3 = \frac{1}{2} (EI)_{PIP} C^2 \tag{13}$$

where

$$(EI)_{PIP} = E_P (I_1 + I_2) + E_C I_C \tag{14}$$

For a hollow pipe with ovalizaton, the moments of inertia are (Calladine 1983)

$$I_i = \pi a_i^3 t_i (1 - \frac{3}{2} \varsigma_i + \frac{5}{8} \varsigma_i^2) \tag{15a}$$

$$I_C = \frac{\pi a_1^4}{4} (1 - \frac{3}{2} \varsigma_1 + \frac{5}{8} \varsigma_1^2) - \frac{\pi a_2^4}{4} (1 - \frac{3}{2} \varsigma_2 + \frac{5}{8} \varsigma_2^2) \tag{15b}$$

Substituting Equations 14 and 15 into Equation 13 gives

$$\begin{aligned} U_3 &= \frac{1}{2} C^2 E_P \pi a_1^3 t_1 (1 + \frac{E_C a_1}{4 E_P t_1})(1 - \frac{3}{2} \varsigma_1 + \frac{5}{8} \varsigma_1^2) \\ &+ \frac{1}{2} C^2 E_P \pi a_2^3 t_2 (1 - \frac{E_C a_2}{4 E_P t_2})(1 - \frac{3}{2} \varsigma_2 + \frac{5}{8} \varsigma_2^2) \end{aligned} \tag{16}$$

Moreover, the strain energy per unit length associated with Poisson's ratio to maintain the circular cross section due to bending is then (Karam & Gibson 1995)

$$\begin{aligned} U_4 &= \frac{1}{2} \int_{a_2}^{a_1} \int_0^{2\pi} (2\sigma_r \varepsilon_r + \tau_{r\theta} \gamma_{r\theta}) r d\theta dr \\ &= \frac{\pi}{16} \frac{\nu_C^2 (5 - 2\nu_C)}{(1+\nu_C)(1-2\nu_C)} E_C C^2 (a_1^4 - a_2^4) \end{aligned} \tag{17}$$

Brazier moment

The final result for the strain energy of the pipe-in-pipe system is expressed by the summation as

$$U = U_1 + U_2 + U_3 + U_4 \tag{18}$$

We can find the optimum value of ζ_1 and ζ_2 for a given value of C from the condition $\partial U / \partial \zeta_i = 0$ and then obtain an expression for M from $M = \partial U / \partial C$. Moreover, the Brazier moment and the ovalization at the Brazier moment can be obtained from $\partial U / \partial C = 0$.

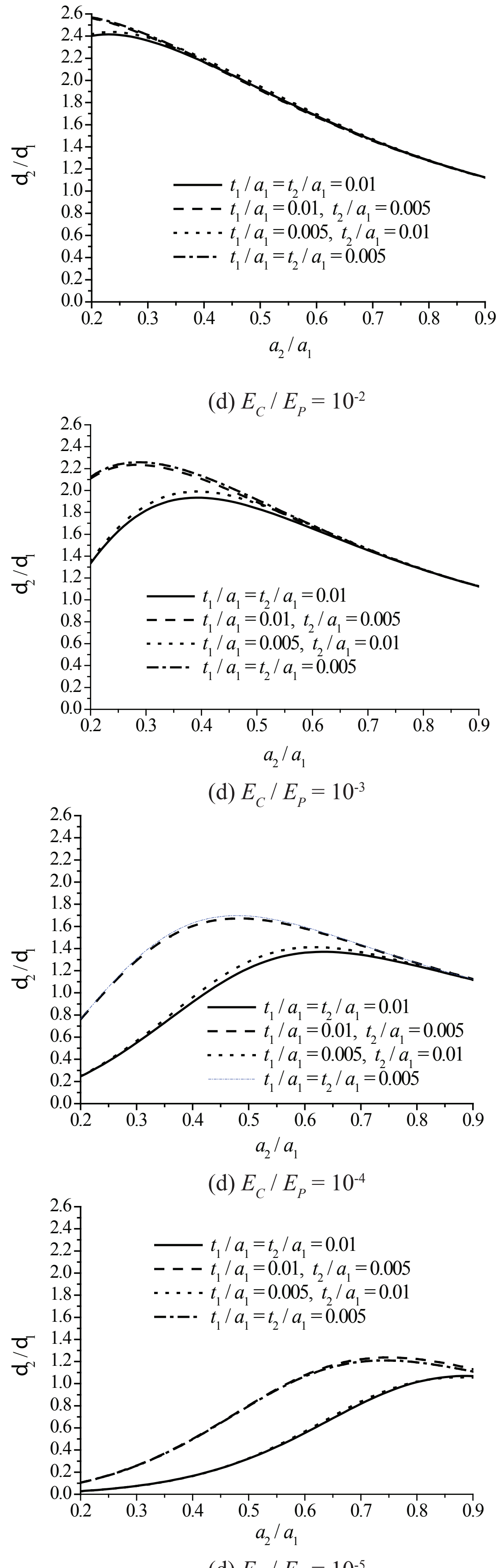

Figure 4. Displacement ratio (Inner to outer pipe, $\nu_P = 0.4$).

Results and Discussion

Ovalization at the Brazier moment

Figures 4a–4d show the plot of the displacement ratio δ_2/δ_1 due to bending against core thickness ratio a_2/a_1 for the various values of outer and inner pipe thicknesses to outer pipe radius ratio and core to pipe stiffness ratio. It is clear from the comparison of these figures that, as the core stiffness increases, the displacement for the inner pipe increases. Moreover, the effect of the change of the outer pipe thickness on the displacement ratio is quite little and this value can be determined by the core thickness and inner pipe thickness ratio.

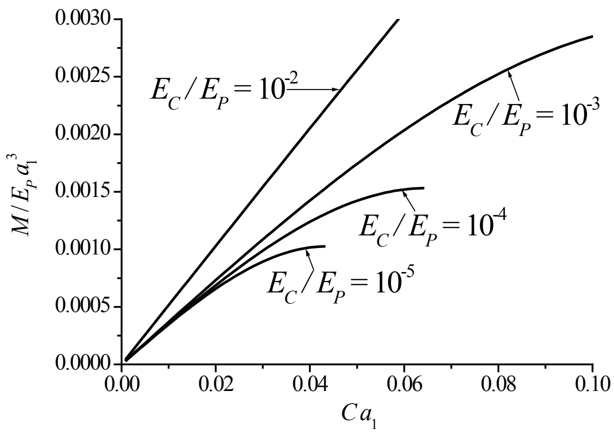

(a) $t_1 / a_1 = t_2 / a_1 = 0.01$, $a_2 / a_1 = 0.5$

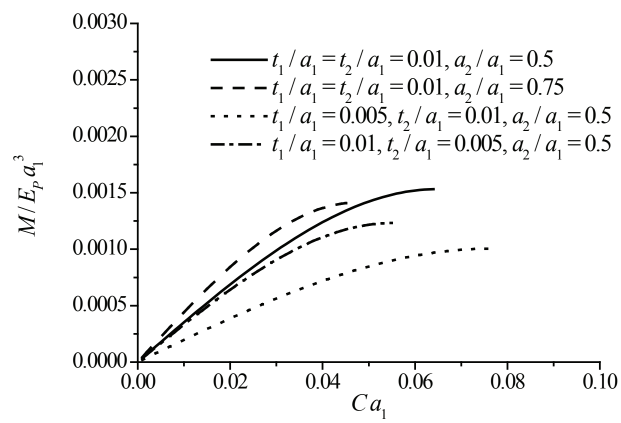

(b) $E_C / E_P = 10^{-4}$

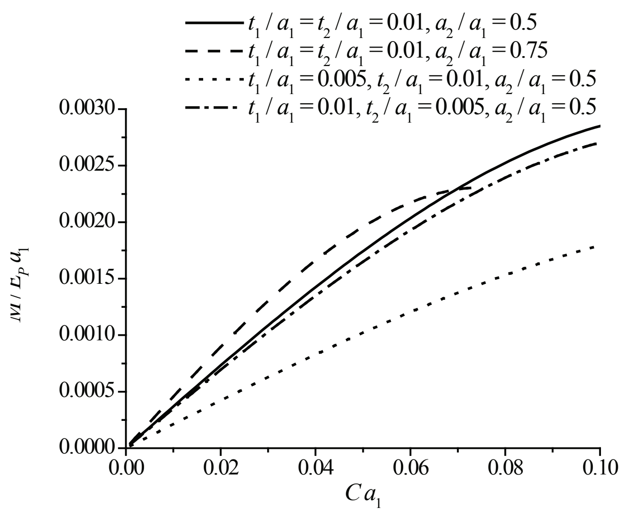

(c) $E_C / E_P = 10^{-3}$

Figure 5. Non-dimensional moment-curvature relationship ($\nu_P = 0.4$).

Moment-curvature relationship and Brazier moment

Figures 5a–5c show the nondimensional bending moment-curvature relationship. In all cases, for small values of Ca_1 we can find that the relationship between bending moment and curvature is almost linear. However, as the curvatures increase, the relation becomes nonlinear and finally the values of M reach maximum, in other words "the Brazier moment." As expected, the Brazier moment increases, with increasing the core thickness. Figures 5b and 5c are the comparison with regard to the different outer/inner pipe thickness and core thickness ratio. The contribution of the outer pipe thickness rather than that for the inner pipe toward bending moment-curvature relationship is significant. In addition, we can find from these figures, that as the core thickness increases, Brazier moment also increases.

Conclusions

This paper presents the bending characteristics of pipe-in-pipe systems analytically by considering the Brazier effect. It should be noted that the outer pipe thickness and the core stiffness, rather than the inner pipe thickness, play an important role in the bending moment-curvature relationship for pipe-in-pipe systems. At the moment, this research is the simplified analytical investigation. However, further studies will address the experimental investigations planned by the authors' research group, and comparisons between analytical and experimental results will be carried out.

Acknowledgment

The support of this work by the Grant-in-Aid for Young Scientists (B) (No. 18760615) of the Ministry of Education, Culture, Sports, Science and Technology (MEXT) in Japan is greatly acknowledged.

References

Brazier, L.G. 1927. On the flexure of thin cylindrical shells and other thin sections. *Proceedings of the Royal Society of London* A116: 104-114.

Calladine, C.R. 1983. *Theory of Shell Structures*. Cambridge: Cambridge University Press.

Karam, G.N. & Gibson, L.J. 1995. Elastic buckling of cylindrical shells with elastic cores – I. Analysis. *International Journal of Solids and Structures* 32: 1259-1283.

Sato, M. & Patel, M.H. 2007. Exact and simplified estimations for elastic buckling pressures of structural pipe-in-pipe cross-sections under external hydrostatic pressure. *Journal of Marine Science and Technology* (in press).

Timoshenko, S.P. & Goodier, J.N. 1970. *Theory of Elasticity*. New York: McGraw-Hill.

Origin and Age of Perennial Ice Within a Block Slope in the Shikaribestu Mountains, Hokkaido, Japan

Yuki Sawada
Institute of Low Temperature Science, Hokkaido University, Sapporo, Japan

Abstract

Borehole drilling and core sampling were conducted at the base of a block slope, where extra-zonal permafrost is preserved by winter air circulation and subsequent formation of the ground ice. A 3.8 m deep borehole displayed a vertical structure of the block slope. The sediment is composed of Sphagnum moss and peat (0–0.1 m depth), boulders (0.1–1.2 m), ice and boulder mixture (1.2–3.2 m), gravelly sand (3.2–3.35 m), and gravelly silt with ice lenses (3.35–3.8 m). Ratios of stable isotopes (δ18O and δD) of the perennial ice show similar linear correlations (gradient 7.5 and intercept 10.5) to the Global Meteoric Water Line, indicating that the ground ice is fed by meteoric water. AMS Radiocarbon datings of the trapped organic materials in the perennial ice indicate that the ground ice started to form between 8411–3728 Cal BP and has accumulated discontinuously throughout the late Holocene. Accumulation of the Sphagnum moss and peat layer on the blocky sediment may contribute to insulation and the gradual growth of the perennial ice.

Keywords: block slope; extra-zonal permafrost; paleoclimate; perennial ice; radiocarbon dating; stable isotope.

Introduction

Permafrost ice has the potential to archive paleo-climatic information within the stable-isotope composition, because most permafrost ice originates from meteoric water. For example, ice-wedge ice in continuous permafrost regions is generally formed by refreezing of snowmelt water. For this reason, stable oxygen isotope signals in the ice wedge have been used as an indicator of paleo-winter temperature (e.g. Mackay 1983, Meyer et al. 2002).

Ground ice in mountain permafrost environments also has a potential for paleoclimate reconstruction (e.g., Steig et al. 1998, Humlum 1999). Humlum (1999) reported that the relict glacier ice within a rock glacier in Greenland exhibits relatively lighter oxygen isotopes, which are indicative of the cooler climate in the little ice age.

Perennial ice bodies are also preserved in block slopes and talus slopes where extra-zonal permafrost is formed by air circulation where mean annual air temperature (MAAT) is positive (Kneisel et al. 2000, Sawada et al. 2003, Sawada 2003, Gude et al. 2003, Delaloye et al. 2003, Gorbunov et al. 2004, Zacharda et al. 2007). Previous studies by the author (Sawada et al. 2003, Sawada 2003) reported that ground ice formed in snowmelt periods and concluded that the ground ice probably originated from refreezing of snowmelt water. If the ground ice is considerably old, ice in the block slope may contain stable isotope signals of past climate changes.

This study presents stratigraphic and stable isotope data from a 3 m long core of ice and boulder mixtures obtained from a block slope in the Shikaribetsu Mountains, Hokkaido Island, Japan. AMS 14C ages of the organic materials in the sediments and ice are measured to determine the age of preserved ice. The oxygen and hydrogen isotope data are used to discuss the origin and formation processes of the perennial ground ice.

Study Area

The study area is located on the summit slope of Mt. Nishi-Nupukaushinupuri (1251 m a.s.l.) in central Hokkaido Island, Japan (Fig.1). This mountain is one of the lava domes which erupted in the last glacial period. MAAT ranged from 0.7°C–1.7°C in 1998–2003. Annual precipitation at the nearest meteorological station (Nukabira, 10 km NW) is 1175.8 mm, an average based on 12 years of data (1979–1990). The drill site is situated on the valley bottom which lies at the base of the block slope (Fig. 1). The lower portion of the block slope is dominated by spruce (Picea glehnii) and dwarf pine (pinus pumila), with ground surface cover of Sphagnum sp. and alpine shrubs (mainly Ledum palustre). Cold air blows during summer and autumn from the hollows opened in the moss mat.

Between 2000 and 2001 the depth of ground ice surface and ground temperatures at the drilling site showed the annual variations of the ground ice and related thermal regime (see for details Sawada et al. 2003, Sawada 2003). In winter the lower block slope was strongly cooled by air circulation driven by the temperature difference between atmosphere and inside of the block slope, while warmer air in the voids of the block slope moved upward and escaped from the top slope. The drained air was compensated by the penetration of colder outside air into the lower and middle part of the block slope (Sawada et al. 2003). Ground ice did not grow in winter, due to the lack of source water. In April, ground ice started to accumulate co-incidentaly with the initiation of the snowmelt (Sawada et al. 2003).

Ice ablation was triggered by heavy rainfall, and it continued until the subsurface was cooled to the freezing point in November 2001 (Sawada 2003). The annual maximum depth of the ground ice (i.e., active layer depth) ranged from -157.8 cm to -143.6 cm between 2001 and 2005 (Sawada unpublished data).

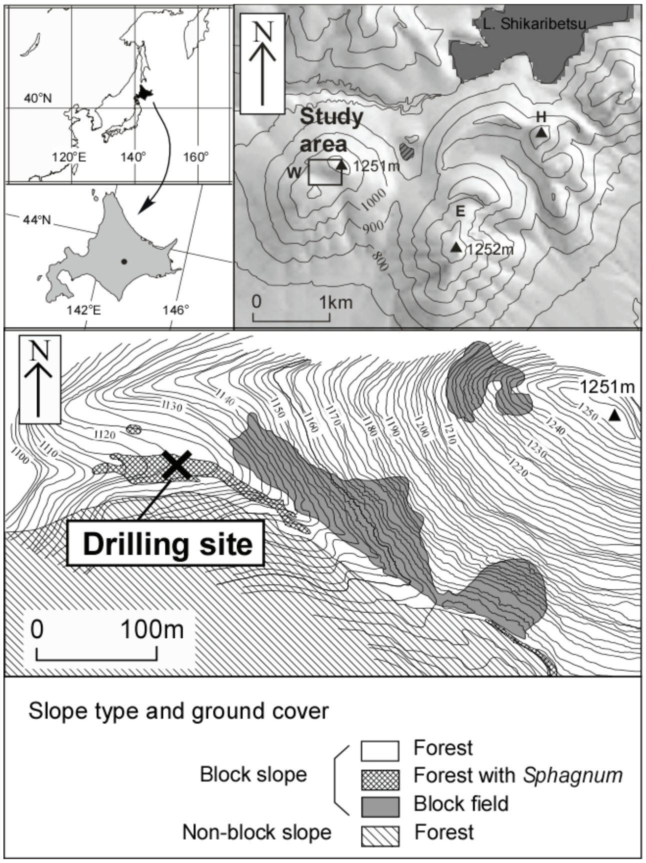

Figure 1. Study area and drilling site.

Methods

Drilling operation

Drilling was conducted on 11 July 2005, when the seasonal ice accumulation reached the annual maximum. The surficial soil and blocks were excavated down to the depth of 1.2 m. Drilling started on the surface of the seasonal ice. A drilling bit with tungsten carbide cutting teeth was used for the ice-predominant part, while a diamond bit with water injection was used for passing through andesite blocks. As a consequence, core samples of the ice and rock mixtures were obtained to the depth of 3.8 m during the 2-day drilling operations.

Sample analysis

The samples were sketched in the cold room at -20°C. Thereafter, these were cut into smaller pieces 2–11 cm in length. The length varied with the material of the samples: shorter length for pure ice, longer samples for ice-boulder mixture. The sample pieces were melted at room temperature. Water and organic materials were separated in the glass vials. AMS 14C datings of organic materials were conducted in Beta Analytic Inc., USA and Paleo Labo Co. Ltd., Japan. The 14C dates were converted into the calendar years with the calibration curve INTCAL04 (Reimer et al. 2004).

Oxygen and hydrogen isotope ratios were measured with the Delta-Plus mass spectrometer and Isoprime-PyrOH mass spectrometer, respectively. Both mass spectrometers are managed at the Institute of Low Temperature Science, Hokkaido University. Stable isotope ratios were given as permil difference to V-SMOW, with errors less than 0.02‰ and 0.5‰ for δ18O and δD, respectively. The results were presented in δ18O-δD diagrams with respect to the Global Meteoric Water Line (GMWL), in which fresh surface water was correlated on a global scale (Craig 1961).

Results

Structure of the core samples

Figure 2 shows sketch and pictures of the sample core. The core is classified into four segments: (A) ice and boulder mixture, (B) boulders, (C) gravelly sand with charcoal fragments, and (D) gravelly silt with ice lenses. Because the maximum thaw depth in the previous year (2004) was -141 cm, the upper 20 cm of ice is interpreted as seasonal ice formed in the spring of 2005.

Segment A contains clear ice and numerous organic materials. The ice displayed a layered structure (Fig. 2) similar to that of the glacier ice. The ice includes organic materials (leaves, branches, and fecal pellets). The fecal pellets piled up on the boundary of the ice layer have rounded shape with a diameter of 2–3 mm. These fecal pellets and plant materials indicate that the voids in the block layer are inhabited by Japanese Pikas (Ochotona hyperborea yesoensis) which commonly live in blocky landforms such as block slopes or moraines. They use the voids as nests or tunnels through which they carry plants (Kawamichi 1969). In addition, Japanese Pikas stock dried plants in the voids to survive in winter (Kawamichi 1969). The presence of the branches, leaves, and fecal pellets within the ice suggests the diets of Japanese Pika in the past.

Segment B does not contain clear ice, and this is probably due to thermal disturbances from drilling with a diamond bit. Because the tungsten bit became unstable at depth, a diamond bit with water injection was used to penetrate this segment. The ice may have melted from the heat of the pouring water.

Segment C consists of gravelly sand. Small particles of charcoal 2–5 mm in diameter are scattered in this layer. Visible ice is absent in this segment.

Segment D is composed of gravelly silt. A number of ice lenses are formed within this layer.

Chronology of the sediments and ground ice

The radiocarbon ages are listed in Table 1. The sediment structure is composed of the upper boulder layer and lower finer materials (sand and silt layers). The charcoal particles within the sand layer (Segment C, Fig. 2) exhibits ages of 8411–8211 Cal BP. There are two possible routes in which the charcoals fall onto the sand layer. One route is direct input to the sand layer. In this case, the accumulation of the boulder layer is considered to occur after the mixing of charcoals with the sand layer. The other is through the voids in the boulder layer. In this case charcoals penetrate into the existing block layer. In both cases the ground ice within the

Table 1. AMS radiocarbon ages of organic remains.

Depth	Host material	Type of organic material	Lab. Number	14C yr BP	Cal. yr BP 2-σ range
−159cm	ground ice	stem	PLD-7814	-65±15	N.A. (1950AD–Present)
−182cm	ground ice	stem	PLD-7815	570±15	633–537
−194cm	ground ice	fecal pellet	PLD-7816	720±15	683–661
−249cm	ground ice	leaf	Beta-213965	3590±40	4065–3728
−324cm	gravelly sand	charcoal	Beta-213966	7530±40	8411–8211

boulder layer is formed after the charcoals are mixed with the sand layer.

Accordingly, the organic materials in the infilling ice (Segment A, Fig. 2) exhibit much younger radiocarbon ages than the charcoals in the sand layer. The oldest age of 4065–3728 Cal BP was obtained from a leaf enclosed within the ice at depth of -249 cm. This leaf was extracted along with fecal pellets from the ice, indicating Japanese Pika stocked leaves in this depth. The age of the leaf also indicates that the ground ice was formed at this depth after the leaf had been transported. Thus, the age of the leaf gives the oldest estimation of the ice that included the leaf.

The ages of the organic materials become younger toward the ground surface. The ages of fecal pellets at -194 cm and stem at -182 cm are 683–661 Cal BP and 633–537 Cal BP, respectively (Fig. 2, Table 1). These two ages indicate that the perennial ice between -194 cm and -182 cm accumulated in 13–15 centuries. The age of stem at -159 cm exhibits a future age, which is apparently affected by recent nuclear testing. Thus, this age of ice shallower than -159 cm is interpreted to be modern (i.e., after 1950 AD).

Stable isotopes

Table 2 shows the isotopic composition of rain, snow, seasonal ground ice, and perennial ground ice samples. These isotope values are also plotted on the δ18O–δD diagram (Fig. 3).

Rain water (N=8) was collected during precipitation events between May and September 2004 at the shore of Lake Shikaribetsu (810 m a.s.l.). The mean isotopic composition of the rainwater was -11.0‰ for δ18O and -78.0‰ for δD. The samples are characterized by the d-excess of 9.7‰ and the slope of 7.4 on the δ18O–δD diagram, which are similar to the GMWL (d-excess of 10 and slope of 8: Craig 1961).

On 17 April 2005, snow cover was sampled at the drilling site (N=5). The snow cover was 2.2 m thick, and the upper 0.2 m started to melt. The isotopic composition of snow differs significantly from that of the rainwater. The mean isotopic composition of snow was -14.7‰ for δ18O and -90.5‰ for δD. The mean d-excess was 27.2‰, and the slope was 7.11. The larger d-excess value of snow indicates non-equilibrium evaporation from the Sea of Japan. In winter, northern Japan suffers westerly prevailing wind which originally blows from Siberia. The cold air causes fast non equilibrium evaporation from the Sea of Japan, where the Tsushima warm current flows from south to north (Waseda & Nakai 1983). Consequently, the winter precipitation has a large

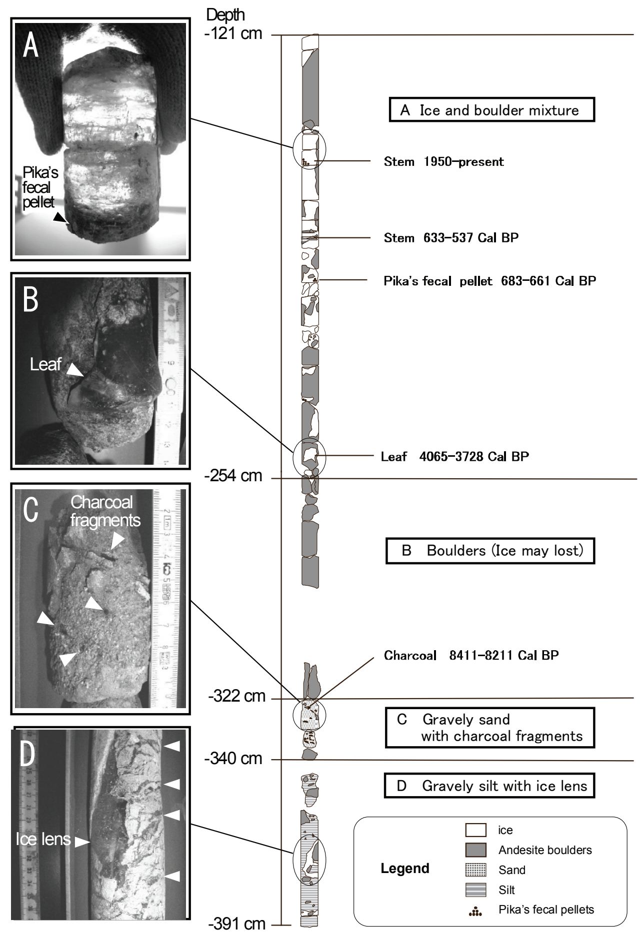

Figure. 2. Stratigraphy of the core samples obtained on the valley bottom.

Figure 2. Stratigraphy of the core samples obtained on the valley bottom.

d-excess value (>20), while the summer precipitation has a small value (<10), because vapor comes from the Pacific Ocean in summer (Waseda & Nakai 1983). Thus, the large d-excess value of snow is thought to originate from vapor from the Sea of Japan in winter.

The mean isotopic composition of seasonal ice formed between April and July 2005 was -12.3‰ for δ18O and -80.5‰ for δD, and mean d-excess was 17.8‰ (Table 2). These values were intermediate between rain and snow water, indicating two possibilities for isotope fluctuations: (1) the recent ground ice was fed by a mixture of rainwater and snowmelt water; (2) the ground ice was fed by snowmelt water, which was isotopically enriched before entering the block slope. Unnikrishna et al. (2002) reported that the initial

Table 2. Minimum, mean and maximum values and standard deviations of stable isotopes (δ18O, δD and d-excess) as well as slopes and intercepts in the δ18O-δD diagram for ground ice and recent precipitation sampled in the study area.

Source	N	slope	Intercept	R^2		$\delta^{18}O$ (‰)	δD(‰)	d-excess(‰)
Perennial ice	19	7.80	13.60	0.98	mean	−11.99	−79.86	16.0
					max.	−11.16	−66.90	18.2
					min.	−14.10	−96.30	14.2
					std. dev.	1.14	9.01	1.2
Seasonal ice formed in 2005 Apr.–Jul.	3	4.99	−19.24	0.99	mean	−12.28	−80.50	17.8
					max.	−10.51	−74.70	20.8
					min.	−13.14	−84.40	14.6
					std. dev.	1.02	5.12	3.1
Rain water in 2004 May–Sep.	8	7.39	3.04	0.98	mean	−10.97	−78.03	9.7
					max.	−4.98	−34.70	17.8
					min.	−18.15	−131.90	0.2
					std. dev.	4.46	33.30	5.4
Snow pack in 2005 Apr.	5	7.11	14.15	0.94	mean	−14.72	−90.52	27.2
					max.	−13.32	−79.80	28.9
					min.	−16.01	−99.70	23.7
					std. dev.	1.09	7.97	2.1

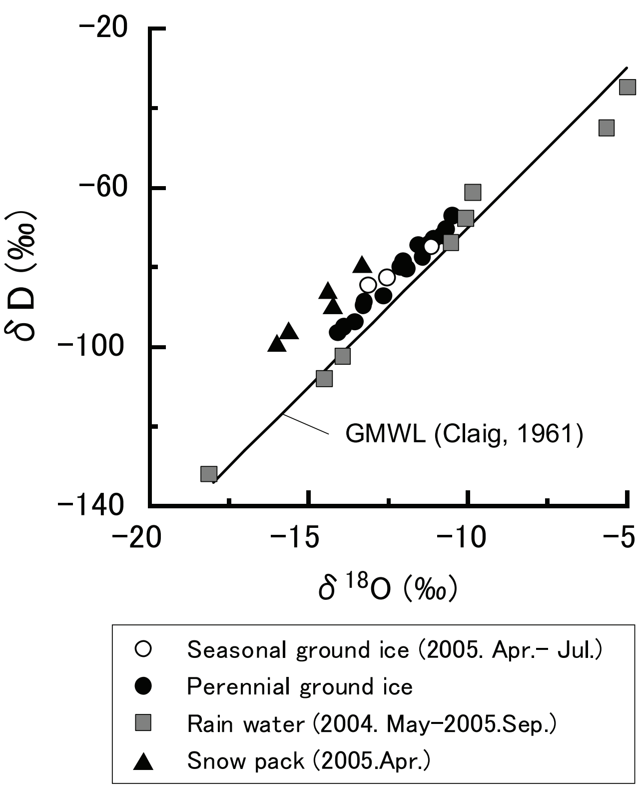

Figure 3. δ18O–δD diagram for rain, snow, seasonal ice, and perennial ice samples. GMWL is the Global Meteoric Water Line.

snowmelt water had higher δ18O than the original snowpack, because it originate from the lower snowpack layers which were isotopically enriched by snowmelt infiltration. This indicates that the rainwater may not be necessary for ground ice, which has a higher (heavier) δ18O than the snowpack.

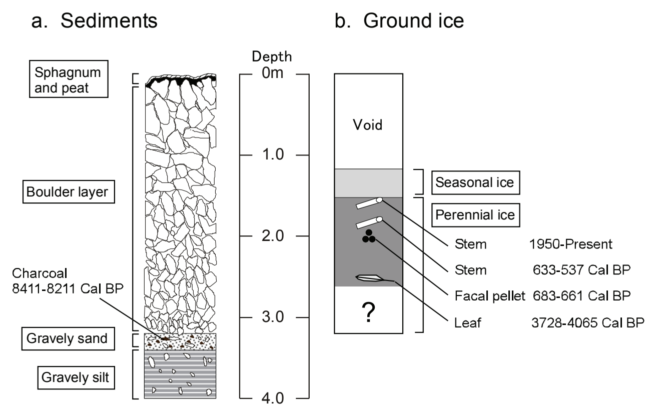

Figure 4. Vertical profiles of (a) sediments and (b) ground ice.

The perennial ground ice also has a smaller range of isotopic composition than rain and snow. The mean isotopic composition of the perennial ice was -11.2‰ for δ18O and -79.9‰ for δD, and mean d-excess was 16.0‰. The ranges were 2.1‰ for δ18O and 23.6 ‰ for δD. These small ranges indicate that the source water of the ground ice is basically unchanged for long periods.

Age and Accumulation Process of the Perennial Ice

The chronology of the sediment and ice of the core samples is shown separately in Figure 4, because the formation ages of these two materials are apparently different. Figure 4a shows the stratigraphy of the sediments. The perennial ice did not formed in the age of the charcoal particle within the sand layer (8411–8211 Cal BP), because the charcoal particles could not enter the sand layer if the above boulder layer was filled with ice. Thus, initiation of the perennial ice is younger than the charcoal age.

The calibrated age of the leaf trapped in the perennial ice at -249 cm depth (4065–3728 Cal BP: Table 1, Fig. 4b) gives the youngest estimation of the ground ice formation. The leaf had been preserved in good condition in the ice, indicating the leaf did not experience any decomposition. Thus, the real age of the ice formation at -249 cm approaches the age of the leaf. From these assumptions, the onset of the ground ice within the block layer can be assumed to be between 8.4–3.7 ka.

The age of organic materials within the perennial ice decreases toward the top (Fig. 4b), indicating the upward accumulation of the ice. Because the top of the perennial ice is determined by the seasonal thaw depth (active layer thickness), this sequence also suggests upward migration of the permafrost table. In the study site, Sphagnum mat, peat, and tephra layers cover the blocky sediments. These organic and volcanic soils may act as an effective insulator to reduce the heat input and to preserve the perennial ground ice even in the positive MAAT environment.

Conclusions

The drilling operation and subsequent geochemical analysis allowed paleoclimate reconstruction from the perennial ground ice preserved in a block slope. The AMS 14C dating of organic materials revealed that the perennial ground ice is preserved at least 3700 years. The 14C age became younger towards the top of the ice, indicating that the law of superposition is applicable to the ground ice sequence in the block slope.

Comparison of the stable isotope compositions between perennial ice, seasonal ice, rain, and snow suggests that the ground ice originates from purely meteoric water, while the isotope composition is changed from the original source water. The perennial ice has the potential to preserve long-term fluctuation in the isotope composition of the meteoric water.

Acknowledgments

This study was supported by the “Leadership fund” of the Institute of Low Temperature Science, Hokkaido University in 2004, by a research fund from the Tokyo Geographical Society in 2005, and by a research fund by Paleo Labo Co. Ltd. in 2006. The author would like to thank Takeshi Nakatsuka for measuring stable isotopes; Hiroshi Adachi and Nobuyuki Nosaka (Geo act Co. Ltd.) for technical guidance for drilling; Atsushi and Sarasa Ono, Katsuhiko Asahi, Yugo Nakamura, Fumitaka Katamura, and Hiroyori Sugiyama for helping the drilling operation; and Takayuki Shiraiwa and Sumito Matoba for helping with ice-core treatment. The author would like to thank the associate editor and two reviewers for constructive comments and language improvement.

References

Craig, H. 1961. Isotopic variations in meteoric waters. Science 133: 1702-1703.

Delaloye, R., Reynard, E., Lambiel, C. & Marescot, L. 2003. Thermal anomary in a cold scree slope (Creux du Van, Switzerland). Proceedings 8th International Conference on Permafrost, 2003, Zürich, Switzerland, 21–25 July, 2003: 175-180.

Gorbunov, A.P., Marchenko, S.S. & Seversky, E.V. 2004. The thermal environment of blocky materials in the mountains of Central Asia. Permafrost and Periglacial Processes 15: 95-98.

Gude, M., Dietrich, S., Hauck, C., Mäusbacher, R., Molenda, R., Ruzicka, V. & Zacharda, M. 2003. Probable occurrence of sporadic permafrost in non-alpine scree slopes in central-Europe. Proceedings 8th International Conference on Permafrost, 2003, Zürich, Switzerland, 21–25 July, 2003: 331-336.

Humlum, O. 1999. Late-Holocene climate in central West Greenland: meteorological data and rock-glacier isotope evidence. The Holocene 9: 581-594.

Kawamichi, T. 1969. Behavior and daily activities of the Japanese Pika, Ochotona hyperborean yesoensis. Jour. Fac. Sci. Hokkaido Univ. Ser. VI, Zool. 17: 127-151.

Kneisel, C., Hauck, C. & Vonder Mühll, D. 2000. Permafrost below the timberline confirmed and characterized by geoelectrical resistivity measurements, Bever Valley, eastern Swiss Alps. Permafrost and Periglacial Processes 11: 295-304.

Mackay, J.R. 1983. Oxygen Isotope Variations in Permafrost, Tuktoyaktuk Peninsula Area, Northwest Territories. Paper 83-1B, Geological Survey of Canada: 67-74.

Mayer, H., Dereviagin A., Siegert, C., Schirrmeister, L. & Hubberten, H.W. 2002. Palaeoclimate reconstruction on Big Lyakhovsky Island, North Siberia - hydrogen and Oxygen isotopes in ice wedges. Permafrost and Periglacial Processes 13: 91-105.

Unnikrishna, P.V., McDonnell, J.J. & Kendall, C. 2002. Isotope variations in a Sierra Nevada snowpack and their relation to meltwater. Journal of Hydrology 260: 38-57.

Reimer, P.J., Baillie, M.G.L., Bard, E., Bayliss, A., Beck, J.W., Bertrand, C.J.H., Blackwell, P.G., Buck, C.E., Burr, G.S., Cutler, K.B., Damon, P.E., Edwards, R.L., Fairbanks, R.G., Friedrich, M., Guilderson, T.P., Hogg, A.G., Hughen, K.A., Kromer, B., McCormac, F.G., Manning, S.W., Ramsey, C.B., Reimer, R.W., Remmele, S., Southon, J.R., Stuiver, M., Talamo, S., Taylor, F.W., van der Plicht, J. & Weyhenmeyer, C.E. 2004. IntCal04 Terrestrial radiocarbon age calibration, 26–0 ka BP. Radiocarbon 46: 1029-1058.

Sawada, Y. 2003. Monitoring of ground-ice formation in a block slope at Mt. Nishi-Nupukaushinupuri, Hokkaido, Japan. Proceedings 8th International Conference on Permafrost, 2003, Zürich, Switzerland, 21–25 July, 2003: 1001-1005.

Sawada, S., Ishikawa, M. & Ono, Y. 2003. Thermal regime of sporadic permafrost in a block slope on Mt. Nishi-Nupukaushinupuri, Hokkaido Island, Northern Japan. Geomorphology 52: 121-130.

Steig, E.J., Fitzpatrick, J.J., Potter, N., Jr. & Clark, D.H. 1998. The geochemical record in rock glaciers. Geografiska Annaler 80A: 277-286.

Waseda, A. & Nakai, N. 1983. Isotopic composition of metric and surface waters in Central and Northeast Japan. Geochemical Journal 17: 83-89. (In Japanese)

Zacharda, M., Gude, M. & Ruzicka, V. 2007. Thermal regime of three low elevation scree slopes in Central Europe. Permafrost and Periglacial Processes 18: 301-308.

Contribution of Self-Potential (SP) Measurements in the Study of Alpine Periglacial Landforms: Examples from the Southern Swiss Alps

Cristian Scapozza
Institute of Geography, University of Lausanne, Switzerland
Pierre Gex
Institute of Geophysics, University of Lausanne, Switzerland
Christophe Lambiel, Emmanuel Reynard
Institute of Geography, University of Lausanne, Switzerland

Abstract

Measurements of streaming potentials were carried out on rock glaciers and talus slopes in a test site of the southern Swiss Alps. After some theoretical considerations and a brief description of the measurement technique, a method of data treatment in high declivity topography is presented. The results of self-potential prospecting measurements are generally in accordance with the geomorphological observations. In particular, the groundwater runoff is influenced by the occurrence of permafrost, which creates surfaces of water migration partially independent from ground porosity.

Keywords: geophysics; rock glacier; self-potential; streaming potentials; Swiss Alps; talus slope.

Introduction

Self-potential (SP) (or spontaneous potential measurements) in the study of periglacial environments is a recent and not well-developed geophysical method in geomorphology, geocryology, and glaciology. Natural electrical potentials measurements have been carried out to monitor the thawing front movement and to study the active layer and permafrost parameters in arctic periglacial environments (e.g., Gahé et al. 1988, Fortier et al. 1993), for the study of subglacial drainage (e.g., Blake & Clarke 1999, Kulessa et al. 2003) or for the investigation of landslides (e.g., Bogoslowsky & Ogilvy 1977, Gex 1993).

In alpine periglacial environments, no studies on streaming potentials associated with groundwater runoff in rock glaciers and talus slopes have been carried out. Rock glacier hydrology has been studied with water tracing (e.g., Tenthorey 1992, Krainer & Mostler 2002) or thanks to borehole logging (e.g., Haeberli 1985, Vonder Mühll 1992), whereas talus slope hydrology is not well known (e.g., Rist & Phillips 2005).

The present paper presents and discusses results of streaming potentials mapping in the Sceru Valley (Fig. 1), in the Eastern part of the Blenio Valley (Lepontine Alps of the Tessin, southern Switzerland). The objectives are to present the measurement technique and a method of data treatment in high declivity topography.

Theory and Methods

Macroscopic streaming potential mapping was realized from field measurements carried out in 2006 and 2007. The method is completed by geomorphological observations and mapping, frequency-domain electromagnetic lateral mapping and 2D resistivity profiling (Geonics EM-16R and EM-31), direct current (DC) resistivity soundings, and

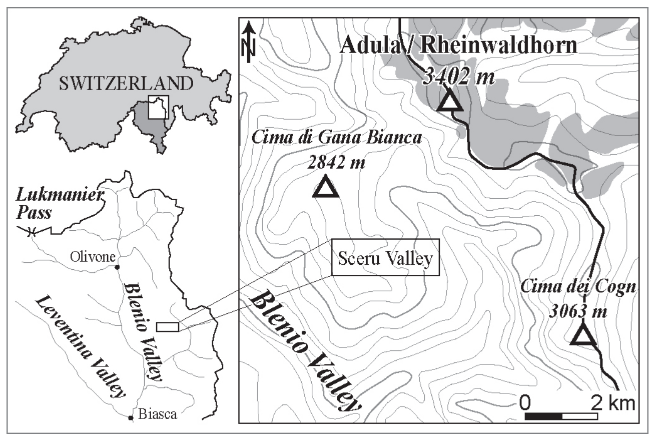

Figure 1. Geographical location of the study area.

thermal prospecting (miniature ground temperature data loggers and spring temperatures). In this paper, only the field measurement technique and the interpretation of large geomorphological structures (> 1000 m^2) are presented.

The streaming potentials

Streaming potentials, or electrofiltration potentials, are natural electrical potentials produced by water flow through a porous and permeable soil (Reynolds 1997). The streaming potentials are directly proportional to the selective filtration of ions (electrofiltration) at the microscopic scale. Water, acting as an electrolyte, creates at the interface mineral-water a positive load flow between the immobile part of the electrical double layer (composed by the Stern layer—in contact with the mineral and with fixed cations, and the Gouy-Chapman diffuse layer—with a lower cations concentration) and the free neutral electrolyte (Revil et al. 2004). The Helmholtz-Smoluchowski law links up the electrofiltration potential (EF) amplitude with the electrolyte characteristics:

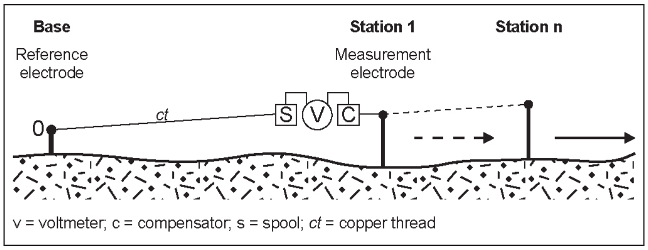

Figure 2. Field acquisition of self-potential data.

$$EF = \frac{\rho \varepsilon \zeta}{4 \pi \eta} \Delta P \tag{1}$$

where ρ is the resistivity, ε the dielectric constant and η the dynamic viscosity of the electrolyte. ζ is the electrical potential of the double layer (zeta potential) and ΔP is the pressure difference between the measurement points of EF.

Ultra-fresh and fresh groundwaters induce the maximum electrofiltration fields (Bogoslowsky & Ogilvy 1973). Indeed, in presence of much conductive water (with a mineral concentration exceeding 5 g/l), the electrolyte short-circuits the spontaneous electrical current.

Self-potential variations are also due to the granulometry and permeability of the soil. In a homogenous and isotropic terrain and where granulometry and permeability are known, the streaming potentials reflect the contours of the water table. In this case, self-potential mapping and inversion can supply information about some characteristics (configuration, direction, and intensity) of seepage flow both in horizontal and vertical planes (Revil et al. 2004).

Measurement of streaming potentials

SP is a passive method. The technique applied in this study is based on the fact that each value of self-potential measured at the ground surface is linked up with one electrode fixed at a base station situated outside of the geomorphological landforms studied. The potential difference (in mV) is measured between the reference electrode and a measurement electrode, which is moved along a traverse (Gex 1993, Reynolds 1997).

The range of the measured potentials is generally comprised between several millivolts (mV) and one volt. Because the sign of the zeta potentials could be positive or negative according to the earth materials, the sign of the difference of voltage measured is an important factor for the interpretation of SP anomalies (Reynolds 1997). For convention, the self-potential value at the reference electrode is zero. SP cartography has been carried out with a distance between every measurement of 3 to 5 m.

The measurement material used in this study was developed at the Institute of Geophysics of the University of Lausanne. The reference electrode of the model non-polarisable with Cu-$CuSO_4$ was realized in PVC and wood. The measurement electrode is fixed on a stick one meter long; its thin section allows us to drive it into the ground comfortably. It is linked up with the reference electrode by an isolated copper wire. A spool, fixed on the back of the operator, permits us to unwind the copper wire. The measurements are carried out with a high impedance (100 MΩ) digital voltmeter. The scale range of the voltmeter is comprised between -2000 and 2000 mV. A compensator is associated with the voltmeter to settle the SP value to the zero at the reference electrode. Finally, the voltmeter is provided with a filter that permits us to stabilize the measurements when the ground presents perturbations to the natural electrical fields. The field data acquisition is schematized in Figure 2.

Very Low Frequency-Resistivity (VLF-R)

The VLF-R technique (see Hoekstra et al. 1975, Hoekstra 1978, McGrath & Henderson 1985) uses electromagnetic energy radiated by a very low frequency (VLF) transmitter. In this study the Hauderfehn transmitter (23.4 kHz) located in Germany was used. The measurement of the horizontal component of the electric field and of the horizontal magnetic component perpendicular to the azimuth of the transmitting station allows the apparent resistivity of the near surface to be determined using the Cagniard (1953) equation:

$$\rho_a = (0.2/f)(E/H)^2 \tag{2}$$

where ρ_a is the apparent resistivity (Ωm), *f* the frequency (Hz), *E* the electric field (mV/km) and *H* the magnetic field (nT). The ratio between *H* and *E* gives a phase angle that changes according to variations of resistivity with the depth.

The field data acquisition was carried out using a Geonics EM-16R instrument.

Field Site Characteristics and Data Acquisition

The Sceru Valley (46°27'N, 9°01'E) is an east-facing glacial cirque situated between 2000–2787 m a.s.l. The morphology and hydrology of the Sceru Valley were studied by Scapozza (2008). The morphology is characterized by the presence of several rock glaciers with different degree of activity, talus slopes, and Lateglacial moraines (Fig. 3).

Permafrost is present in the Piancabella rock glacier and in the lower part of the Gana Rossa talus slope (Scapozza 2008). The hydrology of the southern part of the Sceru Valley is influenced by the presence of rock glaciers. Because of the high porosity of the blocky surface, no subaerial water runoff can be observed (the spring in the lower part of the Gana Rossa talus slope is situated one meter below the ground surface).

In 2006 and 2007, 17 SP profiles were carried out on the Sceru I rock glacier, 2 on the Piancabella rock glacier, 1 on the Gana Rossa talus slope, and 2 on the Sasso di Luzzone talus slope/rock glacier complex. In total, about 1300 SP measurement points were listed.

In the talus slopes and the active rock glacier, several SP profiles were combined with Geonics EM-16R and/or EM-31 mapping along the same traverse.

Results and Discussion

Data treatment

In high declivity topography like the alpine periglacial

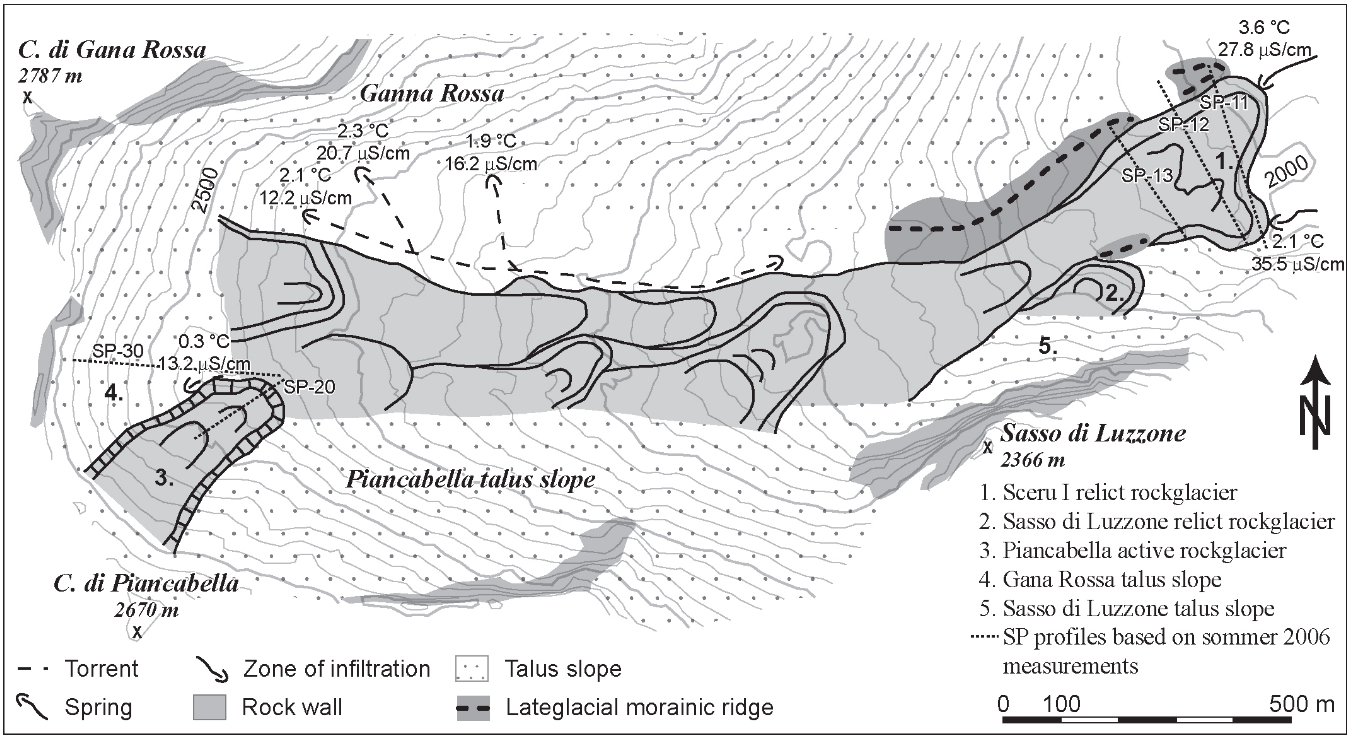

Figure 3. Geomorphological map of the Sceru Valley. For further information, see Scapozza (2008).

environment, the natural streaming potential linked to the slope is important, and its effect on the difference of voltage (in mV) measured by self-potential prospecting is very high. This perturbation, named "Topographic Effect" (TE), has been known to geophysicists for more than 90 years (Ernstson & Scherer 1986). The TE presents, for a constant electric field, an increasing negative potential linked with the elevation in altitude. For these reasons the regional anomaly (due to the TE) has to be subtracted from the measured values, which gives a final residual anomaly. The TE is calculated with a statistical analysis of linear regression between self-potential data and altitude. In practice, the average of the first four values of 11 traverses, measured between 2000–2450 m outside of the body of the Sceru I rock glacier, were used to calculate the TE, with a correlation between SP and altitude of -0.86. The calculated gradient of the TE is -68 mV per 100 m difference in elevation.

SP data were exposed in the form of potential profiles and equipotential maps. For the equipotential maps, a geostatistical interpolation of SP data was made with ordinary kriging. All the SP data (except for profiles SP-20 and SP-30) refer to the reference electrode placed outside the Sceru Valley (Fig. 4). For profiles SP-20 and SP-30, the reference electrode was placed at the Swiss Grid coordinates 720'215/145'660, at 2460 m a.s.l.

Sceru I relict rock glacier

The SP prospecting of this rock glacier shows an almost continuous negative residual anomaly in the northern lobe and another negative residual anomaly in the southern lobe. A zero millivolt residual anomaly is located between the Sceru I rock glacier and the Sasso di Luzzone talus slope/rock glacier complex situated south of it (Fig. 4).

According to the geoelectrical prospecting (2 DC resistivity soundings and one 2D resistivity profile), the bulk resistivity structure of the rock glacier seems to be relatively homogeneous. Indeed, the ground apparent resistivity is comprised between 3–5 kΩm (Scapozza 2008).

The groundwater runoff of two springs with different temperatures and electrical conductivities situated at two different lobes of the rock glacier could be followed by the self-potential prospecting (Figs. 4, 5). The link between the negative anomaly and the groundwater runoff is clearly evidenced in three SP profiles executed in summer 2006 (Fig. 5).

The two continuous anomalies may indicate the presence of two locations of preferential saturated groundwater flow. The two systems are probably independent, as evidenced from the constant difference throughout the year of temperature and conductivity of the two springs situated at the front of the rock glacier. Following this hypothesis, SP measurements would confirm that the two springs are alimented with groundwater of different origin (Fig. 4).

The torrents situated in the northern part of the Sceru Valley possibly feed the northern lobe spring (as pointed out by a warming of water temperatures), whereas the southern lobe spring would be alimented by an important aquifer situated into the Sceru I rock glacier. This water may be stored in the rock glacier for several months. The relatively high water conductivity (compared to the other springs in the valley, see Figure 3) and the constant water temperature (between 2.0°C and 2.2°C) all year long would confirm that the water transfer in this rock glacier is very slow, as it was pointed out by Tenthorey (1992) in a similar environment.

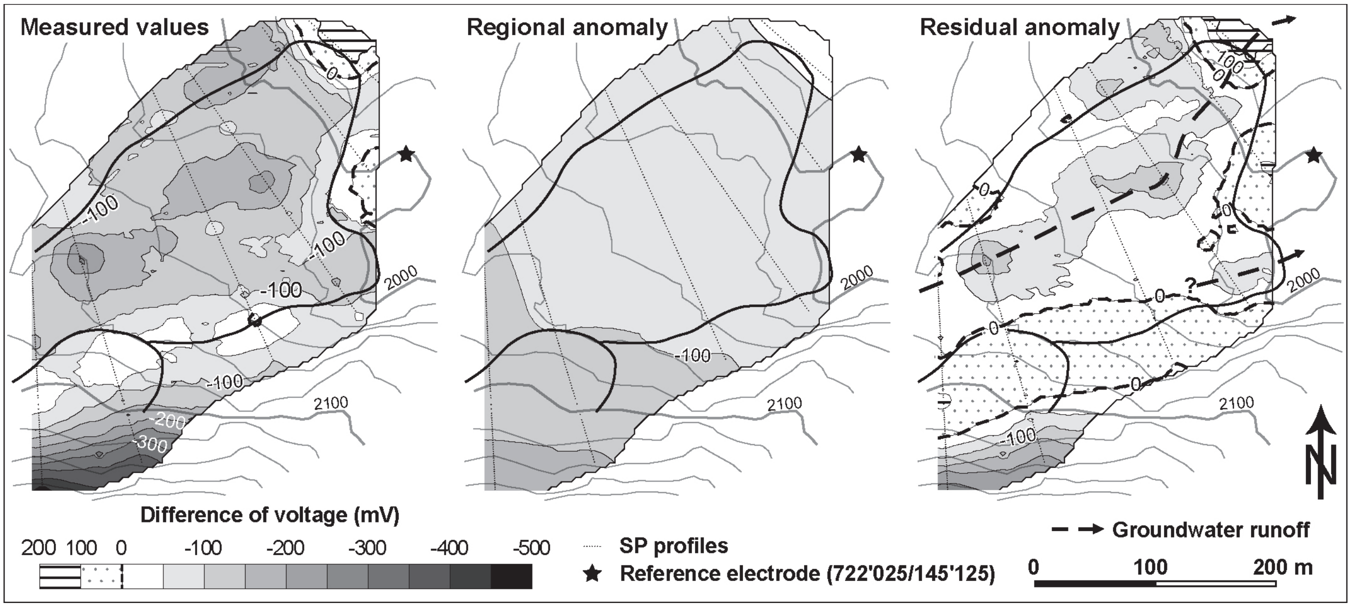

Figure 4. SP equipotential map of the Sceru I rock glacier and the Sasso di Luzzone talus slope/rock glacier complex based on summer 2007 measurements. For topographic names, see Figure 3.

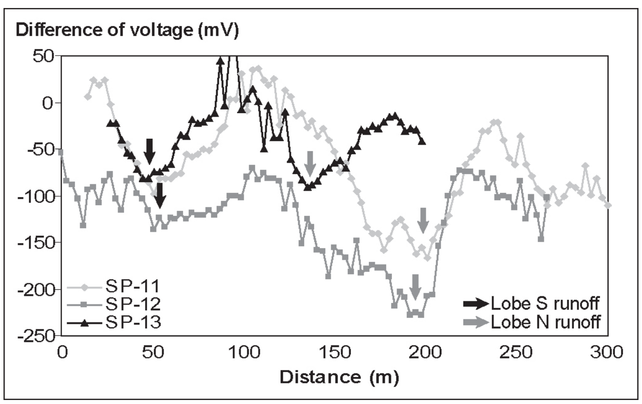

Figure 5. SP profiles executed across the Sceru I rock glacier. The arrows show negative anomalies linked with groundwater runoff. For the location of SP profiles, see the Figure 3.

The cold water temperature of the southern spring may be linked to a process of winter-ascending air circulation (the so-called chimney effect), which facilitates the cooling of the ground in the lower part of a porous sediment deposit (Delaloye & Lambiel 2005).

Piancabella active rock glacier

Prospecting of this landform shows a rise of the SP at the foot of the rock glacier front and a low increase of SP values all along the rock glacier (Fig. 6). Because of the location of the reference electrode (settled to 0) downslope of the rock glacier, the rise of the SP at the front can be interpreted as an important negative residual anomaly of several hundred mV.

A VLF-R tomography performed with the 2LayInv software (Pirttijärvi 2006) allows us to know approximately the active layer depth and the permafrost resistivity. The parameters of the profiling inversion are presented in Figure 6. Maximal VLF-R resistivities are found at the front of the rock glacier, and a decrease of the values toward upslope can be observed. Between 30–70 m, the decrease in the resistivities coincides with a decrease of the active layer depth. At 75 m, an important groundwater runoff has been perceived beneath the surface.

Data from the Piancabella active rock glacier show a connection between changes in SP, changes in active layer properties (particularly, its depth), changes in permafrost structure and/or in bulk resistivity structure (as shown by the VLF-R tomography). Indeed, the correlation between SP and active-layer depth is -0.74, whereas it is -0.85 between SP and permafrost resistivity. The correlation between SP and altitude (in m) is 0.54, which confirms that SP is partially independent from topography.

The permafrost resistivity depends on ground temperature, permafrost ice resistivity and content, and unfrozen water resistivity and content (Haeberli & Vonder Mühll 1996). Thus, it is difficult to separate the effect of change in water conductivity on SP from those on bulk resistivity.

The good connection between SP and permafrost resistivity probably indicates that there is a constant and continuous groundwater flow of constant water electrical conductivity and constant temperature throughout the active layer, and that SP changes are due to changes in the bulk resistivity structure of the rock glacier. This would confirm that the suprapermafrost groundwater runoff is supplied by the melt of annual névés at the root of the rock glacier and by the addition of incidental rainfall (see Tenthorey 1992). It is difficult to know the proportion of ice melt in the active layer and/or at the permafrost table, which is probable for a rock glacier situated at the lower limit of discontinuous permafrost.

Finally, the negative SP residual anomaly at the foot of the rock glacier front evidences an important groundwater runoff. This groundwater runoff is probably linked to suprapermafrost and intra- and subpermafrost water flow, which concentrates at the foot of the rock glacier front (Haeberli 1985).

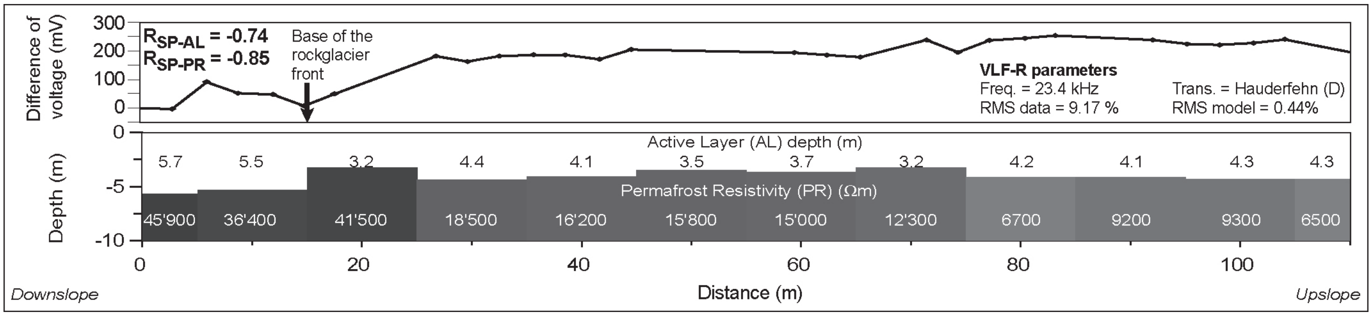

Figure 6. Profile SP-20 (at the top) and VLF-R tomography (below) on the Piancabella rock glacier. The VLF-R profiling inversion was performed with the 2LayInv (©University of Oulu) software (Pirttijärvi 2006).

Gana Rossa talus slope

SP prospecting of the Gana Rossa talus slope (Fig. 7) shows two negative residual anomalies in the lower part of the landform and an important and well-developed positive anomaly between 60–160 m distance. Another positive anomaly is present in the upper part of the talus slope. VLF-R prospecting shows relatively high apparent resistivities (over that 10,000 Ωm) in the lower part and in the middle of the talus slope. According to DC-resistivity, EM-31 and thermal prospecting (Scapozza 2008), permafrost is present only in the lower part of this talus slope (Fig. 7).

The streaming potentials are weakly positively correlated with altitude (R = 0.54), which contrasts with the theory of the TE (see *Data treatment*). Indeed, a test made in the Sasso di Luzzone talus slope (Fig. 3), where permafrost is absent, gives a very high negative correlation between streaming potentials and altitude (R = -0.97). Some results were pointed out by other studies carried out in high declivity slopes (e.g., Jackson & Kauahikana 1988).

Comparison between SP measurements and permafrost distribution shows, for the lower part of the talus slope, a connection between SP residual anomalies and permafrost occurrence. A possible hypothesis to explain this SP positive residual anomaly is the following: the presence of saturated or partially under-saturated permafrost may create a relatively impermeable surface of water runoff, which may modify the direction of the natural streaming potential linked to the slope (which is present between 120–200 m, as pointed out by the negative correlation between streaming potentials and altitude) by the canalization of groundwater flow at the base of the active layer. Following this hypothesis, the negative SP residual anomaly situated at a distance of 25 m may be related to an important water infiltration in the porous sediments, supplied by the melt of annual névés and by the addition of incidental rainfall. Whereas, the negative SP residual anomaly situated at a distance of 50 m may be related to the presence of a talik that would permit an intrapermafrost groundwater flow. The important groundwater runoff in the lower part of the talus is also proved by a spring (Fig. 3). Finally, in the upper part of the talus slope, the SP variations are probably due to the topography of bedrock, which is located only a few meters below the slope surface.

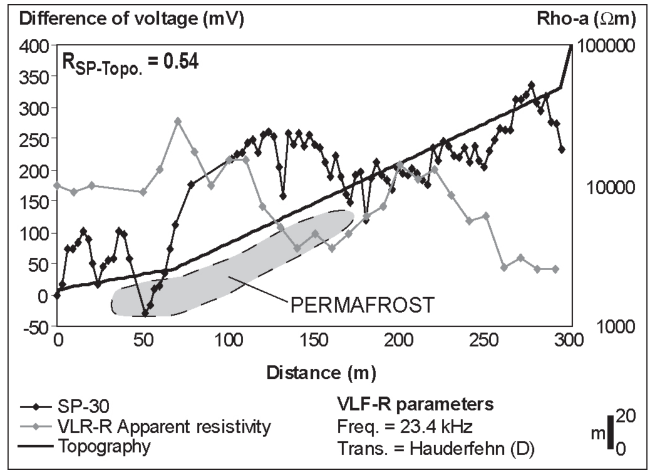

Figure 7. SP profile across the Gana Rossa talus slope.

In conclusion, it is very difficult today to better detail the hydrological and glaciological behavior of this talus slope without short, medium, and long-term thermal and geophysics monitoring at the surface and in boreholes.

Conclusions and Perspectives

The examples discussed show that measurement of streaming potential change on periglacial landforms offers good possibilities for assessing changes in water content and migration. Self-potential measurement could be useful for studying, in accordance with other geophysical methods, the importance of groundwater runoff generated by water infiltration and/or ice melting in permafrost terrains. The repetition of the same SP profile ten months later on a relict and an active rock glacier gave the same results; this confirms that streaming potential monitoring in periglacial landforms is possible. Self-potential monitoring associated with thermal and Electrical Resistivity Tomography (ERT) monitoring could be interesting for quantifying the processes correlated with permafrost degradation in high mountain environments.

Acknowledgments

Special thanks are due to all people who helped in the field, to the Associate Editor and the two anonymous reviewers for their useful feedback, and to Meredith Blake for proofreading the English.

References

Blake, E.W. & Clarke, G.K. 1999. Subglacial electrical phenomena. *Journal of Geophysical Research* 104 (B4): 7481-7495.

Bogoslowky, V.V. & Ogilvy, A.A. 1973. Deformations of natural electric fields near drainage structures. *Geophysical Prospecting* 21: 716-723.

Bogoslowky, V.V. & Ogilvy, A.A. 1977. Geophysical methods for the investigation of landslides. *Geophysics* 42: 562-571.

Cagniard, L. 1953. Basic theory of the magneto-telluric method of geophysical prospecting. *Geophysics* 18: 605-635.

Delaloye, R. & Lambiel, C. 2005. Evidence of winter ascending air circulation throughout talus slopes and rock glaciers situated in the lower belt of alpine discontinuous permafrost (Swiss Alps). *Norsk Geografisk Tidsskrift* 59: 194-203.

Ernston, K. & Scherer, H.U. 1986. Self-potential variations with time and their relation to hydrogeologic and meteorological parameters. *Geophysics* 51: 1967-1977.

Fortier, R., Allard, M. & Seguin, M.-K. 1993. Monitoring thawing front movement by self-potential measurements. *Proceedings of the Sixth International Conference on Permafrost, Beijing, China, July 5–9, 1993*: 182-187.

Gahé, E., Allard, M., Seguin, M.-K. & Fortier, R. 1988. Measurements of active layer and permafrost parameters with electrical resistivity, self potential and induced polarisation. *Proceedings of the Fifth International Conference on Permafrost, Trondheim, Norway, 2–5 August, 1988*: 148-153.

Gex, P. 1993. Mesures d'électrofiltration sur le glissement de la Frasse (Préalpes romandes). *Hydrogéologie BRGM* 3: 239-246.

Haeberli, W. 1985. Creep of mountain permafrost: internal structure and flow of alpine rock glaciers. *Mitteilungen der VAW/ETH Zürich*: 77.

Haeberli, W. & Vonder Mühll, D. 1996. On the characteristics and possible origin of ice in rock glacier permafrost. *Zeitschrift für Geomorphologie N. F.*, Suppl.-Bd. 104: 43-57.

Hoekstra, P. 1978. Electromagnetic methods for mapping shallow permafrost. *Geophysics* 43: 782-787.

Hoekstra, P., Sellmann, P.V. & Delaney, A. 1975. Ground and airborne resistivity surveys of permafrost near Fairbanks, Alaska. *Geophysics* 40: 641-656.

Jackson, D.B. & Kauahikana J. 1988. Regional self-potential anomalies at Kilauea volcano. *Prof. Pap. U.S. Geological Survey* 1350: 947-959.

Krainer, K. & Mostler W. 2002. Hydrology of active rock glaciers: examples from the Austrian Alps. *Arctic, Antarctic, and Alpine Research* 34: 141-149.

Kulessa, B., Hubbard, B. & Brown, G.H. 2003. Cross-coupled flow modeling of coincident streaming and electrochemical potentials and applications to subglacial self-potential data. *Journal of Geophysical Research* 108 (B8): 2381, DOI:10.1029/2001JB001167.

McGrath, P.H. & Henderson, J.B. 1985. *Reconnaissance Ground Magnetic and VLF Profile Data in the Vicinity of the Thelon Front, Artillery Lake Map area, District of Mackenzie.* Paper–Geological Survey of Canada 85-1A: 455-462.

Pirttijärvi, M. 2006. *2LAYINV – Laterally Constrained Two-layer Inversion of VLF-R Measurements*. User's guide, Division of Geophysics, University of Oulu.

Revil, A., Naudet V., Meunier, J.D. 2004. The hydroelectrical problem of porous rocks: inversion of the position of the water table from self-potential data. *Geophysical J. International* 159: 435-444.

Reynolds, J.M. 1997. *An Introduction to Applied and Environmental Geophysics*. Chichester: Wiley, 796 pp.

Rist, A. & Phillips, M. 2005. First results of investigations on hydrothermal processes within the active layer above alpine permafrost in steep terrain. *Norsk Geografisk Tidsskrift* 59 : 157-163.

Scapozza, C. 2008. *Contribution à l'étude géomorphologique et géophysique des environnements périglaciaires des Alpes Tessinoises orientales*. M.S. Thesis. Institute of Geography, University of Lausanne. Published February 28, 2008, on http://doc.rero.ch/

Tenthorey, G. 1992. Perennial nevés and the hydrology of rock glaciers. *Permafrost and Periglacial Processes* 3: 247-252.

Vonder Mühll, D. 1992. Evidence of intrapermafrost groundwater flow beneath an active rock glacier in the Swiss Alps. *Permafrost and Periglacial Processes* 3: 169-173.

Digital Elevation Model of Polygonal Patterned Ground on Samoylov Island, Siberia, Using Small-Format Aerial Photography

M. Scheritz and R. Dietrich
Dresden University of Technology, Institute of Planetary Geodesy, Dresden, Germany
S. Scheller
Dresden University of Technology, Institute of Photogrammetry, Dresden, Germany
W. Schneider and J. Boike
Alfred-Wegener-Institute for Polar- and Marine Research, Potsdam, Germany

Abstract

Accurate land cover, such as meso-scale to high-resolution digital elevation models (DEM), is needed to obtain reliable inputs for modeling the hydrology and the exchange between the surface and atmosphere. Small format aerial photography can be used to acquire high-resolution aerial images using balloons and helicopters. This method presents a low-cost, efficient method to construct a DEM of the polygonal patterned ground on Samoylov Island in the Lena Delta, Northern Siberia (72.2°N, 126.3°E). The DEM should be the foundation for modeling meso-scale hydrological processes on the island and identifying locations of discharge. The whole island could be covered with images taken from heights between 600 m and 800 m. All points of the DEM, with a resolution on the ground of 10 m, have a horizontal and vertical accuracy better than 1.0 m. This accuracy and the resolution depend on the survey height, the resolution of the camera system, the number and the quality of the images, and the algorithms used in the analysis. All listed parameters are explained and discussed in the paper.

Keywords: aerial photography; balloon; digital elevation model; polygonal patterned ground; Samoylov Island.

Introduction

The application of small format aerial photography to acquire high-resolution aerial images is still challenging. Balloons, kites, and helicopters are interesting and valuable tools for aerial photography. Several techniques with their advantages and disadvantages are briefly introduced and discussed in Bigras (1996) and Henry et al. (2002). Boike and Yoshikawa (2003) showed the successful use of balloon aerial photography for mapping snow, ice, and periglacial landforms around Fairbanks and Ny-Alesund, Svalbard. Recently, Vierling et al. (2006) successfully employed a tethered balloon with an altitude up to 2 km to acquire remotely sensed data. Further application fields are briefly explained in Aber and Aber (2002).

The goal of our work was to generate a digital elevation model (DEM, regular or irregular distributed points) of the polygonal patterned ground on Samoylov Island in the Lena Delta, Northern Siberia (72.2°N/126.3°E). The DEM should be the foundation for the modeling of meso-scale hydrological processes on the island for answering questions like: where are polygonal seas, how big are they, and where does the water drain into the Lena?

The landscape of the island is shaped by the micro topography of the wet polygonal tundra. The development of low-centered ice-wedge polygons results in a prominent micro relief with the alternation of depressed polygon centers and elevated polygon rims with elevation differences of up to 0.5 m over a few meters distance. Satellite images with resolutions between 15 m and 30m, such as Landsat (Aber & Aber 2002), do not represent this micro relief sufficiently. Difficulties of using satellite images are discussed in detail by Dare (2005). It is, however, the most important factor for small-scale differences in vegetation type and soil moisture, and is therefore a major variable when considering heat and trace gas fluxes on the meso-scale.

Depending on the general conditions, feasible equipment, cost, and available measurement time, the required horizontal and vertical accuracy of the DEM should be better than 1 m. Since remote-control-aircraft and drones are not permitted in Siberia, we used a tethered helium balloon. In addition it was also possible to take images from a helicopter. The photogrammetric equipment consists of a Nikon D200 with a 14 mm lens, 26 fabric-made targets for ground control points (GCPs), and additional geodetic equipment (tachymeter Elta C30).

This paper presents a low-cost, efficient method to acquire high-resolution aerial images using helium filled balloons. It discusses (1) different steps of obtaining aerial images from a balloon and a helicopter, (2) data analysis, (3) advantages and disadvantages of different assimilation platforms and (4) further improvements to increase the resolution of the DEM and the horizontal and vertical accuracy of the coordinates of each point.

Methods

The motivation mapping of the patterned ground on Samoylov Island was achieved using photogrammetric methods on aerial images with overlapping areas, allowing the determination of 3D coordinates (stereoscopy). There are different methods available ranging from simple stereoscopic methods with two images to a bundle block adjustment (Henry et al. 2002) over all taken images. Here

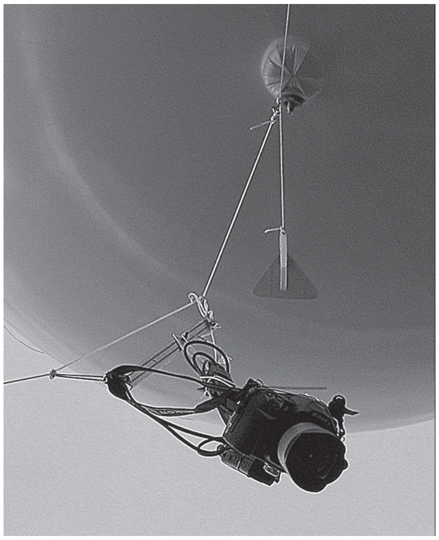

Figure 1. Camera system: Nikon D200, hanging at the tethered helium filled balloon.

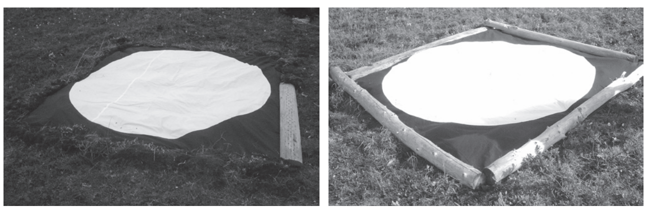

Figure 2. Fabric-made targets used as ground control points with a diameter of 2.5 m.

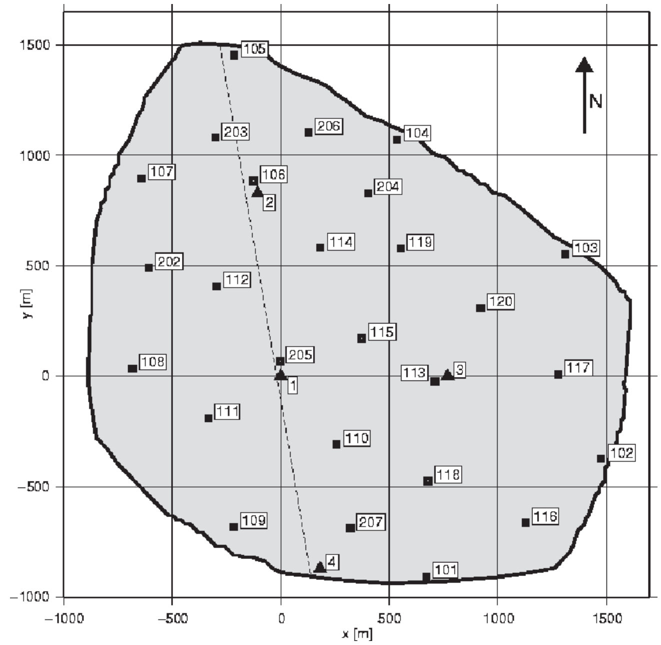

Figure 3. Schematic illustration of Samoylov Island: Network of 26 ground control points (squares); The coordinate (0,0) shows the origin of the local coordinate system with a fixed height of 100 m. The 4 datum points are displayed as triangles. The dashed line separates the flood plain (western part) and the plateau (eastern part).

the former method was used, since the flight path, height, and orientation of the balloon and thus the resulting images were somewhat unpredictable. The data analysis then consisted of two important steps: firstly a separate backward intersection for the calculation of the image orientation and secondly a forward intersection for the calculation of the 3D coordinates of the points of the DEM.

Before the fieldwork was carried out, the optimal camera system and the number of the GCPs was determined. The pre-condition for the DEM was a resolution on the ground better than 10 m with an accuracy in coordinates better than 1 m. Thus prior calculations were done on flight height, the size of the GCPs, the distance between them, and the required number of images covering the whole island. The survey height and the number and size of the GCPs finally were a compromise between the available time for measurement, the investment for the camera system, and the mentioned optimal conditions for resolution and accuracy.

Equipment

The equipment for the aerial photography consists of a Nikon D200 camera with a 14 mm lens (Fig. 1) and 26 fabric-made targets used as GCPs (Fig. 2). The Nikon D200 is a digital mirror reflex camera with a CCD sensor of 10.2 megapixel. With the calculated flight height of 800 m, one pixel maps an area of ~0.12 m² on the ground.

Depending on the flight height, the focal distance of the lens, and the condition that each GCP should represent an area of at least 6 x 6 pixels in the digital images, their diameter had to be greater than 2.0 m (Fig. 2).

To precisely calculate the image orientation, it was necessary to set up enough GCPs on the island to get a minimum of 4 points within each image. Considering the calculated flight height of 800 m, this resulted in at least 20 GCPs (called 101–120) with a spacing of about 500m to get an optimal coverage of Samoylov Island (~5 km²). Six control targets with a diameter of 1.0 m were additionally laid out to condense the point network (point IDs 202–207). The entire network of GCPs is shown in Figure 3.

A local coordinate system on Samoylov Island was fundamental to the photogrammetric fieldwork. Therefore 4 datum points (Fig. 3, point IDs 1–4) were set up, each marked with a 1m iron pipe in the permafrost soil. The distances between these points reached from 800 m to 1200 m. In Figure 3 the coordinate (0, 0) shows the origin of the local coordinate system with a fixed height of 100 m. For setting up the coordinate system we used the tachymeter Elta C30. The repeatability of the coordinates of the datum points was better than +/-2 cm.

Fieldwork

The fieldwork was divided into two parts. Firstly, GCPs were laid out, and their coordinates were surveyed in the local coordinate system. Secondly, aerial photographs were taken using a tethered balloon and a helicopter.

After laying out the GCPs, their registration was conducted

Figure 4. Tethered balloon, filled with helium, diameter 2–3 m.

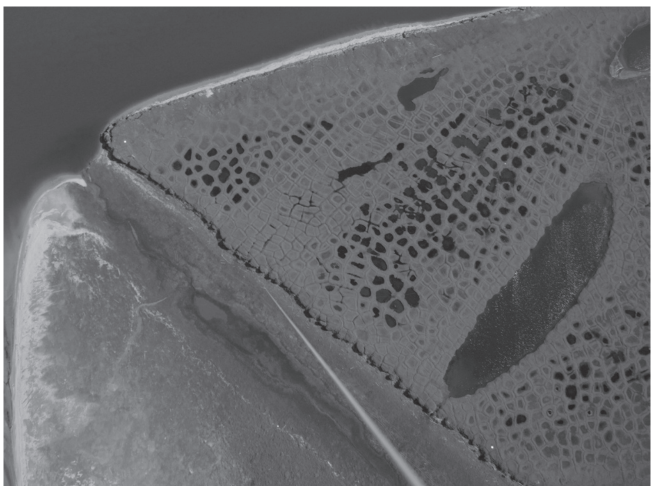

Figure 5. Polygonal patterned ground admitted from a height of ~750 m, in front the rope to the balloon.

in the local coordinate system with help of the tachymeter. The accuracy of the distances between the datum points and the GCPs was better than 1 cm. The coordinates of all GCPs had an absolute accuracy better than +/-5 cm. These accuracies depended on the determination of the center of the GCPs, the accuracy of the angle measurements with the tachymeter, and the distances to the survey points.

The balloon used in mapping the patterned ground on Samoylov Island is depicted in Figure 4, and an example image is given in Figure 5. The interval timer of the camera was adjusted to 1 minute, so the camera could take images for nearly four hours. Using the tethered balloon, one third of the entire island (western part, flood plain, Fig. 3) could be covered from a height of about 800 m.

Additionally, images were captured from a helicopter from altitudes between 600 m and 900 m. Using the helicopter, the middle part of the island could be covered with a flight height of ~600 m, the eastern part with flight heights of nearly 800–900 m.

Table 1. Nikon D200, interior parameters.

Parameter of inner orientation:	
Horizontal size Vertical size	3872 Pixel 2592 Pixel
Pixel size	0.0058mm
Principal point	x_0 = 0.10424mm y_0 = -0.19185mm
Principal distance	c = -13.32284mm
Parameter of distortion dx, dy (without units):	
Radial	a_1 = -0.000495642 a_2 = 1.65615e-006 a_3 = 0.0
Assymetric distortion Tangential distortion	b_1 = 1.72277e-005 b_2 = -1.51355e-005
Affinity Shear	c_1 = 0.000149996 c_2 = 2.72591e-005
r_0 - parameter	r_0 = 8.44

Calibration of the camera system

For the subsequent data analysis it was necessary to determine the parameters of the inner orientation of the camera system (interior parameters: principal distance c, coordinates of the principal point x_0, y_0, parameter of distortion dx, dy). The calibration of the camera system as specified in Luhmann (2000) was conducted before the fieldwork at the Institute of Photogrammetry at the Dresden University of Technology (Table 1).

To verify these camera parameters, a calibration-field was set up on Samoylov Island. Using the Elta C30, the coordinates of these points were measured with a relative accuracy of a few millimeters. The parameters of the inner orientation, that were consecutively determined, were nearly the same as in the laboratory, so the relation between the body of the camera and the objective can be assumed as stable.

Data Analysis

To analyze the collected data, a program was generated based on the algorithms of Luhmann (2000) and Schwidefsky & Ackermann (1976). The program includes the collinearity equations, which correlate the image coordinates (x,y) and the object coordinates (X,Y,Z) for each point:

$$x = x_0 - c \cdot \frac{r_{11}(X - X_0) + r_{21}(Y - Y_0) + r_{31}(Z - Z_0)}{r_{13}(X - X_0) + r_{23}(Y - Y_0) + r_{33}(Z - Z_0)} + dx \qquad (1)$$

$$y = y_0 - c \cdot \frac{r_{12}(X - X_0) + r_{22}(Y - Y_0) + r_{32}(Z - Z_0)}{r_{13}(X - X_0) + r_{23}(Y - Y_0) + r_{33}(Z - Z_0)} + dy \qquad (2)$$

First, a backward intersection was calculated for each single image to determine the outer orientation (perspective center (X_0, Y_0, Z_0) and rotation matrix $\underline{R}$). Approximated parameters of the outer orientation were necessary and could be calculated applying a special algorithm developed by Schwidefsky and Ackermann (1976). The calculation of the outer orientation was successful for all images, which had minimized 4 GCPs.

Second, approximated coordinates for the points of the DEM were determined with help of a regular raster with a step size of 10 m based on the local coordinate system. The height of each point was set up to the average height of all GCPs. With the known outer orientation of the images a backward intersection could be determined for each preliminary point of the DEM, so the approximated positions could be found in the images. Then a search patch was defined around these locations and a matching-algorithm (with sub pixel accuracy) was implemented to locate precisely the same patch in other images. The matching algorithm was calculated with a cross-correlation:

$$k = \frac{\sum_{x'}\sum_{y'} g_1(x',y') \cdot g_2(x+x', y+y')}{\sum_{x'}\sum_{y'} g_1(x',y')^2 \cdot \sum_{x'}\sum_{y'} g_2(x+x', y+y')^2}$$

$$-1 \le k \le 1$$

At each position (x', y') a correlation coefficient k was determined depending on the gray scale value g of each pixel. The output consisted of a correlation image with all calculated values of k. Then, an algorithm was implemented which fitted an ellipsoidal paraboloid in the correlation image to find the exact position of the correlation maximum. At the end a forward intersection was calculated as a least square adjustment to get the exact 3D-coordinates for the points of the DEM.

The output dataset consists of all calculated coordinates, the standard deviation, and the correlation factor for the matching of one point between different images. If the correlation factor is greater than 0.7, and if the accuracy of the coordinates (horizontal and vertical accuracy) is better than 1 m, the point is stored as a point of the resulting DEM of Samoylov Island.

Results

Figure 6 shows the triangulated DEM. The horizontal and vertical accuracy of the coordinates of each point is better than 1.0 m (1σ, i.e., confidence interval of 68%). Polygonal lakes are easy to distinguish, because the algorithm was not able to match over the uniform water surface. Also, areas with bad data coverage are recognizable, for example in the southeastern part of Figure 6. The main reason for this is that the helicopter height changed very fast during the taking of the subsequent images, resulting in changing scaling factors of these images and smaller correlation factors. Other reasons for degraded correlation are poor illumination conditions and insufficient contours. As a result, only few points were found with a correlation larger than 0.7, whereas for most points the correlation factor was lower than 0.5. The island's center and the western and northern part have the best coverage of points. The helicopter was flying over the center at a nearly constant height of 600 m. In addition, the height of the tethered balloon over the flood plain (western part, Fig. 6) was nearly constant, which made the calculations (in particular the matching algorithm) really successful. The estimated points from both datasets could be matched with correlation factors up to 0.99 and with horizontal and vertical accuracies partially better than 0.5 m.

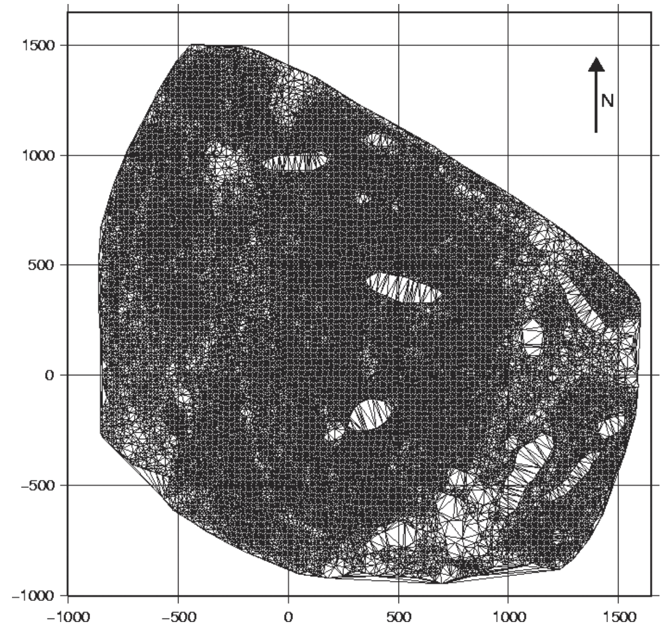

Figure 6. Triangulated irregular DEM with an approximated step size of 10 m of Samoylov Island: x- and y-coordinates are in a local coordinate-system (scale in m).

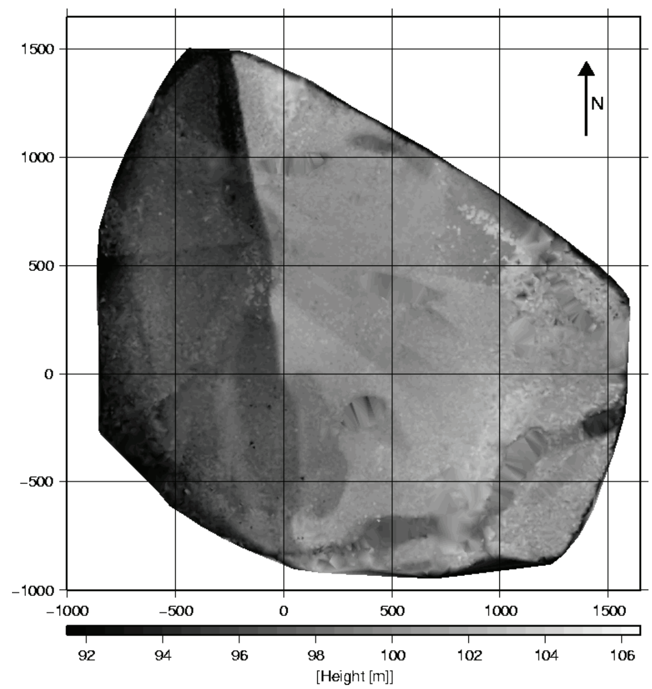

Figure 7. Surface of Samoylov Island: x- and y-coordinates are in a local coordinate system (scale in m). The heights of the points of the DEM are relative heights with respect to the origin of the local coordinate system (0.0) with a height of 100 m.

In Figure 7 the triangulated network from Figure 6 is shown as a surface for the whole island. The flood plain is easy to distinguish, as well as the ridge between the flood plain and the plateau and the cliff line with height differences up to 8 m.

Discussion

The goal of this project was to generate a DEM of the whole of Samoylov Island. The short observation period and the cost of and permission for the equipment formed the boundary conditions for the field work, under which a trade-off between the resolution, accuracy, and practicable amount of work for the acquisition and evaluation of photos had to be found. We finally decided to use a tethered, helium-filled balloon and a camera with a high precision lens (Nikon D200 with 14 mm lens). On the ground, 20 fabric-made targets with a diameter of 2.5 m and 6 targets with a diameter of 1.0 m spanned a network of GCPs.

Taking aerial photographs with a balloon is a low-cost and efficient method to acquire high-resolution aerial images. However, to take images with a balloon-borne camera, a calm day with good illumination conditions is required. Especially the wind speeds limit the observation time – during the 3 weeks of the field work on Samoylov Island we had only 2 days with good weather conditions. Taking images from a helicopter is independent from wind conditions and more stable in maintaining the height and the flight path. But this application is very expensive, and it is also dependent on good illumination conditions.

A sensitive step within the data analysis is the matching algorithm, because different illumination conditions like cloud shadows and different scaling factors of the images are a disadvantage. Also the search patch has to be big enough to get sufficient correlations between different images with high correlation factors. To avoid correlations between neighboring points of the DEM (this would degrade the accuracy of coordinates) the step size has to be at least twice the size of the search patch. Depending on the survey height of 800 m and a search patch of 24 x 24 pixel, the resolution on the ground of the DEM was set to 10 m. Therefore, all points of the generated DEM should be independent from each other.

Under these terms each point of the DEM has a horizontal and vertical accuracy better than 1 m. Naturally there are improvement possibilities to retrieve the micro relief of the polygonal wet tundra, such as the use of more and smaller targets for GCPs concomitant with a lower flight height and thus a higher resolution and accuracy. Furthermore the standard deviation of the coordinates of the DEM improve, if the points can be found in more than 2 images. Therefore, a better and regular image-coverage of the whole island from the same survey heights and good stereoscopic bases (relation between survey height and image-spacing) are a requirement for high resolution DEMs.

Conclusions

The method described in this paper is, depending on the measurement time, cost, and equipment, very useful to measure typical permafrost landscapes with the desired resolution and accuracy. Depending on the survey height and conditions described above, the horizontal and vertical accuracy of each point in the generated DEM of Samoylov Island shown in Figures 6 and 7 is better than 1.0 m for nearly 70% of all triangulated points. The obtained resolution of the DEM amounts to 10 m. Additionally, the combination of images from balloon and helicopter was successful if the flight height was approximately equal.

The meso-scale DEM discussed in this paper is now utilized (at the Alfred Wegener Institute for Polar and Marine Research in Potsdam) to determine the channel routing in a spatially distributed hydrologic model for Samoylov Island. Additionally, it is also possible to generate a orthomosaic (Bitelli & Girelli 2004) with the known parameters of the outer orientation of the images. This methodology provides a good basis for quantification of fluctuating coastlines in permafrost landscapes.

Acknowledgments

This work was funded by the Alfred Wegener Institute for Polar and Marine Research in Potsdam, Germany. We are thankful for the logistical and financial support of the Russian-German research station on Samoylov that made this study possible. We also thank Günter Stoof, Moritz Langer, and Maryvonne Landolt for their assistance in the field and for data discussion and analysis.

References

Aber, J.S. & Aber, S.W. 2002. Unmanned small-format aerial photography from kites for acquiring large-scale, high-resolution, multiview-angle imagery. P*ecora 15/Land Satellite Information IV/ISPRS Commission I/FIEOS 2002 Conference Proceedings.*

Bigras, C. 1997. Kite aerial photography of the Axel Heiberg Island fossil forest. *Proceedings of the First North American Symposium on Small Format Aerial Photography.*

Bitelli, G. & Girelli, V.A. 2004. Low-height aerial imagery and digital photogrammetrical processing for archaeological mapping. *International Archives of Photogrammetry, Remote Sensing and Spatial Information Services*: 498-504.

Boike, J. & Yoshikawa, K. 2003. Mapping of periglacial geomorphology using kite/balloon aerial photography. *Permafrost and Periglacial Processes* 14:0 Wiley InterScience, DOI:10.1002/ 437 pp.

Dare, P. 2005. The use of Small Environmental Research Aircraft (SERAs) for environmental remote sensing. *International Journal of Geoinformatics* 1/3: 19-26

Henry, J.-B., Malet, J.-P., Maquaire, O. & Grussenmeyer, P. 2002. The use of small-format and low-altitude aerial photos for the realization of high-resolution DEMs in mountainous areas: Application to the super-sauze earthflow (Alpes-De-Haute-Provence, France). *Earth Surfaces and Landforms* 27: 1339-1350. DOI:10.1002/esp.411.

Luhmann, Th. 2000. *Nahbereichsphotogrammetrie, Grundlagen, Methoden und Anwendungen*. Heidelberg: Herbert Wichmann Verlag, 571 pp.

Schwidefsky, K. & Ackermann, F. 1976. *Photogrammetrie, Grundlagen, Verfahren, Anwendungen.* Stuttgart: B.G. Teubner, 384 pp.

Vierling, L.A., Fersdahl, M., Chen, X., Li, Zh. & Zimmerman, P. 2006. The Short Wave Aerostat-Mounted Imager (SWAMI): A novel platform for acquiring remotely sensed data from a tethered balloon. *Remote Sensing of Environment* 103: 255-264.

The Yedoma Suite of the Northeastern Siberian Shelf Region: Characteristics and Concept of Formation

Lutz Schirrmeister, Hanno Meyer, Sebastian Wetterich, Christine Siegert
Alfred Wegener Institute for Polar and Marine Research, Telegrafenberg A43, D-14473 Potsdam, Germany
Viktor V. Kunitsky
Permafrost Institute RAS-SB Yakutsk, 677010 Yakutsk, ul. Mersoltnaya, Russia
Guido Grosse
University of Alaska Fairbanks, Geophysical Institute, 903 Koyukuk Drive, Fairbanks, AK 99775, USA
Tatyana V. Kuznetsova, Alexander Yu. Derevyagin
Moscow State University, Geological Faculty, 11991 Moscow, Russia

Abstract

The Yedoma Suite is well exposed along coasts and riverbanks in the northeastern Siberian Arctic. The cryotexture of these mostly ice-supersaturated deposits is similar at most sites—ice bands and reticulated ice lenses. The Yedoma Suite is considered a sequence of buried cryosols, formed under predominantly subaerial conditions. It represents an important terrestrial carbon reservoir (TOC 2–5-wt%). The multimodal grain size distribution does not reflect primarily aeolian accumulation, but rather a mixture of various periglacial transport and accumulation processes based on the concept of nival lithogenesis. The Yedoma Suite age lies in the MIS-3 and MIS-2 periods and, in rare cases, already starts during MIS-4. The palaeoecology of the Yedoma Suite can be summarized in the term "Tundra Steppe," combining both tundra and steppe environmental features. The present occurrence of the Yedoma Suite remains is closely related to low mountain ridges surrounding the northern and northeastern Siberian shelves. The concept of nival lithogenesis is presented, explaining the origin of source material and transport medium.

Keywords: cryolithology; late Pleistocene; northeastern Siberia; palaeo-environment; yedoma.

Introduction

The term *yedoma* is often associated with describing possible reactions of permafrost to global warming (Zimov et al. 2006, Walter et al. 2006, Walker 2007). The word *yedoma* probably originated in Kamchatka and described a boggy site or an elevated meadow-like flat plain. It entered science via the expeditions of Vitus Bering in Siberia during the 18th century. Initially, the term *yedoma* was of geomorphologic origin and described the hills separating thermokarst depressions in East-Siberia, especially in the Yana-Indigirka and Kolyma Lowlands (Kolosov 1947, Baranova & Biské 1964, Mursaev 1984, Tomirdiaro 1980). These mounds were considered to be erosional remnants of former accumulation plains. In this sense, yedoma described a special geomorphological relief type in Siberian permafrost regions, directly formed by thermokarst and thermoerosion (Solov'ev 1959, 1989).

The stratigraphical term *Yedoma Suite* was later adopted for middle Pleistocene horizons in the northeastern Siberian Lowlands (Lavrushin 1963, Vas'kovsky 1963). This stratigraphical position was moved to the late Pleistocene based on faunal studies at the Duvanny Yar site in the Kolyma Lowlands (Sher 1971), which became the stratotype for the Yedoma Suite. This categorization was finally confirmed by the decision of the Interdepartmental Commission on Quaternary Stratigraphy of the Soviet Union in Magadan in 1982 (Sher 1987).

Early genetic conceptions of the Yedoma Suite include glacier-dammed basin sediments (Grosswald 1998), alluvial genesis (Rozenbaum 1981), deltaic formation (Nagaoka et al. 1995), proluvial and slope deposits (Slagoda 2004, Gravis 1969), cryogenic-aeolian (Tomirdiaro et al. 1984, Tomirdiaro & Chernenky 1987), and nival deposits (Galabala 1997) as well as polygenetic origins (Sher et al. 1987).

The deposits of the Yedoma Suite represent unique late Pleistocene palaeoenvironmental archives for a large region of the Northern Hemisphere lacking major glacial records. Within the Russian-German project, System Laptev Sea, these deposits were studied with a multidisciplinary approach (cryolithology, sedimentology, palaeontology, palaeobotany, geochronology, mineralogy, isotope geochemistry, GIS, remote sensing) during the last ten years. We here present a first review of some general results on the overarching features of the Yedoma Suite in the Laptev Sea region and a concept of its formation.

Study Region

Since 1998, we have studied the characteristics of the Yedoma Suite at 15 well-exposed sites on the Laptev Sea and the East Siberian Sea coasts, and in the Lena Delta (Fig. 1). These sites are situated in the lowland plains of the continental shelf on both sides of the current seismically active boundary of the Eurasian and the North American continental plates.

Characteristics of the Yedoma Suite

Occurrence and geomorphology

The occurrence of the Yedoma Suite in the study region is closely related to low mountain ridges (ca. 200 to 400 m a.s.l.) surrounding the northern and northeastern Siberian shelves, which are the major sediment sources for the Yedoma Suite. In the western Laptev Sea and the Lena Delta region the occurrence of the Yedoma Suite is strongly connected with the coastal mountains of the Pronchishchev, Chekanovsky, and Kharaulakh Ridges. Heavy mineral studies at various sites have shown that these ridges are a main source of sediment (Siegert et al. 2002, Schwamborn et al. 2002, Schirrmeister et al. 2003). Therefore, foreland accumulation plains were the areas of the formation of the Yedoma Suite. In the eastern part of the study region, the exposed granite and basalt intrusions on Bol'shoy Lyakhovsky Island and Cape Svyatoy Nos as well as the fault ranges on Bel'kovsky, Stolbovoy, and Kotel'ny Islands serve as source areas for sediments of the Yedoma Suite. The distribution of the ice-rich sequences is easily identified by frequent thermokarst depressions or lakes (Grosse et al. 2005, 2006, 2007).

The Yedoma Suite exposes permafrost cliffs in 10- to 40-m-high horseshoe-shaped thaw slumps or thermocirques along sea coasts and riverbanks (Fig. 2).

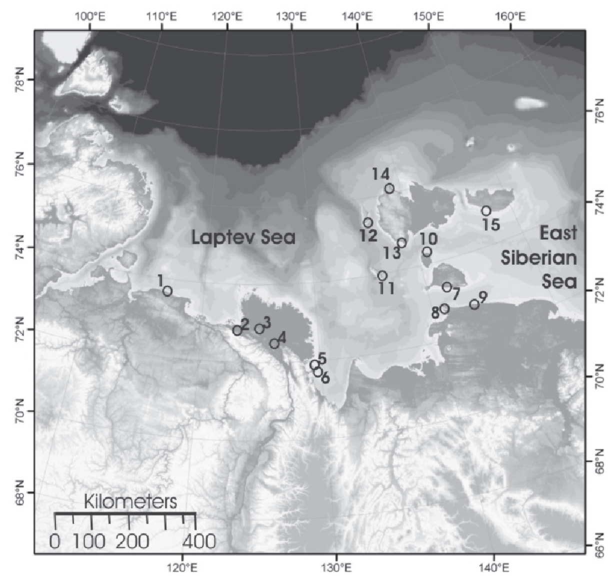

Figure 1. Study sites of the Yedoma Suite between 1998 and 2007. 1: Cape Mamontov Klyk. 2: Ebe Basyn Sise Island. 3: Khardang Island. 4: Kurungnakh Island. 5: Bykovsky Peninsula. 6: Muostakh Island. 7: Bol'shoy Lyakhovsky Island. 8: Syatoy Nos. 9: Oyogos Yar coast. 10: Maly Lyakhovsky Island. 11: Stolbovoy Island. 12: Bel'kovsky Island. 13: Kotel'ny Island. 14: Cape Anisy. 15: Novosibir Island.

Cryolithology

The cliffs are composed of ice wedge bodies and columns of frozen deposits between them, representing vertically or diagonally cut polygonal ice wedge systems. Therefore foliated syngenetic ice wedges of 2–5 m width and 10–40 m height, and separate thermokarst mounds of 2–5 m in diameter and up to 10 m height are the most characteristic features of Yedoma Suite erosion cliffs. Compared to the ice wedges, the intrapolygonal deposits are more resistant to thawing processes because they have a smaller ice content and contain stabilizing peaty paleosol layers alternating with silty-sand layers. These features of continuous permafrost sequences are the result of long-lasting and stable cryogenesis and landscape conditions.

The cryotexture of the Yedoma Suite is quite similar at all of the study sites. The general texture is layered. Ice bands (1–10 cm) alternate with sediment interlayers of variable thickness. These interlayers contain numerous small ice lenses as well as reticulated ice lenses. The frozen sediment sequences are frequently ice-supersaturated, resulting in gravimetric ice contents of 60 to 120% on average (Fig. 3).

Such cryotextures are typical for sediments formed in poorly drained landscapes with a near-surface permafrost table. The formation of these ice bands is a sign of stable surface conditions and stable active-layer depths over a certain time period, resulting in ice aggradation at the top of the permafrost table. The stable isotope signature of ice wedges shows light values for all study sites (site mean

Figure 2. The Yedoma coast at Bol'shoy Lyakhovsky Island. The cliff is about 30 m high (photo: S. Wetterich, July 2007).

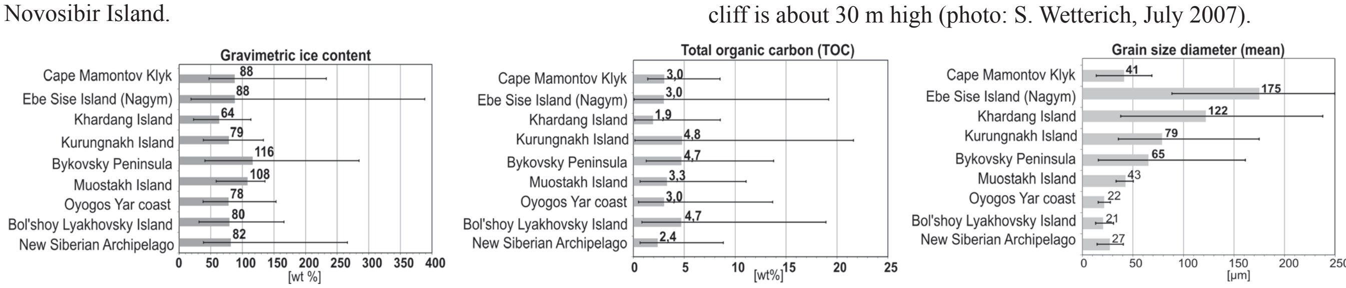

Figure 3. Variation in ice content, TOC content of peat inclusions and sediment, and grain size diameter between various sites of the Yedoma Suite (mean: bar; range: line).

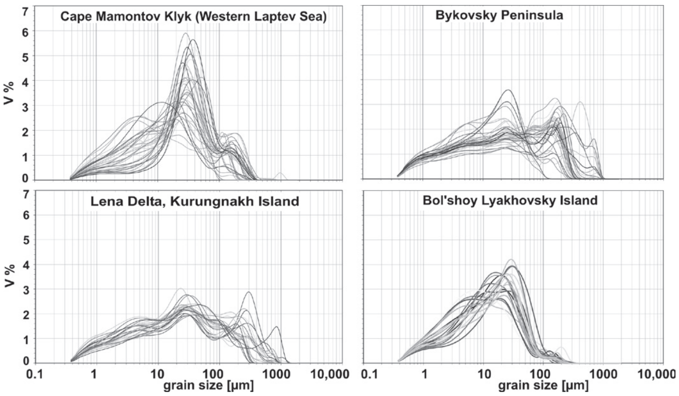

Figure 4. Typical grain-size distribution patterns of the Yedoma Suite at various sites.

values: δD -230 to -260‰, $\delta^{18}O$ -28 to -31‰, d-excess about -6‰) reflecting very cold winter temperatures and moisture sources which are isotopically different from Holocene and modern ones (Meyer et al. 2002a, b).

Organic carbon and grain-size parameters

The Yedoma Suite includes buried cryosols marked by brownish horizons, as well as peat inclusions and/or numerous twigs and leafs. Cryoturbation patterns of 0.5 to 1 m thickness are very common. The organic carbon content is relatively high (1 to > 20 wt%, in average 2 to 5 wt%). Wood fragments and peat are present, with numerous small filamentous rootlets and dispersed organics detritus.

The fine-grained sediments composing the Yedoma Suite are poorly sorted and differ in grain-size parameters from site to site (Fig. 4). Multimodal grain-size distribution patterns reflect a mixture of transport, accumulation, and re-sedimentation processes. Therefore, we conclude that this type of sediment in the Laptev Sea region is not primarily of aeolian origin, a view that is still widely reflected in the scientific literature using the generalizing term "Arctic loess" (e.g., Tomirdiaro 1982, Walker 2007).

Summarizing the special cryolithological and sedimentological characteristics, it is concluded that the frozen deposits of the Yedoma Suite accumulated in a special periglacial facies. The term "Ice Complex" (Soloviev 1959, p. 49) is used for these deposits.

Age determination and stratigraphy

The age of the Yedoma Suite was determined by radiocarbon AMS analyses of about 300 samples and some luminescence datings (Schirrmeister et al. 2002a, 2003, 2008, Grosse et al. 2007, Andreev et al. 2008). The geochronologically determined onset of the Yedoma Suite accumulation varies between about 55 ky BP at the New Siberian Islands and 27 ky BP at the western Laptev Sea coast. The latest deposition is dated between 28 ky BP at the New Siberian Islands and 17 to 13 ky BP in the western Laptev Sea. Unconformities are frequent, up to 20 ky, and probably caused by thermokarst and thermoerosion. The Yedoma Suite predominantly covers the Kargin and Sartan period of the Russian late Pleistocene stratigraphy, which corresponds to the MIS-3 and MIS-2 of the global classification. At Bykovsky Peninsula, the Yedoma Suite is somewhat older, and already started during the Zyryan period (MIS-4) (Meyer et al. 2002a, Schirrmeister et al. 2002b). In general, the lower boundary contrasts sharply with the underlying deposits, which often are fluvial sands with peat layers or loess-like floodplain deposits. These deposits are U/Th and luminescence-dated between 60 and 100 ky). The upper boundary is characterized by separate, locally confined Holocene deposits on top of the Yedoma Suite (Andreev et al. 2004, Krbetschek et al. 2002, Schirrmeister et al. 2003, Grosse et al. 2007).

Table 1. Palaeoenvironmental stages of northeastern Siberian Arctic lowlands during the late Quaternary (inferred from multiproxy analysis of permafrost records, Andreev et al. 2002, 2008).

Allerœd 12 ky	• Tundra with higher bioproductivity • Warming climate • First thermokarst depressions
Sartan 30 - 12 ky	• Sparse grass-sedge tundra • Cold and dry summers, very cold winters • Ice Complex formation
Kargin ca. 50 - 30 ky	• Tundra steppe with high bioproductivity • Relatively warm summers, cold winters • Ice Complex formation
Zyryan ca. 100 - 50 ky	• Sparse grass sedge tundra • Extreme cold and dry climate • Widespread fluvial, lacustrine, and floodplain deposits • Begin of local Ice Complex formation

Palaeoecology (Table 1)

New data for the faunal and floral composition during the formation of the Yedoma Suite in the study region were collected and analyzed within our project "System Laptev Sea" and described in numerous palaeoecological papers (e.g., Andreev et al. 2002, Bobrov et al. 2004, Kienast et al. 2005, Kuznetsova et al. 2003, Sher et al. 2005, Wetterich et al. 2005). The findings are in good agreement with studies; e.g., of Anderson & Lozhkin (2001). The special floral and faunal communities that existed during Yedoma Suite formation disappeared approximately at the Pleistocene-Holocene transition. The palaeo-biosceonosis is called Mammoth Steppe or Tundra Steppe, combining both tundra and steppe features. The climate was more continental in the late Pleistocene Arctic than today, with colder winters and warmer summers and, therefore, stronger seasonal gradients in temperature and precipitation (Meyer et al. 2002a/b, Kienast et al. 2005, Schirrmeister et al. 2002b, 2003, 2008, Wetterich et al. 2008).

Formation of the Yedoma Suite

To explain the formation of the Yedoma Suite, we use the concept of nival lithogenesis proposed by Kunitsky (2007). Several geological processes are important for its formation and can be summarized in four stages (Fig. 6):

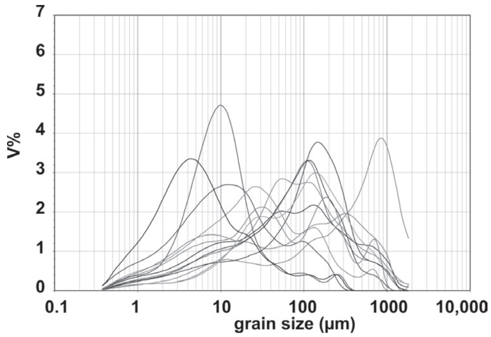

Figure 5. Grain-size distribution curves of clastic remains in various modern snow patches studied around the Laptev Sea.

1. Accumulation of windblown snow together with plant and mineral detritus in numerous perennial snowfields (névés) in topographic features of hills and low mountain ranges (e.g., steep slopes, valleys, cryoplanation terraces, Fig. 6a). Similar processes, but at a smaller scale, are observed today at numerous sites in northeastern Siberia, where nival processes are an essential relief-forming factor (Kunitsky et al. 2002).

2. A concentrated detritus mat forms due to repeated thawing of accumulating snow, transport of detritus by meltwater, and downslope accumulation of plant and mineral debris. Intense freeze-thaw cycles and wet conditions around and below the perennial snowfields support the formation of fine-grained material by frost weathering (Fig. 6b). Such processes are also observed in modern snowfield areas. Grain-size analyses of modern clastic material show similar multimodal patterns as the Yedoma Suite (Fig. 5).

3. Discharge of clastic and organic detritus proceeded by snowfield meltwater runoff. Fine-grained debris was subsequently distributed by alluvial, fluvial, proluvial, and partly also aeolian transport to piedmont plains, cryoplanation terraces or large alluvial fans (Fig. 6c).

4. Ice Complex formation consisted of concurrent processes of sediment accumulation, ground ice segregation, syngenetic ice wedge growth, sediment reworking, peat aggradation, cryosol formation, and cryoturbation (Fig. 6d).

The formation of huge polygonal ice wedge systems and thick continuous sequences of frozen deposits is closely related to the persistence of stable, poorly drained, low-topographic gradient accumulation plains.

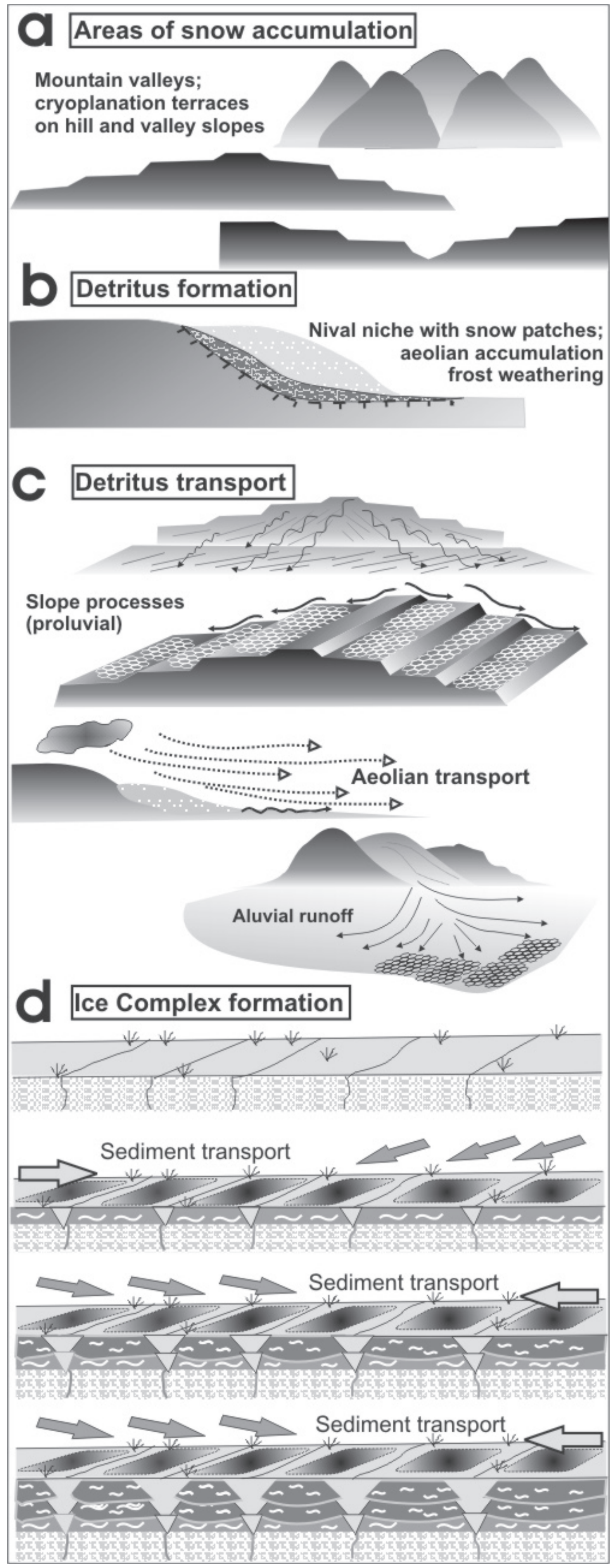

Figure 6. Scheme of Yedoma Suite formation.

Conclusions

The Yedoma Suite is an important paleoenvironmental archive that spans large regional and chronological gaps in the proxy information of the late Pleistocene Arctic. Consistent cryolithological, sedimentological, and palaeo-ecological features (Tab. 2) reflect similar environmental conditions for a wide variety of sites, representing a special periglacial facies.

Concluding, the Yedoma Suite includes a massive carbon and freshwater reservoir susceptible to release by global warming. In order to estimate and calculate the role of these widespread ice- and organic-rich frozen deposits in Siberia in a future warming Arctic, we must improve our knowledge of their characteristics and origin. The specific combination of strongly continental climate and the local landscape permitted syngenetic formation of ice wedges and organic-rich, ice-supersaturated sequences, called Ice Complex or the Ice Complexes of the Siberian Arctic.

Table 2. Typical features of the Yedoma Suite in the shelf region of northeastern Siberian.

Cryolithology	Ice-supersaturated, syngenetic ice wedges, segregation ice
Sediment	Poorly sorted, organic-rich silty sand
Formation age	80 to 12 ky BP
Stratigraphy	(MIS-4) to MIS-2
Palaeoecology	Tundra Steppe/Mammoth Steppe
Climate	High continental, arid
Genesis	Nival lithogenesis, alluvial, proluvial, and aeolian accumulation
Landscape	Lowland plains and cryoplanation terraces
Terminology	Ice Complex deposits compose the Yedoma Suite, which is preserved in Yedoma hills

Acknowledgments

This paper is based on the joint Russian-German science cooperation "System Laptev Sea" supported by the German Ministry of Education and Research. The Russian as well as the German Science Foundation promoted these environmental studies with several projects. We thank all Russian and German colleagues who help us during field work and laboratory studies, but especially S. Kuzmina, M. Grigoriev, W. Schneider, V. Tumskoy, A. Sher, V. Rachold, G. Schwamborn, F. Kienast, P. Tarasov, A. Eulenburg, and U. Bastian. In addition, we thank P.P. Overduin for the native speaker correction as well as D. Froese and one anonymous reviewer for their helpful hints.

References

Anderson, P.M. & A.V. Lozhkin 2001. The stage 3 interstadial complex (Karginskii/middle Wisconsinan interval) of Beringia: variations in paleoenvironments and implications for paleoclimatic interpretations. *Quaternary Science Reviews* 20, 93-125.

Andreev, A.A., Schirrmeister, L., Siegert, C., Bobrov, A.A., Demske, D., Seiffert, M. & Hubberten H.-W. 2002. Palaeoenvironmental changes in northeastern Siberia during the Upper Quaternary: Evidence from pollen records of the Bykovsky Peninsula. *Polarforschung,* 70: 13-25.

Andreev, A.A. et al. 2008. Weichselian and Holocene palaeoenvironmental history of the Bol'shoy Lyakhovsky Island, New Siberian Archipelago, Arctic Siberia. *Boreas* (in review).

Baranova, Yu.P. & Biské, S.F. 1964. *North East USSR: History of Relief Formation in Siberia and Far East*. Moscow: Nauka, 290 pp. (in Russian).

Bobrov, A.A., Andreev, A.A., Schirrmeister, L. & Siegert, Ch. 2004. Testate amoebae (Protozoa: Testacea) as bioindicators in the Late Quaternary deposits of the Bykovsky Peninsula, Laptev Sea, Russia. *Palaeogeography Palaeoclimatology Palaeoecology*, 209: 165-181.

Galabala, R.O. 1997. Pereletki and the initiation of glaciation in Siberia. *Quaternary International*, 41/42: 27-32.

Gravis, G.F. 1969. *Slope Deposits in Yakutia*. Moscow: Nauka, 128 pp. (in Russian).

Grosse, G., Schirrmeister, L., Kunitsky, V.V. & Hubberten, H.-W. 2005. The use of CORONA images in remote sensing of periglacial geomorphology: An illustration from the NE Siberian coast. *Permafrost and Periglacial Processes* 16: 163-172.

Grosse, G., Schirrmeister, L. & Malthus, T.J. 2006a. Application of Landsat-7 satellite data and a DEM for the quantification of thermokarst-affected terrain types in the periglacial Lena-Anabar coastal lowland. *Polar Research* 25: 51-67.

Grosse, G., Schirrmeister, L., Siegert, C., Kunitsky, V.V., Slagoda, E.A., Andreev, A.A. & Derevyagyn, A.Y. 2007. Geological and geomorphological evolution of a sedimentary periglacial landscape in Northeast Siberia during the Late Quaternary. *Geomorphology* 86: 25-51.

Grosswald, M.G. 1998. Late-Weichselian ice sheets in Arctic and Pacific Siberia. *Quaternary International,* 45/46: 3-18.

Kienast, F., Schirrmeister, L., Siegert, C. & Tarasov, P. 2005. Palaeobotanical evidence for warm summers in the East Siberian Arctic during the last cold stage. *Quaternary Research* 63: 283-300.

Kolosov, D.M. 1947. *Problems of Former Glaciation of Northeast Siberia*. SevMorPut, 175 pp. (in Russian).

Krbetschek, M.R., Gonser, G. & Schwamborn G. 2002. Luminescence dating results on sediment sequences of the Lena Delta. *Polarforschung* 70: 83-88.

Kunitsky, V.V., Schirrmeister, L., Grosse, G. & Kienast, F. 2002. Snow patches in nival landscapes and their role for the Ice Complex formation in the Laptev Sea lowlands. *Polarforschung* 70: 53-67.

Kunitsky, V.V. 2007. *Nival lithogenesis and Ice Complex on the territory of Yakutia.* Abstract of the state doctoral dissertation. Permafrost Institute Yakutsk, 46 pp. (in Russian).

Kuznetsova, T.V., Sulerzhitsky, L.D., Andreev, A.A., Siegert, C., Schirrmeister, L. & Hubberten, H.-W. 2003. Influence of Late Quaternary paleoenvironmental conditions on the distribution of mammals fauna in the Laptev Sea region. *Occasional Papers in Earth Sciences* 5: 58-60.

Lavrushin, Yu.A. 1963. *Lowland Rivers Alluvium of the Subartic Region and Periglacial Area of the Continental Glaciation*. Academy of Science USSR 87, 266 pp. (in Russian).

Meyer, H., Derevyagin, A.Y., Siegert, C. & Hubberten H.-W. 2002a. Paleoclimate studies on Bykovsky Peninsula, North Siberia. Hydrogen and oxygen isotopes in ground ice. *Polarforschung* 70: 37-52.

Meyer, H., Siegert, C., Derevyagin, A.Y., Schirrmeister, L. & Hubberten, H.-W. 2002b. Palaeoclimate reconstruction on Big Lyakhovsky Island, North Siberia: Hydrogen and oxygen isotopes in ice wedges. *Permafrost and Periglacial Processes* 13: 91-103.

Mursaev, E.M. 1984. *Glossary of Local Geographical Terms*. Moscow: Mysl, 653 pp. (in Russian).

Nagaoka, D., Saijo, K. & Fukuda, M. 1995. Sedimental environment of the Edoma in high Arctic eastern Siberia. In: K. Takahashi, A. Osawa, & Y. Kanazawa (eds.), *Proceedings of the Third Symposium on the Joint Siberian Permafrost Studies between Japan and Russia,* 8-13.

Rozenbaum, G.E. 1981. Special features of lithogenesis of the alluvial planes in the Eastern Subarctic as related to the problem of the Ice (Yedoma) Complex. In: *Problems of Cryolithology*, 9. Moscow: MSU Press, 87-100. (in Russian).

Schirrmeister, L., Siegert, C., Kunitsky, V.V., Grootes, P.M. & Erlenkeuser H. 2002a. Late Quaternary ice-rich permafrost sequences as a paleoenvironmental archive for the Laptev Sea Region in northern Siberia. *Int. J. Earth Sci.* 91: 154-167.

Schirrmeister, L. et al. 2002b. Palaeoenvironmental and palaeoclimatic records from permafrost deposits in the Arctic region of Northern Siberia. *Quaternary International* 89: 97-118.

Schirrmeister, L., Kunitsky, V.V., Grosse, G., Schwamborn, G., Andreev, A.A., Meyer, H., Kuznetsova, T., Bobrov, A. & Oezen, D. 2003. Late Quaternary history of the accumulation plain north of the Chekanovsky Ridge (Lena Delta, Russia): A multidisciplinary approach. *Polar Geography* 27: 277-319.

Schirrmeister, L. et al. 2008. Periglacial landscape evolution and environmental changes of Arctic lowland areas during the Late Quaternary (Western Laptev Sea coast, Cape Mamontov Klyk) *Polar Research* (in review).

Schwamborn, G., Rachold, V. & Grigoriev. M.N. 2002. Late Quaternary sedimentation history of the Lena Delta. *Quaternary International* 89: 119-134.

Sher, A.V. 1971. *Mammals and Late Pleistocene Stratigraphy of the Northeast USSR and of North America.* Moscow: Nauka, 312 pp. (in Russian).

Sher, A.V., Kaplina, T.N. & Ovander, M.G. 1987. Unified regional stratigraphic chart for the Quaternary deposits in the Yana-Kolyma Lowland and its mountainous surroundings: Explanatory note. In: *Decisions of Interdepartmental Stratigraphic Conference on the Quaternary of the Eastern USSR*. Magadan, 1982. USSR Academy of Sciences, Far-Eastern Branch, North-Eastern Complex Research Institute, Magadan, USSR, 29-69. (in Russian).

Sher, A.V., Kuzmina, S.A., Kuznetsova, T.V., & Sulerzhitsky, L.D. 2005: New insights into the Weichselian environment and climate of the Eastern-Siberian Artic, derived from fossil insects, plants, and mammals. *Quaternary Science Reviews* 24: 533-569.

Siegert, C., Schirrmeister, L. & Babiy, O. 2002. The sedimentological, mineralogical and geochemical composition of Late Pleistocene deposits from the Ice Complex on the Bykovsky Peninsula, Northern Siberia. *Polarforschung* 70: 3-11.

Slagoda, E.A. 2004. *Cryolithogenic Deposits of the Laptev Sea Coastal Plain: Lithology and Micromorphology*. Tyumen: Publishing and Printing Centre “Express,” 119 pp. (in Russian).

Solov’ev, P.A. 1959. *The Cryolithozone in the North Part of the Lena-Amga-Interfluve.* Publ. Academy of Science of the USSR, 144 pp. (in Russian).

Solov’ev, P.A. 1989. Permafrost (Cryolithozone). In: I.A. Matveev et al. (eds.). *Agriculture Atlas of the Yakutian ASSR, 96-97* (in Russian).

Tomirdiaro, S.V. 1982. Evolution of lowland landscapes in northern Asia during Late Quaternary time. In: D.V. Hopkins, J.V. Matthews Jr., Ch.E. Schweger & S.B. Young (eds.), *Paleoecology of Beringia*. New York: Academic Press, 29-37.

Tomirdiaro, S.V., Arslanov, K.A., Chernenkiy, B.I., Tertychnaya, T.V. & Prokhorova, T.N. 1984. New data on formation of loess-ice sequences in Northern Yakutia and ecological conditions of mammoth fauna in the Arctic during the late Pleistocene. *Reports Academy of Sciences USSR* 278, 1446-1449 (in Russian).

Tomirdiaro, S.V. & Chernen’ky, B.I. 1987. Cryogenic deposits of East Arctic and Sub Arctic. AN SSSR Far-East-Science Center, 1-196 (in Russian).

Vas’kovsky, A.P. 1963. Stratigraphic outline of Quaternary deposits in northeastern Asia. In: *Geology of the Koryaksky Mountains.* Moscow: Gostoptekhizdat, 24-53 (in Russian).

Walker, G. 2007. A world melting from the top. *Nature* 446: 718-721.

Walter, K.M., Zimov, S.A., Chanton, J.P., Verbyla, D. & Chapin III, F.S. 2006. Methane bubbling from Siberian thaw lakes as a positive feedback to climate warming. *Nature* 443: 71-75.

Wetterich, S., Schirrmeister, L. & Pietrzeniuk, E. 2005. Freshwater ostracodes in Quaternary permafrost deposits in the Siberian Arctic. *Journal of Paleolimnology* 34: 363-376.

Wetterich, S. et al. 2008. Palaeoenvironmental dynamics inferred from late Quaternary permafrost deposits on Kurungnakh Island (Lena Delta, Northeast Siberia, Russia). *Quaternary Science Review* (in review).

Zimov, S.A., Schuur, E.A.G. & Chapin III, F.S. 2006. Permafrost and the global carbon budget. *Science* 312: 1612-1613.

Mid- to Late-Quaternary Cryogenic Weathering Conditions at Elgygytgyn Crater, Northeastern Russia: Inference from Mineralogical and Microtextural Properties of the Sediment Record

Georg Schwamborn
Alfred Wegener Institut für Polar und Meeresforschung, Potsdam, Germany
Annika Förster
RCOM - DFG Research Center Ocean Margin, Universität Bremen, Bremen, Germany
Bernhard Diekmann
Alfred Wegener Institut für Polar und Meeresforschung, Potsdam, Germany
Lutz Schirrmeister
Alfred Wegener Institut für Polar und Meeresforschung, Potsdam, Germany
Grigory Fedorov
Arctic and Antarctic Research Institute, St. Petersburg, Russia

Abstract

Two sediment-mineralogical properties were tested as proxy data reflecting the intensity of cryogenic weathering. They were applied to lake sediments from Elgygytgyn Crater Lake in Chukotka, Siberia, and to frozen deposits from the catchment that serve as a reference for in situ weathering conditions. (1) The relative amounts of quartz and feldspar in different silt fractions yield the so-called cryogenic weathering index (CWI). High CWI values, as deduced from the samples, are related to the mineralogically selective weathering resulting from freeze-thaw cycles in the upper permafrost. (2) Image analysis of scanning electron micrographs (SEM) of quartz particles allows characterization and semi-quantification of grain morphology and surface features stemming from frost weathering (i.e., flaky surfaces, microcracking). The constant presence of cryogenic weathering signals both in lake sediments and frozen deposits suggests the long-term prevalence of stable permafrost conditions in the area at least since 220 ka.

Keywords: cryogenic weathering; quartz-feldspar ratio; microtextural properties; paleoenvironment reconstruction.

Introduction

Today, the majority of Siberian landmasses are subject to permafrost conditions. This is also the case for most of the Quaternary (Kaplina 1981, Brigham-Grette 2004, Hubberten et al. 2004). Nonetheless, until now no continuous record has been available that could be used to demonstrate variability of permafrost conditions for that time, nor have any suitable proxy data been tested. Such a sediment record could now become available through studies at Elgygytgyn Crater Lake in northeastern Siberia.

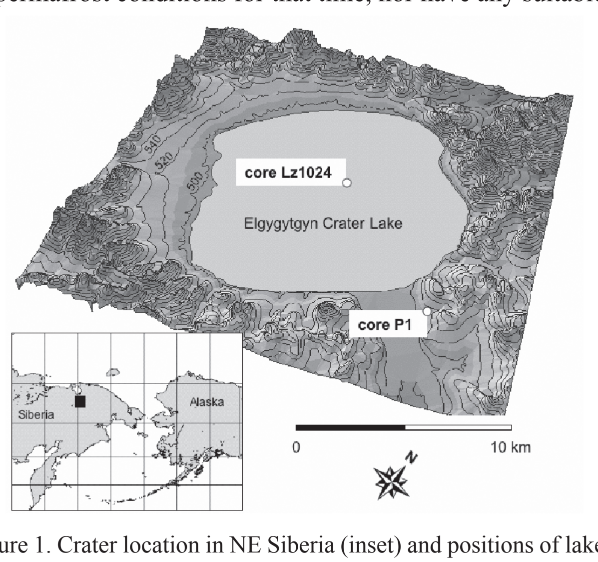

Figure 1. Crater location in NE Siberia (inset) and positions of lake sediment core Lz1024 (67°30.13′N,172°06.46′E) and permafrost core P1. The shoreline is 495 m above sea level.

Frost weathering, slope dynamics, and fluvial outwash are among the main surface processes, and they trigger erosion and detrital sediment transport into the lake basin. Continuous periglacial denudation is assumed for the Quaternary (Glushkova & Smirnov 2007). Tracing signals of cryogenic weathering from the catchment into the lake basin provides a direct land-to-lake linkage within paleoenvironmental reconstruction and will enlighten the permafrost history of non-glaciated NE Siberia. The development of a sediment-mineralogical approach to obtain proxy data for cryogenic weathering is the content of this paper. We use material from former coring into the lake and frozen deposits of the catchment (Melles et al. 2005).

Environmental Setting

Elgygytgyn Crater Lake, 12 km in diameter and 170 m in water depth at maximum (Fig. 1), holds sediments that mirror glacial to interglacial cyclicity and regional environmental change at millennial time resolution (Nowaczyk et al. 2002). The sediments consist of clayey silts and silty clays with occasional sand layers (Asikainen et al. 2007). Based on sedimentological data (physical properties, organic, and isotope geochemistry), distinct climate-related sediment units have been identified that are primarily controlled by fluctuating carbon, nitrogen, and opal contents and linked to a changing extent of lake ice cover; i.e., "cold + moist," "cold + dry," "warm," and "peak warm" (i.e., Eemian interglacial) (Melles et al. 2007). The sediment units alternate in the last 250 kyr, the time span that is covered by the first recovered sediment cores (Juschus et al. 2007, Nowaczyk et al. 2007). We assume a fairly constant surface denudation processes in the confined catchment of the crater lake, which makes the site a natural laboratory for studying the production of weathering debris in the catchment and its subsequent deposition in the adjacent lake sediment column. Longer core retrieval is planned (Melles et al. 2005), which will yield a climate record more than 3 million years old, since the origin of Elgygytgyn Crater is attributed to a meteoritic impact 3.6 M yr ago (Layer 2000). Thus, there will be the potential to identify the assumed onset of permafrost conditions across the Pliocene/ Pleistocene boundary. The altitude of the lake is 495 m above sea level (a.s.l.), and the highest peaks forming the crater walls are about 900 m a.s.l. Local basement rocks are of volcanic origin and are part of the Late Cretaceous Okhotsk-Chukotka volcanic belt (Belyi 1998, Layer 2000, Ispolatov et al. 2004). The rocks consist largely of andesitic to rhyolitic tuffs and ignimbrites of primarily acidic composition. Some subalkaline basaltic andesites have been identified framing the crater lake to the southwest.

Methods

Indicator data for paleo frost weathering: (I) mineral composition

In terms of sedimentology, the destruction of quartz grains is a basic process during the formation of cryogenic debris. As established in experiments, cryogenic disintegration promotes a relative accumulation of quartz grains in the silt fraction (10–50 microns); whereas fresh feldspars and heavy minerals accumulate in the sand fraction (50–100 microns) (Konishchev 1982). This mineralogically selective weathering is active under water-saturated freezing-thawing cycles (Minervin 1982). Expressed in a so-called *Cryogenic Weathering Index* (CWI), the role of cryogenic weathering in frozen soil formation can be estimated (Konishchev 1998):

$$CWI = (Q_1 / F_1) / (Q_2 / F_2) \qquad (1)$$

where Q_1 is quartz content (%) in the fine fraction; F_1 is feldspar content (%) in the fine fraction; Q_2 is quartz content (%) in the coarse fraction; and F_2 is feldspar content (%) in the coarse fraction.

CWI values greater than 1.0 argue for cryogenic weathering that influences the grain-size dependent mineral composition. Comparison of measurements from regionally distributed sediment samples of Arctic Siberia show that warm-climate sediments clearly can be discriminated from cold-climate samples (Konishchev & Rogov 1993). According to that study, Palaeogene-aged samples have CWI values ranging clearly below 1. Towards the Late Neogene and the Early Quaternary, the CWI values reach 1.7. In the lower and middle Pleistocene, values become as high as 3.3. The Eemian has falling values down to 1.7, before values rise again to a maximum of 3 at Weichselian time. Holocene CWI values range from 1.6 to 2.1. Indication of cryogenic weathering according to the CWI has already been implemented into permafrost modeling spanning the last 400 kyr (Romanovskii & Hubberten 2001). In our study, relative quartz and feldspar contents have been determined using standard x-ray diffractometry methods (Ehrmann et al. 1992, Vogt 1997) on a Philips PW 1820 goniometer that used a CoKα radiation (40 kV, 40 mA).

Indicator data for paleo frost weathering: (II) grain morphology and grain surfaces

Grain shapes and grain surface microtextures of mostly quartz and feldspar are well-established means to characterize sedimentary deposits and infer the environmental history from single grain morphology (Krinsley & Doornkamp 1973, Diekmann 1990, Mahaney 2002). Whereas single grain features are well-defined in the case of aeolian, glacial, and fluvial sediments, comparable features associated with mechanical encroachment in frozen ground is only sparsely documented, but appears distinctive (Konishchev & Rogov 1993, Van Hoesen & Orndorff 2004). Angular outlines and micromorphology such as high relief, sharp edges, and articulate steps are most frequent. They have been found in Holocene samples of Elgygytgyn Crater slope deposits (Schwamborn et al. 2006). Here, considerable amounts of grains are characterized by weathered surfaces; flakiness and microcracks were common features when inspected on SEM imagery. The grain surface features are particularly diagnostic for frozen ground sediments, since their production can be directly linked to the destructive effect of thaw-freeze alternation.

Sedimentary material

Lake sediments from core Lz1024 (Fig. 1) down to 12.2 m sediment depth were first measured for grain size distributions of 43 non-turbidite samples using a laser particle analyser (LS200, Beckman Coulter, Inc.). The studied interval spans the last 220 kyr according to the age model of Juschus et al. (2007). In contrast to Konishchev & Rogov (1993), CWI measurements are based on fractions 2–20 microns and 20–63 microns, since first grain size measurements revealed that lake sediments have a major mode at about 20 microns (Fig. 2). Grain shape and grain surface features have been characterized on at least 20 randomly selected quartz grains in each of 28 lake sediment samples. Chemical treatment of the samples followed standard techniques that are outlined elsewhere (Schwamborn et al. 2006). Hereafter, CWI calculations and SEM analysis have been applied.

Frozen deposits were recovered down to 5 m depth in a slope at the crater margin (P1 in Fig. 1). The dated core material shows a correct age-to-depth relation back into the Late Pleistocene (Schwamborn et al. 2006). For CWI calculation, seven samples have been selected that extend over the Holocene. They serve as a reference of in situ cryogenic weathering of the periglacial landscape.

Results and Discussion

Mineral composition

The clayey silts and silty clays from lake sediment core Lz1024 yielded a mean CWI value of 1.6, whereby the minimum value is 1.0 (11.7 m depth), and the maximum value is 3.5 (11.2 m depth) (Fig. 3). The silty sands and sandy silts from permafrost core P1 have a mean CWI value of 1.1, whereby the minimum value is 0.9 (0.7 m depth), and the maximum value is 1.4 (3.7 m depth) (Fig. 3).

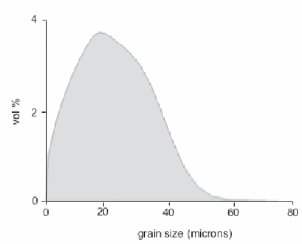

Figure 2. A typical grain size curve of lake sediments displaying the mode at 20 microns (sample from 10.64 m core depth).

All lake sediment CWI values are higher than 1.0 and thus fit well into the range of sediments from the glacial cycles. This argues for the presence of cryogenic conditions throughout the studied time interval. The variability around the mean is independent from sediment units and glacial to interglacial modes (Fig. 3). Several aspects are considered, which influence grain break-up and mixture of cryogenic detritus in the basin. (1) Warm periods are associated with higher temperature gradients in the active layer, thus increasing thermal stress to the grains and subsequent mechanical break-up. (2) Increasing moisture promotes the frequency of microcracking, when water migrates into fissures and subsequently disrupts the grains when crystallizing to ice. Both aspects (1 and 2) are also taking place in soil layers with fluctuating negative temperatures, but to an unknown degree. (3) Varying microclimates at rock surfaces, varying salt concentrations, and biotic encroachment (i.e., lichen growth) contribute to rock fragmentation to an unknown degree (Miotke 1988, Hall & André 2003, Guglielmin et al. 2005). (4) The particle size of source material may vary through time. (5) Soil weathering products that have been eroded and transported into the lake basin are reworked in the

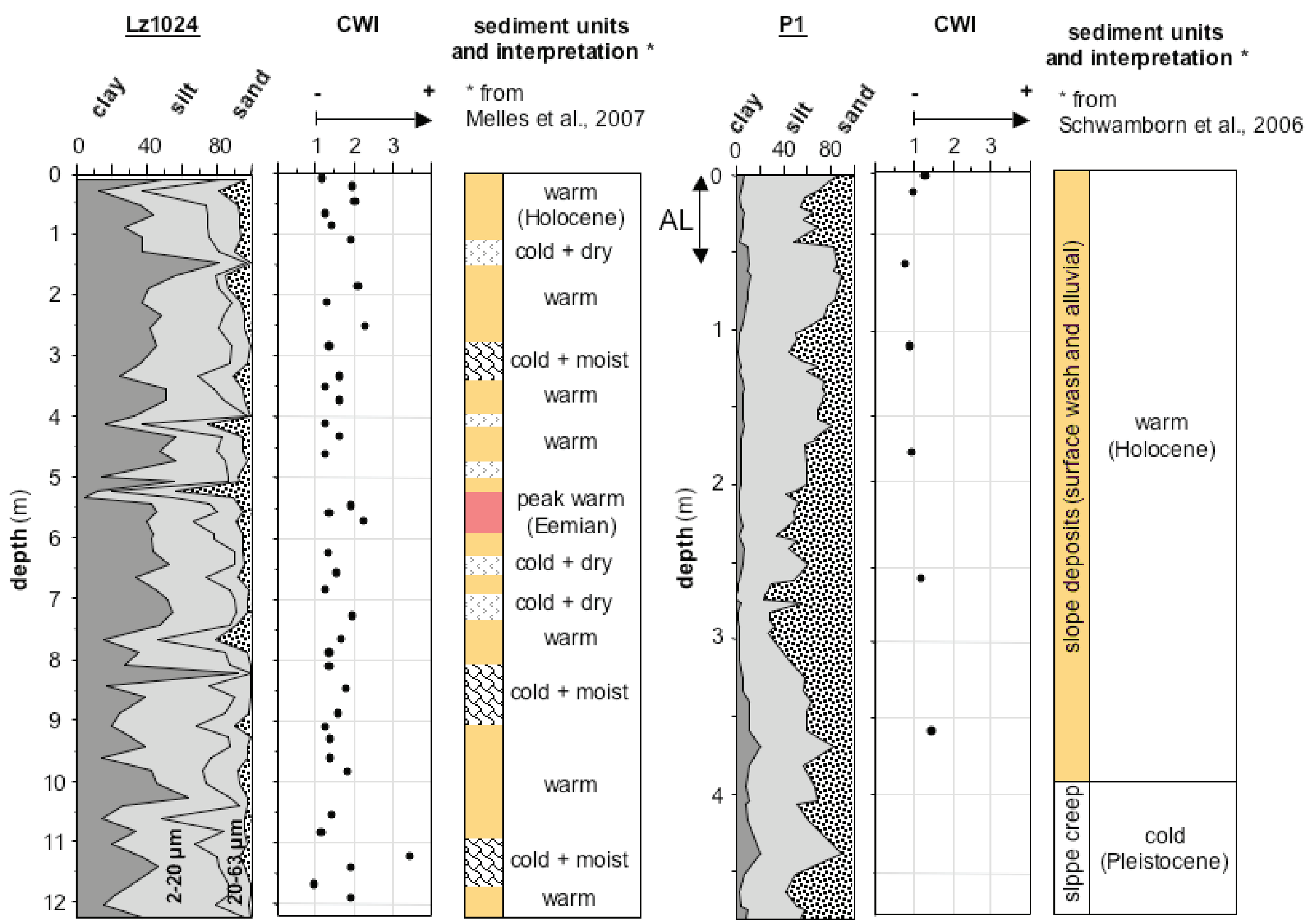

Figure 3. Values of the cryogenic weathering index (CWI) calculated for lake sediment core Lz1024 and permafrost core P1. Basic sediment interpretation schemes are added (see references). AL = Active layer.

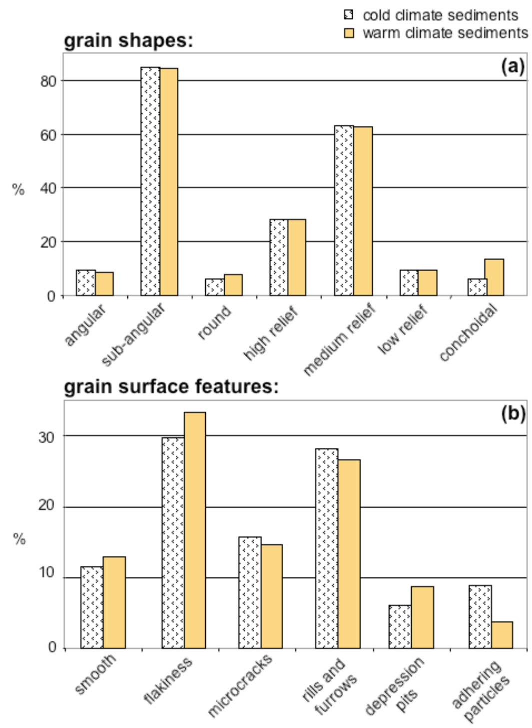

Figure 4. Grain shapes (a) and surface features (b) counted with quartz grains (63–125 microns) from lake sediment core Lz1024 (n=560).

shoals when strong winds from NW or SE lead to a thorough turbulence of the uppermost water column during the open water season. This leads to sediment mixing in the marginal shoals that also may add to blur the original CWI signal. (6) Changing lake levels contribute to sediment mixing, since the exposed and subsequently eroded areas around the lake have changed through time (Glushkova & Smirnov 2007, Schwamborn et al. 2007).

The near-surface permafrost around the lake produces low CWI values under Holocene warm-climate conditions (~1.0). Minor sediment mixing due to transport and reworking processes are associated with the environmental setting of P1 deposits (e.g., hill creep, slope wash, alluvial deposition), since the weathering debris is accumulated in a piedmont setting (Schwamborn et al. 2006).

Grain morphology and grain surfaces

Subangular grains are most common, but angular and round grains can also be found at all lake sediment core depths (Figs. 4, 5). Grains with conchoidal fractures, with smooth surfaces, brittle surfaces, and microcracks occur throughout the lake sediments, but to a lesser extent. Irregular, angular shapes (Fig. 5-1) argue for a short-distance transport, whereas conchoidal features (Fig. 5-4) suggest that pressure occurs either during in situ rock fragmentation or hill creep. Rounded grains (Fig. 5-3) represent the eolian portion that is drifted and deposited in the lake basin. However, estimates of the modern eolian input into the lake sediments yield a portion smaller than 5% (Fedorov pers. com.). V-shaped depression pits occur occasionally and point to grain-to-grain percussion during aquatic transport.

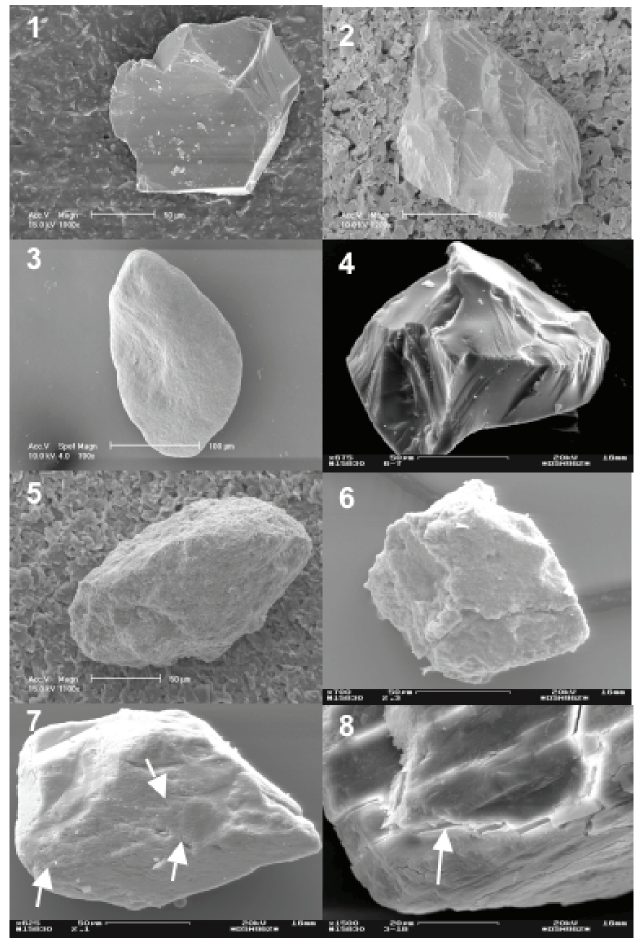

Figure 5. Examples of SEM micrographs from lake sediment quartz grains (63–125 microns); grain shapes: angular (1), subangular (2), rounded (3), conchoidal (4); grain surface features: brittle and flaky surfaces (5 + 6), cryogenic microcracking (7 + 8, see arrows).

Quartz grains exhibit abraded and softened areas, which can act as source areas for silt particles (Figs. 5-5, 5-6). Likewise, microcracks promote separation of silt-sized fragments and conspicuously display the destructive effect of cryogenic widening in the microscale to a varying degree (Figs. 5-7, 5-8). Descriptions of brittle grain surfaces along with microcracks are associated with cryogenic destruction within the thaw-freeze cycles in the uppermost permafrost (Konishchev. & Rogov 1993), or they have been described as crushing features (Van Hoesen & Orndorff 2004). They are present in Elgygytgyn lake sediments, and when medium- to high-relief grains become fragmented due to cryogenic cracking, the connection between SEM and CWI analysis is most obvious.

The discrimination between cold-climate and warm-climate sediments (Fig. 4) does not exhibit prominent quantitative differences between the two. All characteristics can be identified to varying degrees at all sediment depths. Frost weathering features like brittle surfaces and microcracking demonstrate that traces of cryogenic destruction inherited from permafrost processes are well-preserved within the lake sediment column.

For frozen deposits from the catchment, grain micromorphology assessments are already available (Schwamborn et al. 2006). Angular outlines and microfeatures such as high relief, sharp edges, and articulate steps were most common and were consistently observed for all samples. This was linked to short transport distances from their source rocks. Many grains were characterized by rough and weathered surfaces. Flakiness and microcracks were common features. The grain surface textures appear particularly diagnostic for frozen ground sediments, since their production can be directly linked to the destructive effect of thaw–freeze alternation. Frost weathered surfaces and cryogenic cracking point to the sandy grains as the source areas of silt particles. This highlights in situ disintegration, especially of quartz grains, after they were subject to thaw–freeze dynamics (Konishchev and Rogov, 1993).

Conclusions

Despite some blurring effects (e.g., mixing of detritus resulting from weathering and from depositional processes, and sediment reworking in the lake margins due to lake level changes) CWI and SEM analysis can link lake sediments and frozen slope deposits for paleoenvironment interpretation. The studied sediment properties suggest that cryogenic weathering was persistent around Elgygytgyn Crater Lake for at least the last 220 kyr.

An unknown temporal offset between the creation of cryogenic features in the catchment and the material deposition in the lake has to be taken into account when interpreting the timescale within the paleoenvironmental archives.

The combination of grain size, CWI, and SEM results is considered a helpful technique to identify on- and off-set of permafrost conditions in the area when inspecting future drill cores that go beyond 3 M yr back in time.

Acknowledgments

Martin Melles and Olaf Juschus, Cologne University, provided access to the lake sediment samples, Helga Kemnitz, GFZ Potsdam, helped with the SEM facilities. Their assistance is greatly appreciated. Financial support has been granted by the BMBF (German Ministry of Science and Education). The reviewers' comments helped to improve the paper.

References

Asikainen, C.A., Francus, P. & Brigham-Grette, J. 2007. Sedimentology, clay mineralogy and grain size as indicators of 65 ka of climate change from El´gygytgyn Crater Lake, Northeastern Siberia. *Journal of Paleolimnology* 37: 105-122.

Belyi, V.F. 1998. Impactogenesis and volcanism of the El'gygytgyn depression. *Petrology* 6(1): 86-99.

Brigham-Grette, J. 2004. Response to Grosswald and Hughes (2004)–Letter to the Editor, *Quaternary Research* 62: 227-232.

Diekmann, B. 1990. Granulometrie und Sandkornmorphoskopie alpiner Glazialsedimente. *Zbl. Geol. Paläont.* Teil 1, 1989 (9/10): 1407-1421.

Ehrmann, W., Melles, M., Kuhn, G. & Grobe, H. 1992. Significance of clay mineral assemblages in the Antarctic Ocean. *Marine Geology* 107: 249-273.

Glushkova, O.Yu. & Smirnov, V.N. 2007. Pliocene to Holocene geomorphic evolution and paleogeography of the El´gygytgyn Lake region, NE Russia. *Journal of Paleolimnology* 37: 37-47.

Guglielmin, M., Cannone, N., Strini, A. & Lewkowicz, A.G. 2005. Biotic and abiotic processes on granite weathering landforms in a cryotic environment, Northern Victoria Land, Antarctica. *Permafrost and Periglacial Processes* 16: 69-85.

Hall, K. & André, M.-F. 2003. Rock thermal data at the grain scale: applicability to granular disintegration in cold environments. *Earth Surface Processes and Landforms* 28: 823-836.

Hubberten, H.W., Andreev, A., Astakhov, V., Demidov, I., Dowdeswell, J.A., Henriksen, M., Hjort, C., Houmark-Nielsen, M., Jakobsson, M., Kuzmina, S., Larsen, E., Lunkka, J.P., Lysa, A., Mangerud, J., Möller, P., Saarnisto, M., Schirrmeister, L., Sher, A.V., Siegert, C., Siegert, M.J. & Svendsen, J.I. 2004. The periglacial climate and environment in northern Eurasia during the last glaciation. *Quaternary Science Reviews* 23(11-13): 1333-1357.

Ispolatov, V.O., Tikhomirov, P.L., Heizler, M. & Cherepanova, I.Yu. 2004. New 40Ar/39Ar ages of Cretaceous continental volcanics from Central Chukotka: implications for initiation and duration of volcanism within the northern part of the Okhotsk Chukotka volcanic belt (Northeastern Eurasia). *The Journal of Geology* 112: 369-377.

Juschus, O., Preusser, F., Melles, M. & Radtke, U. 2007. Applying SAR-IRSL methodology for dating fine-grained sediments from Lake El´gygytgyn, north-eastern Siberia. *Quaternary Geochronology* 2: 187-194.

Kaplina, T.N., Kartashova, G.G., Nikitin, V.P. & Shilova, G.N. 1983. New data about sand sequence in the Tuostakh depression. *Bulletin of the Comission of Quaternary Studies* 52: 107-122 (in Russian).

Konishchev, V.N. 1982. Characteristics of cryogenic weathering in the permafrost zone of the European USSR. *Arctic and Alpine Research* 14(3): 261-265.

Konishchev, V.N. 1987. Origin of loess-like silt in Northern Siberia. *GeoJournal* 15(2): 135-139.

Konishchev, V.N. 1998. Relationship between the lithology of active layer materials and mean annual ground temperature in the former USSR. *Proceedings 7th International. Conference Permafrost, June 23-27, Yellowknife, Canada,1988*: 591-594.

Konishchev, V.N. & Rogov, V.V. 1993. Investigations of cryogenic weathering in Europe and Northern Asia. *Permafrost and Periglacial Processes* 4: 49-64.

Krinsley, D.H. & Doornkamp, J.C. 1973. *Atlas of quartz sand surface textures*. Cambridge: Cambridge University Press; 91 pp.

Layer, P. 2000. Argon-40/Argon-39 age of the El'gygytgyn impact event, Chukotka, Russia, *Meteoritics & Planetary Science* 35: 591-599.

Mahaney, W.C. 2002. *Atlas of sand grain surface textures and applications*. Oxford: Oxford University Press, 237 pp.

Melles, M., Minyuk, P., Brigham-Grette, J. & Juschus, O. (eds.) 2005. *The Expedition El'gygytgyn Lake 2003 (Siberian Arctic).* Bremerhaven: Reports on Polar and Marine Research 509, 139 pp.

Melles, M., Brigham-Grette, J., Glushkova, O.Yu., Minyuk, P.S., Nowaczyk, N.R. & Hubberten, H.W. 2007. Sedimentary geochemistry of core PG1351 from Lake El´gygytgyn–a sensitive record of climate variability in the East Siberian Arctic during the past three glacial-interglacial cycles. *Journal of Paleolimnology* 37: 89-104.

Minervin, A.V. 1982. In: Konishchev, V.N. & Rogov, V.V. 1993. Investigations of cryogenic weathering in Europe and Northern Asia. *Permafrost and Periglacial Processes* 4: 49-64.

Miotke, F.D. 1988. Microclimate, weathering processes and salt within ice-free continental Antarctica. *Polarforschung* 58(2/3): 201-209.

Nolan, M. & Brigham-Grette, J. 2007. Basic hydrology, limnology, and meteorology of modern Lake El´gygytgyn, Siberia. *Journal of Paleolimnology* 37: 17-35.

Nowaczyk, N.R., Minyuk, P., Melles, M., Brigham-Grette, J., Glushkova, O., Nolan, M., Lozkhin, A.V., Stetsenko, T.V., Anderson, P.M. & Forman, S.L. 2002. Magnetostratigraphic results from impact crater Lake El´gygytgyn, northeastern Siberia: a 300 kyr long high-resolution terrestrial paleoclimatic record from the Arctic. *Geophysical Journal International* 150: 109-126.

Nowaczyk, N.R. & Melles, M. 2007. A revised age model for core PG1351 from Lake El´gygytgyn, Chukotka, based on magnetic susceptibility variations tuned to northern hemisphere insolation variations. *Journal of Paleolimnology* 37: 65-76.

Romanovskii, N.N. & Hubberten, H.W. 2001. Results of permafrost modeling of the lowlands and shelf on the Laptev Sea region, Russia. *Permafrost and Periglacial Processes* 12: 191-202.

Schwamborn, G., Meyer, H., Fedorov, G., Schirrmeister, L. & Hubberten, H.W. 2006. Ground ice and slope sediments archiving Late Quaternary paleoclimate and paleoenvironment signals at the margins of Lake El'gygytgyn impact crater, NE Siberia. *Quaternary Research* 66: 259-272.

Schwamborn, G., Fedorov, G., Schirrmeister, L., Meyer, H. & Hubberten, H.-W. 2007. Periglacial sediment variations controlled by lake level rise and Late Quaternary climate at El'gygytgyn Crater Lake, Arctic Siberia. *Boreas*. DOI: 10.1111/ j.1502-3885.2007.00011.x.

Van Hoesen, J.G. & Orndorff, R.L. 2004. A comparative SEM study on the micromorphology of glacial and nonglacial clasts with varying age and lithology. *Canadian Journal of Earth Sciences* 41: 1123-1139.

Vogt, C. 1997. *Regional and temporal variations of mineral assemblages in Arctic Ocean sediments as climatic indicator during glacial/interglacial changes*. Bremerhaven: Reports on Polar Research 251(30-42), 309 pp.(in German).

Investigation and Monitoring of Tailing Dams in Northeast Russia Using Geoelectrical Methods

Boris M. Sedov
North-Eastern Scientific Research Institute, Far East Branch, Russian Academy of Science, Magadan, Russia
Alexander V. Muslimov
JSC "Ecogeophysics"
Pavel E. Tikhmenev
Omolon Gold Mining Company, Kubaka Mine

Abstract

Geoelectrical methods are recommended for identification and location of seepage zones in permafrost areas. These include vertical electric sounding, and profiling of apparent electric resistances and self-potential. Methods are based on significant specific electric resistance difference between frozen and thawed soils, and self-potential is generated by filtrating flows. Changing the distance between points of vertical electric sounding allows us to build 3D fields of electric resistance $\rho_a(x_i, y_i, z_i)$. Filtration zones appear with low ρ_a values and low (negative) self-potential. Comparison of ρ_a fields measured in different periods allows use to monitor the temperature changes and state of the frozen material, and to forecast and prevent possible seepage with minimum financial effort. Use of the described techniques demonstrate their high efficiency during technical condition determination of water reservoirs dams, technical water retention dams at gold and silver mining enterprises, and at diamond mines.

Keywords: control; dam; filtration; geoelectrical methods; monitoring; permafrost.

Introduction

Northeastern Russia is part of the cryolithozone, with its permafrost base stretching from tens to hundreds of meters in depth. Despite this, the upper soil layer has fluctuating temperatures, often above the melting point. This balanced natural process causes no negative environmental changes. Under technogenic influence, geochemical and thermal changes are much greater then natural factors. In northeast Russia, such negative technogenic effects on soils are caused by hydrotechnical facilities such as tailings and water reservoirs.

Use of cyanide process for gold and silver extraction in Northeast Russia brings up the problem of massive toxic waste storage in permafrost zones. Besides tailings facilities, there are varieties of clean and technical water reservoirs, reservoirs for thermal and hydro-electrical plants, tailings facilities of diamond mines, and more. All these hydrotechnical structures are formed with dams, and are mostly situated in river valleys. Depending on the object's use, dams could be permeable or water retaining. Large volumes of water affect the temperature of the frozen material up to its thaw. Lowering the melting point of frozen material in contact with highly mineralized technical solution can also lead to solution seepage. Investigation of such seepage zones, the determination of their location, and monitoring of technical status of hydro technical structures is successfully performed with use of geoelectrical methods.

Geotechnical Characteristics of Dams and Underlying Base Rock in Permafrost Zones of Northeast Russia

Most rivers at Northeast Russia follow tectonic fault zones. Besides tectonic fracture, vertical cracking as a result of cryogenic deformation appears even in solid bedrock. For example, at Kupol Mine (Central Chukotka), such cracks in basalt are 50–70 m deep and can be traced for hundreds of meters on the surface. Similar cracking in a different rock type were observed in Saha (Yakutia), when tailings facilities for diamond mines were in construction. Granites in the area of the Kolyma River Hydroelectrical Plant have very similar block type form. The absence of tectonic mirrors on joint surfaces within fault zones testifies to the cryogenic genesis of these fractures, as does the absence of tectonic displacement. Such cracks, as a rule, are not filled with ice, but just "capped" with delluvial material 1–2 m at the top. Mostly, such cracks were found during removal of the upper delluvial layer. Filling these cracks at road crossings was not successful, nor was filling with concrete as large amounts were simply draining in.

Basic Technical Peculiarities of Dam Structure in the Russian Northeast

Currently in Northeastern Russia (Yakutia, Chukotka and Magadan Regions), there are number of operating and abandoned tailings facilities and reservoirs. Places in Magadan Region, where geoelectrical investigations were performed, are shown on Figure 1.

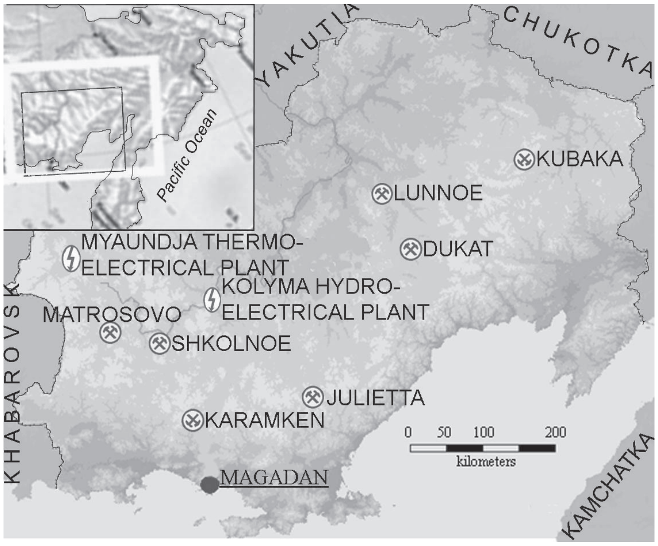

Figure 1. Location of sites where geoelectrical methods were applied to investigate the dam status.

Regardless of design, dams in Russian Northeast are constructed of local materials. Depending on the dam's purpose, there are two different types: permeable (filtering) and watertight (water retaining) (Biyanov 1983) Permeable (filtering) dykes are designed to separate technical solutions and solid parts from sludgy tailings. Sometimes, additional filtering dykes are built on the surface of the tailings for the same reason. Below the filtering core, reclaimed technical water is taken back into the process.

What follows is a general overview of tailings facilities structural peculiarities at various mining enterprises. As a good example, we will describe Kubaka gold mine, the first joint-stock gold mining enterprise with a foreign investor in Magadan Region. During operation from 1997 to 2006, over 90 tons of gold were mined and extracted using the cyanide process. During exploitation, dams were raised to increase the tailings facility capacity. It was situated on the valley side, so no upper dam was needed (Fig. 2). Cleared water was draining through the filtering dyke into a reclaimed water pond, where it was taken into the process again. The water retention dam had a frozen core, formed by over 100 thermo siphons inserted through the dam into bedrock. These were installed in 1998, when geoelectrical sounding showed that dam's core and underlying bedrock had melted zones and technical solution was seeping through. Pipes were filled with carbon dioxide. Foreign engineering companies were developing most sufficient variants of Kubaka deposit mining and foreign investors were implementing them. Kubaka's tailings facilities are example of good handling of a variety of technical challenges. Tailings facilities were inspected with geoelectrical methods several times during operation.

The Kubaka mine was performing a closure procedure during 2007; tailings were caped with 1.5 m of waste rock, 0.5 m of silty shale and 0.3 m of top soil for vegetation. Since waste rock was placed during winter time on frozen tailings, it remained frozen during summer and heavy mining equipment was hauling material on top of capped tailings without sinking. This is a unique example of full reclamation of a tailing facility in Northeast Russia.

Karamken Gold Mine (operated from 1978 to 1995) is situated 100 kilometers north of Magadan. Karamken Mine Tailings facility is situated in the mid-flow of Tumanniy creek. There was a need to prevent inflow of upper creek water into the tailings facility. An impermeable upper dam was guiding into a diversion channel.

In order to maintain impermeability of the upper dam, a row of holes with pipe casing was emplaced. A refrigerator was pumping the cooling agent ($CaCl_2$). Freezing the dam's core created an impermeable barrier. The diversion channel was originally made of concrete U-shaped sections which deformed quickly, and steel lining was placed inside to maintain the level needed for water flow. Its abandoned tailings facility used a different approach for separation of water from the slurry then used at the Kubaka mine. The technical solution was settling and seeping through the dykes and tails and was accumulating at the sump, which was dug at the deepest point of the wooden tunnel and down to the bedrock below the dam.

Currently, despite shut down of the Karamken mine, liquid waste from the Kolyma Refinery is frequently discharged in the Karamken tailings facility.

Tailings facilities at other Magadan region gold and silver mines which use the cyanide process were constructed later then the Karamken and Kubaka facilities. Mostly, they have polymer lining. Tailings facilities of the Vetrenskoe mine was very similar to Kubaka, with reclaimed water sump in the old bed of the diverted creek.

Tailings facilities of Saha (Yakutia) diamond mines have only one watertight dam, the frozen core providing its impermeability. The core is kept frozen by pipes filled with kerosene. Reclaimed water was accumulating in the pond next to the dam.

There are many more plains in Saha (Yakutia) then in the Magadan region, so the areas occupied by diamond mines in Saha (Yakutia) are greater, and dams are lower but longer then tailings facilities in Magadan region mines.

Besides mining enterprises, there are a variety of hydrotechnical structures in the region such as reservoirs for domestic use near towns, and technical water reservoirs for hydro and thermoelectrical plants. The largest volume of water is held by a major dam 150 m high at the Kolyma River Hydroelectrical Plant. The dam is constructed in highly fractured granite, where the fractures have different genesis.

Miaundja Thermo Electrical Plant, built in the early 1950s, has a technical water reservoir. It has a frozen core, which is cooled with air circulating through a wooden tunnel throughout the dam's center during the winter period. The dam is constructed on highly fractured shales.

Dams have a shape of trapezium in cross-section, with the lower face terraced with benches.

Another peculiarity of the Russian Northeast that affects hydrotechnical structures besides permafrost is the high seismicity of some areas in the region.

Tailings facilities, water reservoirs and other hydrotechnical structures bring a local influence to a surrounding frozen material. This includes heat brought with highly thermo conductive water or technical solutions. To protect a dam from melting, extra material is placed from its influenced upper face. This material protects frozen material from heat exchange with water. In addition, heat exchange tailings facilities are influenced by mineralized solution which lowers the ice melting point.

These would be two main reasons for infiltration appearance; through the dam's core as well as through fractured bedrock. A variety of technical accidents on hydrotechnical facilities in Chukotka emphasizes the seriousness of such infiltrations. Roughly every reservoir was loosing water because of infiltrations (Demchenko et al. 2005).

Localizing infiltration zones using non-geophysical methods like drilling is slow and costly, and introduces additional heat to dam's material.

Geoelectrical Methods of Controlling and Monitoring Dams in Northeast Russia

Geoelectrical methods of determining filtration zones is widely used in permafrost free regions; e.g., for mudslides sounding (Bogoslovsky & Ogilvy 1970). Their localization is determined by self-potentials survey, their minimums show the object.

Physical Basis of Geoelectrical Methods for Detection of Seepage and Melting Zones

In permafrost regions, the first applications of geoelectrical methods for determining melted zones in dams and bedrock where performed after several accidents involving water reservoirs (Kadykchan town, Miaundja Thermo Electrical Plant) occurred in permafrost areas of Northeast Russia. Geoelectrical methods from geophysics were used for localization of melting areas and filtration zones. Water flow in a filtration zone creates a field of self-potentials; the magnitude increases with an increase of mineralization level and flow speed. During methods development, the fact of low self-potentials in fresh water filtrations was discovered. Soil resistivity in permafrost studies showed that melting soils increases their conductivity by three orders of magnitude (Frolov 1998, Yakupov 2000). In the case of mineralized solution, resistivity of melted soils is near zero Ω-m. Later, during investigation of seepage zones at the Northeastern (permafrost zone) mining enterprises' tailings facilities, highly mineralized solutions were stated as significant sources of self-potentials as well.

Complex of Geoelectrical Methods for Detection of Dams' Melting and Seepage Zones

Geoelectrical methods from geophysics are used by our team for determination of filtration zones through dams and bedrock, during technical control and monitoring at Northeast Russia (Saha (Yakutia) and Magadan Regions) (Muslimov & Sedov 2006). They include vertical electric sounding (VES), electrical profiling of CD (Schlumberger array), very low frequency (VLF) and self-potential (SP) profiling; all performed on standard equipment. VES uses a symmetrical Schlumberger array (C_1O = 1,5; 2,0; 3,0; 4,5; 6; 9; 12; 16; 20; 30; 40; 80; 110; 150; 200 and 300 m, P_1P_2 = 2; 10 m, C_2 - ∞). Lateral profiling used a half Schlumberger array P_1P = 2.0 m. In winter, we have electrode contact problems and then VES and electric profiling are replaced by alternate current (AC) methods. Time domain electromagnetic survey (TDEM) is search conductor mineralized filtrate. Configuration uses central loop mode and transmitting loop of 20x20 m. The seepage zone has very low resistance. TDEM is faster and cheaper, and can be used all year round since grounding is not needed. Electrical profiling is typically performed on two feeder distances or two different frequencies. This gives the apparent resistances typical for two different depths.

VES, electrical profiling, VLF and TDEM with measuring stations on the dam's crest, benches and lower face is performed as an initial step. Stations interval is 20 m. Electrical profiling of the perimeter may be done as well, if needed. VES measurements are done on dam's crest and benches, as well as at locations which showed low resistances on initial electrical profiling.

Depending on the approach used, geoelectrical sounding results are presented as graphs with resistivity profiles - $\rho_a(x_i)$, pseudo depth plot - $\rho_a(x_i, z_i)$, apparent resistivity contours - $\rho_a(x_i, y_i)$, profile and contours in mV SP, VES curves - $\rho_a(z_i)$ and its interpretation. For technical monitoring of dams, VES provides the most interesting data. It is presented as three dimension (3D) coordinates ρ_a (x_i, y_i, z_i). The developed software allows one to use any "slice" of the collected data for determination of the filtration zones. Mostly, apparent resistance profiles ρ_a (x_i, z_i) and ρ_a (y_i, z_i) along and across the dam body are used. Lateral sections $(z_к)$ ρ_a for different depths ρ_a (x, y, z_n) can be done. Quantitative interpretation (determination of true specific resistance ρ_n) at a certain point with (x_i, y_{ii}, z_i) coordinates is very difficult. This statement is based on the fact that a dam's structure, even if it would be made out of material with invariable resistance, is very complex and does not correspond to conditions required for quantitative interpretation of VES, developed for horizontal stratum of infinite stretch (Hallof 1981). This limitation of VES is valid for any other geological task. The accuracy of the quantitative interpretation is determined by intersecting VESs. Coinciding resistance curves testify that the stratum is horizontal and infinite. Despite quantitative interpretation of VES is not possible, the technical monitoring task was fulfilled successfully, as experimental works results show. Let us describe this statement with the following example. Despite any misrepresentations caused by a complex dam profile, apparent resistances along or across dam's axis will be similar if there are no filtration zones. Only along the dam's flanks, where interfacing environments have some influence, will variations be seen. Abnormally low resistances in the cross section will appear in the filtration (melting) zones, despite their scale, and are very well distinguished on the apparent resistance minimum cross sections. The coordinates of the filtration zone is determined by tracing this zone of low resistances in the row of profiles for the dam's body, or in the bedrock beneath. Besides VES, self-potential profiling along the dam's axis is performed during summer and early autumn. Filtration zones are seen as negatives anomalies. This anomalies SP depend on flow velocity and increases with higher flow velocity.

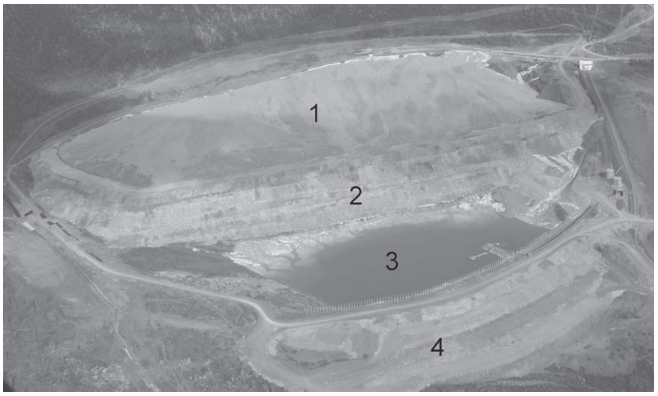

Figure 2. Kubaka Mine tailings facility (Omolon Gold Mining Company, KINROSS GOLD).

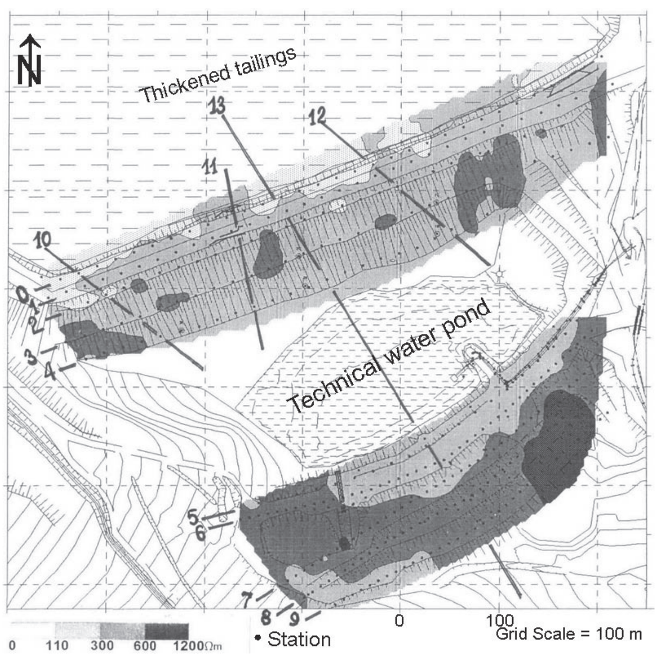

Figure 3. Apparent resistivity contours (Ω-m) for upper (filtering) dyke and lower (water retention) dam, Kubaka Mine (Schlumberger array AO = 2 m).

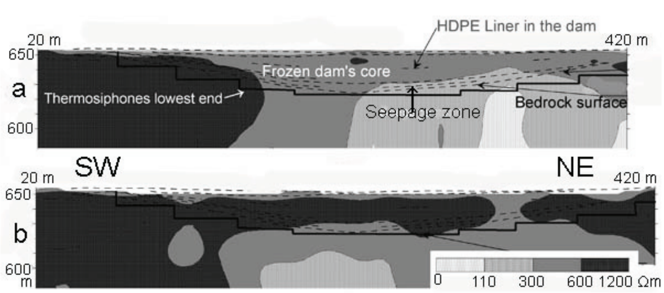

Figure 4. (a) – profile of resistivity in year 1998; (b) – year 2003 (profile position is shown on Fig. 3).

Examples of Determining Location of Filtration and Melting Zones by Geoelectrical Methods for Controlling and Monitoring Dams in Permafrost Regions of Northeast Russia

Using geoelectrical methods described above to locate melting and seepage zones, we will discuss results on specific hydrotechnical structures of different genesis and use. As a very positive example, we will discuss results of monitoring at Kubaka Mine tailings facility (Fig. 2).

It includes thickened tailings (1), filtering dyke (2), reclaimed water pond (3) and water retention dam (4), which holds highly mineralized technical solution.

During seven years, the filtering dyke was built up several times to increase projected capacity. The first year of water retention dam surveying indicated dam instability, and signs of minor seepage of technical solution into the creek below. After geoelectrical control in 1998 was performed on both structures, seepage zones were identified. For seepage zones

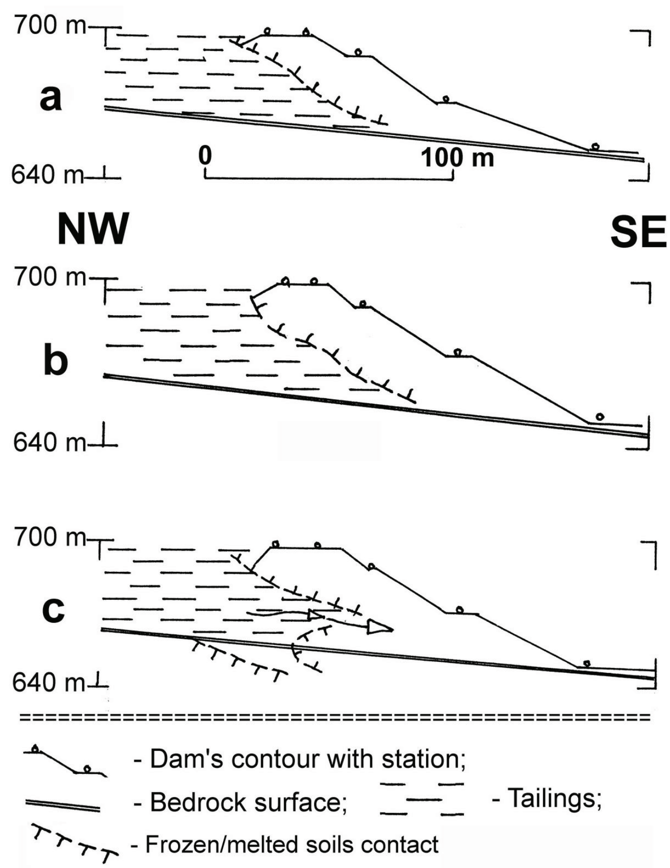

Figure 5. Seepage locations in the upper (filtering) dyke, according to the cross section resistances profiling. Geoelectrical control performed in year 2003.

determination, longitudinal VES profiling was performed (Fig. 3).

Seepage zones were marked with self-potential minimums on the profile, which was compared with VES stations. Later, melted and seepage zone distribution in the dam was confirmed during drilling work to install thermosiphons. The distance between thermosiphons pipes was around 2.0 meters, and they were nailed through the dam into the bedrock. Their bottom line is shown as a step-looking straight line. Figure 4a shows the location of melting and seepage zones four months after the thermosiphons were installed in 1998. Technical solution seepage was stopped after melted zones froze. Soil freezing increased ρ_a (x_i, z_i) and showed clearly during VES. Bedrock resistivity changed insignificantly (Figure 4b). Ceased seepage was marked by negative anomalies of SP disappearance. Geoelectrical methods (VES, SP TDME) were used for melting zones and filtration location in the filtering dyke, as well. Geoelectrical data complex interpretation allowed us to determine the location of filtration zones, pointing out areas blocked with compacted pulp (Fig 5a and 5b). Filtration zones were marked not only with low resistivity ρ_a, but with significantly low SP (Fig. 5c).

On the pseudo plot, melting and seepage zones were shown as areas with minimum apparent resistances.

A 3D apparent resistivity model indicates the distribution of dyke and dam melting zones. Upper face material is influenced with technical solution, and has zones with temperatures above the melting point. This zone is shown as an area with low electric resistance (Fig. 6). The melting and seepage zones pseudo plots for longitudinal profile across Kubaka Mine tailings facility is shown in Figure 7.

Geoelectrical methods of investigation used at others dams in the Magadan Region allowed us to determine seepage zones and to perform adequate measures for their elimination.

Yakutia diamond mine tailings facilities hold low mineralized technical water. A frozen core is usually created with thermosiphons filled with kerosene, and seepage zones appear either in fracture zones of bedrock, or where thermosiphons are not functioning. Seepage of fresh water there is indicated the same way as seepage of technical solution described above; these places demonstrate low electric resistivity (Fig. 8).

A complex of geophysical approaches consisting of VES, apparent resistivity and self-potential profiling were used for seepage determination at Marha' tailings dam ALROSSA. Seepage elimination was achieved with kerosene filled

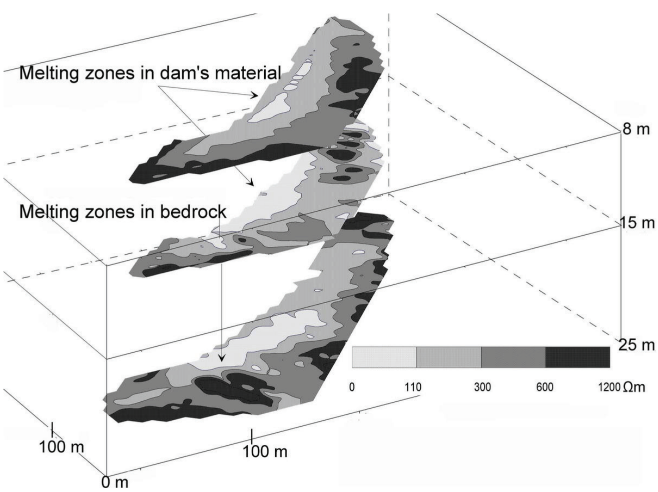

Figure 6. 3D model of showing low resistivity of melted material zones in the dam and bedrock.

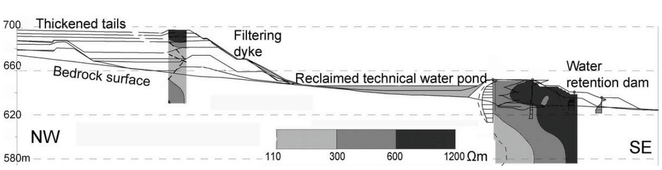

Figure 7. Pseudo plot for longitudinal profile of apparent resistivity across Kubaka Mine tailings facilities.

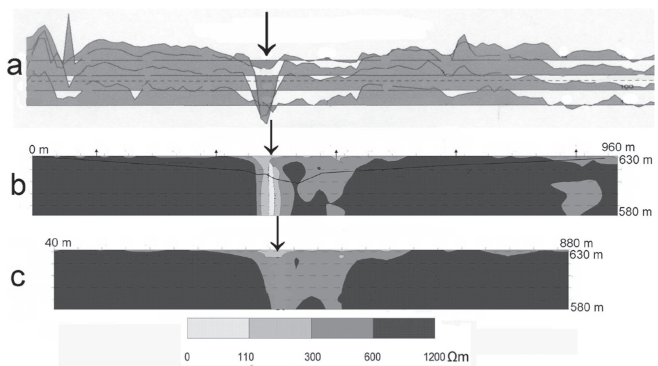

Figure 8. Seepage zone determination with VLF profiling along the crest (Marha Dimond Mine, Saha (Yakutia), ALROSSA). VLF resistivity profiles (a), pseudo plot with melted zone, June 2003 (b), pseudo plot after melted zone congealing, July 2003 (c). Arrows show seepage zone location.

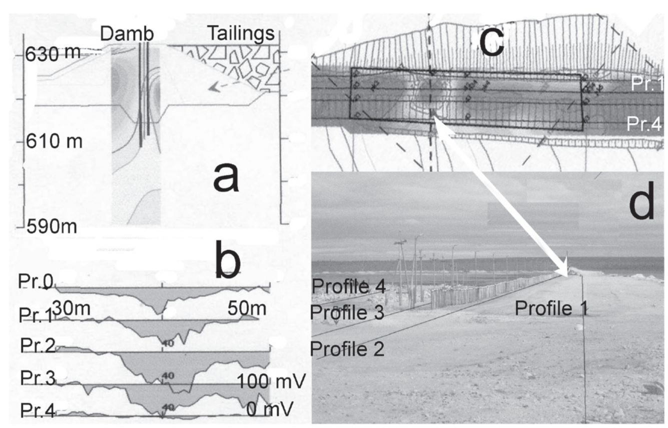

Figure 9. Seepage zone determination with geoelectrical methods (Complex VES, SP and resistivity profiling). Apparent resistivity distribution with depth (a) and on the dam's surface (c) indicates that melted material zone with electric conductivity formed around non-operating thermo needle. Since the dam was constructed with coarse material, seepage occurred in a melted zone, which was distinctly indicated with negative SP anomalies (b). SP and electric resistivity profiles were along the dam's crest (d). Profiles were done using 10 m spacing.

thermo needles and graphical interpretation of achieved results (Fig. 9).

In order to eliminate seepage determined with geoelectrical methods, a new thermo needle was installed and the location refroze. Graphs show self-potential minimums above the seepage zone. The pictures show the dam crest with thermo needles and seepage location with formed depression across.

Conclusions

Experience obtained during several years of using geoelectrical methods for monitoring and controlling the technical status of hydrotechnical structures in the permafrost zone shows high efficiency compared to other methods. They are fast and productive. High resolution mapping allows us to detect melted material zones with volumes as small as 0.1 m^3, in the dam or bedrock beneath it. Measurement can be performed on solid surfaces as well as on the water. Geoelectrical methods of control are remote and do not influence sampled material by introducing heat or highly mineralized technical solutions. This fact is very important for rock material containing ice, when contacting the solution can significantly change the melting point. With all benefits, the described methods are much cheaper then any other.

Acknowledgments

We express our gratitude to JSC “Ecogeophysics” director Alexander Sadikov for fruitful discussions on theories, methods, implementation, and sharing results obtained during geophysical control of structures in permafrost zones of Magadan Region, Chukotka and Saha (Yakutia).

References

Biyanov, G.F. 1983. *Dams in Permafrost Regions*. Moscow: Energoatomizdat, 174 pp.

Bogoslovskiy, V.A. & Ogilvy, A.A. 1970. Natural potential anomalies as a quantitative index of the water seepage from reservoirs. *Geophys. Prosp*. 18: 261-268.

Demchenko, T.V., Krivonogova, N.F., Krivozshekov, V.S. et al. 2005. Hydrotechnikal structures of Chukotka: geocriological and ingineering conditions. *Proceedings of Chikchi Branch of NEISRI FAB RAS, Magadan:* 68 pp.

Frolov, A.D. 1998. *Electrical and Elastic Properties of Frozen Earth Materials*. Pushino, 515 pp.

Hallof, P.G. 1981. *Practical Geophysics for Exploration Geologist.* Compiled by V. Blaricom, Spokane, Northwest Mining Association, 39-154.

Muslimov, A.V. & Sedov, B.M. 2006. Geophysical control and monitoring of technical status of hydrotechnical structures in permafrost region. *Proceedings of International Conference “Modern climatic and ecosystem processes in naturally vulnerable zones (Arctic, aired and mountain zones), Rostov-on-Don:* 233-235.

Muslimov, A.V. & Sedov, B.M. 2006, Geophysical Technique Applied to Control Technical Status of Dams in Permafrost. Geology, Geografy and Biologic Diversity of Northeast Russia. *Proceedings of the Far East Regional Conference Dedicate to the Memory of A.P. Vaskovsky and his 95th Anniversary, Magadan, November 28–30, 2006.* NESC FEB RAS, 252-255

Sharma, P.V. 2002. *Environmental and Engineering Geophysics*. Cambridge University Press, 475 pp.

Yakupov, V.S. 2000. *Investigation of Permafrost by Geophysical Technique.* Yakut Branch of Siberian Branch of RAS, Yakutsk, 335 pp.

Geochemical Analysis of Groundwater Dynamics in Permafrost Regions

Sarah J. Seelen
Water and Environmental Center, University of Alaska Fairbanks, Fairbanks, AK, USA
Kenji Yoshikawa
Water and Environmental Center, University of Alaska Fairbanks, Fairbanks, AK, USA
Tom Trainor
Department of Chemistry & Biochemistry, University of Alaska Fairbanks, Fairbanks, AK, USA
Larry Hinzman
International Arctic Research Center, University of Alaska Fairbanks, Fairbanks, AK, USA

Abstract

The presence or absence of permafrost plays a significant role in balancing the infiltration process between surface water and groundwater. These interactions between surface water and groundwater are poorly understood, yet will have a significant affect on the winter base flow discharge of most Arctic rivers as permafrost degrades. To better understand the base flow variability within the Arctic freshwater system, it is important to document and analyze the geochemical characteristics of groundwater. Spring water from 16 aufeis sites in the foothills of the Alaskan Brooks Range was collected during the summer of 2006. Results indicate that three distinct aquifer systems or hydrologic pathways exist in this region. Major ion chemistry of the waters is dominated by Ca^{2+} and HCO_3^-. Geothermal waters are dominated by SO_4^{2-}. Increased knowledge of geochemical characteristics of base flow will provide more insight into the long-term changes of the hydrologic cycle on the Arctic North Slope of Alaska.

Keywords: Brooks Range; geochemistry; groundwater interactions; PCA; infiltration.

Introduction

The hydrology in the Arctic is responding to an already changing climate. One of the major changes is the degradation of permafrost. As permafrost degrades, surface water and precipitation will infiltrate into the deeper sub-permafrost aquifer for the first time in recent geologic history (Clark et al. 2001). These interactions between the surface water and groundwater are poorly understood and will affect the amount and type of winter base flow reaching the Arctic Ocean. These interactions will also introduce new irregularity into an already sensitive hydrologic cycle. In an effort to better understand the base flow variability within the Arctic freshwater system, it is important to document and analyze the geochemical characteristics of groundwater in the dynamic hydrologic system of the Brooks Range.

Water balance studies are integral to quantifying the amount of water entering the Arctic Ocean from runoff, aufeis fields, and springs of the northern Brooks Range. Traditional thought surrounding water balance studies is that water enters the system from topographic highs and exits at topographic lows. The presence of faults, fractures, and permafrost in this study region introduces complexity to the water balance studies being performed. One of several working hypotheses for this research project is that water enters the watershed from the southern slope of the Brooks Range and then travels through the complex fracture system to emerge on the northern slope as spring water and aufeis fields. Geochemical characteristics, as well as dating, of the water will lead to knowledge of flow paths as these characteristics are indicative of specific water-rock interactions (Gomez et al. 2006).

The spatial expanse and remoteness of the eastern Brooks Range has resulted in a limited number of detailed geological studies, whereas much work has been done on the western and central Brooks Range as a result of the development of Red Dog Mine and National Petroleum Reserve – Alaska (NPRA) (Dumoulin et al. 2004, Kelly et al. 2004, Morelli et al. 2004, Slack et al. 2004). At this time, extrapolation of the subsurface stratigraphy from the drill logs in the west and central Brooks Range has been used in conjunction with limited subsurface evidence from the eastern Brooks Range to conceptualize the subsurface pathways and corresponding water-rock interactions in the study area.

One objective of the project is to collect spring water emerging from known aufeis sites in the foothills of the eastern Brooks Range. Aufeis sites are evidence for subterranean water channels that remain open due to the combination of adequate flow rates and warmer water temperatures. Spring water samples collected during the summer of 2006 were analyzed for major chemical characteristics. The data obtained will later be compared to previous chemical data of similar spring sites in an effort to distinguish whether changes have occurred in the hydrologic system of the Brooks Range. However, this paper will address interpretation of results from only those waters collected during 2006 and their geochemical properties, as well as those of several surface precipitate phases collected at the surface exposures. It is believed that these precipitates will lead to a better understanding of the subsurface water-rock interactions, as they are an indicator of the fluid chemistry (e.g., mineral saturation indices) immediately upon exposure at the surface.

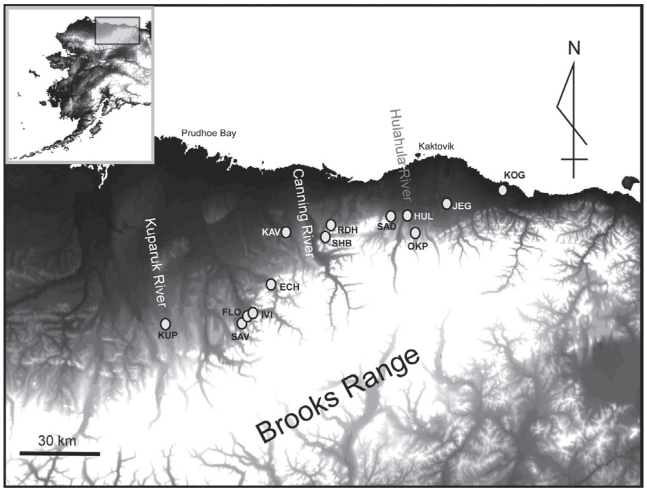

Figure 1. Location map with spring water sites and identifying features.

Methodology

Spring water samples were collected in July of 2006 (Fig. 1). Measurements of pH were conducted in situ with a hand-held meter calibrated at ambient temperatures with pH 4 and pH 7 buffers before and after the sampling trip. Spring water temperature was collected using the same meter. Several liters of water were collected in 1-L HDPE Nalgene bottles. One liter was reserved for alkalinity tests, while the remaining sample volume was then brought back to the lab, filtered through a 0.45um filter, and acidified, if necessary, for further analyses. Alkalinity was determined using HACH method 8203 WAH. Dissolved major cations (Ca^{2+}, Mg^{2+}, Na^{+}, and K^{+}) were analyzed with a Perkin Elmer AAnalyst 300 Atomic Absorption Spectrophotometer; Sr^{2+} was analyzed with an Aglient 7500 CE Inductively Coupled Plasma-Mass Spectrometer. Major anions (Cl^{-}, F^{-}, B^{-}, and SO_4^{2-}) were analyzed with a Dionex LC20 Ion Chromotograph. Hydrothermal precipitates were collected as grab samples in the summer of 2006 at 2 of the 12 spring water sites. The major element compositions of the hydrothermal precipitates were analyzed using a PANAlytical Axios wavelength dispersive x-ray fluorescence (XRF).

Results

Geochemical results indicate that spring waters in the eastern Brooks Range are characterized by varied and distinct water-rock interactions (Table 1). Emerging water temperatures varied by nearly 50°C and pH ranged by a factor of 3. Waters were found to be dominated by either Ca-HCO_3 or SO_4 signature, indicative of the predominant type of water-rock interactions.

Identifying potential flow paths

Principal component analysis (PCA) was used to investigate the underlying relationships among samples. This multivariate statistical analysis reduces the number of variables of a complex system to a lower dimension (from 12 variables to 2 in this case) (Güler et al. 2002). Unscrambler® software was used in calculating principal components (PCs). An initial PCA was created using all sites listing in Table 1. Due to the significant separation between the geothermal springs, OK, RDH1 and RHD2, and the decreased resolution for the remaining spring water sites, it was decided to exclude the geothermal springs to increase the resolution of the remaining spring water sites. The inputs were all those data listed in Table 1, excluding temperature and pH. Figure 2 is the score plot based on these inputs. Principal component one (PC1) explains 50% of the variance and PC2 explains 22% of the variance. PC1 is interpreted to represent flow path interactions. Those samples in the extreme (+) x-direction are subjected to more interactions with material surrounding the flow path while those in the extreme (-) x-direction has little interaction with surrounding material. Those sites lining up on the x-axis indicate site with moderate to limited interactions with surrounding material. The relative distance between sample site SAD and all other sites indicate water at this site interacts with a different type of material or an additional layer than the other sites. SAD water samples have high concentrations of Mg^{2+}, Sr^{2+}, and SO_4^{2-} relative to the others included in this computation.

PC2 is interpreted as segregating the spring sites into groups. Group I sites (IVI, FC, and SAV) not only have similar geochemical characteristics but also spatial proximity (refer to Fig. 1). The same is true for Group II sites (ECH, SHU, and HUL). Sample sites identified to be Group III sites (KUP, JEG, and KAV) are those with a shorter flow distance and, therefore, decreased interactions with more individual, site-specific characteristics.

Precipitates

Several spring water sites had physical evidence of fracture flow through a limestone bedrock formation. Upon surface exposure, the fluids are concentrated during ice-formation, leading to formation of an amorphous precipitate. Spring water site KAV was the most prominent with several mounds of 30 cm in diameter and height. Spring water sites RDH and HUL also had water with a milky-white appearance at the sample site. XRF analysis indicated precipitates at KAV and RDH to be composed principally of CaO (63.76%; 58.24 %), SiO2 (18.6%; 14.9%), and S (17.51%; 26.56%), respectively. The CaO fraction is most likely derived from

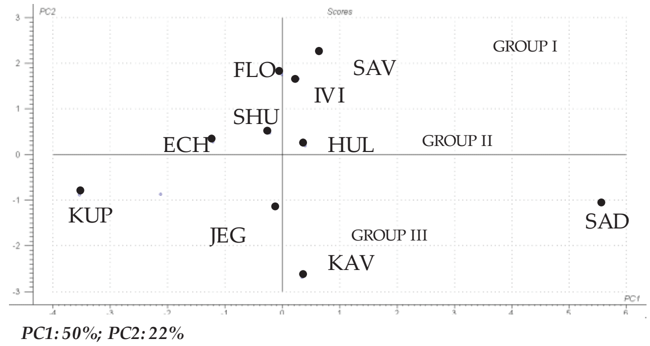

Figure 2. PCA score plot indicating grouped sites.

Table 1. Geochemistry data of spring waters (mg/L).

Sample ID	pH	T (°C)	Na^+	K^+	Sr^{2+}	Mg^{2+}	Ca^{2+}	Cl^-	F^-	Br^-	SO_4^{2-}	Alkalinity as HCO_3^-
IVI	8.02	7.30	2.38	0.132	5.589	8.77	33.8	0.66	0.60	nd†	14.41	97.8
SAV	7.78	7.81	2.12	0.101	8.271	9.83	45.44	0.49	0.66	nd	10.79	110.0
ECH	8.24	0.60	1.85	0.117	2.709	6.38	31.88	0.51	0.27	nd	11.38	80.5
FLO	8.13	6.06	2.23	0.12	6.912	8.52	29.8	0.40	0.61	nd	14.46	96.7
SAD	8.34	13.1	7.3	0.928	15.67	16.57	39.52	1.70	0.73	nd	76.34	108.3
SHU	8.14	5.27	1.68	0.184	11.08	7.64	26.36	0.30	0.42	nd	49.56	90.1
HUL	8.38	3.94	3.11	0.303	1.888	10.33	46.72	0.30	0.39	nd	69.58	85.5
JEG	8.11	8.26	1.6	0.284	3.12	6.4	50.68	0.62	0.00	nd	83.09	124.4
KAV	7.62	0.46	3.42	0.404	1.544	11.17	18.89	0.30	0.00	nd	119.76	147.3
KUP	6.38	1.69	2.13	0.106	0.2725	1.21	4.37	0.20	0.00	nd	2.83	23.3
OKP	8.79	48.1	102.72	5.356	3.079	0.1	1.543	18.00	15.81	nd	196.04	45.6
RDH1§	7.80	3.96	89.92	6.153	13.59	25.68	55.8	83.00	1.01	0.48	75.97	268.3
RDH2	7.54	27.7	96.8	6.585	18.24	22.12	49.12	87.00	1.05	0.55	26.43	248.7

Sites are listed from west to east; †below detection limits; §duplicate samples were collected for this site; ‡additional precipitate grab samples collected.

one of the several limestone lithologies. The emerging temperatures and geochemical characteristics at the spring water sites suggest S and SiO_2 portions are preferentially removed from the flow path as the water reaches the surface. Without more specific subsurface lithologies, it is difficult to determine how similar the flow paths are for the KAV and RDH. Preliminary results based on interpolated subsurface information and multivariate statistical analysis, indicate the two sites do not share flow paths.

The oxide percentages, dominated by CaO, seem to be further evidence of water-rock interaction with carbonate rocks. As the projected infiltration region of the Brooks Range is composed of carbonate rock, it is of little surprise to see a large percentage of the hydrothermal precipitates as CaO. Also of little surprise are the remaining two dominant components, SiO_2 and S. The assumed geothermal properties in the subsurface suggested by well log data, as well as concentrations of Si and S in the spring waters, imply a definite heat source and interaction with sulfide minerals (likely pyrite). Elemental concentrations of Zn, Pb, Zr, Sr, and Ba suggest further comparisons with stratigraphy connections with the region surrounding the Red Dog Mine in the western Brooks Range (Dumoulin et al. 2004, Kelly et al. 2004, Morelli et al. 2004, Slack et al. 2004).

Conclusion

All 12 spring water sites sampled exhibited unique geochemical markers as a result of specific water-rock interactions as the water reached the surface. Using a multivariate statistical technique, PCA, spring water samples were differentiated into groups based on these unique geochemical markers. Precipitate data suggest the type of water-rock interactions that dominate on the path to the surface. Further work is needed to identify potential correlation between spring water sites and fractures as well as subsurface lithologies among those spring water sites grouped according to PCA score plot results.

Acknowledgments

The authors are very grateful to Tevis Underwood and Richard Voss (US Fish and Wildlife Service; ANWR) for providing permit to access Arctic National Wildlife Refuge. Special thanks to the U.S. National Science Foundation (OPP-0229705) for providing funding. Special thanks to Jason Addison, Vanessa Ritchie, and Shane Billings for assistance in sample analysis.

References

Clark, I.D., Lauriol, B., Harwood, L. & Marschner, M. 2001. Groundwater contributions to discharge in a permafrost setting, Big Fish River, NWT, Canada. *Arctic, Antarctic, and Alpine Research* 33: 62-69.

Dumoulin, J.A., Harris, A.G., Blome, C.D., Young, L.E., Johnson, C.A., Kelley, K.D., Leach, D.L. & Anonymous. 2004. Depositional Settings, Correlation, and Age of Carboniferous Rocks in the Western Brooks Range, Alaska: Stable isotopic evidence that barite deposits in the western Brooks Range, Alaska, mark the sites of Mississippian methane seeps. *Geological Society of America, 2003 Annual Meeting in Boulder, CO,* 99: 1355-1384.

Gómez, P., Turrero, M.J., Garralón, A., Peña, J., Buil, B., de la Cruz, B., Sánchez, M., Sánchez, D.M, Quejido, A., Bajos, C. & Sánchez, L. 2006. Hydrogeochemical characteristics of deep groundwaters of the Hesperian Massif (Spain). *Journal of Iberian Geology* 32: 113-131.

Güler, C., Thyne, G.D., McCray, J.E. & Turner, A.M. 2002. Evaluation of graphical and multivariate statistical methods for classification of water chemistry data. *Hydrogeology Journal* 10: 455-474.

Kelley, K.D., Leach, D.L., Johnson, C.A., Clark, J.L., Fayek, M., Slack, J.F., Anderson, V.M., Ayuso, R.A. & Ridley, W.I. 2004. Textural, compositional, and sulfur isotope variations of sulfide minerals in the Red Dog Zn-Pb-Ag deposits, Brooks Range, Alaska: Implications for ore formation. *Economic Geology*, 99: 1509-1532.

Morelli, R.M., Creaser, R.A., Selby, D., Kelley, K.D., Leach, D.L. & King, A.R. 2004. Re-Os sulfide geochronology of the Red Dog sediment-hosted Zn-Pb-Ag deposit, Brooks Range, Alaska. *Economic Geology* 99: 1569-1576.

Slack, J.F., Kelley, K.D., Anderson, V.M.; Clark, J.L. & Ayuso, R.A. 2004. Multistage hydrothermal silicification and Fe-Tl-As-Sb-Ge-REE enrichment in the Red Dog Zn-Pb-Ag district, northern Alaska: Geochemistry, origin, and exploration applications. *Economic Geology* 99: 1481-1506.

Interactions Between Human Disturbance, Demographics of *Betula fruticosa* Pall., and Permafrost in the Vitimskoye Upland, East Siberia

I.R. Sekulich
Institute of General and Experimental Biology SB RAS, Ulan-Ude, Russia

Abstract

The demographic structure of coenopopulations of *Betula fruticosa* Pall. in birch-shrublands is described in relation to off-road vehicle and agricultural disturbance and changes in terrain at the southern limit of continuous permafrost. It was determined that the degree of change in the demographic structure of the shrub affects the dynamics and processes of the permafrost condition. Heavy use of vehicles and ploughing lead to loss of shrubs and to grassy pasture. These changes contribute to major changes in soil temperature, moisture, and drainage conditions, followed by thermokarsting and solifluction. In the case of slight anthropogenic impact, such as the single passage of a tracked vehicle, the birch populations recover and the soil and terrain environment returns to the original condition.

Keywords: anthropogenic disturbances; *Betula fruticosa*; coenopopulations; demography.

Introduction

The major ecostabilizing element in a permafrost ecosystem is vegetative cover. However, the influence of human activity becomes more and more noticeable, and this, first of all, has an effect on vegetation. In this connection, research on the structure of vegetative cover, its stability in relation to anthropogenic disturbances, and its ability to self-recover has become most important.

The study of plant species coenopopulations gives the possibility to reveal the actual reaction of plants to various ecological factors on two levels: the individual level and the populations level.

According to Harper's studies in England (Harper & White 1974, Harper 1977, Harper 1992, etc.) and Rabotnov's, and Uranov's in Russia (Rabotnov 1950, 1964, 1969, 1975, 1978, 1985; Uranov 1960, 1975, 1977) the coenopopulation approach is widely developed, particularly in Russia.

The demographic structure of a plant's coenopopulations is one of the basic criteria of estimation of the modern state of species in coenosis, the level of vital condition of its coenopopulations, the degree of their stability and prospects of development.

Study Area

Our research was performed on the central part of the Vitimskoye upland, which is located in Eastern Siberia in the depths of the Eurasian continent to the east of Lake Baikal (Fig. 1). It is a large isolated area situated at the southern limit of continuous permafrost. The permafrost is the major ecological factor which determines the character and distribution of vegetation here.

Larch forests (from *Larix gmelinii* [Rupr.] Rupr.) and communities formed of low birches or birch-shrublands (in Russia termed *yernik)* are the most widespread here.

The capacity of permafrost in the research area is from 50 m to 250 m with temperatures from 0°C to -3°C, and depth bedding of permafrost in birch-shrublands and lighted larch forests in August-September is about 1.0–1.6 m (Vtorushin & Pigareva 1996).

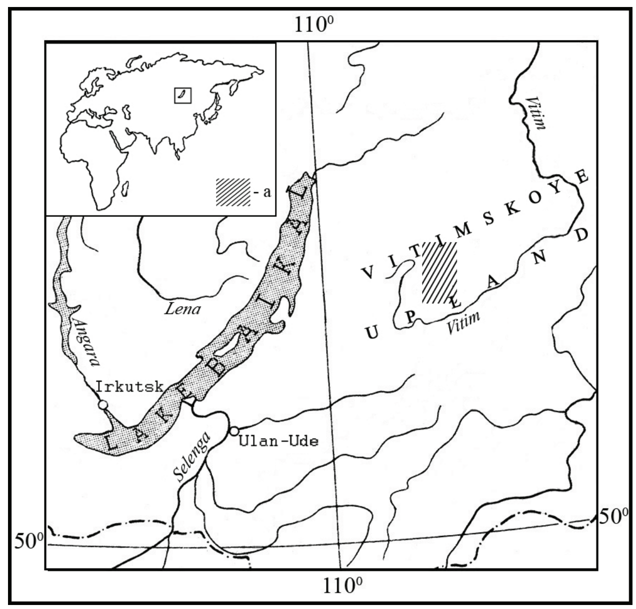

Figure 1. Map of location of research area.

The character of anthropogenic impact on birch-shrublands is developed in the following directions: their total destruction at strip-mining of minerals and ploughing up the earth, influence of track-type transport, and pasturing.

Material and Methods

The object of our research is *Betula fruticosa* Pall. subsp. *montana* M. Schemberg, the basic dominant of birch-shrublands, which occupy hollow inclined slopes, above the floodplain terraces, high parts of valley bottoms; that is, just those sites which are widely used by humans on the Vitimskoye upland.

Research was carried out, spent on model area in 100 square meters on which continuously calculated individuals on age groups.

Table 1. Age stages and age groups of the plants.

The age stages	The age groups	The letter code
latent	seed	sm
pre-generative	germ	pl
	juvenile	j
	immature	im
	virginile	v
generative	young generative	g_1
	mature generative	g_2
	old generative	g_3
post-generative	subsenile	ss
	senile	s

Table 2. Age groups of plants, coefficient of age (m_i) and efficiency of plants (e_i).

Age groups	The coefficient of age (m_i)	The efficiency of plants (e_i)
pl	0.0067	0.0266
j	0.018	0.0707
im	0.0474	0.1807
v	0.1192	0.42
g_1	0.2689	0.7864
g_2	0.5	1
g_3	0.7311	0.7864
ss	0.8808	0.42
s	0.9820	0.1807

The whole life cycle of plants can be divided into the age stages and age groups (Rabotnov 1950) submitted in Table 1. The letter code of each age group has been offered by Uranov (1960).

Determination of age groups is based on a number of complex signs, such as seed or root nutrition of plants, presence of juvenile or adult structures and their quantitative parities at the individuals, seed or vegetative reproduction, a parity and intensity of these processes, a parity of processes of new growth and dying, and degree of basic signs of biomorph generated at the individual.

The age level of the coenopopulations is estimated by the index of age (Δ) proposed by Uranov (1975) and by the index of effectiveness of the populations (ω) proposed by Zhivotovsky (2001). Values of Δ and ω were calculated by the following formulas:

$$\Delta = \sum n_i m_i \Big/ \sum n_i \qquad (1)$$

$$\omega = \sum n_i e_i \Big/ \sum n_i \qquad (2)$$

where n_i is the number of individuals of each age group; m_i is the coefficient of the age group, calculated by Uranov (1975); and e_i is the efficiency of plants of each age group, calculated by Zhivotovsky (2001). Values of m_i and e_i are submitted in Table 2.

Indexes Δ and ω vary from 0 to 1, and the highest value characterized the elder coenopopulation (Uranov 1975, Zhivotovsky 2001).

Results and Discussion

We studied the changes of demographic structure of the coenopopulations of *Betula fruticosa* on sites with partial destruction of vegetative cover as a result of the influence of track transport and pasturing. In estimating the degree of anthropogenic influence on the demographic spectrum of disturbed coenopopulations, it is necessary to compare them with a base spectrum, which, as considered Smirnova (1987), is the modal characteristic of dynamic balance of a coenopopulation. The base spectrum coenopopulations *B. fruticosa* on the Vitimskoye upland is full-constituent, has one peak, with absolute maximum on old generative individuals.

Two variants of modification of the demographic structure were marked.

One of them shows in increase of the quantity of pregenerative individuals at remaining big amount of generative individuals. An age spectrum of such coenopopulations has two peaks, the first maximum on immature individuals and the second maximum on old generative individuals. As an example, the age spectrum coenopopulation in a community of Multiherboso–Betuletum fruticosae is shown (Fig. 2). The community is situated near settlement along a highway and often exposed to influence of track-type vehicle.

At unitary passage of the cross-country vehicle according to mechanical influence, integrity of vegetative cover is broken, shrubbery and herbs are damaged, the moss and lichen cover are destroyed. As a result of these disturbances gaps formed, which are the microecotope for renewal *B fruticosa.* There is a rejuvenation of the coenopopulation at the expense of the big number of young individuals (Table 3). Short-term influence of transport does not effect adult individuals of *B. fruticosa* essentially. After termination of anthropogenic impact, individuals can quickly restore their habitus to former level. It is connected with formation of new suckers from sleeping buds which are on underground xylopodium parts. The growth of these suckers can reach 30–50 centimeters in the first year. At multiple or constant impact of track-type transports, the adult individuals finally perish, which leads to growth of grassy plants (cereals and sedges).

Replacement of birch-shrublands on grassy communities of meadow type leads to change of hydrothermal condition of soil. In space between ruts under the grassy vegetation, the depth of seasonal melting of permafrost is increased, raised soil temperatures, the moisture of soil is decreased. In ruts the temperature is decreased, which is connected with superfluous moisture of a surface (Moskalenko 1999).

Another variant of anthropogenic change occurs with pasturing. There are regressive changes in age structure. As a result of trampling and pasturing the young individuals of

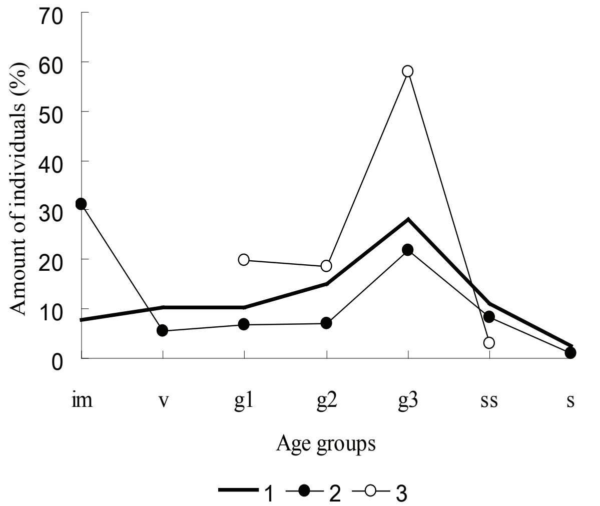

Figure 2. The age spectrums coenopopulations of *Betula fruticosa*. 1 – base spectrum; 2 – community of Multiherboso–Betuletum fruticosae; 3 – community of Kobresio filiformis– Betuletum fruticosae. Characteristic of age groups was explained above.

B. fruticosa disappear from structure of community together with grassy plants. The coenopopulation is presented by old-age plants. A community of Kobresio filiformis–Betuletum fruticosae located on an abrupt slope can be an example of such kind of coenopopulation. The age spectrum here has one peak, but differs from base spectrum. This age spectrum is not full-constituent and presented by old individuals (Fig. 2). This spectrum completely correlated with the regressive coenopopulations type of the spectrum, described by T.A. Rabotnov (1950). The quantity of individuals of *B. fruticosa* in this coenopopulation is small (Table 3). Gradual aging of coenopopulation without young individuals can lead to disappearing. The hydrothermal conditions of soil are changed on the bared sites, therefore cryogenic processes, such as erosion and solifluction, can develop.

The low index of age and index of effectiveness of coenopopulation of *B. fruticosa* occurred in community of Multiherboso–Betuletum fruticosae shows the invasive character of coenopopulation. The high index of age and index of effectiveness in community of Kobresio filiformis–Betuletum fruticosae show, that this coenopopulation mostly consists of old individuals and testifies decreasing of dominant role of species in coenosis (Table 3).

The coenopopulation in community of Multiherboso–Betuletum fruticosae it is considered as young, and the coenopopulation in community of Kobresio filiformis–Betuletum fruticosae – as becoming old according to "delta-omega" classification (Zhivotovsky 2001).

Thus, human-induced disturbances on the demographic structure of coenopopulation *B. fruticosa* in birch-shrublands on the Vitimskoye upland promote development of various geocryological processes, such as bogging, thermokarst, erosion, and solifluction. When the disturbances of demographic structure are slight, fast restoration of coenopopulation and ecological conditions occurs.

Table 3. The quantity, index of age (Δ), and index of effectiveness (ω) of anthropogenic disturbed coenopopulations of *Betula fruticosa*.

Community	Multiherboso-Betuletum fruticosae	Kobresio filiformis-Betuletum fruticosae
The general quantity, pcs. / 100м^2	482,3 ± 17,2	23,3 ± 3,2
The quantity on age groups, pcs. / 100м^2:		
j	89,4 ± 9,6	-
im	149,4±11,7	-
v	25,9±4,1	-
g_1	32,9±4,3	4,6 ±0,6
g_2	34,1±4,3	4,3 ± 0,5
g_3	105,9±6,4	13,7±2,4
ss	40,0 ±3,9	0,7 ±0,1
S	4,7 ±0,6	-
Δ	0,32	0,65
ω	0,43	0,81

Acknowledgments

The author is grateful to Dr. D.V. Sandanov (Institute of General and Experimental Biology, Siberian Divisions, Russian Academy of Sciences, Ulan-Ude) for valuable advice and for help during preparation of this paper.

References

Harper, J.L. & White, J. 1974. The Demography of Plants. *Annu. Rev. Ecology Syst.* 5: 419-463.

Harper, J.L. 1977. *Population Biology of Plants*. New York: Acad. Press, 892 pp.

Harper, J.L. 1992. *Population of Plants.* Oxford: The Alden Press, 892 pp.

Moskalenko, N.G. 1999. *Antropogennaya dynamika rastitel'nosty ravnin kryolytozony Rossii* [*Anthropogenic Dynamics of Vegetation of Flat Lands of Cryolithozone of Russia*]. Novosibirsk: Nauka. The Siberian publishing house of the RAS, 280 pp. (in Russian).

Rabotnov, T.A. 1950. Voprosy izuchenja sostava populjacyi dlja celei fytocenologii [Questions of studying of structure of populations for the purposes of phytocenology]. In: *Problemy botaniki* [*Problems of Botany*]. Moscow: Publishing house of AS SSSR, 465-483 (in Russian).

Rabotnov, T.A. 1964. Opredelenie vozrastnogo sostava populjacyi vidov v soobshestve [Determination of age composition of species populations in a plant community]. In: E.M. Lavrenko & A.A. Korchagin (ed.) *Polevaja geobotanika* [*The Field of Geobotany*]. Moscow- Leningrad: Nauka, 132-145 (in Russian).

Rabotnov, T.A. 1969. Nekotorye voprosy izucheniya cenoticheskih populyacyi [Some problems of study of coenotic populations]. *Bulleten' Moskovskogo obshestva ispytatelei pryrody, otdel biologicheskyi* [*Bulletin* o*f Moscow Society of Naturalists, Biological Series*] 3: 141-149 (in Russian).

Rabotnov, T.A. 1975. Izuchenie cenoticheskih populacyi v celyah vyyasneniya strategyy jyzny [The study of coenotic populations for the purpose of find out of life's strategies]. *Bulleten' Moskovskogo obshestva ispytatelei pryrody, otdel biologicheskyi* [*Bulletin* o*f Moscow Society of Naturalists, Biological Series*] 80(2): 5-17 (in Russian).

Rabotnov, T.A. 1978. On coenopopulations of plants reproducing by seeds. In: *Structure and Functioning of Plant Populations.* Amsterdam, 1-26.

Rabotnov, T.A. 1985. Dynamics of plant coenotic populations. In: J. White (ed.), *The Population Structure of Vegetation.* Dordrecht; Boston; Lancaster, 121-142.

Smirnova, O.V. 1987. *Struktura travjanogo pokrova shirokolistnyh lesov* [*The Grass Layers Structure of Broad-leaved Forests*]. Moscow: Nauka, 207 pp. (in Russian).

Uranov, A.A. 1960. Jyznennoe sostoyanye vyda v rastytel'nom soobshestve [The life state of species in a plant community]. *Bulleten' Moskovskogo obshestva ispytatelei pryrody, otdel biologicheskyi* [*Bulletin* o*f Moscow Society of Naturalists, Biological Series*] 67(3): 77-92 (in Russian)

Uranov, A.A. 1975. Vozrastnoi spektr fytocenopopuljacyi kak funkcija vremeny I energetycheskih volnovyh processov [The age spectrum of phytocoenopopulation as a function of time and power wave of processes]. *Biologycheskye nauki* [*Biological Sciences*] 2: 7-34 (in Russian).

Uranov, A.A. 1977. Voprosy izucheniya structury fytocenozov y vydovyh cenopopulacyi [The questions study of phytocenosis and species coenopopulations]. In: *Cenopopulacyy rasteny.: Razvytye y vzaymootnoshenyya* [C*oenopopulations of Plants. The Development* and interrelations]. Moscow: Nauka, 8-20 (in Russian).

Vtorushin, V.A. & Pigareva, N.N. 1996. *Kryomorfnye pochvy: perspektivy ich effektivnogo ispol'zovaniya* [*Criomorphic Soils: Prospects of their Effective Utilization*]. Ulan-Ude: BSC SB RAS, 295 pp. (in Russian).

Zhivotovsky, L.A. 2001. Ontogeneticheskie sostojanija, effectivnaja plotnost' i klassifikacija populjacyi rastenyi [Ontogenetic states, effective density, and classification of plant populations]. *Ecologija* [*Russian Journal of Ecology*] 1: 3-7 (in Russian).

Permafrost in the South Shetland Islands (Maritime Antarctica): Spatial Distribution Pattern

E. Serrano
Dpt. Geografía, Universidad de Valladolid. Spain
J. López-Martínez
Dpt. Geología y Geoquímica, Universidad Autónoma de Madrid. Spain
J.A. Cuchí
Escuela Politécnica Superior de Huesca, Universidad de Zaragoza. Spain
J.J. Durán
Instituto Geológico y Minero de España. Madrid. Spain
S. Mink
Dpt. Geología y Geoquímica, Universidad Autónoma de Madrid. Spain
A. Navas
Estación Experimental de Aula Dei, CSIC, Zaragoza. Spain

Abstract

Maritime conditions in the South Shetland Islands allow the presence of ice-cemented permafrost and an active layer from 25 cm to more than 1 m thick. In this work permafrost distribution has been studied from detailed geomorphological maps in 14 areas. Periglacial maps derived from the general ones allowed us to differentiate areas where permafrost-related landforms and processes occur and to compile permafrost distribution maps. Field observations and other methods have been used to check mapping interpretations. The spatial location of permafrost-related landforms allowed us to differentiate the following permafrost spatial-distribution pattern: (1) non-existing or sporadic permafrost at altitudes below 20 m a.s.l., (2) mainly discontinuous permafrost between 20 and 40 m a.s.l., and (3) mainly continuous permafrost at more than 70% of ice-free surfaces above 40 m a.s.l. Field observations pointed out important spatial and seasonal local variability in the presence of permafrost.

Keywords: ANTPAS project; geomorphology; Maritime Antarctica; periglacial landforms; permafrost distribution; South Shetland Islands.

Introduction

The South Shetland Islands are located in the Maritime Antarctica, between the Drake Passage and the Bransfield Sea, at 61°59′S/63°20′S, and 57°40′W/62°45′W (Fig. 1). The archipelago occupies about 4700 km^2 and only 10% are ice-free areas. The region has a cold maritime climate with annual mean surface air temperature at the coast line about -2°C, and daily summer temperatures above 0°C. Annual precipitation is between 400 mm/yr and 800 mm/yr and rain occurs in summer.

Studies on permafrost have been carried out on different places in the South Shetland Islands. There are works on Deception Island (López-Martínez et al. 1996, 2000, 2002), Media Luna Island (Corte & Somoza 1954, Serrano & López-Martínez 1997a), Robert Island (Serrano & López-Martínez 1997b, 1998), Nelson Island (Araya & Hervé 1972a, 1972b), King George Island (Simonov 1977, Barsch et al. 1985, Quinsong 1989, Zhu et al. 1996, Serrano & López-Martínez 2004) and Livingston Island (Thom 1978, López-Martínez et al. 1996, Serrano et al. 1996, Bergamín et al. 1997, Ramos 1998, Ramos et al. 2002, Ramos & Vieira 2003, Hauck et al. 2007). These studies provide information about the presence of permafrost and the active layer at different locations and altitudes in different islands. The aim of this work is to show an overview of the permafrost presence and distribution on ice-free areas of the South Shetland Islands from gepomorphological mapping and field observations. It is a contribution to the ANTPAS projects for compiling a map of permafrost in Antarctica. Bockheim (1995) pointed out the necessity to better know the extent of permafrost linked to the soils evolution and the recent global change.

Methods

This work is mainly based on the use of periglacial landforms as indicators of permafrost existence and distribution. Periglacial landforms and processes have been used as indicators of permafrost environments on Arctic and mountain environments with useful results (Black 1976, Washburn 1979, Harris 1982, Karte 1983, Clark 1988, Bockheim 1995, Barsch 1996). On the active layer a widespread group of landforms and processes are developed and relations between landforms, processes, existence, and extension of permafrost have been established (Harris 1982, French 1996). Rock glaciers, patterned ground, protalus lobes, frost mounds, frost creep, and gelifluction features point out the existence of mophodynamic and environmental conditions

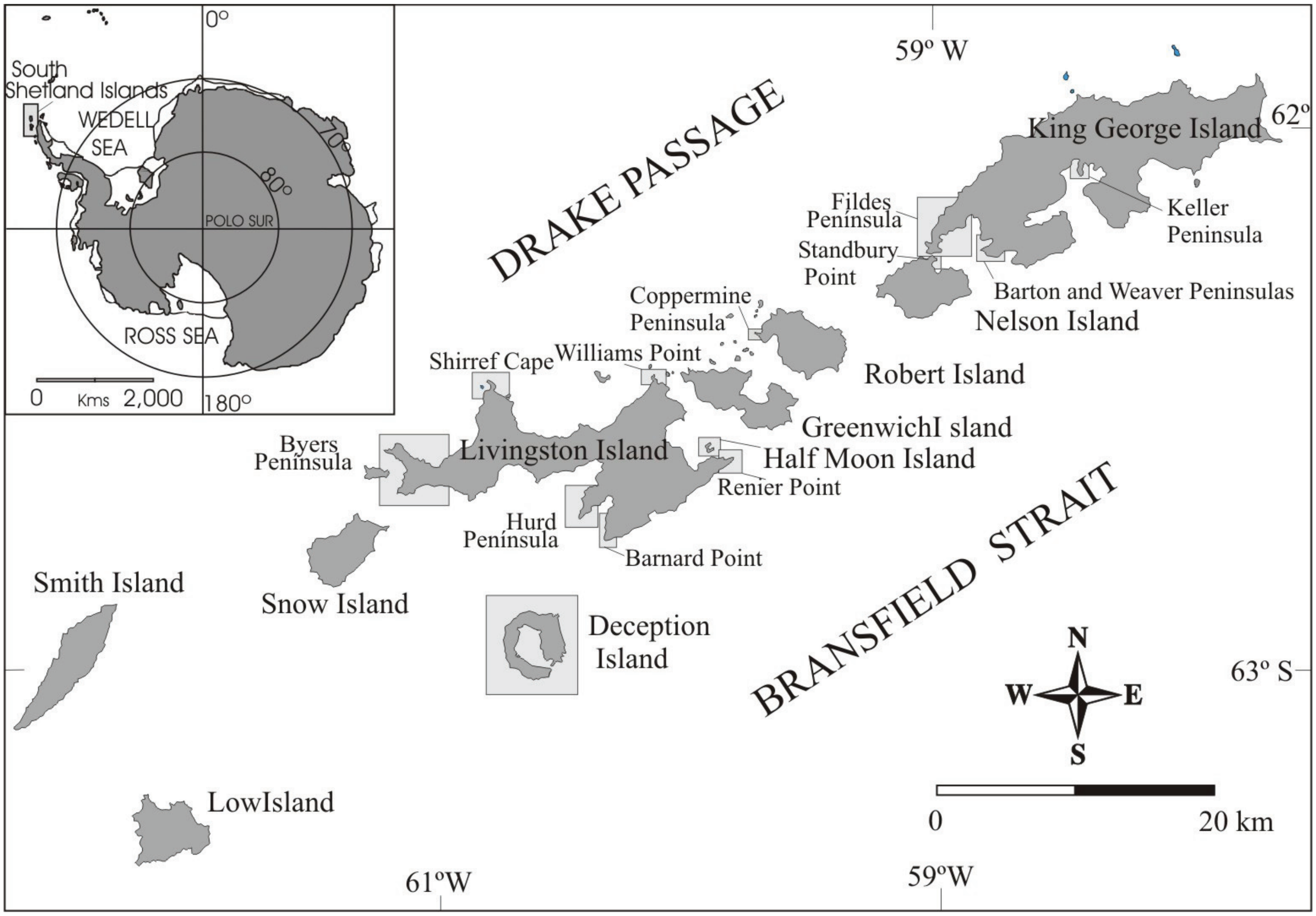

Figure 1. Location map of South Shetland Islands and places where geomorphological maps have been made by our group. Elephant Island not included in the map.

linked to permafrost (Black 1976, Barsch 1978, 1996, Harris 1982, Karte 1983, Haeberli 1985, Clark 1988, Huizjer & Isarín 1997). Differences between permafrost-related periglacial landforms and those periglacial landforms not related to permafrost occurrence have been used in this work to study the distribution and nature of permafrost in the South Shetland Islands. In addition and in order to check the validity of the interpretations in several places other techniques such as BTS measurements, vertical electric sounding, slope transects, mechanical sounding, active layer measurements, and water and permafrost analysis have been used.

Our group has compiled fourteen geomorphological maps between 1:25,000 and 1:10,000 scales (Table 1).

From the geomorphological maps simplified periglacial maps, showing such type of information only, have been made. Landforms valid as indicators of permafrost existence have been selected to deduce permafrost occurrence. The location and altitudinal distribution of permafrost-related landforms have been quantified to produce synthetic simplified maps of permafrost distribution.

Results: Permafrost Distribution

In the study region there is ice-cemented permafrost and the active layer is in general from 25 cm up to more than 1 m thick. Buried or ground ice has been recognized in several places at different altitudes.

Twelve types of landforms related to permafrost have been inventoried in the study areas in the South Shetland Islands and used for permafrost mapping (Table 2). Landforms related to frost heave and frost creep are the most common periglacial landforms in the archipelago. Patterned ground occurs in a wide altitudinal range, mainly between 10–100 m a.s.l. and being the dominant landforms above 25 m a.s.l. Stone fields are located mainly between 10–118 m a.s.l. The permafrost-related landforms and processes comprise 80% of the surface occupied by periglacial shapes on ice-free areas of the South Shetland Islands. Rock glaciers and protalus lobes are indicators of continuous or discontinuous permafrost, and are spread in several peninsulas and other places of the archipelago. Eight active rock glaciers have been identified in the South Shetland Islands but protalus lobes located between sea level and 300 m a.s.l. are more common features (Birkenmajer 1981, 1997, Barsch et al. 1985, Serrano & López-Martínez 2000). The rock glacier fronts have as a mean altitude 13 m a.s.l. and the upper ends 67 m a.s.l. and they are mainly developed below 70 m a.s.l. (Serrano & López-Martínez 2000). The mean altitude of rock glacier upper ends and protalus lobes point out the existence of continuous permafrost, although the fronts are located in

Table 1. Geomorphological maps of the South Shetland Islands compiled by our group.

Place	Island	Scale	Publication
Fildes Peninsula	King George	1:15,000	Not published
Barton and Weaver Pen.	King George	1:10,000	*1
Keller Peninsula	King George	1: 10,000	Not published
Byers Peninsula	Livingston	1:25,000	*2
Hurd Peninsula	Livingston	1:10,000	Not published
Williams Point	Livingston	1:10,000	Not published
Renier Point	Livingston	1:10,000	Not published
Barnard Point	Livingston	1:10,000	Not published
Cape Shirref	Livingston	1:10,000	Not published
Coppermine Pen.	Robert	1:10,000	*3
Deception Island	Deception	1:25,000	*4
Half Moon Island	Half Moon	1:10,000	*5
Standbury Point	Nelson	1:15,000	Not published
Stinker Point	Elephant	1:10,000	Not published

*1, López-Martínez et al. 2002. *2, López-Martínez et al. 1996. *3, Serrano & López-Martínez 1997b. *4, López-Martínez et al. 2000. *5, Serrano & López-Martínez 1997a.

Table 2. Processes and landforms related to permafrost inventoried in the South Shetland Islands.

PROCESSES	LANDFORMS	LANDFORMS ELEVATION
Frost creep Gelifluction	- Protalus lobe - Rock glaciers - Block streams - Ploughing blocks - Gelifluction sheets - Gelifluction lobes - Debris lobes	40-100 m 0-300 m 30-100 m 10-90 m 0->100 m 10-300 m 0-100
Frost heaving Cryoturbation Sorting	- Stone stripes: Coarse stone stripes Fine stone stripes - Stone fields - Patterned ground: Stone circles Earth circles Stone polygons Earth polygons - Frost mounds	45-90 m 10-90 m 10-300 m 45-50 m
Thermokarst	- Melting hollows	40-100 m

areas without permafrost-related landforms.

The altitudinal analysis point out that at very low altitudes (between 0–20 m a.s.l.) patterned ground exists only occasionally. Three rock glacier fronts reach the sea or lowest beaches, permafrost occur at 2.5 m a.s.l. in Deception Island and at 7 m a.s.l. in Livingston Island (López-Martínez et al. 1996, Bergamín et al. 1997). Below 10 m a.s.l. the permafrost indicator features occupy only 12% of the surface with periglacial landforms, insufficient to be considered as discontinuous permafrost. From these data and the mentioned periglacial maps it is possible to deduce that on the lowest beach levels permafrost is sporadic or non-existing. Above 20 m a.s.l. landforms and processes related to permafrost are dominant (72% of periglacial landforms are permafrost-related) and point out a mainly discontinuous permafrost environment. Above 40 m a.s.l. debris lobes, protalus lobes, patterned ground and frost creep processes are dominant and the mean altitude of rock glacier upper ends and the location of all the protalus lobes point out a mainly continuous permafrost environment from 40–300 m a.s.l.

The distribution of the mentioned features allows to differentiate the following altidudinal distribution of permafrost:

- Between 0–20 m a.s.l. Non-existing or sporadic permafrost environments are dominant.
- Between 20–40 m a.s.l., mainly discontinuous permafrost environments are developed.
- Above 40 m a.s.l. mainly continuous permafrost environments are common, being at those altitudes more than 70% of ice free areas surface occupied by permafrost-related landforms and processes.

Field observations pointed out the important spatial and temporary variability in the presence of permafrost. Altitude plays an important role but also topography, soil characteristics, and orientation. Variations in meteorological conditions and snow coverage may change the active layer thickness in different years.

Conclusions

The analysis of permafrost related landforms and processes allowed us to establish the wide distribution of permafrost in the South Shetland Islands but also to assert that not all ice free areas in the archipelago have permafrost environments. The altitudinal analysis of the periglacial landforms denotes a distribution of permafrost environments in three areas with different morphodynamic systems:

- A sporadic permafrost environment (from 2.5–20 m a.s.l.), where less than 15% of the surface is occupied by permafrost related landforms.
- A mainly discontinuous permafrost environment (between 20–40 m a.s.l.)
- A mainly continuous permafrost environment (above 40 m a.s.l.) where more than 70% of periglacial landforms are related to permafrost.

From geomorphological maps it is possible to point out an altitudinal distribution of periglacial landforms and processes characterized by the lack of intense periglacial processes near the sea level, and the domain of permafrost related landforms on higher heights, dominated by the presence of patterned ground.

Acknowledgments

This work has been supported by the Spanish Polar Program (project CGL2005-03256) and it is a contribution to the project Antarctic Permafrost and Soils (ANTPAS) included in the program of the International Polar Year 2007–2008.

References

Araya, R. & Hervé, F. 1972a. Periglacial phenomena in the South Shetland Islands. In: R.J. Adie (ed.), *Antarctic Geology and Geophysics*. Oslo: International Union of Geological Science Series B 1: 105-109.

Araya, R. & Hervé, F. 1972b. Patterned gravel beaches in South Shetlands. In: R.J. Adie (ed.), *Antarctic Geology and Geophysics*. Oslo: International Union of Geological Science, Series B 1: 111-114.

Barsch, D. 1996. *Rock Glaciers. Indicators for the Present and Former Geoecology in High Mountain Environment*. Heidelberg: Springer Verlag.

Barsch, D. 1978. Active rock glaciers as indicators for discontinuous alpine permafrost. An example from the Swiss Alps. *Proceeding of Third International Conference on Permafrost, Edmonton* 1: 349-352.

Barsch. D., Blümel, W.D., Flügel, W.A., Mäusbacher, R., Stäblein, G. & Zick, W. 1985. *Untersuchungen zum Periglazial auf der König-Georg-Insel üdshetland-insel/Antarktika.* Deutsche Physiogeographische Forschungen in der Antarktis. Bericht über die Kampagne 1983/84. Bremenhaven: Reports on Polar Research, nº24. Alfred Wegener Institute, 75 pp.

Bergamín, J.F., Durán, J.J., González-Casado, M. & López-Martínez, J. 1997. Morfología y estructura del basamento pre-Cuaternario de la Caleta Española, Península Hurd, Isla Livingston. *Boletín Real Sociedad Española de Historia Natural (Secc. Geol*.) 93: 189-196.

Birkenmajer, K. 1981. Lichenometric dating of raised marine beaches at Admiralty Bay, King George Island South Shetland Islands, West Antarctica. *Bulletin Academy Polish Science* 29 :119–127.

Birkenmajer, K. 1997. Map of Quaternary geology at Artowsky Station, King George Island, South Shetland Islands (West Antarctica), 1:25,000. *Studia Geológica Polonica* 110: map.

Black, R.F. 1976. Periglacial features indicative of permafrost: ice and soil wedges. *Quaternary Research* 6: 3-26.

Bockheim, J.G. 1995. Permafrost distribution in the southern circumpolar region and its relation to the environment: a review and recommendations for further research. *Permafrost and Periglacial Processes* 6: 27-45.

Clarck, M.J. 1988. *Advances en periglacial geomorphology*. Chichester: Wiley & Son.

Corte, A.E. & Somoza, A.L. 1954. *Algunas observaciones geológicas y criopedológicas en la Antártida*. Buenos Aires: Instituto Antártico Argentino.

French, H.M. 1996. *The Periglacial Environments*. Essex: Longmann.

Haeberli, W. 1985. *Creep of Mountain Permafrost: Internal Structure and Flow of Alpine Rock Glaciers*. Zurich: Mitt. Versuchsants Wasserbau Hydrologie und Glaziologie, ETH nº 77.

Harris, S.A. 1982. Identification of permafrost zone using selected permafrost landforms. *Proceeding Fourth Canadian Permafrost Conference*, *Calgary, Alberta, March 2-6, 1981*, 49-57.

Hauck, C., Vieira, G., Gruber, S., Blanco, J. & Ramos, M. 2007. Geophysical identification of permafrost in Livingston Island, maritime Antarctica, *Journal of Geophysical Research* 112: F02S19, doi:10.1029/2006JF000544.

Huizer, A.S. & Isarin, R.F.B. 1997. The reconstruction of past climates using multiproxy evidence: an example of the weichselian Pleniglacial in northwest and central Europe. *Quaternary Science Review* 16: 513-533.

Karte, J. 1983. Periglacial phenomena and their significance as climatic and edaphic indicators. *GeoJournal* 74: 329-340.

López-Martínez, J. & Serrano, E. 2002. Geomorphology. In: J. López-Martínez, J.L. Smellie, J.W. Thomson & M.R.A. Thomson (eds.), *Geology and Geomorphology of Deception Island.* BAS GEOMAP Series, Sheets 6-A and 6-B, 1:25.000, with supplementary text. Cambridge: British Antarctic Survey, 31-39.

López-Martínez, J., Serrano, E., Rey, J. & Smellie, J.L. 2000. *Geomorphological Map of Deception Island* E. 1:25,000. BAS Geomap series, 7B. Cambridge. British Antarctic Survey.

López-Martínez, J., Serrano, E. & Lee, J.I. 2002. Geomorphological map of Barton and Weaver Penisnulas. King George Island, Antarctica (1:10,000). Seoul. Polar Science Laboratory, Korean Ocean Research and Development Institute KARP.

López-Martínez, J., Ramos, M., Criado, C., Serrano, E. & Nicolás, P. 1996. Anomalías geotérmicas y permafrost en la Isla Decepción, Antártida. *Pro-ceeding of V Simposio de Estudios Antárticos*, *C.I.C.Y.T, Madrid*: 223-234

López-Martínez, J., Thomson, J.W. & Thomson, M.R.A. (eds.). 1996. *Geomorphology of Byers Península, Livingston Island.* BAS GEOMAP Series, Sheet 5-A, 1:25,000, with supplementary text. Cambridge: British Antarctic Survey.

Qingsong, Z. 1989. A comparison of periglacial landforms between the Vestfold Hills, East Antarctica and the Fildes Península of King George Island, west Antarctica. *Proceedings of International Symposium on Antarctic Research*. Beijing: Chinese Committee on Antarctic Research, 74-81.

Ramos, M., Vieira, G., Crespo, F. & Bretón, L. 2002. Seguimiento de la evolución temporal del gradiente térmico de capa activa en las proximidades de la B.A.E Juan Carlos I. In: E. Serrano & García (eds.), *Periglaciarismo en montaña y altas latitudes*. Valladolid: Universidad de Valladolid, 257-276.

Ramos, M. & Vieira, G. 2003. Active layer and permafrost monitoring in Livingston Island, Antarctic. First results from 2000 and 2001. *Proceedings of the Eighth International Conference on Permafrost, Zurich*, *Switzerland*: 929-933.

Ramos, M. & Vieira, G. 2004. Variabilidad térmica de la capa activa y evaluación de la energía perdida por el suelo, durante el proceso de congelación en la isla Livingston (Antártida). Inviernos 2000, 2001, 2002. *Boletín Real Sociedad Española de Historia Natural (Secc. Geol.)* 99: 83-92.

Serrano, E., Martínez de Pisón, E. & López-Martínez, J. 1996. Periglacial and nival landforms and deposits. In: J. López-Martínez, J.W. Thomson & M.R.A. Thomson (eds.), *Geomorphological map of Byers Península, Livingston Island.* BAS GEOMAP Series, Sheet 5-A, 1:25,000, with supplementary text. Cambridge: British Antarctic Survey, 28-34.

Serrano, E. & López-Martínez, J. 1997a. Evolución de las formas de relieve y los depósitos superficiales cuaternarios en la Isla Media Luna. Islas Shetland del Sur. *Boletín Real Sociedad Española de Historia Natural (Secc. Geol.)* 93: 207-218.

Serrano, E. & López-Martínez, J. 1997b. Geomorfología de la Península Coppermine, Isla Robert, Islas Shetland del Sur, Antártida. *Serie Cientifica INACH* 47: 19-29.

Serrano, E. & López-Martínez, J. 1998. Caracterización y distribución de las formas y los procesos periglaciares en las Islas Shetland del Sur (Antár-tida). In: A. Gómez, F. Salvador, L. Schulte & A. García (eds.), *Procesos biofísicos actuales en medios fríos. Estudios recientes*. Barcelona: Universitat de Barcelona, 181-204.

Serrano, E. & López-Martínez, J. 2000. Rock glaciers in the South Shetland Island, Western Antarctica. *Geomorphology* 35: 145-162.

Serrano, E. & López-Martínez, J. 2004. Morfogénesis periglaciar y deglaciación en las penínsulas Barton y Weaver (Islas Shetland del Sur, Antártida). *Boletín Real Sociedad Española de Historia Natural (Secc. Geol.)* 99(1-4): 131-140.

Simonov, I.M. 1977. Physical-geographic description of the Fildes Peninsula (South Shetland Islands). *Polar Geography* 1: 223-242.

Thom, G. 1978. Disruption of bedrock by the growth and collapse of ice lenses. *Journal of Glaciology* 20: 571-575.

Washburn, A.L. 1979. *Geocryology. A Survey of Periglacial Processes and Environments.* London: Edward Arnold.

Zhu, C., Cui, Z. & Zhang, J. 1996. Relationship between the distribution of periglacial landforms and glaciation history, Fildes Península, King George Island, Antarctica. *Permafrost and Periglacial Processes* 7: 95-100.

Effects of Vegetation and Grazing on Soil Temperature, Soil Moisture, and the Active Layer in the Hovsgol Mountain Forest Steppe Zone, Mongolia

Anarmaa Sharkhuu
University of North Dakota, Grand Forks, North Dakota, USA
Natsagdorj Sharkhuu
Institute of Geo-Ecology, Mongolian Academy of Sciences, Mongolia
Bernd Etzelmuller
Department of Geosciences, University of Oslo, Norway
Eva S. Flo Heggem
Department of Geosciences, University of Oslo, Norway
Clyde E. Goulden
Institute of Mongolian Biodiversity and Ecological Studies, Academy of Natural Sciences, Philadelphia, Pennsylvania, USA

Abstract

In this paper we present initial results from observations of the effects of a series of natural vegetation covers and several experimental plots manipulated to mimic local grazing practices on soil temperatures, moisture content, and active-layer thickness in the Dalbay ILTER (International Long Term Ecological Research) study site in the Hovsgol Mountain forest steppe zone, northern Mongolia. We set up experimental plots with three types of treatments—control plot and plots that mimicked light and heavy grazing by clipping vegetation cover. The results show that both live and dead plants (especially moss, shrubs, forest, and dense grass) produce considerable insulation effects, maintaining low permafrost temperatures and protecting soil moisture from high evaporation. Therefore, both natural vegetation cover characteristics and grazing practices are important factors in preventing permafrost degradation in arid mountain environments.

Keywords: active layer; Hovsgol; soil moisture; soil-surface temperatures; soil temperatures; vegetation cover.

Introduction

The mountain forest steppe zone along the eastern shore of Lake Hovsgol Mongolia is characterized by mountains with altitudes of 1700 to 2200 m a.s.l. It is located in the southern fringe of the Siberian continuous permafrost and taiga forest zones. The forest is predominantly Siberian larch (*Larix sibirica*), distributed on crests and north-facing slopes. South-facing slopes and valley bottoms are generally dominated by *Poa* and *Carex* species. Shrubs, lichens, and thick grasses with abundant dead plant materials are widespread on gentle north-facing slopes and along river channels. There are 2–15 cm thick moss layers in the forest and 5–30 cm thick layers of peat in some valley bottoms (Goulden et al. 2006). Discontinuous permafrost is characteristic of the region near the lake. Active-layer depths are highly variable, ranging from 1 to 5 m depending on the topographic setting and vegetation cover. Permafrost thickness is between 5 to 20 m in the valley bottoms and thicker on the forested north-facing slopes. Permafrost is absent on south-facing slopes without forest (Etzelmuller et al. 2006, Heggem et al. 2006).

Permafrost degradation under the influence of climate warming in the Hovsgol region has been more intense during the last 15 years (1991–2006) than the previous 20 years (Sharkhuu et al. 2007). Mean annual air temperature at the Hatgal weather station, located on the most southern shore of the Lake Hovsgol, has increased by 1.86°C during the last 40 years (Nandintsetseg et al. 2006). Within the framework of the International Hovsgol Project supported by the Global Environmental Facility and implemented by World Bank (GEF/WB) in 2002–2006, Norwegian and Mongolian permafrost researchers studied the distribution and thermal conditions of permafrost in the region characterizing topography, snow and vegetation cover, soil texture, and soil moisture. The rate of increase in mean annual permafrost temperature varies from 0.02 to 0.04°Ca^{-1} per year, depending on landscape and ground conditions (Sharkhuu et al. 2007). In addition, human activities such as livestock grazing, anthropogenic forest fires, and some engineering works have led to local intensive degradation of permafrost. In some valleys of the study area especially,, livestock grazing has had negative effects not only on the permafrost but also on the ecosystem. The objective of this study was to estimate these anthropogenic effects, focused on grazing and forest fires. Hence studies on vegetation cover, soil-surface temperature, and active layer thickness were conducted in the Dalbay and Borsog Valleys between 2004 and 2007.

Study Area

The study area includes six valleys (Borsog, Dalbay, Sevsuul, Noyon, Shagnuul, Turag) on the eastern shore of Lake Hovsgol (Fig. 1).

Parts of the eastern shore area have been extensively used for grazing by nomadic families. Grazing is most intense

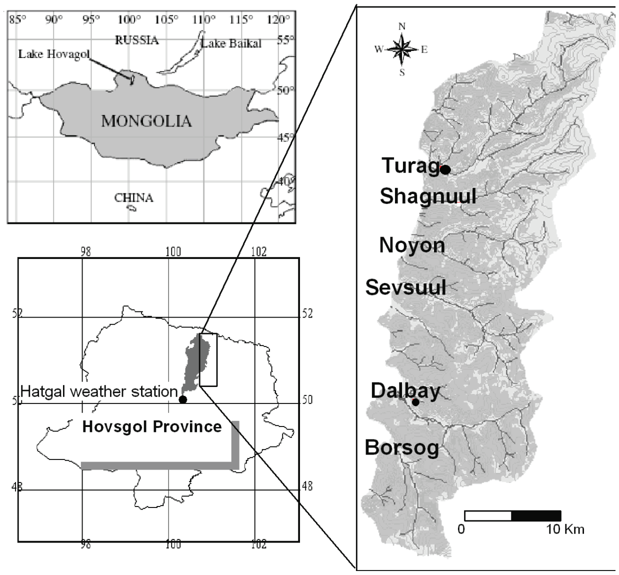

Figure 1. Location of the study sites along the eastern shore of Lake Hovsgol, Mongolia.

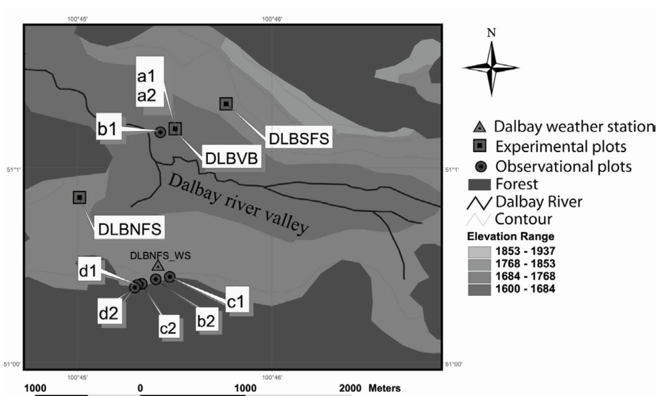

Figure 2. Topographic map of Dalbay Valley showing the locations of the eight plots used to study the effects of natural land-cover types. Points indicate locations of dataloggers used for SST measurements. Several points are overlaid on this map due to the short distance between them (e.g., *a1* and *a2*). Plots used for experimental study were shown as rectangular, labeled DLBSFS (plots on south-facing slope), DLBVB (plots in valley bottom), and DLBNFS (plots on north-facing slopes). Weather station location is illustrated with a triangle, labeled DLBNFS_WS.

in the northern valleys, especially in Turag and Shagnuul Valleys. Sevsuul and Noyon Valleys are only moderately grazed; whereas, Dalbay and Borsog Valleys have little or no pastoral use. Compared with Turag Valley, the present shallow active layer and low permafrost temperatures in Dalbay Valley are apparently insulated from thaw by the thicker vegetation cover (Table 1)

Methods

Natural land-cover plots

In order to estimate the thermal insulative effect of a range of naturally occurring vegetation cover year-round (October 2004–October 2005), soil-surface temperature (SST) recordings at eight observation plots in the Dalbay

Table 1. Vegetation cover and land-use characteristics in the study valleys.

Valley	Borsog	Dalbay	Shagnuul	Turag
Livestock numbers (sheep units)	51	530	3001	3330
Dry plant biomass, gm^{-2}	660	585	48	116
Active-layer thickness, m	2.1	1.4	4.3	4.8
Mean annual permafrost temperature, °C	-0.91	-1.25	-0.56	-0.42
Estimated permafrost thickness, m	35	45	25	20

Valley (Fig. 2) were made. All soil-surface temperature recordings were made at 2–5 cm depth under soil-surface in order to prevent temperature recordings affected by direct sun radiance. These plots represent the range of vegetation available within the valley.

In addition, some observations on the effects of forest fire on soil-surface temperature were made on north-facing slopes with larch forest in Shagnuul Valley Soil-surface temperatures at 2–5 cm depth and ground temperatures at 1 m depth were recorded by UTL-1 datalogger year-round.

Experimental plots

In order to explore effects of grazing on soil temperature, moisture and active layer, three 2×6 m^2 experimental grids were established along a topographic transect (south-facing lower slope, valley bottom, north-facing lower slope) in Dalbay and Borsog Valleys (Fig. 2). Within each grid six 2×2 m^2 plots were established with three different treatments: (*CO*) dead plant material and vegetation cover were both left intact, as control plots; (*CL*) vegetation cover was clipped but dead plant material was not removed (hereafter referred to as clipped plots); and (*CR*) vegetation cover was clipped and dead plant material was removed (hereafter referred to as cleared plots).

Soils within the active layer in valley bottoms and on north-facing gentle slopes consisted of gravelly silt and sands, covered by a 10–20 cm layer of humus. In summer, supra-permafrost waters are usually formed with a thickness of 10 to 30 cm, depending upon the amount of precipitation. Gravelly sands are characteristic of the south-facing slope.

Soil-surface temperature observations at 2–5 cm at each of the experimental plots began in October 2005. Unfortunately, these stopped in late March 2007 after 1½ years of observations, due to low battery power in the loggers. However, during each field season, measurements of soil temperatures and active layer thickness were made in the experimental plots.

UTL-1 dataloggers (interval 1.5 h, accuracy ±0.25°C) were used to record soil surface and soil temperatures for both natural and experimental plots. In addition, the MMT-4 thermistors and probes (accuracy ±0.1°C) were used. Mean winter temperature was calculated from mean December, January, and February temperatures, while mean summer temperature was calculated using June, July, and August means.

Live and dead plant biomass in each experimental plot was sampled from a 0.5×0.5 m^2 area in late June and early September–October of 2006. Biomass was determined after drying the sampled plants at room temperature for more than 48 hours. Dry plant biomass at each Dalbay plot is shown in Table 2. Clipped and cleared (CL and CR, respectively) plots were manually clipped monthly during the summer months of 2006.

Soil moisture in each experimental plot was determined by weight method monthly during summer. Soil samples were taken at each 50 cm depth from surface 0.1 m depth to a depth of 2 m. In addition, we determined soil density by core method to use for a model estimation. Soil samples were obtained using a hand drill (augur) and weighed using a digital balance with an accuracy of 0.1 g. Active layer thickness was measured using a 1.85 m long steel probe and several thaw tubes placed in some of the boreholes in early September and October, 2005–2006.

Table 2. Dry plant biomass (gm^{-2}) at each experimental plot in the Dalbay Valley

Vegetation cover at each site	CO	CL	CR	
			CR_{bj}	CR_{aj}
Grass, forb dry steppe on south-facing slope	340	135	96	118
Forb, grass meadow in valley bottom	625	375	135	160
Grass, forb wet steppe on north-facing slope	560	485	62	36

CO-unclipped control plot; CL-clipped plot with litter left in place; CR-cleared plot (vegetation cover was clipped and litter was removed): CR_{bj}-before July; CR_{aj}-after July.

Results and Discussion

Effect of natural vegetation on soil-surface temperatures

Initial results of quantifying the thermal insulation effect of different vegetation covers on soil-surface temperature are presented in Table 3. In particular, 10 cm thick (*Rhytidium rugosum*) moss cover decreased soil-surface mean summer temperature by 6.4°C as compared to plot without moss cover. Dense 1.8 m (*Salix* sp.) shrubs decreased soil-surface summer temperature by 1.4°C as compared to 0.5 m shrubs, and young dense larch forest decreased soil-surface mean summer temperature by 1.1°C as compared to sparse larch forest. Dense grass decreased soil-surface summer temperature by 2.2°C as compared to mown grass plot. In general, all types of vegetation cover decreased soil-surface summer temperatures by 5–9°C as compared with mown grass plot. Summer temperature differences (R_s) between different types of vegetation cover and mown grass plot are shown in Table 4. The temperatures under sparse forest, 50 cm high shrubs, and dense grass are reduced by 2–4°C. However, mean winter temperatures under dense vegetation cover were increased considerably, due to the accumulation of relatively loose and thick snow. Values of the mean annual temperature and the annual temperature amplitude under

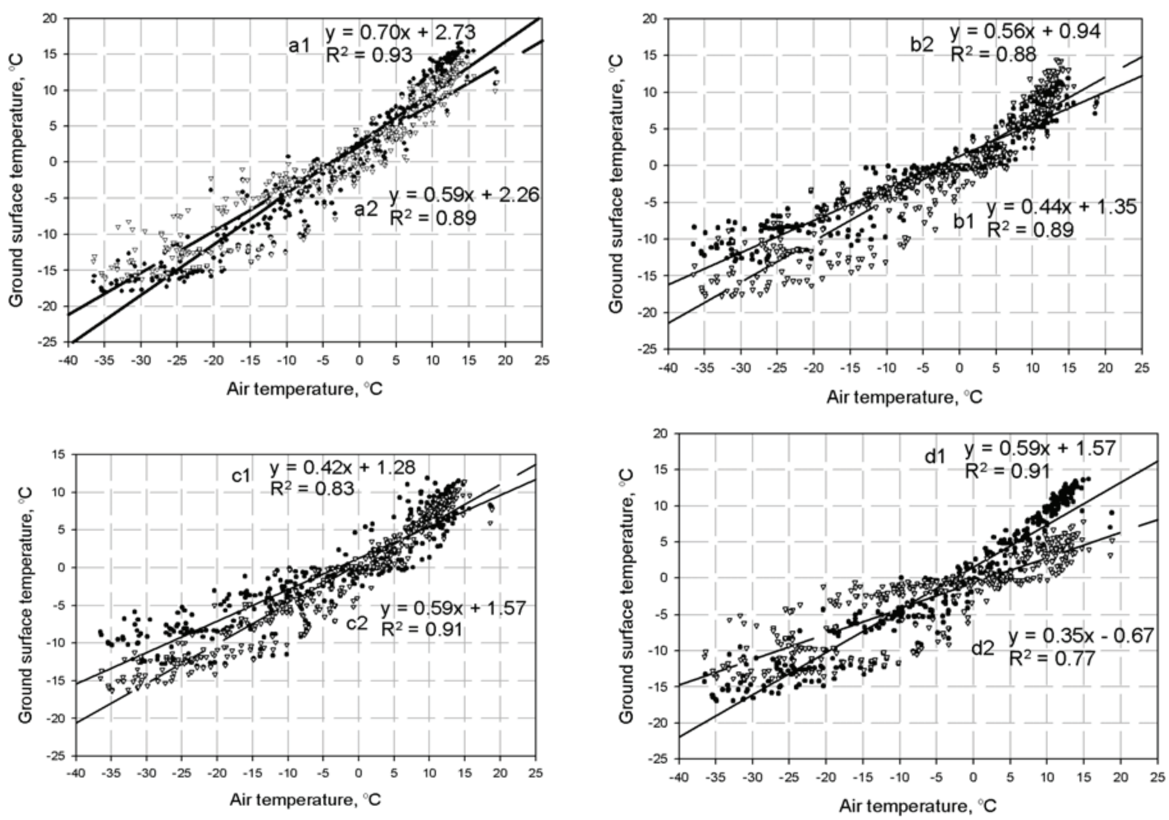

Figure 3. Linear least-squares regressions between daily air temperatures and soil-surface temperatures under different land-cover types at the experimental plots.

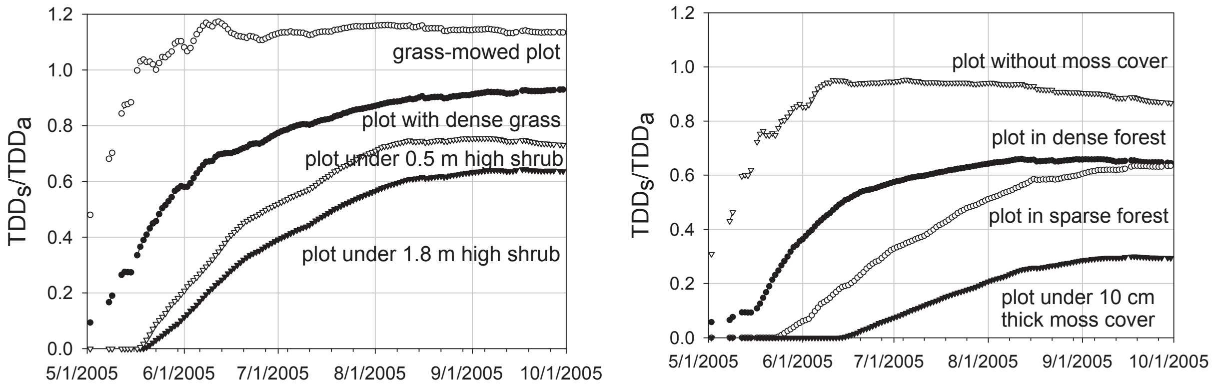

Figure 4. Daily n-factors (ratio of soil-surface to air temperatures) over the course of summer 2005 at each of the eight study plots.

Table 3. Mean soil-surface temperatures, temperature amplitude, summer temperature reduction (Rs) and summer n-factor in plots of different natural land cover in the Dalbay Valley (Oct. 2005 to Oct. 2006).

Plots	Land cover	Mean temperatures, °C			Temperature amplitude	R_s	Summer n-factor
		winter	summer	annual			
d2	10 cm thick moss	-8.6	3.4	0.29	6.8	9.0	0.29
b1	1.8 m high dense shrub	-7.4	7.4	0.63	7.8	5.0	0.63
c2	Dense forest	-11.7	7.5	0.64	10.5	4.9	0.64
c1	Sparse forest	-14.8	8.6	0.72	13.0	3.8	0.72
b2	50 cm high dense shrub	-11.4	8.8	0.73	11.3	3.6	0.73
d1	On moss surface	-11.5	9.8	0.86	11.9	2.6	0.86
a2	Dense grass	-11.1	10.2	0.93	11.9	2.2	0.93
a1	Grass mowed	-13.7	12.4	1.13	14.7	0.0	1.13
Air temperature at Dalbay		-23.9	10.8	-5.3	18.8	-	-

different land-cover types differ by 0.5 to 2.0°C and 3.0 to 7.0°C, respectively.

Linear least-squares regressions between daily air temperatures from the Dalbay automatic weather station and soil-surface temperatures under different land-cover types at the experimental plots were fitted. The linear regression analysis shows that the presence of thick moss is a major factor in insulating the ground from the heat. While slope value of linear regression between daily air temperature and soil-surface temperature under moss cover is 0.35, slope value of regression between air temperature and soil-surface temperature in mown grass plot is 0.70 (Fig. 3). *P* values for r^2 and slopes of all regression analyses were significant (P<0.0001).

Seasonal n-factors (Lunardini 1978), the ratio between thawing degree-days at the soil-surface (TDD_s) and in the air (TDD_a), were calculated for each day at plots of different land covers in Dalbay Valley and are shown in Figure 4. Usually n-factors are calculated using seasonal degree-day sums (Smith & Riseborough 1996). Here, n-factor was calculated using running sum of thawing degree-days at the soil surface and the air to show the seasonal progression.

These observations, though based on just one season of data, clearly demonstrate the importance of vegetation cover on ground thermal regime. In addition, in Shagnuul forest the mean annual surface temperatures were -3.1°C and -3.9°C in burned and unburned forest, respectively.

Effect of vegetation cover manipulation on soil temperatures

The initial results from the experimental plots are presented in Table 5. Compared to the control plots CO, the mean monthly summer soil-surface temperatures in the CR plots (clipped and litter removed) were higher by 0.7–1.7°C on the north-facing slope, by 2.3–2.7°C on the south-facing slope, and by 3.2–5.6°C in the valley bottom, depending upon plant biomass and surface wetness. Meanwhile, the undisturbed presence of dead plant matter (litter) in the valley bottom decreased the temperatures by 0.7–2.0°C. As compared to control plot CO, mean winter soil temperature at a depth of 1.2 m in the CR plot of the valley bottom was higher by 0.3°C, due to accumulation of summer heat into soil. However, the temperature at depth of 0.1 m was lower by 4.3°C due to relatively thin and dense snow accumulation in the clipped and cleared plot. Differences in near-surface soil temperatures between CO and CR plots were higher in summer than in autumn. The difference also decreased gradually with depth. In general, mean annual active layer temperatures in CR plots were significantly warmer than in CO plots.

Effect of vegetation cover manipulation on soil moisture

Not only live vegetation but also dead vegetation reduces near-surface soil moisture evaporation. Soil analysis shows that soil moisture content in CO and CL plots were always

Table 4. Soil temperatures (°C) at the grazing experimental plots in the Dalbay Valley at depths from the surface to 1.2 m.

Topographic position		South-facing		Valley bottom			North-facing	
Plot		CO	CR	CO	CL	CR	CO	CR
Mean soil-surface temperatures for 2006								
June		11.2	13.5	5.7	9.4	10.1	7.2	7.9
July		13.8	16.5	9.2	12.8	14.8	9.9	11.6
August		12.3	14.8	9.2	11.6	12.4	9.9	10.7
Mean winter soil temperatures								
Oct 2006–Mar 2007	0.1 m	-	-	-3.9	-5.5	-8.2	-	-
	0.6 m	-	-	-2.4	-	-2.4	-	-
	1.2 m	-	-	-0.7	-0.8	-0.4	-	-
Soil temperatures								
June 18, 2006	0.1 m	12.5	14.7	3.3	6.0	7.7	2.1	4.5
	0.5 m	7.1	7.4	0.8	1.5	3.5	-	-
Oct 7, 2006	0.1 m	2.3	2.3	0.8	0.9	1.1	-	-
	0.5 m	5.0	5.3	1.7	2.0	2.4	-	-
	1.0 m	5.8	6.0	1.0	1.2	1.4	-	-
Sep 7, 2007	0.1 m	13.0	13.2	9.2	10.1	11.9	8.1	8.8
	0.5 m	9.4	9.8	5.9	6.2	7.0	5.5	5.7

Note: CO – control plot; CL – plot, vegetation cover clipped and dead material left; CR – vegetation cover clipped and dead plant material removed plot

Table 5. Changes in soil moisture content (%),in the experimental plots in the Dalbay Valley.

Date	Depth m	Valley bottom			South-facing	
		CO	CL	CR	CO	CR
Oct 5, 2005	0.1	54.6	-	42.1	-	-
	0.5	45.0	-	36.8	4.7	-
June 18, 2006	0.1	40.9	35.4	32.0	14.1	12.3
	0.5	41.7	33.7	30.1	9.6	8.7
Oct 7, 2006	0.1	61.5	55.1	40.2	20.3	17.8
	0.5	50.2	43.0	35.1	13.8	12.1
	1.0	30.3	27.9	26.2	8.7	8.4
Sep 7, 2007	0.1	42.7	34.4	19.7	4.6	6.1
	0.5	30.5	23.3	18.1	4.6	4.4

higher than in CR plots (Table 5). Due to plant biomass, hydrology, and soil characteristics, the differences in soil moisture content between CO and CR plots ranged from 5% to 20% in the valley bottom and did not exceed 2%–3% on south-facing slope. The difference decreased with depth.

Effect of vegetation cover manipulation on active layer thickness

In 2006 and 2007, the second and third years of the experiment, the thickness of the active layer in the CR plots in the valley bottom and the north-facing slope increased by 40–60 cm due to increased soil-surface temperatures and amplitudes, and decrease in soil moisture content. Each year, active layer thickness increased, though the rate of change decreased after the second year. Active layer thickness in CL plots also increased by about 15 cm (Table 6).

Conclusion

Vegetation cover acts as a cooling factor and reduces mean annual soil-surface temperatures. As compared to the mown

Table 6. Changes in active-layer thickness (cm) in the experimental plots in the Dalbay Valley.

Date	Valley bottom			North-facing slope		
	CO	CL	CR	CO	CL	CR
Oct 5, 2005	123	-	158	103	-	-
June 2006	35	49	61	13	20	29
Oct 7, 2006	125	138	177	102	113	143
Sep 7, 2007	123	140	185	101	116	147

grass site, mean summer soil-surface temperatures decreased by about 2.2°C under dense grass, 3.6°C under sparse forest and dense shrubs, 4.9°C under dense forest and bushes, and by 6.4°C under 10 cm thick moss at the Dalbay observation sites. As compared to Turag Valley where livestock grazing removes vegetation, the low grazing pressure maintains shallower active layer and lower permafrost temperatures in Dalbay Valley. Moss cover, dense grass, and forest are natural insulators, protecting soil moisture from high evaporation and maintaining low soil temperatures. The shallower active layer and low permafrost temperature found in the control (CO) and clipped (CL) plots, in contrast to the cleared plots are caused by live and dead vegetation cover. Thus, the main approach for preserving permafrost and ecosystems, especially in the Hovsgol forest steppe zone, must be based primarily on protecting vegetation cover.

Acknowledgments

These observations were conducted within the framework of the International Hovsgol Project, supported by a grant from the Global Environmental Facility and implemented by the World Bank to the Geo-Ecology Institute, Mongolian Academy of Sciences.

Two anonymous reviewers provided stimulating and helpful comments and suggestions on the draft manuscript. We want to thank all the mentioned persons and institutions.

References

Etzelmuller, B., Heggem, E.S.F., Sharkhuu, N., Frauenfelder, R., Kaab, A. & Goulden C.E. 2006. Mountain permafrost distribution modelling and validation using a multi-criteria approach and DC resistivity tomography in continental Central Asian mountains-example from Hovsgol Area, Northern Mongolia. *Permafrost and Periglacial Processes* 17: 91-104.

Goulden, C.E., Tumurtogoo, O., Karabanov, E. & Mongontsetseg, A. 2006. The geological history and geography of Lake Hovsgol, Mongolia. In: C.E. Goulden et al. (eds.), *The Geology, Biodiversity and Ecology of Lake Hovsgol (Mongolia)*. Leiden, The Netherlands: Backhuys Publisher, 1-20.

Heggem, E.S.F., Etzelmuller, B., Anarmaa, Sh., Sharkhuu, N., Goulden, C.E. & Nandintsetseg, B. 2006. Spatial modeling of ground surface temperatures in the Hövsgöl area, Northern Mongolia. *Permafrost and Periglacial Processes* 17: 375-369.

Lunardini, V.J. 1978. Theory of N-factors. *Proceedings of the Third International Conference on Permafrost, Edmonton, Canada*: 41-46.

Nandintsetseg, B., Greene, J.S. & Goulden, C.E.. 2007. Trends in extreme daily precipitation and temperature in the Lake Hövsgöl basin area, Mongolia. *Int. J. Climatology* 27: 341-347.

Sharkhuu, A., Sharkhuu, N., Etzelmuller, B., Heggem, E.S.F., Nelson, F.E., Shiklomanov, N.I., Goulden, C.E. & Brown, J. 2007. Permafrost monitoring in the Hovsgol mountain region, Mongolia. *J. Geophys. Res.* 112: F02506, doi:10.1029/2006JF000543.

Smith, M.V. & Riseborough, D.W. 1996. Permafrost monitoring and detection of climate change. *Permafrost and Periglacial Processes* 7: 301-309.

Thermal State of Permafrost in Mongolia

Natsagdorj Sharkhuu
Institute of Geo-Ecology, Mongolian Academy of Sciences, Mongolia
Anarmaa Sharkhuu
University of North Dakota, Grand Forks, North Dakota, USA
Vlad E. Romanovsky
Geophysical Institute, University of Alaska Fairbanks, USA
Kenji Yoshikawa
Geophysical Institute, University of Alaska Fairbanks, USA
Frederick E. Nelson
Department of Geography, University of Delaware, USA
Nikolay I. Shiklomanov
Department of Geography, University of Delaware, USA

Abstract

The thermal state of permafrost (TSP) in Mongolia is studied within the framework of mapping and monitoring of permafrost. Main parameters for estimating TSP are mean annual surface temperature (MAST), mean annual ground temperature (MAGT), or mean annual permafrost temperature (MAPT), and permafrost temperature gradient obtained during borehole temperature measurements by movable thermistors and data loggers. In this paper we will analyze and summarize initial data on estimating (1) changes in MAST and MAGT, depending on different natural factors, and (2) trends of increase in MAPT, based on data from 38 GTN-P and CALM borehole measurements in Mongolia. According to the results, the average rate of increase in MAPT in the Hentei and Hangai regions is 0.01°C–0.02°C a year, and in the Hovsgol region it reaches 0.02°C–0.03°C a year. Permafrost degradation under influence of climate warming was more intense during the last 15–20 years than during the previous 15–20 years (1970–1980s).

Keywords: boreholes; ground temperature; Mongolia; permafrost monitoring; soil surface temperature.

Introduction

Mapping and monitoring of permafrost is based mainly on the study of the thermal state of permafrost (TSP) (Kudrayvtsev et al. 1974). Main parameters for estimating TSP are mean annual surface temperature (MAST), mean annual ground temperature (MAGT), or mean annual permafrost temperature (MAPT), and permafrost temperature gradient (PTG). Values of MAGT are estimated by yearly average temperatures at depths of permafrost table or zero amplitude temperatures. They have a close relationship through thermal offset in active layers. For the last 40 years, Sharkhuu (2000) has measured ground temperatures in hundreds of shallow to deep boreholes in Mongolia. The data of borehole temperature measurements are useful for modeling and mapping distribution and thickness of permafrost in Central Asia. During the last 12 years Sharkhuu (2003 and 2005) also conducted permafrost monitoring in Mongolia within the international framework of GTN-P and CALM program (Burgess et al. 2000, Nelson et al. 2004). Initial results on CALM and GTN-P programs in Mongolia are presented in a number of publications (Brown et al. 2000, Sharkhuu 2003, Sharkhuu & Anarmaa 2005, Anarmaa et al. 2007). In addition, the Mongolian Expression of Intent #1129, main components of CALM and GTN-P programs in Mongolia, are part of the Thermal State of Permafrost IPY Project 50. According to the Expression, in 2007–2008 we are to extend boreholes and observations, improve quality of borehole temperature measurements, and generate new permafrost researchers. In this paper we analyze and summarize initial data obtained for mapping and monitoring of permafrost in Mongolia.

Permafrost zones occupy almost two-thirds of Mongolia, predominantly in the Hentei, Hovsgol, Hangai, and Altai Mountains and surrounding areas (Gravis et al. 1974). The territory is characterized by mountainous arid-land permafrost, sporadic to continuous in its extent, and it occupies the southern fringe of the Siberian permafrost zones (Fig. 1). In the continuous and discontinuous permafrost areas, taliks are found on steep south-facing slopes, under large river channels and deep lake bottoms, and along tectonic fractures with hydrothermal activity. In sporadic and isolated permafrost areas, frozen ground is found only on north-facing slopes and in fine-grained and moist deposits. The lower limit of continuous permafrost on south-facing slopes ranges from 1400 to 2000 m in the Hovsgol and Hentei Mountains, and from 2200 to 3200 m in the Altai and Hangai Mountains. The lowest limit of sporadic permafrost is found between 600 and 700 m a.s.l. Most of the permafrost is at a temperature close to 0°C, and thus, thermally unstable. However, average thickness and mean annual temperature of continuous permafrost is 50–100 m and -1°C to -2°C in valleys and depressions, and 100–250 m and -1°C to -3°C on mountains, respectively.

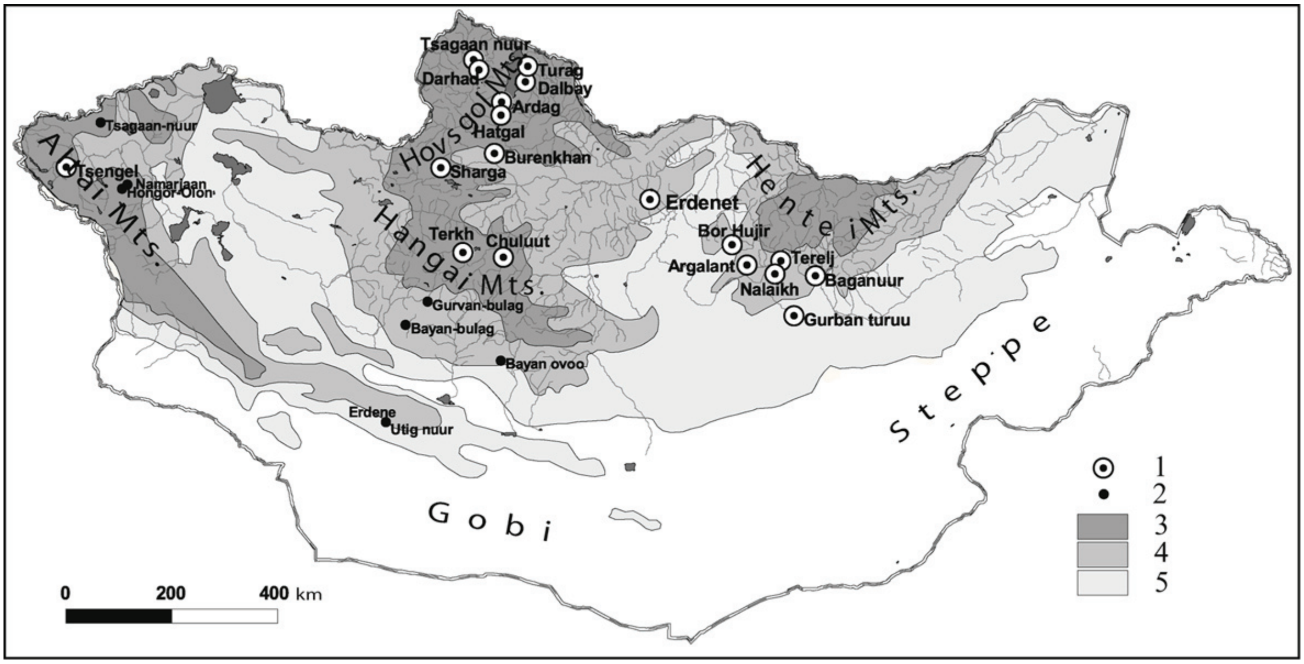

Figure 1. Location of permafrost monitoring boreholes in Mongolia 1 – Permafrost monitoring sites with GTN-P; 2 – Boreholes, planned to drill for permafrost monitoring; 3 – Continuous permafrost and discontinuous permafrost; 4 – Isolated permafrost; 5 – Sporadic permafrost.

Permafrost in Mongolia is characterized mainly by low and moderate ice content in unconsolidated sediments. Ice-rich permafrost is characteristic of lacustrine and alluvial sediments (Gravis et al. 1974, Sharkhuu 2003).

Permafrost in Mongolia is degrading under the influence of climate warming. According to the climate change studies (Natsagdorj et al. 2000), the mean annual air temperature has increased by 1.56°C during the last 60 years. Winter temperature has increased by 3.61°C. and spring-autumn temperature by 1.4°C–1.5°C. However, the summer temperature has decreased by 0.3°C. In the period from 1940–1990, mean annual air temperatures have increased by 1.8°C in northern and western Mongolia, 1.4°C in central Mongolia, and 0.3°C in southern and eastern Mongolia. For example, during the last 40 years mean annual air temperature at Hatgal weather station has increased by 1.86°C. Meanwhile, the air temperature trend was 0.61°C in the period from 1963–1989, and it reached 0.84°C in the period from 1990–2003 (Nandintsetseg & Goulden 2005).

Borehole Temperature Measurements

Methods

Ground temperatures in research boreholes have been measured by using movable thermistor strings and a digital multimeter of the MB-400 type. Temperature accuracy of thermistors of the MMT-4 type was 0.05°C. Temperature measurements in the permafrost monitoring boreholes are made using the same thermistors at the corresponding depths, and carried out on the same dates of any year. In addition, Stow-Away and HOBO, U-12 data loggers have been installed in most of the monitoring boreholes. UTL-1 and TR-52 data loggers have been used for measuring soil surface temperatures. Temperature accuracy of all the loggers is 0.25°C. Terrain and ground characteristics in most of the monitoring and research boreholes are determined in detail. Values of MAGT are estimated at depth of 10 m, although MAGT at depth of zero amplitude temperatures usually ranges from 10 m in fine-grained sediments with high moisture content to 20 m in bedrock and sandy sediments with course fragmental rock. A depth of MAGT also depends on yearly amplitude of soil surface temperatures. Mean winter temperature (MWT) is obtained by average value of air temperatures for December, January, and February. Mean summer temperature (MST) is estimated by the average value of air temperatures for June, July, and August. The frost number (FN) is calculated by a relation of values between thawing degree-days (TDD) and freezing degree-days (FDD) (Nelson & Outcalt 1987). A value of FN > 0.5 indicates more FDD than TDD, and is an indication of permafrost presence. This is, however, dependent on ground conditions, notably the thermal offset to the top of permafrost and therefore is not an absolute confirmation of permafrost existence (Heggem et al. 2006). Values of ground temperature gradient are estimated in the boreholes deeper than 30–50 m. Analysis of surface and ground temperature regime, or changes in MAST and MAGT depending on different natural factors, is made based on scientific methodology, developed at the Geocryology Department of Moscow State University (Kudrayvtsev et al. 1974).

Key study area

There are eight (Baganuur, Nalaikh, Argalant, Erdenet, Burenkhan, Hatgal, Ardag and Dalbay) key study areas with hundreds of geological and geocryological boreholes, where we measured and analyzed changes in MAGT depending on different natural factors. In addition, during the last 40 years ground temperatures have been measured in more than 100 geocryological and engineering-geological boreholes with permafrost in different areas of Mongolia.

Monitoring sites

Monitoring of permafrost in Mongolia, based on studies of TSP within the framework of GTN-P and CALM programs, has been conducted since 1996 and extended from year to year. At present, there are 17 monitoring sites, including 38 GTN-P and CALM boreholes in Mongolia. For the last 5–10 years, some boreholes with an average depth of 10–15 m were drilled in the locations with the temperature measurements which were made 15–40 years ago in old boreholes. We also plan to extend boreholes, especially in the Altai region (Fig. 1). All the monitoring boreholes are situated in natural conditions without thermal disturbance. Most of the monitoring boreholes are instrumented in order to decrease air temperature convection and to protect them from human damage. All the redrilled boreholes are cased by parallel steel and plastic pipes of 3–5 cm diameter with the mouth of the pipe at a depth of about 15–20 cm and covered by soil. The empty space outside of casing pipes is filled with fine sands.

Results and Discussion

Surface temperature regime

Soil surface temperatures in mountainous regions depend on mountain altitudes, slope aspect and steepness, and snow and vegetation covers. Selected data from soil surface temperature recordings on Tsengel (Altai), Solongot (Hangai), and Bogd (Hentei) mountain slopes are presented in Table 1.

Table 1. Year-round recordings of surface temperatures (°C), depending on topography and elevation (H).

Mts	Aspect/ Angle	H, m (a.s.l)	MWT	MST	MAT	A	FN
Altai	flat watershed	3370	-21.5	5.4	-7.48	14.6	0.71
	north/8°	2675	-17.1	10.9	-3.77	12.7	0.59
	north/6°	2400	-20.7	16.4	-1.46	21.3	0.53
	south/10°	2400	-14.0	16.2	1.32	14.7	0.47
	valley bottom	2150	-16.7	16.1	0.11	16.2	0.50
Hangai	flat watershed	2900	-19.7	7.2	-5.77	14.8	0.66
	north/20°	2625	-16.6	8.4	-3.79	13.6	0.61
	north/25°	2230	-17.1	12.3	-1.30	16.5	0.53
	south/25°	2230	-14.6	15.6	1.59	16.5	0.47
	valley bottom	2050	-22.0	15.6	-1.56	20.3	0.53
Hentei	flat watershed	2200	-8.9	10.8	0.02	11.2	0.50
	north/25°	1950	-8.9	7.3	-1.66	8.8	0.57
	south/25°	1920	-13.9	13.5	0.37	15.0	0.49
	north/25°	1600	-17.2	17.5	-0.28	19.3	0.51
	valley bottom	1300	-19.3				

Notes: Mean winter (MWT), summer (MST) and annual (MAT) surface temperatures; FN–frost number; A–amplitude temperature.

There are observed winter air temperature (MWT) inversions in some valleys and depressions which are located at altitudes of 1200 to 1800 m a.s.l in the Hentei Mountain region. A MWT inversion is not characteristic of the Altai high mountains. MST, MAT, and A in all the mountains are decreased in different gradients with mountain surface height. FN is increased with altitude. A south-facing slope, depending on its steepness, is warmer by about 0.5°C–2.0°C than a north-facing slope.

Thermal insulation of snow in severe climate conditions with high soil surface amplitude temperatures is essential (intensive), although average thickness of snow in Mongolia is about 5–20 cm. Experimental observations for studying the thermal insulation effect of snow cover on soil surface temperatures from November to March have been conducted in the Hustai and Terelj areas near Ulaanbaatar and at the Dalbay study site (See Table 2). Thick snow cover of 10–20 cm can warm mean winter surface temperatures by about 3°C–5°C. However, the thermal insulation effect of snow is gradually decreased with an increase in snow density and thickness which is more than 20–40 cm. It should be noted that the warming effect of snow on soil surface in the forest and with thick vegetation cover was more intensive than at open and bare sites.

Experimental observations for studying thermal insulation of different vegetation cover on soil surface temperatures have been conducted at the Dalbay and Hustai study sites (Heggem et al. 2006, Anarmaa et al. 2007). Data from Table 3 show that moss cover, dense grass, and forest are natural insulators, maintaining low soil temperatures. In particular, as compared with the grass mowed site, MSTs under different vegetation cover are decreased by 2°C–9°C. However, MWTs are increased 1°C–5°C, due to accumulation of relatively loose and thick snow in plants. Meanwhile, MSTs under dense

Table 2. Mean winter surface temperatures (T_s) under snow cover with different thickness and density at the Dalbay experimental site.

Data loggers No	M31	M32	M33	M34	M35	M36
Thickness (cm)	40.0	32.9	25.8	18.7	11.6	0
Density (g/cm^3)	0.20	0.17	0.14	0.12	0.10	0
T_s (°C)	-8.5	-8.9	-9.5	-10.9	-12.7	-16.3

Table 3. Mean surface temperatures in single plots with different vegetation cover at Dalbay observation site.

Data loggers under	Mean surface temperatures, °C			
	winter	summer	annual	A
10 cm thick moss	-8.6	3.4	0.29	6.8
1.8 m high dense shrub	-7.4	7.4	0.63	7.8
Dense forest	-11.7	7.5	0.64	10.5
Sparse forest	-14.8	8.6	0.72	13
50 cm high dense shrub	-11.4	8.8	0.73	11.3
On moss surface	-11.5	9.8	0.86	11.9
Dense grass	-11.1	10.2	0.93	11.9
Grass mowed	-13.7	12.4	1.13	14.7
Air temperature	-29.3	10.8	-5.3	18.8

grass, forest, and 10 cm thick moss cover, are colder by 2.2°C, 4.2°C and 6.4°C, respectively. Therefore, the main factor in preserving permafrost and ecosystem in the Hovsgol and Hentei taiga zone must be based, first of all, on protection of vegetation cover (Sharkhuu & Anarmaa 2005).

Ground Temperature Regime

According to general regularities in TSP formation, MAGTs at depths of 10 m are decreased by about 0.4°C–0.6°C for each 100 m rise in mountain altitudes, and increased by 0.8°C–1.0°C for each 100 km moved from north to south. Ground temperature gradient varies from 0.01°C–0.02°C/m on mountain slopes and watersheds to 0.02°C–0.03°C/m in valleys and depressions. Meanwhile, the temperature gradient in unconsolidated sediments is more than in bedrock (Sharkhuu 2000). Changes in MAGTs, depending on different natural factors, are determined as follows:

Data from Table 4 show that forest cover can reduce MAGTs by about 0.5°C–1.2°C. Besides, as compared with south-facing slopes, MAGTs on gentle and steep north-facing slopes are colder by about 0.3°C–0.7°C and 0.8°C–1.5°C, respectively. Thus, north-facing slope and forest cover serve as favorable natural factors for TSP or permafrost existence.

Cold winter air temperatures are able to accumulate in rockfall and talus, which are widespread in the Altai, Hentei and Hovsgol Mountains. As compared with meadow, MAGTs at a depth of 2 m in talus and rockfall were colder by more than 1.7°C and 2.9°C, respectively. Value of low MAGTs in the course fragmental rocks such as rockfall and talus depends on porosity or the empty space in them (Table 5).

The thermal effect of underground waters on MAGT depends on river size, water stream, and water-bearing sediments. Data from Table 6 show that underground water streams along big and medium river valleys in continuous and discontinuous permafrost zones lead to taliks, due to an increase in MAGT. For example, as compared with large rivers, MAGT at a depth of 10 m in water-bearing sediments along medium and small river valleys and near brooks are colder by more than 2°C, 5°C, and 7°C, respectively.

Thermal offset enables permafrost to form and survive even when MASTs are positive (Osterkamp & Romanovsky 1999). Small patches and islands of permafrost in sporadic and isolated permafrost zones of Mongolia are formed as a result of thermal offset caused by differences of ground moisture content and thermal conductivity in the active layer (Sharkhuu 2000, Ishikawa et al. 2005). Observed values of MAGT for the thermal offset at Argalant borehole sites were typically 0.5°C to 1.5°C (Table 7).

Permafrost Temperature Monitoring

Main results on permafrost temperature monitoring in Mongolia are as follows: Permafrost in Mongolia is degrading at various rates, depending on climate and natural factors. In general, permafrost under influence of climate warming was degrading more intensely during the last 15–20 years than during previous 15–20 years (1970–1990). Permafrost degradation in bedrock is more intense than in unconsolidated sediments. For example, a rate of increase in MAPT in the Nalaih borehole with unconsolidated sediments does not exceed 0.02°C/year, but in the Burenkhan borehole with bedrock, it reaches 0.04°C/year (Fig. 2).

Moreover, the increasing permafrost temperature gradients with depth can be addressed as an indicator of recent and former degradation of permafrost (Harris & Haeberli 2003).

Table 4. MAGT depending on vegetation, slope aspect and steepness in Erdenet mountain area.

Slope aspect	Slope angle	Elevation, m	Vegetation	Ground	MAGT at 10 m, °C	Difference
South-facing	10°	1430	grass	bedrock	2.6	0.9
South-facing	10°	1430	forest	bedrock	1.7	
South-facing	15°	1420	forest	bedrock	1.7	0.7
North-facing	15°	1420	forest	bedrock	1	
South-facing	5°	1300	grass	sand	1.8	0.5
North-facing	5°	1300	grass	sand	1.3	

Table 5. Amplitude temperature (A) and MAGT at various depths of meadow, talus, and rockfall in Bogd Mountain.

Depth, m	Meadow		Talus		Rockfall	
	A	MAGT	A	MAGT	A	MAGT
0.5	22	1.08	32	-2.32	42	-2.07
1.0	17	1.19	26	-2.28	39	-2.94
1.5	13	0.62	21	-2.62	37	-3.67
2.0	10	1.17	16	-2.91	36	-4.09

Table 6. MAGT in the boreholes, located in different river valleys near Erdenet area.

Name and size of river	Predominant ground	Water stream	MAGT at 10 m, °C	h, m
Orhon large river	Gravel and pebbles	high	6.5	1.7
Burgaltai medium river	Sandy gravel	medium	4.5	2.3
Chingeltei small river	Gravely sand	low	1.2	2.7
Zunigol brook	Silt and clay	no	-0.4	3.4

Note: h – depth of seasonal freezing of ground.

Table 7. Thermal offset caused by differences of ground moisture content in Argalant boreholes.

Borehole No	Predominant ground	Average moisture, %	MAGT, at 10 m, °C	Thermal offset, °C
26	Sandy loam	12	0.4	0.6
126	Sandy loam	20	-0.2	
58	Loam	11	1.0	1.0
3	Loam	21	0.0	
15	Silt	10	1.2	1.3
18	Silt	23	-0.1	

Figure 3 demonstrates that Darhad site would represent a warming trend during the early 1980s, while the Burenkhan site would respond to warming trends during the early 1960s. Both warming episodes are recorded according to climate data from the Muren, Hatgal, and Rinchinlhumbe weather stations (Anarmaa et al. 2007).

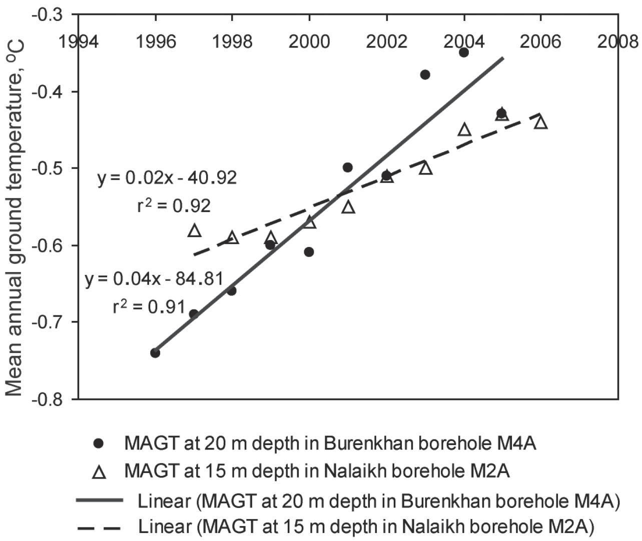

Figure 2. Trend of mean annual permafrost temperatures.

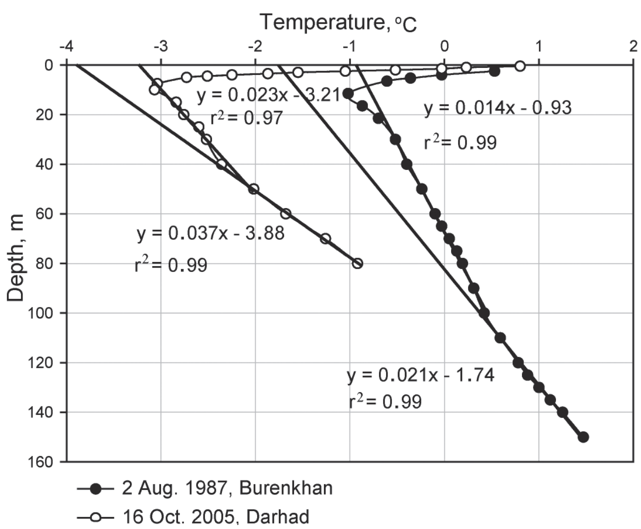

Figure 3. Change in permafrost temperature gradients with depth.

The average rate of increase in MAPT at 10 m depth in the Hovsgol Mountain region reaches 0.02°C–0.03°C/year, but in the Hangai and Hentei Mountain regions it does not exceed 0.01°C–0.02°C/year (Table 8). As compared with central Asia and European mountain territories, average trends of recent degradation of permafrost in Mongolia have almost similar values (Harris & Haeberli 2003, Marchenko 2007). However, as compared with eastern Siberia and Alaska, the average trends have smaller values (Osterkamp & Romanovsky 1999, Gavrilova 2003, Pavlov & Perlshtein 2006).

Conclusions

Main natural factors for determining thermal state and distribution of permafrost in the Altai, Hangai, Hovsgol, and Hentei Mountain regions are altitudes, slope aspect, and sometimes forest cover. The factors in arid land region surrounding the mountains are fine sediments with high moisture content and sometimes course fragmental deposits in mountains. Values of MAST and MAGT under influence of warming (5–20 cm thick snow cover and ground water stream) and cooling (forest and moss covers, fine-grained sediments with high moisture content and course fragmental deposits) factors are reduced within 0.5°C–2.5°C in every factor.

In general, permafrost under influence of climate warming in Mongolia is degrading at different rates. The permafrost in the Hovsgol Mountain region is degrading more intensely than in the Hangai and Hentei Mountain regions. Meanwhile, permafrost degradation under influence of climate warming was more intense during the last 15–20 years than during previous 15–20 years (1970–1980). Studies of TSP are of both scientific and practical significance for mapping and monitoring permafrost.

Acknowledgments

The University of Delaware and the University of Alaska Fairbanks, USA, have provided us with a number of loggers and financial support for conducting CALM and GTN-P programs in Mongolia. We also thank Jerry Brown, IPA president, for coordinating the Mongolian TSP/ INPO for IPY activities.

Table 8. Changes in the mean annual permafrost temperature at 10 m depth in the Hentei, Hangai, and Hovsgol Mountain regions.

Mts region	Hentei				Hangai				Hovsgol			
Borehole No	Baganuur		Argalant		Terkh		Chuluut		Sharga		Tsagaan nuur	
Elevation, m asl	1350		1385		2075		1870		1864		1547	
Land form	Plain of depression		Small valley bottom		High flood plain		Top of the pingo		Wide valley bottom		Lake depression	
Ground	Sandstone		Loam		Gravelly sand		Ice and clay		Gravelly sand		Silt and clay	
Ice content	Low		Medium		Medium		High		Medium		High	
Measured years	1976	2006	1988	2006	1969	2006	1969	2006	1968	2006	1989	2006
MAPT at 10 m	-0.50	-0.09	-0.40	-0.24	-1.96	-1.49	-1.12	-0.80	-2.35	-1.63	-3.91	-3.37
Trend of MAPT, °C/year	0.013	0.013	0.009	0.009	0.015	0.015	0.011	0.011	0.019	0.019	0.032	0.032
	0.01-0.02								0.02-0.03			

References

Anarmaa, Sh., Sharkhuu, N., Etzelmuller, B., Heggem, E.S.F., Nelson, F.E., Shiklomanov, N.I., Goulden, C.E. & Brown, J. 2007. Permafrost monitoring in the Hovsgol mountain region, Mongolia. *J. Geophys. Res.* 112:F02506, doi:10. 1029/2006JF000543.

Brown. J., Hinkel, K.M. & Nelson, F.E. 2000. The Circumpolar Active Layer Monitoring (CALM) Program: Research Designs and Initial Results, *J. Polar Geography* 24(3):258.

Burgess, M., Smith, S.L., Brown, J., Romanovsky, V.E. & Hinkel, K. 2000. Global Terrestrial Network for Permafrost (GTN-P): Permafrost monitoring contributing to global climate observations. *Geol. Surv. Can. Current Res. 2000-E14, 8 pp*.

Gavrilova, M.K. 2003. Recent climatic change in Asia along Yakutia-Mongolia transect. *Papers in Meteorology and Hydrology 25/4. Ulaanbaatar,* 11-17.

Gravis. G.F, Zabolotnik, S.I, Sukhodrovsky, V.L.,.Gavrilova, M.K. & Lisun, A.M. 1974. *Geocryological Conditions in the People's Republic of Mongolia*. Moscow: Nauka Publishing, 200 pp. (in Russian).

Harris, C. & Haeberli, W. 2003. Warming permafrost in Europe. *World Meteorological Organization Bulletin* 52: 252-257.

Heggem, E.S.F., Etzelmuller, B., Anarmaa,S., Sharkhuu, N., Goulden, C.E. & Nandintsetseg, B. 2006. Spatial distribution of ground surface temperatures and active layer depths in the Hovsgol area, Northern Mongolia. *Permafrost and Periglacial Processes* 17: 357-369.

Ishikawa, M., Sharkhuu, N., Zhang, Y., Kadota, T. & Ohata, T. 2005. Ground thermal and moisture conditions at the southern boundary of discontinuous permafrost, Mongolia. *Short Communication in Permafrost and Periglac. Process*. 16: 209-216.

Kudrayvtsev, V.A., Gragula, L.S., Kondratyeva, K.A. & Melamed, V.G. 1974. *Fundamentals of Frost Forecasting in Geological Engineering Investigations.* Moscow: Moscovskogo University, 431 pp. (in Russian).

Marchenko, S.S., Gorbunov, A.P. & Romanovsky, V.E. 2007. Permafrost warming in the Tien Shan mountains, Central Asia. *Global and Planetary Change* 56: 311-327 (available online at www.sciencedirect.com).

Nandintsetseg, B. & Goulden,.C.E. 2005. Recent change in the Northern Mongolia and its impact on ecosystem. *Proceedings of the International Symposium on Terrestrial and Climate Change in Mongolia, Ulaanbaatar, July 26-28, 2005:* 19-21.

Natsagdorj, L., Dagvadorj, D., Batima, P. & Tumurbaatar, D. 2000. Climate change and its impacts in Mongolia. *JEMR Publishing*, 226 pp.

Nelson, F.E, & Outcalt, S.I. 1987. A computational method for prediction and regionalization of permafrost. *Arctic and Alpine Research 19:* 279-288.

Nelson, F.E., Shiklomanov, K.M., Hinkel, K, & Christiansen, H.H. 2004. The Circumpolar Active Layer Monitoring (CALM) Workshop and the CALM 2 Program. *Polar Geogr.* 28: 253-266.

Osterkamp, T.E. & Romanovsky, V.E. 1999. Evidence for warming and thawing of discontinuous permafrost in Alaska. *Permafrost and Periglac. Process.* 10:17-37.

Pavlov, A.V. & Perlshtein, G.Z. 2006. Monitoring and modeling the permafrost dynamics under climate changes. *Abstracts of Asia Conference on Permafrost. Lanzhou, China*, 160-161.

Sharkhuu, N. 2000. Regularities of permafrost distribution in Mongolia. *Transactions of Institute of Geo-Ecology, MAS:,* 217-232 (in Mongolian).

Sharkhuu, N. 2003. Recent changes in the permafrost of Mongolia. *Proceedings of the Eighth International Conference on Permafrost, Zurich, Switzerland:* 1029-1034.

Sharkhuu, N. & Anarmaa, Sh. 2005. Recent degradation of permafrost in Mongolia. *Proceedings of the International Symposium on Terrestrial and Climate Change in Mongolia*, *Ulaanbaatar, Mongolia, July 26-28, 2005*: 99-101.

Thaw Settlement Behavior of Permafrost Along an Oil Pipeline to be Constructed in Northeastern China

Yu Sheng, Zhi Wen, Guoyu Li
State Key Laboratory of Frozen Soil Engineering, CAREERI, CAS, P.R. China
Jiaqian Hao, Wei Wu
Oil Engineering limited, Daqing Oil Field Company, Daqing, P.R. China

Abstract

An oil pipeline is to be constructed in northeastern China, which will transport oil from Russia to Daqing, China. Along the pipeline which runs from north to south, there exists continuous permafrost, discontinuous permafrost, sporadic permafrost, and seasonally frozen soil. A large number of undisturbed permafrost samples were collected to carry out thaw settlement tests in order to predict the potential deformation from thawing of permafrost. Test results include both thaw settlement parameters and the coefficients of compressibility dependent on total water content of samples. Regressive envelopes of the test results are suggested to analyze the relationships between the two parameters and water content for predicting the thaw settlement of permafrost for both fine- and coarse-grained soils. A comparison of thaw settlement parameters obtained using the proposed method and those estimated from specifications was carried out to clarify the thaw settlement behavior of permafrost along the pipeline.

Keywords: coefficient of compressibility; permafrost; pipeline; thaw settlement parameter.

Introduction

A pipeline is to be constructed in northeastern China to transport crude oil from Russia to China, in nearly a straight line in a north-to-south direction within a latitude range from 53°28′N to 46°30′N. The 960 km long, 914 mm diameter pipeline has been designed to be buried at a depth of 1.8 m (from ground surface to top of pipe) along most of the route. The pipeline has to traverse about 450 km of continuous permafrost, discontinuous permafrost, and sporadic permafrost zone from the most north to the south. The oil temperature at the inlet of the pipeline is estimated to be changing between -6°C to +10°C during the year. There will be no temperature control of the oil along the route. According to a preliminary estimate, the underlying permafrost would thaw to a depth of 1.5–4 m in the coming 30 years of service time, depending on the ice content of the permafrost.

Thaw settlement is one of the most critical design issues for a pipeline buried in permafrost. Uneven deformation of the pipe due to thaw settlement of permafrost may induce pipe breakage, especially in a large diameter pipeline. For many existing pipelines in permafrost regions attention was given to engineering permafrost problems in order to optimize design and maintain a good permafrost environment (Greenslade & Nixon 2000, Burgess 1988, Hanna & McRoberts 1988, Hanna et al. 1983, Nixon & Maclnnes 1996). Thaw settlement behavior of permafrost is an essential property for estimating the deformation of pipeline due to permafrost thawing. Some engineering specifications involving permafrost suggest values of thaw settlement based on the ice content of permafrost. However, measured results from tests are not always consistent with the estimated values suggested by the specifications because of the variety of soil type. Also, the compressibility after thaw of the permafrost is generally not considered in any specifications.

In the geological survey for the pipeline, many permafrost samples from boreholes were collected to study the thaw settlement behavior of permafrost. This paper documents the results of thaw settlement tests, which are proposed to be a reference in estimating the thaw settlement of permafrost along the pipeline.

Samples and Testing

Undisturbed frozen samples collected from boreholes were transported to a laboratory for testing. All thaw settlement tests were conducted in a confined condition using a cylinder of 79.8 mm ID and 40 mm height. Samples were carefully trimmed to fit to the test cell. Additional parts of the samples were used to measure their physical properties.

Samples were generally divided into two groups; these were fine-grained silty clay and coarse-grained soils including sand, sand with gravel and strongly weathered sandstone. Soil samples of both groups had a wide range of ice content and bulk density. The average plastic limit and liquid limit of the fine-grained soil were about 12.5% and 31.5%, respectively.

The total thaw settlement strain of a frozen sample generally consists of two components expressed as follows (Tsytovich 1975, McRoberts et al. 1978):

$$\alpha = A_0 + a_0 p \tag{1}$$

where

α is the total thaw settlement ratio, %;
A_0 is the thaw settlement parameter, %;
a_0 is the average coefficient of compressibility, 1/MPa;
p is the pressure applied to the permafrost sample, MPa;
A_0 and a_0 are determined using the thaw settlement test.

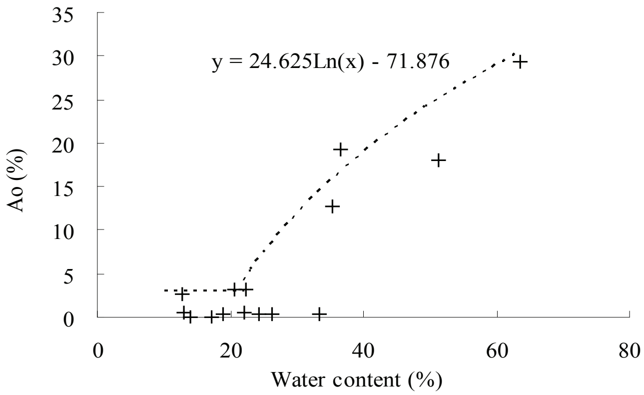

Figure 1. Thaw settlement parameter vs. water content for the fine-grained silty clay.

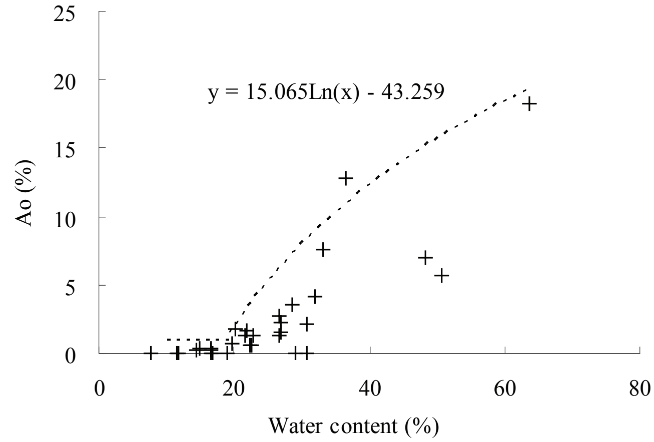

Figure 2. Thaw settlement parameter vs. water content for the coarse-grained soils.

After putting the sample into the test cell, the sample is allowed to thaw under uncontrolled conditions. For the thaw settlement parameter a pressure of about 1 kPa is maintained to overcome the friction between the sample and the cell wall. After the deformation stabilizes, subsequent increments of pressure are applied to determine the coefficient of compressibility. Three pressure stages, 50 kPa, 100 kPa, and 150 kPa are used in the tests. The coefficient of compressibility is determined as the average at the three pressure levels.

Test Results

Thaw settlement parameter A_0

The values of thaw settlement parameter are plotted against the initial water (ice) content of the samples as shown in Figure 1 for the fine-grained silty clay and Figure 2 for the coarse-grained soils. For both groups of soil, the relationship between A_0 and water content shows a two-stage phenomenon. There is a low and comparatively stable value when the water content is less than a certain value (defined as initial water content of thaw settlement for the soil type along the oil pipeline). Once the water content is greater than initial water content of thaw settlement, A_0 starts to increase considerably with the increase in water content. To be safe, it is not thought appropriate to fit a formula to all the test data. A regressive envelope of the data is, therefore proposed to predict A_0 for samples with high water contents. A logarithmic relationship was found to be a good choice (see dotted line in Figs. 1 and 2). The thaw settlement parameters for both soils can be predicted by the following relationships:

For fine-grained silty clay:

$$A_0 = \begin{cases} 3 & w \leq 21\% \\ 24.625\ln w - 71.876 & w > 21\% \end{cases} \tag{2}$$

For coarse-grained soil:

$$A_0 = \begin{cases} 1 & w \leq 19\% \\ 15.065\ln w - 43.259 & w > 19\% \end{cases} \tag{3}$$

where w refers to the initial water content of the samples.

Table 1. A_0 suggested in Specification GB50324-2001.

A_0 (%)	Total water content, w (%)	
	Silty clay	Coarse soil
< 3	$w < w_p+4$	$w < 15$
3~10	$w_p+4 \leq w < w_p+15$	$15 \leq w < 25$
10~25	$w_p+15 \leq w < w_p+35$	$25 \leq w$

Note: w_p is the plastic limit water content.

When the thaw settlement parameter is less than 3%, thaw settlement is generally considered to be negligible. In Equations (2) and (3), the first constant term corresponds to a water content range of less than the initial water content of thaw settlement. The initial water contents of thaw settlement are 21% and 19% for the fine-grained silty clay and coarse-grained soil, respectively.

Comparing Figure 1 with Figure 2, it is found that the value of A_0 for the fine-grained silty clay is greater than that for the coarse-grained soil at the same water content. This means that engineers should pay particular attention to silty clay permafrost soils with high ice content.

Comparison with specifications

In some specifications in China, thaw settlement parameters are suggested for different types of soil. Table 1 lists a typical summary of A_0 according to Specification for Survey of Frozen Soil Engineering Geology (GB50324-2001).

In terms of the classification of A_0 in the specification, water content ranges from test results can be calculated from the proposed predicting formulae. Table 2 lists the results.

It was found that the test results for the fine-grained silty clay roughly agreed with the suggestion in the specification, especially for the permafrost with high water-ice content. For the coarse-grained soils, test results indicated that the water content ranges generally had higher values than those suggested in the specification. In other words, the thaw settlement of coarse-grained permafrost soil would be much lower than that estimated in the specification.

Table 2. Water content ranges from test results in terms of the classification of A_0 in specification.

A_0 (%)	Total water content, w (%)			
	Silty clay		Coarse soil	
	Specification	Test	Specification	Test
< 3	<16.5	< 21	< 15	< 21.5
3~10	16.5~27.5	21~28	15~ 25	21.5~35
10~25	27.5~47.5	28~51	≥ 25	≥ 35

Coefficient of compressibility a_0

Results of the coefficients of the compressibility test are shown in Figures 3 and 4 for the fine-grained silty clay and the coarse-grained soil, respectively. It can be seen that there is a scatter in the test results. Although linear relationships can be used to approximate the test results (solid line in Figures), we suggest that the regressive envelopes of the data provide a reasonable and safe prediction. Logarithmic relationships are found to be quite appropriate for both fine-grained silty clay and coarse-grained soil (shown in dotted line in Figs. 3, 4). Therefore, the coefficient of compressibility for both soils can be predicted according to the following formulae:

For the fine-grained silty clay:

$$a_0 = 0.8514 \ln w - 1.5224 \tag{4}$$

For coarse-grained soil:

$$a_0 = 1.25 \ln w - 2.3146 \tag{5}$$

Although the thaw settlement parameter of the fine-grained silty clay is higher than that of the coarse-grained soil, the coefficient of compressibility of the coarse-grained soil appears to increase faster with increasing water content. This means that the frozen coarse-grained soil has more potential to deform than the fine-grained silty clay when loaded. The total thaw strain of permafrost depends on both A_0 and a_0 for different pressures. Based on the proposed estimate, the total thaw strain can be plotted as shown in Figure 5. It can be seen that if the pressure is less than 100 kPa, the silty clay deforms more than the coarse soil. For pressures greater than 100 kPa, the coarse soil deforms more than the silty clay.

The pipeline is designed to be buried at a depth of about 1.8 m; the depth at the bottom of the pipeline is about 2.7 m. Within the range of 4.0 m below the pipeline, where underlying permafrost may thaw, the soil pressure applied on permafrost is about in the range from 50–150 kPa, which falls within the pressure range of the tests. If an insulation layer is packed around the pipeline to reduce the depth of permafrost thaw, the thaw settlement should be comparatively low. In this case more attention should be paid to the deformation of the frozen silty clay. If there exists a frozen coarse layer with high water content at a deeper location below the pipeline (e.g., 3–4 m below the bottom of the pipeline), the possible deformation from permafrost thawing may be greater than that of the frozen silty clay at the same ice content. Engineers should consider the difference in the thaw settlement

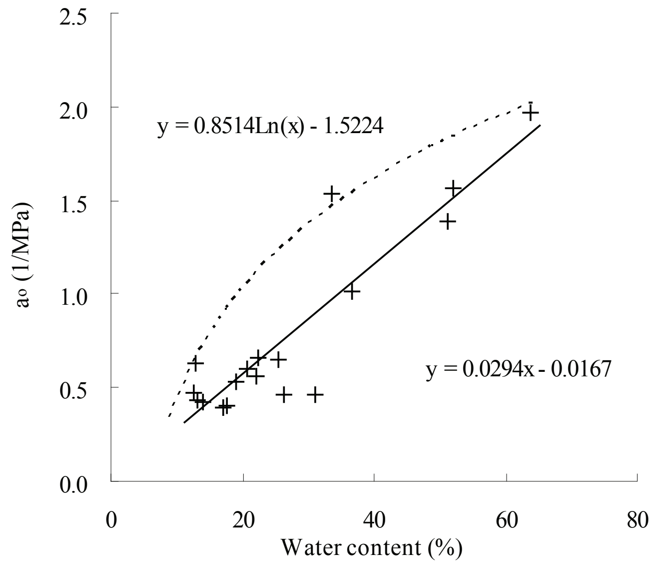

Figure 3. Coefficient of compressibility vs. water content for the fine-grained silty clay.

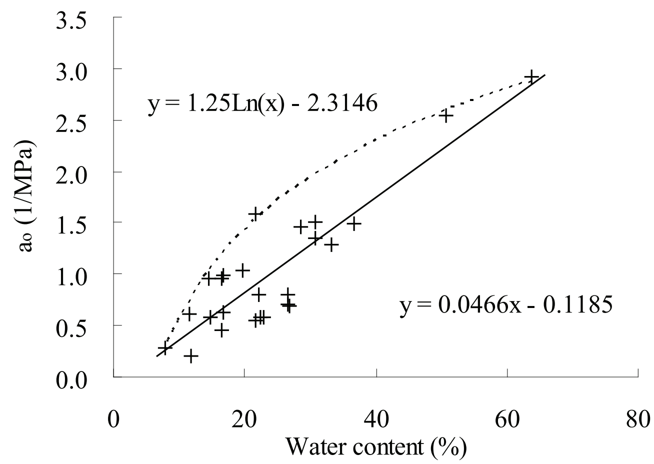

Figure 4. Coefficient of compressibility vs. water content for the coarse-grained soil.

behavior with comprehensive permafrost geological data to optimize the design, so as to choose a reasonable treatment to the permafrost section.

Conclusions

Based on test results, thaw settlement behavior was analyzed for both fine-grained silty clay and coarse-grained soil. Water content appeared to be a dominant factor in the test results. The following suggestions are proposed to provide a guide for the design of the pipeline.

(1) The thaw settlement parameter of the fine-grained silty clay has a high value, which is roughly in agreement with the suggestion in specifications. The thaw settlement parameter of the coarse-grained soil is, however, lower than the value suggested in specifications.

(2) When the water content of the frozen sample is greater than the initial water content of thaw settlement, it was suggested that the thaw settlement parameters of both

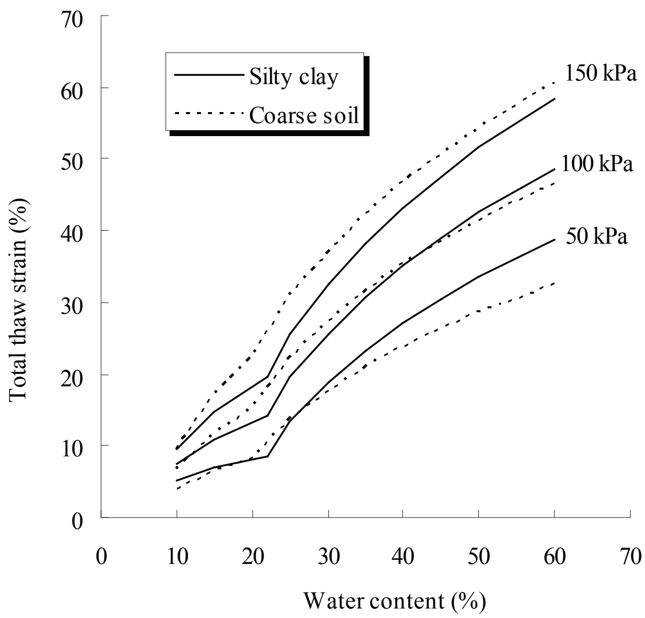

Figure 5. Total strain of the thawed permafrost vs. water content under different pressure.

fine-grained silty clay and coarse-grained soil be predicted using their envelopes of the test results, instead of all data. A logarithmic relationship is proposed to describe the relationship.

(3) The coarse-grained soil has more potential to deform under comparatively high pressures. Its coefficient of compressibility was higher than that of the fine-grained silty clay with increasing water content. Logarithmic envelopes of test results are also useful for predicting the coefficients of compressibility.

Acknowledgments

This work was carried out under the auspices of the Key Directional Project of the CAS Knowledge Innovation Program "Mechanisms and mitigation of frost heaving and thaw settlement of pipeline foundation soils in permafrost regions" (Grant No. KZCX2-YW-311), and Permafrost Research Projects of PetroChina Daqing Oilfield Engineering Company "Assessment and forecast of permafrost conditions along the China-Russia crude oil pipeline route, Thermal/strain analyses on pipeline-soil interactions in permafrost regions."

References

Burgess, M. 1988. Permafrost and terrain preliminary monitoring results, Norman Wells pipeline, Canada. *Proceedings of the 5th International Conference on Permafrost* Vol. 1: 916-921.

Greenslade, J.G & Nixon, D. 2000. New design concepts for pipelines buried in permafrost. *2000 International Pipeline Conference* Vol. 1: 135-143.

Hanna, A.J. & McRoberts, E.C. 1988. Permafrost slope design for a buried oil pipeline. *Proceedings of the 5th International Conference on Permafrost* Vol. 1: 1247-1252.

Hanna, A.J., Saunders, R.J., Lem, G.N. & Carlson, L.E. 1983. Alaska Highway Gas pipeline project (Yukon) section thaw settlement design approach. *Proceedings of the 4th International Conference on Permafrost* Vol. 1: 439-444.

McRoberts, E.C., Law, T.C. & Moniz, E. 1978. Thaw settlement studies in the discontinuously pemafrost zone. *Proceedings of the 3rd International Conference on Permafrost* Vol. 1: 700-706.

Nixon, D. & Maclnnes, K.L. 1996. Application of pipe temperature simulator for Norman Wells oil pipeline. *Canadian Geotechnical Journal* 33: 140149.

Tsytovich, N.A. 1975. *The Mechanics of Frozen Soil.* New York: McGraw-Hill Book Company.

Impact of Surface Air Temperature and Snow Cover Depth on the Upper Soil Temperature Variations in Russia

Artem B. Sherstyukov
All-Russian Research Institute of Hydrometeorological Information - World Data Centre (RIHMI-WDC), Obninsk, Russian Federation

Boris G. Sherstyukov
All-Russian Research Institute of Hydrometeorological Information - World Data Centre (RIHMI-WDC), Obninsk, Russian Federation

Pavel Ya. Groisman
UCAR Project Scientist at National Climatic Data Center, Asheville, North Carolina

Abstract

From 1965–2004, data from all Russian meteorological stations with long-term soil temperature observations at depths 80, 160, and 320 cm were compiled and analyzed. It was found that the prevailing influence on soil temperature variations in the European part of Russia was surface air temperature and in the Asian part of Russia was snow cover depth. By preserving the heat accumulated in the warm season, an observed increase of the winter snow depth in the permafrost zone promotes annual soil temperature increase and therefore may foster the further permafrost degradation associated with on-going regional warming.

Keywords: Eurasia; permafrost; snow depth; soil temperature; warming.

Introduction

According to Izrael et al. (2002), beginning in the mid-1960s, northern Russia experienced climate warming. For the whole of northern Russia, the air temperature rise trend was 0.47ºC/decade. As the sampling stations in Izrael et al. (2006) show, this was accompanied by the soil temperature rise at 80 and 160 cm depths. However, the agreement between air temperature and soil temperature trends has not occurred everywhere. At some stations, soil temperature trends are higher than air temperature trends. The causes of this behavior are to be identified. This work aims at deriving quantitative estimates of the influence of the two major factors of changing climate: air temperature and snow depth, on the soil temperature. The problem is addressed by using data from the network of Russian stations, where soil temperatures have been recorded at depths to 320 cm since 1965.

Temperature rise in the permafrost zone can lead to frozen ground degradation and can change the characteristics of soil toughness. Therefore, the problem of frozen ground degradation is of major practical importance. The Russian permafrost zone contains more than 30% of the developed oil reserves available in Russia; about 60% of natural gas, hard-coal and peat deposits; a significant portion of hydropower resources; deposits of non-ferrous metals, gold and diamond and vast reserves of timber and fresh water. Expensive and vulnerable infrastructure was created here, i.e., petroleum field facilities; main oil and gas pipelines extending thousands of kilometers; mines and pits; and hydroelectric plants. Additionally, settlements and towns, highways and railways, aerodromes, and ports were built in this region (Pavlov et al. 2000). The foundations and base plates of all the structures are supported by pilings frozen in the ground. Melting of frozen ground violates the stability and operational capability of all these engineering facilities (Demchenko et al. 2001).

Analysis and Results

Soil temperature data at depths 80, 160, and 320 cm, as well as air temperature and snow depth data, were analyzed for all Russian meteorological stations for 40 years (for the 1965-2004 period). The monthly data for 150 stations (shown by stars in Fig. 1) were retrieved from the National Roshydromet archive. Thereafter, we conducted multiple correlation analyses searching the factors that control the soil temperature seasonal variations across the Russian Federation.

Correlations, R, between summer soil temperatures at the 160 cm depth and summer air temperatures (mean temperature for June to August) are presented in Figure 1. From the western border of the Russian Federation to 75°E, the Figure shows significant positive R-values (> 0.6). East of 75°E, across West Siberia, southeast Siberia, and at the Far East stations of Sakhalin and Primorie Krai, correlation coefficients (being of the order of 0.4 to 0.5) are still statistically significant at the 0.05 level. The highest positive correlation coefficients (R>0.60) between summer air temperatures and soil temperatures at all depths (with appropriate shifts depending upon the depth, e.g., for 160 cm this shift is around 2 months) are primarily observed outside the permafrost zone. In the vast central part of the permafrost zone, the correlation is close to zero (Fig. 1).

In winter (December to February), the correlations between soil temperatures and air temperatures are weaker and the R-values above 0.6 are absent across the entire nation (Fig. 2). Statistically significant correlation coefficients (0.4 to 0.6) between winter air temperatures and soil temperatures at depths of 80 and 160 cm are observed only over Russia west of the Ural Mountains. Only here in the southernmost part, the impacts of winter air temperature are observed as deep as 320 cm. In winter in the permafrost zone, the impact of long-term surface air temperature changes on soil temperatures is practically unnoticeable at all depths.

The analysis of correlations between winter soil temperatures at different depths and February snow depth shows that significant positive correlation coefficients (0.4 to 0.6) prevail at soil depths of 80 and 160 cm over most of Russia east of the sub-Urals (50°E, with exceptions of the North Siberia Plain, Kamchatka, and southeast Siberia). At the 320 cm soil depth, a significant positive correlation is observed only in small isolated areas in southwest Siberia, Central Yakutia, and Primorie. No significant correlations were found between the February snow depth and winter soil temperatures at all depths over European Russia. The warming influence of snow at each soil depth is recorded over most of Asian Russia, but it becomes weaker as the soil depth increases and is not observed at all in European Russia.

Mean annual soil temperature in different regions is formed in different ways. In European Russia, it is controlled by air temperature changes rather than by snow depth. The warming effect of snow here is practically absent. In Asian Russia, on the contrary, changes in mean annual soil temperature are controlled by snow depth changes rather than by air temperature changes.

The contribution of the mean annual air temperature and the snow depth to the change in mean annual soil temperature was estimated in percent of the total variance of the soil temperature. The analysis of this quantity shows that in European Russia, the main contribution to the total variance is made by the air temperature (23% to 46% of the contribution to the total variance) and the contribution of snow here is minimal (from 0.4% to 8.0%). The impact of snow on the soil temperature in this region is so small that even with negative snow depth trends in northwestern Russia (e.g., in Karelia and Arkhangelsk district; cf. Fig. 3), soil temperature trends are positive and significant.

Tendencies for the increase in mean winter snow depth are observed over most of the Russian territory (mainly in Siberia). But northern regions of European Russia, show a tendency for decreasing snow depth (Bulygina et al. 2007).

Across Asian Russia and in the Urals Region, the values of soil temperature trends are higher than the air temperature trends. Positive soil temperature trends are observed even at the stations with negative air temperature trends (Nizhni Tagil 57.9°N, 60.1°E; Kupino 54.4°N, 77.3°E; Pudino 54.4°N, 79.2°E, and Bokhan 53.2°N, 103.8°E). At the last station (Fig. 4), the contribution of the mean annual air

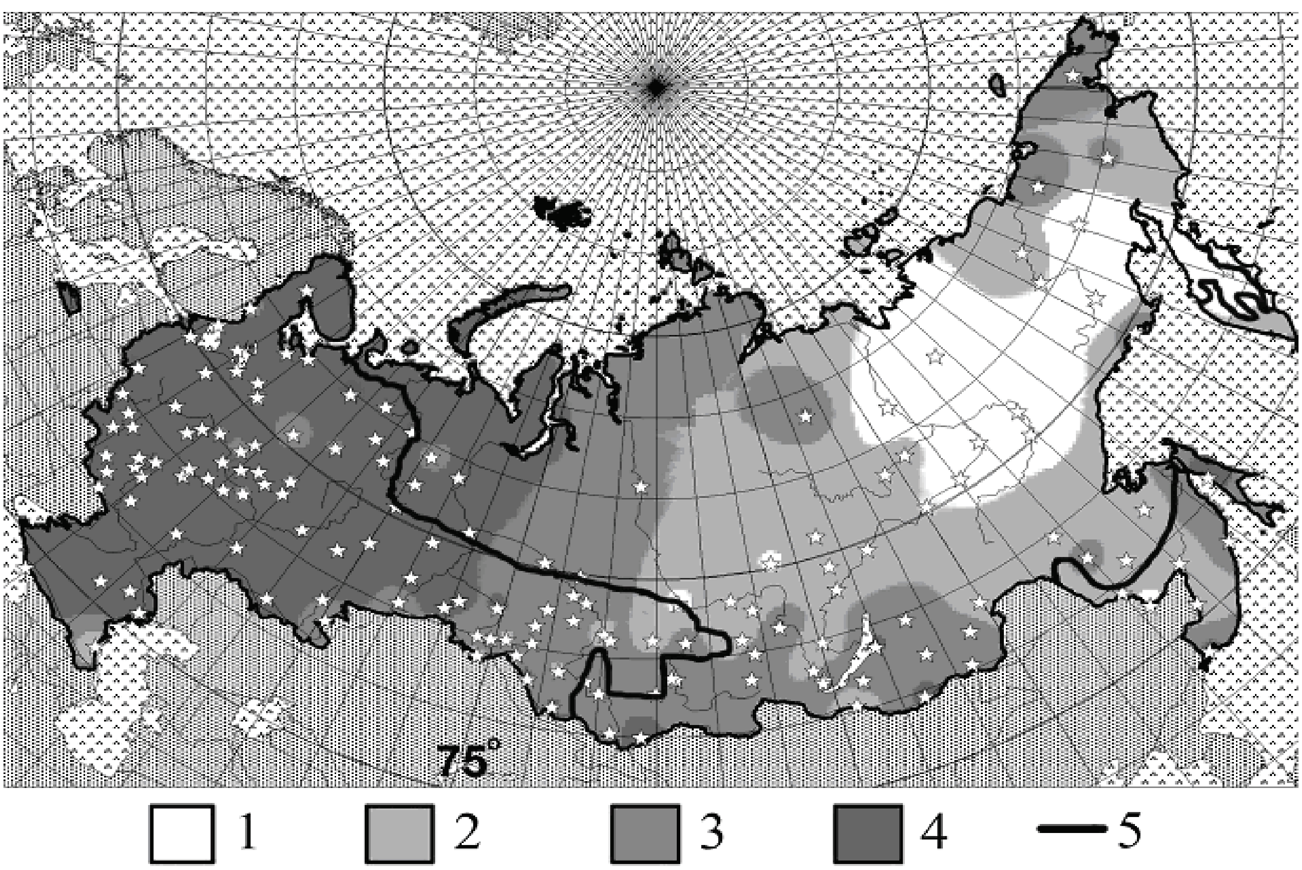

Figure 1. Correlation coefficient (R) between air temperatures and soil temperatures at the 160 cm depth in summer.
1 – 0.1≤k<0.2, 2 – 0.2≤R<0.4, 3 – 0.4≤R<0.6, 4 – 0.6≤R<0.8, 5 – southern border of the permafrost zone.

temperature to the total variance of soil temperatures at 160 cm is only 4.7%, while the contribution of the snow depth is 30%.

A geographical distribution of the contributions of the two factors to the total variance of mean annual soil temperatures at 160 cm is shown as diagrams on the map (Fig. 5). Nearly everywhere in European Russia, the long-term changes in mean annual soil temperature are greatly controlled by air temperature changes (light columns in diagrams, 20% to 50%).

The snow changes here determine no more than 10% of the variance (dark columns in diagrams). In Central Volga, the Urals, and over most of Asian Russia, the long-term changes in mean annual soil temperature are primarily controlled by snow depth changes (10% to 50% of the variance) and air temperature is responsible for less than 10% of soil temperature variability.

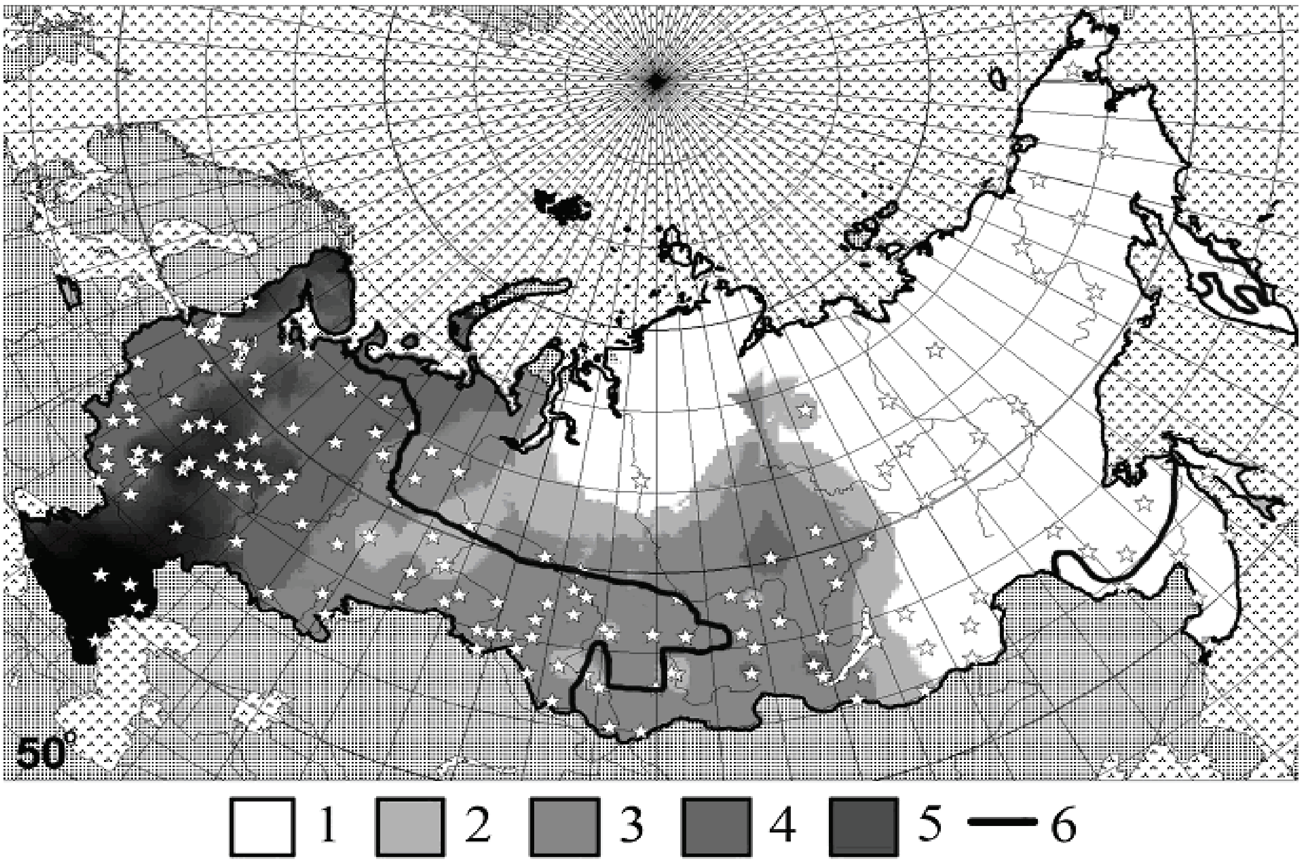

Figure 2. Correlation coefficient (R) between air temperatures and soil temperatures at the 160 cm depth in winter.
1 – $0.1 \le R < 0.2$, 2 – $0.2 \le R < 0.3$, 3 – $0.3 \le R < 0.4$, 4 – $0.4 \le R < 0.5$, 5 – $0.5 \le R < 0.6$, 6 – southern border of permafrost.

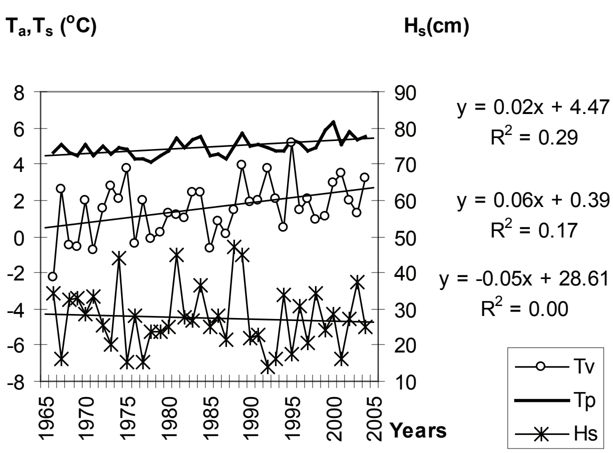

Figure 3. Long-term trends of mean annual air temperatures (T_a), soil temperatures at 160 cm depth (T_p), and snow depth (H_s) at Onega station (63.9°N, 38.1°E, Arkhangelsk district).

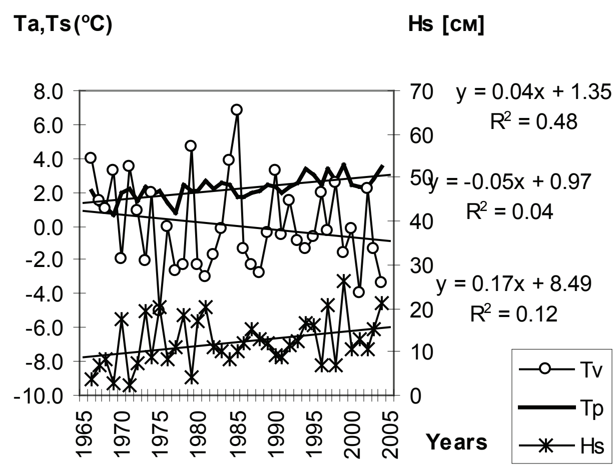

Figure 4. Long-term trends of mean annual air temperatures (T_a), soil temperatures at 160-cm depth (T_p) and snow depth (H_s) at Bokhan station (53°08′N, 103°46′E, elevation 446 m).

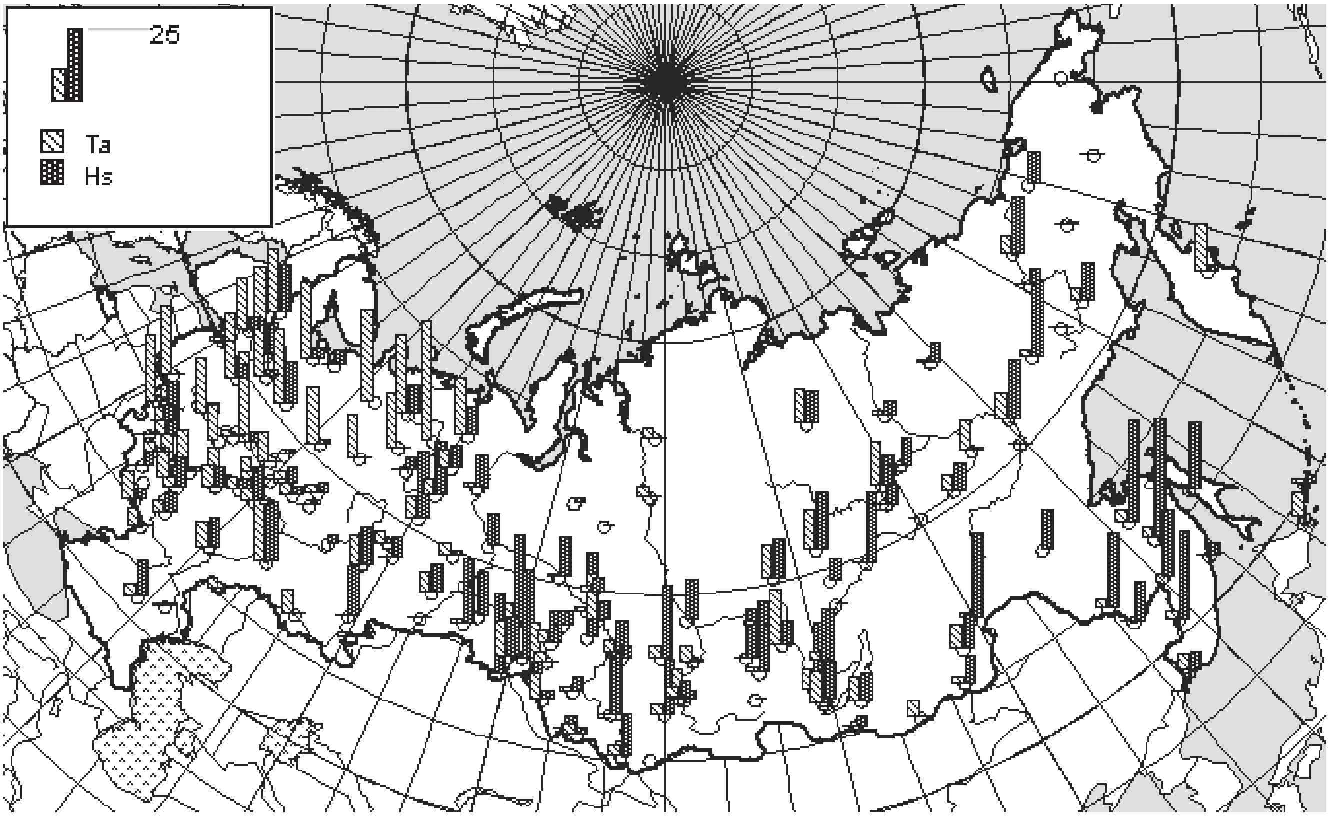

Figure 5. Contribution (in percent of variance) of mean annual air temperature (T_a) and snow depth (H_s) to long-term changes in mean annual soil temperature at 160 cm depth.

At the 320 cm depth, the effect of surface meteorological conditions is very weak and uneven over the Russian territory and is probably controlled by local micrometeorological and soil conditions. The increasing snow accumulation in Siberia results in an additional increase in mean annual soil temperatures and their relatively more rapid increase compared with the lower atmosphere. This fact is of particular importance in the permafrost zone since the increasing snow accumulation here strengthens one of the components likely to contribute to the permafrost degradation.warming.

The impact of long-term changes in air temperatures on soil temperatures in the central regions of the permafrost zone is weak both in summer and in winter. However, in regions with intermittent permafrost, the impact is substantial. The impact of snow depth on soil temperatures is observed throughout the entire permafrost zone of Russia.

Acknowledgments

This research was conducted with the support of the Russian Hydrometeorological Service (Roshydromet) and in the framework of the Northern Eurasia Earth Science Partnership Initiative (NEESPI).

References

Bulygina, O.N., Korshunova, N.N. & Razuvaev, V.N. 2007. Variations in snow characteristics over the Russian territory in the recent decades. *Proc. RIHMI-WDC*, 173: 41-46.

Demchenko, P.F., Velichko, A.A., Golitsin, G.S., Eliseev, A.V. & Nechaev, V.P. 2001. The permafrost fate: seeing the future from the experience of the past. *Prirod* 11: 43.

Izrael, Yu.A., Anokhin, Yu.A., Myach, L.T. & Sherstyukov, B.G. 2006. Analyzing the trends in the change of climate elements under global climate warming in permafrost regions based on meteorological observations. *Meteorology and Hydrology* 5: 27-38.

Izrael, Yu.A., Pavlov, A.V. & Anokhin, Yu.A. 2002. Evolution of the permafrost zone under current global climate change. *Meteorology and Hydrology* 1: 22-32.

Pavlov, A.V. &. Gravis, G.F. 2000. The permafrost and the current climate. *Priroda* 4: 10-18.

The Circumpolar Active Layer Monitoring (CALM) Program: Data Collection, Management, and Dissemination Strategies

N.I. Shiklomanov, F.E. Nelson, D.A. Streletskiy
Department of Geography, University of Delaware, Newark, DE 19716, USA
K.M. Hinkel
Department of Geography, University of Cincinnati, Cincinnati, OH 45221, USA
J. Brown
International Permafrost Association, Woods Hole, MA 02543, USA

Abstract

The Circumpolar Active Layer Monitoring (CALM) program, established in the early 1990s, was designed to observe temporal and spatial variability of the active layer and near-surface permafrost parameters, and their response to changes and variations in climatic conditions. CALM is the world's primary source of information about the active layer. Auxiliary information includes air temperature, soil moisture, soil temperature at different depths, snow cover, soil composition, and landscape characterization and frost heave and thaw subsidence. Metadata include detailed descriptions and photographs for each site. Several groups of sites have been used to create regional maps of active layer thickness. CALM data are distributed through the program's website (www.udel.edu/Geography/calm) and are also archived in and distributed through the Frozen Ground Data Center at the University of Colorado. This paper provides details about the nature, availability, and uses of data from the CALM network.

Keywords: active layer; data analysis; data archive; permafrost; polar regions; sampling design.

Introduction

The Circumpolar Active Layer Monitoring (CALM) program is a network of sites at which data about active layer thickness (ALT) and dynamics are collected. CALM was established in the 1990s to observe and detect the long-term response of the active layer and near-surface permafrost to changes in climate. CALM is among the international permafrost community's first large-scale efforts to construct a coordinated monitoring program capable of producing data sets suitable for evaluating the effects of climate change. Together with the IPA's Thermal State of Permafrost program, CALM comprises GTN-P, the Global Terrestrial Network for Permafrost. The CALM network's history and organizational structure are reported in Brown et al. (2000) and Nelson et al. (2004).

CALM is currently administered through the University of Delaware (UDel) Department of Geography. Analysis, archiving, and distribution of CALM's long-term observations are integral components of the project. Collected measurements are provided by participants to the CALM office at UDel, where they are subsequently incorporated into several databases. The data are distributed through the program's website, and through data products produced by the Frozen Ground Data Center at the University of Colorado. This paper provides details about the nature, availability, and uses of data from the CALM network. Scientific results are presented regularly at national and international meetings and have been published widely in international scientific journals and symposia proceedings. Several edited volumes focused on the CALM program have been published to date (Brown et al. 2000, Nelson ed. 2004a, 2004b). Several papers focused on CALM appear elsewhere in these proceedings.

Distribution of Sites

The distribution of CALM observational sites in the Northern Hemisphere is shown in Figure 1. The CALM network incorporates sites in arctic, subarctic, antarctic, and mountainous regions. Several sites constitute longitudinal and latitudinal transects across northwestern North America, Europe, and the Nordic region, and northeastern and northwestern Russia. Sites in Europe, China, Mongolia, and Kazakhstan provide high-elevation locations. About 70% of the sites are located in arctic and subarctic lowlands underlain by continuous permafrost. Discontinuous and mountainous permafrost areas contain respectively 20% and 11% of sites. The distribution of sites is not uniform, a circumstance attributable to historical circumstances and logistical constraints. The sites were established in regions of extensive economic activity and/or in areas of long-term climatic, permafrost, and ecosystem research. This logistically driven approach to site selection was adopted to insure regularity and periodicity of measurements. Assessment of the representativeness of the CALM network with respect to climatic and environmental conditions is currently in progress, and initial results were reported by Anisimov et al. (2007).

Monitoring Procedures

Three methods are used to determine the thickness of the active layer: (1) Mechanical probing using a graduated metal rod; (2) temperature measurements; (3) frost/thaw tubes.

The method-specific measurement procedure adopted by the CALM program is described in detail at the CALM web site (www.udel.edu/Geography/calm) and by Brown et

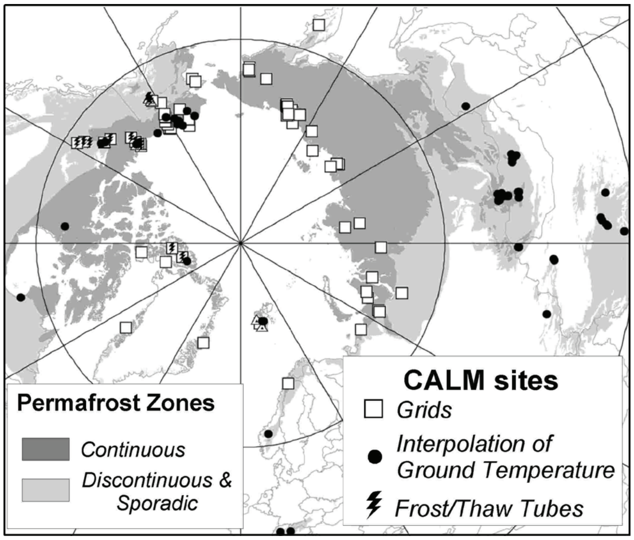

Figure 1. Permafrost distribution and location of CALM sites in the Northern Hemisphere. Sites are grouped according to active layer monitoring methods.

al. (2000). At 86 of the sites the active layer is measured by mechanical probing on regular grids of sampling points ranging from 10×10 m to 1000×1000 m. The time of probing varies from mid-August to the end of September; i.e., when thaw depth is at or near the maximum. More frequent measurements are made at some sites and in some years. The gridded sampling design allows for analysis of intra- and inter-site spatial variability and yields information useful for examining interrelations between physical and biological parameters. Grids are established at undisturbed locations characteristic of dominant environmental conditions. Their size varies depending on site geometry and the level of natural variability of surface and subsurface conditions. In general, 10×10 m to 100×100m size grids are established within relatively homogeneous landscape units. Several sites contain a number of grids representing various landscape units within the area. The 100×100 m to 1000× 1000 m grids usually encompass several characteristic landscapes within the area. CALM adopts a systematic sampling scheme for thaw depth measurements on most grids. The effectiveness of this sampling strategy has been investigated extensively and compared with alternative designs (Nelson et al. 1999). The systematic sampling design involves annual replicate measurement at regularly spaced grid nodes. With a few exceptions, each 10, 100, and 1000 m side grid contains 121 nodes distributed evenly at 1, 10, and 100 m spacing respectively. At some grid nodes thaw depth measurements are not possible due to deep water, roads, or gravel pads. These missing data points are not reported.

At 87 of the sites active layer thickness is determined exclusively by interpretation of ground temperature measurements, obtained by an array of thermistors distributed vertically from the ground surface downward into the permafrost (Romanovsky & Osterkamp 1997, Romanovsky et al. 2003). This method is primarily used in mountain regions and areas with deep (>1.5 m) annual thaw propagation, where spatially oriented measurements by probing are impossible. The depth and spacing of thermistor installation depends on local conditions and the needs of individual research projects.

Liquid- or sand-filled thaw tubes (Nixon & Taylor 1998, Nixon 2000) are employed in 11 Canadian and 3 Alaskan sites. When read periodically, frost tubes provide information about seasonal progression of thaw and maximum seasonal thaw. However, as with temperature measurements, thaw tubes do not provide the information on local variability. Individual thaw tube measurements are highly dependent on location of installation. To address this deficiency, thaw tube measurements are complemented by grid sampling of the active layer.

Data Availability

One of CALM's primary objectives is to develop coherent, quality-controlled datasets of long-term observations on the active layer and upper permafrost, suitable for assessing changes in polar terrestrial ecosystems. At present, the CALM database consists of annual submissions from 168 sites, and includes ALT, soil temperature and moisture (where available), and heave/subsidence data (where available). The majority of available data are distributed through the CALM website maintained by the University of Delaware's Department of Geography. (www.udel.edu/Geography/calm). The web-based summary table contains average ALT at all stations for all years and is linked to metadata and individual data sets. The following subsections provide a brief inventory of available data for specific geographic regions.

Alaska

At 30 out of 41 CALM-designated sites in Alaska periodic active layer observations are conducted on regular grids ranging from 10 m to 1000 m on a side. Geographically, grids are arranged in three north-south transects: (1) Fairbanks to the Beaufort Sea, along the Trans-Alaska Pipeline; (2) Ivotuk to Barrow (Chukchi Sea), and (3) Council and Kougarok, across the Seward Peninsula. These latitudinal transects, positioned from the Bering Sea eastward, encompass areas of steadily increasing continentality from west to east. For 25 of the grids, 10 or more years of consecutive active layer data are available. These include seven sites with 1 km^2 grids (Hinkel & Nelson 2003, Streletskiy et al. 2008), 15 1 ha grids, and three transects with thaw tubes. Two 1 km^2 grids in the Seward Peninsula (Council and Kougarok) and one near Ivotuk have data records dating to 1999. The 1 ha grid at Farmers Loop north of Fairbanks was added to the network in 2005. Pre-1990 data are available for a series of 20 10×10 m Cold Region Research and Engineering Laboratory (CRREL) plots near Barrow (1962–1970, and 1991–2007) and two sites in interior Alaska (Perl Creek, 1969–2007, and Wickersham Dome, 1975–2007).

All grids have data loggers for monitoring air and soil temperatures at various depths. Several sites have installations for continuous monitoring of soil moisture. Detailed spatial characterization of topography and surface and subsurface conditions are available for each spatially heterogeneous 1 km^2 grid. These include DEMs, vegetation, soil, and landform characterization, and organic layer thickness. Annual spatial snow surveys have been conducted at the Barrow 1 km^2 grid, beginning in 1995. In 2000, spatially oriented monitoring of frost heave and thaw subsidence using the Differential Global Positioning System (DGPS) was initiated at three sites representing broad landscape units characteristic of the North Slope of Alaska (Little et al. 2003).

An additional eleven U.S. Geological Survey sites have been established near deep boreholes. At these sites active layer thickness is determined by interpolation of ground temperature measurements. Data from these sites are currently being processed.

Canada

Of the 21 active CALM-designated sites in Canada, 15 are located along the latitudinal transect situated in the Mackenzie River Valley and operated by federal government agencies: Geological Survey of Canada (Nixon et al. 2003) and Agriculture and Agri-Food Canada (Tarnocai 1995, Tarnocai et al. 2004). Several additional long-term, active layer monitoring programs include CALM sites on the Arctic Islands (four sites), and two sites in the Hudson Bay region (Allard et al. 1995, Smith et al. 2001). The spatial active layer observations on grids are conducted at twelve 1 ha and one 1 km^2 grids. The most comprehensive data sets are available for eight 1 ha grids in the Mackenzie River Valley. The data include 10 or more years of active layer observations on grids and thaw tubes, spatial characterization of subsurface conditions (organic layer thickness, organic composition, mineral strata), and several annual snow surveys.

Nordic region

The seven Nordic CALM sites are located in several areas surrounding the North Atlantic: two 1 ha grids in northeast Greenland at Zackenberg; one 1 ha grid in west Greenland on Disko Island (Christiansen 2004); 1 ha grid on the west coast of Svalbard at Kapp Linne (Akerman 1980); four transects constitute two sites at Calypostranda, Svalbard (Repelewska-Pekalowa & Pekalowa 2004); and an alpine-subarctic 1 ha grid in the vicinity of Abisko, northern Sweden. With the exception of Disko and one of the Calypostranda sites, the active layer record for the Nordic region grids is available for 10 or more years. The record for the Abisko site extends back to 1972 and includes thickness of active layer in different landscapes, mean monthly air temperature, and degree days of thawing. The Zackenberg database includes weekly active layer observations for the 1996–2006 thawing periods and snow thickness surveys for selected years.

Russia

Of the 41 CALM sites in Russia, 31 have continuous periodic active layer monitoring. The remaining 10 were either discontinued or are visited only sporadically. All Russian sites have grids ranging from 100 m^2 to 1 km^2. Several sites have supplemental transects that pre-date the establishment of CALM. The Russian CALM network extends from the European tundra of the Pechora and Vorkuta regions to West Siberia and the Lena Delta, eastward to the lower Kolyma River, and to Chukotka and Kamchatka. Most of these sites are within the continuous permafrost zone.

European North: Three 1 ha grids are located in the discontinuous permafrost region of the European tundra: Ayach-Yakha and Talnik near Vorkuta, and Bolvansky in the Pechora lowlands (Mazhitova et al. 2004). Each site has 7 to 11 years of continuous active layer record. The auxiliary data include detailed soil and vegetation characterization, soil temperature, and soil moisture records. Since 1999 periodic, spatially oriented frost heave and ground subsidence measurements using optical leveling are conducted at the Ayach-Yakha site.

West Siberia: Eight active CALM sites are located in West Siberia. The core of the data sets consists of observations from two 1 ha grids at Mare Sale and Vaskiny Dachi in the continuous permafrost zone and 1km^2 Nadym grid in the discontinuous zone (Vasiliev et al. 2008). The active layer observations for Mare Sale are available since 1978 and for Nadym since 1972. The active layer record at the Vaskiny Dachi site dates to 1991. Pre-CALM (1993) observations were performed at the environmentally homogeneous 10 × 10 m plots, and along several transects incorporating the dominant landscape units. Each site has continuous soil temperature records of variable length and detailed spatial landscape, soil, and vegetation characterizations. An additional 1 ha site was established in the continuous permafrost zone in 2005 (Zepalov et al. 2008). During the summer of 2007 four grids were established in the discontinuous permafrost zone in landscapes inadequately represented by the Nadym grid. At present these sites are in the process of being characterized and instrumented.

Central Siberia: In association with the GEWEX Asian Monsoon Experiment (GAME) program in the Siberian Arctic, a 1 km^2 CALM grid was established in 1997 near Tiksi, on the Lena River (Watanabe et al. 2003). The site-specific data base is available in the GAME Siberia website (http://www.hyarc.nagoya-u.ac.jp/game/siberia/index.html). Thaw depth measurements are also available for two 1 ha grids representing different landscapes of the Lena delta since 2004.

Lower Kolyma River: Beginning in 1996, a series of fifteen 1 ha grids spanning a distance of approximately 300 km was established to represent characteristic climatic and environmental conditions in the Kolyma-Indigirka lowlands on the northeast Eurasian tundra (Fyodorov-Davydov et al. 2004). At present, 11 sites are reporting data. Annual active layer and soil temperature observations are carried out at the five most accessible sites situated in close proximity to the North-East Scientific Station in Cherskyi in the transitional zone between taiga and tundra. Logistical problems led to some interruptions in observations at the remaining six sites. All sites have detailed descriptions of surface and subsurface conditions.

Chukotka and Kamchatka Peninsulas: Beginning in 1996, a Mt. Dionisy site was established on the Chukotka Peninsula. A new site was initiated at Lavrentia along the Chukchi Sea coast in 2000 (Zamalodchikov et al. 2004). Both sites consist of 1 ha grids. Annual soil moisture observations and detailed soil characterizations are available for the Lavrentia site. Active layer records are also available for two 1 ha grids on Kamchatka since 2003.

Mongolia

The Mongolian network consists of a series of instrumented boreholes located in the arid land permafrost at the southern fringe of the Siberian permafrost zones. An original network of 12 sites (Sharkuu 2003) was expanded to 37 sites during the last 2–5 years. The majority of the new sites are located in the Hovsgol region. Seventeen boreholes were drilled with depths ranging from 5 to 80 m, and two deep boreholes from the mid-1980s were instrumented for permafrost and active layer monitoring. An additional eight sites were instrumented for shallow ground temperature monitoring (Sharkhuu et. al. 2007). All sites report ground temperature and active layer thickness determined by interpolation of ground temperature profiles obtained in late September and early October.

Mountain permafrost regions

Permafrost occurs in all mountainous regions of the high latitudes and is widespread at higher elevations in mid latitude mountain ranges including the Qinghai-Tibet Plateau. The mountain permafrost is represented in the CALM data base by one site in Norway, one site in Svalbard (Isaksen et al. 2007), two sites in Switzerland (Harris et al. 2001), two sites in Kazakhstan (Marchenko et al. 2007), and six sites on the Qinghai-Tibet Plateau, China (King et al. 2006). All sites consist of boreholes of variable depth. With the exception of Kazakhstan sites, only interpolated active layer values are reported annually.

Southern Hemisphere

The Antarctic Permafrost and Soils (ANTPAS) program (Parsons et al. 2008) incorporates several sites known collectively as CALM-South (CALM-S). Periodic ground temperature monitoring at depths to 2.4 m is conducted at three sites in South Victoria Land, Antarctica and at two others on Livingston Island/South Shetland Islands (Hauck et al. 2007). Data are reported as interpolated maximum annual thaw depth. Detailed site descriptions are available at the ANTPAS website (http://erth.waikato.ac.nz/antpas/). Plans to expand ANTPAS /CALM-S by developing 12 to 15 sites distributed across environmental gradients from the Andes to the subantarctic islands and through the Antarctic Peninsula and Transantarctic Mountains to the McMurdo Dry Valleys are currently under development (Bockheim 2005).

Regional Active Layer Characterization

Several regions with large assemblages of sites and representative of high-latitude climatic/landscape gradients are suitable for spatial data integration. Examples are the North West Siberia region (Yamal-Gydan Peninsulas), the Lower Kolyma River, northcentral Alaska, and the Mackenzie River region (Canada). Each of these regions has been the subject of extensive geocryological research and contains information sufficient to facilitate regional-scale mapping.

At present the CALM database contains two regional (broad-scale) active layer maps compiled from data sampled from multiple sites. The first is a 14-year series of maps (1 km^2 resolution) depicting annual active layer thickness and the probability of the active layer exceeding certain thresholds for the 27,000 km^2 Kuparuk Region in northcentral Alaska (Shiklomanov & Nelson 2002, Anisimov et al. 2002). The second regional compilation is a detailed digital landscape and active layer map of northern West Siberia. The map was compiled in cooperation with the Earth Cryosphere Institute (Russia) and depicts a hierarchy of landscapes units, organic layer thickness, lithology, and the landscape-specific characteristic values of active layer thickness. At present the map is being refined and extended.

Several other regional maps are under construction, including an active layer map for the Kolyma-Indigirka lowlands of Russia, a map of the North Atlantic region, and a map of the Barrow Peninsula on Alaska's North Slope.

Data Use for Models

Active layer observations and auxiliary information from the CALM network provide an extensive circumpolar database which has been used extensively to validate process-based geocryological (e.g., Oelke & Zhang 2003, Shiklomanov et al. 2007) and hydrological (Rawlins et al. 2003) models. Obviously, data obtained from individual observational CALM sites should be used with caution for evaluating model-produced gridded fields, owing to possible discrepancies between the size of observation plots and those of model grid cells. It is well known that active layer thickness and other near-surface permafrost parameters can be highly variable in time and space (e.g., Nelson et al. 1998, Shiklomanov & Nelson 2002). Observational locations may not represent generalized conditions prescribed for the model's grid cells. The use of individual CALM grids or groups of grids representing the diversity of environmental conditions in particular regions can compensate somewhat for such deficiencies. The development/implementation of regional scaling approaches addresses the problem of discordance in resolution between empirical and simulation studies further, and facilitates development of procedures for assimilating geocryological data and modeling results. Shiklomanov et al. (2007) provided an example of a hierarchical approach for evaluating spatial permafrost models. The methodology incorporates empirical data from point locations and observational plots provided through the CALM observational networks, provides regional characterization of permafrost conditions, and can be extended with continental- and circumpolar-scale models.

Conclusions

CALM is the oldest and most comprehensive permafrost-oriented international global-change monitoring program, and has achieved considerable success in this role. Although the CALM network continues to grow in terms of the number of participating sites and the quantity and quality of observations, two outstanding data issues remain to be resolved: (1) Continuation of periodic measurements; this problem relates to difficulties associated with unattended operation of scientific equipment at remote locations and periodic accessibility of sites. For example, approximately one-fourth of Russian sites were discontinued during the last five years due to substantial increases in logistical costs. A large number of sites have suffered from equipment malfunction and vandalism; (2) The methodology of simple sharing of basic data, adopted by CALM in the late 1990s, does not entirely satisfy the growing needs of the increasingly international and interdisciplinary scientific community and general public. Newly developed web-based database and mapping applications provide more advanced, user-friendly vehicles for presenting and sharing geographically referenced information. The first step toward enhancing CALM's archival and dissemination strategies will be to prepare data for the upcoming Circumpolar Active layer Permafrost System (CAPS) Version 3 database compilation developed by the Frozen Ground Data Center and Standing Committee for Data Information and Communication within the IPA (Parsons et al. 2008).

Acknowledgments

The components of the CALM program operating in Alaska, Russia, Mongolia, and Kazakhstan have been supported though the U.S. National Science Foundation's Office of Polar Programs under grants OPP-9732051 to the University of Cincinnati and OPP-0352958 to the University of Delaware. Opinions, findings, conclusions, and recommendations expressed in this paper are those of the authors and other CALM investigators and do not necessarily reflect the views of the National Science Foundation. Transitional (one year) support between USA/NSF grants was provided by the University of Delaware's Center for International Studies. Financial support for CALM activities in other locations has been provided by governmental agencies in the countries of the various CALM investigators. CALM is a collaborative global-change monitoring program and could not exist without good will, generosity, and a spirit of cooperation from scientists from many nations and scientific disciplines.

References

Akerman, J. 1980. *Studies on Periglacial Geomorphology in West Spitsbergen*. Meddelanden Fran Lunds Universitets Geografiska Institution Avhandlingar, 89: 1-297.

Anisimov, O.A., Lobanov, V.A., Reneva, S.A., Shiklomanov, N.I., Zhang, T. & Nelson F.E. 2007, Uncertainties in gridded air temperature fields and effects on predictive active layer modeling. *Journal of Geophysical Research* 112: F02S14, doi:10.1029/2006JF000593.

Anisimov, O.A., Shiklomanov, N.I. & Nelson, F.E. 2002. Variability of seasonal thaw depth in permafrost regions: a stochastic modeling approach. *Ecological Modeling* 153: 217-227.

Bockheim, J. 2005. *International Workshop on Antarctic Permafrost and Soils: Final Report*. November 14-18, 2004, University of Wisconsin, Madison, WI (http://erth.waikato.ac.nz/antpas/pdf/FIN_REP_Ant_Wk3.pdf) , 84 pp.

Brown, J., Hinkel, K.M. & Nelson, F.E. 2000. The circumpolar active layer monitoring (CALM) program: Research designs and initial results. *Polar Geography* 24(3): 165–258.

Christiansen, H.H. 2004. Meteorological control on interannual spatial and temporal variations in snow cover and ground thawing in two northeast Greenlandic Circumpolar-Active layer-Monitoring (CALM) sites. *Permafrost and Periglacial Processes* 15(2): 155-169.

Fyodorov-Davydov, D.G., Sorokovikov, V.A., Ostroumov, V.E., Kholodov, A.L., Mitroshin, N.S., Mergelov, I.A., Davydov, S.P., Zimov, S.A. & Davydova, A.I. 2004. Spatial and temporal observations of seasonal thaw in the Northern Kolyma Lowland. *Polar Geography* 28(4): 308-325.

Harris, C., Haeberli, W., Vonder Muehll, D. & King, L., 2001. Permafrost monitoring in the high mountains of Europe: The PACE Project in its global context. *Permafrost and Periglacial Processes* 12: 3-11.

Hauck, C., Vieira, G., Gruber, S., Blanco, J. & Ramos, M. 2007. Geophysical identification of permafrost in Livingston Island, maritime Antarctica. *Journal of Geophysical Research* 112: F02S19, doi:10.1029/2006JF000544.

Hinkel, K.M. & Nelson, F.E. 2003. Spatial and temporal patterns of active layer thickness at Circumpolar Active Layer Monitoring (CALM) sites in northern Alaska, 1995-2000. *Journal of Geophysical Research* 1089(D2): 8168.

Isaksen, K., Sollid, J.L., Holmlund, P. & Harris C. 2007. Recent warming of mountain permafrost in Svalbard and Scandinavia. *Journal of Geophysical Research* 112: F02S04, doi:10.1029/2006JF000522.

King, L., Herz, T., Hartmann, H., Hof, R., Jiang, T., Ke, C., Wei, Z., Liu, J. & Yi, C. 2006. The PACE monitoring strategy: A concept for permafrost research in Qinghai-Tibet. *Quaternary International* 154: 149-157.

Klene, A.E. 2005. *Climate and Urbanization in Barrow, Alaska*. Ph.D. Dissertation. Department of Geography. Newark, DE: University of Delaware.

Little, J., Sandall, H., Walegur, M. & Nelson, F.E. 2003. Application of differential GPS to monitor frost heave and thaw settlement in tundra environments. *Permafrost and Periglacial Processes* 14(4): 349-357.

Marchenko, S.S., Gorbunov, A.P. & Romanovsky, V.E. 2007. Permafrost warming in the Tien Shan Mountains, Central Asia. *Global and Planetary Change* (3-4): 311-327.

Mazhitova, G., Malkova, G., Chestnykh, O. & Zamolodchikov, D. 2004. Active layer spatial and temporal variability at European Russian circumpolar-active-layer-monitoring (CALM) sites. *Permafrost and Periglacial Processes* 15(2): 123-139.

Nelson, F.E., Shiklomanov, N.I., Christiansen, H.H. & Hinkel, K.M. 2004a. The circumpolar-active-layer-monitoring (CALM) Workshop: Introduction. *Permafrost and Periglacial Processes* 15: 99-101.

Nelson, F.E., Shiklomanov, N.I., Hinkel, K.M & Christiansen, H.H. 2004b. The Circumpolar Active Layer Monitoring (CALM) Workshop and the CALM II Program: Introduction. *Polar Geography* 28(4): 253-266.

Nelson, F.E., Shiklomanov, N.I. & Mueller, G.R. 1999. Variability of active-layer thickness at multiple spatial scales, North-Central Alaska, U.S.A. *Arctic, Antarctic, and Alpine Research* 31(2): 179-186.

Nixon, F.M. 2000. Thaw-depth monitoring. The Physical Environment of the Mackenzie Valley, Northwest Territories: a Base Line for the Assessment of Environmental Change. *Geological Survey of Canada Bulletin* 547, 119-126.

Nixon, F.M. & Taylor, A.E. 1998. Regional active layer monitoring across the sporadic, discontinuous and continuous permafrost zones, Mackenzie Valley, northwestern Canada. In: Lewkowicz, A. G. and Allard, M. (eds.), *Proceedings of the Seventh International Conference on Permafrost.* Quebec: Centre d'Etudes nordiques, Universite Laval, 815-820.

Oelke, C. & Zhang, T. 2003. Comparing thaw depths measured at CALM field sites with estimates from a medium-resolution hemispheric heat conduction model. *8th International Conference on Permafrost: Extended Abstracts on Current Research and Newly Available Information.* Zurich, Switzerland: Department of Geography, University of Zurich, 117-118.

Rawlins, M.A., Vorosmarty, C.J., Lammers, R.B., Frolking, S. & Fekete, B.M. 2003. Simulating pan-Arctic runoff with a macro-scale terrestrial water balance model. *Hydrological Processes* 17(13): 2521-2539.

Repelewska-Pêkalowa, J. & Pêkala, K. 2004. Active-Layer Dynamics at the Calypsostranda CALM Site, Recherche Fiord Region, Spitsbergen. *Polar Geography* 28(4): 326-340

Romanovsky, V.E. & Osterkamp, T.E. 1997. Thawing of the active layer on the coastal plain of the Alaskan Arctic. *Permafrost and Periglacial Processes* 8:1-22.

Romanovsky, V.E., Sergueev, D.O. & Osterkamp, T.E. 2003. Temporal variations in the active layer and near-surface permafrost temperatures at the long-term observatories in northern Alaska. *Proceedings of the Eighth International Conference on* Permafrost, vol. 2. Lisse, A.A. Balkema, 989-994.

Sharkhuu A., Sharkhuu, N., Etzelmüller, B., Heggem, E.S.F., Nelson, F.E., Shiklomanov, N.I., Goulden, C.E. & Brown J. 2007. Permafrost monitoring in the Hovsgol mountain region, Mongolia, *Journal of Geophysical Research* 112: F02S06, doi:10.1029/2006JF000543.

Sharkhuu, N. 2003. Recent changes in the permafrost of Mongolia. *Proceedings of the Eighth International Conference on Permafrost*, 2. Lisse: A.A. Balkema, 1029-1034.

Shiklomanov N.I., Anisimov, O.A., Zhang, T., Marchenko, S.S, Nelson, F.E. & Oelke C. 2007, Comparison of model-produced active layer fields: Results for northern Alaska. *Journal of Geophysical Research* 112, F02S10, doi:10.1029/2006JF000571.

Shiklomanov, N.I. & Nelson, F.E. 2002. Active-layer mapping at regional scales: a 13–year spatial time series for the Kuparuk Region, north-central Alaska. *Permafrost and Periglacial Processes* 13: 219-230.

Streletskiy, D.A., Shiklomanov, N.I., Nelson, F.E. & Klene, A.E. 2008. Long-term active and ground surface temperature trends: 13 years of observations at Alaskan CALM sites. *Proceedings of the Ninth International Conference on Permafrost, Fairbanks, Alaska, June 29–July 3, 2008* (this proceedings).

Vasiliev, A.A., Leibman, M.O. & Moskalenko, N.G. 2008. Active layer monitoring in West Siberia under the CALM II program. *Proceedings of the Ninth International Conference on Permafrost, Fairbanks, Alaska, June 29–July 3, 2008* (this proceedings)

Watanabe, K, Kiyosawa, H., Fukumura, K., Ezaki, T. & Mizoguchi, M. 2003. Spatial and temporal variation in thaw depth in Siberian tundra near Tiksi. *Proceedings of the Eighth International Conference on Permafrost*, 2. Lisse: A.A. Balkema, 1211-1216.

Zamolodchikov, D.G., Kotov, A.N., Karelin, D.V. & Razzhivin, V.Y. 2004. Active-Layer Monitoring in Northeast Russia: Spatial, Seasonal, and Interannual Variability. *Polar Geography* 28(4): 286-307

Zepalov, F.N., Grebenets, V.I., Streletskiy, D.A. & Shiklomanov, N.I. 2008. Active-layer Monitoring at a New CALM Site, Taimyr Peninsula, Russia. *Proceedings of the Ninth International Conference on Permafrost, Fairbanks, Alaska, June 29–July 3, 2008* (this proceedings).

Evaluation of Recent Changes in the Ground Thermal State, Central Yakutia

P.N. Skryabin
Melnikov Permafrost Institute, SB RAS, Yakutsk, Russia
S.P. Varlamov
Melnikov Permafrost Institute, SB RAS, Yakutsk, Russia
Yu.B. Skachkov
Melnikov Permafrost Institute, SB RAS, Yakutsk, Russia

Abstract

Developing an understanding of permafrost evolution in relation to observed climatic warming requires evaluation of changes in the thermal state of near-surface layers. This paper is based on the results of 25 years of geothermal monitoring at 60 sites. The study is focused on the upper permafrost within the depth of annual temperature variation (10–15 m). The integrated research program involves landscape, microclimatic, thermophysical, and hydrothermal methods. Systematization and mapping generalization of permafrost landscapes have been made with indication of the complexity of geocryological conditions. During the last 30 years, the study area has experienced the highest increasing trend in mean annual air temperature in northern Russia. A database has been compiled that includes parameters needed for geocryological predictions. Proposals for cooperation in implementing IPY projects and establishing a single observational network for geocryological monitoring in cold regions of Russia are presented. Experimental research made it possible to quantitatively evaluate the interannual and perennial variability of the active layer thickness and thermal state of the ground within the depth of annual temperature variations.

Keywords: climate; monitoring; permafrost landscapes; temperature regime.

Introduction

Research on the impact of climate warming on permafrost involves a wide variety of issues, including the thermal evolution of upper permafrost. The ground thermal regime is controlled by energy exchange between the ground and atmosphere and is characterized by spatial and temporal variability. Anthropogenic impacts of varying type and magnitude (clear-cutting, fires, removal of surface vegetation and organic mat, etc.) disturb the natural ground thermal state, trigger adverse cryogenic processes and change the ecology of environmental complexes.

In recent years, the development of research on predicted climate warming in many countries has led to an increasing interest in the response of permafrost to projected warming. It may be said without exaggeration that this problem has become one of the most important issues in geocryological research, both in scientific and practical terms.

Most of the research on this problem has been conducted in northern regions of Russia, Canada, Alaska, and Europe (Pavlov 1994, Varlamov et al. 1990, Burgess & Lawrence 1997, Osterkamp et al. 1994, Harris et al. 2000).

Central Yakutia is a region characterized by complicated geocryological conditions, such as continuous permafrost and the presence of water-bearing taliks and polygonal wedge ice. Continuous monitoring of the thermal regime of the ground, which has been implemented by the authors since 1981, illustrates the dynamics of its thermal state in natural and disturbed landscapes. The research project statement and the results of the first stages of its implementation were set out in the authors' early publications (Skryabin et al. 1998, 2001, Varlamov et al. 2002). This report presents a summary of the results obtained during the entire period of observations.

Objectives and Methods of Research

Investigations are conducted on the west and east sides of the Lena River at the latitude of Yakutsk which are characterized by complicated permafrost conditions. Evaluation of changes in thermal state of near-surface layers of permafrost within the frameworks of climatic warming and man-caused impacts (fires, deforestation, embankment), was effected based on integrated data, acquired from regular observations in Chabyda and Yakutsk stations, sites in Tuymaada Valley, and in the northern section of the prospective Tommot-Yakutsk railroad (Fig. 1).

The basis for this research is the variation in temperatures for shallow soils (upper 10–15 m). The main thermal parameters which can indicate an evolution of near-surface layers of permafrost are: seasonally thawed layer thickness (X) and mean annual temperature at corresponding depth (T_x) and at the depth of zero annual amplitude (T_o). It is known that interannual changes in these parameters depend on peculiarities of climatic features (air and surface temperature, precipitation amount, snow depth and density) and terrain conditions (vegetation and ground cover, soils composition, ground water, etc.). The research area shows X variations from 0.5 to 4 meters, and T_0 variations from 0.5 to -6.0°C, depending on terrain conditions.

Experimental observations of varied duration have been carried out since 1981 at 200 localities covering 6 physiographic regions, 9 landscape types, and more than 100 stows. The research involves a variety of integrated

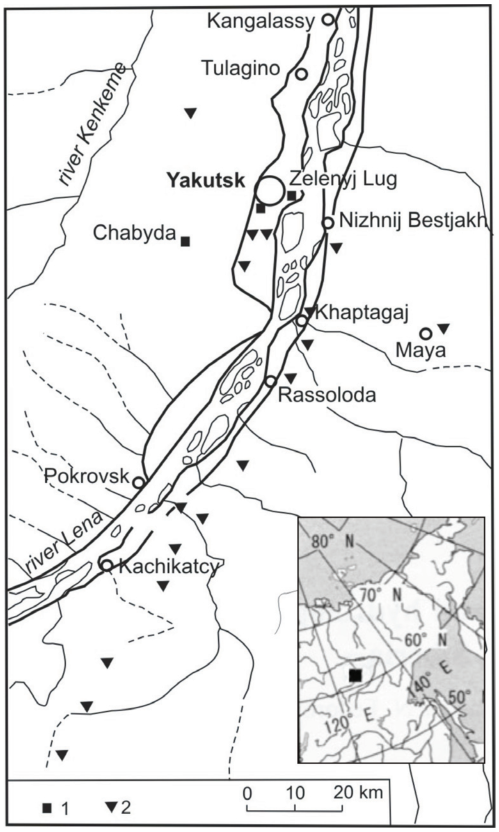

Figure 1. Map of the study area: 1 – stations, 2 – monitoring sites.

techniques and tools used in studying landscape, climate, thermal physics, as well as hydrothermal studies. The project implementation included remote and ground-based sensing of the landscapes, their classification, and mapping summary. The following terrain types were identified in the area covered: flood plain, low-terrace, sand ridge, inter-ridge depression, alas, inter-alas, small valley, upland, and slope.

Long-term records from the nearest weather stations are employed during the study. Snow surveys are carried out in representative permafrost landscapes. The texture and properties of the active layer were determined in test pits. Information on the composition and structure of permafrost soils was obtained from boreholes. Active layer depths are determined by pit measurements, probing with a steel rod, and from soil temperature profiles. To measure temperatures at the snow surface, at the surface and base of the surface vegetation, and in the ground, thermistor and thermocouple sets and cables were used. After installing the cables, the holes were backfilled. Ground temperatures were taken with an accuracy of ± 0.1°C.

Investigations at the Chabyda station included measurements of climatic parameters (air temperature, wind speed, precipitation, evaporation, and snow depth and density) and ground hydrothermal parameters (snow and ground surface temperatures, ground temperature, heat flows, thermal properties of surface covers and ground, and freeze-thaw depths). During the intensive observation period, measurements were made 7 times daily in the warm seasons of 1981 and 1982 and 4 times a day in the cold season of 1982–1983. In the following years, observations were taken once every pentad at 4 standard times and then 1 to 3 times monthly. Since November 1987, measurement frequencies have been reduced at the Chabyda, Yakutsk, and Tyumaada stations, and measurements are now taken on the 15th day of each month. On the east side of the Lena River, observations are made once or twice in the warm and cold seasons. The total number of monitoring locations on the east side of the Lena River is 60.

Results

Central Yakutia is among the areas in Russia that have experienced the highest increasing trends in mean annual air temperature over the last 30 years (up to 0.07°C/yr). Warming of the climate, which was slight in the 1960–1970s became significant in the 1980s. The last decade (1998–2007) has been the warmest in the instrumental record for the region. At Yakutsk, mean annual air temperature increased at a rate of 0.06°C/yr between 1982 and 2007. Mean annual air temperatures were below the normal of -10°C (USSR Hydrometeorological Service 1989) only in four of the last 25 years. All other years were consistently warmer (Fig. 2a).

The rise of the mean annual air temperature is primarily associated with the increasing number of anomalously warm winters which in turn is due to changes in atmospheric circulation. In the period 1982–2007, there were 19 winters with a freezing index higher than the long-term mean. The increase of summer air temperatures was less significant.

In this study, anomalous climatic seasons are defined as those with the average values of climate elements ($\Sigma(-T_{air})$, $\Sigma(+T_{air})$ and h_c^{max}) beyond the average standard deviation σ. If the value is within σ, but it is larger than ½ σ, the season is referred to as warm or cold, and low-snow or snowy. By average winter air temperature, there were 6 normal, 2 warm, 16 anomalously warm winters, and only 1 anomalously cold winter during the observation period. By snow depth, there were 11 normal, 5 anomalously snowy, 4 snowy, 3 low-snow, and 2 anomalously snowy winters.

Variations in X, T_x, and T_o have been studied over 25 years in the Chabyda station, west of the Lena River, where experimental sites were set on the bottom of a small valley (3a, 8a, and borehole 1), gentle slope (5), interfluve (7b), bottom of a drainage depression (8), watershed area (9), moderate north-facing slope (10), and moderate south-facing slope (11).

Active layer depth depends on weather conditions, vegetation, surface cover, soil type, and soil moisture. Interannual variability of active layer thickness is thought to be primarily controlled by the air thawing index and summer precipitation. However, investigations in northern Russia have found no clear correlation between the long-term variations in thaw depth and the air thawing index (Pavlov et al. 2004). Ground conditions, especially soil moisture variations, appear to have significant effects on thaw depth. Data from the Chabyda station indicate that the most

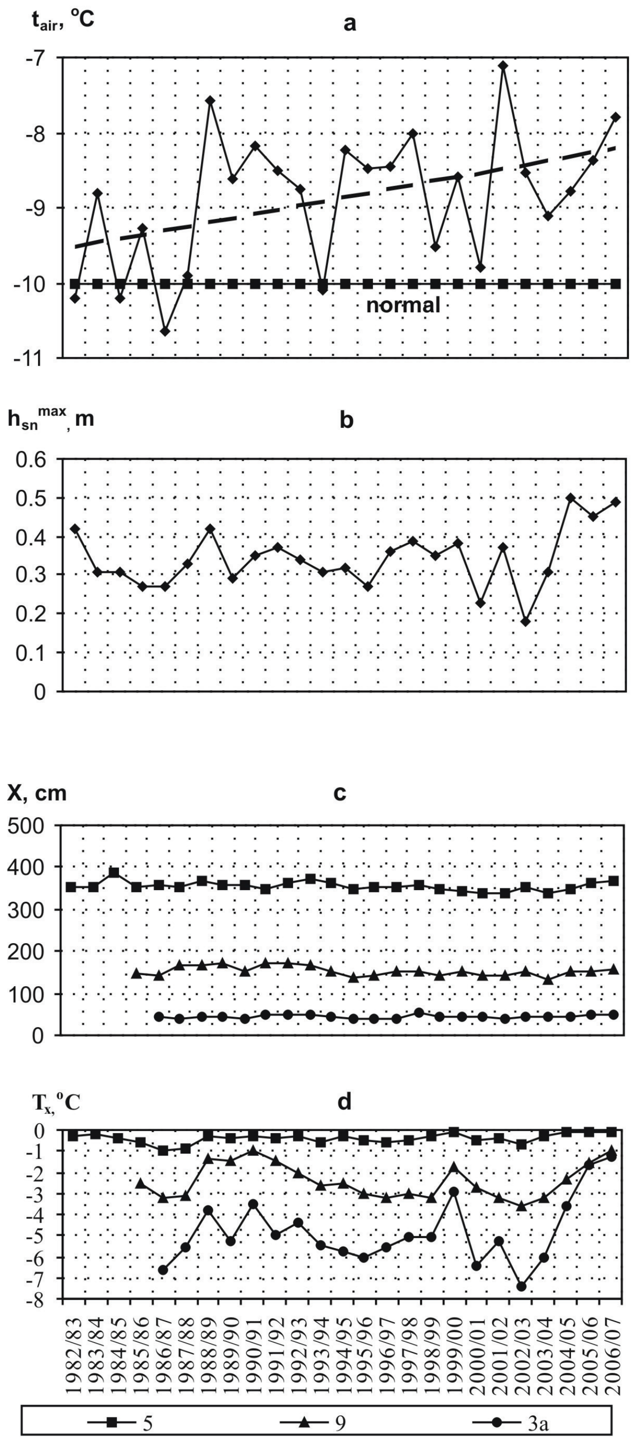

Figure 2. Long-term variations of mean annual air temperature at Yakutsk (a), maximum snow cover depth (b), active layer thickness (c), and mean annual ground temperature (d) in the small valley (3a – bottom of stream valley) and slope (5 – gentle slope, 9 – watershed area) terrain types at the Chabyda station.

significant interannual variations in X (up to 73 cm) occur in small valleys with organic soils. Slope sites on sandy soils show thaw depth variations of 30 to 58 cm. No statistically significant increasing trend in thaw depth has been observed for any of the sites. To the contrary, three sites (5, 6b, and 9) in the slope terrain type show a decreasing trend. The three longest series are given in Figure 2c to illustrate the interannual variations in active layer depth.

Table 1. Variations in mean annual ground temperature (T_x) and its trends in 1986-2007 at the Chabyda station.

Experimen. sites	Soil texture	Mean °C	Max °C	Min °C	Trend T_x, °C/10 yr
Slope terrain type					
5	Sand, sandy silt	-0.4	-0.1	-1.0	0.20
7b	Sandy silt, sand	-1.2	-0.4	-2.2	0.25
9	Sandy silt, clayey silt	-2.4	-1.0	-3.6	-0.10
10	Sandy silt, sand	-1.8	-0.7	-2.8	0.15
11	Sandy silt, sand	-1.0	-0.2	-2.2	-0.10
Small valley terrain type					
Bor. 1	Peat, sand	-2.7	-0.6	-5.1	0.10
3a	Peat, sand	-4.9	-1.3	-7.4	0.80
8	Sand	-3.7	-1.3	-5.5	0.45
8a	Peat, sand	-3.6	-0.1	-6.5	0.65

Depending on terrain and soil conditions, ground temperature is controlled by the same factors as is X. The interannual variation of ground temperature is predominantly related to winter weather factors, such as the air freezing index and snow cover. Table 1 illustrates the complete set of variations in T_x for the warmest and coldest terrain types.

Ground temperature is a better indicator of the long-term changes in the thermal state of near-surface permafrost compared to active layer thickness. The temperature variation was largest in the small-valley areas, as was the thaw depth fluctuation (Fig. 2d). This variation was mainly due to the effect of two winter factors: snow cover conditions and air freezing index. In the continental climate of central Yakutia the first factor appears to be more important. The lowest mean annual permafrost surface temperatures were observed in the winter of 2002–2003 which had an anomalously thin snow cover (see Fig. 2d). In subsequent snowy years (2004–2007) which had the largest snow depths in the last 25 years (0.45 to 0.50 m), the ground temperatures were warmest. Variation in T_x due to anomalous winter conditions can be as high as 1.2–3.5°C. One warm, low-snow winter will cool ground temperatures more than a cold, snowy winter. The effect of one anomalously cold winter will be stronger than that of a few successive anomalously warm winters. However, statistically significant trends in mean annual ground temperature have been observed only for four sites. A positive trend in T_x of 0.2°C per decade was found at site 5, and a negative trend of 0.1°C per decade at site 9. At a depth of 10 m, warming of 0.2°C per decade occurred at site 7b and cooling of 0.1°C per decade at site 9 and 0.1°C per decade at site 11.

On the east side of the Lena River, monitoring of the ground temperature regime has been conducted in 8 terrain types during the last 20 years. The observations have identified the landscapes that are most sensitive to changes of climatic factors. The terrain units have been classified into three sensitivity categories, high, moderate and low, in the following order: small valley → inter-alas, inter-ridge depression, floodplain, slope → low terrace, sand ridge, alas, interfluve. Respective ranges of interannual T_o variations for these categories are 1.0–2.3°C; 0.2–1.2°C and 0.1–0.9°C.

Observational data from 1987 to 2006 show that the trend of mean annual temperatures at the depth of zero annual amplitude varies from negative to positive in different terrain types (Table 2). Negative trends are detected in low terrace, sand ridge, and inter-ridge depression terrain types (up to -0.02°C/yr), while positive trends occur in floodplain and small valley terrain (0.02–0.04°C/yr). Monitoring observations suggest that there is no uniform pattern in t_o variation, and lowering of ground temperature in some landscape units indicates their stability. In the Yakutsk area, snow depth, especially in the early winter, had been decreasing over 20 years until 2004, with a corresponding decrease in its warming effect. This factor, although not alone, has probably been decisive for the ground temperature evolution in the last 20 years. However, during the last three winters of 2005–2007, which had anomalously deep snow and warm air temperatures, there was a notable increase in ground temperature. For northern Alaska, Romanovsky et al. (2003) report increasing trends in air temperature and active layer thickness over the period of 1987 to 2001. Mean annual ground temperatures at several sites increased by 1–2°C over the 15-year period.

Experimental investigations were carried out in order to quantitatively evaluate the anthropogenic impact (ground cover disturbance and stripping, deforestation, fires, etc.) on the thermal regime of the ground in 40 stows within five terrain types.

At an alas site, snow and dwarf-birch/sedge tussock covers were removed in March 1989. This disturbance increased the active layer thickness by 0.4 m and the ground temperature at 10 m depth by 0.4°C (Br. 68 and 186 compared to the undisturbed site. Seven years later, the depth of seasonal thaw was 0.5 m deeper, and T_x was 2.7°C warmer than at the undisturbed site. At an inter-ridge depression site, a moss-lichen layer was stripped in July 1990. The mean annual ground temperature increased by 0.8°C in the second year and by 1.8°C in the third year after disturbance. The depth of seasonal thaw increased by 0.5 by the end of the first summer and by about 1 m, or 2.8 times, by the end of the second summer (Br. 205). At inter-alas sites supporting larch stands, the removal of a *Vaccinium vitis-idea*/moss cover resulted in an increase in upper permafrost temperature of 1 to 0.2°C. Thaw depths increased by less than 0.5 m (Br. 1601). Similar observations conducted from 1984 to 2000 along the Norman Wells oil pipeline in northern Canada indicate that thaw depths increased most rapidly in the first 7 years after disturbance and continued to increase slowly thereafter, reaching depths of 3 to 5 m in fine-grained and organic units and 5 to 7 m in coarse mineral soils (Burgess & Smith, 2003).

Table 2. Variations in mean annual ground temperature (T_0) and its trends in 1987–2006 in landscapes at the right-bank area of the Lena River.

Terrain type	Soil texture	Mean, °C	Max °C	Min °C	Trend T_0, °C/10 yr
Floodplain	Sand, sandy silt	-1.6	-0.8	-2.3	0.2
Low-terrace	Sand, sandy silt	-1.2	-0.1	-2.4	-0.2
Slope	Sand, sandy silt	-1.4	-0.3	-2.4	~0.0
Small valley	Peat, sandy silt	-5.2	-3.6	-6.9	0.4
Sand ridge	Sand	-0.9	0.7	-2.5	0.0…-0.2
Inter-ridge depression	Peat, sand	-2.4	-0.6	-4.1	-0.1…-0.2
Inter-alas	Sandy silt, Clayey silt	-1.4	-0.7	-2.2	~0.0
Alas	Peat, clayey silt	-0.4	-0.1	-0.8	~0.0

In sand-ridge terrain, clear-cutting of pine stands increased thaw depths by 1.8 m and ground temperatures by 1.0°C. In inter-alas terrain, clear-cutting of larch trees resulted in 1°C warming of ground temperatures after 3 years (Br. 12/93).

Removal of pine trees and lichen cover in warm soils (T_o= -0.1…-0.3°C) of well-drained sand ridges resulted in a dry talik (Br. 1324). Clearing of a pine/lichen/ *Arctostaphylos* stand in low-terrace terrain type caused an increase in T_o by 0.3°C and in X by 1 m (Br. 177).

At a sand-ridge site in pine forest burned by a fire in 1987, ground temperatures increased by 0.7–1.5°C during the first two years. From the fourth year after the fire, ground temperatures on the burn began to stabilize with vegetation regrowth. (Br. 13). In low-terrace terrain, the larch stand burned by a fire in 1986 was removed (Br. 166). A considerable increase in T_o, by 0.3–0.5°C, occurred in the first 5 years after the fire. The recovery of vegetation in 6-8 years stabilized the ground thermal state. In an inter-ridge depression, selective tree cutting, surface cover disturbance in 1988, and fire in 1993 (Br. 30) increased T_o by 0.3–1.0°C over 9 years. Gradual cutting of a burned larch stand in inter-alas terrain type resulted in a 1–1.5°C increase in T_o and a 0.7 m increase in thaw depth during 15 years (Br. 56). Selective tree cutting with surface cover disturbance after a 1986 fire in inter-alas terrain (Br. 209) resulted in warming of T_o in the first years. Vegetation recovery lowered ground temperatures (Fig. 3). The T_o difference over the 18-year period was 1.3°C.

Maximum impact on the thermal state of ground results from ground cover stripping and post-fire deforestation in inter-alas type terrain. In inter-alas where wedge ice occurs close to surface, a more intensive thermokarst activity is indicated. The dynamics of the ground thermal state at sites of anthropogenic activity demonstrate dependence on types of impact, their duration, and stages of revegetation during post-anthropogenic period. On the whole, the ground thermal

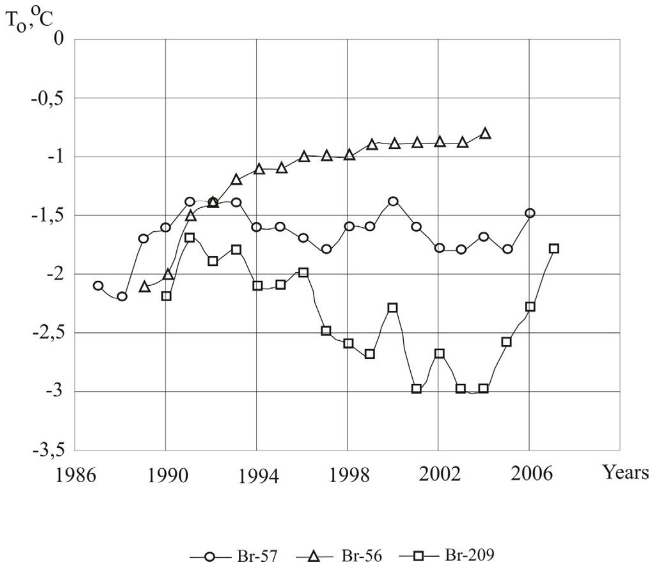

Figure 3. Variations of mean annual ground temperature in the inter-alas terrain unit: larch forest site (Br-57), site of gradual tree removal (Br-56) and burned site with recovering vegetation (Br-209).

state recovery after man-caused damage in sand ridge terrain type is mainly reversible, while in inter-alas type it is either reversible or not.

The database of facts, accumulated during a long period of time is comprised of the following: climatic features, natural and anthropogenic landscapes, content and structure of permafrost, ground cover temperature, temperature, water content ratio, and thermophysical characteristics of ground, seasonal thawing, temperature of water, and bottom sediments in lakes.

Further enhancement of the geothermal monitoring network utilizing automatic loggers is thought to have a great potential. This essential project's feasibility depends on joint Russian and international investigations, pooling human and material resources.

Conclusions

1. Change trends were identified for climate, active layer thickness, and temperatures of natural and anthropogenic landscapes.

2. Small valley and inter-alas terrain types are the most sensitive to man-triggered damage and climatic changes.

3. Long-term dynamics of the ground thermal state illustrate relatively high resistance to climate warming, due to a tendency towards a thinner snow cover during the first half of winter season and, as a result, a lower warming effect.

4. A database was created containing information on landscapes, frozen soils, climate parameters, and ground thermal state.

The results of this study are used in the design and construction of the northern section of the Tommot-Yakutsk railroad. Information obtained is also used in numerical modeling of ground temperature variations and in the Yakutian Permafrost GIS Project.

References

Burgess, M.M. & Lawrence, D.E. 1997. Thaw settlement in permafrost soils: 12 years of observations on the Norman Wells pipeline right of-way. *Proceedings of the Canadian Geotechnical Society Conference, Ottawa*: 77-84.

Burgess, M.M. & Smith, S.L. 2003. 17 years of thaw penetration and surface settlement observation in permafrost terrain along the Norman Wells pipeline, Northwest Territories, Canada. *Proceedings of the Eighth International Conference on Permafrost, Zurich*: 107-112.

Harris, C., Vonder Mohll, D. & Isaksen, K. 2000. The European pace project transect of instrumented permafrost boreholes: preliminary results of permafrost monitoring. *Abstracts Rhythms of Natural Processes in the Earth Cryosphere*, Pushcnino: 256.

Osterkamp, T.E., Zhang, T. & Romanovsky, V.E. 1994. Evidence for a cyclic variation of permafrost temperatures in Northern Alaska. *Permafrost and Periglacial Processes* 5: 137-144.

Pavlov, A.V. 1994. Current changes of climate and permafrost in the Artic and Sub-Artic of Russia. *Permafrost and Periglacial Processes* 5: 101-110.

Pavlov, A.V., Skachkov, Yu.B. & Kakunov, N.B. 2004. Interaction between long-term changes in seasonal thaw depth and meteorological factors. *Earth Cryosphere* VIII(4): 3-11.

Romanovsky, V.E., Sergueev, D.O. & Osterkamp, T.E. 2003. Temporal variations in the active layer and near-surface permafrost temperatures at the long-term observatories in Northern Alaska. *Proceedings of the Eighth International Conference on Permafrost, Zurich*: 989-994.

Skryabin, P.N., Skachkov, Yu.B. & Varlamov, S.P. 2001. Monitoring of thermal state of soils in Central Yakutia. *Proceedings of the Fifth International Study Conference on GEWEX in Asia and GAME (volume 1), Aich Trade Center, Nagoya, Japan*: 170-174.

Skryabin, P.N., Varlamov, S.P. & Skachkov, Yu.B. 1998. *Annual Variability of Ground Thermal Regime in Yakutsk Area.* Novosibirsk: SB RAS Press, 144 pp.

USSR Hydrometeoreological Service. 1989. *Handbook on the USSR Climate, Vol. 24, Yakut ASSR, part 1*. Leningrad: Gidrometeoizdat, 608 pp.

Varlamov, S.P., Skachkov, Yu.B. & Skryabin, P.N. 1990. Interannual variability of ground thermal parameters at Chabyda station, Central Yakutia. In: *Permafrost Changes and Economic Development*. Yakutsk: Permafrost Institute Press, 68-75.

Varlamov, S.P., Skachkov, Yu.B. & Skryabin, P.N. 2002. *Ground Temperature Regime in Permafrost Landscapes, Central Yakutia.* Yakutsk: Permafrost Institute SB RAS Press, 216 pp.

Micromorphological Analyses of Main Genetic Permafrost Types in West Siberia

E.A. Slagoda
Earth's Cryosphere Institute, RAS, Russia
A.N. Kurchatova
Tyumen State Oil & Gas University, Russia

Abstract

The formation of the geomorphological structure on the northern West Siberian plain and the main genetic types of sediments were caused by Arctic Sea regressions during the Pleistocene-Holocene period. Postcryogenic features in the upper part of all terraces testify of climatic cooling in the Latest Pleistocene. During this stage, syngenetic freezing on sites of accumulation and epigenetic freezing of the earlier melted deposits had occurred. Syngenetic sediments are characterized by the postcryogenic voids associated with sedimentary lamination and complex morphology. Walls of voids are coated by clayish particles and iron hydroxides, and filled by oriented mineral grains. The research of epigenetic sediments has shown the deformed sublayers in the form of tongues and displacements of ground blocks. Micromorphological analyses for correlation of cryogenic events in the upper part of Cenozoic sediments sections should be based on the regional database of microtexture of different genetic permafrost types in West Siberia.

Keywords: micromorphological analyses; postcryogenic microtexture; syngenetic and epigenetic permafrost.

Introduction

The present two-layer permafrost on the northern West-Siberian Plain formed during the Late Pleistocene-Holocene. After Arctic Sea regressions, the marine clayish sediments drained and froze as epigenetic permafrost. They were partially transformed to an active layer in subaerial conditions and deeply thawed during the periods of climate warming or sea transgressions (Dubikov 2002). It is possible to distinguish the sequence of cryogenic events using micromorphological features of syngenetic and epigenetic sediments. Results of micromorphological analyses of the main genetic types of permafrost are presented in the report. Samples were taken from sediment sections of exposures and borehole cores (up to 30 m depth) located at the main geomorphological levels within the territory between Nadym and Pur Rivers and on Yamal Peninsula (Fig. 1). Fifty thin soil sections were studied in all.

Study Region

The terrain of the Nadym-Pur watershed is a plain gently inclined to the north and divided by several geomorphological levels consisting of marine and lacustrine-alluvial facies (Baulin et al. 1996, Dubikov 2002).

A flat, slightly wavy plain is located at an elevation of 65–90 m above see level and consists of the loamy Middle Pleistocene Salekhard Suite made of marine and glacial-marine genesis (m,gmQ_{II}^{2-4}). Sediments are characterized by non-clear lamination, lumpy structure, regular distribution, and inclusion of coarse-sized mineral grains, gravels, pebbles as well as sublayers and lenses of sand (Fig. 2, I). Frozen grounds have layered cryostructure. The thickness of ice layers changes from 0.2–4 cm. Thick layered kinds of cryostructure up to 5–6 cm thick have been observed at 4–10 m below the surface and deeper. Total water content in

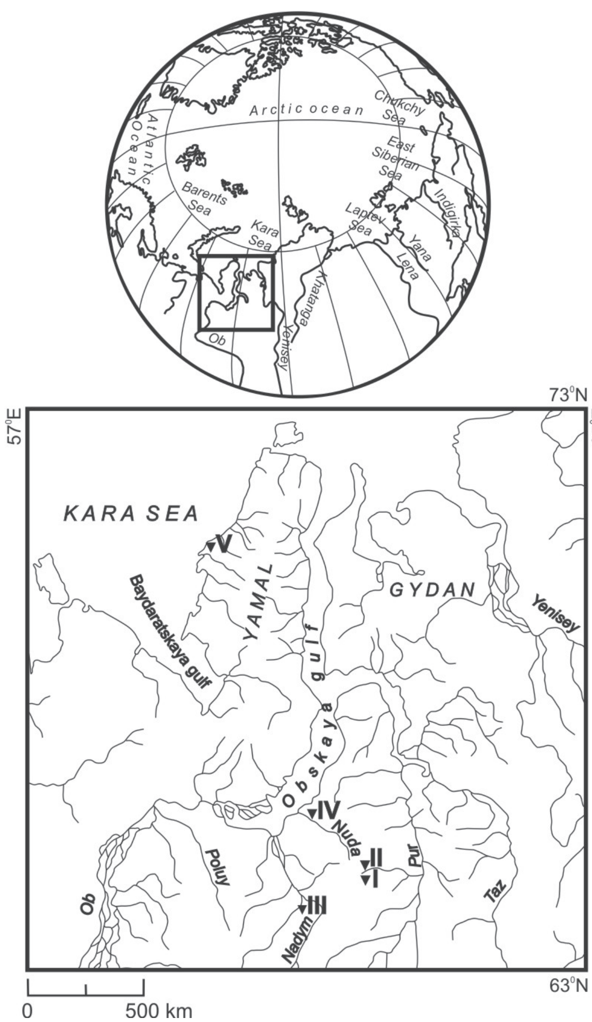

Figure 1. Location of the working sites (I-V) within research area.

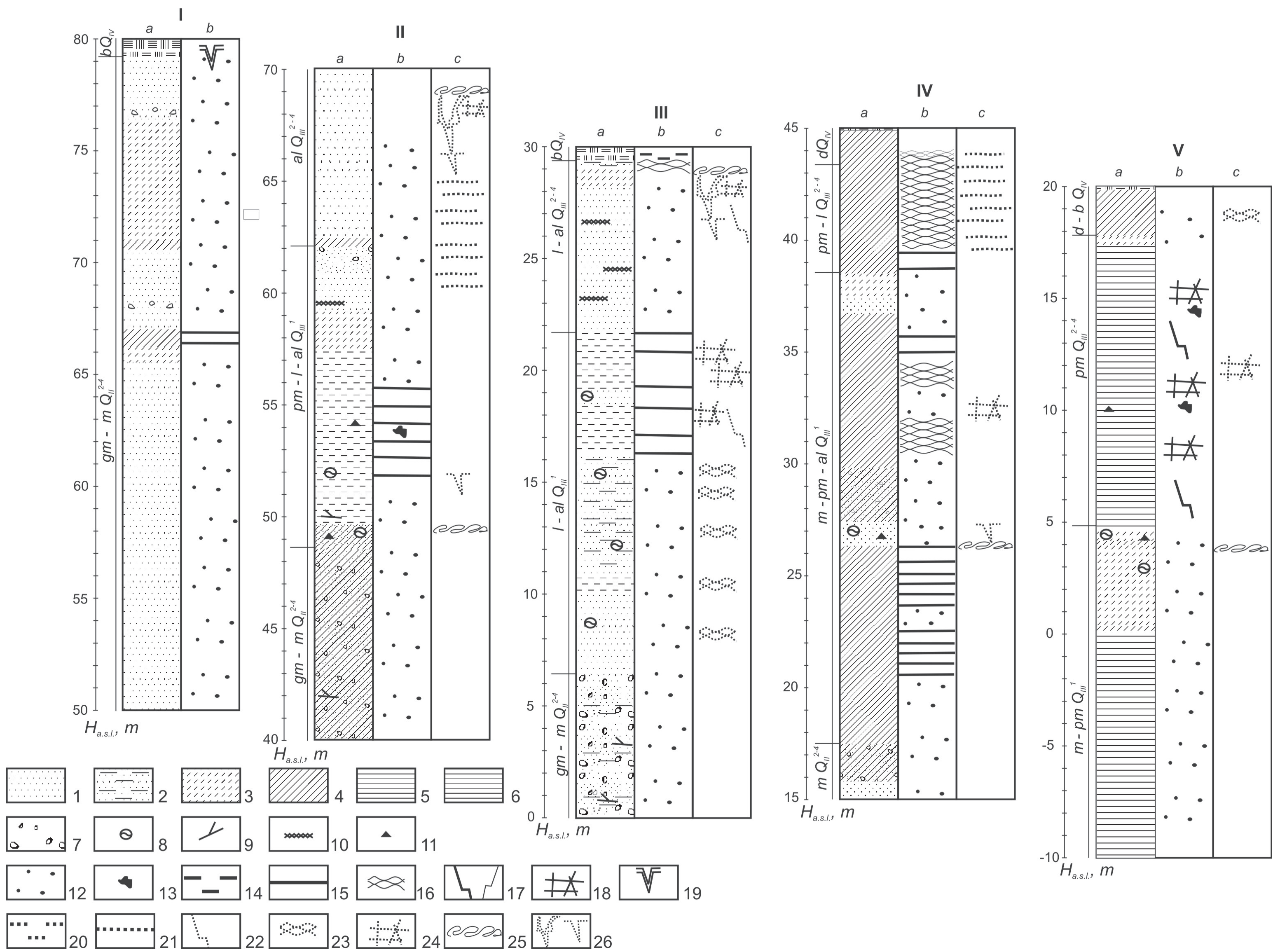

Figure 2. Lithology (a), cryostructure (b), and postcryogenic elements (c) of the main genetic types of permafrost in northern West Siberia. I – the 5th marine terrace; II–III – the 4th and 3rd lacustrine-alluvial terraces; IV – the 3rd marine terrace; V – the 2nd marine terrace. *Lithology: 1 – sand; 2 – silty sand; 3 – sandy-loam; 4 – loam; 5 – silt; 6 – clay; 7 – pebbles; 8 – clayish fragments; 9 – wooden remnants; 10 – allochtonous peat; 11 – carbonized organic debris. Cryostructure: 12 – massive; 13 – massive-agglomerate; 14 – lens-type; 15 – layered; 16 – reticulate-blocky; 17 – vertical veins; 18 – ice wedge. Postcryogenic elements: 20 – lens-type structure; 21 – layered structure; 22 – vertical veins; 23 – reticulate-blocky structure; 24 – reticulate structure; 25 – involution; 26 – ice wedge cast.*

these horizons changes from 30–50%. A massive cryogenic structure with ice-cement is typical for frozen grounds of the drained sites (total water content is 15–25%). On the marsh sites of the flat plain, the Salekhard Suite is overlain by the Holocene palsas.

A flat plain located at an elevation of 55–65 m above sea level (up to 70 m in the southern part) surrounds as a rather narrow strip the highest terrain, and consists of regressive marine series of the Late Pleistocene Kazantsevsky Suite (Q_{III}^{1}). The bottom of the sediment section is presented by light gray homogeneous loams accumulated under shallow sea conditions. Towards the top, they are replaced by sandy loams and silts of lacustrine-alluvial genesis (*lal*), and sometimes form an alternation with layered alluvial sands that are characterized by the presence of thin sublayers and lenses of allochthonous peat and plant detritus. Kazantsevsky sediments have a thickness 15–20 m and are covered by a indurate silty-loamy layer. Frozen loam has layered and reticulate-layered cryogenic structures. Sands have basically a massive cryostructure. Thin-layered cryostructures are widespread (Fig. 2, II). The thickness of ice layers is 0.2–0.7 cm with distance between them of 2–4 cm. Total water content changes from 25–35%, sometimes increasing up to 40%.

3. The third geomorphological level of the West Siberian Plain is located at an elevation of 35–55 m and formed during the Latest Pleistocene ($Q_{III}^{2\text{-}4}$), the Kargian-Sartanian stage of the regional stratigraphy. On the north of the territory, the marine terrace consists of estuary and delta sediments (Fig. 2. IV). On the southern part of the plain, the sediments are presented by an alternation of sands, sandy-loams and loams of the lacustrine-alluvial genesis with a total thickness 10–20 m (Fig. 2, III). Usually, light–grey, slanting layered sands have been observed at the bottom of the section. Small lenses of slightly decomposed fibrous allochthonous peat are distinguished in sands. The layered cryostructure is typical for loam and massive structure for sands. Horizontal and wavy ice layers occurred at the distance 2–3 cm from each other. Their thickness is 0.1–0.2 cm. Total water content is 20–25%.

Permafrost thickness changes south to north from 220–430 km and has a two-layer structure. The thickness of the upper sediment complex is 30–50 m; the second layer was revealed at the depth 70–75 m. The frozen layers are divided by a horizon of thawed and often water-saturated sediments with thickness up to 10–15 m and more. Average annual ground temperature varies from 0.0 to -3.0°C (Baulin et al. 1996).

Complex post-sedimentary deformation structures, extending to depths of 3–4 m below the surface have been observed in many localities within lacustrine-alluvial terraces. The deformations include ice wedge casts, involuted beddings, and sediment-filled kettle-like depressions.

The other working area is located on the territory of the gas-condensate field Kharasavey (West Yamal Peninsula) in a continuous permafrost area with an average annual ground temperature of -4 to -6°C (Vasilchuk et al. 2006).

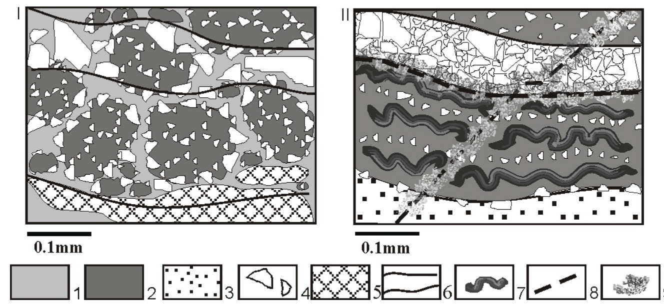

Figure 3. Microstructural scheme of the syngenetic (I) and epigenetic (II) sediments. I – the voids divided the complex aggregates, rock fragments and grains form circular pattern. II – shallow involutions, closed postcryogenic fissures coated by iron.
1 – voids; 2 – fine material; 3 – silt; 4 – debris; 5 – plant remnants; 6 – sediment lamination; 7 – involution; 8 – closed postcryogenic fissures; 9 – ferruginate zone

The thickness of the upper part of cryolithozone within the high terraces is 140–170 m; the lower part is presented by a cryotic saline ground up to the depth of 300 m. Within the gas field, the permafrost thickness and the bottom boundary of cryotic ground are distorted by the thermal influence of gas cupola and a high salinity of marine sediments.

The formation of the terraces on Yamal Peninsula was also associated with Late Pleistocene regressions of the Arctic Sea. The discrete fragments of the first marine terrace ($mQ_{III\text{-}IV}$), located at an elevation of 8–12 m above see level, are extended along the shoreline. The highest third terrace ($mQ_{III}^{2\text{-}3}$) is located at an elevation of 25–35 m a.s.l. and has been observed only in the northeastern part of the territory (Fig. 2, V). The second marine terrace ($mQ_{III}^{3\text{-}4}$), located at an elevation of 12–25 m, consists of loam and clay of the shallow sea with inclusions of a large amount of plant remnants, carbonized organic fragments, and layered sands of lagoon-littoral genesis. Epigenetic permafrost is characterized by massive, massive-agglomerate, and layered cryostructure. The thickness of horizontal, vertical, and broken layers is 0.5–1.5 cm.

Method

As was established and tested on the permafrost objects in the different Arctic regions, the sediments remain postcryogenic textures corresponding to distribution and form of melted-ice inclusions (Slagoda 2005, Konischev et al. 2006, Kurchatova & Slagoda 2006).

Subaerial facies of syngenetic sediments are characterized by microscale fissures which resulted from repeated thermal contraction-expansion in an active layer (Fig. 3, I):

1. mineral grains and debris which have cracked in situ;
2. sediment fragments and blocks which have moved concerning the former texture orientation;
3. complex aggregates of the fine material and debris, and associated with sediment lamination;
4. voids and postcryogenic textures corresponding to aggregates.

Change of structural-textural features of the epigenetic sediments is observed locally near the contact zone of the ice lenses and is characterized by Figure 3, II:

1. ferruginate borders and concentration or dispersion of the fine material observed along the contact zone of the postcryogenic voids, and
2. block-moving of sediment fragments, microfaults of layers without the deep structural unconformity.

The study of macro- and microscale features of sediment structure in the borehole sections was used to determine a type of freezing with complex of facies-genetic analysis.

Results

Salekhard Suite (m, $gmQ_{II}^{2\text{-}4}$) was revealed by boreholes only within Nadym-Pur terrain. Sediments are presented by non-sorted sandy loams with gravel inclusions of 1–2 cm size. Toward the top of the terraces, loams are overlain by small- and fine-grained sands usually with inclined alternation. In the loam layers the microtexture is presented by non-homogeneous material with rare coarse-sized grains included in the silty-clayish fabric. Sandy fraction consists mainly of rounded to subangular quartz grains. Some coarse grains are covered by a clayish coating. Finer material has a chaotic texture. There are fragments of mussels.

Sediments of the *Kazantsevsky Suite* (*la, pmQ_{III}^{1}*) of the third and second terraces are distinguished by finer material of the marine facies to compare with the lacustrine-alluvial ones. However, the common feature of them is a layered structure of sediment and an increase in the sandy fraction towards the top of the section right up to the formation of sandy layers within the lacustrine-alluvial facies.

Silty loam lying at the bottom of lacustrine-alluvial terraces is characterized by banded fabric. Coarse-sized particles often form lenses and sublayers. Particles are mainly presented by rounded quartz grains with hydromica coating. Sediments include a large amount of plant remnants of different decomposition and also fragments of marine fauna. Silts in the middle part of the terrace section have a clear layered structure presented by alternation of mineral sublayers and organic matter. Silts have a reticulate-blocky network cryostructure, and mineral layers have a massive postcryogenic microtexture. In several layers, there are traces of thawing and repeated freezing of sediments. They are presented by deformation of the lamination, tongue-like features of the overlying deposits along the melted ice veins, ferruginate spots, and layers enriched by iron.

The finer material of the second marine terrace on Yamal Peninsula is characterized by a reticulated postcryogenic microtexture that changes into lens-layered ones due to an increase in the quantity of coarse-sized grains. The distinctive feature of Kazantsevsky sediments is a large amount of undestroyed green hydromica particles and clayish rounded debris. There are also sublayers of ferrous diffusion that did not associate with the lamination of clayish plasma. The amount of carbonized organic debris and big plant remnants with good cellular structure (moss?) increases in the loamy-sandy horizon. Similar to lacustrine deposits the

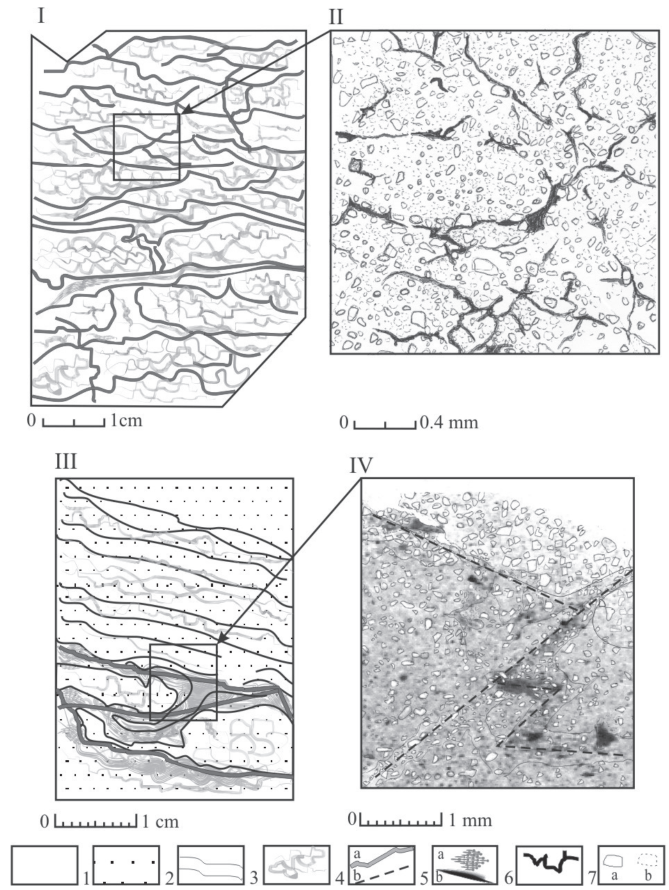

Figure 4. Scheme of macrostructure (I, III) and microstructure (II–IV); I–II – syngenetic sediments of the 3rd terrace, 42 m a.s.l; III–IV – epigenetic sediments of the 2nd terrace, 4 m a.s.l. *1 – silt; 2 – silty-sand; 3 – sediment lamination; 4 – unclear clotted pattern of the fine material underlined by ferruginate; 4 – postcryogenic fissures: a) closed, b) opened; 5 – ferruginate: a) monolith, b) thin soil section; 6 – voids; 8 – debris and coarse-size particles (a) and microaggregates (b).*

shallow-water estuary deposits of the second marine terrace are characterized by layers with sedimentary deformation (involutions).

Karginian-Sartanian sediments (*la, $pmQ_{III}^{2\text{-}4}$*) of the research area are presented by sandy to sandy-loam composition with inclusions of allochthonous peat. Sands of marine and lacustrine-alluvial facies consist of quartz grains with sublayers and lens of the plant detritus. Micromorphological analyses of the shallow-water deposits in the upper part of the third lake-alluvial terrace have shown horizons with clear evidence of syngenetic permafrost. Fine material is characterized by conglomeric fabric with discrete fragments and rounded grains, a circular pattern of coarse-sized grains (orbiculic fabric), lens-type, and layered and reticulate postcryogenic microtexture formed by processes of ground freezing and thawing in a wet active layer.

Sediments in the upper part of the second marine terrace are presented by loam with ferrous spots and a large amount of plant remnants. The micromorphology is characterized by a conglomeric fabric of the complex discrete rounded units consisting of clayish particles and mineral grains. Plant remnants mark sedimentary lamination. An increase in the amount of green hydromica has been observed in the sandy-loamy and loamy layers. Hydromica particles are presented by fresh grains and also by chemically decomposed ones. Plates are split and became colorless around. Iron hydroxides that are the indicators of subaerial oxidation occur in sediments of the upper part of the terraces. Horizons with postcryogenic microtexture of the repeated freezing in the form of downward-penetrating sediment tongues and deformed wedges enriched by finer material along cracks and by oriented mineral grains filling the voids have been observed there.

Conclusions

All marine and lacustrine-alluvial terraces within the research area are overlain by regressive formation with cryogenic and postcryogenic features that testify of climatic cooling in the Late Pleistocene. During this stage the syngenetic freezing on sites of accumulation and epigenetic refreezing of the earlier melted deposits had occurred.

Research of continental and shallow-water marine sediments in northern West Siberia has shown that equally, with direct indicators of syngenetic and epigenetic freezing, the distinct soil micromorphology is formed (Fig. 4):

- Syngenetic permafrost of the different genesis is characterized by postcryogenic voids associated with sedimentary lamination and cryogenic fabric, complex discrete fragments of fine material enclosed by a circular to ellipsoidal pattern of the mineral grains, and coarse-size particles. The walls of the postcryogenic voids are coated by clayish particles and iron hydroxides; the voids are filled by oriented mineral grains.
- Micromorphological analyses of epigenetic permafrost have revealed postcryogenic microtexture in the form of involutions, deformations of sedimentary lamination associated with broken vertical and reticulate-blocky cryostructure.

Permafrost micromorpology can be used for reconstruction of the cryological history of northern West Siberia. The method allows the distinguishing of syngenetic and epigenetic sediments in the section, and therefore, the determination of subaerial conditions of syngenetic stratum accumulation and subaqueous conditions of the cryogenic transformation of the marine facies of epigenetic permafrost.

Results of the micromorphological research for correlation of cryogenic events in sections of upper Cenozoic sediments should be based on the regional database of microtexture of the different genetic permafrost types in West Siberia.

Acknowledgments

This work was supported by the Integration Research Programs (N16; 7.14) of the Russian Academy of Science in the frame of the International Polar Year. Tyumen State Oil and Gas University provided logistical support and drilling. We are also grateful to anonymous reviewers for the constructive comments and assistance in editing this paper.

References

Baulin, V.V., Aksenov, V.I., Dubikov, G.I. et al. 1996. *Engineering-Geological Monitoring of the Gas Fields on Yamal,* Vol. I, II. Tyumen (in Russian).

Dubikov, G.I. 2002. *Composition and Cryogenic Structure of the Permafrost in West Siberia*. Moscow: GEOS (in Russian).

Konischev, V.N., Lebedeva-Verba, M.P., Rogov, V.V. & Stalina, E.E. 2005. *Cryogenesis of the Present-Day and Latest Pleistocene Sediments of Altay and Periglacial Areas in Europe*. Moscow: GEOS (in Russian).

Kurchatova, A.N. & Slagoda, E.A. 2006. Reconstruction of paleocryogenic strata through micromorphological indications. *Proceedings of Asian Conference on Permafrost, Lanzhou, China, August 7–9, 2006:* 115.

Slagoda, E.A. 2004. *Cryogenic sediments of the coastal plain of Laptev Sea: lithology and micromorphology*. Tyumen (in Russian).

Vasilchuk, Y.K., Krylov, G.V., Podborny, E.S. et al. 2006. *Cryosphere of the Oil and Gas Condensate Fields of Yamal Peninsula,* Vol. I. St-Petersburg: Nedra (in Russian).

Ground Temperature and Thaw Settlement in Frozen Peatlands Along the Norman Wells Pipeline Corridor, NWT Canada: 22 Years of Monitoring

Sharon L. Smith, Margo M. Burgess, and Daniel W. Riseborough
Geological Survey of Canada, Natural Resources Canada, Ottawa, Canada

Abstract

A monitoring program along the Norman Wells pipeline corridor has generated 22 years of observations of ground temperature and thaw settlement in frozen peatlands south of Fort Simpson NWT. Thawing beneath the right-of-way (ROW) and associated thaw settlement in response to vegetation clearing, surface disturbance, pipeline construction and operation is still continuing. Where alteration of the ground thermal regime was greater, significant settlement (>2 m) and collapse of peat across the ROW has been observed especially near the edge of a peat plateau. Complete degradation of thin permafrost has been observed in undisturbed terrain adjacent to the ROW which may be a result of the natural evolution of peatlands and recent warming. Thaw depths off-ROW have increased by up to 0.9 m following fires that burned extensive areas of peatlands in 2004.

Keywords: active layer; peatland; permafrost; thaw settlement; thermal regime.

Introduction

Permafrost in the southern portion of the discontinuous zone in western Canada is largely confined to organic terrain. Much of this permafrost likely formed during the Little Ice Age (e.g., Halsey et al. 1995) and has been preserved under subsequent warmer climatic conditions by a thick layer of insulating peat. These frozen peatlands may be particularly sensitive to small changes in the ground thermal regime that may result from construction and operation of infrastructure, forest fires, or climate change. Thawing of ice-rich organic terrain may have implications for infrastructure integrity, hydrological processes, and ecosystems, and it may result in alterations to carbon sources and sinks (ACIA 2005).

The Norman Wells oil pipeline (in operation since 1985), 869 km in length, crosses the discontinuous permafrost zone (Fig. 1) of the Mackenzie Valley, Northwest Territories and northern Alberta. Organic and morainic terrain units dominate the southern portion of the route. Since the mid-1980s the Canadian government and the pipeline company, Enbridge Pipelines (NW) Inc., have collaborated in a permafrost, terrain, and geotechnical research and monitoring program which includes a network of long-term instrumented sites located along the pipeline corridor in organic terrain south of Fort Simpson NWT. This network has generated over 20 years of data on the ground thermal regime and ground movements and provides the opportunity to investigate the response of frozen peatlands to both environmental disturbance and climate change and variability.

This paper focuses on environmental changes at 5 frozen peatland sites, associated with pipeline construction and operation and with natural changes such as fire and climate change and variability. An updated documentation is presented (updates Burgess & Tarnocai 1997) of the evolution of the ground thermal regime both beneath the pipeline right-of-way (ROW) and the adjacent undisturbed terrain over a 22-year period. Changes in thaw depth and settlement of the ground surface are also documented.

Background

Peatlands in the corridor

Peatlands are organic wetlands that have 40 cm or more of peat. They cover over 60% of the terrain along the pipeline corridor south of Fort Simpson (Burgess & Lawrence 2000). The two major classes in the Mackenzie valley are bog and fen, and each has distinctive vegetation assemblages, morphologies, water regimes, and thermal conditions (Aylsworth & Kettles 2000).

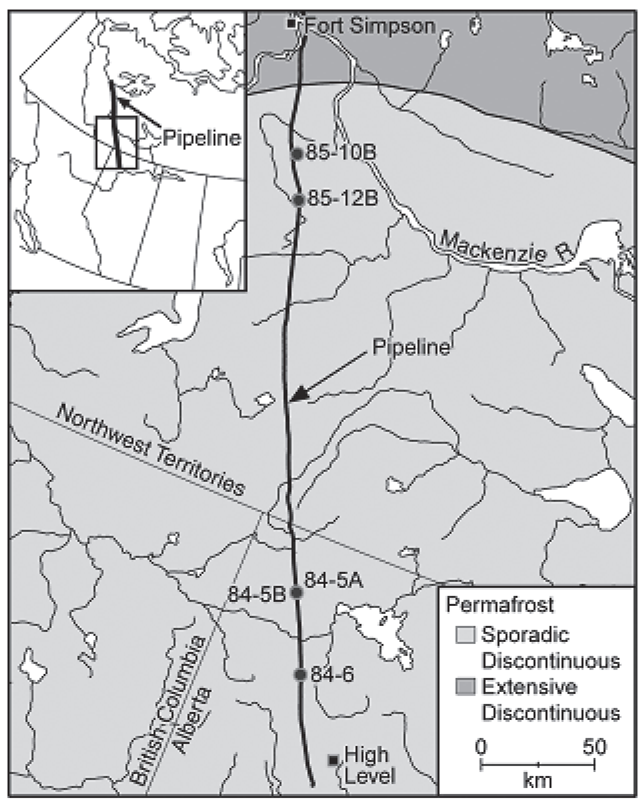

Figure 1. Location of the Norman Wells pipeline and permafrost distribution in the Mackenzie Valley.

Bogs are flat or very gently inclined plains either raised about 1 m above surrounding fens or peat filling slight depressions. Along the pipeline route, the common bog types include peat plateaus, palsa bogs, and collapse scar bogs. Fens and collapse scar bogs are generally unfrozen, while all other bog types are associated with permafrost.

Dominant peat materials of bogs are undecomposed *Sphagnum* and moderately decomposed woody moss peat underlain, in places by moderately- to well-decomposed sedge peat. Heath shrubs are also common. Trees, if present, tend to be low and stunted, forming open canopy forests. Fens are flat to very gently inclined plains which tend to be featureless although some have a reticulate network of low ridges. Dominant peat materials in fens are shallow to deep well- to moderately-decomposed sedge or woody sedge peat. Fens may or may not be vegetated with trees or shrubs (Burgess & Tarnocai 1997).

Bogs commonly developed from fens which in turn formed as organic materials accumulated in lakes or poorly drained depressions. Collapse scars in degrading peat plateaus may develop into fens (Aylsworth & Kettles 2000).

Climate

The Norman Wells pipeline corridor experiences a cold and relatively dry continental climate. Mean annual air temperature, based on 1971–2000 climate normals, is -3.2°C at Fort Simpson and -1.3°C at High Level. Normal annual precipitation is 369 mm at Fort Simpson and 394 mm at High Level with 40–45% falling as snow.

There has been a general increase in air temperature since the mid 1980s (Fig. 2) with the largest changes tending to occur during the winter. A number years with extreme temperatures (>1 standard deviation from normal) have also occurred over the last three decades including extreme warm and dry summers (for example in 1994, 1995, and 2004) that were also associated with forest fires.

Pipeline construction and operation

Pre-construction activities consisted of clearing a ROW up to 25 m wide during the winter mainly between January and March 1983 with the remainder completed by early 1984. Construction occurred over two winters (1983–84 or 1984–85) and involved blading and scraping of the peat surface to provide a stable work platform along the ditchline and travel side of the ROW. A trench about 1 m wide and 1 to 1.2 m deep was excavated for pipe installation. Excavated material (native spoil) was generally mounded over the trench following pipe installation. In peatlands, the native spoil was often blocky frozen peat that was not easily compacted. Although revegetation for erosion control occurred through seeding and fertilizing mineral soils, no revegetation was conducted where peat was greater than 1 to 1.2 m thick (present below the trench bottom).

Oil is chilled as it enters the line at Norman Wells, approximating the temperature of the surrounding permafrost. Although the pipeline operates as an ambient line, the oil warms by 1.5 to 3°C as it passes through the pump station compressors and the temperature remains elevated for more than 20 km downstream. Mean annual pipe temperatures in the southern section of the route have been above 2°C since the second year of operation. A pump station is located just south of Fort Simpson at KP 585, and downstream mean annual pipe temperatures have reached values greater than 6°C (Burgess 1992). During operation, winter pipe temperatures have generally never been below 0°C in the southern peatlands.

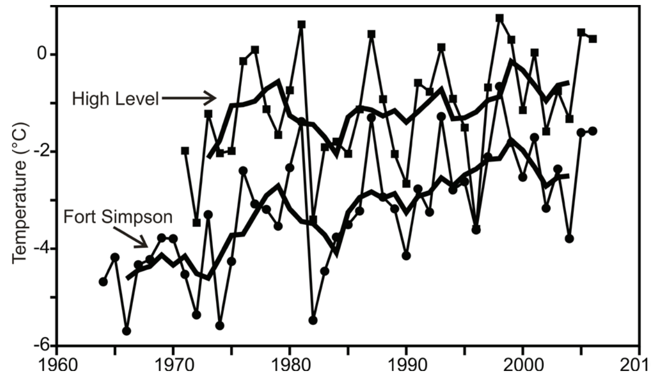

Figure 2. Mean annual air temperature record for the Environment Canada weather station at Fort Simpson, NWT (61°45′N 121°14′W) and High Level Alberta (58°37′N 117°09′W). The 5- year running mean is also shown.

Study sites and instrumentation

A description of the 5 peatland study sites is presented in Table 1. Generally 4 boreholes 5 to 20 m deep were drilled in 1984 or 1985 at each site. Three of these were located on the cleared right-of-way (on-ROW) at varying distances from the pipe and a fourth was located in the adjacent undisturbed terrain (off-ROW), 10–15 m from the edge of the ROW. Temperature cables placed in PVC casing, in each borehole, measure ground temperatures. The accuracy of the temperature sensors is ±0.1K, while the measurement system allows for a resolution of ±0.01K. Details on the site establishment and initial instrumentation are provided in Pilon et al. (1989). Manual measurements of ground temperature were made at monthly to quarterly intervals until 1996. Since 1996, dataloggers have been used at some sites and at least one complete site visit has occurred each fall close to the time of maximum active layer development. Thaw depths based on the maximum annual depth of the 0°C isotherm were determined by interpolation of the ground temperature profile between sensors. At some off-ROW sites a ground temperature sensor has been placed at 2–5 cm depth.

Thaw settlement across the ROW has been determined through level surveys initiated at site establishment and repeated at intervals of 2 to 5 years. The accuracy of these surveys ranges from less than 1 cm for compacted soil surfaces to about 15 cm for softer wet and compressible soils (Burgess & Lawrence 1997).

Observations and Discussion

Initial observations at undisturbed off-ROW sites (Fig. 3) indicate that mean annual ground temperatures in frozen peatlands are close to 0°C (above -0.3°C). Temperature gradients are small or near isothermal within the permafrost although steeper gradients are found below small bodies of permafrost surrounded by unfrozen terrain (e.g., 85-12B, KP608). Permafrost thickness (Table 1) varies from a few metres to greater than 10 m. Thaw depths were initially less than 1 m. The ground thermal regime responds to changes at the ground surface, such as clearing of vegetation related to ROW preparation and pipeline construction. Climate change and variability and natural factors such as fire may also lead to alterations in the ground thermal regime. These factors are discussed below.

Effects related to pipeline construction and operation

Changes in the ground temperature on and off the ROW over the monitoring period observed at a peat plateau near Fort Simpson and one in northern Alberta are shown in Figure 3. Initial observations off-ROW indicate that ground temperatures were colder and permafrost was thicker (10–11 m) at 84-5B (KP783) than at 85-12B (4–7 m). The warmer conditions at 85-12B are due to its lower elevation and also its proximity to the unfrozen fen as the monitoring site is located near the edge of the 2 m high peat plateau.

Over time, temperatures beneath the ROW increased above those in the surrounding undisturbed terrain in response to clearing of the vegetation and other disturbance to the ground thermal regime. This warming of the ground has led to increases in thaw depth (Table 1). At 85-5B, the increase in thaw depth beneath the ROW was about 3 m. At 85-12B, where the disturbance to the ground thermal regime has been greater, the thin permafrost completely degraded beneath the ROW.

The greater amount of warming and thawing beneath the ROW at 85-12B is due to both natural effects and those

Table 1. Characteristics of study sites discussed in this paper (updated from Burgess and Tarnocai 1997). ON and OFF refer to on-ROW and off-ROW, KP refers to kilometre post. The range in thaw depths observed at the site is given. Where the thaw depth is given as less than or greater than a given value, this indicates the depth of thaw is above the shallowest sensor or below the deepest sensor.

Site	KP	Elev m asl	Location	Peat Thickness (m)		Initial Permafrost Base (m)		Initial Thaw Depth (cm)		2006 Thaw depth (cm)	
				ON	OFF	ON	OFF	ON	OFF	ON	OFF
85-10B	588	244	61.3°N 120.9°W	2.4-2.6	2.3	1.8-2.6	2.3	Unfrozen or <100	50-100	Thawed	Thawed
85-12B	608	300	61.2 °N 120.7°W	2.9-3.2	4.8	6.7-7.0	4.5-6.1	50-100	50-100	Thawed	140
84-5A	783	552	59.7°N 119.5°W	3.2-3.7	3.8	14.7	14	<100-200	<100	>500	390 (300 in 2003)
84-5B	783	552	59.7°N 119.5°W	6.6-7.0	6.9	10.7	11.3	<50-200	<100	~400	260 (200 in 2003)
84-6	819	575	59.5°N 119.2°W	4.6-5.5	5.6	6.5-9.8	8.8	50-100	<100	Thawed	Thawed

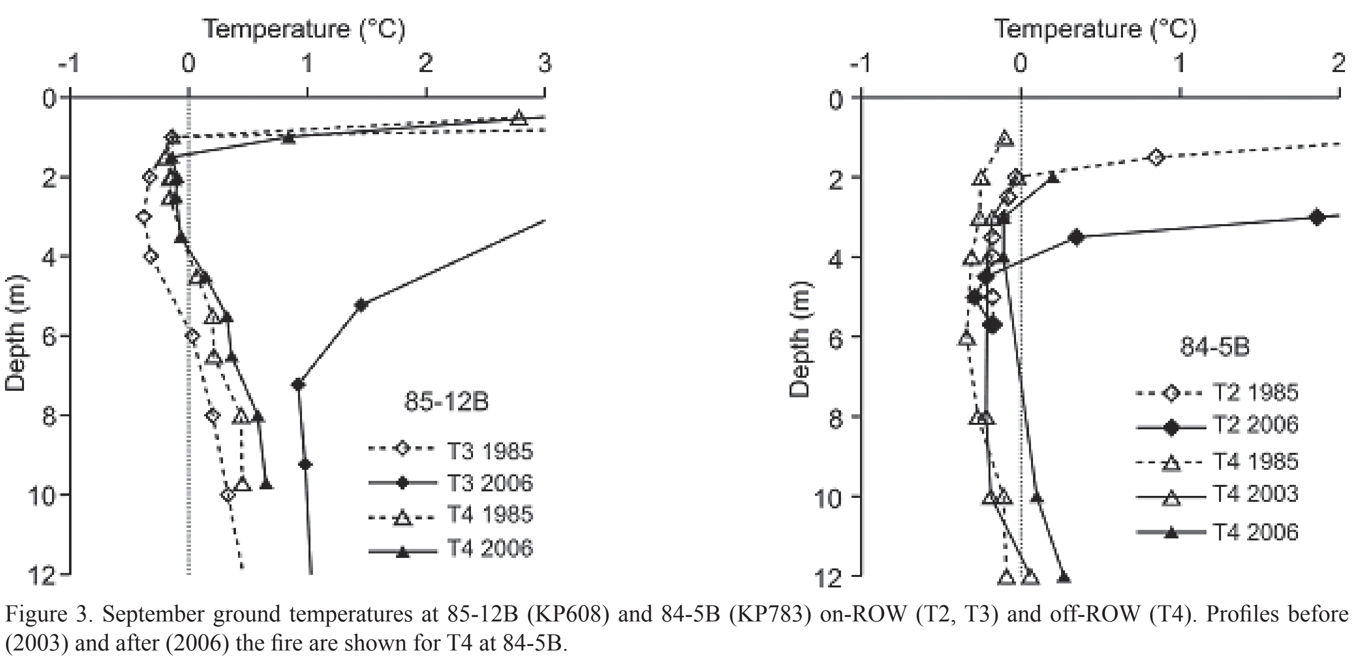

Figure 3. September ground temperatures at 85-12B (KP608) and 84-5B (KP783) on-ROW (T2, T3) and off-ROW (T4). Profiles before (2003) and after (2006) the fire are shown for T4 at 84-5B.

related to environmental disturbance. Since the site is near the collapsing edge of the peat plateau, effects related to the natural evolution of peatlands such as thermal and hydrological erosion will be important (Burgess & Tarnocai 1997). Disturbance due to blading was greater than at 84-5B. In addition, the site is located about 25 km downstream from the pump station, and the ground will be subject to warmer pipe temperatures than at 84-5B which is located much farther south. At 85-10B (KP588), located just a few kilometres south of the pump station, degradation of thin permafrost has also occurred.

Thawing of ice-rich soil can result in thaw settlement. Peat is particularly ice-rich and thaw strains of 30% or more have been determined for the pipeline sites in organic terrain (Burgess & Smith 2003). Surface settlement data obtained through periodic level surveys are presented for three sites in Figure 4. They show the ground surface movements that have occurred across the ROW between 1985 and 2006 (except for 84-6, KP819, where the most recent survey was 2001). At all sites settlement that has occurred on-ROW exceeds that occurring off-ROW due to the greater disturbance and increases in thaw depth that have occurred beneath the ROW.

During the first few years following clearing and construction, the greatest settlement generally occurred near the ditchline. This is partially due to the trenching and settlement of native backfill in the trench. Additional thawing and settlement occurred around the warm pipeline and as the thaw bulb grew, collapse of peat into the trench occurred (Burgess & Tarnocai 1997). Farther from the pipe, settlement was generally less and is mostly associated with thawing of the ground in response to clearance of vegetation. Over time, rates of settlement generally decreased as the thaw progression slowed. However, thaw settlement is still continuing on the ROW 22 years after the initial clearing. The amount of settlement on the ROW has been up to 2 m at the ditchline and up to 0.5 m toward the edge of the ROW.

The greater amount of disturbance related to ROW preparation, trench excavation and warm pipe temperatures has led to greater subsidence and collapse of peat at 85-12B than at 84-5B and 84-6. The higher ice content of the underlying material and higher associated thaw strains at 85-12B are also factors. Proximity to the edge of the peat plateau and the thermal and hydrological erosion along the subsided ditchline at 85-12B has resulted in accelerated collapse of peat into the ditch (Burgess & Tarnocai 1997) and considerable ponding on-ROW which contributed to further thermal disturbance beneath the ROW. Collapse of peat has continued and the area of ponding has enlarged over the 22-year period. By 2006 the area of collapse was found to extend to the edge of the ROW (Fig. 4a), and the trench had widened from an original width of about 1 m to about 16 m. In fact, this area of collapse has extended to the temperature cable (T3) that is near the edge of the cleared ROW and complete degradation of permafrost has occurred (Fig. 3). Although ponding has made it difficult to determine the total amount of settlement that has occurred in the trench area at 85-12B, it is at least 2 m. Toward the ROW edge (right side

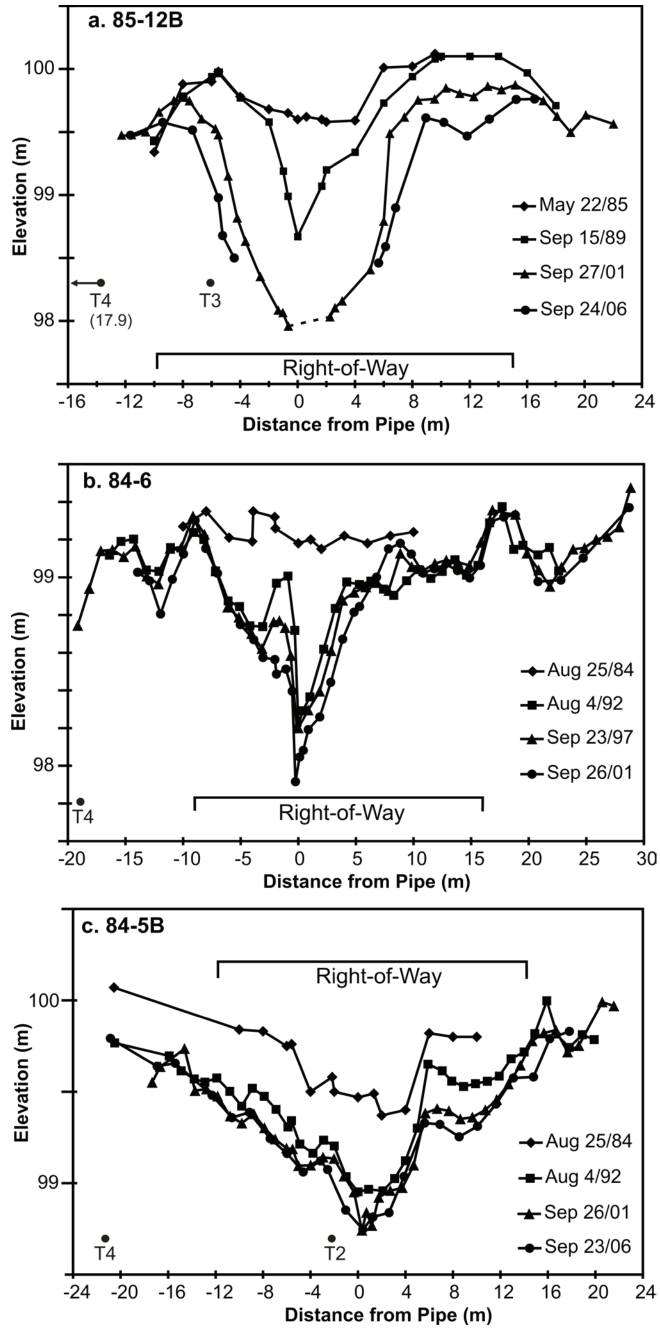

Figure 4. Ground surface elevation (relative to local datum) for peat plateau sites located at (a) KP608, (b) KP819 and (c) KP783.

Fig. 4a) up to 0.6 m of settlement has been observed.

Settlement and collapse of peat is observed to a lesser extent at 84-5B and 84-6. At the most southerly site (84-6), settlement of up to 1.3 m occurred in the trench area between 1984 and 2001. Collapse of peat is also observed and this has occurred over a distance of up to 10 m from the pipe and has extended to the edge of the ROW on one side (Fig. 4b). Farther from the trench, settlement ranges from 0.2 to 0.3 m (right side Fig. 4b). Proximity of this site to the edge of a collapse scar bog is probably also a factor in addition to the disturbance related to the trench excavation, ROW clearing and warming around the pipe.

At 84-5B where permafrost was initially colder and thicker and where effects related to the pipe temperature are less than that at 85-12B, settlement and collapse of peat has been less. Total settlement between 1984 and 2006 within the trench has been about 1m (Fig. 4c) with less collapse, which is limited to about 4 to 5 m from the pipe. Toward the edge of the ROW, settlement up to 0.5 m is observed.

Other effects

The record of ground temperatures at the off-ROW sites provides an indication of the baseline conditions and also the potential effect of climate warming on frozen peatlands. Increases in shallow permafrost temperatures at all off-ROW sites along the pipeline route have been observed over the monitoring period (Smith et al. 2005). The rate of change, however, has varied with smaller changes, or no obvious trend (<0.01°C per year) where permafrost temperatures are close to 0°C, likely due to the latent heat required to thaw the ice-rich soil. In the ice-rich organic terrain south of Fort Simpson, particularly sites with thicker permafrost, the change in ground temperatures at off-ROW sites has been small, but thaw depth has increased at some sites (Table 1). Part of this increase in thaw depth (especially in the first few years following site establishment) is likely due to surface disturbance related to borehole drilling. The general increase in thaw depth, however, is consistent with the increasing air temperature over the monitoring period (Fig. 2) and also the increase in thaw depth observed at other active layer monitoring sites in the Mackenzie Valley in the 1990s (Nixon et al. 2003).

Where permafrost was initially thin, complete degradation of permafrost off-ROW has been observed. At 85-10B, located near the edge of a degrading peatland near Fort Simpson, very warm permafrost less than 3 m thick was present in 1985 (Fig. 5). Ground temperatures then increased, with most warming occurring in the 1990s. The rate of warming was initially slow due to the energy required for phase change. By 2001, ground temperatures were greater than 1°C and permafrost was no longer present (Fig. 5). This warming (and subsequent degradation of permafrost) may be partly due to proximity of the site to the edge of the frozen peatland. Perennially frozen peatlands go through a natural cycle of early (when permafrost development begins), mature (stable), and overmature stages (Burgess & Tarnocai 1997). Thermal degradation results in thawing of ground ice and collapse of peatland surfaces during the later stage. The progression to the latter stages of the natural cycle may therefore be a factor in permafrost degradation at 85-10B.

The loss of permafrost at 85-10B may also be related to extreme warming during the summer of 1998 followed by warm winters over the next three years. Less cooling of the ground during the winter following a period of high heat input may have limited the cooling and freezing of the active layer and resulted in a general warming of the ground (Fig. 5). Both long-term trends in climate and shorter-term variations may be important, therefore, in the maintenance of these marginally frozen peatlands.

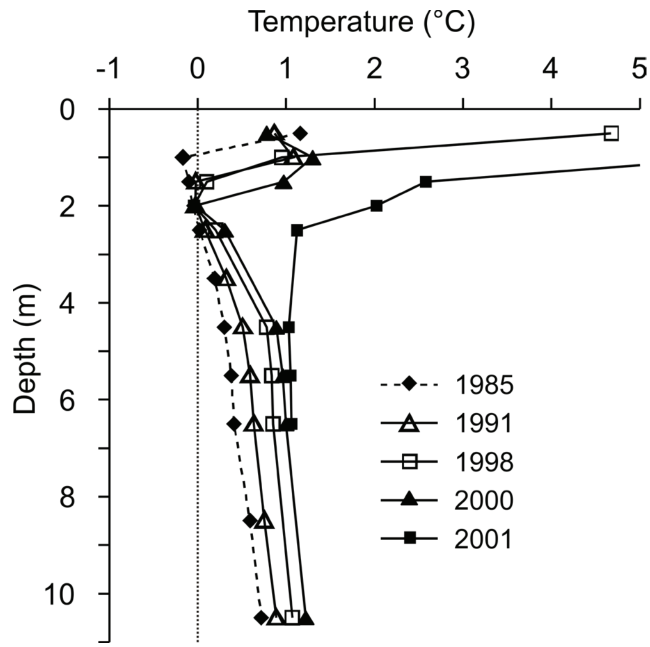

Figure 5. September ground temperature profiles off-ROW at 85-10B (KP588).

Other natural factors are also important in the evolution of the ground thermal regime. Wild fires may have an important influence on permafrost conditions. Burning of vegetation and the organic layer reduces the buffer layer and the surface albedo leading to overall increases in ground surface temperature, which over time propagate to the ground below (e.g., Viereck 1982). In summer 2004 for example, extensive areas of the southern portion of the pipeline corridor were burned. While the ROW acted as a firebreak and was generally not affected by the fire, areas adjacent to the ROW were burned including sites 84-5A and 84-5B. Figure 3 shows the increase in ground temperature and thaw depth (see also Table 1) that occurred in the two years following the fire. Thaw depths increased about 0.5 – 0.9 m over the 2 years following the fire. Analysis of data obtained from the temperature sensor placed at 2 to 5 cm depth at 84-5B indicates that mean annual near-surface ground temperature was about 1°C higher following the fire (2004–2006) than during the 3 years prior to the fire. The level survey data for 84-5B (Fig. 4c) indicates that some settlement did occur off-ROW between 2001 and 2006, but this appears to be limited to within a few metres of the edge of the ROW. Some of this settlement may be related to the burning and subsequent thawing of ground ice. However, a few more years of monitoring will be required to fully assess the impact of the fire in terms of thawing of the frozen peatland and related settlement and collapse of the peat.

These examples of permafrost degradation off-ROW associated with natural causes or climate warming show that during some periods, there may be larger changes in permafrost conditions off-ROW than on-ROW. In addition, some of the changes to permafrost off-ROW may eventually impact the ROW as surface settlement and collapse of peat progresses to the ROW edge in response to thawing.

Summary

Observations from the monitoring program in the Norman Wells pipeline corridor have provided information on the long-term evolution of the thermal regime and ground movements associated with thawing of peatlands in response to environmental disturbance related to pipeline construction and operation and natural factors. Ongoing warming at peatland sites has been observed, with the greater amount of warming occurring beneath the ROW and near the pipe. This warming and thawing of permafrost has led to settlement, particularly within the trench area. At sites where permafrost was initially warm and thin, and also adjacent to the edge of the peat plateau, disturbance to the thermal regime related to both a warm pipe and vegetation clearing has resulted in settlement of up to 2 m. Collapse of peat into the trench is also observed at these sites, in one case extending to the edge of the ROW. The possibility of permafrost thaw, settlement, and collapse of peat extending into the area adjacent to the ROW is also illustrated by these results and indicates that impacts related to infrastructure development may not be confined to the cleared ROW.

Other factors such as climate change and variability and the natural evolution of peatlands are also important. The complete degradation of thin permafrost off-ROW is observed to occur at sites near the edge of the peat plateau (and adjacent to unfrozen terrain). Warmer climate conditions over the last decade have also likely been a factor in thawing of thin permafrost. Forest fires have also resulted in changes to the ground thermal regime, especially in the off-ROW areas, resulting in permafrost thaw and settlement. The effect of fire indicates that changes off- ROW may over time affect ROW conditions should settlement and collapse of peat continue to occur.

The results generated from the monitoring program provide information to improve our understanding of the response of frozen peatlands to environmental disturbance and for planning and design of future infrastructure in similar environments.

Acknowledgments

This project has been supported over the years by: the federal departments of Natural Resources Canada and Indian and Northern Affairs Canada, federal programs of PERD (Panel on Energy Research and Development), NOGAP (Northern Oil and Gas Action Plan) and Northern Energy Development Memorandum to Cabinet, and Enbridge Pipeline (NW) Inc. Numerous colleagues have contributed to data collection and analysis over the life of the monitoring program.

References

ACIA 2005. *Arctic Climate Impact Assessment.* Cambridge University Press, 1042 pp.

Aylsworth, J.M. & Kettles, I.M. 2000. Distribution of peatlands. In: The Physical Environment of the Mackenzie Valley, Northwest Territories: A Base line for the Assessment of Environmental Change *Geological Survey of Canada Bulletin 547*: 49-55.

Burgess, M.M. 1992. Analysis of the pipe and ditch thermal regime, Norman Wells Pipeline. *Proceedings of the 11th International Conference on Offshore Mechanics and Arctic Engineering*. American Society of Mechanical Engineers V: 575-584.

Burgess, M.M. & Lawrence, D.E. 2000. Permafrost and subsurface materials along a north-south transect in the Mackenzie Valley: Observations from the Norman Wells pipeline. In: The Physical Environment of the Mackenzie Valley, Northwest Territories: A Baseline for the Assessment of Environmental Change. *Geological Survey of Canada Bulletin 547*: 127-141.

Burgess, M.M. & Lawrence, D.E. 1997. Thaw settlement in permafrost soils: 12 years of observations on the Norman Wells pipeline right-of-way. *Proceedings of the 50th Canadian Geotechnical Society Conference*, *Ottawa*: 77-84.

Burgess, M.M. & Smith, S.L. 2003. 17 years of thaw penetration and surface settlement observations in permafrost terrain along the Norman Wells pipeline, Northwest Territories, Canada. *Proceedings of Eighth International Conference on Permafrost*, July 2003, Zurich, Switzerland: 107-112.

Burgess, M.M. & Tarnocai, C. 1997. Peatlands in the discontinuous permafrost zone along the Norman Wells Pipeline, Canada. *Proceedings of the International Symposium on Physics chemistry, and Ecology of Seasonally Frozen Soils,* Fairbanks Alaska. US Army Cold Regions and Engineering Laboratory, CRREL Special Report 97-10: 417-424

Halsey, L.A., Vitt, D.H. & Zoltai, S.C. 1995. Disequilibrium response of permafrost in Boreal Continental Western Canada to climate change. *Climate Change* 30: 57-73.

Nixon, M., Tarnocai, C. & Kutny, L. 2003. Long-term active layer monitoring: Mackenzie Valley, northwest Canada. *Proceedings of Eighth International Conference on Permafrost,* July 2003, Zurich, Switzerland: 821-826.

Pilon, J.A., Burgess, M.M., Judge, A.S., Allen, V.S., MacInnes, K.L., Harry, D.G., Tarnocai, C. & Baker, H. 1989. Norman Wells to Zama pipeline permafrost and terrain research and monitoring program: site establishment report. *Geological Survey of Canada, Open File* 2044, 332 pp.

Smith, S.L., Burgess, M.M., Riseborough, D. & Nixon, F.M. 2005. Recent trends from Canadian permafrost thermal monitoring network sites. *Permafrost and Periglacial Processes* 16: 19-30.

Viereck, L.A. 1982. Effects of fire and firelines on active layer thickness and soil temperatures in interior Alaska. *Proceedings of Fourth Canadian Permafrost Conference.* National Research Council, Ottawa, Canada: 123-135.

Systematization of Underground Ice

V.I. Solomatin, N.G. Belova
Moscow State University, Department of Geography, Moscow, Russia

Abstract

This paper examines the history and problems of classification of underground ice. A new approach to genetic classification of ground ice in the permafrost area, taking into account cryolithological, geological, and geographical aspects, is suggested. The general picture of the role of different ice types in permafrost regions is shown.

Keywords: genesis; ice structure; recrystallization; systematization of underground ice; underground ice.

Introduction

Ice with its specific properties has a special place and plays a special role in cold areas of the Earth. These properties reveal themselves in global and micro processes and in events in formation of the Earth's cryosphere.

The basic principles of general systematization of natural ice have been substantiated by Dobrowolsky (1923), Veinberg (1940), Shumskii (1955, 1959) and others. Later, as new facts and theoretical ideas were accumulated, the problem of systematization and structural-genetic conceptions were elaborated (Grave 1951, Pihlainen & Johnston 1963, Katasonov 1965, Popov 1967, Vtiurina & Vtiurin 1970, Mackay 1972, Solomatin 1986, Murton 1999, French 2007 and others).

Ground ice classifications proposed by different authors were based on origin, type, and age of ice formation, relationship between ice formation and formation of the deposit containing ice, source and properties of the water used for ice crystallization, a morphology of ice body, an origin of host deposits, and other characteristics. The classification by Mackay (1972) takes into account the source of water and processes of its movement.

Shumskii (1964) considers ice as a variety of rock. It is necessary to recognize that ice is an unusual rock, the place of which in classifications of rock is hard to describe.

In this paper, the history and problems related to classification of ground ice are examined, and a new approach to genetic classification of ground ice in the permafrost, which takes into account cryolithological, geological, and geographical features, is suggested.

Classification of Ground Ice by Shumskii

The first step in systematization of ground ice is a recognition of its place among the other objects similar in nature and in methodology of study. We already mentioned above that ground ice obviously belongs to rocks, but not what place it occupies among rocks and what class of rocks to which it can be referred. It is clear that ground ice is widespread in absolutely certain geographical space—in the permafrost zone. It is a light mineral and rock, and due to this feature, it lies mainly in the uppermost layers of the lithosphere, at depths of first tens of meters (rarely hundreds) from the surface. Formation of ground ice depends on environmental (facial) and thermal conditions. As with other rocks, ice occupies its own inherent place in the lithosphere, forms unique geological bodies due to specific mechanisms and factors of ice formation, and is characterized by individual features of structure.

Shumskii (1955, 1959, 1964), on the basis of his own studies and analysis of works by Dobrowolski (1923), Veinberg (1940), Tolstikhin (1936) and other founders of glaciology, came to the conclusion that the crystal structure of ice and its formation from a liquid phase during crystallization provides the basis for attributing it to magmatic rock. Also, some types of ice (e.g., glacier ice) have similarities with metamorphic rocks, affected by deep recrystallization and metamorphic transformation of their primary structure. At the same time, the direct analogy of natural ice with magmatic or metamorphic rocks is not completely correct, even though some types of ice are formed by crystallization of the liquid phase and others undergo deep forms of dynamic metamorphism. Ice differs sufficiently from all other rocks in its physical properties and, first of all, in density and thermal properties. Understanding the tentative character of his classification, Shumskii after Veinberg suggested the definition of ice, which is formed from a liquid phase, as *congelation ice*. Shumskii considered glacier ice as metamorphic rock, while snow cover he attributed to sedimentary rocks. The scheme of natural ice classification (including ground ice) suggested by Shumskii, appears to be the least contradictory in the general system of rocks, considering the unique nature of ice-formation processes. Usage of concepts of magmatic and metamorphic rock formation in glaciology establishes important principles and methods of structural-petrographic study, helps to comprehend physical and genetic processes of natural ice formation, and at the same time, allows the use of direct terminological analogies.

Subdivisions of Underground Ice

Applying Shumskii's approach, we can distinguish the following types of ground ice (Table 1):

1. Congelation ice – the analogue of magmatic rocks, the structure of which is determined mainly by processes of crystallization of a liquid phase, with subsequent structural

Table 1. The schematic classification of underground ice.

Group of ice rock	Ice rocks		Physical processes and conditions of formation	Structure
Deposit like ice (buried ice)	All types of primarily surface ice in permafrost		Burial of primarily surface ice in permafrost	The reduced structures of corresponding surface formed ice
Metamorfic ice	Wedge ice	Syngenetic	Dynamic metamorphism of congelation ice of yearly ice veins in thermal crack	Laminated schistose structures
		Epigenetic		
	Regelation-segregation (regelation-migration) ice		Regelation and migration of ice in weakened zones of dislocated frozen soil	Catablastic structures
Congelation ice	Segregated ice		Migration and crystallization of a interfacial water	Hypidiomorphic-granular, less often allotriomorphic-granular structure fabric
	Ice-cement		Crystallization of the free and interfacial water *in situ*	Anisomerous allotriomorphic-granular
	Injection ice		Slow crystallization of free pressurized water in closed and partly closed volumes of a freezing ground	Massive coarse-grained ice fabric of slow not orthotropic crystallization
	Cave ice	Thermokarst-cave ice	Volumetric crystallization of free water in cavities of a ground	Laminated prismatic-granular structures of orthotropic growth
		Incrusted ice	Layer-by-layer crystallization of free water	Laminated fine-grained ice fabric
		Sublimation (hoar) ice	Ice crystal growth from water vapor on cave wall	Conglomerate of crystals
	Crack ice		Crystallization of water in cracks of rock	Prismatic-granular structures of orthotropic growth with axial junction of ice crystal proceeding growth from opposite crack wall

transformations insignificant. Ice of cracks and injective and thermokarst-cave ice can be attributed to this type.

2. Metamorphic ice – first of all wedge ice, the development of which is not limited by formation of elementary vein structure, but includes also the determining role of the subsequent dynamic metamorphism.

3. Buried ice – which remains a still poorly-studied group of underground ice. It is possible to consider this ice as an analogue of sediment.

Of course there are some terminological uncertainties in this interpretation, but not more than in other cases of terminology of ice formation as a geological body. The petrography of buried ice is the result of its formation on the surface and slight changes in ice structure during sediment accumulation. On the other hand, a development of syngenetic wedge ice is also in very close connection with the accumulation of containing deposits. Therefore, the syngenetic ice wedges of Pleistocene sediments, which widely occur in northern Siberia and are up to 30 m tall, should be placed in the classification system between metamorphic (as all ice wedges) and sedimentary ice rocks. The term *sedimentary ice*, however, is used usually for products of snow accumulation (Shumskii 1955, 1964). Therefore, in this classification, we offer the term *deposit like ice* for buried ice and partly for any syngenetic ice.

Modification of Ice Structure with Time

The classification scheme (Table 1) reflects existing uncertainty and terminological inconsistency, which is impossible to avoid if we consider ice (including ground ice) as a type of rock. Shumskii (1955) uses widely the concept of natural ice metamorphism. Thermodynamic conditions, even in the most severe areas of the Earth during parts of the year, are close to a point of phase change of water which determines the unstable condition of ice and its transformation by recrystallization and change in its initial structure.

Ice is always subjected to transformations of any scale due to internal or external stock of free energy. This transformation reveals itself in recrystallization and in different scale changes of primary structures. Especially deep changes of primary ice structure occur during and after dynamic metamorphism, associated with movements of ice masses by external forces. Shumskii (1955) showed that thermometamorphism of ice reaches sufficient results only at temperatures close to a melting point of ice and for ice crystals of smallest size. Rogov (1981) compared size of ice grains in ice veins of ice wedges of Pleistocene and Holocene age and found that size of crystals of Pleistocene ice wedges are greater than in Holocene ice wedges, which shows that the size of ice crystals has increased with time. However, dynamic metamorphism has a more significant influence. The degree of dynamic metamorphism is determined by the origin of ice. For example it has an obvious effect in ice wedges but not in segregation ice, even in layers close to soil surface where tension is maximal.

Every rock undergoes the certain processes of diagenesis, but that does not mean that a structure of the natural ice, which is subjected to deep transformations, has completely lost its primary features with the origin of rock having become unrecognizable. On the contrary, ice as well as other metamorphic rocks, retains features of primary structure, even after intensive metamorphism. For example the sea origin of gneisses is out of doubt, despite intensive thermo and dynamic metamorphic processes through which the rock has passed after sedimentation. So we may say that ice recrystallization is a part of its petrogenesis, and in a certain sense, is an attribute and distinctive feature of its origin. Despite recrystallization, ice masses of different origin, which have formed at the same time and experienced since then identical thermodynamic conditions, preserve features of structure developed during their formation.

Spatial Patterns of Underground Ice-Formation

Because formation of ground ice is determined by thermodynamic conditions of adjacent rocks, patterns and genetic types of ice rocks vary with change in these conditions. In other words, the origin of ice is a function of physiographic conditions and depth of ice-forming horizon. Natural geographical changes and depth of frozen ground in earlier-described sediments should be reflected in permafrost structure (Solomatin 1982, 1996). However, patterns of ground ice predetermined by zonal factors are also affected by azonal lithogenic factors. This should be taken into consideration while studying the formation of ice at spatial boundaries of areas with different genetic types of ground ice.

Conclusions

Underground ice is a special natural mineral and rock. It is the main product and factor of permafrost forming, and is distinct as frozen ground from all other rocks.

The authors try to develop a classification of underground ice, which could help in understanding the general mechanism and spatiotemporal distribution and development of ice-rich permafrost. The classification offered in this paper takes into account the existing ideas, and also is based on initial structural features of different types of underground ice. The general picture of the role of different ice types in permafrost regions has been shown.

References

Dobrowolski, A.B. 1923. Historia naturalna lodu. Warszawa. 191 pp. (in Polish).

French, H.M. 2007. *The Periglacial Environment*. 3rd Ed. Chichester: Wiley.

Grave, N.A. 1951. Geographical distribution of large masses of underground ice in permafrost region. *Proceedings of the Conference on Ice and Snow Investigations.* Moscow: USSR Academy of Sciences Publishing House, 151-218 (in Russian).

Katasonov, E.M. 1965. Cryofacial studies of permafrost and problems of the Quaternary research in Siberia. In: *The Main Problems of Quaternary Studies*. Moscow: Nauka, 286-294 (in Russian).

Mackay, J.R. 1972. The world of underground ice. *Annals of the American Association of Geographers* 62(1): 1-22.

Murton, J.B. 1999. Permafrost: a case study in cryostratigraphy, Mackenzie Delta area, Western Canadian Arctic. In: A.P. Jones, M.E. Tucker & J.K. Hart (eds.), *The Description and Analysis of Quaternary Stratigraphic Field Sections*. Technical Guide 7. Quaternary Research Association, London, 249-266.

Pihlainen, J.A. & Johnston, G.H. 1963. *Guide to a Field Description of Permafrost*. National Research Council, Associate Committee on Soil and Snow Mechanics, Technical Memorandum 79, Ottawa.

Popov, A.I. 1967. *Geocryological Phenomena in the Earth's Crust (Cryolithology)*. Moscow State University, Moscow, 303 pp. (in Russian).

Rogov, V.V. 1981. Structures of wedge ice as an indicator of age of ice. *Problems of Cryolithology,* Issue 9. MSU Publishing, 57-69 (in Russian).

Shumskii, P.A. 1955. *Principles of Structural Glaciology*. Moscow: USSR Academy of Sciences Publishing House, 492 pp. (in Russian).

Shumskii, P.A. 1959. Ground ice. In: *Principles of Geocryology*, Vol. 1. Moscow: USSR Academy of Sciences Publishing House, 274-327 (in Russian).

Shumskii, P.A. 1964. *Principles of Structural Glaciology*. New York: Dover Publications, Inc., 497 pp.

Solomatin, V.I. 1983. Problems of underground ice systematization. *Problems of Cryolithology,* Issue 11. Moscow State University, Moscow, 38-56 (in Russian).

Solomatin, V.I. 1986. Petrogenesis of the underground ices. Novosibirsk: Sciense, 215 pp. (in Russian).

Tolstikhin, N.I. 1936. On classification of ice and ice bearing soils. VI(7): 628-636 (in Russian).

Veinberg, B.P. 1940. *Ice*. Moscow-Leningrad: Gostechizdat: 524 pp. (in Russian).

Vtiurin, B.I. & Vtiurina, E.A. 1969. Genetic classification of ground ice. *Permafrost Research Issue* 9. Moscow: Moscow State University, 165-167 (in Russian).

Nearshore Ground Temperatures, Seasonal Ice Bonding, and Permafrost Formation Within the Bottom-Fast Ice Zone, Mackenzie Delta, NWT

Steven M. Solomon
Natural Resources Canada, Dartmouth, Nova Scotia, Canada
Alan E. Taylor
Alan E. Taylor Geophysics, Sidney, British Columbia, Canada
Christopher W. Stevens
University of Calgary, Calgary, Alberta, Canada

Abstract

The Beaufort Shelf offshore the Mackenzie Delta is characterized by shallow nearshore slopes that result in extensive regions where seasonal bottom-fast ice (BFI) can develop with attendant ground freezing and aggradation of permafrost. Ground temperatures in four 10-m deep boreholes were measured for 2 years along an ~18 km transect from a distributary channel across a nearshore shoal. Maximum BFI thickness in March was 1.05 m with the coldest ground temperatures occurring where BFI was thinnest. Field observations constrained a two-dimensional geothermal model for the study area. The observations and model show the sensitivity of permafrost and ice bonding to subtle changes in bathymetry and to the residency period of BFI. The permafrost table rises beneath shallow water where annual residency of BFI is the greatest, and a subsurface talik develops beneath deeper water where residency is minimal.

Keywords: bathymetry; bottom-fast ice; ground temperature; ice-bonding; nearshore; permafrost.

Introduction

The Mackenzie Delta, located in the western Canadian Arctic (Fig. 1), is under intensive exploration for natural gas, and a proposed gas pipeline may pave the way for production of known reserves in the nearshore off the delta front. Environmentally-sound development of hydrocarbon resources in this region will require an understanding of the processes that govern coastal stability, nearshore morphology, and sediment properties in the extensive, very shallow coastal zone. In water depths <2m during the winter months, sea ice forms and thickens until it contacts the seabed (i.e., becomes "bottom-fast"). Once the ice is bottom-fast, heat is rapidly removed from sediments by conduction via the strong temperature gradient induced by the very cold air temperatures at the ice surface. This facilitates the formation of seasonal frost, and creates conditions conducive to permafrost aggradation into sediments which were formerly unfrozen. This paper reports on recent ground temperatures measured beneath zones of BFI, and on efforts to develop a thermal model for the shallow seabed along a borehole transect.

Study area

Our study transect lies at the northwest edge of the Holocene ("modern") Mackenzie Delta (Fig. 1). The shoreline of the Holocene delta is characterized by lobe-shaped vegetated islands separated by funnel-shaped bays (Hill et al. 2001). The erosional nature of the delta front, drowned morphology, and other features indicate that the Mackenzie Delta is undergoing transgression resulting in limited water depths for sediment accumulation (Hill et al. 2001). However, bar accretion still occurs within large embayments and at the mouths of most distributary channels. In general, the nearshore, seaward of the Holocene delta, is very shallow. Water depths are less than 2 m (relative to chart datum) at distances in excess of 15 km from the shore. Mean tides are 0.3 m and large tides range up to 0.5 m, whereas winds may raise water levels up to 2.4 m (Hill et al. 2001) or lower them by up to 1 m (Henry 1975).

The Mackenzie River is the largest of North American rivers supplying water and sediment to the Arctic Ocean. The abundant supply of freshwater is maintained throughout the year as a surface plume in the summer and as an under-ice freshwater "lake" during the winter (MacDonald & Carmack 1991). Thus the "sea" ice that forms in the winter is primarily formed from Mackenzie River water. Similarly, nearshore sediments deposited beneath the plume have been found to exhibit low pore water salinities (unpublished data).

The Holocene delta is underlain by permafrost to depths of 40–90 m (Judge et al. 1987). Offshore the Holocene delta, the depth to the top of permafrost is variable or absent (e.g., Judge et al. 1987, Pullan et al. 1987). Several drilling transects undertaken in the region have illustrated the nature of the onshore-offshore transition for a range of coastal morphological conditions (Dallimore et al. 1988). As described by Dyke (1991), the thermal state of sediment in the nearshore region depends on the period of time during which the sea ice is bottom-fast. In bottom-fast ice (BFI) zones, permafrost can be aggrading (in shallower water where ice becomes bottom-fast early in the winter) or degrading (where water depths are greater and ice does not become bottom-fast or does so later in the winter). Subtle changes in water depth may play an important role in determining whether or not BFI is present, and therefore can make a significant difference in the thermal state of the nearshore

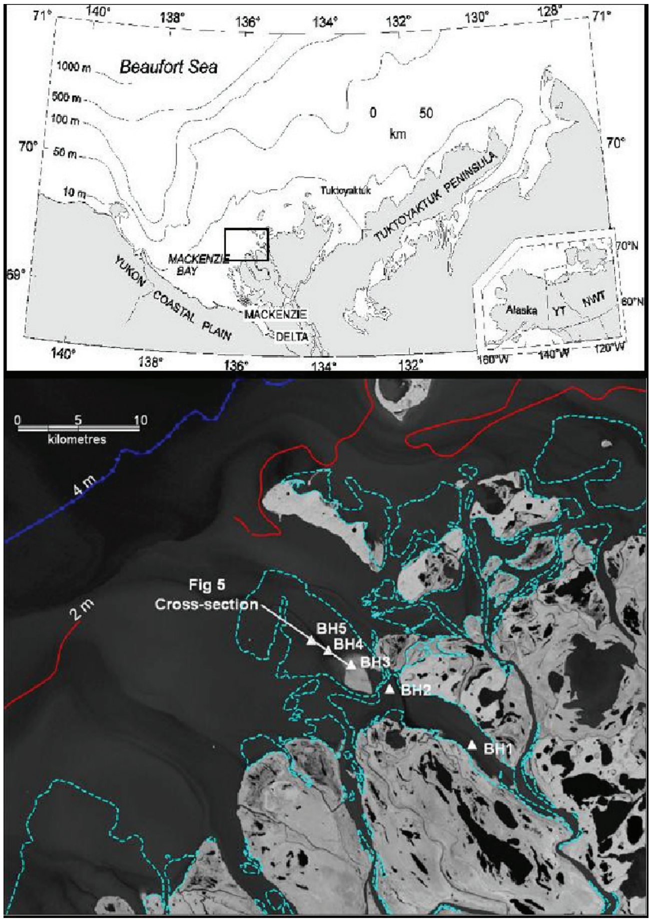

Figure 1 General and detailed location of the study area and boreholes. The Landsat image (lower, composite of summer scenes in 2000-2003) depicts the 2 and 4 m bathymetric contours, the distribution of bottomfast ice (in light blue; as mapped using synthetic aperture radar – Solomon et al. 2005), and the borehole locations (triangles). The 2 m contour is discontinuous due to a lack of data.

sediments since that will determine to what extent (if any) the seabed is coupled through BFI to very cold winter air temperatures (Dyke 1991).

Once the sea ice has become bottom-fast, the active layer above permafrost (or the zone of seasonal freezing) begins to refreeze (e.g., Osterkamp et al. 1989, Dyke 1991, Wolfe et al. 1998). This zone is also characterized by large horizontal spatial variability in temperature and seasonally reversing vertical temperature (Hunter 1988).

Methods

Ground temperature

Ground temperatures were measured in four boreholes drilled to 10 m using a seismic shothole rig. A fifth borehole was drilled in deeper water but not instrumented because of hole problems. Boreholes were located along a transect extending from a partially infilled distributary channel across a large nearshore shoal (Fig. 1). Borehole locations with varying thicknesses of BFI were chosen (Table 1). The boreholes were cased with 2” PVC pipe coupled to 4” pipe for the upper metre. The larger diameter pipe was required to house the 8-channel RBR™ data logger. One borehole (BH3) was completely filled with silicone oil while the remaining boreholes were filled to 7 m (from the bottom). The temperature cable consisted of eight YSI™ thermistors spaced at varying intervals (0.5 m, 0.5 m, 0.5 m, 1 m, 2 m, 2.5 m, 2.5 m) with the uppermost thermistor located approximately 0.5–1.0 m below the riverbed or seabed surface from which all depths are measured; we use the term “seabed” for all boreholes.. An independent temperature logging unit (Vemco™ Minilog) was mounted inside the casing at the seabed surface. Seabed surface temperatures were logged every 3 hours and subseabed temperatures were logged every 8 hours. The YSI thermistors have an accuracy of ±0.1°C and the measurement system can resolve changes in temperature of 0.1°C (S. Smith, pers. com. 2007). The Vemco™ surface temperature loggers are specified to have a resolution of ±0.3°C and an accuracy of ±0.5°C.

Table 1. Borehole characteristics and thermal parameters derived from ground temperature data (2005–06).

			"Depth"	"MAGT$_0$"	"MaxT$_0$"	"MinT$_0$"	"MAGT$_{AL}$"
	Mean BFI thickness 2005-07	Base of ice-bonding (driller)	upper sensor depth	mean annual seabed temperature	maximum annual seabed temperature	minimum annual seabed temperature	mean annual ground temperature at AL depth
	(m)		(m)	(°C)	(°C)	(°C)	(°C)
BH1	0.3	frozen	0.67	0.52	14.83	-17.83	-2.34
BH2	1.0	~5 m	0.60	2.03	14.35	-9.94	-0.28
BH3	0.1	frozen	0.82	-4.24	12.04	-25.55	-3.74
BH4	0.5	frozen	0.86	-1.24	12.41	-15.64	-2.42
	"MaxT$_{AL}$"	"MinT$_{AL}$"	"Z$_{zero-ampl}$"	"T$_{Gzero-ampl}$"	"Z$_{AL}$""	"MaxT$_{AL}$"	"MinT$_{AL}$"
	maximum annual ground temperature at AL depth	minimum annual ground temperature at AL depth	depth of seasonal "zero" temperature amplitude	temperature at depth of seaspnal "zero" temperature	depth of active layer (permafrost below)	maximum annual ground temperature at AL depth	minimum annual ground temperature at AL depth
	(°C)	(°C)	(m)	(°C)	(m)	(°C)	(°C)
BH1	0.00	-12.68	deep	deep	1.80	0.00	-12.68
BH2	0.00	-0.62	3.76	-0.31	2.99	0.00	-0.62
BH3	0.00	-12.74	deep	deep	1.95	0.00	-12.74
BH4	0.00	-11.44	deep	deep	2.13	0.00	-11.44

Borehole positions were surveyed using a geodetic quality global positioning system. The positions were then used to relocate the borehole sites during the recovery of the data loggers.

Finite element geothermal model

Ground thermal modeling was undertaken to investigate the spatial variations in ground thermal conditions that attend BFI, such as the initiation of seasonal seabed freezing and the possibility of the growth of permafrost. The modeling was performed using the software TEMP/W™ (Geo-Slope International Ltd. 2004). This two-dimensional finite-element program combines the physics of heat transfer and phase change in porous media and realistic geologic and temporal boundary conditions to model transient thermal conditions. The model has been verified extensively against analytic solutions and is used widely by the permafrost community.

Boundary conditions, both spatial and temporal, are critical to match observations and for model predictions. The seabed temperatures along the modeled transect throughout the 2005–06 year are crucial “forcing functions” for the numerical model. They were estimated from two sources: (1) the temperature time series from a logger placed at the seabed inside each borehole collar (referred to as BC$_{measured}$), and (2)

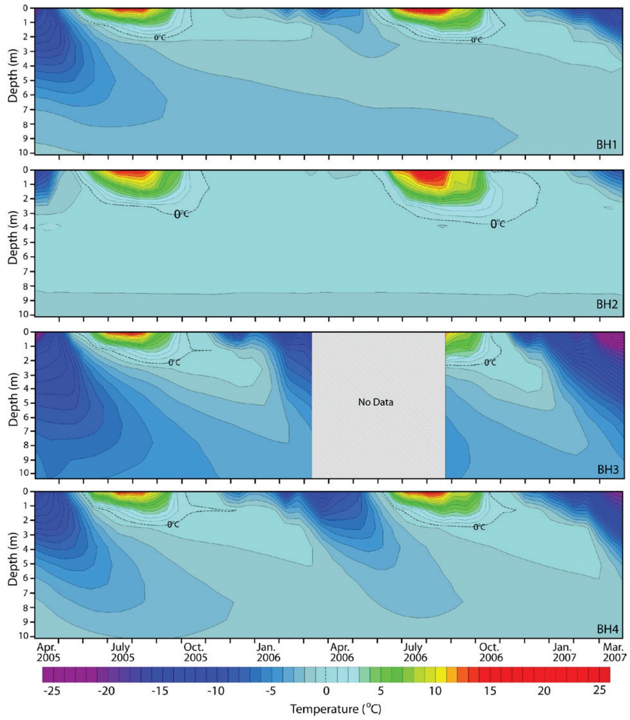

Figure 2 Two years of ground temperature variations for the 4 boreholes are illustrated as depth versus time plots. BH2 (thickest BFI) exhibits the warmest temperatures; BH3 (sub-aerial shoal), the coldest. Part of the data from BH3 is missing due to a malfunctioning data logger.

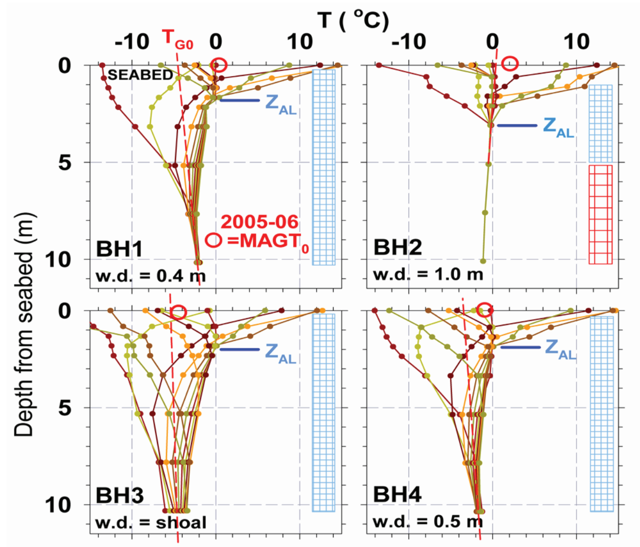

Figure 3 Monthly temperature envelopes for year Mar. 2005 – Mar. 2006 showing diverse character of borehole thermal conditions. Z_{AL}, $MAGT_0$ and T_{G0} are indicated (Table 2). Depth 0 m is at seabed. Hachured, state during drilling: blue = frozen, red=thawed.

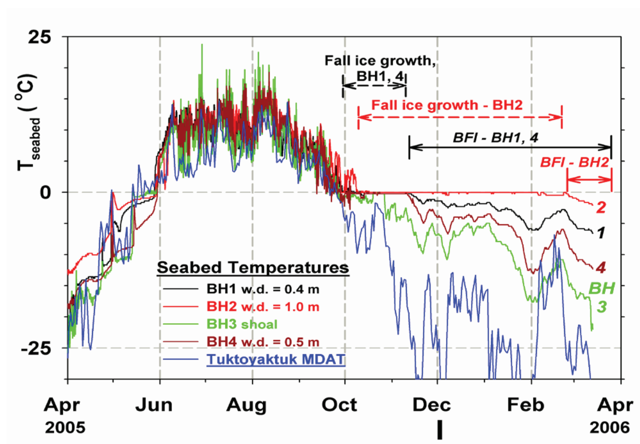

Figure 4 Tuktoyaktuk mean daily air temperatures and seabed temperatures measured at the borehole collars. Onset of fall sea ice freezing (floating), and onset of BFI (grounded) are shown. w.d. = water depth.

a temperature time series developed from Tuktoyaktuk air temperatures, ice thickness growth rates (Menard & Duguay 2006), and near-shore distributary water temperatures (Dyke, pers. com. 2006; $BC_{estimated}$). The first, $BC_{measured}$, is a borehole-specific measurement of temperatures over the periods during which water or BFI covers the seabed along our borehole transect. $BC_{estimated}$ is a regional estimate of seabed conditions based on independent, external data. The latter were used to interpolate conditions between boreholes.

Results

Ground temperatures

The annual ground temperature cycle over the two years of record (2005–2007) is illustrated by Figure 2. Annual ground temperature envelopes ("trumpet curves") calculated from the 2005–06 data were used to calculate a range of parameters pertinent to geothermal interpretations (Table 1, after definitions in Brown & Kupsch 1974).

The general trends in temperature show cooling of the ground in the winter and warming in the spring and summer with illustrated inter-annualinterannual variability. All of the boreholes terminate above the depth of zero annual amplitude and therefore experience changes in ground temperatures that relate to fluctuations in air temperature. The most obvious difference between the four temperature records is the warm and nearly isothermal ground temperatures below 3 m at BH2 (beneath ~1m of BFI) in contrast to colder temperatures at the other three boreholes.

Figure 3 shows plots of mean monthly ground temperatures for 2005–2006 versus depth ("trumpet curves") below the seabed. Permafrost (annual temperatures <0°C, (Brown & Kupsch 1974) underlies an active layer (Z_{AL}) of ~2 m at three of the boreholes (~3 m at BH2, Table 1). Ground temperatures that are below freezing combined with observations made during drilling (March 2005) indicate that the sediments below Z_{AL} in BH1, 3, and 4 are partially or fully frozen throughout the year. Mean annual seabed temperatures ($MAGT_0$) range from ~-4°C on the intertidal shoal (BH3), to >0°C at BH1 and BH2 within the river distributary, and to <0°C offshore at BH4 (Table 1, Fig. 2).

The seabed along the transect experiences a wide range in temperatures, from 14.8°C to -26°C throughout the year,

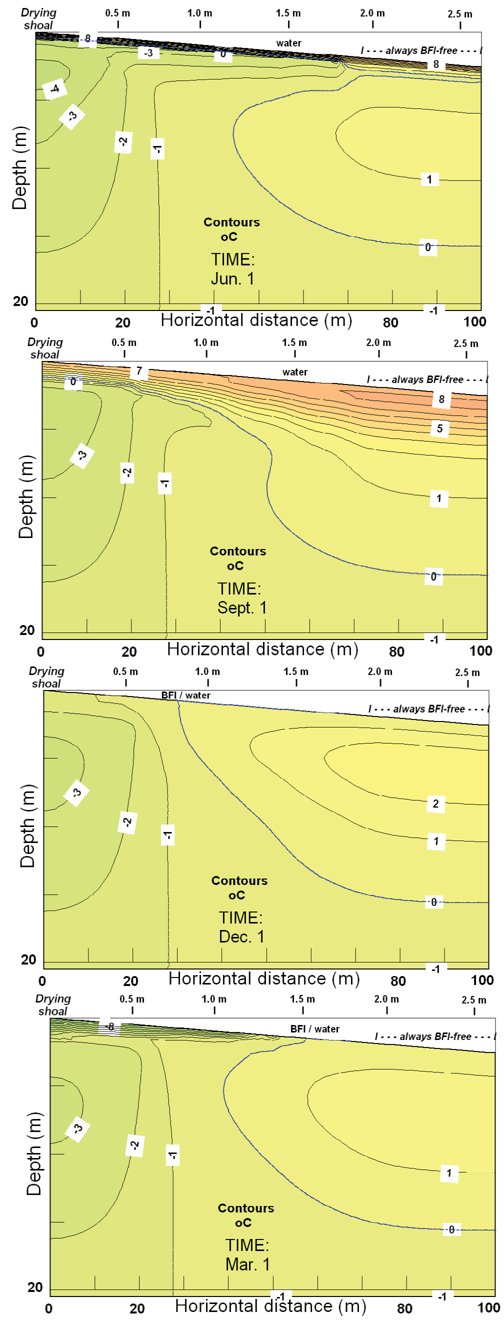

Figure 5 Temperature contours at times indicated for the hypothetical model (using $BC_{measured}$) of linearly increasing water depth (upper scale). The interpreted maximum offshore extent of the seasonal boundary between BFI and a water-covered seabed is shown.

with the greatest annual variation occurring at BH3 where BFI is thinnest (Fig. 4). The rate of change at the seabed is most rapid in the spring coincident with river breakup. As river discharge increases in late May, water overflows onto the surface of bottom-fast ice and under the ice and causes warming of the sea bed. During the open water of summer, the river and seawater are the dominant control on the seabed and riverbed temperatures. During fall and winter, seabed or riverbed cooling occurs more slowly and differs more markedly between boreholes than spring warming. Water cools first to the freezing point, where it remains for several weeks as ice forms. In shallow water, ice becomes bottom-fast relatively early in the winter, allowing low air temperature to penetrate the ice column and freeze the seabed (BH1 and BH4). In deeper water, ice does not become bottom-fast, and therefore, the seabed remains within a narrow range around the freezing point throughout the winter. At intermediate water depths, the onset of BFI is delayed resulting in a shorter duration of BFI than in the shallow water case with proportionally less freezing of the seabed. In the case of BH2, bottom-fast ice conditions were not achieved until mid- February during the winter of 2005–06 (Fig. 4). The late winter ice contact is reflected in the near-isothermal temperatures below 3 m in depth at BH2. Subsequently, freezeback of the active layer also occurs in late winter which results in minimal heat exchange at depth. The following year BFI conditions at BH2 occurred two months earlier (late December), resulting in more rapid freezeback of the active layer and colder shallow ground temperatures (Fig. 2). BH1 and BH4 were bottom-fast early in both the 2005–06 and 2006–07 freeze-up seasons (mid-October to mid-November; Fig. 4). In general, temperatures at the base of BFI correlate with air temperatures but are attenuated to about -2°C to -10°C (Fig. 4).

Numerical modeling

Figure 5 shows the thermal impact of BFI for a modeled scenario in which water depth increases linearly from a shoal to depths beyond maximum seasonal ice thickness. Using a seabed temperature boundary condition based on Figure 4 ($BC_{measured}$) as forcing function, we model the thermal impact on subsurface temperatures throughout the year. An unfrozen seabed is pervasive in summer, with seabed cooling in the fall and nearshore BFI forming in November (compare to Fig. 4). Note how the BFI/seawater boundary moves gradually further offshore during the winter, reaching its maximum extent in late April when sea ice thickness is maximum. In the process, seasonal freezing of the seabed due to BFI develops to ~2 m nearshore and becomes less deep further offshore at the maximum extent of BFI. In May, the spring freshet of warm water floods the ice and detaches it from the seabed, initiating summer open water conditions and thaw of the seasonally-frozen seabed. The effect of BFI is to support offshore permafrost, as indicated by the 0°C isotherms in Figure 5, at shallower sub-seabed depths than in open water areas.

Four zones may be identified in Figure 5: (1) the shoal that is intertidal and over-washed irregularly to create thin BFI, and where frozen sediments occur from the ground surface to >10 m during winter (cf. BH3, Fig. 3), (2) water depths <1/2 of the maximum ice thickness of BFI, where residency of BFI is the longest, and beneath which the permafrost table lies (in this example) at 1 to ~5 m (cf. BH1 and BH4), (3) a transitional zone landward of the BFI-water margin where water depth is somewhat less than the maximum seasonal ice thickness, and (4) water depths > maximum ice thickness where BFI never occurs and beneath which the permafrost table lies deeper (here ~15 m). Note that for a water depth of ~1 m (Zone 3), the model predicts seabed temperatures to be nearly isothermal around -1°C from ~4 to 10 m depth, with a seasonal variation from -8 to +8°C in the upper 4 m. Temperatures at BH2 (Fig. 3) also exhibit an isothermal section <-1°C below 3 m, with a seasonal variation from -14 to +14°C in the upper 3 m.

Discussion

The borehole data presented in this study illustrate the interannual variability in ground temperatures and permafrost conditions within the shallow nearshore environment (Fig. 2) resulting from subtle changes in water depth (Fig. 3). Permafrost *sensu strictu* (<0°C) exists at all boreholes; however, differences in the extent of ice-bonding were found to occur. Drilling data indicates that the sites located beneath the shallowest water (BH1, BH3, and BH4) host ice-bonded permafrost to the maximum drilled depth (10 m), while a deeper water site (BH2) with temperatures marginally below 0°C hosts unfrozen to marginally ice-bonded sediment at depth. Seabed temperatures were found to track variations in air temperature closely with some thermal offset (Fig. 4).

Unique, continuously recorded temperature data collected throughout the fall and winter seasons reveal differences between rates of cooling and warming that are indicative of the processes occurring at those times of year (Fig. 4). Rapid warming at all of the water depths in spring is a response to overflow of warm river water originating at southern latitudes onto the ice surface and eventually melting or floating BFI off the seabed. The relatively slower cooling in the fall is a consequence of ice thickening and the gradual increase in the seaward extent of the zone of bottom-fast ice.

While the borehole temperatures quantify the impact of BFI on the seabed, other unmeasured parameters (sediment type and water content, thermal properties, sediment scour and deposition, snow cover, tidal range, storm surges, etc.) complicate the detailed interpretation of ground temperatures. Numerical modeling of a simplified case provided additional insight into the impact of BFI versus water depth. As described above, the two-dimensional model of a linear increase of water depth in the offshore direction clearly demonstrates the spatial variability of the subsurface thermal and permafrost regime across the complete range of water depths as opposed to the discrete measurements at the boreholes (Fig. 5). Clearly, the impact of residence times of BFI and summer water temperatures on the seabed are primarily a function of water depth. The “end members” are the shoal (thin intertidal BFI) and water deeper than maximum seasonal ice thickness (no BFI and perpetually submarine).

Other investigators have observed similar phenomena. For instance, previous work in the Prudhoe Bay area (e.g., Osterkamp et al. 1989 Osterkamp & Harrison 1982) examined the properties of nearshore permafrost in a narrow bottom-fast ice zone exposed to saline marine waters. They found that development of brines through salt exclusion had a significant effect on the properties of shallow materials. However, as observed in our study, they also noted the presence of an active layer where water depth or ice thickness is about 1.2–1.3 m. Temperature measurements in sediment beneath BFI were made to depths of 2 to 22m in the spring (late May–early June) and fall (November) over the course of one year. These discrete measurements have some similarities to those shown here but lack sufficient temporal detail for in-depth comparisons. The Prudhoe Bay site also differs from our study area in that Prudhoe Bay is far from any major rivers and is in an area of active coastal erosion, where thick onshore permafrost is being transformed into subsea permafrost by erosion and subsequent submergence. In contrast, the Mackenzie Delta study site is likely recording the initiation and evolution of permafrost in an aggradational setting of a freshwater-dominated delta-front of a major river.

A geotechnical investigation undertaken approximately 50 km northeast of the present study site (Hunter & Pullan 1986, Kurfurst & Dallimore 1991) examined ground temperatures across a wide sand flat adjacent to and north of the Mackenzie Delta. A series of 10 temperature cables were installed out to 800 m from the tundra shoreline and were all within the zone of bottom-fast ice. Temperatures recorded in September 1985 and April 1986 show very similar patterns to our data presented above, with a wide range of temperatures at the surface where BFI thickness was relatively thin and a much narrower range where ice was thicker (similar to BH2). Most of their boreholes were drilled to 30 m depth and all were ice-bonded throughout with little annual fluctuation below 12–16 m. Their study differed from ours in that the sand flats are interpreted to overlie older and likely previously frozen material. We believe that our sites are characterized by deposition over unfrozen seabed (based on unpublished drilling results obtained in March 2007).

Conclusions

1. Observations and model results show the importance of the duration of BFI in controlling the temperature regime at the seabed surface.
2. There is a strong seasonality to the influence of BFI with rapid and nearly simultaneous removal of BFI at all four boreholes in spring, and slower, more depth-dependent onset of BFI conditions in the fall.
3. Small changes in water depth causing ongoing natural deposition and erosion or resulting from human intervention (e.g., dredging or trenching) are likely to have dramatic effects on subsea ground temperatures and therefore ice-bonding and permafrost.

Acknowledgments

Funding was provided by Natural Resources Canada, Office of Energy Research and Development, and the Northern Energy Development Project. Logistic support was provided by Aurora Research Institute, Polar Continental Shelf Project, Chevron Canada, and Shell Canada. Field assistance was provided by Dustin Whalen and J.C. Lavergne. Caroline Duschesne and two anonymous reviewers provided comments that improved the paper substantially.

References

Are, F.A. 1988. Thermal abrasion of sea coasts (Parts I and II). *Polar Geography and Geology* 12: 1-157

Brown, R.J.E. & Kupsch, W.O. 1974. *Permafrost Terminology.* Technical Memorandum No. 111. Associate Committee on Geotechnical Research, National Research Council of Canada 14274, 61 pp.

Dallimore, S.R., Kurfurst, P.J. & Hunter, J.A.M. 1988. Geotechnical and geothermal conditions of nearshore sediment, southerm Beaufort Sea, Northwest Territories, Canada. *Proceedings of the Fifth International Conference on Permafrost, Trondheim, Norway, Aug. 2–5, 1988*: 127-131.

Dallimore, S.R. & Matthews, J.V. (eds.), 1997. *The Mackenzie Delta Borehole Project.* Environmental Studies Revolving Funds Report No. 135, Calgary, Canada. CD-ROM.

Dyke, L.D. 1991. Temperature changes and thaw of permafrost adjacent to Richards Island, Mackenzie Delta, N.W.T. *Canadian Journal of Earth Sciences* 28: 1834-1842.

Dyke, L.D., 2005. Shoreline permafrost along the Mackenzie River; In: L.D. Dyke & G.R. Brooks (eds.), *The physical environment of the Mackenzie Valley, Northwest Territories: a base line for the assessment of environmental change*. Geological Survey of Canada, Bulletin 547, 143-151.

Dyke, L.D. & Wolfe, S. 1993. Ground temperatures and recent coastal change at the north end of Richards Island, Mackenzie Delta, Northwest Territories. In: *Current Research, Part E.* Geological Survey of Canada Paper 93-1E, 83-91.

GeoSlope International Ltd. 2004. *TEMP/W, Software for finite element geothermal analysis, Version 6*. Calgary, AB: Geo-Slope International Ltd.

Henry, R.F. 1975. *Storm Surges.* Environment Canada, Beaufort Sea Project. Technical Report 19, 41 pp.

Hill, P.R., Lewis, C.P., Desmarais, S., Kauppaymuthoo, V. & Rais, H. 2001. The Mackenzie Delta: sedimentary processes and facies of a high-latitude, fine-grained delta. *Sedimentology* 48: 1047-1078.

Hunter, J.A.M. 1988. Permafrost aggradation and degradation on Arctic coasts of North America. *Proceedings of the Fifth International Conference on Permafrost, Trondheim, Norway, Aug. 2–5, 1988.* Trondheim: Tapir Publishers, 27-34, 127-131.

Hunter J.A.M., Judge, J.A., MacAulay, H.A., Good, R.L., Gagne, R.M. & Burns, R.A. 1976. *Permafrost and frozen sub-seabottom materials in the southern Beaufort Sea.* Beaufort Sea Technical Report 22, 174 pp.

Hunter, J.A.M. & Pullan, S. 1986. Sub-seabottom temperature measurements. In: P.J. Kurfurst (ed.), *Geotechnical investigations of the near-shore zone, North Head, Richards Island, N.W.T.* Geological Survey of Canada Open File Report 1376, 36-52.

Judge, A.S., Pelletier, B.R. & Norquay, I. 1987. Permafrost base and distribution of gas hydrates. In: B.R. Pelletier (ed.), *Marine Science Atlas of the Beaufort Sea: Geology and Geophysics.* Geological Survey of Canada, Miscellaneous Report 40. Map 39.

Kurfurst, P.J. & Dallimore, S.R. 1991. Engineering geology of nearshore areas off Richards Island, N.W.T.: A comparison of stable and actively eroding coastlines. *Canadian Geotechnical Journal* 28(2): 179-188.

Macdonald, R. & Carmack, E. 1991. The role of large-scale under-ice topography in separating estuary and ocean on an Arctic shelf. *Atmosphere-Ocean* 29:37-53.

Mackay, J.R. 1972. Offshore permafrost and ground ice, southern Beaufort Sea, Canada. *Canadian Journal of Earth Sciences* 9: 1550-1561.

Ménard, P. & Duguay, C.R., 2005. *Thermal modeling of ice growth in support of GSC Mackenzie Delta research*. Contract report submitted to Geological Survey of Canada Atlantic.

Osterkamp, T.E.; Baker, G.C., Harrison, W.D., & Matava, T. 1989. Characteristics of the active layer and shallow subsea permafrost. *Journal of Geophysical Research* 94(C11): 16227-16236.

Osterkamp, T.E. & Harrison, W.D. 1982. Temperature measurements in subsea permafrost off the coast of Alaska. In: H.M. French (ed.), *Proceedings of the Fourth Canadian Permafrost Conference*, *Calgary, Alberta, March 2–6, 1982:* 238-248.

Pullan, S., MacAulay, H.A., Hunter, J.A.M., Good, R.L., Gagne, R.M. & Burns, R.A., 1987. Permafrost distribution determined from seismic refraction. In: B.R. Pelletier (ed.), *Marine science atlas of the Beaufort Sea: geology and geophysics.* Geological Survey of Canada, Miscellaneous Report 40. Map 37.

Solomon, S.M., Fraser, P. & Manson, G. 2005. Nearshore morphology derived from Synthetic Aperture Radar in the Mackenzie Delta region of the Beaufort Sea. *Proceedings of the 12th Canadian Coastal Conference*, *November 6–9, 2005, Dartmouth, Nova Scotia.*

Taylor, A.E., Dallimore, S.R. & Outcalt, S.I. 1996. Late Quaternary history of the Mackenzie-Beaufort region, arctic Canada, from modelling of permafrost temperatures: 1. The onshore–offshore transition. *Canadian Journal of Earth Sciences* 33(1): 52-71.

Wolfe, S.A, Dallimore, S.R. & Solomon, S.M. 1998. Coastal permafrost investigations along a rapidly eroding shoreline, Tuktoyaktuk, N.W.T. *Proceeedings of the Seventh International Conference on Permafrost, June 23–27, Yellowknife, Canada*: 1125-1131.

New Data on the Ice Complex of the Lena-Amga Rivers Plain (Central Yakutia)

Vladimir B. Spektor
Melnikov Permafrost Institute SB RAS
Valentin V. Spektor
Melnikov Permafrost Institute SB RAS
Nadezhda T. Bakulina
State Unitary Enterprise of the Republic Sakha, Central Geologic and Analytic Laboratory

Abstract

Some new forms of buried ice and firn were recovered in the section of the Late Pleistocene deposits by drilling in several near-watershed sites (220–250 m a.s.l.) on the Lena-Amga Rivers Plain (Russia, Central Yakutia). The recovered section consists of three separate horizons of ice and firn formations occurring between 2.5, 5.0, 12.0, 17.0, 33.6, and 39.0 m from the ground surface. The ice and firn horizons are divided by strata of epigenetically frozen sandy silts and silts.

Keywords: Central Yakutia; cryolithology; ground ice.

Introduction

During several cryostratigraphical expeditions to Central Yakutia undertaken by the authors in recent years, two boreholes were drilled in autumn 2004 and spring 2005 to the depths of 50 m on the near-watershed areas (220–250 m a.s.l.) of the Lena-Amga Rivers interfluve. The boreholes located, correspondently, 82 km (62°08'N, 131°18'E) and 94 km (62°04'N, 131°33'E) east of Yakutsk (Fig. 1) recovered strata of wedge ice and horizontally layered ice and buried firn divided by silt and sandy silt horizons.

The investigated area is located on the high Lena-Amga plain (200–300 m a.s.l.) which is restricted to the group of plains separating the Central Siberian Plateau and Prilenskoe Plateau. It is situated within the continuous permafrost zone with ground temperatures at the depth of zero annual variations as low as -3°C to -6°C (Ivanov 1984).

In winter the Siberian anticyclone extends over the whole region resulting in falling of winter temperatures down to -50°C–60°C. The mean annual air temperature in Yakutsk is -10.3°C; mean annual precipitation amounts to 250–300

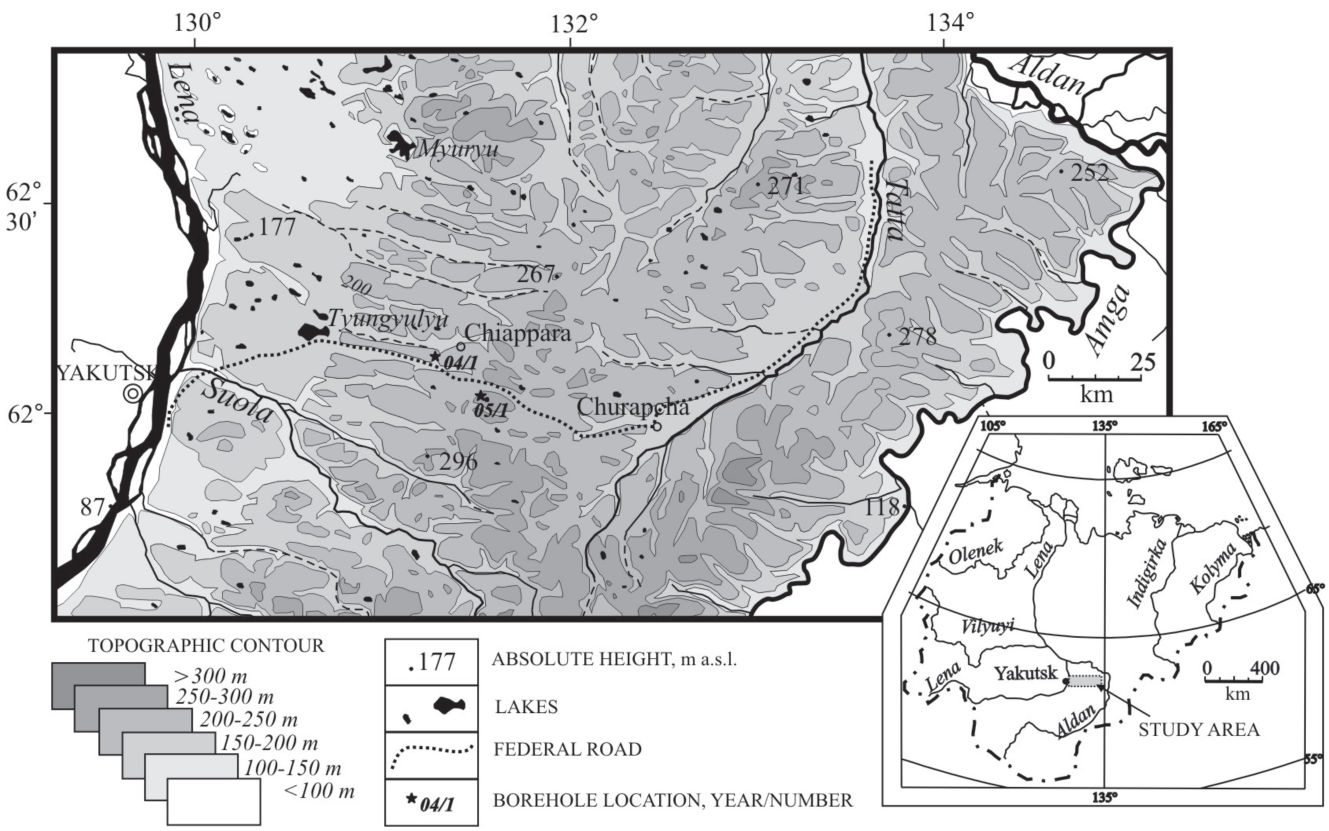

Figure 1. A map view of the study area with the borehole locations within the Lena-Amga Rivers Plain (Central Yakutia).

mm, and the height of snowpack varies between 5–30 cm (Fundamentals 1998). The permafrost thickness may be as much as about 300 m (Ivanov 1984). The upper 150 m of the geological section is loose Quaternary deposits.

According to previous investigations (Solov'ev 1959, Structure 1979, Katasonov 1975, Péwé and Journaux 1983, Ivanov 1984, Spektor & Spektor 2004), a unified stratum of ice complex containing ice wedges and structure ice is widespread on the areal surface. By different accounts the depths of ice complex with syncryogenic ice wedges vary between 10–30 m (Fundamentals 1998) to 50–60 m (Ivanov 1984).

In the course of studies made in 2004–2005, we observed new, not earlier noted, horizontally layered "sedimentary" types of ice, as well as poorly metamorphized buried firn and delineated a rhythmical texture of the upper permafrost section. Probably, similar formations were indicated by P.A. Solov'ev (1959) on the watershed of the Tatta and Amga Rivers (Central Yakutia), which he referred to the category of segregation ice. Later, the same ice forms encountered by P.A. Solov'ev were classified as buried icings (Shpolyanskaya & Streletskaya 2004).

Observation

A most complete and deep section including various forms of buried ice was observed in the borehole drilled in 2004, 82 km east of Yakutsk. The drilling was conducted, successively, by core barrels with reamer bits 147 mm, 127 mm, 108 mm, 89 mm, and 76 mm in diameter. Using air blowing, the core recovery from coring tubes was easy, and the preservation of thin cryostructures inside the core was good. The crushed ground portions up to 20 cm in thickness, caught during tripping process between well-preserved cores, were in a melted state and clearly differed from the rest of the core.

The studied section comprises three irregular intervals of ice and firn formations: upper (2.5–5.0 m from the ground surface), middle (12.0–17.0 m), and lower (33.6–39.0 m) divided by horizons of epigenetically frozen silts and sandy silts. The description of this section is given below. The second borehole drilled in 2005, 94 km east of Yakutsk, recovered buried firn and ice at a depth of 2.8–8.2 from the surface. By its stratigraphic position and cryolithological peculiarities, this horizon can be correlated to the interval 33.6–39.0 m of the 2004 borehole.

The upper ice horizon (2.5–5.0 m) is represented by ice wedge ice. The cored ice wedge had width of not less than 30 cm, and thickness of not less than 2.5 m. The wedge ice is semitransparent and yellowish. It exhibits a vertically layered structure with bands containing different amounts of mineral and organic matter and gas bubbles. The widths of the vertical bands are 1–2 cm.

The middle ice horizon (12.0–17.0 m) is represented by thin, horizontally layered, fine-crystalline and, rarer, coarse-crystalline ice (Fig. 2A). The formation of this type of ice is associated with recrystallization of snow.

The ice has a complex multi-ordered layering. It consists of several packs of layers including: 1_{M*}) packs of clean micro-layered firn, 3–5 cm in thickness, 2_M) packs of thin-layered mineralized firn, 1–2 cm in thickness, and 3_M) packs

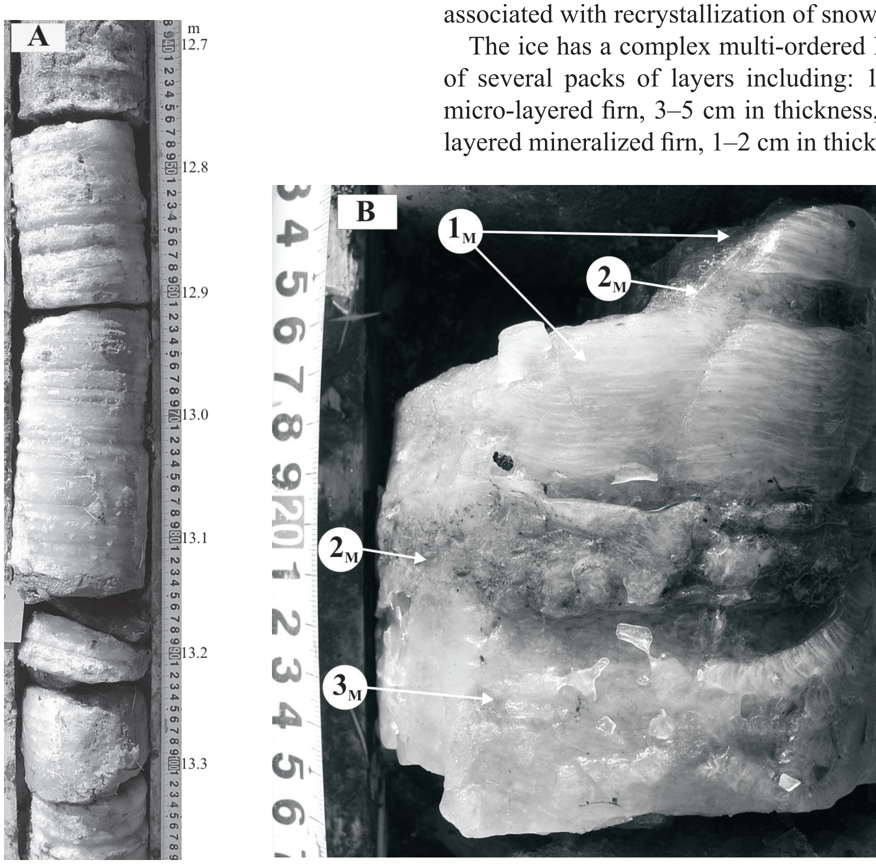

Figure 2. A – The ice core from the middle horizon represented by the horizontally-layered ice (firn) in the interval 12.7–13.4 m from the day surface. B – The multi-ordered layering of ice in the interval of 13.75–13.85 m from the day surface. Index explanation is given in the text.

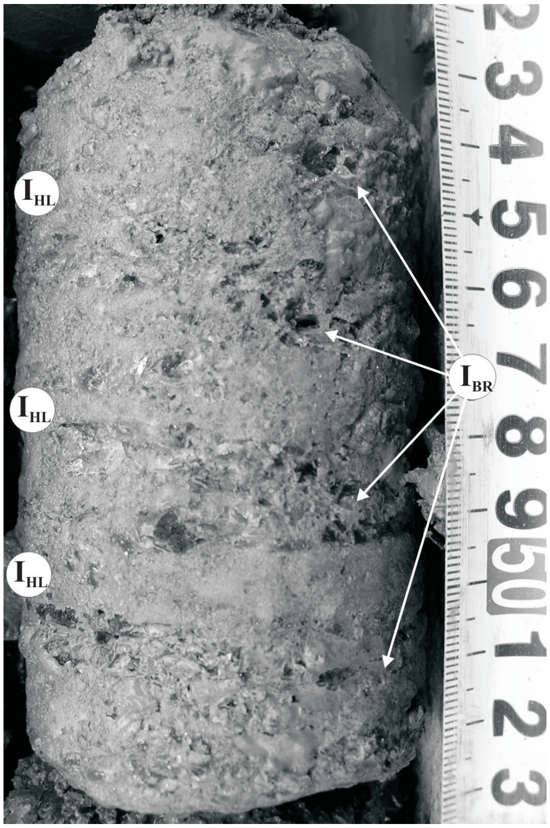

Figure 3. The alternation of ice breccia (I_{BR}) and horizontally-layered ice (I_{HL}) from the lower ice horizon in the interval of 34.02–34.13 m from the day surface.

of brecciated and coarse-crystalline firn, 1–4 cm in thickness ($*_M$ – index of layers, see Fig. 2B).

Separate interlayers of the brecciated and coarse-crystalline firn are 1–3 cm. They consist of partially-melted and rounded crystals of ice of round- or right-angled form up to 5 mm in diameter. Also, sectors with vertically orientated ice crystals, as well as hollows 1 cm in height and several cm in width are marked here.

The lower ice horizon(33.6–39.0 m) consists of big layers with different cryostructures. The upper part of the interval is divided into the layers of 1) horizontally-layered milky fine-crystalline ice (33.60–33.75 m), and 2) the alternation of ice breccia (Fig. 3, index I_{BR}) and horizontally-layered ice (33.75–34.50 m) (Fig. 3, index I_{HL}).

The ice breccia, mineralized in more or less extent, consists of pieces of fine-crystalline ice from the first to 15 mm in size. The pieces are acute-angled, rarer elongated and partly melted. The breccia cement represents milky, semitransparent, coarse-crystalline ice containing mineral particles. The cryostructure of the breccia interlayers is likely massive-agglomerate. The thickness of separate interlayers is 1–3 cm, up to 5 cm in the upper part.

The alteration of horizontally layered mineralized ice bodies and icy silts (ice-ground) is developed down the section (33.5–35.5 m). The layers are often lens-shaped, having first cm in thickness.

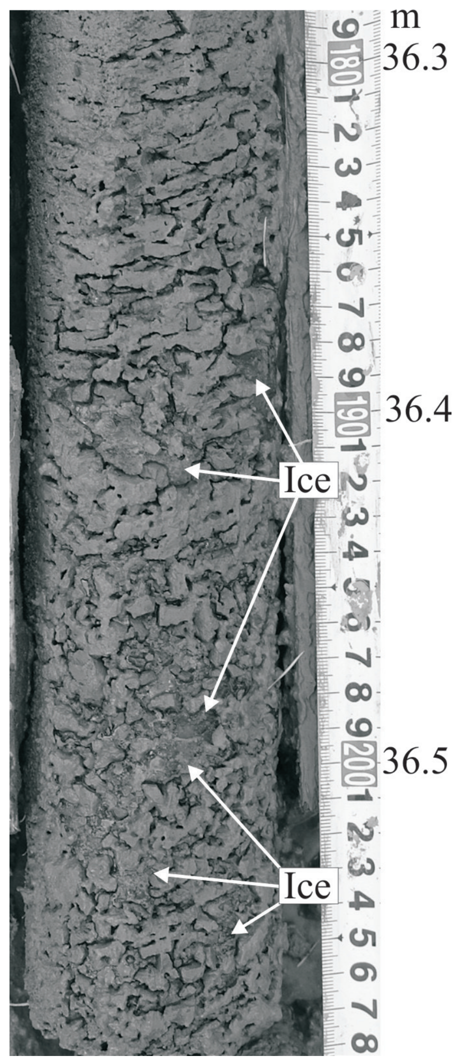

Figure 4. Ice-ground in the interval 36.30–36.58 m from the day surface. Ice, partially melted from the surface, forms the lens-braided structure in the enclosing bluish-grey silts.

Ice-ground with lens-braided cryostructure predominates in the lower part of the interval (35.5–39.0 m) (Fig. 4). This type of ice likely formed due to syncryogenic freezing of unconsolidated silty sediments from a downward direction (Fundamentals 1996).

The uppermost ice horizon is overlain by a stratum of homogeneous yellowish silts, which is developed under a thin soil cover to the depth of 2.5 m. The intervals of 5.0–12.0 m and 17.0–33.6 m are represented by strata of epigenetically frozen silts and sandy silts. A coarse, latticed cryostructure with a predominance of vertical lens ice is characteristic for them. Ice lenses are thicker (up to 3 cm), more frequent, and longer in the layers bedding directly above the ice horizons. The density and thickness of ice lenses decline upward along the section, which becomes almost iceless in the upper parts of these strata. A thin horizontal lens cryostructure appears at the upper contacts with the overlying ice horizons.

Conclusions

In our opinion, the horizontally layered ice strata of the middle and lower ice horizons had formed on the ground surface and present, probably, buried snow fields in contrast to "buried icings." This is supported by their high position on the Lena-Tatta Rivers watershed. The modern icings of the region are, as a rule, restricted to valley bottoms or watershed slopes foot. Besides, these formations are not remnants of modern perennial snowbanks because they are buried under thick (more than 10 m) ground strata. The overlying strata have spore and pollen complexes characteristic of the Late Pleistocene deposits of the region. The presence of various buried firn, ice, and ice-ground formations in the upper portion of the Lena-Amga Rivers plain loose cover points to a more complex, than it was supposed earlier, history of the cryolithozone evolution in the study area.

Acknowledgments

The investigation was made under the support of the Russian Fund of Fundamental Investigations, No. 06-05-65039-a; the Integration program SB RAS No. 71; and the Russian Science Support Foundation.

References

Fundamentals of Geocryology. 1996. E.D. Ershov (ed.), Vol. II. Lithogenous geocryology. Moscow State University. 399 pp. (in Russian).

Fundamentals of Geocryology. 1998. E.D. Ershov (ed.), Vol. III. Regional and historical geocryology of the world. Moscow State University. 575 pp. (in Russian).

Ivanov, M.S. 1984. *Cryogenic Structure of Quaternary Deposits of the Lena-Aldan Depression.* Novosibirsk: Nauka, 126 pp. (in Russian).

Katasonov, E.M. 1975. Frozen-ground and facial analysis of Pleistocene deposits and paleogeogrpaphy of Central Yakutia. In: *Paleogeography and Pleistocene Periglacial Phenomena.* Moscow: Nauka, 16-22 (in Russian).

Péwé, T.L. & Journaux, A. 1983. *Origin and Character of Loesslike Silt in Unglaciated South-Central Yakutia, Siberia, USSR.* Geological Survey Professional Paper 1262: 1-46.

Shpolyanskaya, N.A. & Streletskaya, I.D. 2004. Genetic types of massive ground ices and peculiarities of their distribution in Russian Subarctic. *Earth Cryosphere* 8(4): 56-71 (in Russian).

Solov'ev, P.A. 1959. *Permafrost zones of the northern part of the Lena-Amga Watershed.* Moscow, AN SSSR, 144 pp. (in Russian).

Spektor, V.B. & Spektor, V.V. 2002. On genesis of high Lena-Amga Rivers periglacial plain. *Earth Cryosphere* 6(4): 3-12 (in Russian).

Structure and Absolute Geochronology of the Alas Deposits of Central Yakutia. 1979. E.M. Katasonov (ed.) Novosibirsk: Nauka, 96 pp. (in Russian).

—*Plenary Paper*—

Recent Advances in Permafrost Geotechnics

S.M. Springman
Institute for Geotechnical Engineering, ETH Zurich, Switzerland

L.U. Arenson
BGC Engineering Inc., Vancouver, Canada

Abstract

Tribute is paid to progress in Permafrost Science and Engineering, from a geotechnical point of view, since the Millennium. Advances and concerns will be presented, embellished with thoughts about geotechnical aspects of the Ultimate and Serviceability Limit State requirements for cold regions infrastructure "Soil Structure Interaction," to be able to answer the challenges posed by climate change on a warming planet. Improvements and new developments have been described, briefly, for laboratory testing, physical and coupled numerical modeling. However, recent research progress in geotechnical aspects has not always permeated into practice, and a fundamental need remains to develop, calibrate and validate fully coupled thermo-hydro-mechanical models. This short review paper does not claim to cover all research and developments and will attempt to summarise topical findings in cold regions geotechnics.

Keywords: field Investigation; laboratory testing; modeling, permafrost engineering; review.

Introduction

This paper was commissioned to focus on geotechnical advances in Permafrost Science and Engineering, which can not be decoupled from the effects of global climate change. This has dominated recent work, as researchers seek ways of identifying the hazards to infrastructure in cold regions (ACIA 2005, IPCC 2007, U.S.A. RCPTF 2003), to establish distinct uncertainties through a risk based consideration of sensitivity and consequences and thereby mitigate the risk of permafrost degradation (e.g., Hayley & Horne 2006).

Reliable climate modeling on a regional scale for 30 to 100 years in the future is essential, as geotechnical engineering should also play an important role in integrated strategies. Designers of new infrastructure or rehabilitation measures wish to guarantee that both Ultimate (failure: ULS) and Serviceability (deformation: SLS) Limit States will be achieved throughout the life cycle of their project. Allowable deformations will be dependent upon the structure concerned. Allowable movements are more restrictive for a machinery hall than for a "flexible" pipeline that can sustain greater average and differential settlements.

Hayley & Horne (2006) condemn broad generalisations, which they comment are misleading. The same is true with geotechnical aspects. Each project must be treated on its own merits, to the level of detail required. Some progress has been made on long term solutions to practical issues relating to "Soil-Structure-Environment Interaction." This paper argues that significant fundamental work still remains to be done on geotechnical issues, and outlines contributions required over the next quadrennial. Examples are cited from mainly northern hemisphere polar and mountain permafrost: from America, Canada, Russia, China and Europe.

The authors recognise early literature on topics discussed herein, and have elected to concentrate on recent progress. References of earlier works are in the publications cited.

The Influence of Climate Modeling

When designing structures, engineers are challenged with forecasting future trends in soil properties over the entire expected lifetime. Since the deformation behaviour and strength of foundations in frozen soils depend on soil temperature (e.g., Arenson et al. 2007a), some predictions are required of combinations of permafrost temperatures, active layer thicknesses, freeze thaw cycles or frost penetration. Ultimately, all these parameters, of which further technical detail can be found elsewhere in this conference volume, depend on the climate and hence geotechnical engineers have to understand the strengths and limitations of climate models. Climate trends predicted by such models not only influence the design method, but also form the basis for site investigations and/or monitoring that has to be performed.

In addition to air temperatures, precipitation strongly influences the ground temperatures, and this has increased in toto over the past century, at a rate of about 1% per decade (ACIA 2005, Instanes 2006). Trends in precipitation are hard to assess because precise measurement is difficult in the cold arctic environment. Snow cover extent around the periphery of the Arctic also appears to have decreased.

The latest IPCC report (IPCC 2007) summarises past permafrost and snow conditions, with temperature increasing at the top of the permafrost layer in the Arctic by $\leq 3°C$ since the 1980s. The permafrost base has been thawing at a rate ranging up to 0.04 m/yr in Alaska since 1992 and 0.02 m/yr on the Tibetan Plateau since the 1960s. Permafrost degradation is also causing changes in land surface characteristics and drainage systems. Furthermore, snow cover has decreased in most regions, especially in spring and summer. Where snow cover or snowpack decreased, temperature often dominated; where snow increased, precipitation almost always dominated, reflecting the feedback between snow and temperature. Decline in snow cover area in the mountains of western North America and in the Swiss Alps has been greatest at lower elevations.

Even with physical evidence of ground property changes, predicting the future is challenging. Global climate models (GCMs) do not represent permafrost dynamics and potential critical feedbacks on climate. Nicolsky et al. (2007) and Alexeev et al. (2007) evaluate the land surface scheme Community Land Model (CLM3), against observations, and identify potential modifications to improve fidelity of permafrost and soil temperature simulations. Soil thickness should be > 30 m, to compute annual temperature dynamics cycle for cold permafrost. Decadal-to-century time scales require significantly deeper soil layers, e.g., > 100 m.

Vegetation changes and thermal disturbances in lowland permafrost environments due to forest fire activities, lead to increased active layer depth through reduction of the insulating quality of the surface and potentially greater likelihood of instabilities (Anisimov & Reneva 2006, Dyke 2004). This further complicates prediction of future ground temperature trends and hence the effect on frozen soil properties (Yoshikawa et al. 2003).

Site Investigation and Monitoring

The basis of any geotechnical input is an effective mixture of site investigation and monitoring of response to environmental conditions, especially of deformations in conjunction with thermal details. More progress has been made in the latter area than the former recently, although there remains significant potential for in situ tests in fine grained permafrost, in more advanced forms, or as combinations of pressuremeter, cone penetration (e.g., Buteau et al. 2005, with seismic measurement LeBlanc et al. 2004, 2006) or dilatometer testing in order to determine selected soil parameters such as shear strength, small and large strain stiffness for subsequent modeling. Obtaining basic classification data from disturbed samples, without mineralogical or strength testing, is currently the industry standard (e.g., Couture et al. 2000), with thermal properties estimated empirically from earlier consulting reports.

Sometimes, insitu permeability tests may be helpful if drainage conditions in degrading permafrost are relevant. Using probes to determine associated thermal properties is also advantageous (Overduin et al. 2006). However, thermal disturbances due to drilling, or through variations in thermal contact resistance between sensor and soil, make insitu determination of these properties challenging.

Samples must be extracted with minimal disturbance in terms of melting of the frozen phase and rearrangement of soil grains, and protected during transport for storage and subsequent testing in the laboratory for obtaining accurate soil parameters for constitutive modeling (e.g., Arenson & Springman 2005b). While this does not necessarily pose significant difficulties in polar permafrost, inevitably, this is further complicated by altitude and the blocky nature of the soils encountered when dealing with mountain permafrost. Despite additional expense during drilling, further studies are required on natural soil samples under permafrost conditions to investigate responses under selected stress-strain paths, suitable for a slowly warming environment from below to above zero °C (see laboratory testing).

Geophysical approaches are now common for spatial determination of frozen/unfrozen zones (Hauck et al. 2007, Kneisel & Kääb 2007, Maurer & Hauck 2007, Wu et al. 2005, Musil et al. 2002). Tomographic inversion techniques are adopted to reveal ground structure and for monitoring thaw in the seasonal active layer (Hauck et al. 2003, Ribolini & Fabre 2007). The challenge is to determine geotechnical parameters. This is possible through seismic approaches, although the small strain stiffness obtained can not represent stiffness over the entire strain range to failure and particularly less so in a creeping soil. Consequently, adopting geophysical approaches to determine a ground model and associated parameters is not the sole solution.

In parallel with site investigations, it is essential to plan monitoring experiments to deliver optimal data for design decisions, considering geotechnical aspects in conjunction with predictions of the conditions pertaining over the lifecycle. Monitoring should be used for design of a structure and as a part of ongoing observation that regulates future maintenace requirements. A conservative prognosis should be made of lifetime deformations, including surface deformation fields (e.g., Kääb et al. 2007, Kääb et al. 2005) as well as the deformation fields and structure (e.g., Arenson et al. 2003, Hausmann et al. 2007). GTN-P, CALM, PERMOS 2000-4 provide data of standard temperature measurements with depth, and will not be discussed here.

Inclinometers are effective only when they are able to move with the surrounding soil and when a measuring probe is able to pass through the deflecting tubing (Arenson et al. 2003). Shearing of the tube may occur eventually in slopes demonstrating considerable creep. Recent advances have been made by using TDR cables in a rock glacier to locate a concentrated creep zone, but the data are inconclusive, and the magnitude of strains can not be measured. Novel techniques for fibre optic strain measurements in boreholes, are becoming available and might be valuable in the future.

Laboratory Testing

Some recent papers report the mechanical properties of alpine permafrost both in a natural state (undisturbed) or reconstituted from soil particles extracted by “undisturbed” sampling in boreholes (Vonder Mühll et al. 2003, Arenson et al. 2004, Arenson & Springman 2005a). Issues remain about selecting an appropriate laboratory test to represent stress history and path, as well as to allow for sample heterogeneity and size effects. Interface tests have also been carried out on ice filled joints and between active layer and underlying permafrost (Günzel 2008, Rist 2007, Arnold et al. 2005). Additionally, thermal properties are required to be able to carry out integrated “thermo-hydraulic-mechanical” (THM) modeling, although their determination is well established and will not be discussed further in this paper.

Triaxial testing

Triaxial constant strain rate and constant stress tests have been performed on artificially frozen soil specimens as well as samples won from, for example, rock glaciers (Arenson et al. 2004, Arenson & Springman 2005a). Mainly two types of tests were carried out: constant strain rate (CSR) and constant stress, creep (CSC) tests, to study the effect of the volumetric ice-solid-air fractions, temperature, strain rate and also confining stress on the mobilised shear strength.

Peak shear strengths of artificial samples increased with lower volumetric ice content and faster strain rates. Loading conditions influenced modes of deformation and eventual mechanical failure. The existence of significant percentages of air within the frozen matrix changed mobilised stiffness, strength and volumetric response from ongoing dilatancy, interlocking particles, higher stiffness and strength, in conjunction with increasing volume and rubblisation (see Yasufuku et al. 2003, Da Re et al. 2003 for artificial samples with no air) to lower stiffnesses and strength, with ductile contraction (Arenson & Springman 2005a).

Hydrate bearing soils are important because they contain natural gas (energy resource), and function as a source or sink for atmospheric methane, which may influence global warming (Brouchkov & Fukuda 2002). They are suspected to be a potential factor in the initiation and propagation of submarine slope failures (Anuruddhika & Grozic 2007, Nixon & Grozic 2007). Determining geotechnical properties of such "gassy" deposits may prove to be much more important in future. Tomographic imaging techniques (e.g., Calmels & Allard 2004 determined gas content) offer potential for integration into geotechnical laboratory studies on frozen soils. Other recent advances focus on improved methods of examining cylindrical sample response through the entire stress strain range in triaxial compression, under confining pressures as great as 20 MPa, by including small strain measurement (Da Re et al. 2003) or with radial laser measurements (e.g., Messerklinger & Springman 2007).

Interface testing

Arnold et al. (2005) conducted direct shear tests on active layer material from a 38° rock glacier slope (Pontresina-Schafberg), in support of Rist (2007). Significant dilation under low normal stresses was obtained for elongated rough particles excavated within the active zone, mobilising maximum angles of friction > 60°, and confirming that the active layer was stable for insitu conditions. Replacing the bottom half of the shear box with smooth clean ice reduced the interface friction to just over 30°. It is unlikely that such a smooth surface will form during annual freezing and thawing processes at the base of the active layer. Reliable interface friction values will lie between these two limits.

Rist (2007) created an inclinable sled model filled with active layer material to slide on a permafrost surface to investigate the shear resistance and hence to determine an interface friction angle. Grain size and volumetric water content of an artificial active layer and the degree of ice saturation of the permafrost were varied, with the latter proving to be the most important influencing factor. Soil grains embedded in an ice matrix at the permafrost surface increased the mobilised friction angle by 8° compared to a dry permafrost block, without ice. This implies a probable long term decrease of the active layer slope stability in alpine permafrost terrain under warming conditions.

Günzel (2008) carried out direct shear tests on analogue models of ice filled rock joints to determine the temperature dependent strength. She confirmed earlier findings by Davies et al. (2003) that the strength is lowest for temperatures fractionally below 0°C.

Physical Modeling

Physical modeling offers good opportunities to expose mechanisms of deformation and failure in frozen soil and in interaction with structures. Harris et al. (2003) summarise scaled, centrifuge modeling experiments in fine sandy silt, designed to simulate multi cycle thaw-related gelifluction. They concluded, from considerations of scaling laws, that flow was elastoplastic in nature with a "flow" law based on the "Cam Clay" constitutive model for soils, in which frictional shear strength is dependent on effective stress. Response was not time dependent and viscosity controlled.

Stability of model ice filled jointed rocks has been studied in a geotechnical centrifuge by Davies et al. (2003). Warming rock joints through permafrost degradation can lead to increased instabilities and rock fall events in high mountain permafrost areas. This trend was also noted by Gruber et al. (2004) and Gruber & Haeberli, (2007), who studied Alpine rock walls, and Schwab et al. (2003) for rock avalanches in West Central British Columbia, Canada.

A further series of centrifuge tests (Günzel & Davies 2006) was performed with an ice filled joint within a model rock slope, reinforced by rock bolts, and allowed to thaw. The slope was instrumented with thermocouples, displacement transducers and load cells for observation of stress development and movement during the experiment.

The combination of centrifuge experiments and direct shear tests confirmed that warming of ice inside a joint critical to the stability of a slope could lead to slope failure, even if the slope had an initial safety margin of over 200%, when the joint was filled with "cold" ice or was dry. Reinforcing a slope with pre-stressed bolts should be effective, although the bolts would need to be tested regularly in practice in case of loss of tension during joint closure. The findings from these experiments may offer a valuable means of mitigating the consequences of slope failure in high mountain areas, if the thickness of permafrost ice inside a joint can be assessed and measurements of temperature, displacement, and bolt tension are carried out regularly. Validation of these results with instrumented field tests would be most valuable.

Coupled Modeling

Constitutive and numerical modeling

Existing geotechnical models have become increasingly complex as demands to represent specific aspects of soil response become essential when designing to ULS and SLS. Mohr Coulomb approaches based on one value of cohesion and angle of friction are too simplified to account for the effects of temperature, strain magnitude and rate, relative density and opposing effects of dilatancy and crushing.

Various forms of elastoplasticity offer a modeling basis for coupled thermo-hydro-mechanical (THM) response of soils and rocks. Significant improvements are due to long term investment from the unsaturated soil community (e.g., Sánchez et al. 2002, Khalili et al. 2000). Hydromechanical (HM) aspects are well reproduced by critical state concepts of plasticity. Models for surface cracking at low stresses have also been presented in the literature.

Thermal aspects have mainly been related to temperatures > 0°C, e.g., for radioactive waste disposal. Phase change around 0°C is not covered, although applications such as ground freezing offer interesting perspectives. The representation of thawing and freezing under variable groundwater flow regimes is well modelled (e.g., Pimentel et al. 2007). However links to volume change, ice lensing and the related mechanical behaviour are not yet established.

Recent creep modeling (e.g., Haeberli et al. 2006, Arenson & Springman 2005a) is able to represent time dependent deformations, however, imposing a valid failure criterion remains somewhat empirical. Since large strains have a significant influence on the mobilised strength of frozen geomaterials, establishing insitu strain states is necessary when analysing stability of frozen slopes.

While TH modeling has advanced from one up to three dimensions (Liu et al. 2006), more advanced approaches, (e.g., Zhang et al. 2007a, who couple water flow and heat transfer in soil with water phase change) may still only be available in 1D to date. This can be problematical when the prototype "structure" investigated is multidimensional.

Despite new findings from laboratory and field investigations, no novel constitutive relationships have been presented in recent years for frozen soils. Often only one or two dimensional solutions are adopted, when reality is three dimensional. It is no surprise then that limited progress has been made in developing new numerical models. To the authors' knowledge, none exist for practical engineers to couple thermo-hydro-mechanical processes fully. Mostly, only two elements are modelled and used as an input in the third. Future research efforts should therefore focus on such coupling. Realistic risk assessments in permafrost environments due to changing climatic conditions can benefit significantly from simulation of transient conditions under varying boundary conditions that continuously alter thermal, hydrological and mechanical soil properties. It is important to remember that a true risk analysis incorporates the variability in the predictions, which is extremely challenging for cold region climates.

Challenges for continuum analysis methods lie in the inability to model penetration installation effects or to deal with tension cracking and discontinuities. Future advances are expected in discrete element modeling, in conjunction with validation from physical modeling or field monitoring.

GIS-based modeling

GIS technologies are increasingly powerful and have recently been used for risk assessments or as visualisation tools (Giardino et al. 2004, Heggem et al. 2006, Kneisel et al. 2007, Romanovsky et al. 2006). However, they are only as powerful as the constitutive relationships and the risk determination behind the GIS model when they are used for more than visualisation or database purposes. Insufficient information on the complex interaction between the atmosphere and the ground currently limits the area of applications, which would be a helpful instrument for stakeholders and decision makers.

Phenomena

Frost heave

Frost heave presents severe challenges to owners of infrastructure threatened by temperature and groundwater dependent volume change. Segregation potential or the discrete ice lens theory are still used in practice to estimate frost heave. However, ongoing developments in the laboratory are generating opportunities to achieve greater certainty about soil parameters derived (e.g., Konrad 2005).

Côté & Konrad (2007) demonstrate the use of a heat balance model at the freezing front to compute the frost depth and the frost heave as a routine tool for moderately cold regions pavement designs based on the concept of segregation potential. Studies on the influence of fines on the frost susceptibility of base-course crushed aggregates showed that for a given kaolinite fraction, the segregation potential increases linearly with fines content, until the fines create a matrix in which the coarser particles are embedded (Konrad & Lemieux 2005). Uthus et al. (2006) present frost heave data showing sensitivity, with significantly different heave rates for almost equally graded materials. The occurrence of temperature induced vapour flow in a non-frost-susceptible granular material of pavement base layer was studied by Guthrie et al. (2006). Their laboratory tests demonstrated increased water contents, which may lead to frost heave and thaw weakening behaviour typical of that associated with water ingress through capillary action.

Based on freezing tests on small physical clay models tested under 1g as well as in a centrifuge, Han & Goodings (2006) confirm that low permeability clays experience closed freezing conditions that limit the frost heave.

Improvements in measuring techniques led to detailed observations of ice lens formation and driving mechanisms behind frost heave. Water migrated through the frozen fringe from the unfrozen soil towards the warmest ice lens, while colder ice lenses continued to grow without access to the unfrozen zone, because water was sucked from soil beds between ice lenses (Arenson et al. 2006, 2007b).

Application to road pavements has confirmed again from case histories that frost heave contributes to thermal cracking and unstable permafrost (Dunn & Gross 2006, Mills et al. 2006, Doré et al. 2006). The number of freeze thaw cycles combined with precipitation, particularly on low volume roads in seasonal frost areas, plays a role in the vulnerability of this type of lifeline (Kestler 2003).

Impurities within frozen soils may change thermo-mechanical behaviour completely. Hydrocarbons affect soil properties, such as the unfrozen water content (Siciliano et al. 2007), or the permeability of the permafrost and how contaminants spread (Fourie et al. 2007). They change not only contaminant transport but also the frost heave behaviour of a soil, because chemicals may alter the availability of unfrozen water to migrate towards the freezing front. Laboratory investigations and theoretical considerations have demonstrated the relevance of pore water chemistry on frost heave potential and ice formation (e.g., Beier et al. 2007, Vidstrand 2007, Arenson & Sego 2006b, Arenson et al. 2006, Torrance & Schellekens 2006).

Slope stability

Local physiographic landforms will experience different modes of failure in slopes, despite the same temperature change signatures. Thickening of the active layer and subsequent detachment failures, formation of taliks, debris flows, bi-modal flows, retrogressive slumps, deep seated rotational slides are some of the failure modes reported recently by authors in China, Canada and Russia (Chenji et al. 2006, Wei et al. 2006, Lyle et al. 2004, Dyke 2004, Mazhitova et al. 2004). The presence and exposure of massive ice that released moisture into the slope was found to be critical during permafrost degradation.

Wei et al. (2006) also investigated thaw induced gelifluction in cut slopes along the Qinghai Tibet railway. Thaw slump and retrogressive debris flows developed after only one year, causing unexpected damage to the lifelines. Local erosion due to floods, waves or sea ice (e.g., at lake margins or undercutting coastal tundra blocks; Forbes 2004) or the influence of clay and mineralogy should also be accounted for. Dyke (2004) discussed the loss of both thickness and cohesive strength in an ice bonded surface layer that cracked in tension, due to thaw settlement initiating bending in the ice slab.

Such events are episodic and of a spatially discontinuous nature. Future global climatic conditions will influence site-level slope stability and require transcendence of multiple levels of uncertainty and complexity (Huscroft et al. 2004).

As in any unfrozen geotechnical system, pore water is also the critical element in frozen soil mechanics. An understanding of the pore water pressure response in thawing permafrost is key to ensuring the slopes along linear structures such as roads, railways and pipelines, remain stable. Analysis of over 20 years of pore water pressure data from the Norman Wells pipeline suggests that the sites monitored encountered lower excess pore water pressures than expected and that many slopes experienced long-term drainage as the permafrost degraded (Oswell et al. 2007). Likewise, pore pressure changes induced by sea level rise in coastal regions will cause reduced effective stresses and hence lower stiffness and strength.

But also in other permafrost environments, large slope failures, mainly active layer detachments (e.g., Lewkowicz 2007), are observed that may jeopardise engineered structures. In addition, thermal regime changes can cause slope instability to develop so that mitigation measures must be implemented (e.g., Niu et al. 2005). Field studies on solifluction processes, currently ongoing in Svalbard, highlight the correlation between thaw consolidation, reduced effective stress and pore pressures in the active layer (Harris et al. 2007). These data confirm earlier field measurements by Kinnard & Lewkowicz (2005).

Simple decoupled analyses can be carried out using a combination of conduction and convective heat flow caused by water flow in the active layer. Limit equilibrium slope stability analyses can then be used to examine the effect of degrading permafrost and different water regimes on a traditional global factor of safety. However, neither these nor coupled finite element analyses can represent large strain problems close to the ULS and caution is required in the analysis of the results. Back analysis and verification with field mesurements are crucial in the interpretation of such numerical simulations.

Natural convection

Some progress has been made in numerical TH modeling of natural convection in granular soils in cold regions to demonstrate the cooling generated in embankments or heaps of coarse stones (e.g., Cheng et al. 2007, Lebeau & Konrad 2007, Sun et al. 2007, Arenson & Sego 2006). Ventilation properties (He et al. 2007), wind direction (Zhang et al. 2006, Pham et al. 2008) and embankment surface permeability, geometry of slopes, layers and revetments (Klassen et al. 2007, Sun et al. 2007, 2005, Lai et al. 2004) influence the convection potential, and conditions should be optimised to promote cell formation.

Winter convection effects benefit from embankment surface air permeability, and largely eliminate the 0°C horizon within the subsoil, even after a few summer seasons, apart from at the embankment toe. Davies et al. (2003) have already pointed out that temperatures even marginally below 0°C can still be critical. So, geotechnical implications are that stiffness and strength are raised through reduction of the underlying thaw bulb. Settlements and possibility of failure decrease and the embankment system will be more sustainable, with reduced maintenance costs over the lifetime of the structure. However, load transfer inside embankments brings greater loads onto the toes through arching (e.g., Ellis & Springman 2001), coinciding with zones marginally softened by partial thawing. This must be allowed for in predictions of relative settlement (SLS).

Sun et al. (2005) recognise that reality differs from numerical assumptions made, although many simulations are supported by laboratory and field investigations (e.g., Zhang et al. 2006, 2007a, b, Yu et al. 2006, Goering 2003). Indeed, there is some danger in performing numerical experiments without due consideration of geotechnical effects such as abrasion and long term, often cyclic, mechanical and clastic effects in dense, coarse grained fill (e.g., McDowell 2003). For example, compaction is essential during construction to densify the fill and minimise subsequent settlement. This will cause dilatancy on shearing as well as abrasion and crushing of the coarse stone layers and possible cyclic shakedown (settlements) in long term (Festag 2002). This will lead to fouling, whereby smaller particles will trickle down through the voids creating anisotropy, particularly in respect of water and air permeability in the fill, and will block development of the convection cells over the lifetime of the structure. In addition, layers of low air permeability that form during construction change the formation of convective cells, hence the cooling effect of the embankment/pile. Even though innovative solutions might be derived from numerical modeling with adjacent layers of coarse and fine grained material, the fundamental basics of soil mechanics must not be forgotten, such as maintaining filter relationships to prevent internal erosion.

Soil Structure Interaction – SLS & ULS

Soil Structure Interaction (SSI) represents the inter-dependent reaction between ground and structure, in which both ULS and SLS must be assured. Foundations for typical infrastructure, including linear structures such as pipelines, road pavements, railway beds, communication cables, electrical power lines, or more two dimensional loading problems typical in oil tanks, buildings, airports, embankments, dams, mines, encapsulated landfill sites, are all susceptible to thaw and creep settlement (SLS) and reduced bearing capacity (ULS), under warming planetary conditions, as well as mobility of groundwater (and any related soluble or immiscible contaminants) (e.g., Mills et al. 2006, Mazhitova et al. 2004, Hayley et al. 2004, Cole 2002, Couture et al. 2000). Furthermore, relative or interactive seasonal effects (such as thermal cracking and frost heave, Tighe et al. 2006, frost heave and upheaval of pipelines buried in cold regions, Kanie et al. 2006, Palmer & Williams 2003, or creep of pylons founded on creeping permafrost, Phillips et al. 2007) may threaten the integrity of structures and exacerbate damage.

Mazhitova et al. (2004) call for long term investments in adequate infrastructure in Russia, with consideration of lifetime effects, for oil and gas pipelines, given the potential for serious environmental disasters. Adaptability must also be well thought out, so that design can be enhanced for most vulnerable infrastructure, as geotechnical risk is minimised within an integrated risk approach that considers the entire lifecycle (e.g., Auld et al. 2006).

Solutions that promote improved SSI performance can be described as either active or passive by ensuring the ground remains frozen (e.g., assisted by thermosyphons or thermopiles) or by avoiding, changing or modifying the SSI conditions. Innovative thermosyphon technology that will be operational to 100 m depth, was investigated within a large scale field experiment by Noël & Hockley (2004) and offers tremendous opportunities for future active measures. Managing the effects of thaw in a controlled fashion, or by adding berms to prevent thaw softening developing under the toe of embankments by natural convective air flow are other examples. Numerical modeling confirmed that thermal insulation (e.g., using expanded polystyrene at different embedment depths combined with construction in the cold season, Wang & Dou 2007) can contribute to active measures, although the long term performance at SLS must be guaranteed as well.

Innovative long term solutions are required:

- to place constraints on perennially frozen ground by maintaining a frozen state (Bjella 2006), or
- for structural measures by developing devices to permit superstructures to be realigned on foundations to fulfill SLS requirements (Phillips et al. 2007), or by adopting stabilising measures such as rock bolts and anchors.

Conclusions

Contemporary advances in frozen soil mechanics and geotechnical engineering in cold regions have been described for application to natural permafrost and infrastructure built on or within permafrost. Recent work on field studies, laboratory investigations, physical modeling and coupled simulations are reviewed, in connection with warming planetary conditions, under which permafrost has been recognised as an indicator for climate change. Some phenomena related to frost heave during cyclic freezing and thawing, slope and active layer stability, and convection cooling in coarse granular fill, are discussed within this framework as well.

Urgent need has been identified for ongoing basic geo-technical research in permafrost engineering and science. Investment must be made in site investigations for high risk projects, supported by effective monitoring regimes and advanced laboratory testing to determine key parameters. Challenges were also pinpointed relating to understanding the thermo-hydro-mechanical behaviour of frozen soils and implementing new constitutive relationships into numerical models to represent this behaviour. Physical models, especially those exposed to the correct stresses and environmental conditions, were accepted as providing excellent opportunities for validating and calibrating such codes.

Acknowledgements

The authors thank the conference organisers for their invitation to publish this overview and the anonymous reviewer for his/her helpful comments.

References

ACIA 2005. *Arctic Climate Impact Assessment 2005.* Cambridge, U.K. and New York: Cambridge University Press.

Alexeev, V.A., Nicolsky, D.J., Romanovsky, V.E. & Lawrence, D.M. 2007. An evaluation of deep soil configurations in the CLM3 for improved representation of permafrost. *Geophysical Research Letters* 34: L09502.

Anisimov, O. & Reneva, S. 2006. Permafrost and changing climate: The Russian perspective. *Ambio.* Royal Swedish Academy of Sciences 35(4): 169-175.

Anuruddhika, G.J & Grozic, J.L.H. 2007. An experimental investigation of temperature induced dissociation of methane hydrate in porous soil media. *Proceedings, 60th Canadian Geotechnical Conference,* Ottawa, ON, Canada, October 21-24, 2007: 2062-2067.

Arenson, L., Hoelzle, M. & Springman, S.M. 2003. Borehole deformation measurements and internal structure of some rock glaciers in Switzerland. *Permafrost and Periglacial Processes* 13(2): 117-135.

Arenson, L., Johansen, M.M. & Springman, S.M. 2004. Effects of volumetric ice content and strain rate on shear strength under triaxial conditions for frozen soil samples. *Permafrost and Periglacial Processes* 15(3): 261-271.

Arenson, L.U. & Springman, S.M. 2005a. Triaxial constant stress and constant strain rate tests on ice-rich permafrost samples. *Canadian Geotechnical Journal* 42(2): 412-430.

Arenson, L.U. & Springman, S.M. 2005b. Mathematical description for the behaviour of ice-rich frozen soils at temperatures close to zero centigrade. *Canadian Geotechnical Journal* 42(2): 431-440.

Arenson, L.U. & Sego, D.C. 2006a. Considering convective air fluxes in the design of engineered structures in cold regions. *Proceedings, 59th Canadian Geotechnical Conference,* October 1-4 2006, Vancouver, BC, Canada: 1033-1040.

Arenson, L.U. & Sego, D.C. 2006b. The effect of salinity on the freezing of coarse grained sands. *Canadian Geotechnical Journal* 43(3): 325-337.

Arenson, L.U., Xia, D., Sego, D.C. & Biggar, K.W. 2006. Change in ice lens formation for saline and non-saline Devon silt as a function of temperature and pressure. *Proceedings, 13th International Conference on Cold Regions Engineering,* July 23-26, 2006, Orono, Maine, USA. CD-Rom.

Arenson, L.U., Springman, S.M. & Sego, D.C. 2007a. The Rheology of Frozen Soils. *Applied Rheology* 17(1): 12147-1 - 12147-14.

Arenson, L.U., Take, W.A. & Sego, D.C. 2007b. Measurement of ice lens growth and soil consolidation during frost penetration using particle image velocimetry (PIV). *Proceedings, 60th Canadian Geotechnical Conference,* October 21-24, 2007, Ottawa, ON, Canada. 2046-2053.

Arnold, A., Thielen, A. & Springman, S.M. 2005. On the stability of active layers in alpine permafrost. *Proceedings, 11th International Conference and Field Trip on Landslides* (ICFL), Trondheim, Norway, 1.-10.9.2005: 19-25, Taylor & Francis, Netherlands.

Auld, H., MacIver, D. & Klassen, J. 2006. Adaptation options for infrastructure under changing climate conditions. *Proceedings, Climate Change Technology Conference 2006,* Ottawa, ON, Canada, May 10-12, 2006: CD-Rom.

Beier N., Sego D., Donahue, R. & Biggar, K. 2007. Laboratory investigation on freeze separation of saline mine waste water. *Cold Regions Science and Technology* 48(3): 239-247.

Bjella, K. 2006. Engineering studies for degrading permafrost. *Proceedings, 13th International Conference on Cold Regions Engineering,* July 23-26, 2006, Orono, Maine, USA. CD-Rom.

Brouchkov, A. & Fukuda, M. 2002. Preliminary measurements on methane content in permafrost, central Yakutia, and some experimental data. *Permafrost and Periglacial Processes* 13: 187-197.

Buteau, S, Fortier, R. & Allard, M. 2005. Rate-controlled cone penetration tests in permafrost. *Canadian Geotechnical Journal* 42(1): 184-197(14).

Calmels, F. & Allard, M. 2004. Ice segregation and gas distribution in permafrost using tomodensitometric analysis. *Permafrost and Periglacial Processes* 15: 367–378.

Cheng, G.D., Lai, Y.M., San, Z.Z. & Jiang, F. 2007. The 'thermal semi-conductor' effect of crushed rocks. *Permafrost and Periglacial Processes* 18(2): 151-160.

Chenji, Huzeyong, Doushun & Qianzeyu. 2006. Yin-Yang Slope problem along Qinghai-Tibetan Lines and its radiation mechanism. *Cold Regions Science and Technology* 44(3): 217-224.

Cole, D.M. 2002. Permafrost degradation: problem statement, knowledge gaps and related research activities. Hanover, NH: Cold Regions Research and Engineering Laboratory. ERDC/CRREL LR-02-71.

Côté, J. & Konrad, J.M. 2007. Practical pavement frost heave assessment considering regional specific ground heat flux. *Proceedings, 60th Canadian Geotechnical Conference,* Ottawa, ON, Canada, October 21-24, 2007: 2092-2098.

Couture, R., Robinson, S.D. & Burgess, M.M. 2000. Climate change, permafrost degradation, and infrastructure adaptation: preliminary results from a pilot community case study in the Mackenzie valley. Geol. Survey of Canada. Current research 2000-B2.

Da Re, G., Germaine, J.T. & Ladd, C.C. 2003. Triaxial testing of frozen sand: equipment and example results. *Journal of Cold Regions Engineering* 17(3): 90-118.

Davies, M.C.R., Hamza, O. & Harris, C. 2003. Physical modelling of permafrost warming in rock slopes. *Proceedings, 8th International Conference on Permafrost,* Zurich, Switzerland: 169-174.

Doré, G., Beaulac, I. & Van Gassen, W. 2006 Performance of the Beaver Creek section of the Alaska Highway. *Proceedings, 13th International Conference on Cold Regions Engineering,* July 23-26, 2006, Orono, Maine, USA. CD-Rom.

Dunn, P. & Gross, K. 2006. Standard methods used to mitigate seasonal frost in highway projects. *Proceedings, 13th International Conference on Cold Regions Engineering,* July 23-26, 2006, Orono, Maine: CD-Rom.

Dyke, L. 2004. Stability of frozen and thawing slopes in the MacKenzie valley, NW Territories. Géo-Québec, 57th Canadian Geotechnical Conference, 1G: 31-38.

Ellis, E.A. & Springman, S.M. 2001. Modelling of soil-structure interaction for a piled bridge abutment in plane strain FEM analyses. *Computers and Geotechnics* 28(2): 79-98.

Festag, G. 2002. Experimental investigations on sand under cyclic loading. Constitutive and Centrifuge Modelling: two extremes, Monté Verità. Ed. S.M. Springman. Balkema, Lisse, 269-275.

Forbes, D.L. 2004. Climate-change impacts in the coastal zone: implications for engineering practice. Géo-Québec, 57th Canadian Geotech. Conf., 7A: 10-17.

Fourie, W., Barnes, D.L. & Adhikari, H. 2007. Influence of pore ice on the movement of petroleum and contaminated water through coarse media. *Proceedings, Conference on Assessment and Remediation of Contaminated Sites in Arctic and Cold Climates.* Edmonton AB, Canada, May 6-8, 2007: 99-103.

Giardino, M., Giordan, D. & Ambrogio, S. 2004. GIS technologies for data collection, management and visualization of large slope instabilities: two applications in the Western Italian Alps. *Natural Hazards and Earth System Sciences* 4(2): 197-211.

Goering, D.J. 2003. Passively cooled railway embankments for use in permafrost areas. *Journal of Cold Regions Engineering* 17(3): 119-133.

Gruber, S., Hoelzle, M. & Haeberli, W. 2004. Permafrost thaw and destabilization of Alpine rockwalls in the hot summer of 2003. *Geophysical Research Letters* 31: L13504.

Gruber, S. & Haeberli, W. 2007. Permafrost in steep bedrock slopes and its temperature-related destabilization following climate change. *Journal of Geophysical Research-Earth Surface* 112(F2).

Günzel, F.K. & Davies, M.C.R. 2006. Influence of warming permafrost on the stability of ice filled rock joints. *Proceedings, 6th International Conference on Physical Modelling in Geotechnics,* 343-348.

Günzel, F.K. 2008. Shear Strength of Ice Filled Joints. *Proceedings, Ninth International Conference on Permafrost,* June 29-July 3, 2008, Fairbanks, Alaska, USA (this proceedings).

Guthrie, W.S., Hermansson, Å. & Woffinden, K.H. 2006. Saturation of granular base material due to water vapor flow during freezing: Laboratory experimentation and numerical modeling. *Proceedings, 13th International Conference on Cold Regions Engineering.* July 23-26, 2006, Orono, Maine: CD-Rom.

Haeberli, W., Hallet, B., Arenson, L., Elconin, R.O., Humlum, O., Kääb, A., Kaufmann, V., Ladanyi, B., Matsuoka, N., Springman, S.M. & Vonder Mühll, D. 2006. Permafrost Creep and Rock Glacier Dynamics. Final Report of the IPA/ICSI Task Force. *Permafrost and Periglacial Processes* 17(3): 189-214.

Han, S.J. & Goodings, D.J. 2006. Practical model of frost heave in clay. *Journal of Geotechnical and Geoenvironmental Engineering* 132(1): 92-101.

Harris, C., Luetschg, M., Davies, M.C.R., Smith, F., Christiansen, H.H. & Isaksen, K. 2007. Field instrumentation for real-time monitoring of periglacial solifluction. *Permafrost and Periglacial Processes* 18(1): 105-114.

Harris, C., Davies, M.C.R. & Rea, B.R. 2003. Gelifluction: viscous flow or plastic creep? *Earth Surface Processes and Landforms* 28(12): 1289-1301.

Hauck, C., Vieira, G., Gruber, S., Blanco, J. & Ramos, M. 2007. Geophysical identification of permafrost in Livingston Island, maritime Antarctica. *Journal of Geophysical Research-Earth Surface* 112(F2).

Hauck, C., Vonder Mühll, D. & Maurer, H. 2003. Using DC resistivity tomography to detect and characterize mountain permafrost. *Geophysical Prospecting* 51(4): 273-284.

Hausmann, H., Krainer, K., Bruckl, E. & Mostler, W. 2007. Internal structure and ice content of reichenkar rock glacier (Stubai Alps, Austria) assessed by geophysical investigations. *Permafrost and Periglacial Processes* 18(4): 351-367.

Hayley, D. & Horne, B. 2006. Rationalizing climate change for design of new structures on permafrost. *Proceedings, Climate Change Technology Conference 2006*, Ottawa, ON, Canada, May 10-12, 2006: CD-Rom.

Hayley, D.W., Seto J.T.C., Gräpel, C.K., Cathro, D.C. & Valeriote, M.A. 2004. Performance of two rockfill dams with thermosyphons on permafrost foundations, Ekati Diamond Mine, NT. *Proceedings, 57th Canadian Geotechnical Conference,* Quebec, QC: 5F 32-39.

He, P., Zhang, Z., Cheng, G.D. & Bing, H. 2007. Ventilation properties of blocky stones embankments. *Cold Regions Science and Technology* 47(3): 271-275.

Heggem, E.S.E., Etzelmüller, B., Anarmaa, S. Sharkhuu, N., Goulden, C.E. & Nandinsetseg, B. 2006. Spatial distribution of ground surface temperatures and active layer depths in the Hovsgol area, northern Mongolia. *Permafrost and Periglacial Processes* 17(4): 357-369.

Huscroft, C.A., Lipovsky, P. & Bond, J.D. 2004. Permafrost and landslide activity: Case studies from southwestern Yukon Territory. In: *Yukon Exploration and Geology 2003.* Yukon Geological Survey, 107-119.

Instanes, A. 2006. Impacts of a changing climate on Infrastructure: Buildings, Support Systems, and Industrial Facilities. *Proceedings of the Climate Change Technology Conference 2006,* Ottawa, ON, Canada, May 10-12, 2006: CD-Rom.

IPCC 2007. *Climate Change 2007: The Physical Science Basis Contribution of Working Group I to the Fourth Assessment Report of the IPCC.* Cambridge, U.K. and New York: Cambridge University Press.

Kanie, S., Akagawa, S., Kim, K. & Mikami, T. 2006. Estimation method of frost heaving for chilled gas pipeline buried in frost susceptible soil. *Proceedings, 13th International Conference on Cold Regions Engineering.* July 23-26, 2006, Orono, Maine: CD-Rom.

Kääb, A., Frauenfelder, R. & Roer, I. 2007. On the response of rockglacier creep to surface temperature increase. *Global and Planetary Change* 56(1-2): 172-187.

Kääb, A., Lefauconnier, B. & Melvold, K. 2005. Flow field of Kronebreen, Svalbard, using repeated Landsat 7 and ASTER data. *Annals of Glaciology* 42: 7-13.

Kestler, M.A. 2003. Techniques for extending the life of low volume roads in seasonal frost areas, Transportation Research Board, Washington, D.C.

Khalili, N., Valliappan, S. & Geiser, F. 2000. A fully coupled thermo-hydro-mechanical model for double porous media. European Congress on Computational Methods in App. Sciences Engineering. ECCOMAS.

Kinnard, C. & Lewkowicz, A.G. 2005. Movement, moisture and thermal conditions at a turf-banked solifluction lobe, Kluane Range, Yukon territory, Canada. *Permafrost and Periglacial Processes* 16(3): 261-275.

Klassen, R., Arenson, L.U., Sego, D.C. & Biggar, K.W. 2007. Heat convection modeling in waste rock piles. *Proceedings, 5th Biennial Workshop on Assessment and Remediation of Contaminated Sites in Arctic and Cold Climates* (ARCSACC), May 6-8, 2007, Edmonton, AB, Canada.

Kneisel, C. & Kääb, A. 2007. Mountain permafrost dynamics within a recently exposed glacier forefield inferred by a combined geomorphological, geophysical and photogrammetrical approach. *Earth Surface Processes and Landforms* 32: 1797-1810.

Kneisel, C., Rothenbuhler, C., Keller, F. & Haeberli, W. 2007. Hazard assessment of potential periglacial debris flows based on GIS-based spatial modelling and geophysical field surveys: A case study in the Swiss Alps. *Permafrost and Periglacial Processes* 18: 259-268.

Konrad, J.M. 2005. Estimation of the segregation potential of fine-grained soils using the frost heave response of two reference soils. *Canadian Geotechnical Journal* 42(1): 38-50.

Konrad, J.M. & Lemieux, N. 2005. Influence of fines on frost heave characteristics of a well-graded base-course material. *Canadian Geotechnical Journal* 42(2): 515-527.

Lebeau, M. & Konrad, J.M. 2007. The effects and significance of natural convection in rockfill dams under cold climate conditions. *Proceedings, 60th Canadian Geotechnical Conference,* Ottawa, ON, Canada, October 21-24, 2007: 2084-2091.

LeBlanc, A.M., Fortier, R., Allard M., Cosma, C. & Buteau, S. 2004. Seismic cone penetration test and seismic tomography in permafrost. *Canadian Geotechnical Journal* 41(5): 796-813.

LeBlanc, A.M., Fortier, R., Cosma, C. & Allard, M. 2006. Tomographic imaging of permafrost using three-component seismic cone-penetration test. *Geophysics* 71(5): H55-H65.

Lewkowicz, A.G. 2007. Dynamics of active-layer detachment failures, Fosheim Peninsula, Ellesmere Island, Nunavut, Canada. *Permafrost and Periglacial Processes* 18(1): 89-103.

Lai, Y.M., Zhang, S.J., Zhang, L.X. & Xiao, J.Z. 2004. Adjusting temperature distribution under the south and north slopes of embankment in permafrost regions by the ripped-rock revetment. *Cold Regions Science and Technology* 39(1): 67-79.

Liu Z.Q., Lai, Y.M. & Yu, W.B. 2006. Three-dimensional numerical analysis for temperature characteristic of ventilated embankment with insulated door. *Proceedings, 13th International Conference on Cold Regions Engineering,* July 23-26, 2006, Orono, Maine: CD-Rom.

Lyle, R.R., Hutchinson, D.J. & Preston, Y. 2004. Landslide processes in discontinuous permafrost, Little Salmon Lake (NTS 105L/1 and 2), south-central Yukon. In: *Yukon Exploration and Geology.* Yukon Geological Survey: 193-204.

Maurer, H. & Hauck, C. 2007. Instruments and methods: Geophysical imaging of alpine rock glaciers. *Journal of Glaciology* 53(180): 110-120.

Mazhitova, G., Karstkarel, N., Oberman, N., Romanovsky, V. & Kuhry, P. 2004. Ambio 33(6), Royal Swedish Academy of Sciences: 289-294.

McDowell, G. R. 2003. Micromechanics of creep of granular materials. *Géotechnique* 53(10): 915-916.

Messerklinger, S. & Springman, S.M. 2007. Local radial displacement measurements of soil specimens in a triaxial test apparatus using laser transducers. *Geotechnical Testing Journal* 30(6): GTJ100735.

Mills, B., Tighe, S., Andrey, S., Huen, K. & Parm, S. 2006. Climate change and the performance of pavement infrastructure in southern Canada: Context and case study. *Proceedings, Climate Change Technology Conference 2006,* Ottawa, ON, Canada, May 10-12, 2006: CD-Rom.

Musil, M., Maurer, H., Green, A., Horstmeyer, H., Nitsche, F.O., Vonder Mühll, D. & Springman, S.M. 2002. Case history: Shallow seismic surveying of an Alpine rock glacier. *Geophysics* 67(6): 1701-1710.

Nicolsky, D.J., Romanovsky, V.E., Alexeev, V.A. & Lawrence, D.M. 2007. Improved modeling of permafrost dynamics in a GCM land-surface scheme. *Geophysical Research Letters* 34: L08501.

Niu, F.J., Cheng, G.D., Ni, W.K. & Jin, D.W. 2005. Engineering-related slope failure in permafrost regions of the Qinghai-Tibet Plateau. *Cold Regions Science and Technology* 42(3): 215-225.

Nixon, M.F. & Grozic, J.L.H. 2007. Submarine slope failure due to gas hydrate dissociation: a preliminary quantification. *Canadian Geotechnical Journal* 44(3): 314-325.

Oswell, J., Skibinsky, D. & Radmard, S. 2007. Pore water pressure response to thawing permafrost. *Proceedings, 60th Canadian Geotechnical Conference,* Ottawa, ON, Canada, October 21-24, 2007: 2068-2075.

Overduin, P.P., Kane, D.L. & VanLoon, W.K.P. 2006. Measuring thermal conductivity in freezing and thawing soil using the soil temperature response to heating. *Cold Regions Science and Technology* 45(1): 8-22.

Palmer, A.C. & Williams, P.J. 2003. Frost heave and pipeline upheaval buckling. *Canadian Geotechnical Journal* 40(5): 1033-1038.

Pham, H.N., Arenson, L.U. & Sego, D.C. 2008. Numerical analysis of forced and natural convection in waste-rock piles in permafrost environments. Proceedings, Ninth International Conference on Permafrost, June 29-July 3, 2008, Fairbanks, Alaska, USA (this proceedings).

Phillips, M., Ladner, F., Müller, M., Sambeth, U., Sorg, J. & Teysseire, P. 2007. Monitoring and reconstruction of a chairlift midway station in creeping permafrost terrain, Grächen, Swiss Alps. *Cold Regions Science and Technology* 47(1-2): 32-42.

Pimentel, E., Sres, A. & Anagnostou, G. 2007. Modelling of ground freezing in tunnelling. ITA-AITES World Tunnel Congress "Underground Space: the 4th Dimension of Metropolises," Prague.

Ribolini, A. & Fabre, D. 2007. Shallow active layer temperature and DC resistivity of a rock glacier in the Argentera Massif, Maritime Alps, Italy. *Zeitschrift für Geomorphologie* 51: 55-77.

Romanovsky, V., Marchenko, S., Duguay, C., Zheleznyak, M. & Sergeev, D. 2006. Monitoring and modeling of the Northern Eurasia permafrost dynamics. *Arctic Science Conference Abstracts* 58.

Rist, A. 2007. Hydrothermal processes within the active layer above alpine permafrost in steep scree slopes and their influence on slope stability. Ph.D. thesis. Swiss Federal Institute for Snow and Avalanche Research and University of Zurich, 168 pp.

Sánchez, M., Gens, A. & Olivella, S. 2002. A coupled double structure formulation for THM analysis. Environmental Geomechanics. Monté Verità, eds Vulliet, Laloui, Schrefler, EPFL Press 315-320.

Schwab, J.W., Geertsema, M. & Evans, S.G. 2003. Catastrophic rock avalanches, West-Central British Columbia. *Proceedings, 3rd Canadian Conference on Géotechnique and Natural Hazards,* Edmonton, AB, Canada: 252-259.

Siciliano, S., Schafer, A. & Snape, I. 2007. Liquid water content increases in frozen Antarctic soils that are contaminated with hydrocarbons. *Proceedings, Conference on Assessment and Remediation of Contaminated Sites in Arctic and Cold Climates.* Edmonton AB, Canada, May 6-8, 2007: 92-98.

Sun, B.X., Yang, L.J. & Xu, X.Z. 2007. Onset and evaluation on winter-time natural convection cooling effectiveness of crushed-rock highway embankment. *Cold Regions Science and Technology* 48(3): 218-231.

Sun, B.X., Xu, X.Z. Lai, Y.M. & Fang, M.X. 2005. Evaluation of fractured rock layer heights in ballast railway embankment based on cooling effect of natural convection in cold regions. *Cold Regions Science and Technology* 42: 120-144.

Tighe, S.L., Cowe Falls, L., Haas, R. & MacLeod, D. 2006. Climate impacts and adaptations on roads in Northern Canada. TRB 85th Annual Meeting: CD-Rom.

Torrance, J.K. & Schellekens, F.J. 2006. Chemical factors in soil freezing and frost heave. *Polar Record* 42(220): 33-42.

U.S. Arctic Research Commission Permafrost Task Force. 2003. Climate Change, Permafrost, and Impacts on Civil Infrastructure. Special Report 01-03, U.S. Arctic Research Commission, Arlington VA, USA.

Uthus, L., Hermansson, Å., Horvli, I. & Hoff, I. 2006. A study on the influence of water and fines on the deformation properties and frost heave of unbound aggregates. *Proceedings, 13th International Conference on Cold Regions Engineering,* July 23-26, 2006, Orono, Maine: CD-Rom.

Vidstrand, P. 2007. Density-driven flow beneath a continuous permafrost layer: generic simulations of hydrodynamic effects due to salt rejection. *Proceedings 60th Canadian Geotechnical Conference,* Ottawa, ON, Canada, October 21-24, 2007: 341-346.

Vonder Mühll, D.S., Arenson, L.U. & Springman, S.M. 2003. Temperature conditions in two Alpine rock glaciers. *Proceedings, 8th International Conference on Permafrost,* Zurich, 21-25.7.2003, (2): 1195-1200, Rotterdam: Balkema.

Wei, M., Fujun, N., Satoshi, A. & Dewu, J. 2006. Slope instability phenomena in permafrost regions of Qinghai-Tibet Plateau, China. *Landslides* 3: 260-264.

Wu, T.H., Li, S.X., Cheng, G.D. & Nan, Z.T. 2005. Using ground-penetrating radar to detect permafrost degradation in the northern limit of permafrost on the Tibetan Plateau. *Cold Regions Science and Technology* 41(3): 211-219.

Yasufuku, N., Springman, S.M., Arenson, L.U. & Ramholt, T. 2003. Stress-dilatancy behaviour of frozen sand in direct shear. *Proceedings, 8th International Conference on Permafrost*, Zurich, 21.-25.7.2003, (2): 1253-1258, Rotterdam: Balkema.

Yoshikawa, K., Bolton, W.R., Romanovsky, V.E., Fukuda M. & Hinzman, L.D. 2003. Impacts of wildfire on the permafrost in the boreal forests of interior Alaska. *Journal Geophysical Research* 108 (D1): 8148.

Yu, W.B., Lai, Y.M., Sun, Z.Z., Jin, H.J. & Zhang, X.F. 2006. Experimental studies on the ripped-rock revetment embankment in permafrost regions of the Qinghai-Tibet railroad. *Cold Regions Science and Technology* 45(1): 1-7.

Zhang, X., Sun, S.F. & Xue, Y.K. 2007a. Development and testing of a frozen soil parameterization for cold region studies. *Journal of Hydrometeorology* 8(4): 690-701.

Zhang, M.Y., Lai, Y.M., Yu, W.B. & Huang, Z. 2007b. Experimental study on influence of particle size on cooling effect of crushed-rock layer under closed and open tops. *Cold Regions Science and Technology* 48(3): 232-238.

Zhang, M.Y., Lai, Y.M., Li, S.Y. & Zhang, S.J. 2006. Laboratory investigation on cooling effect of sloped crushed-rock revetment in permafrost regions. *Cold Regions Science and Technology* 46(1): 27-35.

Thermal State of Permafrost in Northern Transbaykalia, Eastern Siberia

Julia Stanilovskaya
Institute of Environmental Geoscience, Russian Academy of Sciences, Moscow, Russia
Julia Ukhova
Institute of Environmental Geoscience, Russian Academy of Sciences, Moscow, Russia
Dmitry Sergeev
Institute of Environmental Geoscience, Russian Academy of Sciences, Moscow, Russia
Irina Utkina
Environmental Analytical Center, "Gazprom" company, Moscow, Russia

Abstract

Temperature monitoring is important for studying the modern permafrost dynamics in mountains of Northern Transbaykalia. The authors combined the permafrost observation with the microclimatic study. The criteria were proposed to estimate the representativeness of each observing site. Middle-scale hypsometric and vegetation maps with other kinds of descriptive information were used. In choosing each monitoring site, it is necessary to take into account the site accessibility, the state of the borehole, and the extent of characterized landscape (limits of homogenous conditions of relief, vegetation, and permafrost). The measurements have shown a 0.5ºC final increase in permafrost temperatures at the 20 m depth from 1987 to 2007.

Keywords: site selection; temperature measurement; temperature observation sites; TSP program.

Introduction

In view of the International Polar Year, the Permafrost Laboratory of the Institute of Environmental Geoscience RAS was involved in the Thermal State of Permafrost (TSP) program with regard to permafrost temperature observations. The permafrost of Northern Transbaykalia is well studied; consequently there was an interest in repeating the measurement characteristics of permafrost. Notice was taken of the boreholes 20 m deep that are located in undisturbed conditions. More than 200 of such boreholes were constructed especially for temperature observations in 1970–80.

The work on logger installation in Northern Transbaykalia started in 2005. While working on logger installation, the question arose, "What principle should we use to choose boreholes and to place loggers in them?" For the rationalized work, it is necessary to zone territory and to allocate sites that are better than the others reflected by geographical conditions. For this purpose, a multifaceted approach has been chosen. Our observation points are considered to be the representative sites.

Basic Assumptions and Research Objective

The aim of the research is substantiation of representative temperature observations under the TSP program. Our purpose is the following:

1. To collect 200 boreholes from different sources constructed especially for temperature observations for 1970–80.
2. To chart the vegetation and hypsometric maps.
3. To give consideration of the borehole construction conditions and the site accessibility.

Research Area

The region of research is located south of the Siberian platform and includes the Kodar Ridge, the Udokan Ridge, and the intermountain of the Chara Depression (Fig. 1).

The coordinates of the Chara settlement are 56.9ºN and 118.4ºW. The Chara Depression extends 120 km southwest to northeast, and its width is 30–35 km. The northwest side of the Chara Depression is formed by the abrupt, almost rectilinear slopes of the Kodar Ridge; the southeast border is formed by foothills slopes of the Udokan Ridge that are smoothly de-

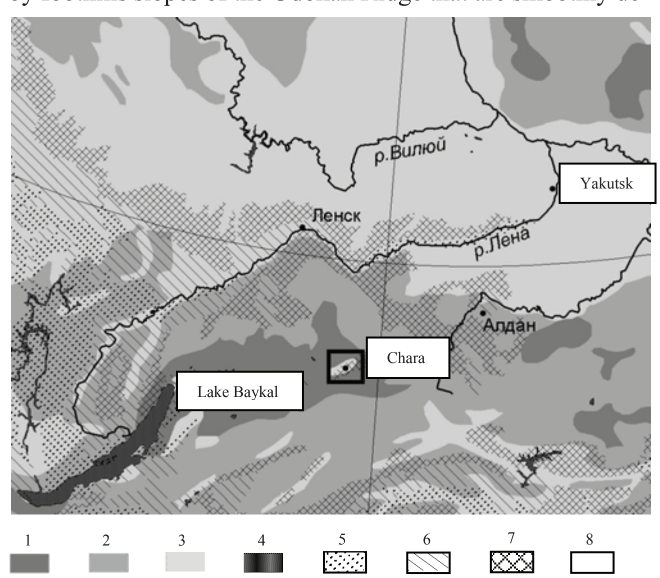

Figure 1. The location of investigation area (shown as a square). 1–3 – Relief types (1, high mountains with glaciers; 2, middle mountains; 3, plaines), 4 – Lakes; 5–8 – Permafrost extent (5, isolated patches; 6, sporadic; 7, discontinuous; 8, continuous). A circumpolar permafrost map was used (Brown et al. 2003).

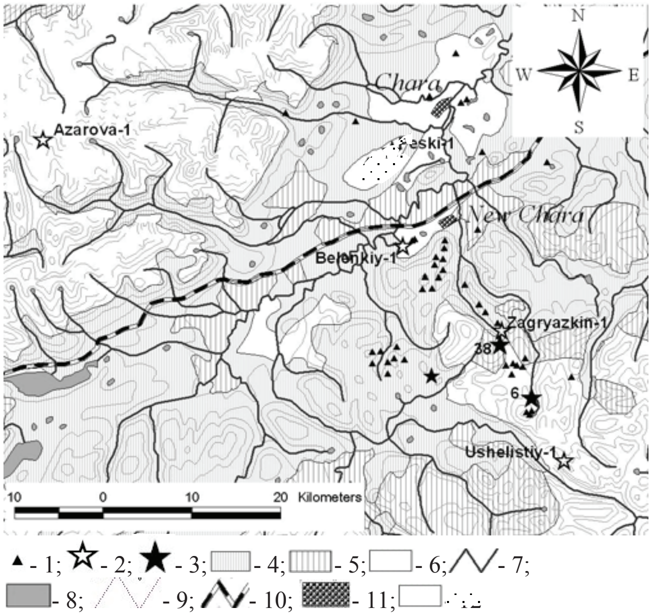

Figure 2. Scheme of investigation region with the location of the original and selected boreholes
1 – original boreholes and wells clusters; 2 – soil temperature observation sites; 3 – actual temperature boreholes. Vegetation: 4 – larch forest; 5 – open woodland; 6 – no forest vegetation (alpine tundra or bogs); 7 – rivers; 8 – lakes; 9 – relief isolines; 10 – railroads; 11 – town; 12 – the Chara Sandy Desert.

scending towards the bottom of the Chara Depression. There are 3 macro levels on investigated territory: the Kodar Ridge with alpine relief and with absolute heights of 3073 a.s.l. (the Peak of the BAM), the Udokan Ridge with golets (smooth mountains) and absolute heights up to 2515 a.s.l. and the Chara Depression with average heights of 600–800 a.s.l. The climate of the territory in question is characterized by extreme continentality with air temperature inversion. The monthly average air temperature in January is -23.9ºC, and in July is +12.5ºC. Average annual precipitation is 700 mm.

Method

The authors used six criteria choosing representative sites: distribution of available boreholes, relief, vegetation, permafrost, state of borehole, and site accessibility.

1. *The distribution of available boreholes*. The mountain permafrost is the science-intensive and engineering-important object of investigation. The intensive permafrost survey was conducted in the Northern Transbaykalia region by the Permafrost Institute in 1960s and by the Chitageologia, the ZabTISIZ, the Chita Institute of Natural Resources and the Moscow State University in the 1970s (Chastkevich 1966, Klimovsky 1966, Nekrasov & Chastkevich 1966, Leibman 1979, Romanovskii et al. 1989, Shesterniov & Yadrishensky 1990).

Regular observations were interrupted in the middle of the 1990s. Figure 2 presents the map showing the location of the original 200 boreholes with the 7 boreholes and monitoring sites selected.

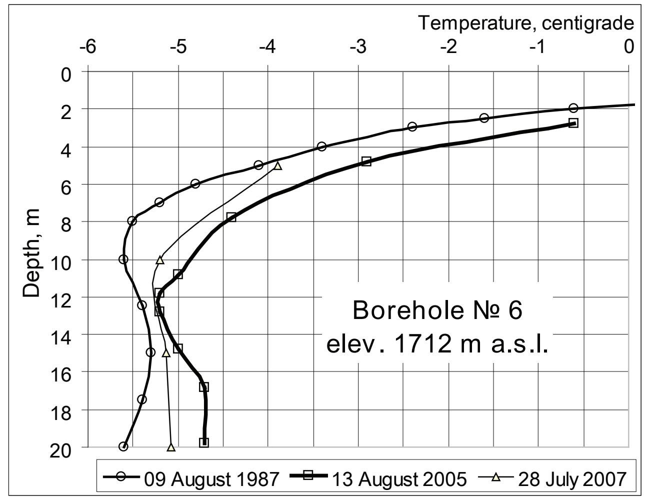

Figure 3. Temperature observation results in the borehole #6 for 1987–2007.

The boreholes are mainly located in the Udokan Ridge, where engineering projects were carried out in the 1970s. Three temperature monitoring sites have been chosen, therefore, including 20 m deep boreholes for 2005–2007. These boreholes are called #6, #38, and Peski-1. The temperature results from #6 and #38 boreholes have been obtained for 2006–2007. The measurements have shown an increase in permafrost temperatures at the scale of 0.5ºC on the 20 m depth for 1987–2006 (Fig. 3).

Figure 4 shows the invasion course of a seasonal wave of temperature fluctuations in coarse debris. The seasonal fluctuations are observed to be 20 meters deep along of low moisture content of rocks and high heat conductivity of quartzitic sandstone.

The Peski-1 borehole is located in the Chara Depression on isolated sandy desert where permafrost is absent. Thus, we have obtained temperatures concerning the Chara Sandy Desert.

There are four active layer observing points with air temperature measurements (kurum's pit – Zagryazkin-1, #5301; Ushelistiy-1; Belenkiy-1; Azarova-1) that were chosen by the authors for 2005–2007. Table 1, which summarizes the characteristics of the chosen boreholes and active layer observing points, is presented at the end of the paper.

The kurum's pit – Zagryazkin-1 (#5301) was produced by scientific and production forces in the 1980s. The authors obtained the temperature data in 2006 (Fig. 5). That allowed for typical block slope detailed information about temperature regime in the active layer where the intensive air convection and water condensation processes are usual.

The kurum's deposits occupy at least 50% of the slope area in the upper belt of The Udokan Ridge and result in a freezing effect on the underlying rocks (Romanovskii et al. 1991, Harris & Pedersen 1998, Gorbunov et al. 2004).

In 2007 three representative sites (Ushelistiy-1; Belenkiy-1; Azarova-1) were established. The active layer observing points have been chosen to proceed from the

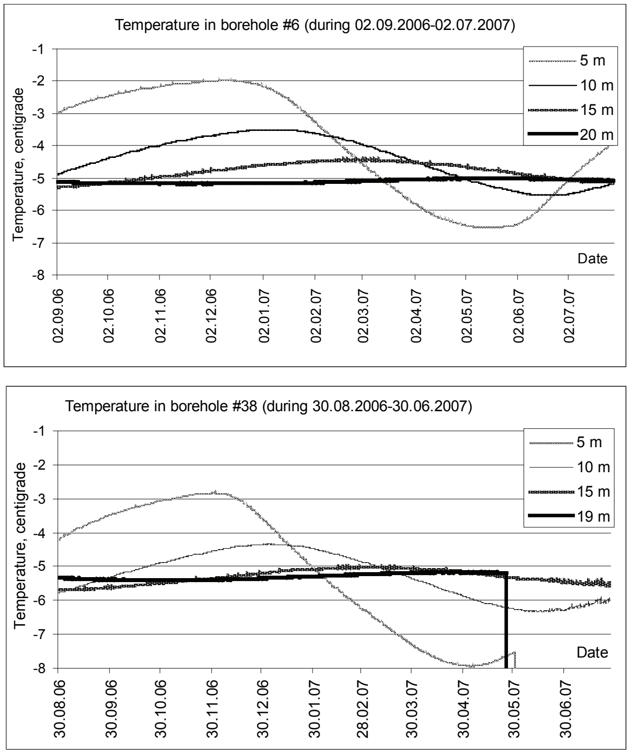

Figure 4. Temperature observations results in the borehole #6 and #38 for 2006–2007 (two channels, 5m and 19m. failed after April 2007).

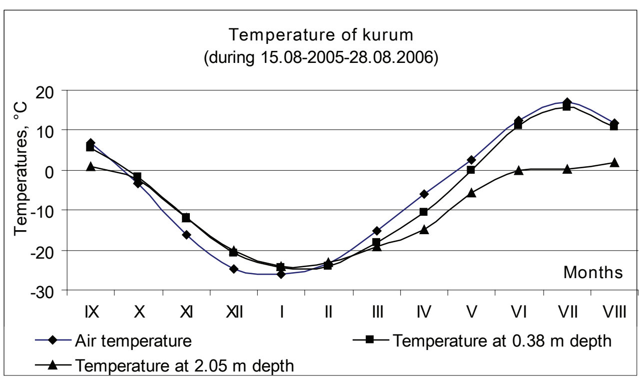

Figure 5. The mean monthly temperature data of kurum's pit in 2006.

premise that the point "Ushelistiy-1" represented the relict ice wedge polygons in the high mountain zone. The point "Belenkiy-1" took advantage of an active layer and relict ice wedge polygons in the Chara Depression. The point "Azarova-1" represented an active layer in moraine near the tongue of the Azarova Glacier in the Kodar Ridge.

The air, soil surface, and active layer temperatures were measured every 3 hours.

2. *The relief*. Whereas we study the alpine region, we take into account the geomorphology of different parts of the region. The orography is the product of tectonical and climate evolution and has a great impact on formation of natural territory conditions. That is why this territory has altitudinal landscape zonality.

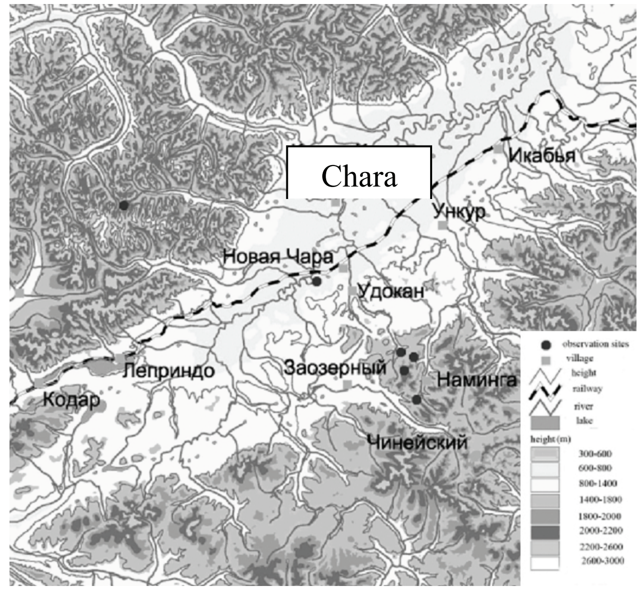

Figure 6. The hypsometric map of investigation territory.

In Figure 6, the hypsometric map is presented. The authors equipped the boreholes and active layer observing points by loggers at dominant heights.

The permafrost observations are based in a range of the heights from 730 m to 2200 m a.s.l. (see Table 1). Viz: Belenkiy-1 on 720 m a.s.l., Peski-1 on 767 m a.s.l., kurum's pit – Zagryazkin-1 (#5301) on 1155 m a.s.l., #6 on 1712 m a.s.l., #38 on 1464 m a.s.l., Ushelistiy-1 on 1651 m a.s.l., and Azarova-1 on 2036 m a.s.l. The height of temperature observation sites are shown in Figure 7.

The monitoring sites are accordingly located in the mountain altitudinal belt, in the upper part of mountain-taiga belt and at the bottom of the Chara Depression.

3. *The landscapes.* All the observing sites represent the nondisturbed landscapes. There are three dominated vegetations—such as "larch forest," "open woodland," and "alpine tundra"—that are presented in Figure 2. Our observing points are located in almost all types of vegetation. For example, the point "Belenkiy-1" is in a bog with larch; the kurum's pit (Zagryazkin-1, #5301) and #38 are in open woodland; the point "Azarova," #6 and Ushelistiy-1 are in alpine tundra. The borehole "Peski-1" is located in the unique Chara Sandy Desert. Knowledge of the cryological conditions is also possible through studying the external physionomical shape of a landscape.

4. *The permafrost*. Northern Transbaykalia is situated in a continuous permafrost zone. Cryological conditions are characterized by high heterogeneity. A local distribution of permafrost varies from sporadic to continuous thickness—from several meters up to 1200 m—and temperature from 0ºC up to -12ºC.

The permafrost conditions are different in depressions and mountains. A maximal thickness of permafrost is found at the foothills of northern expositions and at the bottoms of deep valleys in a depression. Permafrost thickness increases toward watersheds. On watersheds with the dominating

Table 1. The data of the temperature monitoring sites.

Site number/ characteristics	6	38	Peski-1	Zagryazkin-1 (kurum's pit #5301)	Ushelistiy-1	Belenkiy-1	Azarova-1
Latitude and longitude	N56º 36.329' E118º25.591'	N56º 40.017' E118º 21.648'	N56º 50'33.30' E118º 09'15.93'	N56º 40.567' E118º 21.621'	N56º 40.017' E118º 21.648'	N56º 45'39.63' E118º 11'24.53'	N56º 54' 23.33' E117º 34'41.64'
Borehole depth or pit depth (m)	20	19	15.33	2.05	0.33	1.3	1
Elevation (above sea level , m)	1712	1464	767	1155	1651	720	2036
Site slope (angle - degrees, aspect)	15 East-North-East	Flat	Flat	11 South-West	Flat	Flat	Flat
Site topography and local relief	Slope (Top of hill or ridge)	Top of hill or ridge	Plain	Slope	Valley	Valley	Valley
Landform or geo-morphologic description and history of site (age)	Left slope of the the Nirungnacan River – the surface has formed in middle time of Pleistocene. The block slope deposit (kurums)	Left divide surface of the Klyukvenniy River – the surface has formed in middle time of Pleistocene. The stone circles at coarse eluvium's deposits	Sand massif	Low part of the slope; the upper part of the Klyukvenniy River – the glacial valley that has formed in middle time of Pleistocene. The kurum's deposits have originated from a moraine.	Dividing saddle is located between the Ushelistiy Sike and the Ingamakit River of the Udokan Ridge. Pleistocen	First terrace of the Chara River. Pleistocene.	Moraine near the tongue of the Azarova Glacier (the Kodar Ridge)
Geology (brief description of bedrock, sediments)	From the top: 0.0-5.5 m – coarse debris; 5.5-20.0 m – quartzite sandstone of Early Proterozoic Age	From the top: 0.0-3.5 m – coarse debris eluvium with sand; 3.5-19.0 m – quartzite sandstone of Early Proterozoic Age	Sands	From the top: 0.0-2.2 m – active layer in kurum (debris slope) with large blocks (0.2-1.0 m); 2.2-8.0 m – moraine deposits with ice; 8.0-20.0 m – quartzite sandstone of Early Proterozoic Age.	From the top: 0.0-0.38 m – dark-brown peat; 0.38-0.45 m – peat; 0.45-… m ice wedge	From the top: 0.00-0.10 green moss; 0.10-0.20 brown peat; 0.20-1.30 dark-brown clay sand with ice wedges	From the top: 0.0-1.00 m – coarse debris with sand
Dominant site vegetation	Mountain tundra with crustose lichens	Upper limit of mountain taiga – larch tundra-forest with cedar elfin wood shrubs	Sand desert	Large kurum-clearing with crustose lichens (within mountain taiga – larch tundra-forest with "cedar elfin wood" shrubs)	Upper limit of mountain tundra - forest with cedar elfin wood shrubs	Taiga with fire-damaged forest	Alpine tundra
Permafrost presence	Permafrost	Permafrost	No permafrost	Permafrost	Permafrost	Permafrost	Permafrost

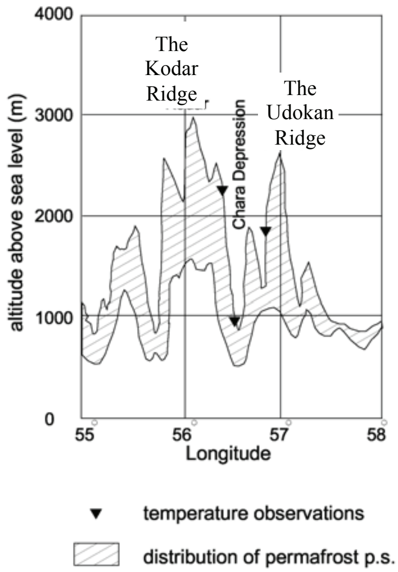

Figure 7. The temperature observation sites on the schematic geocryological profile (cryohydrological conditions, 1984).

heights of 2000–2200 m a.s.l., the thickness of permafrost is 800–900 m, and temperatures are -6 ºC to -8ºC. The point "Azarova-1" was equipped by loggers here. Under peaks with the heights of 2300–2700 m a.s.l., permafrost temperatures are -10ºC … -12ºC, and thickness is 1000–1200 m (Nekrasov & Klimovsky 1978). The Chara Depression is characterized by a most severe environment that promotes continuous development of permafrost at the bottom of the depression with the thicknesses of 100–500 m, with temperatures being -1.5ºC … -6.0ºC (Nekrasov & Klimovsky 1978). In marginal parts of a depression, the thickness of permafrost does not exceed 100–200 m, and an annual average temperature of rocks in most cases is -3ºC. The taliks are distributed within the limits of the Chara Sandy Desert on the left bank of the Chara River and under the riverbeds of large rivers (rivers Chara, Verkhniy and Sredniy Sakukan, etc.). Not far from the Chara Sandy Desert the authors measured temperature in the borehole "Peski-1."

The altitudinal zonality markedly affects the formation of landscape and cryological conditions. The cryological conditions become more severe, the area of taliks decreases, and massive-island distribution of permafrost is replaced by continuous permafrost at the height over 1000 a.s.l. with the altitude increasing.

5. *The state of borehole*. Obviously the good condition of original (old) observation boreholes decreases the expenses of monitoring installation. The boreholes need the special thermal insulation collar to decrease the influence of high thermal conductivity of the steel conductor. If the collar tube is not hermetic, it is possible that ice plugging will form. All sites of actual observation are in good shape.

6. *Accessibility* (mode of transportation: helicopter, road, off-road vehicle, river, etc.). All the temperature observation sites are not far from roads. The real obstacle for the work is the coordinate data absence of the original (old) boreholes. It is difficult to find a small collar in a bush. The active layer observing points have a GPS-affixment.

Conclusions

At the first stage of the TSP program realization in Northern Transbaykalia, the authors obtained a set of observation sites that are almost all located at high-altitude levels, in all landscapes and in all permafrost conditions. This set is unique in Russia, representing the highest altitudinal level of mountain.

Besides the temperature logger installation, the authors have gathered available data on the region (maps, rows of previous monitoring data, descriptions of landscape and natural processes, etc.). This information is important in allocating representative sites on which loggers have already been placed, in estimating the priority of site installation, and in helping to correctly analyze the results of actual permafrost observation. The authors can allocate the most valuable and prime boreholes for temperature measurements analyzing the whole set of boreholes (200 boreholes).

The use of remote sensing materials has been found to be rational at all stages of cryological research and helps to map permafrost and general natural conditions of the territory in tight deadlines and with economic consideration of material resources. It will allow the saving of time and money for expeditions and will improve the accuracy and informativeness of temperature regime monitoring for Northern Transbaykalia.

The results of temperature monitoring will be published on the Internet for practical and educational purposes.

Acknowledgments

This work is supported by grants of Russian Fund of Basic Research (06-05-64959a, 05-05-64390a, 05-05-64215a), National Science Foundation (Polar Earth Science Program, Office of Polar Programs – ARC-0632400, ARC-0520578), NASA THP Discovery Investigation "Current climate changes over Eastern Siberia and their impact on permafrost landscapes, ecosystem dynamics, and hydrological regime," and INTAS 06-1000013-8593 "Evaluating the Recent and Future Climate Change and Glacier Dynamics in the Mountains of Southern Siberia."

Special thanks to Vladislav Podgorbunsky who provided the sustainable fieldwork in the Chara settlement and to all Soviet geologists who conducted the permafrost observation in 1970s and 1980s.

References

Brown, J., Ferrians, O.J., Heginbottom, J.A. & Melnikov, E.S. 2003. Circum-Arctic Map of Permafrost and Ground-Ice Conditions. International Permafrost Association Standing Committee on Data Information and Communication (comp.). *Circumpolar Active-Layer Permafrost System, Version 2.0.* Edited by M. Parsons and T. Zhang. Boulder, CO: National Snow and Ice Data Center/World Data Center for Glaciology. CD-ROM.

Gorbunov, A.P., Marchenko, S.S. & Seversky E.V. 2004. The thermal environment of blocky materials in the mountains of Central Asia. *Permafrost and Periglacial Processes* 15: 95-98.

Klimovsky, I.V. 1966. Geocryological characteristic of the massif of blowing sands in the Chara Depression. Geocryological Condition of Transbaykalian North, Novosibirsk, Nauka, 181-186 (in Russian).

Leibman, M.O. 1979. Vertical geotemperature zonality in the mountain regions adjacent to BAM railroad. Engineering survey in construction, Collected abstracts, Issue 1, PNIIIS, Moscow: 114 (in Russian).

Nekrasov, I.A. & Klimovsky I.V. 1978. Permafrost of BAM. Novosibirsk, Nauka, 119 pp. (in Russian).

Nekrasov, I.A. & Shastkevich, J.G. 1966. Some data about permafrost in Kodar Ridge. Geocryological Condition of Transbaykalian North, Novosibirsk, Nauka, 100-106 (in Russian).

Romanovsky, N.N., Tyrin, A.I. & Sergeev, D.O. 1989. Kurums in the bald mountains. Novosibirsk, Nauka, 150 pp. (in Russian).

Shastkevich, J.G. 1966. Permafrost of high mountain part of Udokan Ridge and conditions of this temperature regime formation. Geocryological Condition of Transbaykalian North, Novosibirsk, Nauka, 24-43 (in Russian).

Shepelev, V.V., Tolstichin, O.N. & Piguzova, V.M. 1984. Cryo-hydrological conditions of Eastern Siberia, Novosibirsk, Nauka, 191 pp. (in Russian).

Shesternyov, D.M. & Yadrichensky, G.E. 1990. Structure and peculiarities of rocks in Udokan's cryolithozone. Novosibirsk, Nauka, 126 pp. (in Russian).

Dry Climate Conditions in Northeast Siberia During the MIS2

Georg Stauch
Department of Geography, RWTH Aachen University, Templergraben 55, D-52056 Aachen, Germany
Frank Lehmkuhl
Department of Geography, RWTH Aachen University, Templergraben 55, D-52056 Aachen, Germany

Abstract

Late Quaternary glaciations in the Verkhoyansk Mountains (NE Siberia) indicate extremely dry conditions during the global Last Glacial Maximum (MIS2). According to geomorphological investigations and IRSL dating results, the last major glaciation in the mountain system occurred before 50 ka. No glaciers were present in the area during the global Last Glacial Maximum. In the early part of the Last Glacial Maximum, precipitation was sufficient for the growth of large mountain glaciers. Precipitation during the stadial is strongly dependent on the size of the western sector of the Eurasian Ice Sheet.

Keywords: glacier; palaeoclimate; Siberia; Verkhoyansk Mountains.

Introduction

The Verkhoyansk Mountains in northeastern Siberia are the easternmost mountain system on the Eurasian continent which receives precipitation mainly from the Atlantic. Therefore the area is quite sensitive to changes on the northern part of the Eurasian continent. However, paleoclimatic studies in the area are very rare and mainly limited to palynological studies (e.g. Andreev et al. 1997, Anderson & Lozhkin 2001, 2002, Anderson et al. 2002, Kienast et al. 2005). Despite that, many new results emerged from the surrounding areas like western Siberia (Svendsen et al. 2004, Hubberten et al. 2004), the Laptev Sea coast (Bauch et al. 1999, Schirrmeister et al. 2002a, b, Grosse et al. 2007) and the Russian Far East (Gualtieri et al. 2000, 2003, 2005, Brigham-Grette 2001, 2003). In this last region Lake El'gygytgyn is located and it revealed a wealth of new information about the palaeoclimate of the area east of the Verkhoyansk Mountains (e.g. Brigham-Grette et al. 2007, Melles et al. 2007).

Quaternary glaciations are good indicators of the paleoclimatic environment as they are sensitive to temperature and moisture changes on a broader timescale. Up to now there have been only a few studies available dealing with Quaternary glaciations in the Verkhoyansk Mountains (Kind 1975, Kolpakov 1979, Kolpakov & Belova 1980). Research in the area was carried out in the 60th and 70th with only poor constraints on absolute dating. A summary of these works has been presented by Zamoruyev (2004). According to these authors the area was shaped by three major glaciations during the last glacial. The last glaciations occurred during the Marine Isotope Stage 2 (MIS2) of the global Last Glacial Maximum (gLGM). Another major ice advance happened during the MIS3 around 32 ka and one in the early part of the last glacial. Every one of the glacial advances in the last glacial was smaller than the previous one. However, new absolute dating results indicate that the morainic deposits in the area are older than previously assumed (Stauch et al. 2007).

Study Area

The Verkhoyansk Mountains (Fig. 1) are located in northeastern Siberia in the zone of continuous permafrost. The mountain range stretches for about 1200 km from the Laptev Sea at 72°N to Central Yakutia at 59°N. To the west, the Verkhoyansk Mountains are bordered by the Lena and Aldan Rivers and to the east by the Jana Highlands. While in the northernmost part, in the Kharaulakh area, maximum elevation is about 1400 m a.s.l., most summits in the south reach elevations of about 2000 to 2400 m a.s.l. The highest summit (2959 m a.s.l.) is reached in the Suntar Chajata, a southern branch of the mountain system. To the west, extended lowlands with elevations between 50 and 400 m a.s.l. stretch along the Verkhoyansk Range.

The climate in the area is extremely continental. Mean monthly air temperature varies between -40°C in January and +20°C in July. Annual precipitation ranges between 220 mm in the lowlands around Yakutsk and up to 700 mm on the western flank of the Verkhoyansk Mountains; on the eastern side of the mountain range the annual precipitation is only up to 200 mm (Lydolph 1977, Shagadenova et al. 2002). In the Verkhoyansk Mountains there are only a few small glaciers, mostly in the area of the Suntar Chajata. The recent snowline is between 2200 and 2400 m a.s.l. (Koreischa 1991, Murzin 2003, Ananicheva & Krenke 2005).

The study area was located in the central Verkhoyansk Mountains between 63°10′N and 66°40′N. The area consists of four large catchment areas on the western side and several smaller ones on the eastern flank of the mountains (Fig. 1) which sum up to an overall area of 150,000 km². The Tumara and Djaunshka valleys were chosen for the field work.

Methods

For the reconstruction of former glaciations, glacial-geomorphological landforms in the central part of the Verkhoyansk Mountains were mapped. Due to the remoteness of the area, without roads and settlements, remote sensing

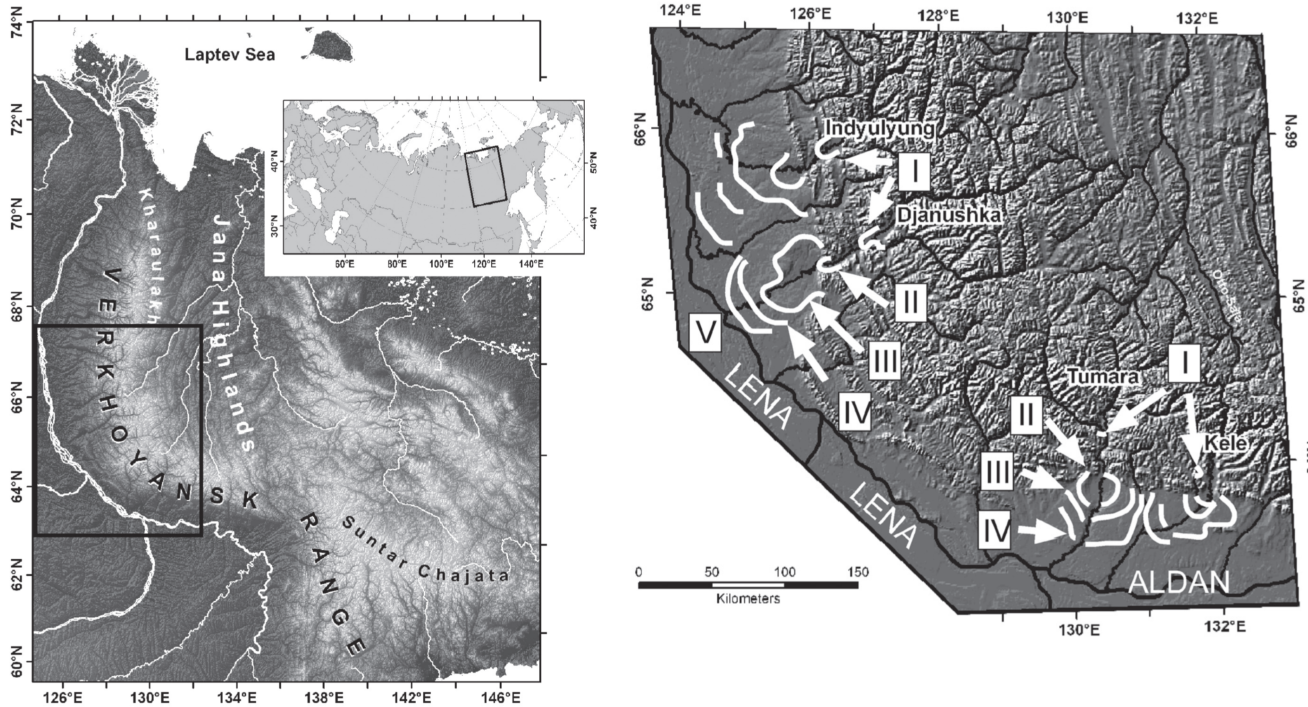

Figure 1. Study area, the Verkhoyansk Mountains (right side) and the central Verkhoyansk Mountains with the selected terminal moraines (left side).

data was utilized for the overall mapping of the region. The results of the image interpretation were in the second stage checked during two field seasons on the western side of the mountains, at which time samples for sedimentological analysis as well as for absolute dating were also taken. We used mainly aeolian cover sediments for IRSL (InfraRed Stimulated Luminescence), however at some points we also dated glacial-fluvial deposits. All samples were processed at the GGA Institute in Hannover, Germany. For a detailed description of the method and the complete table of the IRSL results see Stauch et al. (2007).

For the remote sensing analysis we used Landsat7 Data with a resolution of 30 m and 15 m respectively. A visual image interpretation approach was used for this study (Stauch 2006). This method was useful for identifying terminal moraines inside of the mountains as well as in the southern and western foreland. Besides the field work, crosschecking of the results was done with high resolution Corona images with a resolution of up to 2 m. Both methods showed that Landsat Data was sufficient for mapping of the glacial landforms in the area.

Moraines in the different catchment areas were grouped according to geomorphological criteria and relative position. The geomorphological criteria included degree of weathering and slope wash as well as the number and size of kettle lakes on the surface. Older moraines with a position most distant to the center of glaciation have a smoothed surface with low slope angles, while on younger moraines features of ice decay and moraines of small secondary re-advances are still visible. Kettle lakes are larger on older moraines than on

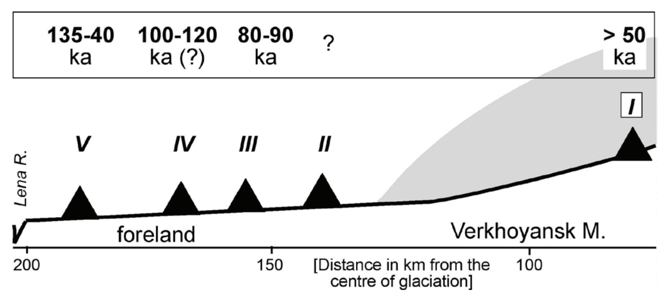

Figure 2. Schematic cross section of the western foreland and the Verkhoyansk Mountains with the ages of the terminal moraines (Stauch et al. 2007).

younger ones. This is caused by longer lasting permafrost processes, which often resemble the former ice margins. Besides morphological criteria these older moraines show distinctive differences in the mineralogical composition of the sediments (Popp et al. 2006, 2007).

Results

Geomorphological mapping revealed four to five sets of terminal moraines on the western and southern side of the Verkhoyansk Mountains. The uppermost moraines (named I, Fig. 1) are located inside of the mountains system about 50 to 80 km away from the supposed center of glaciations, while the other moraines (II to V) have been deposited either at the mountain front or in the foreland (Fig. 2). These later moraines are generally much larger in size than the ones further upstream. On the eastern site the terminal moraines

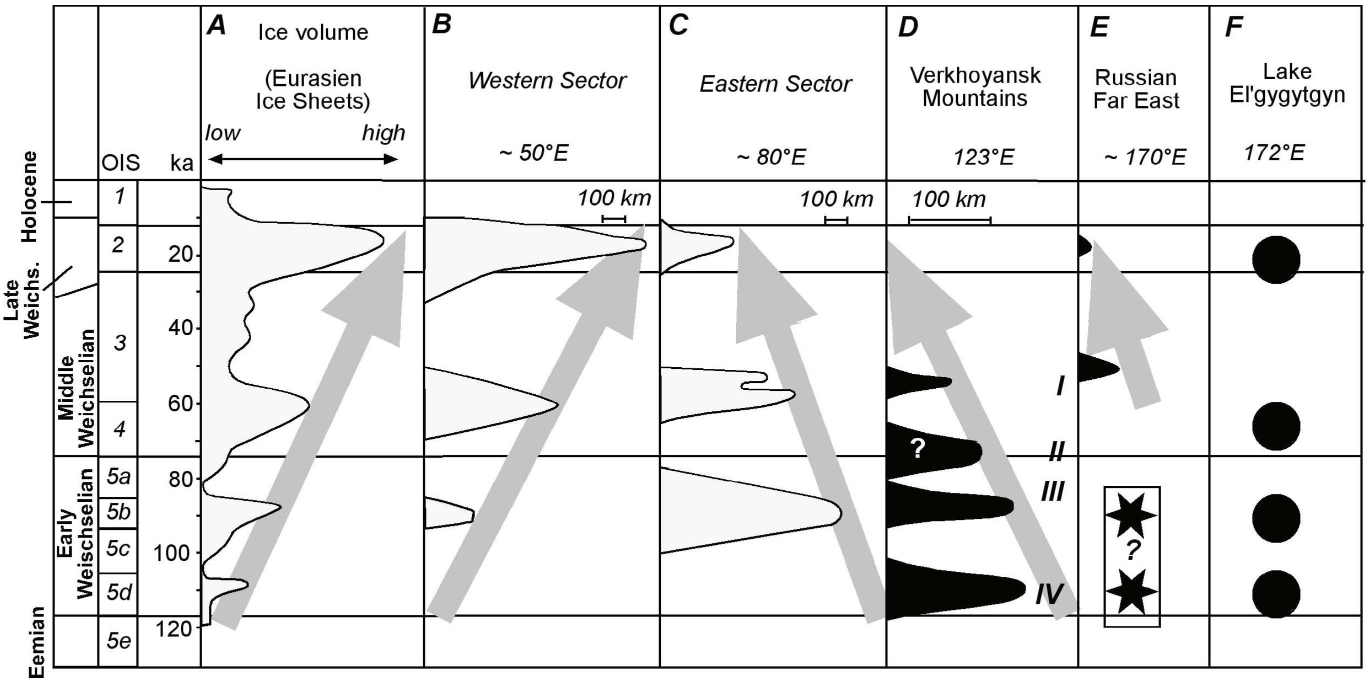

Figure 3. Time distance diagram of glaciations in the northern Asia (A-C: Svendsen et al. 2004, D: Stauch et al. 2007; E: Stauch & Gualtieri *subbm.*, Stars: Brigham-Grette 2001) and cold phases (F: dots) according to Brigham-Grette et al. (2007).

are much smaller and strongly eroded. Therefore, correlation of moraines on the eastern and western side is complicated and mainly based on the relative location of the sediments to the supposed center of glaciations.

However, dating of the moraines revealed that they are much older than previously assumed. Moraine I is older than 50 ka (Fig. 2). Aeolian cover sediments on a glacio-fluvial fan directly upstream of Moraine I in the Tumara catchment has an IRSL age estimate of 52.8 ± 4.1 ka (V09, Stauch et al. 2007). In the Djanushka catchment aeolian sands have been deposited above lacustrine sediments about six kilometers downstream of moraine I. These lacustrine sediments were formed sometime after the retreat of the glacier. The aeolian sediments on the top gave an IRSL age estimate of 39.7 ± 3.1 ka (Dj01). As no terminal moraines could be identified upstream of moraine I in any of the landforms in the northernmost, we suggest that the last studied catchment areas, except some small dubious glacial advance in the Verkhoyansk Mountains occurred before 50 ka. None of our results indicate a glaciation during the global Last Glacial Maximum during the MIS2.

Up to now no absolute ages for the second moraine are available. Aeolian sediments on top of the moraine point to a formation before 46.8 ± 3.1 ka (V17). However, this moraine is older than moraine I according to its stratigraphic position.

The formation of Moraine III presumably finished around 80 to 90 ka. This age estimation is based on two samples. In the Tumara catchment, glacio-fluvial sand in between the till gave an age of 86.9 ± 6.8 ka (V25). At the Djanushka River sand above Moraine III was dated to 92.3 ± 6.5 ka (Dj22).

Four IRSL samples have been dated at Moraine IV in the Tumara catchment. Glacio-fluvial sand at the top of the morainic sediments gave an IRSL age estimate of 97.6 ± 6.8 ka (V29). However, aeolian silt covering these sediments yielded IRSL ages of 123 ± 10 ka (V28) and 107 ± 10 ka (V27). Fluvial sediments on top of glacio-fluvial gravel in front of the moraine resulted in an IRSL age of 107 ± 10 ka. Despite the somewhat dubious due age in one of the profiles, we suppose that the formation of the moraines was completed between 100 and 120 ka.

For the outermost Moraine V two samples from glacial deformed sand between two thin layers of till resulted in IRSL ages of 135 ± 9 ka (DJ30) and 141 ± 10 ka (Dj31).

Discussion

Throughout the late Quaternary, glaciations in the Verkhoyansk Mountains became smaller indicating a reduction in precipitation during the different glacial phases. Comparing the results from the Verkhoyansk Mountains with neighboring regions indicates some continental trends in northern Asia (Fig. 3). Svendsen et al. (2004) compared the development of the western (Finland and western Russia) and the eastern (Arctic Russia, Siberia) sectors with the overall ice volume of the Eurasian Ice Sheets (British Scandinavian and Barents-Kara Ice sheets) throughout the last glacial. Taking all Ice Sheets together there is an overall trend in a growing ice volume during the pace of the last glacial. This trend is also reflected in the waxing of the Ice Sheet in the western sector, where the largest ice extent was reached in the later phase of the glacial during the MIS2.

The eastern sector of the Eurasian Ice Sheet developed the other way round, a large glaciation in the early part of the last glacial and a considerably smaller one during the MIS2. A similar trend can be observed in the Verkhoyansk Mountains. However, while there are multiple glaciations in the early part of the glacial, no glaciation occurred during the last 50 ka. East of the Verkhoyansk Mountains only a few absolute datings are available (Stauch & Gualtieri subbm.). Studies of e.g. the Pekulney Mountains (Brigham-Grette et al. 2003) or the Koryak Mountains (Gualtirie et al. 2000) point to progressively smaller glaciations during the last glacial. The last glaciations occurred during the MIS2. Glacial advances in the early phase of the last glacial are still in debate (Brigham Grette 2001). Similar to the glacial advances in Eastern Siberia, several cold phases have been recognized in a core of Lake El'gygytgyn (Brigham-Grette et al. 2007).

The main factor controlling glaciations in Eastern Siberia was the amount of available precipitation, as much of the continent up to the Verkhoyansk Mountains depends (and depended) on the moisture-bearing winds from the west. During the glaciations this moisture was blocked depending on the size of the western sector of the Eurasian Ice sheet. In the early part of the last glacial, the western part of the Ice Sheet was relatively small leading to major glaciations in western Siberia (eastern sector of the Eurasian Ice Sheet) and to mountain glaciations in the Verkhoyansk Mountains. During the MIS2 the western part of the Eurasian Ice Sheet reached its maximum extent of the last glacial blocking most of the moisture. Therefore, the eastern sector of the Eurasian sector was comparable small, while no glacier developed in the Verkhoyansk Mountains despite very low temperatures. Models of western Siberia show similar results (e.g., Siegert & Marsiat 2001, Siegert & Dowdeswell 2004).

East of the Verkhoyansk Mountains in eastern Russia, the Pacific was at least an additional moisture source which, in turn, led to several mountain glaciations. In Western Siberia and the far east of the Asian continent at least little moisture was available. The environment in Eastern Siberia was cold and very dry during the MIS2.

Acknowledgments

The authors would like to thank the Deutsche Forschungsgemeinschaft (DFG; Le 730/10-1,2) for funding the project. Thanks also to Manfred Frechen for the IRSL dating, and all the Russian and German colleges we worked with in the Verkhoyansk Mountains.

References

Ananicheva, M.D. & Krenke, A.N. 2005. Evolution of climatic snow line and equilibrium line altitudes in the North-Eastern Siberian Mountains (20th Century). *Ice and Climate News* 6: 3-6.

Anderson, P.A. & Lozhkin, A.V. 2001. The stage 3 interstadial complex (Karginskii/ middle Wisconsinan interval) of Beringia: variations in paleoenvironments and implications for paleoclimatic interpretations. *Quaternary Science Reviews* 20: 93-125.

Anderson, P.A. & Lozhkin, A.V. 2002. Palynological and radiocarbon data from late Quaternary deposits of northeastern Siberia. In: P.A. Anderson & A.V. Lozhkin (eds.), *Late Quaternary Vegetation and Climate of Siberia and the Russian Far East (Palynological and Radiocarbon Database)*. Magadan: NESC FEB RAS, 27-34.

Anderson, P.A., Lozhkin, A.V. & Brubaker, L.B. 2002. Implications of a 24,000 yr palynological record for a Younger Dryas cooling and for boreal forest development in Northeastern Siberia. *Quaternary Research* 57: 325-333.

Andreev, A.A, Klimanov, V.A. & Sulerzhitsky, L.D. 1997. Younger Dryas pollen records from Central and Southern Yakutia. *Quaternary International* 41/42: 111-117.

Bauch, H.A., Kassens, H., Erlenkeuser, H., Grootes, P.M. & Thiede, J. 1999. Depositional environment of the Laptev Sea (Arctic Siberia) during the Holocene. *Boreas* 28: 194-204.

Brigham-Grette, J. 2001. New perspectives on Beringian Quaternary paleogeography, stratigraphy, and glacial history. *Quaternary Science Reviews* 20: 15 - 24.

Brigham-Grette, J., Gualtierie, L.M., Yu Glushkova, O., Hamilton, T.D., Mostoller, D. & Kotov, A. 2003. Chlorine-36 and 14C chronology support a limited last glacial maximum across central Chukotka, northeastern Siberia, and no Beringian ice sheet. *Quaternary Research* 59: 386-398.

Brigham-Grette, J., Melles, M, Minyuk, P. & Scientific Party 2007. Overview and significance of a 250 ka paleoclimate record from El'gygytgyn Crater Lake, NE Russia. *Journal of Paleolimnology* 37: 1-16.

Grosse, G., Schirrmeister, L., Siegert, C., Kunitsky, V.V., Slagoda, E.A., Andreev, A.A. & Dereviagyn, A.Y. 2007. Geological and geomorphological evolution of a sedimentary periglacial landscape in Northeast Siberia during the Late Quaternary. *Geomorphology* 86: 25 - 51.

Gualtieri, L., Glushkova, O. & Brigham-Grette, J. 2000. Evidence for restricted ice extent during the last glacial maximum in the Koryak Moutains of Chukotka, far eastern Russia. *Geological Society of America, Bulletin* 112: 1106-1118.

The Fate of Greenland's Permafrost: Results from High-Resolution Transient Climate Simulations

Martin Stendel, Jens Hesselbjerg Christensen, Guðfinna Aðalgeirsdóttir
Danish Meteorological Institute, Copenhagen, Denmark
Ronnie Daanen, Sergey Marchenko, Vladimir Romanovsky
University of Alaska, Fairbanks, Alaska, USA

Abstract

Simulations with global circulation models (GCMs) clearly indicate that major climate changes for Greenland can be expected during the 21st century. Due to their coarse resolution, contemporary global climate models (GCMs) have so far been unable to give a realistic representation of the dynamics of the Greenland ice sheet as well as the permafrost underlying the ice-free regions. Even relatively high-resolution regional climate models (RCMs) may fail in this respect. To improve climate projections, we have therefore conducted a transient simulation for the period 1950–2080 for the whole of Greenland with very high resolution. Based on these simulations, we present modeled changes in permafrost in an unprecedented high resolution.

Keywords: climate change; Greenland; permafrost; regional climate model.

Introduction

There is ample observational evidence for recent warming in high latitudes. Observed changes include air (Moritz et al. 2002) and soil temperature (Majorowicz & Skinner 1997, Osterkamp & Romanovsky 1999, Romanovsky et al. 2002, Osterkamp 2003), vegetation cover (Sturm et al. 2001), sea ice (Bjorgo et al. 1997), glacier mass balance (Arendt et al. 2002) and ice sheets (Rignot & Kanagaratnam 2006). Many of these changes affect the permafrost body (perennially frozen ground) and the seasonally thawed layer between it and the surface, the active layer. Climate change scenarios (e.g., IPCC 2007) indicate that warming due to anthropogenic activities will be greatest in polar regions. Changes involving permafrost may affect infrastructure and regional ecosystems due to thawing of the ground and development of thermokarst depressions (Romanovskii et al. 2000), or they may contribute to the release of large amounts of greenhouse gases.

Model studies with comprehensive coupled ocean-atmosphere general circulation models (AOGCMs) show that the area of the Northern Hemisphere underlain by permafrost could be reduced substantially in a warmer climate (Smith & Burgess 1999, Anisimov et al. 2001, Nelson et al. 2001, Stendel & Christensen 2002). However, thawing of permafrost, in particular if it is ice rich, is subject to a time lag due to the large latent heat of fusion of ice, which implies that permafrost in relict form can persist in deep layers for centuries or even millennia as in western Siberia. State-of-the-art AOGCMs are unable to adequately model these processes for three reasons: even the most advanced subsurface schemes rarely treat depths below 5 m explicitly; soil thawing and freezing processes cannot be dealt with directly due to the coarse resolution of present AOGCMs; and the required simulations covering millennia cannot be conducted due to computer power limitations.

It is important to note that any attempt to model subsurface processes needs information about soil properties, vegetation, and snow cover; but these are hardly realistic on a typical GCM grid. Furthermore, simulated GCM precipitation is often underestimated, and the proportion of rain and snow is incorrect (e.g., Christensen & Kuhry 2000). One possibility to overcome resolution-related problems is to use regional climate models (RCMs). Such an RCM, HIRHAM4 (Christensen et al. 1996), has until now been the only one used for the entire circumpolar domain (ACIA 2005), and it has also been used in this study. No specific treatment of soil freezing and thawing is done in HIRHAM, so the same limitations as for the GCM apply, and so far only studies based on frost indices have been conducted. As for coarser-scale models, these simulations also lack sufficient information about soil properties.

Instead of calculating a degree-day-based frost index from RCM data, we use the regional model to create boundary conditions for an advanced permafrost model. This approach, described in Stendel et al. (2007) in a proof-of-concept study, is novel in two aspects. Firstly, the RCM (and therefore the permafrost model) runs on an unprecedented horizontal resolution of 25 km for the entire region covering Greenland and the surrounding seas. Secondly, while most comparable studies have used "time-slices" due to computer limitations, we here present a fully transient simulation covering the period 1950–2080.

Model Hierarchy and Downscaling Procedure

The models used in this study are briefly described below. The driving AOGCM is the state-of-the-art, coupled ocean-atmosphere model ECHAM5/MPI-OM1 (Roeckner et al. 2003, Marsland et al. 2003, Jungclaus et al. 2006). All the forcing data for the Greenland simulation have been taken from a transient simulation with this model (May 2007) at T63 resolution (~1.8° by 1.8°). ECHAM5 no longer requires a flux correction, as opposed to previous versions

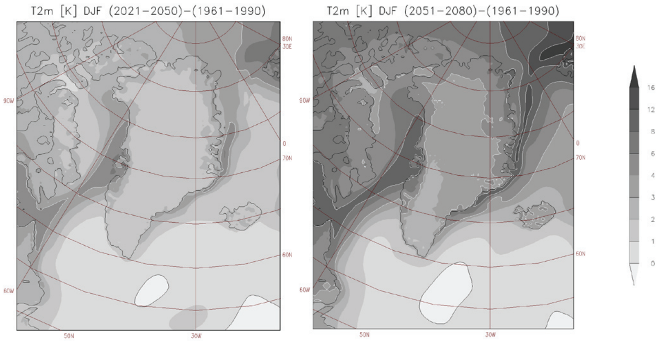

Figure 1. Simulated mean near surface (2 m) air temperature change [K] in HIRHAM4 in winter (December–February). Left panel: 2021–2050 minus 1961–1990, right panel: 2051–2080 minus 1961–1990. Isolines every 4 K.

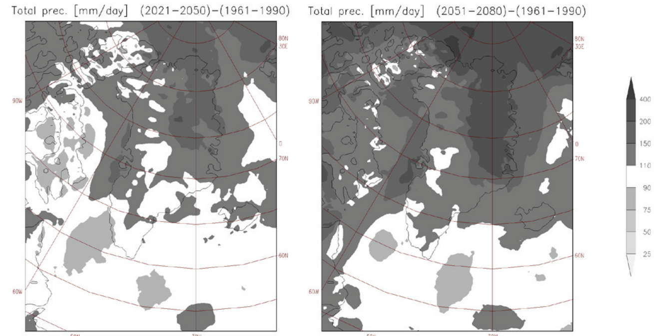

Figure 2. Change in annual precipitation expressed in percent of present-day (1961–1990) precipitation for 2021–2050 (left panel) and 2051–2080 (right panel).

of this model. Walsh et al. (2008) found in a comparison study between 14 of the CMIP3 participating models, that ECHAM5 is a top ranking model with respect to simulating present day conditions in the Arctic, including seasonal sea ice distributions.

The regional model is HIRHAM4 (Christensen et al. 1996), which is based on the adiabatic part of the HIRLAM (High-Resolution Limited Area Model) short-range weather forecast model (Källén 1996). For climate modeling purposes, the standard physical parameterisation of HIRLAM was replaced by that of the global climate model ECHAM4 (the predecessor of ECHAM5), so that HIRHAM4 can be thought of as a high resolution limited area version of ECHAM4. The boundary forcing from the global model (see previous paragraph) is updated every six hours in a region 10 grid points wide with a simple relaxation of all prognostic variables. It has been shown that HIRHAM4 is able to realistically simulate present-day climate (e.g., Christensen et al. 1998).

Varying concentrations of well-mixed greenhouse gases (CO_2, CH_4, N_2O, CFC-11, and CFC-12) as well as ozone (O_3), and sulphate aerosols (SO_4) have been prescribed from observations over the period 1861–2000 and according to the SRES A1B scenario (Nakićenović et al. 2000) thereafter. In this scenario the CO_2 concentration in 2100 is near 700 ppm, and the globally averaged warming with respect to present-day climate is 3.5°C.

To model regional permafrost, we have used the GIPL 1.1 model (Geophysical Institute Permafrost Lab) of the University of Alaska Fairbanks (Sergeev et al. 2003), which is a one-dimensional, spatially distributed, physically based multi processor numerical model for the solution of the non-linear heat transfer equation. The model solves for ground temperatures and active layer thickness. The input data for GIPL 1.1 are air temperature, snow depth and density, soil composition, water content and thermal properties, as well as characteristics of vegetation cover, geomorphologic features, and the geothermal flux as a bottom boundary.

Future Climate Evolution

As discussed above, the driving model for the 25 km HIRHAM simulation is a coupled atmosphere-ocean model; that is, the atmosphere is forced by modeled SSTs and sea ice concentrations rather than by observed ones. This implies that in order to assess variability and change, the considered periods need to be long enough; that is, cover several decades. From the transient simulation covering the complete period 1950–2080, we compare two thirty-year averages for periods in the 21st century (2021–2050 and 2051–2080) to modeled present-day conditions (1961–1990).

Temperature

Figure 1 shows seasonal changes in 2 m air temperature over Greenland for the two periods with respect to present-day conditions. For 2021–2050 a general temperature increase of 3°C in winter and 2°C in summer (not shown) is found. In winter locally larger values up to 6°C along the west coast and 4°C along the east coast and further northeast to Svalbard are simulated, which are related to regions covered with sea ice under present-day conditions but not in future climate. For the second period (2051–2080), warming accelerates considerably, with an increase of 7–8°C along the west and 12°C along the east coast in winter and a maximum increase of more than 18°C in winter at Svalbard's northeast coast, a region which has also been prone to large, recently-observed temperature anomalies.

The predicted temperature changes along the coast of Greenland are larger than in available GCM simulations (including ECHAM5, which provided the driving data for this simulation). We note that sea ice is not a prognostic variable in HIRHAM but is rather interpolated from the driving model. In ECHAM and HIRHAM any sea ice in a grid box is thawed first before near-surface temperatures can increase further. When sea ice retreats, there will be grid cells in HIRHAM free of ice earlier than in ECHAM, just because of the grid size (which is roughly 50 times larger in the GCM). These changes in sea ice cover and the projected increase in the positive phase of the North Atlantic Oscillation (Stendel et al. 2007, Stendel et al. 2008) lead to an increase in wind speed and changes in heat transport from the ocean, compared to the driving model, in particular along the east coast.

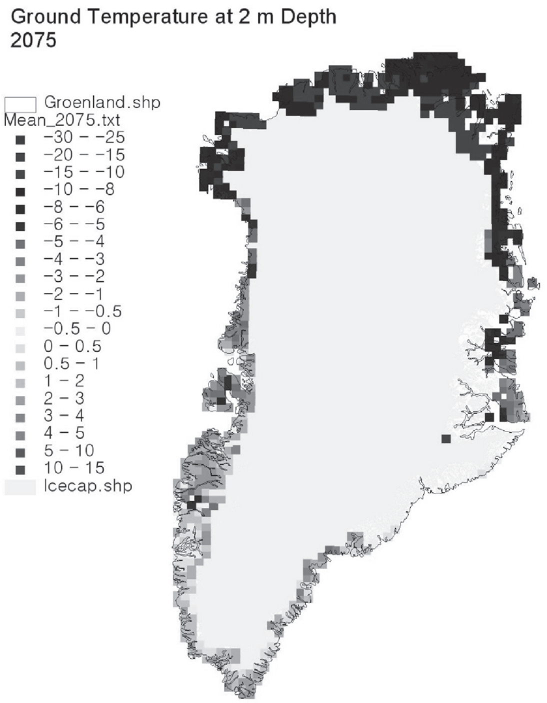

Figure 3. Ground temperatures (°C) at 2 m depth obtained with GIPL for exposed bedrock forced with HIRHAM4. Snapshot for 2075.

As a result, late summer sea ice disappears around 2060 in our simulation (not shown). Winter sea ice generally retreats northward by 100–200 km until 2050 and further (300–400 km) by 2080. Around Svalbard, sea ice totally disappears (even in winter) after 2070.

Precipitation

In Figure 2 precipitation changes are shown. In agreement with ACIA (2005) and Christensen et al. (2007), an increase in precipitation is projected for most of Greenland. With respect to present-day conditions, 15% more precipitation over western and 40% over interior and eastern Greenland are predicted for 2021–2050, while there is an increase of 30%–40% over western and interior and about 60% over eastern Greenland for 2051–2080. A distinct decrease in both snowfall amount and frequency is projected along the coasts except in the north, whereas more snow is projected on the lower parts of the ice sheet, in particular along the east coast (not shown). No information about changes on the ice sheet can be modeled, since it is treated as passive even in the contemporary models. That means that snow is allowed to accumulate on the ice sheet until a predefined maximum snow cover is reached, and no thawing or ablation is taken into account so that in practice the ice sheet is covered by a layer of snow of constant thickness throughout the year.

Permafrost

Rising temperatures, increasing precipitation, and a decrease in the number of snow days all contribute to conditions favorable for permafrost retreat; a decrease in snow depth and duration has the opposite effect. How fast

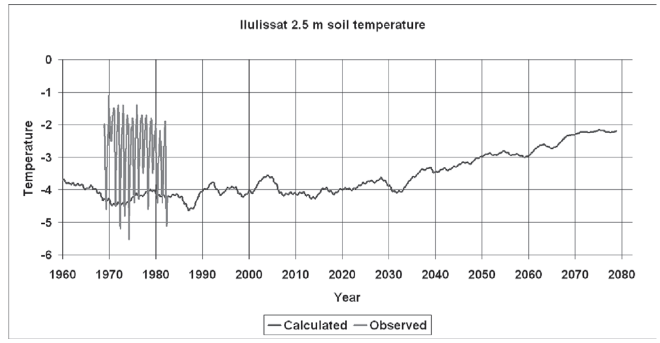

Figure 4. Soil temperature at a depth of 2.5 m in Ilulissat. Blue curve: GIPL 1.1 forced with HIRHAM4. Red curve: observations (van Tatenhove & Olesen 1994).

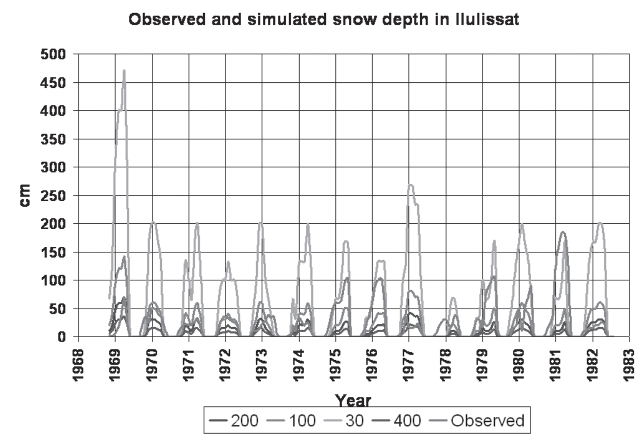

Figure 5. Observed and simulated snow depth (cm) in Ilulissat for mass densities of 30, 100, 200, and 400 kg m^{-3}.

changes in permafrost will take place furthermore depends on soil and vegetation properties, which are not known well on the spatial scale of interest for large parts of Greenland. We have run GIPL 1.1 using variations in snow thermal conductivity and organic layer thickness (Daanen et al. poster, this meeting). As an example, Figure 3 shows a snapshot of the temperature at 2 m depth for 2075.

Figure 4 shows the simulated and observed temperature evolution at 2.5 m depth for Ilulissat, taken from observations during the period 1968 to 1981 (van Tatenhove & Olesen 1994). A cold bias in the model data is obvious. As a consequence, the active layer in the model is too thin, and the permafrost table is too close to the surface, resulting also in a damping of temperature variability compared to the observations.

The model grid point representing Ilulissat is situated on the ice sheet, so an adjacent grid point, 25 km west, was chosen for comparison. This demonstrates that a horizontal resolution of 25 km is not sufficient to successfully model permafrost processes. Despite the strong warming signal in the atmosphere, the warming at the permafrost level is quite moderate. By the end of the period, temperatures at 2 m depth are above or just below freezing south of Maniitsoq and Tasiilaq, respectively, but remain below 0°C further north. This result points out the importance of a realistic simulation of snow depth. The model slightly underestimates the snow cover compared to observations (Fig. 5). However, modeled snow cover is given in water equivalent and thus crucially depends on the mass density. Referring to Raab and Vedin (1995), a density on the order of 100 kg m^{-3} (newly fallen snow) gives reasonable results most of the time. There are, however, indications for winters with much smaller density on the order of 30–50 kg m^{-3}, the cold winters of 1975 and 1981 for example. High values up to 300–400 kg m^{-3} apply at the end of the winter. Of course, warm atmospheric conditions and a decrease in snow cover will eventually lead to permafrost degradation and thawing. However, since Greenland is comparably cold also in summer (when compared to Alaska), and due to the large thermal inertia of the frozen ground, only a part of this warming will be realized within the next decades.

Conclusions

Most state-of-the art GCMs project warming on the order of 2°C–3°C in the southern and larger warming (around 7°C) for the northern part of Greenland. A transient climate simulation at an (for Greenland) unprecedented horizontal resolution of 25 km has been conducted, which was forced by a GCM with a rather high resolution (T63; i.e., roughly 1.8° in latitude and longitude). Our regional model shows considerably stronger temperature increase in regions where sea ice retreats than the driving global model, with largest differences and largest changes along the east coast. Most of Greenland, especially the northeast, is projected to receive more precipitation. In particular at lower elevations, an increasing percentage of this precipitation can be expected to fall as rain rather than snow under present-day conditions. According to the model, present-day permafrost is rather cold in the Ilulissat region, which we have chosen as an example. With ongoing warming, the increase in rainfall events and decrease in snow fall, depth, and duration will lead to a warming of permafrost. Given the existence of marine permafrost along the west coast of Greenland, permafrost degradation can be expected to start at the end of this century.

Acknowledgments

This research was partly funded by the Polar Earth Science Program, Office of Polar Programs, National Science Foundation (ARC-0612533) and by the Danish Environment Agency (Miljøstyrelsen) under grant no. M127/001-0237.

References

ACIA. 2005. *Arctic Climate Impact Assessment.* Cambridge University Press, 1042 pp.

Anisimov, O., et al. 2001. Polar Regions (Arctic and Antarctic). C*limate Change: Impacts, Adaptation and Vulnerability Panel on Climate Change, Contribution of Working Group II of the Intergovernmental, Third Assessment Review.* Cambridge: Cambridge University Press, 801-841.

Arendt, A.A., Echelmeyer, K.A., Harrison, W.D., Lingle, C.S. & Valentine, V.B. 2002. Rapid wastage of Alaska glaciers and their contribution to rising sea level. *Science* 297: 382-386.

Bjorgo, E., Johannessen, O.M. & Miles, M.W. 1997. Analysis of merged SMMR/SSMI time series of Arctic and Antarctic sea ice parameters 1978–1995. *Geophys. Res. Lett.* 24: 413-416.

Christensen, J.H. & Kuhry, P. 2000. High-resolution regional climate model validation and permafrost simulation for the East European Russian Arctic. *J. Geophys. Res.* 105: 29647-29658.

Christensen, J.H., Christensen, O.B., Lopez, P., van Meijgaard, E. & Botzet, M. 1996. *The HIRLAM4 Regional Atmospheric Climate Model.* Danish Met. Inst. Sci. Rep. 96–4.

Christensen, J.H., et al. 2007. Regional climate projections. In: S. Solomon, D. Qin, M. Manning, Z. Chen, M. Marquis, K.B. Averyt, M. Tignor & H.L. Miller (eds.), *Climate Change 2007: The Physical Science Basis.* Cambridge University Press.

Christensen, O.B., Christensen, J.H., Machenhauer, B. & Botzet, M. 1998. Very high-resolution regional climate simulations over Scandinavia–present climate. *J. Climate* 11: 3204-3229.

IPCC. 2007. *Climate Change 2007: The Physical Science Basis.* S. Solomon, D. Qin, M. Manning, Z. Chen, M. Marquis, K.B. Averyt, M. Tignor & H.L. Miller (eds.), Cambridge, United Kingdom and New York, NY, USA: Cambridge University Press, 996 pp.

Jungclaus, J.H., Keenlyside, N., Botzet, M., Haak, H., Luo, J.-J., Latif, M., Marotzke, J., Mikolajewicz, U. & Roeckner, E. 2006. Ocean circulation and tropical variability in the AOGCM ECHAM5/MPI-OM. *J. Climate* 19: 3952-3972.

Källén, E. (ed.) 1996. *HIRLAM Documentation Manual, System 2.5.* Norrköping: Swed. Meteorol. and Hydrol. Inst., 126 pp.

Majorowicz, J.A. & Skinner,W.R. 1997. Potential causes of differences between ground and surface air temperature warming across different ecozones in Alberta, Canada. *Glob. Plan. Change* 15: 79-91.

Marsland, S.J., Haak, H., Jungclaus, J.H., Latif, M. & Roeske, F. 2003. The Max Planck Institute global ocean/sea ice model with orthogonal curvilinear coordinates. *Ocean Modelling* 5: 91-127.

May, W. 2007. Climatic changes associated with a global "2ºC-stabilization" scenario simulated by the ECHAM5/MPI-OM coupled climate model. *Clim. Dyn.* (submitted).

Nakicenovic, N. et al. 2000. *IPCC Special Report on Emissions Scenarios*. Cambridge, UK: Cambridge University Press 599 pp.

Osterkamp, T.E. 2003. A thermal history of permafrost in Alaska. In: M. Phillips, S.M. Springman & L.U. Arenson (eds.), *Proceedings of the 8th Int. Conf. on Permafrost, July 21–25, 2003, Zurich, Switzerland.* Lisse, The Netherlands: A.A. Balkema, 863-868.

Osterkamp, T.E. & Romanovsky, V.E. 1999. Evidence for warming and thawing of discontinuous permafrost in Alaska. *Permafr. Periglac. Proc.* 10: 17-37.

Raab, B. & Vedin, H. 1995. *Climate, Lakes and Rivers: National Atlas for Sweden*. SNA Publishing, 176 pp. +198 plates.

Rignot, E. & Kanagaratnam, P. 2006. Changes in the velocity structure of the Greenland ice sheet. *Science* 311: 986-990.

Roeckner, E. et al. 2003. *The Atmospheric General Circulation Model ECHAM 5. PART I: Model Description.* Max Planck Institute for Meteorology Report 349, 127 pp.

Romanovskii, N.N., Hubberten, H.-W., Gavrilov, A.V., Tumskoy, V.E., Tipenko, G.S. & Grigoriev, M.N. 2000. Thermokarst and land-ocean interactions, Laptev Sea region, Russia. *Permafr. Periglac. Proc.* 11: 137–152.

Romanovsky, V.E., Burgess, M., Smith, S., Yoshikawa, K. & Brown, J. 2002. Permafrost temperature records: indicator of climate change. *Eos* 83: 593-594.

Sergeev, D.O., Tipenko, G.S. & Romanovsky. V.E. 2003. Mountain permafrost thickness evolution under influence of long-term climate fluctuations (results of numerical simulations). In: Phillips, Springman, & Arenson (eds.), *8th International Conference on Permafrost*. Balkema, Zurich, 1017-1021.

Smith, S.L. & Burgess, M.M. 1999. Mapping the sensitivity of Canadian permafrost to climate warming. *Proc. IUGG 99 Symp. HS2, vol. 256*. IAHS Publications, 71-80.

Stendel, M. & Christensen, J.H. 2002. Impact of global warming on permafrost conditions in a coupled GCM. *Geophys. Res. Lett.* 29, 10.1029/2001GL014345.

Stendel, M., Romanovsky, V.E., Christensen, J.H. & Sazonova, T. 2007. Global warming and permafrost: Closing the gap between climate model simulations and local permafrost dynamics *Glob. Plan. Change* 56: 203-214.

Stendel, M., Christensen, J.H. & Petersen, D. 2008. Arctic climate and climate change with a focus on Greenland. In: H. Meltofte, T.R. Christensen, B. Elberling, M.C. Forchhammer & M. Rasch (eds.), *The dynamics of a High Arctic ecosystem in relation to climatic variability and change - Ten years of monitoring and research at Zackenberg Research Station, Northeast Greenland.* Adv. in Ecol. Res., Elsevier. (in press).

Sturm, M., Racine, C. & Tape, K. 2001. Climate change: increasing shrub abundance in the Arctic. *Nature* 411: 546–547.

van Tatenhove, F.G.M. & Olesen, O.B. 1994. Ground temperature and related permafrost characteristics in West Greenland. *Permafr. Perigl. Proc.* 5: 199-215.

Walsh, J.E., Chapman, W.L., Romanovsky, V., Christensen, J.H. & Stendel, M. 2008. Global climate model performance over Alaska and Greenland. *J. Clim.* (In revision).

Detection of Frozen and Unfrozen Interfaces with Ground Penetrating Radar in the Nearshore Zone of the Mackenzie Delta, Canada

Christopher W. Stevens
University of Calgary, Calgary, Alberta, Canada
Brian J. Moorman
University of Calgary, Calgary, Alberta, Canada
Steven M. Solomon
Natural Resources Canada, Dartmouth, Nova Scotia, Canada

Abstract

Multi-frequency Ground Penetrating Radar (GPR) surveys were conducted within the nearshore zone of the Mackenzie Delta to determine the spatial distribution of frozen and unfrozen sediment. Late winter GPR surveys over zones of bottom-fast and floating ice indicate that significant spatial variations in the thermal state of sediments exist. Where ice was bottom-fast, two laterally-continuous high amplitude reflections were verified to represent a transition in thermal state of sediment. These thermally-related interfaces closely correlate with changes in ground temperatures from above freezing to below -0.5°C. At locations where bottom-fast ice thickness was less than 1 m complete freezeback of the active layer occurred. Where bottom-fast ice thickness was greater than 1 m thaw exceeded freezeback of the active layer and a near-surface talik was identified. The depth of seasonal frost decreased towards zones of floating ice, beneath which no near-surface thermal interfaces were resolved.

Keywords: bottom-fast ice; ground penetrating radar; nearshore zone; seasonal frost; thermal interfaces.

Introduction

In the nearshore zone of the Mackenzie Delta (Fig. 1), the occurrence of seasonal frost and the sustainability of permafrost are closely related to the presences of bottom-fast ice (Dyke 1991, Kurfurst & Dallimore 1991, Wolfe et al. 1998). At locations where seasonal landfast ice comes in contact with the sediment bed (bottom-fast ice), heat is readily conducted from the underlying sediment. Several factors control the onset of bottom-fast ice and therefore the extent of heat exchange and ground freezing. Of particular importance are water bathymetry and those influences affecting ice growth (e.g., snowpack thickness). The ice contact time, in part, controls freezeback of the active layer and permafrost cooling (Stevens 2007). The outer delta, seaward of the delta front, is characterized by a shallow-water platform of gentle slope and subtle changes in water depth. As a result, complex thermal structures occur beneath seemingly similar regions of bottom-fast ice.

Under such nearshore conditions, subsurface characterization of the distribution of frozen and unfrozen sediment becomes difficult when solely relying on point-specific measurements such as drill and ground-temperature data. These datasets, although important, can lead to inaccurate correlation between data points and the oversimplification of the current subsurface conditions where rapid changes occur.

The thermal state of ground in this region is important to oil and gas development, as the stability of infrastructure in permafrost environments is greatly dependent on engineering designs that are specific to the existing and naturally changing thermal conditions.

In order to improve the subsurface understanding of ground conditions in the coastal zone, we used Ground Penetrating Radar (GPR) to detect thermal interfaces. Similar GPR surveys conducted over ice-covered rivers (Delaney et al. 1990, Arcone et al. 1992, Arcone et al. 1998) and lakes (Arcone et al. 2006) have identified sub-ice reflections that relate to frozen-unfrozen boundaries.

In this paper we discuss the sources of thermal interfaces detected with GPR in sediments, and characterize the spatial complexity of frozen and unfrozen transitions located beneath bottom-fast ice within the Mackenzie Delta coastal zone.

Detection of frozen and unfrozen sediment

Among the electrical, electromagnetic, and reflection-based geophysical methods utilized for the study of frozen ground, GPR in particular is considered to be a reliable and effective method for identifying thermal interfaces that indicate a change in thermal state (Moorman et al. 2003). In general, two aspects of frozen ground contribute to the wide use and success of GPR in cold regions: the decreased signal attenuation (losses) related to reduced ionic conduction as the phase change of pore water to ice takes place, and the large dielectric contrast that exists between frozen and unfrozen materials (Table 1), which typically causes a highly reflective interface.

The dielectric constant (k) of a material is a function of its ice and liquid water content. As interstitial ice begins to form in the pores of freezing sediments, both the liquid water content and the dielectric constant decreases (Table 1). This results in a large reflection coefficient (-0.34) between

Table 1. Typical dielectric properties of frozen and unfrozen materials. The volumetric unfrozen water content (θuf) for clay is given at various temperatures. (Sources: Patterson & Smith 1981, Davis & Annan 1989).

Material	Dielectric constant	Attenuation dB/m
liquid water	80	0.1
pure ice	3-4	0.01
unfrozen sand	20-30	0.03-0.3
(-1.5°C) frozen sand	4	2
(-0.5°C) clay (θ uf =40%)	27	65
(-1 °C) clay (θ uf =25%)	12	60
(-2 °C) clay (θ uf =17%)	8	47

frozen (*k = 6)* and unfrozen (*k = 25*) sediment (Stevens 2007). As such, the dielectric gradient is mainly controlled by the temperature gradient, textural characteristics of the sediment, and pore-water chemistry.

Study Area

The Mackenzie Delta is located within the western Canadian Arctic (Fig. 1a). Permafrost beneath the upland Pleistocene delta can be in excess of 500 m thick; however, beneath the modern delta plain, permafrost is generally less than 100 m thick (Taylor et al. 1996) with the exception of where channels and lakes restrict cooling of the ground (Smith 1976). Seaward of the delta plain, a shallow-water platform of water depths less than 2 m extends for approximately 17 km. Winter ice growth in this region is commonly in excess of 1 m, and therefore seasonal ice freezes to the sediment bed (bottom-fast ice) over extensive nearshore areas. The thermal regime beneath shallow water in this area has been shown to be regulated by bottom-fast ice, as heat is readily conducted from the ground during the period of ice contact (Dyke 1991).

GPR surveys were conducted from an ice surface over a distributary bar at the mouth of Middle Channel in late March. The area surveyed extended from within Middle Channel to a nearshore location adjacent to Garry Island (Fig. 1b). Fresh water (<0.2 mS/m) and ice dominate this site due to its close proximity to the outflow from Middle Channel. Similarly, pore-water salinity analyzed from sediment cores indicates values below 4 ppt (5 mS/m) within the upper 5 m of sediment. Sediment cores also indicate an overall coarsening upwards sequence of sediment, ranging from silty clay to sandy silt. The low electrical conductivity of ice and water promotes subsurface propagation of EM energy at this site. However, similar application of GPR would be hindered in coastal environments dominated by seawater.

Data Acquisition

A total of 154 line km of GPR data was collected in March of 2005, 2006, and 2007. The GPR surveys were conducted using a PulseEKKO 100 with 100 MHz antennas and a Noggin Plus system with both 500 MHz and 250 MHz antennas. Data from each system were recorded on individual data loggers. The radar systems and corresponding antennas were configured in an array so that simultaneous acquisition of the data could take place by towing the systems at a constant rate of 5 km/hr (Fig. 2). In order to acquire a high density of GPR traces (5 cm/trace) at the towing speed of 5 km/h, low stacking and short time window settings were used. Spatial positioning of each trace was recorded with either a Wide Area Augmentation Service (WAAS) corrected or real-time kinematic GPS unit. The processing of the GPR data included enhancement of weaker reflections using an Automatic Gain Control (AGC).

The subsurface transition in material properties from ice to water and frozen and unfrozen sediment corresponds to significant changes in the propagation velocity of radar waves. This study uses an average velocity of 0.16 m/ns for ice, 0.03 m/ns for water, 0.15 m/ns for frozen sediment, and 0.10 m/ns for unfrozen sediment, based on CMP

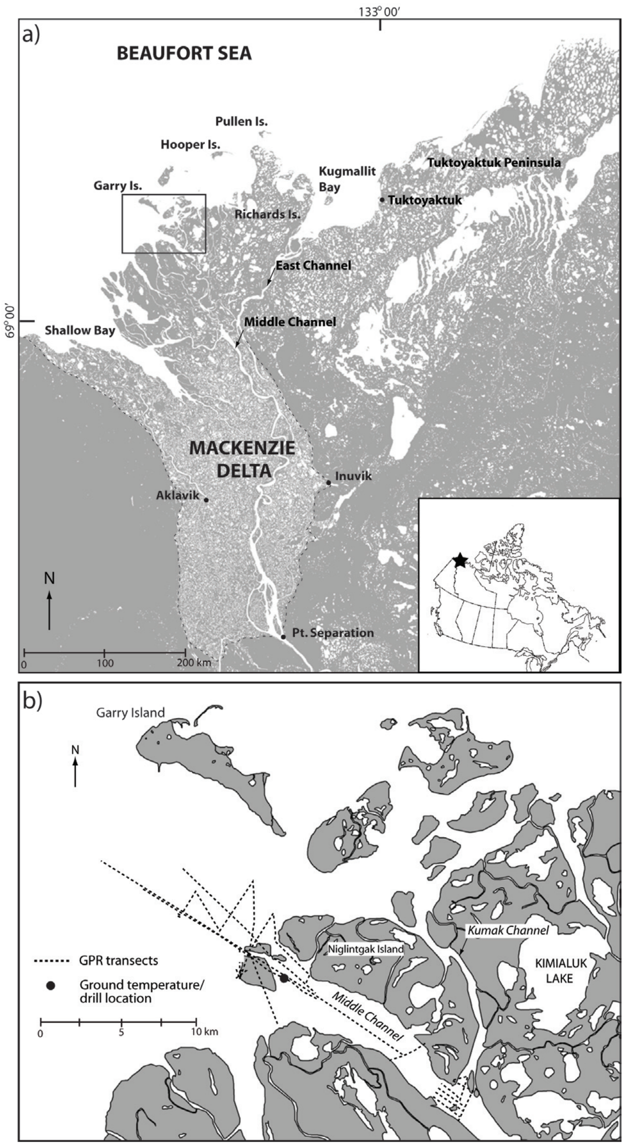

Figure 1. Study area map: a) regional view of the Mackenzie Delta located in the western Canadian Arctic and b) site map showing the orientation of GPR transects surveyed over the distributary bar at the mouth of Middle Channel.

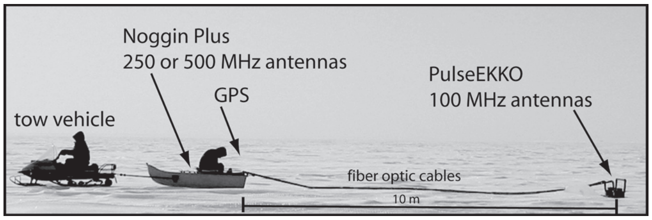

Figure 2. Multi-frequency GPR setup towed behind a snowmachine. GPR systems include a PulseEKKO 100 with 100 MHz antennas and a Noggin Plus systems with 250 and 500 MHz antennas. Positional data was acquired with GPS for each radar trace.

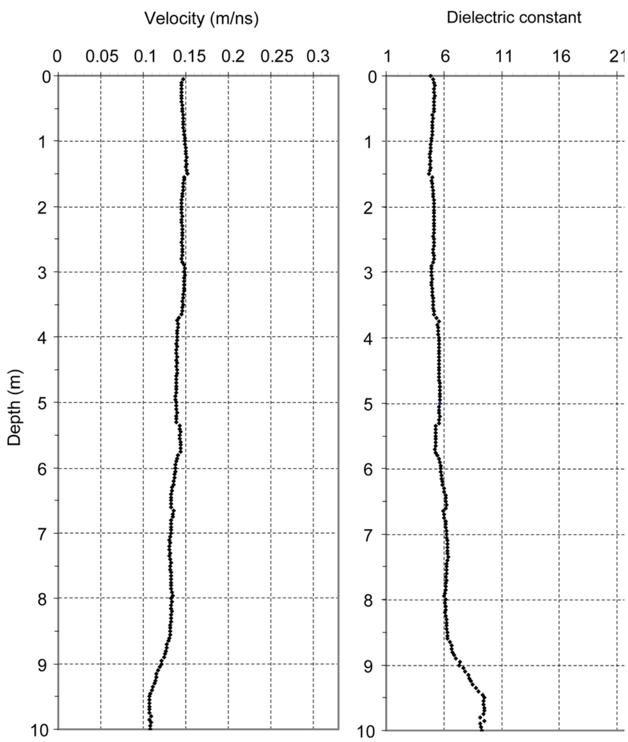

Figure 3. Calculated wave velocities and dielectric constants in frozen sediment obtained from cross-borehole measurements. The average wave velocity in the upper 5 m of sediment was 0.15 m/ns.

measurements, direct drill verification, and cross-borehole radar measurements conducted within the area. The GPR propagation velocities calculated from cross-borehole surveys were relatively consistent within the upper 5 m of sub-bottom sediment and therefore reflect the values used for depth conversions (Fig. 3).

Ground temperature measurements used for this study were recorded up to 10 m beneath zones of bottom-fast ice. Measurements were made every eight hours with RBR™ data loggers and YSI thermistors. The thermistors are accurate to ±0.1°C. Information gained from two years of ground temperature data collected within the study site supports the GPR findings and aids in further radar interpretation where such subsurface verification was not present.

Results and Discussion

Figure 4 shows the GPR trace response to changes in ground temperatures and the thermal state of sediment beneath bottom-fast ice. At this locality, borehole (GSC 2007-301-063) indicates two thermal interfaces 3 m and 5.5 m in depth. Unfrozen saturated sediment in this depth range corresponds to ground temperatures between -0.06°C and -0.48°C. Although these sediments are cryotic, the complete lack of ice bonding observed in core suggests a freezing-point depression.

The radar trace response indicates relatively high amplitude reflection events that correspond to the upper and lower thermal interfaces (Fig. 4). These interfaces exhibit opposing wavelet phase under constant antenna directivity. In this study, antennas were orientated to produce a + - + wavelet phase from the base of the ice. This allowed for a + - + reflection wavelet when transitioning from frozen to unfrozen sediment and - + - phase from unfrozen to frozen sediment. In theory, different reflection polarity occurs when wave impedance is caused by the transition from materials of high-to-low versus low-to-high dielectric constant (Arcone et al. 2006).

In Figure 4, the depth of signal penetration achieved with 250 MHz is limited to the first frozen-unfrozen interface, as a result of high signal attenuation in the unfrozen sediment. The signal attenuation exhibited in fine-grained saturated sediment results from the interaction between the polar water molecules and the charged sediment surfaces. However, greater penetration depths were obtained with lower antenna frequencies (e.g., 100 MHz) which allowed for multiple frozen–to-unfrozen transitions to be imaged up to 10 m in depth.

The upper thermal interface was identified in a cross-sectional profile as a laterally continuous reflection (Fig. 5). Internal reflections resolved from within the zone of frozen sediment represent sedimentary structure. The upper thermal interface was verified to represent the depth of seasonal frost with temperature data. Beneath zones of bottom-fast ice, seasonal frost develops as a result of seasonal cooling in the ground that is prompted by ice contact with the sediment bed (Dyke 1991). Seasonal frost typically extended less than 3 m below the ice surface.

At greater depths, an additional frozen-unfrozen interface (lower thermal interface) was detected using 100 MHz antennas (Fig. 6). This lower thermal interface represents the approximate position of the permafrost table. At locations where the permafrost table remains detectable by late winter, seasonal thaw exceeds freezeback of the active layer and a talik is present.

Similarly, more isolated zones of unfrozen sediment relating to the presence of taliks result from bathymetric depressions in the sediment bed (Fig. 7). At this location, the talik zone corresponds to an area where ice thickness is in excess of 40 cm. The deeper water limits the ice contact time with the sediment bed, as the duration of winter ice growth is extended. Subsequently, seasonal cooling of the ground is less, and thaw exceeds freeze back. These sites demonstrate the relationship that exists between ice thickness and the spatial complexity of frozen-unfrozen zones beneath bottom-fast ice.

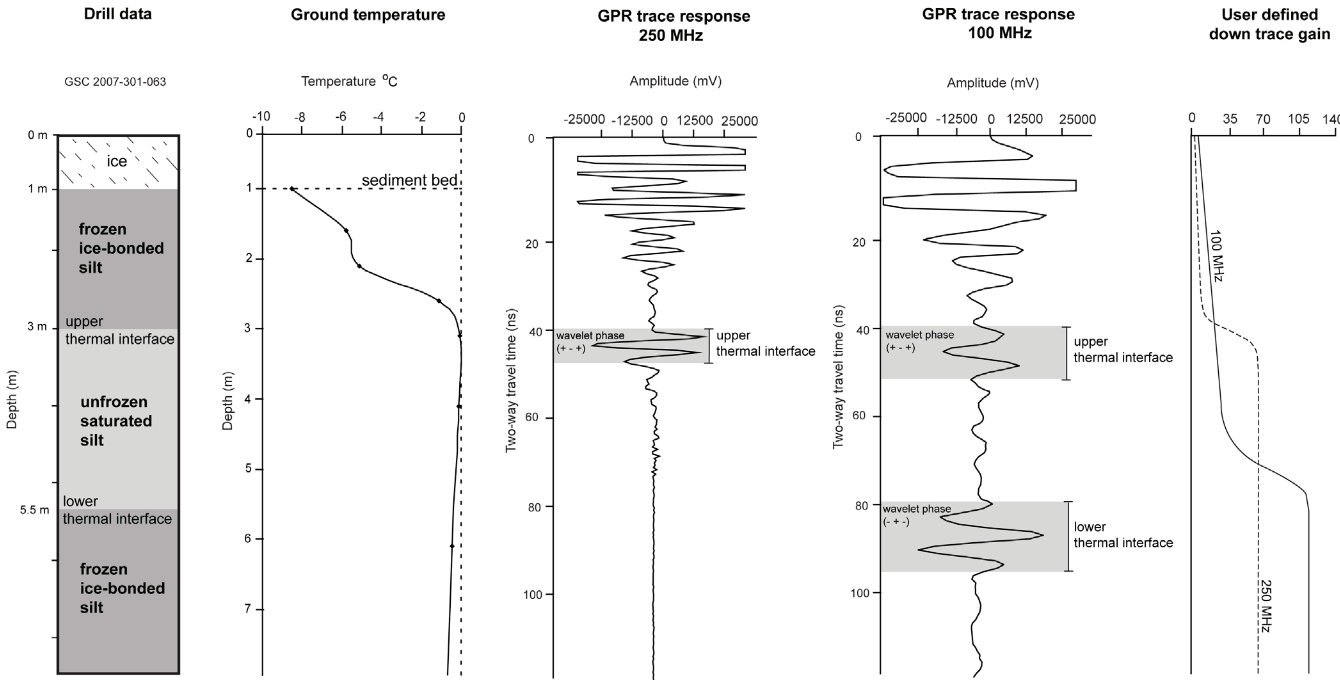

Figure 4. Comparison between drill data, ground temperatures and GPR trace response for 250 and 100 MHz antennas. Drill data at GSC 2007-301-063 indicates a frozen-to-unfrozen interface at 3 m and an unfrozen-to-frozen interface at 5.5 m. The zone of unfrozen sediment corresponds to ground temperatures between -0.06 and -0.48°C. The GPR trace response to these conditions shows two reflective events; an upper thermal interface resolved at 40 ns with 250 MHz, and a lower thermal interface identified at 80 ns with 100 MHz antennas.

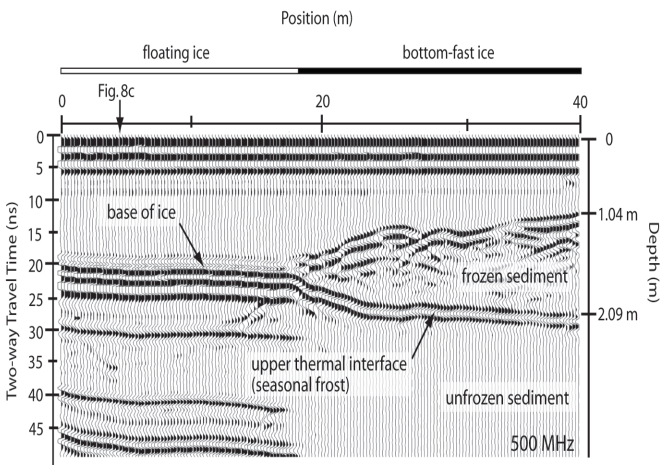

Figure 5. A 500 MHz GPR profile across zones of bottom-fast and floating ice. Beneath the bottom-fast ice an upper thermal interface representing the depth of seasonal frost was detected at 2 m below the ice surface. Ice-bottom multiples are present from 40-50 ns beneath the zone of floating ice.

Interpretations of GPR profiles collected over zones of bottom-fast and floating ice indicate a complex cryostratigraphy with multiple near-surface transitions from frozen to unfrozen sediment occurring over short distances (e.g. <10 m) by late winter. Typically, where bottom-fast ice thickness was less than 1 m, complete active layer freezeback has occurred (Fig. 8a); whereas beneath bottom-fast ice greater than 1 m thick, a talik existed between seasonal frost and the permafrost table (Fig. 8b).

This reflects conditions where seasonal thaw exceeds freezeback of the active layer over one year or a number of years. At locations occupied by floating ice, near-surface sediments were unfrozen to the depth of penetration of the GPR (Fig. 8c). The depth of seasonal frost also decreased towards zones of floating ice, as lateral heat flow restricts the surrounding sediments from freezing.

In general, a strong relationship between bottom-fast ice thickness and nearshore cryostratigraphy exists. As previously noted, the increased duration of ice growth in areas of deeper water restricts the extent of seasonal frost in the ground. This relationship between ice thickness the development of seasonal frost are demonstrated in Figures 6 and 7. The thermal region of the permafrost body is also affected where thaw exceeds complete freezeback of the active layer, as seasonal cooling of the permafrost body is minimal (Stevens 2007). Using this information, the interpretation of GPR profiles also allows the identification of sites where permafrost is potentially degrading.

The variability that exists in the near-surface distribution of frozen and unfrozen sediment may also be influenced by seasonal changes in the rate of ice growth and localized sediment erosion and accretion, which alter the previous water depth.

The GPR reflections from thermal interfaces relate to change in state of pore water, as verified with both drill and ground temperature data (Fig. 4). Therefore, the ability to coherently resolve these two interfaces may be limited where marginally bonded sediments and gradual changes in the dielectric contrast occur over a depth range greater than the transmitted wavelength. Similarly, only under thermal conditions where ice nucleation occurs near 0°C, will GPR reflections correlate with the zero degree isotherm.

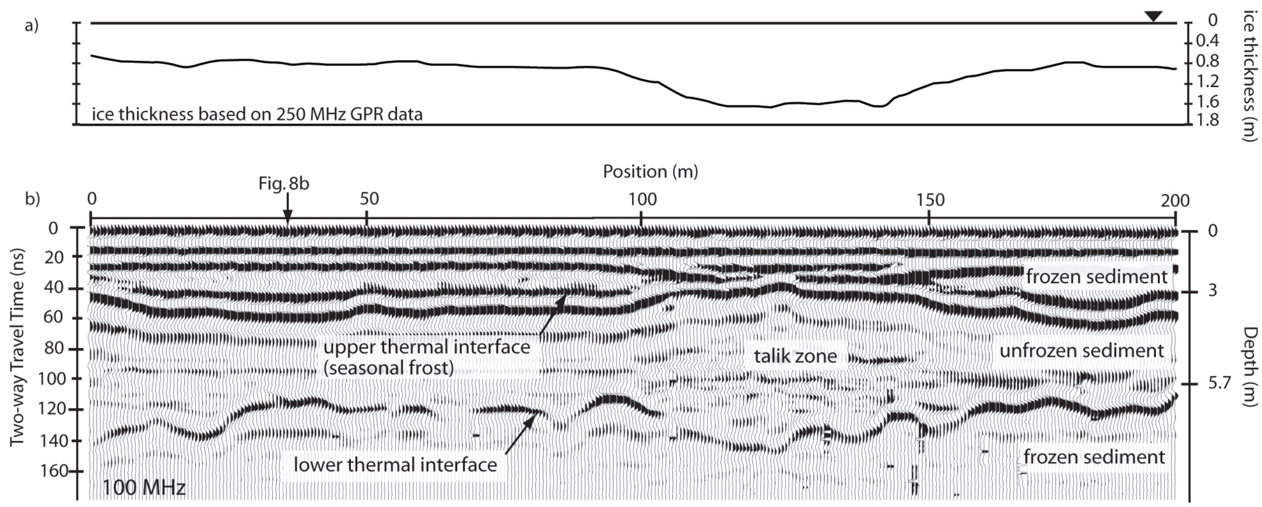

Figure 6. a) Profile of ice thickness obtained across a 200 m section of bottom-fast ice and b) corresponding 100 MHz GPR profile showing both an upper and lower thermal interface which defines a talik zone between ~3 m and 5.7 m.

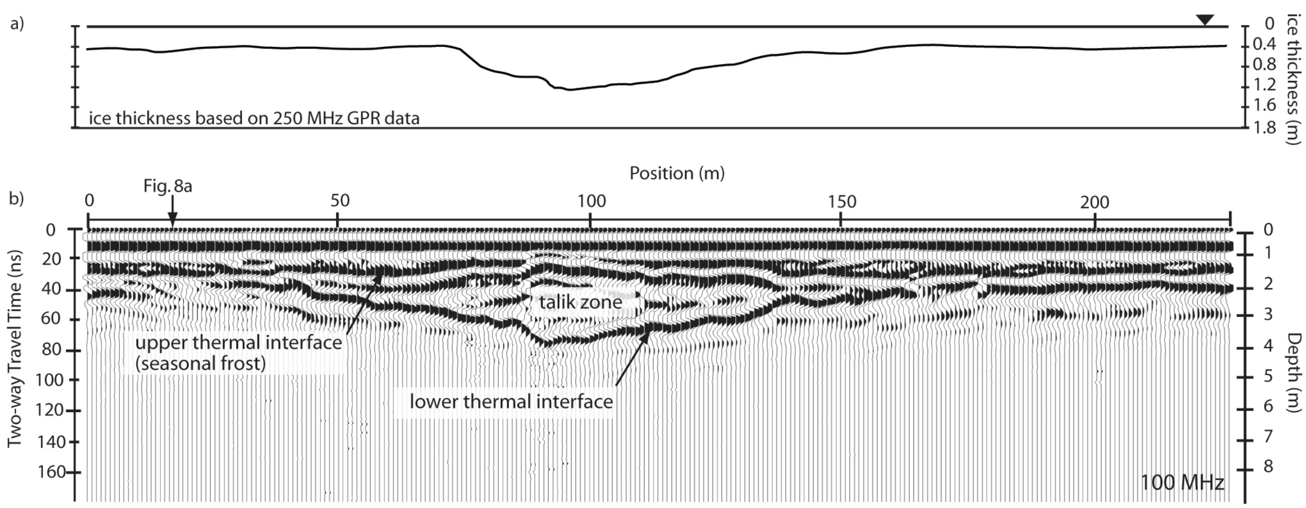

Figure 7. a) Profile of ice thickness obtained across a 225 m section of bottom-fast ice and b) corresponding 100 MHz GPR profile showing the location of an isolated talik. At this location, the talik zone corresponds to ice thickness greater than 40 cm.

Thus, the width of the freezing fringe that is determined by the temperature gradient becomes important to reflection characteristics.

Based on the ground temperature profile presented in Figure 4, a large temperature gradient exists at the upper thermal interface (i.e., the transition from the seasonally frozen to underlying unfrozen sediment). This results in a narrow freezing fringe and a sharp interface between frozen and unfrozen material. This is in contrast to the permafrost table, which exhibited a lower temperature gradient over an equivalent subsurface distance. Therefore, the lower temperature gradient has the potential to cause some misinterpretation of the permafrost table due to more subtle changes in the dielectric properties over the wavelength. In addition, a freezing-point depression would offset the ice nucleation temperature and the recorded position of the permafrost table. As GPR can only resolve changes in the thermal state of pore water and cannot directly detect ground temperatures, the latter information can only be inferred.

Conclusions

Ground penetrating radar surveys conducted within the nearshore zone of the Mackenzie Delta were effective in resolving thermal interfaces up to 6 m beneath zones of bottom-fast ice. With 250 MHz antennas, the depth of penetration was limited to an upper thermal interface which corresponds to the extent of seasonal frost. In contrast, an upper and lower thermal interface delineating talik zones were resolved with 100 MHz antennas. Thermal interfaces closely correlate with frozen-unfrozen transitions of sediment and changes in ground temperatures from above freezing to below -0.5°C.

Complete freezeback of the active layer was exhibited beneath bottom-fast ice less than 1 m thick in contrast to locations where ice was greater than 1 m thick, beneath which talik zones were identified. Sediments were unfrozen at the sediment-water interface where ice remained floating.

The multiple thermal interfaces detected beneath bottom-

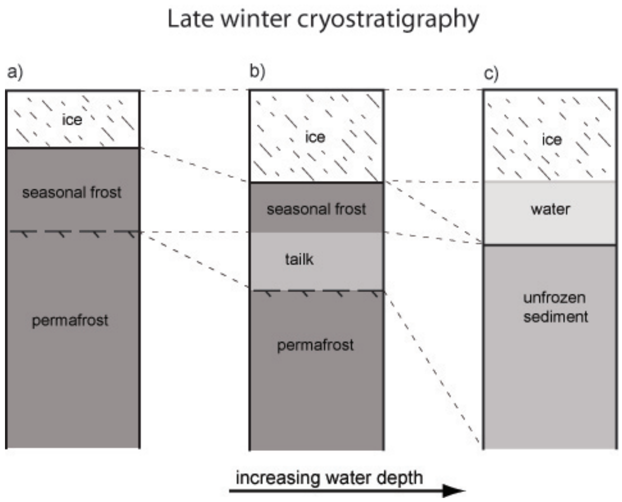

Figure 8. Schematic illustration of late winter cryostratigraphy interpreted from GPR data: a) bottom-fast ice less than 1 m thick characterized by complete freezeback of active layer; b) bottom-fast ice greater than 1 m thick characterized by a talik where thaw exceeds freezeback of the active layer; and c) floating ice where sediments are perennially unfrozen within the upper 3 m of the sediment bed.

fast ice suggest a complex thermal regime that exists at scales not easily characterized by point-source drill and ground-temperature datasets. However, multi-frequency GPR surveys provide high resolution reflection-based data which can detect vertical and spatial variations in the thermal state over large coastal regions. Such subsurface datasets become critical to further understanding permafrost conditions and freeze-thaw processes in the coastal zone.

Acknowledgments

This research was financially supported by the Natural Resources Canada and NSERC. Logistical support was provided by Shell Canada, Chevron Canada, Devon Energy, and the Aurora Research Institute. We also acknowledge Dustin Whalen, J.C. Lavergne, and Jen Bode for assisting with data collection.

References

Arcone, S.A., Chacho Jr., E.F. & Delaney, A.J. 1992. Short-pulse radar detection of ground water in the Sagavanirktok River flood plain in early spring. *Water Resources Research* 28: 2925–2936.

Arcone, S.A., Chacho, E.F. & Delaney, A.J. 1998. Seasonal structure of taliks beneath arctic streams determined with ground-penetrating radar. *Proceedings of the Seventh International Conference on Permafrost, Yellowknife, Canada, June 23-27, 1998*: 19-24.

Arcone, S.A., Finnegan, D.C. & Lanbo, L. 2006. Target interaction with stratigraphy beneath shallow, frozen lakes: Quarter-wave resonances within GPR profiles. *Geophysics* 71: k119-k131.

Davis, J.L. & Annan, P. 1989. Ground-penetrating radar for high-resolution mapping of soil and rock stratigraphy. *Geophysical Prospecting* 27: 531-551.

Delaney, A.J., Arcone, S.A. & Chacho, E.F. 1990. Winter short-pulse radar studies on the Tanana River, Alaska. *Arctic* 43: 244-250.

Dyke, L.D. 1991. Temperature changes and thaw of permafrost adjacent to Richards Island, Mackenzie Delta, N.W.T. *Canadian Journal of Earth Sciences* 28: 1834-1842.

Kurfurst, P.J. & Dallimore, S.R. 1991. Engineering geology of nearshore areas off Richards Island, N.W.T., a comparison of stable and actively eroding coastlines. *Canadian Geotechnical Journal* 28: 179-188.

Moorman, B. J., Robinson, S. D. & Burgess, M.M. 2003. Imaging periglacial conditions with ground-penetrating radar. *Permafrost and Periglacial Process* 14: 319-329.

Patterson, D.E. & Smith, M.W. 1981. The measurement of unfrozen water content by time domain reflectomerty: results from laboratory tests. *Canadian Geotechnical Journal* 18: 131-144.

Smith, M.W. 1976. Permafrost in the Mackenzie Delta. *Geological Survey of Canada*, Paper 75-28: 31.

Stevens, C.W. 2007. Subsurface investigation of shallow-water permafrost. *Unpublished M.Sc thesis* Department of Geography, University of Calgary, Calgary, Alberta 127.

Taylor, A.E., Dallimore, S.R. & Judge, A.S, 1996. Late Quaternary history of the Mackenzie-Beaufort region, Arctic Canada, from modelling of permafrost temperatures. 2. The Mackenzie Delta- Tuktoyaktuk coastlands. *Canadian Journal of Earth Sciences* 33:62-71.

Wolfe, S. Dallimore, S. & Solomon, S.M. 1998. Coastal permafrost investigations along a rapidly eroding shoreline, Tuktoyaktuk, N.W.T. *Proceedings of the Seventh International Conference on Permafrost, Yellowknife, Canada, June 23-27, 1998*: 1125-1131.

Atlas of Northern Circumpolar Soil

Vladimir Stolbovoy
European Commission Joint Research Centre, Institute for Environment and Sustainability, Ispra, Italy
Arwyn Jones
European Commission Joint Research Centre, Institute for Environment and Sustainability, Ispra, Italy
Charles Tarnocai
Agriculture and Agri-Food Canada, Ottawa, Canada
Gabriele Broll
ISPA, Vechta University, Vechta, Germany
Luca Montanarella
European Commission Joint Research Centre, Institute for Environment and Sustainability, Ispra, Italy

Abstract

Cooperation between soil scientists from Canada, European Union, Russia, and the USA has resulted in an Atlas of Northern Circumpolar Soil which brings together soil data for all northern countries to better understand soil resources in these regions. The Atlas aims to raise public awareness of the value of soil in the north and support further research in this area (for example, the European Union's Thematic Strategy for Soil Protection). The Atlas contains a richness of information on soil diversity, the mapping and classification of permafrost-affected soil, the role of soil in the global carbon cycle, and atmospheric concentrations of biospheric greenhouse gases in the past and the future. The publication has fostered cooperation between several countries and bridges the gap between soil science, the permafrost community, policy makers, educators, and the general public. The Atlas is a contribution of the European Union to the International Polar Year 2008.

Keywords: atlas; climate change; cryosols; permafrost; soil.

Introduction

The Arctic plays a key role in the global environment. The region accumulates a huge mass of ice which controls sea level, heat exchange in the atmosphere, and the cold oceanic currents driving atmospheric and oceanic processes. NASA observation shows that perennial Arctic sea ice, which normally survives the summer melt season, has shrunk by 14% between 2004 and 2005. The melting of the ice cap indicates a warming of the marine environments. On the continental land, such a climatic warming will lead to a degradation of the permafrost, which affects the behavior of terrestrial ecosystems including humans (e.g., sinking houses, weakening roads, runways, and pipelines).

While there is considerable research interest in the Arctic region on socioeconomic and broad environmental issues, there is a growing awareness of the importance of soil in the northern circumpolar region. Soil is a surface layer which has resulted from the interaction of climate, relief, parent material, vegetation, and time. As a natural body, soil supports basic physical, chemical, and biological processes in ecosystems and provides principle ecological services for humans. Being sensitive to environmental changes, soil in northern regions is projected to undergo the greatest impact from climate warming. The consequences of changes to the principle soil-forming processes regulating biogeochemical cycles and ecosystems functioning are uncertain at present. In order to draw a reliable picture on the future changes, soil scientists have over the last decades focused efforts to improve the basic and applied knowledge of the circumpolar soil.

One of the specific features of the north circumpolar region is that it is occupied by developed countries (USA, Canada, EU, and Russia) with strong national traditions in soil classifications, survey, and mapping. The diversity of national traditions results in a mosaic of soil inventories, which make joint analysis of soil resources difficult. This situation is a serious constraint for the communication and implementation of agreed environmental policies in the region. Soil scientists have attempted to overcome this gap by focusing on the development of a common circumpolar soil database. All national soil terms and data in this area were combined, correlated, and presented in a common harmonized GIS-compatible database (Tarnocai et al. 2001, Cryosol Working Group 2004). The database has enabled the first estimate of the carbon stock in cryosols (Tarnocai & Broll 2008, Tarnocai et al. 2007, Tarnocai et al. 2006, Tarnocai et al. 2003). It was found that soil in the circumpolar region accumulates about 30% of the world's soil organic carbon. The release of the database stimulated a fundamental review of the knowledge on the permafrost-effected soil. This basic revision has been outlined in Kimble et al. (2004).

However, the soil database, its analysis and related scientific publications address professionals and are too specific for the general public. To bring available information to the latter, a group of scientists from Canada, European Union, Russia, and the USA have collaborated to produce a high quality Atlas on soil in the northern circumpolar regions that is easily readable and graphically stimulating. This publication intends to raise public awareness of the value of soil in northern latitudes supporting further research in this area - for example, Soil Thematic Strategy for Soil Protection in Europe (COM (2006)231, COM(2006)232).

The compilation of the Atlas is a contribution to the Polar Year (IPY) 2007-2008 collaborative science program. This work is included in the IPY CAPP Project #373. It contributes to multidisciplinary approach, incorporating physical and biological sciences, social sciences, and a large education component.

The objective of the paper is to introduce the Atlas of Northern Circumpolar Soil with special emphasis on:

1. Methods and data used;
2. Content of the Atlas;
3. Demonstrate major findings and conclusions.

Methods and Materials

The Atlas is a compilation of different data originating from published and unpublished sources. A substantial portion of the data, including maps, texts, photos, and graphs, is new and was produced specifically for the Atlas. The cartographic coverage originates from a variety of sources: 1) for the North America, Greenland, Mongolia, and part of Kazakhstan: the Northern and Mid Latitude Soil Database (Cryosol Working Group 2004); 2) for Northern Eurasia and Iceland: the Soil Geographical Database of Eurasia (Van Liedekerke et. al. 2004); 3) for China and part of Kazakhstan: Digital Soil Map of the World (FAO 1990). All these databases have been combined to create a single database that covers a circle with the North Pole in the center and limited by 50°N latitude to the south. The database has been translated into the international World Reference Base correlation system (IUSS 2006).

In addition to maps, the Atlas contains explanatory texts illustrated by photographs and graphics that are specially written to address those who are interested in learning more about northern soil characteristics and environments.

Technically, the Atlas is a book of 144 A3 pages illustrated by a mix of text, colored maps, pictures, diagrams, and photographs.

Results

The Atlas (Fig. 1) consists of the following main sections:

1. Introduction
2. The Northern Environment
3. Soil in Northern Latitudes
4. Soil Classification
5. Soil Maps
6. Northern Soils and Global Change
7. Conclusions and Future Perspectives
8. Additional Information

Figure 1. Cover page showing the extent of the northern circumpolar area addressed by the Atlas.

Introduction

This section contains the list of authors, includes acknowledgements, outlines the scope of the Atlas, and presents an overview of EU policy for soil protection within the context of the International Polar Year.

The northern environment

This section is intended to provide the reader with a range of general information on the circumpolar region through a series of documented thematic maps (i.e., sea ice extent, mean annual temperature, mean annual precipitation, permafrost extent, soil temperature, relief, parent material, land cover, population density, permafrost, and patterned ground). Data for this section come from well-distinguished sources. For example, the soil temperature map originates from the US Department of Agriculture; the vegetation patterns were extracted from the Global Land Cover 2000 database; while information on permafrost is provided by the International Permafrost Association.

Soil in northern latitudes

The scope of this section is to provide a basic understanding of what is soil and, in particular, soil in northern regions. The section outlines the main soil functions, especially those related to the principle soil-forming processes in northern latitudes with specific attention being given to cryogenic processes associated with freeze-thaw cycle, cryoturbation, polygonal cracking, and stone sorting. The section also describes soil biodiversity in cold climates.

Soil classification

This section introduces the most widely-used national soil classification systems in the circumpolar region (e.g., Canadian, USA, and Russian). Special attention is paid to the latest version of the World Reference Base for soil classification (IUSS 2006). All classification systems are illustrated by examples of their main concepts, taxonomic systems, and description of the principle soil types. One page of the Atlas is devoted to the correlation and comparison of different classification systems. Examples demonstrate that soil inventories based on the varying concepts used in different soil classifications result in a markedly different outputs (e.g., Cryozems in Russian soil classification are exclusively restricted to highly cryoturbated soils that cover only a part of the Gelisols Order in the USDA Soil Taxonomy, Cryosols in Canadian system and WRB).

The different number of the highest level taxonomic classes is another example of the conceptual differences between national soil classifications: Soil Taxonomy (USDA) uses twelve Orders; the Canadian soil classification system exploits ten soil Orders; the Russian soil classification contains fifteen soil Divisions while the WRB system assigns all soil types to thirty two Reference Soil Groups.

As the conceptual inconsistency is difficult to overcome, many scientists suggest comparing national soil classifications on the basis of physically measured soil parameters (e.g., pH, organic carbon content, base saturation, etc.). Unfortunately this approach has some limitations as soil characteristics are measured differently in different countries. This inconsistency is because of the national traditions, the availability of equipment, economic reasons, etc. For example, the determination of soil organic carbon (SOC) according to the methodology proposed by Walkley–Black (Canada) or Turin (Russia) is based on "wet combustion" (carbon oxidation is performed by dichromate solution). This method recovers about 70%-80% of the total SOC content. Other countries use a dry combustion method, where the soil is heated to 950°C in an oven. In this method the recovery of SOC is 100%. Similar differences can be found in many other analytical methods, such as the detection of soil texture, soil pH, cation exchange capacity, etc. Therefore, an understanding of the methodologies used to measure soil characteristics is crucial for the correlation of national soil classifications.

Other variations in soil characteristics arise from differences in ecological and land-cover interpretations in different countries. For example, the thickness of the peat layer is one of the criteria used to distinguish forest from bog in land cover mapping. In Canada, this threshold is 40 cm, while being 30 cm in Russia. As a result, maps of peat areas using the two approaches look substantially different.

In spite of the differences in national classification schemes and the lack of full coincidence between soil terms, the occurrence of the soil in the same natural zone could be a good basis to correlate soil classifications. For example, Mollisols (the USDA Soil Taxonomy), Chernozems (in Canadian and WRB systems) and Humic-accumulative soils (Russia) are formed under steppe and the prairies vegetation. Therefore, these differently termed soils have many common characteristics and could be regarded as being very close.

The section also contains a description of the Reference Soil Groups of the WRB, illustrated by maps showing the broad distribution patterns of each reference group together with high-quality photographs of characteristic soil profiles and associated landscapes. The section is concluded by examples of soil surveys in the Arctic.

Soil maps

The heart of the Atlas contains 30 plates of soil maps at a scale of 1:3,000,000. The map legend is based on the second level units of the WRB (IUSS 2006). This is the first application of the revised WRB system for this territory. It is important to emphasize that the maps were harmonized at the border between some countries (e.g., USA (Alaska) and Canada, Russia and Finland, Russia and China). All maps contain short explanatory texts aiming to draw the attention to the specific features of this particular circumpolar area.

A short section is devoted to other regions for the world where cold soil can be found, and includes some information on the soil types of Antarctica. The section concludes with an overview of the circumpolar soil database and introduces the basic principles of Geographic Information Systems (GIS) and its use in the Atlas.

Northern soils and global change

This section provides information on the relationship between soil and global change, in particular, climate change. A brief overview of glacial periods is used to introduce the concept of palaeosols that illustrate the ability of soil to preserve indications of past climate change.

The section progresses to consider the role of the circumpolar region in the global carbon cycle, which is highly debated at present. Besides general information, this section demonstrates the special role of the organic and mineral soil types in the north for the sequestration of organic carbon. Through cryoturbation and other pedogenic processes, organic carbon can be moved deep in the soil and preserved from decay by the permafrost for very long periods of time (Fig. 2).

Figure 2. Organic matter translocation by cryoturbation. East European tundra near Vorkuta, Russia. Cryoturbation in permafrost-affected soils removes peat, litter, wood debris, and other kinds of organic matter (fragments of H horizon – the darker parts in the above profile) from the surface deeper into the soil leading to preservation of organic matter in deeper, colder, and less biologically active layers (photo by M. Drewnik).

Such special mechanisms make cryosols and organic-rich soil a unique instrument to mitigate greenhouse gas concentration in the atmosphere. The Atlas explains the processes for the decomposition of vegetation residues and the associated emissions of carbon dioxide and methane, and pays special attention to the potential evolution of organic and mineral soil under present and future climate warming scenarios.

The variation in the characteristics of soil in the northern circumpolar region is striking. The Atlas illustrates this richness through a series of plates devoted to the soil types of Scandinavia, Iceland, Greenland, Canada, Alaska, and Central Siberia.

Conclusions and future perspectives

The last section considers future perspectives for soil in northern areas, raising attention to the need for soil conservation in the area. One page is devoted to the high value of the Atlas as an educational resource. This is supplemented by a glossary of terms, contact information for soil scientists in northern countries, and references for those who wish to know more about the unique world of northern circumpolar soils.

Summary

The Atlas of Northern Circumpolar Soil is the first document of its kind to bring together soil data for all the northern countries in a style designed to better explain and protect soil resources in these areas. The Atlas has fostered cooperation between several countries and bridges the gap between soil science, the permafrost community, policy makers, educators, and the general public.

Core support for the project has been provided by the European Commission's Joint Research Centre (JRC).

References

Cryosol Working Group. 2004. *Northern and Mid-Latitude Soil Database, Version 1*. Data set. Available on-line http://www.daac.ornl.gov] from Oak Ridge National Laboratory Distributed Active Archive Center, Oak Ridge, Tennessee, USA.

EC. 2006. Communication of 22 September 2006 from the Commission to the Council, the European Parliament, the Economic and Social Committee and the Committee of the Regions: Thematic Strategy for Soil Protection (COM [2006] 231 final).

EC. 2006. Proposal for a Directive of the European Parliament and of the Council establishing a framework for the protection of soil and amending Directive 2004/35/EC [COM (2006) 232 final].

FAO. 1990. *Digital Soil Map of the World.* Distributed by UN FAO, http://www.fao.org/

IUSS Working Group WRB. 2006. *World Reference Base for Soils Resources 2006.* World Soil Resources report No. 103. Rome: FAO.

Kimble, J. (ed.). 2004. *Cryosols, Permafrost-Affected Soils*. Berlin Heidelberg : Springer-Verlag, 726 pp.

Van Liedekerke, M., Panagos, P., Darossin, J., Jones, R., Jones, A. & Montanarella, L. (eds.), 2004. *The European Soil Database. Version 2.0*. Ispra, Italy: the EU JRC. CD-ROM.

Tarnocai, C. & Broll, G. 2008. Soil Organic Carbon Stocks in the Northern Permafrost Region and Their Role in Climate Change. *Proceedings of the Ninth International Conference on Permafrost, Fairbanks, Alaska, June 29-July 3, 2008* (this proceedings).

Tarnocai, C., Swanson, D., Kimble, J. & Broll, G. 2007. *Northern Circumpolar Soil Carbon Database.* Research Branch, Agriculture and Agri-Food Canada, Ottawa, Canada.

Tarnocai, C., Lacelle, B., Broll, G., Mazhitova, G., Pfeiffer, E.-M., Stolbovoi, V., Ping, C.L. & Kimble, J.M. 2006. Organic carbon in northern circumpolar soils. *Presented at the World Congress of Soil Science Philadelphia, Pennsylvania, USA, July 9-14, 2006.*

Tarnocai, C., Kimble, J., Swanson, D., Goryachkin, S., Naumov Ye.M., Stolbovoi, V., Jakobsen, B., Broll, G., Montanarella, L., Arnoldussen, A., Orozco-Chavez, F. & Yli-Halla, M. 2001. Soils of Northern and Mid Latitudes. Research Branch, Agriculture and Agri-food Canada, Ottawa, Canada (1:15,000,000 scale map).

Tarnocai, C., Kimble, J. & Broll, G. 2003. Determining carbon stocks in cryosols using the Northern and Mid Latitudes Soil Database. *Proceedings of the Eighth International Conference on Permafrost, 21-25 July 2003, Zurich, Switzerland.* In: M. Phillips, S. Springman, & L. Arenson (eds.), *Permafrost,* volume 2, Lisse/Abingdon/Exton (PA)/Tokyo: A.A. Balkema Publishers, 1129-1134.

Freezing of Marine Sediments and Formation of Continental Permafrost at the Coasts of Yenisey Gulf

Irina D. Streletskaya
Moscow State University, Moscow, Russia
Alexander A. Vasiliev
Earth Cryosphere Institute SB RAS, Tyumen, Russia
Mikhail Z. Kanevskiy
University of Alaska Fairbanks, USA

Abstract

The Quaternary geology of the coasts of Yenisey Gulf is characterized by the prevalence of marine saline sediments. As a rule, the upper parts of coastal sections are of continental origin. Active denudation processes take place in locations with ice-rich sediments, especially where tabular ground ice and ice wedges are present. Massive ground ice bodies with 2–15 m of visible thickness were found in late Pleistocene marine sediments at the Taimyr coasts of Yenisey Gulf. Ice-rich sediments are widespread; they form the "Ice Complex" at the top part of the Quaternary section of west Taimyr. The "Ice Complex" sediments form a geomorphic surface with a height of about 12–15 m a.s.l. These sediments were formed during late Pleistocene sea regression, at a time when the mouth of the Yenisey River was about 300 km to the north from its present location. Ice-rich syngenetic Holocene sediments accumulated mostly at slopes and bottoms of thaw-lake basins and other depressions associated with thawing of Pleistocene ice wedges and tabular massive ice bodies.

Keywords: grain size; heavy minerals; ice wedges; ion composition; quaternary sediments; tabular massive ice.

Introduction

Ground ice studies help to obtain significant paleogeographical information. Huge syngenetic ice wedges, forming specific "Ice Complex" (or "Yedoma") sediments, and tabular massive ice with thicknesses up to 50 m, are unique natural formations. According to most recent publications, "Ice complex" silty sediments of late Pleistocene are polygenetic; they were formed due to aeolian, fluvial, slopewash, nival, and solifluction processes.

"Ice Complex" sediments have been studied mainly in central and northern Yakutia; similar sediments were observed also in Chukotka, West Siberia, Taimyr, Alaska, and Canada (Péwé 1975, Katasonov 1978, Popov et al. 1985, Carter 1988, Romanovskii 1993, Shur et al. 2004). Many publications are also based on studies of tabular massive ice bodies, but numerous hypotheses on their origin are still controversial (Streletskaya et al. 2003). Sections where both tabular and syngenetic ice-wedge bodies can be observed have a special value (Danilov 1969, Trofimov & Vasilchuk 1983, Vasilchuk 2006, Kunitskiy 2007).

Coastal bluffs of the Yenisey Gulf are formed mostly by Quaternary marine and littoral sediments with tabular massive ice bodies (Danilov 1969, Soloviev 1974, Danilov 1978). The upper part of the section is formed by continental sediments with huge ice wedges (Karpov 1986).

Beginning in 2004, we studied permafrost at the coasts of the Yenisey River and Yenisey Gulf between Dudinka and Dikson. This area is located within the continuous permafrost zone (Fig. 1). Our work was aimed at solving the problem of the history of permafrost development during the Pleistocene and Holocene. The purpose of our research included the study of cryogenic structure, chemical and mineralogical composition; estimation of ice content, salinity, grain size, organic carbon content, and age of the Quaternary sediments.

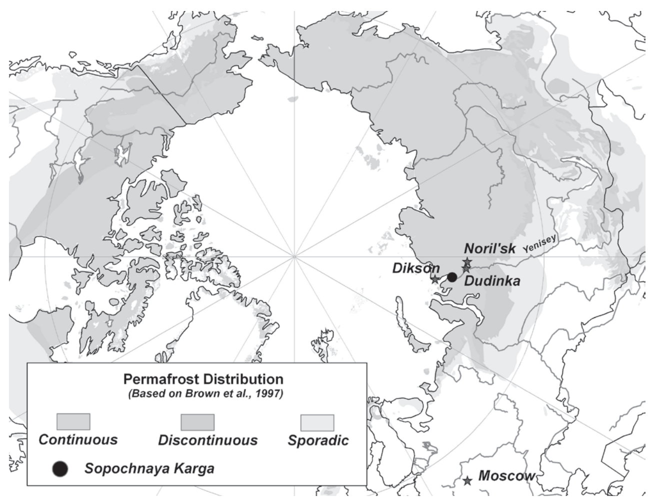

Figure 1. Location of the study area.

During field work, several sections of Quaternary sediments with different types of massive ice were studied (Streletskaya et al. 2005, Streletskaya et al. 2007, Shpolyanskaya et al. 2007). Our research of ground ice and sediments included field investigations and laboratory analyses (chemical, faunistic, micro-pollen and spores, oxygen-isotope, grain size and mineralogical, radiocarbon dating).

Results

One of the most interesting sections was studied in the 30–35 m high coastal bluff located near the "Sopochnaya Karga" Polar Station (71°57′N, 82°41′E), where the tabular massive ice body with a visible thickness of 10–12 m was observed (Fig. 2). This body is overlain by taberal (thawed and refrozen) clayey silts 8–10 m thick. The upper part of section is formed mostly by ice-rich syngenetically frozen silt with a belt-like cryostructure; the cryostructure between ice belts varies from reticulate and ataxitic (suspended) to micro-lenticular. The gravimetric moisture content reaches 80% and more. This layer includes ice wedges that vary from 0.4 m to 3.0 m in width.

The isotope composition (^{18}O) of the intrasedimental ice lenses reaches -17.50‰ to -17.73‰, while the composition of wedge ice varies from -19.04‰ to -20.92 ‰. Wedge ice mineralization reaches 22.04 mg/l, while the silts, including ice wedge, are fresh.

The horizon with ice wedges is underlain by dark-brown peat 1.0–1.5 m thick. The peat transforms with depth into brown organics-rich clayey silt with lenticular-braided, ataxitic (suspended), and micro-lenticular cryostructures (Fig. 2B). Radiocarbon dating of peat samples showed the age 7320 ±130 yr BP (GIN 13056) and 8050 ±60 yr BP (GIN 13055). Thus, radiocarbon dating indicates a Holocene age for the ice wedges.

Peat and peaty silt horizons are underlain by dark-grey silty clay with numerous inclusions of pebbles and boulders. This horizon, which is 10–15 m thick, overlies the body of tabular massive ground ice. Silty clays are characterized by

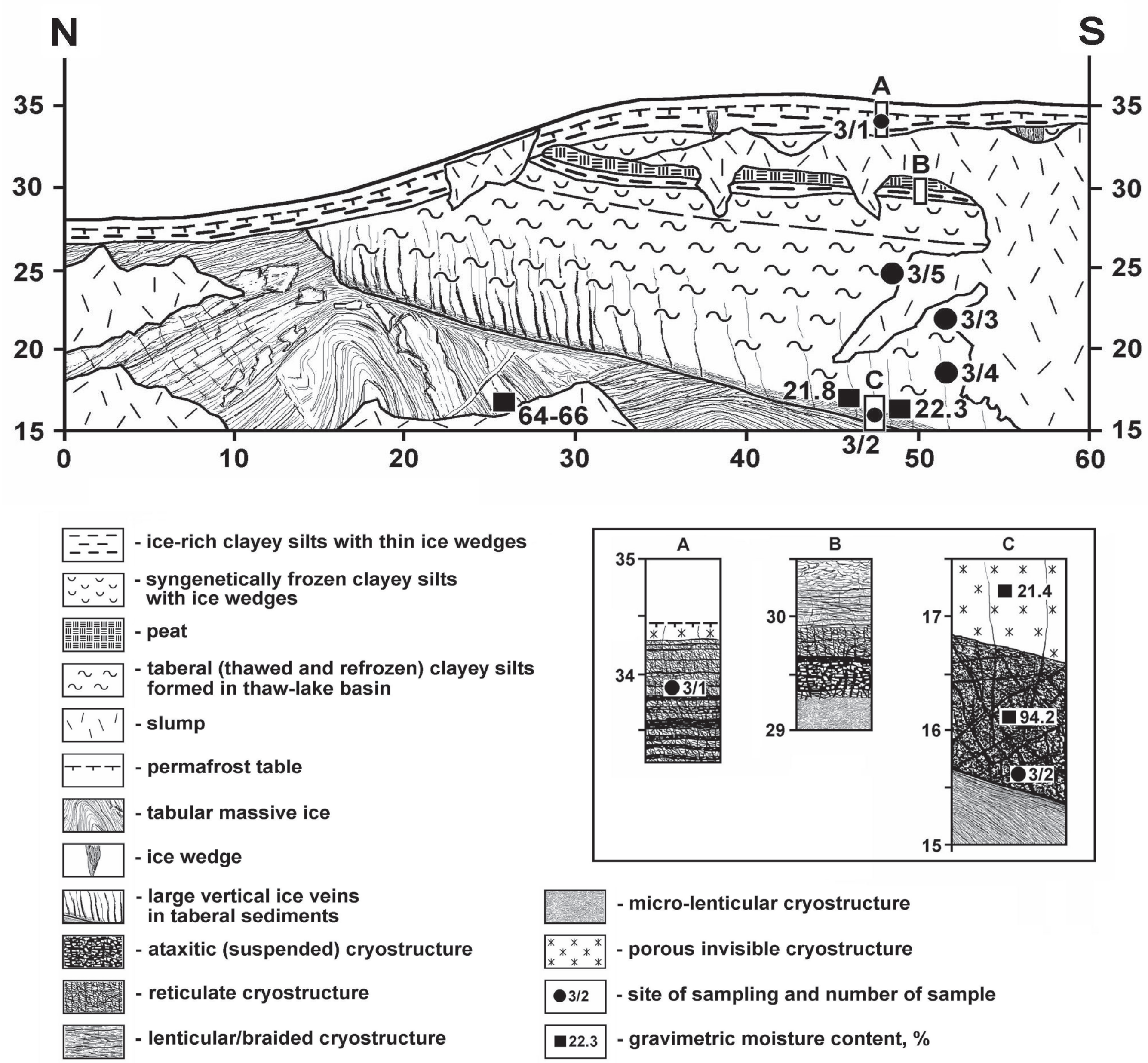

Figure 2. Cryostratigraphic section #3 in the area of "Sopochnaya Karga" Polar Station. Horizontal and vertical scales in meters. A, B, C – details of cryogenic structure.

porous cryostructure; their average gravimetric moisture content is about 22%. At the bottom part of this horizon, above the boundary with the massive ice, thick ice veins, wedging out upwards, were observed. Close to the boundary incline (parallel to the boundary), an ice-rich horizon with the thickness up to 1.2 m was observed. This horizon is characterized by ataxitic (suspended) cryostructure; its gravimetric moisture content reaches 94%.

Silty clays are fresh in general, but their ion composition changes with depth (Fig. 2, samples 3/5, 3/3, 3/4). Bicarbonate-ions and sulfate-ions amounts increase from 0.46 up to 1.92 mg-eqv/l and from 0.18 up to 1.82 mg-eqv/l, respectively. Chlorine-ion content increases from 0.30 up to 0.98 mg-eqv/l. At the boundary with the massive ice body (Fig. 2C, sample 3/2), silty clays contain more soluble salts (salinity is about 0.14%), and contents of bicarbonates and sodium exceeds the contents of all other ions.

A tabular massive ice body is characterized by frequent alternation of folded layers of pure ice and relatively ice-rich soil, with a cryostructure that varies from micro-ataxitic (micro-suspended) to micro-porphyritic (porous visible) with a gravimetric moisture content of 64–66%.

Mineralization of pure ice varies from 46.74 mg/l to 247.87 mg/l. Ion composition shows the prevalence of bicarbonate-ions, which reaches 92% near the upper boundary of the massive ice body and 81.8% at its base. Among cations, sodium-ions prevail, their content increasing towards the center of the massive ice body; ice mineralization and amount of soil inclusions decrease in the same direction. The isotope composition (^{18}O) of the massive ice reaches -22.84‰ to -23.15‰; these values are similar to the composition of wedge ice.

In the section of the other coastal bluff (Fig. 3), also located in the area of “Sopochnaya Karga” Polar Station, three horizons of Quaternary sediments with a total thickness of about 12 m were observed.

The upper part of the section to a depth of 6.2 m is formed by syngenetically frozen silts of alluvial-lacustrine genesis (Fig. 3A). The silts include ice wedges up to 2 m wide. The isotope composition (^{18}O) of the wedge ice varies from -24.46‰ up to -24.84‰. The silts are underlain by ice-poor fine sands and coarse gravelly laminated sands (Fig. 3). At the boundaries of the wedges, strong upward tilting of sands was observed (Fig. 3B). Gravimetric moisture content of

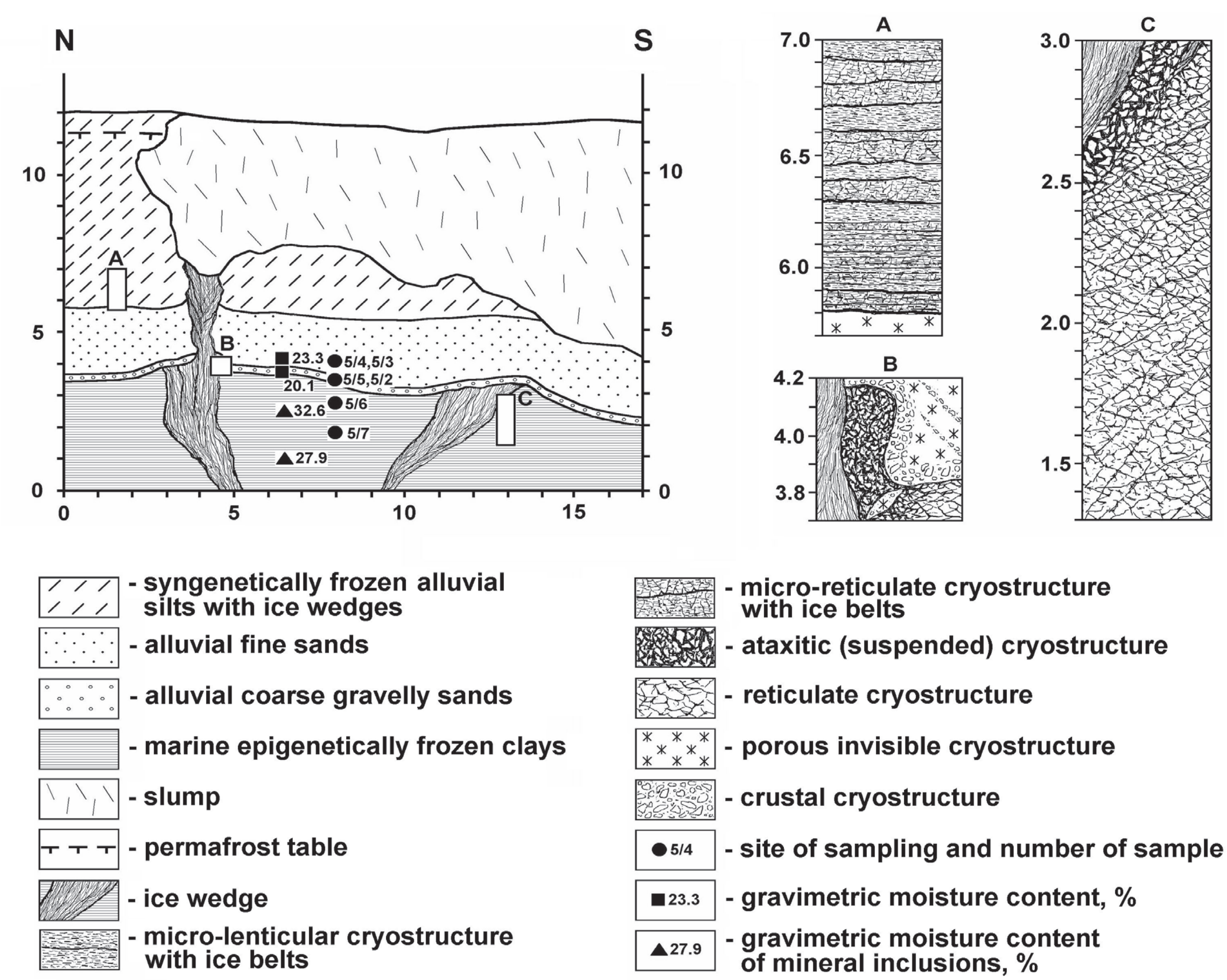

Figure 3. Cryostratigraphic section #5 in the area of “Sopochnaya Karga” Polar Station. Horizontal and vertical scales in meters. A, B, C – details of cryogenic structure.

sands reaches 20–23%. Both silts and sands are fresh. Ion composition shows the prevalence of bicarbonate-ions and sodium-ions.

From a depth of 8.5 m and downward to sea level, dark-gray clays were observed. The clays include ice wedges up to 2 m wide. Sufficient increase in the ice content was observed near the boundaries of the ice wedges (Fig. 3B, C). The clays are saline (salinity is about 0.5%), and the composition of soluble salts is characteristic for marine conditions (chlorine-ion content is 70–85 mg-eqv%, sodium-ion content is 97 mg-eqv%).

Discussion

Analysis of obtained data allows for reconstruction of the freezing conditions of studied strata. In both sections we can see evidence of transformation from marine to continental conditions, which resulted in freezing of Late Pleistocene marine sediments, formation of tabular massive ice, and deposition of syngenetically frozen "Ice Complex" sediments.

We believe that the tabular massive ice body, studied at section #3, could be formed due to an injection of water-soil slurry into epigenetically frozen strata of marine clay. The alternative hypothesis of possible massive ice origin is glacial; it is based on similarity of the studied ice body with the basal ice of modern glaciers (Kanevskiy et al. 2006).

In general, mineralization of the tabular massive ice body is typical for closed taliks: freezing from different directions results in the increase of mineralization near the margins of freezing body. The ion composition is also similar to ion composition of sub-lake taliks. In the studied section, Na/Cl ratio is 3.0–3.7. For example, in sub-lake taliks in Yakutia, this ratio varies from 3.2 to 7.5 (Anisimova 1981).

Development of the thermokarst process resulted in partial thawing of the tabular massive ice body, formation of a thaw bulb beneath the lake, and accumulation of taberal sediments. These sediments formed as a result of thawing and refreezing of epigenetically frozen marine clay. Taberal origin of silty clays can be proved by the absence of lamination, typical for lacustrine sediments, and increase of soluble salts content with depth. Such distribution of soluble salts indicates the process of salts migration towards the freezing front. Originally these sediments were formed at the littoral; marine-type composition of salts transformed to continental as a result of thawing of sediments.

Marine origin of these sediments was also confirmed by complex mineralogy and grain size analysis (Surkov 1993, Surkov 2000). According to this method, the origin of sediments can be distinguished by the patterns of distribution of heavy minerals relating to size and shape of grains (for example, grains of marine sands are better rounded and have a flat shape). Standard patterns for different types of sediments were developed (Surkov 2000); comparison with these patterns allows definition of the origin of sediments and condition of sedimentation.

A study of heavy minerals from the silty clay layer (section #3) shows that this horizon originally was formed in littoral conditions with alongshore currents and big wave activity. Minerals from the tabular massive ice body are well-sorted; the stable assemblage of heavy minerals (magnetite, ilmenite, garnet) indicates a constant source of denudation during the sedimentation process.

Micro-faunistic analysis shows that the foraminifer complex is typical for the low-salinity Arctic basin, which existed presumably in the end of Eemian and after the Eemian stage of the late Pleistocene (Streletskaya et al. 2007). Therefore, the sediments overlaying massive ice and the soil inclusions in the ice itself have the same marine origin and differ sufficiently from the upper horizon with ice wedges.

We believe that talik freezing, triggered by elimination or migration of the lake, started from the surface. An ice-rich layer parallel to the boundary with tabular massive ice (Fig. 2C) was formed due to freezing from below of water-saturated soils at the base of the talik. Simultaneously with the freezing of the talik, the formation of syngenetically frozen soils with micro-lenticular cryostructure started at the surface. The complex mineralogy and grain size analysis of heavy minerals shows that sorting of such minerals as magnetite, ilmenite, garnet, and pyroxene is typical for continental conditions of floodplains with numerous peaty ponds. The prevalence of flat quartz grains with a specific wing-like shape reflects the role of aeolian transportation in sedimentation process (Surkov 1993, Surkov 2000).

Peat accumulation at the bottom of the thaw lake basin during the climatic optimum of the Holocene resulted in the active layer reduction and formation of an ice-rich intermediate layer (Shur 1988) about 0.6 m thick (Fig. 2B). The peat layer was buried beneath syngenetically frozen slope sediments. Termination of slope sedimentation resulted in the formation of the contemporary intermediate layer with thin ice wedges (Fig. 2A).

The formation of silt with syngenetic ice wedges (section #5) started during marine regression at the end of the late Pleistocene, when the mouth of the Yenisey River moved northward more than 300 km in comparison with its contemporary position (Stein 2002). At this period, ice wedge growth occurred in west Siberia, at the west and east coasts of Yamal Peninsula (Forman 2002, Kanevskiy et al. 2005, Vasilchuk 2006), in central parts of Yamal Peninsula, and at Gydan Peninsula (Bolikhovskiy 1987), in different parts of Taimyr at Cape Sabler (*Anthropogen* 1982, Derevyagin et al. 1999) and Labaz Lake (Siegert et al. 1999).

Before syngenetic permafrost formation, the epigenetic freezing of marine clays started, accompanied by frost cracking. In section #5, the transition from sub-aquatic to sub-aerial condition is marked by strong oxidation of the top part of the marine clays sequence; the thickness of the oxidized layer is about 1 m. Clays have a reticulate cryostructure; the size of mineral blocks increases with depth, while their moisture content decreases. It indicates slowing of the freezing rate with depth.

The formation of clays in this section occurred in conditions of marine sedimentation below the level of wave sorting. Properties and composition of the clays show similarity with the silty clays from the previous exposure (Streletskaya et al. 2007).

A break in sedimentation, during which relatively large epigenetic ice wedges formed in the marine clay, was followed by a period of erosion activity. Erosion processes led to truncation of the upper part of clay strata. We could observe several evidences of very cold climate at this period: absence of significant thermokarst features at the surface of truncated ice wedges; light isotope composition of the wedges. The patterns of heavy minerals distribution in overlying sands are shown at the Figure 4. Study of the gravelly sands patterns reveals far transportation of grains by high-energy river flow. Heavy minerals composition and distribution are similar to contemporary alluvial sediments of the Yenisey River in the area of Dudinka city; they differ from contemporary beach deposits of Yenisey Gulf (Streletskaya et al. 2005).

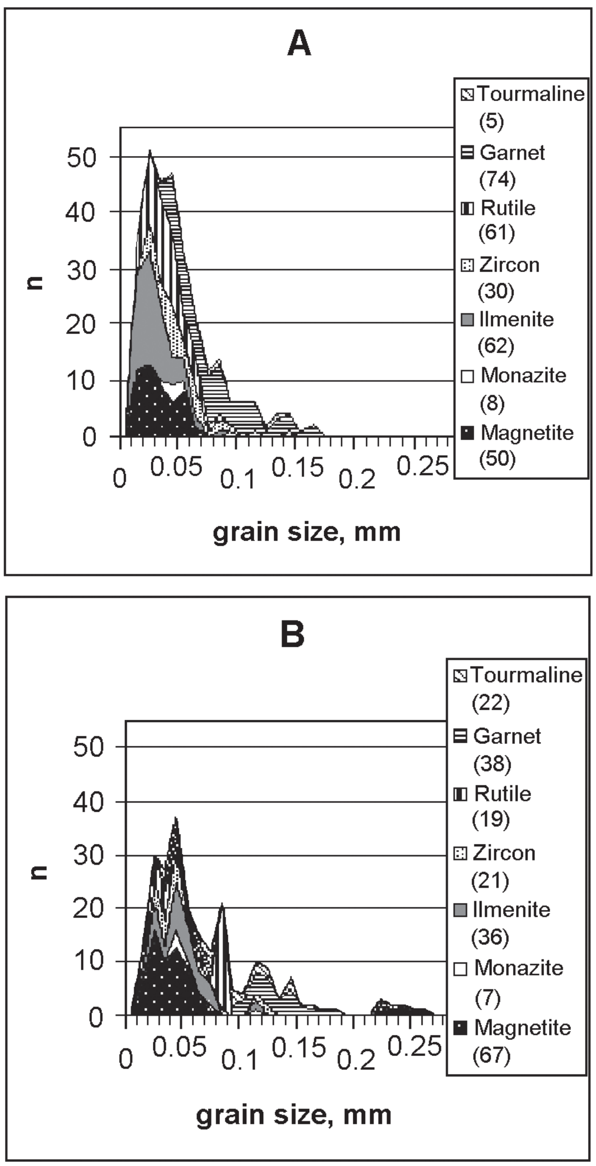

Figure 4. Patterns of heavy minerals distribution vs. thickness of grains (C-axis), Sopochnaya Karga, section #5. Amount of grains is shown in parentheses. A – fine sands; B – coarse gravelly sands.

During the period of alluvial sands accumulation, the growth of part of the ice wedges was terminated (right wedge, Fig. 3). A high sedimentation rate and relatively coarse composition of soils resulted in low ice content and an abrupt decrease in the width of ice wedges still continuing their growth.

We believe that syngenetically frozen silts at the top part of this section have an alluvial-lacustrine genesis. The pattern of heavy minerals distribution showed that they were formed at the floodplain of the big river. The main evidences of a syngenetic type of freezing are the rhythmic cryogenic structure (Fig. 3A); a prevalence of micro-lenticular and micro-reticulate cryostructures; and the occurrence of undecomposed rootlets.

Conclusions

At the coasts of Yenisey Gulf, tabular massive ice bodies are included in littoral clayey sediments of the late Pleistocene, while large syngenetic ice wedges are typical for Late Pleistocene–Holocene continental deposits. Ice-rich sediments are widespread; they form the “Ice Complex” at the top part of the Quaternary section of west Taimyr. The wedges, up to 12 m high, started their development at the end of the late Pleistocene as epigenetic wedges, and continued their growth at the period of syngenetic permafrost formation. They have the same age as thin till deposits of the last glaciation. It confirms the relatively small scale of the last glaciation in Taimyr (Svendsen 2004). Ice-rich syngenetic Holocene sediments accumulated mostly at slopes and bottoms of thaw-lake basins and other depressions associated with thawing of Pleistocene ice wedges and tabular massive ice bodies.

Acknowledgments

We are particularly grateful to Dr. Evgeny Gusev and Dr. Fedor Romanenko for their field assistance, Dr. Boris Vanshtein and Dr. Alexandr Surkov for lab analysis of soil samples, and Dr. Hanno Meyer for lab analysis of isotope composition of ice samples. The work was supported by the “Leading scientific schools of Russia” project 500.2008.5 and by Tyumen Regional Academy.

References

Anisimova, N.P. 1981. *Hydrogeochemical features of the permafrost zone.* Novosibirsk: Nauka, 153 pp. (in Russian).

Anthropogen of Taimyr Peninsula. 1982. Moscow: Nauka, 184 pp. (in Russian).

Bolikhovskiy, V.F. 1987. Yedoma sediments of Western Siberia. In: *New data on Quaternary chronology, XII INQUA Congress (Canada, 1987)*. Moscow: Nauka, 128-135 (in Russian).

Carter, L.D. 1988. Loess and deep thermokarst basins in Arctic Alaska. *Proceedings of the Fifth International Conference on Permafrost.* Tapir publishers, Trondheim, Norway: 706-711.

Danilov, I.D. 1978. *Pleistocene of marine subarctic plains.* Moscow: Moscow University Press, 198 pp. (in Russian).

Danilov, I.D. 1969. Cryofacial structure of Pleistocene sediments of dividing ridges in the lower course of Yenisey River. In: *Problems of Cryolithology 1*, Moscow University Press: 93-105 (in Russian).

Derevyagin, A.Yu., Chizhov, A.B., Brezgunov, V.S., Hubberten, H.-W. & Siegert, C. 1999. Isotope composition of ice wedges at Cape Sabler (Taimyr Lake). *Kriosfera Zemli (Earth Cryosphere)* III (3): 41-49 (in Russian).

Forman, S.L., Ingolfsson O., Gataullin, V., Manley, W.F. & Lokrantz, H. 2002. Late Quaternary stratigraphy, glacial limits and paleoenvironments of Maresale area, Western Yamal Peninsula, Russia, *Quaternary Research* 21: 1-12.

Kanevskiy, M.Z, Streletskaya, I.D. & Vasiliev, A.A. 2005. Formation of cryogenic structure of Quaternary sediments in Western Yamal. *Kriosfera Zemli (Earth Cryosphere)* X (2): 16-27 (in Russian).

Kanevskiy, M., Tumskoy, V., Fortier, D., Jorgenson, T. & Shur, Y. 2006. Structure and properties of basal ice and subglacial till. *Abstracts of Arctic Science Conference "State of the Arctic: Current State of the Arctic – Observations of Arctic Change," Fairbanks, Alaska, 2-4 October 2006*: 37-38.

Katasonov, E.M. 1978. Permafrost-facies analysis as the main method of cryolithology. *Proceedings of the Second International Conference on Permafrost*, *July 13-28, 1973*. *USSR Contribution*. Washington: National Academy of Sciences, 171-176.

Karpov, E.G. 1986. *Ground ice of Yenisey North*. Novosibirsk: Nauka, 133 pp. (in Russian).

Kunitskiy, V.V. 2007. *Nival lithogenesis and Ice Complex in Yakutia.* Author's summary of Dr.S. Thesis. Yakutsk: Permafrost Institute Press, 46 pp. (in Russian).

Péwé, T.L. 1975. *Quaternary geology of Alaska. Geological survey professional paper 835*. Washington: United States Government Printing Office, 145 pp.

Popov, A.I., Rozenbaum, G.E. & Tumel, N.V. 1985. *Cryolithology*. Moscow: Moscow University Press, 239 pp. (in Russian).

Romanovskii, N.N. 1993. *Basics of cryogenesis of lithosphere*. Moscow: Moscow University Press, 336 pp. (in Russian).

Shpolyanskaya, N.A., Streletskaya, I.D. & Surkov, A.V. 2007. Comparative genetic analysis of tabular massive ice and adjacent Pleistocene sediments of the northern part of West Siberia. *Geoecology. Engineering Geology. Hydrogeology. Geocryology* 3: 212-224 (in Russian).

Shur Y.L. 1988. *Upper horizon of the permafrost soils and thermokarst.* Nauka, Siberian Branch, Novosibirsk: 210 pp. (in Russian).

Shur, Y., French, H.M., Bray, M.T. & Anderson, D.A. 2004. Syngenetic permafrost growth: cryostratigraphic observations from the CRREL Tunnel near Fairbanks, Alaska. *Permafrost and Periglacial Processes* 15(4): 339-347.

Siegert, C., Derevyagin, A.Y., Shilova, G.N., Hermichen, W.-D. & Hiller, A. 1999. Paleoclimate indicators from permafrost sequences in the Eastern Taymyr Lowland. In: H.Kassens, H.A.Bauch, I.A.Dmitrenko, H.Eicken, H.-W.Hubberten, M.Melles, J.Thiede, L.A.Timokhov (eds.), *Land-Ocean Systems in the Siberian Arctic. Dynamic and History. Berlin*. Heidelberg: Springer-Verlag, 477-499.

Soloviev, V.A. 1974. Experience of study of the ground ice of Yenisey North aimed on paleo-geographical and neotectonic reconstructions. In: *Natural conditions of West Siberia 4*. Moscow: Moscow University Press, 34-48 (in Russian).

Stein, R. et al. 2002. Siberian river run-off and late Quaternary glaciation in the southern Kara Sea, Arctic ocean: Preliminary results. *Polar Research* 21(2): 315-322.

Streletskaya, I.D. et al. 2007. New results of Quaternary sediment Studies of Western Taimyr. *Kriosfera Zemli (Earth Cryosphere)* XI (3): 14-28 (in Russian).

Streletskaya, I.D., Surkov, A.V. & Semenov, S.V. 2005. Studies of Quaternary sediments of Russian North with the method of complex mineralogy and grain size analysis (Yamal Peninsula, Yenisey River estuary). *Quarter-2005. IV All-Russia Conference on Quaternary researches: Proceedings (Syktyvkar, August 23-26, 2005). Institute of Geology of Komi SC UB RAS*, Syktyvkar, Geoprint: 405-407 (in Russian).

Streletskaya, I.D., Ukraintseva, N.G. & Drozdov, I.D. 2003. A digital database on tabular ground ice in the Arctic. *Proceedings of the Eighth International Conference on Permafrost, 21-25 July 2003, Zurich, Switzerland.* A.A. Balkema Publishers 1: 1107-1110.

Surkov, A.V. 1993. Method of complex mineralogy and grain size analysis and its application for study of sediments. *Geology and Reconnaissance* 3: 36-43 (in Russian).

Surkov, A.V. 2000. *New methods of study of sand-silt component of placers and sedimentary rocks.* Moscow: E. Razumova, 286 pp. (in Russian).

Svendsen, J.I., Alexanderson, H., Astakhov, V. et al. 2004. Late Quaternary ice sheet history of northern Eurasia. *Quaternary Science Reviews* 23: 1229-1271.

Trofimov, V.T. & Vasilchuk, Yu.K. 1983. Syngenetic ice wedges and tabular massive ice in Pleistocene sediments of the northern part of West Siberia. *Bulletin of the Moscow Society of Natural Scientists, Geology Department* 58 (4): 113-121 (in Russian).

Vasilchuk, Yu.K. 2006. *Ice wedges: Heterocyclicity, Heterogeneity, Heterochrony.* Moscow: Moscow University Press, 404 pp. (in Russian).

Thirteen Years of Observations at Alaskan CALM Sites: Long-Term Active Layer and Ground Surface Temperature Trends

Dmitry A. Streletskiy, Nikolay I. Shiklomanov, and Frederick E. Nelson
Department of Geography, University of Delaware, Newark, USA
Anna E. Klene
Department of Geography, University of Montana, Missoula, USA

Abstract

Active layer monitoring is an important component of efforts to assess the affects of global change in permafrost environments. In this study we used data from 13 (1995–2007) years of spatially oriented field observations at a series of 16 representative Circumpolar Active Layer Monitoring (CALM) sites in northern Alaska to examine temporal and spatial trends in active layer thickness and its relation to climatic, surface, and subsurface conditions. The observation strategy consisted of measuring active layer thickness on regular 1-ha and 1-km^2 grids representative of environmental conditions on Alaska's North Slope. The measurement program also involves continuous air and soil temperature monitoring, periodic frost heave and thaw subsidence using Differential Global Position System (DGPS) as well as landscape, vegetation, and soil characterization. This paper showcases CALM observation procedures and analysis designed to monitor processes and detect changes not anticipated in the original CALM protocol of the early 1990s.

Keywords: active layer; Alaska; CALM; Circumpolar Active Layer Monitoring; surface temperature; thaw subsidence.

Introduction

The active layer is the most dynamic part of the permafrost system and undergoes many changes in its properties during each annual cycle. These fluctuations involve variations of ice/water content, thermal conductivity, density, mechanical properties, and solute redistribution (Ershov 2002), all of which are of critical importance for many natural phenomena and processes in permafrost and periglacial environments (French 2007). Most biological and hydrological activities in arctic soils are confined to the layer of seasonal thaw (Hinzman 1991). Active layer monitoring is an important component of efforts to assess the effects of global climate change in arctic environments. The Circumpolar Active Layer Monitoring (CALM) program is a network of sites at which data about active layer thickness (ALT) and related climatic, vegetation, and soil parameters are collected. The CALM network involves more than 160 sites underlain by permafrost in polar regions and selected mountainous environments (Brown et al. 2000, Nelson et al. 2004).

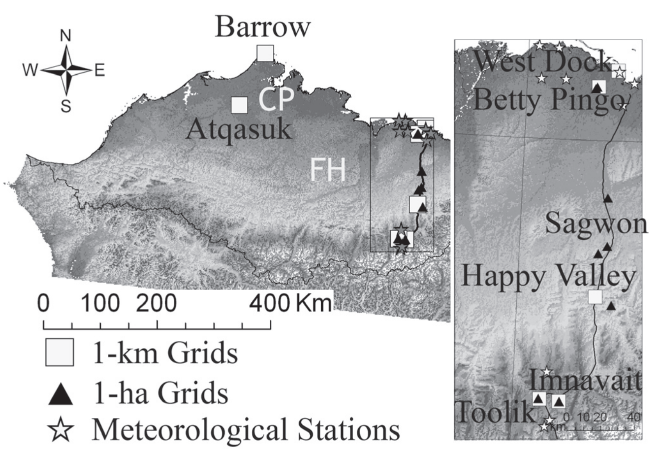

Figure 1. Geographic distribution of Alaskan CALM observational sites used in the present study. Gray tones represent elevation, with brighter shades indicating higher elevations. Physiographic provinces are indicated by white lettering: CP – Coastal Plain, FH – Foothills. Black font is used for name specific sites mentioned in the text.

In this study we used data from 13 years (1995–2007) of extensive, spatially oriented field observations at a series of 16 CALM sites on the North Slope of Alaska to examine landscape-specific temporal trends in active layer thickness and air and soil temperature. CALM strategies are evolving constantly, and this paper showcases CALM observation procedures and analysis designed to monitor processes and detect changes not anticipated in the original CALM protocol of the early 1990s. Details of the analyses and results will be presented in a series of manuscripts currently in preparation.

Study Area

Of the 41 CALM-designated sites in Alaska, 29 are located on the North Slope (Shiklomanov et al. 2008). In this paper we report observed long-term trends of air and ground surface temperature and active layer thickness from 16 sites with continuous records for 13 years (1995–2007).

The sites selected for analysis are distributed along the primary climatic gradient in northern Alaska (Fig. 1). The sites span the regional spectrum of vegetation and terrain conditions in two dominant physiographic provinces: the Arctic Coastal Plain in the north and the Arctic Foothills in the south (Wahrhaftig 1965).

The elevation of the Arctic Coastal Plain increases gradually from north to south, reaching about 100 m at its southern edge. Poor drainage and low relief create conditions for development of thaw lakes. Thaw lakes and thaw-lake basins occupy from 20% to 50% of the area. The coastal plain is dominated by wet sedge polygonal tundra on soils associated with windblown loess deposits (Walker et al. 2003).

The Arctic Foothills province extends between the Arctic Coastal Plain and the Brooks Range and is characterized by hills and plateaus divided by river valleys. The area was glaciated during the Pleistocene, and surface deposits are mostly glacial till with discontinuous loess cover (Bockheim et al. 1998). Differences in underlying deposits create distinct geochemical contrast in soils, leading to differences in vegetation species and organic layer thickness (Walker et al. 1998). Based on soil pH, areas of tundra can be subdivided into acidic (pH <5.5) and nonacidic (pH >5.5) classes. Soils in nonacidic tundra have thinner organic horizons, a significantly thicker active layer, and greater cryoturbation than soils of acidic tundra (Bockheim et al. 1998)

The entire study area lies in the zone of continuous permafrost. The only areas possibly without permafrost are occupied by deep bodies of water that fail to freeze to the bottom in winter (Péwé 1975).

Methodology

Of the 16 CALM sites used in the analysis described in the next section, 9 consist of 1-ha plots established to represent relatively homogeneous examples of the landscape categories found in particular physiographic provinces. The selection of landscapes was guided by a regional landcover map derived from Landsat imagery (Auerbach et al. 1996). The map depicts 5 primary landscape units: wet tundra (WET), moist acidic tundra (MAT), moist nonacidic tundra (MNT), shrublands (SHR), and barrens. Characteristics of the 1-ha sites were described by Shiklomanov & Nelson (2003), and Klene et al. (2001b); their geographic distribution is shown in Figure 1. Beginning in 1995, the active layer has been probed at least annually at the 1-ha sites. The procedure involves pushing a metal rod, calibrated in cm, to the point of refusal, interpreted in most cases to be the frost table. Thaw depth measurements at each site were obtained by probing at 5 m intervals along the plot's two perpendicular and one diagonal transect, resulting in 71 points per plot per probing date. Air and soil surface temperature were measured continuously at two-hour intervals over the 1995–2007 period (data are available for the 1996–2006 period) with an array of Onset™ portable data loggers. At each site one logger is mounted on a mast, with thermistors placed approximately 2 m above the ground in a radiation shield. Seven to ten loggers are distributed over each of the 1 ha plots, with thermistors placed at the vegetation/soil interface at locations representative of microtopographic conditions (Klene et al. 2001b, Klene et al. 2008).

Periodic thaw depth measurements were also conducted at 7 surveyed and georeferenced 1-km^2 grids over the period 1995–2007. These sites were established in northern Alaska during the 1980s and 1990s to monitor long-term ecosystem change (Brown et al. 2000). Four grids (Barrow, Atqasuk, Betty Pingo, and West Dock) are situated on the Arctic Coastal Plain, and the remaining three (Happy Valley, Imnavait Creek, and Toolik Lake) are in the Arctic Foothills (Fig. 1). The 1-km^2 grids were selected to represent more generalized conditions found in each physiographic province. Detailed descriptions of the 1-km^2 sites were provided by Hinkel and Nelson (2003). Each grid consists of a square array of surveyed permanent stakes separated by 100 m, yielding an 11 × 11 array of sampling nodes on each grid. Sampling was conducted by manual probing at each stake, yielding a maximum of 121 data points per grid per probing date. The active layer was not measured at locations where grid points intersect rocks or deep water. A significant portion of the Toolik and Imnavait sites are underlain by coarse glacial material that is impenetrable for metal probes. These sections of the Toolik and Imnavait grids were excluded from the analysis.

Each grid is instrumented for air and ground surface temperature measurements using equipment similar to that at the 1-ha sites. In addition, at each 1-km^2 site ground temperature is monitored at hourly intervals at the standard depths of 0, 5, 10, 15, 20, 25, 30, 35, 45, 70, 95, and 120 cm using Campbell Scientific™ and Measurement Research Corporation instrumentation. Periodic, spatially oriented frost heave and thaw subsidence measurements using Differential Global Position System (DGPS) were initialized in 2001 at 2 Coastal Plain 1-km^2 sites and 1 Foothills 1-ha site (Little et al. 2003, Streletskiy et al. 2005). Measurements are performed twice each year at the beginning (June) and the end (August) of the thawing season, using a hierarchical nested sampling design (Nelson et al. 1999). A series of additional sites were instrumented for measuring air and soil surface temperature at locations chosen to facilitate adequate geographic coverage.

Analytical Results

Air temperatures trends

Air temperature trends from individual sites were analyzed using procedures outlined in Shiklomanov & Nelson (2002). In this paper we present monthly air temperatures, integrated over physiographic provinces.

Regionally, air temperature increases from north to south. Mean annual air temperature over the study period varied between -9.2°C and -12.0°C on the Coastal Plain and between -7.3°C and -10.3°C in the Foothills. Mean summer air temperature (June–August) on the Coastal Plain varies between 5.5°C and 8.7°C, while at Foothills it ranges from 6.8°C to 11.7°C. This climatic pattern demonstrates the pronounced influence of the Arctic Ocean during the summer, throughout the Coastal Plain. Province-specific 12-year (1995–2006) records of mean, minimum, and maximum annual air temperature, as observed at CALM sites, are shown in Figure 2. There is a slight decline in mean and maximum annual air temperature for the Coastal Plain and in maximum annual air temperature for the Foothills.

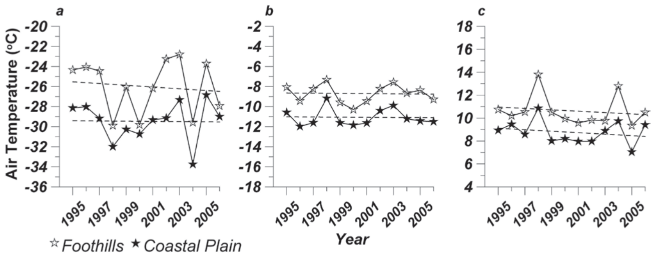

Figure 2. Twelve-year (1995–2006) records of annual minimum (a), mean (b), and maximum (c) monthly air temperature as observed at CALM Coastal Plain and Foothills sites.

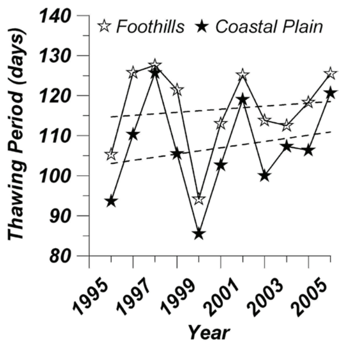

Figure 3. Province-specific 12-year (1995–2006) records of the duration of thawing period, as observed at CALM sites.

Duration of thawing period

The duration of the thawing period was estimated based on analysis of mean daily air temperature at individual sites by counting consecutive days with temperatures above 0.5°C. Results were averaged by physiographic province.

On average, the thawing period on the Coastal Plain is almost 10 days shorter than in the Foothills. However, this difference ranges from 2 to 16 days, depending on the year. Province-specific 12-year records of thaw-period duration, as observed at CALM sites, are shown in Figure 3. Both provinces experienced an increase in the duration of thawing, attributable to both the earlier initiation of the thawing and later freezing.

Effect of vegetation on ground surface temperature

Analysis of ground surface temperature was aimed primarily at evaluating the effects of vegetation and the characteristics of different landscape units on the ground thermal regime. The daily air and soil-surface temperature data obtained at the homogeneous 1-ha sites were used to calculate average differences between surface and air temperature (ΔT) for the warm period (June–August). To evaluate the effect of vegetation on the ground thermal regime further, the landscape-specific values of empirical summer n-factors were calculated. The n-factor, defined operationally as the ratio of the degree-day sum at the soil surface to that in the air (Carlson 1952), has been used in cold regions engineering since the 1950s to estimate soil surface temperature from air temperature records. Estimation of n-factors has been found to be a useful, simple approach for estimating the attenuation of climatic signals by vegetation cover (Klene et al. 2001a, b, Kade et al. 2006). An analysis of winter n-factors for the study sites is presented elsewhere in this volume by Klene et al. (2008).

Table 1. Landscape-specific 12-year (1995-2006) average values of ΔT and n-factors, as estimated from air and ground surface temperature measurements at representative 1-ha CALM sites.

Landscape Unit	Coastal Plain ΔT, °C	Coastal Plain N-factor	Foothills ΔT, °C	Foothills N-factor
Barrens	1.0	1.20	1.6	1.22
MNT	-1.2	0.78	-2.6	0.71
MAT			-3.8	0.52
Shrublands			-3.1	0.57
WET	-2.2	0.66	-2.3	0.74

Values of ΔT and n-factors obtained at individual sites were averaged to represent individual landscapes and physiographic provinces. To account for interannual climatic variability, the annual landscape- and province-specific values of ΔT and n-factor were averaged over a 12-year (1995–2006) period and are presented in Table 1.

The vegetated surfaces in both physiographic provinces show negative values of ΔT and n-factor values of less than unity, indicating the cooling influence of vegetation on ground temperature during the warm period. The distinct values of ΔT and n-factor indicate the distinct thermal influence of landcover types characteristic of the Coastal Plain and Foothills physiographic province. The moist acidic tundra (MAT) of the Foothills province has the largest negative value of ΔT (-3.8°C) and the smallest value of n-factor (0.52). The smallest negative ΔT value (-1.2°C) and highest n-factor value (0.78) were found in moist nonacidic tundra (MNT) of the Coastal Plain. Regionally, values of ΔT and n-factor for similar landscape units vary from north to south in response to the increase in density of the vegetation cover. This effect is evident from differences in ΔT and n-factor for moist nonacidic tundra in two physiographic provinces. The thermal influence of MNT is greater in the Foothills than on the Coastal Plain.

Unvegetated surfaces, which consist of sand, gravel, and bedrock along streams and atop hills and mountains, show positive values of ΔT and values of n-factors of more than unity, indicating a warming influence of barren surfaces on ground thermal regime.

Annual thawing propagation

The annual dynamics of thawing were evaluated by analyzing thawing intensity curves for four 1-km^2 sites. The Barrow and Atqasuk sites were selected to represent the Coastal Plain, while Happy Valley and Toolik are representative of the Foothills. The thawing intensity curves were constructed by calculating a daily increase in thaw depth as a portion of the maximum annual active layer value. The daily values of thaw depth for each site were estimated using ground temperature observations from an array of 12 thermistors, distributed vertically from the surface to 1.2 m depth. The daily depth of thaw penetration was assumed to coincide with the interpolated position of the 0^{o}C isotherm. For the silty soils characteristic of northern Alaska, the correspondence between thaw depth, as determined by

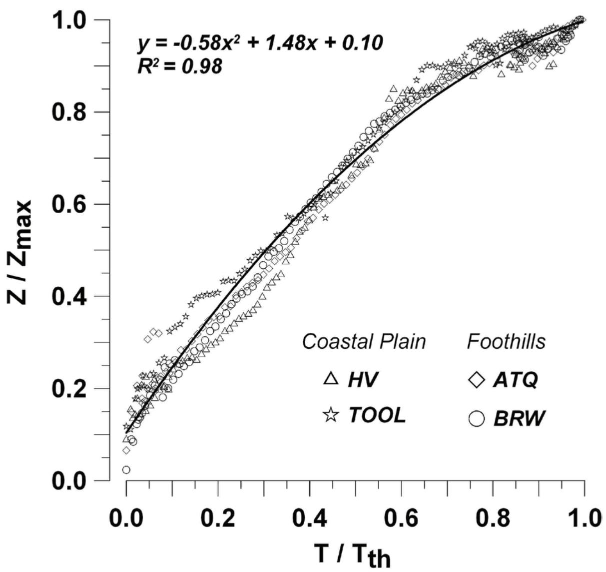

Figure 4. Site-specific 12-year averages of thawing intensity for two coastal plain (Barrow BRW and Atqasuk ATQ) and two foothills (Happy Valley HV and Toolik TOOL) locations. Z is thaw depth at time T and Z_{max} is annual maximum thaw depth achieved over the thaw period T_{th}.

mechanical probing, and the position of the 0°C isotherm is generally quite good (Brown et al. 2000).

The analysis of annual thawing intensity curves indicates that, depending on site and year, 95% to 99% of maximum thaw propagation is reached by mid August, when annual CALM ALT observations by mechanical probing are starting at northern Alaska sites.

To evaluate the physiographic province-specific intensity of annual thaw penetration, independent of interannual variability in climatic conditions, relative increases in thaw depth were plotted as a function of relative time: $Z/Z_{max}=f(T/T_{th})$, where Z is the thaw depth at time T and Z_{max} is the annual maximum thaw depth achieved over thawing period T_{th}. Site-specific 12-year averages of thawing intensity for two coastal plain (Barrow (BRW) and Atqusuk (ATQ)) and two foothills (Happy Valley (HV) and Toolik (Tool)) locations are shown in Figure 4. The thawing intensity curves for all four locations are similar, indicating that the relationship between annual thaw depth propagation and dimensionless time is uniform for different surface, subsurface, and climatic conditions. Figure 4 demonstrates that regardless of location, 44% of annual thaw occurs during the first quarter of the thawing period; during the first half of the thawing period thaw depth reaches 70% of its maximum; after three-quarters of the thawing period, thaw depth is at 88% of its maximum; and that 96% of the active layer has thawed after 90% of the thawing season. These numbers correspond closely to values obtained at three drastically different locations in Russia (Yakutsk, Vorkuta, and Igarka) by Pavlov (1984). The best-fit quadratic equation, presented in Figure 4, can be applied to estimate active layer thickness using thaw depth measurements performed at different times during the summer.

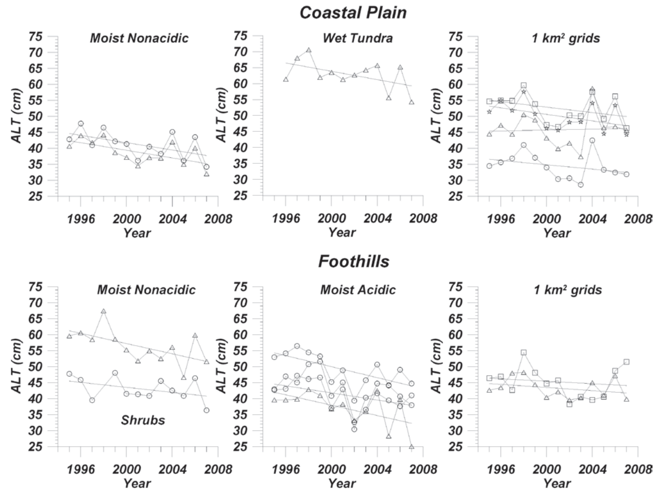

Figure 5. Site-specific 13-year (1995-2007) records of annual active layer thickness. Nine 1-ha sites are grouped by landscape category characteristic of two physiographic provinces. Six 1-km² sites are grouped by physiographic provinces. The Imnavait 1-km² site is not shown due to data quality issues.

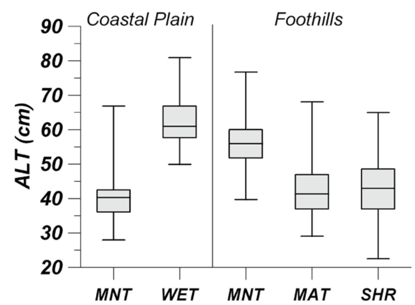

Figure 6. Statistical distribution (box plot) of ALT values for different landscapes characteristic of the two physiographic provinces.

Interannual variability of active layer thickness

The interannual dynamics of active layer thickness were evaluated by analyzing annual, site-specific averages of thaw depth values obtained at the end of the thawing period.

Site-specific 13-year (1995–2007) records of annual active layer thickness for different landscape categories and physiographic provinces are shown in Figure 5. The records indicate a declining active layer trend over the 1995–2007 period for all coastal plain and foothills sites, which generally corresponds to a decline in summer temperature over the same period (Fig. 2c). The maximum values of ALT were recorded in 1998, 2004, and 2006, the years that experienced the warmest summers (Fig. 5). The general agreement between ALT and summer air temperature records stipulates a strong degree of climatic forcing on ALT.

Landscape-specific active layer characteristics

Previous studies, conducted at Alaska CALM sites (Nelson et al. 1998, 1999, Nelson & Hinkel 2003), demonstrated the existence of landscape-specific thermal differences manifested through similar magnitudes of thaw propagation. Although thaw depth can experience significant interannual

Table 2. Landscapes- and province-specific values of active layer thickness.

Landcover categories	Coastal Plain	Foothills
Moist nonacidic tundra	40.0	56.4
Moist acidic tundra		40.5
Moist low shrub tundra		43.0
Wet graminoid tundra	62.9	49.1

variability in response to climatic forcing (Fig. 5), the presence of landform elements shows spatial regularity at the landscape scale and results in landscape-specific thaw depth patterns that repeat on an interannual basis (Nelson et al. 1998, Hinkel & Nelson 2003). Figure 6 shows statistical distributions of ALT, averaged over the 1995–2007 period for different landscapes characteristic of the two physiographic provinces. The landscape- and province-specific mean values of ALT are presented in Table 2.

To evaluate the landscape-specific thermal response to climatic forcing, annual ALT values from representative 1-ha sites were correlated with the square root of degree-days of thawing (DDT), estimated from site-specific air temperature records and accumulated by the date of thaw depth measurements (Shiklomanov & Nelson 2003). A plot of square root of DDT against thaw depth (Fig. 7) yields distinct linear landscape-specific relations, indicating differences in thermal landscape sensitivity to climatic forcing.

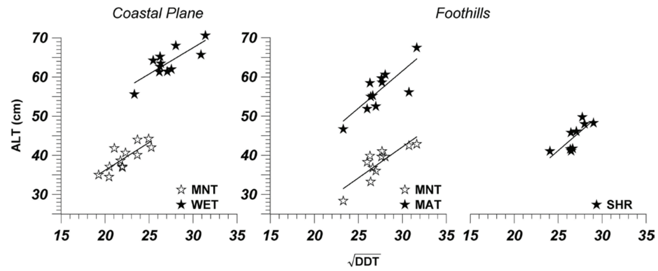

Figure 7. Plot of square root of air DDT against thaw depth for several 1-ha sites characteristic of dominant landscapes in the coastal plain and foothills provinces. Each data point represents annual end-of-thawing season measurements for the 1995–2006 period.

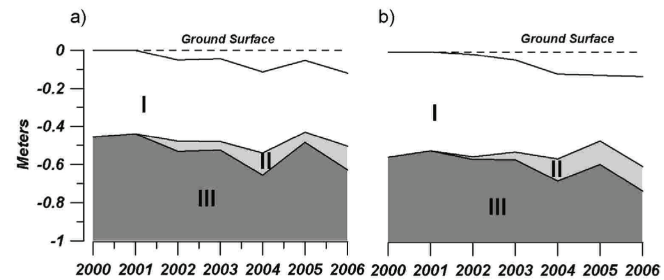

Figure 8. Annual changes in position of ground surface and ALT as measured by mechanical probing for representative Coastal Plain (a) and Foothills (b) CALM sites. I- ALT as measured by probing; II- ALT, corrected for ground subsidence; III-permafrost.

Ground subsidence

Because thaw penetration into an ice-rich layer at the base of the active layer is accompanied by loss of volume (thaw consolidation), straightforward measurement of active layer thickness by such methods as mechanical probing may not always yield accurate estimates of changes in the permafrost system. Periodic thaw subsidence measurements using DGPS technology allowed us to address this problem effectively. Figure 8 shows the results of active layer and ground subsidence measurements over the 2001–2006 period at two locations representative of the coastal plain and foothills physiographic provinces. Total subsidence over the 5-year period was 12 cm at the coastal plain site and 13 cm at the foothills site.

To account for ground subsidence in the active layer record, the annual changes in the position of the ground surface relative to the level in the year 2000 were added to the active layer measurements produced by mechanical probing (Fig. 8). Results from the two sampling locations indicate a monotonic increase in thaw penetration between 2001 and 2006.

Conclusions

The results of 13 years of active layer, air, and ground temperature observations at CALM sites in north-central Alaska indicate that: (1) there is a slight decline in mean and maximum annual air temperature on the Coastal Plain and in maximum annual air temperature in the Foothills. The period of observations was characterized by an increase in the length of the thawing period in both physiographic provinces; (2) the spatially oriented ground surface temperature observations within representative landscapes facilitate evaluation of the effect of ground cover on the ground thermal regime. The distinct values of ΔT and n-factor indicate the distinct thermal influence of landcover types characteristic of the Arctic Coastal Plain and Arctic Foothills physiographic provinces; (3) The results of active layer observations obtained by mechanical probing over 1995–2007 period indicate a pronounced decreasing trend in ALT for all landscape types characteristic of dominant physiographic provinces; (4) Although thaw depth can experience significant interannual variability in response to climatic forcing, the presence of landform elements shows spatial regularity at the landscape scale and results in landscape-specific values of active layer thickness. However, the annual rate of thaw propagation is similar for sites characterized by different surface, subsurface, and climatic conditions; (5) The results of DGPS survey indicate that soil consolidation accompanying penetration of thaw into an ice-rich stratum at the base of the active layer has resulted in subsidence of the surface, accounting for the lack of apparent thickening of the active layer, as traditionally defined.

Acknowledgments

This research was sponsored by the U.S. National Science Foundation grants OPP-9732051, OPP-0352957 and OPP-0352958. We are grateful to M. Walegur, M. Schimek, J. Little, and H. Sandall for their assistance in collecting data, and to VECO Polar Resources and the Barrow Arctic Science

Consortium for providing logistical support. Opinions, findings, conclusions, and recommendations expressed in this paper are those of the authors and do not necessarily reflect the views of the National Science Foundation.

References

Auerbach, N.A., Walker, D.A & Bockheim, J.G. 1996. *Land Cover Map of the Kuparuk River Basin, Alaska.* Institute of Arctic and Alpine Research, University of Colorado, Boulder, CO, USA.

Bockheim, J.G., Walker, D.A., Everett, L.R., Nelson, F.E. & Shiklomanov, N.I. 1998. Soils and cryoturbation in moist nonacidic and acidic tundra in the Kuparuk River Basin, arctic Alaska, U.S.A. *Arctic and Alpine Research* 30(2): 166-174.

Brown, J., Hinkel, K.M. & Nelson, F.E. 2000. The circumpolar active layer monitoring (CALM) program: research designs and initial results, *Polar Geography* 24(3): 165-258.

Carlson, H. 1952. Calculation of depth of thaw in frozen ground. *Frost Action in Soils: A Symposium*. Highway Research Board Special Report 2. Washington, DC: National Research Council.

Ershov, E.D. 2002. *Fundamentals of Geocryology*. Moscow State Univ. Press. 682 pp.

French, H.M. 2007. *The Periglacial Environment*. John Wiley & Sons Ltd., 458 pp.

Hinzman, L.D., Kane, D.L., Gieck, R.E. & Everett, K.R. 1991. Hydrologic and thermal properties of the active layer in the Alaskan Arctic. *Cold Reg. Sci. Technol.* 19(2): 95-110.

Hinkel, K.M. & Nelson, F.E. 2003. Spatial and temporal patterns of active layer thickness at Circumpolar Active Layer Monitoring (CALM) sites in northern Alaska, 1995–2000. *Journal of Geophysical Research* 108(D2): 8168, doi:10.1029/2001JD000927.

Kade, A., Romanovsky, V.E. & Walker, D.A. 2006. The n-factor of nonsorted circles along a climate gradient in arctic Alaska. *Permafrost and Periglacial Processes* 17: 279-289.

Klene, A.E., Nelson, F.E., Shiklomanov, N.I. & Streletskiy D.A. 2008. Interannual variability of winter n-factors in the Kuparuk River Basin, Alaska. *Proceedings of the Ninth International Conference on Permafrost, Fairbanks, Alaska, June 29–July 3, 2008* (this proceedings).

Klene, A.E., Nelson, F.E. & Shiklomanov N.I. 2001. The n-factor as a tool in geocryological mapping: seasonal thaw in the Kuparuk River Basin, Alaska. *Physical Geography* 22: 449-466.

Klene, A.E., Nelson, F.E., Shiklomanov, N.I. & Hinkel, K.M. (2001b). The n-factor in natural landscapes: variability of air and soil-surface temperatures, Kuparuk River Basin, Alaska. *Arctic, Antarctic, and Alpine Research* 33(2): 140-148.

Little, J., Sandall, H., Walegur, M. & Nelson, F.E. 2003. Application of differential GPS to monitor frost heave and thaw settlement in tundra environments. *Permafrost and Periglacial Processes* 14(4): 349-357.

Nelson, F.E., Shiklomanov, N.I., Christiansen, H.H. & Hinkel, K.M. 2004. The circumpolar-active-layer-monitoring (CALM) Workshop: Introduction. *Permafrost and Periglacial Processes* 15: 99-101.

Nelson, F.E., Hinkel, K.M., Shiklomanov, N.I., Mueller G.R., Miller, L.L. & Walker, D.A. 1998. Active-layer thickness in north central Alaska: systematic sampling, scale, and spatial autocorrelation. *Journal of Geophysical Research* 103: 28,963-28,973.

Nelson, F.E., Shiklomanov, N.I. & Mueller, G.R. 1999. Variability of Active-Layer Thickness at Multiple Spatial Scales, North-Central Alaska, U.S.A. *Arctic, Antarctic, and Alpine Research* 31(2): 179-186.

Pavlov, A.V. 1984. *Energy exchange in the Earth landscapes.* Novosibirsk: Nauka, 256 pp. (in Russian).

Péwé, T.L. 1975. *Quaternary Geology of Alaska.* US. Geological Survey Professional Paper 835. 145 pp.

Shiklomanov, N.I., Nelson, F.E., Streletskiy, D.A., Hinkel, K.M. & Brown, J. 2008. The Circumpolar Active Layer Monitoring (CALM) Program: Data Collection, Management, and Dissemination Strategies. *Proceedings of the Ninth International Conference on Permafrost, Fairbanks, Alaska, June 29-July–3, 2008* (this proceedings).

Shiklomanov, N.I. & Nelson, F.E. 2002. Active-layer mapping at regional scales: a 13-year spatial time series for the Kuparuk Region, north-central Alaska. *Permafrost and Periglacial Processes* 13: 219-230.

Shiklomanov, N.I. & Nelson, F.E. 2003. Climatic variability in the Kuparuk region, north-central Alaska: optimizing spatial and temporal interpolation in a sparse observation network. *Arctic* 56: 136-146.

Streletskiy, D.A., Shiklomanov, N.I. & Nelson, F.E. 2005. Monitoring of thaw settlement using a differential global position system approach. In: *Proceedings of the Third Russian Conference on Geocryology*, vol. 2. Moscow: Lomonosov Moscow State University, pp. 163-169.

Wahrhaftig, C. 1965. *Physiographic Divisions of Alaska*, USGS Prof. Pap. 482. Washington, DC: U.S. Govt. Print. Off., 52 pp.

Walker, D.A., Jia, G.J., Epstein, H.E., Raynolds, M.K., Chapin, F.S., Copass, C., Hinzman, L.D., Knudson, J.A., Maier, H.A., Michaelson, G.J., Nelson, F., Ping, C.L., Romanovsky, V.E. & Shiklomanov, N. 2003. Vegetation-soil-thaw-depth relationships along a low-arctic bioclimate gradient, Alaska: Synthesis of information from the ATLAS studies. *Permafrost and Periglacial Processes* 14(2): 103-123.

Walker, D.A., Auerbach, N., Bockheim, J.G., Chapin, F.S. III, Eugster, W., King, J.Y., McFadden, J.P., Michaelson, G.J., Nelson, F.E., Oechel, W.C., Ping, C.L., Reeburgh, W.S., Regli, S., Shiklomanov, N.I. & Vourlitis, G.L. 1998. A major arctic soil pH boundary: implications for energy and trace-gas fluxes. *Nature* 394: 469-472.

Thermal History of Degrading Permafrost in the Source Region of Yellow River, Northeastern Tibet

Tetsuo Sueyoshi
Institute of Low Temperature Science, Hokkaido University, Sapporo, Japan
Atsushi Ikeda
Geoenvironmental Sciences, University of Tsukuba
Norikazu Matsuoka
Geoenvironmental Sciences, University of Tsukuba
Takemasa Ishii
Geological Survey of Japan, National Institute of Advanced Industrial Science and Technology

Abstract

A large part of the source region of the Yellow River (Hunag He) in the northeastern margin of the Tibetan Plateau is underlain by perennially or seasonally frozen ground which has experienced rapid warming in the past decades. Since 2002, we have investigated permafrost distribution in the area to evaluate permafrost degradation and its impacts on groundwater hydrology. It suggested the drastic shrinkage of permafrost area within last the 20 to 30 years, which corresponds to the more than 100 m rise in the lower altitudinal limit of permafrost. This is most likely causing the desertification of the ground surface. In this study, based on the half-century meteorological data from a local observatory, the thermal history of permafrost in the area is investigated by means of a numerical method. The results indicate that some warm permafrost could have existed in the middle of the last century. Considering the time scale of global warming, there is high possibility that the relict permafrost (perennially frozen part beneath the supra-permafrost talik) has widely degraded during the last decades.

Keywords: global warming; numerical modeling; permafrost degradation; Tibet.

Introduction

Recent global warming has raised the temperature of permafrost, which has resulted in the deepening of the active layer and the reversed temperature profile in the high latitudes (e.g., Lachenbruch & Marshall 1986, Harrison 1991, Osterkamp & Romanovsky 1999, Osterkamp 2005, Smith et al. 2005). Warm permafrost in the marginal zone appears to be more sensitive; for instance, the permafrost in Mongolia and the Tibetan (Qinghai-Xizang) Plateau shows rapid thinning in recent decades (e.g., Sharkhuu 1998, Jin et al. 2000).

The source area of the Yellow River (Huang He), located in the northeastern margin of the Tibetan Plateau, appears to be a region broadly underlain by such warm permafrost. Recent studies have reported desertification (degradation of the grassland and meadow vegetation) of the plateau (Wang et al. 2001, Zhang et al. 2004). This has been mainly attributed to the degradation of permafrost (Peng et al. 2003), because there has been no significant change in precipitation during the last half-century (Yang et al. 2004). This study examines this process.

Whereas a few recent reports have indicated rapid degradation of permafrost in the source area of the Yellow River (Zhu et al. 1995, Zhu et al. 1996; Jin et al. 2000, Wang et al. 2000), a large part of the area was considered to have been underlain by permafrost at least until the 1980s (Wang 1987, Wang et al. 1991, Zhou et al. 2000), despite limited evidence. The timescale of the permafrost degradation is therefore of concern to us, to assess the urgency of this environmental change.

In order to verify ongoing degradation of permafrost, we investigated the present geothermal conditions in the source area of the Yellow River (Ikeda et al. 2007, Matsuoka et al. 2004, 2005, 2006), as part of an interdisciplinary research project to model the groundwater circulation and predict near-future water resources of the whole Yellow River basin.

On the basis of the acquired data from field investigations, this paper discusses the ground temperature history of the region using one-dimensional numerical model. The goal of the study is to find a suitable initial condition of the permafrost thickness and to examine its sensitivity to given parameters.

Study Area and Field Study

The fieldwork was undertaken along the R214 road that connects Xining and Yushu in the southeastern part of Qinghai Province (Fig. 1). The elevation varies from 3260–4790 m a.s.l., crossing the boundary between the permafrost and seasonal frost areas (Wang 1987, Zhu et al. 1995). The main study area, Madoi County, is located on an uplifted peneplain composing the northeastern part of the Tibetan Plateau. In this area, valley-fill alluvial plains are widespread between 4200–4300 m a.s.l., and hills rise up to 500 m from the surrounding plains.

The plateau area lies in a transitional zone between

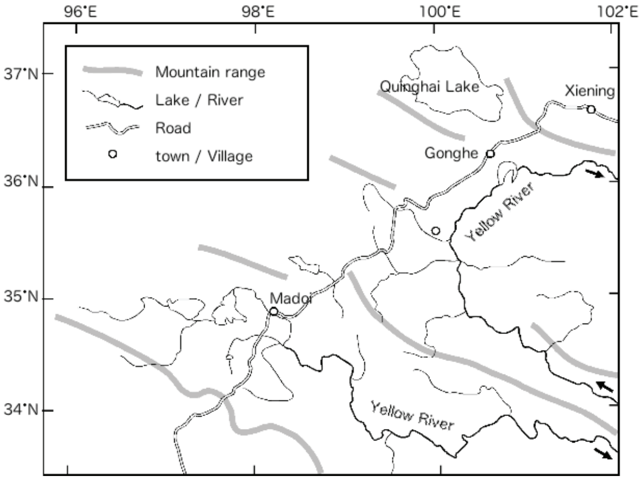

Figure 1. Map of the study area.


Figure 2. Meteorological Station at Madoi borehole site.

discontinuous and sporadic permafrost. Long-term meteorological records at Madoi (98°13′E, 34°55′N, 4273 m a.s.l.; Fig. 1) for 1953–1980 show a cold, dry climate with a mean annual air temperature (MAAT) of -4.1°C, an annual thermal amplitude ranging from -16.8°C in January to 7.5°C in July, and an annual precipitation of 304 mm (Zhou et al. 2000). Decadal mean air temperatures increased by 0.7°C from the 1960s to the 1990s (Yang et al. 2004). More recent records (2001–2005) show further rising MAAT to -2.0°C with an annual thermal amplitude ranging from -13.6°C in January to 9.1°C in July and steady annual precipitation of 304 mm (after WeatherOnline Asia Limited, China). The low precipitation is reflected in shallow winter snow cover (Matsuoka et al. 2005). These conditions favor deep seasonal freezing, whereas the seasonally frozen layer, 2.6 m deep at Madoi, was completely thawed in June 2005 (Matsuoka et al. 2005).

Outcomes from the field study are summarized in previous papers (e.g., Ikeda et al. 2004, Ikeda et al. 2007). Permafrost distribution in the area was examined by ground temperature monitoring and geophysical soundings. Miniature temperature loggers were distributed in the area and recorded year-round ground surface temperatures at hourly intervals. The presence of permafrost was examined from the surface by refraction seismic sounding and one-dimensional (vertical) direct current (DC) resistivity sounding. In addition, a monitoring station was set up at Site Madoi (Fig. 1) with a 8 m-depth borehole for temperature monitoring and meteorological instruments (Fig. 2). During the installation of this borehole, the near-surface stratigraphy of the alluvial plains was directly observed with the recovered cores.

The result suggests that relatively stable permafrost occurs widely above 4300 m a.s.l., that permafrost is mostly absent below 4200 m a.s.l., and that the widespread alluvial plains between 4200–4300 m a.s.l. lack permafrost or have degrading permafrost below a supra-permafrost talik. In contrast, at least until the 1980s, 70%–80% of the plateau surface, that is, the area except for lakes, streams, and nearby swamps, was classified into permafrost terrains (Wang 1987, Wang et al. 1991). Several pits excavated on alluvial plains near Madoi showed that permafrost was generally 15–20 m thick, and the permafrost table lay at about 5 m depth in the early 1980s (Wang 1987). This indicates that permafrost at some places on the plateau began degrading before the 1980s, because the seasonal frost depth rarely exceeds 3 m in the study area (Wang et al. 2000, Matsuoka et al. 2005). From our field study permafrost was completely absent at Site Madoi and its surroundings, indicating that the reported permafrost had considerably disappeared around Madoi after the 1980s, and currently faces a rapid loss of permafrost area, since the elevations mostly belong to a transitional condition between permafrost and seasonal frost environments.

Numerical Modeling

Data

Combining observations and available dataset, the following data were used or referred to for modeling:

(A) data from the borehole (Site Madoi)
(hourly data from 12.08.2004 1500h to 03.08.2006 1000h);

- air temperature, humidity, wind, and snow depth;
- borehole temperature at 7 depths(0.03, 0.3, 1.3, 2.3, 4.3, 6.3 and 7.8 m);
- soil moisture by TDR (0.3, 0.6 and 0.9 m);
- thermal diffusivity, conductivity, heat capacity (0.1 m);

and

(B) other dataset

- monthly mean air temperature at the Madoi meteorological station from 1960 to 2006, and
- 2000-year reconstruction of Northern Hemisphere air temperature (from Jones & Mann 2004).

Model settings

As noted above, we conduct numerical experiments to calculate ground temperature history. The system is one-dimensional thermal conduction with phase change driven by one side (ground surface), so we have to solve an inverse problem of diffusion equation to determine initial values.

Though ground surface temperature history (GSTH) has been commonly reconstructed by the inversion of ground temperature profiles (e.g., Cermak 1971, Lachenbruch &

Marshall 1986, Wang 1992), borehole temperatures are only available for the top 7.8 m, with 7 data points at the study site, too shallow for millennia-scale GSTH reconstruction. Instead, we use the permafrost thickness or complete thaw of the permafrost to compare the model output and observation. Here we seek the initial condition of permafrost at the instant of 1960, the condition in which permafrost survived until the 1980s and its condition and thaw by 2006.

Model settings are shown schematically in Figure 3.

For model equation, the formulation of normal one-dimensional heat conduction is used. Ground temperature variation is described by the following heat conduction equation:

$$\frac{\partial T}{\partial t} = \frac{\partial T}{\partial z}\left(\kappa \frac{\partial T}{\partial z}\right)$$

where T is temperature, t is time, z is depth, and κ is thermal diffusivity, which has different values for frozen and unfrozen soil. Latent heat was considered by introducing an apparent heat capacity. During phase change, the heat capacity of the soil increases, reflecting the amount of latent heat of the soil. Phase change is assumed to occur between 0°C and -0.5°C.

As for finite difference equations, the Multi-point Explicit scheme (Saitoh 1974) was used to solve the equations. Since this is an explicit scheme, grid and time spacing should satisfy the stability condition. In this study the spatial grid and the time step were set to 0.2m and 1 hour, respectively.

Soil properties are set basically according to the observed data. Reflecting the low precipitation, soil water content is constantly low and winter snow depth is also shallow (max. 16 cm). Such conditions yield less sensitivity of ground temperature to the soil water conditions. Volumetric soil water content is assumed to be 10% based on TDR measurements on site. The assumed thermal conductivities of frozen and unfrozen soils are shown in Table 1.

Boundary conditions

To drive the model, upper and lower boundary conditions are needed. The lower boundary condition is given as a flux: based on the global heat flow database (Pollack et al. 1993), constant geothermal heat flow 50mW/m^2 is assumed at the bottom of domain for the whole calculated period. This assumption is not extreme because the whole plateau lies on the stable and old continental crust, with no volcanoes. The area is also located well away from local tectonic activities (e.g., fault system), so a standard value of heat flow was taken. The domain of calculations has 500 m in depth, which is deep enough to guarantee the assumption mathematically.

For the upper (i.e., ground surface) condition, hourly temperature dataset is given to the surface grid, reflecting the seasonal variation and long-term climate change. We used 3 cm-depth temperatures in 2005–2006 at the Madoi station, to which long-term temperature anomalies from the annual mean value are added as an offset. Namely, the surface temperature is given as:

T_S(year, date, hour) = $T_{S,P}$(date, hour) + *Anm.*(year),

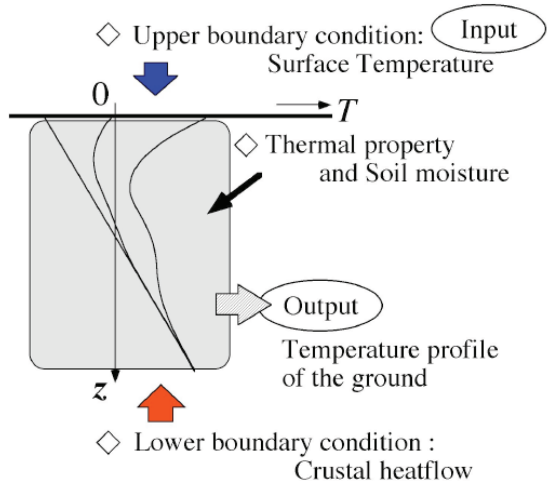

Figure 3. Settings of the one-dimensional model.

Table 1. Thermal conductivities of the soil (Wm^{-1}K^{-1}).

	Depth	Unfrozen	Frozen
Surface	<0.5 m	0.6	0.6
Gravel sediment	<10 m	1.2	1.7
Basement rocks	≥10 m	2.5	3.2

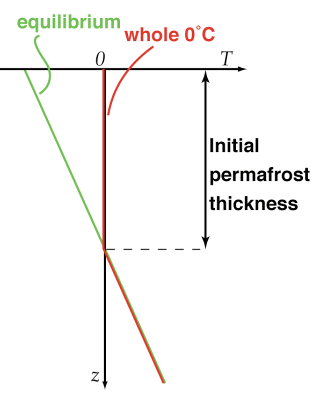

Figure 4. Prescribed initial temperature profile.

where T_S is the ground surface temperature at a certain year/date/hour given to the model, $T_{S,P}$ is the hourly temperature measured on site (i.e., present value), *Anm.* is the anomaly of the annual mean temperature from the present value, for each year. For the period after 1960, monthly mean air temperatures were used to calculate the offset, whereas reconstructed and smoothed data (Jones & Mann 2004) were used for the period before year 1960.

Initial conditions are prepared for two types of runs, illustrated in Figure 4. (1) "Warm permafrost run" is prescribing the initial temperature profile with a certain thickness of warm permafrost at 0°C (i.e., corresponding to the case that the thaw process is in progress). The initial thickness of the warm permafrost is treated as a parameter for this run. (2) "Paleoclimate run" is the long-term calculations based on the reconstructed paleoclimate data for the last 2000 years, which are expected to have reasonable temperature profiles for assumed climate history (see Fig. 5). The offset

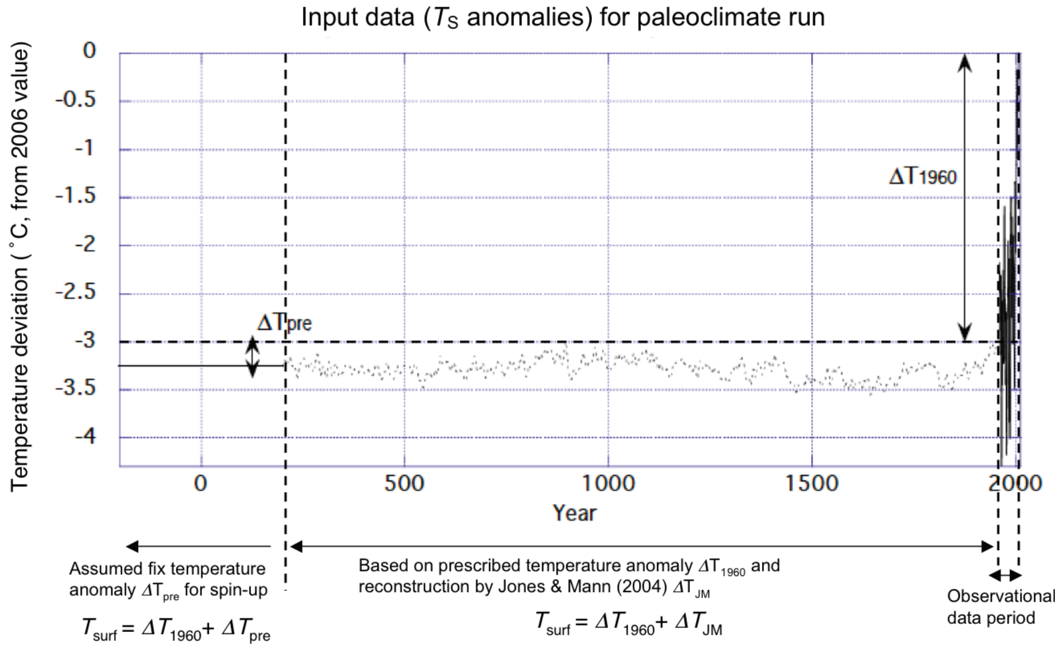

Figure 5. Surface temperature condition for model.

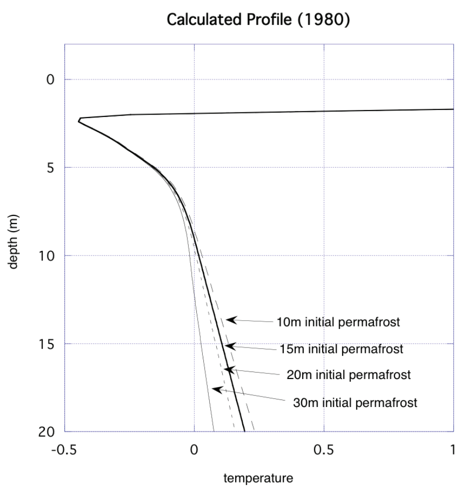

Figure 6. Calculated temperature profiles 1980, starting at warm permafrost conditions.

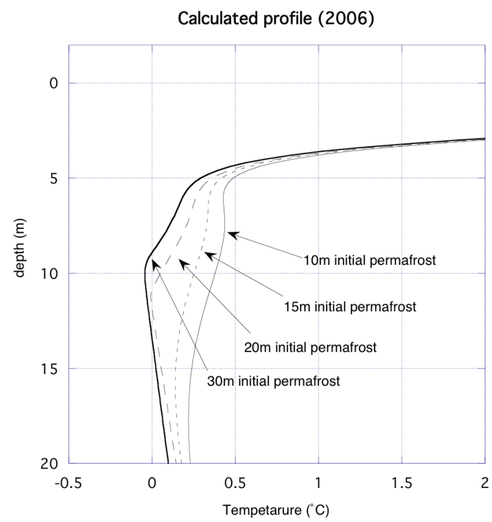

Figure 7. Calculated temperature profiles 2006, starting at warm permafrost conditions.

for the pre-1960 period (ΔT_{1960}) is treated as a parameter to examine the effect of long-term climate, although the 10-year mean (period: 1960–1970) of observed temperature anomaly at Madoi Station can be considered as a standard value.

Soil water content and snow conditions in the paleo-climate runs are assumed to remain unchanged. Recorded precipitation since 1960 was stable in long term, which is partly supports this assumption. The dry condition of the area is considered to be a general geographical setting, mainly due to the blockade of vapor supply by the Himalaya Mountains.

Results

Warm permafrost run

This case is to examine what thickness of warm permafrost can be thawed since 1960. Figures 6 and 7 show the summer temperature profiles in 1980 and 2006 in the model. Permafrost in 2006 can only exist with initial permafrost deeper than 20 m (see Fig. 7).

On the other hand, Figure 6 shows that the permafrost exists for all cases (initial permafrost ≥10 m?) in 1980. Difference in the initial condition produces a slight difference in temperature gradient significantly affects the survival time of permafrost. From this calculation ca. 15 m of permafrost can exist in the 1980s to meet the result of present observations (i.e., it may thaw out by present).

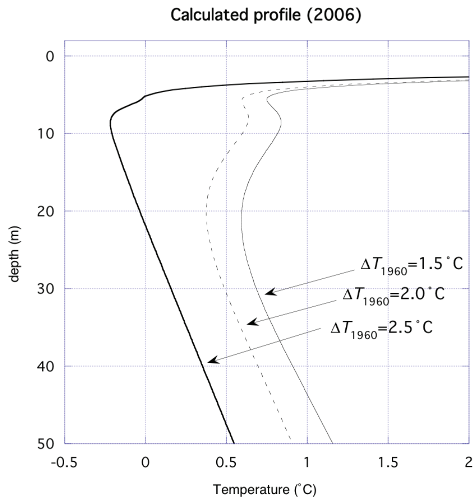

Figure 8. Calculated temperature profiles 2006, under the paleotemperature conditions.

Paleoclimate run

From the parameter study of this run, the effect of pre-1960 climate history to the present condition is examined. Figure 8 shows the temperature profile at 2006 (as before); three profiles correspond to different values of ΔT_{1960}: 1.5°C, 2.0°C, and 2.5°C.

Although the 10-year mean of observed temperature anomaly during the 1960s was 2.5°C, this condition appears to be too cold, leaving thick permafrost (more than 20 m) at 2006. However, as shown in this plot, change in this long-term offset by 0.5°C changes the story completely: the other two cases cannot keep permafrost until the present condition.

In this modeling, the applied trend of paleotemperature is based on the averaged climate for the Northern Hemisphere, which may need reconsideration.

Discussion

Results of this study give a quantitative idea of the timescale of permafrost degradation, which implies that the recent warming climate has played a strong role in causing substantial change in the study area. Although the response of the ground temperature should have delay from the surface (e.g., 10 m-depth temperature lags ca. 10 to 100 years), "Paleoclimate run" shows that the current permafrost condition is strongly affected by the recent climate change. Further accumulation of field and paleoenviroment data would be helpful to discuss more details.

A number of respects have to be improved in modeling. We focus on two topics: thermal properties and paleotemperature input.

One of the uncertainties in modeling lies in thermal properties of the ground. The near-surface layer especially can have a large range of seasonal, and also spatial variation, due to the existence of organic material and differences in the soil water content. In our modeling, the observed values were applied to the near-surface organic layer (Table 1), and they show small seasonal variations through a year, reflecting the dry condition at the observation site. Spatial representativeness of such dry conditions was partly confirmed by the field measurement by portable TDR.

On the contrary, a seasonal difference in thermal conductivity (frozen/unfrozen) appears in wet conditions, which allow more heat flow in winter through the ground surface, compared to summer. This effect cools down the ground temperature effectively in consequence. Therefore, drought of the ground surface can trigger a feedback to cause further thaw of the permafrost.

With respect to the input paleoclimate data, the local paleotemperature history through the last millennia may have significantly larger variability than the reconstruction by Jones and Mann (2004), which was averaged for the whole Northern Hemisphere. Comparing the reconstruction and the recorded temperature since 1960, the hemispherical average has a similar trend with the recorded data, but absolute value of the variation is a few times larger. In general, quantitative paleotemperature data are lacking in the inland continent, but reliable paleoclimate data is essential for further modeling.

Conclusions and Outlook

Ground temperature of the permafrost in the source region of the Yellow River basin was calculated based on the instrumental data, and the response of permafrost to the warming climate was examined quantitatively. The existence of the permafrost in the 1980s, which has been suggested from the previous works, is supported from the modeling results in the case that the permafrost was already the warm (~ 0°C) when it was observed.

It should be noted, however, such a thermal condition of the permafrost is relatively difficult to achieve in dry conditions. If the ground is wet and contains more ice in the permafrost, the thawing process should be slower, and the current distribution of the permafrost, basically lacking up to 4300m, would become hard to explain.

There are still uncertainties in the paleoenvironment of Tibetan plateau, and it is of importance for the prediction of future response of the permafrost to the ongoing climate change. In combination with the paleoclimate study, for example, the reconstruction from lake sediments will be the next step to put the arguments forward. Commencement of deeper borehole temperature measurement, which allows the inversion of surface temperature history (e.g., Pollack & Huang 2000), may also be a candidate of the method to reveal local paleoclimate.

Acknowledgments

We acknowledge Drs. C. Gao, Z. Han, and Mr. J. Ding for logistical help and field assistance. The study was supported by a national program "Sustainable Coexistence of Human Nature and the Earth" founded by the Ministry of Education, Culture, Science, and Technology. We are also thankful for fruitful suggestions by reviewers and the editor.

References

Harrison, W.D. 1991. Permafrost response to surface temperature change and its implications for the 40,000-year surface temperature history at Prudhoe Bay, Alaska. *Journal of Geophysical Research* 96B(1): 683-695.

Ikeda, A., Sueyoshi, T., Matsuoka, N., Ishii, T. & Uchida, Y. 2007. Permafrost sounding (2003–2005) in the source area of the Yellow River, Northeastern Tibet. *Geographical Review of Japan* 80: 259-271.

Ikeda, A., Matsuoka, N. & Sueyoshi, T. 2004. Permafrost survey in the source region of the Yellow River: a preliminary report. *Seppyo* 66: 235-239. (J)

Jin, H., Li, S., Cheng, G., Wang, S. & Li, X. 2000. Permafrost and climatic change in China. *Global and Planetary Change* 26: 387-404.

Jones, P.D. & Mann, M.E. 2004. Climate Over Past Millennia. *Reviews of Geophysics* Vol. 42, No. 2, 6 May 2004.

Lachenbruch, A.H. & Marshall, B.V. 1986. Changing climate: geothermal evidence from permafrost in the Alaskan Arctic. *Science* 234: 689-696.

Liu, S., Lu, A., Ding, Y., Yao, T., Ding, L., Li, G. & Hooke, R.L. 2002. Glacier fluctuations and the inferred climate changes in the A´Nyêmaqên Mountains in the source area of the Yellow River. *Journal of Glaciology and Geocryology* 24: 701-707. (CE)

Lunardini, V.J. 1996. Climatic warming and the degradation of warm permafrost. *Permafrost and Periglacial Processes* 7: 311-320.

Matsuoka N., Ikeda, A., Sueyoshi, T. & Ishii, T. 2004. Permafrost sounding (2003-2004) in the source area of the Yellow River, China. *Annual Report of the Institute of Geoscience, the University of Tsukuba* 30: 33-38.

Matsuoka N., Ikeda, A., Sueyoshi, T., and Ishii, T. 2005. Monitoring frozen ground (2004-2005) at Madoi in the source area of the Yellow River, China. *Tsukuba Geoenvironmental Sciences* 1: 39-44.

Matsuoka, N., Ikeda, A., Sueyoshi, T. & Ishii, T. 2006. Frozen ground monitoring (2004-2006) in the source area of the Yellow River, China. *Tsukuba Geoenvironmental Sciences* 2: 25-30.

Osterkamp, T.E. & Romanovsky, V.E. 1999. Evidence for warming and thawing of discontinuous permafrost in Alaska. *Permafrost and Periglacial Processes* 10: 17-37.

Osterkamp, T.E. 2005. The recent warming of permafrost in Alaska. *Global and Planetary Change* 49: 187202.

Owen, L.A., Finkel, R.C., Haizhou, M., Spencer, J.Q., Derbyshire, E., Barnard, P.L. & Caffee, M.W. 2003. Timing and style of Late Quaternary glaciation in northeastern Tibet. *Geological Society of America Bulletin* 115: 1356-1364.

Peng, X., Wu, Q. & Tian, M. 2003. The effect of groundwater table lowering on ecological environment in the headwaters of the Yellow River. *Journal of Glaciology and Geocryology* 25: 667-671. (CE)

Pollack, H.N. & Huang, S. 2000. Climate Reconstruction from Subsurface Temperatures. *Annual Review of Earth and Planetary Sciences* Vol. 28: 339-365.

Pollack, H.N., Hurter, S.J. & Johnson, J.R. 1993. Heat flow from the Earth's interior: Analysis of the global data set. *Rev. Geophys.* 31: 267-280.

Sharkhuu, N. 1998. Trends of permafrost development in the Selenge River Basin, Mongolia. In: *Proceedings of the Seventh International Conference on Permafrost.* Sainte-Foy: Centre d'études Nordiques, 979-985.

Smith, S.L., Burgess, M.M., Riseborough, D. & Nixon , F.M. 2005. Recent trends from Canadian permafrost thermal monitoring network sites. *Permafrost and Periglac. Process.* 16: 1930.

Wang, G., Qian, J., Cheng, G. & Lai, Y. 2001. Eco-environmental degradation and causal analysis in the source region of the Yellow River. *Environmental Geology* 40: 884-890.

Wang, J. & Derbyshire, E. 1987. Climatic geomorphology of the north-eastern part of the Qinghai-Xizang Plateau, People's Republic of China. *Geographical Journal* 153: 59-71.

Wang, S. 1987. Frozen ground and periglacial features in the southeastern part of Qinghai Province. In: J. Hövermann & W. Wang (eds.), *Reports on the Northeastern Part of the Qinghai-Xizang (Tibet) Plateau by Sino-W. German Scientific Expedition*. Beijing: Science Press, 343-366.

Wang, S., Luo, X. & Guo, P. 1991. The distributive characteristics of frozen ground in the east of Qinghai–Xizang Plateau. *Journal of Glaciology and Geocryology* 13: 131-140. (CE)

Wang, S., Jin, H., Li, S. & Zhao, L. 2000. Permafrost degradation on the Qinghai-Tibet Plateau and its environmental impacts. *Permafrost and Periglacial Processes* 11: 43-53.

WeatherOnline Asia Limited. *WeatherOnline*. http://www.t7online.com (C) (last checked date: November 27, 2006)

Yang, J., Ding, Y., Shen, Y., Liu, S. & Chen, R. 2004. Climatic features of eco-environmental change in the source regions of the Yangtze and Yellow Rivers in recent 40 years. *Journal of Glaciology and Geocryology* 26: 7-16. (CE)

Zhang, S., Wang, Y., Zhao, Y., Huang, Y., Li, Y., Shi, W. & Shang, X. 2004. Permafrost degradation and its environmental sequent in the source regions of the Yellow River. *Journal of Glaciology and Geocryology* 26: 1-6. (CE)

Zhou, Y., Guo, D., Qiu, G. & Cheng, G. 2000. *Geocryology in China.* Beijing: Science Press. (C)

Zhu, L., Wu, Z. & Liu, Y. 1995. Permafrost degeneration in the east of Tibetan Plateau. *Journal of Glaciology and Geocryology* 17: 120-124. (CE)

Zhu, L., Wu, Z., Zang, E., Pan, B., Liu, Y. & Tao, G. 1996. Difference of permafrost degeneration in the east of the Tibetan Plateau. *Journal of Glaciology and Geocryology* 18: 104-110. (CE)

(J): written in Japanese, (C): written in Chinese,
(CE): written in Chinese with English abstract

Permafrost in the *Bibliography on Cold Regions Science and Technology*

Sharon N. Tahirkheli
American Geological Institute, Alexandria, VA, USA

Abstract

The *Bibliography on Cold Regions Science and Technology* has covered approximately 22,000 publications on permafrost and contains an additional 6000 references to the related topic of frozen ground. Permafrost publications are distributed throughout the global scientific literature and are found in peer-reviewed journals, government reports, theses/dissertations, and conference publications. Almost half of the permafrost literature is found in conference proceedings. Coverage of master's theses and doctoral dissertations in the *Bibliography* is limited to a total of two hundred, primarily from U.S. and Canadian institutions. As geographic distribution of permafrost is concentrated in the polar and high-altitude regions of the world, it is no surprise that 9000 publications have been identified in the Russian language. The rest of the literature is published around the globe, including Europe, Canada, the United States, China, and Japan in the north, and Argentina in the south.

Keywords: bibliography; permafrost; publications.

Introduction

The *Bibliography on Cold Regions Science and Technology* is a part of the Cold Regions Bibliography Project (CRBP), jointly sponsored by the U.S. National Science Foundation and the U.S. Army Cold Regions Research and Engineering Laboratory. As part of its scope, the *Bibliography* includes references to publications on all scientific and technical aspects of permafrost including distribution, properties, impacts of current climate change, cold-weather construction, engineering challenges, soil mechanics, hazards, and land use. This paper explores the coverage of permafrost throughout the history of the *Bibliography on Cold Regions Science and Technology* by considering the terminology used, the distributed geographic and linguistic sources of permafrost publications and the variations over time of the frequency of publications.

History of the *Bibliography*

Bibliography on Snow, Ice and Permafrost

The current CRBP evolved from the SIPRE Project. SIPRE stood for the Snow, Ice and Permafrost Research Establishment of the U.S. Army Corps of Engineers and Project was primarily concerned with publishing an annotated bibliography covering snow, ice, and permafrost. Produced at the Library of Congress beginning in 1951 and published as SIPRE Report 12, the *Bibliography on Snow, Ice and Permafrost* was carefully limited to the properties of snow, ice, and permafrost. Only on rare occasions were background materials on peripheral topics included. The objective of the SIPRE Project was to assist SIPRE and other government agencies that were concerned with "various phases of research on the properties of snow, ice and frozen ground." (Library of Congress 1953)

Volumes 16–22 underwent several name and format changes. The SIPRE Report 12 became CRREL Report 12, the *Bibliography on Snow, Ice and Permafrost* became the *Bibliography on Snow, Ice and Frozen Ground* and finally, with Volume 23, the current title, *Bibliography on Cold Regions Science and Technology,* was adopted. With the name changes came an expansion of coverage and an increased emphasis on engineering in a cold environment "including the varied disciplines of engineering and broad coverage of the physical sciences. The disciplines and subject matter remained varied and covered every topic relating to cold regions imaginable" (Liston 2002).

Bibliography on Cold Regions Science and Technology

The CRBP was managed by the Library of Congress until the late 1990s and was published in print as CRREL Report 12 beginning with Volume 23. In 2000, the American Geological Institute (AGI) began compiling the *Bibliography* and producing the current online web-based version of the *Bibliography*. Under the terms of the CRBP Cooperative Agreement between AGI and the U.S. National Science Foundation, all of the publications covered in the CRBP must be obtained and examined. Citations of publications from other bibliographies are helpful in identifying publications for consideration but cannot be used to develop references without access to the original.

The *Bibliography on Cold Regions Science and Technology* now contains more than 218,700 references and is freely available to users via the Internet at http://www.coldregions.org The present-day scope of the *Bibliography* includes "references to scientific and engineering research related to material and operations in a winter battlefield, the nature and impact of cold on facilities and activities, cold-related environmental problems, and the impact of human activity on cold environments" (American Geological Institute 2007).

While permafrost is not explicitly mentioned in the coverage statement, all aspects of permafrost continue to be considered relevant to the *Bibliography* and are included. With the explosion in climate and global change studies, and with the surge in publications expected to result from the International Polar Year 2007–2008, the future expectation is that the number of permafrost publications will show a marked increase over the next several years.

Finding Permafrost in the *Bibliography*

Terminology

An examination of the original volumes of the *Bibliography* quickly reveals that the subject indexes included "permafrost" and "frozen ground" as entries. As the *Bibliography* evolved to the use of a thesaurus of controlled terms, "permafrost" and "frozen ground" remained consistent in their usage as entry points (Engineers Joint Council 1969). This greatly simplifies the attempt to locate the relevant literature within the online database. To locate references to "permafrost" and/or "frozen ground" in the web-based database of the *Bibliography*, the terms were searched directly as part of the entire bibliographic record. This search included "permafrost" and "frozen ground" as parts of the titles, abstracts, keywords, conference titles, publisher names, or notes.

It is useful to note that the controlled vocabulary used in the production of the *Bibliography* contains the following specific types of permafrost as potential additional identifiers: continuous permafrost; discontinuous permafrost; sporadic permafrost; and subsea permafrost. Processes and concepts related to permafrost can also be directly accessed; for example, permafrost heat balance; permafrost origin; permafrost thickness.

For purposes of this study, only the more general terms were chosen. 27,732 references were retrieved with almost 22,000 references containing "permafrost" and close to 6000 containing "frozen ground." Thus 12.6% of the references in the *Bibliography on Cold Regions Science and Technology* are relevant to "permafrost" or "frozen ground."

Publication Date

Overall distribution by date of publication

Permafrost and frozen ground publications were one of the three primary topics in the earliest volumes of the *Bibliography*. Total publishing numbers, however, were substantially lower. For example, in 1955 only 76 publications on permafrost and/or frozen ground were included in the *Bibliography*. Numbers increased dramatically by the late sixties with 470 publications referenced in 1966, and the totals peaked in 1978 and 1983 with 1111 items in both of those years. The rate of publication in the permafrost field has declined slightly from those highs, but varies between 450 to 750 items per year.

When considered as a percentage of the total number of publications added to the *Bibliography* each year, the permafrost/frozen ground publications have varied from as little as 5.73% in 1995 to as much as 27.55% in 1977 with an overall average of 13.52% based on the publication years 1970–2007. Table 1 presents the dates of permafrost/frozen ground publications as a percentage of the total number of publications added to the *Bibliography on Cold Regions Science and Technology*.

Table 1. Percentage of *Bibliography* by date of publication.

Date of Publication	Percentage total references in the *Bibliography*
1970	10.32%
1974	17.27%
1978	17.42%
1982	20.53%
1986	13.08%
1990	10.16%
1994	7.06%
1998	7.36%
2002	7.92%
2006	12.85%
Average percentage	13.52%

Permafrost/frozen ground publications as a percentage of the total number of publications referenced in the *Bibliography* in a given year. Average percentage based on 1970–2007.

Table 2. Publication type.

Type of Publication	Total Count By Type*
Serial	12,818
Conference	10,925
Book	3,437
Report	1,500
Patent	192
Thesis/Dissertation	160
Map	33

*Total will not equal number of permafrost references because some items have multiple types and others have no type provided.

Publication Type

Overall distribution by type of publication

Permafrost and frozen ground publications are found not only in the peer-reviewed literature, but also in what is often referred to as gray literature—government reports, theses/dissertations, and conference publications. References included in the *Bibliography of Cold Regions Science and Technology* are currently tagged as one or more of the following types: serial, book, conference, report, thesis/dissertation, patent, or map. The earlier volumes of the *Bibliography* that were originally produced for a print publication do not always contain equivalent information; however, procedures were developed to determine whether an item was a journal article, map, patent, monograph, conference paper, or technical report. Out of the total references, 940 items could not be categorized and, while not entirely equivalent, for the purposes of this study, monographs were grouped under books.

An examination of the permafrost references in the *Bibliography of Cold Regions Science and Technology* by type of publication (Table 2) reveals several points of interest.

Primary publication types

The primary type of publication included in the

Bibliography that contains permafrost papers is labeled serial. Serials may be of two types: peer-reviewed journals and monographic serials. While serial is the predominant type, conference publications are a very close second, reflecting the importance of these publications to this discipline. More than one-third of the permafrost/frozen ground publications are drawn from conference proceedings. It is worthwhile to note that the *Bibliography*, with a few rare exceptions, does not include abstracts from meetings—only proceedings.

The International Permafrost Conference proceedings are good examples of the significance of conference papers in the literature. The first International Permafrost Conference was held in 1963 and the proceedings contained 102 papers. With 100 or more papers produced at each meeting, the nine conferences represent a major component of the total permafrost literature.

A random selection of twenty papers from conferences produces items from the following workshops and symposia: International snow science workshop; International Congress of the International Association for Engineering Geology and the Environment; USA/CIS joint conference on Hydrologic issues of the 21st Century; Jahrestagung der Schweizerischen Geomorphologischen Gesellschaft; XI glyatsiologicheskii symposium; and the AGU 2004 fall meeting open Northern Eurasia Earth Science Partnership Initiative science session.

Other publication types

Books and book chapters comprise 12.8% of the total permafrost literature while technical/government reports are a healthy 5.8%. Patents, maps, and thesis/dissertations combined are barely a blip in the totals of types of publications. While this may be appropriate for patents, maps and theses/dissertations seem to be underrepresented in the *Bibliography*. The theses/dissertations that are included are primarily from the United States and Canada—not what would be expected if all theses/dissertations on permafrost and frozen ground were included. Maps were seldom included in the *Bibliography* until the CRBP compilation moved to the American Geological Institute. (Tahirkheli 2004)

Document availability

Because of its history in support of research for SIPRE and the Cold Regions Research and Engineering Laboratory, the CRBP was always concerned with the availability of the documents cited in the Bibliography. The Library of Congress provided a microfiche service that provided copies of uncopyrighted materials to requestors. The need to have the documents immediately available has impacted the coverage of the CRBP. Some types of publications such as maps and thesis/dissertations could have been included more frequently without this requirement. Currently, the bibliographers compiling the *Bibliography* cannot include a thesis/dissertation unless the item is easily accessed by the users of the *Bibliography*. For theses/dissertations, this usually means that the document must be available through a microfiche service. With the wider dispersion of electronic publications, this restriction has been relaxed somewhat, and the inclusion of online theses/dissertations is now possible.

The Permafrost Young Researchers Network web site http://www.pyrn.org/ contains approximately 230 citations under consideration for inclusion in the *Bibliography* in the future, depending on availability of the title.

Country/Language of Publication

Distribution by country

Permafrost and frozen ground publications are widely distributed around the globe. Current serial, book, and conference publications added to the *Bibliography* are tagged with an indicator of the country of publication. The earlier volumes of the *Bibliography* and current theses/dissertations and technical reports do not always contain this information; however, procedures were developed to determine the country of publication whenever possible. Approximately 1100 items could not be assigned to a source country. The rest of the permafrost publications identified in the *Bibliography on Cold Regions Science and Technology* were selected by the country of publication and the results are presented in Table 3.

Primary countries producing permafrost publications

Permafrost publications have been identified from 44 separate countries; however, the Former Soviet Union and Russia are the primary sources with a whopping 44.8% of

Table 3. Country of publication.

Country of Publication	Total Count
Former Soviet Union	11,129
United States	5,658
Canada	2,322
Russia	1,307
China	1,264
United Kingdom	1,233
Netherlands	834
International	735
Norway	515
Germany	463
Japan	385
Sweden	142
Poland	131
Finland	98
France	91
Denmark	71
Switzerland	71
Italy	45
Austria	32
Argentina	24
India	21
New Zealand	20
Belgium	17
Australia	11
21 countries	41

Table 4. Language of text.

Language of Text	Total Count
Russian	14,068
English	12,093
Chinese	858
French	217
Japanese	186
German	173
Polish	40
Norwegian	35
Spanish	26
Swedish	23
Finnish	18
Italian	16
Danish	13
Czech	3
Korean	3
Lithuanian	2
Ukrainian	2
Bulgarian	1
Hungarian	1
Serbian	1

the total. The United States is not even a close second with 20.4% and Canada is a distant third with 8.4%.

While both the geographic distribution of permafrost and the distribution of publishing on the topic of permafrost is concentrated in the polar regions (USSR/Russia, Canada, United States), there are significant numbers of permafrost publications being published in countries with high altitude areas including parts of China, Switzerland, and Italy. There are even scattered publications from India and South Africa.

Distribution by language of publication

Distribution by language of publication for permafrost/frozen ground publications is highly concentrated in three languages: Russian, English, and Chinese, which account for 97% of all publications. This distribution only partially mirrors the distribution of publications by country of publication and emphasizes the dominance of Russian and English for the permafrost literature. The languages of the texts are presented in Table 4 in order of prevalence.

Only twenty languages were identified within the *Bibliography*. The language of the text was determined for every permafrost/frozen ground publication.

CRBP Sources

Or, how does the CRBP obtain the publications cited in the Bibliography?

As indicated by the charts of languages of the texts and countries of publication, many sources are necessary to be as complete in coverage as possible. The CRBP uses many online databases and relevant bibliographies. For permafrost, the *Permafrost and Frozen Ground Bibliography, 1978–2003* (available from the Frozen Ground Data Center at the National Snow and Ice Data Center) is a rich source of potential documents (http://nsidc.org/fgdc/biblio/). Of course, as indicated earlier, the CRBP or one of its partners must actually examine the publications and is further required to digitize any uncopyrighted materials that are included.

The CRBP obtains publications in all of the following ways:

Libraries. Both major government and university library collections are mined for possible relevant publications. Some of the libraries mined regularly include:

- U.S. Army Cold Regions Research and Engineering Laboratory Library
- Institute for Arctic and Alpine Research Information Center
- U. S. Geological Survey Library System
- University of Texas at Austin
- Stanford University

Publishers. Many publishers provide both publications and metadata directly to abstracting and indexing services like the one producing the Bibliography.

Open-access Web publications. Many publications are now appearing on the web and are openly available to all users.

Bibliographic partnerships (where several organizations produce similar bibliographies). Partnerships are often formed to assist in broader access to pertinent publications. The American Geological Institute participates in at least a dozen bibliographic partnerships including a significant collaboration with the Scott Polar Research Institute.

Scientists and authors. Interested researchers provide direct information regarding their publications to the *Bibliography* and either links to full-text as posted on their personal web pages or reprints of their articles.

Current opportunities and challenges in maintaining comprehensive coverage

With the growth of web publishing, CRBP faces both new opportunities and challenges. Information about publications is sometimes easier to obtain, and it may even be freely accessible on the web. Publishers often provide citation information electronically. eliminating the need for expensive and time-consuming data entry. On the other hand, some publications appear on the web today and are gone or moved tomorrow. A publication may be launched and die before the publisher communicates with the community about its existence. Even the definition of what a publication is has become somewhat blurred.

The CRBP is continuously adapting to these changes. Suggestions, as well as notification of new publications, are welcome.

International Polar Year 2007–2008

Plans for the Bibliography on Cold Regions Science and Technology

The International Polar Year Publications Database (IPYPD) is in the process of identifying and indexing any permafrost/frozen ground publications that result from the International Polar Year 2007–2008 (IPY). A network of five organizations is collaborating to attempt to compile and provide access to all IPY-related publications through a single database. This network includes the Arctic Science and Technology Information System (ASTIS), the Cold Regions Bibliography Project (CRBP), the Scott Polar Research Institute (SPRI) Library, the Discovery and Access of Historic Literature of the IPYs (DAHLI) project, and National Information Services Corporation (NISC). The IPYPD will include publications that result from research as well as publications that relate to outreach and education. The IPYPD, as part of the IPY Data and Information Service (IPYDIS), is attempting to use the IPY Data Policy to require that researchers report their publications to either ASTIS, CRBP or the SPRI library. Each of these organizations will include records for IPY publications in their existing databases, which are part of the Arctic & Antarctic Regions database distributed by NISC.

Of course, the total number of permafrost/frozen ground publications that will result from the IPY is unknown at this time. Based on previous publishing rates from earlier IPYs, the IPYPD expects an estimated 20,000 total publications. If the percentage of permafrost/frozen ground publications remains stable, then we should expect about 12.6% of the total number of publications or about 2500 permafrost publications to be produced.

In an attempt to locate relevant publications, all of the collaborators are trying to contact researchers through conference presentations and web sites. Instructions for reporting publications are available online at http://www.ipy.org

Conclusions

Based on the above estimates of publication rates in the permafrost literature, the CRBP would expect to add upwards of 600 new permafrost publications over the next twelve months. The data on language, country, and type of publication provide a roadmap for focusing future efforts by the CRBP. When considered from the perspective of country and language of texts, the data regarding permafrost/frozen ground publications highlight the immense contribution to the scientific literature by the Former Soviet Union/Russia. Further examination of the Russian literature is warranted to insure continued coverage and access to this information. The CRBP will focus attention on expanding its connections with relevant organizations in this region. In addition, the International Polar Year and the conferences resulting from activities of the IPY should provide a substantial pool of permafrost/frozen ground literature for future consideration for inclusion in the *Bibliography* over the next decade.

Acknowledgments

The Cold Regions Bibliography Project is supported by the U.S. National Science Foundation and the U.S. Army Cold Regions Research and Engineering Laboratory under Grant No. OPP-0440772. The assistance of AGI staff members MaryAnn Theresa Eitler and Lawrence Berg in the compilation of the data for, and the editing of, this paper is appreciated. The International Polar Year Publications Database is part of the IPY Data and Information Service (IPYDIS).

References

American Geological Institute. Cold Regions Bibliography Project. 2007. http://www.coldregions.org

Engineers Joint Council. 1969. *Thesaurus of Engineering and Scientific Terms.*

Library of Congress, Technical Information Division. 1953. *Annotated Bibliography on Snow, Ice and Permafrost*. SIPRE Report 12, Vol. III, v.

Liston, Nancy C. 2002. The Bibliography on Cold Regions Science & Engineering. In: Kirsten Caning & Vibeke Sloth Jakobsen (eds.), *Poles Apart – Poles On-Line; Proceedings of the 19th Polar Libraries Colloquy.* Copenhagen: Danish Polar Center, 58-62.

Tahirkheli, Sharon N. 2004. Distribution of Source Materials for the Antarctic Bibliography and the Bibliography on Cold Regions Science and Technology. In: Barbara E. Kelcey (ed.), *Polar Research: Let Us Share – Amiqqaaluta; Proceedings of the 20th Polar Libraries Colloquy*. Ottawa: Polar Libraries Colloquy, 160-164

Siberian Woolly Mammoths and Studies into Permafrost in the Russian Empire in the 19th Century

Erki Tammiksaar
Centre for Science Studies, Estonian University of Life Sciences
Ken Kalling
Centre for Science Studies, Estonian University of Life Sciences

Abstract

In 1806 an adjunct of St. Petersburg Academy of Sciences, Michael Adams, brought to the Russian capital a fully preserved skeleton of a woolly mammoth. The mammoth issue became central to research made into aspects of permafrost and of the Ice Age, started in Russia in 1837 by a member of the Academy, Karl Ernst von Baer. For the study of permafrost Baer organized in 1842–45 an expedition to Siberia, headed by Alexander Theodor von Middendorff. All the subsequent expeditions to northern Siberia in 1860–1880s (headed by Friedrich Schmidt, Gerhard von Maydell, Alexander von Bunge *jun*., Eduard von Toll) were among other areas of science aimed at the study of palaeontological remains to establish the once widespread range of the woolly mammoth. In addition, these expeditions contributed much to the study of permafrost, laying foundations for the emergence of the outstanding Soviet school of permafrost studies.

Keywords: Baer, Karl Ernst von; Ice Age; Middendorff, Alexander Theodor von; Russian Empire; woolly mammoths.

Introduction

Mammoths, the conditions in which they lived, and their extinction received much interest among the 19th century scientific community. It could even be stated that the finds of these giant mammals from the Siberian permafrost were the main impulse for studies of prehistoric animals, i.e. for the development of vertebrate palaeontology as such. As the remains of the mammoths were mainly found in the northern and Siberian territories of the Russian Empire, it was the Russian scholars (and among others those of Baltic-German origin) who contributed most to the study of mammoths. One of the topics dealt with in connection with mammoths was their preservation in Siberian permafrost. The present article discusses the importance of mammoth studies on the scholarship on permafrost in the Russian Empire.

Information on Mammoths Prior to the 19th Century

In modern times every new discovery of a well-preserved mammoth is an important event both for science and the media. In the 19th century and before that, finds of well-preserved mammoths caused much attention. But due to the low level of development of natural sciences and little public information about Siberia, superstitious theories on the matter tended to prevail. For example, it was possible to believe the legends of the indigenous people of Siberia. According to legends the mammoths lived like moles underground and died if exposed to the daylight. Ideas that mammoths still existed were found in Chinese sources (Baer 1866). Russian colonists in turn believed that mammoths became extinct during the Great Deluge which carried their bodies to Siberia.

The first confirmed information on the Siberian woolly mammoths was taken to European scholars in the 17th century by Dutch traveler Nicolas Witsen, and by a Russian ambassador to Beijing, Ysbrand Ides. The latter brought with him, to confirm his words, a skull and other bones of a mammoth (Baer 1866).

In the 18th century, the geography and nature of Siberia was studied by several foreigners at the request of the Russian authorities. One should mention Daniel Gottlieb Messerschmidt with his companion Philipp Johann Strahlenberg (Tabber), members of Vitus Bering's second Kamtchatka expedition (1734–1744), Johann Georg Gmelin and Gerhard Müller and also Peter Simon Pallas who headed an expedition group from the St. Petersburg Academy of Sciences (1768–1774). These expeditions all secured information concerning mammoths in different parts of Siberia. Gmelin reported also on the Siberian permafrost (Baer 2001), but the two topics—permafrost and mammoths—were not at this stage linked.

In the end of the 18th century, Russian merchants discovered the islands of New Siberia where a lot of mammoth tusks and teeth were found. Subsequent travels, up to the end of the 19th century, to these islands were mainly aiming at collecting this material for profit.

A Mammoth Skeleton Arrives at St. Petersburg

In 1806, the Russian diplomatic mission to China visited Yakutsk. The team included Michael Adams, an adjunct in zoology, St. Petersburg Academy of Sciences. He heard that at the mouth of the Lena River a wholly preserved mammoth had been found. Adams decided to attempt to profit from this find by going to the site, bringing the mammoth to St. Petersburg, and there placing it on sale. At the site it became evident that the soft tissues of the animal had been lost, partly eaten by scavengers (the mammoth had been discovered in 1799) (Baer 2001). The skeleton of the mammoth was placed in the Zoological Museum of the St. Petersburg Academy of Sciences. In an article published in 1807 in an obscure periodical entitled *Journal du Nord,* data concerning the conditions in which the animal was found were provided by Adams and a local chief named Ossip Schumachow, who had actually made the discovery. The data became more widely known due to a member of the St. Petersburg Academy of Sciences, Wilhelm Gottlob Tilsesius von Tilenau (1815). From him information on the mammoth spread into the works of European scholars, together with a suggestion that mammoths must have been southern animals, the carcasses of which had been carried north by the big Siberian rivers. This idea was supported by a notion that the northern pastures seemed to be too poor for such big animals to feed there. The preservation of the bodies of the animals for a long time was not a matter of concern for the scientists of the day.

The Birth of Permafrost Studies in Russia

At the end of 1837, Karl Ernst von Baer, a natural scientist and member of the St. Petersburg Academy of Sciences in the field of zoology, gave a presentation on the so-called Shergin pit in Yakutsk. This, despite its enormous depth (116 m) did not contain any water due to permafrost. In his presentation Baer analyzed data available to him on the temperature in the pit. He concluded that the observations that had produced these data had to be continued in order to secure more information on this new natural phenomenon in Siberia. Many European scholars (i.e., German geologist Leopold von Buch) were suspicious of Baer's data on the pit stating that in regions in which there was forest and bush growing, the soil could not be permanently frozen, especially if one took into account the theory of a hot core of the Earth (see: Tammiksaar 2002).

Baer in his turn proved that the geothermic observations made in the pit supported current geological theory, proving also that in those geographical regions in which the annual average temperature fell below 0°C the frost entered the soil, causing permafrost (*Boden-Eis*) (Baer 2001).

To defend his arguments, Baer started in 1838 to collect data on this topic not only from literary and archive sources but also from his colleagues who studied the Russian North. As a result he completed by the beginning of 1843 a 218-page manuscript "*Materialine zur Kenntniss des unvergänglichen Boden-Eises in Sibirien.*" This first theoretical study on permafrost remained unpublished for several reasons. In his study von Baer analyzed for the first time the physical characteristics of permafrost and its patterns on the surface and beneath it, characterizing also different formations of ice. Baer also analyzed different landscape formations created by permafrost and tried to fix the distribution of

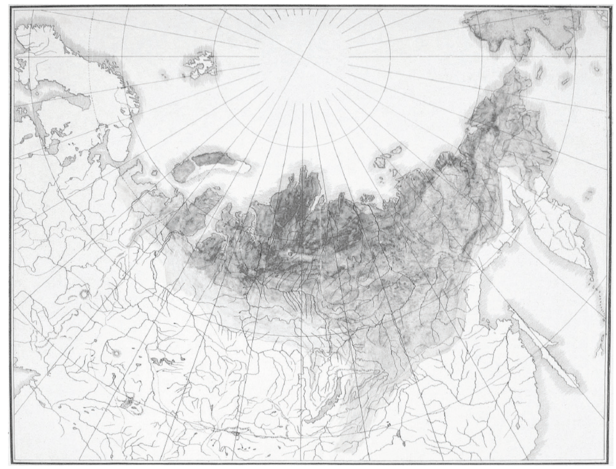

Figure 1. Map of the distribution of the permafrost area in Eurasia compiled by Karl Ernst von Baer (Tammiksaar 2002).

this phenomenon in Siberia and in the whole world (see: Tammiksaar 2001, Tammiksaar 2002). These data were used by Baer in preparing the first map in history of the permafrost areas depicting Eurasia (see Fig. 1). Von Baer also worked out a terminology concerning permafrost. Under *Boden-Eis* he meant permafrost as a physical phenomenon; that is, ice in geological layers. Under *Eis-Boden* he meant the geographic distribution of permafrost (see Baer 2001, Tammiksaar 2002).

Although Baer's manuscript remained unpublished, it was used by his disciple Alexander Theodor von Middendorff. Unfortunately there was no appropriate person in Siberia to run geothermic observations, as Baer had insisted, in the 116 m depth of the Shergin pit. To obtain the necessary data, Baer organised a special expedition with the support of the Academy to study all aspects of permafrost. The leader of the expedition was his countryman Middendorff. The expedition to North Siberia and Far East took place during 1842–1845. Baer gave his manuscript to Middendorff as instruction for the investigation, although many of the arguments set out in it (e.g., the causes of emergence of permafrost-linked surface forms, thickness of ice-cover on the rivers, etc.) still required thorough study (Tammiksaar & Stone 2007). The writings of Middendorff convinced scholars that permafrost really existed and that studies of it were needed. His studies became crucial also for the discipline in Russia, as they served as a starting point for later scholarship on the topic in the region.

Through the studies of Middendorff (Middendorff 1848, 1861) Baer's permafrost terminology spread among European scholars but, due to random and ignorant usage, became corrupted in time, so that a later scholar of permafrost, Eduard von Toll, decided to replace the term *Boden-Eis* with the term *Stein-Eis* (Toll 1895).

Adams' Mammoth, Permafrost, and Ice Age

One of the most important questions to be answered by Middendorff's expedition, according to Baer, was to fix as exactly as possible the physico-geographic and geologic conditions at the site at which Adams' mammoth had been found, Cape Bykovski in Siberia.

It was Baer's guess that mammoth corpses could survive for several thousands of years but only in permafrost. Baer thus viewed it as highly important to specify the geological and geographical circumstances in which Adams's mammoth had been found. The report by Adams on these conditions was internally contradictory, and its French was poor, leading to confusion. Baer could not understand whether the mammoth had been located on the icebergs/river ice heaped on the shore or whether it had melted out from an ice-wall covered with soil. Baer viewed this as a remnant of the Ice Age. Apparently when Adams had arrived at the site, the ice-wall had melted further and was already 30.5 m (100 ft) from the carcass.

In his manuscript Baer discussed Adams' report on the conditions of the mammoth find, and he devoted 30 pages to this. He tried to compare this data with the materials secured by members of the expedition led by Otto von Kotzebue for the search of the Northeast Passage (1815–1818). These were Johann Friedrich Eschscholtz and Adelbert von Chamisso, who had discovered a buried ice sheet in Eschscholtz-Bay (Baer 2001).

In the 1830s, Louis Agassiz and Jean de Carpentier had founded the theory of glaciation of continents. The theory caused controversy among geologists and other natural scientists. There were arguments for and against it, but only a few scholars collected empirical data to explain the theory. One of the few was Baer who was tending to support the theory. To be convinced, he needed more information on the conditions in which Adams' mammoth had been found. Until this was clear, Baer could not decide whether the carcass had survived intact due to ice surviving from the Ice Age (Tammiksaar 2002). Baer had suggested in his manuscript given to Middendorff that the mammoth must have been found on the heaped sea/river-ice (Baer 2001).

Middendorff searched for witnesses concerning the discovery of Adams' mammoth. In Barnaul he met the mining engineer, Slobin, who stated that the mammoth had not been found on the sea-ice but from the permafrost (Baer, 1866). Middendorff also discovered remnants of another mammoth at Taymyr peninsula (at Nizhnaya-Taymyr River) and described, for the first time in the history of mammoth studies, the particular site. This information suggested (at least for Middendorff) that these animals must have lived in the south, meaning that it had to be the rivers that had carried the bodies northward (Middendorff 1860a, b). Thus the information by Slobin became irrelevant for Baer, and he left the whole issue open.

During his expedition Middendorff could not prove the connections of Adams' mammoth with the Ice Age. He admitted that he could find no evidence for an Ice Age in Siberia. Thus he and Baer remained in a tentative position concerning the glacial theory (Baer 1986, Middendorff 1861).

It is not surprising that both Baer and Middendorff could not give simple answers to such a complicated matter. They were lacking hard empirical evidence upon which to draw accurate conclusions. There was also no theoretical basis for their research as permafrost studies were only in their initial stage and it was, in fact, Baer who had started them. There were also no fieldwork results or theory to distinguish ice formations of different origin (sea- and river-ice, glaciers, buried ice, etc.) as up to then a detailed approach to such phenomena had not been possible. The theory of the Ice Age was also in its initial stage.

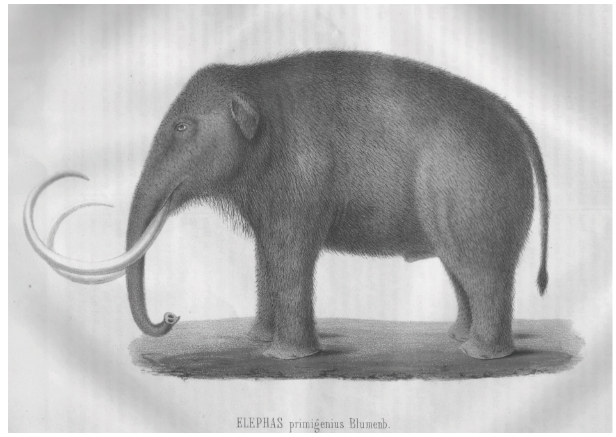

Figure 2. A mammoth drawn by Johann Friedrich Brandt (Brandt 1866a).

On the other hand, the studies of both scholars created a strong basis for future studies of mammoths and permafrost in Russia. It was just a matter of time before a new mammoth find was reported. Middendorff had created, on behalf of the St. Petersburg Academy of Sciences, a prize for those reporting mammoth finds (Middendorff 1860c, Sukhova & Tammiksaar 2005).

Woolly Mammoth as a Northern Species

At the beginning of 1866, Baer received a letter from a mining specialist in Barnaul, Stepan Guliaiev, informing him that near Tazovskaya Guba at the shore of the Arctic Ocean, a wholly preserved mammoth had been discovered. The Academy hurriedly summoned a special commission to organise an expedition to bring the carcass to St. Petersburg. Baer was the head of the commission. He hoped to solve several scientific problems that had remained open after Adams's find had been studied. For Baer it was not the preservation of the soft tissues that was particularly important but the information that might be obtainable from the surviving contents in the animal's digestive tract. He hoped to find remnants of coniferous trees and thus secure support for a theory under which mammoths had been northern animals. Such a find could also give information on the flora in historic times in Siberia (Baer 1866).

In connection with the organisation of the new expedition,Baer published an overview (based on the data of Middendorff (1859, 1860b) and of himself) on all known finds of mammoths in Siberia (Baer 1866). His colleague Johann

Friedrich Brandt, a zoologist, completed an overview on the morphology and living conditions of the extinct animal. In addition Brandt published a drawing to depict a mammoth as understood by him (see Fig. 2) (Brandt 1866a, b). Brandt also stated that mammoths could not have been southern animals but inhabitants of the north, becoming extinct due to climate change and leaving their bodies to survive in the permafrost (Brandt 1866b).

Baer took similar views, but his position was more cautious because of the lack of firm evidence. Baer did not want to rule out the possibility that the mammoths' bodies did not survive only in permafrost but also in ice formed of snow in places not reached by sun. This was possibly confirmed by Adams' case in which there had been ice covered by soil close to where the carcass had been found (Baer 1866).

Friedrich Schmidt, a geologist and later a member in palaeontology of the St. Petersburg Academy of Sciences, was appointed head of the expedition for the search of the mammoth found at Tazovskaya Bay. Arriving at the site, he discovered that the mammoth was not situated at the seashore but on the bank of the Yenissei River. Furthermore the body was badly preserved, and there was no hope of obtaining information on the contents of the digestive tract nor on the physiology of the animal. Yet Schmidt studied thoroughly the place at which the mammoth had been found and concluded that mammoths preserved in permafrost must have been northern mammals (Schmidt 1872). He reported on it to Middendorff (Sukhova & Tammiksaar 2005) and touched on the issue also in the report of his expedition (Schmidt 1869). After that, the scientific community (for example the geologist Count Alexander Keyserling) started to accept the idea that mammoths had not been inhabitants of the southern regions and that the natural conditions of Siberia must have been different in the past (cf. Taube von der Issen 1902, Toll 1895).

The Extinction of Mammoths Becomes Central in Making Broader Conclusions Concerning the Natural Conditions of Siberia

There was, therefore, no doubt that the mammoths had died out due to the chilling of the climate; but how much time the process had taken caused much argument.

In 1871, a member of the St. Petersburg Academy, the geographer Leopold von Schrenck, published a longer article on the issue of the extinction of mammoths based on field studies made by Gerhard von Maydell, a traveler of the Russian Geographical Society, in northeast Siberia studying three mammoth sites between the Indigirka and Kolyma Rivers in 1860–1870s (Schrenck 1871, Maydell 1896).

Schrenck proved that the process of slow ice formation on Siberian rivers, shallow lakes, and swamps during the chilling of the climate was the main reason preventing mammoths from leaving for areas with better conditions, and this finally caused their extinction very quickly. Schrenck also decided that only in very favourable conditions could a mammoth be preserved intact. In most cases bodies would decompose in water or in the atmosphere, and the remnants would be carried by rivers towards the sea in the area between the Indigirka and Lena Rivers. The latter process was still going on (Schrenck 1871).

According to Schrenck, mammoths could remain preserved only if their carcasses fell into the snow beneath the banks which did not melt in summer and finally turned into ice due to temperature changes (Schrenck 1871, Schrenck 1880). Agreeing with Baer in 1860, he considered that the mammoth described by Adams had been preserved in such a way. These two authorities were supported by Alexander von Bunge Jr., who participated in a Russian expedition, dedicated to the International Polar Year (1882–1883), to the delta of the Lena River, and at the request of Schrenck studied the place of Adams' mammoth find (Bunge 1884).

In 1885–1886, during an expedition arranged by the St. Petersburg Academy of Sciences, the region between the Jana and Indigirka Rivers was studied by Bunge and his companion, Eduard von Toll. The main goal of the expedition was to research the New Siberian islands, in which palaeontological finds were abundant (Bunge & Toll 1887). During this expedition the issue of the extinction of mammoths started to interest Toll, especially after seeing the high banks of the Big Lyahhov and Kotelny islands constituted mainly of buried ice/fossil ice (Toll used the term *Stein-Eis*), similar to that described by Adams at the mammoth site at Cape Bykovski. Toll was the first scholar to associate the sites in which mammoths had been found not so much with permafrost as with the occurrence of buried/fossil ice. According to him, the buried/fossil ice was a remnant of the Ice Age in Siberia.

Analysing thoroughly the slightest data on permafrost and traces of the Ice Age between the Lena River and Eschscholtz Bay (the main sources being the works of Baer, Middendorff, Bunge, Schmidt, Maydell, and writings by Erich von Drygalski on the Greenland ice sheet and the results of his two polar expeditions in 1885–1886 and 1893), Toll came to some very important conclusions. He proved that during the Ice Age, one centre of glaciation in Siberia was Cap Sviatoi Nos (east of the Lena River mouth), and this was the reason why after the Ice Age, the New Siberian islands were part of the Asian continent (Toll 1895). Toll named this "mammoth-continent," but this continent was destroyed as a result of gradual melting of the buried ice due to the transgression of the North Polar Sea and the activity of the Siberian rivers (Toll 1899).

Up to then an idea had been dominant (i.e.. Schrenck, Middendorff): the rivers had carried the bodies of the animals to their resting places from the area to the south. Similar conclusions had been made several years earlier by a Russian geologist of Polish origin, Jan Czerski, who had analysed the palaeontological finds and travel reports of Bunge (Tscherski 1893). By the analysis Toll proved that climate in northern Siberia was so warm after the Ice Age that the former continental ice sheet in the "mammoth-continent" was covered with sediments and plants (e.g., Toll found in the same layer bones of mammoth as well as stems of alder**).** This region was a suitable living place for mammoths and other mammals, but the gradual destruction of the continent and the cooling of the climate made the movement of mammoths and other mammals to the south impossible. As a result, the gradual extinction began. It was not catastrophic, for example, due to flood, a sudden fall of temperature, etc.; rather, the living conditions gradually deteriorated. Thus Toll decided correctly that the remnants of the animals had to be younger than the ice sheet in which the carcasses were preserved (Toll 1895). So, unlike his predecessors (Baer, Middendorff, Schrenck, Schmidt, Bunge), Toll came to the conclusion that the places at which extinct mammals were found in Siberia might be linked to regions with buried ice, either on riverbanks or seashore. If in rivers the buried ice submerged formations typical of the permafrost *taryn* (*Aufeis*), then the buried ice on the seashore had to be regarded as a remnant of the former ice sheet of the Ice Age (Toll 1895).

Besides generalisations made on the reasons of extinction of mammoths, Toll analysed the post Ice Age situation in the area east of the Yenissei River. He explained why Middendorff and others could not find traces supporting the glacial theory during their expeditions. According to Toll, the Arctic Ocean during the post Ice Age transgression had destroyed such traces and former glaciers on the low tundra areas and had disconnected the islands of New Siberia from the continent. Only in some regions, starting from the plateau between the Anabar and Olenyok Rivers to Eschscholtz Bay, survived former glaciers degraded into buried ice. In Toll's opinion, fossil ice was clear evidence that could not be explained differently than a remnant of the Ice Age in Siberia (Toll 1895).

Conclusion

The studies of mammoths by the members of the St. Petersburg Academy of Sciences and the expeditions organised by them in the 19th century reveal how complicated the process of scientific work can be in circumstances in which data for drawing conclusions is almost missing and the only information available is indefinite third person accounts. At the beginning of the 19th century the territory of Siberia had been not studied. In the 1830s fresh data started to emerge but initially they were contradictory. There was a need for more thorough and continual research (i.e. to discuss the relations between the mammoth sites with the essence of permafrost and relics of the Ice Age). There was no theoretical basis to link the gathered material into one entity.

That was the reason why Baer, Middendorff, Schrenck, and Bunge could not solve the question of Adams' mammoth, despite the fact that all of them (with the exception of Schrenck) had personally studied, in different parts of Siberia, both permafrost and other ice formations. Only after studies of Bunge, Maydell, and Czerski had enriched knowledge about the natural conditions in Siberia and the physiology of the extinct mammals was it possible for Toll to bind the earlier scholarship into a new entity. Thus Toll, unlike his predecessors, could explain the reasons why mammoths became extinct, as well as explaining other phenomena in Siberia, which all in turn were connected with matters of permafrost in these territories.

These studies at the end of the 19th century made Russia a leader in the theoretical and practical aspects of permafrost studies and created preconditions for the emergence of a special scientific field concerning the matter (*merzlotovedenie*) in the 20th century.

Acknowledgments

The authors wish to thank Ian Stone and Maie Roos for advice and help in arranging the English of the text. This article has been prepared with support of grant no. 7381 of the Estonian Science Foundation.

References

Baer, K.E. v. 1866. Neue Auffindung eines vollständigen Mammuths, mit der haut und den Weichtheilen, im Eisboden Sibiriens, in der Nähe der Bucht des Tas. *Bulletin de l'Académie Impériale des Sciences de St. Pétersbourg* 10: 230-296, 513-534.

Baer, K.E. v. 1986. *Autobiography of Dr. Karl Ernst von Baer*. Jane M. Oppenheimer (ed.). Science History Publications U.S.A. Canton: Watson, XIV+389 pp.

Baer, K.E. v. 2001. *Materialien zur Kenntniss des unvergänglichen Boden-Eises in Sibirien.* In: L. King, (Hrsg) & K.E. v. Baer (eds.) *Materialien zur Kenntniss des unvergänglichen Boden-Eises in Sibirien. Unveröffentliches Typoskript von 1843 und erste Dauerfrostbodenkunde*. Giessen: Universitätsbibliothek, 234 pp.

Brandt, J.F. 1866a. Mittheilungen über die Gestalt und Unterscheidungsmerkmale des Mammuth oder Mamont (*Elephas primigenius*). *Bulletin de l'Académie Impériale des Sciences de St. Pétersbourg* 10: 93-118.

Brandt, J. F. 1866b. Zur Lebensgeschichte des Mammuth. *Bulletin de l'Académie Impériale des Sciences de St. Pétersbourg* 10: 111-118.

Bunge, A. v. 1884. Naturhistorische Beobachtungen und Fahrten im Lena-Delta. Aus Briefen an den Akademiker L. v. Schrenck. *Bulletin de l'Académie Impériale des Sciences de St. Pétersbourg* 29: 422-476.

Bunge, A. v. & Toll, E. v. 1887. Die von der Kaiserlichen Akademie der Wissenschaften ausgerüstete Expedition nach den Neusibirischen Inseln und dem Jana-Lande. *Beiträge zur Kenntniss des Russischen Reiches und der angränzenden Länder Asiens*. Kaiserliche Akademie der Wissenschaften, Folge III: 2, VIII + 412 pp.

Maydell, G. v. 1896. Reisen und Forschungen im Jakutskischen Gebiet Ostsibiriens in den Jahren 1861–1871. *Beiträge zur Kenntniss des Russischen Reiches und der angränzenden Länder Asiens*. St. Petersburg: Kaiserliche Akademie der Wissenschaften, Folge IV: 2, XXV + 800 pp.

Middendorff, A.T. v. 1848. Geothermische Beobachtungen. In: *Dr. A.Th. v. Middendorff's Reise in den äussersten Norden und Osten Sibiriens*. St. Petersburg: Kaiserliche Akademie der Wissenschaften, 1(1): 85-183.

Middendorff, A.T. v. 1860a. O sibirskikh mamontakh. *Vestnik estestvennykh nauk* 26-27: 843-867.

Middendorff, A.T. v. 1860b. Orographie und Geognosie. In: Middendorff, A.T. v. *Dr. A.Th. v. Middendorff's Sibirische Reise*. Uebersicht der Natur Nord- und ost-Sibiriens. St. Petersburg: Kaiserliche Akademie der Wissenschaften, 4(1), Lief. 2: 201-332.

Middendorff, A.T. v. 1860c. Über die Nothwendigkeit von Vorbereitungen für den Empfang vorweltlicher sibirischer Riesenthiere. *Bulletin de l'Académie Impériale des Sciences de St. Pétersbourg* 1: 557-563.

Middendorff, A.T. v. 1861. Klima. *Dr. A.Th. v. Middendorff's Sibirische Reise*. Uebersicht der Natur Nord- und ost-Sibiriens. St. Petersburg: Kaiserliche Akademie der Wissenschaften, 4(1), Lief. 4, 525-783 + LIV pp.

Schmidt, F. 1869. Vorläufige Mittheilungen über die wissenschaftlichen Resultate der Expedition zur Aufsuchung eines angekündigten Mammuthcadavers. *Bulletin de l'Académie Impériale des Sciences de St.-Pétersbourg* 13: 97-130.

Schmidt, F. 1872. Wissenschaftliche Resultate der zur Aufsuchung eines angekündigten Mammuthcadavers von der Kaiserlichen Akademie der Wissenschaften an den unteren Jenissei ausgesandten Expedition. *Mémoires de l'Académie Impériale des Sciences de St. Pétersbourg.* St. Pétersbourg: l'Academie Impériale des Sciences, VII Série, XVIII(1), VI+168 pp.

Schrenck, L. v. 1871. Bericht über neuerdings im Norden Sibirien's angeblich zum Vorschein gekommene Mammuthe, nach brieflichen Mittheilungen des Hr. Gerh. v. Maydell, nebst Bemerkungen über den Modus der Erhaltung und die vermeintliche Häufigkeit ganzer Mammuthleichen. *Bulletin de l'Académie Impériale des Sciences de St. Pétersbourg* 16: 147-173.

Schrenck, L. v. 1880. Der erste Fund einer Leiche von *Rhinoceros Merckii* Jaeg. *Mémoires de l'Académie Impériale des Sciences de St. Pétersbourg.* St. Pétersbourg: l'Academie Impériale des Sciences, VII Série, XXVII(7), V + 55 pp.

Sukhova, N.G. & Tammiksaar, E. 2005. *Aleksandr Fedorovich Middendorf, 1815-1894*. Moskva: Nauka, 331 pp.

Tammiksaar, E. 2001. «Materialien zur Kenntniss des unvergänglichen Boden-Eises in Sibirien» Die erste «Dauerfrostbodenkunde» von Karl Ernst von Baer. In: L. King (Hrsg.) & K. E. v. Baer. *Materialien zur Kenntniss des unvergänglichen Boden-Eises in Sibirien. Unveröffentliches Typoskript von 1843 und erste Dauerfrostbodenkunde*. Giessen: Universitäts-bibliothek, I–XLIV.

Tammiksaar, E. 2002. The contributions of Karl Ernst von Baer to the investigation of the physical geography of the Arctic in the 1830s–1840s. *Polar Record* 38(205): 121-140.

Tammiksaar, E. & Stone, I.R. 2007. Alexander von Middendorff and his expedition to Siberia (1842–1845). *Polar Record* 43(226): 193-216.

Taube von der Issen, H. 1902. *Graf Alexander Keyserling. Ein Lebensbild aus seinen Briefen und Tagebüchern*. Berlin: Reimer, V + 655 pp.

Tilesius von Tilenau, 1815. De skeleto mammonteo Sibirico ad maris glacialis littora anno 1799, effosso, cui praemissiae elephantini generis specie, sum distinctiones. *Mémoires de l'Académie Impériale des Sciences de St. Pétersbourg* 5: 406-513.

Toll, E. v. 1895. Wissenschaftliche Resultate der von der Kaiserlichen Akademie der Wissenschaften zur Erforschung des Janalandes und der Neusibirischen Inseln in den Jahren 1885 und 1886 ausgesandten Expedition. Abtheilung III: Die fossilen Eislager und ihre Beziehungen zu den Mammutleichen. *Mémoires de l'Académie Impériale des Sciences de St. Pétersbourg.* St. Pétersbourg: L'Academie Impériale des Sciences, VII Série, XLII(13), VII + 87 pp.

Toll, E. v. Ocherk geologii Novosibirskikh ostrovov i vazhneishie zadachi issledovaniia poliarnykh stran. *Mémoires de l'Académie Impériale des Sciences de St. Pétersbourg.* St. Pétersbourg: L'Academie Impériale des Sciences, VIII Série, IX(1), IV + 20 pp.

Tscherski, J.D. 1892. Wissenschaftliche Resultate der von der Kaiserlichen Akademie der Wissenschaften zur Erforschung des Janalandes und der Neusibirischen Inseln in den Jahren 1885 und 1886 ausgesandten Expedition. Abtheilung IV: Beschreibung der Sammlung posttertiären Säugethiere. *Mémoires de l'Académie Impériale des Sciences de St.-Pétersbourg.* St.-Pétersbourg: l'Academie Impériale des Sciences, VII Série, XL(1), V + 511 pp.

Soil Organic Carbon Stocks in the Northern Permafrost Region and Their Role in Climate Change

Charles Tarnocai
Research Branch, Agriculture and Agri-Food Canada, Ottawa, Canada

Gabriele Broll
University of Vechta, Vechta, Germany

Abstract

The soil area of the northern permafrost region is approximately $18{,}781 \times 10^3$ km^2, or approximately 14% of the global soil area. Organic soils (peatlands, total depth) and cryoturbated permafrost-affected mineral soils (100 cm) have the highest mean soil organic carbon contents (30–120 kg m^{-2}). Carbon stocks in the northern permafrost region were estimated to be 191 Gt for the 0–30 cm depth and 496 Gt for the 0–100 cm depth. Most of the soil organic carbon stocks occur in permafrost-affected soils, which contain about 70% of the stocks in the 0–100 cm depth. The values calculated here indicate that the organic carbon in soils in the northern permafrost region account for approximately 30% of the global soil organic carbon at the 0–100 cm depth, much of which will be vulnerable to release because of the large temperature increases predicted to result from climate change.

Keywords: carbon content; carbon mass (stocks); climate change; peatlands; permafrost; soils.

Introduction

The importance of permafrost-affected soils in global soil organic carbon stock estimates has been either neglected or poorly handled. This is probably due to the lack of data for these soils and the lack of understanding of the soil-forming processes in permafrost-affected soils. With recognition of the role of cryogenic processes in the genesis of these soils, came an understanding of their function in the sequestration of organic carbon (Van Vliet-Lanoe 1991, Bockheim & Tarnocai 1998, Bockheim 2007). These soils have sequestered carbon for a period of 6–8 thousand years and are still acting as carbon sinks (Tarnocai et al. 2007).

Some estimates of global soil organic carbon stocks are: 1220 Gt (Sombroek et al. 1993), 1395 Gt (Post et al. 1982), 1462 to 1548 Gt (Batjes 1996), and 1576 Gt (Eswaran et al. 1993). Although all of these estimates were based on the 0–100 cm depth, Batjes (1996) did report carbon stocks of 2376–2456 Gt for the 0–200 cm depth.

Post et al. (1982) estimated that the soils in the tundra zone contained, globally, approximately 191.8 Gt of organic carbon. This estimate, however, was based on only 30 samples. Using the, at that time, newly-developed Northern and Mid Latitudes Soil Database, Tarnocai et al. (2003) estimated that the carbon stocks in the 0–100 cm depth of Cryosols (Soil Classification Working Group 1998) in the northern circumpolar region were approximately 268 Gt of organic carbon. In this database, however, coverage of permafrost-affected soils in Eurasia was greatly underestimated.

This paper provides estimates of the organic carbon stocks in both permafrost-affected and nonpermafrost soils in the northern circumpolar permafrost region. The effect of climate change on this carbon is also discussed.

Materials and Methods

Terminology

The U.S. terminology for permafrost-affected (Gelisols) and nonpermafrost soils is used in this paper (Soil Survey Staff 1999).

SOCC (soil organic carbon content) refers to the content of organic carbon in a one meter square soil column. It is expressed as kilograms per square meter (kg m^{-2}).

SOCM refers to the soil organic carbon mass and is expressed as kilograms (kg) or gigatons (Gt).

The northern permafrost region refers to the northern circumpolar permafrost region as outlined by Brown et al. (1997).

The Northern Circumpolar Soil Carbon Database (NCSCD)

This database (Tarnocai et al. 2007) provides the spatial framework and the data needed to determine the organic carbon stocks for soils of the northern permafrost region. The NCSCD contains many thousands of polygons, with each polygon containing one or more named soil or soil taxa that form the basis for determining the carbon stocks.

The North American portion of the NCSCD was compiled from existing soil maps. For remote areas in North America, where more detailed survey maps were unavailable, data from other sources, such as pedon, climate and vegetation data, together with high quality LANDSAT imagery, were used to delineate polygons. The Greenland and Eurasian portion (Russia, Kazakhstan, Mongolia, Scandinavia, Svalbard, and Iceland) was also compiled from small-scale soil maps that had been digitized.

During this process, especially in the case of the Russian maps, the map symbols and classification terms had to be translated into English, and the soil classification terms had to be converted to the US Soil Taxonomy. A special effort was made to harmonize the data and to ensure that no information loss occurred during translation and data conversion, especially for permafrost-affected soils.

Pedon and peatland databases

Data used to calculate soil organic carbon content (kg m^{-2}) were derived from various pedon (soil profile) databases containing numerous pedons and their associated soil attribute data. The Canadian portion of the NCSCD was built up using 3530 pedons. No figures are available for the number of pedons used for the Alaskan portion of the database, but it relies, proportionally, on approximately the same level of supporting data as was used for Canada. Soil data used for the Eurasian portion of the NCSCD is drawn from a number of databases. A pedon database containing information for 253 pedons was developed for the Russian part of the NCSCD. In addition, the West Siberian Lowland Peatland GIS Data Collection, containing data for 90 peat cores (Smith et al. 2000, 2004, Sheng et al. 2004), was also used. Information from Batjes (1996) was also used for Eurasian soils, including Russia, especially where no pedon information was available.

Calculating SOCC and SOCM

Pedons for each soil taxa (Eurasia) or named soil (North America) are selected. These pedons contain all of the data needed to calculate the SOCC. The data for each named soil (North America) are entered into the database and are used to calculate the carbon content of each named soil in the polygon, while data from pedons of each soil taxa (Eurasia) are used to calculate their carbon contents, which are then entered into the database.

The SOCC (kg m^{-2}) was calculated for each named soil (North America) and for the representative pedons for each soil taxa (Eurasia) using the formula:

$$\mathrm{SOCC} = \mathrm{C} \times \mathrm{BD} \times \mathrm{T} \times \mathrm{CF} \tag{1}$$

where C = organic carbon (% weight), BD = bulk density (g cm^{-3}), T = depth of soil layer (0–30 cm and 0–100 cm), including the surface organic layer, and CF = coarse fragments and/or ice content (% weight). The SOCC data are then stored in the database to be used for further calculations or to generate carbon content maps.

The SOCM was then determined by multiplying the SOCC of the specific soil by the area of each such soil component in the polygon.

Results

Soil area

The total soil area of the northern permafrost region is 18,782 × 10^3 km^2 (Table 1). The Eurasian portion covers approximately 65% of the soil area and the North American portion 35%. Gelisols are the dominant soils in the area, covering approximately 54% of the permafrost region with the remainder of the area (46%) being covered by unfrozen soils. The Continuous Permafrost Zone, the largest of the four permafrost zones, covers 54% of the northern permafrost area while the Discontinuous, Sporadic, and Isolated Patches zones cover the remaining 46% of the area. The distribution of the major soil groups for frozen mineral soils (Turbels and Orthels), peat (Histels and Histosols), and unfrozen mineral soils are shown in Figure 1. Perennially frozen and unfrozen mineral soils cover approximately the same areas (40% frozen, 41% unfrozen). Peat soils cover the remaining 19% of the soil area.

Table 1. Areas of all soils in the various permafrost zones.

Permafrost zones	Area (10^3 km^2)		
	North America*	Eurasia	Total
Continuous	2868	7255	10,123
Discontinuous	1443	1649	3092
Sporadic	1149	1444	2593
Isolated patches	1186	1788	2974
Total	6646	12,136	18,782

* Greenland included in the North America calculation.

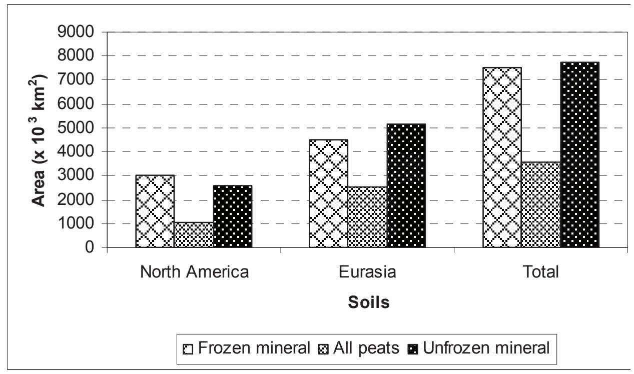

Figure 1. Distribution of major soil groups in the northern permafrost region.

Soil organic carbon content

The mean SOCC values calculated for the northern permafrost region are given in Table 2. Histels (perennially frozen soils) and Histosols (unfrozen peatland soils) have the highest SOCC with average values ranging from 67 to 69 kg m^{-2}. Maximum SOCC values slightly above 100 kg m^{-2} are not uncommon for these soils. The SOCC values for mineral Gelisols (Turbels and Orthels) range from 23 to 32 kg m^{-2}. Turbels have the highest SOCC values, in some cases as much as three times those for unfrozen mineral soils (Table 2).

The standard deviation was greatest (>50) for Histels and Histosols (Table 2). This is probably due to the variability of peat materials, the degree of decomposition, and the mineral (ash) content. Turbels, Orthels, and Spodosols had the second greatest standard deviations (20–27). Their large values were probably due to the various thicknesses of surface organic material associated with these soils and, for Turbels, also to the variability of amounts of cryoturbated organic materials they contained.

Soil organic carbon mass

In the northern permafrost region, the SOCM is approximately 191 Gt in the 0–30 cm depth and 496 Gt in the 0–100 cm depth (Table 3). Approximately 67% of this mass occurs in Eurasia and 33% in North America. The

Table 2. Average carbon contents for soils in the northern permafrost region.

US Taxonomy	Soil organic carbon content ($kg\ m^{-2}$)		
	Mean	SD	No. of pedons
Gelisols			
Histels	66.6	53.3	87
Turbels	32.2	27.4	256
Orthels	22.6	21.4	131
Histosols	69.6	56.9	417
Andisols	25.4*	=	unknown
Spodosols	24.7	20.2	6
Aqu-suborders	20.1	9.7	531
Inceptisols	15.3	9.4	871
Vertisol	13.5	7.3	11
Entisols	9.9	15.8	198
Mollisols	9.6	8.3	422
Natric-suborders	9.1	7.6	67
Alfisols	8.9	6.9	533
Aridisols	3.0*	=	unknown

* SOCC data from Batjes (1996)

Continuous Permafrost zone contains approximately 60% of the carbon mass; the remaining three zones each contain approximately 13%.

The SOCM for all major soil orders is shown in Figure 2. Gelisols are the major SOCM contributors in the permafrost area. They contain approximately 71% of the SOCM at depths of 0–100 cm in the region. Within the Gelisol soil group, the Turbels contain the largest amount (64%) of SOCM in both the 0–30 cm and 0–100 cm depths (Fig. 3).

Peatlands (Histosols and Histels) contain approximately 48% of the SOCM in the northern permafrost region, with the Histosols containing the second largest soil carbon pool (13% of the SOCM).

When the SOCMs of the major soil groups are compared (Fig. 4), the peat soils and frozen mineral soils are the major contributors of SOCM in both North America and Eurasia. The SOCM in the 0–100 cm depth (for both frozen and unfrozen organic and mineral soils) is approximately 239 Gt for organic soils (peatlands) and approximately 256 Gt for mineral soils. It should be pointed out that, although the SOCM values for these soil groups are similar, peatlands cover only 19% of the soil area of the region.

When soil areas and SOCM values of major soil groups were compared, it was found that, although unfrozen and frozen mineral soils cover about the same area, the SOCM values of frozen mineral soils are approximately twice those of unfrozen mineral soils (Fig. 5). Peat soils (unfrozen and frozen) cover about half as much area as the frozen and unfrozen mineral soils, but they contain about 13% more SOCM than the frozen mineral soils and nearly three times more than the unfrozen mineral soils (Fig. 5).

Discussion

Carbon dynamics

The total SOCM at the 0–100 cm depth for soils in the

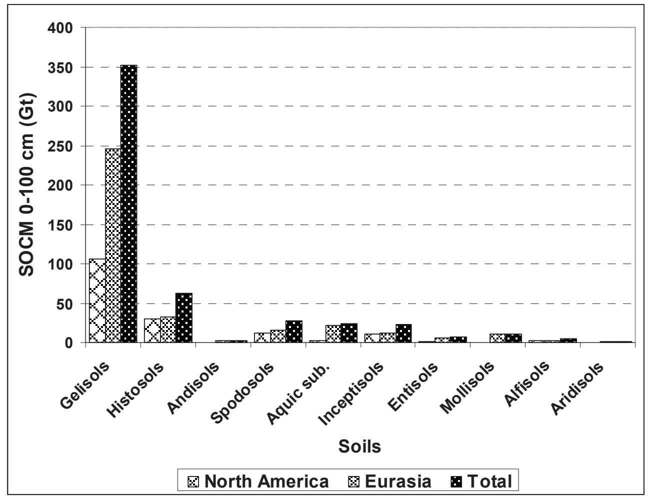

Figure 2. SOCM for the 0–100 cm depth in all soils in the northern permafrost region (SOCM in Vertisols and Natric-suborders is <0.5 Gt).

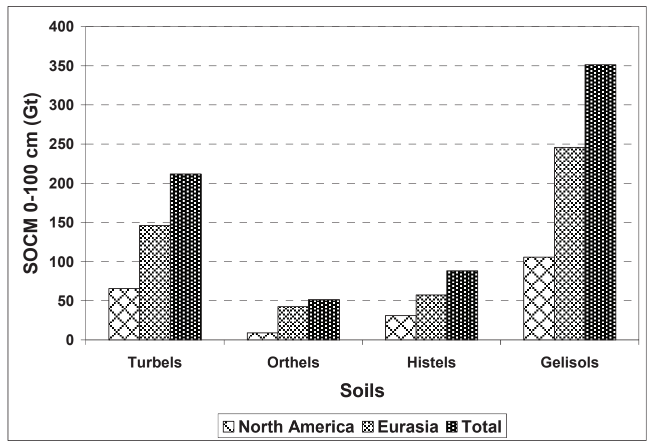

Figure 3. SOCM for the 0–100 cm depth in the three Gelisol suborders and in all Gelisols in the northern permafrost region.

northern permafrost region is approximately 496 Gt, which is about 30% of the global SOCM. The large amount of soil organic carbon in this region is due to the large areas and high carbon content of the peat (organic) soils and cryoturbated mineral soils (Turbels).

Peat soils are composed of organic materials with a high concentration of carbon that has accumulated over a long period of time. Robinson & Moore (1999) found that, in the Sporadic Permafrost Zone, mean carbon accumulation rates in unfrozen bogs (Histosols) and frozen peat mounds (Histels) over the past 100 years were 88.6±4.4 and 78.5±8.8 $g\ m^{-2}$ per year, respectively. They also found that, in the Discontinuous Permafrost Zone, the mean carbon accumulation rate in peat plateaus (Histels) during the past 1200 years was 13.31±2.20 $g\ m^{-2}$ per year, while in unfrozen fens and bogs (Histosols) the comparable rates were 20.34±2.86 $g\ m^{-2}$ and 21.81±3.25 $g\ m^{-2}$ per year, respectively. Radiocarbon dates from the basal peat (the base of the peat deposit, indicating the beginning of peat deposition) suggest that, in North America, the average basal peat date is 7200 ^{14}Cyr BP in the Arctic, 6200 ^{14}Cyr BP in the Subarctic and 6000 ^{14}Cyr BP in the Boreal (Tarnocai

Table 3. Organic carbon mass in all soils in the permafrost zones.

Permafrost zones	Soil organic carbon mass (Gt) North America* 0–30 cm	North America* 0–100 cm	Eurasia 0–30 cm	Eurasia 0–100 cm	Total 0–100 cm
Continuous	31.17	78.29	79.21	220.46	298.75
Discontinuous	12.23	39.69	13.27	37.75	67.44
Sporadic	10.86	26.27	15.50	36.86	63.13
Isolated Patches	12.65	30.60	16.40	36.50	67.10
Total	66.91	164.84	124.38	331.57	496.42

* Greenland included in the North America calculation.

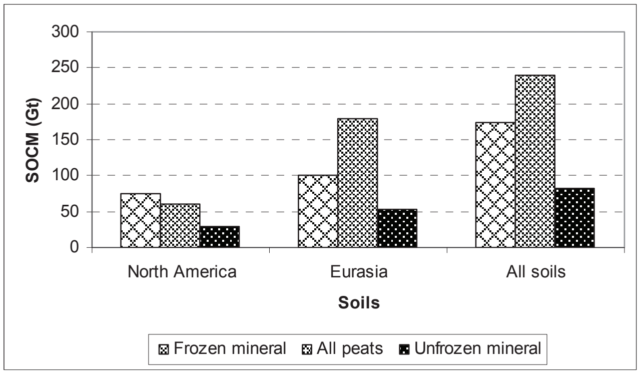

Figure 4. SOCM in major soil groups for the 0–100 cm depth in the northern permafrost region.

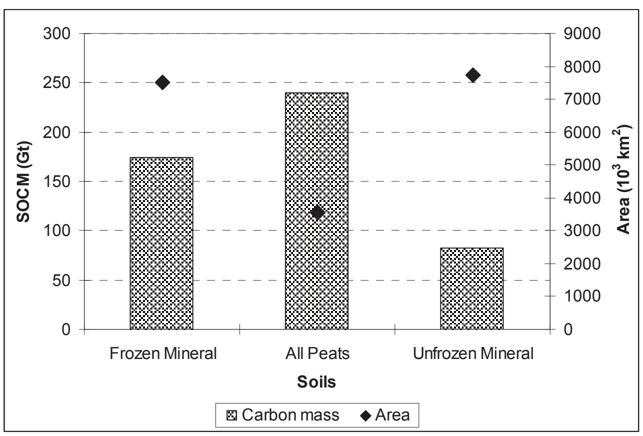

Figure 5. Comparison of the area covered and SOCM in the 0–100 cm depth for the major soil groups.

& Stolbovoy 2006). In Russia, the basal peat dates for the Tundra zone are 2000–3000 ^{14}Cyr BP and for the Taiga zone are 5000–8000 ^{14}Cyr BP (Tarnocai & Stolbovoy 2006).

In mineral soils, Turbels had the highest SOCM, containing approximately 43% of the organic carbon mass occurring in all soils in the northern permafrost region. Cryoturbation, a unique process operating in these soils, is responsible for the high SOCM values. Although the ecosystems in the permafrost region produce much less biomass than do temperate ecosystems, permafrost-affected soils that are subject to cryoturbation (Turbels) have the ability to sequester a portion of this annually-produced biomass and store it for thousands of years. Bockheim (2007) estimated that 55% of the soil organic carbon in the active layer and near-surface permafrost could have resulted from translocation by cryoturbation.

Radiocarbon dates for 50 cryoturbated organic samples from earth hummocks presented by Zoltai et al. (1978) indicate that the dates ranged from 500–11,200 ^{14}Cyr BP. The frequency of dates indicates that the number of samples was constant in the 500–5000 ^{14}Cyr BP range, with a peak occurring in the 3000–3500 ^{14}Cyr BP range. The number of samples decreased in the 5000–11,500 ^{14}Cyr BP range and showed no pattern.

Soluble organic materials also move downward within the soils because of the effects of gravity and the movement of water along the thermal gradient towards the freezing front (Tarnocai 1972, Kokelj & Burn 2005). When these organic materials reach the cold, deep soil layers where very little or no biological decomposition takes place, they may be preserved for many thousands of years.

The SOCC and SOCM values for unfrozen mineral soils in the permafrost region are low because these soils lack a mechanism to move insoluble carbon from the surface into the deeper soil layers. Soluble organic materials, however, may move downward and roots do contribute organic carbon to the subsoil. Trumbore & Harden (1997) reported carbon accumulations of 60–100 g C m^{-2} per year for these soils, but the turnover time, especially because of wildfires, is 500–1000 years. The turnover time for deep carbon, originating mainly from roots, is 100–1600 years (Trumbore & Harden 1997).

Land-use change also has significant effects on soil carbon stocks, especially in northern Europe where large areas are used as pasture (Smith et al. 2005). More research is needed to determine the effect that land-use change will have on northern soils, especially in view of the changing climate and such properties as cryoturbation.

Reliability and uncertainties of carbon data

It is difficult to determine the accuracy of the carbon stocks presented in this paper since no such information has been published for the northern permafrost region.

The North American soil organic carbon estimates were tested by Bhatti et al. (2002), who compared the carbon values generated by both the Carbon Budget Model of the Canadian Forest Sector (CBM-CFS2) and the Boreal Forest Transect Case Study (BFTCS) with the Canadian Soil Organic Carbon Database (CSOCD) (Soil Carbon Database Working Group 1993). They found that the CSOCD generated slightly lower carbon values than the CBM-CFS2 carbon model, but that there was good agreement between the CSOCD- and BFTCS-generated values.

No SOCM data are available for the permafrost region in Eurasia, but Stolbovoi (2000) estimates that the area of permafrost-affected soils in Russia is 307 million ha. He did point out, however, that this value is much less than the total area of the permafrost zone in Russia, which is more than 1,000 million ha. Stolbovoi (2002) reported that the SOCM in Russia is approximately 297 Gt C for the 0–1 m depth and 373 Gt C for the 0–2 m depth. Estimates of Russian peatland areas and the organic carbon stocks they contain are 1162–2730 × 10^3 km^2 and 94–215 Gt, respectively (Botch et al. 1995, Efremov et al. 1998). Although the peatland area (2730 × 10^3 km^2) given by Efremov et al. (1998) is close to that given in this paper, the carbon mass value (118 Gt) is only half that given here. These large variations occur because of the poor inventory and limited amount of reliable pedon data available for these soils. This supports the statement of Efremov et al. (1998) that: "The accuracy of estimates of peat carbon is ± 10 to 15 percent for the European part of Russia and ± 20 to 30 percent for the Asian part of the country."

Climate warming

It is predicted that the average annual air temperature in the permafrost region of Canada will increase 3–4°C by 2020 and 5–10°C by 2050. Such increases have already been observed at seven northern circumpolar climate stations that tracked temperature changes in winter and spring (NOAA 2007)

Various predictions have been made about the effect this large temperature increase will have on soil carbon. The most commonly predicted effects are melting of ice-rich frozen soil materials, higher frequency of wildfires and shoreline erosion.

It is also predicted that the greatest effects of climate warming on Canadian peatlands will occur in the Subarctic and Boreal zones (Tarnocai 2006). Major concerns are the drying of peatlands and an increase in frequency and extent of wildfires. Richie (1987) found that boreal forests in western Canada have a fire return interval of 50–100 years while Kuhry (1994) indicated that, for Sphagnum bogs, the interval is 400–1700 years.

A study similar to that of Tarnocai (2006) was carried out on mineral soils in the permafrost region of Canada (Tarnocai 1999). This study suggests that 12 Gt of organic carbon in Canadian Cryosols could be severely to extremely severely affected by climate warming. This study also suggests that permafrost-affected soils will cease to exist in the southern part of the permafrost region in Canada, and that cryogenic processes will diminish or disappear in southern regions. In these areas, the mechanism for sequestering carbon would cease to operate and a portion of the soil carbon would be released as carbon dioxide and/or methane.

Bockheim (2007), however, suggests that continued warming of the Arctic could accelerate cryoturbation and, thus, enable the soil to store more soil organic carbon than it can at present. Zoltai et al. (1978) suggest that, based on the higher frequency of carbon dates between 3000 ^{14}Cyr BP and 3500 ^{14}Cyr BP, this period coincided with a time of higher soil moisture and lower temperatures with increased cryoturbation. Relict earth hummocks found in the Mackenzie Valley (Zoltai & Tarnocai 1974) suggest that these hummocks were active during the Little Ice Age, but became dormant and cryoturbation ceased when the climate warmed. The soil horizons in these dormant hummocks showed no signs of cryoturbation, although some fossil cryoturbation features remain in the lower part of the soil.

These contradictory findings indicate that we know very little about the complex interactions between soils and climate in these northern regions.

Acknowledgments

We would like to thank Drs. Peter Kuhry, Galina Mazhitova, and Sergey Goryachkin for providing the Russian pedon data. Special thanks are also due to Dr. David Swanson for translating and digitizing the Russian soil maps, which also included Kazakhstan and Mongolia.

References

Batjes, N.H. 1996. Total carbon and nitrogen in the soils of the world. *European Journal of Soil Science* 47: 151-163.

Bhatti, J.S., Apps, M.J. & Tarnocai, C. 2002. Estimates of soil organic carbon stocks in central Canada using three different approaches. *Canadian Journal of Forest Research* 32: 805-812.

Bockheim, J.G. 2007. Importance of cryoturbation in redistributing organic carbon in permafrost-affected soils. *Soil Science Society of America Journal* 71(4): 1335-1342.

Bockheim, J.G. & Tarnocai, C. 1998. Recognition of cryoturbation for classifying permafrost-affected soils. *Geoderma* 81: 281-293.

Botch M.S., Kobak, K.I., Vinson, T.S. & Kolchugina, T.P. 1995. Carbon pools and accumulation in peatlands of the former Soviet Union. *Global Biogeochemical Cycles* 9(1): 37–46.

Brown, J., Ferrians, O.J. Jr., Heginbottom, J.A. & Melinkov, E.S. 1997. *Circum-Arctic Map of Permafrost and Ground Ice Conditions*. 1:10,000,000. United States Geological Survey, International Permafrost Association.

Efremov, S.P., Efremova, T.T. & Melentyeva, N.V. 1998. Carbon storage in peatland ecosystems. In: V.A. Alexeyev & R.A. Birdsey (eds.), *Carbon Storage in Forests and Peatlands of Russia* (Chapter 10).USDA Forest Service, Northeastern Research Station, General Technical Report NE-244, 69-76.

Eswaran, H., Van den Berg, E. & Reich, P. 1993. Organic carbon in soils of the world. *Soil Science Society of America Journal* 57: 192-194.

Kuhry, G.P. 1994. The role of fire in the development of Sphagnum-dominated peatlands in western boreal Canada. *Journal of Ecology* 82: 899-910.

Kokelj, S.V. & Burn, C.R. 2005. Geochemistry of the active layer and near-surface permafrost, Mackenzie delta region, Northwest Territories, Canada. *Canadian Journal of Earth Sciences* 42: 37-48.

NOAA. 2007. Climate indicators – surface air temperatures. Available at: www.arctic.noaa.gov/detect/climate-temps.shtml. Accessed 03 October 2007.

Post, W.M., Emanuel, W.R., Zinke, P.J. & Stangenberger, A.G. 1982. Soil carbon pools and world life zones. *Nature* 298: 156-159.

Ritchie, J.C. 1987. *Postglacial Vegetation of Canada.* New York, NY: Cambridge University Press, 178 pp.

Robinson, S.D. & Moore, T.R. 1999. Carbon and peat accumulation over the past 1200 years in a landscape with discontinuous permafrost, northwestern Canada. *Global Biogeochemical Cycles* 13: 591-601.

Sheng, Y., Smith, L.C., MacDonald, G.M., Kremenetski, K.V., Frey, K.E., Velichko, A.A., Lee, M., Beilman, D.W. & Dubinin, P. 2004. A high-resolution GIS based inventory of the West Siberian peat carbon pool. *Global Biogeochemical Cycles* 18: GB3004, doi:10.1029/2003GB002190.

Smith, J., Smith, P., Wattenbach, M., Zaehle, S., Hiederer, R., Jones, R.J.A., Montanarella, L., Rounsvelle, M.D.A., Reginster, I. & Ewert, F. 2005. Projected changes in mineral soil carbon of European croplands and grasslands, 1990–2080. *Global Change Biology* 11: 2141-2152.

Smith, L.C., Macdonald, G.M., Velichko, A.A., Beilman, D.W., Borisova, O.K., Frey, K.E., Kremenetski, K.V. & Sheng, Y. 2004. Siberian peatlands: a net carbon sink and global methane source since the Early Holocene. *Science* 303 (5656): 353-356.

Soil Carbon Database Working Group. 1993. Soil Carbon Data for Canadian Soils. Ottawa: Land Resource Research Institute, Agriculture Canada, 187 pp. and maps.

Soil Classification Working Group. 1998. *The Canadian System of Soil Classification. 3rd ed. Publication 1646.* Ottawa: Research Branch, Agriculture and Agri-Food Canada, 187 pp.

Soil Survey Staff. 1999. *Soil Taxonomy, a Basic System of Soil Classification for Making and Interpreting Soil Surveys*, Second Ed. Natural Conservation Service, U.S. Department of Agriculture Handbook No. 436. 869 pp.

Sombroek, W.G., Nachtergaele, F.O. & Hebel, A. 1993. Amounts, dynamics and sequestrations of carbon in tropical and subtropical soils. *Ambio* 22: 417-426.

Stolbovoi, V. 2000. Carbon pools in tundra soils of Russia: Improving data reliability. In: R. Lal, J.M. Kimble & B.A. Stewart (eds.), *Global Climate Change and Cold Regions Ecosystems, Advances in Soil Science*. Washington, DC: Lewis Publishers, 39-58.

Stolbovoi, V. 2002. Carbon in Russian soils. *Climate Change* 55(1-2): 131-156.

Tarnocai, C. 1972. Some characteristics of cryic organic soils in northern Manitoba. *Canadian Journal of Soil Science* 52: 485-496.

Tarnocai, C. 1999. The effect of climate warming on the carbon balance of Cryosols in Canada. In: C. Tarnocai, R. King & S. Smith (eds.), *Cryosols and Cryogenic Environments*, special issue of *Permafrost and Periglacial Processes* 10(3): 251-263.

Tarnocai, C. 2006. The Effect of Climate Change on Carbon in Canadian Peatlands. *Global and Planetary Change* 53: 222-232.

Tarnocai, C. & Stolbovoy, V. 2006. Northern peatlands: their characteristics, development and sensitivity to climate change., In: I.P. Martini, A. Martinez Cortizas & W. Chesworth (eds.), *Peatlands: Evolution and Records of Environmental and Climate Changes* (Chapter 2). Amsterdam, The Netherlands: Elsevier B.V., 17-51.

Tarnocai, C., Kimble, J. & Broll, G. 2003. Determining carbon stocks in Cryosols using the Northern and Mid Latitudes Soil Database. In: M. Philips, S. Springman & L.U. Arenson (eds.), *Permafrost*. Lisse, the Netherlands: A.A. Balkema Publishers, Swets & Zeitlinger, 2: 1129-1134.

Tarnocai, C., Swanson, D., Kimble, J. & Broll, G. 2007. Northern Circumpolar Soil Carbon Database. Research Branch, Agriculture and Agri-Food Canada, Ottawa, Canada (digital database).

Tarnocai, C., Ping, C-L. & Kimble, J. 2007. Carbon Cycles in the Permafrost Region of North America. In: A.W. King, L. Dilling, G.P. Zimmerman, D.M. Fairman, R.A. Houghton, G. Marland, A.Z. Rose & T.J. Wilbanks (eds.), *The First State of the Carbon Cycle Report (SOCCR): The North American Carbon Budget and Implications for the Global Carbon Cycle.* A Report by the U.S. Climate Change Science Program and the Subcommittee on Global Change Research. Asheville, NC, USA: National Oceanic and Atmospheric Administration, National Climatic Data Center, 127-138. Available at: http://cdiac.ornl.gov/SOCCR/pdf/sap2-2-finalall.pdf. Accessed 10 Jan 2008.

Trumbore, S.E. & Harden, J.W. 1997. Accumulation and turnover of carbon in organic and mineral soils of the BOREAS northern study area. *Journal of Geophysical Research* 102(D24): 28, 817-28,830.

van Vliet-Lanoë, B. 1991. Differential frost heave, load casting, and convection: converging mechanisms; a discussion of the origin of cryoturbations. *Permafrost and Periglacial Processes* 2: 123-129.

Zoltai, S.C., Tarnocai, C. & Pettapiece, W.W. 1978. Age of cryoturbated organic material in earth hummocks from the Canadian arctic. *Proceedings of the Third International Conference on Permafrost*, *Edmonton, Alberta*: 325-331.

Zoltai, S.C. & Tarnocai, C. 1974. Soils and vegetation of hummocky terrain. Environmental–Social Committee, Northern Pipelines, Task Force on Northern Oil Development, *Report No. 74–5*, 86 pp.

Thermal Impact of Holocene Lakes on a Permafrost Landscape, Mackenzie Delta, Canada

Alan E. Taylor
ASL Environmental Sciences, Inc., Sidney BC V8L 5Y3, Canada
Scott R. Dallimore
Geological Survey of Canada, Sidney BC V8L 4B2, Canada
J. Frederick Wright
Geological Survey of Canada, Sidney BC V8L 4B2, Canada

Abstract

Canada's Mackenzie Delta has experienced Holocene lake development on a permafrost landscape, exerting significant influence on the sub-lake geothermal regime. Two-dimensional finite element geothermal modeling is used to simulate talik formation beneath lakes of various diameters in sand, clayey-silt, and clay. Forward modeling was initiated from a simplifying assumption of thermal steady state at the end of the Wisconsin, and subsequently incorporated the transient effects of Holocene warming and mid-Holocene lake formation, to the present-day. Thermal taliks (>0°C) quickly developed beneath all lakes. In sands, sediments beneath the taliks remained almost entirely ice-bonded to the present time. In contrast, in fine-grained clayey silt, sediments beneath the taliks developed elevated unfrozen water content that eventually extended to the base of permafrost, thus forming chimney-like structures of partially ice-bonded soils that penetrate thick permafrost beneath larger lakes. This characteristic arises from the strong temperature dependence of unfrozen water content in finer-grained sediments.

Keywords: geothermal; lakes; modeling; permafrost; seeps; talik.

Introduction

Lakes and river channels represent dramatic thermal anomalies in terrestrial permafrost environments. In the arctic, the impact of water bodies on permafrost is accentuated because of the large contrast in mean annual ground surface temperature beneath lakes and rivers (if they do not freeze completely in winter) compared to that of the adjacent sub-aerial terrain. The classic study is the analytic model of Lachenbruch (1957), which demonstrates the steady-state (or equilibrium) impact and simple transient effects of lakes on permafrost. Over 30% of the land area of the Mackenzie Delta is occupied by lakes, and large variations in the subsurface geothermal regime are expected from the contrast of warm lakes (mean annual lakebed temperature about +2°C) superimposed on a cold (-6°C or colder) permafrost landscape. Mackay (1963, sect. 76) calculated the thermal disturbance beneath such lakes and W. Brown et al. (1964) presented early field evidence for the presence of a talik beneath a lake in the Mackenzie region. Numerical studies of talik formation beneath lakes have been made by Ling & Zhang (2003) in northern Alaska, and Burn (2002) in the Mackenzie Delta.

In this paper, we use a two-dimensional finite element model to predict the thermal impact of lake formation (during the Holocene) on thick Pleistocene permafrost typical of the Mackenzie Delta, northwestern Canada. The study focuses on the thermal sensitivity of two typical lithologies (sand and clayey silt) to lake diameter (20 m to 4 km), and to time of lake formation (10 kaBP and 6 kaBP). Model outputs are two-dimensional (horizontal and depth) depictions of ground temperatures and unfrozen water contents through the permafrost, and are presented as contours and summary graphs. The model is not calibrated to observed permafrost temperatures or thicknesses at a particular location. Rather, the intent of the paper is to demonstrate the gross impact of the development of hypothetical lakes on permafrost terrain in terms of changes to the local geothermal regime, subsequent development of taliks, and modification of the properties of underlying sediments. Thermal taliks are unfrozen sediments (temperature >0°C) in association with permafrost, and "geophysical taliks" are defined here as frozen sediments (temperature <0°C) which contain sufficient un-crystallized pore water (herein referred to as unfrozen water) so as to be discriminated by geophysical methods.

Extensive permafrost developed in Quaternary sediments of the Pleistocene Mackenzie Delta (principally the Tuktoyaktuk Peninsula and Richards Island) and today is typically 400–700 m in thickness (Judge 1973, Taylor et al. 1982), consistent with late Wisconsinan and Holocene surface temperatures (Taylor et al. 1996). The glacial history is controversial, but the region was mostly unglaciated during the late Wisconsinan (Dyke & Prest 1987). Maximum development of thermokarst lakes occurred in the early Holocene and most lakes have undergone one or more partial drainage events, attaining their present size by ~6 kaBP (Mackay 1992), and lacustrine sediments bordering many present-day lakes reflect this earlier, more extensive lake cover (Rampton 1988). Numerous tundra polygons and pingos are characteristic of poorly drained areas comprising former lake bottoms (Mackay 1963, §64).

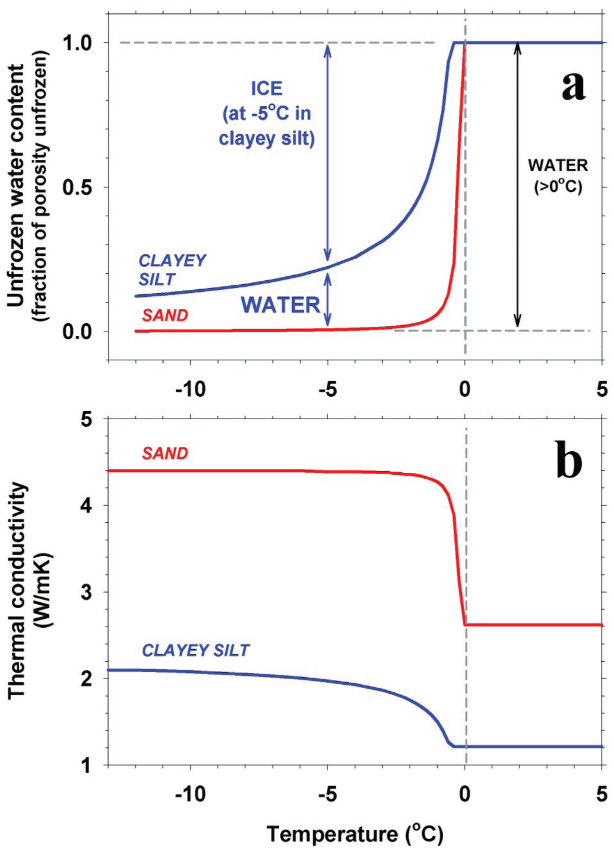

Figure 1. (a) Unfrozen water content and (b) thermal conductivity curves based on laboratory measurements of Mackenzie Delta cores (Dallimore & Matthews 1997) and used in the geothermal modeling.

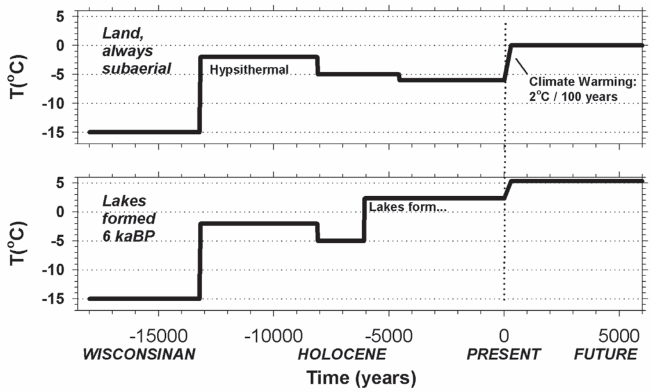

Figure 2. Ground surface/lakebed transient boundary conditions of the model (see Taylor et al. 1996, 63-65; 1999 for development and references).

Model Description

The TEMP/W geothermal modeling software (Geo-Slope International Ltd. 2004) was employed in this work. This two-dimensional finite-element numeric model combines conductive heat transfer and phase-change enthalpies, and accommodates the explicit specification of appropriate geologic properties and temporal boundary conditions. The model has been verified extensively against analytic solutions as well as the pioneering numerical permafrost model of Hwang et al. (1972) and has been used in the permafrost community (e.g., Mottaghy & Rath 2006).

Our problem space extends to a depth of 1000 m along a 14 km hypothetical transect. Lakes of diameter 20 m, 50 m, 100 m, 200 m, 500 m, 1 km, 2 km and 4 km are situated at a spacing that ensures minimal thermal disturbance of adjacent lakes but which is, however, not untypical of the spacing of lakes on Richards Island and the Tuktoyaktuk Peninsula. The goal was to develop, without the advantage of a full 3-dimensional code but with the flexibility of applying quasi-continuous surface boundary conditions, a model that could be applied easily to an actual transect across this region (see Discussion). Water depth in Mackenzie Delta lakes is typically a few meters (Mackay 1963) and is not explicitly considered in the model, except that our results apply only to the central basins of sufficient depth that water does not freeze to the bottom in the winter.

Physical properties

Unfrozen water content as a function of sub-0°C temperature (Smith & Tice 1988) is a primary physical property for permafrost modeling, and refers to pore water that remains in the liquid phase even though its temperature is below 0°C. The Geological Survey of Canada has measured unfrozen water content, porosity, salinity, and grain-size distributions for a suite of some 30 subsurface soils from the Mackenzie-Beaufort area (Dallimore & Matthews 1997). Curves of unfrozen water content as a function of sub-0°,C temperature were chosen that are typical of sand, clayey silt and clay (Fig. 1a). Nowhere does clay fully constitute the entire permafrost section in the Delta, but clay was chosen to compare with sand as geologic "end members" of typical Delta soils. Averages of ~ 2000 measured thermal conductivity values (needle probe method), and unfrozen water content curves from previous field programs (Dallimore 1991, 1992) were used to calculate conductivity-temperature profiles for these three lithologies (Fig. 1b). Thermal heat capacity was calculated from the constituent fractions of soil particles, frozen (ice), and unfrozen water. The phase change temperature assumed for pore water is 0°C. Note that as fine-grained sediments freeze or thaw, the latent heat is distributed over a range of temperatures, according to the unfrozen water content curve (Fig. 1a). TEMP/W fully accommodates such a "distributed" latent heat budget of freeze/thaw. The latent heat of the water is 3.38 x $10^8 J\cdot m^{-3}$; hence for soil volumetric latent heat is less, depending on the porosity.

Boundary conditions

Steady state condition. A geothermal heat flux of 69 $mW\cdot m^{-2}$ (Judge 1973, Majorowicz 1996, Fig. 16) was applied at 1 km depth for all models and times.

Initial and transient surface boundary conditions provide the basic constraints under which the geothermal regime is modeled in the forward sense, from ~13 kaBP through the

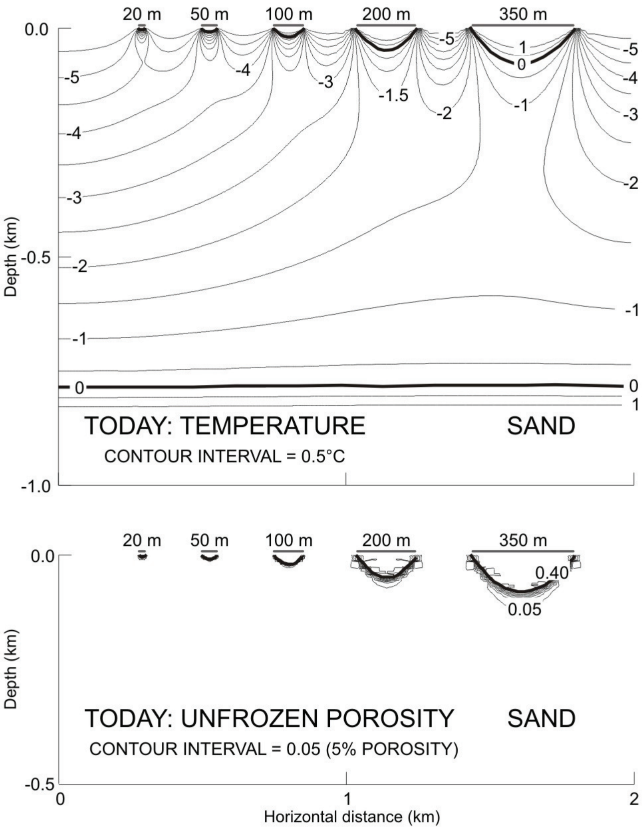

Figure 3a. Modeled present-day temperature vs. depth (upper; contours in °C) and fractional unfrozen volumetric water content (lower) beneath lakes of various sizes (20–350 m diameter) for a sand lithology with volumetric porosity 40%; thus 0.4 designates a totally thawed sand.

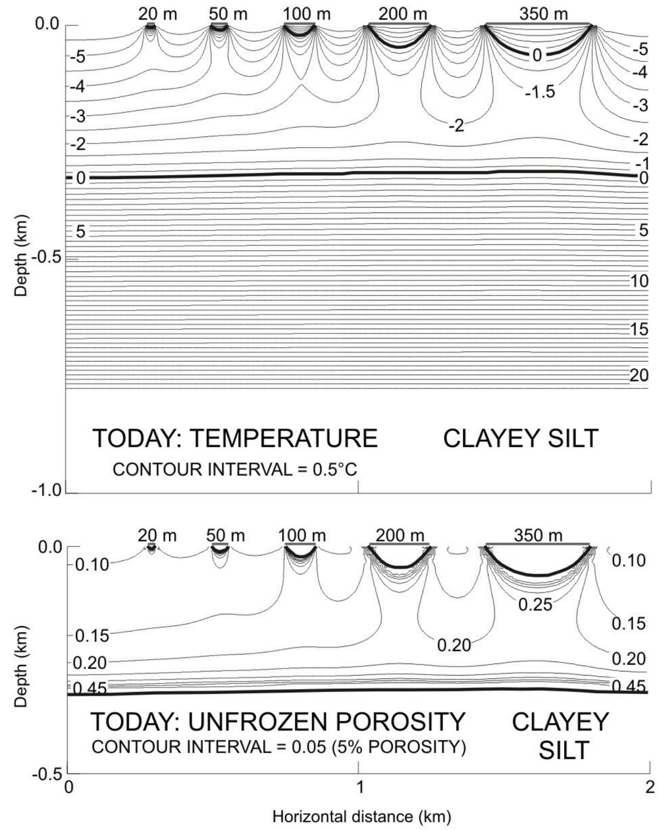

Figure 3b. As above, for a clayey-silt lithology; volumetric porosity 48%; thus, 0.25 indicates sediment in which about half the pore space is unfrozen water.

present to ~13 kaAP (after present). Boundary conditions were developed from the literature for earlier work and were verified through their successful prediction of temperatures measured today (see Taylor et al. 1996 for citations).

Initial conditions provide the geothermal structure at the end of the Wisconsinan from which forward modeling is initiated. Permafrost temperatures at ~13 kaBP were assumed to be in quasi-equilibrium with surface temperatures of -15°C (typical of severe arctic conditions for unglaciated areas) and with the steady state geothermal heat flux.

Transient boundary conditions specify the variation of ground surface temperature through time, forward from the steady state and initial boundary condition at 13 kaBP and at different points along the hypothetical 14-km transect through lakes. Two surface boundary conditions are considered: land that is always subaerial (temperatures variable), and lakes. See Taylor et al. (1996, 63-65) for discussion of subaerial temperatures assumed throughout the Holocene. Lake bottom temperatures were assumed +2.3°C (cf. Burn 2002, +2 to 4°C, 1290). Geological evidence suggests that lakes formed as early as 10,000 to about 6000 years ago (e.g., Mackay 1992); the numerical model applies the subaerial boundary condition prior to those times, and a combination of the subaerial and the lake boundary conditions following lake formation; lakes are assumed to form to full size, a simple "step change" ramped over ~100 years (Fig. 2). The Little Ice Age is not considered. Finally, we invoke a scenario of contemporary climate warming, at 2°C per 100 years for land and half that value for water temperatures for 300 years following the present, thus reaching +0.1°C (land) and +5.3°C (lakes) by 300 aAP. At that time, the transient boundary conditions represent a non-sustainable permafrost environment. Modeling results are saved at frequent time intervals, allowing a depiction of the gross evolution of the two-dimensional ground thermal state.

Model Results

Time slice – present

Figure 3 presents contours of the present transient geothermal regime for lakes formed 6 kaBP in (a) sand, and (b) in clayey silt lithology. The base of permafrost is more than twice as deep in sand due to the effect of higher thermal conductivity (Fig. 1b). Thermal taliks beneath lakes are defined by the upper 0°C isotherm and the base of permafrost is defined by the lower 0°C isotherm. There are two critical observations: (1) Temperature contours are very similar in character for both sand and clayey silt; but (2) the unfrozen water content contours are very different, with <5% volumetric unfrozen water content in sand beneath all lakes regardless of size, whereas >15% unfrozen water content in clayey silt beneath lakes >100 m diameter. The through-

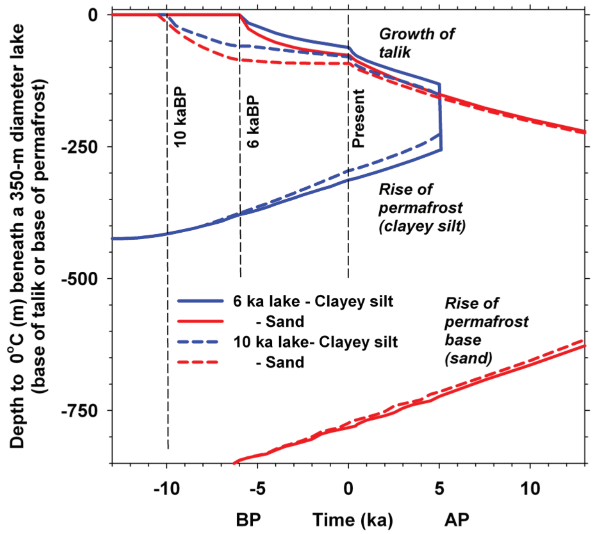

Figure 4. Growth of a talik and rise of permafrost base beneath a 350 m diameter lake, following lake formation at 10 kaBP or 6 kaBP on a permafrost landscape of sand or clayey silt.

going "hourglass" of partially unfrozen soils beneath lakes is absent in sand. These contrasting regimes are directly related to the contrast in unfrozen water content curves in the two lithologies, such that at sub-zero temperatures within a few degrees of 0°C, a comparatively large fraction of pore water remains in the liquid phase in clayey silt compared to sand (Fig. 1a). As a direct result, geophysical taliks (soils having high unfrozen water contents) completely penetrate the permafrost in a clayey silt substrate, while sands underlying lakes of comparable size are almost completely frozen.

Growth of taliks after mid-Holocene lake formation

Figure 4 shows thermal talik development and evolution of permafrost during the Holocene. Today, thermal taliks extend possibly 20 m deeper beneath lakes formed at 10 kaBP than at 6 kaBP. In our model, the 0°C isotherm fully penetrates the permafrost within several hundred years of lake formation on a hypothetical clay lithology (not shown), within ~5 kaAP in clayey silt under contemporary climate warming, and apparently only after several tens of thousand years in sand. The permafrost base rises throughout the Holocene. Many lakes forming ~10 kaBP contracted in size by the mid-Holocene, leaving lacustrine "halos" surrounding some present-day lakes (unit L in Rampton 1988); modeling showed that the geothermal effect at the present time is very small.

Regime beneath lakes and intervening land

Figure 5 depicts the present thermal regime beneath adjacent 100 m and 200 m lakes and the 150 m of land separating them as predicted by the transient model (clayey silt). The expected regime if ground thermal conditions were in equilibrium with today's climate is also shown (lighter

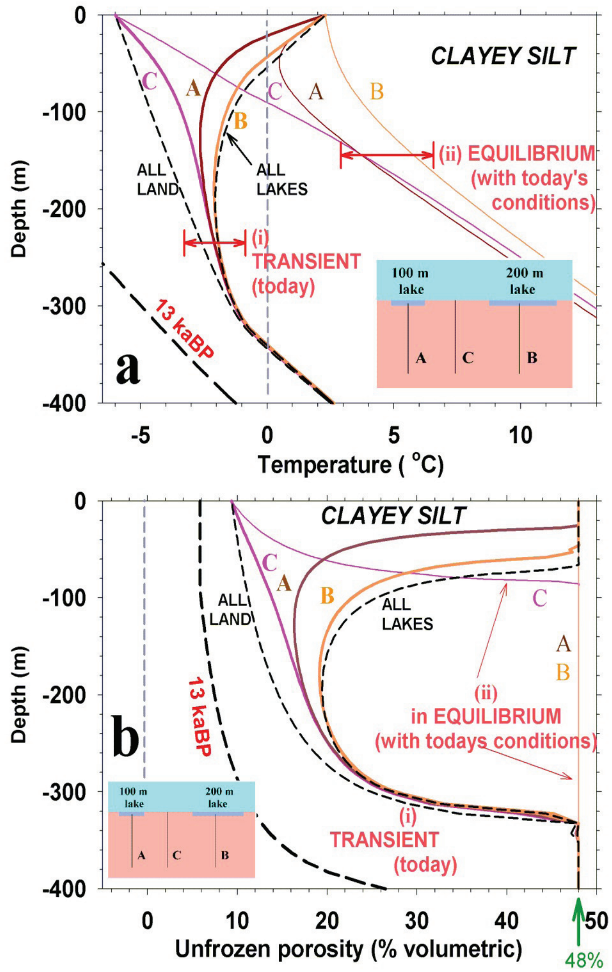

Figure 5. Thermal regime predicted in a clayey silt lithology for today beneath two adjacent lakes (A and B in the insets) and the land separating them (C). (a) transient temperature profiles (i), and equilibrium temperature profiles (ii) for today's surface conditions. (b) volumetric unfrozen water content. Transient profiles labeled "all land" and "all lakes" are bracketing "end member" cases of a landscape that is lake-free or fully inundated.

curves) to demonstrate the fallacy of such an assumption (see "Discussion" for field evidence). Profiles labeled "all land" and "all lake" are the end-member scenarios of the extent of lake coverage and bracket the profiles predicted for a lake-dominated landscape. The temperature profiles beneath lakes 100 m and 200 m in diameter ("A" and "B") contrast to the profile ("C") beneath their shared inter-lake area. Both temperatures and unfrozen water contents deeper than ~300 m appear largely independent of surface conditions (i.e., lakes or land, or Holocene climate change) while at depths less than ~300 m, temperatures reflect the surface environment and Holocene warming. The depth to the base of the sub-lake thermal talik increases from ~ 21 m (100 m diameter lake) to ~40 m (200-m lake, Fig. 5a).

Permafrost with low volumetric unfrozen water content (~6%) underlies all land at 13 kaBP, as predicted by the unfrozen water curve at –15°C for clayey silt (Fig. 1a) and a soil porosity of 48%. The impact of lakes on the modern landscape is to raise the minimum unfrozen water content to ~10% beneath the intervening land between lakes, and to ~16%–20% beneath lakes >100 m in diameter. Hence, almost half the pore space is unfrozen beneath larger lakes situated on clayey-silt sediments, although ground temperatures remain <0°C. Unfrozen water content, and hence sediment permeability within these geophysical taliks, may be sufficiently high to facilitate vertical transport of water and/or gas from deeper horizons to the surface in these environments (e.g., Williams & Smith 1989, §7.5).

The depth to the base of the thermal talik increases with lake diameter, to a maximum of ~50 m under the largest lakes or an "all lake" landscape (clayey silt) and ~85 m (sand), and at present continues to increases at ~4 m/1000 years at present. In contrast, the permafrost base is rising at ~10 m/1000 years (Fig. 4). The depth to the minimum of the unfrozen water content profile is about 4 to 5 times deeper than the depth to 0°C in clayey silt; and the value of the minimum unfrozen porosity is ~20% in clayey silt and <3% in sand. There is little indication of a "geophysical talik" in sand (Fig. 3a, lower).

Discussion and Conclusions

Our finite element geothermal model demonstrates that the present permafrost geothermal regime is in disequilibrium following the onset of the Holocene, and that for lithologies typical of the Mackenzie Delta, the continuous permafrost is not perforated by through-going thermal taliks (i.e., temperatures >0°C) beneath Holocene lakes of any size. However, '"geophysical taliks"' do penetrate the permafrost beneath lakes due to the substantial unfrozen water content of clayey silts at negative temperatures to about -7°C (Fig. 1a). There is some field evidence in support of our interpretation of modeling results and for the presence of both thermal and geophysical taliks beneath lakes. Pre-drainage temperatures beneath the centre of Illisarvik Lake reach -3°C at 84 m with the sub-lake talik extending to ~32 m (Burgess et al. 1982). Temperatures to ~350 m below seabed in the Amauligak geotechnical hole some 80 km offshore in 32 m of water on the Beaufort Shelf are near isothermal at -2.3°C, a good analogy to the "all lakes" model of Figure 5 (Taylor et al. 1989). Beneath a small island in Parsons Lake, permafrost is >300 m deep, similar to depths at several wells surrounding the lake (Judge et al. 1981). Electromagnetic soundings provide some field evidence of the unfrozen water content of sub-talik sediments (Geophysicon 1983, Todd & Dallimore 1998).

Interpretation of 3-dimensional seismic data by Riedel et al. (2006) provides evidence of seismic blanking beneath shallow lakes in the vicinity of Mallik Bay, Richards Island, possibly due to lower seismic velocities in sub-lake sediments containing significant unfrozen water.

The geology of the Pleistocene Mackenzie Delta is largely sands, silts, and clayey silts, at least through permafrost (Dallimore 1992). Where lithology tends towards finer-grained sediments, our model suggests that geophysical taliks may perforate the permafrost beneath lakes, and the elevated unfrozen water content may have implications for the migration of ground water and/or hydrocarbon gases from below permafrost to the surface. In the case of natural gases such as methane, these conduits may provide physical pathways for the transport of greenhouse gases from deep geological sources (conventional hydrocarbon reservoirs and/or gas hydrate deposits) into the atmosphere.

Our model is meant to be a gross prediction of the thermal regime evolving from the initial formation of lakes in the early to mid-Holocene. The gradual *ab initio* enlargement of lakes (e.g., ~1 m/a at 10 ka or 6 kaBP) is not modeled and may be a negligible effect on the subsurface thermal regime today. An inherent assumption in the 2-D model is the "'third dimension" that extends to infinity. Hence, our model more correctly represents a transverse section across a river. For our model, the result is a moderately enhanced talik development arising from the unconstrained third dimension, especially under smaller lakes. An alternative quasi-3D model could be developed in cylindrical symmetry (e.g., Ling & Zhang 2003), better to model details of the thermal impact of an isolated lake but less appropriate to model transects of the closely-spaced lakes of the Mackenzie Delta where we might expect substantial thermal effect of one lake on another (e.g., Figure 3 predicts permafrost temperature between the lakes is higher than away from the lakes).

To the authors' knowledge, there are no "through-permafrost" temperature profiles with which to constrain our model. The intent here is to present a simple model constrained by the literature and reasonable geological assumptions. Current numerical methods enable almost any detail of lake evolution to be modeled; however, the most significant limitation remains the lack of relevant field measurements to constrain the models.

Acknowledgments

This research was supported by the Program of Energy Research and Development, Natural Resources Canada. Comments of two anonymous reviewers helped clarify the presentation. The authors thank Michelle Côté for assistance with the figures.

References

Brown, W.G., Johnston, G.H. & Brown, R.J.E. 1964. Comparison of observed and calculated ground temperatures with permafrost distribution under a northern lake. *Canadian Geotechnical Journal* 1: 147-154.

Burgess, M.M., Judge, A., Taylor, A. & Allen, V. 1982. Ground temperatures studies of permafrost growth at a drained lake site, Mackenzie Delta. In: H.M.

French (ed.), *Proceedings of the Fourth Canadian Permafrost Conference, Calgary.* Nat. Res. Council of Canada. 3-11.

Burn, C.R. 2002. Tundra lakes and permafrost, Richards Island, western Arctic coast, Canada. *Canadian Journal of Earth Sciences* 39: 1281-1298.

Dallimore, S.R. (compiler) 1991. *Geological, Geotechnical and Geophysical Studies along an Onshore-Offshore Transect of the Beaufort Shelf.* Open File 2408. Geological Survey of Canada.

Dallimore, S.R. (compiler) 1992. *Borehole Logs from Joint GSC-Industry Mackenzie Delta Geology/Permafrost Transect.* Open File 2561. Geological Survey of Canada.

Dallimore, S.R. & Matthews, J.V., Jr. 1997. *The Mackenzie Delta Borehole Project.* Environment Studies Research Funds Report No. 135. Calgary, Canada. 1 CD-ROM.

Dyke, A.S. & Prest, V.K. 1987. *Paleogeography of Northern North America, 18,000–5,000 Years Ago.* Map 1703A. Geological Survey of Canada.

Geophysicon, Ltd. 1983. *Detection of Permafrost Base in Permafrost Areas–Transient Electromagnetic Survey in Mackenzie Delta Area, N.W.T.* Open file 83-17. Earth Physics Branch, EMR Canada.

GeoSlope International Ltd. 2004. *TEMP/W, Software for Finite Element Geothermal Analys., version 6,* Calgary, AB: Geo-Slope International Ltd.

Hwang, C.T., Murray, D.W. & Brooker, E.W. 1972. A thermal analysis for structures on permafrost. *Can. Geotech. J.* 9 (1).

Judge, 1973. The prediction of permafrost thickness. *Can. Geotech. J.* 10: 1-11.

Judge, A.S., Taylor, A.E., Burgess, M.M., & Allen, V.S. 1981. *Canadian Geothermal Data Collection–Northern Wells 1978-80.* Earth Physics Branch, Geothermal Series 12, 190 pp.

Judge, A.S., Pelletier, B.R. & Norquay, I. 1987. Permafrost base and distribution of gas hydrates. In: B.R. Pelletier (ed.), *Marine Science Atlas of the Beaufort Sea: Geology and Geophysics.* Miscellaneous Report 40. Map 39. Geological Survey of Canada.

Lachenbruch, A.H. 1957. Thermal effects of the ocean on permafrost. *Geol. Soc. Am. Bull.* 68: 1515-1530.

Ling, F., & Zhang, T. 2003, Numerical simulation of permafrost thermal regime and talik development under shallow thaw lakes on the Alaskan Arctic Coastal Plain, *J. Geophys. Res.* 108(D16): 4511, doi: 10.1029/2002JD003014.

Mackay, J. Ross. 1963. *The Mackenzie Delta area, N.W.T.* Mem. 8. Geogr. Branch, Ottawa, Ontario (reprinted). Misc. Rep. 23. Ottawa, Ontario: Geological Survey of Canada, 202 pp.

Mackay, J. Ross. 1992. Lake stability in an ice-rich permafrost environment: examples from the western arctic coast. In: R.D. Robarts & M.L. Bothwell (eds.), *Aquatic ecosystems in Semi-Arid Regions: Implications for Resource Management.* NHRI, Environment Canada, Saskatoon, Symposium Series 7: 1-26.

Majorowicz, J.A. 1996. Regional geology and geophysical setting: geothermics. In: J. Dixon, (ed.), *Geological Atlas of the Beaufort-Mackenzie Area.* Miscellaneous Report 59. Maps 15 & 16. Geological Survey of Canada.

Mottaghy, D. & Rath, V. 2006. Latent heat effects in subsurface heat transport modelling and their impact on palaeotemperature reconstructions, *Geophys. J. Int*. 164: 236-245, doi:10.1111/j.1365-246X.2005. 02843.

Rampton, V.N. 1988. *Quaternary Geology of the Tuktoyaktuk Coastlands, Northwest Territories.* Memoir 423. Geological Survey of Canada.

Riedel, M., Bellefleur, G., Dallimore, S.R., Taylor, A. & Wright, J.F. 2006. Amplitude and frequency anomalies in regional 3D seismic data surrounding the Mallik 5L-38 research site, Mackenzie Delta, Northwest Territories, Canada, *Geophysic.* 71: B183–B191.

Smith, M.W. & Tice, A.R. 1988. *Measurement of the Unfrozen Water Content of Soils: Comparison of NMR and TDR Methods.* CRREL Report 88-18. U.S. Army Cold Regions Research and Engineering Laboratory, 11 pp.

Taylor, A.E., Burgess, M.M., Judge, A.S., & Allen, V.S. 1982. *Canadian Geothermal Data Collection - Northern Wells 1981.* Earth Physics Branch, Geothermal Series 13: 153 pp.

Taylor, A.E., Judge, A.S. & Allen, V.S. 1989. *Recovery of Precise Offshore Permafrost Temperatures from a Deep Geotechnical Hole, Canadian Beaufort Sea.* Paper 89-1D. Geological Survey of Canada, 119-123.

Taylor, A.E., Dallimore, S.R. & Judge, A.S. 1996. Late Quaternary history of the Mackenzie-Beaufort region, arctic Canada, from modelling of permafrost temperatures: 2. the Mackenzie Delta-Tuktoyaktuk Coastlands. *Canadian Journal of Earth Sciences* 33(1): 62-71.

Todd, B.J. & Dallimore, S.R. 1998. Electromagnetic and geologic transect across permafrost terrain, Mackenzie River delta, Canada. *Geophysics* 63: 1914-1924.

Williams, P.J. & Smith, M.W. 1989. *The Frozen Earth.* Cambridge: Cambridge Univ. Press, 306 pp.

The Impact of Sediments Derived from Thawing Permafrost on Tundra Lake Water Chemistry: An Experimental Approach

M.S. Thompson
Water and Climate Impacts Research Centre, Department of Geography, University of Victoria, Victoria, Canada
S.V. Kokelj
Water Resources Division, Indian and Northern Affairs Canada, Yellowknife, Canada
T.D. Prowse
Water and Climate Impacts Research Centre, Environment Canada, Department of Geography, University of Victoria, Victoria, Canada
F.J. Wrona
Water and Climate Impacts Research Centre, Environment Canada, Department of Geography, University of Victoria, Victoria, Canada

Abstract

Retrogressive thaw slumping can transport ion-rich meltwater and thawing sediment from terrestrial to aquatic systems. Tundra lakes affected by shoreline slumping have elevated ionic concentrations, low dissolved organic matter concentrations, and colour compared to unaffected lakes. To investigate the potential photochemical implications, an in situ microcosm experiment was performed involving the incubation of water from an undisturbed lake with thawed slump sediment. Sediment treatments were 10, 25, and 50% of the total container volume, and containers were incubated in the lake for 52 days during the summer of 2007. Water colour decreased successively with sediment volume, and was highest in the control. Specific conductivity was more than 8 times higher in the 50% sediment treatment water than in the control. Sedimentation of organic matter may explain the low colour in the treatment water. The transportation of thawing permafrost sediment into tundra lakes may rapidly increase water clarity and alter carbon supply.

Keywords: climate change; coloured dissolved organic matter; Mackenzie Delta region; microcosm experiment; retrogressive thaw slumping; tundra lakes.

Introduction

In the uplands east of the Mackenzie Delta, NWT, Canada, thousands of small lakes and ponds are surrounded by terrain underlain by ice-rich permafrost (Mackay 1992, Kokelj et al. 2005). In this region, thawing of the near-surface permafrost commonly leads to the formation of large retrogressive slumps on slopes adjacent to lake shores (Lantz & Kokelj 2008). Solute concentrations in permafrost may be enriched with respect to the overlying active layer (Kokelj & Burn 2003, 2005). The geochemical contrast between the active layer and permafrost is attributed to progressive leaching of soluble materials from seasonally thawed soils and preservation of solutes in underlying frozen sediments, and due to thermally induced migration of water and soluble materials from the base of the active layer into the top of permafrost (Kokelj & Burn 2005). Thaw slumping may release these solutes in the permafrost, with implications for sediment and runoff chemistry (Kokelj & Lewkowicz 1999).

A survey of 298 lakes on five 49 km^2 study plots between Inuvik and the Beaufort Sea indicated that 6 to 17% of the lakes were affected by shoreline slumping (Kokelj et al. 2005). Thaw slumps can be relatively large compared to the size of adjacent lakes. In a sample of 11 first-order upland lakes affected by slumping in the Delta region, the median disturbance area: lake area ratio was 0.48 (Kokelj et al. 2005). The median disturbance size was 1.9 ha, and the median lake size was 4.0 ha. In many cases, disturbance area was almost equivalent to lake area.

Lake chemistry interactions

The water chemistry of small tundra lakes is strongly influenced by lake catchment characteristics, including surficial geology, sediment development, peatland extent, and terrestrial vegetation (Pienitz et al. 1997, Duff et al. 1999, Frey & Smith 2005, Gregory-Eaves et al. 2000, Rühland et al. 2003). In the Mackenzie Delta region, a survey of 22 lakes indicated that those adjacent to retrogressive thaw slumps had elevated ionic concentrations, lower concentrations of dissolved organic carbon (DOC), and were less coloured compared to lake waters in undisturbed areas (Kokelj et al. 2005). Organic carbon supply and related changes in visible and UV light penetration influence the productivity of pelagic algal and bacterial communities (Jones 1992, Teichreb 1999).

Base cations can increase the adsorption and flocculation of coloured dissolved organic matter (CDOM), or humic matter, from the water column (reviewed in Jones 1992, Thomas 1997). Mineral soils, especially clays, that may enter lakes can adsorb humic matter leading to sedimentation (reviewed in Jones 1992, Thomas 1997). This raises the possibility

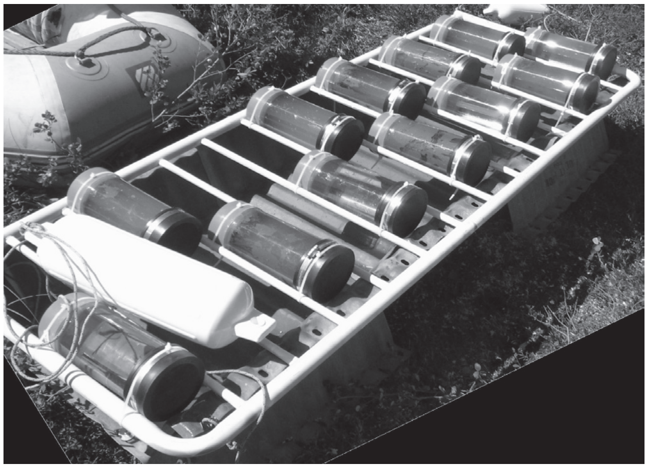

Figure 1. Experimental incubation containers positioned on rack prior to deployment in the lake.

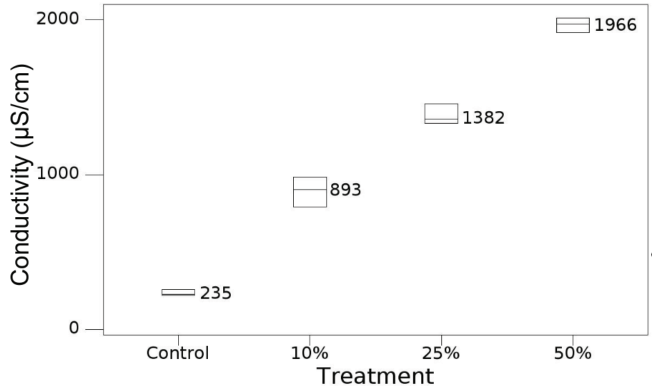

Figure 2. Mean specific conductivity of the incubated lake water in each of the permafrost sediment treatment and control containers (with 95% confidence intervals, mean value provided).

that sediment and soluble ions delivered from terrestrial to aquatic systems by the process of thaw slumping may affect CDOM concentrations and optical properties of water in small tundra lakes.

Here we examine the effects of ion and sediment additions on the colour of lake water by undertaking an incubation experiment. The goal was to test whether exposure of humic lake water to thawed permafrost sediment and associated runoff could produce similar water chemistry conditions characteristic of a "disturbed" lake affected by lake shore thaw slumping.

Methods

Incubation experiment

Recently-thawed sediments and pooled surface runoff were collected on 24 June 2007 from a thaw slump scar located on the shore of a small lake 60 km north of Inuvik. The sediments, comprised of silty clay, were homogenized by mixing with surface water collected from the slump (specific conductivity 2345 µS/cm) to form a saturated slurry. The gravimetric water content of the runoff-sediment mixture was 33% by weight.

The sediment mixture was added to containers constructed from sections of clear acrylic pipe (approximately 10 cm diameter) with a total volume of 2 L. The pipe sections were sealed on one end with a silicone-sealed cap and on the other with a removable rubber "test cap". A spectral scan of the acrylic pipe material indicated that it blocked most UV-B (absorbance at 320 nm = 1.027) and much of the UV-A (absorbance at 380 nm = 0.096) wavelength range. This desirable property of the pipe materials minimized the breakdown of coloured humic substances in lake water by incoming UV radiation (photolysis). The proportion of saturated sediment in each of three replicated container sets was 50, 25 and 10% of the container volume (1.0, 0.5, and 0.2 L respectively).

The incubation containers were installed in a shallow (estimated Z_{max}: 2 m), humic lake within 15 minutes road access of Inuvik, which is unaffected by thaw slumping. Before installation, surface lake water from the same incubation lake site was collected and added to each of these containers, along with a set of replicate control containers, to a total volume of 2 L. The sediment slurry in each container was purposefully not mixed homogeneously with the lake water, since slump materials often enter the lakes as intact blocks. The containers were sealed immediately after the lake water addition, and were attached to a rack apparatus which kept the containers horizontally aligned, approximately 0.75 m below the water surface and elevated approximately 0.75 m above the lake benthos (Fig 1). The containers were installed on 6 July 2007 and were retrieved on 28 August 2007 for a total incubation period of 52 days.

An additional container was filled with distilled and deionized water in order to test the water-tightness of the container seals. Initial specific conductivity of the distilled water was 2 µS/cm; —after incubation it was 20 µS/cm. Specific conductivity in the lake was 219 µS/cm just prior to deployment of the incubation containers.

Analysis

Following retrieval, the containers were removed from the support rack, immediately transported and refrigerated at the Aurora Research Institute lab. Within 3 hours of arrival at the lab, the incubated water was removed from the containers without disturbing the sediment settled at the bottom of each container. Specific conductivity, pH, dissolved oxygen (DO) and oxidation-reduction potential (ORP) of the water was measured using a YSI 556 multiprobe meter (Yellow Springs Instruments, Idaho, USA).

In preparation for measurement of water colour as spectral absorbance, a 125 ml volume of the incubated water was filtered through a 0.45 µm Supor membrane syringe filter (Pall Corporation, NY, USA). Samples were placed in glass containers and kept in a dark refrigerated area until absorbance could be measured. Absorbance was measured across the range 190–900 nm using an Ultrospec 3100 pro spectrophotometer equipped with a 1 cm cuvette (Biochrom, Cambridge, UK). Absorbance measurements at 320 nm (UV-B), 380 nm (UV-A) and 440 nm (PAR, photosynthetically active radiation) were corrected for

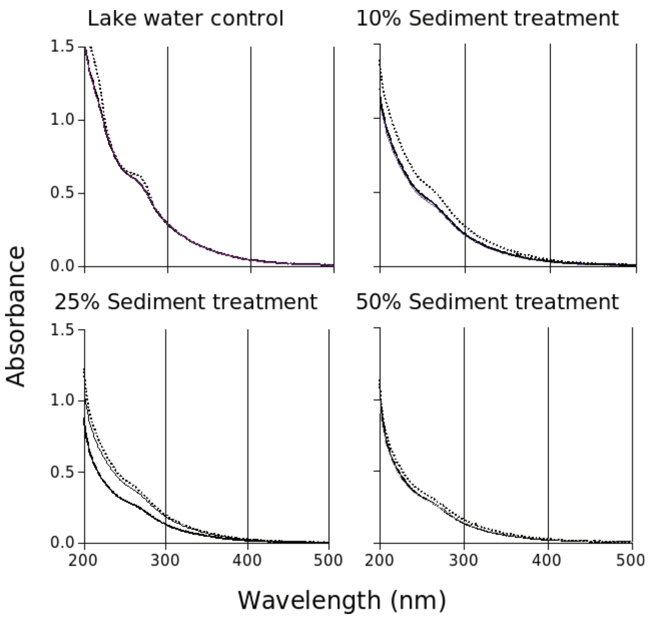

Figure 3. Replicate spectral scans of incubated lake water from the control and each sediment treatment container. For each treatment graph, $n = 3$.

turbidity-related light scattering by subtracting absorbance values at 740 nm. These corrected values were used in statistical analyses.

A one-way analysis of variance (ANOVA) was used to assess the response of the lake water specific conductivity to the sediment treatments. The effect of the sediment treatments on the spectral absorbance of the incubated lake water was tested using a repeated measures ANOVA, including absorbance values at wavelengths in the UV-B (320 nm), UV-A (380 nm) and photosynthetically active radiation (PAR, 440 nm) ranges. Post hoc Tukey tests were used to distinguish between significantly different treatment level. Finally, conductivity and all absorbance measurements were tested for significant Pearson correlations across treatments, with Bonferroni adjusted significance levels. All analyses were completed using SPSS 13.0 (SPSS Inc., Illinois, USA).

Results

Specific conductivity

The measured specific conductivity of the incubated lake water in each of the treatment and control containers are shown in Figure 2. The water at each sediment treatment level and in the control had significantly different mean specific conductivity, with relatively little variation within treatments (one-way ANOVA, $F = 396.23$, $df = 3$, $p < 0.000$). The control and treatment mean specific conductivities were all significantly different from each other (Tukey HSD test).

Water colour

The spectral scan absorbance values for each treatment replicate are shown in Figure 3. Absorbance is generally higher in the control than in all sediment treatments. The greatest difference in the absorbance values between the control and all sediment treatments is apparent in the UV-B and UV-A range (280–320 nm and 320–400 nm, respectively). Differences between the control and treatments in the photosynthetically active radiation range (PAR, 400–700 nm) were lower than observed for the UV range. Relative change in absorbance between the control and treatments for representative wavelengths are provided in Table 1. The change in absorbance across wavelengths in the 25% sediment treatment is somewhat obscured by one low-absorbance replicate (Fig. 3).

There was a highly significant effect of sediment treatment on corrected absorbance at all three representative wavelengths (UV-B, UV-A, PAR) (repeated measures ANOVA, $F = 15.156$, $df = 3$, $p = 0.001$). Error variance between treatments for the 320 nm measurements was not homogeneous and could not be remedied via transformation however, and this must be considered when interpreting the ANOVA results. Post hoc tests found no significant difference ($p > 0.05$) between the control, the 10% and 25% sediment treatment, but did indicate a significant difference between the control and 50% treatment (Tukey's HSD test).

Negative correlations (Pearson's r) between incubated lake water specific conductivity and absorbance values in the UV and PAR range were statistically significant with the exception of the correlation with PAR (corrected $p > 0.05$).

Table 1. Relative decrease in mean spectral absorbance at representative wavelengths of lake water after incubation with thaw slump sediment. Change is relative to the untreated control mean. *PAR* is photosynthetically active radiation. *aX* is absorbance at wavelength X.

Sediment treatment	UV-B (a320)	UV-A (a380)	PAR (a440)
50%	49%	43%	27%
25%	43%	44%	44%
10%	20%	22%	13%

The highest correlation occurred with UV-B absorbance ($r = -0.91$), followed by UV-A ($r = -0.85$) and PAR ($r = -0.64$). Absorbance was strongly positively correlated between the three wavelengths ($r > 0.85$).

Discussion

In the Mackenzie Delta uplands, lakes affected by shoreline thaw slumping contain elevated concentrations of major ions in contrast with lower concentrations in undisturbed lakes (Kokelj et al. 2005). The soluble materials that enrich the lakes are derived from the thawing ion-rich permafrost (Kokelj & Burn 2005). The effect of sediment slurry treatments had a similar effect on lake water specific conductivity in this experiment, as soluble ions were released into solution from the solute-rich slump sediment mixture.

In the natural setting, lakes affected by slumping have clear water in comparison with more coloured water in undisturbed lakes. The experimental response of lake water colour to the sediment treatments suggests that sediment slurry treatments caused the removal of coloured organic materials from the lake water. This is indicated by the lower spectral absorbance in sediment-incubated lake water compared to the lake water control. High-molecular weight CDOM absorbs UV radiation very effectively (Scully & Lean 1994, Laurion et al. 1997), and the relatively high change in absorbance in the 50% and 10% sediment treatments at the UV-B and UV-A wavelengths compared to the PAR wavelength suggests that it is this type of DOM which has been removed from solution in the incubated water.

The within-treatment variability between replicates was relatively large in the 25% and the 10% sediment treatments. This contributed to the heteroscedasticity in the 320 nm absorbance range and the nonsignificant Tukey test between these treatments. Presence of a slight biofilm on a few of the containers walls, variation in sediment-water interface surface area, and variations in possible photolysis rates may contribute to observed within-treatment differences.

Allochtonous (origin outside the lake, terrestrial) DOM content in lake water is linked to catchment conditions, especially the supply (related to catchment vegetation) and the delivery (related to catchment morphology) of carbon (Rasmussen et al. 1989, Pienitz et al. 1997). Subarctic lakes with catchments underlain by permafrost are typically high in DOM because waters are derived from surface runoff through a thin, often organic-rich active layer (Pienitz et al. 1997). Allochtonous DOM usually has a higher molecular weight and is more highly coloured than autochtonous (origin inside the lake) DOM (Lean 1998, Perdue 1998). Catchment-derived carbon is also generally more reactive with metals and base cations due to its more aromatic structure (Perdue 1998). Adsorption of this humic material to fine-grained clay particles readily occurs. Each of these processes can lead to dissolution and sedimentation of the allochtonous DOM. Field observations in conjunction with our experimental results indicate that degradation of permafrost within the catchment can influence the biological and geochemical availability of DOM within lakes (Kokelj et al. 2005).

Organic matter delivered from the lake catchment may be an important source of energy within the lake. For example, bacteria are known to utilize allochtonous sources of carbon as an energy supply (Jones 1992). DOM may also contain phosphorous, often a limiting nutrient for algal and bacterial production (Jones et al. 1988, Klug 2005). Indeed, uptake of DOM by algae and/or bacteria in the experimental containers used here may have contributed to the observed decrease in absorbance, especially if the slump sediment enhanced biological production by providing limiting nutrients (Hobbie et al. 1999). However, the habitat conditions within the incubation containers were likely not representative of *in situ* conditions, so that conclusions concerning biological activity cannot be made here. In addition to the role of DOM as an energy and nutrient source, allochtonous humic material is generally coloured, and capable of attenuating radiation within the water column. This can limit phytoplankton photosynthesis (Jones 1992, Klug 2002), but can also limit the penetration of damaging UV radiation through the water column (Laurion et al. 1997, Lean 1998).

Humic materials in lakes, therefore, can be involved in many interactions between planktonic biota through their effects on nutrient and light quality and supply. The fact that several of these interactions may be competitive or mutually beneficial, makes the ecological outcome of changes in tundra lake conductivity and DOM concentration difficult to predict. However, such shifts have been linked to the overall heterotrophic or autotrophic nature of lakes in northern/cold regions (Jansson et al. 2000). Certainly a reduction in humic matter content due to addition of ion-rich runoff and sediments derived from slumping permafrost appears to be capable of changing the physical and chemical conditions in the pelagic habitat of tundra lakes.

Acknowledgments

The authors gratefully acknowledge: M. Bothwell for advice regarding study design and analyses; D. Lynch for technical and laboratory assistance; T. Carter, W. Hurst, G. King, and P. Mesquita for field assistance. Support was provided by the Natural Sciences and Engineering Research Council, The Northern Scientific Training Program, the Department of Indian Affairs and Northern Development Canada, and the Aurora Research Institute.

References

DeHaan, H. 1992. Impacts of environmental changes on the biogeochemistry of aquatic humic substances. *Hydrobiologia* 229: 59-71.

Duff, K., Laing, T., Smol, J. & Lean, D. 1999. Limnological characteristics of lakes located across arctic treeline in northern Russia. *Hydrobiologia* 391: 205-222.

Frey, K.E. & Smith, L.C. Amplified carbon release from vast West Siberian peatlands by 2100. *Geophysical Research Letters* 32: L09401.

Gregory-Eaves, I., Smol, J., Finney, B., Lean, D. & Edwards, M. 2000. Characteristics and variation in lakes along a north-south transect in Alaska. *Archiv fur Hydrobiologie* 147: 193-223.

Hobbie, J.E., Peterson, B.J., Bettez, N., Deegan, L., O'Brien, W.J., Kling, G.W., Kipphut, G.W., Bowden, W.B. & Hershey, A.E. 1999. Impact of global change on the biogeochemistry and ecology of an Arctic freshwater system. *Polar Research* 18: 207-214.

Jansson, M., Bergstrom, A.-K., Blomqvist, P. & Drakare, S. 2000. Allochtonous organic carbon and phytoplankton/bacterioplankton production relationships in lakes. *Ecology* 81: 3250-3255.

Jones, R.I. 1992. The influence of humic substances on lacustrine planktonic food webs. *Hydrobiologia* 229: 73-91.

Jones, R.I., Salonen, K. & De Haan, H. 1988. Phosphorous transformations in the epilimnion of humic lakes: abiotic interactions between dissolved humic materials and phosphate. *Freshwater Biology* 19: 357-369.

Klug, J. 2002. Positive and negative effects of allochtonous dissolved organic matter and inorganic nutrients on phytoplankton growth. *Canadian Journal of Fisheries and Aquatic Sciences* 59: 85-95.

Klug, J.L. 2005. Bacterial response to dissolved organic matter affects resource availability for algae. *Canadian Journal of Fisheries and Aquatic Sciences* 62: 472-481.

Kokelj, S. & Burn, C. 2003. Ground ice and soluble cations in near-surface permafrost, Inuvik, Northwest Territories, Canada. *Permafrost and Periglacial Processes* 14: 275-289.

Kokelj, S. & Burn, C. 2005. Geochemistry of the active layer and near-surface permafrost, Mackenzie delta region, Northwest Territories, Canada. *Canadian Journal of Earth Sciences* 42: 37-48.

Kokelj, S.V., Jenkins, R.E., Milburn, D., Burn, C.R. & Snow, N. 2005. The influence of thermokarst disturbance on the water quality of small upland lakes, Mackenzie Delta Region, Northwest Territories, Canada. *Permafrost and Periglacial Processes* 16: 343-353.

Kokelj, S.V. & Lewkowicz, A. 1999. Salinization of permafrost terrain due to natural geomorphic disturbance, Fosheim Peninsula, Ellesmere Island *Arctic* 52: 372-385.

Lantz, T.C. & Kokelj, S.V. 2008. Increasing rates of retrogressive thaw slump activity in the Mackenzie Delta region, N.W.T., Canada. *Geophysical Research Letters* (GL032433, in press).

Laurion, I., Vincent, W. & Lean, D.R.S. 1997. Underwater ultraviolet radiation Development of spectral models for northern high latitude lakes. *Photochemistry and Photobiology* 65: 107-114.

Lean, D.R.S. 1998. Attenuation of solar Radiation in Humic Waters. In: D.O. Hessen & L.J. Tranvik (eds.), *Aquatic Humic Substances: Ecology and Biogeochemistry.* Germany: Springer, 109-124.

Mackay, J.R. 1992. Lake stability in an ice-rich permafrost environment: examples from the western arctic coast. In: R.D. Robarts & M.L Bothwell (eds.), *Aquatic Ecosystems in Semi-Arid Regions: Implications for Resource Management.* Saskatoon: Environment Canada, 1-26.

Pienitz, R., Smol, J. & Lean, D. 1997. Physical and chemical limnology of 59 lakes located between the southern Yukon and the Tuktoyaktuk Peninsula, Northwest Territories (Canada). *Canadian Journal of Fisheries and Aquatic Sciences* 5: 330-346.

Perdue, E.M. 1998. Chemical Composition, Structure, and Metal Binding Properties. In: D.O. Hessen & L.J. Tranvik (eds.), *Aquatic Humic Substances: Ecology and Biogeochemistry.* Germany: Springer, 41-61.

Rasmussen, J., Godbout, L. & Schallenburg, M. 1989. The humic content of lake water and its relationship to watershed and lake morphometry. *Limnology and Oceanography* 34: 1336-1343.

Rühland, K., Smol, J., Wang, X. & Muir, D. 2003. Limnological characteristics of 56 lakes in the Central Canadian Arctic Treeline Region. *Journal of Limnology* 62: 9-27.

Scully, N.M. & Lean, D.R.S. 1994. The attenuation of ultraviolet radiation in temperate lakes. *Ergebnisse der Limnologie* 43: 135-144.

Teichreb, C.J. 1999. *Effects of dissolved organic carbon as a bacterial growth substrate and as an ultraviolet-B radiation sunscreen for aquatic microbial foodwebs in Mackenzie Delta lakes, Northwest Territories*. M.Sc. Thesis. Simon Fraser University.

Thomas, J. 1997. The role of dissolved organic matter, particularly free amino acids and humic substances, in freshwater ecosystems. *Freshwater Biology* 38: 1-36.

Identification of Permafrost Landscape Changes Caused by Climate Variability in Central Siberia

Marina Tishkova
Institute of Environmental Geoscience, Russian Academy of Sciences
Sergey Gorshkov
Moscow State University named after M.V. Lomonosov

Abstract

The functioning of natural and natural/man-made ecosystems is impacted by changes in the duration of seasons more than by rising temperatures. Modeling changes in permafrost conditions caused by climate variability requires identifying the types of permafrost landscapes in terms of their sensitivity to climate changes, as well, as studying transformation rules for specific natural complexes. A large amount of data on changes occurring in the lower reaches of the Stony Tunguska River was gathered during field work of 1999–2007. For further analysis, active processes were classified as short-period and long-period, and as local and regional. Landscapes were classified by sensitivity level. Degradation of permafrost landscapes will occur in the order of sensitivity classes. Study of the most sensitive landscapes will be the most interesting for further research and yield the greatest value for monitoring.

Keywords: permafrost; Central Siberia; climate change; permafrost degradation; sensitivity.

Introduction

Woodwell and Mackenzie (1995) suggest that the Earth's climate is not just changing from one equilibrium to another, but probably is moving towards an unbalanced state, which we may already observe each year in the form of catastrophic climate events (Tchebakova 2006). The area of study (Fig. 1) is the low western edge of the Central Siberian Plateau in the lower reaches of the Podkamennaya Tunguska River. It is located in the periphery of discontinuous permafrost in the middle taiga subzone and thus is in an area vulnerable to climate change. The area presents a prime example of landscape ecotone diversity. Changes in many climate and landscape characteristics are evident, and we have been monitoring them in the course of our multi-year observations. In this paper, we discuss instability while recognizing that it is difficult to predict the patterns and rates of change. In order to predict changes in permafrost conditions in the current climate, it is necessary to identify types of permafrost landscapes in terms of sensitivity to climate change. It also is important to study the rules or mechanisms of transformation, patterns of landscape and climate change, and the individual and collective processes for specific natural complexes.

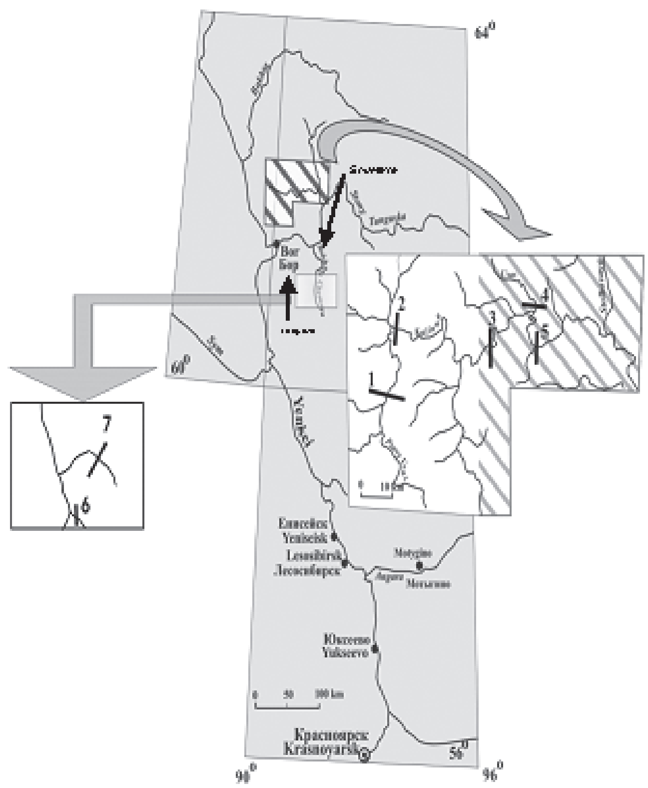

Figure 1. Key areas and transect locations on rivers: (1) Pravy Usas; (2–4) Kulinna; (5) Usas; (6) Bol'shaya Kolonka; (7) Malaya Kolonka; and (8) Bol'shaya Chernaya.

Methods

The methods that we used can be divided into two main categories: evaluation of meteorological data and collection of field data on terrain characteristics.

Meteorological data were evaluated using a range of applied methods. We used air temperature, precipitation, and snow cover data from the weather stations Bor, Vorogovo, Baikit, Yartsevo, and Bakhta. Data are available mainly from the 1980s on, and in some cases from the late 1960s onward. All these locations have high-quality meteorological stations operated by trained personnel. Annual, monthly, and daily data were analyzed using standard statistics tools, such as differential-integral curves, probability/frequency curves, correlation coefficients, etc.

To evaluate the changes in temperature and precipitation over the last 60 years, their time series were approximated by a linear function of $y = ax + b$ type, where y was the value of temperature (precipitation); *a* and *b* were empirical coefficients calculated using the least square method; and *x* was the year. The statistical confidence level was calculated by student criterion. A trend was considered to be statistically significant if the significance level (*P*) was equal to or greater than 0.95.

Landscape responses to the changing climate were evaluated through three main stages. First, we performed a preliminary analysis of satellite images for key areas overlaid with geological, forestry, geomorphology, topography, and fire distribution maps. Second, based on the above, we made our prognosis about the sensitivity of particular landscapes. Third, we confirmed our assumptions by actual field observations. This work was performed using ArcGIS software and GPS instrumentation in the field.

An important element of this combinational method was sampling along landscape transects. The sampling included terrain-unit descriptions, identification of reference soil catenas, detailed descriptions of soil, and measurement of active layer thickness and depth to the top of permafrost using a ground auger. Permafrost and non-permafrost landscapes were differentiated through direct observation using various indicators. Special attention was given to studying rock streams (kurums) and blockfields due to their high information value. In active rock streams we counted the abundance of blocks in an unstable position; in inactive blockfields, we studied forest/vegetation covers and the characteristics of tree stands (percentage of trees in non-vertical positions, the character of tree stand abnormalities, etc). Ground-auger measurements sometimes were of reduced quality, because not all of them were made in survey pits (used as control points for building transects) and many were made from the surface, and thus, liable to some error. Most of our survey pits were dug to the top of permafrost. During the latest field season, we also used temperature loggers but they provided clearly wrong data due to installation mistakes, so we did not use any of those data in our analysis.

Results

Climatic changes

As shown in the Synthesis Report on Climate Change 2001 (Watson et al. 2003), 1980 was an inflection point for positive temperature anomalies in relation to the average temperatures for the period of 1961–1990. Analysis of winter and summer temperatures and precipitation in the northern part of the Central Siberian Plateau shows that during 1980–2000, winters became 1°C warmer in comparison to the period prior to 1980. South of latitude 56°N, especially in the mountains, warming was even more significant, up 2–4°C. Summer warming proved to be as significant as the winter warming (1°C) with a high confidence level and the same scale on the south and on the north (Tchebakova 2006).

The linear trend of air temperatures in the area studied is positive for the past 60 years (data from the Bor village, latitude 61°35′N) (Fig. 2). A considerable increase in annual temperatures started in 1980, and in 1995 the anomaly exceeded a record 3°C. The most significant changes

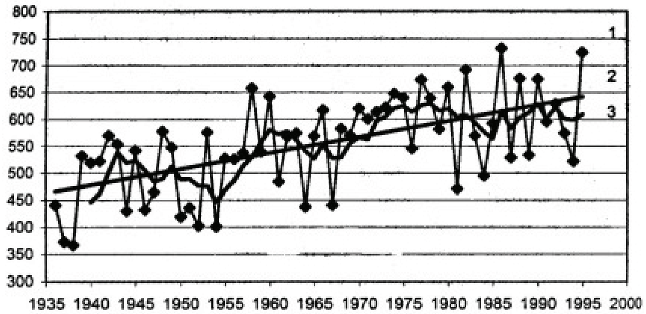

Figure 2. Precipitation at Bor meteorological station: 1 – annual precipitation, 2 – linear trend, 3 – 5-year moving average.

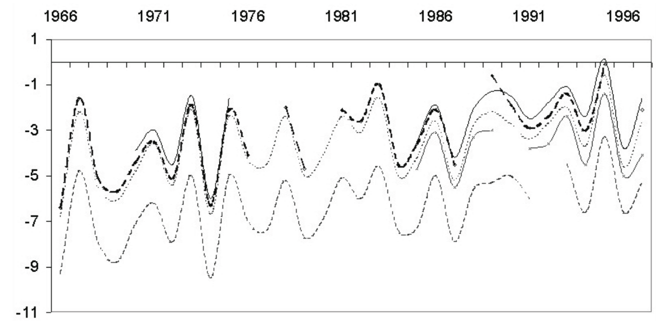

Figure 3. Annual average air temperatures (°C) at Vorogovo, Bor, Bakhta, Baikit, Yartsevo stations.

have occurred during the past 15 years. Analysis of winter (December to March) temperature changes over the past 60 years shows that December temperatures have risen by 3.5°C, and March temperatures have risen by 2.6°C, indicating that winters have become shorter and warmer. Analysis of summer temperature changes also reveals an increase in July and August temperatures. The trend is statistically significant (*P*=0.997 and 0.995 for July and August, respectively). On average, for the time period under consideration, July temperatures rose by 1.9°C, and August temperatures, by 1.1°C. No tendency was observable for June, and May temperatures became somewhat lower. Therefore, winter warming has been more significant than summer warming. A similar situation occurred in the latter half of the 19th century, when contemporaries observed winters becoming essentially less severe, and thawing happened more often (Fedorov 1991).

Annual precipitation for the last 60 years also showed a positive, statistically significant (*P*=0.999) trend, which was even more pronounced than the temperature trend (Fig. 3). The average increase in precipitation was 141 mm. It can be inferred, that this increase was caused by a rise of cyclone activity, especially in the last 20 years of the 20th century. The same process leads to air temperature rises. It should be noted that similar changes of general atmospheric circulation have been traced for the middle latitudes in the European part of Russia (Klimenko 1994). Thus, these changes can be considered global.

Snow accounts for only about 40 per cent of the total annual precipitation (which is 580 mm). There are no apparent trends for changes in snow cover depths.

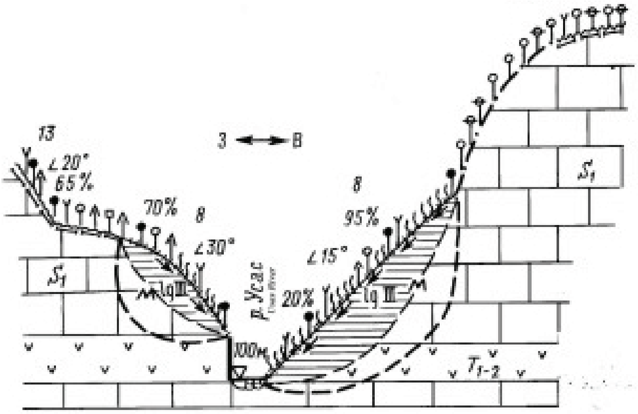

Figure 4. Transect on the Usas River near its mouth.

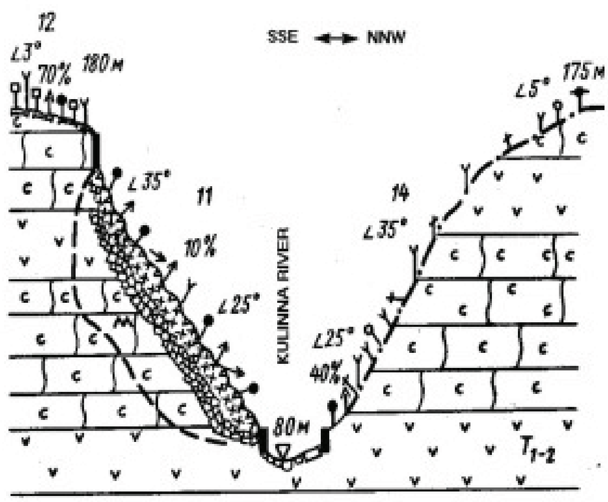

Figure 5. Transect on the Kulinna River near its third line of rapids.

Landscape responses

A large amount of data on changes in Siberian ecosystems was gathered during our field trips between 1999 and 2007. Two representative transects across the valley of the Usas and Kulinna rivers (tributaries of the Bol'shaya Chernaya River), which were sampled during 1999–2003, are shown in Figures 4 and 5.

The Bol'shaya Chernaya River transect crossed the valley with a strongly pronounced hummock swamp under stunted fir-birch taiga with sporadic larch. Hummocks were up to 50 cm in height and covered with true mosses. The depth to the top of permafrost reached 1.05 m under hummocks, and 80 cm under pits, measured from the water surface. This is abnormally deep for such conditions. Evidence of solifluction was abundant on this transect, including at a site by a small creek where soil was probed to a depth of 1.5 m without reaching the top of permafrost.

Observations in rock streams (kurums) on the left bank of the Bol'shaya Lebyazhy'a River about 50 m down from the mouth of the Malaya Lebyazh'a River showed that large rock streams were extremely warm and low in moisture content. At the same time, bi-valley frozen gentle slope deposits (along a zone of a river accumulation that are flooded during the spring floods, and where slope deposits are overlaid with alluvial silts and sands) and hanging bogs kept their permafrost even though it was found at different depths: from the normal depth (0.5–0.7 m) to 1.5 m or deeper. On the whole, data from this and other transects indicate that the top of permafrost has been moving down quite rapidly almost everywhere. Only small areas of bi-valley slope deposits, and hanging peat bogs do not show any signs of permafrost degradation.

During the last observation period, especially recently (in 2006–2007), degradation of cryogenic processes has been clearly tracked in rock streams (kurums). They have been drying out and losing ground ice. In the valley of the Kul'emka River, rock streams have been moving and joining with bottom boulder perluvium, which has a paragenetic connection with rock streams. A similar situation has been observed on the Shumikha River, where a semi-closed rock stream in a birch forest has been joining with an open rock stream on the left cold slope of the river valley.

Systematization of long-term field data shows that with further climate changes, the processes that are already active will only intensify. For further analysis of these processes, we classified them as short-period (fast processes) and long-period (slow), and as local-scale and regional-scale (Table 1).

All these processes manifest an initial response of landscape to climate changes. These primary responses, in turn, will cause secondary changes. For example, the number and the area of forest fires will noticeably increase, vegetation will reorganize, forest/steppe border will shift, the phenological environment will change (which, according to Tchebakova, will affect seed-bearing cycles, cause explosive increases in the numbers of some insects, etc). If the speed of climate change exceeds the adaptive capacity of ecosystems, it will cause a restructuring of all forest hierarchic levels from zonal forests and forest ecosystems to forest forming tree species and populations (Tchebakova et al. 1995, Tchebakova & Parfenova 2003, Tchebakova et al. 2005).

Next Steps

The next steps in our research will include the following:

1) Analyze river run-off data from weather stations and river stations in Bratsk, Boguchany, Motygino, Yeniseisk, Yartsevo, Severoyeniseisk, Vorogovo, Bor, Baikit, Vanavara, Bakhta, Verkhneimbatskoye, Turukhansk, and Tura. These data will be compared with extreme event data, which will make it possible to identify a general rhythmicity of the aggravation and weakening of adverse and catastrophic natural events that reduce the ecological potential of Central Siberia.
2) Evaluate the lowering of the top of the permafrost table and of the process's dependence on particular characteristics of specific terrain units.
3) Select geologic cross-sections with dated syngenetic permafrost structures for detailed documentation and testing. It is necessary to determine the age of permafrost

Table 1. Primary landscape responses to climate warming.

	Short-period	Long-period
Local-Scale	Rock streams (kurums): increase in number of unstable blocks, and increase in number and area of reindeer moss patches left by irrecoverable loss of ice; Rock streams: significant warming of deposit after its water content decreases; Abnormally frequent falls of trees that have creeping root system. Usually it occurs in over-wetted clay soils of visco-plastic consistence and thicknesses of 1.5 m or more; Replacement of solifluction material movements in the lower part of accumulative glacial deposits with local landslide-land creep.	Rock streams : the top of permafrost is going deeper; Rock streams advance towards valley floor as a result of landslide shifts; Solifluction intensifies, especially in areas where slope deposits are in a frozen state and where the thickness of the active layer increases; Drainage improvement on top surfaces and on adjacent gentle slopes (water has disappeared in many pit-ruptures and is often absent in crack-ruptures); General landscape changes with a prevalence of depressive forms which leads to formation of thermokarst lakes; Depletion of underground watercourses under rock streams; Appearance of young fir forests on completely or partially burned out taiga that previously consisted of other tree species.
Regional-Scale	Drying of rock streams. To some degree, drying is also seen in swamped cryogenic-taiga terrain units (e.g., stows, or homogeneous geological and hydrogeological condition).	Thermokarst processes intensify; Wide development of long-frozen rocks which can be evidence of recent permafrost degradation; Solifluction intensifies; The active layer goes down deeper.

(Holocene or Pleistocene) in Central Siberia. This will drive forecasting events resulting from permafrost thawing.

4) Revisit sampling sites.
5) Create a map of permafrost landscapes ranked by sensitivity to climate changes, showing the increased depths to the top of permafrost. This map should also show the estimated times when permafrost will thaw down dozens of meters and cease to impact surface landscapes.
6) Integrate with SEARCH (monitoring of landscape and biological changes as a result of climate change) and TSP (temperature data gathering and evaluation) programs.

Conclusions

Based on the data gathered, landscapes of the region studied can be classified by sensitivity level, where sensitivity is a function of the rate at which landscapes respond to climate change. A slower response indicates a lower sensitivity of the landscape to change.

The *most sensitive* landscapes are terrain units (natural complexes) of "warm" gentle slopes (2–3°) and glacial-related deposits, and low (200–250 m) apical plains, including rock streams. These landscapes are mainly located north of the Podkamennaya Tunguska River. It is an area of Pleistocene moraine and glacio-lacustrine deposits (fine sands, aleurites, loams, and clays). Solifluction in this area is well pronounced. At the end of the summer (1995–1997), the thickness of the active layer did not exceed 0.9–1.0 m; however, during the same period of 2001, the active layer became more than 1.2–1.3 m thick. Thus, there has been a noticeable growth in the depth of the active layer over a few years.

Less sensitive are landscapes of "cold" slopes and slope-related deposits, glacial floodplains, and open rock streams of warm slopes. Mountain and headwater floodplains consisting of slope wash-off material and floodplain alluvial deposits are often swampy, sometimes hummocky, and support dwarf-birch and meadow-bog vegetation growing on alluvial-colluvial bog and meadow-bog cryogenic soils. They are modeled by solifluction and fluvial processes (valley solifluction, alluvial fragment accumulation, bank fragment shifts, and subsiding channel erosion).

The *least sensitive* are multi-factorial permafrost terrain units of cold slopes, including "hanging" peat bogs and forested floodplains of major rivers. "Hanging" bogs are located on moderately steep to steep (25–35°) slopes on hummocky traps and skarns, covered by rock streams and permafrost bogs. Vegetation there consists of scattered trees, alternating with thin cedar pine-spruce-larch forest ("drunken forest"). Our measurements of permafrost depths in "hanging" bogs and floodplains did not show any changes of active layer thickness during the past few years.

We predict that the degradation of permafrost landscapes will occur in the order of the sensitivity classes. The most sensitive landscapes will be the most interesting to study in the course of further research, as they are changing the most rapidly, and their changes will enable us to characterize climate dynamics. The most sensitive landscapes will also yield the highest monitoring value.

Our research showed that it is not annual temperature increases as such, but rather a modification in season durations (changes in intra-annual climate patterns), as well as sharp intra-season fluctuations of temperature and precipitation regimes, which have the greatest impact on the functioning of natural and natural/human-made ecosystems. A rapid downward movement of the permafrost table (5–15 cm/yr) has been occurring since the late 1990s. Permafrost has been moving deeper in most permafrost landscapes. With the depth of the active layer increasing, both solifluction and thermokarst formation have been activated. “Warm” permafrost degrades and rock streams undergo transformation.

Dry and hot weather during the spring season, and followed by severe frosts and different weather fluctuations, which that are not typical for the region with its continental climate, can cause chronic crop setbacks. These in turn influence animal populations. Progressive permafrost degradation can also cause additional emissions of greenhouse gases into the atmosphere and impair biodiversity.

Some of the least sensitive terrain units have not shown any response to climate change yet. However, the processes mentioned, especially solifluction, appear to be a large-scale response to global climate change. It can be considered as a trigger for other natural processes.

If climate change continues at the current rate, it is possible that low-productivity permafrost landscapes will be replaced with highly productive non-permafrost landscapes. With regard to the area of permafrost transition in the zone we studied, this will not cause an ecological disaster, although impacts of such landscape reformation throughout the permafrost zone has not been studied yet.

The work performed is necessary for a comprehensive evaluation of the current and future situation and for the scientifically proven management of natural and natural/man-made systems, consistent with the concept of sustainable development. For the full-fledged and full-scale implementation of what we have intended to do, it is necessary to integrate our research with similar international programs, such as SEARCH and TSP.

Aknowledgments

The research has been performed as part of RFBR Project No. 07-05-00815.

References

Climenko, V.V., Fedorov, M.V., Andreichenko, T.N. & Mikushina, O.V. 1994. Climate on the border between centuries. *Vestnik MEI, N. 3.*

Fedorov, A.N. 1991. *Permafrost landscapes of Yakutia: methods of detection and questions of mapping*. Yakutsk, 140 pp.

Gorshkov, S.P. 2001. First signs of response on the climate warming in periphery of permafrost zone, Central Siberia. *1st European Permafrost Conference, Rome, March 26–28, 2001. Abstracts, 16.*

Gorshkov, S.P. 2006. Prognosis of landscape dynamics in conditions of possible climate change for the lower reaches of the Podkamennaya Tunguska river. In: *Modern Changes in Lithosphere Under the Influence of Natural and Anthropogenic Factors*. Moscow: Nedra, 151-156.

Gorshkov, S.P., Dobrynin, D.V. & Tishkova, M.A. 2001. The resistance of permafrost landscapes to the climate warming in periphery of permafrost zone of Central Siberia. *1st European Permafrost Conference, Rome, March 26–28, 2001. Abstracts:* 24-25.

Gorshkov, S.P, Karrash, H. & Paramonov, A.V. 1998. A geomorphological indication of permafrost and non-permafrost landscapes in the middle taiga in Central Siberia. *Geomorphology* 4.

Gorshkov, S.P. & Tishkova, M.A. 2003. Landscape indication of permafrost degradation in Central Siberia. *Research and New Information*: 43-44.

Gorshkov, S.P. & Tishkova, M.A. 2000. Studying the response of permafrost ecotone to the climate warming (on the example of Central Siberia). *Problems of Regional Geoecology*. Tver, 44-46.

Gorshkov, S.P., Vandenberghe, J., Alexeev, B.A., Mochalova, O. I. & Tishkova, M.A. 2002. *Climate, Permafrost and Landscapes of Middle Yenisei Region*. Scientific edition, Faculty of Geography, Moscow, 96.

Tchebakova, N.M. 2006. *Possible Transformation Of Siberia Vegetation Cover Under Different Scenarios Of Climate Change.* Krasnoyarsk, 60 pp.

Tchebakova, N., Monserud, R., Leemans, R. & Nazimova, D. 1995. Possible vegetation shifts in Siberia under climatic change. In: J. Pernetta, R. Leemans, O. Elder & S. Humphrey (eds.), *Impacts of Climate Change on Ecosystems and Species.* Gland, Switzerland: IUCN, 67-82.

Tchebakova, N. & Parfenova, E.I. 2003. Stand growth and productivity of mountain forests in southern Siberia in a changing climate. In: A. Amaro, D. Reed, and P. Soares (eds.), *Modelling Forest Systems*, Chapter 17.. Wallinford, UK: CAB International, 189-197

Tchebakova, N.M., Rehfeldt, G.E. & Parfenova, E.I. 2005. Impacts of climate change on the distribution of *Larix spp*. and *Pinus sylvestris* and their climatypes in Siberia. Mitigation and Adaptation Stragegies for Global Change. http://dx.doi.org/10.1007/s11027-005-9019-0.

Tchebakova, N.M., Rehfeldt, G.E. & Parfenova, E.I. 2005. Redistribution of vegetation zones and populations of Larix sibirica and Pinus sylvestris in Central Siberia in a warming climate. In: *Proc. of Canadian Tree Improvement Association. 29th Biennal Meeting "Climate Change and Forest Genetics". Eds. G.A. O'Neill and J.D. Simpson. Kelowna, British Columbia. Canada:* 25-42.

Watson, R.T. & the Core Writing Team (eds.). 2003. *Climate Change 2001: Synthesis Report.* Cambridge, UK: University Press, 398 pp.

Woodwell, G.M. & Mackenzie, F.T. (eds.). 1995. *Biotic feedbacks n the global climatic system. Will the warming feed the warming?* 416 pp.

Permafrost in Low Mountains of the Western Chukotka Peninsula

Sergey Titkov
Geological Research Institute for Construction, Moscow, Russia
Vladimir Chernyadyev
Geological Research Institute for Construction, Moscow, Russia
Maria Tsvetkova
Geological Research Institute for Construction, Moscow, Russia

Abstract

The study region is located in the northwest part of the Chukotka Peninsula in the zone of continuous permafrost. Permafrost thickness is from 120–250 m in river valleys and up to 300–350 m on slopes and watersheds. Mean annual ground temperatures are between -4°C and -6.5°C. The ice content of Late Pleistocene-Holocene syncryogenic alluvial, deluvial, eluvial, or solifluction deposits covering the river valleys and slopes is 50%–60%. These types of deposits are characterized by massive fossil ice layers with a typical thickness of 0.5–3.0 m and total area of a separate ice massif up to 30,000 m^2. Thermokarst hollows up to 30 m in diameter are located on sites where the ice surface is less than 1.5 m beneath the ground surface, thus indicating the disposition of the ice body. Frost cracking and frost sorting results in the formation of kurums and patterned ground, such as stone rings and stone stripes that move slowly down slope.

Keywords: continuous mountain permafrost; frozen dam; massive ice layers; patterned grounds; thermal regime of permafrost; thermokarst.

Introduction

A problem of safety in the exploitation of water-engineering systems is especially important in the permafrost zone. The reliability of constructions strongly depends on the consideration of engineering-geological conditions (Biyanov 1983, *Water-Engineering Systems* 2005). Engineering-geocryological investigations in 2007 were carried out in the vicinity of the gold deposit "Mayskoe" at the site of the projected dam for a future water reservoir in order to obtain sufficient data for projecting and construction of the ground dam, pump station, and water pipeline in the zone of continuous permafrost. The study region is widely exploited as a stanniferous and gold-bearing province. Numerous geological expeditions carried out geological exploration in different points of the region (*Engineering Geology of the USSR* 1977, *Geological map of the USSR* 1979, *Chukotka…* 1995.*)*, but it is very poorly investigated by geocryologists. Permafrost researches under similar conditions of low mountains were held in Northern Yakutia (Shur 1988, Kanevskiy 2003).

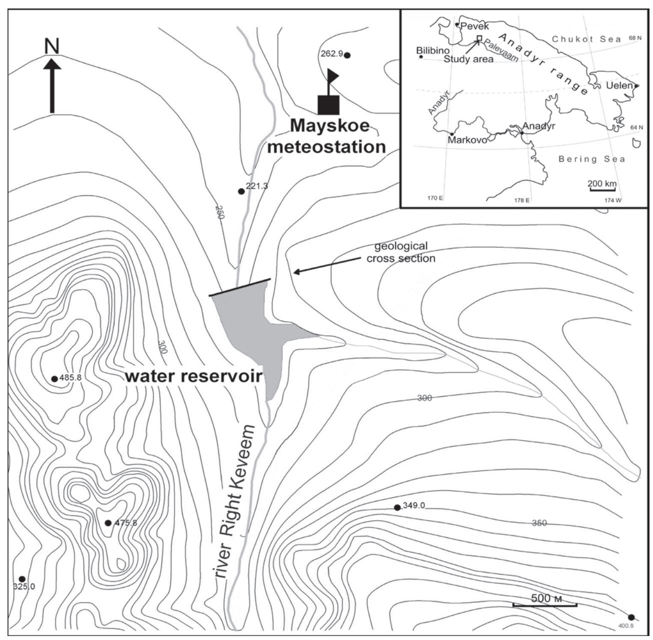

Figure 1. Sketch map of the study area.

Study Area and Methods

The gold ore deposit is located within the Chukotka uplands in the northwest part of the Chukotka Peninsula (68°50′N, 173°40′E) in the northern part of the Anadyr Range, 187 km southeast of the regional center Pevek (Fig. 1).

The study area is situated on a local divide between the rivers Keveem, Pegtymel, and Palevaam, and is characterized by low-mountain relief with gentle slopes and flat watersheds of absolute elevations up to 600 m. Mountain tops rise about 150–250 m above river valley bottoms.

The river valley network is young and has a poorly developed structure. Traces of Late Pleistocene glacial erosion and accumulation are expressed in the presence of exaration and fluvioglacial landforms. The study area is located near the source of the river Right Keveem. The river and its tributaries have fast flow; channels abound with bars and are frequently meandering. The mode of water-flow is extremely changeable in time and depends, basically, on the precipitation regime. The nearest large waterway is the river Palevaam 20 km south of the deposit. During the winter period, it freezes completely as well as other streams and keeps underground runoff along talik zones.

During the engineering-geocryological research, 57 bore holes 20 and 30 m deep along 6 profiles covering the dam and contour of the future water reservoir were drilled. Geophysical investigations revealed linear zones of fractured bedrock located in the vicinity of the projected dam. Laboratory tests of frozen core samples were held to determine physical, mechanical, and thermal physical properties of loose material and solid rocks. The forecast evaluation of the dam and bed of the reservoir has been carried out. The engineering-geocryological map at a scale of 1:2000 has been compiled based on the results of investigations.

Results

Climate

The climate of the area is determined by its location in the northeast of Asia, in the zone of influence of two oceans with the complex atmospheric circulation differing in cold and warm season. The climate is Arctic, transitive from moderately continental to continental. Mean annual air temperature according to the data of the meteorological station "Mayskoe" (~1,5 km north of the site) for the period of 1982–1991 is -13.7°C. The air temperature absolute maximum is 29.5°C in July, and absolute minimum is -45°C in February. Average temperature of July is 9.3°C, that of January -27.8°C. The annual amplitude of average monthly air temperatures is 37.1°C. Winter is long and cold, with strong snow storms, summer is short and cool, but warmer by 7°C than at the coast of the East-Siberian Sea. The positive average monthly air temperature lasts no more than 3.5 months. The duration of the warm period, both in the air and on the ground surface, is less than 30 days in more than 50% of the years.

The annual precipitation is 262 mm and about 60% of this amount is snow. The average thickness of the snow cover depends on surface relief and does not exceed 0.7 m on flat sites. In the rear parts of cryoplanation terraces, in river valley bottoms, and on leeward slopes the snow cover thickness is 2–3 m and more. The snow cover is established in the middle of September and disappears in the end of May. Snow cover density reaches 0.35 g/cm^3. The wind regime is rigid; the average annual wind speed is 3.5 m/s, with maxima in squalls reaching 40 m/s; the annual number of days with a wind speed higher than 15 m/s is 46.

Geological structure

Loose deposits of interstream areas are comprised of eluvial-deluvial and deluvial-solifluction formations, overlapping slopes, and tops of watersheds with a continuous cover. Loose deposit thickness varies from tens of centimeters on narrow watersheds to up to 15–20 m in places where slopes merge into river valleys. The petrographic structure of these sediments is similar to the bedrock. Gradual transitions of one genetic type to another are marked. All types of deposits were formed during the Holocene period (Q_{IV}), except for the bottom layers of eluvial and alluvial sediments, which are of Late Pleistocene age (Q_{III}). According to the analysis of spores and pollen, the most ancient horizons of deposits were generated in the Late Pleistocene interglacial.

Holocene fluvial sediments (aQ_{IV}) are comprised of alluvium of river beds, flood plains, and the first terraces in rivers and brook valleys of 2–3 orders and consist mainly of blocks of a different degree of roundness (up to boulders), gravel and pebble of different size, sand and a sandy-loam material with lenses of peat and ice. The thickness of alluvial layers is 1.5–3.5 m.

Holocene eluvial-deluvial sediments (edQ_{IV}) are developed most widely on gentle spaces of watersheds and flat (1°–3°) slopes. They consist of rubble from 5% up to 30%-40%, or gruss with a sandy-loamy fill (up to 50%-80%). In the direction towards the central part of valleys, the abundance of rubble is reduced up to 5%–10%. The thickness of eluvial-deluvial deposits is 10–15 m in valley boards and 1–2 m in river bed parts of valleys.

Deluvial (dQ_{IV}) and deluvial-solifluction (dsQ_{IV}) deposits are developed on slopes of watersheds with gradient more than 3°. They are presented by blocks, rubble, or gruss with a sandy-loamy fill. The thickness of deluvial deposits is 1–5 m.

Deluvial-colluvial deposits (dcQ_{IV}) are located on slopes of river terraces and erosive benches having a gradient of more than 10° and comprised of sandy loam and loam with a proportion of rubble and gruss of about 30%–50%. The thickness of deluvial-colluvial deposits is up to 2.5 m.

Eluvial deposits (eQ_{III-IV}) underlay the above listed genetic types everywhere and overlay Triassic sandstones and aleurolites. The thickness of continuous cover eluvial deposits is between 1.5 and 7 m. They are comprised of coarse ground with loam and sandy loam; the rubble content is about 30%–40%, and the gruss content about 10%–20%.

Geocryological conditions

The study area is located in northern geocryological zone and characterized by continuous permafrost. The thickness of permafrost is 120–250 m in river valleys; at transition to slopes it increases up to 300–350 m and more, and reaches the greatest values on watersheds (Geocryology of the USSR 1989). The mean annual ground temperature (MAGT) at the depth of 10–12 m is between -4°C in valley bottoms down to -6.5°C on surrounding slopes. The ground temperature on ridges naturally goes down to 7.5°C–8.0°C. Highest temperatures are characteristic for slopes of a southern exposition and the bottoms of valleys. Outside of talik zones, the snow cover is the most essential influence on MAGT; a thick snow cover results in a rise of ground surface temperature by 5°C–6°C in comparison to snowless sites.

Measurements of temperatures in boreholes 3 and 10 in an axial part of the future dam have demonstrated that the

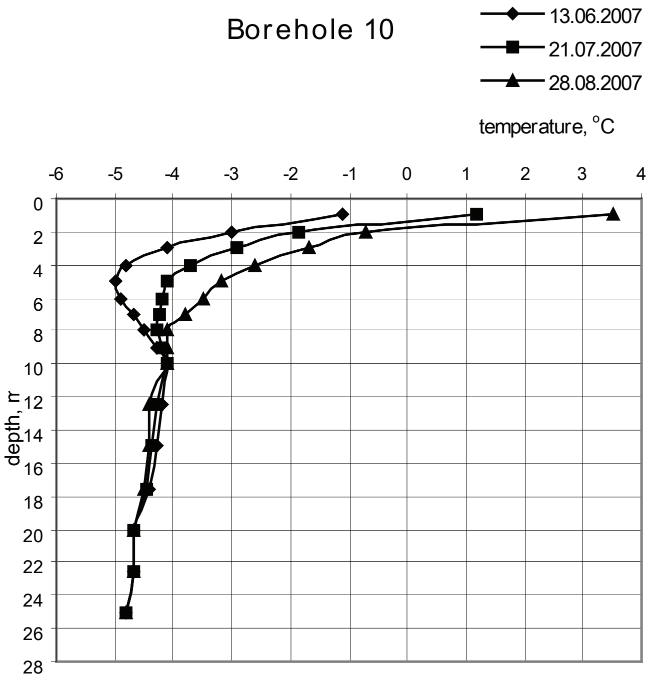

Figure 2. Ground temperature in Borehole 10.

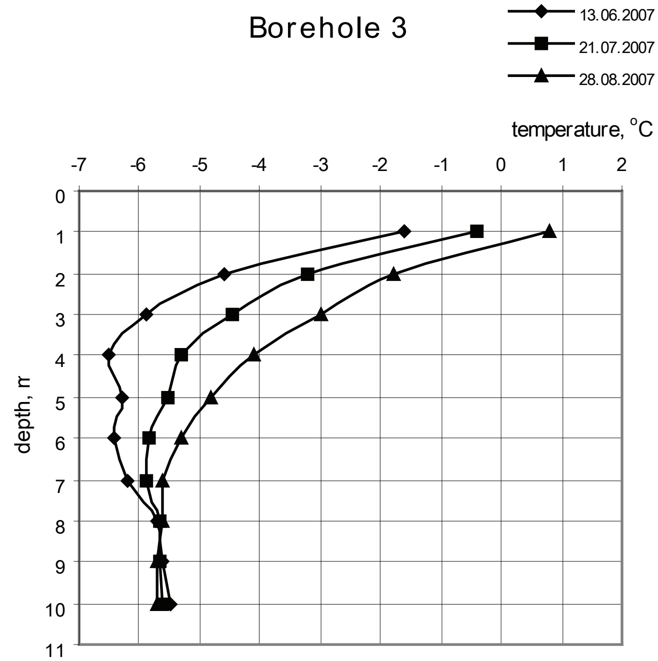

Figure 3. Ground temperature in Borehole 3.

highest MAGT at the depth of 10 m (-4.1°C) is found in the bottom of the river Right Keveem valley in Borehole 10 (Fig. 2).

The ground temperature on the left side of the valley slope was -5.5°C in Borehole 3 (Fig. 3) and -6.5°C on the right side of the valley.

Active layer depth varies from 10–15 cm on sites with thick moss and peat cover to 70–80 cm under swampy areas. At foots of slopes composed of coarse deposits as well as under streamlet beds, active layer thickness is 2–3 m and more.

In a vertical section of frozen ground epigenetic deposits prevail. The characteristic feature of weathered bedrock is its low ice content not exceeding 15%. The average ice content of fissured aleurolites is 5%–6%, decreasing to 1% in monolithic, low-fissured sandstones. The ice content increases up to 10% in strongly fractured aleurolites and argillites where cracks are filled with ice and in sandy-loamy ice-rich ground. Cryogenic structures of the bedrock are massive and crack-like.

Fine-grained deposits contain usually coarse material (up to 30%–40%), and have massive and massive-crust-like cryogenic structures. The ice content does not exceed 10%–15%. Rocks are completely frozen except in separate, localized, fractured, water-saturated zones along tectonic faults.

Late Pleistocene and Holocene deposits are a syncryogenic type of frozen ground formation. These are alluvial, lacustrine, fluvioglacial, swamp, eluvial, deluvial-solifluction and other formations. The ice content often exceeds 50%–60%, and cryogenic structures are lenticular, layered, and recticular.

Loose surface deposits often contain massive ice sheets in the sub-surface. In 2004, drilling in solifluction deposits intersected ice layers that were 1.8–2.0 m thick and had no mineral impurities. The ice sheet was of a layered structure with alternating layers of transparent firm ice and white loose ice 1–2 cm thick. Drilling in 2007 has shown massive ice sheets between 20 cm and 3 m thick occur in an area of about 30,000 m^2 on the left slope of the river Right Keveem valley oriented directly along the axis of a projected dam for a water reservoir (Fig. 4). Ice structure is layered, and the ice contains about 3%–5% fine mineral material.

Massive ice sheets represent, apparently, primary interground ice of segregation-intrusive genesis. They were generated in freezing, water-saturated deposits with constant additional charging by underground water.

Within the limits of the region, permafrost in river valleys has a two-layered structure. In the top part of the section there are friable epigenetic and syngenetic ice-rich and very ice-rich disperse deposits, and in the bottom there is Triassic bedrock frozen epigenetically and having a characteristic, low ice content . The single-layer structure of frozen rock mass is characteristic for epicryogenic bedrock in a mountain part of the region. Cryogenic structures of crack-like type are common for this type of deposit. On highly fissured sites corresponding to zones of constant water saturation before freezing, rocks are characteristic by a high ice content and have crack-vein cryogenic structures. Near the surface, the elevated ice content due to goletz (crust-infiltrated) and segregated ice occurs in most weathered rocks. Crack-like, crust-like, and basal cryogenic structures are most common for this type of deposit.

Numerous cryogenic processes are widely spread in the study area. Frost weathering developed on slopes and watersheds where the snow cover is negligible results in rock destruction and moving of the loose material down slope due

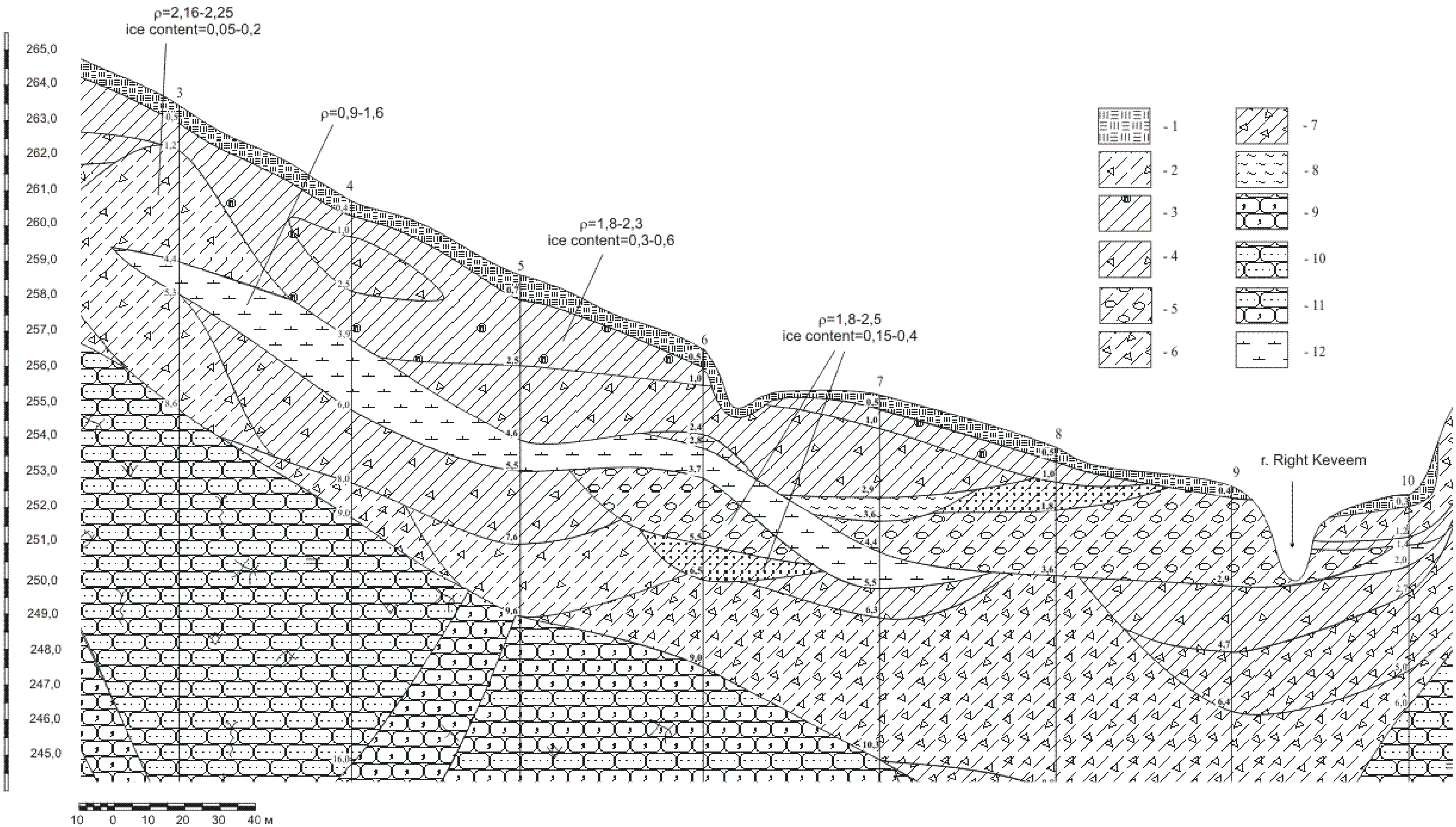

Figure 4. Part of cross section through the left side of the river Right Keveem's valley along the axis of the projected dam. Horizontal and vertical scales in meters. 3… 10 – number of borehole. Lithology: 1 – peat; 2 – sandy-loam with breakstone; 3 – loam; 4 - loam with breakstone; 5 – pebble with sandy-loam; 6 - breakstone with sandy-loam; 7 - breakstone with loam; 8 – silt; 9 – aleurolite; 10 – sandstone; 11 – interleaving of sandstones and aleurolites; 12 – massive ice layer. Ground is frozen from the surface (May 2007).

Figure 5. Stone stripe on the gentle slope surface.

Figure 6. Thermokarst depression – a result of massive ice layer melting.

to active gravitational and deluvial processes. Fine-grained products of the frost weathering accumulate in lower parts of slopes thus forming deluvial and deluvial-solifluction aprons. The surface of slopes is complicated by dells, mud circles, solifluction terraces, and lobes. Dells are the linear hollows 10–12 m wide with flat, swamped bottoms.

On gradual (less than 10°) slopes, solifluction, and deluvial-solifluction slopes, processes of plastic-viscous flow develop. Solifluction occurs in sandy loams and dust-like loams containing sometimes a significant amount of coarse material. The rate of solifluction movement depends on the slope degree, active layer thickness, deposit grain size, etc. Coveral solifluction is a kind of solifluction without surface disturbances when the ground flow is rather uniform and slow. It develops on slopes of 3°–10° and is accompanied by material sorting resulting in the formation of layers of fine and coarse material in longitudinal section.

Frost cracking develops in the active layer and is well defined on the surface in the form of numerous sorted and non-sorted polygons and circles with flat or convex surfaces free of vegetation, 1–3 m in diameter, limited by frost fissures and banks of jacked debris. In non-homogenous friable grounds with a high content of debris (gravel, gruss, pebble), multiple cycles of freezing-thawing result in the frost jacking of coarse material towards the ground surface and its displacement to the fissures located in hollows, thus forming stone rings and polygons. On the slopes, stone rings transform into stone stripes 1.5–2 m wide and 0.4–0.6 m high, divided by convex-plane surfaces covered with turf (Fig. 5).

Thermokarst processes develop by melting out underground ice and ice-rich ground and result in ground subsidence, shallow depressions, and the formation of thermokarst lakes. Thermokarst features are usually closed or semi-closed round-shaped hollows up to several tens of meters in diameter, located predominantly on flat surfaces or gentle slopes. Thermokarst is often caused by the disturbance of natural heat-exchange conditions as a result of technogenic impact or active layer thickness increasing. Thermokarst hollows on the left side of the river Right Keveem valley are connected to the massive ice sheet melting where the ice surface is at a depth of 0.7–1.2 m below the surface (Fig. 6).

The formation of kurums in the study area is a result of a combination of a number of processes. The main factors are cryogenic and gravitational ones. Kurums usually form on deluvial-colluvial slopes of 5°–10° gradient in good conditions of fine-grained material outwash. The thickness of kurums is 1.5–2.5 m, and they consist of clumpy-debris material with sandy-loam fill in the base of the section. This layer is of high ice content, and sometimes lenses of goletz (crust-infiltrated) ice up to 0.5 m thick exist. Kurums move predominantly due to cryogenic creep in the active layer, partly because of plastic deformations of goletz ice in the basal layer.

Discussion

According to the computer modeling, at a constant maximum water level in the future water reservoir, the depth of ground thawing in the upper prism scarp of the dam after one year of operation will be 3.3 m, and by 15 years it will reach 9.9 m. In the seasonal changes of water level in the reservoir assumed by the project, the depth of thawing in the top part of the upper prism scarp will be 1.5 m and should not change during the period of operation while in the bottom part, the depth of thawing will be up to 5.5 m. On the slopes of the lower prism of the dam, the depth of ground thawing during period of operation should remain stable at 1.1–1.5 m.

The depth of frozen ground thawing in the bed of the water basin for 15 years of operation will change from 1.1 m up to 4.9 m. With the presence of ice-rich frozen ground of the relative subsidence 0.2–0.3 (according to engineering-geological researches and laboratory test of frozen ground compressibility in thawing) the total ground subsidence in the water basin bed may be 1.0–1.5 m. It will result in the slipping of the ground of an upper prism and to the infringement of the dam stability. Therefore, replacement of the ice-rich ground to a depth of 1.5–2.0 m is necessary.

During the process of dam and water reservoir construction, the activation of thermokarst, thermal erosion, cryogenic landslides, frost heaving, and frost cracking should be expected.

The most dangerous process in water basin operation is thermokarst. The tendency of global climate warming may lead to the increase of the active layer thickness and, as a result, to the acceleration of massive ice bodies melting (Fig. 6). Thermal subsidence of ice-rich deposits of the water reservoir bed can be up to 1.0–1.5 m.

The activation of frost heaving and frost cracking on the dam surface with low snow cover is possible. It should promote the development of thermal erosion processes during the warm period. To avoid the activation of these processes, predominantly coarse material should be used in the dam construction.

The thermal effect of water filtration through the dam body should be reduced by using a synthetic diaphragm within the dam. It is preferable to erect the dam in the winter time. Additional ground cooling during dam operation should be provided by the application of two-phase hybrid thermosyphons designed so that the dam can be cooled actively as well as passively. As practice shows, installation of air cooling is less effective. Cooling units should be installed on the crest of the dam close to the head race at a distance of 3 m to a depth of at least 15 m. If the dam will be erected in the summer time, freezing thawed ground in the body of the dam using thermosyphons will take one winter season.

For dam stability maintenance, monitoring of the ground thermal regime should be established.

Conclusions

The projected dam for the water reservoir is located in the zone of continuous permafrost. The presence of ice-rich coarse deposits, massive ice sheets, and numerous cryogenic processes significantly complicate conditions of dam construction. The activation of thermokarst, thermal erosion, cryogenic landslides, frost heaving, and frost cracking should be expected in dam and water basin operation.

The dam should be erected in the winter time and supported in the frozen state by two-phase hybrid thermosyphons installed on the surface of the dam near the head race. The complex monitoring of the ground thermal regime should be carried out to provide for the reliable operation of the dam and water reservoir.

Acknowledgments

The authors are grateful to G.P. Pustovoit (Moscow State University) who carried out the computer modeling of the future frozen dam thermal regime dynamics. We also sincerely thank reviewers for editorial assistance and additional language improvement.

References

Biyanov, G.F. 1983. *Dams in the Permafrost Zone.* Moscow: 175 pp. (in Russian).

Chukotka: Natural and Economical Essay. 1995. Moscow: 370 pp. (in Russian).

Engineering Geology of the USSR. Vol. 4. Far East. 1977. Moscow: 502 pp. (in Russian).

Geocryology of the USSR, Vol. 4. Siberia and Far East. 1988. Moscow: Nedra, 516 pp. (in Russian).

Geological Map of the USSR. Scale 1:200 000. Sheet R-59-XXIX, XXX. Geological description. 1979. Magadan: 90 pp. (in Russian).

Kanevskiy, M. 2003. Cryogenic structure of mountain slope deposits, Northern Russia. *Proceedings of VIII International Conference on Permafrost. Zurich.* Philips, Springman, & Arenson (eds.)*:* 513-518.

Shur, Y.L. 1988. *The Top Horizon of Permafrost Strata and Thermokarst.* Novosibirsk: Nauka, 213 pp. (in Russian).

Water-Engineering Systems of Chukotka: Engineering-Geocryological Conditions. 2005. Magadan: 70 pp. (in Russian).

Glacial Ice as a Cryogenic Factor in the Periglaciation Zone of the Composed Rock Glacier Morenas Coloradas, Central Andes of Mendoza, Argentina

Dario Trombotto Liaudat
IANIGLA-CONICET, Mendoza, Argentina
Lucía Arena
Facultad de Matemática, Astronomía y Física, Universidad Nacional de Córdoba, Argentina
Giorgio Caranti
Facultad de Matemática, Astronomía y Física, Universidad Nacional de Córdoba, Argentina

Abstract

The present work focuses on the analyses of glacial ice from thermokarst in relict glacial and degraded Andean permafrost environments (4200 m a.s.l.) in order to reconstruct its environmental or paleoenvironmental history and to understand the processes that generated the Andean rock glaciers. The study area belongs to the Morenas Coloradas rock glacier, situated in the Cordón del Plata (at 33°S approximately), Central Andes, Mendoza, Argentina. An interpretation of the ice samples and an analysis of their internal and crystallographic characteristics is carried out in order to explain the geomorphological and cryogenic history of the landforms. The area of periglaciation—where cryogenic forms are generated—is studied thoroughly. Due to climatic oscillations, these periglacial areas may be identified by thermokarst. The degradation phenomenon helps to build new cryogenic forms like rock glaciers. Different possible environmental scenarios for the genesis of protoperiglacial landforms may be imagined.

Keywords: Central Andes of Mendoza; glacial ice; global warming; periglaciation zone; permafrost; rock glaciers.

Introduction

Rock glaciers, the typical Andean cryogenic mesoforms which characterize creeping mountain permafrost, contain different types of ice that interact with frozen cryosediments, that is to say with sediments of cryogenic origin. From a structural point of view, the types of constitutional ice generally observed are interstitial and segregation ice, but buried massive ice of sedimentary origin is also to be found (Shumskiy 1964, Haeberli & Vonder Mühl 1996). Areas with over 80% of ice (supersaturated permafrost) appear in the structure of the few drillings that have been carried out (Haeberli et al. 1988).

Interstitial ice is a superficial ice found in the first meters of depth in the rock glacier. This kind of ice depends on the diameter of the sedimentary pores which allow for an optimum nucleation of the ice (Van Vliet-Lanoë 1998) and correlates with the size of the particles which induce nucleation (Hobbs' ice, see Anderson et al. 1978), while segregation ice is the kind of ice that creates lenses or layers of few centimeters inside the frozen body (Shumskiy 1964, Trombotto et al. 1999).

But concerning the origin of the ice, periglacial ice is closely linked to different processes (e.g. percolation or regelation), various contributors (e.g. snow, graupel, harsch, or firn) or to other natural manifestations such as glaciers or nivodetritic avalanches. Sedimentary ice in periglacial domain is created mainly by the transformation of snow and graupel which percolate into the open structure of the cryosediments, although snow, harsch, and firn from Andean avalanches also play a decisive role in its creation. This material also incorporates to the frozen sedimentary body of the rock glacier by percolation and burying of the latter under cryosediments. Another origin of the ice is the regelation of glacial ice, after a previous process of melting, which incorporates into the body of rock glaciers as periglacial ice, although the mechanism is fairly unknown.

A parallel process has been observed in the Andes of Mendoza for example, expressed by the fluxion of isolated ice bodies of glacial origin which, favoured by the slope, directly incorporate to the periglacial sedimentary bodies. This is the type of ice we are mostly concerned with in the present work and which shall be analysed and identified, because it contributes to the origin of periglacial landforms.

In general, macroscopical or large scale phenomena may be scientifically interpreted in function of microscopical parameters. In the case of the ice, and as has been shown

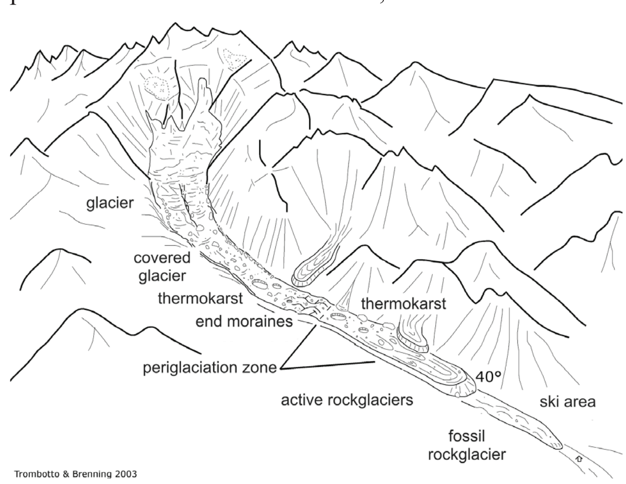

Figure 1. Periglaciation zone.

for glacial ice in thermokarst areas (Arena et al. 2005) microcrystallographical characteristics can be correlated with geomorphological characteristics of the environment in which the ice originated.

This work analyzes ice of a periglaciation zone (Fig. 1), that is to say, an area that used to be glacial and in which periglacial or cryogenic landforms are being generated.

As glaciers retreat to higher altitudes, they leave a large quantity of still frozen morainic or cryogenic sediments behind. At the same time, islands of covered ice may remain. These types of ice, considered 'dead ice' by many authors, are key contributors or perfect natural cryogenic environments for the 'roots' or the genesis of debris rock glaciers. These processes indicate that at the Cordón del Plata, Mendoza, the periglacial level reaches down to 3600 m a.s.l. approximately (Fig. 1). This is a relatively low height considering that 'quasi continuous permafrost' at the same latitude exists only above a height of 4200 m a.s.l. (Trombotto 2000).

The present work also analyzes experimental samples in order to certify natural processes. In particular, microcrystallographical parameters are set up, which allow one to determine whether an ice sample belongs either to regenerated ice of the region close to the active layer, to thermokarst of cryogenic origin (degraded permafrost), or to ancient glacial ice. Moreover, correlations between the mentioned microscopical characteristics and the stress, directions samples underwent in thermokarst, are analyzed. Finally microscopical ice characteristics are linked with environmental and palaeoenvironmental processes.

Study Area

The study area is located in the Cordón del Plata, a mountain range of the Andes of Mendoza. The area is situated between 32°24′S and 33°39′S and 70°14′W and 70°46′W (Fig. 2). The area is glacierized. The Landsat 2000 image reveals glaciers, perennial snow patches, and also snow patches which are mostly considered to be temporary. The entire surface was figured to be 148 km², 119 km² of which correspond to rock glaciers (Trombotto 2003).

Geologically the Cordón del Plata is part of the Cordillera Frontal, limited in the W by the Argentine geological region called Cordillera Principal. In the Cordón del Plata graywacke prevails, sandstone conglomerates from the lower Carboniferous and volcanic rocks of the volcanic Variscian Association of Permian Age. A very important granitico-granodiorhyte batolite as intrusive is associated to the more recent Variscian tectogenesis. The Andean tectonic movement reactivated the entire area during the Tertiary, and it was particularly during that period that sedimentary rocks were deposited as sandstones and conglomerates (Fm Mariño and Mogotes). Three mountain chains may be distinguished in this area: La Jaula in the W, the Cordón del Plata in the central part, to the N and E after which the entire area is named, with El Plata as its highest peak (6310 m a.s.l.), and finally the Cordón Santa Clara in the SW. Taking into account the topographical line of 2000, the study area comprises a surface of approximately 2830 km².

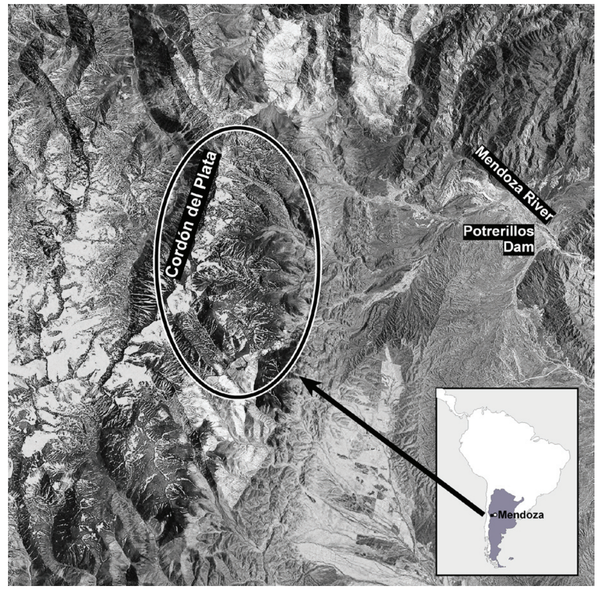

Figure 2. Study area.

The MAAT of the meteorological stations of Aguaditas (1972–1983) at a height of 2225 m a.s.l. and Vallecitos (1976–1985) at a height of 2500 m a.s.l. at its eastern flank are 7.7°C and 6°C respectively. The meteorological station Balcón I at 3560 m a.s.l. on the tongue of a rock glacier at Morenas Coloradas indicates a MAAT of 1.6°C and an annual precipitation between 500 mm (warm period April 2001–April 2002) and 630 mm (1991–1993). The vegetation ranges from shrubs to Andean tundra until 3600 m. Above this height and on rock glaciers vegetation is extremely scarce.

The analyzed ice samples come from a periglaciation zone of the composed rock glacier Morenas Coloradas (with different superposed frozen cryoforms), an area with thermokarst and a detritic cover that varies in thickness between 60 and almost 150 cm. The samples were taken at a height of approximately 4200 m a.s.l. in a tributary valley which unites with the main valley, and where cryosediments meet with the main valley of the composed rock glacier.

Methodology

The natural samples were taken at a glacial valley and rock glacier which are being monitored and investigated at the IANIGLA (Institute of Snow and Ice Research and Environmental Studies) in Mendoza, Argentina, since the 1980s. The extraction of the samples is done by a simple procedure of cutting ice blocks in areas with visible ice. The samples were extracted from two different profiles taken from thermokarst walls perpendicular to each other, according to the imaginary axis of an ovoid (Fig. 3). Before cutting out ice blocks, surfaces were cleaned to a depth of 5 cm. For extraction, blocks or ice monoliths were confectioned in the ice wall. These blocks were carefully oriented according to two fundamental criteria. One is the zenith of the sample itself, in order to identify its positioning within the body of ice, and the other one is the magnetic N of the site, in

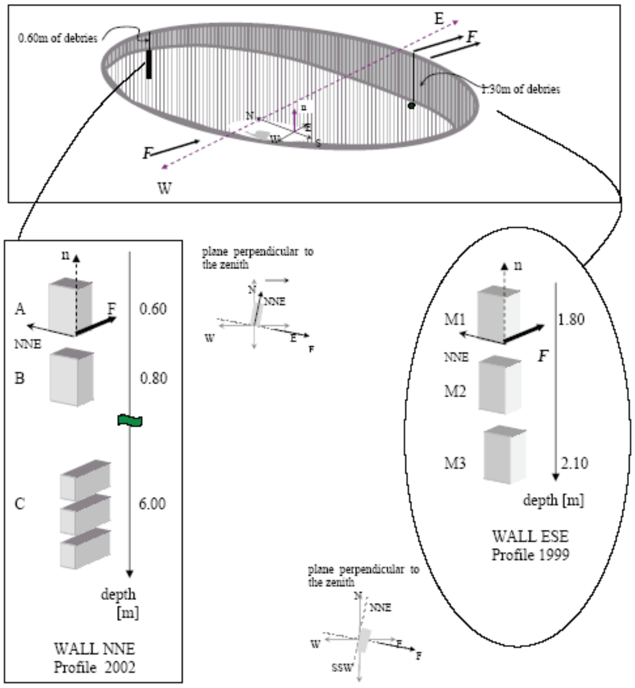

Figure 3. Sketch of thermokarst. F: principal stress, n: zenith.

order to be able to position the entire ice body sampled in the area. The samples were transported to the cold chamber of the LEGAN in Mendoza, where they were classified and preserved at -13°C.

Then thincuts were made of the ice samples, and plastic replicas were created at the University of Córdoba, Argentina. This technique complements the studies of the thincuts and helps to determine size and orientation of the ice crystals, dislocations as well as concentration, orientation and distribution of the bubbles inside the crystals. The method of plastic replication allows the detection of dislocations on the surface of the ice.

Thincuts were made using a xylotome Leitz, model 1400, adapted for ice cuts in the cold chamber. Thincuts were made in the cold chamber of the LEGAN Institute in Mendoza as well as at the University of Córdoba in Argentina. At the same time, laboratory tests of uniaxial statical isothermical compression of the ice core samples extracted from ice from below the base of the active layer of the thermokarst were carried out. These samples, treated in the laboratory, and those extracted from the ice cores and left in natural condition were crystallographically analyzed and compared to each other. It is the aim of these studies to establish a correlation between microcrystallographical and geomorphologically determined characteristics.

Analyzed Ice Characteristics

The most important components of the ice described in the present work are: (1) ice crystals: size and orientation of their C axis, (2) bubbles: areas with bubbles and areas without bubbles. Bubbles are classified into bubbles >50 µm and bubbles <50 µm and microbubbles, (3) defects and dislocations, and (4) presence of particles.

While for the study of the ice crystals (Table I) the size and orientation of their C axis were the important factors, in the case of the bubbles three different types were found and classified as follows:

- Two types of bubbles belong to microbubbles, with a diameter smaller than 0.1 mm
- Another type are macrobubbles with a diameter larger than 0.5 mm

In the first group, bubbles are distinguished according to whether their mean diameter is smaller than 50 µm or larger than 50 µm. This distinction is important because size may influence the migration of the ice crystal edges. If the mean diameter of the bubbles is larger than 50 µm, it was observed that they do not impede or anchor the migration of the grain limit (Arena et al. 1997). The analysis of the bubbles (Table II) in the ice is very important because although some of them may abandon the edge of the grain without producing a remarkable effect, others, if they are small enough, anchor growth of the ice grain. In other cases bubbles of intermediate size may simply slow down their growth. Only at low temperatures and under the phenomenon of isothermic warming in the laboratory, for a long time (over one year), could it be observed that bubbles do not stop the growth of ice crystals.

There are two types of areas considered in the thincuts sections; one was called CB when it contained microbubbles and the other was called SB when it did not contain microbubbles (Table II).

In general (Nassello et al. 1992, Arena 1995) the mean size of ice crystals in areas with microbubbles is smaller, because these anchor the limits of the ice grains. This also occurs in areas with bubbles >50 µm and macrobubbles. It strikes the eye that the bubbles <50 µm are almost spherical while those >50 µm and macrobubbles are not, and thata they can give clues about the main stress directions.

Regarding defects, the density of traces of dislocations holds information for us, for example about the forces of residual stress. The defects were classified into prismatical (P) and hexagonal (H) (Table III). The particles are mainly of mineral and cryogenic origin. They are the product of cryoweathering of cryosediments of glacial or periglacial origin.

Results

The microscopical characterization of glacial ice buried in a thermokarst at a height of 4200 m a.s.l. which displayed ice visible to the naked eye, based on two ice profiles, is shown in the following tables. They summarize the most important results found in crystals, bubbles, and defects of the different analyzed ice samples.

Crystals

The mean size of the grains in an SB area generally increases with depth, except for the case of sample A. On the other hand, polycrystalline samples are more textured, that is to say they have a defined or particular texture which is more pronounced with growing depth of the profile.

Table 1. Crystals.

Sample		Characteristics	D [mm]		Orientation
			SB	CB	
Profile I	M1	Top of profile, sedimentary ice	4.2	0.4	Random
	M2	naturally degraded ice zone (collapse)	5.8	nd	crystallographic axis C perpendicular to n
	M3	glacial ice, stress parallel to F	20	2.6	Crystallographic axis C parallel to F
Profile II	A	Top of the profile, naturally degraded ice zone (collapse)	4	0.4	Crystallographic axis C quasi perpendicular to n
	B	Top of the profile, naturally degraded ice zone (collapse)	2	0.3	Crystallographic axis C is 45° from n and NNE
	C	glacial ice	6	nd	Crystallographic axis C parallel to F

See Figure 1; D= mean diameter; SB= area without microbubbles; CB = area with microbubbles; nd = no data.

Table 2. Bubbles.

Sample		Bubbles				
		d [μm]		N_v [mm^{-3}]	Shape	Orientation
		MBA	MBNA			
Profile I	M1	Nd	500	840	Spherical	Random
	M2	50	Nd	58	Spherical an d elongated	25% elongated parallel to F
	M3	10	Nd	23	Elongated	parallel to n
Profile II	A	20	1250	52	Elongated	parallel to n
	B	20	60	1080	Spherical	45° from n and NNE
					Elongated	45° from n and F
	C	6	<50	465	Spherical	parallel to n
					Elongated	parallel to n

N_v = volumetric bubble density; d = mean bubble diameter; nd = no data; MBA = bubble <50 μm; MBNA = bubble >50 μm.

In M3 and C the crystals take a preferential orientation with the crystallographical axis C parallel to the direction of the flow, while at the top of the permafrost the bubbles appear coincidentally. Those crystals with a size of ≥0.5 cm suggest older age and a glacial origin. The latter are observed in samples taken at greater depth of the profiles.

Bubbles

For the understanding of Table 2 it is helpful to consider that:

- The mean size of the microbubbles which anchor the growth of grains (bubbles <50 μm) decrease with growing depth by a factor of 3 or more, except for sample A.
- The mean size of bubbles which do not anchor the growth of grains (bubbles >50 μm, macrobubbles) changes their shape from spherical to elongated with growing depth, except in the case of sample A.
- In profile I, elongated bubbles have their C axis parallel to “F”, which is the flow direction, in sample M2 (Fig. 4). This is not the case in sample M3 where the prevailing direction is parallel to n.
- In profile II, microbubbles are aligned with the zenith of the samples A and C, but they build an angle of 45° with the zenith of sample B.
- In the samples taken at greater depth, volumetrical density of the bubbles is greater in sample C (profile II) than in M3 (profile I).

Table 3. Defects and dislocations.

Sample		Defect density [x 10^6 mm^{-2}]	
		Hexagonal plane	Prismatic plane
Profile I	M1	2.1 ± 0.5	3.0 ± 1.4
	M2	1.5 ± 0.4	2.6 ± 0.8
	M3	1.5 ± 0.6	2.0 ± 0.1
Profile II	A	2.4 ± 0.7	5 ± 1
	B	0.7 ± 0.2	3 ± 1
	C	0.5 ± 0.2	3 ± 1

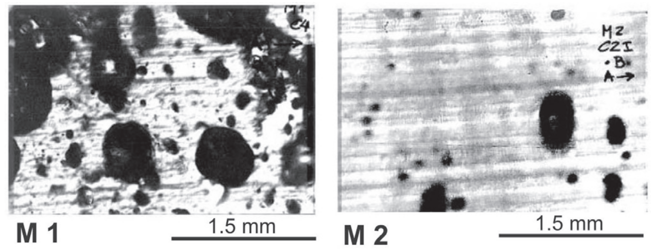

Figure 4. Ice thincuts of profile I (M1 and M2).

Defects, dislocations, and particles

From Table 3 we may deduce that the samples indicate, in the sections analyzed with plastic replicas, that the density of patterns of chemical attack, expressing defects and dislocations, decreases with depth. As to the obtained particles, a lithological study has yet to be made, but it may be supposed that their origin is the local parental rock. In profile II, a majority of a diameter >20 μm prevails. It is assumed that this abundance must have had an important influence in slowing down the growth of the crystals.

Discussion

For reasons of climatic oscillations, ice covered areas express a degradation of glacial ice and formation of thermokarst. Thermokarst are holes or pits and when they are active they are usually filled with melting water, building tiny lakes, unfrozen only in summer. They are a typical characteristic of the irregular landscape of covered glaciers in the Andes of Mendoza. They are also found, less frequently though, on the surface of composed rock glaciers. This phenomenon of degradation of glacial ice contributes to a transformation of the area, making it part of a periglacial landscape. The ice partly melts and then freezes again in the matrix of the structures of periglacial forms.

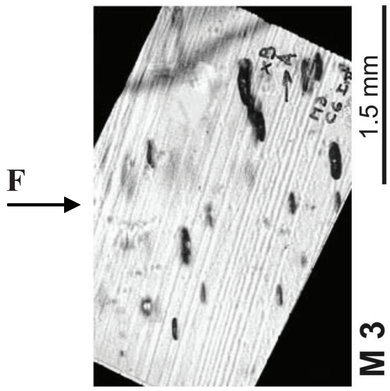

Figure 5. Ice thincut of profile I (M3).

Another important mechanism is the slow movement of small bodies of ice in the form of an "injection." This process is associated with the existence of so-called "dead ice," that is to say, bodies of ice without a connection with the glacier which generated them and which may continue to exist but withdrawn to much higher altitudes. The ice that remains locked in parallel, smaller, and colder valleys with less solar radiation, tends to flow or end up in main valleys with important rock glaciers or composed rock glaciers. In other words it favours periglacial genesis.

Comparing the two ice profiles made in 1999 (profile I) and 2002 (profile II) in a chosen thermokarst, it is easy to observe that M3 of profile I and C of profile II indicate the presence of glacial ice by analyzing the characteristics of their texture. Grains increase in size at growing depth, and their orientation follows the relict flow of the glacier, and the bubbles are elongated perpendicularly to F. In this sense, the C axes of the samples testify to the past glacial flow following the main direction of the stress (F). This way it is possible to prove that the samples taken at depth are correlated and have the pattern that corresponds to the stress of the main direction denominated F (Figs. 3, 5), and that they are of glacial origin.

On the other hand the decrease in the density of the defects indicates that the age of the samples increases with depth. The mean diameter of the bubbles also decreases with depth, following the same principle. Apparently the bubbles try to escape or move upwards, in the direction of n that is, responding to a temperature gradient in a direction normal to the site at the permafrost table. This would also explain the parallel alignment regarding n.

While sample M1 is not textured, M2 shows a texture. The first is indicating a genesis that is different from the second, possibly associated to the thick detritic cover of the profile which acts as an active layer. This ice is mainly of sedimentary origin, generated by solid precipitations which infilter and recrystallize, partly undergoing a liquid state in summer. The textured sample M2, with crystallographical axis C parallel to n, suggests an intervention of a different type of stress with an orientation that is perpendicular to the main stress and which may be due to the collapse phenomenon in connection with thermokarst formation. The shape and the orientation of the bubbles support this idea (Fig. 4). On the other hand in the 2002 profile, sample A is textured, surprisingly with a diameter of grains superior to that of sample B which follows below, indicating most likely that the first sample has been exposed to a higher temperature than the samples of the rest of the thermokarst. This would be a case of degraded ice, a possible effect of local or global warming, and different from the characteristics mentioned above. The size, shape and orientation of the bubbles would also indicate a possible phenomenon of freezing. In addition a remarkable difference between samples A and M1 has to be pointed out, also reaffirmed by the low density of bubbles in sample A which was taken in 2002 and is interpreted as an increase of the mean temperature that affects and creates thermokarst. The special texture of sample B indicates a stress phenomenon geomorphologically observed in a thermokarst environment, which is growing at profile II. But what would be the origin of the ice of profile II? Is it glacial? This question arises when the proper characteristics of the different ice samples are defined. What existed before the ice suffered the variations described? The hypothesis is that it was glacial ice that grew with a sedimentary contribution on top, but that is being transformed and adapted to the present environmental conditions with warming. It would be interesting to reconsider the classification by Shumskiy (1964) according to the processes involved in ice formation.

Conclusions

The microscopical characterization presented in this work helps to classify three different types of ice in an area of periglaciation, or cryogenic processes, which interact with the rock glaciers and may be resumed as follows:

1. Massive ice of glacial origin, indicated by larger ice crystals with a preferential orientation, that is to say with the crystallographic C axis parallel to the flow direction; by elongated or ovoideal bubbles, with low density, also oriented towards the flow direction in some cases and by dislocations in the thincuts or plastic replicas which also indicate the flow direction; in some cases however, like C in profile II, the particles may limit the size of the crystals and influence the interpretation;
2. Sedimentary ice represented by small crystals and by almost spherical bubbles; like in the typical case of M1 and M2, with a high volumetrical density of bubbles and a larger mean diameter; and
3. Regenerated or degraded ice, which is monocrystalline, with bubbles of a large mean diameter but with low volumetrical density of bubbles. This ice is associated with the degradation of permafrost like in A and B of profile II.

On the other hand, as presumed, the layer of sediments has an important role in relation to the penetration of the external caloric wave which interacts with different types of subterranean ice. The phenomena are expressed microscopically and macroscopically.

In profile I, the external caloric wave is impeded and stopped by the thick layer of cryosediments accumulated perpendicularly to the F axis of the main flow and at lower height which interacts with the solid precipitation that falls throughout the year and supports the agradation of ice. However, this is not the case in profile II, where a much thinner layer of a thickness less than 1 m, allows much more external heat to enter and causes a regeneration or transformation of subterranean ice. In addition there are clear signals of collapse processes that preferably affect certain parts (profile II) of the thermokarst perimeter.

Evidently the chosen periglacial area is not in equilibrium, as inferred by the presence of active or reactivated thermokarst. These forms are supposed to be much older, probably from the Middle Holocene when a worldwide warming and a glacial inactivity were produced. This was also registered in South America (Röthlisberger 1986).

The changes caused by present warming, and which affect the structures of the ice, are also clearly observed in the microcrystalline results of the samples. The area of periglaciation extends altitudinally, but also affects lower heights for the contribution of more regenerated ice. It is an area with abundant "dead ice" that is integrating into periglacial forms such as rock glaciers. The "glacial flow" is kept up, hidden, discontinuous and slow, favoured by the inclinaton of the slopes of small colateral valleys.

The periglacial environment is growing or expanding upwards as glaciers disappear, are covered by sediments or are transformed into relict ice. Downwards, that means descending in height and slope downwards, the ice integrates into morainic or cryogenic sediments that fill up valleys and contributes to the formation of new rock glaciers or helps to maintain the existing rock glaciers in activity.

Different environmental situations may be analyzed on the basis of the conclusions. If the environment is considered as continually changing, the "dead ice," as if it were relict ice of glacial origin, does not persist in situ; it keeps flowing as has been pointed out above. This movement is proven by the microscopical characteristics of ice samples taken at great depth of the studied profiles. Sedimentary ice also incorporates into the massive ice in a process of agradation. These types of ice merge from a periglacial environment in the existing periglacial forms that have been observed. The erroneously called "dead ice" partly disappears by degradation and sublimation, but partly plays an essential role for the evolution of periglacial forms at lower altitudes.

The phenomenon of ice agradation would cease if the sedimentary or active layer was very thin and if the mean temperature of the thermokarst increased. These processes, the asymmetry and the deformation of the thermokarst, are represented in the landscape and are expressed in the microcrystallography of the ice, and they may be used as environmental indicators.

These studies allow the reconstruction of three environmental or paleoenvironmental scenarios: (1) old ice expressing its paleoenvironmental background, (2) ice indicating agradation or degradation of the present permafrost environment, and (3) ice expressing geomorphological processes to be expected in the near future.

Acknowledgments

This work was carried out with the financing of project 4664 (PIP 1078/98) by CONICET: "Argentine General and Applied Geocriology." We would especially like to thank José Hernández (IANIGLA) for his permanent cooperation during fieldwork and his logistical support, and Sabine Herfert and Silvina Pereyra for their help with the English version.

References

Anderson, D.M., Pusch, R. & Penner, E. 1978. *Physical and Thermical Properties of Frozen Ground. Geotechnical Engeneering for Cold Regions* (Edited by Andersland & Anderson). McGraw-Hill Book Company: 37-102.

Arena, L.E. 1995. *Crecimiento de grano en hielo puro.* Tesis doctoral FAMAF – Universidad Nacional de Córdoba, Argentina (inédita).

Arena, L., Trombotto, D. & Caranti, G. 2005. Microscopical characterization of thermokarst ice from an area of Andean permafrost, Central Andes of Mendoza, Argentina. *2nd European Conference on Permafrost. Terra Nostra Heft 2005/2,* Potsdam, 55 pp.

Arena, L.E., Nasello, O.B. & Levi, L. 1997. Effect of bubbles on grain growth in ice. *J. Phys. and Chem. B* Vol. 101, Nr. 32, 6109-6112.

Haeberli, W., Huder, J., Keusen, H.-R., Pika, J. & Röthlisberger, H. 1988. Core Drilling through rock glacier-permafrost. *V International Conference on Permafrost, Trondheim. Proceedings Vol.2*, 937-942.

Haeberli, W. & Vonder Mühl, D. 1996. On the characteristics and possible origins on ice in rock glacier permafrost. *Z Geomorph N.F.*, SB104: 43-57.

Nasello, O.B., Arena, L.E. & Levi, L. 1992. Grain growth in pure ice, effects of mobile bubbles. *Phys. Chem. of Ice,* 422–427.

Röthlisberger, F. 1986. *10000 Jahre Gletschergeschichte der Erde.* Verlag Sauerländer, Aarau, 416 pp.

Shumskiy, P.A. 1964. *Part 1, General Geocryology*. Chapter IX, *Ground (subsurface) Ice*. National Research Council of Canada, Techn. Translation 1130, 118 pp.

Trombotto, D. 2000. Survey of cryogenic processes, periglacial forms and permafrost conditions in South America. *Revista do Instituto Geológico*, Vol. 21, Nr.1/2, São Paulo: 33-55.

Trombotto, D. 2003. Mapping of permafrost and the periglacial environment, Cordón del Plata, Argentina. *8th International Conference on Permafrost.* Permafrost, Extended Abstracts, Reporting Current Research and New Information, Edited by W. Haeberli & D. Brandová, Zürich, 161-162.

Trombotto, D., Buk, E. & Hernández, J. 1999. Rock glaciers in the Southern Central Andes (appr. 33° S.L.), Mendoza, Argentina: a review. *Bamberger Geographische Schriften* 19, Selbstverlag des Faches Geographie an der Universität Bamberg, Bamberg, 145-173.

Van Vliet-Lanoë, B. 1998. Frost and soils: implications for paleosols, paleoclimates and stratigraphy. *Catena* 34, 157-183.

Increasing the Bearing Capacity of Pile Foundations by Using Thermostabilizers of Small Diameter in Cryolithozone of Russia

A.N. Tseeva
Yakutsk State Design and Research Institute for Construction, Yakutsk
R.M. Bayasan
VNIIGAS, LLC, InterHeatPipe, Moscow
G.P. Pustovoit
Department of Geocryology, Moscow State University, Moscow
A.P. Okoemova
Yakutagropromprojekt, Open Joint-Stock Company, Yakutsk

Abstract

Three case studies are presented to demonstrate the effect of *InterHeatPipes,* which are small-diameter thermostabilizers, under different permafrost conditions. The installation of the *InterHeatPipes* increases the bearing capacity of piled foundations and therefore provides increased building stability. Thermal disturbances caused by the installation of piles in warm saline permafrost required a quick heat extraction from the ground to provide the required bearing capacity of a multistory business centre in Yakutsk during construction. A series of thermostabilizers were installed that provided very fast ground cooling. Thermostabilizers were also installed to freeze unfrozen soil in the foundation of a nine-story residential building. The third example presents results of a power line tower foundation using thermostabilizers. Supports for power lines are critical because frost heave in warm permafrost often results in uneven lifts of the pile foundation resulting in tilted masts. Ground temperature measurements from the three examples demonstrate how thermostabilizers can be utilized to increase the bearing capacity of the soil.

Keywords: bearing capacity; permafrost; pile foundations; stability; thermostabilizer.

Introduction

Widespread saline and warm frozen grounds, and natural or human-induced taliks cause major problems in the construction of multistory buildings and engineered structures in permafrost environments. Pile foundations are affected by vertical frost heave and pull out forces. Such problems are recorded in Yakutsk, the oldest city among those with a population of more than 50,000 people built on permafrost. The geocryological conditions differ significantly from natural ones. Ground temperature regimes are extremely non-uniform within one construction site and talik zones are common under old buildings promoting permafrost thaw.

Future development of modern northern cities requires the construction of multistory buildings with increased foundation loads, both vertically and horizontally. Seasonal cooling devices in combination with local thermal insulation of the ground surface are efficient in increasing the bearing capacity of the ground for pile installation, freezing talik zones and providing stability of foundations against pull out forces, including frost heave forces. This paper presents the usage of *InterHeatPipe* thermostabilizers as cooling devices on two multistory buildings and a power line foundation.

Site Description

Business centre office building: Block B

The construction site for a new business centre is located in the centre of Yakutsk where previously one-story wooden houses and public buildings were situated. The office building (block B) is 33.0 m x 40.5 m and is located in the centre of the new complex. It is a 13-story building capped by a two-story dome. Structurally, it represents a monolith reinforced concrete framework with a maximum pillar grid distance of 6.0 m x 7.5 m. During site investigations geocryological conditions were identified, characterized by low temperatures, which are typical for the centre of the city of Yakutsk, and high salinity of shallow soil layers. At the depth of zero annual amplitudes (10 m) the ground temperature varied between -3.4 and -5.2ºC, with the lower temperatures measured in places with maximum ground salinity (D_{sal} = 0.58%), and warm temperatures (-3.4ºC) in places with minimum ground salinity (D_{sal} = 0.13%).

According to the Russian construction code (1988) the calculations of the bearing capacity for pile foundations have to consider less favorable conditions: higher ground temperatures (-3.4ºC) at a depth of 10 m, and the maximum depth of saline ground (5.5 m).

The geological section is represented by the following types of soils:

- 0–0.8 m: fill (medium and silty sand, construction waste);
- 0.8–5.5 m: silty sand with the some organic remains, saline;
- below 5.5 m: fine and silty sand of massive cryogenic texture, hard frozen.

Pile clusters of three or four piles combined were designed

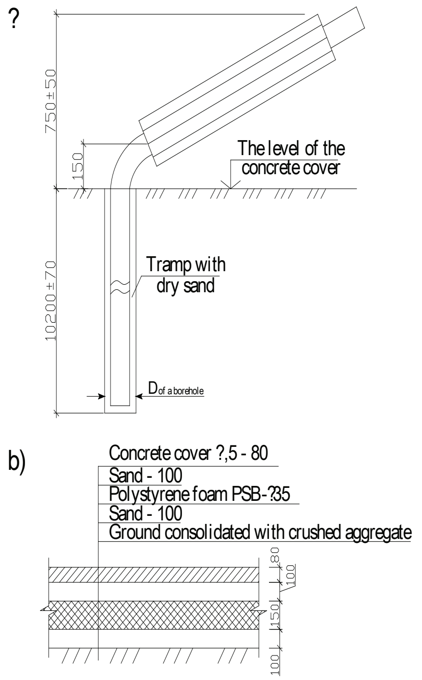

Figure 1. Schematics of the thermostabilizers (a) and the thermal insulation of the ground surface (b) for the business centre.

for the foundations depending on the loads. Square reinforced concrete piles measuring 40 cm x 40 cm were 10 m and 12 m long, and embedded into permafrost to depths between 8.8 m and 10.8 m. The piles were installed into boreholes with diameters larger than the piles. According to the design, borehole pockets should have been filled with cement and sand slurry. The calculated bearing capacities for the pile installation was 1620 kN and 2380 kN, for the 10 m and 12 m long piles, respectively. The calculated pile loads were 1300 kN and 1930 kN.

During the pile installation, water from the thawed layers close to the surface penetrated into the boreholes warming the ground so that the temperatures at 10 m depth increased -2.1 to -2.7ºC. Inspections of the borehole grout showed that piles froze to the saline drilling mud but not to the cement and sand slurry. In addition, the temperatures were significantly higher than calculated. New calculations that considered in situ ground temperatures and salinity increase along the entire length of the piles showed that the bearing capacity of the installed piles was only 610 kN and 856 kN for the 10 m and 12 m long piles, respectively.

Nine-story residential building in the 29th city block in Yakutsk

Until late 1970s there was a lumber-processing plant located on the bank of the Zavodskaya river canal. Later the river canal was filled with lumber-processing waste. A zone of unfrozen ground with high content of organic material formed.

The site mainly consists of upper quaternary alluvial sediments represented by sandy and clayey deposits to a study depth of 26.3 m. Between a depth of 23.5 m and 25.7 m the top of Jurassic sediments formed by siltstones

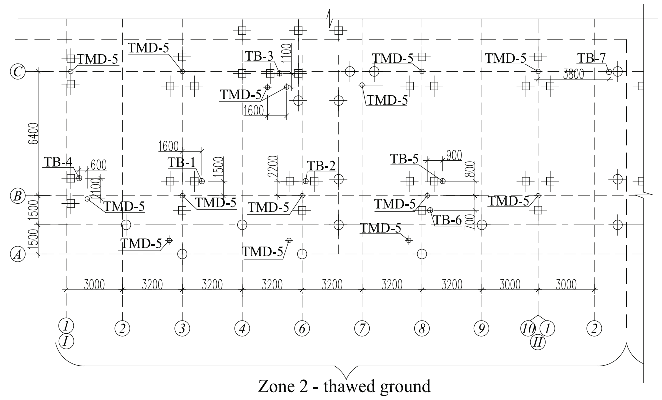

Figure 2. A section of the founda tion scheme of the area with taliks of the 9-story residential building and the scheme of the thermostabilizers (TMD-5) and the location of boreholes (TB-1, 7).

were penetrated. The natural ground is overlain with a fill of sand, sandy loam and loam mixed with chip, bark, board chippings, logs; that is, all sorts of sawing wastes. The inclusions vary from rare to thick and are non-uniform in both horizontal and vertical direction. The thickness of the fill within the site is between 3.9 m and 9.4 m. Some loam sand lenses were also found. These layers are usually saline with organic inclusions. Below the fill the geological section is represented by sands of various ranges; that is, fine, silty, medium, and gravel sands.

Drilling in July/August 2006 revealed both frozen and thawed ground on the site. Thawed ground was penetrated in the active layer as well as at greater depths within the permafrost. Later are inter-permafrost taliks of different thicknesses and distribution. Thawed ground occupies about a third of the site. The origin of the inter-permafrost taliks is initially connected to a former river canal that formed a talik. The river canal was later filled with lumber processing wastes and the surface was leveled with fill, consisting of dry ground that resulted in deep freezing from the surface and a formation of shallow short-term frozen ground. Cast-in-place piles of 650 mm diameter and different lengths are designed for the foundations. The design also suggests that the lower part of the pile to be embedded in permafrost, as well as preconstruction ground freezing.

Power line supports

The site with supports for a power line is situated in the southwestern part of Yakutsk. According to the site investigations the active layer is represented by sandy loams and loams. The ground becomes liquid when it thaws. According to a frost heave parameter the sandy loam is referred to as a highly frost susceptible soil and the loam to an extremely frost susceptible soil.

The frozen ground is represented by silty, fine and medium sands. Ground temperatures measurements carried out in 2001 showed warm temperatures that are not typical for Yakutsk (-0.3 to -0.9ºC at a depth of 10 m). The inclination of the support exceeded the maximum allowable values. The power line supports are sunk-drill piles (two piles under each foot)

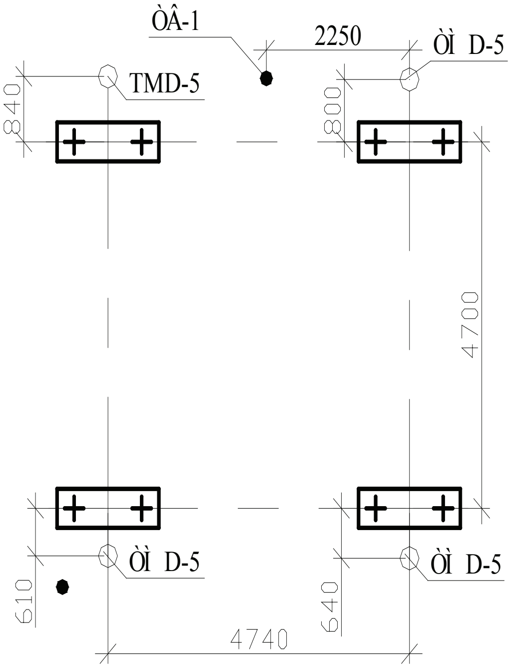

Figure 3. The scheme of the TMD-5 and location of temperature borehole TB-1 near the power line support No. 44.

with a 30 cm x 30 cm cross section and a length of 8 m.

Calculations of foundations showed their instability under vertical forces due to frost heave when the active layer refreezes. The power line supports are subjected to both compressing and pull out forces, therefore, the combination of pull out and vertical forces due to frost heave control heave and tilt of the foundations.

Techniques of Pile Bearing Capacity Increase

To provide the bearing capacity and stability of piles for engineering structures under the above-mentioned permafrost conditions ground temperature control was necessary. Seasonally cooling devices were widely used for heat extraction and to cool down ground temperatures. Thermopiles (Long 1963) and kerosene devices (Gapeyev 1969) are well known. Liquid seasonally cooling devices were used to refreeze thawed ground and to cool plastic frozen grounds (Biyanov et al. 1973), refrigerated piles were installed for multistory buildings in Mirny (Makarov et al. 1978), different types of thermosyphons and thermopiles were further used for numerous constructions in Alaska (Borjesson et al. 2007). In recent years *InterHeatPipe* thermostabilizers of small diameter are widely used for constructions in the Russian north (Lyazghin & Pustovoit 2001, Bayasan et al. 2002). Aluminum thermostabilizers, type TMD-5, with an equivalent diameter of 54 mm have the following advantages compared to other well-known seasonally cooling devices:

- low internal and external thermal resistance where the evaporator and the condenser are located;
- low temperature gradient along the length of the seasonally cooling device;

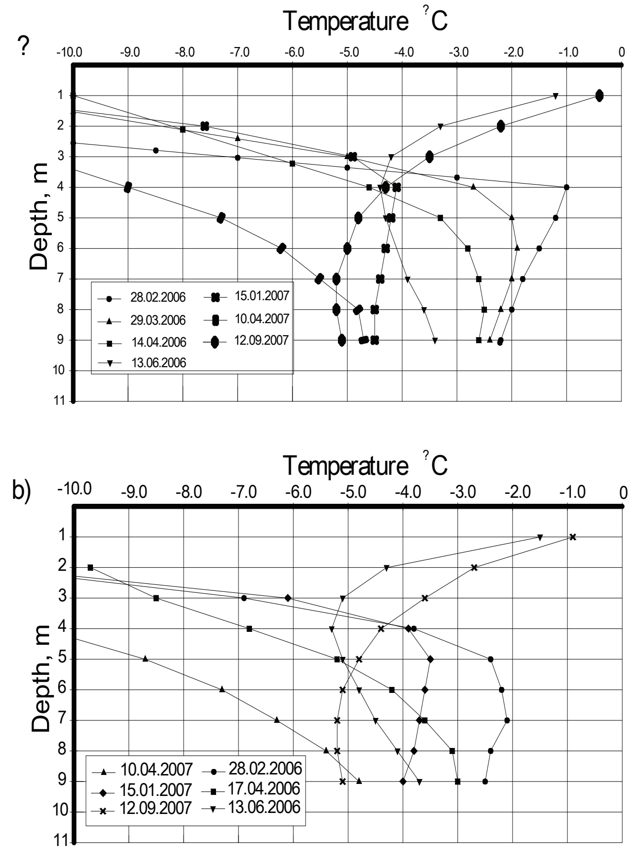

Figure 4. The ground temperatures near piles No. 52 (a) and No. 77 (b) of the business centre building after the installation of the thermostabilizers.

- high rate of freezing and effective cooling;
- short response time, which increases the period of active work of TMD-5 (1.0–1.5 months per season).

In addition to the seasonally cooling devices, the engineering design for ground thermal control includes the use of a thermal insulation. This was recommended and applied in all of the above-mentioned examples.

For the business centre office building, where the ground temperatures increase was recorded and the pile bearing capacity was exceeded, it was designed to install additional piles and to place thermostabilizers TMD-5. The condensators were tilted under the grid, in the centre of pile cluster. To decrease the depth of thawing and, consequently, to expand the adfreezing surface of the piles with the frozen ground the surface was protected with a thermal insulation foam (Fig.1).

Thermostabilizers for the 9-story residential building foundation were designed preliminary to refreeze the thawed ground. Piles will be loaded after the ground around them is frozen. The bearing capacity of the cast-in-place piles in a thawed zone was calculated considering the thawed state of the ground. An air space under the building allows cold air circulation, hence a gradual freezing of thawed ground and the maintenance of the frozen state.

Figure 2 shows a section of the foundation scheme for the area with inter-permafrost taliks where thermostabilizers were installed.

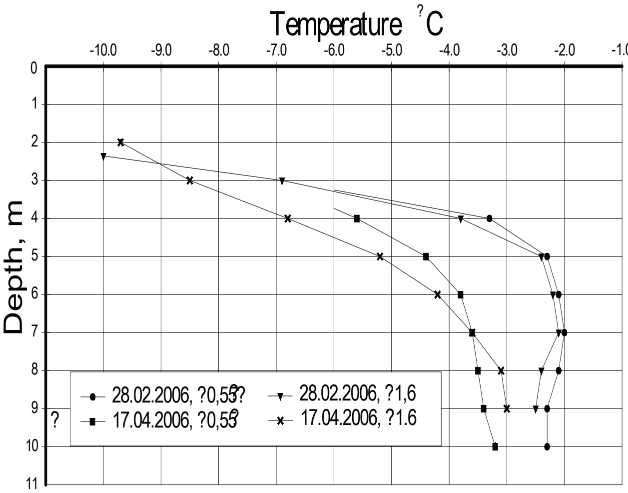

Figure 5. Ground temperature change after the installation of thermostabilizers located at different distances.

To prevent the failure of the power line supports, ground cooling by installing seasonally cooling devices was recommended. Thermostabilizers together with surface thermal insulation are provided to cool down the ground temperatures and to reduce the depth of seasonal thawing. This measure increases the adfreezing surface of the piles with the ground and decreases the surface of piles under the effect of vertical forces due to frost heave. The scheme of the TMD-5 installation is shown in Figure 3.

To measure the performance of the thermostabilizer and monitor ground temperatures boreholes were instrumented with thermistors. In addition, survey points were installed to measure support and foundation deformation.

The thermostabilizers for the business centre office building were installed in March 2006, those for a 9-story residential building in March 2007 and those near the power line supports in December 2006.

Results and Discussion

Figure 4 shows a set of ground temperatures beneath the business centre office building in two representative boreholes. TB-1 (near pile No. 52) is placed at the distance of 1.2 m, TB-2 (near pile No. 77) at the distance of 1.6 m from the TMD-5. Prior to the installation of the thermostabilizers (February 28, 2006) the temperatures at the tip of the pile (at the depth of 9 m) were between -2.2 and -2.5ºC. At the same level the natural ground temperatures reached values between -3.4 and -4.2ºC. Thermostabilizers were installed near pile No. 52 on March 15, 2006, and near pile No. 77 on March 26, 2006. The temperatures decrease as soon as the thermostabilizers had been installed. At the same time in upper permafrost layers (4–7 m) the temperature decrease was even more intensive and continued during the warm season (June 13, 2006)

Some temperature increase was recorded on January 15, 2007, but by the end of the cold season (April 10, 2007) the ground temperatures became much colder than on April 14, 2006 (after thermostabilizers worked for 20–30 days).

The end of a warm period (September for Yakutsk) is typical for the ground temperature regime. According to the temperature distribution on September 12, 2007, permafrost temperatures in both boreholes were low and nearly identical. As it has been stated above, thermistors were installed at a different distances from the thermostabilizers. Figure 5 shows the ground temperature decrease in two boreholes located at the distance of 0.55 m and 1.6 m from the thermostabilizers. Initial temperatures were almost similar and the thermostabilizers were installed on the same day. The figure further shows the intensive decrease in temperature where thermostabilizers were placed close (0.55 m) to the boreholes. However, such a tendency is not typical for the middle layers, which is probably affected by other factors, such as the composition, moisture content and salinity. These factors were not the subject of this investigation.

The data demonstrate that the proposed engineering design allowed the increase of considerably colder ground temperatures and a decrease in depth of seasonal thaw beneath the business centre office building. Ground temperatures lower than the calculated ones allowed the required bearing capacity of the soils and the transfer of calculated loads to piles.

Figure 6 shows typical diagrams of ground temperature changes for the 9-story residential building. As it was stated above, talik zones of different thickness were found below the building; thus ground temperatures were non-uniform. Figure 6a shows the temperature changes in borehole TB-1.

Ground temperatures along the entire depth of the borehole were positive at the end of a warm season (September 10, 2007), but by November 29, 2007, zero degree was recorded at depths below 3 m, and they stayed until January 24, 2008. Similar temperatures were observed in boreholes TB-2 and TB-4. Figure 6b presents the change in ground temperatures in borehole TB-5, where a talik was present at a depth of 7.5–9.5 m. According to the figure, ground cooling with the use of thermostabilizers resulted in subzero temperatures by December 5, 2007, and they continued to decrease (e.g., January 28, 2008). The figure further shows the peculiarities of refreezing thawed ground. Freezing of moist ground is characterized by the latent heat during phase change from water to ice. Therefore, the temperatures remain at about 0ºC (the temperature of water freezing) before ground cooling continuous, which was observed in borehole TB-5. The data obtained demonstrate the efficiency of thermostabilizers when thawed soils are frozen under buildings.

The calculations for made-in-place piles of this building were made with consideration of thawed ground conditions. The purpose of installing thermostabilizers was to reach uniform ground temperatures and to avoid uneven settlements of the foundation. The design also requires the establishment of subzero temperatures before loading of the foundation may begin.

Thermostabilizers were installed near the foundations of each foot of power line supports, subjected to heave deformation. Figure 7 illustrates the change in ground temperatures after the thermostabilizers were installed in the ground under one of the supports.

Thermistors were installed in a borehole located at a

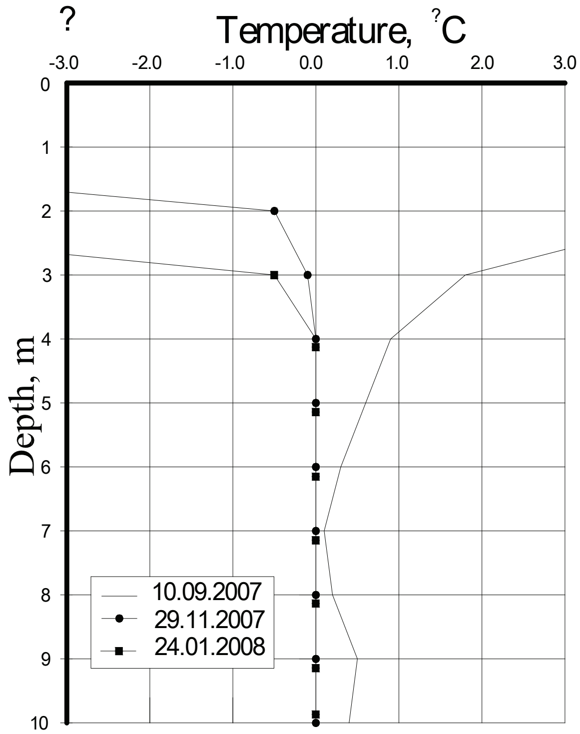

Figure 6. Ground temperature changes in boreholes TB-1 (a) and TB-5 (b) for the 9-story residential building.

rather large distance from the thermostabilizers (2.25 m). Nevertheless, the figure shows the decrease in temperature compared to the initial conditions. In addition to the temperature measurements, foundation deformations were monitored during the winter of 2006–2007, and no vertical deformations were noted for the two supports; that is, the reduction in ground temperature provided the necessary resistance of the foundations against the vertical forces of frost heave.

Conclusions

Small diameter *InterHeatPipe* thermostabilizers were installed under different structures in the city of Yakutsk to improve the ground-bearing capacity. In situ measurements of the temperature regimes of the ground cooled by the thermostabilizers allow for the following conclusions.

- Problems during the installation of the piles for a business centre office building resulted in warming ground temperatures and insufficient bearing capacity. Thermostabilizers and thermal insulation on the ground surface allowed the obtainment of calculated ground temperatures to decrease the depth of seasonal thaw and increase the bearing capacity of the pile foundation.
- Thermostabilizers used to freeze talik zones below a 9-story residential building showed their suitability and the dependency of the talik thickness on the period of temperature decrease.
- Thermostabilizers used to decrease ground temperatures and increase the resistance against vertical forces due to frost heave also eliminated uplift deformation of the pile foundations for a power line support.

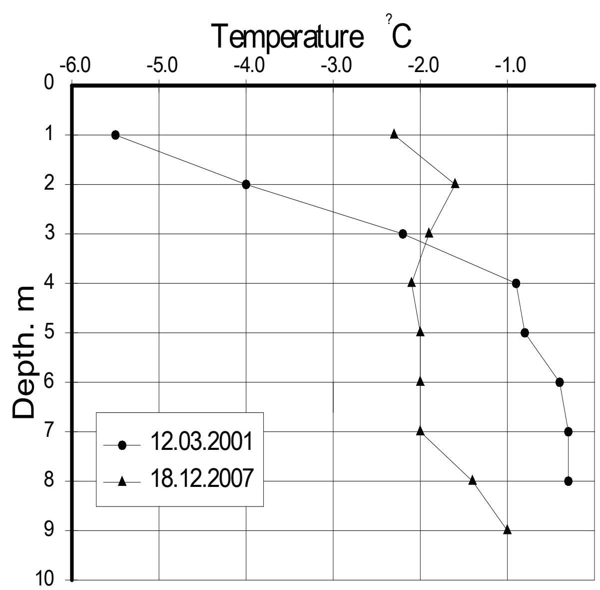

Figure 7. Ground temperatures before (2001) and after (2007) the installation of thermostabilizers the near power line support No. 44.

- The effectiveness of thermostabilizers depends on the initial ground conditions, properties, composition, and temperatures.
- The data obtained confirm the validity of engineering solutions by the use of seasonal cooling devices to increase the bearing capacity and stability of piles in permafrost.

Acknowledgments

The authors express their gratitude to the anonymous reviewers for their careful and thorough examination of the paper, constructive comments, and suggestions for the content change. Assistance with editing the English of the manuscript is greatly appreciated.

References

Bayasan, R.M., Korotchenko, A.T. & Pustovoit, G.P. 2002. The probability, determinism and new technology in the problem of stability of perennially frozen bases. *Bases, Foundations and Soil Mechanics* 5: 26-31.

Biyanov, G.F., Makarov, V.I. & Molochnikov, A.D. 1973. Liquing cooling units for freezing thawed ground and cooling plastically frozen ground for construction in areas with severe climate. *Proceedings of the Second International Conference on Permafrost, Yakutsk, June:* 195-199.

Borjesson, B., Clarke, E.S., Miller, D., Musial, M., Shaw, S.R., Wyman, G.E., Yarmak, E. & Zarling, J.P. 2007. *Permafrost Foundations. State of Practice. Reston.* Virginia: ASCE, 86 pp.

Construction Code SNiP 2.02.04-88. 1991. *Bases and foundations on permafrost*. Gosstroy of the USSR. Moscow: APP CITP, 52 pp.

Gapeyev, S.I. 1969. *Frozen Foundations Strengthening by Cooling.* Leningrad: Stroyizdat, 104 pp.

Long, E.L. 1963. The Long Thermopile. *Proceedings of the First International Conference on Permafrost, Lafayette*: 487-491.

Lyazgin, A.L. & Pustovoit, G.P. 2001. The stability of power line supports against frost heave under conditions of the north of Western Siberia. *Proceedings of the Second Conference of Geocryologists of Russia 4, Moscow*: 172-178.

Makarov, V.I., Plotnikov, A.A. & Chumayevsky, B.F. 1978. Construction of Multi-Storey Buildings on Refrigerated Piles in the City of Mirny. *Proceeding of the Third International Conference on Permafrost, 1, Ottawa*: 820-825.

Recommendations on Design and Calculation of Shallow Foundations in Frost Susceptible Ground. 1985. Gosstroy, the N.V. Gersevanov VNIIOSP, Moscow, 59 pp.

Vegetation Response to Landslide Spreading and Climate Change in the West Siberian Tundra

N.G. Ukraintseva
Institute VNIIST (Institute of the Engineering and Construction of the Oil-Gas Pipeline), Russia

Abstract

Cryogene landslides are widespread and well investigated in the sub-arctic tundra. On the Upper Pleistocene marine plains, active landslide process brings to the surface marine saline deposits saved by permafrost. The landslide-affected slopes present a system of morphologically expressed and often overlapping landslides of different age. Patterns of re-vegetation and "self-stabilization" of landslides as indicators of landslide age have been studied. Natural enrichment of the soil, water, and vegetation in many nutrients leads to anomalous productivity on landslide-affected slopes and to the expansion of high willow shrub to the north. Areas of near-surface distribution of marine saline deposits and old landslides are correlated to the area of high willow shrub tundra. Estimation of cryogenic landslide distribution north of Western Siberia has been studied using methods of landscape indications. Spreading of cryogenic landslides further to the north may be an indication of a warming tendency in the Aarctic climate.

Keywords: cryogenic landslides; marine deposits; willow shrub.

Introduction

Special interest in studying the process of cryogenic sliding has arisen after a mass descent of landslides in many areas of the Russian and North American Arctic regions in 1988–1991. Landslide processes affect the surface of marine plains and terraces. The permafrost table serves as a "mirror" for sliding masses; therefore, the majority of researchers name them "cryogenic landslides" or "active-layer detachments" (Levkovicz 1990, Harry & Dallimore 1989, Leibman 1995, Poznanin 2001). The cryogenic landslides are developing on surfaces built of fine-grained marine sediments with high salinity. Outcropping of frozen salty marine sediments took place due to seasonal sliding of the thawed water-saturated ground over the permafrost table. This process leads to sediment desalinization and enrichment of the active layer with salts (Dubikov 2002, Leibman 1995, Ukraintseva et al. 2003).

The purpose of the present study is to estimate the distribution of cryogenic landslides in the north of the Western Siberia using methods of landscape indication.

Study Area and Methods

The basic area of research is the region of the Bovanenkovsky gas refinery (between the Mordyjaha and Naduyaha Rivers) and projected gas pipeline "Yamal Center" in western and central Yamal. The author's research materials from the Peljatkinsky gas refinery (Lake Pelyatka, southern Gudan) and the coast of the Yenisey Gulf (Shajtansky, western Taimyr) are used also.

The research station of "Vaskiny Dachi" is located in typical tundra of central Yamal. Since 1991, field groups from the Earth Cryosphere Institute of the Russian Academy of Sciences (Tyumen) have been studying cryogenic landslides (with participation of the author). The technique of field sampling and laboratory analysis of samples is described in the paper by Ukraintseva et al. (2003).

Figure 1. Study area: research station Vaskiny Dachi in central Yamal Peninsula is marked by the star.

In the area of the Bovanenkovsky gas field, 10 key sites within landscapes of IV, III, and II marine plains and terraces in the valleys of Nadujjaha, Seyaha, and Mordiyaha Rivers were explored. The large-scale landscape map of the Bovanenkovsky area was made using GIS-Technologies (Drozdov & Ukraintseva 2000). A method of landscape indication was applied to determine the relative age of landslides slopes (young and ancient) in each landscape.

The landscapes map of the north of Western Siberia published in 1991 (with scale 1:1,000,000) was used for extrapolation of the obtained data to all typical tundra. The legend of the landscape map of the Bovanenkovsky gas field was generalized and made consistent with the legend of the published map. This allowed the extrapolation of calculation results according to the principle of landscape analogies and estimation of a fraction of landslide slopes in landscape areas of typical (sub-arctic) tundra.

Spatial distribution various vegetation communities was evaluated using an analysis of the distribution of Nenets'

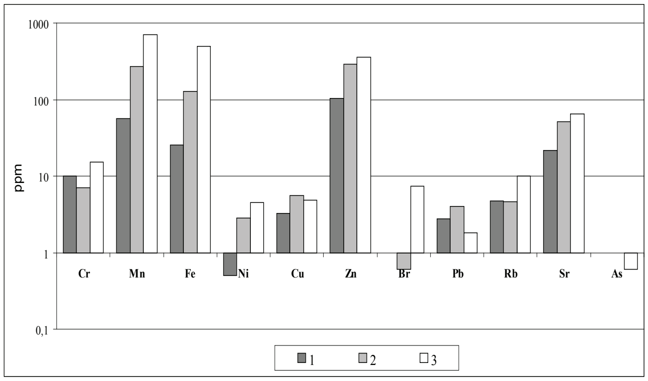

Figure 2. Trace element composition in various structural parts of willow. 1–willow trunk; 2–willow branches; 3–willow leaves.

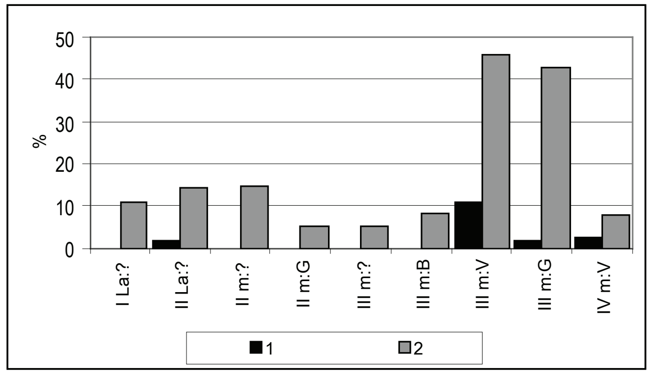

Figure 3. Landslide-affected slopes in structure of landscapes of the Bovanenkovsky gas field (Melnikov & Grechishchev 2004). 1–young slopes; 2–old and ancient slopes.

names (toponyms) on topographic maps of northwestern Siberia with a scale of 1:1,000,000 (with insertion of several larger scale pieces).

Landslides in the Subarctric Tundra

Biogeochemical features of landslide-affected slopes

In the region of typical tundra where salted marine loams and clays lie close to a surface, cryogenic landslides of sliding are widespread on the Upper Pleistocene marine plains and terraces and have been studied in detail. Extended landslide slopes represent a system of morphologically expressed landslides of different ages quite often overlap each other. In comparison with background conditions, biogeochemical features of ecosystems of landslide slopes vary significantly. The main features of landslide processes in the regions of interest were described earlier:

- Mechanical displacement of land, mixing, and increase of heterogeneity (vertical and lateral) of granulometric structure of the active layer (Ukraintseva & Leibman 2007);
- Periodic activation and recurrence of landslide descent, leading to change of a longitudinal profile of a slope and position of the permafrost table (Ukraintseva et al. 2003);
- Destruction of topsoil layer and vegetation cover along the sliding surfaces, and burial of organic soils on the landslide bodies (Ukraintseva & Leibman 2007);
- Desalination of the marine premafrost and enrichment of the soil-vegetation cover with dissolvable salts (mineral nutrients), accelerating "self-stabilization" process of the landslide-affected slopes (Ukraintseva et al. 2003);
- Age of the landslides defined by the radiocarbon dating of buried organic matter, varies from 0–30 till 1500–2000 (Leibman et al. 2000).
- Increase of fertility of the soils enriched by nitrogen, potassium and organic matter: peat soils prevail in ancient landslide slopes with thickness of organic layer 20 cm or more (Ukraintseva & Leibman 2007);
- Change of structure and increase of the phyto-mass storage on the surface of the landslide slopes represented by high willow shrubs (Ukraintseva & Leibman 2000, Ukraintseva 2004).

The rich microelement structure of the substratum promotes zinc accumulation in leaves and trunks (Fig. 2), and raises the frost resistance of willow. Due to this, willows form steady communities in unusually high latitudes (up to 70°N, –72°N). This is confirmed by conclusions of other researchers who refer to willow bushes as pioneer plants which spread out into natural or human-caused bare soil tundra (Andreev 1970, Burn & Friele 1989, Geertsema & Pojar 2007, Matsuda et al. 1988, McKendrick 1987, Pospelova & Pospelov 2000, Rebristaya et al. 1995, Sturm et al. 2001, Ukraintseva & Leibman, 2000).

The next step in research of the landslide processes is an estimation of their spatial distribution.

Landscape indicators of landslide-affected slopes

On large-scale aerial images, -only young landslides (younger than 100 years old) can be detected. Old and ancient landslides are expressed weakly in morphological structure and do not have direct pattern on the image. For mapping of PLAITS on aerial images, the indirect method—the method of landscape indication based on studying of spatial and temporal variation of a vegetation cover—is applied.

In the investigated areas, the dominating community of hill tops and stable slopes is bush-grass-moss and bush-lichen-moss tundra—the background communities of typical tundra. The vegetation cover on the landslide slopes sharply differs from the background.

There are three basic stages of re-vegetation of landslides, and there are three gradations of landslide' relative ages, respectively: young, old, and ancient (Ukraintseva et al. 2003, Rebristaya et al. 1995). On *young* surfaces of landslides (10–15 years after a landslide occurred), bare soil sites alternate with pioneer meadow groupings of *Phippsia concinna, Tripleurospermum Hookerii*, etc. At the same time, some short bushes (willow, dwarf birch) still remain on young landslides; mosses degrade and wilt, and pioneer plants (cereals, a sedge, a horsetail) appear. On *old* landslides (from 100–300 till 1000 years old), the second stage of re-vegetation is observed—meadow communities with participation of mosses and active renewal of a willow (0.3–1 m height). And finally, associations of *Salix glauca* and *S. lanata* (height: 1.5–2 m) are characteristic for *ancient* landslides (from 1000

Table 1. Landslide slope area in typical tundra of Western Siberia.

Regions	Area, kм^2	Fraction of area in the zone %	Fraction of landslide slopes in the area %	Fraction of landslide slopes in the zone %
11	4946	4,94	20,28	1,00
12	19337	19,31	30,19	5,83
13	18103	18,07	1,83	0,33
14	8767	8,75	31,92	2,79
15	3063	3,06	0,46	0,01
16	13500	13,48	15,92	2,15
17	20764	20,73	9,54	1,98
18	11677	11,66	19,11	2,23
Total	100161	100,00	-	16,32

to 2000 years old (Leibman et al. 2000)—sparse moss-grass willows on surfaces of sliding and dense grass-moss willows on landslide bodies. High willows occupy the most area on the landslide slopes.

Successive stages of re-vegetation of landslides determine choice of landscape indicators. Two last stages of landslide re-vegetation are poorly distinguishable on aerial images, merging together and creating a small grey texture of bush communities. Thus, the landscape indicators of old and ancient landslides (older than 100–300 years) are high willows (an index *6n*), and modern young landslides are identified by pioneer meadow communities with bare soil surfaces (an index *6p*).

Distribution of landslide-affected slopes on the Bovanenkovsky gas field

On a large-scale landscape map of the Bovanenkovsky gas field (Drozdov & Ukraintseva 2000), the relative age of landslide slopes (young and ancient) in the structure of each landscape is calculated. The maximum distribution of landslide slopes is characteristic for large-hill thermodenudation areas of III marine plain (III m: V = about 57%). The fraction of young landslides from the total area of landslide slopes for all districts does not exceed 20–30% that indicates some attenuation of process (Fig. 3).

Landslide slopes in typical tundra

The map of natural complexes of nnorthwestern Siberia (scale 1:1,000,000) published in 1991 was used for extrapolation of the received data on all typical tundra. In the region of typical tundra, eight landscape areas are allocated, for each of which the histogram of morphological structure—a percentage of landscape and land area—is determined. This allowed extrapolation of results of calculations by a principle of landscape analogies. The legend for a landscape map of the Bovanenkovsky gas field was generalized and is made consistent with a legend of the published map.

Evaluation of the distribution of landslide slopes in typical tundra of western Siberia is presented in Table 1.

Areas of landslide processes occupy more than 16% of a total area of typical tundra zone. It is a high percentage, considering that landslides occur only in the most elevated locations. The maximum activity of landslide development—over 30% of the area—is characteristic for central Yamal (area 12) and western Gudan (area 14), where hilly sites (V) consisting of permafrost marine loam and clay with salinity over 0.5% (Dubikov 2002) prevail. Landslide slopes occupy about 15–20% of the area of Western Yamal (area 11), Gydansky ridge (area 16), and Tanamo-Yenisey valley (area 18). The structure of these areas almost does not concede to the first two, but the fraction of sand covering salted marine clay increases. The fraction of landslide slopes is minimal in low, strongly boggy, mainly sandy areas (A) with widely-developed river network: east Yamal (area 13), valleys of the rRivers Juribej (area 15) and Tanama (area 17) on Gudan Peninsula.

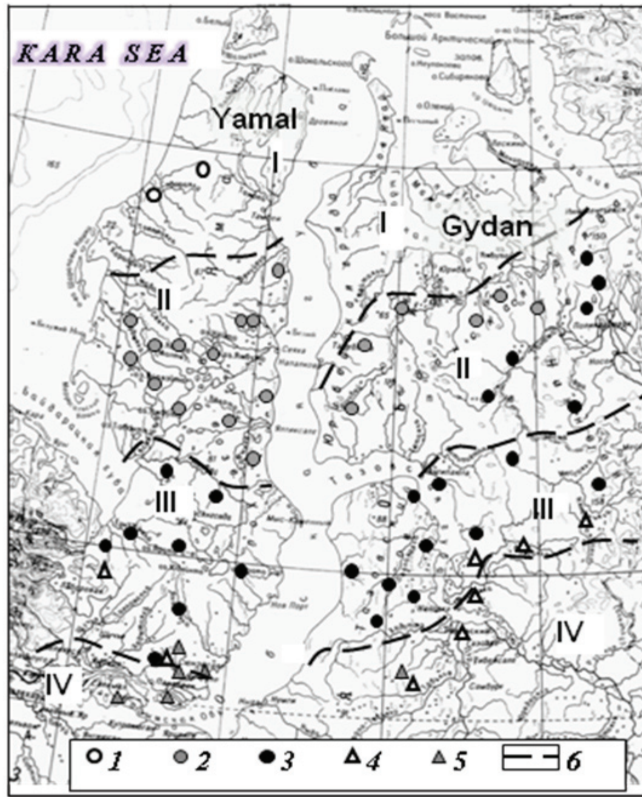

Figure 4. Nenets toponymics (denominations) on the West Siberian topographical map. 1–*pyasyada, tartsya (*nude); 2–nero, *nerka,, neruta* (willow shrub, willow canopy, *Salix sp.*); 3–*pae, paya* (alder shrub, *Alnus fruticosa*); 4–*kharv* (larch, *Larix sibirica*); 5–*khadita* (fir, *Picea obovata*); 6–limits of subzones. Zone and subzone: I-arctic tundra; II–typical (subarctic) tundra; III–southern (low) tundra; IV–forest-tundra.

Willow tundra in Nenets toponymics

The main feature of toponymics of the Nenets people living in the Far North in severe climatic conditions is their deep penetration into nature. To survive in tundra, every Nenets knows (notices) seasonal rhythms of nature and is able to predict the approach of sharp changes of weather and extreme natural phenomena by monitoring the behavior of animals or the state of the vegetation. Figure 4 shows zone borders from the map of northwestern Siberia and the distribution of Nenets toponymics characterising the vegetative cover.

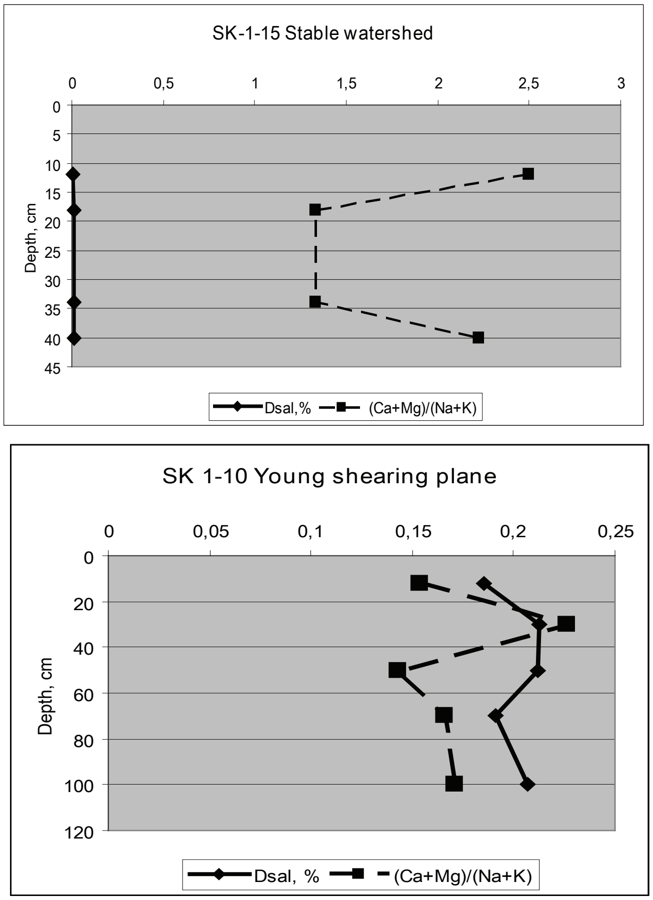

Figure 5. Salinity and cation ratio in active layer profiles on Cape Shaitansky, Western Taimyr. Top panel–stable watershed; bottom panel–young shearing plane.

Thus, the typical terms for the Arctic tundra are *pyasyada* (bald) and *tartsya* (nude). In typical tundra, the names *nero*, *nerka*, *neruta*, and *neromo* (willow shrub, willow canopy) are very common. Borders of southern tundra are underlined by various names with a root base of *pae* or *payu,* corresponding to alder shrubs. The northern limit in the spread of these names on the Yamal Peninsula is the lower part of River Juribej. And it was 40 km from the mouth of Juribej, where the first and the most northern curtains of alder shrubs have been observed on the aerial images.

Toponymic areas repeat outlines of natural zones and subzones, being a little displaced to the north. In the eastern (Prienisejsky) part of the region, the warming effect of the Yenisey River accounts for the especially considerable displacement of toponymic area of alder and larch to the north.

Toponymic areas of alder shrubs and tree species are not in the focus of the present study of landslide slopes distribution. They are shown on the map to illustrate high correlation of Nenets' toponymics to the nature laws. The alder shrub is not an indicator of subzones in southern tundra since it grows mainly in valleys of the rivers (dependent sites). Willow tundra, on the contrary, is widespread on the watersheds (independent sites) where they can be the indicator of ancient landslide activity (Ukraintseva 2004).

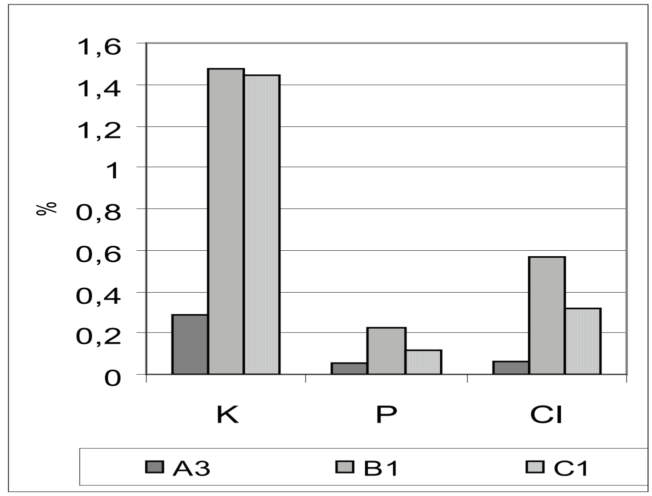

Figure 6. Potassium, phosphorous, and chlorine in grasses on Cape Shaitansky. A3–stable site; B1–shearing plain; C1–landslide body.

Landslides in the Arctic Tundra

Cryogen landslides with glide faces formed by the roof of the salty marine permafrost are widespread on the Yamal and Gudan Peninsulas, on the Taimyr coast of the Yenisey Gulf (from Dixon to Cape Shaitansky), as well as on the islands of the Canadian Archipelago (Ukraintseva et al. 2004, Harry & Dallimore, 1989, Lewkowicz et al 1990). Bare landslide surfaces with salt outcrops are well observed and overgrown with pioneer grasses and herbs with halophytes (vegetation cover varies from 10% to 80%). Landslide age being estimated by vegetation development ranges from a few to several dozen years.

Cryogen landslides are studied in Yenisey Gulf near Cape Shaitansky. The salinity and marine cation ratio (Dubikov 2002) in active layer witnesses the marine origin of sediments (Fig. 5). A joint plot of vertical distribution of salinity and cation ratio clearly illustrates the degree of diagenetic transformation of the marine deposits. On the young shearing plane, the saline marine clay got into the active layer only recently, and its desalination is still in the initial stage. The values of clay salinity on the young shearing plane profile (Fig. 5, bottom panel) are close to 0.2%, which is higher than cation ratio values (salinity curve is to the right from the cation ratio curve). The active layer of stable watershed and slopes was long-term flushed due to drainage and precipitation during the warm seasons of the year. In these areas, the salinity of the active layer is close to zero (Fig. 5, top panel), and the salinity curve is to the left from the cation ratio curve.

Grasses growing on the shearing plain and landslide bodies were considerably more enriched with chlorine, phosphorous, and potassium relative to stable areas, therefore marking leaching of these elements in stable conditions (Fig. 6).

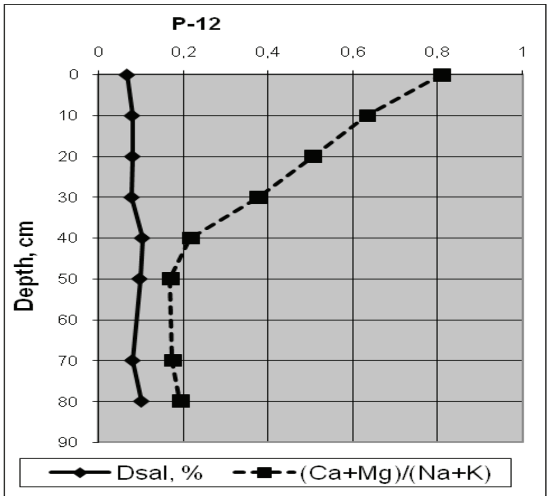

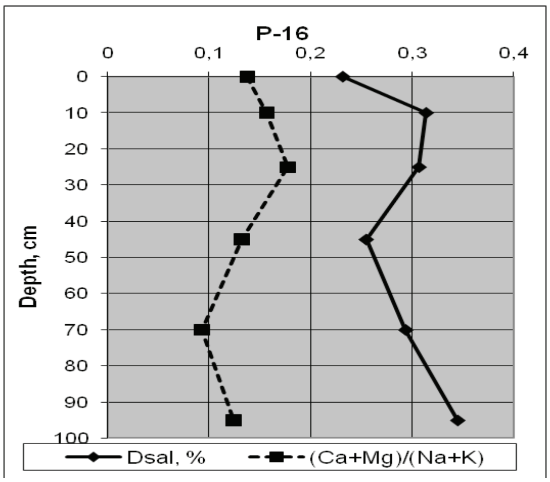

Figure 7. Salinity and cation ratio in active layer profiles on Pelyadkinsky gas field, Southern Gydan. Top panel–young shearing plane; bottom panel–the same shearing plane after repeated landslide event.

Landslides in the Low (Southern) Tundra

The 10–20-year-old landslide events have been studied in 2003–2005 in the Pelyatkinsky gas field located in southern tundra. Salinity and ratios of continental and marine cations also showed the initial marine origin of the sediments in these areas (Fig. 7). Unlike typical and arctic tundra, landslide events in southern tundra bring already significantly diagenetically reworked marine sediments to the active layer (Fig. 7, top panel); thus, cryogen sliding in these areas can be traced by thick layers of diagenetically reworked deposits. After repeated landslide events on the same slope in 2004, the saline marine layer has been exposed at the surface (Fig. 7, bottom panel). As a result, the saline marine permafrost lies twice as deep compared to modern thaw-depth: at 2.5 m depth or even deeper.

The slope is overgrown with low dwarf birch and undershrub-moss tundra. Despite the long-term desalination process, chlorine content is still higher in horsetail and willow leaves inhabiting shearing plains and landslide bodies as compared to the stable background surface (Fig. 8).

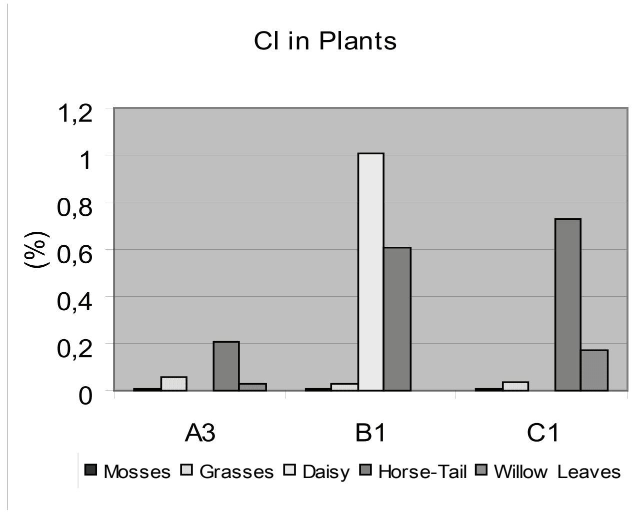

Figure 8. Chlorine in plants. For sites, see comments to Figure 6.

Conclusions

In the arctic tundra, young cryogenic landslides formed by the roof of the saline marine permafrost are widespread. Bare landslide shearing planes with salt outcrops are well observed and overgrown with pioneer grasses and herbs with halophytes. Landslide age estimated from vegetation development ranges from a few to several dozen years.

In the typical (subarctic) tundra, cryogen landslides are mostly widespread and extensively investigated. Areas of cryogenic landslide slopes have been evaluated using the landscape indicator technique, and they occupy close to 16% of the total area of the subzone. The cryogenic landslide process is the leading landscape-forming process in the typical tundra of western Siberia.

Maximum landslide activity (more than 50% of the area) is characteristic for the elevated plains of central Yamal and western Gydan, formed by permafrost marine loam and clay with 0.5% salinity and higher. The fraction of young landslide slopes (10–100 years old) is estimated not to exceed 5–30%. This is an indication of the gradual decay of landslide processes in these areas.

In the southern (low) tundra, cryogenic landslides have been active since the Holocene Hypsitermal (7000–8000 years ago). At the present time, the desalination process of landslide slopes is finished. The slopes are covered with thick mosses and high willow shrubs partially replaced by dwarf birch. Thick layers of old diagenetically reworked deposits containing a mixture of iron-enriched and buried organic-enriched sediments might be the only indicators that cryogenic sliding took place on these hill slopes.

Thus, during the Holocene, landslide processes slowly moved further north, causing the consequent spread of willow communities with high bio-productivity to the north. Southern tundra (at present the process is finished) formed 5000–8000 years ago; typical tundra (active process, widespread high willows), 2000–0 years ago; and arctic tundra (the beginning stage, young landslide slopes with grass cover and sparse willow restoration), 20–30 years ago. The indicator of the final stage of the landslide process is the replacement of high willow shrubs by typical zonal vegetation with a thick lichen-moss-litter layer.

Therefore, the presented study has demonstrated that the dynamic process of cryogen sliding caused by increase of heat, moisture, and seasonal thaw-depth is moving to the north. This can be considered as an additional indication of the global warming tendency in the arctic climate.

Acknowledgments

The author is grateful to Elena Korobova and Tatiana Smirnova for assistance in paper preparation, and to the crew of the research vessel "Akademik Boris Petrov" who participated in the fieldwork. The author also acknowledges A. Savichev, S. Sorokin, and R. Grishina for chemical analyses of samples.

References

Andreev, V.N. 1970. Some geographical laws in the distribution of above-surface phytomass in tundra zone in connection with progress to the north of tree-shrubs vegetation. In: *Biological Basis of Nature Usage in the North*. Syktyvkar: Komi Publisher (in Russian).

Burn, C.R. & Friele, P.A. 1989. Geomorphology, Vegetation Succession, Soil Characteristics and Permafrost in Retrogressive Thaw Slumps near Mayo, Yukon Territory. *Arctic* 42(1): 31-40.

Geertsema, M. & Pojar, J.J. 2007. Influence of landslides on biophysical diversity—A perspective from British Columbia. *Geomorphology* 89(1): 55-69.

Drozdov, D.S. & Ukraintseva, N.G. 2000. *The map of natural geocryosystem of Bovanenkovo gas field (landscape map).* E.S. Melnikov (ed.). Earth cryosphere Institute SB RAS.

Dubikov, G. I. 2002. *Structure and a cryogenic structure of frozen thicknesses of Western Siberia*. Moscow: GEOS, 246 pp.

Harry, D.G. & Dallimore, S.R. 1989. Permafrost, Ground Ice and Global Change in the Beaufort Sea Coastlands. Moscow: GEOS 3, 48-53.

Leibman, M.O. 1995. Preliminary results of cryogenic landslides study on Yamal Peninsula, Russia. *Permafrost and Periglacial Processes* 6: 259-264.

Leibman, M.O., Archegova, I.B., Gorlanova, L.A. & Kizyakov, A.I. 2000. Stages of cryogenic landslides on Yugorsky and Yamal Peninsulas. *Earth Cryosphere* IV(4): 67-75 (in Russian).

Leibman, M.O. & Egorov, I.P. 1996. *Climatic and Environmental Controls of Cryogenic Landslides, Yamal, Russia. Landslides.* Rotterdam: Balkema Publishers, 1941-1946.

Lewkowicz, A. 1990. Morphology, frequency and magnitude of active-layer detachment slides, Fosheim peninsula Ellesmere Island, N.W.T., Permafrost-Canada. *Proceedings of the Fifth Canadian Permafrost Conference,* Quebec: Collection Nordicana, 54.

Matsuda, K. et al. 1988. Observations of Geomorphic and Vegetational Changes Caused by Thermal Erosion of an Involuted Hill in Tuktoyaktuk, N.W.T., Canada. In: *Characteristic of the massive ground ice body in the Western Canadian Arctic related to paleoclimatology, 1984-1985.* Hokkaido: Inst. Low Temp. Sci., Hokkaido Univ.

McKendrick, Jay D. 1987. Plant Succession on Disturbed Sites, North Slope, Alaska, U.S.A. *Arctic and Alpine Research* 19 (4): 554-565.

Melnikov, E.S. (ed.). 1991. *Map of natural geosystem of the North Western Siberia.* 1:1,000,000. Novosibirsk: Map Publishing House, 6 sheets.

Melnikov E.S. & Grechishthev S.E. 2002. *Permafrost and Development of Oil and Gas Regions.* Moscow: GEOS, 402 pp.

Pospelova, E.B. & Pospelov, I.N. 2000. Relic high shrub communities near the northern border (the central part of Byrranga mountains, Taymyr Peninsula). *Novosti Akademii nauk, seriya geographicheskaya,* (4): 92-97.

Poznanin, V. L. 2001. Morphology, the mechanism of formation and dynamics active-layer detachments on the central Yamal. In: *Problems of environment and natural resources.* Moscow: VINITI (2), 78-92.

Rebristaya, O.V., Khitun, O.V., Chernyadyeva, I.V. & Leibman, M.O. 1995. Dynamics of vegetation on the cryogenic landslides at the central part of Yamal Peninsula. *Botanical Journal* 80(4): 31-48 (in Russian).

Sturm, M., Racine, C. & Tape, K. 2001. Increasing shrub abundance in the Arctic. *Nature* 411: 546-547.

Ukraintseva, N.G. & Leibman, M.O. 2000. Productivity of willow-shrub tundra in connection with landslide activity. In: *30th Arctic Workshop, March 15-19 2000*. Boulder, CO USA: INSTAAR, University of Colorado, 150-152.

Ukraintseva, N.G., Streletskaya, I.D., Ermokhina, K.A. & Yermakov, S.Yu. 2003. Geochemical properties of plant-soil-permafrost system at landslide slopes, Yamal, Russia. In: M. Phillips, S.M. Springman & L.U. Arenson (eds.), *Proceedings of the Eighth International Conference on Permafrost, Zurich, Switzerland, July 20-25, 2003*: 1149-1154.

Ukraintseva, N.G. 2004 Spreading of cryogenic landslides in typical tundra subzone of Western Siberia. In: Moscow, GEOS (ed.), *Sergeevsky chteniya* (6): 211-214

Ukraintseva, N.G., Shuvalova, E.M. & Smetanin, N.N. 2005. Cryogenic landslides in the area of Bovanenko gas field: spread, peculiarities, consequence. *Proceedings of the 3th Conference of the Russian Geocryologist. Moscow, 1–3 July 2005*. Moscow: MSU. V.2, teil 3, 178-185 (in Russian).

Ukraintseva, N.G. & Leibman, M.O. 2007. Cryogenic landslides (active-layer detachments) and fertility of tundra soils on Yamal Peninsula, Russia. *Proceedings of the First North American Landslide Conference Vail, Colorado, June 3-–8, 2007:*1605-1615. Conference CD.

Permafrost Occurrence in Southernmost South America (Sierras de Alvear, Tierra del Fuego, Argentina)

Marcos Valcárcel-Díaz
Department of Geography, University of Santiago de Compostela, Santiago de Compostela, Spain
Pedro Carrera-Gómez
Department of Geography, University of Santiago de Compostela, Santiago de Compostela, Spain
Ramón Blanco-Chao
Department of Geography, University of Santiago de Compostela, Santiago de Compostela, Spain
Augusto Pérez-Alberti
Department of Geography, University of Santiago de Compostela, Santiago de Compostela, Spain

Abstract

Several lines of evidence indicate that permafrost is present at elevations above ca. 775 m a.s.l. in the Mount Alvear region of the Sierras de Alvear, Fuegian Andes, Argentina. Ground temperatures recorded to depths of 1.3 m in sorted circles remain near 0°C in late summer and suggest perennial frozen ground at a depth of approximately 1.5 to 2 m. Three active rock glaciers occur in the upper Alvear Valley. On the flat surface to the east of the Alvear Glacier, sorted circles are located in the centres of poorly-defined polygons. The latter are interpreted to reflect either joint widening in underlying bedrock or thermal-contraction cracking in bedrock. Collectively, this evidence suggests the presence of permafrost on the higher summits of the Fuegian Andes.

Keywords: Argentina; Fuegian Andes; ground thermal regime; mountain permafrost; rock glacier.

Introduction

The distribution and characteristics of mountain permafrost in the southernmost Andes are, to date, poorly known. This contribution provides both geomorphological and instrumental (ground temperature records) evidence for the occurrence of permafrost in the high levels of the Sierras de Alvear, Tierra del Fuego, Argentina (Fig. 1). The central sector of the Fuegian Andes is characterized by the presence of a wide variety of cryogenic landforms related to ground freezing and/or to nivation activity (e.g., frost-heaved clasts, patterned ground, debris lobes, clast pavements, and protalus ramparts) (Valcárcel-Díaz et al. 2006), and to permafrost occurrence (rock glaciers). According to Corte (1997), the lower limit of permafrost in the Fuegian Andes is located at 900 m a.s.l.

The research presented in this contribution has focused on an unnamed summit and the upper Alvear Valley (54°40′S, 68°02′W), both located ca. 2.5 km to the E of Mount Alvear and the Eastern Alvear Glacier, at elevations ranging from 775 to 1077 m a.s.l. The summit is a nearly flat, clast-covered surface with occasional rock outcrops. The upper Alvear Valley shows steep slopes and is bounded by an arête and a near-vertical rock wall. The bedrock is composed of Late-Jurassic basalts, porphyrites, and slates (Olivero & Martinioni 2001). Southern Tierra del Fuego climate is cold-temperate and wet (Tuhkanen 1992). Air temperature measured from January 2005 to January 2006, at 1050 m a.s.l. near the upper col of the Alvear Valley was -2°C. No precipitation data are available for these mountains. Snowfalls are frequent and may take place year-round, even during summer. Strong and persistent winds blow on the summit area, where gusts exceeding 140 km/h have been recorded. Vegetation cover is extremely scarce and is limited to communities of lichens and mosses.

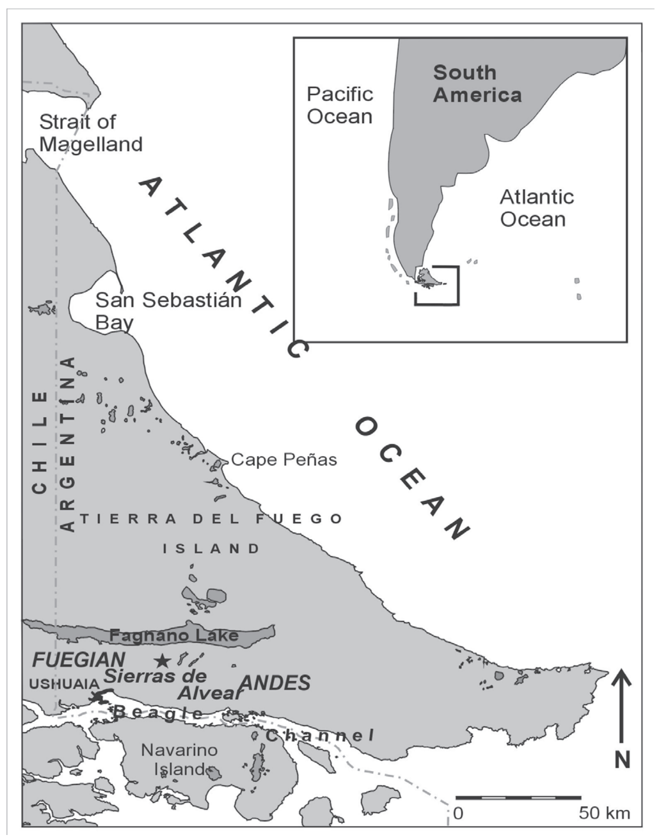

Figure 1. Location of the Sierras de Alvear.

Geomorphological Observations

A geomorphological survey, focused on the identification of potentially active landforms indicative of permafrost, was carried out in the summit area and the upper Alvear Valley.

The nearly flat summit is almost entirely covered by a sheet of rock rubble, composed of basalt and porphyrite angular clasts, overlying solid bedrock. The thickness of the rubble sheet is roughly estimated to exceed 1 m. However, small outcrops of bedrock occur, showing evidence of widespread and intense mechanical weathering. Poorly defined polygons, 4 to 5 m wide, delimited by shallow furrows or trenches 30 to 50 cm deep, have developed in the underlying bedrock. Small depressions or stone pits have formed in the intersections of the furrows. Sorted circles (“stony earth circles”), composed of an exterior border of coarse clasts enclosing an inner sector of sands, silts, and isolated larger clasts, occur in the centers of the polygons (Fig. 2). The latter are interpreted to reflect either joint or fracture widening in underlying bedrock or thermal-contraction cracking of the bedrock. Although it has yet to be proven if the polygons are presently active, the inner nonsorted circles show present-day activity related to seasonal freezing.

Three rock glaciers occur at the foot of the northwestern ridge of the upper Alvear Valley. According to shape, one is complex, the second is lobate, and the third is tongue-shaped. All of them are of reduced dimensions, but nevertheless, seem to be presently active. As the tongue-shaped rock glacier is better-developed than the others, the geomorphological survey was conducted on it. This is a small, talus-derived rock glacier 150 m long, 70 m wide, and 22 m high (Fig. 3). It is located at the foot of a southwest-facing, near-vertical rock wall, and it extends downwards to 775 m a.s.l. The root area grades into a steep talus slope (mean gradient is 36°). It is predominantly composed of angular, slate blocks, embedded in finer debris, and it is directly connected with its source area. The shales that form the rock wall are densely jointed and foliated, being highly susceptible to frost weathering and favoring talus production. Under present climatic conditions, talus production is considerable. Transport of debris from the talus to the root area of the rock glacier seems to be steady. This landform shows some of the features stated by Barsch (1996) as to be distinctive of active rock glaciers, e.g., steep front and side slopes (mean gradient is 38°), and exposure of fine, light-colored, unweathered material in the front and side slopes.

Figure 2. Oblique aerial view of nonsorted circles and polygons developed on the summit surface. Arrow indicates shallow borehole site.

Figure 3. View of the tongue-shaped rock glacier of the upper Alvear Valley. Arrows indicate the front slope of the complex rock glacier.

Methods

A shallow borehole equipped with thermistor probes was set up in the summit area. The aim was to get temperature records that could prove the occurrence of permafrost. Due to logistical problems, a similar borehole could not be drilled in the tongue-shaped rock glacier of the upper Alvear Valley.

The borehole is 2 cm in diameter, and it was made in the centre of a nonsorted circle located at 1057 m. a.s.l. (Fig. 2), using a battery-powered drill. Drilling was mainly conducted through a thick layer of frost-weathered rock rubble, up to a depth of 130 cm. Further deepening of the drill hole was impeded by the presence of solid bedrock. Thermistor probes were fixed with adhesive tape to a wooden rod 1.5 cm in diameter. The rod was then inserted into the drill hole, and the probes were installed at depths of 1, 5, 10, 20, 35, 70, 100, and 130 cm. Only the records corresponding to the probes located at depths of 1, 70, and 130 cm will be discussed in this paper. Temperature probes have a resolution of 0.03°C and an accuracy of ±0.25°C. Data were read and stored hourly using “U12” multi-channel data loggers (from Onset Computer Corp.).

The time span covered by the temperature records extended from mid-February 2006 to the end of January 2007.

Results

Figure 4 shows the temperature curves obtained from the shallow borehole of the summit. Ground temperature evolution at the surface (1 cm depth) is mainly characterized by the occurrence of short-term fluctuations throughout

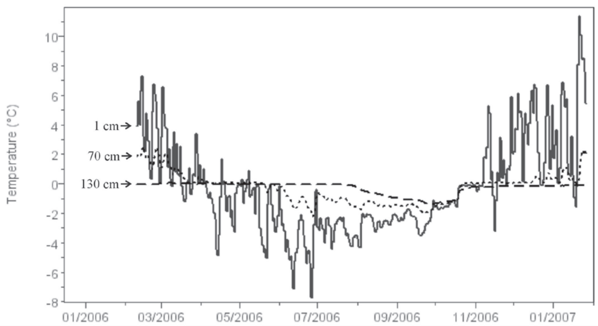

Figure 4. Temperature curves displaying daily mean values, obtained at depths of 1, 70, and 130 cm in the shallow borehole of the summit.

the year, including winter. The mean temperature of the recording period was -0.3°C. Minimum temperature occurred in early winter (end of June) and was -7°C. Temperature at the end of the winter (mid-September) was slightly below -3°C. Seasonal freezing extended from early April to early November and was interrupted on three occasions by daily above zero fluctuations. The end of the seasonal freezing (period from mid-October to early November) was characterized by an increase in temperature, attaining a nearly constant value close to 0°C, probably due to snow melting and heat transfer by percolating melt water. Daily frost mainly takes place during late spring and summer.

The evolution of ground temperature at a depth of 70 cm during the seasonal freezing period, shows a general trend similar to that at 1 cm depth. Surface daily fluctuations have been filtered at this depth, and the mean temperature was -0.28°C. Similar to the upper thermistor, the minimum temperature occurred in early winter (end of June) and in this case was -2.3°C. Seasonal freezing was not interrupted and extended from mid-May to early November. Two zero curtains occurred immediately before (from mid-April to mid-May) and after (from the end of October to mid-December) the seasonal freezing period.

Ground temperature at a depth of 130 cm continuously remained below 0°C, except from a short period of 20 days with positive values (from early to mid-March), in which a maximum temperature of 0.05°C was attained. The mean temperature was -0.28°C, and the minimum temperature occurred in early spring (end of September) and was -1.39°C. Short-term temperature fluctuations have been completely filtered at this depth, and only the annual cooling and warming cycle is observed.

Discussion

Evidence of the occurrence of perennial frozen ground in the summit area is provided by the temperature records obtained in the shallow borehole. Ground temperature at a depth of 1.3 m remained subzero almost year-round (mean temperature was -0.28°C), except for a short period in late summer (from early to mid-March), when it experienced slightly above 0°C values.

Winter short-term fluctuations observed in the surficial level of the borehole suggest the presence of a thin snow cover. The summit is swept by persistent and strong winds, limiting snow cover build-up. Direct exposure to the cold atmosphere throughout winter takes place, allowing deep frost penetration into the ground. Bearing this evidence in mind, permafrost is estimated to occur at depths below ca. 1.5 –2 m in the summit area.

The occurrence of permafrost in the upper Alvear Valley can only be inferred from the geomorphological evidence of activity observed in rock glaciers.

It is difficult to establish the lower altitudinal limit of the permafrost belt with the currently available data. However, if we consider the active rock glaciers of the upper Alvear Valley as permafrost indicators, then we can propose the approximate lower limit of discontinuous permafrost. This limit is roughly indicated by the elevation reached by rock glacier fronts (Barsch 1996). In our case, the lower limit of discontinuous permafrost would be at ca. 800–775 m a.s.l. Patches of sporadic permafrost could exist at lower elevation in particularly suitable topoclimatic locations.

The suggested limit is lower than that proposed by Corte (1997), who estimated the lower limit of permafrost in the mountains of Tierra del Fuego to be at 900 m a.s.l.

Conclusions

Preliminary observations suggest the occurrence of permafrost at 1057 m. a.s.l. in the unnamed summit located to the E of Mount Alvear and the Eastern Alvear Glacier, at depths below ca. 1.5–2 m. However, a longer time series from the summit borehole is needed to obtain definitive results.

The lower limit of the discontinuous permafrost in the studied area is tentatively placed at ca. 800–775 m a.s.l., according to the elevation reached by the front of active rock glaciers.

Further research is needed in order to gain a better understanding about mountain permafrost distribution and characteristics in the Sierras de Alvear. Proposed future work comprises geoelectric surveys and the drilling and equipment of new shallow boreholes (particularly in the rock glaciers of the the upper Alvear Valley).

Acknowledgments

The authors want to thank Professor Hugh M. French for his help and valuable suggestions during the 2007 field season. Thanks are also due to Mr Luis Lavado, helicopter pilot, for his logistical support. Two anonymous reviewers provided valuable comments that helped to improve the initial version of the paper. Their advice is greatly appreciated. This research has been funded by the Ministerio de Educación y Ciencia (Spain) projects CGL2004-03380/BOS and POL2006-09071, and it is a contribution to the International Polar Year.

References

Barsch, D. 1996. *Rockglaciers. Indicators for the Present and Former Geoecology in High Mountain Environments*. Berlin: Springer-Verlag, 331 pp.

Corte, A. 1997. *Geocriología. El Frío en la Tierra*. Mendoza, Ediciones Culturales de Mendoza, 398 pp.

Olivero, E.B. & Martinioni, D.R. 2001. A review of the geology of the Argentinian Fuegian Andes. *Journal of South American Earth Sciences* 14: 175-188.

Tuhkanen, S. 1992. The climate of Tierra del Fuego from a vegetation geographical point of view and its ecoclimatic counterparts elsewhere. *Acta Botanica Fennica* 145: 1-64.

Valcárcel-Díaz, M., Carrera-Gómez, P., Coronato, A., Castillo-Rodríguez, F., Rabassa, J. & Pérez-Alberti, A. 2006. Cryogenic landforms in the Sierras de Alvear, Fueguian Andes, Subantarctic Argentina. *Permafrost and Periglacial Processes* 17(4): 371-376.

Appearance of Heinrich Events on Pollen Plots of Late Pleistocene Ice Wedges

Alla C. Vasil'chuk
Geography Department, Lomonosov's Moscow University, Moscow, Russia

Yurij K. Vasil'chuk
Geography and Geology Departments, Lomonosov's Moscow University, Moscow, Russia

Abstract

The palynological characteristics of large ice wedges and surrounding syngenetic yedoma sediments at three locations in the Lower Kolyma River Valley in northeast Yakutia are presented. AMS ^{14}C dating of micro-organic and pollen concentrates from the ice wedges reveal sharp oscillations of pollen and spore spectra, and permit correlation of these rhythms with Heinrich events. The variability of global, regional, and local pollen components in yedoma sediments linked with periodical rhythms is discussed.

Keywords: ice wedge; Heinrich events; pollen; Yakutia.

Introduction

Coolings of the North Atlantic Ocean associated with Heinrich events appeared throughout the various natural systems at global and regional scales. For example, traces of Heinrich events are recorded in sediments of Lake Baikal as variations in diatoms and Fe(II)/Fe(III) ratios (Grygar et al. 2006), and maximum terminal position of glaciers in the Swiss and Austrian Alps (Ivy-Ochs et al. 2006). Regional response of Siberian landscapes linked to the North Atlantic's thermohaline circulation is indicated by oxygen-isotope analysis of syngenetic ice wedges and by pollen data from well-dated cross-sections of ice-wedge complexes. Simulation of Late Pleistocene circulation (Sarnthein et al. 2002, Lowe et al. 2006) shows that there was positive feedback for the northern Eurasian region. We suppose that Heinrich Events were characterized as times of low summer temperatures. Hence pollen spectra could be potential archives of Heinrich Events. Pollen is well preserved in ice-wedge ice because of low temperatures, the stable conditions of this closed system and the low microbial activity. ^{14}C dating of fossil pollen grains contained in ground ice could therefore provide new information about past environments. The pollen concentration in ice wedges is very similar to those of Arctic ice caps: approximately 10 to 1000 grains/l. As with Arctic ice caps (Bourgeois 2000), the pollen assemblages from ice wedges in arctic and subarctic tundra comprise a high percentage of far-travelled pollen, primarily tree pollen. The regional tundra pollen input is essential also, and the local pollen contribution is very small. The penecontemporaneous pollen grains and spores are also found in ice wedges (Vasil'chuk et al. 2003, 2005a, b, Vasil'chuk 2005, 2007).

To interpret the pollen variations in ice wedges and their host sediments we apply Yu.Vasil'chuk's (1992) multistage model of large syngenetic ice-wedge ice formation. The ice wedges develop as large pulses of subaquaeous deposition alternate with subaerial conditions of ice-wedge growth. The main water source for ice wedges is snowmelt water during the subaerial stage and mixtures of snowmelt, river or lake water during the subaqueous stage. Water enters frost cracks in spring, when snow melting and flooding take place. During the subaqueous stage "reworked" pollen and spores may enter into ice wedges.

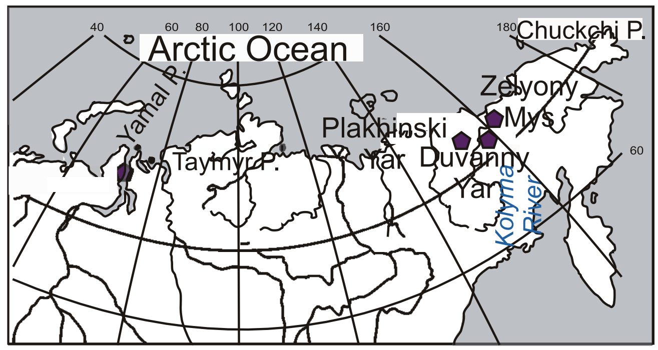

Figure 1. Location of ice-wedge sections in the Lower Kolyma River area of northeast Yakutia: Duvanny Yar, Plakhinskii Yar, and Zelyony Mys.

Regional Setting

The locations of the study sites in the Lower Kolyma River area of northeast Yakutia are shown in Figure 1. Vertical cross-sections through ice-wedge complexes were examined at Duvanny Yar, (69°N, 158°E); at Plakhinskii Yar, on the left bank of the Stadukhinskaya stream (68°40'N, 160°17'E); and At Zelyony Mys (70°N, 160°E), in northern taiga near the boundary with forest tundra. The mean winter air temperature is -22°C. This sequence with a depth of 22–24 m is especially valuable for palaeogeographical reconstruction because of the abundance of multistage ice wedges. The dominance of herb immature pollen indicates a very short vegetation period.

Results and Discussion

The Plakhinskii Yar exposure reveals syngenetic permafrost sediments with thick ice wedges. Here we present the results of a palynological study of ice wedges (16 samples) and the surrounding sediments (30 samples).

The pollen plot from sediments is dated by ^{14}C from 26 to 11 kyr BP, and the ice wedges are dated from 17 to 11 kyr (Fig. 2).

The sediments are characterized by a dominance of immature herb pollen (55.8–97.0%). Two intervals of very short vegetation periods are identified on the pollen plot: 24–21 kyr BP (9–12 m) and 17–11 kyr BP (3–6 m).

Larix pollen is found at a depth of 6.3 m in the sediments and also in the ice wedge at a depth of 8.2–8.8 m. The difference may be the depth of frost cracking at that time.

Every maximum of immature pollen comes before a local maximum of *Artemisia* and *Pinus pumila*. The pollen spectra of ice wedges show regional vegetation changes from 14 to 17 kyr; i.e., during the first Heinrich event. The *Artemisia* maximum (36.6%) coincides with a local maximum of immature pollen (42.2%) and a minimal amount of *Betula nana* pollen.

In the upper part of the plot the *Artemisia* content decreases and *Poaceae* increases together with *Selaginella sibirica* and *Pinus pumila.*

There are three development stages of vegetation cover. The first stage is single *Larix* trees, *Betula* sect. *Nanae* and *Poaceae-Artemisia* grass tundra. The second stage is the maximum development of herbaceous nival meadows (a very short vegetation period) with *Artemisia.* The third stage is grassland tundra.

Because the ^{14}C dates approximately correlate with H1, we suggest that pollen phase changes indicate this global climatic change. The structure of H2, according to ^{14}C-dates (21–23 kyr BP), can be followed only in the pollen plot of the sediments. The indicator of most extreme conditions is the maximum immature pollen, comes before the local *Artemisia* maximum (Vasil'chuk 2005, 2007).

The *Zelyony Mys* 36 m exposure of ice wedges occurs in loamy syngenetic sediments. There is no organic material in the upper 10 m. The lower 26 m consist of three layers of high and low peat content. Large ice wedges have shoulders at levels of peaty layers. The tops of small ice wedges are located at the level of the shoulders. The cryogenic structure is caused by subaqueous conditions of sedimentation and subaerial freezing of the sediment, together with peaty layers and ice-wedge growth (Vasil'chuk 1992).

According to the ^{14}C-dates, the duration of the subaerial stage is about 2–3 kyr, and that of the subaqueous one is about 1–1.5 kyr. From 37 to 27 kyr BP there were three subaerial periods. Gophers' holes mark subaerial horizons, when ice wedges grew in width. Seeds from the holes are dated at 30.5 and 32.8 kyr.

Figure 3 shows the results of a palynological study of ice wedges (11 samples) and the surrounding sediments (45 samples). The pollen plot of the sediments is dated by ^{14}C from 36–38 to 22–23 kyr BP, and the ice wedges date from 27 to 13 kyr. Every maximum of immature pollen corresponds with a local maximum of *Selaginella sibirica* and a local minimum of *Pinus pumila*. Most *Varia* is represented by *Brassicaceae* and *Rosaceae*. The seeds and pollen of *Potentilla nivea L., Draba cinerea Adam., Ranunculus repens L.*, are found in gophers' holes at a depth of 5–15 m (Vasil'chuk 2005).

Simultaneous changes in both local and regional components indicate regional or global changes of seasonal vegetation conditions. Maxima of *Pinus sibirica* are located immediately under peaty layers. Peaty layers contain high concentrations (up to 26%) of shrub pollen, mainly *Betula* sect. *Nanae*. But shrub remains have not been found.

There are three rhythms in the pollen plot of sediments, expressed by variations of local and regional components. At the base of the lower rhythm, the maximum percentages of *Selaginella sibirica* (about 40%) are replaced with maximum percentages of *Artemisia* (14.2%), *Poaceae* (16.4%) and *Betula* sect. *Nanae* (18.1%).

The most unfavorable conditions (very short vegetation season) are recorded by maximum percentages of unmatured pollen in the peaty layer at a depth of 24–22 m. The peat contains "reworked" organic material, as indicated by inverted ^{14}C dates. There is no penecontemporaneous pollen, but the content of coal particles is about 250%. Then the percentages of unmatured herb pollen decreases from 87 to 19%. Simultaneously there are increases in the content of *Pinus sylvestris* (21%) and *Betula* sect. *Nanae*. (19%) together with twin peaks of *Selaginella sibirica (*37–41%).

We suggest that sediments at a depth of 22 m accumulated at the erosion level caused by H3, about 29–27 kyr BP.

The next rhythm has another structure. The peak of *Betula* sect. *Nanae* (22.5%) is replaced with a maximum of *Pinus sylvestris* (19.8%), *Selaginella sibirica* (29.2%) and a very low content of *Poaceae.* This "suggests an" increase of the accumulation rate of sediments at the thermal minimum and subsequent improvement of vegetation season conditions.

Due to difference of the scales between the plots of sediment and ice wedges, we can look after regional changes of pollen rain of this rhythm at the pollen plot of the ice wedge. The maximum *Poaceae* and *Selaginella sibirica* is replaced by a *Pinus sylvestris* peak conterminous with maximum percentages of *Varia* at a depth of 20–18 m. According AMS-^{14}C dates of ice and the similar variations of regional components, we suggest that this rhythm coincides with H2 (about 23 kyr BP).

In the upper part of the pollen plot, *Pinus sylvestris* pollen disappears. The same variation of pollen is observed as at Plakhinskii Yar, and is correlated with H2. The *Artemisia* maximum is replaced by a peak of immature *Varia* pollen. The content decreases and *Poaceae* increases together with *Selaginella sibirica* and *Pinus pumila.* The final stage of H2 is absent in the ice-wedge record.

In the *Duvanny Yar exposure* large syngenetic ice wedges occurred in a 55 m thick section of loam (Fig. 4). The wedges are up to 3–3.5 m wide in the bottom of the cross-section, and up to 1.0–1.5 m wide in the upper part.

On the basis of more than 50 ^{14}C conventional dates of the host sediments we conclude that ice-wedge formation occurred from 37 to 17 kyr BP (Fig. 4). The age of the beginning of sediment accumulation is confirmed by a ^{14}C date of 31,200 yr BP from ice-wedge ice at a height about 6 m above sea level (Fig. 3), as well as by AMS ^{14}C dating of

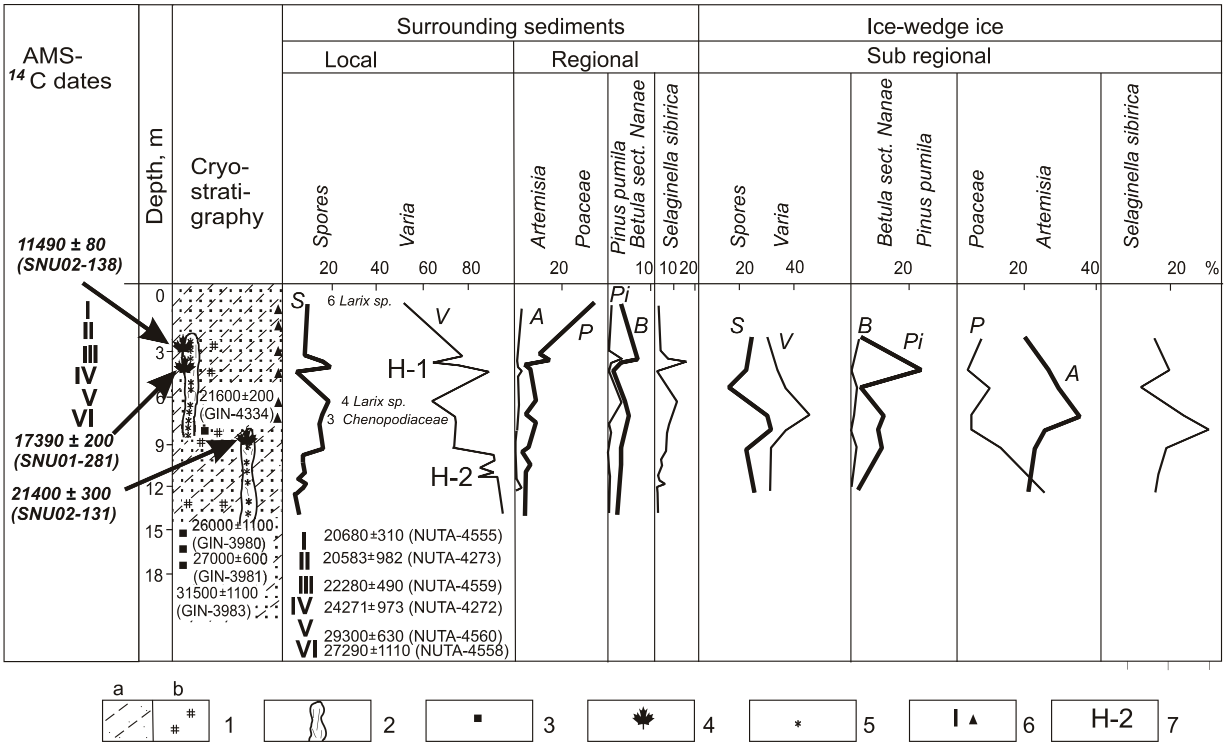

Figure 2. Pollen and spores plot of Plakhinskii Yar ice-wedge cross-section (after Vasil'chuk 2007 with corrections): 1 – sediments: a – sandy loam, b – peat remains in edoma sediments, 2 – large syngenetic ice wedges 3 – sampling point in surrounding sediments for radiocarbon dating; 3 – 4 sampling point of for AMS radiocarbon dating; 3 –of micro organic from ice-wedge ice 4 – of pollen concentrate from ice-wedge ice, 5 – 6 – sampling point for palynological analysis: 5 – from surrounding sediments, 6 – from ice-wedge ice; 7 - a cold phase of Heinrich events on pollen curve. Latin letters near to pollen curves indicate first letter of the name of the appropriate plant. NUTA – radiocarbon dates of Fukuda et al. (1997).

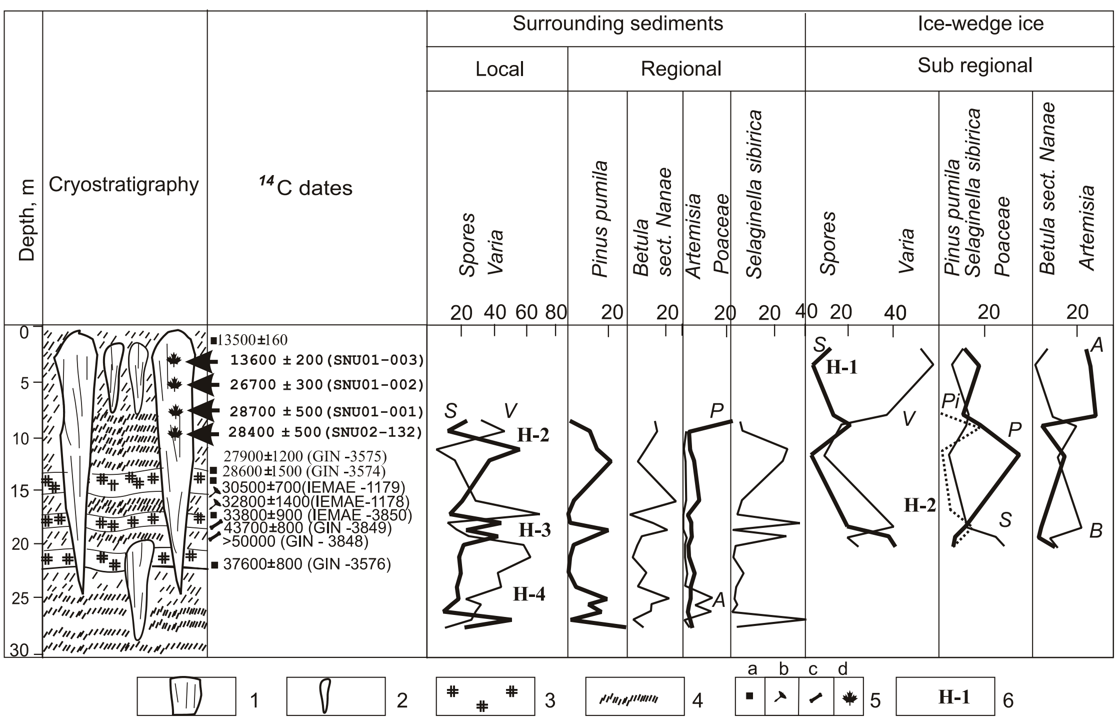

Figure 3. Pollen and spores plot of the Zelyony Mys ice-wedge cross-section: 1 – large syngenetic ice wedge 2 – small buried ice wedge 3 – peat remains; 4 – sandy loam; 5 – sampling point for ^{14}C dating: a – rootlets, b –seeds, c – bones; d – micro organic remains ≤ 200µm; 6 – cold phase of Heinrich events on pollen curve. Latin letters near the pollen curve indicate first letter of the name of the appropriate plant.

separate fractions of plant organic material separated using a microscope from samples of mixed plant detritus.

Here we present the results of a palynological study of sediments (93 samples) and their contained ice wedges (23 samples). The pollen plot of sediments dated by ^{14}C is from 31 to 14 kyr BP. The ice wedges have been dated from 25 to 14 kyr BP (Vasil'chuk 2007, Vasil'chuk & Vasil'chuk 1998, Vasil'chuk et al. 2004).

A main feature of the Duvanny Yar pollen plot is the stable ratio between local components. This suggests that sediment accumulation took place during stable local conditions. Various herbs and *Selaginella sibirica* represent local vegetation. Minimal salt concentrations correspond to high percentages of *Varia* and *Poaceae*, whereas maximum salt concentration corresponds with a peak of *Selaginella sibirica*.

Larix pollen is found in ice wedges, indicating that larch occurred as isolated trees in that vegetation community. The three small peaks of Artemisia percentages (4.5–5.1%) indicate short-term dry periods. It is possible to assume that the sediment at the depth of 15–19 m accumulated at 27–29 kyr BP and corresponds to H3. It is also possible to correlate an increase of *Poaceae* with a warm phase, and a subsequent maximum of Artemisia with H2 (21–23 kyr BP). In the upper part of the plot is observed a typical distribution of the components for H1 (16.5–14 kyr BP).

Pollen spectra of ice wedges demonstrate regional peculiarities of two rhythms of vegetation cover changes. The lower one, at a depth of 11.6–21 m, is similar to the lower rhythm of the ice-wedge plot of Zelyony Mys. The maximum spores percentages correspond with the *Poaceae* peak, which is replaced by *Artemisia* and then by *Varia* peak. We equate this rhythm with H2 (21–23 kyr BP).

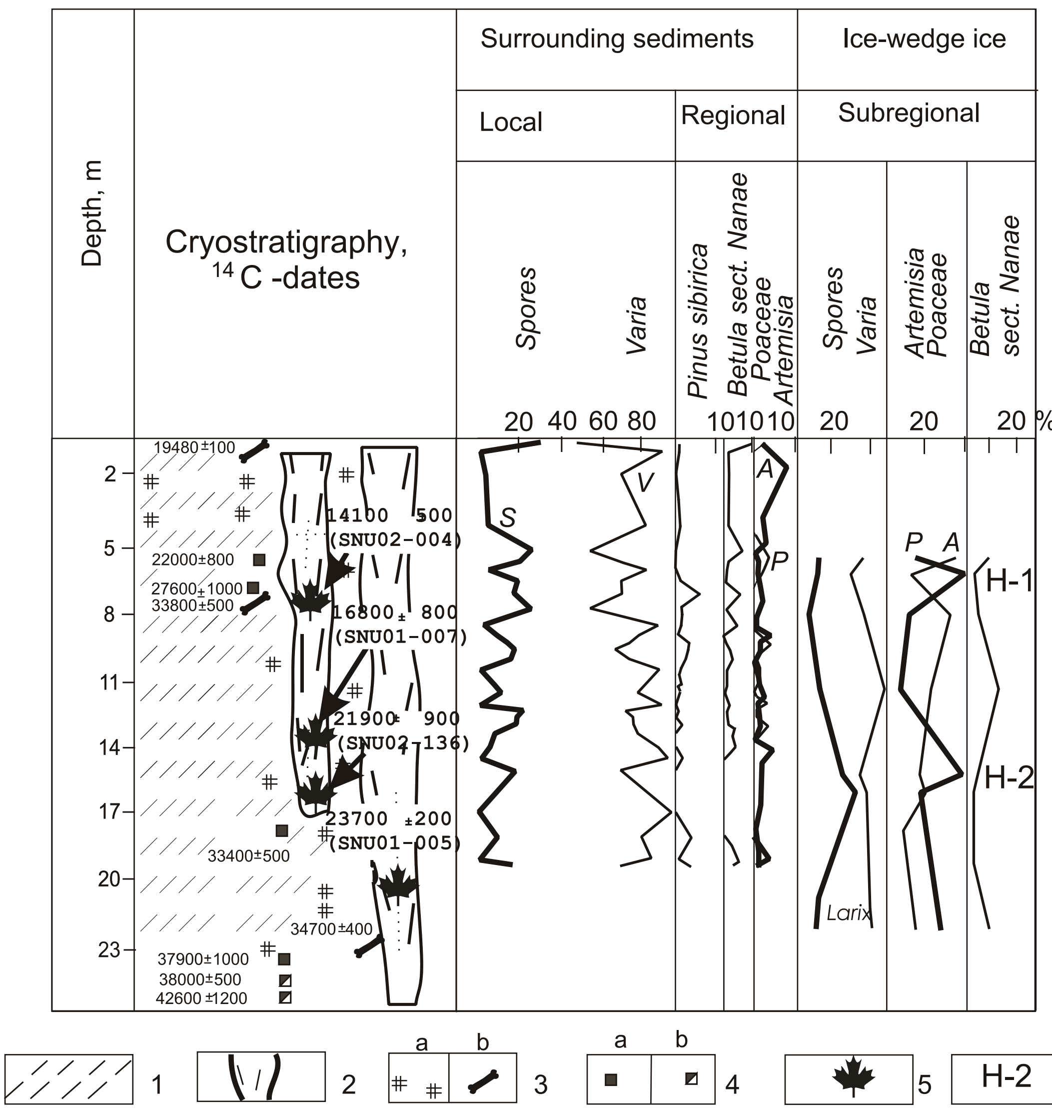

Figure 4. Pollen and spores plot of Duvanny Yar ice-wedge cross-section (after Vasil'chuk 2007 with corrections): 1 – sandy loam; 2 — large syngenetic ice wedge; 3-a – plant remains and peat, b – bones; 4 – sampling point for radiocarbon dating: a – rootlets, b –branches; 5 – sampling point from ice-wedge ice: for AMS ^{14}C dating, of pollen concentrate; 6 – a cold phase of Heinrich events on pollen curve. Latin letters near to pollen curves indicate first letter of the name of the appropriate plant.

The structure of upper rhythm (11.6–5.5 m) is similar to variations of the main components observed in ice wedges of Plakhinskii Yar. The fluctuations of the contents of *Poaceae* and *Artemisia* pollen are opposite. The *Betula* sect. *Nanae* peak follows Artemisia. This rhythm corresponds to H1 (16.5–14 kyr BP).

Changes of vegetation cover are found at the same time intervals. They may correspond with Heinrich events (Bond et al. 1997, Veiga-Pires et al. 1999, Vidal et al. 1999, Ivy-Ochs et al. 2006, Parnell et al. 2007, Sepulchre et al. 2007). Every event has a specific appearance.

H1 is divided into three phases on the basis of pollen plots of the syngenetic sediments and ice wedges. The first pollen phase corresponds to relatively high temperatures and normal humidity, nival meadows and Pleistocene mesic tundra with a mosaic of shrubs and trees (*Betula* and *Larix*).

The second phase corresponds to low temperatures during the vegetation growth season, a very short vegetation season, low humidity and a maximum distribution of nival meadow vegetation (*Varia* and *Selaginella sibirica* or *Bryales*). The regional pollen rain is characterized by a prevalence of Artemisia pollen. The third phase corresponds to relatively high temperatures and increased humidity. *Poaceae* and *Varia* are prevalent and *Pinus pumila* pollen is represented in the regional pollen rain.

H2 is expressed by a change of a combination of peaks of *Poaceae* and *Selaginella sibirica,* by maximum immature pollen of *Varia* and then by the appearance of *Pinus sylvestris* pollen. This rhythm in the Lower Kolyma plain was asymmetrical.

The warm phase before the thermal minimum was relatively dry and long in comparison with the thermal minimum stage. A difference between the local and regional pollen rain was observed. The maximum distribution of vegetation of nival meadows took place simultaneously with the appearance of *Pinus* pollen.

H3 is characterized by consecutive changes of local peaks of *Betula* sect. *Nanae*, *Poaceae* and *Artemisia* and the disappearance of *Pinus pumila*.

H4 is characterized by an absolute maximum of *Selaginella sibirica*, then a sharp decrease of the total concentration of pollen and then twin peaks of *Poaceae* and *Artemisia* and *Betula* sect. *Nanae* pecentages growth.

These sharp oscillations of pollen and spores caused by global changes are recorded in other pollen plots of polygonal ice-wedge complexes of northern Eurasia. It is possible to find millennial scale events in Holocene ice-wedge complexes also as manifestations of a pervasive millennial-scale climate cycle operating independently of the glacial-interglacial climate state (Bond et al. 1997).

Acknowledgments

The authors are grateful to H. Jungner, J. van der Plicht and J.-C. Kim for ^{14}C dating of pollen and micro inclusions in ice-wedge ice and organic material in host sediments.

Dr. Julian Murton kindly commented on and greatly improved the original manuscript.

The work is partially financed by Russian Foundation for Basic Research (grants 05–05–64814 and 07-05-01100).

References

Bond, G., Showers, W., Cheseby, M., Almasi, P., deMenocal, P., Priore, P., Cullen, H., Hajdas, I. & Bonani, G. 1997. A pervasive millennial-scale cycle in North Atlantic Holocene and glacial climates. *Science* 278: 1257-1266.

Bourgeois, J.C. 2000. Seasonal and interannual pollen variability in snow layers of arctic ice caps. *Review of Palaeobotany and Palynology* 108(1-2): 17-36.

Fukuda, M., Nagaoka, D. et al. 1997. Radiocarbon dating results of organic materials obtained from Siberian pernafrost areas. Reports of Institute of Low Temperature Science. Sapporo. Hokkaido University: 17-28.

Grygar, T., Kadlec, J., Pruner, P., Swann, G., Bezdicka, P., Hradil, D., Lang, K., Novotna , K. & Oberhänsli, H. 2006. Paleoenvironmental record in Lake Baikal sediments: environmental changes in the last 160 ky. *Palaeogeography Palaeoclimatology Palaeoecology* 237: 240-254.

Ivy-Ochs, S., Kerschner, H., Kubik, P.W. & Schluchter, C. 2006. Glacier response in the European Alps to Heinrich Event 1 cooling: the Gschnitz stadial. Journal of Quaternary Science 21(2): 115-130.

Lowe J.A., Gregory J.M., Ridley J., Huybrechts P., Nicholls R.J. & Collins M. 2006. The role of sea-level rise and the Greenland ice sheet in dangerous climate change: implications for the stabilisation of climate. In: J. Schellnhuber, W. Cramer, N. Nakicenovic, T. Wigley & G. Yohe (eds.), *Avoiding Dangerous Climate Change*. Cambridge: Cambridge University Press, 29-36.

Parnell, J., Bowden, S., Andrews, J.T. & Taylor, C. 2007. Biomarker determination as a provenance tool for detrital carbonate events (Heinrich events?): Fingerprinting Quaternary glacial sources into Baffin Bay. *Earth and Planetary Science Letters* 257(1-2): 71-82.

Sarnthein, M., Kennett, J.P., Allen, J.R.M., Beer, J., Grootes, P., Laj, P., McManus, J., Ramesh R. & SCOR-IMAGES Working Group 117. 2002. Decadal-to-millennial-scale climate variability chronology and mechanisms: summary and recommendations. *Quaternary Science Reviews* 21(10): 1121-1128.

Sepulchre, P., Ramstein, G., Kageyama, M., Vanhaeren, M., Krinner, G., Sanchez-Goni, M.-F. & d'Errico, F. 2007. H4 abrupt event and late Neanderthal presence in Iberia. *Earth and Planetary Science Letters* 258: 283-292.

Vasil'chuk, A.C. 2005. *Pollen spectra formation features in permafrost areas of Russia*. Moscow: Moscow University Press, 247 pp.

Vasil'chuk, A.C. 2007. *Palynology and chronology of polygonal ice wedge complexes in Russia permafrost area*. Ed.: Member of the Russian Academy of Natural Sciences, Professor Yurij K.Vasil'chuk. Moscow: Moscow University Press, 488 pp.

Vasil'chuk, A.C., Kim, J.-C. & Vasil'chuk, Yu.K. 2003. First radiocarbon dating of pollen and spores from syngenetic ice-wedge ice. *Proceedings of the Eighth International Conference on Permafrost, Zurich, Switzerland, 21–25 July 2003*: 1167-1172.

Vasil'chuk, A., Kim, J.-Ch. & Vasil'chuk, Yu. 2005a. AMS ^{14}C dating of pollen concentrate from Late Pleistocene ice wedges from the Bison and Seyaha Sites in Siberia. *Radiocarbon* 47(2): 243-256.

Vasil'chuk, A.C., Vasil'chuk, Yu.K. Kim, J.-Ch., van der Plicht J. & Sulerzhitsky, L.D. 2005b. Appearance of Heinrich events in radiocarbon dated pollen and spores diagrams of ice-wedge ice and its surrounding Edoma sediments of Kolyma River. *Terra Nostra. 2nd European Conference on Permafrost. June 12-16, 2005. Potsdam, Germany. Abstracts.* AWI: 28-29.

Vasil'chuk, Yu.K. 1992. *Oxygen isotope composition of ground ice application to paleogeocryological reconstructions)* (in Russian, with English the contents, all figure captions and appropriate summary). Theoretical Problems Department, Russian Academy of Sciences and Moscow University publ., Moscow. V. I, 420 pp.; V. II, 264 pp.

Vasil'chuk, Yu.K. & Vasil'chuk, A.C. 1998. ^{14}C and ^{18}O in Siberian syngenetic ice wedge complexes. *Radiocarbon* 40(2): 883-893.

Vasil'chuk, Yu.K., van der Plicht, J., Jungner, H., Sonninen, E. & Vasil'chuk, A.C. 2000. First direct dating of Late Pleistocene ice-wedges by AMS. *Earth and Planetary Science Letters* 179(2): 237-242.

Vasil'chuk, Yu.K., Kim, J.-C. & Vasil'chuk, A.C. 2004. AMS ^{14}C dating and stable isotope plots of Late Pleistocene ice-wedge ice. *Nuclear Instruments and Methods in Physics Research*. *Section B: Beam Interactions with Materials and Atoms* 223-224: 650-654.

Veiga-Pires, C.C. & Hillaire-Marcel, C. 1999. U and Th isotope constraints on the duration of Heinrich events H0 – H4 in the southeastern Labrador Sea. *Paleoceanography* 14(2): 187-199.

Vidal, L., Schneider, R.R., Marchal, O., Bickert, T., Stocker, T.F. & Wefer, G. 1999. Link between the North and South Atlantic during the Heinrich events of the glacial period. *Climate Dynamics* 15(12): 909-919.

Dansgaard-Oeschger Events on Isotope Plots of Siberian Ice Wedges

Yurij K. Vasil'chuk and Alla C. Vasil'chuk
Geology and Geography Department, Lomonosov's Moscow University, Moscow, Russia,

Abstract

Hydrogen and oxygen isotope records with a resolution of 100–200 years were obtained from ice-wedge ice at four locations in Siberia. Micro-organic inclusions and pollen concentrates from ice wedges allowed precise AMS radiocarbon dating of the isotope records and comparison with GISP2 and GRIP ice cores. Separate Dansgaard-Oeschger events are distinguished within the ice-wedge ice and correlated with the Greenland ice cores.

Keywords: Dansgaard-Oeschger events; ice wedge; radiocarbon; stable isotope.

Introduction

Isotope records of Siberian ice wedges have become available from 50 sequences of syngenetic permafrost sediments of northern Eurasia (Vasil'chuk 1992, 2006). Late Pleistocene and Holocene syngenetic ice wedges have been studied throughout the Yamal Peninsula to the Chukotka and Magadan regions, and from northern Yakutia to the Aldan and Vilyui River valleys and to the Chara depression (Trans-Baikal Region) (Vasil'chuk 1992). At first we inferred a local origin for dramatic cyclic oscillations of stable isotope values within ice-wedge ice. However, the first radiocarbon dates of micro inclusions, alkaline extract and pollen concentrate directly in ice-wedge ice (Vasil'chuk 1992, 2006, Yu.Vasil'chuk et al. 1999, 2000, 2001, 2004, Vasil'chuk & Kotlyakov 2000) have fixed stable isotope curves of ice wedges onto a ^{14}C scale, allowing us to evaluate the duration of the oscillations.

A variety of multi-millennial oscillations from ice wedges with a dominant periodicity of ca. 1.5 kyr was obtained. Several parameters of ice-wedge isotope curves show some correlation with the GISP2 and GRIP $\delta^{18}O$ records (Dansgaard et al. 1993, Grootes et al. 1993, Jouzel et al. 2007), although not all of the same amplitude or frequency. Such changes might be associated with the response of winter temperatures in Siberia to freshwater anomalies in the North Atlantic, which dramatically reduce the transport of the meridional overturning cell. This paper addresses this question with ice wedge records dated by ^{14}C AMS. Four ice-wedge complexes are located in Yakutia, and one is in northwest Siberia. This enables us to follow the changes depending on longitude and distance from the Atlantic.

Regional Setting

We present several cross-sections with syngenetic ice wedges studied in detail. The Seyaha cross-section is located in typical tundra of northwest Siberia. Sections at Duvanny Yar, Plakhinskii Yar and Bison are located in forest tundra in the Lower Kolyma River Valley in northeastern Yakutia, and one at Mamontova Gora is located in taiga in Central Yakutia (Fig. 1). The ice wedges of these cross-sections have been dated directly by ^{14}C AMS.

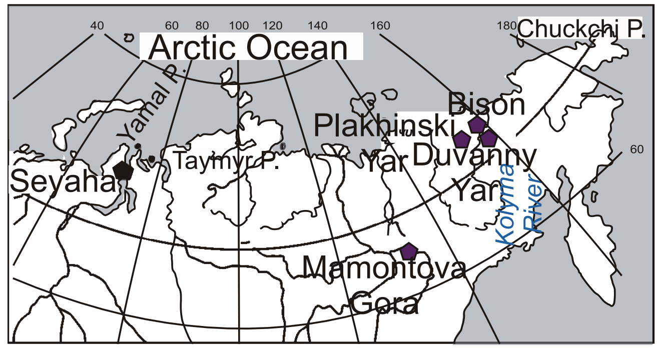

Figure 1. Location of Siberia ice wedge sections: Seyaha cross-section (70°10′N, 72°34′E, Yamal Peninsula, northwest Siberia), Duvanny Yar (69°N, 158°E, Lower Kolyma River, northeast Yakutia), Plakhinskii Yar (69°40′N, 160°17′E, Lower Kolyma River, northeast Yakutia), Bison (68°15′N, 150°45′E) (Lower Kolyma River, northeast Yakutia).

Dating Strategy

Many parts of cross-sections from modern permafrost areas can be dated by ^{14}C; however, date-inversions are common in permafrost, and this requires a special study.

In Arctic regions inversion of dates on different fractions of organic material is more likely the rule than anthe exception (Vasil'chuk & Vasil'chuk 1997). Contamination by old material is the main problem in ^{14}C dating of permafrost sediments because of the low decay rate of organic material and repeated re-deposition of old organic material (Nelson et al. 1988). The search for the most reliable subject for dating is a prominent part in a dating strategy for syngenetic permafrost sediments. So we suppose that the youngest ^{14}C date from a number dates of various fractions of the same sample or from the same layer is the most reliable method for determining the apparent age of syngenetic permafrost sediments and ice wedges.

Several different fractions were dated in the ice wedges, including organic micro-inclusions, alkali extracts and pollen concentrates. The micro-inclusions most likely originated from contemporaneous plant material and in most cases provided the youngest dates. Alkali extracts were older than micro-inclusions, with the difference between them ranging from 1100 years to more than 7900 years. It is evident that there is a correlation between ^{14}C-dates of pollen concentrate and re-deposited pollen and spores content. The youngest date corresponded to the minimum amount of re-deposited pollen and spores. This indicates a high probability of old organic contamination in organic material within permafrost. In a case like that it is impossible to calibrate AMS dates from ice-wedge complexes. So the comparison of ice-wedge isotope profiles with GRIP and GISP curves is approximate and the correlations could be done with shifts of 1500–2000 years.

However, in such a case where pollen concentrate from syngenetic ice wedges was relatively free from organic particles and contained well-preserved pollen and spores of typical Late Pleistocene tundra plants (dwarf birch and especially thin-walled pollen such as *Salix* or *Liliaceae*), the pollen concentrate ^{14}C date was the youngest (Vasil'chuk et al. 2005). The youngest numbers of ^{14}C AMS dates are utilized for dating of isotope profiles. The majority of them are the dates of micro-organic material; some dates are from pollen concentrate (Fig. 2, Table 1). In any case, the youngest date was picked as a base of ^{14}C scale.

AMS dating of ice wedges confirms the vertical stratification of ice-wedge ice, that is, where younger ice is located above older ice (i.e., syngenetic accumulation).

Results

Hydrogen and oxygen isotope records from ice-wedge ice with a resolution of 100–200 years were obtained from well-dated Siberian cross-sections. In each case the isotope profile was sampled along the axis of a single ice wedge.

1. Seyaha cross-section: the $\delta^{18}O$ values range from -25.0 to -20.4‰ (modern ice wedge $\delta^{18}O$ values range from -19.0 to -17‰). Direct ^{14}C AMS dates of micro-inclusions from ice are from 14,700 to 20,900 yr BP.
2. Duvanny Yar cross-section: $\delta^{18}O$ values range from -32.7 to -28.7‰ (modern ice wedge $\delta^{18}O$ values range from -24 to -27‰). Direct ^{14}C AMS dates of micro-inclusions from ice are from 14,100 to 25,900 yr BP.
3. Plakhinskii Yar cross-section: $\delta^{18}O$ values range from -34.7 to -28.7‰ (modern ice wedge $\delta^{18}O$ values range from -24 to -27‰). Direct ^{14}C AMS dates of micro inclusions from ice are from 11,400 to 21,400 yr BP.
4. Bison cross-section: $\delta^{18}O$ values range from -33.79 to -28.7‰ (modern ice wedge $\delta^{18}O$ values range from -24 to -27‰). Direct ^{14}C AMS dates of micro inclusions and pollen from ice are from 26,400 to 32,600 yr BP.
5. Mamontova Gora cross-section: the $\delta^{18}O$ values range from -29.0 to -25.4‰ (modern ice wedge $\delta^{18}O$ values range from -19.0 to -17‰). Direct ^{14}C AMS dates of micro inclusions from ice are from 18,900 to 13,900 yr BP. ^{14}C dating of stable isotope records from the ice-wedge ice shows millennial scale changes of isotope composition. These oscillations can be compared with Greenland ice-sheet records. The plots from each ice-wedge system could be separated into episodes correlating with Dansgaard-Oeschger events lasting 1–2.5 kyr (Fig. 2). AMS ^{14}C dates of the ice yields the age of the stable isotope shift.

The key points for the comparison of the ice-wedge ice record are found at the GISP2 and GRIP $\delta^{18}O$ records as positive shifts at the stable isotope curves.

The large $\delta^{18}O$ oscillations recorded in the Seyaha ice-wedge ice are ^{14}C dated to between 20,900 and 14,000 yr BP (Fig. 2a). A positive shift of $\delta^{18}O$ values of almost 4‰ and then a negative one of 4.2‰ from 17 to 15 m depths (dated about 17–15 kyr BP) in ice-wedge ice corresponds to a warm oscillation of D/O event 1 in the Greenland record: the Bølling and Allerød episodes.

Detailed AMS dating of Bison ice-wedge ice is based on 6 micro-organic dates and 5 pollen concentrate dates, allowing selection of the youngest dates from 32,600 up to 26,400 yr BP (Fig. 2b). The stable isotope record of this cross-section can be compared with some parts of the GISP2 ice core. Several episodes can be correlated with from 3 to 7 D/O events lasting 1–2 kyr. However, the shift of $\delta^{18}O$ values in this section is negligible (from -33.2 up to -32‰). This fact could be caused by reduced climatic response on global changes.

Similar to the Seyaha stable isotope profile, a significant oscillation of $\delta^{18}O$ values is observed in the upper part of Plakhinskii Yar ice-wedge ice record, which is ^{14}C dated 21,400–11,400 yr BP (Fig. 2c). A positive shift of $\delta^{18}O$ values of almost 4‰ and then a negative one of 3.5‰ from 4.5 to 1.5 m depths (dated about 15–11.5 kyr BP) in ice-wedge ice corresponds to D/O event 1 and possibly D/O event 2.

Oscillating $\delta^{18}O$ values are observed in the middle part of Duvanny Yar ice-wedge ice record, which is ^{14}C dated 23,700–14,100 yr BP (Fig. 2e). A positive shift of $\delta^{18}O$ values of about 4‰ and then a negative one in ice-wedge ice corresponds to D/O event 1. A second oscillation in underlying ice dated about 22,000–23,000 yr BP probably corresponds with to D/O event 2.

The 3‰ oscillation of $\delta^{18}O$ values in the Mamontova Gora ice-wedge ice is dated about 14,000–15,000 yr BP (Fig. 2f). It may correspond to D/O event 1.

Discussion and Conclusions

Ice-wedge ice originates from snow. Such ground ice is a natural archive of climatic changes. There are some differences, however, between the palaeotemperature interpretation of ice cores and ice-wedge ice. Ice cores are repositories of past precipitation.

One of the backbones of ice-core palaeoclimate reconstructions is the use of δD and $\delta^{18}O$ stable isotopes in the ice, which have classically been interpreted as indicating local to regional temperature (Dansgaard 1964).

The tritium concentration is low in all ice samples. It does not exceed 1.5 TU, indicating the absence of any exchange processes of Late Pleistocene ice-wedge ice with the external environment and high preservation of primary properties of ice-wedge ice, including its isotope characteristics.

The starting point for the analysis is to decide on criteria for defining DO events and determining the transition times.

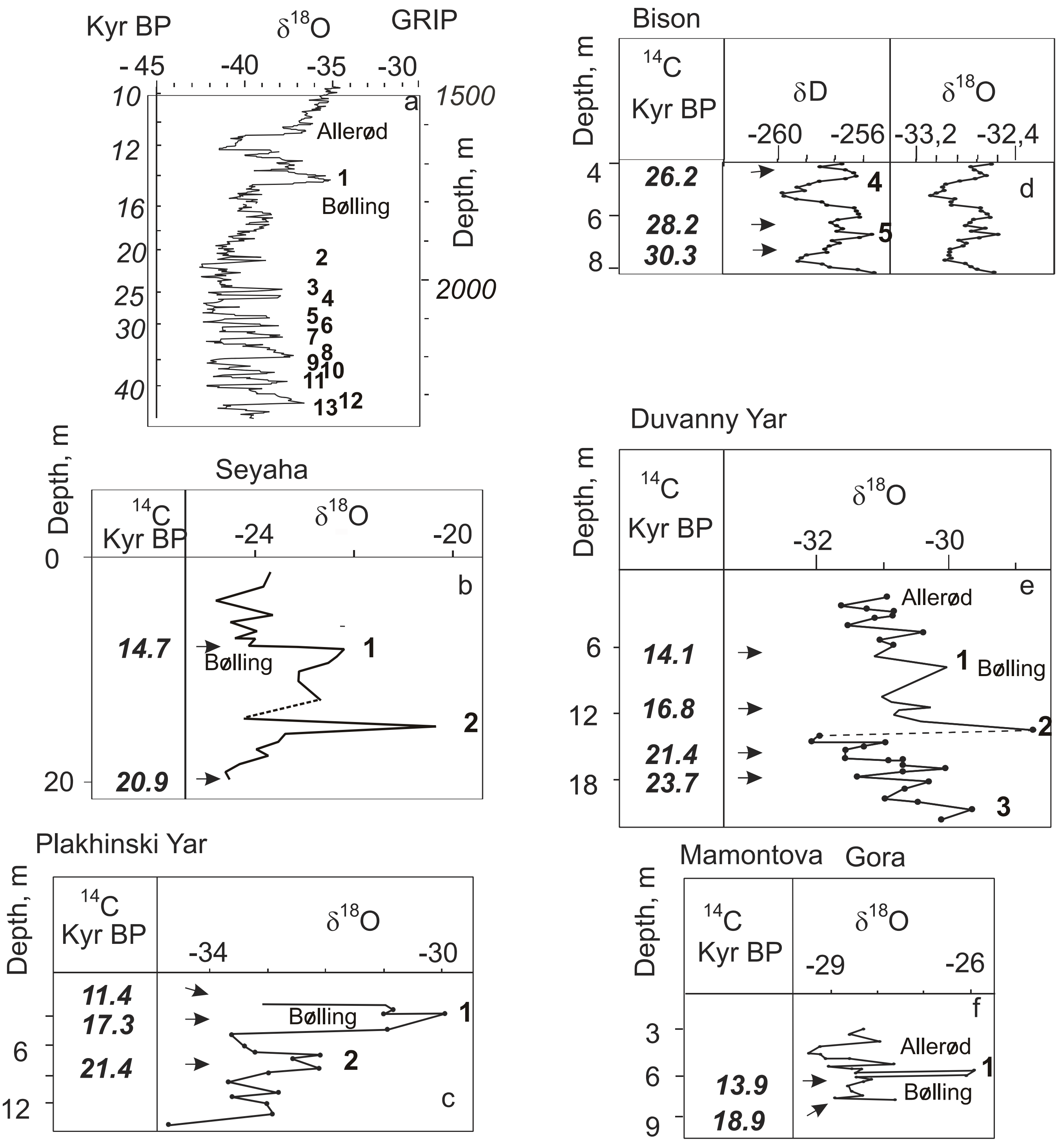

Figure 2. Comparison of Dangaard-Oeschger events of Siberian ice-wedge ice: a – fragment of GRIP ice core (Dansgaard et al. 1993); b – Seyaha cross-section, Yamal Peninsula; c – Plakhinskii Yar, Lower Kolyma River; d – Bison, Lower Kolyma River; e – middle part of Duvanny Yar; Lower Kolyma River; f – Mamontova Gora, Aldan River. Numbers – suggested number of D/O event.

The "canonical" numbered DO events were identified visually (Dansgaard et al. 1993). Schulz (2002) defined the DO events from a positive 2 permil anomaly in the 12 kyr highpass filtered isotope signal. By that DO9 is disregarded. Rahmstorf (2003) defined a criterion for increase of 2 per mil within 200 years on the 2 m sampled record (approx. 100 years lowpass). In this way DO9 is omitted and an event "A" in the Allerød period is included. Alley et al. (2001) use a bandpass procedure by which 43 events in the glacial period were defined. Ditlevsen et al. (2005, 2007) defined first upcrossings of an upper level following upcrossings of a lower level as a criterion. In this way the critical dependence on the (arbitrary) lowpass filter and crossing levels is to a large extent avoided (Ditlevsen et al. 2005). Using this

Table 1. Direct AMS radiocarbon dates of organic micro inclusions from Siberian ice wedge.

Field number	Depth, m	AMS ^{14}C data BP	Lab. Number	$\delta^{13}C$, ‰
Seyakha ice-wedge complex				
363–YuV/27	1,8	14550 ± 100	GrA-10538	–25.7
363–YuV/87	12.0	14720 ± 100	GrA-10539	–26.3
363–YuV/125	20.6	20960 ± 140	GrA-10536	–26.1
Plakhinsii Yar ice-wedge complex				
311-YuV/6	3.9	13130 ± 130	SNU02-129	–23.3
311-YuV/18	3.9	11490 ± 80	SNU02-130	–30.4
311-YuV/21	4.5	17390 ± 200	SNU01-281	–40.4
311-YuV/29	8.6	21400 ± 300	SNU02-131	–25.9
Bison ice-wedge complex				
378–YuV/90	4.0	29500 ± 500	GrA–16802	–26.5
		26200 ± 300*	SNU02-147	
378–YuV/101	6.3	30430 ± 1500	GrA-12893	–26.1
378–YuV/100	7.6	32600 ± 700	GrA-16808	–26.1
		28200 ± 600*	SNU02-150	
378–YuV/102	7.6	30750 ± 550	GrA-16804	–26,2
		35600 ± 800*	SNU02-124	
378–YuV/103	7.6	30350 ± 550	GrA-16807	–26,3
Mamontova Gora ice-wedge complex				
335-YuV/24	2.6	17040 ± 100	SNU01-283	–31.5
335-YuV/27	3.2	19800 ± 600	SNU01-284	–40.9
335-YuV/33	5.0	19050 ± 180	SNU01-285	–29.8
335-YuV/13	5.7	16190 ± 250	SNU02-142	–22.9
335-YuV/12	5.9	13950 ± 200	SNU02-141	–23.1
335-YuV/5	6.9	18400 ± 400	SNU02-140	–32.4
335-YuV/2	7.2	18900 ± 200	SNU02-139	–26.8
Duvanny Yar ice-wedge complex				
320-YuV/15	7.0	14100 ± 500	SNU02-004	–30.3
320-YuV/17	11.6	20100 ± 1400	SNU02-137	–24.1
320-YuV/8	13.0	16800 ± 800	SNU01-007	–46.7
320-YuV/3	16.3	25800 ± 300	SNU01-006	–35.4
320-YuV/2	16.8	21900 ± 900	SNU02-136	–37.8

* AMS ^{14}C dating of pollen concentrate

criterion several additional DO events are identified, such as DO2, which is split into two separate events.

The sampling of ice-wedge ice for isotope analysis with a vertical interval of 10–15 cm and a horizontal interval of 3–5 cm corresponds to a resolution of 60–100 years according to layer counting and ^{14}C AMS dating. The isotope records of ice wedges are shorter in comparison with Greenland ice cores. Moreover, ice-wedge records may contain gaps when ice-wedge formation stopped.

Having ^{14}C dated organic micro-inclusions in ice-wedges we can attempt to compare their stable isotope records with such records in polar ice. In the GRIP ice core, $\delta^{18}O$ values from 35 to 25 kyr BP range from -38‰ to -43‰ (Dansgaard et al. 1993) This is a factor of two higher than that in simultaneous Bison ice wedges (from -33.25 to -32.40‰). Such sharp excursions could be caused by Atlantic ice cover changes, especially in summer, whereas winter conditions were much more stable. The 100-year resolution of the Bison ice wedge isotope record shows changes of mean winter temperatures of the air. A number of matching points can be identified between the GRIP core and two fragments of ice wedges in Bison (see Fig.2). It is enough to identify similar sequences of major and minor events in the interval 35–25 kyr BP as in GRIP.

The d_{exc} values differ from those inherent in modern snow, d_{exc} – about 10‰. It is supposed that there was a difference in the mode of evaporation above the oceans during the Late Pleistocene, confirming the earlier data on small d_{exc} values for Late Pleistocene ice-wedge ice in comparison with Late Pleistocene Antarctic ice (Jouzel et al. 2007). Slight isotope variations of Bison ice-wedge ice do not give sufficient evidence for division into warm and cold periods from 25 to 35 kyr BP.

Late Quaternary climate instability implies rapid, closely linked changes in the Earth's environmental systems: hydrosphere, atmosphere, cryosphere and biosphere. Ice-wedge ice is one of the natural archives reflecting climatic changes. Direct AMS ^{14}C dating of ice-wedges enabled comparison of their stable isotope contents with those in polar ice. Ice wedges, however, cover a shorter time span than ice cores. By means of AMS ^{14}C-dating, paleoenvironmental proxies from ice wedges can be "stacked".

Variations of stable isotope ratios in ice wedges are similar to those in the ice cores. The range of $\delta^{18}O$ values from ice-wedge ice is about 2‰, indicating precipitation during wintertime and mean winter temperatures. In polar ice cores $\delta^{18}O$ is proportional to the difference between the mean annual temperature of the air above the inversion layer from which it was precipitated and the temperature of the precipitation source region. Atlantic ice cover changes especially in summer, whereas winter conditions were much more stable.

Several other ice-wedge sections have previously been analyzed (Vasil'chuk et al. 2005, Vasil'chuk 2006). At Zelyony Mys (69°N, 160°E, Lower Kolyma River) the ^{14}C dates range from 13,600 to 28,400 yr BP, and $\delta^{18}O$ values range from -34.1 to -29.4‰. At Mamontova Gora (64°N., 134°E, Aldan River) the ^{14}C dates range from 13,900 to 18,400 yr BP, and $\delta^{18}O$ values range from -29.4 to -25.9‰. At Phoenix (68°34'N, 158°34'E, Magadan Region) the youngest ^{14}C date is 11,000 yr BP, and $\delta^{18}O$ varies from -32.2 to -32.6‰ at the top to -24.9‰ at the bottom.

The most negative isotopic shifts are observed between 16.5–14 and 11–12 kyr BP. They demonstrate that a single spectral peak (indicating a ~1500 yr cycle) is characteristic of the records in both the Greenland ice sheet and Siberian ice wedges.

Especially interesting is the coincidence of D-O events 1 and 2 with distant ice-wedge sequences at Seyaha and Duvanny Yar.

Diverse palaeoclimatic evidence, including marine sediment data, pollen profiles, and glacial snow line data, indicates that the effects of at least some events were felt on a global scale (Broecker 1993). Recently well-dated curves with identifiable D-O events have been obtained for the last 10–60 kyr. Dansgaard-Oeschger events are described in the southern Aegean Sea (Geraga et al. 2005), by coccolithophores from the Gulf of Cadiz (NE Atlantic) and Alboran Sea (W Mediterranean) (Colmenero-Hidalgo et al. 2004), in bottom sediments in the Okhotsk Sea (Goldberg et al. 2005), and in the northern area of the East China Sea (Ijiri et al. 2005). Isotope records of Siberian ice wedges also demonstrate millennium scale oscillations (Vasilchuk et al. 2004). Stable oxygen and hydrogen isotope analysis of the ice in combination with adequate radiocarbon dates is one of the best tools available to obtain palaeotemperature information for the last 40 thousand years.

Several episodes lasting 1–2.5 kyr can be distinguished in isotope plots from each ice-wedge system. The AMS dates yields a precise age of the observed stable isotope shift. The ice-wedge records for northern Siberia are consistent in providing a chronological framework for this region. A ~1500 yr cycle characterizing both the Greenland ice sheet and Siberian ice wedges is observed.

Acknowledgments

The authors are grateful to Prof. H.Jungner, Dr. J. van der Plicht and Prof. J.-C.Kim for ^{14}C dating of pollen and micro inclusions in ice-wedge ice and organic material in host sediments, Prof. M.Geyh, Dr. W.Papesch, Prof. D.Rank and E.Sonninen for stable isotope analyses, and Dr. J.Murton for improvements to the final text.

The work is partially financed by Russian Foundation for Basic Research (grants 05–05–64814 and 07-05-01100).

References

Alley, R.B., Anandakrishnan, S. & Jung, P. 2001. Stochastic resonance in the North Atlantic. *Paleoceanography* 16: 190-198.

Broecker, W.S. 1993. *The glacial world according to Wally*. Palisades: Lamont-Doherty Earth Observatory of Columbia University. 318 pp.

Colmenero-Hidalgo, E., Flores, J.-A., Francisco, J. Sierro, F.J., Ángeles Bárcena, M., Löwemark, L., Schönfeld, J. & Grimalt, J.O. 2004. Ocean surface water response to short-term climate changes revealed by coccolithophores from the Gulf of Cadiz (NE Atlantic) and Alboran Sea (W Mediterranean). *Palaeogeography, Palaeoclimatology, Palaeoecology* 205(3–4): 317-336.

Dansgaard, W. 1964. Stable isotopes in precipitation. *Tellus* 16(4):436-468.

Dansgaard, W., Johnsen, S.J., Clausen, H.B., Dahl-Jensen, D., Gundestrup, N.S., Hammer, C.U., Hvidberg, C.S., Steffensen J.P., Sveinbjornsdottir A.E., Jouzel, J. & Bond, G. 1993. Evidence for general instability of past climate from a 250-kyr ice-core record. *Nature* 364(6434): 218-220.

Ditlevsen, P.D., Kristensen, M.S. & Andersen, K.K. 2005. The Recurrence Time of Dansgaard-Oeschger Events and Limits on the Possible Periodic Component. *Journal of Climate* 18: 2594-2603.

Ditlevsen, P.D., Andersen, K.K. & Svensson, A. 2007. The DO-climate events are probable noise induced: statistical investigation of the claimed 1470 years cycle. *Climate of the Past* 3: 129-134.

Geraga, M., Tsaila-Monopolis, S., Ioakim, C., Papatheodorou G. & Ferentinos, G. 2005. Short-term climate changes in the southern Aegean Sea over the last 48,000 years. *Palaeogeography, Palaeoclimatology, Palaeoecology* 220(3–4): 311-332.

Goldberg, E.L., Gorbarenko, S.A., Shaporenko, A.D., Bosin, A.A., Leskov, V.Yh. & Chebykin, E.P. 2005. Instability of last glacial climate from SRXFA data for bottom sediments in the Okhotsk Sea. *Nuclear Instruments and Methods in Physics Research Section A: Accelerators, Spectrometers, Detectors and Associated Equipment* 543(1): 284-287.

Grootes, P.M., Stuiver, M., White, J.W.C., Johnsen, S. & Jouzel, J. 1993. Comparison of oxygen isotope records from the GISP2 and GRIP Greenland ice cores. *Nature* 366(6454): 552-554.

Ijiri, A., Luejiang Wang, L., Oba, T., Kawahata, H., Huang, C.-Y. & Huang, C.-Y. 2005. Paleoenvironmental changes in the northern area of the East China Sea during the past 42,000 years. *Palaeogeography, Palaeoclimatology, Palaeoecology* 219(3–4): 239-261.

Jouzel, J., Masson-Delmotte, V., Cattani, O., Dreyfus, G., Falourd, S., Hoffmann, G., Minster, B., Nouet, J., Barnola, J. Chappellaz, M.J., Fischer, H. et al. 2007. Orbital and Millennial Antarctic Climate Variability over the Past 800,000 Years. *Science* 317: 793-796.

Nelson, R.E., Carter, L.D. & Robinson, S.W. 1988. Anomalous radiocarbon ages from a Holocene detrital organic lens in Alaska and their implications for radiocarbon dating and paleoenvironmental reconstructions in the Arctic. *Quaternary Research* 29(1): 66-71.

Rahmstorf, S. 2003. Timing of abrupt climate change: A precise clock. *Geophysical Research Letters* 30(10): 1029-1032.

Raisbeck, G.M., Yiou F., Jouzel, J. & Stocker, T.F. 2007. Direct north-south synchronization of abrupt climate change record in ice cores using beryllium 10. *Climate of the Past Discussions* 3: 755-769. www.clim-past-discuss.net/3/755/2007/

Schulz, M. 2002. On the 1470-year pacing of Dansgaard-Oeschger warm events. *Paleoceanography.* 17(2): 1014 –- 1023.

Vasil'chuk, A., Kim, J.-Ch. &Vasil'chuk, Yu. 2005. AMS ^{14}C Dating of Pollen Concentrate from Late Pleistocene Ice Wedges from the Bison and Seyaha Sites in Siberia. *Radiocarbon.* 47(2): 243-256.

Vasil'chuk, Yu.K. 1992. *Oxygen isotope composition of ground ice application to paleogeocryological reconstructions* (in Russian, with English the contents, all figure captions and appropriate summary). Theoretical Problems Department, Russian Academy of Sciences and Moscow University publ., Moscow, V. 1, 420 pp., V. 2, 264 pp.

Vasil'chuk, Yu.K. 2006. *Ice wedge: Heterocyclity, Heterogeneity, Heterochroneity*. Moscow: Moscow University Press: - 404 pp.

Vasil'chuk, Yu.K. & Vasil'chuk, A.C. 1997. Radiocarbon dating and oxygen isotope variations in Late Pleistocene syngenetic ice-wedges, northern Siberia. Pe*rmafrost and Periglacial Processes* 8(3): 335-345.

Vasil'chuk, Yu.K., van der Plicht, J., Jungner, H. & Vasil'chuk, A.C. 1999. AMS-dating of Late Pleistocene and Holocene syngenetic ice-wedges. *Eighth International Conference on Accelerator Mass Spectrometry, Abstracts*, *Palais Auersperg, Vienna, Austria, 6-–10 September*: 141.

Vasil'chuk, Yu.K. & Kotlyakov, V.M. 2000. *Principles of Isotope Geocryology and Glaciology. A Comprehensive Textbook*. Moscow University Press. 616 pp.

Vasil'chuk, Yu.K., van der Plicht, J., Jungner, H. & Vasil'chuk, A.C. 2000. AMS-dating of Late Pleistocene and Holocene syngenetic ice-wedges. *Nuclear Instruments and Methods in Physics Research. Section B: Beam Interactions with Materials and Atoms* 172: 637-641.

Vasil'chuk, Yu.K., Vasil'chuk, A.C., Rank, D., Kutschera, W. & Kim, J. 2001. Radiocarbon dating of $\delta^{18}O$ – δD plots in Late Pleistocene ice – wedges of the Duvanny Yar (Lower Kolyma River, northern Yakutia). *Radiocarbon* 43(2B): 541-553.

Vasil'chuk, Yu.K., Kim, J.-C. & Vasil'chuk, A.C. 2004. AMS ^{14}C dating and stable isotope plots of Late Pleistocene ice-wedge ice. *Nuclear Instruments and Methods in Physics Research*. *Section B: Beam Interactions with Materials and Atoms* 223-224: 650-654.

Vasil'chuk, Yu.K., Kim, J.-Ch., van der Plicht, J., Papesch, W. & Vasil'chuk, A.C. 2005. AMS-dating Dansgaard-Oeschger events in Siberian ice-wedge ice. *Tenth International Conference on Accelerator Mass Spectrometry. AMS-10. Conference Agenda & Abstracts, Berkeley, California, September 5–10, 2005*: 35-36.

Active Layer Monitoring in West Siberia Under the CALM II Program

A.A. Vasiliev
Earth Cryosphere Institute SB RAS, Tyumen, Russia
M.O. Leibman
Earth Cryosphere Institute SB RAS, Tyumen, Russia
N.G. Moskalenko
Earth Cryosphere Institute SB RAS, Tyumen, Russia

Abstract

Active-layer monitoring in northern West Siberia started in 1972 at the Nadym site. Sites at Marre-Sale polar station in 1978 and Vaskiny Dachi polygon followed in 1991. Measurements are obtained within dominating landscape units and aimed at establishing active layer and ground temperature changes in various bioclimatic zones and landscapes. In 1993 the CALM (Circumpolar Active Layer Monitoring) project was launched, and monitoring began on the 100 x 100 m CALM grids at Nadym and Vaskiny Dachi and 1000 x 1000 m grid at Marre-Sale. The focus was on the active-layer dynamics in connection to climate change. Results obtained at the CALM grids, as well as at previously established sites and transects, facilitate estimation of the main factors involved in active-layer dynamics on various landscape units of the Tundra and Northern Taiga bioclimatic subzones under climate fluctuations. Results reveal that active-layer depth in mires is very sensitive to climate changes, while peatlands are least sensitive.

Keywords: active layer; climate change; ground temperature; monitoring; northern taiga; typical tundra.

Introduction

The northern part of the West Siberian lowland is characterized by relatively flat topography, variable drainage, marine and continental climate, and well developed latitudinal zonality (Melnikov 1983). Northern West Siberia is divided into three bioclimatic subzones according to the thermal and moisture balances: northern taiga, forest-tundra, and tundra. Surficial geology is dominated by sandy-clayey Pleistocene deposits. Permafrost distribution is continuous north of 67°N and discontinuous south of this latitude.

Active layer monitoring in northern West Siberia has been ongoing at the Nadym site (Northern Taiga subzone) since 1972, at Marre-Sale since 1978, and at the Vaskiny Dachi site since 1991 (both in Typical Tundra subzone, coastal and inland localization) (Fig. 1). The Marre-Sale and Vaskiny Dachi research sites are in the continuous permafrost zone, while permafrost distribution at Nadym is discontinuous.

Active layer/landscape interrelations are largely controlled by the composition and moisture content of the constituent soils. The maximum active layer is characteristic of sands, especially in recent blowouts that lack vegetative cover and are well drained. In the northern taiga, the maximum active layer may also occur in mires and dry tundra with peaty hummocks. The minimum active layer is found at the sites with relatively thick organic cover, mainly on fine-grained soils in poorly drained environments.

Observations are performed at environmentally homogeneous sites 10 x 10 m in size and along transects several hundred meters long that cross dominant landscape units (Table 1). Active-layer and permafrost temperatures are measured in boreholes up to 10 m deep at the same sites. Studies are aimed at establishing active-layer and ground temperature changes in bioclimatic subzones and landscape units within the context of climate change.

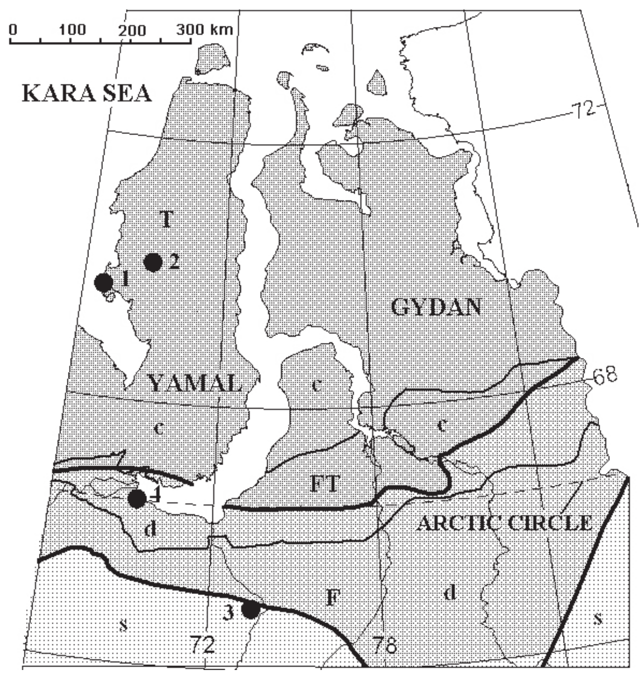

Figure 1. Location of the Marre-Sale (1), Vaskiny Dachi (2), and Nadym (3) research sites, and Salekhard weather station (4). Permafrost zones: c – continuous, d – discontinuous, s – sporadic.

In 1993–1995, observations following the protocol of the CALM (Circumpolar Active Layer Monitoring) project started on the 100 x 100 m CALM grids at Nadym and Vaskiny Dachi and on 1000 x 1000 m at Marre-Sale. The primary focus was on the active-layer dynamics in connection to climate change (Brown et al. 2001). The active layer studies within the framework of the CALM project were conducted for a number of years both on CALM sites, and on additional grids and profiles (Table 1).

Table 1. Metadata summary for CALM grid and additional grids and transects.

Research site	Observation unit	Unit size, m	Years of record
Marre-Sale	CALM grid (R3*), borehole 2 m deep	1000x1000	1995-2007
	Grid 1, borehole 10 m deep	10x10	1978-2007
	Grid 17, borehole 10 m deep	10x10	1978-2007
	Grid 36, borehole 10 m deep	10x10	1987-2007,
Vaskiny Dachi	CALM grid (R5*), borehole 2 m deep	100x100	1993-2007, 1999-2007
	Transect boreholes 5-10 m deep	320	1989-2006 1989-1993
Nadym	CALM grid (R1*), borehole 2 m deep	100x100	1997-2007
	transects 5x200 m	1000	1972-2007
	18 grids, boreholes 10 m deep	10x10	1972-2007

* CALM grid numbers are given as in (Brown et al. 2001).

Methods

Northern West Siberian north is known for wide distribution of saline marine deposits, and thus measuring the active layer in this area is not trivial. The salinity of clay in the active layer in the Typical Tundra subzone may be as high as 1.6% (Leibman & Streletskaya 1997). Some parts of the slope were subjected to landsliding that removed washout deposits to expose saline clay. Salinity in the active layer strongly correlates with the age of a landslide event (Ukraintseva et al. 2000).

In fine-grained soils mechanical strength changes gradually with decreasing unfrozen water content. When clayey soil is saline, the changes are much less apparent. At the same time, the freezing point departs from zero. Thermal measurements to determine the 0°C temperature position, when compared to insertion of a metal probe, show that in clayey soils the probe is inserted to a depth of 5 cm to 25 cm deeper than that of the 0°C isotherm depth (Leibman 1998); by comparison, Mackay (1977) measured a difference of 23 cm in early summer. In sand and silt the probe insertion can be even less than the 0°C isotherm depth due to higher mechanical resistance of the sandy-silty thawed layer. The probe can be inserted into the clay to a depth where ground temperatures are -0.5°C to -1.0°C according to our measurements (-0.6°C to -0.9°C in Mackay 1977).

CALM protocol (Brown et al. 2001) was applied from 1993–1995. Replicate thaw-depth measurements were performed using a metal probe in late August or early September, when the depth of seasonal thaw was close to maximum. The measurement error for the probe is about 1 cm. At the same time, in aeolian sands of the Marre-Sale grid in the warmest years the active layer depth may exceed the probe length (>160 cm). At Vaskiny Dachi, measurement error can be large owing to the presence of saline soils. In warm years thaw depth (or depth of penetration) at some Vaskiny Dachi probing points exceeds the probe length (180 cm) in the clayey active layer with the surface recently exposed by landsliding (Leibman 1998). Accordingly in this study, observations from such probing points were eliminated from calculations to better follow the interannual dynamics of active layer depth. The thaw index was calculated using monthly averages from weather records at the nearest meteorological stations.

A landscape survey was performed at each site based on the classification suggested in Melnikov et al. (1983). Determined were: structure of vegetative complexes and coverage as suggested in Moskalenko (1999); organic layer thickness by direct field measurements in similar areas adjacent to the probing point; density, moisture content, and chemical properties of soils, grain size, water content by volumetric weighting, and ionic analysis in water extraction. Geochemical tests were performed at Vaskiny Dachi to locate probing points with erroneous measurements due to recent landsliding.

Most of these methods were used since the 1970s and were improved within the framework of the CALM project. Measuring along the transects and within the landscape units started in the 1970s. Transects were set to cross the majority of the landscape units according to the results of a landscape survey. This approach is most common in the geocryological surveys in Russia, allowing us to extrapolate key site monitoring data to regions of similar landscape structure. This method helps when using remotely sensed imagery to map parameters not directly measured from space.

Climate

According to the climate zoning of the Russian Arctic (Prick 1971), the northern West Siberian lowland belongs to the Eastern region of the Atlantic sector of the Arctic Ocean. This region is subject to the strong impact of circulation processes from the mid-latitudes, specifically the Icelandic depression, and is subdivided into three zones. The northern tundra subzone of northern Yamal and Gydan peninsulas is characterized by marine arctic climate. The middle zones of typical and southern tundra of the Yamal, Gydan, and Tazovsky peninsulas are territories with marine sub-Arctic climate. The southern zone of forest-tundra and northern taiga is of moderate-continental climate.

The most important climatic parameters affecting permafrost dynamics are air temperature and snow cover depth. Northern West Siberia, due to climatic zoning mentioned above, is characterized by highly variable mean annual air temperature. At the Kara sea coast, mean annual air temperature decreases from -7.6°C on the southwestern coast of the Kara sea (Ust-Kara weather station, 69°12′N, 65°07′E) up to -11.3°C on the northeastern coast of Gydan (Gyda weather station, 70°53′N, 78°31′E) (Temperature of air and soils 1966). Inland there are few weather stations with short-term records. Within the study area, the southernmost inland station is Nadym, with the highest mean annual air temperature (-5.7°C). Calculations based on the short-term air temperature records show that the mean annual air temperature at Central Yamal decreases eastward, with a minimum at the main watershed of Yamal and at Vaskiny Dachi as low as -9°C (Belopukhova et al. 1989). At Marre-Sale the weather station mean annual air temperature is about -8°C.

Permafrost dynamics, including that of the active-layer depth, is linked to air temperature fluctuations. It is generally accepted that climate warming has been observed during the last 30–35 years (Pavlov 2003). Warming is more intensive inland, while along the coasts it is less expressed (Pavlov & Malkova 2005).

Figure 2 shows a time series of the mean annual air temperature at the West Siberian weather stations Salekhard, Marre-Sale, and Nadym. One can see that starting in the 1970s, there is a mean annual air temperature increase. Warming is rather synchronous across the entire region, though with local deviations. However, the degree differs. According to estimates by Pavlov & Malkova (2005) for northern West Siberia maximum warming is noted on the Tazovsky peninsula (Nadym area), exceeding 1.5°C. The least warming is in northern Yamal (0.7°C).

In analyzing long-term records for diurnal air temperature we noted that in the past 25 years in the tundra zone, the warm period has increased by 5–6 days, while in the northern taiga it increased by 15–17 days. The duration of the cold period decreased accordingly.

The thermal regime of permafrost is strongly affected by the thickness and regime of snow accumulation. In Marre-Sale the average perennial snow depth is 20–30 cm, while at Nadym it is as high as 50–60 cm, with year to year deviation. Total snow thickness tends to increase northward in West Siberia.

Results and Discussion

Results of active layer measurements at the monitoring sites located on the dominant landscape units are presented as Figures 3 and 4. The graphs show that active layer dynamics generally follow the sum of positive air temperatures, or thawing degree-days (DDT). However, one can see that short-term active layer records cannot characterize real trends in active layer evolution due to the oscillating nature of active layer dynamics. Still, it is apparent from the time series that all the landscape units show a tendency to increase over time since the 1970s until the recent. Trends of active-layer deepening within similar landscape units in the typical tundra are of smaller magnitude compared to the northern taiga. In the peatlands, active-layer changes are small, while in the mires and wet tundra they are much higher (Vasiliev et al. 2003, Melnikov et al. 2004). The same climate warming in the northern taiga is two times greater compared to the typical tundra.

Climate warming affects ground temperature, so permafrost reaction to climate change can be expressed in

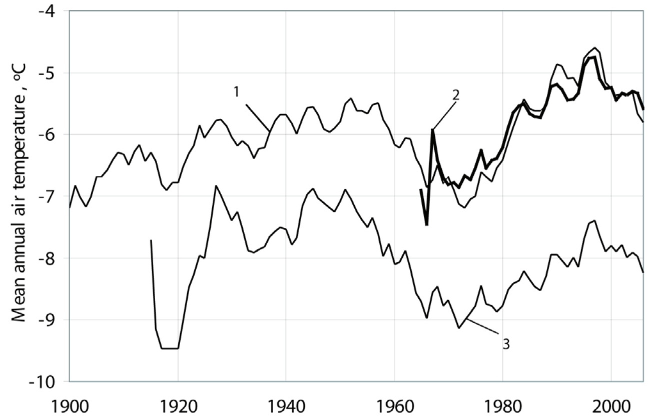

Figure 2. Ten-year moving averages of mean annual air temperature for Salekhard (1), Nadym (2), and Marre-Sale (3) weather stations.

mean annual ground temperature dynamics. In northern West Siberia the depth of zero annual temperature amplitude is about 10 m, the depth of most boreholes at the research sites. Results from the Marre-Sale and Nadym borehole temperature measurements, collected under conditions of changing climate at a depth of ~10 m, are shown in Figure 5. These traces also show oscillations that are similar to those for the active-layer depth. However, the mean annual ground temperature increase is more clearly marked since the 1970s. It is especially well observed at the Nadym site. At this station, in peatlands, the mean annual ground temperature rose from -0.9°C to -0.1°C. In the mires the mean annual ground temperature rose from -0.3°C to -0.1°C. Thus, in the discontinuous permafrost zone of the West Siberian northern taiga, recent climate warming has already caused a critical ground temperature increase approaching entire permafrost degradation.

In the typical tundra subzone, a ground temperature increase is observed as well. As snow cover here is less thick and its impact is not very pronounced, ground temperature shows a strong correlation with air temperature (Fig. 6). As a first approximation, the linear trend is applied. The slope of the straight-line approximation differs for each landscape unit. We suppose that the slope trend characterizes the annual ground temperature response of a particular landscape unit to climate fluctuations. The maximum slope is typical of flat peatlands, whereas the minimum slope is typical of mires. All other landscape units are characterized by intermediate values of annual ground temperature versus annual air temperature.

Conclusions

The study of permafrost reaction to climate change through active-layer depth dynamics was initiated within the framework of the CALM program. The response to climate changes of dominant landscape units in typical tundra and northern taiga subzones, as manifested by the active-layer depth, is evaluated quantitatively.

The active layer depth in mires is very sensitive to climate

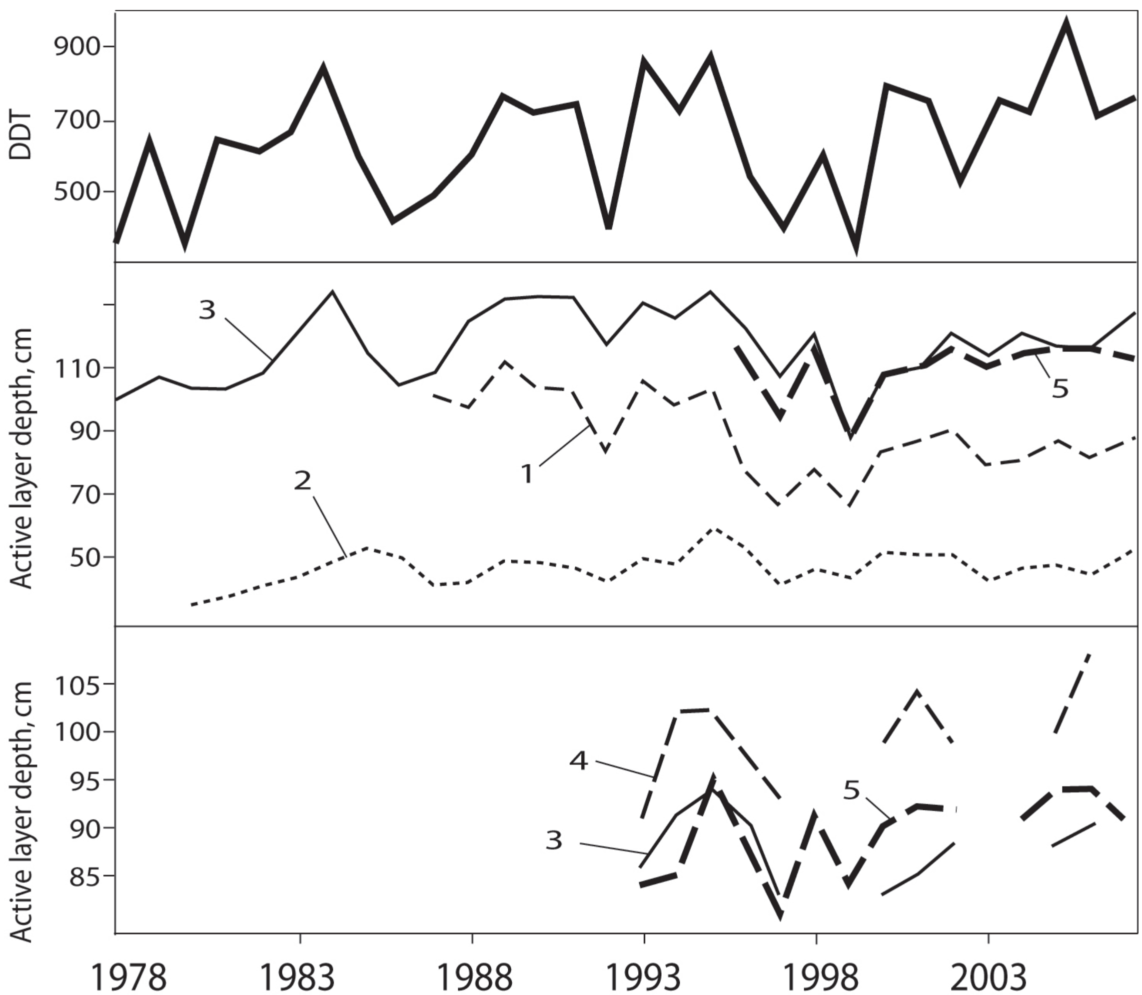

Figure 3. Time series of thaw index (DDT, upper pane), and average active layer depths on the dominating landscape units and CALM grid average in Marre-Sale (middle pane) and Vaskiny Dachi (lower pane): 1, mire; 2, peatland; 3, wet tundra; 4, dry tundra; 5, CALM grid average.

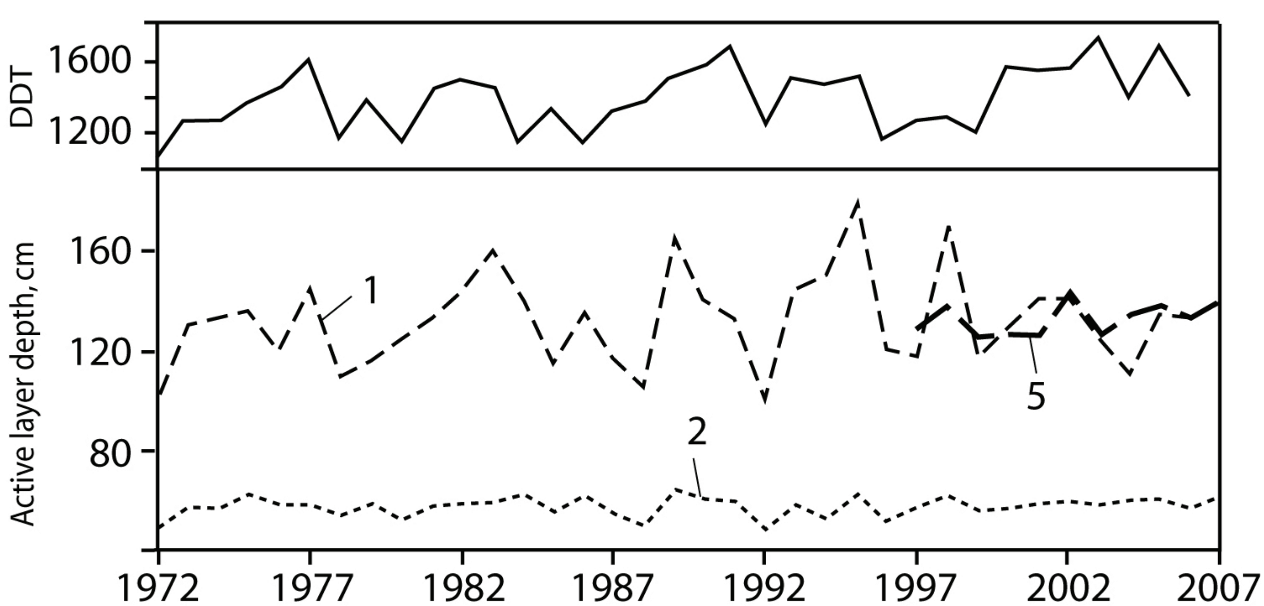

Figure 4. Time series of DDT (upper pane), and average active layer depths (lower pane) on the dominating landscape units and CALM grid average in Nadym area: 1, mire; 2, peatland; 5, CALM grid average.

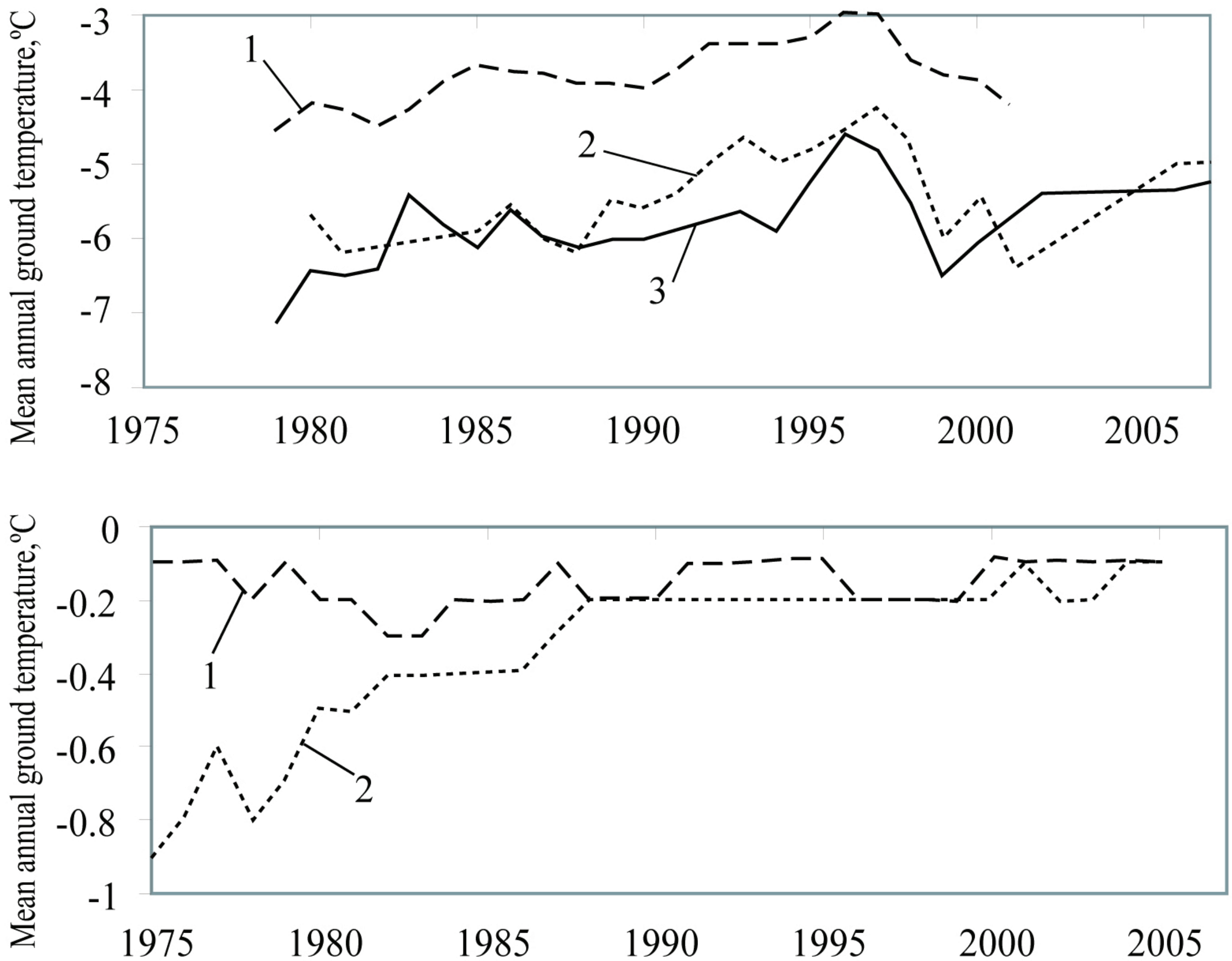

Figure 5. Time series of average ground temperature (depth of ~10 m) at Marre-Sale (upper pane) and Nadym (lower pane) sites: 1, mire; 2, peatland; 3, wet tundra.

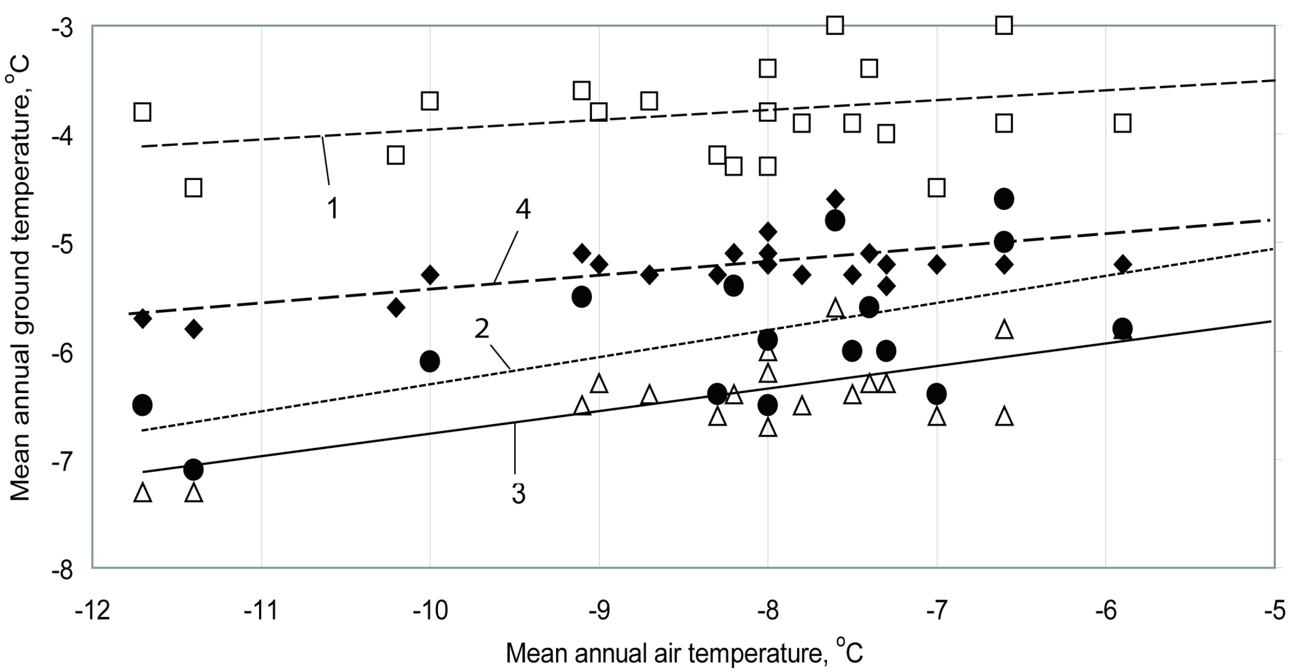

Figure 6. Correlation of mean annual air and ground temperature in Marre-Sale: 1, mire; 2, peatland; 3, wet tundra; 4, dry tundra.

change, while peatlands are least sensitive. And vice versa, the average annual ground temperature of permafrost changes considerably in the peatlands, while only minor changes are noted in mires. The landscape response to climate change expressed through the active layer is opposite to the response expressed through the average annual ground temperature.

Thus, analysis of the monitoring data allows us to conclude that the reaction of permafrost landscapes in northern West Siberia to climate change can develop in two directions. For some landscape units maximum increase of the active-layer depth is observed under the minimum change of mean annual ground temperature. For other landscapes with maximum change of mean annual ground temperature, minimum change of the active layer depth is characteristic. We cannot expect coincidence of both parameter maxima or minima within any environment.

Acknowledgments

This study was supported by the U.S. National Science Foundation (Grant # OPP-9732051), and Russian Academy of Sciences, Siberian Branch (Program of Fundamental Research SB RAS "Evolution of natural and Technogenic Geosystems in Cryolithozone").

References

Belopukhova, E.B., Leibman, M.O. & Tkacheva, L.A. 1989. Impact of climatic parameters on the ground temperature and active-layer depth on Yamal Peninsula. In: *Engineering Investigations for Construction in Yakutian Republic.* Yakutsk: GOSSTROI RSFSR, 111-112 (In Russian).

Brown, J., Hinkel, K.M. & Nelson, F.E. 2001. The Circumpolar Active Layer Monitoring (CALM) program: research designs and initial results. *Polar Geography* 24: 165-258.

Melnikov, E.S. (ed.) 1983. *Landscapes of permafrost zone in the West Siberian gas province*. Novosibirsk: Nauka, 185 pp. (in Russian).

Melnikov, E.S., Leibman, M.O., Moskalenko, N.G. & Vasiliev, A.A. 2004. Active layer monitoring in West Siberia. *Polar Geography* 28(4): 267-285.

Pavlov, A.V. 2003. Permafrost–climate changes in the Russian North: observations, prediction. *Transactions of RAS, Geographic Series* 6: 22-29 (in Russian).

Pavlov, A.V. & Malkova, G.V. 2005. *Contemporary Changes of Climate in Northern Russia*. Novosibirsk: Academic Publishing House "GEO," 54 pp. (in Russian).

Pavlov, A.V. & Moskalenko, N.G. 2002. The thermal regime of soils in the North of Western Siberia. *Permafrost and Periglacial Processes* 13(1): 43-51.

Prick, Z.M. 1971. Climatic zoning of the Arctic. In: *Transactions of AARI 304*: Leningrad, 72-84 (in Russian).

Leibman, M.O. 1998. Active layer depth measurements in marine saline clayey deposits of Yamal Peninsula, Russia: procedure and interpretation of results. *Permafrost. Seventh International Conference, June 23-27, 1998, Proceedings, Yellowknife, Canada-1998*: 635-639.

Leibman, M.O. & Streletskaya, I.D. 1997. Land-slide induced changes in the chemical composition of active-layer soils and surface-water runoff, Yamal Peninsula, Russia. In: I.K. Iskandar, E.A. Wright, J.K. Radke, B.S. Sharratt, P.H. Groenevelt & L.D. Hinzman (eds.), *Proceedings of the International Symposium on Physics, Chemistry, and Ecology of Seasonally Frozen Soils, Fairbanks, Alaska, June 10-12, 1997.* CRREL Special Report 97-10, CRREL, Hanover: 120-126.

Mackay, J.R. 1977. Probing for the bottom of the active layer. Report of activities, Part A; *Geological Survey of Canada*, Paper 77-1A: 327-328.

Moskalenko, N.G. 1999. *Anthropogenic Vegetation Dynamics of Cryolithozone Plains*. Novosibirsk: Nauka, 280 pp. (n Russian).

Temperature of air and soils. 1966. In: *Reference Book of USSR Climate* 24 (II). Leningrad: Gidrometeoizdat, 404 pp. (in Russian).

Ukraintseva, N.G., Leibman, M.O. & Streletskaya, I.D. 2000. Peculiarities of landslide process in saline frozen deposits of central Yamal, Russia. In: E. Bromhead, N. Dixon & L.-L. Ibsen (eds.) *Landslides. Proceedings of VIII International Symposium on Landslides* 3, London: Thomas Telford, 1495-1500.

Vasiliev, A.A., Moskalenko, N.G. & Brown, J. 2003. A new approach for interpreting active layer observations in the context of climate change: a West Siberian example. In: *Proceedings, Eighth International Conference on Permafrost Zurich, Switzerland, July 21-25 2003, Extended Abstracts*: 169-170.

Relation Between Soil Temperature and Late 20th Century Climatic Change in Yakutia

I.S. Vasiliev
Melnikov Permafrost Institute, SB RAS, Yakutsk, Russia

Abstract

This report presents analysis of the relationships of mean annual soil temperature at a depth of 1.6 m to air freezing index and snow depth, based on data from 40 weather stations in Yakutia. These relationships are discussed for the regional groups distinguished on the basis of linear trends in soil temperature. In the high-latitude lowland regions showing a negative trend, the decrease in mean annual soil temperature, with the freezing index remaining stable, is attributed to the persistence of snow cover long after the onset of positive air temperatures retarding soil warming, rather than to the increased snow depth and density. In the regions with a positive trend, the increase in mean annual soil temperature is caused by the weakening of the Asian anticyclone in winter. In the mountainous regions, soil temperatures are determined by local temperature-controlling factors, showing a decrease in cold landscapes and an increase in warm landscapes.

Keywords: freezing index; mean annual soil temperature; snow depth; trend.

Introduction

Changes in mean annual air temperature in the high latitudes of the Northern Hemisphere have been analyzed during the last 30 years by many investigators, using various approaches (Climate Change 1990, Ghil & Vautard 1991, Zhang & Osterkamp 1993, Pavlov 1994, 1997, Drozdov & Lugina 1996, Varlamov & Skachkov 1996, Balobaev 1997, Zukert & Zamolodchikov 1997, Gavrilova & Cherdonova 1997, Varlamov et al. 1998, Fedorov and Svinoboev 2000, Gedalof & Smith 2001, Harris 2002, 2005, and others).

Along with assessing the changes in air temperature, it is important to determine the responses of near-surface permafrost, particularly upper soil layers, to climatic variation. Pavlov (1997) reported data from several sites near Igarka and Vorkuta, indicating an increase in the mean annual permafrost temperatures to a depth of 10 m. Other studies also indicate a warming trend in ground temperature in Russia, on the North Slope of Alaska, along the Arctic coasts of Canada, and in the Northern Hemisphere as a whole (Osterkamp & Romanovsky 1999, Gilichinsky et al. 2000, Chudinova et al. 2001, 2003, Izrael et al. 2002, 2006, Frauenfeld et al. 2004, 2006, Smith et al. 2003). For Yakutia, it was shown previously (Vasiliev 1999) that linear trends in soil temperature at 1.6 m were of opposite sign in different regions (Fig. 1), which were provisionally grouped into three zones based on the character of soil temperature variation (Fig. 2).

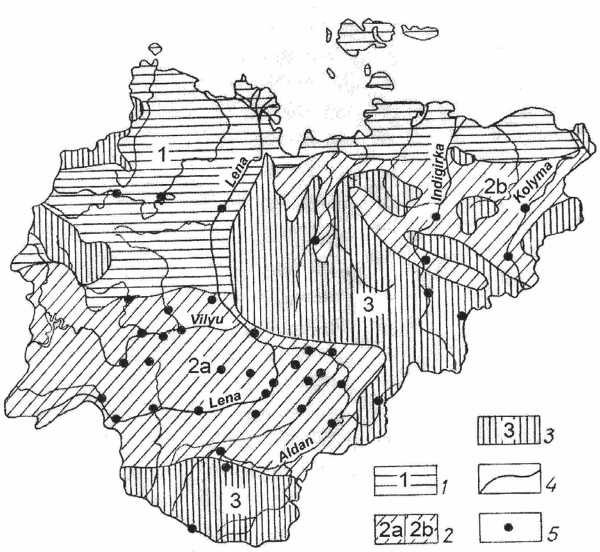

Figure 1. Map showing the location of soil temperature measurement sites and the regional groups identified based on linear trends: 1 – regions with negative trends; 2(a, b) – regions with positive trends; 3 – mountainous regions with opposing trends; 4 – group boundaries; 5 – weather stations.

This report presents analysis of the relationships of mean annual soil temperature at a depth of 1.6 m ($T_{m\ 1.6}$) to air freezing index ($\sum_{at}<0$) and snow depth (h_s).

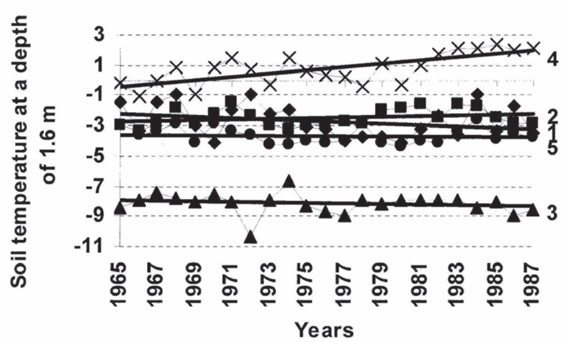

Figure 2. Variations and linear trends of mean annual soil temperature at 1.6 m for the Jarjan (1), Pokrovsk (2), Predporozhnaya (3), Gorelyy (4) and Nagornyy (5) weather stations.

Method

Regular instrumental measurements of soil temperature have been made in Yakutia since 1931. Soil temperature records of various lengths are available from 50 weather stations. However, the relocation of sites and the discontinuance of measurements introduce inhomogeneities into the temperature series. Of the 50 stations, only 16 continue to make soil temperature observations, 12 stations were closed by 1987, 9 stations by 1989 and 3 by 1994. Moreover, in the 1970s–1980s, instruments were relocated at 12 stations. Only homogeneous data sets from the same sites can provide a general picture of how the parameters under discussion have varied in the region. Therefore, soil temperature records from 40 weather stations for only the period from 1965 to 1987 have been used in the present study. Data on air freezing index and snow depth, which are compared to soil temperature, cover the same period (Fig. 3).

Results

Relations between $T_{m\,1.6}$, $\sum_{at}<0$ and h_s have been analyzed for the three regional groups distinguished in the previous study: (1) northern plains with a negative trend of $T_{m\,1.6}$; (2a) southwestern and central plains and (2b) northeastern plains and intermontane depressions, where $T_{m\,1.6}$ shows a steady increasing trend; and (3) mountains, exhibiting either stable or opposing $T_{m\,1.6}$ trends.

1. The northern plains with a negative trend of $T_{m\,1.6}$ include the tundra and north-taiga areas of western Yakutia and the tundra areas of eastern Yakutia (see Fig. 2, line 1). Air freezing indices were temporally stable at most stations of the region (Fig. 3, plot 1a), while snow depths slightly increased during the study period. The linear trend in h_s is 0.14–0.36 cm per year (Saskylakh, Sukhana and Siktyakh stations). At Jarjan, no trend is noted, although some increase in h_s occurred in the 1980s (Fig. 3, plot 1b). In the northernmost areas, increased snow depth is known to have a cooling effect on the soil thermal regime (Dostovalov & Kudryavtsev 1967, p. 252). The negative effect of snow cover in these regions can be due to three main reasons. First, snow density increases from south to north up to 0.2–0.3 g/cm^3 in mid winter and to 0.35–0.4 g/cm^3 in late winter. The high snow densities are caused by strong winds with speeds increasing to 20 m/s during snow storms. The frequency of storm winds is 20–40 days/yr in northern Yakutia, increasing to 60–80 days/yr on the Arctic islands. It is known that the higher that snow density is, the lower is the insulating effect of snow cover, even with increased thickness. Second, snow cover disappears as late as mid-June in northern Yakutia and late June on the Arctic islands, and the duration of the snow-covered season is 230–240 days in the north and 290–300 days on the Arctic islands. Under these severe climatic conditions, snowmelt occurs very slowly after air temperatures rise above 0ºC, thus retarding soil warming. This 2–3 week delay results in a decrease in mean annual permafrost temperature. Third, it is a common knowledge that the snow cover of long duration increases the albedo and this also has a negative effect on mean annual ground temperature. With no changes in $\sum_{at}<0$, the decrease in $T_{m\,1.6}$ therefore appears to result from the persistence of snow cover long after the onset of positive air temperatures retarding soil warming, rather than to the increased snow depth and density. The soils in northern Yakutia showed a rise in the early 1980s, while according to Pavlov (1997) the mean annual soil temperatures in northern West Siberia began warming a decade earlier. Although Jarjan records indicate a negative linear trend of temporal $T_{m\,1.6}$ variation (see Fig. 2, plot 1), its extremely low values (–4ºC) occurred at $\sum_{at}<0$ = –6000 degree-day/year or lower and h_s = 20 cm or less (see Fig. 4, plots 1a and 1b).

2a. In western Yakutia, winters have become milder with a decrease in $\sum_{at}<0$ at 3-9 degree-day/year. According to the graphical relationship, h_s increased at a trend of 0.18–1.18 cm/year (Berdigestyakh and Vilyuisk stations). In Central Yakutia, where h_s shows temporal stability, winters also tend to become milder, resulting in increased $T_{m\,1.6}$. This is attributed to the general weakening of the Asian anticyclone. The plot constructed from the Pokrovsk weather station data indicates that $T_{m\,1.6}$ increases to –1.3ºC at $\sum_{at}<0$ = –5300 degree-day/year and h_s = 40 cm and decreases to –3.4ºC at $\sum_{at}<0$ = –5700 and h_s < 30 (Fig. 4, plots 2a and 2b). In southwestern Yakutia, trends toward lower $\sum_{at}<0$ and greater h_s, resulting in increased $T_{m\,1.6}$, suggest stronger winter advection in the westerlies.

2b. The northeastern plains of the north-taiga zone and the major intermontane depressions also show a positive trend in $T_{m\,1.6}$. Winters became much warmer throughout the region, where $\sum_{at}<0$ decreased at a rate of 13.6–27 to 59 degree-day per year (Batagai, Srednekolymsk, Delyankir and Ust-Moma). During winter, these areas are predominantly under the influence of the Asian anticyclone and the cyclones bringing precipitation from the Pacific Ocean (Kazurova 1961, Gavrilova & Cherdonova 1997). Because the winter snow cover is thin, its insulating effect is small. At the same time, a decrease in h_s of 0.13–0.4 cm per year is observed in the region (Batagai and Zyrianka stations). The reduction of $\sum_{at}<0$ is accompanied by an increase in $T_{m\,1.6}$ despite a tendency toward thinner h_s, which can also be explained by the instability or lesser influence of the Asian anticyclone.

3. In the mountainous regions, the changes in $\sum_{at}<0$ suggest a warming throughout the region during winter. Decreasing trends of 13.6–15.9 degree-day/year in $\sum_{at}<0$ and 0.09–0.36 cm/year in h_s are found. The plot for the Predporozhnaya weather station (Fig. 4, plots 3a and 3b) indicates that $T_{m\,1.6}$ varies inter-annually from–6.7 to–10.3ºC, when $\sum_{at}<0$ increases from –6500 to –6600 degree-day/year and и h_s decreases from 35 to 10 cm. $T_{m\,1.6}$ shows a closer relationship to h_s than to $\sum_{at}<0$. At this site characterized by relatively cold winter temperatures, cooling of $T_{m\,1.6}$ is associated with the decreasing trend in already shallow snow depth.

In the northern and central parts of the Aldan Plateau, the increase in $T_{m\,1.6}$ is directly related to the reduction of $\sum_{at}<0$ and the increase in h_s. At the Gorelyy weather station, a trend of $T_{m\,1.6}$ was 0.09ºC per year during the period from 1966 to 1985 (Fig. 2, line 4). The linear relationship for this site

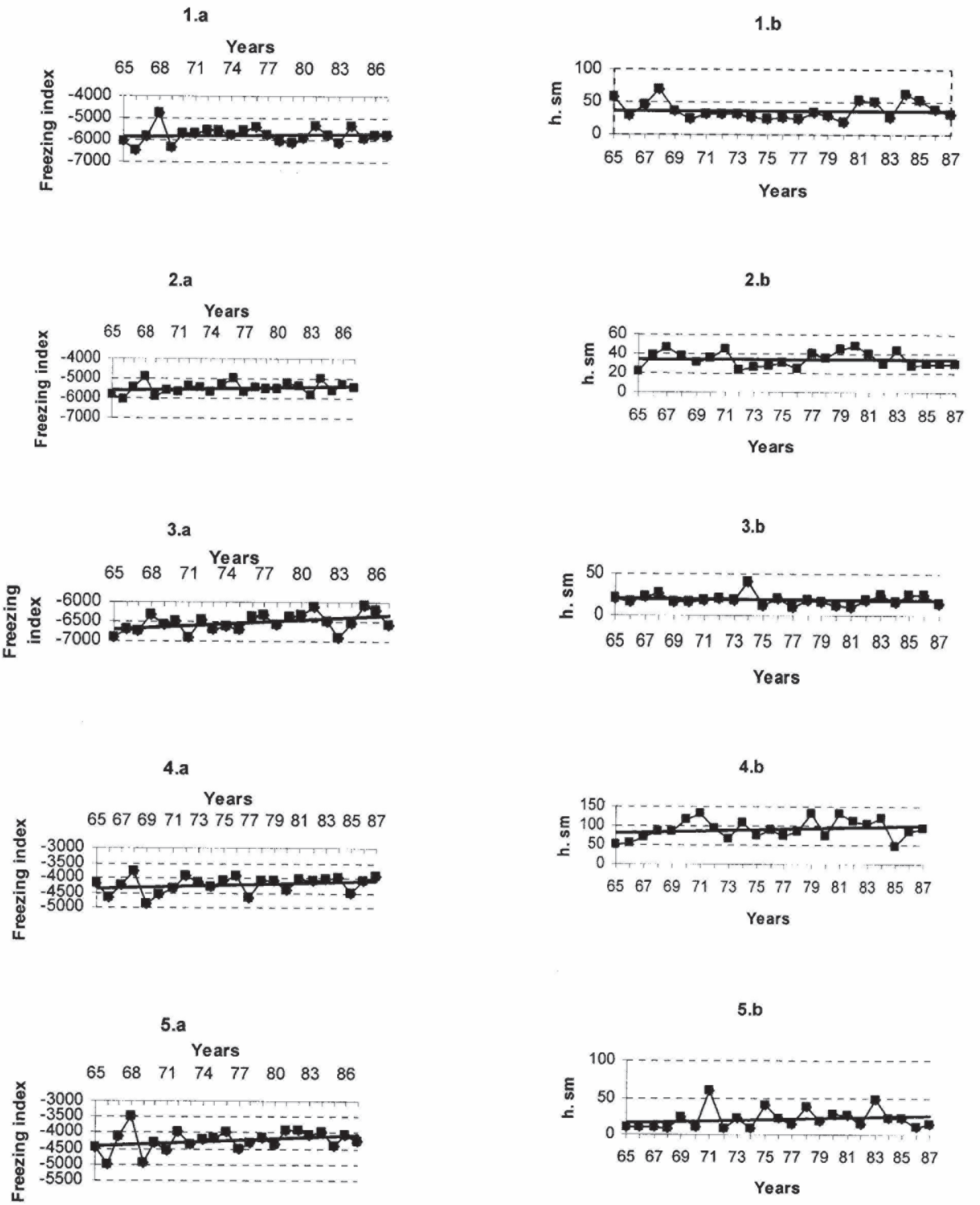

Figure 3. Variations of mean annual freezing index (a) and snow depth (b) for the same station (see Fig. 1).

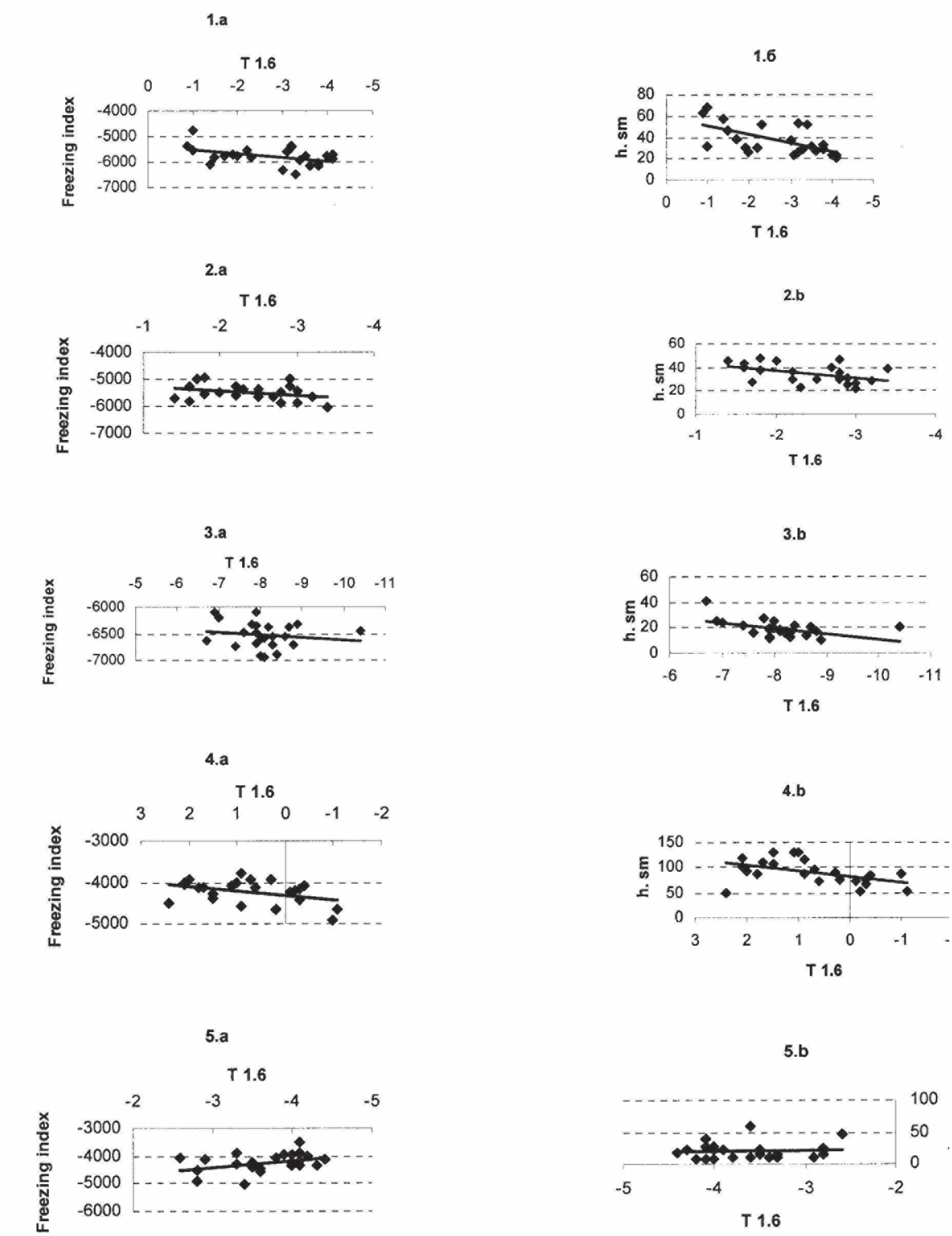

Figure 4. Relation of mean annual soil temperature variation at 1.6 m to air freezing index (a) and snow depth (b) for the same stations (see Fig. 2).

shows that $T_{m\ 1.6}$ increases from –1 to +2.4ºC with changes in $\sum_{at}<0$ from –4400 to –4000 degree-day/year and in h_s from 70 to cm (Fig. 4, plots 4a and 4b).

In the southernmost part of Yakutia, on the northern megaslope of the Stanovoy Range, $T_{m\ 1.6}$ is found to be temporally stable exhibiting a very slight negative trend (0.01ºC per year) at Nagornyy (Fig. 2, line 5). Comparison of $T_{m\ 1.6}$ with $\sum_{at}<0$ variation (Fig. 4, plot 5a) leads to the misleading conclusion that $T_{m\ 1.6}$. decreases with decreasing $\sum_{at}<0$. The slight progressive decrease in $T_{m\ 1.6}$ with positive trends in $\sum_{at}<0$ and h_s (see Fig. 4, plot 5b) is attributed to the persistence of snow cover long after the onset of positive air temperatures, because the station is located at a relatively high elevation (861 m a.s.l.) on a north-facing slope. Besides, the Timpton valley narrows here to 800 m, while shortly downstream it is 2–2.5 km wide, resulting in strong local winds which can also cause significant soil cooling. Thus, in the mountainous regions, some decrease in $\sum_{at}<0$ and increase in h_s do not lead to an increase in $T_{m\ 1.6}$.

Conclusions

● In the northern regions of Yakutia, the decreasing trend in $T_{m\ 1.6}$, with the freezing index remaining stable, appears to be due to the persistence of snow cover long after the onset of positive air temperatures retarding soil warming, rather than to the increased snow depth and density.

● In the north of Yakutia, a recent rise of $T_{m\ 1.6}$ occurred in the early 1980s, while in northern East Siberia an increase was observed since the early 1970s.

● In the middle-taiga areas of western and central Yakutia, in the north-taiga areas of eastern Yakutia, and in the intermontane basins, the increase of $T_{m\ 1.6}$ is attributed to the instability or lesser influence of the Asian anticyclone. In southwestern Yakutia, it is caused by stronger advection of the westerlies.

● In the mountains, $T_{m\ 1.6}$ variation under present climate are largely determined by local temperature-forming factors, showing a decrease in cold landscapes and an increase in warm landscapes.

References

Balobaev, V.T. 1997. Global changes of the Earth's climate and permafrost (in Russian). *Nauka i Obrazovanie* 2(6): 82-90.

Chudinova, S.M., Bykhovets, S.S., Fedorov-Davydov, D.G., Sorokovikov, V.A., Gubanov, V.S., Barry, R.G. & Gilichinsky, D.A. 2001. Response of temperature regime of Russian north to climate changes during second half of XX century (in Russian). *Kriosfera Zemli* V(3): 63-70.

Chudinova, S.M., Bykhovets, S.S., Fedorov-Davydov, D.G., Sorokovikov, V.A., Barry, R., Zhang, T. & Gilichinsky, D.A. 2003. Features of soil warming versus recent climate warming in Russia (in Russian). *Kriosfera Zemli* VII(3): 23-30.

Climate Change. 1990. The IPCC Scientific Assessment. Report of Working Group I of the International Panel on Climate Change. New York: Cambridge Univ. Press, 364 pp.

Dostovalov, B.N. & Kudryavtsev, V.A. 1967. *Permafrost Science (Obshchee merzlotovedenie)* (in Russian). Moscow: Izd-vo Moskovskogo Universiteta, 404 pp.

Drozdov, O.A. & Lugina, K.M. 1996. Non-uniformity of climate variation effects in the sectors and zones of the Northern Hemisphere (in Russian). *Vestnik St.-Petersburgskogo Universiteta* 1(7): 44-57.

Fedorov, A.N. & Svinoboev, A.N. 2000. Changes in near-surface air temperature in the Republic of Sakha (Yakutia). In: *Climate and Permafrost: Integrated Investigations in Yakutia (Klimat i merzlota: kompleksnye issledovania v Yakutii)* (in Russian). Yakutsk: Permafrost Institute Press, 68-75.

Frauenfeld, O.W., Zhang, T. & McCreight, J.L. 2006. Northern Hemisphere freezing/thawing index variations over the 20th century. *Int. J. Climatol.* 27: 4763.

Frauenfeld, O.W., Zhang, T., Barry, R.G. & Gilichinsky, D.A. 2004. Interdecadal changes in seasonal freeze and thaw depths in Russia. *J. Geophys. Res.,* 109, D05101, doi 10. 1029/2003 JD004245.

Gavrilova, M.K. & Cherdonova, V.S. 1997. Pacific atmospheric circulation processes in Yakutia. *Proceedings of International Workshop on Energy and Water Cycle in GAME-Siberia, 1995: Research Report of JHAS (3). Nagoya*, 9-12.

Gedalof, Z. & Smith, D.J. 2001. Interdecadal climate variability and regime-scale shifts in Pacific North America. *Geo. Res. Lett.* 28: 1515-1518.

Ghil, M. & Vautard, R. 1991. Interdecadal oscillations and the warming trend in global time series. *Nature* 350: 324-327.

Gilichinsky, D.A., Bykhovets, S.S., Sorokovikov, V.A., Fedorov-Davydov, D.G., Barry, R.G., Zhang, T., Gavrilova, M.K. & Alekseeva, O.I. 2000. Use of the data of hydrometeorological survey for century history of soil temperature trends in the seasonally frozen and permafrost areas of Russia (in Russian). *Kriosfera Zemli* IV(3): 59-66.

Harris, S.A. 2002. Global heat budget, plate tectonics and climatic change. *Geografiska Annaler* 84A: 1-10.

Harris, S.A. 2005. Thermal history of the Arctic Ocean environs adjacent to North America during the last 3.5 Ma and a possible mechanism for the cause of the cold events (major glaciations and permafrost events). *Progress in Phys. Geography* 29(4): 218-237.

Izrael, Y.A., Pavlov, A.V. & Anokhin, Y.A. 2002. Permafrost evolution related to current global climatic change (in Russian). *Meteorologia i Gidrologia* 1: 22-34.

Izrael. Y.A., Pavlov, A.V., Anokhin, Y.A., Myach, L.T. & Shershtyukov, B.G. 2006. Statistical evaluation of variations of climate parameters in the Russian permafrost zone (in Russian). *Meteorologia i Gidrologia* 5: 27-38.

Kazurova, N.S. 1961. Synoptic processes in Yakutia in different seasons and their brief characterization. In: *Issues of Yakutia Geography (Voprosy geografii Yakutii)* (in Russian). Yakutsk: Knizn. izd-vo,. 19-26.

Osterkamp, T. E. & Romanovsky, V.E. 1999. Evidence for warming and thawing of discontinuous permafrost in Alaska. *Permafrost and Periglacial Processes* 10: 17-37.

Pavlov, A.V. 1994. Prediction of permafrost evolution in relation to global change of contemporary climate. In: *Current Issues in Hydrogeology, Engineering Geology and Ecology (Sovremennye problemy gidrogeologii, inzhenernoy geologii I ecologii)* (in Russian). Moscow: VSEGINGEO, 135-151.

Pavlov, A.V. 1997. Permafrost and climate monitoring in Russia: methodology, observational results and prediction (in Russian). *Kriosfera Zemli* 1(1): 47-58.

Smith, S.I., Burgess, M.M. & Taylor, A.E. 2003. High Arctic permafrost observatory at Alert, Nunavut – analysis of a 23 year data set. *Proceedings of the Eighth International Conference on Permafrost, Zurich, Switzerland, 21-25 July, 2003*: 1073-1078.

Varlamov, S.M., Kim, E.S. & Han, E.C. 1998. Recent temperature variations in East Siberia and the Russian Far East (in Russian). *Meteorologia i Gidrologia* 1: 19-28.

Varlamov, S.P. & Skachkov, Y.B. 1996. Spatiotemporal variability of climatic elements. In: V.T. Balobaev, M.K. Gavrilova, & A.N. Fedorov (eds.), *The Influence of Climate on Permafrost Landscapes in Central Yakutia (Vlianie klimata na merzlotnye landshafty Centralnoi Yakutii)* (in Russian). Yakutsk: Permafrost Institute Press, 11-36.

Vasiliev, I.S. & Torgovkin, Y.I. 1996. The influence of climate on temperature and thickness of thawing soils. In: V.T. Balobaev, M.K. Gavrilova, & A.N. Fedorov (eds.), *The Influence of Climate on Permafrost Landscapes in Central Yakutia (Vlianie klimata na merzlotnye landshafty Centralnoi Yakutii)* (in Russian). Yakutsk: Permafrost Institute Press, 37-45.

Vasiliev, I.S. 1992. Changes in climate elements and active layer thickness in western Yakutia. In: *Natural Resource Management in Permafrost Regions (Ratsionalnoe prirodopolzovanie v kriolitozone)* (in Russian). Moscow: Nauka, 43-46.

Vasiliev, I.S. 1999. Response of soil temperatures to recent climatic variations (in Russian). *Meteorologia i Gidrologia* 2: 98-104.

Zhang, T. & Osterkamp, T.E. 1993. Changing climate and permafrost temperatures in the Alaskan Artic. *Proceedings of the Sixth International Conference on Permafrost, Beijing, China. July 5-9*. Vol. 1, 783-788.

Zukert, N.V. & Zamolodchikov, D.G. 1997. Long-term trends of air temperature and precipitation in Russian tundra zone (in Russian). *Meteorologia i Gidrologia* 1(1): 47-58.

Approaches to Allocation of Terrain Complexes (Landscapes) in the Areas of Thermokarst Development

Alexandra Veremeeva
Institute of Physicochemical and Biological Problems in Soil Science, Russian Academy of Sciences, Pushchino, Moscow Region, Russia

Stanislav Gubin
Institute of Physicochemical and Biological Problems in Soil Science, Russian Academy of Sciences, Pushchino, Moscow Region, Russia

Abstract

Evaluation of organic matter content and the amount of greenhouse gases released in polar areas of Northern Yakutia, as well as the study of polar landscape stability in the face of climate warming, now demand systematization of the data on landscape structure of the Northern Yakutia lowlands. In this study, such systematization is performed on the basis of classifying and mapping major terrain complexes in the northern Kolyma Lowlands.

Keywords: global warming; landscape; mapping; permafrost; terrain complex; thermokarst.

Introduction

Active research in the Kolyma Lowlands started in the late 1950s. The greatest interest in this territory lies in the peculiarities of its formation during the Pleistocene. A considerable number of publications are devoted to the origin and stratigraphy of the Pleistocene deposits, Pleistocene flora and fauna, and to general paleo-reconstructions.

Since the 1990s, the Kolyma Lowland has become a key region for studies of possible permafrost degradation, which can be triggered by global warming. Degradation of permafrost is likely to be followed by significant release of methane and carbon dioxide (Rivkina et al. 1996, Rivkina et al. 2006, Walter et al. 2006). To answer the questions triggered by these studies, it is necessary to calculate the quantity of organic matter and amount of greenhouse gases released from it, and then to forecast future development of thermokarst. This, in turn, demands conducting studies of modern landscapes and systematization of present day concepts of the terrain structure. Detailed landscape studies for the northern Kolyma Lowland have not yet been implemented. To fill this gap, we set a task to define and distinguish the major landscapes types (Terrain Complexes) of the northern Kolyma Lowland, to classify them, to identify patterns of their distribution, and to map them using Geographic Information Systems for acquiring the desired parameters.

Objects and Methods of Research

Objects of research

Our investigations are based on field data, collected during expeditions to this region (1980-2000), the studies of A.N. Fedorov (Fedorov 1991), and the permafrost-landscape map of Yakutian ASSR at 1:2500000 scale edited by P.I. Melnikov (1991). After analysis of field data, existing maps and publications, we selected the key study region for our research, which is a 6500 km^2 area in the Kolyma Lowlands located between the Alazeya River and Chukochya River in their middle flows (central coordinate is 69°30′N, 156°0′E). The region is located within the continuous permafrost zone; it belongs to the Alazeya-Kolyma lake-thermokarst province (Fedorov 1991). Comparison of the key region structure with the structure of other Northern Yakutia lowland areas shows that it is typical and reflects major patterns of tundra landscape development in the Holocene impacted by active thermokarst processes.

The key study region is characterized by flat and gently sloping thaw-lake depressions (thaw-lake basins), and the remnants of the Late Pleistocene surface formed by ice-rich deposit with polygonal ice wedges (named in the literature *Ice Complex* or *yedoma*). Based on paleogeographical data, we presume that during the Pleistocene the region was a flat plain underlain by ice-rich silts with ice wedges. At the Late Pleistocene-Holocene boundary, the active structural change began as a result of climate warming. Under the impact of thermo-erosional and thermokarst processes, the Ice Complex areas have been reduced, and they now represent different stages of thermokarst evolution. Some surfaces (relatively high elevation yedoma remnants) have not yet been reworked by thermokarst and have the thickest strata with ice wedges. Other surfaces have been partly reworked, and some have been transformed into thaw-lake basin depressions due to thawing of ground ice.

Methods of research

Allocation and mapping of landscapes first requires the determination of the basin mapping unit. A.N. Fedorov recommended distinguishing the hierarchy of local territorial geosystems on the basis of identifying leading factors among different characteristics, and considers the resulting boundaries to be absolute (Fedorov 1991). Another approach is suggested by Gr.A. Isachenko (Isachenko & Reznikov 1996, Isachenko 1998), who distinguish within a particular landscape different types of units characterized by relatively stable parameters:

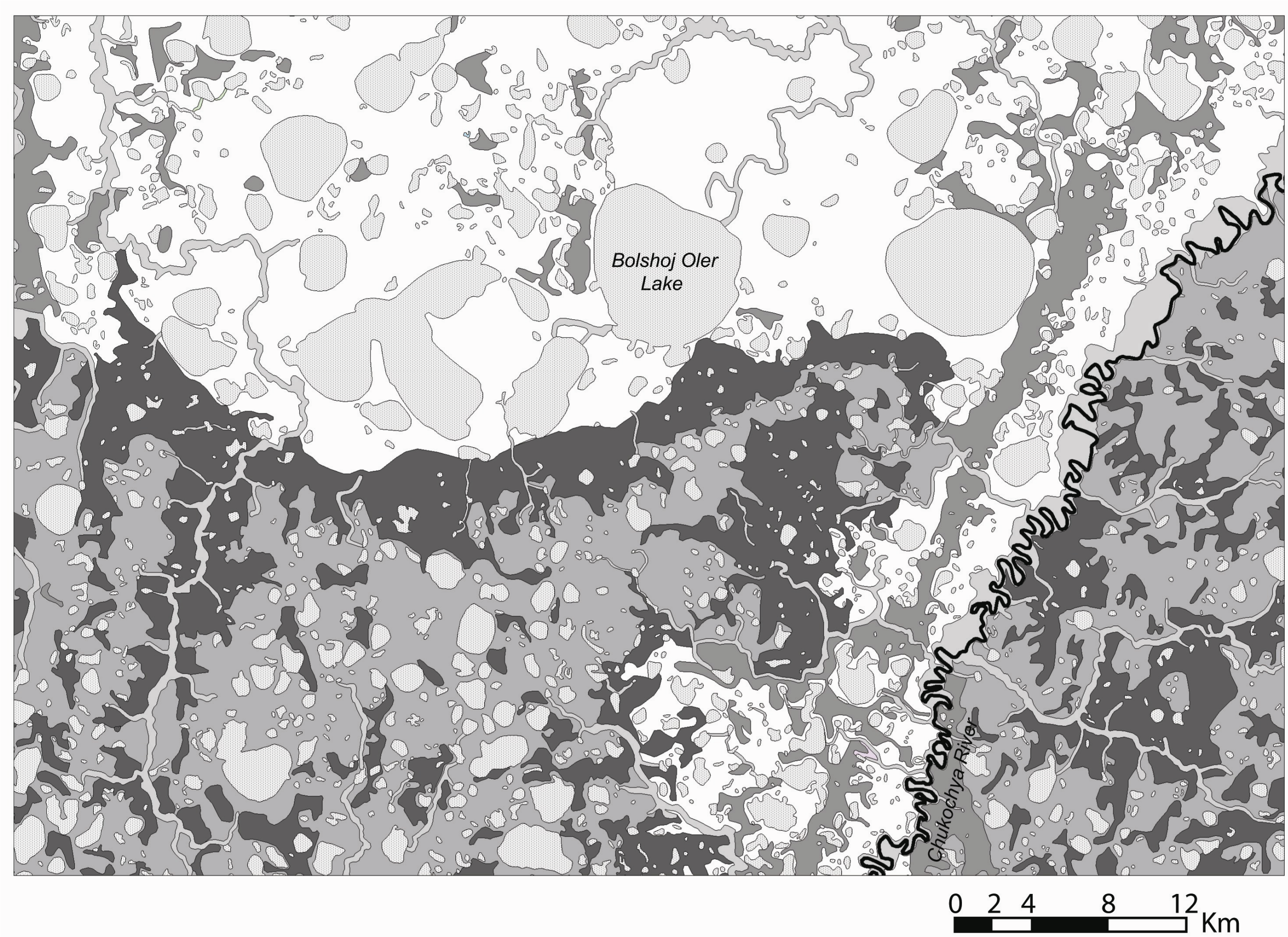

Type of terrain	Index	Depth of permafrost table (m)	Sediments	Absolute elevations, m	Prevailing soils	Dominant type of vegetation
1. Drained surface of Yedoma remnants (gradient 0-15º) with initial forms of developing thermokarst (High Yedoma)		0.5–0.6	Ice-rich Late Pleistocene silts with polygonal ice wedges (Ice Complex)	40–80	Cryosols, gleysols	Gramineous-dryas, sedge-herbaceous shrub-moss
2. Slightly drained surface of Yedoma remnants (gradient 0-10º), with initial forms of developing thermokarst (Low Yedoma)		0.4–0.5	Ice-rich Late Pleistocene silts with polygonal ice wedges and overlaid with taberal deposits (thawed and refrozen sediments)	20–40	Gleysols histosols	Sedge-Herbaceous shrub-moss
3. Waterlogged flat surface with polygonal nano- and mesorelief, and numerous small lakes (Upper thaw-lake depressions)		0.2–0.4	Ice-rich lacustrine-alas deposits of thaw-lake basins with partially remained polygonal ice wedges	20–40	Gleysols histosols	Sedge-cotton grass, Herbaceous shrub- moss
4. Heavily waterlogged flat surface with polygonal nano- and mesorelief, and numerous lakes (Low thaw-lake depressions)		0.2–0.3	Ice-rich lacustrine-alas deposits of thaw-lake basins	10–30	Histosols, Gleysols	Sedge-moss
5. River valleys complex (with terraces)		0.3–0.8	Fluvial silty-sandy deposits	0–20	Fluvisols, histosols	Moss-shrub, Sedge-moss

Figure 1. Portion of terrain complexes map of the key study region.

1. similar position in relief (single meso-scale landform);
2. similar composition and cryogenic structure of subsurface layers;
3. similar drainage conditions.

These characteristics determine the hydrographical network, distribution of lakes and bogs, soils and vegetation. They also define the so-called “rigid design” of the territory, which acts as a reference frame for study of long-term (hundreds of years) processes of landscapes development (Isachenko & Reznikov 1996). This approach corresponds to our tasks including the forecasting of terrain evolution at the onset of global warming.

Figure 1 shows the landscape map based on topographic maps of 1:200000 scale and confronted with Landsat 7 ETM+ satellite images. For charting, we used MapInfo 7.0 and ArcView 3.2. Topographic maps of 1:200000 scale are most useful for our task because they show every substantial roughness while, at the same time, make it possible to cover large territories. Another important property of this scale is its comparativeness with existing satellite images.

Results

On the basis of Isachenko’s (1998) approach, we have distinguished five major types of terrain complexes in the key region: high yedomas, low yedomas, upper thaw-lake depressions, low thaw-lake depressions and river valleys. We have charted the digital landscape map of the key region at a 1:200,000 scale (Fig. 1). Analysis of the map shows that the largest part of the territory is the interstream area between the Alazeya River and the Chukochya River. In the north is located an extensive low thaw-lake depression. It is filled with many lakes (as large as 50 km^2); the surface is flat so the drainage is limited. Within the depression only small remnants (not larger then 4 km^2) of low yedoma are still preserved. Only along the major river valleys are vast remnants of low yedoma present, some of them as large as 50 km^2. Southward the territory of upper thaw-lake basins is located. There are a number of high yedoma remnants found here (with areas not larger then 6 km^2). Large areas of yedoma are adjacent to river valleys and low thaw-lake depressions. The right bank of the Chukochya River is also an upper thaw-lake basin, where large areas of high yedoma are preserved (up to 60 km^2). The latter are being drained by tributaries of the Chukochya River. The presence of vast high yedoma here is associated with exposed Oler sequence deposits containing low ice content and lacking polygonal ice wedges (Sher 1971). Thus, it determines the greater ruggedness of the surface and therefore the better drainage of the territory.

Table 1 shows that most common types of terrain complexes are thaw-lake depressions formed due to thawing ice wedges. They occupy 64.8% of the territory. The area of low and upper thaw-lake basins is 34.8% and 30.0%, respectively, of the total area of the key region. The area occupied by lakes in the upper and lower thaw-lake depressions makes up 21.5% and 29.3%, respectively, of the terrain complex area. High and low yedomas occupy about 26.5% of the territory, and the lake percentage of terrain complexes is 5.4 and 3.2%, respectively.

Lakes are classified according to the area on three groups within each terrain complex: large (>1 km^2), medium (0.1 to 1 km^2) and small (<0.1 km^2) (Table2).

Table 1. Areas occupied by terrain complexes and lakes.

Terrain complexes	Area of terrain complex (with lakes), sq km	Percentage of total area, %	Area of lakes, sq km	Percentage of total area of terrain complex, occupied by lakes, %
High Yedoma	1181.0	18.1	63.5	5.4
Low Yedoma	548.7	8.4	17.8	3.2
Upper thaw-lake depressions	1956.6	30.0	420.0	21.5
Low thaw-lake depressions	2274.3	34.8	665.8	29.3
River valleys	567.1	8.7	18.0	3.2
Total classified area	6527.7	100	1185.1	18.2

Table 2. Distribution of different groups of lakes (number and square) within separate terrain complex.

Groups of lakes	Number	In % of total lake number for terrain complex	Area, sq km	In % of total lake area	In % of terrain complex area
High Yedoma					
<0.1 km^2	204	56.4	11.1	17.4	0.9
0.1–1 km^2	151	41.7	38.4	60.5	3.2
>1 km^2	8	2.2	14.0	22.1	1.2
Low Yedoma					
<0.1 km^2	60	58.3	3.0	16.7	0.5
0.1–1 km^2	41	39.8	9.5	53.2	1.7
>1 km^2	3	2.9	5.3	30.0	1.0
Upper thaw-lake depressions					
<0.1 km^2	551	45.8	29.7	7.1	1.5
0.1–1 km^2	563	46.8	185.9	44.3	9.5
>1 km^2	90	7.5	204.4	48.7	10.4
Low thaw-lake depressions					
<0.1 km^2	373	42.1	22.0	3.3	1.0
0.1–1 km^2	408	46.1	133.2	20.3	5.9
>1 km^2	104	11.8	502.6	76.4	22.1
River valleys					
<0.1 km^2	78	60.5	4.1	22.8	0.7
0.1–1 km^2	49	38,0	10,3	57,1	1,8
>1 km^2	2	1,6	3,6	20,2	0,6

Lakes with areas of more than 1 km^2 occur sporadically within yedomas, and medium lakes predominate here by total area. Small lakes, which existence is connected with the initial stages of thermokarst development, prevail by number. Within the high yedoma terrain complex are found small thermokarst depressions, filled by medium lakes. Large lakes dominate in low thaw-lake basins. They occupy 22.1% of the area of low thaw-lake basins and 76% of summarized area of lakes within this landscape. In upper thaw-lakes basins, areas of large and medium lakes are comparable (10.4 and 9.5% respectively). It demonstrates the potential of increasing the area of medium lakes from climate warming and thawing of polygonal ice wedges.

Conclusions

Allocated terrains (all types except river valleys) represent different stages in the regional development. High yedoma are the remnants of the Late Pleistocene surface. At the end of Pleistocene and the beginning of the Holocene at 12 kyr BP (Schirmaister et al. 2002), as a result of climate warming the active modeling of initial landscape and the formation of vast thaw-lake basins had begun. The most active stage of thermokast development, characterized by maximum total area occupied by thaw-lake basins (present upper thaw-lake depressions), took place 7–5 kyr BP (Kachurin 1961, Grosse 2005). A substantial proportion of thaw-lake basins formed during this time later underwent further development from thermokarst and thermo-erosional process, especially at watershed locations. On that part of the region where thermokarst processes ceased or stopped, low yedomas were formed with partly melted polygonal ice wedges overlain by tabular deposits.

The next stage of active thermokarst development and formation of low thaw-lake basins took place in the late Holocene 3000–700 years ago (Baulin et al. 1967, Chekhovsky & Shamanova 1976).

The present age is characterized by climate cooling (Schirrmeister et al. 2002), which is confirmed by the absence of track of thermokarst activation during the past 50 years (Voskresensky 2001). More than 80% of the initial Late Pleistocene plains are modeled by thermokarst and thermo-erosional processes. Slopes of yedomas and thaw-lake depressions are gradually flattening and overgrowing by vegetation. The total portion of thaw-lake basins area in the region of research is 18.2%. It is commensurable with other regions with Ice Complex: Bykovsky Penninsula (lower course of river Lena – 14.4%, (Grosse 2005), and the Barrow Peninsula (Alaska) – 22% (Hinkel et al. 2003).

In case the global warming scenario is realized, the most stable areas will be low thaw-lake depressions because at these areas polygonal ice wedges have already melted out, and peat layers with a thick moss mat formed at the surface protects the permafrost substrate from incoming warmth.

Upper thaw-lake basins are subject to partial surface modeling in case of the onset of global warming. Polygonal ice wedges, although partly melted, still exists here; activation of thermokarst and thermo-erosional processes causes further melting and an increase of lake areas is likely.

Even more unstable during climate warming by thermokarst activation will be yedomas. Low yedomas will be more stable then high yedomas because polygonal ice wedges in low yedomas are located deeper, the peat and moss mat is thicker, and permafrost is more resistant to thermokarst (waterlogged areas are more frequent here).

High yedomas are the most unstable areas and are highly susceptible to thermokarst and thermo-erosional processes because polygonal ice wedges are very close to the surface, which in turn is characterized by free drainage. Peat and vegetation are uncommon and don't provide thermal insulation.

The information obtained about terrain structure and terrain complex distribution and evolution patterns helps to forecast thermokarst development in the northern Yakutia coastal lowlands at the onset of global warming.

This study is the first stage of northern Kolyma Lowland landscapes research. We consider it as a basis for other studies of northern coastal lowlands of Yakutia.

References

Baulin, V.V., Belopukhova, E.B., Dubikov, G.I. & Shmelev, L.M. 1976. *Geocryological conditions of Western Siberia Lowland*. Moscow: Nauka Press, 214 pp (in Russian).

Chekhovsky, A.L. & Shamanova, I.I. 1976. Forming of taliks under the thermokarst lakes of Western Siberia. *Proceedings of PNIIS.* Moscow, 49: 64-73 (in Russian).

Fedorov A.N. 1991. *Permafrost landscapes of Yakutia: method of allocation and problems of mapping*. Yakutsk, Russia, 140 pp. (in Russian).

Grosse, G. 2005. *Characterisation and evolutional of periglacial landscapes in Northern Siberia during the Late Quarternary – Remote sensing and GIS studies*. Dissertation. Potsdam, 126 pp.

Hinkel, K.M., Eisner, W.R., Bockheim, J.G., Frederick, E.N., Peterson, K.M. & Dai, X. 2003. Spatial extent, age, and carbon stocks in drained thaw lake basins on the Barrow Peninsula, Alaska. *Arctic, Antarctic and Alpine Research* 35: 291-300.

Isachenko, Gr.A. 1998. *Field landscape research methods and landscape-ecology mapping*. St.-Petersburg State University Press, 112 pp. (in Russian).

Isachenko, Gr.A. & Reznikov, A.I. 1996. *Taiga of the European Russia north-west: landscape dynamics*. St.-Petersburg State University Press, 140 pp. (in Russian).

Kachurin, S.P. 1961. Thermokarst on USSR territory. Moscov, Academy of Science Press, 291 pp. (in Russian).

Permafrost-landscape map of Yakutian ASSR of 1:2500000 scale. 1991. Edited by Melnikov P.I. Moscow, 2 pp. (in Russian).

Rivkina, E.M., Kraev, K.V., Krivushin, K.S., Laurinavichus, K.S., Fyodorov-Davydov, D.G., Kholodov A.L., Shcherbakova, V.A. & Gilichinskyy, D.A. 2006. *Methane in permafrost of Northeastern Arctic*. *Cryosphere of Earth* 3: 23-42 (in Russian).

Rivkina, E.M. & Gilichinskyy, D.A. 1996. Methane as a paleoindicator for genesis and dynamics of frozen layers. *Lithology and Minerals* 4: 183-193 (in Russian).

Schirrmeister, L., Siegert, C., Kuznetsova, T., Kuzmina, S., Andreev, A.A., Kienast, F., Meyer, H. & Bobrov, A. 2002. Paleoenvironmental and paleoclimatic records from permafrost deposits in the Arctic region of Northern Siberia. *Quaternary Internetional* 89: 97-118.

Sher, A.V. 1971. *Mammals and Stratigraphy of the Pleistocene of the Extreme Northeast of the USSR and North America.* Moscow: Nauka Press, 310 pp. (in Russian).

Voskresensky, K.S. 2001. *Modern relief forming processes at plains of North of Russia*. Moscov State University Press, Geographic Department, 260 pp. (in Russian).

Walter, K.M., Zimov, S.A., Chanton, J.P., Verbyla, D. & Chapin III, F.S. 2006. Methane bubbling from Siberian thaw lakes as a positive feedback to climate warming. *Nature*. V (443): 71-75.

Numerical Studies of Permafrost Effects on Groundwater Flow

Patrik Vidstrand
Chalmers University of Technology, Gothenburg, Sweden

Jens-Ove Näslund
Swedish Nuclear Fuel and Waste Management Company, Stockholm, Sweden

Juha Hartikainen
Helsinki University of Technology, Espoo, Finland

Abstract

Despite the inferred present global warming trend, future climate during the long life-span of a nuclear waste repository could well include periods of permafrost development in all of Sweden. The occurrence of permafrost in soil and bedrock can alter significantly surface boundary conditions that affect groundwater recharge and discharge as well as the deeper circulation of groundwater in the bedrock presently investigated for the potential to accommodate nuclear waste. Within the safety assessments, generic studies on deep groundwater circulation in the presence of permafrost have been conducted. The present study includes a compilation of future permafrost scenarios and their implications on the groundwater flow. The results suggest that for a location where unfrozen taliks are present, sporadic permafrost will reduce while continuous permafrost will enhance groundwater flow. The study, although generic in character, is conclusive on the importance of permafrost in controlling both local and regional groundwater flow systems.

Keywords: climate scenario; groundwater flow; permafrost; taliks.

Introduction

Over the life-span of relevance for a nuclear waste geological repository, climate models predict future climatic situations that result in permafrost development, glacial conditions, and changes in shoreline elevation with possibilities for both elevated and submerged situations. Conditions of permafrost as surface boundary cause changes within the subsurface environment in hydrogeological properties as well as in the hydrogeochemistry.

Permafrost is defined as ground that is at or below 0°C for at least two consecutive years (French 1996). This definition has the implication that permafrost does not necessarily need to be frozen ground. However, the greatest impact on the subsurface hydrology from permafrost is the phase change related to the freezing of water. Frozen water creates an almost impervious stratum, which inhibits groundwater recharge but also the possibility of discharge, highlighting the possibility of high groundwater pressure beneath the permafrost (McEwan & de Marsily 1991, Boulton et al. 1993, Haldorsen & Heim 1999). One possible change due to permafrost is a re-organization of the regional as well as local groundwater flow regimes caused by the occurrence of frozen and nonfrozen areas within the ground.

This study mainly addresses the possible effects of different upper boundary conditions. The different scenarios considered are based on climate scenarios for the Forsmark site in Northern Uppland, Sweden; with special attention to the SFR geological repository for low and intermediate radioactive substances.

Even though the study is a hydrogeological flow study, it was not intended to create a realistic representation of the "true" groundwater flow situation. The purpose was instead to provide a safety analysis with quantification of, and uncertainty indicators for, the possible effects of different upper boundary conditions. Overall, the strategy was to use simplified models in the simulation of scenario cases to provide the safety analysis with relative flux values and uncertainty ranges.

Site Description

The site for this study is found in the Forsmark area in Northern Uppland, on the east coast of Sweden; some 200 km northwest of Stockholm. The site is one of the candidate sites for siting a nuclear waste deep geological repository in Sweden, but also hosts an active repository for low and intermediate nuclear waste (SFR).

The corrected precipitation in Forsmark for the measurement period August 1, 2003, to July 31, 2004, was

Figure 1. Location of the study area.

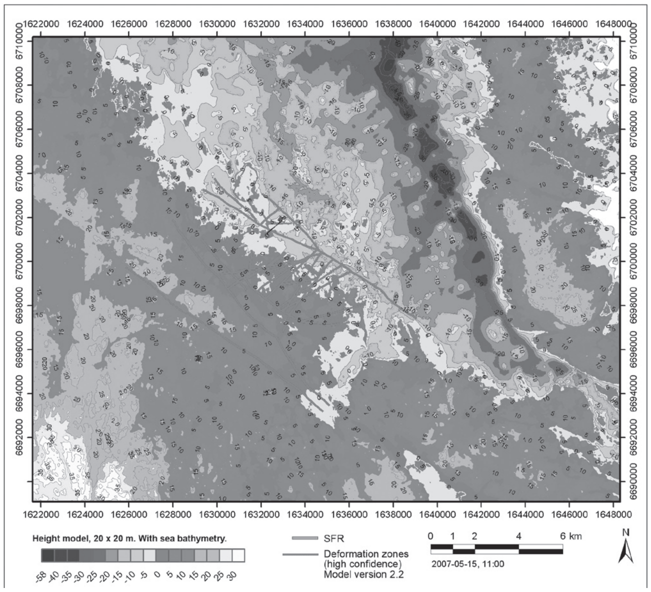

Figure 2. Local topography of the SFR region and the high confidence large-scale deformation zones as defined in the site investigation program.

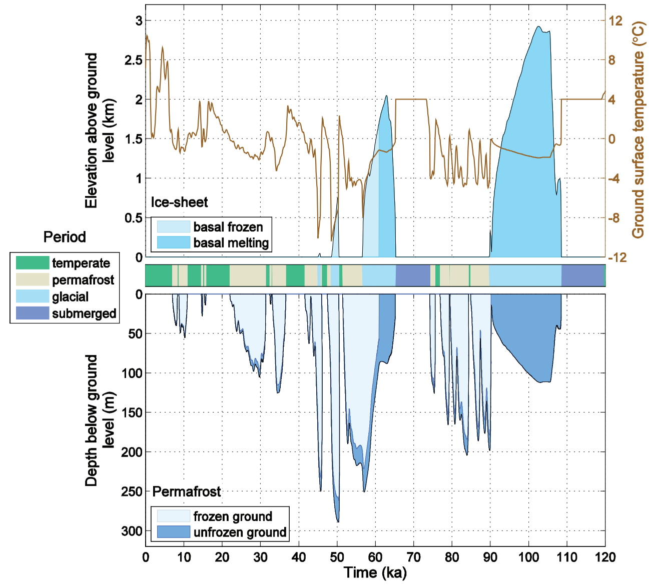

Figure 3. A climate scenario for the Forsmark region, including prevailing climate domains and climate related variables for a timeframe of 120,000 years in the future.

630 mm. The total "potential evapotranspiration" as reported in Lindborg (2005) was 472 mm for the same period. These numbers are in alignment with the long-term statistics from the Swedish Meteorological and Hydrological Institute (SMHI) for nearby stations as reported in Larsson-McCann et al. (2002). Based on these numbers, the net precipitation and the ground hydraulic properties indicate an excess of water in order to keep the groundwater table close to the surface. A permafrost environment may be significantly dryer as compared to present day conditions. However, the topography and geology at the site support a groundwater table close to the surface even if the net recharge is decreased to only one tenth. Hence, it is justified to assume a fully saturated subsurface and a groundwater table close to the surface as well as a prescribed pressure boundary condition at the surface also during permafrost conditions.

The local topography of the SFR region and the high-confidence large-scale deformation zones as defined in the site investigation programme is presented in Figure 2.

Future Climate and Permafrost Development

Climate-related changes, such as changes in shoreline elevation and development of permafrost and ice sheets, are the most important naturally occurring external factors affecting a nuclear waste repository in a time perspective from tens to hundreds of thousands of years.

It is not possible to predict the evolution of the climate in a 100,000-year time perspective with enough confidence for a safety assessment. However, the extremes within which the climate of Sweden may vary can be estimated with reasonable confidence. Within these limits, characteristic climate-related conditions of importance for repository safety can be identified. The conceivable climate-related conditions can be represented as *climate-driven process domains* (Boulton et al. 2001) where such a domain is defined as *a climatically determined environment in which a set of characteristic processes of importance for repository safety appear.* In the following, these climate-driven process domains are referred to as *climate domains.*

The identified relevant climate domains are named as

- *The temperate domain*
- *The permafrost domain*
- *The glacial domain*

The purpose of identifying climate domains is to create a framework for the assessment of issues of importance for repository safety associated with particular climatically determined environments that may occur in Sweden. If it can be shown that a repository fulfills the safety requirements independent of the prevailing climate domain, and the possible transitions between them, then the uncertainty regarding their exact timing in the future is less important. In addition to these climate domains, it is necessary to consider the periods for which the site is submerged by the Baltic Sea.

Figure 3 shows an example of a future scenario at Forsmark in a 120,000-year time frame in the future (SKB 2006). The scenario based on the evolution of the last glaciation, the Weichselian, and involves all the three climate domains. The permafrost domain is defined as periglacial regions that contain permafrost. It is a cold region without the presence of an ice sheet. The permafrost can occur in sporadic, discontinuous, or continuous forms. Regions belonging to the permafrost domain are not necessarily the same as regions with a climate that *supports* permafrost; i.e., as long as permafrost is present and not underlying an ice sheet, the region is defined as belonging to the permafrost domain, regardless of the prevailing temperature at the ground surface. Thereby, the climate in the permafrost domain can be warm diminishing permafrost. This way of defining the

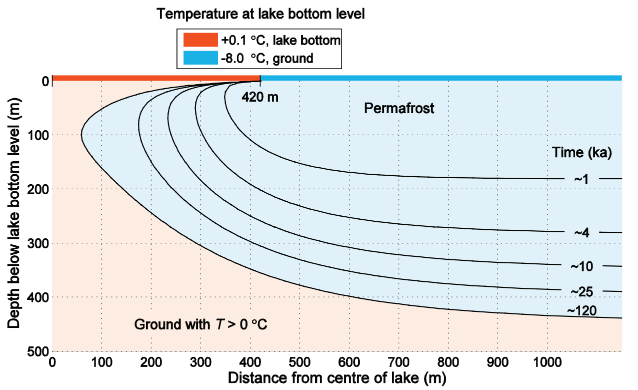

Figure 4. Evolution of permafrost in the vicinity of a circular lake of radius of 420 m at Forsmark when a constant lake bottom temperature of +0.1ºC, and a constant ground temperature of –8ºC at lake bottom level are assigned.

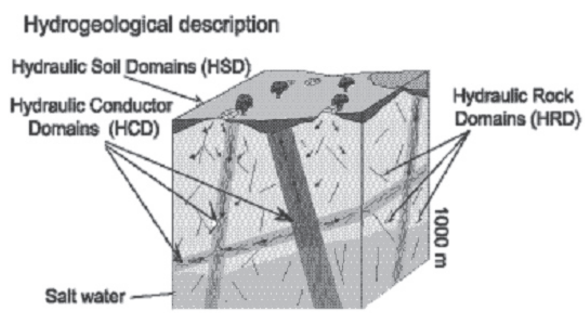

Figure 5. The Quaternary deposits and the crystalline bedrock are divided into separate hydraulic domains named the Hydraulic Soil Domains (HSD), Hydraulic Rock Mass Domains (HRD), and Hydraulic Conductor Domains (HCD). Within each domain, the hydraulic properties are represented by mean values or by spatially distributed statistical distributions (after Rhén et al. 2003).

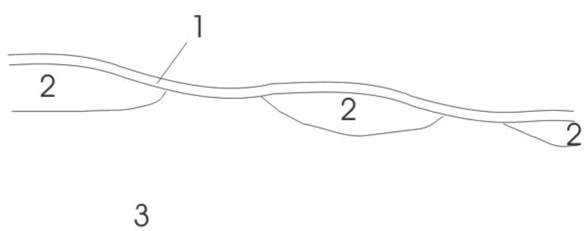

Figure 6. Illustration of conceptual model when permafrost is present.

domain is used because the presence of permafrost is more important for the safety function of the repository than the actual temperature at the ground surface. In general, the permafrost domain has a climate colder than the temperate domain and warmer than the glacial domain.

Large water bodies affect permafrost development and the presence of taliks. A talik can exist beneath a water body when its bottom temperature remains above the freezing point. Figure 4 demonstrates that an open talik can survive beneath a circular shallow lake, if its radius is greater than the thickness of ambient permafrost (SKB 2006).

Hydrogeological Numerical Flow Modeling

Basis

The computer code DarcyTools has been developed for simulations of groundwater flow and mass transport in porous and fractured media; the code uses continuum equations. Detailed descriptions of the concepts, methods, and equations of DarcyTools are documented in Svensson et al. (2004).

The modeling methodology used in this study followed SKB´s system approach for hydrogeological modeling (Rhén et al. 2003), which herein is much simplified. This approach divides the geosphere into three types of Hydraulic Domains, representing the Quaternary deposits, or Hydraulic Soil Domain (HSD), the fracture zones (HCD), and the rock mass between the fracture zones (HRD) (Fig. 5).

This study was conducted in two dimensions, even though such an approach is not necessarily well suited to the representation of fracture systems. Also, the study did not concentrate on a surface hydrology and, hence, did not include any soil cover (soil domain). The bedrock is in principle assumed to be a homogeneous porous medium with isotropic characteristics.

Common to all cases is no-flow boundary conditions on the lateral (side) boundaries and at the bottom for the sake of simplicity; sensitivity studies where the lateral boundaries were specified as hydrostatic showed no change in the results. The model is a fresh water model. The upper boundary is a spatially distributed specified pressure boundary assessed for the different surface conditions (climate domains); i.e., the groundwater table is fixed close to or at the ground surface. All simulations are steady-state.

All assigned hydrogeological properties are homogeneous within their specified model domains (Fig. 6):

- Unfrozen bedrock [3] (deep bedrock) has a hydraulic conductivity of $3 \cdot 10^{-8}$ m/s;
- Frozen bedrock [2] (permafrost) has a hydraulic conductivity of $3 \cdot 10^{-14}$ m/s;
- An active layer [1], if present, has a hydraulic conductivity of $3\ 10^{-4}$ m/s.

An active layer is present for all cases with assumed maximum infiltration capacity. Sensitivity to less available water has been tested where the active layer is removed and replaced with no-flow bodies along the surface boundary.

Reference case

These results are considered to be a representation of the present-day conditions. However, the simulations are a simplification in terms of conceptual model as well as flow dimensions and hydrogeological properties.

For simulations of the reference case, the hydraulic conductivity was specified as a homogeneous value of $3 \cdot 10^{-8}$ m/s. The upper boundary has a prescribed pressure at ground surface, which mimics a case of maximum infiltration (groundwater recharge). The regional topographic gradient is 3 m per km, but applies in combination with a more local gradient created by a sinusoidal surface with a wavelength of 5 km and amplitude of 10 m. Further, the groundwater throughout the domain is taken to be fresh water.

Figure 7. Permeability structure of the reference case. The four dots in the right upper model domain corner indicate the locations for synthetic repositories through which the flow is investigated.

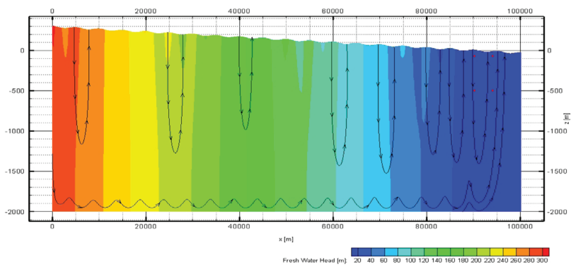

Figure 8. Fresh water heads of the steady-state solution of the reference case.

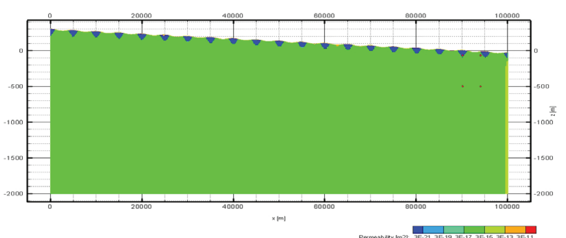

Figure 9. Conceptual model for the case of sporadic permafrost.

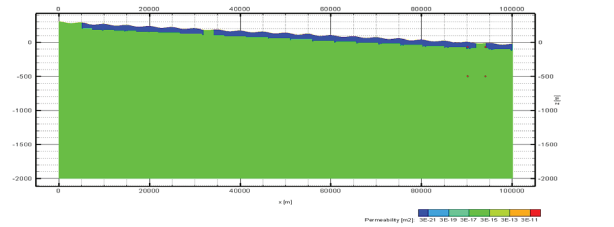

Figure 10. Conceptual model for the case of continuous permafrost.

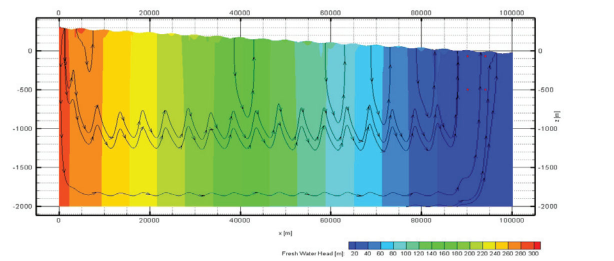

Figure 11. Fresh water heads of the steady-state solution for the sporadic permafrost case.

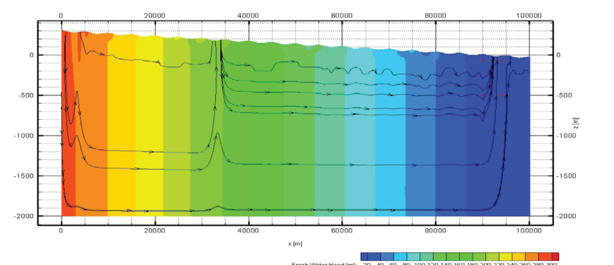

Figure 12. Fresh water heads of the steady-state solution for the continuous permafrost case.

Figure 8 presents the fresh water head of the steady-state solution of the reference case. The head situation along with the illustrative streamlines indicates the strong influence of the local topographic gradient. However, these results are strongly dependent on the shape of the local topography; for a case with only a regional gradient the flow also is regional with discharge only in the sea. A smaller local topographic variation yields more regional flow as compared with the reference case. These effects also affect the magnitude of the flux and were hence the subject of the sensitivity study presented below.

It should be noted that regions located beneath sea elevation (zero m altitude) all have a fresh water head of zero independent of where the sea bottom is located.

Permafrost cases

The sporadic permafrost case is illustrated below (Fig. 9). The maximum depth of permafrost is 100 m. The chosen maximum permafrost depth is used since it is adequate for illustration purposes.

The continuous permafrost case is illustrated below (Fig. 10). The maximum depth of permafrost is again due to illustrative reasons set to 100 m. Open taliks are located between the extensive areas of permafrost.

Figure 11 presents the fresh water head of the steady-state solution of the maximum infiltration case for sporadic permafrost. The maximum infiltration case is conducted with a fully saturated active layer on top of all frozen regions. The head situation along with the illustrative streamlines indicates the influence of the patches of frozen ground on the regional flow.

Figure 12 presents the fresh water head of the steady-state solution of the maximum infiltration case for continuous permafrost. The head situation along with the illustrative streamlines indicates the strong influence of the open taliks and of the regional topographical gradient. The flow is from one open talik toward the next, downstream, open talik. The results further indicate that a talik located along the regional gradient acts as a discharge location but also, at the same time, recharges water into the system.

Discussion

Two different groundwater flow scenarios involving the presence of permafrost have been studied. These are (1) a sporadic permafrost distribution, in which the groundwater within local topographic highs is frozen, and (2) a continuous permafrost distribution, in which extensive permafrost exists all over the model domain, only locally bypassed by open taliks (i.e., unfrozen regions in the permafrost).

The sporadic permafrost produces a situation where the regional groundwater flow becomes more important and the flow driven by local topographical differences becomes less important. This yields a smaller total flow for the sporadic permafrost scenario as compared with the reference case.

The continuous permafrost case yields an increase in the water flux all over a talik where discharge of water is occurring; a situation where a talik contains regions of both recharge and discharge is possible according to the conceptual model used, but is more likely to occur in regional up-stream locations than at the location of SFR repository. However, after emerging from the sea by shoreline displacement, when permafrost first is encountered, the location of SFR will be on a hill side. The location is more on the shaded side and hence it is possible for it to have early permafrost development. Hence the location may become frozen relatively early. However, the location of the shoreline when the first permafrost arrives is not well determined, and for a situation in which the SFR is still beneath water at that time, a talik could be formed above it. A sensitivity test of the location of the measurement volume within a talik indicates that a continuous permafrost situation could enhance the water flux through the facility by up to one order of magnitude.

The continuous permafrost situation may have a smaller impact, if the amount of available water is small, an effect different from that found in the sporadic permafrost case. A situation with less available water is mimicked by replacing the active layer with no-flow bodies (frozen) along the surface boundary. However, the decrease of flow in a dry scenario is not so large that it counteracts the effect of a talik in increasing the flow.

Even though it was not an investigated issue of the study it is, as expected, clear that for both the sporadic and continuous permafrost cases the total flow of groundwater through the model domain is decreased as compared to the reference case. This effect is most dominant when no active layer is part of the simulations. However, as described above this does not by necessity mean that the flow through the investigated generic repository volume is decreased.

In relation to thermal permafrost simulations, it should be noted that for most simulated episodes of possible future permafrost the frozen groundwater has reached a depth exceeding that of the SFR repository. If the ground surrounding the repository is frozen, the groundwater flow becomes negligible, but other problems arise, such as possible failures of the buffer material.

Conclusions

The upper boundary conditions have a significant impact on the groundwater flow in the geosphere. Permafrost and the development from sporadic permafrost to continuous permafrost yield increased groundwater flows in unfrozen parts of the domain. The increase is one order of magnitude or less. In the permafrost, the flow is negligible.

The characteristic of the surface in regard to being a recharge or discharge area affects the results. In general, a discharge area will experience an increase in groundwater flow under changed conditions.

Acknowledgments

The economic support for this work provided by the Swedish Nuclear Fuel and Waste Management Company (SKB) and Bergab is greatly acknowledged.

Further, the review work by Professor M. Thorne, Professor L.O. Ericsson, and Dr. J-O Selroos of the main report published by SKB is acknowledged. The main report could be downloaded from www.skb.se under Publications (Hydrogeological flux scenarios at Forsmark, R-07-63).

The anonymous reviewer is acknowledged for improving the clarity of the paper.

References

Boulton, G.S., Kautsky, U., Morén, L. & Wallroth, T. 2001. I*mpact of Long-Term Climate Change on a Deep Geological Repository for Spent Nuclear Waste.* SKB TR-99-05, Stockholm, Sverige: Svensk Kärnbränslehantering AB.

Boulton, G.S, Slot, T., Blessing, K., Glasbergen, P., Leijnse, T. & van Gijssel, K., 1993. Deep circulation of groundwater in overpressured subglacial aquifers and its geological consequences. *Quaternary Science Review* 12(9): 739-745.

French, H.M, 1996. *The Periglacial Environment,* 2nd ed.. Addison Wesley Longman Limited.

Haldorsen, S. & Heim, M. 1999. An arctic groundwater system and its dependence upon climatic change: An example from Svalberg, *Permafrost and Periglacial Processes*10(2): 137-149.

Larsson-McCann, S., Karlsson, A., Nord, M., Sjögren, J., Johansson, L., Ivarsson, M. & Kindell, S. 2002. *Meteorological, Hydrological and Oceanographical Information and Data for the Site Investigation Program in the Communities of Östhammar and Tierp in the Northern Part of Uppland.* SKB TR-02-02. Stockholm, Sverige: Svensk Kärnbränslehantering AB.

Lindborg, T. (ed.) 2005. *Description of Surface Systems Preliminary Site Description Forsmark Area – Version 1.2.* SKB R-05-03. Stockholm, Sverige: Svensk Kärnbränslehantering AB.

McEwan, T. & de Marsily, Gh. 1991. *The Potential Significance of Permafrost to the Behaviour of a Deep Radioactive Waste Repository.* SKI Technical Report 91:8. Stockholm, Sweden: Swedish Nuclear Power Inspectorate.

Rhén, I., Follin, S. & Hermansson, J. 2003. *Hydrogeological Site Descriptive Model – a Strategy for its Development During Site Investigations.* SKB R-03-08. Stockholm, Sverige: Svensk Kärnbränslehantering AB.

SKB, 2006. *Climate and Climate-related Issues for the Safety Assessment SR-Can*. SKB TR-06-23. Stockholm, Sverige: Svensk Kärnbränslehantering AB.

Svensson, U., Kuylenstierna, H-O. & Ferry, M. 2004. *DarcyTools Version 2.1. Concepts, Methods, Equations and Demo Simulations.* SKB R-04-19, Stockholm, Sverige: Svensk Kärnbränslehantering AB.

Geomorphological Observations of Permafrost and Ground-Ice Degradation on Deception and Livingston Islands, Maritime Antarctica

Gonçalo Vieira
Centre of Geographical Studies, University of Lisbon, Portugal
Jerónimo López-Martínez
Autonomous University of Madrid, Spain
Enrique Serrano
Department of Geography, University of Valladolid, Spain
Miguel Ramos
Department of Physics, University of Alcalá de Henares, Spain
Stephan Gruber
Department of Geography, University of Zurich, Switzerland
Christian Hauck
University of Karlsruhe, Germany
Juan José Blanco
Department of Physics, University of Alcalá de Henares, Spain

Abstract

The Antarctic Peninsula is experiencing one of the fastest increases in mean annual air temperatures (ca. 2.5ºC in the last 50 years) on Earth. If the observed warming trend continues as indicated by climate models, the region could suffer widespread permafrost degradation. This paper presents field observations of geomorphological features linked to permafrost and ground-ice degradation at two study areas: northwest Hurd Peninsula (Livingston Island) and Deception Island along the Antarctic Peninsula. These observations include thermokarst features, debris flows, active-layer detachment slides, and rockfalls. The processes observed may be linked not only to an increase in temperature, but also to increased rainfall, which can trigger debris flows and other processes. On Deception Island some thermokarst features may be related to anomalous geothermal heat flux from volcanic activity.

Keywords: active layer; Antarctic; debris flow; permafrost; thermokarst.

Introduction

The Antarctic Peninsula is experiencing the strongest warming signal in the Southern Hemisphere, with mean annual air temperatures (MAAT) increasing ca. 3ºC since 1951 (Marshall et al. 2002, Meredith & King 2005, Turner et al. 2005). However, the region of strongest warming is limited in area, with the highest increases near Faraday/Vernadsky Stations and lesser increases near the northern tip of the Peninsula and the Orcadas Islands (King & Comiso 2003, Turner et al. 2007). Global Climate Model (GCM) projections for 2001–2100 suggest that the strongest warming will extend into the Antarctic continent, with values even greater than those expected on the Antarctic Peninsula (Chapman & Walsh 2007).

The strong atmospheric warming in the Antarctic Peninsula region has had a substantial effect on glaciers in the last few decades, especially on ice-shelves along the eastern coast (Scambos et al. 2003). The collapse of Larsen-B in 2002 is the most well-known example, but the retreat of mountain and outlet glaciers has been also reported. On Livingston Island (Hurd Peninsula) glaciers have been retreating and equilibrium-line elevations increasing (Ximenis et al. 1999, Molina et al. 2007).

Permafrost is central to the carbon cycle and to the climate system, especially due to CH_4 and CO_2 release following permafrost degradation in organic-rich sediments (Anisimov et al. 1997, Osterkamp 2003). The active-layer thickness and dynamics are also important factors in polar ecology. Since most exchanges of energy, moisture, and gases between the atmospheric and terrestrial systems occur through the active layer, its thickening has important ramifications on geomorphic, hydrologic and biological processes (Nelson & Anisimov 1993). Furthermore, permafrost degradation can cause terrain instability and increase geomorphological hazards and damage to infrastructures. According to the International Panel on Climate Change (IPCC), regions underlain by permafrost have been reduced in extent, and a warming of the ground has been observed in many areas (Anisimov et al 2001, Lemke et al 2007). Permafrost is, therefore, recognized by the (World Climate Research Programme/World Meteorological Organization (WCRP/WMO) as a key element of the Earth System in which research efforts should focus. However, compared with the Arctic, very little is known about the distribution, thickness, and properties of permafrost in Antarctica. The scarcity of data on Antarctic permafrost is reflected in the last IPCC

Figure 1. Location of Deception and Livingston Islands in the Antarctic.

report (Lemke et al. 2007) where it is not even mentioned. The main problem is the limited network of boreholes for monitoring permafrost temperatures and the paucity of active-layer monitoring sites. Turner et al. (2007) mention a reduction in permafrost extent in the Antarctic Peninsula region.

In general, increasing air temperatures will have a direct influence on ground-temperature regimes and, therefore, on permafrost and ground ice. A major consequence of warming of the lower atmosphere is an increase in active-layer thickness, which induces permafrost degradation and amplifies the rates of geomorphic processes. As a consequence, thermokarst features are prone to occur in ice-rich and unconsolidated sediments, active-layer detachment slides and debris flows on sloping ground, and an increase in rockfall activity may occur in rocky terrain.

The northerly location of the Antarctic Peninsula region and the oceanic setting result in a milder and moister climate than in the interior of the Antarctic continent. The northern Antarctic Peninsula is roughly located between the MAAT isotherms of -1 to -8ºC at sea level and, therefore, the northern tip of the Peninsula and especially the South Shetland islands are close to the environmental limits of permafrost occurrence (Bockheim 1995). If the observed warming trend continues, as indicated by climate models, the region might suffer widespread permafrost degradation.

Monitoring of ground temperatures is essential for assessing the reaction of permafrost to global change, but in remote areas the drilling and maintenance of boreholes is problematic. Geomorphological surveying enables identification of the processes related to permafrost degradation and provides important information for assessing the influence of climate change on ground temperatures. However, other techniques are needed, such as geophysical surveying, monitoring of active-layer depths, micrometeorological measurements, and modelling to achieve a more complete overview of the response of permafrost to regional warming.

This paper joins together inputs from two groups researching in the South Shetlands. The group of the Autónoma de Madrid and Valladolid universities (i.e., Serrano & López-Martínez 2000, Smellie et al. 2002, Serrano 2003) has been focusing on geomorphological surveying and mapping of the periglacial processes in the South Shetlands (Fig. 1). The group at the universities of Alcalá de Henares, Lisbon, Zurich, and Karlsruhe (Ramos & Vieira 2003, Vieira & Ramos 2003, Ramos et al. 2007, Hauck et al. 2007) has been monitoring ground temperatures and modelling spatial distribution of permafrost. In this paper a synthesis of observations on geomorphic processes that are seemingly related to permafrost and ground-ice degradation from Hurd Peninsula (Livingston Island) and Deception Island is presented. The next step is a geomorphological and climatological monitoring programme, which is planned to start in 2008–09.

Climate of the South Shetlands

The climate of the South Shetlands is cold-oceanic at sea level with frequent summer rainfalls and a moderate annual temperature range. Mean annual air temperatures are close to -2ºC at sea level and average relative humidity is very high, ranging from 80 to 90% (Simonov 1977, Rakusa-Susczewski 1993). The weather conditions are dominated by the influence of the polar frontal systems, and atmospheric circulation is variable, with the possibility of winter rainfall occurring as far south as Rothera Station (Turner et al. 2007). Temperature data from Hurd Peninsula recorded by our group for the period of 2003–05 at 20 m a.s.l. show values comparable to those at Arctowski Station on King George Island. From April to November average daily temperatures stay generally below 0ºC and from December to March temperatures are generally slightly above 0ºC. Two contrasting seasons in terms of freezing and thawing are, therefore, defined. At 275 m a.s.l. on Reina Sofia Hill the recorded mean annual air temperatures were of ca. -4.2ºC. This corresponds to a lapse rate of -0.8 ºC/100 m and to a freezing season that is about one month longer than at sea level. The climate on Deception Island is similar to Hurd Peninsula.

Geomorphological Setting and Permafrost Distribution

Deception Island

Deception Island is an active stratovolcano with a large collapsed caldera; the most recent eruptions occurred in 1967, 1969, and 1970 (Smellie et al. 2002). In some places there are fumaroles and ground temperature anomalies from continued volcanic activity. Mean annual air temperature at sea level is close to -2ºC. The volcano rim rises to 539 m a.s.l. at Mount Pond, and the island is glaciated to a large extent. As a result of recent eruptions, the island has been covered by volcanic ash and debris, and many of the glaciers remain ash-covered today. Pyroclastic deposits covered snow, and buried snow is still present at some sites. The pyroclastic deposits are very porous and insulating, and give rise to a thin active layer, which varies from 30 to 90 cm in thickness.

Figure 2. Thermokarst bumpy terrain in Deception Island (arrow).

Figure 3. Thermokarst hollows in Deception Island.

On lower valley slopes, exposures of fossil snow (buried-ice) with perennially frozen ice-cemented volcanic debris on top can be observed, testifying to post-eruption aggradation of permafrost. At these sites, ice-cemented permafrost also occurs under the buried-ice layer.

Buried-ice is widespread on Deception Island, especially along the lower slopes, and ice-cemented permafrost occurs down to sea level. Geophysical surveying and trenches show that the permafrost inside the caldera thins near sea level and is absent on beaches near the shore.

Hurd Peninsula (Livingston Island)

Hurd Peninsula is comprised of mountainous terrain and is located on the southern coast of Livingston Island. About 90% of the island is glaciated, with ice-free areas occurring at low altitude, generally on small peninsulas with rugged relief. Our study focused on ice-free areas of the northwestern part of Hurd Peninsula in the vicinity of the Spanish Antarctic Station Juan Carlos I. The bedrock is a low-grade metamorphic turbidite sequence with alternating layers of quartzite and shales; conglomerates and breccias occur in some areas (Miers Bluff Formation). Dolerite dykes and quartz veins are frequent (Arche et al*.,* 1992), with the surficial lithology being very heterogeneous (Pallàs 1996).

The geological setting on Hurd Peninsula is substantially different to that of Deception Island. On the former, bedrock outcrops are prevalent, with only a thin cover of diamictite. Therefore, studying permafrost distribution is much more complex than at Deception, since frozen bedrock is very difficult to identify without a good network of boreholes. Observations from boreholes and geophysical surveying (Electrical Resistivity Tomography and Refraction Seismics Tomography) will allow a first insight into permafrost distribution, and a dense network of boreholes is planned for installation in 2007/08.

The observations indicate that continuous permafrost is present in diamictite and bedrock at least at 275 m a.s.l. At 115 m a.s.l. permafrost probably occurs only at some locations and seems to be controlled by late-lying snow patches. At this altitude in diamictite deposits, during summer, the ground thaws at least down to 1 m depth. On Hurd Peninsula, the limit between continuous and discontinuous permafrost in bedrock is probably located between these two altitudinal limits, 115 and 275 m a.s.l. However, it is possible that at 115 m the active layer is thicker than 1 m. At 35 m a.s.l. ground temperature data indicate that permafrost may be absent in bedrock, or that the active layer is thicker than 2.3 m.

Ice-cored sediments are widely distributed on Hurd Peninsula and occur down to sea level. These are likely of glacigenic origin, but in several cases still show active deformation giving origin to rockglaciers, mostly of the protalus or moraine-derived types.

Permafrost and Ground-Ice Degradation Features

Thermokarst

Thermokarst features have been observed at different sites on Deception Island. Two types of features occur, including thermokarst bumpy terrain and thermokarst hollows.

Bumpy terrain consists on a series of depressions with a small depth/width ratio that cover the terrain continuously (Fig. 2). They appear on the upper parts of the slopes inside the caldera. Preliminary observations suggest that they are more frequent on slopes below 100–150 m a.s.l.

Bumpy terrain is related to the thaw of buried-ice derived from buried snow patches. It is not yet clear if the depressions are solely the consequence of atmospheric warming or if they relate to a dynamic situation mainly induced by the thinning of the insulating layer of pyroclastic material being eroded. The thinning of the sedimentary cover, which is stronger in upper sector of the slopes, induces a decrease of the thermal insulation of the buried-ice layer, allowing for thawing. On the lower slope, the sedimentary cover is thickest due to the accumulation of material transported from upslope. There, a permafrost layer above the buried-ice layer can be observed which is probably linked to an increasing insulation effect due to sediment accretion.

Thermokarst hollows are features of decimetric to metric size and occur isolated or in small groups (Fig. 3). Their depth/width ratio is larger than the bumpy terrain, but they were not studied in detail yet. They appear in flat or

Figure 4. Debris-flow tracks in a talus slope on Hurd Peninsula (Livingston Island).

Figure 5. Debris flows depositing over the surface of the Las Palmas Glacier in Hurd Peninsula (Livingston Island).

gentle sloping terrain. No trenches were excavated, nor was geophysical surveying conducted in these features. They are probably related to localized degradation of massive ice. Their origin is not clear yet, since they can result from a climatic influence, but may also relate to changes in ground heat flux due to the volcanic activity. Geophysical surveying of these thermokarst hollows will be conducted in 2007/08.

Debris flows

Sub-aerial present-day debris-flow activity is a geomorphic process that has been poorly analysed in the literature for maritime Antarctica. Recent debris-flow tracks and deposits have been observed at several sites both on Livingston (Vieira & Ramos 2003) and Deception Islands (Figs. 4, 5, 6). Debris-flow activity is initiated by the saturation of surface unconsolidated material that flows along a channel in the slope, reworking the slope material.

In several mountain regions in the northern hemisphere an increase or altitudinal change in debris-flow activity has been linked to permafrost degradation (Jomelli et al. 2004). In maritime Antarctica, the widespread distribution of permafrost, together with the mountainous terrain and its proximity to the climatic limits of permafrost, a similar consequence of increasing air temperatures is to be expected.

Figure 6. Debris flow tracks in Deception Island.

Figure 7. Active layer detachment slide on Deception Island.

However, rainfall episodes may also be a triggering mechanism for debris flows. The lack of monitoring data does not allow us to precisely define the origin of the debris-flow activity and, therefore, in 2008/09 a monitoring programme for debris-flows will be implemented.

On Deception Island debris-flow tracks are widespread, at least in the inner slopes of the caldera. These are erosional slopes built up of volcanoclastic material. The debris flows form on the upper parts of the slopes and seem to be related to permafrost degradation, since this area is also at a similar geomorphological setting to the bumpy terrain features. The tracks are tens to a few hundred metres long. The predominantly gravely grain-size of the slope material and moderate slope angle limit the downslope movement of the flow; therefore, the debris generally does not contribute significantly to the valley floors. In the 2007/08 campaign a systematical mapping of the debris-flow tracks will be conducted in order to detect their spatial pattern and controlling factors.

On Hurd Peninsula several debris-flow tracks have been observed and one of them is known to have occurred in late spring. Debris flows on Hurd affect mainly talus slopes and lateral moraines. Due to the steep slope angles and slope length they reach more than a hundred metres in length and have been observed being deposited on top of glaciers (Fig. 5).

Active-layer detachment slides

Active-layer detachment slides form from the presence of an impermeable frozen layer at depth. Several small slides of metric dimension have been observed affecting the surface of the ice-cored moraine of the Argentine lobe of Hurd glacier in January 2000 and are related to the degradation of the ice-rich till on the very steep inner slope of the moraine. Other ice-cored moraines near sea level have been detected using electrical resistivity tomography and refraction seismics tomography and they can be subject to these processes of degradation in the near future if the current climate trend continues.

On Deception Island small detachment slides were also found on steep slopes. The mass movements were under 40 m^2 in area (Fig. 7).

Rockfalls

Rockfalls in the mountain permafrost zone have been pointed out as a consequence of permafrost degradation, especially relating to the melting of ice filling rock wall fractures (Davies et al. 2001, Kaab et al. 2005, Gruber & Haeberli 2007). Rockfalls occur on both Hurd Peninsula and Deception Island; however, without proper monitoring it is difficult to access the influence of permafrost degradation on their origin.

Conclusions

The South Shetland Islands are a privileged area to study climate change and its effects on landscape dynamics. Permafrost is widespread and occurs down to sea level. On Deception Island permafrost is continuous throughout most of the area, but on the Hurd Peninsula continuous permafrost likely occurs only above ca. 150 m a.s.l. In the same area discontinuous and sporadic permafrost exist down to sea level, especially in the form of ice-cored moraines and rock glaciers. The mean annual air temperatures at sea level are close to -2ºC, positioning the archipelago near the climatic limit of permafrost. This fact, together with the warming that affects the Antarctic Peninsula region should be responsible for permafrost degradation.

This paper describes landforms and geomorphic processes related to permafrost and ground-ice degradation that seem to result from climate change. Where ground-ice occurs, thermokarst hollows, bumpy terrain, and active-layer detachment slides have been found. The first occurs on flat or gentle sloping ground and the latter on moderate to steep slopes. Debris-flow activity was observed to be widespread on slopes of both. Their genesis has still to be assessed, since they can be linked either to ground warming or to heavy rainfall events. On Deception Island heat flux anomalies caused by volcanic activity can also generate permafrost degradation features. These anomalies are of small areal extent and their locations are known.

The observations presented here are preliminary and constitute a starting point for a new approach that will emphasize monitoring of geomorphological activity in order to detect the influence of climate change on present-day processes. Another interesting issue to be analysed is the control of changing geothermal heat fluxes on permafrost degradation in Deception Island and to assess on the possibility of using permafrost degradation features as indicators of changes in volcanic activity.

Acknowledgments

This study was conducted as part of the project PERMAMODEL within the Spanish Antarctic Program CICyT (CGL2004-20896-E/ANT). This research is included in the IPY project ANTPAS – Antarctic and Sub-Antarctic Permafrost, Soils and Periglacial Processes. G. Vieira was funded by the Fundo de Apoio à Comunidade Científica (FCT) and Fundação Calouste Gulbenkian.

References

Anisimov., O. A., Shiklomanov., N. I. & Nelson, F.E. 1997. Global warming and active layer thickness: results from transient general circulation models. *Global and Planetary Change* 15: 61-67.

Arche, A., López-Martínez, J. & Martínez de Pisón, E. 1992. Sedimentology of the Miers Bluff Formation, Livingston Island, South Shetland Islands, in *Recent Progress in Antarctic Earth Science*, edited by Y. Yoshida et al., 357-362, Terrapub., Tokyo.

Bockheim, J.G. 1995. Permafrost distribution in Southern circumpolar region and its relation to the environment: a review and recommendations for further research. *Permafrost and Periglacial Processes* 6, 27-45.

Chapman, W.L. & Walsh, J.E. 2007. A synthesis of Antarctic temperatures. Journal of Climate 20(16): 4096-4117.

Davies, M.C.R., Hamza, O. & Harris, C. 2001. The effect of rise in mean annual temperature on the stability of rock slopes containing ice-filled discontinuities. *Permafrost and Periglacial Processes* 12: 137-144

Gruber, S. & Haeberli, W. 2007. Permafrost in steep bedrock slopes and its temperature-related destabilization following climate change. *Journal of Geophysical Research* 112.

Hauck, C., Vieira, G., Gruber, S., Blanco, J. & Ramos, M. 2007. Geophysical identification of permafrost in Livingston Island, Maritime Antarctica. *Journal of Geophysical Research* 112.

Jomelli, V., Pech, V.P., Chochillon, C. & Brunstein, D. 2004. Geomorphic Variations of Debris Flows and Recent Climatic Change in the French Alps. *Climatic Change* 64(1–2): 67-102.

Kaab, A., Reynolds, J.M. & Haeberli, W. 2005. Glaciers and permafrost hazards in high mountains. In: U.M. Huber, H.K.M. Bugmann, & M.A. Reasoner (eds.). *Global Change and Mountain Regions – An overview of current knowledge*: 225-234.

King, J.C. & Comiso, J.C. 2003. The spatial coherence of interannual temperature variations in the Antarctic Peninsula. *Geophysical Research Letters* 30(2): 1040.

Lemke, P., Ren, J., Alley, R.B., Allison, I., Carrasco, J., Flato, G., Fujii, Y., Kaser, G., Mote, P., Thomas, R.H. & T. Zhang, 2007: Observations: Changes in Snow, Ice and Frozen Ground. In: S. Solomon, D. Qin, M. Manning, Z. Chen, M. Marquis, K.B. Averyt, M. Tignor & H.L. Miller (eds.) *Climate Change 2007: The Physical Science Basis. Contribution of Working Group I to the Fourth Assessment Report of the Intergovernmental Panel on Climate Change*. Cambridge, UK & New York, NY: Cambridge University Press.

Marshall, G.J., Lagun, V. & Lachlan-Cope, T.A. 2002. Changes in Antarctic Peninsula tropospheric temperatures from 1956 to 1999: A synthesis of observations and reanalysis data. *International Journal of Climatology* 22: 291–310.

Meredith, M.P. & King, J.C. 2005. Rapid climate change in the ocean west of the Antarctic Peninsula during the second half of the 20th century. *Geophysical Research Letters* 32.

Molina, C.; Navarro, F.J.; Calvet, J. García-sellés, D. & Lapazaran, J.J. 2007. Hurd Peninsula glaciers, Livingston Island, Antarctica, as indicators of regional warming: Ice-volume changes during the period 1956–2000. *Annals of Glaciology* 46: 43-49.

Nelson, F.E. & Anisimov, O.A. 1993. Permafrost zonation in Russia under anthropogenic climate change. *Permafrost and Periglacial Processes* 4(2): 137-148.

Osterkamp, T.E. 2003. Establishing Long-term permafrost observatories for active-layer and permafrost investigations in Alaska: 1977-2002. *Permafrost and Periglacial Processes* 14: 331-342.

Pallàs, R. 1996. *Geologia de l'Illa de Livingston (Shetland del Sud, Antàrtida). Del Mesozoic al Present.* PhD thesis, Universitat de Barcelona.

Ramos, M. & Vieira, G. 2003. Active layer and permafrost monitoring in Livingston Island, Antarctic. First results from 2000 and 2001. In: M. Phillips, S.M. Springman & L.U. Arenson (eds.), *Permafrost. Proceedings of the Eight International Conference on Permafrost, 21-25 July 2003, Zurich, Switzerland*: 929-933.

Rakusa-Susczewski, S. 1993. *The maritime Antarctic coastal ecosystem of Admiralty Bay*. Department of Antarctic Biology. Polish Academy of Sciences, Warsaw.

Scambos, T.A., Hulbe, C. & Fahnestock, M.A. 2003. Climate-induced ice shelf disintegration in the Antarctic Peninsula. *Antarctic Research Series* 79: 79-92.

Serrano, E. 2003. Paisaje natural y pisos geoecologicos en las áreas libres de hielo de la Antártida Marítima (Islas Shetland del Sur). *Boletín de la A.G.E.* 35: 5-32.

Serrano, E. & López-Martínez, J. 2000. Rock glaciers in the South Shetland Islands, Western Antarctica, *Geomorphology* 35: 145-162.

Smellie, J.L., López-Martínez, J. et al. 2002. *Geology and geomorphology of Deception Island.* BAS Geomap Series Sheets 6-A and 6-B, 1:25 000. Cambridge: British Antarctic Survey.

Simonov, I.M. 1977. Physical geographic description of Fildes Peninsula (South Shetland Islands). *Polar Geography* 1: 223-242.

Turner, J., Colwell, S.R., Marshall, G.J., Lachlan-Cope, T.A., Carleton, A.M., Jones, P.D., Lagun, V., Reid, P.A. & Iagovkina, S. 2005. Antarctic climate change during the last 50 years. *International Journal of Climatology* 25: 279-294.

Turner, J., Overland, J.E. & Walsh, J.E. 2007. An Arctic and Antarctic perspective on recent climate change *International Journal of Climatology* 27(3): 277-293.

Ximenis, L., Calvet, J., Enrique, J., Corbera, J., Fernández de Gamboa, C. & Furdada, G. 1999. The measurement of ice velocity, mass balance and thinning-rate on Johnsons Glacier, Livingston Island, South Shetland Islands, Antarctica. *Acta Geologica Hispanica* 34(4): 403-409.

Vieira, G. & Ramos, M. 2003. Geographic factors and geocryological activity in Livingston Island, Antarctic. Preliminary results. In: M. Phillips, S.M. Springman & L.U. Arenson (eds.), *Permafrost. Proceedings of the Eight International Conference on Permafrost, 21–25 July 2003, Zurich, Switzerland*: 1183-1188.

Effect of Wildfire and Fireline Construction on the Annual Depth of Thaw in a Black Spruce Permafrost Forest in Interior Alaska: A 36-Year Record of Recovery

Leslie A. Viereck
University of Alaska Fairbanks, Fairbanks, Alaska
Nancy R. Werdin-Pfisterer
University of Alaska Fairbanks, Fairbanks, Alaska
Phyllis C. Adams
US Forest Service, Pacific Northwest Research Station, Portland, Oregon
Kenji Yoshikawa
University of Alaska Fairbanks, Fairbanks, Alaska

Abstract

Maximum thaw depths were measured annually in an unburned stand, a heavily burned stand, and a fireline in and adjacent to the 1971 Wickersham fire. Maximum thaw in the unburned black spruce stand ranged from 36 to 52 cm. In the burned stand, thaw increased each year to a maximum depth of 302 cm in 1995. In 1996, the entire layer of seasonal frost remained, creating a new active layer depth at 78 cm. An unfrozen soil zone (talik) remained between the two frozen layers until 2006 when the entire profile remained frozen. Permafrost returned to the burned site by the formation of a layer of seasonal frost that remained frozen through subsequent years. The fireline displayed a similar pattern with a maximum thaw of 266 cm in 1995 and the establishment of a continuous frozen layer at 69 cm, but the upper frozen layer became discontinuous after several years.

Keywords: active layer; boreal forest; disturbance; fire effects; permafrost.

Introduction

The 1971 Wickersham fire burned 6313 ha in an open black spruce (*Picea mariana* [Mill.] BSP) forest underlain with permafrost in the boreal forest of interior Alaska. As a part of the fire suppression effort, 113 km of fireline were constructed with heavy equipment which removed most of the organic layer and resulted in an increase in depth of thaw. This fire provided an opportunity for long-term studies of the effects of fire and fireline construction on the rate and pattern of permafrost degradation and subsequent recovery. The annual thawing of the active layer in undisturbed vegetation at the site was also documented and vegetation change following the fire was observed. This is one of the longest records of annual active layer measurements in the boreal forest of North America (Brown et al. 2000). Initial results of this study were reported 12 years after the fire (Viereck 1982) and again 33 years after the fire (Viereck et al. 2004).

When wildfire burns through a northern black spruce forest, there is usually a subsequent increase in soil temperature and depth of thaw due largely to reduction in organic layer depth and subsequent loss of thermal insulation (Van Cleve & Viereck 1981, Mackay 1995, Swanson 1996, Burn 1998). Reduced heat loss from decreased evapotranspiration and a lowering of the surface albedo after wildfires also contribute to higher ground surface temperature and an increase in active layer thickness (Mackay 1995, Burn 1998, O'Neill et al. 2002).

We hypothesized that a continuous increase in the active layer would occur initially at the burned site, followed by the return of a shallow active layer by a gradual freezing back from the lower depth (Fig. 1).

This long-term study presents results of 36 years of annual measurements of the active layer in a burned black spruce site, a fireline in which the organic layer was removed, and in an adjacent undisturbed black spruce forest underlain by ice-rich permafrost. The purpose of this paper is to compare annual depth of thaw among these three sites and to document the recovery of vegetation, soil organic layers, and permafrost after fire and fireline construction.

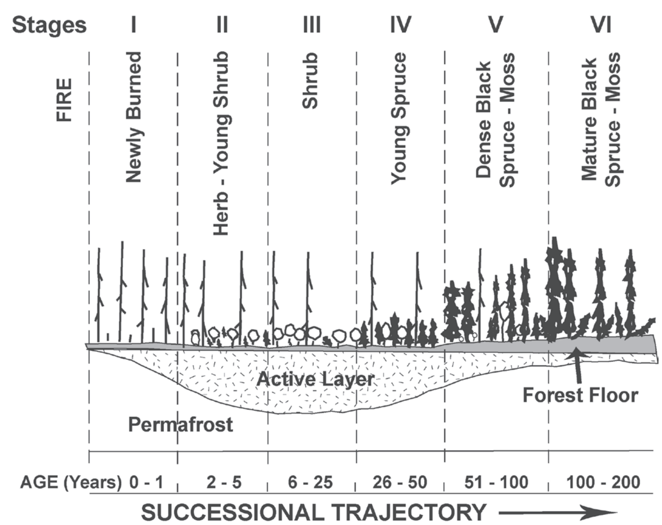

Figure 1. Succession model showing vegetation and active layer changes in a burned black spruce stand. Model modified from Van Cleve & Viereck (1981).

Methods

Study area

The Washington Creek Fire Ecology Research Area, located 50 km northwest of Fairbanks in interior Alaska (65°10′N, 147°54′W, 335 m elevation), was established to study the effects of the June 1971 Wickersham fire. The fire was ignited by lightning and burned 6313 ha in an open black spruce stand underlain by permafrost (Viereck & Dyrness 1979).

The vegetation prior to the fire was a 100- to 150-year-old open black spruce/lichen stand with a moss-derived organic layer 25 to 30 cm thick. The burn severity was originally classified as heavy, but later reduced to moderate. All of the trees and above-ground parts of the mosses, lichens, herbs, and shrubs were killed by the fire, but below-ground parts of some herbs and shrubs remained alive. Approximately one third (10 to 15 cm) of the organic layer was removed by the fire (Viereck & Dyrness 1979). At the time of the fire (June 24–30), the organic layer would have been thawed to only 20 to 30 cm. The soil is in the Saulich series with an active layer that varied from 40 to 50 cm.

Climate

Continuous climate records are not available from the site; the long-term weather record was obtained from the Weather Bureau's Fairbanks airport site. The Fairbanks record was compared with short-term climate studies at the Wickersham site. These include weather records kept at the study site from November 1971 to September 1980 and at the adjacent Washington Creek Fire Ecology Research site from January 1977 to September 1999.

From these records, we have estimated that the mean annual temperature at the Wickersham site is 1°C to 2°C colder than at the Fairbanks airport. Summer months tend to be cooler than Fairbanks, but winter months are warmer because of the lack of a cold inversion layer present during extreme cold spells in Fairbanks (Viereck 1982). The air temperatures at the Fairbanks airport have risen considerably during the period of this study (Hinzman et al. 2006). Since air temperatures at other weather stations in interior Alaska have also risen (Osterkamp & Romanovsky 1999), air temperatures at the Wickersham site are likely to have warmed, but there are no recent measurements to confirm this.

Maximum snow depths for each year at the Fairbanks airport are reported here. Based on only two winters of snowfall records available from the Wickersham fire (1977 and 1980), snow accumulation at the study site is usually about 25 cm greater than in Fairbanks (Viereck 1982).

Experimental design

A 25 m wide fireline was constructed up and down the slope between a heavily burned black spruce stand and an unburned stand, which before the fire was continuous and very similar to the stand that was burned. Most but not all of the organic layer was removed by the bulldozers in the construction of the fireline.

Three study sites were established in: 1) the heavily burned stand, 2) the fireline where vegetation and organic material were removed down to the frozen layer, and 3) the adjacent unburned black spruce stand that served as a control to compare the fireline and burned areas. At each site, 10 permanent probe points were established at 2 m intervals across the slope and perpendicular to the fireline. Maximum thaw depths were measured annually from 1971 to 2006 at each sample point using a metal probe.

A permanent transect of fixed points at 1 m intervals was established across the fireline from the burned stand on the north side to the unburned stand on the south side. At the center of this transect were ten poles that were used as probe sites to obtain the average thaw for the fireline. Across the entire width of the fireline, active layer depths were measured annually. Levels to the soil surface of the transect were made with a theodolite at intervals of three to five years, and changes in surface level relative to a fixed point were measured. Using these surface levels, it was possible to plot the profile of the surface and the depth of the active layer annually across the transect.

In 2002, a 6.5 m deep borehole was drilled in the burned site and a string of thermistors installed at 25 and 50 cm intervals to record temperatures. These temperatures have been logged both manually and with a logger at intermittent periods between 2002 and the present.

Vegetation

The vegetation of each of the sites was recorded at varying intervals. In the early years of the study, the vegetation of the burned and unburned stands was determined with a 20-plot system (Viereck 1982). In 1980, 1995, and 2004, vegetation of the burned, unburned, and fireline sites was measured by plots centered on the ten active layer probe sites. Moss, lichen, herb, and shrub percent cover was measured in 1 m^2 plots centered on the probe poles. Shrub cover was measured on 4 m^2 circular plots centered on the probe poles. Tree density and diameters were measured on larger circular plots.

Organic layer thickness

The thickness of the organic layer was originally measured in the 20 vegetation plots in the burned and unburned stands. Organic layer thickness of the fireline transect was assumed to be negligible at the beginning of the study. Organic layer thickness was remeasured along the probe lines in 1980, 1995, and 2004.

Results

Vegetation

The general vegetation type is a black spruce/moss/lichen community (*Picea mariana* / feathermoss / *Cladonia*–open needleleaf forest community) (Viereck 1982). Previous to the fire, the vegetation consisted of an open canopy of black spruce with an average diameter of 5.2 cm at 1.3 m height, a density of 1240 trees/ha and 45% canopy cover. In 1971, the age of most of the trees was 70 years, but there were a few scattered trees of 135 to 140 years in the stand. There was an open tall shrub layer of *Salix pulchra* and *Betula glandulosa* and a low shrub layer of *Ledum groenlandicum* and *Vaccinium vitis-idaea*. The moss and lichen layer was made up primarily of *Pleurozium schreberi* and scattered *Sphagnum* species, and several species of *Cladonia* and *Peltigera* (Viereck 1982).

Unburned control site: Vegetation data recorded in 1980, 1995, and 2004 at the control site showed that the stand did not change significantly during that period and was similar to that recorded in 1971. Cover of the black spruce canopy was 22% in 2004. There was an open tall shrub layer of 8% mostly of *Salix pulchra* and *Betula glandulosa* and a low shrub layer of 47% *Ledum groenlandicum* and *Vaccinium vitis-idaea*. The moss and lichen layer of 95% cover was made up primarily of *Sphagnum girgensohnii*, *Pleurozium schreberi* and *Cladonia rangiferina.*

Burned site: Revegetation was slow for the first 9 years following the fire, probably as a result of the 10 to 20 cm organic layer that remained after the fire and provided a poor seedbed for invading pioneer species (Viereck 1982). Early revegetation was primarily from roots and underground rhizomes that had survived the fire. *Equisetum sylvaticum* and *Calamagrostis canadensis* and an occasional *Epilobium angustifolium* provided nearly 70% cover by 1980. Early successional mosses, *Ceratodon purpureus* and *Polytrichum juniperinum*, covered 35% of the surface. A few black spruce seedlings had become established, but provided less than 1% cover.

From 1980 to 2004, development of the site toward a mature black spruce stand continued at a somewhat faster pace. Black spruce reestablished with a cover of 17%. The tall shrub cover of *Betula glandulosa* and *Salix pulchra* reached 12%, while a low shrub layer primarily of *Ledum groenlandicum* and *Vaccinium vitis-idaea* developed a cover of 40%. The herbaceous layer of 55% cover is still dominated by *Equisetum sylvaticum* with some scattered clumps of *Calamagrostis canadensis*. The moss layer with 55% cover is still dominated by *Polytrichum juniperinum*, but feather mosses have developed a combined cover of 20%. Although *Ceratodon purpureus* has disappeared from the stand, the first small clumps of *Sphagnum* species (<1% cover) are now present in the stand. There has not been a significant return of any lichens to the stand after 36 years.

Fireline site: Invasion of herbaceous species and shrubs by seed was rapid in the first nine years after the fireline construction because of the exposed mineral soil and the wet condition of the surface. Herbaceous species of wet habitats accounted for nearly all of the 52% herbaceous cover. Since 1980, the herbaceous cover has been reduced drastically to 31% in 1995 and 18% in 2004. Tall shrub cover was nearly constant at 33% to 36% from 1980 to 2004. The moss layer changed dramatically throughout the 36-year period. Total moss cover dropped from 75% in 1980 to 44% in 2004. As of 2004, no lichens had established on the fireline. Although a few black spruce seedlings established near the edge of the fireline transect in the first few years following the fire, they had achieved a cover of only 4% by 2004.

Organic layer thickness

Unburned control site: The study area, situated on Saulich silt loam soils, originally had a combined organic layer thickness of 25 to 30 cm at the time of the fire (Viereck 1982). The profile was comprised of decaying mosses and litter (O1 and O2 layers). The organic layer of the unburned control stand was measured again in 1980 and 1995. The organic layer consisted of mosses and peat, formed primarily of *Sphagnum*. The average thickness of these layers was 33 cm, ranging from 16 to 45 cm.

Burned site: In the burned stand, the fire removed an average of 10 cm of the organic layer, although depths were variable (Viereck 1982). In 1980, the organic layer consisted of a 0 to 3 cm thick moss layer overlying a 1 to 2 cm layer of dark humus. By 1995, the organic layer consisted of 3 cm of mosses, primarily *Polytrichum* species, overlying 5 cm of dry, decaying mosses and the previously developed 2 cm layer of humus for a total organic layer of 10 cm. In 2004, the organic layer still consisted of 3 cm of moss, but the decaying moss layer had decreased to 3 cm and the humus layer had increased to 6 cm, for a total organic layer of 12 cm.

Fireline site: The irregular organic layer of the fireline is difficult to characterize. Although most of the organic layer was removed by the fireline construction, pockets and areas of the original humus layer remained. The surface of the fireline remained very wet, and several semi-aquatic mosses and *Sphagnum* species developed quickly. By 1980, the organic layer consisted of approximately 5 cm of live and decaying mosses overlying 4 to 5 cm of humus, for a total organic layer of 9.3 cm. The overall organic layer thickness was less in 1995 with a small decrease in both the moss and the humus layers. However, by 2004, the overall organic layer had increased to 12 cm. Although the humus layer had decreased since 1995, a fibrous layer of decayed sedges and grasses had developed to account for the increase.

Active layer thickness

The primary objective of this study was to document the changes in the annual depth of thaw (the active layer) following the 1971 fire (Fig. 2).

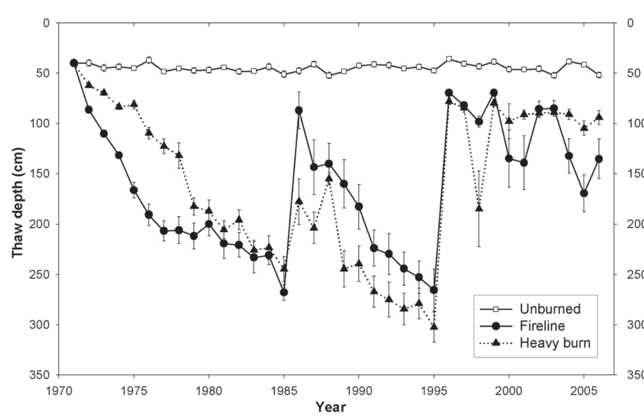

Figure 2. Maximum thaw depth of an unburned black spruce stand, a burned black spruce stand, and a fireline from 1971 to 2006. Values represent the mean (n = 10) and standard error.

Unburned control site: Maximum thaw ranged from 36 cm in 1996 to 52 cm in 1988, 2003, and 2006. The average thaw depth over the 36-year period was 45 cm. There was a tendency for deeper thaws to be associated with higher snowfall the previous winter and higher thawing degree days the following summer. For example, the minimum thaw depth of 36 cm in 1996 followed a previous cold winter with low snowfall through the month of January.

Burned site: Annual maximum thaw depth increased rapidly in the first 14 years following the fire to a maximum depth of 245 cm in 1985. In 1986, however, seasonal frost remained in 3 of the 10 probe sites resulting in an average thaw of 178 cm. An upper layer of frozen soil remained at some of the probe sites for the next 2 years resulting in an average thaw of only 155 cm in 1988. These upper layers melted out completely in 1990 and the depth of thaw continued to increase to 302 cm in 1995. In 1996, following a winter with light snow and cold temperatures, the upper seasonal frost layer remained at all 10 probe sites, giving an average thaw of only 78 cm. This upper layer has remained frozen, except in 1998 when 4 of the probe sites reached the bottom thaw layer of over 300 cm, to give an average thaw depth of 185 cm. From 1998 to 2006, the upper layer has remained frozen, and the thaw depth has ranged from 80 to 105 cm.

Mean annual temperatures and snow depths from the Fairbanks International Airport (Fig. 3) show that the two summers when seasonal frost first remained (1986 and 1996) followed winters of low snowfall. In addition, 1996 had a below average mean annual temperature.

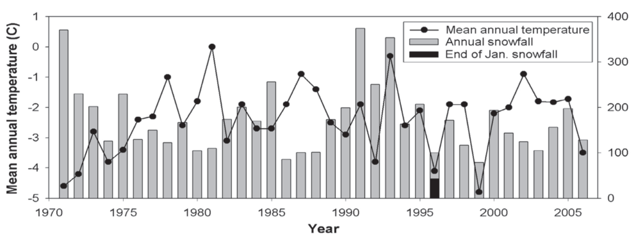

Figure 3. Mean annual temperature and mean annual snowfall for Fairbanks, Alaska from 1971 to 2006.

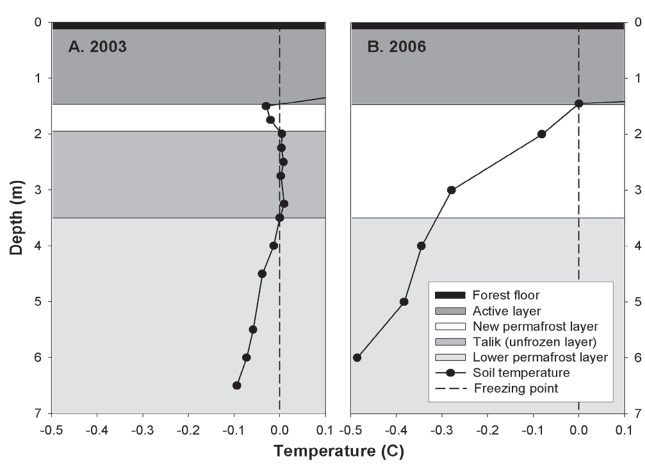

Figure 4. Soil temperature profiles from the burned site borehole, A) 2003 profile shows a new frozen layer approximately 50 cm thick extending from 1.4 to 1.9 m below the active layer, B) 2006 profile shows complete freezing of the talik and new permafrost extending 1.45 m below the present active layer.

Fireline site: For the first 25 years following the fire, the thaw depth under the fireline followed much the same pattern as the burned site. There was an annual increase in thaw depth from 1971 to a maximum of 268 cm in 1985. In 1986, the upper layer of seasonal frost remained frozen across the entire fireline. For the next six years, the upper seasonal frost layer began to thaw, and the number of probe points that penetrated through to the lower frozen layer increased from three in 1987 to all ten of the probe points in 1992, when the thaw depth approached the pre-1986 level. This condition continued until 1995 when a thaw depth of 266 cm was recorded.

In 1996, a winter of light snow and below average temperatures (Fig. 3) resulted in a seasonally frozen layer that persisted throughout the following summer. The average depth of thaw in 1996 was only 69 cm. Unlike the burned area, the shallow layer of frozen soil did not remain along the probe line. From 1997 through 2006, there was an increase in the number of probe points that reached the pre-1996 level. By 2006, only 2 points along the probe line had thaw depths less than 100 cm, and the average thaw depth of all 10 points was 135 cm.

At this time, it is impossible to predict if the upper frozen layer will continue to melt or if a light snow year with cold temperatures, such as occurred in 1996 and 2006, will result in the reestablishment of a continuous upper frozen layer.

Borehole profile

The thickness of the upper frozen layer was impossible to determine using our probing method. In 2002, we drilled a 6.5 m deep borehole in the burned site near the probe line and installed a series of thermistors to obtain temperatures throughout the soil profile.

A temperature profile from the borehole during the period of maximum thaw in September of 2003 (Fig. 4A) shows an active layer of 1.4 m. The new frozen layer was approximately 50 cm thick and extended from 1.4 to 1.9 m below the current active layer. This new permafrost layer divided the active layer and the talik formation. The talik temperatures were very close to 0°C. Below 3.4 m, the temperatures of the original permafrost layer decreased to -0.1°C at the bottom of the borehole (6.5 m). The lower permafrost depth stabilized at 3.5 to 4.0 m, and an unfrozen soil zone (talik) remained between the two frozen layers. However, in September of 2006, the temperature profile (Fig. 4B) shows the disappearing talik layer. The permafrost temperature at 6 m depth is more than 0.3ºC colder after 3 years. The new permafrost development, since 1996, accelerated the refreezing of the talik layer. As a result of the three years of permafrost aggradations, the ground temperature profile is becoming similar to the pre-fire thermal conditions.

Fireline cross section

To better understand the changes in thaw depth across the fireline, cross sections of the fireline were measured

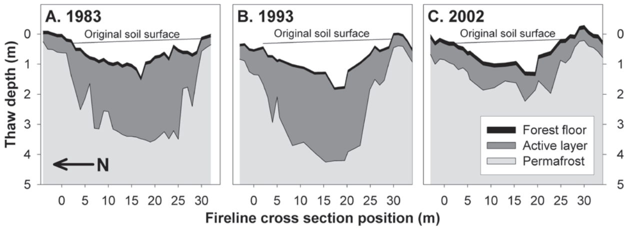

Figure 5. Cross section of the fireline in A) 1983, B) 1993, and C) 2002, showing considerable lowering of the original surface, and the reestablishment of permafrost in an uneven band across the entire fireline.

periodically during the 36 years of the study. Changes prior to 1980 are described by Viereck (1982). Figure 5 shows the cross section in 1983; 1993, when thaw was near the maximum; and 2002, the most recent cross section where the new layer of seasonal frost had persisted.

Surface: Figure 5 shows a considerable lowering of the surface level over time through subsidence and erosion. In 1983 (Fig. 5A), the surface lowered about 1 m through erosion and subsidence with slightly more on the northern side of the fireline. By 1993 (Fig. 5B), a small intermittent stream that formed from water captured upslope in the fireline had created a ditch that was approximately 75 cm deeper than the surrounding surface. The 2003 profile of the surface (Fig. 5C) shows that there has been some filling of the ditch and a slight rise in the surface of the fireline, which may be the result of vegetation buildup, deposition, and expansion due to the refreezing of water into ice in the newly frozen upper layer.

Depth of thaw: The cross sections in Figure 5 show that the depth of maximum annual thaw and the reestablishment of permafrost occur in an uneven band across the fireline. In 1983 (Fig. 5A), the deepest thaw occurs near the middle of the fireline beneath the small stream. There is a very steep rise of the permafrost on the south side of the fireline, due perhaps to the shading of that side of the fireline by trees to the south. The cross section in 1993 (Fig. 5B) shows that the thaw is fairly even across the middle of the fireline and rises sharply on both edges to the level of the active layer in the adjacent undisturbed vegetation. By 2002 (Fig. 5C), the upper surface of the newly developed permafrost is uneven, but in general follows the surface layer.

Estimated fireline cross section: Figure 6 illustrates a conceptual fireline cross section during the late 1990s and early 2000s, when the upper zone of permafrost (newly established in 1996) was intact. It shows the surface of the fireline, lowered through erosion and subsidence, and the uneven surface of the new upper frozen layer. The base of this layer is estimated from the measured thickness in the burn site (approximately 150 cm) at a similar period. Below this is an unfrozen layer of talik that is surrounded above and below by the permafrost in the adjacent unburned area. For the base of the talik, we have used the depth of thaw taken in 1995 when the thaw was at its deepest. Below the talik is the zone of permafrost that was there before the fire and reaches an unknown depth.

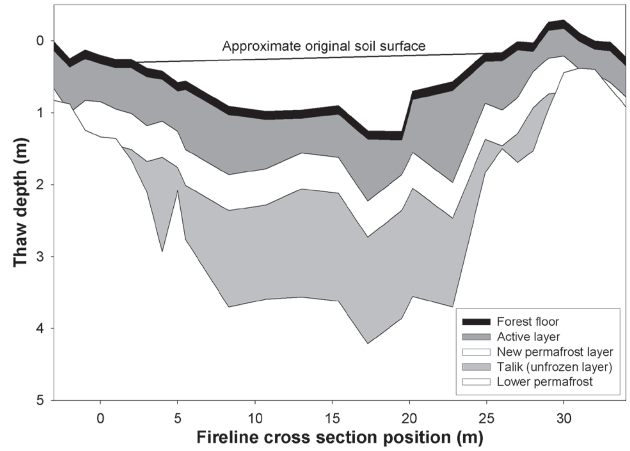

Figure 6. Conceptual fireline cross section during the period (1996–2003) that the upper zone of newly established permafrost was intact.

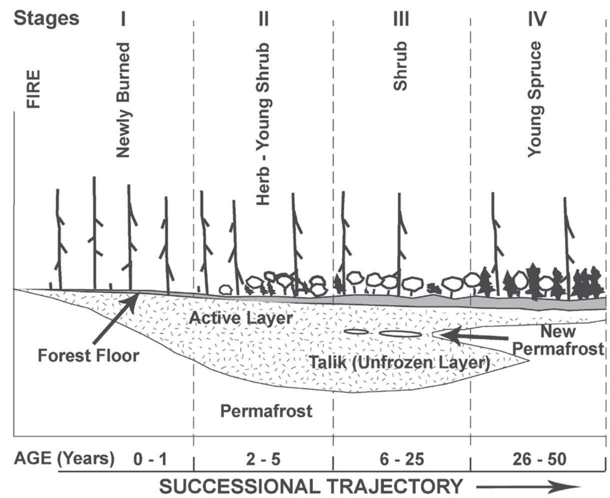

Figure 7: Successional changes observed in vegetation and the active layer at the burned site following the Wickersham fire.

Conclusion

Long-term observations such as those made on active layer and vegetation changes over the last 36 years at the Wickersham fire site are extremely valuable for developing an understanding of the effects of fire and fireline construction in the boreal forest of Alaska. We originally hypothesized that a shallow active layer would return to the burned site by a gradual freezing back from the lower depth (Fig. 1). We expected to observe a continuous increase in the active layer to a maximum depth during the first 30 to 50 years after the fire. Next, a gradual decrease in the active layer was expected to return the active layer to its approximate pre-fire depth 100 years following the fire. Other long-term measurements of active layer recovery following wildfire in the southern Yukon Territory (Burn 1998) and near Inuvik, N.W.T., Canada (Mackay 1995) reported that permafrost aggraded upward in a return to pre-fire conditions.

Surprisingly, a layer of seasonal frost formed at the Wickersham burned site that eventually remained frozen throughout the entire year and continued to remain frozen for the next ten years (Fig. 7). The active layer did increase for the first 25 years following the fire as originally hypothesized. However, an upper layer of seasonal frost remained frozen 17 years after the fire and then became discontinuous for the next 10 years. Since 1996, the seasonal frost layer has remained frozen. This created a new permafrost layer with an active layer of 90 cm and an unfrozen talik layer between the upper and the lower frozen layers. This new permafrost layer accelerated the refreezing of the talik layer, and by 2006, the talik layer disappeared (Fig. 4B) and the permafrost has returned to the pre-fire thermal conditions.

Another important observation of this study is that under present climate conditions, permafrost is reforming at the Wickersham fire site on the burned stand but not on the fireline. The increased maximum thaw depth pattern for the two sites is similar, with a maximum thaw of 266 cm for the fireline and 302 cm for the burned site in 1995 (Fig. 2). Also, the development of an upper frozen zone in 1986 and 1996 was similar. The difference on the fireline is that the upper frozen zone has become intermittent, but it may be rejuvenated by another cold snowless year.

In addition to the permafrost differences at the burned and fireline sites, there is a significant difference in rate of vegetation recovery between the burned area and the fireline. The vegetation of the burned area is beginning to have many features of the original black spruce stand, whereas the fireline has remained very different with few features and species of the original stand.

Acknowledgments

This work was funded by the Bonanza Creek Long Term Ecological Research program (funded jointly by the National Science Foundation and USDA Forest Service, Pacific Northwest Research Station).

References

Brown, J., Hinkel, K.M. & Nelson, F.E. 2000. The Circumpolar Active Layer Monitoring (CALM) Program: Research designs and initial results. *Polar Geography* 24(3): 166-254.

Burn, C.R. 1998. The response (1958-1997) of permafrost and near-surface ground temperatures to forest fire, Takhini River valley, southern Yukon Territory. *Canadian Journal of Earth Sciences* 35: 184-199.

Hinzman, L.D., Viereck, L.A., Adams, P.C., Romanovsky, V.E. & Yoshikawa, K. 2006. Climate and permafrost dynamics of the Alaskan boreal forest. In: Chapin, F.S. III, Oswood, M.W., Van Cleve, K., Viereck, L.A. & Verbyla, D.L. (eds.), *Alaska's Changing Boreal Forest*. New York: Oxford University Press, 39-61.

Mackay, J.R. 1995. Active layer changes (1968 to 1993) following the Forest-Tundra Fire near Inuvik, N.W.T., Canada. *Arctic and Alpine Research* 27(4): 323-336.

O'Neill, K.P., Kasischke, E.S. & Richter, D.D. 2002. Environmental controls on soil CO_2 flux following fire in black spruce, white spruce, and aspen stands of interior Alaska. *Canadian Journal of Forest Research* 32: 1525-1541.

Osterkamp, T.E. & Romanovsky, V.E. 1999. Evidence for warming and thawing of discontinuous permafrost in Alaska. *Permafrost and Periglacial Processes* 10: 17-37.

Swanson, D.K. 1996. Susceptibility of permafrost soils to deep thaw after forest fires in interior Alaska, U.S.A., and some ecologic implications. *Arctic and Alpine Research* 28(2): 217-227.

Van Cleve, K. & Viereck, L.A. 1981. Forest succession in relation to nutrient cycling in the boreal forest of Alaska. In: West, D.C., Shugart, H. & Botkin, D.B. (eds.), *Forest Succession Concepts and Application*. New York: Springer Verlag, 185-211.

Viereck, L.A. 1982. Effects of fire and firelines on active layer thickness and soil temperatures in interior Alaska. *Proceedings of the Fourth Canadian Permafrost Conference, Calgary, Alberta, March 2–6, 1981*: 123-135.

Viereck, L.A. & Dyrness, C.T. 1979. Ecological effects of the Wickersham Dome fire near Fairbanks, Alaska. USDA Forest Service, Pacific Northwest Forest and Range Experiment Station. General Technical Report PNW-90, 71 pp.

Viereck, L.A., Werdin, N.R., Yoshikawa, K. & Adams, P.C. 2004. Effect of wildfire and fireline construction on the annual depth of thaw in a black spruce-permafrost forest in interior Alaska: a 33-year record. *International Boreal Forest Research Association Conference, Fairbanks, Alaska, May 3–7, 2004*: poster presentation.

Investigation of the Permafrost Environment for Pile Installation at Fort Wainwright, Alaska

Ted S. Vinson

Professor (Emeritus), Department of Civil Engineering, Oregon State University, Corvallis, Oregon, USA

Abstract

During 2004, 516 piles were driven to -18 m (59 ft) for housing units on Fort Wainwright, Alaska. Nearly 93% of the piles encountered permafrost compared to the contractor's estimate of 15%. Owing to the substantial difference between the actual and estimated number of piles that encountered permafrost, an investigation was undertaken to determine if the prediction of the percentage of piles that would encounter permafrost could have been improved prior to pile driving. Very limited data was available. No borings within 100 m (330 ft) of the housing units were advanced to a depth of 18 m (59 ft). Notwithstanding this fact, a topographic surface was generated using commercially available mapping software from four borings which encountered permafrost and six borings advanced to 14.5 m (47.5 ft) in thawed material at the project site. When the building footprints were projected on the predicted surface, it was estimated that greater than 80% of the piles would encounter permafrost.

Keywords: degrading permafrost; mapping; pile driving; topographic surface.

Introduction

During the period July 6 to October 16, 2004, 516 piles were driven as foundation elements for four housing units on Fort Wainwright, Alaska. The piles were driven to a design tip elevation of -18 m (-59 ft) on an approximate two hectare (five acre) tract to the west of an existing housing complex on Alsace Loop. A total of 129 piles were driven at each housing unit (i.e., 4 units x 129 piles per unit = 516 piles). The 2-cm (8-in.) diameter piles were driven with a hardened steel driving shoe welded to the pile tip to prevent damage during high driving resistance. Of the 516 piles driven, 479 piles experienced high driving resistance when permafrost (typically frozen sand and/or gravel) was encountered at depths ranging from 6 to > 15 m (19 to > 50 ft). When permafrost was encountered, it required a substantial change in the installation procedure. Specifically, the pile was cut, a tricone (or roller) drilling bit was inserted in the pipe pile, a hole was advanced (i.e., predrilled) to the pile tip elevation or beyond, the cut section of the pile was welded back onto the pile, and the pile was driven through the permafrost to the design tip elevation. Of the 479 piles encountering permafrost, 24 were completed without predrilling, 362 required one predrilling operation and 93 required two predrilling operations.

Nearly 93% of the piles at the four housing units, designated as Buildings C, D, F, and H, encountered permafrost. The pile foundation contractor, based on a "conventional" interpretation of the pre-bid boring logs, estimated 15% of the piles would encounter permafrost. More specifically, the contractor noted "Six of the forty (40) test borings in or near the four buildings where pile foundations were specified indicated the existence of permafrost" Consequently, [6/40] x 100% = 15% of the piles would encounter permafrost.

Owing to the substantial difference between the estimated compared to the actual number of piles that encountered permafrost, an investigation was undertaken to determine if the prediction of the permafrost surface and the percentage of piles that would encounter permafrost could have been improved prior to pile driving. The results of the investigation are reported herein.

Geologic Conditions, History of Surface Disturbance and Modification, Boring Logs

Fort Wainwright is situated in the Tanana River Valley, to the south and east of Fairbanks, on the broad floodplain of the Tanana and Chena Rivers. The Tanana basin was filled through alluvial processes with deposits of silt, sand, and gravel, in excess of 180 m (590 ft) deep near the Tanana River. A mantel of 1–5 m of aeolian silt to silty fine sand may overlie these alluvial deposits in the Fort Wainwright area. At the project, site there is a silt-to-silty sand layer of approximately 1–5 m (3–16 ft) depth overlying clean sand and/or gravel to a depth greater than approximately 16 m (53 ft) (maximum boring depth).

Fairbanks and Fort Wainwright are in a discontinuous permafrost zone. The occurrence and characteristics of permafrost in a discontinuous zone can vary dramatically. On Fort Wainwright moss-dominated black spruce forests on lowlands or lower slopes are generally underlain by permafrost. Romanovsky (2006) reports the typical thickness of permafrost around Fairbanks is about 50 meters (165 ft), but varies between a few meters to 150 m (490 ft) and more.

Removal of the vegetative cover in an area underlain by permafrost will cause the permafrost to degrade. Pewe & Reger (1983) report that past surface disturbances have increased the depth of permafrost in the Fairbanks area by 7–12 m (23–40 ft). Linell (1973) reported that on a research site in the Fairbanks area underlain by frozen silt, when the trees and brush were removed, the permafrost level, initially at -1.1 m (-3.6 ft), degraded to -4.7 m (-15.4 ft) after 26

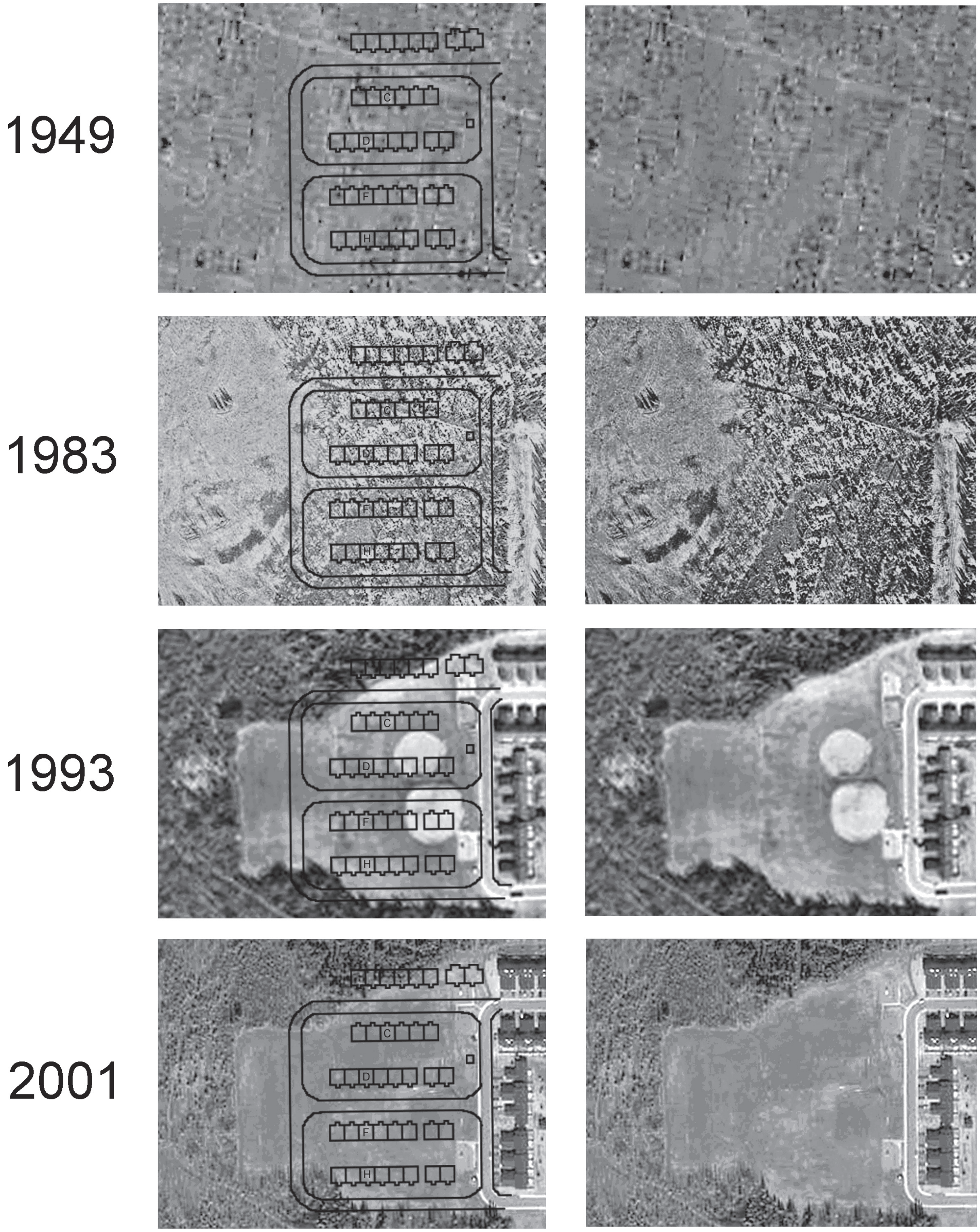

Figure 1. Comparison of 1949, 1983, 1993, and 2001 airphotos of the project site. The left frames show the project site with the building structures and roads superimposed. The right frames are without building structures and roads. North is at the top of the photographs.

years. In the same study, when the trees, brush, and surface vegetation were removed, the permafrost level degraded to -6.7 m (22 ft) after 26 years. Studies by the Defense Mapping Agency Hydrographic/Topographic Center (1978) indicate that permafrost at Fort Wainwright in cleared areas occurs at 8–13 m (26–43 ft) below the ground surface. Cleared areas were defined as areas where surface vegetation has been removed. It is apparent from past studies in the Fairbanks area that the amount and rate of degradation is dependent on a number of factors.

The preceding reported thaw depth estimates are based on conduction as the heat transfer mode. Convective heat transport associated with groundwater flow will cause thawing of permafrost. Conduction and convection heat transfer modes acting in concert have resulted in permafrost thawing in the Fairbanks and Fort Wainwright area greater than the values noted above.

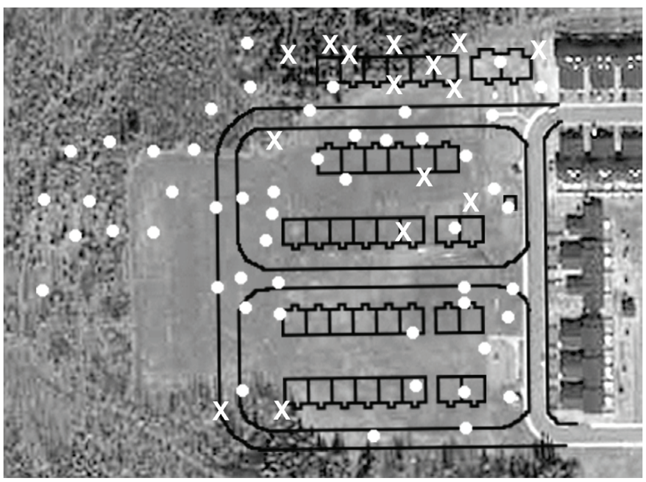

Figure 2. Schematic of borings, buildings, and roads on the 2001 airphoto. Circles indicate permafrost thawed to a depth greater than the boring was advanced; X indicates permafrost was encountered.

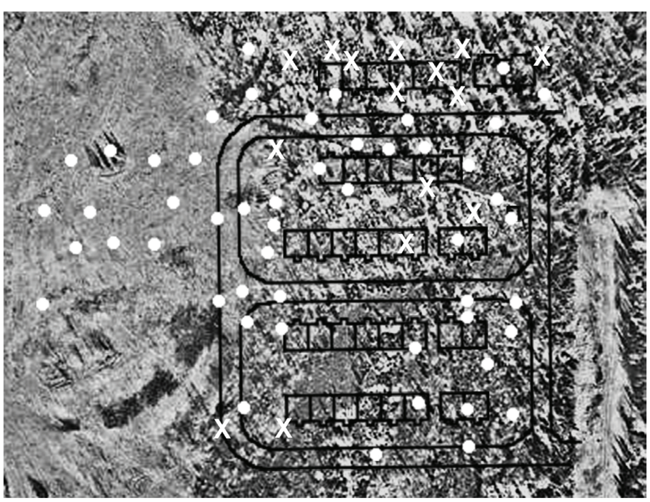

Figure 3. Schematic of borings, building, and roads on the 1983 airphoto. Circles indicate permafrost thawed to a depth greater than the boring was advanced; X indicates permafrost was encountered. The similarity in the surface vegetation over the project site is apparent.

Fort Wainwright (formerly Ladd Field) was established in 1939. Figure 1 shows 1949 and 1983 airphotos of the project site in which the surface vegetation and trees prior to surface disturbance and modification are clearly visible. It is apparent that significant surface disturbance did not occur on the project site prior to 1983. Considering the character of the vegetation, it is likely the project site was completely underlain by permafrost at a relatively shallow depth prior to surface disturbances. Based on boring logs presented in the March 2003 Geotechnical Report for the project, in "Black spruce woods with moss on the ground" permafrost occurred at a depth of less than 1 m (3.3 ft). Evidence of a substantial change in surface cover is shown in the 1993 airphoto taken approximately two years after construction activities were initiated for a housing complex on Alsace Loop to the east of the project site. The 2001 airphoto shows the likely site condition when the geotechnical investigation was conducted at the project site (2002–2003). The central portion of the site was a recreational facility (e.g., softball fields and playground). An old excavation was present at the mid-eastern portion of the site. There was evidence that a large portion of the site was graded in the past. It was reported that the open areas are fill material.

The boring logs for the project site provide evidence of permafrost degradation in the 10- to 12-year period from the early 1990s to 2002–2003. The boring locations are shown in Figure 2 overlain on the 2001 airphoto of the site.

Following a review of the boring logs in the general vicinity of Buildings C, D, F, and H, 17 borings were advanced through thawed material to a depth of approximately 7 m (23 ft). The correct interpretation of the 17 boring logs is that permafrost has degraded to a depth of at least 7 m (23 ft) at the location of the borings. It cannot be assumed that permafrost is absent at these locations or permafrost has thawed to a depth of 18 m (59 ft) (i.e., design depth of pipe pile). Six borings were advanced to a depth of approximately 14.5 m (47.5 ft), indicating that permafrost had degraded to a depth of at least 14.5 m (47.5 ft) at these locations. Three borings which were in the "footprints" of Buildings C, D, and H, indicated permafrost was present at depths of 1.5, 6.5, and 9.5 m, respectively. A fourth boring west of Building C indicated permafrost at a depth of 14.2 m (46.6 ft). Figure 3 shows the boring locations superimposed on the 1983 airphoto. As previously noted, there was very little difference in the character of the surface vegetation

Table 1. Borings in the footprint and close proximity of Buildings C, D, F, and H.

Building	Borings in Building Footprint	Borings within 10 m of Building Footprint	Total Number of Applicable Borings
C	1	5	6
D	1	2	3
F	1	1	2
H	1	1	2

from 1949 (and likely much earlier) up to the initiation of construction activities at the project site in the early 1990s. This implies that permafrost was very likely at a relatively shallow depth over most of the project site prior to the early 1990s.

The number of borings in the footprint and close proximity of Buildings C, D, F, and H is given in Table 1. It is apparent that very limited data is available to estimate the permafrost surface beneath the buildings. Furthermore, and equally significant, is the fact that no borings within 100 m (330 ft) of any proposed building were advanced to the tip elevation of the pipe piles (18 m, 59 ft).

Use of Pile Driving Records to Plot Topographic Map of Permafrost Surface

The driving record for the 479 piles which experienced high driving resistance when permafrost (typically frozen sand and/or gravel) was encountered at depths ranging from 6 to >15 m (20 to >50 ft) may be used to create a topographic map of the surface of the permafrost at the project site. Each pile location was assigned an X and Y coordinate. The Z coordinate is the depth at which permafrost was encountered during pile driving. A topographic surface is produced using a surface generation algorithm. A contour map can be plotted on the topographic surface or projected to the ground surface. The topographic surface and contour map shown in Figure 4 is believed to be an accurate depiction of the actual permafrost environment at the site. The irregular character of the surface and depth of thaw strongly suggests that both conduction and convection heat transport processes are occurring at the project site. Figure 5 presents the contour map together with the footprints of Buildings C, D, F, and H. It is apparent that permafrost at a depth of 18 m (59 ft) underlies all of Buildings C and D, and 85+% of Buildings F and H. This is in excellent agreement with the occurrence of permafrost at a depth of 18 m (59 ft) or less from the pile driving records.

Comparison of Permafrost Surface at Site to the Record provided by Boring Logs

Figure 6 shows a contour map of the depth to permafrost from the pile driving record and the locations of borings advanced in the area. Borings which encountered permafrost and borings advanced in thawed material are shown. The number adjacent to the boring locations indicates either the depth to permafrost or the maximum depth to which thawed material was encountered. By comparing the depths shown adjacent to the borings to the contour intervals it is possible to establish if the boring logs indicated a site condition that was different than the conditions actually encountered. For the fifteen borings that were inside the boundary of the contour map, there are no apparent contradictions. At the locations where 12 borings were advanced to an approximate 7 m (23 ft) depth and thawed ground was reported, permafrost was encountered at a greater depth during the pile driving

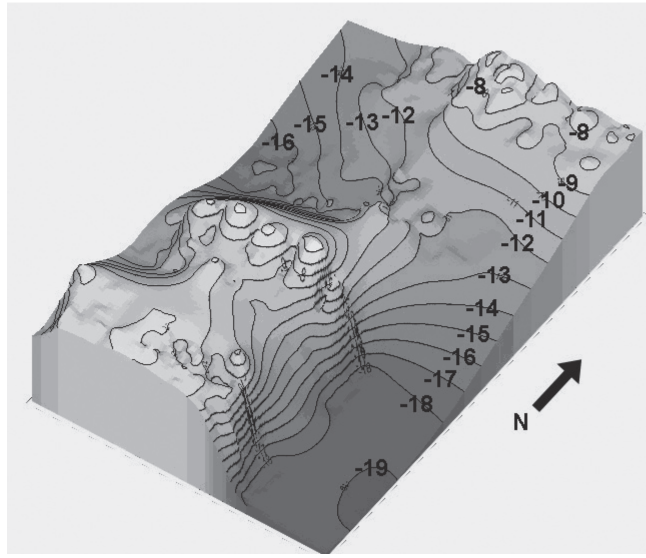

Figure 4. Topographic surface of permafrost based on the pile driving records. The irregular character of the surface strongly suggests that conduction and convection heat transport processes are occurring at the project site. The depth in meters is shown on the contour lines.

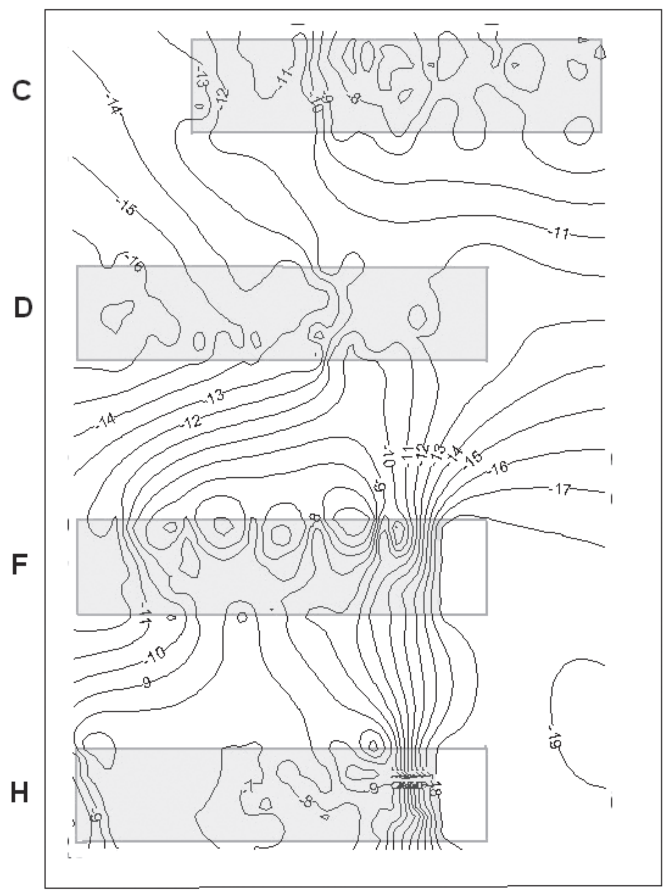

Figure 5. Contour map together with the footprints of Buildings C, D, F, And H. The shaded area represents the occurrence of permafrost at a depth of 18 m (59 ft) or less. It is apparent that permafrost at a depth of 18 m (59 ft) underlies all of Buildings C and D, and 85+% of Buildings F and H. The depth in meters is shown on the contour lines.

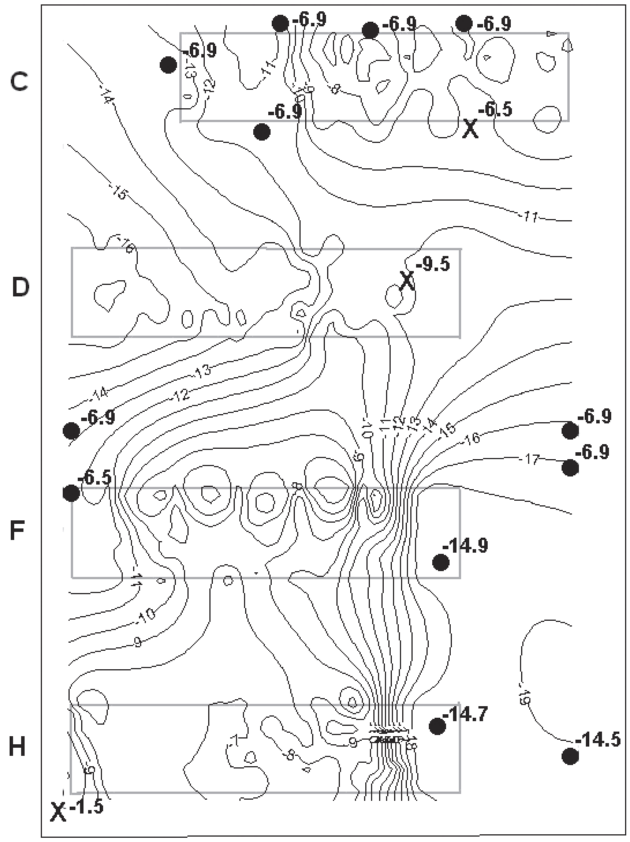

Figure 6. Contour map of the depth to permafrost from the pile driving record. Circles indicate permafrost thawed to a depth greater than the boring was advanced; X indicates permafrost was encountered. The number adjacent to the boring location indicates either the depth (m) to permafrost or the maximum depth to which thawed material was encountered. North is at the top of the figure.

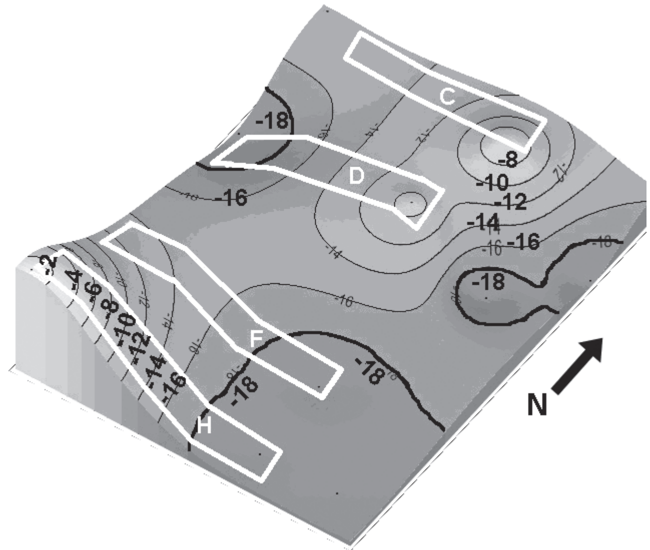

Figure 7. Topographic surface developed from boring logs with the Kriging surface mapping algorithm. The -18 m (59 ft) elevation is shown as a bold contour line. A distortion of the building footprint occurs when it is projected on the topographic surface, and the footprint no longer appears to be rectangular or at the correct distance from adjacent structures.

operation. For the three borings that indicated permafrost would be encountered at a specific location, permafrost was encountered during the pile-driving operation at the approximate depth indicated by the borings. An assertion of a “Differing Site Condition” is without merit.

Use of Boring Logs to Plot Topographic Map of Permafrost Surface

A topographic surface of the permafrost may be predicted from the boring logs provided in the contract documents. Figure 7 shows a surface produced using 4 borings which encountered permafrost at the project site together with 6 borings advanced to approximately 14 m (46 ft) in thawed material. For the borings advanced to approximately 14 m (46 ft), it was assumed that permafrost was at a depth of 20 m (66 ft). The predicted surface is in very good general agreement with the actual surface (see Fig. 4). A very satisfactory topographic surface can be generated from the boring logs with one of three commonly used topographic mapping algorithms considered in the investigation (i.e., Kriging, linear equations, and inverse distance). A fourth method (i.e., triangulation) was less satisfactory. When the building footprint is projected on the topographic surface and the area inside the building footprint with permafrost at a depth of 18 m (59 ft) or less is noted, it represents the area over which permafrost would be encountered during pile driving. To estimate the area it is convenient to display the permafrost surface contour map with the footprint of the buildings (Fig. 8). It is apparent from Figure 8 that all of Building C is underlain by permafrost at a depth less than or equal to 18 m and approximately 90%, 70%, and 70% of the piles in Buildings D, F, and H, respectively, would be underlain by permafrost at a depth less than or equal to 18 m. Based on the results presented in Figure 8, a reasonable estimate of the piles that would encounter permafrost at a depth less than or equal to 18 m would be greater than 80%.

Summary and Conclusions

It is highly probable that the entire housing unit project site was underlain by permafrost at a shallow depth prior to the establishment of Fort Wainwright. Permafrost degradation was initiated when surface disturbance and modification occurred (primarily) in the early 1990s.

It is apparent that very limited data was available to estimate the depth of permafrost beneath the buildings. No borings within 100 m (330 ft) of the housing units were advanced to a depth of 18 m (59 ft). Notwithstanding these facts, it is possible to generate a topographic surface of the permafrost using commercially available software and the 4 borings which encountered permafrost at the project site, together with 6 borings advanced to approximately 14 m (46 ft) in thawed material. For the borings advanced to approximately 14 m (46 ft), it was assumed that permafrost was at a depth of 20 m (66 ft). When the building footprints are projected on the predicted topographic surface, and the

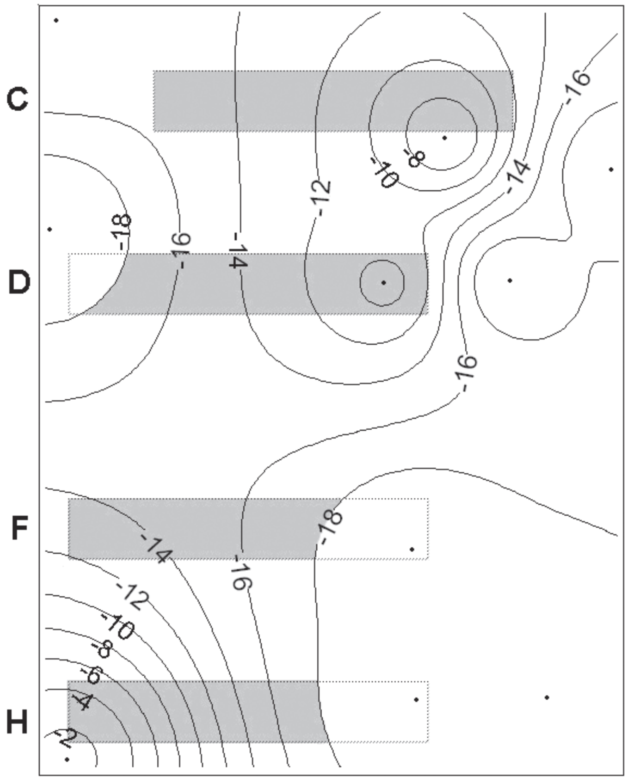

Figure 8. Contour map with emphasis on the -18 m permafrost surface elevation. The shaded area represents the occurrence of permafrost at a depth of 18 m (59 ft) or less. All of Building C is underlain by permafrost at a depth less than 18 m and *approximately* 90%, 70%, and 70% of the piles in Buildings D, F, and H, respectively, would be underlain by permafrost at a depth of 18 m (59 ft) or less. Based on the results, a reasonable estimate of the piles that would encounter permafrost at a depth less than or equal to 18 m would be approximately 80%. North is at the top of the figure.

area inside the building footprints with permafrost at a depth of 18 m (59 ft) or less is noted, a reasonable estimate of the piles that would encounter permafrost would be greater than 80%. The predicted surface compares very favorably with the actual surface plotted from the 479 piles that encountered permafrost.

It is neither logical nor reasonable in the permafrost environment in which the piles were to be installed at Fort Wainwright to conclude that 15% would encounter permafrost. The possibility that permafrost could exist over the entire project site at a depth less than 18 m (59 ft) should have been anticipated. Studies relating to degrading permafrost in the Fairbanks area have been reported in the scientific and engineering literature for more than three decades. Based on available information, it is without precedent that permafrost in the Fairbanks area at an initial depth of 1 m would degrade to a depth of 18 m (59 ft) in 10 to12 years (with conduction as the heat transfer mode; in the absence of convective heat transport, e.g., groundwater flow).

The logs of the borings advanced in the thawed materials do not confirm the *non*existence of permafrost. Prior to surface disturbance and modification, permafrost was present over nearly the entire project site at a very shallow depth. The permafrost did not disappear in the 10- to 12-year period following surface disturbance and modification. To correctly interpret the likely subsurface conditions at the project site the permafrost must be thought of as a surface that is changing with time and not a feature that is present or exclusively absent even in a discontinuous permafrost zone.

Acknowledgments

Steve Young, Corvallis, Oregon, assisted in the data reduction, and executed the software used to perform the topographic mapping. Charles Wilson and Greg Carpenter, U.S. Army Corps of Engineers, Anchorage, Alaska, provided information related to the geotechnical conditions at the site. Miles Illichmann, U.S. Army Corps of Engineers, Fairbanks, Alaska, provided the photographs shown herein and valuable insight into the history of the project site. Steve Pinnell and Blake Marchand, Pinnell Busch, Inc., Portland, Oregon, reviewed the project report written by the author that is the basis for this paper. The contribution of these individuals is gratefully acknowledged.

References

Defense Mapping Agency Hydrographic/Topographic Center. 1978. Fort Wainwright, Alaska, Terrain Analysis, prepared for the Terrain Analysis Center, U.S. Army Engineer Topographic Laboratories, Fort Belvoir, Virginia, September.

Linell, K.A. 1973. Long-term effects of vegetative cover on permafrost stability in an area of discontinuous permafrost. *Proceedings of the Second International Conference on Permafrost*, *Yakutsk, USSR, July 13-28, 1973*: 688-693.

Pewe, T.L. & Reger, R.D. (Eds.) 1983. Guidebook to permafrost and Quaternary geology along the Richardson and Glenn Highways between Fairbanks and Anchorage, Alaska. *Proceedings of the Fourth International Conference on Permafrost, Fairbanks, Alaska, July 18–22, 1983*: Guidebook 1.

Romanovsky, V.E. 2006. How rapidly is permafrost changing and what are the impacts of these changes? Arctic Theme Page, National Oceanic and Atmospheric Administration.

Stone Polygons in Southern Colorado, USA: Observations of Surficial Activity 1975–2004

John D. Vitek
Office of Graduate Studies & High Altitude Research Program (HARP), Texas A&M University, College Station, TX, USA
Netra Raj Regmi
HARP & Geology & Geophysics Department, Texas A&M University, College Station, TX, USA
Daniel Humbolt
Electrical & Computer Engineering, Texas A&M University, College Station, TX, USA
John R. Giardino
HARP, Geology & Geophysics Department, Geography Department, & Water Management & Hydrological Sciences Program, Texas A&M University, College Station, TX, USA

Abstract

Small stone polygons occupy a depression at 3865 m in the Sangre de Cristo Mountains, southern Colorado, USA. Vertical photographs were collected between 1975 and 2004 to document natural change on the surface of these polygons. Over time, the stones in the core region of these small polygons moved in multiple directions rather than directly toward the edges of the polygons. Clearly, movement results from freeze-thaw forces in three-dimensions within the polygons and from forces generated by water freezing in the stone gutters. Smaller polygons formed within the larger unit. Some stones observed in 1975 disappeared by 2004, essentially moved into the edges of the polygon and rotated such that identification becomes difficult. Measured horizontal displacements reached 29 cm, although the average is 7.4 cm for all stones. Maps of change and vectors of motions reveal the dynamic aspects of three dimensional forms subjected to intense freeze-thaw in an alpine environment.

Keywords: displacement; frost processes; repeat photography; stone polygons.

Introduction

Stone polygons, forms of patterned ground that are common in arctic and alpine areas, are generally attributed to intense freeze-thaw processes (Washburn 1956). In the years since Washburn's comprehensive review, numerous researchers have reported on many aspects of patterned ground in various locations (Washburn 1979, French 1996, Hallet et al. 2004) and attributed them to numerous processes of formation. Additional research will be cited with specific information as this paper is developed rather than simply listing them in this introduction. Vitek (1983) reported on seven years of surficial activity observed on stone polygons found in a small depression in glacial till at 3865 m in the Blanca Massif of the Sangre de Cristo Mountains in south-central Colorado. This paper extends the record of those initial observations to 30 years. In total, observations were made 22 times from 1975–2004. On several occasions, observations could not be obtained because the stone polygons in the 850 m^2 depression in a cirque were underwater from snowmelt and precipitation.

Since the site was first observed in 1975 until the last visit in 2004, standing water during the growing season is a major deterrent to grasses occupying the depression. Occasionally small tufts of grass appear but seldom do they survive the harsh winters. The lack of vegetation suggests that frost processes are not impeded and readily move stones around the surfaces of the polygons. The site is very remote, a five hour hike from the nearest road, and is not on any marked trail, nor would a causal hiker venture into this area because of the lack of access to high peaks, i.e. those above 4300 m .a.s.l. Aside from an occasional small animal print embedded in the center of a polygon, the site has been virtually undisturbed. Every effort was made during photography to retain the site as undisturbed.

This paper presents observations, analyses of these observations, and discusses the forces involved in creating these stone polygons and movements of stones in the center of several polygons. How these observations relate to published research will be described in the discussion section along with suggestions for future research at this site. Whereas these observations represent changes in a surficial plane, stone polygons are three-dimensional phenomena. Within the centers of these small polygons, smaller polygons have been observed; they form either from desiccation drying or are the remnants of frost polygons left over from winter. Movement vectors reveal that motion is possible in many directions rather than just toward the edges of the polygons. We present only total change from 1975– 2004 in this paper rather than the incremental changes that are possible with the data that have been collected. Greater detail will be published in a subsequent paper.

Study Area

The Sangre de Cristo Mountains are located in south-central Colorado (Fig. 1). Extensively glaciated during the Pleistocene, the Blanca Massif portion of the range contains numerous sites with patterned ground. Large stone polygons (Vitek & Tarquin 1984, Berta 1988, Vopata et al. 2006) are

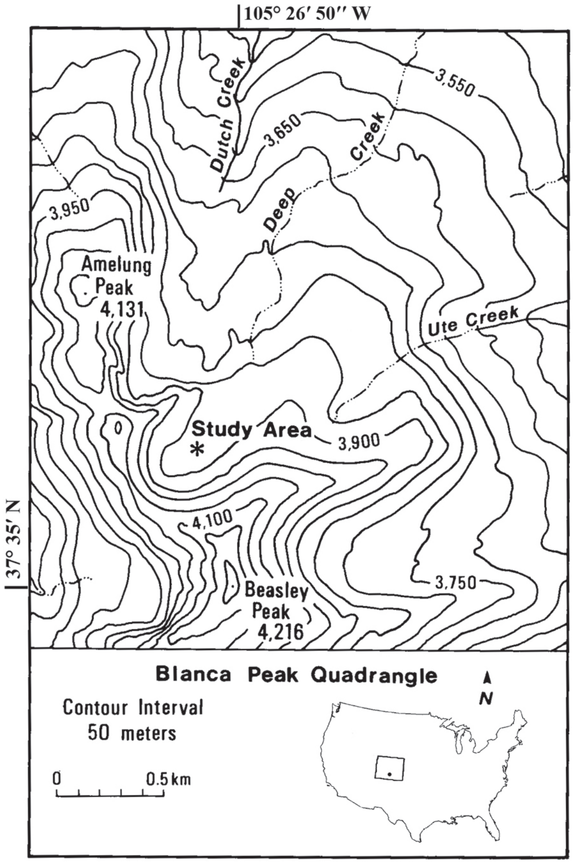

Figure 1. Location of the study area in southcentral Colorado.

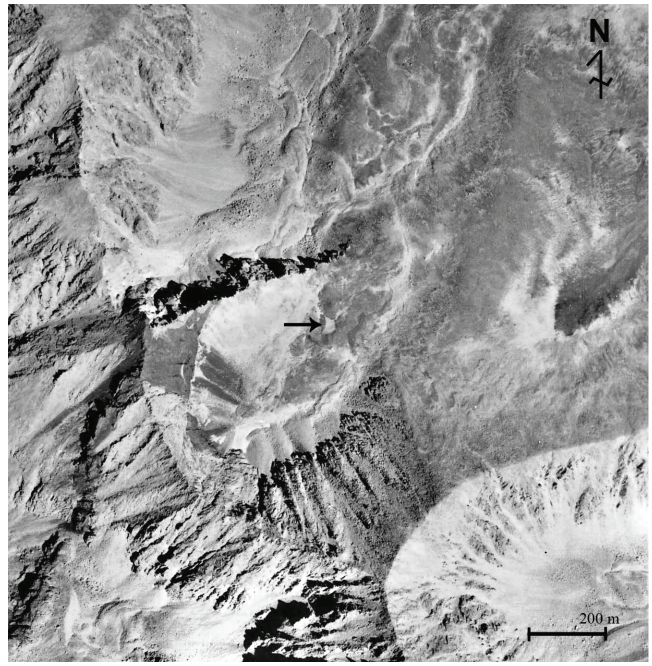

Figure 2. August 31, 1974, aerial photograph of the study area.

Figure 3. July 31, 2004, ground view of the study site with colleagues for scale.

prevalent in numerous locations above the tree line, including sites on ridges above 3900 m .a.s.l. The location of these stone polygons, shown on an aerial photograph (Fig. 2), is precisely 37°36′27.89″N, 105°26′54.51″W, with these values read from an image on Google Earth©. At approximately 180 m above the tree line, the climatic conditions of the site can be classified as alpine tundra, but exact temperature and moisture conditions have not been monitored. When the site was first observed in 1975, it was covered by water. Within several weeks after the initial observation, however, the water evaporated and/or infiltrated through the glacial till (the frost table or permafrost may have lowered sufficiently to allow the water to drain) and revealed the stone polygons that have been photographed since 1975 (Fig. 3).

Methodology

Repeat photography is a viable technique for observing surficial change (Graf 1985, Kull 2005). In some instances changes occur rapidly, but some changes occur so slowly that photographic records can be used to confirm change. Over the years, every effort was made to take these hand-held photographs at approximately the same time of day to keep shadows constant. Colored slides and black-and-white photographs were collected on every trip to the site. The same Pentax camera was used for all black-and-white photography, and two different Nikons were used to record colored slides of the polygons. A 50 mm lens was used on both cameras. In 2004, digital images were acquired of the site in addition to traditional film medium. A steel ruler was positioned in every photograph to provide a consistent scale. J. Vitek took the photographs in every year but one. In this manner, any variation in the distance from the camera to the surface of a polygon was minimized.

The analyses for Vitek (1983) required making maps of the locations of stones from photographic prints and overlaying a map from one year over the photograph of the next year to detect change. The process was slow and only as accurate as the cartographic representation of the photographic image. Minor scale changes were made during the photographic process to create images that could be compared.

Fast forward into the twenty-first century and high speed computing. Digital images can be processed with software and provide a wealth of data about surficial change that occurs between two sets of imagery. ERSI ArcGIS 9.0©

is used to digitize, analyze, and layout the stone polygon images of 1975 and 2004. Identifiable structures and features on the largest stones found around the edges of the polygons were recognized and were used in the geo-referencing process. The structures chosen are mainly mafic inclusions, fractures, stone edges and stone corners. Geo-referencing of the images was done in the same coordinate system (UTM, Zone 13 N) and the same spatial extent. The scales of all the geo-referenced images are defined according to the metal scale placed on a stone polygon and measured during photography in 1975. After geo-referencing, all the boundaries of the stones were mapped as polygons. For each stone in 1975, a point, primarily the edges of the stone, and polygon centroids were marked and tracked to positions in the 2004 image. The magnitudes and directions of the movement of these points are represented by vector lines. The lengths of these vector lines and area of the polygons were calculated. Finally, the stone polygons from both dates and the vectors of movement were overlaid and the layouts of stone movement were created. The position of a stone in 2004 can be visually linked to its position in 1975. We believe that computer-generated and compared images yield results that are significant because images that are compared can be aligned more precisely than with manual mapping.

All images were converted to digital images for these analyses because of the ease of comparing such images. Although the stone polygons were not disturbed during the observation period, individual stones are lost only because we could no longer positively identify them at a new location. For the purpose of this paper, we chose to compare several images from 1975 against the images of the same sites collected in 2004. An initial assumption that the large stones forming the edges of the polygons do not move was easily discredited. Some large stones that formed the edges of the polygons have moved, but the analyses considered such changes in calculating the movement of the stones in the centers of the polygons for this paper.

Observations

We never knew before making the trek from the base camp at 3110 m to the site at 3865 m if the depression in which the stone polygons formed would contain water or would be dry. Water over the stone polygons excluded photographic data being collected on individual stone polygons. Often, water was observed in the gutters between polygons but below the level of the centers. During dry summers, water completely disappeared from this site. We can assume that water was lost to evaporation as well as drainage into the till once it was no longer frozen. The annual depth of frost penetration is unknown and no information exists on permafrost in this area. A trench dug to a meter in depth in August of 1983 revealed a frozen surface. Whether the ice survived until the next summer is unknown.

A site visit in March of 1978 was made to assess the conditions of the depression in late winter. Interestingly, lacustrine ice over the site had already begun to thaw, but needle ice, isolated patches of lacustrine ice, and frozen centers were observed in several polygon centers that were exposed above the level of the lacustrine ice. Stones on the surfaces of the polygons, therefore, are subjected to more forces than the simple freeze-thaw introduced into the till by temperature fluctuations. The variety of forces at work will be evaluated in the discussion section. No effort was made to visit the site during the winter because the depth of snow was impassable in the main valley and the total distance and time to walk to the site doubled in such severe conditions.

Figure 4. Photograph of site D taken on August 6, 1975. Metal scale is 150 mm.

Figure 5. Photograph taken of site D on July 31, 2004. Metal scale is 150 mm.

For this paper, the same four-stone polygon centers presented in Vitek (1983) are re-assessed. Photographic data also exist for 12 additional stone polygons and will be used in conjunction with a complete analysis of this site at a later date. Figure 4 is a photograph of site D collected on August 6, 1975, and Figure 5 is the same sited on July 31, 2004. Scanning and comparing these two images generates Figure 6. Figure 7 shows the vectors of motion for stones in polygon D using the center of each stone as the position of reference.

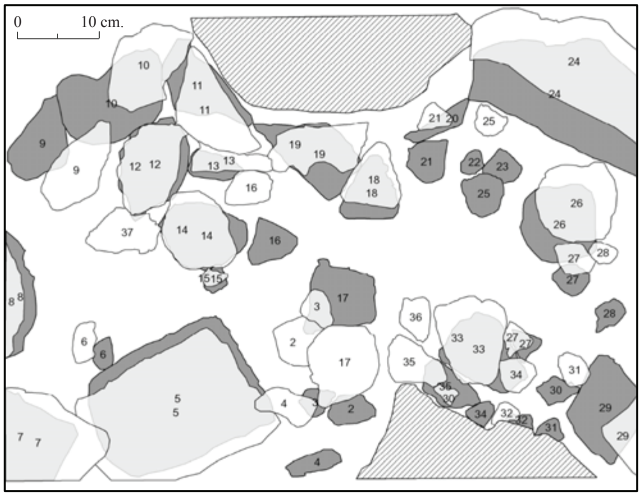

Figure 6. Map of stone movements at site D observed from 1975–2004. Gray tone is 1975 position; white is 2004. Stripe is a stable stone from 1975–2004.

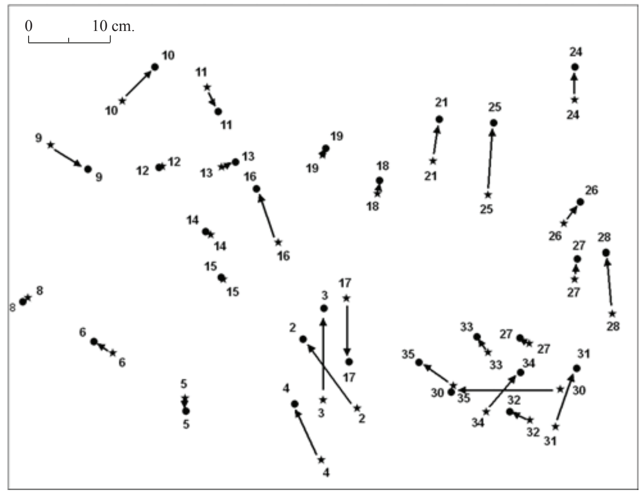

Figure 7. The amount and direction of movement of stones in polygon D, 1975–2004.

Results

Observing this site over 30 years reveals how slowly freeze-thaw processes operate in an alpine environment to rearrange the surficial appearance of the polygons. Given that the site has been free of glaciers since the end of the Pleistocene, approximately 11,000 years have been available for various freezing processes to reorganize the till left behind by the glacier. The absence of trees at this elevation and the current absence of grass and other alpine plants in the depression allows frost processes to be active. In close proximity to the depression with active stone polygons, large relict stone polygons (Vitek & Tarquin 1984) probably ceased to develop once grass was able to stabilize the centers of the polygons. Grass was observed growing over some stone gutters between the relict polygons. The frequent presence of water in this depression (probably for a significant amount of time each year), therefore, is the primary reason why the site remains active and free of vegetation.

Stones in the centers of the polygons were identified in 1975 and mapped using the system discussed in the Methodology section. Table 1 is a comparative summary of the observations made in four centers of stone polygons that were photographed in 1975 and 2004. Perhaps the most important observation in Table 1 is the number of stones that could not be easily identified in 2004 compared to the initial positions in 1975. Movement of a stone plus rotation often makes it impossible to conclude the fate of a particular stone. Such stones are reported as "lost" and the amount of movement cannot be calculated. Even if the stone is resting with others along the edges of the polygon, it was considered "lost" if precise identification was not possible. The number of "lost" stones may be minimized when a comparison is made between every photograph available for each site, a total of 22 iterations being possible. Movement of an individual stone ranged from only the slightest degree of movement to 29 cm in one instance (polygon C) with the

Table 1. Summary of measurements for 1975–2004.

Site	N (1975–2004)*	Mean Disp.	SD	Range
A	57 – 36	7.69 cm	4.53	1.0 –16 cm
B	40 – 27	7.67 cm	5.78	1.8 – 19.9 cm
C	52 – 23	8.65 cm	7.99	1.0 – 29 cm
D	37 – 30	5.59 cm	3.89	1.0 – 15.7 cm

* N is the number of stones observed in 1975 and those relocated in 2004; Mean Disp. is the mean displacement observed; and SD is the standard deviation.

average distance moved for all stones that were re-identified in 2004 being 7.4 cm. Figure 6 shows the position of stones in polygon D in 1975 and 2004, respectively. If all stones could be located, we believe that the average distance moved would significantly increase.

The level of analysis possible is a function of the size of stone selected and whether it can be relocated during the next time period, or in this case, after 30 years. Many stones were deemed too small to trace even yearly because when rotation occurred positive identification was difficult, if not impossible. Moreover, assumptions about the direction of movement (toward the edge of the polygon) are not correct in that stones were moved toward the center of the polygon as observed in every polygon. No stone was physically identified by lifting it from the site. Interpretation to relocate a stone was based on viewing each site in color, and black-and-white images. If one were to continue the study, perhaps some type of marker could be added to each stone without disturbing it.

On a yearly average basis, stone movement is about 0.25 cm. Hence, years of observation really are necessary to detect significant change in the arrangement of stones in stone polygons. Whereas this focus has been on the visual changes in the surface, essentially a plane, the centers of stone polygons are three dimensional because sorting over the history of the feature has concentrated fine material (sand, silt and clay) in the core and stones were noticeably absent in the center of the core of one polygon that was excavated. Other research has shown how stone polygons function as three-dimensional systems such that stones are sorted to the surface and edges of the polygon. This concept is expanded in the discussion section.

Discussion

In the 25 years since the fourth Permafrost Conference was held in Fairbanks, significant contributions have been made to the literature on patterned ground. Detailed measurements by Hallet (1998) of motion within sorted circles demonstrated how frost processes operate. Hallet's instrumented efforts from 1983–1997 on Spitsbergen represent the best effort to interpret change in patterned ground at a low elevation, high latitude location. He measured vertical heave, the rapid settling of fines, a preferential subsidence of borders, and was able to conclude that convection occurred in the sorted circles. He observed that a small residual difference in displacement remains after each full-year cycle and over time pattern evolves. Gleason et al. (1986) demonstrated that sorted patterned ground can arise from density-driven Rayleigh free convection in water saturated soils that are frozen. With the presence of water in the alpine depression that we studied, observations confirmed that a small average yearly displacement is capable of sorting material given sufficient time. An ample supply of water is transformed into ice (needle, lacustrine, and ground), thereby, generating re-occurring forces that transform till into sorted stone polygons.

Kessler & Werner (2003) developed a numerical model to explain how stones and soil self-organize in polar and high alpine environments to create patterned ground.

They demonstrated that frost heave can act in a number of different orientations within the surface based upon the nature of the material encountered. Lateral sorting and stone domain squeezing are the feedback mechanisms that develop stone polygons. They stated that polygons are enhanced by rapid freezing. At our alpine site, the centers of the stone polygons can be squeezed as frost penetration occurs from the surface and through the sides (gutters) given that ample air spaces are prevalent in the stone gutters between centers. If water occupies these gutters, however, the centers will be squeezed by water freezing within the gutter and material in the core of the stone polygons will, therefore, freeze from the surface and the sides. How the water in the stone gutters (and subsequently ice) contacts the core material of the stone polygon will definitely impact how the core freezes and how much heaving occurs. Hence, the presence or absence of water in the depression during the dominant freeze-thaw periods (fall and spring) will have a significant impact on the forces generated in the till. Fowler & Noon (1997) noted that differential frost heave depends on the soil heaving characteristics and the rate of frost penetration. Observations at our site suggests that the rate of frost penetration will be extremely variable because of the variation in the sizes of stones that formed the gutters and the sides of the polygons in addition to the size of stones on the surface and the sediment composition of the core. In actuality, every site will exhibit such variability and, thereby, complicate formulation of models to replicate the processes involved in formation. Without precise temperature and moisture values for the site, including the presence or absence of water during freezing, one can only hypothesize about the frost processes that contribute to stone motion from the forces generated by freezing and thawing.

Fang & Hager (2002) believe that the stones represent large sources of noise in a non-linear reaction-diffusion type of model. Regardless of the model used, the variability of the sizes of stones in the centers and in the gutters of stone polygons complicates any model because nothing is uniform in any setting with stone polygons. The role of differential frost heave (Peterson & Krantz 2003) is dependent upon heat transfer in the system. The variable sizes of the stones in the till in this depression create complexities that would be difficult to model. Penetration of the freezing plane in three dimensions is very irregular and would result in thrusts and heaves in multiple directions. These forces are reflected in the observation of stones moving in the multiple directions in the centers of the polygons not just toward the edges.

Ugolini et al. (2006) assessed how fines were segregated in the development of patterned ground. They mentioned that airborne fines, plus those produced by weathering, contribute to the core of fine material segregated by frost processes. We believe that fines at this site can be attributed, in part, to aeolian transport because sand dunes occur in the San Luis Valley immediately west of the site. Detailed analyses of the silts and clays would be necessary to confirm the source of the fines in the centers of the polygons. Although radiocarbon techniques have been used to date patterned ground (Jeong 2006), no efforts were made to date these stone polygons. The absence of lichens on stones within the depression also provides an indication of the dynamic nature of the site. Vitek & Tarquin (1984) observed and measured lichens found on large inactive stone polygons nearby that indicated the stones in the gutters were stable for at least 2500 years based upon a growth rate curve for lichens from another location in Colorado (Benedict 1979).

Gleason et al. (1986) observed that the depth of the active layer at the onset of convection corresponded to the depth of sorting. Holness (2003) reported similar relationships for sorted circles in the maritime Subantarctic. Convection cells may account for certain features of the circles, including regularity of form morphology, but differential frost heave contributes to movement within the circles. He noted that increasing frost penetration was highly correlated with the distance between fine centers and also the depth of sorting. At our site, the short distances between centers suggests shallow depth of sorting, perhaps a function of the thin till layer over the bedrock surface of this glacial cirque.

Conclusions

Stone polygons are common in arctic and alpine areas in which freeze-thaw processes dominate. Observing one site on 22 occasions over 30 years yields information about the rate at which the surface is changing. Although 30 years is less than 0.27% of the total time since deglaciation, these observations do demonstrate change. For some stones in the system, change is significant whereas it is not for others. We also observed secondary polygons forming within the fines of the cores and we observed stones on the surface moving in directions other than toward the edges of the polygons. Whereas repeat photography of the surface of the centers reflects two-dimensional change, forces acting on these polygons do so in three dimensions – the surface and through the sides (the gutters). Variability between each polygon is a function of how these forces act at each site. Whereas the average total movement of the stones observed was 7.4 cm from 1975–2004, the average yearly rate of motion was only 0.25 cm for stones relocated in 2004. The passage of time, however, makes change easier to detect.

To increase the complexity of the study would require significant resources for instruments and transportation to the site in all seasons. We believe that the data collected thus far provide a unique glimpse of the two-dimensional changes that can occur. Additional research on this unique alpine site in southern Colorado is possible because it has not been disturbed.

Acknowledgments

Friends who made the five-hour hike to the site to assist with data collection include Mark Vitek, Mark Gregory, Marshall Cossman, Phil Ward, Lance Salisbury, Pam Tarquin, and Ellen Rose. Our sincere thanks for your help.

References

Benedict, J.B. 1979. Fossil ice wedges polygons in the Colorado Front Range: Origin and significance. *Geol. Soc. Am. Bull.* 90:173-197.

Berta, S. 1988. Three-dimensional characteristics of stone polygons in a periglacial environment. *Abstracts with Programs, Geol. Soc. Am.* 20(7): 184.

Fang, M. & Hager, B.H. 2002. Stone polygons: self-organization assisted by noise. *AGU Abstracts* #U72B-0018.

Fowler, A.C. & Noon, C.G. 1997. Differential frost heave in seasonally frozen soils. *Proceedings on the International Symposium on Physics, Chemistry, and Ecology of Frozen Soils.* Special Report-Corps of Engineers, US Army CRREL, 247-252.

French, H.M. 1996. *The Periglacial Environment.* Second Edition. London: Longman, 341 pp.

Gleason, K.J., Krantz, W.B., Caine, N., George, J.H. & Gunn, R.D. 1986. Geometrical aspects of sorted patterned ground in recurrently frozen soils. *Science* 232: 216-220.

Graf, W.L. 1985. Geomorphic measurements from ground-based photographs. In: A.F Pity (ed.), *Geomorphology Themes and Trends*. Totowa, NJ: Barnes & Noble, 211-225.

Hallet, B. 1998. Measurement of soil motion in sorted circles, Western Spitsbergen. *Proceedings of the Seventh International Conference on Permafrost, Yellowknife, Canada*, *June 23-27, 1998*: 415-420.

Hallet, B., Putkonen, J., Sletten, R. S. & Potter, N.J. 2004. Permafrost process research in the U.S. since 1960. *Developments in Quaternary Science* 1: 127-145.

Holness, S.D. 2003. Sorted circles in the maritime Subantarctic, Marion Island. *Earth Surface Processes and Landforms* 28(4): 337-347.

Jeong, G.Y. 2006. Radiocarbon ages of sorted circles on King George Island, South Shetland Islands, West Antarctica. *Antarctic Science* 18(2): 265-270.

Kessler, M.A. & Werner, B.T. 2003. Self-organization of sorted patterned ground. *Science* 299: 380-383.

Kull, C.A. 2005. Historical landscape repeat photography as a tool for land use change research. *Norsk Geografisk Tidsskrift* 59:253-268.

Peterson, R.A. & Krantz, W.B. 2003. A mechanism for differential frost heave and its implications for patterned-ground formation. *Journal of Glaciology* 49(164): 69-80.

Ugolini, F.C., Corti, G. & Certini, G. 2006. Pedogensis in the sorted patterned ground of Devon Plateau, Devon Island, Nunavut, Canada. *Geoderma* 136: 87-106.

Vitek, J.D. 1983. Stone polygons: observations of surficial activity. *Proceedings of the Fourth International Conference on Permafrost*, National Academy Press, Washington, DC: 1326-1331.

Vitek, J.D. & Tarquin, P. 1984. Characteristics of relict stone polygons, Sangre de Cristo Mountains, Colorado, USA. *Zeitschrift fuer Geomorphologie* 28(4): 455-465.

Vopata, J., Aber, J.S. & Kalm, V. 2006. Patterned ground in the Culebra Range, southern Colorado. *Emporia State Research Studies* 43(1): 8-21.

Washburn, A.L. 1956. Classification of patterned ground and review of suggested origins. *Geological Society of America Bulletin* 67: 823-865.

Washburn, A.L. 1979. *Geocryology*. London: Edward Arnold, 406 pp.

Transformations of Cryogenic Structure of Frozen Clay Soils at Shear

S.S. Volokhov
Faculty of Geology, Moscow State University, Vorobievy Gory, 119899, Moscow, Russia

Abstract

This report presents research results regarding the process of ice segregation in frozen clay soils at shear under creep conditions. It is demonstrated that the process of ice segregation takes place in the shearing area only at the stage of frozen soil failure and is related to crack formation during shear. When soils were subjected to continuous creep deformation, no increase in ice content was observed. It is concluded that the formation of a film of ice within the soil shear surface has a strengthening effect.

Keywords: creep; failure shear; migration; moisture; segregation.

Introduction

Transformation of cryogenic structure of frozen soils at shear is the subject of works by Vyalov (1959), Tsytovich (1975), Roggensack & Morgenstern (1978), Yershov et al. (1981), Chuvilin et al. (1994), and others. It is demonstrated by Roggensack & Morgenstern (1978) that as a result of shear of frozen clay samples at a constant deformation velocity of frozen clay samples at temperatures from -1°C to -1.5°C, ice schliers are formed in the shearing area orientated along the shear planes. Similar results are obtained in Yershov et al. (1981) and Chuvilin et al. (1994) under shear tests of bentonite, polymineral, and kaolinite clays in creep conditions at a temperature of -3°C. Moreover, Savigny & Morgenstern (1986) reported a growth of new ice lenses in ice-rich soils along shear surfaces at triaxial compression. This research is far from being complete. The issue of the nature of unfrozen water migration and of ice segregation in the shearing area is still of present interest.

Scientific literature contains evidence of the fact that unfrozen water migration may result from changing of the pore geometry and the interfacial energy of soil particles at formation of dislocations, microfractures, and other defects (Sakharov 1994, Komarov 1999). This suggests that unfrozen water migration and ice segregation at shear in frozen soils happens due to formation of microfractures when shearing stress exceeds the long-term strength; i.e., in divergent creep conditions, at deformation velocities comparable with unfrozen water migration velocities. Verifying this hypothesis is the subject of the present research.

Research Methods

Kaolinite clay (Chelyabinsk), polymineral clay (Gzhel), and loam (Yamal) were tested. The tests were performed on samples of soils of disturbed structure. The samples of frozen soils were prepared in work rings from a soil paste, consolidated for 2 days under a step load increasing until it reached 0.2 MPa, cooled for 4 h at a temperature of 0°C, and frozen for one day in a low-temperature cabinet (-30°C). They were then maintained at the experiment temperature (-3°C or -1°C) for one day. The values of total moisture content and density of the samples were, respectively, 37%–38% and 1.68 g/cm3 for kaolinite clay, 30% and 1.86 g/cm3 for polymineral clay, and 29%–30% and 1.85 g/cm3 for loam. The samples were of cylindrical form and had a diameter of 71.4 mm and a height of 35–37 mm.

Single-plane shear apparatus PRS (Fig. 1) designed by NIIOSP (Sadovsky 1967) was used for shear tests on frozen soils. The test scheme is shown on Figure 2. The research was carried out at constant shear loads in conditions of convergent and divergent creep. In convergent creep cases the duration of the experiments was up to 30 days, and in divergent creep cases the samples were brought to failure. The tests were carried out at normal load of 0.1 MPa with double replication. The experiments were performed in a refrigerating chamber NKR at temperatures -3°C and -1°C maintained within the accuracy of ±0.1°C. One of the two tested samples was used for studying the transformation of cryogenic structure, the other one for studying the changes in the total moisture content of the frozen soil.

Research on cryogenic structure of soil samples was performed by means of an optical microscope. Distribution of the total moisture content along the height of the samples was determined by division into 12 layers, each about 3 mm thick. Each layer was then divided by two cutting rings of different diameter into three areas: the edge area, the intermediate area, and the central area (Fig. 3). For

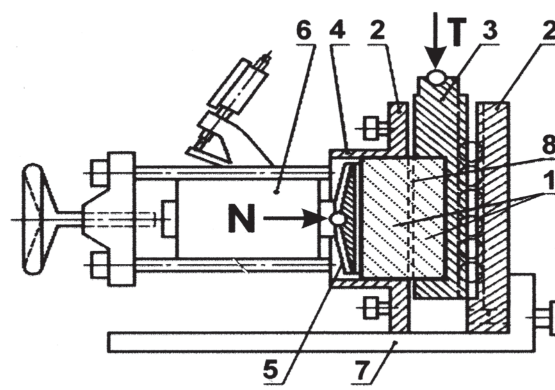

Figure 1. Single-plane shear apparatus PRS. 1 – sample of frozen soil, 2 – shear cell, 3 – mobile carriage, 4 – work rings, 5 – lateral stamp, 6 – dynamometer, 7 – supporting plate, 8 – apparatus clearance. N – normal load, T – shear load.

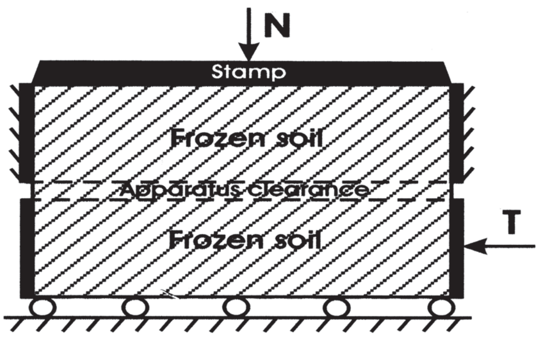

Figure 2. Scheme of shear test. N – normal load, T – shear load.

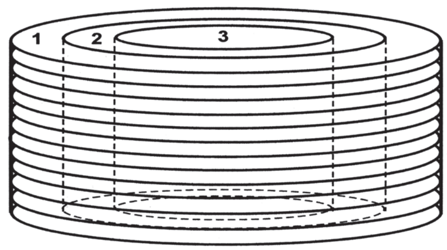

Figure 3. Scheme of frozen samples cutting. 1 – the edge area, 2 – the intermediate area, 3 – the central area.

each of them, a curve of total moisture content distribution according to sample height was plotted. Comparison was made between the tested samples and of samples which had not undergone shear.

Research Results

In order to verify the hypothesis stated above regarding the nature of ice segregation in the shearing zone, analysis was undertaken of transformation of cryogenic structure and of moisture content in frozen soils which had undergone constant loads, both being under the value of the limit of long-term shear strength and exceeding this value. Thus, the tests were performed under convergent creep and divergent creep conditions. In the latter case, the samples were brought to failure.

The results of this research are demonstrated with the kaolinite clay example. Tests of polymineral clay and loam samples had similar results.

An example of the initial cryogenic structure of frozen kaolinite clay samples at a temperature of -3°C before the shear test is demonstrated in Figure 4. In general, the samples had a massive cryogenic texture, with ice pocket and air bubble inclusions. Increase of ice content from the centre of the samples to their peripheral areas is indicated. The soil in the centre of the samples was more solid, almost without ice inclusions. Detached ice schliers parallel to the exterior surfaces of the samples could be seen in the edge areas. The patterns of the initial total moisture content distribution are demonstrated on Figure 5. The diagrams show that moisture content increased from the central part of the sample towards the edges. It was connected with moisture migration at soil freezing.

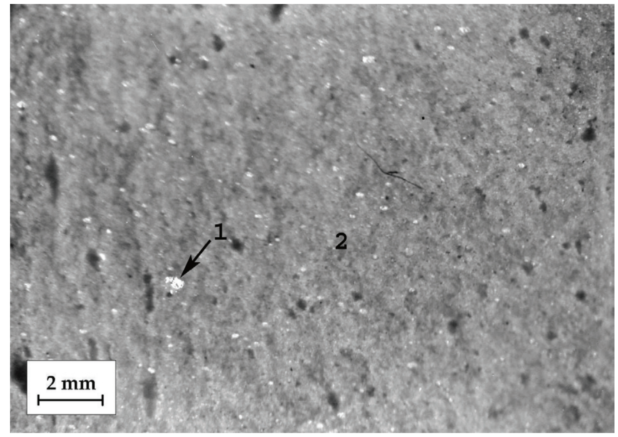

Figure 4. Initial cryogenic structure of cross section of frozen kaolinite clay samples before the shear test. Temperature -3°C. 1 – ice, 2 – mineral skeleton.

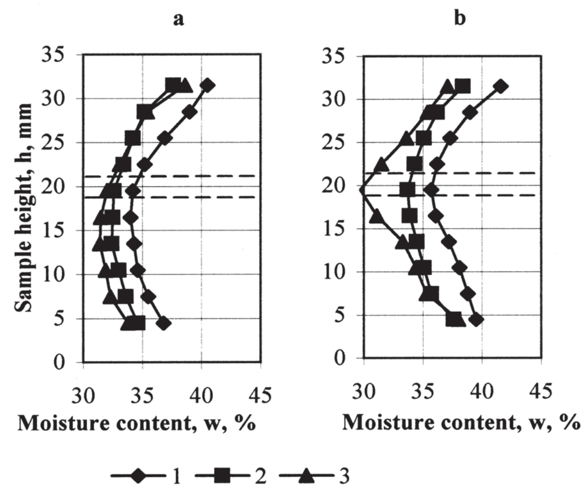

Figure 5. Initial total moisture content distribution in the samples of frozen kaolinite clay. 1 – in the edge area, 2 – in the intermediate area, 3 – in the central area. Dashed lines show a position of apparatus clearance.

Tests were performed on frozen kaolinite clay samples at the temperature -3°C, by means of constant shear loads of 0.5 and 0.45 MPa. The shear load of 0.5 MPa corresponded to the limit of long-term shear strength achieved by step-stress tests. When a shear load of 0.5 MPa was applied, sample failure was achieved in 29 days. At that load, the transient creep stage lasted for about 7 days. When the load of 0.45 MPa was applied, convergent creep was observed for 29 days. A duplicate test of the samples under the load of 0.5 MPa was carried out, with an interruption after 7 days, i.e., in the end of the transient creep stage.

The results showed that increase of the total moisture content (Fig. 6c) and formation of ice schliers in the shearing area (Fig. 7c) was observed only in the samples brought to failure. In this case, the schliers originated at the lateral surface, in the zone of apparatus clearance, and had an angle to it equal to approximately 45°. The moisture increased by 3%–5% in the upper edge area of the samples.

In convergent creep conditions, and at the transient stage

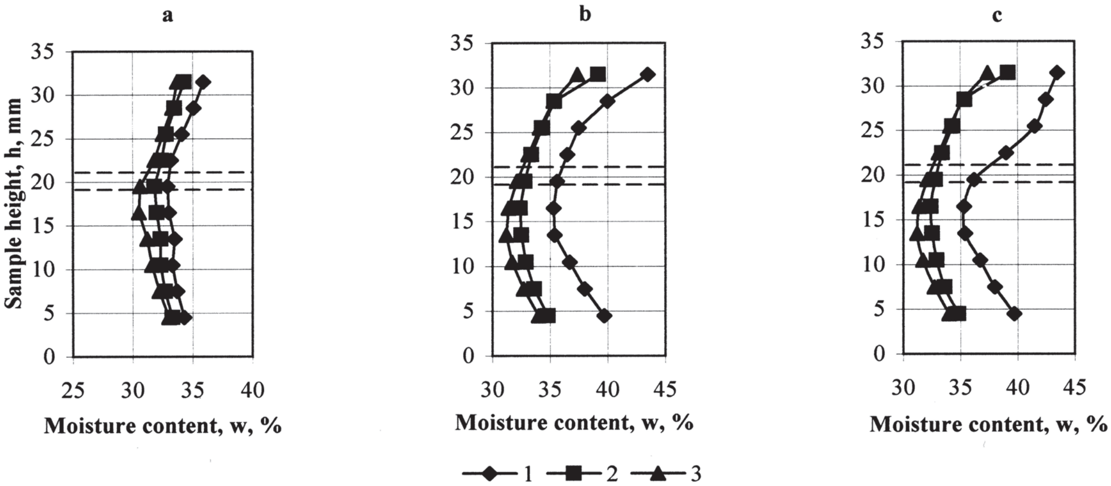

Figure 6. Total moisture content distribution in frozen kaolinite clay samples after shear tests under shear loads: a – 0.45 MPa (29 days), b – 0.5 MPa (7 days), c – 0.5 MPa (29 days). Temperature -3°C. 1 – in the edge area, 2 – in the intermediate area, 3 – in the central area. Dashed lines show a position of apparatus clearance.

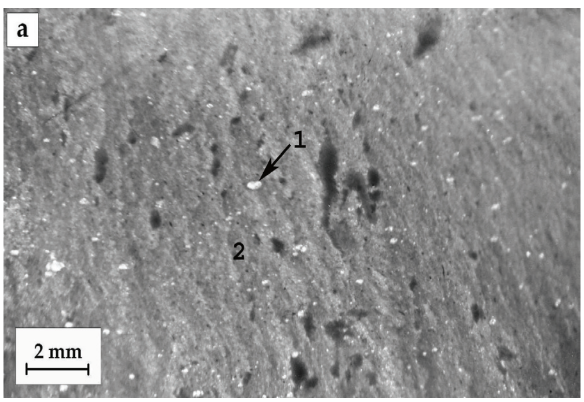

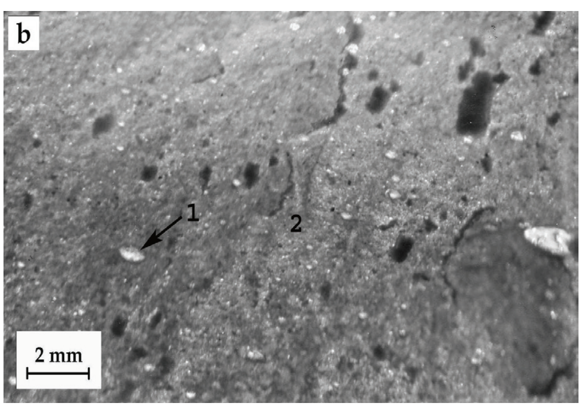

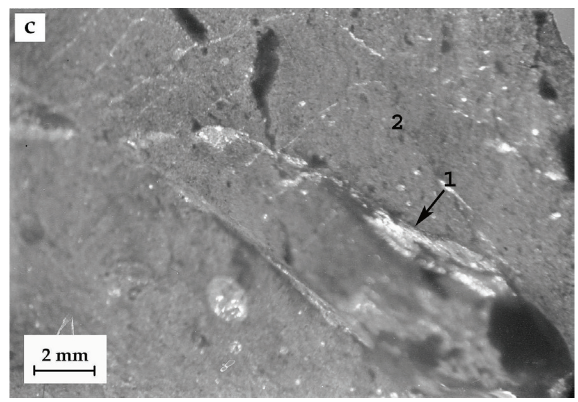

Figure 7. Cryogenic structure of cross section of frozen kaolinite clay samples after shear tests under shear loads: a – 0.45 MPa (29 days), b – 0.5 MPa (7 days), c – 0.5 MPa (29 days). Temperature -3°C. 1 – ice, 2 – mineral skeleton.

at divergent creep, no changes in the moisture distribution along the height of the samples (Fig. 6a, b) or in the cryogenic structure (Fig. 7a, b) of the frozen soil occurred. Thus, redistribution of moisture and formation of schliers in the shearing area took place only at the stages of steady-state creep and progressing flow; i.e., at the stage of sample failure.

The tests of frozen kaolinite clay were also done at the temperature of -1°C, under constant shear loads of 0.1, 0.3, and 0.4 MPa, and under a step load increasing until it reached 0.4 MPa. The tests lasted for 18 to 21 days. Failure of samples was achieved only under constant shear load of 0.4 MPa. In this case, increase of moisture occurred in the edge area (by 6%) and in the intermediate area (by 1%–2%), in the shear zone defined by apparatus clearance. A reduction in moisture content (Fig. 8d) was observed in the layers adjacent to the zone of shearing. Apparently, the unfrozen water migrated from those areas to the soil shear surface where a nearly solid layer of ice (Fig. 9) was formed. At lower loads (0.1 and 0.3 MPa) and at a step load increasing up to 0.4 MPa, convergent creep was observed and no changes in the cryogenic structure or total moisture content were recorded (Fig. 8a, b, c). As the work of Volokhov (2005) demonstrates, under shear tests of kaolinite clay at the temperature of -3°C, the shear surface does not coincide with the plane of the shear apparatus clearance but has an angle of gradient to it equal to about 45°, originating at the lateral surface of the samples and reaching their frontal surface. Here, displacement of a cuneal-shaped part of the sample takes place, overthrusting the other part of the sample (Fig. 10a). At the temperature of -1°C, the soil shear zone is arc-shaped confined to the clearance of the apparatus (Fig. 10b). It appears from this

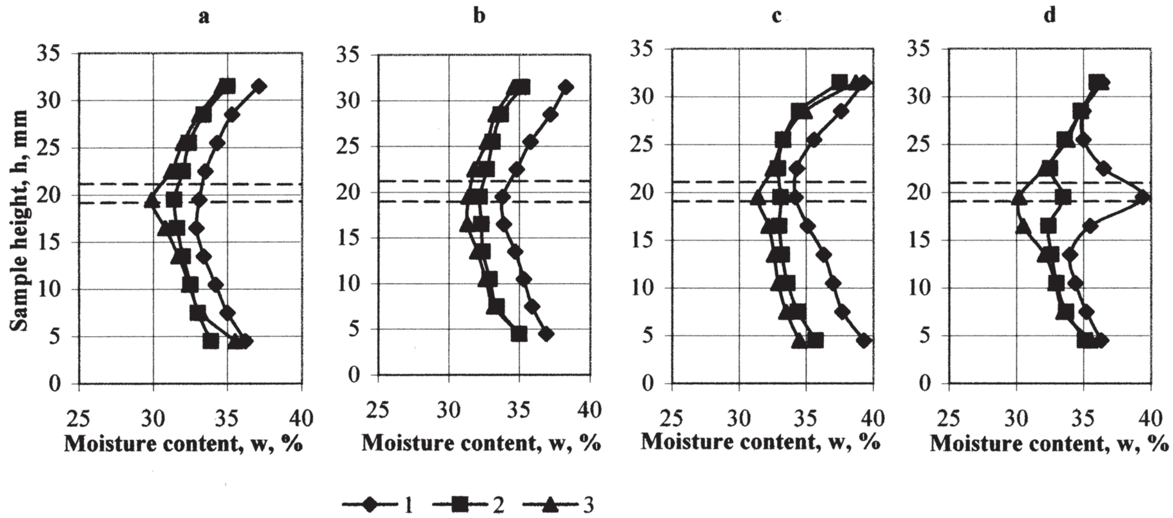

Figure 8. Total moisture content distribution in frozen kaolinite clay samples after shear tests under shear loads: a – 0.1 MPa, b – 0.3 MPa, c – a step load increasing until it reached 0.4 MPa , d – 0,4 MPa. Temperature -1°C. 1 – in the edge area, 2 – in the intermediate area, 3 – in the central area. Dashed lines show a position of apparatus clearance.

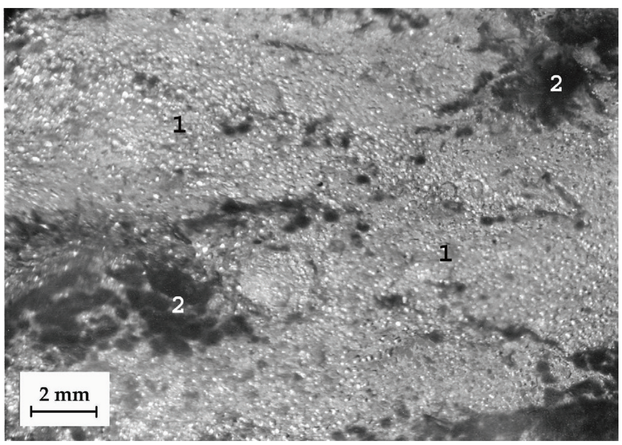

Figure 9. Cryogenic structure of soil shear surface of the frozen kaolinite clay sample. Temperature -1°C. 1 – ice, 2 – mineral skeleton.

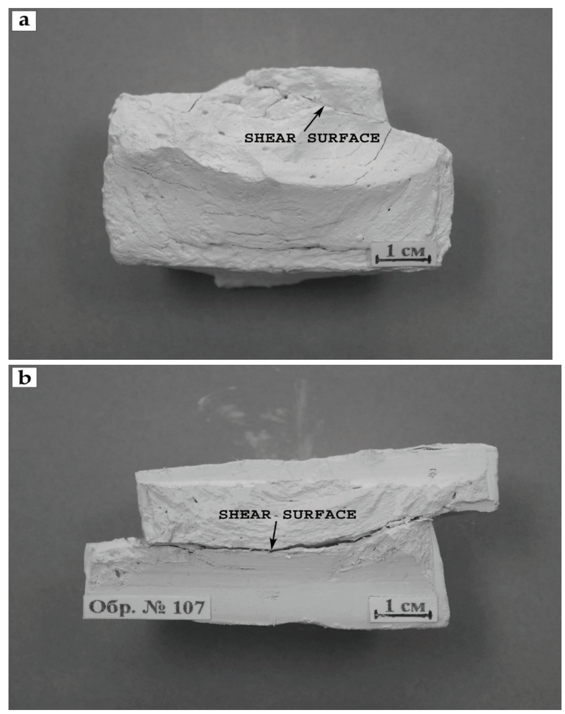

Figure 10. Character of failure of frozen kaolinite clay samples at temperatures: a – 3°C, b – 1°C.

that the aforementioned changes in the cryogenic structure and in moisture content of frozen kaolinite clay occur in the zone of soil shear dislocation.

Thus, this research has provided the following results.

1. In convergent creep conditions, no changes in the cryogenic structure or in distribution of the total moisture content occur. Ice segregation and an increase of total moisture content happen only in divergent creep conditions; i.e., under failure of samples.

2. In divergent creep conditions, ice segregation occurs in the shear area only at the stages of steady-state creep and progressing flow; i.e., at the stage of frozen soil failure. It is not recorded at the transient creep stage.

3. In all of the cases, ice segregation is confined not to the clearance plane of the shear apparatus, but to the shear surface within the soil, irrespective of its alignment in relation to the clearance of the shear apparatus. In this soil shear surface, an ice film develops.

4. Maximal increase of the total moister content of frozen soils and formation of ice schliers at shear is characteristic for the edge area of the samples. As for the central area of the samples, such changes are not present.

Analysis of Results

The results achieved allow conclusions to be drawn concerning the nature of unfrozen water migration and of ice segregation in the shearing area. Changes in the cryogenic structure and in moisture content of frozen clay samples occurred only at the failure stage and their confinement to the sample shear surface suggests that processes of unfrozen water migration to the shearing area and ice segregation in it are related to formation of microfractures at the failure stage. Formation of cracks in the soil is accompanied by formation of new surfaces and increase of interfacial energy of the mineral or ice components of frozen soil. It can cause unfrozen water migration from the areas having lower specific interfacial energy to the microfractures with high values of specific interfacial energy; i.e., under the effect of thermodynamic water potential gradient. Continuous deformation of frozen soil under steady-state creep and progressing flow, and the formation of new microfractures must provide for inflow of unfrozen water to the shearing area from adjacent areas of soil. Freezing of excessive water in the microfractures results in formation and growth of ice schliers there.

Apparently, the described process can go on provided that the unfrozen water migration velocity and the velocity of microfracture formation are commensurate. This is possible at rather low strain rates during frozen soil failure stages, provided that the duration of the stages is significant.

Verification of the hypothesis on the leading role of crack formation in the process of ice segregation at shear is based on the fact that this process occurs mainly in the edge area of the samples and does not affect their central area. This may be related to the fact that shearing of samples begins at the lateral surface at low crack formation velocities. The central area of the samples remains unaffected by the failure process. Therefore, unfrozen water has time to migrate to the shearing zone, filling the cracks in the edge area and freezing there. Advance of the cracks to the central area of samples occurs at high strain rates so that moisture has no time to migrate into them; therefore no changes in the cryogenic structure and in moisture content of the samples takes place in this area of the samples. This process is possible only within a certain range of strain rates at the stage of frozen soil failure.

The conclusion can be made regarding the role of ice segregation in forming of frozen soil strength. Ice schliers appearing in the cracks serve to bond cracks, preventing their advancement and decelerating frozen soil failure. If this process did not occur, frozen soil would be destroyed faster. Consequently, it plays a strengthening role.

Acknowledgments

The work was carried out with the financial support of RFFR RAS (project № 05-05-64310).

References

Chuvilin, E.M., Roman, L.T., Tsyrendorjieva, M.D. & Degasyuk, V.N. 1994. Experimental study of structural and textural transformations in frozen rocks during shear. *Geoecology* 3: 69-75.

Komarov, I.A. 1999. *Thermodynamic of Freezing and Frozen Disperse Grounds. Doctoral Dissertation, Abstract.* Moscow: Lomonosov Moscow State University Press, 52 pp.

Roggensack, W.D. & Morgenstern, N.R. 1978. Direct shear tests on natural fine-grained permafrost soils. *Proceedings of the Third International Conference on Permafrost*, *Edmonton*, *Alberta*, *Canada*, *July10-15*, *1978*: 729-735.

Sadovsky, A.V. 1967. Determination of adfreezing strength of soil with concrete by method of plane shear. In: *Works of the Nord Department of SRI Bases.* Syktyvkar 3: 70-79.

Sakharov, I.I. 1994. Structural and textural transformations in freezing rocks and their relation to moisture migration processes. *Geoecology* 1: 56-64.

Savigny, K.W. & Morgenstern, N.R. 1978. Creep behavior of undisturbed clay permafrost. *Canadian Geotechnical Journal* 23(4): 515-526.

Tsytovich, N.A. 1975. *The Mechanics of Frozen Ground.* Washington DC: Scripta Book Company, 426 pp.

Vialov, S.S. 1959. *Rheological Properties and Bearing Capacity of Frozen Soils.* Moscow: Izdatelstvo Akademii Nauk SSSR, CRREL Translation, Hanover, NH, 219 pp.

Volokhov, S.S. 2005.The character of frozen clay soils failure at shear. *Proceedings of the Third Russian Conference on Geocryology*, *MSU*, *Moscow*, *June 1-3*: 27-32.

Yershov, E.D., Lebedenko, Y.P., Yershov, V.D. & Kondakova, O.A. 1981. Migration of moisture and segregation ice exudation in frozen soils under strain gradient during shear. *Engineering Geology* 6: 104-112.

PERMOS – A Comprehensive Monitoring Network of Mountain Permafrost in the Swiss Alps

Daniel S. Vonder Mühll
PERMOS Coordination Office, University of Zurich and SystemsX.ch, ETH Zurich, Switzerland

Jeannette Noetzli
PERMOS Coordination Office, Glaciology, Geomorphodynamics and Geochronology, Department of Geography, University of Zurich, Switzerland

Isabelle Roer
PERMOS Coordination Office, Glaciology, Geomorphodynamics and Geochronology, Department of Geography, University of Zurich, Switzerland

Abstract

Permafrost Monitoring in Switzerland (PERMOS) has been built up since the early 1990s. After a 6-year pilot phase starting in 2000, PERMOS has taken root. In 2007, all potential PERMOS elements were evaluated based on the criteria and categorised into (A) approved element, (B) element subject to verification in the next two years, and (C) no PERMOS element. The concept "PERMOS 2007" was updated and adapted accordingly. All approved elements will fulfill defined technological and methodological standards. Hence, in 2010, PERMOS will be a sound, sustainable observation network with two types of PERMOS stations: (1) drill sites building the basis of the monitoring network, and (2) kinematic sites, where systematic observations of permafrost geomorphodynamics are performed, allowing for an integral assessment of the permafrost state in the Swiss Alps. PERMOS is presently active in four regions: Upper Engadine, Bernese Oberland, Matter Valley, and "Quatre Vallées."

Keywords: active layer; monitoring; mountain permafrost; permafrost temperature; rock glacier creep velocity.

Introduction

PERmafrost MOnitoring Switzerland (PERMOS) has taken root and passed from first steps in the 1990s (Haeberli et al. 1993) through its pilot phase (2000–2006) (Vonder Mühll et al. 2001, 2004) and has now reached its implementation phase (2007–2010).

Low-latitude high-altitude mountain permafrost is governed mainly by climate conditions, in particular mean annual air temperature but also snow precipitation. Climate change therefore has an impact on mountain permafrost that is also an important indicator for environmental changes. According to IPCC assessments (IPCC 2007), circumpolar but also mountain regions will be affected much more strongly than the global average. Therefore, the Global Terrestrial Network for Permafrost (GTN-P) that is currently being established within the worldwide climate-monitoring program (GCOS/GTOS) of the World Meteorological Organization (WMO) and others (FAO, UNEP, UNESCO, ICSI) increases in importance. PERMOS is one early component of GTN-P. Moreover, it complements the glacier monitoring network in Switzerland, which was already established towards the end of the 19th century.

In contrast to glaciers and snow, systematic scientific investigation of Alpine permafrost only was started in the early 1970s by the Barsch group of the University of Basel. Since the late 1980s and after the drilling through the Murtèl-Corvatsch rock glacier in 1987 (Haeberli et al. 1988; Vonder Mühll & Haeberli 1990), a number of Swiss institutes started performing research on low-latitude mountain permafrost. An important and valuable contribution was the EU-funded project PACE (Permafrost and Climate in Europe; Harris et al. 2003). These various activities formed the basis for establishing PERMOS, which officially started in 2000 under the umbrella of the Swiss Academy of Sciences (SAS) with support of the Federal Office for Environment (FOE) for a pilot-phase which ended in 2006.

As for the four years from 2007 to 2010, the Federal Office for Environment, the Swiss Academy of Sciences, and the Federal Office for Meteorology signed a contract to implement PERMOS within the responsible federal monitoring structures in Switzerland. This means that after an evaluation, the PERMOS-approved sites will be updated to a technological and methodological standard, and a 50% position is financed for coordination and reporting.

Goals and Strategy

The main goal of PERMOS is to document the state of permafrost in the Swiss Alps on a long-term basis, and hence, temporal permafrost variations. In fact, this is perfectly complementary to the glacier monitoring network. The Cryosphere Commission of the Swiss Academy of Sciences is presently setting up an integral cryosphere monitoring concept which includes all relevant parts of the Alpine cryosphere: snow, glaciers, and permafrost.

As simple as this task is to formulate, as difficult it is to implement. In contrast to glaciers and snow, permafrost is invisible. Moreover, permafrost characteristics change within short distances in low-latitude mountain regions such

Table 1. “Priorities for GGD” according to the IPA- resolution of August 1995 (Hegginbottom 1995, p 13).

PARAMETER*	APPLICATIONS: Process understanding	Engineering design	GCM validation	Change detection	Impact evaluation
Geometry					
Permafrost extent	M	H	H	H	M
Permafrost thickness (shallow†)	H	H	H	H	H
Permafrost thickness (deep†)	M	M	L	H	L
Active layer thickness	H	H	M	H	H
Ground ice extent	H	H	M	M	H
Lateral /vertical displacement	H	H	L	H	H
Thermal State					
Temperature (shallow†)	H	H	H	H	H
Temperature (deep †)	M	M	M	H	L
Properties (Soil/Rock)					
Moisture content (water/ice)	H	H	M	H	H
Bulk density	H	H	H	L	L
Texture	H	H	L	M	M
Chemistry (water/ice)	M	M	L	M	M
Trace gases	H	L	H	M	M

* Site descriptions include location, geology, geotechnical properties, vegetation, etc. Metadata includes techniques, equipment, precision, post-processing, data ownership, etc.
† For permafrost thickness and temperature, the demarcation between “shallow” and “deep” is taken as the local depth of zero annual amplitude.
H, M, L = High, moderate, or low priority.

as the Alps. The observed parameters were chosen according to the “Priorities for Global Geocryological Database (GGD),” released by the IPA resolution in August 1995 (Hegginbottom 1995, Table 1). The strategy has been set up in a pragmatic way; PERMOS is based on infrastructure (equipped drillings, ground surface temperature sites, and observation of permafrost creep at various rock glaciers) that was established within research projects. New and explicit PERMOS sites will be placed only after available and existing stations are updated to a common standard. New stations will be located in regions where gaps occur. Ideally, each climate region of the Alps is covered by four PERMOS stations.

Pilot Phase (1990s–2006)

The pilot phase aimed to (1) ensure continuation of established time series, (2) check, improve, and adapt observations, and (3) propose a monitoring concept that allows maintenance over decades.

Initial PERMOS observations

In 1999, three items were defined to be observed during the pilot phase:

(1) borehole measurements (temperature, deformation)
(2) lower boundary of permafrost distribution (BTS)
(3) aerial photographs to document surface characteristics

After three years, first corrections were made based on gained experiences of the monitoring and ongoing research projects: (a) drill sites will be complemented by permanent electrodes to regularly record Electrical Resistivity Tomographies (ERT) following the principles according to Hauck and Vonder Mühll (2003); (b) it turned out that the annual lower boundary of permafrost distribution could not be determined by combining the bottom temperature of the snow cover (BTS) and ground surface temperature (GST). Consequently, permafrost pattern is determined in few areas every 10 years only. In addition, GST sites were complemented with a number of single-channel-temperature-loggers mounted in steep walls (Gruber et al. 2003); (c) Creep processes and behaviour of alpine rock glaciers are only poorly understood so far. However, recent studies (Kääb et al. 2006, Roer 2003) indicate that creep velocities vary considerably (see Fig. 1). Arenson et al. (2002) report even annual variations. Therefore, creep velocity of selected rock glaciers shall be determined by photogrammetry and geodetic surveys.

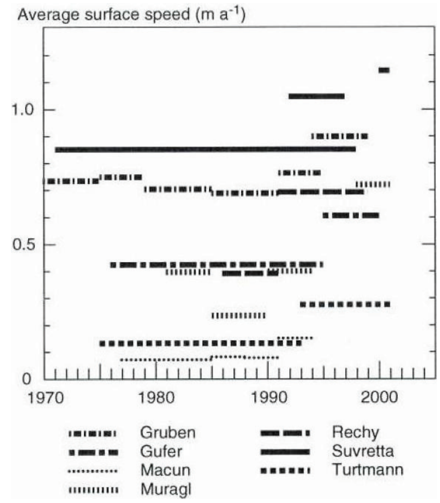

Figure 1. Creep velocities of seven rock glaciers determined by photogrammetry (Kääb et al. 2006). Note the marked variations, e.g., of Muragl rock glacier.

Types of PERMOS Sites

Following the adaptations and in discussing the monitoring results, it was decided to focus on two types of PERMOS sites: drill sites and kinematic sites.

Drill sites

Each drill site of PERMOS shall be composed of:

- One or several borehole(s) that is (are) at least some 15 m deep, equipped with a thermistor string attached to a data logger. Sensors are recommended to be at the following depths [m]: 0.0, 0.4, 0.8, 1.2, 1.6, 2.0, 2.5, 3.0, 4.0, 5.0, 7.0, 9.0, 11, 13, 15, 20, 25, 30, 40, 50, 60, 70, 80, 85, 90, 92, 94, 96, 98, 100 with temporal interval of 6 hours down to 5 m depth, farther down, once every day.
- Snow thickness and air temperature shall be measured as a minimum for climate parameters.
- Geophysical monitoring consists of at least 20 fixed installed electrodes to regularly record ERTs.
- Single-channel-temperature loggers recording ground surface temperatures in at least 15 spots with (flat and oblique) and without (steep rock walls) a snow cover in winter in the region (distributed at various altitude, exposure, locality within a few kilometers).

Kinematic sites

Rock glacier creep is observed either by photogrammetry using aerial photos, by geodetic survey, or differential GPS. Each rock glacier is equipped individually according to the applied methodology and movement pattern.

PERMOS 2007–2010

The updated concept was discussed, elaborated, and approved by the PERMOS community. A comprehensive evaluation of each potential PERMOS element was conducted in 2007.

Evaluation and applied criteria

During the pilot phase, each potential monitoring element was included and, to a limited amount, financially supported. While at the beginning of the pilot phase only few sites were available, the number increased. Consequently, each potential element was evaluated according to various criteria. Approved elements shall be recorded for the next several decades. The base line was to continue rather few elements on a standardized high quality and technology level and to omit redundancies.

The following set of criteria was elaborated within the expert Cryosphere Commission SAS:

(a) Relevance towards the overall aim to document the permafrost state in the Swiss Alps;
(b) Importance towards society and politics; i.e., contribution to understanding issues related to environment, climate change, and natural hazards;
(c) Importance for research and academic education;
(d) Feasibility in terms of accessibility.

In addition, time series were assessed according to length and temporal resolution, quality (accuracy, gaps), site characteristics, representativeness, accessibility, contribution to the GHOST tier structure (Cilhar et al. 1997), additional parameters available, and particular remarks.

The evaluated elements were allocated to one of the following categories:

(A) PERMOS approved: the element will be recorded for the next several decades, and a large part will be funded by PERMOS. The site will be updated to the technological and methodological standard.

(B) Retention: the element is part of PERMOS. Particular requirements and open questions are addressed. The element will be re-evaluated in 2009.

(C) Rejected: the element is rejected and no longer financially supported by PERMOS. It is up to the institution to continue the time series.

Network in 2007

In the evaluation, all drill sites that are not fully equipped according to the above-mentioned composition were B-rated, and similarly most "GST sites." Within the updated concept, these two elements will be merged into one "drill site" until 2010. Presently, PERMOS consists of 9 A-rated drill sites, 9 A-rated GST sites, which will be updated and transferred into "standard PERMOS drill sites." All B-rated elements (6 drill sites, 3 GST sites, and 5 kinematic sites) are subject to additional installation or further strategical aspects and a re-evaluation in 2009 (see Table 2). Figure 2 shows the geographical distribution of the elements in 2007.

PERMOS Partners

A comprehensive monitoring network must be set up among interested partners from academia and administration. Academia provides the permafrost know-how and the link to ongoing research projects, while administration is responsible for monitoring and provides political links.

The pilot phase allowed for setting up a concept with parameters and elements that could be adapted according to gained experiences and new research results. After some 15 years, PERMOS complements the Swiss glacier monitoring network and Swiss snow observation, data of which all are being complied to contribute to cryological monitoring.

In general, funding institutions are skeptical to invest in monitoring programs, since they cannot fund "infinite" long-term projects. Also, universities cannot carry such programs, since their core activities are research and education. However, both research funding institutions and universities were key to setting up PERMOS. Research projects funded by the Swiss National Science Foundation (SNSF) and the European Commission, and from ETH Zurich and SFISAR Davos also, have established important milestones without which PERMOS would not exist. Still, the maintenance of the elements is being carried by the university institutes and has been supported since 2000 by the financing partners.

In fact, the success of PERMOS is based on a go-together of the academic institutions involved in permafrost research in Switzerland and the financial support of the SAS: University of Zurich (coordination), ETH Zurich, SFISAR Davos, the Universities of Berne, Fribourg, Lausanne, and the Academia Engadina Samedan.

This, in turn, triggered the commitment of the authorities, which are officially in charge of climate and environmental monitoring: the Federal Office for Environment (FOE) and the Federal Office for Climatology (MeteoSwiss).

Monitoring Results

Most important results from monitoring consist of comparing elements from one time interval to another. However, many details of involved processes that are modeled are based on data provided by monitoring sites. In particular, numerical and statistical models are calibrated using one part of monitoring data. It is therefore neither possible nor intelligent to distinguish or separate permafrost monitoring and research.

PERMOS drill sites are located in different terrain and lithologies. Murtèl-Corvatsch is a rock glacier site with a coarse, blocky surface layer and permafrost below the active layer consisting of almost pure ice. The Schilthorn drill site is on schist bedrock with a shallow weathered clay-rich debris layer of some decimeters in thickness. The same climate

Table 2. PERMOS elements 2007.

(1) Drill sites and GST sites

Name	borehole	GST
Flüela	A	A
Lapires	A	A
Murtèl-Corvatsch	A	A
Schafberg / Mt Barba Peider	A	A
Schilthorn	A	A
Gentianes	A/B	C
Matterhorn	A/B	C
Stockhorn	A/B	A
Tsaté	A/B	C
Arolla / Mt. Dolin	B	B
Dreveuneuse	B	C
Gemsstock	B	C
Les Attelas	B	C
Muragl	B	C
Jungfrau	B/C	A
Alpage de Mille / Aget	C	A
Gemmi	C	A
Réchy	C	B
Yettes Condjà	C	B

(2) Kinematic sites

Name	air photo	terrestr surv
Gemmi-Furggentälti	A	yes
Gruben	A	no
Muragl	A	yes
Murtèl	A	no
Réchy	A	yes
Gianda Grischa	B	no
Gross Gufer	B	no
Turtmann Grueo1	B	yes
Yettes Condjà	B	yes
Suvretta	B/C	no

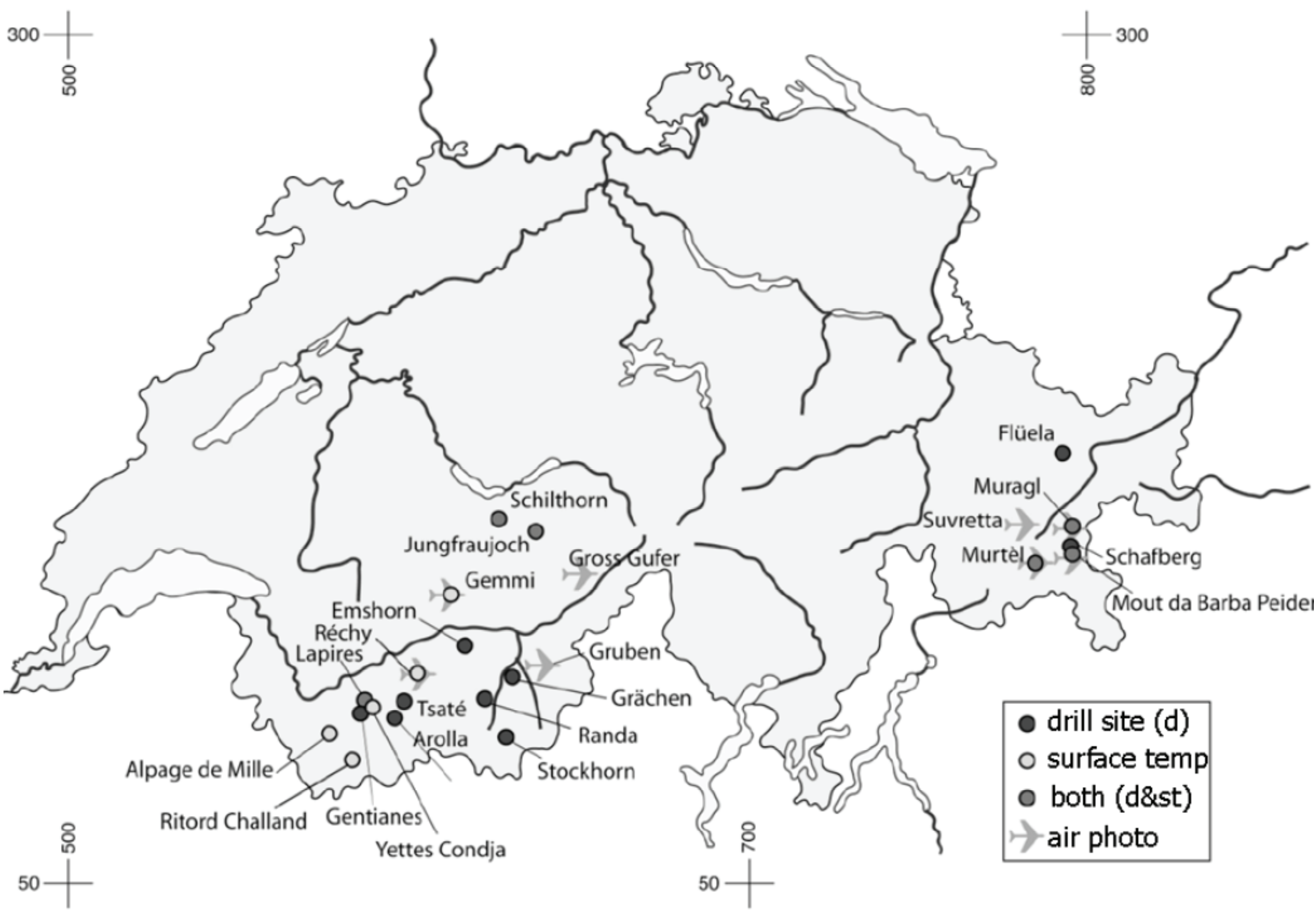

Figure 2. PERMOS sites in 2007 where different parameters are measured.

signal causes different reactions of the thermal regime at such different locations.

Process understanding

In winter 2006/2007, snow cover was only thin, and mean monthly temperatures were 1°C to 3°C warmer than normal. Permafrost temperatures were influenced differently: in steep walls where snow cannot accumulate, air temperatures caused a warming. At permafrost sites with usually a significant snow cover, lacking snow led to a cooling of subsurface temperatures.

Active layer

The thickness of the active layer is mainly influenced by summer weather conditions. Recorded in summer 2003 was an active layer almost twice as thick as in the years before and afterwards (Fig 2). Within PERMOS, maximal active layer thicknesses and the corresponding date are recorded. Several PERMOS sites are integrated into the CALM network (Brown et al. 2000).

Permafrost temperatures

Permafrost temperatures at about 10 m depth are

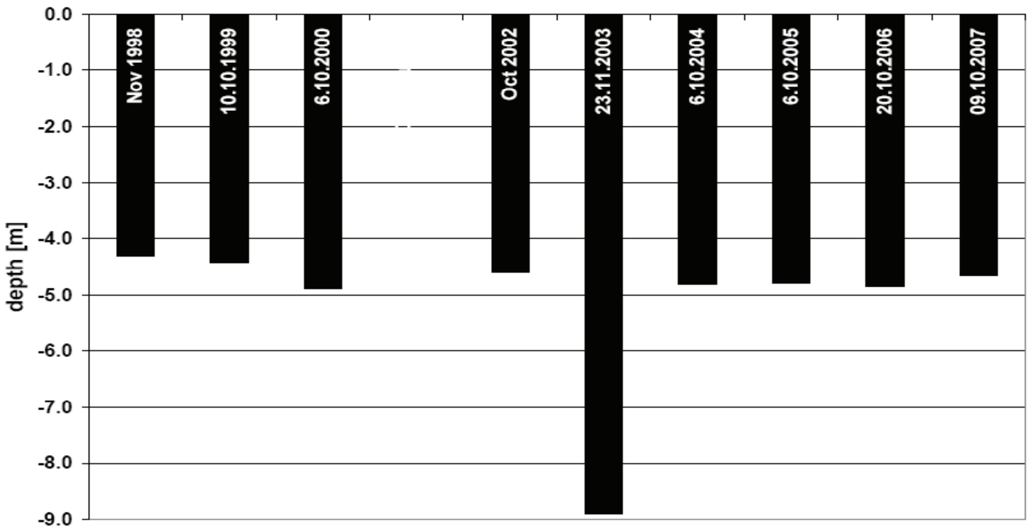

Figure 3. Depth and date of the active layer thickness at borehole Schilthorn 51/1998. In the extremely warm summer 2003 permafrost thawed down to almost 9 m.

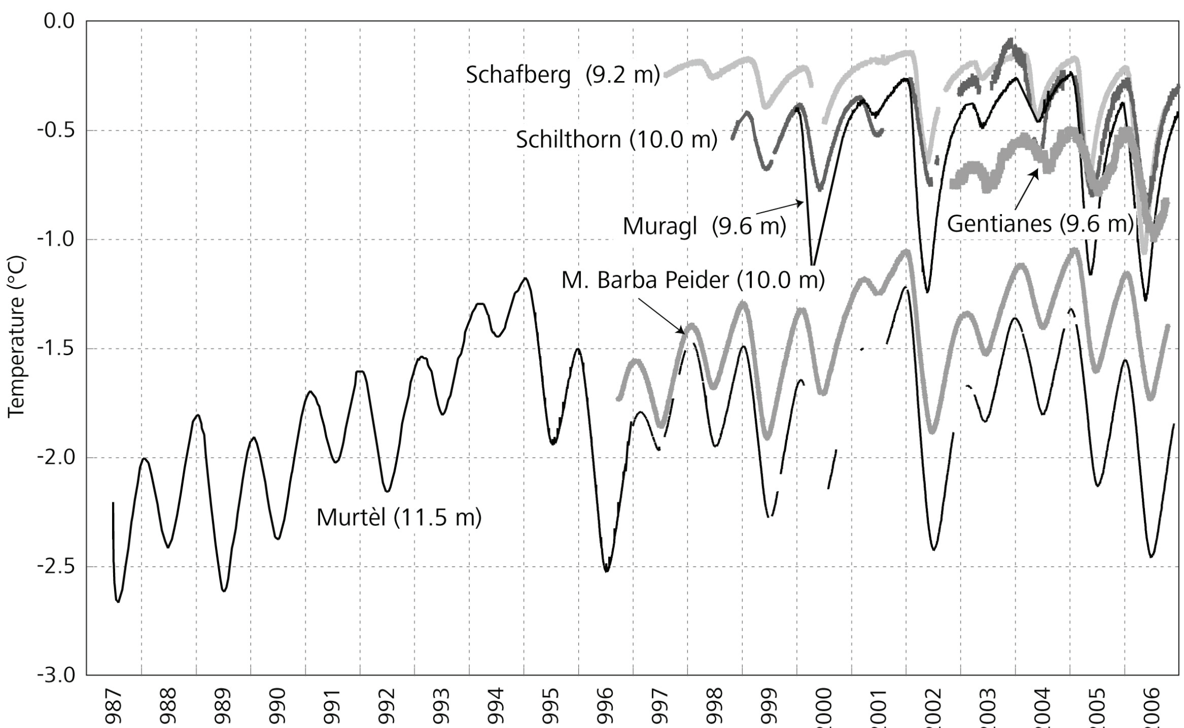

Figure 4. Permafrost temperature of a number of PERMOS elements at about 10 m depth.

characterized by a nice sinusoidal shape and a phase lag of about half a year. High frequency “noisy” parts of the temperature signal are largely filtered out, and differences of the various localities are damped as well. Therefore, these graphs are used for comparison of the various drill sites and also to determine region-specified trends.

Figure 4 shows a compilation of temperatures at about 10m depth from a number of drill sites, all located on flat or oblique terrain with a snow cover in winter. At these sites, snow characteristics govern mainly thermal regime.

Conclusions

A comprehensive monitoring network must be set up among interested partners from academia and administration. Academia provides the permafrost know-how and the link to ongoing research projects, while administration is responsible for monitoring and provides political links.

The pilot phase allowed for setting up a concept with parameters and elements that could be adapted according to gained experiences and new research results. After some 15 years, PERMOS has found its place by complementing the Swiss glacier monitoring network and Swiss snow observation, data of which all are being complied to contribute to cryological monitoring.

Acknowledgments

Obviously, PERMOS as a monitoring program involves many contributors and depends on key persons that support the efforts, and on financial support. The Swiss Academy for Sciences (SAS), the Federal Office for Environment (FOE), and the Federal Office for Climatology (MeteoSwiss) finance PERMOS based on a signed contract. Equally important are the contributions of the academic institutions, providing synergies from research and education projects.

References

Arenson, L.U., Hoelzle, M. & Springman, S.M. 2002. Borehole deformation measurements and internal structure of some rock glaciers in Switzerland. *Permafrost and Periglacial Processes* 13: 117-135.

Brown, J, Nelson, F.E. & Hinkel, K.M. 2000. The circumpolar active layer monitoring (CALM) program research designs and initial results. *Polar Geography* 3: 165-258.

Cihlar, J., Barry, T.G., Ortega Gil, E., Haeberli, W., Kuma, K., Landwehr, J.M., Norse, D., Running, S., Scholes, R., Solomon, A.M. & Zhao, S. 1997. *GCOS/GTOS plan for terrestrial climate-related observation. GCOS 32, version 2.0*. WMO/TD-796, UNEP/DEIA/TR, 97-7.

Gruber, S., Hoelzle, M. & Haeberli, W. 2004. Rock wall temperatures in the Alps - modeling their topographic distribution and regional differences, *Permafrost and Periglacial Processes* 15(3): 299-307.

Haeberli, W., Huder, J., Keusen, H.-R., Pika, J. & Röthlisberger, H. 1988. Core drilling through rock glacier-permafrost. *Proceedings of the Fifth International Conference on Permafrost, Trondheim, Norway,* 2: 937-942.

Haeberli, W., Hoelzle, M., Keller, F., Schmid, W., Vonder Mühll, D. & Wagner, S. 1993. Monitoring the long-term evolution of mountain permafrost in the Swiss Alps. *Proceedings of the Sixth International Conference on Permafrost, Beijing, China,* 1: 214-219.

Harris, C., Vonder Mühll, D., Isaksen, K., Haeberli, H., Sollid, J.L., King, L., Holmlund, L., Dramis, F., Guglielmin, M. & Palacios, D. 2003. Warming permafrost in European mountains. *Global and Planetary Change* 39: 215–225.

Hauck, C. & Vonder Mühll, D. 2003. Inversion and interpretation of 2-dimensional geoelectrical measurements for detecting permafrost in mountainous regions. *Permafrost and Periglacial Processes* 14(4): 305-318.

Heginbottom, J.A. 1995. Report of the IPA Data Workshop. *Frozen Ground* 18: 12-13.

IPCC. 2007: Climate change 2007: impacts, adaptation and vulnerability. *Contribution of Working Group II to the Fourth Assessment Report of the Intergovernmental Panel on Climate Change. M.L. Parry, O.F. Canziani, J.P. Palutikof, P.J. van der Linden & C.E. Hanson (eds.),* Cambridge, UK: Cambridge University Press, 976 pp.

Kääb, A., Frauenfelder, R. & Roer, I. 2006. On the response of rockglacier creep to surface temperature variations. *Global and Planetary Change*.

Roer, I. 2003. Rock glacier kinematics in the Turtmanntal, Valais, Switzerland - observational concept, first results and research perspectives. *Proceedings of the Eighth International Conference on Permafrost, Zürich, Switzerland,* 2: 971-975.

Vonder Mühll, D. & Haeberli, W. 1990. Thermal characteristics of the perma-frost within an active rock glacier (Murtèl/Corvatsch, Grisons, Swiss Alps). *Journal of Glaciology* 36(123): 151-158.

Vonder Mühll, D., Delaloye, R., Haeberli, W., Hoelzle, M. & Krummenacher, B. 2001. Permafrost Monitoring Switzerland PERMOS - *1. Jahresbericht 1999/2000, Glaciological Report (Permafrost) of the Glaciological Commission (GC) of the Swiss Academy of Sciences (SAS)* 1: 32 pp.

Vonder Mühll, D., Nötzli, J., Makowski, K. & Delaloye, R. 2004. Permafrost in Switzerland 2000/2001 and 2001/2002. *Glaciological Report (Permafrost) of the Glaciological Commission (GC) of the Swiss Academy of Sciences (SAS)* 2/3: 80 pp.

Methane Cycle in Terrestrial and Submarine Permafrost Deposits of the Laptev Sea Region

Dirk Wagner, Katharina Koch
Alfred Wegener Institute for Polar and Marine Research, Research Unit Potsdam, Potsdam, Germany
Andreas Gattinger
Helmholtz Zentrum München-German Research Center for Environmental Health, Neuherberg, Germany
André Lipski
Universität Osnabrück, Abteilung Mikrobiologie, Osnabrück, Germany

Abstract

Permafrost environments within the Siberian Arctic are natural sources of the climate-relevant trace gas methane. In order to improve our understanding of present and future carbon dynamics in high latitudes, we studied the activity and biomass of the methanogenic communities in terrestrial and submarine permafrost deposits. For these investigations, permafrost cores of Holocene and Late Pleistocene age were drilled in the Laptev Sea region. A high CH_4 concentration was found in the upper 4 m of the Holocene deposits, which correlates well with the methanogenic activity and biomass. Even the incubation of core material at -3°C and -6°C showed a significant CH_4 production (range: 0.04–0.78 nmol CH_4 h^{-1} g^{-1}). The results indicated that the methane in permafrost deposits originated from modern methanogenesis by cold-adapted methanogenic archaea. Microbial-generated methane in permafrost sediments is, so far, an underestimated factor for future climate development.

Keywords: Laptev Sea; methane; methanogenesis; permafrost deposits; phospholipid biomarker; psychrophiles.

Introduction

The Arctic plays a key role in Earth's climate system, as global warming is predicted to be most pronounced at high latitudes and because one third of the global carbon pool is stored in ecosystems of the northern latitudes. Global warming will have important implications for the functional diversity of microbial communities in these systems. It is likely that temperature increases at high latitudes will stimulate microbial activity and carbon decomposition in Arctic environments, and accelerate climate change by increasing trace gas release (Melillo et al. 2002, Zimov et al. 2006). Currently, the functioning of microbial communities and their impact on changing environmental conditions are not adequately understood, and the potential methane release from frozen sediments is not adequately quantified.

Methane is chemically very reactive and more efficient in absorbing infrared radiation than carbon dioxide. Estimates of methane emissions from arctic and sub-arctic wetlands range between 10 and 39 Tg a^{-1}, or between 2.2 and 8.6% of global methane emissions (Bartlett & Harriss 1993, Cao et al. 1998). Methane, as a powerful greenhouse gas, contributes to about 20% of global warming (IPCC 2001).

In general, temperature is one of the most important variables regulating the activity of microorganisms. The growth potential, as well as the molecular, physiological and ecological aspects of microbial life at low temperatures, has been investigated in many studies (e.g., Gounot 1999, Wagner 2008). Certain key processes of the methane cycle are carried out exclusively by highly specialised microorganisms such as methanogenic archaea and methane oxidising bacteria. The microbial methane production (methanogenesis) in the active layer of permafrost is the terminal step during the anaerobic decomposition of organic matter, while the methane oxidation is the primary sink for methane in Arctic wetlands (Wagner et al. 2005).

However, there are only a few studies investigating the geochemistry and microbiology of permafrost deposits, which were mainly done in Siberia and Canada. Direct bacterial counts in the order of 10^7 to 10^8 were reported for permafrost deposits from Northeast Siberia (Rivkina et al. 1998). Shi and colleagues (1997) found viable bacteria in permafrost sediments up to 3 million years in age in the Kolyma-Indigirka lowlands. Most of the isolated bacteria showed mesophilic growth characteristics. In contrast, the minimum temperature for growth of permafrost bacteria was recently calculated to be -20°C (Rivkina et al. 2000). Furthermore, molecular life markers and low numbers of methanogens were found in the Mallik gas hydrate production research well (Colwell et al. 2005, Mangelsdorf et al. 2005). However, methanogenic activity could not be detected in the permafrost sediments using radiolabelled ^{14}C-substrates.

For the understanding and assessment of recent and future carbon dynamics in high latitudes, we have to answer the question: "What will happen to the carbon stored in permafrost, in the event of a climate change?" From this view point, we studied the methane concentration, the quantity and quality of organic matter, and the activity, biomass and diversity of methanogenic communities in permafrost deposits of the Laptev Sea region.

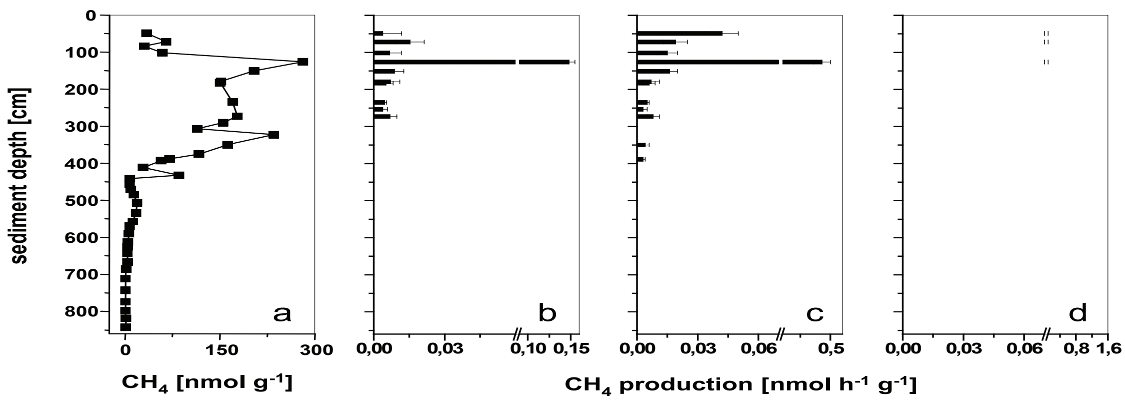

Figure 1. Vertical profiles of methane concentration (a), and methane production rates determined at 5°C without any additional substrate (b), with acetate (c) with hydrogen (d) as methanogenic substrates.

Study Sites

Within the scope of long-term studies on carbon dynamics in the Siberian Arctic, several expeditions were carried out by the Alfred Wegener Institute for Polar and Marine Research.

The Holocene permafrost core was drilled during the LENA 2001 expedition on the main study site Samoylov Island (72°22′N, 126°28′E, Pfeiffer & Grigoriev 2002). Samoylov, with the Russian-German Research Station, is located in the active part of the Lena Delta (Hubberten et al. 2006). The Lena Delta lies at the Laptev Sea coast between the Taimyr Peninsula and the New Siberian Islands. Continuous permafrost, which occurs throughout the investigation area, extends to depths of about 100–300 m (Yershov 1998), with active layer thicknesses between 30 and 60 cm depth.

The submarine permafrost cores of Late Pleistocene age were recovered in the framework of the COAST expedition from the western Laptev Sea along a transect running perpendicular to the coastline (Rachold et al. 2007). The Laptev Sea region is characterised by an arctic continental climate with low mean annual air temperature of about -15°C and low summer precipitation of <198 mm. Further details of the study sites were described previously in Wagner et al. (2003) and Rachold et al. (2007).

Drilling of Permafrost Deposits

The drilling of an 850 cm long core was carried out with a portable gasoline powered permafrost corer without using drilling fluid to avoid microbiological contamination of the permafrost samples. A mixing of the permafrost sediments was not observed due to the frozen state of the core material. The individual core segments, which were up to 50 cm in length, were placed immediately after removal from the corer into plastic bags and stored at about -8°C in the permafrost cellar of the Research Station Samoylov. After drilling of the core, the borehole temperature was monitored with a string of 9 thermistors. The cores were transported in a frozen state to Potsdam, Germany. During transport, the temperatures in the containers were monitored by micro data loggers. The storage temperature in the Potsdam laboratory was -22°C.

Core segments were split along their long axis into two halves under aseptic conditions with a diamond saw in an ice laboratory at -22°C. Afterwards, one half of the core was cleaned with a sterile knife for lithological and geocryologically descriptions. Subsequently, one half was cut into segments of about 10–30 cm length according to the lithology and the geocryology. Small pieces (approx. 10 g) of each sub-sample were taken for analysing the methane concentration in the frozen sediments. The remaining material of each sub-sample was thawed at 4°C and homogenized under anoxic and sterile conditions for analysis of the sediment properties and the microbial activities and biomarkers. Sub-samples for the different analyses were placed into sterile plastic Nalgene boxes. Separated samples were used directly for the experiments (methane concentration, methane production rates, and biomarker analysis) or were freeze-dried for the organic carbon analyses. The second half of the core is kept as an archive in the ice core storage at the Alfred Wegener Institute.

Methanogenesis in Terrestrial Permafrost

Our results show significant amounts of methane in the first four meters of frozen sediments (up to 282 nmol CH_4 g^{-1} sediment, Late Holocene, 5000 yr BP until today) and only trace amounts of methane in the bottom section of the core (0.4–19 nmol CH_4 g^{-1} sediment; Middle Holocene, 9000–5000 yr BP; and Early Holocene, 11500–9000 yr BP; Fig.1a). Different amounts of methane in different aged permafrost deposits from northeastern Eurasia were reported by Rivkina & Gilichinsky (1996). They detected methane in modern (Holocene) and old permafrost deposits (Middle and Early Pleistocene, 1.8–0.78 mill. yr BP), but not in Late Pleistocene ice complexes (ice rich permafrost, 130000–11500 yr BP). They concluded from their findings that methane cannot diffuse through permafrost sections. If methane is unable to diffuse through permafrost from deeper deposits, it must either be entrapped during the deposition of the sediments or originate from recent methane production by methanogenic archaea (methanogenesis) in the frozen ground.

The analyses of methane production in selected sediment samples at 5°C, revealed activity only in permafrost layers with significant concentrations of methane (upper 4 m of the sediments; Fig. 1b). An important finding from the activity analyses is that no methane production was detectable in the bottom part of the permafrost section (>4 m) characterized only by traces of methane. This was also the case after addition of acetate or H_2/CO_2 as energy and carbon source (Fig. 1c, d). This indicates that the absence of methanogenesis does not depend on deficiency of methanogenic substrates in the Middle and Early Holocene deposits. Methane was only found in permafrost sediments with verifiable methane production activity.

The investigation of phospholipids as molecular biomarkers for *Bacteria* (PLFA) and *Archaea* (PLEL) shows a vertical profile with the same trend as the methane concentration. Specifically, significant amounts of phospholipids were determined in the upper Late Holocene deposits (<4 m sediment depth), which correlates ($r = 0.632$, $P = 0.05$) with the highest amount of methane (Fig. 2). In contrast, the biomarker concentrations in the Middle and Early Holocene permafrost sediments (>4 m sediment depth) drastically decreased to values below 10 nmol g^{-1} sediment, which corresponds with the detected traces of methane. Phospholipids are compounds of cell membranes that rapidly degraded after cell death (Harvey et al. 1986, White et al. 1979). They are regarded as appropriate biomarkers for viable microorganisms (e.g., Ringelberg et al. 1997, Zelles 1999). Therefore, the positive correlation of methane concentration with viable bacteria and archaea gives us the first strong evidence of recent methanogenesis under in situ conditions in permafrost deposits.

Although only a few psychrophilic strains of methanogenic archaea have been isolated, there are some indications of methanogenic activity in cold permafrost environments (Kotsyurbenko et al. 1993, Ganzert et al. 2006). However, the incubation of permafrost samples from 45–63 cm depth at sub-zero temperatures with acetate and hydrogen as methanogenic substrates, indicated a relatively high methane production rate under permafrost temperature conditions. At a temperature of -3°C, a significant increase in methane production was found, which rose linearly to headspace concentrations of about 1000 ppm (with acetate) and 2500 ppm (with hydrogen) during 300 h after the initiation of the experiment. At a temperature of -6°C, methanogenesis was lower; however, after a lag phase of about 300 h, a significant increase to 200 ppm (with acetate), and 500 ppm (with hydrogen) within 200 h, was observed. The calculated activity of methanogenic archaea with hydrogen reached values of 0.78 ± 0.31 nmol CH_4 h^{-1} g^{-1} and 0.14 nmol CH_4 h^{-1} g^{-1} at incubation temperatures of -3°C and -6°C, respectively. This was 2.5 and 3.5 times higher compared to the activity with acetate (0.31 ± 0.04 nmol CH_4 h^{-1} g^{-1} and 0.04 ± 0.01 nmol CH_4 h^{-1} g^{-1}) at the corresponding temperatures.

The quality of organic carbon is a limiting factor in the microbial metabolism process. Our results reveal a high organic carbon content (on average 2.4%) for the Holocene permafrost deposits (Table 1). However, the quantity of organic matter in permafrost ecosystems provides no information on the quality, which determines the availability of organic compounds as energy and carbon sources for microorganisms (Hogg 1993, Bergman et al. 2000). For this purpose, the humification index (HIX), which is a qualitative parameter, can give suitable information with regard to microbial metabolism. Wagner and colleagues (2005) demonstrated that the availability of organic carbon in permafrost soils decreased with increasing HIX. This is in agreement with the present study. It was shown for the permafrost sequence that the HIX increased continuously with depth. This indicates that the organic carbon is less available for microorganisms with depth because of the higher degree of humification. Consequently, at this point, we can summarize that the zone with significant concentrations of methane and activity of methanogenic microorganisms is characterized by the highest concentration of high quality organic carbon.

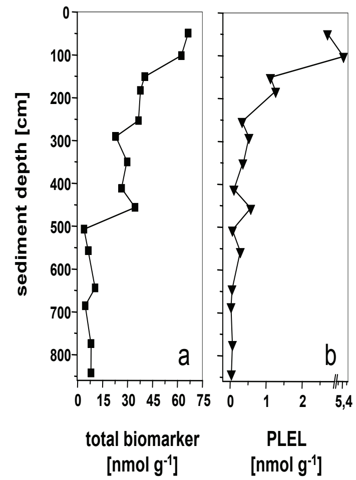

Figure 2. Vertical profiles of total lipid biomarkers (a) and phospholipid ether lipids (PLEL, b) within the Holocene permafrost core.

In contrast to the results of the soil-ecological variables (methane production activity, PLEL biomarker concentration, TOC, HIX), we do not achieve any hint for a possible entrapment process of methane during sedimentation, which was deduced from data of paleoclimate research carried out in the same study area (Andreev et al. 2004, Andreev & Klimanov 2005).

More than 20 percent of the terrestrial Arctic is characterized by ice rich permafrost (Zhang et al. 1999). Large areas, mainly dominated by continuous permafrost, exist in Siberia with thicknesses up to 900 m (Yershov 1998). The present study revealed that considerable parts of these cold habitats are recent sites of methane production, probably catalyzed by specific cold-adapted methanogenic archaea. This increasing reservoir of climate-relevant trace gases becomes of major importance against the background of global warming which could result from a thawing of permafrost area up to 25% until 2100 (Anisimov et al. 1999) and subsequent disposal of the methane reservoirs into the atmosphere. Additionally, the results show that an increase of the permafrost temperature would lead to substantial rise in microbiologically-produced methane in the frozen ground. This would further strengthen the contribution of permafrost to the atmospheric methane budget.

Table 1. Borehole temperature, total organic carbon (TOC), and humification index (HIX, dimensionless) of the Holocene permafrost deposits from Samoylov Island.

Depth [cm]	T [°C]	TOC [%]	HIX
49	-1.9	4.82	3.71
72		2.50	5.74
84		3.64	5.33
102	-4	4.47	6.39
126		4.91	5.47
151		4.01	3.80
179		2.63	5.62
183	-7.4	3.42	6.64
235		n.d.	6.88
254		2.54	5.69
273		1.65	8.13
291		3.11	6.95
307	-9.4	0.87	0.68
323		1.88	6.08
350		2.11	6.83
375		2.49	8.01
389		n.d.	8.07
393	-12.5	n.d.	7.65
412		1.19	6.42
433		1.57	7.06
442		2.46	8.34
456		2.90	n.d.
471		3.00	7.65
485		2.54	8.10
507	-12.8	1.85	n.d.
534		2.27	8.25
557		2.49	8.70
570		2.65	7.80
590	-12.7	2.52	6.65
613		2.39	9.20
626		1.92	8.42
644		1.51	9.10
667		1.85	9.08
686		0.96	9.58
712		0.61	9.23
743		1.25	11.29
774		1.04	8.38
798	-11.5	1.69	9.11
819		1.97	9.46
843		2.56	8.42

n.d. = not detected

Methanogenesis in Submarine Permafrost

Coastal erosion and sea level rise created the shallow shelf of the Laptev Sea whose bottom is formed by the formerly terrestrial permafrost (Rachold et al. 2007). Flooding of the cold (-5 to -15°C) terrestrial permafrost with relatively warm (-0.5 to -2°C) saline sea water changed the system profoundly and resulted in a warming of the permafrost. Therefore, we consider submarine permafrost as a natural laboratory for studying the impact of environmental changes on permafrost habitats.

First results obtained from submarine permafrost deposits of the Laptev Sea shelf revealed methane concentrations of up to 284 nmol CH_4 g^{-1} sediment (Fig. 3a). Highest methane values were found in the layers with the highest amount of organic carbon (up to 9%). Extremely low $\delta^{13}CH_4$ values of -75 ‰ indicated active methanogenesis in this zone (Knoblauch, pers. com.). According to the studies of Rivkina & Gilichinsky (1996), who did not find any significant amounts of methane in Late Pleistocene permafrost sediments, it can be concluded that our findings in submarine permafrost are also a result of recent methanogenesis. This interpretation is supported by first data of DNA-based analyses of methanogenic communities in the sediments, which revealed a higher diversity and abundance of methanogens within the core segment with the highest amount of methane (Fig. 3b).

Conclusions

This work shows, for the first time, that methanogenic archaea do not only survive in permafrost habitats, but also can be metabolicly active under in situ conditions. Due to the sub-0°C experiments and the in situ temperatures of permafrost sediments, we can conclude that the methanogenic community is dominated by psychrotolerant or even psychrophilic microorganisms. Despite this adaptation to cold environments, we show that a slight increase of the temperature can lead to a substantial increase of methanogenic activity. In the event of degradation of terrestrial or submarine permafrost sediments, this would lead to an extensive expansion of the methane deposits with subsequent impacts on total methane emissions. A future in-depth characterization of the metabolism of these cold-adapted methanogens will reveal biotic and abiotic factors which influence the methane production activity of these organisms.

Methane of microbial origin in perennially frozen deposits probably represents an unconsidered source for the global methane budget. Methane release to the atmosphere from frozen ground is mediated by ongoing permafrost degradation through enhanced thermokarst formation and accelerated coastal erosion in the Arctic. Although the change in permafrost conditions by global warming is examined in the framework of several international projects (e.g., ACD: Arctic Coastal Dynamics, CALM: Circumpolar Active Layer Monitoring), these investigations should be linked more closely with microbiological process studies and biodiversity research. Microbial parameters important

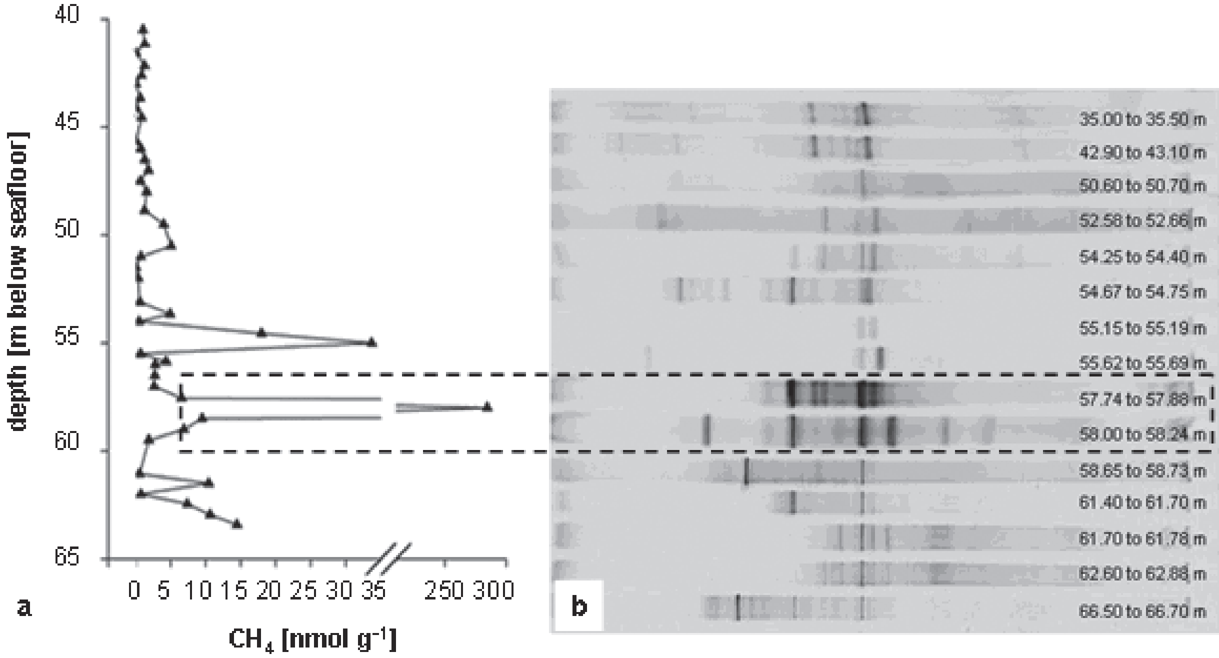

Figure 3. Vertical profiles of methane concentration (a), and DGGE fingerprinting of 16S rRNA genes (b) amplified from the submarine permafrost sediments (between 35.0 and 66.7 m depth).

for the assessment of the carbon turnover (e.g., cell numbers, activities, biodiversity and stability of microbial communities) should be analysed at observation areas in the Arctic, where long-term ongoing monitoring programs are undertaken. The evaluation of microbiological data and their correlation with climatic and geochemical results represents the basis for the understanding of the role of permafrost in the global system, in particular feedback mechanisms related to material fluxes and greenhouse gas emissions in the scope of a warming Earth.

Acknowledgments

The authors wish to thank the Russian-German field parties during the expeditions LENA 2001 and COAST, especially Dimitri V. Melnitschenko (Hydro Base Tiksi), Dimitry Yu. Bolshiyanov (Arctic and Antarctic Research Institute) and Waldemar Schneider (Alfred Wegener Institute for Polar and Marine Research) for their logistic support as well as Volker Rachold (IASC, formerly AWI) and Eva Pfeiffer (University of Hamburg, formerly AWI) for their leadership of the expeditions COAST and LENA 2001, respectively.

References

Andreev, A. & Klimanov, A. 2005. Late-Glacial and Holocene in Chapter 5 East Siberia (based on data obtained mainly in Central Yakutia). *Geological Society of America Bulletin* 382: 98-102.

Andreev, A., Tarasov, P., Schwamborn, G., Ilyashuk, B.P., Ilyashuk, E.A., Bobrov, A.A., Klimanov, V.A., Rachold, V. & Hubberten, H.W. 2004. Holocene paleoenvironmental records from Nikolay Lake, Lena River Delta, Arctic Russia. *Palaeogeography, Palaeoclimatology, Palaeoecology* 209: 197-217.

Anisimov, O.A., Nelson, F.E. & Pavlov, A.V. 1999. Predictive scenarios of permafrost development under conditions of global climate change in the XXI century. *Earth Cryology* 3: 15-25

Bartlett, K.B. & Harriss, R.C. 1993. Review and assessment of methane emissions from wetlands. *Chemosphere* 26: 261-320.

Bergman. I., Klarqvist, M. & Nilsson, M. 2000. Seasonal variation in rates of methane production from peat of various botanical origins: effects of temperature and substrate quality. *FEMS Microbiology Ecology* 33: 181-189.

Cao, M., Gregson, K. & Marshall, S. 1998. Global methane emission from wetlands and its sensivity to climate change. *Atmospheric Environment* 32: 3293-3299.

Colwell, F.S., Nunoura, T., Delwiche, M.E., Boyd, S., Bolton, R., Reed, D.W., Takai, K., Lehman, R.M., Horikoshi, K., Elias, D.A. & Phelps, T.J. 2005. Evidence of minimal methanogenic numbers and activity in sediments collected from the JAPEX/JNOC/GSC et al. Mallik 5L-38 Gas Hydrate Production Research Well. In: S.R. Dallimore & T.S Collett (eds.),Scientific Results from Mallik 2002 Gas Hydrate Production Research Well Program, Mackenzie Delta, Northwest Territories, Geological Survey of Canada, Microbiology section, Canada Bulletin 585: 1-11.

Ganzert, L., Jurgens, G., Münster, U. & Wagner, D. 2006. Biodiversity of methanogenic archaea in permafrost environments of the Laptev Sea coast. FEMS *Microbiology Ecology* 59: 476-488.

Gounot, A.M. 1999. Microbial life in permanently cold soils. In: R. Margesin & F. Schinner (eds.), *Cold-Adapted Organisms*. Berlin: Springer, 3-16.

Harvey, H.R., Fallon, R.D. & Patton, J.S. 1986. The effect of organic matter and oxygen on the degradation of bacterial membrane lipids in marine sediments. *Geochimica et Cosmochimica Acta* 50: 795-804.

Hogg, E.H. 1993. Decay potential of hummock and hollow Sphagnum peats at different depths in a Swedish raised bog. *Oikos* 66: 269-278.

Hubberten, H.W., Wagner, D., Pfeiffer, E.M., Boike, J. & Gukov, A.Yu. (2006) The Russian-German research station Samoylov, Lena Delta – a key site for polar research in the Siberian arctic. *Polarforschung* 73: 111-116.

IPCC 2001. Climate change 2001: The scientific basis. Contribution of the working group I to the third assessment report of the Intergovernmental Panel on Climate Change. J.T. Houghton, Y. Ding, D.J. Griggs, M. Nogner, P.J. van der Linden, X. Dai, K. Maskell & C.A. Johnson. (eds.), Cambridge, New York: Cambridge University Press, 881.

Kotsyurbenko, O.R., Nozhevnikova, A.N. & Zavarzin, G.A. 1993. Methanogenic degradation of organic matter by anaerobic bacteria at low temperature. *Chemosphere* 27: 1745-1761.

Mangelsdorf, K., Haberer, R.M., Zink, K.-G., Dieckmann, V., Wilkes, H. & Horsfield, B. 2005. Molecular indicators for the occurrence of deep microbial communities at the JAPEX/JNOC/GSC et al. Mallik 5L-38 Gas Hydrate Production Research Well. In: S.R. Dallimore & T.S. Collett (eds.) *Scientific Results from Mallik 2002 Gas Hydrate Production Research Well Program, Mackenzie Delta, Northwest Territories,*. Geological Survey of Canada, Microbiology section. Canada Bulletin 585: 18-29.

Melillo, J.M., Steudler, P.A., Aber, J.D., Newkirk, K., Lux, H., Bowles, F.P., Catricala, C., Magill, A., Ahrens, T. & Morrisseau, S. 2002. Soil warming and carbon-cycle feedbacks to the climate system. *Science* 298: 2173-2176.

Pfeiffer, E.M. & Grigoriev, V. (eds.). Russian-German Cooperation System Laptev Sea 2000: The Expedition Lena 2001. *Reports on Polar Research* 426, 186 pp.

Rachold, V., Bolshiyanov, D.Y., Grigoriev, M.N., Hubberten, H.-W., Junker, R., Kunitsky, V.V., Merker, F., Overduin, P. & Schneider, W. 2007. Nearshore arctic subsea permafrost in transition. *EOS* 88: 149-156.

Ringelberg, D.B., Sutton, S. & White, D.C. 1997. Biomass, bioactivity and biodiversity: microbial ecology of the deep subsurface: analysis of ester-linked phospholipid fatty acids. *FEMS Microbiology Reviews* 20: 371-377.

Rivkina, E.M., Friedmann, E.I., McKay, C.P. & Gilichinsky, D. 2000. Metabolic activity of permafrost bacteria below the freezing point. *Applied Environmental Microbiolology* 66: 3230-3233.

Rivkina, E.M. & Gilichinsky, D.A. 1996. Methane as a paleoindicator of the dynamics of permafrost deposits. *Limnology and Mineral Resources* 31: 396-399.

Rivkina, E.M., Gilichinsky, D., Wagener, S., Tiedje, J., Shcherbakova, V. & McGrath, J. 1998. Biochemical activity of anaerobic microorganisms from buried permafrost sediments. *Geomicrobiology* 15: 187-193.

Shi, T., Reevers, R., Gilichinsky, D. & Friedmann, E.I. 1997. Characterization of viable bacteria from Siberian permafrost by 16S rDNA sequencing. *Microbial Ecology* 33: 167-179.

Wagner, D., Kobabe, S., Pfeiffer, E.-M. & Hubberten H.-W. 2003. Microbial controls on methane fluxes from a polygonal tundra of the Lena Delta, Siberia. *Permafrost Periglac. Process.* 14: 173-185.

Wagner, D. 2008 Microbial communities and processes in Arctic permafrost environments. In: P. Dion & C.S. Nautiyal (eds.), *Microbiology of Extreme Soils*. *Soil Biology* 13, Berlin: Springer, 133-154.

Wagner, D., Lipski, A., Embacher, A. & Gattinger, A. 2005. Methane fluxes in extreme permafrost habitats of the Lena Delta: effects of microbial community structure and organic matter quality. *Environmental Microbiology* 7: 1582-1592.

White, D.C., Davis, W.M., Nickels, S., King, J.D. & Bobbie, R.J. 1979. Determination of the sedimentary microbial biomass by extractible lipid phosphate. *Oecologia* 40: 51-62.

Yershov, E.D. 1998. *General geochryology*. Cambridge: Cambridge University Press, 580 pp.

Zelles, L. 1999. Fatty acid patterns of phospholipids and lipopolysaccharides in the characterisation of microbial communities in soil: a review. *Biology and Fertility of Soils* 29: 111-129.

Zhang, T., Barry, R.G., Knowles, K., Hegnibottom, J.A. & Brown, J. 1999. Statistics and characteristics of permafrost and ground-ice distribution in the Northern Hemisphere. *Polar Geography* 2: 132-154.

Zimov, S.A., Schuur, E.A.G. & Chapin III, F.S. 2006. Permafrost and the global carbon budget. *Science* 312: 1612-1613.

Importance of Glacier-Permafrost Interactions in the Preservation of a Proglacial Icing: Fountain Glacier, Bylot Island, Canada

Pablo A. Wainstein
Department of Geography, University of Calgary, Alberta, Canada
Brian J. Moorman
Department of Geography, University of Calgary, Alberta, Canada
Ken Whitehead
Department of Geography, University of Calgary, Alberta, Canada

Abstract

Fountain Glacier is hydrologically unique in the Canadian Arctic for the large perennial icing in its proglacial valley. It is hypothesized that the icing holds information on the glacier hydrology and the role permafrost has on the overall hydrological system. A spring first observed in 1991, down valley from the glacier, is thought to be supplied by pressurized subglacial water. Aerial and geophysical surveys have been used in conjunction with thermal-hydrological modeling to study the spring's stability and longevity of the icing. Results indicate that there is a well established temporal relationship between changes experienced by the glacier and the icing. It is suggested that the relationship between glacier and permafrost, is an unstable equilibrium, where the glacier drives the system out of equilibrium by altering the proglacial hydraulic conditions as it retreats, whereas the growth of permafrost restores the system back to a new hydro-thermal balance.

Keywords: Bylot Island; glacial hydrology; glacier; GPR; icing; naled.

Introduction

A major issue in glacial hydrology is to determine the way water flows in the glacial environment and the interactions it has with the surrounding ground, which are mainly controlled by the local hydrology, geology and topography.

However, in the High Arctic, where the permafrost is continuous, the interaction between the flow of glacial meltwater and the surrounding ground is mainly governed by temperature. Subzero temperature regimes promote the formation of permafrost and cold glacier ice fringes which, frozen to the glacial bed, act as effective water barriers, enabling the storage of pressurized subglacial flow.

Icings and associated features are often observed on proglacial floodplains in the High Arctic. These occur where water, flowing through a network of subglacial and intra-permafrost passages, comes to the surface and freezes in layers. Studies have pointed out that water could mainly come from two sources: (1) subglacial long-term storage; or (2) interconnected supraglacial or marginal ice dammed lakes (Pollard et al. 1999, Hodgkins 2004). It has been commonly accepted that the formation of some icings are related to polythermal glaciers, such as Fountain Glacier on Bylot Island, that have a temperate base, under which water can be stored in a network of interconnected cavities (Pollard et al. 1999, Yde & Knudsen 2005). However recent research by Hodgkins et al. (2004) has presented evidence supporting the existence of icings in front of Scott Turnerbreen Glacier in Svalbard, believed to be a cold based glacier.

Field observations suggest that the icing in front of Fountain Glacier is a perennial feature that partially degenerates throughout the melt season as a result of thermal and hydraulic erosion. However, once the ablation season is over and air temperatures become negative, a delicate hydrostatic and thermal balance enables its regeneration by allowing an uninterrupted liquid water supply throughout the winter.

This paper describes the glacier-permafrost interactions that lead to the preservation of a proglacial icing on Bylot Island, Canada; and proposes that subglacial water storage is responsible for supplying water to the icing through a proglacial talik. Additionally, it is suggested that the slow overall thinning of the proglacial icing is directly related to the retreat and thinning of Fountain Glacier.

Study Area

Bylot Island (Fig. 1a) is located at the eastern margin of the Canadian Arctic, north of Baffin Island, at approx 73°N, 78°W. It is roughly 180 km in length and 100 km in width; with a 4,500 km^2 icefield covering the centre of the island.

Even though the island has been studied by a few authors (e.g., Zoltai et al. 1983, Moorman 1998, 2000a, b, 2003, Irvine-Fynn 2004, Fortier & Allard 2004) it is still considerably unexplored.

Mountain areas are composed mainly of crystalline Canadian Shield bedrock, while the lowlands that receive the flowing glaciers mainly consist of poorly consolidated sandstone and mudstone of Cretaceous-Tertiary age.

The climate of Bylot Island can be considered as an arctic desert. It has a mean annual temperature of -15°C, a mean annual precipitation of 225 mm and the average local snow depth was measured to be less than 80 cm near the terminus of Fountain Glacier (Moorman & Michel 2000a, b,

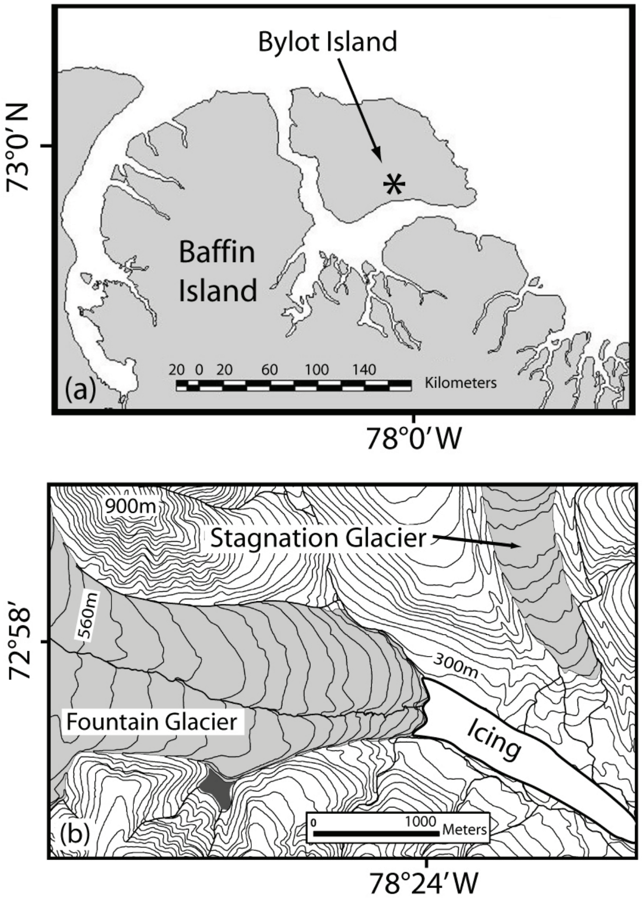

Figure 1. (a) Location of Bylot Island on the northern edge of Baffin Island, Canadian Arctic and (b) topography of the study area in the region of Fountain and Stagnation Glaciers.

Moorman 2003). The island is located in a zone of continuous permafrost (Zoltai et al. 1983) with estimated thicknesses being between 200 and 400 m (Moorman 2003). The coupled action of the strong presence of permafrost and the low precipitation makes the hydrology highly dependent on glacial conditions (i.e., ice melt and dynamics). The island's air and ground temperature regimes directly influence the preservation of hydrologic features in ice, ice cored moraines and proglacial plains. Klassen (1993) and McCuaig (1994) have presented evidence suggesting that Bylot Island has not experienced glacial advances in more than 40,000 years. Its glaciers currently show signs of retreat from their Neoglacial maximum at the end of the Little Ice Age.

Field observations were carried out on the lower ablation zone of Fountain Glacier and the adjacent section of the icing located on its proglacial plains (Fig. 1b).

Methodology

Glacial retreat and thinning

The quantification of the retreat and thinning of Fountain Glacier was obtained through the comparison of the following images and Digital Elevation Models (DEM):

- Aerial photographs obtained in 1958 and 1982 were georeferenced using a second order polynomial, and resampled to a standard pixel size of 5 m.
- A CV580 radar image was acquired over the area of interest in May 1995 by the Canada Centre for Remote Sensing. This image was already terrain-corrected and had a pixel resolution of 5 m.
- A 15 m-resolution orthorectified panchromatic Landsat ETM image was obtained in 2001.

All four images were re-sampled to UTM zone 17X, NAD 83 and given a pixel size of 5 m. Vectors were then drawn representing the position of the glacier snout on each of the four dates.

- A 5 m gridded DEM was generated for the lower part of Fountain Glacier from 20 m contours available as a vector layer from the 1:50,000 Canvec vector coverage, derived from the 1982 photography.
- A second DEM was generated from DGPS positions obtained in the summer of 2007.

The 2007 DEM was then subtracted from the 1982 DEM to establish the amount of thinning which has occurred over the ablation zone of Fountain Glacier over the last 25 years.

Icing thinning

Ground Penetrating Radar (GPR) surveys were carried out on the proglacial icing in front of Fountain Glacier during the summer of 2007. Transverse survey lines were established all over the extent of the icing following a zigzag pattern. Additionally, a longitudinal line was surveyed through the middle section of the icing in order to tie the transverse profiles together.

Survey lines were conducted using a Pulse Ekko Pro GPR System (Sensors and Software) with 200 MHz antennas in parallel broadside configuration. The profiles were acquired in continuous mode using a 400V transmitter and a stacking of 16, which allowed an average step size of 12 cm. A Garmin GPS receiver was connected to the GPR unit allowing the continuous acquisition of positional data while the radar profile was collected. Radar data was then filtered for low frequency signal saturation and enhanced with an Automatic Gain Control (AGC).

A Common Mid Point (CMP) survey was also acquired in order to determine the wave propagation velocity for the icing ice and convert time-based profiles to depth.

The base of the icing was delineated using ReflexW software and a contour map of the icing showing ice thickness was then generated.

Based on GPR surveys conducted in 1993 with a Pulse Ekko IV System (200MHz antennas), Moorman & Michel (2000) produced an ice thickness map of the proglacial icing. Both maps were compared and a contour map was generated showing the changes in ice thickness over the period from 1993 to 2007.

Spring activity and location

The spring activity and location was determined through the comparison of:

- Image extracted from an aerial video shot in 1991.

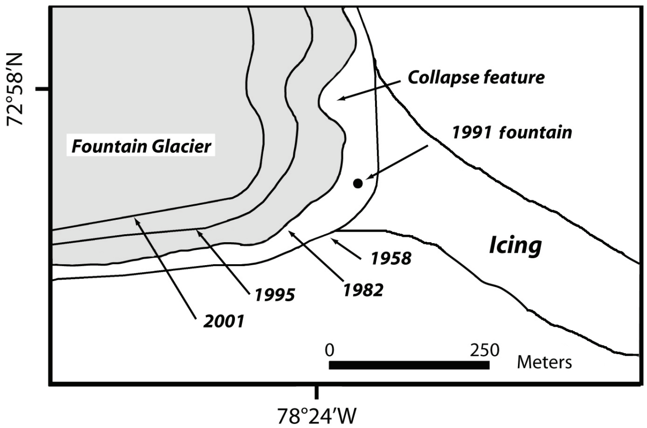

Figure 2. Temporal variation of Fountain Glacier's terminus. The retreat rate has increased considerably since 1982 when a collapse feature on the northern half of the snout was first observed.

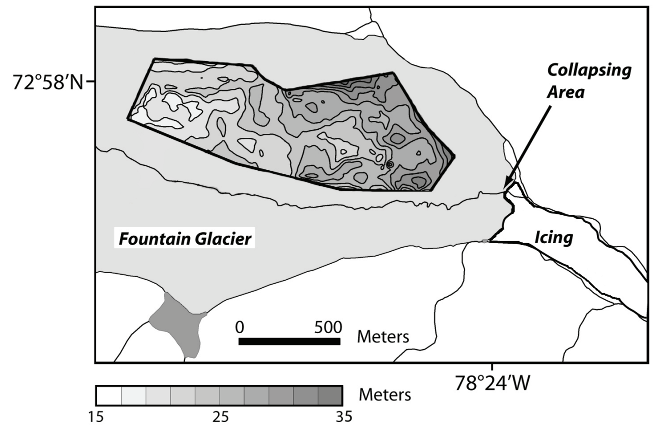

Figure 3. Contour map showing the thinning experienced by Fountain Glacier during the last 25 years (1982–2007). Contour interval is 2 m. The glacier's outline corresponds to its 1982 position.

- Georeferenced aerial photograph acquired in 1982.
- Icing map created by Moorman & Michel (2000) in 1993.
- Field observations conducted in 1991, 1993, 1994, 1995, 1999, 2001, 2003 and 2007.

Glacial Behavior

Fountain Glacier (Fig. 1b) has a total catchment area of 72 km^2 (Walter 2003). The glacier is 16 km long, its elevation ranges from 255 m a.s.l. to 1758 m a.s.l. and its average surface slope is 5.5° (Walter 2003).

The snout of Fountain Glacier terminates in a 20–30 m cliff face overlooking the proglacial plain where the icing is situated. It is flanked by vegetated moraines which tend to be considerably smaller than the ones surrounding neighboring glaciers, such as Stagnation Glacier.

The glacier's surface is generally smooth, with few moulins and crevasses, characteristic of polythermal glaciers subjected to subzero temperature regimes. As such, the superficial hydrology of Fountain Glacier mainly consists of marginal streams and a deeply incised meandering channel in the lower 3 km of the ablation area that discharges a large percentage of the supraglacial meltwater. This deeply cut and strongly meandering supraglacial stream is an indication that some hydraulic features are reoccupied annually (e.g., Moorman & Michel 2000a).

Although the glacier's englacial and subglacial hydrology has not been thoroughly studied, signs of preserved englacial conduits have been observed by Ground Penetrating Radar (GPR) surveys and corroborated with field observations on the glacier's margins. Radar profiles have also shown areas of higher concentration of noise, interpreted as water-rich temperate ice towards the base of the glacier. Although there were no observations of subglacial channels flowing from Fountain Glacier in 2007, continuous water chemistry measurements showed that water turbidity considerably increased towards the end of June, suggesting the beginning of the emergence of subglacial flow.

Even though the proglacial plains are reworked seasonally by meltwater erosion, there are a few signs of high water pressure events. A roughly 5 m-high, water-transported boulder was deposited on the southern side of the proglacial plain between field observations made in 1996 and 1999. These observations support the hypothesis that Fountain Glacier may sporadically exhibit water outbursts as a result of the sudden release of subglacially stored pressurized water. This affects the area's morphology, including the permafrost that surrounds the glacier terminus.

Until recently (since the Little Ice Age) the glacier has not presented marked retreats, slowly losing mass via ice melting and sublimation only during the short ablation summer period. However, this appears to have changed in the last few years. The terminus has shown important signs of activity, retreating about 60 m between 1958 and 1982, giving an average retreat rate of about 2.5 m per year over this period (Fig. 2).

Between 1982 and 1995, it retreated about 80 m, which gives an average retreat rate of about 6 m per year. On average, the retreat rate has more than doubled in speed over a period of 13 years. Between 1995 and 2001 the glacier receded 60 m more at an average rate of 10 m per year. Although imagery is not yet available for 2007, preliminary field observations support the hypothesis that this trend will continue and that the rate of retreat is still increasing.

During the period 1958 and 1982, a collapse feature began to develop in the northern half of the glacier's snout very close to the effluent point of the incised supraglacial stream shown in Figure 1b. Before the collapse, the glacier's snout showed a mild slope ramp, characteristic of undisrupted termini. The collapse feature is clearly shown by a distinct curve in the contour lines representing the glacier's position in 1982. The collapse feature has become more predominant throughout the years, severely increasing the snout's slope.

The long-observed equilibrium of Fountain Glacier has not only been disrupted by recession but also by thinning (Fig. 3).

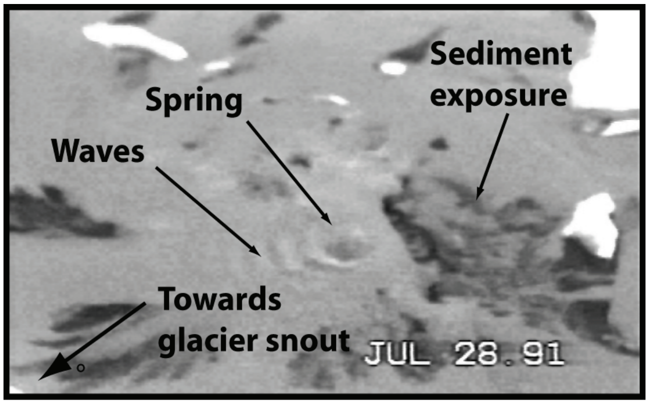

Figure 4. Image extracted from a video shot during a helicopter flight over the proglacial plains of Fountain Glacier in 1991. Note the spring activity shown by the presence of concentric waves on the water surface.

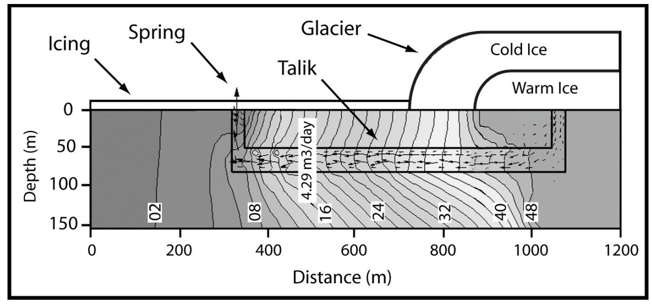

Figure 5. Thermal hydrological modeling of the generation and preservation of the proglacial icing. The model shows a stable liquid water flow through the proglacial talik after 10 years of modeling iterations. The talik is 30 m thick and the spring is located at approximate 300 m from the glacier terminus which is the maximum attainable distance for the talik to be preserved. Contour lines represent hydraulic head with an interval of 2 m.

Although there is insufficient data to determine the thinning rates over the last 50 years, the comparison of the 1982 DEM and field observations collected during 2007 shows that the upper surveyed area had thinned by around 15–20 m, while the section nearest the snout showed the greatest thinning, typically between 25 and 30 m. On average Fountain Glacier appears to have thinned between 0.6 and 1.2 m per year over the last 25 years.

Icing and Spring Activity

Fountain Icing is a proglacial icing located at an elevation of approximately 260 meters above sea level. It presents well developed candle ice and is considerably debris free. The icing extends for over 11 km from the terminus of Fountain Glacier down valley until the margins of Sirmilik Glacier; although aerial photographs show that only the section closest to Fountain Glacier (500 m wide by 1.2 km long) has had perennial ice cover since 1948 (Moorman & Michel 2000b). This last section presents a valley bottom profile characteristic of outwash plains, with some areas emerging through the icing surface. The sub-icing topography varies considerably and is continuously being reworked by water erosion during the melting season.

As in glaciers, field observations show that meltwater tends to concentrate in channels that grow bigger at the expense of smaller ones. As such, the icing has historically presented a main supra-icing channel that drains the majority of the meltwater. Aerial and field photographs show that this channel was located on the north side of the icing until the glacier collapse feature began to develop. Some time before 1999, when the collapse feature was big enough and the glacier's terminus ramp had become steepened, this main drainage channel shifted towards the southern side of the icing. The prevalence of drainage channels on the margins of the icing has promoted a dome shape surface recognized by Moorman & Michel (2000b).

During the fall and winter, when freezing temperatures prevail, the icing is rebuilt. Field observations conducted during early June and late August show that even though the icing is significantly eroded by the end of one melting season, it is totally replenished by the beginning of the subsequent one. By the end of the ablation season, superficial water flow rapidly decreases leaving only groundwater sources as an option for the icing to regenerate.

Fountain Glacier, originally named B26, got its unofficial name from the presence of a fountain, first observed during over flights in 1991(Fig. 4). The spring emerged strongly at a distance of roughly 50 meters from the glacier's terminus, flooding the proglacial plains, which at that time promoted the partial erosion of the icing that covered the proglacial valley.

It is hypothesized that pressurized subglacial storage is responsible for supplying water to the icing through a proglacial talik that connects the glacier to the spring, promoting the regeneration of the icing during the freezing winter. Simplified finite element thermal-hydrological models support the hypothesis that liquid water may indeed flow, even under harsh arctic winter conditions, by means of a proglacial talik, which is preserved unfrozen by the heat produced by pressurized flowing water. Although the model shows that the talik begins a slow freeze-back process after some time, high water pressure episodes such as the one that occurred in 1991 cause a thermal enlargement of the talik (Fig. 5).

Aerial photograph comparison suggests that the icing did not extend all the way to the terminus of the glacier before 1991 (Moorman & Michel 2000) when the spring was first observed. However, field observations conducted in 1993 determined that the area flooded by the spring activity in 1991 had become covered by icing ice, and that an ice blister had developed in the former location of the fountain. Marks of small supra-icing streams radiating out were observed (Fig. 6). The ceasing of the spring activity, the development of the collapse feature on the glacier snout and an increasingly consistent glacial retreat appear to have occurred around the same time. From this time onwards the icing has thinned considerably.

The thinning of the icing allowed the exposure of what is

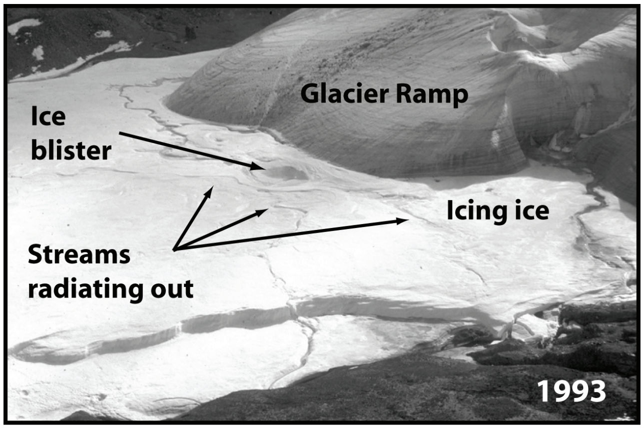

Figure 6. Oblique aerial photograph showing the ice blister adjacent to the terminus of Fountain Glacier. A series of radiating streams have been presumably fed by water flowing from a spring under the blister.

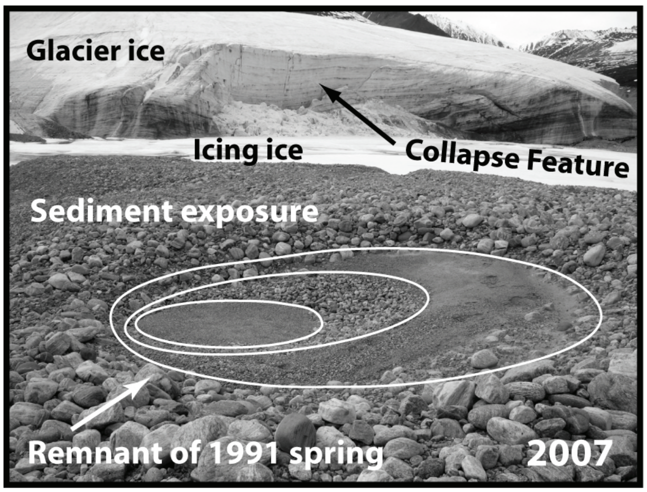

Figure 7. Circular feature embedded in a sediment exposure in front of Fountain Glacier. The feature has been interpreted as the remnants of the spring observed in 1991 which resulted in the icing blister observed in 1993.

inferred to be the remnants of the spring observed in 1991. Figure 7 shows a circular sediment feature embedded in a sediment exposure located in the same area where the spring was observed. In fact, its position taken by GPS closely aligns with the position presented by the map created in 1993 by Moorman & Michel (2000b). The remnant feature consists of three well-sorted sediment rings devoid of fines. Additionally, marks of incipient channels radiating out from the circular feature were observed. As such, based on its location, sediment characteristics and morphology, it has been concluded that the feature is in fact the remnants of the spring observed in 1991.

The subtraction between the ice thicknesses measured by Moorman & Michel (2000b) in 1993 and those obtained in the summer of 2007 reveals a considerable thinning of the icing, by almost 10 m in some areas (Fig. 8). These areas are included within the zones of perennial ice, and as such it is suggested that the icing's thinning is the result of the closure of the spring that once supplied liquid water year

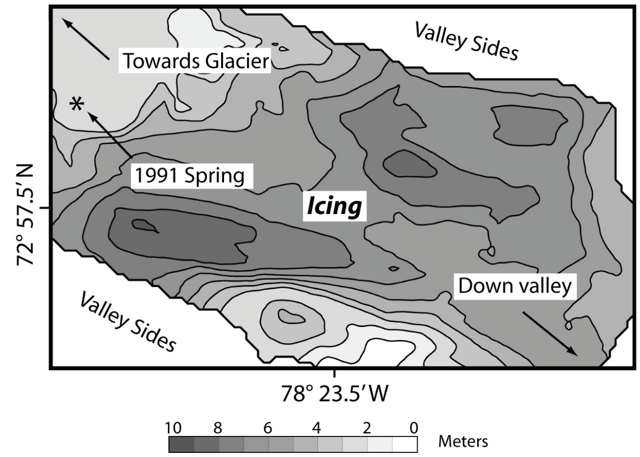

Figure 8. Contour map showing the thinning experienced by the Fountain Glacier Icing during the last 15 years (1993–2007). Contour interval represents 1 m of change in the ice thickness.

round. The total volume lost is 507,075 m^3 over a surveyed area of 94,813 m^2, giving an average thinning of 5.3 m.

It is worth noting that even though the icing has experienced a considerable overall thinning, it is still being rebuilt every winter. This supports the idea that another routing for groundwater has been established, presumably closer to the glacier.

Discussion and Conclusions

The growth and preservation of the Fountain Glacier icing depends on the balance between the glacial system and the surrounding permafrost. Field observations show there is a well established temporal relationship between changes experienced by the glacier and the icing.

The cold impermeable margin of Fountain Glacier results in the year round pressurized storage of liquid water used in the regeneration of the proglacial icing. It was observed that after the collapse of the terminus, the winter spring flow was dramatically reduced, resulting in the thinning of the perennial icing.

The hydrology and dynamics of Fountain Glacier have a considerable effect on the characteristics and response of the proglacial talik responsible for connecting the subglacial environment with the proglacial plain. Figure 9 illustrates a conceptual model that links the reaction of the icing and permafrost systems to the retreat and collapse of Fountain Glacier. It is suggested that the icing is rebuilt by water running through a proglacial talik which needs to remain unfrozen in order to deliver the necessary water year round.

Preliminary results from thermal-hydrological modeling of the proglacial talik suggest that there is a maximum distance between the glacier snout and the point of water expulsion (spring) that can be attained if the talik is to remain unfrozen. The talik is kept unfrozen as a result of a balance between the energy extracted by the subzero air temperature regime and the incoming energy produced by the friction of the pressurized water flow through the sediments (Fig. 5).

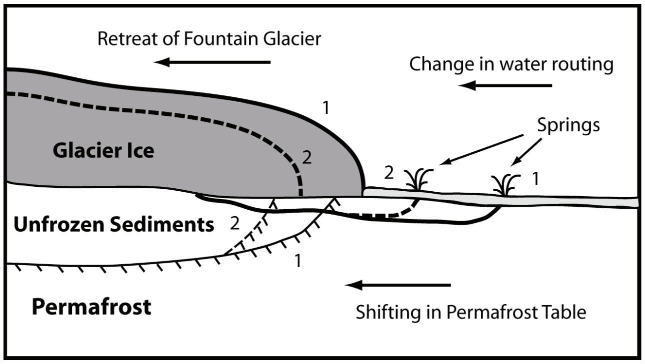

Figure 9. Schematic diagram showing changes in icing and permafrost table as a result of variations in glacial dynamics. (1) Shows the old equilibrium position whereas (2) is the new equilibrium attained.

As such, the retreat and collapse of the glacier terminus exposes a new portion of the proglacial plain to cold air temperatures, altering the talik energy balance, resulting in freeze back and reduction of the spring activity. However, field observations show that the icing is replenished every winter; supporting the hypothesis that a new water routing is readily established as the system attains a new equilibrium position.

It is suggested that the relationship between the two systems, glacier and permafrost, is an unstable equilibrium, where changes in the behavior of either of the two will have considerable effects on the characteristics of the icing. The glacier is considered the dominant factor able to drive the icing out of equilibrium by altering the hydraulic conditions needed to maintain an open talik. Permafrost is the secondary factor that promotes talik freezeback upon the retreat of the glacier, leading to a decrease of water flow through the talik. This hydro-thermal disturbance results in abandonment of the portion of the talik furthest from the glacier terminus. It appears that the closest portion of the talik is preserved, enabling the establishment of a new spring. As such, glacier retreat will promote the up-valley movement of the spring, maintaining a constant distance between the point of water emergence and the glacier snout.

The remotely-sensed data, field observations and finite element modeling demonstrate how the preservation of the icing is a function of the balance between hydrological and thermal regimes that change over a number of time scales. In the short term, seasonal variations in water pressure result from changes in summer temperatures and glacial discharge; that subsequently control the seasonal accretion and erosion of the icing. Over the longer term, glacial retreat and thinning affects the glacier's hydrology and the proglacial subsurface thermal regime. This alters the talik thermal equilibrium at the decadal scale and results in shifts in the spring equilibrium location and discharge.

Finally, steady state thermal disequilibrium (resulting from the gradual talik freezeback) and short high-water pressure events results in intermittent hydrological changes that can affect the icing over the short, medium or long-term.

Acknowledgments

This work was supported by the Natural Sciences and Engineering Research Council of Canada (NSERC) through a research grant held by Dr. Brian Moorman, by the Polar Continental Shelf Project (PCSP), and Alberta Ingenuity.

References

Fortier, D. & Allard, M. 2004. Late Holocene syngenetic ice-wedge polygons development, Bylot Island, Canadian Arctic Archipelago. *Canadian Journal of Earth Sciences* 41: 997-1012.

Hodgkins, R., Tranter, M. & Dowdeswell, J. A. 2004. The characteristics and formation of a High-Arctic proglacial icing. *Geografiska Annaler* 86: 265-275.

Irvine-Fynn, T.D.L. 2004. *A non-invasive investigation of polythermal glacial hydrology: Stagnation Glacier, Bylot Island, Nunavut, Canada*. M.S. Thesis. Calgary: Department of Geography, University of Calgary, 389 pp.

Klassen, R.A. 1993. *Quaternary Geology and Glacial History of Bylot Island, Northwest Territories*. Ottawa, Ontario: Geological Survey of Canada, 93 pp.

McCuaig, S.J. 1994. *Glacial chronology of the South Bylot and Salmon River lowlands, NWT, using erratic dispersal patterns, cosmogenic dating and lichenometry*. M.S. Thesis. Ottawa, Ontario: Carleton University, 140 pp.

Moorman, B.J. 1998. *The development and preservation of tabular massive ground ice in permafrost regions*. Ph.D. Thesis. Ottawa, Ontario: Carleton University, 308 pp.

Moorman, B.J. & Michel, F.A. 2000a. The burial of ice in the proglacial environment on Bylot Island, Arctic Canada. *Permafrost and Periglacial Processes* 11(3): 161-175.

Moorman, B.J. & Michel, F.A. 2000b. Glacial hydrological system characterization using ground-penetrating radar. *Hydrological Processes* 14(15): 2645-2667.

Moorman, B.J., Robinson, S.D. & Burgess, M.M. 2003. Imaging periglacial conditions with ground-penetrating radar. *Permafrost and Periglacial Processes* 14(4): 319-329.

Pollard, W., Omelon, C., Andersen, D. & McKay, C. 1999. Perennial spring occurence in the Expedition Fiord area of western Axel Heiberg Island, Canadian High Arctic. *Canadian Journal of Earth Sciences* 36: 105-120.

Walter, F.S.A. 2003. *Glacier fluctuations and glacier hypsometry on Bylot Island, Nunavut, Canada, using remote sensing methodology*. M.S. Thesis. Calgary: Department of Geography, University of Calgary, 159 pp.

Yde, J.C. & Knudsen, N.T. 2005. Observations of debris-rich naled associated with a major glacier surge event, Disko Island, West Greenland. *Permafrost and Periglacial Processes* 16: 319-325.

Zoltai, S.C., McCormick, K.J. & Scotter, G.W. 1983. *A natural resources survey of Bylot Island and adjacent Baffin Island, Northwest Territories*. Ottawa: Parks Canada, 176 pp.

Isolation and Identification of Cold-Adapted Fungi in the Fox Permafrost Tunnel, Alaska

Mark P. Waldrop
United States Geological Survey, Geologic Division, Menlo Park, CA, USA
Richard White III
United States Geological Survey, Geologic Division, Menlo Park, CA, USA
Thomas A. Douglas
Cold Regions Research and Engineering Laboratory, Fort Wainwright, AK, USA

Abstract

Permafrost microbiology is important for understanding biogeochemical processes, paleoecology, and life in extreme environments. Within the Fox, Alaska, permafrost tunnel, fungi grow on tunnel walls despite below freezing (-3°C) temperatures for the past 15,000 years. We collected fungal mycelia from ice, Pleistocene roots, and frozen loess. We identified the fungi by PCR, amplifying the ITS region of rRNA and searching for related sequences. The fungi within the tunnel were predominantly one genus, *Geomyces,* a cold-adapted fungi, and has likely "contaminated" the permafrost tunnel from outside. We were unable to obtain DNA or fungal isolates from the frozen loess, indicating fungal survival in permafrost soils can be strongly restricted. *Geomyces* can degrade complex carbon compounds, but we are unable to determine whether this is occurring. Results from this study suggest *Geomyces* may be an important colonizer species of other permafrost environments.

Keywords: Fox tunnel; fungi; *Geomyces*; ice wedge; loess; permafrost.

Introduction

The permafrost tunnel near Fox, Alaska, was constructed in the early 1960s to examine mining, tunneling, and construction techniques in permafrost. The tunnel was constructed, and continues to be maintained, by the U.S. Army Cold Regions Research and Engineering Laboratory. The tunnel consists of ice-cemented loess, massive ice, and ice wedges that have been dated from 12 kbp to 40 kbp. The permafrost present in the tunnel is syngenetic with multiple exposures of primary and secondary ice features (Bray et al. 2006, Shur et al. 2004). Fungal growth has been observed on the interior walls. The interior walls, ice wedges, and hanging roots within the tunnel are covered with white fungal mycelia all year. Although the temperature in the permafrost tunnel has remained below freezing (approximately -3°C) for at least the past 15,000 years (Katayama et al. 2007) microbial activity is still present. The tunnel is also very dry and there is no evidence of liquid water. As a consequence, the organisms that grow in the tunnel must be adapted to cold and dry environments.

Observational evidence, such as fungal growth appearing from drilled holes and nails, suggests that the fungal organisms were contaminants brought in from outside the tunnel either from air contamination or on sampling equipment. Fungal growth was observed not only on the loess-rich interior walls, but mycelia often completely carpeted ice wedges. The widespread nature of the fungi throughout the tunnel suggests that it can be transported by air currents. It may also be possible that the fungi occurs on ice surfaces and around drill holes because it is moisture-limited. When a hole is drilled, ice-cemented material is exposed and immediately starts to melt and then sublimate. Therefore, when a hole is drilled, moisture is liberated, and fungal growth at these sites should be possible.

Our research objective was to determine the identity of the fungal organism(s) covering the interior walls and ice wedges of the permafrost tunnel. Understanding their taxonomy could help us understand the microbiology of permafrost environments and determine the range of environmental parameters in which the some fungi can grow. A secondary objective was to determine whether the identified organisms have important characteristics related to biogeochemical processes or human health.

Methods

Soil sampling

To determine the identity of the fungal organisms throughout the permafrost tunnel and on different substrates, five samples were collected from interior walls, hanging roots, and ice wedges. Three samples were taken from the interior walls by scraping the fungus gently with the end of a sterile plastic centrifuge tube. When doing this it was common for loess particles to enter the tube (Figs. 1a, b, d). One sample was taken from an ice wedge in the ceiling in the side corridor (winze) of the tunnel (Fig. 1c). The mycelial "mat" was covering the ice wedge and was easily collected with tweezers and placed in a sterile centrifuge tube (Fig. 1c). The fourth sample was taken from a root hanging from the ceiling of the main adit where the adit and winze separate near the entrance (Fig. 1e). The root was covered in mycelia and the root was broken off with tweezers and placed in a sterile centrifuge tube. The tubes were frozen that same day and later transported to the USGS in Menlo Park for isolation and molecular characterization. We also sampled loess samples from the wall using a serrated metal drill corer (keyhole corer) that had been sterilized using ethanol. In the lab, we further attempted to minimize any potential contamination by scraping of the exterior of the core with sterile razor blades and sampling the interior of the frozen loess core. Carbon and nitrogen concentrations of loess were quantified on oven-dried material (105°C, 48 h) on a Carlo Erba C/N analyzer.

Soil preparation

Soil or fungal flocs were weighed out into 2 ml microcentrifuge tubes (Eppendorf Inc., Westbury, NY) in 0.5 g increments. Under sterile technique, 1.5 ml of DNase/RNase free water (Eppendorf Inc., Westbury, NY) was added to the soil samples or fungal mat. The soil slurry was vortexed for 10 minutes. The slurry was then centrifuged at 10,000 rpm for 1 minute. The supernatant was then serially diluted 10-fold, 100-fold and 1000-fold. These serial dilutions were then plated onto standard potato dextrose agar plates (Difco Inc., Lawrence, KS). As a control the wet soil from the previous step and the dry soil from the original sample were also plated onto potato dextrose agar plates (Difco Inc., Lawrence, KS).

Growth conditions

Plates of each dilution were grown at 0, 4, 20, and 37°C in the dark for 28–31 days. Fungal growth did not occur at 20 or 37°C but did occur at 0 and 4°C. Fungal isolates that appeared on the 4°C plates were isolated onto fresh potato dextrose plates. This step of removing isolates from plates took another 2–3 months of replica plating until there was no difference in isolate morphology. Pure cultures were tested for pH sensitivity at various pHs ranging from 2–8 on potato dextrose agar (Difco Inc., Lawrence, KS) over a period of one month. Growth was only observed at pH 5 and 6.

DNA isolation

Single isolates were removed from agar plates by scraping, placed in liquid nitrogen, and homogenized with a mortar and pestle. DNA was isolated from the homogenized samples following gram-positive bacteria DNA isolation protocol from a Purelink Genomic DNA mini kit (Invitrogen Inc., Carlsbad, CA). There was no fungal protocol with this kit. The isolated DNA was quantified using a standard Picogreen dsDNA assay (Invitrogen Inc., Carlsbad, CA). We also attempted to extract DNA from loess samples in bare (no mycelia) areas using a Powersoil DNA extraction kit (Mo Bio, Inc.), but agarose gel electrophoresis and the picogreen dsDNA assay showed that there was no measurable DNA in the extract. PCR was also tried but was not successful.

PCR conditions

Fungal DNA from isolates was amplified using ITS1-ITS4 primers in a PCR reaction using 0.5 to 1.0 µl of genomic fungal DNA. BSA at a final concentration of 1µg/ml was used to bind to common PCR inhibitors. Thermocycler parameters were an initial melting step 95° (10 minutes one cycle), followed by 40 cycles of 95° (1 minute), 53° (30s), and 72° (1 minute. PCR was concluded with a long extension step of 72° (10 minutes), and then the PCR reactions were placed in the -20°C freezer.

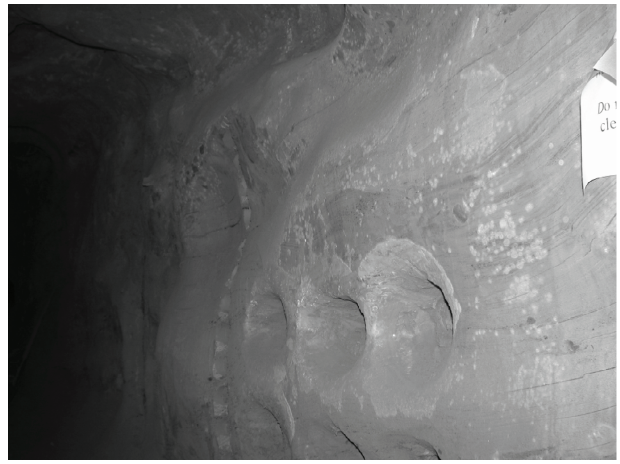

Figure 1a. Fungi on tunnel walls where previous core samples had been taken (sample FG1).

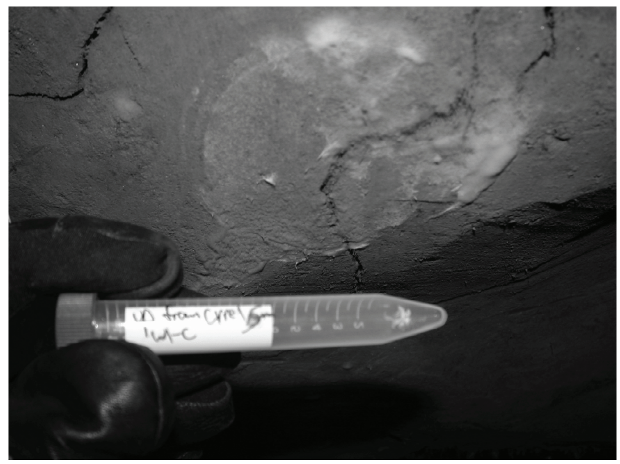

Figure 1b. Sample taken from tunnel ice-cemented loess wall (sample FG2).

Figure1c. Fungal mycelia carpeting ice wedge (sample FG3).

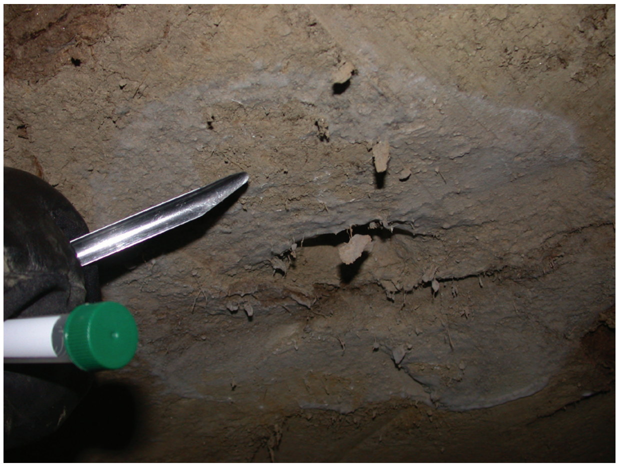

Figure 1d. Fungal mycelia on a loess wall where a previous core had been collected (sample FG5).

Figure 1e. Fungi taken from alder tree root hanging from ceiling (sample FG6)

Sequence analysis

Amplified DNA was sequenced at a commercial lab (MClab, San Mateo, CA), and results were imported into Geneious software (Biomatters Ltd., New Zealand). Sequences were examined for quality and Blast searched on the NCBI database. The three best matches were recorded.

Restriction analysis

Restriction analysis was performed on the PCR products in order to determine if the sequences were of the same or different organisms. PCR products were digested overnight with the enzyme CFO1. BSA was added at a concentration of 10 µg/µl to aid in enzymatic digestion. Digests were then run on a 3% gel for 90 min at 75 volts, with a 100 bp ladder (NEB Inc, Ipswich, MA), and negative controls. The gel was stained in ethydium bromide, rinsed for 20 min, and digitally photographed on a UV light table.

Results and Discussion

White mycelia are present on tunnel walls, ice wedges, and plant roots within the permafrost cave near Fox, Alaska, (Figs. 1a–f). The fungal organisms sampled and isolated from multiple locations within the Fox permafrost tunnel were all of the same genus, *Geomyces*. Two of the organisms were identified as *Geomyces pannorum*, while three other samples were closely associated with *Geomyces* strain FMCC-4 (Table 1). Restriction digests of the PCR products produced different restriction patterns for most of the organisms (Fig. 2). The restriction patterns for sample FG1 and FG2 were the only two samples to be identical to each other. Except for FG1 and FG2, all samples had unique restriction patterns, indicating that they had slightly different DNA sequences. Therefore, although they were all the same genus, they differed at the species or strain level.

The physiology of *Geomyces* is such that it is very well adapted to growth in the cold, dark, and dry conditions of the permafrost tunnel. Fungi are generally well suited for growing in dry habitats due to their hyphal growth form an unique forms of osmoprotection. Additionally, *Geomyces* is one of only a few fungal organisms known for growth below freezing, which would be a necessity for any organism living within this frozen environment (Ozerskaya et al. 2005, Panikov & Sizova 2007). *Geomyces* was not capable of growth at 20°C or above, but grew well, albeit slowly, at 4°C. *Geomyces* is considered to be a psychrotrophic fungi, which is an organism that can grow at 0°C, but its optimum growth rate is above 20°C. (Gilichinsky et al. 2005, Robinson 2001). Our results indicate that our isolates could not grow at 20°C or above, and therefore they should be considered psychrophilic fungi.

Geomyces is a commonly observed fungi in boreal and arctic ecosystems that can survive in permafrost environments due to its ability to grow at cold temperatures, its ability to withstand moisture stress and high salt tolerance (Lydolph et al. 2005, Robinson 2001). *Geomyces* has the ability to break down keratin, a compound contained within hair and nails, as well as cellulose, present in plant tissues (Freiedrich et al.). Because *Geomyces* is a kerinatinolytic fungi, it has been used as an indicator of the presence of ancient megafauna (due to the presence of hair and nails in some permafrost). The use of *Geomyces* as an “indicator species” is supported by this study because of the visible presence of ancient megafauna (generally bones) contained within the Pleistocene loess deposits (Willerslev et al. 2004). Cellulose may also be present in this permafrost environment due to the visible presence of plant roots, although *Geomyces* appeared no more dense on plant roots than on the loess tunnel walls.

Geomyces appeared to be capable of much more extensive growth on ice wedges compared to either roots or ice-cemented loess walls (compare Fig. 1c with others). The growth forms of *Geomyces* differed between the ice wedge and the permafrost tunnel walls. *Geomyces* often formed thin brittle mycelial sheets over the entire surface of the ice wedge that could be easily sampled with a small metal instrument. The ice wedges were dark in color and exhibited elevated DOC dissolved organic carbon concentrations (18.4 to 68.5 ppm; Douglas & Cai, unpublished data) which is probably a strong source of carbon substrate for the fungi.

Table 1. Identification of four fungal isolates taken from the interior of the Fox permafrost tunnel. BLAST results matched with the 18S rRNA gene, partial ITS1, 5.8S rRNA, ITS2, and 28S partial sequence.

Sample	Source	Colony Description	Best Identity	Homology	E score	Accession number
FG1	Loess wall	White to yellow colored, spiked hairy circular arrangement	1. *Geomyces* sp. BC7	94%	4e-156	DQ317337
			2. *Geomyces* sp. LC-03-010	94%	2e-154	DQ402527
			3. *Geomyces pannorum* strain VKM	94%	2e-154	DQ189224
FG2	Loess wall	White, pink to light rust colored powdery small circular arrangement	1. Uncultured fungus clone	86%	3e-70	EF434070
			2. Uncultured fungus clone	86%	3e-70	EF433976
			3. *Geomyces* sp. FMCC-4	86%	3e-70	DQ499474
FG3	Ice wedge	White to gray colored, smooth, hairy, powdery, linearly arranged	1. Uncultured fungus clone	97%	0.0	EF434070
			2. Uncultured fungus clone	97%	0.0	EF433976
			3. *Geomyces* sp. FMCC-4	97%	0.0	DQ499474
FG5	Loess wall	White, smooth colonies, powdery, linearly arranged	1. *Geomyces pannorum* strain 857	99%	0.0	DQ189229
			2. *Geomyces pannorum* strain 2236	99%	0.0	DQ189228
			3. *Geomyces pannorum* strain VKM	98%	0.0	DQ189224
FG6	Plant root	White, smooth colonies, powdery, linearly arranged	1. *Geomyces pannorum* strain VKM	94%	0.0	DQ189229
			2. *Geomyces pannorum* strain VKM	94%	0.0	DQ189228
			3. *Geomyces* sp. BC-7	94%	0.0	DQ317337

On ice-cemented loess walls, *Geomyces* tended to have a spotty distribution. Growth was generally circular emanating from previously sampled areas, and the mycelia could not be easily sampled without breaking off loess particles from the walls. The growth of *Geomyces* on loess walls tended to be associated with disturbance or points of contamination, where people would, for example, place nonsterile sampling instruments on their surface. The loess walls had carbon and nitrogen concentrations of 2.75% and 0.25%, respectively, and had moisture contents ranging from 18 to 55%. Root samples were not examined for nutrient content, but organic tissues can generally range from 40 to 50% carbon and 1 to 5% N. Therefore, these substrates had enough C and N for microbial growth.

Surprisingly, no other genus of organism except *Geomyces* was isolated from the tunnel. It is possible that given our growth conditions for isolation, we selected for this organism, although we attempted isolation at multiple pH and temperature ranges. This does not preclude other organisms from being present in the tunnel, but it is a strong indication that all of the organisms visible within the tunnel are *Geomyces*. Restriction analysis showed that we isolated several species or strains of *Geomyces*. Although all of our isolates were of the same genus, restriction analysis showed that there were slight differences in their ITS or ribosomal sequences (Fig. 2). It is likely the fact that the isolated *Geomyces* fungi is common in boreal soils, can grow well at cold temperatures, and can be easily dispersed in air that allows it to be the dominant (or only) fungal organism visibly present on the walls of the permafrost tunnel.

We also attempted to isolate DNA from the ice-cemented loess walls in order to compare the fungal DNA present within the loess to the isolates. However, we were either unsuccessful at extracting DNA or the concentration of DNA within the ice-cemented loess walls was so low that we could not measure it, even using sensitive fluorometric techniques. We have been successful at extracting DNA from surface permafrost loess samples (1 m below the soil surface in boreal forests), which leads us to conclude that DNA concentrations within the tunnel loess walls were so low as to be unquantifiable. Our inability to extract DNA from loess in the Fox tunnel may have been due to the fact that few organisms survive frozen conditions for long periods of time (Panikov & Sizova 2007), and DNA quality in frozen soils is reduced over millennia (Willerslev et al. 2004).

We suspect that *Geomyces* in the Fox tunnel is a contaminant from outside the tunnel, rather than an organism that was present in the extant permafrost that has begun to grow on disturbed tunnel walls. *Geomyces* is a common soil organism associated with black spruce (Filion et al. 2004) and therefore is probably very prevalent in the surrounding environment. *Geomyces* growth is observed primarily around sampling holes, metal nails, and areas where the soil has been disturbed by human activity. This could have been caused by using nonsterile tools during sampling. Alternatively, small amounts of soil moisture that are released upon sampling the frozen walls (heat produced by friction between sampling equipment and wall) would permit water-limited fungi to grow rapidly in disturbed areas. The door to the Fox permafrost tunnel is often open and there is good air circulation through the tunnel. Therefore, it would be possible for organisms to contaminate the tunnel from outside.

There are some minor human health aspects to consider with regard to *Geomyces*. It is considered an indoor mold that reduces the air quality within some buildings. It is also found

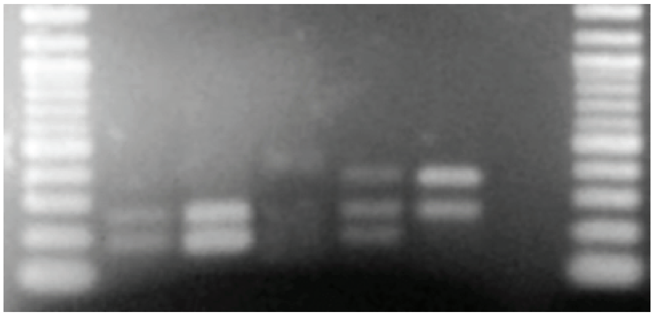

Figure 2. Restriction analysis of PCR products of the four isolates. Lanes 1 and 8 are 100 bp ladders. From left to right the samples in each lane are FG1, FG2, FG3, FG5, FG6, and a negative control.

in household dust, damp walls, and archived paper such as in libraries. It is not considered dangerous. However, one variety of *Geomyces, Geomyces pannorum var pannorum* is suspected in creating slight skin and nail infections (Bloom et al. 2007).

Cold-adapted fungi and biogeochemical cycling

Carbon and nitrogen cycling within thawed permafrost soils is an important area of global change research (Zimov et al. 2006). This study highlights two factors that make permafrost environments unique microbiologically which, in turn, are important for biogeochemical cycling.

First, results from the permafrost tunnel and permafrost studies at the ground surface indicate that fungal abundance in permafrost soils is very low (Gilichinsky et al. 2005, Waldrop et al., unpubl.). Microbial diversity in permafrost soil is also likely to be restricted because fewer organisms are able to withstand frozen temperatures for long periods of time. Therefore, as permafrost soils thaw, what will be the fungal organisms that enter into this new biological niche? Likely it will be cold-adapted organisms not unlike *Geomyces* in this study. Therefore, the study of cold-adapted fungi in C and N cycling is an important area of future research.

Secondly, the temperature response of microbial activity in cold permafrost environments with low fungal diversity may have to be carefully evaluated. Normally, microbial activity increases with temperature, but cold-adapted fungi, such as *Geomyces*, may have faster growth rates and enzyme activities at low temperatures than at higher temperatures (Robinson 2001). An area of further study will be to determine the fungal organisms that act as primary colonizers of permafrost soils as they thaw. Could low microbial diversity in permafrost soils affect the efficiency or rate of biogeochemical processes as permafrost soils thaw? Given that soil microorganisms mediate biogeochemical cycles and the lack of data on permafrost microbiology, there is certainly a strong research need in this area.

Acknowledgments

I would like to acknowledge the U.S. Army Cold Regions Research and Engineering Laboratory for sampling assistance.

References

Bloom, E., Bal, K., Nyman, E., Must, A. & Larsson, L. 2007. Mass spectrometry-based strategy for direct detection and quantification of some mycotoxins produced by *stachybotrys* and *aspergillus spp.* in indoor environments. *Applied and Environmental Microbiology* 73: 4211-4217.

Bray, M.T., French, H.M. & Shur, Y. 2006. Further cryostratigraphic observations in the CRREL permafrost tunnel, Fox, Alaska. *Permafrost and Periglacial Processes* 17: 233-243.

Filion, M., Hamelin, R.C., Bernier, L. & St-Arnaud, M. 2004. Molecular profiling of rhizosphere microbial communities associated with healthy and diseased black spruce (*picea mariana*) seedlings grown in a nursery. *Applied and Environmental Microbiology* 70: 3541-3551.

Gilichinsky, D., Rivkina, E., Bakermans, C., Shcherbakova, V., Petrovskaya, L., Ozerskaya, S., Ivanushkina, N., Kochkina, G., Laurinavichuis, K., Pecheritsina, S., Fattakhova, R. & Tiedje, J.M. 2005. Biodiversity of cryopegs in permafrost. *FEMS microbiology ecology* 53: 117-128.

Katayama, T., Tanaka, M., Moriizumi, J., Nakamura, T., Brouchkov, A., Douglas, T.A., Fukuda, M., Tomita, F. & Asano, K. 2007. Phylogenetic analysis of bacteria preserved in a permafrost ice wedge for 25,000 years. *Applied and Environmental Microbiology* 73: 2360-2363.

Lydolph, M.C., Jacobsen, J., Arctander, P., Gilbert, M.T.P., Gilichinsky, D.A., Hansen, A.J., Willerslev, E., & Lange, L. 2005. Beringian paleoecology inferred from permafrost-preserved fungal DNA. *Applied and Environmental Microbiology* 71: 1012-1017.

Ozerskaya, S.M., Ivanushkina, N.E., Kochkina, G.A., Fattakhova, R.N. & Gilichinsky, D.A. 2005. Mycelial fungi in cryopegs. *International Journal of Astrobiology* 3: 327-331.

Panikov, N.S. & Sizova, M.V. 2007. Growth kinetics of microorganisms isolated from Alaskan soil and permafrost in solid media frozen down to -35 degrees C. *FEMS Microbiology Ecology* 59: 500-512.

Robinson, C.H. 2001. Cold adaptation in arctic and antarctic fungi. *New Phytologist* 151: 341-353.

Shur, Y., French, H.M., Bray, M.T. & Anderson, D.A. 2004. Syngenetic permafrost growth: Crystallographic observations from the CRREL tunnel near Fairbanks, Alaska.. *Permafrost and Periglacial Processes* 15: 339-347.

Willerslev, E., Hansen, A.J. & Poinar, H.N.. 2004. Isolation of nucleic acids and cultures from fossil ice and permafrost. *Trends in Ecology & Evolution* 19: 141-147.

Zimov, S.A., Schuur, E.A.G. & Chapin, F.S. 2006. Permafrost and the global carbon budget. *Science* 312: 1612-1613.

A Web-Based Arctic Geobotanical Atlas and a New Hierarchy of Maps of the Toolik Lake Region, Alaska

D.A. Walker, H.A. Maier, and E.M. Barbour
Alaska Geobotany Center, Institute of Arctic Biology, University of Alaska Fairbanks, AK 99775, USA

Abstract

Accurate maps of arctic terrain at multiple scales are needed for spatial analyses, modeling and monitoring of permafrost responses to a changing climate. A new *Arctic Geobotanical Atlas* (AGA) is a web-based multi-scale (plant-to-planet) collection of geobotanical maps and supporting data. A new set of geobotanical maps focuses on the area around the University of Alaska's Toolik Lake Research Field Station in the vicinity of Toolik Lake Alaska, and includes the Upper Kuparuk River region (published at 1:63,360 scale), the Toolik Lake area (published at 1:20,000 scale), and a map of a 1.2-km^2 intensive research grid on the south side of the Toolik Lake (published at 1:5000 scale). We present an overview of the AGA and descriptions of the new maps and mapping methods.

Keywords: GIS; geomorphology; NDVI; remote-sensing; tundra; vegetation.

Introduction

Vegetation distribution is a key variable for predicting the thickness of the active layer and other properties related to permafrost. Most importantly the vegetation mat acts as an insulating blanket above the mineral soil and prevents deep heat penetration in the summer (Walker et al. 2003). Vegetation maps of CALM grids are being used for modeling active layer depths at local scales within 1-km areas (Nelson et al. 1998), and a vegetation map of the entire Kuparuk River basin was used to model regional scale patterns of active layer depth (Nelson et al. 1997, Hinzman et al. 1998). The vegetation is also strongly related to snow distribution (Evans et al. 1989), another variable that strongly influences permafrost temperatures (Zhang et al. 1997). Maps of vegetation at several scales would be highly useful for monitoring and modeling active layer and permafrost temperatures at site and regional scales.

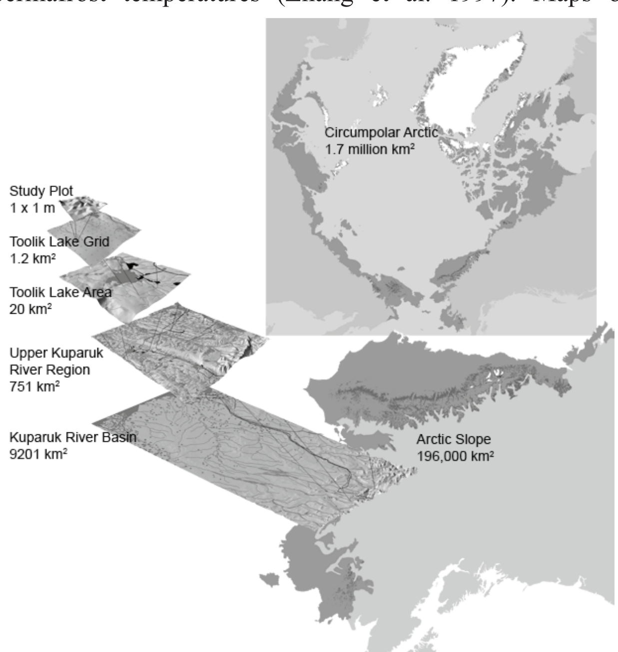

Figure 1. Hierarchy of digital elevation models for the Toolik Lake region in the AGA. Geobotanical maps of the upper Kuparuk River, Toolik Lake area, and Toolik Lake grid are presented in this paper.

The Arctic Geobotanical Atlas

The Arctic Geobotanical Atlas (AGA) is a web-based archive of geobotanical maps that is being developed to aid such studies and other studies that require detail spatial information of the vegetation and other geobotanical information at several scales. The term "geobotany" refers to the science of the relationship of plants to the Earth (Rübel 1927).

The AGA contains a hierarchy of maps and supporting data at seven scales ranging from 1:10 scale (1 m^2 plots) of local areas near Toolik Lake and Imnavait Creek, Alaska to 1:7,500,000 scale for the entire Arctic (Fig. 1). Diverse geobotanical themes include vegetation, geology, topography, landforms, lake cover, and surficial geomorphology. Students and researchers can view thematic maps and download the data by several methods including a map server and SwathViewer software developed at the Geographic Information Network of Alaska (GINA), or they can explore the Arctic using Google Earth. They can also view and print out pdf versions of the original published maps. The map legends are linked to extended descriptions and photographs of the map units.

Other features of the AGA include: (1) an *image library* with photos of the various map units and plant species mentioned in the atlas; (2) a *map catalog* whereby users can select maps according to region of interest, scale of interest, theme or topic of interest, or year of interest; (3) a *glossary* with links to scientific terms used in the atlas; (4) a *bibliography* linked to pdf versions of the references; and (5) a *supporting data* section with links to the original plot-level vegetation and soils data used to describe the map units. The AGA currently includes maps and data from the following projects:

Circumpolar Arctic Vegetation Map (CAVM)

The CAVM covers the global region north of the arctic treeline. It contains maps and descriptions of the vegetation, bioclimate subzones, floristic provinces, topography, landscapes, lake cover, substrate pH, and plant biomass. This section also contains an area analysis of the map by bioclimate subzones and countries (CAVM Team 2003, Walker et al. 2005).

Alaska Arctic Tundra Vegetation Map (AATVM)

The AATVM is a plant community-level map of Arctic Alaska derived from the CAVM. It portrays the dominant plant communities across all of Arctic Alaska, in contrast to the physiognomic-level mapping of the CAVM (Raynolds et al. 2006).

Toolik Lake/upper Kuparuk River basin hierarchy of maps

The Toolik Lake Field Station is a flagship US Arctic Observatory. The upper Kuparuk River basin is a key region for terrestrial arctic research associated with the station. Numerous maps have been prepared to support the research in the area, including that of the Arctic Long-Term Ecological Research (LTER) program and the Department of Energy's R4D studies at Imnavait Creek (Reynolds & Tenhunen 1996). Several maps in the region have been published previously, including geobotanical maps of the Imnavait Creek study areas (Walker & Walker 1996), a Landsat-derived vegetation map of the entire Kuparuk River watershed (Muller et al. 1998) and a Star3i digitial elevation model of the entire Kuparuk River watershed (Nolan 2003). Here we present the maps of upper Kuparuk River region, the Toolik Lake area, and the Toolik Lake research grid (see Fig. 1).

New Maps of the Toolik Lake Area

A new set of geobotanical maps of three areas in the vicinity of the Toolik Lake Research Station have been added to the AGA. A portion of the maps will also be published as a map sheet in the Biological Papers of the University of Alaska (Walker & Maier 2008 in review). The new maps include the Upper Kuparuk River region (Fig. 2, 3) (published at 1:63,360 scale), a map of the 20 km^2 area surrounding Toolik Lake (Fig. 4) (published at 1:20,000 scale), and a map of a 1.2-km^2 intensive research grid on the south side of the Toolik Lake (Fig. 5) (published at 1:5000 scale).

Maps of the upper Kuparuk River region

The 751-km^2 upper Kuparuk River region has terrain typical of the southern Foothills of the Brooks Range, including landscapes affected by three major glacial events

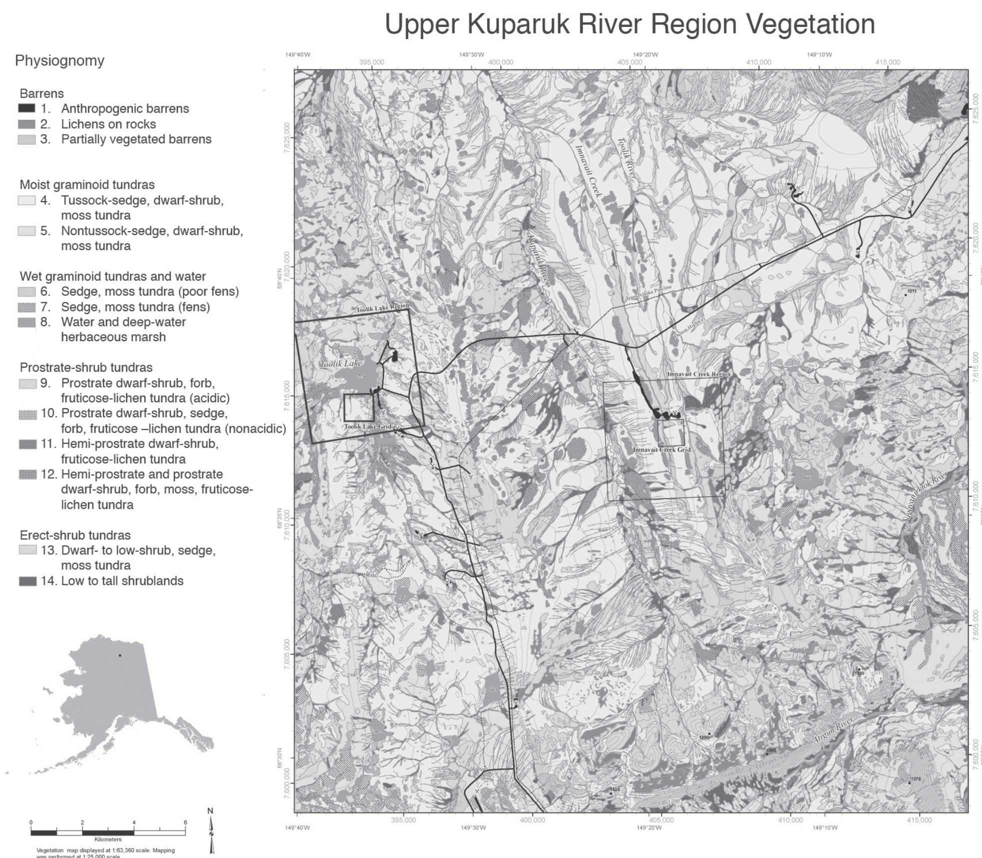

Figure 2. Vegetation of the upper Kuparuk River region. The color version of the map published at 1:63,360 scale has an expanded legend that includes dominant plant communities with GIS codes, typical microsites where each vegetation map unit is found, and area summaries for each map unit (Walker and Maier 2008). A color version also can be found at http://www.arcticatlas.org/. The black rectangles on the vegetation map delineate the boundaries of the Toolik Lake Area, and Toolik Lake Grid (Figs. 4, 5). The location of the mapped area is shown at actual scale as the small black rectangle on the inset map of Alaska.

(Hamilton 2003). The region includes the Toolik Lake and the Imanvait Creek research areas and a stretch of the Dalton Highway and Trans-Alaska Pipeline from the Galbraith Lake airstrip to Slope Mountain. A black and white rendition of the vegetation map of this region is shown in Figure 2.

The vegetation portrayed on the map is derived from a geobotanical database of the region. The base map for the geobotanical map was a 1:25,000-scale black-and-white orthophoto-topographic map that was prepared especially for the mapping project by Vexcel Corp., Denver, CO, in 1994 from stereo pairs of 1:60,000-scale 9 x 9-inch color-infrared aerial photographs that were obtained by NASA in 1982. The base map was prepared without ground-control points, but was registered as closely as possible to the 1:63,360 USGS map of the region. Vegetation and other geobotanical features were mapped by photo-interpretation onto 1:25,000-scale enlargements of the 1982 NASA aerial photographs.

No formal accuracy assessment was performed, but 320 of the map polygons representing 3.2% of the total map polygons, and about 16% of the total map area were checked on the ground during helicopter-assisted transects in 1994.

Geobotanical variables coded for each map polygon included: primary vegetation, secondary vegetation, tertiary vegetation, landform, surface deposit, primary surficial geomorphology, and secondary surficial geomorphology. (Secondary and tertiary types are subdominant types that cover more than 30% of a map polygon.) The geobotanical map was made using methods and legends specially developed for northern Alaska (Walker et al. 1980, 1986, 1989). The geographic information system (GIS) was developed using Arc/Info software and followed the integrated terrain-unit mapping approach (Dangermond & Harnden 1990). The resulting geobotanical maps were presented at conferences in 1996 (e.g., Walker & Walker 1996), but remained unpublished until now. In 2007 the map boundaries were modified to register with a recent digital elevation model (DEM) of the Kuparuk River region (Nolan 2003) and a 1989 SPOT image of the region. The legends were also modified to better fit the hierarchy of maps in the *Arctic Geobotanical Atlas*.

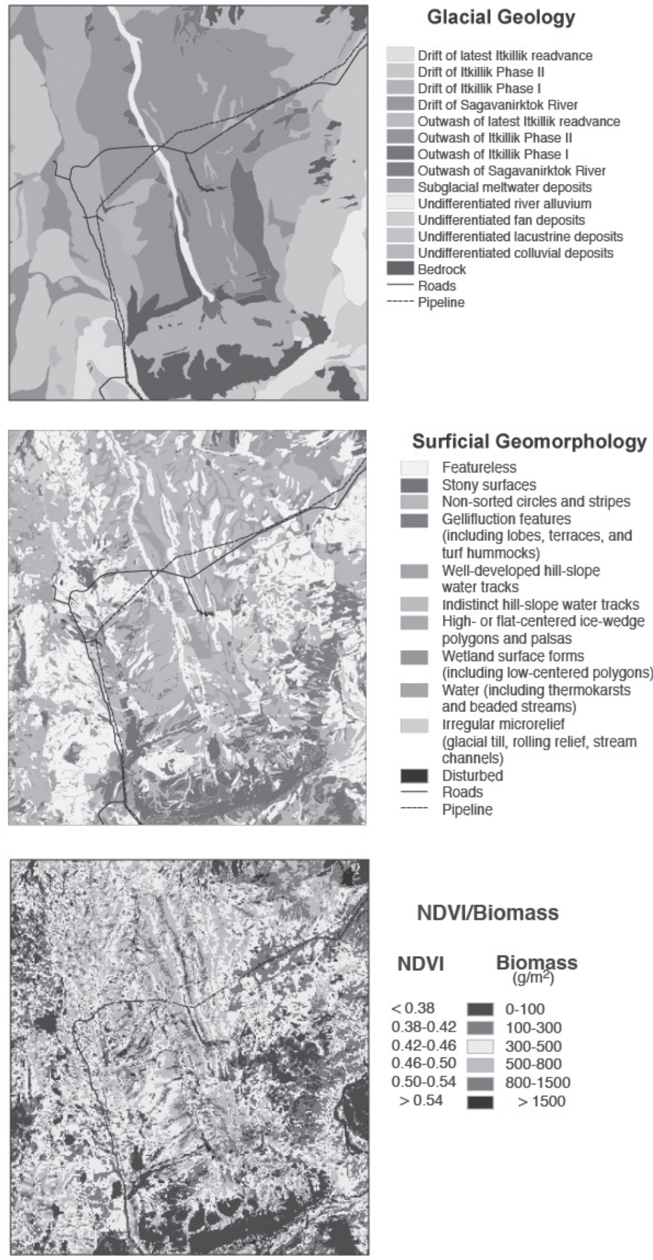

Figure 3. Glacial geology (derived from Hamilton 2003), surficial geomorphology, and NDVI/biomass (derived from Shippert et al. 1995) maps of the upper Kuparuk River region. Color versions can be found at http://www.arcticatlas.org/.

The vegetation of the region was studied and mapped as part of the Arctic Long-Term Ecological Research (LTER) project at Toolik Lake (Walker et al. 1994, Walker & Walker 1996), and the Department of Energy R4D (Response, Resistance, Resilience and Recovery of vegetation from Disturbance) project at Imnavait Creek (Walker & Walker 1996).

Fifty-seven plant communities and land-cover types were recognized during the mapping of the upper Kuparuk River region and are designated by the numeric GIS codes that are included in the expanded legend (not shown here). These were grouped into the 14 physiognomic map units shown on the map, which are compatible with the Circumpolar Arctic Vegetation Map (CAVM Team et al. 2003) and the Alaska Arctic Tundra Vegetation Map (Raynolds et al. 2006). Photos and explanations of the geobotanical mapping units and the supporting field data and metadata can be found on the AGA web site http://www.arcticatlas.org/.

The other maps on the front side of the published map sheet include a false color-infrared satellite image derived from the French SPOT (Système Probatoire d'Observation de la Terre) satellite (not shown), glacial geology (Hamilton 2003), surficial geomorphology, and a map of greenness and biomass as portrayed by the Normalized Difference Vegetation Index (NDVI) (Shippert et al. 1995) (Fig. 3), all published at 1:226,576 scale.

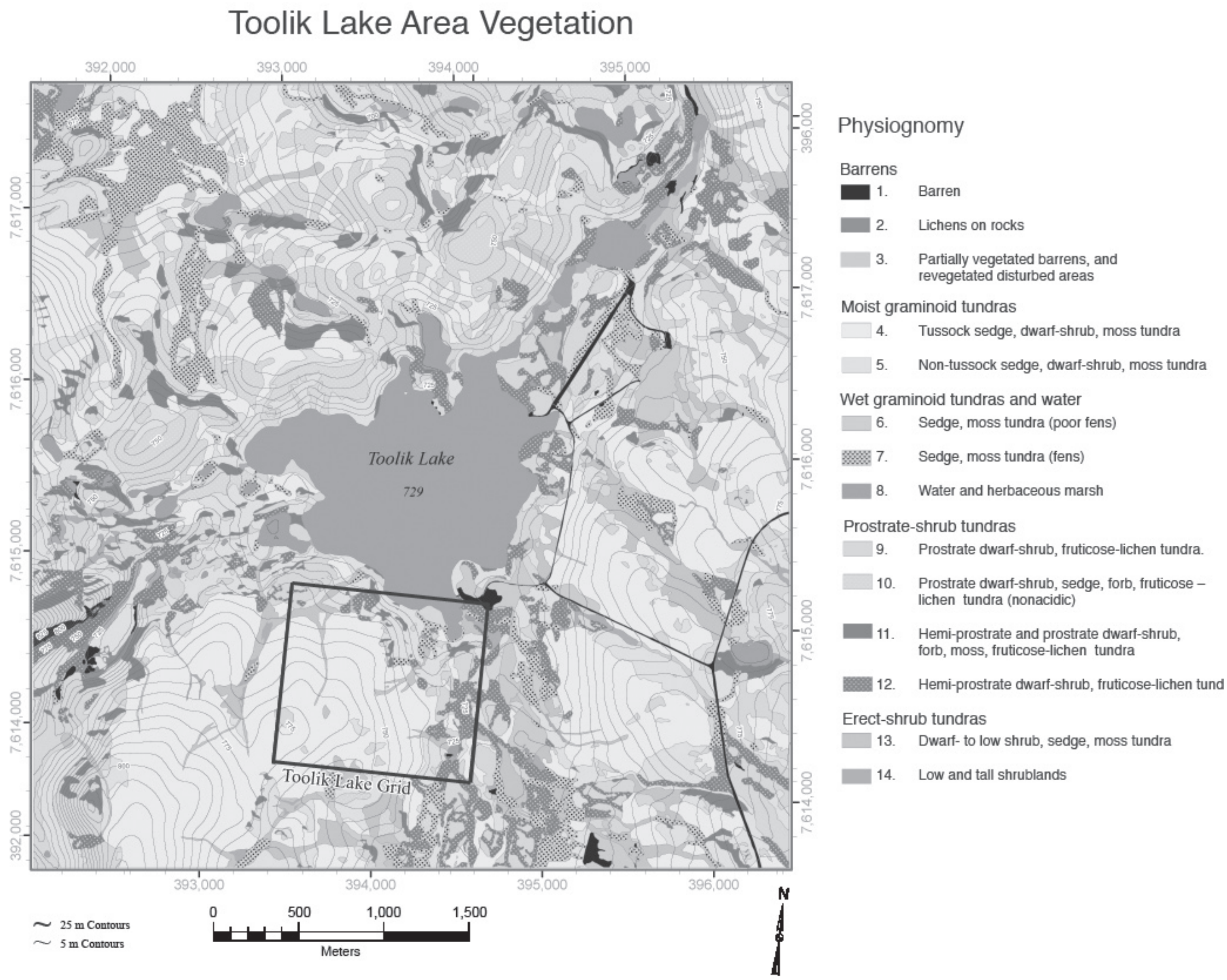

Figure 4. Vegetation map of the Toolik Lake region. The black rectangle delineates the boundary of the Toolik Lake Grid (Fig. 5). A color version can be found at http://www.arcticatlas.org/.

Maps of the Toolik Lake area and grid

The reverse side of the published map sheet shows more detailed vegetation maps of the 20 km^2 area centered on Toolik Lake (Fig. 4) and a 1.2 km^2 intensive research grid on the south side of Toolik Lake (Fig. 5). The Toolik Lake map includes terrain that stretches from the Dalton Highway on the east side of Toolik Lake to Jade Mountain on the west. It includes the Toolik Lake Field Station, the old pipeline construction camp pad and airstrip on the northeast side of the lake, and the primary terrestrial research areas on the south, west, and east side of the lake, as well as several smaller research lakes in the immediate vicinity of Toolik Lake. The area contains surfaces that were glaciated during the Late Pleistocene during the Itillik I and Itillik II glaciations.

The vegetation legend for the Toolik Lake area (Fig. 4) is essentially the same as for the map of the Upper Kuparuk River region but the map shows more detail corresponding to the variations in terrain. Fifty-one landcover and vegetation types were recognized in the field and later grouped into the 14 physiognomic units on the map. The units portray the physiogonomy (dominant plant growth forms) of the major plant communities in each mapped polygon.

The map of the Toolik Lake Grid (Fig. 5) focuses on the 1.1 km^2 research grid on the south side of Toolik Lake. This area is one of the principal intensive research areas at the Toolik Lake Field Station. It includes many experimental research sites where long-term measurements are being made, such as snow-fence study sites and greenhouse experimental sites. The grid was constructed in 1989 to provide geographic referencing for the experimental plots and to provide a sampling scheme for periodic measurements of snow, active layer, and the plant communities.

Sixty-five plant communities were recognized in the field and were then grouped into the 25 units appearing on the map. The vegetation units are primarily at the plant-community level (compared to the physiogonomic level for the maps of the Upper Kuparuk River Region and the Toolik Lake region).

Details of the methods for both maps, including sources for aerial photos, orthophoto topographic map, and the other geobotanical variables that were mapped are in the Arctic Geobotanical Atlas http://www.arcticatlas.org/.

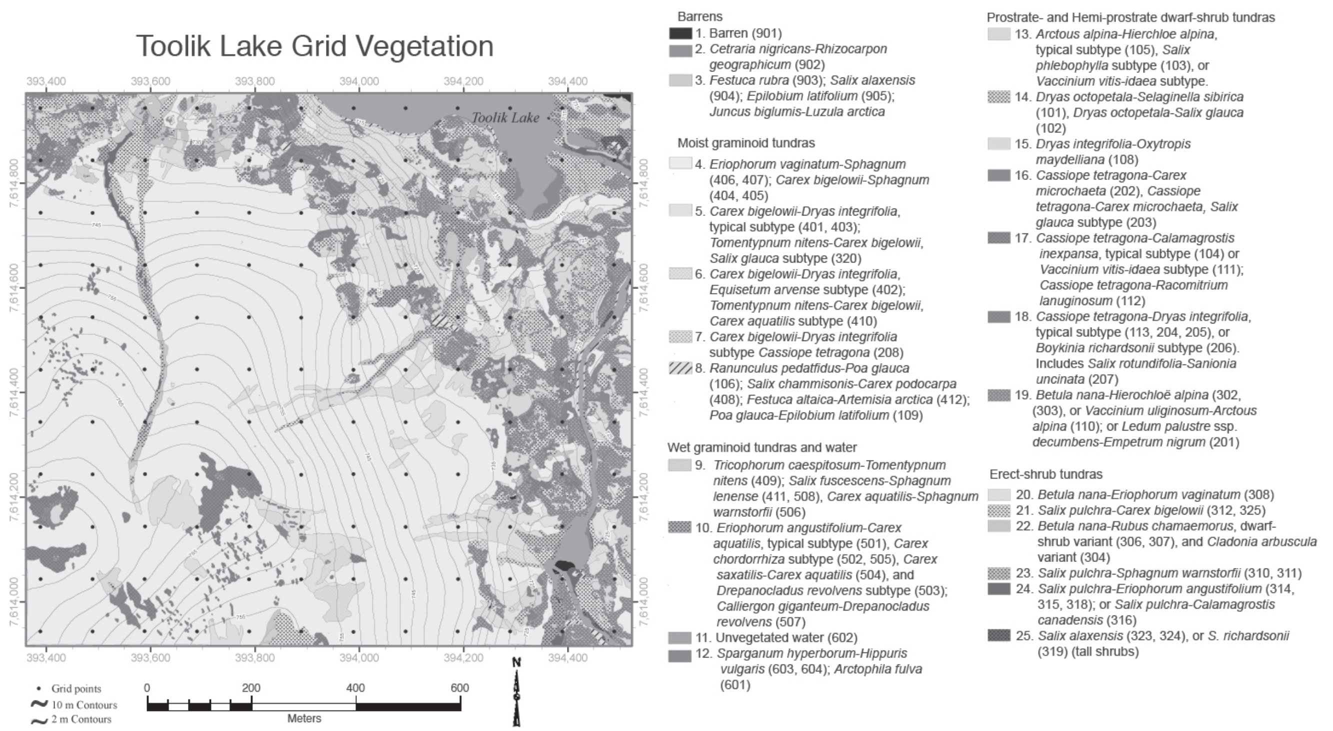

Figure 5. Vegetation map of the Toolik Lake grid. The grid points are spaced at 100-m intervals. A color version can be found at http://www.arcticatlas.org/. The grid is also a component of the Circumpolar Active Layer Monitoring (CALM) program (Brown et al. 2000).

Conclusion

The maps presented here lend themselves well to permafrost-related studies because of the long history of permafrost and active-layer studies in the Toolik Lake region (e.g., Osterkamp 2003, Raynolds et al. 2008 in press, Romanovsky et al. 2008, Walker et al. 2003, 2008 in press) and the clear need to conduct such studies in areas with detailed maps of vegetation, topography, and other terrain information at a variety of scales. Maps at similar scales to those presented here have been extensively for active layer studies and modeling in northern Alaska (Nelson et al. 1997, 1998, Hinzman et al. 1998). The hierarchic nature of the map legends allows results of plot-level studies conducted at Toolik Lake to be extrapolated to much broader regions up to and including the circumpolar tundra region.

Acknowledgments

The maps and website were developed at the Alaska Geobotany Center in the Institute of Arctic Biology and in collaboration with other groups at the University of Alaska Fairbanks, including: Water and Environmental Research Center, Geographic Information Network of Alaska, and Toolik Lake Field Station. Many people have helped in the production of the AGA including Nancy Auerbach, Andrew Balser, Jason Grimes, Tom Heinrichs, Julie Knudson, Leanne Lestak, Corinne Munger, Martha Raynolds, Lael Rogan, Dan Stahlke, and Scott Vockeroth. Funding for the mapping and the AGA came from the Toolik Lake LTER project, the DOE R4D program, and NSF Grants ARC-0425517, ARC-0225517, and ARC-0531180.

References

Brown, J., Hinkle, K.M. & Nelson, F.E. 2000. The circumpolar active layer monitoring (CALM) program: research designs and initial results. *Polar Geography* 24: 165-258.

CAVM Team. 2003. *Circumpolar Arctic vegetation map.* 1:7,500,000. Conservation of Arctic Flora and Fauna (CAFF) Map No. 1. Anchorage, Alaska. U.S. Fish and Wildlife Service.

Dangermond, J. & Harnden, E. 1990. Map data standardization: A methodology for integrating thematic cartographic data before automation. *ARC News* 12: 16-19.

Evans, B.M., Walker, D.A., Benson, C.S., Nordstrand, E. A. & Petersen, G.W. 1989. Spatial interrelationships between terrain, snow distribution and vegetation patterns at an arctic foothills site in Alaska. *Holarctic Ecology* 12: 270-278.

Hamilton, T.D. 2003. *Glacial Geology of Toolik Lake and the Upper Kuparuk River Region.* Biological Papers of the University of Alaska No. 26. Fairbanks, AK: University of Alaska Printing Services.

Hinzman, L.D., Goering, D.J. & Kane, D.L. 1998. A distributed thermal model for calculating soil temperature profiles and depth of thaw in permfrost regions. *Journal of Geophysical Research—Atmospheres* 103: 28,975-28,991.

Muller, S.V., Walker, D.A., Nelson, F., Auerbach, N., Bockheim, J., Guyer, S. & Sherba, D. 1998. Accuracy assessment of a land-cover map of the Kuparuk River basin, Alaska: considerations for remote regions. *Photogrammetric Engineering & Remote Sensing* 64: 619-628.

Nelson, F.E. & Hinkle, K.M. 1998. Active-layer thickness in north central Alaska: Systematic sampling, scale, and spatial autocorrelations. *Journal of Geophysical Research—Atmospheres* 103: 28,963-28,973.

Nelson, F.E., Shiklomanov, N.I., Mueller, G.R., Hinkle, K.M., Walker, D.A. & Bockheim, J.G. 1997. Estimating active-layer thickness over a large region: Kuparuk River Basin, Alaska, *Arctic, Antarctic, and Alpine Research* 29: 367-378.

Nolan, M. 2003. Distribution of the Star3i DEM of the Kuparuk River watershed (on CD-ROM). Boulder, CO: Joint Office of Scientific Support.

Osterkamp, T.E. 2003. Establishing long-term permafrost observations for active layer and permafrost investigations in Alaska 1977-2002. *Permafrost and Periglacial Processes* 14: 331-342.

Raynolds, M.K., Walker, D.A. & Maier, H.A. 2005. *Alaska Arctic vegetation map*, Scale 1:4,000,000. Conservation of Arctic Flora and Fauna (CAFF) Map No. 2. Anchorage, AK: U.S. Fish and Wildlife Service.

Raynolds, M.K., Walker, D.A., Munger, C.A., Vonlanthen, C.M. & Kade, A.N. 2008, in press. A map analysis of patterned-ground—vegetation relationships along a North American Arctic transect. *Journal of Geophysical Research—Biogeosciences*.

Reynolds, J.F. & Tenhunen, J.D. (eds.) 1996. *Landscape Function and Disturbance in Arctic Tundra*. Berlin: Springer-Verlag.

Romanovsky, V.E., Marchenko, S.S., Daanen, R., Sergeev, D.O. & Walker, D.A. 2008. Soil climate and frost heave along the permafrost/ecological North American Arctic transect. *Ninth International Conference on Permafrost, Fairbanks, Alaska, June 29-July 3, 2008* (this proceedings).

Rübel, E. 1927. Ecology, plant geography, and geobotany; their history and aim. *Botanical Gazette* 84: 428-439.

Shippert, M.M., Walker, D.A., Auerbach, N.A. & Lewis, B.E. 1995. Biomass and leaf-area index maps derived from SPOT images for Toolik Lake and Imnavait Creek areas, Alaska. *Polar Record* 31: 147-154.

Walker, D.A., Binnian, E., Lederer, N.D., Nordstrand, E. & Webber, .J. 1989. Terrain, vegetation and landscape evolution of the R4D research site, Brooks Range Foothills Alaska. *Holarctic Ecology* 12: 238-261.

Walker, D.A., Epstein, H.E., Gould, W.A., et al. 2008 in press. Biocomplexity of small patterned-ground features along the North American Arctic Transect. *Journal of Geophysical Research - Biogeosciences.*

Walker, D.A., Everett, K.R., Webber, P.J. & Brown, J. 1980. *Geobotanical Atlas of the Prudhoe Bay Region, Alaska*. CRREL Report 80-14. U.S. Army Cold Regions Research and Engineering Laboratory.

Walker, D.A., Jia, G.J., Epstein, H.E., Raynolds, M.A., Chapin III, F.S., Copass, C.D., Hinzman, L., Knudson, J.A., Maier, H., Michaelson, G.J., Nelson, F., Ping, C.L., Romanovsky, V.E. & Shiklomanov, N. 2003. Vegetation-soil-thaw-depth relationships along a low-arctic bioclimate gradient, Alaska: synthesis of information from the ATLAS studies. *Permafrost and Periglacial Processes* 14: 103-123.

Walker, D.A. & Maier, H.A. 2008. *Geobotanical Maps in the Vicinity of the Toolik Lake Field Station, Alaska.* Biological Papers of the University of Alaska, No. 28.

Walker D.A., Raynolds M.K., Daniëls F.J.A., et al. 2005. The circumpolar Arctic vegetation map. *Journal of Vegetation Science* 16: 267-282 + appendices.

Walker, D.A., & Walker, M.D. 1996. Terrain and vegetation of the Imnavait Creek Watershed. In: J.F. Reynolds & J.D. Tenhunen (eds.), *Landscape Function and Disturbance in Arctic Tundra*. Berlin: Springer-Verlag, 73-108

Walker, D.A., Weber, P.J., Walker, M.D., Lederer, N.D. & Meehan, R.H. 1986. Use of geobotanical maps and automated mapping techniques to examine cumulative impacts in the Prudhoe Bay Oilfield, Alaska. *Environmental Conservation* 13: 149-160.

Walker, M.D., Walker, D.A. & Auerbach, N.A. 1994. Plant communities of a tussock tundra landscape in the Brooks Range Foothills, Alaska. *Journal of Vegetation Science* 5: 843-866.

Lake Modification in a Permafrost Region, the Colville River Delta, Alaska

H. Jesse Walker
Louisiana State University, Baton Rouge, USA

Abstract

The Colville River Delta, like most deltas of the world, contains a variety of lakes. They range in size from small ponds (less than 0.0125 km^2 in area) that occupy low-centered ice-wedge polygons to large lakes (five of which are larger than 2.0 km^2) that occupy abandoned river channels. As the delta's distributaries migrate, they not only destroy ice wedges and the polygons the ice wedges helped create, but also tap lakes causing them to drain. After tapping, lakes become sedimentary traps and subject to rapid fill. Not all tapping is the result of the river, because the lakes themselves (especially the larger ones) tend to expand with time due to the physical and thermal erosion of their banks. Lake expansion into an ice-wedge polygonal field results in the melting of adjacent ice wedges, the production of an inverted relief and a serrated lake border.

Keywords: delta; erosion; flooding; ice wedge; lakes; permafrost

Introduction

The North Slope of Alaska extends from the crest of the Brooks Range northward to the Arctic Ocean. It is a part of the area dominated by continuous permafrost and has a surface much of which is covered with lakes and ice-wedge polygons. It drains into the Arctic Ocean via a number of rivers, the longest of which is the Colville River (Fig. 1). At its mouth the Colville has constructed a delta that is about 600 km^2 in area (Fig. 2). The delta supports a variety of forms many of which are similar to their counterparts in more temperate regions. However, most of these deltaic forms are impacted by snow, ice, and permafrost in addition to the typical processes, such as those caused by wind and river flow, dominating elsewhere.

The Delta's Lakes

Unlike on the general tundra surface of the North Slope where oriented lakes are common, the delta has a highly varied lake system. The delta's lakes range in size from small ponds to those that are more than 2 km^2 in area (Fig. 3) and in shape from circular and rectangular to sinuous and elongated. They vary in depth from a few centimeters to more than 10 m. Those that are deeper than 2 m usually do not freeze to the bottom during winter and have a permafrost-free zone (talik) beneath them. The delta's lakes vary in age from newly formed to some that have lasted hundreds of years, and they also vary in genesis from those formed in association with ice-wedge polygons and sand dunes to those resulting from river channel migration.

Basically all of the delta's lakes are ephemeral because of the continuous migration of the delta's distributaries which not only aids in the creation of lakes but inevitably leads to their destruction.

The types and distribution of lakes within the Colville Delta

The lakes and ponds of the delta exhibit a variety of types including ice-wedge polygons, abandoned channels, terrace flank depressions, and ice-scour holes (Dawson 1975). The most common are those ponds that occupy low-centered polygons. They are present on most surfaces except newly deposited areas such as sandbars and mudflats. Many of the delta's lakes fit into the thaw-lake category in that they

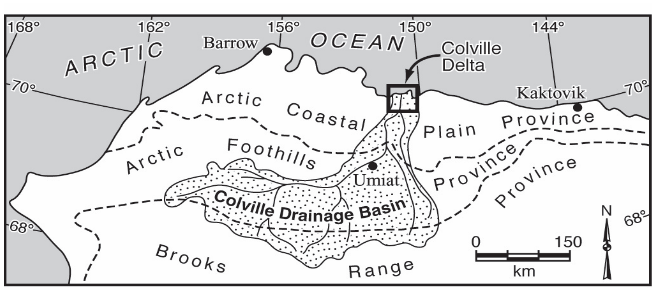

Figure 1. Regional map of the North Slope, Alaska, showing the Colville River Basin and Delta.

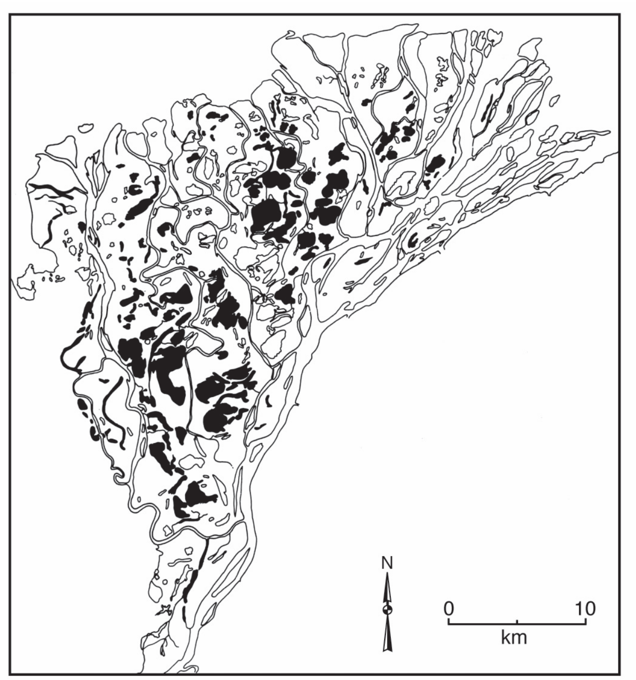

Figure 2. The Colville River Delta showing lake distribution Those lakes subject to flooding are in black.

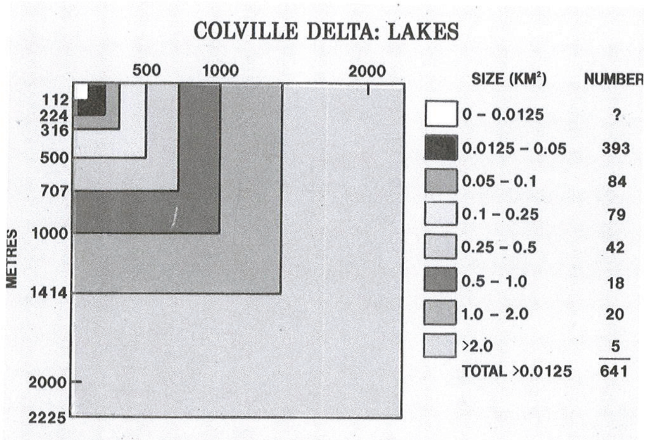

Figure 3. The numbers and sizes of lakes in the Colville River Delta.

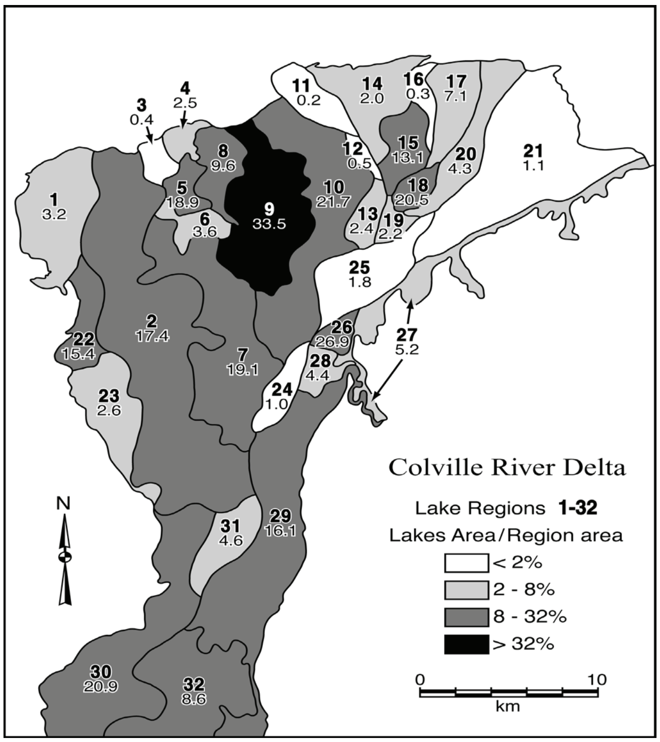

Figure 4. A regional map of the Delta's lakes with percentage of surface area occupied by lakes with areas more than 0.0125 km^2.

exhibit subsidence following the thawing of permafrost (Hopkins 1949, Jorgenson & Shur 2007).

Although the most distinctive characteristic of the delta is often considered to be its lakes, there is great variation in their occurrence within the delta (Fig. 4). The area with the most lake coverage is a north-south band through that part of the delta impacted by meandering distributaries, whereas the least coverage is especially in the northeast part of the delta which is characterized by braided drainage.

Perched Ponds and the Active Layer

One of the characteristics of permafrost is that it prohibits percolation and thus, under the right conditions, can serve as an aquiclude. The Colville River Delta with its varied relief provides a number of situations where perching can occur. The best examples are found within sand dune complexes throughout much of the delta. However, in a sense, the ponds present in low-centered polygons (especially those near a river channel) are perched in that they are perennial lakes with a surface level lying at an elevation above what would be the normal level of the water table in a permafrost-free environment.

Within the Colville Delta, local relief is more varied within sand dune complexes than elsewhere. Further, the delta is an ideal location for the formation of dunes because of the extensive sandbars that form along its channels. This is especially true of the main channel on the east side of the delta. Because the prevailing wind is from the northeast, dunes are best developed in left-bank locations. Dunes nearest the river channel tend to be active, whereas those away from the bank are usually stable and are covered with vegetation. Stabilized dunes, over time, become rounded and smooth, a type of relief that does not favor pond formation. Active dunes on the other hand have a varied relief that often provides ideal conditions for pond formation.

The dunal systems of the delta provide two types of perching: inter-dune and intra-dune ponds. Inter-dune ponds form between dune ridges, whereas intra-dune ponds form within dune ridges. During several field seasons in the 1960s and 1970s, detailed studies of inter-dune ponds were made (Walker & Harris 1976).

The pond selected for repetitive measurements (including active layer thickness and water stage and temperature) is near a field camp on Putu Channel, 3 km north of the head of the delta (Fig. 5). Putu Pond, as we named it, lies in an elliptical basin that is about 96 m long and 31 m wide (Fig. 6, 7). The pond at its maximum extent, which occurs during the snowmelt period, has an area of about 300 m^2 and a depth of 1.3 m. The lowest edge of the basin is about 6 m above the mudflat of Putu Channel, an ideal perching situation. The vegetation in the basin includes a variety of aquatic plants, moss, grasses, flowering plants, and willows that are up to 2 m tall. However, the steep sides of the dune are vegetation free and composed of coarse-textured sand.

During most of the year the area is blanketed with snow, which in the basin itself is several meters thick. The lake freezes to the bottom, and the active layer is frozen for some 7 to 8 months. Although wind, even during winter, removes snow from the crest of the dune, the snow in the basin remains intact until snowmelt begins. The rate of snowmelt varies; snow in the willows lasts much longer than it does elsewhere in the basin. Measurements indicated that active layer thaw began almost immediately after snowmelt exposed the surface. The actual deepening of the active layer varied mainly because of the nature of the vegetation cover (Fig. 8).

Once the active layer begins to thaw, percolation occurs through the coarse sand that makes up the riverbank. Thus during the short summer period, the lake not only lost water to evaporation but also to percolation. However, the lake was sufficiently deep so that it has never dried up.

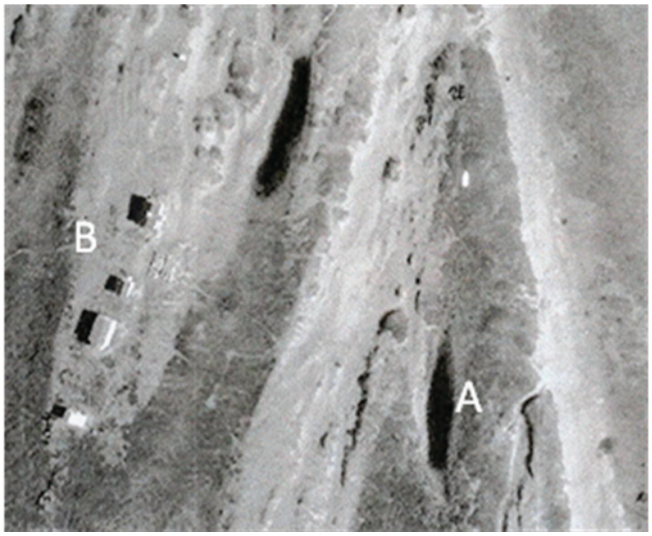

Figure 5. Air photograph of perched lakes in sand dunes at Camp Putu. A. Lake Putu, B. Research cabins.

Figure 6. Ground-level photograph of Lake Putu. Scale is shown in Figure 7.

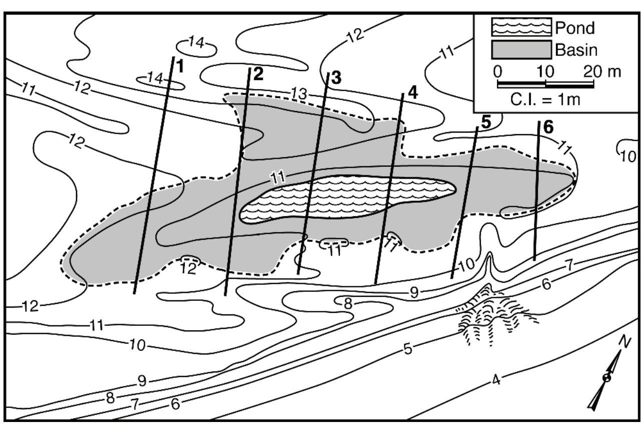

Figure 7. Map showing characteristics of Lake Putu. Lines 1 – 6 are basin transects.

Although perched ponds are less common in stabilized dunes than in active dunes, a few can be found in the delta (Fig. 9). It is not known what initiated the pond illustrated in Figure 9; however, some such ponds begin as blowouts, possibly when ground squirrel dens have been enlarged by bears. Once initiated, thermal degradation increases the pond's depth due to subsidence.

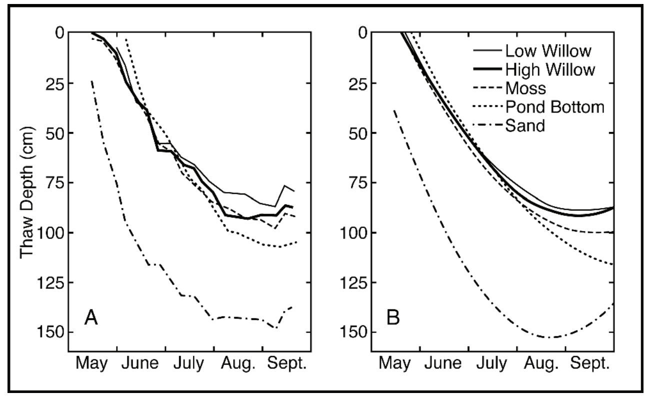

Figure 8. Seasonal development of active layer during 1973 of Lake Putu. A. Actual measurements, B. Calculated trends.

Figure 9. Photograph of intra-dune pond.

Ice Wedges and Lake Expansion

Many of the lakes in the Colville Delta are bordered by ice-wedge polygons which are subject to erosion by wind-generated waves, ice scour, and temperature-induced thaw. These processes are much less active than those accompanying a flooding river so that lake-bank retreat, even in the larger lakes, is relatively small. Another difference is that the eroded or thawed materials from a lake's shoreline remain in the lake. In Figure 10, the importance of wind-wave erosion is demonstrated by the repetitive saw-like form of the irregular shoreline. The predominating northeast wind causes wave action, which thermally erodes the ice-wedge polygons along the shoreline. The resulting form contrasts with that of the relatively smooth channel shoreline (Fig. 10).

Many of the low-center polygons that surround lake basins have water levels that are lower than lake levels. When the ice wedges facing the lakes melt and the ridges around the polygons collapse, lake water invades creating an inverted relief with a highly irregular bench around the lake margin (Fig. 11).

Expansion of lakes by physical and thermal erosion frequently results in the elimination of barriers between adjacent lakes so that they join. The resulting combination often produces a lake that has an irregular shape.

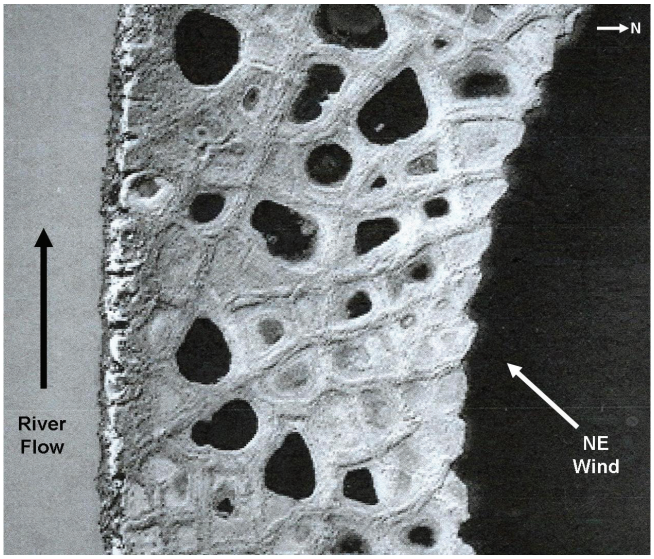

Figure 10. A 1981 air photograph of the upper Nechelik Channel and an adjacent lake illustrating the contrast between river and lake shorelines.

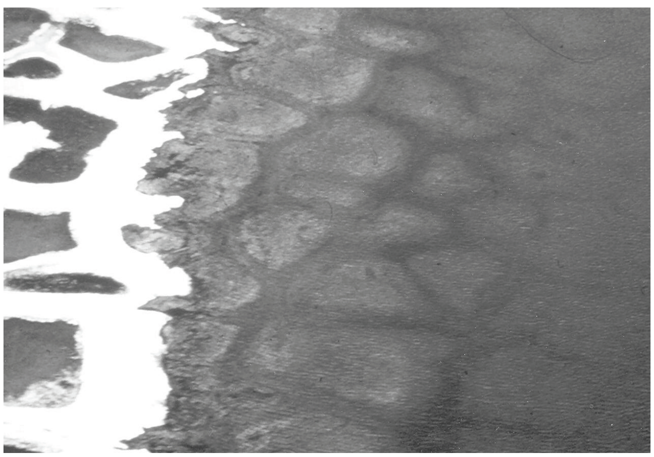

Figure 11. Photograph of the inversion of shoreline relief as ice wedges melt.

Figure 12. Photograph of the erosion and drainage of ice-wedge polygons.

Lake Tapping

One of the most distinctive changes in delta morphology occurs because of the tapping or breaching of lakes by migrating river channels. An examination of the delta's shorelines in 1971 (Ritchie & Walker 1974) showed that 59% are erosional, 35% are depositional, and 6% are neutral. Rates of retreat vary from an average of a fraction of a meter to two or more meters per year (Walker et al. 1987). In the process not only are the materials of which the banks are composed removed, but any ponds or lakes that the banks previously protected are breached. If the river banks are high and the lakes (usually ice-wedge polygons) are perched at the top above floodwater level, bank erosion, especially via ice wedges, causes the ponds to drain (Fig. 12). Often within peat banks, ice-wedge melting progresses inward from the bank, draining additional ponds (see McGraw, this Proceedings).

Once tapping occurs, lake drainage follows and the former lake level, if the lake bottom is below the level of the river, subsequently fluctuates with river stage. It then serves as a settling basin and begins to fill with the sediment transported into it by the river. The coarsest material is deposited near the lake entrance, and the fines are spread throughout the lake basin. The nature of the deposition is such that the lake basin becomes segmented as it fills. As the river continues to erode lakeward, the entrance channel is enlarged and the near-river deposits begin to be eroded.

Another morphologic/hydrologic change that occurs with lake tapping is the creation of a scour hole at the entrance to the lake. These scour holes as well as lake morphology changes are illustrated in the discussion below of Lake Nanuk (Polar Bear), Lake Tuttut (Caribou), and Lake 35.

Within the delta there are examples of virtually every stage in the life history of tapped lakes from those recently tapped to those nearing complete destruction.

Lake Nanuk and Lake Tuttut

Lake Nanuk (Polar Bear Lake) and Lake Tuttut (Caribou Lake) were two of the delta's largest lakes until they were tapped by migrating river channels (Roselle 1988). Lake Nanuk faced the Nechelik Channel whereas Lake Tuttut, which is just east of Lake Nanuk, faced Sakoonang Channel. It is not known just when Lake Nanuk was tapped, but it was probably in the late 1930s or 1940s based on the width of the entrance channel and the smallness of the lake delta displayed on 1948 photographs. In contrast, however, Lake Tuttut was tapped in 1971 at the time a field crew was working in the delta (Fig. 13).

Subsequent to tapping, two major events occurred: the lakes began to fill with sediment and the entrances began to enlarge. Because Lake Nanuk faces a channel that carries (at least during flood) some 25% of the delta's discharge it is filling at a much more rapid rate than Lake Tuttut whose facing channel only carries about 2% (Arnborg et al. 1966). Although the low-water stage of Lake Tuttut displays extensive bottom material, most of it is the result of the fact that it was sufficiently shallow to begin with so that once drainage occurred bottom materials became exposed.

In 1962, depth measurements were made by boat in Lake Nanuk between its southern- and northern-most points, a condition that today, because of this shallow depth, would be

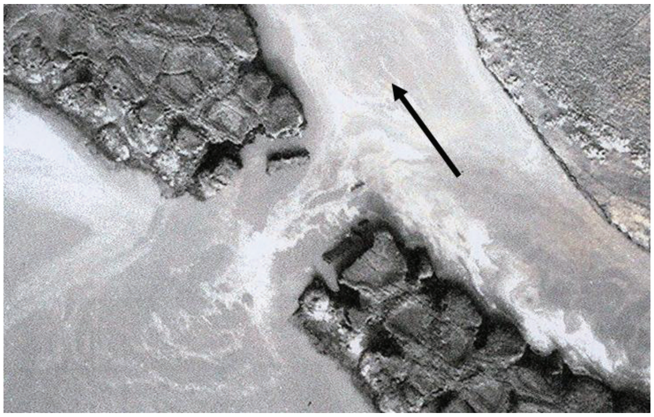

Figure 13. Photograph of Lake Tuttut entrance.

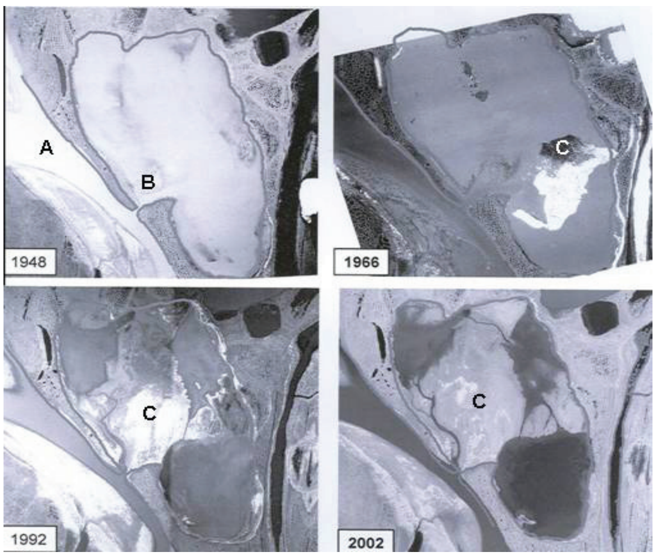

Figure 14. The depositional sequences in Lake Nanuk from 1949 to 2002. A. River channel, B. Lake entrance, C. Lake deposits.

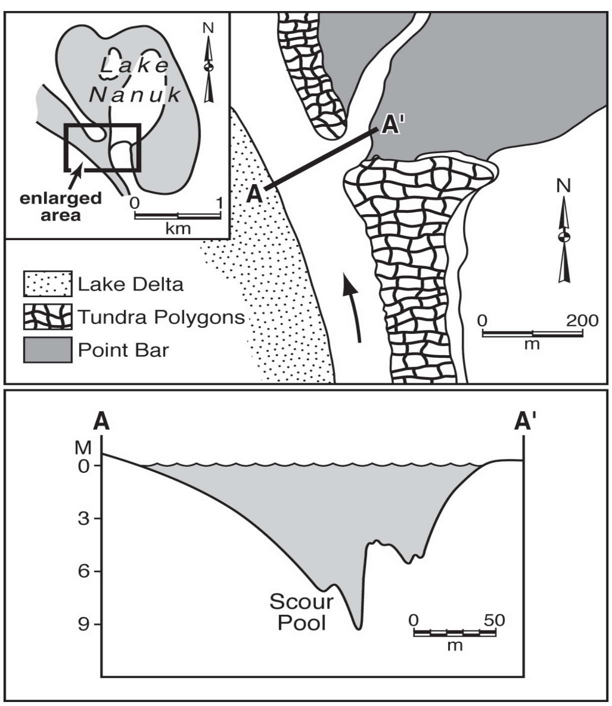

Figure 15. Scour hole at Lake Nanuk's entrance.

impossible (Fig. 14). In addition to showing the amount of fill that has occurred during the past 70 or so years, Figure 14 also shows the evolution of the entrance (also exit) channel with time. Such a long, winding channel is a typical feature of tapped lakes after they begin to fill. The channel in Lake Tuttut shows the same feature.

Upon tapping, lakes, most of which have levels some 2 m above normal river level, drain rapidly enlarging the opening and developing a scour hole at their mouths (Fig. 15).

Lake 35

Lake 35 (the number given the lake in a catalog of lakes made in the 1970s) is located in the northcentral part of the delta (Walker 1978). The changes that have occurred through the tapping of Lake 35 are among the most distinctive changes to have happened in the delta in the last century. The changes include not only the development of a scour hole, the exposure of shallow bottom areas, the creation of a lake delta, and widening of the inlet (outlet), but also the addition of other lakes to the system and the rearrangement of river channel flow. These changes are diagramed in Figure 16. The locations of the changes that are discussed below are indicated by the letters A, B, and C in Figure 16:1.

When the first air photos of the delta were made, Lake 35 and its adjacent lakes were essentially distinct and not impacted by the river, even during flood stage (Fig. 17). The exact dates of the initiation of various events are unknown because their recognition depends on the dates of photo coverage or field observation. Although, in 1949 there was some overflow and percolation along ice wedges between some of the lakes, the first major change was the tapping of Lake 35 a few years before 1970. By 1971 a small delta had formed, and at low water a bench was visible along both the south and north sides of the lake.

By 1981 (Fig 16:2) the adjacent lakes were all connected by irregular water courses through ice-wedge polygons as

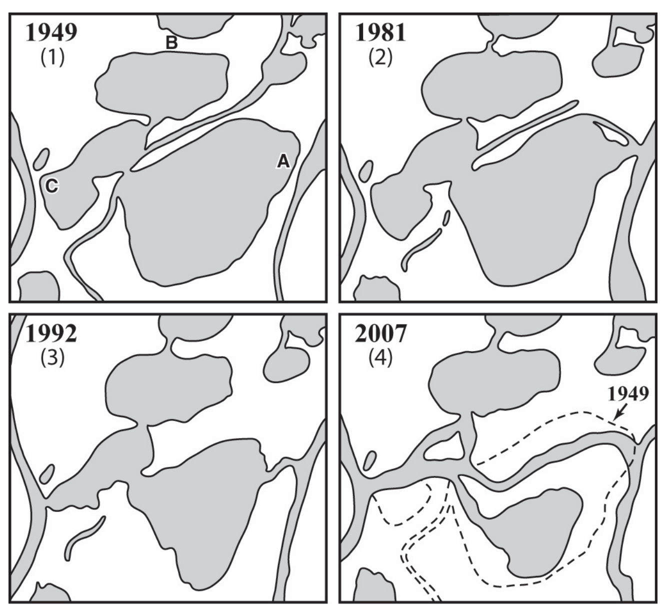

Figure 16. The modification of Lake 35 between 1949 and 2007, explanation in the text.

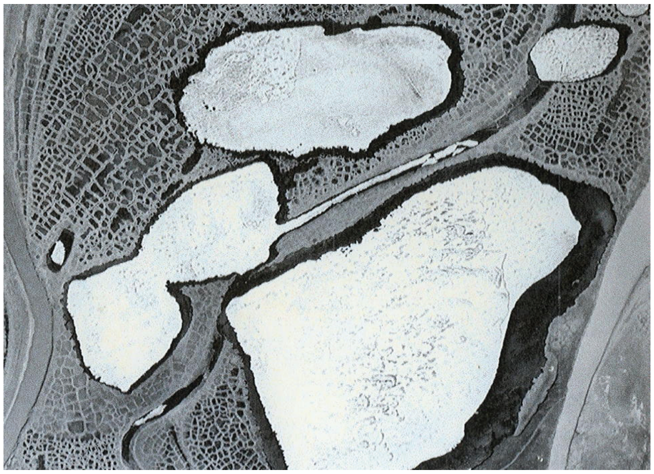

Figure 17. Lake 35 prior to tapping (See Fig. 16:1 A).

exampled at Figure 16:1 B, the lakes were still distinctive, the exposed shore areas around Lake 35 had expanded, and Lake 35's delta had shifted northward.

Eleven years later (Fig. 16:3) tapping had occurred at location C. It appears that, in this case, much of the erosion that caused the rupture was the result of floodwaters flowing through Lake 35 from east to west. Further, by this time, deposition in Lake 35 had reduced the actual water surface to less than half its original size.

The impact of this flow from east to west continued to increase so that by 2007 (Fig. 16:4), Lake 35 had become channelized. Because so much water and sediment was now being carried toward the west, the original distributary that caused the initial tapping some 40 years earlier ceased flowing north at low stage.

Conclusions

Although there are other types of lakes and ponds in the delta, such as those formed as toeheads at channel bifurcation points, the most distinctive relationships between permafrost and ice wedges with lakes are those associated with perching and ice-wedge polygons and with the processes of riverbank and lake bank erosion.

Lake tapping not only alters a lake's morphology, but also, through deposition, creates ideal conditions for former taliks to become frozen and for new sets of ice-wedge polygons to develop.

Acknowledgments

The research for this paper, which is based in part on field work conducted in the Colville River Delta since 1961, was supported by a number of organizations both financially and logistically. Included are: ONR, AINA, the North Slope Borough, the town of Nuiqsut, ARCO, Conoco Phillips, ABR, and Louisiana State University. To all of them, I extend my thanks. The assistance of Molly McGraw, Clifford Duplechin, and Mary Lee Eggart, and the suggestions made by two anonymous reviewers are much appreciated.

References

Arnborg, L., Walker, H.J. & Peippo, J. 1966. Water discharge in the Colville River, 1962. *Geografiska Annaler* 48: 195-210.

Dawson, A.G. 1975. *Landforms of the Colville River Delta, Alaska, as Interpreted from Aerial Photographs*. Unpublished thesis, Louisiana State University, 93 pp.

Hopkins, D.M. 1949. Thaw lakes and thaw sinks in the Imuruk lake area, Seward Peninsula, Alaska. *Journal of Geology* 57: 119-131.

Jorgenson, M. T. & Shur Y. 2007. Evolution of lakes and basins in northern Alaska and discussion of the thaw lake cycle. *Journal of Geophysical Research-Earth Surface* 112 (F2): F02S17.

McGraw, M. 2008. The degradation of ice wedges in the Colville River Delta and their role in pond drainage. *Proceedings of the Ninth International Conference on Permafrost*, Fairbanks, Alaska.

Ritchie, W. & Walker, H. 1974. Riverbank forms of the Colville River Delta. In: J.C. Reed & J.E. Sater (eds.), *The Coast and Shelf of the Beaufort Sea*. Washington, D.C.: The Arctic Institute of North America, 545-562.

Roselle, D.L. 1988. *Morphology and sedimentation of Arctic tapped lakes*. Unpublished thesis, Louisiana State University, 109 pp.

Walker, H.J. 1978. Lake tapping in the Colville River Delta, Alaska. In: R.J.E. Brown, *Proceedings, Third International Conference on Permafrost*. Ottawa, National Research Council of Canada, 233-238.

Walker, J., Arnborg, L. & Peippo, J. 1987. Riverbank erosion in the Colville Delta, Alaska. *Geografiska Annaler* 69A: 61-70.

Walker, H. & Harris, M. 1976. Perched ponds: An arctic variety. *Arctic* 29: 223-238.

Submarginal Glaciotectonic Deformation of Pleistocene Permafrost

Richard Waller
Research Institute for the Environment, Physical Sciences & Applied Mathematics, Keele University, Staffordshire, U.K.
Julian Murton
Department of Geography, University of Sussex, Brighton, U.K.
Colin Whiteman
School of Environment and Technology, University of Brighton, Brighton, U.K.

Abstract

Recent advances in our understanding of glacier-permafrost interactions provide an alternative hypothesis to interpret Pleistocene glaciotectonic sequences in regions where permafrost no longer exists. Instead of necessarily forming under unfrozen subglacial conditions, some glaciotectonic sequences may have formed by submarginal deformation of warm, partially-frozen permafrost. An example from North Norfolk, U.K., suggests that an ice sheet during Marine Isotope Stage 12 advanced across permafrost terrain, deforming it beneath the margin. Such a scenario can help explain some features whose formation under unfrozen conditions is problematic, including (1) the substantial thickness of the deforming layer and (2) the preservation of stratified intraclasts. Accordingly, glacial geologists should remain open to the possibility of glacier-permafrost interactions when interpreting glacigenic sequences. Such a re-interpretation could have major implications for reconstructing basal thermal regimes and modeling palaeo-ice sheets.

Keywords: basal thermal regime; eastern England; glacier-permafrost interaction; glaciotectonic deformation; Pleistocene permafrost.

Introduction

Whilst the ability of glaciers to deform their substrates has long been recognized (Lamplugh 1911), the glaciological significance of glaciotectonic deformation was not fully appreciated until the late 1970s (e.g., Boulton & Jones 1979). Since then, numerous papers have inferred the process at many Pleistocene localities and demonstrated its widespread occurrence beneath former continental ice masses (e.g., Hart et al. 1990, Clark 1994, Benn & Clapperton 2000). In addition, it is has been invoked to explain states of fast ice flow (e.g., Hart & Smith 1997, Truffer et al. 2000), ice streaming (Alley et al. 1986), high sediment fluxes (Dowdeswell & Siegert 1999), and the creation of distinctive glacial landforms and sediments (Boulton 1987, Benn & Evans 1996).

The majority of this research has assumed that sediment deformation only occurs beneath warm-based ice, when subglacial sediments are unfrozen and water-saturated. This stems from the widespread assumption that basal processes are inactive at subfreezing temperatures (e.g., Paterson 1994) and by inference that cold-based glaciers are slow moving and geomorphologically ineffective (Kleman 1994). Recent research has demonstrated, however, that cold-based glaciers can slide over and deform their beds (Echelmeyer & Zhongziang 1987, Cuffey et al. 1999) and therefore actively erode and deposit (Atkins et al. 2002). This conclusion is supported by work in high-latitude Pleistocene glacial environments where thick sequences of deformed permafrost provide evidence of extensive glacier-permafrost interaction beneath former ice sheets (Mackay et al. 1972, Astakhov et al. 1996, Murton et al. 2004).

Whilst the implications of glacier-permafrost interactions are being explored within glaciology (e.g., Cutler et al. 2000), little attempt has been made to consider their potential implications for interpreting Pleistocene glacigenic sequences. But if we consider deformation under partly-frozen conditions as an alternative hypothesis, it may help to explain features difficult to reconcile with deformation under entirely unfrozen conditions.

We suggest here that submarginal deformation of permafrost can help to explain key aspects of the well-known glaciotectonic sequences of North Norfolk, U.K.

Processes and Products of Subglacial Sediment Deformation

Whilst the importance of subglacial sediment deformation is widely acknowledged by glaciologists and glacial geologists, the identification of an appropriate flow law for subglacial tills remains elusive and controversial. To date, four flow laws have been applied to subglacial sediment rheology: (1) linear viscous, (2) non-linear viscous, (3) non-linear Bingham, and (4) Coulomb-plastic (Kavanaugh and Clarke 2006). Models one to three consider tills as viscous fluids. In model one, the strain rate is linearly related to the shear stress, and the till viscosity is independent of porewater pressure. Models two and three are both non-linear, with porewater pressure determining the till's shear resistance, and the latter incorporating a yield strength determined by the Mohr-Coulomb failure criterion (Boulton & Hindmarsh 1987). Model 4 differs from the first three models in that it treats tills as plastic materials, with no permanent deformation occurring until a yield strength (again based on the Mohr-Coulomb failure criterion) is surpassed, after which they experience infinite strains. The choice of flow law is highly significant, as it represents a key control on the dynamic behavior of glaciers and ice sheets. However, there is currently conflict between the strong evidence for the Coulomb-plastic model derived from studies at modern-day glaciers and the geological evidence for the viscous fluid models, illustrated by contrasting deformation profiles.

Initial research at modern-day glaciers suggested that subglacial tills behaved like viscous fluids, with both field measurements (Boulton & Hindmarsh 1987) and geophysical data (Alley et al. 1986) suggesting that subglacial sediments deformed pervasively in layers several metres thick. Subsequent work, however, has favoured a Coulomb-plastic rheology, with new observations and borehole measurements suggesting that subglacial sediment deformation is restricted to thin shear zones only a few tens of centimetres thick (e.g., Iverson et al. 1995; Engelhardt & Kamb 1998; Fuller & Murray 2002). For example, recent work by Kavanaugh & Clarke (2006) at the Trapridge Glacier, British Columbia, concluded that the Coloumb-plastic model provided the closest match to the field instrument records. The model, in turn, predicted a deformation depth of 0.35 m, in close accordance with the measured depth of ~0.3 m.

Geological evidence has also been widely employed, both to infer the existence of subglacial sediment deformation beneath former ice sheets and to reconstruct the sediment deformation profile. Cited evidence includes a range of structures that belie varying amounts and styles of deformation involving both ductile and brittle failure (see Hart 1995, Boulton et al. 2001, & Evans et al. 2006 for lengthier reviews). At low strains, folds are commonly developed where compression occurs on the up-glacier flank of an obstacle. As shear strains increase, the folds are progressively attenuated and boudinaged, which can generate a tectonically-laminated deposit, which in turn can later be re-folded. The shearing can affect pre-glacial materials to generate glacitectonites (Banham 1977). Ultimately, high strain deformation can homogenize sediments and form so-called deformation tills (Benn & Evans 1996); in this case, clast fabrics (van der Meer 1993, Hart 1994) and micro-scale structures provide the only evidence of the sediment's strain history, although the ability of the former to infer strain history remains controversial (Benn 2007).

Geological evidence has frequently been used to infer pervasive deformation within a deforming layer several metres thick (e.g., Hart et al. 1990, Alley 1991), supporting a viscous fluid model of till rheology. But such a conclusion is increasingly difficult to reconcile with the results of field-based investigations at modern-day glaciers. Whilst this paradox has been used to argue that subglacial deformation is less extensive or deep-seated than originally thought (e.g., Piotrowski et al. 2001), this paper considers an alternative hypothesis, that the geological evidence may instead indicate subglacial deformation under contrasting thermal conditions.

Glaciotectonic Deformation of Permafrost

The deforming-bed model was originally limited to the situation where warm-based glaciers overlie thawed beds (see Alley 1991). Consequently, ice-sheet models commonly include the boundary condition that basal velocities are zero where the temperature of the basal ice falls below the pressure melting point (e.g., Payne 1995). There is growing evidence, however, that this assumption is not universally applicable. Echelmeyer & Zhongxiang (1987), for example, found that over 60% of the surface motion of the cold-based Urumqi No. 1 Glacier in China was accommodated via the deformation of ice-rich subglacial sediment with an effective viscosity two-orders of magnitude lower than the overlying ice. This demonstrates the ability of glaciers to couple with subglacial permafrost.

Permafrost that has never thawed since it was overridden and deformed by Pleistocene ice sheets provides an important touchstone for interpreting glaciotectonic sequences in regions where permafrost no longer exists. Previous work has highlighted evidence for glacier-ice thrusting near the northwest limit of the Laurentide ice sheet in western Arctic Canada (Mathews & Mackay 1960, Mackay et al. 1972), and for a deformable bed of permafrost beneath the southern Kara ice sheet in western Siberia (Astakhov et al. 1996). More recently, we have detailed the stratigraphy and glaciotectonic structures of permafrost in the Tuktoyaktuk Coastlands of western Arctic Canada (Murton et al. 2004). Several important observations arise from these studies.

First, the thickness of glaciotectonically-deformed permafrost is substantial. Astakhov et al. (1996) reported thicknesses of tens of metres from the western Yamal Peninsula and the lower Yenissei region, and Murton et al. (2004) reported thickness of at least 5–20 m from the Tuktoyaktuk Coastlands (Fig. 1a, 1b). Second, ductile deformation of warm, ice-rich materials is inferred from recumbent and S-shaped folds, sand lenses and layers (Fig. 1c), whereas there is less evidence for brittle failure in the form of pinch-and-swell structures and ice-filled tension gashes. Third, submarginal erosion of permafrost is indicated by (1) incorporation of rafts of massive ice (Fig. 1d) and smaller ice clasts into frozen glacitectonite (Fig. 1b), and (2) angular unconformities (décollement surfaces) beneath the glacitectonite (Fig. 1a). Adjacent layers of frozen silt, clay, and sand have deformed around some ice clasts, giving the latter the misleading appearance of 'dropstone-like' structures. Overall, the permafrost was probably warm, ice-rich, and contained limited amounts of liquid water – a type of easily deformable permafrost termed 'plastic frozen ground' (Tsytovich 1975).

A Reconsideration of the Glaciotectonic Sequences of North Norfolk

The coastal cliffs of northeast Norfolk exhibit a complex sequence of glacial sediments (e.g., Lee et al. 2004). Banham (1968, 1977, 1988) recognized evidence for glaciotectonic processes, a conclusion supported by Hart & Boulton (1991), Hart & Roberts (1994), and, in part, by Lunkka (1994); the latter author also recognized evidence for subaqueous processes. Lunkka's conclusions, and those of Roberts and Hart (2005), probably reflect the influence of Eyles et al. (1989), who interpreted the whole sediment pile in glaciomarine terms. Eyles et al.'s interpretation, however, has received little support, and Roberts and Hart (2005) have re-affirmed their view that the 'Laminated Diamict' at West Runton is

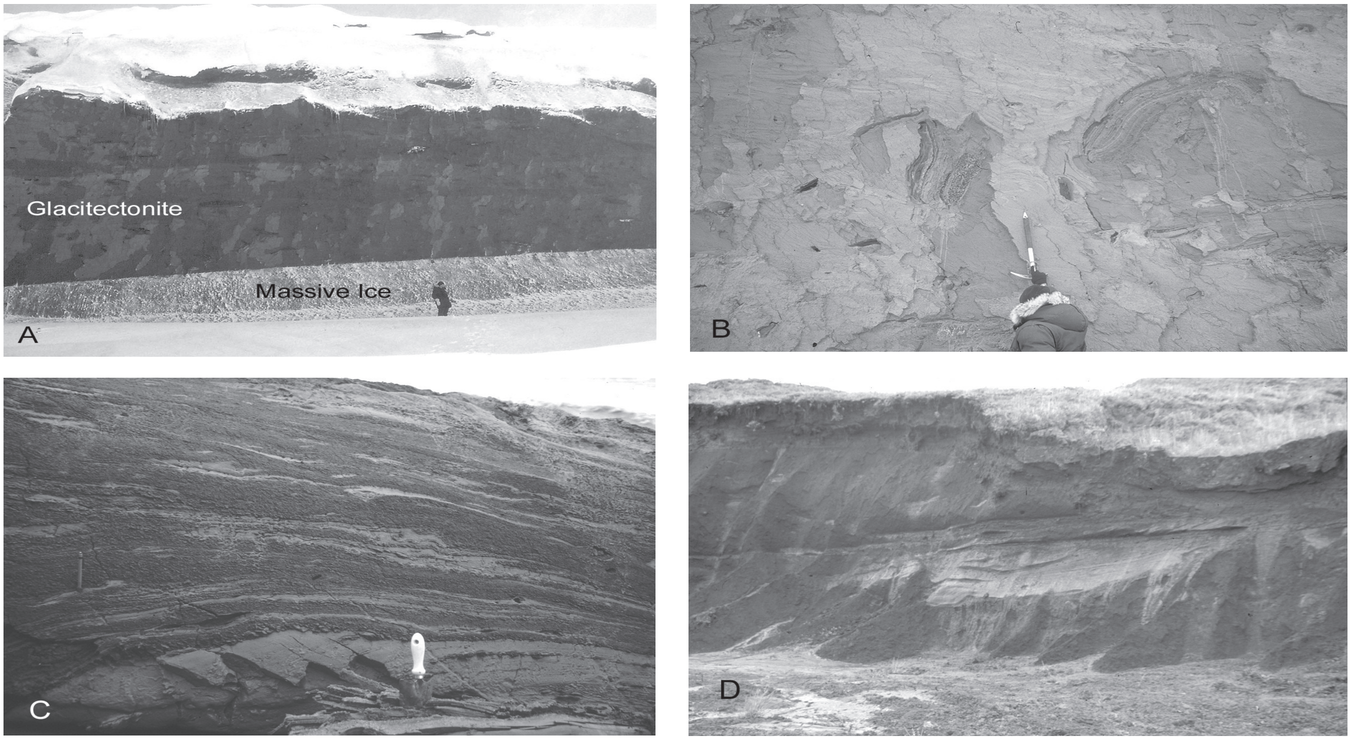

Figure 1. Glaciotectonically-deformed permafrost in the Canadian Arctic: (A) frozen glacitectonite above massive ice at Pullen Island - note intervening angular unconformity (69º46′25″N, 134º24′18″W, figure for scale), (B) close-up of chaotically-orientated and deformed sand lenses and ice clasts at Pullen Island (figure for scale), (C) sand lenses and fold noses between silty clay at North Head (69º43′22″N, 134º26′08″W), (D) raft of massive ice (~14 m long) within frozen glacitectonite at Liverpool Bay (69º50′10″N, 129º20′12″W).

essentially a subglacially-deformed sediment package, although the primary depositional process of some of the sediment may have been subaqueous. They recognize two types of stratified diamict, Type 1 and Type 2. While both types of laminae are said to be the product of "primary extensional glaciotectonism, with ductile, intergranular pervasive shear and brittle shear, … the lateral continuity of Type 2 laminae and the presence of dropstone-like structures supports a primary subaqueous origin with secondary subglacial deformation" (p. 123). Preservation of Type 2 laminae is attributed to "low strain at the lower interface of the deforming bed" (p. 138). In an earlier iteration of this material (Roberts and Hart in Lewis et al. 2000), these authors noted that the presence of ice wedge pseudomorphs implied subaerial permafrost conditions during the onset of glaciation.

Remarkably, none of the work mentioned above has paid significant attention to the existence of pre-glacial permafrost. Wedge-shaped structures do occur at several horizons in the pre-glacial sediments (West 1980), but many are small and isolated, and both Worsley (1996) and Preece (2000) have questioned their permafrost origin. They could be hydrofractures, water-escape structures or soft-sediment deformations. Nevertheless, the largest wedge-shaped structures in these sediments possess convincing ice wedge-pseudomorph characteristics associated with permafrost (Whiteman 2002). They extend downwards from the upper surface of the pre-glacial sediments and have been correlated to the widespread, Anglian periglacial soil-stratigraphic-unit known as the Barham Soil (Rose et al. 1985). There can be no doubt that cold permafrost subject to thermal contraction cracking was an integral component of the Norfolk landscape prior to glaciation. Less certain are the thickness, ice content, and temperature of the permafrost.

We suggest that submarginal deformation occurring under partially-frozen conditions at temperatures close to, but slightly below, the pressure melting point ("warm permafrost") represents an alternative hypothesis for interpreting the glaciotectonic sequences of North Norfolk. This hypothesis may elucidate some features that are hard to explain if the substrate was entirely unfrozen:

First, the prevailing model of an unfrozen deforming layer ≤15 m thick (Hart et al. 1990) appears increasingly at odds with observations from modern glaciers that suggest that even under thick ice, deformation is restricted to layers a few tens of cm thick or at most, 1–2 m thick (Engelhardt & Kamb 1998). Whilst the incremental stacking of thin, deforming layers at the ice margin might create a thick sequence of deformed sediments (e.g., Evans & Hiemstra 2005, Benediktsson et al. in press), this cannot account for the size and coherence of the structural features observed at West Runton, for example. In contrast, the presence of a thick and pervasively-deformed sequence (Fig. 2a) is entirely consistent with deformation at subfreezing conditions, as documented by the authors in the western Canadian Arctic (Murton et al. 2004) and by Astakhov et al. (1996) in Western Siberia.

Second, the streamlined sand lenses at West Runton (Fig. 2b, c, e, g, Hart et al. 1990, Lunkka 1994) are difficult to reconcile with high-strain deformation under unfrozen

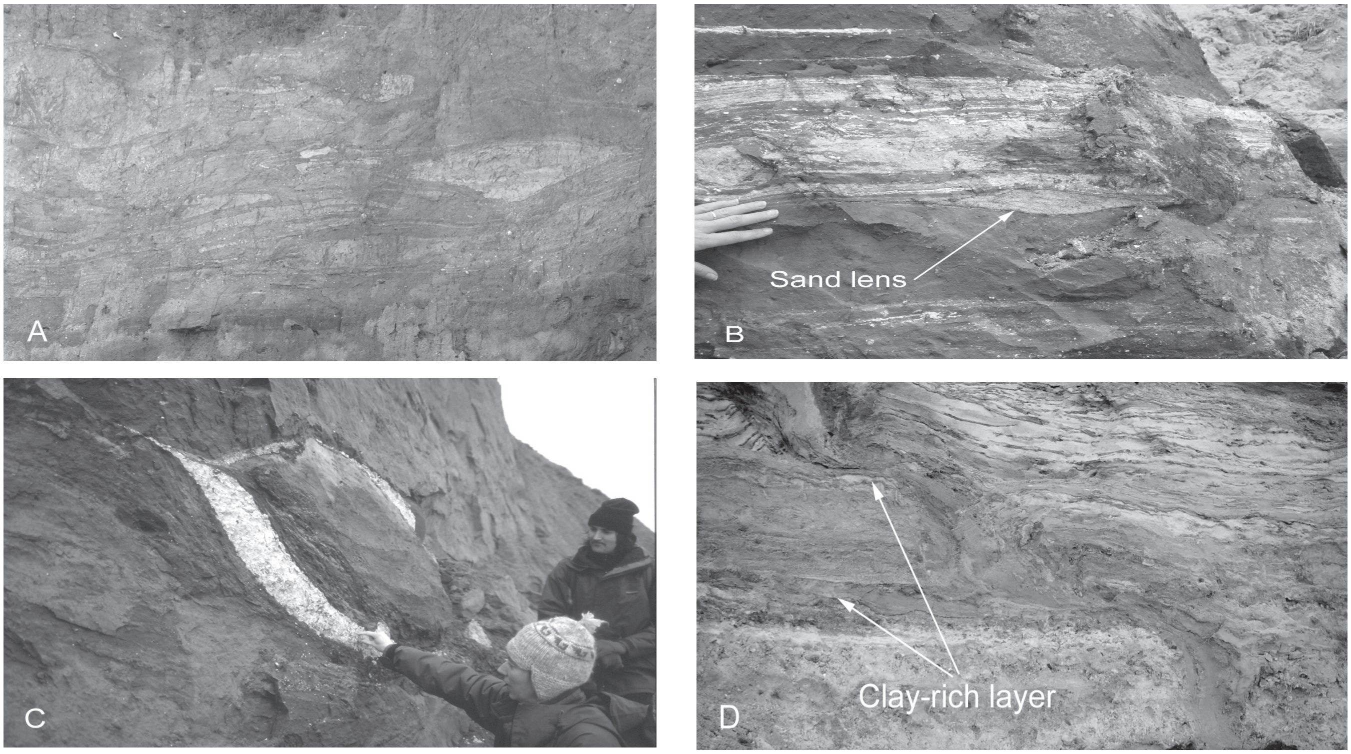

Figure 2. Glaciotectonic features in Northern Norfolk: (A) streamlined lenses, pods and folds at Weybourne (52º56′25″N, 1º08′42″E, area depicted ~10 m across), (B) stratified and streamlined sand lens at West Runton (52º56′25″N, 1º15′21″E, hand for scale), (C) streamlined sand lens surrounded by chalk, West Runton (figures for scale), (D) sheared ice wedge pseudomorph, West Runton (area depicted ~0.8 m across).

conditions. If the fine-grained till surrounding the sand lenses experienced high porewater pressures, then the lenses could not have been well drained and therefore able to act as more resistant masses. Also, it is difficult to envisage how they could have remained intact as they lacked any cohesion (see also Piotrowski et al. 2001). In contrast, the survival of recognizable intraclasts within an actively deforming till, and the associated rheological heterogeneity, are easy to explain if deformation takes place at temperatures below, but close to, the pressure melting point. The presence and quantity of liquid water, and therefore the mechanical properties of frozen ground at these relatively warm temperatures, are strongly grain-size dependent (Williams & Smith 1989). Consequently, if such a sequence was overridden by ice, deformation would occur preferentially within the fine-grained till matrix (which contains liquid water), whilst the sand intraclasts should remain frozen and largely intact. This prediction is consistent with field observations of subglacially-deformed permafrost in the western Canadian Arctic, showing streamlined and occasionally boudinaged sand lenses within a pervasively deformed till matrix (Murton et al. 2004, Fig. 2c). Menzies (1990) has similarly argued that undeformed, sand intraclasts within a deformation till in Ontario, Canada must have been frozen when deformation took place, producing a "block-in-matrix" mélange.

Observation of a sheared ice wedge pseudomorph at West Runton provides additional evidence for a grain-size-related variation in rheology. The pseudomorph has been displaced by several centimeters where it transects clay-rich layers, whilst those parts situated within sand-rich layers have not been substantially deformed (Fig. 2d). This is consistent with the findings of Astakhov et al. (1996), who found deformation within permafrost sequences to be restricted to ice-rich or clay-rich layers.

Finally, the deformed permafrost hypothesis is consistent with the pre-glacial history of the region. There is extensive evidence that the area was characterized by permafrost conditions immediately prior to glaciation. Therefore, the ice would have initially advanced over frozen ground, probably warming it from cold to warm permafrost. Cutler et al. (2000) have modeled interactions between the Green Bay lobe of the southern Laurentide Ice Sheet and pre-existing permafrost and concluded that glacier-permafrost interactions would have persisted for 80–200 km up-glacier of the margin, and could have remained intact for up to a few thousand years beneath the advancing ice.

Discussion

With recent research suggesting that subglacial permafrost has been more widespread than previously thought (Cutler et al. 2000) and that glaciers can couple with ice-rich materials (Astakhov et al. 1996, Bennett et al. 2004, Murton et al. 2004), it seems highly likely that there should be evidence of this process within the geological record.

At present, the alternative hypothesis advocated in this paper remains speculative. Whilst there is clear evidence for deformation under subfreezing conditions in high-latitude regions where permafrost has remained intact, we currently lack any sedimentological criteria with which to recognize glacier-permafrost interactions in areas where the permafrost has subsequently thawed. More detailed investigation of the origin and significance of undeformed intraclasts within pervasively deformed sequences might provide a useful starting point as a research avenue amenable both to field and laboratory testing.

If such criteria, capable of distinguishing between deformation under unfrozen and partly-frozen conditions can be developed, then the potential applications are highly significant. They could enable the basal boundary conditions of past ice sheets to be reconstructed on the basis of geological evidence, thereby providing an opportunity to independently test the predictions both of numerical ice-sheet models and geomorphological inverse models.

Conclusions

Recent research indicates that subglacial sediment deformation and erosion can remain active at subfreezing temperatures, allowing some glaciers to couple with and deform permafrost beneath their margins. Submarginal deformation of past permafrost may explain some problematic features of the glaciotectonic sequences in North Norfolk, previously attributed to deformation of an unfrozen substrate. Deformation under subfreezing conditions should be considered as an alternative hypothesis elsewhere, particularly in ice-marginal settings where pre-glacial permafrost is known to have occurred. It is hoped that further research on the products of glacier-permafrost interactions will help to identify geological criteria for distinguishing between deformation of permafrost and that of unfrozen materials.

References

Alley, R.B. 1991. Deforming-bed origin for southern Laurentide till sheets? *Journal of Glaciology* 37: 67-76.

Alley, R.B., Blankenship, D.D., Bentley, C.R. & Rooney, S.T. 1986. Deformation of till beneath Ice Stream B, Antarctica. *Nature* 322: 57-59.

Astakhov, V.I., Kaplyanskaya, F.A. & Tarnogradsky, V.D. 1996. Pleistocene permafrost of West Siberia as a deformable glacier bed. *Permafrost & Periglacial Processes* 7: 165-191.

Atkins, C.B., Barrett, P.J. & Hicock, S.R. 2002. Cold glaciers erode and deposit: evidence from the Allan Hills, Antarctica. *Geology* 30: 659-662.

Banham, P.H. 1968. A preliminary note on the Pleistocene stratigraphy of northeast Norfolk. *Proceedings of the Geologists' Association* 79: 507-512.

Banham, P.H. 1977. Glacitectonites in till stratigraphy. *Boreas* 6: 101-105.

Banham, P.H. 1988. Polyphase glaciotectonic deformation in the contorted drift of Norfolk. In: D. Croot (ed.), *Glaciotectonics: Forms and Processes*. Balkema, Rotterdam: 27-32.

Benediktsson, Í.Ö., Möller, P., Ingólfsson, O., van der Meer, J.J.M., Kjær, K.H. & Krüger, J. In press. Instantaneous end moraine and sediment wedge formation during the 1890 glacier surge of Brúarjökull, Iceland. *Quaternary Science Reviews*.

Benn, D.I. 2007. Interpreting glacial sediments. In: P.G. Knight (ed.), *Glacier Science and Environmental Change*. Oxford: Blackwell Publishing, 434-439.

Benn, D.I. & Clapperton, C.M. 2000. Pleistocene glaciotectonic landforms and sediments around central Magellan Strait, southernmost Chile: evidence for fast outlet glaciers with cold-based margins. *Quaternary Science Reviews* 19: 591-612.

Benn, D.I. & Evans, D.J.A. 1996. The recognition and interpretation of subglacially-deformed materials. *Quaternary Science Reviews* 15: 25-32.

Bennett, M.R., Waller, R.I., Midgley, N.G., Huddart, D., Gonzalez, S., Cook, S.J. & Tomio, A. 2003. Subglacial deformation at subfreezing temperatures? Evidence from Hagafellsjökull-Eystri, Iceland. *Quaternary Science Reviews* 22: 915-923.

Boulton, G.S. 1987. A theory of drumlin formation by subglacial sediment deformation. In: J. Menzies & J. Rose (eds.), *Drumlin Symposium*. Rotterdam: Balkema, 25-80.

Boulton, G.S. & Jones, A.S. 1979. Stability of temperate ice caps and ice sheets resting on beds of deformable sediment. *Journal of Glaciology* 24: 29-42.

Boulton, G.S. & Hindmarsh, R.C.A. 1987. Sediment deformation beneath glaciers: rheology and geological consequences. *Journal of Geophysical Research* 92: 9059-9082.

Boulton, G.S, Dobbie, K.E. & Zatsepin, S. 2001. Subglacial sediment deformation beneath glaciers and its coupling to the subglacial hydraulic system. *Quaternary International* 86: 3-28.

Clark, P.U. 1994. Unstable behaviour of the Laurentide ice sheet over deforming sediment and its implications for climate change. *Quaternary Research* 41: 19-25.

Cuffey, K.M., Conway, H., Hallet, B., Gades, A.M. & Raymond, C.F. 1999. Interfacial water in polar glaciers, and glacier sliding at -17°C. *Geophysical Research Letters* 26: 751-754.

Cutler, P.M., MacAyeal, D.R., Mickelson, D.M., Parizek, B.R. & Colgan, P.M. 2000. A numerical investigation of ice-lobe/permafrost interaction around the Southern Laurentide Ice Sheet. *Journal of Glaciology* 46: 311-325.

Dowdeswell, J.A. & Siegert, M.J. 1999. Ice-sheet numerical modeling and marine geophysical measurement of glacier-derived sedimentation on the Eurasian Arctic continental margins. *Geological Society of America Bulletin* 111: 1080-1097.

Echelmeyer, K. & Zhongxiang, W. 1987. Direct observation of basal sliding and deformation of basal drift at subfreezing temperatures. *Journal of Glaciology* 33: 83-98.

Engelhardt, H. & Kamb, B. 1998. Basal sliding of Ice Stream B, West Antarctica. *Journal of Glaciology* 44: 223-230.

Evans, D.J.A. & Hiemstra, J.F. 2005. Till deposition by glacier sub-marginal, incremental thickening. *Earth Surface Processes & Landforms* 30: 1633-1662.

Evans, D.J.A. Phillips, E.R., Hiemstra, J.F. & Auton, C.A. 2006. Subglacial till: Formation, sedimentary characteristics and classification. *Earth-Science Reviews* 78: 115-176.

Eyles, N, Eyles, C.H. & McCabe, A.M. 1989. Sedimentation in an ice-contact subaqueous setting: the mid-Pleistocene "North Sea Drifts" of Norfolk, UK. *Quaternary Science Reviews* 8: 57-74.

Fuller, S. & Murray, T. 2002. Sedimentological investigations in the forefield of an Icelandic surge-type glacier: implications for the surge mechanism. *Quaternary Science Reviews* 21: 1503-1520.

Hart, J.K. 1994. Till fabric associated with deformable beds. *Earth Surface Processes & Landforms* 19: 15-32.

Hart, J.K. 1995. Subglacial erosion, deposition and deformation associated with deformable beds. *Progress in Physical Geography* 19: 173-191.

Hart, J.K., Hindmarsh, R.C.A. & Boulton, G.S. 1990. Styles of subglacial glaciotectonic deformation within the context of the Anglian ice sheet. *Earth Surface Processes & Landforms* 15: 227-241.

Hart, J.K. & Boulton, G.S. 1991. The interrelations of glaciotectonic and glaciodepositional processes within the glacial environment. *Quaternary Science Reviews* 10: 335-350.

Hart, J.K. & Roberts, D.H. 1994. Criteria to distinguish between subglacial glaciotectonic and glaciomarine sedimentation, I. Deformation styles and sedimentology. *Sedimentary Geology* 91: 191-213.

Hart, J.K. & Smith, 1997. Subglacial deformation associated with fast ice flow, from the Columbia Glacier, Alaska. *Sedimentary Geology* 111: 117-197.

Iverson, N.R., Hanson, B., Hooke, R.LeB. & Jansson, P. 1995. Flow mechanism of glaciers on soft beds. *Science* 267: 80-81.

Kavanaugh, J.L. & Clarke, G.K.C. 2006. Discrimination of the flow law for subglacial sediment using in situ measurements and an interpretation model. *Journal of Geophysical Research* 111: F01002, doi:10.1029/2005JF000346.

Kleman, J. 1994. Glacial landforms indicative of a partly frozen bed. *Journal of Glaciology* 40: 255-264.

Lamplugh, G.W. 1911. On the shelly moraine of the Sefstrom glacier and other Spitsbergan phenomena illustrative of the British glacial conditions. *Proceedings of the Yorkshire Geological Society* 17: 216-241.

Lee, J.R., Booth, S.J., Hamblin, R.J.O., Jarrow, A.M., Kessler, H., Moorlock, B.S.P., Morigi, A.N., Palmer, A., Pawley, S.J., Riding, J.B. & Rose, J. 2004. A new stratigraphy for the glacial deposits around Lowestoft, Great Yarmouth, North Walsham and Cromer, East Anglia, UK. *Bulletin of the Geogical Society of Norfolk* 53: 3-60.

Lewis, S.G., C.A.Whiteman & R.C. Preece (eds). 2000. *The Quaternary of Norfolk and Suffolk: Field Guide.* London: Quaternary Research Association,.

Lunkka, J.P. 1994. Sedimentation and lithostratigraphy of the North Sea Drift and Lowestoft Till Formations in the coastal cliffs of northeast Norfolk, England. *Journal of Quaternary Science* 9: 209-233.

Mathews, W.H. & Mackay, J.R. 1960. Deformation of soils by glacier ice and the influence of pore pressure and permafrost. *Royal Society of Canada Transactions* LIX, Series III, Section 4: 27-36.

Mackay, J.R., Rampton, V.N. & Fyles, J.G. 1972. Relic Pleistocene permafrost, western Arctic, Canada. *Science* 176: 1321-1323.

Menzies, J. 1990. Sand intraclasts within a diamicton mélange, southern Niagara Peninsula, Ontario, Canada. *Journal of Quaternary Science* 5: 189-206.

Murton, J.B., Waller, R.I., Hart, J.K., Whiteman, C.A., Pollard, W.H. & Clark, I.D. 2004. Stratigraphy and glaciotectonic structures of permafrost deformed beneath the northwest margin of the Laurentide Ice Sheet, Tuktoyaktuk Coastlands, Canada. *Journal of Glaciology* 49: 399-412.

Payne, A.J. 1995. Limit cycles in the basal thermal regime of ice sheets. *Journal of Geophysical Research* 100(B3): 4249-4263.

Paterson, W.S.B. 1994. *The Physics of Glaciers* (3rd Ed.). Oxford: Pergamon Press, 480 pp.

Piotrowski, J.A., Mickelson, D.M., Tulaczyk, S., Krzyszkowski, D. & Junge, D.W. 2001. Were deforming subglacial beds beneath past ice sheets really widespread? *Quaternary International* 86: 139-150.

Preece, R.C. 2000. Molluscan evidence for differentiation of interglacials within the 'Cromerian Complex'. *Quaternary Science Reviews* 20: 1643-1656.

Roberts, D.H. & Hart, J.K. 2005. The deforming bed characteristics of a stratified till assemblage in north East Anglia, UK: investigating controls on sediment rheology and strain signatures. *Quaternary Science Reviews* 24: 123-140.

Rose, J., Allen, P., Kemp, R.A., Whiteman, C.A. & Owen, N. 1985. The early Anglian Barham Soil in southern East Anglia. In: J. Boardman (ed.), *Soils and Quaternary Landscape Evolution.* Chichester: Wiley, 197-229.

Truffer, M.A., Harrison, W.D. & Echelmeyer, K.A. 2000. Glacier motion dominated by processes deep in underlying till. *Journal of Glaciology* 45: 213-221.

Tsytovich, N.A. 1975. *The Mechanics of Frozen Ground*. Washington DC: Scripta Book Company, 426 pp.

van der Meer, J.J.M. 1993. Microscopic evidence of subglacial deformation. *Quaternary Science Reviews* 12: 553-587.

West, R.G. 1980. *The Pre-glacial Pleistocene of the Norfolk and Suffolk Coasts*. Cambridge: Cambridge University Press, 203 pp.

Whiteman, C.A. 2002. Implications of a Middle Pleistocene ice-wedge cast at Trimmingham, Norfolk, Eastern England. *Permafrost and Periglacial Processes* 13: 163-170.

Williams, P.J. & Smith, M.W. 1989. *The Frozen Earth: Fundamentals of Geocryology*. Cambridge: Cambridge University Press, 306 pp.

Worsley, P. 1996. On ice-wedge casts and soft sediment deformations. *Quaternary Newsletter* 78: 1-7.

—Plenary Paper—

Simulations of Present Arctic Climate and Future Regional Projections

John E. Walsh
International Arctic Research Center, University of Alaska Fairbanks

Abstract

Projections of changes in permafrost require credible projections of the atmosphere that overlies terrestrial regions containing permafrost. The critical atmospheric variables for permafrost are surface air temperature and precipitation, especially snowfall. In this study, global climate models used in the Intergovernmental Panel on Climate Change (IPCC) Fourth Assessment Report are ranked on the basis of their simulations of regional Arctic temperature, precipitation and sea level pressure. When evaluated by the root-mean-square error relative to an atmospheric reanalysis, the models that perform best over the pan-Arctic and broader Northern Hemisphere domains are generally found to have the smallest errors over permafrost areas (e.g., Alaska). However, even the highest ranking model has some areas in which its simulations are problematic. The changes of temperature and precipitation projected by the highest ranking models are generally larger than the changes projected by the other models used by the IPCC.

Keywords: Arctic; climate; climate models; permafrost; temperature.

Introduction

Global climate models are the most widely used tools for projections of climate change over the timescale of a century. The periodic assessments by the Intergovernmental Panel on Climate Change (IPCC) have relied heavily on global model simulations of future climate driven by scenarios of increasing greenhouse gas concentrations. The global model simulations show a polar amplification of the greenhouse-driven warming and of other variations in climate (Serreze & Francis 2006, Wang et al. 2007), although the ratio of the models' projected changes to the natural variability is not necessarily greater in the Arctic than in lower latitudes (Kattsov & Sporyshev 2006).

Given the likelihood that the Arctic will experience greater climate changes than most other regions over the next century, the credibility of the model simulations of Arctic climate becomes a key issue when, for example, atmospheric simulations are used to drive projections of changes in permafrost. The absence of databases for validation of future climate simulations increases the importance of evaluations of models' ability to simulate recent climate, for which syntheses of observational data are available.

Greenhouse-driven climate change largely represents a sensitivity to forcing, i.e., the radiative forcing associated with carbon dioxide, methane, water vapor and other radiatively active gases, as well as associated changes in cloudiness. Hence the models' sensitivity to forcing is an essential consideration in assessing the credibility of climate projections. While changes in the radiative forcing associated with increasing greenhouse gases have thus far been relatively small (only a few Watts per square meter, IPCC 2007), a far more potent change in forcing occurs each year through the seasonal cycle of solar radiation. In the present paper, we place the models' ability to capture the *seasonal cycle* of present-day climate at the core of a strategy for evaluating the models' simulation of Arctic climate. Our evaluation is motivated by regional applications of the climate model output in the Arctic, specifically in the regions such as Alaska and Greenland where permafrost may be vulnerable to a warming climate. These regions have surface states that can be fundamentally altered by relatively small climate changes of temperature and precipitation, especially during the cold season when precipitation determines the depth and density of the snowpack that insulates the soil.

Models and Methodology

Our evaluation is based on the 20th-century simulations by the fifteen of the models used in the Fourth Assessment Report (AR4) of the Intergovernmental Panel on Climate Change (IPCC. 2007). For those models with ensembles of 20th-century simulations, only one (the first archived) simulation is used. Also, output from about seven additional models that were added to the IPCC archive after this study began is not included here. The output used here consists of the monthly grids of surface air temperature and precipitation for 1958–2000, which is a subperiod of the 20th-century simulations by these models and is also the period spanned by the validation fields (see below). The models are listed in Chapman & Walsh (2007, their Table 1). Most of the model simulations were begun in the 1800s and continued through 2000 with prescribed greenhouse gas concentrations and, in some cases, estimated sulfate aerosols and variable solar forcing (see discussion in Wang et al. (2007)). The simulations were continued through the 21st century with forcing prescribed from the IPCC's greenhouse scenarios (A2, A1B, B1, etc.). For the evaluation performed in this study, we use the output from the 20th-century simulations.

The IPCC model output is compared here against the European Centre for Medium-Range Weather Forecasts (ECMWF) Re-Analysis, ERA-40, which directly assimilates sea level pressure (SLP) observations and some air temperature observations into a reanalysis product spanning 1958–2000. Precipitation is computed by the model used in the data assimilation. The ERA-40 is one of the most consistent and

Table 1: Summary of performance rank derived from the models' RMSE for three variables: temperature, precipitation and sea level pressure over three domains: Alaska, pan-Arctic (60-90ºN) and the Northern Hemisphere extratropics (20-90ºN). An integrated rank, defined as the sum of ranks over the three domains and the three variables, is included in the right-most column.

Overall Rank	Model										
1	MPI ECHAM5	13	1	1	5	3	3	1	1	1	29
2	GFDL CM2.1	6	3	5	2	1	2	5	4	2	30
3	MIROC 3.2	2	4	3	7	6	8	10	3	5	48
4	UKMO HADCM3	11	8	6	3	2	9	4	6	7	56
5	CCCMA 3.1	12	11	10	4	8	2	8	2	4	61
6	GFDL CM2.0	6	9	14	1	10	6	4	8	4	62
7	MRI CGM2.3.2A	11	13	7	6	5	4	2	11	6	65
8	CNRM CM3	1	5	5	12	12	13	7	12	11	78
9	NCAR CCSM3	8	2	2	9	8	7	15	15	13	79
10	INMC 3.0	7	6	10	10	13	12	9	7	9	83
11	NCAR PCM1	14	13	14	8	5	10	6	5	12	87
12	CSIRO MK3.0	6	14	12	11	11	5	11	9	9	88
13	IPSL CM4	11	7	12	13	9	11	14	11	15	103
14	GISS E R	6	10	10	14	14	15	13	14	14	110
15	IAP_FGOALS1_0_G	15	15	15	15	15	14	12	13	10	124

accurate gridded representations of these variables available, and it compares favorably with other reanalyses of the Arctic (Bromwich et al. 2007). It is therefore, a logical choice for observational analyses from which we determine the model biases of late-twentieth-century surface air temperatures, precipitation and SLP. (Data and documentation for the ERA-40 can be found online at http://www.ecmwf.int/research/era/Products.). While the ERA-40 reanalysis was performed at T106 (~125 km) resolution with 60 levels, we use the version of the output archived on a 2.5° latitude x 2.5° longitude grid for compatibility with the climate model output. This grid resolution, to which the varios model grid configurations were interpolated, is typical of the resolution of the global climate models.

To facilitate GCM intercomparison and validation against the reanalysis data, all monthly fields of GCM temperature, precipitation and SLP are interpolated to the common 2.5° × 2.5° latitude–longitude ERA-40 grid. Our evaluation of the models' simulated fields uses monthly, seasonal, and annual climatological means for the late-twentieth-century period 1958-2000.

The core statistic of our validation is the root-mean-square error (RMSE) evaluated from the differences between ERA-40 and each model for each grid point and calendar month. In all cases, the differences are between climatological means for the 1958–2000 period. The RMSE calculations are performed for each of the fifteen models, for each calendar month, and area-weighted for each of three domains: Alaska, the "pan-Arctic" polar cap (60–90°N) and a middle-high latitude "Northern Hemisphere" domain (20-90°N). The Alaska domain is contained within the Arctic and Northern Hemisphere domains (except for a small portion of southeastern Alaska), so the results for the various domains are not independent. The reason for our choice of the three overlapping domains is that, although our primary interest is in the models' performance for a region that contains permafrost (Alaska), the simulation of present-day and future climate in Alaska will depend on the simulation of regions from which weather systems move toward Alaska. In particular, the larger-scale circulation over much of the Northern Hemisphere influences Alaska via advection and teleconnections, so credible simulations of future changes will depend on the models' ability to capture the large-scale circulation of the pan-Arctic and Northern Hemisphere domains.

As a seasonally inclusive measure of the models' success in simulating the regional and larger-scale climates, we sum the RMSE values over the 12 calendar months. In this respect, we are evaluating the models' ability to simulate the seasonal cycle and hence the models' sensitivities to the cycle of solar forcing. While success in capturing this sensitivity does not guarantee a realistic sensitivity to greenhouse gas forcing (infrared radiation), one may view a climate model's ability to respond to seasonally varying solar radiation as a prerequisite for a realistic response to perturbations of infrared radiation.

After summation of the regional mean RMSEs over the 12 calendar months, the sums are used to rank the models. The model with the smallest 12-month sum of the RMSE is ranked #1 for that variable and region, while the model with the largest 12-month sum of the RMSE is ranked #15. The ranks can then be summed over different variables and/or different domains, depending upon a user's priorities for variables and regional emphasis. The raw RMSE values for individual months also enable users to assess the utility of a particular model for a particular month or season.

Results

Present climate

This paper's main objective is an identification of the models that are most successful at simulating the seasonal cycle of the climates of Alaska and the Arctic. Information on the variables most relevant to permafrost is contained in Figures 1 and 2, which show the 12-month mean RMSEs of the different models, arranged in order of increasing RMSE, for the surface air temperature (Fig. 1) and precipitation (Fig. 2). Each figure contains a separate display for the three domains discussed earlier: (a) Alaska, (b) the pan-Arctic, 60–90°N, and (c) the extratropical Northern Hemisphere 20–90°N. It is apparent from these figures, especially Figure 1 for temperature, that the models vary widely in their ability to capture the seasonal climates of Alaska. For example, the yearly averaged RMSE of temperature over Alaska varies from 2.9°C in MPI-ECHAM5 to 11.0°C in IAP-FGOALS. The range for the pan-Arctic domain (60–90°N) is even greater, from 2.9°C to 13.6°C. While the ranges are smaller for the other variables, the RMSEs still vary across the models by nearly a factor of two for precipitation and by more than a factor of two for sea level pressure. Similar ranges are found for the larger domains, i.e., the pan-Arctic and hemispheric polar caps.

A noteworthy feature of Figures 1 and 2 is the tendency for some models to rank highly for both Alaska and the larger domains, although there are exceptions. Table 1 provides a synthesis of the model performance based on the RMSE metric. This table ranks the models from 1 (smallest RMSE) to 15 (largest RMSE) for each variable and domain. As in Figures 1 and 2, these ranks are based on RMSEs summed over all twelve calendar months, so they incorporate the models' successes or failures in capturing the seasonal cycle.

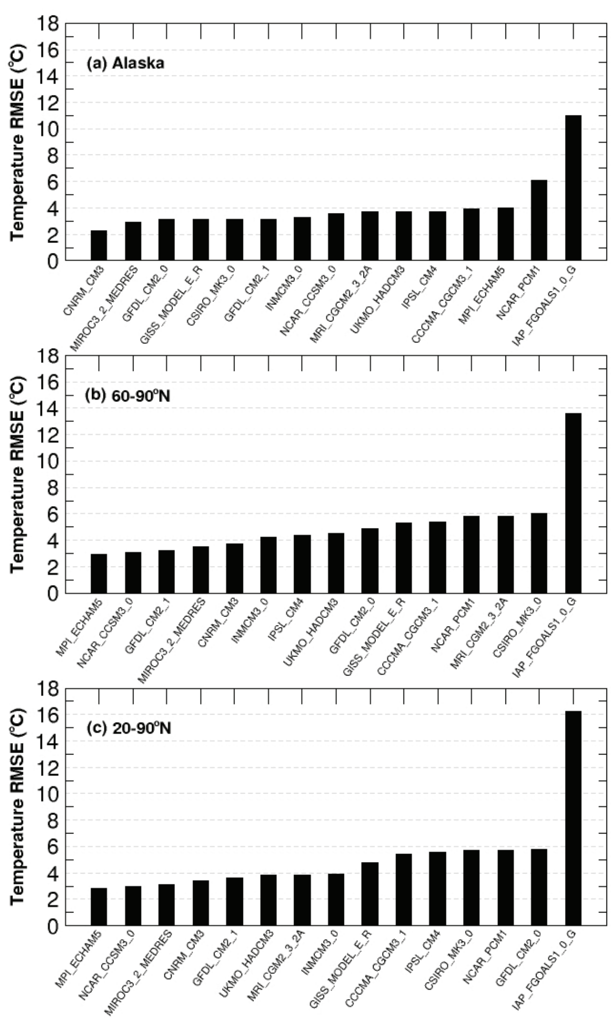

Figure 1. Area-averaged and annually-average Root Mean Square Error (RMSE) of simulated monthly mean (1981–2000) temperatures from 15 models for (a) Alaska, (b) 60–90°N, and (c) 20–90°N.

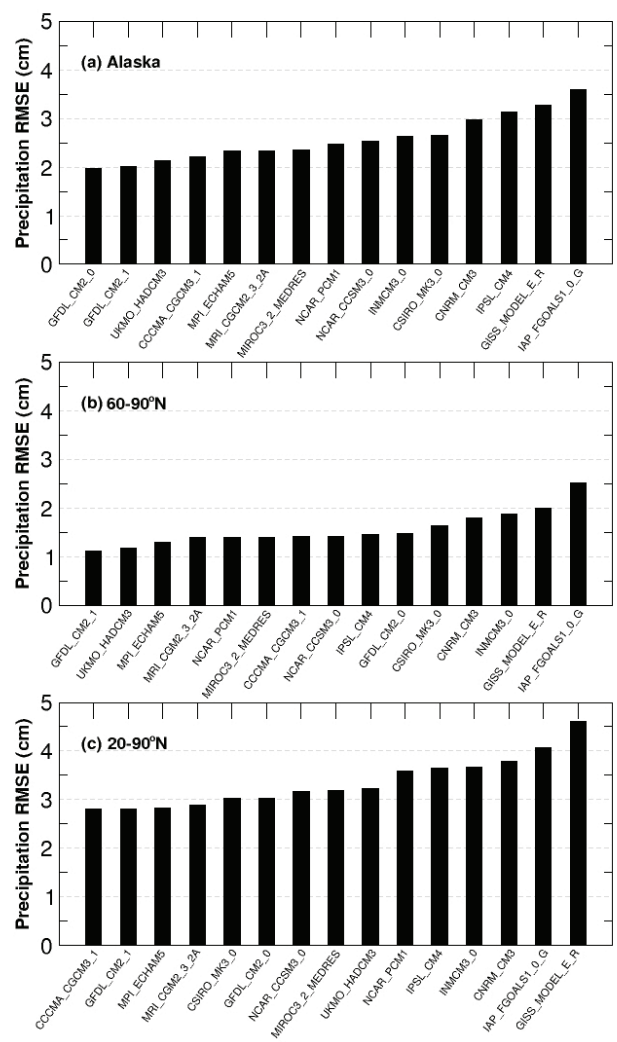

Figure 2. Area-averaged and annually-average Root Mean Square Error (RMSE) of simulated monthly mean (1981–2000) precipitation from 15 models for (a) Alaska, (b) 60–90°N, and (c) 20–90°N.

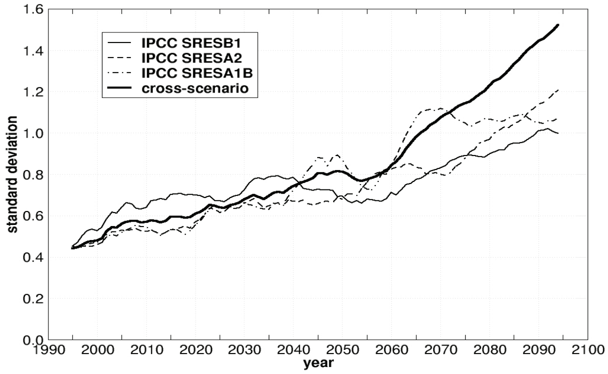

Figure 3. Across-model variability, expressed as 11-year running standard deviations of annual surface air temperature for three greenhouse gas forcing scenarios: IPCC SRES B1, A1B and A2. Also plotted is the across-scenario variability, expressed as the 11-year running standard deviation of surface air temperature across the three IPCC scenarios.

The right-most column of Table 1 is the sum of all 9 ranks (3 domains x 3 variables) of the models. We refer to this column as our "integrated rank". Because the domains are nested, this "integrated rank" effectively double-weights the model performance over the Arctic polar cap (60–90°N) and triple-weights the model performance over the Alaskan (i.e., Alaska is included in both larger domains).

It is apparent from Table 1 that, according to our metric and the integrated rank derived from it, two models outperform the others by a considerable margin. These two top-ranking models are MPI-ECHAM5 and GFDL-CM2.1. Both models consistently rank in the top five for all regions and variables, with the exception of temperatures over Alaska. As a cautionary note, MPI-ECHAM5 shows a large negative bias (and hence RMSE) of temperature during January-March over Alaska, illustrating that potentially important regional errors can be present in even the best-performing models. The MIROC3.2-MEDRES and UKMO-HADCM3 models are the third and fourth models in integrated rank, followed by the CCCMA-CGCM3.1 and GFDL-CM2.0 models.

The top-ranking models for Alaska are GFDL-CM2.0, GFDL-CM2.1, UKMO-HADCM3, MPI-ECHAM5, MIROC3.2-MEDRES (in a tie with CCCMA-CGCM3.1 and MRI-CGM2.3.2A). There is substantial overlap among the top performers for the larger domains (pan-Arctic and Northern Hemisphere) and the other subregional domains not discussed here (e.g., Siberia and Greenland).

Projected changes

A key issue underlying model evaluation is the possibility of a relationship between the models' projected greenhouse changes and the relative accuracy of the simulations of present-day climate. Before addressing this question directly, we highlight uncertainties in future projections by distinguishing the effects of uncertainties in the future greenhouse forcing scenarios (A2, A1B, B1) and uncertainties inherent in the across-model variance. In order to assess the relative contributions of these two sources of uncertainty, we evaluated (1) the intermodel variability for each scenario, expressed as centered 11-year running means of across-model standard deviations of annual temperature change; and (2) the across-scenario variability, expressed as standard deviations of projected temperature change across the three scenarios. The temporal evolution of these two measures of variability is plotted in Figure 3. The across-model and across-scenario variances in the projected temperatures are comparable through the first half of the 21st century, but the increases in variability associated with the choice of greenhouse gas scenario begin to outpace those of across-model variability by about year 2070. By the end of the 21st century, the across-scenario variability is about 50% greater than the across-model variability.

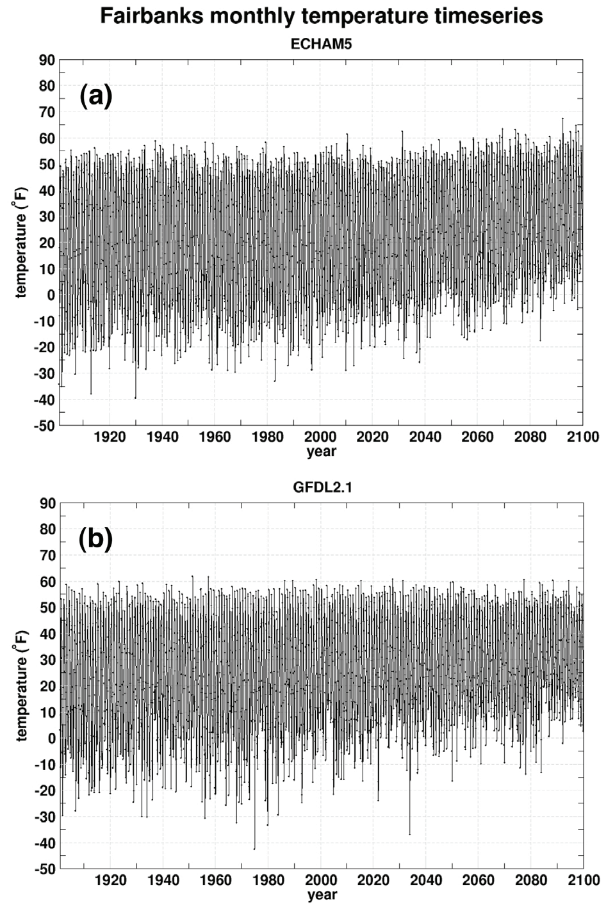

Figure 4. Monthly temperatures (ºF) at the grid cell containing Fairbanks, AK in the A1B simulations by the (a) MPI ECHAM5 and (b) GFDL CM2.1 models.

In order to illustrate the projected temperature changes, we show in Figure 4 the two time series of projected temperatures for a grid cell (near Fairbanks, Alaska) in which discontinuous permafrost is now present. The two models chosen for Figure 4 are MPI ECHAM5 and GFDL CM2.1, which have the highest integrated ranks in Table 1. It is apparent from Figure 4 that warming occurs in both models (as in all the other models). However, the warming

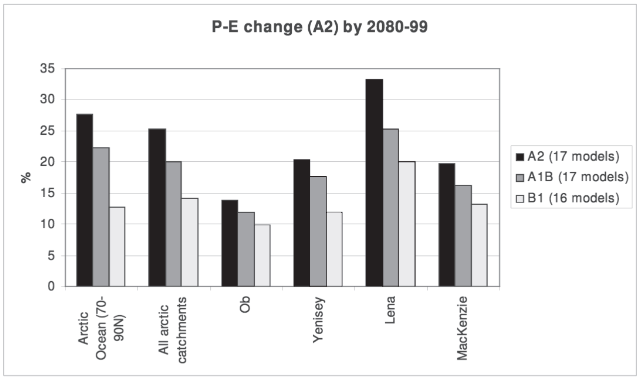

Figure 5. Percentage changes of annual mean P-E (river discharge) in A2, A1B and B1 scenarios for 2080-2099 over different regions (watersheds): the Arctic Ocean (70–90ºN), all Arctic Ocean terrestrial watersheds, the Ob, the Yenisey, the Lena, and the Mackenzie.

that is readily apparent in both the minimum (winter) and maximum (summer) temperatures in the MPI ECHAM5 model is apparent primarily only in the coldest (winter) months in the GFDL model. Most of the models show this seasonal asymmertry of the warming at Arctic locations For example, in the GFDL CM2.1 simulation, the temperature of the coldest winter month increases from about -25˚C (-12˚F) in the early 1900s to about -12˚C (+10˚F) by the 2090s. There is, however, considerable interannual variability. This interannual variability is obscured by temporal (e.g., decadal) or multi-model averaging.

Figure 5 shows the percentage increase in precipitation less evapotranspiration (P-E), averaged over various Arctic terrestrial drainage basins and over the Arctic Ocean (70-90ºN), for the 2080–2099 time slice relative to the 1980-1999 time slice for the A2, A1B and B1 scenarios. The strongest relative increase of P-E (a 33% increase in the A2 scenario) is projected for the Lena Basin, which is largely underlain by permafrost. The weakest relative change is shown for the Ob Basin, which is largely devoid of permafrost. P-E is also projected to increase over the Arctic Ocean, although the increased input of freshwater by P-E over the Arctic Ocean represents only about half the increase of P-E from projected river discharge (P-E over the surrounding Arctic terrestrial drainage basins). While the increase of P-E over the Arctic Ocean is largest in summer and autumn, the increases of P-E over the terrestrial drainage basins are largest in the winter, implying an increase of snowfall. Because snow insulates permafrost during winter, the effect of increased snowfall on permafrost may act to enhance the direct effects on permafrost of warming of the air temperature (Zhang 2005).

Figure 6a shows the models' projected warming for 60–90°N plotted as a function of the integrated rank of the models. The warming is defined here as the area-weighted linear change in surface air temperature from 2000 to 2099. While there is considerable scatter in the warming, there is a tendency for the highest-ranking models to simulate the greatest warming over the 60–90°N zone. The projected

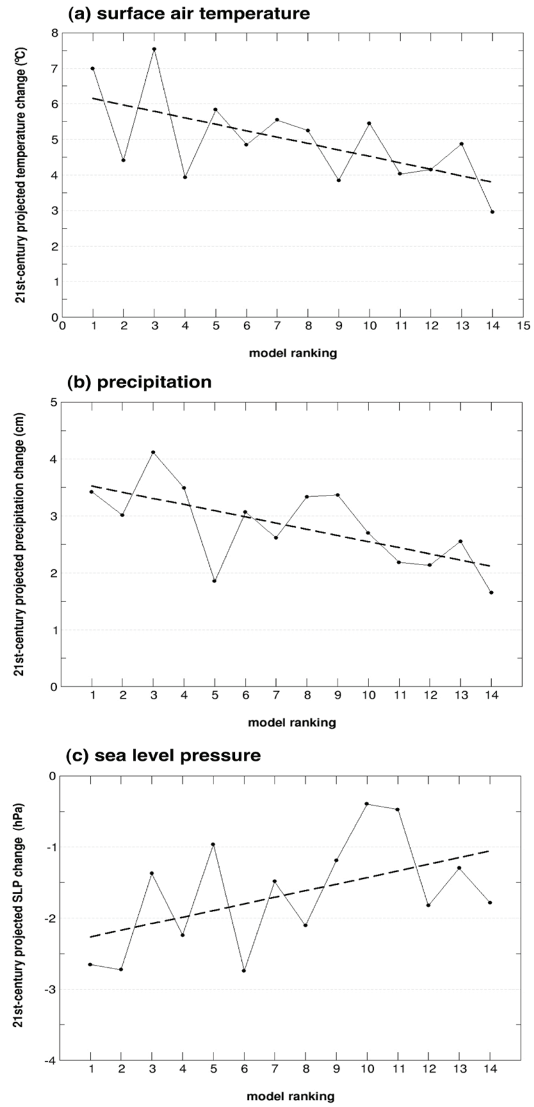

Figure 6. Projected change of (a) surface air temperature (ºC), (b) precipitation (cm) and (c) sea level pressure (hPa) averaged over 60–90ºN for 2081–2100 relative to 1981–2000. Changes are plotted vs. model performance rank (x-axis). Linear best fit is shown as a dashed line in each plot.

changes of precipitation (Fig. 6b) show a similar dependence on the models' integrated ranks, with better performing models projecting larger increases of Arctic precipitation than the lower-ranking models. While there is more scatter in the corresponding SLP results (Fig. 6c), there is a tendency for larger 21st century decreases in Arctic sea level pressure to be projected by higher-ranking models than by lower-ranking models.

Conclusion

This study has emphasized model simulations of climate over Alaska, which we have chosen because it contains large areas of permafrost. Model performance over Alaska is generally neither better nor worse than the performance over the pan-Arctic and Northern Hemisphere domains. During winter and autumn, the temperature errors over Alaska are somewhat smaller, but the precipitation errors are generally larger, than over the larger domains. The specific models that perform best over the larger domains tend to be the ones that perform best over Alaska. Although not shown here, model performance over other permafrost areas (e.g., Greenland) appears to be comparable to the same models' performance over Alaska.

In the context of permafrost, the most important results of the model simulations are the trends toward a warmer and wetter climate. A wetter climate implies more snowfall during winter. To the extent that snow cover insulates the soil during winter, the changes in the two main controls of permafrost temperatures will favor a warming of permafrost in areas such as Alaska. (Osterkamp 2007) However, the warming also implies a shorter snow season. A high priority for research is the determination of net effect of two competing changes of snow: larger snowfall rates during the cold season, but a shorter snow season.

There is a tendency for the models with the smaller errors to simulate a larger greenhouse warming over the Arctic. Since several models have substantially smaller systematic errors than the other models, the differences in warming imply that the choice of a subset of models may offer a viable approach to narrowing the uncertainty and obtaining more robust estimates of future climate change in regions such as Alaska and the broader Arctic. The results obtained here suggest that the uncertainty might be narrowed by eliminating models with the weaker projected warming in the Arctic, as those models tend to have the largest errors in simulations of the present-day climate. Such an approach has already been suggested by Overland & Wang (2007) and Kattsov & Sporyshev (2006), and will be pursued in future assessments of Arctic change.

A key limitation of this study is the coarse resolution of the global climate models, which are not able to resolve many of the topographic features that are crucial to permafrost distribution. The differences between north-facing and south-facing slopes within a grid cell represent one such example. In order to include finer-scale features, it will be necessary to employ either (a) statistical downscaling approaches using algorithms trained on observational data, perhaps including permafrost measurements, or (b) regional climate models, which effectively provide a "dynamical downscaling". Since regional climate models are driven at their lateral boundaries by the output from global models, and since statistically downscaling of projections requires global or regional model output, the global model assessment described here has relevance to downscaling approaches. Moreover, the permafrost community is generally ahead of the global climate modeling community in the sophistication of modules used to simulate permafrost. Given that this situation is likely to persist as permafrost models improve, the optimum strategy for projecting future changes of permafrost may be to utilize off-line permafrost simulations driven by downscaled output (including snowfall) from large-scale models.

Acknowledgments

This work was supported by the National Science Foundation, Office of Polar Programs through Grant OPP-06533 and by Grant OPP-0327664, the Cooperative Agreement between the National Science Foundation and the International Arctic Research Center.

References

Bromwich, D.H., Fogt, R.L., Hodges, K.I. & Walsh, J.E. 2007. A tropospheric assessment of the ERA-40, NCEP and JRA-25 global reanalyses in the polar regions. *Journal of Geophysical Research* 112: D10111, doi:10.1029JD007859.

Chapman, W.L. & Walsh, J.E. 2007. Simulations of Arctic temperature and pressure by global climate models. *Journal of Climate* 20: 609-632.

IPCC (Intergovernmental Panel on Climate Change). 2007. *The Physical Basis of Climate Change*. Working Group I, Fourth Assessment Report of the Intergovernmental Panel on Climate Change, Cambridge University Press, Cambridge, U.K., 1099 pp.

Kattsov, V.M. & Sporyshev, P.V. 2006. Timing of global warming in IPCC AR4 AOGCM simulations. *Geophysical Research Letters* 33: L23707, doi:10.1029/2006GL027476.

Kattsov, V.M., Walsh, J.E., Chapman, W.L., Govorkova, V.K., Pavlova, T.V. & Zhang, X. 2007. Simulation and projection of Arctic freshwater budget components by the IPCC AR4 global climate models. *Journal of Hydrometeorology* 8: 571-589.

Osterkamp, T.E. 2007. Causes of warming and thawing permafrost in Alaska. *EOS, Transactions of the American Geophysical Union 88:* 522.

Overland, J.E. & Wang, M. 2007. Future climate of the North Pacific Ocean. *EOS, Transactions of the American Geophysical Union* 88: 178-182.

Serreze, M.C. & Francis, J. 2007. The Arctic amplification debate. *Climatic Change* 76: 241-264.

Wang, M., Overland, J. E., Kattsov, V., Zhang, X. & Pavlova, T. 2007. Intrinsic versus forced variation in coupled climate model simulations over the Arctic during the twentieth century. *Journal of Climate* 20: 1093-1107.

Zhang, T. 2005. Influence of the seasonal snow cover on the ground thermal regime: An overview. Rev. Geophys. 43: RG4002, doi10.1029/2004RG000157.

The Freezing Process Deformation of Soil Under Higher Confining Pressure

Dayan Wang, Wei Ma, Zhi Wen
State Key Laboratory of Frozen Soil Engineering, Cold and Arid Regions Environmental and Engineering Research Institute, CAS, Lanzhou, China

Abstract

This paper describes results from a series of laboratory tests carried out after the samples subjected to the K_0 consolidation process, which could simulate the deep soil stratum-forming history. The observed results from these tests have shown that the high of the soil sample under higher confining pressure decreases with the soil temperature decreasing, and the downtrend will stop and keep a constant when the temperature reaches a desired level. The variation of the specimen size depends on the confining pressure, soil temperature, and soil type. For soil under the same temperature level, the higher the initial confining pressure, the smaller the variation of the specimen size. For a soil under the same confining pressure level, however, the high of the higher negative temperature soil specimen will reduce unceasingly. When the soil temperature is lower than -5°C, the fluctuation of the soil temperature hardly influences the final high of the soil specimen. In addition, the high variation of the loess sample is much less than the sand sample under the same other factors.

Keywords: artificial frozen soil; higher confining pressure; K_0 consolidation.

Introduction

Ground freezing has been recognized by mining and civil engineers as undoubtedly the most effective and consistently reliable method of providing temporary support and of preventing groundwater from flowing into deep excavations. Its uses does not deplete aquifer reserves by continuous pumping, nor does it pollute or alter the groundwater regime in any way, thus eliminating any adverse affect on adjacent structures, installations, and populations. Frozen wall design and construct, based on how to reasonably choose the physical-mechanical parameter of artificially frozen soils, is a key factor affecting the application of this technology. Therefore, in the last 20 years, a lot of research has been carried out in relation to the test techniques, physical parameters, mechanical characteristics, and freezing temperature of deep soils (Cui et al. 1998, Ma et al. 1993, 1995, 1999, 2000, Ma & Chang 2002, Zhou et al. 1999, Wang et al. 2002), and drawn a series of significant results. Although the obtained results could resolve some practical difficulties arising from the application of artificially frozen soil construction, we could not obtain the reasonable strength theory and the constitutive model of frozen soil forming in the deep alluvium. Generally, the mechanical properties of the frozen soils are influenced by its physical characteristics. The study of soil deformation properties in the process of freezing under higher confining pressure is involved in the stability of the surface construction and is particularly important for establishing the constitutive model of artificially frozen soil forming under the deeper stratum. However, very few experimental data on this problem exist because of the technical difficulties; for example, how to restore the tested soil to the original state of deep alluvium and then freeze it in the laboratory, and the time-consuming nature of the above-mentioned process. Guided by the earlier studies, this paper was designed to study the features of deep soil deformation during freezing under different negative temperature, initial confining pressure, and soil type. Among these, the initial confining pressure represents the degree of the stratum depth.

Preparation of Specimens and Test Procedure

The soils used in the current study were typical Lanzhou loess and Lanzhou sand, and their engineering properties are shown in Table 1a and Table 1b. The testing scheme is found in Table 2.

Table 1a. The basic physical properties of sand specimens.

Soil type	Composition of grains (%)				Dry density	Water content
Lanzhou	＞0.5	0.5～0.05	0.05～0.005	＜0.005	g/cm^3	%
sands	25.6	54.23	8.04	12.13	2.0	10.5

Table 1b. The basic physical properties of loess specimens.

Soil type	Composition of grains (%)				Liquid limit (%)	Plastic limit (%)	Dry density (g/cm^3)	Water content (%)
Lanzhou	＞0.1	0.1～0.05	0.05～0.005	＜0.005				
loess	1.7	5.4	58.6	34.3	24.6	17.7	1.78	16.5

The procedure for preparing the sample is generally performed according to the Specification of Soil Test (GB/T50123–1999) issued by the Ministry of Water Resources, PRC. All the specimens, typically 61.8 mm in diameter and 125 mm in height, were compacted in 6 layers, with a relevant density and water content according to the different soil types, shown in Table 1. The specimen was then covered with rubber sleeves to prevent evaporation of water, and put into the K_0 consolidating instrument, which was developed by our laboratory and used the working principle of oil side-limiting control with the greatest confining pressure of 15 MPa and the lowest temperature of -60°C. In this chamber, the specimen could experience drained triaxial compression before freezing. This process can simulate an increase of overburden, and restores the loading history and initial stress states of soils in the field.

To assure that the soil sample does not laterally deform, the static lateral pressure coefficient of the tested soils was obtained from preliminary experimental study (Ma & Cui 2000). The consolidating pressures were controlled at a certain rate, shown in Table 2. When the confining pressure reached the desired pressure, the loading process stopped and began to lower the temperature. The axial deformation was automatically measured by the axial pressure system monitoring the changes of axial displacement, and the data were collected continually by computer.

Table 2. The controlling parameters of this experiment.

Soil type	K_0	Speed of the axial loading（MP/s）	Speed of the radial Loading (MP/s)
sands	0.32	10×10^{-5}	3.2×10^{-5}
loess	0.34	10×10^{-5}	3.4×10^{-5}

Results and Discussion

Influence of soil temperature on the deformation

Temperature is a key factor in the study of frozen soil formation, for frozen ground is defined as soil or rock having a temperature below 0°C. The data presented in Figure1 show the ΔH with the time, where ΔH is defined as the variation of sample height obtained in the freezing process. From Figure 1, we can conclude that the high of the loess sample became sharply reduced with the ambient temperature decrease. When the sample temperature is consistent with the ambient temperature, the variation of the sample height is related to the frozen soil temperature status. The lower the surrounding temperature, the more steady the deformation of the sample, and the shorter the time needed to reach stabilization. With

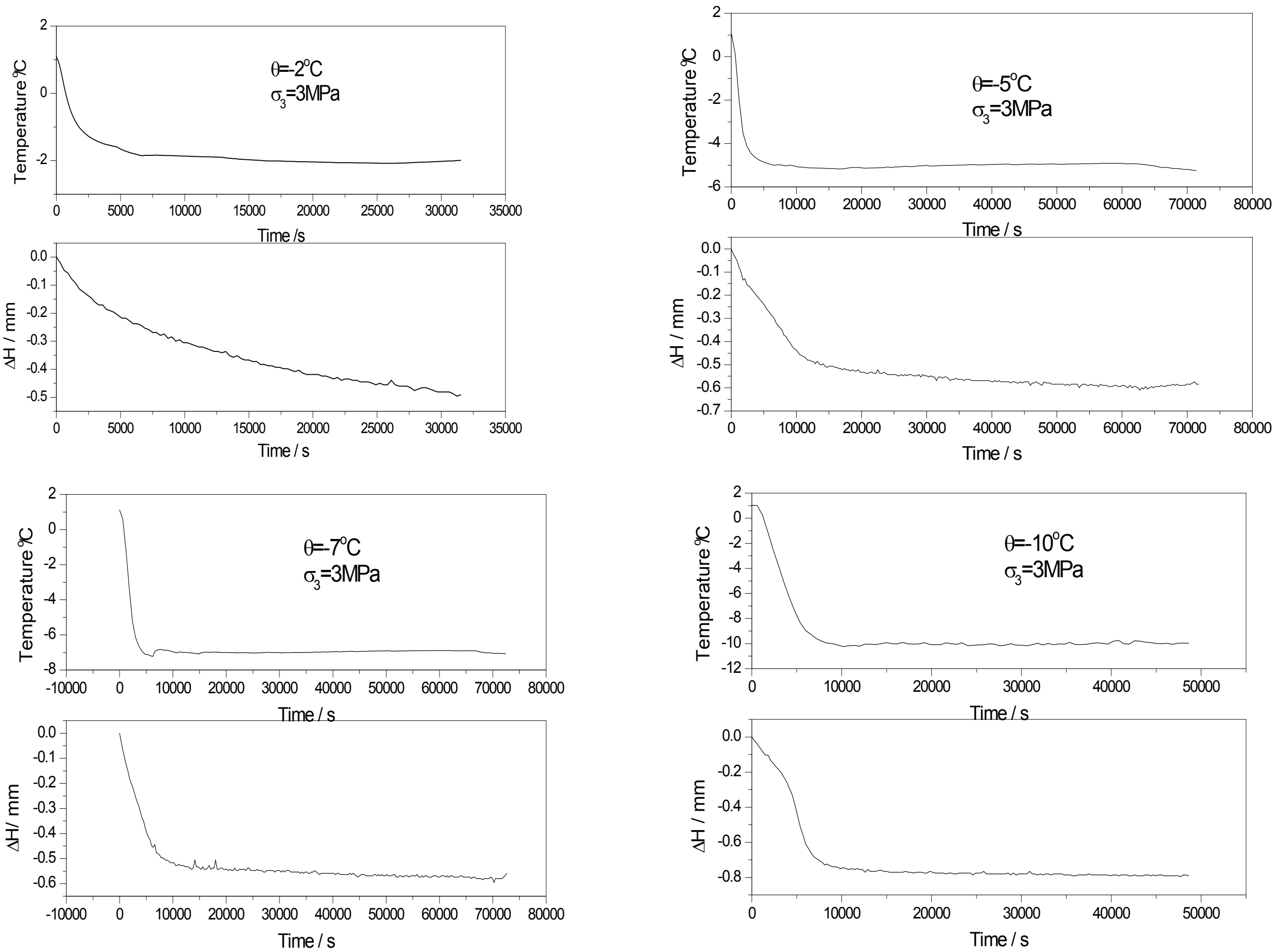

Figure1. Effect of the frozen soil temperature on the variation of loess specimen high in the process of freezing.

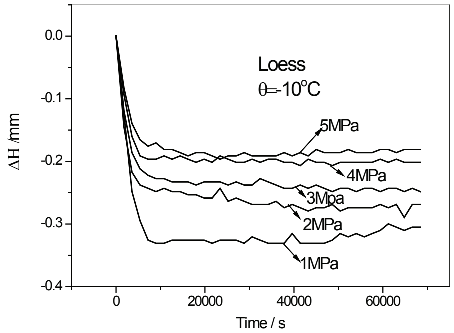

Figure 2. Effect of the initial confining pressure on the variation of loess specimen high in the process of freezing.

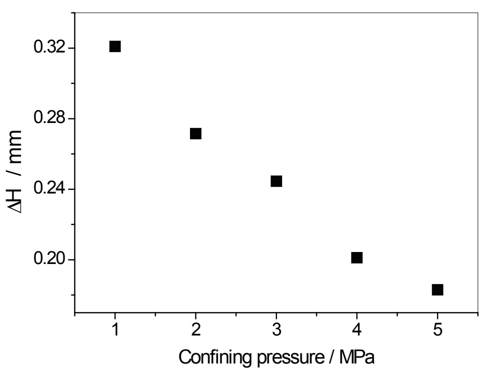

Figure 3. The variation of loess specimen high versus the initial confining pressure.

respect to soil frozen to a temperature lower than -5°C under the same initial confining pressure, the time that the sample deformation reaches stabilization almost equals the time of the surrounding temperature reaching the desired temperature. The sample high variation is about 0.6 to 0.8 mm and independent of the soil temperature. However, for frozen soil with a temperature higher than -5°C, the axial deformation progresses ceaselessly, even though the soil temperature is equal to the surrounding temperature.

Influence of the initial confining pressure on the deformation

Figure 2 shows the variation of the sample high with time from the lowering temperature to -10°C process on the loess subjected to K_0 consolidated to confining pressure σ_3 of 1~5MPa, respectively. From Figure 2, we can conclude that the sample high reduces sharply with the surrounding temperature dropping, and then stops and holds a constant when the sample temperature equals the surrounding temperature. The variation of frozen sample high was heavily influenced by the condition of the initial confining pressure. If the variation of the sample high was taken as the deformation resulted from freezing the soil, we can find from Figure 3 that the deformation of the sample after having been frozen was linearly decreased with the initial confining pressure increase.

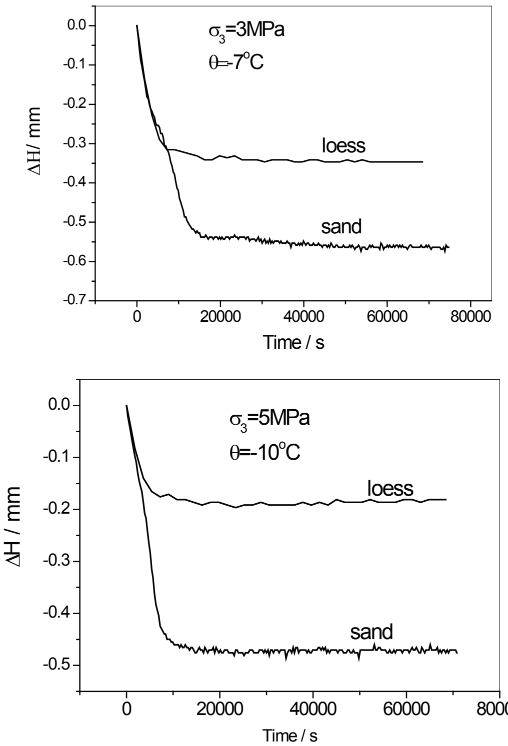

Figure 4. Comparison of the specimen high variation of the two types of soils used in this study.

Table 3. Comparison of the specimen high variation of the two types of soils used in this study.

confining stress	1MPa	2MPa	3MPa	4MPa	5MPa
sand	0.7214	0.5858	0.5364	0.6541	0.471
loess	0.3209	0.2715	0.2445	0.2012	0.183
differential value	0.4	0.314	0.2919	0.453	0.288

Influence of the soil type on deformation

The variation of deformation in the freezing process is affected by characteristics of the soil type. It can be concluded from Figure 4 that the deformation of the sample is larger than that of the loess sample under the same initial confining stress and negative temperature, despite the sample's high decrease when the temperature drops to -7°C or -10°C. After the loess sample and the sand sample experienced the K_0 consolidation process under initial confining stress varying from 1 to 5MPa and completely frozen, a comparison of the variation sample high obtained that the deformation of sand sample is larger than that of loess under the same other condition, and the difference is about 0.3 to 0.4 mm (see Table 3). This suggests that, even for the samples consolidated to the same confining pressure and frozen at the same negative temperature by the same method in the process of using artificial ground freezing to reinforce ground, the soil group would heavily influence the deformation of the freezing soil, causing differential settlement of the ground surface. The builder must consider this point in the design.

Conclusions

It is important to recognize that the deep artificial ground freezing process could cause stratum settlement. This study simulated the deep artificial ground freezing process in the laboratory by K_0 consolidation and presented the findings of a comprehensive study of the effects of the stratum depth, frozen soil temperature, and soil group on settlement expressed by the sample deformation. The following conclusions can be drawn:

1. When the surrounding temperature drops to lower than 0°C, the high of the soil sample subjected to K_0 consolidation will decrease with the temperature decreasing. Until the temperature reaches the desired temperature, the variation of soil sample high stops and keeps a constant level. Therefore, freezing the deep soil could lead to settlement of surface ground. The magnitude of settlement is decided by the soil depth, frozen soil temperature, and soil group.
2. In the process of freezing, deformation of the soil sample was linearly decreased with the initial confining stress increase; namely, with the stratum becoming deep, the sample deformation produced by freezing the soil will decrease.

Sample deformation caused by the freezing process was affected by the soil group. In the range of the studied confining pressure, the deformation of sand was always larger than that of loess. The differential value is about 0.3 to 0.4 mm.

Acknowledgments

This research was supported by the Project for Incubation of Specialists in Glaciology and Geocryology of the National Nature Science Foundation of China (J06309966), the key Program of the National Natural Science Foundation of China (No.50534040), the Talent Training Program for Young Scientists in West China of the Chinese Academy of Sciences, the Special President Scholarship of CAS for Postgraduate Students, and the PYRN Educational Stipend.

References

Cui, G. 1998. Mechanics of frozen soil for deep alluvium: A new field of frozen soil mechanics. *Journal of Glaciology and Geocryology* 20(2): 97-100 (in Chinese).

Ma, J. & Cui, G. 2000. Experimental study of K_0 consolidation in deep alluvium. *Annual Report of State Key Laboratory of Frozen Soil Engineering*, Vol. 9. Gansu Province: Xinhua Press, 135-142 (in Chinese).

Ma, W., Wu, Z. & Zhang, C. 1993. Strength and yield criteria of frozen soil. *Proceedings of the Sixth International Conference on Permafrost, South China*. Beijing: University of Technology, 432-435.

Ma, W., Wu, Z. & Chang, X. 1995. Effect of confining pressure on strength behaviour of frozen soil. *Chinese Journal of Geotechnical Engineering* 17(5): 7-11 (in Chinese).

Ma, W., Wu, Z., Zhang, L. & Chang, X. 1999. Analyses of process on the strength decrease in frozen soils under high confining pressure. *Cold Regions Science and Technology* 29(1): 1-7.

Ma, W., Wu, Z. & Chang, X. 2000. Effect of consolidation process on stress-strain characters of frozen soils. *Rock and Soil Mechanics* 21(3): 198-201 (in Chinese).

Ma, W. & Chang, X. 2002. Analyses of strength and deformation of an artificially frozen soil wall in underground engineering. *Cold Regions Science and Technology* 34(1): 11-17.

Wang, D., Ma, W. & Chang, X. 2004. Analyses of behavior of stress-strain of frozen Lanzhou loess subjected to K0 consolidation. *Cold Regions Science and Technology* 40: 19-29.

Zhou, G., Cui, G., Cheng, X. et al. 1999. An experimental frame for geomechanical engineering simulation and its application. *Chinese Journal of Geotechnical Engineering* 21(6): 715-718.

Tower Foundation Engineering in a Patchy Permafrost Area Along the 110-kV Power Transmission Line from Amdo to Damxung, Tibet, China

Guoshang Wang
Gansu Electric Power Design Institute, Lanzhou 730000, China

Fengxian Yu, Weidong Cao, Xiaoqi Meng, Yong Liu, Changjin Yang, Yueming Guo
Southwest Electric Power Design Institute, Chengdu 61002, China

Huijun Jin, Xiaoli Chang, Qihao Yu, Jianming Zhang
State Key Laboratory of Frozen Soils Engineering, Lanzhou 730000, China

Abstract

The 110 kV power transmission line from Amdo to Damxung, Tibet, is in the patchy permafrost zone in southcentral Tibet. Frost heave/thaw settlement of the tower foundation soil was one of the major challenges for geotechnical design and construction. Surveys on frozen ground conditions were conducted for assessing frost hazards. The thermal and strain/stress interactions of tower foundation and soils were monitored, tested in situ and in the laboratory, and analyzed. Shallow oblique and straight concrete-column foundations and thermosyphon-cooled pile foundations were proposed and adopted with proven mitigative results. Tower site selection and ground improvement were proven most cost-effective. Data-bank and engineering measures, as well as experiences from the 110 kV power line were very helpful for the design and construction of the proposed 400 and 750 kV power transmission lines and other linear foundation engineering in warm, elevational permafrost regions on the Qinghai-Tibet Plateau.

Keywords: frost-hazard mitigation; ground-improvement; 110-kV power-line; permafrost; site-selection; tower foundation.

Introduction

Towers for transmission lines are commonly either self-supporting or guyed. A tower supported on the top of frost zone will experience frost heave with the presence of frost-susceptible soil and available moisture. The seasonal vertical movement may be detrimental. If the heave is differential between footings supporting the tower, the tower will tip and/or the structure will be unevenly stressed. The guyed tower might experience an overstressing of the guys or of their anchors. Differential footing settlements may occur during thaw-weakening in spring. If the tower is on a slope, progressive downslope movement may occur with successive freeze-thaw cycles.

Granular material may be used to control or eliminate detrimental vertical movement. Due to the intense winter cold, it is usually impractical to make the mat thick enough to completely prevent frost penetration or heave in the underlying frost-susceptible mat, particularly when the mat is naturally well-drained. However, the magnitude of frost heave may be substantially reduced by a relatively modest surcharge, consisting of the weight of the gravel plus the load from the structure (U.S. Department of Defense 2004). Pile foundation with flanged sleeves to isolate the pile from frost heave forces also can be used.

However, studies closely related to the tower foundations of power transmission lines are limited. Myska & How (1978) presented a case study for installation of pile foundations for a microwave tower system, Gillam-Churchill, Manitoba, Canada. This is a route of about 250 km in the continuous and widespread permafrost zones. In this case study, grouted rod anchors for the tower guys were installed without pre-design subsurface investigations, and the subsurface investigations for the foundations were conducted concurrently, using anchor installation drilling equipment. Precast concrete piles were installed in augered holes. To avoid on-site concreting, the pile caps were constructed of pre-fabricated structural steel.

The 110 kV transmission line from Damxung to Amdo in southcentral Tibet originally was to supply the power needed for engineering construction and operation of the Qinghai-Tibet Railway system at an average elevation of 4500 m. It was the first 110-kV transmission line in the permafrost region on the Qinghai-Tibet Plateau. The 281-km line starts from Damxung in the south and via Nagqü, ends at Amdo in the north, of which 173 km is from Damxung to Nagqü and 108 km from Nagqü to Amdo (Fig. 1). The line traverses regions of patchy permafrost, extensive taliks, and seasonally frozen ground in the vicinity of the southern lower limit of permafrost on the Qinghai-Tibet Plateau.

Large amounts of then-existing data, research papers and reports, previous engineering experiences, and lessons learned were collected and analyzed for the route selection and for the subsequent preliminary and detailed designs for construction for this unprecedented power line on the Qinghai-Tibet Plateau. These data and studies generally included, but were not limited to, published research and review papers on permafrost and cold regions engineering, frozen ground engineering geology reports for the design, construction, and operation of the Qinghai-Tibet Highway, the Golmud to Lhasa fiber-optic cables and an oil products

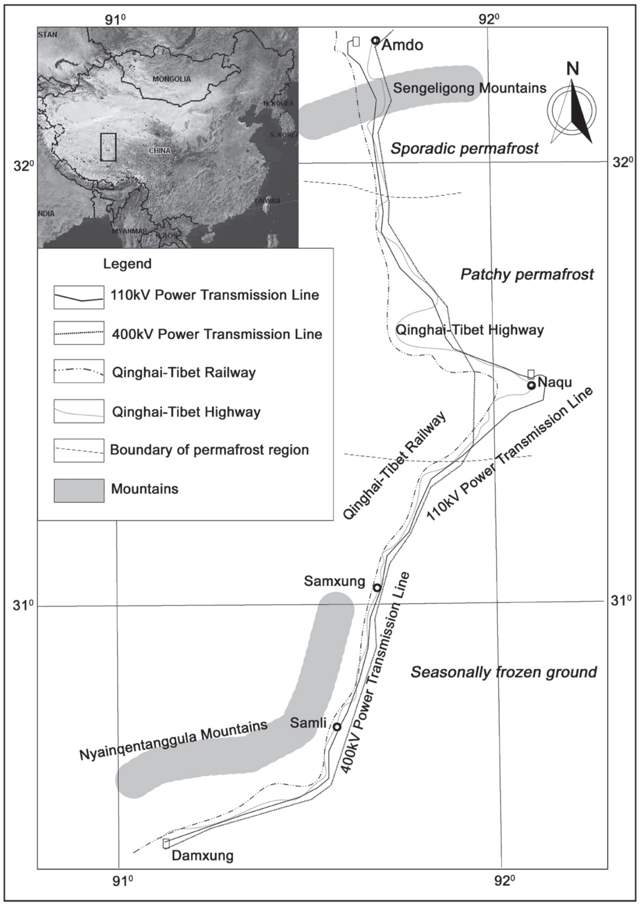

Figure 1. Sketch map of the study region from Amdo to Damxung on the Qinghai-Tibet Plateau.

Figure 2. Landscape of patchy permafrost zone north of Amdo on the Qinghai-Tibet Plateau, with the 110 kV power transmission line crossing the Amdo River in southern front of the Shengeligongshan Mountains.

pipeline. Experts on frozen ground engineering from the Cold and Arid Regions Environmental and Engineering Research Institute, Chinese Academy of Sciences were consulted and their advice sought for in situ engineering surveys, design, and construction. Data on meteorology related to the Qinghai-Tibet Railway, then under construction, also were gathered and analyzed. The planning of the power line began in September 2002. All preliminary and construction designs were completed, reported, reviewed, and delivered by December 2003.

The majority of the power line route is located in areas impacted by seasonal frost, but some sections also are affected by warm, patchy, and ice-rich permafrost. Therefore, it was highly desirable to clearly delineate the interfaces and depths of frozen ground in order to cost-effectively design and build the transmission line tower foundations. Frost heave and thaw settlement are the two most frequently occurring hazards, which can induce abnormal differential deformation strains and stresses in frozen soil foundations and subsurface infrastructures. However, studies on the impacts of frozen ground on the safety and long-term stability of tower foundations for transmission lines were very limited in China before the early 2000s.

Power transmission lines are very important for construction of key engineering projects and for the sustainable societal and economic development in a region. However, the constraints for their engineering reliability and long-term stability are very exacting. Although the power transmission lines share some common features with other linear engineering projects, their survey, design, and construction for the frozen ground engineering geology are unique and site-specific because of the large distance between towers and the elevation/suspension nature of power lines compared to other linear engineering infrastructures such as roads and pipelines. The related surveys, selection of foundation types, design, and construction of tower foundations directly or indirectly affect the safety, integrity, long-term stability, profitability, and societal benefits. Therefore, differential frost heaving and thaw settlement are paid great attention during all phases (surveys, design, and construction) of power-line foundation engineering.

Because of its proximity to the southern lower limit of the plateau-elevation permafrost, potentials of frost heaving, sensitivity to thaw settlement of foundation soils, and depths of seasonal frost and thaw penetration in tower foundation soils vary markedly, even over short distances. Adverse cryogenic hazards resulting from freeze-thaw processes occur extensively and frequently. Their impacts on tower foundations are complicated and highly uncertain in various spatio-temporal scales due to their migratory nature. Therefore, the boundaries and depths of the permafrost table or seasonal frost penetration and frozen or unfrozen soils, as well as adverse cryogenic features, should be well understood in order to provide reliable criteria for designing cost-effective tower foundations and/or mitigative measures of hazardous foundation soils.

Frozen Ground Along the Power Line Route

The elevation along the power line route ranges from 4200 m to 4980 m. The topography is gentle and open, with relative relief generally less than 500 m. The annual mean air temperatures generally are colder than 0°C. Frozen ground, predominantly seasonally frozen ground, is found

Table 1. susceptibility classification of permafrost (revised from State Forestry Administration 2001).

coefficients	δ <1	1< δ <3	3< δ <10	10< δ <25	δ >25
Thaw-sensitivity	Insensitive	Weakly sensitive	Sensitive	Very sensitive	Collapsing

extensively at all terrains from Nagqü to Damxung, and permafrost is generally found in the Amdo area.

Patchy permafrost

Patchy permafrost is generally connected with the active layer in areas north of Amdo, but it is separated from the active layer by a talik layer in the south (Wang & Wang 1982). Permafrost at elevations above 4700 m between Amdo and Damxung occurs in the Shengeligongshan Mountains, in intermontane basins in the vicinity of Highway Maintenance Squad Stations (HMSSs) 119, and 121 to 124 along the Qinghai-Tibet Highway, in the wetlands in the Liangdaohe River Basin (Figure 1). Patchy permafrost generally occurs in locations with better moisture conditions, fine-grained soils, and good vegetative cover favoring the development and protection of permafrost (Jin et al. 2007a, 2007b) (Fig. 2). Hazardous periglacial phenomena such as frost mounds and icings also are well developed.

Seasonally frozen ground

Seasonally frozen ground generally is found in intermontane basins between the Shengeligongshan Mountains and HMSSs 119, between HMSSs 121 and 122, 122 and 124, where permafrost occurs. The depths of seasonal frost penetration are 3.7–3.9 m in the Amdo area, 2.8–3.0 m in the Nagqü area, and 1.2–1.5 m in the Damxung area, as revealed by meteorological data. Ground surveys also confirm that seasonal frost penetration depths vary greatly from 1.2–4.0 m from Amdo to Damxung.

Hazardous periglacial phenomena

Pingos, seasonal frost mounds, and icing generally occur in concentrated small areas from HMSS 119 to the Liangdaohe River. Most of their occurrence is controlled by active faults (Wu et al. 2004, 2005, Jin et al. in press). Retrogressive thermal slumps also are found in very limited areas and are avoided.

Frozen Ground Engineering Geology

Classification of frozen soils for engineering purposes

On the basis of ice content, frozen soils were divided into 5 types: ice-poor, ice-medium, ice-rich, ice-saturated permafrost, and ice layers with soil inclusions. On the basis of frost heaving coefficients, the frost-heave susceptibility of soils was similarly divided into five grades: non-frost heave, weak frost heave, frost heave, strong frost heave, and very strong frost heave (State Forestry Administration 2001).

Frost heaving of seasonally frozen ground

The magnitude of vertical frost heave differs significantly with depth, even in a uniform soil layer, due to moisture migration and subsequent ice segregation. Generally, the major frost heaving occurs at depths less than two-thirds of the maximum depth of the seasonal frost penetration (State Forestry Administration 2001).

Moisture and the content of fine-grained soil are the major factors leading to frost heave in foundation soils. Drainage conditions of excess water from the foundation soil also influence frost-heave forces. To mitigate the impact of frost heave, one needs to eliminate the effect of soil moisture by using lubricants (generally hydrophobic material such as bitumen mixed with 5% used machine oil, industrial vaseline, or heavy oil) on the walls of the tower foundation, separating foundation and soil. When foundation soils are rich in soil moisture or water supply, mixing and heating of coarse sands with used oil (1:6 in weight), placing a 20-cm-layer of this mixture around the foundation, and compacting well offered one solution. Drainage controls such as ditches and a water-retaining berm on the shaded side of the tower, especially on the slope in the permafrost regions, can be applied to prevent re-entry of ground water to tower foundation soils. The effect of fine-grained soil can be reduced by replacing it with well-compacted, clean gravel (the <0.074 mm clay less than 12%) within 0.5 m around the foundations outer surface. Refills for bedrock tower locations should be well-compacted gravels, and the outer surface of the tower foundation should be lubricated.

On the basis of coefficients (δ), which are a percentage of volumetric settlement of vertical column of tested soil, the thaw-sensitivity of permafrost, can be divided into five grades as in Table 1.

Research on Frozen Subsoil

Analysis of frost-heave forces

The normal frost-heave forces toward the bottom of foundation were mitigated by deeper (greater than maximum frost or thaw penetration depth) burial of the tower foundation. The mitigative effect was enhanced using with well-compacted gravel to a depth of 0.3–0.5 m beneath the tower foundation.

For tower foundation in areas impacted by seasonally frozen ground, a lubricant separating foundation wall from subsoil was used for tower location with weak frost- heaving subsoils. For subsoils with frost heave to very strong frost heave susceptibility, a mixture of used oil and coarse sand was placed within 0.2 m around the foundation and compacted well after lubricating the foundation walls. The impact of fine-grained soil also was mitigated by clean gravel refill within 0.5 m around the foundation outer surface. Drainage control ditches on the shady side of the tower also were used on the slopes to cut off the surface water supply to foundation soils. Deeper burial of the tower foundation, compacted

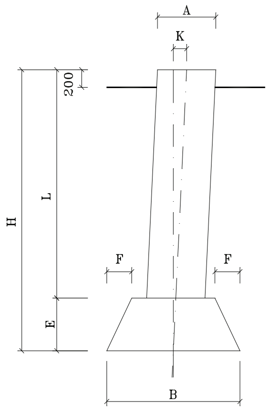

Figure 3. Sketch map of the oblique reinforced concrete column foundations for the power line tower.

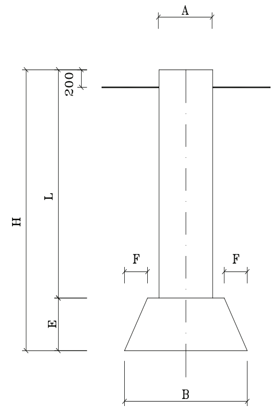

Figure 4. Straight reinforced concrete column foundation with constant cross-section.

gravel, reinforced structural integrity, and spatial stiffness were used to reduce deformation of foundation soils.

Soils above the permafrost table subjected to tangential seasonal frost-heave forces were mitigated using similar approaches. After the in-situ concrete-pouring during construction, permafrost temperatures beneath the bottom of the foundation rose, leading to thawing or thinning of permafrost. Therefore, the bearing capacity of unfrozen soils was used in design for safety. Deeper burial of tower foundation also was used to alleviate deformation of foundation soils.

In addition, the foundations were poured shortly after excavation, keeping the permafrost temperature as close to the original as possible. Thick ground-ice layers beneath tower foundations were removed. Local environmental and geological conditions were protected as cost-effectively as possible. Abandoned construction materials or soils were removed from around the tower foundations, and the ground surface was re-vegetated.

Design of Tower Foundations

Shallow foundation

Oblique column foundations of reinforced concrete (Fig. 3) to distribute the stresses were used extensively for the transmission line in montane areas. Frost-heave force was generally small, because the freezing of the subsoil generally lasted less than two months and resulted in very shallow (<1 m) seasonally frozen ground. Wind speed is generally less during the cold season, and frost-heave force is less than the anchorage force of the bottom of the foundation, satisfying the safety criteria for tower foundations.

Straight, reinforced concrete column foundation with constant cross-section (Fig. 4) also was used. Because the freezing time of subsoil was still short in shallow (<2 m) seasonally frozen soil regions, frost-heave forces were mainly affected by the subsoil features and moisture contents, satisfying the safety requirement of the transmission lines.

Straight reinforced concrete column foundation with variable cross-section areas (Fig. 5) was used where the subsoil freezing is long in deep (>2 m) seasonally frozen soil regions. This form of foundation more reasonably balanced the loads, made full use of material and effectively minimized the side surface area, such as to use the cylinder column, to reduce the tangential frost-heave forces.

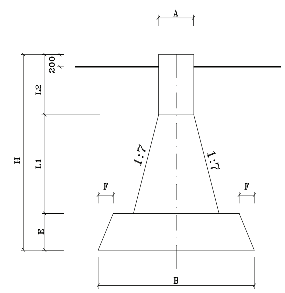

Figure 5. Straight reinforced concrete column foundation with variable cross-section.

Pile foundation

Pile foundations were suitable for frozen subsoil under all geological conditions. When the upper structure of foundation burdens was heavy and constraints for differential settlement deformation were critical, pile foundations were usually embedded in the permafrost layer to obtain higher bearing capacity with minor changes in the ground temperature field (Heilongjiang Province Academy of Cold Area Building Research 1989). Pile foundations were divided into drilled-hole driven-in pile, inserted-in pile, and cast-in-situ pile. Pile foundations were used in deep (>4 m) seasonally frozen soil regions and in permafrost wetlands. The advantages of pile foundation include minor damage to the environs and significantly-reduced disturbance to frozen subsoil. However, the disadvantages include more precise engineering requirements and higher investment.

In critically important situations, thermal or thermosyphon-cooled pile foundations (Figs. 6, 7, 8) were adopted to supplement other techniques for maintaining the stability of the subsoil. Thermal pile foundation included pile foundations where the pile itself was the thermosyphon, and pile foundations where the thermosyphon(s) were inserted

Figure 6. Thermosyphon-cooled tower of power transmission line in alpine meadow in the vicinity of Damxung along the Qinghai-Tibet Highway. The thermosyphons were installed in each of the four feet of the tower supported by mat/pile foundation.

Figure 7. Enlarged picture for details of the thermosyphon-cooled tower foundation.

into or around the pile foundation. Both kinds of foundation were used in warm permafrost to maintain the ground temperatures at the predesigned conditions and subsequent long-term stability of the frozen subsoil.

Tower foundation types and improvement of subsoils

Selection of tower foundation types:

Tower foundations were placed in non-frost or weakly frost-susceptible soil zones, such as the top of mountains with bedrock, slopes and lowlands with coarse-grained soils with the least possible soil moisture content.

Subsoil improvement:

a) Replace with non-frost or weakly frost-susceptible soils, such as clean gravels and sands, with less than 12% to 15% clayey particles. Refill depth 80% of the maximum depth of frost penetration, extended about 0.3–0.5 m on side wall of the foundation.

b) Physical and chemical smearing of 2–5 mm thick hydrophobic material such as heavy oil, bitumen mixed with 5% used machine oil, or industrial vaseline on wall of the foundation to reduce cohesion between the foundation and subsoil. Wrap the outside of the foundation with bituminous felt or impervious geotextiles and thickness of about 0.2–0.3 m of sand or gravel placed around the foundation.

c) Insulating material such as EPS, furnace slag, sod, or humic soil (peat) spread on the surface.

d) Drainage control to avoid water collection established at the sides of foundation. Excessive water drained by ground gutter or basal pipe/culverts.

e) Structure methods included deep anchored foundations. Burial depth of iron tower foundation should be 0.3–0.5 m more than the maximum depth of frost penetration to increase the anchorage forces of the foundations.

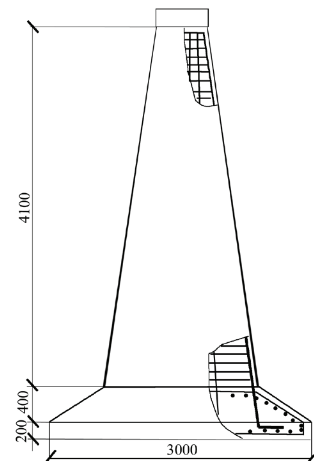

Figure 8. Sketch of reinforced concrete piling of tower foundation beneath the tower of Figures 3 and 4.

Operation Status

The 440-km long Amdo-Damxung power line was the largest electric network construction project. Construction started in April 2003, and was completed and put into operation in December. As a result of the project, the Central Tibet and Nagqü Power Networks were combined, greatly benefiting the local inhabitants and providing the critical needs for building the Qinghai-Tibet Railway.

During the early operation period, frequent power outrages were experienced due to bird and wind hazards. Some appreciable deformations and settlement were observed after the pouring of the concrete during construction. The deformations were later adjusted during the tower foundation installation processes. In addition, during construction in July and August 2003, the tower foundation subsoils at several sections were soaked by rain storms, resulting in differential settlement and horizontal displacement of tower foundations. It was soon rehabilitated and monitored afterwards, with satisfactory performance. Monitoring results during 2004–2007 indicated that the foundations in frozen ground were in designed condition.

Summary, Conclusions, and Prospects

a) The 110 kV power transmission line from Amdo to Damxung, Tibet Autonomous Region, China, is located in the patchy permafrost zone where frost heaving and thaw settlement were two challenging problems for design and construction of the line.

b) Surveys and assessment of frozen ground conditions for engineering geology were conducted for the evaluation of the potential of differential frost heaving and thaw settlement of tower foundation soils along the route.

c) The thermal and strain/stress of tower foundation and subsoils were analyzed for proper design and construction of the 110 kV power line.

d) Oblique and straight reinforced concrete column foundations and ordinary and thermosyphon-cooled pile foundations were proposed and adopted where appropriate. Tower site selection and ground improvement also were proven cost-effective.

e) Basic site selection principles included using bedrock foundations on mountain slopes and tops and coarse soils with least possible soil moisture on gentle slopes and lowlands.

f) Ground improvement measures generally included refilling with non- or weakly frost-susceptible soils, surface treatment to enhance water-proofing of foundation surfaces, insulation materials to decrease thaw penetration depths, drainage control to reduce frost heaving potential, and deep or bolted tower foundations exceeding the maximum depth of frost penetration.

g) The data bank and engineering measures, as well as experiences from the 110 kV power line would be very helpful for the proposed construction of 400 and 750 kV power transmission lines and other linear foundation engineering in warm, elevational permafrost.

Acknowledgments

Professor Emeritus Max C. Brewer from the U.S. Geological Survey, Alaska, provided generous assistance in English editing of the paper. The authors are very grateful for his generous assistance.

References

Heilongjiang Province Academy of Cold Area Building Research. 1989. *Code for Design of Building Foundation in Permafrost Area* (JGJ118-89). Beijing, China: China Architecture & Building Press, 243 pp.

Jin, H., Yu, S., Jin, R. & Sun, G. 2007a. Symbiosis of marshes and permafrost in the Xing'anling Mountains, Northeastern China. *Chinese Geographical Science* 17(4): 376-382. doi:10.1007/s11769-007-0376-3.

Jin, H., Yu, Q., Wang, S. & Lü, L. 2007b. Changes in permafrost environments along the Qinghai-Tibet engineering corridor induced by anthropogenic activities and climate warming. *Cold Regions Science and Technology* 49(2), doi:10.1016/j.coldregions.2007.07.005

Jin, H., Wei, Z., Ji, Y., Yu, Q., Lü, L., Wang, S. & Wu, Q. 2008. Assessment of frozen ground conditions for engineering geology along the Qinghai-Tibet Railway and Highway, China. *Engineering Geology* (in press).

Myska, A.D. & How, G.T.S. 1978. Installation of pile foundations for a microwave tower system, Gillam-Churchill, Manitoba. In: National Research Council of Canada (sponsored), *Proceedings of the Third International Conference on Permafrost, Edmonton, Alberta, Canada, July 10–13, 1978,* Vol. 1: 827-832.

State Forestry Administration, P.R. China. 2001. *Code for Engineering Geological Investigation of Frozen Ground* (GB50324-2001). Beijing, China: China Planning Press, 181 pp.

U.S. Department of Defense. 2004. *Foundations for Structures: Arctic and Subarctic Construction.* Unified Facilities Criteria (UFC), UFC 3-130-04. Washington, DC, USA, 4-147 to 4-152.

Wang, J. & Wang, S. 1982. *Features of Permafrost in the Southern Section of the Qinghai-Tibet Railway (South of Tanggula Mountain)*. The Geographical Society of China Conference on Glaciology and Geocryology (Cryopedology Vol.). Beijing, China: Science Press, 44-53.

Wu, Z., Barosh, P.J., Hu, D., Wu, Z., Zhao, X., Ye, P. & Wang, J. 2004. Hazards posed by active major faults along the Golmud-Lhasa railway route, Tibetan Plateau, China. *Engineering Geology* 74: 163-182.

Wu, Z., Barosh, P.J., Hu, D., Wu, Z., Ye, P., Liu, Q. & Zhou, C. 2005. Migrating pingos in the permafrost region of the Tibetan Plateau, China and their hazard along the Golmud-Lhasa Railway. *Engineering Geology* 79: 267-287.

Hydraulic Conductivity in Frozen Unsaturated Soil

Kunio Watanabe
Graduate school of Bioresources, Mie University, Japan
Tomomi Wake
Graduate school of Bioresources, Mie University, Japan

Abstract

Freezing experiments of silt and sand columns were carried out, and water and heat flows were observed. To estimate unsaturated hydraulic conductivity of soils, $K(h)$, at above-freezing and subzero temperatures, Darcy's law was solved under a non-isothermal condition with ice formation. $K(h)$ steeply decreased with decreasing soil water pressure, h, and more gradually decreased with soil freezing. The results show that the hydraulic model, in which water content became constant under $h< -10^5$ cm, underestimated the $K(h)$ of frozen soil, and suggest that the impedance factor, which reduced $K(h)$ for frozen soil, is not necessary when accurate soil water and soil freezing characteristics are available. The hydraulic model, which can express two types of soil water flow, such as capillary and film flows, appears to be useful for expressing the hydraulic properties of soils under the freezing process.

Keywords: soil freezing characteristic; soil water characteristic; TDR; unsaturated hydraulic conductivity; water and heat flows.

Introduction

Knowledge of water flow in frozen and thawing ground is important to investigating water and solute redistributions in soil during winter (Baker & Spaans 1997) and in studying the mechanism of frost heaving (Wettlaufer & Worster 2006). Changes in soil properties, such as hydraulic conductivity, have also received research attention. For example, changes caused by ground freezing have been examined by applying an artificial soil-freezing technique to stabilize soil and form a barrier against hazardous waste (McCauley et al. 2002). Moreover, a major concern of hydrological and climate modeling is how to express change in soil hydraulic properties.

Burt & Williams (1976) and Horiguchi & Miller (1983) measured the steep decrease in hydraulic conductivity with soil freezing, although within a small temperature range. Using oil as a fluid, McCauley et al. (2002) measured saturated hydraulic conductivity of frozen soil at various temperatures. However, few experimental studies have examined the unsaturated hydraulic conductivity of frozen soil, $K_f(h)$. The unsaturated hydraulic conductivity of unfrozen soil, $K(h)$, is usually expressed by the formula proposed by Brooks & Corey (1964), Clapp & Hornberger (1979), or van Genuchten (1980). For frozen soil, Harlan (1973) used $K(h)$ instead of $K_f(h)$, assuming the same film-water geometry between frozen and unfrozen soils. However, numerical simulations have suggested that this assumption overestimates water flow near the freezing front (Harlan 1973, Taylor & Luthin 1978, Jame & Norum 1980). Guymon & Luthin (1974) and Tao & Gray (1994) expressed $K_f(h)$ from $K(h)$ by subtracting ice content from saturated water content. When the soil is frozen, the presence of ice in some pores may block water flow. To account for this blocking, several impedance factors have been introduced (James & Norum 1980, Lundin 1990, Smirnova et al. 2000). However, Black & Hardenberg (1991) criticized the use of an impedance factor, stating that it is a potent and wholly arbitrary correction function for determining $K_f(h)$. Newman & Wilson (1997) also concluded that an impedance factor is unnecessary when an accurate soil water characteristic curve and relationship between $K(h)$ and soil water pressure are defined.

Measuring unsaturated hydraulic conductivity for frozen soil remains difficult, and a complete expression for $K_f(h)$ is still not available. In addition, the model for $K_f(h)$ should be correlated with the soil water characteristics and soil freezing characteristics for ease of use in numerical simulations (Watanabe et al. 2007). In this experiment, we estimated $K_f(h)$ from water and heat flow measurements in a frozen soil column and discuss a model for $K_f(h)$.

Theory

Assuming that vapor and ice flows are negligible, variably saturated water flow in above-freezing and subzero soil is described using a modified Richards equation as follows (Noborio et al. 1996, Hansson et al. 2004).

$$\frac{\partial\theta(h)}{\partial t}+\frac{\rho_i}{\rho_l}\frac{\partial\theta_i(T)}{\partial t}=\frac{\partial}{\partial z}\left(K(h)\frac{\partial h}{\partial z}+K(h)+K(h)\gamma h\frac{\partial T}{\partial z}\right) \quad (1)$$

where θ is volumetric liquid water content, θ_i is volumetric ice content, t is time, z is a spatial coordinate, ρ_i is density of ice, ρ_w is density of water, h is the water pressure head, T is temperature, and γ is the surface tension of soil water. The terms in parentheses on the right-hand side of equation (1) represent the water flux, J_w, obtained from the change in the amount of liquid water and ice. Thus, if we measure the pressure and temperature gradient, $K(h)$ [or $K_f(h)$ at subzero temperature] would be derived as

Table 1. Experimental conditions and physical properties of soil.

		FSi	TDS
Bulk density	g cm^{-3}	1.18	1.45
θ when packed	m^{3}m^{-3}	0.40	0.15
θ saturation	m^{3}m^{-3}	0.569	0.36
Thermal conductivity*	W m -		
at θ = 0.00 (frozen)	^{1}K^{-1}	0.20(0.20)	0.25(0.25)
at θ = 0.17 (frozen)			0.96(1.50)
at θ = 0.24 (frozen)			
at θ = 0.29 (frozen)		0.52(0.55)	1.06(1.05)
Saturated hydraulic cond.			50.6
	cm h^{-1}	0.66(0.76)	
		0.25	
van Genuchten parameter			
θ_r	m^{3}m^{-3}	0.03	0.015
α	m^{-1}	0.16	3.36
n		1.38	7
l		0.552	-0.5
Durner parameter			
θ_r	m^{3}m^{-3}	0.06	0
α_1	m^{-1}	0.35	3.466
n_1		3.10	6.40
l		–0.08	-0.5
α_2	m^{-1}	0.011	0.027
n_2		1.70	1.40
w_2		0.461	0.105

*The value for thermal conductivity is average of 2 to 20°C for unfrozen soil and -5 to -20°C for frozen soil.

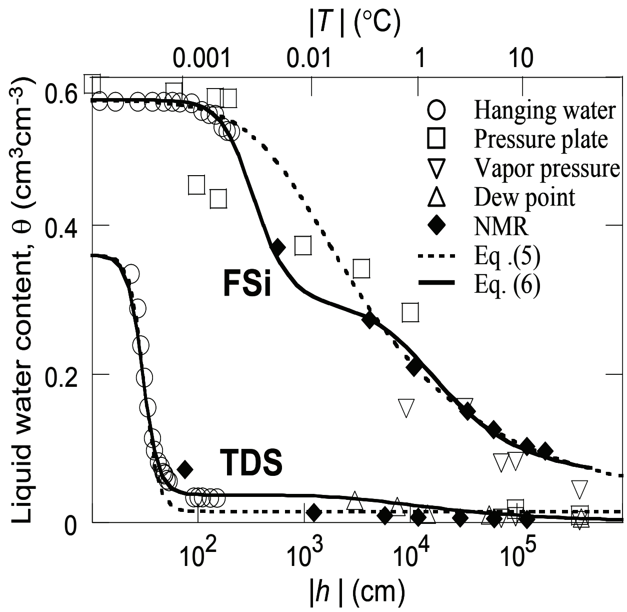

Figure 1. Soil water characteristics measured by hanging water, pressure plate, vapor pressure, and chilled mirror dew point measurement methods, and soil freezing characteristics measured by pulsed NMR measurement for FSi and TDS (in thawing process).

$$K(h) = -\frac{J_w}{\left(\frac{\Delta T}{\Delta z}\gamma h + \frac{\Delta h}{\Delta z} + 1\right)} \tag{2}$$

The value of h in unfrozen soil can be obtained from the soil water characteristics (relationship between θ and h) when measuring the profile of θ, while h in frozen soil can be calculated from the temperature profile derived from the generalized form of the Clausius–Clapeyron equation by assuming a differences between ice and water. Specifically, the ice pressure is sometimes assumed to equal zero gauge pressure (Williams & Smith 1989, Hansson et al. 2004):

$$\frac{dP}{dT} = \frac{L_f}{v_l T} \tag{3}$$

where P is the pressure (= $\rho_w gh$), g is the acceleration due to gravity, L_f is the latent heat of freezing, and v_l is the specific volume of water. Thus, equation (3) gives the soil freezing characteristics (relationship between θ and T) from the soil water characteristics and vice versa.

Material and Methods

The samples used in this study were Fujinomori silt (FSi) and Tottori dune sand (TDS). Figure 1 shows the soil water characteristics measured by several physical methods (Jury & Horton 2004) for both soils as well as soil freezing characteristics measured by pulsed nuclear magnetic resonance (NMR) measurement and depicted by equation (3). FSi is highly susceptible to frost and retains much liquid water even when $|h| > 10^4$ cm ($T < -1$°C), while for TDS, θ = 0.03 when $|h| > 10^2$ cm ($T < -0.01$°C).

The TDS were preliminarily washed in deionized water, and the FSi was passed through a 2 mm screen. Each sample was mixed with distilled and deionized water and packed into an acrylic column with an internal diameter of 7.8 cm and a height of 35 cm. Table 1 lists the experimental conditions and physical properties of the samples. Fifteen copper-constantan thermocouples and seven time domain reflectometry (TDR) probes were inserted into each column, and the side wall of the column was insulated. The TDR was preliminarily calibrated for measuring unfrozen water content by comparison to the pulsed NMR measurement. The column was settled at an ambient temperature of 2°C for 24 h to establish initial water and temperature profiles and then frozen from the upper end by controlling temperature at both ends of the column (T_L = -8°C and T_H = 2°C). During the experiment, no water flux was allowed from either end, and profiles of temperature, water content, and solute concentration (EC_a) were monitored using thermocouples and TDRs. A series of experiments with different durations of freezing were then performed for each freezing condition (i.e., same freezing rate and temperature gradient). At the end of the experimental series, the sample was cut into 2.5 cm intervals to measure the total water content by the dry-oven method. From thermocouples and TDR readings, it was confirmed that each column had the same temperature and water profiles during the series of experiments.

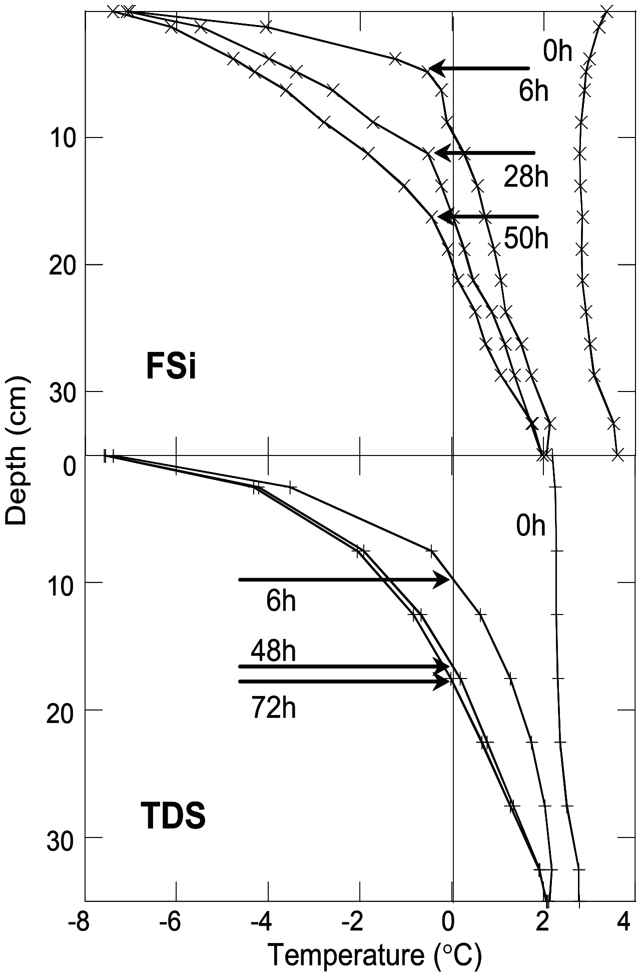

Figure 2. Temperature profiles for FSi (0, 6, 28, 50 h after freezing started) and TDS (0, 6, 48, 72 h after freezing started). Arrows represent the freezing front.

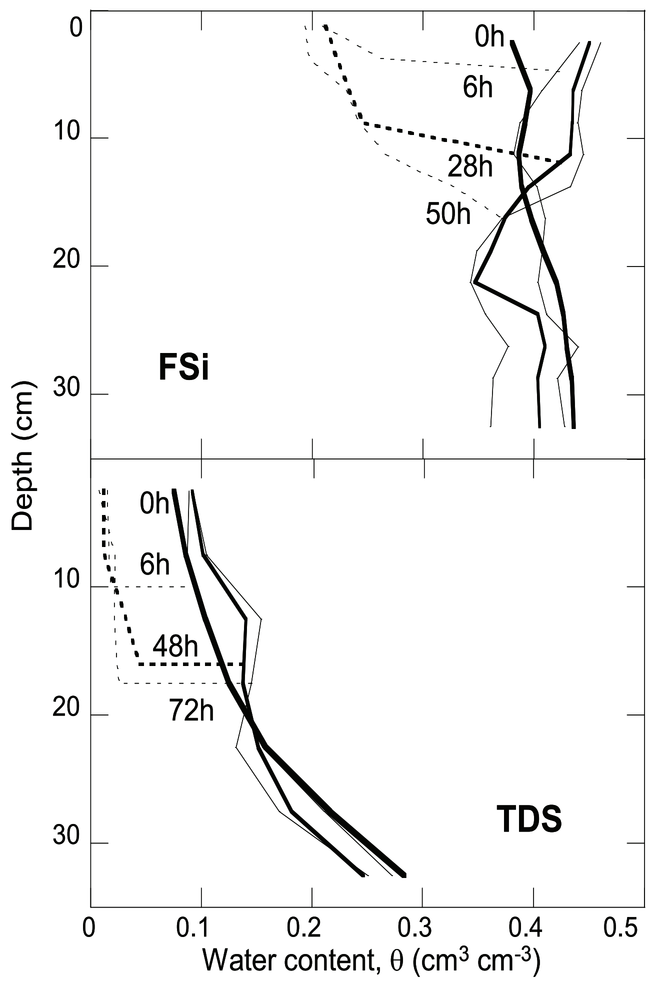

Figure 3. Moisture profiles for FSi and TDS at the same freezing time as shown in Figure 2. The solid line and dashed line represent total water and unfrozen water contents, respectively.

Results

Heat and water flow

Figure 2 shows temperature profiles of the freezing soils. When both ends of the column were set at different temperatures, the soil near the column ends quickly reached the required temperatures. In FSi, the advancing rate of the 0°C isotherm was 1.57, 0.34, and 0.16 cm h^{-1} for 0–6, 6–24, and 24–48 h, respectively, and approximately 0.25°C lowering of the freezing point was observed. The freezing rate of TDS was similar to that of FSi, although TDS had larger thermal conductivity (Table 1). Even after 72 h, the temperature profile of the subzero area in TDS did not reach a linear shape as in FSi and in the unfrozen area in TDS.

Figure 3 presents water profiles in FSi and TDS at the same freezing time as shown in Figure 2. The solid line indicates total water content, θ_t, measured by the dry-oven method, and the dashed line indicates unfrozen water content measured by TDR. The ice content, θ_i, was obtained by subtracting the unfrozen water from the total water content. FSi had a relatively vertical initial θ profile, having similar θ values for h <100 cm (Fig. 1). An increase of θ_t, decrease of θ in the frozen area, and decrease of θ in the unfrozen area with the advancing freezing front were observed, implying that the soil water flowed not only through the unfrozen area, but also the frozen area. The gradient of the initial θ profile of TDS corresponded to its soil water characteristics (Fig. 1). In TDS, the soil water in the unfrozen area flowed to and accumulated near the freezing front because of suction at the freezing front caused by ice formation. Water flow in the unfrozen area continued 48 h or later after freezing began, although there was no apparent advance of the freezing front. Meanwhile, much less water flow was observed in the frozen area.

The profile of water flux, J_w, was then calculated by developing θ profiles (Fig. 3) with the boundary condition of no water flux. In early stage of freezing (0–6 h), soil water in almost the entire column moved upward at about J_w = 0.04 cm h^{-1} for FSi and J_w = 0.01 cm h^{-1} for TDS. The progression of the peak observed in the J_w profile coincided with the freezing front. In the frozen area, J_w in SFi was ≥10 times larger than that in TDS and exponentially decreased as the temperature decreased ($J_w = 0.007|T|^{-0.69}$ for FSi and $0.0012|T|^{-1.45}$ for TDS).

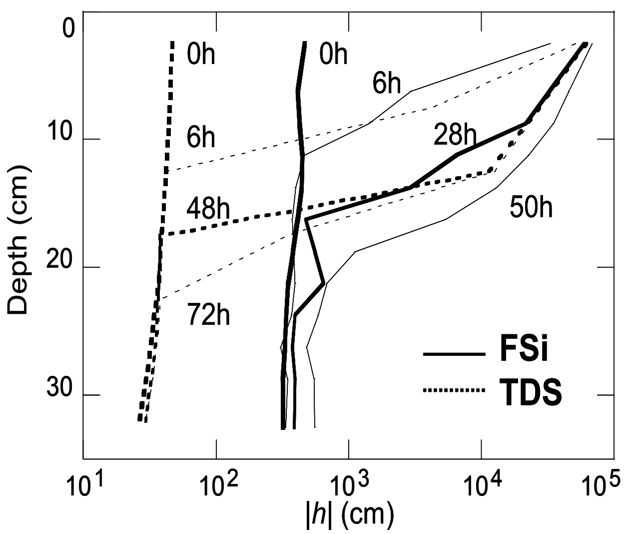

Figure 4. Profile of soil water pressure estimated from Figures 2 and 3.

Change in hydraulic conductivity

Figure 4 shows the profile of soil water pressure h estimated by the soil water characteristics (Fig. 1) with the θ profile (Fig. 3) and equation (3) with the temperature profile (Fig. 2). Solute effect was negligible during the experiments, since very low solute concentration was confirmed by TDR (EC_a) readings. Note that for equation (3) there was discontinuity in the h profiles near 0°C, especially for unsaturated soil; therefore, we used linear interpolation to connect the closest calculated h values between the unfrozen and frozen areas. With freezing, $|h|$ steeply increased ($h < -10^3$ cm). A larger difference in h between unfrozen and frozen areas was observed in TDS than in FSi.

The non-isothermal version of Darcy's law (Eq. 2) could consequently by solved with the J_w, T, and h profiles, obtaining the relationship between the unsaturated hydraulic conductivity, $K(h)$, at above-zero and subzero temperatures with the soil water pressure, as shown in Figure 5. In the range $h > -10^3$ cm (unfrozen), $K(h)$ decreased steeply with increasing $|h|$, while it decreased gradually in the range $h < -10^3$ cm (frozen). Similar $K(h)$ was observed when different freezing conditions were applied (T_L = -5°C and T_H = 5°C in Fig. 5 for TDS). These changes were clearer for $K(h)$ of TDS, which agreed well with the value obtained using the evaporation method (Sakai & Toride 2007). In the frozen area, $K(h)$ in FSi was about 10 times larger than that in TDS, which is why more water flow was observed in frozen FSi. Figure 6 shows the relationship between $K(h)$ and liquid (unfrozen) water content measured by TDR. In frozen TDS, $K(h)$ decreased steeply from 10^{-5}–10^{-8} cm h^{-1} with decreasing θ from 0.04–0.01 cm^3 cm^{-3}, while $K(h)$ of frozen FSi decreased more gradually.

The $K(h)$ of frozen soil also correlated with temperature T and with ice content θ_i. The decrease of $K(h)$ with lowering T and θ_i was well fitted by power law as $K(h) = 3 \times 10^{-6}\,|T|^{-1.49}$ and $K(h) = 2.3 \times 10^{-8}\,\theta_i^{-2.42}$ for FSi, and $K(h) = 0.7 \times 10^{-6}\,|T|^{-1.75}$ and $K(h) = 8.2 \times 10^{-14}\,\theta^{-6.96}$ for TDS. This power law relationship was consistent with the relationship between J_w and $|T|$ mentioned above. The θ_I–T relationship is sometimes expressed by power law (Anderson & Tice 1972) and can be converted through equation (3) to a θ -h relationship, which may also be expressed by power law (Brooks & Corey 1964). The shape of the formula indicating $K(h)$ may arise from the soil water characteristics (θ-h) and soil freezing characteristics (θ_i-T).

Discussion

Soil freezing characteristics

Soil freezing characteristics are sometimes interpreted from the surface force, pore curvature, when solute effect is negligible (Dash et al. 1995, Watanabe & Mizoguchi, 2002). The surface force accounts for the power law shape of soil freezing characteristics and the effect of the curvature known as the Gibbs–Thomson effect, which creates a shoulder to the soil freezing characteristics by means of the freezing temperature depression, $T_m - T$ depending on the soil pore radius r:

$$T_m - T = \frac{T_m \sigma}{\rho_i L_f r} \tag{4}$$

where T_m is the freezing temperature of bulk water and σ is the ice-water interface free energy. In the soil pore size distribution, two peaks are presumed: one from pores among the soil particles (r = 5–50 μm) and the other from pores on the particle surface (r = 3–10 nm). These peaks would yield two shoulders to the soil freezing characteristics around -0.001 to -0.1°C and -2.5 to -10°C, respectively. By converting the soil freezing characteristics to soil water characteristics through equation (3), the warmer shoulder would correspond to air entry. In the range from water saturation to the other (colder) shoulder, soil water will flow predominantly as capillary flow, but will change to film flow at h lower than the colder shoulder. Soil water characteristic models proposed by Brooks & Corey (1964) and van Genuchten (1980) (Eq. 5) are intended to express unsaturated soil with moderate h and give the constant θ (defined as resident water content, θ_r) at extremely low h. These models, therefore, cannot express the area around the colder shoulder, which is an important portion for soil freezing characteristics (Fig. 1). Durner (1994) combined two van Genuchten models, which express different soil water characteristics, to describe water retention in a soil having a dual porosity distribution (Eq. 6):

$$S_e = \left(1 + |\alpha h|^n\right)^{-m} \tag{5}$$

$$S_e = w_1\left[1 + (\alpha_1 h)^{n_1}\right]^{-m_1} + w_2\left[1 + (\alpha_2 h)^{n_2}\right]^{-m_2} \tag{6}$$

where $S_e = (\theta - \theta_r)(\theta_s - \theta_r)^{-1}$, $m = 1 - n^{-1}$, $w_1 = 1 - w_2$, θ_s is saturated water content, α and n are empirical parameters,

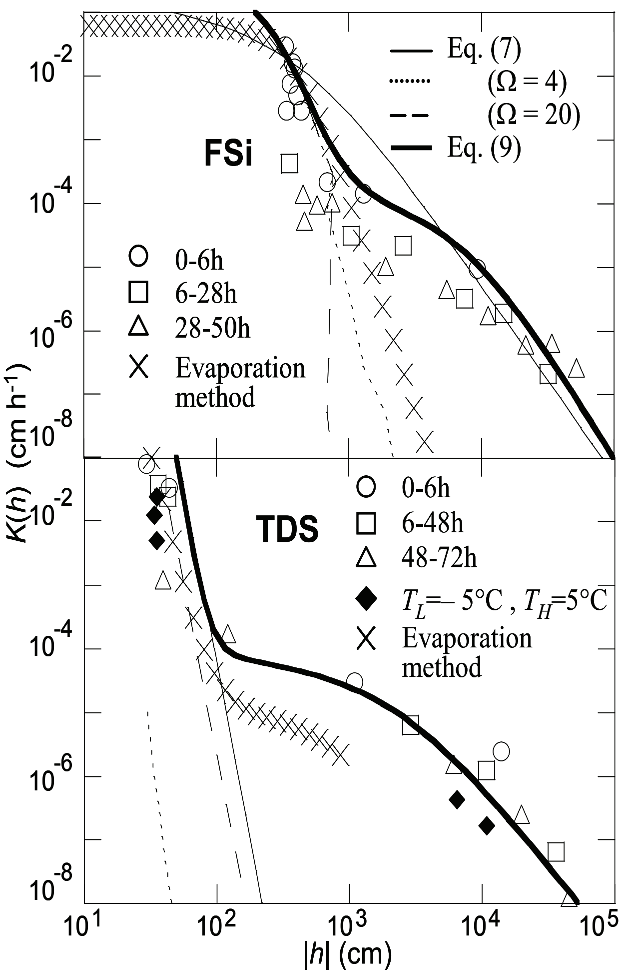

Figure 5. Relationship between unsaturated hydraulic conductivity [$K(h)$] and soil water pressure at above-zero and subzero temperature. Table 1 lists the parameters for equations (7) and (9).

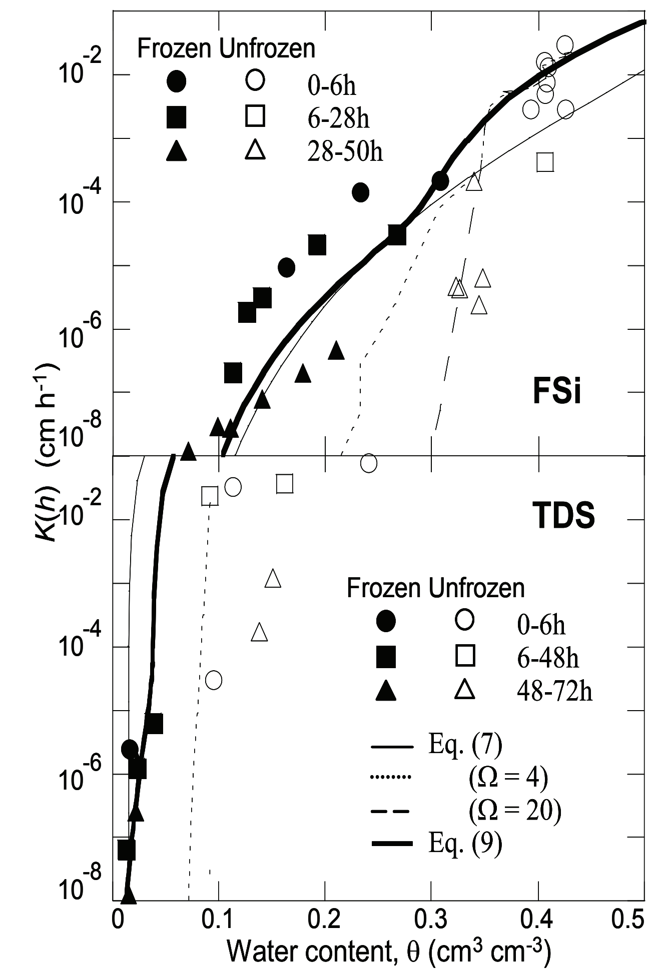

Figure 6. Relationship between unsaturated hydraulic conductivity, $K(h)$, and soil water content at above-zero and subzero temperature. Table 1 lists the parameters for equations (7) and (9).

and w_2 is the weighting factor. Using the parameters listed in Table 1, equation (6) was well fitted to a wide range of soil water characteristics, including soil freezing characteristics, for FSi and TDS (Fig. 1).

Unsaturated hydraulic conductivity for frozen soils

The unsaturated hydraulic conductivity for unfrozen soil, $K(h)$, is often derived from equation (5) (van Genuchten 1980) as follows:

$$K(h) = K_s S_e^l \left[1-\left(1-S_e^{1/m}\right)^m\right]^2 \tag{7}$$

where l is the pore-connectivity coefficient. For frozen soil, $K(h)$ is sometimes reduced by an impedance factor Ω (Lundin 1990, Hansson et al. 2004):

$$K(h)_{frozen} = 10^{-\Omega\theta_i/(\theta_t-\theta_r)} K(h) \tag{8}$$

Applying equations (7) and (8) to our measured $K(h)$ verified that equation (7) could not fit the gradient change of $K(h)$ around $h = 10^{-3}$ cm for FSi and underestimated $K(h)$ at $h < -10^2$ cm for TDS (Fig. 5). The impedance factor might be useful for expressing the steep decrease of $K(h)$ near 0°C, if equation (5) were fitted to the whole range of soil water characteristics (FSi in Figs. 5, 6). However, use of an impedance factor requires caution since it will underestimate $K(h)$ as freezing progresses.

The design of equation (7) was based on the bundle of capillary tube model in which water flow decreases with square decrease in the pore (tube) radius, as Poiseuille flow, and produces a linear reduction in $K(h)$ on a log–log scale when θ is constant. On the other hand, film water can be regarded as the flow proportional to the first or less root of film thickness. The $K(h)$ of frozen soil consequently has a lower grade than that of unfrozen soil. Thus, the Durner model was again applied to $K(h)$, taking care that θ did not become constant at $10^{-3} < h < 10^{-6}$ cm ($-0.1 < T < -100$°C).

$$K\left(S_e\right) = K_s\left(w_1 S_{e1} + w_2 S_{e2}\right)^l \times \frac{\left(w_1\alpha_1\left[1-\left(1-S_{e1}^{1/m_1}\right)^{m_1}\right] + w_2\alpha_2\left[1-\left(1-S_{e2}^{1/m_2}\right)^{m_2}\right]\right)^2}{\left(w_1\alpha_1 + w_2\alpha_2\right)^2} \tag{9}$$

Equation (9) showed good agreement with the $K(h)$ obtained from the column freezing experiment (Figs. 5, 6). This model was originally used for explaining water flow containing two different flow rates, such as among and within soil aggregates. Our results suggest that this model is also suitable for soils under freezing-thawing processes, in which soil water flow changes from capillary flow to film flow.

Conclusion

The sand and silt columns were frozen directionally, and the water and heat flows during soil freezing were measured. The flows depended on the soil types. Unsaturated hydraulic conductivity for frozen and unfrozen soils was estimated by solving Darcy's law under non-isothermal conditions with ice formation, although further consideration of the precision of flux measurements and limits of the Clausius-Clapeyron equation may be required. Hydraulic conductivity steeply decreased with decreasing soil water pressure and water content in unfrozen soil but more gradually decreased in frozen soil. In both unfrozen and frozen states, the silt had higher hydraulic conductivity than the sand, resulting in more water flow during silt freezing.

The shapes of soil water characteristics and soil freezing characteristics were discussed from the viewpoint of the pore size distribution. Use of an impedance factor for calibrating the hydraulic conductivity of frozen soil, which has sometimes created unstable numerical simulations, appears to be unnecessary when the hydraulic model can appropriately express both the soil water and freezing characteristics. Rather, the results suggest that the Durner model is useful for expressing the hydraulic properties affected by the change in the type of water flow during soil freezing.

References

Anderson, D.M. & Tice, A.R. 1972. Predicting unfrozen water content in frozen soils from surface area measurements. *Highway Res. Record*, 393: 12-18.

Baker, J.M. & Spaans, E.J.A. 1997. Mechanics of meltwater movement above and within frozen soil. *Proceedings of International Symposium on Physics, Chemistry, and Ecology of Seasonally Frozen Soils. U.S. Army CRREL Special Report* 97-10, 31-36.

Black, P.B. & Hardenberg, M.J. 1991. Historical perspectives in frost heave research, the early works of S. Taber and G. Beskow. *CRREL Special Report*, 91-23.

Brooks, R.H. & Corey, A.T. 1964. Hydraulic properties of porous media. *Hydrol. Paper 3*. Colorado State Univ., Fort Collins, CO, USA.

Burt, T.P. & Williams, P.J. 1976. Hydraulic conductivity in frozen soils. *Earth Surface Processes* 1: 349-360.

Clapp, R.B. & Hornberger, G.M. 1979. Empirical equations for some soil hydraulic properties. *Water Resour. Res.* 14: 601–604.

Dash, J.G., Fu, H. & Wettlaufer. J.S. 1995. The premelting of ice and its environmental consequences. *Rep. Prog. Phys.* 58: 115-167.

Durner, W. 1994. Hydraulic conductivity estimation for soils with heterogeneous pore structure. *Water Resour. Res.* 30(2): 211-223.

Guymon, G.L., Berg, R.L. & Hromadka, T.V. 1993. Mathematical model of frost heave and thaw settlement in pavement. *CRREL Report* 93-2.

Hansson, K., Šimůnek, J., Mizoguchi, M., Lundin, L.C. & van Genuchten, M.Th. 2004. Water flow and heat transport in frozen soil: Numerical solution and freeze-thaw applications. *Vadose Zone Journal* 3: 693-704.

Harlan, R.L. 1973. Analysis of coupled heat-fluid transport in partially frozen soil. *Water Resour. Res.* 9: 1314-1323.

Horiguchi, K & Miller, R.D. 1983. Hydraulic conductivity of frozen earth materials. *Proceedings of the Fourth International Conference on Permafrost*, Fairbanks, 504-509.

Jame, Y.W. & Norum, D.I. 1980. Heat and mass transfer in freezing unsaturated porous media. *Water Resour. Res.* 16: 811-819.

Jury, A.W. & Horton, R. 2004. *Soil Physics*, Hoboken: John Willey & Sons Inc., 384 pp.

Lundin, L.-C. 1990. Hydraulic properties in an operational model of frozen soil. *J. Hydrol.* 118: 289-310

McCauley, C.A., White, D.M., Lilly, M.R. & Nyman, D.M 2002. A comparison of hydraulic conductivities, permeabilities and infiltration rates in frozen and unfrozen soils. *Cold Regions Sci. Tech.* 34: 117-125.

Newman, G.P. & Wilson, G.W. 2004. Heat and mass transfer in unsaturated soils during freezing. *Can. Geotech. J.* 34: 63-70.

Noborio, K., McInners, K.J. & Heilman, J.L. 1996. Two-dimensional model for water, heat and solute transport in furrow-irrigated soil: I. Theory. *Soil Sci. Soc. Am. J.* 60: 1001-1009.

Sakai, M & Toride, N. 2007. Optimum conditions for predicting unsaturated hydraulic properties using the evaporation method. *J. Jpn. Soc. Soil Phys*. 106: 33-46.

Smirnova, T.G., Brown, J.M., Benjamin, S.G. & Kim, D. 2000. Parameterization of cold-season processes in the MAPS land-surface scheme. *J. Geophys. Res.* 105: 4077-4086.

Tao, Y.X. & Gray, D.M. 1994. Prediction of snowmelt infiltration into frozen soils. *Numerical Heat Transfer, Part A: Applications* 26: 643-665.

Taylor, G.S. & Luthin, J.N. 1978. A model for coupled heat and moisture transfer during soil freezing. *Can. Geotech. J.* 15: 548-555.

van Genuchten, M.Th. 1980. A closed-form equation for predicting the hydraulic conductivity of unsaturated soils. *Soil Soc. Am. J.* 44: 892-898.

Watanabe, K. & Mizoguchi, M. 2002. Amount of unfrozen water in frozen porous media saturated with solution. *Cold Reg. Sci. Tech.* 34: 103-110.

Watanabe, K. Toride, N., Sakai, M. & Šimůnek, J. 2007. Numerical modeling of water, heat and solute transport during soil freezing. *J. Jpn. Soc. Soil Phys.* 106: 21-32.

Wettlaufer, J.S. & Worster, M.G. 2006. Premelting dynamics. *Annu. Rev. Fluid. Mech.* 38: 427-452.

Williams, P.J. & Smith, M.W. 1989. *The Frozen Earth: Fundamentals of Geocryology*. Cambridge: Cambridge University Press, 360 pp.

Sounding Ice and Soil Wedge Structures with Ground-Penetrating Radar

Tatsuya Watanabe
Geoenvironmental Sciences, University of Tsukuba, Tsukuba, Japan

Norikazu Matsuoka
Geoenvironmental Sciences, University of Tsukuba, Tsukuba, Japan

Hanne H. Christiansen
Department of Geology, the University Centre in Svalbard, Longyearbyen, Norway

Atsushi Ikeda
Geoenvironmental Sciences, University of Tsukuba, Tsukuba, Japan

Abstract

Ground-penetrating radar (GPR) was used to sound subsurface structures below troughs delimiting non-sorted polygons in Svalbard. On marine terraces, a single hyperbolic reflection spreads downward from the ground surface, which represents an active layer soil wedge. Some large troughs are underlain by double hyperbolic reflections extending downward from the ground surface and the frost table, which correspond to a soil wedge and an underlying ice wedge, respectively. On fluvial terraces, a hyperbolic reflection extends downward from the frost table, which represents an ice wedge; the width of the hyperbola corresponds to the width of an ice wedge. The hyperbolic reflections originate from the contrast in water content between the wedge filling and the host material. These results indicate that GPR is useful for distinguishing ice and active layer soil wedges in terms of depth of the hyperbola and for estimating the width of ice wedges without excavation.

Keywords: ground-penetrating radar; ice wedge; non-sorted polygon; soil wedge; Svalbard.

Introduction

Non-sorted polygons are one of the most widespread periglacial landforms in Svalbard. Most of them occur on the bottoms and slopes of inland valleys, uplands surrounding the valleys (Sørbel et al. 2001, Tolgensbakk et al. 2001), and on strandflats (Åkerman 1980, 1987). Direct excavation and drilling revealed that ice wedges are predominant in Adventdalen (inland valley), while active layer soil wedges are more common in Kapp Linné (strandflat) despite similar surface patterns (Matsuoka & Hirakawa 1993). Thus, surface patterns cannot indicate the presence of ice wedges. Since direct methods are time consuming, more convenient methods are required to relate surface geometry to subsurface wedge structures.

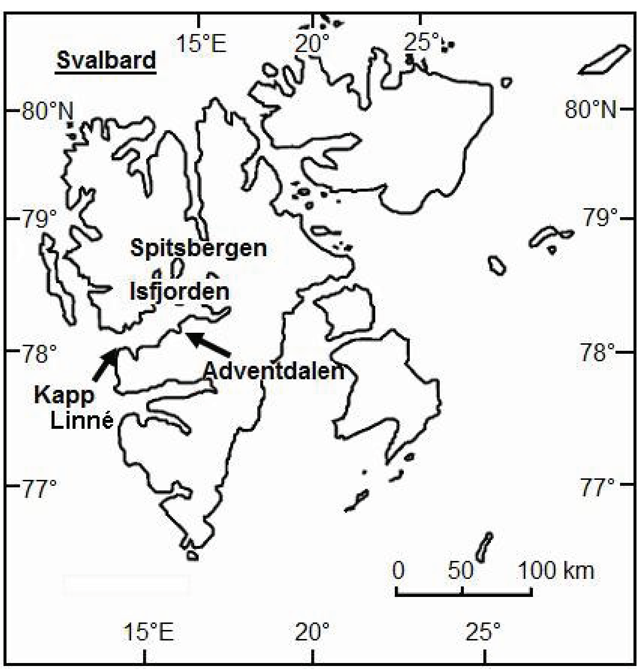

Figure 1. Locations of the study areas.

Ground-penetrating radar (GPR) is a useful tool for imaging near-surface structures. GPR has been applied to permafrost studies since the 1970s to identify areas of massive ground ice (e.g., Dallimore & Davis 1987), internal structure of rock glaciers (e.g., Berthling et al. 2000) and pingos (Ross et al. 2005, Yoshikawa et al. 2006), and to determine the depth of the permafrost table and ice wedges (Hinkel et al. 2001). A recent GPR study attempted to visualize near-surface structures in permafrost with three-dimensional images (Munroe et al. 2007). We also applied GPR to visualize subsurface wedge structures, and particularly to distinguish ice wedges from active layer soil wedges in Svalbard. Furthermore, ice wedge width was estimated from the reflection patterns of radar signal.

Study Sites

Svalbard is an archipelago situated between 74°N to 81°N and 10°E to 35°E. The largest island is Spitsbergen, which covers an area of 38,000 km^2 (Fig. 1).

Kapp Linné is located at the southern edge of the mouth of Isfjorden, central Spitsbergen (Fig. 1). The area is located on a wide strandflat composed of a sequence of raised marine terraces with beach ridges, small lakes, and bogs. The strandflat emerged above sea level after the Lateglacial deglaciation (11–5.5 ka BP) (Landvik et al. 1987). A number of relatively small polygons (5–15 m in diameter) developed on the raised beach ridges consisting of gravely sand and lacking vegetation. The polygons are mostly highcentered and delimited by narrow and shallow troughs. The mounds and troughs are well distinguished by the presence of vegetation only in the latter. The troughs mostly lack well-defined rims at both sides except for some extraordinarily large ones. Åkerman (1980) mapped most of the troughs underlain by active layer soil wedges but extraordinary large ones having ice wedges. Similar mounds and troughs also sporadically occur on the bogs which are composed of peat and covered with vegetation. However, they rarely constitute polygonal patterns and are usually obscured by full vegetation. Åkerman (1980) classified them as ice wedge polygons. The mean annual air temperature (MAAT) is −4.9°C in Kapp Linné (Åkerman 1996). Permafrost is nearly continuous except for a karst area (Salvigsen et al. 1985). The active layer thickness varies from 0.3 m in the bogs to 2 m on the raised beach ridges (Åkerman 1980).

Adventdalen is a broad, U-shaped valley joining Isfjorden at Longyearbyen (Fig. 1). The lowermost 15 km of the valley bottom is covered with fluvial sediments composed of branched river flood plain deposits (Tolgensbakk et al. 2001). Large, low-centered, hexagonal polygons are widespread on the Adventelva river terrace, where the fluvial sediments are covered with fine-grained loess about 3 m thick. The polygons are typically delineated by troughs a few centimeters to 40 cm deep and 20–100 cm wide. The variation in trough size probably represents different generations of thermal contraction cracks constituting a complex polygonal network (Christiansen 2005). MAAT is -6.5°C (1961–1990) at Svalbard Lufthavn (airport) in Longyearbyen (Hanssen-Bauer et al. 1990). Permafrost is continuous, and its thickness is estimated to be 220 m at Janssonhaugen, located in the upper Adventdalen (Isaksen et al. 2001). The thickness decreases to less than 100 m approaching the sea (e.g., Humlum et al. 2003). The active layer thickness in Adventdalen is about 1 m in the fine-grained loess (Christiansen & Humlum 2003).

Methods

Surveys were conducted in late June and late July 2007 in Kapp Linné and in early July 2006, end of July, and middle of August 2007 in Adventdalen. The numbers of survey lines in Kapp Linné and Adventdalen are 44 and 36, respectively. The GPR used in this study was a Noggin Smart Systems, produced by Sensors & Software Inc. The system consists of a cart, an antenna box (Noggin 250), an odometer wheel, a digital video logger, and a battery. The 250 MHz signal was applied to the survey of wedge structures. The resolution is enough to display the target, although the radar signal tends to attenuate in thawed fine-textured sediments.

The GPR antenna transmits electromagnetic pulses into the ground. The transmitted wave is reflected at geological boundaries that have an electromagnetic impedance contrast. The two way travel time (TWT) for the reflected waves is recorded and plotted on a diagram. Radar records were processed with the RADPRO for Windows version 3.0 (Korea Institute of Geoscience and Mineral resources). Processing included conversion of TWT to the depth scale, removal of the direct ground wave during radar acquisition, topographic modification, and gain adjustments. Converting TWT to the depth scale requires the radar transmission velocity in the layer or layers above the reflector. The velocity was determined by direct depth measurements or a point-source reflection analysis. The latter permits estimation of the radar transmission velocity using the shape of hyperbolic patterns produced by point structures (Moorman et al. 2003). The GPR images were compared with the results of direct excavation and/or drilling at six troughs. Soil samples were taken at these troughs to determine the grain size distribution and water content to interpret GPR images, because the contrast of water content, which mainly depends on the difference in grain size distribution at a depth, results in different dielectric constants.

Results and Interpretations

Kapp Linné: Marine terraces

The GPR profiles across polygon troughs developed on beach ridges displayed strong horizontal and hyperbolic reflections (Fig. 2a). The point-source reflection analysis using the hyperbolic reflections estimated that the propagation velocity was around 0.065–0.090 m/ns. This velocity indicates that the horizontal reflections were located at about 1 m depth, which corresponded to the depth of the frost tables revealed by excavation. This coincidence demonstrates that the estimated velocity was reasonable, although the velocity was slightly small for sandy materials. Most of the polygon troughs were accompanied by a hyperbolic reflection extending downward from just below the ground surface. Ice wedges tend to show strong hyperbolic reflections (Hinkel et al. 2001), while the hyperbolas in Kapp Linné are located at depths too shallow for ice wedges. In fact, two excavated troughs on a marine terrace displayed active layer soil wedges restricted within the upper 20–40 cm depth of the active layer (Fig. 2b). The GPR profiles also displayed minor hyperbolic reflections below polygon mounds, which appear to be produced by large stones in the marine sediment.

The GPR profiles of four extraordinarily large troughs were characterized by double hyperbolic reflections extending downward from the ground surface and at about 1 m depth, respectively (Fig. 3a). The upper reflection corresponds to that of active layer soil wedges below smaller polygon troughs. In contrast, the lower reflection may indicate the presence of an ice wedge, because the top of the hyperbola approximates the permafrost table. An excavation conducted in late July exposed a soil wedge just below the trough, surrounded by marine sand partly containing gravels (Fig. 3b). The width of the wedge approximates that of the trough (ca. 80 cm). Despite consisting of similar material to the surrounding marine sediments, the

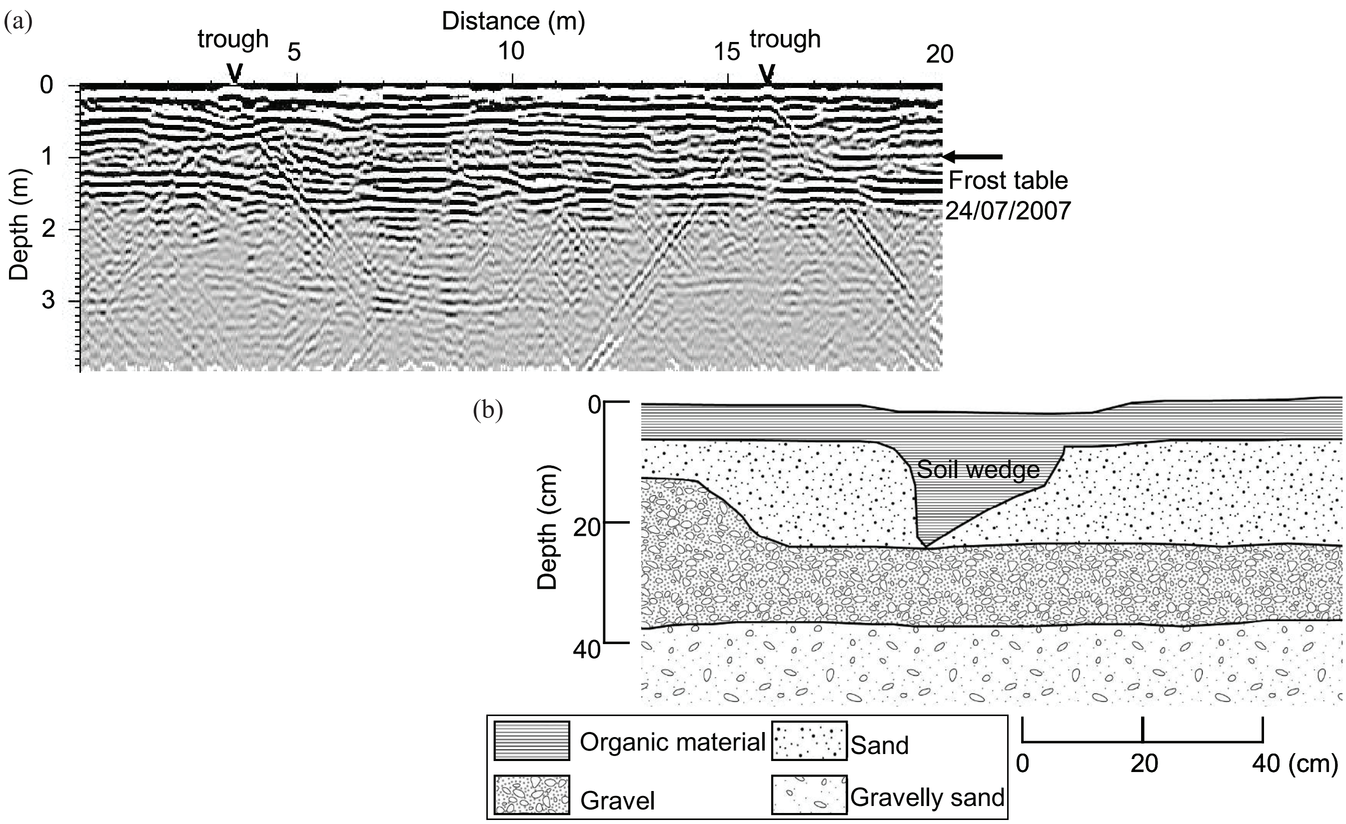

Figure 2. (a) A GPR profile across two polygon troughs on a marine terrace in Kapp Linné. (b) The cross section of the trough at the 16 m point along the above profile.

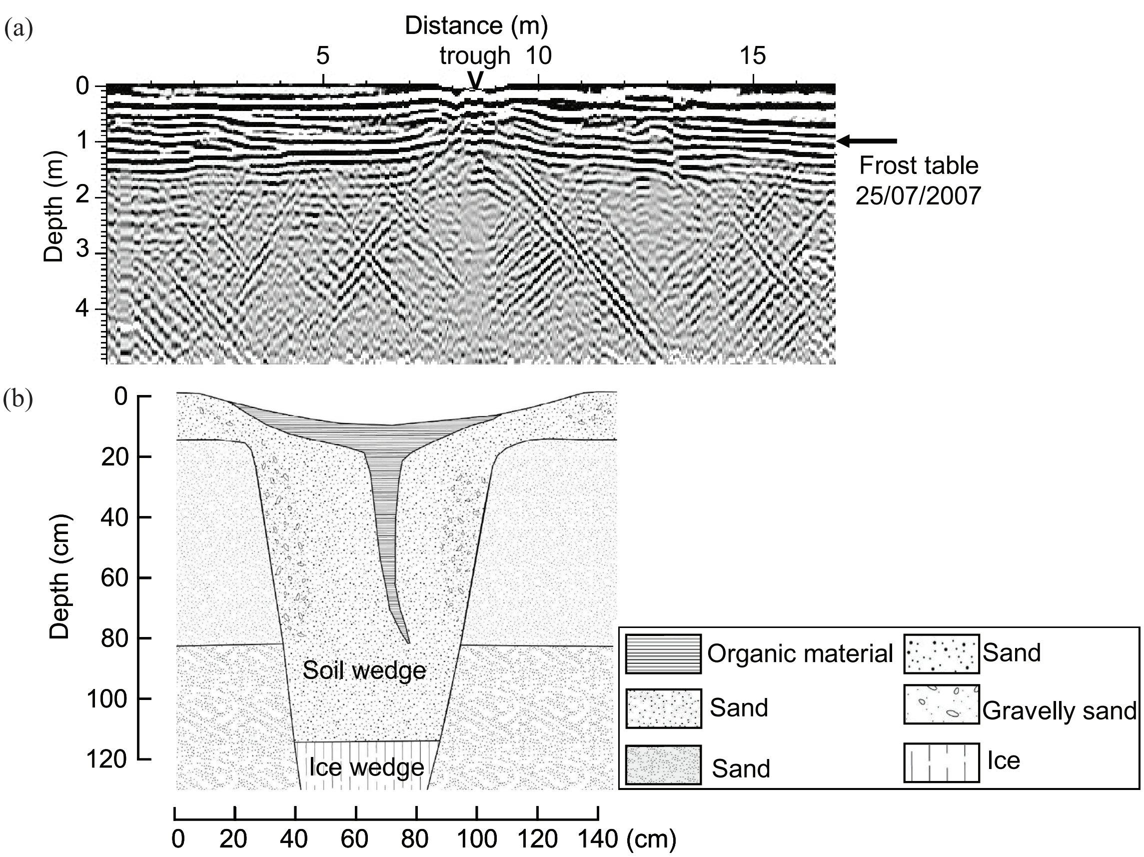

Figure 3. (a) A GPR profile across an extraordinarily large polygon trough on a beach ridge in Kapp Linné. (b) The cross section of the trough.

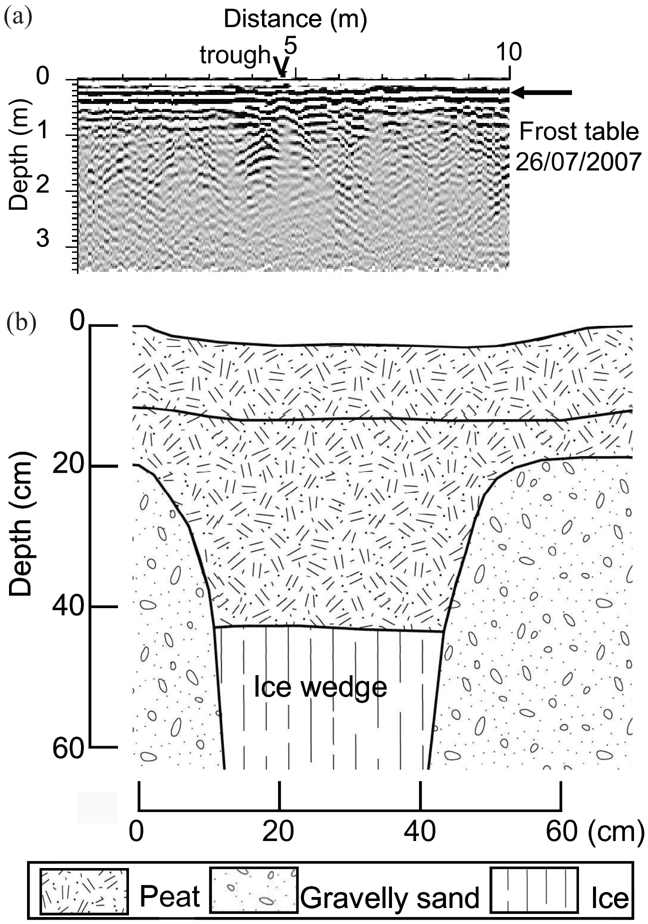

Figure 4. (a) A GPR profile across a polygon trough on a bog site in Kapp Linné. (b) The cross section of the trough.

wedge filling is distinguished by a difference in color. A thin organic layer covers the trough and intrudes into the wedge filling to about 80 cm depth. This intrusion may have originated from the latest cracking activity. The soil wedge extends below the frost table (at ca. 105 cm depth). Further drilling into the permafrost confirmed the presence of an underlying ice wedge which penetrates deeper than 270 cm. The ice wedge corresponds to the lower GPR reflection.

Kapp Linné: Bogs

GPR profiles of widely spaced polygon troughs in bogs showed a narrow hyperbolic reflection underlying a strong horizontal reflection, although the wet surface significantly attenuated the radar signals (Fig. 4a). The propagation velocity was estimated to be around 0.070 m/ns by the point-source reflection analysis using the hyperbolic reflection. This velocity suggests that the top of the hyperbola lay at about 0.3 m depth. Such a hyperbolic reflection may indicate the presence of an ice wedge. The drilling and excavation in late July actually confirmed the presence of a narrow ice wedge reaching 130 cm depth. The excavation displayed a peat layer about 20 cm thick overlying marine sediments. A peat wedge penetrates into the marine sediment below the trough. The active layer thickness was thin and varied from 25 cm in the wedge to 35 cm in the marine sediment. The shallow frost table corresponded to the strong horizontal reflection on the GPR profile. An ice wedge with a top width of 30 cm occurred below the peat intrusion. The top of the ice wedge was located at 40 cm depth. Such a structure agrees with the narrow hyperbolic reflection. The trough lacked a double hyperbola pattern, although the peat intrusion formed an active layer soil wedge above the ice wedge. This is probably due to the difficulty in resolving two features which are so close to each other with a 250 MHz antenna.

Adventdalen: Fluvial terraces

GPR profiles displayed two kinds of reflections: (1) multiple horizontal reflections, which are slightly deformed below troughs; and (2) hyperbolic reflections, which underlie horizontal reflections below troughs (Fig. 5). The point-source reflection analysis using the hyperbolic reflections estimated that the radar velocity was about 0.050 m/ns, which was lower than the values of ice wedges in Kapp Linné. This is probably due to the low propagation rate in the poorly drained loess material. The estimated velocities suggest that the tops of the hyperbolic reflections were located at 1.2 m depth, regardless of the size of the polygon trough. A series of drilling holes across two polygon troughs reproduced the structure of the ice wedges. The drilling revealed that ice wedges were about 1.9 m wide below well-developed troughs (Fig. 5a) and about 0.5 m wide below shallow troughs (Fig. 5b). Below the shallow troughs, the centre of the ice wedge did not agree with the new crack at the ground surface. This relationship was correctly shown in the GPR profile (Fig. 5b), which indicates that the ice wedge has unevenly developed. The top of a hyperbola roughly corresponded to an edge of the ice wedge, which means that the width of hyperbola top represents the width of an ice wedge. The disturbance of the horizontal reflections below the trough may have originated from thermal contraction cracks filled with air and meltwater.

Influences of Grain Size and Water Content on GPR Profiles

Both of the ice and soil wedges showed strong hyperbolic reflections. This means that the dielectric constant is considerably different between ice and frozen soil and between a soil wedge and the host sediment. The dielectric constant varies with material of solids and air and water contents. In particular, the dielectric constant of water significantly affects the composite dielectric constant of soil, because water has an extremely high dielectric constant compared to other substances. These influences were evaluated by measurements of grain size distribution and water content of soils.

Figure 6 summarizes the grain size distribution of soils at 4 sites. The soil samples were taken from both the soil wedge and the host sediment. In Kapp Linné, the composition of the soil-wedge filling is different from that of the marine sediment. Below a marine terrace where a single hyperbola occurs by a soil wedge, the wedge filling is significantly finer than the marine sediment. Below a beach ridge where the double

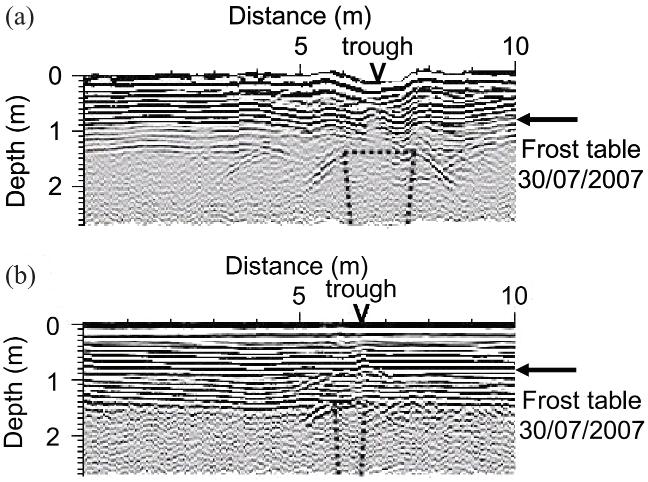

Figure 5. Subsurface structures below low-centered polygons on a fluvial terrace in Adventdalen. (a) A GPR profile across a large polygon trough. (b) A GPR profile across a small polygon trough. The broken lines illustrate ice wedges indicated by drillings.

hyperbolic reflections occur, the wedge and host sediment show similar mean grain sizes, but the wedge filling ranging from gravel to silt, shows a wider size distribution than the host sediment. The difference may result in a different porosity and influence the dielectric constant. A large difference in grain size occurs between samples derived from the bog site, although the soil wedge lacks a hyperbolic reflection. This may result from soil wedge too thin to be detected by 250 MHz signals. In contrast, the samples obtained from the Adventdalen river terrace indicate similar grain size distributions between the soil wedge and the host loess. This probably explains why double hyperbolic reflections did not occur at the Adventdalen study site, where the soil wedges are filled with similar material to the host sediments.

Table 1 shows water contents in and around the soil wedge below the marine terrace at Kapp Linné in summer. The ground surface was dry when the samples were collected. The soil wedge has significantly higher water content than the surrounding materials. This is probably because the organic materials composing the soil wedge have a high water retention capacity, while the marine sediments are highly drained. The contrast probably induces strong reflections.

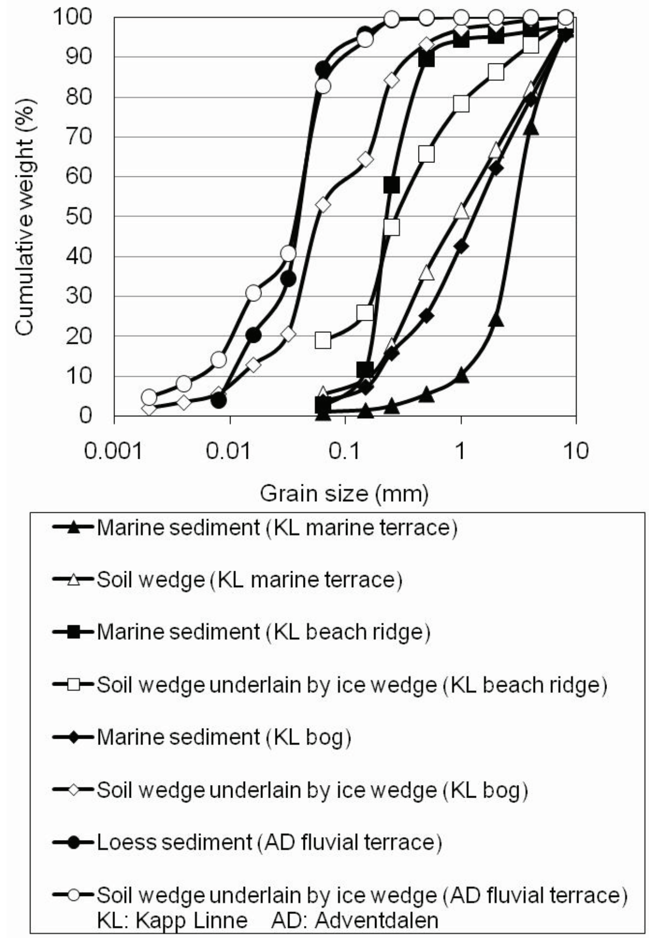

Figure 6. Grain size distribution in soil wedges and the host materials.

Table 1. Volumetric water contents in a soil wedge and the host materials at the Kapp Linné marine terrace site. Samples were taken on July 24, 2007.

Sampling point	*Water content (%)*
Soil wedge (organic)	40.8
Sand layer below soil wedge	15.7
Sand layer aside of soil wedge	8.8
Gravel layer below soil wedge	6.2

Conclusions

The GPR profiles across non-sorted polygons show characteristic reflections representing ice and soil wedges. Hyperbolic reflections extending downward from the ground surface represent active layer soil wedges. Such a sharp reflection is considered to originate from the different water content between the soil wedges and the host sediments. Ice wedges show hyperbolic reflections extending downward from the frost table. The width of the hyperbola roughly coincides with the width of an ice wedge determined by drilling. Where a soil wedge in active layer is underlain by an ice wedge, troughs are underlain by double hyperbolic reflections extending downward from the ground surface and the frost table.

These results indicate that GPR is useful for distinguishing ice and active layer soil wedges, in terms of the depth of hyperbolic reflections, and for estimating the width of ice wedges without excavation or drilling down to permafrost.

Acknowledgments

We thank Ole Humlum and UNIS students for their cooperation in the field, UNIS technical staff for their assistance in transporting equipment and safety guidance, and H. Miura for permission to use GPR systems in the National Institute for Polar Research.

References

Åkerman, J. 1980. *Studies on Periglacial Geomorphology in West Spitsbergen*: Meddelanden från Lunds Universitets Geografiska Institution Series Avhandlinger 89, 297 pp.

Åkerman, J. 1987. Periglacial forms of Svalbard: a review. In: J. Boardman (ed.), *Periglacial Processes and Landforms in Britain and Ireland*. Cambridge: Cambridge University Press, 9–25.

Åkerman, J. 1996. Slow mass movements and climate relationships, 1972–1994, Kapp Linné, West Spitsbergen. In: M. G. Anderson & S. M. Brooks (eds.), *Advances in Hillslope Processes* 2. Chichester: Wiley, 1219–1256.

Berthling, I., Etzelmüller, B., Isaksen, K. & Sollid, J.L. 2000. Rock glaciers on Prins Karls Forland. II:–GPR soundings and the development of internal structures. *Permafrost and Periglacial Processes* 11: 357–369.

Christiansen, H.H. 2005. Thermal regime of ice-wedge cracking in Adventdalen, Svalbard. *Permafrost and Periglacial Processes* 16: 87–98.

Christiansen, H.H. & Humlum, O. 2003. Active layer monitoring in Ny Ålesund and in Adventdalen in the CALM Network. In: J.L. Sollid & H.H. Christiansen (eds.), *Permafrost, Periglacial Features and Glaciers in Svalbard, Excursion Guide*. Oslo: University of Oslo, 97–100.

Dallimore, S.R. & Davis, J.L. 1987. Ground probing radar investigation of massive ground ice and near surface geology in continuous permafrost. *Geological Survey of Canada Paper* 87-1A: 913–918.

Hanssen-Bauer, M., Soløs, M.K. & Steffensen, E.L. 1990. The climate of Spitsbergen. *Klima: Norwegian Meteorological Institute Report 39/40*. Oslo: Norwegian Meteorological Institute, 1–40.

Hinkel, K.M., Doolittle, J.A., Bokheim, J.G., Nelson, F.E., Paetzold, R., Kimble, J.M. & Travis, R. 2001. Detection of subsurface permafrost features with ground-penetrating radar, Barrow, Alaska. *Permafrost and Periglacial Processes* 12:179–190.

Humlum, O., Instanes, A. & Sollid, J.L. 2003. Permafrost in Svalbard: a review of research history, climatic background and engineering challenges. *Polar Research* 22: 191–215.

Isaksen, K., Holmund, P., Sollid, J.H. & Harris, C. 2001. Three deep alpine-permafrost boreholes in Svalbard and Scandinavia. *Permafrost and Periglacial Processes* 12: 13–25.

Landvik, J., Mangerud, J. & Salvigsen, O. 1987. The late Weichselian and Holocene shoreline displacement on the west-central coast of Svalbard. *Polar Research* 5: 29–44.

Matsuoka, N. & Hirakawa, K. 1993. Critical polygon size for ice-wedge formation in Svalbard and Antarctica. *Proceedings of the Sixth International Conference on Permafrost 1*, *Beijing, China, July 5–9, 1993*: 449–454.

Moorman, B.J., Robinson, S.D. & Burgess, M.M. 2003. Imaging periglacial conditions with ground-penetrating radar. *Permafrost and Periglacial Processes* 14: 319–329.

Munroe, J.S., Doolittle, J.A., Kanevskiy, M.Z., Hinkel, K.M., Nelson, F.E., Jones, B.M., Shur, Y. & Kimble, J.M. 2007. Application of ground-penetrating radar imagery for three-dimensional visualization of near-surface structures in ice-rich permafrost, Barrow, Alaska. *Permafrost and Periglacial Processes* 18: 309–321.

Ross, N., Harris, C., Christiansen, H.H. & Brabham, P. Ground-penetrating radar investigations of open system pingos, Adventdalen, Svalbard. *Norsk Geografisk Tidsskrift* 59: 1–11.

Salvigsen, O. & Elgersma, A. 1985. Large-scale karst features and open taliks at Vardeborgsletta, outer Isfjorden, Svalbard. *Polar Research* 3: 145–153.

Sørbel, L., Tolgensbakk, J., Hagen, J.O. & Høgvard, K. 2001. Geomorphological and Quaternary geological map of Svalbard 1:100,000. Sheet C9Q Adventdalen. *Temakart No. 31/32.* Tromsø: Norwegian Polar Institute, 57–78.

Tolgensbakk, J., Sørbel, L. & Høgvard, K. 2001. Geomorphological and Quaternary Geological Map of Svalbard 1:100,000. sheet C9Q Adventdalen. *Temakart No. 31/32*. Tromsø: Norwegian Polar Institute.

Yoshikawa, K., Leuschen, C., Ikeda, A., Harada, K., Gogineni, P., Hoekstra, P., Hinzman, L., Sawada, Y. & Matsuoka, N. 2006. Comparison of geophysical investigations for detection of massive ground ice (pingo ice). *Journal of Geophysical Research* 111: E06S19, doi: 10.1029/2005JE002573.

Modeling Forecasting on Permafrost Changes in Northeastern China

Zhi Wei, Huijun Jin, Jianming Zhang, Yanjun Ji, Sizhong Yang, Ruixia He
State Key Laboratory of Frozen Soils Engineering, Cold and Arid Regions Environmental and Engineering Research Institute, Chinese Academy of Sciences, Lanzhou, China

Shaopeng Yu
Department of Geography, Harbin College, Harbin, China

Abstract

In northeastern China, mean annual air temperature (MAAT), as a main control factor, increased by 1°C between 1975 and 2000 as compared to 1951–1975 with a warming rate of 0.04°C/yr. In the absence of adequate borehole temperature data, geographic factors such as latitude, longitude, elevation, aspect, and slope were used to describe the present distribution of permafrost and to model scenarios of its potential future changes. The result showed that latitude is the primary factor that determines the distribution of MASST, enabling an equivalent latitude model (ELM) to be constructed and a GIS-based map of present-day MASST distribution to be drawn. Future permafrost changes 50 years from now were then estimated by finite-element modeling. The results indicate that permafrost thickness would not change greatly, apart from some south-oriented slopes, but that permafrost degradation would primarily be caused by increasing mean annual ground temperature.

Keywords: finite element; forecast; mean annual soils surface temperature; modeling, northeastern China.

Introduction

Permafrost in northeastern China (NE China) is warm, thin, and sensitive to atmospheric warming. Research on permafrost in northeastern China was initiated in the early 1950s. During the 1960s and 1970s numerous regional investigations, together with local studies for specific purposes such as water supply, road construction, or coal-mining, were conducted in order to meet the needs of economic development. The boundaries of continuous (>65% occupation), discontinuous (50%–60%), and sporadic permafrost (5%–30%) were empirically determined to correlate with the -5°C, -3°C, and 0°C isotherms of mean annual air temperature, respectively. This pattern has strongly changed during about 30 years of ongoing atmospheric temperature rise and heavy direct impacts from human activities. The most influencing human activities are unceasing deforestation, frequent forest fire, and some large-scale constructions. All these natural and non-natural realities affected the existing and developing conditions of permafrost in NE China. (Zhou & Wu 1965, Guo & Li 1981, Guo et al. 1981, Dai 1982, Northeastern China Permafrost Research Taskforce 1983, Guo & Huang 1989, Peng & Cheng 1990, Lu et al. 1993, Gu & Zhou 1994, Zhou et al. 1996). Degradation of permafrost in northeast China has been of considerable concern during the past decade (Gu & Zhou 1994, Chen & Yin 1996, Wang et al. 1996, Zhou et al. 1996). Many major engineering and environmental projects such as express highways and high-speed railways, the proposed China-Russia Crude Oil Pipeline from Skovorodino, Russia to Daqing, China, or a hydropower project near the Heilongjiang (Amur) River, necessitate an understanding of the status and possible future evolution of permafrost in the NE China over the next 30–50 years. This paper analyzes the effects from increasing MAAT, introduces a concept of MASST zonality, and presents a preliminary forecast concerning the future trends of permafrost conditions in NE China.

Changes of MAAT and MASST

Climate change and permafrost condition

Long-term (1951–2000) monthly air temperature records of 117 meteorological stations (Fig. 1a) in regions with continuous or discontinuous permafrost or seasonally frozen ground within the study area of NE China showed a pronounced warming tendency comparable with warming trends observed in northward zones in Siberia (Yang et al. 2000). In the 1970s, the southern limit of permafrost (SLP) and boundaries between different types of continuous, discontinuous, and sporadic permafrost in NE China were determined by Northeastern China Permafrost Cooperation Group (NCPCG) (Guo et al. 1981). Comparison of the two time intervals 1951–1975 and 1976–2000 illustrates the notable long-term warming trend (Figs. 1a, b).

The pattern of isotherms is quite similar during both time periods but documents a shift in MAAT of about +1°C between the two considered time intervals. This change will definitely affect permafrost: its existence, distribution, thermal condition, and active layer depth. Using the MAAT range of -1°C and +1°C for southern limit of permafrost occurrence (SLP), its climate-induced northward displacement can be estimated at 40–120 km in accordance with previous studies (Jin et al. 2007).The principal cause of the observed permafrost degradation in NE China is atmospheric warming which has occurred since the end of the 19th century. Based on decadal average air temperatures (DAATs) from northeastern China, this change can be divided into three main periods: (1) persistent warming from the end of the 19th century to the 1940s; (2) quasi-stable

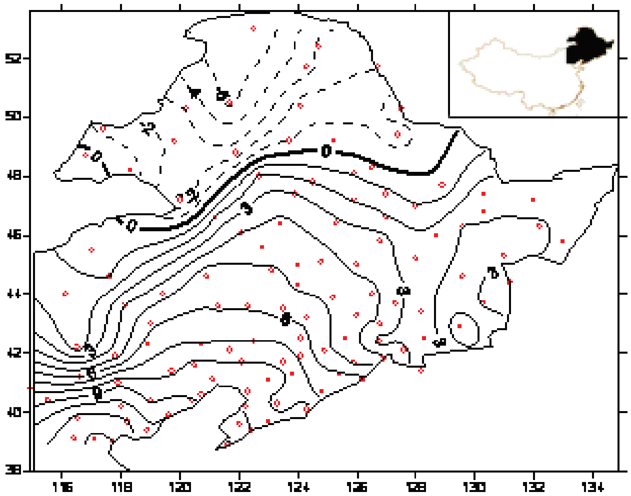

(a)

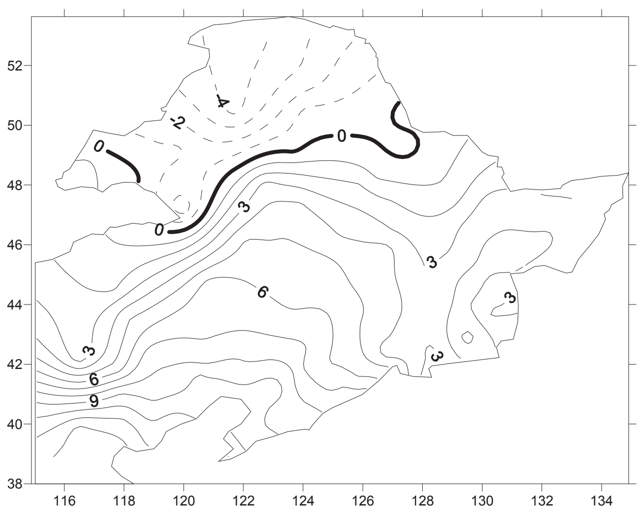

(b)

Figure 1. Mean annual air temperature isotherms during 1951–1975 (a) and 1976–2000 (b) in NE China; the embedded circles are the distribution of 117 meteorological stations in study area of NE China.

average temperatures during the 1950s to the 1970s; and (3) a second persistent warming from 1970 to 2000, particularly during 1991–2000a (Qin 2002).

Soils surface temperature and climate change

Mean annual soils surface temperatures (MASST) are primarily influenced by air temperature. In order to better understand their changes in the study area as related to conditions of atmospheric warming, data for the time period 2000–2004 from all 47 systematically observed, national meteorological stations in northeastern China and some of those in the Meng'gu and He'bei provinces in the North China district were employed to analyze the relation between MAAT and MASST. The statistical analysis identified a strong relation between the two (Fig. 2), with MASST being on average about 1.7°C higher than MAAT. Strong correlation between air and ground surface temperatures indicates that higher air temperatures induced a corresponding heat absorption and ground warming over the past decades.

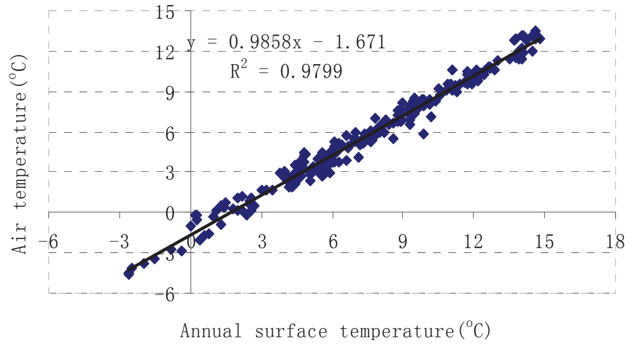

Figure 2. The correlation analysis between mean annual air temperature and soil surface temperatures.

Equivalent Latitude Model for MASST

In its spatial distribution, MASST is basically controlled by latitude (Table 1), but according to the former relative studies, permafrost condition in NE China is very different with topography such as aspect and slope at almost the same location (Brown 1973, Liu et al. 1993). These variations reflected from different mean annual ground temperature (MAGT), permafrost thicknesses, and depths of active layer (Tables 2, 3), so aspect and slope were taken into account to constitute equivalent latitude (Haugen et al 1993):

$$\varphi' = \sin^{-1}(\sin k \cosh \cos \varphi + \cos k \sin \varphi) \tag{1}$$

where k is slope of the surface (°); h is surface aspect (°); φ and φ' are actual latitude and equivalent latitude of the spot (°).

Measured data and previous articles proved that snow has a much greater influence than vegetation on the thermal condition of permafrost, and show a unconspicuous influence if acting together (Fig. 3); but it is a complicated process how snow affects, so MASST is used in the model to remove snow influence.

When replacing the actual latitude with so-calculated "equivalent latitude," the partial correlation between MASST and equivalent latitude increases to 0.957 compared to the previous 0.938. According to trends in altitude changes, a two-section equation was used in the model simulation. This provided more satisfactory results (R^2=0.972>0.957; F=190.86>148.68) (Fig. 4). The two-section equation (Jin et al 2007) is:

$$Ts = \begin{cases} 72.153 - 0.684\varphi' - 0.265\theta - 0.007h & h \le 250m \\ 60.369 - 1.105\varphi' - 0.015\theta - 0.005h & h > 250m \end{cases} \tag{2}$$

where: T_s is mean annual soils surface temperature (°); θ and h is longitude (°) and altitude (m) of the spots; φ' is equivalent latitude of the spots (°).

From Figure 4, the simulant essentially reflected the MASST, F test value is 190.86, indicate that the equivalent latitude model is relatively exact and can be used to predict the MASST distribution. Based on Equation 2, a GIS-based

Table 1. Partial correlations between MASST and three elementary geographic factors.

		Latitude/°	Longitude/°	Altitude/m
Mean annual soils surface temperature/°C	Pearson correlation	0.938	-0.552	-0.805
	Sig.(2-tailed)	0.000(**)	0.000(**)	0.000(*)
	Total stations	47		

**Correlation is significant at the 0.01 level (2-tailed).

Table 2. The permafrost thickness changes to slope in NE China.

Topography (Different slope)	Lowland in river valley			Foothill			Mountain slope
Borehole No.	$H_{4\text{-}7}$	$H_{1\text{-}3}$	$H_{5\text{-}24}$	$H_{z\text{-}1}$	$H_{z\text{-}2}$	$H_{z\text{-}3}$	$H_{z\text{-}10}$
Permafrost table/m	0.3-0.8	0.3-0.8	0.3-1.0	1.0-2.5	1.0-3.0	1.0-2.5	1.0-3.0
Permafrost base/m	112.65	122.6	130	31	14.9	25	16

Table 3. The affect of aspect on permafrost conditions in NE China.

items	East–West-oriented valley			South–North-oriented valley		
	S-oriented slope	lowland	N-oriented slope	W-oriented slope	lowland	E-oriented slope
MAGT/℃	0~ -1.0	-2.0~ -4.2	-1.0~ -2.0	0~ -1.0	-2.0~ -4.2	0~ -0.5
PTH/m	0~20	50~150	20~50	10~30	50~100	0~20
SMTH/m	2.0~4.0	0.5~1.0	1.0~1.5	1.0~2.0	0.5~1.0	1.0~3.0

MAGT – mean annual ground temperature; PTH – permafrost thickness; SMTH – seasonal melted thickness.

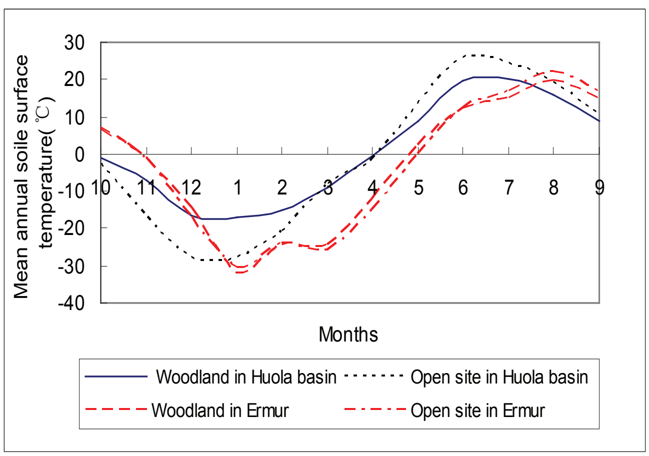

Figure 3. Influence of snow and vegetation on MASST (Huola basin cleaned snow in winter).

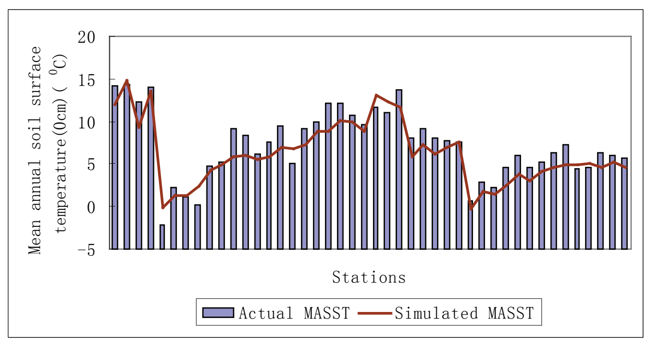

Figure 4. Simulated MASST compared to measured data.

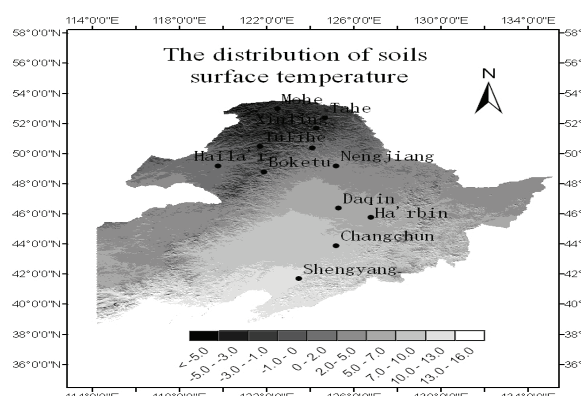

Figure 5. The distribution of MASST in NE China.

MASST distribution map was drawn using C++ programs (Fig. 5). The DEM and other digital data were taken from GTOPO 30 with a horizontal grid spacing of 30 arc seconds (approximately 1 kilometer), Center for Earth Resources Observation and Science (EROS), U.S. Geological Survey (USGS 2007).

The w-shaped pattern of MASST-isotherms is due to elevation effects, as the Da and Xiao Xing'anling Mountains are relatively higher than their surroundings in the western and eastern parts of the study area, ranging from 1000 to 1400–1500 m a.s.l. in the middle section from A'ershan to Yi'ershi and to the source of the Zhuo'er River, but decreasing northward to 500–600 m a.s.l. in the section from Mangui to Gulian. In contrast, the Xiao Xing'anling Mountains are gentler in topography, with meandering river channels, elevations of 500–600 m a.s.l., and few peaks higher than 800 m a.s.l. Large quantities of eroded debris from the steeper eastern slopes have been carried by deeply incised rivers to the Nenjiang River Plain, which lies between the two mountain ranges, with the elevation ranging from several meters to 200–300 m a.s.l.

Permafrost Change with Global Warming

Mathematical model for calculation

On the basis of the MASST distribution, permafrost changes can be calculated using finite element methods of heat diffusion at depth and characteristic surface boundary conditions. The main control equation is:

$$\rho.C\frac{\partial T}{\partial t}=\frac{\partial}{\partial x}(\lambda\frac{\partial T}{\partial x})+\frac{\partial}{\partial y}(\lambda\frac{\partial T}{\partial y}) \qquad (3)$$

In this equation:

$$C=\begin{cases} C_u & (T>T_p) \\ C_f+\dfrac{C_u-C_f}{T_p-T_b}(T-T_b)+\dfrac{L}{(1+W)}\dfrac{\partial W_i}{\partial T} & (T_b\le T\le T_p) \\ C_f & (T<T_b) \end{cases}$$

$$\lambda=\begin{cases} \lambda_u & (T>T_p) \\ \lambda_f+\dfrac{\lambda_u-\lambda_f}{T_p-T_b}(T-T_b) & (T_b\le T\le T_p) \\ \lambda_f & (T<T_b) \end{cases}$$

where ρ is natural density of soils (kg/m3); C is apparent specific heat of soils (J/(kg.K); C_u, C_f are specific heats of thawed and frozen soils; λ is apparent conductivity of soils (J/(m.h.k)); λ_u, λ_f are conductivities of thawed and frozen soils; L is latent heat (K/kg); W, W_i is total water content or ice content (%); T_p and T_b are the upper and lower critical temperature related to phase changing (°C); T is temperature (°C); t is time (h); x and y are spatial variables (m).

Geometrical model for forecasting calculation

An additional geometrical model considered effects from human activities within a distance of 30 m, mainly relating to deforestation in connection with road construction, creation of fire insulation zones, or installing electrical transforming line (Fig. 6); with an additional 30 m added to each side, the total width considered is 90 m. Some borehole data in NE China approved that the gradient at depths greater than 30m is less than 0.004°C/m (Li et al. 1996). The bottom boundary was therefore chosen at this depth.

Boundary conditions

The surface boundary of calculation area presented as:

$$T=T_0+\alpha\cdot t+A\sin\left(\frac{2\pi\cdot t}{8760}+\frac{\pi}{2}\right) \qquad (4)$$

where T is SST (0 cm) (°C); T_0 is MASST (°C); α is increment of MASST, is 0.048 within 50-year period in the future (°C/a); t is time duration; A is amplitude of SST (°C, 18.5°C for the forest surface); $\pi/2$ is the initial phase (corresponding to the warmest part of the year).

In the IPCC WG2 report (Chapter 10–Asia) (IPCC 2007), the minimum future increase in surface air temperature will be 1.4°C (2010a–2039) and 2.5°C (2040–2069), then the surface air temperature would be 2.4°C higher after 50 years in NE China, atmospheric model of A1, A1B, and A2 also examined its increment of 0.026, 0.027, and 0.05, and synthesized α = 0.048 in connection with the actual increment. Therefore the soil surface temperature would be with an approximately same increment based on former 50-year linear relation without any large change in atmospheric circulation.

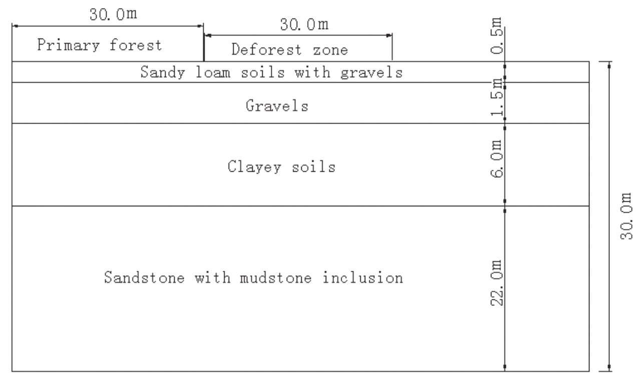

Figure 6. The geometrical model in calculation.

The mean annual ground temperature of present-day stable permafrost temperature regime is inferred from 200 years ahead. Calculated results (Fig. 7) indicated that present MAGT is near to MASST, future MAGT in different MASST zonal areas would increase in various extents: about 0.5°C, 0.4°C, and 0.3°C where the present MASST is -2.0°C, -1.5°C, and -1.0°C, slightly in -0.5°C and 0°C zones, because the nearer to the phase-change area, the more slowly permafrost temperature will change, but much more of that together with anthropic activities: In contrast, the permafrost table deepens most where present MASST is 0°C, the increment ranged from 1.2 m to 0.2 m in 5 different MASST zones (Table 4). Permafrost thickness would not change greatly apart from some south-oriented slopes and areas around 0°C in MAGT. The permafrost degradation would mainly take in place in the form of increasing in mean annual ground temperature.

Conclusion

Mean annual air temperature (MAAT) in NE China increased by about 1°C from 1976–2000 as compared to 1951–1975 with a yearly 0.04°C increase, i.e., higher than mean warming rate of 0.026°C/a estimated by IPCC for the Northern Hemisphere. Mean annual soil surface temperature (MASST) is linearly related to MAAT and may therefore have risen at the similar rate if there aren't any large changes in surroundings. This inevitably caused permafrost warming.

Climatic warming and increased human activity during the last century are both thought to be responsible for the degradation of permafrost in NE China. Extensive and increasing human activity for resource exploitation, agriculture, and economic development have accelerated the processes.

Table 4. Changes of MAGT (at 15 m deep location) and table of permafrost in different zones, present and within next 50 years.

MASST zonal area /°C	Mean annual ground temperature /°C (-15 m)			Permafrost table /m		
	Present	GW	GW+MA	Present	GW	GW+MA
0.0	0.06	0.07	0.10	3.00	4.20	5.85
-0.5	-0.50	-0.45	-0.40	2.80	3.40	5.20
-1.0	-0.99	-0.77	-0.64	2.65	3.10	4.70
-1.5	-1.44	-1.11	-0.86	2.50	2.80	4.00
-2.0	-2.03	-1.56	-1.12	2.40	2.60	3.20

GW – in the scenario of global warming; GW+MA – in the scenario of global warming plus human activities.

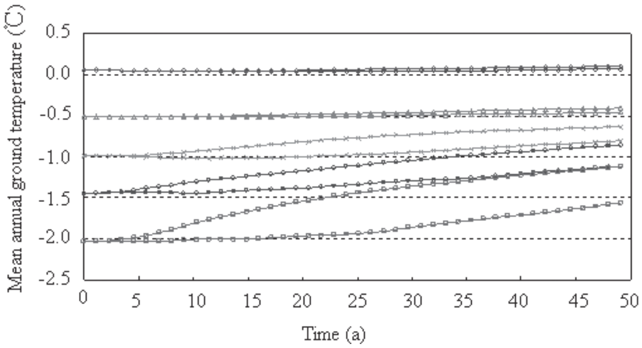

Figure 7. Calculated changing process of permafrost with various MAGT (down to 15 m) in different MASST zonal area within coming 50 years in NE China, under global warming and added anthropic activities (upper and lower line for each case).

A forward projection of atmospheric warming trends revealed that mean annual permafrost temperature would more strongly increase in zones of relatively cold MASST of around -2.0°C than in zones of warm to temperate permafrost. The permafrost table, on the other hand, is expected to deepen most strongly (about 12 m) in zones with MASST near 0°C. These effects are considerably enhanced by effects from direct human impact. Changes in permafrost thickness would be limited, and increasing mean annual ground temperatures are likely to be the predominant manifestation of permafrost degradation.

Acknowledgments

Genuine acknowledgment goes to Doctor Xujun Han for support and help in the accomplishment of the equivalent latitude model in GIS. Data supplied by 1st Team, Forest Design and Research Institute, Hei'long'jiang province.

References

Brown, R. 1973. Influence of climatic and terrain factors on ground temperature at three locations in the permafrost region of Canada. *Proceeding of the Second International Conference on Permafrost (North American Contribution), Yakutsk, USSR, July 13–28, 1973*: 27-34.

Chen, Y. & Yin, Y. 1996. Impacts of forest industry development in the Da Xing'anling Mountains on the seasonally thawed layer overlying permafrost. *Proceeding. of the Fifth Chinese Conference on Glaciology and Geocryology (Vol. 2), Lanzhou, August 18–22, 1996*: 1087-1091.

Dai, J. 1982. Features of permafrost temperature in northern part of the Da-Xing'anling Mountains. *Journal of Glaciology & Geocryology* 4(3): 53-63 (in Chinese).

Gu, Z. & Zhou, Y. 1994. Changes of permafrost in the Amu'er area of the Da-Xing'anling Mountains. In Y.W. Zhou & Z.X. Yang (eds.), *Impacts and Countermeasures of Forest Fire in the Da-Xing'anling Mountains*. Beijing: Science Press, 156-161.

Guo, D., Wang S. & Lu G. 1981. Division of permafrost regions in Da'xiao Hingganling northeast China. *Journal of Glaciology & Geocryology* 3(3): 1-9 (in Chinese).

Guo, D. & Huang Y. 1989. The role of geological structure in the formation of permafrost in the Hola Basin, northeastern China. *Journal of Glaciology & Geocryology* 11(3): 216-222 (in Chinese).

Guo, D. & Li Z. 1981. Geological evolution and age of formation of permafrost in northeastern China since the late Pleistocene. J*ournal of Glaciology & Geocryology* 3(4): 1-6 (in Chinese).

Haugen, K., Greeley, H. & Collins, M. 1993. Permafrost mapping using GRASS. *Proceeding of Six International conference on permafrost, (Vol. 2): Beijing, July 5–9*: 1128-1131.

IPCC, 2007. http://ipcc-wg2.ucar.edu.

Jin, H.J., Yu, Q., Lü, L., Guo, D.X., He, R.X., Yu, S.P., Sun, G.Y. & Li, Y.W. 2007. Degradation of permafrost in the Xing'anling Mountains, Northeastern China. *Permafrost & Periglacial Process* 18: 245-258.

Jin, H.J., Zhang, J.M. & Tong, C.J. 2007. *Final Report on the Assessment and Prediction of Frozen Ground Engineering Geology Along the Mo'he to Daqing Oil Pipeline.* PetroChina DOE & CAS CAREERI (eds.): 100-120.

Li, Y., Tong, C. & Zhang, L. 1996. Computation of the permafrost thickness in Yitulihe observations field. *Proceeding of the Fifth Chinese Conference on Glaciology and Geocryology (Vol.2), Lanzhou, August 18–22*: 1143-1148.

Liu, Q., Sun, K. & Cui, S. 1993. Study of the law of the distribution of permafrost and vegetation in Da Higgan Ling. *Journal of Glaciology & Geocryology* 15(2): 246-251.

Lu, G., Weng, B. & Guo, D. 1993. Geographical southern limit of permafrost in Northeastern China. *Journal of Glaciology & Geocryology* 15(2): 214-218 (in Chinese).

Northeastern China Permafrost Research Taskforce. 1983. Major features of permafrost distribution in northeastern China. *Proceeding of the Second Chinese Conference on Geocryology, Lanzhou, October 12–15:* 36–42.

Peng, H. & Cheng, G. 1990. Ice wedges in the Da Xing'anling Mountains, northeastern China and their implications in paleo-climatology. *Proceeding of the Fourth Chinese Conference on Glaciology & Geocryology, Lanzhou, October 6–9,1988:* 9-16.

Qin, D. (ed.). 2002. *Features and Evolution of Environments in Western China: Assessment of the Evolution of Environments in Western China.* Beijing: Science Press, 41–49.

USGS. 2007. http://edc.usgs.gov/.

Wang, C., Zhang, B. & Liu, F. 1996. Marks and phenomena of permafrost degradation in northern China. *Proceedings of the Fifth Chinese Conference on Glaciology and Geocryology (Vol. 2), Lanzhou, August 18–22, 1996:* 1063–1070.

Yang, D., Kane, D.L. & Hinzman L. 2002. Siberian Lena River hydrological regime and recent change, *Journal Geophysical Research* 107 (D23): 1-10.

Zhou, Y. & Wu, Z. 1965. Permafrost in the northern part of the Da-Xing'anling Mountains. In: *Monograph on the Geocryological Expedition Along the Qinghai-Tibet Highway*, Appendix. Beijing: Science Press, 20-25.

Zhou, Y., Gao, X. & Wang Y. 1996. The ground temperature changes of seasonally freeze-thaw layer and climate warming in northeast permafrost in northeast China in the past 40 years. *Proceeding. of the Fifth Chinese Conference on Glacialogy and Geocryology, (Vol.1), Lanzhou, Ausust 18–22, 1996:* 3-10.

Thermokarst Lakes in Central Yakutia (Siberia) as Habitats of Freshwater Ostracods and Archives of Palaeoclimate

Sebastian Wetterich
Alfred Wegener Institute for Polar and Marine Research, Telegrafenberg A43, D-14473 Potsdam, Germany
Lutz Schirrmeister
Alfred Wegener Institute for Polar and Marine Research, Telegrafenberg A43, D-14473 Potsdam, Germany
Hanno Meyer
Alfred Wegener Institute for Polar and Marine Research, Telegrafenberg A43, D-14473 Potsdam, Germany
Christine Siegert
Alfred Wegener Institute for Polar and Marine Research, Telegrafenberg A43, D-14473 Potsdam, Germany

Abstract

Thermokarst lake deposits are useful archives of climatic and environmental changes in the past, and can contain palaeo-bioindicators such as pollen, plant macro-fossils, diatoms, chironomids, and ostracods. Nevertheless, such studies from permafrost regions including thermokarst lake deposits are still rare. We studied late Holocene ostracods from an excavation of deposits of the Alas Myuryu in Central Yakutia. In order to apply modern data to fossil records, we also studied the present-day relationships between the environmental setting and the geochemical properties of ostracods in six thermokarst lakes of the same region. The fossil ostracod record reflects lake-level fluctuations in the composition and stable isotope data ($\delta^{18}O$, $\delta^{13}C$) of both species. The modern ostracod communities of thermokarst lakes in Central Yakutia are broadly similar to those of Holocene age. Geochemical stable isotopes studies in both modern host water and ostracod calcite are a prerequisite for further interpretation of the fossil records.

Keywords: Central Yakutia; Holocene; ostracods; thermokarst lakes.

Introduction

Thermokarst is a common phenomenon of the cryolithozone generally caused by extensive melting processes of ground ice in the underlying permafrost. Widespread thermokarst processes have been climatically driven and intensified during warm periods in the Quaternary, especially since the Holocene (e.g., Katasonov 1979). They are responsible for the formation of numerous depressions in the landscape surface (alases), which are often occupied by thermokarst lakes. These landscape forms are typical for Central Yakutia (e.g., Soloviev 1973). The deposits of thermokarst lakes frequently contain fossil remains of bio-indicators, e.g., freshwater ostracods, which can be used for palaeoenvironmental reconstructions. Cyclic water level changes in the lakes are related to regional climatic variations (e.g., Nemchinov 1958).

Freshwater ostracods are crustaceans, usually less than 3 mm long, with a bi-valved carapace made of low-magnesium calcite. Changes in climatic and hydrological parameters influence the diversity of freshwater ostracods as well as the geochemical composition of ostracod calcite. In general, several geochemical properties of the calcareous shells of ostracods contain environmental information about the water chemistry and stable isotope composition of the host water at the time of shell formation (e.g., Griffiths & Holmes 2000). In particular, $\delta^{18}O$ and $\delta^{13}C$ records of ostracod calcite provide a highly localized and temporally restricted reflection of the isotopic composition of water, making them useful tools in palaeolimnology (Griffiths & Holmes 2000). The $\delta^{18}O$ of carbonates serves as proxy for temperature of the water, the isotopic composition of which is also influenced by precipitation, drainage basin hydrology, and the precipitation/evaporation ratio (P/E) (Kelts & Talbot 1990). The $\delta^{13}C$ of carbonates reflects changes in the isotopic ratio of the total dissolved inorganic carbon (TDIC) (Griffiths & Holmes 2000). Changes in $\delta^{13}C$ are attributed to changes in aquatic productivity within a lake, CO_2 exchange rates between atmosphere and water TDIC, as well as to the photosynthesis/respiration ratio within the lake (Leng & Marshall 2004).

In this respect, we present here the first combined study of modern and late Holocene ostracod assemblages from Central Yakutia. The first description of ostracods from this area was given by Pietrzeniuk (1977). Further regional studies were carried out on freshwater ostracods of the North Yakutian Lena River Delta, Laptev Sea (Wetterich 2007). In addition, Arctic freshwater ostracod associations were palaeoecologically analyzed in late Quaternary permafrost sequences from Bykovsky Peninsula, Laptev Sea (Wetterich et al. 2005).

Study Area

The studied lakes are situated on the Lena-Amga interfluve and around Yakutsk in Central Yakutia, in East Siberia (Fig. 1). The region belongs to the southern foreland of the Verkhoyansk Mountain Range. The fieldwork on an excavation of the late Holocene deposits of the Alas Myuryu (62°43′N, 131°08′E) was performed in summer

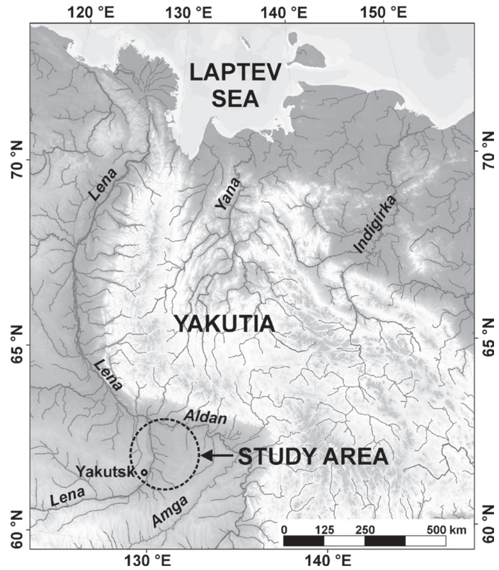

Figure 1. Schematic map of Russia showing the study site on the Lena-Amga interfluve in Central Yakutia (East Siberia). Map compiled by G. Grosse (UAF) using data from GLOBE Task Team (1999).

1997. Six modern thermokarst lakes (between 61°32′N and 62°19′N, 129°32′E and 132°12′E) were sampled in summer 2005 under the auspices of the Russian-German expedition "Central Yakutia 2005" (Wetterich et al. 2007).

Central Yakutia is characterized by a strong continental climate with low annual precipitation (222 mm) and a high temperature gradient over the year (mean temperature in January -37.6°C and in July 19.3°C) and a mean annual air temperature of -8.7°C (Meteorological station Yakutsk; RIHMI-World Data Centre: http://www.meteo.ru).

Materials and Methods

The late Holocene ostracod assemblages of the Alas Myuryu were recovered from a 1.4-m-deep excavation of lake deposits at the desiccated margin of the lake. The sediment samples were freeze-dried, wet sieved through a 0.250 mm mesh size, and then air-dried. About 200 g of each sediment sample was sieved for further ostracod analysis.

Living ostracods were caught at the lake bottoms in the littoral zone of six thermokarst lakes using a plankton net and an exhaustor (Viehberg 2002) in July and August 2005. The ostracods were preserved in 70% alcohol and afterwards counted and identified under a binocular microscope by soft body and valve characteristics.

The stable isotope analyses of oxygen ($\delta^{18}O$) and carbon ($\delta^{13}C$) were performed at the isotope laboratories of the Alfred Wegener Institute (AWI, Potsdam and Bremerhaven, Germany) and the GeoForschungsZentrum (GFZ, Research Centre for Geosciences, Potsdam, Germany).

For $\delta^{18}O$ and $\delta^{13}C$ analyses on fossil and modern valves of adult ostracods we used mass spectrometers (Finnigan MAT 251 at AWI and MAT 253 at GFZ) directly coupled to automated carbonate preparation devices (Kiel II and IV, respectively). Only clean valves of adult specimens were used. Particles adhered to valves were removed with a fine brush under microscope. To ensure enough material for isotope analysis (50–100 mg $CaCO_3$), multi-valve samples of single species have been created. The reproducibility as determined by standard measurements is better than ±0.08% (1σ) for $\delta^{18}O$ and ±0.06% (1σ) for $\delta^{13}C$.

The rain and lake water samples for $\delta^{18}O$ and δD were analyzed by equilibration technique (Meyer et al. 2000) using a mass spectrometer (Finnigan MAT Delta-S at AWI). The water samples for $\delta^{13}C$ analysis on TDIC were preserved by adding HgCl until analysis using a mass spectrometer (Finnigan MAT 252 at AWI). The reproducibility of these data derived from standard measurements is better than ±0.1‰ ($1\ \sigma$).

The values are expressed in delta per mille notation (δ, ‰) relative to the Vienna Standard Mean Ocean Water (VSMOW) for water isotopes ($\delta^{18}O$, δD) and relative to the Vienna Pee Dee Belemnite standard (VPDB) for $\delta^{13}C$ on TDIC and carbonate isotopes.

The dating of organic matter and calcareous valves from seven samples (Table 1) was undertaken at the Leibniz Laboratory for Radiometric Dating and Stable Isotope Research, University of Kiel (Germany) using radiocarbon Accelerator Mass Spectrometry (AMS).

Results and Interpretation

Fossil ostracods

The late Holocene ostracod assemblage consists of 22 species (Fig. 2). The most abundant species during the periods recovered are *Candona candida*, *Fabaeformiscandona rawsoni*, *Ilyocypris lacustris*, and *Limnocythere inopinata*. According to the modern ecological requirements of these species, some facts can be concluded for the living conditions of the fossil assemblage. Most of the species show a great adaptation to changes in both temperature and salinity regime, and are mostly typical for shallow water. The tolerance to temperature ranges from cold stenotherm to warm stenotherm with a great part of thermoeuryplastic (temperature tolerant) species. Furthermore, concerning changes in salinity, most of the species have oligo- to mesohaline ranges; i.e., 0.5 to 18‰ total salt content in the host waters (Meisch 2000). In general, the habitat of the fossil ostracods was a shallow-water environment with significant changes in temperature and salinity, which are linked to lake-level changes. Three periods of different lake conditions are distinguishable (Fig. 2). However, the geochronology of the fossil record from the excavation at the lake margin of the Alas Myuryu does not yield age relations for periods B and C. Whereas period A is well-defined by three dates between about 4300 to 1500 yr BP, period B lacks direct dates, and period A was only dated in its upper part with about 300 yr BP. Furthermore, the lower part of period A is complicated by two rejected ages, which are most likely caused by re-deposition during lake-level changes after sedimentation. Therefore, geochronological interpretation of the fossil data is weak and needs further dates. Nevertheless, late Holocene variations of the lake stages are reflected in taxonomical and geochemical data of the periods A to C (Fig. 2).

Period A (about 4300 to 1500 yr BP) is characterized by moderate water level fluctuations, which are also reflected in the changes in ostracod abundance and diversity. The $\delta^{18}O$ data of *F. rawsoni* with relative ^{18}O-depleted values between about -11 to -8‰ are most likely a sign of a higher P/E due to lower evaporation that caused a generally higher lake level. The shifting $\delta^{13}C$ values of *F. rawsoni* between about -2 to 1.5‰ indicate variable aquatic productivity during period A.

The following period B (after about 1500 yr BP) shows a short-time distinct decrease (at a depth of 58–63 cm) in the abundance of all species which appeared before. That was apparently caused by drying up of the water body. The appearance of *Plesiocypridopsis newtoni* shortly before and during period B (Fig. 2) points to higher salinity, since this species tolerates and even prefers brackish conditions (Meisch 2000). The $\delta^{18}O$ data of *F. rawsoni* reflect drastic changes in the isotopic composition of the lake with shifts between about -12 and -9‰ in a very short time. Afterwards, during a gradual flooding the species composition changed again.

In period C (about 300 yr BP) the species *F. acuminata*, *F. hyaline,* and *F. lepnevae* became common, and moderate lake-level fluctuations took place. In accordance with the $\delta^{18}O$ data of *F. rawsoni*, with relative ^{18}O-enriched values between about -9 to -6‰, the P/E ratio was lower (E>P) and that generally suggests higher evaporation and/or lower precipitation, resulting in a generally lower lake-level compared to period A. The $\delta^{13}C$ values of *F. rawsoni* between about -4 to -1‰ are relatively ^{13}C-depleted and can imply a general lowering in aquatic productivity compared to period A.

Modern ostracods

In six thermokarst lakes of Central Yakutia we observed 15 ostracod species (Fig. 3). In total, up to 250 adult specimens per lake were caught. The highest diversity per lake includes six species. The most abundant species from the fossil assemblages were found, but they are rare in the modern dataset. The dominant modern species are *Candona weltneri* in combination with *C. muelleri jakutica* and/or *F. rawsoni* (Fig. 3).

The studied lakes are shallow, without visible in- or outflows, and mainly fed by precipitation and meltwater from

Table 1. AMS dates of deposits of the Alas Myuryu. Rejected ages in brackets.

Lab No.	Sample No.	Depth [cm]	Material	uncal. Ages [yr BP]	cal. Ages* [yr BP] Max	cal. Ages* [yr BP] Min
KIA20827	J-97-6/161	10-15	Ostracods	275 ± 25	285	330
KIA8180	J-97-6/164	19-21	Reed leafs	285 ± 30	349	456
KIA8179	J-97-6/156	35-40	Grass and moss	(1935 ± 30)	(1820)	(1949)
KIA20828	J-97-6/156	35-40	Ostracods	(2100 ± 30)	(1995)	(2146)
KIA20829	J-97-6/147	75-80	Gastropods	1505 ± 30	1329	1417
KIA8178	J-97-6/141	105-110	Plant detritus	1945 ± 30	1823	1950
KIA20830	J-97-6/138	120-125	Gastropods	4280 ± 30	4822	4880

* Calibrated ages were calculated using the software "CALIB 5.0." Calibration data set: intcal04.14c (Stuiver & Reimer 1993, Reimer et al. 2004).

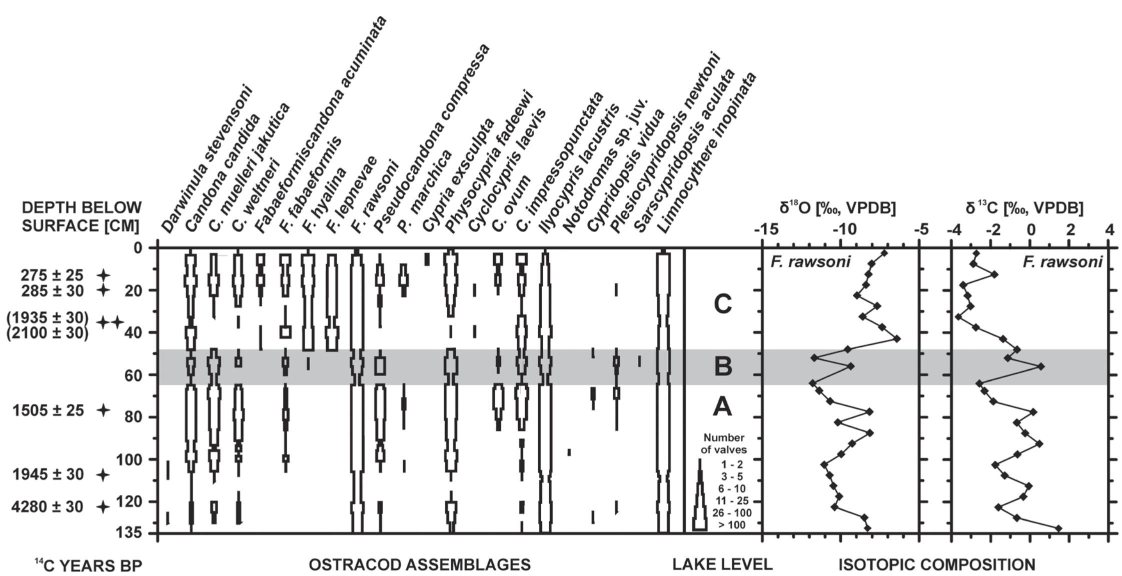

Figure 2. Ostracod assemblages and isotopic composition of ostracod valves from late Holocene lake deposits of the Alas Myuryu: A - Period of moderate lake-level fluctuations; B - Period of drastic lake-level fluctuations; C - Period of moderate lake-level fluctuations. Rejected AMS dates from deposited material are marked in brackets. Width of bars indicates ostracod number (see key).

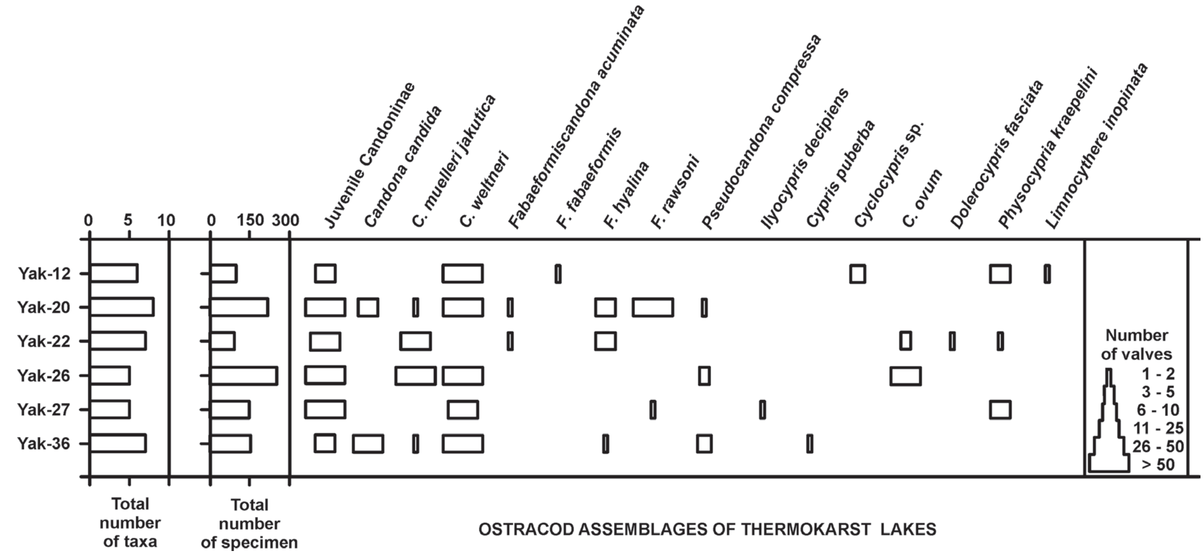

Figure 3. Modern ostracod assemblages from six thermokarst lakes on the Lena-Amga interfluve. Width of bars indicates ostracod number (see key).

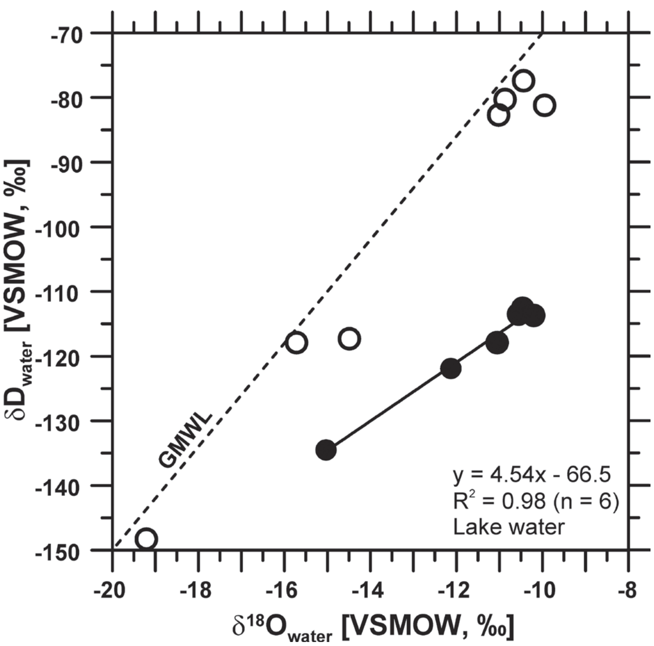

Figure 4. Isotopic composition of rain water (open circles) from Yakutsk in August 2005 and the studied lakes (filled circles) on the Lena-Amga interfluve.

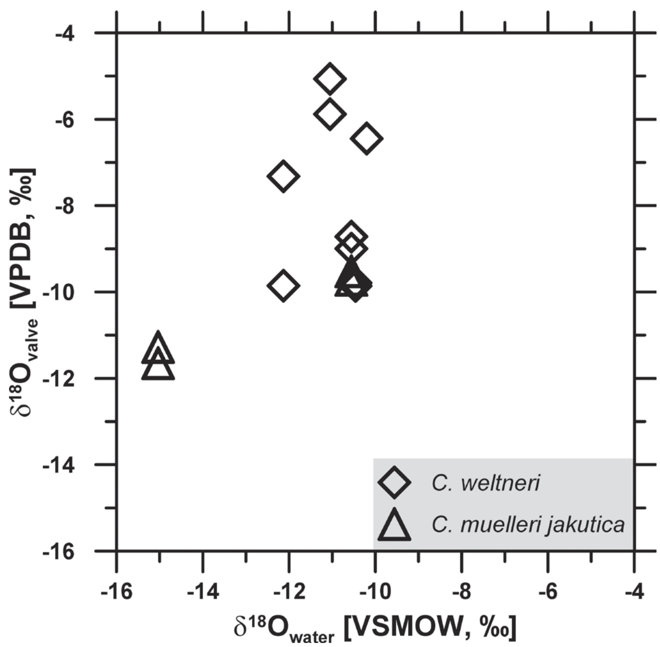

Figure 5. Stable isotope composition of $\delta^{18}O$ in ostracod calcite and host waters for female and male specimen of adult *C. weltneri* and *C. muelleri jakutica*.

the underlying permafrost. The high temperature variation in the surface lake waters during the fieldwork ranged from 12°C up to 26°C, and the ionic content expressed as electrical conductivity reached from 0.36 to 0.92 mS/cm.

The results of oxygen and hydrogen isotope analyses of the lake waters are shown in a $\delta^{18}O$ - δD plot (Fig. 4) with respect to the Global Meteoric Water Line (GMWL), which correlates fresh surface waters on a global scale (Craig 1961). Furthermore, in Figure 4 the stable isotope data of seven rainwater samples from August 2005 taken in Yakutsk are presented. Lake water samples are shifted below the GMWL, and this deviation reflects evaporation in the studied water bodies, as indicated by a slope of 4.54 (R^2 = 0.98; shown in Fig. 4).

The geochemical analyses of ostracod calcite ($\delta^{18}O$, $\delta^{13}C$) were performed on valves of the most common species, *C. weltneri* and *C. muelleri jakutica*. The $\delta^{18}O$ of host waters varies between about -15 to -10‰, whereas the $\delta^{18}O$ of ostracod calcite is generally shifted to ^{18}O-enriched values and ranges between about -12 to -5‰ (Fig. 5). The shift between $\delta^{18}O$ in host waters and ostracod calcite includes metabolic (vital) and temperature effects. Vital offsets on the isotopic composition of several species of Candoninae of up to 3‰ were already proposed by other studies, (Xia et al. 1997, von Grafenstein et al. 1999, Keatings et al. 2002, Wetterich et al. 2007). The temperature-dependence of $\delta^{18}O$ fractionation is reflected by the variation of the shift within a species, where increased temperatures correspond to smaller

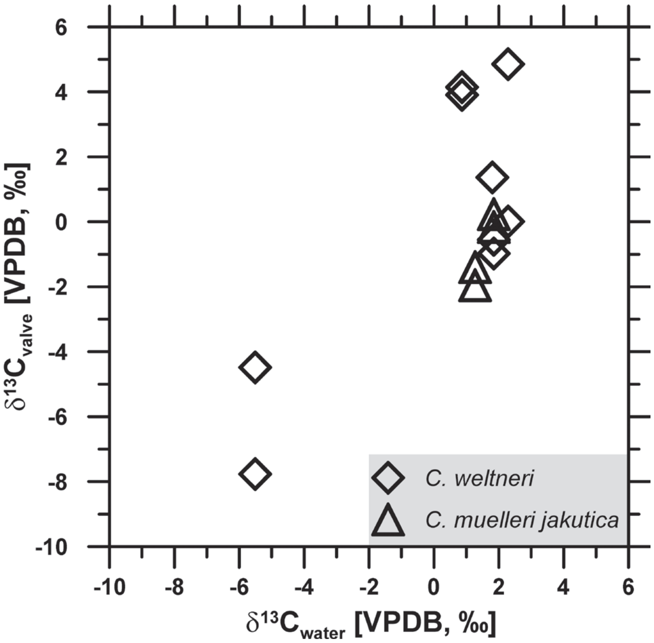

Figure 6. Stable isotope composition of $\delta^{13}C$ in ostracod calcite and ambient waters for female and male specimen of adult *C. weltneri* and *C. muelleri jakutica*.

shifts (e.g., Leng & Marshall 2004). The observed variation in the shift can be explained by different temperatures of the host water at the time of calcification.

The $\delta^{13}C$ of the studied host waters TDIC shows two different ranges at about -5.5‰ and between 1 to 2.5‰. The corresponding $\delta^{13}C$ data on ostracod calcite show considerable scatter from about -8 to -4‰ and -2 to 5‰, respectively. The scatter in $\delta^{13}C$ indicates the influence of complex abiotic and biotic effects at different times of shell secretion on $\delta^{13}C$ fractionation, as is expected in natural waters.

Discussion

For the late Holocene, Wolfe et al. (2000) detected a similar pattern of cellulose-inferred lake water $\delta^{18}O$ in a North Yakutian lake sediment record. They found most ^{18}O-depleted values between 2000 and 500 yr BP due to probably cooler conditions and less influence of evaporation. After 500 yr BP, the data change to relative ^{18}O-enriched values, as it is also recorded in the $\delta^{18}O$ record of ostracod calcite in period C, indicating a warming trend with higher evaporation.

The observed modern ostracod assemblages from Central Yakutian thermokarst lakes are characterized by species with preferences for lower water temperatures and lower salinities (e.g., *C. candida*, *C. muelleri jakutica*, *C. welterni*, *F. hyalina*, *F. rawsoni*). The most common species, *C. weltneri,* is described as cold stenothermal to oligothermophilic and oligohalophilic (Meisch 2000). Other species are tolerant to changes in temperature and salinity. In comparison to Arctic ostracod assemblages (Wetterich et al. 2007) from North Yakutia (Lena River Delta, Laptev Sea), the Central Yakutian fauna generally lacks strictly cold-adapted species such as *F. harmsworthi*, *F. pedata*, and *Tonnacypris glacialis*. Nevertheless, other species, such as *C. candida*, *C. muelleri jakutica,* and *F. hyaline,* are common in both regions. The $\delta^{18}O$ record of ostracods from North and Central Yakutia shows differences. The $\delta^{18}O$ in valves of Arctic ostracods is relatively more ^{18}O-depleted and ranges between about -20 to -13‰ (Wetterich et al. 2007), whereas the $\delta^{18}O$ of the Central Yakutian ostracods ranges between about -12 to -5‰. This general tendency in the $\delta^{18}O$ records reflects the general lower temperatures and lower evaporation in the north with higher P/E rations as compared to Central Yakutia.

Comparing the Central Yakutian $\delta^{13}C$ records of modern and late Holocene ostracods, we observe a reversed pattern, in which the fossil data are relatively more ^{13}C-depleted (mostly lighter than 0‰) than the modern ones (mostly heavier than 0‰). That may imply generally higher aquatic productivity today as compared to the late Holocene, since plants preferentially fix $^{12}CO_2$ during photosynthesis thereby leaving TDIC enriched in ^{13}C (Griffiths & Holmes 2000). The generally lower range in ostracod $\delta^{13}C$ between -2 to -11‰ from modern North Yakutian ponds (Wetterich et al. 2007) as compared to Central Yakutia may point to dominance of organic matter decay in the northern waters, since these microbiological processes release ^{13}C-depleted CO_2 and lower $^{13}C/^{12}C$ ratios in TDIC (Griffiths & Holmes 2000).

Conclusions

Periodic short- and mid-term climate variability leads to significant changes in hydrological conditions; e.g., to drastic water-level changes in thermokarst lakes of Central Yakutia, as it was first described by Nemichov (1958). A drying-up period of the thermokarst lake within Alas Myuryu in the late Holocene was observed in both taxonomical and geochemical properties of fossil freshwater ostracods. The uncertain geochronology of the record presented here renders unclear the relationship between lake changes as reflected by ostracod data and the Holocene environmental history. Nevertheless, freshwater ostracods are useful indicators for reconstruction of aquatic conditions in the past.

The modern ostracod assemblage reflects today's environmental conditions that are characterized by moderate lake-level variations due to evaporative effects during the summer season. The high variability in the modern $\delta^{18}O$ and $\delta^{13}C$ data of ostracod calcite underscores the need for further studies in this context.

Acknowledgments

We thank Hedwig Oberhänsli and Birgit Plessen (GFZ, Potsdam, Germany) as well as Ulrike Herzschuh, Andreas Mackensen (AWI Potsdam and Bremerhaven, Germany), and Lyudmila Pestryakova (University of Yakutsk, Russia) for help during fieldwork and analytical work. We are very grateful to Erika Pietrzeniuk (formerly Museum of Natural History Berlin, Germany) who performed the work on the fossil ostracods. The paper benefited by critical comments from two anonymous reviewers and by English language correction from Paul Overduin (AWI Potsdam, Germany).

References

Chivas, A.R., De Deckker, P., Cali, J.A., Chapman, A., Kiss, E. & Shelley, J.M.G. 1993. Coupled stable-isotope and trace element measurements of lacustrine carbonates as paleoclimatic indicators. In: P.K. Swart, K.C. Lohmann, J. McKenzie & S. Savin (eds.) *Climate Change in Continental Isotopic Records.* Geophysical Monograph 78: 113-121.

Craig, H. 1961. Isotopic variations in meteoric waters. *Science* 133: 1702-1703.

GLOBE Task Team 1999. The global land one–kilometre base elevation (GLOBE) digital elevation model, version 1.0. Boulder CO: NOAA, National Geophysical Data Center.

Griffiths, H.I. & Holmes J.A. 2000. *Non-marine ostracods and Quaternary paleoenvironment*. Quaternary Research Association, London, 179 pp.

Katasonov, E.M. 1979. *Structure and Absolute Geochronology of Alas Deposits in Central Yakutia*. Moscow: Nauka, 94 pp. (in Russian).

Keatings, K.W., Heaton, T.H.E. & Holmes, J.A. 2002. Carbon and oxygen fractionation in non-marine ostracods: Results from a "natural culture" environment. *Geochimica et Cosmochimica Acta* 66: 1701-1711.

Kelts, K. & Talbot, M.R. 1990. Lacustrine carbonates as geochemical archives of environmental change and biotic/abiotic interactions. In: M.M. Tilzer & C. Serruya (eds.). *Large Lakes: Ecological Structure and Function*. Madison: Science and Technology Publishers, 288-315.

Leng, M. & Marshall, J.D. 2004. Palaeoclimate interpretation of stable isotope data from lake sediment archives. *Quaternary Science Reviews* 23: 811-831.

Meisch, C. 2000. *Freshwater Ostracoda of Western and Central Europe*. Heidelberg, Berlin: Spektrum Akademischer Verlag, 522 pp.

Meyer, H., Schönicke, L., Wand, U., Hubberten, H.-W. & Friedrichsen, H. 2000. Isotope studies of hydrogen and oxygen in ground ice-experiences with the equilibration technique. *Isotopes in Environmental and Health Studies* 36: 133-149.

Nemchinov, A.G. 1958. About periodic lake level changes in Central Yakutia. *Scientific reports of the Yakutsk branch of the Soviet Academy of Science* 1: 30-37 (in Russian).

Pietrzeniuk, E. 1977. Ostracoden aus Thermokarstseen und Altwässern in Zentral-Jakutien. *Mitteilungen aus dem Zoologischen Museum in Berlin* 53: 331-362 (in German).

Reimer, P.J., Baillie, M.G.L., Bard, E., Bayliss, A., Beck, J.W., Bertrand, C.J.H., Blackwell, P.G., et al. 2004. IntCal04 Terrestrial Radiocarbon Age Calibration, 0–26 Cal Kyr BP. *Radiocarbon* 46: 1029-1058.

Soloviev, P.A. 1973. Thermokarst phenomena and landforms due to frost heaving in Central Yakutia. *Biuletyn Peryglacjalny* 23: 135-155.

Stuiver, M. & Reimer, P.J. 1993. Extended (super 14) C data base and revised CALIB 3.0 (super 14) C age calibration program. *Radiocarbon* 35: 215-230.

von Grafenstein, U., Erlenkeuser, H. & Trimborn, P. 1999. Oxygen and carbon isotopes in modern freshwater ostracod valves: assessing vital offsets and autecological effects of interest for palaeoclimate studies. *Palaeogeography Palaeoclimatology Palaeoecology* 148: 133-152.

Wetterich S., Schirrmeister, L., Meyer, H., Viehberg, F.A. & Mackensen, A. 2007. Arctic freshwater ostracods from modern periglacial environment in the Lena River Delta (Siberian Arctic, Russia): Geochemical applications for palaeoenvironmental reconstructions. *Journal of Paleolimnology* (DOI 10.1007/s10933-007-9122-1).

Wetterich, S., Schirrmeister, L. & Pietrzeniuk, E. 2005. Freshwater ostracodes in Quaternary permafrost deposits from the Siberian Arctic. *Journal of Paleolimnology* 34: 363-376.

Wetterich, S., Herzschuh, U., Pestryakova, L., Daibanyrova, M. & Ksenofontova, M. (2007). Limnological studies in Central and North-east Yakutia in summer 2005. In: B. Diekmann, S. Wetterich, & F. Kienast (eds.), *Russian-German Cooperation Yakutsk-Potsdam: The Expedition Central Yakutia 2005.* Reports on Polar and Marine Research 550: 259-264.

Wolfe, B.B., Edwards, T.W.D, Aravena, R., Forman, S.L., Warner, B.G., Velichko, A.A. & MacDonald, G.M. 2000. Holocene paleohydrology and paleoclimate at treeline, North-Central Russia, inferred from oxygen isotope records in lake sediment cellulose. *Quaternary Research* 53: 319-329.

Xia, J., Ito, E. & Engstrom, D.R. 1997. Geochemistry of ostracode calcite 1: An experimental determination of oxygen isotope fractionation. *Geochimica et Cosmochimica Acta* 61: 377-382

Hydrology, Hydrochemistry, and Vegetation of a High Arctic Wetland Complex

Ming-ko Woo
School of Geography and Earth Sciences, McMaster University, Hamilton, ON, Canada L8S 4K1
Dan K. Thompson
School of Geography and Earth Sciences, McMaster University, Hamilton, ON, Canada L8S 4K1
Xiu Juan Guan
Department of Geography, University of Saskatchewan, Saskatoon, SK, Canada S7N 5A5
Kathy L. Young
Department of Geography, York University, Toronto, ON, Canada M3J 1P3

Abstract

A wetland complex on Ellesmere Island, Canada, typical of many such complexes in the polar oases, consists of patches that include tundra pond, ice wedge trough, wet meadow, and mesic ground. In the spring, overland flow generated by snowmelt filled the topographic depressions and flooded the wetlands, flushing out the chemicals in the surface ice formed in the previous season. As floodwater receded and the surface flow connections were severed, wetland patches were largely separated. Vertical processes of evaporation and rainfall dominated. The diverse hydrological and chemical environments that emerged were possibly responsible for the different vegetation assemblages on the wetland complex. For High Arctic wetlands, permafrost significantly influences the thermal, hydrological, and chemical regimes. Frozen ground favours surface runoff, but restricts hydrological linkages among wetland patches. Shallow thaw allows prolonged active-layer saturation, and ground ice melt or thermokarst alters the concentration of various ions.

Keywords: High Arctic; hydrochemistry; hydrology; tundra pond; vegetation; wetland.

Introduction

Wetlands occur in small patches or extensively as wetland complexes in the High Arctic (Woo & Young 2003, 2006). The existence of wetlands is predicated upon frequent excess of water with gains greater than losses so as to maintain a high water table to facilitate the development of ponds or hydrophytic vegetation. The presence of permafrost enables prolonged retention of water in the wetlands, as the frozen soil limits percolation and has only a shallow thawed layer that does not require a large amount of water to saturate.

Cowell et al. (1978) noted that the formation of wetland in permafrost areas is favoured by shading and insulation provided by vegetation, peat which insulates the frozen substrate, and the lack of water movement largely due to low gradients. While the factor of vegetation cover is less important in the tundra and polar desert than in the forested areas, the presence of peat is a major consideration in retarding ground thaw (Yi et al. 2007). Poor drainage allows frequent saturation that is requisite for wetland occurrence. While the hydrology and the vegetation of Arctic wetlands have been studied (e.g., Bliss 1977, Bowling et al. 2003, Rovansek et al. 1996) and hydrochemical sampling of wetland and pond waters (e.g., Keatley et al. 2007) has been made across the Arctic, there has not been an integrative investigation on the hydrology, hydrochemistry, and vegetation of a wetland complex. It is proposed that these wetland characteristics are interrelated, and the present study examines these several aspects at a High Arctic wetland in Canada. Results of this study are applicable to other wetlands in the continuous permafrost region.

Study Area and Methods

The study area is located near Eastwind Lake on Fosheim Peninsula, Ellesmere Island, Nunavut, Canada (80°08′N, 85°25′W) (Fig. 1). This High Arctic site has a polar oasis climate that is generally warmer than the polar desert (Edlund & Alt 1989, Woo & Young 1997). The weather station at Eureka, 20 km away, measured 76 mm annual precipitation, though this value may be an underestimation due to poor gauge catch (Woo et al. 1983).

The wetland complex where the study was undertaken in 2005 occupies a shallow depression at the foot of a long slope. This topographic setting favours the collection and storage of surface and subsurface runoff. The wetland complex drains northwestward via a small channel. Within the wetland complex are six tundra ponds and wet grounds criss-crossed by ice-wedge polygons (Fig. 2). Two lines of palsa-like features follow the rims of the polygons to deflect the paths of the surface runoff from the hill slope to the ponds. The entire area is underlain by fine-grained diamict to a depth of at least 2 m. The diamict has a high carbonate content, while the wetland complex lies below the Holocene marine limit (Bell 1996) so that the soils have a high salt content. In the wet meadow and mesic ground, a 0.1 m layer of organic litter and peat lies atop silt and clay. Part of the mesic ground and the pond rims have also a thin peat layer below mineral soil, likely buried during the last glaciation.

Hydrological methods are given in detail in Woo & Guan (2006). A vegetation survey (presence/absence) was conducted in July 2005 for the main terrain types following

Figure 1. Location of the study site on Fosheim Peninsula, Ellesmere Island, Nunavut, Canada.

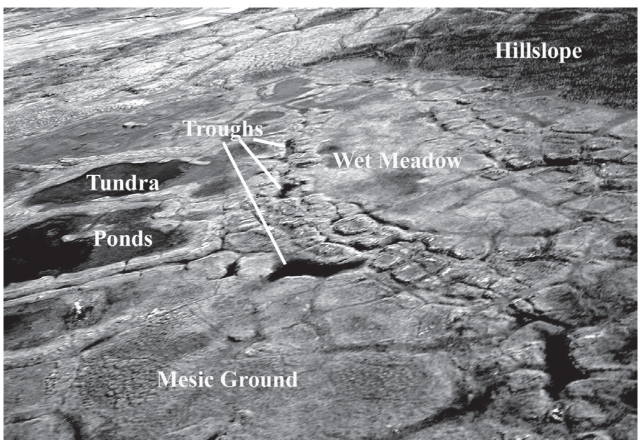

Figure 2. Photograph of the wetland complex showing hill slope, tundra ponds, ice-wedge troughs, mesic, and wet meadow sites.

the approach of Edlund et al. (1990) to determine the floristic diversity of the wetland-complex.

Water samples were collected once every six days from the start of overland flow on June 2 until mid-August. Samples were taken from the water in the northern ice wedge trough and from one of the six tundra ponds. Water was also sampled from a pool in the wet meadow and from a 15-cm diameter pit dug down to the frost table in the mesic area. In the pond, daily electrical conductivity measurements were combined with pond volume estimates to yield total solute load values in units of mS m^{-3} cm^{-1}. All water samples were kept cool (~4ºC) and in the dark prior to field analyses. Immediately after collection, samples were analyzed for total Fe. Hach FerroVer pre-measured reagents were used for total Fe measurements. The FerroVer reagent acidifies and extracts colloidal iron and iron sorped to organic matter otherwise not detected in analyses for "dissolved" iron. Samples were acidified to pH 2.5 using concentrated nitric acid before filtration through a 0.45 µm glass microfibre filter, prior to cation (Ca^{2+}, Mg^{2+}, Na^{+}, K^{+}) analysis at York University in Toronto, Ontario, using a Spectra-10 Atomic Absorption Spectrometer. This technique yields concentrations as a sum of the dissolved, colloidal, and acid-soluble suspended constituents.

Hydrological Processes

Throughout the long and cold winter, the dominant hydrological processes were the accumulation and redistribution of snow. By early June, just prior to the onset of snowmelt, the snow was unevenly distributed, as governed largely by terrain. The uplands and slopes had 163±65 mm, the wet meadows accumulated 95±4 mm, the mesic site had 80±8 mm, while the tundra ponds collected 68±18 mm of snow (all in snow water equivalent unit). From the melt period until the onset of freezeback, the magnitude of various hydrological processes varied, giving rise to strong seasonality in the wetland hydrological behaviour. The melt period occurred when the winter snow cover melted within about 10 days, generating substantial overland flow on most hill slopes and across the wetland. This was the major event that flooded large parts of the study area, infilling depressions and ponds and saturating the thinly thawed soils. Lateral surface flow enhanced hydrological connectivity across the landscape and evaporation was effective at this time around the summer solstice. Evaporation rate from the ponds averaged 2.7 mm d^{-1} and was 2.5 mm d^{-1} for the saturated areas. Ground thaw accelerated soon after the snowmelt season and the thawed active layer was able to accommodate more infiltration. A deepening of the frost table together with high evaporation loss led to a drop in the water table. Surface flow ceased, first on the hill slopes, then the mesic ground, and finally the wet meadows and between the tundra ponds.

Subsurface flow in the active layer was meager due to the shallow thaw, the low gradient (an elevation drop of 10 m over a distance of 1625 m) and the low hydraulic conductivity once the water level fell into the mineral soil layer (pumping tests and falling head tests yielded hydraulic conductivity values of 10^{-2} to 10^{-4} m s^{-1} in the organic layer and 10^{-6} to 10^{-7} m s^{-1} in the mineral substrate). The curtailment of hydrological connectivity is a major consideration in the wetland complex, as individual wetland patches became largely separated from their surroundings. Only vertical processes of rainfall, evaporation, and to a limited extent, ground ice melt controlled the water balance of the wetland patches. In summer, different types of wetland exhibited divergent hydrological behaviour. The wet meadows were no longer flooded, and the pools of water shrank as the water table dropped (Fig. 3). The ponds not only had lower water levels, but drying along their edges allowed wet meadows to emerge. Only the ice-wedge troughs with a steady supply of water from ground ice melt and confined by high rims retained water throughout the summer. The mesic ground often had dry patches between the wet areas that had a water table below the surface, partly maintained by meager subsurface flow from hill slopes. Summer rain was seldom sufficient (total of 27 mm in 2005) to rejuvenate surface flow, though a rainfall event in the following year raised the pond levels to the point of overflow (Woo & Guan 2006).

Table 1. Average pH, electrical conductivity (μS cm^{-1}) and concentration of selected major ions (μmol L^{-1}) for four types of wetland waters in the 2005 summer. Standard deviations are shown in brackets.

	Tundra pond	Wet meadow	Mesic ground	Ice wedge
pH	6.8 *(0.2)*	7.0 *(0.1)*	6.2 *(0.2)*	6.8 *(0.2)*
EC	151 *(62)*	116 *(30)*	194 *(26)*	170 *(42)*
Ca^{2+}	257 *162)*	185 *(91)*	170 *(60)*	368 *(200)*
Mg^{2+}	203 *(96)*	181 *(59)*	232 *(47)*	230 *(61)*
K^{+}	92 *(23)*	25 *(8)*	107 *(36)*	143 *(25)*
Na^{+}	184 *(84)*	136 *(17)*	219 *(17)*	148 *(15)*
no. of samples	15	13	13	15

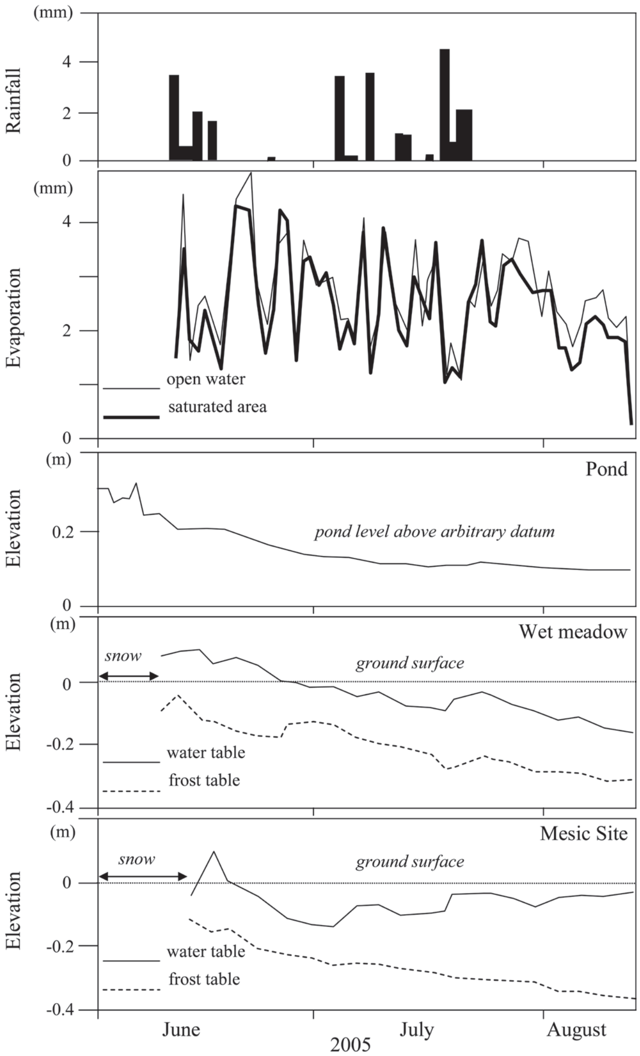

Figure 3. Daily rainfall, pond evaporation, pond water level, frost and water tables of wet meadow and mesic ground.

Hydrochemical Processes

The mean values and seasonal changes in the concentration of selected ions (Ca^{2+}, Na^{+}, K^{+}) and pH for four types of wetlands are shown in Table 1 and Figure 4. In the spring season, extensive inundation by snow meltwater runoff of low ionic concentration (electrical conductivity-

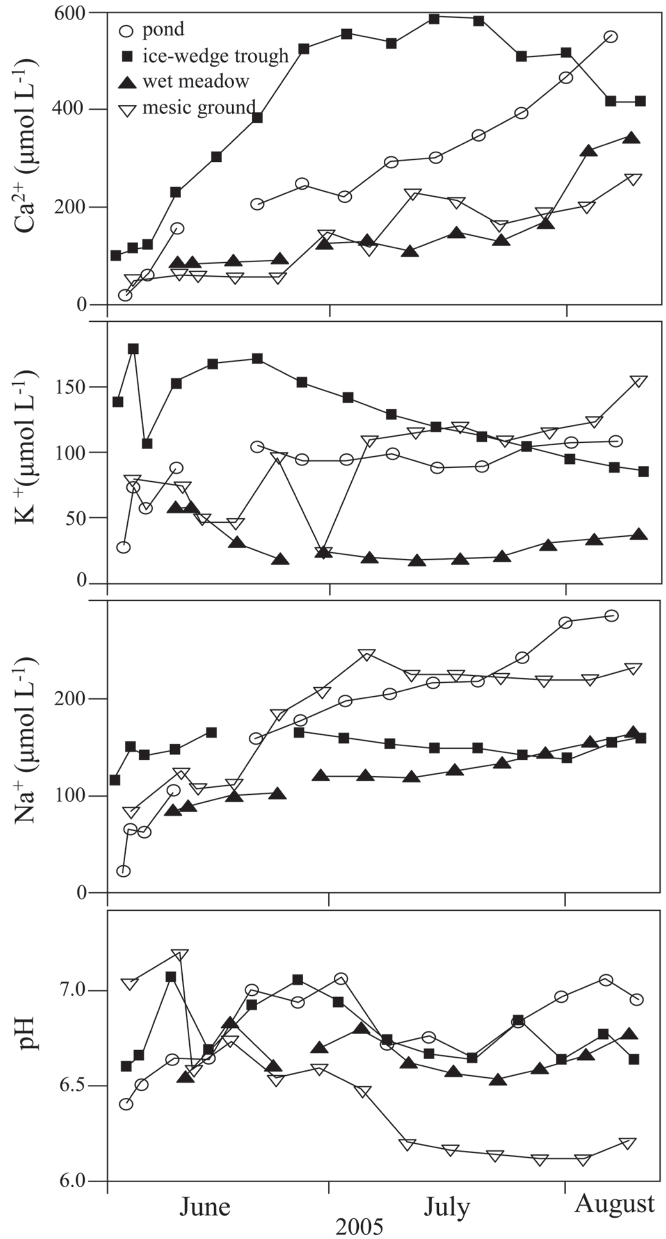

Figure 4. Seasonal change in concentration of selected major ions (Ca^{2+}, Na^{+}, K^{+}) and pH in the water of four types of wetlands (pond, ice wedge trough, wet meadow, and mesic ground).

EC = 13±7 μS cm^{-1}, pH = 6.0±0.6) homogenized the hydrochemical environment of the entire wetland complex. The hydrochemistry of different wetland types was similarly low in ionic concentrations, except for potassium in the ice-wedge troughs. Its initial high value may be attributed to the trough water being in contact with the organic soil exposed on the trough walls. Later in the thaw season, however, the concentration declined as plant growth took up more K^{+} from the trough water. With the cessation of snowmelt runoff, a weakening of hydrological connectivity between the wetland patches and their surroundings became a major consideration in the evolution of wetland hydrochemistry. Rainfall was low (27 mm) and the rainwater has low chemical concentrations (Ca^{2+} = 20±16 μmol L^{-1}, equivalent to 10 μS

cm^{-1}) so that rainfall dilution of the wetland waters was not a major consideration.

Evaporation was effective in reducing the amount of water stored in the wetland. Thus, while the solute load remained relatively unchanged during the summer, a continuous loss of water to evaporation caused a distillation of solute cations, responsible largely for their increasing concentrations after the snowmelt season. This effect is typically evident in the tundra ponds which showed a steady increase in all cations concentrations but not in the total load (Fig. 5). Without surface runoff, both the input of chemicals and the export of soluble ions were limited by the low subsurface flow. By late summer, the in situ suprapermafrost groundwater which is a mixture of meteoric and soil water, and meltwater from seasonal ground ice and from wedge-ice (samples of ground ice showed an electrical conductivity of 233 μS cm^{-1}) had enhanced chemical concentrations compared with the spring conditions. A decrease in pH from late July onwards was possibly related to senescence of the pond vegetation that started around the same time, leading to leaching of organic acids from the plants.

Of particular interest was a thermokarst collapse event along an ice-wedge trough. Prior to the collapse, Ca^{2+} alone increased while K^+ declined steadily, a pattern seen only in the trough (Fig. 4). Afterwards, the concentration of Fe increased from 47 to 276 μmol L^{-1}, and of Na^+ from 149 to 160 μmol L^{-1}, but the concentrations of the other cations measured were reduced. The iron is likely to be colloidal Fe, but our analyses cannot differentiate between its soluble and colloidal forms. The thermokarsting episode showed an abrupt addition of constituents from the soil and ground ice, and an influx of ice meltwater that quickly altered the chemical content of the water in the trough.

In summary, hydrochemical behaviour of the wetlands is strongly influenced by the hydrological processes. Surface and subsurface runoff bring in or remove chemicals; vertical processes of snowmelt and direct rainfall on the wetland add atmospheric fallout (both dry and wet) while ground ice melt (including thermokarst) contributes chemicals from the soil and the ground ice to the water. The addition of water from horizontal and vertical fluxes may dilute or increase the chemical concentration, but evaporation reduces the water volume, thus increasing the concentration but not the chemical load. Vegetation growth further modifies the water chemistry.

Vegetation

Climate, geology, and topography control the hydrological and hydrochemical behaviour which, together with the soil factor, govern the wetland ecology. Different ecological settings give rise to distinct vegetation niches (Table 2). The non-wetland hill slopes have good drainage and are covered by a large diversity of vascular plants ranging from grasses to a variety of saxifrages. The mesic areas experience more frequent saturation than the hill slopes, and the vegetation typically reflects these conditions with the presence of cotton-grass (*Eriophorum scheuchzeri*), mosses and a range of graminoid species. The wet meadows lack the diversity

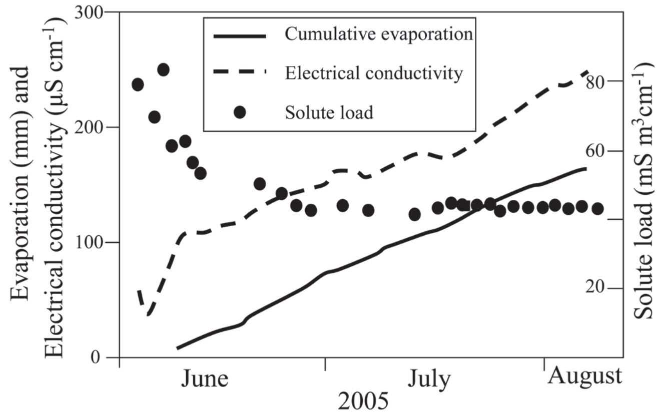

Figure 5. Cumulative evaporation, electrical conductivity, and solute load in tundra pond.

in vascular plants when compared to the mesic sites, but contain various algae species, some graminoids, and cotton-grass (e.g., *Eriophorum scheuchzeri* and *Eriophorum angustifolium*) which reflect their saturated substrate, as was typically noted by other ecologists (Bliss & Matveyeva 1992, Edlund & Garneau 2000). Rims of the ponds experience drying in the summer, and vascular diversity here is comparable to the drier hill slopes. These small strips also appear to represent a transition zone from flooded pond sites with the presence of cotton-grass and algae. As the ponds shrink, the emergent plants include grasses and sedges such as *Alopecurus alpinus, Agrostis mertensi, Calamagrostis neglecta, Carex misandra,* and cotton-grasses such as *Eriophorum scheuchzeri and Eriophorum angustifolim.* Only a few vascular plants exist in these flooded zones (e.g. *Lycopodium alpinum, Pedicularis hirsuta*). The water-filled troughs of the ice-wedge polygons have low vascular diversity (e.g. *Salix arctica, Saxifraga cernua*) and are more typical of flooded sites dominated by mosses and graminoids.

Roles of Permafrost

Permafrost plays an important role in affecting the hydrology and hydrochemical evolution of arctic wetlands, thus also exerting an indirect influence on the development of wetland vegetation.

(1) Ground saturation and water storage: Frozen soil prevents or limits deep percolation, and most hydrological and hydrochemical activities in the High Arctic are restricted to the shallow thawed zone. A thin active layer does not accommodate much water so that where drainage is poor, as in low gradient terrain, the ground is frequently saturated to form wetlands. Annually, rapid release of ample snow meltwater to the thinly thawed soil enables replenishment of surface water storage and homogenization of the chemical conditions of the wetland complex.

(2) Runoff and hydrological connectivity: The extremely poor hydraulic conductivity of permafrost restricts hydrological linkages while low gradient further limits lateral subsurface flow, so that the hydrochemistry of the wetland patches evolves differentially in the thaw season. In the long run, divergent hydrological regimes and

Table 2. Plant species found in the study area.

Species	Hill slope	Mesic Ground	Wet meadow	Pond rim	Pond	Polygon trough
Alopecurus alpinus	x	x	x	x	x	
Agrostis mertensi				x	x	
Algae sp.			x	x	x	
Calamagrostis neglecta	x	x	x	x	x	
Carex saxatilis				x		
Carex supine						x
Carex bigelowii		x				
Carex misandra	x	x	x	x	x	
Carex sp.	x	x	x	x	x	x
Cassiope tetragona	x					
Draba sp.		x		x	x	x
Dryas integrifolia	x	x		x		x
Eriophorum scheuchzeri		x	x	x	x	x
Eriophorum angustifolium			x	x	x	x
Fungii sp.				x		
Graminoid sp.	x	x	x	x	x	x
Juncus biglumis				x		
Lichen sp.	x			x		
Lycopodium alpinum					x	
Melandrium apetalum	x	x	x	x		
Moss sp.	x	x	x	x	x	x
Papaver radicatum	x	x		x		
Pedicularis flammea	x			x		
Pedicularis hirsute	x	x	x	x	x	
Polygonum viviparum		x	x	x		
Potentilla nivea	x	x		x		
Oxyria digyna	x	x		x		
Salix arctica	x	x	x	x		x
Saxifraga cernua	x		x	x		x
Saxifraga oppositifolia	x			x		
Saxifraga tricuspidata	x					
Stellaria longipes	x	x		x		

hydrochemical environments lead to the development of different vegetation assemblages. The vegetation itself has feedback on the chemistry as previously discussed.

(3) Ground ice melt: Although the amount of water provided by the melting of ground ice is small relative to other water sources, it nonetheless is important in affecting the water chemistry due to the ionic constituents of the thawing soil and of the ice-water. Ground ice contribution may come steadily through the seasonal thaw of the active layer or arrive rapidly through occasional thermokast events that inject new chemicals and add ice melt water to the wetland environment in relatively short periods.

Conclusion

The wetland complex in the polar oasis of Ellesmere Island shows strong interactions among the hydrology, hydrochemistry, vegetation, and permafrost. A large influx of snow meltwater in the spring leads to general flooding and replenishment of wetland storage. The floodwater also homogenizes the hydrochemistry across the wetland complex. Shallow ground thaw maintains saturated conditions and prevents drainage of the tundra ponds but limits subsurface flow, hence restricting hydrological connectivity among the wetland patches. Vertical processes of rainfall, evaporation, and ground ice melt dominate in the post-snowmelt period. These processes concentrate or dilute the chemical concentration of the wetland waters, leading to divergent chemical evolution paths of the hydrologically isolated wetland patches. Vegetation development represents a long-term response to the divergent physical and chemical environments within the complex. Vegetation growth and the formation of peat significantly reduce the ground thermal conductivity while the abundance of seasonal ground ice in the wetland soils requires much latent heat for ground thaw (Woo et al. 2006a). These conditions give rise to a thinner active layer than in the mineral soils. Such feedback mechanisms among wetland soil saturation, vegetation growth and peat formation, and shallow seasonal thaw, sustain the presence of the arctic wetlands (Woo et al. 2006b).

Acknowledgments

This study was supported by the Natural Sciences and Engineering Research Council of Canada. Logistical support was provided by the Polar Continental Shelf Project of Natural Resource Canada. We thank the reviewer for helpful comments that improved this article.

References

Bell, T. 1996. The last glaciation and sea level history of Fosheim Peninsula, Ellesmere Island, Canadian High Arctic. *Canadian Journal of Earth Sciences* 33: 1075-1086.

Bliss, L.C. 1977. *Truelove Lowland, Devon Island, Canada: A High Arctic Ecosystem*. Edmonton, Alberta: University of Alberta Press, 714 p.

Bliss, L.C. & Matveyeva, N.V. 1992. Circumpolar arctic vegetation. In: Chapin, S.F. III, Jeffries, R.L., Reynolds, J.F., Shaver, G.R., Svoboda, J. and Chu, E.W. (eds.), *Arctic Ecosystems in a Changing Climate*. San Diego: Academic Press, 59-89.

Bowling, L.C., Kane, D.L., Giech, R.E. & Hinzman, L.D. 2003. The role of surface storage in a low-gradient Arctic watershed. *Water Resources Research* 39 (4): 1087, DOI: 10.1029/2002WR001466.

Cowell, D.W., Jeglum, J.K. & Merriman, J.C. 1978. Preservation of seasonal frost in peatlands, Kinoje Lakes, southern Hudson Bay Lowland. *Proceedings, Third International Conference on Permafrost, Edmonton, Alberta,* Vol. 1: 453-459.

Edlund, S.A. & Alt, B.T. 1989. Regional congruence of vegetation and summer climate patterns in the Queen Elizabeth Islands, Northwest Territories, Canada. *Arctic* 42: 3-23.

Edlund, S.A. & Garneau, M. 2000. Overview of vegetation zonation in the Arctic. In: M. Garneau & B.T. Alt (eds.), *Environmental Response to Climate Change in the Canadian High Arctic*. Geological Survey of Canada Bulletin 529, 113-127.

Edlund, S.A., Woo, M.K. & Young, K.L. 1990. Climate, hydrology and vegetation patterns, HWC, Ellesmere Island, Arctic Canada. *Nordic Hydrology* 21: 273-286.

Keatley, B.E., Douglas, M.S.V. & Smol, J. 2007. Limnological characteristics of a High Arctic oasis and comparisons across Northern Ellesmere Island. *Arctic* 60: 294-308.

Rovansek, R.J., Hinzman, L.D. & Kane, D.L. 1996. Hydrology of a tundra wetland complex on the Alaskan Arctic Coastal Plain. *Arctic and Alpine Research* 28: 311-317.

Woo, M.K. & Guan, X.J. 2006. Hydrological connectivity and seasonal storage change of tundra ponds in a polar oasis environment, Canadian High Arctic. *Permafrost and Periglacial Processes* 17: 309-323.

Woo, M.K. & Marsh, P. 1977. Effect of vegetation on limestone solution in a small High Arctic basin. *Canadian Journal of Earth Sciences* 14: 571-581.

Woo, M.K., Mollinga, M. & Smith, S.L. 2006a. Simulating active layer thaw in a boreal environment. *Geographie Physique et Quaternaire* 60: 9-17.

Woo, M.K. & Young, K.L. 1997. Hydrology of a small drainage basin with polar oasis environment, Fosheim Peninsula, Ellesmere Island, Canada. *Permafrost and Periglacial Processes* 8: 257-277.

Woo, M.K. & Young, K.L. 2003. Hydrogeomorphology of patchy wetlands in the High Arctic, polar desert environment. *Wetlands* 23: 291–309.

Woo, M.K. & Young, K.L. 2006. High Arctic wetlands: their occurrence, hydrological characteristics and sustainability. *Journal of Hydrology* 320: 432-450.

Woo, M.K., Young, K.L. & Brown, L. 2006b. High Arctic patchy wetlands: hydrologic variability and their sustainability. *Physical Geography* 27: 297-307.

Yi, S., Woo, M.K. & Arain, A. 2007. Impacts of peat and vegetation on permafrost degradation under climate warming. *Geophysical Research Letters* 34: L16504, DOI: 10.1029/2007GL030550.

Soil and Permafrost Temperature Data Obtained During the First International Polar Year, 1882–1883

Kevin R. Wood
Joint Institute for the Study of the Atmosphere and Ocean, University of Washington, Seattle, USA
Dmitry A. Streletskiy
Dept. of Geography, Center for Climatic Research, University of Delaware, Newark, USA

Abstract

Synoptic meteorological data from Arctic stations established during the first International Polar Year (IPY-1) have recently been collected and digitized. The research program at seven of fourteen stations included ground temperature observations at regular depth intervals. We have analyzed data obtained at the IPY-1 stations at Jan Mayen, Sodankylä, Finland, and at Malyye Karmakuly and Sagastyr, Russia. Descriptive records and more fragmentary data are available for most stations. Initial comparisons indicate that ground temperatures are consistent with surface air temperature (SAT) observations obtained using well-calibrated standard instruments. Using these data, we compare ground-temperature observations with contemporary measurements made at nearby locations.

Keywords: climate change; ground temperature; historical data; permafrost; Polar Year.

Introduction

Ground temperature measurements were recorded at seven of fourteen research stations established in the Polar Regions during the first International Polar Year (IPY-1) (Fig. 1) (Heathcote & Armitage 1959). Time series data were collected in soil at four or more levels down to 1.6 or 2.0 m depth where possible. Measurements were made with calibrated instruments and recorded values tracked variations in surface air temperature (SAT) as expected. The two U.S. stations were not equipped for systematic observation of ground temperature, but at Point Barrow a shaft was sunk to a depth of 37.5 feet for the purpose of obtaining the temperature of the earth, which at the bottom was reported to be a near-constant 12°F (-11.1°C) (Ray 1885). Descriptive observations covering a wide range of cryosphere-related features are commonly found in expedition reports, including notes on ice and ice-processes that were features of the regional landscape. All data obtained during IPY-1 were published *en extenso* by each of the national expeditions. There has been renewed interest in historical data of this type in recent years due to the potential value they hold for improving our understanding of climate change and its impact on the environment.

We present an analysis of the four most complete ground temperature data sets recorded during IPY-1 in the Northern Hemisphere. These were obtained by the Austro-Hungarian expedition at Jan Mayen (von Wohlgemuth 1886); the Finnish expedition at Sodankylä (Lemström & Biese 1886); and by the Russian expeditions at Malyye Karmakuly, on Novaya Zemlya, and Sagastyr, in the Lena River delta (Lenz 1886a, 1886b). Descriptive records obtained at these locations are discussed. Data and an extensive image collection are available at: www.arctic.noaa.gov/aro/ipy-1.

Inspired by Carl Weyprecht (1838–81), the aim of IPY-1 was to investigate those fundamental problems in geophysics which could only be studied effectively through a program of coordinated observation at a widely distributed network of stations anchored in Polar Regions (Weyprecht 1875).

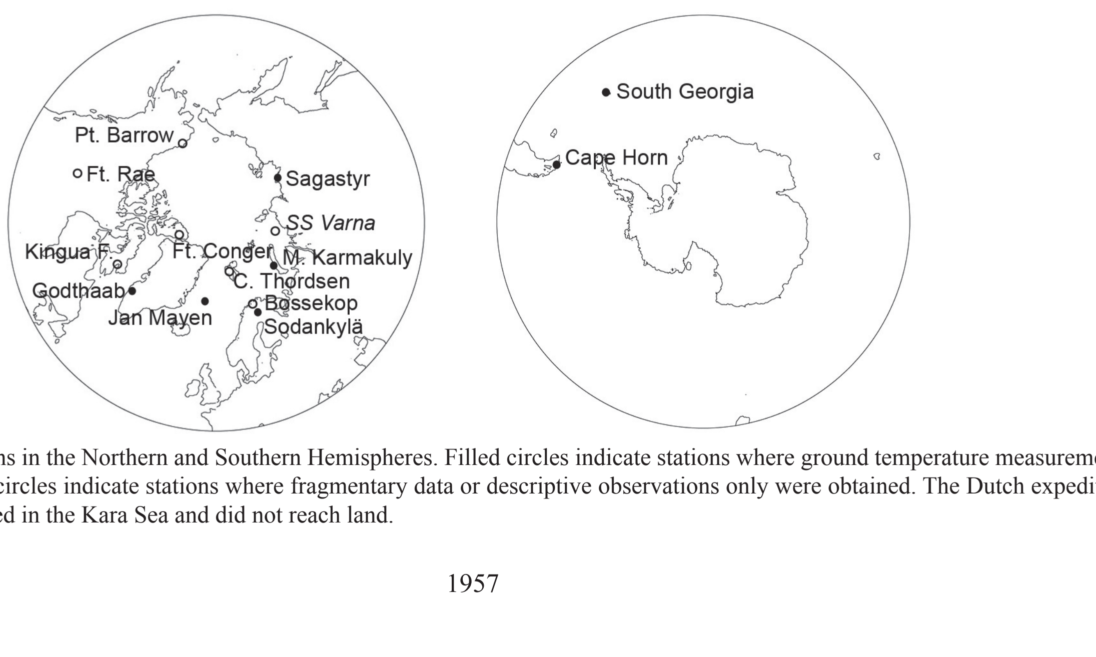

Figure 1. IPY-1 stations in the Northern and Southern Hemispheres. Filled circles indicate stations where ground temperature measurements were obtained. Open circles indicate stations where fragmentary data or descriptive observations only were obtained. The Dutch expedition (SS *Varna*) was trapped in the Kara Sea and did not reach land.

The three main fields of inquiry were meteorology, terrestrial magnetism, and the aurora. The science plan of IPY-1 also encompassed a wide range of additional subjects under the heading of optional observations. In addition to the ground temperature data discussed here, research was undertaken in a variety of subject areas including ethnology, natural history, and oceanography.

It is not surprising that ground temperature and related geocryological studies were undertaken during IPY-1 given the interest in the subject over the previous 40 or more years and the personal involvement of H. Wild, the president of the International Polar Commission (IPC) in this research area (Wild 1878), and G. Wild, president of the Russian Polar Commission and noted permafrost scientist (Baker 1982, Shiklomanov 2005).

Direct comparisons between IPY-1 and modern ground temperature regimes proved to be impossible, primarily due to a lack of modern data at these stations. Landscape transformation was also a factor, especially at Sodankylä, where a reservoir now covers the station site. Since the data were collected simultaneously, we are able to discuss the spatial variability between stations. Given the connection between upper level ground temperatures and synoptic meteorology, we also draw some tentative conclusions about where IPY-1 observations fall within the spectrum of recent monthly mean SAT variability.

Data and Methods

The most complete time series of ground temperature observations in soil obtained during IPY-1 were recorded at Jan Mayen (71.00°N, 008.47°W), Sodankylä (67.41°N, 026.6°E), Malyye Karmakuly (72.38°N, 052.7°E), and Sagastyr (73.38°N, 124.08°E). Two years of observations were recorded at Sodankylä and Sagastyr. A temperature time series in rock was obtained at Godthaab, and fragmentary data of various types were obtained at Cap Thordsen, Fort Rae, and Point Barrow. We have concentrated our analysis on the first four data sets. Data collected at the two Southern Hemisphere stations have not been addressed.

Details on the methods adopted at each station and descriptions of the ground cover and soil type are provided in the expedition reports cited above. An idea of the different environments around each station can also be gleaned from Figure 2 and other graphical information in the reports.

The most detailed metadata available for the four stations relates to the Russian station at Sagastyr. Given that procedures at this station and the stations at Malyye Karmakuly, and Sodankylä were all initiated by H. Wild, IPC president and director of the Central Physical Observatory in St. Petersburg, we can expect that many particulars are common to these three stations. In general, separate holes were excavated to 40, 80, and 160 cm and either glass or wooden tubes inserted. The earth thermometers themselves were enclosed in brass cylinders with their bulbs embedded in a mixture of brass filings and tallow. The cylinders were then attached to wooden sticks that were placed in each tube.

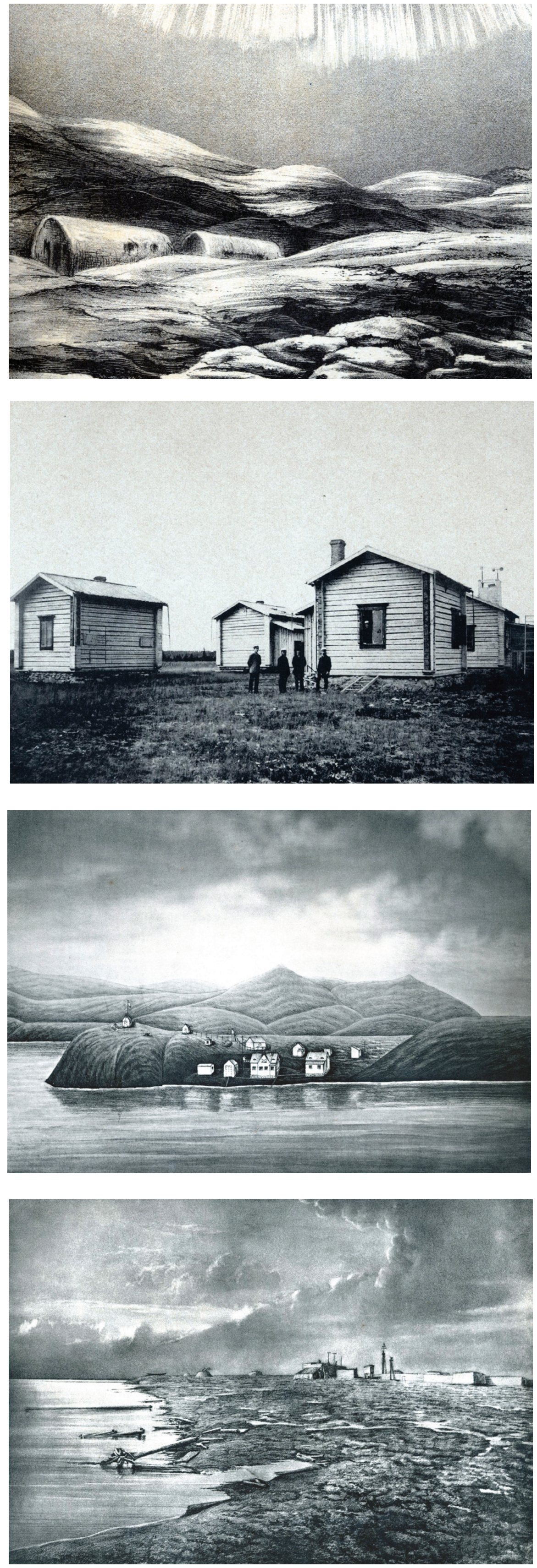

Figure 2. IPY-1 stations and surrounding terrain (from top): Jan Mayen, Sodankylä, Malyye Karmakuly, and Sagastyr.

The tubes were then closed with brass caps. Thermometers at the ground surface were installed horizontally, usually on two small brackets. Surface instruments were often buried in snow and were susceptible to breakage when the snow was removed each time they were read. Instruments on the surface and at 40 cm were read hourly, while the deeper ones were read less frequently (either 3x or daily). Thermometers were calibrated at a range of temperatures against standard instruments at the Central Physical Observatory and verified more frequently at the station at the 0°C calibration point.

The Sagastyr station was established on a small island on the northern edge of Lena River delta. A. Bunge, one of the expedition scientists, noted the dynamic effects of the river upon the terrain in the delta (Lenz 1886a). Old islands were continually being eroded and new ones created. The ground was generally composed of sandy soils overlaid with peat, the thickness of which Bunge suggested was proportional to the length of time the place was undisturbed. The vegetation around the station was dominated by mosses and lichens, with sparse dwarf-shrubs (mostly *Salix polaris*). The data record was interrupted in the summer of 1883 due to meltwater infiltrating from the surface and refreezing in the tubes at deeper levels which prevented the extraction of the thermometers. The location was also moved at this time to an area less susceptible to the building-induced snow drift that was problematic during the first year. Several reported changes of equipment produced small inhomogeneities in the record, but these had minimal influence on the interpolated mean annual ground temperature (MAGT) at particular depths.

The expedition to Malyye Karmakuly was dispatched hurriedly and was not prepared for as thoroughly as the others (Barr 1985). Here, soil temperatures were measured at the standard depths in gravelly soil characteristic of the island.

Wooden tubes rather than glass were used. Continuous snow cover at the measurement site was registered from 6 October 1882 to 25 May 1883. The measurements at 160 cm were interrupted on 30 May, again due to the infiltration and freezing of meltwater, as was the case in Sagastyr.

The metadata for Sodankylä is sparse. The earth thermometers were located about 20 m south of the buildings shown in Figure 2, on flat grassy terrain about 300 m from the Kitala River. Instruments at the surface and 40 cm were read hourly; others were read at least daily but the interval was not clear in the report. In the second year, observations were taken three times daily (0600, 1400, and 2200). Training

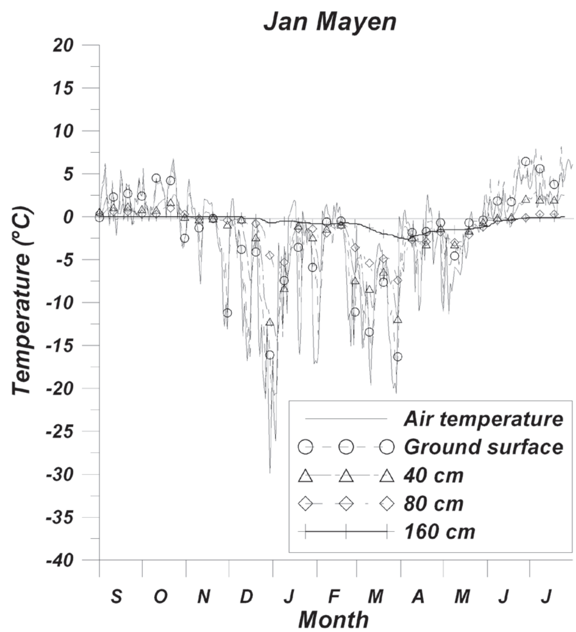

Figure 3. Air and ground temperatures observed at Jan Mayen, 1882–1883. Markers are placed at 10-day intervals throughout.

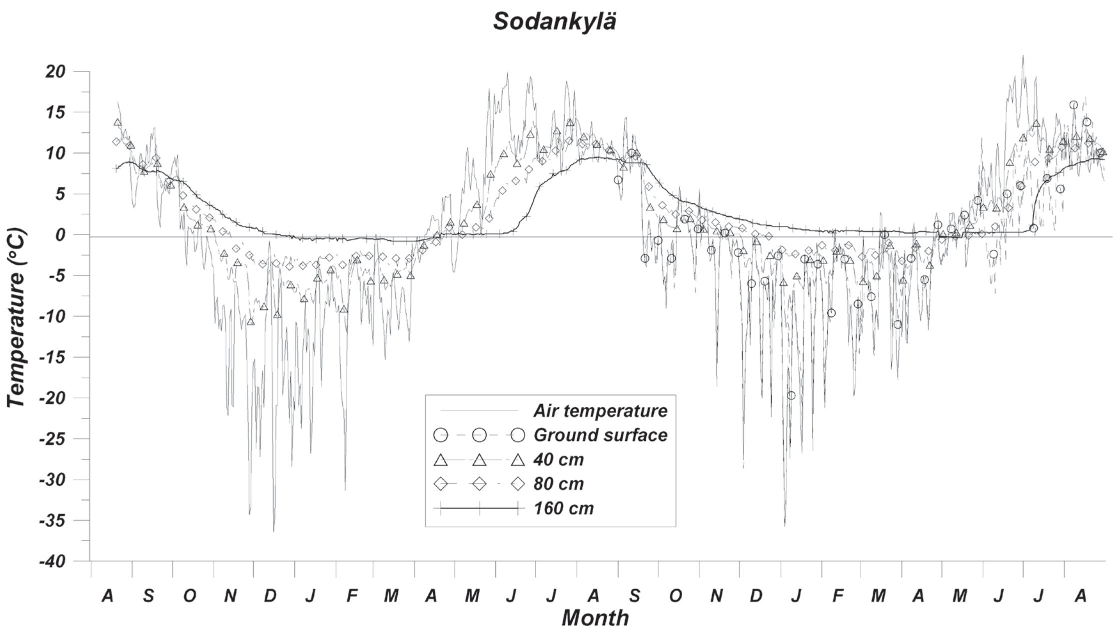

Figure 4. Air and ground temperature measurements at Sodankylä, 1882–1884. Note the difference between the years, which is especially clear in the 160 cm temperature curve. During the second year, the temperature at this level remained above freezing, but then did not warm appreciably until 7 July, nearly four weeks later than in 1883. This is a hallmark of a warmer, snowier winter followed by a cold spring.

and equipment, including glass tubes and thermometers, were provided by the Central Physical Observatory in St. Petersburg. The methods followed at Sodankylä most likely resembled those used at Sagastyr.

At Jan Mayen, rather different procedures were used. Temperatures were recorded at 6 levels down to 1.56 m depth, but the thermometers were graduated in whole degrees and read once per day at 1130. The thermometers were constructed such that they could be buried vertically in the ground while their scales remained above the surface where they could be read. Frozen ground was encountered at 80 cm depth. The expedition's standard thermometers were verified at the Kew Observatory in Great Britain, and they were, in turn, used to calibrate the earth thermometers at the station. We have interpolated the Jan Mayen data to match the standard depth intervals used at the other three stations.

The four stations were located where distinct types of climate and permafrost occur in the Arctic, from seasonal freezing to low temperature permafrost. At Jan Mayen and Sodankylä, the climate can be generally characterized as maritime type, with relatively warm winters and cool summers, even though both are geographically within the Arctic. The milder climate at these stations is due primarily to the dynamics of the atmospheric circulation over the North Atlantic and the influence of the warm ocean currents of the Atlantic Drift. The climate of Fennoscandia is more sensitive to fluctuations in large-scale circulation of the sort indicated by the North Atlantic Oscillation (NAO) (e.g., Thompson & Wallace 2001). The climate at Malyye Karmakuly, and especially Sagastyr, tends toward the more severe arctic-continental type with low temperatures and high amplitude variability. At the latter station, the Siberian high-pressure area is an important factor in winter, which tends to limit the influence of warm advection from the West.

Analysis

Four time series plots of ground temperature data were produced and these are briefly interpreted with respect to mean SAT and other key factors. Differences between subsequent years are pointed out. Gaps in the data were interpolated between other depth levels with data using standard polynomial interpolation.

Jan Mayen

The mean annual air temperature (MAAT) below -2.0°C that was registered at Jan Mayen was enough to form a thin layer of frozen ground (Fig. 3). Despite this there is a sharp attenuation of climatic signal with depth which implies that this layer is unstable to climatic fluctuations. It is possible that the ground at 150 to 200 cm depth was frozen for more than two years, meaning that permafrost was present. This would be consistent with the fact that frozen ground was encountered below 80 cm during the placement of the earth thermometers, but it is also possible that this layer could thaw completely during a warmer year. An interesting feature is the prolonged presence of a zero-degree curtain at 160 cm.

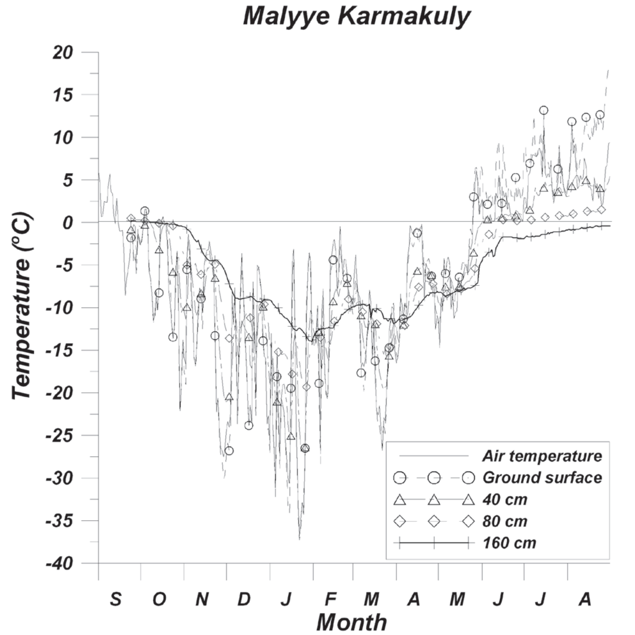

Figure 5. Air and ground temperature observations at Malyye Karmakuly, 1882–1883.

Assuming that there was no instrumental error involved, one possible explanation is that there was a massive body of ground ice present below the study site.

Sodankylä

Despite its position above the Arctic Circle, the climate at Sodanklyä is relatively mild, with MAAT just below 0°C. Even though MAAT during IPY-1 was slightly above the value of the reference climatology (1968–1997) the winter cold signal was enough to create seasonal freezing during the two years of observation. The depth of freezing was down to 165 cm during the first winter and 190 cm during the second (Fig. 4). The difference can be attributed to the fact that the cold climatic signal expressed as Degree-Days of Freezing (DDF) of the second winter was less than 80% of the first winter. This resulted in less penetration of cold into the ground.

A marked difference in meteorology between 1882–83 and 1883–84 was noticed by both scientists and the local inhabitants, who considered 1882–83 much more representative of the typical climate than the following year. The second winter was warmer than the first, but the spring and early summer were much colder. There were also 201 days of rain or snow precipitation during the second year compared to 134 days during the first, which could also have affected the ground temperature regime (GTR).

Malyye Karmakuly

Malyye Karmakuly is located on the west coast of Novaya Zemlya, where North Atlantic circulation patterns also influence the climate, but to a somewhat lesser extent than in Fennoscandia. The MAAT observed in 1882–83 was -6.6°C, which is 1.4° below the reference climatology value of

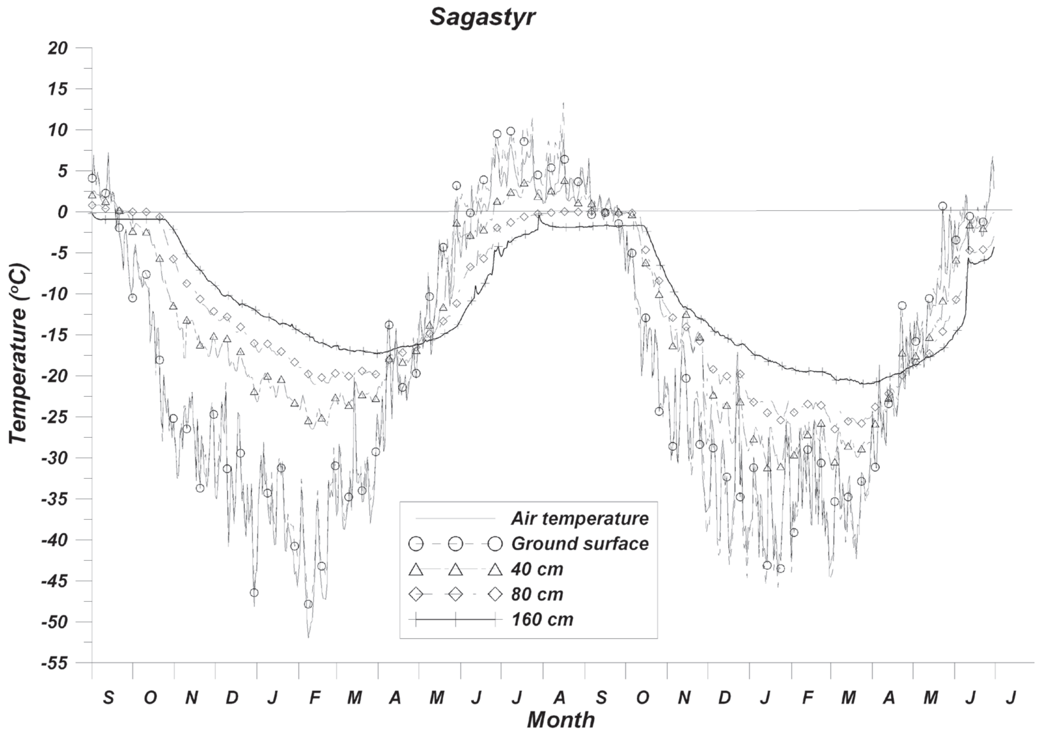

Figure 6. Air and ground temperature measurements at Sagastyr, 1882–1884. While there were differences in the meteorology of the two years, the difference in GTR is primarily due to the reduction in snow cover resulting from the relocation of the instruments away from an area of building-induced snow drift.

-5.1°C. The GTR at this location was more favorable for the formation of permafrost than either Jan Mayen or Sodankylä. This is because of the lower MAAT and greater range of air temperature expressed as Mean Annual Amplitude (MAAA) here. The mean annual ground temperature (MAGT) at 160 cm was -6.0°C at this location, but daily values were still highly sensitive to synoptic meteorology. There was no zero-curtain feature like in the locations discussed previously. Based on the ground temperature gradient, the interpolated permafrost depth was about 12 m in 1883.

Sagastyr

The overall pattern of variability in SAT anomalies at Sagastyr over the two year period was similar to the pattern observed at Sodankylä. The second winter was warmer than the first, especially February, while the spring was cooler. Notwithstanding the warmer winter, MAGT was lower during the second year. This is most likely the result of the drastic change in snow cover that resulted from the shift in location. During the first year, the depth of the snow drift next to the thermometers reached nearly 2 m compared to an accumulation of ~25 cm in the open tundra. The GTR at the second location was quite different due to much less snow cover. MAGT the second year was more than 3.0°C colder even though MAAT was 0.6°C warmer. This clearly demonstrates the critical role snow cover plays with respect to the GTR.

It is also quite interesting to note that SAT in all seasons at Sagastyr was apparently much colder than the mean of the recent climatology (1968–1997). There were no positive anomalies in the entire 22 months of record, and 18 months were more than one standard deviation below the reference means. SAT records at every other IPY-1 station in the Northern Hemisphere showed fluctuations about the mean of the reference climatology that were generally consistent with month-to-month variations in the large-scale atmospheric circulation patterns, particularly the NAO. The nearest modern station with data comparable to Sagastyr was Tiksi, about 200 km south, but an average displacement of more than ~2.5°C in the reference anomaly values would be required to bring Sagastyr observations into line with the rest of the IPY-1 monthly anomalies.

Discussion

There were distinct differences in GTR evident between the IPY-1 stations studied. Both SAT and ground temperatures decreased toward the north and east, consistent with regional climatology. The GTR at Jan Mayen and Sodankylä was much warmer than either Malyye Karmakuly or Sagastyr where MAGT ranged between -5°C and -10°C. Expected exponential attenuation of the temperature signal with depth and delayed phase shifts proportional to depth below the surface can be seen in the data.

If the GTR data from IPY-1 are broadly representative, then we can see that permafrost landscapes situated in the Atlantic-maritime climate zone would have been more sensitive to climate fluctuations even at that time than those toward the East with a more polar-continental type climate. This speculation is supported to some extent in that marked changes in permafrost landscapes were reported during the climate warming that occurred in this region early in the 20th century (Jensen 1939, Wood & Overland, in prep.). This region has certainly experienced changes in vegetation, hydrological regime, and geomorphologic processes during the recent period, and this process would likely expand in the case of increased warming as the boundary of the less-sensitive region to the eastward shifted in response.

We also note that the month-to-month fluctuations in SAT and GTR during the winter were often consistent with large-scale variability in atmospheric circulation. In February 1883, for example, the NAO index was 2.4 and the SAT anomaly distribution over the Atlantic and northern Europe closely resembled the canonical pattern (e.g., Hurrell 1995). Positive SAT anomalies occurred at Jan Mayen, Sodankylä, and Malyye Karmakuly; the effect on GTR is particularly evident at the latter station. However, the effects of increased westerly advection did not extend as far as Sagastyr, where SAT was especially low during this month. It would be reasonable to expect that GTR in Fennoscandia and northern Russia would be sensitive to those fluctuations in atmospheric circulation that produce well-known SAT anomaly patterns in winter.

Historical data such as these we have been discussing are particularly interesting now in light of the large environmental impacts that have been observed in the Arctic and elsewhere associated with a warming climate. The practical use of this type of data, however, is encumbered by a number of well-known issues, not least of which is the lack of comparable site-specific modern data. Even without the ability to make direct comparisons, we can certainly use historical information to study questions suited to the material and also to discover where new investigations might be leveraged by historical resources.

Acknowledgments

This publication was supported in part by the NOAA Arctic Research Office and JISAO under cooperative agreement NA17RJ1232, Contribution #1478.

References

Baker, F. 1982. The first International Polar Year. *Polar Record* 21(132): 275-285.

Barr, W. 1985. The expeditions of the first International Polar Year, 1882-83. In *Technical Paper No. 29*, 223. Calgary: Arctic Institute of North America.

Heathcote, N.H.d.V. & Armitage, A. 1959. The First International Polar Year (1882-1883). In *Annals of the International Geophysical Year*, ed. ICSU. London; New York: Pergamon Press.

Hurrell, J.W. 1995. Decadal trends in the North Atlantic Oscillation: Regional temperatures and precipitation. *Science* 269: 676-679.

Jensen, A.S. 1939. Concerning a change of climate during recent decades in the Arctic and Subarctic regions. *Kgi. Dansk. Vid. Selsk. Biol. Medd.* 14.

Lemström, S. & Biese, E. (eds.) 1886. *Observations Fait aux Stations de Sodankylä et Kultala*. Helsingfors: L'Imprimerie des Hértiers de Simelius.

Lenz, R. (ed.) 1886a. *Beobachtungen der Russischen Polarstation an der Lenamündung*: Russischen Geographischen Gesellshaft.

Lenz, R. (ed.) 1886b. *Beobachtungen der Russischen Polarstation auf Nowaya Semlja*: Russischen Geographischen Gesellshaft.

Ray, P.H. 1885. *Report of the International Polar Expedition to Point Barrow, Alaska*. Washington, D.C.: Government Printing Office.

Shiklomanov, N.I. 2005. From exploration to systematic investigation: development of geocryology in 19th- and early 20th-century Russia. *Physical Geography* 26(4):249-263.

Thompson, D.W.J. & Wallace, J.M. 2001. Regional Climate Impacts of the Northern Hemisphere Annular Mode. *Science* 293: 85-89.

von Wohlgemuth, E.E. (ed.) 1886. *Österreichische Polarexpedition nach Jan Mayen. Beobachtungs-Ergebnisse*. Wien: Der Kaiserliche-Königliche Hof- und Staatsdruckerei.

Weyprecht, C. 1875. Fundamental principles of scientific Arctic investigation. An address delivered before the 48th meeting of German naturalists and physicians at Graz, on the 18th of September 1875.

Wild, H. 1878. Über die Bodentemperaturen in St. Petersburg und Nukuss. *Repertorium für Meteorologie* VI(4): 1-88.

Wood, K.R. & Overland, J.M. In Prep. Early 20th century Arctic warming in retrospect.

The Monitoring Network of Permafrost Conditions and Embankment Performance Along the Qinghai-Tibet Railway

Qingbai Wu
State Key Laboratory of Frozen soil Engineering, Cold and Arid Regions Environmental and Engineering Research Institute, Chinese Academy of Science, Lanzhou

Yongzhi Liu
State Key Laboratory of Frozen soil Engineering, Cold and Arid Regions Environmental and Engineering Research Institute, Chinese Academy of Science, Lanzhou

Hui Yu
State Key Laboratory of Frozen soil Engineering, Cold and Arid Regions Environmental and Engineering Research Institute, Chinese Academy of Science, Lanzhou

Abstract

Some effective engineering measures (crushed-rock-based embankment, crushed-rock cover, U-type crushed-rock embankment, and thermal pile in the embankment) have been used to mitigate the impact of engineering disturbance on the thermal regime of permafrost and to avoid permafrost thawing and surface subsidence affecting railway performance. A network of 43 automated sections was installed in 2004 along the Qinghai-Tibet Railway to monitor at regular intervals the ground temperature at different locations (in the embankment shoulders and slope foot and in the permafrost underneath the embankment and away from the embankment) for studying the thermal regime of permafrost. The thawing front location in the embankment and ground underneath the embankment also can be monitored based on temperature data. In addition to this network, 12 subsidence benchmarks and one 20 m deep pile as a reference benchmark in each section were also installed for monitoring the surface subsidence of the railway embankment. Recent monitoring results of two years showed that the roadbed was stable during observed periods. Under the crushed-rock-based embankment and the embankment with thermal piles, the permafrost temperatures decreased and permafrost tables were raised noticeably; but the temperature of permafrost under the embankment with a crushed-rock revetment was slightly decreased, and the permafrost table was basically unchanged.

Keywords: embankment performance; monitoring network; permafrost conditions; Qinghai-Tibet Railway; subsidence; temperature.

Introduction

Surface disturbance from engineering construction and other human activities can cause significant permafrost warming and thawing by altering the surface energy balance. Permafrost thawing can result in ground surface subsidence, which can disrupt infrastructure stability and operations in cold regions (Smith & Burgess 1999, Nelson et al. 2001). As a consequence, understanding, evaluation, and anticipation of changes in permafrost under engineering construction are of great scientific interest.

Of the 1142 km of the Qinghai-Tibet Railway (QTR) from Golmud to Lhasa, about 542 km go through continuous permafrost regions. In the 542 km of continuous permafrost regions, there are 275 km in warm permafrost (mean annual ground temperature is higher than -1.0°C), with 134 km of high ice content (including ice-rich frozen soil, saturated-ice frozen soil, and ice with soil), and 171 km in cold permafrost (mean annual ground temperature is lower than -1.0°C), with 97 km of high ice content (Wu et al. 2004). Widespread, warm, ice-rich permafrost along the QTR is easily subject to thaw settlement caused by climate warming and engineering construction, which can affect the stability of highways or railways in permafrost regions (Wu et al. 2004, 2005a, Cheng & Wu 2007). To prevent ground ice near the permafrost table from thawing caused by climate warming and engineering effects, some effective measures, such as crushed-rock-based embankments, crushed-rock cover, and substituting a bridge for embankments, were applied to cool the permafrost under embankments (Ma et al. 2002, Cheng 2005, Wu et al. 2006). The results of permafrost variation during the QTR construction indicated that these measures could effectively reduce the thermal impact of climate warming and engineering disturbance (Wu et al. 2005b, Ma et al. 2006, Cheng et al. 2007). However, under the long-term effect of climate warming and thermal disturbance of engineering, whether these measures can maintain the long-term effect of cooling the permafrost is an important issue for roadbed stability in permafrost regions along the QTR.

The main objective of this article is to introduce the long-term monitoring system of permafrost condition and embankment performance along the Qinghai-Tibet Railway. We first discuss the principles of the long-term monitoring system setup, then the systematic composition and monitoring methods. We focus on roadbed deformation and variation of the permafrost table under embankments with various engineering measures. The relationship between roadbed stability and permafrost variation under embankments caused by the thermal disturbance of engineering were investigated.

Principles of Monitoring Network Setup

The goal of the long-term monitoring network for the Qinghai-Tibet Railway in permafrost regions is mainly to monitor permafrost changes, including artificial permafrost table, permafrost temperature, freezing and thawing process under embankments with and without engineering measures and under the natural surface, roadbed deformation and the variation of seasonal freezing depth under the embankment in seasonally frozen soil areas and thawed areas of permafrost regions. The principles of the long-term monitoring network setup mainly included the following factors:

Permafrost thermal stability

Permafrost thermal stability is one of the most important factors in roadbed stability, including the mean annual ground temperature (MAGT) of permafrost and the frozen soil types (ice content). The permafrost regions along the Qinghai-Tibet Railway are divided into four areas by the MAGT: (1) extremely unstable areas of warm permafrost where the MAGT is higher than -0.5°C, (2) unstable areas of warm permafrost where the MAGT ranges from -0.5°C to -1.0°C, (3) basically stable areas of cold permafrost where the MAGT ranges from -1.0°C to -2.0°C, and (4) stable areas of cold permafrost where the MAGT is lower than -2.0°C. Each area defined by the MAGT could be further divided into two sub-areas by ice content near the permafrost table: (1) ice-rich permafrost areas including ice-rich permafrost, saturated ice permafrost, and ice layer with soil; and (2) ice-poor permafrost areas. We focused on establishing some monitoring sections in warm, ice-rich permafrost areas, where many measures were applied to decrease the permafrost temperatures under embankments.

Engineering measures

The application of engineering measures for the Qinghai-Tibet Railway was to effectively cool the permafrost temperature under embankments. Under the effect of climate warming and engineering construction, the long-term impact of engineering measures on permafrost under embankments is closely related to roadbed stability.

Some measures that were focused on included (1) crushed-rock-based embankment with length up to 142 km, (2) embankment with crushed-rock cover with length up to 156 km, (3) U-type crushed-rock embankment; (4) embankment with thermal piles, and (5) general embankment.

The goals of the permafrost monitoring network on the QTR were to investigate permafrost variations (under the natural surface and the embankments) and surface deformation of the embankment. So, the monitoring network is divided into two parts: one is to investigate the variation of active layer thickness—the soil temperatures at the ground surface as well as near the permafrost table and the MAGT under climate warming; the other is to investigate the variation of the permafrost table—the temperature under the embankments and the total deformation on railway surface under the effect of the railway.

Monitoring Sites Description

According to the principles of the monitoring network setup, 43 monitoring sections were established in 2004, including the monitoring of road surface deformation and permafrost temperatures under the embankment and natural surface. In each section, the permafrost temperatures under both the right and left shoulders of the embankment, under the embankment slope foot, and under the natural surface away from the railway were monitored. Additionally, 12 deformation benchmarks were installed on the road surface for each section. All of these instruments comprised the deformation monitoring system in each site. Meanwhile, two weather stations will be established at the Kaixinling and Tanggula Mountains in 2008. Together with a weather station at Beiluhe basin, they will consist of a weather system in the whole monitoring network along the Qinghai-Tibet Railway.

These 43 monitoring sites along the 542 km of the QTR, from Xidatan to Anduo, span about 3.4 latitudinal degrees and about 2.6 longitudinal degrees on the eastern Qinghai-Tibet Plateau (Fig. 1). The elevation of these sites vary from 4423 m a.s.l. at Xidatan site to 5080 m a.s.l. at the Tanggula Mountain site, with an average elevation of about 4713 m a.s.l. All monitoring sites are located in the permafrost region except the XD1 site, located in seasonal frozen soil areas near the northern limit of permafrost. Among the sites located in permafrost regions, the QH1 and ZH1 sites are in thaw areas of the permafrost region, and the ZR1, XQ1, and WT1 sites are in degraded areas of the permafrost region, where the MAGT is higher than 0°C. These observed sites are distributed in various terrains, including high altitude mountains, high plains, and basins from north to south of the plateau. In the high altitude mountains along the QTR, that is, the Kunlun Mountains, Kekexili Mountains, Fenghuo Mountains, Tanggula Mountains, and Touerjiu Mountains, the MAGTs are lower than -1.5°C or -2.0°C, the active layer thickness ranges from 1.2 m to 2.0 m, the permafrost thickness is larger than 60 m, and ice-rich permafrost exists from the permafrost table to 10 m deep below the ground surface. In the high plain along the QTR, that is, the high plain of the Chumaer River, the MAGTs range from -0.5°C to -1.5°C, the active layer thickness ranges from 2.0 m to 3.0 m, the permafrost thickness is lower than 50 m, and ice-rich permafrost is widespread from the permafrost table to 10 m deep below the ground surface. In the basins along the QTR, that is, the Beilu River, Wuli, Tuotuo River, Buqu River, Zajiazangbu River and Anduo, the MAGTs are higher than -0.5°C, exceptionally lower than -0.5°C, most of the active layer thickness is larger than 3 m, but some is exceptionally lower than 2.5 m, permafrost thickness ranges from 10 m to 25 m, and thaw area is widespread.

The areas in the high plain and in the basin are key sections for monitoring permafrost variation under the embankment and the total deformation of road surface due to warm, ice-rich permafrost.

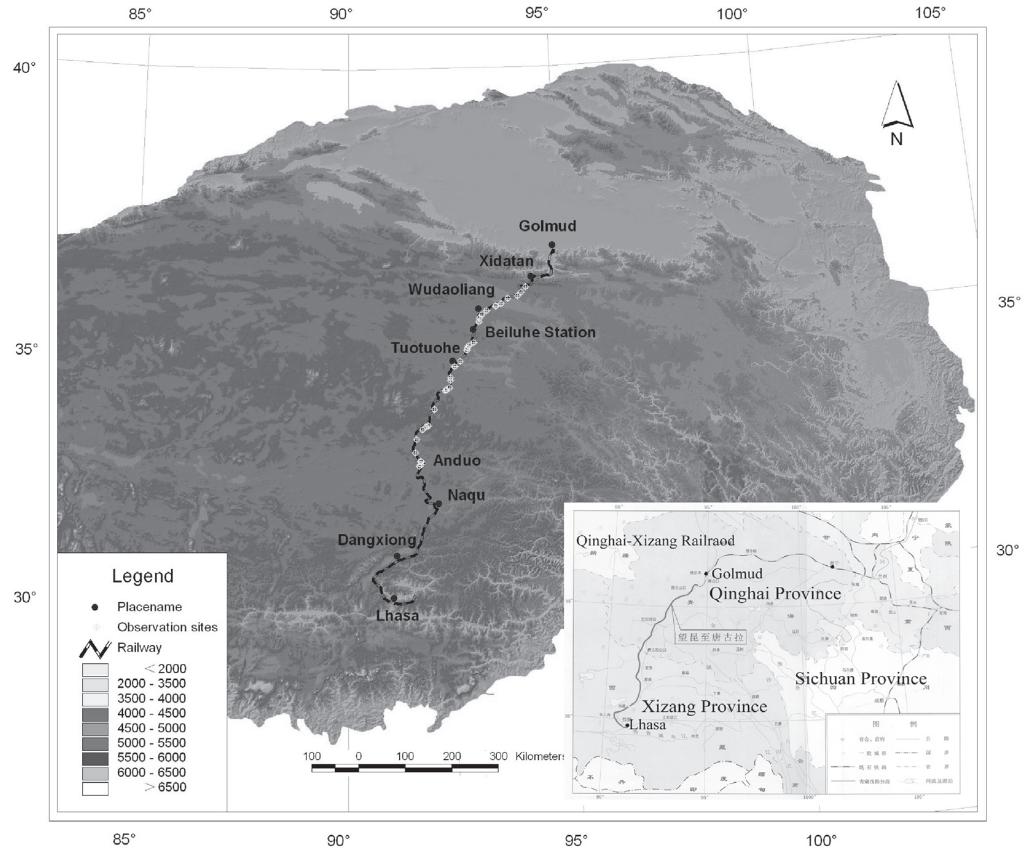

Figure 1. Monitoring network of the permafrost along the Qinghai-Tibet Railway.

Measuring Methods

Soil temperature measuring method

Soil temperatures were measured in three embankment locations: from the road surface to 20 m deep through the borehole at the right and left shoulders, from the natural surface to 8 m deep through the borehole at the embankment slope foot, and from the natural surface to 18 m deep through the borehole at a place away from the railway (Fig. 2). All measurements were obtained by a string of thermistors installed with the interval of 0.5 m from each other along the borehole, except at the places away from the railway. There the thermistors were installed at depths of 10, 20, 40, 80, 120, 160, and 200 cm from the surface to 2 m deep, and with the interval of 0.5 m from 2 m to 18 m deep. These thermistors, with sensitivities of ±0.05°C, were made by the State Key Laboratory of Frozen Soil Engineering (SKLFSE). The in situ measurement data acquisitions were automatically conducted by the Datataker of DT500 series (made in Australia). Well-trained technicians and professionals manually download the data from the Datataker every two months, and they check the operational condition of the equipment, including power, communication, etc., every month.

Deformation measuring method

Total deformation of embankment surface monitoring consists of two parts in each site. One part is constructed of 12 thin-steel benchmarks inserted 20 cm deep from the embankment surface. The other part is constructed of standard piles, as a reference benchmark, buried 20 m deep under the embankment near the deformation benchmarks (Fig. 3). Relative elevations of the deformation benchmarks and the reference benchmark are measured by electronic theodolite. The absolute heights are calculated by comparison of the elevation differences between deformation benchmarks and the reference benchmark. The deformation measurements of the embankment surface are conducted on day 20 of every month by well-train technicians and professionals, strictly following the standard guideline.

Estimation method of active layer thickness and permafrost table

Active layer thickness (ALT) under the natural surface or the artificial permafrost table under the embankment can be estimated by soil temperature data measured by the methods mentioned above. The ALT can be estimated by various methods: mechanical probing, temperature measurements, visual measurements, etc. (Brown et al. 2000). The soil temperature measurement method is available in our study. The maximum thawing depth can be shown by the profile of the soil temperature versus the depth-mapped base on the data of the daily soil temperature during any time extent, commonly several months from August to November. The

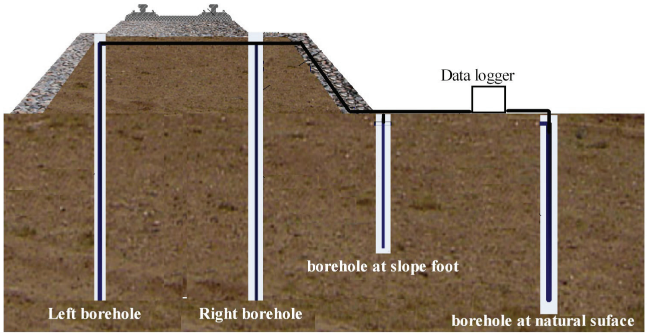

Figure 2. Section of the permafrost temperature observed site; depth of borehole at both left and right shoulders is 20 m, at the slope foot is 8 m, and at the natural surface is 18 m. Generally, the borehole at the natural surface is away from the railway.

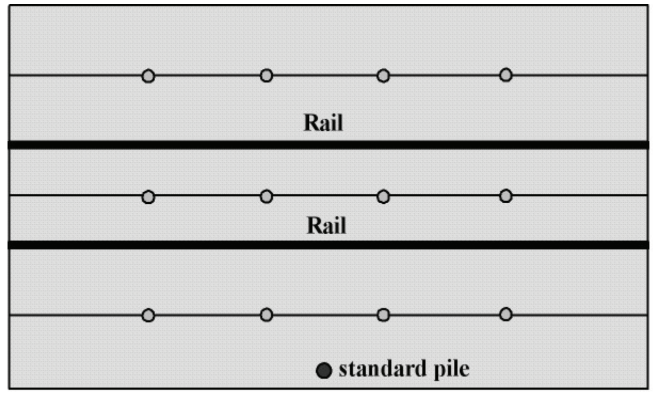

Figure 3. Planform of thin-steel benchmarks setup of the deformation in embankment surface in each section. Grey solid circles are thin-steel benchmarks of deformation, and black solid circles are standard piles as a reference benchmark of deformation.

deepest intersection between the profile mentioned above and the 0°C axes is the deepest depth of soil thawing in summer, which is the active layer thickness from the ground surface. The artificial permafrost table under the embankment is estimated by the same method.

Results

Permafrost variation and deformation for general embankment

Table 1 shows the variation of the artificial permafrost table under the general embankment and deformation of the embankment surface. During the period of observation, the artificial permafrost table rose, ranging from 0.55 m to 0.9 m under the right shoulder of the embankment and from 1.1 m to 2.9 m under the left shoulder of the embankment for KM1, CR2, CR5, LD1, WL3, and WQ1 sites; the artificial permafrost table dropped, ranging from -0.35 m to -4.1 m for CR1, YH1, YH2, DB1, RR1, and AD3 sites. However, the sections where the artificial permafrost table dropped are located in extremely warm permafrost regions where mean annual ground temperature is high, up to -0.5°C, except at the CR2 site. This indicates that extremely warm permafrost could gradually thaw if special design methods are not used.

However, deformation of the embankment surface seems to be unrelated to the variation of the artificial permafrost table (Table 1). The amount of average deformation at the sections of CR1, CR5, WQ1, and AD3 is larger than 20 mm, and only CR1 and AD3 sites found that the artificial permafrost table dropped during observed periods. Drilling data show that the deformation of embankment surface obviously depends on ice content of permafrost. The ice content of permafrost is more than 30% for these sites.

Permafrost variation under crushed-rock-based embankment

Table 2 shows the variation of the artificial permafrost table under a crushed-rock-based embankment. During observed periods, the artificial permafrost table under the embankment rose except at the left shoulder of the WL1 and TG1 sites, ranging from 0.05 m to 3.35 m. The artificial permafrost table under the left shoulder of the embankment was still deeper than the permafrost table under the natural surface. These results indicate that using a crushed-rock-based embankment is effective in raising the artificial permafrost table under the embankment. The cause of the artificial permafrost table under the left shoulder of the embankment for WL1 and TG1 sites is unclear, and probably is related to the crushed-rock-based embankment construction.

Permafrost thawing under embankments resulted in subsidence of the embankment. For WL1 and TG1 sites, the average deformation at the left shoulder of the embankment surface was more than 10 mm—up to 15 mm and 32 mm, respectively, during observed periods. For other sites, the average deformation is lower to 2 mm, indicating that the roadbed is stable.

The monitoring results before 2006 testified that the artificial permafrost table was not only raised, but also the temperatures had a trend of decreased permafrost temperatures under the crushed-rock-based embankment (Wu et al. 2005b, Ma et al. 2007), indicating that it is a good engineering measurement to avoid permafrost thaw.

Discussion and Summary

The network that monitors permafrost conditions and embankment performance along the QTR began to run in 2005, and some very useful data have been obtained successfully, including variation of the permafrost temperature, active layer under the natural surface, artificial permafrost table, temperature under the embankment, and total deformation of railway surface. These helpful data can be used to investigate and analyze the relationship between roadbed stability and permafrost variation under the embankment. The data about active layer can be used to investigate spatial features of active layer thickness along the QTR. These data are useful also for understanding the response of permafrost and active layer to climate warming and engineering construction.

To check permafrost variation in the early stage of the QTR operation, we first analyzed the obtained data of these 43 sites. The results of two recent years showed that

Table 1. Rising of permafrost table under embankment and deformation on embankment surface.

Site	Location	MAGT (°C)	PT(m)	H(m)	APT(m)		△H(m)		Aver. Def. (mm)
					Right	Left	Right	Left	
KM1	Kunlun Mts.	-3.17	1.9	1.0	2.35	1.75	0.55	1.15	-2
CR1	Chumaerhe high plain	-0.75	1.1	5.5	7.5	5.5	-0.90	0.90	34
CR2		-0.90	5.1**	4.0	7.3	5.0	0.90	2.90	0
CR5		-0.50	4.7	2.8	7	5.0	0.50	2.50	20
LD1		-0.65	4.0	0.9	4.9	4.5	0.00	0.40	3
YH1	Yamaerhe	-0.50	2.95	4.2	7.5	7.75	-0.35	-0.60	1
YH2		-0.24	5.22	2.4	11.7	9.0	-4.10	-1.38	2
WL3	Wuli Basin	-0.54	2.8	3.6	6.2	5.6	0.20	0.80*	12
DB1	100daoban	-0.12	4.5	4.0		9.0		-0.50	0
WQ1	Wenquan	-0.40	3.1	3.0	5.5	5.0	0.60	1.10	31
RR1	Riazangbuqu	-0.27	5.3	5.0	11.5	11.3	-1.20	-1.00	0
AD3	Anduo	-0.20	2.3	3.5	5.8	6.2	0.00	-0.40	88

MAGT means mean annual ground temperature, PT means permafrost table, APT means artificial permafrost table in 2006, H means height of embankment, and ΔH means the rising value of artificial permafrost table during observed periods. Aver. Def. means average deformation of embankment surface. All data used in this table is before Oct. 2007. ** The temperatures at the slope foot of embankment are a reference due to no temperature data under natural surface.

Table 2. Variation of artificial permafrost table after the CRBE construction.

Site	MAGT (°C)	PT(m)	H(m)	APT(m)		△H (m)	
				Right	Left	Right	Left
CR3	-1.5	2.7	3.10	3.6	<0*	2.1	>2.7*
WD1	-1.48	1.85	3.2	2.65*	2.1	2.4*	2.95
KK1	-2.4	1.8	4.0	2.45	3.1	3.35	2.4
HL3	-1.28	2.3	3.5	3.2	3.72	2.6	2.08
WL1	-0.5	3.2	3.70	5.8*	7.1	1.1*	-0.2
KL1	-0.67	2.35	3.40	4.4	4.85	1.35	0.9
BB1	-0.33	2.4	5.7	4.5	6.5	3.6	1.6
TG1	-1.24	2.85	4.4	7.2	7.8	0.05	-0.55

All signs are the same as that in Table 2. * means the value under roadbed centerline. <0 means artificial permafrost table entered into embankment.

the total roadbed deformation was smaller than 10 mm, which indicates roadbed stability. Under the crushed-rock-based embankment and the embankment with thermal piles, permafrost temperatures were noticeably decreased, and the permafrost table was noticeably raised. Under the embankment with crushed-rock revetment, permafrost temperatures were slightly decreased, and the permafrost table was basically stable. However, the following problems deserve more attention:

- For all observed sites, the permafrost temperatures were uneven due to the radiation difference of the two embankment slopes. The permafrost table depth under the sun-side slope of the embankment is greater than that under the shade-side slope, and the permafrost table slope inclining to the sun-side slope of the embankment could be deformed possibly, resulting in roadbed crack.
- The thaw layer between the upper permafrost and the seasonal freezing layer occurred under the embankment in the warm permafrost areas where the MAGT is higher than -0.5°C. The thickness of the thaw layer ranged from 50 cm to 150 cm with an average of 85 cm, which could potentially result in larger deformation of the roadbed.
- The frozen layer which would not thaw within a year formed under the left shoulder (shade-side) of the embankment in both of the seasonal frozen soil areas and the thaw areas of permafrost regions. This frozen layer formation beneath the left side of the embankment could be an inducement to roadbed damage.
- The permafrost temperatures under the slope foot of the embankment were higher than those under the natural surface. Under the thermal effect of the railway, the active layer thickness under the slope foot of the embankment was larger than that under the natural surface. Rainfall could accumulate here possibly because of the lateral thermal influence.

Acknowledgments

Many technicians contributed greatly during construction of the permafrost monitoring network along the QTR, and the authors are very thankful. This research was funded by the Outstanding Youth Foundation Project, the National Natural Science Foundation of China (Grant No. 40625004).

References

Brown, J, Hinkel, K.M. & Nelson, F.E. 2000. The Circumpolar Active Layer Monitoring (CALM) program: research designs and initial results. *Polar Geography* 24(3): 165-258.

Cheng, G. 2005. A roadbed cooling approach for the construction of Qinghai–Tibet Railway. *Cold Regions Science and Technology* 42: 169-176.

Cheng, G.D. & Wu, T. 2007. Responses of permafrost to climate change and their environmental significant, Qinghai-Tibet Plateau. *J. Geophys. Res.* 112: F02S03, dio:10.1029/2006/ JF000631.

Cheng, G.D., Sun, Z.Z. & Niu, F.J. 2007. Application of the roadbed cooling approach in Qinghai–Tibet railway engineering. *Cold Regions Science and Technology*: doi:10.1016/j.coldregions. 2007.02.006.

Ma, W., Cheng, G.D. & Wu, Q.B. 2002. Preliminary study on technology of cooling foundation in permafrost regions. *Journal of Glaciology and Geocryology* 24(5): 579-587.

Ma, W., Shi, C.H., Wu, Q.B., Zhang, L.X. & Wu, Z.J. 2006. Monitoring study on technology of the cooling roadbed in permafrost region of Qinghai-Tibet Plateau. *Cold Regions Science and Technology* 44(1): 1-11.

Ma, W., Feng, G.L., Wu, Q.B. & Wu, J.J. 2007. Analyses of temperature fields under the embankment with crushed-rock structures along the Qinghai-Tibet Railway. *Cold Regions Science and Technology:* doi:10.1016/j.coldregions.2007.08.001.

Nelson, F.E., Anisimov, O.A. & Shiklomanov, N.I. 2001. Subsidence risk from thawing permafrost. *Nature* 410: 889–890.

Smith, S.L. & Burgess, M.M. 1999. Mapping the sensitivity of Canadian permafrost to climate warming, in Interaction between Cryosphere, Climate and Greenhouse Gases. *Proceeding of the IUGG~99 Symposium HS2, Birmingham,* IAHS Publ. 256: 71-80.

Wu, Q.B., Cheng, G.D. & Ma, W. 2004. The impact of climate warming on Qinghai-Tibetan Railroad. *Science in China, Series D* 47(Supp. I): 122-130.

Wu, Q.B., Dong, X.F. & Liu, Y.Z. 2005a. Responses of permafrost on the Qinghai-Tibet Plateau to climate change and engineering action. *Journal of Glaciology and Geocryology* 27(1):50-54. (In Chinese with English abstract).

Wu, Q.B., Zhao, S.Y., Ma, W., Liu, Y.Z. & Zhang, L.X. 2005b. Monitoring and analysis of cooling effect of block-stone embankment for Qinghai-Tibet Railway. *Chinese Journal of Geotechnical Engineering* 27(12): 1386-1390.

Wu, Q.B., Cheng, G.D., Ma, W., Niu, F.J. & Sun, Z.Z. 2006. Technical approaches on ensuring permafrost thermal stability for Qinghai-Xizang Railroad construction. *Geomechanics and Geoengineering*, 1(2): 119-128.

Freezing/Thawing Index Variations During the Last 40 Years Over the Tibet Plateau

Tonghua Wu, Lin Zhao, Shuxun Li, Changwei Xie, Qiangqiang Pang, Wengang Zhang
Cryosphere Research Station on the Qinghai-Tibet Plateau, Cold and Arid Regions Environmental and Engineering Research Institute, Chinese Academy of Sciences

Abstract

This paper presents the freezing/thawing index variation over the Tibet Plateau based on the analysis of the mean monthly air temperature and ground surface temperature data from 101 meteorological stations during the period of 1961 to 2000. The statistical results showed that the mean annual air and ground surface freezing indices equal 959 and 780 degree-days, respectively, and that the mean annual air and ground surface thawing indices equal 2494 and 3532 degree-days, respectively. The multivariate regression analysis results indicated there is a high correlation between the freezing/thawing index and the latitude and elevation on the plateau. On a decadal scale, the annual air freezing indices indicated a decrease of 146 degree-days during the last four decades. As to the annual ground surface freezing indices, the values indicated a decrease of 95 degree-days. Moreover, the annual air thawing index displayed an increase of 209 degree-days, and the annual ground surface thawing index also displayed an increase of 150 degree-days since 1961. The decrease of freezing index and the increase of thawing index may be responsible for the permafrost degradation in recent years on the plateau.

Keywords: freezing index; permafrost; thawing index; Tibet Plateau.

Introduction

In permafrost regions, the annual air and ground freezing and thawing indices are of great significance in predicting and mapping permafrost distribution (Nelson & Outcalt 1987) and active layer thickness (Nelson et al. 1997, Shiklomanov & Nelson 2002, Zhang et al. 2005). Both of the indices are also important parameters for engineering design in cold regions (Steurer 1996). Generally, the annual freezing and thawing indices are defined as the cumulative number of degree-days below and above 0°C for a year (Permafrost Subcommittee 1988). Among the four main types of freezing and thawing indices which have been used, the annual freezing and thawing indices may be representative of the freezing and thawing climatology (Legates & Willmott 1990). A recent study also demonstrated the validity of approaching the freezing/thawing index by means of calculations of mean monthly air temperature data, which is originally defined based on daily observations (Frauenfeld et al. 2007).

This paper aims to provide the variations of annual air and ground surface freezing/thawing indices from 1961 to 2000 on the Tibet Plateau. The estimation of the annual freezing/thawing index would contribute to an understanding of climate change and variations in ground thermal regime on the plateau.

Data and Methods

We collected the mean monthly air and ground surface temperature data at 101 meteorological stations from 1961 to 2000 on the Tibet Plateau (Fig. 1). The air temperature is based on the observations at 1.5 m above the ground, and the

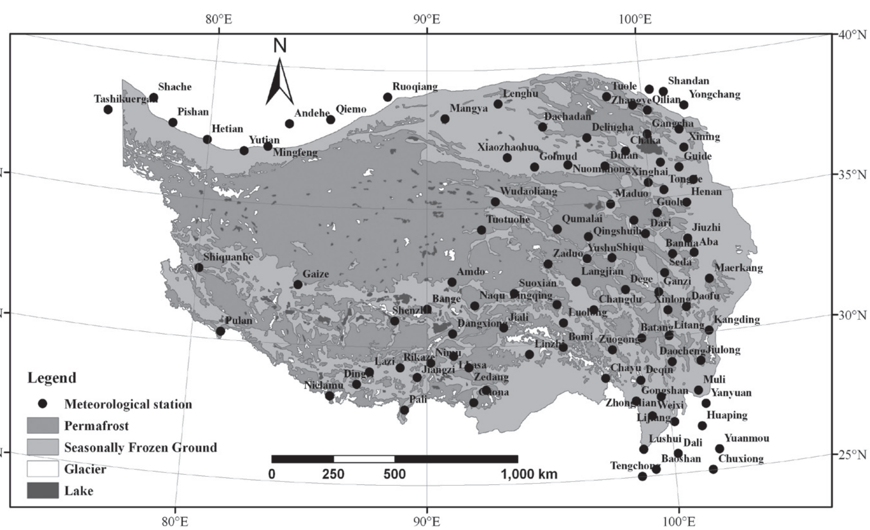

Figure 1. Permafrost distribution and the locations of meteorological stations on the Qinghai-Tibet Plateau.

ground surface temperature is based on the measurements at 0 cm of earth surface.

The annual air and ground surface freezing indices are calculated as the following equations (Frauenfeld et al. 2007). The duration in estimating the freezing index includes those months when temperatures were below 0°C degree:

$$FI_a = \sum_{i=1}^{M_F} \left|\overline{T}_{ai}\right| \cdot D_i, \ \ \overline{T}_{ai} < 0\,^{\circ}\mathrm{C} \tag{1}$$

$$FI_s = \sum_{i=1}^{M_F} \left|\overline{T}_{si}\right| \cdot D_i, \ \ \overline{T}_{si} < 0\,^{\circ}\mathrm{C} \tag{2}$$

where FI_a and FI_s are the annual air and ground surface freezing indices; M_F are those months when the mean monthly temperature is below 0°C; D is the number of days in the month of M_F.

Similarly, the annual air and ground surface thawing indices are calculated as the following equations. The duration in estimating the thawing index includes those months when temperatures were above 0°C degree:

$$TI_a = \sum_{i=1}^{M_T} \overline{T}_{ai} \cdot D_i, \ \ \overline{T}_{ai} > 0\,^{\circ}\mathrm{C} \tag{3}$$

$$TI_s = \sum_{i=1}^{M_T} \overline{T}_{si} \cdot D_i, \ \ \overline{T}_{si} > 0\,^{\circ}\mathrm{C} \tag{4}$$

where TI_a and TI_s are the annual air and ground surface freezing indices; M_T are those months when the mean monthly temperature is above 0°C; D is the number of days in the month of M_T.

The FI_a, FI_s, TI_a, and TI_s are calculated for each year from 1961 to 2000. Then the decadal values of those indices are obtained for avoiding great interannual fluctuations (Thompson 1963, Shur & Slavin-Borovskiy 1993).

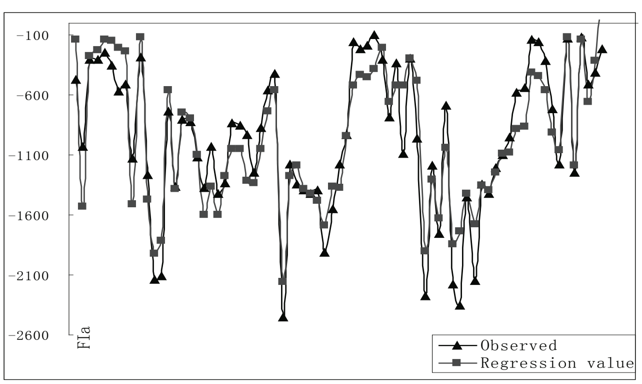

Figure 2. Regression analyses for the air freezing indices.

Table 1. Analysis of variance for the regression model of air freezing indices.

Source	Sum of squares	df	Mean square	F	Sig.
Regression	23443987.090	2	11721993.545	187.842	0.000(a)
Residual	4493051.921	72	62403.499		
Total	27937039.012	74			

Results

Variations of air and ground surface freezing indices

Among the 101 meteorological stations, there are 26 stations where monthly mean air temperature and monthly mean ground surface temperature are above 0°C. Therefore, the remaining 75 stations are selected for the calculation of freezing index on the plateau. The statistical results indicated that the mean annual air freezing index during the 40 years was 959 degree-days and that the mean annual ground surface freezing index was 780 degree-days. The maximum value of air freezing index occurred at Wudaoliang station, which is located at the hinterland of the plateau, equaling 2450 degree-days. The maximum value of ground surface freezing index also occurred at Wudaoliang station, which equals 1792 degree-days. The minimum value of air freezing index occurred at Lhasa station, which is located in the south of the plateau, equaling 97 degree-days. The minimum value of ground surface freezing index occurred at Zhongdian station, which is located in the southeast of the plateau, equaling 42 degree-days.

The calculated annual air and ground surface freezing indices showed a close correlation with the altitude (h) and the latitude (φ). As shown in Figures 2 and 3, validation with FI_a and FI_s from field data shows good correlation (R_{af}=0.916 and R_{sf}=0.943). We used the multivariate regression method to determine the function between air and ground surface freezing indices and the latitude and elevation. The analyses of variance indicated a high significance level (Tables 1 and 2).

$$FI_a = 8029.077 - 192.541\varphi - 0.738h \tag{5}$$

$$FI_s = 6513.638 - 162.230\varphi - 0.537h \tag{6}$$

Table 3 showed the interdecadal variations of air and ground surface freezing indices (degree-days) at nine stations

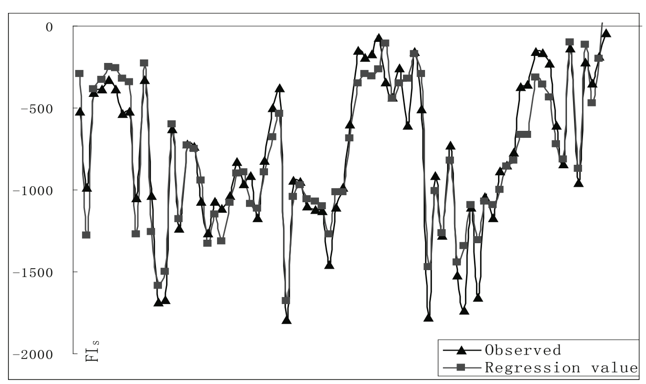

Figure 3. Regression analyses for the ground surface freezing indices.

Table 2. Analysis of variance for the regression model of ground surface freezing indices.

Source	Sum of squares	df	Mean square	F	Sig.
Regression	14206138.964	2	7103069.482	287.283	0.000(a)
Residual	1780197.600	72	24724.967		
Total	15986336.564	74			

Table 3. Interdecadal variations of air and ground surface freezing indices (degree-day) at nine selected stations.

Station name	$F_{af}60$	$F_{af}70$	$F_{af}80$	$F_{af}90$	$F_{af}mean$	$F_{sf}60$	$F_{sf}70$	$F_{sf}80$	$F_{sf}90$	$F_{sf}mean$
Golmud	1120	809	709	707	836	999	809	742	763	829
Wudaoliang	2562	2406	2443	2389	2450	1912	1732	1853	1670	1792
Amdo	2069	1851	1831	1896	1912	1712	1388	1328	1389	1454
Naqu	1779	1514	1517	1382	1548	1265	1063	1115	997	1110
Tuotuohe	2316	2179	2374	2238	2277	1841	1702	1882	1695	1780
Zaduo	1228	1198	1151	1156	1183	987	922	877	882	917
Qumalai	1842	1729	1781	1689	1760	1335	1298	1302	1175	1277
Maduo	2274	2252	2155	2050	2183	1657	1619	1330	1470	1519
Qingshuihe	2383	2369	2333	2331	2354	1737	1788	1674	1740	1735

located in permafrost regions where there is seasonally frozen ground. The data showed an obvious decrease in the air and ground surface freezing indices since the 1960s.

On a decadal scale, the average values of air freezing index in the 1960s, 1970s, 1980s, and 1990s are 1047, 960, 928, and 901 degree-days, respectively. As a signal of climatic warming on the plateau, the air freezing index on the plateau indicated a decrease of 146 degree-days during the past 40 years. While the average values of ground surface freezing index in the 1960s, 1970s, 1980s, and 1990s are 838, 785, 753, and 743 degree-days, respectively. The ground surface freezing index on the plateau also showed a decrease of 95 degree-days since 1961. This conclusion coincides with the general opinion of greater warming in winter than in summer on the plateau during the last 40 years.

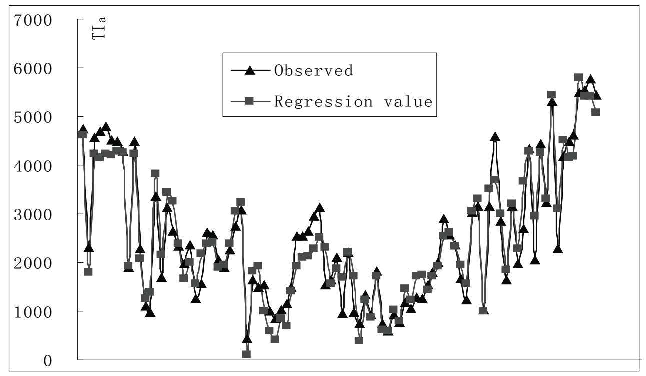

Figure 4. Regression analyses for the air thawing indices.

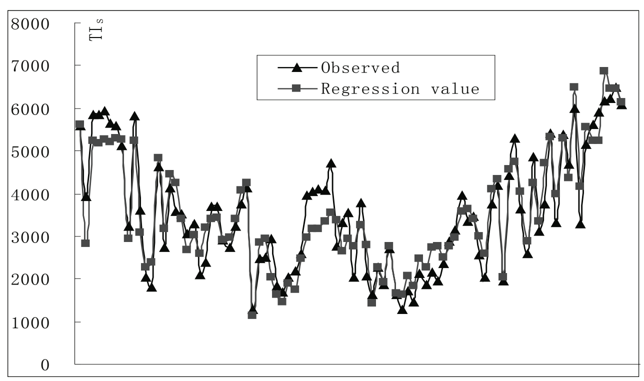

Figure 5. Regression analyses for the ground surface thawing indices.

Variations of air and ground surface thawing indices

We also excluded 9 stations where air temperature and ground surface temperature showed great difference with the other stations. Most of them are located in the southeast of the plateau with a low elevation and high monthly temperature. The remaining 92 stations were selected to calculate the thawing indexes on the plateau. The averaged air thawing index on the plateau is estimated at 2494 degree-days, and the averaged ground surface thawing index is estimated at 3532 degree-days. The minimum value of air and ground surface thawing indices also occurred at the hinterland of the plateau, while the maximum value occurred in the northwest of the plateau, where the West Kunlun Mountain range is situated.

Similar to the freezing index, the calculated annual air and ground surface thawing indices also showed close correlation with the altitude (h) and the latitude (φ). As shown in Figures 4 and 5, Validation with TI_a and TI_s from observed data also shows good correlation (R_{at}=0.961 and R_{st}=0.937). We also used the multivariate regression method to determine the function between air and ground surface thawing indices and latitude and elevation. The analyses of variance indicated a high significance level (Tables 4 and 5).

$$TI_a = 11971.781 - 157.441\varphi - 1.370h \tag{7}$$

$$TI_s = 13130.046 - 161.442\varphi - 1.366h \tag{8}$$

Table 4. Analysis of variance for the regression model of air thawing indices.

Source	Sum of squares	df	Mean square	F	Sig.
Regression	160157223.662	2	80078611.831	538.553	0.000(a)
Residual	13233611.063	89	148692.259		
Total	173390834.725	91			

Table 5. Analysis of variance for the regression model of ground surface thawing indices.

Source	Sum of squares	df	Mean square	F	Sig.
Regression	160228386.337	2	80114193.168	320.168	0.000(a)
Residual	22270071.547	89	250225.523		
Total	182498457.884	91			

Table 6. Interdecadal variations of air and ground surface thawing indices (degree-day) at nine selected stations.

Station name	$F_{at}60$	$F_{at}70$	$F_{at}80$	$F_{at}90$	$F_{at}mean$	$F_{st}60$	$F_{st}70$	$F_{st}80$	$F_{st}90$	$F_{st}mean$
Golmud	4417	4500	4503	4609	4507	5563	5666	5594	5784	5652
Wudaoliang	934	940	944	1041	965	1764	1790	1748	1951	1813
Amdo	1883	1950	1953	2082	1967	2866	2949	3085	3304	3051
Naqu	2319	2345	2321	2500	2371	3277	3219	3188	3428	3278
Tuotuohe	1476	1464	1512	1666	1530	2942	2777	2852	3196	2942
Zaduo	1018	905	1002	1063	997	1796	1771	1800	2001	1842
Qumalai	821	803	832	888	836	1578	1663	1649	1862	1688
Maduo	1082	1106	1171	1217	1144	2093	2184	2176	2286	2185
Qingshuihe	1423	1473	1507	1566	1492	2439	2443	2701	2793	2594

Table 6 implies the interdecadal variations of air and ground surface thawing indices (degree-days) at nine stations. The data show an obvious increase in the air and ground surface thawing indices since the 1960s.

On a decadal scale, the average values of air thawing index in the 1960s, 1970s, 1980s, and 1990s are 2433, 2472, 2488, 2584 degree-days, respectively, which indicate an increase of 209 degree-days in the last 40 years. Similarly, the average values of ground surface thawing index are much higher than the air thawing index. The ground surface thawing indices in the 1960s, 1970s, 1980s, and 1990s are 3448, 3485, 3539, 3657 degree-days, respectively, which show an increase of 150 degree-days. Compared with the variations of air and ground surface freezing indices, the amplitude of changes in thawing index on the plateau was much less than that of freezing index.

Changes of permafrost and active-layer thickness

The observation results of borehole temperature data from sporadic permafrost regions and discontinuous permafrost regions both indicated that permafrost on the Tibet Plateau has undergone significant degradation during the past 40 years (Cheng & Wu 2007). From the 1970s to the 1990s, the ground temperature in sporadic permafrost regions and seasonally frozen ground regions has risen by 0.3–0.5°C, while the permafrost temperature in discontinuous permafrost regions has risen by 0.1–0.3°C. The permafrost where mean annual ground temperature was 0–-0.5°C has been accelerating in warming and thinning (Jin et al. 2000, Wang et al. 2000).

In the recent 10 years, the thickness of the active-layer on the Tibet Plateau showed an increasing tendency, with increasing velocity approximating 3.1 cm/yr in discontinuous permafrost regions and 8.4 cm/yr in sporadic permafrost regions (Wu et al. 2005).

To a great extent, the recent changes of permafrost and active-layer thickness could attribute to the significant decrease in the air and ground surface freezing indices and great increase in the air and ground surface thawing indices.

Conclusions and Discussion

We calculated the freezing and thawing indices based on monthly air temperature and ground surface temperature data on the Tibet Plateau, provided that the freezing and thawing indices can be reliably calculated based on monthly data. The calculation results showed that the 1961–2000 air and ground surface freezing indices which represent the cold-season temperature climatology displayed a drastic decrease, while the thawing indices which are reminiscent of the warm-season temperature climatology showed a significant increase on a decadal scale. Meanwhile, the freezing and thawing indices on the plateau both illustrated close correlation with latitude and altitude. The analysis provided a basis for estimating the temporal and spatial variations of permafrost distribution and active-layer thickness on the plateau.

All of the calculations conducted above are based on the validity of using monthly air temperature data and ground surface temperature data to obtain freezing and thawing indices. Although the idea of utilizing monthly rather than daily temperature values to calculate the freezing and thawing indices is already an acceptable method in estimating degree-days variations (Nelson & Outcalt 1987, Zhang et al. 1996, Brown et al. 2000), the precision of using monthly data is still not assessed on the plateau until now. This would be the focus of our following work.

Acknowledgments

We are grateful to the Cryosphere Research Station on the Qinghai-Tibet Plateau, Chinese Academy of Sciences for obtaining the monthly data. This study was supported by the 973 Key Projects for Basic Research (No. 2007CB411506 and No. 2007CB411505) and the Chinese National Science Foundation (No. 40471026 and No. 40701029).

References

Brown, J., Hinkel, K.M. & Nelson, F.E. 2000. The Circumpolar Active Layer Monitoring (CALM) program: Research designs and initial results. *Polar Geography* 24(3): 163-258.

Cheng, G. & Wu, T. 2007. Responses of permafrost to climate change and their environmental significance, Qinghai-Tibet Plateau. *Journal of Geophysical Research-Earth Surface* 112: F02S03, doi:10.1029/2006JF000631.

Frauenfeld, O.W., Zhang T. & McCreight, J.L. 2007. Northern Hemisphere freezing/thawing index variations over the twentieth century. *International Journal of Climatology* 27: 47-63.

Jin, H., Cheng, G. & Zhu, Y. 2000. Chinese geocryology at the turn of the twentieth century. *Permafrost Periglacial Processes* 11(1): 23-33.

Nelson, F.E. & Outcalt, S.I. 1987. A computational method for prediction and regionalization of permafrost. *Arctic and Alpine Research* 19(3): 279-288.

Nelson, F.E., Shiklomanov, N.I., Mueller, G.R., Hinkel, K.M., Walker, D.A. & Bockheim, J.G. 1997. Estimating active-layer thickness over a large region: Kuparuk River basin, Alaska, U.S.A. *Arctic and Alpine Research* 29(4): 367-378.

Legates, D.R. & Willmott, C.J., 1990. Mean seasonal and spatial variability in global surface air temperature. *Theoretical and Applied Climatology* 41: 11-21.

Permafrost Subcommittee 1988. *Glossary of Permafrost and Related Ground-Ice Terms.* Associate Committee on Geotechnical Research, National Research Council of Canada.

Shiklomanov, N.I. & Nelson, F.E. 2002. Active-layer mapping at regional scales: a 13-year spatial time series for the Kuparuk Region, North-Central Alaska. *Permafrost and Periglacial Processes* 13: 219-230.

Shur, Y.L. & Slavin-Borovskiy, V.B. 1993. N-factor maps of Russian permafrost region. *Proceedings of the Sixth International Conference on Permafrost, Vol. 2, Beijing, China, July 5–9, 1993*: 564-568. Wushan, Guangzhou, China: South China University of Technology Press.

Steurer, P.M. 1996. Comparison of probability distributions used in estimating the 100-year return period of the air-freezing index. *Journal of Cold Regions Engineering* 10: 23-35.

Thompson, H.A. 1963. Freezing and thawing indices in Northern Canada. *Proceedings of the First Canadian Conference on Permafrost*. NRC of Canada, Ottawa: 18-36.

Wang, S., Jin, H. & Li, S. 2000. Permafrost degradation on the Qinghai-Tibet Plateau and its environmental impacts. *Permafrost and Periglacial Processes* 11(1): 43- 53.

Wu, Q., Lu, Z. & Liu, Y. 2005. Permafrost monitoring and its recent changes in Qinghai-Tibet Plateau. *Advances in Climate Change Research* 1(1): 26-28.

Zhang, T., Osterkamp, T.E. & Stamnes, K. 1996. Some characteristics of the climate in northern Alaska, U.S.A. *Arctic and Alpine Research* 28(4): 509-518.

Zhang, T., Frauenfeld, O.W., Serreze, M.C., Etringer, A.J., Oelke, C., McCreight, J.L., Barry, R.G., Gilichinsky, D., Yang, D., Ye, H., Feng, L. & Chudinova, S. 2005. Spatial and temperal variability in active layer thickness over the Russian arctic drainage basin. *Journal of Geophysical Research-Atmospheres* 110: D16101, doi:10.1029/2004JD005642.

Hydrological Dynamics of the Active Layer in the Permafrost Region, Qinghai-Tibetan Plateau

Changwei Xie, Lin Zhao, Yongjian Ding, Tonghua Wu
Cold and Arid Regions Environmental and Engineering Research Institute, Croyosphere Research Station on the Qinghai-Tibet plateau, Chinese Academy of Sciences

Abstract

Due to recent climate warming, the heat energy absorbed by the ground surface of the permafrost in the Qinghai-Tibetan plateau region has increased, thereby, leading to a continuous rise in ground temperature and the persistent increase in the thickness of the active layer. In recent years, with an increase in the thickness of the active layer, a large amount of shallow water diffused downward and thus resulted in the migration of water, enriching deeper horizons. Water infiltration carried much heat and increased heat storage in the deep subsoil; hence the freezing time was delayed. The positive feedback relation between the increase in active layer thickness and the water-heat transfer toward the deep soil exerted a profound influence on surface water resources.

Keywords: active layer; changes; hydrological effects; permafrost; Qinghai-Tibet Plateau; water-heat coupling.

Introduction

Traditionally, the active layer has been defined as the surficial layer above permafrost which thaws during summer (Burn 1998). The active layer serves as an energy-water exchange passage between the permafrost and the outer atmosphere. It is also a most sensitive zone for the response of permafrost to climate change. The Qinghai-Tibetan plateau (QTP) is a concentrated, distributed region of continuous permafrost at the word's highest altitude. Under the background of recent global warming, the active layer of permafrost has been affected by a series of changes, such as increase in thickness, vegetation degradation, and swamp drainage. These changes exert a profound influence on the regional ecosystems, hydrological environment, and even engineering construction (Ding et al. 2000). The increase in the thickness of the active layer of permafrost on the QTP has been verified by the data observed in the past few decades, and an increasing trend in active-layer thickness has been even more obvious in recent years. Such a trend is roughly consistent with the changes of the permafrost in other arctic regions (Osterkamp & Romanovsky 1997, Tarnocai et al. 2004). Studies show that in a 20-year period from the 1970s to the 1990s the active layer thickness has increased by 80–100 cm in the Chumar River valley (Tong et al. 1996). It has also been demonstrated that the increase in active-layer thickness was significantly larger in the high-temperature permafrost region than in the low-temperature permafrost region; the mean thickening rate of active layer in the <-1.5°C low temperature region was 3.1cm/yr, while that in the >-1.5°C high-temperature region was 8.3 cm/yr, and the largest thickening rate was 12.6 cm/yr (Wu et al. 2005). Existing studies and observation data show that the rise in the ground temperature of permafrost and the increase in the thickness of the active layer are a basic trend explaining the variations in permafrost in the QTP at present. Permafrost as an impermeable stratum adjusts the regional hydrological processes mainly through the dynamic changes of the active layer. The increase trend of active-layer thickness will inevitably lead to the lowering of the freeze-thaw surface and water drawdown in the active layer, which enhances precipitation infiltratration into deep subsoil, reduces surface runoff, and increases subsurface flow (Yang, et al. 2000).

Several questions need to be answered about this deepening. For example, what is the internal mechanism for the hydrological process variations caused by the thickness changes of the active layer under the present global warming background? What are the influences of the increase in active layer thickness and the rise in ground temperature on water-heat transfer processes? What is the feedback mechanism for the water-heat coupling process to the dynamic changes of the active layer? In response to the water-heat changes in the active layer of permafrost in QTP region, since the 1970s the cryosphere research station on the Qinghai-Tibetan plateau, Chinese Academy of Sciences, has selected more than ten observation sites. They are distributed within a 5 km section on both sides of the Qinghai-Tibetan Highway, from the northern limit of the permafrost-Xidatan to the southern limit of permafrost-Liangdaohe (Table 1). Of these, six sites have a continuous record of 8 years and 4 sites have an observation history of two years.

Temperature of the active layer was measured by a Pt resistance probe with an observation error of ±0.1°C. Soil moisture content was measured by TDR probe, with an observation error of ±0.5%. The buried depths of the probes were different at different sites, and the maximum buried depth of the probes exceeds by 20 cm the largest active layer depth at the observation site. The data were recorded automatically at one hour intervals by a data logger. This paper attempts to analyze the influences of the increase in active layer thickness, the rise in ground temperature on the water-heat transfer processes, and the impact on the regional hydrological environment.

Table 1. The locations of study sites on the Qinghai-Tibet Plateau.

Serial number	Latitude (N °)	Longitude (E °)	Altitude (m)	Amount ofObservation layers	Thickness of active layer in 2006(cm)	Place name	Observation begin time
QT01	35.1449	93.0426	4740	12	155	Kekexili	2005.8
QT02	34.8229	92.9218	4620	10	72	Beiluhe 1	2005.8
QT03	34.8231	92.9219	4620	10	221	Beiluhe 2	2005.8
QT04	33.070	91.9400	5100	10	>300	Tanggula	2005.8
QT05	33.9560	92.3381	4660	10	303	Kaixinlin	2005.8
QT06	33.7717	92.2387	4670	10	250	Tongtianhe	2005.8
QT07	32.5766	91.8593	5133	10	-*	Taoerjiu	2005.8
QT08	35 1226	93 0673	4619	10	-*	Wudaoliang	2005.8
Ch01	34.7290	92.8946	4820	12	165	Fenhuoshan	1998.5
Ch02	35.4332	93.5988	4488	12	260	Suolandajie	1998.5
Ch03	34.4706	92.7270	4620	12	280	Wuli	1998.5
Ch04	31.8180	91.7368	4850	12	115	Liandaohe1	1998.5
Ch05	31.8180	91.7368	4808	12	240	Liandaohe2	1998.5
Ch06	35.6212	94.0625	4750	12	145	Konlongshan	1998.5

* apparatus had been destroyed

Water-Heat Changes in Active Layer During the Freeze-Thaw Processes

Ground temperature changes

According to the annual freeze-thaw processes, the annual variations in the active layer can be divided into four stages: summer thawing stage, autumn freezing stage, winter temperature-falling stage, and spring temperature-rising stage (Zhao et al. 2000). In this environment, during the summer thawing stage the interior of the active layer had a positive ground temperature gradient, the ground temperature was significantly higher in the shallow layer than in the deep layer, the active layer and the underlying permafrost were in a heat-absorbing state, and the internal temperature exhibited a rising trend. Generally, several days after the atmospheric temperature reached the annual maximum value, the ground temperature below the depth of 10 cm also reached the annual maximum value. With an increase in active layer depth, the time at which the annual ground temperature in different horizons reached the maximum value was delayed. As the climate turned cold and the ground surface temperature fell below 0°C, the active layer entered the autumn freezing period and the ground temperature gradient became negative. The ground temperature was higher in the deeper layer than in the shallower layer, the active layer started to release heat to the atmosphere, and the ground temperature started to drop. Other studies have shown that both the positive and negative ground temperature gradients in the active layer could be maintained for more than 100 days, while the period of no ground temperature gradient lasts only 10–30 days or so in the autumn freezing process and spring temperature thawing period (Ding et al. 2000). Figure 1 is the pattern of annual ground temperature variations at different depths in the active layer of permafrost at the CN1 observation point on the QTP in 2003. The thickness of the active layer in 2003 was 147 cm.

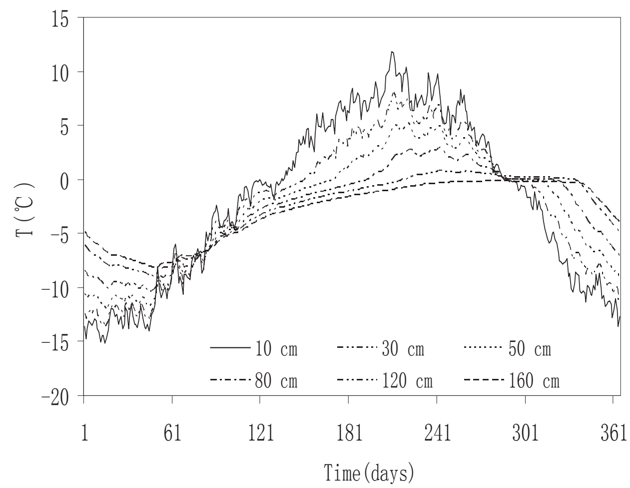

Figure 1. Pattern of annual ground temperature variations at different depths in the active layer of permafrost at CN1 point on the QTP in 2003(the temperatures at 12 levels were measured and the graph showed the data of 6 levels).

Figure 2 shows the ground temperature isoline in the active layer of permafrost at the CN1 observation point in 1999 and 2006. The observation point is located at the north slope of Mt. Fenghuoshan on the QTP, where continuous permafrost exists. It can be seen that the curves are wide near the 0°C isoline, suggesting that the transformation of the two phases of ice and water during the thawing and freezing course is a slow process, and during the process the soil temperature is prolonged at 0°C. But as the soil is entirely thawed or frozen, the isoline density obviously increases, and the ground temperature variation with time significantly speeds up. It can be seen from the annual variation of the 0°C isoline that about 100 days or more were required for the active layer to thaw entirely, but to freeze-back to the surface only required 10 days or so. The statistical results at different observation sites on the QTP show that the thawing time was far larger

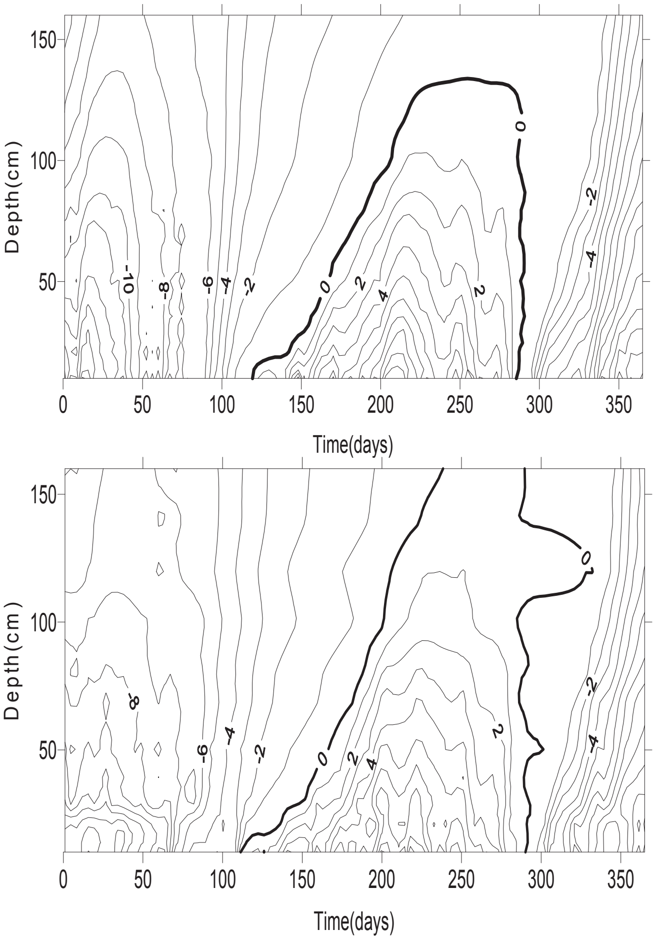

Figure 2. Ground temperature isoline at the different depth in the active layer of permafrost at CN1 observation point on the QTP in 1999 (upper) and 2006 (lower).

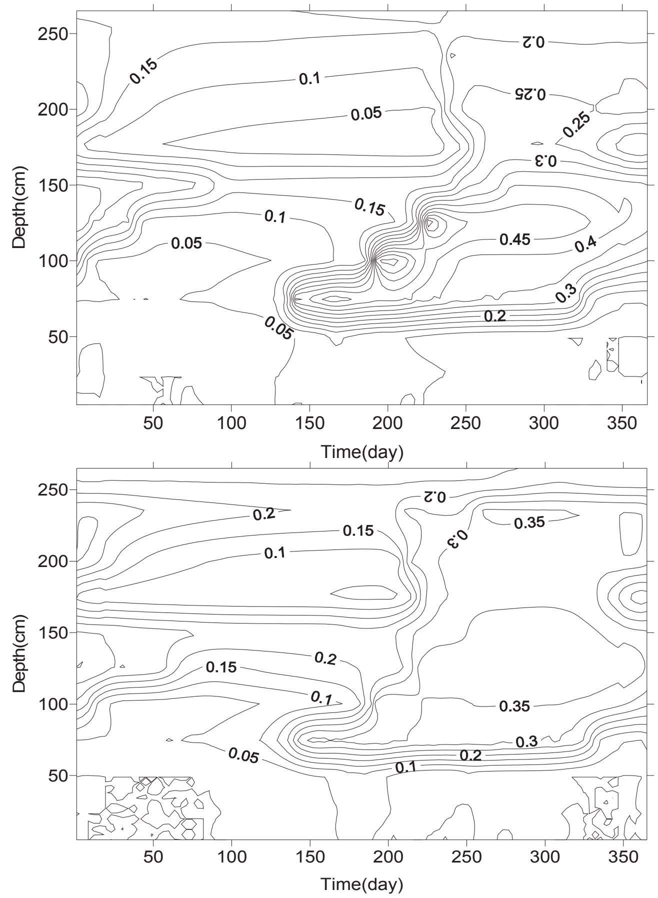

Figure 3. Soil water isoline at different depth in the active layer of permafrost at CN2 observation point on QTP in 2000 (upper) and 2006 (lower).

than the freezing time, but in some other places, such as in northeastern China, the freezing time of the active layer is approximately as long as the thawing time (Zhou et al. 2000).

Water change during the thawing process

As the frozen soils started to thaw, the solid water changed into liquid water and was redistributed in the active layer. In the meantime, activities of precipitation and evaporation, etc., in the active layer took place. Due to the limitations of the equipment, the soil water study in this paper was confined to the changes in liquid water; solid water cannot be discussed. Figure 3 shows the soil water isoline at CN2 in 2000 and 2006. It can be seen that the density of isolines during the soil freezing or thawing periods is very high. Water content changes rapidly near the thawing or freezing front. During the thawing period the soil water content increases rapidly, while in the freezing period it decreases quickly. The correlation statistics of soil temperature and water data at different depths and different observation points show that as the ground temperature drops belows 0°C, soil water gradually increases, with increasing ground temperature, and reaches a maximum value at a ground temperature of 0°C. As the ground temperature exceeded 0°C, soil water tended to decrease with increasing ground temperatures (Fig. 4). It can be seen from Figure 4 that the water contents at different horizons in the active layer all reached a maximum value at a ground temperature of 0°C; as the soil temperature exceeded 0°C, soil water tended to decrease, and such a trend was quite obvious in the shallow soil layer.

This phenomenon can be explained as follows: first, instrumentation can only measure liquid water as the frozen solid water gradually melts and the ground temperature gradually approaches 0°C, the percentage of liquid water continuously increases until it is entirely changed into liquid water. The changes in water content in 0°C soil are mainly caused by this process. Second, it results from the water-heat coupling action during the thaw-freeze period of the active layer. The simultaneous transfer process of water and heat in the active layer is called the water-heat coupling process. In this process, material (water) and energy are transferring simultaneously (Zhao et al. 2000). The temperature gradient is an important factor controlling the soil water transfer.

As soil is entirely thawed, gravity promotes water infiltration; when the ground temperature gradually rises to form a ground temperature gradient, water will migrate

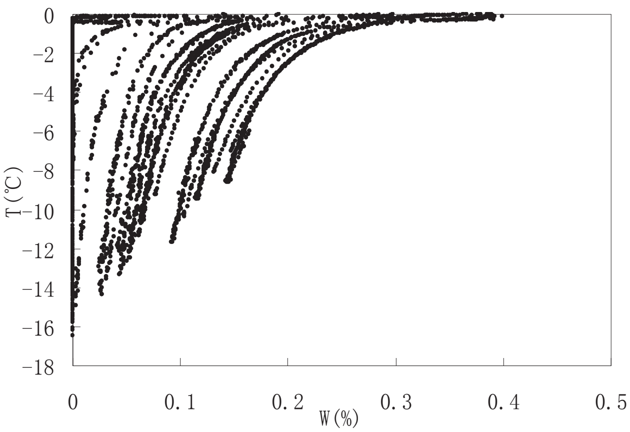

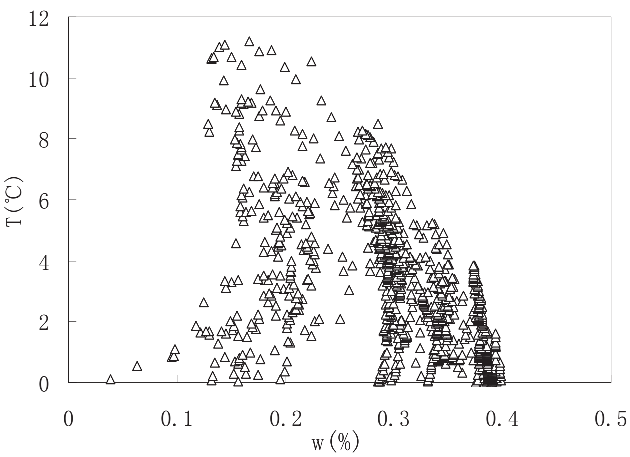

Figure 4. The scatter diagram showing the change trend of water content when soil temperature is below 0°C (upper) and above 0°C (lower) in the active layer of permafrost on QTP (CN1 observation point in 1999).

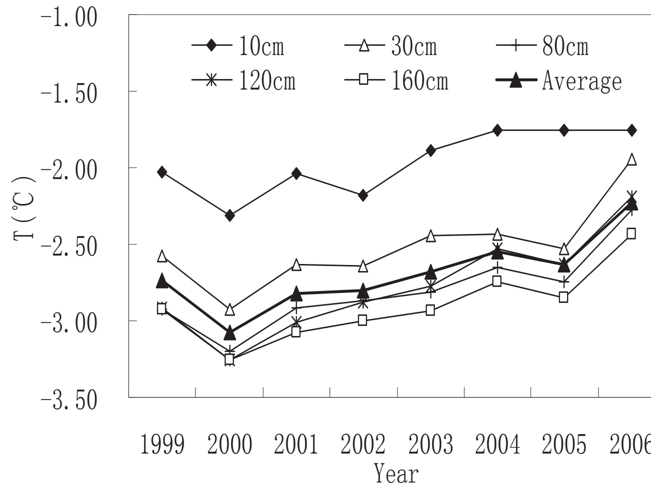

Figure 5. Change of the ground temperatures at different levels during 1999–2006 in CN1 observation site (the temperatures at 12 levels were measured and the graph showed the data of 5 levels and the average value of 12 levels).

to the ground surface; this results in water concentration at the freezing front. Soil water migration in any form is accompanied by heat transfer. This can be clearly seen from the isoline changes in Figures 2 and 3.

Water-Heat Changes and Their Hydrological Effects in Recent Years

As the thickness of the active layer increased, the temperature in it also continuously rose. Taking the CN1 site as an example, the temperature in the active layer at this area has been recorded since May 1998. The statistics of annual mean temperature at different horizons show that the temperature at various horizons rose at different rates over the last 10 years (Fig. 5). The ground temperature at the bottom of the active layer exhibited a steady temperature-rising trend, while that of the shallow layer was more variable.

As viewed from the fluctuated variations of ground temperature at different horizons, in September the rising trend of ground temperature close to the permafrost table could not be affected by the annual fluctuation changes of air temperature, while the variations in the upper active layer apparently coincided with the fluctuation changes of annual mean air temperature. Of course, viewed from the annual mean value of ground temperature, the ground temperature at the bottom of the active layer could be affected by annual air temperature fluctuations.

In December, the general trend of the ground temperature fluctuation changes in the deep layer was consistent with that in the shallow layer. The main reason for this is that the downward transfer of surface heat is a slow process. When the thawing reaches a maximum value in September, the temperature at the lowest part of the active layer still changes. Statistical data reveal that the mean ground temperature in the active layer at the CN1 observation point increased by 0.4°C since 1998, the rising amplitude of ground temperature was significantly higher in the deep layer than in the shallow layer (Fig. 5). The largest rise in temperature occurred at a depth of 120 cm. The freezing time at this depth also significantly changed. It can be seen from Figure 2 that soil at a 120 cm depth froze in the middle of September 1999, and the duration of ground temperature higher than 0°C was 71 days. In 2006, this duration increased to 124 days, while the freezing period was delayed to the end of November, and the thickness of the active layer exceeded the initial observed depth.

Measured data indicate that the 120 cm depth was the horizon with the highest moisture content, and it also had the highest heat storage. Climate warming leads to an increase in energy input in the active layer, but energy storage delays the freezing time of the region with the highest water content. If the annually received energy is persistently greater than the released energy during the freezing period, the winter freezing front cannot reach the bottom of the active layer and therefore a discontinuous layer can be formed in the active layer. The presence of the discontinuous layer will further promote the downward migration of water and thus change the spatial distribution pattern of water in a permafrost region. This is one of the most striking feedbacks of the water-heat coupling process.

Analysis on the vertical profile in the active layer in recent years shows that the water distribution in the active layer has changed and is triggered by a rise in ground temperature. The downward transfer of originally stored water in the dry and shallow soil layer caused the downward migration of the water-enriching zone. A comparison of water isolines of 2000 and 2006 at CN2 point is shown in Figure 3. It can be seen that in 2000 the soil water-enriching zone was located at a depth of 100–150 cm, and the maximum water content was 60% or so (volumetric ratio). As the depth of the active layer increased from 235 cm in 2000 to 270 cm in 2006, the soil water content in the 100–150 cm layer decreased below 40%, while the water content in the 200–250 cm soil layer, which originally had a lower water content, greatly increased, thereby forming two soil water-enriched zones. As a rule, the increase in active-layer thickness led to soil water migration from the shallower layer to the deeper layer, and the downward migration of water carried more heat to the bottom of the active layer. Therefore the freezing time of the bottom of the active layer was delayed and the thickness of the active layer further increased.

Conclusion

It can be seen from the above analysis that under the background of climate warming the increase in active-layer thickness and the rise in ground temperature are favorable to downward migration of soil water. In turn, the water heat coupling action causes a positive feedback to active-layer changes. The intensification of the downward migration trend of soil water will inevitably lead to a decrease in surface runoff yield and an increase in regional groundwater storage. The decrease in surface soil water content strengthens the infiltration of precipitation; on the other hand it promotes soil water loss to evaporation. In one word, the rise in ground temperature in the active layer and the increase in active-layer thickness are unfavorable to the storage of surface water resources in the permafrost, and they likely have a negative effect on regional runoff yield. Of course, this final point needs further study.

Acknowledgments

We would like to express our gratitude to the Cryosphere Research Station on the Qinghai-Tibet Plateau, Chinese Academy of Sciences, for the observation data collection and logistic support. This work was supported by a grant from the Major State Basic Research Development Program of China (973 Program, No.2007CB411506) and the Chinese National Fundamental Research Program (No. 40701029).

References

Burn, C.R. 1998. The Active Layer: Two contrasting definitions. *Permafrost Periglac. Process.* Vol 9: 411-416.

Charles T., Nixon, F.M. & Kutny, L. 2004 Circumpolar-Active-Layer-Monitoring (CALM) sites in the Mackenzie Valley, Northwestern Canada. *Permafrost and Periglac. Process.* 15: 141–153.

Ding, Y.J., Ye, B.S., Liu, S.Y. et al. 2000. Macro-scale monitoring study of permafrost hydrology in Tibetan Plateau. *Bulletin of Science* Vol. 45(2): 208-214.

Osterkamp, T.E. & Romanovsky, V.E. 1997. Freezing of the active layer on the coastal plain of the Alaskan Arctic *Permafrost Periglac. Process* Vol. 8: 23-44.

Perfect, E. & Williams, P.J. 1980. Thermally induced water migration in frozen soils. *Cold Region Science and Technology* Vol. 9(3): 101-109.

Tong ,C.J. & Wu, Q.B. 1996. The effect of climate warming on the Qinghai-Tibet Highway. *Cold Regions Science and Technology* Vol. 24: 101~10.

Wu, Q.B., Lu, Z.J. & Liu, Y.Z. 2005. Permafrost monitoring and its recent changes in Qinghai-Tibet Plateau. *Advances in Climate Change Research* Vol. 1(1): 26-28.

Yang, Z.N., Liu, X.R., Zeng, Q.Z. et al. 2000. *Frozen Soil Hydrology in China.* Beijing: Science Press, 90-12.

Zhao, L, Cheng, G.D., Li, S.X. et al. 2000.Thawing and freezing processes of active layer in Wudaoliang Region of Tibetan Plateau. *Chinese Science Bulletin* Vol. 45(23): 2181-218

Zhou, Y.W., Guo, D.X., Qiu, G.Q. et al. 2000. *Geocryology in China.* Beijing: Science Press: 37-41.

Variation of Atmospheric Methane Over the Permafrost Regions from Satellite Observation During 2003 to 2007

Xiaozhen Xiong
Perot Systems Government Services, Fairfax, Virginia; and Satellite Meteorology & Climatology Division, Center for Satellite Applications and Research, National Environmental Satellite, Data, and Information Service, NOAA, USA
Chris Barnet
Satellite Meteorology & Climatology Division, Center for Satellite Applications and Research, National Environmental Satellite, Data, and Information Service, NOAA, USA
Eric Maddy, Xingpin Liu
Perot Systems Government Services, Fairfax, Virginia; and Satellite Meteorology & Climatology Division, Center for Satellite Applications and Research, National Environmental Satellite, Data, and Information Service, NOAA, USA
Mitch Goldberg
Satellite Meteorology & Climatology Division, Center for Satellite Applications and Research, National Environmental Satellite, Data, and Information Service, NOAA, USA

Abstract

Thawing permafrost as a major source of climate feedback could accelerate climate change by releasing methane (CH_4) into the atmosphere. However, current estimation of CH_4 emissions from thawing permafrost or northern wetlands has large uncertainty. The Atmospheric Infrared Sounder (AIRS) on EOS/Aqua platform provides a measurement of global CH_4 in the mid-upper troposphere. Based on more than four years' AIRS data in high northern hemisphere, it is found (1) a significant CH_4 increase when the surface temperature becomes above the freezing point; (2) a decreasing trend of -1.3 ppbv/year in Canada-Alaska and -3.9 ppbv/year in Siberia from August 2003 to 2007; (3) a lower CH_4 in 2005; and (4) a possibly large unknown source in Siberia between Jan to March. This study demonstrates that a long-term monitoring of CH_4 using AIRS and other satellites will enable us to better study the CH_4 trend and its relation with thawing permafrost.

Keywords: AIRS; High Northern Hemisphere; methane; northern wetlands; thawing permafrost.

Introduction

As one of the most important greenhouse gas next to carbon dioxide (CO_2), CH_4 is about 20 times more powerful at warming the atmosphere than CO_2 by weight, and plays an important role in atmospheric chemistry. CH_4 is highly variable in the northern hemisphere, and its concentration over the globe has been observed to rise dramatically since the preindustrial era (Dlugokencky et al. 1995). However, the increase rate of CH_4 varies significantly, for example, an anomalous increase of the growth rate of CH_4 was observed in 1998, and the anomalous increase of the growth rate of CH_4 was partially attributed to wetland emission (Dlugokencky et al. 2001). As the largest single source wetlands emission contributes CH_4 around 100–230 Tg/yr (IPCC, 2001), which represents ~20–45% of total methane emissions (~500 Tg/yr). However, the emission of CH_4 from wetlands is dominated by climate, and as demonstrated from model simulations, ±1°C changes in temperature could lead to ±20% changes in the CH_4 emission from wetlands, and ±20% changes in the precipitation alter CH_4 emission by about ±8% (Walter et al. 2001).

The permafrost thaw beneath wetlands and lakes may enhance methane production and emission by biological decomposition of organic matter previously sequestered in permafrost. i.e., permafrost degradation may lead to environments that produce methane. Since the Arctic is vulnerable to climate changes, the accelerated thawing of subarctic peatland permafrost, as observed in the discontinuous permafrost zone of northern Canada (53–58°N) over the last 50 years (Payette et al. 2004), may lead to the increase of CH_4 emission to the atmosphere. Field measurements showed that CH_4 emission from mires increased by about 22–66% over the period of 1970 to 2000 and this increase was associated with the permafrost and vegetation changes (Christensen et al. 2004). The world's northern wetlands as a much larger source of CH_4 were observed to release more CH_4 into the atmosphere than previously believed. For instance, Walter et al. (2006) observed a large emission through ebullition from Siberia thaw lakes, which increases present estimates of CH_4 emissions from northern wetlands by 10 to 63%. The thawing permafrost along the margins of the thaw lakes is the primary source of CH_4 released from the lake. Since the impacts to CH_4 emissions from northern wetlands and thawing permafrost are hard to isolate, later in this paper we just refer to emissions from these regions in the High Northern Hemisphere (HNH) as emissions from wetlands/thawing permafrost.

Current ground-based measurements of CH_4 emissions and CH_4 concentration in the atmosphere are sparse and not representative at large scales, particularly in the subarctic wetlands and permafrost regions. Sampling of the vertical variation of CH_4 in the atmosphere is much more sparse than current ground-based measurement. Therefore, space-borne measurements are crucial, as they provide the large spatial and temporal coverage needed to help us better understand the variation of CH_4 and its relation with surface emission in hemispheric scale. CH_4 in the middle atmosphere to near the tropopause region was observed from Halogen Occultation Experiment (HALOE) measurement on Upper Atmosphere Research Satellite *(*UARS*)*, and its most sensitive region is in the stratosphere to near tropopause (Schoeberl et al. 1995, Park et al. 1996). CH_4 total columns were recently observed by the SCanning Imaging Absorption spectroMeter for Atmospheric CHartographY (SCIAMACHY) instrument on board the European Space Agency's environmental research satellite (ENVISAT) (Frankenberg et al. 2005). Compared with SCIAMACHY which uses the absorption spectra of solar radiation in the near-infrared, AIRS is a nadir cross-track scanning infrared spectrometer on EOS/AQUA with 2378 channels at high spectral resolution (Aumann et al. 2003), and is most sensitive to CH_4 in the middle to upper troposphere. Moreover, the sensitivity of SCIAMACHY in the HNH is worse than that in lower latitudes due to large solar zenith angles at high latitudes. A combination of both AIRS and SCIAMACHY may provide more information on the CH_4 than either of them separately, but to combine these two data sets to derive CH_4 requires taking into account their difference in spatial resolution and many other aspects and is outside the scope of this paper.

This paper attempted to utilize AIRS observation of CH_4 from August 2003 to 2007 to investigate its seasonal variations and trend in the HNH, particularly in Canada, Alaska, and Siberia which are mostly underlain by wetlands and permafrost. The relation between AIRS CH_4 with surface temperature is also investigated. Through a combination of AIRS data with model simulation, a trend in the past four years was derived. This study demonstrates the value of satellite observations of CH_4 to the study of the effect of permafrost on climate change. However, it is still preliminary considering some uncertainties and caveats in current retrieval, the limited validation in the HNH and only a few years' data available.

Data and Method

AIRS on EOS/AQUA is a nadir cross-track scanning infrared spectrometer with about 200 channels near the absorption band of CH_4 around 7.6 μm at high spectral resolution ($\lambda/\Delta\lambda = 1200$, ~0.5 cm^{-1}), and the noise equivalent change in temperature (NeΔT), referred to 250K target temperature, ranges from 0.14K in the critical 4.2 μm lower tropospheric sounding wavelengths to 0.35K in the 15 μm upper tropospheric sounding region (Aumann et al. 2003). The spatial resolution of AIRS is 13.5 km at nadir, and in a 24-hour period AIRS nominally observes the complete globe once per day and once per night. In order to retrieve CH_4 in both clear and partial cloudy scenes, 9 AIRS pixels in the footprint of an Advanced Microwave Sounding Unit (AMSU) pixel are used to derive the cloud cleared radiance in this field of regard (FOR), from which the retrieval is made with the spatial resolution of about 45 km. The atmospheric temperature profile, water profile, surface temperature and surface emissivity required as inputs in CH_4 retrieval are derived from other AIRS channels.

A detailed description of CH_4 retrieval from AIRS can be obtained from Xiong et al. (2007), in which over 70 AIRS channels sensitive to CH_4 but less sensitive to water vapor and HNO_3 are selected for CH_4 retrieval. The most sensitive region is in the middle to upper troposphere at about 300–400 hPa in the HNH. Validation using *in situ* aircraft observations of NOAA Earth System Research Laboratory, Global Monitoring Division (ESRL/GMD) shows the bias of the retrieved CH_4 profiles is -1.4% ~ +0.1% and its rms difference is about 0.5–1.6% (Xiong et al. 2007). In this paper, the AIRS data in the retrieval are in 3 x 3 degrees in latitude and longitude.

Data of *in situ* observation of CH_4 mixing ratio at the Marine Boundary Layer (MBL) at Barrow, Alaska are obtained from *ftp://ftp.cmdl.noaa.gov/ccg/ch4/in-situ/brw* (GLOBALVIEW-CH_4, 2005). The global CH_4 concentration data from transport model simulations, as reported by Houweling et al. (2006), were obtained using a source scenario (S3) as input to the atmospheric transport model TM3 (Heimann & Körner 2003). Model simulations have been performed on 3.75° x 5° for the period 2001–2004 with meteorological fields derived from the NCEP reanalysis (Kalnay et al. 1996).

Due to the change of information content inherent in the infrared observation, which is related to the atmospheric temperature-moisture profiles, the averaging kernels have to be used to convolve the model data as below (Rodgers 2000, Xiong et al. 2007):

$$\hat{x} \approx Ax + (I - A)x_a \tag{1}$$

where $\hat{x}$ is the convolved CH_4 mixing ratio profile, x is the profile from model simulations, and x_a is the first-guess profile ("*a priori*"), which is a function of latitude and pressure but does not vary with time and longitude (Xiong et al. 2007). I is the identity matrix, and A is the averaging kernels (Maddy & Barnet 2007). Difference between AIRS observation with the model convolved data will reflect the biases between satellite observation and the model simulation (as a "truth") but taking into account the retrieval scale associated with the variation of information content in satellite observation. To analyze the seasonal variation of CH_4 from August 2003 to 2007, the average needs to be removed for both AIRS and model data. Thus, the difference between AIRS observation and model convolved data after removing their mean values individually will remove the systematic bias between AIRS and the model. By using the model data in 2004 only and the averaging kernels from every satellite observation from August 2003 to 2007, we obtained convolved data using Equation (1). Such data can be used as a "baseline," which considers the retrieval scales but no annual variation in the "truth," to drive the trend of CH_4 from its difference with AIRS observation.

Results and Discussion

Spatial and vertical distribution of CH_4 in the HNH

In the HNH, the ground surface is usually frozen and covered by the snow in the winter and early spring, so emissions of CH_4 from the wetlands/permafrost are very low, if not zero, during this period. As snow starts to melt in the late spring, soil temperature increases above the freezing point, and vegetation grows quickly into the summer; hence, CH_4 emission starts to increase in the late spring or early summer. The maxima of CH_4 emission occurs around July (Zhuang et al. 2004)., and the most CH_4 emissions from wetlands/thawing permafrost occur in June, July and August (JJA). For example, Figure 1 shows the averaged distribution of AIRS CH_4 at 200–300 from June to August 2004 in North America and Eurasia, respectively. It is evident that CH_4 is enhanced in Siberia and Canada-Alaska, which are mostly underlain by wetlands and permafrost. For further analysis, we chose two regions in Canada-Alaska (60–70°N, 165–90°W) and Siberia (50–70°N, 75–170°E).

The seasonal variation of mean CH_4 profiles averaged in Canada-Alaska and Siberia from 2004 to 2007 is shown in Figures 2a and 2b, respectively. Since the sensitivity of AIRS is low in the lower troposphere and stratosphere, the profiles shown are from 150 to 500 hPa only. Here, only the daytime profile (from the ascending node at 1:30pm LST) of each day is used, as the information content of AIRS in daytime is relatively larger than that in the nighttime (Xiong et al. 2007). Evidently, CH_4 starts to increase from June to August in both Canada-Alaska and Siberia. However, the maxima of CH_4 occurs in early spring in Siberia, which is possibly due to the leakage of natural gases, and worthy of further study. In late spring, CH_4 observed from AIRS is low, which is consistent with ground-based measurement of CH_4 in Barrow, Alaska. As indicated by Dlugokencky et al. (1995), the reason for the low CH_4 in late spring can be attributed to the break-down of atmospheric inversion in the HNH, allowing dilution of northern air with the air from the upper level.

Seasonal variation of CH_4 in the HNH from August 2003–2007 and its relation with surface temperature

Figure 3 shows the seasonal variation of CH_4 at 300 hPa (after removing the average) from AIRS observation and models from August 2003 to 2007. Here the model data are fixed in 2004, and then convolved using the averaging kernels corresponding to each AIRS observation. One common feature at both regions is the increase of CH_4 in June every year. The period for the increase of CH_4 has a good correlation with the increase of surface temperature (*Tsurf*). The decrease of CH_4 in the summer also follows the decrease of surface temperature, but with a delay of about 2–3 weeks.

Compared to the model convolved data in 2004, CH_4 from AIRS in Canada-Alaska is much higher than that from the model, which may be associated with the large forest fires in 2004. In Siberia, the maxima of CH_4 from AIRS occur mostly from January–March each year, and they are much higher than those from model convolved data. This large difference between AIRS and the model indicates a possible unknown, strong source occurring in the winter to early spring in Siberia. One possibility is the gas leakage in Siberia, and this gas leakage or other sources are not well characterized in the model, if they are included at all.

Trend of CH_4 in the HNH and its relation with surface temperature

Figure 4 shows the difference of the seasonal variation (after removing the mean) of AIRS CH_4 minus the model convolved data and the trend. Since most emissions occur from May to October, the data in this period (red) are fitted

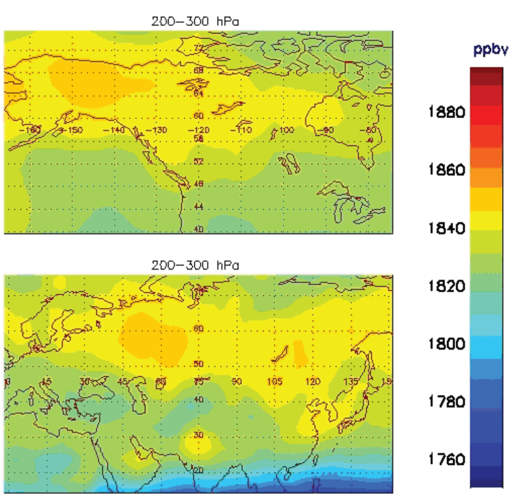

Figure 1. Seasonal averaged distribution of AIRS CH_4 in layer 200–300 hPa in June, July and August 2004 over North America (upper) and Eurasia (right). Enhancement of CH_4 CH_4 is evident over Canada-Alaska and Siberia which are underlain by wetlands and permafrost.

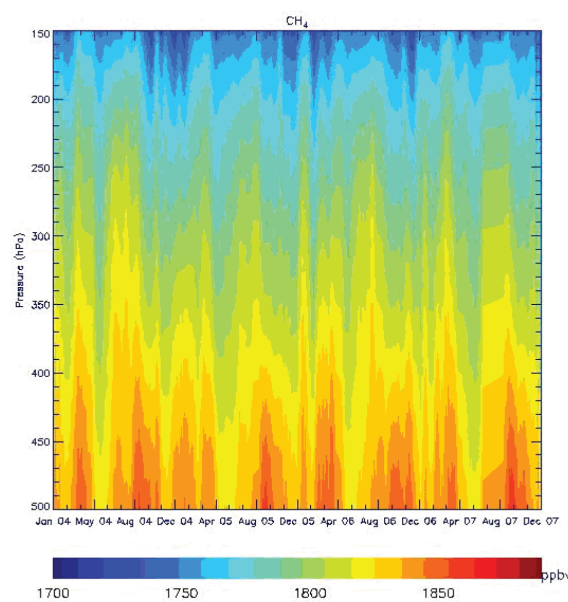

Figure 2a. Seasonal variation of CH_4 profiles (using daytime data from ascending node only) from 2004 to 2007 at Canada-Alaska.

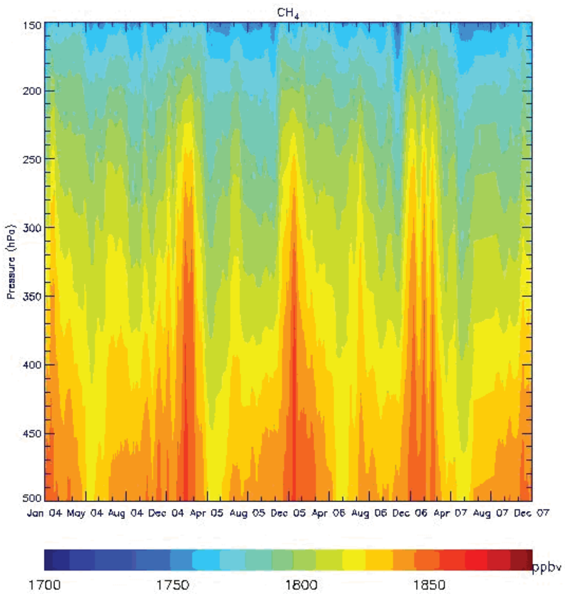

Figure 2b. Same as Figure 2a, but in Siberia.

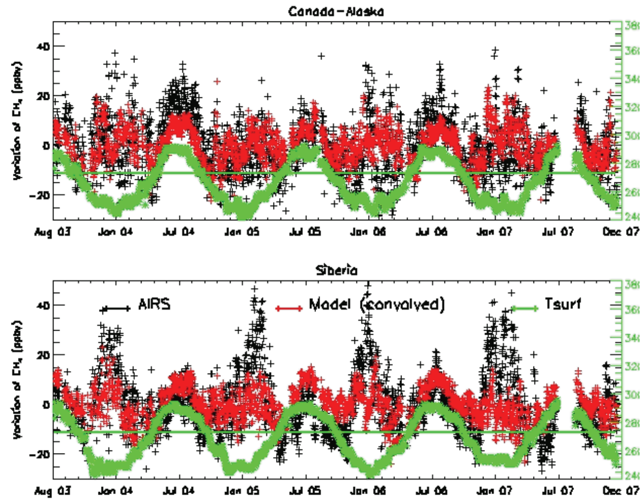

Figure 3. Seasonal variation of CH_4 (300 hPa) from AIRS (black), model convolved (red), and surface temperature (Tsurf, green) at Canada-Alaska and Siberia. There is a good correlation between CH_4 and Tsurf in the summer.

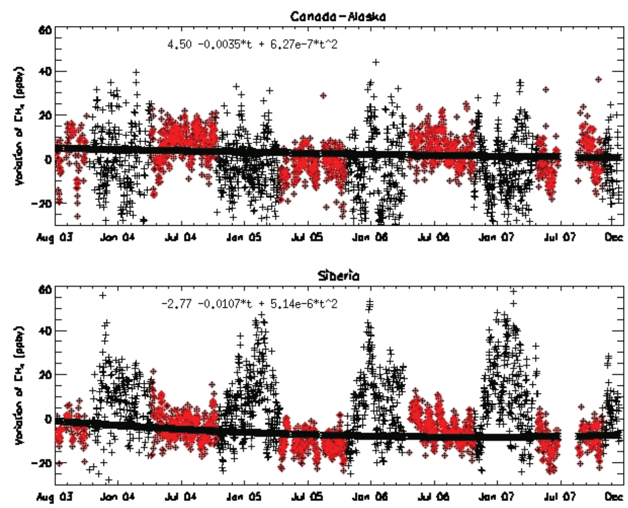

Figure 4. Trend of CH_4 (300 hPa) derived as the difference of AIRS observation minus the model convolved data (model data are fixed to 2004) at Canada-Alaska and Siberia. Black solid lines are the second-order polynomial fitting to their differences from May to October (red), and the legends are the equations.

using a second order polynomial of date (starting from Aug. 6, 2003), as shown in the solid line. The equations are given in the legends of Figure 4. The CH_4 trend is about -1.3 ppbv/year in Canada-Alaska and -3.9 ppbv/year in Siberia.

We note that in Figure 4, in the summer of 2005, CH_4 is biased lower than the fitting in both regions. This indicates that CH_4 emission in 2005 is smaller than that in 2004 and 2006. If this argument, based on satellite observation, is reasonable, lower CH_4 in 2005 may exist in the ground-based observation since its variation has a closer link with surface emission than CH_4 in the mid-upper troposphere observed by satellite. Therefore, we analyzed the seasonal variation of CH_4 measured by NOAA/ESRL/GMD in Barrow, Alaska and the surface temperature retrieved from AIRS. The hourly CH_4 observed at MBL were used to compute the daily average in Figure 5 (upper panel). In agreement with AIRS observation, CH_4 at the MBL in the summer of 2005 is lower than that of 2004 and 2006. Analysis of surface temperature provides more evidence to lower emission of CH_4 from high northern wetlands/thawing permafrost in 2005 as the surface temperature from June to September in 2005 is lower than that at 2004 and 2006 (Fig. 5). Further study of the trend of CH_4 emission from high northern wetlands/permafrost from model simulations may help to validate whether this observed trend from AIRS is reasonable.

Uncertainty analysis

It is important to keep in mind some uncertainties and caveats in current AIRS retrievals and limited validation made in the HNH. As addressed in Xiong et al. (2007), the uncertainty of CH4 retrieval corresponding to a noise equivalent bias in AIRS radiances can be evaluated by putting a noise equivalent bias to the observed radiance in CH4 channels, and then comparing the differences in their retrieved profiles. As an example, Figure 6 (upper left panel) shows the mean retrieved bias resulted from a noise equivalent bias based on two days' AIRS data (in 3 x 3 degree) in the HNH above 50°N. These two days are chosen randomly, and one is Aug. 10, 2004 (summer) and another one is Feb. 15, 2005 (winter). The largest bias is 24.9±6.0 ppbv at 350–400 hPa, and below 600hPa the bias is less than 10 ppbv. The standard deviation for all cases, represented by the error bar in the figure, is mostly less than 10 ppbv. A similar methodology is used to estimate the uncertainties of retrieval due to errors in temperature-moisture profiles and surface temperature. The mean CH4 biases resulted from the AIRS temperature and moisture profile biases are mostly less than 10 ppbv. The errors in cloud clearing could be the largest source of uncertainty, however an examination to the variation of AIRS retrieved CH4 within 200 km in the same granule and its relation with cloud amount, and

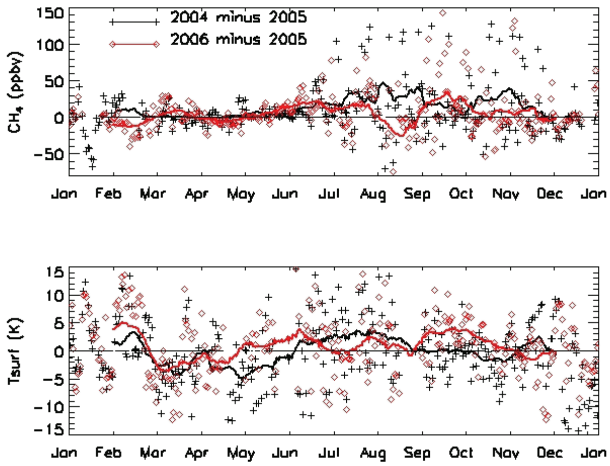

Figure 5. Difference of CH_4 at the MBL in 2004 and 2006 minus that in 2005 in Barrow, Alaska (upper). Lower CH_4 in the summer of 2005 is consistent with the lower CH_4 in the middle to upper troposphere observed from AIRS. Lower panel is surface temperature (Tsurf) in 2004 and 2006 minus that in 2005 at Canada-Alaska. Lower Tsurf from June to September in 2005 may indicate the lower emission of CH_4 from high northern wetlands/thawing permafrost in 2005.

found the difference of CH4 between clear cases (with the cloud fraction less than 0.1) and cloudy cases (with the cloud fraction over 0.8) is usually less than 1.0%. Since the magnitude of the seasonal variation of CH4 (see Fig. 3) is significantly larger than the uncertainties of the retrieval, these uncertainties should not undermine the conclusions.

We noted that there are some correlations between the retrieved CH_4 with the surface temperature and water vapor amount. Therefore, variation of water vapor and temperature profiles make the interpretation of the retrieval results complicated, and the averaging kernels have to be taken into account in the interpretation of the variation of CH_4 from AIRS, and in the comparison of AIRS with model simulation and/or other observations. A better retrieval of CH_4 also depends on a more accurate computation of radiance from the radiative transfer model, and further improvement to current model is required (Xiong et al. 2007).

It is almost impossible to isolate the impact of wetland emissions and emissions from thawing permafrost on the seasonal variation and trend illustrated above; therefore, it is hard to say whether the observed trend is related to the thawing permafrost. This will require long-term monitoring of CH_4 from satellite and more model studies.

Conclusion

Satellite observations using AIRS, show that the CH_4 in middle to upper troposphere increases in the summer in regions that are mostly underlain by the northern wetlands and permafrost, and that this increase has a good relation with the surface temperature. Preliminary analysis using AIRS observation from August 2003 to 2007, in conjunction with model simulation, shows a small but negative trend of CH_4 of -1.3 ppbv/year in Canada-Alaska and -3.9 ppbv/year in Siberia. Moreover, lower trend of CH_4 in 2005 is observed from AIRS which is in good agreement with the lower CH_4 from ground-based observation and lower surface temperature in 2005. These results have demonstrated that AIRS can provide valuable information of CH_4 in the middle to upper troposphere. Further use of AIRS CH_4 appropriately in conjunction with model simulation will provide a way to better estimate source emissions from wetlands and/or permafrost in the HNH. NOAA plans to utilize the Infrared Atmospheric Sounding Interferometer (*IASI*) (2006–2021) and the Cross-track Infrared Sounder (*CrIS*) (2009–2023) to derive atmospheric CH_4 in the same method as used for AIRS for the next 20 years. These long-term observations will be useful to monitor the trend of CH_4 associated with the thawing of permafrost and climate warming.

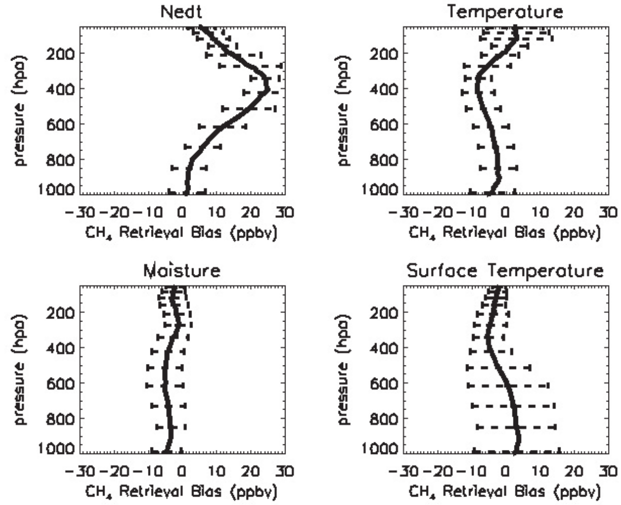

Figure 6. The mean bias of the retrieved CH_4 profiles in the HNH assuming a radiance bias equivalent to the noise of the AIRS *NeΔT* for CH_4 channels (upper left), AIRS biases in temperature (upper right) and moisture profile, and a bias in surface temperature of 2 k. Two days' AIRS data in Aug. 20, 2004, and Feb. 15, 2005 are used. Solid lines are the mean bias, and dashed lines represent the standard deviation.

Acknowledgments

This research was supported by funding from NOAA Office of Application and Research Climate Program. The views, opinions, and findings contained in this paper are those of the authors and should not be construed as an official National Oceanic and Atmospheric Administration or U.S. Government position, policy, or decision. The model data were provided by Dr. Sander Houweling at the Netherlands Institute for Space Research.

References

Aumann, H.H., Chahine, M.T., Gautier, C., Goldberg, M.D., Kalnay, E., McMillin, L.M., Revercomb, H., Rosenkranz, P.W., Smith, W.L., Staelin, D.H., Strow, L.L. & Susskind, J. 2003. AIRS/AMSU/HSB on the Aqua mission: Design, science objectives, data products, and processing systems. *IEEE Trans. Geosci. Remote Sens.* 41:.253-264.

Christensen, T.R., Johanson, T., Akerman, H.J. & Mastepanov, M. 2004. Thawing sub-arctic permafrost: Effects on vegetation and methane emissions. *Geophys. Res. Lett*. 31:L04501, doi: 10.1029/2003GL018680.

Divakarla, M., Barnet, C., Goldberg, M.D., McMillin, L., Maddy, E.S., Wolf, W.W., Zhou, L. & Liu, X. 2006. Validation of Atmospheric Infrared Sounder temperature and water vapor retrievals with matched radiosonde measurements and forecasts. *J. Geophys. Res.* 111: doi:10.1029/2005JD006116.

Dlugokencky, E.J., Steele, L.P., Lang, P.M. & Masaire, K.A. 1995. Atmospheric methane at Mauna Loa and Barrow observatories: Presentation and analysis of in situ measurements. *J. Geophys. Res.* 100: 23, 103-23, 113.

Dlugokencky, E.J., Walter, B.P., Masaire, K.A., Lang, P.M. & Kasischke, E.S. 2001. Measurement of an anomalous global methane increase during 1998. *Geophys. Res. Lett.* 28: 499-502.

Frankenberg, C., Meirink, J.F., van Weele, M., Platt, U. & Wagner, T. 2005. Assessing methane emissions from global space-borne observations. *Science* 308: 1010-1014, doi:10.1126/science.1106644.

Heimann, M. & Körner, S. 2003. The global atmospheric tracer model TM3, Max Planck Institute of Biogeochemistry, Model description and user's manual. Release 3.8a.

Intergovernmental Panel on Climate Change. 2001. Climate Change 2001: The Scientific Basis. New York: Cambridge University Press, 881 pp.

Kalnay, E. et al. 1996. The NCEP/NCAR 40-year Reanalysis Project. *Bull. Amer. Meteor. Soc*. 77: 437-471.

Maddy, E.S. & Barnet, C. D. 2008. Vertical resolution estimates in Version 5 of AIRS operational retrievals. IEEE TGRS, Accepted.

Park, J.H., Russell, J.M. III, Gordley L.L., Drayson, S.R., Benner, D.C., McInerney J.M., Gunson, M.R., Toon, G.C., Sen, B., Blavier, J.F., Webster, C.R., Zipf, E.C., Erdman, P., Schmidt, U. & Schiller, C. 1996. Validation of Halogen Occultation Experiment CH_4 measurements from the UARS. *J. Geophys. Res.* 101(D6): 10,183-10,204.

Payette S., Delwaide, A., Caccianiga, M. & Beauchemin, M. 2004. Accelerated thawing of subarctic peatland permafrost over the last 50 years. *Geophys. Res. Lett.* 31:L18028, doi: 10.1029/2004GL020358.

Rodgers, C.D. 2000. Inverse Methods for Atmospheric Sounding. *World Sci*., Hackensack, N. J.

Schoeberl, M.R., Luo, M. & Rosenfield, J.E. 1995. An analysis of the Antarctic Halogen Occultation Experiment trace gas observations. *J. Geophys. Res.* 100: 5159-5172.

Walter, B.P., Heimann, M. & Mattews, E. 2001. Modeling modern methane emissions from natural wetlands. 1. Model description and results. *J. Geophys. Res.* 106: 34,189-34,206.

Walter, K.M., Zimov, S.A., Chanton, J.P., Verbyla, D. & Chapin, F.S. III. 2006. Methane bubbling from Siberian thaw lakes as a positive feedback to climate warming. *Nature* 443: 71-75.

Xiong, X., Barnet, C.D., Maddy, E., Sweeney, C., Liu, X., Zhou, L. & Goldberg, M. 2007, Characterization and Validation of Methane Products from the Atmospheric Infrared Sounder (AIRS). *J. Geophys. Res.* doi:10.1029/2007JG000500, in press.

Zhuang, Q., Melillo, J.M., Kicklighter, D.W., Prinn, R.G., McGuire, A.D., Steudler, P.A., Felzer, B.S. & Hu, S. 2004. Methane fluxes between terrestrial ecosystems and the atmosphere at northern high latitudes during the past century: A retrospective analysis with a process-based biogeochemistry model. *J. Geophys. Res.* doi:10.1029/2004GB002239.

Numerical Analysis of a Thermosyphon Foundation of High-Voltage Transmission Towers in a Permafrost Region

Xue-yan Xu , Lin-lin Yu, Li-yue Wang
School of Civil Engineering, Harbin Institute of Technology, Harbin 150090, China

Abstract

A new-model thermosyphon foundation (the portion of thermosyphon under ground is wrapped with concrete) is applied in the project, because this special foundation can bear the loads from superstructure, preserving permafrost soil from thawing. Research contents: According to the conditions of permafrost regions and considering global warming, the thermal and mechanical finite element model of thermal pipe foundation is made with the function of thermal and nonlinear mechanical analysis of ANSYS. Temperature distributions are compared between a thermosyphon foundation and a traditional pole foundation. The thermal calculation results indicate that the natural permafrost table rises by 0.5 m, and the inner temperature lowers by 2°C, in comparison to those with a traditional foundation. This proves the distinct permafrost-preserving effect of thermal pipes. In response to the distributions of the temperature fields of ten years in permafrost regions, it is concluded that the permafrost-preserved effect of thermal pipes is in direct ratio to working years. With the increase of areas ratio, pile space, and pile length, a better cooling effect is obtained; when the spacing between thermal pipes is 4 m, the cooling effective is optimum. On the basis of the above thermal analysis, the appropriate design parameters of a thermosyphon foundation are presented.

Keywords: design parameters; global warming; permafrost-preserved effect; temperature fields; thermosyphon foundation.

Introduction

The permafrost area of the Northern Hemisphere is about 25% of the land surface. In China, permafrost is about 22.4% of the country (Zhou et al. 2000). The Direct-Current (±500 kV) Transmission Project will be built from Hu Lun Bei Er to Liao Ning Province, and it will pass across the permafrost region (Daxing'an Mountain Range, A Er Mountainous Region, and the northwest of SongNen Plain). When the project is constructed, disturbed frozen soil and the seasonally thawed layer will have great influence on the thermal regime of the permafrost region. Often permafrost in these regions is ice-rich and makes large deformation for consolidation if thawing occurs. Global warming tends to warm the permafrost in these regions and makes it susceptible to thaw. (Mingyi Zhang et al. 2005). So it is very significant and practical to study the design method to ensure the construction security and the regular service of the project.

So far, in China, systemic test research and numerical calculations have not been conducted on the combination of the bearing capacity of the foundation of the transmission tower with the permafrost-preserving effect.

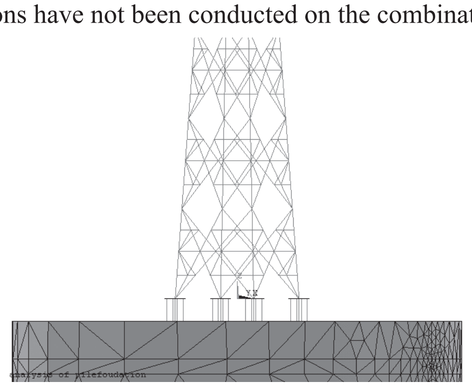

Figure 1. Sketch of the connection of tower and thermosyphon foundation.

In this paper, we consider the effect of global warming on a thermosyphon foundation (one thermosyphon pile under each tower foot, total of four) shown in Figure 1. In order to research the cooling effects of different pile spacing distances with or without a thermosyphon, we have used numerical modeling by ANSYS. Some numerical simulations are carried out during the course of this study. Namely, the temperature fields of a traditional pile foundation and a thermosyphon foundation have been analyzed under the assumption that the average atmosphere temperature will be warmed by 1°C in 10 years.

Governing Equations, Numerical Model, and Boundary Conditions

The thermal convection of foundations is the process of heat transfer. In the analysis, circular cylindrical coordinates are introduced and then the corresponding governing equations as follows (Yuanming Lai et al. 2004).

Energy: $$\rho c \frac{\partial T}{\partial t} + \rho_w c\left(u_z \frac{\partial T}{\partial z} + u_r \frac{\partial T}{\partial r}\right) = \lambda\left(\frac{\partial^2 T}{\partial z^2} + \frac{\partial^2 T}{\partial r^2}\right) + s_3 \tag{1}$$

where c and λ are specific heat and coefficient of heat conductivity separately, T is temperature, t is time, and s_3 is heat source of the whole system.

Continuity and energy:

$$\lambda_f \frac{\partial T_f}{\partial n} - \lambda_n \frac{\partial T_u}{\partial n} = L\rho \frac{\partial \xi}{\partial t} \tag{2}$$

Table 1. Thermal-physical parameters of soil used in numerical simulation.

	Temp. (℃)	-10	-5	-2	-1	-0.5	0	15
Fine sand	ρ(kg/m³)	1680	1680	1680	1680	1680	1680	1680
	W_u(%)	0.44	1.1	1.76	3.3	4.84	22	22
	λ(J/m · ℃ · h)	5760	5760	5760	5760	5760	4680	4680
Marl soil	ρ(kg/m³	1600	1600	1600	1600	1600	1600	1600
	W_u (%)	2.2	5.4	6.3	7.4	8.1	30	30
	λ(J/m · ℃ · h)	5004	5004	5004	5004	5004	2304	2304
Mud stone	ρ(kg/m³)	1890	1890	1890	1890	1890	1891	1890
	W_u (%)	4.4	5.5	6.6	7.7	8.8	35	35
	λ(J/m℃ · h)	8640	8640	8640	8640	8640	5544	5544

$$T_f(\xi(t), t) = T_u(\xi(t), t) = T_m \tag{3}$$

where *f* and *u* indicate frozen state and thaw state separately. *t* is time; *L* is critical heat; ξ is interface between freeze and thaw; T_m is the temperature of freezing front; *n* is normal vector of frozen-thaw interface.

In this study, numerical solutions are obtained using a two-dimensional finite ANSYS model through the function of the thermal and nonlinear mechanical analysis.

According to the engineering geological exploration and requirements of The Direct-Current (±500 kV) Transmission Project, the simplified computational domain including thermosyphon foundation is shown in Figure 2, 18 m depth, 30 m width, the distance between two thermosyphon foundations is 6 m. And there are no thermal flows on boundaries E–F and D–G; that is, $q = 0$.

The thermal-physical parameters of the three kinds of soils (A, B, and C) used in numerical simulation are shown in Table 1.

The temperature at the native surface E–D is changed according to the follow expression:

$$T_a = -1.0 + \frac{1}{50 \times 365 \times 24} t + 10 \sin\left(\frac{2\pi}{8760} t + \frac{\pi}{2}\right) \tag{4}$$

where, *t* is working time of the thermosyphon foundation, and is given in hours for ten years.

The temperature on the sub-permafrost boundary (18 m depth) F–G is -2.5°C.

In this study model, the thermosyphon Φ 89 (7.5 m long totally) is simplified to a 7.5 m long line, and divided into three parts, and the finite width in computation area is concrete in the results Figures 6a–h. The first one is aboveground (1.5 m length), that is, the condensation part; the second one is 3.0 m underground, which is heat-insulating; the third one, the bottom part, namely the evaporation part, is 3.0 m, and when air temperature is higher than the temperature of the thermosyphon foundation, its density of heat flow is 0; on the contrary, it starts to work, and then the density of heat flow changes as the air temperature does, and the refrigerating output per second is changed according to the following expression:

$$q = \frac{T_s - T_a}{R_s + R_f} \tag{5}$$

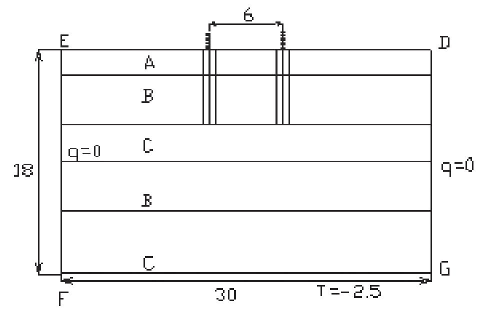

Figure 2. The simplified computational domain. A is fine sand; B is marl soil; C is mud stone (unit: m).

where, q is refrigerating output per second, T_s is average ground temperature, T_a is air temperature, R_s is thermal resistance on the soil-syphon interface, R_f is thermal resistance of the radiator on the air-syphon interface (cooling portion).

$$R_f = 1 / A\alpha \tag{6}$$

where, A is the effective area of the cooling portion of the thermosyphon; α is the heat-release coefficient of the cooling portion of the thermosyphon.

$$R_s = \frac{\ln\left(2r / D\right)}{2\pi\lambda L_e} \tag{7}$$

where, D is the outside diameter of the thermosyphon; L_e is length of cooling portion of the thermosyphon; λ is the coefficient of heat conductivity of the soil; r is the maximum radiator of area influenced by the thermosyphon.

The heat transfer quantity of the thermosyphon bar is expressed as follows:

$$Q = M \Delta T(t) \tag{8}$$

where, Q is heat transfer quantity, M is heat transfer quantity, and it is altered as follows:

$$M = \begin{cases} \dfrac{1}{R_s + R_f} & T_a - T_s \geq 1 \\ 0 & T_a - T_s \leq 1 \end{cases} \tag{9}$$

ΔT(t) is the difference in temperature between soil around the thermosyphon foundation and the inner thermosyphon.

In this analysis, the 10-year simulation starts on July 15, 2007, when the high-voltage transmission tower is applied according to the requirements of the project. We choose the representative calculation results on autumnal equinox and spring equinox. On autumnal equinox, the seasonal thaw layer is the deepest, and the thermosyphon works because of the temperature difference; on spring equinox, the active layer is frozen totally, and the thermosyphon stops working.

Numerical Results and Comparisons

Characteristics of the temperature fields of thermosyphon foundation

The temperature field of (traditional) foundation is shown in Figure 3. It can be seen that the initial temperature distribution is even in the same soil layer. The temperature field in Figure 3 also shows the temperature field of traditional foundation.

Figures 4 and 5 are the temperature distributions of soil next to a traditional foundation and a thermosyphon foundation on autumnal equinox and spring equinox along depth. It is evident that the natural permafrost table rises by 0.5 m and the average temperature decreases by 2°C due to the permafrost-preserving effect of the thermosyphon foundation.

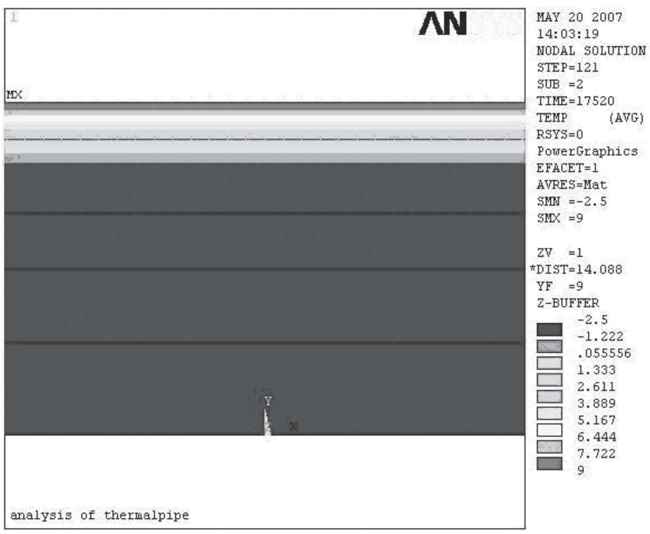

a) Isotherm of autumnal equinox.

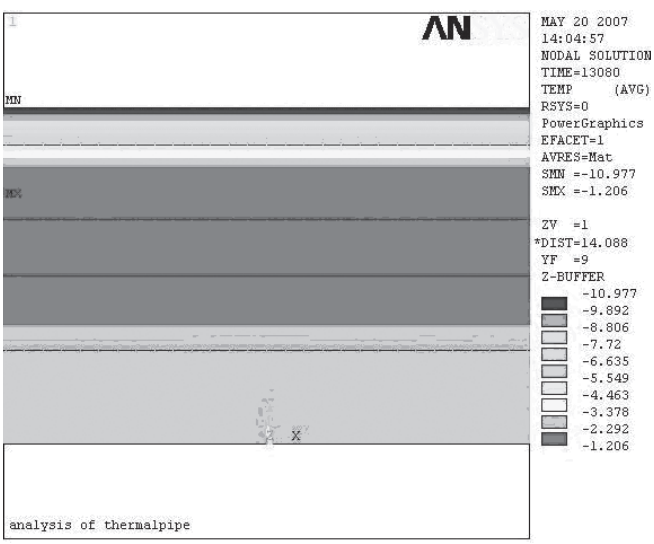

b) Isotherm of spring equinox.

Figure 3. Temperature field of (traditional) foundation.

Figures 6a–6f separately display isotherms of the thermosyphon foundation on autumnal equinox and spring equinox in the second, fifth, and tenth working year. From Figure 6b, it can be seen that the isotherms of the thermosyphon foundation change in evidence, which reveals that the thermosyphon has worked; however the affected region is only as big as twice the diameter of the thermosyphon foundation on the first spring equinox after the first cold season.

As shown in Figures 6a, 6d, and 6f, with the working years going, the influenced region surrounding the thermosyphon foundation has become wider and deeper and relative temperatures descend obviously, especially for the soil layers around the bottom of the thermosyphon foundation; so it is demonstrated that the cooling effect becomes more powerful.

From Figures 6a, 6c, and 6e, because of the heat-absorbing effect of the evaporation part of the thermosyphon, there is an approximate elliptic low-temperature (isotherm of -4.2°C to -4.9°C) region, and we can state that cold power stored in the soil near the thermosyphon foundation increases greatly; therefore, the stability of the foundation can be protected effectively from rising air temperatures in permafrost regions.

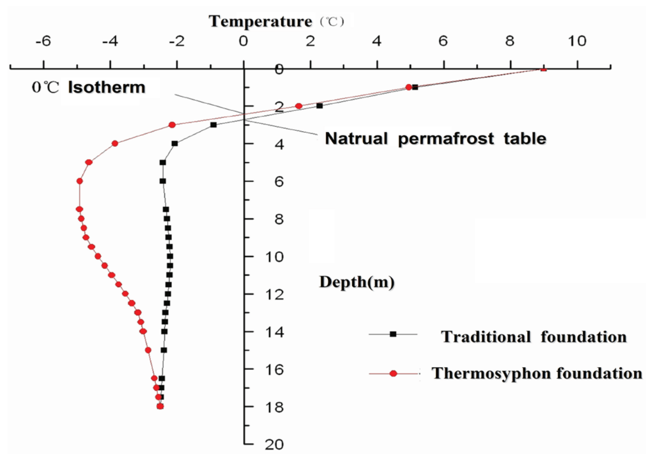

Figure 4. Temperature distributions of the two kinds of pile foundations on autumnal equinox.

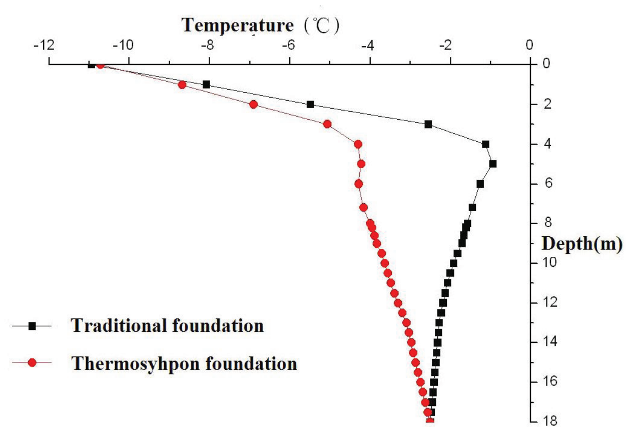

Figure 5. Temperature distribution of the two kinds of pile foundations on spring equinox.

Figures 6a–6f show that it is obvious that the cooling effect of the thermosyphon foundation gets stronger and better as working time goes, per annum. Through each cold season's cooling effect and each warm season's heat-absorbing effect, cooling power gradually increases in the thermosyphon foundation each year, which illuminates that the longer the working time of a thermosyphon foundation, the better the permafrost-preserving effect will be in the application life.

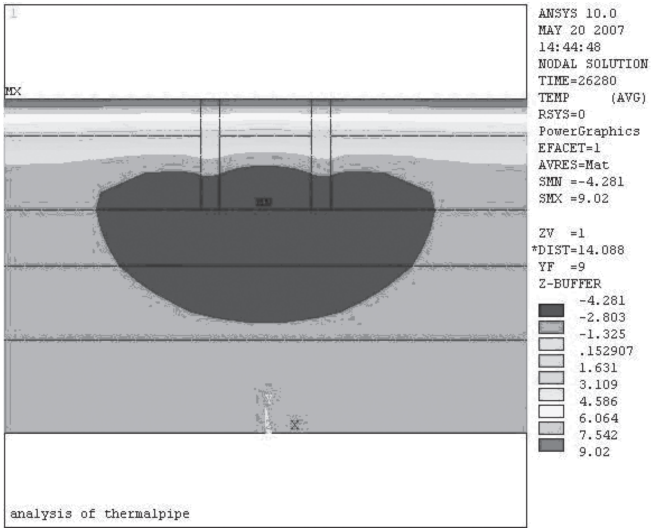

a) Isotherm on the second autumnal equinox.

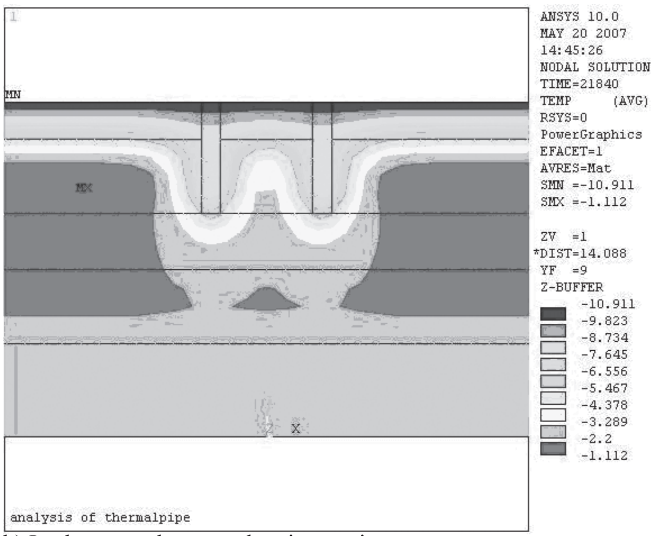

b) Isotherm on the second spring equinox.

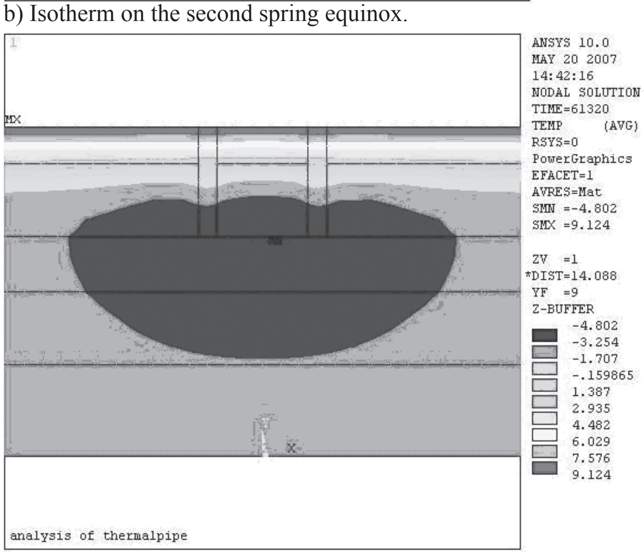

c) Isotherm on the fifth autumnal equinox.

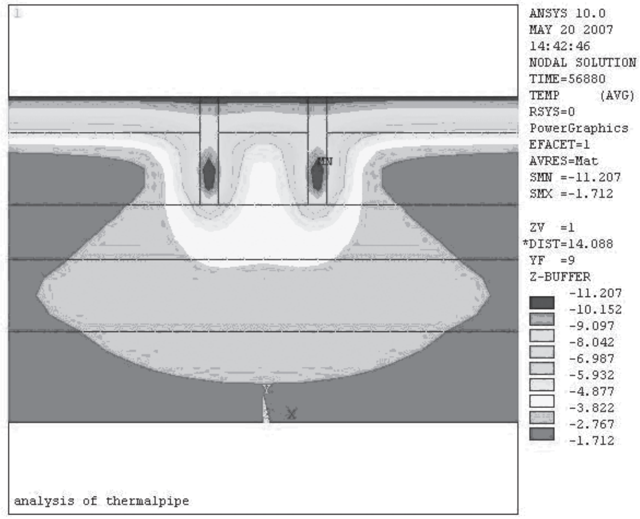

d) Isotherm on the fifth spring equinox.

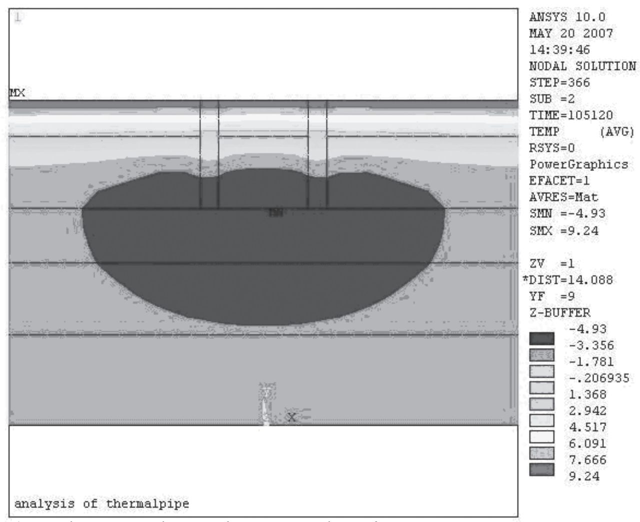

e) Isotherm on the tenth autumnal equinox.

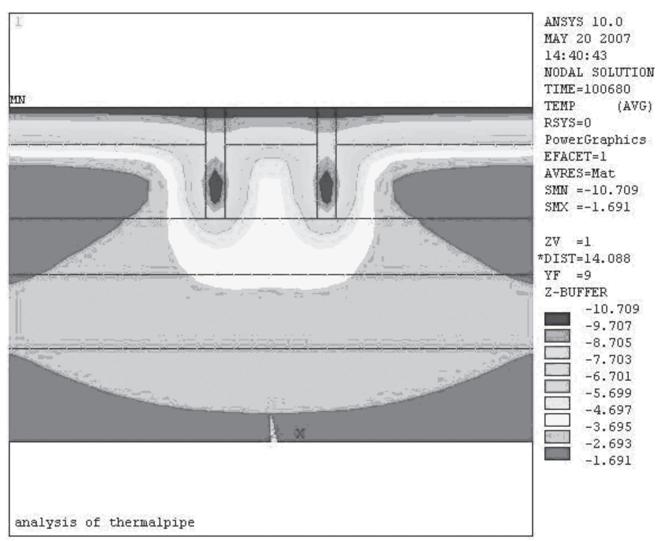

f) Isotherm on the tenth spring equinox.

Figure 6. Isotherms of the thermosyphon foundation in different years (the second, the fifth, and the tenth year taken, for instance).

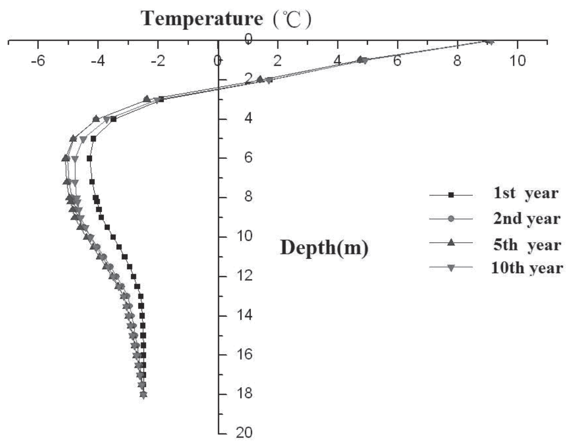

a) Temperature distribution on autumnal equinox.

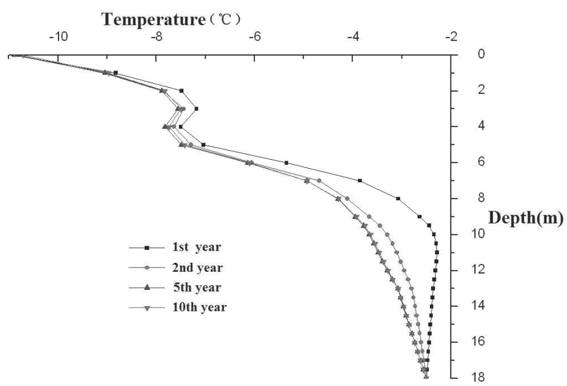

b) Temperature distribution on spring equinox.

Figure 7. Temperature distributions in different years.

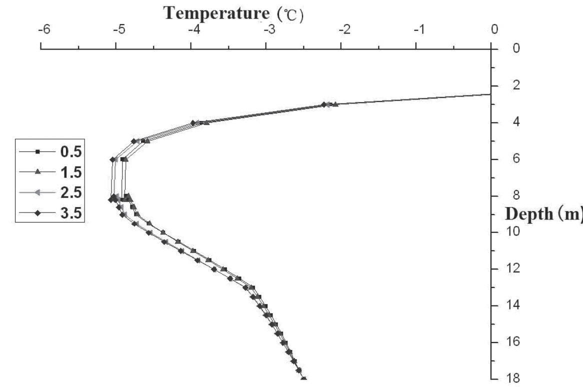

Areas ratio:

Figure 8. Temperature distribution with different ratios of areas (0.5, 1.5, 2.5, 3.5) on the tenth autumnal equinox.

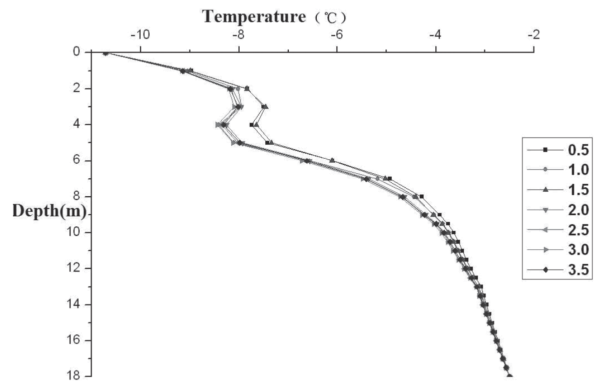

Figure 9. Temperature distribution with different ratios of areas (0.5, 1.0, 1.5, 2.0, 2.5, 3.0, 3.5) on the tenth spring equinox.

Figure 7 is temperature distribution in which is as far as the diameter of thermosyphon foundation away from the foundation, along depth in different years. The average temperature in year 1 is apparently higher than those in other years, and as working time goes, it continuously drops but the falling range becomes smaller and smaller. At the same time, there is a rising trend for the temperature of permafrost due to the influence of global warming. For the cooling effect of thermosyphon foundation, the natural permafrost table keeps in a certain level, so the foundation is safe and steady enough to sustain structures.

The influence of parameters of thermosyphon foundation on temperature field

The article investigates the influence of parameters (areas ratio, length, pile space) of thermosyphon foundation on temperature fields to gain reasonable design parameters. The total calculation time is ten years. Areas ratio is defined with the surface area of the condensation part divided by that of the evaporation part.

Influence of areas ratio on temperature field

Figures 8 and 9 separately show temperature fields that are one diameter away from the thermosyphon foundation with different ratios of areas, such as 0.5, 1.5, 2.5, and 3.5 along depth on the tenth autumnal equinox and spring equinox. It is clear that the temperature of soil layers near to the foundation changes slightly with areas ratio 0.5–1.5, distinctly with 1.5–2.0, less with 2.0–3.5. From Figure 7, we can state that from -3 m to the bottom, namely the evaporation part, the temperature of soil layers near to this part is greatly affected by the variation of areas ratio, and the temperature falling range rises with areas ratio increasing, especially from 1.5 to 2.0, so that we choose 2.0 as the reasonable ratio of areas in the study.

Due to the limitation of the transmission tower structure, the length of condensation part is not appropriate to be changed, so the length of evaporation part varies with 3.0 m, 3.5 m, 4.0 m, 4.5 m, 5.0 m for calculation. Figure 10 represents temperature distributions with different lengths of thermosyphon Φ89 pile along depth on the tenth autumnal equinox, from which we can see that the temperature falling range of soil increases, as well as the cooling efficiency, with the evaporation part becoming longer. Meanwhile, the influencing region is getting wider and deeper. In view of facts such as project cost, design requirements and so on, the article suggests that the reasonable length of evaporation part is 3 m.

The pile spaces for numerical analysis between thermosyphon Φ89 piles are 3.0 m, 4.0 m, 5.0 m, and 6.0 m with areas ratio 2.0, and all these chosen spaces(3.0 m, 4.0 m, 5.0 m, and 6.0 m) are limited by the structural sizes. All these data points are node points in the analysis. Figure 11 shows temperature distributions (below 0°C) of the foundation with different pile spaces along depth. It reveals that when pile space is 3.0 m the cooling effect of thermosyphon founda-

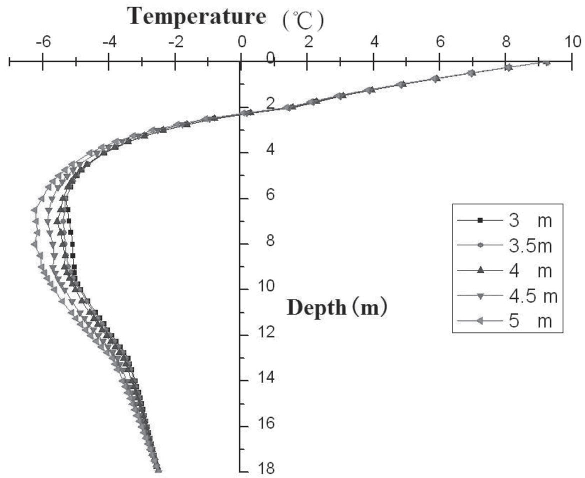

Figure 10. Temperature distributions with different lengths of thermosyphon.

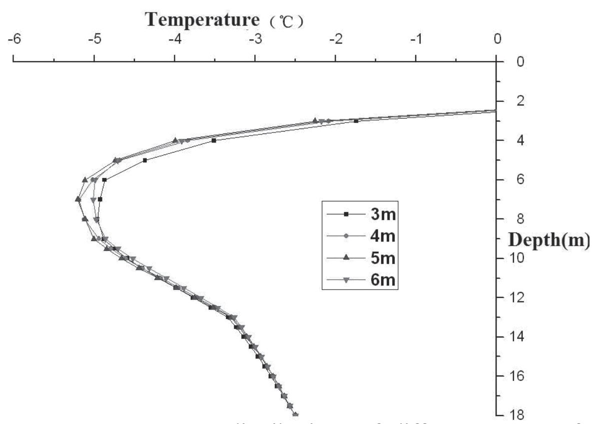

Figure 11. Temperature distributions of different spaces of the thermosyphon.

tion decreases, but increases with pile space getting large; the cooling effect with pile space 6.0 m is not as good as that with 4.0 m or 5.0 m, and 4 m is optimum, because the mutual influence (i.e. group action of piles) between thermosyphon φ89 piles turns strong with small pile space, but if the pile space is too large, there will be a weak region (with relatively high temperature) between two thermosyphon piles. According to the calculation result and the type of transmission tower applied in this project, 6.0 m is the best pile space, and in order to reinforce the cooling effect, it can be considered to add a thermosyphon pile in the central zone of the four ones with the pile space among them about 4.0 m.

To sum up, as a result of the cooling effect, the average temperature of permafrost with the thermosyphon foundation is lower than that with a traditional foundation.

After ten years, the natural permafrost table moves up 0.5 m owing to the thermosyphon foundation. Although ten years of global warming makes permafrost near the ground surface degenerate, from the above analysis and figures, it can be stated that permafrost surrounding the bottom part of the thermosyphon foundation can be refrozen completely in cold seasons; a big central frozen zone is formed with -5.2°C; after the tenth whole warm season the temperature of this zone is even -3.7°C. Therefore, the permafrost-preserving effect of a thermosyphon is strong enough to keep the whole structure stable and resistant to the influence of global warming.

Conclusions

Based on the continuity equation, momentum equation, and energy equation, the temperature characteristics of a thermosyphon foundation of a high-voltage transmission tower in permafrost regions are calculated and analyzed using FEM with the aid of ANSYS, and reasonable design parameters are obtained considering global climatic warming. The results provided a theoretical basis for the design of a thermosyphon foundation. It can be concluded that: (1) Under the stated climatic conditions and the project requirements, the temperature fields of a thermosyphon foundation and traditional foundation compared on autumnal equinox and spring equinox reveal that the natural permafrost table rises by 0.5 m due to the cooling effect of the thermosyphon pile, and the average temperature of soil near to the foundation drops by 2°C, which proves that the thermosyphon foundation has a distinct permafrost-preserving effect. (2) The temperature fields of a thermosyphon foundation in the first year and the tenth year are also compared, and the average temperature in the tenth year is 2.0°C lower than in the first year, which indicates that the cooling effect increases as working years pass. (3) The influence of the design parameters of a thermosyphon—for instance, areas ratio, pile length, and pile space on temperature fields—is analyzed in ten years. The computation results suggest that the temperature of soil layers near the foundation changes slightly with areas ratio 0.5–1.5, distinctly with 1.5–2.0, less with 2.0–3.5, so this paper chose 2.0 as the reasonable areas ratio. In order to satisfy the project requirements and economy, the appropriate length of the evaporation part is taken as 3.0 m. According to the analysis stated above, 4 m is the optimum pile space, and considering the type of transmission tower applied in this project, 6.0 m is the best pile space. In order to reinforce the cooling effect, a thermosyphon pile can be added in the central zone of the four ones with the pile space among them about 4.0 m.

Acknowledgments

This research was supported by the National Science Fund (No. 40571032), the Research Fund for The Direct-Current (±500 kV) Transmission Project from Hu Lun Bei Er to Liao Ning Province.

References

Lai, Y., Wang, Q. & Niu, F. 2004. Three-dimensional nonlinear analysis for temperature characteristic of ventilated embankment in permafrost regions. *Cold Regions Science and Technology* 38: 165-184.

Zhang, M., Lai, Y., Liu, Z. & Gao, Z. 2005. Nonlinear analysis for the cooling effect of Qinghai-Tibetan Railway embankment with different structures in permafrost regions. *Cold Regions and Technology* 42: 237-249.

Zhou, Y.W., Guo D.X., Qiu, G.X. et al. 2000. *Geocryology in China.* Beijing: Science Press, p. 37(in Chinese).

"Permafrost Is No Excuse": Geoarchaeology and Zooarchaeology of the Little John Paleoindian Site, Alaska/Yukon Borderlands

David R. Yesner
University of Alaska Anchorage
Kristine J. Crossen
University of Alaska Anchorage
Norman A. Easton
Yukon College

Abstract

Permafrost deposits have affected archaeological excavations in interior and northern Alaska in numerous ways. Here we consider a new geoarchaeological context for Paleoindian sites in eastern Beringia: permafrost-shattered bedrock colluvium which has sealed deep loess deposits within swales between bedrock knobs. These loess deposits contain paleosols with early archaeological materials, including Nenana complex artifacts and Late Pleistocene megafauna. They are often underlain by additional permafrost. In order to discover such deeply buried deposits, it may be necessary to excavate through bedrock colluvium. Under such situations, "permafrost is no excuse." These principles are illustrated by recent excavations at the Little John Paleoindian site in the Alaska/Yukon Borderlands.

Keywords: Beringia; Little John site; Nenana complex; Paleoindian archaeology; permafrost; Pleistocene megafauna.

Introduction

Numerous archaeological excavations in interior and northern Alaska have encountered permafrost conditions either prior to or during excavation, and have been forced to develop methodologies to confront that situation. Permafrost interacts with archaeology in two ways: by creating unique preservation conditions for organic materials, and by creating difficult conditions for excavation to retrieve those materials. In northern Alaska, conditions which allowed for the development of permafrost "freezers" for storing meat and other organic materials by Inupiaq people have also created conditions for organic preservation over periods of hundreds to thousands of years. Excavation in northern Alaskan coastal sites in areas of permafrost (e.g., St. Lawrence Island) often yields not only bone, ivory, and wood, but also food remains and rendered seal, whale, or fish oil, some of which still emits odors when newly exposed. Long-term preservation of such organic residues allows an additional source of materials for radiocarbon dating, although calibrated date corrections to account for the marine reservoir effect frequently add several hundred years to dates, whether produced by standard or AMS methods. Preservation of categories of material culture such as clothing is generally only possible under permafrost conditions, as was the case in the Utqiagvik project in the Barrow region. Human bodies have also preserved in ice, again in the Utqiagvik site, and on St. Lawrence Island. In the former case, soft tissue pathologies (e.g., pneumoconiosis due to soot inhalation) and even evidence of late-life pregnancy could be determined. In the latter case, tattooed symbols were visible, similar to those of the Pazyryk bodies, encased in ice within kurgans (traditional burial mounds) in the Altai and upper Yenisei River regions of westernmost Beringia.

All of these unique discoveries come at a methodological expense. Excavation through permafrost is difficult, and requires the use of specialized archaeological techniques. Traditionally, until 30 years ago, sites were only excavated a few centimeters at a time as the surface was exposed and allowed to thaw. The use of such techniques meant that even some well-known Paleoindian site excavations in interior Alaska were abandoned because of difficulties or slowness of these procedures. The Utqiagvik project experimented with warm water thawing of the surface, and the gradual extraction of organic materials such as clothing from the ice. This technique was extremely successful, and has become the standard in recent years.

The results of ice on archaeological materials embedded in soft sediments such as loess (fine-grained glacial silt) are somewhat an issue of debate. While it is recognized that ice may preserve organic remains, it is also possible that higher permafrost tables result in a greater degree of cryoturbation, frost jacking, and displacement if not destruction of materials. For example, at the Broken Mammoth site near Big Delta in interior Alaska (Fig. 1), there is excellent preservation of organic material (bone, ivory, eggshell) in paleosols at the base of a 2 m loess deposit, dated from 9500 to 12,000 ^{14}C yr BP (Fig. 2); this has been suggested by some to have been at least partly the result of a higher permafrost table in the Late Pleistocene and/or Early-to-Mid Holocene. However, in our view, this preservation is more likely attributable primarily to the calcareous nature of the loess and the depth of the loess, with the latter retarding the downward mobilization of acidic ions in the soil column as a result of rainfall percolating through the coniferous needle mat associated with the contemporary (2–3,000 year old?) closed spruce forest (Holmes 2001, Yesner & Pearson 2002). Today, there is no permafrost present at the Broken Mammoth site, although it is found both to the north of the site (in the vicinity of Richardson) and to the south (in Shaw

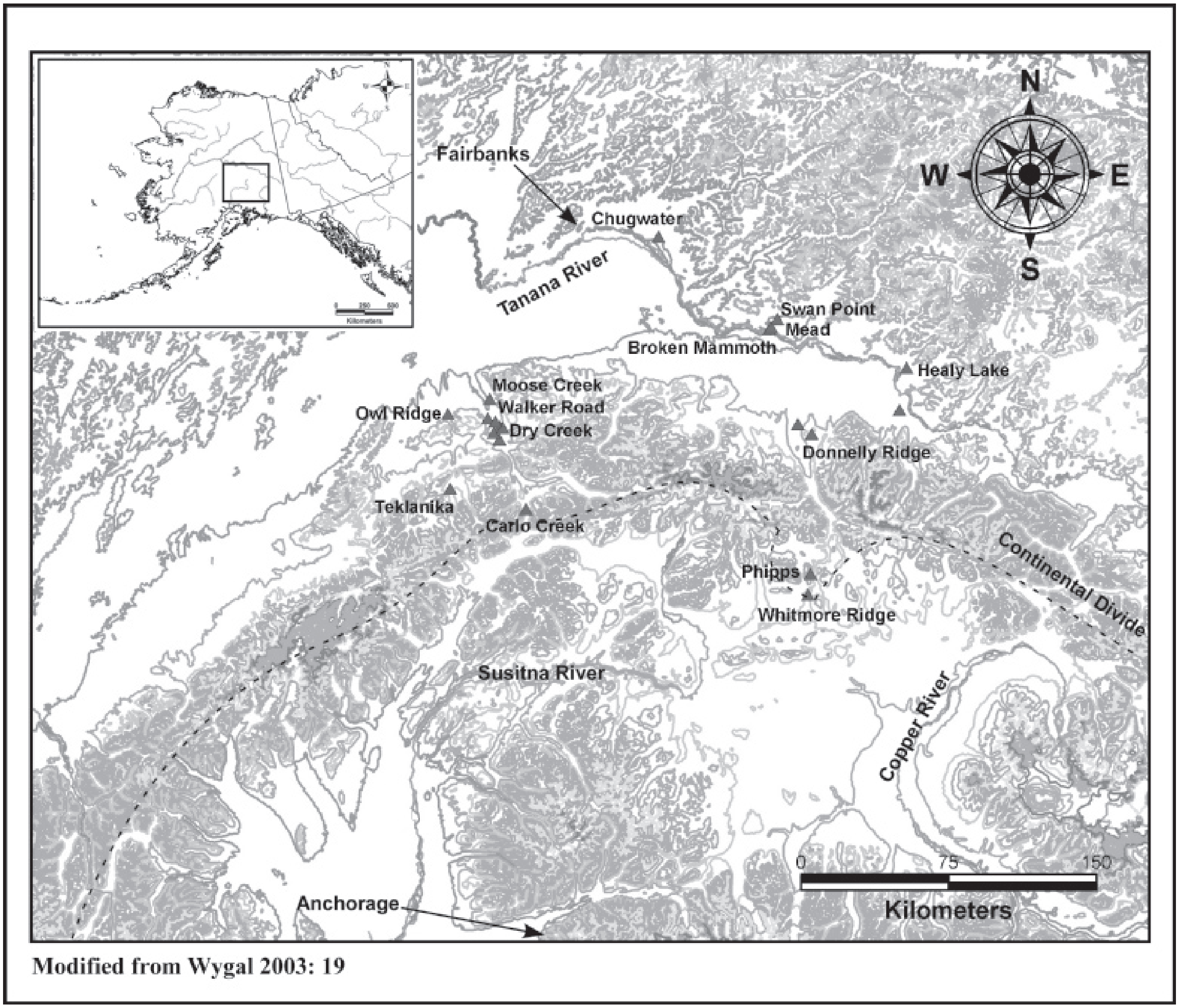

Figure 1. Early sites in Interior Alaska.

Creek Flats). This may be related to the fact that the site is on a south-facing slope, which has produced a microhabitat of relict Beringian flora in the site vicinity, including sage (*Artemisia* sp.). The result is that stratigraphic layers at the site are extremely flat lying, with even relatively thin (<5 cm thick) paleosols traceable horizontally over 30 meters or more. This suggests no previous experience with a higher permafrost table, a condition which differs strongly from Late Pleistocene/Early Holocene archaeological sites found elsewhere in interior Alaska (e.g., the Dry Creek, Walker Road, Moose Creek, Panguingue Creek, Owl Ridge, and Teklanika West sites in the Nenana Valley/Denali Park region; and the Chugwater and Gerstle River Quarry sites in the Tanana Valley region), all of which display evidence of cryoturbation, including distortion of archaeological stratigraphy (Powers & Hoffecker 1989, Hoffecker et al. 1993). Some of these sites also contain gleyed soils which are linked to reduced ions resulting from permafrost table saturation of the soil column.

The Little John Site, KdVo-6

Located just off the Alaska Highway, approximately 2 km due east of the International Boundary, the Little John Site occupies a knoll overlooking Mirror Creek, the easternmost tributary of the Tanana River basin. Unglaciated during the Wisconsin (Rampton 1971), this site contains evidence of human occupation from the Late Pleistocene to the recent past.

The western area of the site exhibits a geoarchaeological context similar to that of northern Alaskan sites or sites in the Tangle Lakes region of interior Alaska, with shallow, gravelly deposits entraining a basal loess layer at no more than 30–40 cm depth, directly overlying frost-shattered bedrock (West 1967, 1996). An archaeological component associated with this thin, shallow loess contains abundant microblades, burins on microblades, several core tablets, and irregular core fragments (although as yet no complete microcores). It also contains numerous scrapers and a limited bifacial industry, which may suggest that it be assigned to the Northern Archaic or the "Late Denali complex." Unfortunately, this area of the site is so far undated, due to a lack of datable organic material.

The eastern portion of the Little John site presents a completely different geoarchaeological context. In terms of paleogeomorphology, this portion of the site represents a swale between two bedrock knobs which has served as a sediment trap throughout the Late Quaternary. Here, a combination of frost jacking and gravitational processes has produced a series of colluvial episodes in which blocks of bedrock have become dislodged and transported into the swale. The last of these episodes, about 10–30 cm below surface, has produced a frost-shattered bedrock "pavement" in some areas which is extremely difficult to excavate through, but which may have helped preserve some of the underlying package of sediments. Underlying this colluvium is at least 30 cm to 40 cm of brunisol strata overlying 40 cm to 60 cm of (probably colluvially reworked) loess containing thick (10–30 cm), darkly stained paleosols. These paleosols also exhibit evidence of B horizon eluviation, indicative of gleyed conditions associated with a formerly higher permafrost table; a similar phenomenon can be seen at the Gerstle River Quarry site in the central Tanana valley to the NW. There are additional lenses of colluvial frost-jacked bedrock found within the loess, including some materials near the base of the loess that are Late Pleistocene or Early Holocene in age. There is also permafrost in some units at the base of the loess. The paleosols within the loess contain a diverse assemblage of culturally modified fauna, with AMS assays to date on three samples dating to 8890 +/-50 RCYBP (Beta 182798), 9530 +/-40 RCYBP (Beta 217279), and 9550 +/-50 RCYBP (Beta 218235). None of these bone samples, however, was from the lowest paleosol stringer within the loess, from which will have dates available shortly from new, stratigraphically-lower bone samples.

Nenana complex materials

The artifact assemblage from the eastern area of the site is assignable to the Nenana Complex or Early Beringian Tradition, previously established for the lower Tanana Valley and Nenana Valley areas (Bever 2006, Easton & MacKay 2007). It contains four teardrop-shaped Chindadn points, two biconvex bifacial knives, other large bifaces, macroblades, a variety of scraper forms, waste flakes, and two chisel-like bone tools; some of these are directly associated with dated fauna (see below). These materials are all characteristic of Denali assemblages in interior Alaska, including both the Nenana and central Tanana valleys.

Zooarchaeological and paleoecological data

Fauna identified to date from the palesol complex (cf. Hutchinson et al. 2007) include the following taxa: bison (cf. *Bison priscus*), elk or wapiti (*Cervus elaphus*), caribou (*Rangifer tarandus),* moose (*Alces alces*), hare (*Lepus sp.*)*,* swan (*Cygnus sp.*) and other as yet unidentified birds, rodents, and canids. This diverse faunal assemblage indicates a broad-spectrum subsistence strategy, similar to that

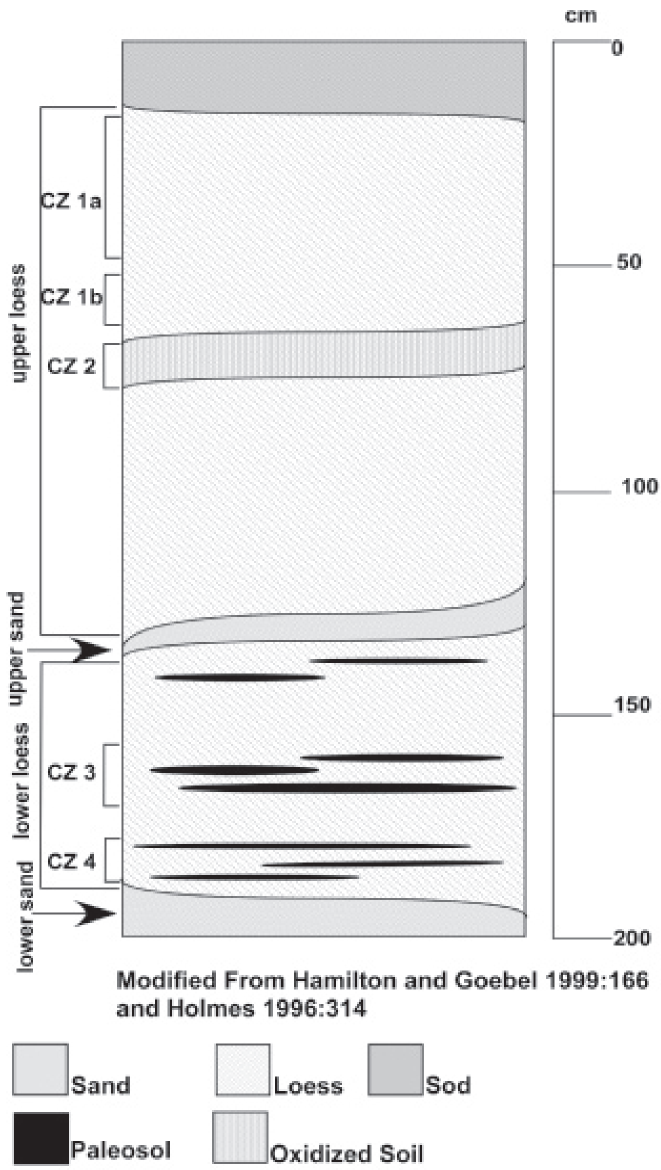

Figure 2. Broken mammoth profile.

displayed at a few other Late Pleistocene/Early Holocene sites in the central Tanana valley and Nenana valley with good bone preservation (Broken Mammoth, Mead, Swan Point, Dry Creek).

A core sample from a lake called *Yihkah Männ'* (~5 km from the Little John site) indicates that a transition from herb tundra ("tundra-steppe") to shrub tundra occurred ~11,000 ^{14}C yr BP, perhaps some 500–1000 years later than in the Tanana Valley (MacIntosh 1997). Occupation of the Little John site may correspond with this transition (cf. Bigelow & Powers 2001, Hoffecker & Elias 2007). The importance of this transition was to provide not only a more mesic, ameliorated environment for human occupation of the region, but also wood resources (especially with the appearance of *Populus* at ~11,000 ^{14}C yr BP) for hunting technology, dwellings, and other purposes. Simultaneously, these mesic conditions allowed soil formation and the entrainment of archaeological materials which might otherwise not have been preserved.

A successive eastward movement of Nenana and Denali culture bearers adapted to the subsistence opportunities offered by the shrub tundra environment of the Tanana Valley may explain the appearance of these complexes in the southwest Yukon. The Little John site extends the range of the Nenana complex to the far southeast edge of Beringia during the terminal Pleistocene.

Summary and Conclusions

Archaeological excavation in interior Alaska has provided data for Early Eastern Beringian archaeological assemblages (~12,000 to 9000 C^{14} yr BP) typically entrained in paleosols within deep loess units deposited on bedrock or river gravel terraces above river floodplains. In the middle Tanana Valley, deep, calcareous loess deposits have resulted in excellent faunal preservation at some of sites (e.g., the Broken Mammoth and Mead sites). New work at the Little John site in the upper Tanana Valley, Yukon Territory, extends the eastern Beringian record another 250 km eastward, and simultaneously provides a new geoarchaeological context within which early (Nenana Complex or Early Beringian Tradition) sites with excellent faunal preservation are found: fine-grained sediments deeply buried in swales between bedrock knobs above the valley floor. Discovery of additional such early sites may, however, be difficult, because such deeply buried deposits may be similarly covered by extensive sheets of colluvially-transported bedrock fragments, a fact of life in a region dominated by permafrost activity.

Acknowledgments

The authors would like to thank Daniel Stone and Rita Eagle for supervising the 2007 field season at the Little John Paleoindian site. The University of Alaska Anchorage and Yukon College provided joint funding for the 2007 excavations, with partial support for graduate students from IPY and EPSCOR initiatives. We also thank the White River First Nation, based in Beaver Creek, Yukon Territory, for permission to undertake excavations on their ancestral lands. The slogan of the Little John project is “Permafrost is no Excuse.”

References

Bever, M.R. 2006. Too little, too late? The radiocarbon chronology of Alaska and the peopling of the New World. *American Antiquity* 71: 595-620.

Bigelow, N.H. & Powers, W.R. 2001. Climate, vegetation, and archaeology 14,000–9000 cal yr BP in central Alaska. *Arctic Anthropology* 38: 171-195.

Easton, N.A. & MacKay, G. 2007. Early bifaces from the Little John Site (KdVo-6), Yukon Territory, Canada. In: R. Carlson (ed.), *Projectile Point Sequences in Northwestern North America*. Burnaby: Simon Fraser University Press (in press).

Hoffecker, J.F., Powers, W.R. & Goebel, F.E. 1993. The colonization of Beringia and the peopling of the New World. *Science* 259: 46-53

Hoffecker, J.F. & Elias, S.A. 2007. *Human Ecology of Beringia.* New York: Columbia University Press, 290 pp.

Holmes, C.E. 2001. Tanana Valley archaeology circa 14,000 to 9,000 BP. *Arctic Anthropology* 38: 154-170.

Hutchinson, V., Easton, N.A. & MacKay, G. 2007. *Faunal remains from the Little John Site (KdVo-6): An Early Holocene Assemblage from the Yukon–Alaska Borderlands*. Paper presented at the Annual Meeting of the Alaska Anthropological Association, Fairbanks.

MacIntosh, G.D. 1997. *Paleoecology of the Scottie Creek District*, Beaver Creek, Yukon. M.A. Thesis. Department of Geology, University of Alaska Fairbanks.

Powers, W.R. & Hoffecker, J.F. 1989. Late Pleistocene settlement in the Nenana Valley, central Alaska. *American Antiquity* 54: 263-287.

Rampton, V. 1971. Late Pleistocene glaciations of the Snag Klutlan area, Yukon Territory. *Arctic* 24: 277-300.

West, F.H. 1967. The Donnelly Ridge site and the definition of an early core and blade complex in central Alaska. *American Antiquity* 32: 360-382.

West, F.H. (ed.) 1996. *American Beginnings: The Prehistory and Paleoecology of Beringia*. Chicago: University of Chicago Press, 576 pp.

Yesner, D.R. & Pearson, G.A. 2001. Microblades and migrations: Ethnic and economic models in the peopling of the Americas. In: R.G. Elston & S.L. Kuhn (eds.), *Thinking Small: Global Perspectives on Microlithization*. Arlington, VA: Archaeological Papers of the American Anthropological Association 12: 133-161.

Stable Isotope Composition of Ice in Seasonally and Perennially Frozen Mounds

Kenji Yoshikawa
Water and Environmental Research Center, Institute of Northern Engineering, University of Alaska Fairbanks

Abstract

Ice-cored mounds develop in regions of continuous and discontinous permafrost. Isotopic composition not only clarifies the growth process of the ice, but also indicates groundwater environments, such as open or closed environments and residual water fraction. Isotope stratigraphy of ice cores from the various types of frozen mounds (open- and closed-system pingos, palsas, icing blisters, frost blisters) can be applied to reconstruct the growth mechanism of each mound. An ice-cored mound in an open hydrological environment (such as an open-system pingo or a frost blister) froze relatively fast (enrichment of isotope ratio) at the top of the ice layer and remained an open environment during the main growth period. However, a major part of the ice (60% or more) was formed in a closed environment by continuous downward freezing. At the end of the growth period, a discontinued groundwater supply and slow freeze-up was followed by Rayleigh distillation. Palsas and closed-system pingos were in a semi-closed environment during the entire period.

Keywords: frost blister; icing blister; ice core; pingo; palsa; stable isotope.

Introduction

Ice-cored mounds are known for their unusual growth process and ice structure. However, a detailed physical mechanism for the formation of such mounds is still poorly understood. This study discusses the isotopic characteristics of ice from ice-cored mounds around Alaska, Canada, and Svalbard. Isotopic composition can indicate the groundwater source and physical environment of the ice development. The stable isotopic composition of ice formation is relatively well-studied for lake ice (Gibson & Prowse 2002), river ice (Gibson & Prowse 1999), and frost blister ice (Michel 1986), especially by Canadian scientists. Clark & Fritz (1997) reviewed well-documented surface and groundwater isotope studies. These well-documented isotopic works are useful in the study of ground ice processes. Isotope stratigraphy can be applied in reconstructing growth mechanisms with a variety of ice-cored-mound signals to understand differences between and the developmental process for these mounds. Definitions for each type of permafrost mound follow the terminology used by the Associate Committee on Geotechnical Research (1988).

Isotope study for permafrost mounds

The term *pingo* is an Eskimo word for a conical, more or less asymmetrical mound or hill, with a circular or oval base and commonly fissured summit. Pingos occur in areas of continuous and discontinuous permafrost, have a core of massive ground ice covered with soil and vegetation, and exist for at least two winters. A pingo has two general types of origin based on hydrological environments: open system (hydraulic) and closed system (hydrostatic). Mackay (1990) reported stable isotope results from one of the closed-system pingos at the Tuktoyaktuk Peninsula area. The isotope value slowly trends lighter, with a $\delta D/\delta^{18}O$ ratio of about 6. Yoshikawa (1993) reported oxygen isotope results from one of the Svalbard open-system pingos. The $\delta^{18}O$ values remain at -13‰ from top to bottom of the ice core except where there is dilation crack ice.

Two basic differences between pingos and seasonal frost mounds are (1) the time necessary for development and (2) the stability of ice conditions. Seasonal frost mounds are less than a decade old because their ice is situated over (or near) the thawing zones. Therefore, ice conditions are unstable in frost mounds.

Icing mounds and icing blisters are formed by hydraulic pressure during winter. These ice formations are usually continuous during the winter. In High Arctic regions, some icing mounds have been reported to exist longer than a decade (Sharp 1942). Excellent stable isotope studies for seasonal frost mounds were reported by Michel (1986) and Clark & Lauriol (1997). Michel (1986) successfully collected frost blister isotope signals as an entire fractionation process at North Fork Pass, Canada. The present study examines several ice cores from the same site at North Fork Pass.

The purpose of this study is to identify and characterize groundwater discharge and freezing processes of the different types of ice-cored mounds in permafrost regions. The source of water, freezing rate, and groundwater pressure are fundamental parameters. Stable isotopes were applied to reveal these parameters in understanding the formation process of the mounds.

Methods

During 2001 and 2006, ice samples from locations in Alaska, Canada, and Svalbard were taken to examine three open-system pingos, one closed-system pingo, two palsas, four icing blisters, and four frost blisters. Table 1 and Figures 1 and 2 show the sample sites and their profiles. In Table 1, the numbers in column $\varepsilon^{18}O_{i\text{-}w}$ are the values for fractionation relationships for ^{18}O in water-ice reactions. Ground ice was obtained using a portable drill core sampler (5-cm diameter stainless steel hollow Stein auger with hand or 1 kW electric drill). Obtained samples were analyzed

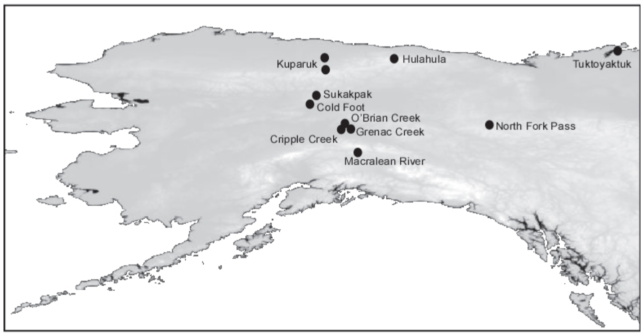

Figure 1. Sample sites in Alaska and Yukon, Canada.

for stable isotopes at the Alaska Stable Isotope Facility at the Water and Environmental Research Center (WERC), University of Alaska Fairbanks (UAF), using Pyrolysis Elemental Analysis-Isotope Ratio Mass Spectrometry (pyrolysis-EA-IRMS) DeltaV system. This method utilizes a ThermoFinnigan MAT high-temperature elemental analyzer (TC/EA) and Conflo III interface with a DeltaV Mass Spectrometer. The pyrolysis reactor consists of a reaction tube packed with glassy carbon/graphite and silver wool. Other TC/EA conditions are as follows: Pyrolysis tube temperature 1450°C, He flow rate 120 mL/min, GC column 3 m 5Å mol sieve and GC oven temperature 75°C to 100°C. Water from ice samples in the amount of 0.2 µL are injected into the TC/EA with a CTC Analytics A200SE liquid autosampler. The sample is pyrolyzed into H_2 and CO gases, then separated chromatigraphically. These gases are then transferred to the IRMS, where the isotopes are measured.

The values $\delta^2H_{V\text{-}SMOW}$ and $\delta^{18}O_{V\text{-}SMOW}$ are reported in reference to international isotope standards. The typical quality control scheme involves analyzing laboratory working standards every seven replicate samples. Each sequence batch is calibrated to NIST standards to confirm quality assurance. NIST standards are analyzed in replicate throughout the sequence.

The freezing of water in a closed system is a good example of Rayleigh distillation (Fig. 3, closed circles). During the closed-system freezing process, ice is progressively enriched; however, such enrichment does not occur in an open-system environment.

Results

The series of the ice-core signature contain a unique isotope value that reveals freezing processes. Figure 4 shows perennial ice-cored-mound results. Closed-system pingos (Mackay 1990) and palsas show a similar gradually decreasing trend of oxygen isotopes. Thus, frozen ice at an early stage is heavier than that at a later stage. The isotopic structure of the palsa is considered a semi-closed hydrological environment, similar to a closed-system pingo. However, an open-system pingo does not have this trend. The values of $\delta^{18}O$ are nearly constant for all sampling points deeper than 2 m at different horizons except for the sample of the upper 2 m of ice. As the water of the open-system pingo continuously comes from sub-permafrost and/or a talik, the value of $\delta^{18}O$ does not change (ca. -16‰) when the water source is constant. However, the early stage of the open-system pingo has complicated signals. This upper layer indicates rapid freezing similar to the frost blister. Figure 5 shows the relationship between δD and $\delta^{18}O$ from various ice-cored mounds and spring water adjacent to the mounds. The local water sources are at the local meteoric water line (LMWL). The freezing process of the mounds follows Rayleigh-type evolution.

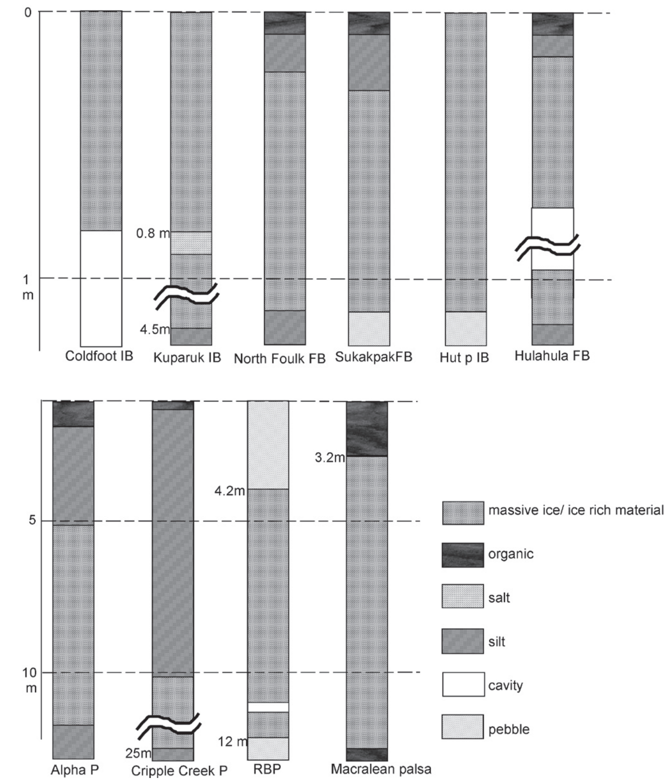

Figure 2. Drill logs for sampling frost mounds (FB: frost blister; IB: icing blister; P: pingo). Palsa samples taken include the organic layer up to 3.2 m, and focus on the ice layer below 3.2 m.

Figure 6 shows seasonal ice-cored mound results. All of the signals have similar trends. At the top of the ice, the isotope value is quickly enriched 2–3‰, which is the equilibrium fractionation factor to the ice. When freezing continues, ice formed from the depleted water preserves this trend of increasingly lighter oxygen isotope values. These mounds are produced through doming of groundwater due to hydraulic pressure. Once the dome shape is established, the downward freezing continues forming ice in a water-filled cavity under closed-system conditions. Some frost blisters are observed in a over several winters. Sukakpak frost blister (Fig. 6) is a good example. This ice core (2 m) indicated two times of enrichment.

During the winter of 2005–2006, one icing blister near Cold Foot (in the south-facing foothills of the Brooks Range) developed 2 m in height and about 30 m in diameter (Fig. 7). The details of ice grain size and C-axis measurements were observed. The upper 20 cm of the icing blister had overflow of white ice with very fine random crystals (<2

Table 1. A list of the sampled frost mounds (FB: frost blister; IB: icing blister; OP: open-system pingo; CP: closed-system pingo).

site	type	ice sample thickness (m)	$\varepsilon^{18}O_{i-w}$	δD/δ18O slope	location	permafrost	MAGST	size (D/H)	reference
Hulahula	FB	1.4	-2.17	4.06	69° 9'50.86"N/144°35'19.46"W	cold	-7.79	20/4.5	
Sukakpak Mountain	FB	1.5	1.68	5.74	67°36'20.21"N/149°46'42.08"W	warm	-1.11	10/0.8	
Sukakpak Mountain	FB	1.5	3.3	6.13	67°36'20.21"N/149°46'42.08"W	warm	-1.11	12/1.1	
North Fork Pass	FB	1.5	-3.09	4.68	64°28'31.87"N/138°11'48.30"W	moderate	ND	15/1.5	Michel 1986
Coldfoot	IB	1.5	2.37	6.5	67°30'3.76"N/149°51'29.07"W	warm	ND	30/1.5	
Kuparuk	IB	0.6	-1.11	5.64	68°58'42.14"N/149°42'49.42"W	moderate	ND	5/0.5	
Svalbard	IB	1.2	0.08	na	78°10'34.55"N/ 16°16'50.57"E	cold	-5.7	8/1.2	
Cripple Creek	OP	4	1.7	5.46	64°48'33.66"N/148° 2'48.60"W	warm	-1.00	55/10	
O'Brian Creek	OP	8	1.4	5.63	64°54'4.85"N/147°54'25.19"W	warm	ND	100/6.5	
Grenac Creek	OP	6.5	na	5.33	64°53'52.47"N/147°45'5.25"W	warm	ND	80/6	
Tuktoyaktuk	CP	na	na	7.34	69°40'24.32"N/130°46'16.84"W	cold	ND	50/12	Mackay 1990
Svalbard	OP	5	na	na	78°10'34.55"N/ 16°16'50.57"E	cold	-5.7	60/9.6	Yoshikawa 1993
Kuparuk	Palsa	1	na	6.78	68°47'21.72"N/149°36'12.61"W	moderate	ND	10/0.5	
Macralean	Palsa	6	0.32	na	63° 7'27.22"N/146°29'55.72"W	warm	ND	80/4.5	

The numbers for $\varepsilon^{18}O_{i-w}$ are the values for the difference in 18O between water (spring) and uppermost (oldest) ice. Permafrost conditions are classified by zero annual amplitude permafrost temperature: warm (0° ~ -2ºC), moderate (-2° ~ -4ºC), and cold (< -4ºC). Size is indicated by diameter (D) and height (H) ratio.

mm). The stratification extended from below the overflow ice to the base of the cavity, with three layers of different ice crystal size. The icing blister ice had two major joint thresholds by the iron extraction (Fig. 7b). This chemical extraction indicated discontinuity of the freezing process. Ice crystals have a candle-like, slender, enlongated shape. There were several air bubbles inside the crystals (Fig. 7a). The long-axis orientation demonstrates the direction in which the crystals grew, which was vertically toward the freezing front. Once the dome shape was established, downward freezing stopped at least two times; however, the water-filled cavity froze under the closed system conditions (Fig. 6: IB Cold Foot).

Frost blisters from both the south- and north-facing foothills of the Brooks Range were sampled to the bottom of the ice. Drilling was performed June 2, 2004, at the Hulahula River frost blister to obtain an ice core. Below the 188 cm of ice and overburden was a large water-filled cavity 262 cm in height. This pressured cavity was developed by groundwater artesian water which continues to flow and discharge as a spring (Fig. 8). The isotope signals from this core did not reveal a Rayleigh distillation curve for ice that indicates open-system conditions during freezing in the water-filled cavity.

Sukakpak Mountain (in the south-facing foothills of the Brooks Range) and North Fork Pass, Yukon Territory, Canada, are two of the most well-studied areas for frost blisters (Brown et al. 1983, Michel 1986). For this study, six frost blisters were drilled at these two sites. The frost blisters at Sukakpak Mountain are considered to be at least 5–10 years old, but no more than 20 years old. The locations of previously studied frost blisters from the 1980s (Brown et al. 1983) were confirmed, but the frost blisters have completely disappear.

The grain size and shape of ice crystals in perennial and seasonal ice-cored mounds were different. Seasonal mound ice usually has small, enlongated ice crystals, the average crystal size being 1–5 mm. Perennial mound ice has big crystals (30–200 mm), and there are fewer bubbles observed

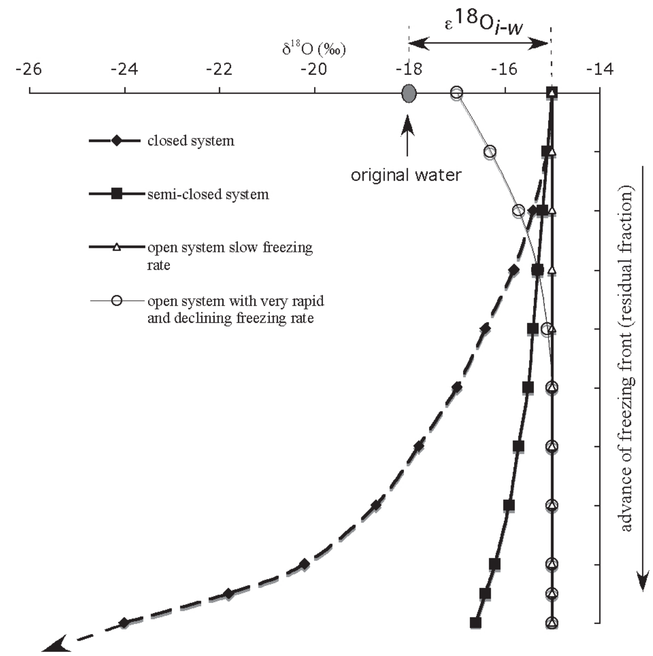

Figure 3. $\delta^{18}O$ versus freezing condition and water source effects (after Gibson & Prowse 1999).

in each crystal. Open-system pingos can be separated into two sections based upon grain size and isotope signals. The upper part of pingo ice is similar to that of a frost blister; the lower part consists of massive ice with bigger crystals.

The petrofabric analyses of icing mounds show that the c-axis orientations are normal for crystal elongations, with crystal growth along the basal plane in an a-axis direction (Pollard & French 1985). Mackay & Stager (1966) reported that in closed-system pingo ice beneath 5.5 m of overburden, the *c*-axis tended to point toward the pingo center. The isotope results also support development of ice formation similar to the petrofabric analyses results. The isotope analysis indicated the last residual water body in the ice core was located at the lower center of the mound. Ice-fabric analysis of the three samples taken from the basal pingo ice shows a changing *c*-axis pattern from the edge of the pingo

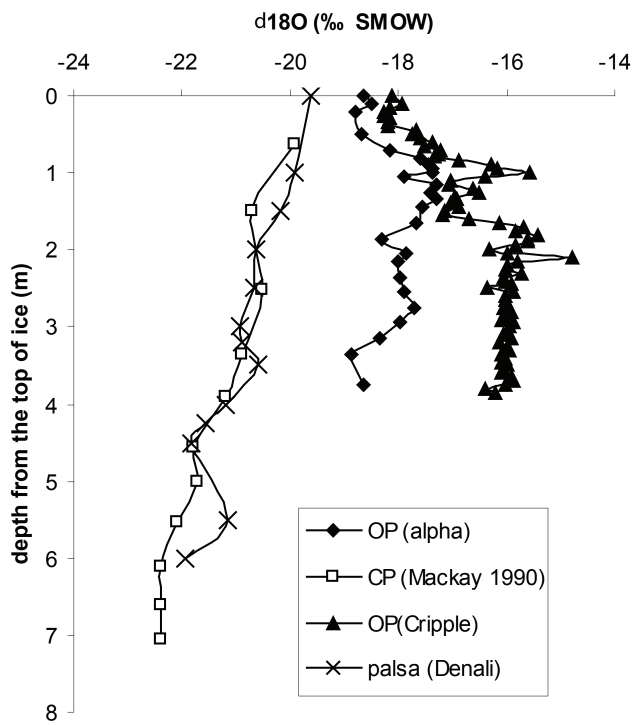

Figure 4. Oxygen isotope results versus ice thickness for perennial ice-cored mounds. Signals from an open-system pingo (OP) are quite different from those of a closed-system pingo (CP) and palsa.

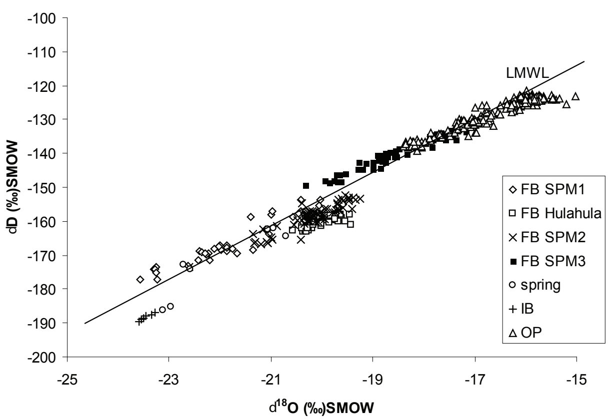

Figure 5. δD and δ[18]O relationship from various ice-cored mounds in Interior Alaska. LMWL is from Fairbanks.

to its center. The lattice orientation apparently coincides with vertically oriented columnar ice crystals. However, usually there is a maximum of four *c*-axis concentrations at the center of the pingo, which indicates that the ice received a strong force after crystallization due to residual water. As a result, pingo ice has significant pressure at the center. The edge of the ice has only a small amount of this force (Yoshikawa 1993).

Discussion

One of the important processes of closed-system freezing is chemical extraction or enrichment. Mackay (1990) reported

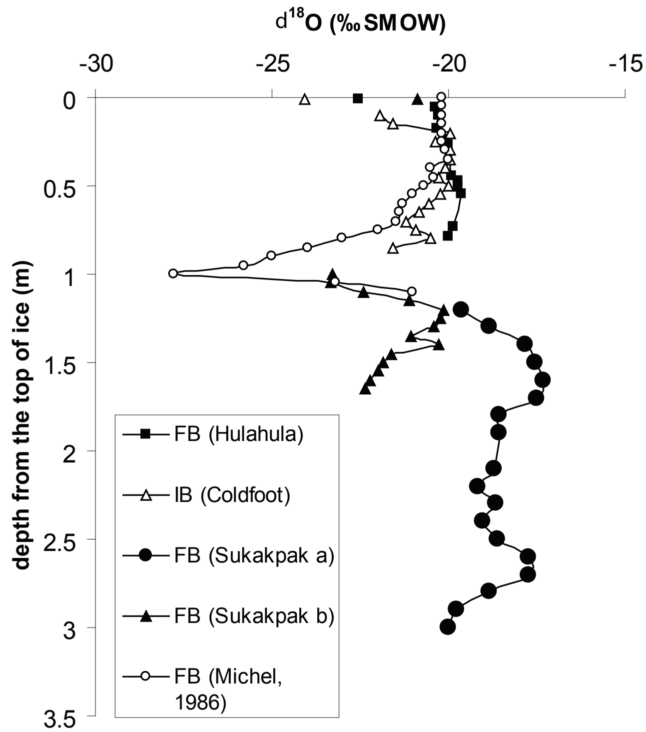

Figure 6. Oxygen isotope results against fraction (ice thickness) of the remaining ice on seasonal ice-cored mounds.

several layers of high ion concentrate in the closed-system pingo ice body. The isotope fraction analysis can detect this layer associated with delayed freezing (residual water) by the descending freezing point. Chemical extraction or salt precipitation during the freezing process is commonly observed in icing formation during the winter period. An icing blister from the Kuparuk River area, which was examined for this study, had developed only a week before the drilling sample was taken. The blister is 50 cm in height and 20 m in diameter. A highly concentrated and pressurized mineral layer was found 80 cm below the surface. This mineral layer is relatively easy to see from the air (Fig. 9). During core sampling 80 cm below the surface, about 5 cm of the cavity was found to have minerals with yellow fine form (bubbles) throughout, rising to the ground surface (Fig. 9, lower right). The majority of the minerals consists of carbon and calcium. Calcium and alkalinity concentrations indicate 14 times enrichment, and total carbon indicated 10 times. Isotope results follow chemical enrichments and indicated closed conditions for freezing both from the top down (Fig. 10, between 25–80 cm) and from the bottom up (Fig. 10, between 80–180 cm). The isotope fractionation demonstrates this freezing process. These enrichments are examined in terms of the Rayleigh distillation model (Fig. 11). The equilibrium-type curve of the fractionation factor (α) is 1.0028 for oxygen and 1.0206 for hydrogen (O'Niel 1968). However, the models show both oxygen and hydrogen, indicating the existence of non-equilibrium conditions (α = 1.006 for oxygen, α = 1.030 for hydrogen) (Fig. 11). The reason for the higher number in the fractionation factor (α)

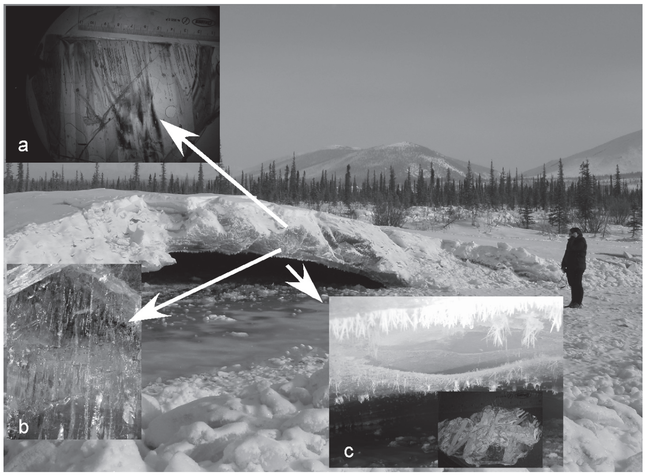

Figure 7. Icing blister transect profile near Coldfoot. Three layers of enlongated ice crystals (a) with bubbles contained in a majority of the ice body. Iron-extracted layer (b) was observed in the lower 20 cm. Needle-shaped crystals develop at the bottom.

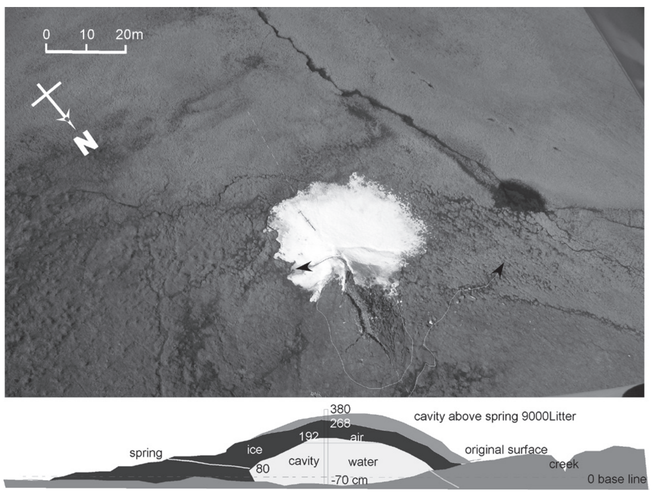

Figure 8. Diagram (lower) and aerial view (upper) of frost/icing blister at Hulahula River.

is unknown. It may be caused by the continual addition of water while freezing, resulting in a partially open system which will affect the fractionation.

The source water for this icing blister has high alkalinity (200–300mg/L) and was observed precipitating during the freezing process. This icing blister is not associated with hydraulic pressure from the groundwater; rather it is formed by hydrostatic pressure caused by freezing of the residual ion-rich water. There are a number of days that reach the freezing (thawing) point during spring months in this area. The unfrozen mineral-rich layer can associate with and move to an unfrozen layer.

Conclusions

Stable isotope signals from different types of ice-cored mounds (open- and closed-system pingos, palsas, icing blisters, frost blisters) were studied in relation to mound formation. An open-system ice-cored mound, such as an

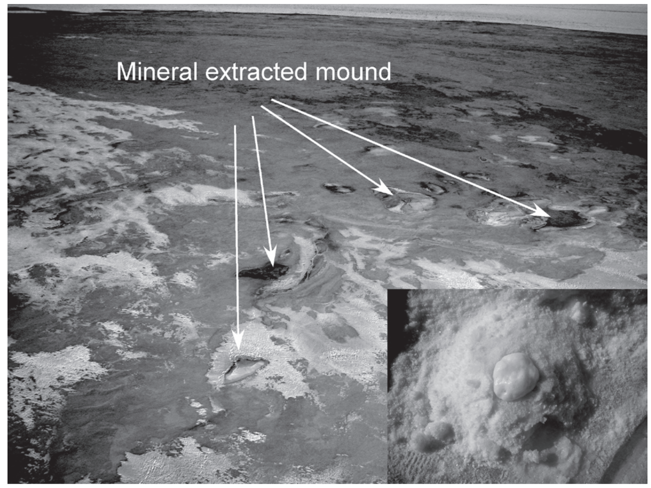

Figure 9. Salt extraction mounds (dark spots) are found at the Kuparuk River icing site during the spring period (April). After the drilling operation, highly concentrated minerals with yellow fine form rose to the ground surface (bottom right).

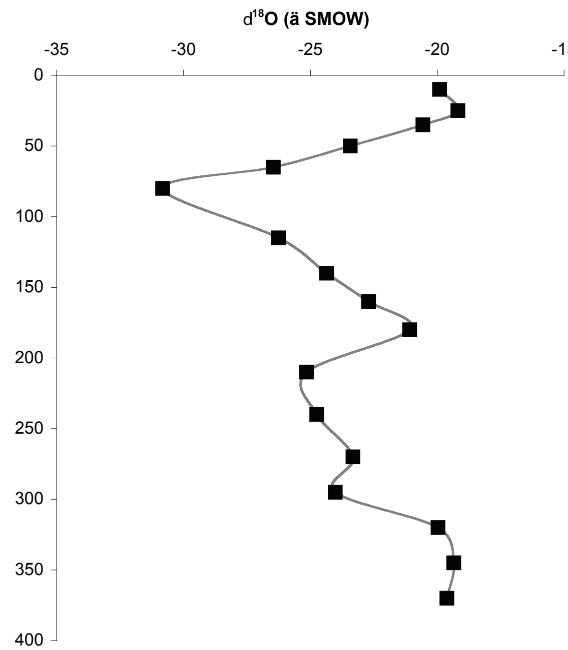

Figure 10. Strong (top down and bottom up) freezing process is observed between 30 cm and 180 cm depth. This is closed-system fractionation, where ice is progressively enriched under Rayleigh distillation of isotope signals and high concentrated ion layer at 80–110 cm.

open-system pingo or frost blister, freezes relatively fast with delayed enrichment of the isotope ratio at the uppermost ice layer. Once the stable freezing point is reached, the isotope value remains the same as that of an open environment.

The ice cores from palsas and closed-system pingos have signals of a semi-closed environment. The reservoir seems much bigger than the other closed-system mounds, but still follows Rayleigh distillation during freezing of the water. Icing blisters and frost blisters have very similar isotopic

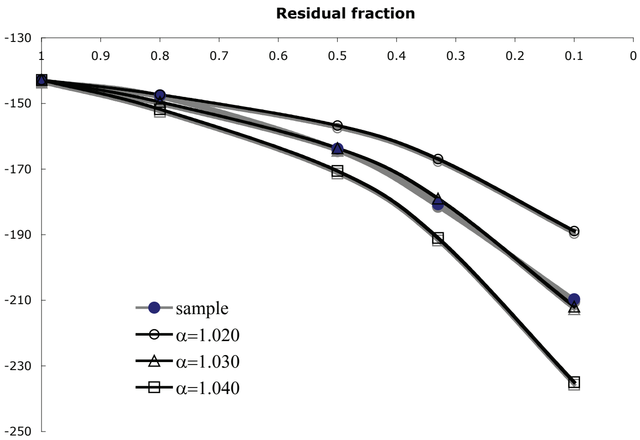

Figure 11. Sample value and calculated δD value for estimation of the fraction.

signals and ice structures. They develop (uplift) relatively quickly with a pressurized water source. The mound consists mainly of ice and water (cavity filling water). The water freezes downward following Rayleigh distillation. However, during the freezing process, especially with an icing blister, the chemical extraction involves dropping freezing point.

This study classifies the perennial and seasonal ice-cored mounds of four different stable isotope types by ice formation: 1) superimposed/crack ice, typically observed open-system condition; 2) upper part of frost blister, open system-pingo ice, rapid freezing with delaying enrichment; 3) open-system freezing ice, constant values of the isotope signals, and 4) semi-closed (or closed) freezing, following the Rayleigh distillation curve. Each of these isotope signals plays a critical role in revealing the growth mechanism of ice formation.

Acknowledgments

This project was funded by the National Science Foundation, Office of Polar Programs, Arctic System Science Program (ARC-0229705). We would like to thank Mr. Tohru Saito (University of Alaska Fairbanks), Dr. Atsushi Ikeda (University of Tsukuba), VECO Polar Resources for logistical support, and Tim Howe and other Water and Environmental Research Center staff members and students at the University of Alaska Fairbanks for help with laboratory analyses and field support.

References

Brown J., Nelson, F., Brockett, B., Outcalt, S.I. & Everett, R. 1983. Observations on ice-cored mounds at Sukakpak Mountain, southcentral Brooks Range, Alaska. *Proceedings of the Fourth International Conference on Permafrost, Fairbanks, Alaska, July 17–22*: 1983.

Clark, I.D. & Fritz, P. 1997. *Environmental Isotopes in Hydrogeology*. New York: Lewis Publishers, 328 pp.

Clark, I.D. & Lauriol, B. 1997. Aufeis of the Firth River Basin, Northern Yukon, Canada: Insights into permafrost hydrogeology and karst**.** *Arctic and Alpine Research* 29(2): 240-252. doi:10.2307/1552053.

Gibson, J.J. & Prowse, T.D. 1999. Isotopic characteristics of ice cover in a large northern river basin. *Hydrol. Process* 13: 2537-2548.

Gibson, J.J. & Prowse, T.D. 2002. Stable isotopes in river ice: Identifying primary over-winter streamflow signals and their hydrological significance. *Hydrol. Process* 16: 873–890. doi:10.1002/hyp.366.

Mackay, J.R. 1979. Pingos of the Tuktoyaktuk Peninsula, Northwest Territories. *Geographie physique et Quaternaire* 33: 3-61.

Mackay, J.R. 1990: Seasonal growth bands in pingo ice. *Canadian Journal of Earth Sciences* 27: 1115-1125.

Mackay, J.R. & Stager, J.K. 1966. The structure of some pingos in the Mackenzie Delta area, N.W.T., Ottawa. *Geogr. Bull.* 8: 360-368.

Michel, F.A. 1986. Isotope geochemistry of frost-blister ice, North Fork Pass, Yukon, *Canada. Canadian Jour. Earth Sci*. 23: 543-549.

Müller, F. 1959. Beobachtungen ber Pingos. *Meddelelser om Grønland.* 153: 1-127.

O'Niel, J.R. 1968. Hydrogen and oxygen isotope fractionation between ice and water. *Journal of Physical Chemistry* 72: 3683-3684.

Pollard W.H. 1988. Seasonal frost mounds. In: M.J. Clark (ed.), *Advances in periglacial geomorphology*. Chichester: John Wiley & Sons Ltd., 201-229.

Pollard, W.H. & French, H.M. 1985. The internal structure and ice crystallography of seasonal frost mounds. *Journal of Glaciology* 31: 157-162.

Seppälä, M. 1972. The term "palsa." *Zeitschrift für geomorphologie* 16: 463.

Washburn, A.L. 1983. What is a palsa? In: H. Poser & E. Schunke (eds.), *Mesoformen des reliefs im Heutingen periglazialraum. Gottingen, Mathematish, physikalische Klasse, Drilte folge,* nr. 35, 34-47.

Yoshikawa, K., 1993. Notes on open-system pingo ice, Adventdalen, Spitsbergen. *Permafrost and Periglacial Processes* 4: 327-334.

Hydrologic Status of High Arctic Ponds in a Continuous Permafrost Environment, Somerset Island, Nunavut, Canada

Kathy L. Young
Geography Department, York University, Toronto, Ontario, Canada, M3J 1P3
Anna Abnizova
Geography Department, York University, Toronto, Ontario, Canada, M3J 1P3

Abstract

In 2004, a suite of ponds, 71 in total, situated in moraine, coastal, and bedrock-wetland terrains were surveyed, in order to assess their sustainability in a continuous permafrost, polar desert environment. Snow cover, ground thaw, water table, and water quality were measured. In 2005 and 2006, detailed hydrological studies were undertaken on a selection of these ponds. The 2004 results indicate that snow depth, melt, frost table, and water table variations exist between the ponds located in the different geomorphic settings. Electrical conductivity of water varied due to differences in Na^{+}, Mg^{2+} and Ca^{2+}. The 2005 and 2006 results signaled the importance of pond substrate (e.g., texture, colour) in modifying ground thaw, vertical seepage, and evaporation rates. Terrestrial linkages of ponds to late-lying snowbeds, wet meadows, and streams sustain pond levels during dry, warm episodes, but not frost cracks which can divert water from ponds. Ponds in this extensive wetland might show a range of responses to future climate change.

Keywords: climate change; continuous permafrost; extensive wetland; High Arctic; ponds; wetland hydrology.

Introduction

Wetlands are important ecological sites in the High Arctic. They are often the only zones where sufficient grasses and sedges exist to supply northern ungulates, such as muskox and caribou, with sufficient grazing grounds. They also provide food and water for migratory birds and help to cleanse and store water. Permafrost is critical to their existence; it serves to maintain water tables near the ground surface and allows for the growth of hydric vegetation. Despite the ecological importance of wetlands, a limited understanding of their hydrology and chemical status still exits. Progress has been made in understanding small patchy wetlands lying in continuous permafrost terrain (e.g., Woo & Young 2003, Young & Woo 2003a, b), but less information exists about extensive wetlands. Woo & Young (2006) recognize three groups: periglacial polygonal areas (low-centered polygons, ice-wedge cracks), glacial terrain, and coastal zones. A recent study by Woo & Guan (2006) focused on the first type: tundra thaw ponds, lying within a polar oasis environment (warm/dry; see Woo & Young 1997). They found that linkages between ponds and the surrounding landscape were good at the time of snowmelt (shallow thaw), but connectivity dropped off with deep ground thaw and prolonged evaporation.

Here, an extensive wetland-complex, underlain by continuous permafrost and possessing a polar desert climate (cool/wet; see Woo & Young 1997) is examined. It is characterized by numerous ponds, lakes, wet meadows, streams, and dry ground, and encompasses a range of surfaces: glacial terrain, bedrock, and coastal zones. The region is considered ecologically significant to migratory birds (Latour et al. 2005), but a clear understanding of the area's present and future sustainability has not yet been achieved.

Here we report on the characteristics of the typical ponds situated in three broad geomorphic zones (moraine, bedrock, and coastal) in relation to several environmental factors (e.g., snow, sediment, frost, water tables, and water quality). Detailed hydrological studies conducted on a selection of these ponds (small to large in area) during 2005 and 2006 are useful in confirming and understanding these spatial patterns. Finally, our study provides an indication of how these ponds might respond to future climate change.

Study Area

The study area is located in an extensive low-gradient wetland complex situated on the southern shore of Creswell Bay, Somerset Island, Nunavut (72°43′N, 94°15′W). Continuous permafrost exists here, and active layers approach 0.40 m in boggy areas and about 1.0 m in sandy and gravely zones. There are no continuous climate records from Somerset Island, but the area is considered to have a polar desert climate similar to Resolute, Bay, Cornwallis Island (200 km to the north) with its long, cold, dry winters and brief, cool, damp summers (Dyke 1983).

The study encompasses about 23 km^2, and the site contains two contrasting landscapes, the northern part being modified by beach and coastal processes and the southern section showing evidence of glacial and periglacial influence (Brown & Young 2006). Figure 1 provides an aerial photograph, depicting the general area. Letters indicate ponds in the main geomorphological zones (moraine, bedrock, and coastal). Ponds in the moraine area exist both in an upper plateau area (>40 m a.s.l) and at a lower elevation (c.a. 25 m) with the latter fed by a stream draining the upland. Lingering snowbeds are typical of the west bedrock ponds, while major and minor frost cracks running generally east-west across the landscape are typical in the coastal wetland zone (see Fig. 2).

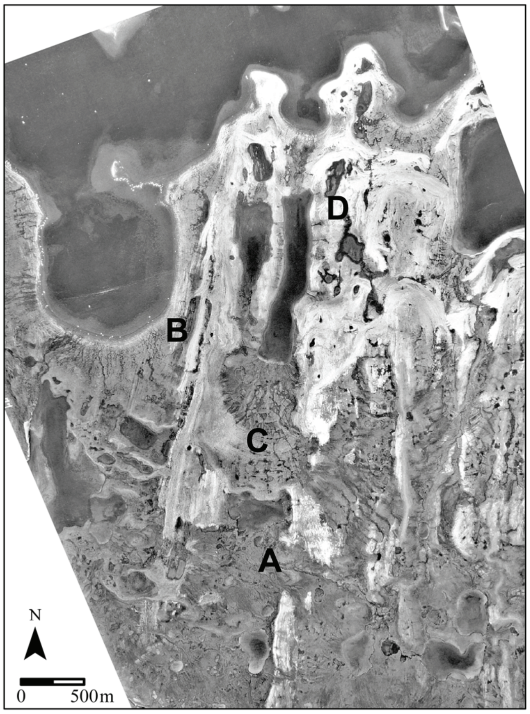

Figure 1. Aerial photograph of the study area: A-moraine zone; B-west bedrock zone; C-coastal area; and D-east bedrock zone. Creswell Bay is at the top of the diagram, and an Automatic Weather Station (AWS) is located near A.

Figure 2. Photographs of typical ponds in the study area: A-Moraine; B-West Bedrock; C-Coastal and D-East Bedrock pond. Note frost crack adjacent to Coastal pond and late-lying snowbed beside the West Bedrock pond.

In 2005 and 2006, at least three ponds (small, medium, and large) were selected from each zone for detailed study (late May to early August).

Methodology

Fieldwork 2004

Ponds dominate the landscape, so an earlier map of this region (Brown & Young 2006) was used as a guide to select the study ponds. In total 71 ponds ranging in size (small-median 510 m^2, medium-median 1,710m^2, and large-median 11,624 m^2) were examined. Due to logistical constraints (traveling by foot), we selected eight of these ponds to conduct detailed snow surveys in early June 2004. These ponds represented the three main geomorphic areas: in total, four moraine ponds with one situated on the upper plateau; two coastal ponds; one west bedrock pond and one small east bedrock pond. Snow surveys (i.e., snow depths, density) were conducted at each pond site. A physically-based snowmelt model described by Woo & Young (2004) was used to model melt for the ponds in 2004. Meteorological information (net radiation, incoming and outgoing solar radiation, air temperature, relative humidity, precipitation, and wind speed and direction) obtained at the AWS was used to drive the model.

During the post-snowmelt period, a comprehensive survey of the 71 ponds was conducted from July 18–July 25. The ponds occurring in the main geomorphic regions: moraine, west and east bedrock, and coastal are examined here. Position and area of ponds was determined using a Garmin 12 XL GPS (±3 m). The frost table divides the zones between thawed and frozen ground and provides an indication of water storage and seepage potential. Development of the thaw zone usually develops rapidly after the snow cover is depleted, but is also influenced by temperature gradients, surficial materials, and ice content. At each pond site, frost table position was measured by probing with a frost rod (±5 mm) until frozen ground was encountered. Three measurements at each pond site were made: 1 m from shore, 1 in the center of the pond, and then 1 between the center of the pond and the shore. Water table, the height of the water level above or below the ground surface, was determined adjacent to frost table measurements with a metric ruler (±5 mm). Estimates of water and frost tables for each pond at the time of sampling were averaged prior to analysis (see Fig. 4). Presence of plants (i.e., type and amount) was recorded, and a soil core of the near-shore sediment was obtained (250 cm^3). This soil sample allowed volumetric soil moisture to be determined, and was used to assess organic content (loss on ignition), soil color, and grain size (Sheldrick & Wang 1993).

Water quality information is helpful in determining relative water sources and periods of dilution and drying. The pH and water temperature were measured with a Hanna #18424±0.01 type meter. The electrical conductivity was measured with an YSI 30 ±0.1 µS/cm meter. A water sample was obtained from each pond, kept cool and returned to the York University Biogeochemistry Laboratory. Here the samples were analyzed for major cations (Ca^{2+}, Mg^{2+}, Na^+, and K^+) using a Spectra-10 Atomic Absorption Spectrometer, and laboratory standards and blanks were run to ensure quality control. The means and standard deviation of samples are reported. A Student t-test with unequal variance ($\alpha = 0.05$) was used to assess differences between ponds and aid in the discussion.

Fieldwork 2005, 2006

A detailed water balance framework was employed to investigate the hydrology of typical ponds (small to large) lying within the three broad geomorphic zones. Similar to 2004, snow surveys were conducted to determine initial pond and catchment's snow amount (in snow water equivalent units). Snowmelt was modeled and confirmed in the field with ablation measurements. In August 2004, perforated and screened water wells were placed along transects at each study site, dissecting both the pond and its catchment. Water tables were measured routinely in these wells at least every other day in 2005, 2006. Frost table was measured adjacent to these wells twice a week. Groundwater movement was estimated using the Darcy's approach. Soil moisture was measured both indirectly (Theta Probe) and directly (gravimetrically). Evaporation loss was determined using the Priestley-Taylor approach, with meteorological data supplied from the main AWS, and a portable AWS station which roved between the pond sites. Pond shrinkage was accounted for in the evaporation estimates. Streamflow both into and out of the moraine zone was estimated using the velocity-area approach. Retreat of a late-lying snowbed, which continued to supply moraine ponds with meltwater after the main melt period, was quantified on a daily basis. All ponds and their catchments were surveyed with a Total Survey Station in July 2005. In 2005 and 2006, no measurements were made of west bedrock ponds. Here, logistical and time constraints prevented these types of detailed measurements.

Results and Discussion

July 2004 was colder than 2005 and 2006, and much rain fell towards the end of July. In 2005, rain events were more frequent but of shorter duration than in 2006. Poor conditions during the early part of the season in 2006 resulted in greater rain and snow.

Environmental factors

Snowfall in the High Arctic usually occurs from September until May. Spatial variation in snow coverage and variations in the timing and duration of melt is important in the initiation of water for runoff, in defining the pattern and timing of ground thaw, and for providing waters for evaporation and/or infiltration.

Table 2 indicates the range of snow water equivalent (SWE, mm) for the study ponds in 2004. Initiation and duration of melt is also shown. For comparison, snow data from medium-sized ponds (2005, 2006) are also presented. Snow amount varies amongst the different pond types and within the same zones due to subtle differences in topography. However, snow amounts are still higher than that observed for a polar oasis environment (Woo & Guan 2006), but timing of melt and duration is generally later and longer. Hence, these ponds experience a polar desert climatic regime.

Ponds in the lee of slopes (e.g., a moraine pond-258 mm w.e.) can accumulate much snow, being sheltered from high winds. Other ponds on exposed ridges (e.g., west bedrock pond-58 mm w.e) have less snow due to steady winds redistributing snow. Topographic depressions (east bedrock-124 mm w.e.) provide shelter from wind and are effective in capturing much snow. Table 2 indicates that snow accumulation patterns are typical from one year to the next, though variations in amount can exist. Melt duration also varies amongst the sites. Some pond sites with shallow snow become isothermal and melt out earlier (e.g. west bedrock, 2004) than other sites with much snow (e.g. moraine, east bedrock, 2004).

Soil texture and organic content are important factors in the evolution of ground thaw and storage capacity. Fine soils (e.g., silts/clays) with high organic contents can hold considerable ground ice and can store much water, delaying thaw as ice melts and energy is consumed in evaporation. Once vegetation and organic materials start to dry out, they can serve as an effective insulator delaying the thaw of ice further and even encouraging permafrost growth. While coarse soils can contain ground ice, these soils and areas with little vegetation or organic cover will generally experience enhanced thaw (e.g., Woo & Xia 1996; Young & Woo 2003a). Figure 3 provides an assessment of grain-size distribution and organic content of surveyed ponds (small to large).

Table 1. Summary of climatic conditions.

Year/Month	Ta (°C)	PPT (mm)	Thaw Days
2004			
July	3.8	37.7	117
2005			
June	1.2	8.1	36
July	4.8	31.8	145 (121*)
Aug.	5.0	6.7	15
2006			
June	0.6	47.0	15
July	5.6	21.2	138 (till JD 207)

*Thaw days up until JD 207 (July 26).

Table 2. Range of snow conditions for study ponds: SWE (mm), initiation and duration of melt; 2005 and 2006 data are for medium-sized ponds.

Year/Ponds	SWE (mm)	Initiation of Melt	Melt Duration (days)
2004			
Moraine	77-258	June22 (JD 174)	6-9
Coastal	101-108	June 21 (JD 173)	8
East Bedrock	124	June 21 (JD 173)	9
West Bedrock	58	June 10 (JD 162)	11
2005			
Moraine	148	June 7 (JD 163)	10
Coastal	163	June 4 (JD 155)	9
East Bedrock	258	June 8 (JD 159)	14
2006			
Moraine	115	June 12 (JD 163)	10
Coastal	122	June 11 (JD 162)	9
East Bedrock	163	June 12 (JD 163)	11

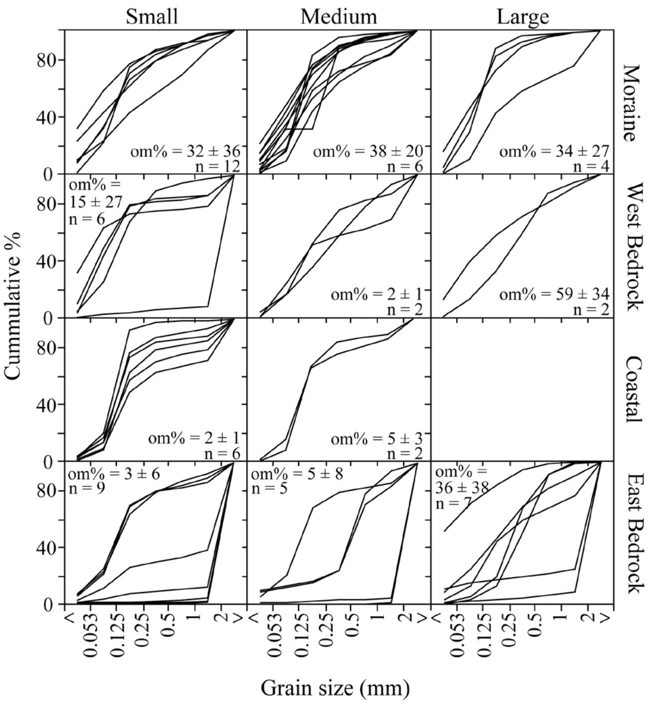

Figure 3. Grain size analysis and % organics (±standard deviation, and sample size [n]) of soil samples obtained at surveyed ponds (small to large).

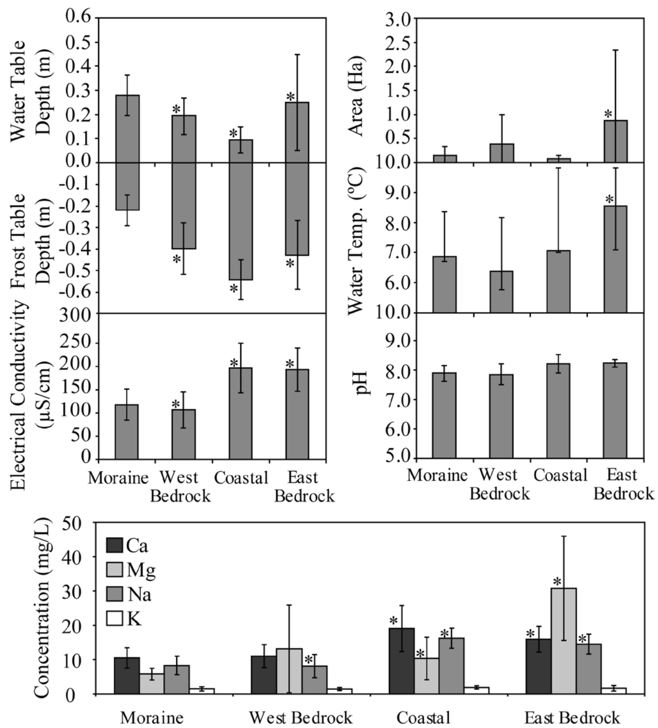

Figure 4. Selected environmental factors of all surveyed ponds. Significant differences of coastal and bedrock ponds to moraine ponds are indicated by an asterisk (*). Analysis is based on Student T-tests (α=0.05). Standard deviation bars are plotted.

Moraine ponds have a high amount of fines, while coastal ponds comprise fine sands and have the most uniform soil texture. West bedrock pond substrates are generally coarse, and soil texture is most variable in the east bedrock ponds. This reflects a longer period for these ponds to accumulate fine sediments through the dissolution of rocky material.

Moraine pond soils contain high organic contents, arising from extensive wet meadows with grasses and sedges surrounding most ponds in this area. In small and medium ponds (both bedrock types and coastal), organic percentages are low, reflecting the sparse vegetation coverage around these pond-types. However, as pond size increases, organic content also rises. The slow accumulation of fines in these areas eventually gives rise to a prolific wet-meadow community.

Environmental response

Figure 4 indicates a range of environmental factors which were measured over a short time span (mid-July to early August 2004). All ponds surveyed (small to large) are grouped here for analysis. A similar diagram for "small" ponds emerged, but these results are not reported here. The data indicate that we sampled more "large" east bedrock ponds, with some much larger than the other ponds.

The position of the frost table defines the position of the water table and can influence the presence of both surface and subsurface flow. Moraine ponds had the shallowest thaw (0.2 m) at the time of sampling, an observation which is supported by process studies in 2005 and 2006 (see Fig. 5). The frost table is deepest in the coastal ponds and is indicative of the coarser soils here and the lack of vegetation. Frost tables in the west and east bedrock ponds are all deeper than moraine ponds, arising from their coarser substrate, which enhances deeper thaw and vertical seepage. Some east bedrock ponds also possess black (blue-green algae) substrates (e.g. 5YR 2.5/1). This dark surface triggers two processes. Radiation penetration through clear pond water can be absorbed by this dark surface (α = 0.10, 2005), and the heat generated can then be used to warm the water and enhance evaporation, leading to lower water levels. It can also accelerate ground thaw and vertical seepage by elevating the thermal gradient at the water/substrate interface (see Oke 1987).

Water table is an important indication of the balance between water inputs and losses in a pond. High water tables may encourage runoff and sustain evaporation, and its persistence throughout a dry summer is indicative of lateral water inputs (i.e., surface and/or groundwater). Low water tables in the absence of rain can suggest an isolated system where vertical processes dominate; evaporation and/or seepage to the subsurface. Landscape alterations, such as erosion of a pond rim or an enlarged drainage outlet, may also encourage pond drainage and desiccation (e.g., Woo & Guan 2006).

Figure 4 indicates that water tables in the moraine ponds are greater than the other ponds. This is a reflection of the materials (greater % of fines and organics) which give rise to shallow frost tables, ensuring elevated water tables (Young & Woo 2003a). This area, especially the low-lying area, also received much water from a stream which drained the upland area. Several ponds in this area were also adjacent to late-lying snowbeds which continued to supply this area with meltwater long after the seasonal snowpack had disappeared (Fig. 5).

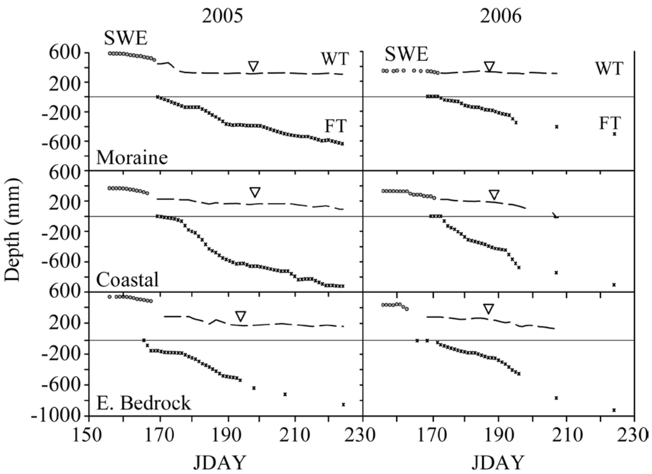

Figure 5. Seasonal patterns of frost and water table at the medium-sized ponds in 2005 and 2006.

Coastal ponds have the lowest water tables, owing to the higher proportion of coarser materials here and less vegetation, two factors which promotes deeper thaw and vertical water seepage. Frost cracks which dissect this zone serve as "sinks" during dry episodes, channeling water out of the ponds by setting up a hydraulic gradient (i.e., reversal of flow). Groundwater outflow from these ponds was estimated to be 1.3 x 10^{-2} m^3/d per unit m in 2005 and 2.8 x 10^{-2} m^3/d per unit m in 2006.

Water tables are higher in the east bedrock ponds. Many ponds occur in slight topographic depressions which are effective in trapping and sheltering much snow. Deeper snow prolongs melt, and delays ground thaw and evaporation losses. In warm years, ground-ice melt from the surrounding rocky catchment helps to maintain water levels (e.g., 2006).

All ponds are slightly alkaline owing to the underlying bedrock materials: limestone and dolostone. Water temperatures are the highest in the east bedrock ponds due to the dark substrate of most ponds here, which readily absorbs radiation and warms the waters. This pattern was similarly repeated in 2005 and 2006. Cooler water prevails at the other sites, which suggests frequent additions of cool water; i.e., stream water recharging ponds (e.g., moraine), and/or meltwater from late-lying snowbeds (e.g., west bedrock).

Electrical conductivity of the bedrock ponds and the coastal ponds are significantly different than the moraine ponds. Deeper thaw and shallower water tables ensure that waters have prolonged contact with the substrate, allowing additional solutes to be absorbed. Nearness to the sea allows salts and aerosols to be easily carried by sea breezes, fog, and rain, helping to elevate levels. Electrical conductivities are dampened in moraine ponds owing to high water tables, which are maintained by shallow ground thaw and the continual recharge by stream water and melting of late-lying snowbeds. West bedrock ponds have slightly lower electrical conductivities than the moraine ponds. Steady meltwater inputs from snowbeds, which lie in the breaks-of-slopes above many of these ponds, is effective in diluting pond waters.

Higher electrical conductivity values at the east bedrock and coastal pond sites can be attributed to higher values of Ca^{2+}, Mg^{2+}, and Na^+ at these sites. Elevated values of Ca^{2+} and Mg^{2+} reflect the bedrock type and greater ground thaw. Na^+ is much higher at the bedrock ponds owing to its nearness to the ocean and occurrence of sea breezes. The west bedrock ponds are on the west side of a NE-SW bedrock ridge lying adjacent to an inlet of Creswell Bay (see Figs. 1, 2). Winds blew from the NW in 2004, about 40% of the time and likely were effective in transferring sodium into these ponds.

All sites had low values of K^+, less than 5 mg/L. This is a common occurrence, given that any available K^+ is readily taken up by plants.

Response to climate change

The recently published ACIA (2005) suggests that arctic regions will be significantly affected by climate warming, with increases in precipitation (likely rainfall) and warmer temperatures. It is postulated that these ponds, despite occurring within a small landscape, will likely respond differently to these anticipated changes. For example, warmer and drier summers might mean the disappearance of many of the late-lying snowbeds which now feed several ponds both in the moraine and bedrock zones. These late-lying snowbeds are vulnerable to short-term changes in climate (Woo & Young 2003) and can disappear from the landscape, depriving downslope areas and ponds of water (Brown & Young 2006). Given the likelihood that these snowbeds will be vulnerable to shifting and changing climatic conditions, then it is probable that the electrical conductivity levels and solutes will also shift. The electrical conductivity levels of west bedrock ponds are now similar to moraine ponds largely due to the diluting effect of the late-lying snowbeds. However, with no additional meltwater inputs in the summer period, these waters will become more comparable to east bedrock ponds where electrical conductivity values are twice as high.

The ponds able to sustain themselves the best will be the low-lying moraine ponds. The occurrence of fine soils with much organics is able to promote ground ice and shallow thaw. Continual discharge of stream water into this zone, along with melting late-lying snowbeds, ensures elevated water tables, and buffers most of these ponds against warmer and drier summers.

Coarse and darkened substrates encourage ground thaw and vertical seepage. If water supplies are not sufficient to overcome losses, then many of these types of ponds might disappear. One other possibility is that emergent grasses may start to encroach and transform ponds into wet meadows. This process was observed for a small pond near Eastwind Lake, Ellesmere Island, in 2005. Others have noticed similar trends (e.g., Smith et al. 2005).

It is postulated that large ponds in all areas will likely sustain themselves in a warmer climate. They often have more fine material than smaller ponds and are linked to both wet meadow areas and smaller ponds which can funnel water into their watersheds during melt and rainfall events.

Summary and Conclusions

This pond survey undertaken in 2004 reveals the following:

(1) Within a polar desert wetland-complex, there can be significant differences in the types of ponds existing. Response of the ponds in terms of water table position, ground thaw, and water quality is strongly controlled by the substrate type, topography (level versus depression), and linkages with other water sources (streams, frost cracks). Ponds found in moraine areas tend to have fine substrates, higher water tables and shallower ground thaw than ponds occurring in coarse textured areas (e.g. coastal, east bedrock), unless additional sources of water are available (e.g., west bedrock ponds-meltwater from late-lying snowbeds). Higher conductivities and solute levels are common in the coastal and east bedrock ponds where water inputs are limited.

(2) It is likely in a warmer/drier climate that the ponds which possess a greater percentage of fine materials and organics and receive additional contributions of water aside from snowmelt and rainfall (e.g., stream water recharge, meltwater from late-lying snowbeds, groundwater inflow) will be able to sustain themselves in the future. It is the "isolated" ponds, shallow and poorly defined ponds (wind-swept), and/or ones with coarse and/or dark substrates which will be the most susceptible to demise.

(3) It is expected that the low-lying moraine zone of this wetland-complex will remain little changed; ponds receive multiple sources of water and have much fine sediments and organics to minimize thaw and maintain relatively high water tables. The coastal and east bedrock ponds, especially small ones, will be the most vulnerable. Years with low snowfall, little rain, and warm summers may see many of these ponds dry up and/or be overtaken by emergent grasses.

(4) The west bedrock ponds can be considered to be in "transition." Presently, they behave much like moraine ponds. Water tables are elevated despite coarse bedrock, with water being supplied by melting late-lying snowbeds. However, these snowbeds are vulnerable to warm/dry years and can be severely reduced in size or disappear completely from the landscape (Brown & Young 2006, Woo & Young 2006). In the long-term, climate warming will likely result in the disappearance of these snowbeds, and when this occurs, west bedrock ponds will begin to behave like the east bedrock ponds.

Acknowledgments

Funding for this project was provided by NSERC and NSTP. Logistical support from PCSP is gratefully acknowledged. Excellent field assistance was provided by Dan Thompson and Markus Anastasiades. Laboratory assistance by Jackson Langat is also appreciated. The authors are grateful to an anonymous reviewer whose suggestions have improved the paper.

References

ACIA (Arctic Climate Impact Assessment). 2005. Impacts of a warming Arctic: Arctic climate impact assessment. Cambridge: Cambridge University Press, 1042 pp.

Brown, L. & Young, K.L. 2006. Assessment of three mapping techniques to delineate lakes and ponds in a Canadian High Arctic wetland complex. *Arctic* 59: 283-293.

Dyke, A. 1983. Quaternary geology of Somerset Island, District of Franklin. Geological Survey of Canada, Memoir 404.

Latour, P.B., Machtans, C.S. & Beyersbergen, G.W. 2005. Shorebird and passerine abundance and habitat use at a High Arctic breeding site: Creswell Bay, Nunavut. *Arctic* 58: 55-65.

Oke, T. 1987. *Boundary Layer Climatology* (3rd edition). London: Meuthen and Co., 435pp.

Sheldrick, B.H. & Wang, C. 1993. Particle size distribution: Soil sampling and methods of analysis. In: M.R. Carter (ed.), *Canadian Society of Soil Science.* Boca Raton: Lewis Publishers, 499-511.

Smith, L.C., Sheng, Y., MacDonald, G.M. & Hinzman, L.D. 2005a. Disappearing Arctic lakes. *Science* 308: 1429.

Woo, M.K. and Xia, Z.J. 1996. Effects of hydrology on the thermal conditions of the active layer. *Nordic Hydrology* 27: 129-142.

Woo, M.K. & Young, K.L. 1997. Hydrology of a small drainage basin with polar oasis environment, Fosheim Peninsula, Ellesmere Island, Canada. *Permafrost and Periglacial Processes* 8: 257-277.

Woo, M.K. & Guan, X.J. 2006. Hydrological connectivity and seasonal storage change of tundra ponds in a polar oasis environment, Canadian High Arctic. *Permafrost, Periglacial Processes* 17: 309-323.

Woo, M.K. & Young, K.L. 2006. High Arctic wetlands: Their occurrence, hydrological characteristics and sustainability. *Journal of Hydrology* 320: 432-450.

Woo, M.K. & Young, K.L. 2004. Modelling arctic snow distribution and melt at the 1-km grid scale. *Nordic Hydrology* 35: 295-307.

Woo, M.K. & Young, K.L. 2003. Hydrogeomorphology of patchy wetlands in the High Arctic, polar desert environment. *Wetlands* 23: 291-309.

Young, K.L. & Woo, M.K. 2003a. Frost table development beneath patchy wetlands in a continuous permafrost, High Arctic setting. *Proceedings, Eighth International Conference on Permafrost, Zurich, Switzerland July, 2003:* 1265-1270.

Young, K.L. & Woo, M.K. 2003b. Thermo-hydrological responses to an exceptionally warm, dry summer in a High Arctic environment. *Nordic Hydrology* 34: 51-70.

Recent Comparative Investigations and Monitoring of Permafrost of the Eastern and Western Qinghai-Tibet Plateau, China

Qihao Yu
State Key Laboratory of Frozen Soil Engineering, Cold and Arid Regions Environmental and Engineering Research Institute, Chinese Academy of Sciences, Lanzhou 730000, China

Kurt Roth
Institute of Environmental Physics, University of Heidelberg, Heidelberg D-69120, Germany

Huijun Jin
State Key Laboratory of Frozen Soil Engineering, Cold and Arid Regions Environmental and Engineering Research Institute, Chinese Academy of Sciences, Lanzhou 730000, China

Abstract

To further understand the degradation process of permafrost on the Qinghai-Tibet Plateau (QTP) and its environmental impacts, a Sino-German joint team conducted a pilot research project in the interior and on the eastern and western parts of the QTP. Preliminary results show that characteristics of surface landscapes have important influences on heat and mass transfer in soils. Major differences between cold (<-4°C) permafrost in the Tianshuihai Lake region and warm (>-1°C) permafrost in the interior and eastern QTP lie in their features of lithology, ice content, and ground temperature. The ecological environments in the Tianshuihai region have changed greatly in the past 30 years: large areas of vegetation have degenerated or vanished with considerable surface soil salinization. Extensive occurrences of small pingos, unsorted circles, sand wedges, and polygonal ground, and other periglacial phenomena were identified in the Tianshuihai area. Geophysical surveys indicate that topography, vegetation, and surface moisture conditions have substantial impact on the permafrost table and ground ice.

Keywords: environments; permafrost; Three Rivers Sources; Tianshuihai area; vegetation.

Introduction

The Qinghai-Tibet Plateau (QTP) is considered the third largest cold region on earth and is the source region of most major rivers in Asia (Zhou 2000). The source region of theThree Rivers (Yangtze, Yellow, and Lancang-Mekong) is in the interior and on the eastern part and feeds about 6×10^{10} m^3 of water per year into the three rivers. The water flow volume in the source of each of the Three Rivers respectively accounts for 49%, 15% and 1% in the total volume of each river (Li et al. 2006). The cold-region hydrological processes, especially the modification of hydrologic cycling by climate warming, have attracted increasingly more public attention in recent years. To understand the degradation of permafrost and its environmental impact in the source regions of the Three Rivers in the interior and eastern QTP, as well as in the Tianshuihai region in the Western Kunlun Mountains on western QTP, a series of preliminary research and field investigations have been conducted.

The source region of the Three Rivers is in the continuous and discontinuous plateau permafrost zones, where cold climate and permafrost produce a special hydrologic cycle, cryogenic phenomena, and fragile ecological environments (as shown in Fig. 1). The changes in cold-region ecological environments have directly impacted the water storage. Major ecosystems, such as the paludified alpine meadows, grasslands, and steppes degraded markedly between the 1970s and 1990s (Cao et al. 2006). Degradation of permafrost and ecological environments represented by aeolian desertification has been accelerated since the 1990s because of persistent regional droughts and overgrazing (Cheng & Wang 1998, Wang et al. 2000, Yang et al. 2004, Jin et al. 2007). In recent years, the aggravated ecological environment in the source region of the Yellow River has been seriously impacting its regional sustainable development, and could be one of the primary reasons for the decreasing runoff of the Yellow River from Qinghai Province, and for the increasing soil and water erosion (Kang 1996, Cheng et al. 1998). Thus, permafrost degradation modes and processes, and their ecological impacts are subjects of major research (Jin et al. 2006).

The distribution and degradation of permafrost in regions along the the Qinghai-Tibet Highway and Railway have been studied in more detail using meteorological measurements and the established long-term monitoring systems (Li et al. 2005, Wu et al. 2005, Jin et al. 2006, Cheng & Wu 2007). However, these observation systems are close to regions frequently and significantly impacted by human activities, and vast regions in the west and east remain unknown due to difficult access to and subsequent paucity of data.

The active layer is the crucial link between the climate and permafrost during the permafrost degradation process and can buffer climatic impact on permafrost. However, other than along the Qinghai-Tibet Highway, the heat, moisture, and mass transfer processes in permafrost soils had not been studied in detail (Li & He 1990, He 1991, Li et al. 1998). There also are remarkable differences between cold (<-4°C) permafrost in the Tianshuihai Lake region in the western Kunlun Mountains and warm (>-1°C) permafrost in the interior and eastern parts of the QTP.

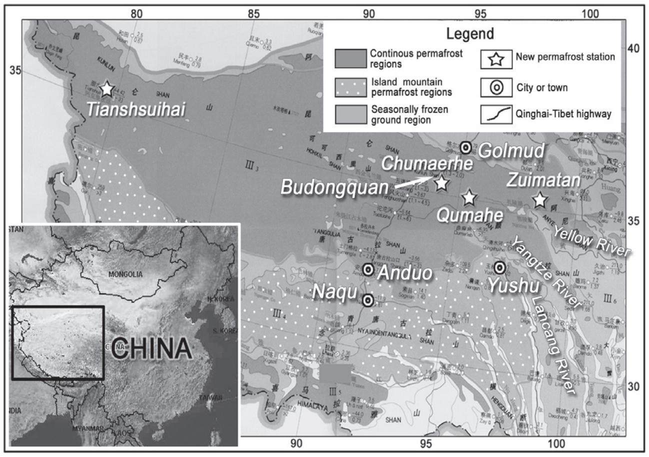

Figure 1. The extent of permafrost on Qinhai-Tibet Plateau in China and the positions of new permafrost stations established on QTP in the Sino-German joint research project.

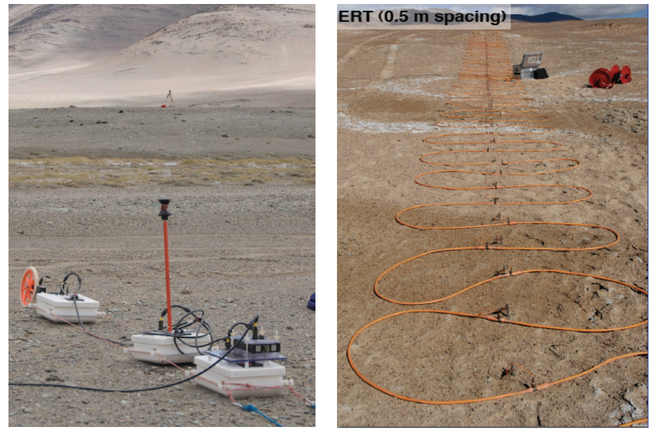

Figure 2. Some of the geophysical methods used in permafrost investigation in this project. The left is ground penetrating radar, and the right is electrical resistivity tomography.

Two joint teams from the Institute of Environmental Physics, University of Heidelberg, Germany, and the Cold and Arid Regions Environmental and Engineering Research Institute, Chinese Academy of Sciences conducted field investigations on the degradation of permafrost on the QTP and its environmental impacts in the source regions of the Three Rivers, in the east from August to October in 2006, and in the Tianshuihai Lake region in the Western Kunlun Mountains in August to September 2007. Three long-term monitoring stations were established in Zuimatan, Qumahe, and Chumaerhe along the access road from Yushu, along National Highway 214 (Xi'ning to Yushu section) to Budongquan along National Highway 109 (Golmud to Lhasa section) in 2006; a long-term monitoring station was established in Tianshuihai (Fig. 1). These stations are the very first in these regions.

Methods

Conventional exploratory methods such as hand-dug pits, water and soil sampling, in situ measurements of soil moistures and temperatures, and surface surveys were augmented with new geophysical investigation methods (Fig. 2), such as electrical resistivity tomography (ERT), new multi-channel ground penetrating radar (GPR), electromagnetic survey (EMS), and DC-resistivity (Arcone et al. 1998, Jared et al. 2003, Pettersson & Nobes 2003, Sass 2000, Schwamborn et al. 2000, Yu & Cheng 2003). They were applied for investigating the structures of the active layer, permafrost, cryogenic phenomena and vegetative differentiations, distribution of ground water tables and soil moistures, migration of salts, the physical properties of permafrost in the vicinity of the permafrost table, and the thickness of permafrost.

Results and Discussion

1) Based on investigations in the source regions of Three Rivers, three sites with representative landscapes were instrumented for soil and weather data as shown in Figure 1.

The landscape at the Chumaerhe Station is characteristic of barren land with sparse vegetation, but rich in ground water. The Qumahe Observation Plot is more densely vegetated and is covered by about 20 cm of peat layer. The Zuimatan Observation Site is sparsely vegetated, with saline soils and groundwater. The three sites were chosen along a gradient of the permafrost; with Chumaerhe in the continuous permafrost region, Qumahe in the patchy permafrost region and Zuimatan at the edge of the patchy permafrost region. In addition to measurements of wind direction and speed, air temperature, precipitation, and net radiation, there are profiles of temperature sensors and of CS616 and TDR100 soil moisture sensors down to the ice table at depths between 1.3 m and 2.8 m. The interval of the temperature sensors is 10 cm to 20 cm, and that of the moisture sensors is 20 cm to 40 cm. Furthermore, there are borehole temperature sensors from 3 m to 15 m with intervals between 0.5 m and 1.0 m (Table 1).

2) In Three Rivers source region and Tianshuihai Lake area, water and soil samples at different depths were collected in the active layer of various surface landscapes for studying the cryogenic phenomena and migration of salts.

Early data on ground temperatures at three stations in the east from early September to mid-October 2006 were read (Fig. 3). As indicated from the change in ground temperature, geomorphic units and surface landscapes have important influences on ground temperatures. The highest ground temperature is at the Chumaerhe Station, and the lowest is at the Qumahe Station. The temperature was always positive in this period, while the other two started freezing from the bottom. This shows that more vegetation in Qumahe tends to shade solar radiation onto the ground surface in summer, which helps in protection of permafrost by reducing surface heating (Fig. 3b). However, the freeze-up of ground is significantly later at the Zuimatan Station (Fig. 3a).

The Tianshuihai Lake region is the center of low air temperatures in China, and it could be the last region of permafrost degradation on the QTP in future (e.g. Li & Chang 1999). Continued research in this region is important

Table 1. The positions and observations of the comprehensive observation stations.

Stations	Chumaerhe (No.1)	Qumahe (No.2)	Zuimatan (No.3)	Tianshuihai
Characters	Discontinuous vegetation, shallow organic soil	Continuous vegetation, thick organic soil	Slight saline soil at surface, salty ground water	Slight saline soil at surface, no vegetation
Permafrost table	2.45	1.25	2.65	1.6
Ground water table	1.51	—	2.05	1.4
Latitude	93°57′E	94°47′E	99°08′E	79°32′ E
Altitude	35°11′N	34°54′N	35°22′N	35°24′N
Elevation	4443m	4447m	4187m	4840m
Observations	Net radiation, precipitation, air temperature at depth 2 m, atmospheric pressure wind speed, wind direction ground temperature, soil moisture.			

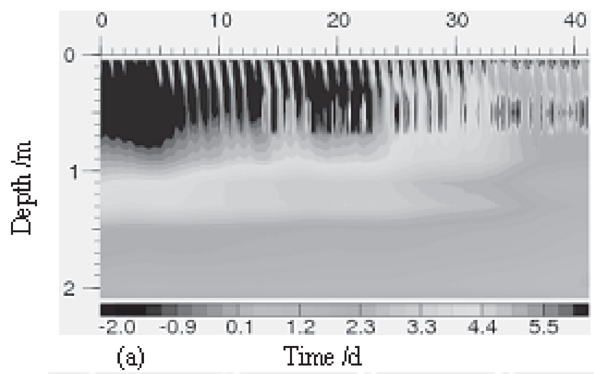

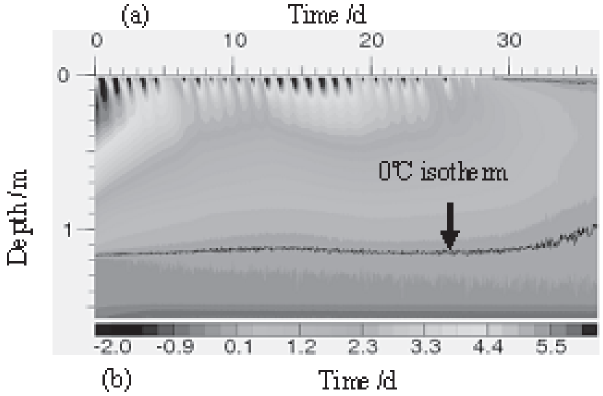

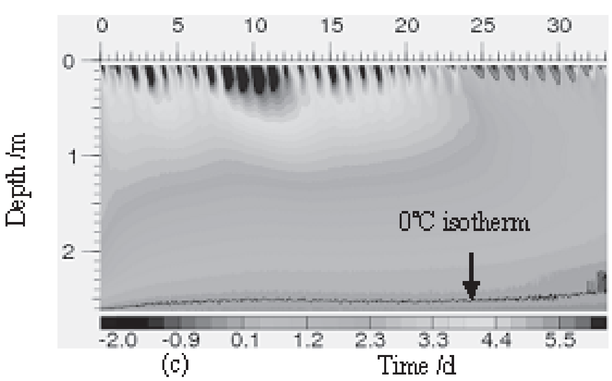

Figure 3. The ground temperature for the three weather stations are from Sept-Oct 2006. a. Chumaerhe station; b. Qumahe station; c. Zuimatan station.

for better understanding of existing permafrost conditions on the QTP as a whole and of its developing trends.

3) In the continuous permafrost region of Tianshuihai Lake area (79°26′E, 35°45′N, 4952 m to 79°59′E, 34°53′N, 5055 m) in Xingjiang Uygur Autonomous Region, although there is little precipitation, plenty ofsuprapermafrost water exists at the opened areas in alluvial-fluvial plains, and the ground water table is only about 1.0 to 1.2 m. Most of the surface is sparsely vegetated or completely barren; the coverage is generally less than 5% even on the gentle slopes. The ground ice was probably formed in the relict permafrost during the Late Quaternary, and the drainage patterns and mass and salt migration control the distribution of vegetation and permafrost. During the last 40 years, vegetation has changed significantly. For example, there was thick vegetation, and wild animals (like bronco) were at Tielongtan (79°40′E, 35°03′N, 4958 m) in the 1960s and 1970s, but it is barren land now (Li et al. 1998).

4) The geology and permafrost along the Xinjiang-Tibet Highway (K513~K650) significantly differ from those in the interior and on the eastern QTP.

Along the 80-km-long segment of the highway on the Tielongtan fluvial plain, the active layer is gravelly and with high ice content, sometimes even consisting of ice layers with soil inclusions on the gentle mountain slopes. Along the 30-km-long Gyttja section in the Tianshuihai Lake area, the soil consists of clayey sands with gravels or sandy clay. Dirty ice layers with volumetric ice content greater than 90% at depths of 1.0–1.4 m, are common.

5) At the Tianshuihai Lake region, permafrost is saline. The salinity of soils is low at the alluvial-proluvial fans; it is high on the gently sloped mountains, and even water at the low ground is salty. However, cryopegs were not detected during the investigation in the Tianshuihai area, whereas they are common on the northern QTP.

6) Extensive and various relict cryostructures, such as sand wedges and involutions, formed by soil movement during the freeze-thaw cycles were found in both research regions, and they have important influences on vegetation (Fig. 4) (Jin et al. 2007). There are many other periglacial phenomena, such as pingos and unsorted circles, and others, on the Tianshuihai Lake terraces and recently dried lakebeds (Fig. 5).

7) GPR exploration results show that landscape, vegetation distribution, and soil moisture content can significantly influence the permafrost table and ground -ice content. The coverage of small sand dunes, vegetation, and soil moisture conditions in or near ground surface are favorable for permafrost development and protection, while roads and tracks, as well as other human activities can lead to permafrost degradation (Fig. 6).

8) Geophysical methods, such as eletromagnetic survey

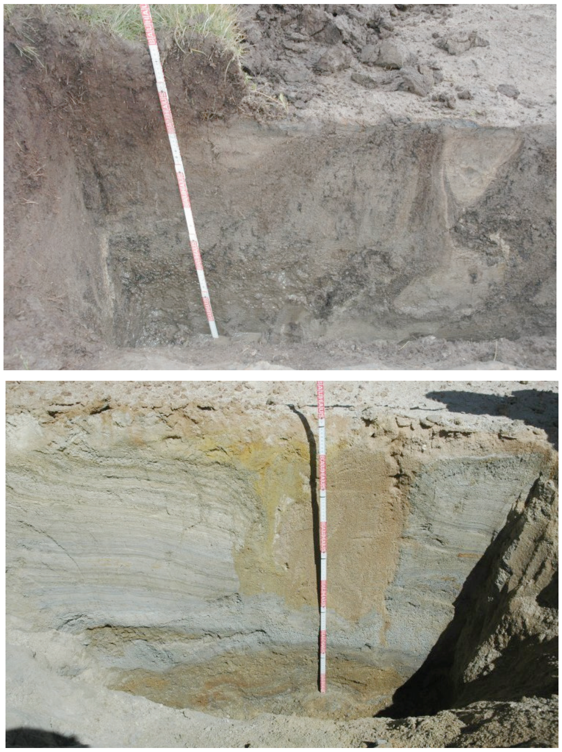

Figure 4. The upper picture is the involution found in river sources region, and the lower picture is the sand wedges found on the second Tianshuihai Lake terrace.

Figure 5. The landscape of cryogenic phenomena in Tianshuihai regions, the upper photo is pingo, the lower photo is unsorted circles.

(EMS), can better reveal the thickness of permafrost, especially for permafrost thicker than 50 m.

The EMS investigation results show that the thickness of permafrost is about 100 m in the Tianshuihai Lake area. Mean annual ground temperatures measured at depths from 15 m to 20 m in boreholes are about -2°C to -4°C. Considering the ground temperature gradient, the survey data with EMS should have good consistency with the average ground temperature.

9) The latest geophysical techniques have proven indispensable and effective tools for field permafrost research, particularly for revealing subsurface soil structures, moisture conditions, and other properties of permafrost, using various geophysical methods or their combinations.

Detailed information on the processes in the active layer and on the spatio-temporal changes of the permafrost table, such as soil strata and moisture contents, depth of the permafrost or ground water table, and distribution of ground ice can be obtained using GPR (better with multi-channel GPR) and ERT. To reveal the permafrost table and base, ERT is better for shallow permafrost, but EMS is better for thick permafrost. Soil moisture and salinity have strong influences on applicability and results of geophysical methods. In general, the quality of GPR survey data from areas with high soil moisture and salinity are usually poor and difficult (if not impossible) to interpret; ERT, EMS and DC-resistivity can provide viable alternatives under this circumstance. In dry areas, the situation is reversed.

The data and samples from field investigation and

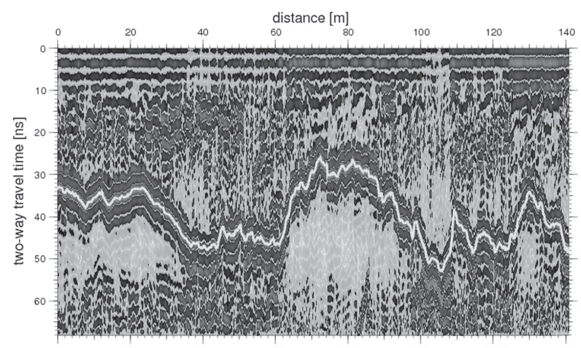

Figure 6. The investigation result of GPR in Tianshuihai.

monitoring are being studied. In the future, plans with emphasis on study of the western Kunlun Mountains will be executed. Further plans call for a north to south transect study through the permafrost province of the Tanggula Mountains and for construction of a third biodiversity transect in China, for the very important study of permafrost and cold-region ecology and biodiversity.

Acknowledgments

This research was supported by the Deutsche Forschungsgemeinschaft (DFG, Grant No. RO 1080/10-2), Chinese Academy of Sciences 100 Talents Project (Grant No. 0481811), National Science Foundation of China Outstanding Youth Foundation Project (Grant No. 40625004). Professor Yu Sheng, Dr. Ute W., Mr. Philip S., Mr. Tobias P. with

Univeristy of Heidelberg, and Mr. Xichai Pan, Mr. Zhi Wei, Miss Xiaoli Chang, Miss Ruixia He and Miss Yang Bai with State Key Laboratory of Frozen Soils Engineering, Cold and Arid Regions Environmental and Engineering Research Institute, Chinese Academy of Sciences also participated in fieldwork and some data analyses. Their assistance is thus acknowledged.

References

Arcone, S.A., Lawson, D.E., Delaney, A.J., Strasser, J.C. & Strasser, J.D. 1998. Ground-penetrating radar reflection profiling of groundwater and bedrock in an area of discontinuous permafrost. *Geophysics* 63(5): 1573-1584.

Cao, W.B., Wan, L. & Zeng, Y.J. 2006. Impacts of global warming on the eco-environments in the headwater region of the Yellow River. *Earth Science Frontiers* 13(1): 40-47 (in Chinese).

Cheng, G.D. & Wang, G.X. 1998. Eco-environmental changes and causal analysis in the source regions of Yangtze, Yellow and Lancang-Mekong Rivers. *Advance in Earth Science* 13 (Suppl.): 24-31 (in Chinese).

Cheng, G.D. & Wu, T.H. 2007. Response of permafrost to climate change on the Qinghai-Tibetan Plateau and its environmental impacts. *Journal of Geophysical Research* 112: F02S03.

He, Y.X. 1991. The permafrost investigation with electronic sound method along Xingjian–Tibetan Highway. *Journal of* Glaciology *and Geocryology* 13(3): 255-259 (in Chinese).

Jin, H.J., Zhao, L., Wang, S.L. & Jin, R. 2006. Modes of degradation and thermal regimes of permafrost along the Qinghai-Tibet Highway. *Science in China* 49 (D11): 1170-1183.

Jin, J.H., Chang. X.L. & Wang, S.L. 2007. Evolution of permafrost on the Qinghai-Tibet Plateau since the end of the Pleistocene. *Journal of Geophysical Research* 112: F02S09 DOI: 10.1029/2006JF000521.

Kang, X.C. 1996. Analysis on the climate change characteristics in the Tibetan Plateau regions. *Journal of Glaciology and Geocryology* 18(Suppl.): 281-288 (in Chinese).

Li, L., Zhao X., Wang, Q.C. & Wang, Z.Y., 2005. Mapping and analyses of permafrost change in the Qinghai Plateau using GIS. *Journal of Glaciology and Geocryology* 27(3): 320-328 (in Chinese).

Li, S.D. & He, Y.X. 1990. Features of permafrost in the West Kunlun Mountains. *Proceedings of Fourth National Conference on Glaciology and Geocryology*, Beijing: Science Press, 1-8 (in Chinese).

Li, S.D., He, Y.X. & Wang, Y.X. 1998. Permafrost and periglacial environments in the Karakorum and Kunlun Mountains. *Glaciers and Environments in the Karakorum and Kunlun Mountains*. Beijing: Science Press, 181-215 (in Chinese).

Li, X. & Cheng, G.D. 1999. A GIS-aided response model of high-altitude permafrost to global change. *Science in China* 42(D 1): 72-79.

Li, Y.B., Yang, G.H. & Wang, D.X. 2006. Dryness (aridity) and wetness changes in climate during the recent decades in the source regions of Yangtze, Yellow and Lancang-Mekong Rivers. *Journal of Northwest Sci-Tech University of Agriculture and Forestry* (Natural Sciences) 34(3): 3-77 (in Chinese).

Pettersson, J.K. & Nobes, D.C. 2003. Environmental geophysics at Scott Base: ground penetrating radar and electromagnetic induction as tools for mapping contaminated ground at Antarctic research bases. *Cold Regions Science and Technology* 37: 187– 195.

Sass, O. 2006. Determination of the internal structure of alpine talus deposits using different geophysical methods (Lechtaler Alps, Austria). *Geomorphology* 80: 45–58

Schwamborn, G., Rachold, V. & Schneider, W. 2000. Ground penetrating radar and shallow seismic -stratigraphy and permafrost investigations of Lake Nikolay, Lena Delta, Arctic Siberia. In: *Proceedings, 8th International Conference on Ground Penetrating Radar*. Washington DC, USA: SPIE-The International Society for Optical Engineering, Vol. 4084: 783-789.

Wang, G.X., Sheng, Y.P. & Cheng, G.D. 2000. Eco-environmental changes and causal analysis in the source regions of the Yellow River. *Journal of Glaciology and Geocryology* 22(3): 200-205 (in Chinese).

Wu, Q.B., Lu, Z.J. & Liu, Y.Z. 2005, Permafrost monitoring and its recent changes on the Qinghai-Tibet Plateau. *Advances in Climate Change Research* 1(1): 26-28 (in Chinese).

Yang, J.P., Ding, Y.J., Chen, R.S. & Sheng, Y. 2004. Permafrost change and its effect on eco-environment in the source regions of the Yangtze and Yellow Rivers. *Journal of Mountain Science* 22(3): 278-285 (in Chinese).

Yu Q.H. & Cheng G.D. 2003. The progress of permafrost investigation with geophysical methods in China. In: M. Phillips, S.M. Springman & L.U. Arenson (eds.), *Proceedings, 8th International Conference on Permafrost*, *21-25 July 2003, Zurich, Switzerland*. Lise, Abingdon, Exton, PA, Tokyo: A. A. Balkema Publishers, 1271-1276.

Zhou Y.W., Guo D.X., Qiu G.Q. & Cheng G.D. 2000. *Geocryology in China*. Beijing: Science Press, 37-45 (in Chinese).

Severity of Climate Conditions in the Russian Federation

S. I. Zabolotnik
Melnikov Permafrost Institute, SB RAS, Yakutsk, Russia

Abstract

This paper evaluates the severity of permafrost and climate conditions and the distribution of permafrost in the Russian Federation. It presents a permafrost and climate severity map of the Russian Federation, drawn on the basis of long-term air temperature records from over 3000 weather stations. The map delineates 6 environmental-climatic zones at a 1250°C·day interval. The mapping shows that the most extreme conditions occur north of 60°N latitude in Yakutia, where the so-called Cold Pole of the Northern Hemisphere is located, and in the adjacent parts of Krasnoyarsk Krai and Magadan Oblast. The permafrost of these regions has the lowest temperatures and largest measured thicknesses. Harsh conditions exist in the remainder of these provinces, in Chukotka, northern West Siberia, and the adjacent Arctic islands. The least cold areas are located in the southwestern part of European Russia where only seasonal freezing of soils is observed and no permafrost exists.

Keywords: air freezing index; climatic conditions; permafrost.

Introduction

The Russian Federation extends across the whole of northern Asia and much of north-eastern Europe. Because of its northern location, Russia has a cold climate and widespread permafrost which underlies about 65% of the country (Shepelev & Shatz 2005). Permafrost is a natural integral indicator of environmental and climatic conditions. The frozen ground greatly influences human life and activities. For example, the existence of ground ice poses many engineering problems for the construction and maintenance of buildings and facilities; the great thicknesses of permafrost, reaching 1000–1500 m in Yakutia, make water supplies difficult to obtain; the development of cryogenic processes require additional measures and costs for agricultural developments. In view of these harsh conditions, there is a continuing need for comprehensive appraisal of the natural environment in which humans live and work. Such assessment requires an aggregate indicator that would be able to measure both the permafrost conditions and the extremity of the environment.

At the first stage, the indicator selected was the degree of climate severity since permafrost is a product of climate, and its formation, distribution, temperature, and thickness largely depend on the intensity and duration of winter cold. It is defined as the sum of negative (below 0ºC) air temperatures during the year (air freezing index), which was used as a basic mapping criteria. Then, the climate severity index was correlated with the distribution and type of frozen ground within the identified zones.

The climate severity zonation of Russia has been an issue for a long time. The problem remains unsolved and is still much debated.

The first subdivision of Russia into the regions of the Far North and territories equated to it was undertaken in 1932 in order to stimulate industrial development of the northern and remote eastern regions by providing incentive payments. The list of Far North areas included the Kola Peninsula, Murmansk Okrug, Yakut Autonomous Republic, Kamchatka Oblast, as well as the Okhotsk, Koryak, and Chukotka Okrugs of the Far East Krai.

This list has been continuously revised by adding more areas. At present, 28 federal units are categorized as the regions of the Far North and equivalent areas and 41 units use regional coefficients. In 2002, the additional burden on federal and local budgets for the cost of "non-northern" territories reached 65 billion rubles (Zhukov 2005). The regions where employees are entitled to northern allowances (0% to 80% increase to wages depending on the length of employment) or regional coefficients (fixed regional rates of extra wage payment) now comprise more than 88% of the total area of the Russian Federation.

Huge financial expenditures for extra wage payments in the federal units, which do not incorporate areas with the far northern and equivalent regions status, generated a need to improve the labour compensation system and to introduce changes into the current legislation. The State Duma Committee for North and Far East Affairs resolved to revise existing criteria and to develop a science-based system for assessing living conditions. For this purpose, an interdepartmental working group was established including representatives from regional governments and parliaments, as well as those from relevant research institutions, including the Melnikov Permafrost Institute at Yakutsk.

State of the Problem

Some work on this topic was done in 1998, when the Federal Ministry of Economy and Trade together with the Institute of Geography Russian Academy of Sciences (RAS), and the Institute of Economic Problems, RAS Kola Scientific Centre devised a methodology for environmental and climatic zonation of Russia. Much consideration in this document was given to zonation criteria.

Earlier, the Institute of Geography proposed "a new version of the method that takes into account both zonal and azonal factors affecting the selection of indicators and criteria of extremity of environmental and social conditions

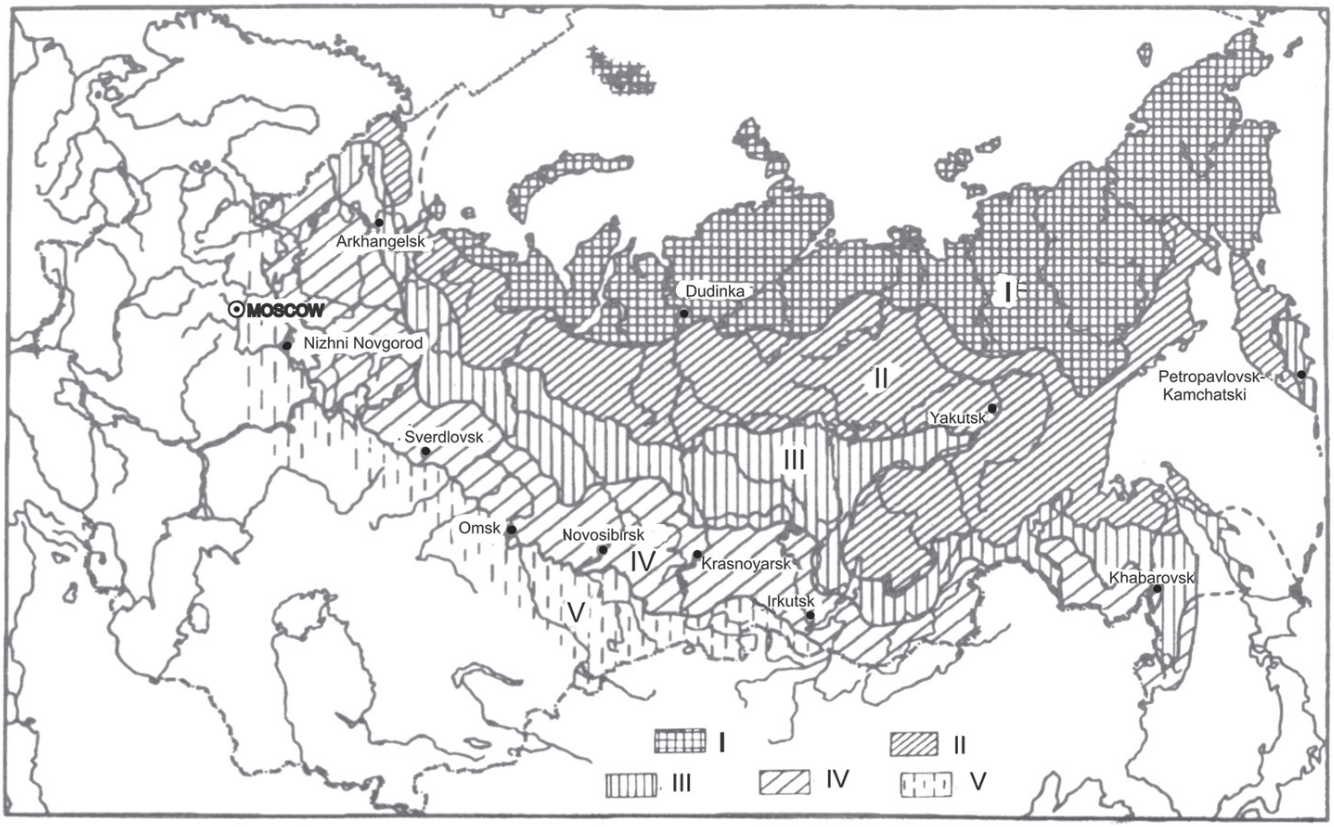

Figure 1. Zonation of environmental and climatic conditions affecting human life with consideration of azonal factors, Northern and Eastern Russia (after Zolotokrylin et al. 1992). I – absolutely unfavorable; II – extremely unfavorable; III – unfavorable; IV – relatively unfavorable; V – favorable.

of life" (Zolotokrylin et al. 1992). The new scheme was applied for zoning and mapping the Russian North and East (Fig. 1). Four unfavorable zones were distinguished in this map, based on a large number of indicators. However, analysis of the final product gives rise to many questions. For example, why are the populated centers with very different environmental conditions which show a range of 11°C in mean annual air temperature, *t* (*USSR Climate References* 1964–1967) placed into the same extremely unfavorable zone (zone II)? This zone includes Murmansk (t = +0.3°C), Salekhard (t = -6.4°C), Turukhansk (t = -7.0°C), Yakutsk (t = -10.3°C), Magadan (t = -4.7°C) and Palana in Kamchatka (t = -2.8°C). Similar examples can be found for other zones. The difference in living conditions among these populated centers is obvious and needs no comment.

The understanding that "the map was inadequate in reflecting the azonal factors that affect human life, such as strong winds, high humidity, frequent fogs in coastal areas, paludification, and others" (Krenke et al. 2001) caused a need for further work. The author analyzed seven bioclimatic indices, applied clothing insulation and seasonal freeze and thaw depths as azonal factors, and adjusted the zone boundaries in relation to geobotanical and permafrost physiographical boundaries. As a result, a new map of unfavorable zones was produced (Krenke et al. 2001). This map also has shortcomings. For one, the northernmost absolutely unfavorable zone (I) was significantly extended to the south to include the Okhotsk coastal areas with Ayan (t = –2.7°C to -3.3°C) and all the localities listed above except the coldest one, Yakutsk. All these localities were within the extremely unfavorable zone (II) of the earlier map (see Fig. 1).

The usefulness and necessity of the multiple-factor taking into account different environmental parameters is beyond question. However, these two maps seem to have over-estimated the role of secondary parameters, leading to such results. In order to avoid misjudgments in future, it is necessary to re-examine and re-define the significance of each comparison factor.

A few such attempts were made by Gavrilova et al. (2003, 2004). Building on the earlier works, they proposed "the number of days below 5°C" as "an additional criteria of nordicity." The results obtained were reflected in two maps: "Climate and Economic Subdivision of the North" (Gavrilova et al. 2003) and "Zonation of the Russian North" (Gavrilova et al. 2004). These maps, however, take no account of such important factors as the length of a period of extreme cold temperature (e.g., below -40°C). As a result, the later map (Gavrilova et al. 2004) places the northern part of the Kola Peninsula with the ice-free port of Murmansk where winters are as mild as in Moscow (long-term mean winter temperature, t_{win} is -6.8°C to -7.0°C at both localities (*USSR* Vol. 2 1965, *USSR* Vol. 8 1964) into the absolute unfavorable (Arctic) zone (1). Palana in Kamchatka,

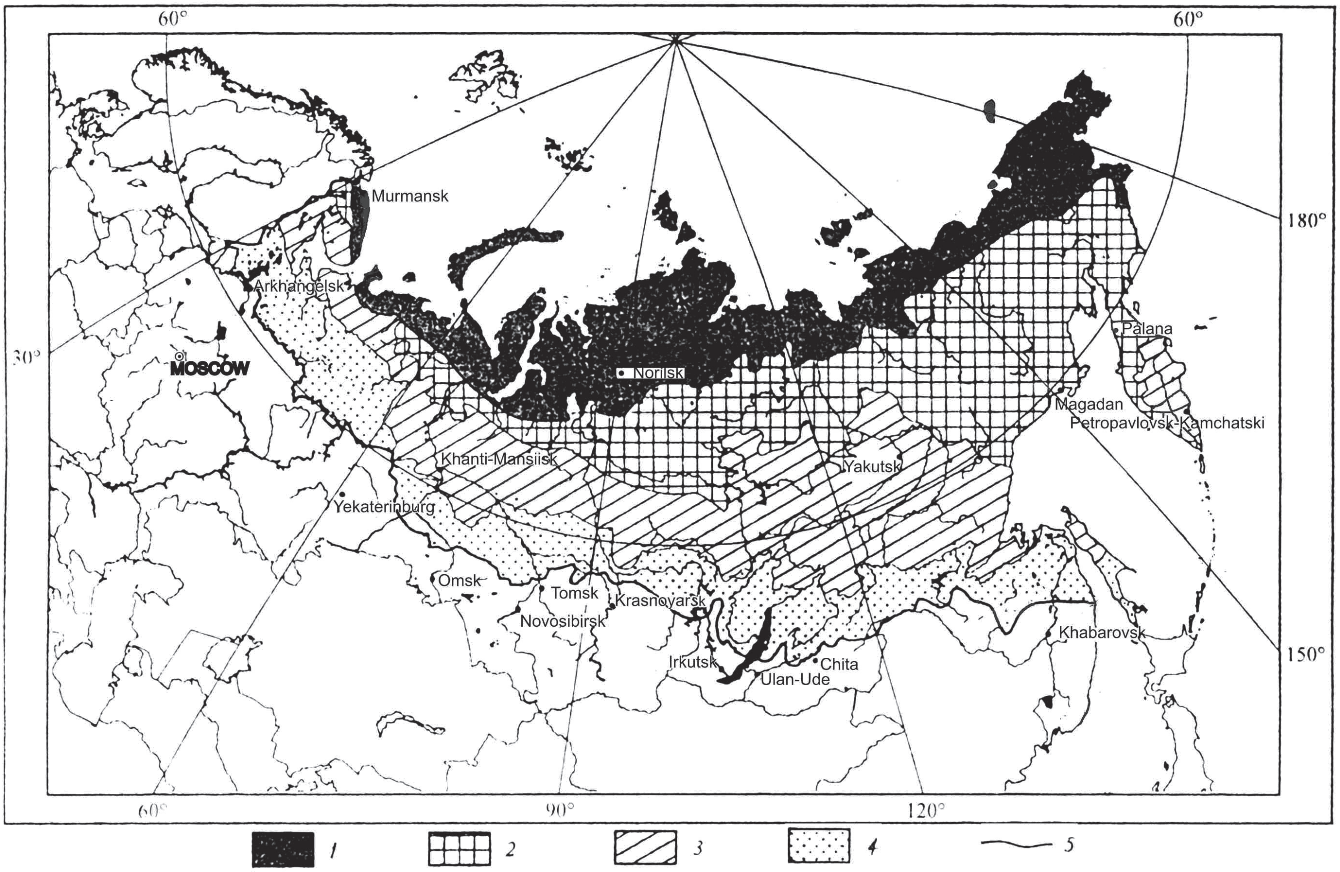

Figure 2. Zonation of the Russian North (after Gavrilova et al. 2004). 1 – Far North– absolutely unfavorable (arctic) zone, 2 – Far North equivalent – extremely unfavorable (subarctic) zone, 3 – North – unfavorable zone, 4 - North equivalent - relatively unfavorable zone, 5 – limit of the North.

and Magadan, where t_{win} is -10.4°C (*USSR* Vol. 27 1966) and -14.2°C (*USSR* Vol. 33 1966) respectively, are in the extreme unfavorable (Subarctic) zone (2), while northerner and much colder Yakutsk where t_{win} = -26.5°C (*USSR* Vol. 24 1966) is in the most southern of the three enumerated zones – unfavorable zone 3 (Fig. 2).

It is obvious that shortcomings in the zonation schemes result from the fact that all investigators try to incorporate a large number of different (often incomparable) environmental parameters into a single scheme, and such attempts are not always successful. Besides, it is time to abandon efforts to regionalize the North only, because, conditions for life in the Altai and Sayan Mountains in southern Russia, for example, are much worse than in Chukotka. The present author shares M.A. Zhukov's view that "zonation should be made not for the North …, but for the whole country based on the main significant unfavorable factors … And unfavorable conditions should be taken into account where conditions are unfavorable, not where it is the North, South, West, or East" (Zhukov 2005).

Attempts to regionalize the entire territory of Russia have been made before, based, among others, on the air freezing index. The Working Group's report contains a map (author not given), which delineates the areas with the air freezing indices (Στ) of 0°C·days to -4000°C·days (five zones) and below -4000°C·days (one zone). The latter zone includes all regions where the freezing index varies from -4000°C to -7700°C·days; i.e., the range of variation is nearly the same as in the first five zones combined. Resultantly, the same climatic zone includes Oymyakon (the air freezing index is -7300°C days to -7670°C·days), Yakutsk (Στ = -5550°C days to -5575°C·days), and Anadyr (Στ = -3570°C days to -4200°C·days) (*USSR* Vol. 24 1966, *USSR* Vol. 33 1966), which is totally incorrect.

Results

The particular climatic qualities of a territory are the most important factors affecting human activities and quality of life. Their effects are not at all uniform. In relatively favorable regions, including much of European Russia and the southern parts of West Siberia and the Far East, the climate variation is not so great as to exert a strong effect on the human organism. But in the continental areas of East Siberia, Yakutia, and the adjacent northwestern part of Magadan Oblast, the climate harshness increases so greatly, that all indicators showing the possibility of long outdoor activity and residence change radically.

To demonstrate this, published air temperature data from all Russian weather stations were analyzed (*USSR Climate*

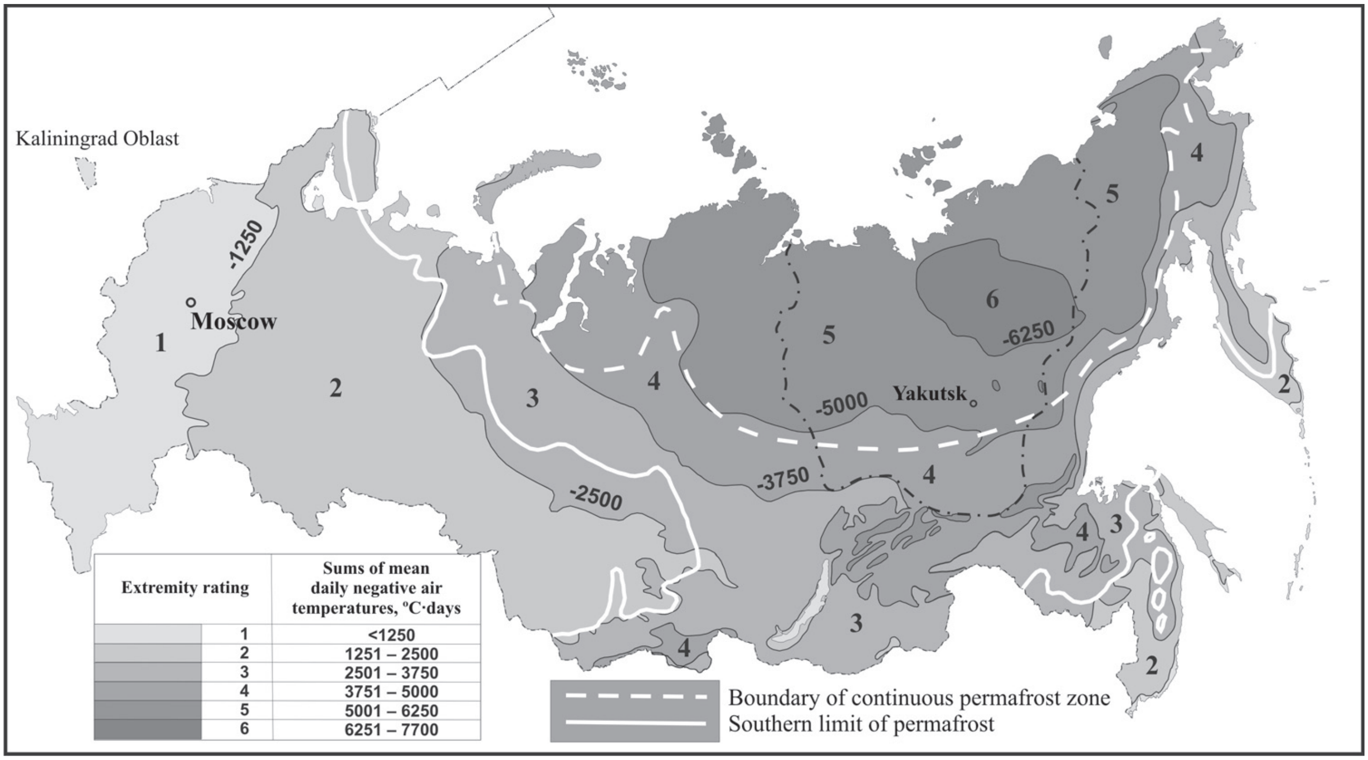

Figure 3. The permafrost and climate severity map of the Russian Federation. Dot-and-dash line – boundary of the Republic of Sakha (Yakutia).

References 1964–1967). For each weather station the average air freezing index for the whole period of record (τ), which in many cases exceeded 100 years, was calculated. The air freezing indices (Στ) for more than 3000 stations were drawn on a base map, and interpolated and extrapolated accounting for topography. This work resulted in "The Permafrost and Climate Severity Map of the Russian Federation" at a scale of 1:5,000,000. This map is presented, in a reduced form, in Figure 3. The map provides a climatic severity rating and identifies six zones, as in the earlier mapping schemes, but with equal air index intervals.

It is shown that absolutely extreme conditions (score 6) occur in the northeastern mountainous part of Yakutia and in the adjacent part of Magadan Oblast where Στ varies from -6251°C·days to -7669°C·days (Fig. 3). This zone is smallest in size and occupies only 3% of the country. At the same time, it is the coldest zone where the coldest places of the Northern Hemisphere, Verkhoyansk and Oymyakon, are located. The mean annual air temperature at these populated centers is -15.7°C to -17.0°C, and the minimum temperatures are -68°C to -70°C (*USSR* Vol. 24 1966). The mean winter air temperatures (for the persistent period of freezing temperatures) vary from -24.5°C to -32.5°C in the zone.

Extreme conditions (score 5, Στ = -5001°C·days to -6250 °C·days) are characteristic of the arctic archipelagos of Severnaya Zemlya and the New Siberian Islands, the vast areas of East Siberia, Yakutia, Magadan Oblast, and Chukotka Autonomous Okrug, as well as the high mountainous areas of northern Buryatia, Chita Oblast, Amur Oblast, and Khabarovsk Krai. Winters are very cold in these regions, with average temperatures varying from -17.0°C to -27.5°C. This zone covers extensive areas in northeastern Russia, comprising 22.4% of the area of the country.

The regions with severe conditions (score 4, Στ = -3751°C·days to -5000°C·days) are Franz Josef Land, islands in the Kara Sea, northern West Siberia, central East Siberia, southern Yakutia, the mountainous parts of Tuva and Altai, the northern parts of Buryatia, Irkutsk, Chita and Amur Oblasts, and Khabarovsk Krai, as well as parts of Magadan and Kamchatka Oblasts, Chukotka Autonomous Okrug, and Wrangel Island. This zone fringes the previous zone semi-circularly, intruding to the mountains of Trans-Baikal and Pre-Amur, and comprises about 18.2% of the area of Russia. Winters are still cold in this zone, with mean temperatures ranging from -13.5°C to -24.0°C.

The zone of unfavorable conditions (score 3, Στ = -2501°C days to -3750°C days borders all the above zones in the west, south, and east (Fig. 3). It covers about 22.5% of the area of the country and includes the Novaya Zemlya and Vaigach Islands, the eastern part of Nenets Autonomous Okrug, the northern Urals, northwestern and southern areas of West Siberia, and parts of Krasnoyarsk, Khabarovsk and Primorsky Krais, Magadan and Kamchataka Oblasts, and Chukotka. Winters are still long, especially in the Arctic islands, but now not so cold. The mean winter temperatures vary from -10.5°C to -20.5°C.

Temperate conditions (score 2, Στ = -1251°C·days to -2500 °C·days) are characteristic of much of the North-western and Privolzhsky Federal Districts, the southern part of the Urals Federal District and southwestern part of the Siberian Federal District. To the east, such conditions are found along the southern edge of Lake Baikal and in a small part of southern Chita Oblast. In the Far East, the temperate zone includes Khabarovsk Krai, most of Primorsky Krai, Sakhalin, and Kamchatka, and narrow coastal areas of Magadan Oblast and Anadyr Bay in Chukotka. This zone is largest in size (approximately 25% of the area of the country), and winters are relatively mild. The mean winter air temperatures vary from -6.5°C to -16.5°C.

The zone of relatively favorable living conditions (score 1, Στt above -1250°C·days) in the proposed map includes only those areas where the mean air temperatures for the cold season (t<0°C) are above -8.5°C. This zone occupies the Kola Peninsula coast in the Barents Sea, the northern part of the Onega Peninsula, the southwestern coasts of Onega Bay in the White Sea, Kaliningrad Oblast, the Central Federal District, southwestern Privolzhsky District, and Southern Federal District in the European part of Russia. Virtually all of Siberia, the Far East, and Chukotka have more severe conditions. Relatively favorable conditions are found here only along the sea coasts in Primorsky Krai, in southern parts of Sakhalin, along southeastern coasts and the southernmost part of Kamchatka, and on the Kuril and Komandorskie Islands. The relatively favorable zone lies mostly in the west of the country (Fig. 3), and its total area comprises about 9% of the Russian Federation.

In addition to climate severity analysis, the character of permafrost distribution within the identified zones was evaluated by the present author together with V.V. Kunitsky, M.M. Shatz and V.V. Shepelev (Shepelev et al. 2007).

The evaluation shows continuous permafrost in the areas with absolutely extreme or extreme conditions where Στt is -5001°C·days to -7669°C·days (zones 5 and 6 on Fig. 3).

In zone 4 with severe conditions (Στt of -3751°C·days to -5000°C·days), either continuous (mainly in the northern parts) or discontinuous permafrost and permafrost islands occurs. It should be noted that, except the Barents Sea islands, "the continuous permafrost zone lies entirely within the Asian part of Russia" (Shepelev & Shatz 2005).

In the areas with unfavorable conditions (see Figure 3, zone 3) where Στt ranges from -2501°C·days to -3750°C·days, permafrost islands mostly occur.

In zone 2 with temperate conditions (Στt of -1251°C·days to -2500°C·days), permafrost is of limited occurrence and exists as islands or isolated patches in the European North and in the Sayan foothills in the southeast of the country. The zone is generally free of permafrost, as is zone 1 with relatively favorable conditions (Στt > -1250°C·days) where only seasonal freezing of soils is observed, and permafrost never exists (Fig. 3).

For the purpose of illustration, permafrost zone boundaries from Baranov's (1977) Geocryological Map of the USSR were overlain on the present map. Although Baranov's map was published 30 years ago, it remains one of the best frozen-ground maps for Russia and former Soviet Union republics. More recent maps only add details for individual areas or refinements to the limits of seasonal and perennial frost which can not be reflected on this small-scale map.

Comparison shows that the presented map radically differs from all the earlier maps. The major distinction is that this map shows, for the identified zones, both the real extreme conditions with the coldest and thickest permafrost and the areas with milder and relatively favorable conditions where permafrost occurs as isolated patches or is absent. For example, Yakutia has always, now and 100 years ago, been the coldest region in Russia with the largest measured depth of permafrost (up to 1500 m). But the earlier classifications placed only the northern part of Yakutia in the absolutely and extremely unfavorable zones. Moreover, these zones included the Kola Peninsula coasts washed by the warm Gulf Stream (Figs. 1, 2) with the open sea near Murmansk where permafrost never forms, and the continental areas of the peninsula where only patches of frozen ground less than 50 m in thickness are encountered (*Geocryology of USSR* 1988).

As for the problem of defining the Far North and equivalent areas and the territories with regional coefficients, their total area is within a reasonable range. The geographic location of the Russian Federation is such that most of the country has difficult climatic conditions. The regionalization presented in this paper shows that the regions with extreme, severe, and unfavorable conditions, where the air freezing index ranges from -2500°C·days to -7700°C·days, occupy little more than 66% of the country. If the zone of temperate living conditions is added, the total area will reach 91%.

Conclusions

The present work is not yet sufficient to provide a basis for establishing regional coefficients in the entire Russian Federation. For this purpose, it is necessary to investigate in greater detail the effect of many other natural factors. In particular, more detailed consideration should be given to the geocryological situation in the regions and to their impact on human life and activities. Nevertheless, the proposed map can help compare temperature conditions with permafrost and other environmental factors, as well as value at the validity of previous elaborations.

References

Baranov, I.Y. 1977. *The Geocryological Map of the USSR*. Scale 1:5,000,000. Moscow: USSR Agency for Geodesy and Cartography, 4 sheets, 62×92 cm.

Gavrilova, M.K., Fedorova, E.N. & Lazebnik, O.A. 2003. Zoning the Russian North by discomfort for living. *Nauka i Obrazovanie* 2(30): 16-24.

Gavrilova, M.K., Fedorova, E.N. & Lazebnik, O.A. 2004. On the problem of delineating boundaries and zoning the Russian North. *Bulletin of Russian Geographical Society* 136(1): 63-69.

Geocryology of USSR. 1988. European Part of the USSR. In: E.D. Ershov (ed.), Moscow: Nedra, 358 pp.

Krenke, A.N., Zolotokrylin, A.N. & Vinogradova, V.V. 2001. Zonation of the Russian North and East based on environmental and climatic conditions for living. In: V.M. Kotlyakov (ed.), *Regional Aspects in the Development of Russia under Global Environmental and Climatic Changes*. Moscow: NTs ENAS, 65-74.

Shepelev, V.V. & Shatz, M.M. 2005. Zonation of Russia based on living conditions and geocryological environment. *Nauka i Obrazovanie* 4(40): 72-79.

Shepelev, V.V., Zabolotnik, S.I., Kunitsky, V.V. & Shatz, M.M. 2007. Permafrost-related factors in zonation of the Russian North. In: V.V. Philippov (ed.), *Zonation of the North of the Russian Federation*. Yakutsk: Permafrost Institute SB RAS Press, 14-26.

USSR Climate References. 1964–1967. Part II. Air and Soil Temperatures. Leningrad: Gidrometeoizdat.

——, Volume 1. 1965. Archangel and Vologodsk Oblasts, Karelian and Komi ASSR: 358 pp.

——, Volume 2. 1965. Murmansk Oblast: 144 pp.

——, Volume 3. 1965. Karelian ASSR. Leningrad, Pskov and Novgorod Oblasts: 343 pp.

——, Volume 6. 1965. Lithuanian SSR and Kaliningrad Oblast RSFSR.

——, Volume 8. 1964. Yaroslavl, Kalinin, Moscow, Tula, Vladimir, Smolensk, Kaluga and Ryazan Oblasts: 355 pp.

——, Volume 9. 1965. Perm, Sverdlovsk, Chelyabinsk, Kurgan Oblasts and Bashkir ASSR: 362 pp.

——, Volume 12. 1965. Tatar ASSR, and Ulyanovsk, Kuibyshev, Penza, Orenburg and Saratov Oblasts.

——, Volume 13. 1966. Volgograd, Rostov and Astrakhan Oblasts; Krasnodar and Stavropol Krais; and Kalmyk, Kabardino-Balkaria, Chechen-Ingush and North Ossetia ASSR.

——, Volume 15. 1966. Dagestan ASSR, Azerbaijan SSR and Nakhichevan ASSR.

——, Volume 17. 1965. Tyumen and Omsk Oblasts: 276 pp.

——, Volume 20. 1965. Kemerovo, Novosibirsk and Tomsk Oblasts and Altai Krai: 396 pp.

——, Volume 21. 1967. Krasnoyarsk Krai and Tuva ASSR: 504 pp.

——, Volume 22. 1966. Irkutsk Oblast and Western Buryat ASSR: 360 pp.

——, Volume 23. 1966. Buryat ASSR and Chita Oblast: 320 pp.

——, Volume 24. 1966. Yakut ASSR: 398 pp.

——, Volume 25. 1966. Khabarovsk Krai and Amur Oblast: 312 pp.

——, Volume 26. 1966. Primorsky Krai: 220 pp.

——, Volume 27. 1966. Kamchatka Oblast: 184 pp.

——, Volume 28. 1965. Tambov, Bryansk, Lipetsk, Orel, Kursk, Voronezh and Belgorod Oblasts.

——, Volume 29. 1964. Ivanovo, Kostroma, Kirov, Gorky Oblasts; Mari, Udmurt, Chuvash and Mordovian ASSR: 208 pp.

——, Volume 33. 1966. Chukotka National Okrug and Magadan Oblast: 288 pp.

——, Volume 34. 1966. Sakhalin Oblast: 205 pp.

Zhukov, M.A. 2005. Struggle for the "norths," or a Long road to common sense. *Nauka i Obrazovanie* 4(40): 141-145.

Zolotokrylin, A.N., Kantsebovskaya, I.V. & Krenke, A.N. 1992. Zonation of Russia territory based on environmental extremity for life. *Tidings of the Academy of Sciences, Geographical Series* 6: 16-30.

Recent Climate and Active Layer Changes in Northeast Russia: Regional Output of Circumpolar Active Layer Monitoring (CALM)

Dmitry Zamolodchikov
Center for Ecology and Productivity of Forests, Russian Academy of Sciences, Moscow, Russia
Anatoly Kotov
Scientific Center, Chukotka, Anadyr, Russia
Dmitry Karelin
Center for Ecology and Productivity of Forests, Russian Academy of Sciences, Moscow, Russia
Vladimir Razzhivin
Komarov Botanical Institute, Russian Academy of Sciences, St. Petersburg, Russia

Abstract

This paper presents recent observations of active layer changes at three CALM (Circumpolar Active Layer Monitoring) tundra sites in northeastern Russia (Chukotka region). Results show that regional changes of climate became evident after 2000. In the Anadyr area (CALM sites R9 and R11) air temperatures in June–September significantly increased from 7.4°C (1901–2000) to 9.3°C (2001–2007), with corresponding increase in accumulated thawing degree days (DDT). At the Lavrentiya site (R27), DDT in 2001–2007 rose by 217°C as compared to 1929–2000. After 2000, all sites demonstrate significantly greater end-of-season grid-averaged thaw depths in response to the increase of incoming warmth. Annual values of edaphic factors display significant positive trend (0.03 y^{-1}) at R9 (P = .026) and no trends at R11 and R27. This demonstrates a different response of the active layer in local ecosystems to warming. Analysis shown that microhabitats with shallower thaw depths are more sensitive to warming.

Keywords: active layer; monitoring; Northeast Russia; permafrost; tundra.

Introduction

The CALM (Circumpolar Active Layer Monitoring) network includes three sites in the northeastern part of the Russian Federation (Chukotka peninsula). All sites are located near the Russian coast of the Bering Strait in the continuous permafrost zone (Fig. 1). The Cape Rogozhny site (R9) was established in 1994 on the northern coast of Onemen Bay (64°49′N 176°50′E) off the Bering Sea, and is the closest to the coast of the Chukotka CALM sites. Site R11 (Mount Dionisiya, 64°34′N 177°12′E), operating since 1996, is 25 km to the south of Anadyr city and about 11 km from the nearest seacoast. The direct distance between these two sites is 33 km. Both sites are dominated by cotton grass tussocks on Gleyi-Histic Cryosols. Site R27 was initiated in 2000 in the vicinity of Lavrentiya settlement (65°36′N 171°03′W), 3 km from the coast of the Bering Strait. The direct distance between the Lavrentiya site and the above-mentioned sites in the Anadyr area is 560 km. Within the landscape of the Lavrentiya site, wet sedge-*Salix* mosses tundra on Gleyi-Histic Cryosols are dominant. More detailed site descriptions are available in our earlier papers (Zamolodchikov et al. 2004).

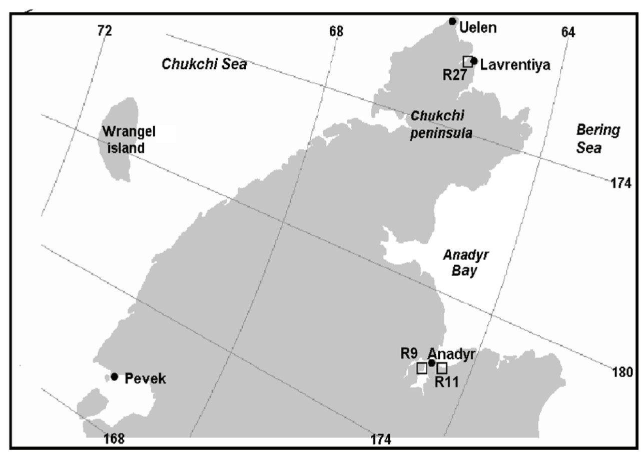

Figure 1. CALM sites in Northeast Russia: R9–Cape Rogozhny; R11–Mount Dionisiya; R27–Lavrentiya.

Methods

The standard sampling design recommended under the CALM program (Brown et al. 2000) was applied, with minor modifications, at all northeastern CALM sites. Permanent 100x100 m grids were established, with 10 m intervals between grid nodes marked with stakes (121 per grid). Thaw depth was measured at each grid node using a steel rod. Grids at the Cape Rogozhny and Mt. Dionisiya sites had one measurement replication per node, with four replications per node at the Lavrentiya grid. The active-layer was measured once each year at the end of the warm season at the Cape Rogozhny and Mt. Dionisiya sites, whereas the Lavrentiya grid was monitored throughout thaw season, with a maximum of four complete replications over the season.

An additional set of parameters was monitored at the three sites in order to estimate the influence of different natural controls over the temporal and spatial variability of the active layer. At the Cape Rogozhny site, we inventoried the surface characteristics of microhabitats such as tundra, vehicle tracks, and frost boils. At Mt. Dionisiya, the relative areas occupied by tundra vegetation, water tracks, and frost boils was determined accompanied by grid leveling. The most comprehensive set of additional parameters was collected on the Lavrentiya grid including a topographic survey, qualitative characteristics of microhabitats, measurements of volumetric soil moisture, projective cover of vegetation, moss cover, and organic layer thickness.

The Cape Rogozhny and Mt. Dionisiya grids are presently equipped with temperature data loggers measuring air and soil temperatures to a depth of 1 m. The Lavrentiya grid is equipped with a 21X Campbell data logger, recording a wide spectrum of meteorological characteristics. Unfortunately, these data loggers were not initiated at the very beginning of site occupation. It is therefore not surprising that in further analyses we used climate data from the nearest long-term government weather stations. The nearest to sites R9 and R11 is the weather station at Anadyr city (the direct distance from this weather station to the sites is 25 and 30 km, respectively), and for the Lavrentiya site (R27) it is the weather station in the native settlement of Uelen (direct distance of 85 km). Previously it was shown that air temperatures at the sites are well correlated with the temperature data from the nearest weather stations (Zamolodchikov et al. 2004).

In addition to observations made according to the CALM protocol (Nelson et al. 1996), several other geocryological and ecological surveys were conducted at the sites. Detailed descriptions of cryolithological structure and cryogenic processes were compiled for Cape Rogozhny site (Kotov et al. 1998, Kotov 2001). Mt. Dionisiya was one of the official sites of the International Tundra Experiment (ITEX; Arft et al. 1999), a program designed to examine variability in arctic and alpine plant species response to increased temperatures. The Lavrentiya site is the location of intensive year-round investigations of CO_2, water vapor fluxes, and energy balance using the eddy-covariance technique (Zamolodchikov et al. 2003).

Results

Regional climate changes become evident after the year 2000 (Fig. 2). Near the sites R9 and R11, the Anadyr weather station recorded a mean annual air temperature of -7.6°C in the 1901–2000 period and -6.3°C in 2001–2006, which is significantly warmer (P < .05). Warm season (June–September) mean air temperature increased from 7.4°C in 1901–2000 to 9.3°C in 2001–2007. The corresponding increase in accumulated thawing degree days (DDT) was 214°C at Anadyr region (R9, R11). The same tendencies could be found in data taken from other long-term weather stations in the region. For example, in the Lavrentiya area (R27), mean DDT values in 2001–2007 increased by 217°C compared to the 1929–2000 period.

After the year 2000, all three sites demonstrate a clear trend of increased of end-of-season grid-averaged thaw

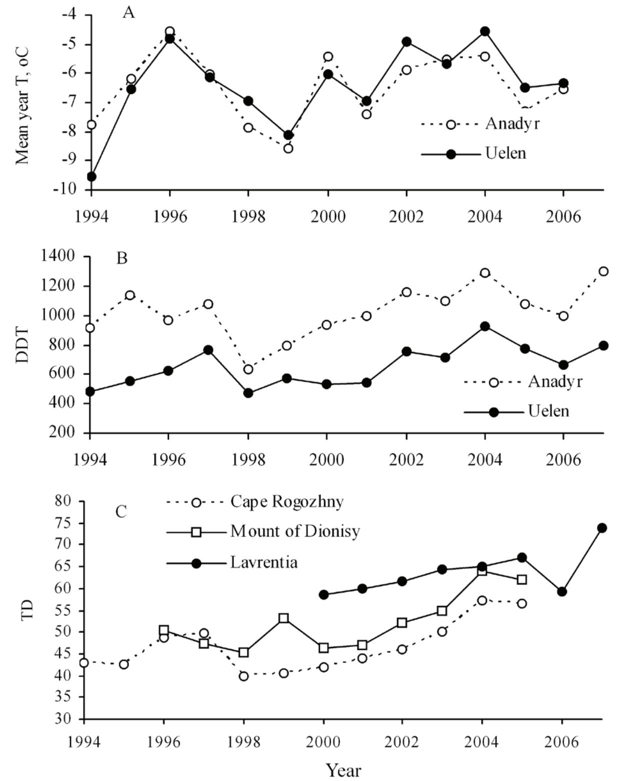

Figure 2. Mean air temperature dynamics (A) and accumulated thawing degree-days (B) at Anadyr and Uelen weather stations, and mean end-of-season depth of thaw (C) at the CALM sites in East Chukotka (Russia). Missing thaw depth data points in Anadyr sites in 2006–2007 (C) are due to logistical problems.

depths. Thus, in 2000, thaw depths were 42 cm at R9, 46 cm at R11 and 59 cm at R27. Five years later, thaw depth increased by 15 cm (35%) and 16 cm (34%) at Anadyr sites R9 and R11, respectively. Thaw depth increased by 15 cm (21%) at Lavrentiya site R27 by 2007.

The specificity of thawing processes at different sites can be characterized by the so-called edaphic factor (E), estimated as a rate, or coefficient of proportionality, between thaw depth and the square root of DDT (Nelson & Outcalt 1987). This approach was very effective in application to different sites at circumpolar Arctic sites (Hinkel & Nelson 2003; Mazhitova et al. 2004; Zamolodchikov et al. 2004, and many others). For the period of observation, mean edaphic factors were estimated as 1.49 at the R9 site, 1.70 at R11, and 2.43 at R23. It was found that the values of E display positive interannual trends (0.02–0.03 y^{-1}) at tussock tundra sites R9 (P = 0.026) and R11 (P = 0.25), though not significant in the latter case, and have no significant trend (P = 0.56) at site R27 (sedge-Salix moss tundra).

The R9 grid exhibits rather low spatial variability in active-layer thickness. The average annual coefficient of spatial variation (CV) is only 0.11. The R11 and R27 sites demonstrate more expressed spatial variability within the grid, with CV coefficients of 0.20 and 0.21, respectively. This is about twice the value observed on the R9 grid.

The interannual node variability (INV, %) reflects the level of interannual changes of spatial thaw depth distributions (Hinkel & Nelson 2003). R11 and R27 grids have similar INV estimates (21 and 19%, respectively). The R9 site demonstrates the greatest interannual node variability (29%). We note that CALM grids in East Chukotka have significantly greater INV values, as compared to East European tundra sites (Mazhitova et al. 2004).

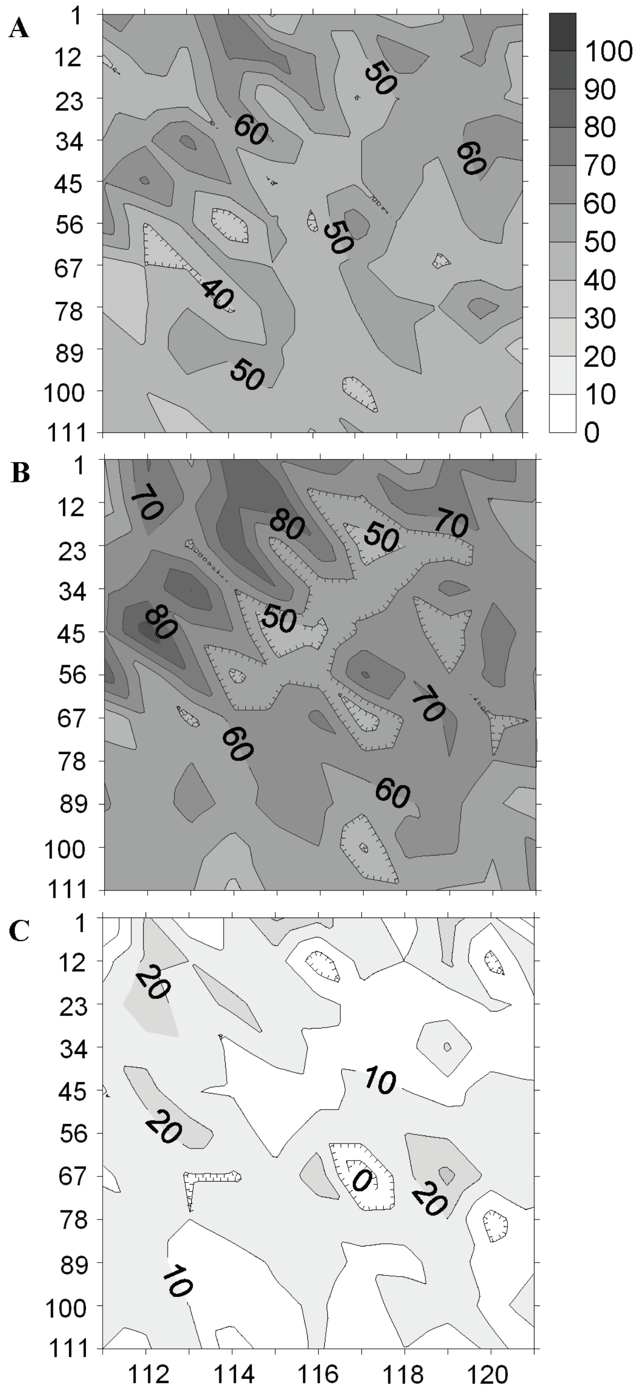

Figure 3.Thaw depth patterns and increments (cm) at the Mt. Dionisiya grid (R11). Parameters are mapped over the grid area using triangulation with linear interpolation algorithm; grid node numbers are shown on left and bottom margin. A: thaw depth, August 21, 1996; B: thaw depth, September 14, 2005; C: increments of thaw depth between 1996 and 2005.

Nonuniform rates of thawing in different habitats is one possible factor of interannual spatial variability. Spatial distributions of interannual thaw depth increments (Figs. 3C, 4C) are essentially different from those of thaw depth (Figs 3A, 3B, 4A, 4B). To put it another way, maximum thaw depth at a given location within the plot does not necessarily result in the maximum incremental increase in thaw under warming conditions.

The question arises as to whether different grid nodes demonstrate different rates of thawing. To answer this question, grid nodes were grouped and ranked by thaw depths measured in the first year of observation for each grid. The first group included the 40 nodes (33%) with the shallowest thaw depth, the second group had 41 nodes with intermediate thaw depths, and the third group incorporated the 40 nodes with the deepest thaw. Table 1 shows the average thaw depths by groups at the beginning and the end of the observation periods on different grids.

The results show that at all CALM grids, the maximum incremental increase were observed at nodes with the shallowest initial thaw depth. Hence, microhabitats with shallow thaw depths are more sensitive to warming. This is also evident from the negative coefficients of correlation between incremental thaw increase and initial thaw depths values. The correlations were highly significant for grids R9 (R = -0.47, P < 0.01) and R27 (R = -0.30, P < 0.01), but not significant for R11 (R = -0.11, P = 0.21).

Discussion

We have shown a well-defined general tendency for increasing thaw depth at all East Chukotka tundra CALM sites within the last 10–15 years of observations. This is due to a significant rise in mean annual temperature and accumulated thawing degree days. The recent tendency of increased summer temperatures are observed in most regions of the Russian Arctic (Pavlov & Malkova 2005).

The anomalous year of 2006 demonstrates a

Table 1. Incremental change in thaw depth by node groups at CALM grids in northeastern Russia.; see text for explanation.

Grid, periods of observations	Grid nodes grouped by thaw depth at first year	Average thaw depth, cm		Thaw depth increment, cm
		first year	last year	
R9, 1994–2005	low	38	54	16
	medium	43	56	13
	high	48	59	11
R11, 1996–2005	low	40	53	13
	medium	49	61	11
	high	62	72	11
R27, 2000–2007	low	46	64	19
	medium	58	73	15
	high	72	86	14

disproportionately low thaw depth at the Lavrentiya site (Fig. 2C) if compared to the Uelen weather station temperature data only (Fig. 2A, B). The explanation is due to the influence of local weather conditions. The Gulf of Lavrentiya, adjacent to the experimental site, is part of the Bering Strait. Throughout most of the summer season of 2006, the Gulf was completely blocked with ice due to prevailing winds from the Arctic Ocean. This resulted in a well-expressed local cooling effect. This was not the case in other regions of the Chukotka peninsula, as is apparent from the corresponding values of mean annual temperatures at the Uelen and Anadyr weather stations (Fig. 2A).

In the following year (2007), the average thaw depth at the Lavrentiya site returned to the overall general tendency. In doing so, the deepest active layer measurement for all years of observation and at all sites was recorded (Fig. 2C). In 2007, the Anadyr weather station recorded the greatest annual sum of thawing degree days for the entire period of 108 years of observation since 1899, which exceeded 1300°C. This DDT sum matches the normal range characteristic of the northern geographical zone of boreal forest (north taiga).

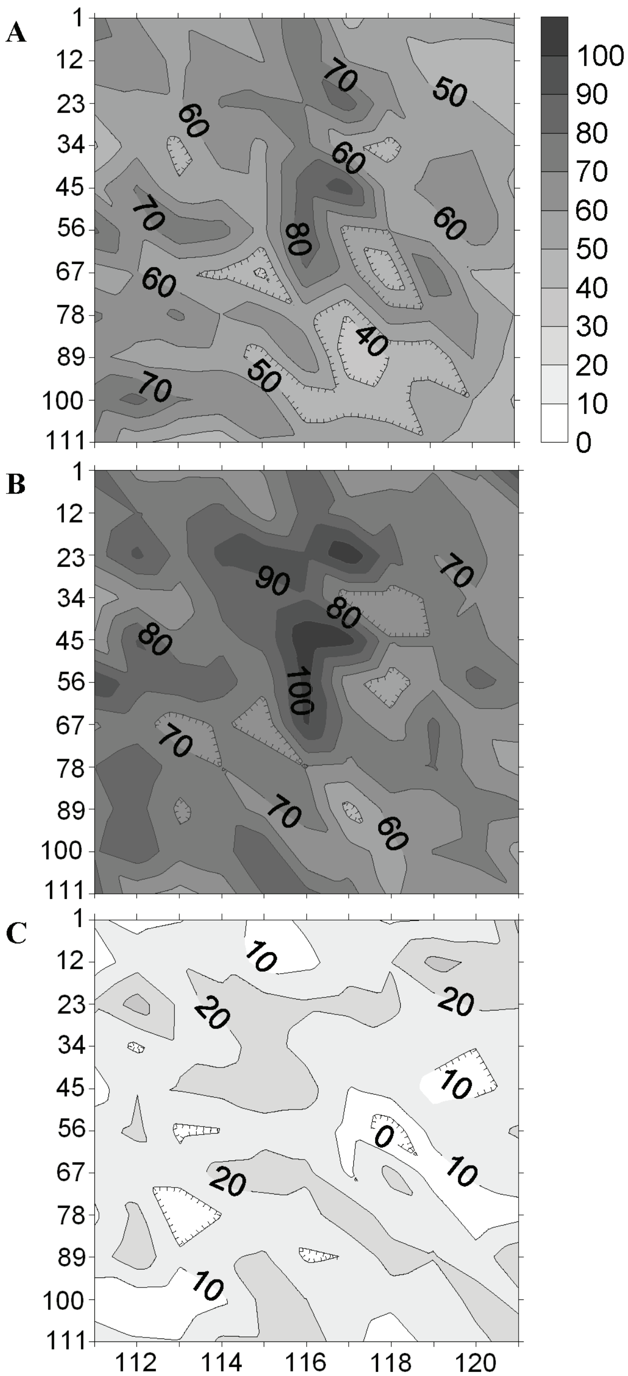

Figure 4. Thaw depth spatial patterns and increments (cm) at the Lavrentiya grid (R27). Parameters are mapped over the grid area using triangulation with linear interpolation algorithm; grid node numbers shown at left and bottom margins. A: thaw depth, September 29, 2000; B: thaw depth, September 25, 2007; C: increments of thaw depth between 2000 and 2007.

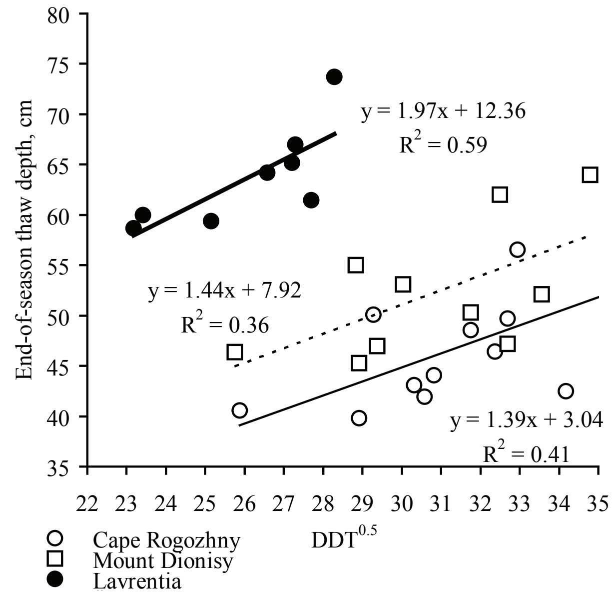

Figure 5. End-of-season thaw depth (cm) vs. accumulated thawing degree days ($DDT^{0.5}$) at East Chukotka CALM sites (Russia).

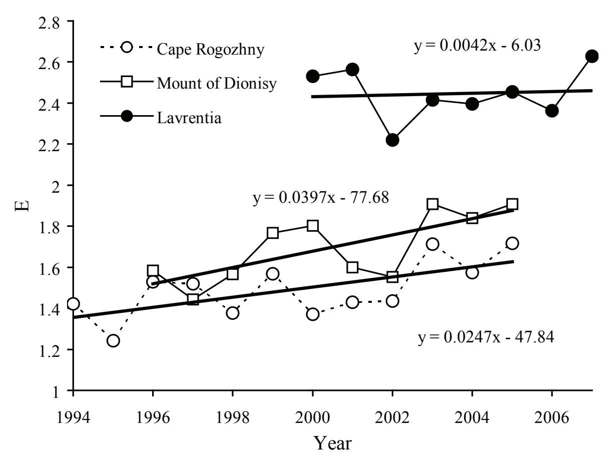

Figure 6. Interannual changes of calculated edaphic factors (E) at East Chukotka sites (Russia). Missing data points in curves for the Anadyr sites (trend lines below) are due to logistical problems in 2006–2007.

The average thawing-degree-days sums during the periods of observations at both Anadyr experimental sites are almost 1.5 times greater than at the Lavrentiya site (Fig. 5). The latter site is located much further north and is a substantially colder climate (Fig. 2B). Despite this fact, the average interannual thaw depth at the Lavrentiya site is significantly greater than at the two sites in the Anadyr region. According to our data, we believe that the difference is mostly due to the greater storage of aboveground phytomass, including more developed moss and lichen mats, bodies of *Eriophorum* tussocks, dwarf-shrub and shrub layers, and litter reserves in tussock tundras. All these factors result in better insulation.

Nevertheless, in spite of overall long-term trend of thaw depth increase, different local ecosystems could demonstrate site-specific reactions. The so-called edaphic factor *E* (the rate of active layer thickness to incoming warmth) is supposed to be an estimate of the response rate of a permafrost layer in a given ecosystem to external warming. Factor *E,* as a general property of a given soil and vegetation complex, defines a slope of a direct proportion between the rate of soil thawing and the accumulated sum of incoming warmth depending on soil structure and its other important characteristics (Brown et al. 2000). Hence, this factor is bound to demonstrate a relatively constant value in a given ecosystem. However, as is shown in Figure 6, it is not true in all cases.

In the wet sedge-Salix mosses coastal ecosystem of the Lavrentiya site, the rate of soil thawing during the entire period of observations remains constant (Fig. 6). At least one of two tussock tundra sites in the Anadyr area (Cape Rogozhny, R9) demonstrates a highly significant linear trend for this rate to increase ($P = .026$). The positive nature of this tendency suggests that, in contrast to other two ecosystems, continuous warming more affects the latter ecosystem, which possibly fails this growing pressure and degrades, or begins to change adaptively.

The spatially more heterogeneous Lavrentiya and Mount Dionisiya sites possibly remain more stable and relatively tolerant to recent warming. Such a well-expressed reaction of the Cape Rogozhny ecosystems may be also due to more intense local anthropogenic stress (pressure of all-terrain vehicles in the past), as compared to the other sites.

As was shown, the greater the depth of seasonal thaw at a given microhabitat, the less the anticipated impact of warming. This means that a given micro- and meso-habitat structure of ecosystem (i.e., the degree of its spatial heterogeneity) can seriously impact the average rate of thawing within the landscape. Under extended rise of temperature, this could offset the warming effect in permafrost ecosystems.

To estimate the stability and significance of the trends and patterns found, it is highly desirable to continue monitoring using the CALM design.

Acknowledgments

We devote this paper to the memory of Dr. Anatoly Kotov, our friend and colleague. The study was supported by NSF grants OPP-9732051 and OPP-0352958. Thanks are also due to O.D. Tregubov, Yu.A. Vertebsky (Anadyr), G.M. Zelensky (Lavrentiya), and A.I. Ivaschenko (Moscow State University) for logistical support and assistance in the field.

References

Arft, A.M., Walker, M.D., Gurevitch, J., Alatalo, J.M., Bret-Harte, M.S., Dale, M., Diemer, M., Gugerli, F., Henry, G.H.R., Jones, M.H., Hollister, R.D., Jonsdottir, I.S., Laine, K., Levesque, E., Marion, G.M., Molau, U., Molgaard, P., Nordenhall, U., Raszhivin, V., Robinson, C.H., Starr, G., Stenstrom, A., Stenstrom, M., Totland, O., Turner, P.L., Walker, L.J., Webber, P.J., Welker, J.M. & Wookey, P.A. 1999. Responses of tundra plants to experimental warming: meta-analysis of the International Tundra Experiment. *Ecological Monographs* 69(4): 491-511.

Brown, J., Hinkel, K.M. & Nelson, F.E. 2000. The Circumpolar Active Layer Monitoring (CALM) program: research design and initial results. *Polar Geography* 24(3): 165-258.

Hinkel, K.M. & Nelson, F.E. 2003. Spatial and temporal patterns of active layer thickness at circumpolar active layer monitoring (CALM) sites in northern Alaska, 1995-2000. *Journal of Geophysical Research* 102(D2): 8168, doi: 10.1029/ 2001JD000927.

Kotov, A.N, Brazhnik, S.N., Galanin A.V., Maslov, V.Ya. & Samokhvalov V.D. 1998. Organization of ecological monitoring at "Onemen" research station. In: *Chukotka: Nature and Human*. Chukotka North-East Scientific Center, Far-East Branch, Magadan: Russian Academy of Sciences, 93-111. (in Russian).

Kotov, A.N. 2001. Stratigraphy, composition and constitution of massive ground ice bodies of tabular type on northern coast of Onemen Bay (Chukotka). In: *Materials of the Second Conference of Russian Geocryologists*, *June 6–9, 2001.* Moscow: Lomonosov State University, 218-225. (in Russian).

Mazhitova, G., Malkova (Ananjeva), G., Chestnykh, O. & Zamolodchikov D. 2004. Active layer spatial and temporal variability at European Russian Circumpolar Active Layer Monitoring (CALM) sites. *Permafrost and Periglacial Processes.*15: 123-139.

Nelson, F.E. & Outcalt, S.I. 1987. A computational method for prediction and regionalization of permafrost. *Arctic and Alpine Research* 19(3): 279-288.

Nelson, F., Brown, J., Lewkowicz, T. & Taylor, A. 1996. Active layer protocol. In: U. Molau & P. Molgaard, (eds.), *ITEX Manual, Second Edition*. Copenhagen: International Tundra Experiment, 14-16.

Pavlov, A.V. & Ananjeva, G.V. 2004. Assessment of recent air temperature changes in the territory of the cryolithozone of Russia. *Kriosfera Zemli* VIII(2): 3-9. (in Russian).

Zamolodchikov, D.G., Karelin, D.V., Ivaschenko, A.I., Oechel, W.C. & Hastings, S.J. 2003. CO_2 flux measurements in Russian Far East tundra using eddy covariance and closed chamber techniques. *Tellus* 55B(4): 879-892.

Zamolodchikov, D.G., Karelin, D.V., Ivaschenko, A.I. & Lopes de Gerenyu, V.O. 2005. Micrometeorological assessment of biogenic fluxes of carbon dioxide in typical tundra ecosystems of Eastern Chukotka. *Eurasian Soil Science* 38(7): 759-763.

Zamolodchikov, D.G., Kotov, A.N., Karelin, D.V. & Razzhivin, V.Yu. 2004. Active layer monitoring in Northeast Russia: spatial, seasonal, and interannual variability. *Polar Geography* 28(4): 286-307.

N-Factors and Soil Temperatures Adjacent to the Vertical Support Members on the Trans Alaska Pipeline System

John P. Zarling
Zarling Aero and Engineering and University of Alaska Fairbanks, Fairbanks, Alaska, USA

Steve Sorensen
BP Exploration, Prudhoe Bay, Alaska, USA

Melody Shangin
Alyeska Pipeline Service Company, Fairbanks, Alaska, USA

Abstract

This paper describes the results from several data logger systems that were installed along the above-ground portion of the Trans Alaska Pipeline System (TAPS) which transverses Interior Alaska and discontinuous permafrost terrain. These data logger systems record air, ground surface, and subsurface ground temperatures using thermistor strings. From these freezing and thawing data, n-factors are calculated and are presented for a few sites. Several of the instrumentation sites also included installing a pressure transducer in the heat pipe within the thermal vertical support members (VSM). These heat pipes are used to cool the ground around VSM during winter and can be used as thermometers to sense the temperature at the base of thermal VSM. The heat pipe pressure-derived temperature measurements correlate well with subsurface thermistor data. Reading heat pipe pressures has been adopted as a strategy for determining permafrost temperatures along the TAPS in the discontinuous permafrost region.

Keywords: data loggers; heat pipes; *n*-factors; permafrost; pipeline; temperatures.

Introduction

Design of the Trans Alaska Pipeline System (TAPS) began in 1970, and construction of the access road, pipeline, marine terminal, and pump stations started in 1974. The pipeline went into operation in 1977. The 800 mile (1270 km) pipeline has its origin at Prudhoe Bay on the North Slope of Alaska and its terminus at the ice-free port of Valdez. About one half on the pipeline is built above ground where it crosses non-thaw stable permafrost. North of the Brooks Range, where the climate is the coldest, the permafrost is continuous. South of the Brooks Range, where the climate is warmer, the permafrost is discontinuous across most of Alaska's Interior. Along the southern portion of Interior Alaska, in the Copper River Basin, discontinuous permafrost transitions to sporadic permafrost and to seasonal frost before reaching Valdez. Thermal issues relating to permafrost design of the TAPS were presented by Jahns (1983).

The above-ground pipeline is supported by bents formed by two to four piles, a cross-beam with a sliding shoe riding on the cross beam and attached to the pipe. The piles on each end of the crossbeam are called vertical support members or VSM. Bents are generally spaced approximately 60 ft (18.3 m) apart.

In the non-thaw stable discontinuous permafrost zone, each VSM has two heat pipes installed which are called thermal VSM. These heat pipes are one-way heat transfer devices that extract thermal energy from the ground during the winter when the air temperatures are less than the ground temperatures. During the summer, the heat pipes become inactive.

Much of the field testing of thermal VSM that occurred during the design phase of the pipeline was conducted in the early 1970s when the climate conditions were somewhat colder than present, with a large portion of this testing occurring near Fairbanks, Alaska. Figure 1 shows freezing and thawing indices for the last 55 years for Fairbanks. Based on a linear least squares best fit trend line through these data, the average freezing index has decreased about 11%, and the average thawing index has increased about 8% over the last 35 years. Because a safety factor of two was applied to conservative thermal design criteria, the constructed above-ground pipeline system continues to perform well, despite warming trends. This is evidenced by the very small number of VSM which have undergone measurable settlement or heave.

Throughout the operating life of the pipeline, more than 80 sites along the TAPS rout have monitored subsurface soil temperatures. However, air temperatures at these sites were not monitored. As a proactive measure to evaluate the above-ground pipeline support system under current climate conditions, Alyeska Pipeline Service Company (APSC) initiated an additional ground and air temperature monitoring program in 2003. This program consists of the installation of data loggers and temperature measuring sensors at over 40 sites along the pipeline, from fairly continuous permafrost regions just south of the Brooks Range to sporadic permafrost regions near the Little Tonsina River north of Big Thompson Pass. Each data logger site monitors air temperature, ground surface temperature, and sub-surface ground temperatures. Several of the data loggers also monitor the pressure inside the heat pipes (thermosyphons) installed in the thermal VSM.

Data from these sites have been analyzed in terms of air

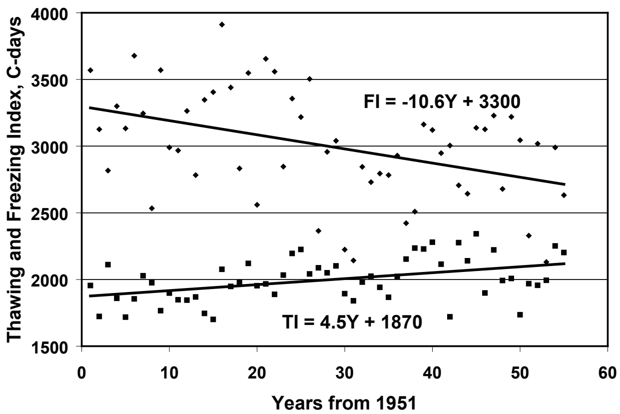

Figure 1. Freezing and thawing index data and trends for Fairbanks, Alaska beginning in 1951.

Figure 2. Installation of photovoltaic panel, battery box, data logger enclosure on VSM and thermistor string enclosure.

and surface freezing and thawing degree days and indices. From these data, freezing and thawing n-factors have been calculated and are presented for three of the data logger sites near Fairbanks. These n-factors are commonly used by engineers to predict depths of freeze or thaw. Many of these sites are undisturbed during the winter months, i.e., there is no snow removal. Surfaces are typically graveled, with either sparse grasses and/or brush growing, but growth is controlled by mowing from time to time (see Fig. 2).

Because the working fluid inside the heat pipes is in the two phase region, the heat pipes can be used as thermometers. The measured pressure inside a heat pipe can be converted to temperature of the liquid pool at its base. Thermistor strings have also been installed adjacent to several vertical support members that have pressure transducers installed. During the summer season when the heat pipes are non-operational and soil temperatures surrounding the VSM have come to equilibrium, the temperatures measured by these two methods are almost equal. During the winter months, the base of heat pipe temperatures are colder than the soil temperatures adjacent to the vertical support member, as expected when the heat pipes are operational. Graphs are presented showing air temperature, base of heat pipe temperature, and soil temperature surrounding the VSM.

Instrumentation System

Power for each of the instrumentation systems consists of a nominal 20 watt solar voltaic panel connected through a charge controller to a sealed 12-volt, 100 amp-hour lead acid battery. The data logger system is a Campbell Scientific CR10X data logger coupled to an AM/16/32 multiplexer housed in a fiberglass all weather enclosure. Air temperatures are measured with a thermistor housed in a Campbell Scientific six gill radiation shield. Ground surface temperatures and ground temperatures at depth are measured using thermistors. Ground surface temperature thermistor strings use two-pair direct burial telephone cable which has a polyethylene jacket providing mechanical protection over the range of temperatures experienced under arctic conditions. Air and vertical ground thermistor strings are single pair or multi-pair, respectively, Halar coated conductors, with a Halar outer jacket. The thermistors are 16,320 ohms at 0°C, +/- 0.1C°, YSI P/N 44034. KPSI pressure transducers with a range of 0 to 600 psia (0 to 4.1 MPa), or programmable Honeywell PPT pressure transducers with a range of 0 to 1,000 psia (0 to 6.9 MPa) were used to measure heat pipe pressures. Because the nominal output-range of the pressure transducers are 0 to 5 volts, a Campbell Scientific VDIV2.1 voltage divider is used to reduce the input voltage to match the CR10X's 0 to 2.5 volt input range. The photovoltaic panel, polyethylene battery box, and all-weather enclosure are mounted to Unistrut. The Unistrut supporting the photovoltaic panel and enclosure are banded to the VSM, and the battery box is banded to the cross-beam as shown in Figure 2.

Data were retrieved from the data logger by swapping SM4 storage modules, or downloaded using Campbell Scientific's PConnect software with a Palm handheld or by directly connecting to a laptop computer through the data logger's serial port.

N-Factor Results

N-factors are empirically determined and used to estimate ground surface temperatures based on air temperatures. These factors are used in the modified Berggren method for depth of freeze and thaw calculations. Geotechnical finite element thermal modeling programs typically use n-factors to arrive at an annual surface temperature variation. To determine an *n*-factor, the air and surface temperatures are measured at a chosen site. The freezing and thawing degree days are calculated based on the following relationships:

$TDD = T_{AVE} - 0^0 C$ if $T_{AVE} < 0^OC$ and
$FDD = 0^0 C - T_{AVE}$ if $T_{AVE} > 0^OC$

From these data, air and surface freezing and thawing indices are calculated on a seasonal basis, using the cumulative method. Then the ratio of the surface and air freezing indices and surface and air thawing indices are calculated from measured and recorded temperatures to arrive at the site-specific *n*-factor. The equations stating these relationships are:

$$n_F = \frac{Surface \cdot Freezing \cdot Index}{Air \cdot Freezing \cdot Index}$$ and

$$n_T = \frac{Surface \cdot Thawing \cdot Index}{Air \cdot Thawing \cdot Index}$$

A compilation of measured n-factors has been published by (Lunardini 1978). However, there have been very few *n*-factors published for surfaces other than paved and gravel roads, and airport runways and taxiways.

Air and surface temperature data have been collected at most of the sites for the last four years. Three of the instrumented sites are along a section of above-ground pipeline between Chena Hot Springs Road and Nordale Road, northeast of Fairbanks. This section of above-ground pipeline is usually referred to as the Love Road site.

The Love Road site is typical for a low-lying, non-thaw stable permafrost area in Interior Alaska. It is a marshy lowland flood plain area, underlain by ice-rich silt with more than 95% typically passing a no. 200 sieve (Pearson 1977). The natural vegetation around the gravel pad area consists of tussocks, mosses, tamarack, black spruce, and willows and other brushy plants, as well as various varieties of grasses. This area represented a "worst case scenario" in terms of thermal stability design in a warmer permafrost horizon. During construction, the natural ground was covered with a gravel work pad to allow installation of VSM supports and the pipeline. The work pads have been maintained over the years by application of additional gravel surfacing. The northern end of this section of pipeline was the first above-ground pipeline constructed, with the work pad placed in March of 1974 and 14 VSM in early October of 1974 (Pearson 1977). It is also the area where initial field testing of several pre-construction heat pipes was performed. Twelve of the VSM became part of the pipeline, with production heat pipes installed in these VSM in March of 1975 (Pearson 1977). Table 1 identifies the three instrumented sites as A, B, and D, with their corresponding pipeline mileposts. Soil temperature data for the VSM at Site A, at elevations below the surface of the gravel pad, were recorded from 1974 through 1976 (Pearson 1977).

Air temperature and ground surface temperature curves are shown in Figure 3 for Site A. The n-factors for the three sites A, B, and D, along this section of pipeline are presented in Table 2, beginning with winter 2003–4 through summer 2007.

Thermistor strings at the Love Road Sites A and C were installed to a depth of 18 m and within 0.8 m of the VSM on the drive lane side of the work pad. An additional thermistor string, Site B, was installed to a depth of 18 m at the mid-point between bent C and the bent station immediately north (upstream). Whiplash curves are shown in Figures 4 and 5 for the thermistor strings installed at Sites B and C.

Comparing Figures 4 and 5 shows the ground cooling effect provided by the heat pipes in the thermal VSM. It is also noted, that the top of the permafrost next to the thermal VSM is about 2 m below the ground surface after 30 years of pipeline operation. Midway between bents, the top of the permafrost has receded to about 4 m below the ground surface nearly 30 years after pile placement. Design phase calculations predicted 3.3 m of seasonal thaw after 20 years of operation (Jahns et al. 1978) and from 4 m to 6 m of thaw after 20 to 30 years of operation, (Jahns 1983).

The top of the permafrost was at a depth of about 2 m

Table 1. Site location in miles from Prudhoe Bay and comments about location.

Site	Mile Post	Comments
A	456.130	VSM/Bent Station at preconstruction test site
B	456.183	Thermistor string 18 m north of Site C
C	456.189	VSM/Bent Station adjacent to preconstruction test site
D	458.178	VSM/Bent Station at transition to below ground

Table 2. Year and *n*-factors for Sites A, C, and D.

Year and N-Factor		Site A	Site C	Site D
2003–4	N_F	.22	.17	N.A.
2004	N_T	1.08	1.07	1.12
2004–5	N_F	.21	.18	.25
2005	N_T	1.04	1.08	1.09
2005–6	N_F	N.A.	0.35	0.48
2006	N_T	1.02	1.10	1.09
2006–7	N_F	.0.34	0.32	0.49
2007	N_T	1.04	1.07	1.09

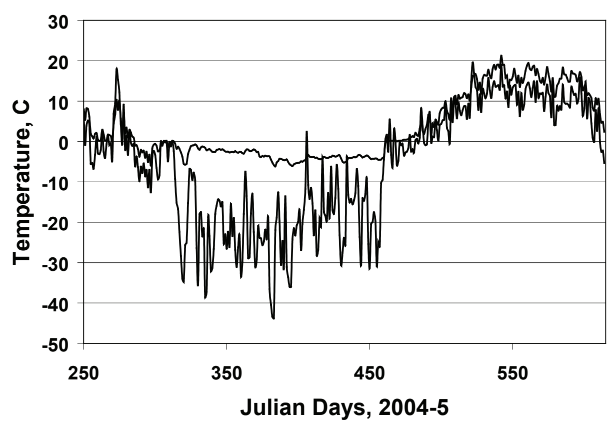

Figure 3. Air (highly variable curve) and ground surface temperatures for instrumentation Site A near Fairbanks. The soil surface temperature measured 6 m from VSM.

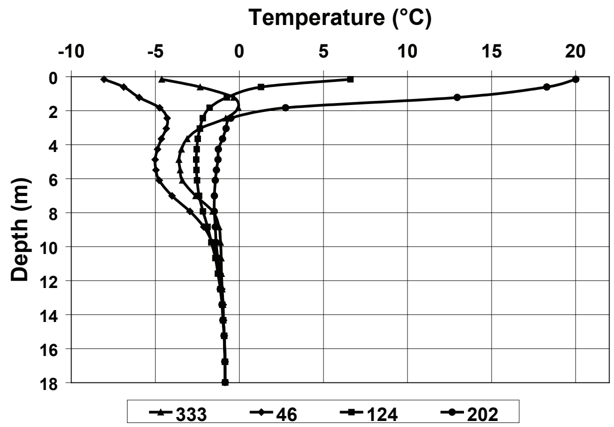

Figure 4. Site C whiplash curves for Julian days 46, 124, 202, and 333 within 1 m of thermal VSM in 2004.

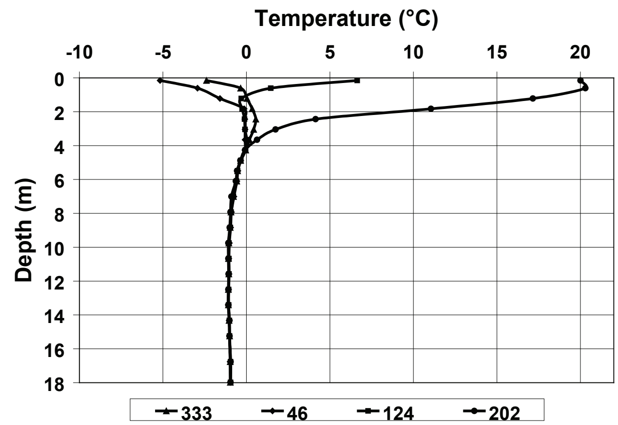

Figure 5. Site B whiplash curves for Julian days 46, 124, 202, and 333 midway between bent stations in 2004.

in October of 1976 (Pearson 1977). In 2004, the top of the permafrost had receded to about 4 m midway between bents as shown by the whiplash curves in Figure 5. The temperature at a depth of 8 m beneath the work pad was about -0.5°C in October of 1976. Figure 5 indicates about the same temperature at a depth of 8 m in 2004.

End of summer temperatures at 8 m depth in October 1976 adjacent to the VSM at Site A were about -2.2°C. The warm side trumpet curve shown in Figure 6 in 2003–2004 shows similar recorded temperatures at the 8 m depth.

Figure 6 shows the cold side and warm side trumpet curves for Site A. It is observed the ground temperatures at depth are about 1°C colder at this site than Site B referenced in Figure 4 which is about 92 m away. There is a remote gate valve close to Site A, which is supported by four thermal VSM which provide greater combined ground cooling in the immediate area. It is worth noting, that installing free-standing heat pipes next to existing thermal VSM is a way to mitigate potential climate warming effects and have been successfully employed at a few locations on the TAPS.

Heat Pipes as Thermometers

The 124,300 heat pipes installed in the VSMs of TAPS were manufactured by the McDonnell Douglas Corporation. The heat pipes are 2-inch (51 mm) OD steel pipe below the top of the VSM and 3-inch OD pipe above the top of the VSM. Inside diameter is a uniform 1.5-inches (38 mm). Heat pipes with a 4-foot (1.22 m) long extruded aluminum fin were made in lengths of 28 ft (8.5 m) to 37 ft (11.3 m) in 3-foot (0.9 m) increments. Heat pipes with a 6-foot (1.83 m) long extruded aluminum fin were manufactured in lengths from 42 ft (12.8 m) to 75 ft (22.9 m) in 3-foot (0.9 m) increments. These heat pipes were originally charged with anhydrous ammonia.

In 1983, (Johnson 1983), six years following completion of TAPS, it was reported that many of the heat pipes were experiencing an accumulation of non condensable gas inside the units. The gas was determined to by hydrogen. During operation, the hydrogen is swept by the ammonia vapor

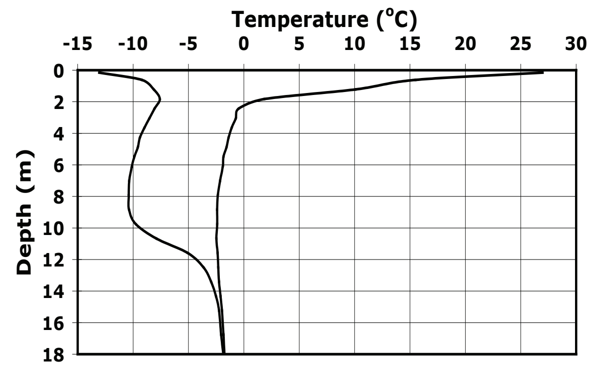

Figure 6. Site A cold and warm side trumpet curves for the period of 2003 to 2005 at 1 m from the thermal VSM.

to the top of the heat pipe. The ammonia then condenses, leaving the hydrogen behind, partially blocking the top finned section from condensing additional ammonia. Using infrared camera technology, the amount of blockage or "cold topping" is determined. In the 1980s through the 1990s, getter pins were installed in the top of the heat pipes to absorb the hydrogen. The getter pins contained a metal halide, zirconium dimanganese. When the getter pins became saturated with hydrogen, non-condensable gas blockage would return. In 2001, Sorensen et al. (2003), developed a program of bleeding-off the ammonia and non-condensable gas and recharging with carbon dioxide. This process required the installation of a valve at the top of the heat pipe.

The pressure transducers were attached to valves installed above the finned section of the heat pipes. A thread-o-let was welded on the side of the steel pipe above the fins, and a hole drilled through the heat pipe wall to within 1/8 inch of breaking through. A hot tapping tool was then attached to the thread-o-let, and the final drilling was completed through the wall of the heat pipe. The ammonia was bled off, and the heat pipe was evacuated and purged with nitrogen before the final charge of carbon dioxide was performed.

Because the working fluid in the heat pipe is in the two phase region, pressure and temperature are not independent

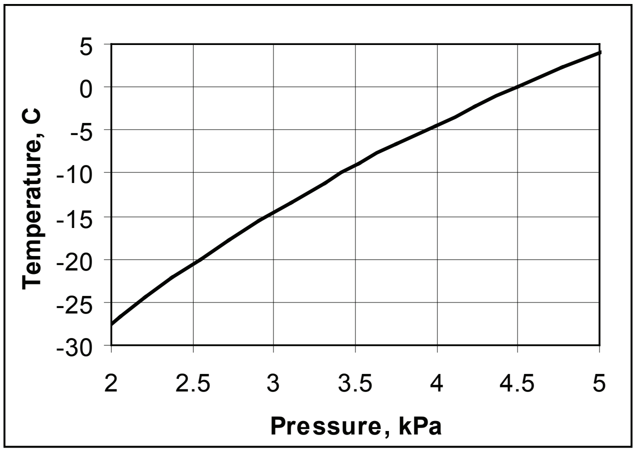

Figure 7. Saturation temperature–pressure relationship for carbon dioxide.

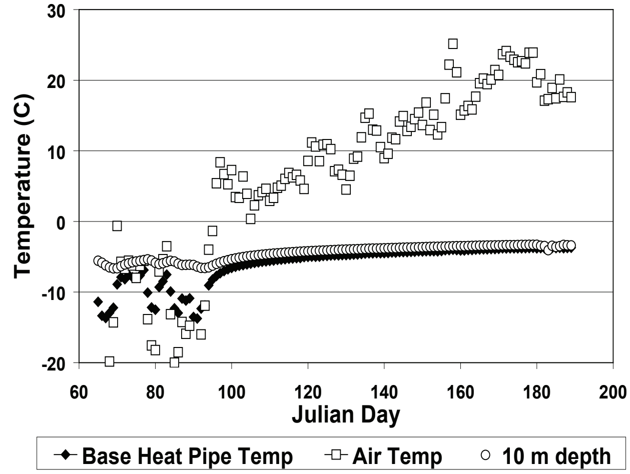

Figure 8. Comparison of air, base of heat pipe, and ground temperature near base of VSM.

properties for a single component fluid. Therefore, by measuring the pressure inside the heat pipe, the temperature is readily determined by referencing the thermodynamic tables of the specific working fluid. At those instrumented sites where the temperature at the base of the VSM was desired, a hot taping operation was performed to bleed-off the ammonia, and then the heat pipe was recharged with carbon dioxide. The saturation temperature–saturation pressure relationship for carbon dioxide is shown in Figure 7. The pressure indicated by the pressure transducer was corrected for the hydrostatic head of vapor in the heat pipe to arrive at the pressure at the liquid pool vapor interface at the base of the heat pipe. Then, using a chart as shown in Figure 7, the temperature at the base of the heat pipe was established.

When the air temperature is colder than the ground temperature surrounding the VSM, the heat pipe operates and removes heat from the ground. When the air temperature is warmer than the ground temperature surrounding the VSM, the heat pipe ceases to reject heat.

Figure 8 shows air temperature, base of heat pipe temperature, and the ground temperature as measured by a thermistor at the same elevation as the base of the heat pipe. This thermal VSM is at the northern end of the Love Road site. Temperatures of air, base of heat pipe, and ground at the 10 m depth are plotted in the Figure for Julian days 65 through 195. During the winter, it is seen that when the air temperature is coldest, the base of heat pipe temperature is warmer, and the temperature of the surrounding ground the warmest. It is noted that there are a few days during the winter period that the outdoor air temperature exceeded the ground temperature and the heat pipe would become inoperative. When the heat pipe ceases to function in the spring of the year, the base of heat pipe temperature and the surrounding ground temperature trend to equilibrium. It is observed that the temperature measured by the thermistor and the temperature calculated from measuring the heat pipe pressure (refer to Fig. 7) are almost exactly the same.

By measuring the pressure in the heat pipe during or after maintenance is performed, the temperature of the permafrost at the bottom of the VSM can be determined. Measurements in late summer using this method have revealed that most VSM base temperatures remain below freezing, even in cases of severe cold topping. In many cases, where temperatures are initially near or slightly above freezing during maintenance, re-freezing tends to occur within one to two years, even in sporadic permafrost areas. In addition, the method assists in providing a relatively dense map of late summer subsurface temperatures along the TAPS right-of-way that would be difficult to achieve by any other method.

Conclusions and Discussion

The Campbell Scientific data loggers and multiplexers have proven to be very reliable. A few intermittent problems that occurred initially with respect to data logging among the 40 sites included flooding of one data logger due to stream icing/overflow, broken thermistor lead wires at two sites due to frost heave and settlement, and low battery voltage in valleys where the sun does not shine on the photovoltaic panels for several months during mid-winter at two locations. Because batteries are mounted on the crossbeams of the bents, they are exposed to ambient temperatures. Their capacities are decreased with decreasing temperature, and their charging efficiency is also decreased at low temperatures Many researchers bury batteries beneath the snow to avoid exposure to low ambient temperatures. However, in this case, mounting the batteries on the crossbeams provided greater security and allowed better access for periodic maintenance. All of these challenges were addressed early in the project to ensure effective monitoring.

The thawing *n*-factors are lower than typical thawing n-factors for gravel surfaces (Lunardini 1978). Early morning and late evening shading by trees and brush along the sides of the right-of way, daily shading of the ground from the shadow cast by the pipeline, and ground shading by vegetation are all causes for the lower thawing *n*-factors.

The freezing *n*-factors show more variation from year to year. The amount and timing of the snow cover has the major effect on the freezing n-factors. Early and deep snow covers yield lower freezing n-factors.

The trumpet and whiplash curves presented for sites A, B, and C show no significant changes in temperature from the data presented by Pearson (1977). The heat pipes installed in the VSM have been effective in maintaining reduced permafrost temperatures around the VSM. The drive lane for this section of pipeline serves as a summer and winter recreational trail. Wintertime activities include dog mushing, Nordic skiing, and snowmobiling, which tend to compact the snow. Additionally, APSC plows this section of drive lane from time to time in the winter for access to the two remote gate valves along this section. The effects of compacting and/or removing snow enhance cooling of the ground as the thermal resistance of the snow is reduced.

Using the heat pipes as thermometers is a very effective method of determining the late summer base of heat pipe temperatures. This tends to be a more cost effective method of obtaining these temperatures in comparison to the installation of thermistor strings.

The dynamics of heat pipe cooling in thermal VSM as a function of time and air temperature is better understood. Thanks to the early work by others at the Fairbanks sites during design of the pipeline, a good comparison of long-term thermal data is possible. By evaluating thermal conditions at several sites in a region, *n*-values have been determined for use in trending and predictive maintenance of thermal VSM.

Acknowledgments

The authors would like to acknowledge Christopher Swaim, Commissioning Engineer, Pipeline Maintenance Engineering, and Wiley Splain, Engineer II, Integrity Management Engineering, both with the Alyeska Pipeline Service Company, for the installations of the data logger systems, and Tracy Shields for downloading and analyzing some of the data. The authors would also like to thank the Alyeska Pipeline Service Company for permission to publish this paper.

References

Jahns, H.O. 1983. Pipeline Thermal Considerations. *Proceeding of the Fourth International Conference on Permafrost. Vol. 2. Fairbanks, Alaska, USA.*: 101-111.

Jahns, H.O., Miller, T.W., Power, L.D., Rickey, W.P., Taylor, T.P. & Wheeler, J.A., 1978. Permafrost protection for pipelines. *Proceeding of the Second International Conference on Permafrost. Yakutsk, Russia*. North America Contribution. National Academy of Science. Washington DC: 673-683.

Lunardini, V.J. 1978 Theory of n-factors and correlation of data. *Proceeding of the Third International Conference on Permafrost, Vol. 1. Edmonton, Alberta, Canada*: 40-46.

Johnson, E.R. 1983. Performance of the Trans-Alaska Oil Pipeline *Proceeding of the Fourth International Conference on Permafrost*. *Vol. 2. Fairbanks, Alaska, USA.:*109-111.

Pearson, S.W. 1977. Thermal Performance Verification of Thermal Vertical Support Members for the Trans-Alaska Pipeline. ASME Winter Annual Meeting, Atlanta, Georgia. Paper 77-WA/HT-34. 1-9.

Riseborough, D.W. 2003. Thawing and freezing indices in the active layer. *Proceeding of the Eighth International Conference on Permafrost. Vol. 1. Zurich, Switzerland*: 953-958.

Sorensen, S., Smith, J. & Zarling, J. 2003. Thermal performance of TAPS heat pipes with non-condensable gas blockage. *Proceeding of the Eighth International Conference on Permafros*t. *Vol. 1. Zurich, Switzerland*: 1097-1102.

Study of Western Taymyr Permafrost in the Framework of the IPY Education Program

Alexandra M. Zemskova
Lomonosov Moscow State University, Faculty of Geography, Dept. of Cryolithology and Glaciology, Moscow, Russia

Abstract

A 10-day course on Permafrost and Periglacial Geomorphology of Western Siberia and Western Taymyr (PPG), as part of the framework of the IPY education program, was jointly developed by faculty of the Geography Department of Moscow State University and researchers from the Earth Cryosphere Institute. The course was held at the end of July and beginning of August 2007 aboard the *Fedor Naianov* vessel, which sailed on Yenisey River from the town of Dudinka to the port of Dikson on the Arctic coast. The course attracted six Russian upper-level undergraduate and graduate students from Moscow State and St. Petersburg State Universities. The main topics of the course were (1) landscape-specific permafrost conditions and characteristics of the lower Yenisey River region, (2) ground ice and cryolithology, (3) Quaternary history of Western Taymyr, and (4) field methods of geomorphologic investigations. The course consisted of extensive field excursions at nine stops along the Yenisey and a lecture series and laboratory work aboard the ship.

Keywords: ground ice; IPY education program; landscapes; permafrost; Quaternary deposits; Western Taymyr.

Introduction

The expedition was organized under the supervision of two doctors of science: Irina D. Streletskaya (Lomonosov Moscow State University, Faculty of Geography, Dept. of Cryolithology and Glaciology, Moscow, Russia) and Aleksander A. Vasiliev (The Earth Cryosphere Institute SB RAS, Tyumen, Russia).

The young participants of the expedition were Alexandra M. Zemskova, Mikhail N. Ivanov, Ivan V. Kopytov, Sergey A. Simonov (Lomonosov Moscow State University, Faculty of Geography, Dept. of Cryolithology and Glaciology, Moscow, Russia), Maria A. Medvedeva, and Alexandra G. Cherkasheva (St Petersburg State University, Faculty of Geography, St. Petersburg, Russia) (Fig. 1).

Students participated in applied geocryology, geomorphology, biology, and Quaternary research. This included the study of the spatial distribution of major landscapes, vegetation, and soil along the prime climatic gradient from Dudinka to Dikson; the study of geological cryogenic structures of Pleistocene sediments; collection of characteristic vegetation, soil, and sediment samples; and collection of ground ice samples for isotopic analysis. Contemporary cryogenic processes of the Western Taymyr coastal zone were studied, including coastal dynamics, ice wedges, thermokarst, etc.

Figure 1. Our research group: Maria A. Medvedeva, Aleksander A. Vasiliev, Alexandra M. Zemskova, Alexandra G. Cherkasheva, Ivan V. Kopytov, Irina D. Streletskaya, Sergey A. Simonov, Mikhail N. Ivanov.

Study Area

The study area was along the Yenisey River from Dudinka to Dikson Island. The eastern coast of the Yenisey Gulf from Sopochnaya Karga Cape to Dikson Island is the northwest periphery of the Taymyr Peninsula. Geographical characteristics of the region are influenced by the high latitude and the cold Kara Sea currents (Fig. 2).

Despite a general increasing trend of summer precipitation from north to south, the difference is not large: Ust'-Port, 137 mm; Igarka, 213 mm. The radiation balance in the warm period varies by latitude: Dikson Island, 891.7 MW; Turuhansk, 1218.3 MW.

The radiation balance during the cold period at Dikson Island is equal to 380.9 MW and in Turuhansk, 255.3 MW. The difference in the degree-hour sum for the cold period in the north and in the south is not more than 25%. The precipitation variance from north to south is large: Gol'chiha, 107 mm, and Igarka, 294 mm. The reason for this contrast is in the barrier for the western air masses, such as Putorana Plato. The Yenisey River valley is the territory of increased snow accumulation. Changes in topography effect the development of cryogenic processes.

The northern portion of the described region has relief with stepped construction. We can observe continuity of

Figure 2. The map with the route of research: 1 - Dudinka, 2 – Sopkarga, 3 – Vorontsovo, 4 – Budenovsk, 5 – Dixon, 6 – Krest'yanka, 7 – Narzoi, 8 – Zverevsk, 9 – Innokentevskoe.

relief levels from interfluve to river valley. Formation of these levels is connected with the presence of Pleistocene sea basins, lake reservoirs, and rivers. According to the main exogenic processes, which form contemporary relief, it is possible to substract three types of relief in this area: Pleistocene marine terraces; Pleistocene-Holocene, lake-limnetic accumulative depressions; and alluvial terraces.

The continuity of landscape zones with its own complex of cryogenic processes goes from the south to the north. The southern zone of low-bush tundra stretches from the latitude of Dudinka to Karaul. The northern zone of moss-lichen tundra extends close to 72°N latitude. Finally the arctic zone extends northward to the town of Dikson. (Tumel' 1988, Popov & Tumel' 1989).

Our research was in the northern part of this region. This polar region of the permafrost distribution consists of a tundra zone that stretches for 450 km from Dudinka latitude to the coast of the Kara Sea. Permafrost is continuous here. The permafrost thickness is greatest at the mouth of the Yenisey River: from 10 m to 600 m. Minimal thickness is observed at the low inundable levels where contemporary permafrost is forming. The annual average air temperature spectrum is wide: from 0°C to -9°C or -10°C. To the north from Ust'-Port the average air temperature is -7°C to -9°C.

Quaternary history of Western Taymyr

Mesozoic aqueous rocks crop out only to the North from Kuznecovskiy Cape. To the south Pleistocene sediments have practically solid sedimentary cover above the bedrock. The intensive erosion of bedrock came before the Quaternary period, therefore the overdeepening of the Yenisey valley was 380 m lower than contemporary sea level. The thickness of Pleistocene sediments increases regularly from 100 to 200–400 m from south to the north. Quaternary deposits are as follows: alluvial, marine, glacial-marine, fluvio-glacial, glaciolacustrine, and deluvial- soliflual Pleistocene-Holocene sands, loams, and clays (Troickiy 1966).

Methods

Seven scientific-educational field trips have been undertaken by the participants of the expedition. We were doing observations, collecting samples of frozen ground and ice for different analyses, and making some field measurements (e.g., evaluation of the moisture content of frozen samples). For study of the contemporary permafrost state, ground ice specifics, and paleogeographical reconstructions a complex of field and laboratory methods has been used: geomorphological, cryolithological, geobotanical, landscape, geological, paleontological, radiocarbon, isotopic,

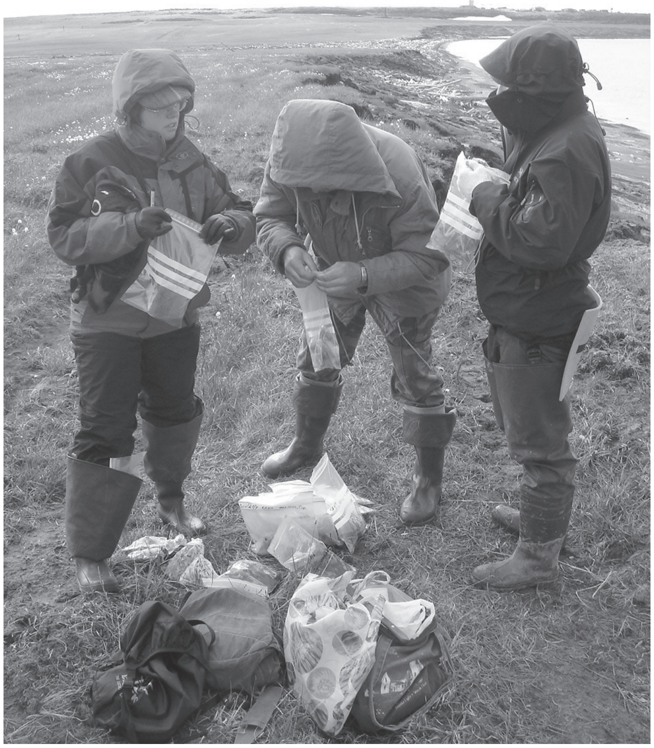

Figure 3. Packing samples of ice from the ice wedges.

optically stimulated luminescence (OSL), geochemical, pellet-mineralogical analysis by the Surkov method, and sporo-pollen analysis. For these purposes, samples of frozen ground, snow, and ice were collected from coastal exposures (Fig. 3).

Geothermal survey methods were used in two wells equipped with loggers to monitor the temperature regime of the Western Taymyr accumulative land forms (alluvial spits). The boreholes are situated at the flat coast of the Sopochnaya Karga lagoon.

During the expedition students acquired fieldwork skills (describing boreholes and transverse sections, defining ice fraction, and collecting and registering of samples) and field and cameral treatment of collected materials (evaluation of solid natural moisture content, herborization, and sorting of samples).

Field Observations

During the expedition, Pleistocene-Holocene deposits in the coastal exposure of the east bank of the Yenisey River and Yenisey Bay were studied. The two types of frozen rocks showed epigenic type (freezing after the rock forming) and syngenetic type (freezing synchronously with sediment formation). The Samarovskaya (MIS (marine isotopic stage) 10) moraine deposits of middle Pleistocene, Sanchugovskie (MIS 8-6) marine and Kazancevskie (MIS 5) (Late Pleistocene) glacial-marine, marine and coastal-

Figure 4. Ice complex (coastal area of Sopochnaya Karga polar station).

Figure 5. Collecting the samples of ice from the "ice complex."

marine deposits of Late Pleistocene refer to the epicryogenic type. As usual, the Middle-Pleistocenic deposits are characterized by comparatively low ice content: up to 20% in volume and massive or nonregular cryogenic structure. The Late Pleistocene Kazancevskie deposits have greater ice content—up to 50%—and tabular massive ground ice with visible thickness more than 10 m were found (Figs. 4, 5).

Late Pleistocene-Holocene deposits of ice complex and Holocene deposits of contemporary deluvium and accumulative marine and fluvial formations refer to the syncryogenic type of permafrost. Ice complex deposits are characterized by high ice content—up to 80% in volume—and lenticular-stratified cryostructure (Karpov 1986). They contain polygonal ice wedges 4 m wide in the upper part of the section and up to 12 m high (Fig. 6).

Contemporary cryogenic processes of the Western Taymyr coastal zone were also studied. They are the following: coastal dynamics, ice wedges, thermokarst, etc. It is possible to see that for the last several decades the permafrost gas degraded in the explored region. Two wells were equipped with loggers for temperature regime monitoring of Western

Figure 6. Ice wedges near the Dikson.

Taymyr accumulative land forms (alluvial spits). The boreholes are situated at the flat coast of the Sopochnaya Karga lagoon.

Conclusions

Natural conditions at the Yenisei delta and at the Yeniseyskiy Bay coastal area from Sopochnaya Karga polar station to Dikson were studied.

Research methods in arctic landscapes, plant formation and soil covering, transverse sections of permafrost thicknesses have been taught in real, natural settings. Areal differentiation and variability of dominant landscapes, plant formations, soil cover in relation to the nature climatic zone at the Dudinka–Dixon transect have been studied. Geology aspects and cryolithological specifics of Middle-Late Pleistocene and Holocene deposits of Western Taymyr were studied too.

The samples of snow and ice from ice wedges and ice complex for study of isotopic composition of ground ice have been selected. Samples for optically stimulated luminescence (OSL) analysis of sand deposits have been selected with the purpose to determine absolute age of Middle-Late Pleistocene deposits.

Solids and ice samples were collected for laboratory study of their properties. We get new data for different parameters such as grain texture, mineralization of soils, spore-pollen compound and OSL, and radiocarbon age. Isotopic sampling was done almost for the first time ever at this part of Taymyr Peninsula.

Detailed data about flora specifics and their ratios in the different natural and climatic zonality—from forest tundra to arctic tundra—were collected.

Unique deposits of ice complex, inclosing repeated-wedge ice of great thickness, have been defined. It is established that the ice complex of Western Taymyr is represented by Late Pleistocene-Holocene sabulous deposits, the youngest deposits in the transverse section.

We plan to continue our observations on loggers. This will help to get new data about offshore permafrost on the lowland accumulative forms of relief (beach, bay bar); the speed and dynamic of permafrost formation; and how permafrost follows annual air temperature; that is, its reaction on climate changes.

Our research helps to improve the methods of field investigation and the use of new technologies and methods in the field. Results of these analyses would apply as a foundation for master and Ph.D. student work.

This expedition is a first step in international research group organization to do research work in this region.

But of course, some things need to be improved. If our group were able to use more portable technical equipment (e.g., modern GPS, salinity meter – to compare water in the Yenisey River and Yenisey Bay and ground, different soil and meteorological portable equipment, etc.) it could have made information, that we got more accurate and our trip would have been even more informative and productive. This would be useful because the region of our investigations is unique and poorly studied.

Acknowledgments

Research has been sponsored by ConocoPhillips Russia, Inc., and by the Oceanology Institute in Saint Petersburg. Special thanks to Elena Zemskova, to the management of the Great Arctic Reserve, to Mrs. A. F. Lubnina and Mr. G. I. Lubnin for lectures and for historical and ecological tour arrangements in the town of Dikson. I also express thanks to the reviewers of this paper for their comments and editorial changes.

References

Karpov, E.G. 1986. *Ground Ice of Yeniseyskiy North.* Novosibirsk: Nauka, 133 pp.

Saks, V.N. & Antonov, K.V. 1945. Quaternary deposits and geomorphology of Ust'-Yeniseyskiy port region. *Proceedings of the Glavsevmorput' Mining-and-Geological Administration.* Issue 16, N: Nauka, 56-117.

Troickiy, S.L. 1966. *Quaternary Deposits and Relief of Yeniseyskiy Bay Flat Coastal Areas and Neighboring Part of Byrranga Mountains*. Moscow: Nauka, 207 pp.

Tumel', N.V. 1988. *Cryolithological Research at the Educational Field Practice.* Moscow: Moscow State University, 97 pp.

Active Layer Monitoring at a New CALM Site, Taimyr Peninsula, Russia

F.N. Zepalov, V.I. Grebenets
Moscow State University, Moscow, Russia

D.A. Streletskiy, N.I. Shiklomanov
University of Delaware, Newark, USA

Abstract

The Circumpolar Active Layer Monitoring (CALM) site was established in the Taymir Peninsula to compensate for some deficiencies in the CALM observational network in Russia. The regular active layer measurements were initiated in 2005 followed by detailed characterization of landscapes and surface conditions. Periodic frost heave and thaw subsidence measurements by optical leveling were initiated in 2007. A short three-year period of observations allowed for only preliminary conclusions. The grid-average ALT for the study period is 87 cm. The thickness of the active layer varies from 45-50 cm to 125-150 cm, depending on landscape-specific conditions. The maximum thickness of the active layer is observed at landscapes represented by sparsely-vegetated patterned ground and dry hillocks. The minimum ALT was found in the polygonized peatlands. In the near future we intend to extend the observational program to include air and ground temperature monitoring. The establishment of complementary sites in underrepresented landscapes is currently under consideration.

Keywords: active layer thickness; CALM; Taimyr Peninsula.

Introduction

The active layer is the most dynamic and sensitive part of the climate-permafrost system. Knowledge of spatial and temporal characteristics of the active layer and factors affecting its long-term behavior and spatial pattern is required for assessing and predicting environmental conditions and socio-economic development of permafrost regions. Active layer investigations have a long history in Russia (Shiklomanov 2005) and include both empirical (Garagulya 1985, Kudryavstsev 1979) and modeling studies (Feldman 1977, Anisimov et al. 2002, Malevsky-Malevich et al. 2006).

Beginning in the 1990s systematic, standardized active layer and shallow permafrost observations were initiated under the international Circumpolar Active Layer Monitoring (CALM) program (Brown et al. 2000, Nelson et al. 2004). The series of 41 CALM sites that constitute the Russian portion of the network extends from the European tundra of the Pechora and Vorkuta regions to Chukotka and Kamchatka (Shiklomanov et al. 2008). However, the area adjacent to the Taimyr Peninsula, which constitutes a vast portion of Russian permafrost regions, is largely underrepresented by CALM. Two sites established in the Taymur region in the early 1990s were discontinued due to logistical circumstances (Fig. 1). To compensate for this CALM network deficiency, in 2005 a new Talnah site was established on the Taimyr Peninsula, in the Norilsk Industrial Region. This report provides a detailed description of the Talnah CALM site, observational methodology, and initial results obtained over the 2005-2007 period.

Study Area

The Talnakh grid (R32 according to CALM classification) is located (69°26′01″N, 88°28′03″E) in the northern part of Eastern Siberia on the Taimyr Peninsula (Fig. 1) at the Noril-Rybnin interfluve, about 2.5 km southeast of the settlement of Talnakh (Norilsk Industrial Region). Kharaelakh Ridge of the Putorana Mountains lays 1.5 km north of the site. The site is situated on a fluvial terrace, characterized by loamy soils and underlain by low-temperature, continuous permafrost (Sheveleva & Khomichvskaya 1967, Ershov 1991). The climate of the region is temperate continental with prolonged, snowy winters and short, cool summers (Tushinskiy & Davydova 1976). On average, the period with negative mean daily air temperatures extends 245 days. Mean annual air temperature is –9.8°C. Mean air temperature of the coldest month (January) is -27.6°C, of the warmest month (July), +13.4°C. Average annual wind speed is 6.3 m/s and the annual sum of precipitation is 340 mm/yr. The climatologically average maximum snow-cover thickness is 80 cm.

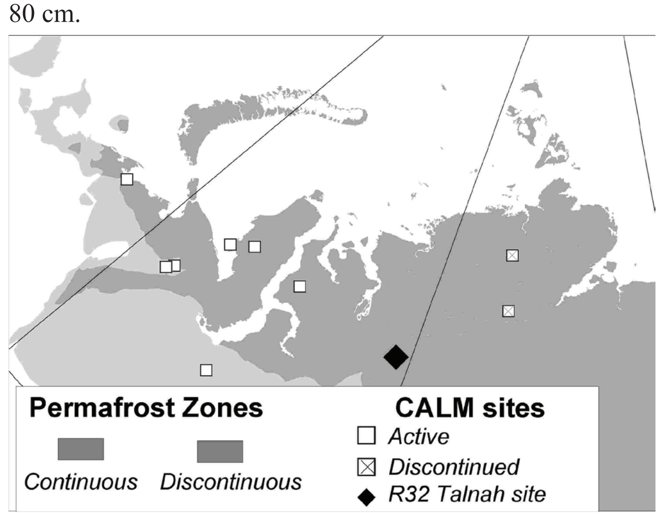

Figure 1. Distribution of permafrost zones (Brown et al. 1997) and location of CALM sites in Russian European North, West Siberia and Taimyr Region.

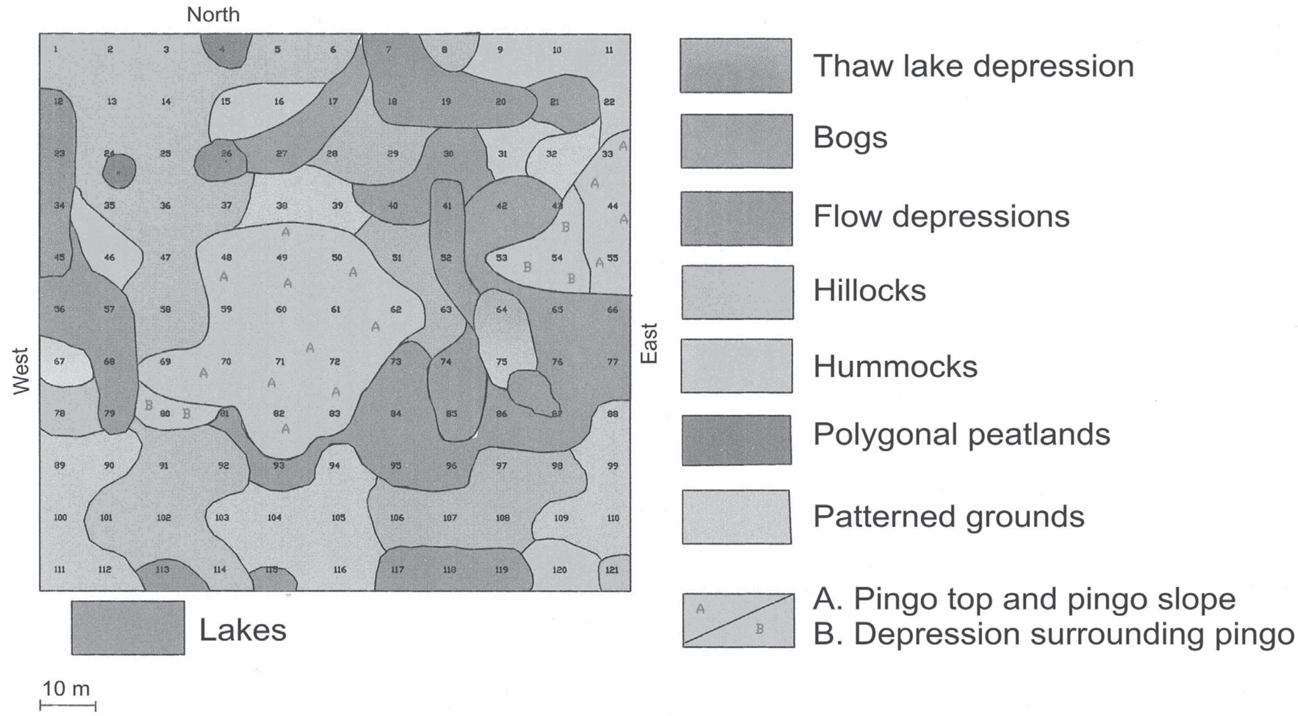

Figure 2. Results of landscape classification within the R32 Talnakh 1-ha CALM site.

Sediments primarily consist of loam with small intrusions of pebbles and overlain by a thin peat layer. The grid is situated on subhorizontal surface with elevation decreasing in a southeast direction. A small frost mound (pingo) 30 m in diameter and 1.5 m high occupies a portion of the site. The frost mound is surrounded by flow depressions and polygonized peatlands. The size of the polygons varies from 6 to 8 m across. Hummocks up to 20 cm in height and hillocks up to 60-70 cm in height are widely present. Typical tundra vegetation occupies the site and consists of shrubs, dwarf-shrub and sedges. Mosses and lichens are largely absent from the site. The environmental and geocryologic conditions of the site closely correspond to those of the southwestern part of the Taimyr Peninsula.

Methodology

A regular 100 x 100 m (1 ha) grid was established at the site in the summer of 2005 according to recommendations provided by CALM protocol (Brown 2000).

The establishment of the grid was followed by detailed characterization of landscapes and surface conditions. Nine main landscape categories, characteristic of the south-western part of the Taimyr Peninsula are contained within the grid (Fig. 2).

Periodic annual active layer measurements were initiated in 2005 at grid nodes separated by 10 m, yielding an array of 11 x 11 nodes across the grid (Fig. 2). The measurements are performed by mechanical probing using a graduated metal rod. As a rule, each point is probed twice. However, if the difference between two measurements is significant, additional observations are taken at close proximity to the sampling point. An average value is calculated for each sampling point, yielding a total of 121 data values for the grid per probing date.

During the 2007 field season the optical leveling of grid nodes was initiated following CALM-approved procedure described in detail at the CALM website (http://www.udel.edu/Geography/calm/research/MazhitovaMethod.pdf).

Records of major climatic parameters are available from the Russian meteorological station, Alykel Airport, located 50 km west of the grid. In the near future we intend to instrument the Talnah site for continuous air and ground temperature monitoring.

Results and Discussion

The Digital Elevation Model (DEM) of the site for the year 2007 is shown in Figure 3. DEM indicates a slight increase in elevation in the northwest direction. The optical leveling will be continued annually and will be used to evaluate changes in the position of the ground surface associated with frost heave and thaw subsidence.

To analyze the spatial distribution of the active layer thickness, grid-node values of ALT were interpolated using krigging technique to produce annual maps of ALT. Annual ALT maps for the 2005-2007 period and map of three-year averages are shown in Figure 4. The summary statistics for three years of available ALT measurements are presented in Table 1.

The maximum three-year grid average ALT is 87.3 cm, with the minimum 50 cm and the maximum 126.5 cm; standard deviation is relatively small and does not exceed 15 cm (Fig. 4).

Constructed annual maps of ALT show high spatial variability of this parameter, despite the fact that the variation of the summer climatic signal expressed as Degree-Days of Thawing on a moment of measurements did not exceed 10% and on average was around 980°C·days.

To evaluate landscape-specific contributions to overall active layer pattern, the ALT values, as measured at each particular landscape presented in Figure 2, were analyzed. The landscape-specific statistical distributions of ALT values, obtained over a three-year period and representing both temporal and spatial ALT variability, are shown in Figure 5.

The highest degree of variability was encountered at patterned ground features represented by frost mounds. It

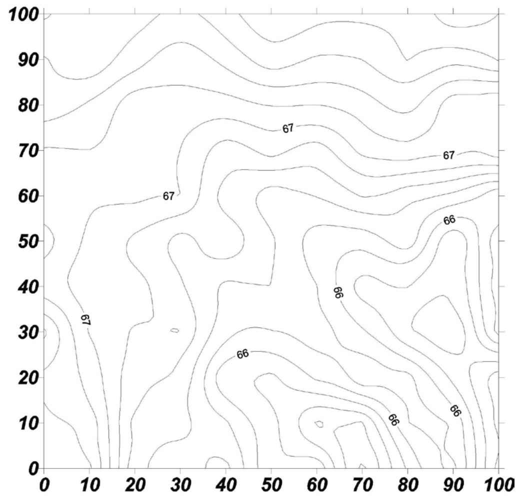

Figure 3. Digital elevation model developed by optical leveling. Isolines are given at 0.2 m interval. In-between grid interpolation performed by krigging.

Table 1. Annual ALT statistics for the R32 Talnakh site.

Year	2005	2006	2007
Mean	81.3	90.8	89.5
Minimum	49.0	42.5	49.0
Maximum	150.0	164.0	150.0
St.Deviation	19.0	22.4	19.9

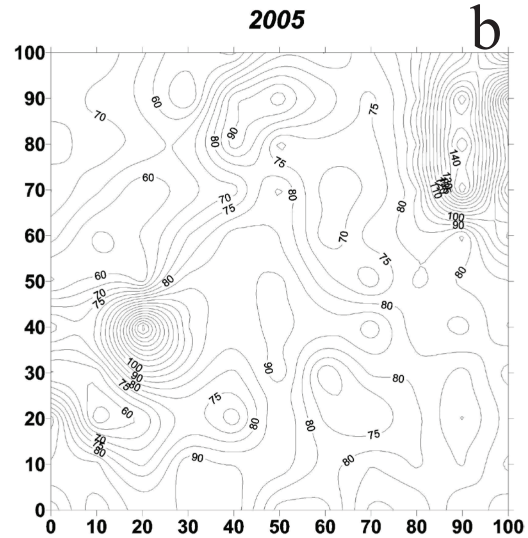

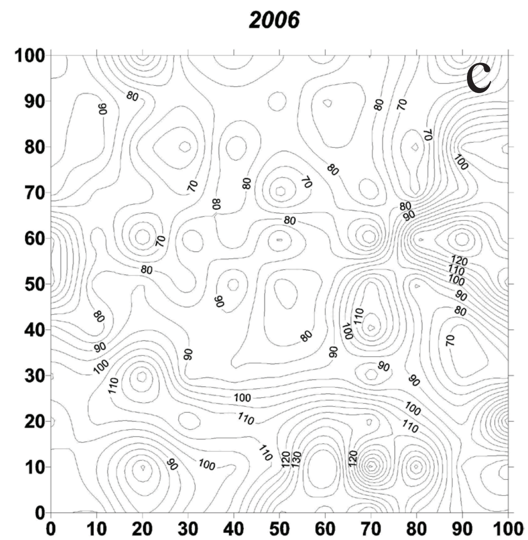

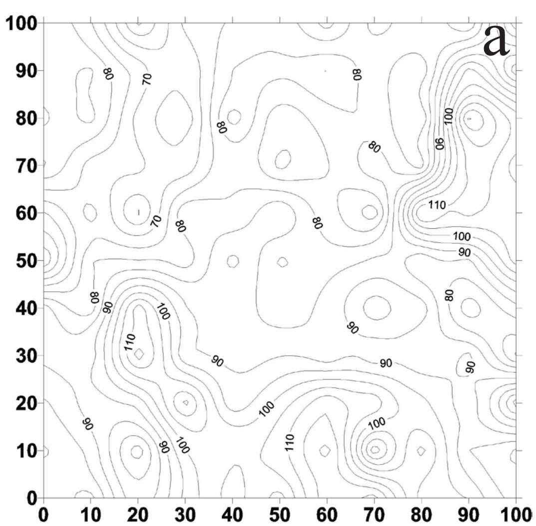

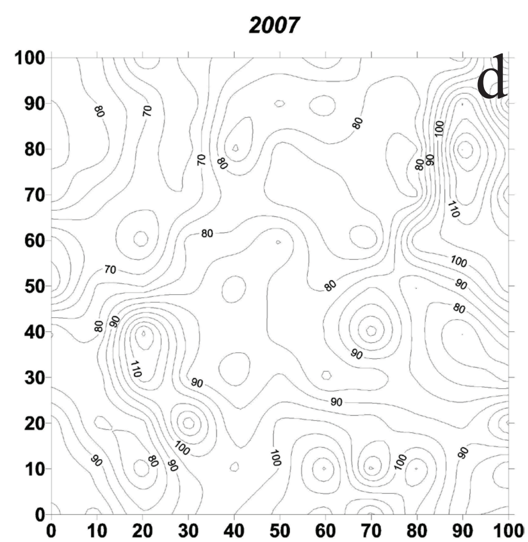

Figure 4. Results of annual ALT surveys at R32 Talnakh grid for 2005 (b), 2006 (c), 2007 (d) and average values of ALT for 2005-2007 period (a). Isolines are given at 5 cm intervals.

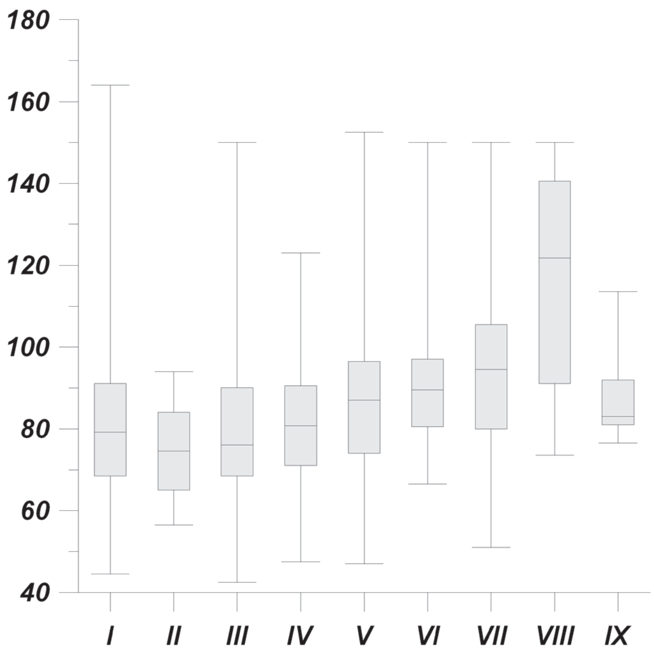

Figure 5. Box-whisker plots of ALT in characteristic landscape units. I – Hillocks, II – Polygonal peatland, III – Hummocks, IV – Flow depressions, V – Bogs, VI – Pingo, VII – Patterned ground, VIII – Depression surrounding pingo, IX – Thaw lake depression.

Table 2. Average (2005–2007) values of ALT for characteristic landscape units. Landscapes are identified in captions for Figure 5.

Unit	I	II	III	IV	V	VI	VII	VIII	IX
ALT	82	74	80	81	90	92	95	114	87

can be attributed to sparse vegetation cover and thin organic layer characteristic of these landscapes. Dense vegetation and thick organic layer significantly mitigate the influence of variability in climatic forcing resulting in less temporally and spatially heterogeneous active layer. This effect is illustrated by small ALT variations, observed at densely- vegetated, polygonized peatlands and thaw lake depressions. These landforms are also characterized by thick accumulations of peat. The high degree of active layer variability observed at hillocks and hummocks can be largely attributed to significant differences in ALT values obtained from the tops of hummocks and from interhummock depressions. The high spatial heterogeneity of the active layer in a tussocky and hummocky landscape was observed in Alaska and reported by Nelson et al. (1999). Flow depressions, surrounding frost mounds, are characterized by a high degree of variability around mean, but a relatively small range of values. This can be explained by the relatively small sample of points representing this landscape unit.

The landscape-specific three-year means of ALT are presented in Table 2. The highest value of 114 cm was observed at flow depressions, which are subject to convectional heat transfer by running water. The thinnest ALT (74 cm) is characteristic of polygonized peatlands with dense vegetation cover and thick organic layer.

Conclusions

The Talnah CALM site was established in the Taymir Peninsula to compensate for some deficiencies in the CALM observational network in Russia. Regular active layer measurements were initiated in 2005. A short, three-year period of observations allowed for only preliminary conclusions. The grid-average ALT for the study period is 87 cm. The thickness of the active layer varies from 45–50 cm to 125–150 cm, depending on landscape-specific conditions. The maximum thickness of the active layer is observed at landscapes represented by sparsely-vegetated patterned ground and dry hillocks. The minimum ALT was found in the polygonized peatlands. Periodic heave and subsidence measurements by optical leveling were initiated in 2007. In the near future we intend to extend the observational program at the Talnah site to include air and ground temperature monitoring. The establishment of complementary sites, characteristic of regional landscapes underrepresented by the Talnah site, is currently under consideration.

Acknowledgments

This study was conducted as part of the research and educational plan of the Department of Geography at Moscow State University. We are also grateful to the U.S. National Science Foundation for their partial financial support through an OPP-0352957 grant, administered by the University of Delaware.

References

Anisimov, O.A., Shiklomanov, N.I. & Nelson, F.E. 2002. Variability of seasonal thaw depth in permafrost regions: a stochastic modeling approach. *Ecological Modeling* 153(3): 217-227.

Brown, J., Hinkel, K.M. & Nelson, F.E. 2000. The circumolar active layer monitoring (CALM) program: Research designs and initial results. *Polar Geography* 24(3): 165–258.

Brown, J., Ferrians, O.J., Heginbottom, J.A. & Melnikov, E.S. 1997. *Circum-Arctic Map of Permafrost and Ground-ice Conditions.* Circum-Pacific Map Series, Report: CP- @0045, 1 sheet.

Ershov, E.D. & Kondrateva, K.A. 1991. *The Geocryological Map of the USSR*. Scale 1:2,500,000. Moscow: GUGK, 1 p.

Feldman, G.M. 1977. Forecast of ground temperature regime and development of cryogenic processes. Nauka: Novosibirsk, 192 pp. (in Russian).

Garagulya, L.S. 1985. Metodika prognoznoy otsenki antropogennih izmeneniy merzlotnih usloviy. Izd. Moscovskogo Universiteta. 224 pp. (in Russian).

Kudryavtsev, V.A., Garagula, L.S., Kondrat'yeva, K.A. & Melamed, V.G. 1974. Osnovy merzlotnogo prognoza. Moscow State University Press, 431 pp. (in Russian).

Malevsky-Malevich, S.P., Molkentin, E.K., Nadyozhina, E.D., Pavlova, T.P. & Semioshina, A.A. 2006. Validation problems of permafrost evolution modeling. *Proceedings of International Conference: Earth Cryosphere Assessment: Theory, Applications and Prognosis of Alterations, Tumen'* Vol. 1, 78-82.

Nelson, F.E., Shiklomanov, N.I., Christiansen, H.H. & Hinkel, K.M. 2004. The circumpolar-active-layer-monitoring (CALM) Workshop: Introduction. *Permafrost and Periglacial Processes* 15: 99-101.

Nelson, F.E., Shiklomanov, N.I. & Mueller, G.R. 1999. Variability of Active-Layer Thickness at Multiple Spatial Scales, North-Central Alaska, U.S.A. *Arctic, Antarctic, and Alpine Research* 31 (2): 179-186.

Sheveleva, N.S. & Khomichevskaya, L.S. 1967. *Geocryological Conditions of Enisey North.* Moscow, Nauka, 126 pp.

Shiklomanov, N.I., Nelson, F.E., Streletskiy, D.A., Hinkel, K.M. & Brown, J. 2008. The Circumpolar Active Layer Monitoring (CALM) program: data collection, management, and dissemination strategies. *Proceedings of the Ninth International Conference on Permafrost, Fairbanks, Alaska, June 29-July 3, 2008* (this proceedings).

Shiklomanov, N.I. 2005. From exploration to systematic investigation: Development of geocryology in 19th- and early-20th-century Russia. *Physical Geography* 26(4): 249-263.

Tushinskiy, G.K. & Davydova, M.I. 1976. *Physical Geography of the USSR.* Moscow: Prosveschenie, 543 pp.

Experimental Study on Mechanisms of Subgrade Deformation in Permafrost Regions Along the Qinghai-Tibetan Railway

Jianming Zhang
State Key Laboratory of Frozen Soil Engineering, Cold and Arid Regions Environmental and Engineering Research Institute, Chinese Academy of Sciences, Lanzhou, China

Xiaojie Ma
Zhejiang College of Construction, Hangzhou, China

Bo Zheng
China Academy of Railway Science, Beijing, China

Abstract

Field observations at the Beiluhe test site along the Qinghai-Tibetan Railway indicate that, even though the permafrost table under the embankment has moved up since the railway was built, the embankment still has suffered quite a lot of settlement, and the settlement has been mainly due to deformation of the warm and ice-rich frozen soils under the original permafrost table. In order to understand the mechanism of the subgrade deformation in permafrost regions, pressure meter tests were conducted under the embankment, and compression tests were carried out in the laboratory. Based on the test results, the settlement in the embankment at the Beiluhe test site was estimated taking into consideration the compression of the warm and ice-rich permafrost. Over the next 50 years, the estimated settlement in the embankment is about 40 cm, even though the permafrost under the embankment will not thaw at all.

Keywords: embankment settlement; permafrost regions; Qinghai-Tibetan Railway; warm and ice-rich frozen soils.

Introduction

In permafrost regions, the construction of a roadway embankment changes not only the thermal regime of the permafrost under the embankment but the stress state in the subsoil as well. With the adjustment of both temperature and stress in the subsoil, the stability of the embankment will inevitably be modified, and settlement of the embankment takes place. According to experience gained from the Qinghai-Tibetan Highway, the settlement of a roadway embankment in permafrost regions is generally composed of three parts: (1) compression of the fill, which depends on the material of the embankment and the density of the fill; (2) consolidation of the active layer, which is controlled by the soil type and its water content; (3) thaw settlement of the permafrost, which is related to the thickness of the embankment and the ice content in the permafrost. Of the three kinds of deformations, the thaw settlement of permafrost under the embankment is the most significant for the stability of the roadway embankment (Wu et al. 1988, Wu & Liu 1989, Yu & Yan 1986).

During the construction of the Qinghai-Tibetan Railway in 2001, many measures were taken to protect the permafrost in the subsoil. Among them the most common practice was to build an embankment thick enough to prevent the permafrost from thawing. However, field observations from 2002 to 2005 at Beiluhe test site along the railway indicated that, even though the permafrost table under the embankment has moved up since the railway was built, the embankment has still suffered quite a lot of settlement, and the settlement has been mainly due to deformation of the ice-rich frozen soils under the original permafrost table. In order to understand the mechanism of this kind of deformation and to estimate the settlement of the railway embankment in the future, pressure meter tests were conducted under the embankment in the summer of 2005, and compression tests on ice-rich frozen soils under a stepped temperature rise were carried out in the laboratory in 2006. In this paper, we present the field observation data, the test results, and then an estimate of the settlement of the railway embankment in the coming 50 years.

Field Observation

Test section

Since 2002, after the embankment was built, six test sections have been set up at Beiluhe test site along the railway to monitor the ground temperature under the embankment and the layered settlement of the subgrade. The layout of the test sections is shown in Figure 1, and the permafrost conditions at each section are given in Table 1.

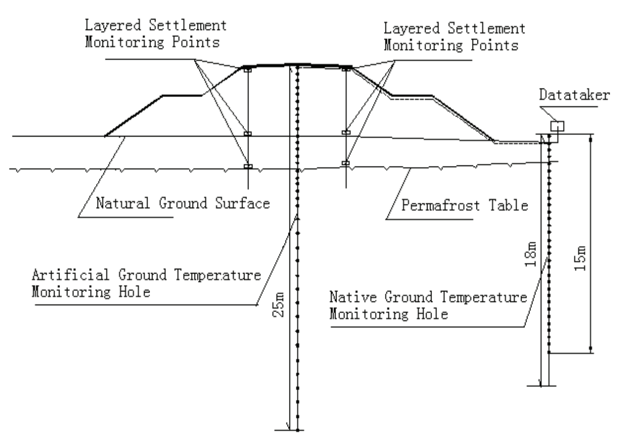

Figure 1. Component layout at the test section.

Table 1. Permafrost conditions at each test section.

Test section (km+m)	Embankment thickness (m)	Permafrost table in natural ground (m)	Mean annual ground temperature (℃)	Thickness of ice-rich frozen soils (m)
DK1136+520	2.9	2.2	-0.74	4.4
DK1136+540	4.5	2.0	-0.78	3.5
DK1136+580	5.0	1.9	-1.01	5.6
DK1136+755	3.0	2.0	-0.46	2.0
DK1136+775	4.2	2.0	-0.45	3.0
DK1136+800	5.4	2.3	-0.46	4.5

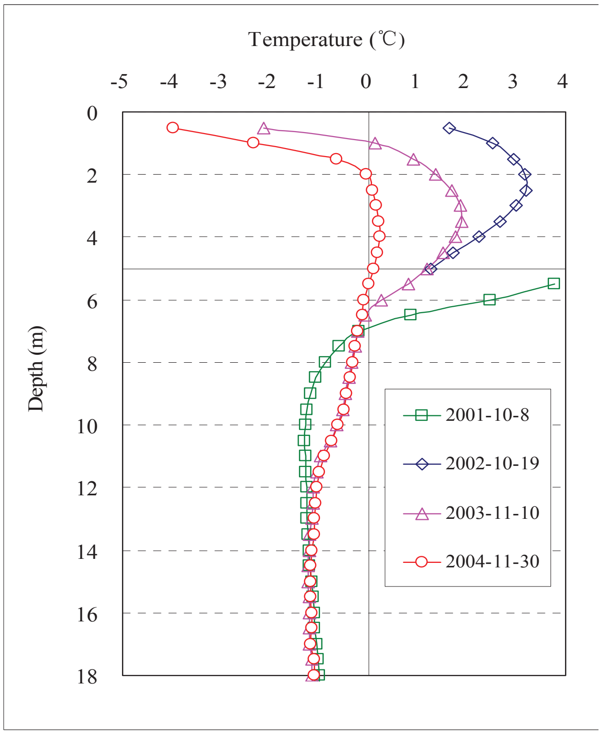

Figure 2. Ground temperature profiles in the embankment.

Ground temperature

Figure 2 shows the typical ground temperature profiles at the centerline of the embankment at DK1136+580 during 2001 to 2004 in the seasons of max. thawing depth. It can be seen that, though the permafrost table under the embankment has moved up gradually since the embankment was built, the ground temperature under the original permafrost table also rose remarkably at the same time. The ground temperature rise will certainly cause changes in mechanical properties of the permafrost, resulting in settlement of the embankment.

Embankment settlement

Figure 3 presents layered settlement processes of the embankment at DK1136+580 from 2002 to 2005. Taking a close look at the processes, we can see that the difference in settlement between the roadway surface and the natural ground surface, which is the compression of the fill, is rather small. The difference between the ground surface and the original permafrost table, which is the consolidation of the active layer, is also small. However, the settlement at the

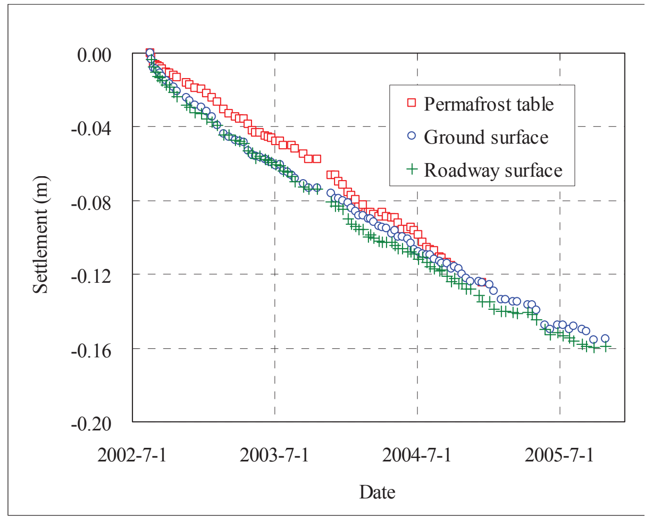

Figure 3. Layered settlement processes of the embankment.

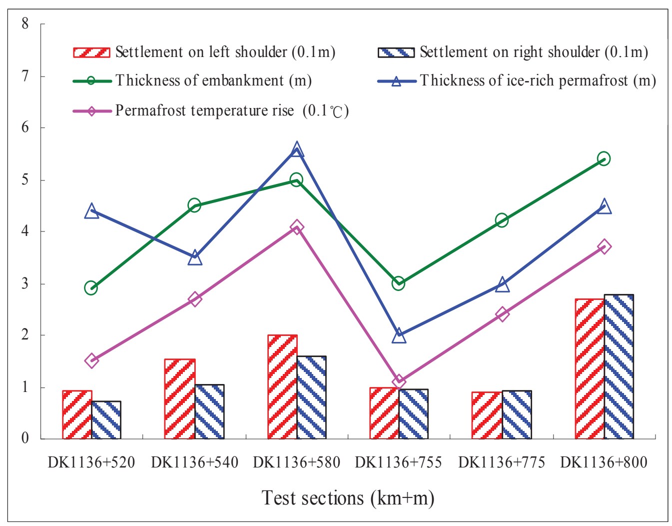

Figure 4. Embankment settlement and permafrost conditions in the subgrade.

original permafrost table is much larger. It is clear that the total settlement of the roadway embankment is largely due to the deformation of the warm and ice-rich frozen soils under the original permafrost table.

Discussion

Figure 4 shows the total settlement values at each of the six test sections and the possible factors which have an effect on the settlement, such as the thickness of embankment and

Table 2. Soil conditions of the pressure meter tests.

Test position	Under embankment				Natural ground	
Depth (m)	1.4	2.1	3.6	4.0	3.6	4.7
Soil type	Silty clay					
Temp. (℃)	-0.25	-0.31	-0.50	-0.69	-0.85	-0.89
Moisture (%)	20.8	101	36	63.9	37.3	24.5
Density (g/cm^3)	2.27	1.39	2.09	1.66	2.07	2.12

the thickness of ice-rich permafrost in the subgrade, as well as the temperature rise of the ice-rich permafrost due to the construction of the embankment. In this figure, it can be seen that the settlement values relate well with the factors at most of the test sections. At the sections with thicker embankment, thicker ice-rich permafrost, and more temperature rise, the settlement of embankment is greater.

Pressure Meter Test

Test condition

In order to investigate the variation of mechanical properties of the permafrost in the subgrade, pressure meter tests were carried out under the railway embankment as well as in the adjacent natural ground in September 2005. The device used in the tests was a TEXAM pressure meter made by ROCTEST with a metallic probe of 58mm in diameter. The tests were performed in the strain controlled mode, and the test conditions are given in Table 2. In the table, it is obvious that, at the same depth below the original ground surface, the soil temperatures under the embankment are always higher than those in the natural ground.

Test result

Figure 5 and Figure 6 show the pressure meter test results of shear modulus and max. pressure, respectively, at different depths under the embankment and in the natural ground. It is evident that both the shear modulus and the max. pressure in the subgrade are lower than those in the natural ground. This means the mechanical properties of the permafrost in the subgrade have been changed considerably since the railway embankment was constructed. It also confirms that the settlement of the embankment was mainly due to the deformation of the ice-rich frozen soils under the original permafrost table caused by temperature rise in the subgrade.

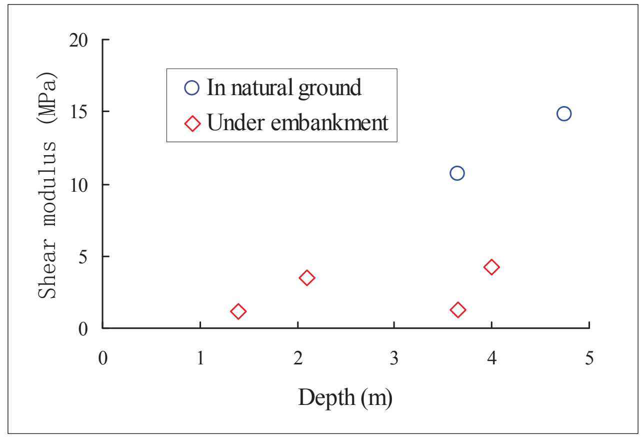

Figure 5. Comparison of shear modulus between under embankment and in natural ground

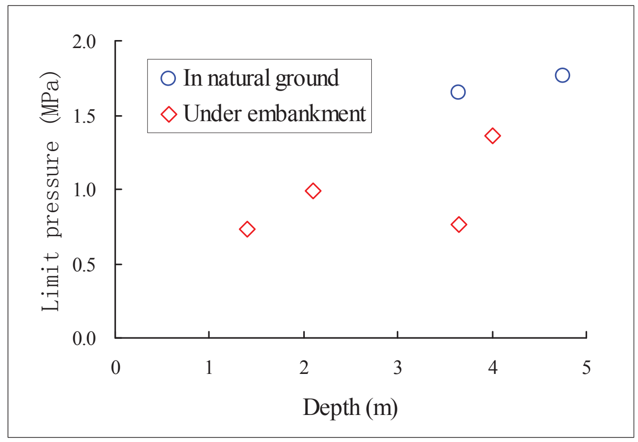

Figure 6. Comparison of max. pressure between under embankment and in natural ground

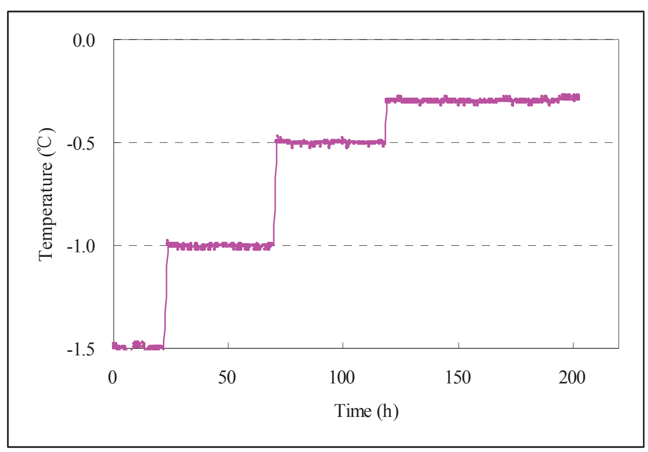

Figure 7. Temperature process in the compression test.

Compression Test

Test condition

In order to determine the compressibility of the ice-rich frozen soils caused by temperature rise, compression tests were carried out in the laboratory. The soil samples of silty clay from the test sections were prepared with water contents of 40% and 80%, respectively, and the water contents were kept constant during the tests. The tests were performed in an oedometer with a diameter of 61.8mm and a height of 40mm. In order to understand the influence of temperature on the compressibility of frozen soil, the load was kept constant in each test, and the temperature was controlled in a stepped rise mode as shown in Figure 7.

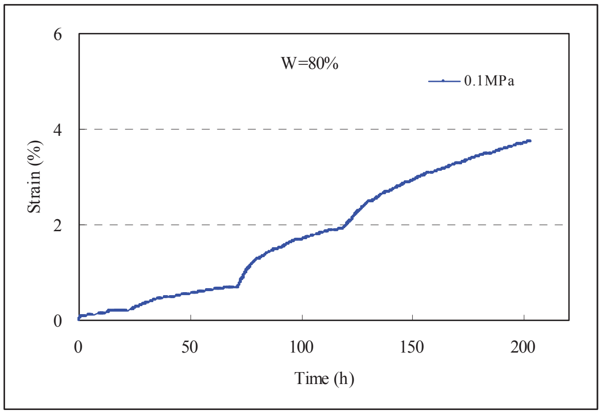

Figure 8. Deformation process in the compression test.

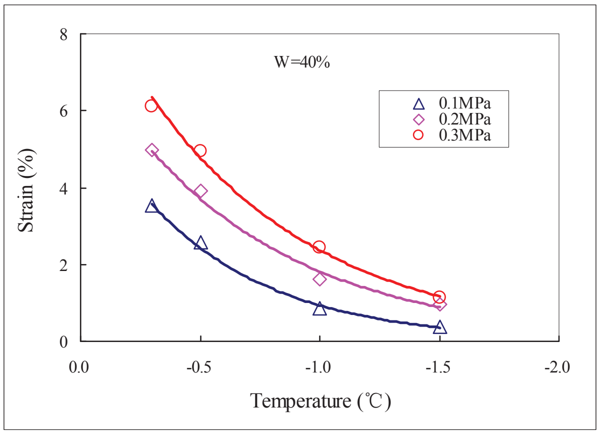

Figure 9. Total compressibility vs. temperature step.

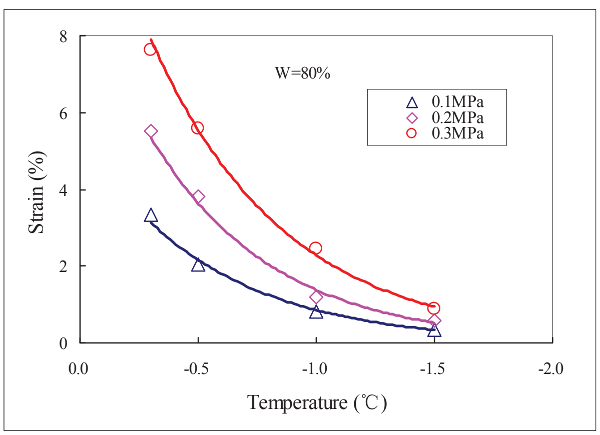

Figure 10. Total compressibility vs. temperature step.

Test result

Figure 8 shows the deformation process of the frozen soil with water content of 80% and under pressure of 0.1MPa, corresponding to the temperature steps shown in Figure 7. It is apparent that, even under such low stresses, the frozen ice-rich, silty clay can produce quite a lot of deformation during the temperature rise process, especially when close to 0°C. Figure 9 and Figure 10 present the test results of compressibility under different temperature steps and different pressures. It should be noted that the compressibility is more sensitive to pressure when temperature approaches 0°C.

Settlement Estimation

Calculation model

Based on the test results and concepts mentioned above, we can estimate the settlement of the railway subgrade in permafrost regions. According to experience obtained from both the Qinghai-Tibetan Highway and the Qinghai-Tibetan Railway, the settlement of the subgrade must include both the thaw settlement and the compression of the permafrost under the embankment, and it should be calculated as:

$$S = S_1 + S_2 + S_3 = \sum_{i=1}^{n} A_i \cdot h_i + \sum_{i=1}^{n} \alpha_i \cdot P_i \cdot h_i + \sum_{j=1}^{m} \Delta\alpha_j^{\Sigma} \cdot P_j \cdot h_j$$

where S is the total settlement of the subgrade, S_1 is the thaw settlement of the permafrost, S_2 is the consolidation of the permafrost after thawing, and S_3 is the compression of the warm and ice-rich permafrost. In detail, A is the thaw-strain parameter of permafrost, h is the thickness of soil strata assumed in the calculation, α is the compression coefficient of thawed soil, P is the pressure applied on the soil strata, and $\Delta\alpha^{\Sigma}$ is the variation of the compression coefficient of frozen soil caused by temperature change.

According to the geological conditions at Beiluhe test site, the permafrost profile adopted in the calculation is shown in Figure 11. The compressible layer is the ice-rich frozen soil under the embankment from 2 to 8 m below the natural ground surface. The mechanical parameters of the ice-rich frozen soil in the subgrade are: A=0.084, α=0.45MPa. The variation of a^S with temperature is shown in Figure 12, and h is taken as 0.25 m referring to the calculation of the ground temperature profiles over the next 50 years.

Ground temperature prediction

Before the settlement of the subgrade is estimated, it is necessary to predict the ground temperature profiles under the embankment. According to the numerical model to calculate heat transfer in frozen ground (Zhang et al. 2006), the ground temperature profiles in the centerline of the embankment over the next 50 years in the seasons of max. thawing depth are shown in Figure 13. In this figure, it is clear that the ground temperature in the subgrade will increase with the service life of the railway embankment.

Calculation result

Based on the subgrade deformation model and the ground temperature profiles, the settlement of the subgrade in future can be calculated. Figure 14 presents the estimate of the subgrade settlement processes for different embankment thickness. It can be seen that the settlement increases with increase in embankment thickness, and it will be about 40 cm by the end of the next 50 years even though the permafrost under the embankment does not thaw at all.

Conclusions

The results of both pressure meter tests and compression tests confirm that the warm and ice-rich permafrost in the railway subgrade can produce quite a lot of deformation

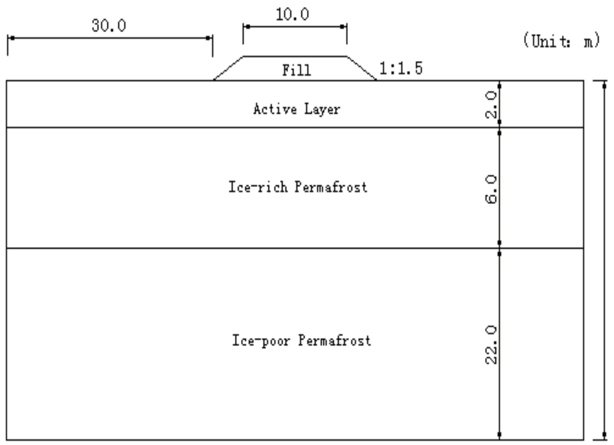

Figure 11. Permafrost profile under the embankment.

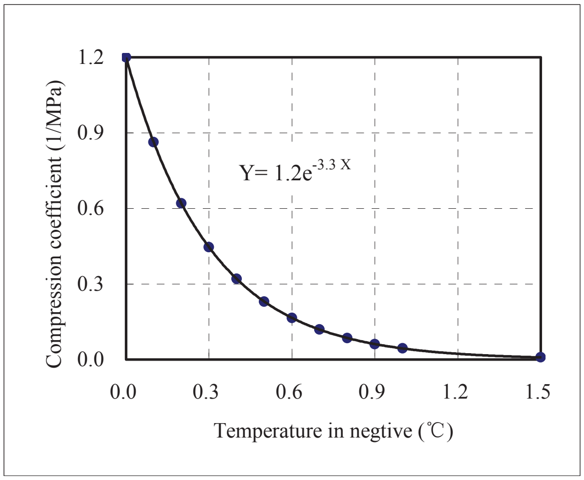

Figure 12. Relationship between compression coefficient of frozen soil and temperature.

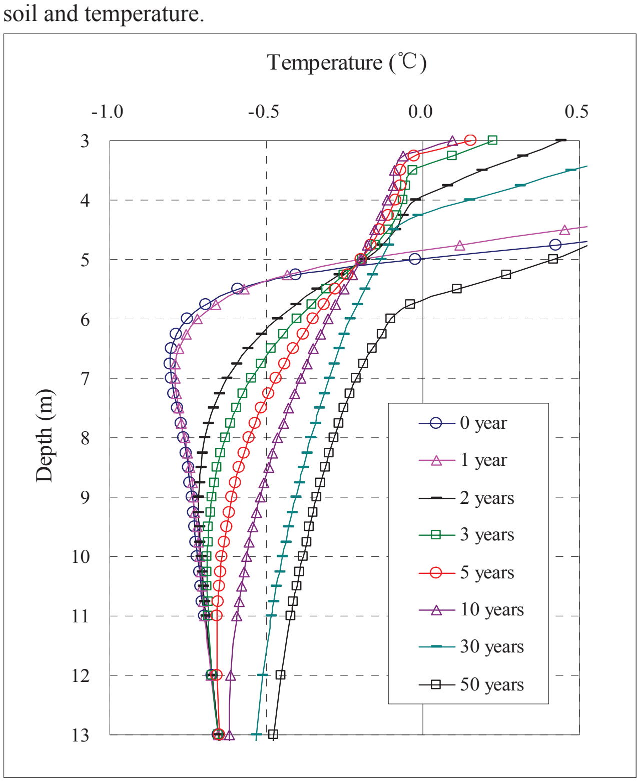

Figure 13. Prediction of the ground temperature under embankment (embankment thickness: 3 m, MAGT: -0.5°C).

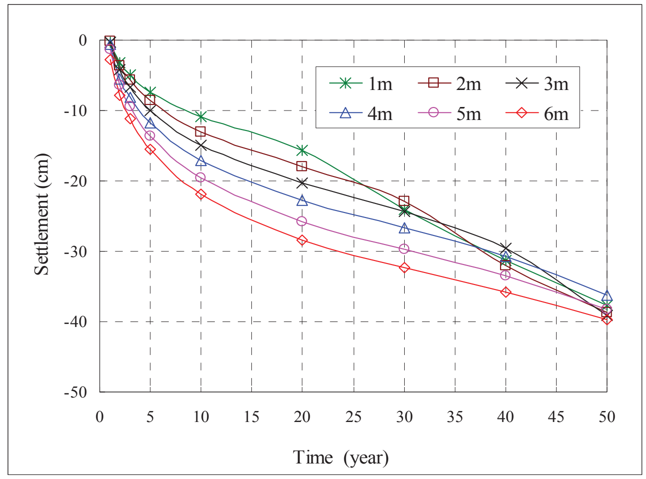

Figure 14. Estimate of the subgrade settlement process (embankment thickness: 1~6m, MAGT: -0.5°C).

due to the temperature rise in the subgrade, even though the permafrost table under the embankment moves up after the railway is built. The estimate of the subgrade settlement indicates that the settlement increases with the increase in embankment thickness and ground temperature. Therefore, if this kind of deformation is to be controlled, active cooling measures must be taken to lower the ground temperature in the subgrade. The traditional method of increasing the embankment thickness is ineffective and even worse for the stability of the railway subgrade in the warm and ice-rich permafrost regions.

Acknowledgments

This work was supported by the Knowledge Innovation Program of Cold and Arid Regions Environmental and Engineering Research Institute, Chinese Academy of Sciences (2004104), the Knowledge Innovation Important Program of the Chinese Academy of Sciences (KZCX3-SW-351), and the National Natural Science Foundation of China (40730736).

References

Wu, Z.W., Cheng, G.D., Zhu, L.N. & Liu, Y.Z. 1988. *Roadbed Engineering in Permafrost Regions*. Lanzhou: Lanzhou University Press, 61-84.

Wu, Z.W. & Liu, Y.Z. 1989. Forecasting of deformation of asphalt paved frozen roadbed of the Qinghai-Xizang Highway. *Proceedings of the 3rd Chinese Conference on Permafrost*. Beijing: Science Press, 333-338.

Yu, W.X. & Yan, Q.P. 1986. Primary analysis of the subgrade deformation along the Qinghai-Xizang Highway in permafrost regions. *Journal of Xi'an Highway University* 1986 (1): 49-70.

Zhang, J.M., Zhang, J.Z. & Liu, Y.Z. 2006. Study on the reasonable embankment height of the Qinghai-Tibetan Railway in permafrost regions. *China Railway Science* 27(5): 28-34.

Designing the Height of the Qinghai-Tibet Highway in Permafrost Regions

Jinzhao Zhang
Laboratory of Cold Regions Road Engineering, The First Highway Survey and Design Institute of China, Xi'an, 710068
Fujun Niu
State Key Laboratory of Frozen Soil Engineering, Cold and Arid Regions Environmental and Engineering Research Institute, CAS, Lanzhou, China 730000
Shuangjie Wang
Laboratory of Cold Regions Road Engineering, The First Highway Survey and Design Institute of China, Xi'an, 710068
Yongguo Zhao
Laboratory of Cold Regions Road Engineering, The First Highway Survey and Design Institute of China, Xi'an, 710068

Abstract

The Qinghai-Tibet Highway is a significant engineering structure built in the permafrost regions of China. When the highway was initially constructed in the 1950s and permafrost was encountered, the road embankment was just paved with the nearby materials. Since the 1970s, the highway has been rebuilt or repaired on a large scale three times, mainly to treat problems caused by the permafrost. Along with continuous repairing activities, research work was carried out three times, focusing on embankment stability and permafrost status. In the first research work before 1979, the main factor considered in the embankment height designing was the buried depth of the local permafrost table. In the second research work during 1979–1985, when it was paved with asphalt, the embankment height was increased and a permafrost-protecting principle was adopted. In the third research work after 1985, roadbed problems along the whole length were investigated. The investigation showed that 152 km of the highway were damaged by settlement. To avoid future thaw settlement, comprehensive remedy methods were applied to actively protect the permafrost and, subsequently, the roadway.

Keywords: designing principle; embankment height; permafrost; roadbed; Qinghai-Tibet Highway.

Introduction

The total length of the Qinghai-Tibet Highway (QTH) is 1937 km from Xi'ning of the Qinghai province to Lhasa of the Tibet Autonomous Region. The length of the section from Golmud to Lhasa, which is a second-class highway, is 1150 km. The highway is very important, as more than 85% of materials and more than 95% of passengers to Tibet were transported this way since 1954. The highway crosses a permafrost area with a length of more than 630 km from Xidatan Valley to Andou County (Fig. 1), where the average elevation is over 4500 m a.s.l.

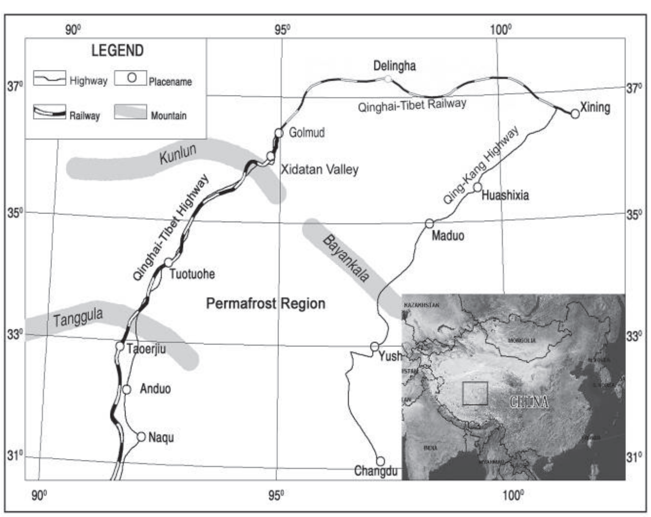

Figure 1. The location of the QTH and permafrost distribution in the Qinghai-Tibet Plateau.

The QTH was initially constructed in the 1950s, and then about 20 years later, an asphalt layer was paved on the surface. Since the 1990s, the highway has been rebuilt or repaired greatly three times, and research work has been carried out which focuses on the embankment design principle and height. Though some problems of the QTH have not been thoroughly solved so far, the average driving speed can be 60 to 100 km/h now. Such a speed is the highest value in the servicing history of the highway.

Embankment Height Designing of the QTH Before 1979

The QTH research group drafted an Asphalt Layer Construction Manual of the QTH in Permafrost Regions in October 1978. In the report, it was pointed out that there were more than 100 km of ice-saturated and massive-ice permafrost along the highway. As the underlying permafrost was not effectively treated during roadbed construction, some problems, including thaw slumping, roadbed deformation, and frost boiling, occurred when the road was opened to service. The problems were eliminated after repair and remedy over 20 years. However, it was pointed out that the heat balance would be destroyed again if the asphalt layer were paved. Also, new diseases would occur if the permafrost were not protected effectively. It was also pointed out that a filling-but-not-cutting principle should be followed in roadbed construction in permafrost regions, except in icy soil, ice-poor soil, and seasonally frozen ground sections. Embankments in ice-poor and icy soil regions may be designed without any special structure. The frozen ground should be properly protected in sections of ice-rich permafrost. Necessary measures were suggested to protect the underlying frozen ground in ice-saturated permafrost regions, and to strictly protect massive-ice permafrost regions. These prescripts indicated that the design principle during this period was to protect the permafrost in roadbed construction.

The results of the field experiments along the highway showed that the sandy surface lowered the permafrost table with a value of 15–25cm. The relation between embankment height (H) and the depth of permafrost table (h) was

$$h = 0.95H - 0.15 \tag{1}$$

However, the permafrost table lowered 25–30 cm under the black asphalt surface. Considering the different thermodynamic conditions of asphalt and gravel surface, suggestions on the embankment height were given as listed in Table 1, based on monitored results (QTH Research Group 1978).

According to Table 1, the maximum embankment height of QTH was less than 1.5 m. Based on the principle of protecting permafrost and suggestions on the embankment height, an embankment design scheme between Wudaoliang (mileage of K3007) and the Tanggula Mountain (mileage of K3350) was recommended. At the same time, it was confirmed that a black asphalt surface can be paved on the embankment in permafrost regions.

Embankment Height Designing of the QTH from 1979 to 1985

Since 1979, black road surface was mainly paved in permafrost regions where geological conditions were poor and frozen damage easily occurred. In order to ensure the quality of the project, the embankment height was suggested to be increased to protect the underlying frozen ground, based on engineering practice and observation. Some methods were proposed such as: (1) a principle of protecting frozen ground should be followed in permafrost regions; (2) embankment height should be increased to counteract the influence of black road surface, and two lateral sides should be protected too; (3) necessary embankment height should be determined,, keeping the permafrost table stable or a little lowered in regions where the frozen ground has low ice-content (lower than the ice-content in ice-rich soil), instead of keeping the roadbed totally frozen. To practice these methods, the permafrost along the way was classified into 4 classes. Two sets of embankment height value were suggested in 1980 and 1981 (QTH Research Group 1978, 1981). The values were listed in Tables 2 and 3.

Comparing the values listed in Tables 2 and 3, the embankment height was higher in 1980 and 1981 than that in 1978 and 1980. At same time, the embankment height values suggested in 1981 were higher up to 1.0 m than those in 1980. The embankment height values suggested in 1980 were based on considerations of frozen soil types and embankment soils. The values suggested in 1981 were based on considerations of frozen soil types, permafrost table, and topography. Therefore, the values of 1981 were increased in accord with protecting frozen soil and status of the QTH.

The repair design in this period was changed according to the suggested height values in 1980. Then part of the embankment was repaired considering investment capacity and building time.

Along with progress of research work on the QTH, some other suggestions were proposed, such as the filling soils could be cut from the nearby ground as it was lack of sand and stone materials along the highway, but it was strictly

Table 1. Suggested embankment height in different permafrost regions (unit: m).

Permafrost	Embankment soil		
	Silty clay and clay	Sand and sandy soil	Gravel soil
Ice-rich soil	0.5- 0.8	0.5 - 0.8	0.5 - 0.8
Ice-saturated soil	0.8 - 1.0	0.8 - 1.1	0.8 - 1.2
Massive ground-ice	1.0 - 1.2	1.1 - 1.3	1.2 - 1.4

Table 2. The suggested minimum embankment height for protecting the underlying permafrost in 1980 (unit: m)

Permafrost	Embankment soil		
	Silty clay and clay	Sand and sandy soil	Gravel soil
Ice-rich soil	0.8- 1.0	0.9 - 1.1	1.0 - 1.2
Ice-saturated soil	0.9 - 1.2	1.0 - 1.3	1.2 - 1.5
Massive ground-ice	1.1 - 1.4	1.2 - 1.5	1.3 - 1.7

Table 3. The suggested minimum embankment height for protecting the underlying permafrost in 1981 (unit: m).

Permafrost	Depth of the natural permafrost table /m	Critical height H_0 /m	Design height /m	Topography
Icy soil	>2.5	1.0	（0.6~0.7）H_0	Valley zone
Ice-rich soil	2.0- 2.5	1.0 - 1.3	H_0	High plateau regions
Ice-saturated soil	1.6 - 2.0	1.3 - 1.6	(1.1 - 1.2) H_0	High plateau and river terrace
Massive ground-ice	>1.2~≤1.8	1.4 - 1.8	(1.2 - 1.3) H_0	Mountain regions
Massive ground-ice	≤1.2	>1.8 - 2.0	(1.2 - 1.3) H_0	Frozen peat soil island

restricted to excavating filling materials within 10 m away from the road slope toe. According to different engineering geological conditions, permafrost along the highway was classified into five types: ice-poor soil, icy soil, ice-rich soil, ice-saturated soil, and massive ground-ice. In determining an embankment height designing formula suggested in this period, deformation compressed by seasonal thawing layer and traffic loads were also considered. The calculating method was given as the formula below, and the relevant parameters were listed in Table 4, 5, and 6 (Yu & Wu 1986).

$$H_d = mH_c + S \tag{2}$$

where H_d is the designed embankment height and H_c is the critical minimal height; m is corrected comprehensive coefficient. It is determined by frozen soil type, the permafrost table, and water-containing status of seasonal thawing layers, and its values are suggested in Table 4. The value is suggested to adopt the higher one when the buried depth of the permafrost table is shallow and the ground-ice is rich; contrarily, it is suggested to adopt the lower one.

S is the compressed deformation value of the seasonal thawing layers and is determined with the formula below.

In the maximum thawing season:

$$s = \sum_{1}^{n} a_{0i}\delta_{0i} \tag{3}$$

During the freezing period:

$$s = \sum_{1}^{N} A_{0i}h_i + \sum_{1}^{N} a_{0i}\delta_{0i}h_i \tag{4}$$

where N is the number of seasonal thawing layers above the embankment bottom; h_i is the thickness of the i layer; δ_{0i} is the average total stress of i layer, which equals to average appending stress and weight stress; A_{0i} and a_{0i} is thawing subsidence coefficient and frost-heave coefficient of i layer correspondingly. The values of A_{0i} and a_{0i} were listed in Table 5 and 6.

The embankment design principle and embankment height suggested in 1985 were reasonable at that time; however, it was not widely applied as asphalt-paving work was finished in 1985. It was only used in the embankment repair in a section from the Kulun Mountains (mileage of K2898) to Wudaoliang (mileage of K3007) in 1986.

Embankment Height Designing of the QTH after the 1990s

The QTH crosses 630 km of permafrost region, of which 83.6% is continuous permafrost and 16.4% is island permafrost. Engineering geology conditions of frozen soil along the highway are complex and variable, as they are controlled by many factors. On one hand, the air temperature in the Qinghai-Tibet Plateau gradually increased from 1962 to 1999 with a value of 0.02–0.03ºC/a during wintertime. The value changed to 0.01–0.02ºC/a during summertime

Table 4. Corrected comprehensive coefficient *m* of formula (2).

Frozen soil type	Icy soil	Ice-rich soil	Ice-saturated soil	Massive ground-ice
m	0.6 - 0.7	0.9 - 1.0	1.1 - 1.2	1.15 - 1.25

Table 5. Thawing subsidence coefficient.

Frozen soil type	Icy soil	Ice-rich soil	Ice-saturated soil	Massive ground-ice
Thawing index A / %	<5	5≤ - <10	10≤ - <40	≥40

Table 6. Frost-heave coefficient of seasonally thawing layer.

Frost-heaving type of seasonally thawing layer	Sections with permafrost table buried deep, coarser soil with low moist content	Seasonally thawing layer above ice-rich soil	Seasonally thawing layer above ice-saturated soil	Seasonally thawing layer above massive ground-ice
Frost-heaving coefficient a_{0i} / %	1.0 - 1.5	1.5 - 2.0	2.0 - 3.0	3.0 - 5.0

(Wei et al. 2003). On the other hand, the permafrost was in degradation, influenced by global warming (Wu et al. 2000, 2003). Especially as the black road surface absorbed radiation energy, the situation of the underlying frozen ground was worsening and resulted in new problems. According to statistical data in 1990, the total length of damaged section caused by thawing deformation was 152 km, which was 24% of the total length in the permafrost region. Aiming at solving the problems, the Ministry of Communication approved the First Repair Project Plan to repair the 339 km section of the QTH with serious problems. The designed embankment height in the project still followed the principle of protecting permafrost. It was designed following the principle that the settlement caused by lowering of the permafrost table should be less than the maximum displacement of the road surface in servicing life of the asphalt pavement. The embankment height was increased 30 cm based on formula (2), considering global warming influences on permafrost, so to avoid new damages. During the repair, the neighboring environment was required to be recovered. The suggested embankment height values were listed in Table 7 during the time.

In the first repair project, a longitudinal crack with a width of 15–20 cm and a length of 300 m appeared in the embankment of a section from mileage K3403 to K3409, north to Anduo in winter, 1993. Longitudinal cracks with a width of 15–25 cm and a length of 500 m also appeared in sections of K2932–K2935 and K2947–K2951 in winter, 1995. The total length of the highway damaged by longitudinal cracking was up to 14 km according to an investigation in April 1997. It was found that more than 80% of longitudinal

Table 7. The minimum embankment height of roadbed suggested in 1991 (unit: m).

Frozen soil type	Icy soil	Ice-rich soil	Ice-saturated soil	Massive ground-ice
Embankment height	1.5	1.8	2.2	2.6

Figure 2. Longitudinal cracks and settlement developed in the embankment of the QTH.

Figure 3. Crack damage of the concrete surface layer.

cracks along with settlement appeared in the sun-facing side of the embankment (Fig. 2). The embankments once seriously damaged on Kunlun Mountains Pass, Kekexili Mountains, Fenghuoshan and Tanggulashan Mountains Pass had less damage this time, while the embankments in Chuma'erhe Plateau, Beiluhe Basin, Wuli, Kaixinling to Tongtianhe and north of Anduo regions suffered more longitudinal cracking and subsidence deformation. Sections of these regions possessed more than 95% of the total length damaged by longitudinal crack. Based on analysis of ground temperature data of the QTH for many years, it was found that when the mean annual ground temperature (MAGT) was lower than -1.5ºC, the longitudinal cracking and embankment deformation were minor, while when the MAGT was higher than -1.5ºC, such problems were serious. This indicated that MAGT has a close relationship to the embankment problems. As the longitudinal crack problems were very serious, paving with a concrete surface layer was tested to see if it was able

Table 8. Height values of embankment with asphalt surface suggested in 1995 (unit: m).

Designing principle	Protecting frozen ground (low temperature district)			Controlling thawing rate(high temperature district)		
Frozen soil type	Icy soil	Ice-rich soil	Ice-saturated soil	Icy soil	Ice-rich soil	Ice-saturated soil
Embankment height	1.6 - 2.0	1.8 - 2.6	2.4 - 3.2	1.8 - 2.4	2.2 - 3.2	2.6 - 3.4

to resist crack damage. The tested results showed that such a surface could not solve the problem when the roadbed was not stable enough. The concrete layer was damaged seriously, too (Fig. 3). Therefore, the surface damages were mainly caused by deformation of the embankment.

The first repair project of the QTH was finished in 1995, and survey and design work for the second repair project was soon followed. In order to use index of ground temperature to evaluate the roadbed stability, researchers suggested -1.5ºC as the dividing value for classifying high-temperature permafrost (warm permafrost) and low-temperature permafrost (cold permafrost), considering the ground thermal regime along the highway. As the different temperature districts were divided, a new principle was proposed, as (Zhang 1996) protecting the frozen ground, controlling the thawing rate, and comprehensive treatment. In low-temperature permafrost regions, embankment designing should follow the principle of protecting the frozen ground. In high-temperature regions, it should follow the principle of controlling thawing rate. Comprehensive treatments can be used to avoid roadbed problems in poor geological condition sections. According to the principle, the minimal embankment height is given in Table 8. It was also suggested that on the basis of considering frozen soil type, geomorphology, and water conditions along the two sides, an additional embankment on the slopes be constructed 0.8–1.5 m in height and 2–3 m in width.

Maintaining and Repairing Project from 2002 to 2004

Construction of the Qinghai-Tibet Railway (QTR) started in 2001. This project was regarded as one of the four major projects in West China. The railway construction depended very much on the QTH to transport workers, materials, prefab concrete structures, machines, etc. This greatly increased traffic load on the highway. Though the highway was a second-class way, it was hard to support too much, as its main part was in permafrost regions. To ensure the railway construction, 12.2 billion Yuan were invested to carry out a large-scale repair project of the QTH from 2002 to 2004. According to research and statistics in 2001, embankments of the QTH with serious subsiding deformations and longitudinal cracks were mainly in warm and ice-rich permafrost regions. The total length of such sections was 60 km. The sections had never been reconstructed or repaired, and the embankment

Figure 4. Thermosyphone installed along the QTH to treat thawing settlement.

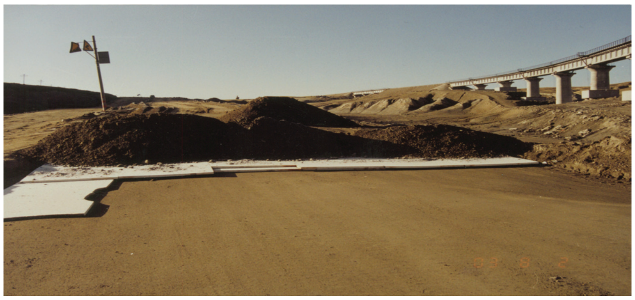

Figure 5. Insulation layer installed along the QTH to keep the underlying permafrost.

was somewhat high. High embankment might cause new problems, which mainly resulted from disturbance of the surrounding environment. The designing principles in this period included: (1) recovering the damaged permafrost environment of both sides of the road; (2) using artificial ground-freezing methods (such as thermosyphone, Fig. 4) and increasing heat resistance (such as using EPS, XPS material, Fig. 5) to treat the subsiding and cracking problems; (3) properly adjusting the roadbed according to actuality of embankment and bearing capacity of surface layer; (4) strengthening drainage structure. The route-change section was designed according to the recommended values for asphalt surface roads in 1995. Focusing on treating roadbed problems in warm and ice-rich permafrost regions, some field experimental research work was carried out at same time. The work included study on the genesis and mechanism of roadbed settlement and longitudinal cracks, and new construction methods for highways in permafrost regions and their engineering effects. The new methods included thermosyphone embankments, crushed-stone embankments, duct-ventilated embankments, and also thermal-insulated embankments. Some testing sites were constructed along the highway during the time. Among the testing sites, some of them were installed to study the reasonable embankment height along both the QTH and the Qinghai-Tibet Railway (QTR). In the Beiluhe region, several testing embankments with different height were studied (Cheng et al. 2004). The tested results showed that the minimum embankment height has a close relationship to the surface conditions of the roadway and the local mean annual air temperatures. The minimum embankment height needed to be increased when the mean annual air temperature was higher. There was no minimum embankment height effective unless the local

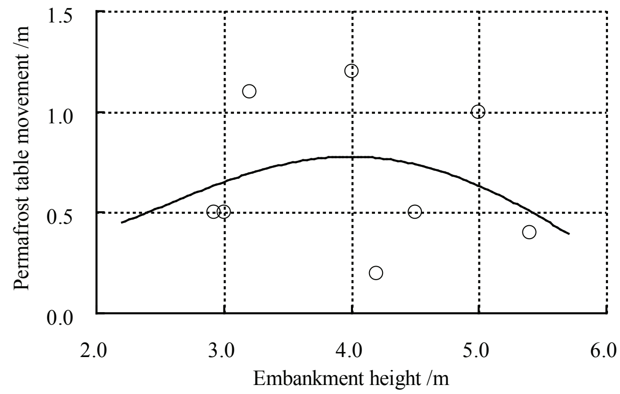

Figure 6. Relation of permafrost table movement with embankment height (Cheng et al. 2004).

mean annual air temperature was lower than a critical value (-3.8°C). That means no matter how high the embankment was, the permafrost table under the roadway would fall.

The tested results of relationship between the permafrost table movement and embankment height is drawn in Figure 6. The figure indicates that when the embankment rose to a certain range the permafrost table would drop but not rise. Therefore, the range of the applied height was a function of properties of the fill materials, the surface conditions, and the mean annual air temperatures.

Now after years of study, a comprehensive design principle for determining embankment height and protecting roadbed stability in permafrost regions is proposed. It suggests that in low-temperature regions, the permafrost is recommended to be protected. Some methods such as increasing the height, installing an insulation layer, or installing the side berm, can be applied. The height values may be referred to the data listed in Table 8. In high-temperature regions, the critical height values are not the controlling index of embankment design. Some methods, including crushed stone embankment, thermosyphone associatex with insulation layer embankment, duct-ventilated embankment, and land bridge, can be adopted. Certainly a minimal height of embankment to install the structures mentioned above is necessary.

Conclusions

(1) The Qinghai-Tibet Highway was constructed in the 1950s. Permafrost was not considered at that time, and roadbed problems were rooted thereby. After that, large-scale repair was carried out three times to maintain the roadbed stability. The embankment height was an important research content during the past, and it was suggested differently during different time.

(2) The suggested embankment height before 1979 was mainly based on considering the depth of the permafrost table, along with kinds of frozen ground and soil fill materials.

(3) The suggested embankment height value was increased from 1979 to 1985, as a permafrost-protecting principle, and the critical minimal height was proposed.

(4) The influences of global warming and ground temperature on roadbed stability were considered after the 1990s. District division of permafrost according to the ground temperature was applied, and different designing principles were proposed after that.

(5) In the last maintenance and repair projects of the highway from 2002 to 2004, the permafrost environment, new construction methods, and drainage systems were considered. The permafrost-protecting principle was confirmed. To realize the principle, some of the new methods were tested, and their effectiveness was evaluated. Now the Qinghai-Tibet Highway is in its best servicing status in history.

Acknowledgments

This work was supported in part by the Chinese Natural Science Fund (No. 40471023), the National Science Supporting Project of the Ministry of Science and Technology of China (2006BAC07B02), and the grant of the Knowledge Innovation Programs of the CAS (No. KZCX1-SW-04, KZCX-XB-10).

References

Cheng, G.D. Zhang, J.M. & Sheng, Y. 2004. Principle of thermal insulation for permafrost protection. *Cold Regions Science and Technology* 40: 71-79.

Research group of QTH. 1978. Construction of black road surface of QTH on permafrost regions. *Research Report of the First Highway Survey and Design Institute of China,* Xi'an.

Research group of QTH. 1980. Embankment height of asphalt roadbed surface of the QTH. *Research Report of the First Highway Survey and Design Institute of China,* Xi'an.

Research group of the QTH. 1981. Embankment height of asphalt roadbed surface of QTH . *Research Report of the First Highway Survey and Design Institute of China,* Xi'an.

Wei, Z.G., Huang, R.H. & Dong, W.J. 2003. Inter-annual and inter-decadal variations of air temperature precipitation over the Tibetan Plateau. *Chinese Journal of Atmospheric Sciences* 27(2):157-170.

Wu, Q.B., Li, X. & Liu, W.J. 2000. The Prediction of Permafrost Change along the Qinghai–Tibet Highway, China. *Permafrost and Periglacial Processes* 11(4): 371-376.

Wu, Q.B., Shi, B. & Fang, H.Y. 2003. Engineering geological characteristics and processes of permafrost along the Qinghai-Xizang (Tibet) Highway. *Engineering Geology* 68: 387-396.

Yu, W.X. & Wu, J.M. 1986. Embankment height of asphalt roadbed surface of the QTH. *Journal of Xi'an Highway Institute*: 1986 (1): 25-42

Zhang, J.Z. 1996. Discussion on embankment height designing principles of QTH with asphalt road surface in permafrost regions. *Proceeding of the Fifth Symposium on Glaciology and Geocryology of China*. Lanzhou: Gansu Culture Press, 383-387.

Modeling Long-Term Dynamics of Snow and Their Impacts on Permafrost in Canada

Yu Zhang and Wenjun Chen
Canada Center for Remote Sensing, Natural Resources Canada, Ottawa, Canada
Daniel W. Riseborough
Geological Survey of Canada, Natural Resources Canada, Ottawa, Canada

Abstract

Seasonal snow, controlled mainly by temperature and precipitation, has a significant impact on ground temperature; therefore, it is essential to integrate snow dynamics for assessing the impacts of climate change on permafrost. In this study, we simulated snow dynamics in a permafrost model over the years 1850–2100 in Canada at a spatial resolution of 0.5° latitude/longitude. We validated the results by comparing them with snow measurements at climate stations. This long-term spatial modeling shows that snow depth would be thinner in eastern and northern Canada, and the duration of snow cover would be shorter almost everywhere in Canada by the end of the 21st century, causing a 1°C–2°C warming of annual mean ground temperature compared to changes in the annual mean air temperature. That means the concurrent change in snow condition would reduce the amount of permafrost degradation in response to climate warming.

Keywords: climate change; ground temperature; model; permafrost; snow dynamics.

Introduction

Annual mean ground temperature near the surface at high latitudes is usually several degrees warmer than the annual mean air temperature due to the insulating effects of snow (Zhang 2005, Zhang et al. 2005, Goodrich 1982). Changes in air temperature and precipitation would directly alter snow dynamics through changes in snowfall, snow density, and snowmelt. Therefore, it is essential to integrate snow dynamics in assessing the impacts of climate change on ground temperature and permafrost.

Some of the permafrost modeling studies used measured snow-depth or snow-water equivalent (SWE) as input. However, field, satellite, and climate station data are usually limited in temporal and spatial coverage, especially for observations of snow density, which is critical for quantifying the insulating properties of snow. Therefore, modeling the dynamics of snow is essential for assessing the impacts of climate change on permafrost and for other applications, such as estimating the feedbacks of snow on climate system, assessing avalanche risks, quantifying flooding and other hydrological processes, and modeling ecosystems and soil biogeochemistry.

Snow models can be categorized based on the purpose for which the models are developed. Models for snow avalanche risks consider the details of the mechanical features of snowpack and their changes (e.g., Bartelt & Lehning 2002); models for the impacts of snow on hydrology and flooding pay more attention to the spatial distribution of the total SWE and the rate of snowmelt; models for the impacts of snow on ground temperature and permafrost are concerned primarily with the thermal effects of the snow, while snow models for climate systems consider the thermal and hydrological effects of snow and the effects on surface energy processes, especially albedo. Tempo-spatial scales also vary significantly depending on the models' purposes.

Although it is recognized that snow cover has significant effects on ground temperature and permafrost, few permafrost models integrate snow dynamics. The major challenges include the following: (1) The model should have the capacity to simulate the dynamics of snow depth and snow density, since both are important for the thermal effects of snow on the ground. (2) The response of permafrost to climate change could take centuries; therefore, long-term climate data are needed to drive the models. (3) Detailed climate station data usually have limited spatial coverage. Monthly data are usually the only available historical climate datasets with long-term and spatial coverage.

Recently, we developed a process-based model—NEST, a model for northern ecosystem soil temperature—to quantify the impacts of climate change on permafrost, including the concurrent changes of snow (Zhang et al. 2003). Monthly climate data were down-scaled to run the model over the years 1850-–2100 in Canada at a spatial resolution of 0.5° latitude/ longitude (Chen et al. 2003, Zhang et al. 2006). In this paper, we describe the procedures and validation of the snow sub-model, and then analyze the simulated long-term patterns of snow dynamics in Canada and the effects on ground temperature and permafrost. The simulated distribution and changes in soil temperature and permafrost conditions have been presented in other papers (Chen et al. 2003, Zhang et al. 2005, 2006, 2008a, b).

Methods and Data

The NEST model

The NEST model was developed to simulate the transient response of ground thermal regime to climate change. It explicitly considered the effects of different ground

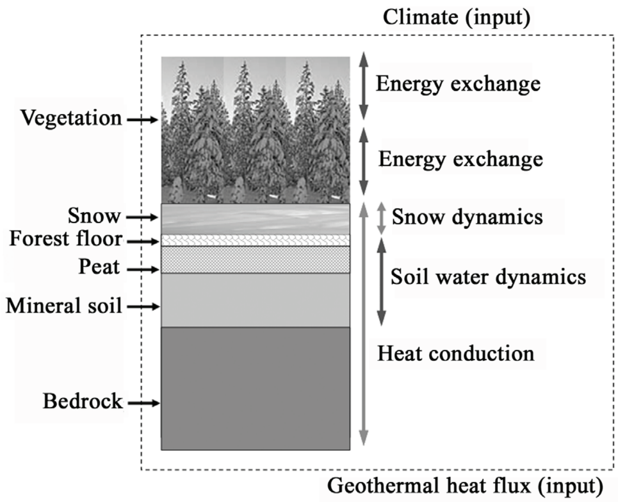

Figure 1. The components and processes considered in the NEST model (Zhang et al. 2003, 2008a)

conditions, including vegetation, snow, forest floor or moss layers, peat layers, mineral soils, and bedrock (Fig. 1). The dynamics of the ground temperature were simulated by solving the one-dimensional heat conduction equation. The upper boundary conditions (the ground surface or snow surface when snow is present) were determined based on the energy balance, and the lower boundary conditions (at a depth of 120 m) were defined based on the geothermal heat flux. The ground profile was divided into 63 layers with the thickness of the layers increased gradually from 0.1 m for top layers to 4.8 m close to the lower boundary. Soil water dynamics, including phase change, were simulated, and their effects on energy balance and on soil thermal properties were considered as well. A detailed description of the model and its validation were provided by Zhang et al. (2003).

The snow sub-model

The dynamics of snow were integrated in the NEST model. The thickness of the snow was determined based on snow density and the amount of snow (in SWE) on the ground, calculated as the cumulative difference between snowfall and snowmelt. Daily snowfall was determined by precipitation and air temperature (discussed below), and the density of fresh snow was estimated using air temperature. Snowmelt was determined based on the available energy calculated from the energy balance on the surface. The snowpack was divided into layers of about 0.1 m in thickness. The profile of snow density and its change with time were simulated considering compaction and destructive metamorphism, following Kongoli & Bland (2000). The equations and the calculation procedures were described by Zhang et al. (2003). Since the spatial resolution of this study (0.5° latitude/longitude) was much coarser than the fetch scale of blowing snow, wind effects on snow redistribution were not considered in this study.

Precipitation was designated as rainfall or snowfall based on air temperature. Measurements from climate stations in Canada show that snowfall occurs over a range of air temperatures around 0°C, and the range differs from place to place. Rather than defining a constant critical air temperature, we used a probability distribution function, similar to the approach of Riseborough and Smith (1993), to designate precipitation as rainfall or snowfall

$$P_s = 1 - 1/\{1 + \exp[-k(T_a - T_0)]\} \quad (1)$$

where P_s is the probability of precipitation as snowfall in a day. T_a is daily mean air temperature (°C), k is a parameter determining the slope of the frequency changing with air temperature around 0°C, and T_0 is the temperature at which rainfall and snowfall are equally likely. We selected 37 climate stations across the whole Canada landmass and determined the parameters k and T_0 for each station using historical daily measurements of temperature and the fractions of rainfall and snowfalls. Except for one station on the west coast, k was closely correlated with mean annual vapor pressure (V in mb), and T_0 was correlated with the total precipitation from October to December (P in mm)

$$k = -0.0517V + 0.7605 \qquad (r=0.78, n=36) \quad (2)$$

$$T_0 = -0.0135P + 2.2928 \qquad (r=0.74, n=36) \quad (3)$$

V and P were calculated as long-term averages. The above statistical relationships are probably related to the regional climate conditions and weather systems (e.g., wet and mild southeast Canada frequently has rainfalls when air temperature is below 0°C, while the Prairies, Yukon, and high Arctic frequently have snowfalls when air temperature is above 0°C. T_0 is also related to annual total precipitation ($r = 0.66$, $n = 36$) but not as significant as for the precipitation from October to December). Equations 2 and 3 were used for each grid except for the west coast region, where k and T_0 were assigned according to the station data (k = 0.8, T_0 = 0.7). For each day with precipitation, a random number from 0 to 1 was generated. If this number was smaller than P_s calculated based on the daily air temperature, the precipitation was assigned as snowfall, otherwise the precipitation was assigned as rainfall (We did not consider the cases with mixed rainfall or snowfall in a day, since such cases are relatively few).

Data

Inputs to the model include information about vegetation (land cover types, leaf area index), ground conditions (thickness of organic layers, texture of the mineral soils, soil organic carbon content in mineral soils, ground ice content, and the geothermal heat flux) and atmospheric climate (air temperature, precipitation, solar radiation, vapor pressure, and wind speed). Climate data from 1901 to 2002 were from Mitchell and Jones (2005). Six climate scenarios were selected for the 21st century, generated by six general circulation models (GCMs): NCAR, CGCM, CSIROM, GFDL, HadCM, and ECHAM. These six scenarios covered most of the possible range of GCM projected scenarios for Canada (Zhang et al. 2008b). A

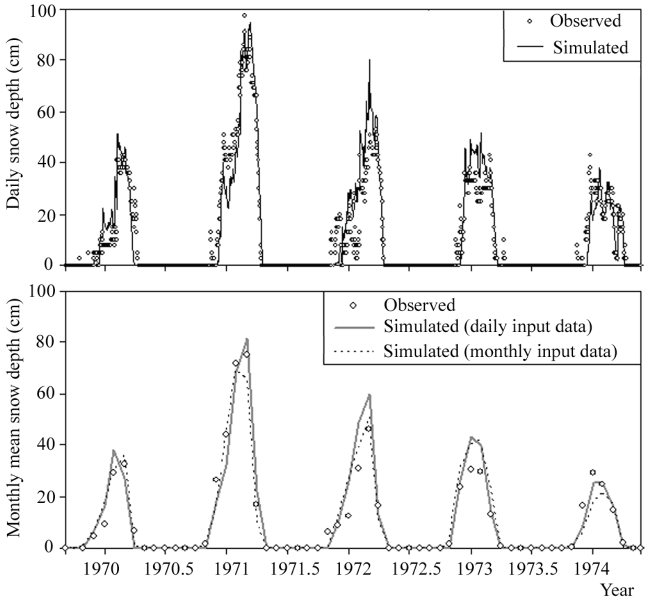

Figure 2. Comparisons between the measured and simulated snow depth at Ottawa climate station. a) comparing daily snow depth between the measured (circles) and the simulated (curves) using daily climate data as input. b) comparing monthly mean snow depth between the measured (circles) and the simulated using daily climate data as input (gray curves) and using month climate data as input (dash curves).

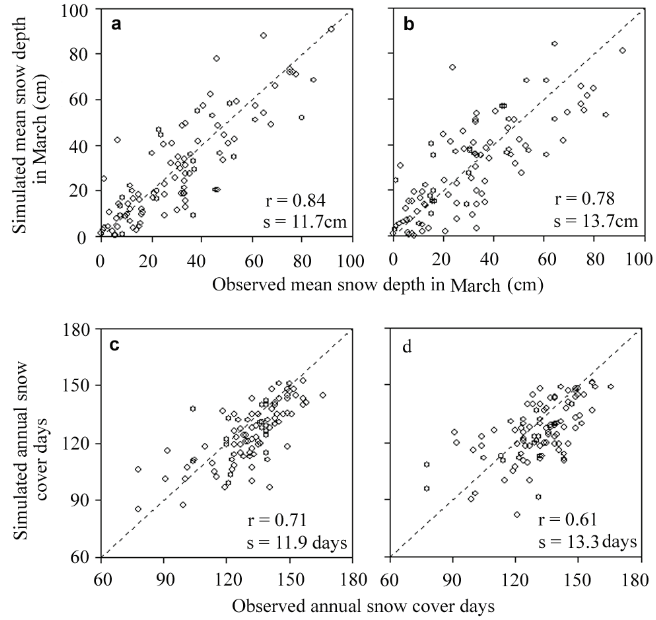

Figure 3. Comparisons between the simulated and the measured mean snow depth in March (a and b) and snow-cover days in a year (c and d) for Ottawa climate station from 1901 to 1999. The left panels (a and c) were simulated using daily climate data as input, and the right panels (b and d) were simulated using monthly climate data as input. *r* is correlation coefficient, and *s* is standard deviation.

detailed description of the vegetation and ground input data were provided by Zhang et al. (2006, 2008b). Several studies indicate that the current climate warming in Canada began largely from the end of the Little Ice Age (circa 1850) (Overpeck et al. 1997). Therefore, we initialized the model in 1850 assuming the ground thermal regime was in equilibrium with the atmospheric climate. We then simulated continuously from 1850 to 2002, and then from 2002 to 2100 under six climate change scenarios. Climate for 1850–1900 was extrapolated linearly from the data during 1901–1990. During the simulation, the monthly climate data were down-scaled to half-hourly to accommodate the short time-step requirement of the NEST model (Chen et al. 2003).

We validated the model using measured snow depth at climate stations. First, we validated the model by comparing measured daily snow depth with the simulated using daily climate data as input. We then ran the model using monthly climate data as input (derived from the daily observations and then down-scaled to half hourly in the model) and compared the simulated monthly snow depth with the observations. We selected the Ottawa climate station (45.4°N, 75.7°W) since this station has a long and continuous record of snow depth and other climate variables. Finally, we compared the nationwide simulation results with observations at 1670 climate stations which have at least 20 years of measurements. The daily and monthly climate station data were from Environment Canada (1999, 2000).

Result and Analysis

Comparing with measurements

Using daily climate data as input, the model was able to capture the observed patterns of snow-depth variation (Fig. 2a). The major difference was usually caused by the errors in defining precipitation as rainfall or snowfall. For dates on which daily measurements of snow depth were available from the snow database (Jan. 1, 1961, to Dec. 31, 1999; only monthly data were available in the database before 1961), the correlation coefficient between measured and simulated daily snow depth was 0.88 (n = 14149, standard deviation was 5.7 cm). A similar positive validation was presented for the Whitehorse climate station (60.9°N, 135.7°W) and for two boreal forest sites in Canada (Zhang et al. 2003).

Snow usually reaches the maximum depth in March in most of Canada. Figure 3a shows a comparison between measured and simulated mean snow depth in March using daily climate data as input (data from 1901 to 1999). It shows that the model can well capture the long-term variation patterns. Figure 3c shows a comparison between observed and simulated snow-cover days (days with snow depth >0 cm) in a year using daily climate data as input.

Using monthly climate data as input, the model could still capture seasonal patterns of snow dynamics (Fig. 2b). Monthly mean snow depths simulated using monthly and daily climate data as inputs were similar, and both are comparable to the observed monthly mean snow depth. The model could also capture the long-term (from 1901 to 1999) pattern of the snow depth in March using monthly data as

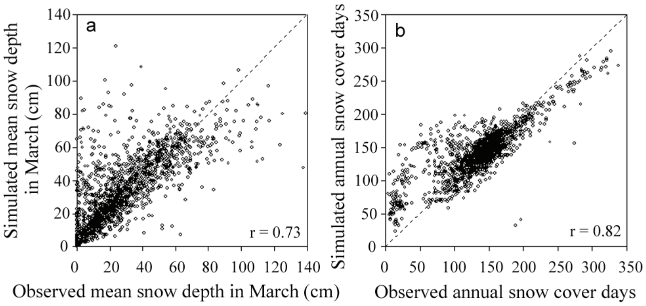

Figure 4. Comparisons between the simulated and observed mean snow depth in March (a) and mean annual snow-cover days (b) for 1670 climate stations in Canada. Each dot represents a climate station comparing between the observed and the simulated using the grid climate coving this station. The data for each station were averaged for all the observational years.

input (Fig. 3b), although the modeling skill was less than using daily climate data as input. Similarly, the simulated annual snow-cover duration and its long-term change using monthly climate data as input were also comparable with the measurements, although the relationship was not as good as when using daily climate data as input (Fig. 3d).

Figure 4 compares simulated and measured mean snow depth in March and the annual snow-cover days (averaged for all years with measurements) at about 1670 climate stations across Canada. The simulation was conducted using gridded monthly climate data as input. These results show that the simulated spatial distributions of snow-depth and snow-cover days were generally comparable with station measurements, although there were differences for some stations, especially in the province of British Columbia, where the terrain is complex and mountainous. This is mainly due to the differences between station and grid climate data. Local conditions could have significant effects on precipitation and snow conditions, while the model results were for average conditions in grid cells.

Changes in snow conditions in Canada over 1850-–2100

Figure 5 shows the spatial distributions of changes in mean snow depth in March and annual snow-cover days from the 1850s to the 1990s and from the 1850s to the 2090s simulated using the HadCM and CSIROM scenarios, in which the simulated difference between changes in soil and air temperatures were smallest and biggest, respectively (and the simulated snow conditions are near the extremes of the six GCMs). Snow depth in northern and eastern Canada would be thinner by the end of the 21st century, while becoming thicker in some regions in the western and southwestern regions. The annual snow-cover duration would be shorter almost everywhere in Canada by the end of the 21st century. On average for the major permafrost regions of Canada (latitude higher than 55°N), the mean snow depth in March shows a general decline over 1850–2100. The annual snow-cover duration shows a more consistent decline, with a more significant reduction during the 21st century (Fig. 6). These changes in thickness and duration of snow cover would affect the soil thermal conditions and permafrost.

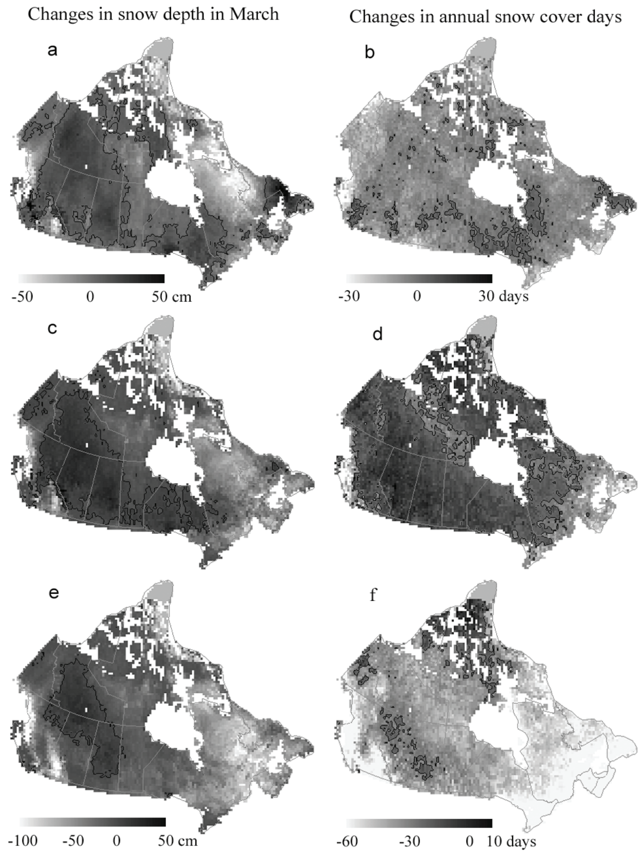

Figure 5. Simulated spatial distributions of changes in mean snow depth in March (the left panels) and annual snow-cover days (the right panels) from the 1850s to the 1990s (a, b), and from the 1850s to the 2090s (c–f) simulated using the scenarios of HadCM (c, d) and CSIROM (e, f). The uniform grey area at the top is glacier, which was not simulated.

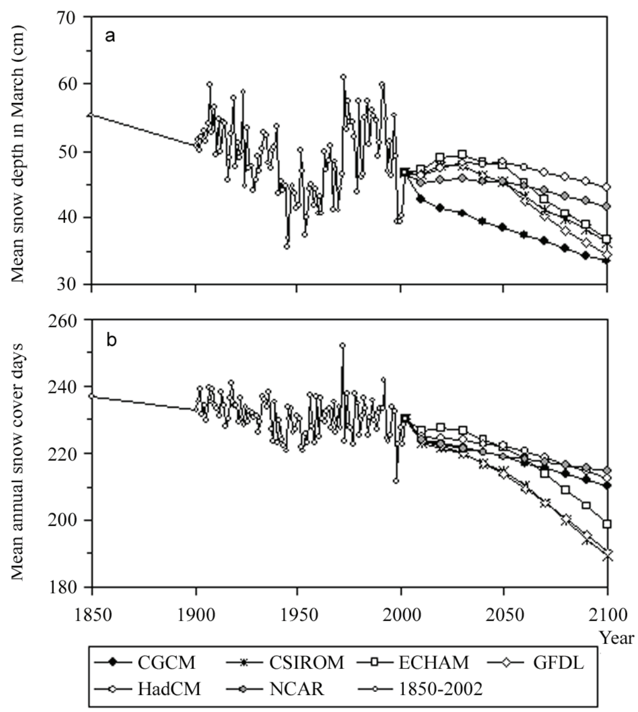

Figure 6. Simulated changes in mean snow depth in March and mean snow-cover days in a year in Canada with latitude higher than 55°N.

Effects of snow change on soil temperature and permafrost

Annual mean soil temperature near the ground surface generally responded strongly to the changes in air temperature, but they were not exactly in parallel. From 1850 to 2100, the rate of the increase in soil temperature near the ground surface was 1°C–2°C smaller than that of the air temperature, and the difference mainly occurred during the 21st century when warming was more significant (Figs. 7a, 7b).

Rates of change in air and soil temperatures were not significantly different in the summer months (Figs. 7c, 7d). The difference mainly occurred in winter months, with a much smaller increase in soil temperature than in air temperature (Figs. 7e, 7f), due mainly to the changes in snow conditions (snow depth and annual snow-cover days). As a result, the amount and the rate of permafrost degradation would be smaller than the estimates based on air temperature alone, although the influence of this seasonal differentiation would have little effect on the summer thaw depth. As for the possible effects on the southern boundary of permafrost under equilibrium conditions, a difference of 1°C–2°C in annual mean temperature is equivalent to about 100–200 km distance in latitudinal direction (the typical latitudinal air temperature gradient in Canada is about 0.01°C/km).

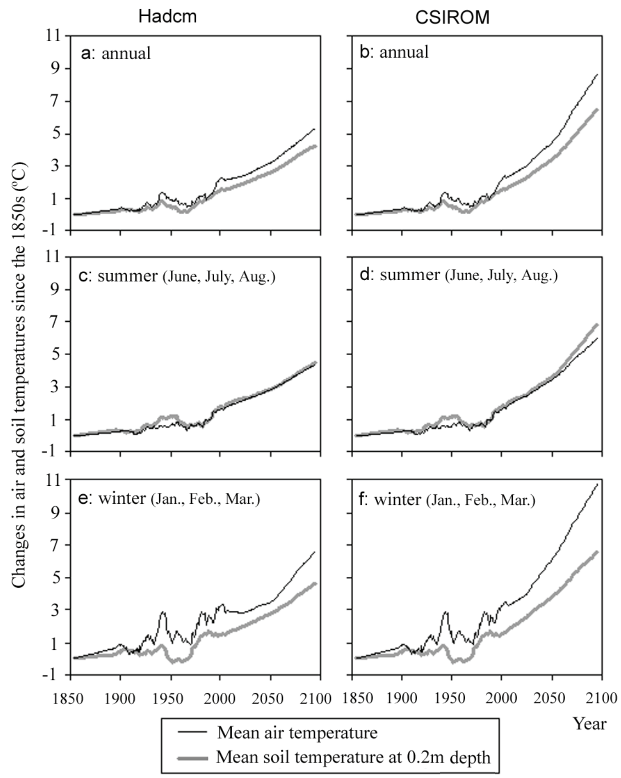

Figure 7. Changes in mean air and soil temperatures since the 1850s in Canada with latitude higher than 55°N. The values are calculated as 10-year running averages minus the averages in the 1850s.

Discussion

Climate station measurements in Canada from 1946 to 1995 show that snow cover and snow depth in spring are decreasing, especially in March (Brown & Braaten 1998). Earlier ablation of snow in spring would mean shorter annual snow-cover duration, which is in agreement with the simulated trend of this study. A shorter snow season was also simulated by GCMs for the 21st century (Räisänen 2007). The simulated decrease pattern of snow depth during the 21st century is generally consistent with GCM projections reported by Christensen et al. (2007). Räisänen (2007) found that SWE generally increases in coldest areas but decreases in other places during the 21st century, with the -20°C isotherm broadly defining the borderline. Our results show a more complex pattern in Canada, with a reduction in northern and eastern regions. The simulated changes in snow-cover days were stronger and more consistent than the simulated changes in snow depth during the 21st century, probably because the former is more dependent on temperature, while the latter is more directly affected by precipitation, which was projected to increase in most high latitudes during the 21st century. Statistical analysis also shows that temperature variations and trends play a significant role in variability and trends of snow-cover area in the Northern Hemisphere in the 20th century (Lemke et al. 2007). Our simulation shows that average snow-cover days in a year could be reduced by 13 to 37 days during the 21st century, which is comparable to the projected increase of 20–50 days in growing season length in the high latitudes (Wrona et al. 2005).

Field measurements and modeling studies have shown that the mean annual soil temperature near the ground surface can be several degrees warmer than the mean annual air temperature in permafrost regions, mainly due to snow-cover, which could last for about half of a year in these cold regions (Goodrich 1982, Zhang, 2005, Zhang et al. 2005). Reduction in the depth and duration of snow cover would reduce the insulating effects of snow, thereby reducing the difference between the annual means of soil and air temperatures. In other words, the increase in annual mean soil temperature in these cold regions would be smaller than that of the air temperature with climate warming (Zhang et al. 2005). On average for all the landmass of Canada with latitudes higher than 55°N, the mean annual soil temperature in the 1850s was about 3°C warmer than the annual mean air temperature. With a 1°C–2°C smaller increase in annual mean ground temperature than the air temperature over 1850–2100, the annual mean ground temperature on average for Canada would be only 1°C–2°C warmer than the annual mean air temperature by the end of the 21st century.

We used the general patterns of climate scenarios without considering the interannual variations for the 21st century. The large fluctuation during 1901–2002, when observations were available, shows that the actual variation pattern of snow depth in the 21st century could be different from the simulated general patterns because of the year by year fluctuations of climate. In addition, climate stations are sparser and the years of observations shorter in higher latitudes. This would induce errors in input data and the simulation results. In the current model, we did not consider snow drift by wind and the changes in vegetation conditions from year to year. For a more realistic simulation, especially at fine spatial resolutions, these features will need to be considered.

Conclusions

This study shows that it is necessary and possible to integrate the dynamics of snow when simulating the long-term impacts of climate warming on ground thermal regimes and permafrost. Comparisons with climate station measurements showed that the model not only could simulate snow dynamics using daily climate data as input, but also captured the seasonal patterns and long-term changes of snow using monthly climate data. Driven by monthly grid climate data, the simulated spatial distribution of snow in Canada was comparable with the measurements at climate stations.

This long-term simulation shows that snow depth would be thinner in northern and eastern Canada and annual snow-cover duration would be shorter almost everywhere in Canada by the end of the 21st century. These decreasing trends in snow-cover days and in snow depth were mainly due to the increase in air temperature. The simulated increase in annual mean ground temperature was 1°C–2°C less than that of the annual mean air temperature, due mainly to the concurrent change in snow conditions. This study shows that the interaction between air temperature and snow conditions would reduce permafrost degradation by a noticeable amount in response to climate warming.

Acknowledgments

The authors thank Richard Fernandes and Fuqun Zhou for the internal critical review of the paper. This study is supported by the climate change program in Natural Resources Canada and Canada's IPY funding (CiCAT).

References

Bartelt, P.B. & Lehning, M., 2002. A physical SNOWPACK model for the Swiss avalanche warning: part I. Numerical model. *Cold Reg. Sci. Technol*. 35, doi:10.1016/S0165-232x(02)99974-5.

Brown, R.D. & Braaten, R.O. 1998. Spatial and temporal variability of Canadian monthly snow depths, 1946–1995. *Atmosphere-Ocean* 36: 37-45.

Chen, W., Zhang, Y., Cihlar, J., Smith, S.L. & Riseborough, D.W. 2003. Changes in soil temperature and active-layer thickness during the twentieth century in a region in western Canada. *J. Geophys. Res.* 108 (D22): 4696, doi:10.1029/2002JD003355.

Christensen, J.H. et al. 2007. Regional climate projections. In: Solomon, S. et al. (eds.), *Climate Change 2007: The Physical Science Basis. Contribution of Working Group I to the Fourth Assessment Report of the Intergovernmental Panel on Climate Change*. Cambridge, UK, and New York, USA: Cambridge University Press.

Environment Canada. 1999. Canadian daily climate data (CD-ROM).

Environment Canada. 2000. Canadian snow data CD-ROM. CRYSYS Project, Meteorological Service of Canada, Downsview, ON, Canada.

Goodrich, L.E. 1982. The influence of snow cover on the ground thermal regime. *Can. Geotech. J.* 19: 421-432.

Kongoli, C.E. & Bland, W.L. 2000. Long-term snow depth simulation using a modified atmosphere-land model. *Agric. For. Meteorol.* 104: 273-287.

Lemke, P. et al. 2007. Observations: Changes in snow, ice and frozen ground. In: Solomon S. et al. (eds.), *Climate Change 2007: The Physical Science Basis. Contribution of Working Group I to the Fourth Assessment Report of the Intergovernmental Panel on Climate Change*. Cambridge, UK, and New York, USA: Cambridge University Press.

Mitchell, T.D. & Jones, P.D. 2005. An improved method of constructing a database of monthly climate observations and associated high-resolution grids, *Int. J. Climatol.* 25: 693-712. doi:10.1002/joc.1181.

Overpeck, J. et al. 1997. Arctic environmental changes of the last four centuries. *Science* 278: 1251-1256.

Räisänen, J. 2007. Warmer climate: less or more snow? *Clim. Dyn*. doi:10.1007/s00382-007-0289-y (in press).

Riseborough, D.W. & Smith, M.W. 1993. Modelling permafrost response to climate change and climate variability. *Proceedings, Fourth International Symposium on Thermal Engineering and Science for Cold Regions.* Hanover, New Hampshire, U.S.A.: 179-187.

Wrona, F.J., Prowse, T.D. & Reist, J.D. 2005. Freshwater ecosystems and fisheries. In: *Arctic Climate Impact Assessment*. Cambridge University Press.

Zhang, T. 2005. Influence of the seasonal snow cover on the ground thermal regime: An overview. *Rev. Geophys.* 43, RG4002. doi:10.1029/2004RG000157.

Zhang, Y., Chen, W. & Riseborough, D.W. 2008a. Disequilibrium response of permafrost thaw to climate warming in Canada over 1850–2100. *Geophys. Res. Lett.* 35, L02502, doi:10.1029/ 2007GL032117.

Zhang, Y., Chen, W. & Riseborough, D.W. 2008b. Transient projections of permafrost distribution in Canada during the 21st century under scenarios of climate change. *Global and Planetary Change* 60: 443-456, doi:10.1016/j.gloplacha.2007.05.003.

Zhang, Y., Chen, W. & Riseborough, D.W. 2006. Temporal and spatial changes of permafrost in Canada since the end of the Little Ice Age. *J. Geophys. Res.* 111, D22103, doi:10.1029/2006JD007284.

Zhang, Y., Chen, W., Smith, S.L., Riseborough, D.W. & Cihlar, J. 2005. Soil temperature in Canada during the twentieth century: complex responses to atmospheric climate change, *J. Geophys. Res. 110*, D03112, doi:10.1029/2004JD004910.

Zhang, Y., Chen, W. & Cihlar, J. 2003. A process-based model for quantifying the impact of climate change on permafrost thermal regimes. *J. Geophys. Res.* 108(D22), 4695, doi:10.1029/2002JD003354.

—Plenary Paper—

Regional Changes of Permafrost in Central Asia

Lin Zhao
Cryosphere Research Station on the Qinghai-Tibet Plateau and State Key Laboratory of Cryospheric Sciences, Cold and Arid Regions Environmental and Engineering Research Institute, Chinese Academy of Sciences

S.S. Marchenko
Geophysical Institute, University of Alaska Fairbanks, AK 99775-7320, USA

N. Sharkhuu
Geo-Ecology Institute, Mongolian Academy of Sciences

Tonghua Wu
Cryosphere Research Station on the Qinghai-Tibet Plateau and State Key Laboratory of Cryospheric Sciences, Cold and Arid Regions Environmental and Engineering Research Institute, Chinese Academy of Sciences

Abstract

Recent progress in research about permafrost changes induced by climatic warming in Central Asia is summarized in this paper. Most permafrost in Central Asia is located on the Qinghai-Tibet Plateau in China, the Tien Shan Mountain regions in China, Kazakhstan, and Kyrgyzstan, Pamir and mountain regions in Tajikistan and Mongolia. Monitoring of the permafrost thermal regime has been carried out in all these regions in the past several decades. Accompanying climate warming, the thermal regime of permafrost changed greatly in all the permafrost regions in central Asia. Permafrost in the Tibetan Plateau is widespread, and occupies about 1.5 million square kilometers. In the continuous permafrost regions on the plateau, the annual mean temperature has risen by 0.1–0.2°C, while in the discontinuous permafrost regions the annual mean temperature has risen by 0.2–0.5°C from 1995 to 2002. The thickness of the active layer has increased by 0.15 to 0.50 m between 1996 and 2001 and residual thaw layers recently. The average rate of increase in mean annual permafrost temperatures is from 0.2°C to 0.4°C per decade in Hovsgol Mountains of Mongolia. Permafrost has been degrading more intensively during the last 15 years (since 1990s) than during the previous 15–20 years (1970s and 1980s). Permafrost occupies about 0.16 million square kilometers in the Tien Shan Mountain regions. Geothermal observations during the last 30 yr indicate an increase in permafrost temperatures from 0.3°C up to 0.6°C. During the same period, average active-layer thickness increased by 23% in comparison to the early 1970s.

Keywords: Central Asia; climate changes; Mongolia; permafrost changes; Qinghai-Tibet Plateau; Tien Shan Mountains

Introduction

The most recent report of the Intergovernmental Panel on Climate Change (IPCC) provided a comprehensive assessment of the climatic changes that have occurred during the last 100 years. The report indicated that the global average surface temperature has increased dramatically, especially since about 1950 (IPCC 2007). Permafrost was identified as one of the key indicators of climate change (WMO 1997). Permafrost measurements are particularly important for determining the long-term terrestrial responses to surface climate change. Climate warming during the 20th century has a great influence on the contemporary thermal state of permafrost. Recent changes in permafrost conditions related to climate warming have been documented in Alaska, Canada, Europe, Siberia, and the high mountains of Central Asia (Jorgenson et al. 2001, Walker 2007, Osterkamp 2007, Camill 2005, Isaksen et al. 2007, Oberman & Mazhitova 2001, Cheng & Wu 2007, Marchenko et al. 2007, Sharkhuu et al. 2007).

Changes in the permafrost thermal regime can have significant impacts on local hydrology, land surface energy and moisture balances, carbon exchange between the land and the atmosphere, and ecosystems, as well as engineering infrastructure in cold regions (Cheng & Zhao 2000, Nelson et al. 2001, Zhang et al. 2005, Zimov et al. 2006a, b). It is, therefore, of great importance to study the permafrost dynamics of past decades. This paper summarizes recent response of permafrost to climatic changes in Central Asian regions, primarily on the Qinghai-Tibet Plateau, the mountain permafrost regions of Mongolia, and in the Tien Shan Mountains.

Study Region and Methods

The Central Asian region is the largest area underlain by alpine permafrost in the world, and includes the territories of southern Siberia, Mongolia, China, Kazakhstan, and adjacent countries (Fig. 1) (Brown et al. 2001). The mountain permafrost area of Central Asia is estimated to be 3.5×10^6 km^2, about 15% of the total areal extent of permafrost in the Northern Hemisphere (UNEP/GRID-Arendal 2007). Under climatic warming and increasing human activities in this region, the permafrost has been undergoing great changes. Here, we present a historical overview of recent permafrost investigations on the Qinghai-Tibet Plateau, Tien Shan Mountains, and Mongolia.

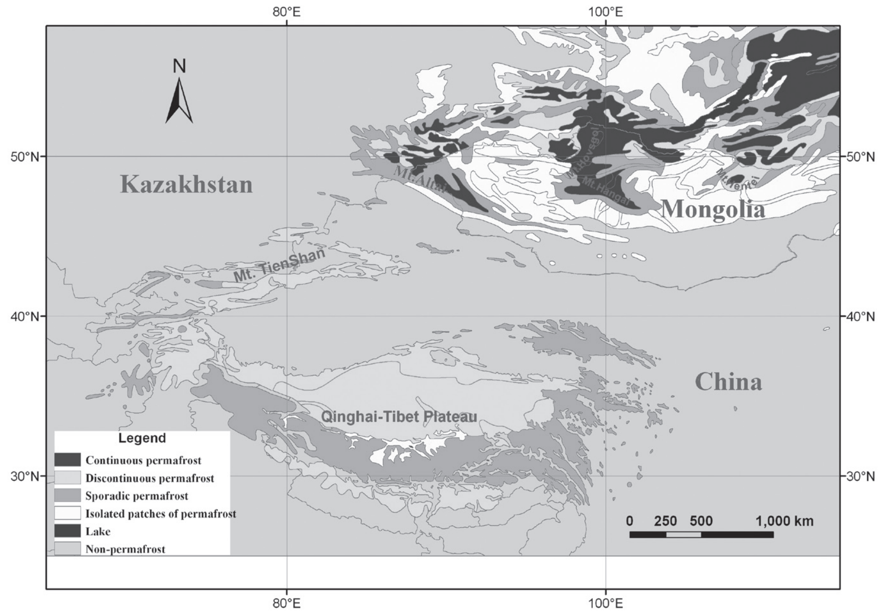

Figure 1. Permafrost distribution in the Central Asian regions (Brown et al. 2001).

Qinghai-Tibet Plateau in China

Systematic permafrost investigations on the Qinghai-Tibet Plateau began in 1954 when the Qinghai-Tibet Highway from Golmud to Lhasa was paved. In the early 1960s, intensive field investigations were conducted along the Qinghai-Tibet Highway to assess geological engineering conditions related to permafrost. Zhou and Du (1963) described permafrost characteristics, distribution, temperature, ground ice distribution, and related periglacial phenomena in detail along the highway. In 1974, a more systematic survey of permafrost was conducted by several research institutions and universities to solve the challenging problems involved in constructing a gas pipeline and the Qinghai-Tibet Railway in permafrost regions. After this survey, the work team summarized knowledge about permafrost distribution and characteristics, thermal and physical properties of frozen ground on the plateau, the thermal regime of permafrost and calculations related to permafrost, and the application of geophysical methods in permafrost studies (Tong & Li 1983). Permafrost on the Qinghai-Tibet Plateau was classified as predominantly continuous permafrost (continuity from 70% to 90%), widespread island permafrost (continuity from 30% to 70%), and sparse island permafrost (continuity less than 30%) (Zhou et al. 2000). During the 1980s, geocryologists and engineers made great progress involving the regularity of permafrost distribution, mechanisms of ground-ice formation, moisture and salt migration during the freezing and thawing process of frozen ground, and application of remote sensing techniques in periglacial geomorphic studies (Cheng 1982). After many field surveys and much analysis, the regularities of altitudinal, latitudinal, and continental mountain permafrost zonation based on the mean annual ground temperature (MAGT) of permafrost and mean annual air temperature (MAAT) were summarized and subsequently applied by the international permafrost community (Cheng and Wang 1982, Cheng and Dramis, 1992, King et al. 1992). In 1989, the Cryosphere Research Station on the Qinghai-Tibet Plateau was established in Golmud, Qinghai Province to perform long-term and continuous observations on permafrost temperatures and related climatic factors. To satisfy the needs for solving engineering problems in cold regions, further understanding the regularities of permafrost formation and evolution, and assessing the environmental significance of permafrost regions, the State Key Laboratory of Frozen Soil Engineering affiliated to Chinese Academy of Sciences was established in 1991. In the 1990s, permafrost studies on the plateau were improved to create a more detailed and comprehensive science that includes mapping of permafrost and seasonally frozen ground, conducting long-term programs of monitoring the thermal regime of permafrost and the active layer, exploring the thermal, physical and mechanical properties of frozen ground, investigating cold region hydrology and engineering, and especially assessing the impacts and feedbacks of permafrost degradation on engineering infrastructures, the climate system, and related aspects of the environment. Zhang (2005) summarized the historical development of permafrost studies from the 1950s to the present on the Qinghai-Tibet Plateau. A permafrost monitoring network along the Qinghai-Tibet Highway (Fig. 2) has been established, and includes 18 boreholes with depths from 20 to 127 m, 13 sets of active layer measurements systems, 4 automatic weather stations, and 2 eddy covariance systems to collect related data (Cheng & Wu 2007).

Mongolia

Permafrost regions occupy about two-thirds of the territory of Mongolia, predominantly in Altai, Hovsgol, Khangai, and Khentei mountainous regions, which are located in the southern reaches of the Siberian permafrost regions (Fig.

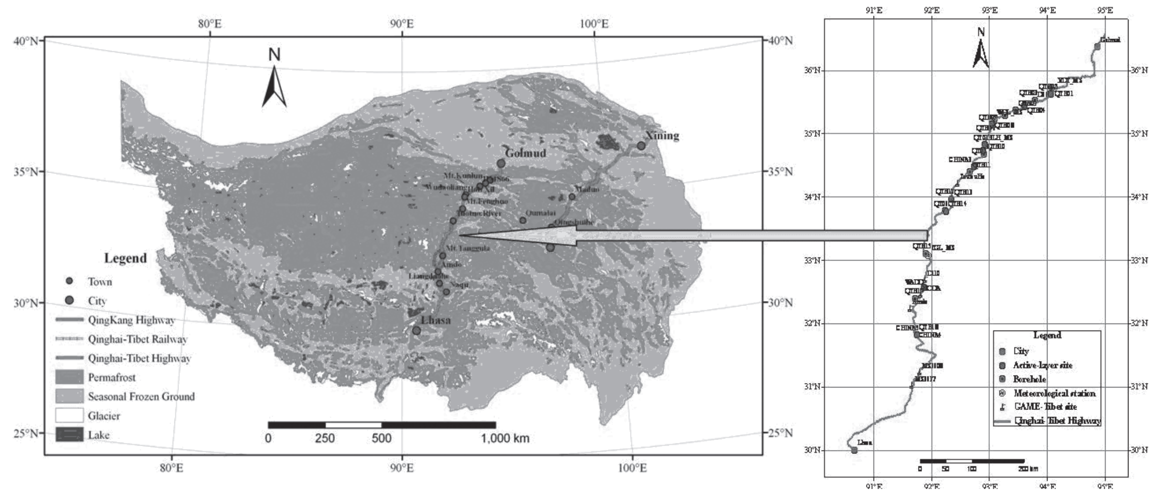

Figure 2. Permafrost monitoring network along the Qinghai-Tibet Highway.

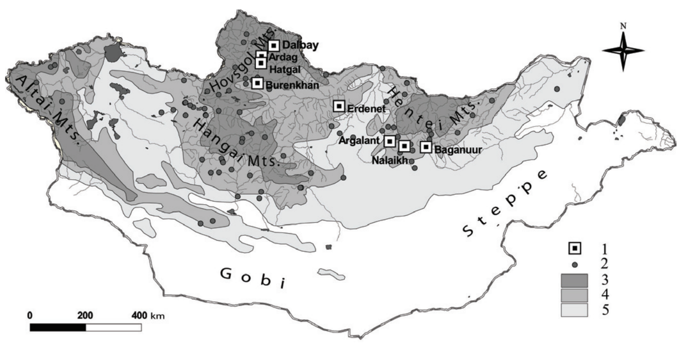

Figure 3. Permafrost distribution and the monitoring network in Mongolia (Sharkhuu et al. 2007).

3). Generally, permafrost temperatures in most regions of Mongolia are close to 0°C, and are thus very sensitive to climatic changes (Sharkhuu et al. 2006). In order to assess the responses of permafrost to recent climatic warming and human activities, Mongolian scientists began systematic observations of permafrost in 1996. The observation sites belong to the Circumpolar Active Layer Monitoring (CALM) and Global Terrestrial Network for Permafrost (GTN-P) programs. Furthermore, some cryogenic processes and phenomena are observed at different sites. Active layer depth and mean annual soil temperature at different levels are measured on the same dates of each year. Temperature data loggers and thaw tubes have been installed in some of the boreholes.

At present, there are fourteen sites for permafrost observations in Mongolia. Five of the sites are in Khentei (Baganuur, Nalaikh, Argalant, Terelj, and Gurvanturuu), two in Khangai (Terkh and Chuluut), six in Hovsgol (Sharga, Burenkhan, Hatgal, Ardag, Hovsgol Project, and Darhad), another site (Tsengel) is in the Altai mountains (Fig. 3). The depth of six boreholes ranges from 50 m to 80 m. So far, there are 37 boreholes belonging to the CALM network and the GTN-P program in Mongolia. Observations on periglacial processes, including thermokarst lakes, frost heaving, and icings, have been carried out seven sites in Hovsgol, Khangai, and Khentei mountains.

Tien Shan Mountains in Kazakhstan

The alpine permafrost region in the Tien Shan Mountains belongs to the Asian high-mountain permafrost area (Marchenko et al. 2007). It is estimated that permafrost in the Tien Shan Mountains formed about 1.6 million years ago due to its high elevation (Aubekerov and Gorbunov 1999). The permafrost in the Tien Shan Mountains has undergone repeated aggradation and degradation since the Holocene. Relict permafrost is found in many places in this region (Gorbunov 1996). Furthermore, mountain permafrost and associated periglacial landforms contain a large amount of ground ice. Moraines, rock glaciers, and other coarse blocky material have especially high ice content (40% to 90% by volume). Preliminary evaluation indicates that the total volume of ground ice is about 320 km^3 (Gorbunov and Ermolin 1981). Water derived from thawing permafrost could, therefore, become an important source of water for vegetation in this region.

The earliest reference to the occurrence of permafrost in the Tien Shan Mountains was in a Russian report in 1914 (Bezsonov 1914). Systematic investigations of mountain permafrost in the Tien Shan Mountains began in the mid-1950s (Gurbonov 1967, Gurbonov 1970). Traditionally, the alpine permafrost area of the Tien Shan Mountains is divided into altitudinal sub-zones of continuous, discontinuous, and sporadic permafrost (Gurbonov 1978, Gurbonov 1988). The earliest permafrost temperature measurements in the Northern Tien Shan began in 1973. Many methods have been used to observe permafrost temperatures, including measuring the active layer's thermal regime and thickness and spring water temperatures and DC resistivity soundings (Gurbonov & Nemov 1978, Zeng et al. 1993, Gorbunov et al. 1996). Permafrost investigations in the Inner Tien Shan were conducted from 1985 to 1992. Ground temperature measurements were conducted in 20 boreholes in the Ak-Shiyrak massif, and in more than 25 boreholes in the Kumtor valley. Thermistor sensors MMT-4 with a sensitivity 0.02°C and an accuracy less than 0.05°C were used during the observations (Ermolin et al. 1989, Marchenko et al. 2007).

Recent Climatic Changes in Central Asia

In Central Asia, including the Qinghai-Tibet Plateau, the air temperature is strongly affected by changes in the winter and spring snow cover. It is predicted that the area-averaged annual mean warming would be about 3°C in the decade of the 2050s over the land regions of Asia as a result of future increases in atmospheric concentration of greenhouse gases (IPCC 2007). Recent atmospheric warming particularly affects terrestrial systems where surface and sub-surface ice are involved. The retreat of glaciers and changes in permafrost in the central Asia in recent years is unprecedented as a consequence of climate warming. Kharlamova and Revyakin (2006) considered the oldest weather station in Asia, the Barnaul station as a benchmark for central Asia with 166 years measurement of air temperature. The statistical analysis showed that the MAAT has increased by 2.8°C over the 166-year period (1.8°C/100yr). The climatic warming in Central Asia is rather noticeable. The trend of MAAT from 1838 to 1958 amounts to 0.015°C/yr and 0.034 °C/yr from 1959 to 2003. During the last 166 years, the MAAT of the warm season (from April to October) has increased by 2.3°C (1.4°C/100yr) and of 3.4°C (2.2°C/100yr) warming found in the cold season (November to March). The most pronounced warming occurred in January (4.8°C), March (4.4°C), and April (4.5°C). The fourth IPCC assessment report (IPCC 2007) also documented that all of Asia is very likely to warm during this century and that the warming is likely to be well above the global mean in Central Asia. The long-term observation results in precipitation amount showed a significant increase in Central Asia from 1900 to 2005 (IPCC 2007).

Many previous studies have demonstrated that dramatic climatic warming has occurred on the Qinghai-Tibet Plateau (Liu and Hou 1998, Yao et al. 2000, Liu and Chen 2000, Duan et al. 2006, Wang et al. 2007). Liu & Chen (2000) collected monthly surface air temperature data from 97 meteorological stations above 2000 m a.s.l. on the plateau. Analysis of the temperature series indicated that most of the territory of the Qinghai-Tibet Plateau has undergone significant warming since the mid-1950s. The statistically significant warming trends in MAAT ranging from 0.016°C/yr to 0.032 °C/yr were found between 1955 and 1996. There is also a tendency for the warming trend to increase more in the high-elevation regions than in the surrounding low-elevation regions. It is evident that the Qinghai-Tibet Plateau region is among the most sensitive to global climatic changes. Wu (2005) analyzed inter-decadal changes of MAAT from 101 meteorological stations on the Qinghai-Tibet Plateau over the 1961–2000 period. Their statistical results indicate that there are 94 stations where the NAAT has increased. The MAAT has increased by about 0.70°C with a trend of 0.017°C/yr over the entire plateau during the last 40 years, which is much greater than the mean value in China (0.005°C/yr).

Based on systematic observations at 25 meteorological stations established beginning in 1936 in Mongolia, Batima and Dagvadorj (2000) it appears that the annual air temperature in Mongolia has increased by 1.56°C (0.026°C/yr) during the last 60 years. Winter temperature has increased by 3.61°C and the spring-autumn temperature by 1.4°C to 1.5°C. Furthermore, winter warming is more pronounced in high mountains and in open valleys (Batima et al. 2005). In the Altai Mountains, the MAAT has increased with a trend of 0.03°C/yr during the last 50 years. Summer precipitation has increased by 11% while spring precipitation has decreased by 17% from 1940 to 1998. The mean annual precipitation in Mongolia has displayed little increasing trend during the past 50 years.

Aizen et al. (1997) analyzed climatic data from 110 sites in the Tien Shan Mountains from 1940 to 1991. Their results show that the MAAT increased by an average rate of 0.01ºC/yr over the entire Tien Shan Mountains and by 0.006ºC/yr in the northern Tien Shan Mountains below 2000 m. The rise in air temperature was greater, especially in the central Tien Shan Mountains (0.012°C/yr) and in the high altitudes of the peripheral northern and western regions. Mean annual precipitation has increased 100 mm, or about 12-14%, during the past 52 years. Research also indicates that the average trend of MAAT ranges from 0.006°C/yr to 0.032°C/yr in different parts of the Tien Shan Mountains during the last 70 years (Dikih 1997, Marchenko et al. 2007).

Permafrost Changes

Qinghai-Tibet Plateau

The results outlined above indicate that extensive permafrost degradation has occurred during the past several decades on the Qinghai-Tibet Plateau. Evidence includes the thickened active layer, thinned permafrost, increased permafrost temperatures, talik formation, and disappearance of permafrost islands (Cheng & Wu 2007). In areas of discontinuous permafrost, the MAGT has increased by 0.1°C to 0.3°C (Wang et al. 2000, Cheng & Wu 2007) and active-layer thickness has increased during the 1980s and 1990s by several centimeters to 1 m, even 2 m at some sites (Wang & Zhao 1997). Observations of ground temperature at the Kunlun Pass site and Mt. Fenghuo site showed a warming trend in permafrost from 1996 to 2002 (Fig. 4). In undisturbed permafrost regions, the permafrost surface temperature has increased by about 0.1°C to 0.7°C from 1996 to 2001 and the thickness of the active layer has increased by 10–40 cm (Wu & Liu 2004, Yang et al. 2004). Temperature at the permafrost surface and at the depth of 6 m rose at different rates from 1996 to 2001 (Table 1) (Wu et al. 2005). The change in cold (<-1.5°C) permafrost is greater than that in warm (>-1.5°C) permafrost under the effect of climate warming. However, warm permafrost is very susceptible to climatic warming and the thermal regime of warm permafrost will be impacted more directly and immediately by surrounding warming (Wu et al. 2007).

In the sporadic permafrost regions, ground temperature measurements at Xidatan, located in the vicinity of the northern altitudinal lower limit of permafrost (i.e., the zone above which permafrost occurs), indicate that the MAGT at 20 m depth increased by 0.2–0.3°C in the same period and

Table 1 Permafrost observation from 7 sites on the plateau (Wu et al. 2005).

Site	ALT* (m)		TTOP (°C)		TP_6* (°C)	
	1996	2001	1996	2001	1996	2001
Kunlun Pass No.1	1.09	1.50	-3.05	-2.68	-3.19	-2.90
Kunlun Pass No.2	1.22	1.40	-3.08	-2.78	-3.06	-2.77
Mt. Fenghuo	1.26	1.60	-3.73	-3.36	-3.67	-3.48
Wudaoliang	2.53	2.75	-1.82	-1.75	-1.63	-1.50
HohXil	1.64	2.00	-2.14	-1.63	-2.01	-1.69
HMS 66	1.94	2.40	-0.82	-0.63	-0.91	-0.83
Cumar Riverside	3.24	3.50	-0.43	-0.30	-0.56	-0.40

TP6* denotes permafrost temperature taken at 6 m depth. ALT is the abbreviation of Active Layer Thickness.

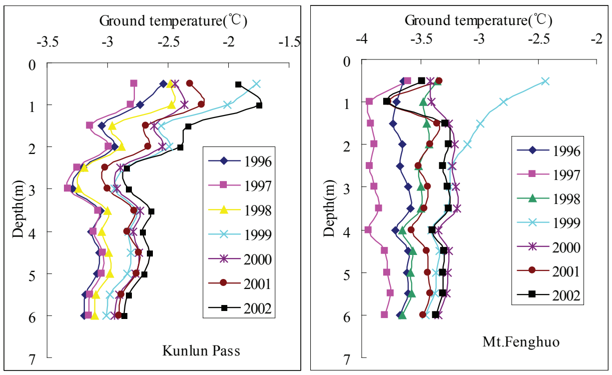

Figure 4. Variations of permafrost temperatures in the Kunlun Pass and the Mt. Fenghuo from 1996 to 2002.

permafrost has disappeared at some locations. The base of permafrost rose by about 4 m from 1983 to the end of the 1990s. A borehole was drilled in 1983 to a depth of 30 m at the Cryosphere Research Station on the Qinghai-Tibet Plateau (CRSQTP) site (35°43′N, 94°05′E) to monitor changes in permafrost temperature. The measurements indicate that ground temperatures at depths of 12–20 m have risen by 0.15–0.36°C and soil temperatures at depths from 5 to 10 m increased by about 0.2°C between 2001 and 2003. The permafrost base monitored from a borehole profile at the Jingxiangu Valley (10 km south of the CRSQTP site) has risen by 10–15 m and the MAGT has increased by 0.5–0.8°C over the last 20 years.

The Amdo-Liangdaohe section of the Qinghai-Tibet Highway is located in the vicinity of the southern lower altitudinal limit of permafrost and is underlain by sporadic permafrost. Permafrost has decreased in area by 35.6% and the lower altitudinal limit of permafrost has risen by 50-80 m. The southern boundary of permafrost has been displaced northward by 1.0–2.0 km over the past 30 years (Wang and Zhao 1997). A 19.53 m borehole was drilled near Amdo in July 1975 to monitor permafrost change. Drilling records indicate that the permafrost table was at a depth of 3.5 m and that the thickness of permafrost was 6.5 m. However, temperature measurements made in July 1989 demonstrate that the MAGT had increased by 0.1–0.2°C and no frozen layer was detected. Another borehole was drilled in June of 1975 to the south of the Highway Maintenance Squad (HMS) 124. Records show that the permafrost table was at a depth

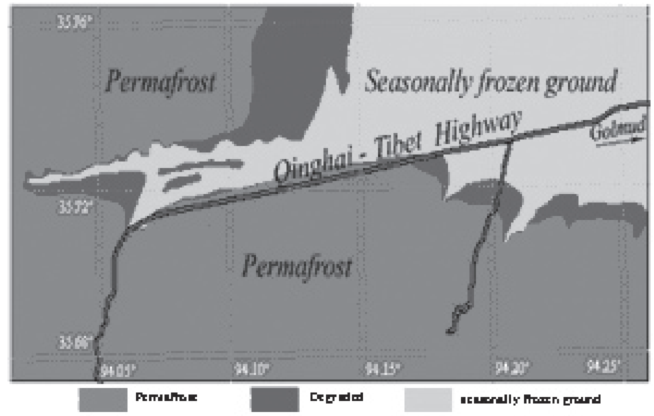

Figure 5. Permafrost change in Xidatan during the last 30 years.

of 3 m and the thickness of permafrost was 5.5 m. However, ground temperature records taken in 1989 indicate that the MAGT had increased by 0.2–0.3°C and permafrost had completely disappeared (Cheng & Wu 2007). The Qinghai-Kang (West Sichuan) Highway travels through the hilly terrain of eastern Qinghai-Tibet Plateau, which is underlain by sporadic and discontinuous permafrost. Approximately 300 km of the Qinghai-Kang Highway is over permafrost. Recent studies reveal that permafrost along the highway in the eastern part of the plateau is undergoing degradation. Taliks have developed at Madoi, Qingshuihe, and the Huashixia Permafrost Station. To the east of Huashixia, a 2.2 m test pit was dug in a marsh at an elevation of 4230 m in June 1992. At that time, soil was thawed to a depth of 0.60 m; ice was found from 0.60 to 1.20 m. A thawed layer was located between 1.20 and 1.60 m; soil was frozen below. A 7 m borehole was drilled near Qingshuihe in May 1995. The borehole records indicate that the ground was frozen to a depth of 1.5 m and a talik was located between 1.5 and 3.0 m. The layer below was frozen from 3 to 7 m. Another borehole, 154.88 m deep, was drilled in 1990 at Qingshuihe. The drilling records indicate that a talik was located between 1.50 and 15.34 m and the layer below was frozen from 15.34 to 37.32 m. A number of boreholes and test pits were drilled or dug to map the distribution of permafrost along the Qinghai-Kang Highway in the 1960s and 1990s. It appears that the lower altitudinal limit of permafrost along the highway rose by approximately 50-100 m over a 30-year period. Ground Penetrating Radar investigations in the northern plateau indicated that the lower altitudinal limit of permafrost has risen by 25 m and permafrost shrank in area considerably over the last 30 years (Fig. 5) (Wu et al. 2005).

Based upon field observations of permafrost temperatures, Wu (2005) discovered that the annual rate of increase in MAGT is 0.042 to 0.065°C/yr for stable permafrost (MAGT <-3°C), 0.016 to 0.098°C/yr for quasi-stable permafrost (MAGT between -0.5 and -3°C), and 0.011 to 0.041°C/yr for unstable permafrost (MAGT >-0.5°C), respectively. It is estimated that the base of permafrost rose at a rate of 0.1 to 0.2 m per decade on average during the last four decades throughout the plateau (Zhao et al. 2003). This trend is expected to continue under the current climate conditions.

Mongolia

The preliminary results of observation indicated that permafrost is degrading to a different extent depending on the regional and local changes in climate and human activities. The change of permafrost condition in bedrock is greater than that in unconsolidated sediments, in ice-poor substrates greater than that in ice-rich ones, on south-facing slopes greater than that on north-facing slopes, and at sites influenced by human activities greater than those undisturbed ones. In generally, permafrost degradation during the last 15-20 years (from 1990s to 2000s) was more intensive than that during the 1970s to 1990s. Spatially, permafrost in the Hovsgol Mountains changed more intensively than that in the Khentei, Khangai Mountains (Sharkhuu et al. 2006).

The Hovsgol Mountain region of northern Mongolia is located at the southern fringe of the Siberian continuous permafrost zone. Monitoring results obtained through measuring ground temperatures and active layer thickness in boreholes indicate that the average rate of increase in mean annual permafrost temperatures is from 0.02°C/yr to 0.04°C/yr. The observation results from selected Sharga, Hatgal, Tsagaan-nuur, and Burenkhan long-term monitoring sites (Fig. 3) showed an apparent trend of increase in mean annual permafrost temperatures at a depth of 10–15 m during the measurement period, ranging between 0.026 and 0.045°C/yr (Fig. 6). The highest rate, 0.042°C/yr with an increasing trend (r^2=0.91, P<0.0001) in permafrost temperatures during the last 11 years, is observed in the Burenkhan 1 borehole on a mountain slope composed of high thermal conductivity bedrock. Moreover, MAGTs in the Burenkhan mountain area have increased by 0.027°C/yr on south-facing slope, while 0.019°C/yr on north-facing slope, 0.023°C/yr in the upper watershed and 0.011°C/yr in the valley bottom (Sharkhuu et al. 2007).

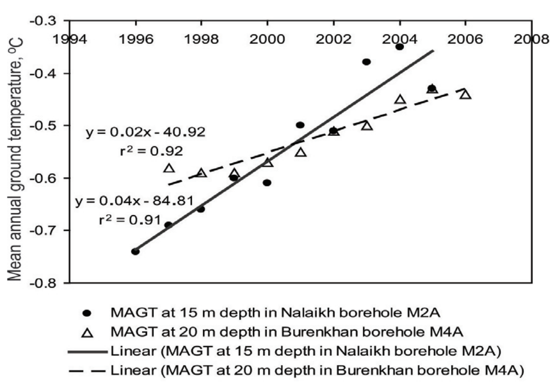

Figure 6. Trend of mean annual permafrost temperatures.

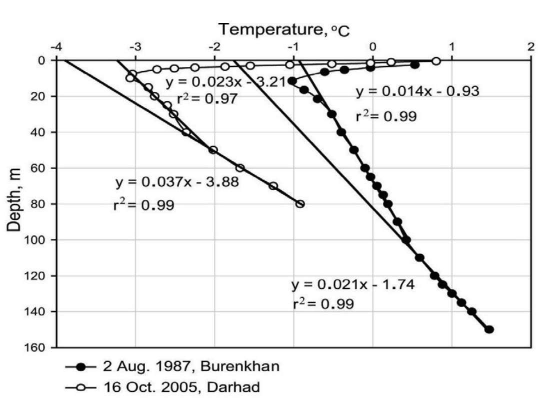

Figure 7. Change in permafrost temperature gradients with depth.

Increasing temperature gradients in the Dahard and Burenkhan 2 deep boreholes (Fig. 7) support the hypothesis that the observed change in thermal gradient with depth in addition to lithological factors might be associated with a warming temperature pulse. The Darhad site would be considered as a benchmark of warming trend in the early 1980s, while the Burenkhan site would be considered as a benchmark of warming trend in the early 1960s. Estimated trends of the increase in mean annual permafrost temperatures over 20–30 years in Mongolia are 0.01–0.02°C/yr in the Hangai and Hentei region, and 0.02–0.04°C/yr in the Hovsgol region (Sharkhuu et al. 2006).

Observation of thermokarst processes at Chuluut (in Khangai Mountain region) and Nalaikh (in Khentei Mountain region) during the last 30 years showed that subsidence of 3–10 cm/yr has taken place in the land surface. The maximum subsidence of land surface amounts to 20 to 40 cm/yr during the formation of a thermokarst pond at the Chuluut site. Until late August of 2004, active layer thickness on 5-meter-high pingo in Nalaikh has deepened to 1.50 m from 1.35 m in 1998, and the southeastern side of the pingo has subsided. The subsiding trend of the ice-rich lacustrine clays by the Chuluut River bank is estimated to be 15-30 cm/yr (Sharkhuu et al. 2006).

Tien Shan Mountains

There is some evidence indicating that climatic changes in the 20th century have exerted a significant impact on the thermal condition of mountain permafrost in the Tien Shan Mountains. The geothermal observations during 1974–1977 and 1990–2004 indicate that permafrost has been warming during the last 30 years (Fig. 8). Ground temperatures increased by 0.2–0.3°C at undisturbed sites, and up to 0.6°C at those influenced by human activities. In the northern Tien Shan Mountains, average active layer thickness has increased from 3.2 to 3.4 m in the 1970s to a maximum of 5.2 m in 1992 and to 5.0 m in 2001 and 2004 (Fig. 8),

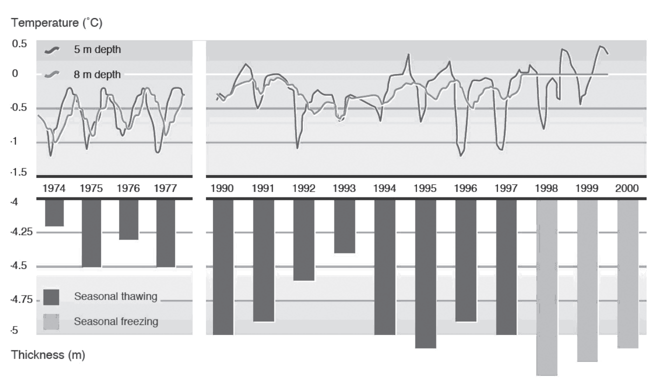

Figure 8. Permafrost temperatures and active layer thickness variations during 1974-1977 and 1990-2000 measured in Borehole K1, 3328 a.s.l., northern Tien Shan Mountain (Marchenko et al., 2007).

a major increase from the early 1970s (Marchenko et al. 2004). As a result of a deep ground thawing, a talik between 5 and 8 m in depth at different sites has formed. Permafrost temperatures in the Inner Tien Shan Mountains have also increased by 0.1°C over 1986-1993 both in the valley and on the mountain slopes (Marchenko et al. 2007).

Summary

Extensive climatic warming has taken place in Central Asia. MAAT has increased with a trend of 0.017°C/yr on the Qinghai-Tibet Plateau during the last 40 years, 0.026°C/yr in Mongolia in the past 60 years, and 0.01°C/yr over the entire Tien Shan Mountains over the 1940–1991 period. The climatic changes occurring in Central Asia have had a pronounced influence on the thermal condition of permafrost. In the different permafrost regions in Central Asia, permafrost degradation has occurred as shown by increasing ground temperatures, thickening of the active layer disappearance of permafrost patches, formation of taliks and development of thermokarst terrain. Permafrost degradation will impact engineering infrastructure, surface and subsurface hydrology, ecosystems, and will even feedback to climatic changes by means of emission of stored carbon from permafrost. In the high-mountains regions of Central Asia, the further near-surface permafrost degradation will probably accompany a transformation in environmental conditions and may lead to slope instability and permafrost-related hazards such as landslides, thermakarst, and glacial lake outburst causing mudflows.

Acknowledgments

We express our gratitude to Dr. Jerry Brown, the president of the International Permafrost Association, for all his help. This paper would not have been possible without his kindly help. Thanks for all the suggestions from Dr. Frederick E. Nelson, Dr. Douglas Kane, and other anonymous reviewers. Thanks for the support from the Chinese Key Basic Research development Project (973 Project: No. 2005CB422003), the Chinese National Science Foundation (No. 40471026), and the Innovation Project of the Chinese Academy of Science (KZCX3-SW-345, KZCX3-SW-351).

References

Aizen, V.B., Aizen, E.M., Melack, J. & Dozier, J. 1997. Climatic and hydrologic changes in the Tien Shan, Central Asia. *Journal of Climate* 10(6): 1393-1404.

Aubekerov, B. & Gorbunov, A.P. 1999. Quaternary permafrost and mountain glaciation in Kazakhstan. *Permarost and Periglacial Processes* 10: 65-80.

Batima, P. & Dagvadorj, D. (eds.). 2000. *Climate Change and Its Impacts in Mongolia.* Mongolia: JEMR Publishing, 1-227.

Batima, P., Natsagdorj, L., Gombluudev, P. & Erdenetsetseg, B. 2005. Observed climate change in Mongolia. AIACC Working Paper. No. 12: 1-25.

Bezsonov, A.I. 1914. Preliminary report on organizing and performance of the soil investigation in the Asian Russia in 1913. St. Petersburg, 245-260.

Brown, J., Ferrians, O.J., Heginbottom, J.A. & Melnikov, E.S. 1998 (revised February 2001). Circum-arctic map of permafrost and ground ice conditions. Boulder, CO: National Snow and Ice Data Center/World Data Center for Glaciology. Digital media.

Camill, P. 2005. Permafrost thaw accelerates in boreal peatlands during late-20th century climate warming. *Climatic Change* 68: 135-152.

Cheng, G. 1982. Formation of massive ground ice near the permafrost surface. *Science in China* (Series B) 3: 281-287.

Cheng, G. & Dramis, F. 1992. Distribution of mountain permafrost and climate. *Permafrost and Periglacial Processes* 3: 83-92.

Cheng, G. & Wang, S. 1982. On zonation of mountain permafrost in China. *Journal of Glaciology and Geocryology* 4: 1-17.

Cheng, G. & Wu, T. 2007. Responses of permafrost to climate change and their environmental significance, Qinghai-Tibet Plateau. *Journal of Geophysical Research-Earth Surface* 112, F02S03, doi: 10.1029/2006JF000631.

Cheng, G. & Zhao, L. 2000. The problems associated with permafrost in the development of the Qinghai-Xizang Plateau. *Quaternary Science* 20(6): 521-531 (in Chinese with English abstract).

Dikih, A.N. 1997. Globalnoe poteplenie klimata, ego proyavlenie na Tyan-Shane i reaktcia lednikov. (Global climate warming event in the Tien Shan and glaciers reaction). Data of Glac. Studies. Moscow, vol. 83, pp. 135-139 (in Russian).

Duan, A., Wu, G., Zhang, Q. & Liu, Y. 2006. New proofs of the recent climate warming over the Tibetan Plateau as a result of the increasing greenhouse gases emissions. *Chinese Science Bulletin* 51 (11): 1396-1400.

Ermolin, E.D., Nemov, A.E. & Popov, M.V. 1989. Geotermicheskaya harakteristika mestorojdeniya Kumtore. (Geothermal characteristic of the Kumtor gold mine). Geocryological Investigations in the Mountains of USSR, Yakutsk, pp. 31-40 (in Russian).

Gravis, G.F., Melnikov, E.S., Guo, D.X., Li, S.X., Li, S.D., Zhao, L., Nan, Z.T., Sharkhuu, N., Gorbunov, A.P., Marchenko, S.S. & Seversky, E.V. 2003. Principles of classification and mapping of permafrost in Central Asia. *Proceedings of the 8th International Conference on Permafrost,* Zurich, Switzerland. Balkema, Lisse, 297-302.

Gorbunov, A.P. 1967. Vechnaya Merzlota Tyan-Shanya (Permafrost of the Tien Shan). Ilim, Frunze (in Russian).

Gorbunov, A.P. 1970. Kriogennye yavleniya Tyan-Shanya (Cryogenic phenomena of the Tien Shan). Gidrometeoizdat, Moscow (in Russian).

Gorbunov, A.P. 1978. Permafrost investigations in high-mountain regions. *Arctic and Alpine Research* 10: 283-294.

Gorbunov, A.P. 1988. The alpine permafrost of the USSR. *Proc. Of Fifth Int. Conf. on Permafrost*, Vol. 1. Tapir, Trondheim, Norway, 154-157.

Gorbunov, A.P. 1996. Monitoring the evolution of permafrost in the Tien Shan. *Permafrost and Periglacial Processes* 7(3): 297-298.

Gorbunov, A. & Ermolin, E. 1981. Ground ice of Central Asian Mountains. *Glaciers Studies*, Moscow 41: 59-62 (in Russian).

Gorbunov, A.P. & Nemov, A.E. 1978. K issledovaniu temperature rykhlooblomochnyh tolscsh vysokogornogo Tyan-Shanya (On temperature research of loose deposits in the Tien Shan high mountains). Cryogenic Phenomena of High Mountains. Nauka, Novosibirsk, 92-99 (in Russian).

Gorbunov, A.P., Seversky, E.V. & Titkov, S.N. 1996. Geocriologicheskie Usloviya Tyan-Shanya i Pamira (Geocryological Conditions of the Tien Shan and Pamir). Permafrost Institute publishers, Yakutsk (in Russian).

IPCC, 2007: *Climate Change 2007: The Physical Science Basis.* Contribution of Working Group I to the Fourth Assessment Report of the Intergovernmental Panel on Climate Change. Edited by S. Solomon D. Qin, M. Manning, Z. Chen, M. Marquis, K.B. Averyt, M. Tignor & H.L. Miller. Cambridge, U.K., and New York: Cambridge University Press, 996 pp.

Isaksen, K., Sollid, J.L., Holmlund, P. & Harris, C. 2007. Recent warming of mountain permafrost in Svalbard and Scandinavia. *Journal of Geophysical Research* 112, F02S04, doi:10.1029/2006JF000522.

Jin, H., Yu, Q., Lu, L., Guo, D., He, R., Yu, S., Sun, G. & Li, Y. 2007. Degradation of permafrost in the Xing'anling Mountains, Northeastern of China. *Permafrost and Periglacial Processes* 18: 245-258.

Jorgenson, M.T., Racine, C.H., Walters, J.C. & Osterkamp, T.E. 2001. Permafrost degradation and ecological changes associated with a warming climate in central Alaska. *Climatic Change* 48: 551-579.

Kharlamova, N.F. & Revyakin, V.S. 2006. Regional climate and environmental change in Central Asia. Vogtmann H. & Dobretsov N. (eds.), Environmental Security and Sustainable Land Use, with special reference to Central Asia. Netherland: Springer, 19-26.

King, L., Gorbunov, A.P. & Evin, M. 1992. Prospecting and mapping of mountain permafrost and associated phenomena. *Permafrost and Periglacial Processes* 3: 73-82.

Liu, X. & Chen, B. 2000. Climatic warming in the Tibetan Plateau during recent decades. *International Journal of Climatology* 20: 1729-1742.

Liu, X. & Hou, P. 1998. Relationship between the climatic warming over the Qinghai-Tibet Plateau and its surrounding areas in recent 30 years and the elevation. *Plateau Meteorology* 17: 245-249 (in Chinese with English abstract).

Marchenko, S.S., Gorbunov, A.P. & Romanovsky, V.E. 2007. Permafrost warming in the Tien Shan Mountains, Central Asia. *Global and Planetary Change* 56: 311-327.

Marchenko, S.S., Gurbunov, A.P. & Romanovsky, V.E. 2004. Permafrost degradation in the Tien Shan Mountains, Central Asia. American Geophysical Union, Fall Meeting 2004, abstract #A13B-0109.

Nelson, F.E., Anisimov, O. & Shiklomanov, N. 2001. Subsidence risk from thawing permafrost. *Nature* 410: 889-890.

Oberman, N.G. & Mazhitova, G.G. 2001. Permafrost dynamics in the north-east of European Russia at the end of the 20th century. *Norwegian Journal of Geography* (55): 241-244.

Osterkamp, T.E. 2007. Characteristics of the recent warming of permafrost in Alaska. *Journal of Geophysical Research* 112, F02S02, doi:10.1029/2006JF000578.

Sharkhuu, N. 2003. Recent changes in the permafrost of Mongolia. *Proceedings of the 8th International Conference on Permafrost,* Zurich, Switzerland. Balkema, Lisse, pp 1029-1034.

Sharkhuu, N. & Sharkhuu, A. 2006. Monitoring of Permafrost in Mongolia. *Proceedings of Asian Conference on Permafrost,* Abstracts, Lanzhou, China, 184-186.

Sharkhuu, A., Sharkhuu, N., Etzelmuller, B., Heggem, E.S.F., Nelson, F.E., Shiklomanov, N.I., Goulden, C.E. & Brown, J. 2007. Permafrost monitoring in the Hovsgol mountain region, Mongolia. *Journal of Geophysical Research* 112, F02S06, doi: 10.1029/2006JF000543.

Sodnom, N. & Yanshin, A.L. 1990. Geocryology and geocryological zonation of Mongolia. Digitized 2005 by Parsons, M.A. Boulder, Colorado, USA, National Snow and Ice Data Center/World Data Center for Glaciology, Digital Media.

Tong, B. & Li, S. 1983. Characteristics and controlling factors of permafrost distribution on the Qinghai-Tibet Plateau. Special Issue of Professional Papers on Permafrost Research on the Qinghai-Tibet Plateau. Beijing, China, Science Press, 1-11.

UNEP, 2007. Global Outlook for Ice and Snow. In: J. Eamer (ed). Norway: UNEP/GRID-Arendal, 235 pp. Also available at: http://www.unep.org/geo/geo_ice/.

Walker, G. 2007. A world melting from the top down. *Nature* 446: 718-721.

Wang, S., Jin, H., Li, S. & Zhao, L. 2000. Permafrost degradation on the Qinghai-Tibet Plateau and its environmental impacts. *Permafrost and Periglacial Processes* 11: 43-53.

Wang, S., Yin, Y., Zheng, D. & Yang, Q. 2007. Climatic trends over the Tibetan Plateau during 1971-2000. *Journal of Geographical Sciences* 17(2): 141-151.

Wang, S. & Zhao, X. 1997. Environmental change in patchy permafrost zone in the south section of Qinghai-Tibet Highway. *Journal of Glaciology & Geocryology* 19: 231-239 (in Chinese with English abstract).

World Meteorological Organization (WMO). 1997. Global Climate Observing System: GCOS/GTOS Plan for terrestrial climate-related observations, Version 2.0. GCOS-32, WMO/TD-No. 796, UNEP/DEIA/TR97-7, WMO, Geneva, Switzerland, 130.

Wu, Q. & Liu, Y. 2004. Ground temperature monitoring and its recent change in Qinghai-Tibet Plateau. *Cold Regions Science and Technology* 38: 85-92.

Wu, Q., Dong, X. & Liu, Y. 2005. Response of permafrost to climate change and engineering activity along the Qinghai-Tibet Highway. *Journal of Glaciology and Geocryology* 27(1): 50-54 (in Chinese with English abstract).

Wu, Q., Dong, X., Liu, Y. & Jin, H. 2007. Responses of permafrost on the Qinghai-Tibet Plateau, China, to climate change and engineering construction. *Arctic, Antarctic, and Alpine Research* 39 (4): 682-687.

Wu, T. 2005. A study on responses of permafrost to global climate change in Qinghai-Tibetan Plateau. Ph.D. Thesis, 117 pp., Graduate University of Chinese Academy of Sciences, Beijing, China (in Chinese with English abstract).

Yang, J., Ding, Y., Chen, R. & Shen, Y. 2004. Permafrost change and its effect on eco-environment in the source regions of the Yangtze and Yellow Rivers. *Journal of Mountain Science* 22(3): 278-285.

Yao, T., Liu, X. & Wang, N. 2000. Amplitude of climatic changes in Qinghai-Tibetan Plateau. *Chinese Science Bulletin* 45(13): 1236-1243.

Zeng, Z., Wang, S. & Nemov, A.E. 1993. Some new data of DC electrical soundings of permafrost in the Northen Tian Shan. *Studies of alpine permafrost in central Asia, Northern Tien Shan* Vol. 1. Yakutsk Institute, Yakutsk, 37-41.

Zhang, T. 2005. Historical overview of permafrost studies in China. *Physical Geography* 26(4): 279-298.

Zhang, T., Frauenfeld, O.W., Serreze, M.C., Etringer, A.J., Oelke, C., McCreight, J.L., Barry, R.G., Gilichinsky, D., Yang, D., Ye, H., Feng, L. & Chudinova, S. 2005. Spatial and temperal variability in active layer thickness over the Russian arctic drainage basin. *Journal of Geophysical Research-Atmospheres* 110: D16101, DOI:10.1029/2004JD005642.

Zhao, L., Cheng, G. & Li, S. 2003. Changes of frozen-ground and its environmental engineering effects on the Qinghai-Tibet Plateau. In: Zheng Du (ed.), *The Formation Environment and Development of Qinghai-Tibet Plateau*. Shijiazhuang: Heibei Science and Technology Press, 143-150 (in Chinese).

Zhou, Y. & Du, R. 1963. Preliminary investigation of permafrost on the Qinghai-Tibet Plateau. *Science in China* 2: 23-34.

Zhou, Y., Guo, D., Qiu, G., Cheng, G. & Li, S. 2000. *Geocryology in China.* Beijing, China: Science Press.

Zimov, S.A., Davydov, S.P., Zimova, G.M., Davydova, A.I., Schuur, E.A.G., Dutta, K. & Chapin, F.S. 2006a. Permafrost carbon: Stock and decomposability of a globally significant carbon pool. *Geophysical Research Letter* 33: L20502, doi: 10.1029/2006GL027484.

Zimov, S.A., Schuur, E.A.G. & Chapin, F.S. 2006b. Permafrost and the global carbon budget. *Science* 312: 1612-1613.

Monitoring Permafrost Changes on the Qinghai-Tibet Plateau

Lin Zhao, Tonghua Wu, Yongjian Ding, Changwei Xie
Cryosphere Research Station on the Qinghai-Tibet Plateau, Cold and Arid Regions Environmental and Engineering Research Institute, Chinese Academy of Sciences

Abstract

This paper summarizes recent research conducted on permafrost changes on the Qinghai-Tibet Plateau. Long-term temperature data were collected and analyzed for assessing the variations of permafrost thermal regimes. The field investigations indicated that the lower altitudinal limit of permafrost has moved up by 50 to 100 m over the plateau during the last 20 years. Research also indicated that the thinning and disappearance of permafrost has taken place in the southern and northern limit of the plateau. The mean annual temperature of permafrost has risen in the continuous permafrost regions, as well as in the discontinuous permafrost regions with different annual rate of increase in mean annual soil temperatures. Permafrost degradation has significant influence on greenhouse gas emission, local hydrology, and ecology on the plateau. The extensively occurring climatic warming on the plateau could be responsible for the permafrost degradation during the past decades.

Keywords: climatic warming; environmental significance; permafrost degradation; Qinghai-Tibet Plateau.

Introduction

Recently more and more attention has been paid to permafrost degradation all around the world under scenarios of climatic warming. A large amount of research based on long-term continuous temperature observations indicates that the permafrost on the Earth is undergoing extensive warming (Osterkamp 2007, Isaksen et al. 2007, Cheng & Wu 2007, Walker 2007). Variations in the permafrost thermal regime in cold regions have exerted profound impacts on the local hydrology, the surface energy and moisture balance, carbon emission, engineering constructions, as well as on the whole ecosystem (Cheng & Zhao 2000, Nelson et al. 2001, Zhang et al. 2005, Zimov et al. 2006).

The permafrost area in the Qinghai-Tibet Plateau covers about 1.50 x 10^6 km^2 and is the largest mid-latitude permafrost zone in the world. This permafrost was formed during the late Pleistocene (Fig. 1). Research has shown that the permafrost has been degrading and shrinking in areal extent with a general tendency of warming during the Holocene (Jin et al. 2007). In this paper, we have summarized some recent observation results about the evolution of permafrost on the plateau.

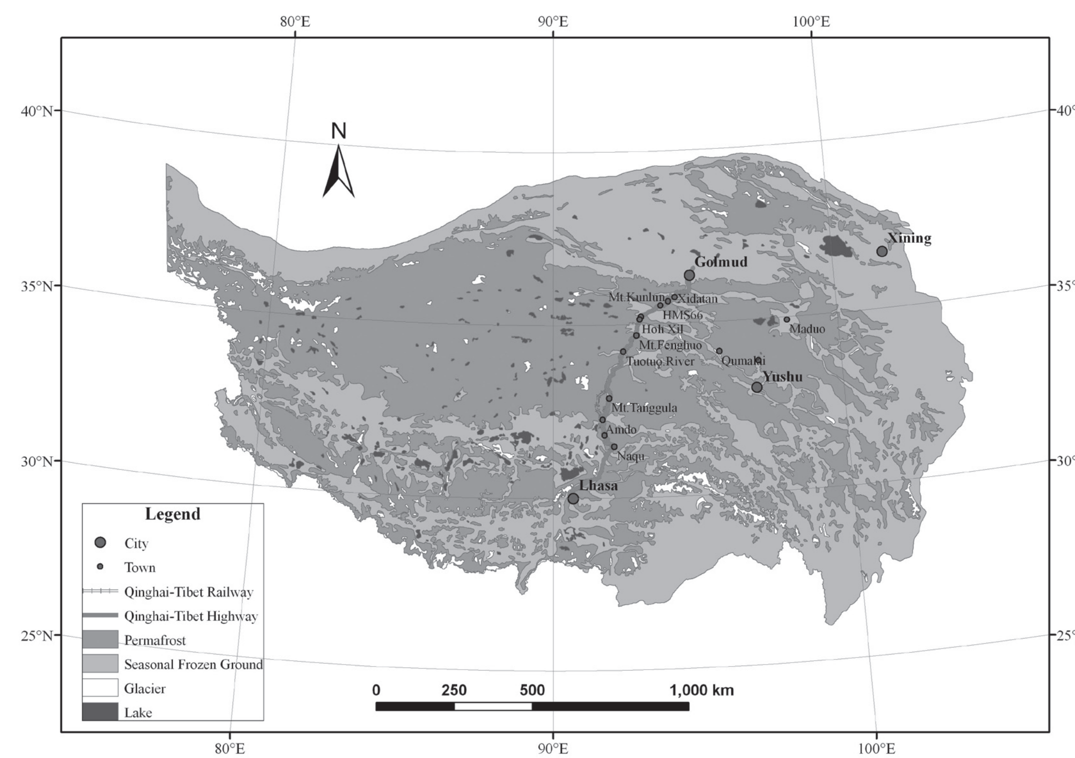

Figure 1. Permafrost distribution and the locations of study sites on the Qinghai-Tibet Plateau.

Site Conditions and Methods

Over the last 40 years Chinese researchers and engineers have established a permafrost monitoring network along the Qinghai-Tibet Highway (Fig 2). Eighteen boreholes, whose depths range from 20 to 127 m, have been drilled along the Qinghai-Tibet Highway to monitor the thermal regime of permafrost. Calibrated thermistor thermometer sensors were installed on cables at certain depth intervals and were put into these boreholes. Initially, soil temperatures at different levels were measured manually three times per month and then averaged over a year. The precision of the temperature data was estimated to be within 0.01°C. In 1998 automatic temperature data loggers were installed to collect temperature data at different depths. Since then the temperature readings have been automatically recorded 12 times per day at 2-hour intervals. We selected those sites whose measurements are continuous to be analyzed and discussed in this paper.

Furthermore, thirteen integrated monitoring sites were installed to collect soil temperature, moisture content, and heat flux data within the active layer. Some of these sites are close to the above-mentioned boreholes. Four automated weather stations and two eddy covariance systems were set up to measure parameters including air temperature, soil temperature and moisture content, precipitation, wind speed and direction, surface evaporation, radiation and CO_2 fluxes. All sites are in undisturbed natural conditions and represent the predominant types of landscape on the plateau. This paper focuses on the recent research carried out on the Qinghai-Tibet Plateau on permafrost warming and its environmental implications.

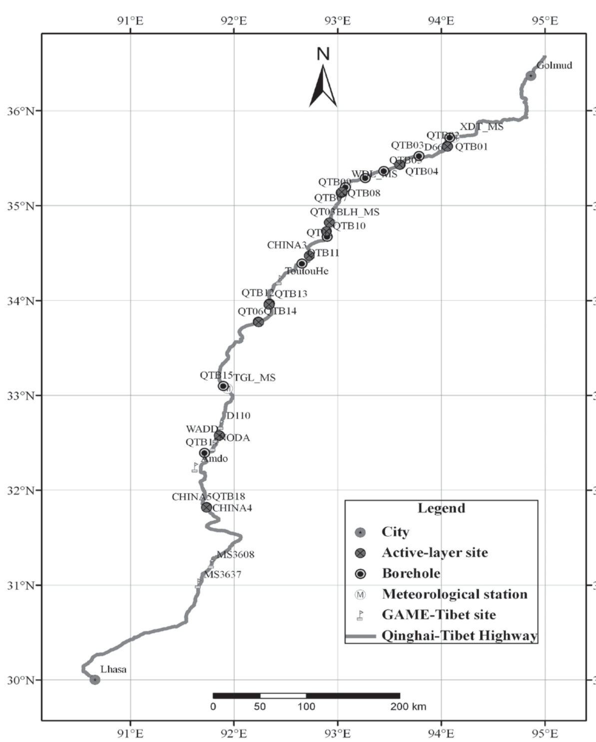

Figure 2. Permafrost monitoring network along the Qinghai-Tibet Highway.

Results and Analysis

It is apparent that permafrost on the Qinghai-Tibet Plateau has undergone severe degradation during the past decades. Various observation data indicates that the mean annual ground temperature has increased and that the active-layer has thickened; talik and thermokarst development and disappearance of sporadic permafrost has occurred in some regions.

Borehole drillings and testpit excavations on the plateau in the 1970s and 1990s indicated that the lower altitudinal limit of permafrost has uplifted by 50 to 100 m (Wang et al. 1997) (Table 1). Ground-penetrating radar investigations at the northern limit of the continuous permafrost zone on the plateau also showed an uplift of 25 m for the lower altitudinal limit in the past 20 years (Wu et al. 2005). In the 1960s ground temperature data taken from a borehole drilled in Xidatan, which is the northern lower limit of permafrost on the plateau, suggested the existence of permafrost at depths between 11.4 m and 16.0 m; but no frozen layer was observed at the same site in 1975 (Wang et al. 1996). The Amdo-Liangdaohe section of the Qinghai-Tibet Highway is located in the vicinity of the southern lower limit of the continuous permafrost zone on the plateau. The temperature observations from a 19.53 m deep borehole drilled in 1975 indicated that the permafrost table was at a depth of 3.5 m and that the permafrost thickness was about 6.5 m. However, temperature measurements in 1989 showed that the permafrost has disappeared (Zhao et al. 2004).

Observed ground temperature changes in the discontinuous permafrost regions on the plateau

The Xidatan site is located in the transitional area from the discontinuous permafrost zone to the continuous permafrost zone. Another 30 m deep borehole was drilled in 1998 as a long-term observation site. The borehole site is situated at a down-faulted basin in the west section of the Kunlun Mountains. The surficial geology consists of fluvial sands and gravel. The available meteorological data in 1976 showed that the mean annual air temperature was -2.9°C. We installed the thermistor thermometers (precision was

Table 1. Changes in the lower altitudinal limit of permafrost on the Qinghai-Tibet Plateau.

Site	Latitude	Lower altitudinal limit (m)		Uplift of altitude (m)
		1960s	1990s	
North slope of southern Mt. Qinghai	36°25′N	3650-3700	3700-3800	50-100
North slope of Mt. Heka'nanshan	35°49′N	3800-3840	3860-3900	60
North slope of Mt. Ngola	35°25′N	3850	3900	50
Southwest slope of Mt. Animaqing	34°35′N	4180	4250	70

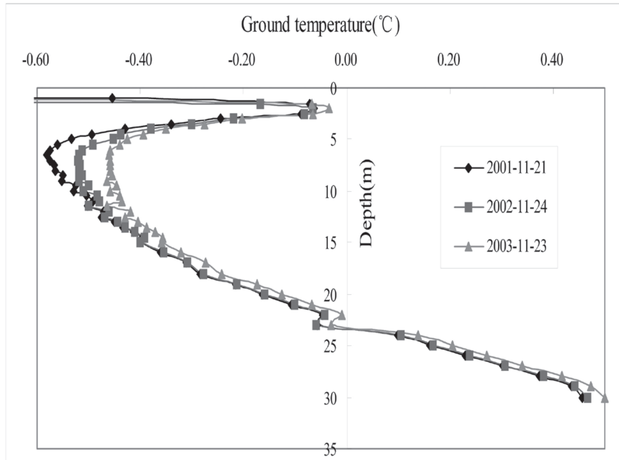

Figure 3. The changes of soil temperature at the Xidatan site.

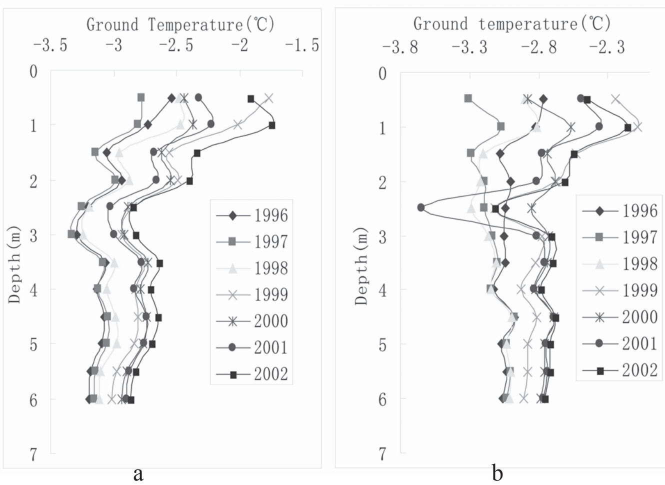

Figure 4. The changes of MAST at the Mt. Kunlun sites.

0.01°C) in the borehole. The available observation results in November of 2001 to 2003 indicated that the permafrost temperature had increased by 0.04~0.10°C on average (Fig. 3). The change in ground temperatures at a depth of 5 m to 8 m was estimated to be more than 0.10°C during the 3 years.

Observed ground temperature changes in the continuous permafrost regions on the plateau

Mt. Kunlun sites

In 1995 two boreholes were drilled to a depth of 6 m in 1995 in an undisturbed plain. The observation results indicated that the upper ground temperatures of permafrost were between -3.5°C and -2.0°C. The mean annual soil temperatures (MAST) in one borehole had increased by 0.50°C in the 7 years, which annual rate of increase in mean annual soil temperatures amounts to 0.086°C/yr. The MAST at a depth of 1 m had risen by 0.98°C. The ground temperatures at different levels showed a clear warming trend although there was some fluctuation (Fig. 4a). The MAST in the other borehole had increased by 0.34°C on average at an annual increase rate of 0.072°C/yr from 1996 to 2002 (Fig. 4b). The MAST at a depth of 1 m had risen by 0.66°C. We think the sudden decrease in the value of soil temperature at a depth of

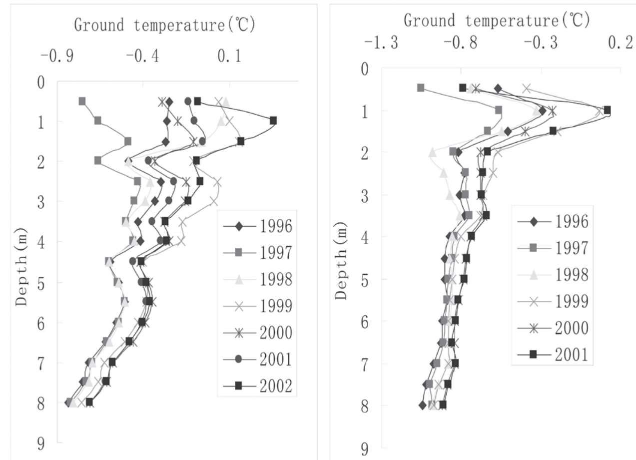

Figure 5. The changes of MAST at the HMS 66 sites.

2.5 m results from the un-recalibration or malfunction of the sensor. And the soil temperatures at both sites had increased greatly at depths of 0.5 m to 2.0 m.

HMS 66 sites

The HMS (Highway Maintenance Squad) 66 site is located in a plain near the Xieshui stream, a branch of the Chumaer River. The ground surface is covered by sand and gravel, and sand dunes can be found in this region. The observation records showed that the mean annual ground temperature in the borehole was approximately -0.6°C to -0.7°C. The mean annual soil temperatures in this site also displayed a warming tendency from 1996 to 2001. The collected observation data from two 8 m deep boreholes also showed that the soil temperatures in 7 years had increased by 0.11°C with an annual increasing rate of 0.030°C/yr at one borehole, and by 0.22°C with an annual increasing rate of 0.041°C/yr at the other borehole (Fig. 5). The mean annual soil temperatures were mostly higher than -1.0°C, which was delimited as high-temperature permafrost. From Figure 5 we can conclude that permafrost warming has taken place from 1996 to 2001.

Hoh Xil site

An 8 m deep borehole was drilled in 1995 to measure the ground temperatures at this site. The results showed that the MAST is between -1.3°C and -2.2°C. The ground temperatures had increased by 0.26°C ~ 0.89°C in the 7 years; the annual increase rate amounted to 0.098°C/yr. The MAST above 5 m depth had increased by 0.67°C, while the MAST between the 5 m to 8 m levels by 0.34°C during the 7 years. Soil temperatures at different levels showed a clear warming trend (Fig. 6).

Wudaoliang site and Mt.Fenghuo site

The Wudaoliang site is located in hilly land with an elevation of about 4735 m a.s.l. The soil profiles are composed of eolian and solifluction deposits. The permafrost table is located between 1.5 m to 1.8 m in this site, and the vegetation is alpine meadow with the coverage of about 50%

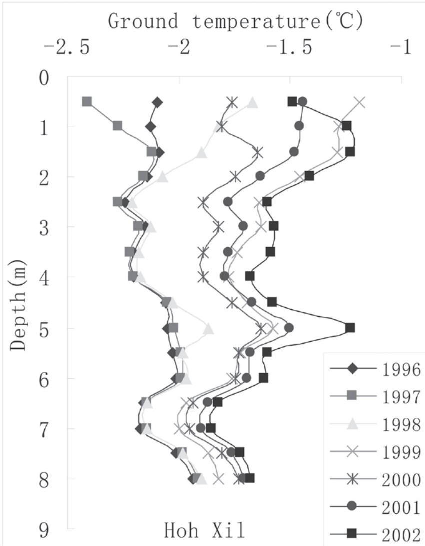

Figure 6. The changes of MAST at the HMS 66 sites.

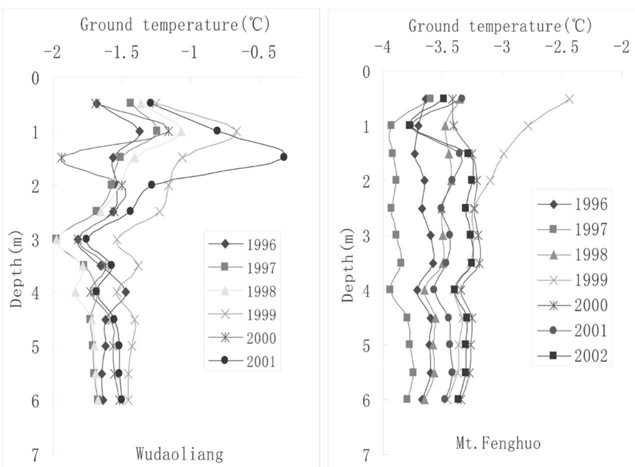

Figure 7. The changes of MAST at the Wudaoliang site and the Mt. Fenghuo site.

(Zhao et al. 2000). Observation results from the 6 m deep borehole at theWudaoliang site indicated that the MAST has increased by 0.07~0.57°C, from 1996 to 2001 with an annual increasing rate of 0.047°C/yr (Fig. 7). The drastic fluctuation in the value of soil temperature at a depth of 1.5 m in 2000 and 2001 results from the malfunction or the un-recalibration of the sensor.

The Mt. Fenghuo site is located in the hinterland of the Qinghai-Tibet Plateau. The permafrost temperatures at the Mt. Fenghuo site were lower than -3.5°C, which were delimited as low-temperature permafrost. The MAST at the Mt. Fenghuo site has increased by 0.32°C on average with an annual increasing rate of 0.065°C/yr (Fig. 7).

Mt.Tanggula sites

There are two boreholes whose ground temperatures were very close to 0°C drilled to the south of Tanggula Mountain. The observation results from a 10.8 m deep borehole indicated that the MAST had increased by 0.01°C~0.07°C from 1999

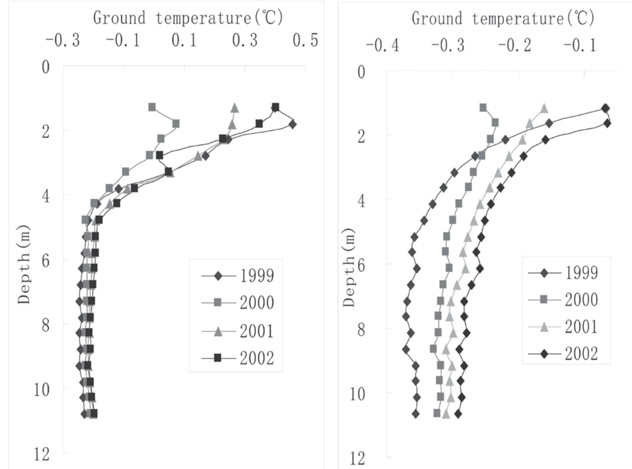

Figure 8. The changes of MAST at the Mt.Tanggula sites.

to 2002. The observation results from another 10.65 m deep borehole indicated that the MAST had increased by 0.06~0.10°C over the 4 years. The annual increasing rates of MAST were 0.011°C/yr and 0.027°C/yr respectively (Fig. 8). At both boreholes, mean annual temperatures of the lower layer of permafrost have changed steadily, and permafrost will disappear if the warming continues.

The environmental implications of permafrost degradation on the plateau

The experiments to measure the emission of CH_4 and CO_2 from the permafrost regions of the plateau indicated that the CO_2 exchange between the ground and atmosphere is characterized by emission, while the CH_4 exchange is characterized by absorption (Lin et al. 1996). Jin et al. (1999) estimate that methane emission from the wetland on the plateau amounts to 0.7–1.0 Tg per year.

Permafrost degradation closely interacts with hydrological and thermal processes near the ground surface, as well as with other components of the ecosystem. Permafrost degradation also results in the lowering of local water tables and lake water levels and the shrinking of wetlands and grazing grasslands (Cheng & Zhao 2000). Cao et al. (2006) concluded that the deterioration of marshy meadows at the source area of the Yellow River results from the lowering supra-permafrost water table.

Climatic Change on the Qinghai-Tibet Plateau

Using mean monthly air temperature data for 1961–2000 at 101 weather stations located all over the plateau and adjacent regions (Fig. 9), we analyzed the decadal changes of mean annual air temperature in the study regions during these 40 years. The results indicated that there are 19 stations where the mean annual air temperature has increased by more than 1.0°C, 50 stations where it increased by 0.5°C–1.0°C, and 25 stations where the mean annual air temperature had increased by 0.0°C–0.5°C (Fig. 9).

Among the above-mentioned 101 weather stations, we analyzed the data of 4 stations located in permafrost regions

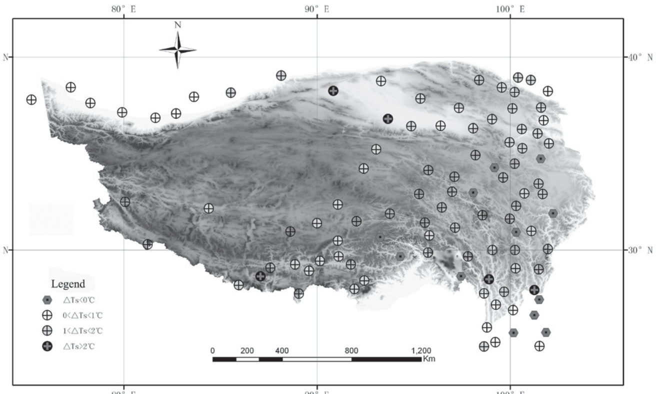

Figure 9. Location of the 101 weather stations with mean monthly air temperature observations on the Qinghai-Tibet Plateau and adjacent regions.

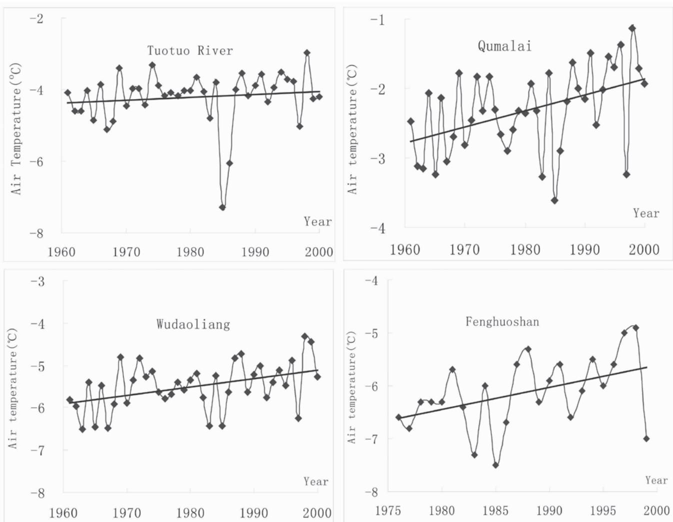

Figure 10. The changes of mean annual air temperature during the last several decades at the stations located in permafrost regions.

to reveal the climate changes occurring in permafrost zones. The results showed the mean annual air temperature in Tuotuo River increased by 0.46°C, 0.79°C in Qumalai, 0.68°C in Wudaoliang from 1961 to 2000, and 0.65°C in Mt. Fenghuo from 1975 to 2000 (Fig. 10). The climatic warming has occurred predominantly in winter. The mean annual increasing rates of air temperature at those 4 stations amounted to 0.022°C/yr. The dramatic increase of air temperature in winter decreased the seasonally frozen depth and deepened the active layer, which finally led to the permafrost degradation. With no doubt the extensively occurring climatic warming during the last decades is one of the principal factors leading to permafrost degradation on the plateau.

Conclusions

Observation results from most sites on the Qinghai-Tibet Plateau indicate that extensive permafrost degradation has taken place during the last years. In the northern and southern lower limits of the discontinuous permafrost regions, permafrost has thinned and disappeared in some areas, and the lower limit of permafrost has risen in altitude. In the hinterland of the plateau where continuous permafrost regions predominate, the ground temperatures have displayed an obvious warming tendency in recent years. In general, the annual rate of increase in MAST is 0.042°C to 0.065°C/yr for low-temperature permafrost (mean annual ground temperature is lower than -3.0°C), 0.016°C to 0.098°C/yr for the permafrost whose mean annual ground temperature is between -0.5°C and -3.0°C, and 0.011°C to 0.041°C/yr for high-temperature permafrost (mean annual ground temperature is higher than -0.5°C). Previous studies indicated that freezing and thawing processes have great impacts on carbon absorption and emission on the plateau. In the mean time, the regional lowering of ground water tables triggered by degrading permafrost is likely mainly responsible for the deteriorating environment on the plateau, as evidenced by dropping lake water levels, shrinking wetlands, and degenerating grasslands.

Based on the analysis of the decadal changes of mean annual air temperature, we revealed that extensive climatic warming has occurred on the plateau during the last decades. Records from weather stations in permafrost regions also indicated that mean annual air temperature has increased especially in winter. The observed climatic warming could be responsible for permafrost degradation.

Acknowledgments

We would like to express our gratitude to the Cryosphere Research Station on the Qinghai-Tibet Plateau, Chinese Academy of Sciences for the observation data collection and logistic support. Especially we thank Dr. Stephen Robinson and another anonymous reviewer for their constructive comments and suggestions to improve this manuscript. This work was supported by a grant from the Major State Basic Research Development Program of China (973 Program, No.2007CB411506) and the Knowledge Innovation Project of the Chinese Academy of Sciences (No. KZCX3-SW-345 and KZCX3-SW-351).

References

Cao, W., Wan, L., Zeng, Y., Hu, F. & Chen, J. 2006. Impacts of global warming on the eco-environment in the headwater region of the Yellow River. *Earth Science Frontiers* 13(1): 40-47.

Cheng, G. & Wu, T. 2007. Responses of permafrost to climate change and their environmental significance, Qinghai-Tibet Plateau. *Journal of Geophysical Research* 112: F02S03, doi: 10.1029/2006JF000631.

Cheng, G. & Zhao, L. 2000. The problems associated with permafrost in the development of the Qinghai-Xizang Plateau. *Quaternary Science* 20(6): 521-531.

Isaksen, K., Sollid, J.L., Holmlund, P. & Harris, C. 2007. Recent warming of mountain permafrost in Svalbard and Scandinavia. *Journal of Geophysical Research*, 112: F02S04, doi:10.1029/2006JF000522.

Jin, H., Chang, X. & Wang S. 2007. Evolution of permafrost on the Qinghai-Xizang (Tibet) Plateau since the end of the late Pleistocene. *Journal of Geophysical Research* 112: F02S09, doi:10.1029/2006JF000521.

Jin, H. & Cheng, G. 1997. Methane emissions in permafrost regions. *Journal of Glaciology & Geocryology* 12(3): 276-283.

Lin, Q., Jin, H., Cheng, G. & Li, N. 1996. CH_4 and CO_2 emission from permafrost surface in Wudaoliang in the Tibetan Plateau. J*ournal of Glaciology & Geocryology* 18(4): 325-330.

Nelson, F., Anisimov, O. & Shiklomanov, N. 2001. Subsidence risk from thawing permafrost. *Nature* 410: 889-890.

Osterkamp, T.E. 2007. Characteristics of the recent warming of permafrost in Alaska. *Journal of Geophysical Research* 112: F02S02, doi:10.1029/2006JF000578.

Walker, G. 2007. A world melting from the top down. *Nature* 446: 718-721.

Wang, S. 1997. Study of permafrost degradation in the Qinghai-Xizang plateau. *Advance in Earth Science* 12(2): 164-167.

Wang, S., Zhao, X. & Guo D. 1996. Response of permafrost to climate change in the Qinghai-Tibet Plateau. *Journal of Glaciology & Geocryology* 18(Supplement): 157-165.

Wu, T., Li, S., Cheng, G. & Nan Z. 2005. Using ground-penetrating radar to detect permafrost degradation in the northern limit of permafrost area on the Tibetan Plateau. *Cold Regions Science and Technology* 41: 211-219.

Zhang, T., Frauenfeld, O.W., Serreze, M.C., Etringer, A.J., Oelke, C., McCreight, J.L., Barry, R.G., Gilichinsky, D., Yang, D., Ye, H., Feng, L. & Chudinova, S. 2005. Spatial and temporal variability in active layer thickness over the Russian arctic drainage basin. *Journal of Geophysical Research-Atmospheres* 110: D16101, DOI:10.1029/2004JD005642.

Zhao, L., Cheng, G. & Ding Y. 2004. Studies on frozen ground of China. *Journal of Geographical Sciences* 14(4): 411-416.

Zhao, L., Cheng, G., Li, S., Zhao, X. & Wang, S. 2000. Thawing and freezing processes of active layer in Wudaoliang region of Tibetan Plateau. *Chinese Science Bulletin* 45(23): 2181-2186.

Zimov, S., Schuur, E. & Chapin, F. 2006. Permafrost and the global carbon budget. *Nature* 312: 1612-1613.

Impact of Freezing on Water Migration in Silty Clay Samples

Shu-ping Zhao
State Key Laboratory of Frozen Soil Engineering, CAREERI, CAS, Lanzhou, Gansu 730000, China
Jian-feng Zheng
State Key Laboratory of Frozen Soil Engineering, CAREERI, CAS, Lanzhou, Gansu 730000, China
Wei Ma
State Key Laboratory of Frozen Soil Engineering, CAREERI, CAS, Lanzhou, Gansu 730000, China
Yi-bin Pu
State Key Laboratory of Frozen Soil Engineering, CAREERI, CAS, Lanzhou, Gansu 730000, China

Abstract

A group of tests were conducted to study the impact of freezing on the re-distribution of water and on dry density in silty clay soil samples. Tests determined that freezing has nearly no influence on dry density. Tests also show that, in those standard samples with evenly distributed water content initially, the water content will be re-distributed following freezing. The extent of water re-distribution in a sample is determined by the soil type, the state of saturation, and the freezing method. For water-unsaturated Lanzhou Loess samples, a great amount of water appears to have migrated during radial freezing or axial freezing, and the maximum range of water content in one specimen reaches 4.46%. For water-saturated Lanzhou Loess and water-unsaturated Beiluhe Soil frozen by the axial method or the radial method, and for water-saturated Beiluhe Soil specimens frozen by the axial freezing method, water migration is minor and the range of water content in each specimen is less than 2%.

Keywords: axial freezing; radial freezing; silty clay; water migration; water-saturated; water-unsaturated.

Introduction

Laboratory mechanical experiments are usually performed to evaluate mechanical properties of frozen soil for geotechnical engineering as well, as to obtain a variety of parameters for the modeling of constitutive relationship. Standard cylindrical soil samples with a diameter and a length being twice the diameter are usually used in laboratory mechanical experiments. The soil samples include two types: undisturbed samples which are drilled in-situ directly, and remoulded samples which are made and frozen under artificial cryogenic environment indoors. A large number of studies show that water migration toward freezing front will occur during the soil freezing process (Solomatin & Xu 1994, Butler et al. 1996, Spaans & Baker 1996, Newman & Wilson 1997, Zhao et al. 1997, Stahli et al. 1999, Dawson et al. 1999, Brouchkov 2000, Brouchkov 2002, Iwata & Hirota 2005, Qi et al. 2006). Even if rapidly freezing method and close system are applied to making remoulded frozen soil samples, there still exists slight moisture migration. The effect caused by this migration might be possibly ignored if the results of mechanical tests on remoulded frozen soil samples are used in engineering. However, in theoretic modeling which assumes an ideally evenly moisture distribution throughout soil sample, a more precise measurement is required. In this context moisture migration should be taken into account. This paper will be dedicated to the study of moisture redistribution in remoulded frozen silty clay samples in association with a specific specimen-preparing method and varying freezing approaches.

Table 1. The physical properties of test soils.

	Liquid limit	Plastic limit	Plastic index
Lanzhou Loess	29.36	14.92	14.44
Beiluhe Soil	32.88	17.50	15.38

Test Preparation

Materials

The materials used in this investigation are remoulded silty clay from the Donggang town of Lanzhou City, termed *"Lanzhou Loess"* in this paper, and from the Beiluhe area of the Qinghai-Tibet plateau, referred to here as "*Beiluhe Soil*." Their physical properties and particle distribution curves are shown in Table 1 and Figure 1, respectively. Both of them are classified as CL based on the Unified Soil Classification System.

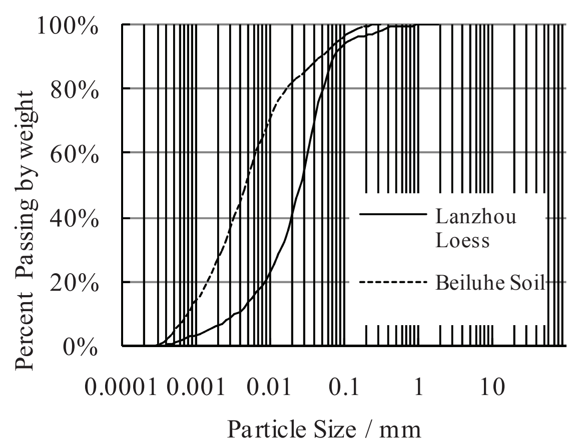

Figure 1. The particle distribution curves of test soils.

Testing apparatus

All samples were prepared using the Standard Specimen Instrument (Fig. 2a) designed by Zhao (1998) consisting of mainframe, control system, mould, and drain system. Press-poles and press-caps of various sizes are assembled with high precision load sensors. The maximum loading capacity is up to 180 kN. In this test, a press-pole with a loading capacity of 30 kN was used. The nominal size of the soil specimen is 61.8 mm in diameter by 125 mm long.

Moulding

Our earlier tests (Zheng et al. in press) found that the dry-density distribution in samples prepared by the pressure method was better than that in samples prepared by the layered-bumping method which has been widely adopted in literature (Zhu & David 1987, Zhao et al. 1998, Yang et al. 2000). In this paper the pressure method is used to make soil samples.

First, raw soil samples were air-dried, ground and sifted with a 2 mm sieve. Second, distilled water was added to dry soil to form a moist soil with the equired water content. After storage overnight to allow for moisture equilibration, the moist soil was carefully put into the mould. Third, the press-pole was descended to compact the moist soil, with the descending velocity adjusted through the control system. A higher velocity was used at the very beginning, and then at a constant but lower velocity after the press cap touches soil sample. The pressing lasted a certain time, after which the sample was turned over and pressed with the same lower speed. The overall pressing time periods are 8 h and 4 h, respectively, for Lanzhou Loess and Beiluhe Soil. In this way, water-unsaturated specimens can be obtained.

After compaction, partial specimens were deaerated under a vacuum of 73 mm Hg and then water saturated with distilled water for more than 12 h. The set-up for Water-saturation is shown in Figure 2b.

Both water-unsaturated and water-saturated specimens were put into special moulds. The moulds were then placed into a freezing cabinet and quickly frozen in a close system (without water supply) with an upper boundary temperature of lower than -30°C. Two freezing approaches were used: axial freezing and radial freezing. The axial freezing approach is to use a heat-insulated sponge to pack peripheral and bottom parts of the moulds so that specimens are frozen downwards. The radial freezing approach places plastic caps to both ends of a specimen, causing the specimen to be frozen from the exterior to the center. After freezing more than 24 h, the specimens were removed from the moulds.

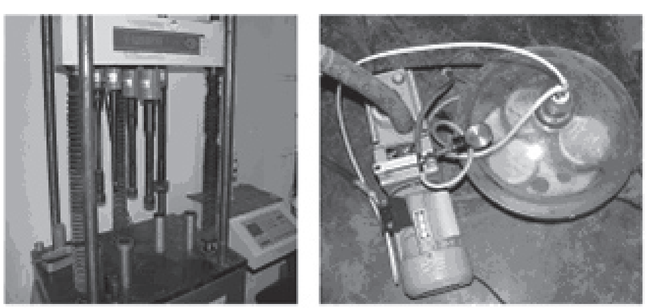

(a) (b)

Figure 2. Standard specimen instrument and set-up for water-saturation.

Testing procedure

Each specimen was partitioned vertically into four layers to test the dry density. The inner part (symbolized as part A in Fig. 3) and outer part (symbolized as part B in Fig. 3) of each layer were detached to test water content. For each specimen, four dry density values and eight water content values can be obtained.

Test Results

The dry density distribution in specimens

To study the dry density distribution, the mean value (ME), standard deviation (SD) and range (R) for each specimen were calculated and shown in Tables 2 and 3.

Tables 2 and 3 show a similar change trend of dry density in Lanzhou Loess and Beiluhe Soil from the unfrozen to frozen states. The standard deviations observed in all specimens are small. Moreover, there are minor variations in standard deviation for each group of specimens (unfreezing, axial and radial freezing), which proves that the freezing process has nearly no influence on dry density distribution.

The water content distribution in specimens

To analyze the water content distribution, the mean value (ME), standard deviation (SD) and range (R) were calculated and are shown in Tables 4 and 5.

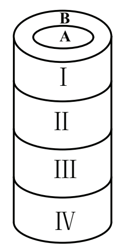

Figure 3. The sampling scheme for testing dry density and water content.

Table 2. The dry density (g/cm^3) distribution in Lanzhou Loess.

		Water unsaturated				Water saturated			
Specimen no.		1#	2#	3#	4#	1#	2#	3#	4#
Un-freezing	ME	1.725	1.705	1.705	1.698	1.690	1.693	1.700	
	SD	0.015	0.022	0.015	0.015	0.014	0.019	0.019	
	R	0.03	0.06	0.04	0.04	0.04	0.05	0.05	
Radial freezing	ME	1.761	1.761			1.734	1.715	1.691	1.687
	SD	0.018	0.006			0.016	0.008	0.009	0.006
	R	0.044	0.015			0.04	0.021	0.025	0.015
Axial freezing	ME	1.763	1.757	1.753	1.744	1.721	1.723		
	SD	0.009	0.003	0.009	0.001	0.003	0.017		
	R	0.024	0.007	0.025	0.027	0.008	0.042		

Table 3. The dry density (g/cm^3) distribution in Beiluhe Soil.

		Water unsaturated				Water saturated			
Specimen no.		1	2	3	4	1	2	3	4
Un-freezing	ME	1.863	1.850	1.803	1.863	1.813	1.805	1.747	1.761
	SD	0.008	0	0.029	0.004	0.011	0.005	0.006	0.008
	R	0.02	0	0.07	0.01	0.03	0.01	0.017	0.02
Radial freezing	ME	1.768	1.769			1.802	1.793	1.742	1.762
	SD	0.016	0.019			0.013	0.017	0.013	0.011
	R	0.037	0.045			0.031	0.044	0.031	0.028
Axial freezing	ME	1.775	1.768			1.792	1.805	1.801	1.792
	SD	0.011	0.018			0.008	0.005	0.017	0.009
	R	0.03	0.03			0.021	0.013	0.04	0.023

Table 4. The water content (%) distribution in Lanzhou Loess.

		Water unsaturated				Water saturated			
Specimen no.		1	2	3	4	1	2	3	4
Un-freezing	ME	16.29	14.30	14.15	14.49	21.79	21.75	21.68	
	SD	0.35	0.15	0.17	0.05	0.54	0.66	0.72	
	R	0.95	0.47	0.54	0.19	1.57	2.11	2.40	
Radial freezing	ME	15.56	15.68			20.34	20.87	21.65	21.37
	SD	1.31	1.56			0.45	0.43	0.39	0.42
	R	3.20	3.48			1.4	1.49	1.19	1.44
Axial freezing	ME	15.34	15.65	15.33	14.98	20.67	20.52		
	SD	1.54	1.73	1.28	1.52	0.27	0.49		
	R	3.91	4.46	3.33	3.61	0.77	1.41		

Table 4 shows that in the water-unsaturated Lanzhou Loess samples, the initial water content distributes evenly, and R of water content for each sample is less than 1%. In the process of freezing, a significant amount of water migration was observed with both the radial and axial freezing approaches. The maximum difference of water content between different positions of a specimen can reach up to 4.46%. This difference will make sense, especially when we study the impact of water content on frozen soil mechanical or thermal characteristics through indoor experiments. Therefore, in such a case, we should take into account water content variations inside a specimen rather than using simple mean water content.

Table 4 also suggests that the amounts of SD and R in the water-saturated state are larger than those in water-unsaturated for Lanzhou Loess. However, after axial or radial freezing, SD and R of water content will decrease. Each R for samples of frozen water-saturated Lanzhou Loess is less than 1.5%, indicating to some degree that moisture in frozen water-saturated Lanzhou Loess is evenly distributed. These results are in accordance with the conclusion of Liu et al. (2002).

Table 5 shows the initially even water content distribution in water-unsaturated Beiluhe Soil, with R of water content for each sample being less than 1%. Only minimal water migration was observed during the axial or radial freezing process. The R of water content for each sample is still under 1% after freezing.

Table 5. The water content (%) distribution in Beiluhe Soil.

		Water unsaturated				Water saturated			
Specimen no.		1	2	3	4	1	2	3	4
Un-freezing	ME	16.00	16.28	16.33	16.12	18.54	18.63	19.96	19.51
	SD	0.23	0.13	0.13	0.23	0.75	0.21	0.63	0.37
	R	0.71	0.45	0.46	0.73	2.29	0.70	1.67	1.15
Radial freezing	ME	15.30	15.50			18.69	19.02	19.61	19.18
	SD	0.24	0.23			0.68	0.68	1.05	0.86
	R	0.59	0.57			1.95	1.71	2.81	2.44
Axial freezing	ME	15.82	15.82			18.90	18.55	18.44	18.68
	SD	0.32	0.28			0.64	0.56	0.52	0.41
	R	0.97	0.71			1.93	1.53	1.63	1.43

Table 6. The mean value and range of water content (%) for the inner and outer parts of Lanzhou Loess.

	Specimen no.		Unfreezing		Radial freezing		Axial freezing	
			ME	R	ME	R	ME	R
Water unsaturated	1	Inner	16.47	0.88	14.31	0.60	14.03	2.80
		Outer	16.10	0.48	16.81	1.33	16.65	0.93
	2	Inner	14.33	0.35	14.13	0.24	14.21	3.18
		Outer	14.27	0.41	17.23	0.59	17.10	1.31
	3	Inner	15.22	0.47			14.22	2.07
		Outer	15.06	0.29			16.45	0.99
	4	Inner	14.51	0.13			13.75	2.84
		Outer	14.47	0.12			16.22	0.78
Water saturated	1	Inner	21.93	1.37	20.29	0.95	20.70	0.74
		Outer	21.65	1.44	20.39	1.40	20.68	0.59
	2	Inner	21.94	1.30	20.80	0.57	20.54	1.18
		Outer	21.55	1.97	20.95	1.49	20.50	1.34
	3	Inner	21.95	1.32	21.68	0.99		
		Outer	21.40	2.19	21.62	1.15		
	4	Inner			21.08	0.69		
		Outer			21.65	0.95		

Table 5 also shows that SD and R for water-saturated Beiluhe Soil samples are larger than those for water-unsaturated samples. The SD and R of water content will increase after radial freezing, but decrease after axial freezing. The R for water-saturated Beiluhe Soil samples frozen by the axial freezing approach is less than 2%.

The water migration in specimens

To study the direction of water migration, the water content of the inner part and outer parts were collected. The mean value (ME) and range (R) were then calculated, and results are shown in Tables 6 and 7.

A number of similar change trends in water content can be found for these two types of soils in Tables 6 and 7. First, for unfrozen water-unsaturated samples, there is small variation of the mean water content between inner and outer positions of a specimen. Meanwhile, the R of water content in both inner and outer parts is rather small. After water-saturating, a similarly small variation of mean value of water content

Table 7. The mean value and range of water content (%) for the inner and outer parts of Beiluhe Soil.

	Specimen no.		Unfreezing		Radial freezing		Axial freezing	
			ME	R	ME	R	ME	R
Water unsaturated	1	Inner	16.05	0.51	15.07	0.16	15.57	0.7
		Outer	15.95	0.71	15.53	0.13	16.07	0.39
	2	Inner	16.37	0.30	15.28	0.14	15.59	0.53
		Outer	16.19	0.22	15.73	0.12	16.05	0.23
	3	Inner	16.42	0.19				
		Outer	16.25	0.32				
	4	Inner	16.28	0.46				
		Outer	15.95	0.38				
Water saturated	1	Inner	18.74	1.84	18.06	0.43	18.33	0.84
		Outer	18.35	1.97	19.32	0.93	19.46	0.69
	2	Inner	18.81	0.31	18.37	0.22	18.02	0.34
		Outer	18.45	0.26	19.66	0.68	19.07	0.61
	3	Inner	20.41	1.4	18.70	0.52	18.02	0.74
		Outer	19.52	0.13	20.52	1.81	18.87	0.64
	4	Inner	19.58	1.13	18.44	0.83	18.34	0.31
		Outer	19.44	0.79	19.93	1.38	19.02	0.77

between inner and outer parts was preserved. But a larger R of water content at either the inner or outer parts appears, proving that the degree of water supply at different position along the axial direction differs. Secondly, for all unfrozen samples, the mean value for the central inner part is slightly larger than that for the outer part, while for all frozen samples, the mean value for the outer part is larger than that for the inner part, implying that water moves outwards during the freezing process.

Table 6 shows that when the water-unsaturated Lanzhou Loess samples were radial frozen, there is a distinguishing difference between mean water content in the inner and outer parts of a same specimen, along with invariant R statistics in those parts. This observation indicates water has migrated outwards along the radial direction. When the water-unsaturated samples were axially frozen, not only was there is great difference between ME at inner and outer parts, but also R at both parts are large, proving water has migrated along radial and axial direction at the same time.

Table 6 also shows that, when water-saturated Lanzhou Loess samples were frozen by the radial or axial freezing approach, there is still little difference between the ME of the inner and outer parts; moreover, R in both parts decreases. These results prove that water moves mainly along the axial direction and makes the water content distribution more uniform.

Table 7 shows that, when the water-unsaturated Beiluhe Soil samples were frozen by radial or axial freezing, there is still little variation between the ME in the inner and outer parts, and that R in both parts is still small. This proves that there is nearly no water migration during the freezing process.

Table 7 also shows that when the water-saturated Beiluhe Soil samples were frozen by radial freezing, the difference between the mean value of water content of the inner and outer parts clearly increase, while R in both parts is still as much as that for unfrozen water-saturated samples. This proves that the water moves mainly along the radial direction.

Furthermore, the following result can also be observed in Table 7. When water-saturated Beiluhe Soil samples were frozen by axial freezing, the variation between the mean value of the water content in the inner and outer parts increases slightly, and R in both parts decrease.

The influence of soil type on water migration

If specimens are prepared by the pressure method, the longer the pressing time, the more uniform the samples will be. The pressing time is 8h and 4h for Lanzhou Loess and Beiluhe Soil, respectively, which proves that it is easier to obtain uniform specimens with Beiluhe Soil.

For water-unsaturated samples, there is obvious water migration in Lanzhou Loess, and there is nearly no water migration in Beiluhe Soil. The main reason can be expressed as follow. The particle-size analysis results show that silty particles and clay particles account for 77.73% and 13.55% by weight in Lanzhou Loess, while accounting for 40.79% and 52.78% in Beiluhe Soil. Lanzhou Loess mainly consists of silty particle, which can form better channel for water migration. In Beiluhe Soil, the percentage of silty grain and clay grain both occupy higher proportions. The grain gradation is good; it is therefore difficult to form channels for water migration.

For water-saturated samples, water migration in Beiluhe Soil is more obvious than that in Lanzhou Loess. Beiluhe Soil contains more fine grains with lower thermal conductivity, so the freezing front penetrates more slowly during freezing and there is enough time for water migration.

If those samples with water content R of less than 2% can be considered as feasible, then, both water-saturated Lanzhou Loess and water-unsaturated Beiluhe Soil--frozen by the axial or radial freezing approach--can meet this requirement. The water-saturated Beiluhe Soil specimens frozen by the axial freezing approach also meets this requirement. However, for the water-unsaturated Lanzhou Loess, the internal unevenness of water content must be considered.

Conclusions

To summarize the test results, the following conclusion can be drawn.

The water content distribution in specimens prepared by the pressure method is uniform. The degree of water supply at different position along the axial direction differs during the water- saturating process.

For all unfrozen samples, the mean value of water content for the inner part is slightly larger than that for the outer part, while for all frozen samples, the mean value for the outer part is larger than that for the inner part, implying that water moves outward during the freezing process.

The freezing process has nearly no influence on dry density distribution.

For water-unsaturated Lanzhou Loess samples, in the process of freezing a significant amount of water migration was observed with both the radial and axial freezing approaches. The maximum difference in water content between different positions of a specimen can be up to 4.46%. This difference will make sense, especially when we study the impact of water content on frozen soil mechanical or thermal characteristics, through indoor experiments. Therefore, in such cases, we should take into account internal water content variation rather than simple average water content of a specimen.

For water-saturated Lanzhou Loess and water-unsaturated Beiluhe Soil, proper specimens can be obtained by the axial or radial freezing approaches. The water-saturated Beiluhe Soil specimens frozen by the axial freezing method also meets the requirement.

Acknowledgments

The project is supported by the National Natural Science Foundation of China (No. 40501016), the National Natural Science Fund for Talent Training in Basic Research (No. J0630966), and the Western Project Program of the Chinese Academy of Sciences (No. KZCX2-XB2-10).

References

Brouchkov, A. 2000. Salt and water transfer in frozen soils induced by gradients of temperature and salt content. *Permafrost andPperiglacial Processes* 11(2): 153-160.

Brouchkov, A. 2002. Nature and distribution of frozen saline sediments on the Russian Arctic coast. *Permafrost and Periglacial Processes* 13(2): 83-90.

Butler, A.P., Burne, S. & Wheater, H.S. 1996. Observations of 'freezing-induced redistribution' in soil lysimeters. *Hydrological Processes* 10(3): 471-474.

Dawson, R. Sego, D. & Pollock, G. 1999. Freeze-thaw dewatering of oil sands fine tails. *Canadian Geotechnical Journa*l 36(4): 587-598.

Iwata, Y. & Hirota, T. 2005. Monitoring over-winter soil water dynamics in a freezing and snow-covered environment using a thermally insulated tensiometer. *Hydrological Processes* 19(15): 3013-3019.

Liu, Z.L., Li, H.S. & Zhu, Y.L. 2002. A distinguish model for initial and additional micro-damages on frozen soil. *Journal of glaciology and geocryology* 24(5): 676-680.

Newman, G.P. & Wilson G.W. 1997. Heat and mass transfer in unsaturated soils during freezing. *Canadian Geotechnical Journa*l 34(1): 63-70.

Qi, J.L., Vermeer, P.A. & Cheng, G.D. 2006. A review of the influence of freeze-thaw cycles on soil geotechnical properties. *Permafrost and Periglacial Processes* 17(3): 245-252.

Solomatin, V.I. & Xu, X.Z. 1994. Water migration and ice segregation in the transition zone between thawed and frozen soil. *Permafrost and Periglacial Processes* 5(3): 185-190.

Spaans E.J.A. & Baker, J.M. 1996. The soil freezing characteristic: Its measurement and similarity to the soil moisture characteristic. *Soil Science Society of America Journal* 60(1): 13-19.

Stahli, M., Jansson, P.E. & Lundin, L.C. 1999. Soil moisture redistribution and infiltration in frozen sandy soils. *Water Resource Research* 35(1): 95-103.

Yang, S.L., Sandven, R. & Lin, L. 2000. Improved preparing technique of silt sample. *Chinese Journal of Geotechnical Engineering* 22(3): 379-380.

Zhao, J.J. 1998. *Development of standard specimen instrument and frost heave model* (Article for the Degree of Master). Lanzhou: Lanzhou Glacier and Frozen Soil Research Institute, Chinese Academy of Science.

Zhao, L.T., Gray, D.M. & Male, D.H. 1997. Numerical analysis of simulationeous heat and mass transfer. *Journal of Hydrology* 200(1-4): 345-363.

Zhao, Z.Y., Zhou, C.E. & Cao, X.R. The simple sample-preparing method and its application in engineering. *GuangDong GongLu JiaoTong* 93(1): 57-60.

Zheng, J.F., Zhao, S.P & Ma, W. Study on the specimen-preparing method for remoulded silty clay samples. *Journal of Glaciology and Geocryology (*in press).

Zhu, Y.L. & David, L.C. 1987. *Creep and strength behavior of frozen silt in uniaxial compression*. U.S. Army Cold Regions Research and Engineering Laboratory, CRREL Report 87-10: 3-6.

Variation of CO_2 Concentrations in the Active Layer in Alpine Grasslands Soil on the Qinghai-Tibet Plateau

Yong-hua Zhao
Cold and Arid Regions Environment and Engineering Research Institute, CAS; Observation and Research Station of Qinghai-Tibet Plateau, CAREERI, CAS, Lanzhou Gansu730000, China

Lin Zhao
Cold and Arid Regions Environment and Engineering Research Institute, CAS; Observation and Research Station of Qinghai-Tibet Plateau, CAREERI, CAS, Lanzhou Gansu730000, China

Tian-yun Wu
Cold and Arid Regions Environment and Engineering Research Institute ,CAS; Observation and Research Station of Qinghai-Tibet Plateau, CAREERI, CAS, Lanzhou Gansu730000, China

Abstract

CO_2 concentrations from 0 to 180 cm in active layer soil were measured by static dark enclosed chamber technique from January in 2006 to January in 2007 in alpine grassland located on the Qinghai-Tibet Plateau. Results revealed: (1) CO_2 concentrations increasing gradually from 0 cm to 140 cm depth, and feebly decreasing from 140 cm to 180 cm. The ranges of CO_2 concentrations changed successively from 1138 to 3162 ppm. (2)Seasonal variations from 0 to 100 cm depth showed the highest concentrations occurring in the active layer thawing period and lowest occurring in the frozen period. The CO_2 concentration's seasonal changing ranges at deeper layers were all significantly higher than those at surface layers, but the deeper (100–180 cm) layers did not show clear trends. The variations of CO_2 concentrations in the soil were hardly explained by soil temperature at any depth. A significant correlation was found between CO_2 concentrations and active layer unfrozen-water content.

Keywords: active layer; alpine grasslands soil; CO_2 concentrations; Qinghai-Tibet Plateau; variation.

Introduction

Global warming has been of great concern, and the accumulation of greenhouse gases in soils is assumed to be responsible for the rise in mean global temperatures (Crowley 2000). As one of the most effective greenhouse gases, carbon dioxide (CO_2) is a maximum atmospheric trace gas and responsible for almost 63.7% (Rodhe 1990) of anticipated annual global warming undergoing an atmospheric concentration exceeding 367 ppm (IPCC 2001). Some evidence from the literature indicated that the elevated atmospheric CO_2 could affect many belowground processes of grassland such as grassland types, root respiration, and soil microbes (Pietikainen et al. 1999).

There are many sources of CO_2, but the most important natural source of atmospheric CO_2 is assumed to be microbial activities in environments like soil and water (Andersen et al. 2001). The partial pressure of CO_2 in the soil may differ greatly from that in the atmosphere. Due to the respiratory activity of plant roots and soil biota, the higher CO_2 concentration can be measured compared to that in the atmosphere. Several studies have shown that a high spatial variation of the CO_2 efflux from the soil can be efficiently explained by fine root and microbial biomass distribution, and by physical and chemical soil properties (Pangle & Seiler 2002, Maestre & Cortina 2003). Much of that heterogeneity occurs within short distances (Stoyan et al. 2000) and is especially high in areas where the distribution of ecological factors and organisms is markedly patchy (Maestre & Cortina 2003).

In comparison to data on atmospheric CO_2 enrichment, surprisingly, less is known about soil CO_2. To our knowledge, however, there is no study on temporal and spatial variation in permafrost soil on Qinghai-Tibet Plateau.

The mean altitude of the plateau is more than 4000 m above sea level with an area about 2,500,000 km^2. Great uplift of the plateau since the Late Cenozoic has been strongly affecting the physical environment of the plateau itself and its neighboring regions. Meanwhile, the plateau is also a sensitive trigger of climate change in Asian monsoon region, which is closely related to the global change (Zheng and Zhu 2000). Due to the topographic features and the characteristics of the atmospheric circulation, typical alpine zones of forests, meadows, grasslands, and deserts appear in succession from southeast to northwest in the plateau. Alpine grassland is one of the most important ecosystems on the Qinghai-Tibet Plateau because of its large area. Besides, the area is special for its lack of human activity. It provides an ideal scientific field for understanding on CO_2 exchanges in a soil-plant-atmosphere profile.

Freeze–thawing fluctuations are common characters in cold areas. Their effects on soil biogeochemical processes are a subject of major ecological interest, because it is often suggested that freeze–thawing events may be a major factor contributing to the microbial release of C in plant available form (Lipson et al. 1999, Grogan & Jonasson 2003). Furthermore, since plant productivity is often strongly limited by nutrient availability (Vitousek et al. 1991), freeze–thawing effects on soil nutrient transformations may substantially influence the C balance of cold ecosystems. Freezing and subsequent thawing of soils often results in an initial flush of microbial respiration and CO_2 effluxes (Muller et al. 2002). Laboratory incubation studies indicate that freeze–thawing cycles can lyse a substantial proportion of microbial cells, resulting in C releases into the surrounding soil, that may be immobilized by surviving microbes as they consume the enhanced supply of C substrate (Skogland et al. 1988). Thus, the extent and biogeochemical significance of freeze–thawing processes to overall ecosystem C cycling remains unclear, and may vary substantially depending on the character of the plants and temperature the freeze–thawing process is largely uninvestigated. Most of the above conclusions have been based on studies of soils without freeze–thawing process on the Qinghai-Tibet Plateau. CO_2 fluxes responses to freeze–thawing are clearly important, since soils in cold ecosystems generally contain large CO_2 concentrations (Zhao et al. 2005). Therefore, studies on the variations of CO_2 concentrations in active layer are necessary to fully evaluate freeze–thawing processes effects on whole ecosystem C cycles.

Materials and Methods

Site description

The experimental site is at Beiluhe Experimental Station, Cold and Arid Regions Environmental and Engineering Research Institute, Chinese Academy of Sciences (34°51.24′N, 92°56.39′E, 4628 m a.s.l.). The station is located in continuous permafrost area with cold and dry climate condition, and top soil is frozen from September to April of the next year. The annual average temperature is -5.2°C with the lowest temperature of -37.7°C and the highest of 23.2°C.

The sampling site is located in an area near the station. The soil, under typical vegetation type (alpine grassland) was collected, and its basic chemical and physical properties were analyzed.

The sampling site is at a river bank where the vegetation type was alpine grassland under which Cab-Gel-Sandic Entisols had developed (Chinese Soil Taxonomy, Gong et al. 1999). About 70% of the ground was covered by the dominant plants such as *Avena fatua, Kobresia pygmea, Aster asteroids, Astragalus melilotoides, and Saussurea arenaria*. The parent material of the soil at 0–100 cm was aeolian sand and at the 100–140 cm depth, alluvial sand over red residual of the Tertiary at 140–180 cm. The contents of $CaCO_3$ and clay along the profile illustrated $CaCO_3$ moved downward slightly, but the clay did not, reflecting unintensive soil water movement. The high clay content at the 140–160 cm layer should be ascribed to the parent material. There was no groundwater at the 0–180 cm depth when soil sampling.

Experimental design

CO_2 concentrations at different layers in the soil were examined thrice (1 d) a month from January 2006 to January 2007. On each sampling day, CO_2 concentrations were measured between 10:00 and 16:00. At each depth, three samples were taken by sampling pipes. All gas samples were taken with polypropylene syringes equipped with three-way stopcocks into 12 mL polyethylene vacuum vials for CO_2 concentration analyses (Maljanen et al. 2001). The samples were transported to the lab frozen, and were analyzed using gas chromatography.

We gathered the soil gas samples at the depths of 0.1, 0.2, 0.4, 0.6, 0.8, 1.0, 1.2, 1.4, 1.6, and 1.8 m from the soil through soil gas samplers, which were similar to Burton's facilities (Burton & Beauchamp 1994). Our gas samplers were made of stainless steel tubes. The outside tube has an exterior diameter of 16 mm, and the diameter of the inside pipes was 8 mm. The tops of the inside pipes were tightened by three-way stopcocks, thereby separating the inner soil gases from the outer atmosphere. The sampling plots were selected on typical plant community and coverage of the study area, and the example wells were dug on January 2006. Samplers were put in each well osculated to the soil profiles in order to get the exact CO_2 concentrations at different soil layers. Gas samples were gathered from each of the airtight pipes with polypropylene syringes into 12 mL polyethylene vacuum vials. Furthermore, the soil temperature and moisture content were also measured using temperature and moisture content probes during the experimental time.

Sample analyses

The Total Soil Organic Carbon (TOC) was analyzed using a Shimazu 5000A, and its standard analytical procedure for TOC was adopted. The Microbial Biomass Carbon (MB-C) was measured by extracting 20 g of defrosted soil with 40 ml K_2SO_4 solution for 1 h under shaking at 200 rpm. After extraction, the soil suspensions were filtered. MB-C was measured by directly determining TOC using the Shimazu 5000A at 680°C. The Water Dissolved Organic Carbon (WDOC) was measured by the method described by Wu et al. (2003). CO_2 concentrations were analyzed within 30 days by a gas chromatography (GC) (Type: Hewlett-Packard 6890), which was equipped with a flame-ionization detector (FID).

Results and Discussion

Soil carbon characteristics

Soil moisture increased gradually with depth from values of about 3.61% at the surface to 13.75% at 1.5 m. The root system here was stronger than the plain area due to the frigid climate.

The TOC content in the soil profiles decreased as the depth increased, and the trends could be described as exponential processes. It decreased dramatically in the 0–60 cm depths and then slowly in the lower layers with the depth increasing.

The TOC mass (0–180 cm) in the soil was 69.64 Mg C ha^{-1}, of which 66.11 Mg C ha^{-1} was in the 0–100 cm depth. About 94.4% of TOC in the solum was in the upper 0–100 cm layers and only a little below the layers. Even though the solum of this site was composed of loam or sandy loam which favor water percolation, the soil moisture in the layers below

100 cm were saturant the whole year and it was near saturant in the 50–100 cm layers most of a year, due to the permafrost layer beneath 180 cm (Zhao et al. 2000). The excess water prohibited root growth, and thus nearly all of the TOC was located in the upper 60 cm layer. The distribution of root residual along the profile was both a reflection of the soil water regime and an explanation of the TOC distribution in the layers: totally 9.23 Mg C ha^{-1} as root residual and all of it was in the 0–40 cm layers. Beside the soil water regime, the high content of pebble or particles larger than 2 mm in the layers below 40 cm definitely influenced the root growth and therefore the TOC distribution along the profile.

The WDOC contents declined dramatically with depth increasing, and it was significantly higher in the 0–40 cm layers than the lower layers. Also, in the soils MB-C was detected only in the 0–20 cm layers, and it was much higher in the 0–10 cm layer than the 10–20 cm layer.

CO_2 concentration in soil profile

Soil CO_2 concentrations increased gradually with depth, and the highest CO_2 concentration was found at the depth of 150 cm; the lowest CO_2 concentration occurred at the 10 cm, which is similar to the researches at the agriculture (Burton & Beauchamp 1994). In general, the mean concentrations in the atmosphere were all much lower than the CO_2 concentrations in the soil, which introduced a CO_2 emission from the alpine grassland soil to the atmosphere in our study area. Furthermore, the standard deviations of CO_2 concentrations in the atmosphere were all much lower than those in the soil. The ranges of CO_2 concentrations changed successively from 1138 to 3162 ppm in soil, which are less than the range in Chinese Loutu soil and the soil under alpine grassland in the Wudaoliang region of the Tibetan Plateau, and is less than the range in soil of farmland and grassland that has been reported.

The particle size distribution of soil has been described as the dominant independent variable determining CO_2 concentrations. It has been clearly demonstrated that CO_2 in soils is produced by microbe processes. But things are more complex than this, because the amount of CO_2 produced by either transfer processes or the activity and amount of microbe depends on the prevailing oxygen conditions; maximum yields of the gas occur only in a narrow range of low oxygen concentrations (Bange 2000). Some previous studies suggested that higher CO_2 concentrations were caused by increased CO_2 production from aerobic conditions rather than by increased production from anaerobic conditions in soils (Dowrick 1999). At the same time, the soil aperture, which is produced by particle size heterogeneity, controls the amount of CO_2 in soil.

Temporal variations of CO_2 concentrations

Over the one-year measurement period, concentrations tended to be positively correlated with the active layer freezing-thawing processes, with highest CO_2 levels occurring in thawing conditions, and lowest values in frozen, soil temperature also exerted an important control.

Soil CO_2 concentrations varied significantly during the study period, both temporally and with depth. Seasonal variation of CO_2 concentrations in the soil during the sampling period were the greatest at superstratum depths (Fig. 2). This was quite different and provided an interesting contrast to some previous studies (Bouton & Beauchamp 1994). Their experiments were carried out in the areas with strong human impacts. Production of CO_2 at topper soil changed widely with human activities including fertilizer application, farming, and land-use changes (Hadietal. 2000, Pathak & Nedwell 2001). But our study site was located at a remote plateau with little human activities. CO_2 concentrations in the surface layers kept a more stable state than those in the deeper layers, whereas the diffusion of CO_2 in deeper layers was lacking efficient pathways. The seasonal variation of CO_2 concentrations in soil showed a very clear pattern, with the higher CO_2 concentration occurring at the thawing period (from summer mid-autumn to the mid-autumn) and the lower concentrations during the frozen period (spring and winter). During the experimental period, variations of

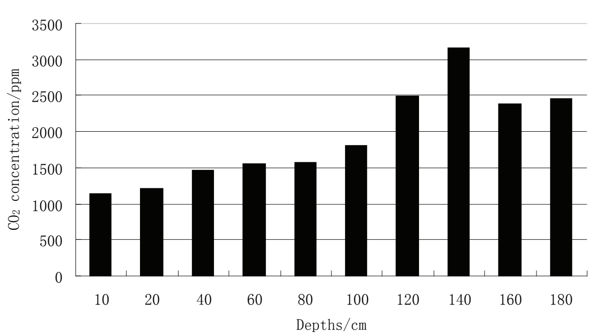

Figure 1. The average CO_2 concentration in soil depths.

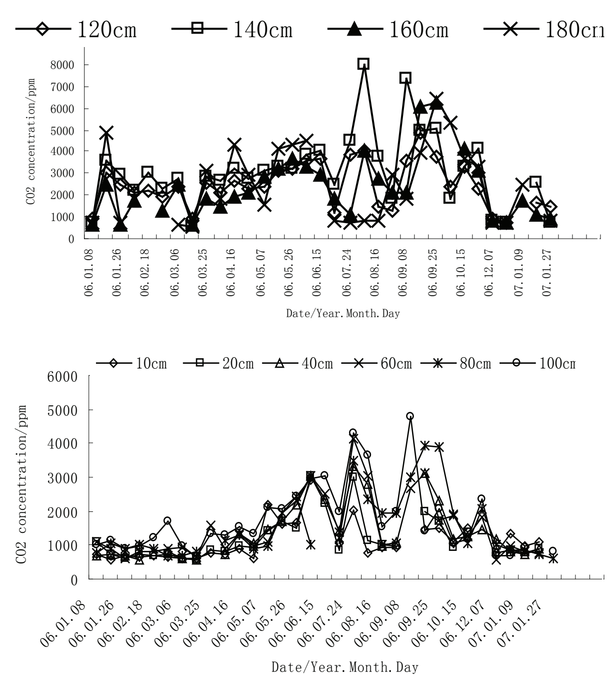

Figure 2. Variation of CO_2 concentrations at different depths in the soil.

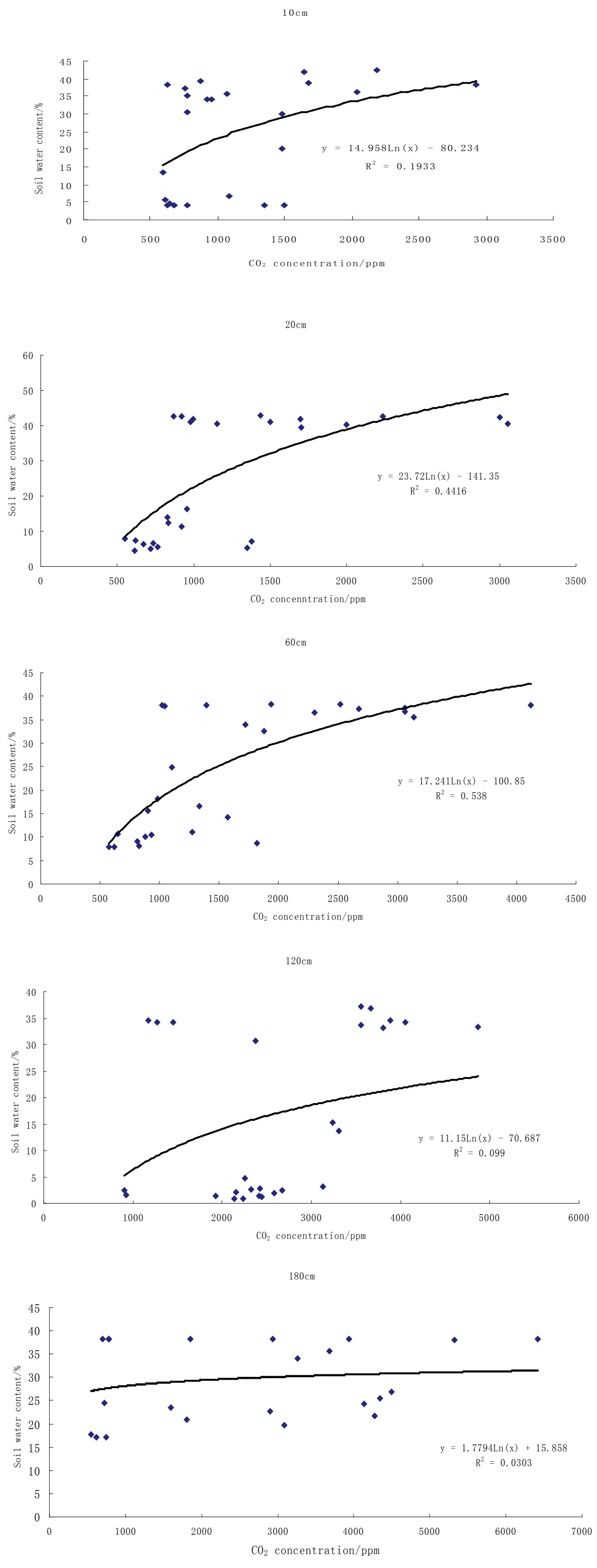

Figure 3. Correlations between CO_2 concentrations and soil water content at different depths in the soil.

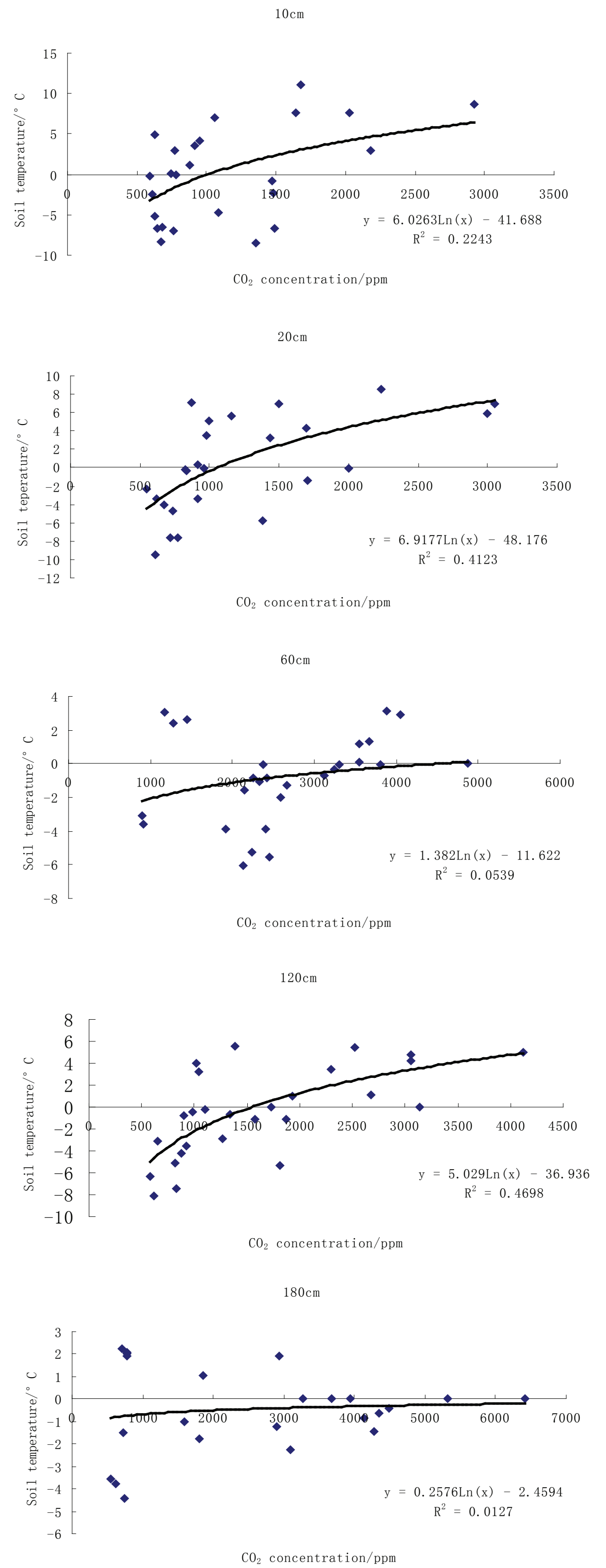

Figure 4. Correlations between CO_2 concentrations and soil temperature at different depths in the soil.

CO_2 concentrations in soil showed different ranges at all depths: the ranges of deeper layers (120–180 cm) larger than which in topper soils (10–100 cm). It may be caused by the variations of particle size distribution and unfrozen-water content in the bottom of active layers. The highest ranges occurred in the 140 cm depth layer, which was the pebble layer in the soil. It is well known that CO_2 concentrations in soil was the direct lie on the CO_2 producing processes and the storage conditions, so the CO_2 concentrations and its variability in the pebble layer were large.

Although mean CO_2 concentrations varied widely with depth in the soil, the seasonal variations of concentrations showed significant correlation between soil water contents in surface soil (10–60 cm).The most interesting result is the correlation between CO_2 concentrations at surface layers increased with depth, and the most significant correlation (R^2=0.54, P<0.01) (Fig. 3) was found at 60 cm depth layers where the greater mass of WDOC was measured. The WDOC, which have effect on CO_2 production and transportation procedures, were easily disturbed by the soil water contents at soil surface; on the contrary, the soil water contents showed more stable state at deeper layers relatively because of unfrozen-water content was near saturation.

Furthermore, the soil temperature has influences on CO_2 concentrations at the soil surface layers, but we can find influences 1.2 m deep in the soil. The situation in the surface layers in soil is relatively simpler than the soil deeper layers, so the CO_2 procedures here were only dominated by the temperature. That is the reason why the correlation between CO_2 concentration variations at surface layers was more significant than that at bottom layers. A significant correlation (R^2= 0.47, P<0.01) was also found between CO_2 concentrations and soil temperature at 1.2 m in depth during the study period (Fig. 4). This implied that the variation of CO_2 concentrations in the layer was the most direct driving force of soil particle size distribution (sandy loam). It is known that the terrestrial C cycles are driven by the activities of microorganisms. The frozen water in the form of an ice layer represents a diffusion barrier which reduces CO_2 supply to the microorganisms and partly prevents the release of the CO_2.

Conclusions

CO_2 concentrations increase gradually from 0 to 140 cm depth in soil, and feebly decrease from 140 cm to 180 cm. The ranges changed successively from 1138 to 3162 ppm. Seasonal variations in the 0 to 100 cm depth soil showed almost the same seasonal pattern, with the highest concentrations occurring in the active layer thawing period and lowest concentrations occurring in the active layer thawing period. The seasonal variations of CO_2 concentrations in the 100–180 cm layers did not show clear trends, but it can be explained by temperature and unfrozen-water content in soil. There was a significant correlation between CO_2 concentrations changing and active layer unfrozen-water content.

Acknowledgments

This study is financially supported by the projects of National Foundation for Sciences (40701033) and (40471025). The efforts of Mr. Zhixue Ma and Mr. Zesheng Gao are appreciated for their help in locating study sites. Ms. Yuemei Li and Ms. Donghui Wang are appreciated for their assistance in laboratory analyses. Dr. Guojun Sun is sincerely appreciated for his efforts in identification of plant species. This study was conducted at the Beiluhe Experimental Station and Germud Experimental Station of Chinese Academy of Sciences.

References

Actuat, B. *Chem* 81: 42-48.

Andersen, K., Kjar, T. & Revsbech, N.P. 2001. An oxygen insensitive microsensor for nitrous oxide. *Sensor*.

Bange, G.W. 2000. It'snota gas. *Nature* 408: 301-302.

Bouma, T.J. & Bryla, D.R. 2000. On the assessment of root and soil respiration for soils of different textures: interactions with soil moisture contents and soil CO_2 concentrations. *Plant Soil* 227: 215-221.

Brooks, P.D., Williams, M.W. & Schmidt, S.K. 1998. Inorganic nitrogen and microbial biomass dynamics before and during spring snowmelt. *Biogeochemistry* 43: 1-15.

Crowley, T.J. 2000. Causes of climate change over the past 1000 years. *Science* 298: 270-277.

DeLuca, T.H. & Keeney, D.R. 1992. Effect of freeze–thaw events on mineralization of soil nitrogen. *Biology and Fertility of Soils* 14: 116-120.

Fang, C. & Moncrieff, J.B. 2001. The dependence of soil CO_2 efflux on temperature. *Soil Biol. Biochem.* 33: 155-165.

Grogan, P. & Jonasson, S. 2003. Controls on annual nitrogen cycling in the understorey of a sub-arctic birch forest. *Ecology* 84: 202–218.

Hamada, Y. & Tanaka, 2001. Dynamics of carbon dioxide in soil profiles based on long-term field observation. *Hydrol. Process* 15: 1829-1845.

Lipson, D.A. & Monson, R.K. 1998. Plant-microbe competition for soil amino acids in the alpine tundra: effects of freeze–thaw and dry-rewet events. *Oecologia* 113: 406-414.

Lipson, D.A., Schmidt, S.K. & Monson, R.K., 1999. Links between microbial population dynamics and nitrogen availability in an alpine ecosystem. *Ecology* 80: 1623-1631.

Maestre, F.T. & Cortina, J., 2003. Small-scale spatial variation in soil CO_2 efflux in a Mediterranean semiarid steppe. *Appl. Soil Ecol.* 23: 199-209.

Muller, C., Martin, M., Stevens, R.J., Laughlin, R.J. & Kammann, C. 2002. Processes leading to N_2O emissions in grassland soil during freezing and thawing. *Soil Biology & Biochemistry* 34: 1325-1331.

Pangle, R.E. & Seiler, J. 2002. Influence of seedling roots, environmental factors and soil characteristics on soil CO_2 efflux rates in a 2-year-old loblolly pine (Pinus taeda L.) plantation in the Virginia Piedmont. *Environ. Pollut.* 116: 85-96.

Rayment, M.B. & Jarvis, P.G. 2000. Temporal and spatial variation of soil CO_2 efflux in a Canadian boreal forest. *Soil Biol. Biochem.* 32: 35–45.

Skogland, T., Lomeland, S. & Goksoyr, J. 1988. Respiratory burst after freezing and thawing of soil: experiments with soil bacteria. *Soil Biology & Biochemistry* 20: 851-856.

Stoyan, H., De-Polli, H., Bohm, S. et al. 2000. Spatial heterogeneity of soil respiration and related properties at the plant scale. *Plant Soil* 222: 203-214.

Teepe, R., Brumme, R. & Beese, F. 2000. Nitrous oxide emissions from frozen soils under agricultural, fallow and forest land. *Soil Biol Biochem* 32:1807-1810.

Zhao, L., Cheng, G.D., Li, S.X. et al. 2000. Freezing and thawing process of active layer in permafrost region near Wu Dao Liang on Qinghai-Tibetan Plateau. *Chinese Science Bulletin* 45(11): 1205-1211.

Cost Impact of Climate Change-Induced Permafrost Degradation on Building Foundations in Inuvik, Northwest Territories

F. Zhou, A. Zhang
Canada Centre for Remote Sensing, Enhancing Resilience in a Changing Climate Program, Natural Resources of Canada, Ottawa, Canada

E. Hoeve
EBA Engineering Consultants Ltd., Yellowknife, Canada

Abstract

Permafrost degradation due to climate warming can impact buildings supported on permafrost. This paper describes a methodology used to evaluate impacts and costs for adaptation, considering soil profile, geothermal response, foundation type, mode of deformation, and building age, type, and service life to determine if and when foundation adaptation would be warranted, and at what likely cost. As Inuvik is predicted to experience the largest impact in the Northwest Territories, with 40 to 75% of existing buildings potentially impacted during their remaining service life, this case is described. The estimated cost without adaptation ranges from \$52M, under a moderate climate warming scenario, to \$121M, under an aggressive climate warming scenario. "Informed adaptation" (where the costs of remedial measures are considered in the context of the remaining service life and value of the building) was the most economical approach, reducing the cost impacts to about two-thirds of these costs.

Keywords: climate change; cost assessment; foundations; permafrost degradation.

Introduction

The stability of building foundations in many northern communities relies on the strength of the underlying permafrost. The Intergovernmental Panel on Climate Change (IPCC) projected that by 2100, air temperature will likely increase globally by 2.0°C to 4.5°C, based on a range of greenhouse gas emission scenarios (Solomon et al. 2007). Temperature increases in the north are predicted to be higher than the global average. Air temperature increases can be expected to bring about permafrost degradation, thereby impacting foundation systems in northern communities.

The impact of climate warming on foundation systems was recognized as a community issue in the Canadian north, and a lack of specific information was identified as a concern (Eamer et al. 2003). Studies of the climate change impacts on community housing, especially quantitative assessments, have been very limited and adaptation cost estimates are rare.

In Canada, the only previous studies (Robinson et al. 2001, Couture et al. 2002) dealt with the compilation and documentation of the infrastructure, geotechnical, and borehole data for two of the 32 communities in the Northwest Territories (Norman Wells, Tuktoyaktuk). While these studies identified permafrost degradation to have potential negative impacts on the foundation systems of these communities, no follow-up investigations or analyses were undertaken.

Khrustalev (2000, 2001) indicated that temperature increases could result in a significant decrease in the service life and potential failure of foundations. Nelson et al. (2001, 2002) mapped the hazard potential associated with thawing permafrost under global warming. The maps were created using a dimensionless thaw-settlement index, computed using the projected percentage change in active-layer thickness and the ground ice content. The resulting maps depicted areas of "low," "moderate," and "high" hazard potential. They then superimposed the locations of existing infrastructure on the hazard map to obtain a general assessment of the susceptibility of engineered works to thaw-induced damage. However, the spatial resolution of this mapping was rather coarse (0.5° by 0.5°), thus producing only a macro-view, which could not be used for foundation impact assessment at the community level.

This paper summarizes an approach to obtain quantitative estimates of the potential physical and cost impacts of climate change, and the associated timeframe, on existing building foundations in the Northwest Territories, using Inuvik as an example. This represents a portion of a broader project by Natural Resources Canada, which developed similar estimates for five communities. The overall objective of the study summarized in this paper was to take science and engineering-based information and put it into a form that could be considered at the planning and policy level to assist in determining the resources to be expended towards mitigation.

Methodology

A multiple accounts analysis (MAA) of the 32 communities in the Northwest Territories was used to rank the sensitivity of building foundation infrastructure in these communities to climate change. MAA is well suited to situations where a variety of factors affect an outcome, and it provides an overall framework in which such factors, described quantitatively or qualitatively, may be taken into account. MAA has been previously used fully or in part to identify most acceptable options in various development projects (e.g., Robertson & Shaw 2004).

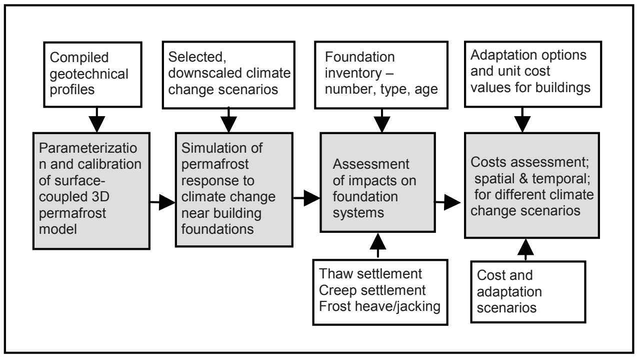

Figure 1. Methodology for foundation impact assessment.

In this case, thermal, physical, and infrastructure sensitivities were considered. The Inuvik region in general, and the community of Inuvik in particular, were determined to have the highest overall sensitivities (EBA 2005, Hoeve 2005).

Based on the MAA assessment, five representative communities were selected among the 32 for a more detailed analysis: Inuvik, Tuktoyaktuk, and Paulatuk in the continuous permafrost zone and Norman Wells and Tulita in the extensive, discontinuous permafrost zone. The selection was designed to represent a range of sensitivities, geographic regions, and population sizes. Only the results from Inuvik are summarized in this paper.

Figure 1 illustrates the methodological framework of the overall study leading to the cost assessment for the selected case communities.

Geotechnical profiles

Generalized geotechnical profiles were compiled to represent areas within which the subsurface was assumed to have geotechnical properties, such as soil texture, hydraulic and thermal properties, water/ice content, and the thickness of each layer, that are horizontally uniform or vary within only a narrow range. The impacts of permafrost degradation were assessed for each sub-area, considering the temporal and spatial distribution of foundation systems.

Climate change scenarios selection and downscaling

From among the many scenarios produced with the aid of General Circulation Models (GCMs) (IPCC 2001), three were chosen (CGCM 1 GHG + aerosol, HadCM3 SRES A2 and B2) that roughly represent an upper, a middle, and a lower level of the impact of greenhouse gases emissions on future air temperature trends. Thus, with these scenarios, the simulated geothermal dynamics should accordingly have an upper and lower bound as well as a middle range.

In this study, the selected GCMs were downscaled by using the Statistical Downscaling Model (SDSM) tool (Wilby & Dawson 2004). Six climatic variables were downscaled—air temperature, precipitation, solar shortwave and longwave radiation, wind speed, and water vapour pressure—for input into the model.

Surface-coupled three-dimensional geothermal model

A physical, process-based, surface-coupled, three-dimensional finite-element geothermal model (SC3D) was developed. Driven by climate variables, and constrained by ground surface condition, geothermal gradient, and geotechnical profile characteristics, the model transforms the changes in climate variables into ground surface temperature dynamics by computing surface energy and water balance including snow. The model mimics the three-dimensional flux of heat and water that occurs around and underneath the building. The model also represents the building's effects on these processes through dynamically differentiating the solar radiation, precipitation, and snow cover received by the ground surface at different locations underneath and around the building, and it reflects the modification of the natural geothermal regime by the building. Zhou et al. (2006) provides a detailed description of the model, the required input data, and results of its validation.

Modeling of permafrost changes

The modeling space was specified as a cube, 22 m by 18 m in plan and 100 m deep. The "building" was specified as a typical residential house, with an enclosed area of 14 m by 10 m, and a height of 5 m with a 0.5 m high air space under the floor.

The finite-element mesh was uniform in both X and Y directions, on a 2 m grid. To capture the details of heat and water transfer near the ground surface and to achieve computational efficiency, the vertical cell size was 10 cm for upper layers, and it increased downward to 4 m at the bottom of the modeling space.

Following the protocol recommended in IPCC-TGIA (1999), the period of 1961–1990, with actual data, served as a benchmark, and the projected period 2010–2069 was used to assess the changes due to climate warming with respect to the benchmark. The IPCC recommended three assessment periods: 2010–2039, 2040–2069, and 2070–2099. The period of 2010–2069, representing two of these recommended periods, was chosen because it covers the expected service life of all the existing buildings (constructed before 2005).

The simulation employed a daily time step. From recorded vertical temperature profiles, two indices of permafrost condition were computed: mean annual ground temperature and active layer thickness.

Impact of permafrost degradation on building foundations

The rate of permafrost degradation determines the degree of soil deformation in response to climate change. In this study, three types of terrain instability due to permafrost degradation were taken into account in the estimation of the impacts: thaw settlement and creep settlement, and frost-jacking. The rate of permafrost degradation was quantified through increasing mean annual ground temperature and deepening active layer thickness. The former was considered mainly in creep settlement analysis, and the latter is used for the calculation of thaw settlement and frost-jacking.

For pile foundations, the assessment took into account all the three types of terrain instability. Only thaw and creep settlements were involved in estimating the impact on shallow foundations, which would include surface footings or buried spread footings.

Differential settlements were obtained as a result of the varying geothermal response below various portions of the building. The ground below the centre of the building was coldest and the ground at the south corners/side was the warmest.

A critical part of the physical impact assessment concerns the thresholds at which damage to building systems is considered to occur. The maximum allowable total settlement of a building was set at 30 mm, and allowable differential settlement between adjacent foundation supports at 10 mm over a 3 m span during the service life of the building (CFEM 1992). Thus, if settlement of a building is 30 mm or higher or if differential creep settlement is more than 10 mm over the horizontal distance of 3 m, the building was regarded to be at risk.

For pile foundations, the frost-jacking and resisting forces were evaluated. If at any location under the building, the frost-jacking force exceeded the resisting force (sum of pile resistance and dead load), the building was considered at risk of frost-jacking.

Cost assessment

Typical building sizes, foundation configurations and unit costs for the most appropriate rehabilitation technique applicable to each foundation type were determined (EBA 2006, Hoeve et al. 2006).

Foundation inventories were prepared to characterize individual buildings within each geotechnical profile area by age (grouped at 5-year intervals), replacement cost and present value. A depreciation factor of 5% per year was used to determine present value. The age distribution was determined by examination of historical air photos. It should be noted that the compilation of inventories was office-based, incorporating assumptions based on experience and judgment, and not including site visits, except as documented by Robinson et al. (2001) and Couture et al. (2002) for Tuktoyaktuk and Norman Wells.

Commercial/institutional buildings were considered to have a longer service life (65 years) than residential buildings (50 years). If the age of a building reached these thresholds, the building was considered to retire "maturely." If a younger building was assessed at risk due to permafrost degradation, it would either be forced to retire prematurely or to undergo an adaptation.

The cost study considered three responses (Fig. 2):

Response 1 – mature retirement: a building will reach the end of its service life without detrimental impact induced by climate warming. In this scenario, no action will be needed and no cost will be incurred. As no cost would occur in Response 1, it is not considered further.

Response 2 – no action: a building is assessed to be at risk, but no action will be taken. The building will be forced to retire early and cost of the premature retirement would be incurred, equal to the residual value of the building. Therefore, the cost will be the total asset value of all impacted buildings at the age when the buildings would be assessed at risk.

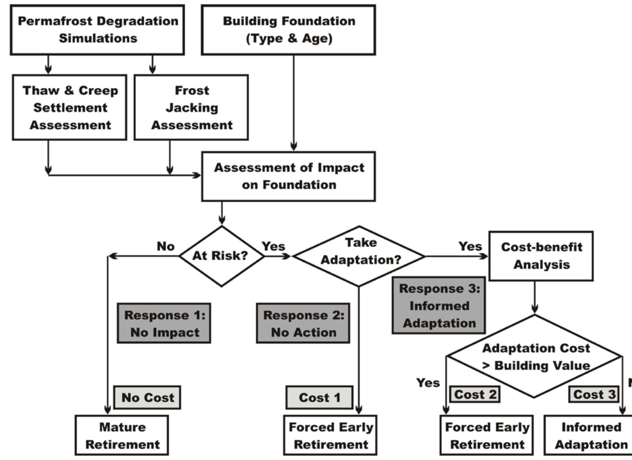

Figure 2. Procedures for impact and cost assessment.

Response 3 – informed-adaptation: when a building is assessed to be at risk, a cost-benefit analysis is conducted to determine what actions should be taken and when. The cost-benefit analysis thus compares the adaptation cost and asset value of the building under consideration when it is assessed at risk.

If a building at risk is approaching the end of its service life, the cost of the impact (forced premature retirement) would be relatively low. Conversely, if a building is at risk in its early service life, the cost of the impact would be relatively high and adaptation may be warranted. The cost-benefit analysis thus aims to minimize total costs of the climate change impacts, i.e., the sum of Cost 2 and Cost 3 is less than Cost 1.

The foregoing procedure was applied to each category of building/foundation type in each geotechnical profile, over each time increment and for each case community. Details are presented in Zhou et al. (2007).

Assessment Results for Inuvik

Inuvik is located on the East Channel of Mackenzie Delta, approximately 100 km from the Arctic Ocean, at latitude 68°19′N and longitude 133°29′W. In 2003, it had a population of 3688.

Typical geotechnical profiles

Geotechnical data from 17 evaluations was reviewed to develop typical subsurface soil profiles in the Inuvik area. The community was divided into two sub-areas of generally similar subsurface stratigraphy. The extent of Profiles 1 and 2 within the community are shown on Figure 3. Profile 3 was developed for the area located west of town along the Dempster Highway out to and including the Inuvik airport.

The soil profiles and associated thermal properties were described in EBA (2004) and are summarized in Figure 4.

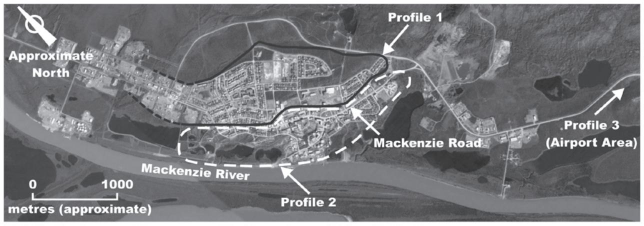

NOTE: Background image provided courtesy of Google Earth and is for visual presentation purposes only.

Figure 3. Location of geotechnical profiles for Inuvik.

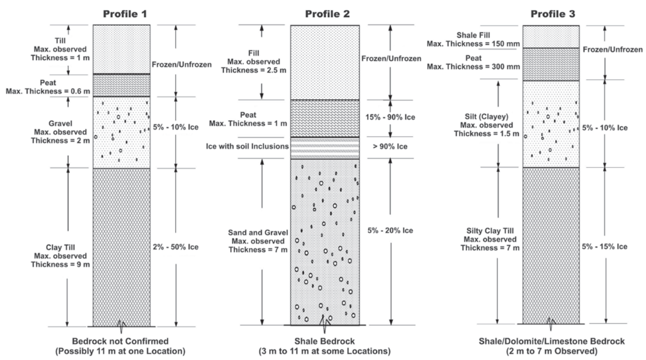

Figure 4. Geotechnical profiles for Inuvik.

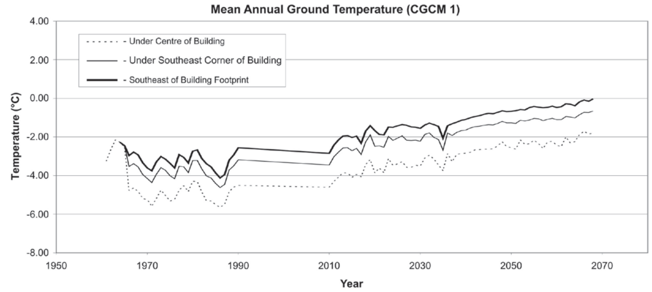

Figure 5. Mean annual ground temperatures for Inuvik, Profile 1.

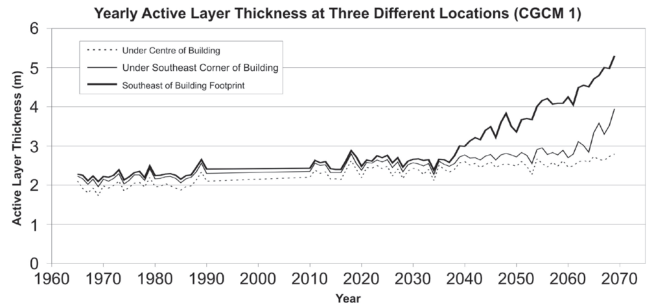

Figure 6. Active layer thickness response for Inuvik, Profile 1.

Building age distribution

The temporal distribution of buildings over about 5-year increments were compiled by examining air photos. The majority of the buildings are located in the Profile 1 and Profile 2 areas. The area of Profile 1 has about 600 residential and 60 commercial buildings and encompasses the newer development areas. Profile 2 is in a mature area of the community and the number of buildings has remained stable since the late 1970s, with about 400 residential and 40 commercial/institutional buildings. The area of soil Profile 3 has exhibited growth, but only has about 30 commercial/institutional buildings and negligible residential buildings.

Ground temperature trends under climate change scenarios

The model was calibrated with ground temperature data from a power station in Inuvik, a site within the Profile 2 area. Cables were installed in 1995, extending under the building, at the perimeter of the building and away from the building (EBA 1996). Regular data were available for four years, with sporadic data available for another six years. The model was initialized and run from 1961 through the period where measurements were available.

Permafrost simulations were conducted for the baseline period (1961–1990) and two projected periods (2010–2039, 2040–2069). The simulations through the baseline period were driven by actual climate data, and the simulations during the projected periods were driven by the downscaled GCM data.

The intervening period, 1991–2009, was not modeled, because it was not called for in the IPCC-TGIA (1999) protocol and because the input data, either actual or projected, were not complete.

Figure 5 shows the mean annual ground temperature response (average for depths 1 m to 10 m) at three locations, derived from the CGCM 1 scenario, which is the most severe. The locations for which results are plotted range from the maximum mean annual ground temperature at a point outside the building footprint to the minimum mean annual ground temperature under the centre of the building. The intermediate point represents the warmest under the building, with the southeast and southwest corners being approximately the same.

The simulation began in 1961, and the building effect was introduced in 1965. The building caused an immediate and substantial change in the temperature regime, and this effect was strongest underneath in the centre of the building. Figure 5 also suggests that the temperature differential did not increase over time. Once the thermal regime stabilized, the building exerted an approximately constant additional effect on the near-surface temperature profile.

Figure 6 shows the change in active layer thickness derived from the CGCM 1 scenario. It indicates that the projected active layer thickness did not change substantially between 2010 and 2040 for all the locations. However, the active layer thickness became deeper at a faster rate away from the building after about 2040, at the south corner around 2065, and there was little change under the centre of the building during the modeling period.

The results in Figure 6 seem to suggest that the shading effect of a building, on solar radiation and snow cover, has a more dominant effect on active layer thickness than increasing air temperature.

The analyses indicate that, over the long term, ground temperature changes more or less in step with air temperature but changes in the active layer lag behind changes in ground temperature. This is attributable to the latent heat that must be overcome for an active layer response in ice-rich soil.

Table 1. Summary of impacted buildings in Inuvik.

	Profile 1		Profile 2		Profile 3		Inuvik Overall	
Total Buildings	659		448		34		1141	
Scenario	Buildings Impacted							
	#	%	#	%	#	%	#	%
CGCM1	393	60	441	98	16	47	850	74
HadCM3 A2	5	1	441	98	5	14	451	40
HadCM3 B2	5	1	441	98	14	42	460	40

Table 2. Cost impacts in Inuvik for three climate scenarios.

Climate Change Scenario	Response 3 (2005 C$M)					Response 2 (2005 C$M) (Cost 1)
	Premature Retirement (Cost 2)		Adaptation (Cost 3)		Total	
	Res.	Com.	Res.	Com.		
CGCM1	15.3	5.4	4.0	55.3	80.0	121.3
HadCM3 A2	9.0	4.1	1.3	21.5	36.0	52.3
HadCM3 B2	9.0	4.9	1.3	24.5	40.0	56.3

Impacts on building foundations

Table 1 summarizes the number of buildings impacted for the three climate change scenarios and within the three geotechnical profiles. Among the 1141 buildings in Inuvik (as of 2005), 659 buildings are located in Profile 1, 448 in Profile 2, and 34 in Profile 3. The buildings in Profile 2 are most severely affected. This is because the baseline (1961–1990) active layer in Profile 2 is deeper, at about 3 m, compared to about 2.5 m and 1.5 m for Profiles 1 and 3.

The fraction of buildings in Profiles 1 and 3 that would be affected ranged from around 15% (Profile 3 with HadCM3 A2) to 60% (Profile 1 with CGCM1 GHG+aerosol). Buildings in Profile 3 would be the least impacted due to a shallower active layer and lower mean annual ground temperature. These results reflect the importance of the geotechnical conditions on the susceptibility of building foundations, the impact being modulated by the climate change scenario employed.

The differences between climate change scenarios (CGCM1 GHG+aerosol and HadCM3 A2 or HadCM3 B2) are rather strong: about 74% of all buildings would be impacted under CGCM1 scenario, compared to approximately 40% for the two HadCM3 scenarios. This difference represents about 400 buildings, mostly located in Profile 1.

Cost impacts

Table 2 summarizes the distribution of costs to community buildings for the three climate scenarios. Results of Responses 2 and 3 are shown. Based on the Response 3 (informed adaptation, Fig. 2), cost-benefit analysis was used to determine whether or not adaptation measures were warranted for each impacted building. The results show that CGCM1 scenario would bring about the highest cost of approximately C$80M, and HadCM3 A2 and HadCM3 B2 would result in the cost about C$36M and C$40M, respectively. The costs were also broken down to the costs due to premature retirement (Cost 2) or costs for adaptation (Cost 3). The results show that, under CGCM1 scenario, about 74% of the total cost would be for adaptation. Under climate change scenarios HadCM3 A2 and HadCM3 B2, about 64% of the total cost would be due to adaptation.

Under all climate change scenarios, the higher adaptation costs are associated with commercial/institutional buildings. The highest premature retirement costs are associated with residential buildings. This is partially attributable to the longer service life of commercial/institutional buildings, but is also a result of the magnitude of adaptation costs relative to residential building value. Commercial/institutional buildings are more likely to warrant adaptation than residential buildings.

The table also lists the costs of the no action scenario in which impacted buildings are assumed to retire prematurely with no attempt at adaptation (Cost 1, Response 2). Although the total number of impacted buildings in Responses 2 and 3 are the same, the total cost of informed adaptation ($80M) is only about two-thirds of the no-adaptation scenario ($121M) under CGCM 1 scenario. This relationship held true for the HadCM3 A2 and B2 scenarios.

To help put these costs into perspective, the total replacement cost of the building infrastructure in Inuvik was calculated to be about $1.2 billion and the present value of the buildings was calculated to be about $250 million, in 2005 dollars.

The analysis shows that "informed adaptation" is the preferable management response to dealing with impacts of climate change on building foundations in Inuvik.

Acknowledgments

The authors are grateful to Josef Cihlar for his advice on the study and for his guidance. Thanks also go to Yu Zhang and Fred Wright for advice on permafrost modeling and Richard Fernandes' research group for providing climate data; the NWT Housing Corporation, the Government of the NWT, and Departments of Public Works and Services and Municipal and Community Affairs who contributed community infrastructure data. Funding was by the Climate Change Impact and Adaptation Directorate with support by the Earth Sciences Sector, Natural Resources Canada.

References

Canadian Foundation Engineering Manual. 1992. Third Edition. Canadian Geotechnical Society, Technical Committee on Foundations, 512 pp.

Couture R., Robinson, S.D., Burgess, M.M. & Solomon, S. 2002. *Climate change, permafrost, and community infrastructure: A compilation of background material form a pilot study of Tuktoyaktuk, Northwest Territories.* Geological Survey of Canada, Open File 3867, May 2002.

Eamer C., Johnson, P.G. & Love, C. 2003. C-CIARN North online workshop on Climate Change and Infrastructure: summary report. *Weathering Change Vol. 1, No. 4*, 2003.

EBA Engineering Consultants Ltd. 1996. *Geotechnical Investigation, Volcano Boiler Foundation Improvements*. Report submitted to the Northwest Territories Power Corporation, January 1996.

EBA Engineering Consultants Ltd. 2004. G*eotechnical Characterization for Inuvik, NWT*. Report submitted to Natural Resources Canada, November 2004.

EBA Engineering Consultants Ltd. 2005. *Assessment of foundation sensitivity to climate change in the Northwest Territories.* Report submitted to Natural Resources Canada, January 2005.

EBA Engineering Consultants Ltd. 2006. *Estimated Costs for Foundation Adaptation in the Northwest Territories–Draft.* Report submitted to Natural Resources Canada, January 2006.

Hoeve, E., Zhou, F. & Zhang, A. 2005. *Assessment of Building Foundation Sensitivity to Climate Change in the Northwest Territories.* Presentation at Adapting to Climate Change in Canada 2005, Montreal, Quebec. PowerPoint summary available at: http://adaptation2005.ca/abstracts/hoeve_e.html

Hoeve E., Zhou, F. & Zhang, A. 2006. Potential Cost Impacts for Adaptation of Building Foundation Infrastructure in the Northwest Territories. *Engineering Institute of Canada–Climate Change Technology Conference, Ottawa, Canada, May 2006.*

Intergovernmental Panel on Climate Change (IPCC). 2001. *Climate change 2001: Synthesis Report*. Geneva, Switzerland: Intergovernmental Panel on Climate Change, 84 pp.

IPCC-TGCIA. 1999. *Guidelines on the Use of Scenario data for Climate Impact and Adaptation Assessment. Version 1.* Prepared by T.R. Carter, M. Hulme & M. Lal. Intergovernmental Panel on Climate Change, Task Group on Scenarios for Climate Impact Assessment, 69 pp.

Khrustalev, L.N. 2000. Allowance for climate change in designing foundations on permafrost grounds. *International Workshop on Permafrost Engineering, Longyearbyen, Norway, 18–21 June, 2000*. Tapir Publishers, 25–36.

Khrustalev, L.N. 2001. Problems of permafrost engineering as related to global climate warming. In: R. Paepe & V.P. Melnikov (eds.), *NATO Advanced Workshop on Permafrost Response on Economic Development, Environmental Security and Natural Resources, Novosibirsk, Russia, 12–16 November 1998*. Kluwer Academic Publishers, 407–423.

National Research Council (NRC). 1962. *Engineering site information for Inuvik, NWT.* Technical Paper No. 135. Division of Building Research.

Nelson, F.E, Anisimov, O.A. & Shiklomanov, N.I. 2001. Subsidence risk from thawing permafrost. *Nature* 410: 889-890.

Nelson, F.E, Anisimov, O.A. & Shiklomanov, N. I. 2002. Climate change and hazard zonation in the circum-arctic permafrost regions. *Natural Hazards* 26(3): 203-225.

Robertson, A. & Shaw, S. 2004. Use of multiple accounts analysis process for sustainability optimization. *Proceedings of the SME Annual Meeting, February 23-25, Denver, CO:* 7pp.

Robinson, S.D., Couture, R. & Burgess, M.M. 2001. C*limate change, permafrost, and community infrastructure: A compilation of background material form a pilot study of Norman Wells, Northwest Territories.* Geological Survey of Canada, Open File 3913. January 2001.

Solomon, S., Qin, D., Manning, M., Alley, R.B., Berntsen, T., Bindoff, N.L., Chen, Z., Chidthaisong, A., Gregory, J.M., Hegerl, G.C., Heimann, M., Hewitson, B., Hoskins, B.J., Joos, F., Jouzel, J., Kattsov, V., Lohmann, U., Matsuno, T., Molina, M., Nicholls, N., Overpeck, J., Raga, G., Ramaswamy, V., Ren, J., Rusticucci, M., Somerville, R., Stocker, T.F., Whetton, P., Wood, R.A. & Wratt, D. 2007. 2007: Technical Summary. In: *Climate Change 2007: The Physical Science Basis. Contribution of Working Group I to the Fourth Assessment Report of the Intergovernmental Panel on Climate Change.* Cambridge, United Kingdom, and New York, NY, USA: Cambridge University Press.

Wilby, R.L. & Dawson, C.W. 2004. *Using SDSM version 3.1 - A Decision Support Tool for the Assessment of Regional Climate Change Impacts.* User Manual.

Zhou, F., Zhang, A., & Li, R. 2006. *Surface-coupled 3-D permafrost model for impact assessment on building foundations in Northern Canada due to permafrost degradation.* Presented at the first Asian Conference on Permafrost, Lanzhou, China, 2006.

Zhou, F., Zhang, A., Li, R., Hoeve, E. & Majid, A. 2007. *Potential climate change-induced permafrost degradation and building foundations: An assessment of impacts and costs for five communities in the Northwest Territories.* Report (V.3) distributed to stakeholders for feedback, September 2007.

Iron-Oxides and Pedogenesis of Modern Gelisols and Paleosols of the Southern Lena Delta, Siberia, Russia

Sebastian Zubrzycki
University of Hamburg, Hamburg, Germany
Sebastian Wetterich
Alfred Wegener Institute for Polar and Marine Research, Potsdam, Germany
Lutz Schirrmeister
Alfred Wegener Institute for Polar and Marine Research, Potsdam, Germany
Anastasia Germogenova
Moscow State University, Moscow, Russia
Eva-Maria Pfeiffer
University of Hamburg, Hamburg, Germany

Abstract

Five exposures on two arctic islands in southern Lena Delta, Russia, were investigated in order to determine the development of iron-oxides under different pedogenic conditions in permafrost-affected paleosols and to prove their application for describing environmental conditions during pedogenesis of buried soils and the predominant paleoclimate during their development. The samples were collected from the active layer on Samoylov Island as well as from Late Pleistocene and Holocene paleosols on Kurungnakh Island. The amounts of iron extractable by dithionite (Fe_d) and by oxalate (Fe_o) were determined for all samples. The extracts were conducted to determine the forming conditions of paleosols and their iron-oxide contents and to compare them with modern permafrost-affected soils. The iron-oxide amounts characterize well the sedimentation conditions and the paleoclimate of the investigated paleosols. As contributing factors, the organic matter content and the inundation were identified. Additionally, in modern soils, translocation processes within the polygon affect the conditions of the different Fe-fractions.

Keywords: environmental and climate change; Gelisols; iron-oxides; Lena Delta; paleosols; Siberia.

Introduction

Permafrost-affected soils (Gelisols or Cryosols) cover nearly one-fourth of the terrestrial surface in the northern hemisphere. Staudies have been conducted for more than 100 years (Goryachkin et al. 2004). The first studies were exploratory in nature in order to find land for agriculture. Pedoscientists study permafrost-affected soils to learn more of their active physico-chemical processes (Tarnocai 2004). Spatial distribution, genesis and properties of different Cryosols are presented in details by Kimble 2004. However, this does not imply that these soils have been sufficiently investigated.

Pedogenesis in permafrost regions takes place in the active layer above the permafrost table only during the short summer period. On one hand, the cold conditions hinder strong pedogenesis; on the other hand, permafrost preserves records of former soil conditions.

Spatial distribution and genesis of soils in the southern Lena Delta provide a basis for evaluation of the impact of environmental and climate change on permafrost landscapes.

The objective of this study was to prove if crystallized iron-oxides are a useful criterion for estimating environmental conditions of pedogenesis of buried soils and paleoclimate during their development.

Morphological and analytical data are taken into account to understand both properties and genesis of buried soils in ice rich permafrost sediments (so called ice complex) and modern soils in the southern Lena Delta.

Identifying different forms of iron-oxides helps to understand the environment in which active pedogenesis took place. In general paleosols are often characterized by their iron-oxides fractions, and this data facilitates an estimate of the relative age of a given soil-sequence (Arduino et al. 1984, Arduino et al. 1986, Bäumler 2001).

During expeditions to the Lena Delta in 2002 and 2007 investigation of several soil profiles were carried out to determine the development of iron-oxides under different pedogenic conditions in permafrost-affected paleosols and to prove their application for description of environmental conditions of pedogenesis of buried soils and predominant paleoclimate during their development. For understanding the processes of modern pedogenesis, from the active layer of young soils were investigated.

Investigation Area

The study sites are located on Samoylov Island (72°22′N, 126°28′E) and Kurungnakh Island (72°20′N, 126°18′E). The islands are situated at one of the main Lena River channels, the Olenyokskaya Channel in the southern part of Lena Delta (Fig. 1). The Lena Delta is located in northeastern Siberia, where the Lena River cuts through the Verkhoyansk

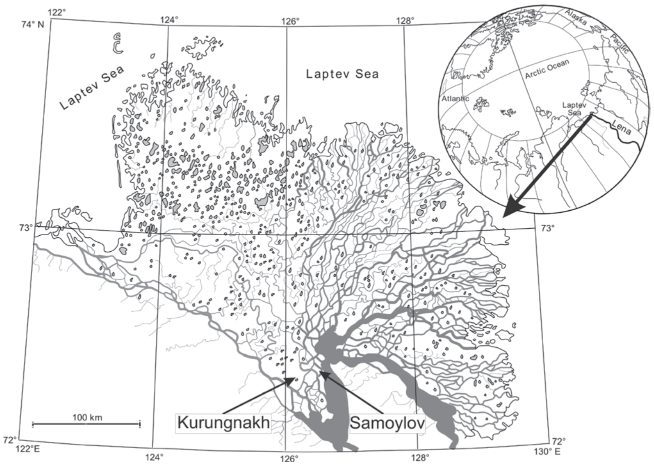

Figure 1. Map of the Lena Delta with study sites.

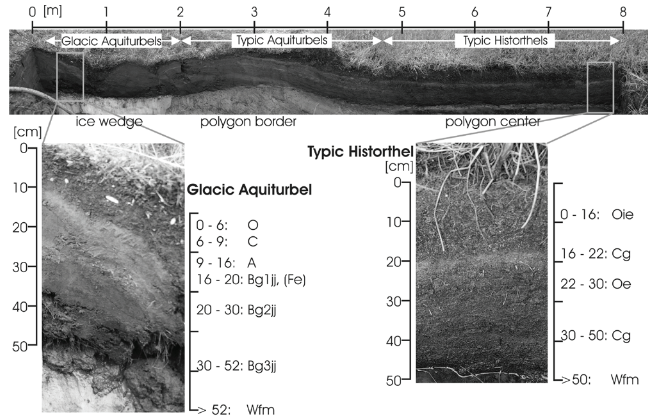

Figure 2. Soil-cross-section of a half of a low-centered polygon on Samoylov Island with the soil-complex of Glacic Aquiturbel and Typic Historthel, according to U.S. Soil Taxonomy.

Mountains Ridge and discharges into the Laptev Sea, which is part of the Arctic Ocean.

Samoylov Island can be divided into two major geomorphological units (Akhmadeeva et al. 1999): the relative young floodplain (0 to 4 m a.r.l. [about river level]) in the western part which is flooded annually in spring, and the higher-elevated (1 to 12 m a.r.l.) river terrace of Late Holocene age, the "first" terrace in the eastern part (Pavlova & Dorozhkina 1999). The first terrace is flooded only during extreme high-water events (Kutzbach 2005).

Kurungnakh Island belongs to the third river terrace complex (up to 55 m a.r.l.) of the Lena Delta. The third terrace is the oldest terrace in the delta. It was formed in Middle and Late Pleistocene (Schwamborn et al. 2002, Kuzmina et al. 2003). This terrace forms autonomous islands along the Olenyokskaya and Bykovskaya Channels. The Kurungnakh Island is located at the southeastern part of Olenyokskaya Channel (Schwamborn et al. 2002).

The climate in the Lena Delta is high-arctic with continental influence and characterized by low temperatures and low precipitation. The mean annual air temperature, measured by the meteorological station in Tiksi located about 110 km (68 stat. mi.) to the southeast directly at the coast of the Laptev Sea, was -13.6°C (7.5°F) during the 30-year period 1961–1990; the mean annual precipitation in the same period was 319 mm. The average temperatures of the warmest month August and the coldest month January were 7.1°C (44.8°F) and -32.4°C (-26.3°F), respectively (ROSHYDROMET 2007), demonstrating the extreme climatic contrasts between polar day and polar night for continental Polar Regions.

Material and Methods

The main soil unit of the first terrace above the floodplains of Samoylov Island is covered mainly by polygonal wet sedge tundra with soil-plant-complexes which consist of ice rich ground, wet and cryoturbated Gelisols (Glacic Aquiturbels) and very wet organic rich Gelisols (Typic Historthels). Typic Historthels are Gelisols that have more than 40%, by volume, organic materials from the surface to a depth of 50 cm (Soil Survey Staff 2006). According the WRB-Classification the Gelisols were classified as Glacic Turbic Cryosols and Haplic Histic Cryosols (Food and Agriculture Organisation, 2006). Typic Historthels were formed in depressed centers of low-centered ice-wedge polygons characterized by high water saturation to the soil surface and high organic matter accumulation due to anaerobic conditions.

Glacic Aquiturbels formed at the elevated borders of the polygons are characterized by prolonged inundation but with less organic matter accumulation and pronounced cryoturbation. Thus Glacic Aquiturbels are Gelisols that have one or more horizons showing cryoturbation in the form of irregular, broken or distorted horizon boundaries, involutions, and accumulation of organic matter on top of the permafrost and ice wedges. They have within 50 cm of the mineral soil surface redox depletions and also aquic conditions during normal years and a glacic layer with its upper boundary within 100 cm of the mineral soil surface (Soil Survey Staff 2006).

Beside these wet and organic rich soils various sandy soil complexes such as Psammorthels and Psammoturbels are typical along the eroded cliffs. They are drier than the Aquiturbels and Historthels (Pfeiffer et al. 1999, Pfeiffer et al. 2000, Pfeiffer et al. 2002). Psammorthels and Psammoturbels are soils that have less than 35%, by volume, rock fragments and a texture of loamy fine sand or coarser in all layers within the particle-size control section (Soil Survey Staff 2006). In the erosional cliff area thermal erosion results in formation of high-centred polygons which are often covered with eolian sands.

Glacic Aquiturbels and Aquic Histurbels are common on Kurungnakh Island as on Samoylov Island. These modern soils are compared with paleosols such as Histels of different degree of decomposition, iron-rich Aquorthels and Aquiturbels of exposures on both islands.

For investigations of paleosols three exposures of 2.1, 2, and 1.2 m thickness were selected on the third terrace of Lena Delta on Kurungnakh Island. The samples were taken during the expedition "LENA 2002" (Kuzmina et al. 2003).

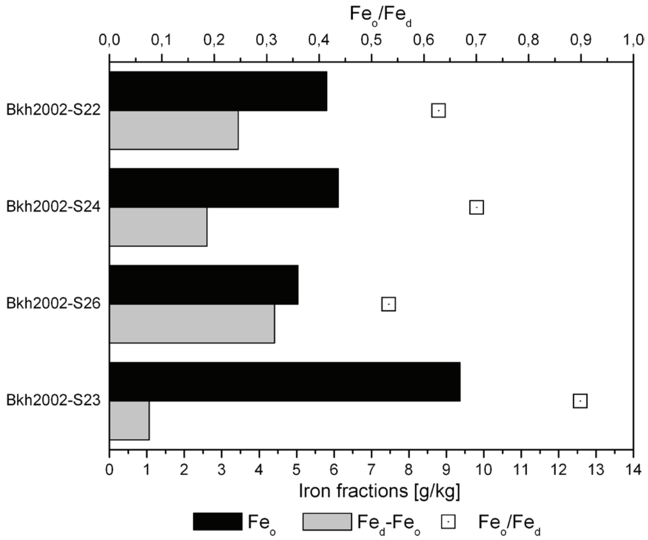

Figure 3. Values of Fe_o, Fe_d-Fe_o, and Fe_o/Fe_d in different soil horizons of profile Bkh2002-S22 to S26. Late Pleistocene paleosol, Kurungnakh Island.

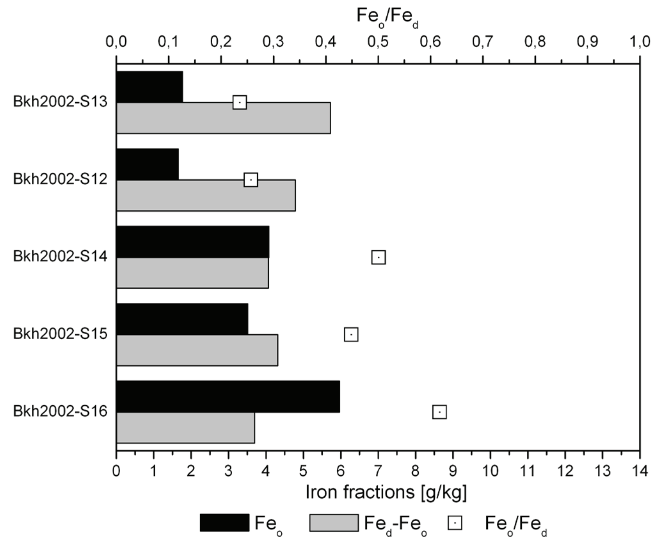

Figure 4. Values of Fe_o, Fe_d-Fe_o, and Fe_o/Fe_d in different soil horizons of profile Bkh2002-S12 to S16. Late Glacial paleosol, Kurungnakh Island.

The third terrace was formed in Middle and Late Pleistocene (Schwamborn et al. 2002). We collected samples of different ages from 5.8 to 40 ky BP (Schirrmeister et al. 2003, Wetterich et al. subm.).

Samples of modern soils have been taken on Samoylov Island during the expedition 'LENA – New Siberian Islands – 2007' in summer 2007 from the active layer of a low-centered polygon (Fig. 2).

Samples were collected from each layer of individual exposures. Pedological descriptions including Munsell soil color, fresh weight and other morphological remarks were made in the field. All analyses were done on the <2mm fraction and data are expressed on an oven-dry basis (105°C).

For pH determination a soil suspension with 0.01 M $CaCl_2$ was prepared and measured after an equilibration time of one hour with pH-Meter Schott CG820.

Total organic carbon (TOC) and nitrogen (N) were determined by VarioMax Elementaranalysator (Elementar Analyse Systeme GmbH).

A special consideration is given to different pedogenically formed iron-oxides to compare recently formed cryosols with paleosols of deeper sediment layers of both islands.

Oxalate-extractable iron (Fe_o) was determined by the method of Schwertmann (1964) at room temperature, in dark with acid ammonium oxalate at pH 3.25. Dithionite-extractable iron (Fe_d) was determined by the DCB method of Mehra & Jackson (1960) with dithionite-citrate buffered by bicarbonate at pH 7.3. Iron in all extracts was determined by Atomic-Absorption-Spectrometer.

To make an estimation of the degree of pedogenesis and relative age of a soil-horizon using analysis of different forms of Fe the following fractions were used: Fe_o as "active" Fe-oxides, probably ferrihydrite, (Fe_d - Fe_o) as Fe-oxides in less "active" well crystallized form, probably goethite and the ratio Fe_o/Fe_d as a degree of activity and pedogenesis.

Results and Discussion

Bkh2002-soil-sample series, Kurungnakh Island (Expedition 2002)

This sample collection represents the paleosols of the third terrace of Lena Delta. The lowest part of the third terrace consists of fluvial sands with low organic matter content (Schwamborn et al. 2002, Wetterich et al. subm.). The accumulation conditions were shallow water similar to the modern flood plains (Schirrmeister et al. 2003). The pedogenesis was characterized by hydromorphic conditions scarce vegetation and a cold dry climate. The unit was radiocarbon dated to >57 ky BP (Schirrmeister et al. 2003). The sand unit is covered by ice complex deposits (17 – 29.5 m a.r.l.). The profile Bkh2002-S22 to S26 (24 – 26.1 m a.r.l.) belongs to the ice complex sequence that was formed during the Late Pleistocene regression (Schwamborn et al. 2002). It is composed of fine grained poorly sorted sediments, thick peaty paleosols and large ice wedges (about 5 m wide and 20 m high). The thick peat layers were found in the lower part of the ice complex. They are thinner in the upper part where sand lenses were often observed. According to radiocarbon ages the entire ice complex sequence was formed between 44 and 17 ky BP in connection with niveo-eolian and slope processes (Schirrmeister et al. 2003, Wetterich et al. subm.). Pedogenesis during this time mirrors relatively warm and wet interstadial climate with tundra-steppe vegetation. Climate conditions with high production of organic matter are clearly recognizable in the extracted iron-oxide values that vary from 5 to 9.4 g/kg for active not crystallized oxides (Fe_o) and 1.1 to 4.4 g/kg for crystallized oxides (Fe_d-Fe_o) (Fig. 3).

High amounts of organic matter as they were found in the peaty paleosols with TOC values from 3.5 to 7.1% (Tab. 1) hinders the transformation of active iron-oxides to more crystallized oxides or even leads to formation of Fe-organic complexes (Cornell & Schwertmann 2004).

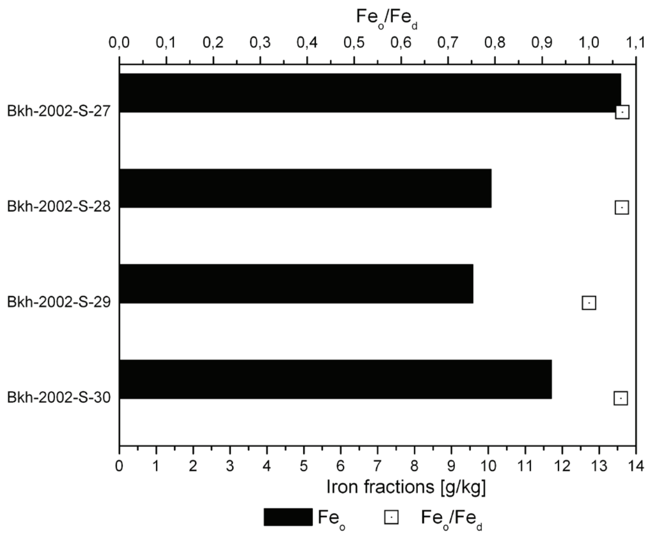

Figure 5. Values of Fe_o, and Fe_o/Fe_d in different soil horizons of profile Bkh2002-S27 to S30. Early Holocene paleosol, Kurungnakh Island.

According to the high amount of Fe_o-fraction the Fe_o/Fe_d ratio is relatively high with amounts from 0.5 to 0.9. The highest ratio was measured in the Bkh2002-S23 sample of a peat layer (TOC – 7.1%) that was formed during the wettest and warmest conditions that existed between ca. 44 and 38 ky BP (Schirrmeister et al. 2003).

The pH values vary from 6.9 to 5.5 whereby the moderate acid one was found in the peat horizon with the highest Fe_o/Fe_d ratio.

The ice complex is covered by two younger units dated to 17 – 8 ky BP and 6 – 3 ky BP respectively. The first one (29.5 – 33.5 m a.r.l.) was formed under very cold and dry climate with scarce steppe-like vegetation and dry soil conditions (Schirrmeister et al. 2003, Wetterich et al. subm.). It consists of poorly sorted silt deposits with low organic matter content. In this unit Bkh2002-S12 to S16 were sampled (29 – 31 m a.r.l.).

Values of the extracted iron-oxides vary from 1.7 to 6 g/kg and 3.7 to 5.7 g/kg for Fe_o-oxides and Fe_d-Fe_o-oxides respectively (Fig. 4). The Fe_o/Fe_d ratio is relatively low in the samples Bkh2002-S13 and S12 with 0.24 and 0.26. With increasing altitude the ratio decreases. The highest ratio of 0.62 was found in Bkh2002-S16 (29 m a.r.l.) sampled of a mixed horizon of sand and peat. Under dry and cold late glacial climate conditions with scarce vegetation and low organic matter content pedogenesis can progress but less intense well-expressed by relatively low iron activity ratio and high amounts of better crystallized iron-oxides indicating dry soil conditions with distinct iron-oxide crystallization.

The TOC values vary from 1.1 to 4.7% and pH values show low variability in the sandy horizons (7.4–7.3). In the mixed horizon there are weakly acid conditions (6.7) corresponding to higher content of organic matter (TOC–4.7%) similar to the last sample of the ice complex profile (Bkh2002-S23).

Samples of the last profile were taken from the youngest unit that was formed in Mid Holocene (6 ky BP). It was comprises of 4 samples (Bkh2002-S27 - S30) taken from

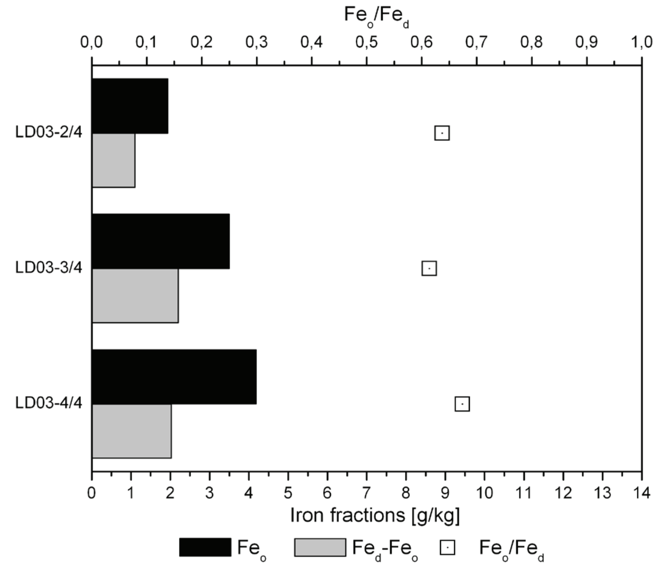

Figure 6. Values of Fe_o, Fe_d-Fe_o, and Fe_o/Fe_d in different soil horizons of profile LD03-2/4 to 4/4. Modern Gelisol Typic Historthel, Samoylov Island.

the 33.5 to 34.7 m a.r.l. The values of not crystallized active iron-oxides and Fe-organic complexes are very high and vary from 9.6 to 13.6 g/kg (Fig. 5). Crystallized iron-oxides were not verifiable, because of negative Fe_o-Fe_d values.

The Fe_o/Fe_d ratio is about 1 and the highest described in this paper. The pH values are acid (4.4 to 4.9) and correspond to the high organic matter content (TOC 3 to 4.6%) throughout the entire profile that consists of grey silt sediments with peat lenses. These sediments with high amounts of organic matter developed because of warmer climate, which caused a vegetation change to tundra-like. According to paleoenvironmental reconstructions (Wetterich et al. subm.) the pedogenesis took place under wet local conditions during this period.

LD-soil-sample series, Samoylov Island (Expedition 2007)

This sample collection which is composed of two active layer profiles represents recent pedogenesis on the first terrace of Lena Delta. The first terrace is of Holocene age and the young floodplains are assumed to represent the active part of Lena Delta. Maximum altitude is 12 m a.r.l. representing the oldest parts of the first terrace. The first terrace is formed by fluvial sediments that change from organic-rich sands at the bottom to silty-sandy peats towards the surface including several layers of eolian sands (Akhmadeeva et al. 1999, Schwamborn et al. 2002). This terrace is characterized by active ice wedge growth, low- and high-centered polygons, and thermokarst lakes.

The investigated profiles were sampled at a cross-section of a typical low-centered polygon (Fig. 2). These modern soils were classified by using U.S. Soil Taxonomy (Soil Survey Staff 2006).

In the polygon center a Typic Historthel (LD03-2/4 – 4/4) (11.85 – 11.5 m a.r.l.) and at polygon rim a Glacic

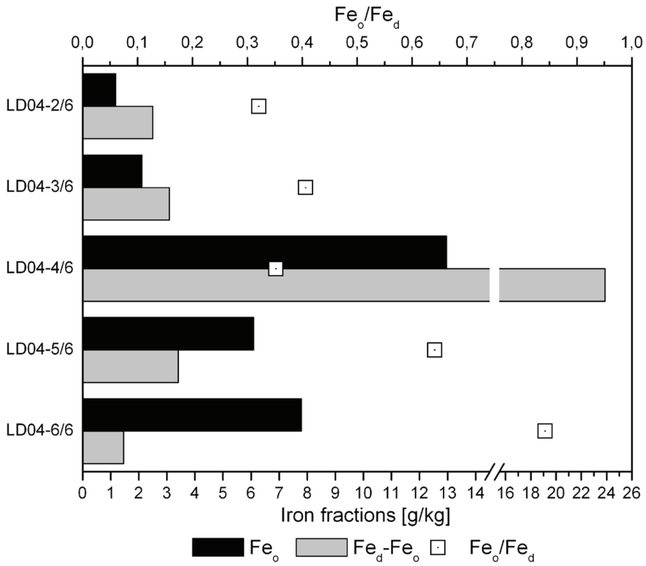

Figure 7. Values of Fe_o, Fe_d-Fe_o, and Fe_o/Fe_d in different soil horizons of profile LD04-2/6 to 6/6. Modern Gelisol Glacic Aquiturbel, Samoylov Island.

Aquiturbel (LD04-2/6–6/6) (11.95–11.5 m a.r.l.) were selected (Figs. 6, 7).

In the polygon center the values of the oxalate extractable iron-oxides (Fe_o) vary from 1.9 to 4.2 g/kg and for crystallized iron-oxides from 1.1 to 2.2 g/kg where the lowest values (Fe_o - 1.9 g/kg, Fe_d-Fe_o – 1.1 g/kg) were found in C-horizon (sample LD03-2/4) containing an eolian sand band at the altitude of 11.85 m a.r.l. (Fig. 6) with very slightly decomposed organic matter with C/N of 25. (Table 1). All horizons of this profile are rich in organic matter (TOC values from 1.8 to 5.5 %) and high C/N values from 23 to 25.2. Due to the organic matter the Fe_o/Fe_d ratio is relatively high. The pH values are strongly acid (4.5 – 4.8) and show low variability (Table 1).

The Fe_o values of the investigated Glacic Aquiturbel (LD04-2/6–6/6) vary from 1.18 to 12.96 g/kg and values of less active iron-oxides vary from 1.1 to 23.87 g/kg. The particularly high values were extracted from the Bg1jj-horizon (sample LD04-4/6) containing an iron band (Figs. 2, 7). This iron band can probably be considered as an enrichment horizon due to element redistribution among recent soil profiles by downward-translocation of mobile iron (Fiedler et al. 2004).

Relatively low values of iron-oxides in C- and A-horizon (samples LD04-2/6 and 3/6) support this hypothesis (Fig. 7) when they are regarded as eluvial horizons. The Fe_o/Fe_d ratio is low in the upper part of the profile. The value increases with increasing depth below ground surface. The upper horizons are first aerated during the slow process of thawing in spring and summer. This leads to the transformation of active iron-oxides to more crystallized oxides in the upper part. The pH values vary from 4.6 to 5.8 with strongly acid values in horizons Bg2jj and Bg3jj (samples LD04-5/6 and 6/6). The organic matter content (TOC) is lower than in the polygon center and shows values from 1.5 to 2.3% (Tab. 1).

Table 1. Analysis data of different soil horizons. Bkh2002: paleosol samples, Kurungnakh Island. LD: modern soil samples, Samoylov Island.

Soil sample	Altitude [m]	pH [$CaCl_2$]	TOC [%]	C/N
Bkh2002 - S27	34.70	4.9	4.6	18.1
Bkh2002 - S28	34.50	4.4	3.6	17.9
Bkh2002 - S29	34.00	4.6	3.8	19.7
Bkh2002 - S30	33.50	4.5	3.0	17.6
Bkh2002 - S13	31.00	7.4	1.7	10.9
Bkh2002 - S12	30.50	7.4	1.1	8.3
Bkh2002 - S14	30.00	7.4	1.4	10.1
Bkh2002 - S15	29.50	7.3	1.6	10.6
Bkh2002 - S16	29.00	6.7	4.7	12.7
Bkh2002 - S22	26.10	6.8	4.3	12.8
Bkh2002 - S24	25.00	6.4	4.2	13.4
Bkh2002 - S26	24.50	6.9	3.5	11.7
Bkh2002 - S23	24.00	5.5	7.1	15.1
LD04-2/6	11.95	5.8	1.6	15.9
LD04-3/6	11.90	5.8	2.3	15.9
LD04-4/6	11.85	4.6	2.1	14.6
LD04-5/6	11.80	4.7	1.9	14.0
LD04-6/6	11.70	4.8	1.5	15.4
LD03-2/4	11.85	4.5	1.8	25.2
LD03-3/4	11.80	4.8	5.5	24.5
LD03-4/4	11.70	4.8	4.2	23.0

Conclusions

The differences in values and ratios of extractable iron-oxides suggest that changes in forms of iron-oxides depend on the main soil material and water conditions. The influence of organic matter on iron-oxide transformation from young and active to more crystallized oxides is in evidence.

Paleosols show clear differentiation according to their stratigraphic position and paleoenvironmental conditions.

Soils that developed under relatively warm and wet interstadial climate (44–38 ky BP) and during the Early Holocene Climatic Optimum (8–6 ky BP) are characterized by relatively low values of well crystallized iron-oxides due to climatically caused high production of vegetation and the negative effect of the organic matter on the crystallization progress. Dry stadial climatic conditions as they were predominant at the end of Late Pleistocene (about 17 ky BP) associated with lower production of biomass and higher aeration of soil horizons principally lead to the formation of varying iron-oxides with relatively high values of the well crystallized fraction.

The results of the investigated modern soils from the active layer are comparable with those of the paleosols. The organic matter content and the seasonal inundation play a major role for Fe-transformation in modern soils. Further elements of modern soils are affected by translocation processes within the polygon. Detailed considerations of processes taking place in polygons during thawed periods have to be included in further investigations.

This approach promises to be more effective when applied to iron-oxides. The identification of texture and minerals and the radiocarbon dating of all samples will be finished. The analysis is still in progress.

Acknowledgments

This paper is based on the joint Russian-German science cooperation "System Laptev Sea" supported by the German Ministry of Education and Research. We thank the University of Hamburg and the Alfred Wegener Institute for Polar and Marine Research for financial support. We thank all Russian and German colleagues who helped us during fieldwork and laboratory studies. In addition, we thank Leon von Below for English language correction as well as two anonymous reviewers for their helpful comments.

References

Ahhmadeeva, I., Becker, H., Friedrich, K., Wagner, D., Pfeiffer, E.-M., Quass, W., Zhurbenko, M. & Zöller, E. 1999. Investigation site 'Samoylov'. *Reports on Polar and Marine Research* 315: 19-21.

Arduino, E., Barberis, E., Carraro, F. & Foro, M.G. 1984. Estimating relative Ages from Iron-Oxide/Total-Iron Ratios of Soil in the Western Po Valley. Italy. *Geoderma* 33: 39-52.

Arduino, E., Barberis, E., Ajmone Marsan, F., Zanini, E. & Franchini, M. 1986. Iron Oxides and Clay Minerals within Profiles as Indicators of Soil Age in Northern Italy. *Geoderma* 37: 45-55.

Bäumler, R. 2001. *Vergleichende bodenkundliche Untersuchungen in Hochasien und Kamtschatka*. Berlin: Gebr. Borntraeger. 215 pp.

Cornell, R.M. & Schwertmann, U. 2004. *The Iron Oxides.* Weinheim: Wiley-VCH, 663 pp.

Fiedler, S., Wagner, D., Kutzbach, L. & Pfeiffer, E.-M. 2004. Element Redistribution along Hydraulic and Redox Gradients of Low-Centered Polygons. Lena Delta. Northern Siberia. *Soil Science Society of America Journal* 68: 1002-1011

Food and Agriculture Organisation. 2006. *World reference base for soil resources 2006*. FAO, Rom. 128 pp.

Goryachkin, S.V., Karavaeva, N.A. & Makeev, O.V. 2004. The History of Research of Euroasian Cryosols. In: Kimble, J.M. (ed.). *Cryosols. Permafrost-Affected Soils*. Berlin: Springer Verlag, 17-28.

Kimble, J.M. (ed.) 2004. *Cryosols. Permafrost-Affected Soils*. Berlin: Springer Verlag, 726 pp.

Kutzbach, L. 2005. *The Exchange of Energy. Water and Carbon Dioxide between Wet Arctic Tundra and the Atmosphere at the Lena River Delta, Northern Siberia*. (PhD Thesis) Hamburg: University of Hamburg. 141 pp.

Kuzmina, S., Wetterich, S. & Meyer, H. 2003. Paleoecological and sedimentological studies of Permafrost deposits in the Central Lena Delta (Kurungnakh and Samoylov Islands). *Reports on Polar and Marine Research* 466: 71-81.

Mehra, O.P. & Jackson, M.L. 1960. Iron oxide removal from soils and clays by dithionite-citrate systems buffered with sodium bicarbonate. *7th National Conference on Clays and Clay Minerals*: 317-327.

Munsell. 1975. *Soil Color Chart*. Baltimore: Kollmogen Corporation.

Pavlova, E. & Dorozhkina, M. 1999. Geological-geomorphological studies in the northern Lena river delta. *Reports on Polar and Marine Research* 315: 112-126.

Pfeiffer, E.-M., Akhmadeeva, I., Becker, H., Friedrich, K., Wagner, D., Quass, W., Zhurbenko, M. & Zöllner, E. 1999. Modern processes in permafrost affected soils. *Reports on Polar and Marine Research* 315: 19-79.

Pfeiffer, E.-M., Wagner, D., Becker, H., Vlasenko, A., Kutzbach, L., Boike, J., Quass, W., Kloss, W., Schulz, B., Kurchatova, A., Pozdnyakov, V. & Akhmadeeva, I. 2000. Modern processes in permafrost affected soils. *Reports on Polar and marine Research* 354: 22-54.

Pfeiffer, E.-M., Wagner, D., Kobabe, S., Kutzbach, L., Kurchatova, A., Stoof, G. & Wille, C. 2002. Modern processes in permafrost affected soils. *Reports on Polar and Marine Research* 426: 21-41.

ROSHYDROMET. 2007.10.10. Russian Federal Service for Hydrometeorology and Environmental Monitoring. Weather Information for Tiksi. http://www.worldweather.org/107/c01040.htm.

Schirrmeister, L., Grosse, G., Schwamborn, G., Andreev, A.A., Meyer, H., Kunitsky, V.V., Kuznetsova, T.V., Dorozhkina, M.V., Pavlova, E.Y., Bobrov, A.A. & Oezen, D. 2003. Late Quaternary History of the Accumulation Plain North of the Chekanovsky Ridge (Lena Delta, Russia): A Multidisciplinary Approach. *Polar Geography* 27(4): 277-319.

Schwamborn, G., Rachold, V. & Grigoriev, M.N. 2002. Late quaternary sedimentation history of the Lena Delta. *Quaternary International* 89: 119-134.

Schwertmann, U. 1964. Differenzierung der Eisenoxide des Bodens durch photochemische Extraktion mit saurer Ammoniumoxalat-Lösung. *Zeitschrift für Pflanzenernährung, Düngung und Bodenkunde* 105: 194-202.

Soil Survey Staff. 2006. *Keys to Soil Taxonomy.* 10th ed. Washington, DC: U.S. Department of Agriculture & Natural Resources Conservation Service. 332 pp.

Tarnocai, C. 2004. Northern Soil Reasearch in Canada. In: Kimble, J.M. (ed.). *Cryosols. Permafrost-Affected Soils*. Berlin: Springer Verlag, 29-43.

Wetterich, S., Kuzmina, S., Kuznetsova, T., Andreev, A.A., Kienast, F., Meyer, H., Schirrmeister, L. & Sierralta, M. 2008. (subm.). Paleoenvironmental dynamics inferred from late Quaternary permafrost deposits on Kurungnakh Island (Lena Delta, Northeast Siberia, Russia). Submitted to *Quaternary Science Reviews*.

Author Index

Subject Index